The Role of Tidal Interactions and Mergers on the Evolution of Intermediate Redshift Galaxies

Sinan Deger

B.S. Physics, Middle East Technical University 2008

M.S. Physics, Middle East Technical University 2011

Submitted to the graduate degree program in Department of Physics & Astronomy and the Graduate Faculty of the University of Kansas in partial fulfillment of the requirements for the degree of Doctor of Philosophy.

Committee members

Gregory Rudnick, Chairperson

Thomas Cravens

Hume Feldman

Bruce Twarog

Justin Blumenstiel, External Reviewer

Date defended: June 21, 2019

The Dissertation Committee for Sinan Deger certifies
that this is the approved version of the following dissertation :

The Role of Tidal Interactions and Mergers on the Evolution of Intermediate Redshift Galaxies

Gregory Rudnick, Chairperson

Date approved: September 27, 2019

Abstract

In this work, we present our analysis attempting to constrain the prevalence of tidal interaction and merger (TIM) events on the evolution of intermediate redshift galaxies. The main focus of this work is the effect of such events on the star formation properties of galaxies. Such an undertaking requires the precise selection of tidal interactions and mergers (TIMs), in a wide range of environments to account for environmental effects. As such, in the first part of this work we study the fraction of tidal interactions and mergers with well identified observability timescales ($f_{\rm TIM}$) in group, cluster, and accompanying field galaxies and its dependence on redshift (z), cluster velocity dispersion (σ), and environment. We analyze images from the Hubble Space Telescope (HST), and catalogs from the ESO Distant Cluster Survey (EDisCS) for our work. Our data sample consists of 11 clusters, 7 groups, and accompanying field galaxies at $0.4 \leq z \leq 0.8$. We select our TIM sample using both a visual classification of galaxy morphologies and an automated method, the $G-M_{20}$ method. We calibrate this method using the visual classifications that were performed on a subset of our sample. After this calibration, we label visual TIMs also picked by our $G-M_{20}$ selection criterion as "$G-M_{20}$ TIM ", and gather our visually undisturbed galaxies plus the visual TIMs that are not $G-M_{20}$ selected under the "undisturbed "label. Our tests indicate that these subpopulations are well-seperated in the $G-M_{20}$ space, and that our results are robust against different $G-M_{20}$ TIM selection criteria.

Next, we investigate whether the fraction of $G-M_{20}$ TIMs, or $f_{\rm TIM}$, shows any strong trends with redshift (z), cluster velocity dispersion (σ), and the global environment the in which our galaxies reside. We find marginal evidence for a trend between $f_{\rm TIM}$ and z, in that higher z values correspond to higher $f_{\rm TIM}$. However, we also cannot rule out the null hypothesis of no correlation at higher than 68% confidence. No trend is present between $f_{\rm TIM}$ and σ. We find that $f_{\rm TIM}$ shows suggestive peaks in groups, and tentatively in clusters at $R > 0.5 \times R_{200}$, implying that $f_{\rm TIM}$ gets

boosted in these intermediate density environments. However, our analysis of the local densities of our cluster sample does not reveal a trend between $f_{\rm TIM}$ and density, except for a potential enhancement at the very highest densities. We also perform an analysis of projected radius-velocity phase space for our cluster members. Our results reveal that tidal interactions and mergers (TIM), and undisturbed galaxies only have a 6% probability of having been drawn from the same parent population in their velocity distribution and 37% in radii, in agreement with the modest differences obtained in $f_{\rm TIM}$ at the clusters.

After classifying our sample into $G-M_{20}$ TIMs and undisturbed galaxies, we investigate the stellar populations of our sample. To this purpose, we perform a full spectral fitting on the deep EDisCS spectroscopy data. We use the publicly available pPXF code for the spectral fitting, obtaining the details of the stellar populations, and the gas present in our sample, as results of our spectral fitting. We extract the fraction of the total stellar mass contained in stellar populations of different ages in our sample from this information. We also derive age-sensitive spectral indices, the strength of the narrow 4000Å break strength, $D_{n,4000}$, and the Balmer Hδ absorption line index using the results of the spectral fitting.

The final part of our analysis attempts to combine our morphological analysis, and our stellar population analysis. We search for trends in our $G-M_{20}$ TIMs and undisturbed galaxies with respect to the ages of their stellar populations. We find that our $G-M_{20}$ TIM galaxies are predominantly star-forming, as derived from multi-band photometric data. A larger fraction of the $G-M_{20}$ TIM galaxies also have features in their galaxy spectra indicating that their light is dominated by young stars. We then analyze the mass-weighted age fractions in the last 0.5 Gyr ($f_{Age<0.5\ \rm Gyr}$), and between 0.5 Gyr and 1 Gyr ($f_{0.5<Age<1.0\ \rm Gyr}$). Our results imply an enhanced $f_{Age<0.5\ \rm Gyr}$ value for the $G-M_{20}$ TIMs. This time interval is comparable in length to merger timescales reported by many studies, thereby this result is indicative of the TIM event boosting the star formation of these galaxies.

Acknowledgements

With hopefully many accomplishments to follow the completion of this work, one thing I know with certainy that I will be unable to do is to adequetly show my appreciation for everyone that helped me through this journey. Below is a humble attempt, and a beginning of unwavering effort, to make sure they know this work is completed, and this acknowledgement section is being written thanks to their support and at times unearned belief in me.

I would like to begin with the most futile attempt of them all, and that is acknowledging the Değer family. My mother Hamide, father Nuri, and brothers Sadık and Sedat, whom I had to move away from, and thereby had to miss everyday, for this work to be mapped on to reality. They have shown time and again that there is no place on this planet far enough where their support will not reach me. I came to rely on this indefatigable support, and their resolute faith in me more times than I can count. It is almost unfair that I get to put my name on the title page, which I can only justify because I decidedly performed more merger classifications than they did. Thank you so, so much, and I hope that this work serves as a source of happiness for all of you.

Next, I would like to express my gratitude to all my professors at KU, starting with my dissertation committee. A very special thank you to Drs. Justin Blumenstiel, Tom Cravens, Hume Feldman, and Bruce Twarog, for all your help, and invaluable guidance through the dissertation process. I would also like to appreciate Hume, Bruce, and Dr. Barbara Anthony-Twarog for always having an open door, the patience when I did not deliver the best I could, many invaluable advice, and guidance in picking a direction to move towards. I am eternally grateful for the opportunity to meet all of you. Barbara and Bruce, I am sorry I showed my gratitude by making you endure so many G-M_{20} plots. I hope that the spectral fitting analysis at least slightly made up for that. Finally, to all my other professors who taught me so much, and were instrumental for the completion of this dissertation, thank you.

I can only hope that anyone who joins a completely new department, in a completely new city, in a completely new country, in a completely new continent is as lucky as I am. Because what I found at KU Department of Physics & Astronomy was more than just a group of people working at a university department. I found an environment full of support, care, and respect. And of course, patience. They had to start from teaching me the correct pronunciation of our building, to give an idea as to what I mean when I say patience (I still think that Malott should be pronounced Malott, and not Malott, though). I already mentioned my professors, and now I would like acknowledge other past and present members of the department. Kristin Rennels, Joel Sauerwein, Kim Hubbel, Bob Curry, Dr. Jennifer Delgado, Alan Feltz, and Kayla Wegley, thank you for all your help, your never-ending patience, and the much needed support.

Graduate school is tough, I proudly wrote in words probably never uttered before. Yet, the friendships formed through it alone makes this journey one of utmost value for me. First, I am grateful to the current and past members of our research group with whom I shared many, many enlightening discussions on galaxy evolution. And also many discussions that had very little to do with galaxy evolution, for which I am equally thankful. Many thanks to Justin Mann, Mindy Townsend, Jennifer Cooper, Brittany Henke, and Matt Russell, and I look forward to discussing the mysteries of the universe with you again. Next comes dear friends from different research groups, who shared a very similar path nonetheless. James Castle, Donald Lee-Brown, Nesar Ramachandra, and Maulik Nariya, thank you for everything. I would not have believed it if someone told me I would meet so many incredible individuals halfway around the world, and thank you all for showing me that I would have been sorely mistaken.

I also had the good fortune of having many wonderful friends back in Turkey, who took it upon themselves to provide an international outlet for me to complain about life in copious amounts. Cihangir Tezcan, Murat Tolga Ertürk, Can Kartoğlu, Bulutay Güneş, Mertcan Özbakır, and Selçuk Bilmiş, and Onur Keskin currently (conveniently) residing in the beautiful Cambridge MA, all of whom have made my life orders of magnitude better for decades. Thank you for making sure I never felt alone, thank you for the support, and that you were always there to give me a much

needed push to walk this path, whenever I needed it.

I would like to dedicate the closing paragraph to my PhD advisor, Prof. Greg Rudnick. I will start simple. This work would not have been possible if not for his carefully calibrated administration of patience/impatience. His belief that I can succeed, and much needed encouragement and guidance to ensure that I do, have been fundamental in me being here, writing these words. His passion made my journey through this field that was previously all but unknown to me one of immense enjoyment. And yes, this includes even the aforementioned merger classifications, which is saying quite a lot. I have learned so much from him during this time, the scope of which is decidedly not limited to the field of galaxy evolution. I find it therefore befitting, in this section conveniently titled "Acknowledgements", for me to at least try to acknowledge my utmost gratitude to him for making me a better scientist in every respect. My hope is that I will have the chance to keep discussing science, in all its aspects, with him in what is to come after this dissertation. If past experience is any indicator, such discussions would mainly consist of him promptly terminating my excitement over my fascinating results by pointing out something I have not thought of before. But, such are the perils of the search for the truth! So thank you, Greg, for making it so that there is too many reasons for me to acknowledge here.

Sinan Deger

Contents

List of Figures

List of Tables

Chapter 1

Introduction

1.1 Characteristics of the Galaxy Population in the Universe

A crucial observation made in the past decade is that local galaxy populations show a bimodal distribution in color-magnitude, and color-stellar mass spaces. Observations from large surveys, such as the Sloan Digital Sky Survey (SDSS), show that galaxies generally reside in a red and a blue sequence (Strateva et al., 2001; Baldry et al., 2004, 2006; Blanton & Moustakas, 2009; Whitaker et al., 2011; Schawinski et al., 2014). Another such observation is that galaxies can also be split into two broad morphological classes; disk galaxies featuring spiral arms ("late-type galaxies"), and elliptical galaxies with higher central concentration (bulge) of light that lack such features ("early-type galaxies"). This scheme was established by Hubble (1926, 1936) and Sandage (1961). Though the variety in morphological classes has increased over the years (see Sandage (2005) for a historical account), this broad classification remains useful nonetheless. These morphological types also generally correlate with the star-forming properties of galaxies, in that the majority of spiral galaxies are blue and star-forming, and most of the elliptical galaxies are red and quiescent (Holmberg, 1958; Roberts & Haynes, 1994; Conselice, 2014).

In recent years, surveys investigating star forming galaxies revealed an interesting result: There is a strong correlation between the star formation rates (SFR's) of star-forming galaxies, and their stellar masses, in that star-forming galaxies with higher stellar mass also have higher SFR's. Galaxies that reside on this relation are said to form the "star-formation main sequence"(Brinchmann et al., 2004; Noeske et al., 2007). This correlation has been shown to hold for at least the redshift range of $0.0 < z < 2.5$ (Noeske et al., 2007; Elbaz et al., 2007; Daddi et al., 2007; Wuyts et al.,

2011; Karim et al., 2011; Whitaker et al., 2012). Similar analyses found that this trend evolves with time as well, galaxies on the star-formation main sequence in the distant universe are producing stars at a higher rate compared to the main sequence galaxies in the local universe (Whitaker et al., 2012). Connectedly, the cosmic star-formation rate density of the universe also drops as we approach to today (Lilly et al., 1996; Madau et al., 1998; Le Floc'h et al., 2005; Schiminovich et al., 2005; Hopkins & Beacom, 2006). A collection of multiple surveys by Madau & Dickinson (2014) reveal that the peak star-formation rate density of our universe has been at around $z = 1.9$, or about 3.5 billion years after the Big Bang.

1.2 Observing Star Formation in Galaxies

Following the demographics of star-forming galaxies we presented in the previous section, we now briefly discuss the methods commonly used to detect and analyze the stellar content of galaxies, starting with photometry. Photometric surveys measuring the integrated colors of galaxies, which are sensitive to their star-formation histories, have played a crucial role in galaxy evolution research. Photometry surveys measure the flux received in a set of passbands, or filters, which are defined at certain wavelength values. An early example for a set of filter definitions is the Johnson UBV system (Johnson & Morgan, 1953). A collection of photometric measurements in multiple passbands measured on the same object is called the spectral energy distribution, or SED. Extracting key galaxy features such as their redshifts, stellar masses, or the ages of their stellar populations, by performing a fit to the SED has been a key component of astronomy research over the last decades (Couch et al., 1983). A few examples to SED fitting codes are the iSEDfit suite by Moustakas et al. (2013), which we use to derive the stellar masses of our sample (see §2.2 for details), FAST by Kriek et al. (2009), Prospector by Leja et al. (2017), and CIGALE by Boquien et al. (2019).

One way such techniques derive galaxy properties is by making use of synthetic stellar population libraries to find the model which minimizes the chi-square (χ^2) of the SED fit, or the best-fitting model. Another way is to employ a Bayesian approach that investigates the full pos-

terior probability distribution as a function of the input model parameters, such as the ages or the stellar masses of the models. By doing so, the Bayesian approach takes into account the entire input model grid, and not just the best-fitting model, when extracting physical properties. The physical properties are then determined by weighting all the models in terms of their goodness-of-fit (such as χ^2), with the best-fitting models having higher weights. Of the examples we included above, iSEDfit and CIGALE allow for a Bayesian approach when fitting SEDs.

An early example for a photometric survey was performed by Butcher & Oemler (1978), who presented evidence for a significantly higher fraction of blue (or possibly star forming) galaxies in distant clusters compared to nearby clusters. This observation, commonly referred to as the "Butcher-Oemler Effect", has been confirmed by various other photometric studies since then (Rakos & Schombert, 1995; Margoniner & de Carvalho, 2000; Margoniner et al., 2001; Urquhart et al., 2010).

Spectroscopy, on the other hand, measures the flux received covering a continuous range in wavelength. Data gathered this way provides invaluable information as to the composition of galaxies, as a galaxy spectrum is the superposition of the spectra of all its stars, modified by emission and absorption from the gas and dust lying between the stars.

Following Butcher & Oemler (1978), spectroscopic studies of the same galaxies have found a significant fraction of these have strong emission lines, confirming that the blue colors observed by Butcher & Oemler (1978) are due to star formation (Dressler & Gunn, 1983; Lavery & Henry, 1986; Couch & Sharples, 1987; Poggianti et al., 1999). Furthermore, spectroscopic studies have uncovered certain aspects not accesible to the photometric studies. Dressler & Gunn (1983) was the first to observe a group of galaxies with no emission lines, but strong hydrogen Balmer absorption lines. They inferred that these galaxies had a recent intense period of star formation that ended abruptly, and were at a post-starburst state (referred to as E+A galaxies), and the strong Balmer absorption lines were due to significant amounts of A-type stars present in the galaxy (see §4.2 for further discussion).

Finally, we very briefly mention an instrument that has been essential to this work, the Hubble

Space Telescope (HST), in the context of this section. The high-resolution imaging capabilities of HST has made an immeasurable impact on extragalactic astronomy research. In the context of the discussion in this section, HST allowed for the matching of observations summarized above with the detailed morphologies of galaxies. HST follow-up observations to the studies above found that the blue star forming galaxies also have disky morphologies, and some of them have disturbed morphologies due to interactions and mergers (Couch et al., 1994, 1998; Dressler et al., 1994, 1997). We discuss the effects of galaxy-galaxy interactions and mergers on galaxy evolution, and triggering star formation in subsequent sections of this chapter.

For the work we present in this thesis, we use both the multiband photometry (Pelló et al., 2009; Rudnick et al., 2009), and the deep spectroscopy of ESO Distant Cluster Survey (EDisCS) (Milvang-Jensen et al., 2008). This data set has been used in various other papers by members of the EDisCS collaboration, related to the concepts we described in this section, including analyses of morphologies and environment (Desai et al., 2007; Just et al., 2010; Kelkar et al., 2017; Deger et al., 2018), the environments of E+A galaxies Poggianti et al. (2009), and evolution of star formation as a function of environment Poggianti et al. (2006); Finn et al. (2010). In a recent paper, connecting spectral indices measured from galaxy spectra and environment, Rudnick et al. (2017) analyzed the EDisCS spectroscopy to compare [OII] emission line strengths between inhabitants of different environments. They find a significant difference in the fractions of galaxies with [OII] emission between galaxies residing in cluster and group (or dense environments, see §1.3 for brief descriptions of environment types) environments, and in the field. This difference reveals itself when galaxies with old stellar populations are considered. Rudnick et al. (2017) proposes multiple scenarios to explain this observation, one of which is especially related to the subject matter of this work, which is a scenario where the progenitor gas content gets decoupled from the merger remnant in denser environments, especially in groups and infall regions of clusters.

As we outline in §1.7, this work aims to compare modifications to the star formations of EDisCS galaxies measured from their spectra, with morphological disturbencese attributable to TIM events measured from HST images. In Chapter 4, we describe our spectral fitting scheme

using the full spectrum fitting code pPXF (Cappellari & Emsellem, 2004; Cappellari, 2017). In Chapters 5 and 6 we discuss the stellar populations of our sample, in light of the spectral fitting, and the color indices derived from the EDisCS photometric data. We also use high-resolution HST images to identify disturbed morphologies due to TIM events, the details of which we present in §2.3.

1.3 Environments of Galaxies

The past few decades have witnessed the shaping of the question of "nature versus nurture"in galactic evolution. This question addresses whether the above properties of galaxy populations we observe today are the result of intrinsic mechanisms, or the result of their environments and the interactions they underwent. It is highly likely that both of these play a role, but it is still unclear if either one is the dominant factor in shaping galactic evolution.

Before we discuss important correlations with environment, we introduce the types of environment we analyze in this work. We introduce these environments in order of highest density to the lowest, as follows: The most populous and the most massive aggregations of galaxies are called "galaxy clusters". Some early work into the observation of clusters go back to Abell (1958), where 1682 galaxy clusters were selected. Next, intermediate density environments called "groups" are a less massive and less populous aggregation of galaxies. We make the disctinction between galaxy clusters and groups in terms of their velocity dispersions (σ), with groups being defined as those structures with $\sigma < 400\,\mathrm{km\,s^{-1}}$ (see §2.1 for details). Finally, galaxies that are not members of either of these aggregations are referred to as "field galaxies". These three classes form what we refer to as the "global environment" of galaxies in this work. We also make use of the term "local environment" to refer to the immediate neighborhood of galaxies, irrespective of their global environment. We discuss our local density definition in §3.5.

An important observation that helped shape the "nature versus nurture"scheme is the so-called morphology-density relation. The fractions of galaxies with "early-type"morphology, or galaxies that are classified as ellipticals (E's) and lenticulars (S0's) are found to peak in dense environments,

whereas the fractions of spiral and irregular (Irr) galaxies show a comparable decrease (Dressler, 1980; Dressler et al., 1997). This comparable change implies that the increase in early-types has been in expense of transforming late-type galaxies. The fraction of early types depends both on global environment (Dressler, 1980; Dressler et al., 1997; Fasano et al., 2000; Blanton & Moustakas, 2009; Just et al., 2010; Vulcani et al., 2010), and local environment (Dressler, 1980; Postman et al., 2005; Wilman et al., 2009; Tasca et al., 2009). Likewise the fraction of passive galaxies is also higher in denser global (Lewis et al., 2002; Gómez et al., 2003; Balogh et al., 2004; Hogg et al., 2004; Poggianti et al., 2006; Gerke et al., 2007) and local environments (Lewis et al., 2002; Gómez et al., 2003; Balogh et al., 2004; Kauffmann et al., 2004; Poggianti et al., 2008). Though the main culprit for these observations eludes identification as of yet, there is significant effort to pinpoint the exact mechanics at play.

1.4 Processes Playing a Role in the Evolution of Galaxies

Multiple processes have been proposed as candidates to explain the observations we have discussed above. One such process is ram pressure stripping, which occurs when the hot intracluster medium acts as a source of drag for galaxies moving through it, which can strip the cold gas within the galaxies (Gunn & Gott, 1972; Mori & Burkert, 2000; Quilis et al., 2000; Bekki, 2009). This process is most effective in the denser regions of galaxy clusters, and has been observed in members of nearby clusters such as the Virgo and Coma clusters (Vollmer et al., 2001; Boselli & Gavazzi, 2006, 2014; Boselli et al., 2016), and for simulated galaxies (Kronberger et al., 2008). Observations and simulations both indicate that ram pressure stripping is capable of perturbing the gas supply of galaxies at timescales of 100-200 Myr (Vollmer et al., 2004; Roediger & Hensler, 2005; Boselli & Gavazzi, 2006; Crowl & Kenney, 2008).

Another mechanism, referred to as either “strangulation" or “starvation", occurs when the hot gas reservoir bound to a galaxy is stripped when the galaxy falls into a dense environment such as a cluster. After losing access to this reservoir to replenish its gas content, the galaxy will consume whatever fuel it has left for star formation and will gradually show lower and lower star formation

rate (SFR) as it runs out of fuel (Larson et al., 1980; Bekki et al., 2002; Boselli & Gavazzi, 2006). This process acts slower compared to ram pressure stripping, and requires a timescale of the order of a gigayear to modify the star formation of galaxies(Larson et al., 1980; Bekki et al., 2002). Both of these processes result in the depletion of gas in galaxies and may result in the presence of passive disks (Bundy et al., 2010; Cantale et al., 2016b), potentially also with larger bulges (Kawata & Mulchaey, 2008). Due to the high velocity dispersions of cluster environments, encounters between member galaxies occur at high speeds. Changes to the internal energy of galaxies after such encounters make them more and more susceptible to disruptions by later encounters with other members or by the tidal interactions with the cluster potential, either of which is capable of alterations to morphology. The cumulative effect of these high speed encounters is called “galaxy harassment" (Richstone, 1976; Farouki & Shapiro, 1982; Moore et al., 1998). Finally, the process of the central galaxy of a halo accreting satellite galaxies that lost their momentum due to dynamical friction is called “galactic cannibalism". The most massive central galaxies of halos almost invariably have elliptical morhologies, possibly due to many such events (Ostriker & Tremaine, 1975; White, 1976; Hausman & Ostriker, 1978). Even though these processes underline the importance of environment, environmental factors may not represent the entire picture. Examples of transition galaxies, such as E+A galaxies (galaxies with strong Balmer absorption lines but a lack of emission lines, see §1.2) can be found in the field (Zabludoff et al., 1996), demonstrating that a dense environment is not a necessary condition. They suggest that cluster specific environmental effects, such as interaction with the cluster gravitational potential or intraculster medium are not responsible for the production of E+A galaxies.

1.5 How Mergers Affect Galaxy Evolution

We focus on another candidate process for our work, namely galaxy mergers and galaxy-galaxy interactions. While related to cannibalism, in the context of our analysis tidal interactions and mergers are those events that can occur between satellite galaxies, and also between a satellite and central. Mergers are a likely suspect in explaining the observed transformation in morphology,

as merger events are usually violent events that trigger drastic change. Toomre & Toomre (1972) proposed that elliptical galaxies can be the outcome of the merging of two disk galaxies. This morphological transformation via mergers has been subsequently demonstrated in many simulations since then (Barnes & Hernquist, 1996; Naab & Burkert, 2003; Lotz et al., 2008b). On the other hand, multiple papers argued that it is possible for merger remnants to retain a disk structure after major merger events, and even potentially have active star formation on the disk (Springel & Hernquist, 2005; Robertson et al., 2006). Simulations of major mergers (Barnes, 2004; Cox et al., 2006) and observations of local gas-rich mergers (Schweizer, 1982) indicate that merger events are capable of putting galaxies in states of intense star formation called starbursts, where galaxies have much higher star formation rates (SFRs) compared to their normal production (Larson & Tinsley, 1978; Rodighiero et al., 2011).

Many studies investigated how mergers and interactions transform galaxies. Bekki (1998) investigates the effects of mergers by performing numerical simulations of mergers of unequal mass between gas-rich disk galaxies. They find a significant amount of the gas is exhausted during the merger event, due to starbursts that the merger triggers, and the outcome is one gas-poor S0 galaxy. They then argue that their results provide insight into the evolutionary link between blue spirals and red S0's. Their analysis also provides a clue as to the connection between E+A galaxies in intermediate redshift clusters and red S0 galaxies in local clusters today. Brinchmann & Ellis (2000) investigates the mass assembly of distant field galaxies, and derive the time evolution of stellar mass density per morphology type. They find a decline in the stellar mass associated by irregular galaxies, accompanied by an increase in that of elliptical galaxies. They propose that the abundance of peculiar galaxies decline in time due to transformation into elliptical systems as a result of mergers. Christlein & Zabludoff (2004) show that models that generate early-type S0 galaxies by fading the disks of late-type galaxies fail to generate the bulge and disk luminosities they studied, and that bulge enhancement models are in good agreement with their clusters. They further conclude that their results are in favor of galaxy interactions and mergers, which can play a role in bulge enhancement. Johnston et al. (2014) on the other hand finds it is possible to fade

disks and grow bulges through centrally-concentrated star formation. Wilman et al. (2009) also emphasizes the importance of bulge growth, and proposes minor mergers (we give the definition of minor mergers in the next section) as a favored mechanism to explain S0 production. They also find that the fraction of S0's in their sample is much higher in groups compared to the field, and they propose galaxy groups to be the prominent environment in S0 production. This may be expected as groups have moderately high densities and low velocity dispersions, and are thus conducive sites for mergers. Just et al. (2010) also finds that S0 type galaxies, which are likely products of mergers, are evolving in number faster in galaxy groups than in clusters. This suggests that the galaxies that will later on fall into a cluster are preprocessed in these moderate density environments, which host conditions favorable for merger-based morphological transformation. (Zabludoff & Mulchaey, 1998; Fujita, 2004; Cortese et al., 2006; Dressler et al., 2013; Abramson et al., 2013; Vijayaraghavan & Ricker, 2013).

The vast improvements in computational power over the last decade has opened a new venue to explore galaxy formation and evolution: high-resolution, large-scale cosmological simulation suites. One such example is the hydrodynamical simulation suite Illustris (Vogelsberger et al., 2014; Genel et al., 2014). The results from the Illustris simulations have been used for comparison with observations in many different ways, including the comparison of simulated versus observed morphologies of galaxies (Dickinson et al., 2018; Rodriguez-Gomez et al., 2019), comparison in colors (Sales et al., 2015), and quenching of star formation due to environment (Bluck et al., 2016). As for mergers, Rodriguez-Gomez et al. (2017) investigated the role of mergers in shaping the morphologies of Illustris galaxies, and found mergers to be an important transformational mechanism for massive galaxies ($M_* > 10^{11}\mathrm{M}_\odot$), but that their importance starts to diminish at lower masses.

1.6 Identification of Galaxy Mergers

Two main methods are commonly used in the identification of galaxy mergers; the "close pair"method, and by visually searching for galaxies showing disturbed morphologies. The "close pair"method looks for galaxies in close proximity in projected space, and relative velocity (Burkey et al., 1994;

Carlberg et al., 2000; Kartaltepe et al., 2007). The latter method inspects for morphological disturbances caused by merger events, and is the method used in this work. Before we describe this method in detail, we introduce the following terminology commonly used to classify mergers of different mass ratios. A major merger indicates an event where the stellar mass ratios of the merging galaxies are 1:4, or higher. The term minor merger is used when the merging galaxies this ratio is less than 1:4. Even if the mass ratios of the merging galaxies are lower, minor mergers are nonetheless still play a role in the evolution of galaxies. They are more common than major mergers (Lotz et al., 2010b), various high-resolution simulations have shown that they play a significant role in triggering star formation in the early universe (Somerville et al., 2001), and in modifying the stellar mass of galaxies (Guo & White, 2008; Genel et al., 2009).

We now introduce the merger identification technique we used for our analysis. Galaxy interactions have a variety of visible effects on morphologies of galaxies. Detection of these alterations has been a prime tool in the identification and study of galaxy interactions and mergers. The morphological detection of mergers is enabled by the asymmetries and distortions in the structures of galaxies that result from gravitational interactions, and from the compression and heating of the gas that results from hydrodynamical effects. Visual identification of these morphological disturbances is therefore common practice in galaxy interaction research (Abazajian et al., 2003; Schawinski et al., 2007; Kartaltepe et al., 2015; Kelkar et al., 2017). Such methods are subjective, and also are not immune to misclassification, as not every visually asymmetric/distorted galaxy is the result of interactions. Likewise, some signatures of merging, such as diffuse tidal tails are hard to identify long after the merger has occurred, causing incompleteness in some merger classifications. Recent years have seen extensive improvement in automated methods that is based on quantifying these distortions (Abraham et al., 1996; Conselice, 2003; Lotz et al., 2004; Hoyos et al., 2012; Freeman et al., 2013). Automated methods have multiple advantages over visual classification in that they are easily reproducible, are faster compared to visual identification methods, especially for large sample sizes, and can easily be run on large simulation suites to assess the detection efficiency (Lotz et al., 2010b,a). A shortcoming these methods suffer from is that they

are susceptible to both missing asymmetric features (incompleteness), and contamination due to noisy measurements which becomes especially prevalent at low signal-to-noise ratios. They therefore require careful calibration, as accurate merger detection is key to measuring the prevalence of galaxy mergers and their role in galaxy evolution. That is why we decided to use an automated method which we calibrate using a visually classified subsample.

Most automated methods utilize nonparametric parameters to quantify morphology. Unlike parametric methods of quantifying the morphologies of galaxies, which assume an underlying light profile for galaxies (de Vaucouleurs, 1948; Sérsic, 1963), nonparametric methods aim to quantify the major morphological features of galaxies without apriori assumptions about the underlying form. A widely used method measures galaxy structures through the three nonparametric parameters of concentration (C), asymmetry (A), clumpiness (S) (*CAS* system) (Conselice, 2003). The C paramater quantifies how concentrated the light of galaxies are, by comparing the amount of light in the center with the outer parts. A measures how asymmetric a galaxy is by subtracting the galaxy rotated 180 from its center from its prerotated image. S measures the patchiness of the light distribution in galaxies, and is computed as the ratio of the amount of light contained in clumpy regions to the total light of the galaxy. Conselice (2003) finds that merging galaxies are those with a high asymmetry that is also higher than the value of the clumpiness. One main shortcoming of this method is that it is only sensitive to major mergers (Lotz et al., 2008b, 2010b; Conselice, 2014).

The automated method we use for this analysis is the $G-M_{20}$ method (details in Lotz et al. (2004), brief explanation in §2.3). The $G-M_{20}$ space is formed by two nonparametric measures of morphology. Very briefly, G, or the Gini coefficient in the way it is used for astronomical purposes, is a measure of how equally the light is distributed among the pixels of a galaxy image (Lotz et al., 2004). In this coefficient, egalitarian light distributions would have a G value of 0, and the complete opposite case where the entire flux is concentrated in one pixel would have a G value of 1. M_{20} is defined as the normalized second-order moment of the brightest 20% of the galaxy's flux. Higher M_{20} values indicate higher spatial separation amongst the brightest 20% pixels, and is

especially sensitive to merger signatures such as double nuclei. We describe our merger selection using the $G-M_{20}$ method in §2.3. Unlike the *CAS* system, the $G-M_{20}$ method is sensitive to identifying minor mergers, down to stellar mass ratios of 9:1 between merging galaxies the (Lotz et al., 2010b).

An important physical quantity to understand how galaxies evolve is the merger rate, which is the number of mergers occurring per unit time. The merger rate is found as the ratio of the merger fraction to the merger timescale. The merger timescale can be derived by analyzing simulated merger events, and measuring the amount of time the event is detected as a merger (Cox et al., 2006, 2008; Lotz et al., 2008a, 2010a,b) Despite much effort, measurements into the merger rates and its evolution with redshift still show considerable disagreement (Lotz et al., 2011). This stems from both differences between the methodologies of studies deriving merger fractions (Bundy et al., 2004; Kartaltepe et al., 2007; Bundy et al., 2009; Bridge et al., 2010), and poorly constrained merger timescales. We discuss the details of the derivation of our merger fraction in §2.3, and our future plans to derive a merger timescale in §7.1.

1.7 This Work

In this work we analyze galaxy tidal interaction and merger (TIM) events using the ESO Distant Cluster Survey (EDisCS) sample of cluster, group, and field galaxies with Hubble Space Telescope (HST) imaging at a redshift range of $0.4 \leq z \leq 0.8$ (White et al., 2005). To understand the role TIMs play in galaxy evolution it is vital to study them in different environments, so as to separate the effects due the TIM process from those due to the environment. Our sample allows us to study mergers at multiple environments of varying density, such as galaxy groups, clusters, and the accompanying field. In the first part of this thesis we present our merger detection, and our analysis of merger fractions. This study is complementary to those of Desai et al. (2007), Just et al. (2010), and Vulcani et al. (2011), who studied the morphological fractions in the EDisCS systems. We on the other hand are directly exploring the mergers that potentially drove this transformation.

We used a visual merger classification from Kelkar et al. (2017) that was performed on the

subset of our sample with spectroscopic redshifts. We then measured G and M_{20} values for our entire catalog, including those with photometric redshifts. Using our visually classified sample we calibrated a tidal interaction and merger (TIM) decision boundary on the $G-M_{20}$ space. We then calculated the fraction of tidal interactions and mergers ($f_{\rm TIM}$) of our clusters, groups, and field galaxies and analyzed the dependence of $f_{\rm TIM}$ on redshift, velocity dispersion, and both global and local environment. We used the local density measures derived by Poggianti et al. (2008) for the spectroscopic cluster members of EDisCS for our analysis of the dependence of $f_{\rm TIM}$ on local density. Finally, we examined where tidal interactions and mergers lie with respect to undisturbed galaxies in projected radius-velocity phase space.

Next, we attempt to match the signs of morphological transformations with changes in the recent star formation histories of our sample. We extract the detailed stellar population distributions of our sample by performing a spectral fitting of the EDisCS spectroscopy. This allows us to extract age-sensitive spectral indices, and analyze the characteristics of the $G-M_{20}$ TIMs and undisturbed galaxies in terms of stellar age content.

The work consists of the following sections; we split the contents of our publication, Deger et al. (2018), detailing our TIM selection and investigating trends with astronomical parameters, into Chapters 2 and 3. In 2 we describe the two approaches taken in our analysis for merger identification; namely visual classification and $G-M_{20}$ classification (Abraham et al., 2003; Lotz et al., 2004) to obtain $f_{\rm TIM}$. We present our results for the variation of $f_{\rm TIM}$ with redshift, velocity dispersion, and global and local environment in §3. Next, in Chapter 4 we present the details of the spectral fitting we have performed on the EDisCS spectroscopy. We analyze the age diagnostics of our sample in Chapter 5. In Chapter 6 we discuss the results of our star formation analysis, in connection with our morphological analysis. Finally, we summarize and provide a general conclusion to this work, together with possible future work, in Chapter 7. In Appendix A, we provide a table containing our cluster, group, and field members, and their morphological classes as derived in 2. Finally, in Appendix B we present a table containing the spectral indices we derived in Chapter 4. Throughout the thesis we assume $H_0 = 70$ km s^{-1} Mpc^{-1}, and use AB magnitudes.

1.8 Commonly Used Terminology

We finalize this chapter by listing the descriptions of terminology commonly used in the following chapters.

- **TIM:** Abbreviation for "Tidal Interaction and Merger".
- **Visual Undisturbed:** A galaxy showing no visual evidence of undergoing a TIM event. See §2.3 for details, and Figure 2.3 for examples.
- **Visual TIM:** A galaxy visually classified as a TIM via a visual inspection of its Hubble image. See §2.3 for details, and Figure 2.3 for examples.
- G**:** The Gini coefficient, as applied to astronomy (details in Lotz et al. (2004), brief explanation in Chapter 1 and §2.3).
- M_{20}**:** The normalized second-order moment of the brightest 20% of the galaxy's flux (details in Lotz et al. (2004), brief explanation in Chapter 1 and §2.3).
- $G-M_{20}$ **TIM:** A galaxy both visually classified as TIM, and also identified as TIM by our TIM selection criterion on the $G-M_{20}$ space. See 2.3 for details.
- f_{TIM}**:** The fraction of $G-M_{20}$ TIMs in our sample. See 2.3 for details.
- $\mathrm{EW}(\mathrm{H}\delta_{\mathrm{A}})$**:** The equivalent width of Balmer $H\delta$ absorption line. We provide a more detailed discussion in 4.2.
- $D_{n,4000}$**:** The evolution of the narrow 4000Å break strength. We provide a more detailed discussion in 4.2.
- $f_{(\mathrm{Age\,Interval})}$**:** The fraction of stellar mass contained in stellar populations of ages bounded by the age interval. We used age intervals of (Age < 0.5 Gyr), (0.5 < Age < 1.0 Gyr), (Age < 1 Gyr) in this work. See §5.3 for more information.

- **Global Environment:** Cluster, group, or field membership of galaxies. We describe our global environment selection in §2.1.

- **Local Environment:** Immediate neighborhood of galaxies, irrespective of their global environment. We discuss our local density estimation in §3.5

Chapter 2

Selection of the TIM Subpopulation of the EDisCS-HST Sample

In this chapter we present the data selection as described in Deger et al. (2018). In §2.1 we introduce the ESO Distant Cluster Survey, and provide details concerning our sample selection. In §2.2 we describe the method we used to derive the stellar masses of our sample, and the mass completeness criterion we applied. We present the details of the morphological classification we used for this work, both the visual classification and the automated method of quantitative morphology we used, in §2.3. We present our sample with this morphological classification in §2.4. Finally, we discuss the false positives and negatives of our morphological selection in §2.5.

2.1 Sample

ESO Distant Cluster Survey (EDisCS, White et al. (2005)) is a detailed photometric and spectroscopic survey of clusters, groups, and field galaxies, with structures drawn from the Las Campanas Distant Cluster Survey (LCDCS; Gonzalez et al. (2001)). The EDisCS fields have either BVIK, BVIJK, or VRIJK photometry depending on the redshift estimate of the original cluster candidate. The sample was also observed with extensive FORS2 spectroscopy on the Very Large Telescope (ESO) (Halliday et al., 2004; Milvang-Jensen et al., 2008). To study the morphological content of the EDisCS sample, we used Hubble Space Telescope (HST) Advanced Camera for Surveys (ACS) imaging in the F814W filter (depths of 1 orbit at cluster outskirts, 5 orbits at cluster core) of 10 of the highest redshift clusters from Desai et al. (2007). We make use of these 10 fields with HST ACS images plus photometric and spectroscopic catalogs for the analysis presented in this work.

Table 2.1: The EDisCS-HST Sample - Cluster, Group, and Field Members

Structure Name	Redshift	σ	$N_{phot+spec}$	N_{spec}
CL1040.7-1155	0.7043	418^{+55}_{-46}	24	10
CL1054.4-1146	0.6972	589^{+78}_{-70}	71	24
CL1054.7-1245	0.7498	504^{+113}_{-65}	57	16
CL1138.2-1133	0.4796	732^{+72}_{-76}	-	13
CL1138.2-1133a	0.4548	542^{+63}_{-71}	-	7
CL1216.8-1201	0.7943	1018^{+73}_{-77}	102	36
CL1227.9-1138	0.6357	574^{+72}_{-75}	54	12
CL1232.5-1250	0.5414	1080^{+119}_{-89}	82	31
CL1354.2-1230	0.7620	648^{+105}_{-110}	36	8
CL1354.2-1230a	0.5952	433^{+95}_{-104}	-	6
Clusters Total			429	163
CL1037.9-1243	0.5783	319^{+53}_{-52}	-	7
CL1040.7-1155a	0.6316	179^{+40}_{-26}	-	2
CL1040.7-1155b	0.7798	259^{+91}_{-52}	-	2
CL1054.4-1146a	0.6130	227^{+72}_{-28}	-	4
CL1054.7-1245a	0.7305	182^{+58}_{-69}	-	7
CL1103.7-1245a	0.6261	336^{+36}_{-40}	-	7
CL1103.7-1245b	0.7031	252^{+65}_{-85}	-	5
Groups	-	-	-	34
Field $0.4 \leq z < 0.6$	-	-	85	22
Field $0.6 \leq z < 0.8$	-	-	93	47
Field Total			178	69

Column 1: Structure Name. Column 2: Cluster Redshift. Column 3: Cluster velocity dispersion. Column 4: Number of phot+spec members. Column 5: Number of spectroscopically confirmed members. Numbers are given after quality cuts described in §2.1 are applied.

Our sample consists of 11 galaxy clusters, 7 groups, and the accompanying field galaxies at $0.4 \leq z \leq 0.8$. Following Poggianti et al. (2009) we define galaxy groups as structures with $\sigma < 400\,\mathrm{km\,s^{-1}}$. The catalog of objects that have spectroscopic redshifts will be addressed as the "spectroscopic sample" throughout. Likewise, the catalog of objects that only have photometric redshifts (Rudnick et al., 2009; Pelló et al., 2009) will be referred to as the "photometric sample". The other sample we use for our analysis consists of these two samples together, the spectroscopic sample plus galaxies identified as members or field galaxies using photometric redshifts from the EDisCS catalog, to which we will refer to as the "phot+spec sample" throughout.

For galaxy groups we only use our spectroscopic sample. Our groups are poorer systems with a lower contrast against the background than the clusters, and precise redshift values are needed for clear identification of their members. The modest precision of even our good photometric redshifts would result in too high of a contamination from non-members if only using photometric redshifts to assign group membership.

In obtaining our results we chose to exclude certain structures from the analysis of our samples. CL1227.9-1138a is a poorer side structure in the same field as the targeted cluster CL1227.9-1138, with a much lower number of spectroscopic membership. It only had two spectroscopic members remaining after the application of our sample selection criteria. Due to this low sample size this structure has been excluded from our analysis.

CL1354.2-1230a is a cluster where we used the spectroscopic sample only. It has a small number of members and attempting to pick this structure using our photometric sample would have suffered from high contamination.

CL1138.2-1133 and CL1138.2-1133a are two clusters in the same field. Both these clusters are at $z < 0.5$, and therefore outside of the redshift interval where we have reliable photometric redshifts as our photometry does not extend shortward of the 4000Å break for those systems. Hence we only used these two clusters for our spectroscopic analysis.

CL1138.2-1133a and CL1354.2-1230a are too off-center in our spectroscopic observations to probe out to $0.5 \times R_{200}$. Therefore we exclude them from any analysis that depends on the radial

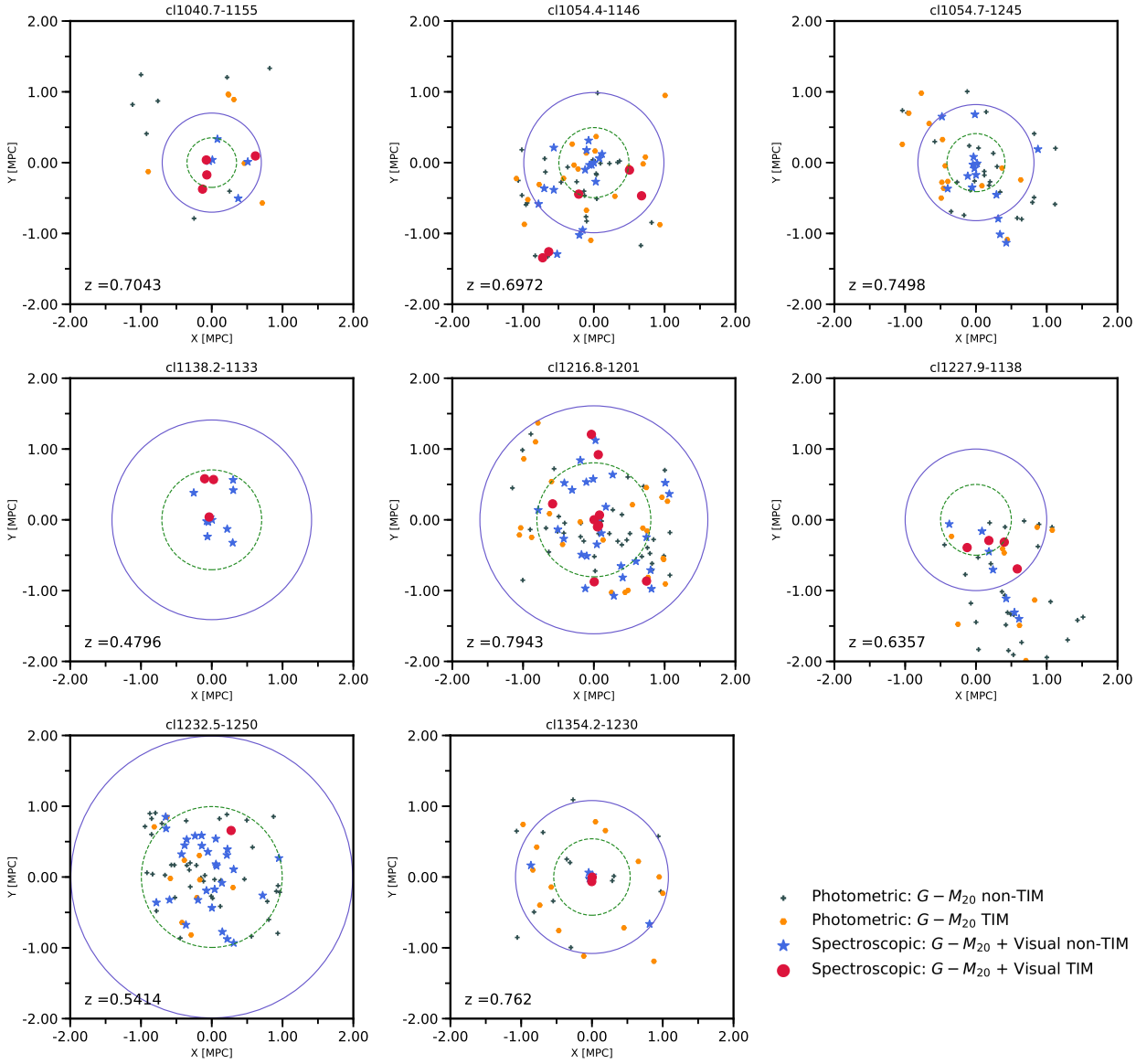

Figure 2.1: X-Y plots for the cluster members in our sample. All plots are centered at the brightest cluster galaxy of the individual cluster. In every plot, red circles are visually classified TIM that also reside above our TIM selection line ($G-M_{20}$ + Visual TIM, see Figure 2.4), blue stars are either visually classified undisturbed spectroscopic members or visually classified TIM below our line ($G-M_{20}$ + Visual non-TIM), orange points are photometric members above our line (Photometric $G-M_{20}$ TIM), and gray plus signs are photometric members below our line (Photometric $G-M_{20}$ non-TIM). The solid blue ring in each plot shows R_{200} for each cluster, and the green dashed circle has a radius of $0.5 \times R_{200}$. Cluster CL1138.2-1133 uses only its respective spectroscopic catalogs, as discussed in §2.1. Some clusters, such as CL1232.5-1250, do not have HST data that extends out to full R_{200}. We don't show CL1138.2-1133a and CL1354.2-1230a here, for reasons discussed in §2.1.

distribution or velocity distribution. We do include them in analyses that include the clusters as aggregates. We note that excluding these two systems does not affect any of our conclusions. CL1227.9-1138 has a brightest cluster galaxy (BCG) that is off-center compared to the rest of the members (see Figure 2.1), but since there is spectroscopic observations out to R_{200} we included this cluster in any radial distribution analysis.

We choose field galaxies for our spectroscopic sample and photometric sample in a similar fashion. In each sample, we define our field galaxies to be within $\Delta z = 0.2$ of the cluster redshift, excluding galaxies that are cluster members. As described in Milvang-Jensen et al. (2008), galaxies within a $\Delta z = 0.2$ slice around the cluster redshift form a magnitude limited sample that is unbiased by SED type. For the spectroscopic sample, this results in pure and complete field and cluster samples. For the photometric redshift sample, Pelló et al. (2009) showed that our photometric redshift cut is 90% complete in selecting cluster members independent of SED type. The high membership completeness of our photometric redshift selection ensures that our our photometric field sample will have little contamination by cluster members. Due to the same reasoning as for our cluster galaxies, we also limit our field sample to $z > 0.5$. Hence in our phot+spec sample, field galaxies with $z < 0.5$ are coming from our spectroscopic sample only.

2.2 Stellar Masses, Stellar Mass Completeness, and Final Galaxy Sample

We made use of the iSEDfit suite for the calculation of our stellar masses (for detailed information on iSEDfit see Moustakas et al. (2013)). iSEDfit uses the redshift and observed photometry of galaxies to derive their stellar mass via a statistical likelihood analysis of a large ensemble of model SEDs. For our spectroscopic sample the masses were calculated at the galaxy spectroscopic redshifts. For our photometric cluster members masses were calculated with their redshifts fixed at the cluster redshift, where for the field galaxies masses were calculated at their photometric redshifts. We used a stellar mass cut of $\log_{10}(M_*/M_\odot) > 10.4$ to both our photometric and spectroscopic samples (Rudnick et al., 2017). Above this limit we are mass complete. The $G - M_{20}$ code (more details on the $G - M_{20}$ method in §2.3 has a quality flag indicating whether the measurement can

be trusted. Any objects that failed to pass this test was taken out of our sample as well. We mapped the distribution of objects for which a flag was raised across all our fields (17 objects total), and found via visual inspection that the distribution is spatially uniform. The rejection is not biased towards whether the object resides in a 1 orbit or 5 orbit depth region. After these quality cuts, there are a total of 163 cluster members in our spectroscopic sample, and 429 cluster members in our photometric+spectroscopic sample. Our samples sizes after these quality cuts is shown in Table 2.1. Our spectroscopic cluster plus group sample, and all spectroscopic field galaxies are shown in a U-V color versus stellar mass plot in Figure 2.2. The galaxies in both panels are after all the quality cuts described above, except for the stellar mass cut. This plot also shows galaxies according to their visual class. The galaxies are split by their visual classification as determined by Kelkar et al. (2017) and as described in detail §2.3.

2.3 Morphological Classification

We chose to make use of two different techniques to quantify the morphologically disturbed features in our galaxy sample, an automated method and visual classification of galaxies. These two methods have particular strengths that complement the intrinsic weaknesses of each other. Interactions between galaxies leave an imprint on the morphologies of the galaxies involved, and visually identifying these is a common method in merger analysis. This procedure invariably suffers from subjectivity, as visual morphological distortions a galaxy displays may have multiple causes. Automated methods are generally faster methods that carry the advantage of being reproducible. However, such methods can miss certain signatures of merger events and hence suffer from incompleteness. They also require careful calibration to increase completeness and to reduce contamination.

For our case, we use the visual classification method to calibrate our automated method of choice. The automated morphology analysis we use for this work uses G (Abraham et al., 2003), the Gini coefficient and M_{20} (Lotz et al., 2004) as parameters. Briefly, G is a measure of how the flux is distributed among the pixels of the target galaxy, and M_{20} is defined as the normal-

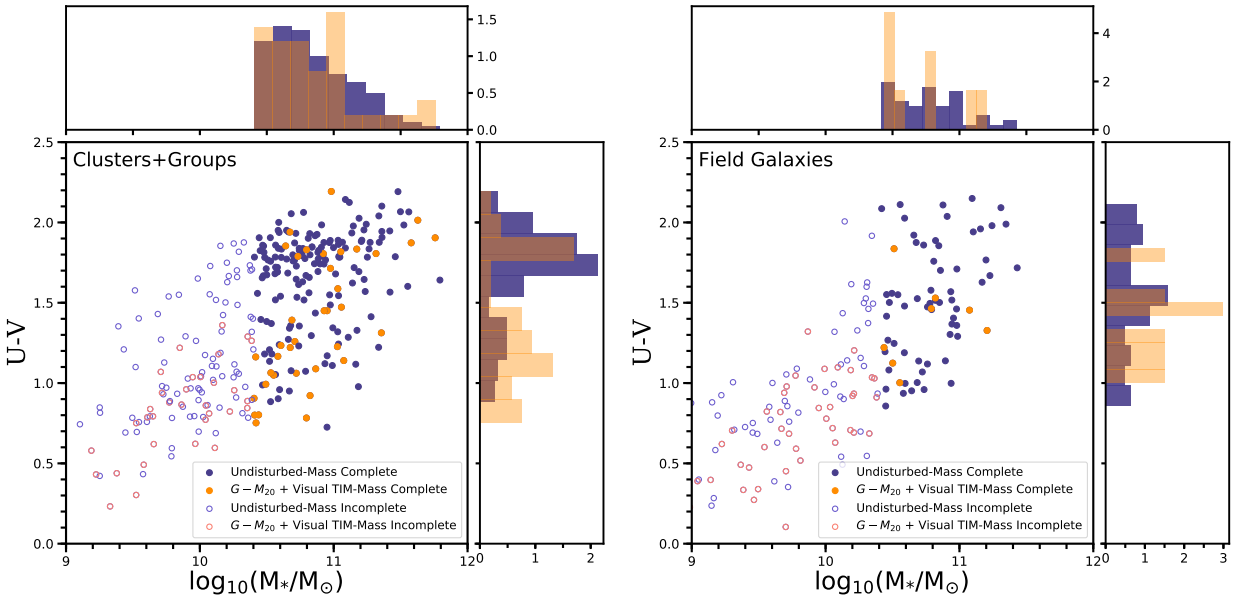

Figure 2.2: U-V color versus stellar mass plots of our spectroscopic samples. All galaxies in *both panels* have visual classifications. Galaxies shown in these plots have passed all quality cuts detailed in §2.1, except for the stellar mass completeness cut. In both panels, galaxies below our mass completeness limit of $\log_{10}(M_*/M_\odot) = 10.4$ are shown using open circles, galaxies above this threshold are shown in full circles. While we are complete below this limit for our photometric sample, we adopt the 10.4 limit to allow us to straightforwardly combine both samples. In both panels orange circles are visually classified TIM that are also classified as $G - M_{20}$ TIM, as explained in §2.3. Purple circles are galaxies visually classified as undisturbed or visual TIM that were not $G - M_{20}$ TIM. The normalized histograms for both panels show the number density of these classes, with colors being the same as the respective symbols. *Left panel* – Our aggregate sample of spectroscopic cluster and group members. *Right panel* – Our spectroscopic field galaxy sample.

ized second-order moment of the brightest 20% of the galaxy's flux (further details in Lotz et al. (2004)). This method, henceforth referred to as the $G-M_{20}$ method, is a nonparametric measure of morphology and hence does not assume any analytic functions for the light distribution of the measured object. This brings applicability of the method to irregular galaxies as well. The method has been shown to be effective especially at picking up bright double nuclei, which might be indicative of a merger event. Lotz et al. (2004) showed that this method is able to detect morphological disturbances even at low signal-to-noise ratio (S/N). Furthermore, Lotz et al. (2010b) compares observability time scales at various baryonic mass ratios for different tests of morphology, namely $G-M_{20}$, $G-A$ and A (asymmetry, Conselice (2003)). They conclude that the merger detection timescale of $G-M_{20}$ does not drop significantly even at baryonic mass ratios of around 10:1, and that it is, therefore, just as capable of detecting 9:1 mass ratio minor mergers as 1:1 major mergers (Lotz et al., 2010b). This favors the use of $G-M_{20}$ for detection of minor mergers. Hence another clear advantage the use of this method grants us is the well determined timescales of merger events, which we plan to use for future analysis.

In order to calibrate the completeness and contamination of our $G-M_{20}$ classification, we use the visual classification of Kelkar et al. (2017) for galaxies from our sample with spectroscopic redshifts. In Kelkar et al. (2017) three identifiers independently classified structural disturbances in order to control for variation between the identifiers. Every galaxy in our spectroscopic sample was classified into classes of minor/major mergers, strong/weak interaction and strong/mild tidal features and undisturbed (non-interacting galaxies), independent of morphology. A classification of merger or interaction required at least one visually nearby neighbor, whereas tidal features did not require any since tidal features can remain intact after the merger is complete. In Figure 2.3 we present examples of our visual classification scheme. Even with the best of efforts, no visual classification of morphology is foolproof. It is unfitting to appropriate every morphological asymmetry a galaxy displays to interactions with another galaxy. Regardless, classes other than undisturbed still have a higher probability of being the result of some form of galaxy-galaxy gravitational interaction or merger event. Therefore for the purposes of our merger analysis, all classes except for

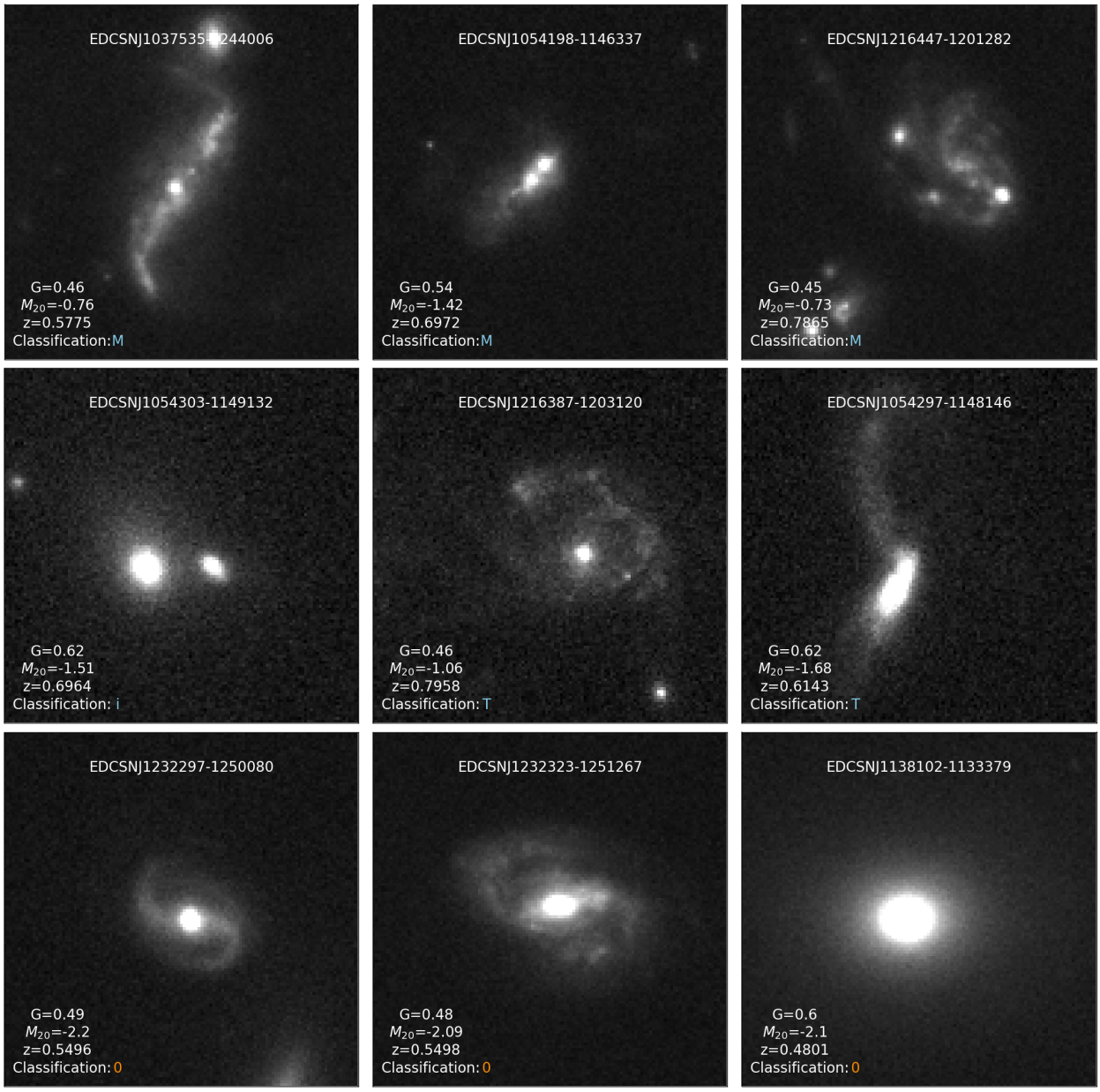

Figure 2.3: Example postage stamps from the EDisCS-HST spectroscopic sample for which we performed a visual classification of morphology. Every panel shows a $6'' \times 6''$ region. Every panel shows the galaxy ID on top, then G, M_{20}, redshift, and its visual classification info at the bottom. M/m denote major/minor mergers, I/i denote strong/weak interactions, T/t denote strong/mild tidal features, and 0 denotes undisturbed galaxies (Kelkar et al., 2017). Light blue color for the visual class is used to indicate that the object is a $G - M_{20}$ identified TIM (see Figure 2.4 for the line, and §2.3 for its derivation), and orange color to indicate that it is below our line and hence is not identified as a $G - M_{20}$ TIM.

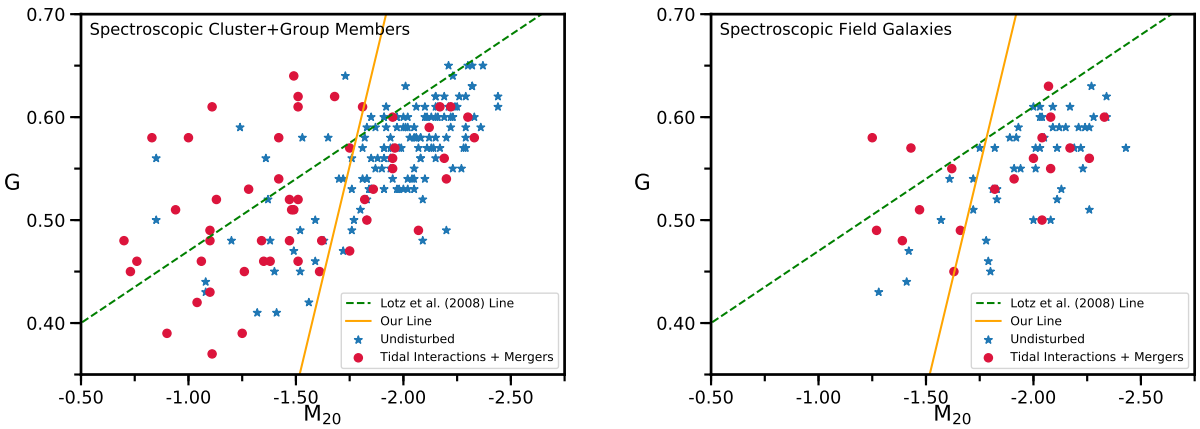

Figure 2.4: The $G - M_{20}$ plots of our spectroscopic sample. All galaxies in *both panels* have visual classifications. *Left panel* – All spectroscopically confirmed cluster and group member galaxies are shown together. Red circles are galaxies that are visually classified as TIM as described in §2.3. Blue stars are galaxies that show no sign of interaction and are hence classified as undisturbed. The orange line corresponds to the highest purity value obtained through our calibration detailed in §2.3, whereas the green dotted line is the merger selection line from L08. *Right panel* – Spectroscopically confirmed field galaxies. Symbols are the same as in the left panel. In both panels we see that our line picks many visually classified TIM that would have been left out by the L08 line.

undisturbed are considered under one composite tag and will hence be referred to as "tidal interactions and mergers", or TIM for short. After careful examination of the visual classifications of Kelkar et al. (2017), we reclassified three of the galaxies in our sample. These new classifications are given in Table A.1.

For our analysis, we rely on both a visual classification and an automated classifier of galaxy morphology, in hopes of combining the particular strengths of both methods. The G and M_{20} values we measured for this sample together with their visual classes (TIM and undisturbed) are shown in Figure 2.4. Our results reveal that the selection line used by (Lotz et al. (2008a); L08) to separate merging galaxies from nonmergers is missing a substantial fraction of our visually classified mergers. L08 uses a lower stellar mass cut compared to ours and their line is optimized to avoid selecting low mass, high gas fraction irregular galaxies that are not undergoing an interaction or merger event. Our higher mass cut ensures that our analysis is not contaminated by such galaxies. To address this issue we decided to utilize the visual classifications to calibrate our merger selec-

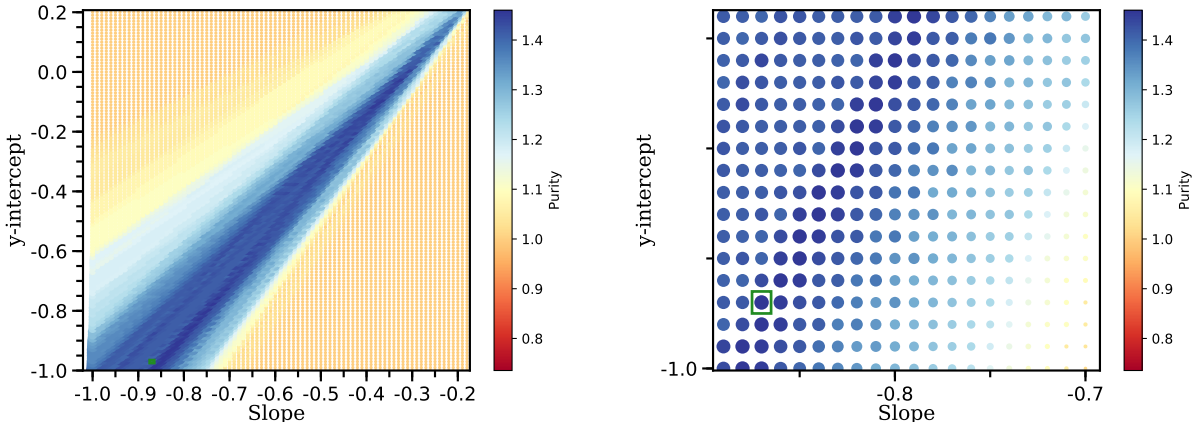

Figure 2.5: Purity plot we used for the calibration of our line. The right panel is a zoom-in to a region of the left panel where our highest purity value resides (shown inside the green box). The plot has been obtained by calculating values of purity (as defined in §2.3) at different y-intercept and slope values. Larger and darker blue points represent higher purity results. We had only one result with the highest purity value of 1.46, which corresponded to -0.87 for the slope, and -0.97 for the y-intercept. Those values have been used for our merger selection line for all $G-M_{20}$ plots in this work. We also tested purity values close to our highest value and using these did not change the results of our analysis in a significant way.

tion criteria with the $G-M_{20}$ method. We derived a selection line with the premise of maximizing the number of mergers above and maximizing the number of nonmergers below it. We first define purity ρ as

$$\rho = \frac{N_{above}^{VisTIM}}{N_{total}^{VisTIM}} + \frac{N_{below}^{VisUnd}}{N_{total}^{VisUnd}}, \tag{2.1}$$

where *VisTIM* and *VisUnd* is used for objects visually classified as tidal interactions and mergers, and undisturbed, respectively, above and below to denote above and below the selection line. We optimized our line by requiring maximum purity, which we obtained by varying values of y-intercept and slope of the selection line. In Figure 2.5 we show the purity value as a function of slope and y-intercept of the line obtained from our spectroscopic sample. The line with maximum purity is used in our G versus M_{20} plots, and for all subsequent calculations of $f_{\rm TIM}$. We show the $G-M_{20}$ plots with this line for our spectroscopic cluster and group members (left panel), and our field sample (right panel) in Figure 2.4. Using a plot where both these samples were plotted together, we find that that among the galaxies that remain above this selection line, 60% are

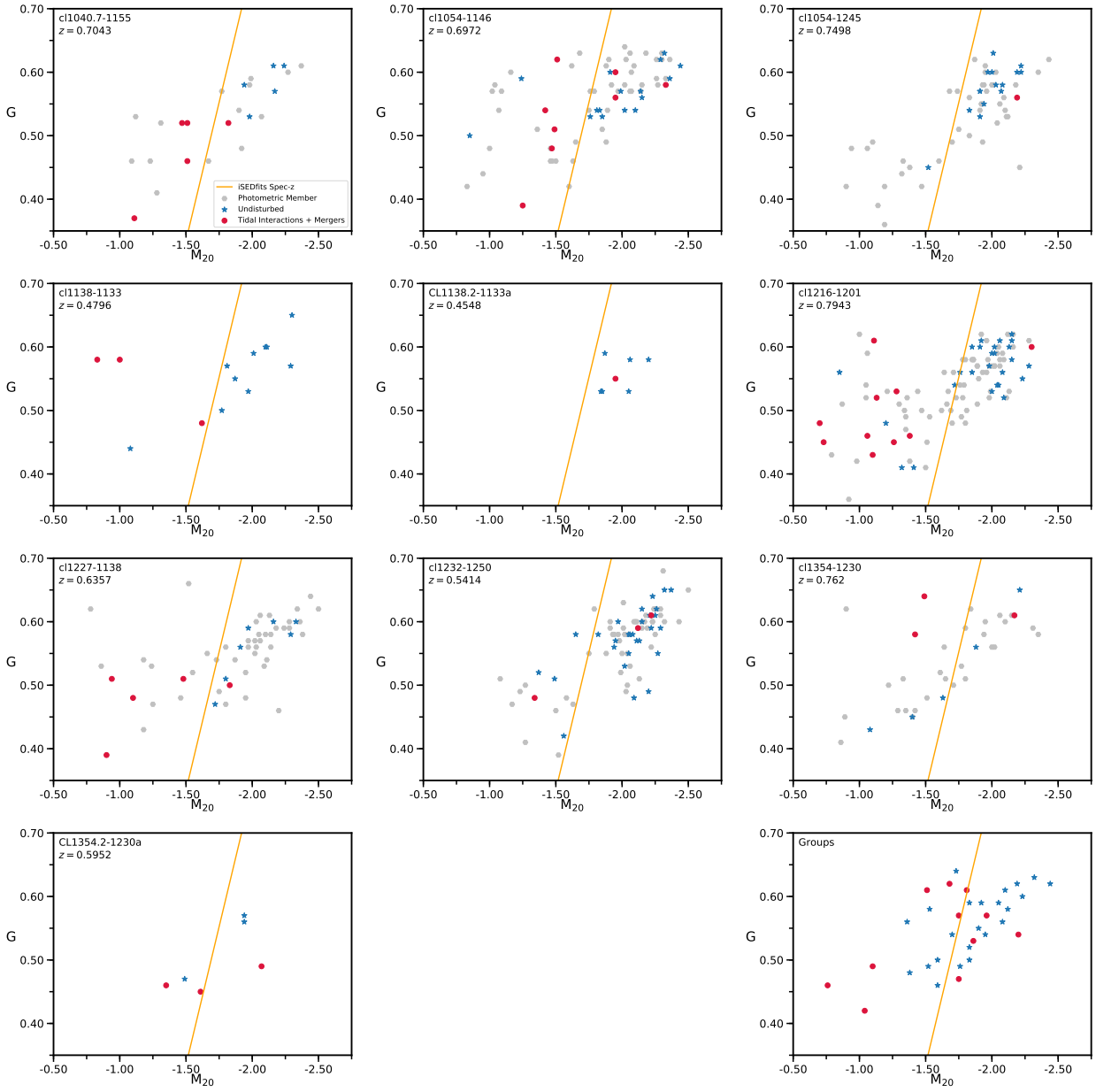

Figure 2.6: $G-M_{20}$ plots for all of our individual clusters and an aggregate plot of our groups. Red data points are visually classified TIM in our spectroscopic sample, blue data points are undisturbed galaxies in our spectroscopic sample. Gray circles are our members that only have photometric redshifts and hence lack visual classification. The line is our calibrated TIM decision boundary, see §2.3 for its derivation. As discussed in §2.3, CL1227.9-1138a has been excluded from any following analysis as it only contains two members that satisfy our selection criteria.

tidal interactions and mergers (TIM). As we describe in more detail below, we are concerned with identifying TIM with well established observability timescales. Therefore, for the purpose of this analysis we regard the objects visually classified as TIM that reside below our line as part of our undisturbed population. Hence we define the fraction of tidal interactions and mergers with well identified observability timescales, or $f_{\rm TIM}$, for samples with visual classification as

$$f_{\rm TIM} = \frac{N_{above}^{VisTIM}}{N_{total}}, \tag{2.2}$$

where N_{above}^{VisTIM} is the number of objects visually classified as tidal interactions and mergers above our line, and N_{total} is the total number of objects in the sample. By using a sample with visual classifications, we explicitly correct for the contamination by symmetric galaxies above our line. We applied a correction factor $C = N_{above}^{VisTIM}/N_{above}$ calculated using our visually classified spectroscopic sample to the $G-M_{20}$ TIM fraction of samples we do not have visual classifications for, to account for the visually symmetric galaxies that would be identified as TIM by the $G-M_{20}$ technique. The TIM fraction for our photometric sample, for which a visual classification has not been performed, is hence calculated as

$$f_{\rm TIM}^{p} = \frac{N_{above}^{p}}{N_{total}^{p}} \times C, \tag{2.3}$$

where the superscript p is to symbolize that this $f_{\rm TIM}$ calculation has been used for our photometric sample only. As also mentioned above, we find $C = 0.60$ from the $G-M_{20}$ distribution of our entire spectroscopic sample.

In future work we plan to couple the observability timescale of the mergers with a study of the stellar populations in our galaxies to determine the relative timing of morphological transformation and star formation quenching. In this study we therefore have deliberately chosen to only optimize our selection based on obtaining a clean sample of mergers above our dividing line, as those galaxies will have the most well constrained observability timescales, unlike “true" mergers below our line. In other words, our goal is not to measure a total merger fraction, but rather to

isolate a sample of mergers with a well identified observability timescale.

2.4 Distribution of Our Sample in the $G - M_{20}$ space

In this subsection we explore the discriminatory power of both G and M_{20} and find that the disturbed and undisturbed populations are significantly separated in both parameters. Our line and the distribution in $G - M_{20}$ space of our spectroscopic and photometric cluster members, and our aggregate group members is presented in Figure 2.6.

The best purity value we obtained from our code was a single value, corresponding to a y-intercept of -0.97 and slope of -0.87. As is evident from Figure 2.5, there are many other outcomes close to our purity value corresponding to different y-intercept and slope values. In order to test the robustness of our results, we drew 10^5 random combinations of (y-intercept, slope)$_{\rm test}$. For each combination we also drew a random purity $1 \leq \rho_{\rm test} \leq \rho_{\rm max}$, where $\rho_{\rm max}$ is the maximum purity over all y-intercepts and slopes. If $\rho_{\rm test}$ was less than or equal to the purity corresponding to (y-intercept, slope)$_{\rm test}$, we kept the (y-intercept, slope)$_{\rm test}$ pair. Otherwise we discarded it and drew another (y-intercept,slope)$_{\rm test}$. This resulted in $\sim 10^4$ sets of (y-intercept,slope)$_{\rm test}$. We find that the same visual TIM galaxies are isolated by most of the accepted lines. We demonstrate this by plotting a random subset of the accepted lines on the $G - M_{20}$ space of our entire spec sample in Appendix C. We then calculated the TIM fraction per global environment at every accepted (y-intercept, slope) pair to assess the impact of different lines on our analysis in §3.3. All of our results presented in §3.3 computed using the best purity line are within the 68% confidence interval of the distribution in $f_{\rm TIM}$ we derive using this procedure. Furthermore, at every (y-intercept, slope)$_{\rm test}$, we performed a two sample KS Test comparing the distribution of $G - M_{20}$ TIM and undisturbed objects (where the $G - M_{20}$ TIM and undisturbed populations are picked relative to (y-intercept, slope)$_{test}$ each time) in $\Delta V/\sigma$ and R_{proj}/R_{200}. Here ΔV is the peculiar velocity, σ is the velocity dispersion of the galaxy cluster, R_{proj} is the projected radius from the cluster center, and R_{200} is the radius at which the density inside becomes 200 times the critical density. The KS p-values we report in §3.4 for the best purity line are close in value to the peak of the distribution in each case.

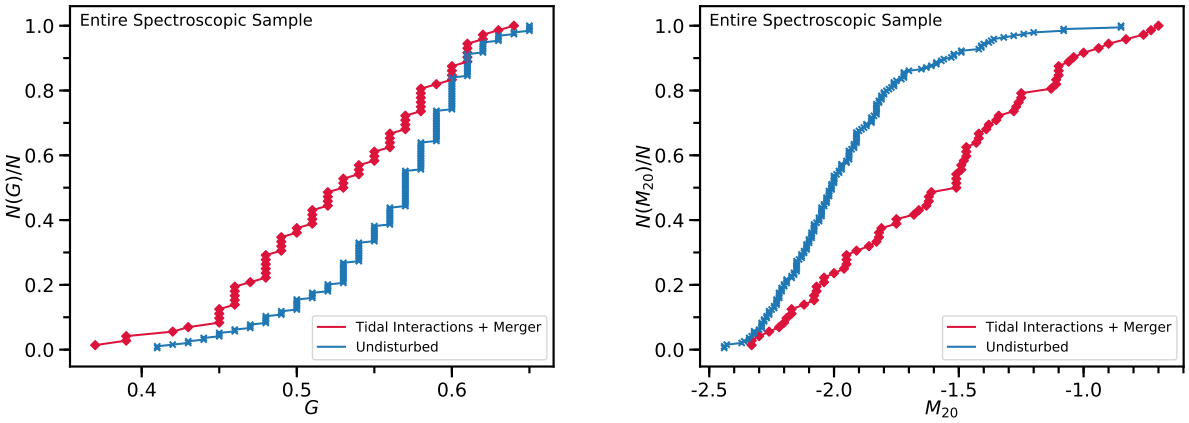

Figure 2.7: Cumulative histograms for our spectroscopic sample which includes every galaxy from both panels of Figure 2.4. In both panels the red line is for tidal interactions and mergers, and blue line is for our undisturbed galaxies. *Left panel* – The cumulative histogram for G. *Right panel* – The cumulative histogram for M_{20}. The KS test result is 0.0003 for the left panel, and 10^{-10} for the right panel.

Therefore we decided to use the line corresponding to our best purity value for the entire analysis presented in this work.

We further investigate the distributions in G and M_{20} by plotting cumulative histograms of the TIM and undisturbed galaxies using our entire spectroscopic sample in Figure 2.7. We ran a Kolmogorov-Smirnov test (KS test) for both panels. We found that the KS p-value over the G parameter for the TIM and undisturbed galaxies is 0.0003, showing that the probability that these classes are drawn from the same parent distribution in G is 0.03%. The KS p-value is significantly smaller for the M_{20} parameter, which we found to be 10^{-10}. Hence the probability that the TIM and undisturbed galaxies are drawn from the same parent distribution in M_{20} is significantly less than 1%. These results indicate that the M_{20} parameter is especially effective at separating TIM galaxies from undisturbed galaxies and that G, while still having discriminatory power, is less effective.

We finalize this section by investigating the distribution of lines accepted as a result of the test we describe at the end of §2.3. We show a subsample of such lines in Figure 2.8. We chose to display only values with $\rho > 1.35$ to emphasize the region spanned by the higher purity lines. Our test preferentially accepts (y-intercept, slope) values with higher purities, so $\rho > 1.35$ draws

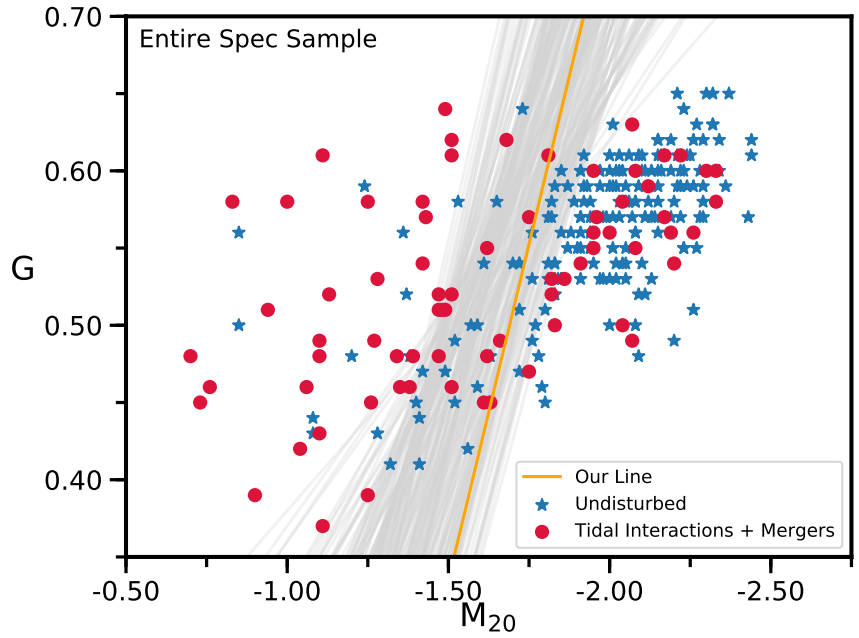

Figure 2.8: Distribution of a random subsample of accepted lines (gray lines), shown on the $G - M_{20}$ plot of our entire spectroscopic sample. The orange line is the line with maximum purity ($\rho = 1.46$), and is the line we used for the analysis of this entire work. To emphasize the region isolated by lines corresponding to high purity, we only plot the accepted lines with purity values larger than 1.35. Our test shows that such draws already dominate the distribution of accepted lines. Furthermore, for visual clarity, we also display only every twentieth accepted line.

already form the majority of the distribution of accepted lines. For visual clarity we plot every twentieth accepted line. We also display our line of maximum purity plotted on this distribution. Our results show that the same visual TIM galaxies remain above most of the accepted lines. Due to this result, combined with the results we presented at the end of §2.3, we chose to perform the entire analysis of this work using the maximum purity line.

2.5 False Positives and False Negatives of Our TIM Selection

Every automated method of merger detection suffers from incorrect classifications. We give some examples of such detections from our sample in this section. We present in Figure 2.9 some of the galaxies that Kelkar et al. (2017) visually classified as undisturbed, but are picked as TIM by the $G-M_{20}$ method. These are the undisturbed galaxies that remain above our selection line, or the false-positives of the $G-M_{20}$ detection. We also present some of the galaxies that Kelkar et al. (2017) visually classified as having merger signatures, but remain below our selection line, in Figure 2.10. So these form the false-negatives of the $G-M_{20}$ detection. Galaxies undergoing mergers will move on the $G-M_{20}$ space as their morphologies get altered by the merger event. They will be detected as mergers by the $G-M_{20}$ method only during a certain period of the merging process (Lotz et al., 2010b,a). It should be noted that stages too early and too late in the merger process are prone to avoid detection by automated methods, and are also challenging to identify by visual methods. The left panel in Figure 2.10 might be an example to a late stage event, that avoided detection the $G-M_{20}$ and hence resided below our line.

Figure 2.9: Galaxies visually classified as undisturbed but lie above our merger selection line, or false-positives. Visual classes and colors the same as in Figure 2.3. All images show galaxies with a neighboring object. These objects cause a variance in the flux distribution and therefore increase the M_{20} value. This in turn pushes the object above our line.

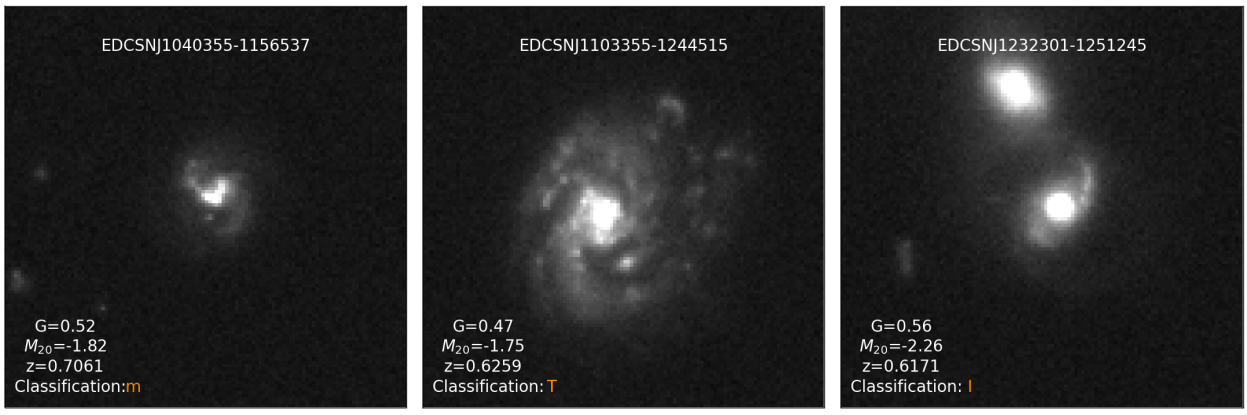

Figure 2.10: Galaxies visually classified as TIM but lie below our merger selection line, or false-negatives. Visual classes and colors the same as in Figure 2.3. As discussed in the text, these galaxies might be at a stage when they avoid classification as mergers by the $G-M_{20}$ method.

Chapter 3

Characteristics of the TIM Population

In this chapter we present the analysis we have detailed in Deger et al. (2018), where we study the distribution of the TIM population in our sample. After getting the fraction of tidal interactions and mergers with well identified observability timescales ($f_{\rm TIM}$) for our spectroscopic and photometric catalogs, we looked at the dependence of $f_{\rm TIM}$ on redshift, cluster velocity dispersion, global environment, and local environment. We present our findings from each of these in the subsequent subsections. Most errors have been obtained through bootstrapping respective catalogs, except for spectroscopic errors attributed to the merger fractions of CL1054.7-1245 and CL1138.2-1133a which didn't have any visually classified TIM galaxies above our selection line. We calculated errors for these clusters using the binomial error formulas as given in Gehrels (1986). For all other structures, we confirmed that the error we obtain from bootstrapping of respective samples is equal to the error we obtain from the same binomial error formula. We present a table showing $f_{\rm TIM}$ values in Table 3.1.

3.1 $f_{\rm TIM}$ versus Redshift

Our findings for how $f_{\rm TIM}$ varies with redshift are shown in Figure 3.1. The left plot shows results from our spectroscopic sample. It displays each cluster from this sample we used for our analysis, members from these clusters binned in equal redshift intervals, and field galaxies binned in two redshift bins containing roughly equal numbers of galaxies. The right plot shows results from our phot+spec sample. We obtained a weighted fit of the cluster data for both plots, which we present with the confidence intervals on the fit.

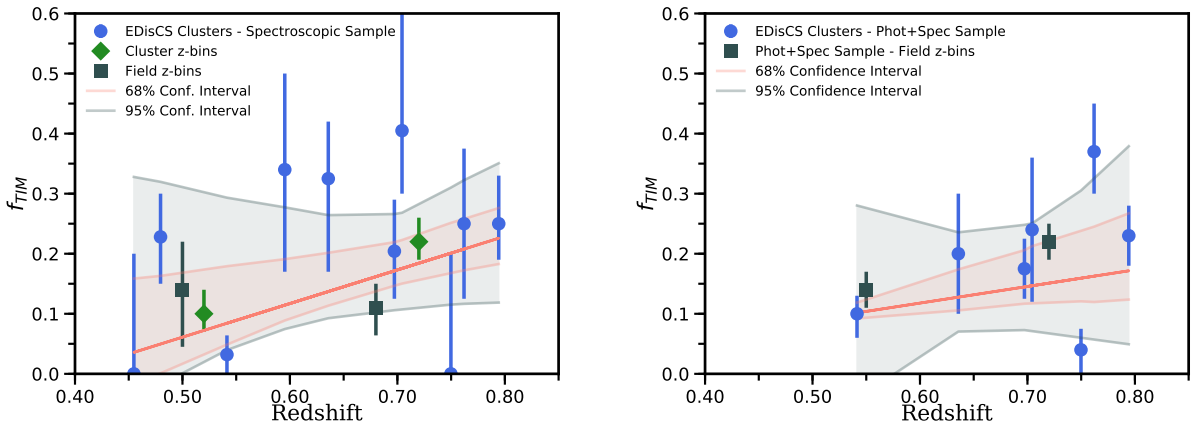

Figure 3.1: *Left panel* – Evolution of $f_{\rm TIM}$ for our spectroscopic sample. Blue circles are the clusters in our spectroscopic sample, green diamonds are galaxies from these clusters in redshift bins of $0.45 < z < 0.6$ and $0.6 < z < 0.8$. Dark gray squares are spectroscopically confirmed field galaxies in bins of $0.4 < z < 0.6$ and $0.6 < z < 0.8$. *Right panel* – Evolution of $f_{\rm TIM}$ for our phot+spec sample. Blue circles are the clusters, and dark gray squares are field galaxies in bins of $0.4 < z < 0.6$ and $0.6 < z < 0.8$. We obtain the red fitted line via a weighted linear regression algorithm for both panels. In both panels, error bars in $f_{\rm TIM}$ are the 68% confidence limits obtained through a bootstrapping of the $G - M_{20}$ catalogs of respective clusters. Finally, for both panels, the pink and light gray lines above and below the fit are the 68% and 95% confidence limits of the fit respectively. The best fit line in both plots show an increasing $f_{\rm TIM}$ with redshift. However, we cannot rule out no evolution $f_{\rm TIM}$ at more than 68% confidence for either sample. The Spearman rank p-values, at 0.42 for the clusters in the left panel, and 0.29 for the clusters in the right panel, further point to our results being consistent with no evolution of $f_{\rm TIM}$ with z.

Table 3.1: $f_{\rm TIM}$ Results

Structure Name	$f_{\rm TIM}^{\rm phot+spec}$	$f_{\rm TIM}^{\rm spec}$
CL1040.7-1155	$0.24^{+0.12}_{-0.12}$	$0.40^{+0.2}_{-0.1}$
CL1054.4-1146	$0.17^{+0.05}_{-0.05}$	$0.20^{+0.9}_{-0.075}$
CL1054.7-1245	$0.04^{+0.035}_{-0.04}$	$0.0^{+0.2}_{-0.0}$
CL1138.2-1133	-	$0.23^{+0.07}_{-0.08}$
CL1138.2-1133a	-	$0.0^{+0.2}_{-0.0}$
CL1216.8-1201	$0.23^{+0.05}_{-0.05}$	$0.25^{+0.08}_{-0.06}$
CL1227.9-1138	$0.20^{+0.10}_{-0.10}$	$0.32^{+0.10}_{-0.14}$
CL1232.5-1250	$0.10^{+0.03}_{-0.04}$	$0.03^{+0.03}_{-0.03}$
CL1354.2-1230	$0.37^{+0.08}_{-0.07}$	$0.25^{+0.125}_{-0.125}$
CL1354.2-1230a	-	$0.34^{+0.16}_{-0.17}$
Field	$0.18^{+0.02}_{-0.02}$	$0.12^{+0.04}_{-0.05}$
Groups	-	$0.20^{+0.06}_{-0.05}$
Cluster: $R > 0.5 \times R_{200}$	$0.25^{+0.02}_{-0.02}$	$0.23^{+0.06}_{-0.05}$
Cluster: $R < 0.5 \times R_{200}$	$0.14^{+0.02}_{-0.03}$	$0.16^{+0.04}_{-0.04}$
Cluster: $R < 0.15 \times R_{200}$	$0.16^{+0.04}_{-0.03}$	$0.24^{+0.06}_{-0.06}$

Column 1: Structure Name. Column 2: TIM fraction in the phot+spec sample. Column 3: TIM fraction using the spectroscopic sample only.

While the best fit line in both panels show an increasing $f_{\rm TIM}$ with redshift, we cannot rule out a non-evolving $f_{\rm TIM}$ at more than 68% confidence for either sample. This is reinforced by the results of a Spearman rank test, which gives a p-value of 0.42 for the clusters in spectroscopic sample (blue data points in Figure 3.1, left panel), and 0.29 for the clusters in the phot+spec sample (blue data points in Figure 3.1, right panel), indicating that there is a 42 and 29% chance respectively that a random sample would show as strong a correlation as ours. Thus our results are consistent with no evolution of $f_{\rm TIM}$ with redshift. We finalize this section by stating that our results rule out a line with a slope greater than 1.23 $\Delta f_{\rm TIM}/\Delta z$ for the spec, and a line with a slope 1.36 $\Delta f_{\rm TIM}/\Delta z$ for our phot+spec sample at a 99.5% confidence level. Thus, we can also rule out at high confidence very strong evolution in $f_{\rm TIM}$. Furthermore, our results rule out lines with slopes less than -1.65 $\Delta f_{\rm TIM}/\Delta z$ for the spec, and less than -1.96 $\Delta f_{\rm TIM}/\Delta z$ for our phot+spec sample with 99.5% confidence.

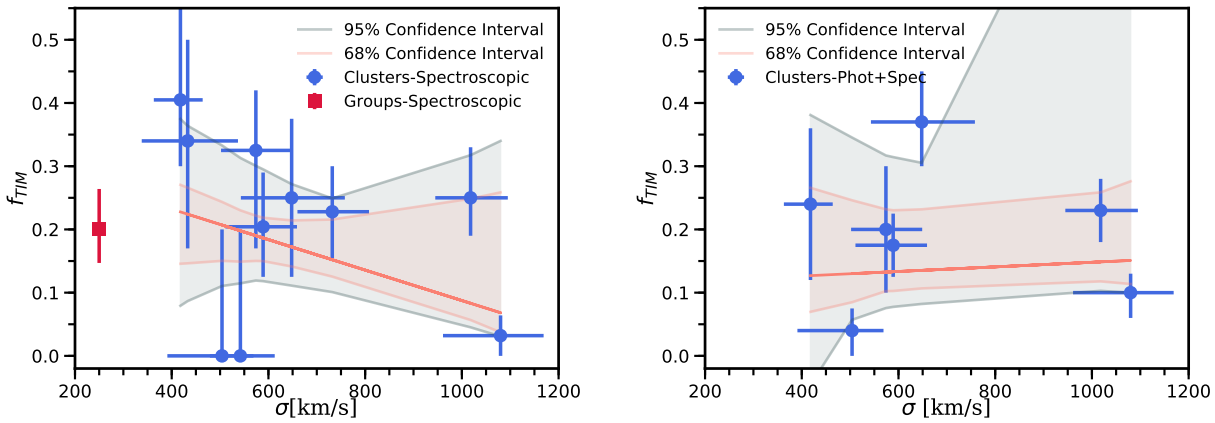

Figure 3.2: *Left panel* – $f_{\rm TIM}$ versus velocity dispersion results for our spectroscopic sample. Blue circles are the clusters in the spectroscopic sample. The red square data point is the $f_{\rm TIM}$ value of our aggregate group sample shown at the mean σ of our groups. *Right panel* – $f_{\rm TIM}$ versus velocity dispersion results for our phot+spec sample. Blue circles are the clusters in our phot+spec sample. We do not present a group result for our photometric sample, as explained in §2.1. For both panels the error bars are the 68% confidence limits obtained through a bootstrapping of the $G-M_{20}$ catalogs of the respective clusters or groups. We obtain the red fitted line via a weighted linear regression algorithm for both panels. The pink and light gray lines above and below the fit are the 68% and 95% confidence limits of the fit respectively. These reveal that our data are completely consistent with no dependence on velocity dispersion. The Spearman rank p-values of the left and right panels are 0.37 and 0.93, respectively, in support of this conclusion.

3.2 $f_{\rm TIM}$ versus Velocity Dispersion

We present our findings for how $f_{\rm TIM}$ varies with velocity dispersion in Figure 3.2. The left panel of the figure shows results from our spectroscopic sample and the right panel from our phot+spec sample. In the plot for our spectroscopic sample we display the result for groups at a σ value that is the average of the individual group σ values. The right panel does not present a data point for groups, as discussed in §2.1. Similar to Figure 3.1, we also present a weighted best fit to the cluster data in both panels, and the 68% and 95% confidence limits of the fit. In both panels we see that our results are fully consistent with no correlation of $f_{\rm TIM}$ with σ. The Spearman rank test results also point out to a probable no correlation with σ. We obtain a Spearman rank p-value of 0.37 for our spectroscopic sample (left panel, Figure 3.2), and 0.93 for our phot+spec sample (right panel, Figure 3.2), indicating that there is a 37 and 93% chance respectively that a random

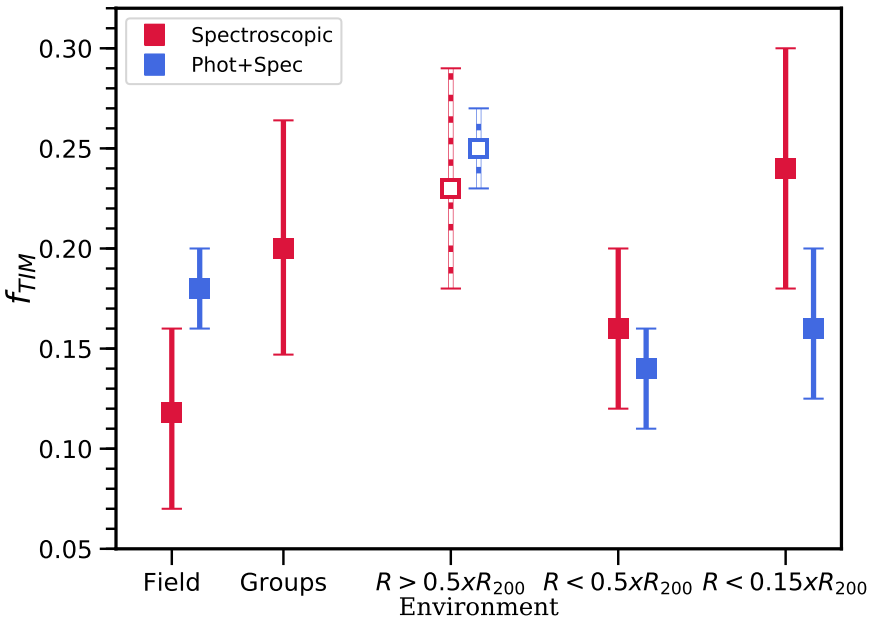

Figure 3.3: $f_{\rm TIM}$ of our spectroscopic and phot+spec samples at different environments. Red and blue markers represent our spectroscopic and phot+spec samples respectively. Error bars are obtained by bootstrapping catalogs per each composite data point. The group result only uses spectroscopic sample as discussed in §2.1. We split our cluster members into three regions according to clustercentric radius, namely $R < 0.5 \times R_{200}$, $R > 0.5 \times R_{200}$, and $R < 0.15 \times R_{200}$. Our sample is not equally represented in $R > 0.5 \times R_{200}$, therefore we present our results for that region as open squares with dashed error bars. The plot shows that $f_{\rm TIM}$ has suggestive peaks at groups, and at radii in clusters larger than $0.5 \times R_{200}$.

uncorrelated sample would show as strong a correlation as ours. We therefore conclude that there is no significant trend of $f_{\rm TIM}$ with velocity dispersion for either sample. Finally, we find that our results rule out lines with slopes greater than a slope of 9×10^{-4} $\Delta f_{\rm TIM}/\Delta\sigma$ for our spectroscopic sample, and a slope of 2×10^{-3} $\Delta f_{\rm TIM}/\Delta\sigma$ for our phot+spec sample at a 99.5% confidence level. Similarly, we are able to rule out at a 99.5% confidence level lines with slopes less than -6×10^{-4} $\Delta f_{\rm TIM}/\Delta\sigma$ for the spec, and -7×10^{-4} $\Delta f_{\rm TIM}/\Delta\sigma$ for our phot+spec sample.

3.3 $f_{\rm TIM}$ in Different Environments

In Figure 3.3 we show how our $f_{\rm TIM}$ values vary across environment. This figure shows the $f_{\rm TIM}$ results using our spectroscopic and phot+spec samples for field galaxies, groups (using the spec-

troscopic sample only, see §2.1 for an explanation of why only the spectroscopic sample has been used for groups), and our cluster result in three radial bins, $R < 0.5 \times R_{200}$, $R > 0.5 \times R_{200}$, and and $R < 0.15 \times R_{200}$. We remark that while the random uncertainties are smaller for our phot+spec sample, the spectroscopic sample has lower systematic uncertainties due to the more precise determination of membership. Our results show that $f_{\rm TIM}$ has a peak at $R > 0.5 \times R_{200}$ in clusters for our phot+spec sample. We find that $f_{\rm TIM}$ has peaks at groups, at $R > 0.5 \times R_{200}$ and $R < 0.15 \times R_{200}$ in clusters for our spectroscopic sample, though these peaks are weaker and are of low significance. Here we note that for some of our clusters, our data does not extend to the full R_{200}, so our clusters are not equally represented in the cluster outskirt result (see Figure 2.1). For example, CL1232.5-1250, one of our most massive and lowest $f_{\rm TIM}$ clusters does not have HST coverage past $0.5 \times R_{200}$. Since the result at this radius is inevitably affected by this unequal representation, we present it with a caveat and plot our findings with different markers in Figure 3.3. We also note that we excluded CL1354.2-1230a and CL1138.2-1133a from the cluster outskirts and core results, as discussed in §2.1.

3.4 Phase Space Analysis

We performed a phase space analysis using cluster members from our spectroscopic sample to observe whether TIM and undisturbed galaxies show any trends. We limit our analysis to our clusters as they are the only systems with sufficient member counts for a precise determination of σ and R_{200}. From our clusters we additionally excluded CL1354.2-1230a and CL1138.2-1133a for this analysis, as discussed in §2.1. The distribution of our sample in the phase space is shown in Figure 3.4. The plot displays the phase space distribution of our undisturbed and $G-M_{20}$ TIM galaxies. The solid orange line is from Mahajan et al. (2011), and it signifies the region where most virialized galaxies reside. Since the majority of our galaxies are inside the virialized region, it is difficult to draw conclusions with respect to the virialized nature of the subpopulations.

We present cumulative histograms of $|\Delta V|/\sigma$ and R_{proj}/R_{200} for our two classes in Figure 3.5. We further investigate the environmental dependence of our sample by performing the Kolmogorov-

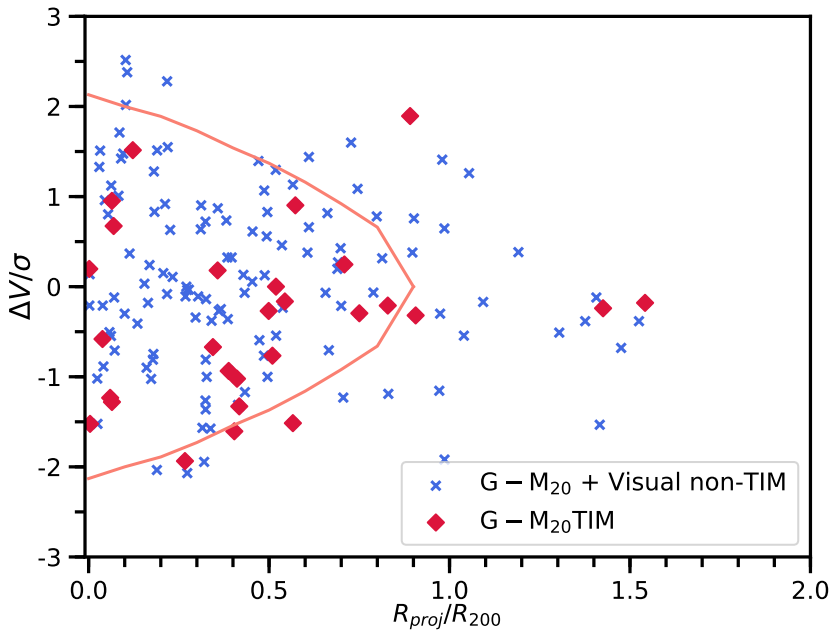

Figure 3.4: Phase space analysis of our spectroscopic sample. Red circles are cluster members from our spectroscopic sample visually classified as TIM that also reside above our TIM selection line ($G-M_{20}$ TIM), blue crosses are galaxies visually classified as undisturbed, or visually classified TIM that reside below our line. The orange solid line from Mahajan et al. (2011) indicates the region where the majority of virialized galaxies lie. No significant trend is apparent in the phase space. We further investigate this in Figure 3.5.

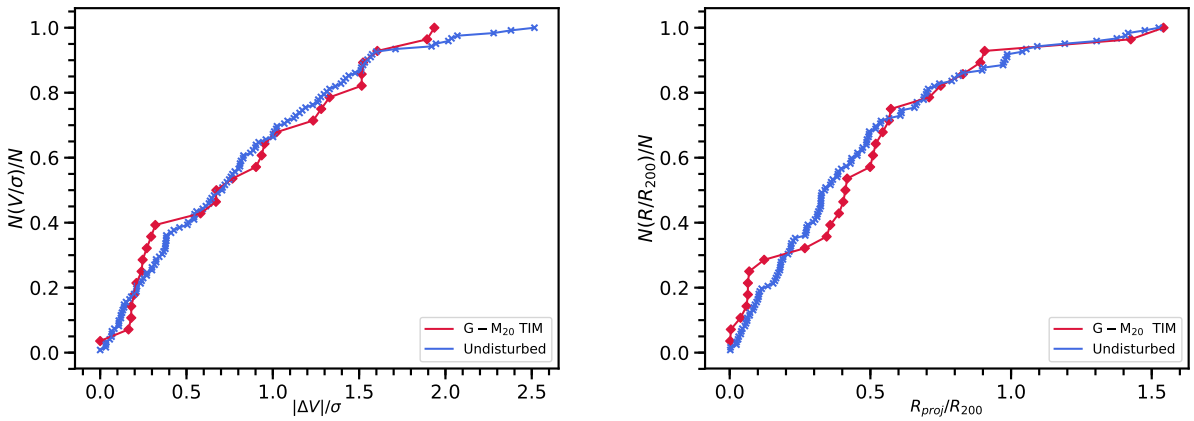

Figure 3.5: *Left panel* – The cumulative histogram of $|\Delta V|/\sigma$ for the sample we used in our phase space plot, Figure 3.4. The colors represent the same populations as in the phase space plot, red for $G-M_{20}$ TIM, and blue for undisturbed galaxies. *Right panel* – The cumulative histogram of R_{proj}/R_{200} for the sample we used in our phase space plot, Figure 3.4. Red and blue colors represent the same populations as in the left panel. KS test results show that there is a 6% and 37% probability that our samples are drawn from the same distribution when their $\Delta V/\sigma$ and R_{proj}/R_{200} values are compared, respectively.

Smirnov (KS test) for our undisturbed and $G-M_{20}$ TIM samples, comparing their $\Delta V/\sigma$ and R_{proj}/R_{200} values. The KS test shows that there is a 6% probability that our TIM and undisturbed galaxies have been drawn from the same parent population in their $\Delta V/\sigma$ distribution. For the R_{proj}/R_{200} values the KS test finds that the probability is 37%. These results are comparable in statistical significance to results from our analysis of $f_{\rm TIM}$ in clusters (in Figure 3.3), where we found that the sample of cluster members with higher radii have a moderately higher $f_{\rm TIM}$ value compared to the members closer to the cluster core.

3.5 Local Density Analysis

In §3.3 we presented our findings for how the $f_{\rm TIM}$ varies according to global environment. Here we present the results of the local density analysis of our sample, using values derived by Poggianti et al. (2008). In their paper they measured the local density via a projected tenth nearest neighbor analysis for the spectroscopic cluster members of the EDisCS sample. As described below, it is not possible to measure accurate local densities for group and field galaxies in our sample and so we

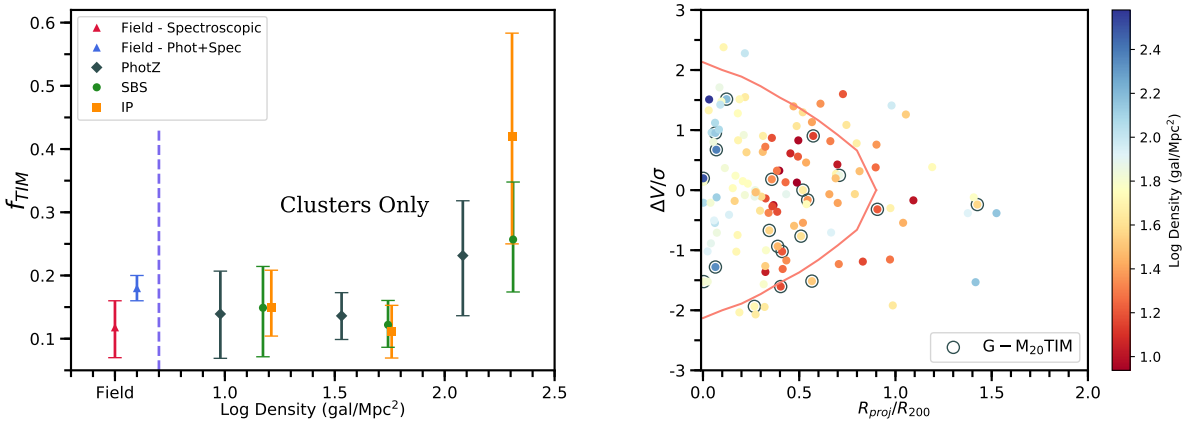

Figure 3.6: *Left panel* – The local density versus $f_{\rm TIM}$ plot for our spectroscopic cluster members, using the three different measures derived in Poggianti et al. (2008). The local densities are given as the logarithm of the number of galaxies per Mpc^2. We calculated the $f_{\rm TIM}$ within three equal size bins for each measure, and the markers are displayed at the centers of their respective bins. Green circles show the result with the SBS local density measure, orange squares for the IP measure, and gray diamonds for the PhotZ measure. Please see text in §3.5 and Poggianti et al. (2008) for the details. We also display the $f_{\rm TIM}$ results for our field samples, from Figure 3.3, to the left of our local density results. We note that we did not measure local density for our field samples, and the field results here are presented at an arbitrary point on the LogDensity axis (we indicate this region of the plot with the vertical purple line). Our results show a mild boost in $f_{\rm TIM}$ at the highest density bins. *Right panel* – The phase space plot of the IP local density measure. The color bar represents the local density in the IP measure per spectroscopic cluster member, red colors for lower density and blue for higher. The orange line is as described in §3.4. We note the diversity in local density values within the $0.5 \times R_{200}$ of the cluster environment, ranging from the lowest values all the way to the highest.

restrict ourselves to the local density measurements for cluster members. Poggianti et al. (2008) made use of the EDisCS photometric catalogs to derive the local density per spectroscopic cluster member using three different methods. The first method uses every galaxy in the photometric catalogs with the sample corrected using a statistical background subtraction (SBS). The other two methods use different ways of determining photometric membership, one requiring the integrated probability that the galaxy is within $\pm 0.1z$ of the cluster to be above a certain threshold for two different photometric redshift codes (hyperz, Bolzonella et al. (2000), and the code of Rudnick et al. (2001), and the other accepting a galaxy as a cluster member if its best photometric estimate using the hyperz code (Bolzonella et al., 2000) is within $\pm 0.1z$ of the cluster redshift. We label these measures as IP and PhotZ here respectively. We remark that the IP method is the accepted method of determining photometric redshift-based membership in EDisCS (Pelló et al., 2009), and that the photometric redshifts we use and present in this work comes from this method. We refer the interested reader to Poggianti et al. (2008), and subsequently to Pelló et al. (2009) and Rudnick et al. (2009), for the details of each method. We note that Poggianti et al. (2008) excluded some galaxies from their analysis for which reliable local densities could not be measured. For galaxies close to the edges of the field, the circular region containing the ten nearest neighbors extends off the image, hence these objects were taken out of the analysis. We therefore end up with a local density measure for 134 out of the 163 spectroscopic cluster members we use in our analysis. There are excluded objects from each of our 10 fields, with no bias towards rejecting more from a particular field.

We present the $f_{\rm TIM}$ versus local density plot in Figure 3.6, left panel, for all three measures of local density. For comparison purposes we also included our field $f_{\rm TIM}$ results from §3.3 for both of our samples to this plot, at an arbitrary point on the local density axis. Even though we do not measure their local densities, our field samples are reasonable choices to represent low local densities, as they exclude all group and cluster members. We find a mild boost in $f_{\rm TIM}$ at the highest density bin with the most significant increase seen for the IP density measure. This tentative enhancement is in agreement with the potentially higher $f_{\rm TIM}$ result at $R < 0.15 \times R_{200}$, in Figure 3.3.

We attempt to better understand the trends in $f_{\rm TIM}$ in the IP measure by looking at the distribution of local density values in the phase space, we show our results in the right panel of Figure 3.6. The plot reveals the diversity in the local density values at $R < 0.5 \times R_{200}$. The distribution does not show a monotonic decrease in local density with increasing radius. This nonmonotonic behavior could explain why we observe a flat relation in $f_{\rm TIM}$ in low and intermediate local densities in our clusters, as opposed to the tentative enhancement we find in clusters at $R > 0.5 \times R_{200}$, in Figure 3.3.

We have a small number of spectroscopic members per group and our photometric redshifts are not adequate to select a high completeness sample of group members (see §2.1). Therefore any local density estimate in our groups would suffer from significant systematic uncertainties, and we therefore choose not to compute local densities for our groups. Cooper et al. (2005) finds that a contiguous and relatively high sampling rate is essential for accurate local density measurements. Our field sample lacks this high sampling rate in the spectroscopic sample and supplementing it with photometric redshifts would induce significant systematic errors. Hence we do not calculate the local density for our field sample. We only present the $f_{\rm TIM}$ results from §3.3 on Figure 3.6.

3.6 Discussion

Our results imply that $f_{\rm TIM}$ does not depend strongly on redshift. The weighted best fits in our $f_{\rm TIM}$ versus redshift plots (Figure 3.1) reveal a tentative correlation for both our spectroscopic and photometric samples, but we cannot rule out the null hypothesis above 68% confidence in either case. We also find no correlation between $f_{\rm TIM}$ and cluster velocity dispersion (Figure 3.2). This result goes against the simplistic expectation that merger fraction should be higher for dense systems with lower velocity dispersion.

When we separate our galaxies into environmental classifications based on their position in the cluster, or their inclusion in clusters, groups, or the field (Figure 3.3), we find that $f_{\rm TIM}$ shows its most significant peak at $R > 0.5 \times R_{200}$ in clusters for our phot+spec sample. Our spec sample shows tentative peaks of low significance at groups, at $R > 0.5 \times R_{200}$ and $R < 0.15 \times R_{200}$ within

the cluster environment. We relate this tentative enhancement within the innermost parts of the clusters to trends in local density later in this section. The high uncertainties in the group $f_{\rm TIM}$ due to low sample size inhibits us from being able to more definitively conclude that groups have higher $f_{\rm TIM}$. However, assuming this result holds let us consider its origin. Our groups have lower velocity dispersions than our clusters, yet have relatively high galaxy density, making them especially conducive for galaxy mergers and interactions to occur. Our results are therefore potentially in support of the preprocessing scheme, where groups serve as a preprocessing stage for the evolution of cluster galaxies (Zabludoff & Mulchaey, 1998; Fujita, 2004; Cortese et al., 2006; Dressler et al., 2013; Abramson et al., 2013; Vijayaraghavan & Ricker, 2013). Likewise, the outer regions of our clusters have lower galaxy-galaxy velocities and therefore may also host regions with an enhanced merger and interaction probability. We note that our sample is not equally represented outside of $0.5 \times R_{200}$, which may have an effect on the peak we see in $f_{\rm TIM}$ at cluster outer regions. We clearly need more TIM measurements in different environments to conclusively determine how $f_{\rm TIM}$ depends on detailed environment.

When we analyze the local environment of our spectroscopic cluster members (Figure 3.6), we see that $f_{\rm TIM}$ remains constant over the majority of the range of the cluster environment, with only a tentative enhancement in the highest density regions. The potential elevation of $f_{\rm TIM}$ at the highest local densities is driven mostly by the elevated $f_{\rm TIM}$ in the very centers of the clusters at $R < 0.15 \times R_{200}$, seen in our spectroscopic cluster members. The marginal enhancement we see in $f_{\rm TIM}$ at $R > 0.5 \times R_{200}$ is likely not reflected in the $f_{\rm TIM}$ versus local density plot because of the non-monotonic relation of local density and radius (Figure 3.6). As the phase space diagram of one of our local density measures displays (Figure 3.6), there is a high diversity in density values around $R = 0.5 \times R_{200}$. As discussed in §3.5, we are unable compute local densities reliably for the field or group galaxies, which limits our ability to understand how $f_{\rm TIM}$ behaves at intermediate and low densities outside of the cluster.

The potentially elevated $f_{\rm TIM}$ values in the outskirts of the cluster and in groups are broadly consistent with a picture in which galaxies are morphologically transformed before their passage

through the cluster core, and perhaps even before their entry into the cluster. Thus, the morphology-density relation might not be driven by processes specific to clusters. As far as our results for the core regions of clusters, it is not clear what drives the marginal elevation in $f_{\rm TIM}$ at $R < 0.15 \times R_{200}$, although it is possible that the much higher densities make conditions favorable for high-speed tidal interactions without actually increasing the merger and interaction rate. Given the marginal signal we cannot make any more definitive statements at this time. Similar to our results, Adams et al. (2012) find that the fraction of tidally disturbed galaxies drops within $0.5 \times R_{200}$. Within the considerable uncertainties of our $f_{\rm TIM}$ measurements, this agrees with our result that $f_{\rm TIM}$ drops within $0.5 \times R_{200}$, but may be inconsistent with the slight increase in $f_{\rm TIM}$ that we see at the very highest densities and smallest ($R < 0.15 \times R_{200}$) clustercentric radii. If this discrepancy turns out to be real, it could be due to the different tidal interaction and merger classification techniques, or because their clusters are older and more dynamically developed, and therefore better at removing the faint tidal features that they measure.

Our results for global environment is broadly consistent with the conclusion we draw from an analysis of the phase space of our spectroscopic cluster members. When considering the cumulative distribution of $|\Delta V|/\sigma$ (Figure 3.5) we find only a 6% KS probability that TIM and undisturbed galaxies are drawn from the same distribution. The cumulative distribution of radii shows a higher KS probability, of 37% in this case, that the two samples are drawn from the same population. Nonetheless, these two phase space results are consistent with the modest differences in $f_{\rm TIM}$ seen in the environment plot. In our analysis we have assumed that the merger observability timescale is the same in all environments and at all redshifts in our study. For example, we have not accounted for the potentially shorter lifetimes of some TIM signatures, e.g. tidal tails, via interaction with the cluster tidal environment. Accounting for this particular effect would serve to enhance the $f_{\rm TIM}$ in cluster cores compared to our measured value. We will explore the implications for this phase space distribution in a future study that constrains the visibility timescale of our $G - M_{20}$ merger classification and compare it to the infall histories of our clusters as derived by simulations.

Chapter 4

Spectral Diagnostics of the EDisCS Spectra

To properly constrain the effects of TIM events on the star formation history our sample, we extract the stellar and gas kinematics, and the age distributions of the stellar populations of our sample via a spectral fitting. We give the details of the methods we use in this section. In §4.1 we present our spectral fitting methodology in detail. We discuss our data quality assurance efforts in §4.1.1, and the tests we have performed to assert the credibility of pPXF results in §4.1.2. We give the definitions of age-sensitive spectral indices we used in our analysis in §4.2. Finally, we conclude this chapter by providing examples of our spectral fitting in §4.3.

4.1 Method

We perform the full spectral fitting of our sample using the Penalized Pixel-Fitting (pPXF, Cappellari & Emsellem (2004), Cappellari (2017)) code. pPXF extracts the velocity distributions of the stars and the gas, and the details of the stellar populations in a given galaxy, by fitting its full spectrum with a linear combination of simple stellar population (SSP) models. Briefly, an SSP model is a collection of stars born at the same time, according to an initial mass function (IMF), from the same initial chemical composition. All the stars within an SSP therefore have the same metallicity value. This population is evolved to a certain age, keeping track of the stars that complete their lives, and the stars still are alive. We use the MILES stellar library (Vazdekis et al., 2016) as the template set for our spectral fitting. The library includes 144 total SSP models at 24 different ages, each of these having six metallicity values. The SSP's were generated using a Kroupa IMF (Kroupa, 2001). When fitting a galaxy, pPXF attempts to find the optimal weights for

the linear combination of these templates that best fit the galaxy spectrum, and outputs the mass weights of the templates. As the MILES templates are normalized to one solar mass, our fitting obtains mass-weighted fractions and not luminosity-weighted ones.

A major advantage of using the pPXF method is the regularization of template weights (more details in Cappellari (2017), Section 3.5). This procedure dampens noise-driven high frequency variations in the attempted fit, reducing the impact of noise on the best fit solution. In general, there are more than one solution consistent with the data. The regularization process preferentially selects the smoothest solution within the set of degenerate solutions equally consistent with the data. This prevents the best fit solution to be solely determined by a few stellar templates. Runs we have performed without utilizing the regularization feature returned grids with only a few non-zero weights, meaning that the entire integrated galaxy spectrum was fit with only a few SSP's, making the age-metallicity space physically non-realistic. Galaxies generally do not form their stars in modes of multiple bursts, and starbursts (see Chapter 1) are generally rare (Rodighiero et al., 2011) Regularization is therefore necessary for any use of the pPXF method that aims to study star formation histories and stellar populations of galaxies. It is important to note that regularization does not force the solution to be smooth. If required by the data, fit attempts with regularization will still return as sharp an age-metallicity space as the non-regularized attempt (e.g. for spectra featuring sharp star-bursts). Regularization will only favor smooth solutions when they are equally consistent with the data as non-smooth ones (Cappellari, 2017).

pPXF has built-in capabilities that can account for dust extinction. When fitting our spectra, we also use the dust reddening feature of pPXF, which uses a Calzetti et al. (2000) extinction curve. pPXF does not allow the use of multiplicative Legendre polynomials to correct the shape of the continuum for fits with dust reddening. Adding multiplicative polynomials can correct for potential incorrect flux calibrations, and therefore incorrect estimates of galaxy continuum levels. (Milvang-Jensen et al., 2008) details the careful flux calibration of the EDisCS spectra, and reports very high accuracy for our multi-object spectroscopy. We also choose not to include any additive Legendre polynomials for our fitting, as they alter line strengths and can obstruct the accurate

determination of the stellar populations.

4.1.1 Data Quality Assurance and Flagging

In this subsection we describe our efforts to ensure the credibility of the pPXF fit. First, we summarize our data processing and quality assurance. We begin by remarking that we tested the pPXF fit results using the full EDisCS spectra (987 spectra total), and not just the overlap with the EDisCS-HST sample (see §2.1), which is the data set we use for the analysis presented in this work. This larger sample size provided us with a better medium to investigate the quality of the pPXF fits.

The MILES stellar templates have a rest wavelength range of [3540Å, 7409Å]. The high wavelength end of this range is above the wavelength coverage of our spectra, but we have some galaxies that have data in wavelength values less than 3540Å. Therefore, as a first step for the fitting, we mask our spectrum to match the range of the MILES templates. The loss of around 100Å of data from a small subset of our galaxies very likely does not cause a significant issue for our analysis, as this is too small a range to critically affect the spectral fit, and it does not contain any spectral features of importance for our goals.

Another important data quality assurance step is the masking of unrealistic flux spikes that are present at the ends of a portion of our spectrum. We visually inspected the entire data set, and applied a wavelength mask to any spectrum that has these spikes, to make sure the fit is not affected by these spurious flux values.

Even with every effort, some of the spectra are not possible to be salvaged due to critical flaws. These can be caused due to low signal-to-noise ratio, or due to a sky line on top of a spectral feature of interest. We visually detected and flagged such spectra, and extract these from our final sample. Out of the 987 total spectra we have inspected, there were a total of 201 spectra we have flagged as unreliable. There are a total of 84 such objects in the spectroscopic sample we define in §2.1, and taking these out results in a total sample size of 182 quality-assured galaxies for our stellar populations analysis. The final sample, together with spectral index measures we derive, is given

in Table B.1.

We remark that the quality assurance flag we introduce here only pertains to the capability of extracting reliable spectral indices from a given spectrum. As such, this does not affect the spectroscopic sample we defined in §2.1, and used for the analysis in §3, for which the only requirement was the estimation of a reliable spectroscopic redshift. For any analysis that follows this chapter we only use the subsample of the spectroscopic sample that passes the quality assurance procedure detailed here, as the upcoming analysis requires the reliable detection of spectral indices.

We found that pPXF would fit low significance emission lines with very high velocity dispersion (1000 km/s) line configurations. To ensure physically meaningful emission line profiles we have limited the maximum velocity dispersion for the gas component at 400 km/s, so pPXF did not attempt to fit any lines broader than this limit.

4.1.2 Assessing the Accuracy of the pPXF Age Estimates

Before we analyzed the results of our spectral fitting with pPXF, we performed tests to assess the accuracy of the pPXF stellar population age estimates. We first determined how well pPXF could recover a single template age and metallicity when expressed as a mock observation with realistic spectral resolution and noise. To maintain similarity with our data, as a first step, we have convolved the MILES stellar libraries given at $FWHM = 2.51$Å to the FWHM of the FORS2 instrument, $FWHM = 6.0$Å. To do this we smoothed the template spectrum to the resolution of our data using a Gaussian kernel. Next, we added a Gaussian noise to the template, to make the procedure closer to actual measurements. We then fit this smoothed, noise-added spectrum with pPXF, using the full library. pPXF was able to recover the underlying template extremely well, only having minute residuals due to the smoothing and added noise. Following this, we perform a test attempting to fit random linear combinations of MILES templates. We made linear combinations of a young (Age < 0.5 Gyr), and an old (Age > 1 Gyr) stellar population, and added noise to the combined spectrum as in the single population test. pPXF managed to find the existence of two stellar populations, with the fit results showing two separate peaks in the age distributions.

We then tested our pPXF fitting using the MILES stellar library with a synthetic spectra generated by BC03, to assess whether this library is able to recover populations generated by a different code. Our fit results show that pPXF was able to recover the ages of BC03 generated SSP's accurately.

We tested the results of our fitting allowing the templates to be drawn from the entire metallicity range of the MILES library, and only allowing templates with a lower limit of $Z_{\odot}/10$ to be drawn. We found that this selection changes the detailed weights of the templates in age-metallicity space, but also found that none of the results presented in Chapter 5 are significantly affected by this choice. We decided to use the fitting where we only allow templates with metallicity values $Z > Z_{\odot}/10$, as this range is more appropriate for our massive galaxies at intermediate redshift. Furthermore, we performed another fitting where we change our metallicity limit to $Z > Z_{\odot}/5$, and found that this selection yields age estimates similar to the $Z > Z_{\odot}/10$ case, especially for ages younger than 0.5 Gyr. We also constrain the age of the stellar templates used for the fitting to be less than the age of the universe at the spectroscopic redshifts of each galaxy.

4.2 Spectral Indices as Age Indicators

The spectrum of galaxies carry age-sensitive features that can provide evidence for the existence of young or old stellar populations. One such feature is the 4000Å break, a strong discontinuity occurring at the rest-frame 4000Å region, is an index that increases as the stellar populations of galaxies get older. This break is the result of the accumulation of many spectral lines, specifically spectral lines present in the atmospheres of cool stars, in a relatively small wavelength range. These lines will be ionized in hot stars, making the 4000Å break small for young stellar populations and large for stellar populations with old and cool stars (Rudnick et al., 2000; Kauffmann et al., 2003). The strength of the 4000Å break with the wavelength windows of Balogh et al. (1999), $D_{n,4000}$, is defined as

$$D_{n,4000} = \int_{4000}^{4100} F_\nu d\lambda \Big/ \int_{3850}^{3950} F_\nu d\lambda, \tag{4.1}$$

where F_ν is the galaxy flux given in units of frequency. We favor this definition of the 4000Å over the original definition by Bruzual A. (1983), as it is less sensitive to dust reddening by virtue of its shorter-wavelength baseline.

Another age-sensitive spectral index of importance for this work is the emission line free Balmer $H\delta$ absorption line, EW($H\delta_A$). Galaxies that experienced a period of heavy star formation activity, or a starburst, that ended 0.1-1 Gyr ago will feature high EW($H\delta_A$) values (Kauffmann et al., 2003). The peak strength of this index occurs when the massive O and B stars produced in the star formation activity terminate their evolution, and the light from the galaxy is dominated by A stars. We derive $D_{n,4000}$, and the equivalent width (definition below) of EW($H\delta_A$), and use these as age indicators in our analysis of the stellar populations of our sample in Chapter 5. We show the evolution of these indices for an SSP model with solar metallicity in Figure 4.1. The results in this figure are generated using the stellar population synthesis code by Bruzual & Charlot (2003) (which we will refer to as BC03 models the rest of the text). The left panel shows the evolution of $D_{n,4000}$, and that its value increases as the population gets older. The right panel shows how EW($H\delta_A$) evolves with time, and that this feature has its peak value before 1 Gyr.

The equivalent width of a spectral line is the width of the rectangle that has the height of the continuum, and has the same area as the spectral line. First, we determine a continuum level by fitting a line to the flux within the two continuum windows at either side of the feature bandpass. For absorption lines, the equivalent width is defined as

$$W_\lambda = \int_{\lambda_1}^{\lambda_2} \frac{F_C - F_\lambda}{F_C} d\lambda, \tag{4.2}$$

where F_C is the flux value of the continuum, F_λ is the observed flux per unit wavelength, and $\lambda_1 \& \lambda_2$ describe the feature bandpass. The equivalent width of emission lines is defined by the same expression but with a negative sign. We show the continuum region and feature bandpass

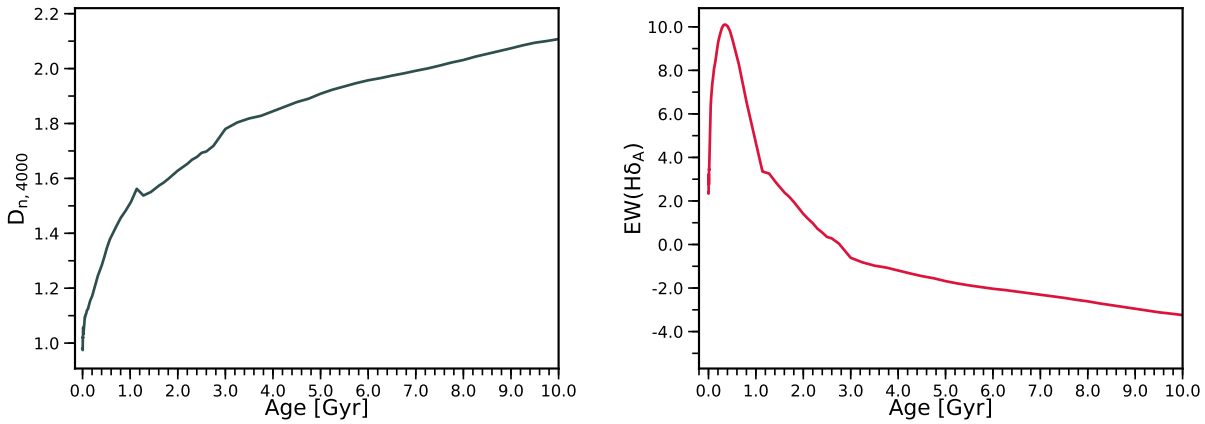

Figure 4.1: *Left panel* – The evolution of the narrow 4000Å break strength, $D_{n,4000}$, for a BC03 SSP model with solar metallicity. As discussed in §4.2, the value of this index increases as the stellar population gets older. *Right panel* – The evolution of the equivalent width of Balmer $H\delta$ absorption line, EW($H\delta_A$), for a BC03 SSP model with solar metallicity. This measure has its peak value before the population is 1 Gyr old, and after about 0.1 Gyr after the population is generated.

Table 4.1: Spectral Index Definitions

Index	Blue Continuum (Å)	Feature Bandpass	Red Continuum (Å)
$D_{n,4000}$	3850-3950	-	4000-4100
[OII]	3653-3713	3713-3741	3741-3801
Hδ	4030-4082	4082-4122	4122-4170
Hγ	4283-4319	4367-4419	4319-4363
Hβ	4827-4847	4876-4891	4847-4876

Column 1: Name of the spectral index. Column 2: Blue continuum window for the spectral index. Column 3: Feature bandpass Column 4: Red continuum window for the spectral index. Wavelength values are all given in Angstroms.

definitions for every spectral index we derive in Table 4.1.

pPXF features a library of emission line central wavelenths, and the spectral fit procedure returns the best fitting Gaussian at these locations. Within the common wavelength range of our data and the MILES stellar library, our fit returns the [OII] λ3726, [OII] λ3729, [OIII] λ5007 forbidden lines, and the Hβ, Hγ, Hδ Balmer lines. We derive the emission line equivalent widths using the this best fit to the galaxy gas component.

4.3 Example pPXF Fits

We demonstrate the results of the fitting procedure using two example galaxies from our sample of 182 galaxies total. In Figure 4.2 we present a galaxy with no signs of young (<1 Gyr old) stellar content. This galaxy features a strong 4000Å break strength, $D_{n,4000}$, and a low EW($H\delta_A$). Furthermore, in Figure 4.3 shows very weak levels of nebular emission. Figure 4.4 shows that this galaxy mainly also contains stars with high metallicities. The age fraction versus the logarithm of age plot we obtain by summing this grid over metallicities is shown in Figure 4.5. For comparison, we present an example elliptical galaxy in Figure 4.6, borrowed from Sparke & Gallagher (2007). We see that this galaxy shares critical characteristics with the galaxy we show in Figure 4.2. Our galaxy also features prominent CaII K and H absorption lines, and the G band at 4300 Å. Even if we do not present a quantitative treatment of the absorption lines of these heavy elements in our analysis, the old templates in the MILES libraries have these features in their spectra, and therefore pPXF uses them when estimating the mass-weighted age fractions.

Next, we present the star formation history (SFH) of this galaxy derived using the mass-weighted age fractions in Figure 4.7. To obtain this, first we obtain how much stellar mass is produced in each age bin by multiplying the mass-weighted age fractions with the total stellar mass of the galaxy. Next, we calculate the amount of time elapsed in the log age bins from Figure 4.5. Dividing the stellar mass produced in a bin by the time elapsed within the bin gives the star formation rate. The SFH we present in Figure 4.7 shows a decreasing star formation with time, and it reaches zero at around 1 Gyr.

An item of importance we need to discuss here is the signal-to-noise (S/N) ratios we present in each panel of our emission line fits, such as in Figure 4.3. As part of the fitting procedure, pPXF returns the formal 1σ uncertainty of the emission line fit for each gas component. However, the code documentation indicates that these values are only to be trusted in case the reduced chi-squared value of the fit is approximately one. We have found cases where the S/N derived using the pPXF uncertainty values were unexpectedly high, and therefore chose not to report the S/N values in this way. Instead, we derive the uncertainty in the flux values of each emission line

by performing a statistical sampling of the fit, utilizing the input galaxy spectrum and its errors. At each iteration of this procedure, we go to every single point of the discrete galaxy spectrum and generate a Gaussian distribution, where the data point serves as the mean, and its error as the standard deviation. We then draw a random point from this newly generated Gaussian distribution, and set it as the data point. We repeat this procedure until every point of the spectrum is modified in this way. Next, we perform a pPXF fit on this modified spectrum, and obtain the new fits to the emission lines, and the new gas flux values. We repeat this procedure 100 times, resulting in a distribution of flux values for each gas component within the spectrum. We use the 68% confidence interval of this distribution as the the formal 1σ error of the fit, and derive the S/N using this value instead of what pPXF returns via a fit to the original spectrum. We find that this procedure eliminates the unexpectedly high S/N ratios due to the unreliable errors returned by pPXF. However, this only corrects for the inaccurate estimation for the S/N values, and does not prohibit pPXF from subtracting low significance emission lines from the spectrum when fitting to obtain the stellar component. We discuss how we tested for the accuracy of our results in §5.7.

We finalize this section by presenting a galaxy that contains young stellar populations. Figure 4.8 shows a galaxy spectrum with spectral signatures indicating the presence of young stars. Contrary to the example we show in Figure 4.2, this galaxy features a low $D_{n,4000}$, and a high EW($\mathrm{H}\delta_{\mathrm{A}}$), indicative of its light being dominated by young stellar content. Similar to the old galaxy, we present the emission lines, age-metallicity grid, mass-weighted age fractions versus log(age), and the SFH of this galaxy in Figures 4.9-4.12. The SFH in Figure 4.12 implies that this galaxy has not formed any stars between 200-400 Myr before when it was observed, but started forming stars again at a rate of roughly 10 $\mathrm{M}_{\odot}/\mathrm{yr}$, around the age of 100 Myr. We note that the spike in star is potentially modified due to a systematic present in the pPXF fitting code when using MILES stellar libraries. We discuss the implications of this in Chapter 5, and in §5.7. Finally, we present the same figures in this subsection for the entire sample that pass the quality assurance checks we describe in §4.1.1 in Appendix C.

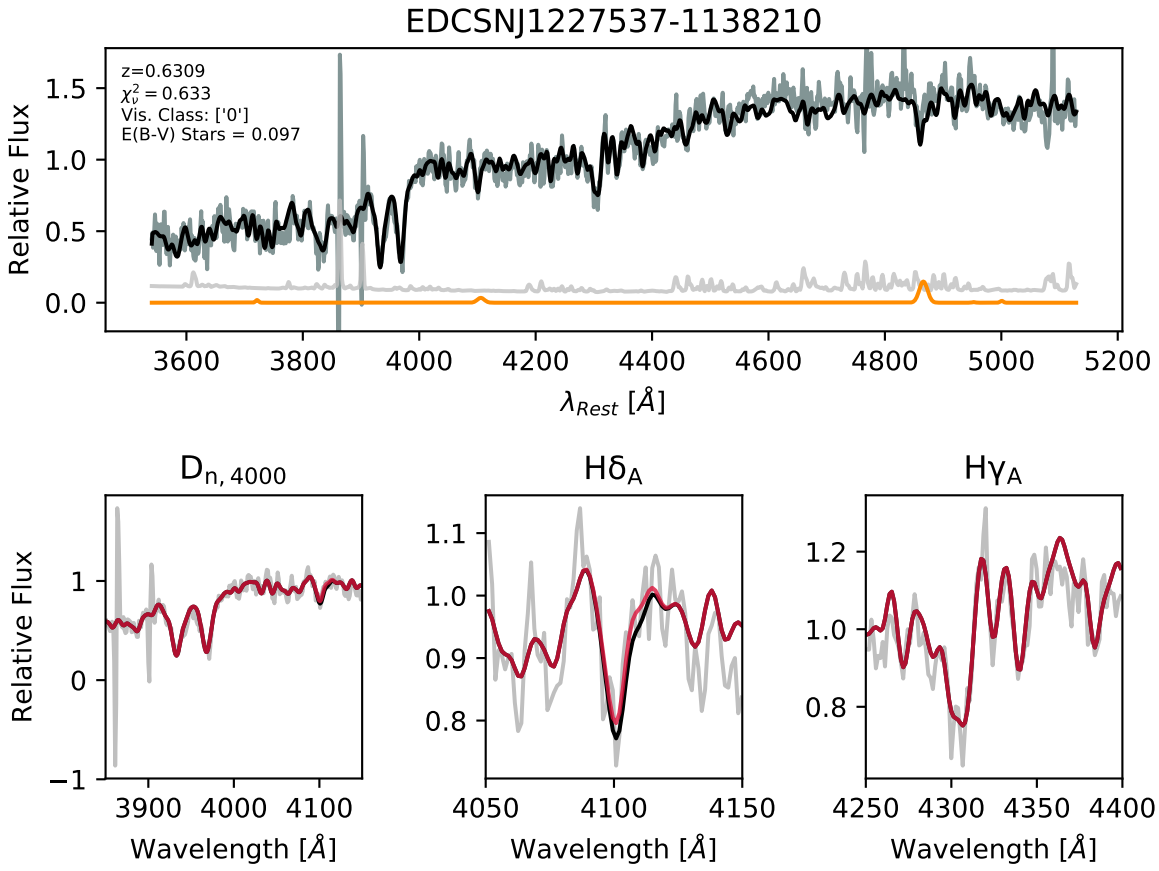

Figure 4.2: *Top panel* – The pPXF fit to the spectrum of EDCSNJ1227537-1138210, as described in §4.3. The dark gray line is the galaxy spectrum de-redshifted to its rest frame wavelength. The black line plotted on top of the galaxy spectrum is the pPXF fit to the stellar content only, i.e. after emission lines have been removed. The orange line is the fit to the gas component, and the light gray line behind it is the error in the galaxy flux. *Bottom panels* – The bottom left, middle, and right panels are zoomed views of a selection of spectral features. Shown here from left to right are the narrow definition of the 4000Å break, the $H\delta$ absorption line, $H\delta_A$, and the $H\gamma$ absorption line, $H\gamma_A$. The black line is the same as the top panel. The red line in these panels is the pPXF best fit to the spectrum, which is the sum of the fits to the stellar content and the gas content. As explained further in §4.3, this galaxy does not show evidence of a significant amount of young stars.

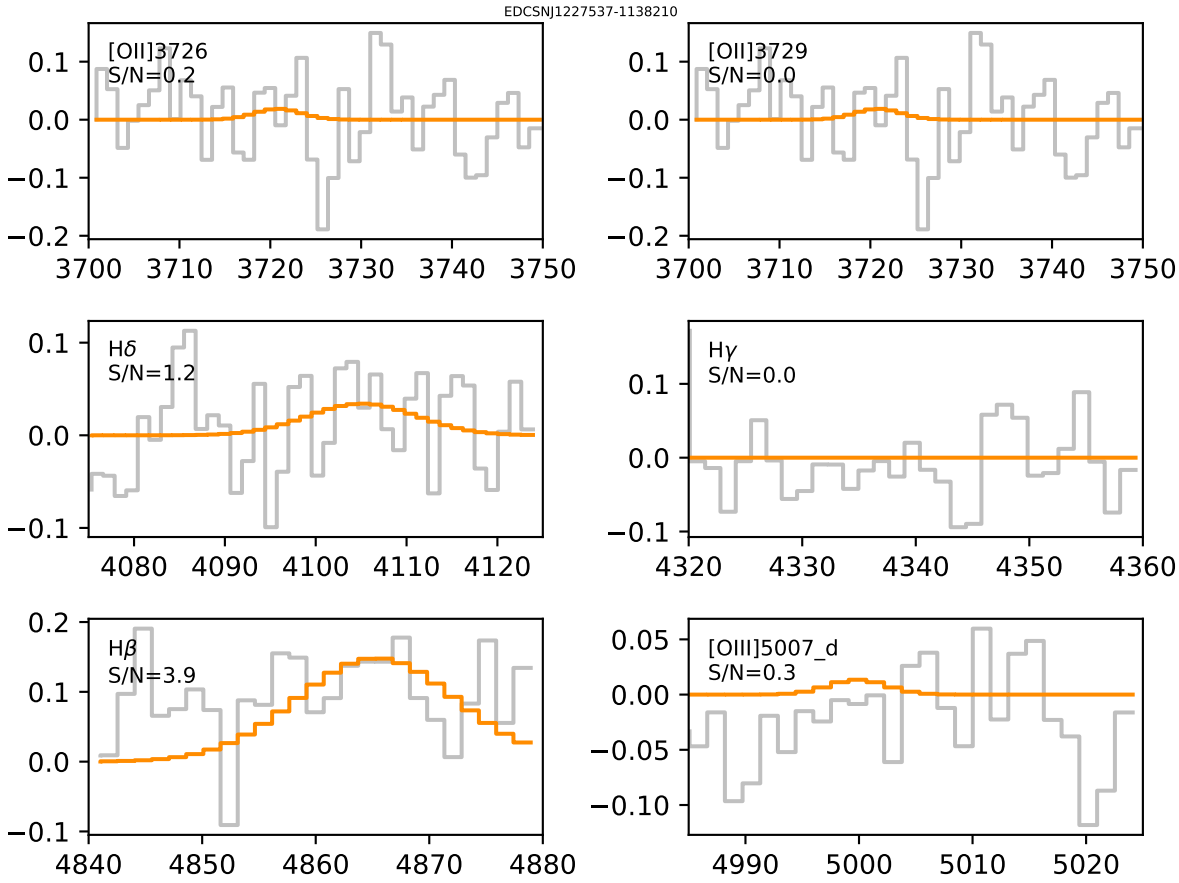

Figure 4.3: The pPXF fit to the gas emission lines of EDCSNJ1227537-1138210. The gray line is the flux of the galaxy that remains after the pPXF best fit to the stellar component (black line in Figure 4.2) is subtracted, and the orange line is the pPXF fit to this gas component (same as the orange line in Figure 4.2). This galaxy has weak levels of emission of low significance, as signified by the signal-to-noise (S/N) ratios included in the panels.

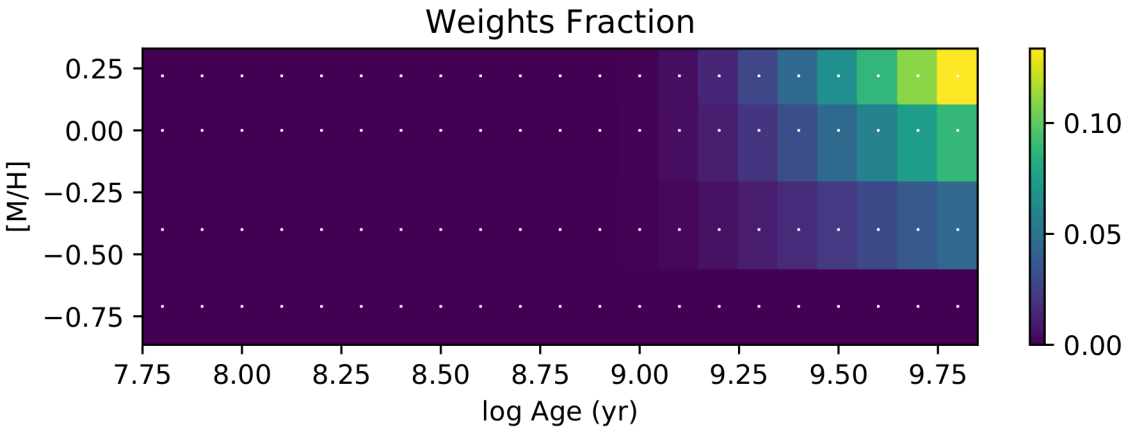

Figure 4.4: The pPXF age-metallicity grid to the spectrum of EDCSNJ1227537-1138210, as described in §4.1. The x-axis shows the logarithm of the age, in units of years. As explained further in §4.3, this galaxy shows no evidence towards the presence of young stars. The pPXF fit also indicates that this galaxy does not have a significant amount of young stellar populations.

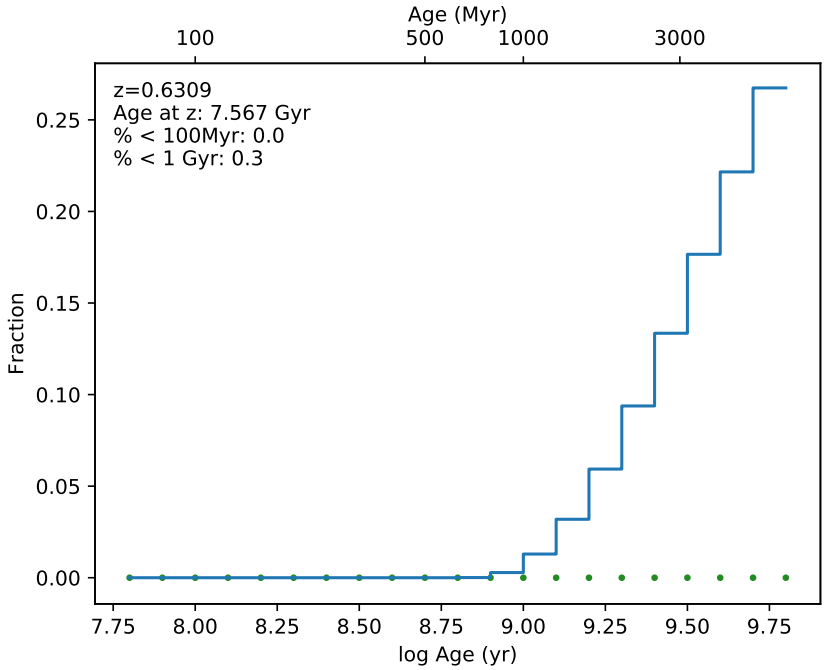

Figure 4.5: The pPXF mass-weighted age fractions of EDCSNJ1227537-1138210, derived by summing over the metallicities of Figure 4.4. We see that this galaxy shows no presence of young stars, in support of the age diagnostics we discussed in §4.1.

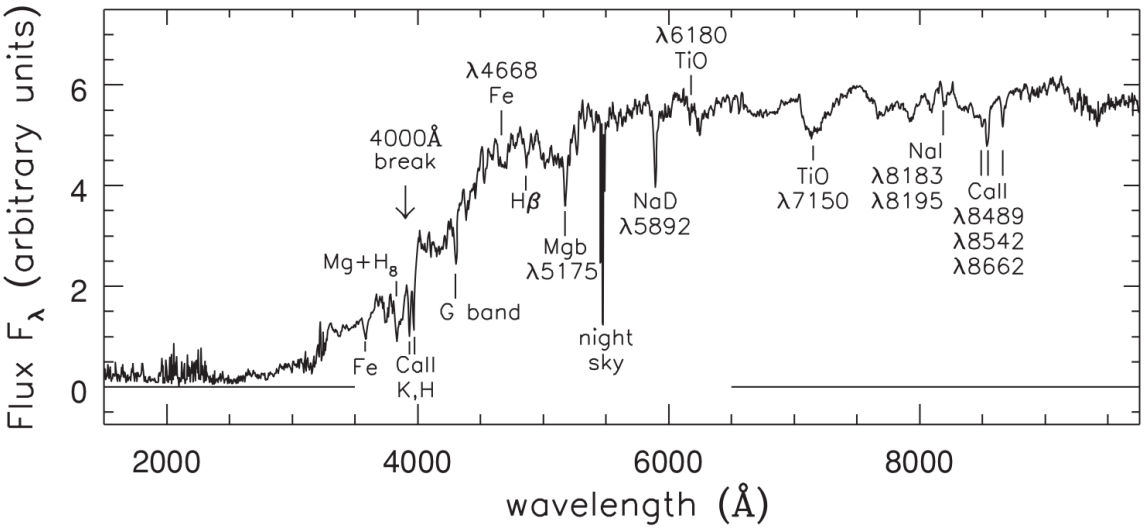

Figure 4.6: Example spectrum of an elliptical galaxy, borrowed from Sparke & Gallagher (2007). We notice the similarity this spectrum has with the galaxy we present in Figure 4.3, within their common wavelength range. As in this example, our galaxy also features strong CaII K and H absorption lines, and the G band at 4300 Å.

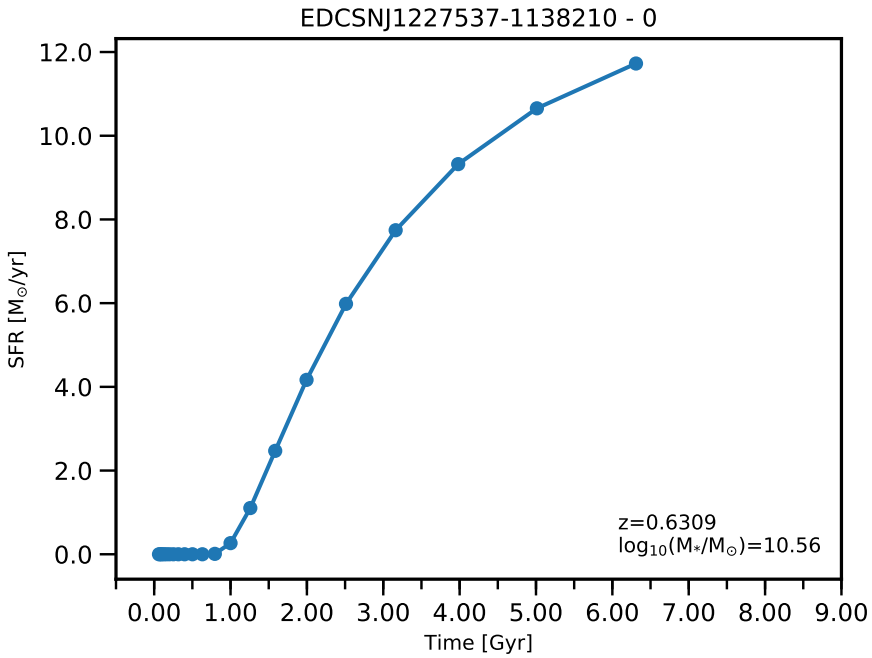

Figure 4.7: The star formation history (SFH) of EDCSNJ1227537-1138210, which we derive by using the pPXF mass-weighted age fractions shown in Figure 4.5. The star formation rate is given in units of solar masses per year. We discuss how we derive the SFH in §4.3. Confirming our findings in the plots above, this galaxy has no star formation past 1 Gyr.

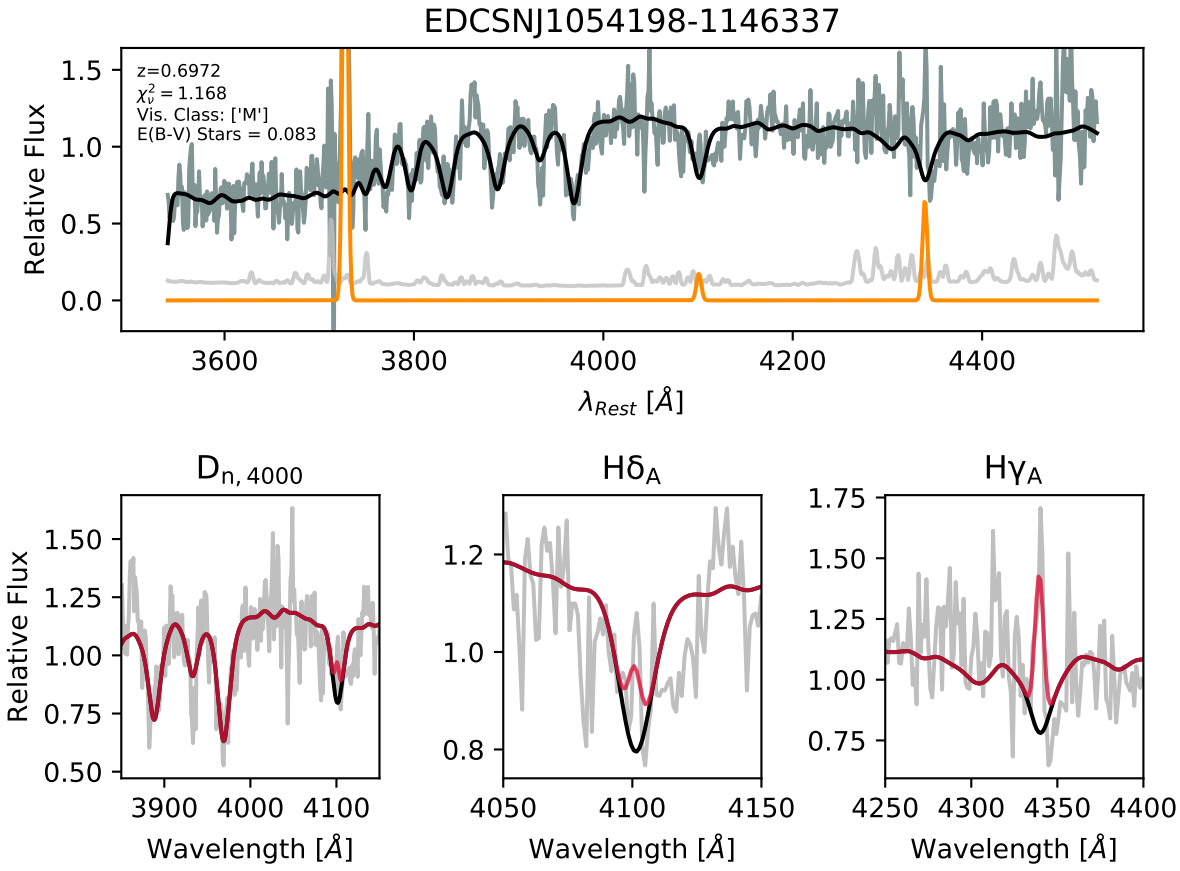

Figure 4.8: The pPXF fit to the spectrum of EDCSNJ1054198-1146337, as described in §4.1. Panels and lines are the same as in Figure 4.2. As explained further in §4.3, this galaxy shows evidence pointing towards the presence of young stars.

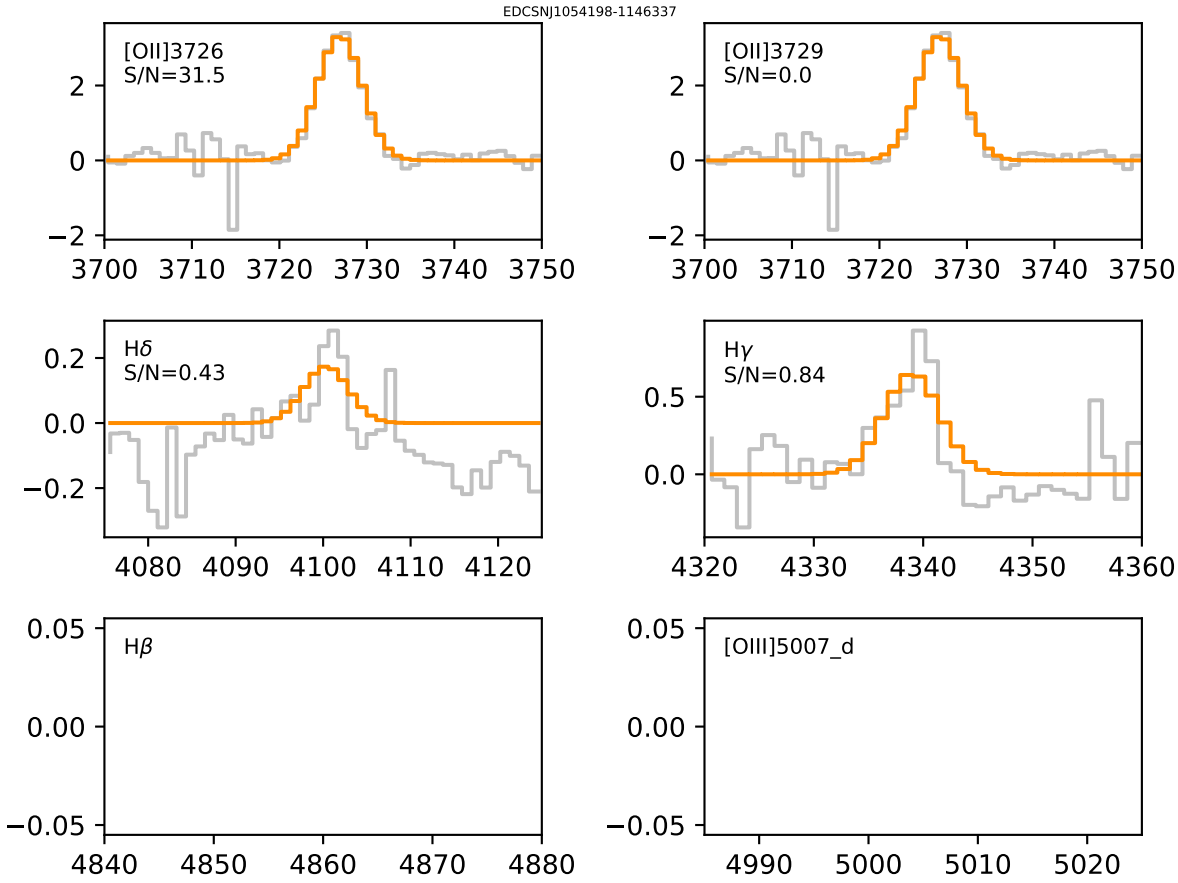

Figure 4.9: The pPXF fit to the gas emission lines of EDCSNJ1054198-1146337. The gray line is the flux of the galaxy that remains after the pPXF best fit to the stellar component is subtracted (black line in Figure 4.8), and the orange line is the pPXF fit to this gas component (same as the orange line in Figure 4.8). Hβ and [OIII]λ5007 are outside the wavelength range of the galaxy spectrum, hence their panels are empty.

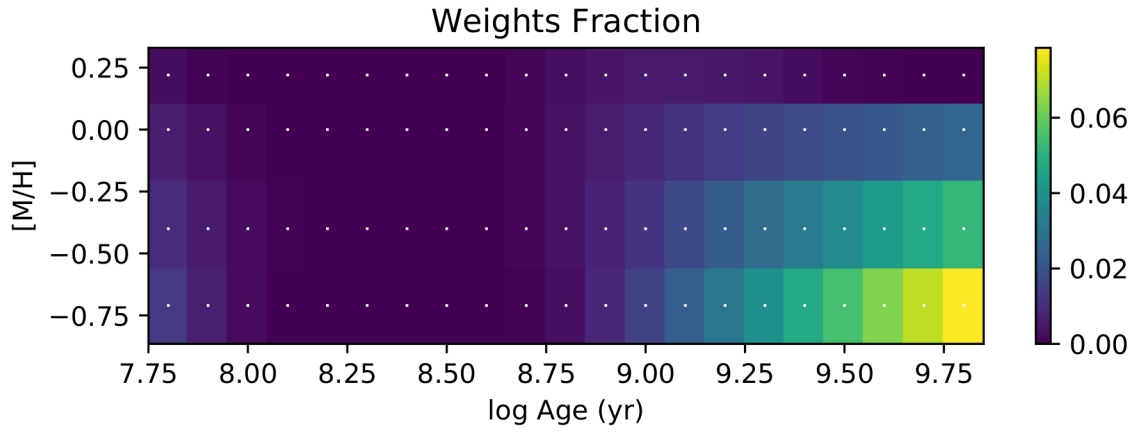

Figure 4.10: The pPXF age-metallicity grid to the spectrum of EDCSNJ1054198-1146337, as described in §4.1. As explained further in §4.3, this galaxy shows evidence pointing towards the presence of young stars.

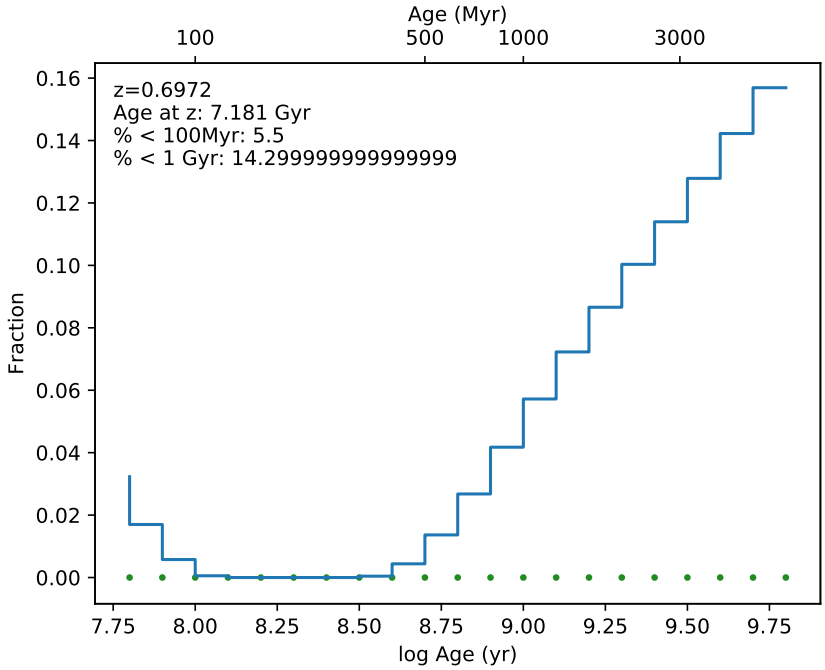

Figure 4.11: The pPXF age fractions of EDCSNJ1054198-1146337, derived by summing over the metallicities of Figure 4.10. As explained further in §4.3, this galaxy shows evidence pointing towards the presence of young stars, seen as the bump in the fraction of stars younger than 0.1 Gyr here.

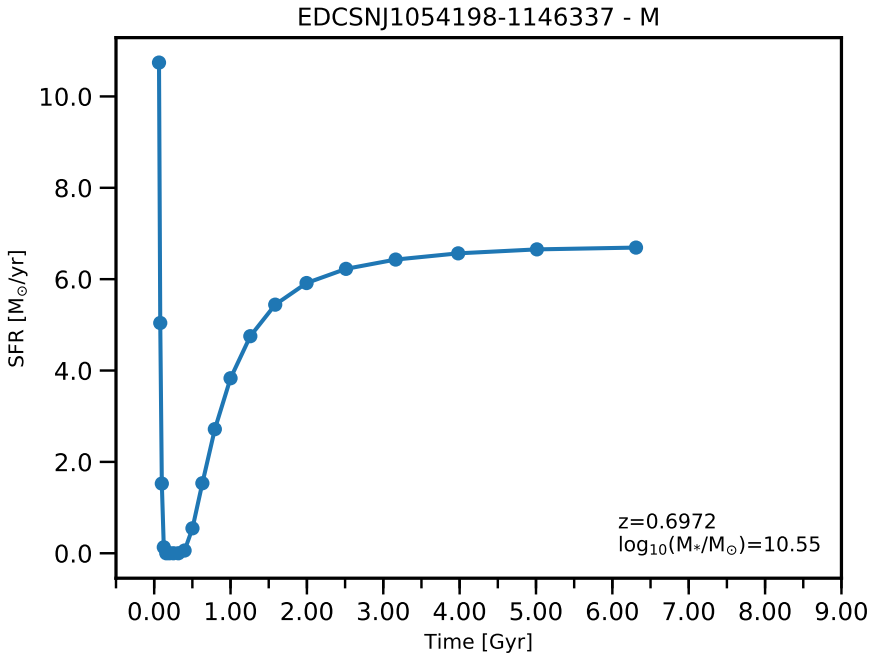

Figure 4.12: The star formation history (SFH) of EDCSNJ1054198-1146337, which we derive by using the pPXF mass-weighted age fractions shown in Figure 4.5. The “M ”in the title of the plot next to the galaxy id indicates that this galaxy is a visually classified merger. We discuss how we derive the SFH in §4.3. Confirming our findings in the plots above, this galaxy has a relatively high star formation rate in its last 100 Myr.

Chapter 5

Stellar Populations of the EDisCS Sample

Here we present the results of the stellar population analysis of our sample. In §5.1 we study our sample in EW($H\delta_A$) and $D_{n,4000}$ derived in §4.1 utilizing our deep spectroscopy. In §5.2 we show photometric diagnostics of the stellar population age, utilizing $(U-V)$ and $(V-J)$ plots, obtained using the multi-band EDisCS photometry, and describe how we classify our sample into star-forming or quiescent. We present the results using the mass-weighted age fractions we derived as a result of our spectral fit in §5.3. Next, in §5.4, we analyze the results of these three sections in conjunction. We revisit the $G-M_{20}$ space with star-forming and age diagnostics in §5.5, and revisit the phase space in §5.6.

We note that the entire analysis presented in this chapter uses the part of our spectroscopic sample that pass the quality checks we detail in §4.1.1.

5.1 EW($H\delta_A$) versus $D_{n,4000}$

In this section we present our analysis of two age-sensitive spectral indices we derived in Chapter 4, the equivalent width of Hδ Balmer absorption line, EW($H\delta_A$), versus $D_{n,4000}$. We derive the narrow 4000Å break strength, $D_{n,4000}$, following the wavelength window definitions of Balogh et al. (1999) (see 4.1 for details). We present the EW($H\delta_A$) versus $D_{n,4000}$ plot of our entire spectroscopic sample that pass the quality assurance checks we described in §4.1.1, including members from clusters, groups, and the field, in the top panel of Figure 5.1. As we describe in §4.2, galaxies whose light mainly comes from young and old stars occupy different regions of the EW($H\delta_A$)-$D_{n,4000}$ plane. Galaxies whose light is dominated by old stars reside in the lower

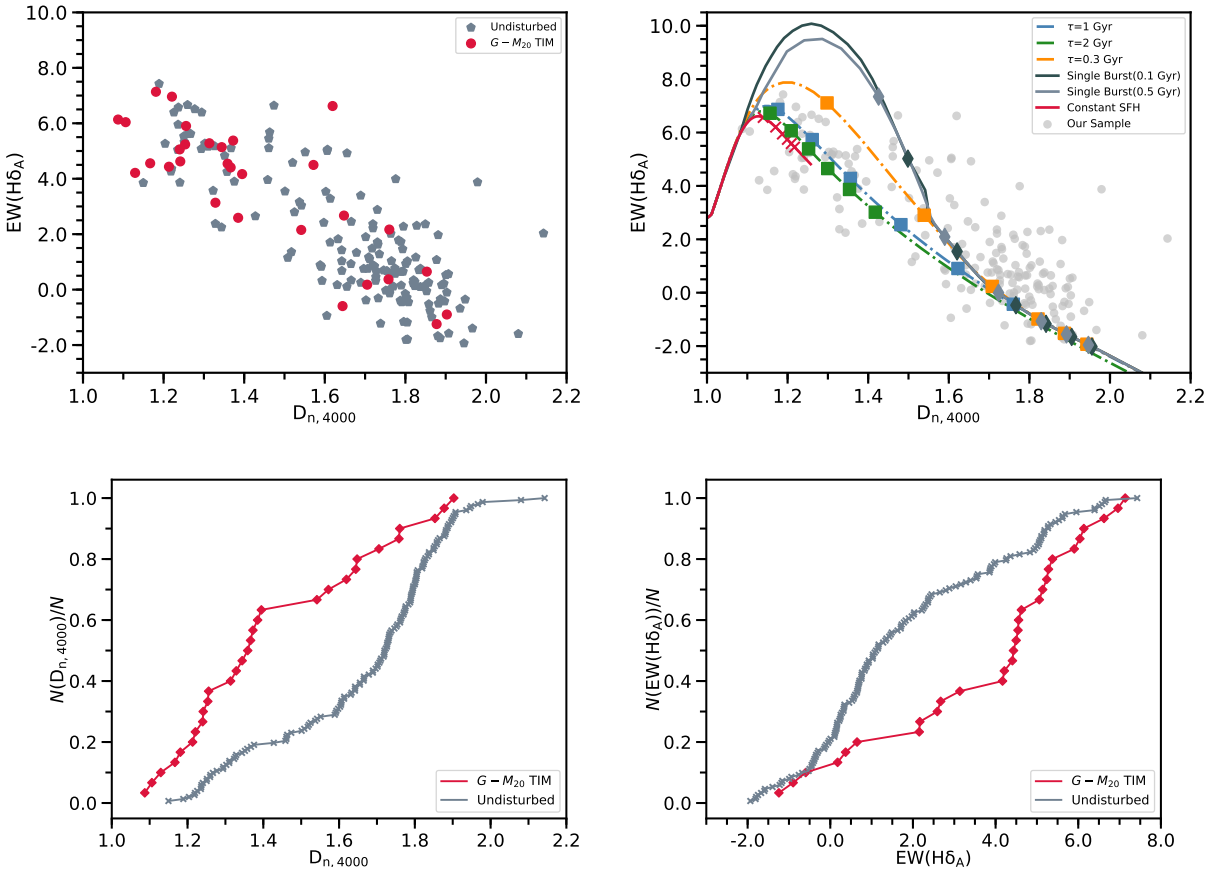

Figure 5.1: *Top left panel* – Equivalent width of Balmer $H\delta$ absorption line, EW($\mathrm{H}\delta_\mathrm{A}$) versus $D_{n,4000}$ plot for our sample. Gray markers represent the undisturbed objects, and the red markers are for the $G-M_{20}$ TIM galaxies. *Top right panel* – BC03 tracks showing the evolution of different models on the EW($\mathrm{H}\delta_\mathrm{A}$)-$D_{n,4000}$ plane, plotted on top of our sample (gray markers). Presented here are evolution tracks for a constant star formation rate model (red curve), two different single burst models (black curve: burst duration of 0.1 Gyr, gray curve: burst duration of 0.5 Gyr), and three different exponentially declining models (orange curve: timescale of 0.3 Gyr, blue curve: timescale of 1 Gyr, green curve: timescale of 2 Gyr). All models are evolved until a redshift of 0.6, which is approximately the median redshift value of our sample. 1 Gyr time periods are shown on the tracks as markers of the same color. Note that the upper limit of the y-axis is different for this panel, to make room for the burst models to fit. *Bottom left panel* – Cumulative histogram comparing $G-M_{20}$ TIM and undisturbed galaxies in their $D_{n,4000}$ distribution. Gray lines with markers represent the undisturbed objects, and the red lines with markers are for the $G-M_{20}$ TIM galaxies. *Bottom right panel* – Cumulative histogram comparing $G-M_{20}$ TIM and undisturbed galaxies in their EW($\mathrm{H}\delta_\mathrm{A}$) distribution. Lines and markers denote the same classes as the bottom left panel.

right, and the fraction of young stars in a galaxy increases as we move towards the upper left. We demonstrate this by providing the EW($H\delta_A$)-$D_{n,4000}$ evolution tracks of SSP's in the top left panel of Figure 5.1. Shown here are model tracks generated using the stellar population synthesis code by Bruzual & Charlot (2003) (BC03). We have generated multiple stellar populations, all with solar metallicity, but with different star formation histories and plotted their evolutionary tracks over our sample. The models we have generated include a model with constant star formation rate, two models generated in a single burst having burst durations of 0.1 Gyr and 0.5 Gyr, and three exponentially declining models with timescales of 0.3 Gyr, 1 Gyr, and 2 Gyr. These model tracks are the same as in the analysis presented in Rudnick et al. (2017). All the tracks start at the top left part of the EW($H\delta_A$)-$D_{n,4000}$ plane, and move towards the lower right as their stellar populations get older. Every model is evolved until a redshift of 0.6, which is roughly the median redshift of our sample. We notice that the constant star formation model fails to generate the distribution of our population, as its track stops before reaching a significant portion of our sample. The other models overlap with our sample well. We discuss the implications of this further in Chapter 6.

Visual inspection shows that the $G-M_{20}$ TIMs and undisturbed galaxies are distinguishable in their distribution on this space. The bottom right of the plane is dominantly populated by undisturbed galaxies. We display the distribution of these classes in these indices as cumulative histograms at the bottom row of Figure 5.1. The left cumulative histogram shows their distribution in $D_{n,4000}$, and the right in EW($H\delta_A$), revealing that the $G-M_{20}$ TIMs and undisturbed galaxies have different distributions in the EW($H\delta_A$)-$D_{n,4000}$ space. This is further reinforced by the two sample KS test results, finding a KS p-value of 6×10^{-5} when comparing the distribution of these two classes in $D_{n,4000}$, and 10^{-4} in EW($H\delta_A$). This leads us to conclude that the subpopulations of $G-M_{20}$ TIM and undisturbed galaxies are extremely unlikely to have been drawn from the same parent population in $D_{n,4000}$ and EW($H\delta_A$).

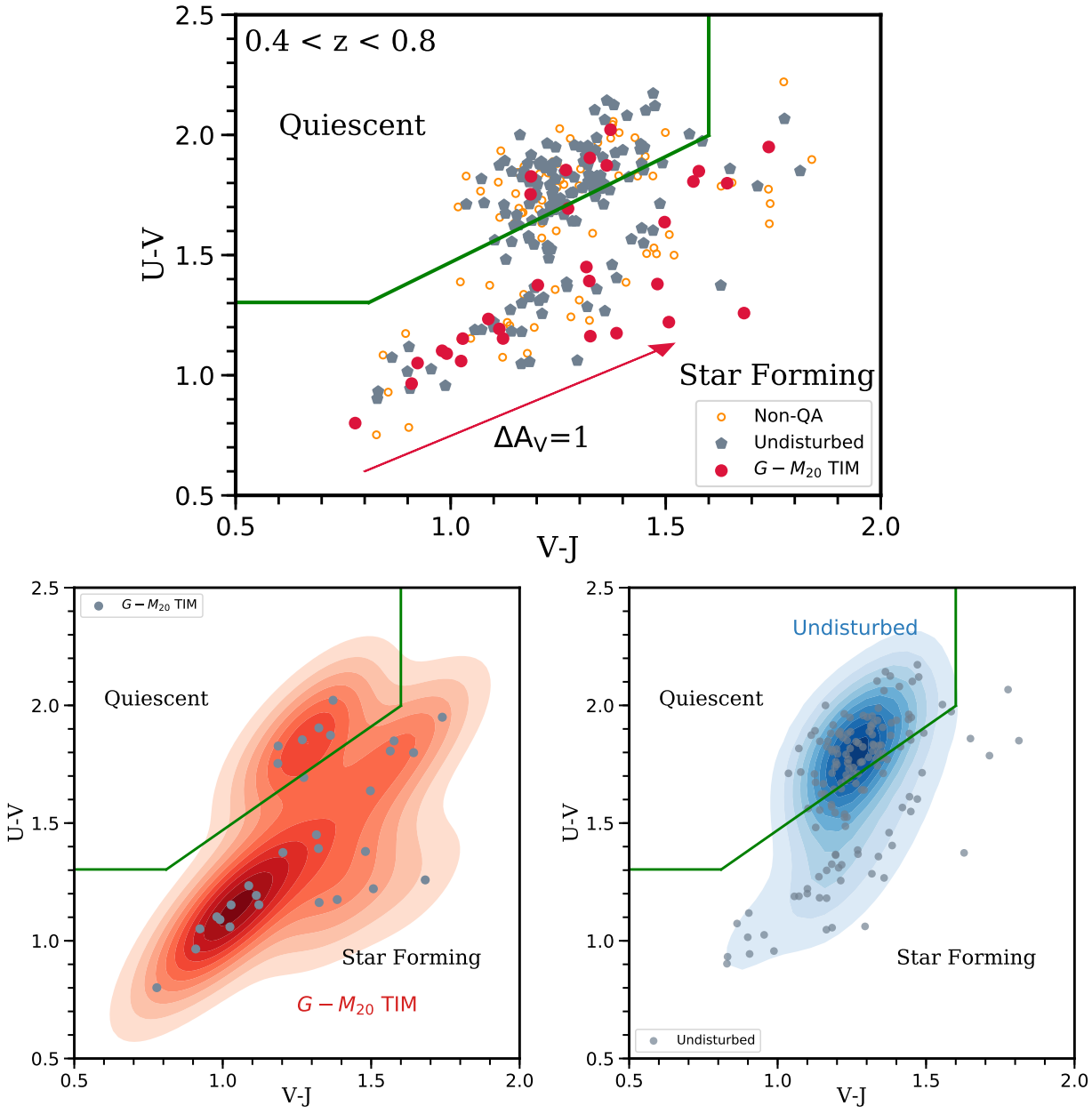

Figure 5.2: *Top left panel* – $(U-V)$ vs $(V-J)$ color plot for our entire, mass-complete spectroscopic sample. Blue stars represent the undisturbed objects, and the red circles are the $G-M_{20}$ TIM galaxies. The orange rings are the members of our spec sample that did not pass the quality assurance checks we describe in §4.1.1, but still have reliable redshift estimates. We note that the *UVJ* colors of these galaxies come from their photometry, and are therefore robust regardless of the problems they have in their spectra. The green line that separates the quiescent and star forming populations is from Williams et al. (2009), for the redshift range of $0.5 < z < 1.0$. The red dust vector indicates an extinction of $A_V = 1$mag. *Bottom left panel* – Bivariate kernel density estimate plot showing the distribution of $G-M_{20}$ TIMs on the *UVJ* diagram. Only the $G-M_{20}$ TIMs that pass the quality checks detailed in §4.1.1 are plotted. *Bottom right panel* – Bivariate kernel density estimate plot showing the distribution of undisturbed galaxies on the *UVJ* diagram. Only the undisturbed galaxies that pass the quality checks detailed in §4.1.1 are plotted. We note that the highest density regions do not correspond to the same number density in the bottom panels.

5.2 Photometric Age Diagnostics

Before presenting our results, we briefly summarize a technique commonly used to classify galaxies into star-forming and quiescent. For this classification we will make use of the multiband photometry of our data. One reason why we do not use our spectroscopic data to perform this classification is that the most reliable tracer of star formation in a galaxy spectrum, the Balmer ($H\alpha$ emission line at 6563 Å, falls outside of the range of our spectroscopic data. Even with measurements of ($H\alpha$, careful correction for dust reddening is essential for accurate estimations of star formation rates. The method we will describe and utilize here is powerful because it is much less susceptible to selecting dust reddened galaxies as quiescent ones.

Previous work (Wuyts et al., 2007; Williams et al., 2009) has shown that quiescent and star-forming galaxies form a bimodal distribution in the $(U-V)$-$(V-J)$ color-color space. Quiescent galaxies occupy a highly concentrated locus redder in $(U-V)$ color than in $(V-J)$, whereas star-forming galaxies form a distinct star forming strip extending through the UVJ diagram diagonally. Galaxies that are red due to dust reside at the redder colors both in $(U-V)$ and $(V-J)$, or at the red end of the star-forming strip, as dust affects these color indices in a similar fashion. Quiescent galaxies selected using the UVJ diagram therefore are red due to old stellar populations and a lack of active star formation, and not due to dust reddening.

In this subsection we present the results of the $(U-V)$ versus $(V-J)$ analysis of our sample. The top panel in Figure 5.2 shows the rest-frame $(U-V)$ versus $(V-J)$ color-color plot. We also include the galaxies in our spectroscopic sample with reliable redshift estimates that did not pass the quality assurance checks of §4.1.1 as empty markers in this panel. Via visual inspection, we conclude that their distribution is uniform on the space spanned by our data, and that their exclusion does not bias our results. We classify galaxies as quiescent if they reside within the top left window defined by the Williams et al. (2009) line, and star-forming if outside this partition. The bottom left and right panels of Figure 5.2 show the bivariate kernel density estimate (KDE) contour plots for the $G-M_{20}$ TIM and undisturbed subpopulations, displaying the best-fitting bivariate Gaussian kernels for the distribution of these classes. This is thus a two-dimensional

density estimate of these two classes on the UVJ diagram. Even if the number densities are not the same, these provide a visual representation of the distribution of $G-M_{20}$ TIM and undisturbed galaxies. These plots reveal that the distributions of $G-M_{20}$ TIM and undisturbed galaxies on the UVJ space are distinct. The undisturbed galaxies predominantly reside within the quiescent section of the plot, with their fraction at the quiescent section being much higher than the fraction of $G-M_{20}$ TIMs. The origin of this discrepancy, or whether it is caused by the TIM event that $G-M_{20}$ TIMs are going through is not immediately clear. We discuss this further in Chapter 6.

In Figure 5.3, we demonstrate the star-forming and quiescent populations defined from the UVJ diagram on the $(U-V)$-color versus stellar mass plot. This plot shows the contamination of galaxies that are red due to dust, at around $(U-V)=1.6$. The strong bimodal trend only reveals itself when $(U-V)$-color is plotted with the $(V-J)$ color. This validates the use of the bicolor UVJ plot, to make the classification into star-forming and quiescent more cleanly and with higher purity.

5.3 Ages of the Stellar Populations in the EDisCS-HST Sample

One of the crucial results of our spectral fitting is the amount of mass contained in stellar populations of different ages in our galaxies. As we present in detail in Chapter 4, we extract this information from the age-metallicity weights returned by pPXF, for stellar templates of known ages and metallicities. As an analysis of the metallicities is outside the primary scope of this work, we sum over the metallicities in the weights matrix, and obtain the distribution of the mass-weighted stellar ages.

A main goal of this work is correlating TIM signatures with changes in the stellar populations, and to do so requires constraining both timescales adequately. One aspect that hinders the process of constraining the precise effects of TIMs in galaxy evolution is the difficulty in constraining merger timescales. Previous work utilizing the $G-M_{20}$ method for merger detection in N-body hydrodynamics simulations quotes merger timescales of 0.2-0.6 Gyr (Lotz et al., 2008b), and 0.2-0.4 Gyr (Lotz et al., 2010b,a). These analyses use simulations to track the G and M_{20} values of

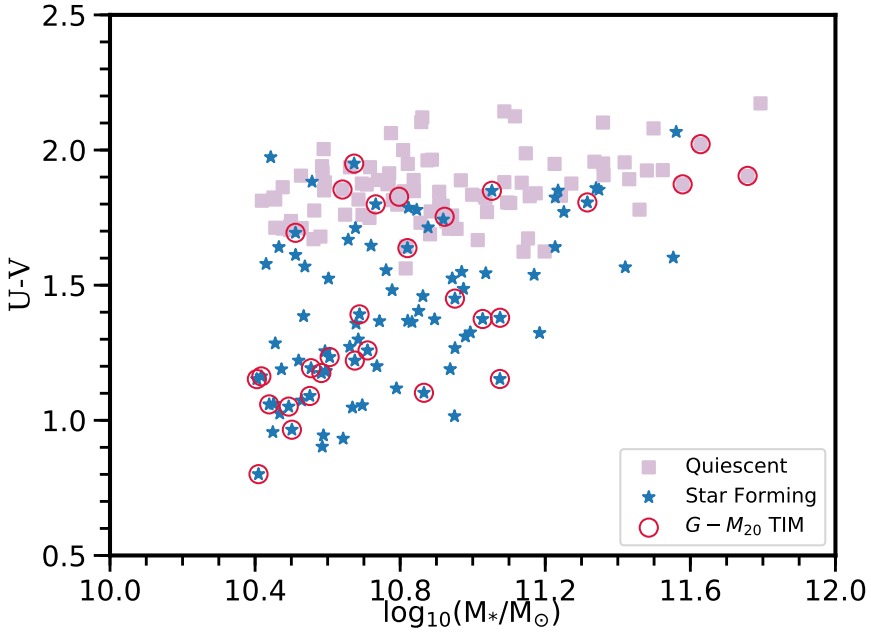

Figure 5.3: The $(U-V)$ color versus log stellar mass ($\log_{10}(M_*/M_\odot)$) plot. Blue stars represent galaxies residing at the star forming strip of the UVJ diagram, and purple squares are within the quiescent section. We indicate the visually classified TIM galaxies with a red ring around the data points.

merging galaxies as a function of time. The amount of time the merger event is selected as a $G-M_{20}$ merger, or remains above the selection threshold on the $G-M_{20}$ space, determines the observability timescale of the merger event. These results are shown to be robust against influence from many parameters, including the baryonic mass fractions, and the total mass fractions of the merging galaxies. Nonetheless, these timescales have a non-negligible range. With this in mind, and to be able to probe the shape of the SFH in a relatively large time range, we decided to analyze the fraction of stellar mass contained in four age intervals in our galaxies. We derive the fraction of stellar populations younger than 1 Gyr ($f_{Age<1.0\ \mathrm{Gyr}}$), between 1 and 0.5 Gyr ($f_{0.5<Age<1.0\ \mathrm{Gyr}}$), 0.5 Gyr ($f_{Age<0.5\ \mathrm{Gyr}}$), and 0.1 Gyr ($f_{Age<0.1Gyr}$) for our sample. This helps sample a wide time range to look for signatures of TIM-enhanced or -suppressed star formation activity. We choose not to look at ages higher than 1 Gyr, based on the observability timescales of merger events we quote above. Furthermore, determining the age distribution of galaxies becomes increasingly difficult and thereby inaccurate at older ages, especially with the the spectral indices contained in our wavelength range, and with the S/N of our data. The time period higher than 1 Gyr is outside of the range where we expect to see the effects of TIM events on the star formation of galaxies. Careful examination of the results for $f_{Age<0.1Gyr}$ reveals that for part of our sample, the star-formation histories show an atypical behavior. For these galaxies the star formation rate is zero for the 100-400 Myr interval, and then shows significant increase in the last 100 Myr. We conclude that this behavior is not realistic, and is a result of the fitting procedure. We discuss the possible causes for this in §5.7. We therefore decided to discard the results for the $f_{Age<0.1Gyr}$ case. This timescale is also relatively shorter than the merger timescale we quoted above, and therefore is not an ideal timescale to gauge the effects of TIM on star formation. Our analysis that follows will focus on comparing the mass-weighted age fractions at the age intervals of $f_{Age<0.5\ \mathrm{Gyr}}$, $f_{0.5<Age<1.0\ \mathrm{Gyr}}$, and $f_{Age<1.0Gyr}$.

This selection of age intervals results in two intervals of length 0.5 Gyr, and one of length 1 Gyr. To account for the unequal time intervals and to be able to compare them on equal footing, we derive the relative star formation rate of our galaxies during these periods, by dividing mass-

weighted age fraction with the length of the time interval, $f(\Delta t)/\Delta t$. $\Delta t = 0.5$ Gyr for $f_{Age<0.5\text{ Gyr}}$ and $f_{0.5<Age<1.0\text{ Gyr}}$, giving us the relative star formation rate in these time intervals in units of 1/Gyr. Using the relative star formation rates during these periods instead of age fractions themselves allows for the comparison of our results on equal footing, since the results for $f_{Age<1.0Gyr}$ would otherwise be biased by the time period being twice as long.

In Figure 5.4 we present the cumulative histograms for the $G-M_{20}$ TIM and undisturbed galaxies at these three age intervals. Furthermore, we have calculated the two sample KS p-values comparing these classes in all three, and found their respective p-values to be 2×10^{-4} for $f_{Age<1.0\text{ Gyr}}/\Delta t$, 3×10^{-4} for $f_{Age<0.5\text{ Gyr}}/\Delta t$, and 1.5×10^{-2} for $f_{0.5<Age<1.0\text{ Gyr}}/\Delta t$. The small p-values indicate that the $G-M_{20}$ TIM and undisturbed galaxies are unlikely to have been drawn from the same parent population in $f_{Age<1.0\text{ Gyr}}/\Delta t$ and $f_{Age<0.5\text{ Gyr}}/\Delta t$. The KS p-value is higher for $f_{0.5<Age<1.0\text{ Gyr}}/\Delta t$, indicating that the distributions of these classes are more similar in their relative star formation rates at $0.5 < t < 1$ Gyr.

5.4 Spectral Indices and Star Formation Indicators

In this section we analyze the age sensitive spectral indices we have derived together with the photometric diagnostics of our sample. We first examine the distribution of the UVJ-classified star-forming and quiescent galaxies on the EW($H\delta_A$)-$D_{n,4000}$ plane, in §5.4.1.

5.4.1 UVJ Classifications on the EW($H\delta_A$)-$D_{n,4000}$ Plane

As detailed in §5.2, we divide our sample into star-forming and quiescent using the UVJ diagram. In this subsection we revisit the EW($H\delta_A$) versus $D_{n,4000}$ plane when our sample is separated into star-forming and quiescent.

We present the EW($H\delta_A$) versus $D_{n,4000}$ plot with the star-forming and quiescent classification in Figure 5.5. Our results reveal that the star-forming galaxies preferentially reside at the high-EW($H\delta_A$) and low-$D_{n,4000}$ part of the plot, and the quiescent galaxies at the low-EW($H\delta_A$) and

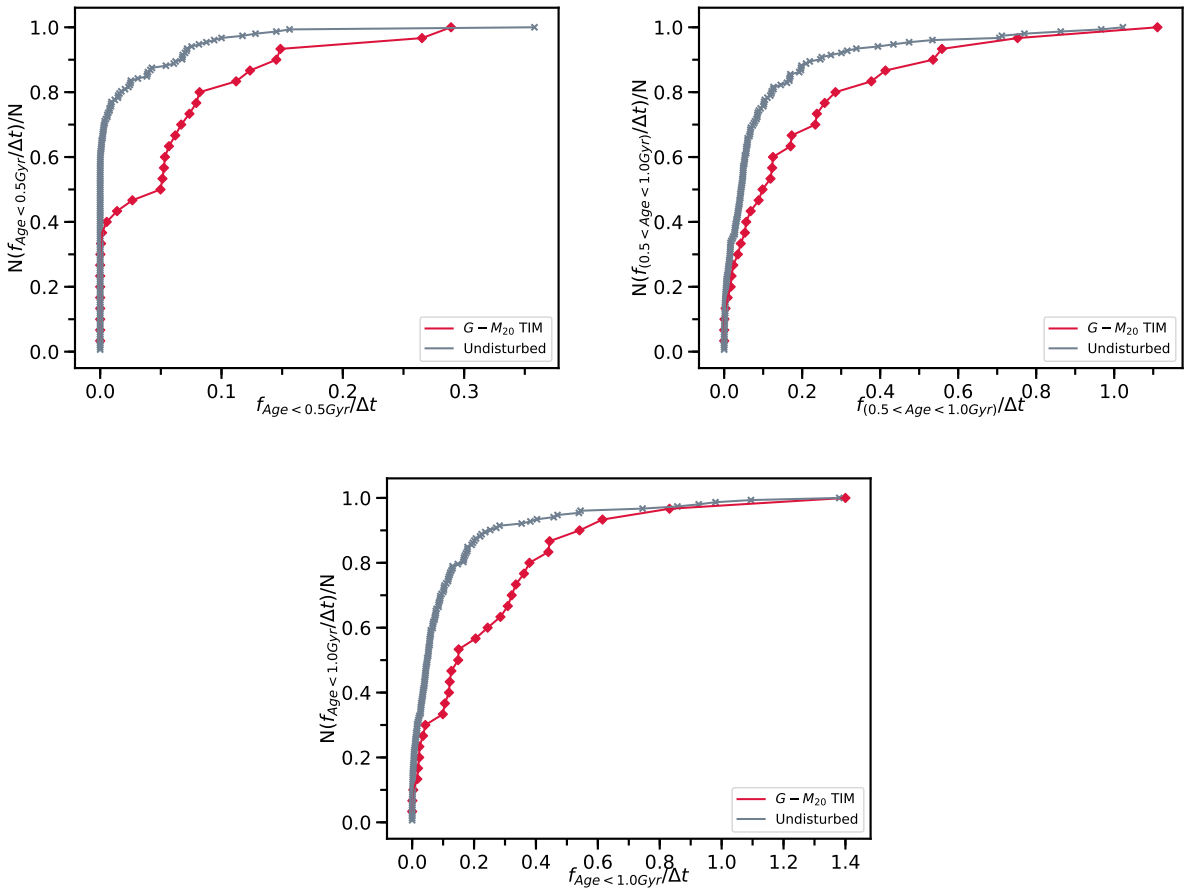

Figure 5.4: Cumulative histograms for $G-M_{20}$ TIMs and undisturbed galaxies in their relative star formation rates at the three age intervals; in their last 1 Gyr ($f_{Age<1.0\ \mathrm{Gyr}}/\Delta t$, Δt = 1 Gyr, bottom panel), last 0.5 Gyr ($f_{Age<0.5\ \mathrm{Gyr}}/\Delta t$, Δt = 0.5 Gyr, upper left panel), and between 0.5 Gyr and 1 Gyr ($f_{0.5<Age<1.0\ \mathrm{Gyr}}/\Delta t$, Δt = 0.5 Gyr, upper right panel). Gray line and markers represent the undisturbed galaxies, red line and markers represent the $G-M_{20}$ TIMs. KS p-values comparing these morphological classes are 3×10^{-4} for $f_{Age<0.5\ \mathrm{Gyr}}/\Delta t$, 1.5×10^{-2} for $f_{0.5<Age<1.0\ \mathrm{Gyr}}/\Delta t$, 3×10^{-4} for $f_{Age<1.0\ \mathrm{Gyr}}/\Delta t$.

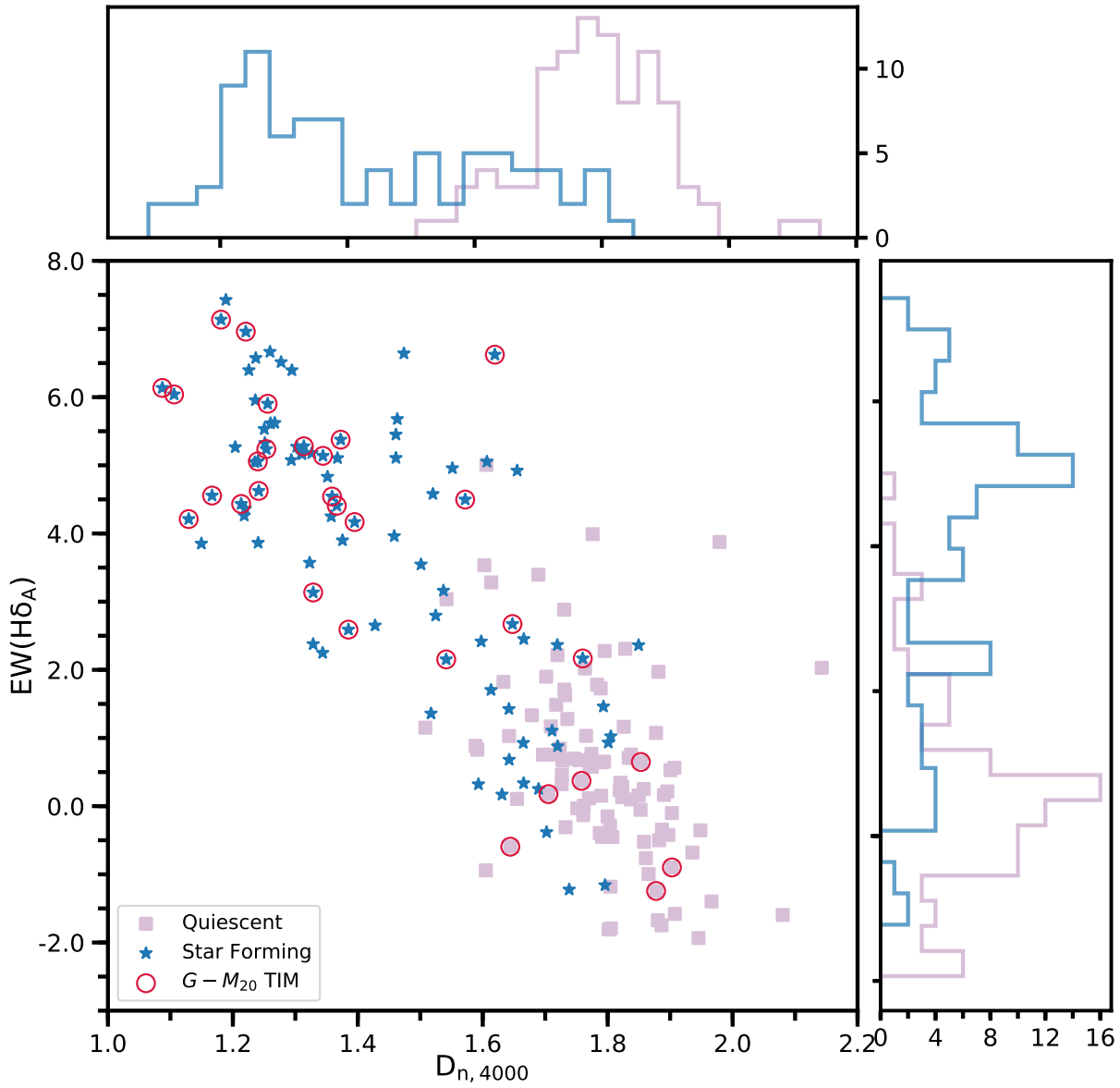

Figure 5.5: EW($H\delta_A$) versus $D_{n,4000}$ plot when galaxies are classified into star-forming and quiescent, according to their positions in Figure 5.2. Blue stars represent galaxies residing at the star forming strip, and purple squares are within the quiescent section. We indicate the $G-M_{20}$ TIM galaxies with a red ring around markers. Side-histograms exhibit the distribution of star-forming (blue histogram), and quiescent (purple histogram) in EW($H\delta_A$) in the right panel, and in $D_{n,4000}$ in the top panel.

high-$D_{n,4000}$. The star-forming population is more spread in both measures, whereas the quiescent population is more concentrated. None of our galaxies with $D_{n,4000} < 1.5$ or EW($H\delta_A$) > 5.0 are quiescent.

Next, we exhibit some results using an empirical measure derived from the distribution of our sample on the EW($H\delta_A$)-$D_{n,4000}$ space. For its derivation, we follow the prescription as described in Rudnick et al. (2017), which we summarize here. On this space, we estimate a best-fitting straight line going through our data points, and then choose an arbitrary line perpendicular to it, slightly above our data at the top left of the panel. We find that this new line that is perpendicular to the EW($H\delta_A$)-$D_{n,4000}$ relation of our sample has a slope of 7.2. Then, we calculate the distance of each of our galaxies to this new line. Even though the absolute values of this measure is not meaningful, as they depend on the arbitrary line chosen above the EW($H\delta_A$)-$D_{n,4000}$ relation, the relative values are indicative of EW($H\delta_A$)-$D_{n,4000}$ positions, and therefore ages of galaxy stellar content. Lower values of the distance measure indicate high-EW($H\delta_A$) and low-$D_{n,4000}$, implying young stellar populations; higher values indicate low-EW($H\delta_A$) and high-$D_{n,4000}$, implying old stellar populations. In effect, it is a diagnostic helpful in reducing the information contained in two age-sensitive parameters to one. We make use of this parameter in the analysis that follows, to illustrate the EW($H\delta_A$)-$D_{n,4000}$ positions of our sample on plots such as the $G-M_{20}$ plot.

We first show the UVJ plot color-coded by the distance measure in Figure 5.6. The plot reveals that the galaxies on the star-forming section of the plot dominantly have lower values of the measure, with the lowest values mainly residing at the blue end of the $(U-V)$ and $(V-J)$ colors. Galaxies in the dust extincted end of the star-forming strip have lower distances compared to the galaxies with no dust extinction. We find mainly intermediate values in this measure close to the border separating star-forming and quiescent galaxies. This potentially illustrates an evolutionary track; moving from the star-forming strip to the quiescent section, and moving down the EW($H\delta_A$)-$D_{n,4000}$ at the same time. Next, we find that moving towards redder $(U-V)$ colors results in an increase in the distance measure, irrespective of the galaxy being a $G-M_{20}$ TIM or undisturbed. This becomes especially pronounced when moving to redder $(U-V)$ in the quies-

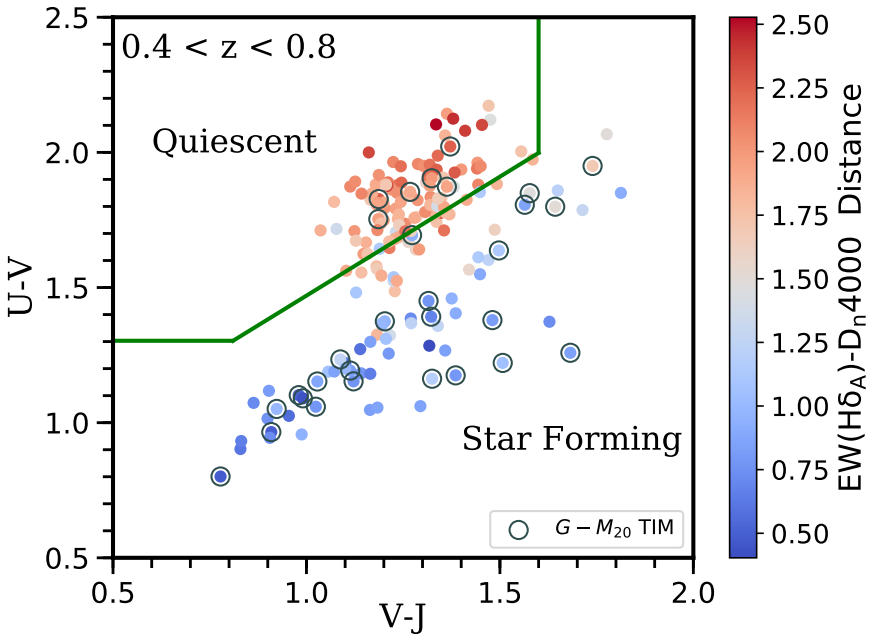

Figure 5.6: The UVJ diagram color-coded by the EW($H\delta_A$)-$D_{n,4000}$ distance measure, as described in Rudnick et al. (2017). Lower values, or blue marker colors indicate a galaxy with high-EW($H\delta_A$) and low-$D_{n,4000}$. Higher values, or red marker colors indicate a galaxy with low-EW($H\delta_A$) and high-$D_{n,4000}$. We indicate the $G-M_{20}$ TIMs with a black ring around data points.

cent section, the galaxies with the highest value of the distance measure, or oldest stellar content, reside close to the highest $(U-V)$ value. We will discuss this result further when we plot the UVJ-diagram with different fractions of stellar ages in §5.4.2.

Finally, we show the $(U-V)$ color versus stellar mass plot color-coded by the distance measure in Figure 5.7. This plot displays a high concentration of low fraction values at the blue end of the $U-V$ color. Red $(U-V)$ colors are mainly occupied by galaxies with high EW($H\delta_A$)-$D_{n,4000}$ distances, but with much more variance in the distribution. The high stellar mass end of $U-V$ colors are mainly high EW($H\delta_A$)-$D_{n,4000}$ distance galaxies.

5.4.2 Stellar Age Distributions on the UVJ Diagram

Having introduced key results of our spectral fitting, the mass-weighted age fractions and consequently the relative star formation rates, in §5.3, we now investigate how galaxies with different

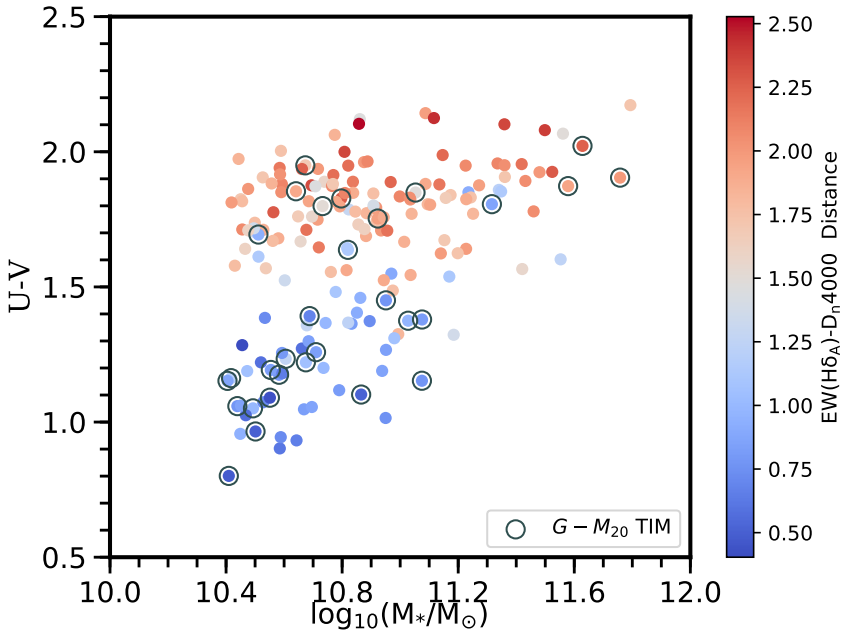

Figure 5.7: The $(U-V)$ color versus stellar mass ($\log_{10}(\mathrm{M}_*/\mathrm{M}_\odot)$) plot color-coded by the EW($\mathrm{H}\delta_\mathrm{A}$)-$D_{n,4000}$ distance measure. Lower values, or blue marker colors indicate a galaxy with high-EW($\mathrm{H}\delta_\mathrm{A}$) and low-$D_{n,4000}$ values. Higher values, or red marker colors indicate a galaxy with low-EW($\mathrm{H}\delta_\mathrm{A}$) and high-$D_{n,4000}$. We indicate the $G-M_{20}$ TIMs with a black ring around data points.

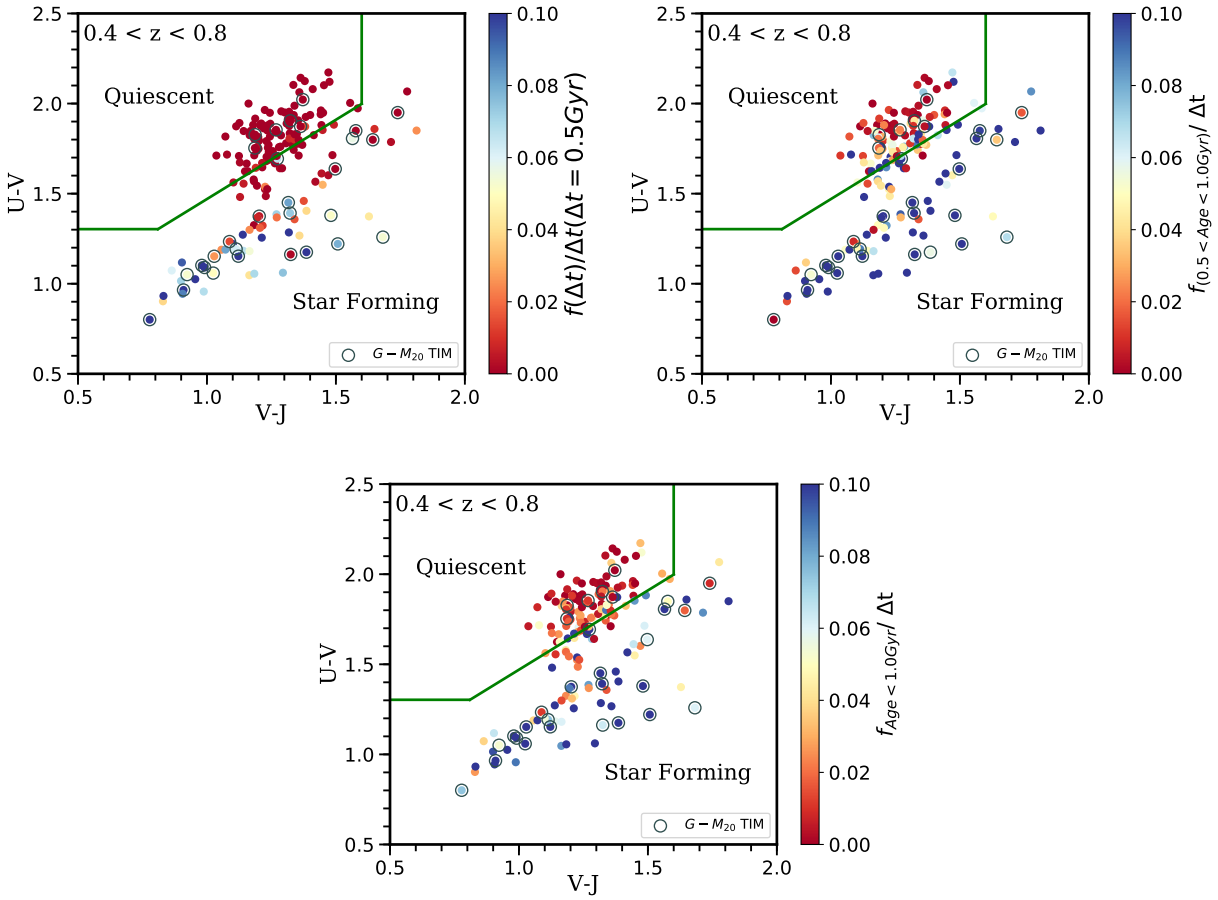

Figure 5.8: The UVJ-diagram color-coded by the ratio of the mass-weighted age fractions to the time interval, which equals to the relative star formation rate in that period. The age fractions are the three we introduced in §5.3, namely the fraction of stellar populations younger than 1 Gyr ($f_{Age<1.0\ \mathrm{Gyr}}$, bottom panel), 0.5 Gyr ($f_{Age<0.5\ \mathrm{Gyr}}$, top right panel), and between 0.5 and 1 Gyr ($f_{0.5<Age<1.0\ \mathrm{Gyr}}$, top left panel). The time interval, or Δt, is 0.5 Gyr for the top two panels, and 1 Gyr for the bottom panel. The colorbar maximum range for each panel has been set at 0.10, to avoid the color scale to be skewed by few galaxies with very high fractions. We indicate the $G-M_{20}$ TIMs with a black ring around data points.

stellar content is distributed in some of our plots we examined above. We start by reexamining the UVJ diagram with respect to the star formation rates in the three age periods defined in §5.3. Figure 5.8 shows our results for $f/\Delta t$ at these three separate age intervals. In this section and the sections below, instead of plotting the age fractions directly, we plot $f/\Delta t$, to account for the unequal time intervals. This converts these fractions to relative star formation rates, allowing each panel to be compared directly. We show this plot with $f_{Age<0.5\text{ Gyr}}$ and $f_{0.5<Age<1.0\text{ Gyr}}$ values directly in Chapter 6, when we compare these two periods in terms of star formation activity.

The plots all reveal that the higher rate values predominantly reside on the UVJ star-forming strip. All the galaxies in the quiescent section have zero star formation rate measured in their last 0.5 Gyr. This result indicates that the galaxies we classify as quiescent using their multi-band photometry also do not show any signs of star formation activity in at least their last 0.5 Gyr, as determined by our analysis of their deep spectroscopy. This changes as we look at the interval between 0.5 and 1 Gyr before the U-, V-, J-band magnitudes of these galaxies were measured. In the interval between 0.5 to 1 Gyr, we start to see galaxies with active star formation in the quiescent section, and close to the edge of the quiescent section. These galaxies have had star formation in the interval between 0.5 to 1 Gyr, but no star formation in their last 0.5 Gyr. This potentially implies these galaxies moved from the star-forming part of the UVJ diagram to the quiescent part in their last 0.5 Gyr. Some of the galaxies with low star formation activity in the last 0.5 Gyr might be in this state of transition at the time of the measurement. A good example to such a transition state is the E+A galaxies we introduced in §1.2. Galaxies in this category have had their star formations terminated recently, and are transitioning from blue galaxies to red ones. Several spectroscopic surveys find that they are much more common at intermediate redshifts, around $z \sim 0.6$, compared to low redshifts (Dressler & Gunn, 1983; Couch & Sharples, 1987; Tran et al., 2003, 2004; Poggianti et al., 2009). This is around the median redshift of our sample.

The result for the last 1 Gyr of our sample, which combines the results of the two periods we have discussed above, roughly outlines an evolutionary track on the UVJ diagram. Galaxies with the most star formation activity reside on the star forming strip, intermediate rates of star

formation close to the quiescent selection line, and galaxies with mainly low star or zero star formation activity higher up in the quiescent section. Non-zero rates for galaxies in or close to the quiescent section are mainly driven by their star formation activity between 0.5 to 1 Gyr. Finally, we also find some galaxies that have higher star formation activity in their last 0.5 Gyr, compared to their activity in 0.5 to 1 Gyr. We comment on these results further in Chapter 6.

We continue this analysis by investigating the relative star formation rates at these intervals on the $(U-V)$ color-stellar mass plane. We present our findings in Figure 5.9, one panel for each of the three age intervals. The top left panel shows that galaxies with redder $(U-V)$ colors, at $(U-V) > 1.5$, mainly have low star formation activity in their last 0.5 Gyr. The distribution at $(U-V) < 1.5$ shows a mixture of rates, with a clear trend not visually apparent. The results for the period between 0.5 to 1 Gyr, top right panel, also show the relative star formation rate estimates blended in this space. At the highest $(U-V)$ values, the galaxies with higher star formation activity generally have low stellar masses. Low and high fractions are mixed at red $(U-V)$ color, for the entire stellar mass range. This attests to the advantage of using the UVJ-diagram to classify star-forming and quiescent galaxies, as some of the high fraction galaxies at high $(U-V)$ are pushed out of the quiescent selection with the inclusion of the $(V-J)$ color information. Similarly, in the bottom panel of Figure 5.9, displays no strong trend apart from a rough separation of high rates at the blue, and lower fractions at the red $(U-V)$ color.

5.4.3 Stellar Age Distributions on the $\mathrm{EW}(\mathrm{H}\delta_\mathrm{A})$-$D_{n,4000}$ Plane

After revisiting the color-color, and color-stellar mass spaces when the star-forming properties of galaxies are considered in §5.4.2, we now reexamine the $\mathrm{EW}(\mathrm{H}\delta_\mathrm{A})$-$D_{n,4000}$ plane. In order to do so, we plot our sample on this plane color-coded by the relative star formation rates per interval, which is obtained by dividing the mass-weighted stellar age fractions by the length of the time interval. We show our results for the three age intervals in Figure 5.10.

Our results for the last 0.5 Gyr of our sample (Figure 5.10, top left panel) find the galaxies with highest relative star formation rates mainly reside at the top left part of the $\mathrm{EW}(\mathrm{H}\delta_\mathrm{A})$-$D_{n,4000}$

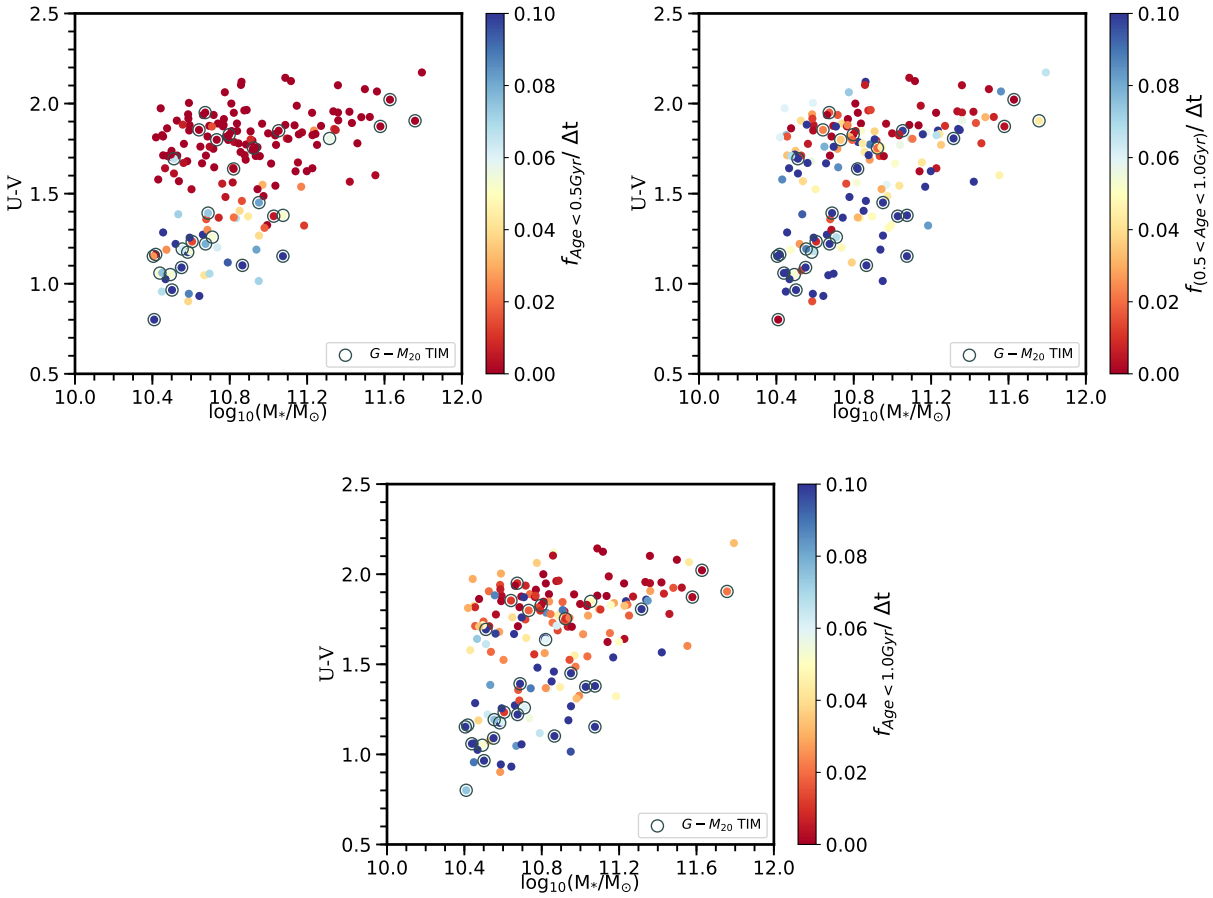

Figure 5.9: The $U-V$ versus stellar mass plot, color-coded by the ratio of the mass-weighted age fractions to the time interval, or the relative star formation rate in that period. The age fractions are the three we introduced in §5.3, namely the fraction of stellar populations younger than 1 Gyr ($f_{Age<1.0\text{ Gyr}}$, bottom panel), 0.5 Gyr ($f_{Age<0.5\text{ Gyr}}$, top right panel), and between 0.5 and 1 Gyr ($f_{0.5<Age<1.0\text{ Gyr}}$, top left panel). The time interval, or Δt, is 0.5 Gyr for the top two panels, and 1 Gyr for the bottom panel. The colorbar maximum range for each panel has been set at 0.10, to avoid the color scale to be skewed by few galaxies with very high fractions. We indicate the $G-M_{20}$ TIMs with a black ring around data points.

plane. As we discussed above, this region is also where we expect galaxies whose light is dominated by young stars. We start to see more intermediate rates going towards the bottom right of the panel on the EW($H\delta_A$)-$D_{n,4000}$ relation. Galaxies at the bottom half of this plot show no significant star formation activity in their last 0.5 Gyr. Towards the bottom of the EW($H\delta_A$)-$D_{n,4000}$ relation is where galaxies whose stellar content is dominated by old stars resides. Therefore, the distribution of galaxy star formation rates in their last 0.5 Gyr in this panel is in agreement with the characteristics of the age-sensitive spectral indices that form this plane. We find galaxies that have produced stars 0.5 Gyr before they were observed at the top left, and those with no significant star formation activity during this period at the bottom right.

Deriving this rate for the period between 0.5 to 1 Gyr (Figure 5.10, top right panel) reveals non-zero values during this period in galaxies that had zero rates in their last 0.5 Gyr. There are many galaxies in the bottom half of the panel that produced stars in the period between 0.5 to 1 Gyr. That these galaxies all have zero rates, and no significant fraction of young stars in their last 0.5 Gyr implies their star formation quenched some time during this interval.

Finally, we look at the interval covering these two periods, the last 1 Gyr of our galaxies. During this period, we see galaxies with high rates at the top left, intermediate values in the middle, and low values in the bottom right. This plot reveals an evolutionary scheme on the EW($H\delta_A$)-$D_{n,4000}$ plane, with galaxies having significant fractions of stars younger than 1 Gyr decidedly on the top left, intermediate values in the middle, and low values at the lower right. This result is in close association with the model evolutionary tracks we have shown in Figure 5.1. Furthermore, comparing the the top panels, we detect a population of possible post-starburst galaxies between EW($H\delta_A$) values of 4.0 and 7.0, and $D_{n,4000}$ values of 1.4 and 1.8. As the BC03 model tracks show, SSP's formed through bursts and exponentially declining SFH's follow tracks with an important difference at young ages on the EW($H\delta_A$)-$D_{n,4000}$. Burst models reach higher EW($H\delta_A$) values than the exponentially declining models. Models with bursts undergo their evolution through the general region we point out here. We discuss this further in Chapter 6.

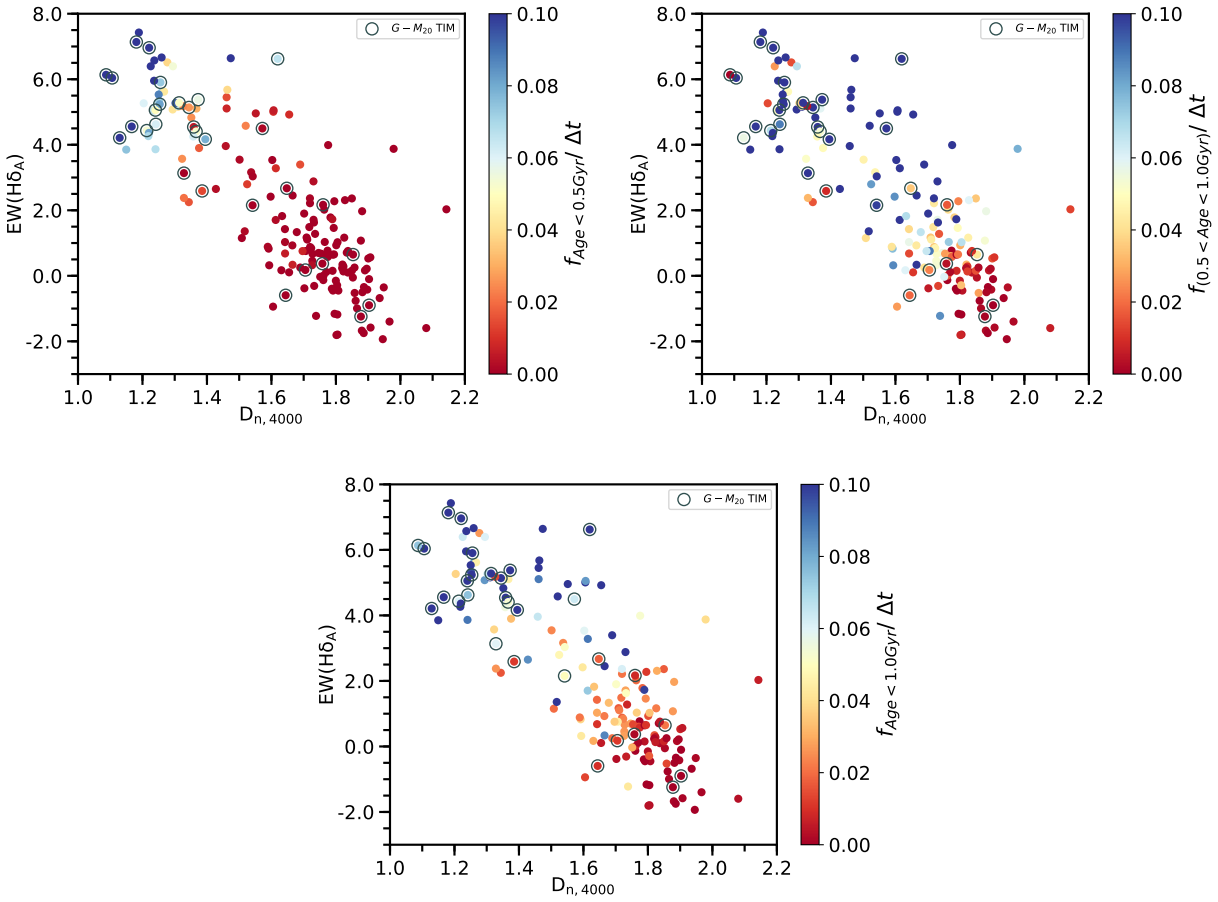

Figure 5.10: The EW($H\delta_A$) versus $D_{n,4000}$ plot, color-coded by their relative star formation rates within the intervals we introduced in §5.3. We show the relative star formation rate in the last 1 Gyr ($f_{Age<1.0Gyr}/\Delta t$ with $\Delta t = 1Gyr$, bottom panel), in the last 0.5 Gyr ($f_{Age<0.5Gyr}/\Delta t$, $\Delta t = 0.5Gyr$, top left panel), and between 0.5 and 1 Gyr ($f_{0.5Gyr<Age<1.0Gyr}/\Delta t$, $\Delta t = 0.5Gyr$, top right panel). The colorbar maximum range for each panel has been set at 0.10, to avoid the color scale to be skewed by few galaxies with very high fractions. We indicate the $G - M_{20}$ TIMs with a black ring around data points.

5.5 The $G-M_{20}$ Space and Stellar Populations

In this section we examine the relation between the non-parametric morphology measures of G and M_{20}, and the star formation indicators we introduced in this chapter. In Figure 5.11 left panel, we show the star-forming and quiescent galaxies on the $G-M_{20}$ plot. In the right panel we plot our sample on the $G-M_{20}$ space color-coded by the distance measure we introduced in §5.4.1. These plots reveal a few remarkable features of the $G-M_{20}$ selection. We briefly list these here, in no particular order, and leave further discussion to Chapter 6. In §2.3, we discussed that the majority of undisturbed galaxies reside at the the high G, low M_{20} part of the space. Figure 5.11 left panel reveals the majority of the galaxies at this section are quiescent. We find that star-forming galaxies are spread in their positions throughout the $G-M_{20}$ space, but larger in fraction at high M_{20} values. Every galaxy above our line (orange line in Figure 5.11, see §2.3 for its derivation) and below the Lotz et al. (2008b) line are star-forming. These are reflected by the EW($H\delta_A$)-$D_{n,4000}$ distance measure, as the galaxies in this section all have low distance values, indicating the presence of a significant fraction of young stellar populations. As we go towards higher G values above our line, we start to see an increase in the number of galaxies that are in the quiescent section of the UVJ diagram. At the highest G values their fractions become higher than the star-formers. Furthermore, galaxies with higher G values here predominantly have high EW($H\delta_A$)-$D_{n,4000}$ measures, indicating the existence of old stellar populations in these galaxies, and a lack of young stars. This trend brings into light new characteristics about the $G-M_{20}$ selection of TIMs. We investigate this further below with the age fraction plot, shown in Figure 5.12.

We finalize this subsection by examining the distribution of star formation activity on the $G-M_{20}$ space. We show the results of this analysis in Figure 5.12, one panel for each time interval we describe in §5.4.2. The top left panel examines the star formation rate in the last 0.5 Gyr of our sample. Below our line (orange line in Figure 5.12) and at high G values we find that many of the galaxies do not have star formation activity, or a noteable amount of stellar populations younger than 0.5 Gyr. This is the same subpopulation we found to be quiescent, and to have low values of the distance measure in Figure 5.11. Above our TIM selection line, and at lower G values, we

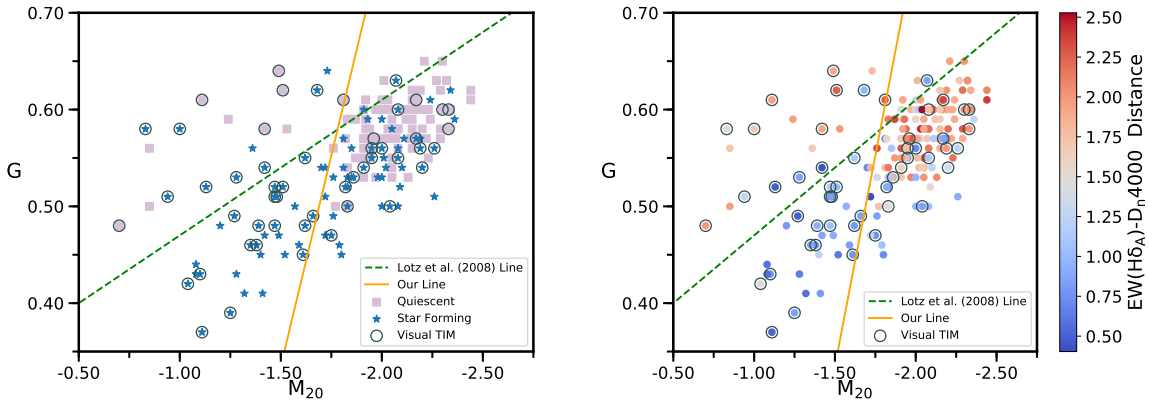

Figure 5.11: *Left panel* – The $G-M_{20}$ plot when galaxies are classified into star-forming and quiescent, according to their positions in Figure 5.2. Blue stars represent galaxies residing at the star forming strip, and purple squares are within the quiescent section. We indicate the visually classified TIM galaxies with a black ring around the data points. *Right panel* – The $G-M_{20}$ plot color-coded by the distance measure defined in §5.4.1. Lower values, or blue marker colors indicate a galaxy with high-EW($H\delta_A$) and low-$D_{n,4000}$ values. Higher values, or red marker colors indicate a galaxy with low-EW($H\delta_A$) and high-$D_{n,4000}$. We indicate the $G-M_{20}$ TIMs with a black ring around data points. Note that this is different from Figures 5.8, 5.9, and 5.10, where the black rings indicate the $G-M_{20}$ TIMs.

see that most of our galaxies have non-zero star formation rates in their last 0.5 Gyr. This changes dramatically as we move towards higher G values, where every galaxy above G = 0.5 shows little to no star formation activity in their last 0.5 Gyr.

Investigating this further, we look at the relative star formation rate of our sample between 0.5 to 1 Gyr, in the top right panel. We find that the galaxies above our line at high G values now show presence of stars formed between 0.5 to 1 Gyr. At low G values most galaxies above our line have high relative star formation rates during the same period. It is difficult to comment on the distribution of rates below the line, where galaxies from the entire range of rates reside. However, we note that at low G values and close to our line, most galaxies have preferentially high rates. The same galaxies also have low EW($H\delta_A$)-$D_{n,4000}$ distance measures, as seen in the right panel of Figure 5.11, in line with this result.

Finally, we examine the relative star formation rate of our galaxies in the period covering their last 1 Gyr, combining the two periods we have discussed above. Similar to the results above, we see an interesting trend above our line. In this region, galaxies with high star formation rate in

their last 1 Gyr have low G values, and those with low and intermediate rates reside in higher G values. Though a complete investigation of what causes this is beyond the scope of this work, as this would require a detailed analysis involving simulations that track the $G-M_{20}$ values of mergers, we comment on the possible origins of this trend in Chapter 6. Mainly driven by their star formation activity between 0.5 to 1 Gyr, we find that the galaxies below our line show a mixture of rates in their last 1 Gyr, with no trends immediately apparent.

5.6 The Phase-space and Stellar Populations

In §3.4, we have analyzed the projected radius-velocity phase space for our cluster members. We now revisit the phase space in light of the star-formation analysis we have performed in this chapter. Same way as the previous sections, we investigate the distribution of relative star formation rates of our galaxies during three different time periods, plotted on the phase space. We plot the $G-M_{20}$ TIM (Figure 5.13, left panels) and undisturbed (Figure 5.13, right panels) subpopulations in different panels to visually probe any trends easier.

The results for the last 0.5 Gyr (top panels of Figure 5.13) show that the majority of the undisturbed cluster members have not had any significant star formation during this period. Apart from a few galaxies, almost every undisturbed galaxy in the cluster environment has a significant lack of stars younger than 0.5 Gyr. The small sample size of $G-M_{20}$ TIMs that are also cluster members makes the inference of a decisive trend difficult. They tentatively show an enhancement of galaxies with higher young population fractions towards higher clustercentric radius.

The plots observing the period between 0.5 to 1 Gyr (middle panels, Figure 5.13), on the other hand, show a significantly different distribution of relative star formation rates. We find that the undisturbed cluster members show a wide range of star formation activity, and also reveal a trend in clustercentric radius. We find that in small projected radii, e.g. $R_{proj}/R_{200} < 0.3$, the majority of our undisturbed cluster members have low or intermediate star formation activity between 0.5 to 1 Gyr. But when we go to higher radii, especially at $R_{proj}/R_{200} \sim 0.5$, we find that the majority of galaxies have had active star formation between 0.5 to 1 Gyr prior to our observation. This implies

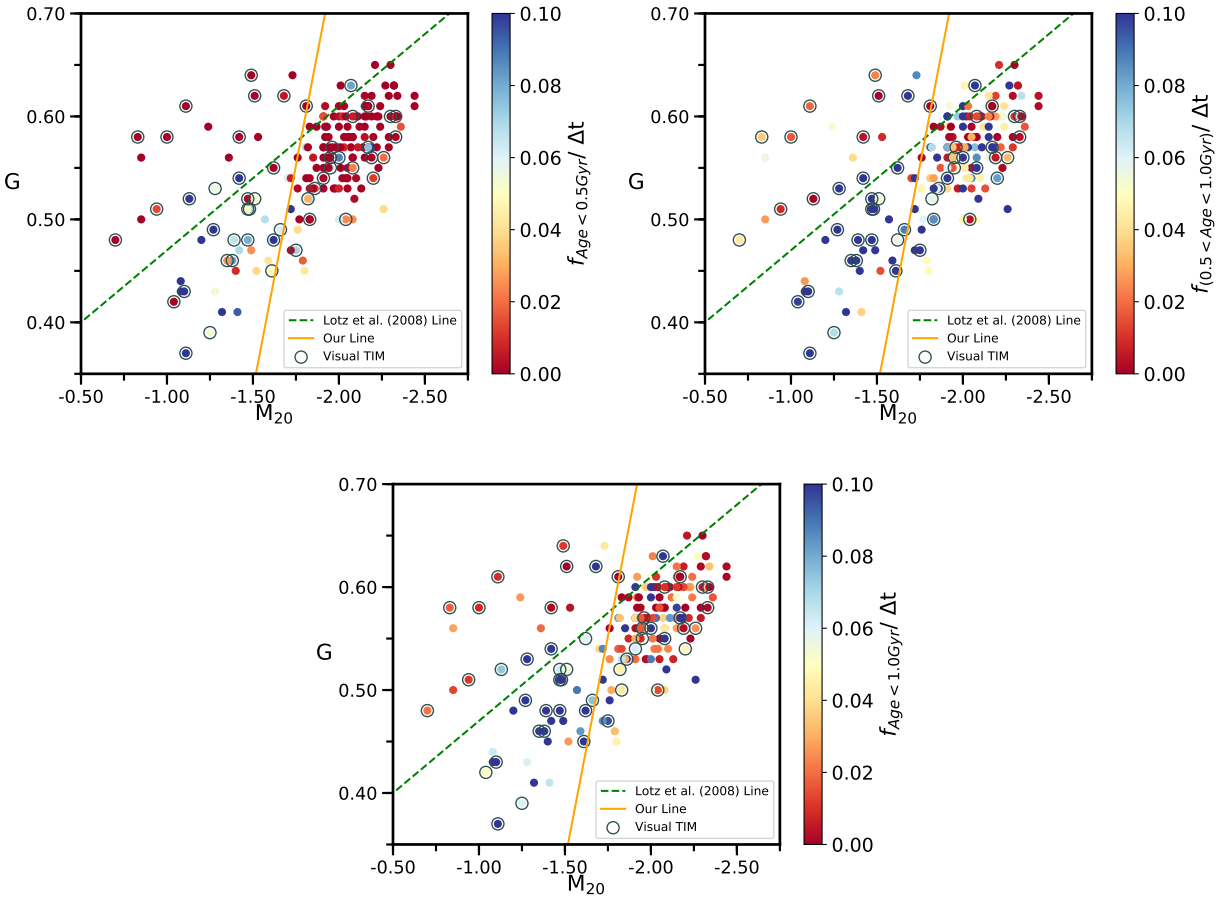

Figure 5.12: The $G-M_{20}$ plots color-coded by their relative star formation rates in the three age intervals introduced in §5.3. We show the star formation rate in the last 1 Gyr bin ($f_{Age<1.0Gyr}/\Delta t$, $\Delta t = 1Gyr$, bottom panel), in the last 0.5 Gyr ($f_{Age<0.5Gyr}/\Delta t$, $\Delta t = 0.5Gyr$, top left panel), and between 0.5 and 1 Gyr ($f_{0.5Gyr<Age<1.0Gyr}/\Delta t$, $\Delta t = 0.5Gyr$, top right panel). The colorbar maximum range for each panel has been set at 0.10, to avoid the color scale to be skewed by few galaxies with very high fractions. We indicate the visually classified TIM galaxies with a black ring around the data points. Note that this is different from Figures 5.8, 5.9, and 5.10, where the black rings indicate the $G-M_{20}$ TIMs.

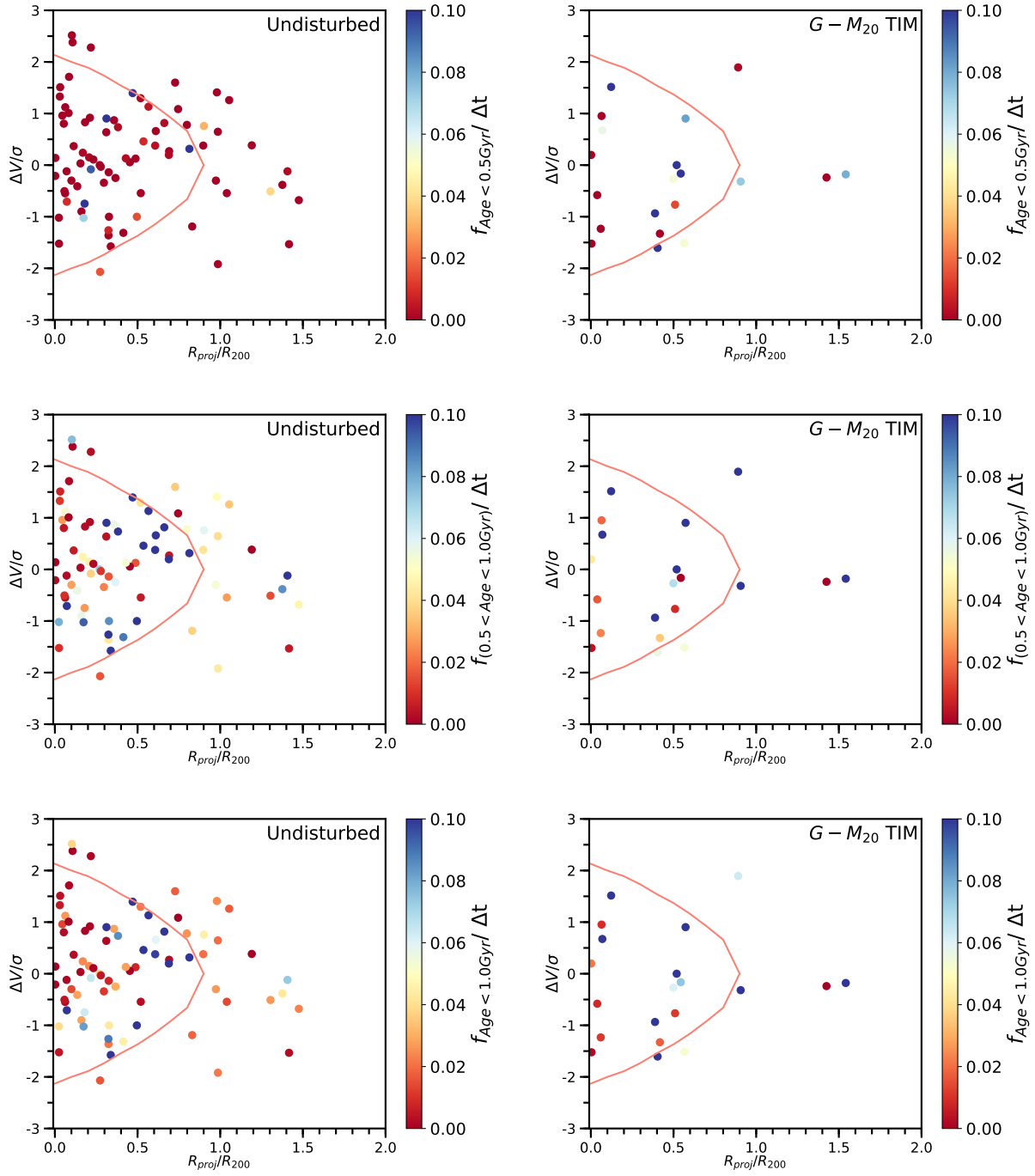

Figure 5.13: The phase space plots (see §3.4 for details) color-coded their relative star formation rates in the three age intervals introduced in §5.3. Note that there are less galaxies plotted here compared to the previous figures in this chapter, as we are analyzing only the cluster environment for the phase space analysis (see §3.4 for details). We show the star formation rate in the last 1 Gyr ($f_{Age<1.0Gyr}/\Delta t$, $\Delta t = 1Gyr$, bottom panel), in the last 0.5 Gyr ($f_{Age<0.5Gyr}/\Delta t$, $\Delta t = 0.5Gyr$, top left panel), and between 0.5 and 1 Gyr ($f_{0.5<Age<1.0Gyr}/\Delta t$, $\Delta t = 0.5Gyr$, top right panel). The colorbar maximum range for each panel has been set at 0.10, to avoid the color scale to be skewed by few galaxies with very high fractions. Left panels display the phase space distributions of undisturbed galaxies, and right panel display the $G - M_{20}$ TIMs. The orange solid line from Mahajan et al. (2011) indicates the region where the majority of virialized galaxies lie, in both panels.

an environmental effect on the star formation of our cluster members. We investigate this more in depth in Chapter 6.

5.7 Caveats

The cumulative histogram for $f_{Age<1.0\ \mathrm{Gyr}}$ in Figure 5.4 shows that our sample includes galaxies for which the total stellar mass contained in stars younger than 1 Gyr is notably high. We remark that at our redshift range, for galaxies with our stellar mass limit, it is unlikely that a galaxy in our sample with our stellar mass limit of $\log_{10}(M_*/M_\odot) > 10.4$ formed more than 50% of its stellar mass budget in the last 1 gyr. Studies show that, on average, galaxies of our mass range have formed more than half of their stellar mass content before z = 1 (Bundy et al., 2005; Mortlock et al., 2011), before the median redshift of our sample at z = 0.6. These likely imprecise estimates of the age fractions are due to the integrated spectrum being dominated by recently formed stars. At a given mass young stars are much brighter than old ones. As a result of this, the best fitting pPXF models to such spectra heavily favor younger templates, causing the high $f_{Age<1.0\ \mathrm{Gyr}}$, even when the young stars may not dominate the total stellar mass content. We therefore present our results using the $f_{Age<1.0\ \mathrm{Gyr}}$ with this caveat in mind. As no part of our analysis uses the specific values of age fractions directly, we chose not to exclude these galaxies from our sample.

Another caveat we would like to make concerns the robustness of our statistical tests. In our analysis we compare the $G-M_{20}$ TIMs and undisturbed galaxies, but the fraction undisturbed galaxies (152 undisturbed galaxies total) in our sample is higher than the $G-M_{20}$ TIMs (30 $G-M_{20}$ TIMs total). Tests like the two sample KS test can suffer from low accuracy when performed on small samples. However, the number of $G-M_{20}$ TIMs in our sample is still safely above the threshold where this inaccuracy starts to be an issue. As long as our $G-M_{20}$ TIMs are an unbiased representation of their parent population, the cumulative histograms we have presented are also reliable. In our analysis, we have not found any evidence pointing to our particular $G-M_{20}$ TIMs being a biased selection. We therefore conclude that our results are robust against the uneven total numbers in these classes.

We would also like to note that we are using the stellar masses for our sample as defined in §2.2, which are the results of an SED fitting using the photometric data of our sample. We do not derive the stellar masses of our galaxies using the pPXF fit to the spectroscopic data. pPXF does not return the total stellar mass when fitting spectra, but this can be derived using the mass normalization of the stellar templates, and the mass-weighted age fractions. We chose to use the same masses as described §2.2, or as published in Deger et al. (2018), for easier comparison between results.

We detailed how we derived the S/N ratio of gas emission line fits by a statistical sampling of pPXF runs in §4.3. At the end of that discussion we briefly mentioned that we do not use these corrected S/N values to put restrictions on whether emission lines should be subtracted from the spectrum prior to the stellar component fit, or not. pPXF does not provide an easy way to define constraints based on the S/N of the emission line fit. Therefore, as it stands, for the analysis presented in this work every emission line fit by pPXF is subtracted from the total spectrum before fitting for the stellar component. Here we discuss how we tested the robustness of our results following this choice. To test whether subtracting low significance emission lines affects our conclusions, we reran pPXF by making it ignore the gas components of certain spectral elements. As it is especially important for the analysis presented in this work, we performed another spectral fitting by excluding the Hδ emission line from the gas component fit. pPXF therefore did not subtract an emission line at the location of Hδ when fitting for the stellar component. We then derived EW(H$\delta_{\rm A}$) using this new fit, or the raw EW(H$\delta_{\rm A}$), so to speak, and compared these values with our original ones. We found that the residuals in the majority of cases are around zero, with the median residual being 0.56, and the standard deviation being 0.92. Next, we revisited the EW(H$\delta_{\rm A}$)-$D_{n,4000}$ plot with the raw EW(H$\delta_{\rm A}$), color coded by the mass weighted age fractions. We found that our results for this plot did not qualitatively change in any way that would affect our conclusions. We therefore chose to use the approach where every emission line fit by pPXF is subtracted prior to the stellar component fit, as this approach correctly subtracts many well-defined lines. Only a small fraction of galaxies are potentially affected by subtracting a fit of low significance, and as mentioned, this does not affect the conclusions of our analysis.

Here we address the SFR boost we detect in the last 100 Myr's of our galaxies that we briefly discussed in §5.3. This caveat pertains to the significant enhancement in SFR in the last 100 Myr of our galaxies when it is preceded by 200-300 Myr of no star formation activity. This implies that the star formation activity has been rejuvenated to a significant level in the last 100 Myr. We detect this in only a small subset of our galaxies, and these are all objects with evidence of young stellar populations as they all reside at the top left part of the EW($H\delta_A$)-$D_{n,4000}$ plane. Even if these galaxies show evidence of having young stellar content, this sharp increase in a relatively short timescale is suspicious. A likely explanation is that the very young (< 100 Myr old) stars in these galaxies dominate the spectrum in a way that our pPXF fit overestimates the fraction of 100 Myr and younger population, and underestimates the fraction of 200-400 Myr. As such, we decided not to probe the star formation activity in the last 100 Myr, and decided only to present our results analyzing the last 0.5 Gyr. This extended timescale accounts resolves the issue of the sudden spike, and is a timescale suitable to test the effects of TIM on the star formation, since it is comparable to the merger timescales we discuss in §5.3.

We note that we find some of these galaxies to be $G - M_{20}$ TIMs, such as the example we discuss in §4.3. For such a galaxy, this could potentially indicate a merger-induced star formation period, preceded by a period of no star formation activity. However, we find similar enhancements in the SFR's of undisturbed galaxies as well, in almost equal numbers.

Chapter 6

Effects of TIM on the Star Formation of Our Sample

In this chapter we combine the analyses we have performed on the quantitative morphologies of our sample in Chapter 3, and the analysis on the stellar populations of our sample in Chapter 5. One crucial definition we made in Chapter 3, and in Deger et al. (2018), is that of our morphological classes. Our first class, the $G-M_{20}$ TIMs (tidal intereactions and mergers), are galaxies both showing morphological signatures of TIM, and remain above our TIM selection line calibrated to select maximum purity on the $G-M_{20}$ space (details in §2.3). The undisturbed class is comprised of galaxies showing no visual evidence of undergoing TIM events, and the visual TIM that remain below our $G-M_{20}$ selection line. This two step selection is mainly motivated by future work we plan to do analyzing the outputs of merger simulations by Lotz et al. (2010b,a) (more explanation on this below). A TIM selection based on both visual signatures and quantitative morphological parameters allow us to select a high purity sample, for which we can also constrain the TIM observability timescales.

We discuss the star-formation properties of these two morphological classes, $G-M_{20}$ TIMs and undisturbed galaxies, in this chapter. We remark that the results we present below use the subset of the spectroscopic sample that passes the quality diagnostics described in §4.1.1.

6.1 Star Formation Diagnostics from Spectroscopy and Photometry

In Chapter 5, we have presented our analysis attempting to identify the young and old stellar populations in our galaxies. To accomplish this, we made use of the multiband photometry data, age sensitive spectral indices derived from its spectroscopic data, and mass-weighted age fractions

and star formation histories we extracted via a spectral fitting of the full galaxy spectra. To probe the modifications to the star formation history in the last 1 Gyr, we perform our analysis in three age intervals: We derive the fraction of stellar populations younger than 1 Gyr ($f_{Age<1.0\ \mathrm{Gyr}}$), 0.5 Gyr ($f_{Age<0.5\ \mathrm{Gyr}}$), and between 0.5 and 1 Gyr ($f_{0.5<Age<1.0\ \mathrm{Gyr}}$) for our sample. Next, to account for the uneven time periods in these three fractions, we derive the star formation rates (SFRs) in these in these time periods as $(f(\Delta t)/\Delta t$. Here we discuss some of the implications of our results.

First, we investigate the distribution of our galaxies on a plane formed by the two age-sensitive spectral indices we calculated, equivalent width Balmer Hδ absorption line, EW(Hδ_{A}), and the strength of the 4000Å break, $D_{n,4000}$. Our examination of the $G-M_{20}$ TIMs and undisturbed galaxies on the EW(Hδ_{A})-$D_{n,4000}$ plane shows that the distributions of these subpopulations are distinguishable, in both parameters. Two sample KS test p-values indicate that $G-M_{20}$ TIMs and undisturbed galaxies are very unlikely to have been drawn from the same parent population in either parameter. The $G-M_{20}$ TIMs preferentially reside on the part of the EW(Hδ_{A})-$D_{n,4000}$ plane populated by galaxies having a significant fraction of young stars. The fraction of undisturbed galaxies are much higher on the part of the plane where galaxies with old stellar population reside.

Next, we performed photometric diagnostics of the stellar ages of our sample. We have utilized the $(U-V)$ versus $(V-J)$ color-color plot, or the UVJ diagram, to classify our galaxies into star-forming and quiescent. The strength of the UVJ diagram lies in its ability to distinguish between galaxies that are red due to their stellar content being dominated by old stars, and galaxies that are red due to dust extinction. This provides a medium to seperate star-forming and quiescent subpopulations, effectively eliminating contamination in this classification due to dusty galaxies. When classified into star-forming and quiescent this way, we find that the our $G-M_{20}$ TIMs are predominantly star-forming. The quiescent section of the UVJ diagram is dominated by undisturbed galaxies. The star-forming strip contains both $G-M_{20}$ TIMs and undisturbed galaxies, roughly in equal amounts. We explore the possibility of an enhancement in star formation activity in $G-M_{20}$ TIMs by taking a closer look at mean mass-weighted age fractions in §6.2 below.

One trend we observe in Figure 5.12 is that above our line, the G parameter acts as a seperator

between galaxies of different star formation rates. Above our line irrespective of morphological class, galaxies with high G, or less egalitarian light distribution, have lower relative star formation rates in their respective time periods, and those with low G have higher rates. Top left panel shows that all the galaxies with high G are already quenched in their last 0.5 Gyr. These galaxies are also towards the bottom right of the EW($H\delta_A$)-$D_{n,4000}$ plane (see Figure 5.11), indicating their light is dominated by old stars. Lotz et al. (2008a) find late-type galaxies tend to reside below their merger selection line at the high M_{20} end (green dotted line in the G versus M_{20} plots), and early-types at the low M_{20} end. One possible explanation for the trend in G is that mergers between different morphology types have distinct tracks through the $G-M_{20}$ space. Simulations tracking the G and M_{20} values of merging galaxies could shine a light on this trend in star formation rates in G. We discuss this further in §7.1.

6.2 Enhancement and Suppression of Star Formation

In this section we comment on whether the star formation of our sample of intermediate redshift galaxies has been modified by TIM events by comparing their star formation activity in their last 0.5 Gyr, and the period between 0.5 and 1 Gyr. Our primary focus on Chapter 5 has been the overall star formation rate of our galaxies calculated in these time bins, but in this section we will solely focus on the fraction of stellar mass they have between the ages of 0 to 0.5 Gyr, and 0.5 Gyr to 1 Gyr. Another major focus of this section is also attempting to observe the differences between $G-M_{20}$ TIMs and undisturbed galaxies, in an attempt to explain the trends we discussed in §6.1

We begin by revisiting the age diagnostic plots from Chapter 5, the UVJ diagram and EW($H\delta_A$)-$D_{n,4000}$ plot, plotted using age fractions instead of star formation rates. These will help illustrate the positions of galaxies with different age fractions on these two age diagnostic plots. We present these plots in Figure 6.1, top panels for $f_{Age<0.5\text{ Gyr}}$, and bottom panels for $f_{0.5<Age<1.0\text{ Gyr}}$. We note that these plots are almost exactly the same as the star formation rate plots we presented in Figures 5.8 and 5.10, except that here we do not divide the mass-weighted age fractions by the time interval $\Delta t = 0.5$ Gyr, which changes the colors of individual points with non-zero values.

We decided to put the versions with $f_{Age<0.5\ \mathrm{Gyr}}$ and $f_{0.5<Age<1.0\ \mathrm{Gyr}}$ here, to make the analysis that follows visually more accesible on these plots. The general trends we have discussed for relative star formation rates in §5.4.2, and §5.4.3, hold identically for these plots as well, since the only difference is the values on the colorbar scale. To briefly revisit our results, we find that the galaxies with highest $f_{Age<0.5\ \mathrm{Gyr}}$ values reside in the high EW($\mathrm{H}\delta_\mathrm{A}$) and low $D_{n,4000}$ part of the top left panel, indicating the existence of young stars. All of these same galaxies are on the star-forming strip of the UVJ diagram. Galaxies with high, intermediate, and low $f_{0.5<Age<1.0\ \mathrm{Gyr}}$ values respectively reside on the top left, middle, and bottom right of the EW($\mathrm{H}\delta_\mathrm{A}$)-$D_{n,4000}$ plane.

Next, we illustrate the distribution of stellar mass fraction contained in stars younger than 0.5 Gyr, and at ages of 0.5 to 1 Gyr of our total sample, in Figure 6.2. In the top left panel we see that there are many more galaxies with higher $f_{0.5<Age<1.0\ \mathrm{Gyr}}$ than $f_{Age<0.5\ \mathrm{Gyr}}$, which reside above the one-to-one line. This suggests that our galaxies were generally producing more stars in the time period between 0.5 to 1 Gyr before our observations, than in their last 0.5 Gyr, for both $G-M_{20}$ TIMs and undisturbed galaxies. This result is to be expected for galaxies with declining star formation histories, which generally holds true for galaxy populations. However, the decline we see for the majority of our sample is much more steep than literature values, such as the trends in (Whitaker et al., 2012). Though some significant differences between $f_{0.5<Age<1.0\ \mathrm{Gyr}}$ and $f_{Age<0.5\ \mathrm{Gyr}}$ are possible in rapidly quenching galaxies, we believe the number of galaxies with significant changes in the top left panel of Figure 6.2 is too high to solely be accounted for by this transitioning population. It is possible that what we see stems from a systematic issue present in the spectral fitting. We will investigate the roots of this as part of our future work with this analysis. As a reminder, note that we discuss the few galaxies with very high $f_{Age<1.0\ \mathrm{Gyr}}$ values in §5.7. This plot shows that these values are mainly being driven by their high $f_{0.5<Age<1.0\ \mathrm{Gyr}}$ values. Our reasoning for using these is the same as our discussion §5.7 for galaxies with high $f_{Age<1.0\ \mathrm{Gyr}}$ values. There is a subpopulation of galaxies which have higher $f_{Age<0.5\ \mathrm{Gyr}}$ than $f_{Age<1.0\ \mathrm{Gyr}}$, and we note that the two objects with the highest values are both $G-M_{20}$ TIMs. We present the distribution in age fractions as histograms in the top right panel.

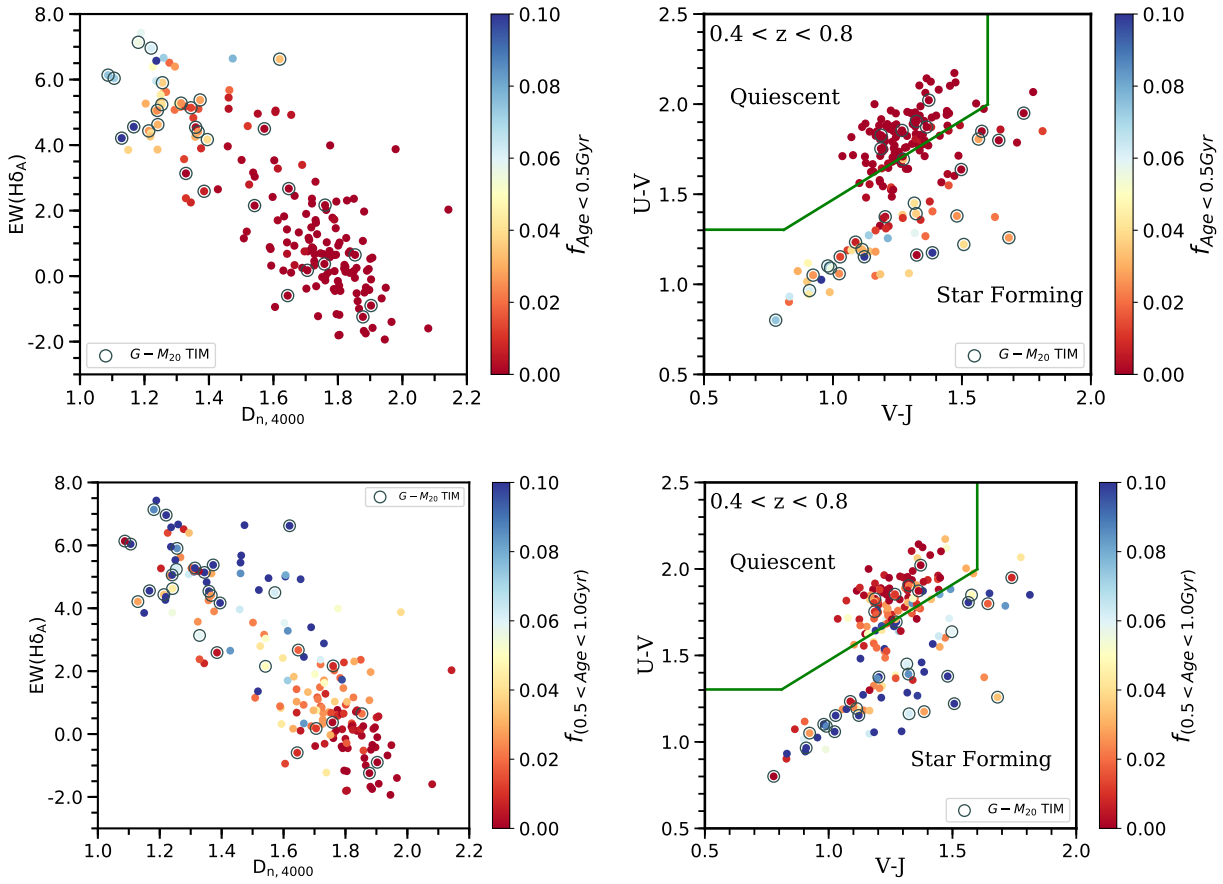

Figure 6.1: *Top left panel* – The EW($H\delta_A$) vs $D_{n,4000}$ plot, color coded by the amount of stellar mass contained in stars younger than 0.5 Gyr. *Top right panel* – The $(U-V)$ vs $(V-J)$ color-color plot, color coded by the amount of stellar mass contained in stars younger than 0.5 Gyr. *Bottom left panel* – The EW($H\delta_A$) vs $D_{n,4000}$ plot, color coded by the amount of stellar mass contained in stars between the ages of 0.5 and 1 Gyr. *Bottom right panel* – The $(U-V)$ vs $(V-J)$ color-color plot, color coded by the amount of stellar mass contained in stars between the ages of 0.5 and 1 Gyr. We indicate the $G-M_{20}$ TIMs with a black ring around data points, in all panels. Furthermore, the colorbar maximum range for each panel has been set at 0.10, to avoid the color scale to be skewed by few galaxies with very high fractions, in all panels. The difference between these panels and Figures 5.8 and 5.10 is that we present only the mass-weighted age fractions here, and not the star formation rates in these intervals.

Next, we compare the distributions of $G-M_{20}$ TIMs and undisturbed galaxies in $f_{Age<0.5\ \mathrm{Gyr}}$ and $f_{0.5<Age<1.0\ \mathrm{Gyr}}$ via cumulative histograms in the bottom panels. We also calculate the two sample KS p-value comparing the two classes, and find the p-value to be 3×10^{-4} for $f_{Age<0.5\ \mathrm{Gyr}}$, and 1.5×10^{-2} for $f_{0.5<Age<1.0\ \mathrm{Gyr}}$. These values indicate that the distributions of these two classes in terms of their stellar content in these two periods is unlikely to have been drawn from the same parent distribution, especially in $f_{Age<0.5\ \mathrm{Gyr}}$. The simplistic implication here is that the TIM events are playing a role in transforming the star formation histories of our $G-M_{20}$ TIMs, when compared with undisturbed galaxies. Our ability to reject the null hypothesis is lower for the $f_{0.5<Age<1.0\ \mathrm{Gyr}}$ case. This could potentially indicate that the TIM events affect the star formation histories of our galaxies more significantly in the last 0.5 Gyr, than it does in the period 0.5 Gyr before that. This is to be expected from the merger timescales we present in §5.3, with 0.6 Gyr being an upper limit to the values we quote. This upper limit has been obtained by Lotz et al. (2008a) for their own merger selection criteria, but granted that it holds true for our selection as well, it is safe to assume that any TIM signature on star formation is more likely to be observed in the last 0.5 Gyr of our galaxies. This is also the time period where we find the more significant difference between the distributions of $G-M_{20}$ TIMs and undisturbed galaxies, indicative of TIM events modifying the star formation histories. Careful calibration of timescales is needed to make a robust claim for results when we use our entire sample. We discuss how we plan to approach this problem in 7.1.

Next, we investigate the difference in the fraction of stars produced in these two time periods. We analyze the two morphological classes in their difference of $f_{Age<0.5\ \mathrm{Gyr}}$ and $f_{0.5<Age<1.0\ \mathrm{Gyr}}$, or the difference of the total stellar mass produced between 0.5 Gyr and 1 Gyr with the stellar mass produced in the last 0.5 Gyr, in Figure 6.3. The left panel is normalized histograms, and the right panel is cumulative histograms, both showing the distributions of $G-M_{20}$ TIMs and undisturbed galaxies in ($f_{0.5<Age<1.0\ \mathrm{Gyr}}$ - $f_{Age<0.5\ \mathrm{Gyr}}$). We use this difference to detect an increase or decrease of total amount of stars produced in these periods. We find that only a small subset of our sample have negative values in this difference, which we also observed in the top left panel of Figure 6.2. Visually, the distributions are similar. This is reinforced by the relatively high value

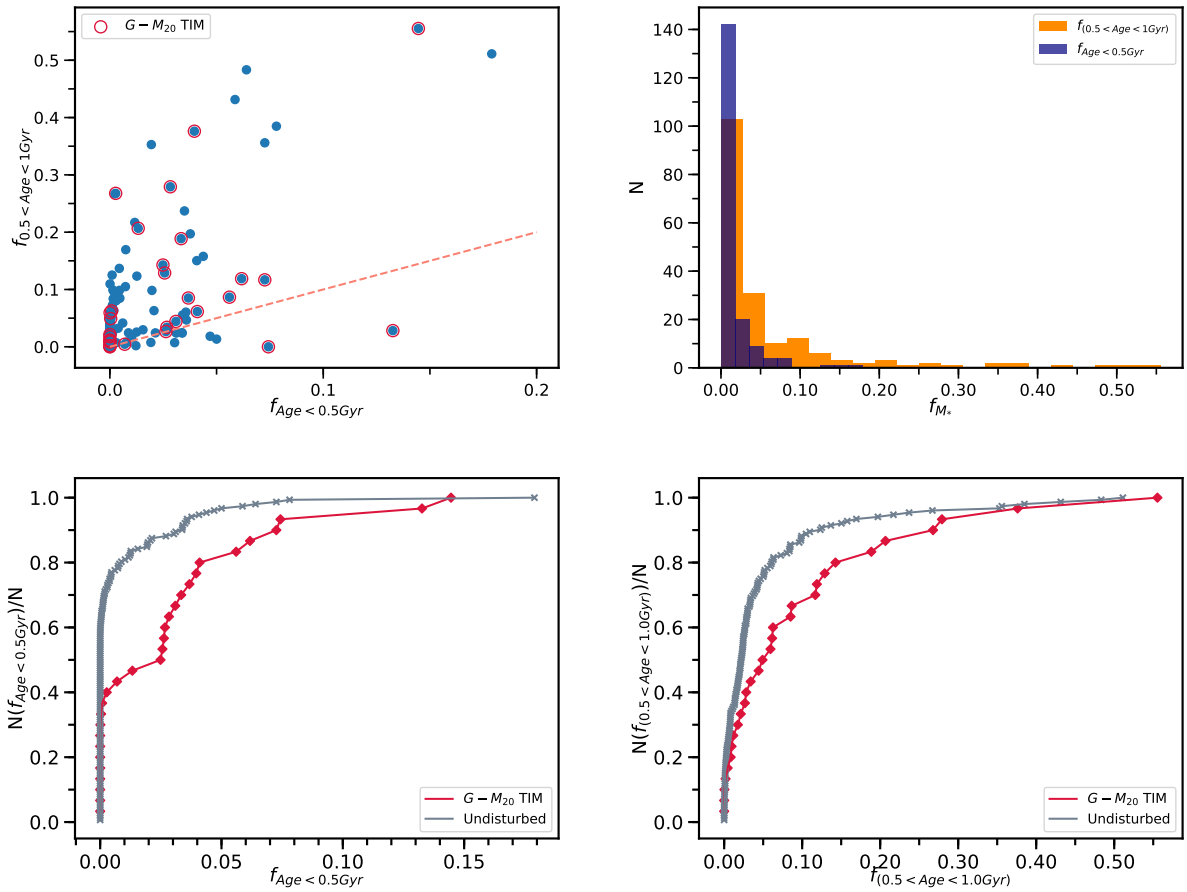

Figure 6.2: *Top left panel* – The $f_{0.5<Age<1.0\ \mathrm{Gyr}}$ versus $f_{Age<0.5\ \mathrm{Gyr}}$ plot for our sample. The dotted line is the one-to-one ($y = x$) line. We denote the $G-M_{20}$ TIMs with a red ring around data points. *Right panel* – Histograms representing the distributions of our sample in $f_{Age<0.5\ \mathrm{Gyr}}$ (blue bars), $f_{0.5<Age<1.0\ \mathrm{Gyr}}$ (orange bars). *Bottom left panel* – Cumulative histograms comparing the $G-M_{20}$ TIMs and undisturbed galaxies in their distribution in $f_{Age<0.5\ \mathrm{Gyr}}$. Two sample KS p-value for the same comparison is 3×10^{-4}. *Bottom right panel* – Cumulative histograms for the $G-M_{20}$ TIMs and undisturbed galaxies in their distribution in $f_{0.5<Age<1.0\ \mathrm{Gyr}}$. The KS p-value for this panel is 1.5×10^{-2}.

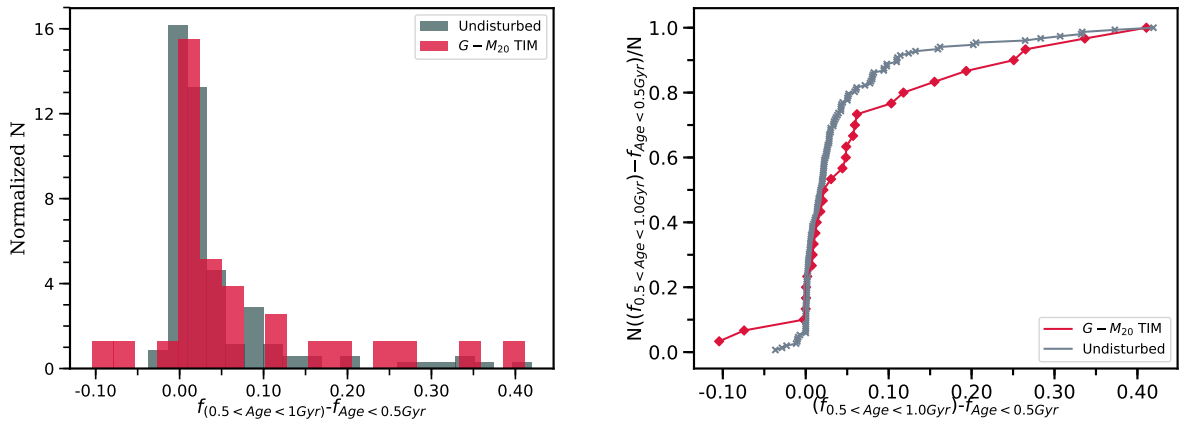

Figure 6.3: *Left panel* – The normalized histogram showing the distribution of $G-M_{20}$ TIMs (red histogram) and undisturbed galaxies (gray histogram) in ($f_{0.5<Age<1.0\ \mathrm{Gyr}}$ - $f_{Age<0.5\ \mathrm{Gyr}}$). *Right panel* – Cumulative histograms showing the distribution of $G-M_{20}$ TIMs (red histogram and markers) and undisturbed galaxies (gray histogram and markers) in ($f_{0.5<Age<1.0\ \mathrm{Gyr}}$ - $f_{Age<0.5\ \mathrm{Gyr}}$. The KS p-value for the same comparison in these panels is 0.12, meaning there is a 12% probability that these two morphological classes are drawn from the same parent distribution in ($f_{0.5<Age<1.0\ \mathrm{Gyr}}$ - $f_{Age<0.5\ \mathrm{Gyr}}$).

of the KS test p-value of 0.12, meaning that when their ($f_{0.5<Age<1.0\ \mathrm{Gyr}}$ - $f_{Age<0.5\ \mathrm{Gyr}}$) values are considered, the probability that our $G-M_{20}$ TIM and undisturbed samples are random draws from the same parent population is 12%. We therefore cannot reject the null hypothesis that these two morphological classes are drawn from the same distribution with high confidence, when we inspect the difference in the fraction of stars they have produced in these two time periods. This implies that for the last 1 Gyr, there is no evidence for a substantial difference in the SFHs of $G-M_{20}$ TIMs and undisturbed galaxies. Similar to the situation we discussed above, the length of this time period might potentially be what drives this low significance. The amount of star formation enhancement or suppression due to the TIM event, if any, might be imperceptible when probed as the ($f_{0.5<Age<1.0\ \mathrm{Gyr}}$ - $f_{Age<0.5\ \mathrm{Gyr}}$) difference, over our entire sample.

A crucial test into whether the TIM event has a significant effect on the star formation of our sample comes from comparing the distributions of star-forming $G-M_{20}$ TIM and undisturbed galaxies. This allows us to directly compare the SFHs of galaxies that are UVJ classified as star-forming, in these two periods. A key point motivating this choice is that the merger timescales by

Lotz et al. (2008a, 2010b) are derived for star-forming galaxies only, hence analyzing this subpopulation is important for investigating the effects of TIM on star formation. We therefore investigate the distribution of only star-forming $G-M_{20}$ TIM and undisturbed galaxies, in Figure 6.4, in $f_{Age<0.5\text{ Gyr}}$ and $f_{0.5<Age<1.0\text{ Gyr}}$. We also run two-sample KS tests for these panels, and find p-value of 0.2 $f_{0.5<Age<1.0\text{ Gyr}}$ for the distribution of these two classes when only their star-forming population is considered. This result suggests that we cannot reject the null hypothesis that the $G-M_{20}$ TIM and undisturbed galaxies are drawn from the same sample in their $f_{0.5<Age<1.0\text{ Gyr}}$ values. On the other hand, we find the KS p-value to be 0.01 when their $f_{Age<0.5\text{ Gyr}}$ value is considered, remarkably smaller than the $f_{0.5<Age<1.0\text{ Gyr}}$ value. This low value indicates that the star-forming $G-M_{20}$ TIM and undisturbed galaxies do have distinguishable star formation properties in their last 0.5 Gyr. This comparison is important, because as we discuss above, the last 0.5 Gyr is when we expect to observe the effects of TIM events shaping the evolution of galaxies. The distribution in the left panel in Figure 6.4 indicates that in star-forming galaxies, the $G-M_{20}$ TIM have formed more stars than the undisturbed galaxies in the last 0.5 Gyr. This is potentially in support of a TIM enhanced star-forming scenario.

Next, we plot the mean of $f_{Age<0.5\text{ Gyr}}$ and $f_{0.5<Age<1.0\text{ Gyr}}$ for our entire sample, and only the UVJ-selected star-forming galaxies, in Figure 6.5. This plot shows an enhancement in $\langle f_{Age<0.5\text{ Gyr}}\rangle$ of the $G-M_{20}$ TIMs, for both the total sample and the star-forming sample. This result has a 1.9σ confidence for the star-forming sample. This vanishes for $\langle f_{0.5<Age<1.0\text{ Gyr}}\rangle$, indicating that on average, the $G-M_{20}$ TIMs and undisturbed galaxies have similar fractions of stars between the ages of 0.5 and 1 Gyr. These results are aligned with the results we find above, that the $G-M_{20}$ TIMs show evidence of enhanced star formation in their last 0.5 Gyr.

6.3 Effects of Environment on Star Formation

In this subsection we discuss any trends we see on the star formation of our galaxies due to the environment in which they reside. We begin by investigating whether the mean age fractions show any trends with global environment. For easy comparison, we make use of the same global

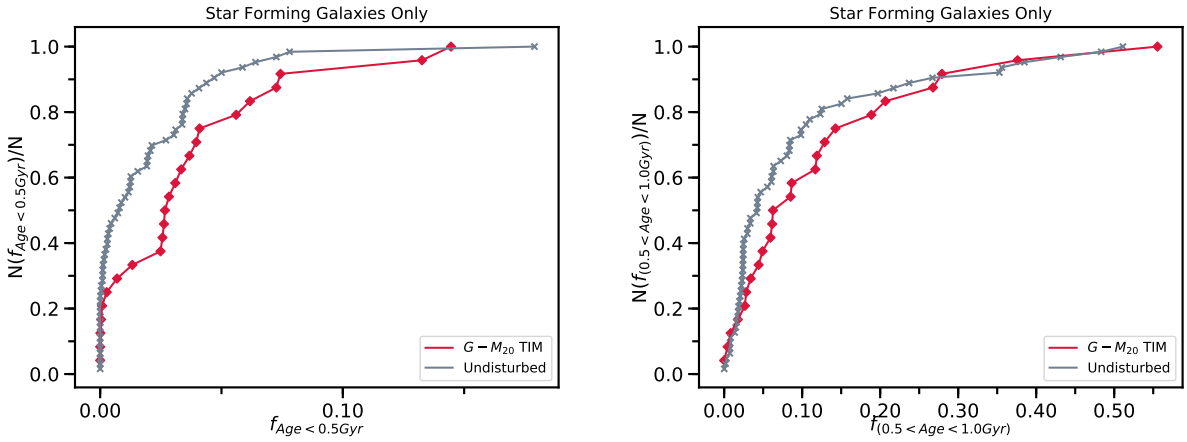

Figure 6.4: *Left panel* – Cumulative histograms showing the distribution of the star-forming $G-M_{20}$ TIMs (red histogram and markers) and the star-forming undisturbed galaxies (gray histogram and markers) in $f_{Age<0.5\text{ Gyr}}$. The two-sample KS p-value comparing these same populations is 0.01, indicating we can reject the null hypothesis that these samples come from the same population at high confidence. *Right panel* – Cumulative histograms showing the distribution of the star-forming $G-M_{20}$ TIMs (red histogram and markers) and the star-forming undisturbed galaxies (gray histogram and markers) in $f_{Age<0.5\text{ Gyr}}$. The two-sample KS p-value comparing these same populations is 0.2, which indicates that the star-forming $G-M_{20}$ TIM and undisturbed galaxies are likely drawn from the same distribution.

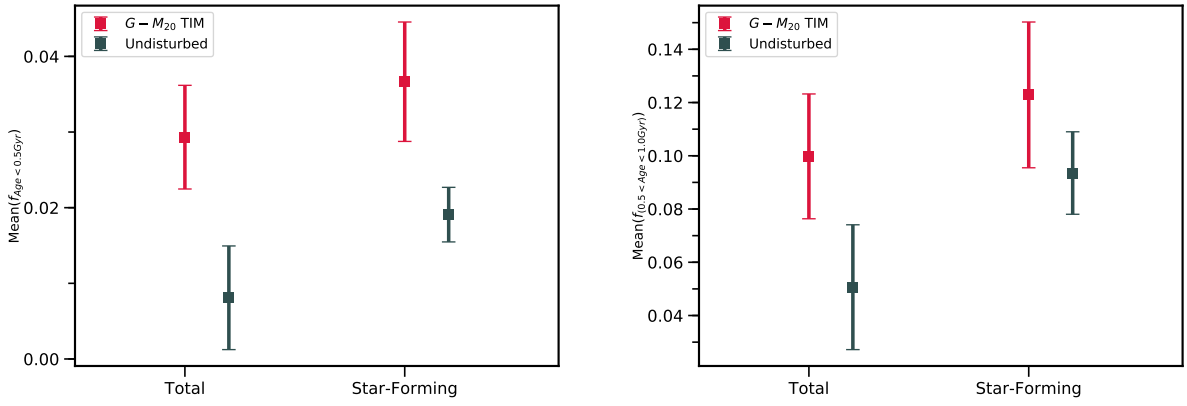

Figure 6.5: *Left panel* – Mean $f_{Age<0.5\text{ Gyr}}$ of the $G-M_{20}$ TIM (red markers) and undisturbed galaxies (gray markers), for only the star-forming galaxies (right), and the total sample (left). *Right panel* – Mean $f_{0.5<Age<1.0\text{ Gyr}}$ of the $G-M_{20}$ TIM (red markers) and undisturbed galaxies (gray markers), for only the star-forming galaxies (right), and the total sample (left).

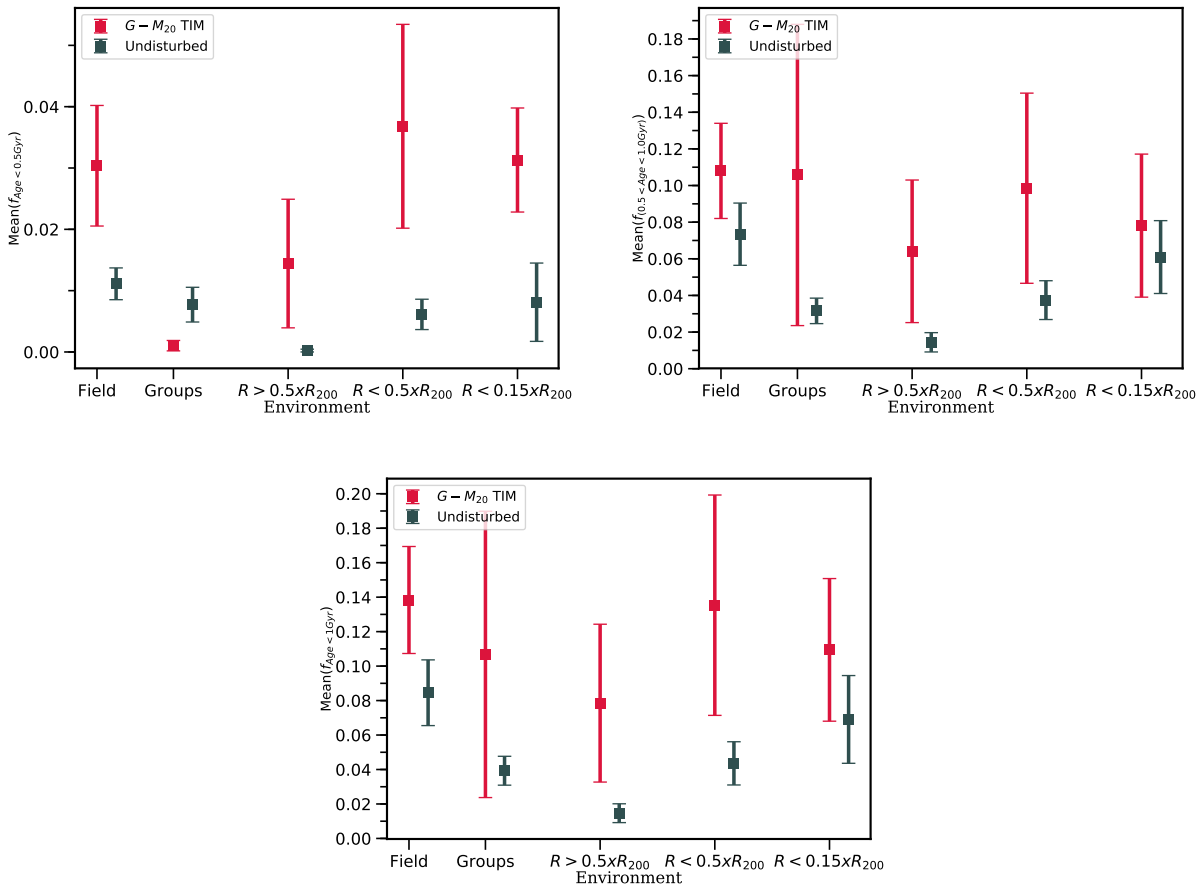

Figure 6.6: Mean $f(\Delta t)$ versus global environment plots for fractions of stellar content younger than 0.5 Gyr ($f_{Age<0.5\text{ Gyr}}$, left panel), between 0.5 and 1 Gyr ($f_{0.5<Age<1.0\text{ Gyr}}$, right panel), and younger than 1 Gyr ($f_{Age<1.0\text{ Gyr}}$, bottom panel). Red markers represent $G-M_{20}$ TIMs, and gray markers represent undisturbed galaxies. The error bars denote the error in the mean value for each data point. The environment bins we analyze consist of the field, the group environment, and the cluster environment split into three radial bins; $R<0.5\times R_{200}$, $R>0.5\times R_{200}$, and $R<0.15\times R_{200}$.

environment definitions we made in §3.3. We present the mean age fractions for $G-M_{20}$ TIM and undisturbed galaxies in the three age intervals, with their errors in the mean, in Figure 6.6, three left panels. The $\langle f_{Age<0.5\ \mathrm{Gyr}} \rangle$ values are comparable across every environment. The high errors of the $G-M_{20}$ TIMs, due to low number counts, hinder our ability to draw strong conclusions about the effect of environment on these age fractions. Our results are in agreement with the null hypothesis of no correlation for every age fraction, at every environment. However, these plots also show that the $G-M_{20}$ TIM values are elevated above the values of undisturbed galaxies, albeit tentatively, at almost every environment. This potentially supports a scenario where star formation rates are transformed by the $G-M_{20}$ TIM event itself, irrespective of the environment in which they occur.

Next, we plot the mean mass-weighted age fractions versus global environment plot, binning our two morphological classes together, and look at the total inhabitants of these environments irrespective of whether they are $G-M_{20}$ TIMs or undisturbed. We present this plot in Figure 6.7. We use the same global environment definitions in §3.3, and in Figure 6.6, for this plot. This plot reveals an interesting trend, in that the mean age fraction values are ordered according rough density estimates of the environment bins. This value is lowest in the densest environment, at $R < 0.15 \times R_{200}$ of clusters. It shows a slight increase in the intermediate density environments of groups, and the $R < 0.5 \times R_{200}$ bin within clusters. This is followed by yet another slight increase at radii $R > 0.5 \times R_{200}$, and this value is comparable to the field value. The error bars are large, and hence these results are tentative and of low statistical significance. This picture is in alignment with well known results of denser environments having galaxies with older stellar populations (Blanton & Moustakas, 2009). Performing our age distribution analysis with a larger sample size has the potential to provide more decisive insights into the role environment plays on quenching star formation.

We finalize this section by investigating only the UVJ-selected star-forming galaxies in mean age fraction versus global environment plot. We present our findings in Figure 6.8. Focusing on only the star-forming population makes our sample size even smaller, and due to this the error bars are even larger compared to Figure 6.7. This plot shows no apparent trend in global environment

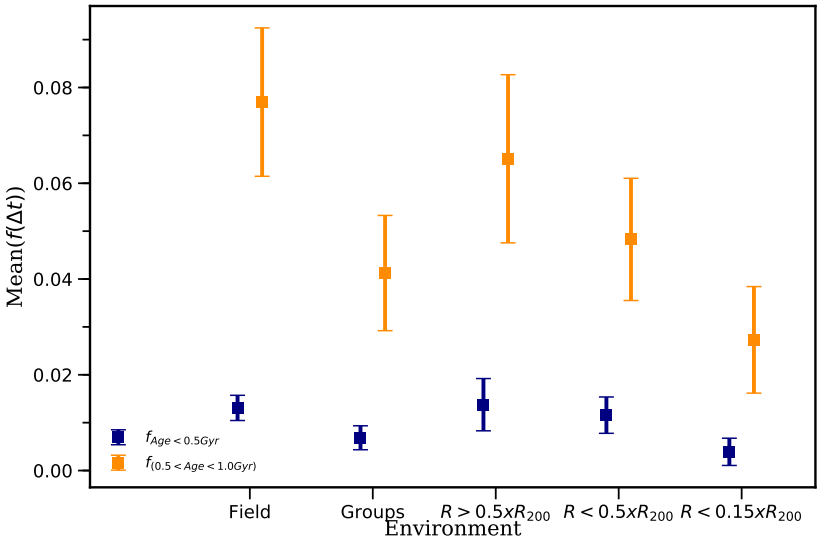

Figure 6.7: Mean $f(\Delta t)$ versus global environment plots for fractions of stellar content younger than 0.5 Gyr ($f_{Age<0.5\text{ Gyr}}$, dark blue markers), between 0.5 and 1 Gyr ($f_{0.5<Age<1.0\text{ Gyr}}$, orange markers). We plot every galaxy that reside in these environment bins, irrespective of whether they are $G-M_{20}$ TIM or undisturbed. The error bars denote the error in the mean value for each data point. The environment bins are the same as Figures 3.3 and 6.6.

in mean age fraction for these two time periods. This could indicate that their global environment has not had a significant effect on the star-formation of these galaxies. The similar amount of stars they produced between $0.5 < t < 1.0$ Gyr has fallen down to similar values, irrespective of environment. However, the lack of trend in this figure means that the enhancements in the field, and at $R > 0.5 \times R_{200}$ we found for the total sample vanish when we consider only the star-forming galaxies. This implies that some of UVJ quiescent galaxies have had a more significant decrease in the amount of stars they produced going from $0.5 < t < 1.0$ Gyr to $t < 0.5Gyr$. It is possible that the environment had an impact on the star formation of these galaxies, especially for those cluster members in $R > 0.5 \times R_{200}$. On the other hand, as we discuss in §6.2 in regards to Figure 6.2, the picture we see here could be affected by potential systematic issues with the spectral fitting. As future work, we will investigate the drop we see between these two age intervals, and attempt to determine what causes it.

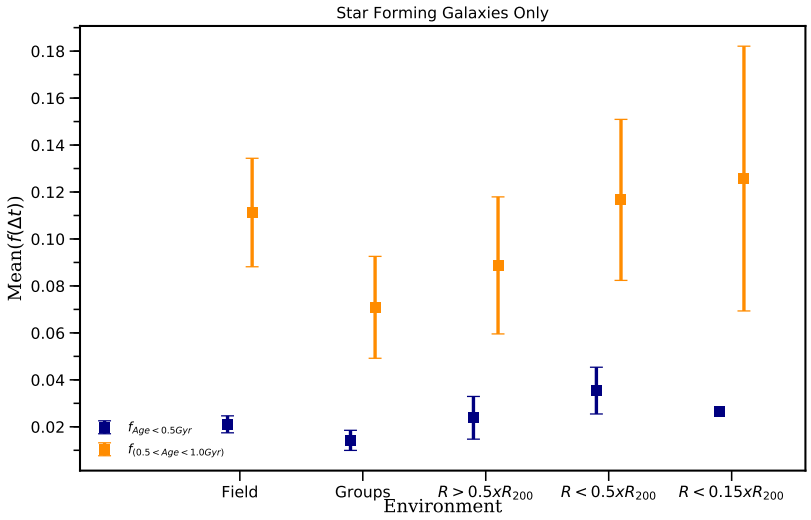

Figure 6.8: Mean $f(\Delta t)$ versus global environment plots for star-forming galaxies only, in fractions of stellar content younger than 0.5 Gyr ($f_{Age<0.5\text{ Gyr}}$, dark blue markers), between 0.5 and 1 Gyr ($f_{0.5<Age<1.0\text{ Gyr}}$, orange markers). We plot every galaxy that reside in these environment bins, irrespective of whether they are $G-M_{20}$ TIM or undisturbed. The error bars denote the error in the mean value for each data point. The environment bins are the same as Figures 3.3 and 6.6.

Chapter 7

General Conclusions

In this work, we have attempted to quantify and constrain the prevalence of tidal interactions and mergers (TIMs) in shaping the star-formation histories of a sample of galaxies at $0.4 \leq z \leq 0.8$. First, we presented our analysis of tidal interactions and mergers (TIM) in the EDisCS cluster, group, and field galaxies. For our analysis we make use of a visual identification of morphological signatures indicative of tidal interactions and mergers, performed on every galaxy in our sample that has a spectroscopic redshift. We then calibrated a line selecting TIM with high purity in the $G - M_{20}$ space using this visual classification. We showed that both G and M_{20} are effective at identifying visually disturbed galaxies. For our galaxies with photometric redshifts, for which a visual classification was not performed, we used a correction factor derived using the visual classification of our spectroscopic sample. We then derived $f_{\rm TIM}$, the fraction of TIM objects with well identified observability timescales utilizing the selection line we calibrated, and analyzed its dependence on redshift, velocity dispersion, and both global and local environment. We also analyzed the projected radius-velocity dispersion phase space distribution of our spectroscopic cluster sample. Following this analysis, we performed a full spectrum fitting to analyze the stellar populations of our sample. As a result, we have extracted mass-weighted age fractions of our sample, and derived age-sensitive spectral indices, such as Balmer Hδ absorption line, and the strength of the 4000Å break, $D_{n,4000}$. Using the mass-weighted age fractions of stars we have investigated the star formation rates of our galaxies in three time periods, in their last 1 Gyr, last 0.5 Gyr, and between 0.5 Gyr and 1 Gyr. We have also separately analyzed the mass-weighted age fractions of our two morphological classes in their last 0.5 Gyr, and between 0.5 Gyr and 1 Gyr. Our conclusions are as follows.

1. We find tentative evidence that $f_{\rm TIM}$ increases with increasing redshift. However, we cannot rule out at more than 68% confidence that there is no evolution in redshift for either of our samples. Our results do rule out very strong evolution of $f_{\rm TIM}$ with high confidence. Our results rule out any line with slopes outside of $[-1.65, 1.23]$ for the spectroscopic sample, and outside of $[-1.96, 1.36]$ for the phot+spec sample with 99.5% confidence.

2. $f_{\rm TIM}$ shows no trend with velocity dispersion for either sample.

3. $f_{\rm TIM}$ has a potentially higher value in our groups and our cluster outskirts, compared to the field and cluster cores. We tentatively conclude that $f_{\rm TIM}$ is enhanced in these environments.

4. Our results are also statistically consistent with the cluster core playing no strong role in enhancing $f_{\rm TIM}$. However, given the limited precision of our $f_{\rm TIM}$ values, we also cannot strongly rule out a more significant trend with clustercentric radius.

5. We perform a phase space analysis of our cluster members, an environment where we can measure R_{200} and σ reliably, and find a marginally significant difference in the velocity distributions of the TIM and undisturbed galaxies. This supports our tentative identification of the outskirts of clusters as potentially being the site of an enhanced fraction of tidal interactions and mergers. However, it is also worth noting that the radial distribution of TIM and undisturbed galaxies does not differ significantly. Clearly we need more clusters with $f_{\rm TIM}$ estimates to make stronger constraints.

6. Except for an elevated $f_{\rm TIM}$ value of low significance at the highest density bin for one of our local density measures, our results show no trend between $f_{\rm TIM}$ and local density within the cluster environment.

7. The $G-M_{20}$ TIM and undisturbed galaxies are distinguishable in their distributions in both of the age-sensitive spectral indices we utilize, EW($\rm H\delta_A$), and $D_{n,4000}$. We find the two-sample KS p-values to be 6×10^{-5} when comparing the distribution of these two classes in $D_{n,4000}$, and 10^{-4} in EW($\rm H\delta_A$). This difference is due to the $G-M_{20}$ TIMs preferentially

residing on the part of the EW($H\delta_A$)-$D_{n,4000}$ plane populated by galaxies having a significant fraction of young stars, and the undisturbed galaxies having much higher fractions on the part of the plane populated by galaxies that dominantly have old stars.

8. We analyze the $G-M_{20}$ TIM and undisturbed galaxies in the fraction of stellar mass they have in stars younger than 0.5 Gyr ($f_{Age<0.5\ \mathrm{Gyr}}$), and between the ages of 0.5 Gyr and 1 Gyr ($f_{0.5<Age<1.0\ \mathrm{Gyr}}$). Our results find that these classes are unlikely to have been drawn from the same parent sample in their $f_{Age<0.5\ \mathrm{Gyr}}$ distribution, and in $f_{0.5<Age<1.0\ \mathrm{Gyr}}$. We find no evidence for star formation enhancement in $G-M_{20}$ TIMs as measured by the difference of the fractional stellar mass produced during these periods, ($f_{0.5<Age<1.0\ \mathrm{Gyr}}$ - $f_{Age<0.5\ \mathrm{Gyr}}$).

9. When we only examine the UVJ-selected star-forming galaxies, we find that we are unable to reject the null hypothesis that the star-forming $G-M_{20}$ TIM and undisturbed galaxies are drawn from the same sample in their $f_{0.5<Age<1.0\ \mathrm{Gyr}}$ values. This changes when we investigate their $f_{Age<0.5\ \mathrm{Gyr}}$ values, where we find these morphological classes have a distinguishable distribution, and they are unlikely to have been drawn from the same parent distribution for this measure. This potentially indicates a TIM-enhanced star formation scenario UVJ-selected star-forming galaxies in their last 0.5 Gyr. However, given that we do not see such elevation for the full sample, this result is tentative. Careful calibration of timescales is needed to make a definitive claim about TIM modifications to the star formation histories of intermediate redshift galaxies. We discuss our plans for the derivation of a merger timescale in §7.1.

10. We calculate the $\langle f(\Delta t)\rangle$ (mean of the fractional mass contained in stars with ages within Δt) of the $G-M_{20}$ TIM and undisturbed galaxies as a function of environment. The high errors of the $G-M_{20}$ TIMs, due to low number counts, hinder our ability to draw strong conclusions about the effect of environment on these age fractions. We find that $G-M_{20}$ TIM $\langle f(\Delta t)\rangle$ values are higher than the values for the undisturbed galaxies, albeit tentatively, at every environmental bin we consider. However, we cannot reject the null hypothesis of no

correlation for any $\langle f(\Delta t) \rangle$, at any of the global environments we consider. This potentially indicates that the tentative enhancement in star formation for the last 0.5 Gyr we find in the star-forming $G - M_{20}$ TIMs can likely not be attributed to environmental factors, but to the TIM event itself.

7.1 Future Work

An important future work item would be attempting to boost the signal of the results in our work by using a larger sample similar in its properties to our sample. For example, a larger sample size in group members would be invaluable in pinpointing the role of the group environment in transforming star-forming properties in our analysis. Applying this analysis to similar surveys such as CANDELS, CLASH, or Frontier Fields, within our redshift range would reduce the uncertainties in our analysis due to sample size.

While our limited number of galaxies prevents us from drawing more robust conclusions, this analysis lays the groundwork for future studies that will make stronger constraints. For example, this analysis can be readily applied to any data set with excellent image quality and precision redshifts. Space-based missions like Euclid and WFIRST will be the prime candidates thanks to their high resolution and grism-based redshifts. LSST will also have very precise photometric redshifts and good image quality and this technique should be possible for lower redshift samples where the ground-based seeing results in sufficient physical resolution. Finally deconvolution methods such as in Cantale et al. (2016a) can be applied to ground-based imaging surveys making it possible to carry out analysis on these surveys to much larger distances.

As future work, we intend to analyze the outputs of galaxy merger simulations presented in Lotz et al. (2010b,a). These simulations track the G and M_{20} values of merging galaxies as a function of time. The amount of time the merger event is selected as a $G - M_{20}$ merger, or remains above the selection threshold on the $G - M_{20}$ space, determines the observability timescale of the merger event. The final values are quoted after averaging the timescales of the merger event at many viewing angles, and also for events of varying stellar mass ratios between merging galaxies.

Lotz et al. (2010b,a) use the green dotted line in our $G - M_{20}$ figures as their merger selection. Similarly, we plan to first constrain a merger timescale with our selection line on the $G - M_{20}$ space. We also plan to investigate the simulated SFHs of the merging galaxies, and their UVJ color evolution, to better understand our results so far.

In §6.2 and §6.3, we discussed how the star formation rates of some galaxies show too steep a change, going from $0.5 < t < 1$ Gyr to $t < 0.5$ Gyr, compared with literature values. We plan to look into the star formation histories of these galaxies further, and investigate whether these modifications are caused by a physical process, or whether they are the result of a systematic aspect of our spectral fitting. An initial approach will be to test our fitting with a different library of stellar templates, to compare with our current star formation histories derived using the MILES templates.

Both parts of our TIM selection process is fitting for the application of machine learning techniques. First, we make use of a visual classification of interaction and merger signatures as the initial step for our TIM selection. Neural networks have shown remarkable success in visual classification in a variety of different situations, surpassing human identifiers overwhelmingly in speed, and in cases where human subjectivity is an issue, even in accuracy (e.g. cancer detection). Using a well-calibrated neural network for merger detection will benefit not only from higher speeds of classification, also from less identifier subjectivity.

Secondly, we rely on two morphological parameters, G and M_{20}, for a pure selection of TIM with a well-identified merger timescale. Methods such as random forest classifiers or gradient boosting are capable of using many more parameters, for binary or multiclass classification, which can in turn increase purity. It is yet unclear how these methods can be used jointly with a determination of the merger timescale, and I believe this to be an important venue to research further by applying these techniques to state of the art simulations. A precise calculation of merger rates is crucial for a considerable time span of the universe, which requires a precise determination of merger timescales, and merger fractions.

Appendix A

Cluster, Group and Field Members of the EDisCS Sample

Here we present our spectroscopic and photometric sample in more detail. Table A.1 contains every spectroscopic cluster and group member, and field galaxy that passes all our quality cuts. Groups according to our definition have $\sigma < 400\,\mathrm{km\,s^{-1}}$. We remind that we applied a stellar mass completeness cut of $log(M_*/M_\odot) > 10.4$ to obtain this sample. For other details, we refer the reader to §2.1. The table shows the galaxy ID, name of the field the galaxy is in, galaxy spectroscopic redshift, galaxy stellar mass, G and M_{20} values, and its visual classification. Table A.2 contains every photometric cluster member and field galaxy that passes all our quality cuts. Stellar mass completeness cut is the same as the spectroscopic sample. The table shows the galaxy ID, name of the field the galaxy is in, galaxy stellar mass, and its G and M_{20} values.

Table A.1: Spectroscopic Cluster & Group Members, and Field Galaxies

Galaxy ID	Field Name	Redshift	$\log_{10}(M_*/M_\odot)$	G	M_{20}	Vis. Class
Cluster Members						
EDCSNJ1040415-1156559	cl1040.7-1155	0.7007	10.49	0.52	-1.51	I
EDCSNJ1040410-1155590	cl1040.7-1155	0.7079	10.87	0.37	-1.11	m
EDCSNJ1040409-1156282	cl1040.7-1155	0.6997	10.72	0.46	-1.51	I
EDCSNJ1040407-1156015	cl1040.7-1155	0.703	11.15	0.58	-1.94	0
EDCSNJ1040402-1155587	cl1040.7-1155	0.7031	10.92	0.61	-2.16	0
EDCSNJ1040396-1155183	cl1040.7-1155	0.7046	10.93	0.57	-2.17	0
EDCSNJ1040369-1157141	cl1040.7-1155	0.7052	11.04	0.61	-2.24	0
EDCSNJ1040356-1156026	cl1040.7-1155	0.7081	11.25	0.53	-1.98	0

A.1 *(continued)*

Galaxy ID	Field Name	Redshift	$\log_{10}(M_*/M_\odot)$	G	M_{20}	Vis. Class
EDCSNJ1040355-1156537	cl1040.7-1155	0.7061	10.97	0.52	-1.82	m
EDCSNJ1040346-1155511	cl1040.7-1155	0.7088	10.42	0.52	-1.47	i
EDCSNJ1054323-1147213	cl1054.4-1146	0.7019	10.99	0.56	-1.95	i
EDCSNJ1054316-1147400	cl1054.4-1146	0.6908	10.97	0.54	-2.02	0
EDCSNJ1054311-1149250	cl1054.4-1146	0.6966	10.67	0.48	-1.47	i
EDCSNJ1054309-1147095	cl1054.4-1146	0.6998	11.01	0.57	-2.14	0
EDCSNJ1054303-1149132	cl1054.4-1146	0.6964	11.63	0.62	-1.51	i
EDCSNJ1054296-1147123	cl1054.4-1146	0.6981	11.36	0.63	-2.32	0
EDCSNJ1054296-1145499	cl1054.4-1146	0.6994	10.5	0.57	-1.99	0
EDCSNJ1054292-1149179	cl1054.4-1146	0.6968	10.47	0.6	-1.91	0
EDCSNJ1054264-1147207	cl1054.4-1146	0.6963	10.71	0.39	-1.25	i
EDCSNJ1054263-1148407	cl1054.4-1146	0.7014	10.92	0.54	-1.81	0
EDCSNJ1054259-1148307	cl1054.4-1146	0.6962	10.91	0.59	-1.24	0
EDCSNJ1054255-1146331	cl1054.4-1146	0.6942	10.58	0.56	-2.15	0
EDCSNJ1054255-1146441	cl1054.4-1146	0.7048	11.04	0.58	-2.33	i
EDCSNJ1054254-1145547	cl1054.4-1146	0.6977	11.55	0.54	-2.1	0
EDCSNJ1054251-1145360	cl1054.4-1146	0.6945	10.61	0.53	-1.85	0
EDCSNJ1054250-1146238	cl1054.4-1146	0.6968	11.42	0.62	-2.29	0
EDCSNJ1054247-1146238	cl1054.4-1146	0.7004	10.72	0.5	-0.85	0
EDCSNJ1054244-1146194	cl1054.4-1146	0.6965	11.5	0.61	-2.44	0
EDCSNJ1054242-1146564	cl1054.4-1146	0.6903	10.68	0.59	-2.36	0
EDCSNJ1054237-1146107	cl1054.4-1146	0.6962	10.58	0.54	-1.83	0
EDCSNJ1054233-1146024	cl1054.4-1146	0.698	10.6	0.53	-1.76	0
EDCSNJ1054209-1145141	cl1054.4-1146	0.7020	11.28	0.6	-1.95	M
EDCSNJ1054198-1146337	cl1054.4-1146	0.6972	10.55	0.54	-1.42	M

A.1 *(continued)*

Galaxy ID	Field Name	Redshift	$\log_{10}(M_*/M_\odot)$	G	M_{20}	Vis. Class
EDCSNJ1054182-1147240	cl1054.4-1146	0.6965	10.98	0.51	-1.49	m
EDCSNJ1054478-1244244	cl1054.7-1245	0.7517	10.53	0.53	-1.91	0
EDCSNJ1054471-1246412	cl1054.7-1245	0.7522	10.7	0.6	-2.0	0
EDCSNJ1054445-1246173	cl1054.7-1245	0.7498	10.77	0.6	-1.97	0
EDCSNJ1054440-1246390	cl1054.7-1245	0.7496	10.72	0.55	-1.94	0
EDCSNJ1054439-1245556	cl1054.7-1245	0.7531	10.84	0.6	-2.22	0
EDCSNJ1054438-1245409	cl1054.7-1245	0.7568	11.12	0.58	-2.03	0
EDCSNJ1054437-1246028	cl1054.7-1245	0.7572	10.45	0.57	-2.07	0
EDCSNJ1054436-1244202	cl1054.7-1245	0.7463	10.91	0.58	-2.08	0
EDCSNJ1054435-1246152	cl1054.7-1245	0.7525	11.09	0.57	-1.91	0
EDCSNJ1054433-1245534	cl1054.7-1245	0.7468	10.65	0.57	-1.91	0
EDCSNJ1054409-1246529	cl1054.7-1245	0.7496	10.91	0.54	-1.83	0
EDCSNJ1054407-1247385	cl1054.7-1245	0.7482	10.88	0.6	-2.19	0
EDCSNJ1054404-1248083	cl1054.7-1245	0.7483	10.59	0.45	-1.52	0
EDCSNJ1054398-1246055	cl1054.7-1245	0.7482	11.23	0.56	-2.19	I
EDCSNJ1054396-1248241	cl1054.7-1245	0.7478	10.94	0.63	-2.01	0
EDCSNJ1054356-1245264	cl1054.7-1245	0.7493	11.19	0.61	-2.22	0
EDCSNJ1138130-1132345	cl1138.2-1133	0.4791	10.72	0.55	-1.87	0
EDCSNJ1138116-1134448	cl1138.2-1133	0.4571	10.77	0.58	-2.06	0
EDCSNJ1138113-1132017	cl1138.2-1133	0.4748	10.73	0.58	-0.83	I
EDCSNJ1138110-1133411	cl1138.2-1133	0.4825	10.59	0.53	-1.97	0
EDCSNJ1138109-1134170	cl1138.2-1133	0.4759	10.53	0.57	-1.81	0
EDCSNJ1138107-1133431	cl1138.2-1133	0.4764	10.68	0.59	-2.01	0
EDCSNJ1138106-1133312	cl1138.2-1133	0.4775	10.67	0.58	-1.0	I
EDCSNJ1138104-1133319	cl1138.2-1133	0.4844	10.53	0.57	-2.29	0

A.1 *(continued)*

Galaxy ID	Field Name	Redshift	$\log_{10}(M_*/M_\odot)$	G	M_{20}	Vis. Class
EDCSNJ1138102-1133379	cl1138.2-1133	0.4801	11.14	0.6	-2.1	0
EDCSNJ1138086-1136549	cl1138.2-1133	0.4519	10.83	0.55	-1.95	m
EDCSNJ1138078-1133592	cl1138.2-1133	0.4769	10.52	0.44	-1.08	0
EDCSNJ1138069-1134314	cl1138.2-1133	0.4819	10.81	0.6	-2.11	0
EDCSNJ1138069-1132044	cl1138.2-1133	0.4798	10.48	0.65	-2.3	0
EDCSNJ1138068-1132285	cl1138.2-1133	0.4787	10.59	0.5	-1.77	0
EDCSNJ1138065-1136018	cl1138.2-1133	0.4561	10.44	0.53	-1.85	0
EDCSNJ1138056-1136287	cl1138.2-1133	0.4561	10.58	0.53	-1.84	0
EDCSNJ1138031-1134278	cl1138.2-1133	0.4549	10.69	0.59	-1.87	0
EDCSNJ1138024-1136024	cl1138.2-1133	0.4585	10.59	0.53	-2.05	0
EDCSNJ1138022-1135459	cl1138.2-1133	0.4541	10.77	0.58	-2.2	0
EDCSNJ1216522-1200595	cl1216.8-1201	0.7882	10.71	0.6	-1.91	0
EDCSNJ1216504-1200480	cl1216.8-1201	0.7886	11.07	0.43	-1.1	M
EDCSNJ1216498-1201358	cl1216.8-1201	0.7882	10.72	0.56	-2.08	0
EDCSNJ1216490-1201531	cl1216.8-1201	0.7998	10.66	0.41	-1.32	0
EDCSNJ1216490-1200091	cl1216.8-1201	0.7863	10.88	0.54	-2.05	0
EDCSNJ1216480-1200220	cl1216.8-1201	0.7859	10.86	0.54	-2.04	0
EDCSNJ1216470-1159267	cl1216.8-1201	0.7971	10.82	0.6	-2.02	0
EDCSNJ1216468-1202226	cl1216.8-1201	0.7987	11.04	0.55	-2.23	0
EDCSNJ1216464-1203257	cl1216.8-1201	0.7966	10.56	0.58	-2.15	0
EDCSNJ1216462-1202253	cl1216.8-1201	0.7866	10.74	0.53	-2.0	0
EDCSNJ1216462-1200073	cl1216.8-1201	0.7847	10.66	0.59	-2.0	0
EDCSNJ1216456-1158383	cl1216.8-1201	0.7925	10.98	0.45	-1.26	I
EDCSNJ1216454-1200017	cl1216.8-1201	0.7996	11.04	0.61	-2.15	0
EDCSNJ1216452-1203134	cl1216.8-1201	0.7933	10.41	0.52	-1.13	M

A.1 *(continued)*

Galaxy ID	Field Name	Redshift	$\log_{10}(M_*/M_\odot)$	G	M_{20}	Vis. Class
EDCSNJ1216453-1201176	cl1216.8-1201	0.7955	11.76	0.48	-0.7	I
EDCSNJ1216451-1158493	cl1216.8-1201	0.7969	11.04	0.54	-1.72	0
EDCSNJ1216449-1202036	cl1216.8-1201	0.7938	10.79	0.41	-1.41	0
EDCSNJ1216449-1201203	cl1216.8-1201	0.8035	11.52	0.57	-1.98	0
EDCSNJ1216448-1201309	cl1216.8-1201	0.7984	11.32	0.53	-1.28	I
EDCSNJ1216447-1201282	cl1216.8-1201	0.7865	10.82	0.45	-0.73	M
EDCSNJ1216446-1201089	cl1216.8-1201	0.8001	10.92	0.61	-1.11	i
EDCSNJ1216443-1201429	cl1216.8-1201	0.7918	11.36	0.56	-0.85	0
EDCSNJ1216438-1200536	cl1216.8-1201	0.7945	11.36	0.56	-1.76	0
EDCSNJ1216429-1159536	cl1216.8-1201	0.7951	10.82	0.61	-1.92	0
EDCSNJ1216428-1203395	cl1216.8-1201	0.7955	11.42	0.52	-2.09	0
EDCSNJ1216420-1201509	cl1216.8-1201	0.7941	11.46	0.6	-2.3	i
EDCSNJ1216419-1202440	cl1216.8-1201	0.8028	10.59	0.48	-1.2	0
EDCSNJ1216417-1203054	cl1216.8-1201	0.8012	10.78	0.56	-1.85	0
EDCSNJ1216401-1202352	cl1216.8-1201	0.8022	11.15	0.62	-2.15	0
EDCSNJ1216387-1203120	cl1216.8-1201	0.7958	11.36	0.46	-1.06	T
EDCSNJ1216387-1201503	cl1216.8-1201	0.8008	11.07	0.59	-2.02	0
EDCSNJ1216382-1202517	cl1216.8-1201	0.79	11.19	0.6	-2.13	0
EDCSNJ1216381-1203266	cl1216.8-1201	0.7939	11.26	0.57	-2.28	0
EDCSNJ1216364-1200087	cl1216.8-1201	0.7868	10.9	0.61	-2.06	0
EDCSNJ1216359-1200294	cl1216.8-1201	0.7929	10.93	0.6	-1.85	0
EDCSNJ1228025-1135219	cl1227.9-1138	0.638	10.82	0.47	-1.72	0
EDCSNJ1228001-1136095	cl1227.9-1138	0.6325	10.42	0.39	-0.9	t
EDCSNJ1227581-1135364	cl1227.9-1138	0.6383	11.0	0.6	-2.16	0
EDCSNJ1227572-1135552	cl1227.9-1138	0.6336	10.8	0.48	-1.1	M

A.1 *(continued)*

Galaxy ID	Field Name	Redshift	$\log_{10}(M_*/M_\odot)$	G	M_{20}	Vis. Class
EDCSNJ1227571-1136178	cl1227.9-1138	0.6333	10.77	0.51	-1.8	0
EDCSNJ1227566-1136545	cl1227.9-1138	0.6391	10.66	0.58	-2.29	0
EDCSNJ1227551-1135584	cl1227.9-1138	0.6333	10.61	0.51	-0.94	I
EDCSNJ1227548-1137529	cl1227.9-1138	0.6369	11.23	0.6	-2.33	0
EDCSNJ1227541-1138174	cl1227.9-1138	0.6345	11.56	0.5	-1.83	I
EDCSNJ1227537-1138210	cl1227.9-1138	0.6309	10.56	0.56	-1.91	0
EDCSNJ1227533-1136527	cl1227.9-1138	0.6347	10.69	0.51	-1.48	T
EDCSNJ1227531-1138340	cl1227.9-1138	0.6345	10.48	0.59	-1.97	0
EDCSNJ1232384-1251324	cl1232.5-1250	0.5349	10.56	0.57	-2.13	0
EDCSNJ1232370-1248239	cl1232.5-1250	0.5401	10.74	0.58	-2.06	0
EDCSNJ1232370-1248495	cl1232.5-1250	0.5381	10.47	0.6	-1.97	0
EDCSNJ1232365-1251264	cl1232.5-1250	0.5393	10.71	0.59	-2.29	0
EDCSNJ1232347-1249462	cl1232.5-1250	0.5408	10.51	0.57	-1.95	0
EDCSNJ1232343-1249265	cl1232.5-1250	0.5395	10.77	0.6	-2.15	0
EDCSNJ1232341-1252213	cl1232.5-1250	0.5394	10.65	0.64	-2.23	0
EDCSNJ1232340-1249138	cl1232.5-1250	0.5306	10.79	0.61	-2.25	0
EDCSNJ1232327-1249057	cl1232.5-1250	0.5327	10.57	0.42	-1.56	0
EDCSNJ1232323-1251267	cl1232.5-1250	0.5498	11.03	0.48	-2.09	0
EDCSNJ1232318-1249049	cl1232.5-1250	0.5408	10.5	0.62	-2.15	0
EDCSNJ1232317-1249275	cl1232.5-1250	0.542	11.14	0.56	-1.94	0
EDCSNJ1232311-1251061	cl1232.5-1250	0.5526	10.48	0.55	-2.27	0
EDCSNJ1232309-1249408	cl1232.5-1250	0.5485	11.34	0.59	-2.22	0
EDCSNJ1232303-1251441	cl1232.5-1250	0.55	10.57	0.58	-1.65	0
EDCSNJ1232299-1251034	cl1232.5-1250	0.5493	10.41	0.58	-2.05	0
EDCSNJ1232297-1250080	cl1232.5-1250	0.5496	10.67	0.49	-2.2	0

A.1 *(continued)*

Galaxy ID	Field Name	Redshift	$\log_{10}(M_*/M_\odot)$	G	M_{20}	Vis. Class
EDCSNJ1232297-1249120	cl1232.5-1250	0.5412	10.58	0.65	-2.32	0
EDCSNJ1232296-1250119	cl1232.5-1250	0.5509	10.97	0.55	-2.05	0
EDCSNJ1232287-1252369	cl1232.5-1250	0.5432	11.24	0.57	-2.11	0
EDCSNJ1232288-1250490	cl1232.5-1250	0.547	10.82	0.58	-2.08	0
EDCSNJ1232280-1252528	cl1232.5-1250	0.5448	10.47	0.51	-1.49	0
EDCSNJ1232281-1249480	cl1232.5-1250	0.5301	10.57	0.58	-1.82	0
EDCSNJ1232280-1249353	cl1232.5-1250	0.5449	11.21	0.52	-1.37	0
EDCSNJ1232275-1248540	cl1232.5-1250	0.5424	11.03	0.48	-1.34	M
EDCSNJ1232273-1251080	cl1232.5-1250	0.5369	10.61	0.59	-2.12	T
EDCSNJ1232271-1253013	cl1232.5-1250	0.5445	10.88	0.61	-2.21	0
EDCSNJ1232271-1250195	cl1232.5-1250	0.5404	10.91	0.65	-2.37	0
EDCSNJ1232250-1251551	cl1232.5-1250	0.5399	10.73	0.61	-2.22	i
EDCSNJ1232228-1251168	cl1232.5-1250	0.5432	10.74	0.62	-2.26	0
EDCSNJ1232204-1249547	cl1232.5-1250	0.546	11.21	0.53	-2.02	0
EDCSNJ1354175-1230391	cl1354.2-1230	0.7632	10.47	0.43	-1.08	0
EDCSNJ1354164-1231599	cl1354.2-1230	0.5937	11.24	0.47	-1.49	0
EDCSNJ1354159-1232272	cl1354.2-1230	0.5929	10.46	0.57	-1.94	0
EDCSNJ1354144-1231514	cl1354.2-1230	0.5946	10.4	0.46	-1.35	m
EDCSNJ1354118-1232499	cl1354.2-1230	0.5946	10.44	0.45	-1.61	i
EDCSNJ1354114-1230452	cl1354.2-1230	0.5947	11.16	0.49	-2.07	i
EDCSNJ1354106-1230499	cl1354.2-1230	0.7634	11.03	0.61	-2.17	i
EDCSNJ1354102-1230527	cl1354.2-1230	0.7593	11.34	0.45	-1.4	0*
EDCSNJ1354101-1231041	cl1354.2-1230	0.7612	10.97	0.56	-1.88	0
EDCSNJ1354098-1231098	cl1354.2-1230	0.7573	10.64	0.64	-1.49	i
EDCSNJ1354098-1231015	cl1354.2-1230	0.7562	11.58	0.58	-1.42	i

A.1 *(continued)*

Galaxy ID	Field Name	Redshift	$\log_{10}(M_*/M_\odot)$	G	M_{20}	Vis. Class
EDCSNJ1354097-1230579	cl1354.2-1230	0.7562	11.27	0.65	-2.21	0
EDCSNJ1354026-1230127	cl1354.2-1230	0.5942	10.5	0.56	-1.94	0
EDCSNJ1354025-1232300	cl1354.2-1230	0.7576	10.99	0.48	-1.63	0
Group Members						
EDCSNJ1037548-1245113	cl1037.9-1243	0.5789	11.09	0.59	-2.05	0
EDCSNJ1037535-1244006	cl1037.9-1243	0.5775	11.06	0.46	-0.76	M
EDCSNJ1037535-1241538	cl1037.9-1243	0.5789	10.88	0.58	-1.53	0
EDCSNJ1037531-1243551	cl1037.9-1243	0.5788	10.48	0.5	-1.59	0
EDCSNJ1037527-1243456	cl1037.9-1243	0.5807	10.8	0.61	-1.81	m
EDCSNJ1037525-1243541	cl1037.9-1243	0.5772	10.84	0.59	-1.83	0
EDCSNJ1037521-1243392	cl1037.9-1243	0.5799	11.05	0.42	-1.04	M
EDCSNJ1040471-1153262	cl1040.7-1155	0.7792	10.53	0.49	-1.1	M
EDCSNJ1040420-1155525	cl1040.7-1155	0.6308	10.95	0.49	-1.76	0
EDCSNJ1040409-1157230	cl1040.7-1155	0.6316	10.67	0.46	-1.59	0
EDCSNJ1040343-1155414	cl1040.7-1155	0.7807	11.48	0.63	-2.32	0
EDCSNJ1054308-1147557	cl1054.4-1146	0.615	10.68	0.48	-1.38	0
EDCSNJ1054297-1148146	cl1054.4-1146	0.6143	11.03	0.62	-1.68	T^*
EDCSNJ1054249-1147556	cl1054.4-1146	0.6139	10.93	0.61	-1.51	I
EDCSNJ1054197-1145282	cl1054.4-1146	0.6127	11.05	0.49	-1.52	0^*
EDCSNJ1054525-1244189	cl1054.7-1245	0.7283	11.17	0.57	-1.75	T
EDCSNJ1054466-1247161	cl1054.7-1245	0.7302	10.43	0.64	-1.73	0
EDCSNJ1054457-1246373	cl1054.7-1245	0.7302	10.86	0.5	-1.83	0
EDCSNJ1054451-1247336	cl1054.7-1245	0.7305	10.89	0.57	-1.96	i
EDCSNJ1054450-1244089	cl1054.7-1245	0.7305	10.86	0.53	-1.86	i
EDCSNJ1054387-1243048	cl1054.7-1245	0.7314	10.78	0.58	-2.12	0

A.1 *(continued)*

Galaxy ID	Field Name	Redshift	$\log_{10}(M_*/M_\odot)$	G	M_{20}	Vis. Class
EDCSNJ1054350-1243344	cl1054.7-1245	0.7293	10.74	0.55	-1.9	0
EDCSNJ1103438-1247251	cl1103.7-1245	0.6238	10.52	0.61	-2.1	0
EDCSNJ1103413-1244379	cl1103.7-1245	0.7038	11.17	0.6	-2.23	0
EDCSNJ1103401-1244377	cl1103.7-1245	0.7032	10.6	0.52	-1.83	0
EDCSNJ1103386-1247210	cl1103.7-1245	0.6276	11.18	0.54	-2.2	I
EDCSNJ1103373-1246364	cl1103.7-1245	0.703	10.54	0.56	-1.36	0
EDCSNJ1103372-1245215	cl1103.7-1245	0.6251	10.93	0.62	-2.19	0
EDCSNJ1103365-1244223	cl1103.7-1245	0.7031	11.79	0.56	-2.08	0
EDCSNJ1103363-1246220	cl1103.7-1245	0.6288	11.11	0.54	-1.95	0
EDCSNJ1103357-1246398	cl1103.7-1245	0.6278	10.74	0.59	-1.92	0
EDCSNJ1103355-1244515	cl1103.7-1245	0.6259	10.95	0.47	-1.75	T
EDCSNJ1103349-1246462	cl1103.7-1245	0.6257	11.34	0.62	-2.44	0
EDCSNJ1103339-1243415	cl1103.7-1245	0.7004	10.53	0.54	-1.7	0
Field Galaxies						
EDCSNJ1038014-1242267	cl1037.9-1243	0.7424	11.09	0.6	-2.33	i
EDCSNJ1037495-1246452	cl1037.9-1243	0.5327	10.98	0.57	-2.43	0
EDCSNJ1037430-1244080	cl1037.9-1243	0.487	10.55	0.49	-1.66	t
EDCSNJ1037448-1245026	cl1037.9-1243	0.4456	10.46	0.55	-1.94	0
EDCSNJ1037534-1246259	cl1037.9-1243	0.4948	10.81	0.61	-2.17	0
EDCSNJ1037571-1246441	cl1037.9-1243	0.6184	10.54	0.53	-1.81	0
EDCSNJ1037580-1241553	cl1037.9-1243	0.6836	10.5	0.49	-1.27	M
EDCSNJ1037576-1242041	cl1037.9-1243	0.7775	10.99	0.61	-2.09	0
EDCSNJ1037529-1246428	cl1037.9-1243	0.6452	10.66	0.58	-1.89	0
EDCSNJ1040422-1154417	cl1040.7-1155	0.7613	11.17	0.55	-2.08	I
EDCSNJ1040424-1154443	cl1040.7-1155	0.7614	10.51	0.48	-1.39	I

A.1 *(continued)*

Galaxy ID	Field Name	Redshift	$\log_{10}(M_*/M_\odot)$	G	M_{20}	Vis. Class
EDCSNJ1040351-1156435	cl1040.7-1155	0.5384	10.89	0.45	-1.8	0
EDCSNJ1040399-1157135	cl1040.7-1155	0.6308	10.47	0.5	-2.08	0
EDCSNJ1040391-1157386	cl1040.7-1155	0.6311	10.76	0.48	-1.78	0
EDCSNJ1040410-1156134	cl1040.7-1155	0.6303	10.82	0.55	-1.62	t
EDCSNJ1040355-1153214	cl1040.7-1155	0.5214	10.51	0.53	-1.83	0
EDCSNJ1040467-1154041	cl1040.7-1155	0.7821	10.91	0.57	-2.03	0
EDCSNJ1040380-1154147	cl1040.7-1155	0.7791	11.35	0.57	-2.11	0
EDCSNJ1040419-1155198	cl1040.7-1155	0.7388	10.44	0.45	-1.63	t
EDCSNJ1040494-1157385	cl1040.7-1155	0.5362	10.79	0.57	-1.43	t
EDCSNJ1054206-1144284	cl1054.4-1146	0.7255	10.85	0.55	-2.01	0
EDCSNJ1054238-1146477	cl1054.4-1146	0.7619	11.24	0.59	-2.12	0
EDCSNJ1054252-1148269	cl1054.4-1146	0.7622	10.64	0.57	-2.19	0
EDCSNJ1054194-1145180	cl1054.4-1146	0.5207	10.68	0.5	-2.04	t
EDCSNJ1054239-1145236	cl1054.4-1146	0.7408	11.2	0.63	-2.27	0
EDCSNJ1054174-1145346	cl1054.4-1146	0.5204	11.21	0.58	-1.25	M
EDCSNJ1054338-1146388	cl1054.4-1146	0.7613	10.85	0.51	-2.26	0
EDCSNJ1054378-1248214	cl1054.7-1245	0.7742	10.73	0.57	-1.75	0
EDCSNJ1054474-1242572	cl1054.7-1245	0.6349	10.79	0.52	-1.83	0
EDCSNJ1054437-1245471	cl1054.7-1245	0.6315	10.59	0.43	-1.28	0
EDCSNJ1054487-1245052	cl1054.7-1245	0.6189	10.78	0.57	-2.01	0
EDCSNJ1054353-1246528	cl1054.7-1245	0.6932	11.43	0.53	-2.13	0
EDCSNJ1103477-1247428	cl1103.7-1245	0.7657	10.58	0.44	-1.41	0
EDCSNJ1138100-1136361	cl1138.2-1133	0.4389	10.5	0.61	-2.0	0
EDCSNJ1138078-1134468	cl1138.2-1133	0.5282	10.59	0.6	-2.34	0
EDCSNJ1138045-1135118	cl1138.2-1133	0.5798	10.59	0.56	-2.0	i

A.1 *(continued)*

Galaxy ID	Field Name	Redshift	$\log_{10}(M_*/M_\odot)$	G	M_{20}	Vis. Class
EDCSNJ1216467-1159378	cl1216.8-1201	0.6669	10.45	0.57	-2.17	M
EDCSNJ1216446-1202358	cl1216.8-1201	0.6698	10.48	0.57	-1.82	0
EDCSNJ1216502-1200038	cl1216.8-1201	0.6659	10.59	0.6	-2.03	0
EDCSNJ1216445-1201533	cl1216.8-1201	0.6703	10.94	0.63	-2.07	T
EDCSNJ1216372-1200419	cl1216.8-1201	0.6606	10.94	0.58	-2.05	0
EDCSNJ1216449-1202139	cl1216.8-1201	0.6691	10.94	0.59	-2.24	0
EDCSNJ1227585-1135250	cl1227.9-1138	0.5439	10.82	0.59	-2.09	0
EDCSNJ1227543-1136008	cl1227.9-1138	0.6802	11.08	0.51	-1.47	t
EDCSNJ1227453-1137005	cl1227.9-1138	0.6789	10.98	0.46	-1.79	0
EDCSNJ1227589-1139039	cl1227.9-1138	0.4911	10.47	0.59	-2.26	0
EDCSNJ1227578-1136570	cl1227.9-1138	0.4679	10.94	0.6	-2.28	0
EDCSNJ1227552-1137559	cl1227.9-1138	0.4893	10.79	0.57	-2.22	0
EDCSNJ1227599-1138116	cl1227.9-1138	0.7076	10.68	0.59	-1.93	0
EDCSNJ1227592-1139142	cl1227.9-1138	0.4678	10.98	0.52	-2.11	0
EDCSNJ1227548-1139394	cl1227.9-1138	0.7548	10.56	0.54	-1.72	0
EDCSNJ1228009-1138122	cl1227.9-1138	0.7081	11.31	0.58	-2.04	T
EDCSNJ1227558-1139556	cl1227.9-1138	0.4885	10.72	0.59	-2.21	0
EDCSNJ1232339-1249205	cl1232.5-1250	0.6797	10.42	0.55	-1.91	0
EDCSNJ1232326-1249355	cl1232.5-1250	0.4186	10.86	0.6	-2.04	0
EDCSNJ1232301-1251245	cl1232.5-1250	0.6171	10.82	0.56	-2.26	I
EDCSNJ1232315-1251578	cl1232.5-1250	0.4171	10.96	0.55	-2.23	0
EDCSNJ1232333-1250121	cl1232.5-1250	0.4155	10.74	0.5	-2.0	0
EDCSNJ1232339-1252010	cl1232.5-1250	0.7295	10.88	0.54	-1.91	t
EDCSNJ1232373-1249247	cl1232.5-1250	0.6778	10.46	0.51	-1.72	0
EDCSNJ1232365-1253082	cl1232.5-1250	0.6579	10.7	0.47	-1.42	0

A.1 *(continued)*

Galaxy ID	Field Name	Redshift	$\log_{10}(M_*/M_\odot)$	G	M_{20}	Vis. Class
EDCSNJ1354107-1231236	cl1354.2-1230	0.6183	10.69	0.58	-1.92	0
EDCSNJ1354073-1233158	cl1354.2-1230	0.789	11.16	0.59	-2.15	0
EDCSNJ1354139-1229474	cl1354.2-1230	0.6865	10.76	0.6	-2.08	i
EDCSNJ1354009-1233233	cl1354.2-1230	0.6622	10.45	0.5	-1.57	0
EDCSNJ1354123-1233380	cl1354.2-1230	0.6164	10.93	0.53	-1.82	M
EDCSNJ1354178-1230335	cl1354.2-1230	0.565	10.44	0.54	-1.61	0
EDCSNJ1354164-1229192	cl1354.2-1230	0.6846	11.23	0.62	-2.34	0
EDCSNJ1354091-1233426	cl1354.2-1230	0.7913	11.1	0.61	-2.03	0

Table A.2: Photometric Cluster Members and Field Galaxies

Galaxy ID	Field Name	$\log_{10}(M_*/M_\odot)$	G	M_{20}
Cluster Members				
EDCSNJ1040506-1154108	cl1040.7-1155	11.32	0.6	-2.27
EDCSNJ1040495-1153125	cl1040.7-1155	10.7	0.61	-2.37
EDCSNJ1040488-1155078	cl1040.7-1155	10.76	0.54	-1.9
EDCSNJ1040486-1156217	cl1040.7-1155	11.26	0.46	-1.23
EDCSNJ1040473-1154038	cl1040.7-1155	11.16	0.48	-1.92
EDCSNJ1040426-1157532	cl1040.7-1155	11.03	0.53	-2.07
EDCSNJ1040383-1153176	cl1040.7-1155	10.67	0.59	-1.99
EDCSNJ1040382-1153506	cl1040.7-1155	10.79	0.52	-1.31
EDCSNJ1040381-1153518	cl1040.7-1155	10.83	0.46	-1.09
EDCSNJ1040380-1157000	cl1040.7-1155	10.89	0.46	-1.67
EDCSNJ1040374-1154010	cl1040.7-1155	10.63	0.53	-1.12
EDCSNJ1040361-1156054	cl1040.7-1155	10.7	0.41	-1.28
EDCSNJ1040337-1157231	cl1040.7-1155	11.09	0.57	-1.77

A.2 *(continued)*

Galaxy ID	Field Name	$\log_{10}(M_*/M_\odot)$	G	M_{20}
EDCSNJ1040328-1152599	cl1040.7-1155	10.87	0.58	-1.98
EDCSNJ1054345-1146503	cl1054.4-1146	10.83	0.61	-1.62
EDCSNJ1054343-1146541	cl1054.4-1146	10.67	0.57	-2.06
EDCSNJ1054338-1147230	cl1054.4-1146	11.49	0.62	-2.3
EDCSNJ1054338-1145541	cl1054.4-1146	11.2	0.63	-2.18
EDCSNJ1054335-1148197	cl1054.4-1146	10.61	0.44	-0.95
EDCSNJ1054332-1147414	cl1054.4-1146	10.56	0.57	-2.07
EDCSNJ1054331-1147379	cl1054.4-1146	10.93	0.59	-2.26
EDCSNJ1054330-1147315	cl1054.4-1146	11.05	0.63	-1.68
EDCSNJ1054320-1149211	cl1054.4-1146	11.22	0.58	-1.92
EDCSNJ1054315-1147019	cl1054.4-1146	10.91	0.58	-1.04
EDCSNJ1054308-1146114	cl1054.4-1146	10.94	0.62	-2.26
EDCSNJ1054307-1146375	cl1054.4-1146	10.46	0.57	-1.79
EDCSNJ1054304-1149226	cl1054.4-1146	10.78	0.58	-2.15
EDCSNJ1054287-1146574	cl1054.4-1146	10.73	0.63	-2.06
EDCSNJ1054284-1146500	cl1054.4-1146	10.89	0.57	-1.02
EDCSNJ1054278-1146280	cl1054.4-1146	10.57	0.6	-2.07
EDCSNJ1054272-1145430	cl1054.4-1146	10.48	0.48	-1.46
EDCSNJ1054270-1146240	cl1054.4-1146	10.66	0.51	-1.36
EDCSNJ1054266-1146566	cl1054.4-1146	10.86	0.49	-1.88
EDCSNJ1054265-1146316	cl1054.4-1146	10.83	0.57	-1.09
EDCSNJ1054257-1147149	cl1054.4-1146	10.67	0.58	-2.27
EDCSNJ1054256-1147235	cl1054.4-1146	11.0	0.63	-2.3
EDCSNJ1054254-1148048	cl1054.4-1146	10.41	0.62	-1.9
EDCSNJ1054254-1147523	cl1054.4-1146	11.24	0.33	-1.04

A.2 *(continued)*

Galaxy ID	Field Name	$\log_{10}(M_*/M_\odot)$	G	M_{20}
EDCSNJ1054254-1148135	cl1054.4-1146	10.88	0.54	-1.75
EDCSNJ1054254-1146005	cl1054.4-1146	10.63	0.57	-1.76
EDCSNJ1054248-1148509	cl1054.4-1146	10.43	0.46	-1.46
EDCSNJ1054245-1146139	cl1054.4-1146	10.59	0.61	-1.88
EDCSNJ1054243-1146168	cl1054.4-1146	11.03	0.61	-2.09
EDCSNJ1054243-1145565	cl1054.4-1146	10.59	0.42	-0.83
EDCSNJ1054241-1146407	cl1054.4-1146	10.98	0.64	-2.02
EDCSNJ1054241-1145283	cl1054.4-1146	10.44	0.46	-1.5
EDCSNJ1054241-1146427	cl1054.4-1146	11.02	0.57	-2.14
EDCSNJ1054240-1147297	cl1054.4-1146	10.72	0.58	-2.02
EDCSNJ1054239-1144031	cl1054.4-1146	10.43	0.54	-1.89
EDCSNJ1054235-1146205	cl1054.4-1146	10.46	0.57	-1.97
EDCSNJ1054224-1146208	cl1054.4-1146	11.09	0.62	-2.36
EDCSNJ1054217-1147249	cl1054.4-1146	10.65	0.49	-1.65
EDCSNJ1054213-1146186	cl1054.4-1146	10.94	0.59	-2.33
EDCSNJ1054211-1146162	cl1054.4-1146	10.47	0.51	-1.85
EDCSNJ1054199-1146282	cl1054.4-1146	10.62	0.46	-1.47
EDCSNJ1054183-1149011	cl1054.4-1146	10.94	0.62	-2.03
EDCSNJ1054180-1146217	cl1054.4-1146	10.8	0.48	-1.0
EDCSNJ1054177-1146083	cl1054.4-1146	10.6	0.6	-1.16
EDCSNJ1054169-1148162	cl1054.4-1146	10.45	0.42	-1.6
EDCSNJ1054158-1148203	cl1054.4-1146	10.72	0.46	-1.63
EDCSNJ1054151-1144080	cl1054.4-1146	10.61	0.54	-1.07
EDCSNJ1054528-1245171	cl1054.7-1245	10.47	0.48	-1.06
EDCSNJ1054528-1244126	cl1054.7-1245	10.96	0.58	-2.0

A.2 *(continued)*

Galaxy ID	Field Name	$\log_{10}(M_*/M_\odot)$	G	M_{20}
EDCSNJ1054522-1244173	cl1054.7-1245	11.01	0.62	-2.43
EDCSNJ1054520-1244178	cl1054.7-1245	10.72	0.57	-1.74
EDCSNJ1054504-1243398	cl1054.7-1245	10.48	0.48	-0.94
EDCSNJ1054494-1244376	cl1054.7-1245	10.4	0.42	-1.47
EDCSNJ1054487-1245119	cl1054.7-1245	10.84	0.49	-1.7
EDCSNJ1054479-1246592	cl1054.7-1245	10.95	0.46	-1.33
EDCSNJ1054478-1246292	cl1054.7-1245	10.83	0.49	-1.1
EDCSNJ1054477-1245080	cl1054.7-1245	10.68	0.57	-1.68
EDCSNJ1054476-1246405	cl1054.7-1245	10.41	0.46	-1.6
EDCSNJ1054474-1245580	cl1054.7-1245	10.59	0.44	-1.32
EDCSNJ1054471-1246276	cl1054.7-1245	10.86	0.42	-1.19
EDCSNJ1054466-1247248	cl1054.7-1245	11.11	0.49	-1.93
EDCSNJ1054459-1246290	cl1054.7-1245	10.75	0.6	-2.03
EDCSNJ1054450-1247318	cl1054.7-1245	10.64	0.62	-1.87
EDCSNJ1054446-1243367	cl1054.7-1245	10.81	0.51	-1.75
EDCSNJ1054443-1245198	cl1054.7-1245	11.29	0.45	-2.21
EDCSNJ1054442-1246441	cl1054.7-1245	11.35	0.53	-2.12
EDCSNJ1054437-1246270	cl1054.7-1245	10.88	0.56	-2.09
EDCSNJ1054432-1245541	cl1054.7-1245	10.75	0.55	-1.92
EDCSNJ1054432-1245241	cl1054.7-1245	10.53	0.57	-1.96
EDCSNJ1054427-1246359	cl1054.7-1245	10.54	0.39	-1.14
EDCSNJ1054424-1246085	cl1054.7-1245	11.1	0.6	-2.35
EDCSNJ1054424-1246157	cl1054.7-1245	10.66	0.55	-2.06
EDCSNJ1054422-1244154	cl1054.7-1245	10.47	0.5	-1.83
EDCSNJ1054418-1246350	cl1054.7-1245	10.58	0.54	-1.91

A.2 *(continued)*

Galaxy ID	Field Name	$\log_{10}(M_*/M_\odot)$	G	M_{20}
EDCSNJ1054417-1246282	cl1054.7-1245	10.66	0.55	-1.93
EDCSNJ1054413-1245341	cl1054.7-1245	10.57	0.58	-1.93
EDCSNJ1054408-1245594	cl1054.7-1245	10.74	0.58	-2.18
EDCSNJ1054404-1246478	cl1054.7-1245	10.49	0.6	-1.95
EDCSNJ1054402-1246022	cl1054.7-1245	10.76	0.42	-0.9
EDCSNJ1054395-1248181	cl1054.7-1245	10.78	0.45	-1.38
EDCSNJ1054383-1247373	cl1054.7-1245	10.48	0.61	-1.95
EDCSNJ1054378-1246245	cl1054.7-1245	10.47	0.36	-1.19
EDCSNJ1054377-1247394	cl1054.7-1245	10.63	0.54	-2.1
EDCSNJ1054363-1247075	cl1054.7-1245	10.64	0.56	-1.83
EDCSNJ1054361-1246580	cl1054.7-1245	10.8	0.53	-2.11
EDCSNJ1054361-1244568	cl1054.7-1245	10.66	0.58	-2.01
EDCSNJ1054335-1247110	cl1054.7-1245	10.59	0.58	-1.94
EDCSNJ1054334-1245246	cl1054.7-1245	10.98	0.52	-2.04
EDCSNJ1216554-1200183	cl1216.8-1201	10.65	0.58	-1.86
EDCSNJ1216546-1201460	cl1216.8-1201	10.71	0.51	-0.87
EDCSNJ1216544-1201328	cl1216.8-1201	11.1	0.49	-1.53
EDCSNJ1216541-1203104	cl1216.8-1201	10.91	0.57	-1.89
EDCSNJ1216542-1159077	cl1216.8-1201	10.53	0.61	-1.96
EDCSNJ1216540-1159240	cl1216.8-1201	10.74	0.42	-0.98
EDCSNJ1216532-1201359	cl1216.8-1201	11.14	0.52	-1.78
EDCSNJ1216530-1201504	cl1216.8-1201	10.51	0.36	-0.92
EDCSNJ1216531-1158378	cl1216.8-1201	10.86	0.52	-1.98
EDCSNJ1216525-1158523	cl1216.8-1201	10.41	0.52	-1.05
EDCSNJ1216522-1158170	cl1216.8-1201	10.89	0.51	-1.3

A.2 *(continued)*

Galaxy ID	Field Name	$\log_{10}(M_*/M_\odot)$	G	M_{20}
EDCSNJ1216512-1201331	cl1216.8-1201	10.48	0.58	-1.8
EDCSNJ1216509-1202177	cl1216.8-1201	10.41	0.58	-1.86
EDCSNJ1216508-1201063	cl1216.8-1201	10.51	0.45	-1.51
EDCSNJ1216506-1200064	cl1216.8-1201	10.43	0.53	-1.67
EDCSNJ1216502-1159425	cl1216.8-1201	10.76	0.48	-1.8
EDCSNJ1216498-1201392	cl1216.8-1201	11.2	0.57	-2.02
EDCSNJ1216497-1201117	cl1216.8-1201	10.89	0.52	-2.11
EDCSNJ1216492-1202036	cl1216.8-1201	10.61	0.62	-1.0
EDCSNJ1216490-1201426	cl1216.8-1201	11.21	0.62	-2.12
EDCSNJ1216489-1201239	cl1216.8-1201	11.14	0.56	-1.96
EDCSNJ1216470-1201216	cl1216.8-1201	10.93	0.54	-1.05
EDCSNJ1216469-1201494	cl1216.8-1201	10.46	0.59	-2.04
EDCSNJ1216469-1201241	cl1216.8-1201	11.14	0.6	-2.05
EDCSNJ1216465-1201574	cl1216.8-1201	10.78	0.59	-2.08
EDCSNJ1216457-1158368	cl1216.8-1201	10.54	0.5	-1.62
EDCSNJ1216452-1202262	cl1216.8-1201	10.45	0.56	-1.93
EDCSNJ1216451-1202531	cl1216.8-1201	10.52	0.5	-1.69
EDCSNJ1216447-1201234	cl1216.8-1201	10.76	0.58	-2.09
EDCSNJ1216447-1201434	cl1216.8-1201	11.26	0.53	-2.13
EDCSNJ1216446-1201139	cl1216.8-1201	10.58	0.57	-2.0
EDCSNJ1216445-1201132	cl1216.8-1201	11.12	0.42	-1.38
EDCSNJ1216443-1201201	cl1216.8-1201	11.03	0.53	-1.99
EDCSNJ1216441-1201553	cl1216.8-1201	10.51	0.43	-0.79
EDCSNJ1216434-1201434	cl1216.8-1201	10.68	0.52	-1.73
EDCSNJ1216431-1203334	cl1216.8-1201	10.81	0.53	-1.21

A.2 *(continued)*

Galaxy ID	Field Name	$\log_{10}(M_*/M_\odot)$	G	M_{20}
EDCSNJ1216429-1200591	cl1216.8-1201	10.57	0.55	-1.9
EDCSNJ1216423-1201576	cl1216.8-1201	10.99	0.62	-1.92
EDCSNJ1216418-1202044	cl1216.8-1201	10.58	0.58	-1.97
EDCSNJ1216418-1201081	cl1216.8-1201	11.25	0.61	-2.28
EDCSNJ1216414-1203332	cl1216.8-1201	10.78	0.53	-1.44
EDCSNJ1216412-1201554	cl1216.8-1201	10.46	0.58	-1.85
EDCSNJ1216410-1203293	cl1216.8-1201	10.48	0.41	-1.5
EDCSNJ1216411-1159579	cl1216.8-1201	10.65	0.51	-1.89
EDCSNJ1216408-1201433	cl1216.8-1201	10.59	0.5	-1.81
EDCSNJ1216405-1200496	cl1216.8-1201	10.83	0.49	-1.35
EDCSNJ1216393-1202262	cl1216.8-1201	10.81	0.49	-1.77
EDCSNJ1216392-1201333	cl1216.8-1201	10.52	0.56	-1.71
EDCSNJ1216391-1200154	cl1216.8-1201	10.8	0.57	-1.89
EDCSNJ1216388-1200176	cl1216.8-1201	10.67	0.5	-1.47
EDCSNJ1216387-1201386	cl1216.8-1201	10.74	0.5	-1.34
EDCSNJ1216386-1202099	cl1216.8-1201	10.58	0.57	-2.02
EDCSNJ1216385-1203051	cl1216.8-1201	10.78	0.47	-1.35
EDCSNJ1216383-1202205	cl1216.8-1201	10.63	0.54	-1.79
EDCSNJ1216381-1202515	cl1216.8-1201	11.23	0.6	-2.16
EDCSNJ1216380-1202393	cl1216.8-1201	10.56	0.62	-2.16
EDCSNJ1216379-1201545	cl1216.8-1201	10.43	0.54	-1.76
EDCSNJ1216368-1200357	cl1216.8-1201	10.59	0.58	-1.78
EDCSNJ1216367-1202298	cl1216.8-1201	11.42	0.59	-1.06
EDCSNJ1216366-1202317	cl1216.8-1201	10.94	0.52	-1.36
EDCSNJ1216366-1202253	cl1216.8-1201	11.11	0.48	-1.7

A.2 *(continued)*

Galaxy ID	Field Name	$\log_{10}(M_*/M_\odot)$	G	M_{20}
EDCSNJ1216365-1159452	cl1216.8-1201	10.67	0.58	-2.06
EDCSNJ1216364-1203174	cl1216.8-1201	10.65	0.51	-1.66
EDCSNJ1216361-1200431	cl1216.8-1201	11.0	0.56	-1.64
EDCSNJ1216358-1203011	cl1216.8-1201	10.71	0.57	-2.06
EDCSNJ1216358-1201415	cl1216.8-1201	10.48	0.57	-1.98
EDCSNJ1228031-1136039	cl1227.9-1138	11.52	0.64	-2.44
EDCSNJ1228025-1140247	cl1227.9-1138	10.84	0.59	-2.24
EDCSNJ1228022-1135468	cl1227.9-1138	10.65	0.55	-1.66
EDCSNJ1228021-1140299	cl1227.9-1138	10.49	0.56	-1.8
EDCSNJ1228013-1138450	cl1227.9-1138	11.3	0.54	-1.18
EDCSNJ1228007-1140469	cl1227.9-1138	11.64	0.53	-1.24
EDCSNJ1228003-1137041	cl1227.9-1138	10.84	0.53	-2.09
EDCSNJ1227596-1138024	cl1227.9-1138	10.52	0.55	-2.02
EDCSNJ1227589-1138408	cl1227.9-1138	10.7	0.58	-2.05
EDCSNJ1227586-1136295	cl1227.9-1138	10.48	0.49	-1.75
EDCSNJ1227586-1139362	cl1227.9-1138	11.1	0.46	-2.2
EDCSNJ1227585-1140265	cl1227.9-1138	11.29	0.52	-1.55
EDCSNJ1227570-1135193	cl1227.9-1138	10.81	0.56	-1.97
EDCSNJ1227569-1136423	cl1227.9-1138	11.17	0.6	-2.36
EDCSNJ1227554-1137391	cl1227.9-1138	10.49	0.59	-2.28
EDCSNJ1227553-1136118	cl1227.9-1138	10.7	0.48	-1.46
EDCSNJ1227551-1136202	cl1227.9-1138	10.88	0.66	-1.52
EDCSNJ1227550-1135278	cl1227.9-1138	11.09	0.56	-2.14
EDCSNJ1227550-1137464	cl1227.9-1138	11.43	0.62	-2.34
EDCSNJ1227548-1138463	cl1227.9-1138	11.16	0.59	-2.18

A.2 *(continued)*

Galaxy ID	Field Name	$\log_{10}(M_*/M_\odot)$	G	M_{20}
EDCSNJ1227546-1138212	cl1227.9-1138	10.51	0.57	-2.06
EDCSNJ1227545-1139383	cl1227.9-1138	11.32	0.54	-2.11
EDCSNJ1227542-1138246	cl1227.9-1138	10.95	0.61	-2.13
EDCSNJ1227538-1139470	cl1227.9-1138	10.51	0.47	-1.8
EDCSNJ1227538-1138257	cl1227.9-1138	10.99	0.56	-2.03
EDCSNJ1227530-1138474	cl1227.9-1138	11.2	0.62	-0.78
EDCSNJ1227527-1139218	cl1227.9-1138	11.07	0.58	-2.14
EDCSNJ1227524-1135155	cl1227.9-1138	10.67	0.58	-2.38
EDCSNJ1227521-1139587	cl1227.9-1138	10.51	0.43	-1.18
EDCSNJ1227510-1137559	cl1227.9-1138	10.56	0.53	-0.86
EDCSNJ1227506-1135282	cl1227.9-1138	10.68	0.54	-1.73
EDCSNJ1227505-1136072	cl1227.9-1138	11.19	0.48	-1.95
EDCSNJ1227504-1135224	cl1227.9-1138	10.42	0.57	-1.97
EDCSNJ1227503-1140297	cl1227.9-1138	10.65	0.52	-1.95
EDCSNJ1227493-1139524	cl1227.9-1138	10.94	0.54	-1.87
EDCSNJ1227488-1137593	cl1227.9-1138	10.88	0.61	-2.06
EDCSNJ1227486-1135281	cl1227.9-1138	10.61	0.6	-2.03
EDCSNJ1227486-1135342	cl1227.9-1138	10.49	0.47	-1.25
EDCSNJ1227482-1140258	cl1227.9-1138	11.17	0.6	-2.28
EDCSNJ1227465-1139168	cl1227.9-1138	11.18	0.62	-2.5
EDCSNJ1227452-1138369	cl1227.9-1138	10.75	0.57	-2.02
EDCSNJ1227444-1138305	cl1227.9-1138	11.19	0.58	-2.1
EDCSNJ1232401-1248452	cl1232.5-1250	11.15	0.53	-2.06
EDCSNJ1232398-1250269	cl1232.5-1250	10.46	0.55	-1.75
EDCSNJ1232394-1248165	cl1232.5-1250	10.98	0.59	-1.91

A.2 *(continued)*

Galaxy ID	Field Name	$\log_{10}(M_*/M_\odot)$	G	M_{20}
EDCSNJ1232391-1249025	cl1232.5-1250	10.76	0.49	-2.03
EDCSNJ1232391-1248278	cl1232.5-1250	10.69	0.55	-2.0
EDCSNJ1232390-1250300	cl1232.5-1250	10.76	0.62	-2.25
EDCSNJ1232387-1248459	cl1232.5-1250	10.64	0.41	-1.27
EDCSNJ1232384-1251509	cl1232.5-1250	10.58	0.62	-2.29
EDCSNJ1232386-1248154	cl1232.5-1250	10.89	0.6	-2.23
EDCSNJ1232376-1248384	cl1232.5-1250	11.23	0.51	-2.13
EDCSNJ1232371-1250322	cl1232.5-1250	10.87	0.65	-2.5
EDCSNJ1232369-1248246	cl1232.5-1250	10.4	0.47	-1.17
EDCSNJ1232364-1250394	cl1232.5-1250	11.13	0.51	-1.08
EDCSNJ1232362-1250098	cl1232.5-1250	10.64	0.58	-2.05
EDCSNJ1232358-1250099	cl1232.5-1250	10.67	0.58	-2.25
EDCSNJ1232357-1251214	cl1232.5-1250	11.35	0.62	-2.24
EDCSNJ1232349-1252505	cl1232.5-1250	10.55	0.52	-1.99
EDCSNJ1232347-1252164	cl1232.5-1250	10.61	0.46	-1.5
EDCSNJ1232343-1249594	cl1232.5-1250	10.99	0.48	-1.58
EDCSNJ1232340-1248326	cl1232.5-1250	10.68	0.59	-2.19
EDCSNJ1232339-1250106	cl1232.5-1250	10.94	0.62	-2.26
EDCSNJ1232336-1250207	cl1232.5-1250	10.79	0.61	-2.18
EDCSNJ1232334-1250578	cl1232.5-1250	10.63	0.58	-1.97
EDCSNJ1232335-1250052	cl1232.5-1250	10.86	0.61	-2.29
EDCSNJ1232333-1252436	cl1232.5-1250	10.46	0.47	-1.63
EDCSNJ1232325-1250105	cl1232.5-1250	11.02	0.6	-2.43
EDCSNJ1232325-1251214	cl1232.5-1250	10.6	0.5	-1.27
EDCSNJ1232321-1249489	cl1232.5-1250	10.47	0.39	-1.52

A.2 *(continued)*

Galaxy ID	Field Name	$\log_{10}(M_*/M_\odot)$	G	M_{20}
EDCSNJ1232320-1250423	cl1232.5-1250	10.47	0.49	-1.23
EDCSNJ1232319-1250383	cl1232.5-1250	10.88	0.58	-2.02
EDCSNJ1232315-1250454	cl1232.5-1250	10.96	0.56	-2.22
EDCSNJ1232313-1250327	cl1232.5-1250	10.69	0.59	-2.01
EDCSNJ1232304-1251184	cl1232.5-1250	11.53	0.61	-2.22
EDCSNJ1232302-1251229	cl1232.5-1250	10.71	0.57	-1.98
EDCSNJ1232299-1250418	cl1232.5-1250	10.6	0.6	-1.91
EDCSNJ1232290-1251407	cl1232.5-1250	10.8	0.6	-2.15
EDCSNJ1232292-1248278	cl1232.5-1250	10.68	0.58	-1.93
EDCSNJ1232290-1250437	cl1232.5-1250	10.55	0.6	-2.17
EDCSNJ1232281-1248188	cl1232.5-1250	10.79	0.6	-2.1
EDCSNJ1232272-1250593	cl1232.5-1250	11.1	0.62	-1.79
EDCSNJ1232255-1250409	cl1232.5-1250	10.41	0.55	-2.04
EDCSNJ1232252-1248313	cl1232.5-1250	10.76	0.68	-2.31
EDCSNJ1232245-1252467	cl1232.5-1250	10.44	0.6	-2.23
EDCSNJ1232243-1249307	cl1232.5-1250	10.81	0.59	-2.15
EDCSNJ1232221-1251299	cl1232.5-1250	10.41	0.58	-1.94
EDCSNJ1232219-1252098	cl1232.5-1250	10.98	0.55	-1.88
EDCSNJ1232212-1248234	cl1232.5-1250	10.93	0.6	-2.32
EDCSNJ1232208-1251077	cl1232.5-1250	11.31	0.5	-2.04
EDCSNJ1232206-1252401	cl1232.5-1250	10.56	0.63	-2.01
EDCSNJ1232206-1250553	cl1232.5-1250	10.9	0.6	-2.11
EDCSNJ1232203-1251098	cl1232.5-1250	10.5	0.6	-2.09
EDCSNJ1354192-1232556	cl1354.2-1230	10.54	0.61	-2.15
EDCSNJ1354193-1229343	cl1354.2-1230	11.05	0.62	-1.84

A.2 *(continued)*

Galaxy ID	Field Name	$\log_{10}(M_*/M_\odot)$	G	M_{20}
EDCSNJ1354185-1229217	cl1354.2-1230	11.31	0.5	-1.22
EDCSNJ1354172-1230479	cl1354.2-1230	10.87	0.48	-1.51
EDCSNJ1354171-1232073	cl1354.2-1230	10.64	0.51	-1.8
EDCSNJ1354168-1230046	cl1354.2-1230	10.42	0.46	-1.29
EDCSNJ1354164-1231544	cl1354.2-1230	10.48	0.51	-1.65
EDCSNJ1354160-1229367	cl1354.2-1230	10.63	0.5	-1.71
EDCSNJ1354149-1231202	cl1354.2-1230	10.52	0.51	-1.33
EDCSNJ1354147-1231467	cl1354.2-1230	10.65	0.59	-2.31
EDCSNJ1354140-1232426	cl1354.2-1230	10.65	0.77	-1.65
EDCSNJ1354130-1230274	cl1354.2-1230	10.59	0.6	-2.1
EDCSNJ1354126-1230338	cl1354.2-1230	10.8	0.58	-1.94
EDCSNJ1354125-1233145	cl1354.2-1230	10.7	0.56	-2.02
EDCSNJ1354122-1228350	cl1354.2-1230	11.09	0.61	-2.06
EDCSNJ1354108-1233308	cl1354.2-1230	10.44	0.45	-0.89
EDCSNJ1354103-1231039	cl1354.2-1230	10.68	0.6	-1.95
EDCSNJ1354093-1229167	cl1354.2-1230	10.59	0.46	-1.42
EDCSNJ1354081-1229334	cl1354.2-1230	11.19	0.52	-1.61
EDCSNJ1354072-1231083	cl1354.2-1230	11.0	0.58	-2.35
EDCSNJ1354070-1230595	cl1354.2-1230	10.43	0.53	-1.77
EDCSNJ1354058-1232373	cl1354.2-1230	11.0	0.62	-0.9
EDCSNJ1354039-1230317	cl1354.2-1230	10.59	0.45	-1.4
EDCSNJ1354020-1233406	cl1354.2-1230	10.7	0.56	-1.64
EDCSNJ1354014-1229441	cl1354.2-1230	10.62	0.59	-1.8
EDCSNJ1354013-1231011	cl1354.2-1230	10.43	0.46	-1.35
EDCSNJ1354011-1231288	cl1354.2-1230	10.6	0.56	-2.0

A.2 *(continued)*

Galaxy ID	Field Name	$\log_{10}(M_*/M_\odot)$	G	M_{20}
EDCSNJ1354008-1231321	cl1354.2-1230	11.04	0.41	-0.86
	Field Galaxies			
EDCSNJ1038017-1242248	cl1037.9-1243	11.27	0.42	-1.27
EDCSNJ1037584-1243336	cl1037.9-1243	11.05	0.6	-2.18
EDCSNJ1037582-1241336	cl1037.9-1243	10.61	0.47	-1.08
EDCSNJ1037559-1246161	cl1037.9-1243	10.84	0.59	-2.11
EDCSNJ1037558-1245275	cl1037.9-1243	10.93	0.63	-2.26
EDCSNJ1037517-1246153	cl1037.9-1243	10.84	0.57	-2.23
EDCSNJ1037501-1244278	cl1037.9-1243	10.47	0.58	-1.93
EDCSNJ1037423-1242167	cl1037.9-1243	11.66	0.7	-0.8
EDCSNJ1040403-1153391	cl1040.7-1155	10.94	0.57	-1.86
EDCSNJ1040368-1156356	cl1040.7-1155	10.72	0.58	-1.72
EDCSNJ1054338-1147158	cl1054.4-1146	10.77	0.61	-2.07
EDCSNJ1054335-1148242	cl1054.4-1146	11.17	0.49	-1.29
EDCSNJ1054262-1148495	cl1054.4-1146	11.0	0.59	-2.2
EDCSNJ1054243-1145430	cl1054.4-1146	10.67	0.5	-1.67
EDCSNJ1054240-1148300	cl1054.4-1146	10.47	0.49	-1.38
EDCSNJ1054233-1147247	cl1054.4-1146	10.98	0.61	-2.07
EDCSNJ1054191-1148441	cl1054.4-1146	10.71	0.62	-2.28
EDCSNJ1054173-1146301	cl1054.4-1146	11.12	0.46	-0.97
EDCSNJ1054521-1245027	cl1054.7-1245	10.47	0.51	-1.8
EDCSNJ1054469-1246075	cl1054.7-1245	10.62	0.47	-1.43
EDCSNJ1054451-1245528	cl1054.7-1245	10.5	0.56	-2.14
EDCSNJ1054446-1247596	cl1054.7-1245	10.48	0.61	-2.29
EDCSNJ1054445-1246051	cl1054.7-1245	10.72	0.61	-2.09

A.2 *(continued)*

Galaxy ID	Field Name	$\log_{10}(M_*/M_\odot)$	G	M_{20}
EDCSNJ1054445-1245536	cl1054.7-1245	10.65	0.6	-2.06
EDCSNJ1054445-1246244	cl1054.7-1245	10.57	0.54	-1.75
EDCSNJ1054426-1248008	cl1054.7-1245	10.5	0.51	-1.94
EDCSNJ1054416-1248203	cl1054.7-1245	10.99	0.6	-2.52
EDCSNJ1054386-1244107	cl1054.7-1245	10.44	0.51	-1.31
EDCSNJ1054381-1244408	cl1054.7-1245	10.71	0.5	-1.61
EDCSNJ1054378-1245513	cl1054.7-1245	10.74	0.49	-1.1
EDCSNJ1054373-1245097	cl1054.7-1245	11.35	0.53	-1.02
EDCSNJ1054367-1245124	cl1054.7-1245	10.79	0.58	-2.25
EDCSNJ1054364-1244288	cl1054.7-1245	10.71	0.46	-1.25
EDCSNJ1054345-1242544	cl1054.7-1245	10.72	0.61	-2.0
EDCSNJ1138195-1136068	cl1138.2-1133	10.66	0.6	-2.07
EDCSNJ1138188-1135111	cl1138.2-1133	10.42	0.57	-1.8
EDCSNJ1138186-1135089	cl1138.2-1133	10.65	0.59	-2.03
EDCSNJ1138185-1136236	cl1138.2-1133	10.92	0.59	-1.79
EDCSNJ1138183-1136167	cl1138.2-1133	11.21	0.52	-1.65
EDCSNJ1138182-1136265	cl1138.2-1133	11.39	0.59	-2.17
EDCSNJ1138168-1133018	cl1138.2-1133	10.91	0.6	-1.99
EDCSNJ1138154-1134211	cl1138.2-1133	11.09	0.5	-2.07
EDCSNJ1138150-1136038	cl1138.2-1133	11.38	0.63	-2.51
EDCSNJ1138131-1136331	cl1138.2-1133	10.59	0.6	-2.06
EDCSNJ1138127-1135161	cl1138.2-1133	10.53	0.58	-1.83
EDCSNJ1138122-1135255	cl1138.2-1133	10.66	0.7	-0.96
EDCSNJ1138113-1131448	cl1138.2-1133	10.54	0.51	-1.86
EDCSNJ1138101-1132310	cl1138.2-1133	10.67	0.45	-1.36

A.2 *(continued)*

Galaxy ID	Field Name	$\log_{10}(M_*/M_\odot)$	G	M_{20}
EDCSNJ1138090-1134132	cl1138.2-1133	10.48	0.45	-1.66
EDCSNJ1138087-1133225	cl1138.2-1133	10.9	0.65	-2.43
EDCSNJ1138077-1137026	cl1138.2-1133	10.45	0.59	-1.95
EDCSNJ1138023-1134036	cl1138.2-1133	10.46	0.56	-1.94
EDCSNJ1216551-1201240	cl1216.8-1201	10.65	0.57	-1.1
EDCSNJ1216547-1202091	cl1216.8-1201	10.87	0.49	-2.09
EDCSNJ1216546-1202166	cl1216.8-1201	10.79	0.63	-2.35
EDCSNJ1216545-1202109	cl1216.8-1201	10.79	0.58	-2.18
EDCSNJ1216530-1200450	cl1216.8-1201	10.67	0.62	-2.06
EDCSNJ1216502-1201147	cl1216.8-1201	11.25	0.51	-1.29
EDCSNJ1216486-1202115	cl1216.8-1201	10.52	0.63	-1.86
EDCSNJ1216486-1201110	cl1216.8-1201	10.99	0.6	-1.93
EDCSNJ1216486-1201185	cl1216.8-1201	11.16	0.41	-1.58
EDCSNJ1216477-1158596	cl1216.8-1201	11.05	0.5	-1.73
EDCSNJ1216467-1158478	cl1216.8-1201	11.15	0.56	-2.14
EDCSNJ1216465-1159330	cl1216.8-1201	10.88	0.57	-1.9
EDCSNJ1216449-1202158	cl1216.8-1201	10.61	0.58	-2.07
EDCSNJ1216448-1200064	cl1216.8-1201	10.44	0.5	-1.51
EDCSNJ1216440-1202383	cl1216.8-1201	10.98	0.45	-1.56
EDCSNJ1216436-1200070	cl1216.8-1201	10.85	0.57	-2.02
EDCSNJ1216431-1202241	cl1216.8-1201	10.43	0.5	-2.02
EDCSNJ1216428-1201380	cl1216.8-1201	10.63	0.49	-1.39
EDCSNJ1216423-1203412	cl1216.8-1201	10.45	0.58	-1.4
EDCSNJ1216387-1202566	cl1216.8-1201	11.0	0.6	-2.3
EDCSNJ1216388-1201292	cl1216.8-1201	10.98	0.54	-2.03

A.2 *(continued)*

Galaxy ID	Field Name	$\log_{10}(M_*/M_\odot)$	G	M_{20}
EDCSNJ1216366-1203019	cl1216.8-1201	10.58	0.48	-1.72
EDCSNJ1216364-1203027	cl1216.8-1201	11.24	0.56	-1.85
EDCSNJ1216360-1203137	cl1216.8-1201	10.76	0.6	-2.25
EDCSNJ1228027-1137275	cl1227.9-1138	10.88	0.49	-1.71
EDCSNJ1227551-1138432	cl1227.9-1138	11.07	0.67	-0.8
EDCSNJ1227516-1135101	cl1227.9-1138	10.6	0.53	-1.8
EDCSNJ1227513-1139461	cl1227.9-1138	11.18	0.6	-1.49
EDCSNJ1227491-1139478	cl1227.9-1138	10.43	0.38	-1.09
EDCSNJ1232388-1253191	cl1232.5-1250	13.28	0.94	-2.45
EDCSNJ1232347-1248448	cl1232.5-1250	10.77	0.47	-1.47
EDCSNJ1232338-1250133	cl1232.5-1250	10.56	0.52	-1.24
EDCSNJ1232339-1248243	cl1232.5-1250	11.07	0.48	-1.05
EDCSNJ1232322-1252276	cl1232.5-1250	10.51	0.47	-0.8
EDCSNJ1232303-1248563	cl1232.5-1250	11.27	0.43	-1.03
EDCSNJ1232269-1250179	cl1232.5-1250	10.52	0.43	-1.18
EDCSNJ1232256-1251245	cl1232.5-1250	10.45	0.6	-2.0
EDCSNJ1232253-1250116	cl1232.5-1250	10.57	0.58	-2.07
EDCSNJ1232234-1252228	cl1232.5-1250	10.56	0.57	-2.06
EDCSNJ1232227-1248216	cl1232.5-1250	10.69	0.43	-1.26
EDCSNJ1232221-1248212	cl1232.5-1250	10.41	0.54	-1.83
EDCSNJ1354182-1232584	cl1354.2-1230	10.52	0.59	-2.26
EDCSNJ1354129-1232379	cl1354.2-1230	10.5	0.63	-2.01
EDCSNJ1354119-1233066	cl1354.2-1230	11.29	0.63	-2.5
EDCSNJ1354118-1232547	cl1354.2-1230	10.44	0.5	-1.75
EDCSNJ1354112-1230511	cl1354.2-1230	10.43	0.58	-1.85

A.2 *(continued)*

Galaxy ID	Field Name	$\log_{10}(M_*/M_\odot)$	G	M_{20}
EDCSNJ1354067-1232431	cl1354.2-1230	10.84	0.56	-1.59
EDCSNJ1354063-1232490	cl1354.2-1230	11.66	0.62	-2.49
EDCSNJ1354052-1233546	cl1354.2-1230	10.46	0.64	-2.32
EDCSNJ1354053-1230455	cl1354.2-1230	11.04	0.59	-2.35
EDCSNJ1354038-1233250	cl1354.2-1230	11.04	0.57	-1.98
EDCSNJ1354021-1229569	cl1354.2-1230	11.14	0.58	-1.61
EDCSNJ1354016-1231124	cl1354.2-1230	10.82	0.58	-2.15
EDCSNJ1354016-1230045	cl1354.2-1230	10.98	0.65	-1.18
EDCSNJ1354015-1230353	cl1354.2-1230	10.54	0.61	-2.11
EDCSNJ1354012-1231300	cl1354.2-1230	10.83	0.4	-0.94
EDCSNJ1354011-1232507	cl1354.2-1230	10.61	0.49	-1.76

Appendix B

Spectral Indices

We present tables showing the spectral indices we derived in Chapter 4 in this appendix. The sample in Table B.1 are the galaxies that pass the quality assurance checks we describe in §4.1.1.

Table B.1: Spectroscopic Indices

Galaxy ID	Vis. Class	$\log_{10}(M_*/M_\odot)$	$D_{n,4000}$	EW($H\delta_A$)	$f_{Age<0.1Gyr}$	$f_{Age<0.5Gyr}$	$f_{Age<1.0Gyr}$
EDCSNJ1037527-1243456	m	10.8	1.88	-1.24	0.0	0.0	0.0
EDCSNJ1037548-1245113	0	11.09	1.77	0.77	0.0	0.0	0.0
EDCSNJ1037535-1241538	0	10.88	1.79	0.15	0.0	0.0	0.004
EDCSNJ1037525-1243541	0	10.84	1.9	-0.1	0.0	0.0	0.0
EDCSNJ1037521-1243392	M	11.05	1.54	2.15	0.0	0.0	0.05
EDCSNJ1040409-1157230	0	10.67	1.29	5.08	0.021	0.021	0.084
EDCSNJ1040420-1155525	0	10.95	1.31	5.16	0.02	0.02	0.118
EDCSNJ1040343-1155414	0	11.48	1.82	0.34	0.0	0.0	0.016
EDCSNJ1054297-1148146	T	11.03	1.36	4.54	0.003	0.003	0.27
EDCSNJ1054450-1244089	i	10.86	1.46	5.45	0.0	0.007	0.112
EDCSNJ1054457-1246373	0	10.86	1.78	3.99	0.0	0.0	0.052
EDCSNJ1054451-1247336	i	10.89	2.14	2.03	0.0	0.0	0.007
EDCSNJ1054466-1247161	0	10.43	1.59	0.32	0.0	0.0	0.043
EDCSNJ1103372-1245215	0	10.93	1.73	-0.31	0.0	0.0	0.007
EDCSNJ1103386-1247210	I	11.18	1.52	2.8	0.006	0.006	0.047
EDCSNJ1103349-1246462	0	11.34	1.85	-0.05	0.0	0.0	0.002
EDCSNJ1103357-1246398	0	10.74	1.51	1.15	0.0	0.0	0.02

B.1 *(continued)*

Galaxy ID	Vis. Class	$\log_{10}(M_*/M_\odot)$	$D_{n,4000}$	EW($H\delta_A$)	$f_{Age<0.1Gyr}$	$f_{Age<0.5Gyr}$	$f_{Age<1.0Gyr}$
EDCSNJ1103355-1244515	T	10.95	1.25	5.33	0.036	0.036	0.096
EDCSNJ1103365-1244223	0	11.79	1.68	1.33	0.0	0.0	0.033
EDCSNJ1103339-1243415	0	10.53	1.2	5.27	0.03	0.03	0.038
EDCSNJ1103401-1244377	0	10.6	1.24	5.04	0.034	0.034	0.058
EDCSNJ1103373-1246364	0	10.54	1.64	1.42	0.0	0.0	0.019
EDCSNJ1103413-1244379	0	11.17	1.64	1.03	0.001	0.001	0.029
EDCSNJ1040346-1155511	i	10.42	1.57	4.5	0.0	0.001	0.063
EDCSNJ1040415-1156559	I	10.49	1.37	4.41	0.024	0.026	0.053
EDCSNJ1040369-1157141	0	11.04	1.69	0.25	0.0	0.0	0.021
EDCSNJ1040396-1155183	0	10.93	1.9	0.53	0.0	0.0	0.008
EDCSNJ1040407-1156015	0	11.15	1.95	-0.35	0.0	0.0	0.002
EDCSNJ1040355-1156537	m	10.97	1.37	5.11	0.015	0.016	0.045
EDCSNJ1040402-1155587	0	10.92	1.82	0.28	0.0	0.0	0.005
EDCSNJ1040410-1155590	m	10.87	1.11	6.04	0.067	0.073	0.189
EDCSNJ1040356-1156026	0	11.25	1.72	0.88	0.0	0.0	0.018
EDCSNJ1054254-1145547	0	11.55	1.5	3.54	0.001	0.001	0.024
EDCSNJ1054244-1146194	0	11.5	1.97	-1.4	0.0	0.0	0.001

B.1 *(continued)*

Galaxy ID	Vis. Class	$\log_{10}(M_*/M_\odot)$	$D_{n,4000}$	EW($H\delta_A$)	$f_{Age<0.1Gyr}$	$f_{Age<0.5Gyr}$	$f_{Age<1.0Gyr}$
EDCSNJ1054198-1146337	M	10.55	1.18	7.14	0.055	0.056	0.143
EDCSNJ1054242-1146564	0	10.68	1.34	2.25	0.008	0.008	0.016
EDCSNJ1054296-1147123	0	11.36	1.84	0.1	0.0	0.0	0.002
EDCSNJ1054323-1147213	i	10.99	1.79	1.46	0.0	0.0	0.024
EDCSNJ1054316-1147400	0	10.97	1.66	0.93	0.0	0.0	0.022
EDCSNJ1054292-1149179	0	10.47	1.61	1.7	0.0	0.001	0.074
EDCSNJ1054296-1145499	0	10.5	1.6	3.53	0.0	0.0	0.059
EDCSNJ1054233-1146024	0	10.6	1.54	3.16	0.001	0.001	0.024
EDCSNJ1054250-1146238	0	11.42	1.9	-0.42	0.0	0.0	0.001
EDCSNJ1054255-1146331	0	10.58	1.75	0.7	0.0	0.0	0.028
EDCSNJ1054309-1147095	0	11.01	1.73	0.67	0.0	0.0	0.026
EDCSNJ1054255-1146441	i	11.04	1.82	0.23	0.0	0.0	0.002
EDCSNJ1054259-1148307	0	10.91	1.88	1.07	0.0	0.0	0.027
EDCSNJ1054263-1148407	0	10.92	1.85	2.36	0.0	0.0	0.018
EDCSNJ1054303-1149132	i	11.63	1.9	-0.9	0.0	0.0	0.0
EDCSNJ1054311-1149250	i	10.67	1.39	4.17	0.011	0.04	0.416
EDCSNJ1054237-1146107	0	10.58	1.86	-0.52	0.0	0.0	0.014

B.1 *(continued)*

Galaxy ID	Vis. Class	$\log_{10}(M_*/M_\odot)$	$D_{n,4000}$	EW($H\delta_A$)	$f_{Age<0.1Gyr}$	$f_{Age<0.5Gyr}$	$f_{Age<1.0Gyr}$
EDCSNJ1054247-1146238	0	10.72	1.6	-0.94	0.0	0.0	0.014
EDCSNJ1054264-1147207	i	10.71	1.21	4.43	0.025	0.027	0.061
EDCSNJ1054398-1246055	I	11.23	1.7	-0.38	0.0	0.0	0.003
EDCSNJ1054435-1246152	0	11.09	1.83	0.71	0.0	0.0	0.001
EDCSNJ1054404-1248083	0	10.59	1.28	6.51	0.019	0.019	0.027
EDCSNJ1054436-1244202	0	10.91	1.78	1.78	0.0	0.0	0.019
EDCSNJ1054438-1245409	0	11.12	1.95	-1.93	0.0	0.0	0.0
EDCSNJ1054433-1245534	0	10.65	1.98	3.88	0.0	0.0	0.04
EDCSNJ1054437-1246028	0	10.45	1.59	0.83	0.0	0.0	0.038
EDCSNJ1054445-1246173	0	10.77	1.77	1.03	0.0	0.0	0.037
EDCSNJ1054396-1248241	0	10.94	1.72	0.84	0.0	0.0	0.023
EDCSNJ1054478-1244244	0	10.53	1.76	2.02	0.0	0.0	0.02
EDCSNJ1054439-1245556	0	10.84	1.73	0.46	0.0	0.0	0.026
EDCSNJ1054471-1246412	0	10.7	1.73	2.88	0.0	0.001	0.101
EDCSNJ1054407-1247385	0	10.88	1.75	0.67	0.0	0.0	0.014
EDCSNJ1138113-1132017	I	10.73	1.65	2.67	0.0	0.0	0.018
EDCSNJ1138068-1132285	0	10.59	1.83	2.31	0.0	0.0	0.03

B.1 *(continued)*

Galaxy ID	Vis. Class	$\log_{10}(M_*/M_\odot)$	$D_{n,4000}$	EW($H\delta_A$)	$f_{Age<0.1Gyr}$	$f_{Age<0.5Gyr}$	$f_{Age<1.0Gyr}$
EDCSNJ1138102-1133379	0	11.14	1.89	-0.34	0.0	0.0	0.0
EDCSNJ1138069-1134314	0	10.81	1.81	-0.45	0.0	0.0	0.002
EDCSNJ1138099-1132035	X	10.58	1.13	4.21	0.115	0.133	0.161
EDCSNJ1138104-1133319	0	10.53	1.65	0.11	0.0	0.0	0.006
EDCSNJ1138078-1133592	0	10.52	1.23	6.4	0.05	0.05	0.063
EDCSNJ1138069-1132044	0	10.48	1.76	-0.13	0.0	0.0	0.0
EDCSNJ1138130-1132345	0	10.72	1.76	0.01	0.0	0.0	0.008
EDCSNJ1138106-1133312	I	10.67	1.76	2.17	0.0	0.0	0.008
EDCSNJ1138110-1133411	0	10.59	1.89	0.16	0.0	0.0	0.003
EDCSNJ1138109-1134170	0	10.53	1.26	5.62	0.034	0.036	0.083
EDCSNJ1138086-1136549	m	10.83	1.31	5.18	0.033	0.034	0.058
EDCSNJ1138116-1134448	0	10.77	1.79	-0.45	0.0	0.0	0.0
EDCSNJ1138024-1136024	0	10.59	1.82	0.13	0.0	0.0	0.006
EDCSNJ1138022-1135459	0	10.77	1.8	-1.18	0.0	0.0	0.0
EDCSNJ1138065-1136018	0	10.44	1.63	0.17	0.0	0.0	0.03
EDCSNJ1138031-1134278	0	10.69	1.88	-1.67	0.0	0.0	0.001
EDCSNJ1227533-1136527	T	10.69	1.26	5.9	0.033	0.037	0.122

B.1 *(continued)*

Galaxy ID	Vis. Class	$\log_{10}(M_*/M_\odot)$	$D_{n,4000}$	EW($H\delta_A$)	$f_{Age<0.1Gyr}$	$f_{Age<0.5Gyr}$	$f_{Age<1.0Gyr}$
EDCSNJ1227548-1137529	0	11.23	1.79	-0.39	0.0	0.0	0.0
EDCSNJ1228025-1135219	0	10.82	1.43	2.65	0.0	0.002	0.085
EDCSNJ1227541-1138174	I	11.56	1.6	2.42	0.0	0.0	0.043
EDCSNJ1227551-1135584	I	10.61	1.38	2.59	0.007	0.007	0.011
EDCSNJ1227537-1138210	0	10.56	1.8	-1.79	0.0	0.0	0.003
EDCSNJ1227581-1135364	0	11.0	1.9	0.22	0.0	0.0	0.001
EDCSNJ1227566-1136545	0	10.66	1.94	-0.68	0.0	0.0	0.0
EDCSNJ1216447-1159162	?	10.95	1.25	5.24	0.007	0.041	0.102
EDCSNJ1216470-1159267	0	10.82	1.61	5.01	0.0	0.004	0.141
EDCSNJ1216429-1159536	0	10.82	1.73	0.32	0.001	0.001	0.028
EDCSNJ1216454-1200017	0	11.04	1.88	1.97	0.0	0.0	0.028
EDCSNJ1216490-1200091	0	10.88	1.71	0.76	0.0	0.0	0.045
EDCSNJ1216504-1200480	M	11.07	1.17	4.56	0.105	0.145	0.7
EDCSNJ1216522-1200595	0	10.71	1.69	3.4	0.0	0.007	0.177
EDCSNJ1216453-1201176	I	11.76	1.85	0.65	0.0	0.0	0.021
EDCSNJ1216498-1201358	0	10.72	1.74	-1.22	0.0	0.0	0.043
EDCSNJ1216420-1201509	i	11.46	1.91	0.56	0.0	0.0	0.005

B.1 *(continued)*

Galaxy ID	Vis. Class	$\log_{10}(M_*/M_\odot)$	$D_{n,4000}$	EW($H\delta_A$)	$f_{Age<0.1Gyr}$	$f_{Age<0.5Gyr}$	$f_{Age<1.0Gyr}$
EDCSNJ1216401-1202352	0	11.15	1.59	0.89	0.001	0.001	0.021
EDCSNJ1216462-1200073	0	10.66	1.67	2.45	0.0	0.0	0.11
EDCSNJ1216480-1200220	0	10.86	1.72	2.22	0.0	0.0	0.021
EDCSNJ1216438-1200536	0	11.36	1.91	-1.58	0.0	0.0	0.001
EDCSNJ1216462-1202253	0	10.74	1.46	5.11	0.003	0.004	0.089
EDCSNJ1216419-1202440	0	10.59	1.47	6.64	0.046	0.078	0.463
EDCSNJ1216428-1203395	0	11.42	1.52	1.36	0.0	0.001	0.126
EDCSNJ1216448-1201309	I	11.32	1.37	5.38	0.006	0.028	0.308
EDCSNJ1216443-1201429	0	11.36	1.73	1.71	0.0	0.0	0.028
EDCSNJ1216449-1202036	0	10.79	1.3	5.27	0.047	0.047	0.065
EDCSNJ1216417-1203054	0	10.78	1.55	4.96	0.0	0.002	0.269
EDCSNJ1216452-1203134	M	10.41	1.09	6.14	0.074	0.074	0.074
EDCSNJ1216464-1203257	0	10.56	1.79	1.73	0.0	0.002	0.098
EDCSNJ1216446-1201089	i	10.92	1.64	-0.59	0.0	0.0	0.009
EDCSNJ1216449-1201203	0	11.52	1.8	-1.81	0.0	0.0	0.004
EDCSNJ1216490-1201531	0	10.66	1.26	6.66	0.046	0.073	0.429
EDCSNJ1232343-1249265	0	10.77	1.8	2.28	0.0	0.0	0.012

B.1 *(continued)*

Galaxy ID	Vis. Class	$\log_{10}(M_*/M_\odot)$	$D_{n,4000}$	EW($H\delta_A$)	$f_{Age<0.1Gyr}$	$f_{Age<0.5Gyr}$	$f_{Age<1.0Gyr}$
EDCSNJ1232317-1249275	0	11.14	1.77	0.12	0.0	0.0	0.001
EDCSNJ1232296-1250119	0	10.97	1.87	-0.99	0.0	0.0	0.001
EDCSNJ1232288-1250490	0	10.82	1.86	-0.76	0.0	0.0	0.0
EDCSNJ1354175-1230391	0	10.47	1.24	6.57	0.155	0.179	0.69
EDCSNJ1354098-1231098	i	10.64	1.71	0.18	0.0	0.0	0.012
EDCSNJ1354098-1231015	i	11.58	1.76	0.37	0.0	0.0	0.002
EDCSNJ1354097-1230579	0	11.27	1.84	0.76	0.0	0.0	0.005
EDCSNJ1354102-1230527	0	11.34	1.66	4.92	0.0	0.005	0.103
EDCSNJ1354106-1230499	i	11.03	1.8	-0.15	0.0	0.0	0.003
EDCSNJ1354118-1232499	i	10.44	1.24	5.06	0.025	0.025	0.168
EDCSNJ1354026-1230127	0	10.5	1.71	1.17	0.0	0.0	0.017
EDCSNJ1354144-1231514	m	10.4	1.34	5.14	0.008	0.013	0.22
EDCSNJ1354159-1232272	0	10.46	1.8	-0.29	0.0	0.0	0.017
EDCSNJ1354164-1231599	0	11.24	1.35	4.83	0.0	0.013	0.136
EDCSNJ1038014-1242267	i	11.09	1.7	0.75	0.0	0.004	0.036
EDCSNJ1037430-1244080	t	10.55	1.24	4.62	0.031	0.031	0.075
EDCSNJ1037448-1245026	0	10.46	1.74	1.28	0.0	0.0	0.008

B.1 *(continued)*

Galaxy ID	Vis. Class	$\log_{10}(M_*/M_\odot)$	$D_{n,4000}$	EW($H\delta_A$)	$f_{Age<0.1Gyr}$	$f_{Age<0.5Gyr}$	$f_{Age<1.0Gyr}$
EDCSNJ1037534-1246259	0	10.81	1.89	-1.75	0.0	0.0	0.0
EDCSNJ1037580-1241553	M	10.5	1.22	6.96	0.036	0.062	0.181
EDCSNJ1040422-1154417	I	11.17	1.52	4.58	0.0	0.012	0.229
EDCSNJ1040424-1154443	I	10.51	1.62	6.62	0.0	0.033	0.222
EDCSNJ1040351-1156435	0	10.89	1.27	5.62	0.021	0.021	0.046
EDCSNJ1040399-1157135	0	10.47	1.32	3.57	0.013	0.013	0.038
EDCSNJ1040410-1156134	t	10.82	1.33	3.13	0.0	0.0	0.059
EDCSNJ1040355-1153214	0	10.51	1.46	3.96	0.0	0.002	0.065
EDCSNJ1040467-1154041	0	10.91	1.61	3.28	0.0	0.005	0.089
EDCSNJ1040380-1154147	0	11.35	1.61	5.05	0.001	0.003	0.083
EDCSNJ1054206-1144284	0	10.85	1.71	1.11	0.0	0.0	0.022
EDCSNJ1054238-1146477	0	11.24	1.72	1.49	0.0	0.0	0.021
EDCSNJ1054252-1148269	0	10.64	1.24	5.95	0.056	0.064	0.547
EDCSNJ1054194-1145180	t	10.68	1.33	5.18	0.012	0.012	0.014
EDCSNJ1054239-1145236	0	11.2	1.73	1.63	0.0	0.0	0.05
EDCSNJ1054338-1146388	0	10.85	1.46	5.68	0.004	0.019	0.372
EDCSNJ1054437-1245471	0	10.59	1.29	6.39	0.023	0.027	0.061

B.1 *(continued)*

Galaxy ID	Vis. Class	$\log_{10}(M_*/M_\odot)$	$D_{n,4000}$	EW($H\delta_A$)	$f_{Age<0.1Gyr}$	$f_{Age<0.5Gyr}$	$f_{Age<1.0Gyr}$
EDCSNJ1054487-1245052	0	10.78	1.77	0.6	0.0	0.0	0.015
EDCSNJ1054353-1246528	0	11.43	1.85	0.16	0.0	0.0	0.008
EDCSNJ1138100-1136361	0	10.5	1.54	3.04	0.0	0.001	0.051
EDCSNJ1138078-1134468	0	10.59	1.86	0.25	0.0	0.0	0.001
EDCSNJ1138045-1135118	i	10.59	1.25	5.53	0.044	0.044	0.202
EDCSNJ1216467-1159378	M	10.45	1.15	3.85	0.038	0.038	0.235
EDCSNJ1216446-1202358	0	10.48	1.63	1.82	0.0	0.0	0.034
EDCSNJ1216445-1201533	T	10.94	1.22	4.36	0.041	0.041	0.191
EDCSNJ1216372-1200419	0	10.94	1.8	0.93	0.0	0.0	0.015
EDCSNJ1216449-1202139	0	10.94	1.83	1.16	0.0	0.0	0.023
EDCSNJ1227543-1136008	t	11.08	1.31	5.28	0.02	0.026	0.155
EDCSNJ1227453-1137005	0	10.98	1.38	3.9	0.009	0.009	0.033
EDCSNJ1227552-1137559	0	10.79	1.77	0.58	0.0	0.0	0.009
EDCSNJ1227599-1138116	0	10.68	1.8	-1.16	0.0	0.0	0.0
EDCSNJ1227548-1139394	0	10.56	1.67	0.34	0.0	0.003	0.087
EDCSNJ1232339-1249205	0	10.42	1.75	-0.03	0.0	0.0	0.03
EDCSNJ1232326-1249355	0	10.86	2.08	-1.6	0.0	0.0	0.003

B.1 *(continued)*

Galaxy ID	Vis. Class	$\log_{10}(M_*/M_\odot)$	$D_{n,4000}$	EW($H\delta_A$)	$f_{Age<0.1Gyr}$	$f_{Age<0.5Gyr}$	$f_{Age<1.0Gyr}$
EDCSNJ1232301-1251245	I	10.82	1.33	2.38	0.01	0.01	0.026
EDCSNJ1232315-1251578	0	10.96	1.88	-0.5	0.0	0.0	0.001
EDCSNJ1232333-1250121	0	10.74	1.36	4.25	0.031	0.031	0.055
EDCSNJ1232339-1252010	t	10.88	1.72	2.36	0.0	0.0	0.062
EDCSNJ1232373-1249247	0	10.46	1.19	7.43	0.025	0.059	0.49
EDCSNJ1232365-1253082	0	10.7	1.22	4.26	0.023	0.035	0.272
EDCSNJ1354107-1231236	0	10.69	1.79	0.64	0.0	0.0	0.0
EDCSNJ1354073-1233158	0	11.16	1.7	1.9	0.0	0.0	0.051
EDCSNJ1354139-1229474	i	10.76	1.64	0.68	0.0	0.003	0.01
EDCSNJ1354009-1233233	0	10.45	1.24	3.86	0.034	0.034	0.089
EDCSNJ1354164-1229192	0	11.23	1.8	1.02	0.0	0.0	0.034
EDCSNJ1354091-1233426	0	11.1	1.79	0.65	0.0	0.0	0.011

Appendix C

Spectral Fitting Results

We list the results of the spectral fitting performed on the sample that pass the quality assurance checks we describe in §4.1.1. The details of each panel are presented in §4.3.

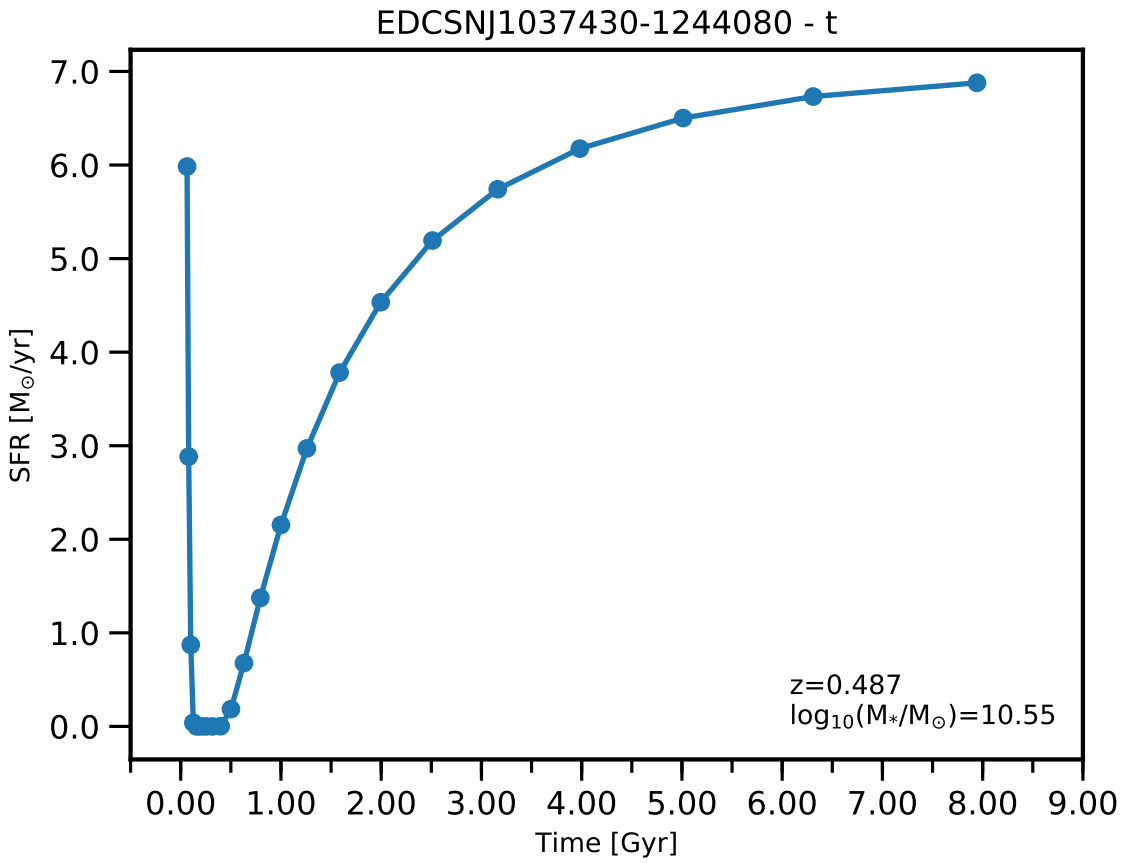
EDCSNJ1037430-1244080 - t
SFR [M⊙/yr]
Time [Gyr]
z=0.487
log10(M*/M⊙)=10.55
0.0
1.0
2.0
3.0
4.0
5.0
6.0
7.0
0.00
1.00
2.00
3.00
4.00
5.00
6.00
7.00
8.00
9.00

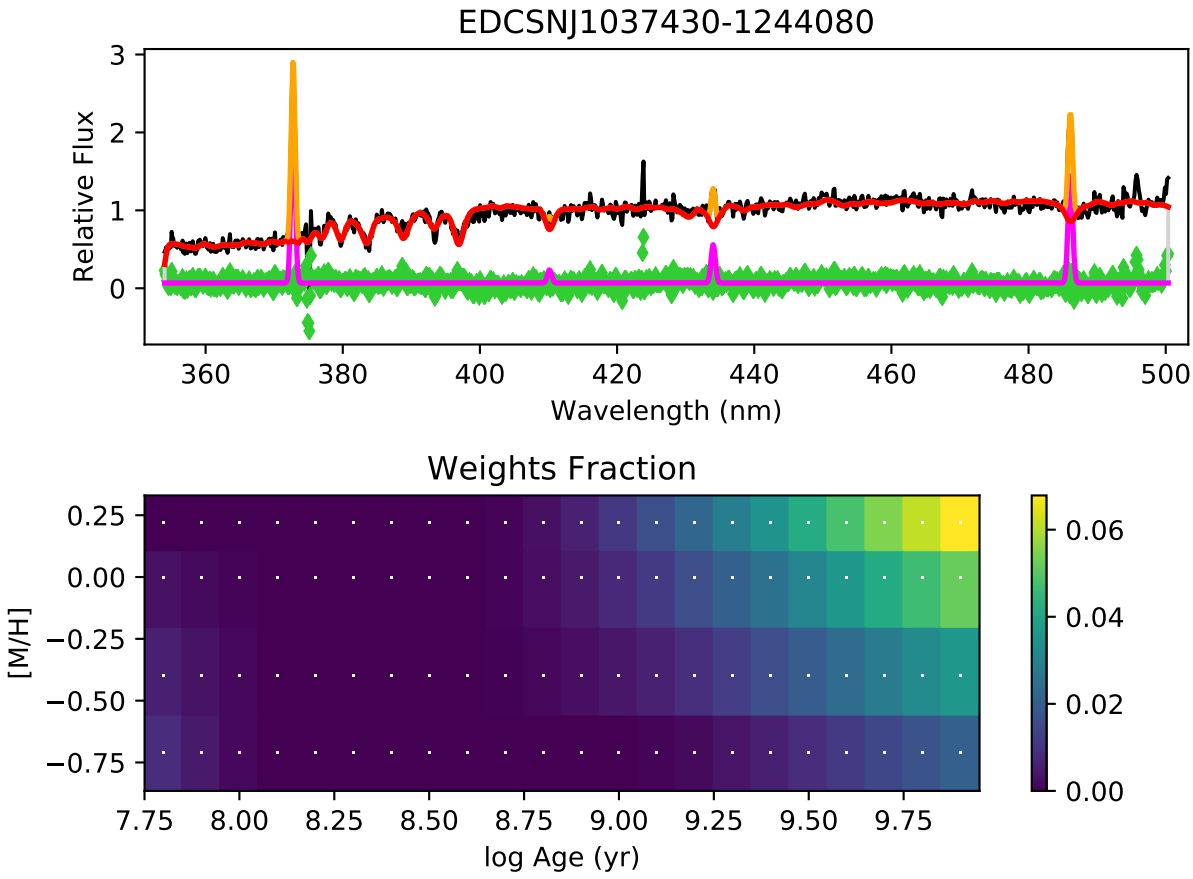
EDCSNJ1037430-1244080
Relative Flux
3
2
1
0
360
380
400
420
440
460
480
500
Wavelength (nm)
Weights Fraction
[M/H]
0.25
0.00
−0.25
−0.50
−0.75
7.75
8.00
8.25
8.50
8.75
9.00
9.25
9.50
9.75
log Age (yr)
0.06
0.04
0.02
0.00

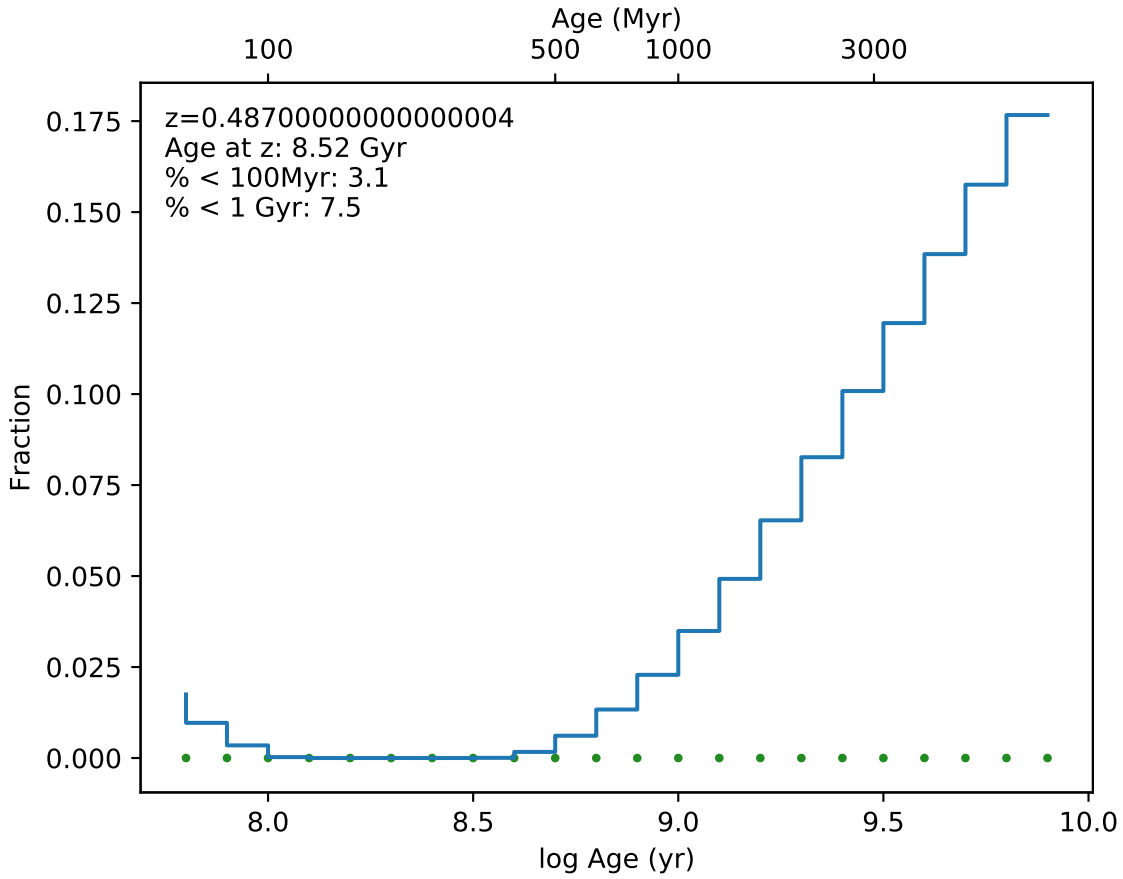
Age (Myr)
100
500
1000
3000
z=0.48700000000000004
Age at z: 8.52 Gyr
% < 100Myr: 3.1
% < 1 Gyr: 7.5
Fraction
0.175
0.150
0.125
0.100
0.075
0.050
0.025
0.000
8.0
8.5
9.0
9.5
10.0
log Age (yr)

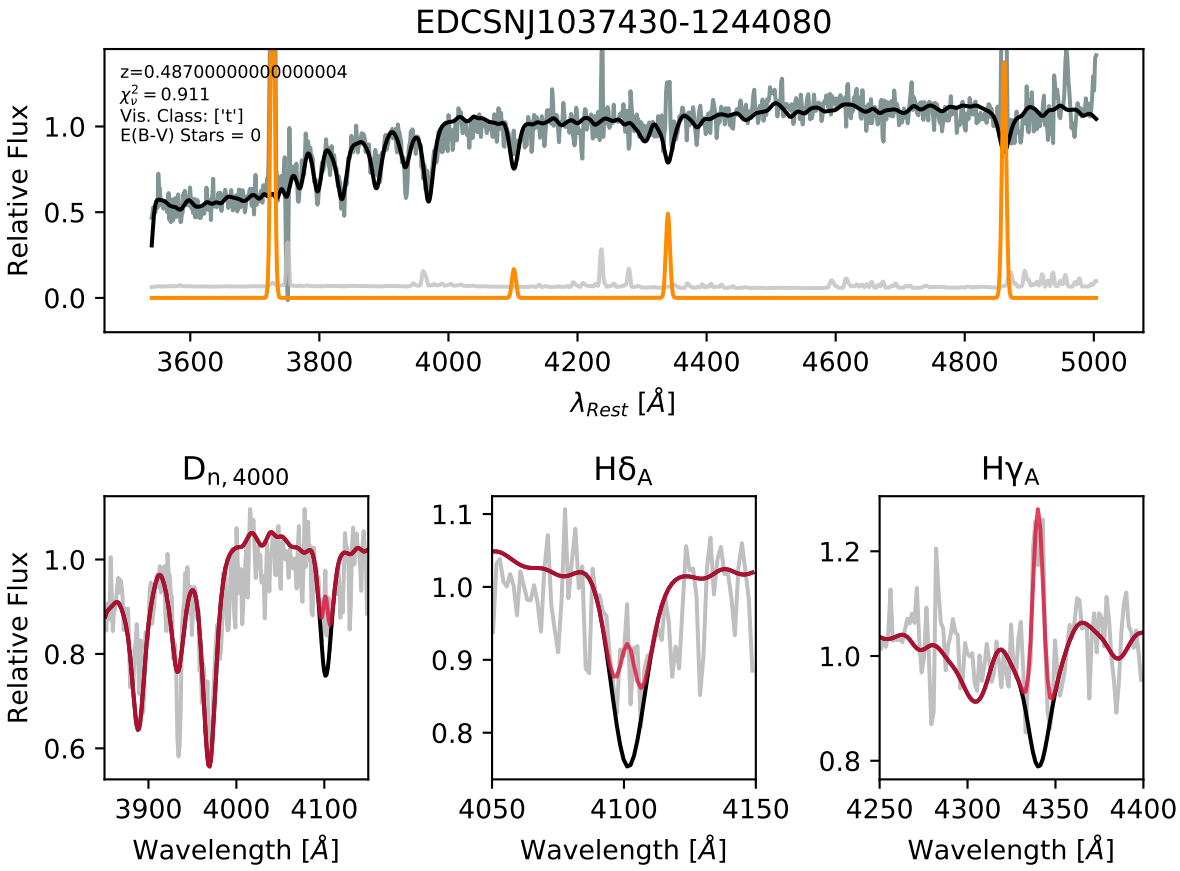
EDCSNJ1037430-1244080
z=0.48700000000000004
$\chi^2_\nu = 0.911$
Vis. Class: ['t']
E(B-V) Stars = 0
Relative Flux
1.0
0.5
0.0
3600
3800
4000
4200
4400
4600
4800
5000
λ_{Rest} [Å]
$D_{n,4000}$
$H\delta_A$
$H\gamma_A$
Relative Flux
1.0
0.8
0.6
3900
4000
4100
Wavelength [Å]
1.1
1.0
0.9
0.8
4050
4100
4150
Wavelength [Å]
1.2
1.0
0.8
4250
4300
4350
4400
Wavelength [Å]

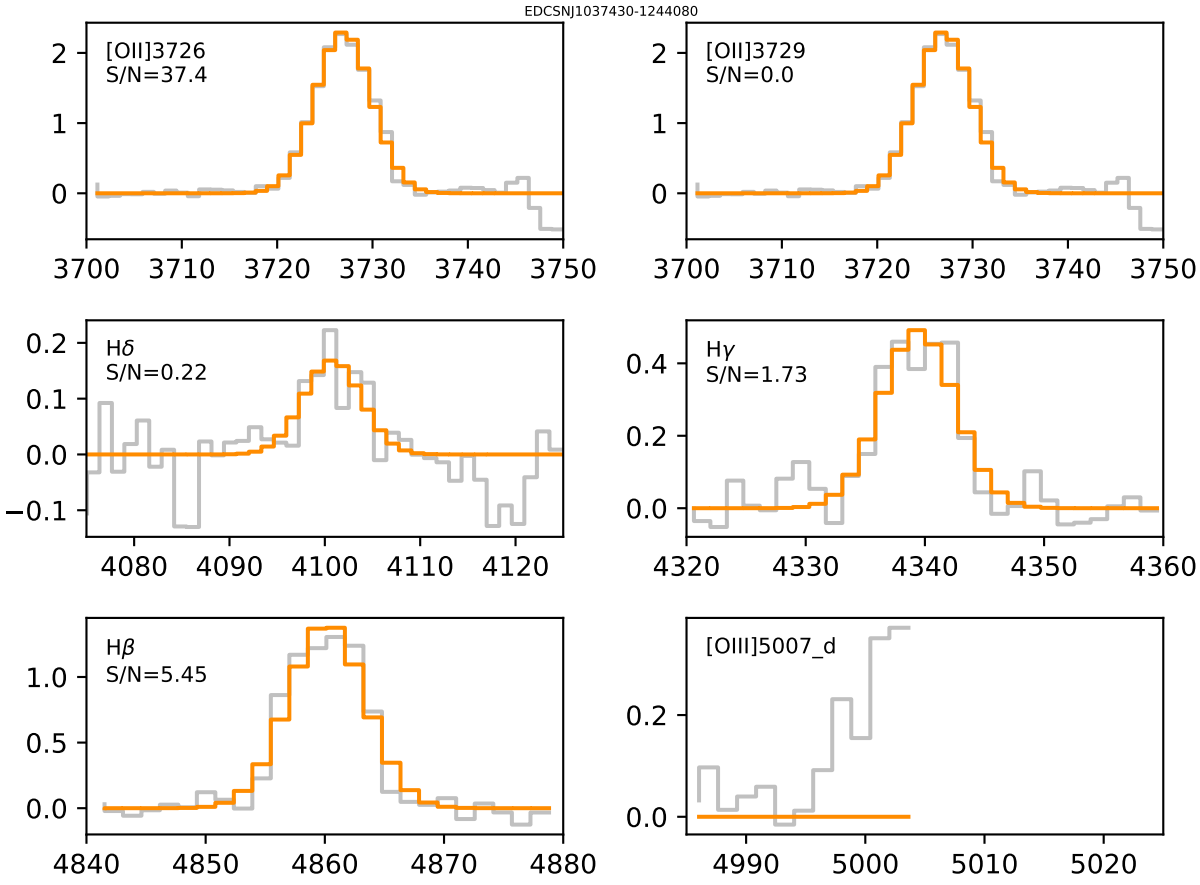
EDCSNJ1037430-1244080
[OII]3726
S/N=37.4
[OII]3729
S/N=0.0
Hδ
S/N=0.22
Hγ
S/N=1.73
Hβ
S/N=5.45
[OIII]5007_d

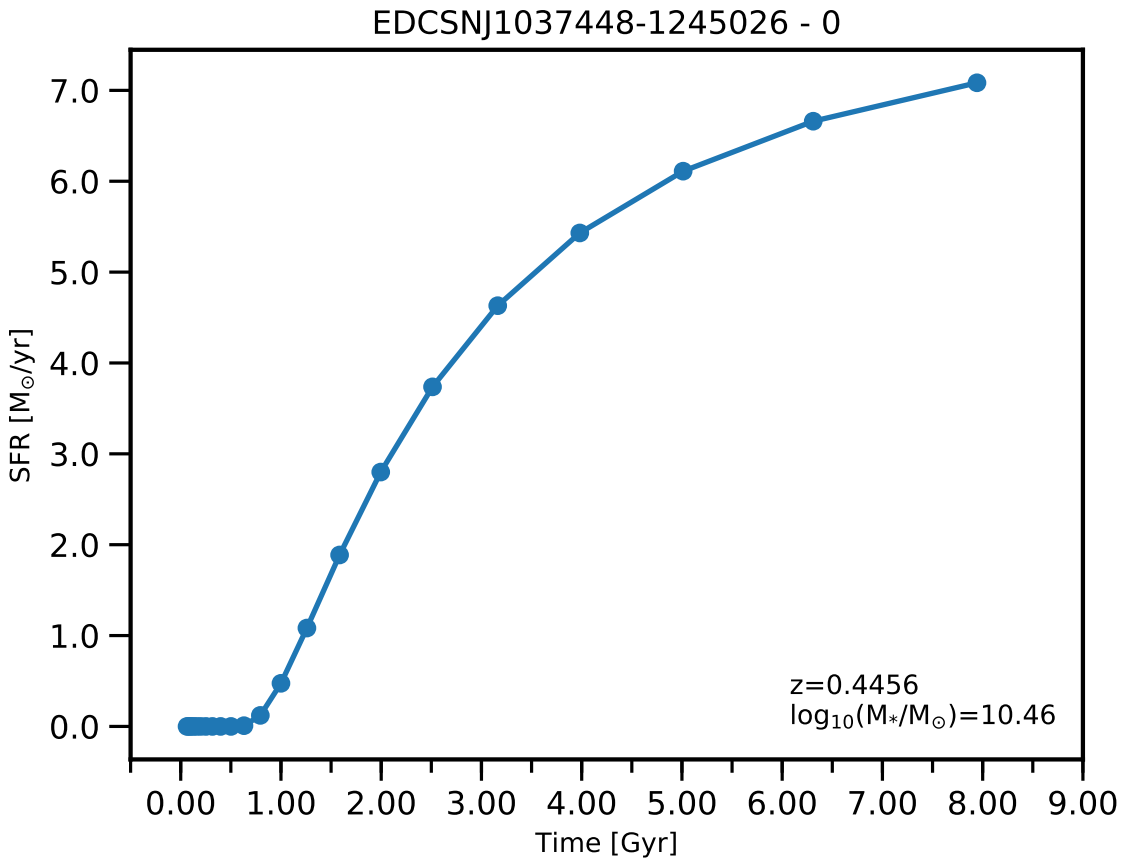
EDCSNJ1037448-1245026 - 0
SFR [M⊙/yr]
Time [Gyr]
z=0.4456
log10(M*/M⊙)=10.46
0.0
1.0
2.0
3.0
4.0
5.0
6.0
7.0
0.00
1.00
2.00
3.00
4.00
5.00
6.00
7.00
8.00
9.00

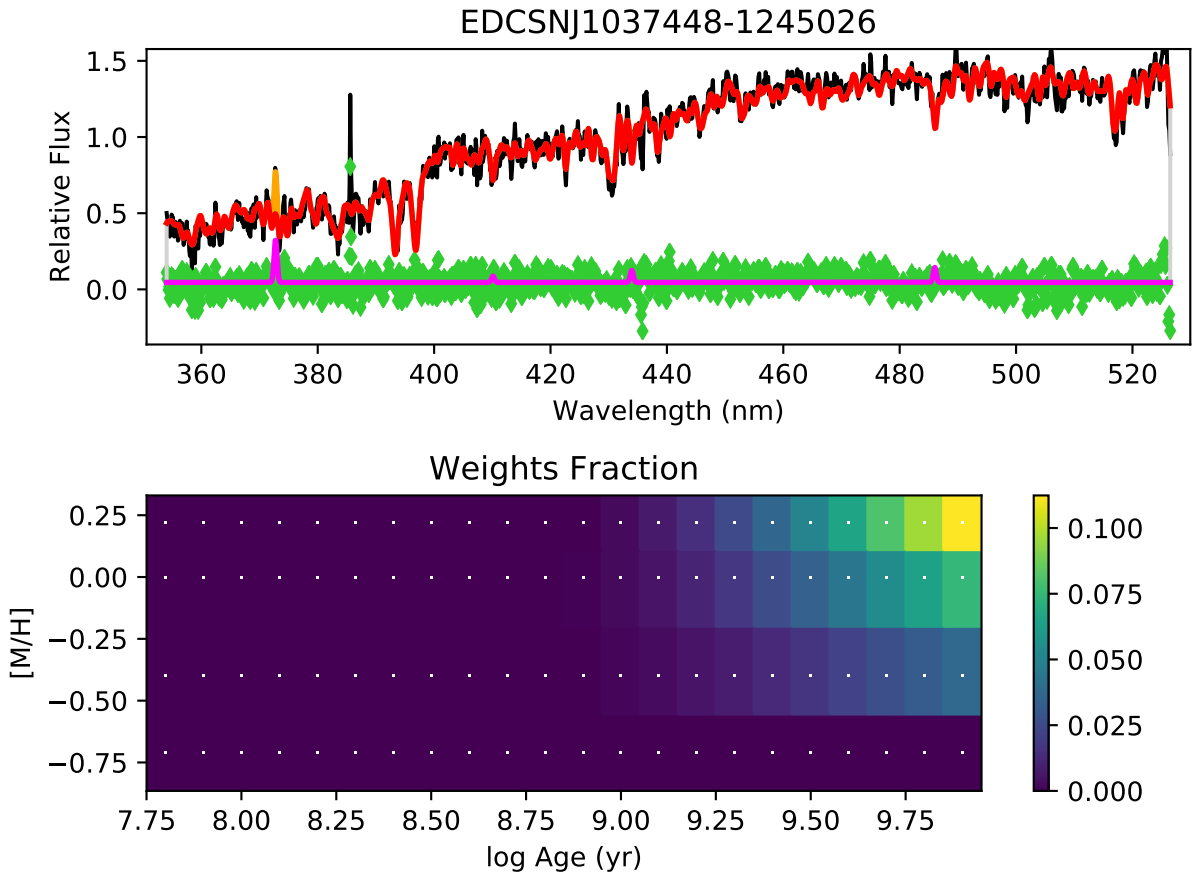
EDCSNJ1037448-1245026
Relative Flux
1.5
1.0
0.5
0.0
360
380
400
420
440
460
480
500
520
Wavelength (nm)
Weights Fraction
[M/H]
0.25
0.00
−0.25
−0.50
−0.75
7.75
8.00
8.25
8.50
8.75
9.00
9.25
9.50
9.75
log Age (yr)
0.100
0.075
0.050
0.025
0.000

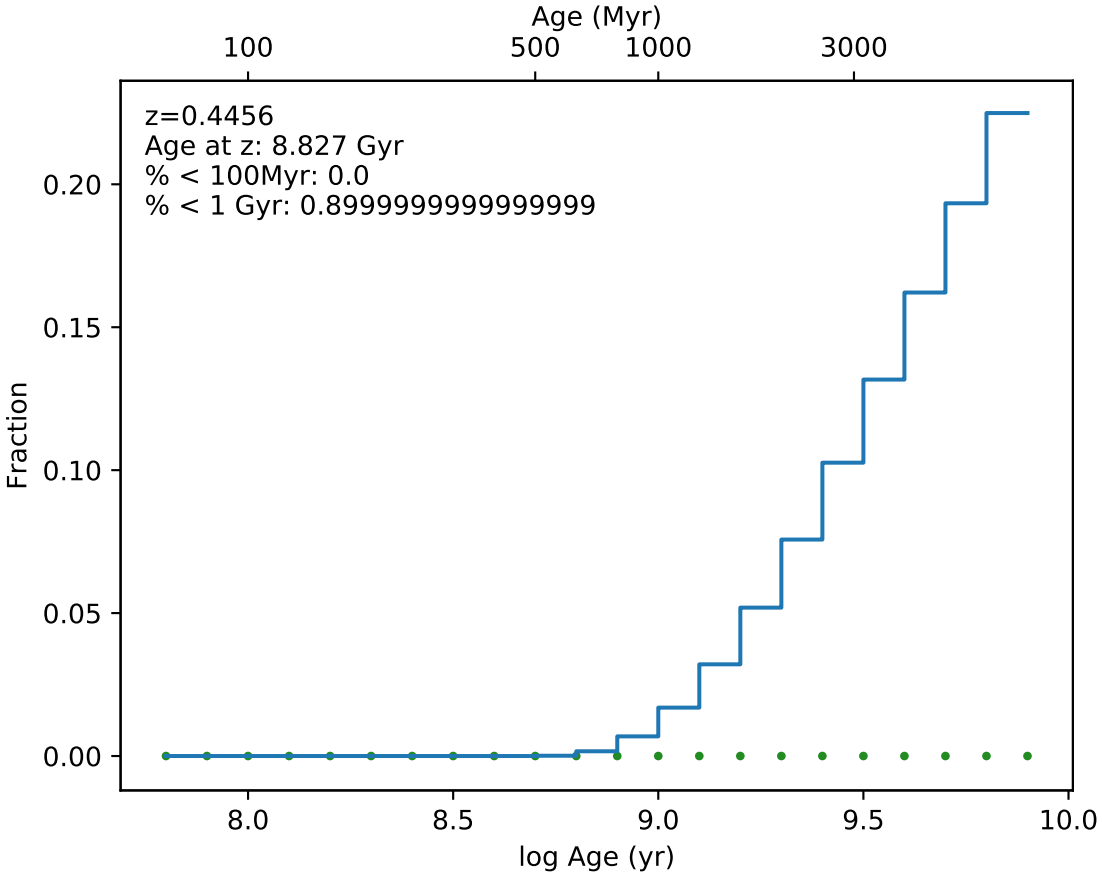
Age (Myr)
100
500
1000
3000
z=0.4456
Age at z: 8.827 Gyr
% < 100Myr: 0.0
% < 1 Gyr: 0.8999999999999999
Fraction
0.20
0.15
0.10
0.05
0.00
8.0
8.5
9.0
9.5
10.0
log Age (yr)

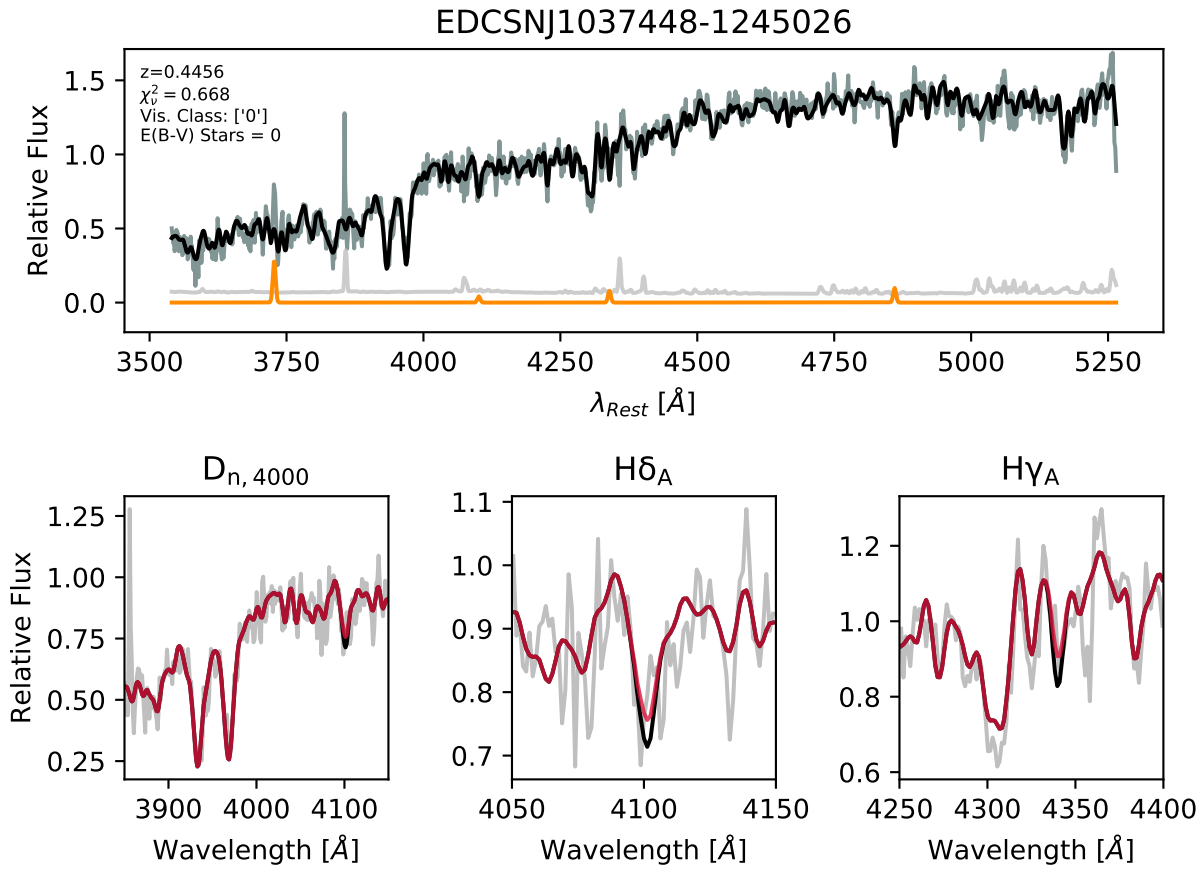
EDCSNJ1037448-1245026
z=0.4456
$\chi^2_\nu = 0.668$
Vis. Class: ['0']
E(B-V) Stars = 0
Relative Flux
λ_{Rest} [Å]
$D_{n,4000}$
$H\delta_A$
$H\gamma_A$
Wavelength [Å]

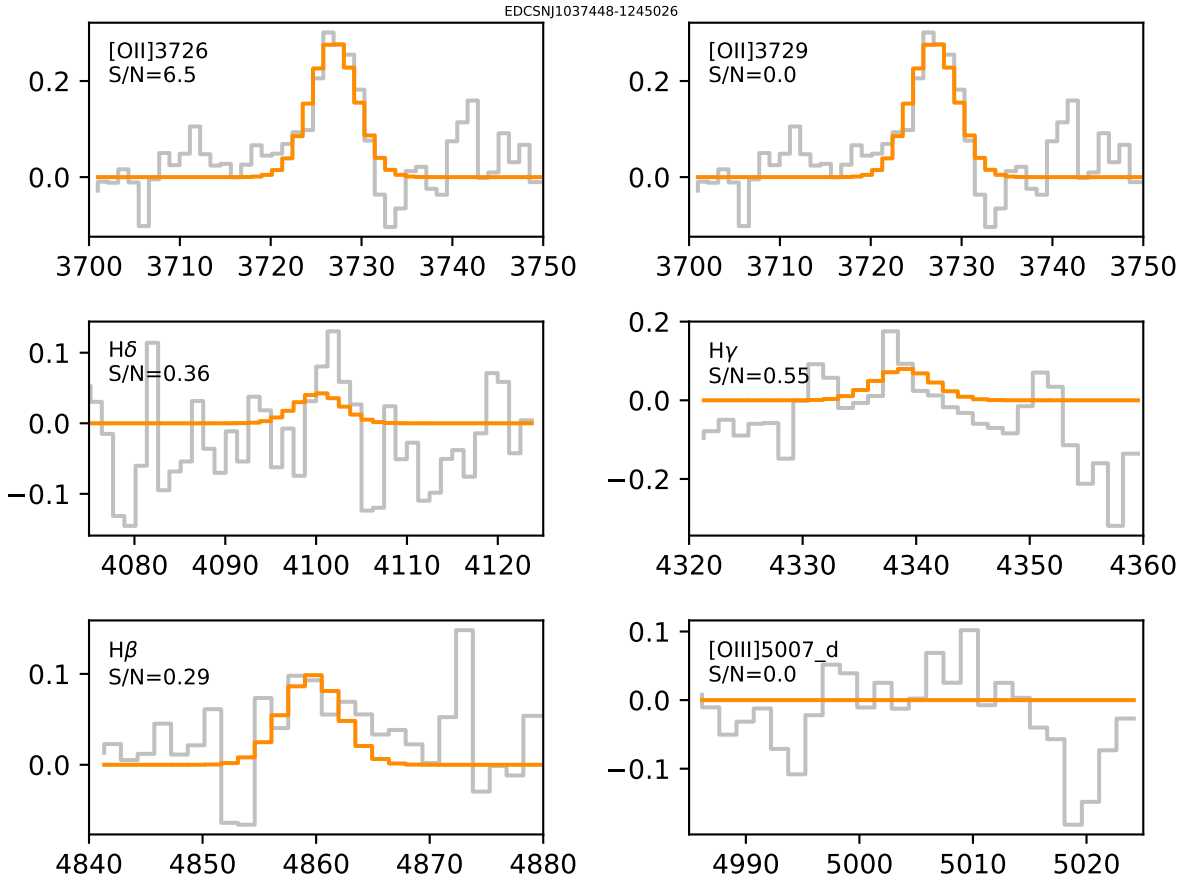
EDCSNJ1037448-1245026
[OII]3726
S/N=6.5
[OII]3729
S/N=0.0
Hδ
S/N=0.36
Hγ
S/N=0.55
Hβ
S/N=0.29
[OIII]5007_d
S/N=0.0

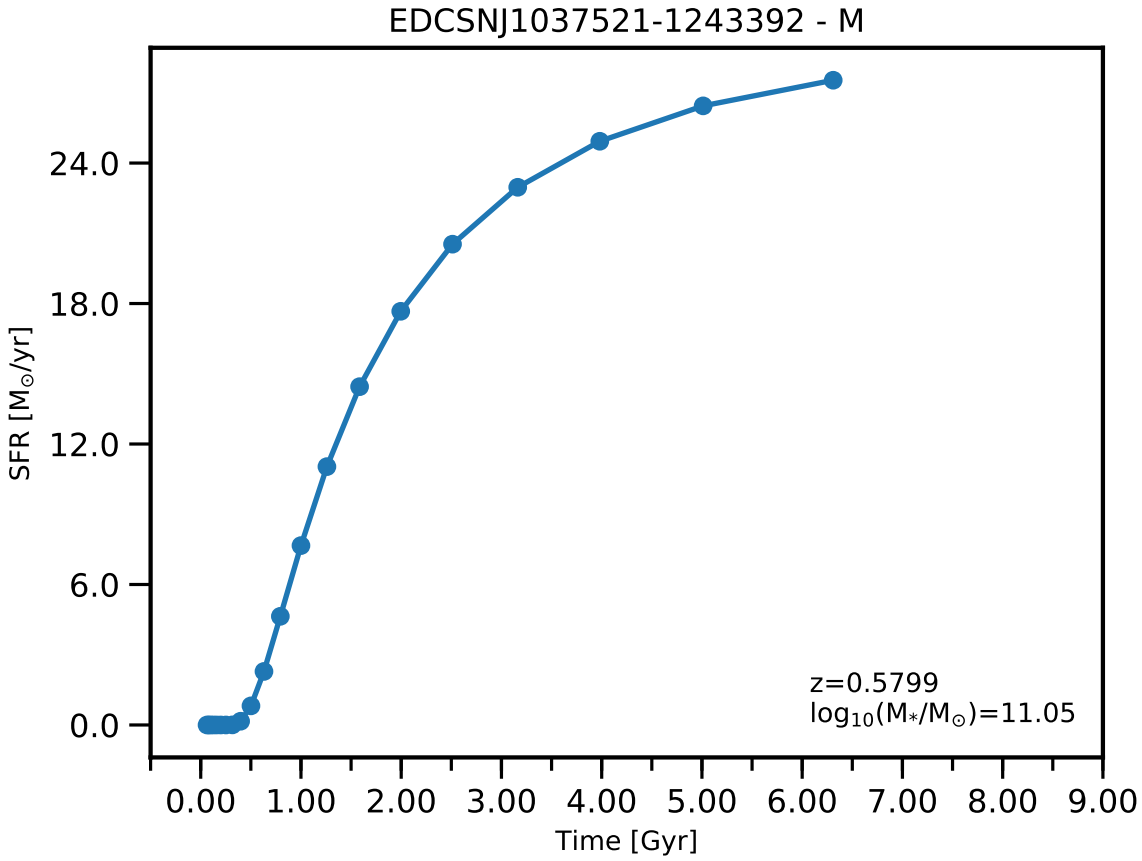
EDCSNJ1037521-1243392 - M
SFR [M⊙/yr]
24.0
18.0
12.0
6.0
0.0
0.00
1.00
2.00
3.00
4.00
5.00
6.00
7.00
8.00
9.00
Time [Gyr]
z=0.5799
log10(M*/M⊙)=11.05

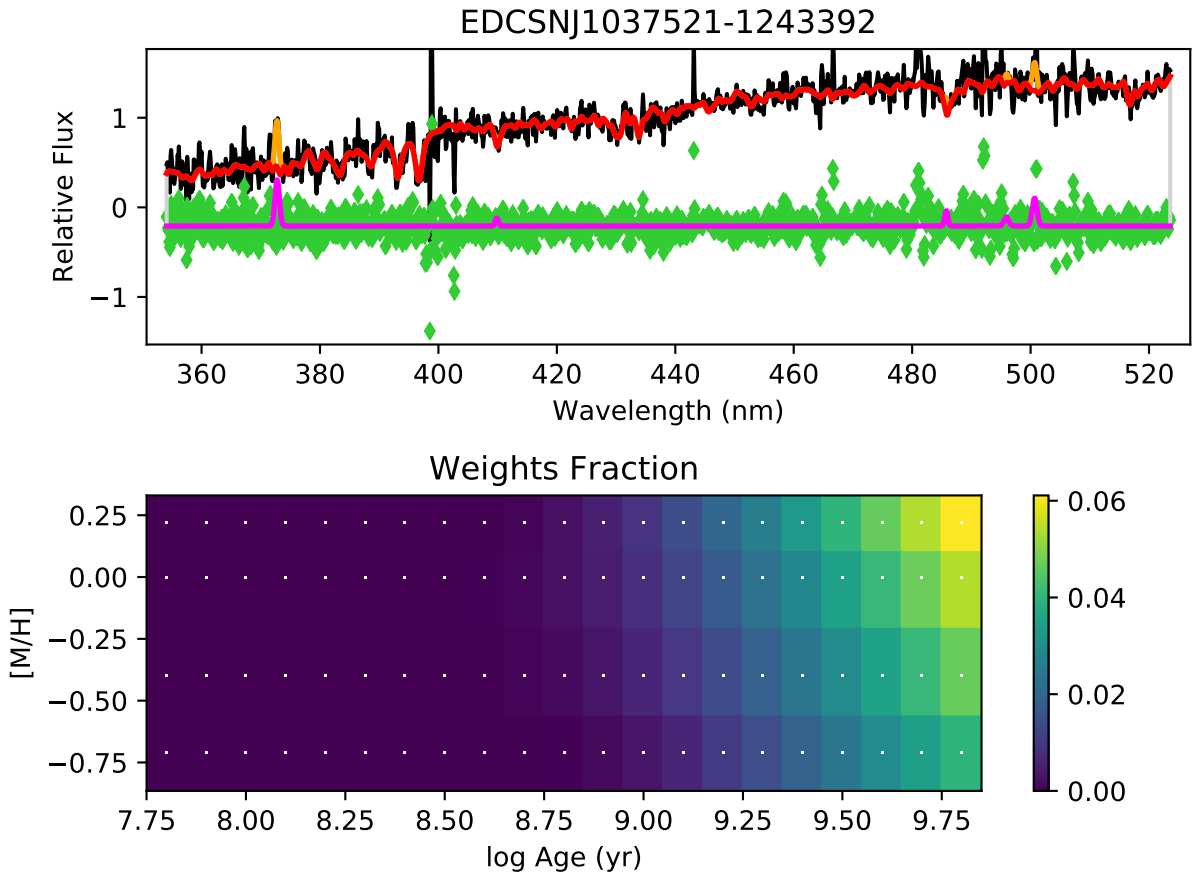
EDCSNJ1037521-1243392
Relative Flux
1
0
−1
360
380
400
420
440
460
480
500
520
Wavelength (nm)
Weights Fraction
[M/H]
0.25
0.00
−0.25
−0.50
−0.75
7.75
8.00
8.25
8.50
8.75
9.00
9.25
9.50
9.75
log Age (yr)
0.06
0.04
0.02
0.00

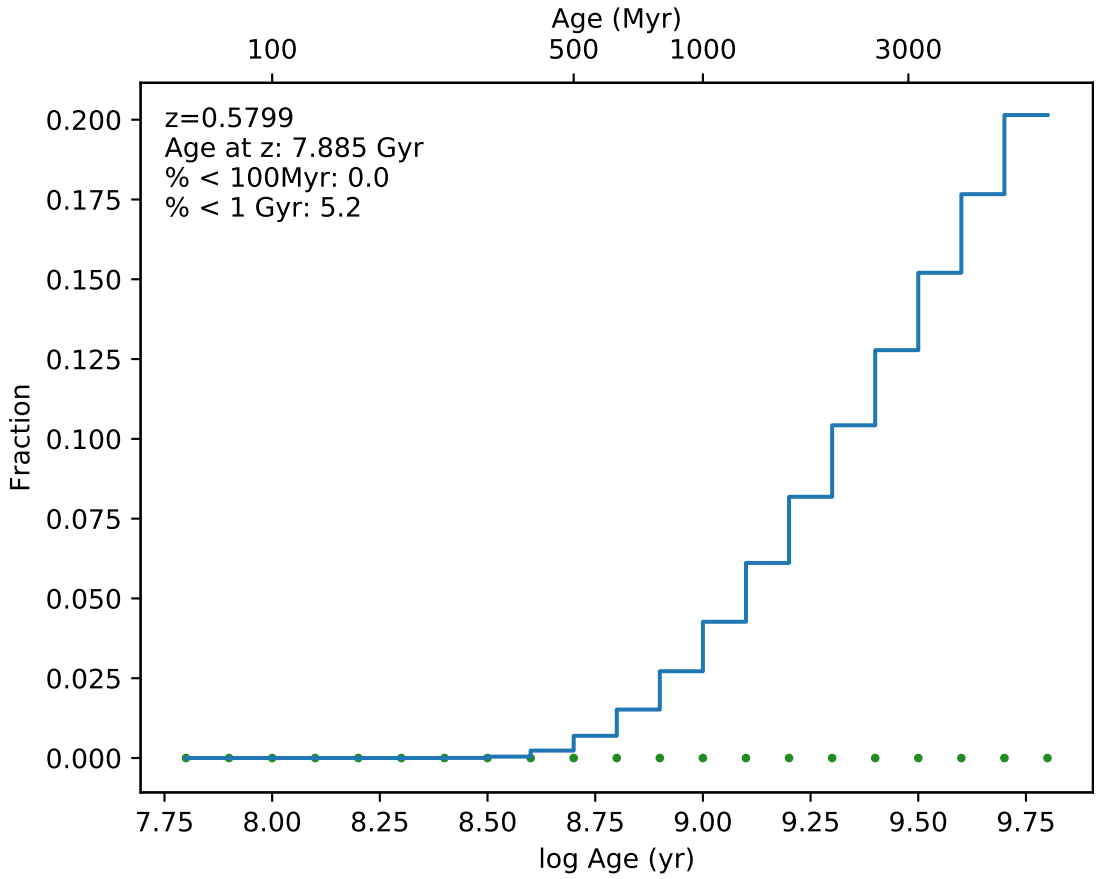
Age (Myr)
100
500
1000
3000
z=0.5799
Age at z: 7.885 Gyr
% < 100Myr: 0.0
% < 1 Gyr: 5.2
Fraction
0.200
0.175
0.150
0.125
0.100
0.075
0.050
0.025
0.000
7.75
8.00
8.25
8.50
8.75
9.00
9.25
9.50
9.75
log Age (yr)

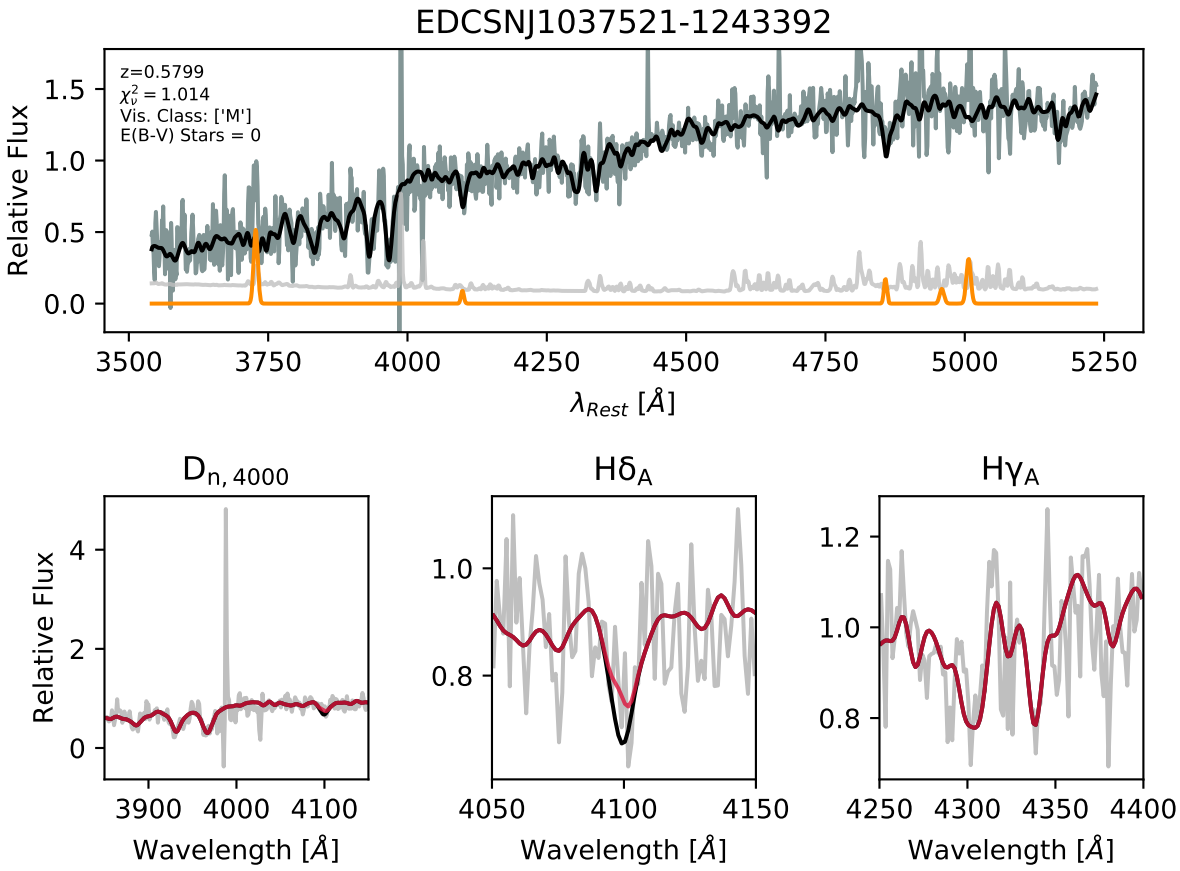
EDCSNJ1037521-1243392
z=0.5799
$\chi^2_\nu = 1.014$
Vis. Class: ['M']
E(B-V) Stars = 0
Relative Flux
λ_{Rest} [Å]
$D_{n,4000}$
$H\delta_A$
$H\gamma_A$
Wavelength [Å]

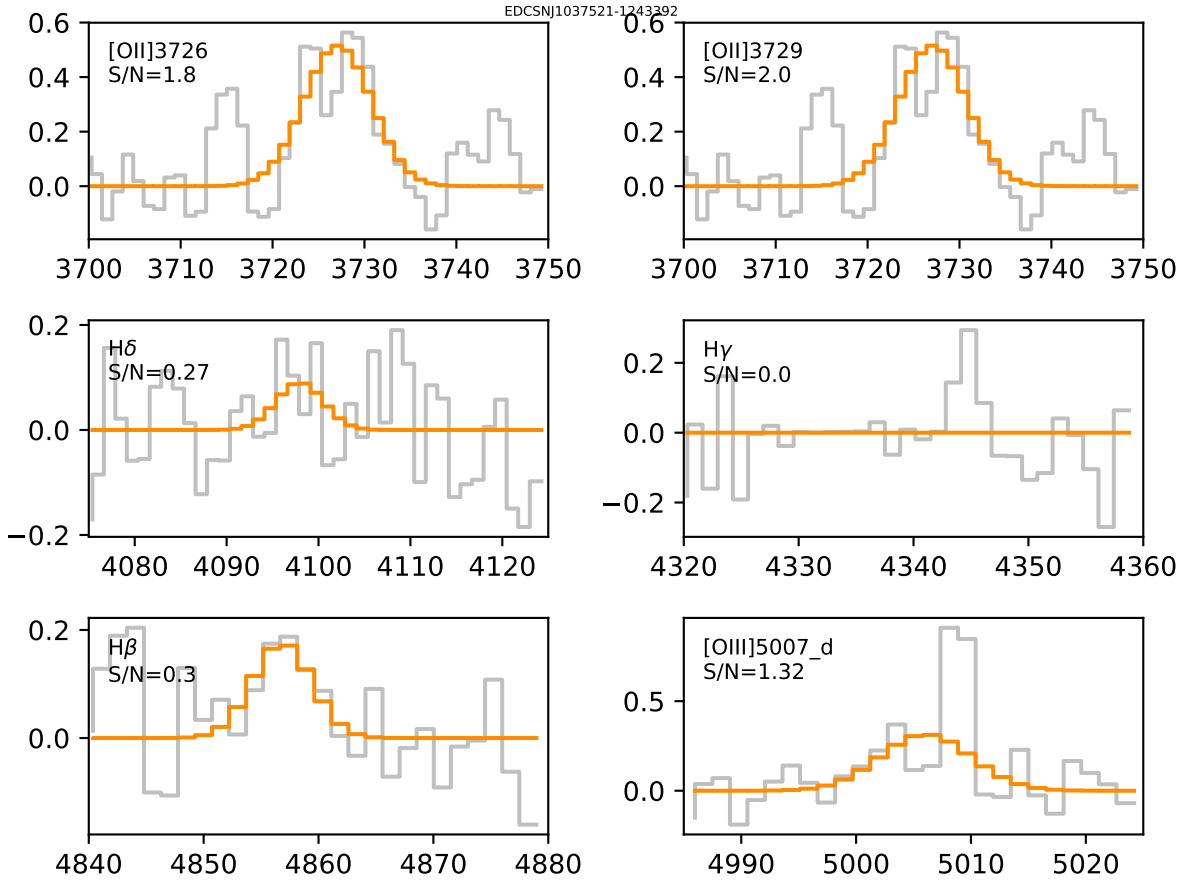
EDCSNJ1037521-1243392
[OII]3726
S/N=1.8
[OII]3729
S/N=2.0
Hδ
S/N=0.27
Hγ
S/N=0.0
Hβ
S/N=0.3
[OIII]5007_d
S/N=1.32

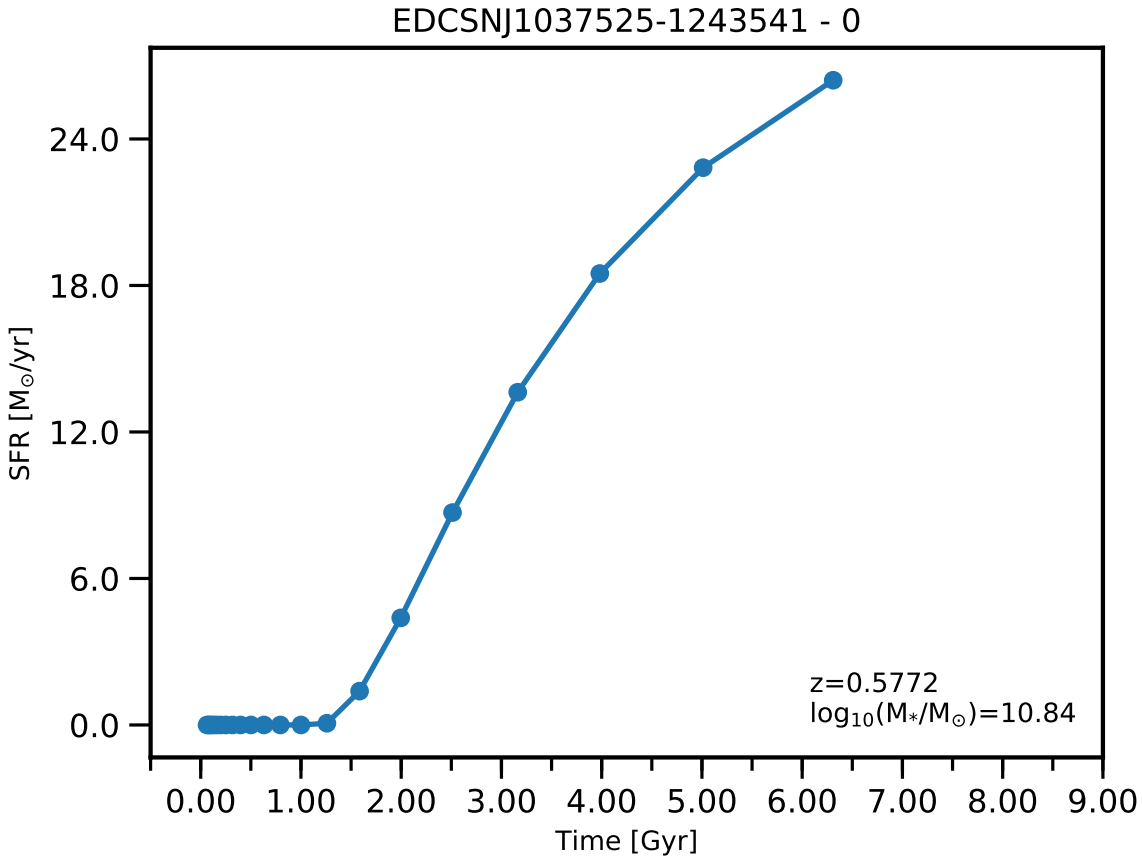
EDCSNJ1037525-1243541 - 0
SFR [M⊙/yr]
24.0
18.0
12.0
6.0
0.0
0.00
1.00
2.00
3.00
4.00
5.00
6.00
7.00
8.00
9.00
Time [Gyr]
z=0.5772
log10(M*/M⊙)=10.84

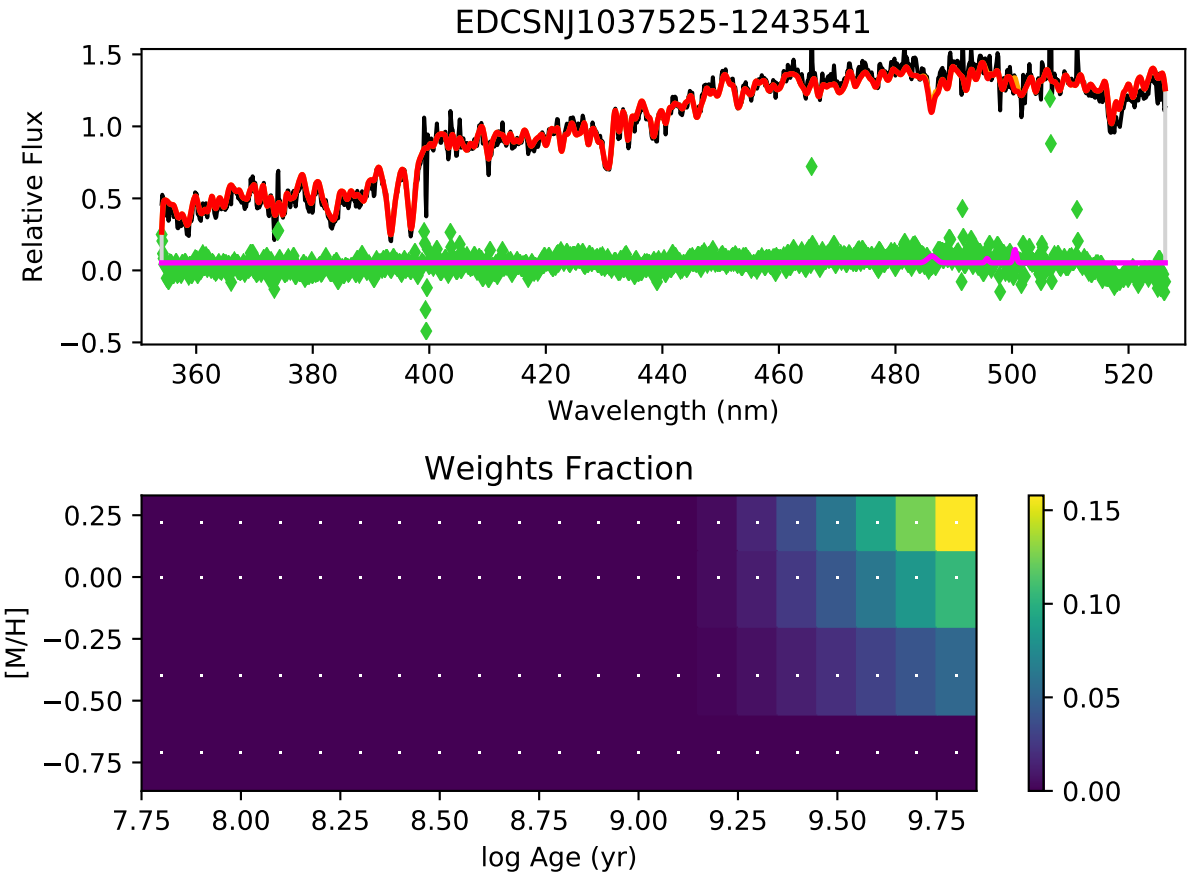
EDCSNJ1037525-1243541
Relative Flux
1.5
1.0
0.5
0.0
−0.5
360
380
400
420
440
460
480
500
520
Wavelength (nm)
Weights Fraction
[M/H]
0.25
0.00
−0.25
−0.50
−0.75
7.75
8.00
8.25
8.50
8.75
9.00
9.25
9.50
9.75
log Age (yr)
0.15
0.10
0.05
0.00

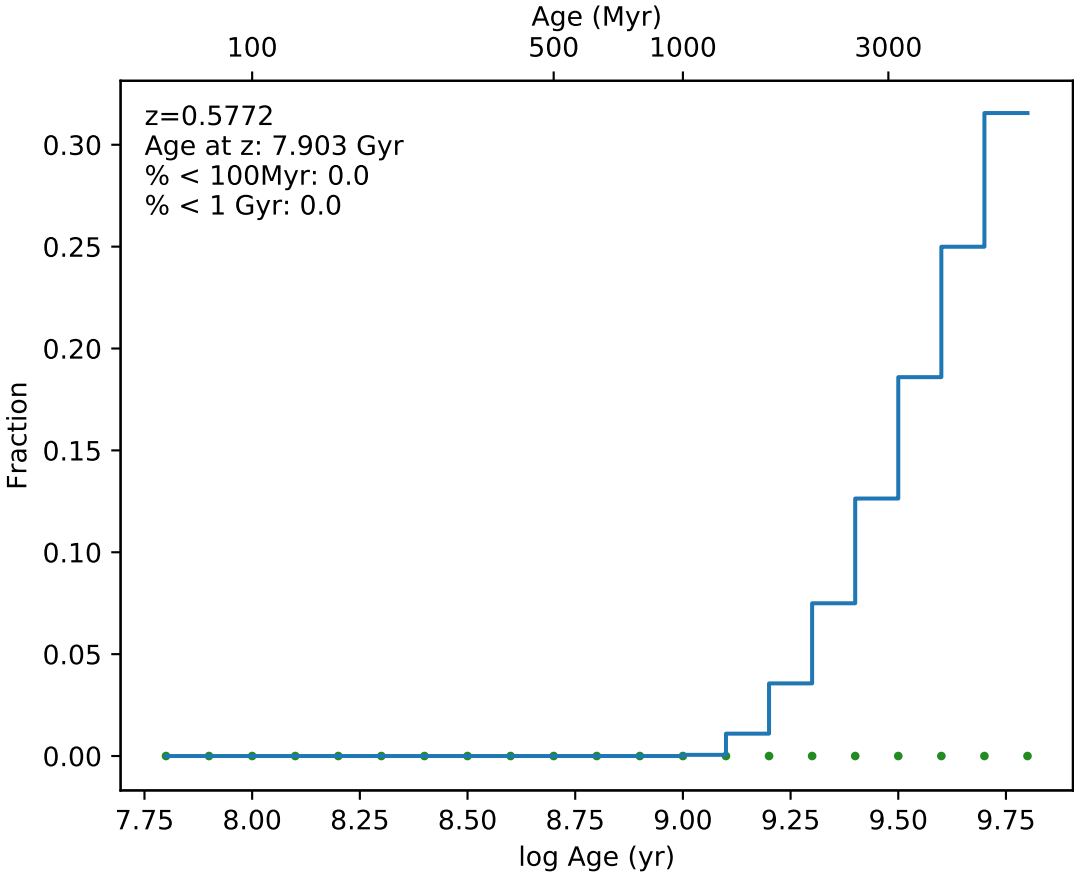
Age (Myr)
100
500
1000
3000
z=0.5772
Age at z: 7.903 Gyr
% < 100Myr: 0.0
% < 1 Gyr: 0.0
Fraction
0.30
0.25
0.20
0.15
0.10
0.05
0.00
7.75
8.00
8.25
8.50
8.75
9.00
9.25
9.50
9.75
log Age (yr)

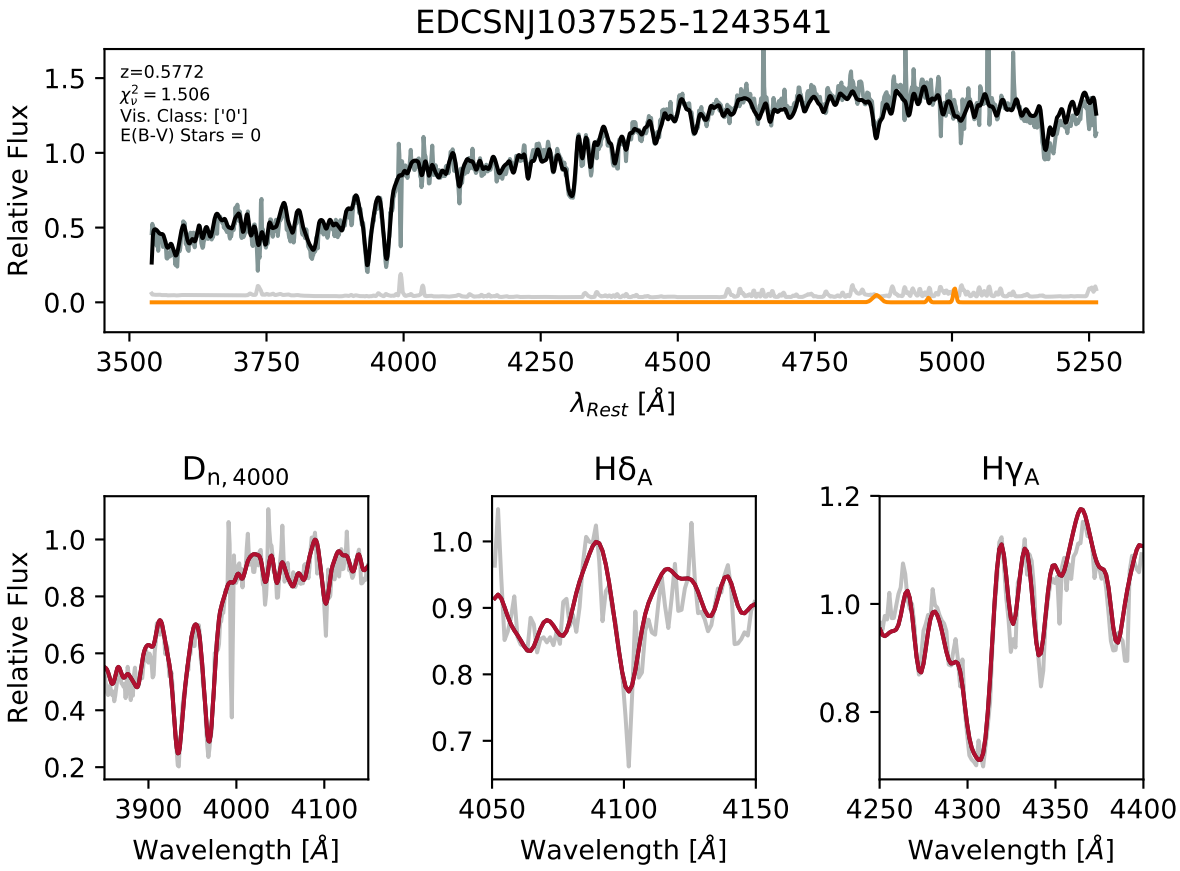
EDCSNJ1037525-1243541
z=0.5772
$\chi^2_\nu = 1.506$
Vis. Class: ['0']
E(B-V) Stars = 0
Relative Flux
λ_{Rest} [Å]
$D_{n,4000}$
$H\delta_A$
$H\gamma_A$
Wavelength [Å]

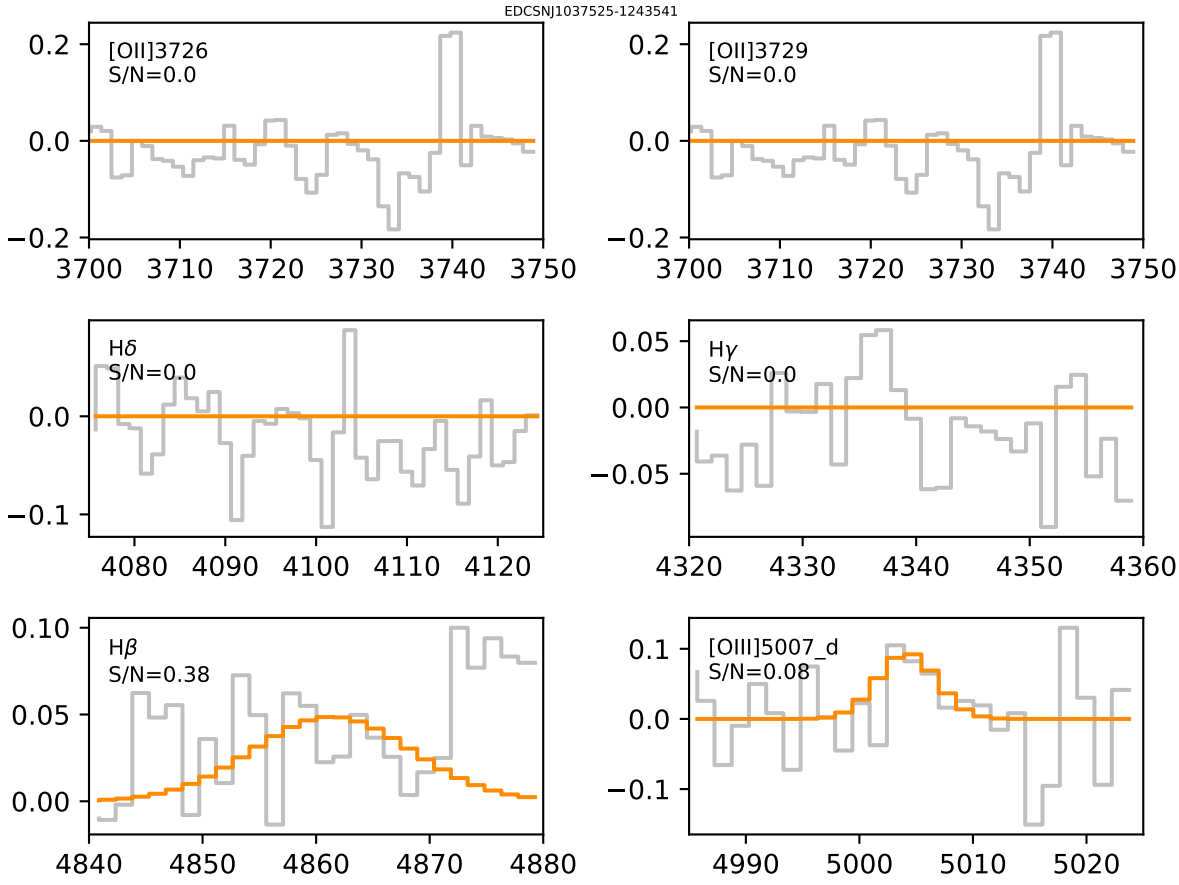
EDCSNJ1037525-1243541
[OII]3726
S/N=0.0
[OII]3729
S/N=0.0
Hδ
S/N=0.0
Hγ
S/N=0.0
Hβ
S/N=0.38
[OIII]5007_d
S/N=0.08

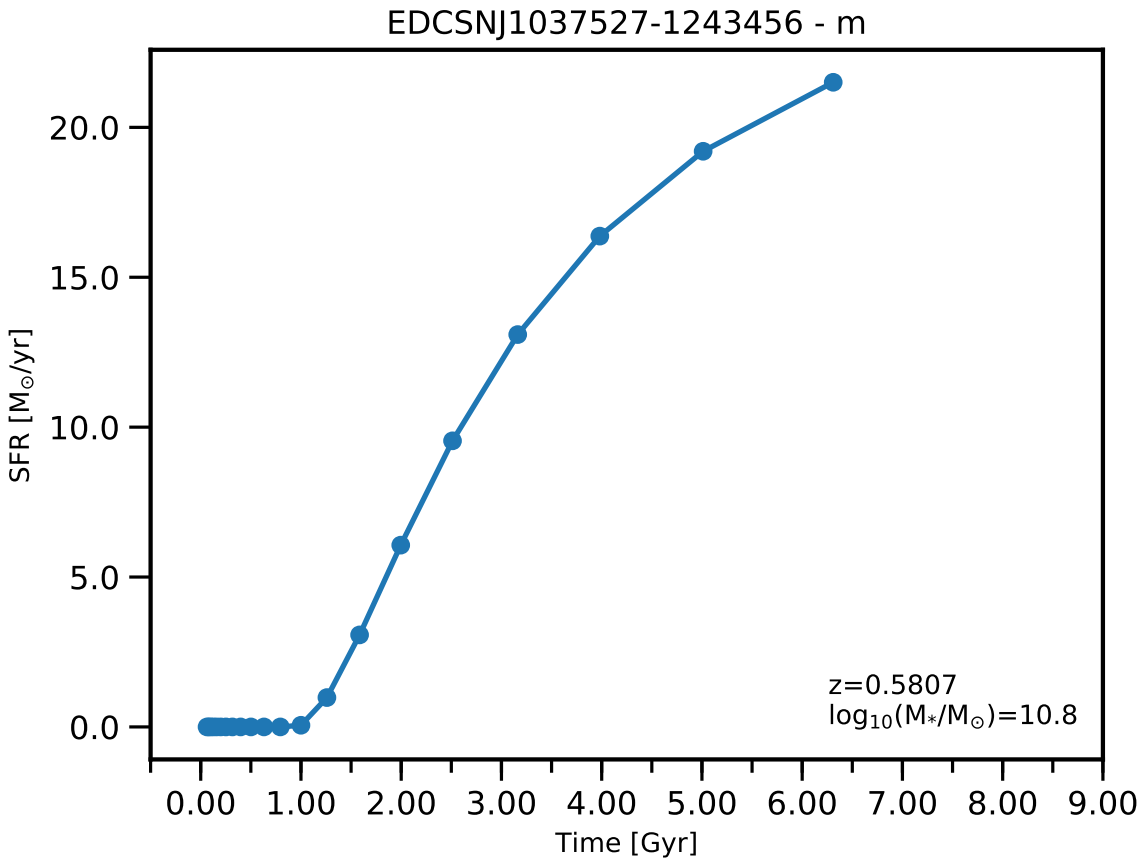
EDCSNJ1037527-1243456 - m
SFR [M⊙/yr]
20.0
15.0
10.0
5.0
0.0
0.00
1.00
2.00
3.00
4.00
5.00
6.00
7.00
8.00
9.00
Time [Gyr]
z=0.5807
log10(M∗/M⊙)=10.8

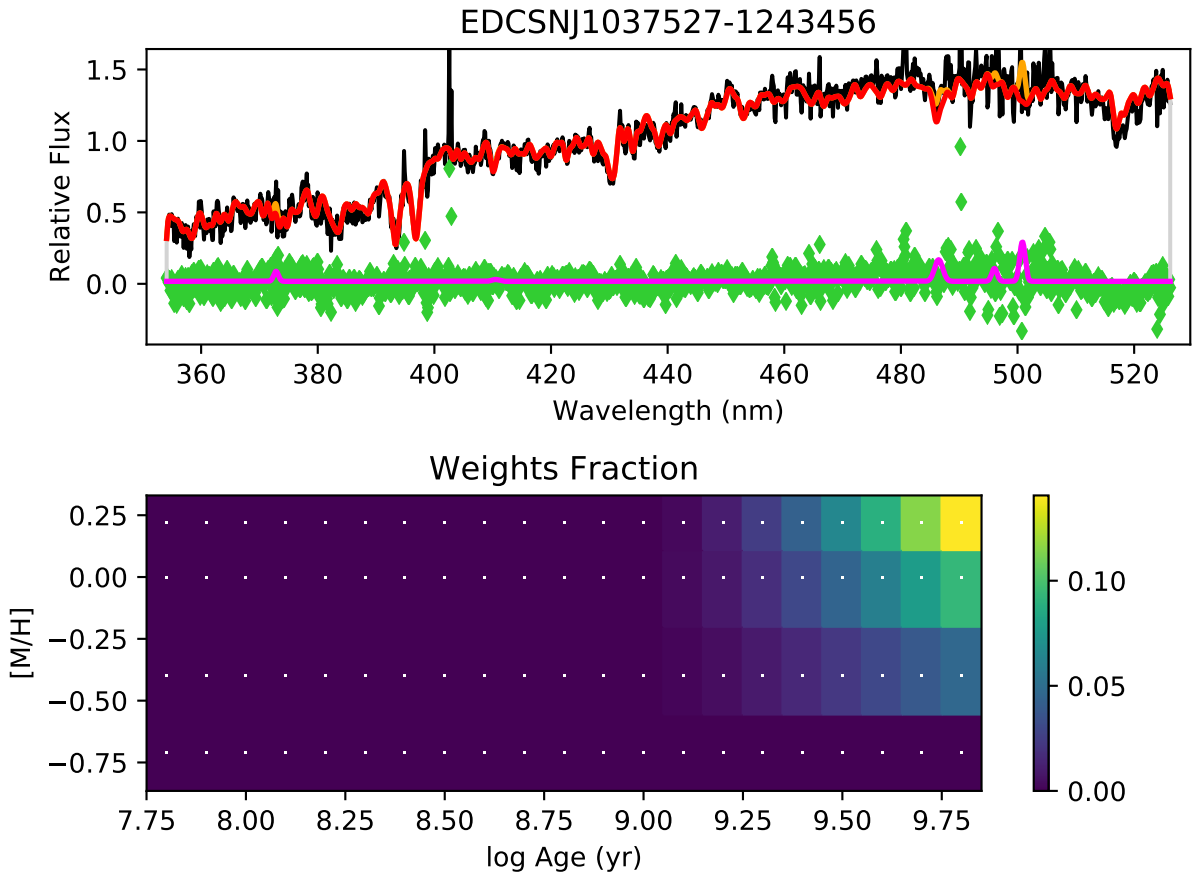
EDCSNJ1037527-1243456
Relative Flux
1.5
1.0
0.5
0.0
360
380
400
420
440
460
480
500
520
Wavelength (nm)
Weights Fraction
[M/H]
0.25
0.00
−0.25
−0.50
−0.75
7.75
8.00
8.25
8.50
8.75
9.00
9.25
9.50
9.75
log Age (yr)
0.10
0.05
0.00

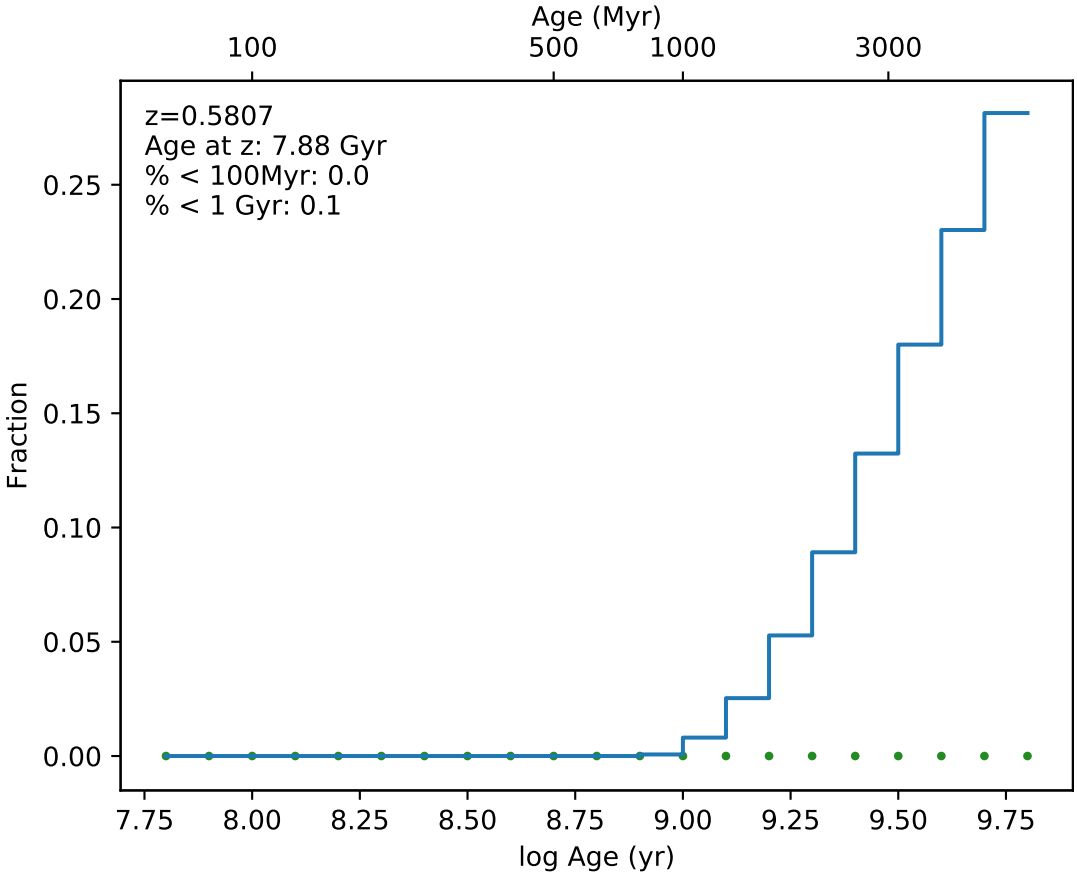
Age (Myr)
100
500
1000
3000
z=0.5807
Age at z: 7.88 Gyr
% < 100Myr: 0.0
% < 1 Gyr: 0.1
Fraction
0.25
0.20
0.15
0.10
0.05
0.00
7.75
8.00
8.25
8.50
8.75
9.00
9.25
9.50
9.75
log Age (yr)

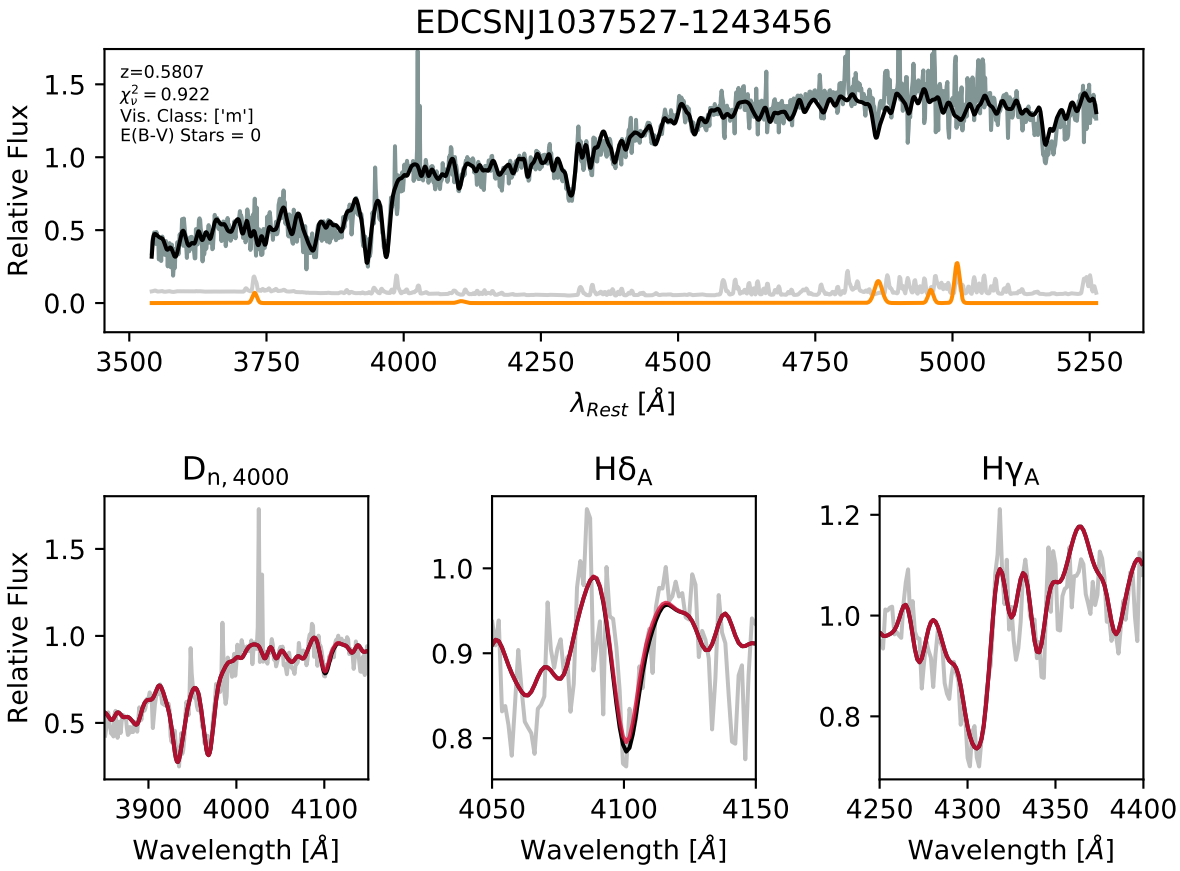
EDCSNJ1037527-1243456
z=0.5807
$\chi^2_\nu = 0.922$
Vis. Class: ['m']
E(B-V) Stars = 0
Relative Flux
λ_{Rest} [Å]
$D_{n,4000}$
$H\delta_A$
$H\gamma_A$
Wavelength [Å]

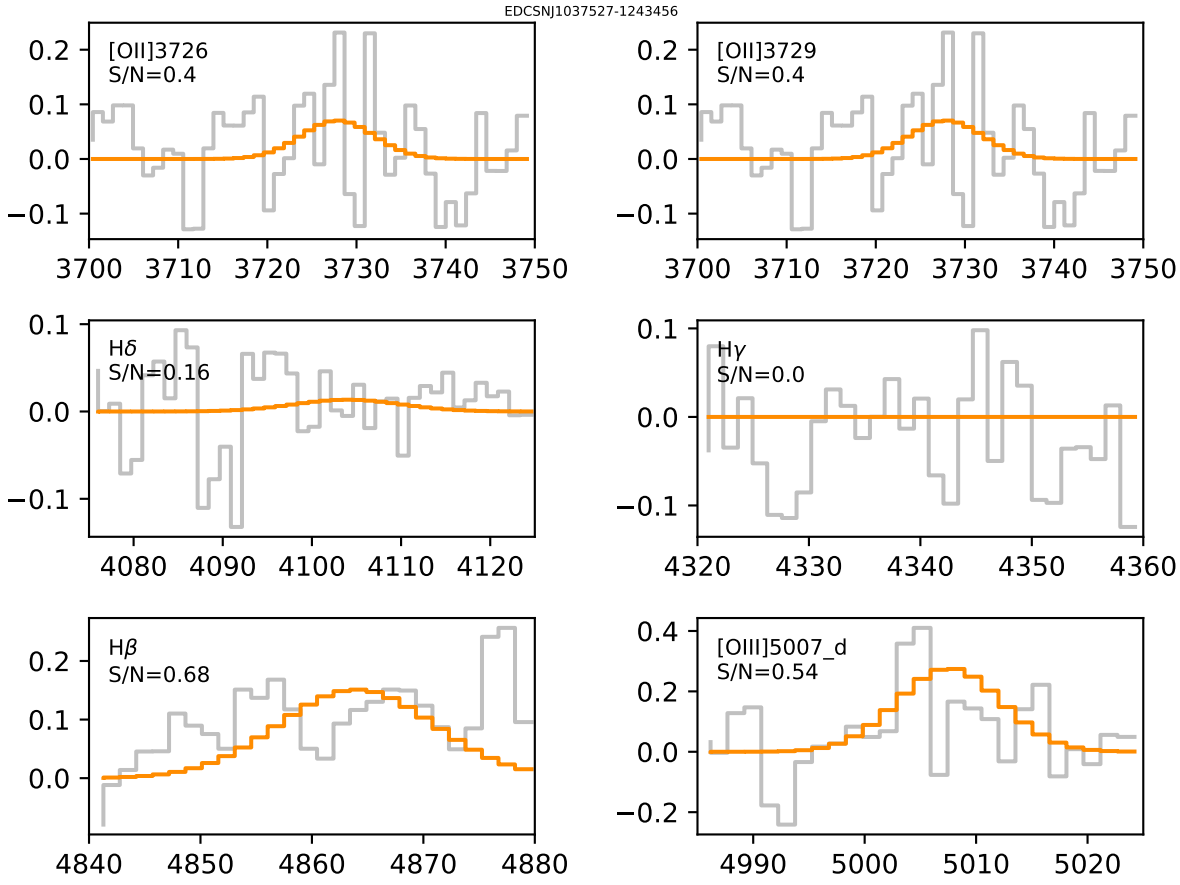
EDCSNJ1037527-1243456
[OII]3726
S/N=0.4
[OII]3729
S/N=0.4
Hδ
S/N=0.16
Hγ
S/N=0.0
Hβ
S/N=0.68
[OIII]5007_d
S/N=0.54

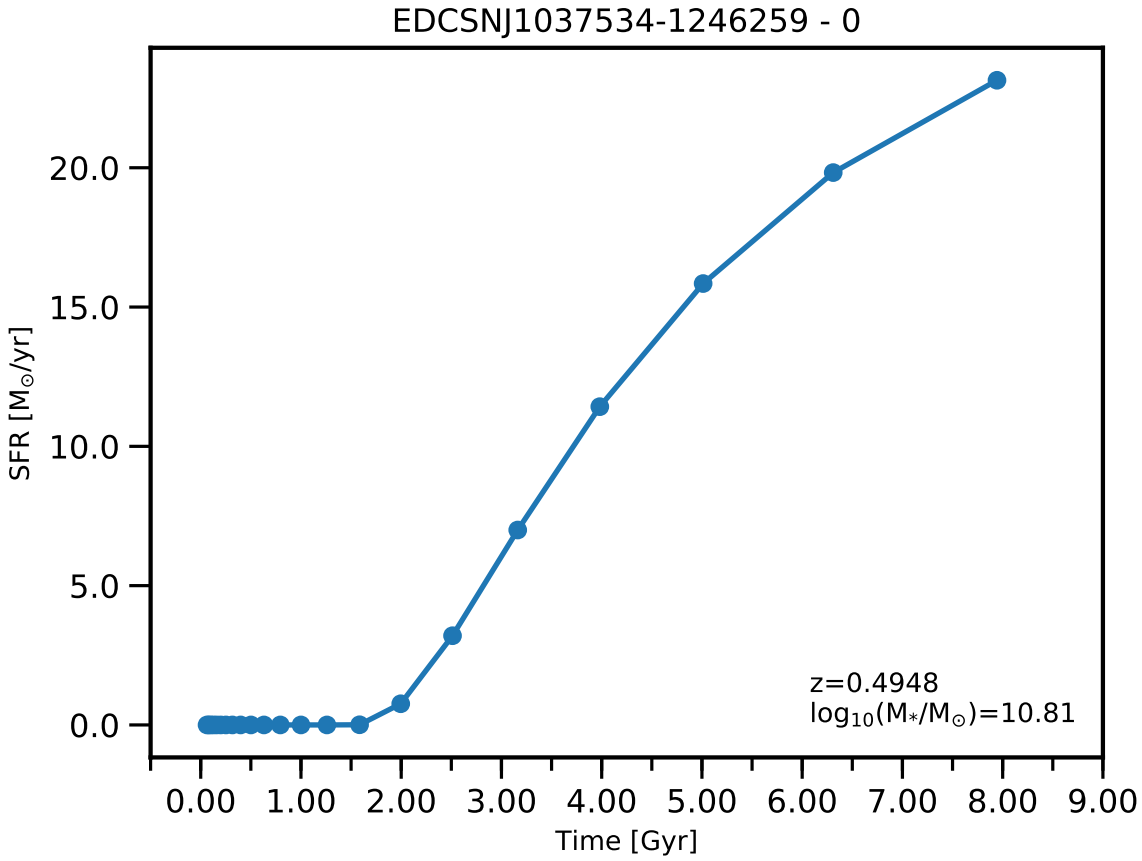
EDCSNJ1037534-1246259 - 0
SFR [M⊙/yr]
20.0
15.0
10.0
5.0
0.0
0.00
1.00
2.00
3.00
4.00
5.00
6.00
7.00
8.00
9.00
Time [Gyr]
z=0.4948
log10(M*/M⊙)=10.81

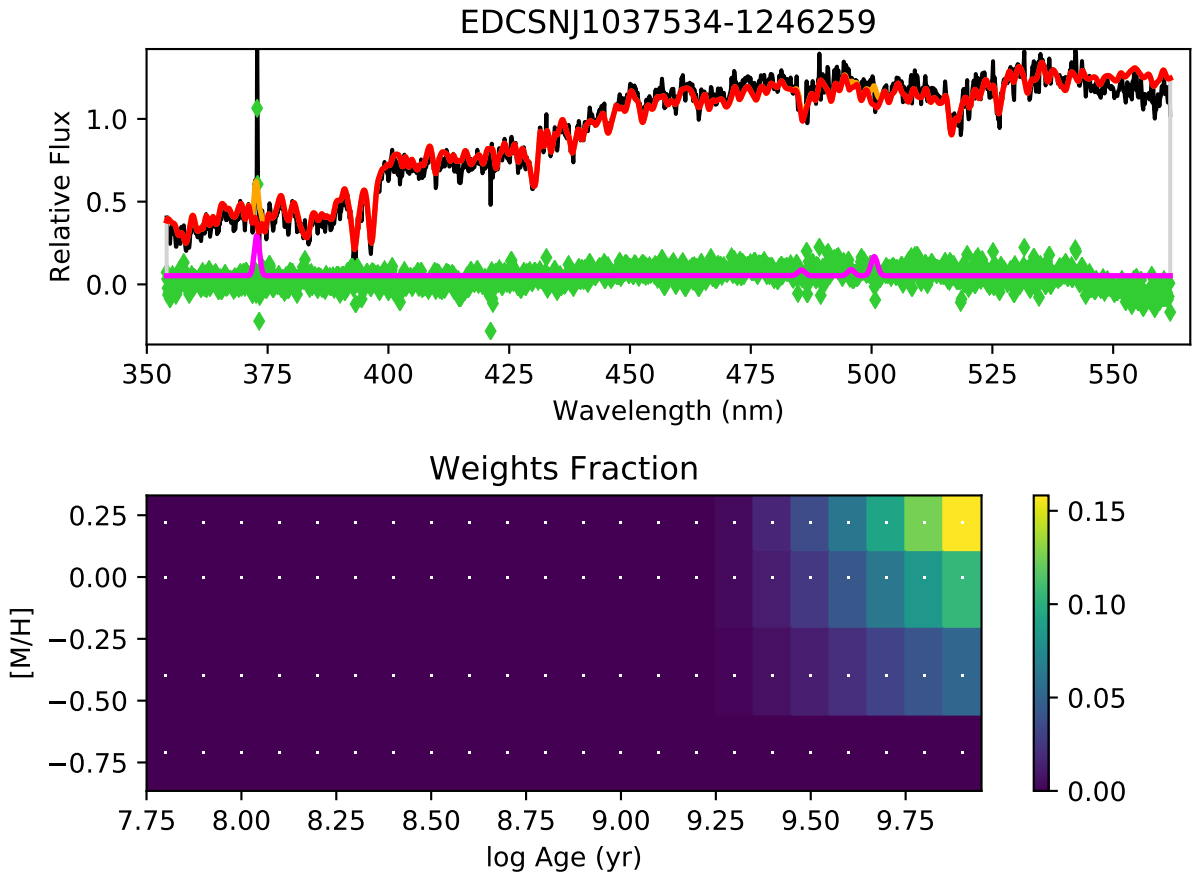
EDCSNJ1037534-1246259
Relative Flux
1.0
0.5
0.0
350
375
400
425
450
475
500
525
550
Wavelength (nm)
Weights Fraction
[M/H]
0.25
0.00
−0.25
−0.50
−0.75
7.75
8.00
8.25
8.50
8.75
9.00
9.25
9.50
9.75
log Age (yr)
0.15
0.10
0.05
0.00

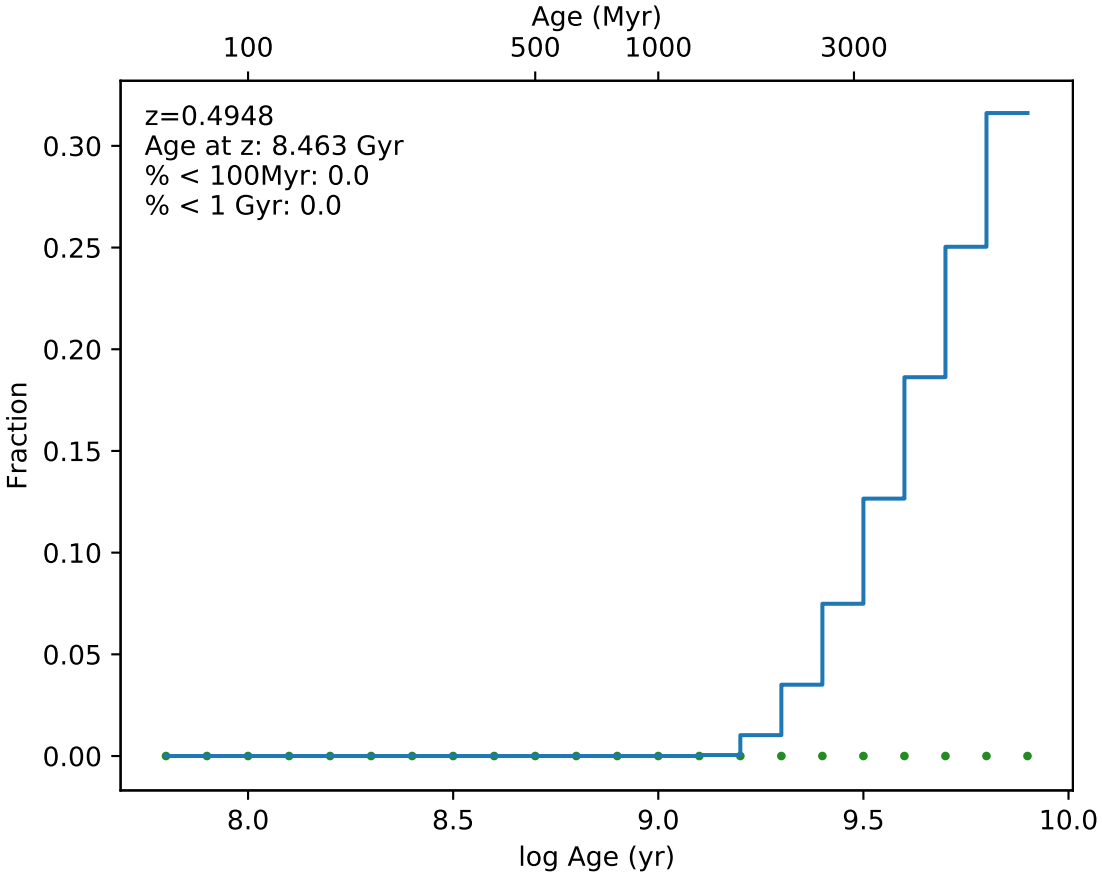
Age (Myr)
100
500
1000
3000
z=0.4948
Age at z: 8.463 Gyr
% < 100Myr: 0.0
% < 1 Gyr: 0.0
Fraction
0.30
0.25
0.20
0.15
0.10
0.05
0.00
8.0
8.5
9.0
9.5
10.0
log Age (yr)

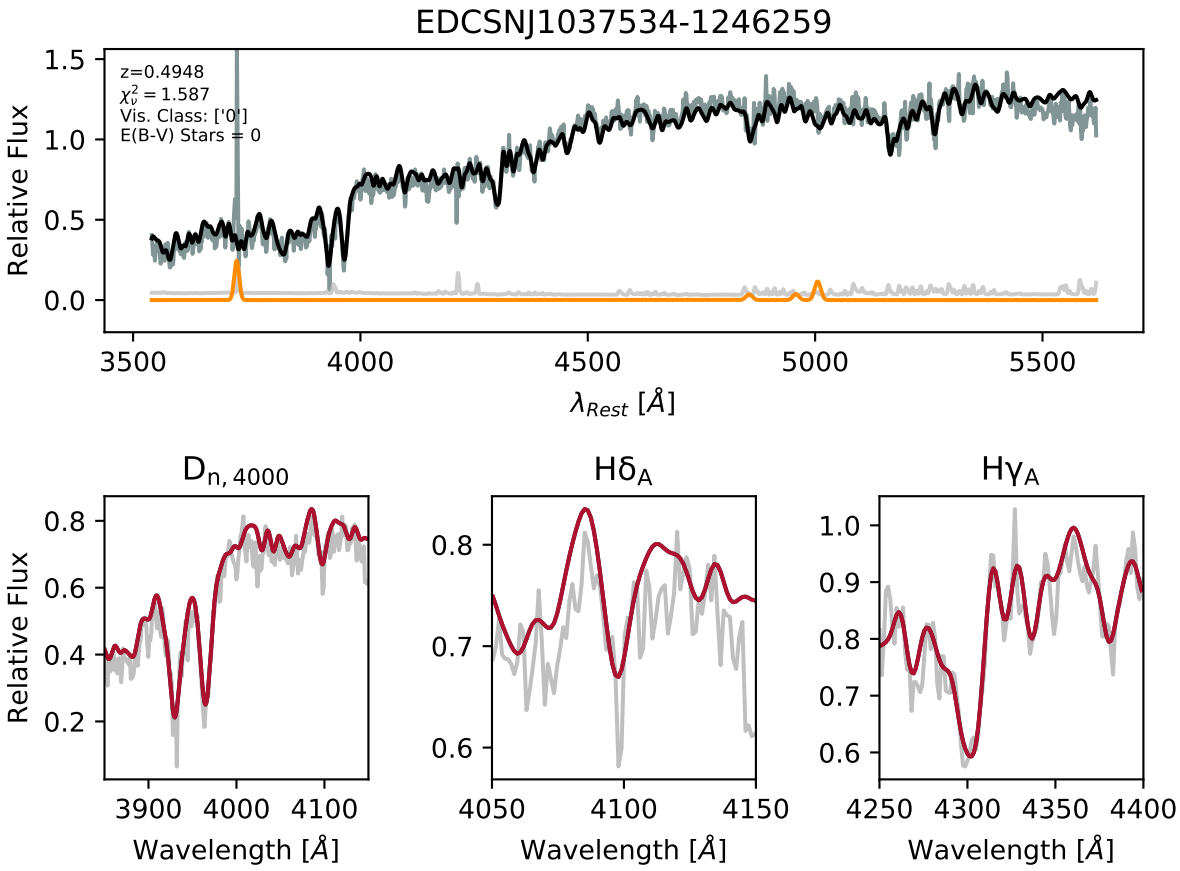
EDCSNJ1037534-1246259
z=0.4948
$\chi^2_\nu = 1.587$
Vis. Class: ['0']
E(B-V) Stars = 0
Relative Flux
λ_{Rest} [Å]
$D_{n,4000}$
$H\delta_A$
$H\gamma_A$
Wavelength [Å]

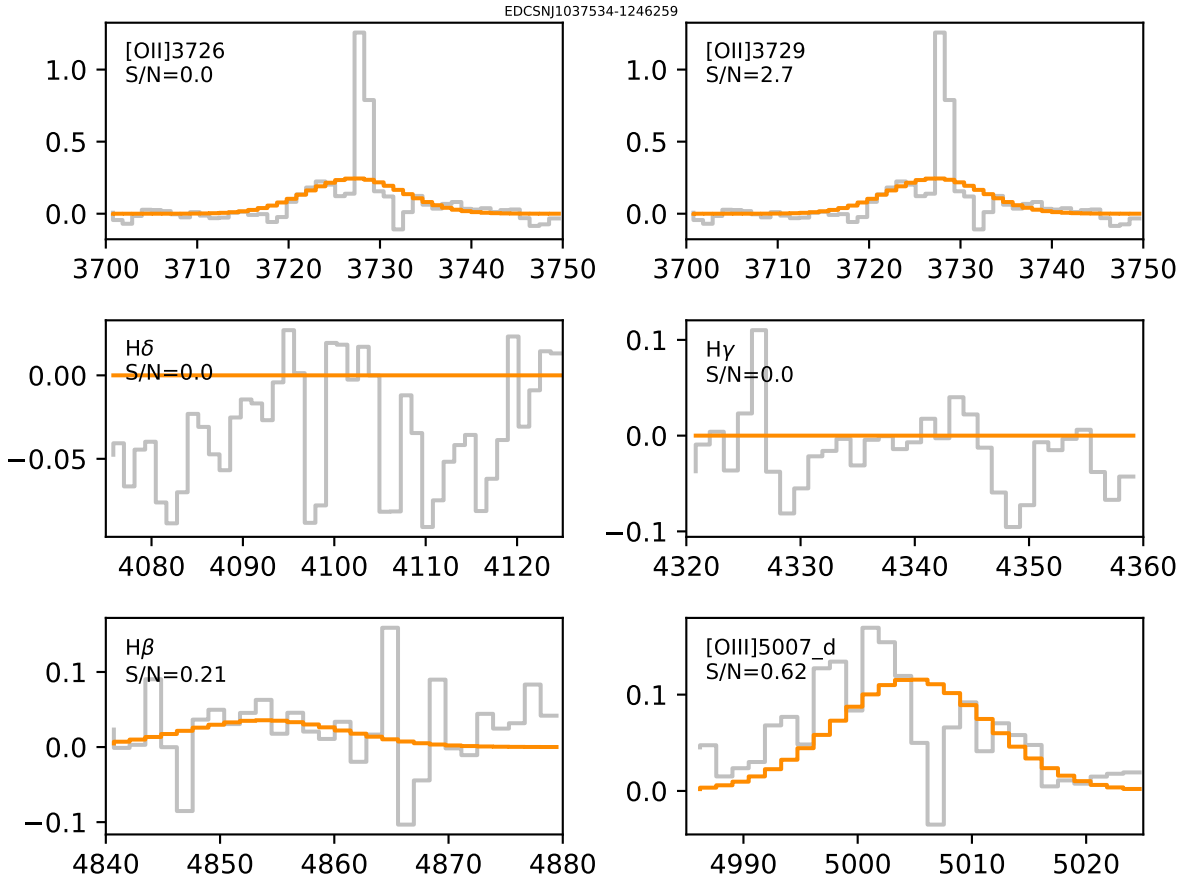
EDCSNJ1037534-1246259
[OII]3726
S/N=0.0
[OII]3729
S/N=2.7
Hδ
S/N=0.0
Hγ
S/N=0.0
Hβ
S/N=0.21
[OIII]5007_d
S/N=0.62

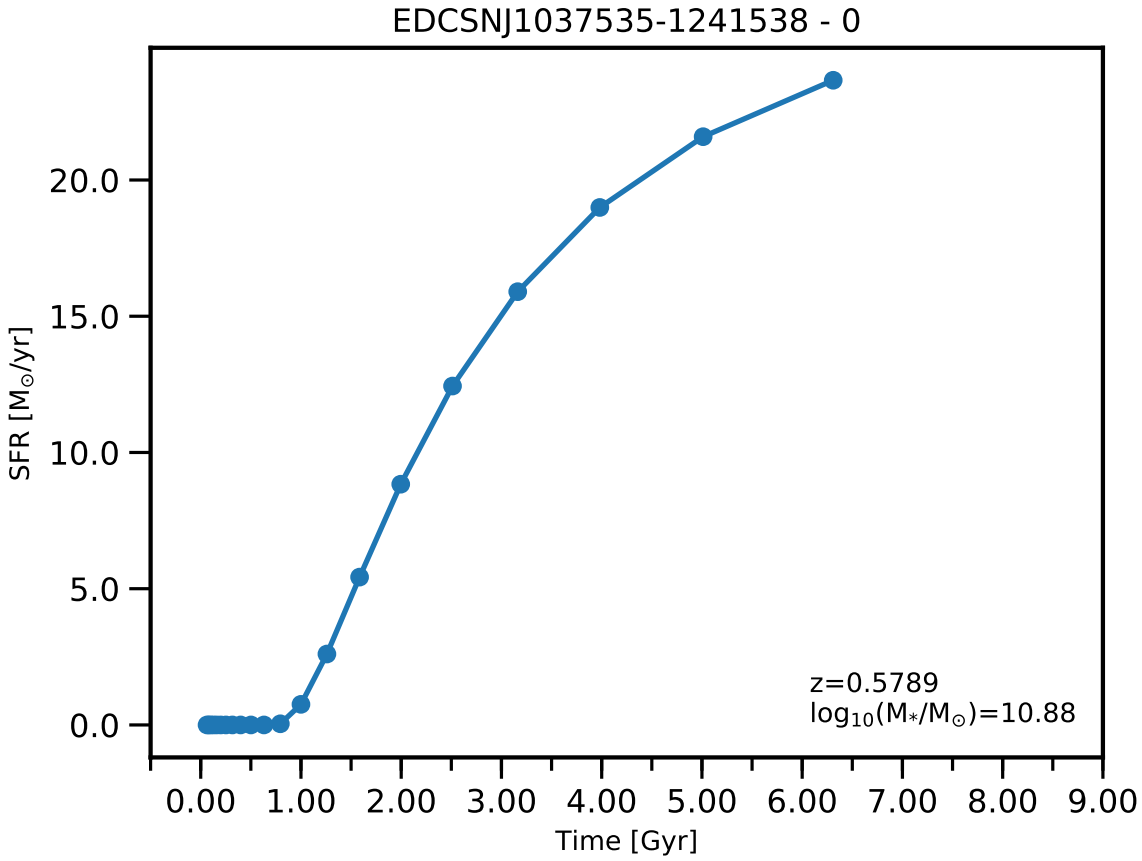
EDCSNJ1037535-1241538 - 0
SFR [M⊙/yr]
20.0
15.0
10.0
5.0
0.0
0.00
1.00
2.00
3.00
4.00
5.00
6.00
7.00
8.00
9.00
Time [Gyr]
z=0.5789
log10(M*/M⊙)=10.88

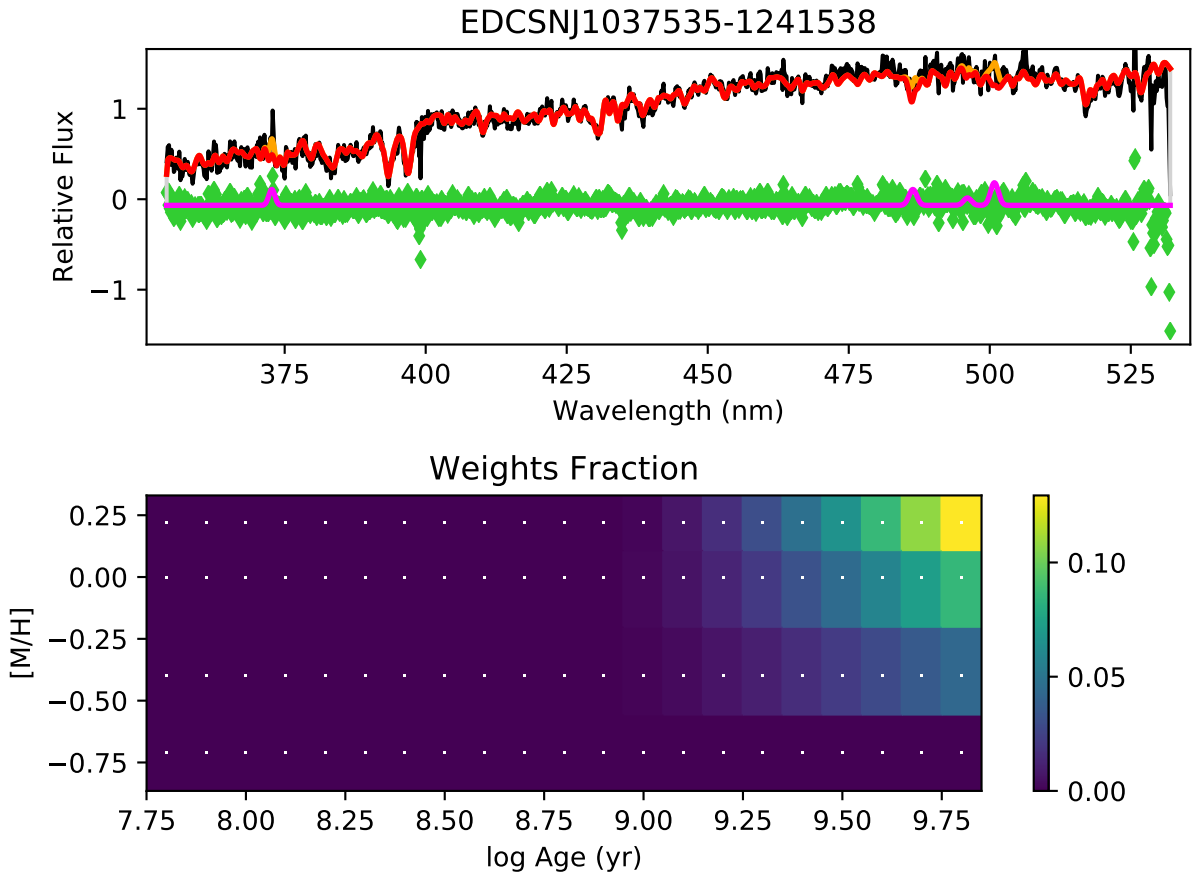
EDCSNJ1037535-1241538
Relative Flux
1
0
−1
375
400
425
450
475
500
525
Wavelength (nm)
Weights Fraction
[M/H]
0.25
0.00
−0.25
−0.50
−0.75
7.75
8.00
8.25
8.50
8.75
9.00
9.25
9.50
9.75
log Age (yr)
0.10
0.05
0.00

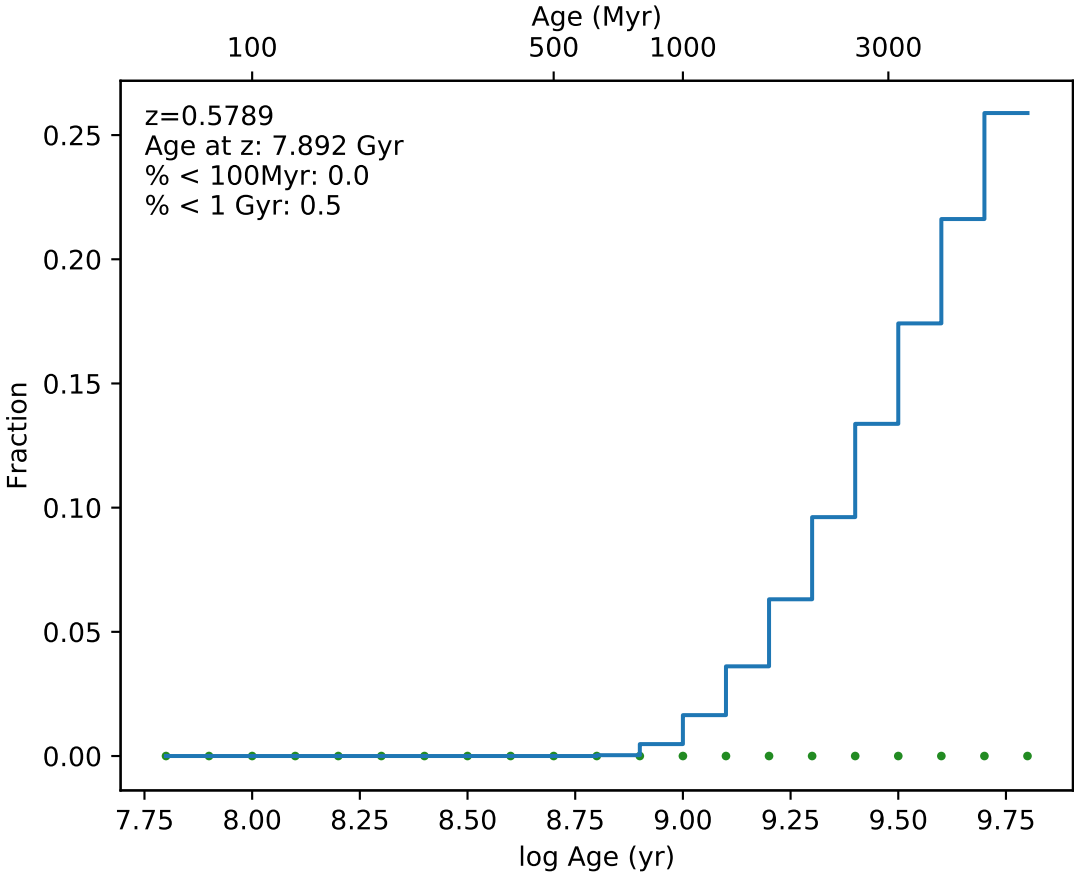
Age (Myr)
100
500
1000
3000
z=0.5789
Age at z: 7.892 Gyr
% < 100Myr: 0.0
% < 1 Gyr: 0.5
Fraction
0.25
0.20
0.15
0.10
0.05
0.00
7.75
8.00
8.25
8.50
8.75
9.00
9.25
9.50
9.75
log Age (yr)

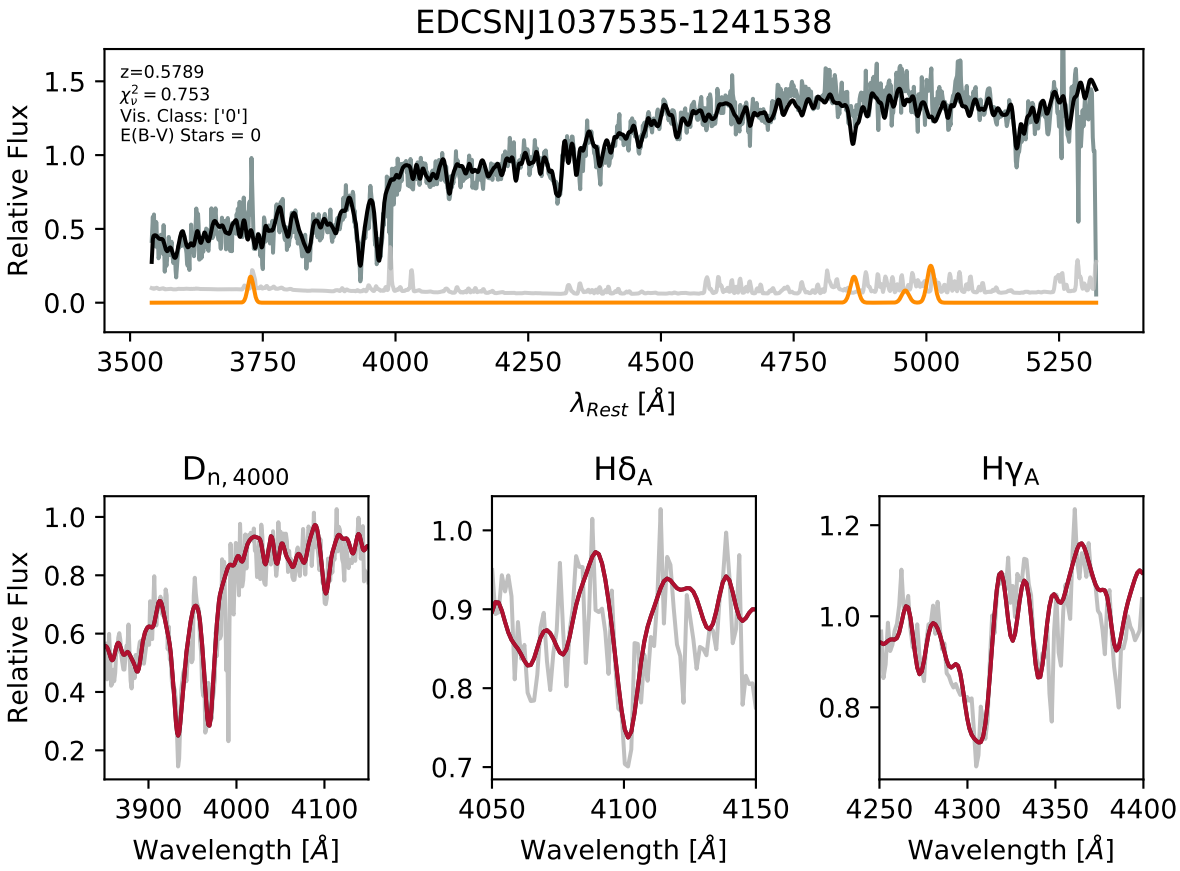
EDCSNJ1037535-1241538
z=0.5789
$\chi^2_\nu = 0.753$
Vis. Class: ['0']
E(B-V) Stars = 0
Relative Flux
λ_{Rest} [Å]
$D_{n,4000}$
$H\delta_A$
$H\gamma_A$
Wavelength [Å]

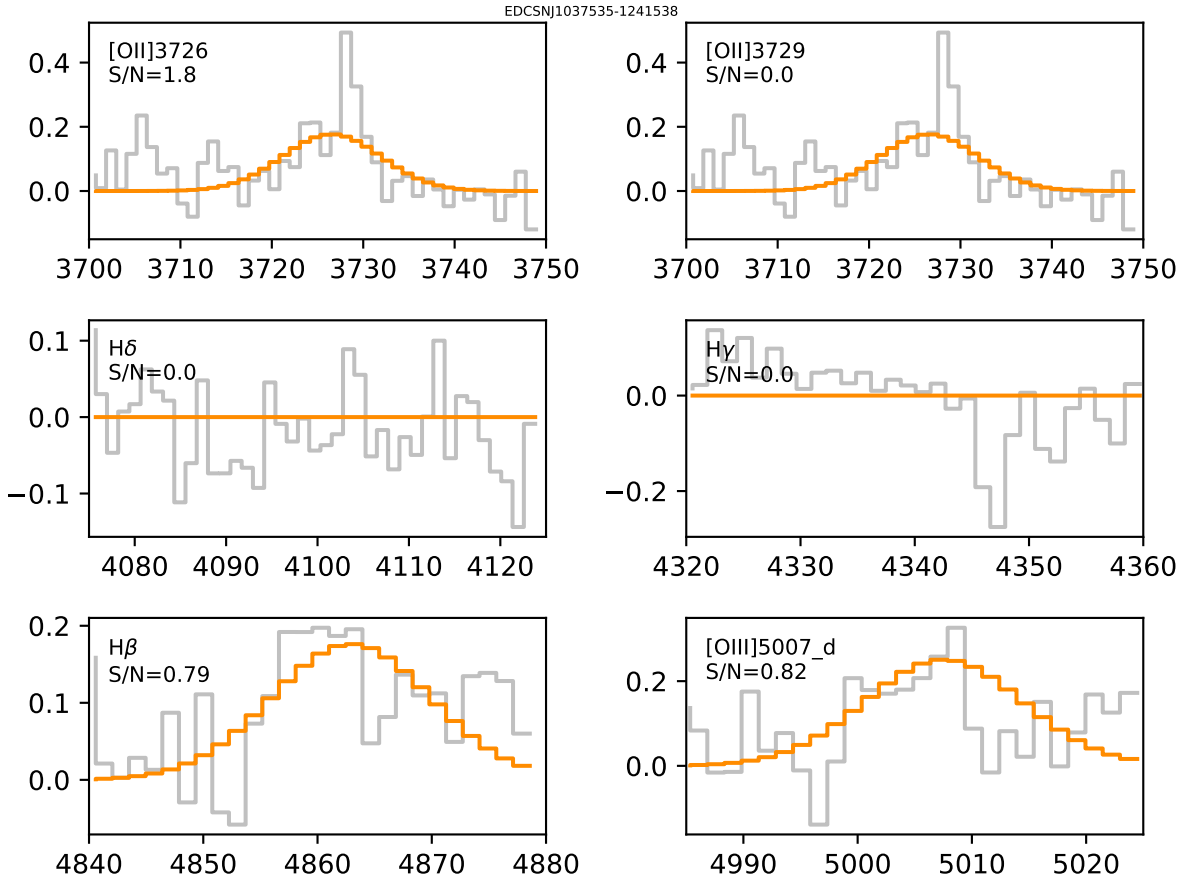
EDCSNJ1037535-1241538
[OII]3726
S/N=1.8
[OII]3729
S/N=0.0
Hδ
S/N=0.0
Hγ
S/N=0.0
Hβ
S/N=0.79
[OIII]5007_d
S/N=0.82

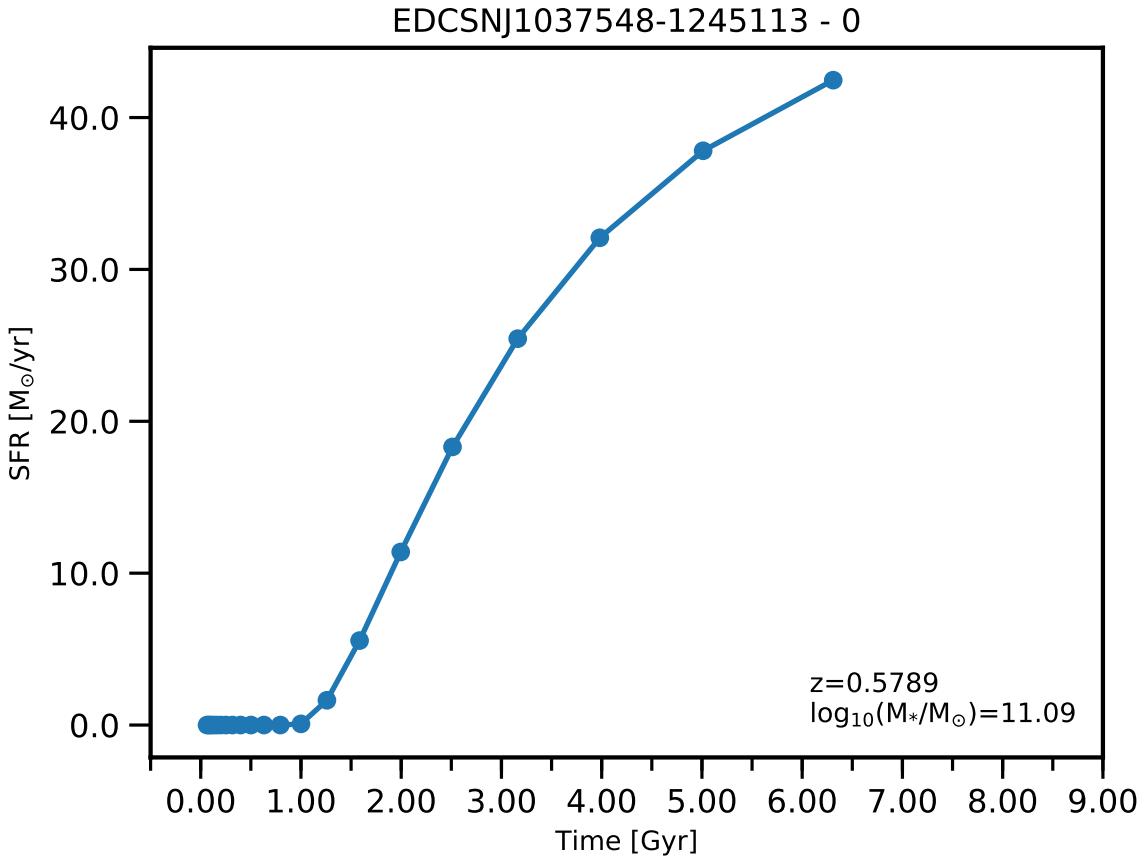
EDCSNJ1037548-1245113 - 0
SFR [M⊙/yr]
40.0
30.0
20.0
10.0
0.0
0.00
1.00
2.00
3.00
4.00
5.00
6.00
7.00
8.00
9.00
Time [Gyr]
z=0.5789
log10(M*/M⊙)=11.09

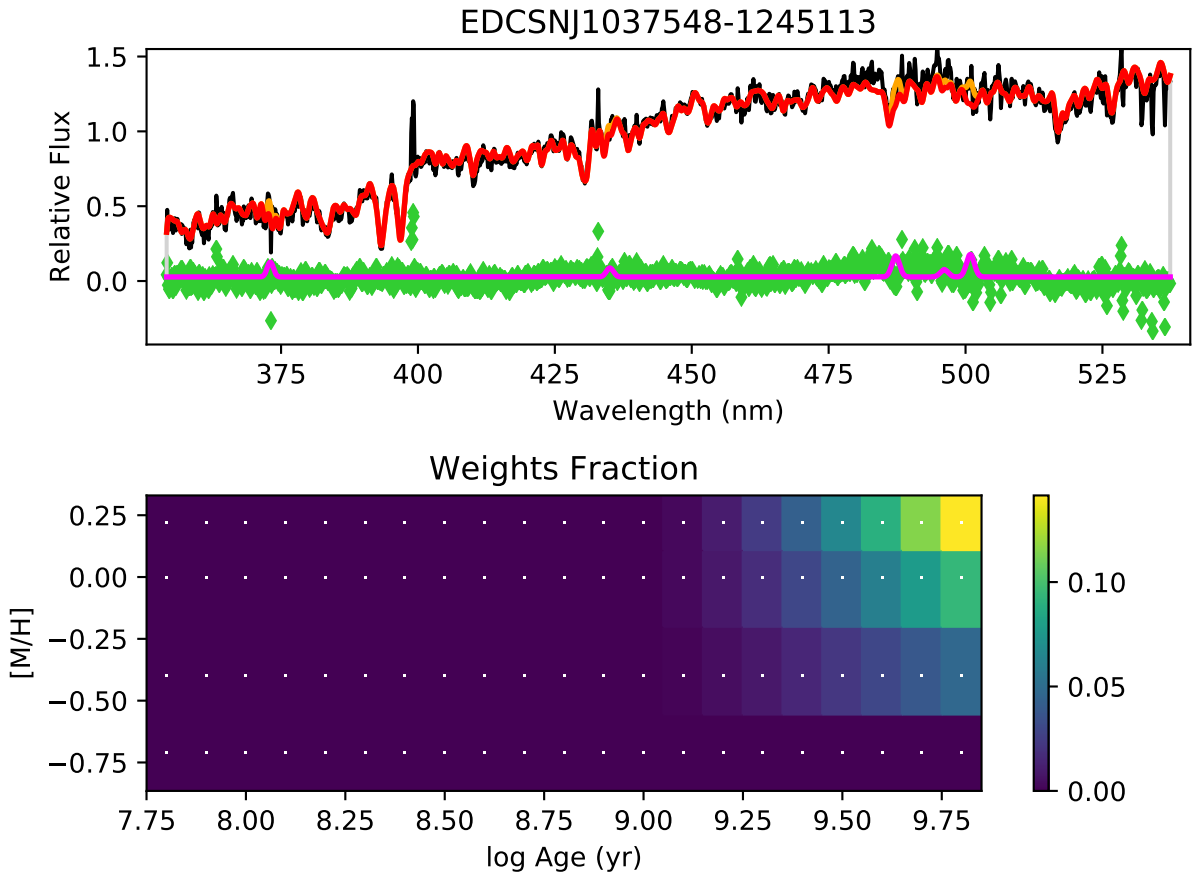
EDCSNJ1037548-1245113
Relative Flux
1.5
1.0
0.5
0.0
375
400
425
450
475
500
525
Wavelength (nm)
Weights Fraction
[M/H]
0.25
0.00
−0.25
−0.50
−0.75
7.75
8.00
8.25
8.50
8.75
9.00
9.25
9.50
9.75
log Age (yr)
0.10
0.05
0.00

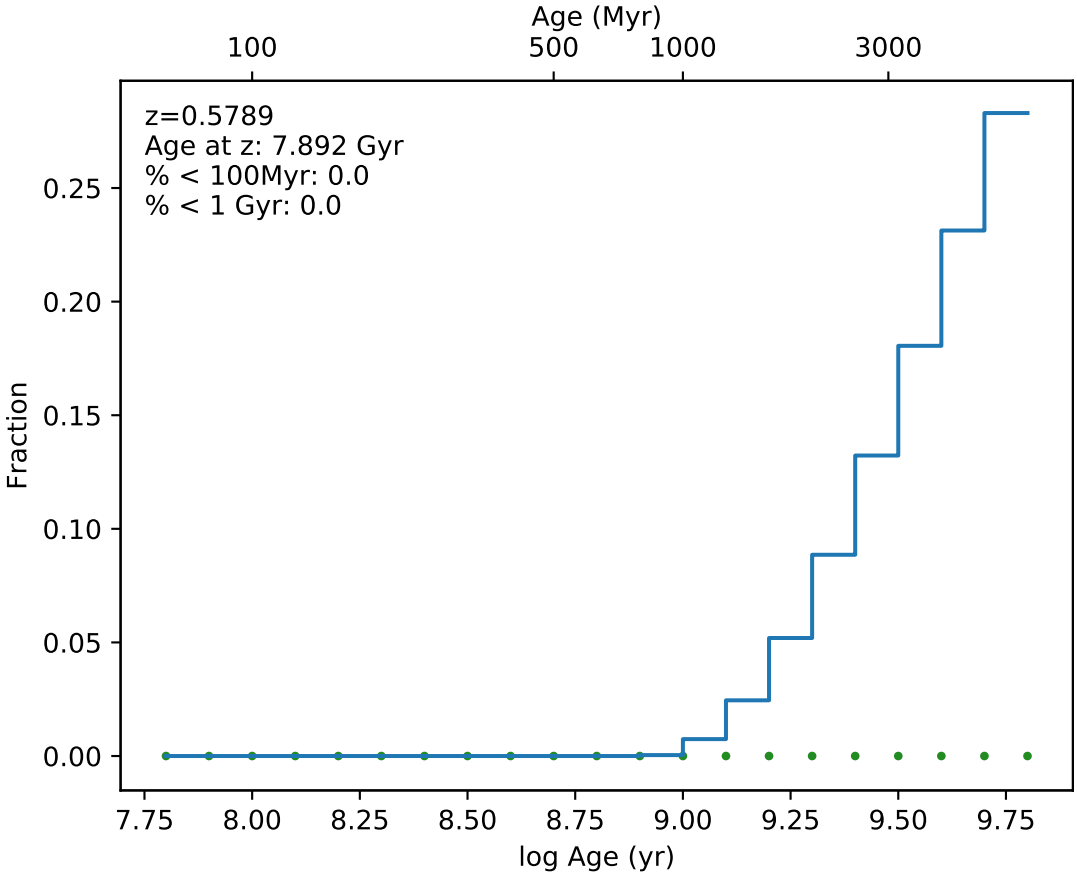
Age (Myr)
100
500
1000
3000
z=0.5789
Age at z: 7.892 Gyr
% < 100Myr: 0.0
% < 1 Gyr: 0.0
Fraction
0.25
0.20
0.15
0.10
0.05
0.00
7.75
8.00
8.25
8.50
8.75
9.00
9.25
9.50
9.75
log Age (yr)

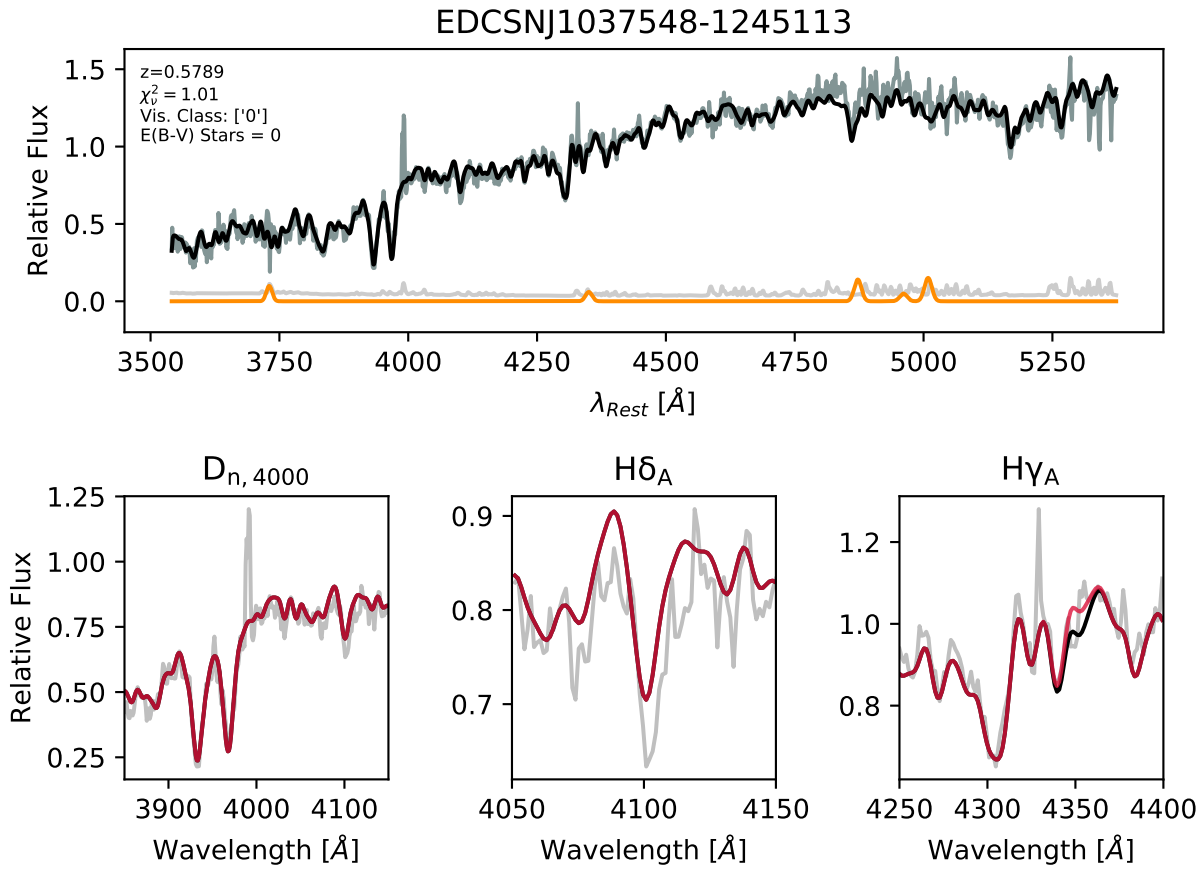
EDCSNJ1037548-1245113
z=0.5789
$\chi^2_\nu = 1.01$
Vis. Class: ['0']
E(B-V) Stars = 0
Relative Flux
λ_{Rest} [Å]
$D_{n,4000}$
$H\delta_A$
$H\gamma_A$
Wavelength [Å]

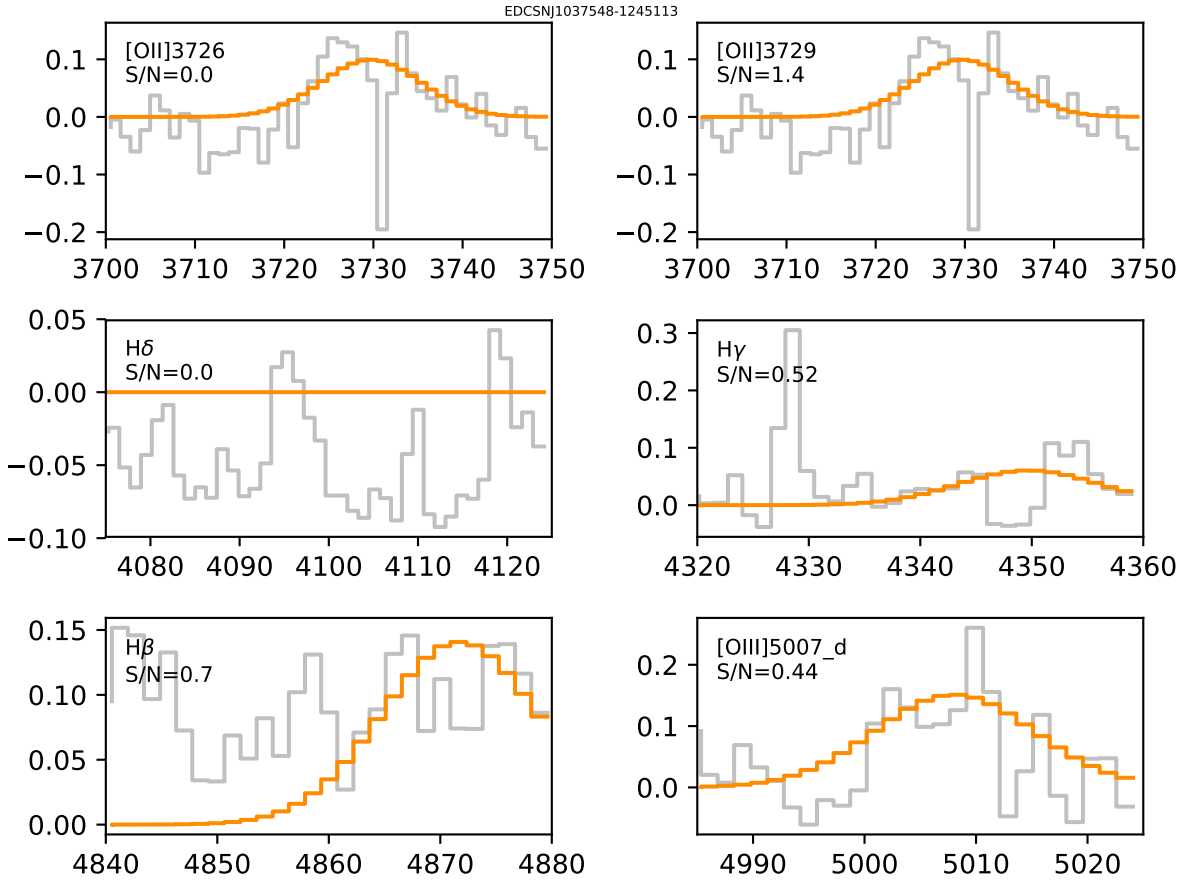
EDCSNJ1037548-1245113
[OII]3726
S/N=0.0
[OII]3729
S/N=1.4
Hδ
S/N=0.0
Hγ
S/N=0.52
Hβ
S/N=0.7
[OIII]5007_d
S/N=0.44

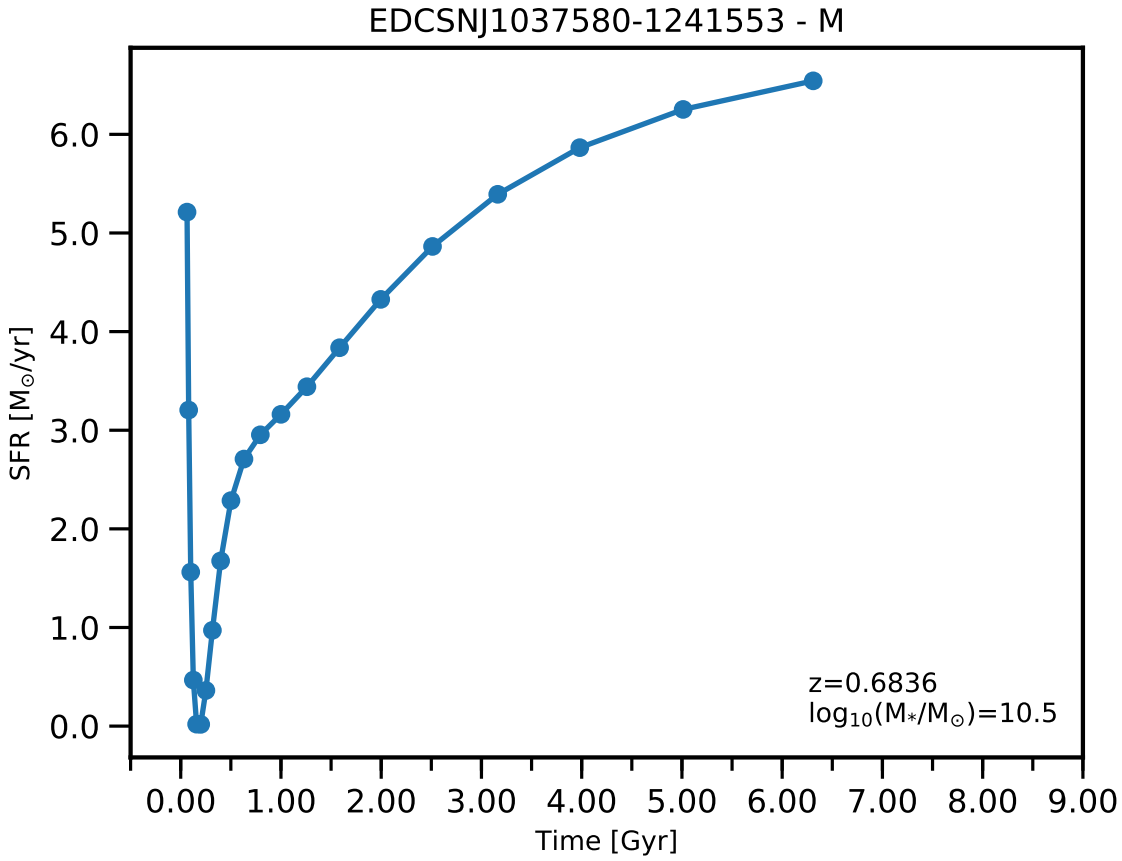
EDCSNJ1037580-1241553 - M
SFR [M⊙/yr]
Time [Gyr]
z=0.6836
log10(M*/M⊙)=10.5
0.0
1.0
2.0
3.0
4.0
5.0
6.0
0.00
1.00
2.00
3.00
4.00
5.00
6.00
7.00
8.00
9.00

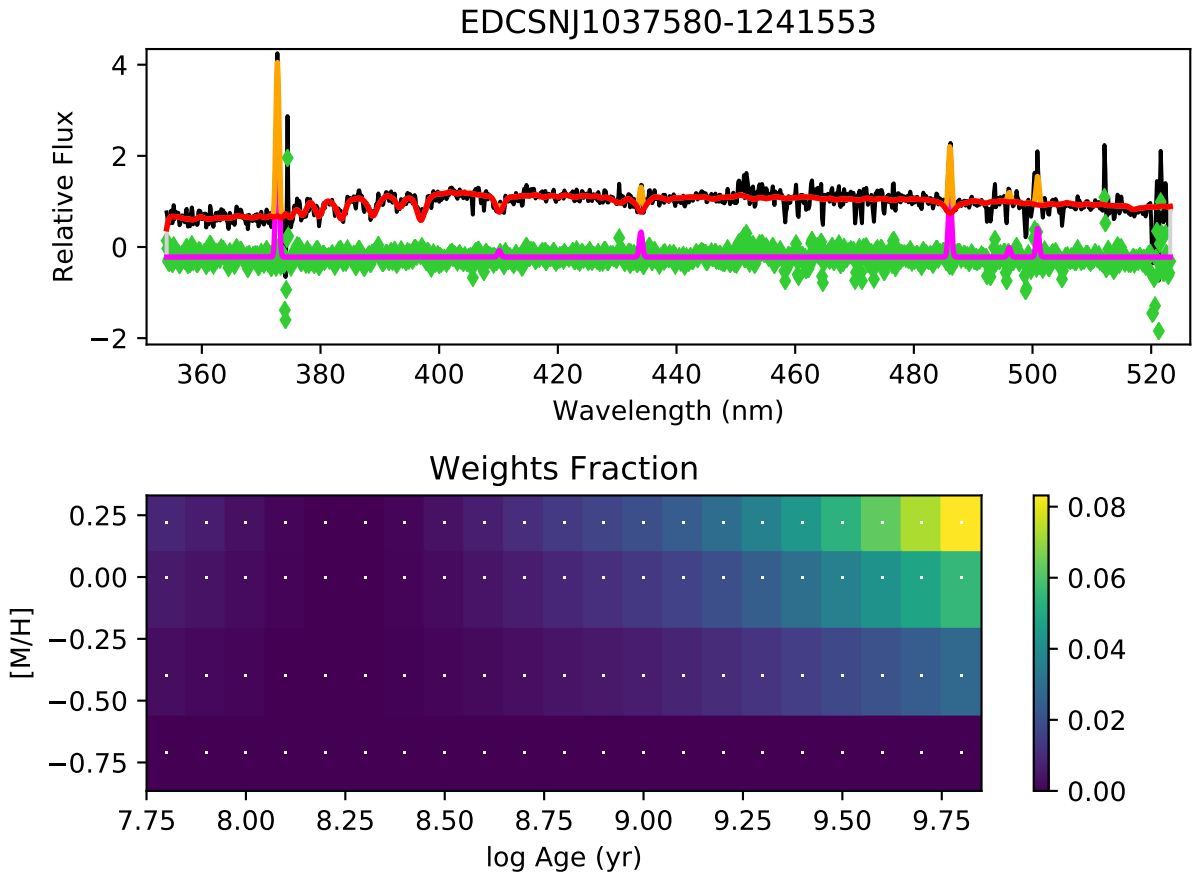
EDCSNJ1037580-1241553
Relative Flux
4
2
0
−2
360
380
400
420
440
460
480
500
520
Wavelength (nm)
Weights Fraction
[M/H]
0.25
0.00
−0.25
−0.50
−0.75
7.75
8.00
8.25
8.50
8.75
9.00
9.25
9.50
9.75
log Age (yr)
0.08
0.06
0.04
0.02
0.00

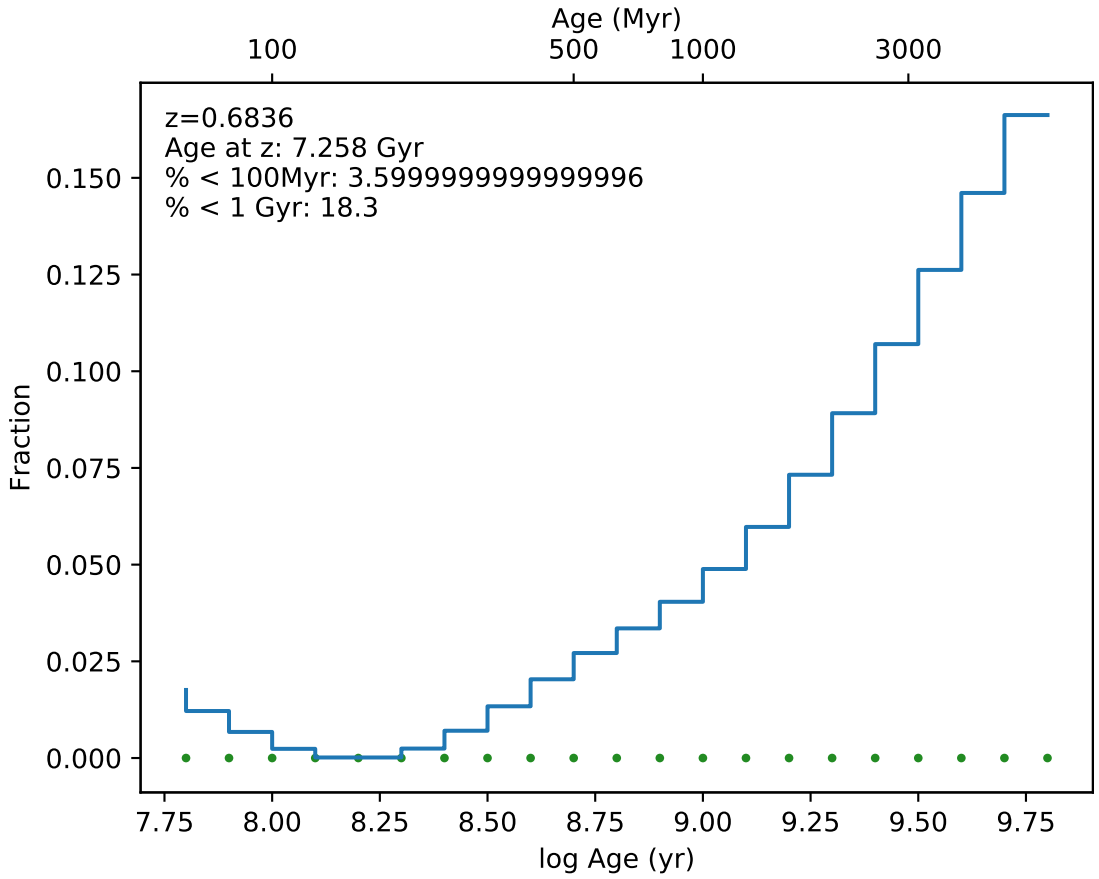
Age (Myr)
100
500
1000
3000
z=0.6836
Age at z: 7.258 Gyr
% < 100Myr: 3.5999999999999996
% < 1 Gyr: 18.3
Fraction
0.150
0.125
0.100
0.075
0.050
0.025
0.000
7.75
8.00
8.25
8.50
8.75
9.00
9.25
9.50
9.75
log Age (yr)

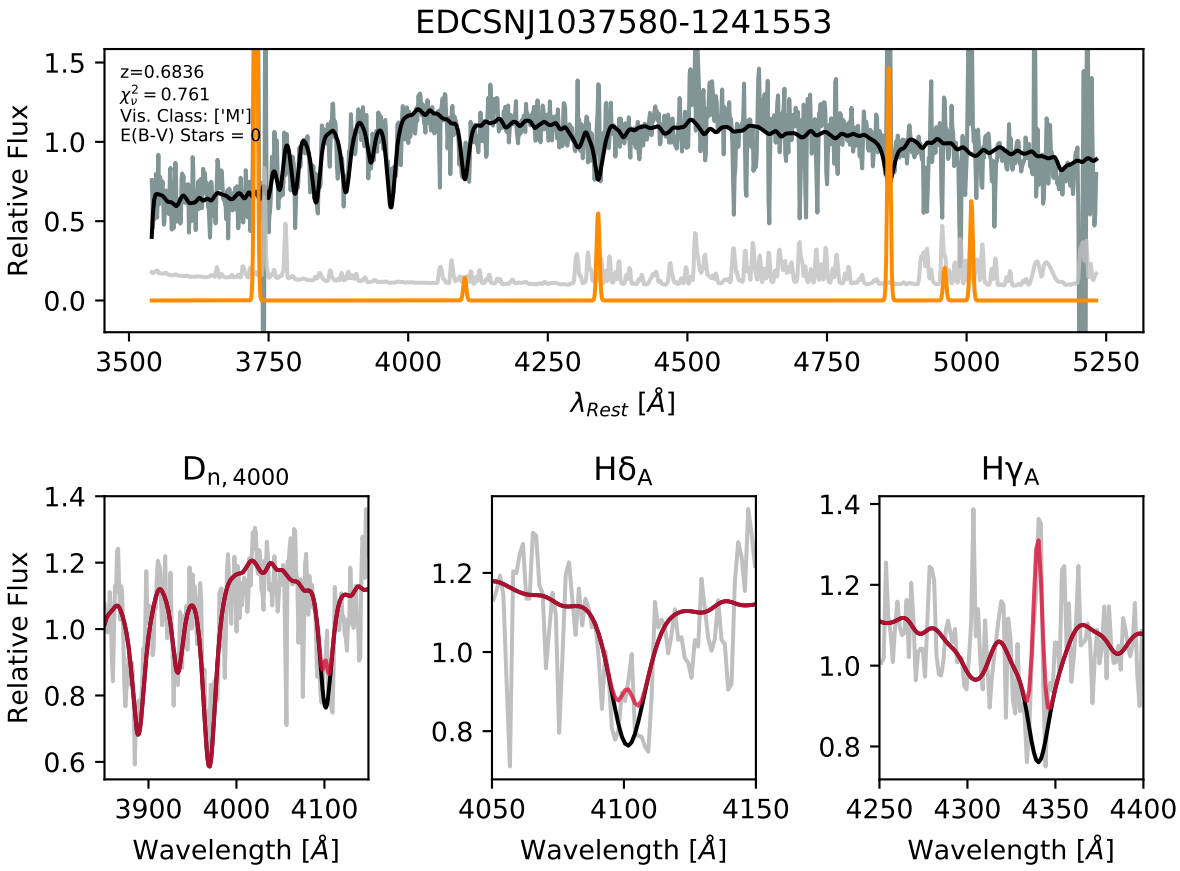
EDCSNJ1037580-1241553
z=0.6836
$\chi^2_\nu = 0.761$
Vis. Class: ['M']
E(B-V) Stars = 0
Relative Flux
λ_{Rest} [Å]
$D_{n,4000}$
$H\delta_A$
$H\gamma_A$
Wavelength [Å]

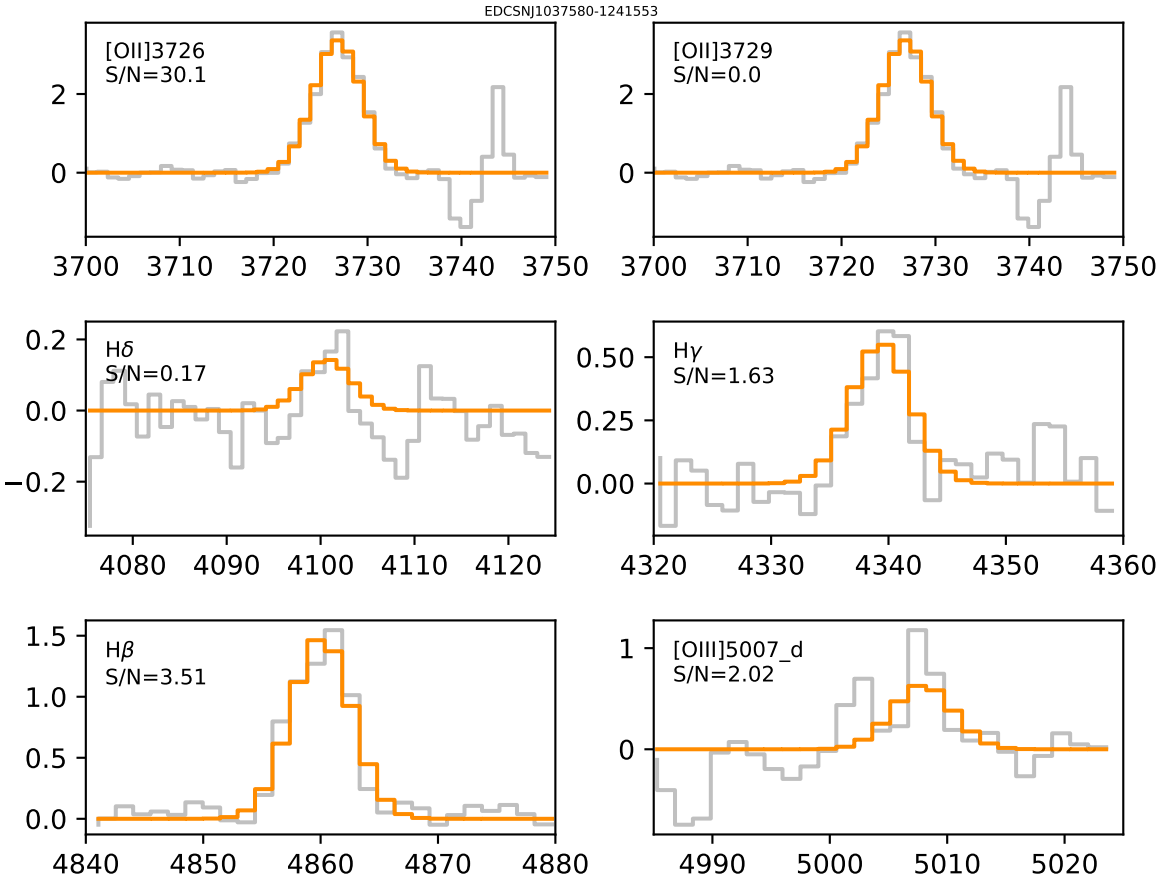
EDCSNJ1037580-1241553
[OII]3726
S/N=30.1
[OII]3729
S/N=0.0
Hδ
S/N=0.17
Hγ
S/N=1.63
Hβ
S/N=3.51
[OIII]5007_d
S/N=2.02

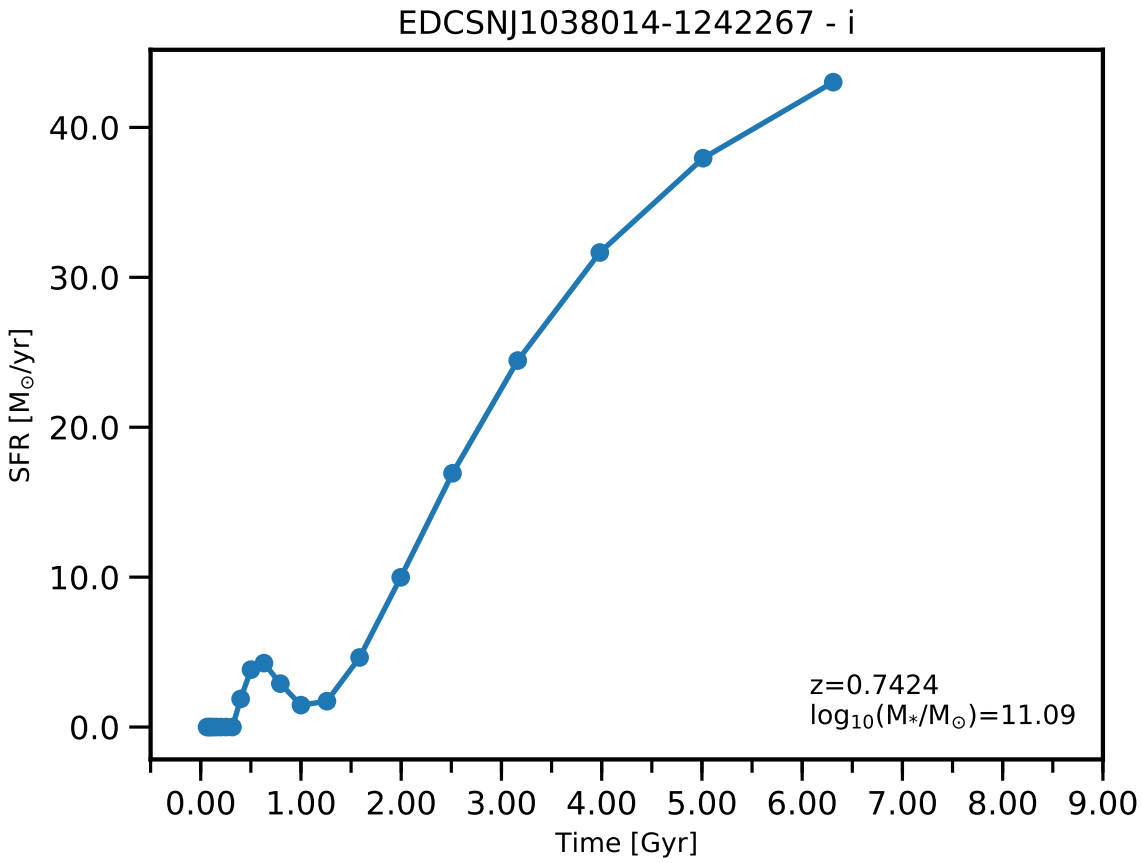
EDCSNJ1038014-1242267 - i
SFR [M⊙/yr]
40.0
30.0
20.0
10.0
0.0
0.00
1.00
2.00
3.00
4.00
5.00
6.00
7.00
8.00
9.00
Time [Gyr]
z=0.7424
log10(M*/M⊙)=11.09

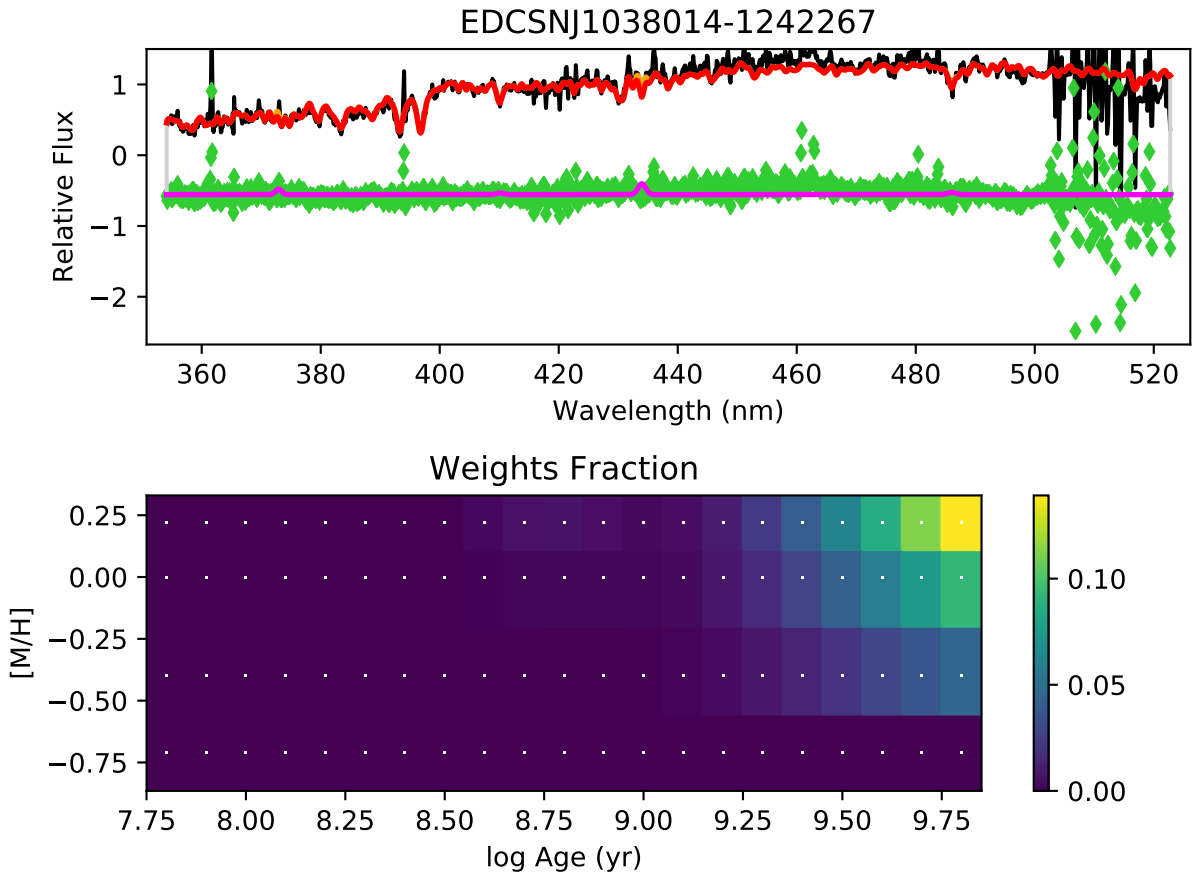
EDCSNJ1038014-1242267
Relative Flux
1
0
−1
−2
360
380
400
420
440
460
480
500
520
Wavelength (nm)
Weights Fraction
[M/H]
0.25
0.00
−0.25
−0.50
−0.75
7.75
8.00
8.25
8.50
8.75
9.00
9.25
9.50
9.75
log Age (yr)
0.10
0.05
0.00

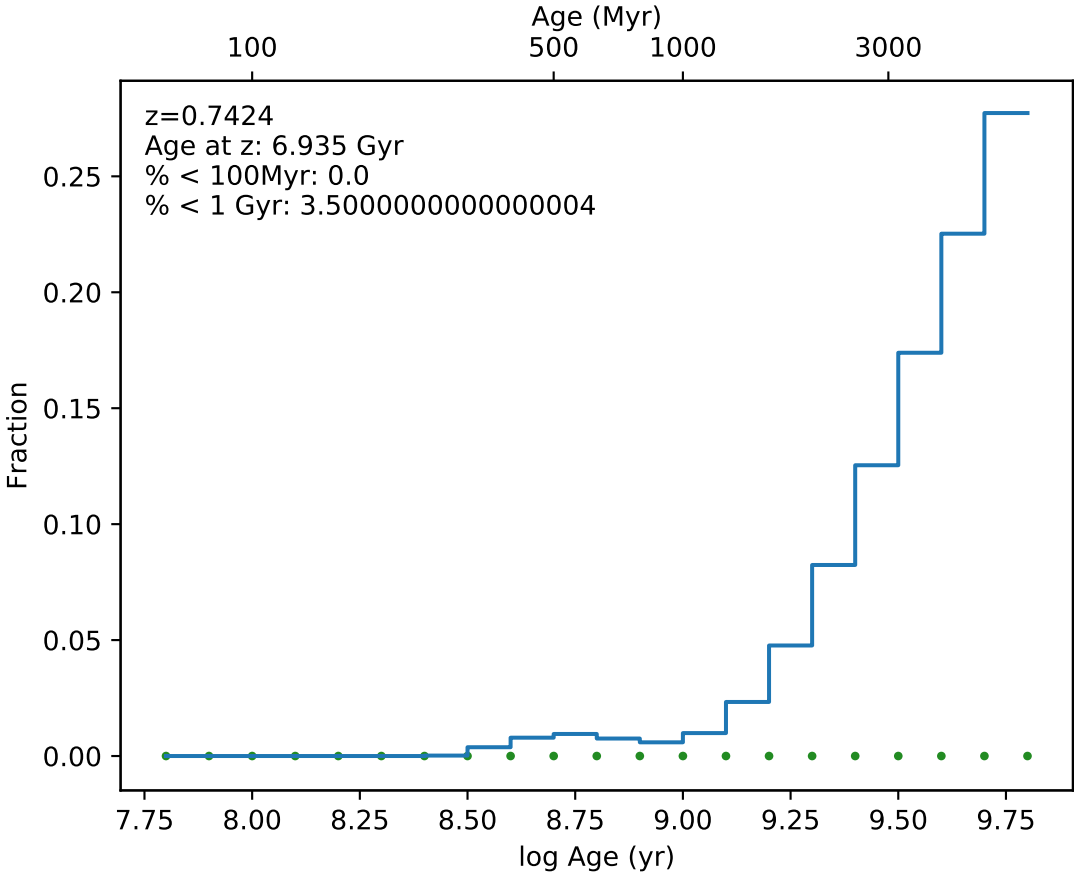
Age (Myr)
100
500
1000
3000
z=0.7424
Age at z: 6.935 Gyr
% < 100Myr: 0.0
% < 1 Gyr: 3.5000000000000004
Fraction
0.25
0.20
0.15
0.10
0.05
0.00
7.75
8.00
8.25
8.50
8.75
9.00
9.25
9.50
9.75
log Age (yr)

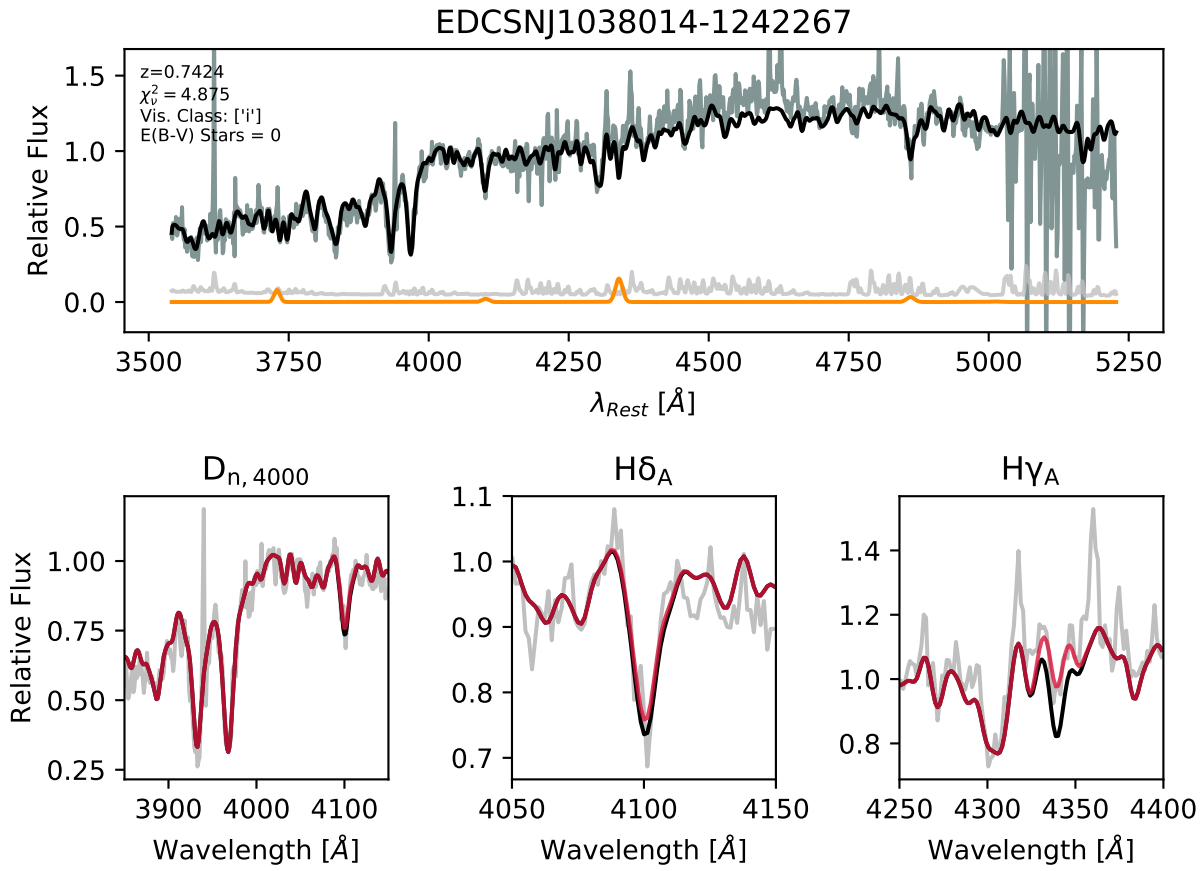
EDCSNJ1038014-1242267
z=0.7424
$\chi^2_\nu = 4.875$
Vis. Class: ['i']
E(B-V) Stars = 0
Relative Flux
λ_{Rest} [Å]
$D_{n,4000}$
$H\delta_A$
$H\gamma_A$
Wavelength [Å]

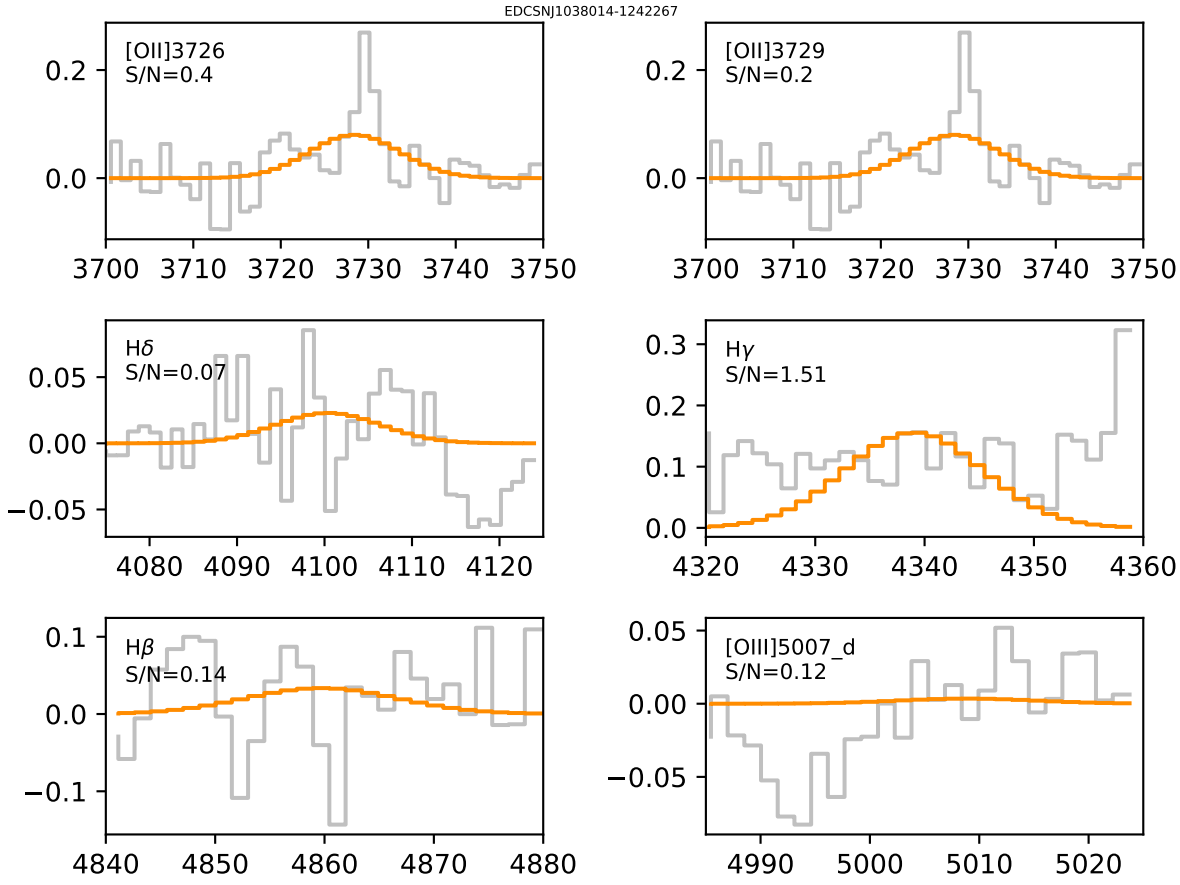
EDCSNJ1038014-1242267
[OII]3726
S/N=0.4
[OII]3729
S/N=0.2
Hδ
S/N=0.07
Hγ
S/N=1.51
Hβ
S/N=0.14
[OIII]5007_d
S/N=0.12

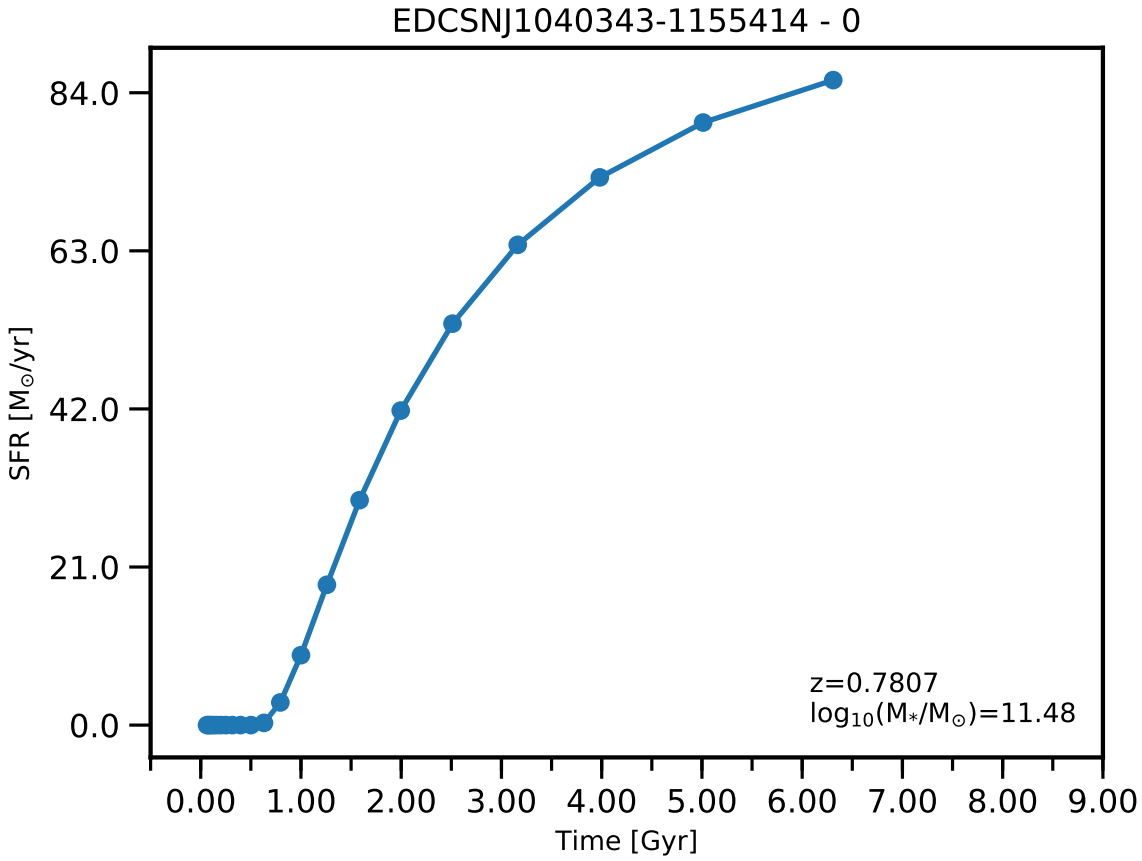
EDCSNJ1040343-1155414 - 0
84.0
63.0
42.0
21.0
0.0
SFR [M⊙/yr]
0.00
1.00
2.00
3.00
4.00
5.00
6.00
7.00
8.00
9.00
Time [Gyr]
z=0.7807
log10(M*/M⊙)=11.48

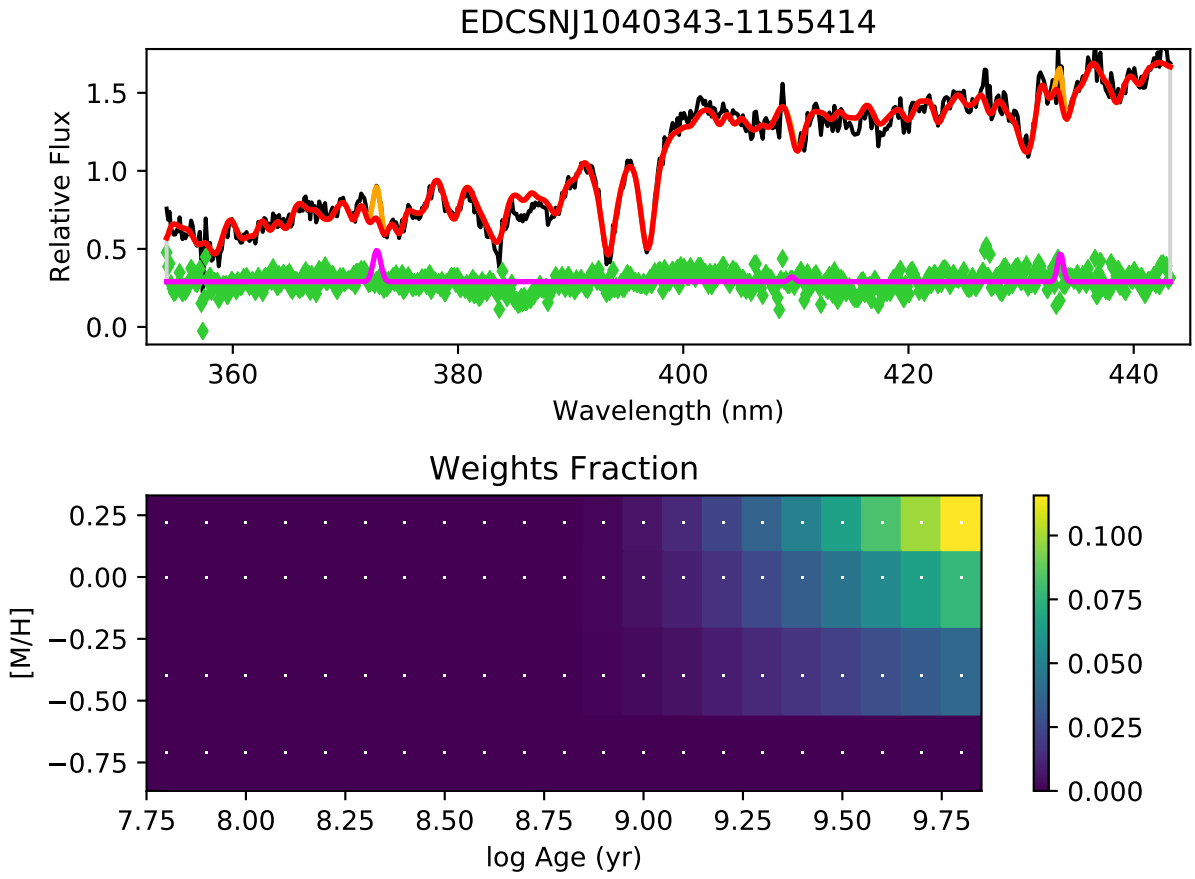
EDCSNJ1040343-1155414
Relative Flux
1.5
1.0
0.5
0.0
360
380
400
420
440
Wavelength (nm)
Weights Fraction
[M/H]
0.25
0.00
−0.25
−0.50
−0.75
7.75
8.00
8.25
8.50
8.75
9.00
9.25
9.50
9.75
log Age (yr)
0.100
0.075
0.050
0.025
0.000

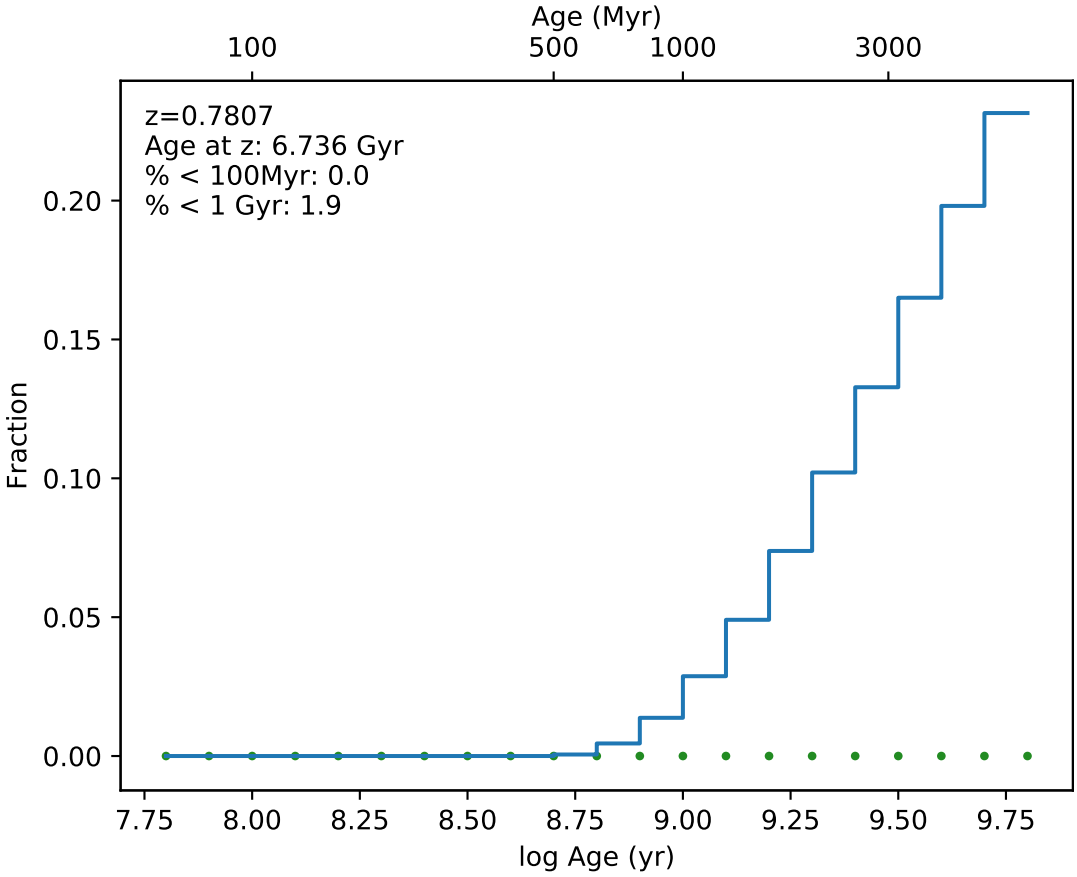
Age (Myr)
100
500
1000
3000
z=0.7807
Age at z: 6.736 Gyr
% < 100Myr: 0.0
% < 1 Gyr: 1.9
Fraction
0.00
0.05
0.10
0.15
0.20
7.75
8.00
8.25
8.50
8.75
9.00
9.25
9.50
9.75
log Age (yr)

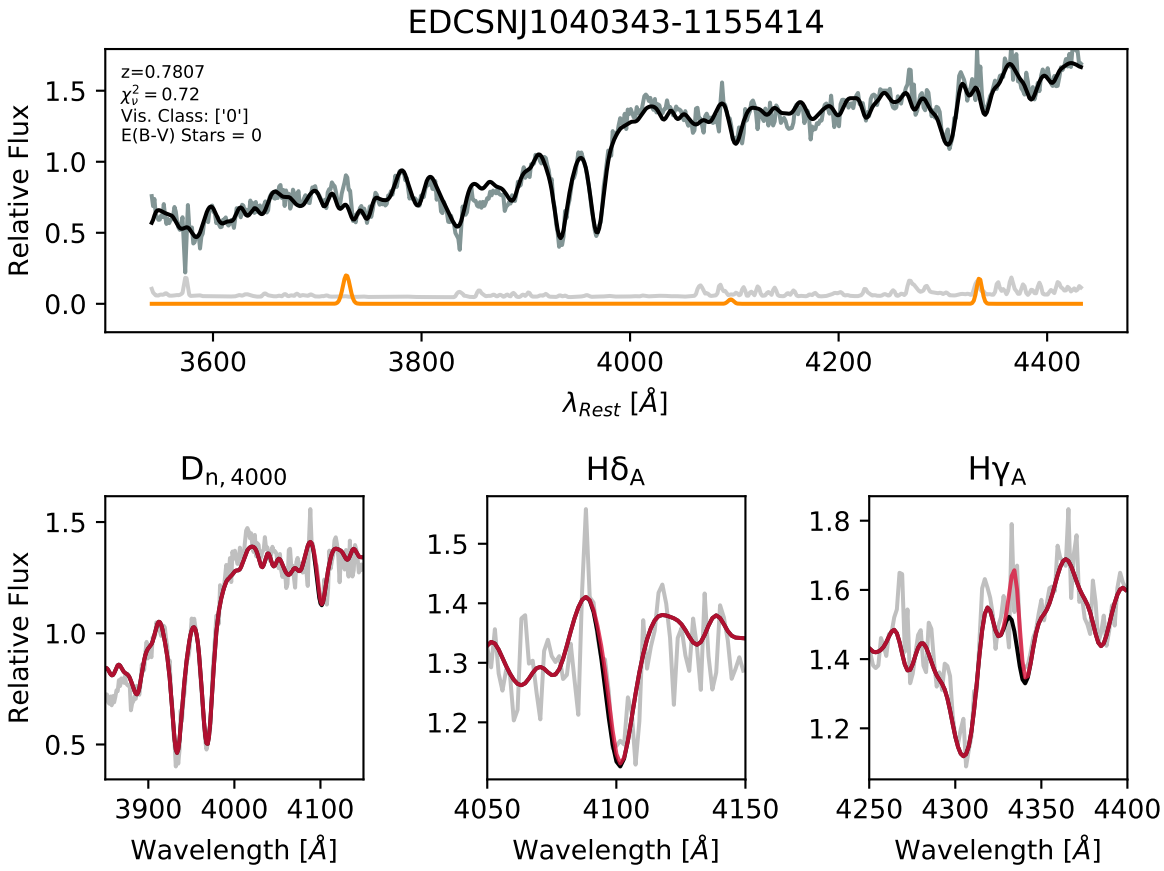
EDCSNJ1040343-1155414
z=0.7807
$\chi^2_\nu = 0.72$
Vis. Class: ['0']
E(B-V) Stars = 0
Relative Flux
λ_{Rest} [Å]
$D_{n,4000}$
$H\delta_A$
$H\gamma_A$
Wavelength [Å]

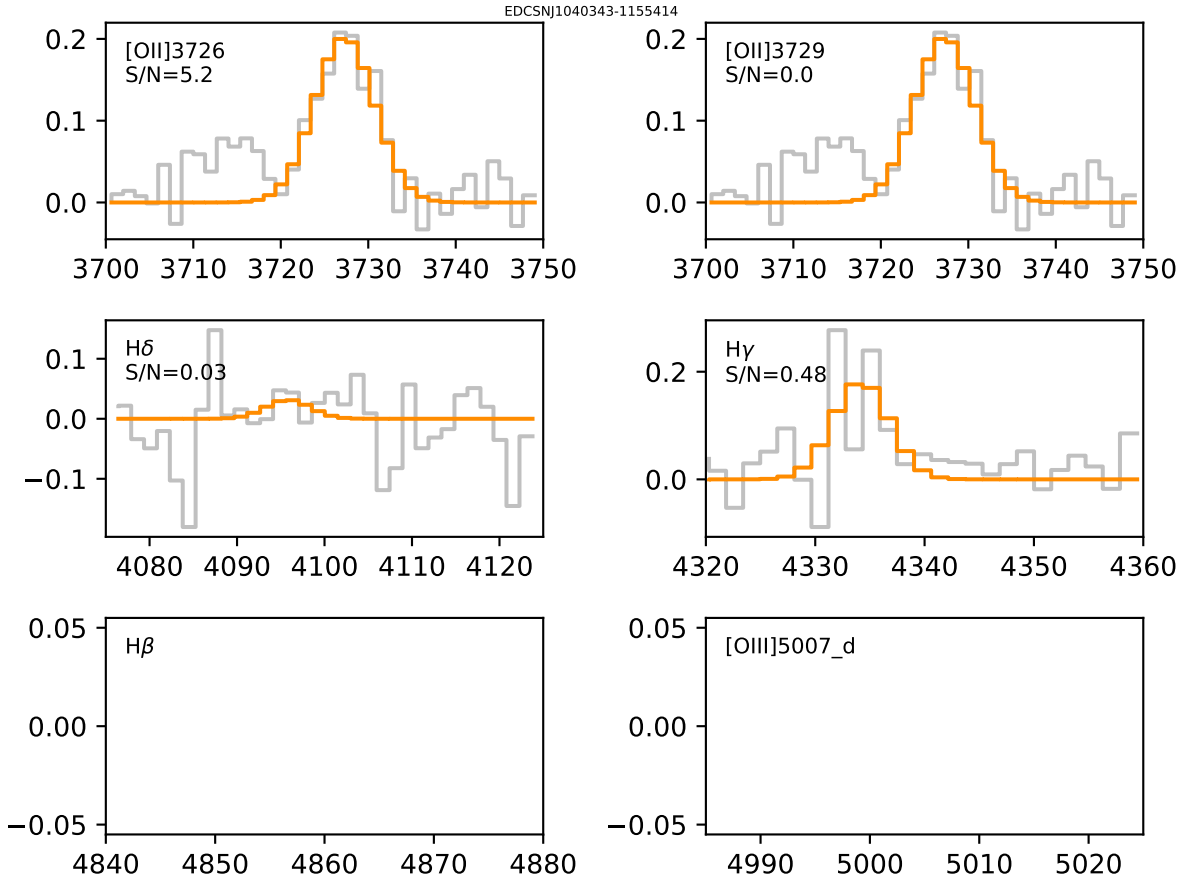
EDCSNJ1040343-1155414
[OII]3726
S/N=5.2
[OII]3729
S/N=0.0
Hδ
S/N=0.03
Hγ
S/N=0.48
Hβ
[OIII]5007_d

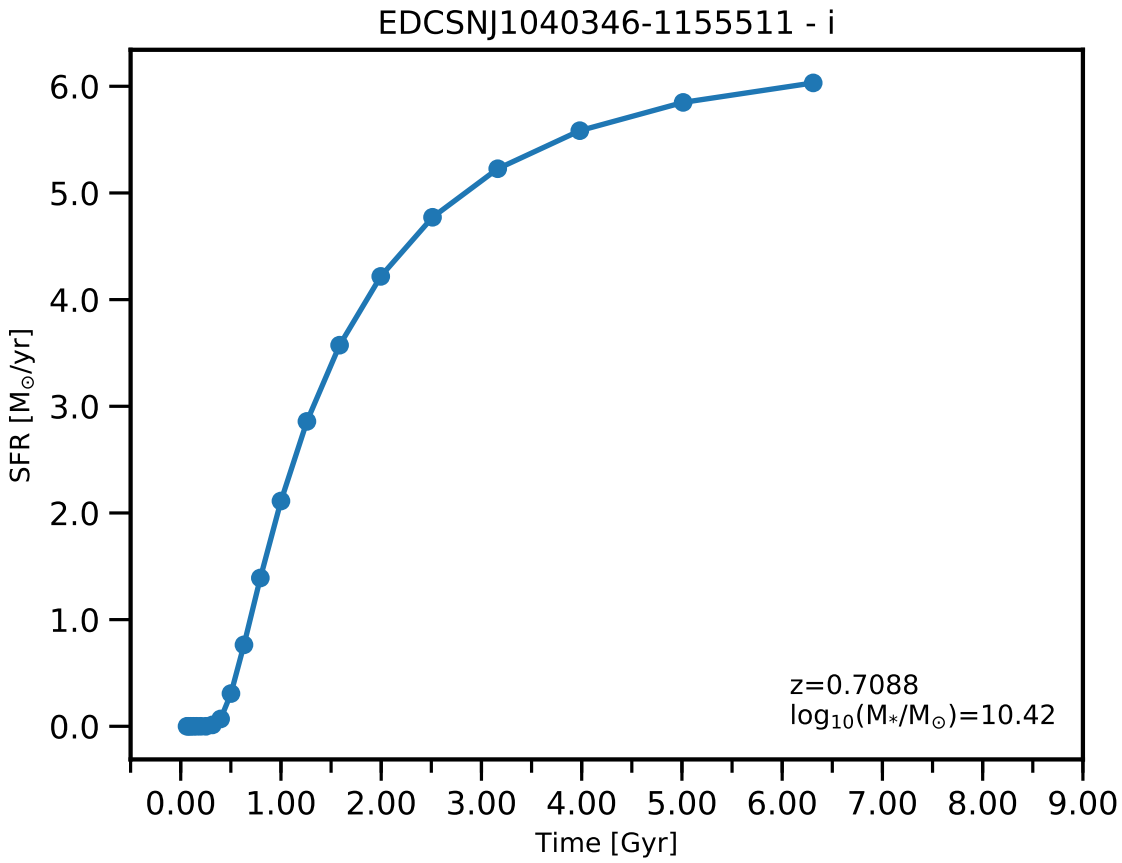
EDCSNJ1040346-1155511 - i
SFR [M⊙/yr]
Time [Gyr]
z=0.7088
log10(M*/M⊙)=10.42
0.0
1.0
2.0
3.0
4.0
5.0
6.0
0.00
1.00
2.00
3.00
4.00
5.00
6.00
7.00
8.00
9.00

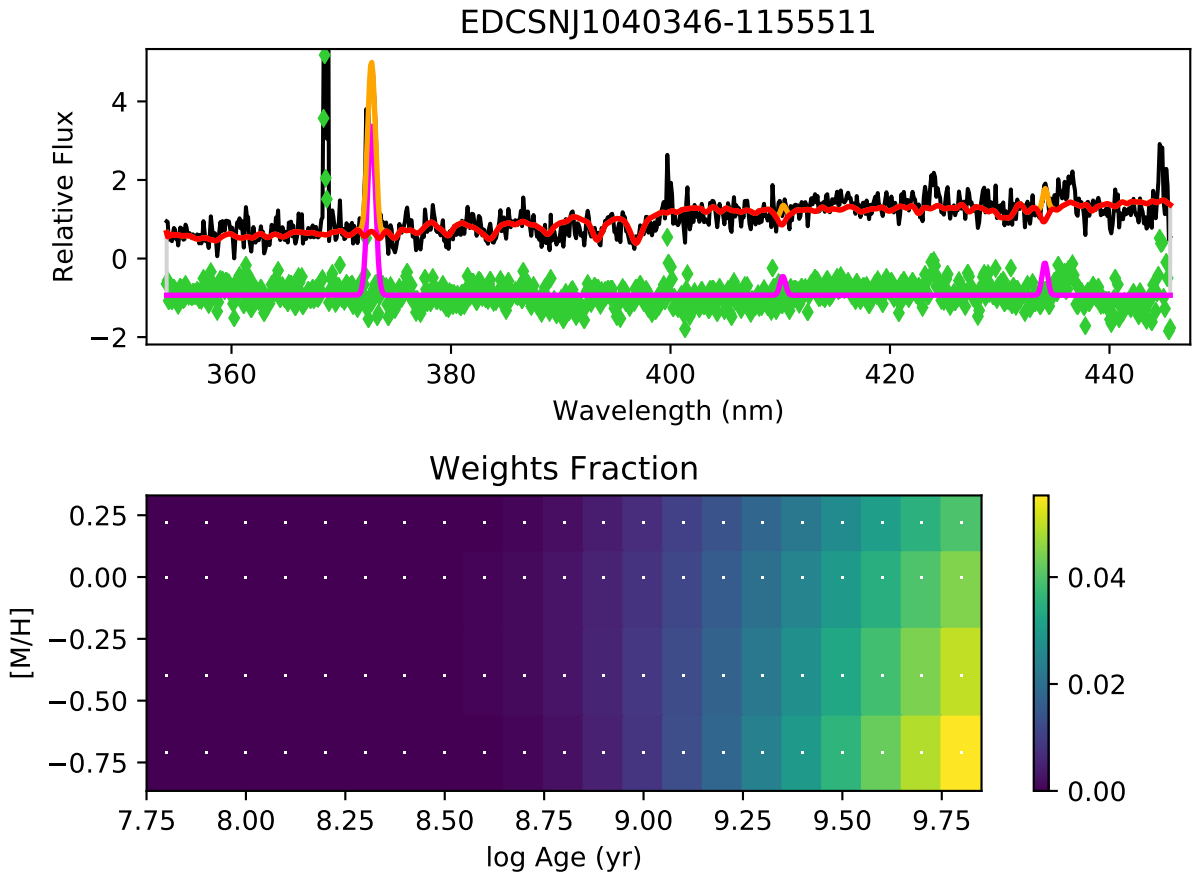
EDCSNJ1040346-1155511
Relative Flux
4
2
0
−2
360
380
400
420
440
Wavelength (nm)
Weights Fraction
[M/H]
0.25
0.00
−0.25
−0.50
−0.75
7.75
8.00
8.25
8.50
8.75
9.00
9.25
9.50
9.75
log Age (yr)
0.04
0.02
0.00

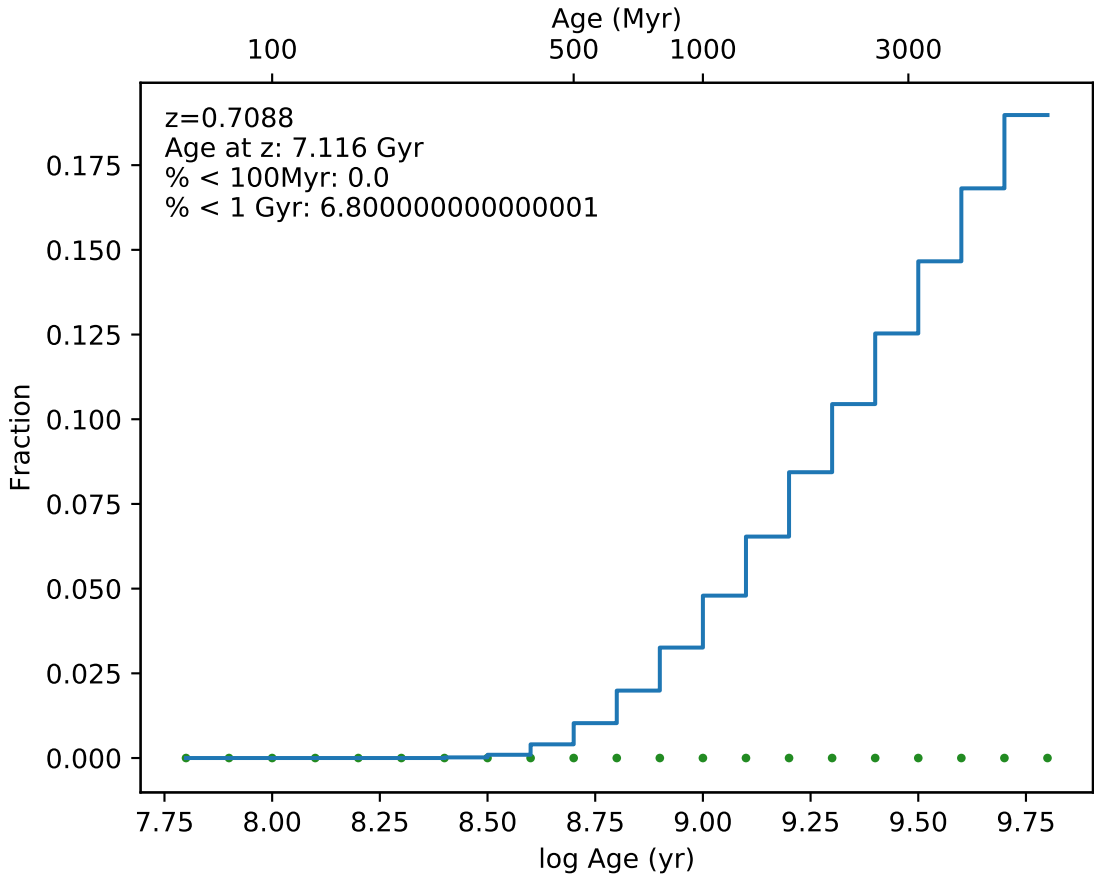
Age (Myr)
100
500
1000
3000
z=0.7088
Age at z: 7.116 Gyr
% < 100Myr: 0.0
% < 1 Gyr: 6.800000000000001
Fraction
0.175
0.150
0.125
0.100
0.075
0.050
0.025
0.000
7.75
8.00
8.25
8.50
8.75
9.00
9.25
9.50
9.75
log Age (yr)

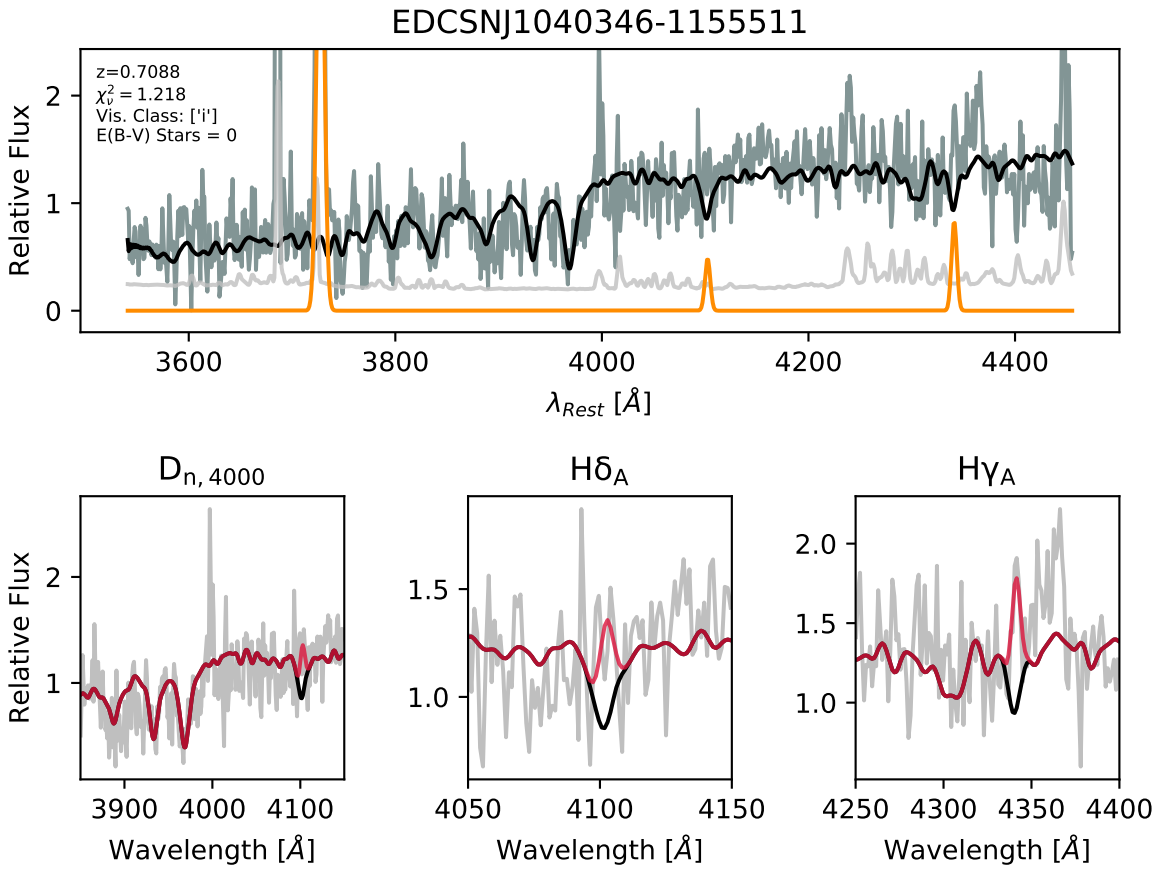
EDCSNJ1040346-1155511
z=0.7088
$\chi^2_\nu = 1.218$
Vis. Class: ['i']
E(B-V) Stars = 0
Relative Flux
λ_{Rest} [Å]
$D_{n,4000}$
$H\delta_A$
$H\gamma_A$
Wavelength [Å]

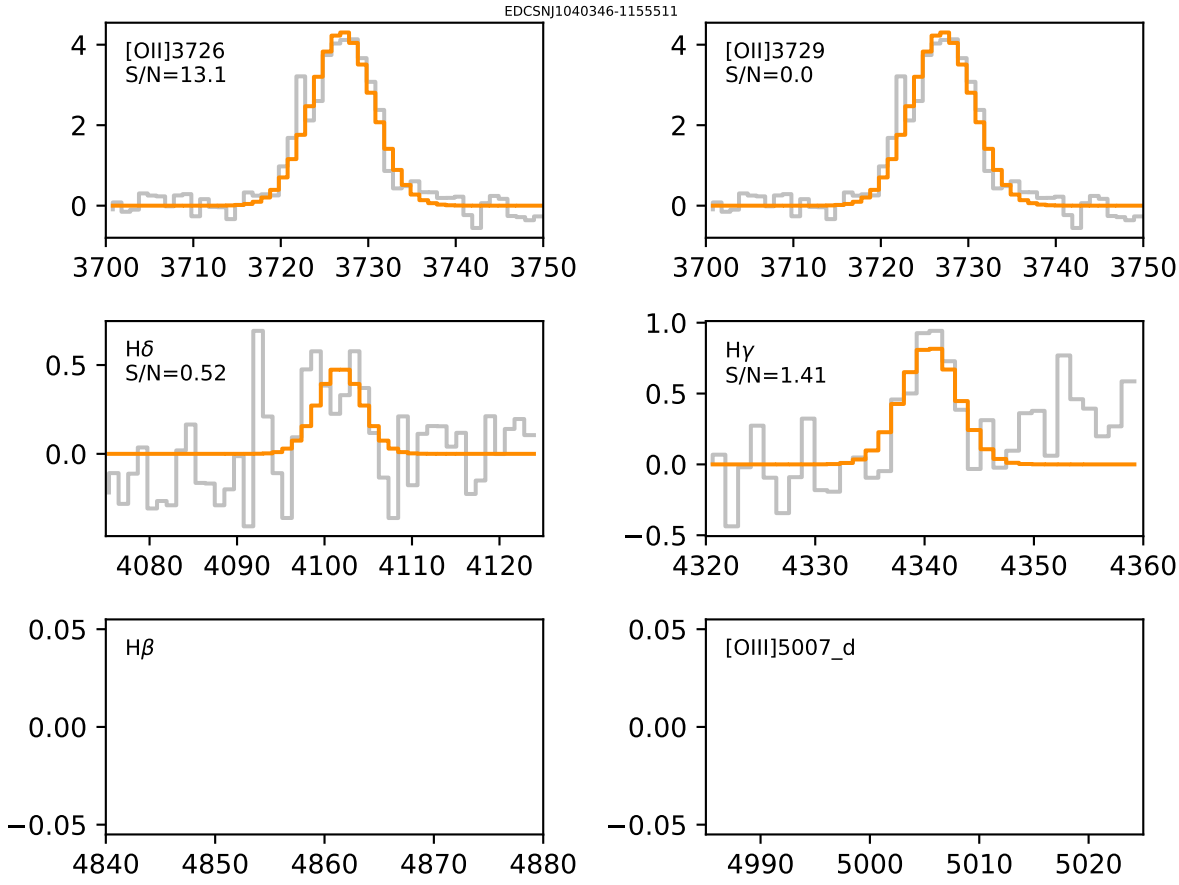
EDCSNJ1040346-1155511
[OII]3726
S/N=13.1
[OII]3729
S/N=0.0
Hδ
S/N=0.52
Hγ
S/N=1.41
Hβ
[OIII]5007_d

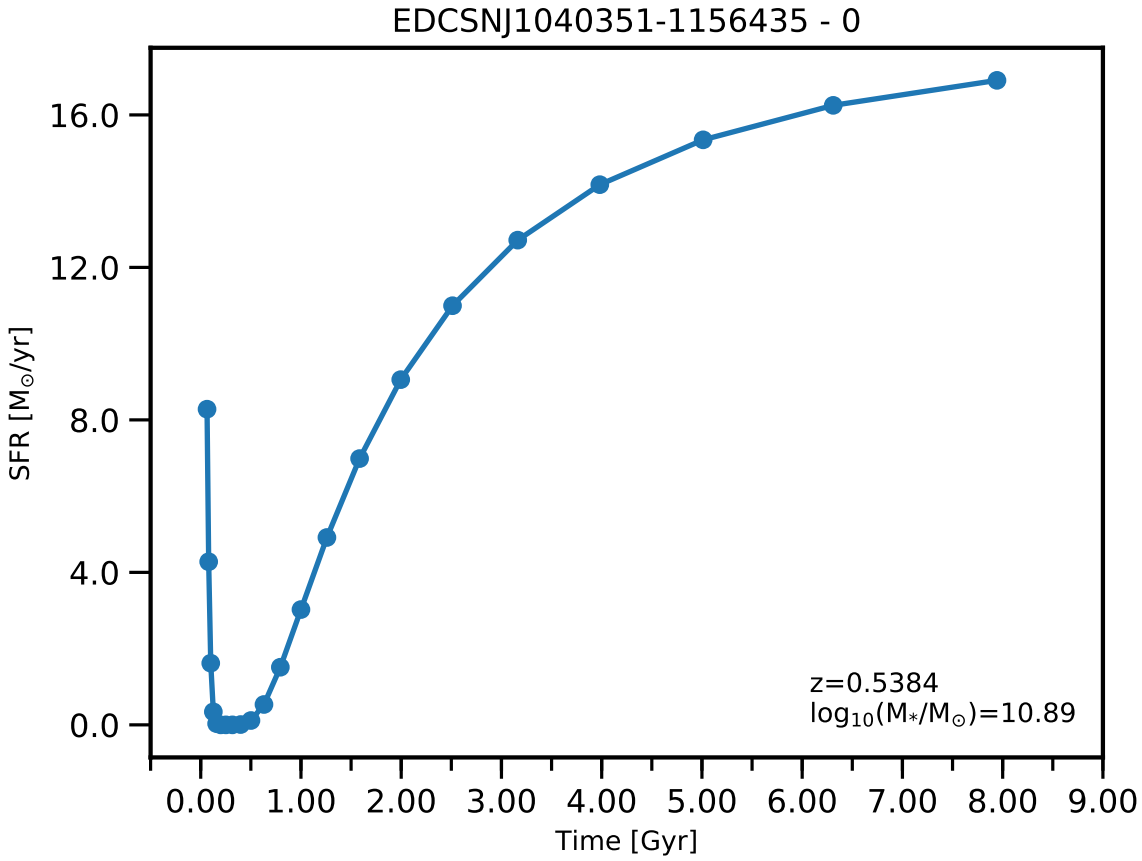
EDCSNJ1040351-1156435 - 0
SFR [M⊙/yr]
16.0
12.0
8.0
4.0
0.0
0.00
1.00
2.00
3.00
4.00
5.00
6.00
7.00
8.00
9.00
Time [Gyr]
z=0.5384
log10(M*/M⊙)=10.89

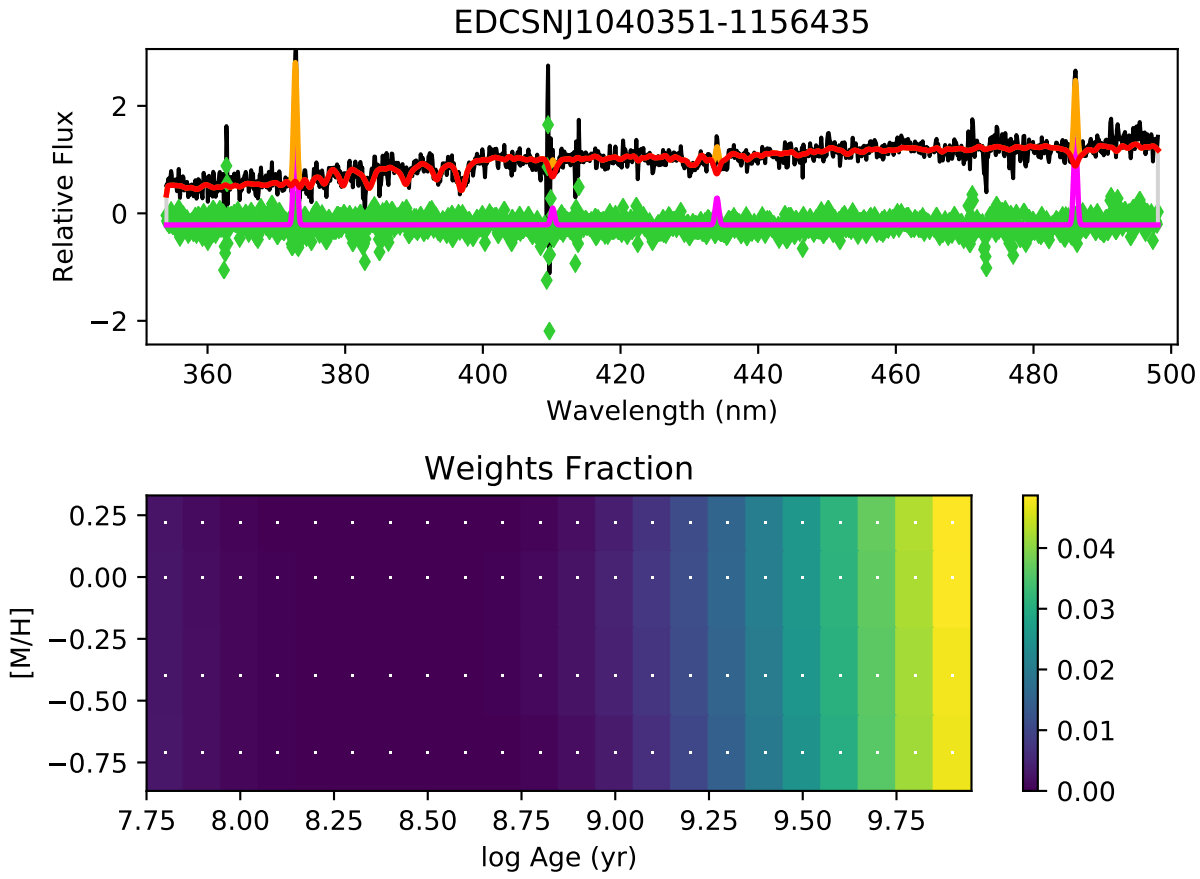
EDCSNJ1040351-1156435
Relative Flux
2
0
−2
360
380
400
420
440
460
480
500
Wavelength (nm)
Weights Fraction
[M/H]
0.25
0.00
−0.25
−0.50
−0.75
7.75
8.00
8.25
8.50
8.75
9.00
9.25
9.50
9.75
log Age (yr)
0.04
0.03
0.02
0.01
0.00

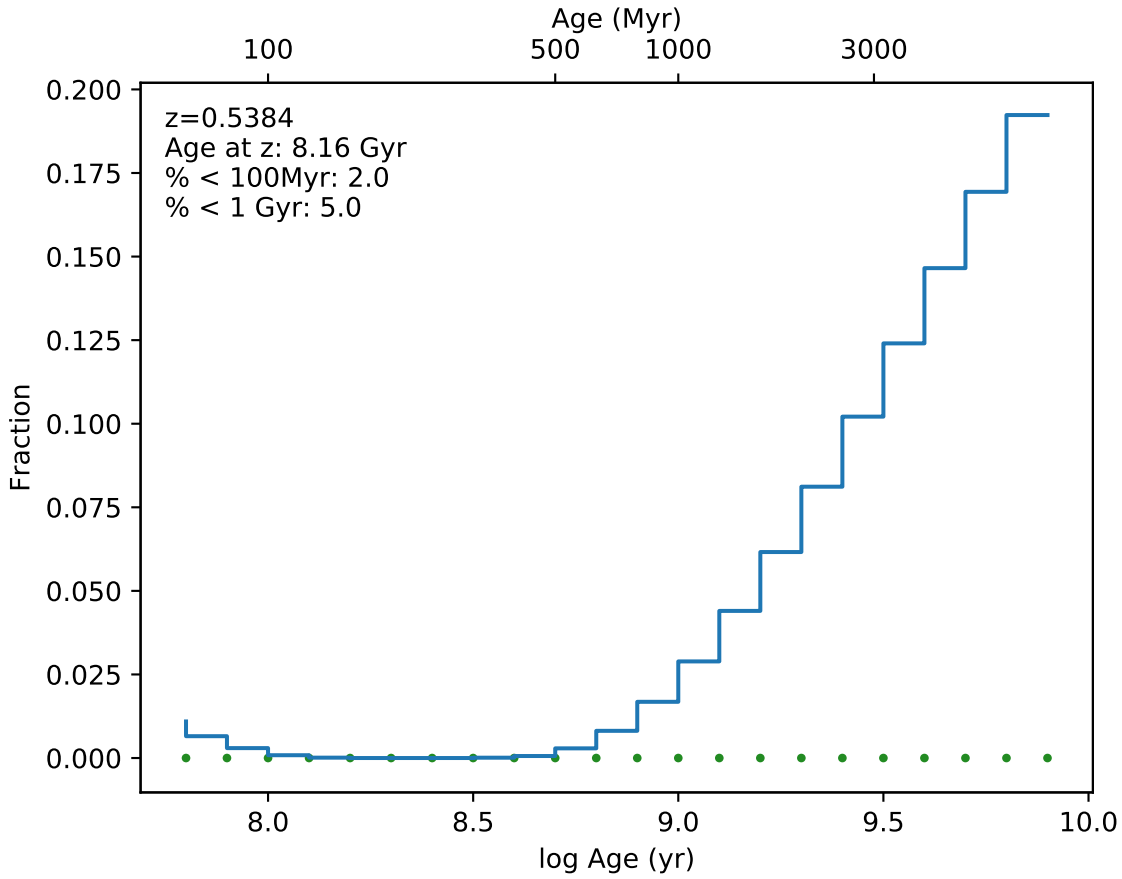
Age (Myr)
100
500
1000
3000
z=0.5384
Age at z: 8.16 Gyr
% < 100Myr: 2.0
% < 1 Gyr: 5.0
Fraction
0.200
0.175
0.150
0.125
0.100
0.075
0.050
0.025
0.000
8.0
8.5
9.0
9.5
10.0
log Age (yr)

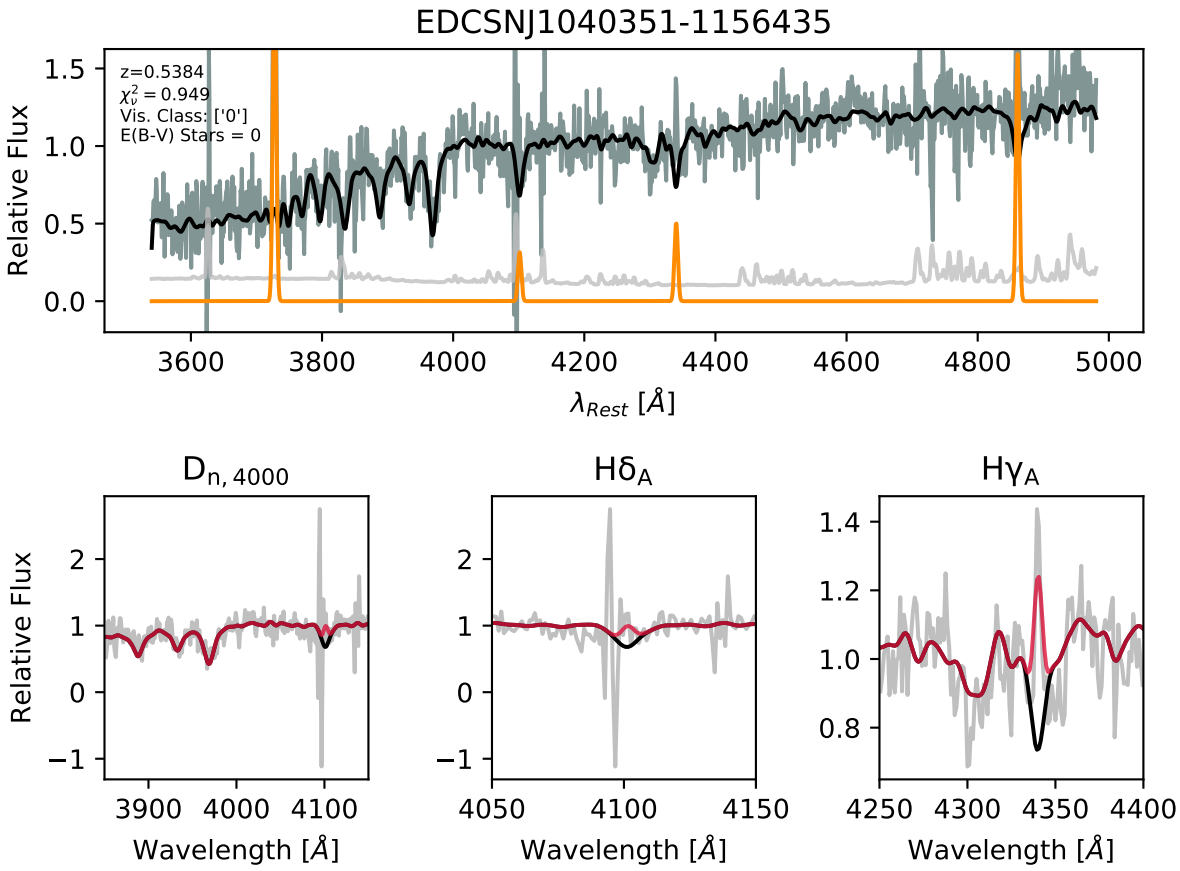
EDCSNJ1040351-1156435
z=0.5384
$\chi^2_\nu = 0.949$
Vis. Class: ['0']
E(B-V) Stars = 0
Relative Flux
λ_{Rest} [Å]
$D_{n,4000}$
$H\delta_A$
$H\gamma_A$
Wavelength [Å]

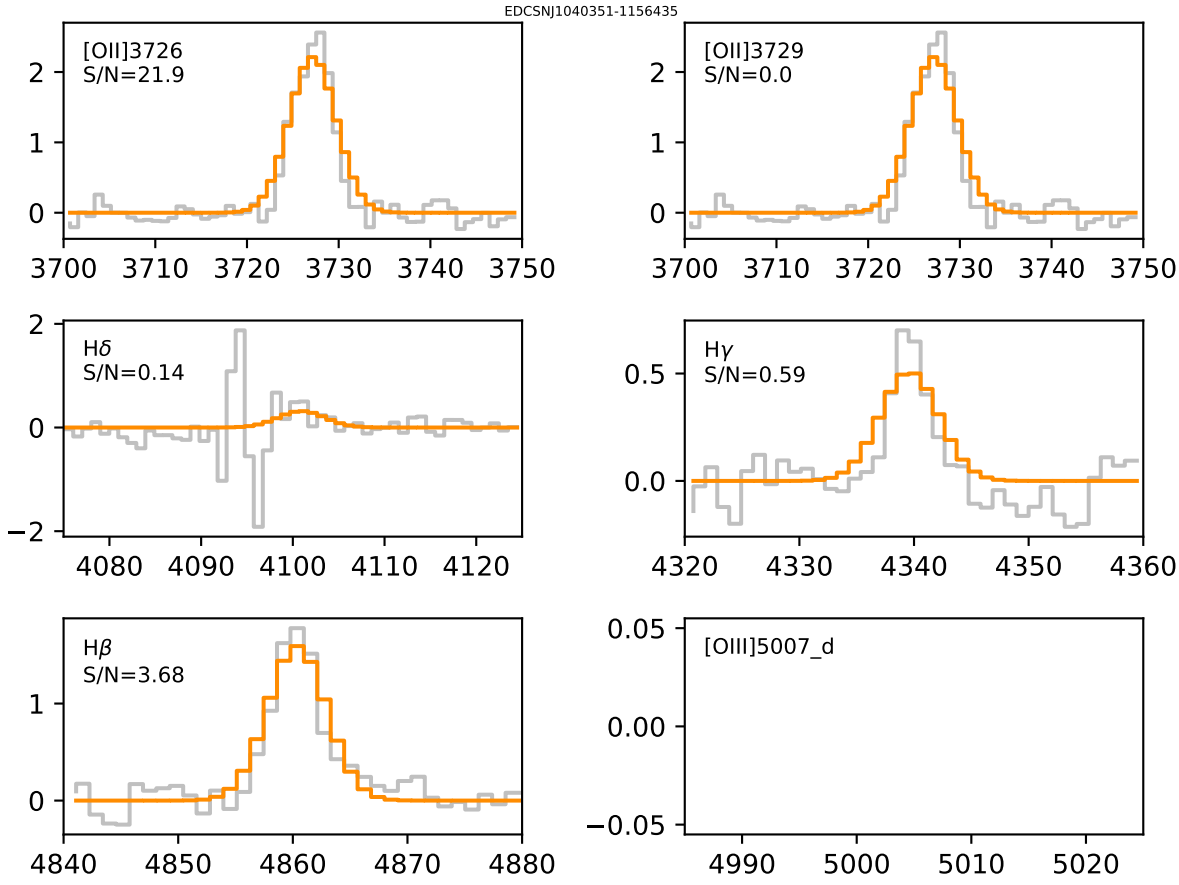
EDCSNJ1040351-1156435
[OII]3726
S/N=21.9
[OII]3729
S/N=0.0
Hδ
S/N=0.14
Hγ
S/N=0.59
Hβ
S/N=3.68
[OIII]5007_d

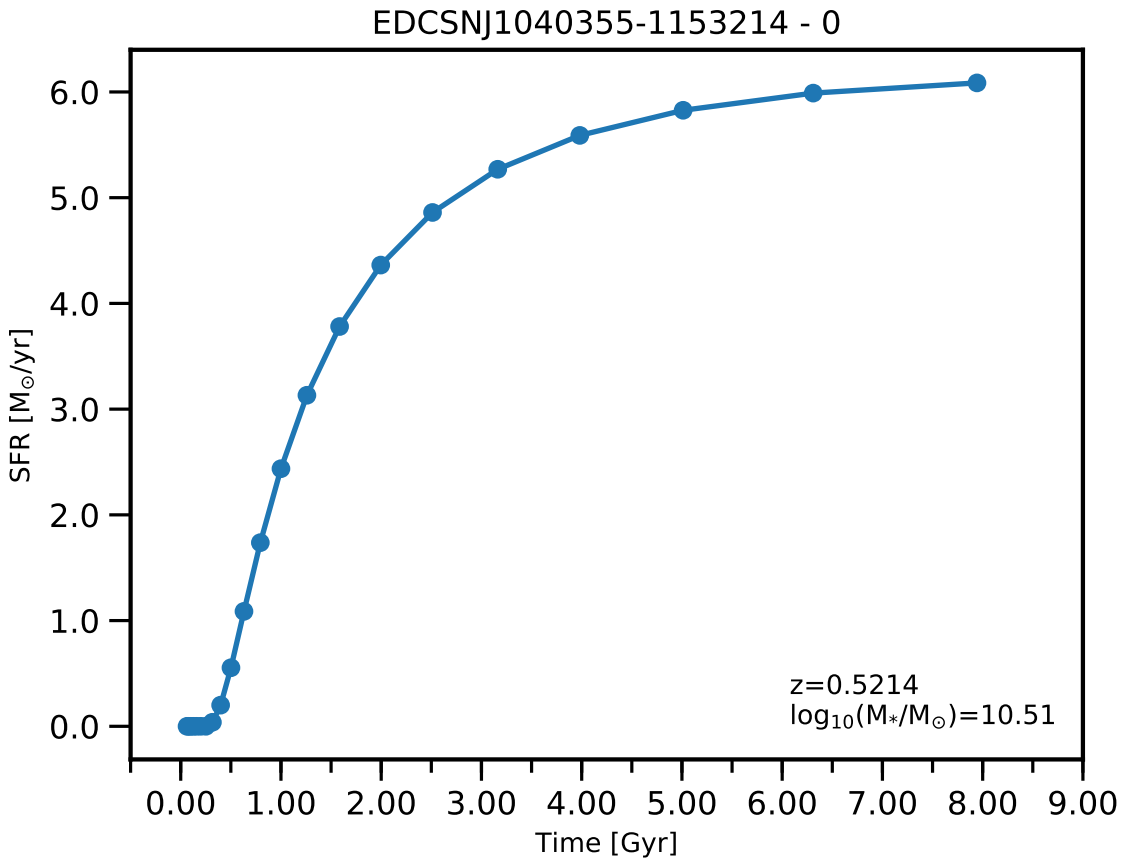
EDCSNJ1040355-1153214 - 0
SFR [M⊙/yr]
Time [Gyr]
z=0.5214
log10(M*/M⊙)=10.51
0.0
1.0
2.0
3.0
4.0
5.0
6.0
0.00
1.00
2.00
3.00
4.00
5.00
6.00
7.00
8.00
9.00

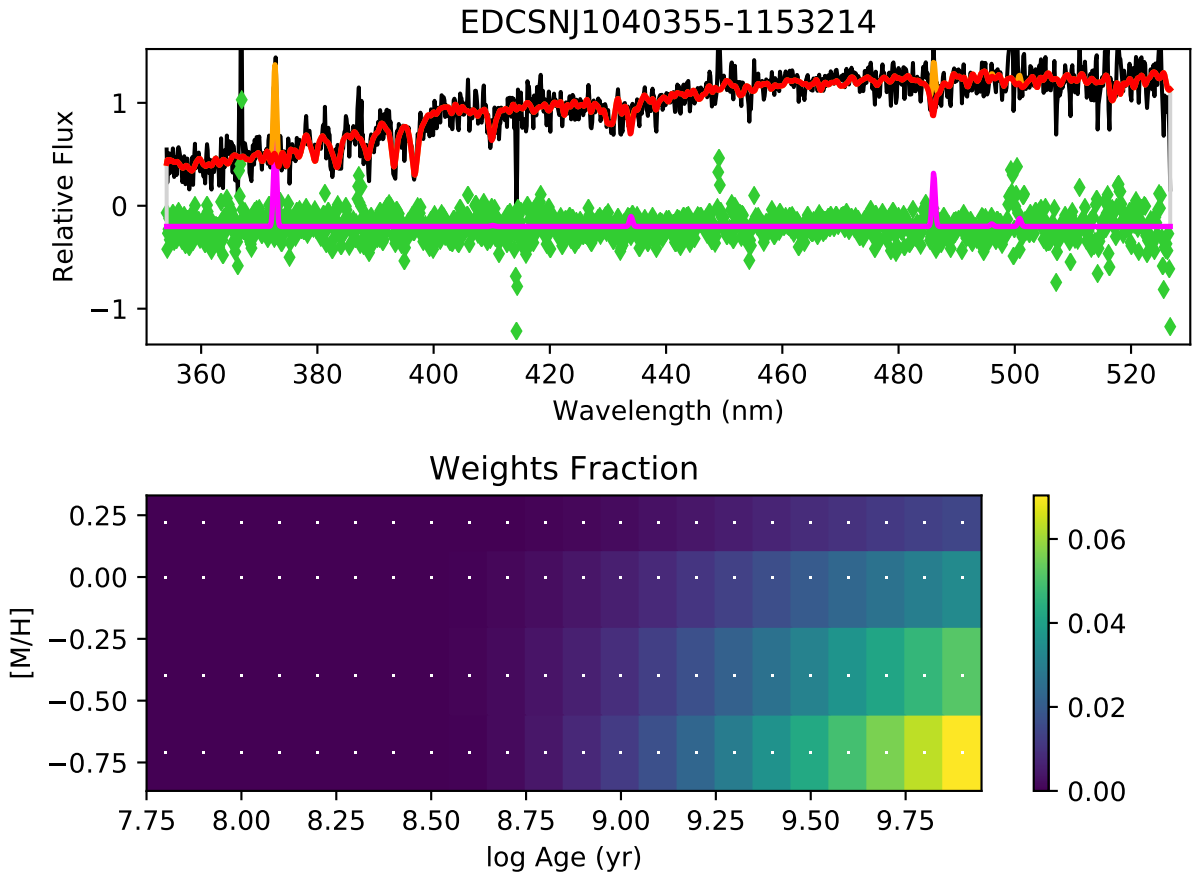
EDCSNJ1040355-1153214
Relative Flux
1
0
−1
360
380
400
420
440
460
480
500
520
Wavelength (nm)
Weights Fraction
[M/H]
0.25
0.00
−0.25
−0.50
−0.75
7.75
8.00
8.25
8.50
8.75
9.00
9.25
9.50
9.75
log Age (yr)
0.06
0.04
0.02
0.00

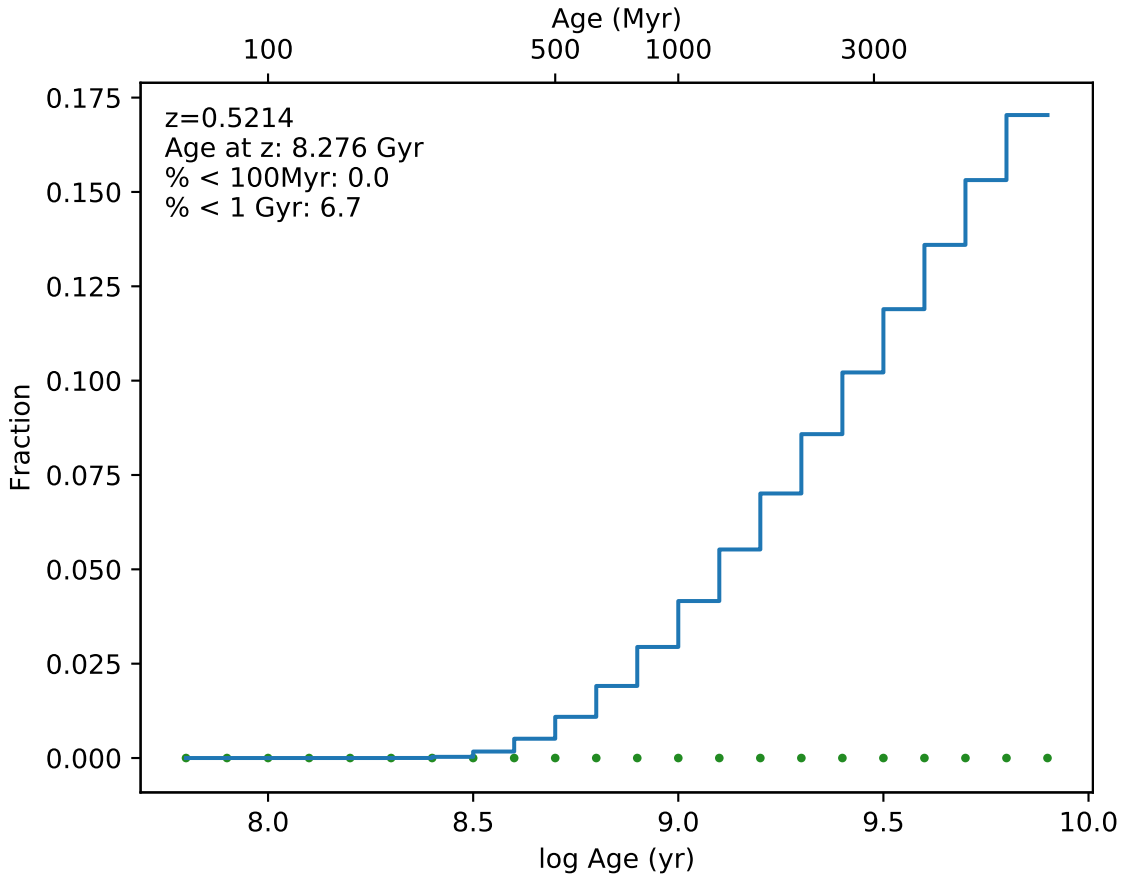
Age (Myr)
100
500
1000
3000
z=0.5214
Age at z: 8.276 Gyr
% < 100Myr: 0.0
% < 1 Gyr: 6.7
Fraction
0.175
0.150
0.125
0.100
0.075
0.050
0.025
0.000
8.0
8.5
9.0
9.5
10.0
log Age (yr)

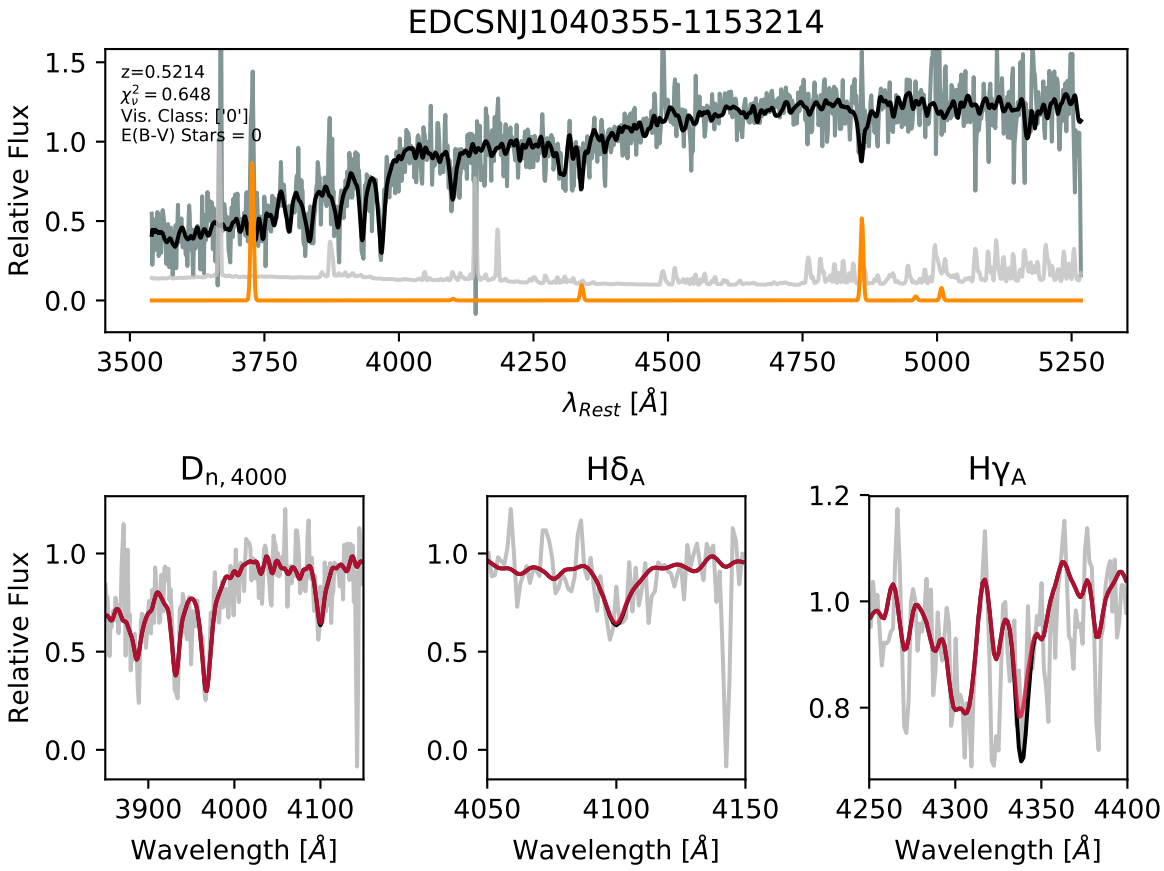
EDCSNJ1040355-1153214
z=0.5214
$\chi^2_\nu = 0.648$
Vis. Class: ['0']
E(B-V) Stars = 0
Relative Flux
λ_{Rest} [Å]
$D_{n,4000}$
$H\delta_A$
$H\gamma_A$
Wavelength [Å]

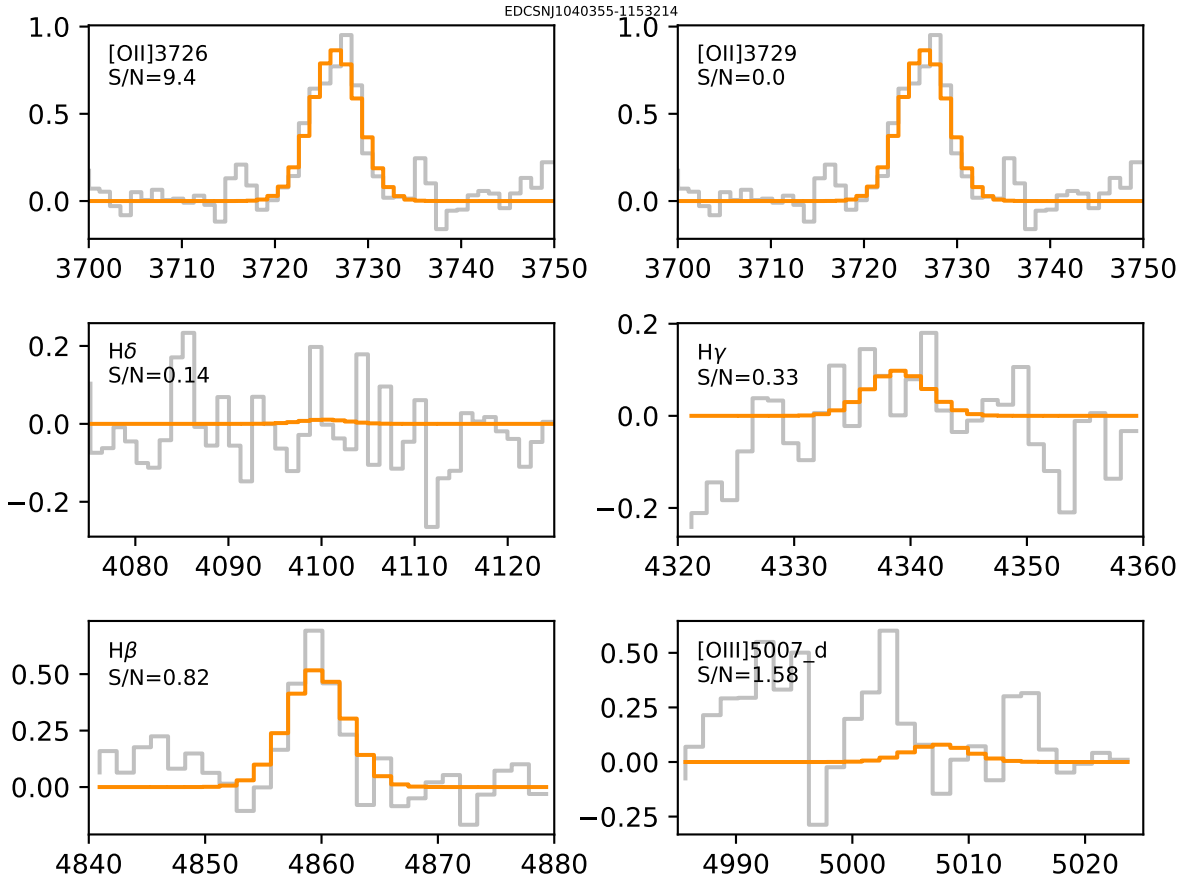
EDCSNJ1040355-1153214
[OII]3726
S/N=9.4
[OII]3729
S/N=0.0
Hδ
S/N=0.14
Hγ
S/N=0.33
Hβ
S/N=0.82
[OIII]5007_d
S/N=1.58

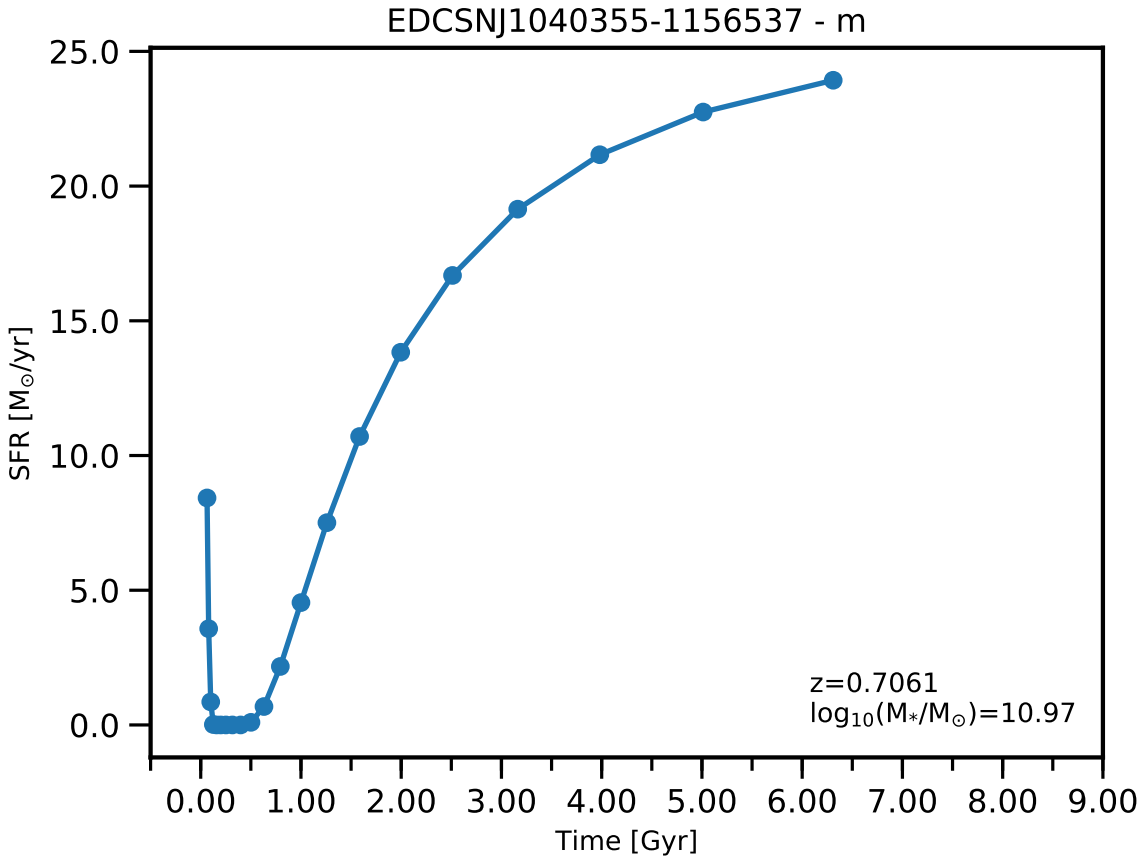
EDCSNJ1040355-1156537 - m
SFR [M⊙/yr]
Time [Gyr]
z=0.7061
log10(M*/M⊙)=10.97
0.0
5.0
10.0
15.0
20.0
25.0
0.00
1.00
2.00
3.00
4.00
5.00
6.00
7.00
8.00
9.00

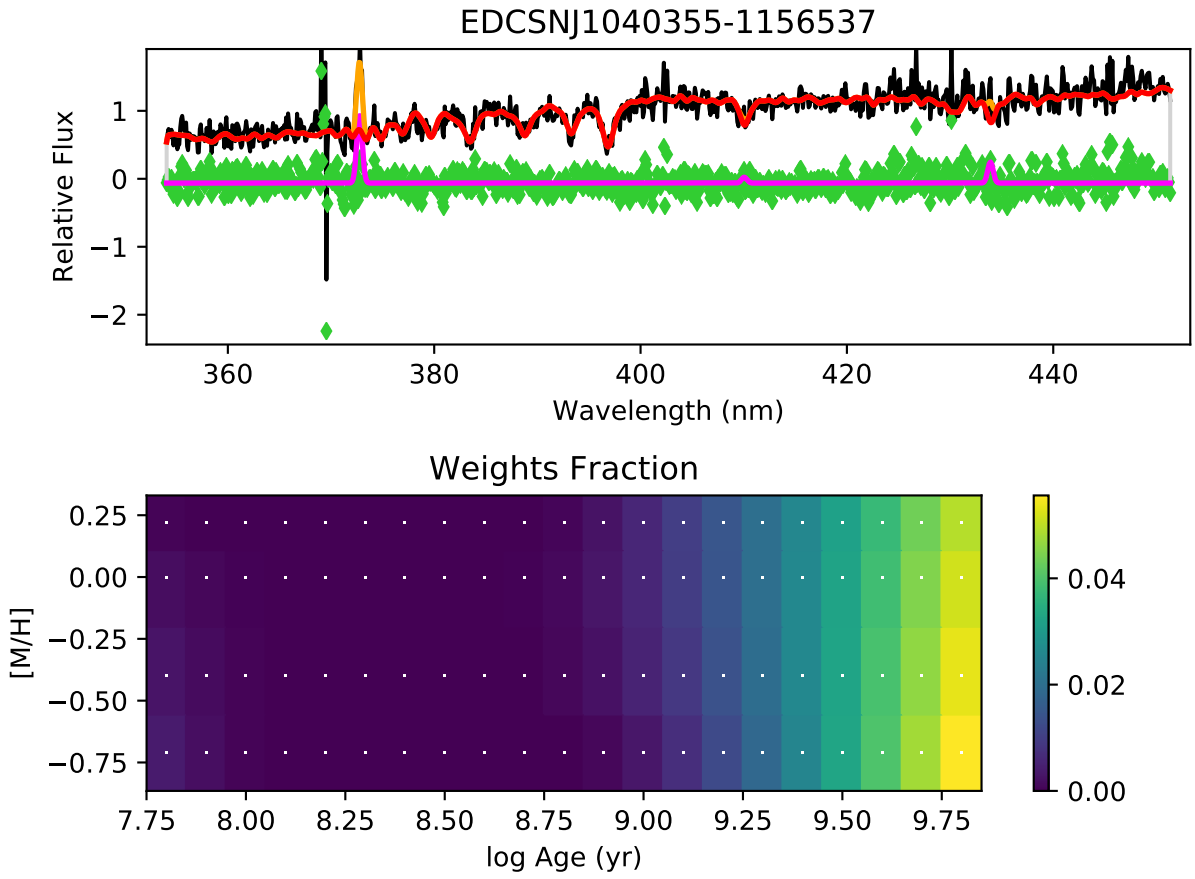
EDCSNJ1040355-1156537
Relative Flux
1
0
−1
−2
360
380
400
420
440
Wavelength (nm)
Weights Fraction
[M/H]
0.25
0.00
−0.25
−0.50
−0.75
7.75
8.00
8.25
8.50
8.75
9.00
9.25
9.50
9.75
log Age (yr)
0.04
0.02
0.00

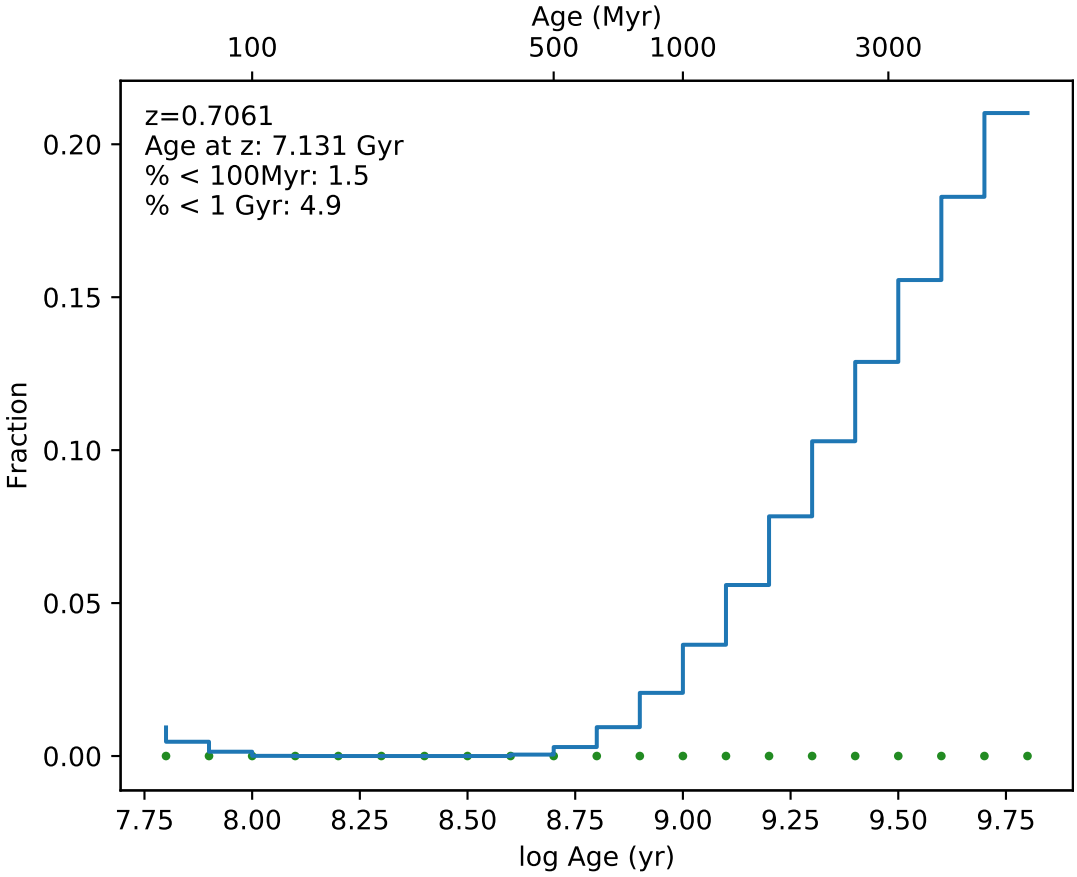
Age (Myr)
100
500
1000
3000
z=0.7061
Age at z: 7.131 Gyr
% < 100Myr: 1.5
% < 1 Gyr: 4.9
Fraction
0.20
0.15
0.10
0.05
0.00
7.75
8.00
8.25
8.50
8.75
9.00
9.25
9.50
9.75
log Age (yr)

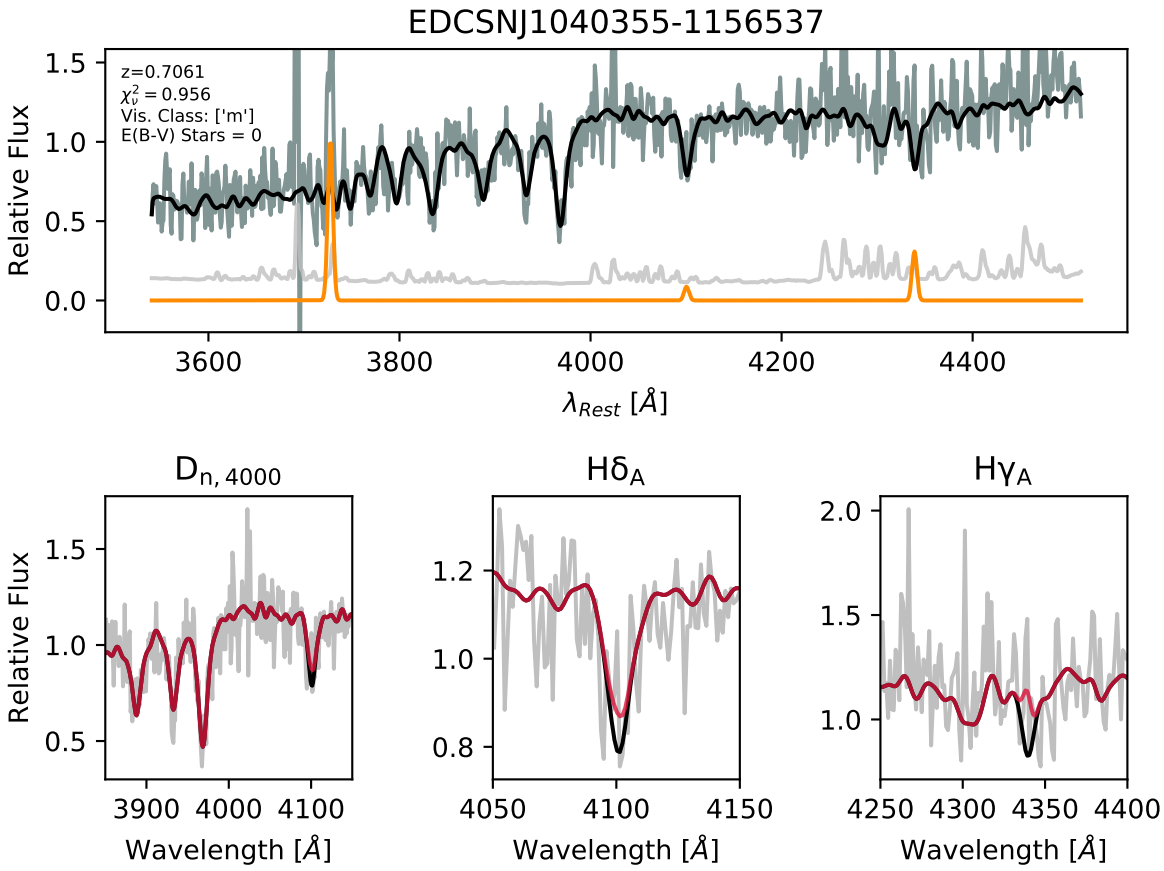
EDCSNJ1040355-1156537
z=0.7061
$\chi^2_\nu = 0.956$
Vis. Class: ['m']
E(B-V) Stars = 0
Relative Flux
λ_{Rest} [Å]
$D_{n,4000}$
$H\delta_A$
$H\gamma_A$
Wavelength [Å]

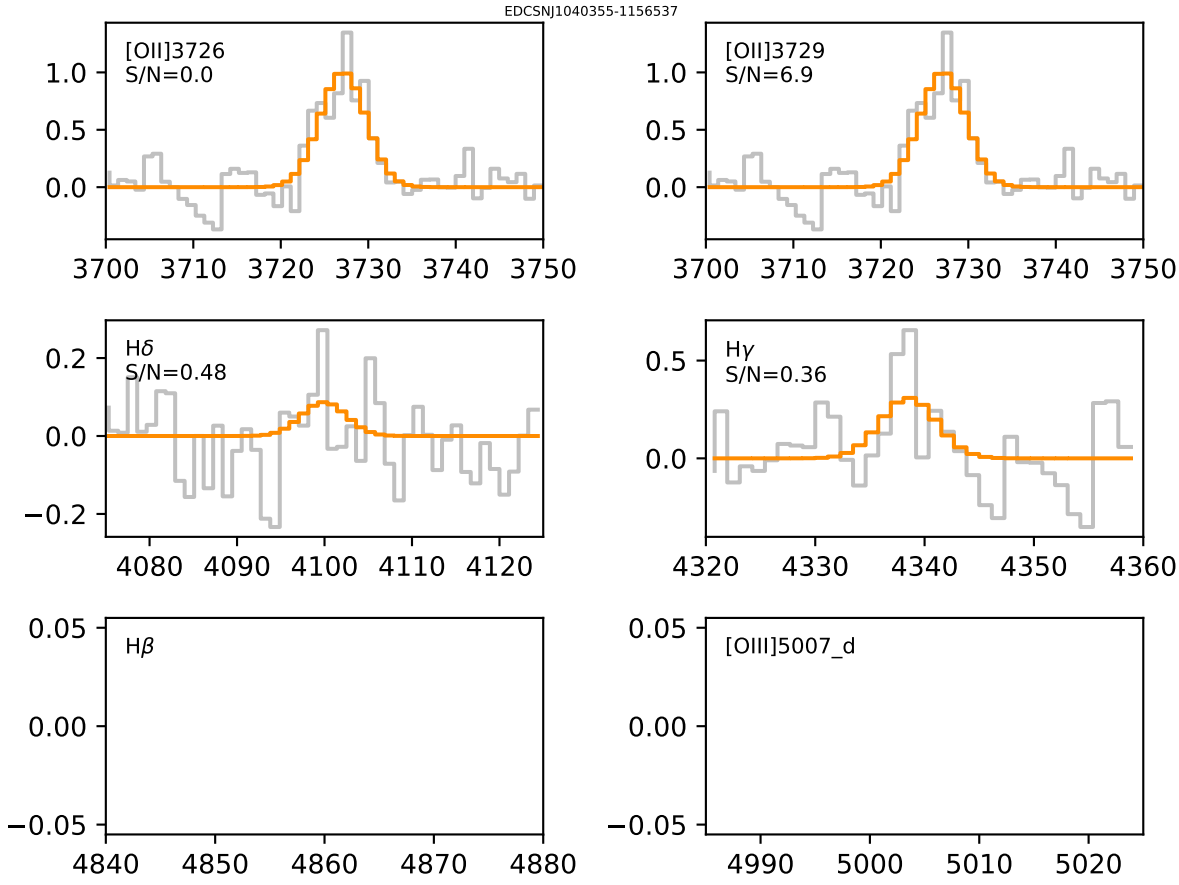
EDCSNJ1040355-1156537
[OII]3726
S/N=0.0
[OII]3729
S/N=6.9
Hδ
S/N=0.48
Hγ
S/N=0.36
Hβ
[OIII]5007_d

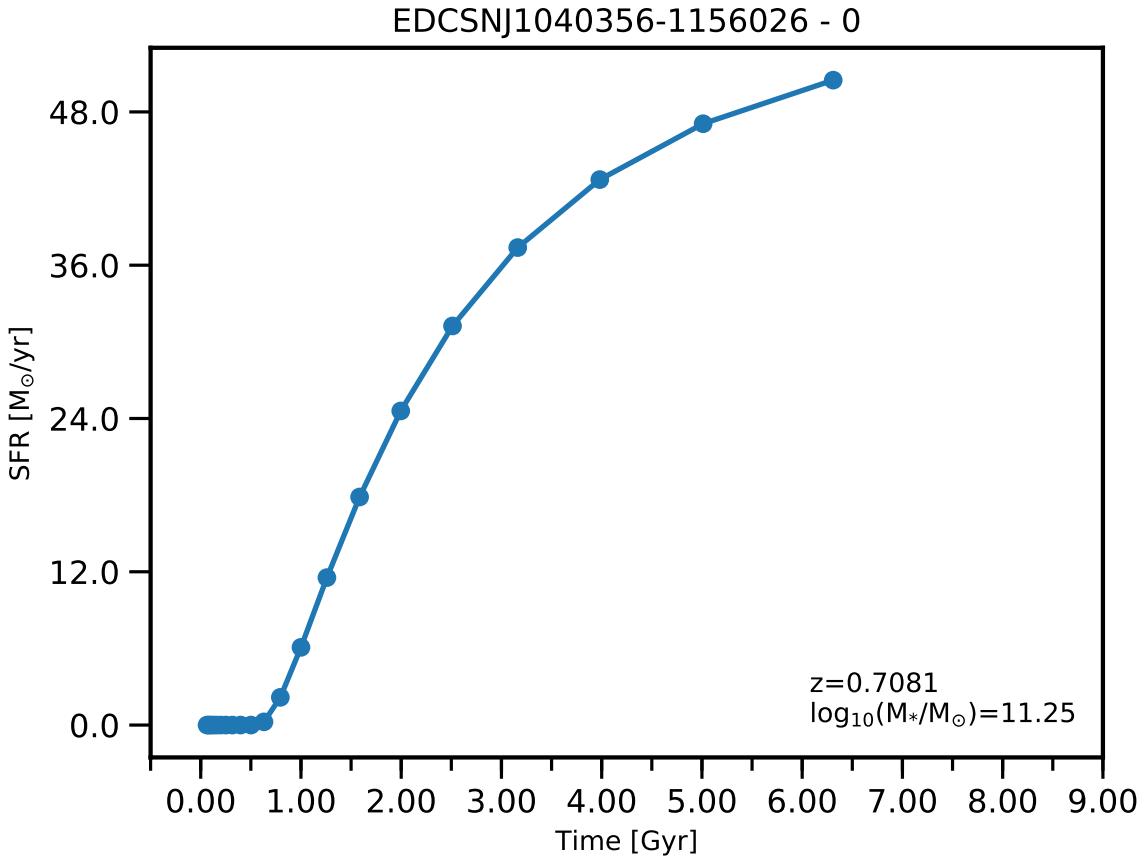
EDCSNJ1040356-1156026 - 0
48.0
36.0
24.0
12.0
0.0
SFR [M⊙/yr]
0.00
1.00
2.00
3.00
4.00
5.00
6.00
7.00
8.00
9.00
Time [Gyr]
z=0.7081
log10(M*/M⊙)=11.25

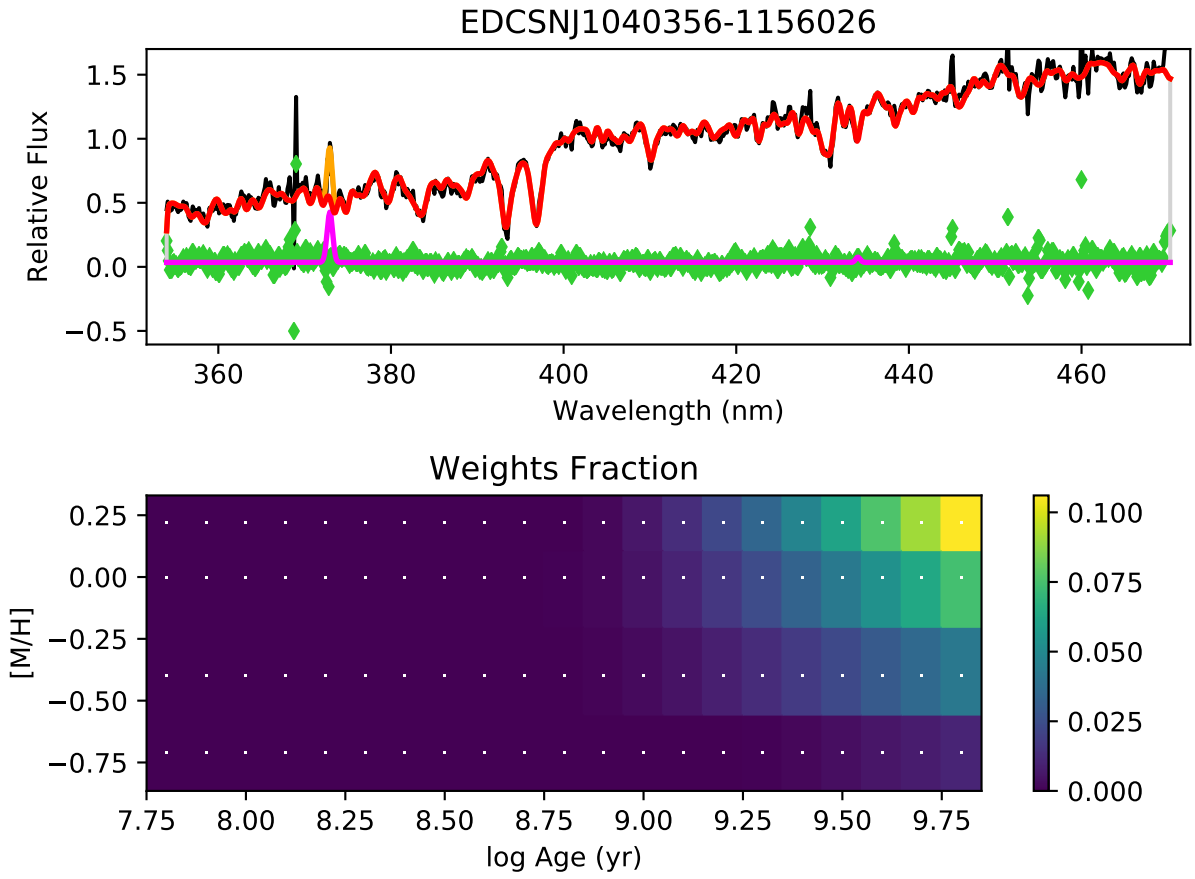
EDCSNJ1040356-1156026
Relative Flux
1.5
1.0
0.5
0.0
−0.5
360
380
400
420
440
460
Wavelength (nm)
Weights Fraction
[M/H]
0.25
0.00
−0.25
−0.50
−0.75
7.75
8.00
8.25
8.50
8.75
9.00
9.25
9.50
9.75
log Age (yr)
0.100
0.075
0.050
0.025
0.000

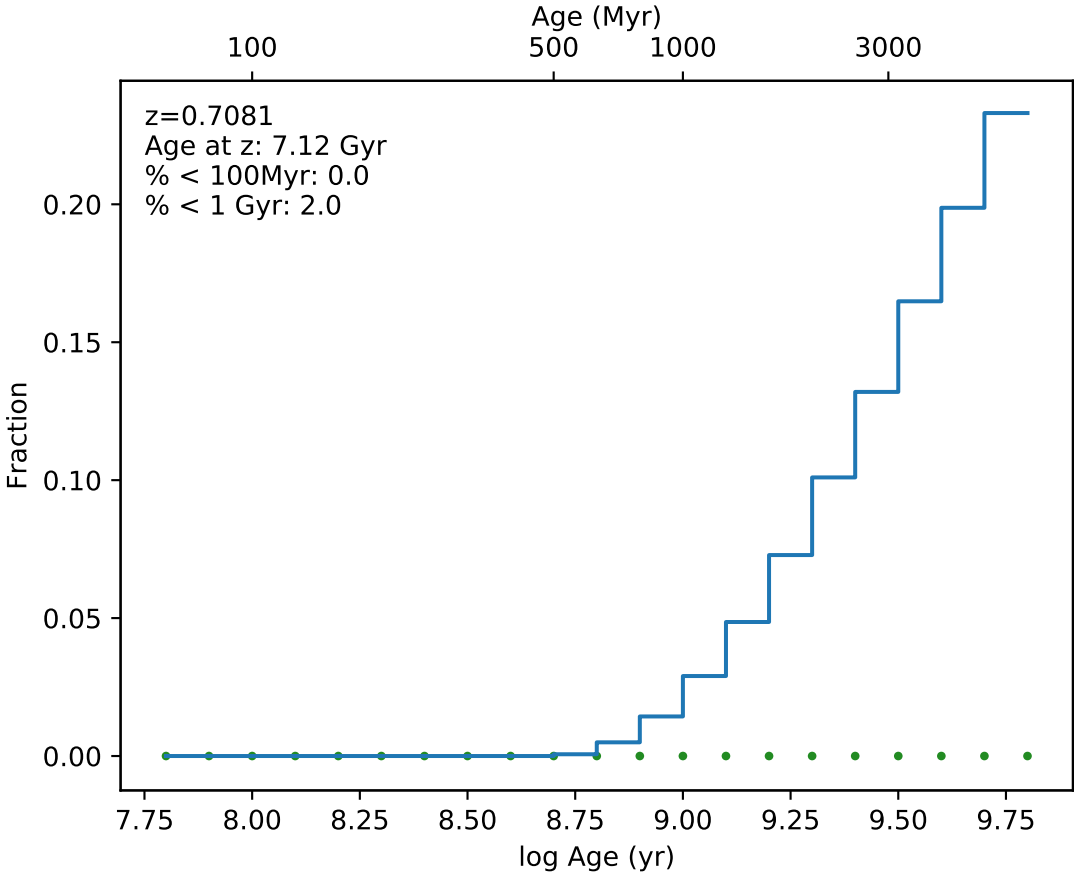
Age (Myr)
100
500
1000
3000
z=0.7081
Age at z: 7.12 Gyr
% < 100Myr: 0.0
% < 1 Gyr: 2.0
Fraction
0.00
0.05
0.10
0.15
0.20
7.75
8.00
8.25
8.50
8.75
9.00
9.25
9.50
9.75
log Age (yr)

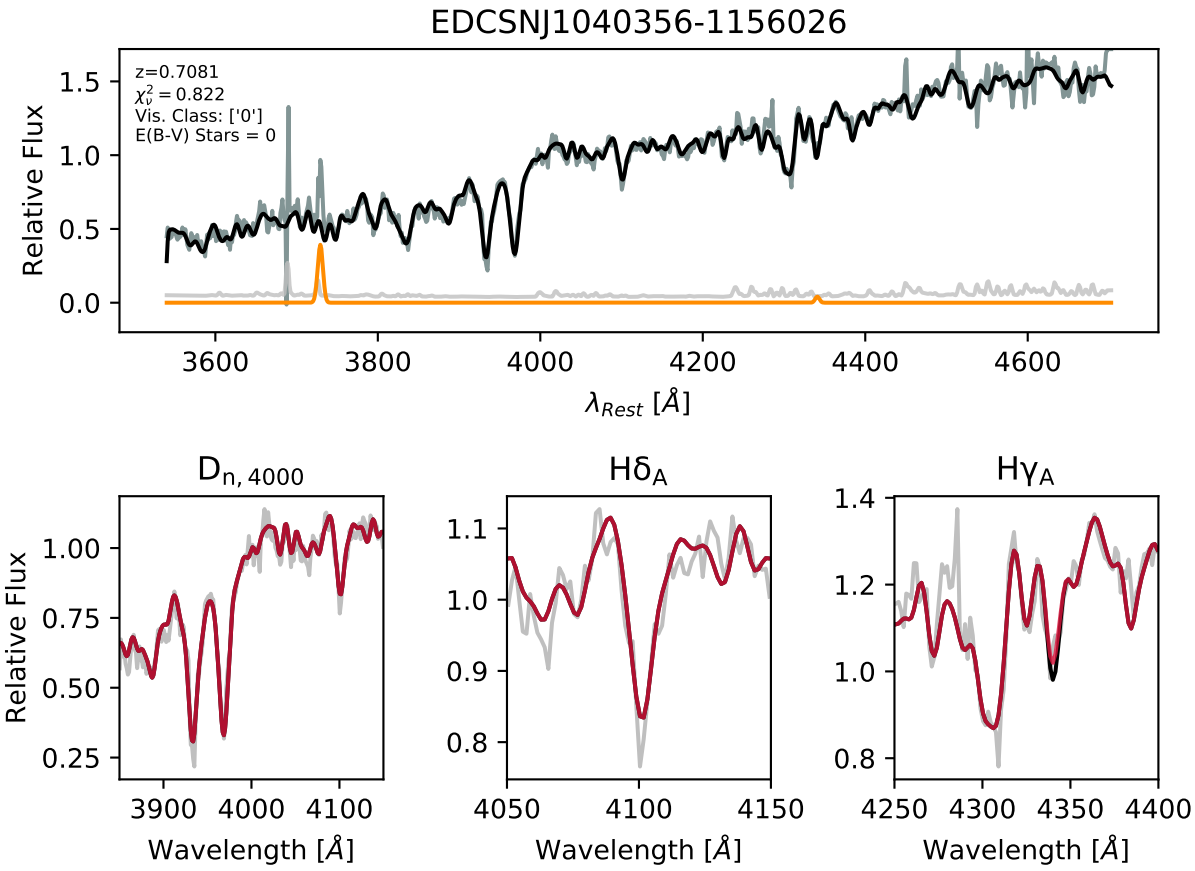
EDCSNJ1040356-1156026
z=0.7081
$\chi^2_\nu = 0.822$
Vis. Class: ['0']
E(B-V) Stars = 0
Relative Flux
1.5
1.0
0.5
0.0
3600
3800
4000
4200
4400
4600
λ_{Rest} [Å]
$D_{n,4000}$
$H\delta_A$
$H\gamma_A$
Relative Flux
1.00
0.75
0.50
0.25
3900
4000
4100
Wavelength [Å]
1.1
1.0
0.9
0.8
4050
4100
4150
Wavelength [Å]
1.4
1.2
1.0
0.8
4250
4300
4350
4400
Wavelength [Å]

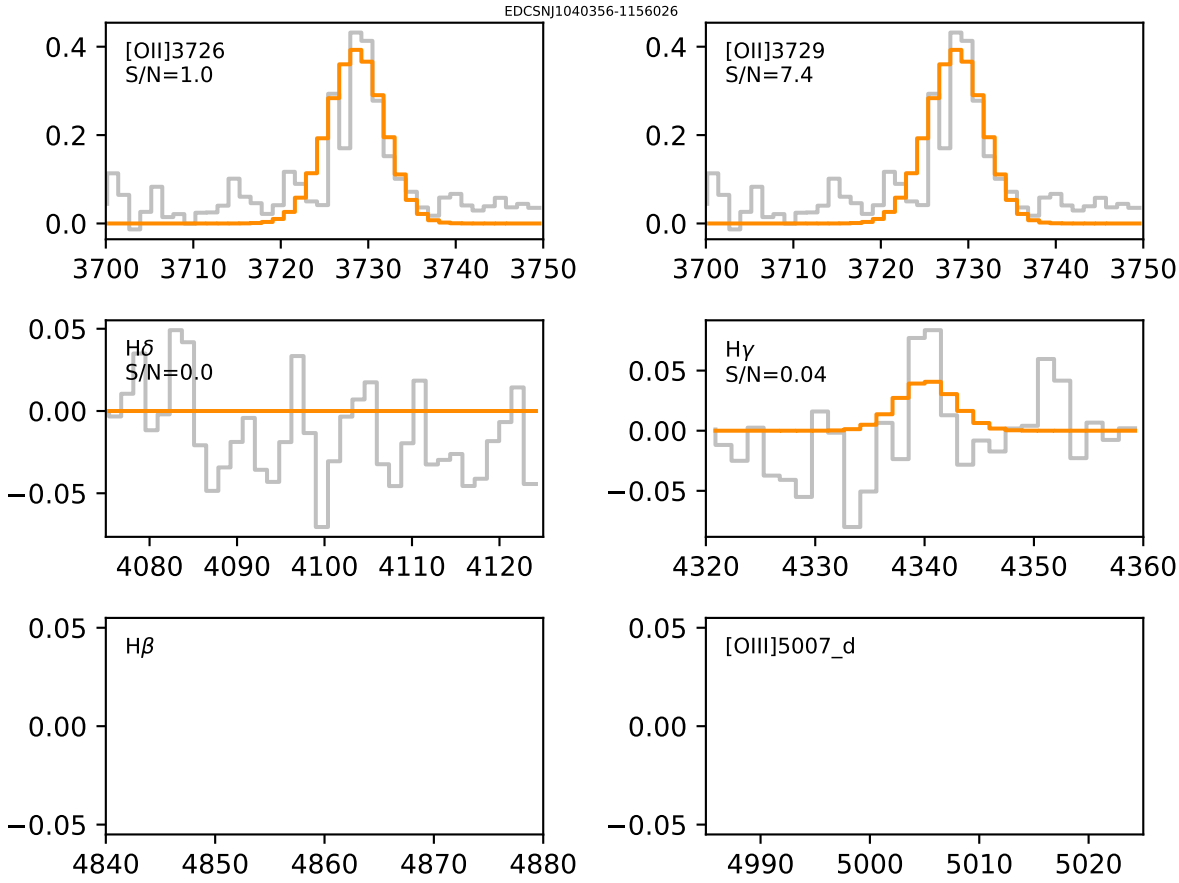
EDCSNJ1040356-1156026
[OII]3726
S/N=1.0
[OII]3729
S/N=7.4
Hδ
S/N=0.0
Hγ
S/N=0.04
Hβ
[OIII]5007_d

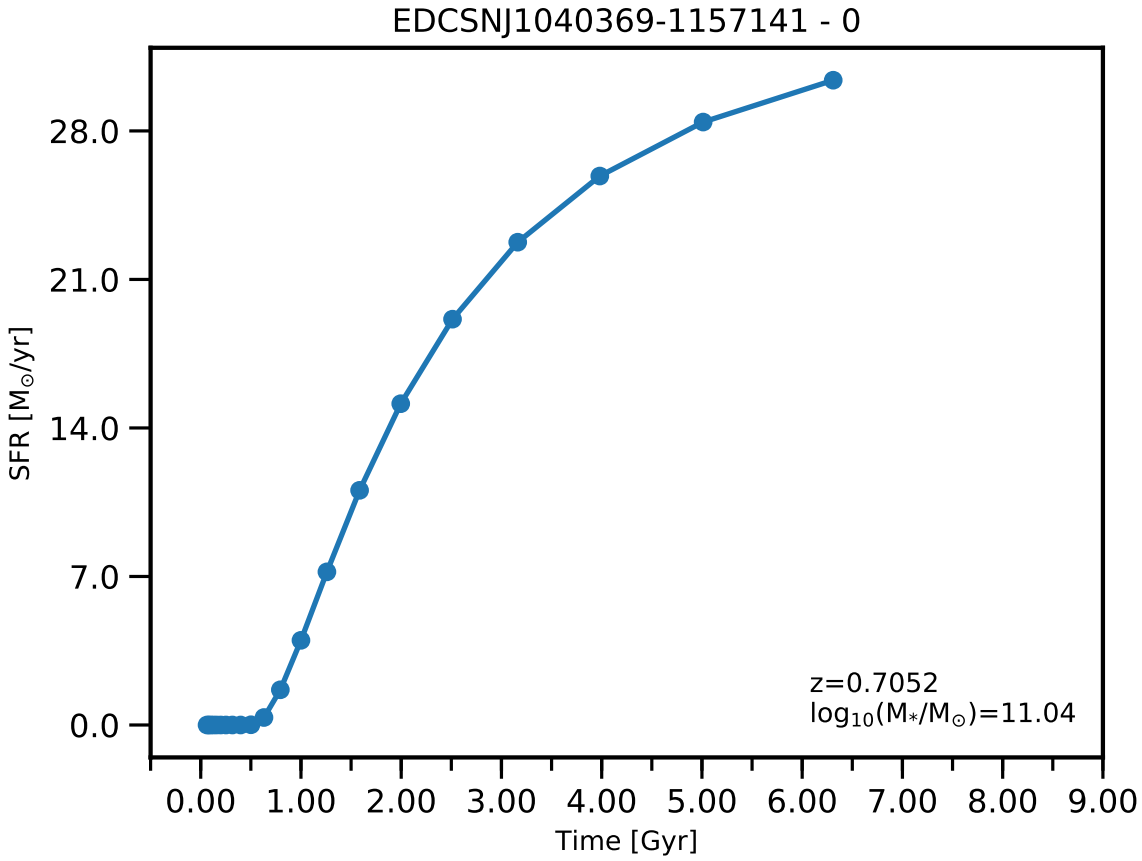
EDCSNJ1040369-1157141 - 0
SFR [M⊙/yr]
28.0
21.0
14.0
7.0
0.0
0.00
1.00
2.00
3.00
4.00
5.00
6.00
7.00
8.00
9.00
Time [Gyr]
z=0.7052
log10(M*/M⊙)=11.04

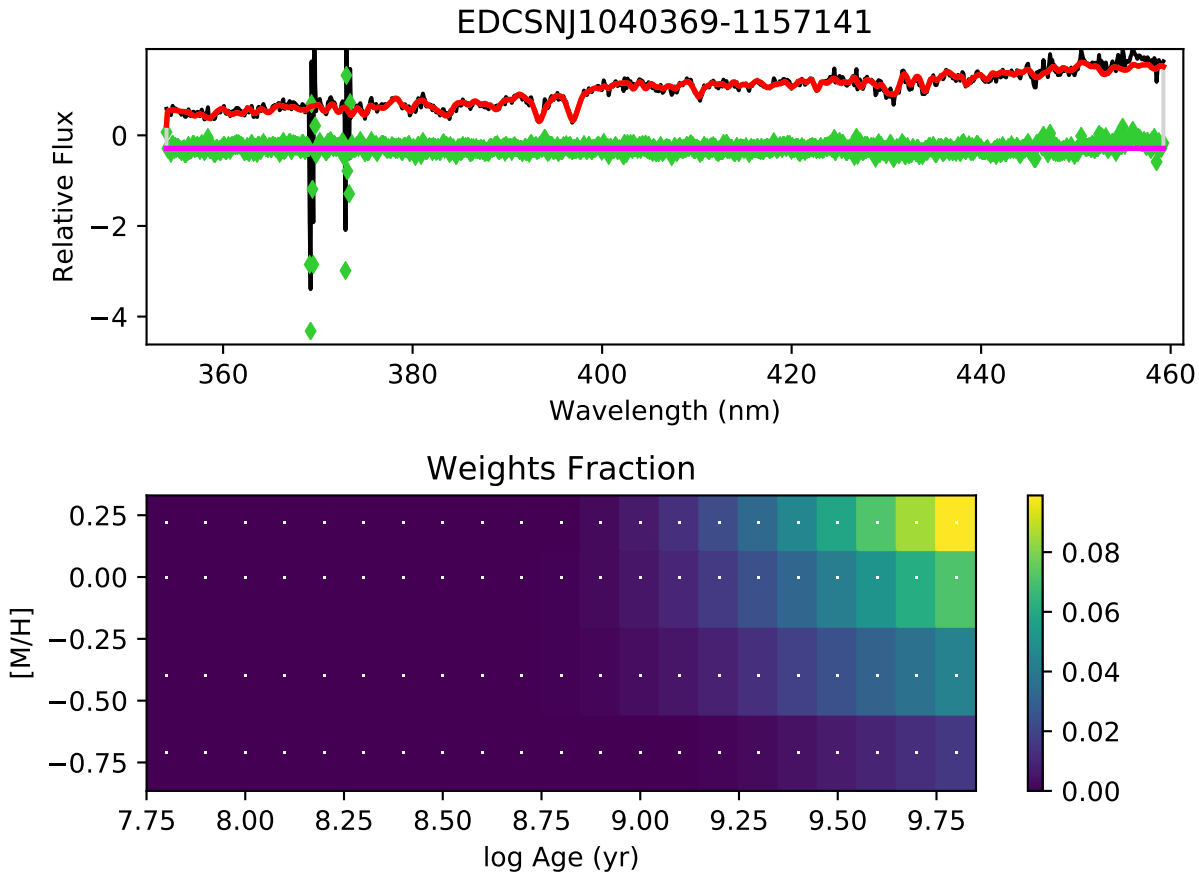
EDCSNJ1040369-1157141
Relative Flux
0
−2
−4
360
380
400
420
440
460
Wavelength (nm)
Weights Fraction
[M/H]
0.25
0.00
−0.25
−0.50
−0.75
7.75
8.00
8.25
8.50
8.75
9.00
9.25
9.50
9.75
log Age (yr)
0.08
0.06
0.04
0.02
0.00

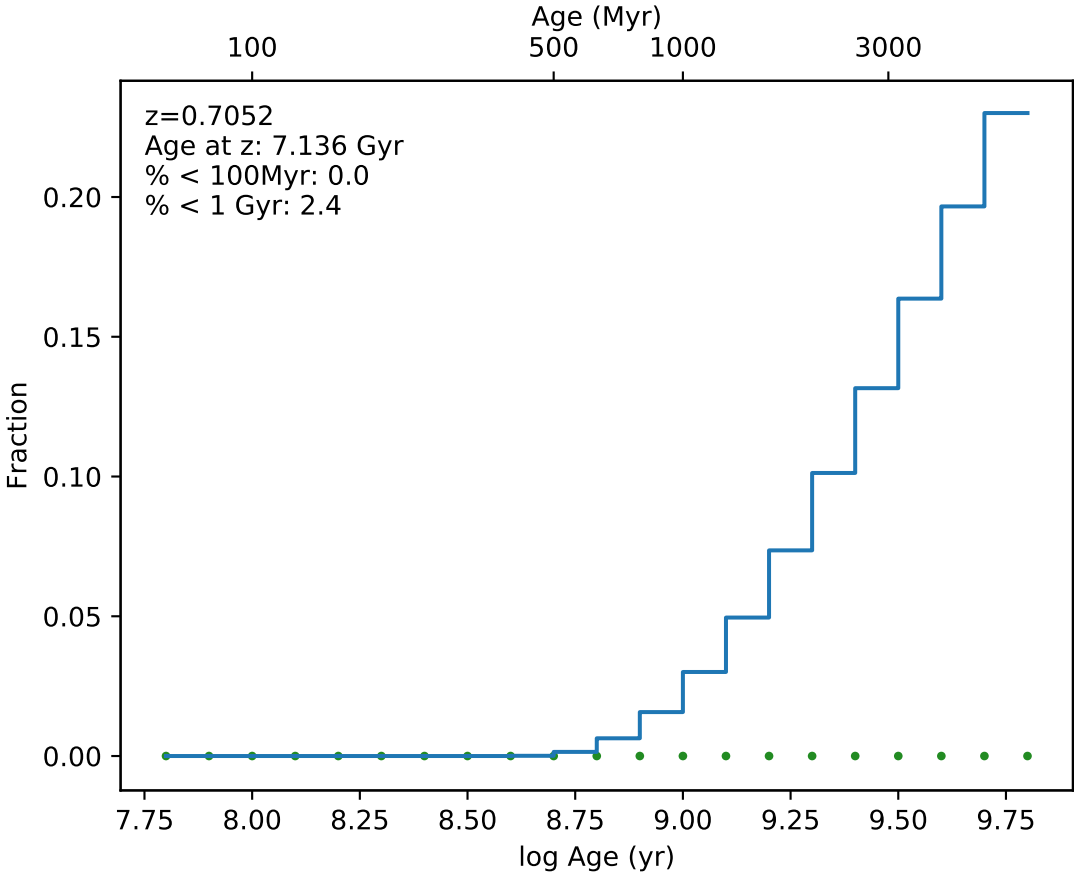
Age (Myr)
100
500
1000
3000
z=0.7052
Age at z: 7.136 Gyr
% < 100Myr: 0.0
% < 1 Gyr: 2.4
Fraction
0.00
0.05
0.10
0.15
0.20
7.75
8.00
8.25
8.50
8.75
9.00
9.25
9.50
9.75
log Age (yr)

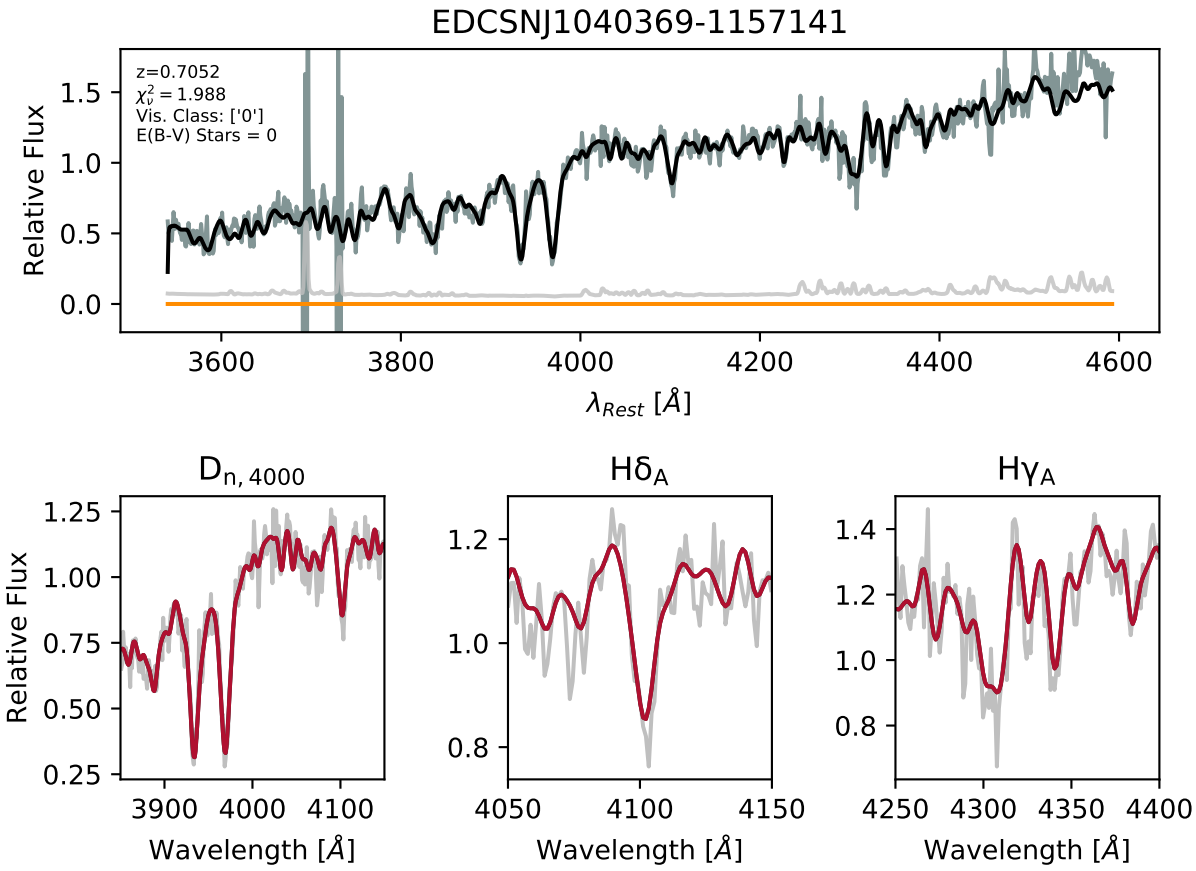
EDCSNJ1040369-1157141
z=0.7052
$\chi^2_\nu = 1.988$
Vis. Class: ['0']
E(B-V) Stars = 0
Relative Flux
λ_{Rest} [Å]
$D_{n,4000}$
$H\delta_A$
$H\gamma_A$
Wavelength [Å]

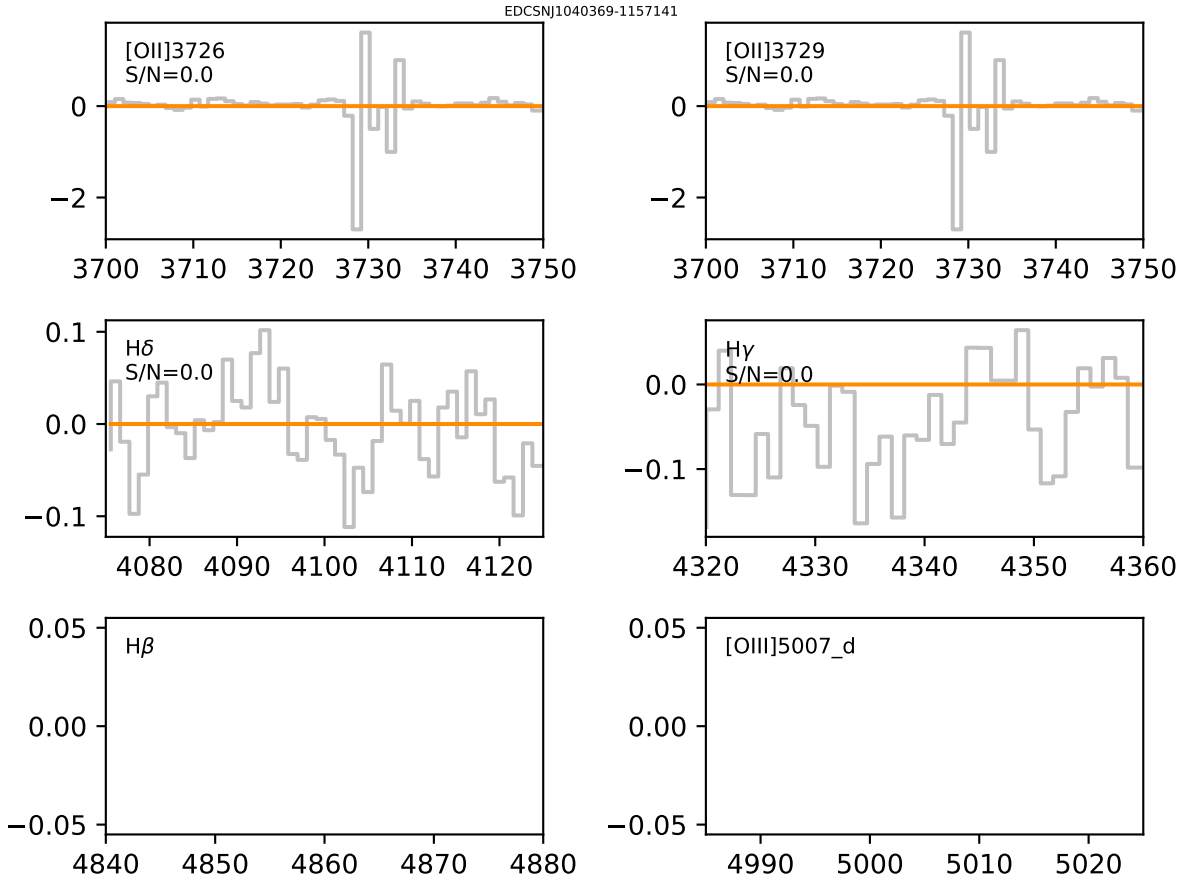
EDCSNJ1040369-1157141
[OII]3726
S/N=0.0
[OII]3729
S/N=0.0
Hδ
S/N=0.0
Hγ
S/N=0.0
Hβ
[OIII]5007_d

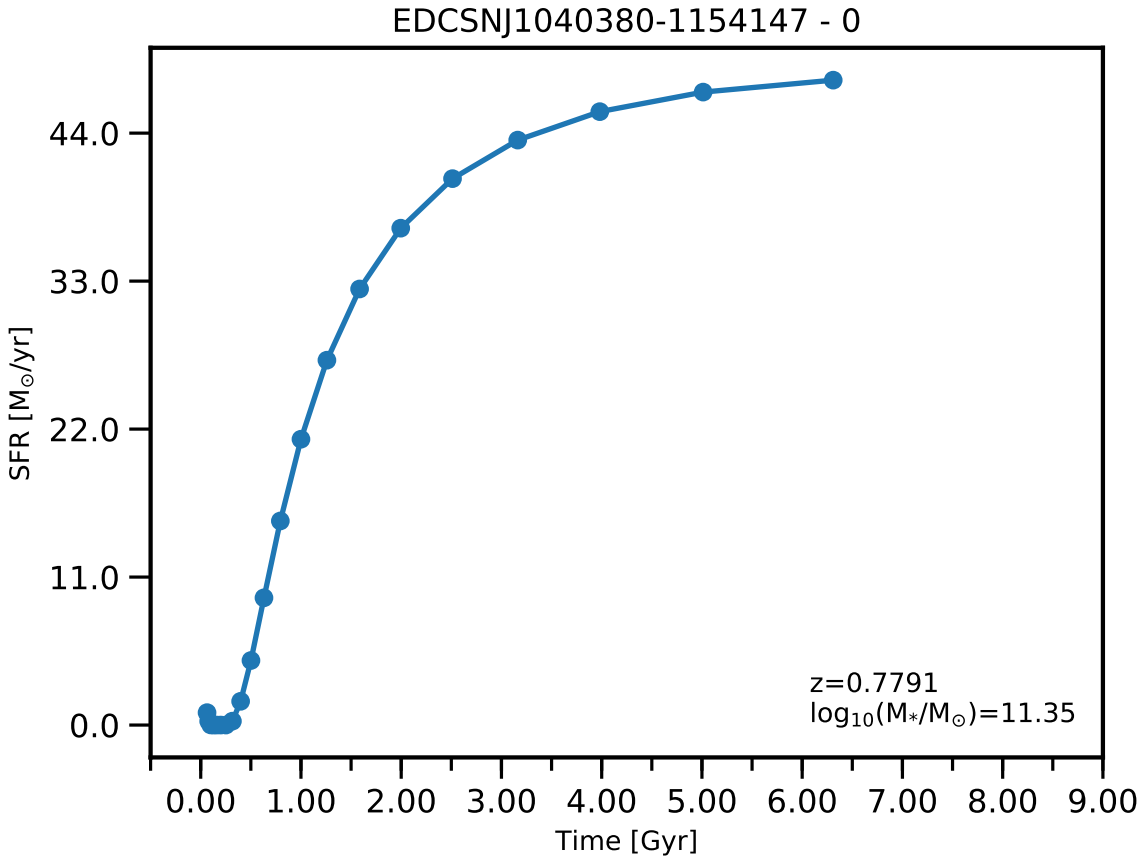
EDCSNJ1040380-1154147 - 0
SFR [M⊙/yr]
44.0
33.0
22.0
11.0
0.0
0.00
1.00
2.00
3.00
4.00
5.00
6.00
7.00
8.00
9.00
Time [Gyr]
z=0.7791
log10(M*/M⊙)=11.35

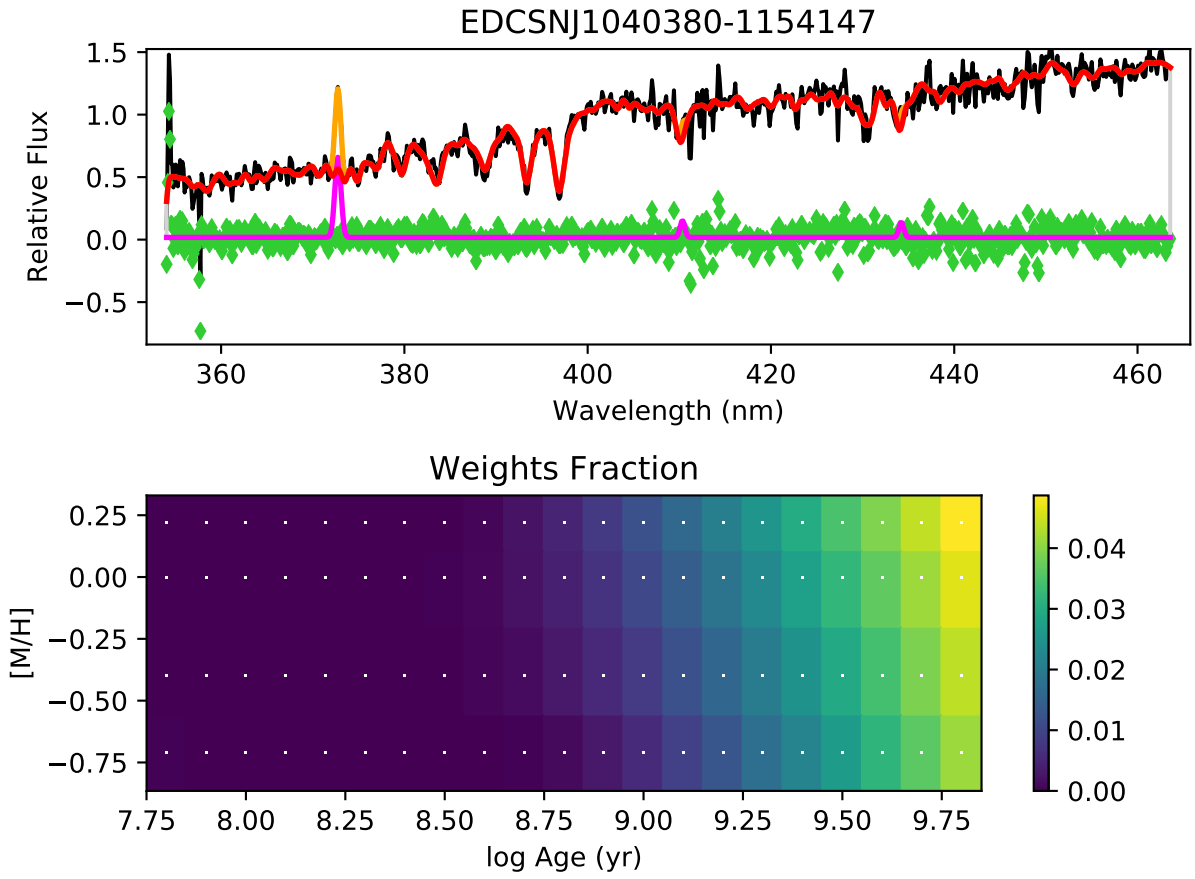
EDCSNJ1040380-1154147
Relative Flux
1.5
1.0
0.5
0.0
−0.5
360
380
400
420
440
460
Wavelength (nm)
Weights Fraction
[M/H]
0.25
0.00
−0.25
−0.50
−0.75
7.75
8.00
8.25
8.50
8.75
9.00
9.25
9.50
9.75
log Age (yr)
0.04
0.03
0.02
0.01
0.00

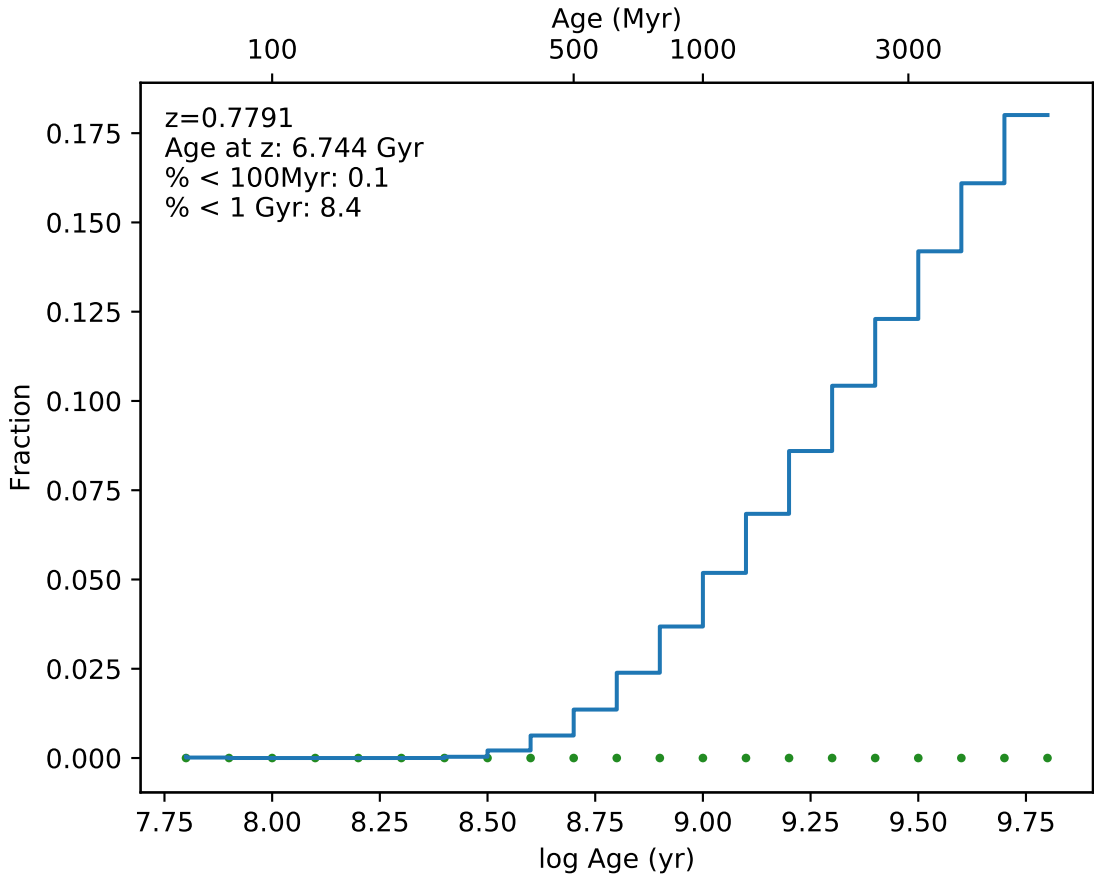
Age (Myr)
100
500
1000
3000
z=0.7791
Age at z: 6.744 Gyr
% < 100Myr: 0.1
% < 1 Gyr: 8.4
Fraction
0.175
0.150
0.125
0.100
0.075
0.050
0.025
0.000
7.75
8.00
8.25
8.50
8.75
9.00
9.25
9.50
9.75
log Age (yr)

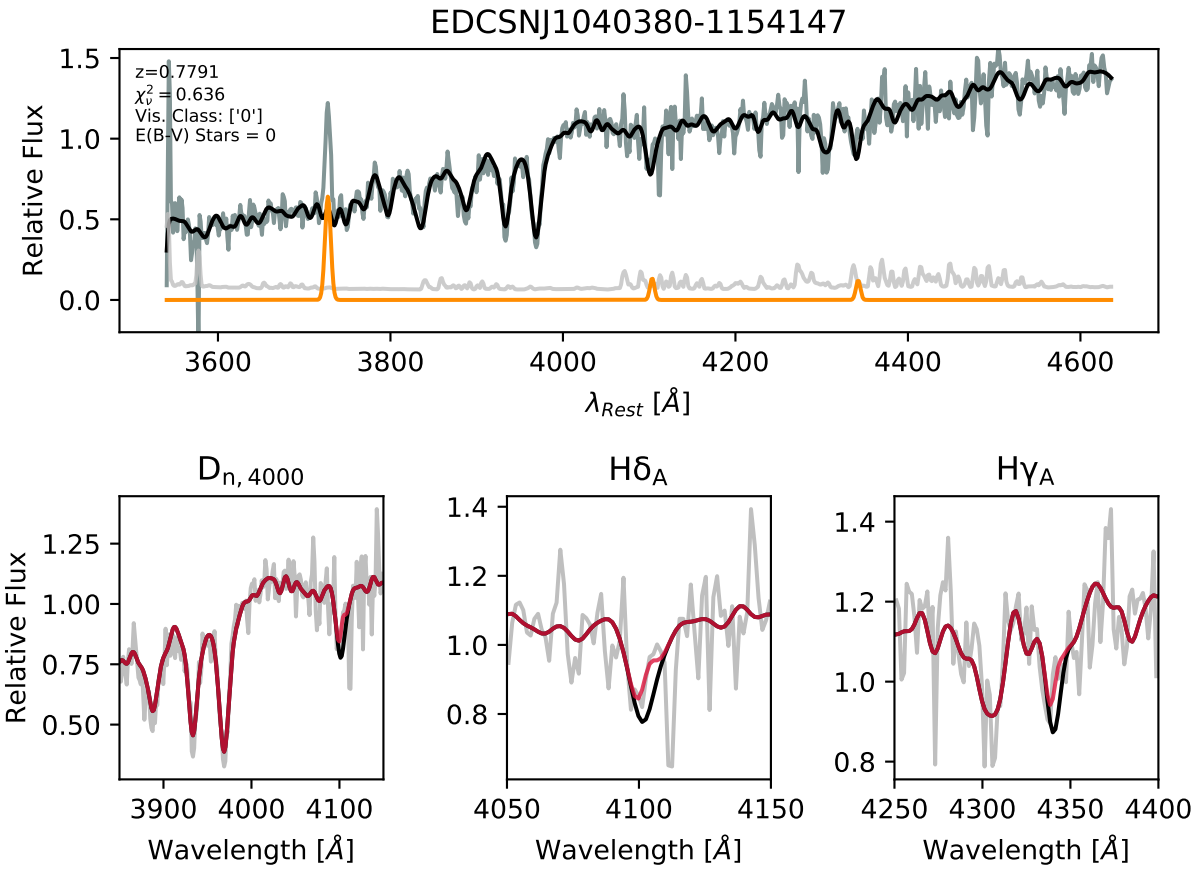
EDCSNJ1040380-1154147
z=0.7791
$\chi^2_\nu = 0.636$
Vis. Class: ['0']
E(B-V) Stars = 0
Relative Flux
λ_{Rest} [Å]
$D_{n,4000}$
$H\delta_A$
$H\gamma_A$
Wavelength [Å]

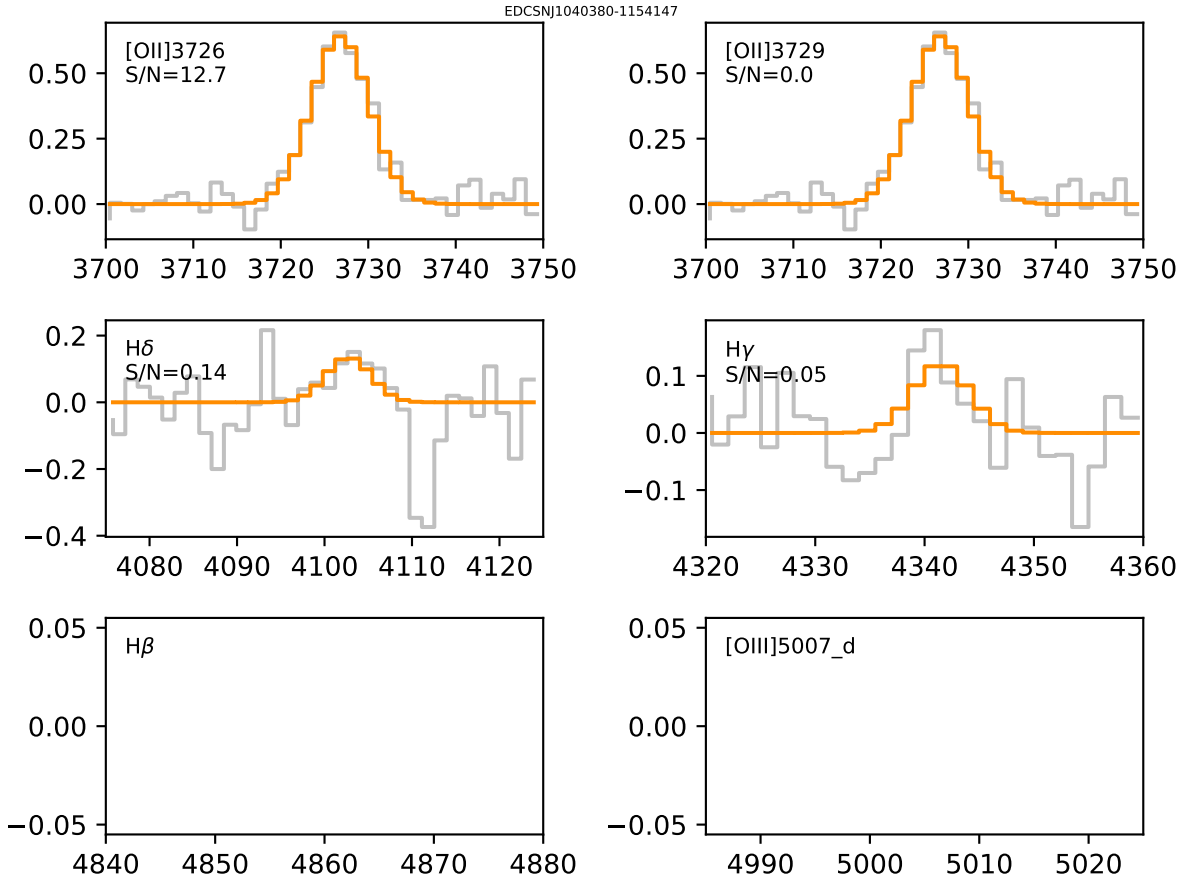
EDCSNJ1040380-1154147
[OII]3726
S/N=12.7
[OII]3729
S/N=0.0
Hδ
S/N=0.14
Hγ
S/N=0.05
Hβ
[OIII]5007_d

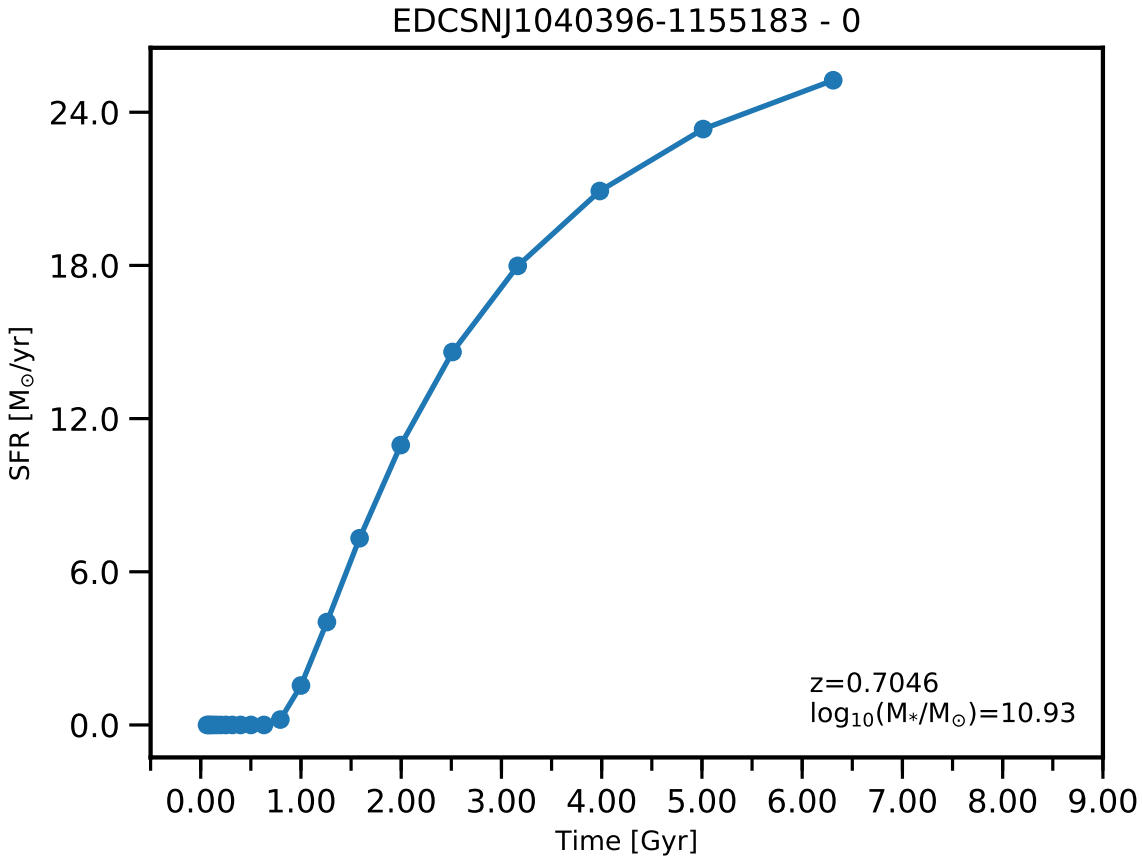
EDCSNJ1040396-1155183 - 0
24.0
18.0
12.0
6.0
0.0
SFR [M⊙/yr]
0.00
1.00
2.00
3.00
4.00
5.00
6.00
7.00
8.00
9.00
Time [Gyr]
z=0.7046
log10(M*/M⊙)=10.93

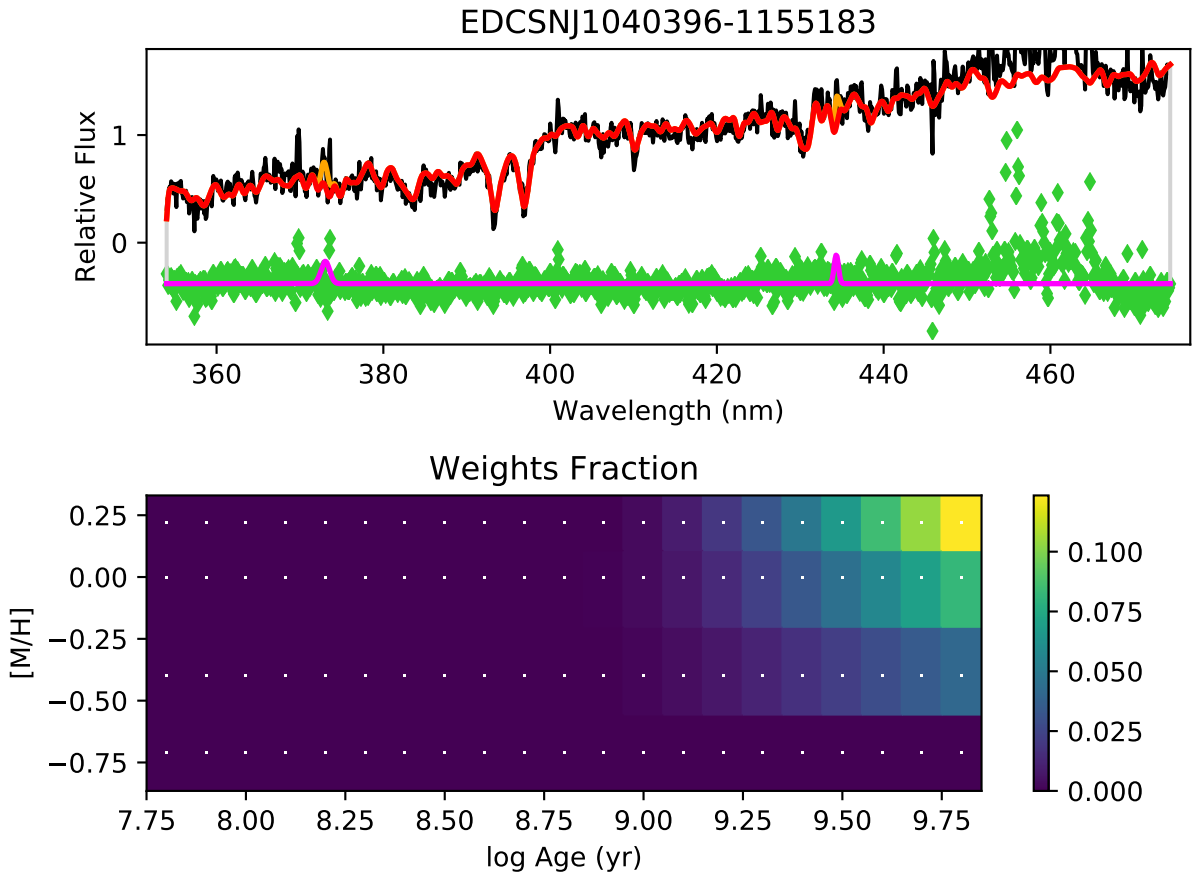
EDCSNJ1040396-1155183
Relative Flux
1
0
360
380
400
420
440
460
Wavelength (nm)
Weights Fraction
[M/H]
0.25
0.00
−0.25
−0.50
−0.75
7.75
8.00
8.25
8.50
8.75
9.00
9.25
9.50
9.75
log Age (yr)
0.100
0.075
0.050
0.025
0.000

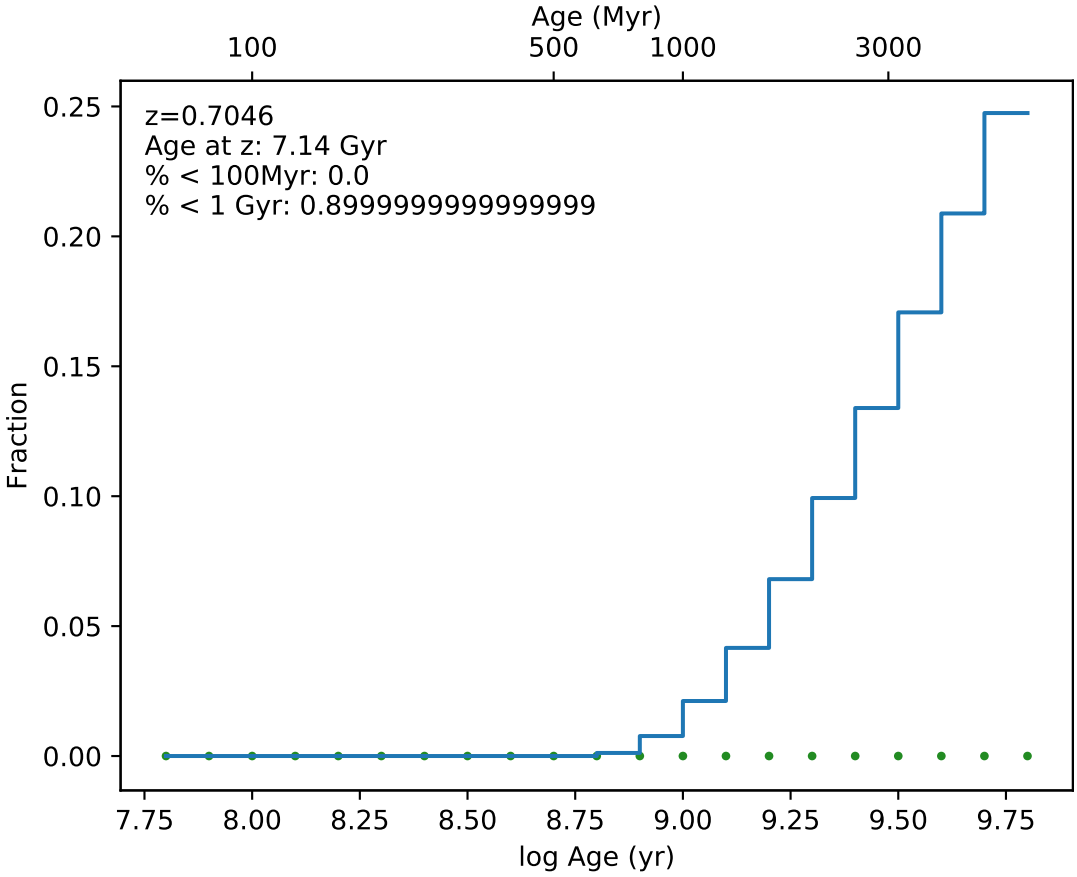
Age (Myr)
100
500
1000
3000
z=0.7046
Age at z: 7.14 Gyr
% < 100Myr: 0.0
% < 1 Gyr: 0.8999999999999999
Fraction
0.25
0.20
0.15
0.10
0.05
0.00
7.75
8.00
8.25
8.50
8.75
9.00
9.25
9.50
9.75
log Age (yr)

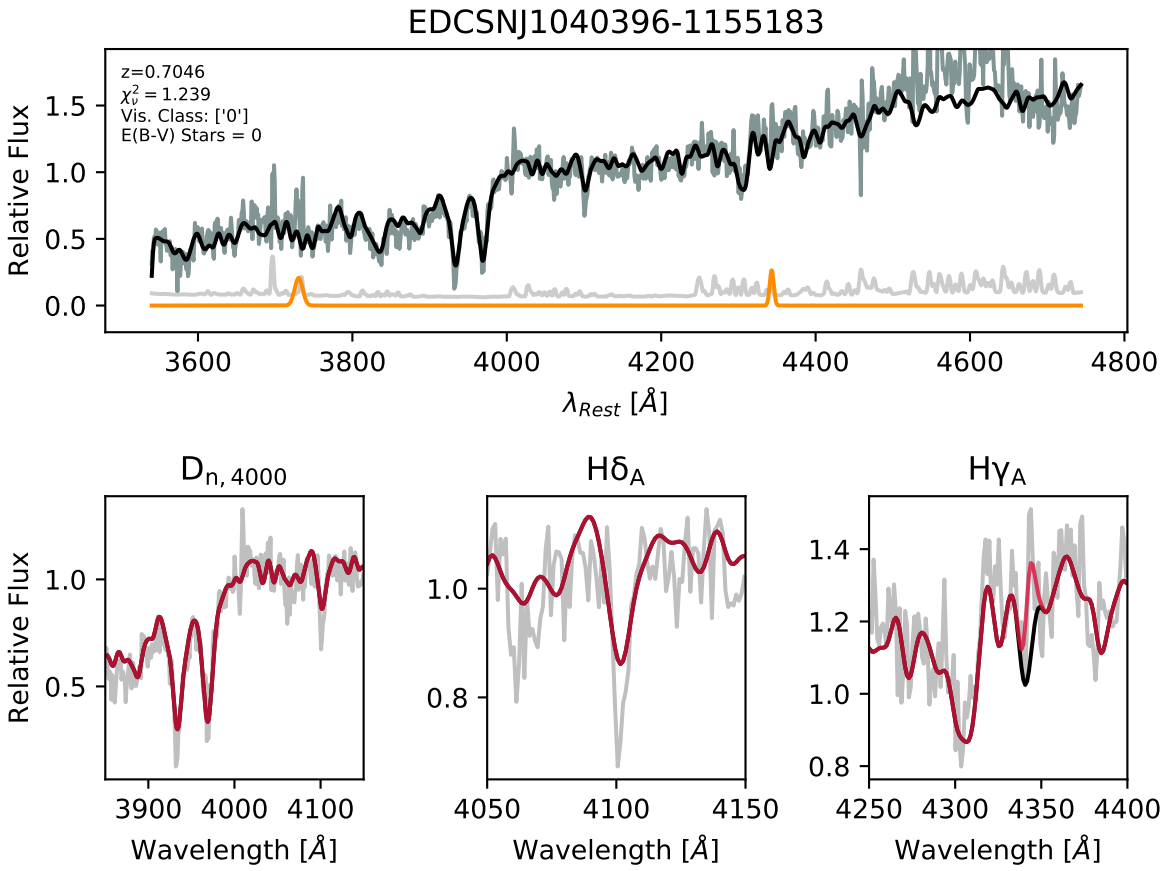
EDCSNJ1040396-1155183
z=0.7046
$\chi^2_\nu = 1.239$
Vis. Class: ['0']
E(B-V) Stars = 0
Relative Flux
λ_{Rest} [Å]
$D_{n,4000}$
$H\delta_A$
$H\gamma_A$
Wavelength [Å]

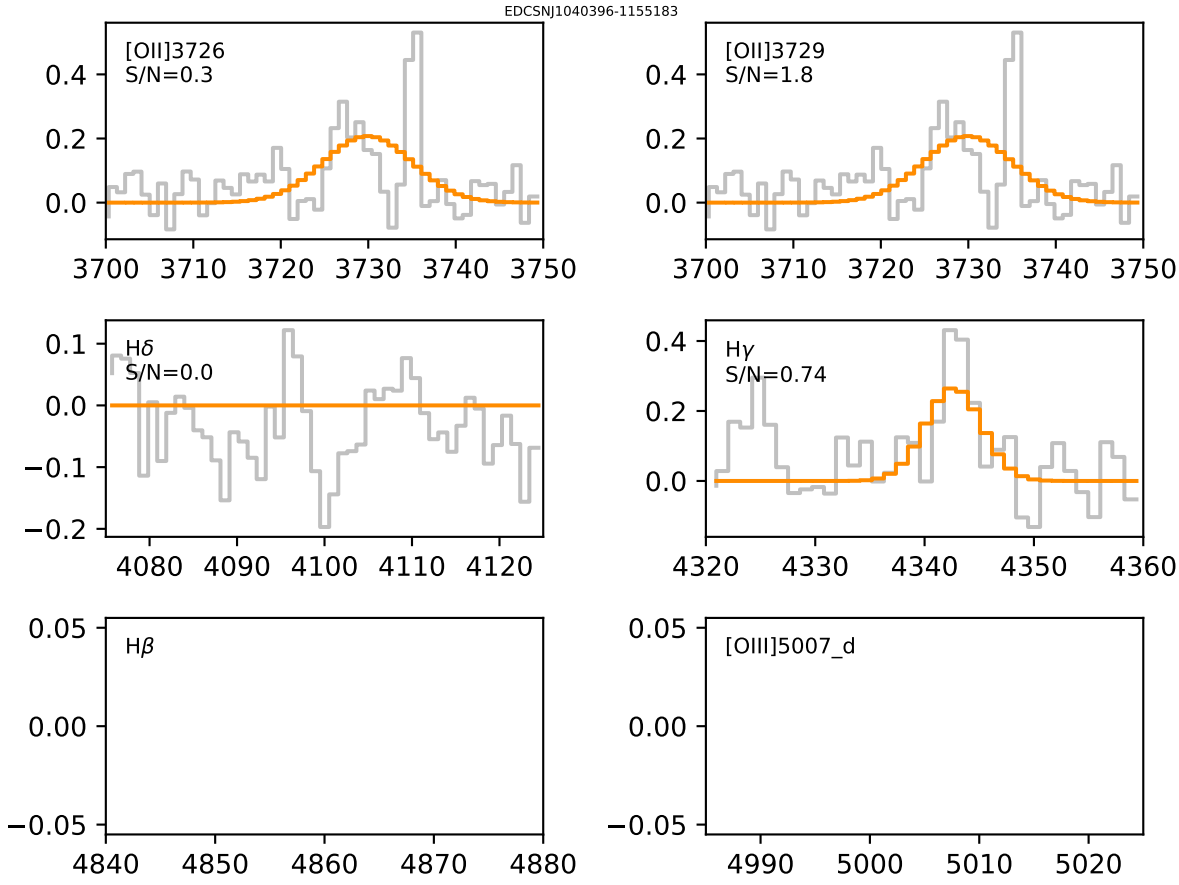
EDCSNJ1040396-1155183
[OII]3726
S/N=0.3
[OII]3729
S/N=1.8
Hδ
S/N=0.0
Hγ
S/N=0.74
Hβ
[OIII]5007_d

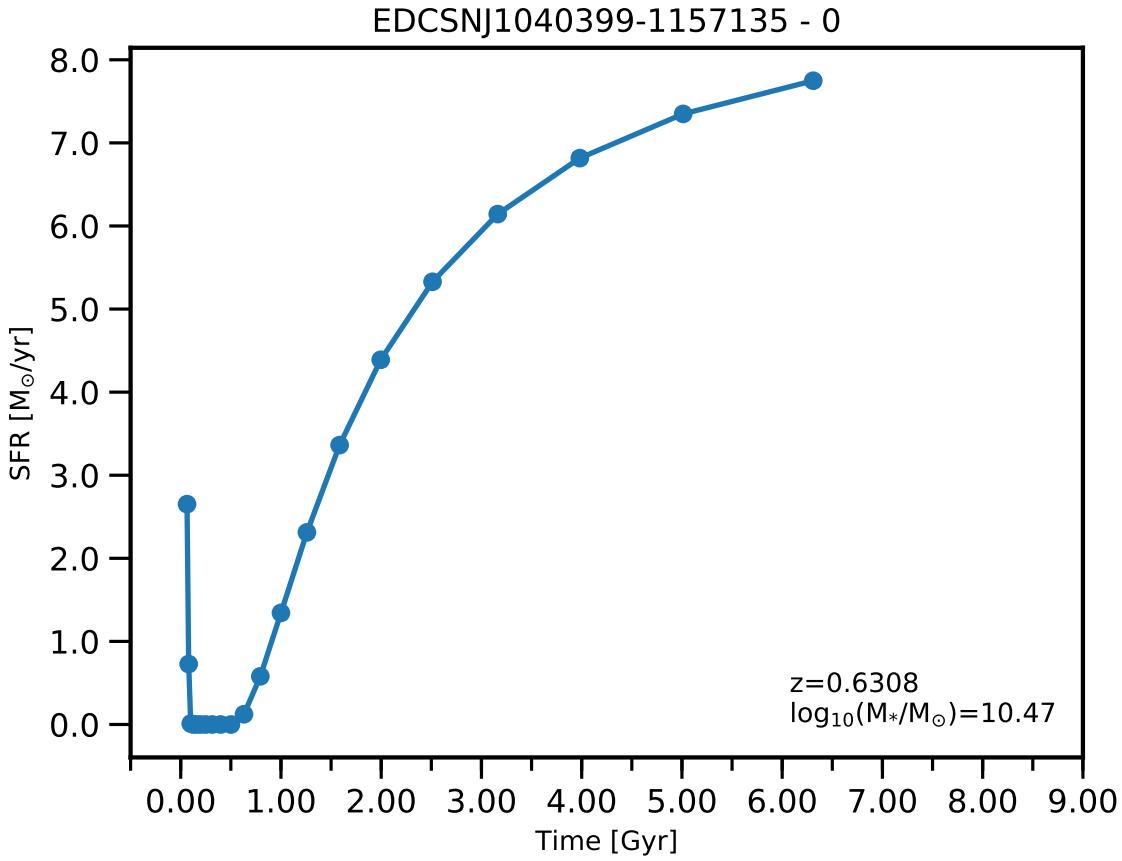
EDCSNJ1040399-1157135 - 0
SFR [M⊙/yr]
Time [Gyr]
z=0.6308
log10(M*/M⊙)=10.47
0.0
1.0
2.0
3.0
4.0
5.0
6.0
7.0
8.0
0.00
1.00
2.00
3.00
4.00
5.00
6.00
7.00
8.00
9.00

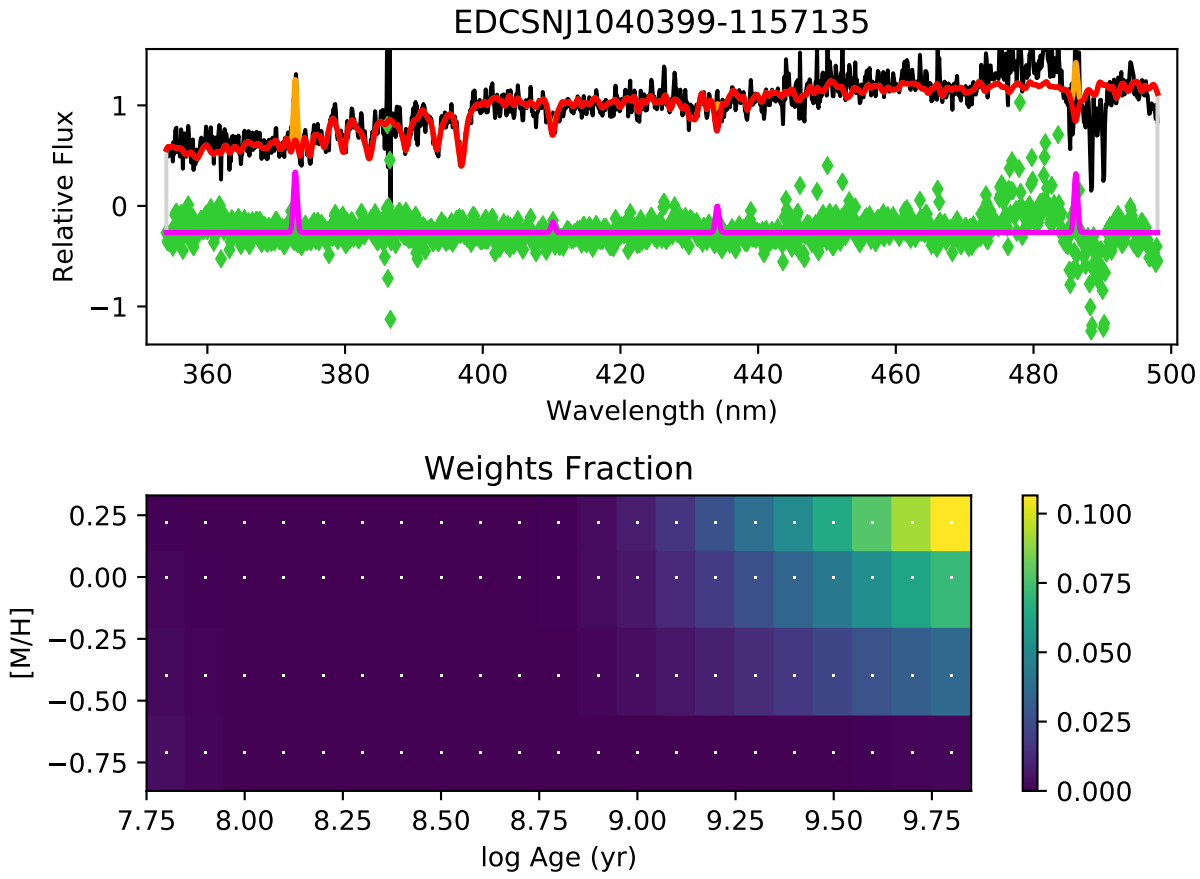
EDCSNJ1040399-1157135
Relative Flux
1
0
−1
360
380
400
420
440
460
480
500
Wavelength (nm)
Weights Fraction
[M/H]
0.25
0.00
−0.25
−0.50
−0.75
7.75
8.00
8.25
8.50
8.75
9.00
9.25
9.50
9.75
log Age (yr)
0.100
0.075
0.050
0.025
0.000

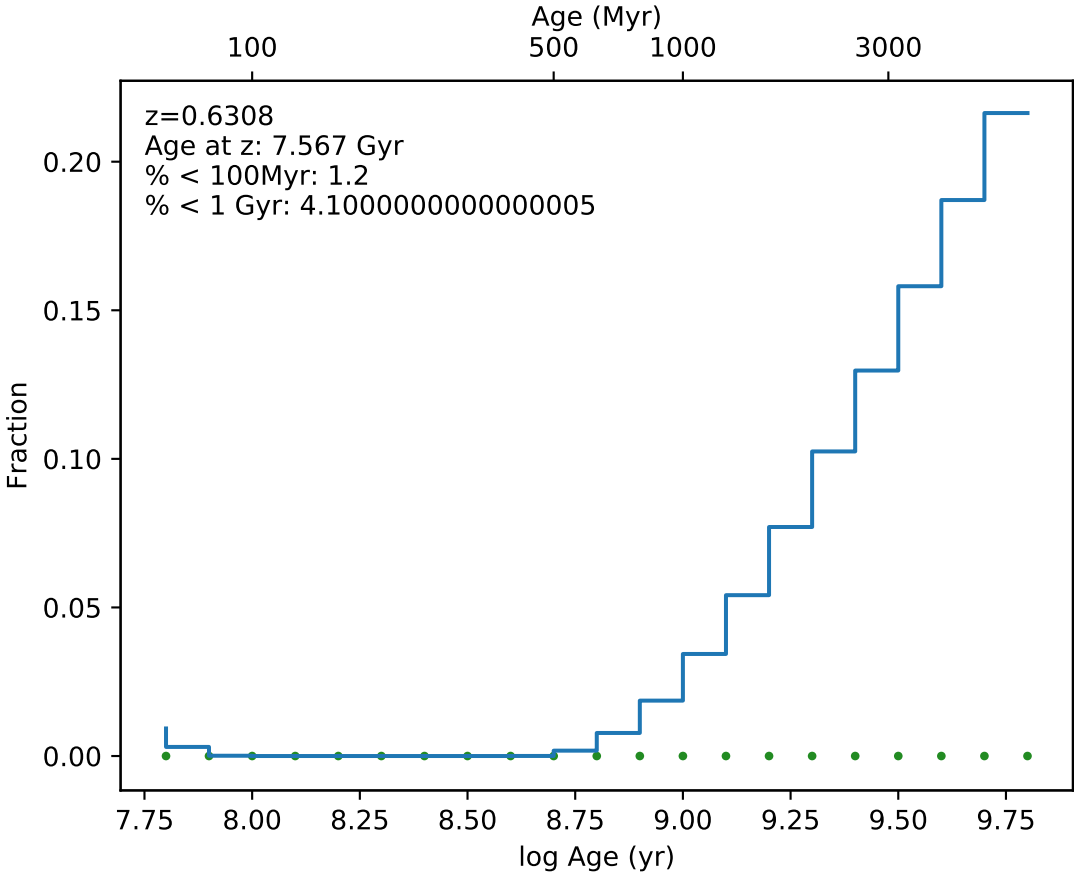
Age (Myr)
100
500
1000
3000
z=0.6308
Age at z: 7.567 Gyr
% < 100Myr: 1.2
% < 1 Gyr: 4.1000000000000005
Fraction
0.20
0.15
0.10
0.05
0.00
7.75
8.00
8.25
8.50
8.75
9.00
9.25
9.50
9.75
log Age (yr)

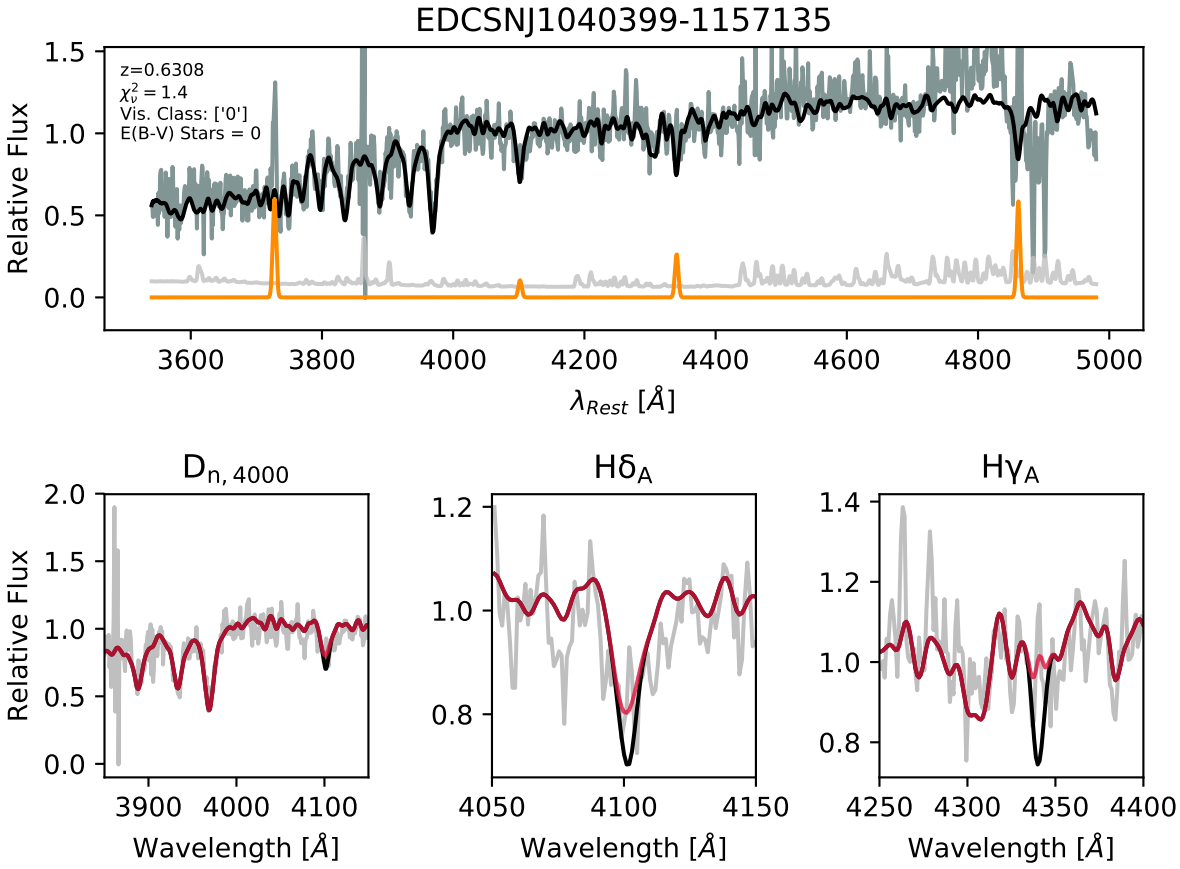
EDCSNJ1040399-1157135
z=0.6308
$\chi^2_\nu = 1.4$
Vis. Class: ['0']
E(B-V) Stars = 0
Relative Flux
λ_{Rest} [Å]
$D_{n,4000}$
$H\delta_A$
$H\gamma_A$
Wavelength [Å]

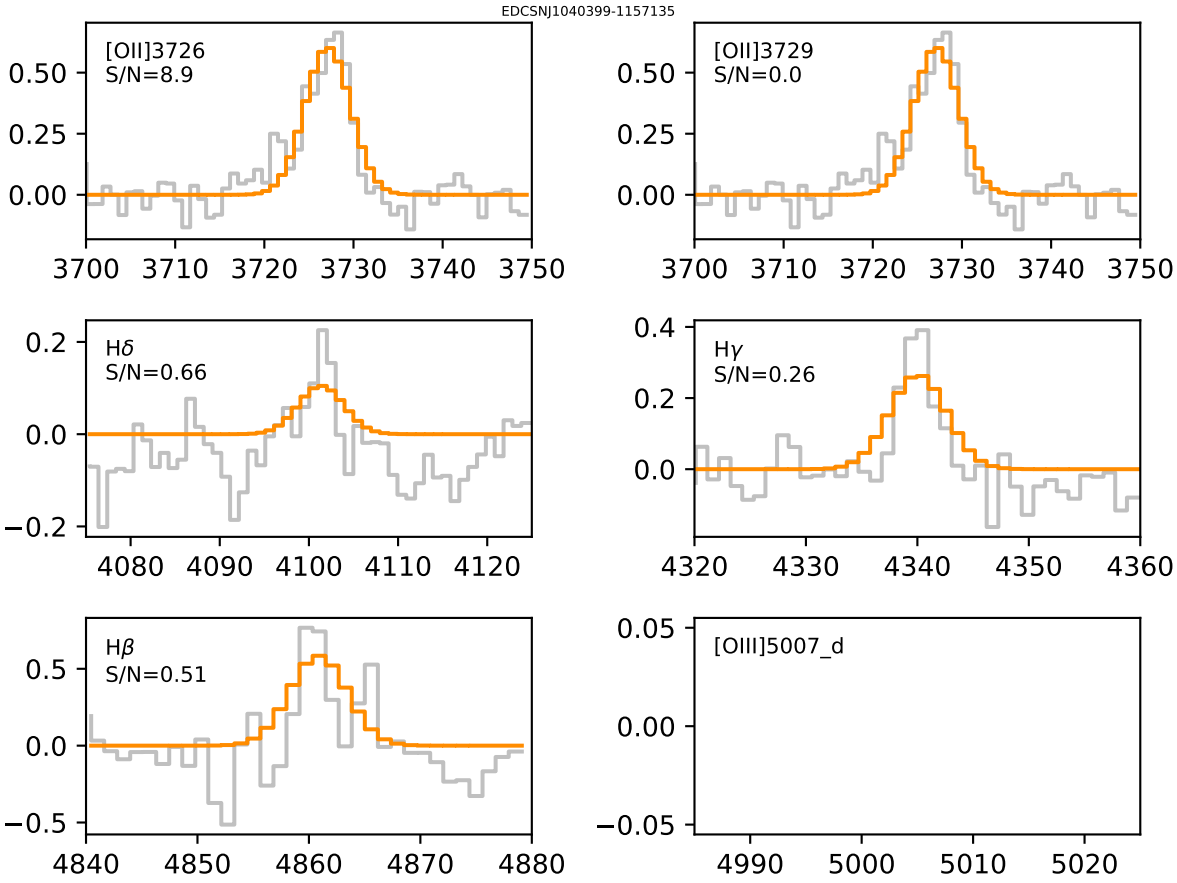
EDCSNJ1040399-1157135
[OII]3726
S/N=8.9
[OII]3729
S/N=0.0
Hδ
S/N=0.66
Hγ
S/N=0.26
Hβ
S/N=0.51
[OIII]5007_d

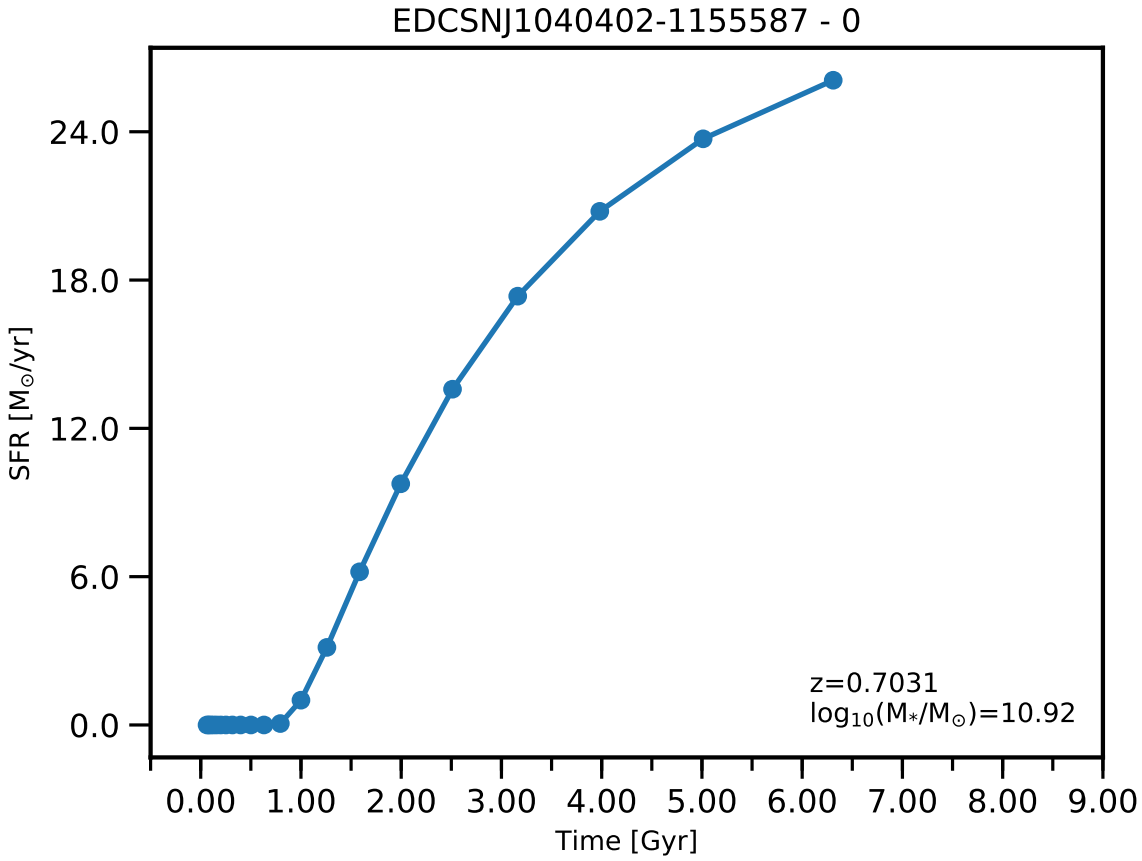
EDCSNJ1040402-1155587 - 0
SFR [M⊙/yr]
24.0
18.0
12.0
6.0
0.0
0.00
1.00
2.00
3.00
4.00
5.00
6.00
7.00
8.00
9.00
Time [Gyr]
z=0.7031
log10(M*/M⊙)=10.92

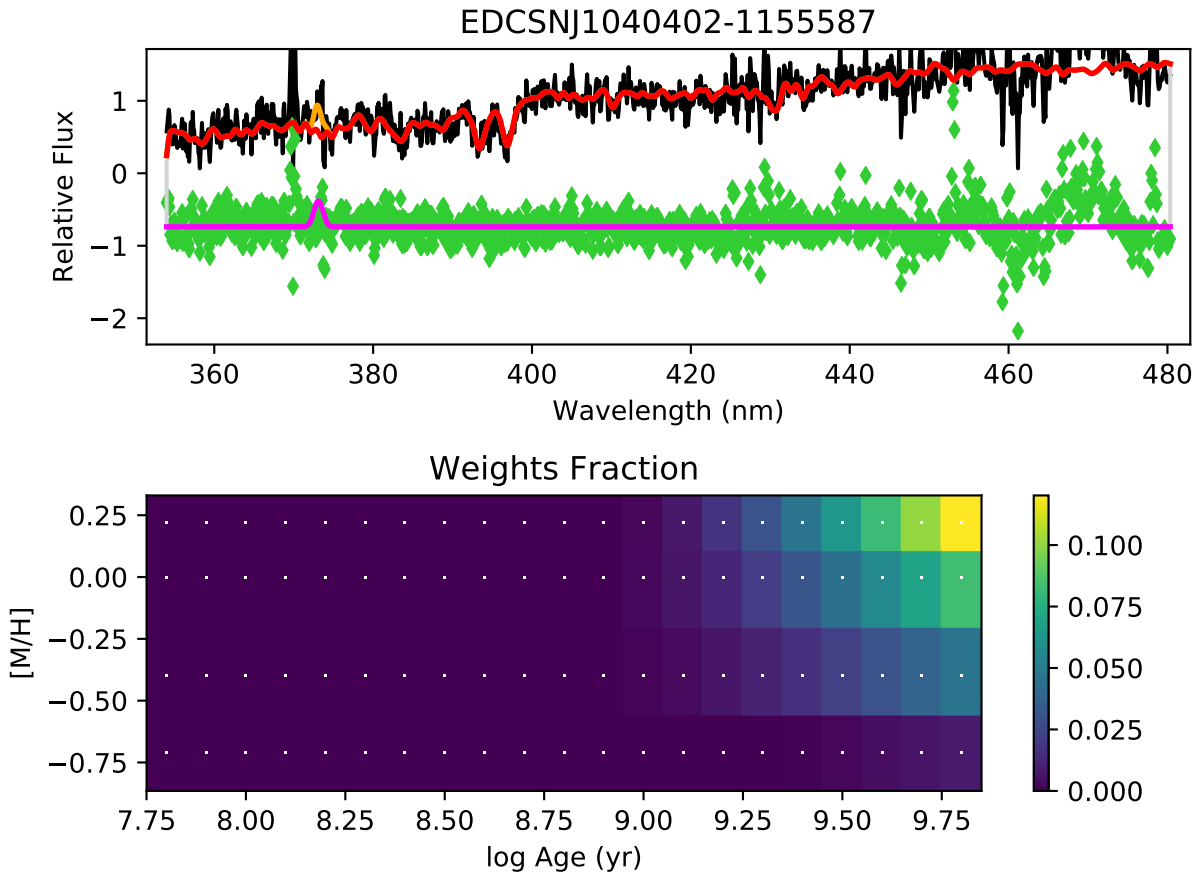
EDCSNJ1040402-1155587
Relative Flux
1
0
−1
−2
360
380
400
420
440
460
480
Wavelength (nm)
Weights Fraction
[M/H]
0.25
0.00
−0.25
−0.50
−0.75
7.75
8.00
8.25
8.50
8.75
9.00
9.25
9.50
9.75
log Age (yr)
0.100
0.075
0.050
0.025
0.000

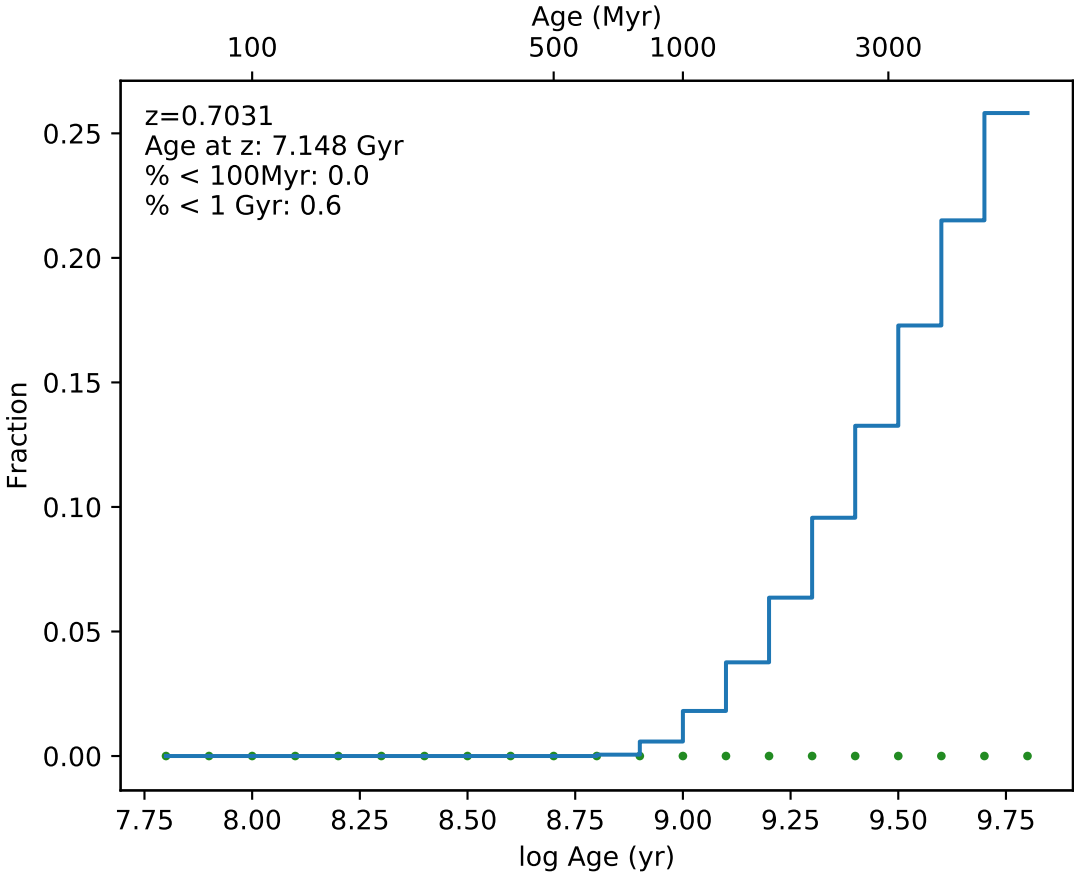
Age (Myr)
100
500
1000
3000
z=0.7031
Age at z: 7.148 Gyr
% < 100Myr: 0.0
% < 1 Gyr: 0.6
Fraction
0.25
0.20
0.15
0.10
0.05
0.00
7.75
8.00
8.25
8.50
8.75
9.00
9.25
9.50
9.75
log Age (yr)

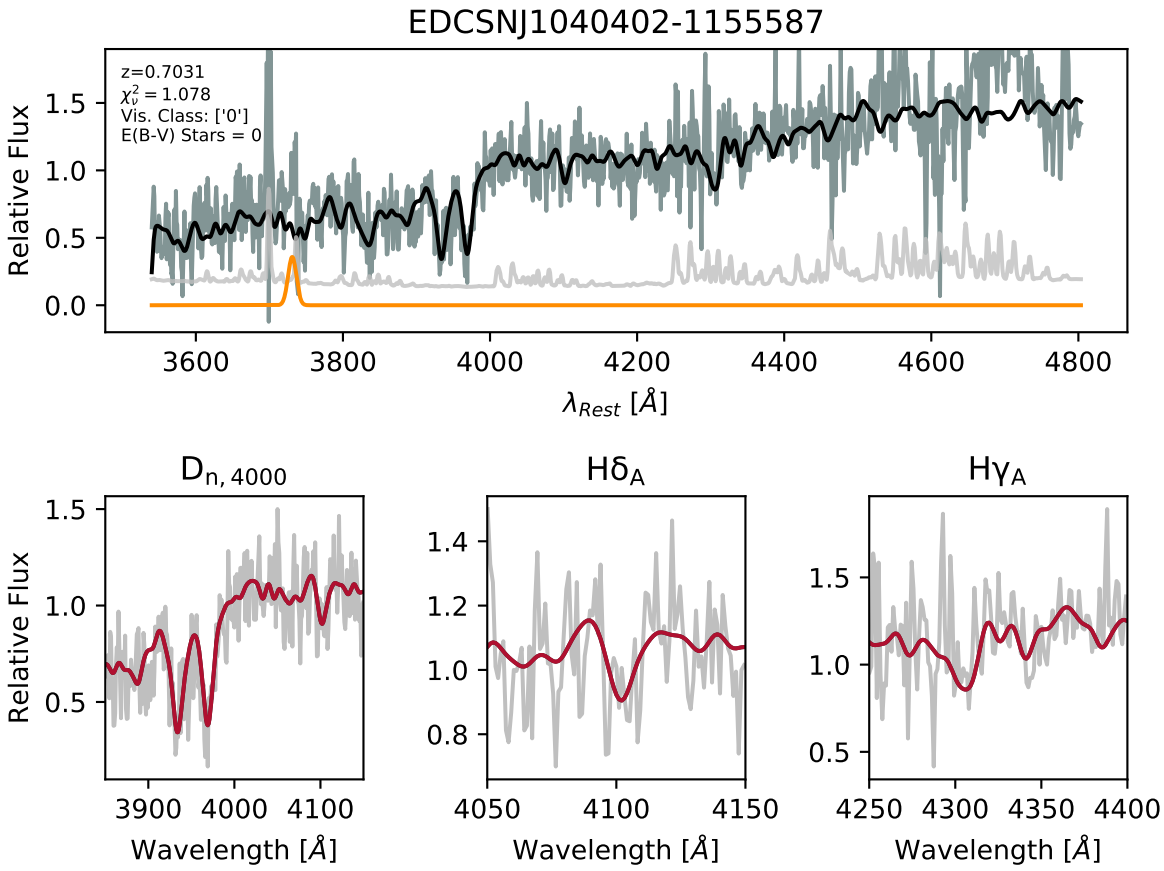
EDCSNJ1040402-1155587
z=0.7031
$\chi^2_\nu = 1.078$
Vis. Class: ['0']
E(B-V) Stars = 0
Relative Flux
λ_{Rest} [Å]
$D_{n,4000}$
$H\delta_A$
$H\gamma_A$
Wavelength [Å]

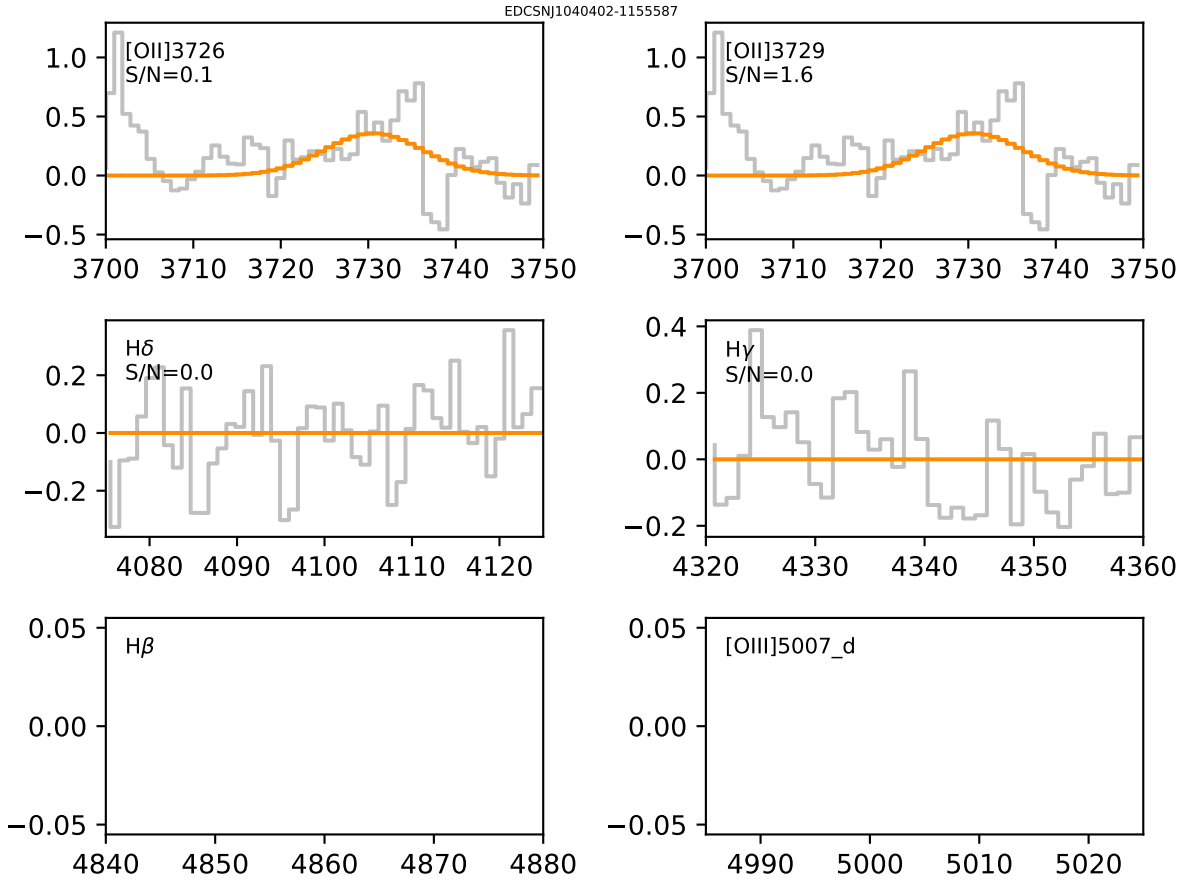
EDCSNJ1040402-1155587
[OII]3726
S/N=0.1
[OII]3729
S/N=1.6
Hδ
S/N=0.0
Hγ
S/N=0.0
Hβ
[OIII]5007_d

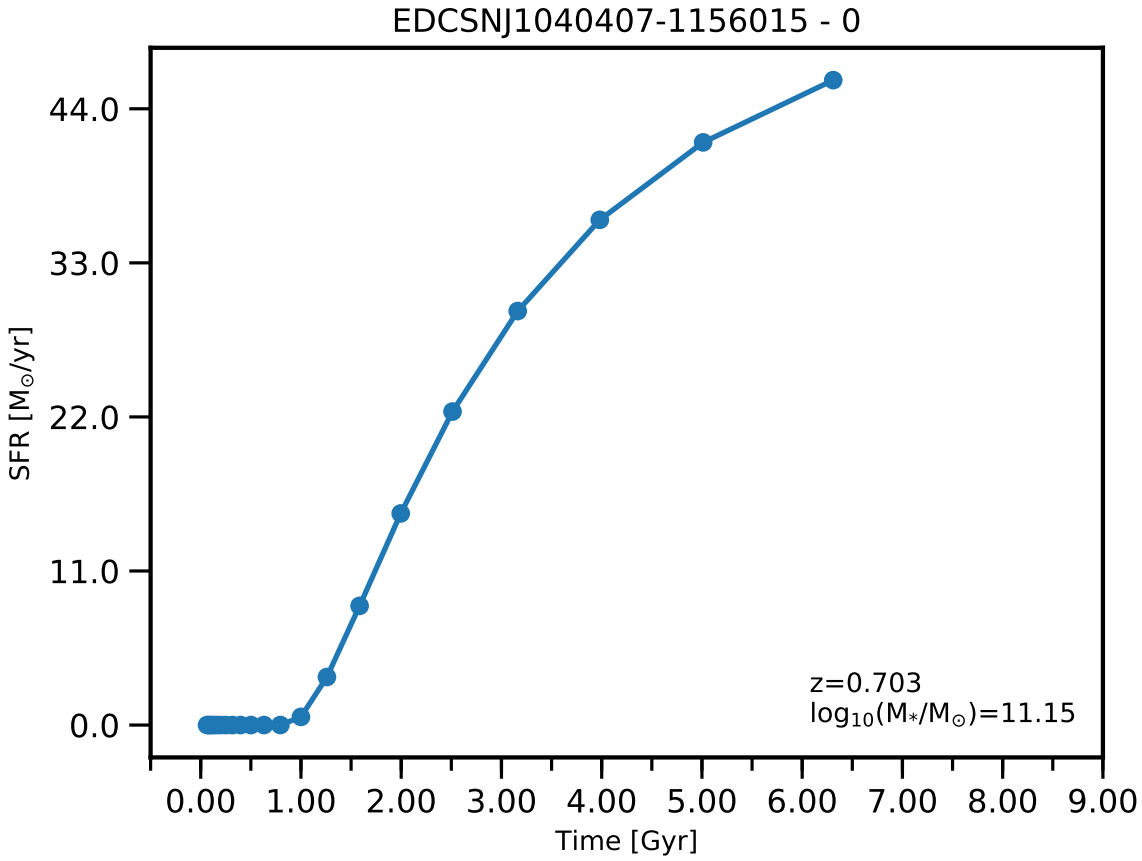
EDCSNJ1040407-1156015 - 0
SFR [M⊙/yr]
44.0
33.0
22.0
11.0
0.0
0.00
1.00
2.00
3.00
4.00
5.00
6.00
7.00
8.00
9.00
Time [Gyr]
z=0.703
log10(M*/M⊙)=11.15

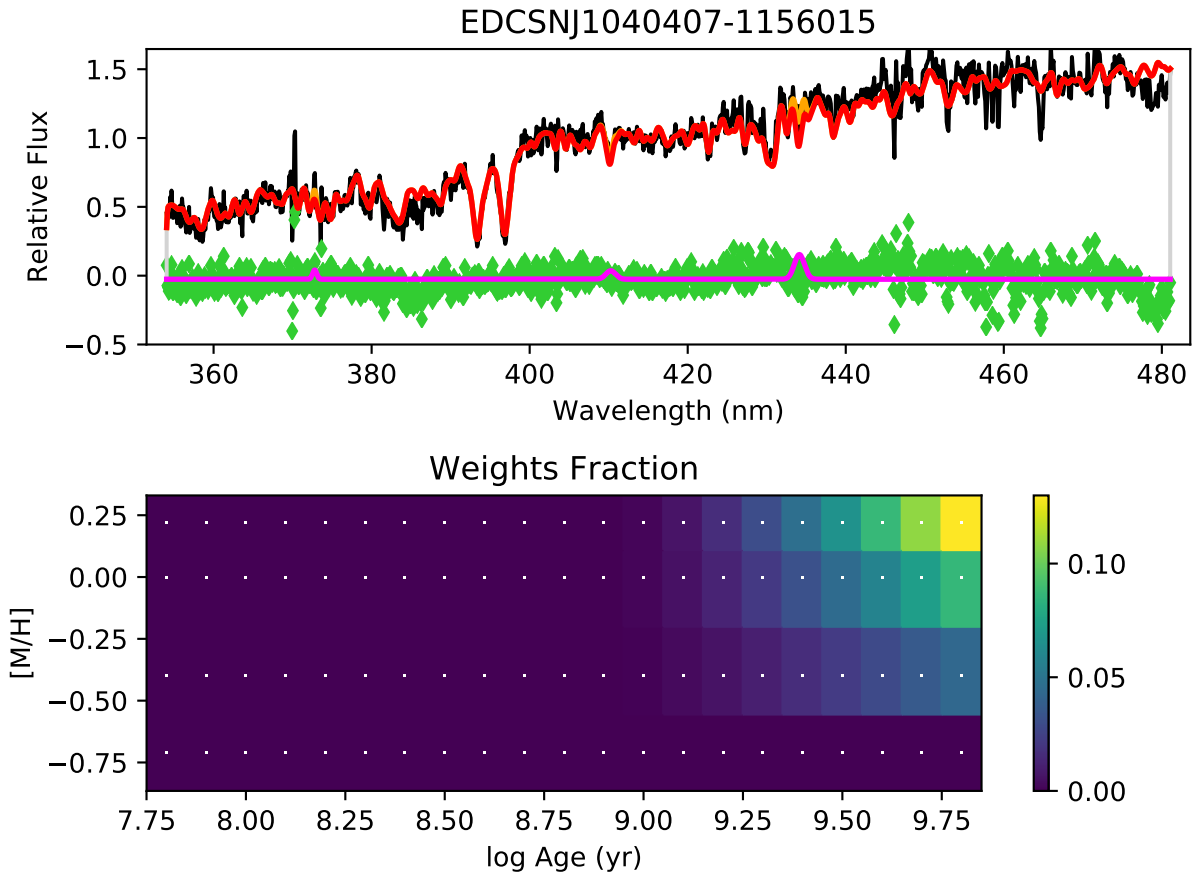
EDCSNJ1040407-1156015
Relative Flux
1.5
1.0
0.5
0.0
−0.5
360
380
400
420
440
460
480
Wavelength (nm)
Weights Fraction
[M/H]
0.25
0.00
−0.25
−0.50
−0.75
7.75
8.00
8.25
8.50
8.75
9.00
9.25
9.50
9.75
log Age (yr)
0.10
0.05
0.00

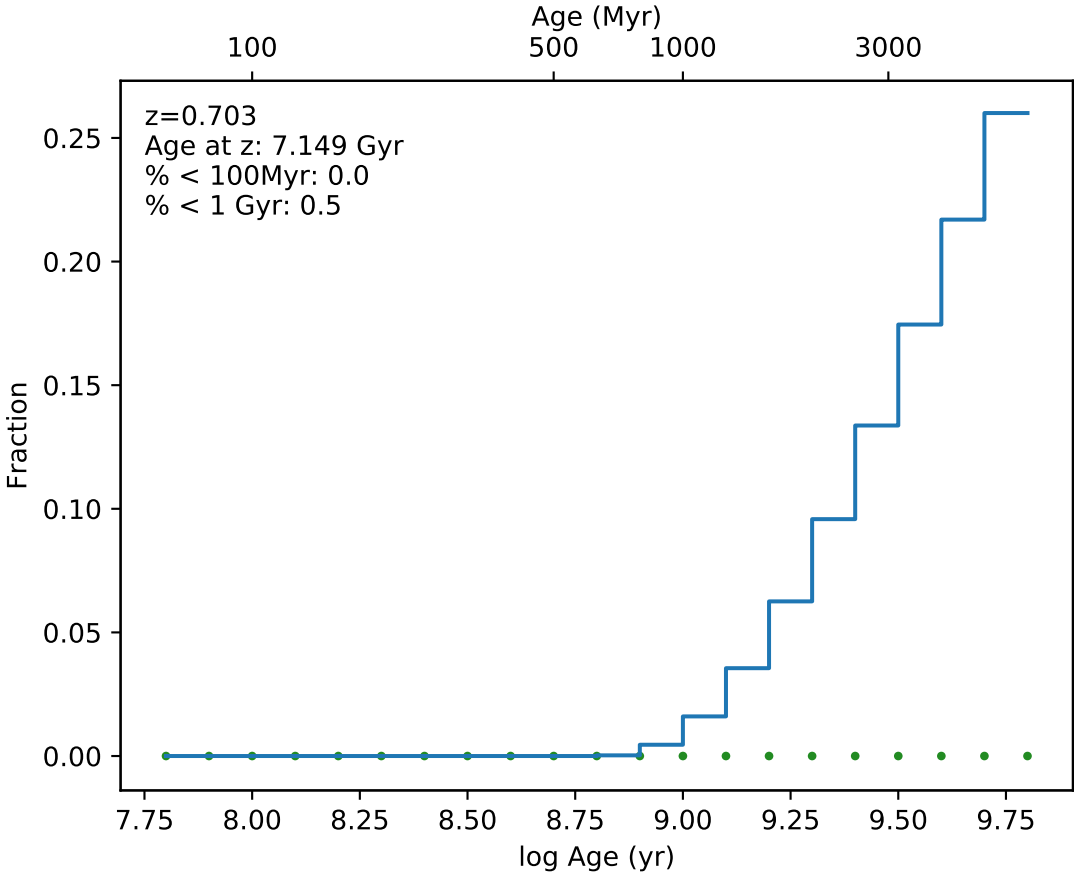
Age (Myr)
100
500
1000
3000
z=0.703
Age at z: 7.149 Gyr
% < 100Myr: 0.0
% < 1 Gyr: 0.5
Fraction
0.25
0.20
0.15
0.10
0.05
0.00
7.75
8.00
8.25
8.50
8.75
9.00
9.25
9.50
9.75
log Age (yr)

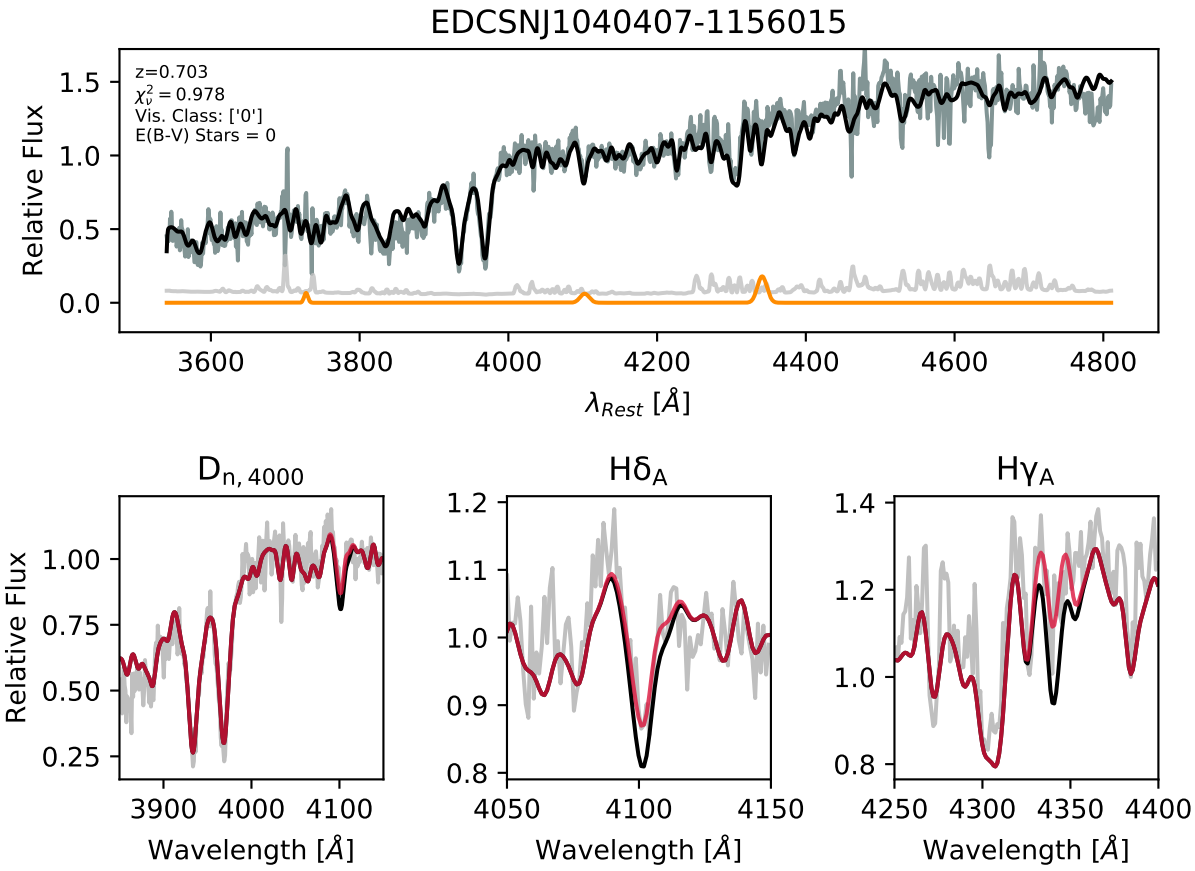
EDCSNJ1040407-1156015
z=0.703
$\chi^2_\nu = 0.978$
Vis. Class: ['0']
E(B-V) Stars = 0
Relative Flux
λ_{Rest} [Å]
$D_{n,4000}$
$H\delta_A$
$H\gamma_A$
Wavelength [Å]

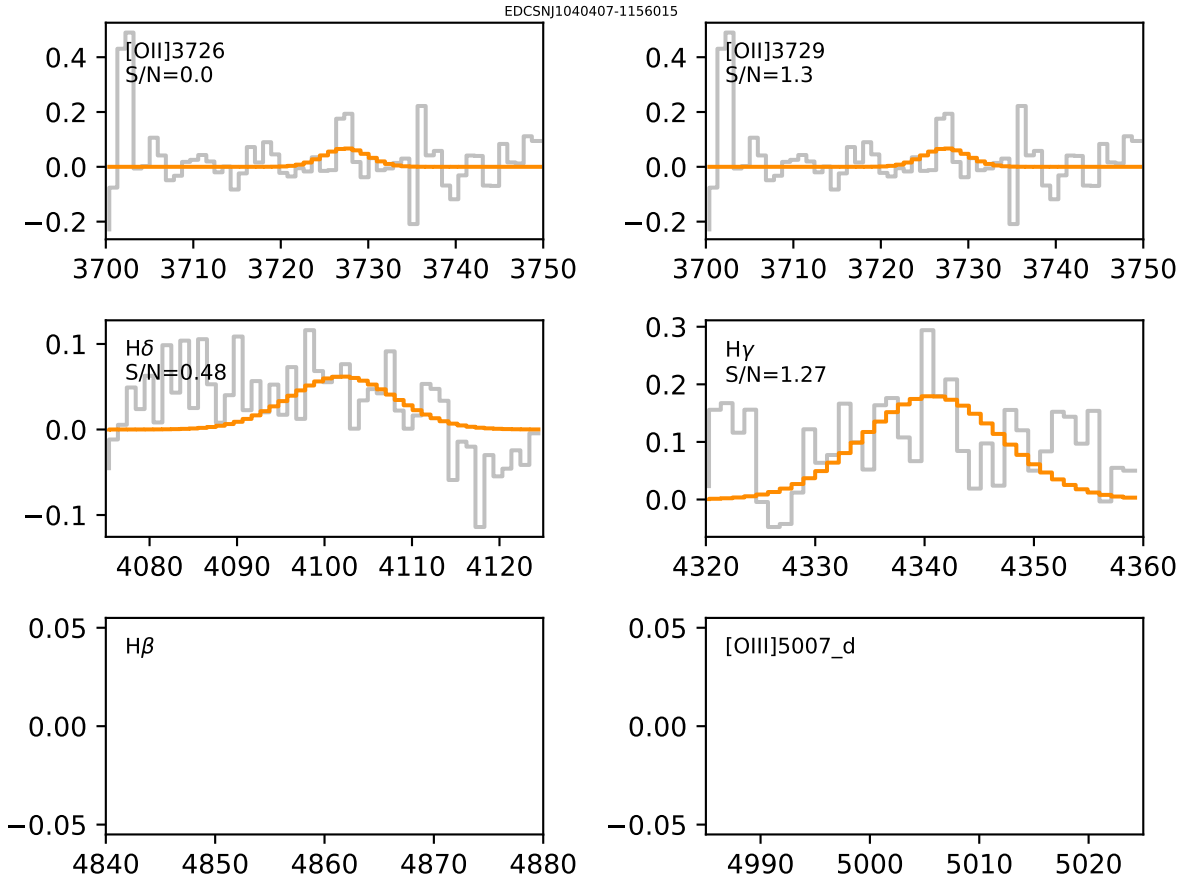
EDCSNJ1040407-1156015
[OII]3726
S/N=0.0
[OII]3729
S/N=1.3
Hδ
S/N=0.48
Hγ
S/N=1.27
Hβ
[OIII]5007_d

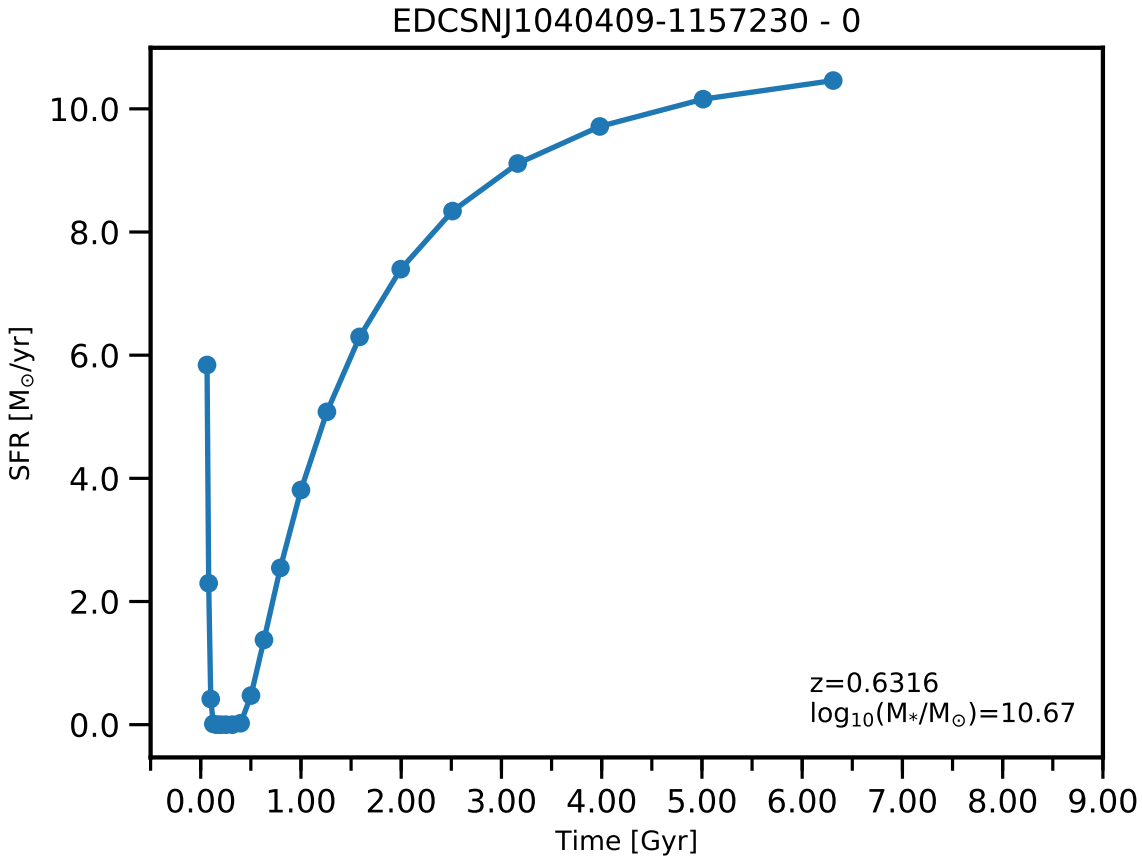
EDCSNJ1040409-1157230 - 0
SFR [M⊙/yr]
10.0
8.0
6.0
4.0
2.0
0.0
0.00
1.00
2.00
3.00
4.00
5.00
6.00
7.00
8.00
9.00
Time [Gyr]
z=0.6316
log10(M*/M⊙)=10.67

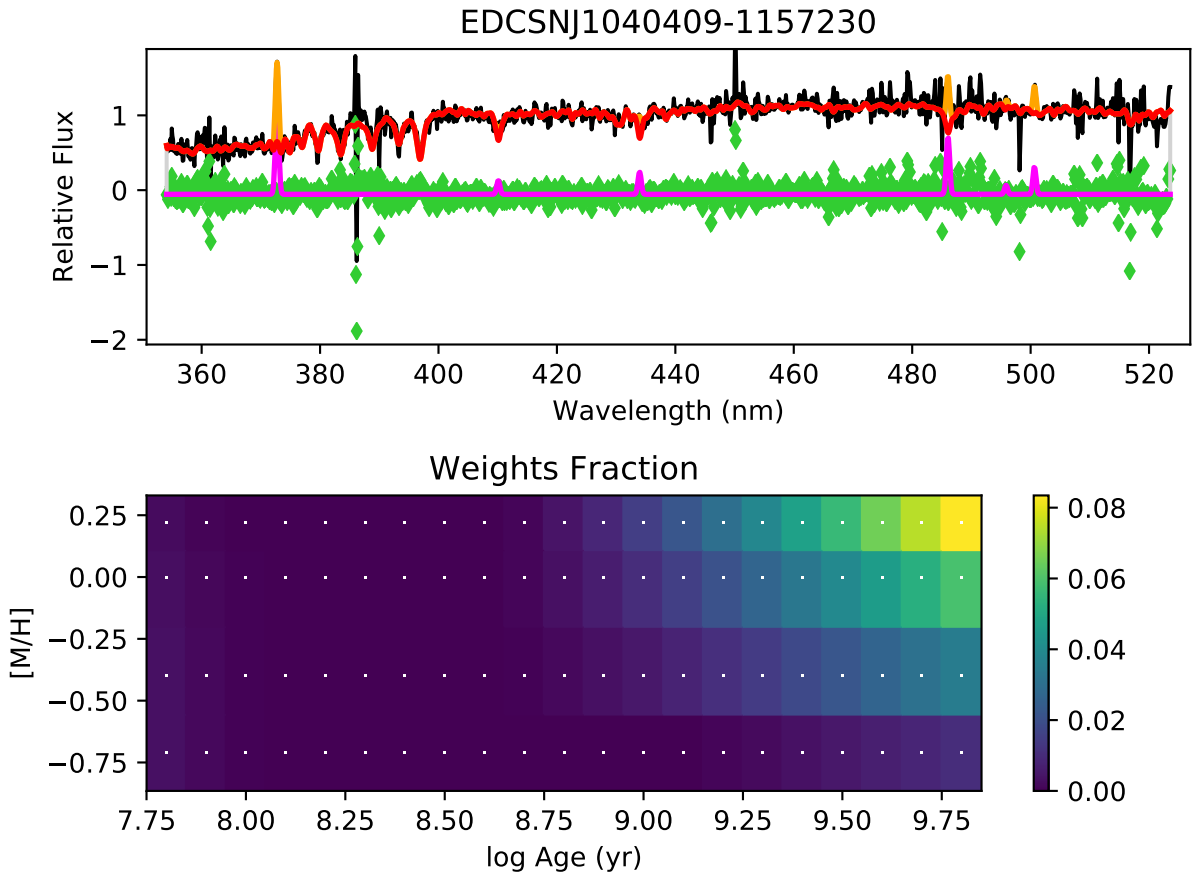
EDCSNJ1040409-1157230
Relative Flux
1
0
−1
−2
360
380
400
420
440
460
480
500
520
Wavelength (nm)
Weights Fraction
[M/H]
0.25
0.00
−0.25
−0.50
−0.75
7.75
8.00
8.25
8.50
8.75
9.00
9.25
9.50
9.75
log Age (yr)
0.08
0.06
0.04
0.02
0.00

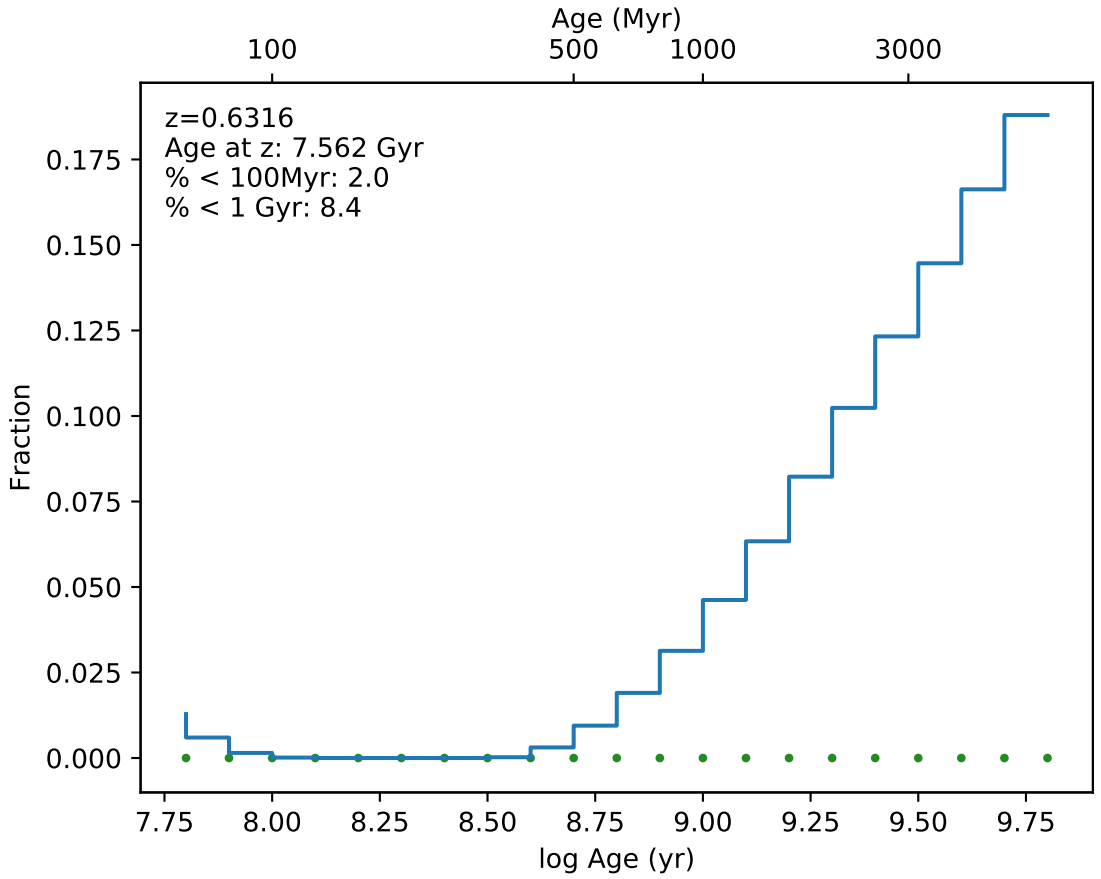
Age (Myr)
100
500
1000
3000
z=0.6316
Age at z: 7.562 Gyr
% < 100Myr: 2.0
% < 1 Gyr: 8.4
Fraction
0.175
0.150
0.125
0.100
0.075
0.050
0.025
0.000
7.75
8.00
8.25
8.50
8.75
9.00
9.25
9.50
9.75
log Age (yr)

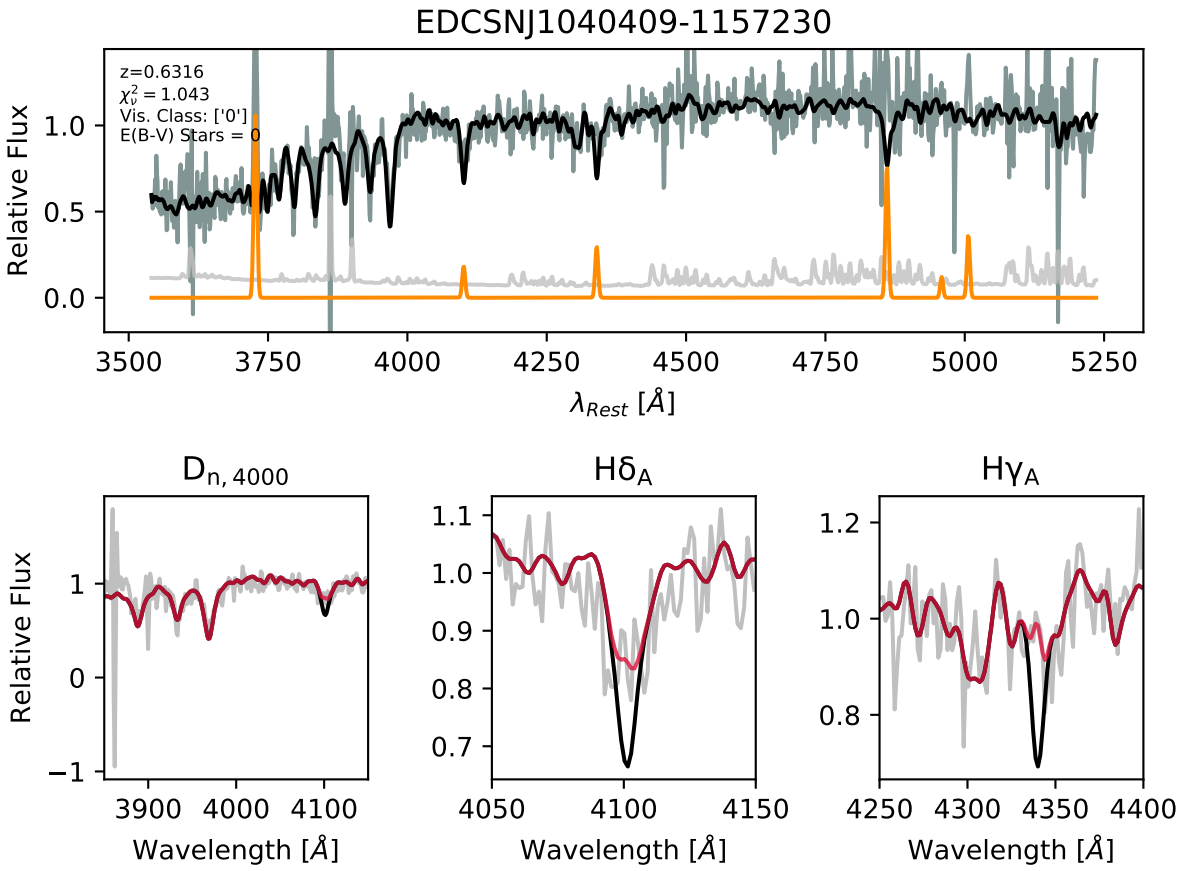
EDCSNJ1040409-1157230
z=0.6316
$\chi^2_\nu = 1.043$
Vis. Class: ['0']
E(B-V) Stars = 0
Relative Flux
1.0
0.5
0.0
3500
3750
4000
4250
4500
4750
5000
5250
λ_{Rest} [Å]
$D_{n,4000}$
$H\delta_A$
$H\gamma_A$
Relative Flux
1
0
−1
3900
4000
4100
Wavelength [Å]
1.1
1.0
0.9
0.8
0.7
4050
4100
4150
Wavelength [Å]
1.2
1.0
0.8
4250
4300
4350
4400
Wavelength [Å]

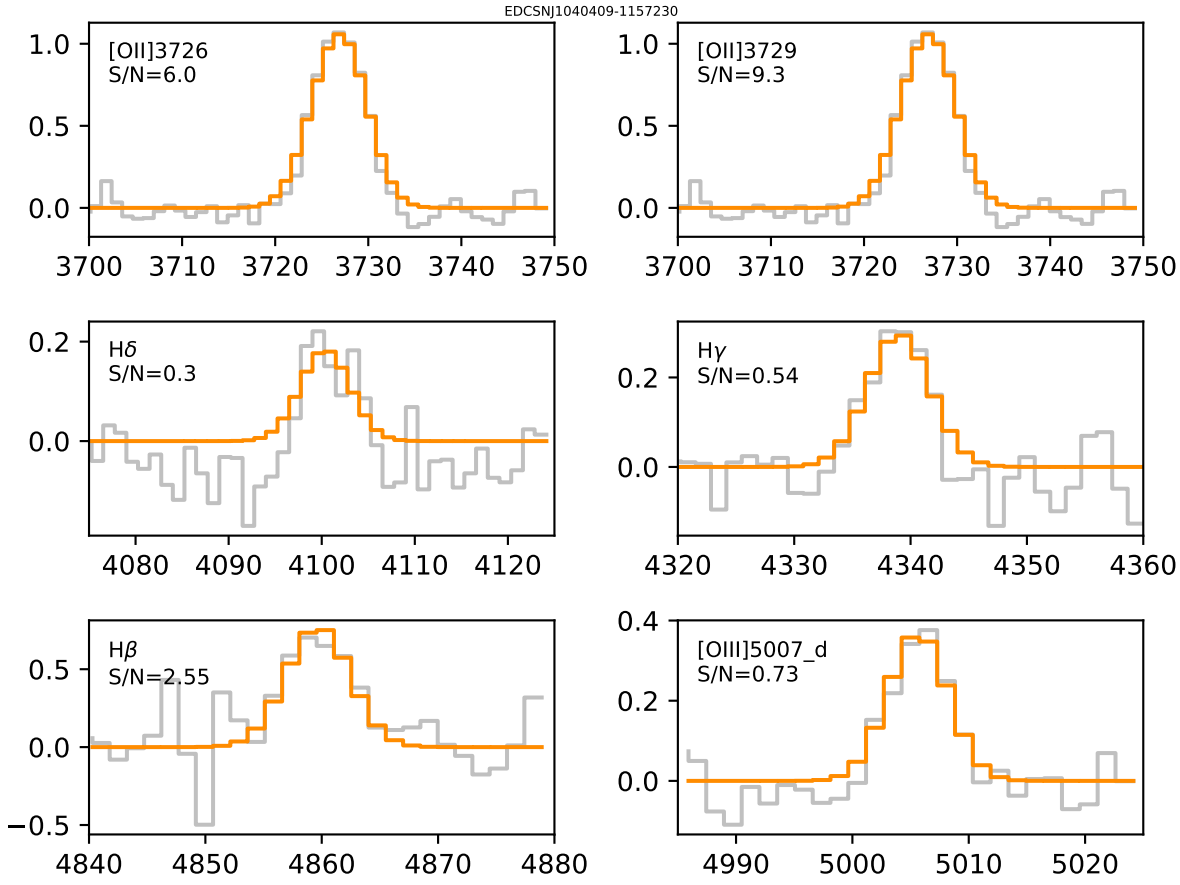
EDCSNJ1040409-1157230
[OII]3726
S/N=6.0
[OII]3729
S/N=9.3
Hδ
S/N=0.3
Hγ
S/N=0.54
Hβ
S/N=2.55
[OIII]5007_d
S/N=0.73

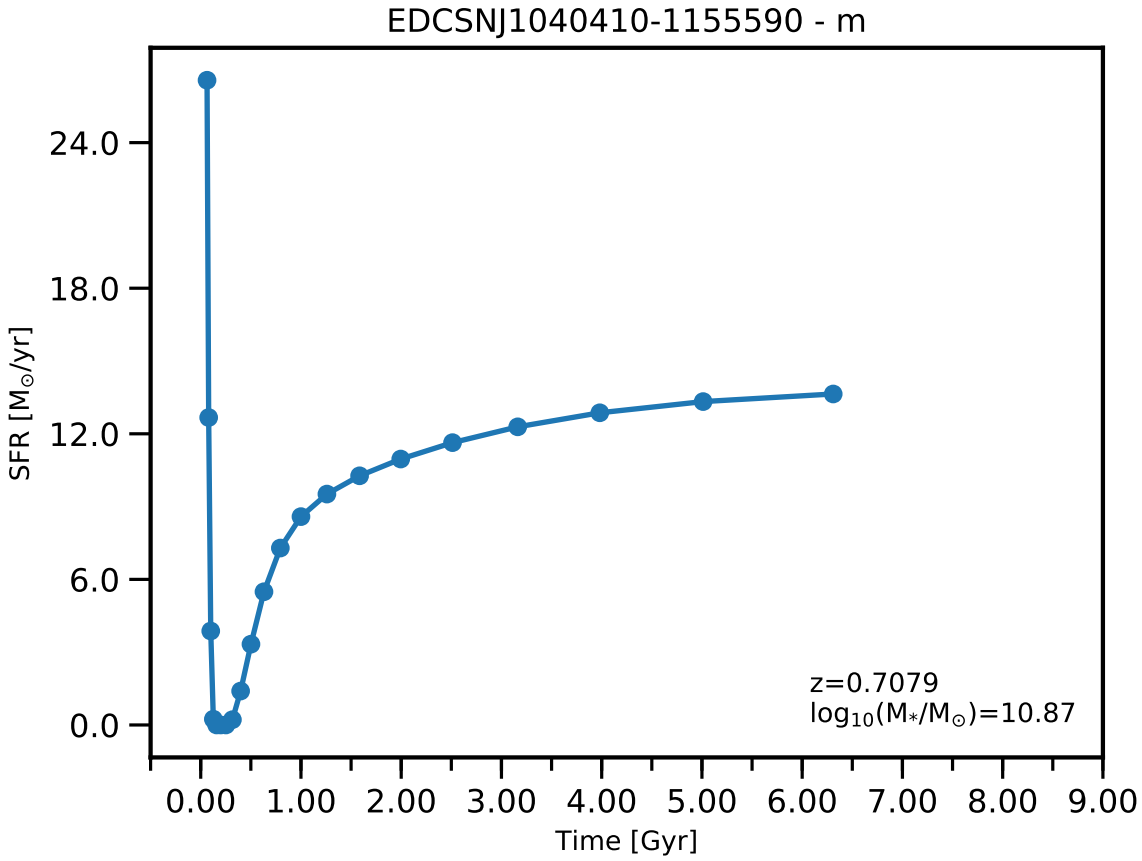
EDCSNJ1040410-1155590 - m
SFR [M⊙/yr]
24.0
18.0
12.0
6.0
0.0
0.00
1.00
2.00
3.00
4.00
5.00
6.00
7.00
8.00
9.00
Time [Gyr]
z=0.7079
log10(M*/M⊙)=10.87

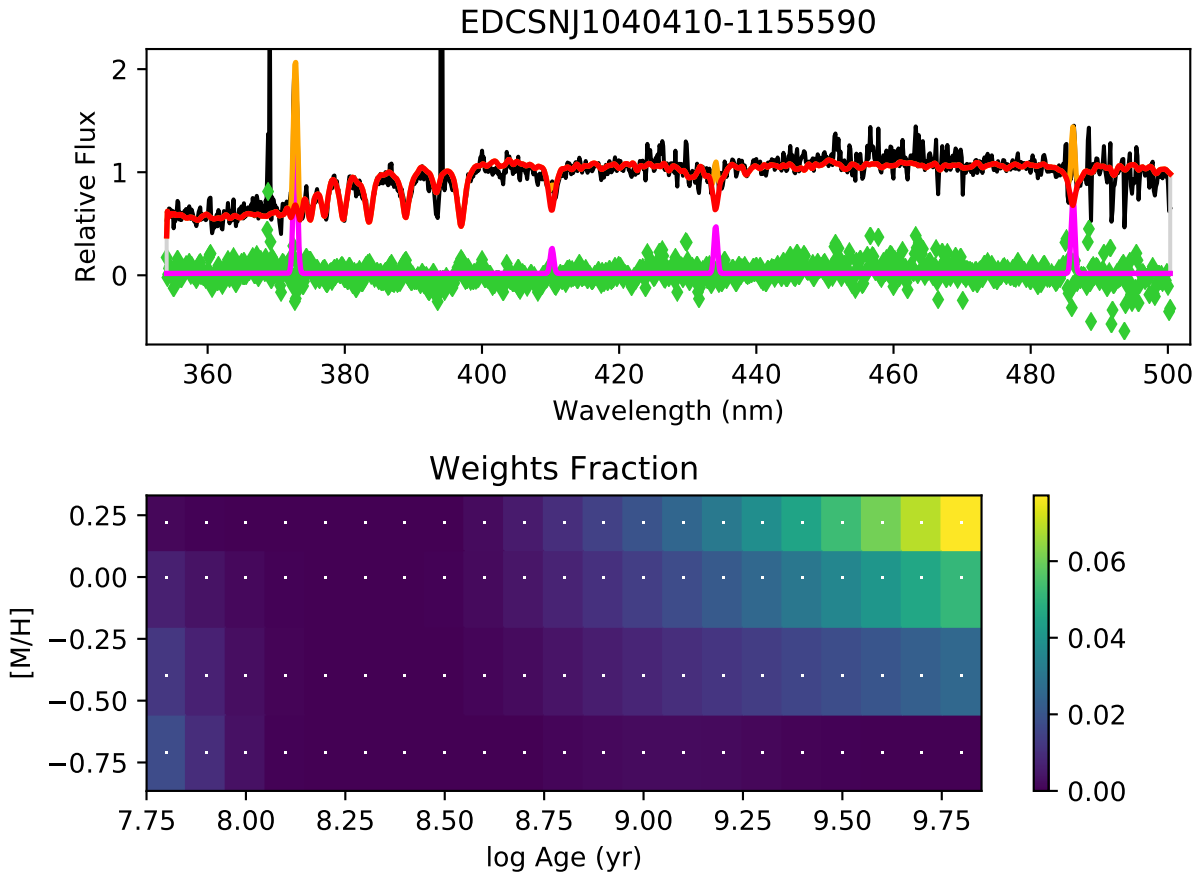
EDCSNJ1040410-1155590
Relative Flux
2
1
0
360
380
400
420
440
460
480
500
Wavelength (nm)
Weights Fraction
[M/H]
0.25
0.00
−0.25
−0.50
−0.75
7.75
8.00
8.25
8.50
8.75
9.00
9.25
9.50
9.75
log Age (yr)
0.06
0.04
0.02
0.00

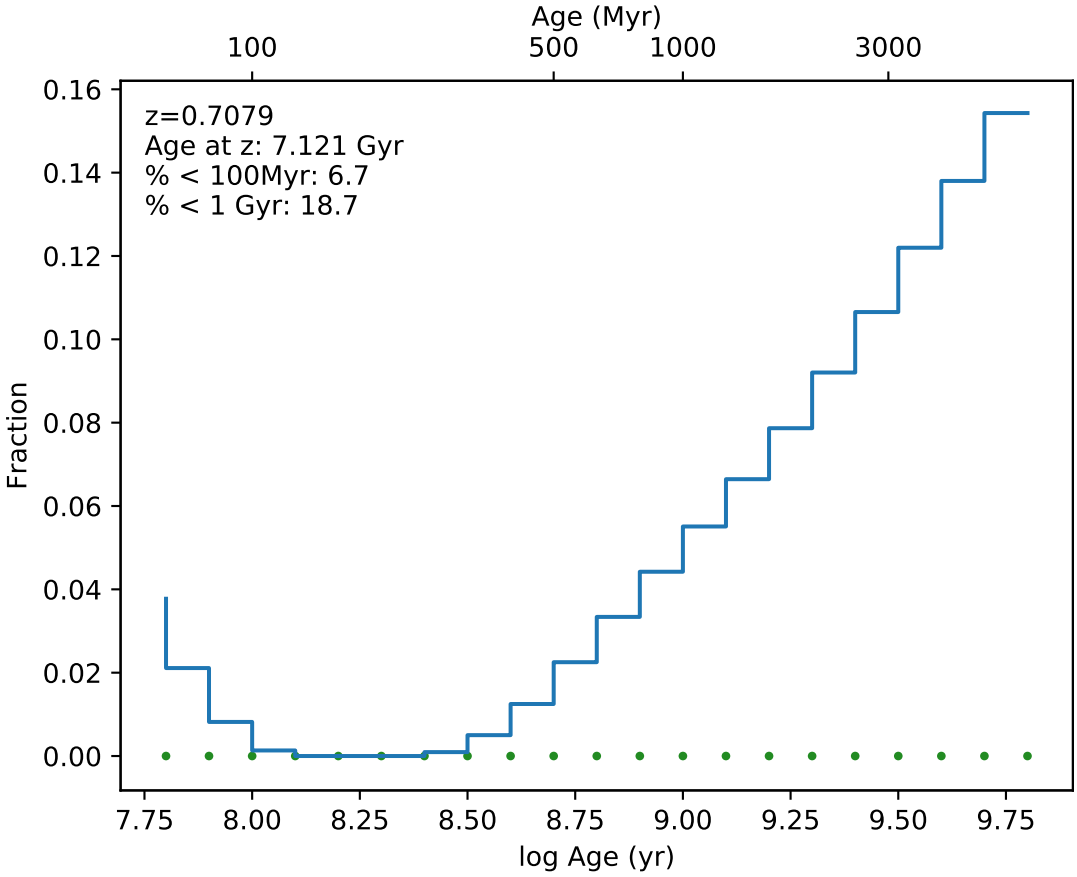
Age (Myr)
100
500
1000
3000
z=0.7079
Age at z: 7.121 Gyr
% < 100Myr: 6.7
% < 1 Gyr: 18.7
Fraction
0.16
0.14
0.12
0.10
0.08
0.06
0.04
0.02
0.00
7.75
8.00
8.25
8.50
8.75
9.00
9.25
9.50
9.75
log Age (yr)

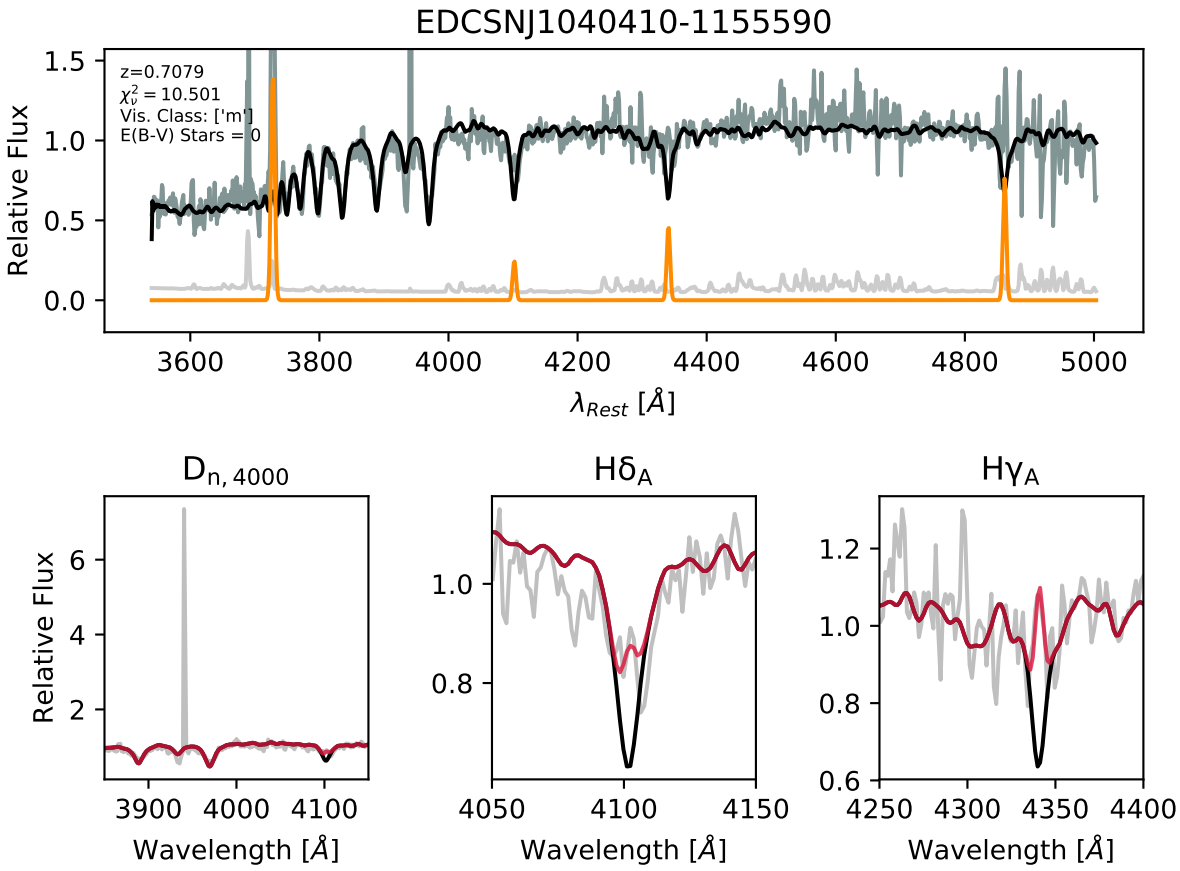
EDCSNJ1040410-1155590
z=0.7079
$\chi^2_\nu = 10.501$
Vis. Class: ['m']
E(B-V) Stars = 0
Relative Flux
λ_{Rest} [Å]
$D_{n,4000}$
$H\delta_A$
$H\gamma_A$
Wavelength [Å]

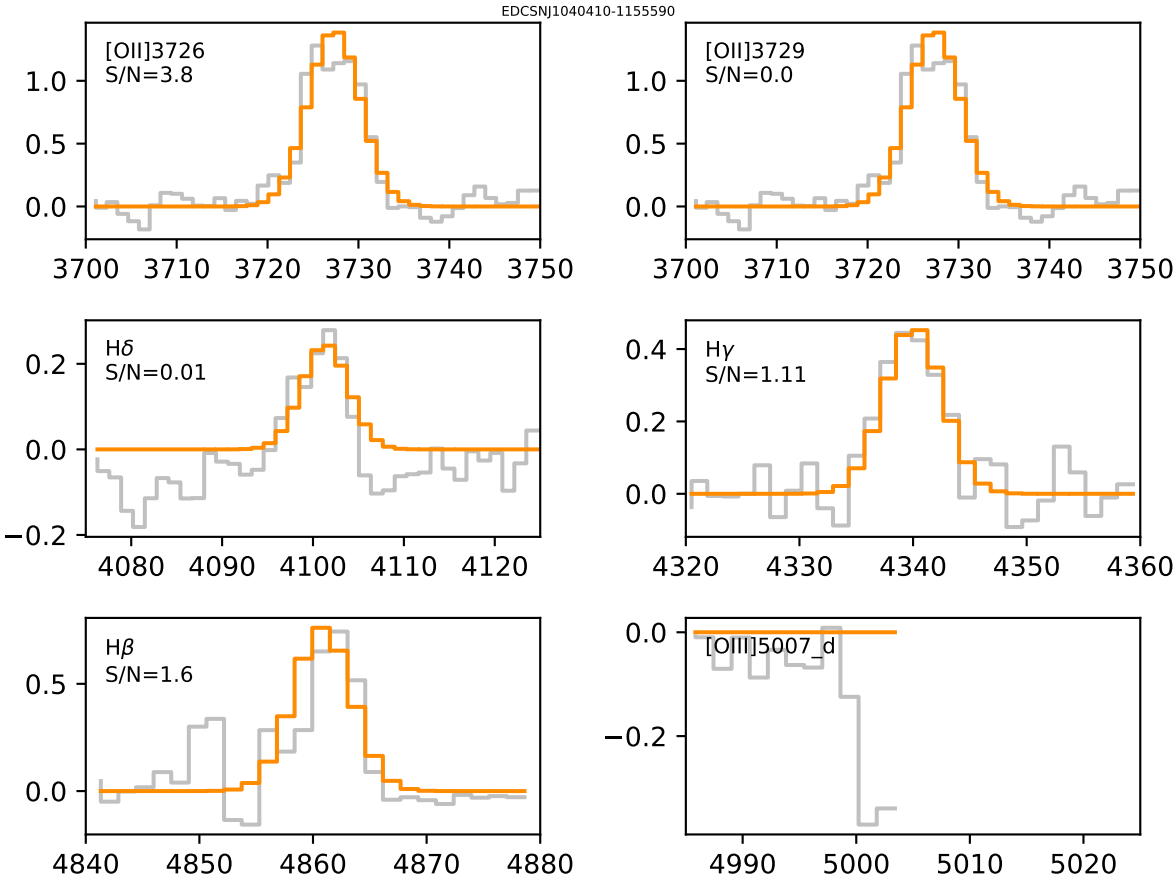
EDCSNJ1040410-1155590
[OII]3726
S/N=3.8
[OII]3729
S/N=0.0
Hδ
S/N=0.01
Hγ
S/N=1.11
Hβ
S/N=1.6
[OIII]5007_d

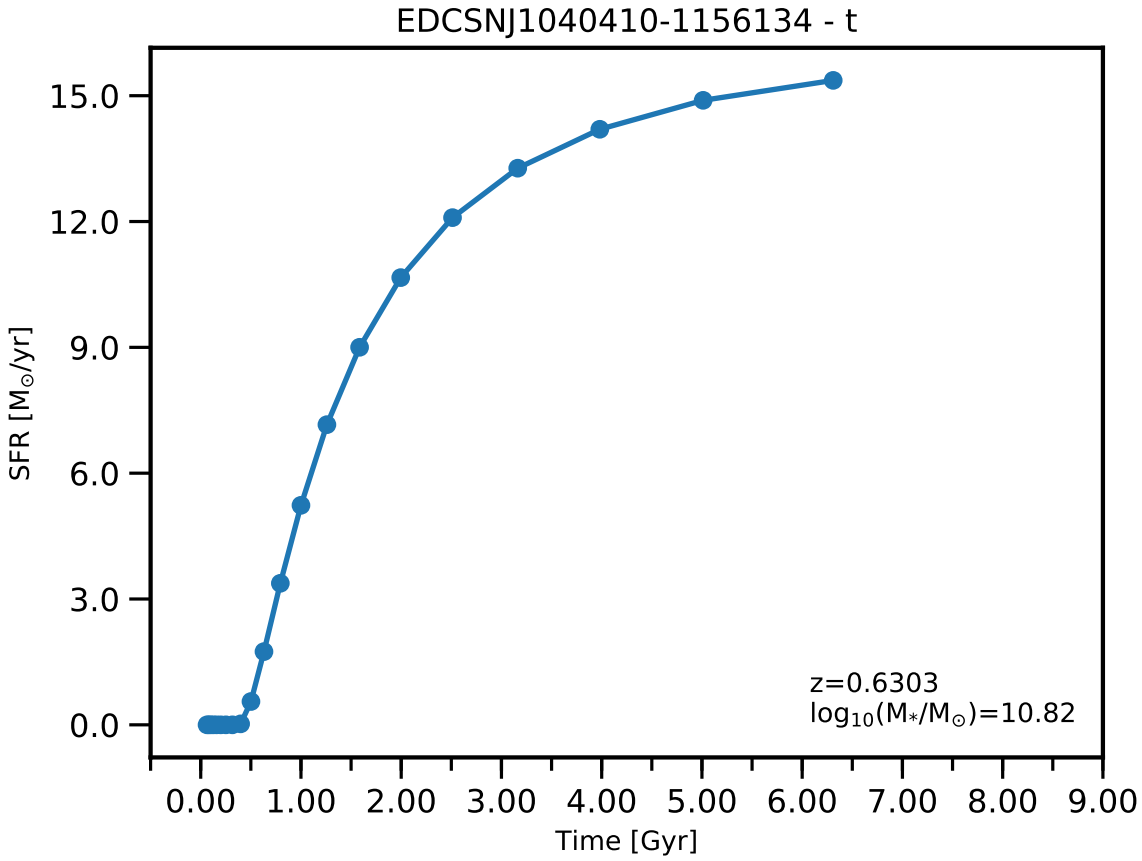
EDCSNJ1040410-1156134 - t
SFR [M⊙/yr]
15.0
12.0
9.0
6.0
3.0
0.0
0.00
1.00
2.00
3.00
4.00
5.00
6.00
7.00
8.00
9.00
Time [Gyr]
z=0.6303
log10(M*/M⊙)=10.82

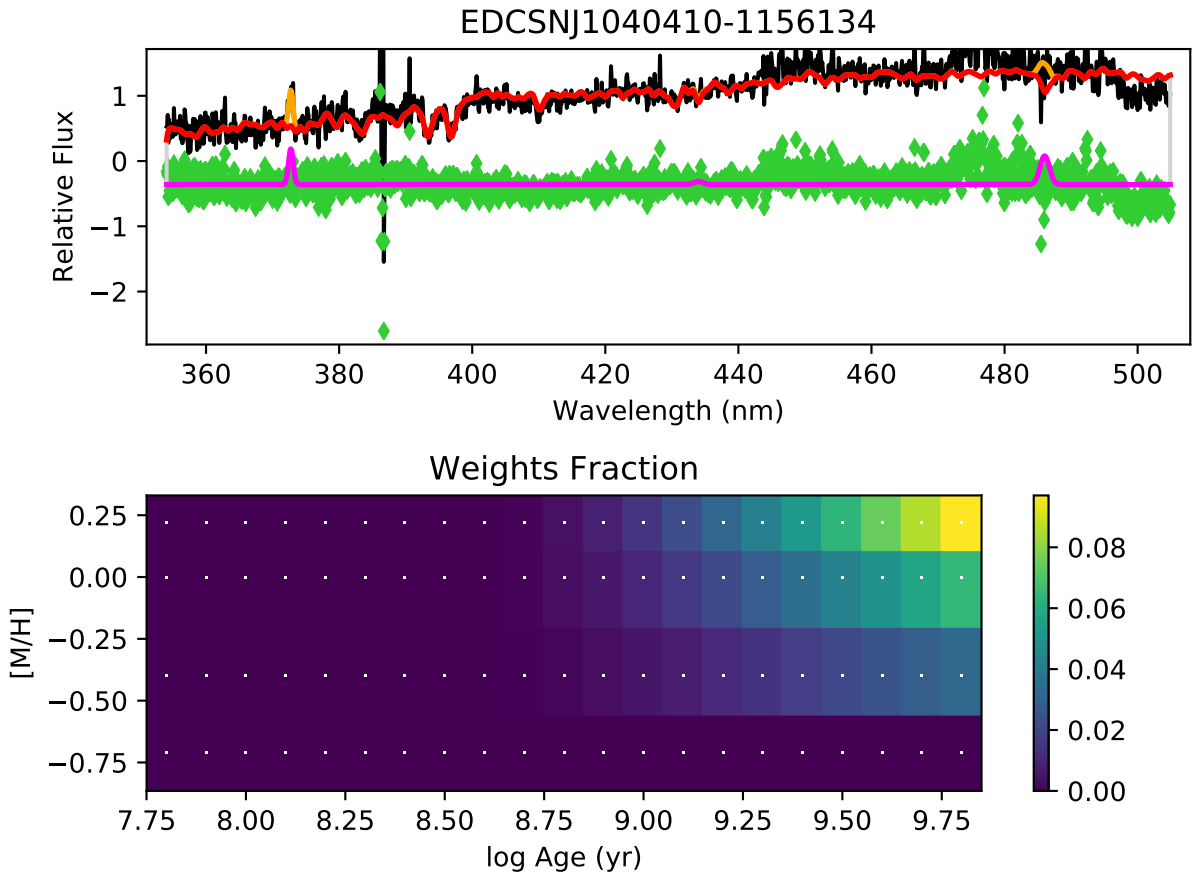
EDCSNJ1040410-1156134
Relative Flux
1
0
−1
−2
360
380
400
420
440
460
480
500
Wavelength (nm)
Weights Fraction
[M/H]
0.25
0.00
−0.25
−0.50
−0.75
7.75
8.00
8.25
8.50
8.75
9.00
9.25
9.50
9.75
log Age (yr)
0.08
0.06
0.04
0.02
0.00

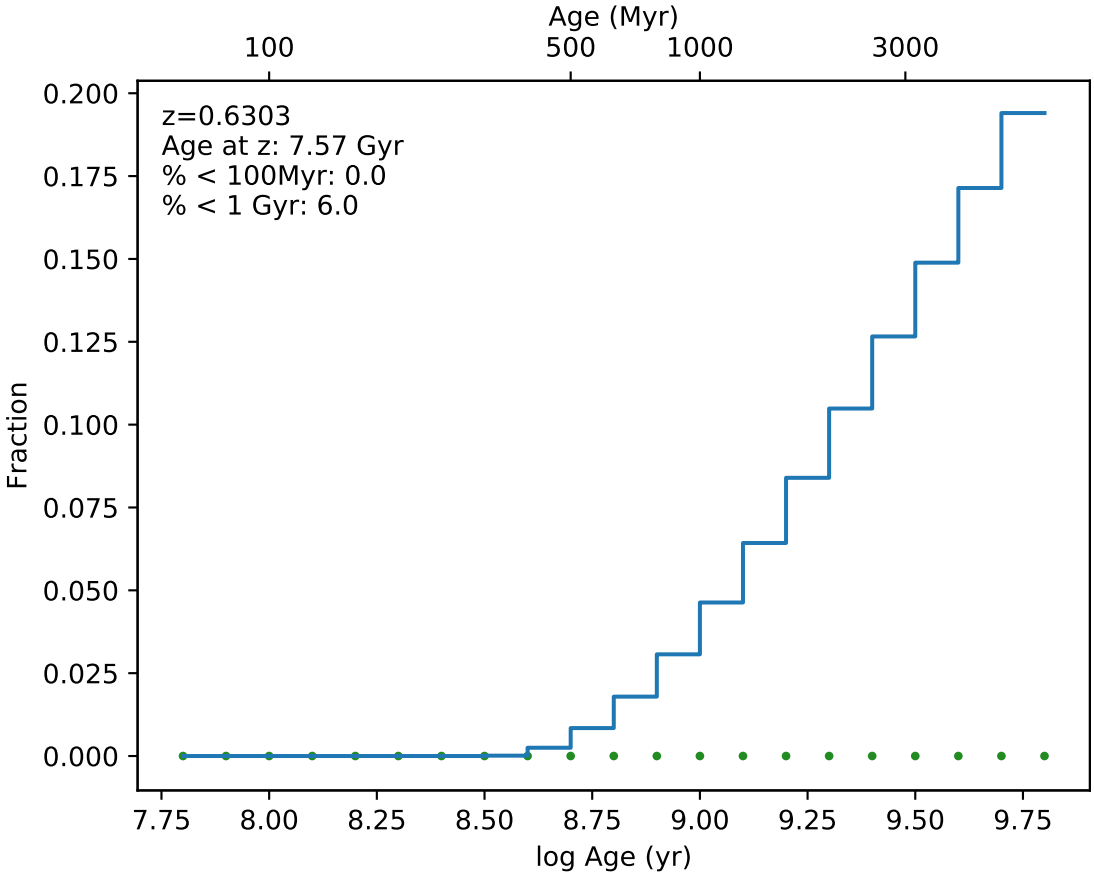
Age (Myr)
100
500
1000
3000
z=0.6303
Age at z: 7.57 Gyr
% < 100Myr: 0.0
% < 1 Gyr: 6.0
Fraction
0.200
0.175
0.150
0.125
0.100
0.075
0.050
0.025
0.000
7.75
8.00
8.25
8.50
8.75
9.00
9.25
9.50
9.75
log Age (yr)

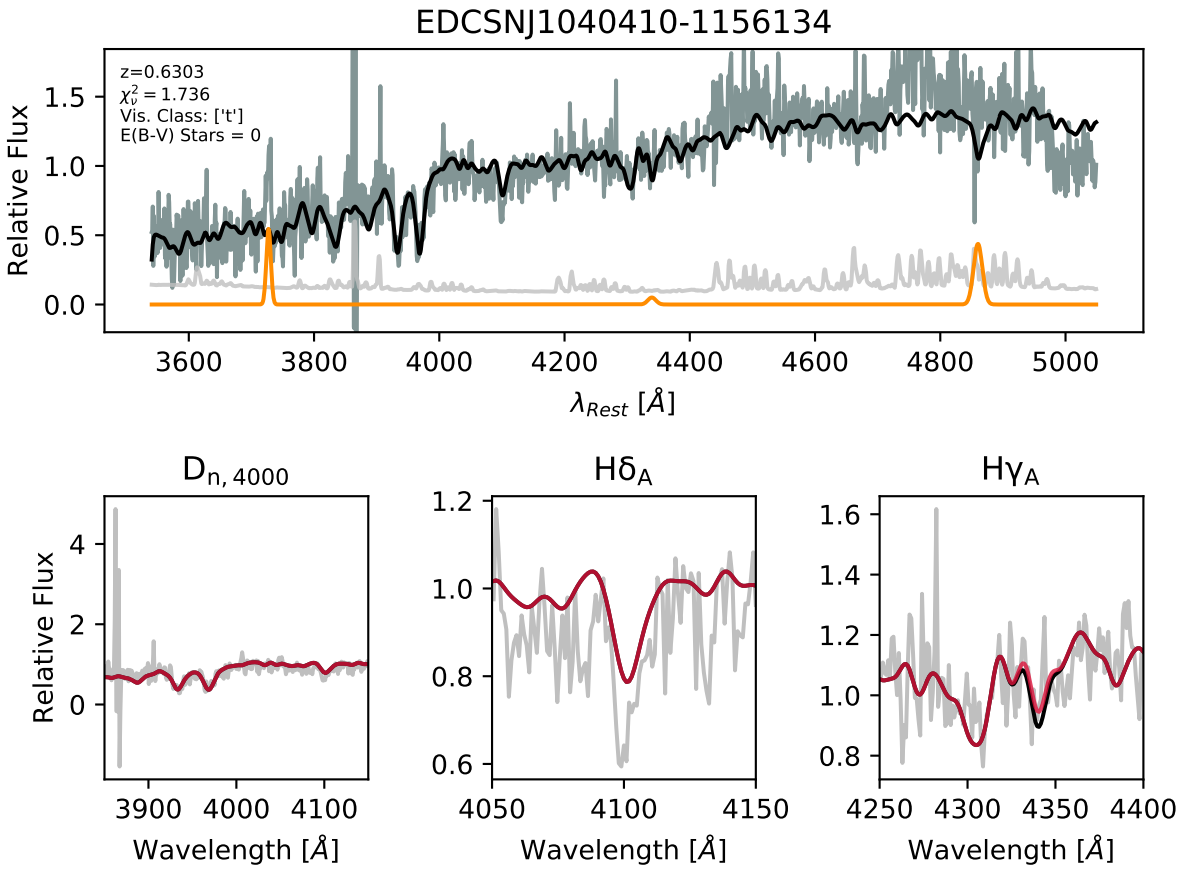
EDCSNJ1040410-1156134
z=0.6303
$\chi^2_\nu = 1.736$
Vis. Class: ['t']
E(B-V) Stars = 0
Relative Flux
λ_{Rest} [Å]
$D_{n,4000}$
$H\delta_A$
$H\gamma_A$
Wavelength [Å]

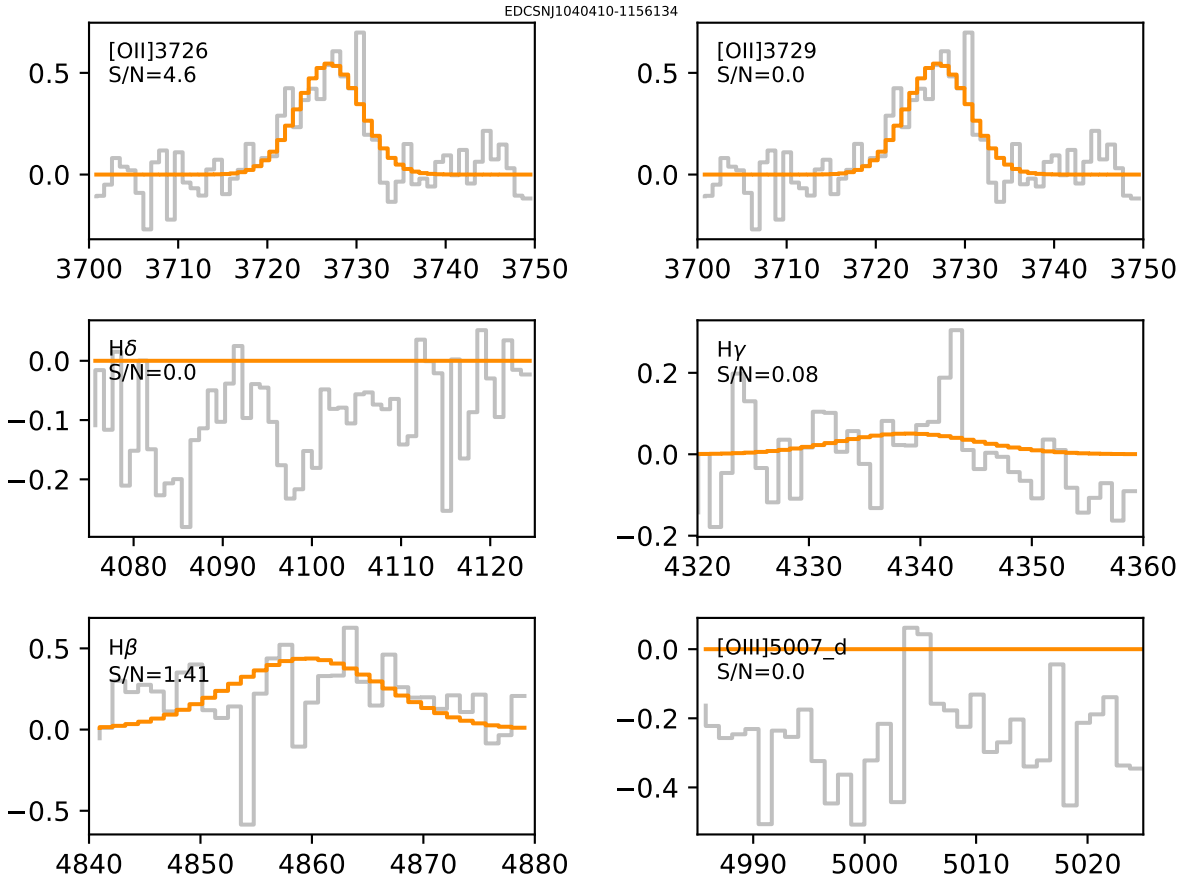
EDCSNJ1040410-1156134
[OII]3726
S/N=4.6
[OII]3729
S/N=0.0
Hδ
S/N=0.0
Hγ
S/N=0.08
Hβ
S/N=1.41
[OIII]5007_d
S/N=0.0

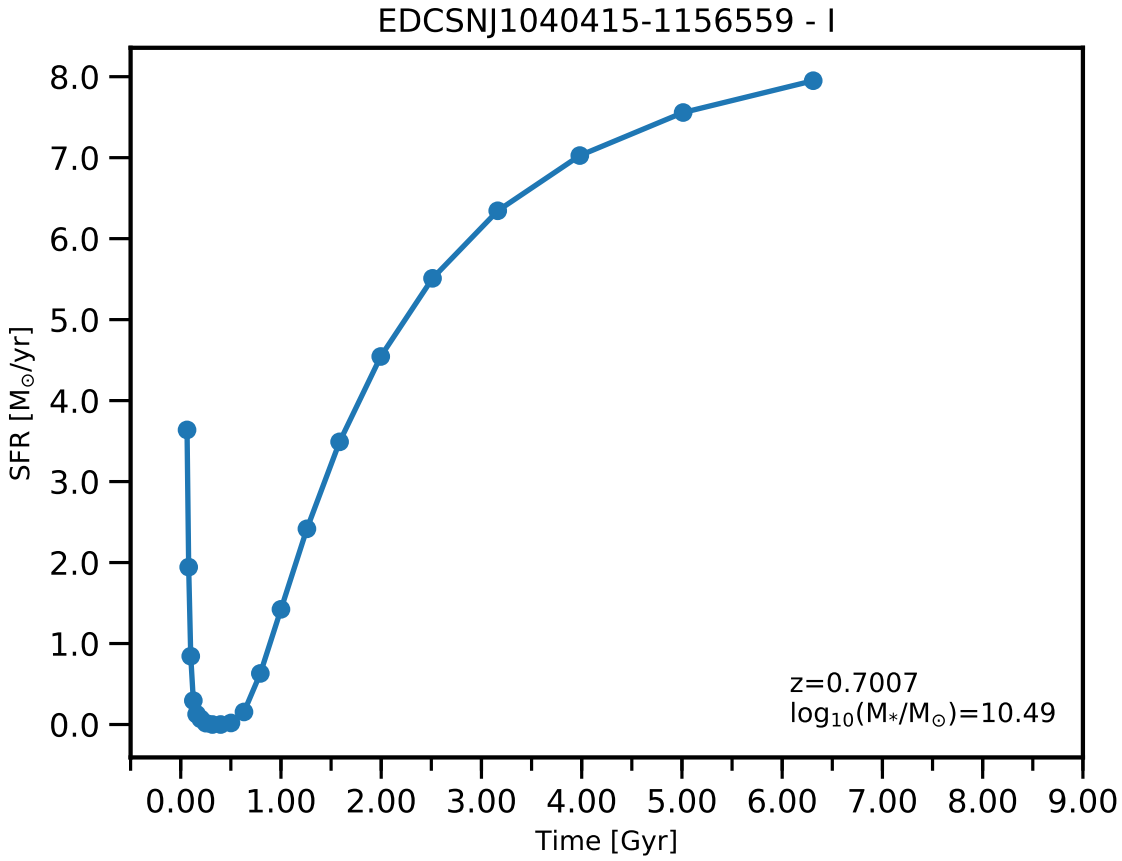
EDCSNJ1040415-1156559 - I
SFR [M⊙/yr]
Time [Gyr]
z=0.7007
log10(M*/M⊙)=10.49
0.0
1.0
2.0
3.0
4.0
5.0
6.0
7.0
8.0
0.00
1.00
2.00
3.00
4.00
5.00
6.00
7.00
8.00
9.00

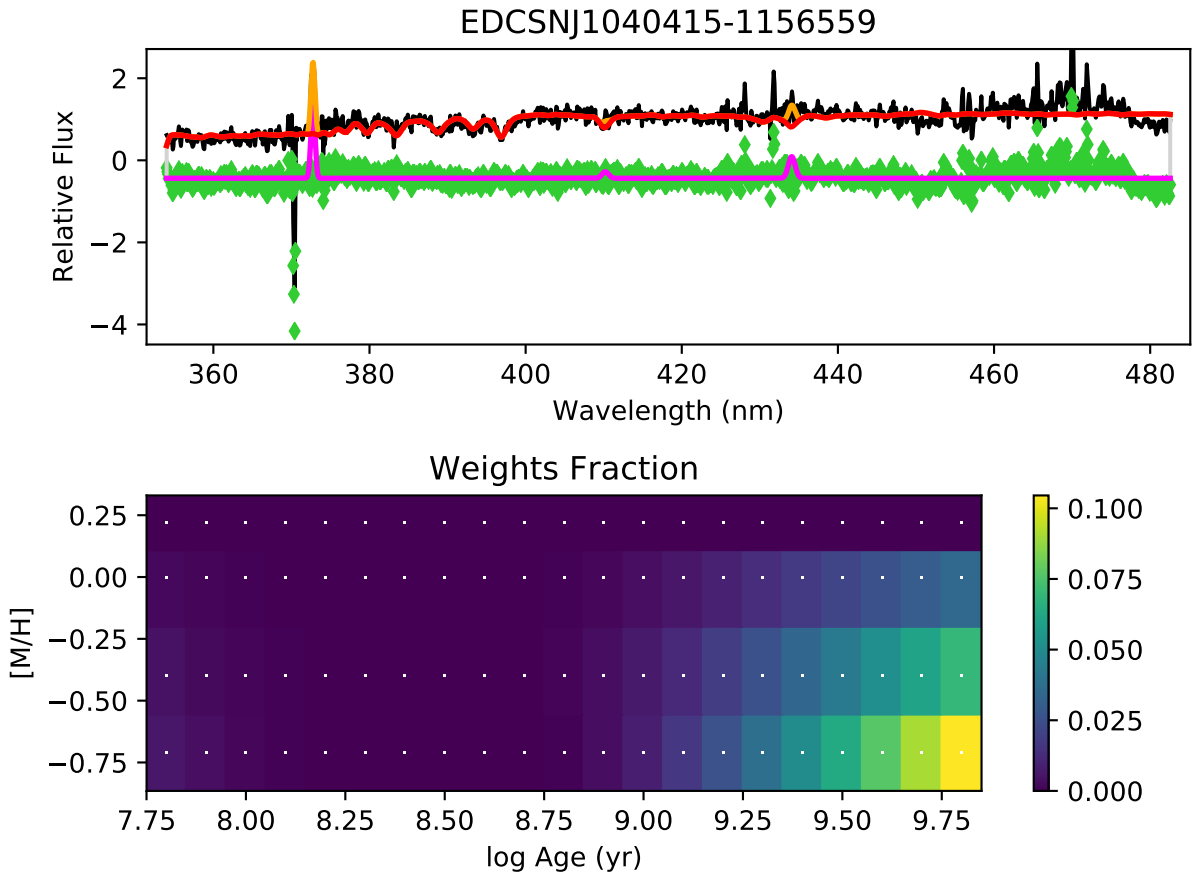
EDCSNJ1040415-1156559
Relative Flux
2
0
−2
−4
360
380
400
420
440
460
480
Wavelength (nm)
Weights Fraction
[M/H]
0.25
0.00
−0.25
−0.50
−0.75
7.75
8.00
8.25
8.50
8.75
9.00
9.25
9.50
9.75
log Age (yr)
0.100
0.075
0.050
0.025
0.000

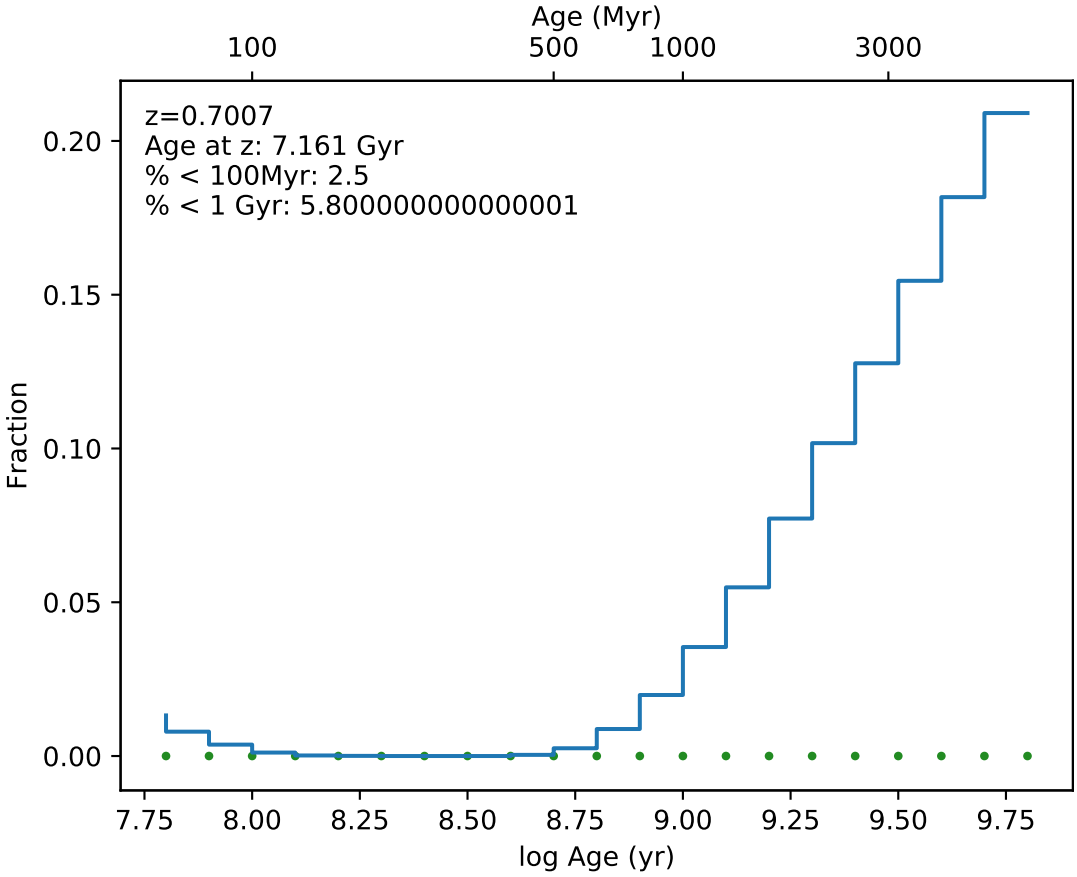
Age (Myr)
100
500
1000
3000
z=0.7007
Age at z: 7.161 Gyr
% < 100Myr: 2.5
% < 1 Gyr: 5.800000000000001
0.20
0.15
0.10
0.05
0.00
Fraction
7.75
8.00
8.25
8.50
8.75
9.00
9.25
9.50
9.75
log Age (yr)

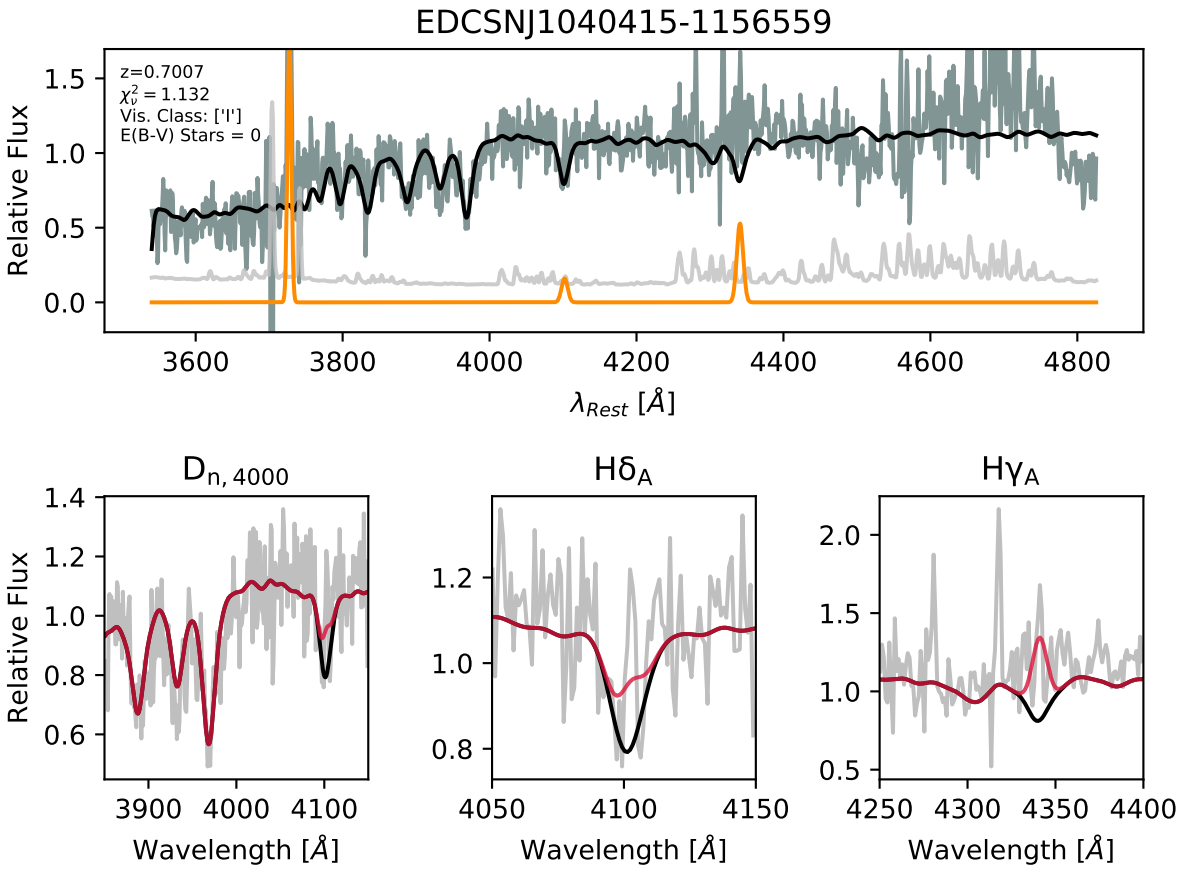
EDCSNJ1040415-1156559
z=0.7007
$\chi^2_\nu = 1.132$
Vis. Class: ['I']
E(B-V) Stars = 0
Relative Flux
λ_{Rest} [Å]
$D_{n,4000}$
$H\delta_A$
$H\gamma_A$
Wavelength [Å]

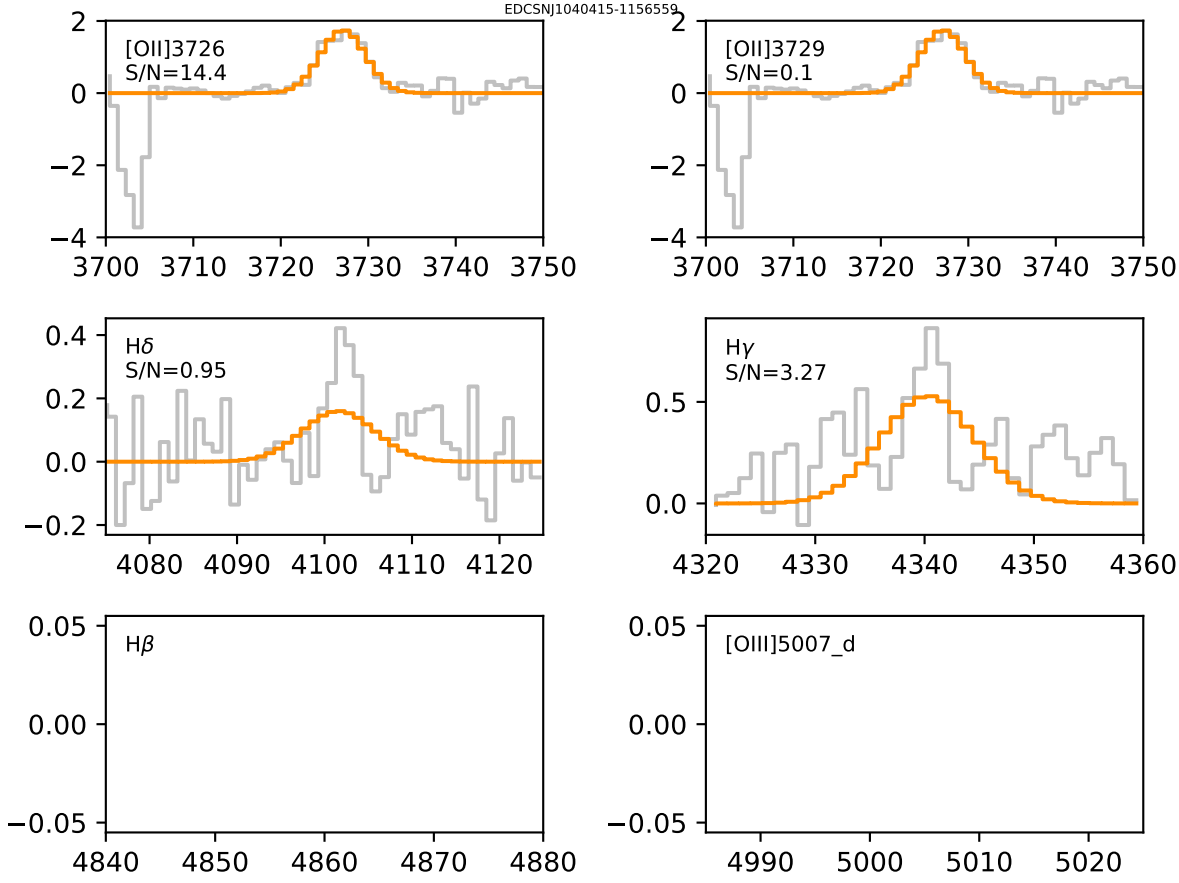
EDCSNJ1040415-1156559
[OII]3726
S/N=14.4
[OII]3729
S/N=0.1
Hδ
S/N=0.95
Hγ
S/N=3.27
Hβ
[OIII]5007_d

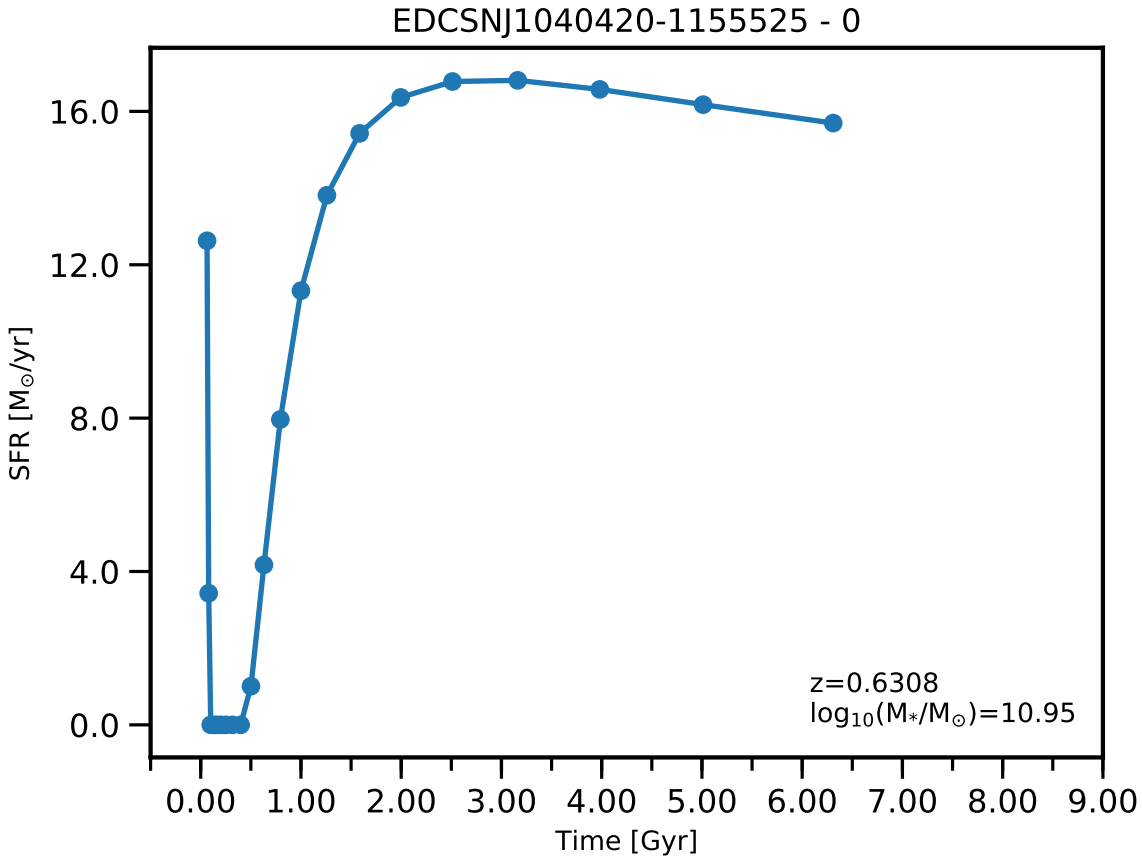
EDCSNJ1040420-1155525 - 0
SFR [M⊙/yr]
16.0
12.0
8.0
4.0
0.0
0.00
1.00
2.00
3.00
4.00
5.00
6.00
7.00
8.00
9.00
Time [Gyr]
z=0.6308
log10(M*/M⊙)=10.95

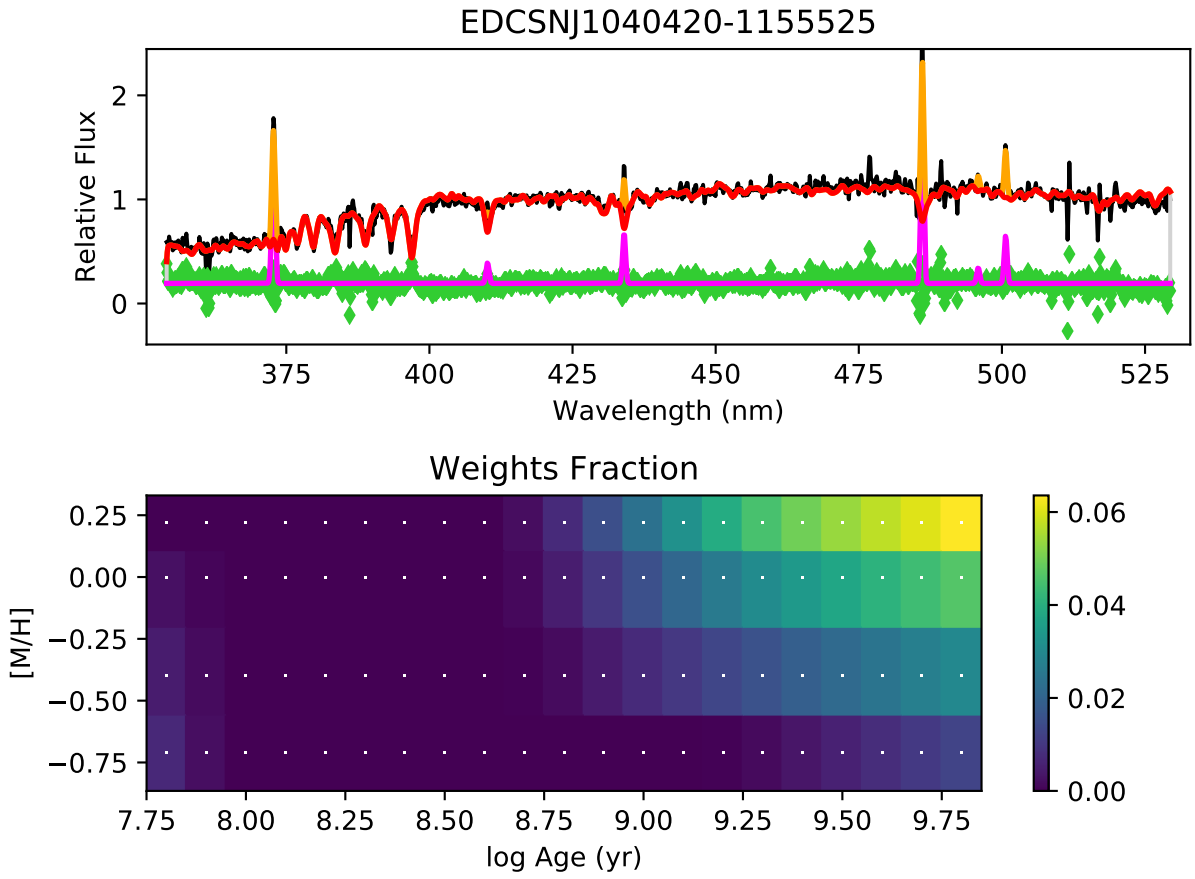
EDCSNJ1040420-1155525
Relative Flux
Wavelength (nm)
Weights Fraction
[M/H]
log Age (yr)

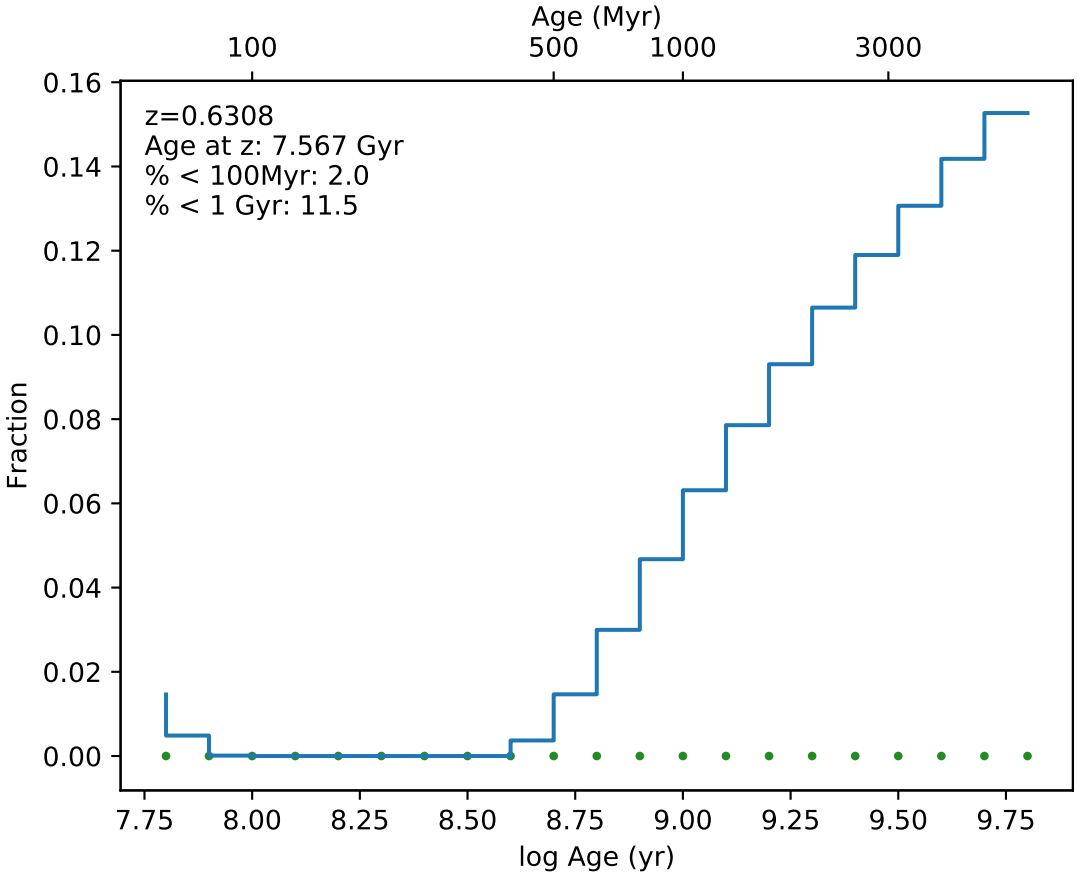
Age (Myr)
100
500
1000
3000
z=0.6308
Age at z: 7.567 Gyr
% < 100Myr: 2.0
% < 1 Gyr: 11.5
Fraction
0.16
0.14
0.12
0.10
0.08
0.06
0.04
0.02
0.00
7.75
8.00
8.25
8.50
8.75
9.00
9.25
9.50
9.75
log Age (yr)

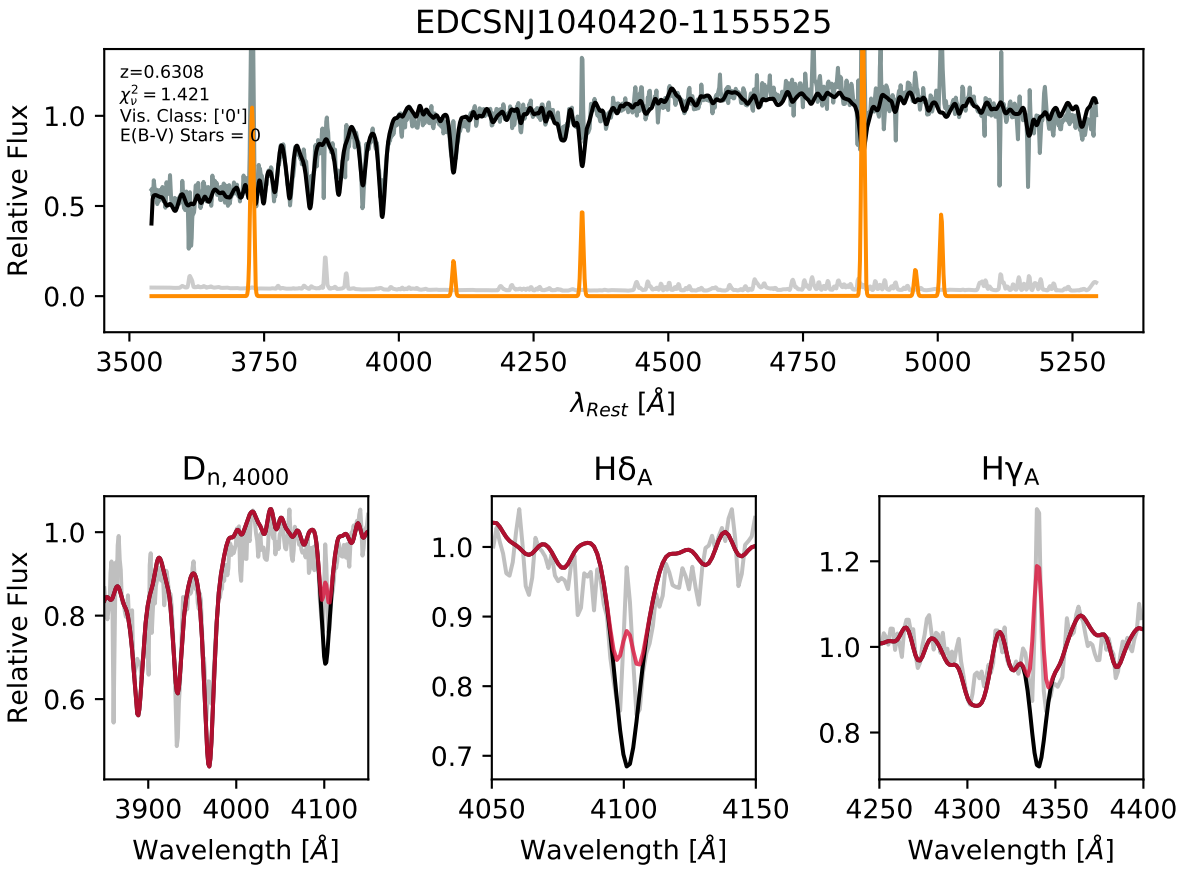
EDCSNJ1040420-1155525
z=0.6308
$\chi^2_\nu = 1.421$
Vis. Class: ['0']
E(B-V) Stars = 0
Relative Flux
1.0
0.5
0.0
3500
3750
4000
4250
4500
4750
5000
5250
λ_{Rest} [Å]
$D_{n,4000}$
$H\delta_A$
$H\gamma_A$
Relative Flux
1.0
0.8
0.6
3900
4000
4100
Wavelength [Å]
1.0
0.9
0.8
0.7
4050
4100
4150
Wavelength [Å]
1.2
1.0
0.8
4250
4300
4350
4400
Wavelength [Å]

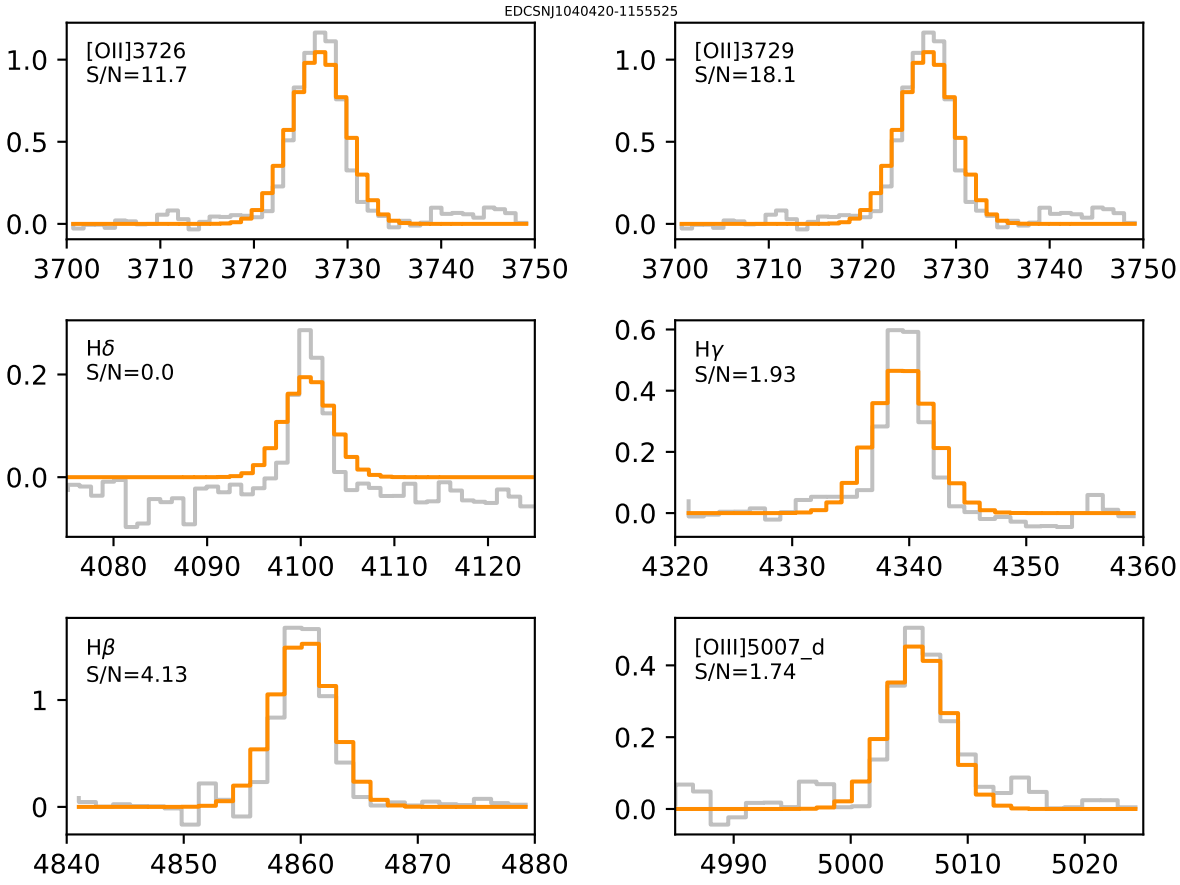
EDCSNJ1040420-1155525
[OII]3726
S/N=11.7
[OII]3729
S/N=18.1
Hδ
S/N=0.0
Hγ
S/N=1.93
Hβ
S/N=4.13
[OIII]5007_d
S/N=1.74

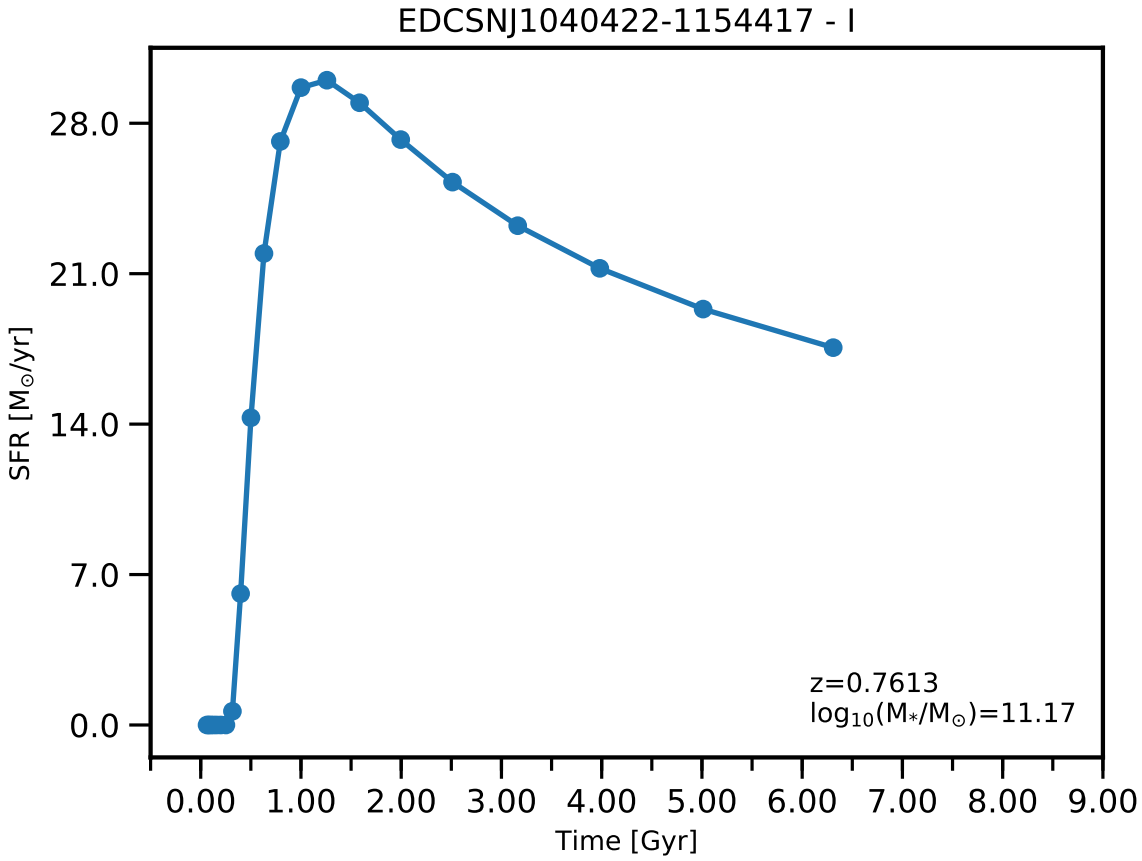
EDCSNJ1040422-1154417 - I
SFR [M⊙/yr]
28.0
21.0
14.0
7.0
0.0
0.00
1.00
2.00
3.00
4.00
5.00
6.00
7.00
8.00
9.00
Time [Gyr]
z=0.7613
log10(M*/M⊙)=11.17

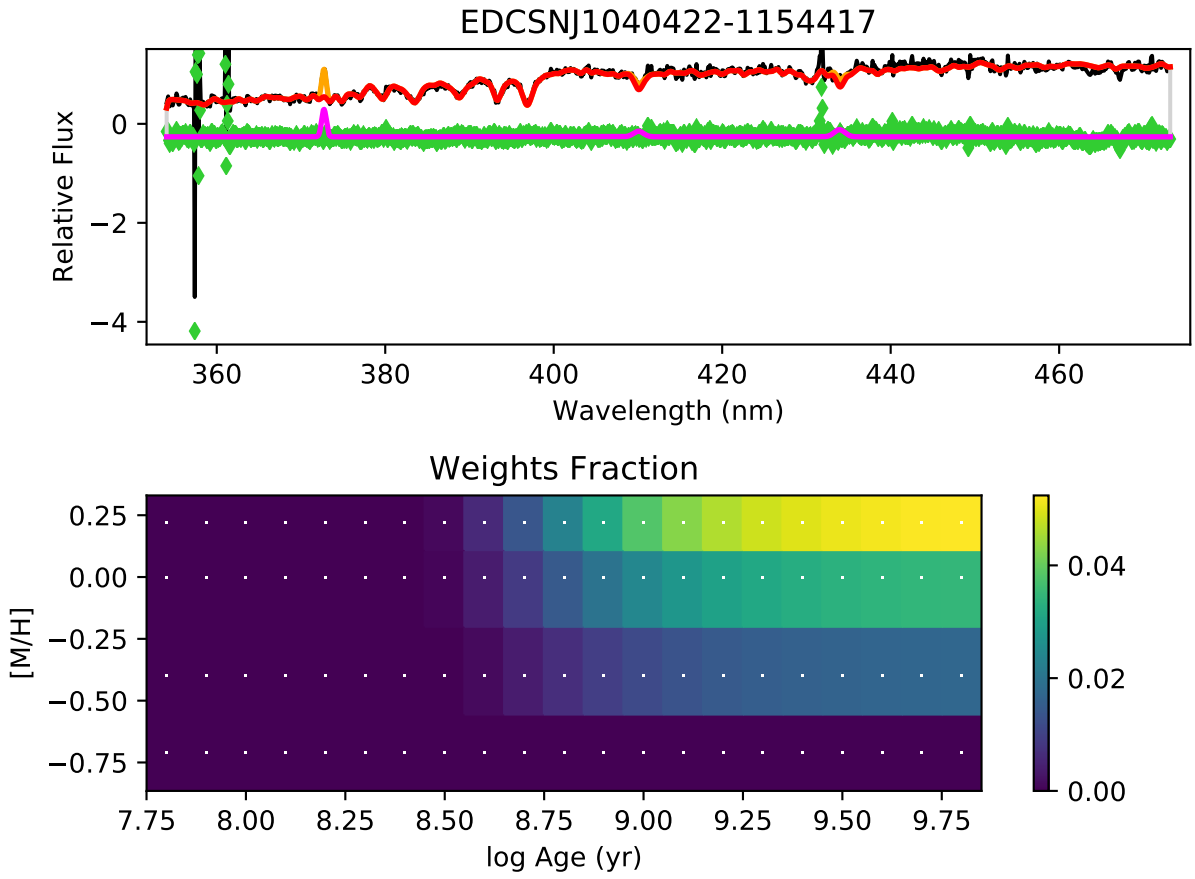
EDCSNJ1040422-1154417
Relative Flux
0
−2
−4
360
380
400
420
440
460
Wavelength (nm)
Weights Fraction
[M/H]
0.25
0.00
−0.25
−0.50
−0.75
7.75
8.00
8.25
8.50
8.75
9.00
9.25
9.50
9.75
log Age (yr)
0.04
0.02
0.00

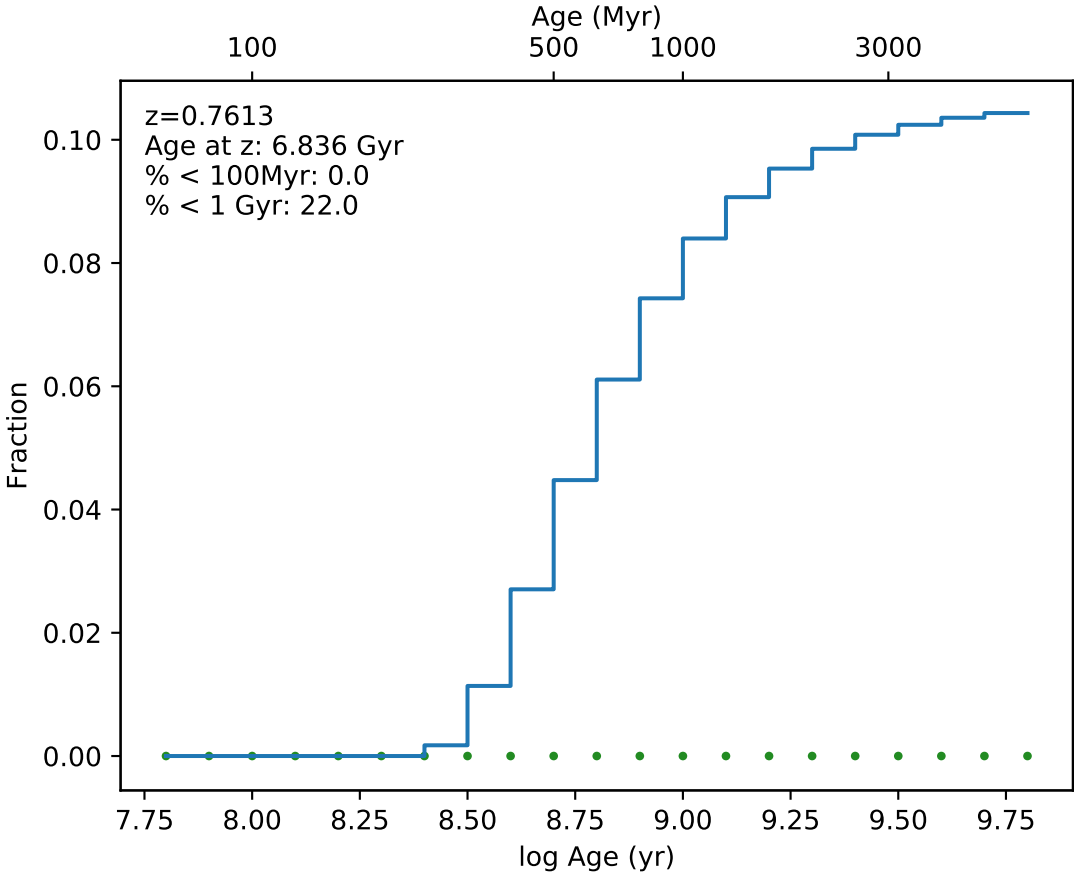
Age (Myr)
100
500
1000
3000
z=0.7613
Age at z: 6.836 Gyr
% < 100Myr: 0.0
% < 1 Gyr: 22.0
Fraction
0.10
0.08
0.06
0.04
0.02
0.00
7.75
8.00
8.25
8.50
8.75
9.00
9.25
9.50
9.75
log Age (yr)

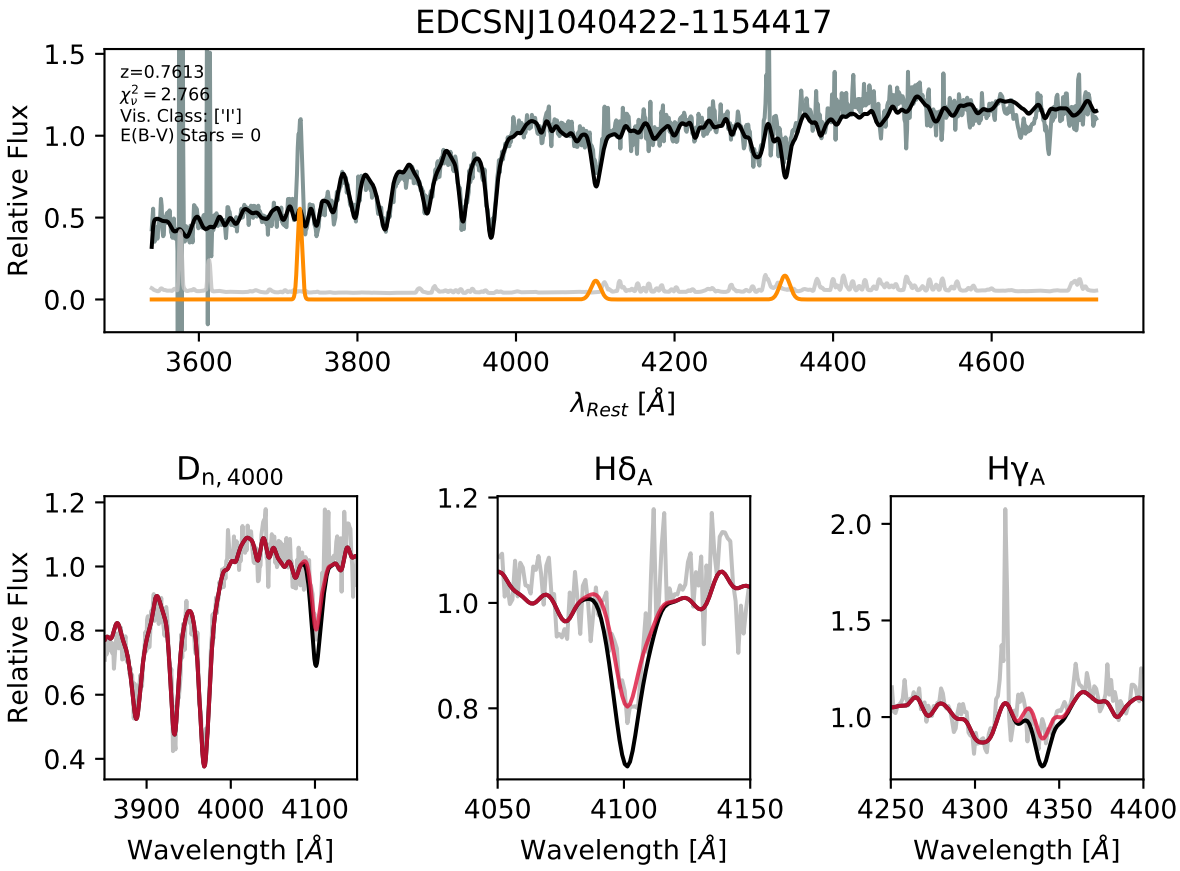
EDCSNJ1040422-1154417
z=0.7613
$\chi^2_\nu = 2.766$
Vis. Class: ['I']
E(B-V) Stars = 0
Relative Flux
λ_{Rest} [Å]
$D_{n,4000}$
$H\delta_A$
$H\gamma_A$
Wavelength [Å]

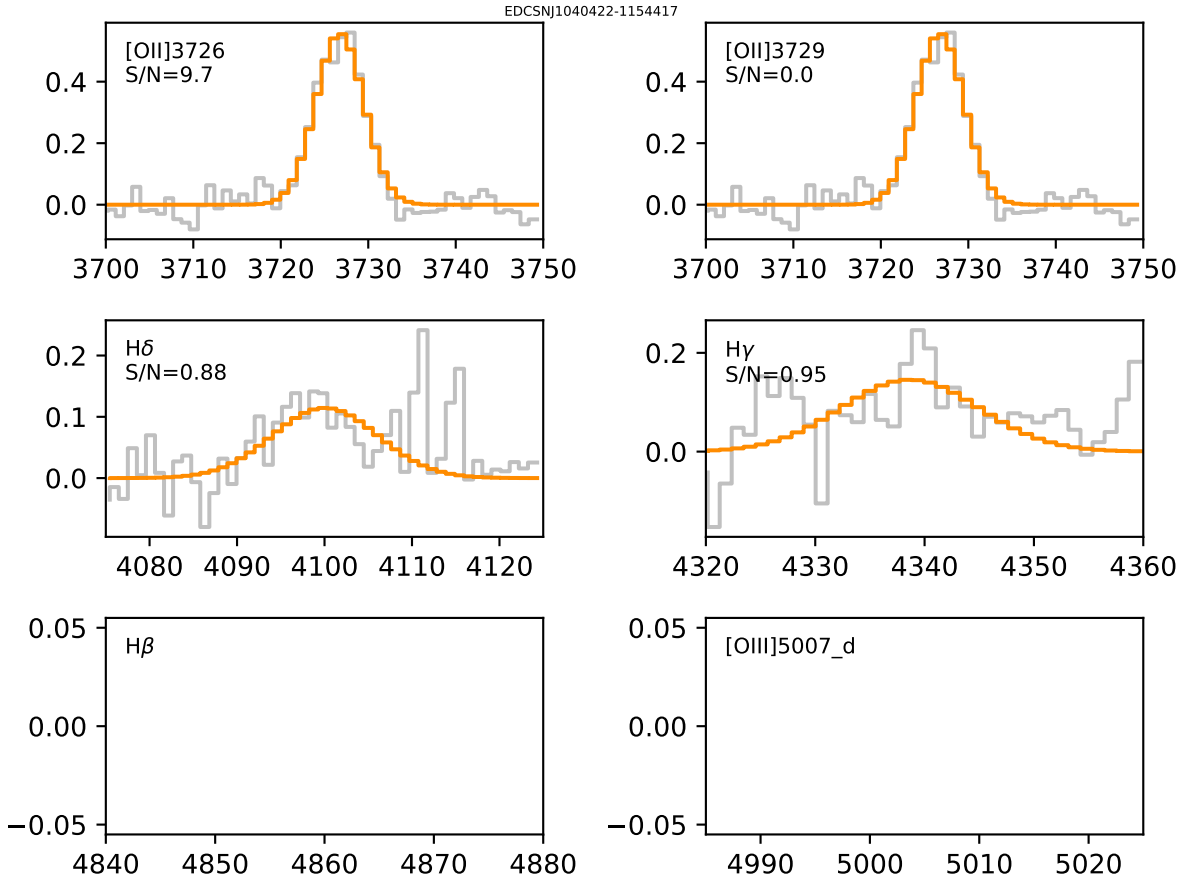
EDCSNJ1040422-1154417
[OII]3726
S/N=9.7
[OII]3729
S/N=0.0
Hδ
S/N=0.88
Hγ
S/N=0.95
Hβ
[OIII]5007_d

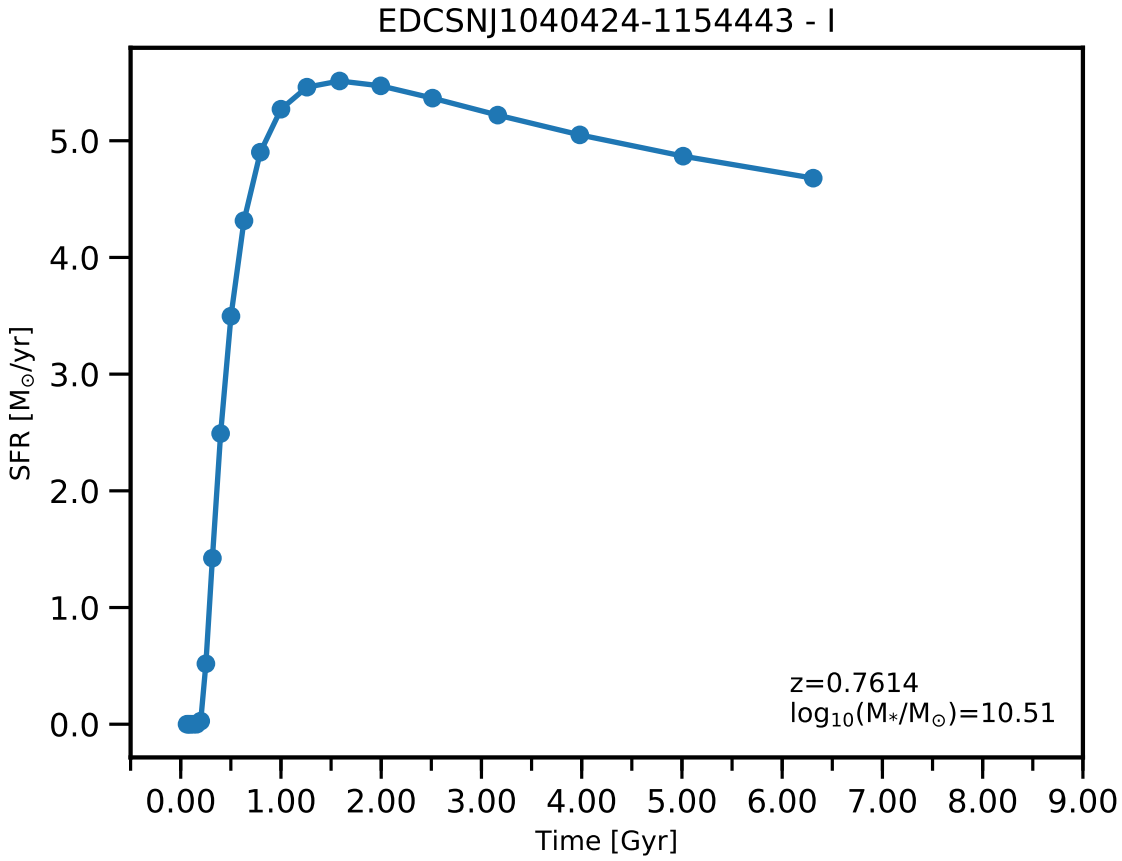
EDCSNJ1040424-1154443 - I
SFR [M⊙/yr]
0.0
1.0
2.0
3.0
4.0
5.0
0.00
1.00
2.00
3.00
4.00
5.00
6.00
7.00
8.00
9.00
Time [Gyr]
z=0.7614
log10(M*/M⊙)=10.51

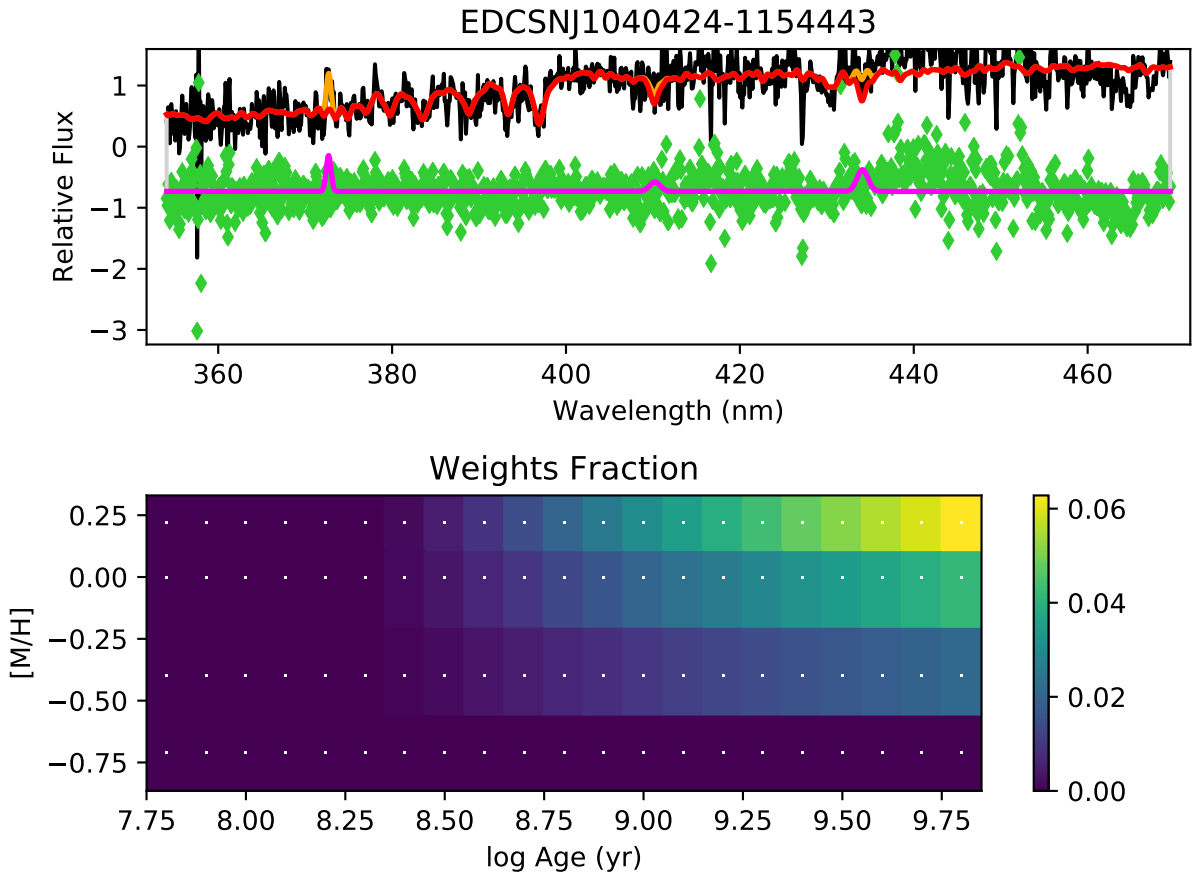
EDCSNJ1040424-1154443
Relative Flux
1
0
−1
−2
−3
360
380
400
420
440
460
Wavelength (nm)
Weights Fraction
[M/H]
0.25
0.00
−0.25
−0.50
−0.75
7.75
8.00
8.25
8.50
8.75
9.00
9.25
9.50
9.75
log Age (yr)
0.06
0.04
0.02
0.00

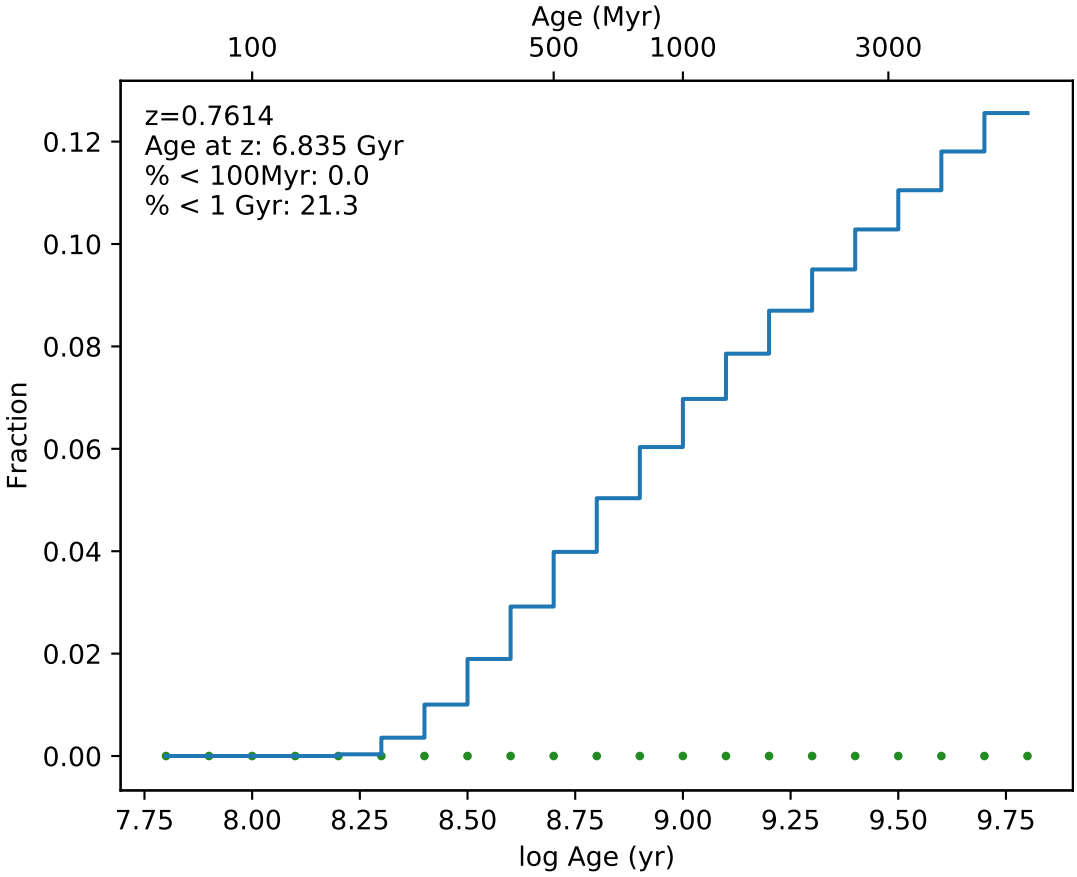
Age (Myr)
100
500
1000
3000
z=0.7614
Age at z: 6.835 Gyr
% < 100Myr: 0.0
% < 1 Gyr: 21.3
Fraction
0.12
0.10
0.08
0.06
0.04
0.02
0.00
7.75
8.00
8.25
8.50
8.75
9.00
9.25
9.50
9.75
log Age (yr)

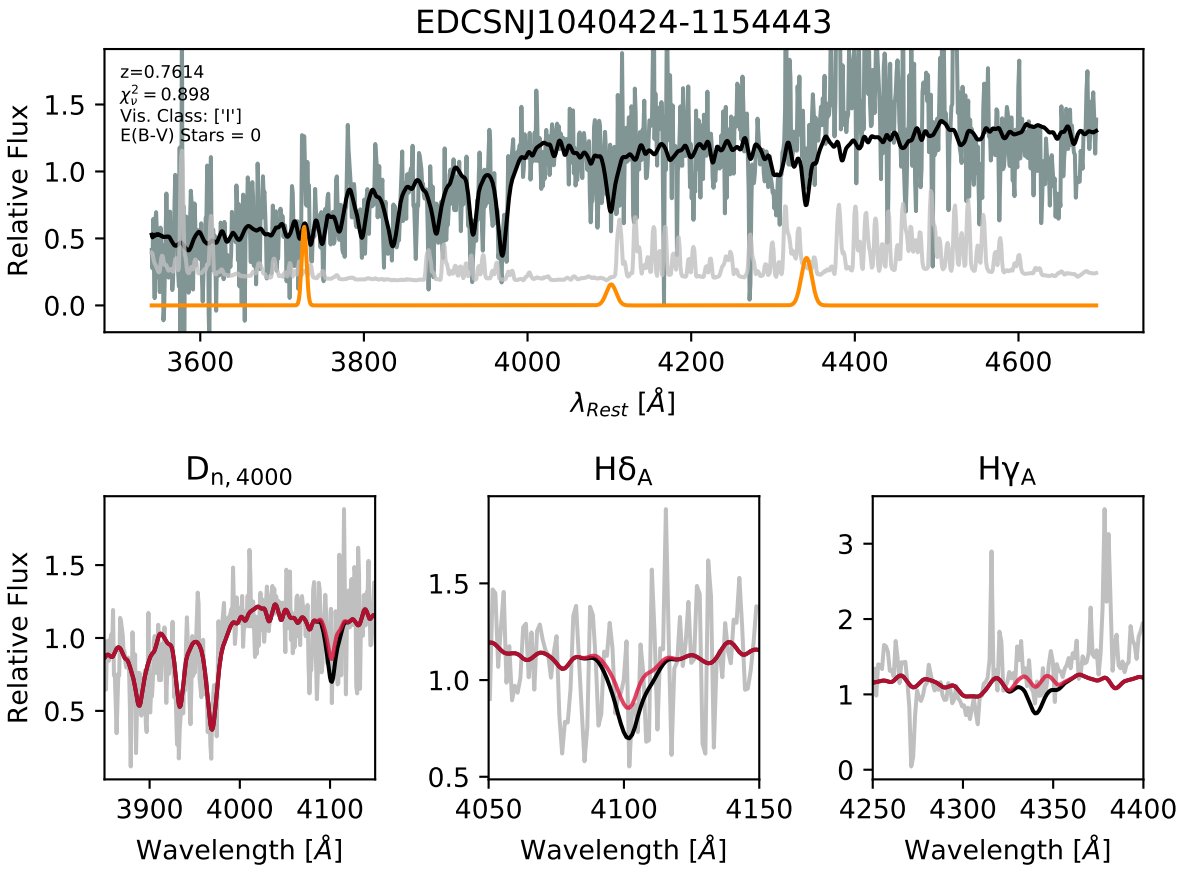
EDCSNJ1040424-1154443
z=0.7614
$\chi^2_\nu = 0.898$
Vis. Class: ['I']
E(B-V) Stars = 0
Relative Flux
λ_{Rest} [Å]
$D_{n,4000}$
$H\delta_A$
$H\gamma_A$
Wavelength [Å]

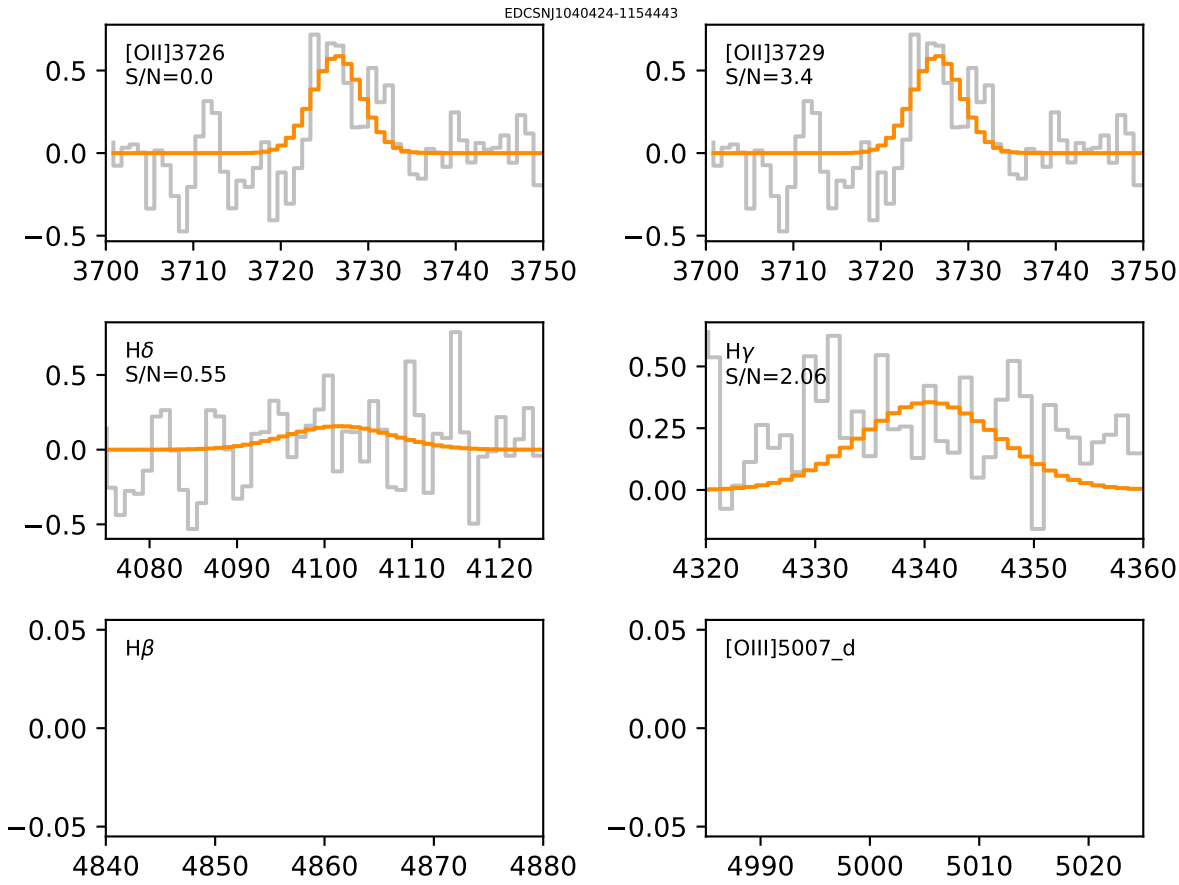
EDCSNJ1040424-1154443
[OII]3726
S/N=0.0
[OII]3729
S/N=3.4
Hδ
S/N=0.55
Hγ
S/N=2.06
Hβ
[OIII]5007_d

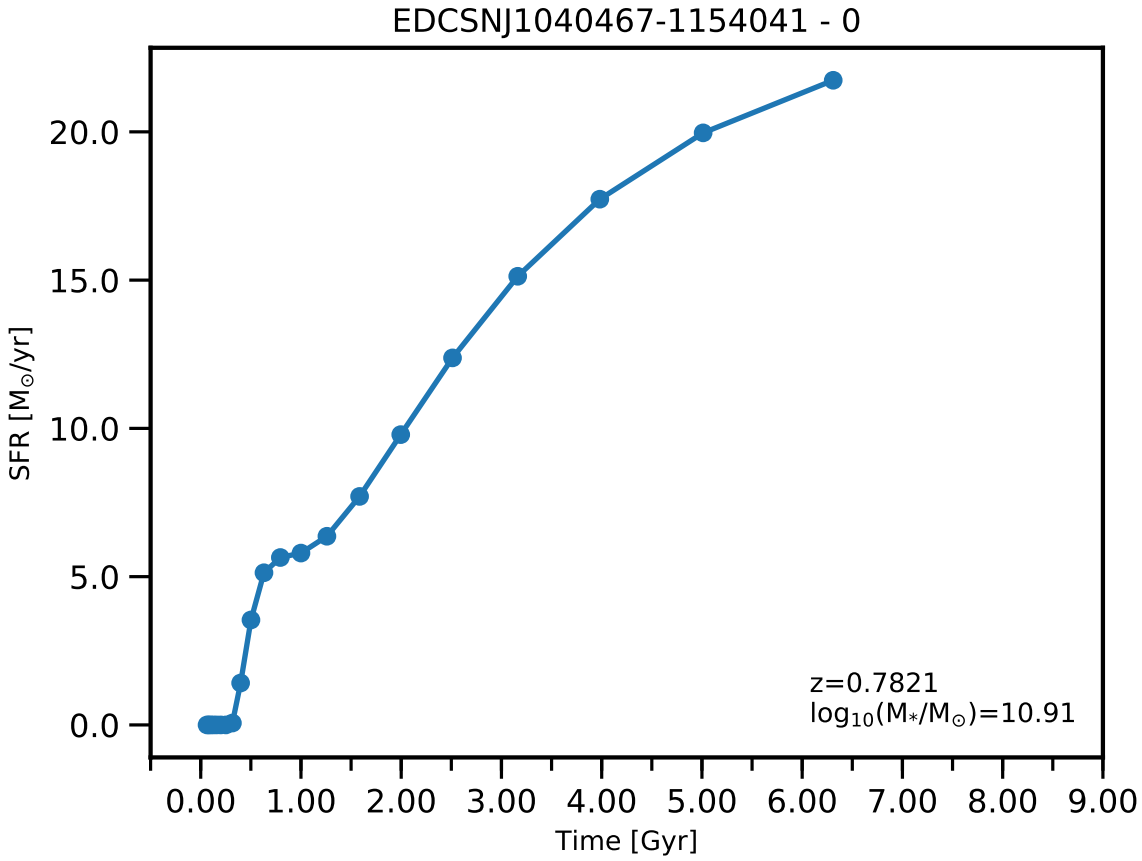
EDCSNJ1040467-1154041 - 0
SFR [M⊙/yr]
20.0
15.0
10.0
5.0
0.0
0.00
1.00
2.00
3.00
4.00
5.00
6.00
7.00
8.00
9.00
Time [Gyr]
z=0.7821
log10(M*/M⊙)=10.91

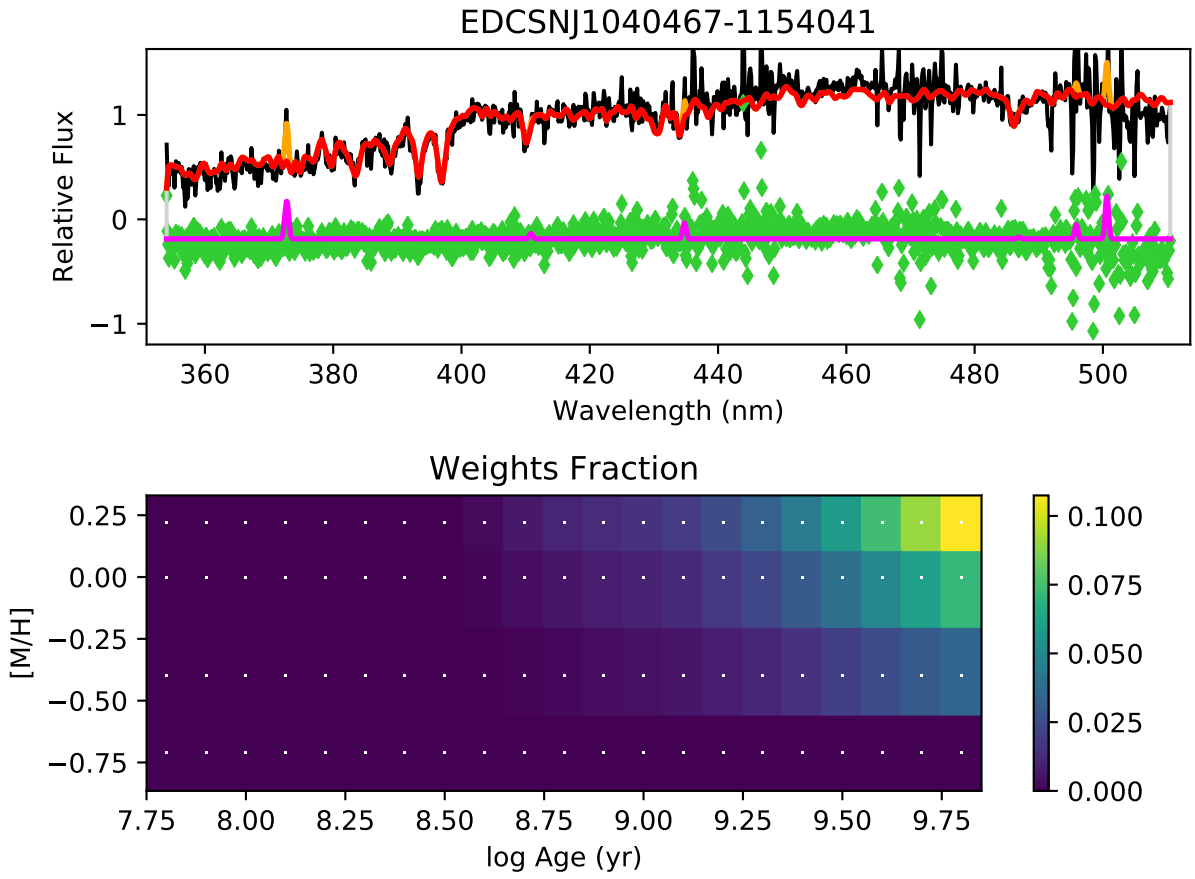
EDCSNJ1040467-1154041
Relative Flux
1
0
−1
360
380
400
420
440
460
480
500
Wavelength (nm)
Weights Fraction
[M/H]
0.25
0.00
−0.25
−0.50
−0.75
7.75
8.00
8.25
8.50
8.75
9.00
9.25
9.50
9.75
log Age (yr)
0.100
0.075
0.050
0.025
0.000

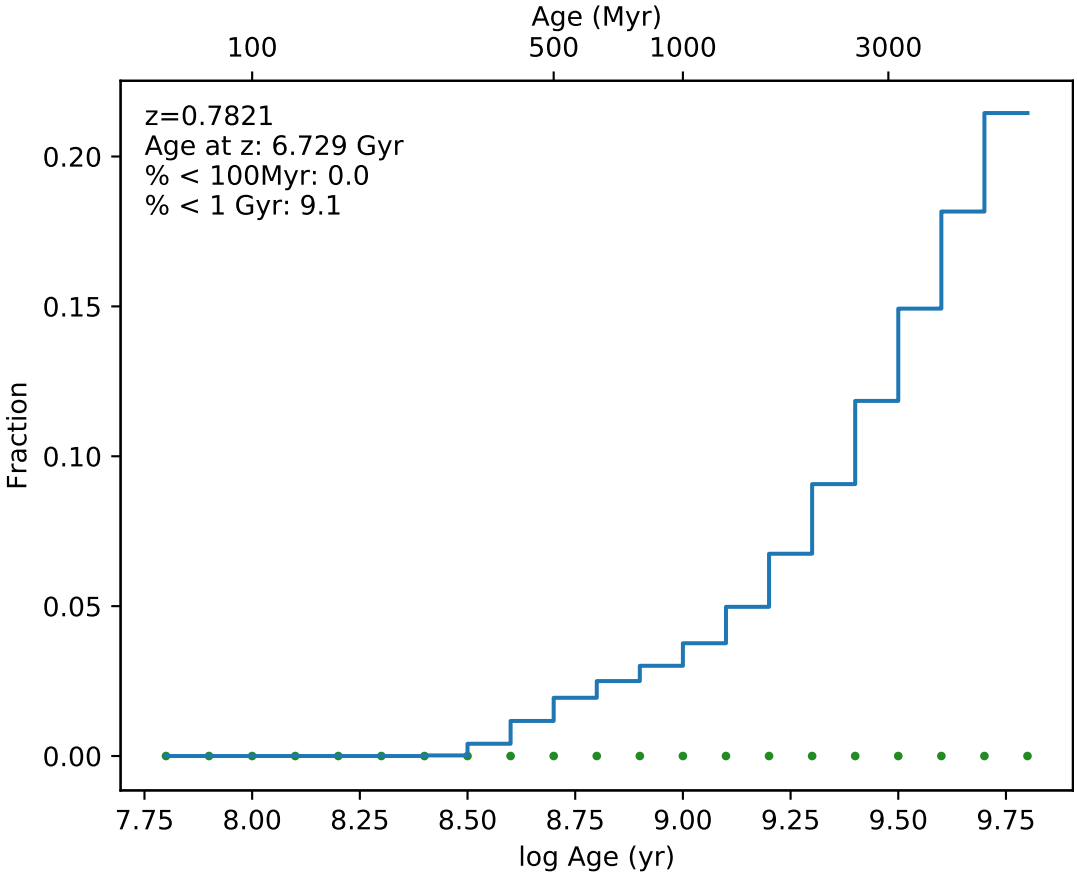
Age (Myr)
100
500
1000
3000
z=0.7821
Age at z: 6.729 Gyr
% < 100Myr: 0.0
% < 1 Gyr: 9.1
Fraction
0.20
0.15
0.10
0.05
0.00
7.75
8.00
8.25
8.50
8.75
9.00
9.25
9.50
9.75
log Age (yr)

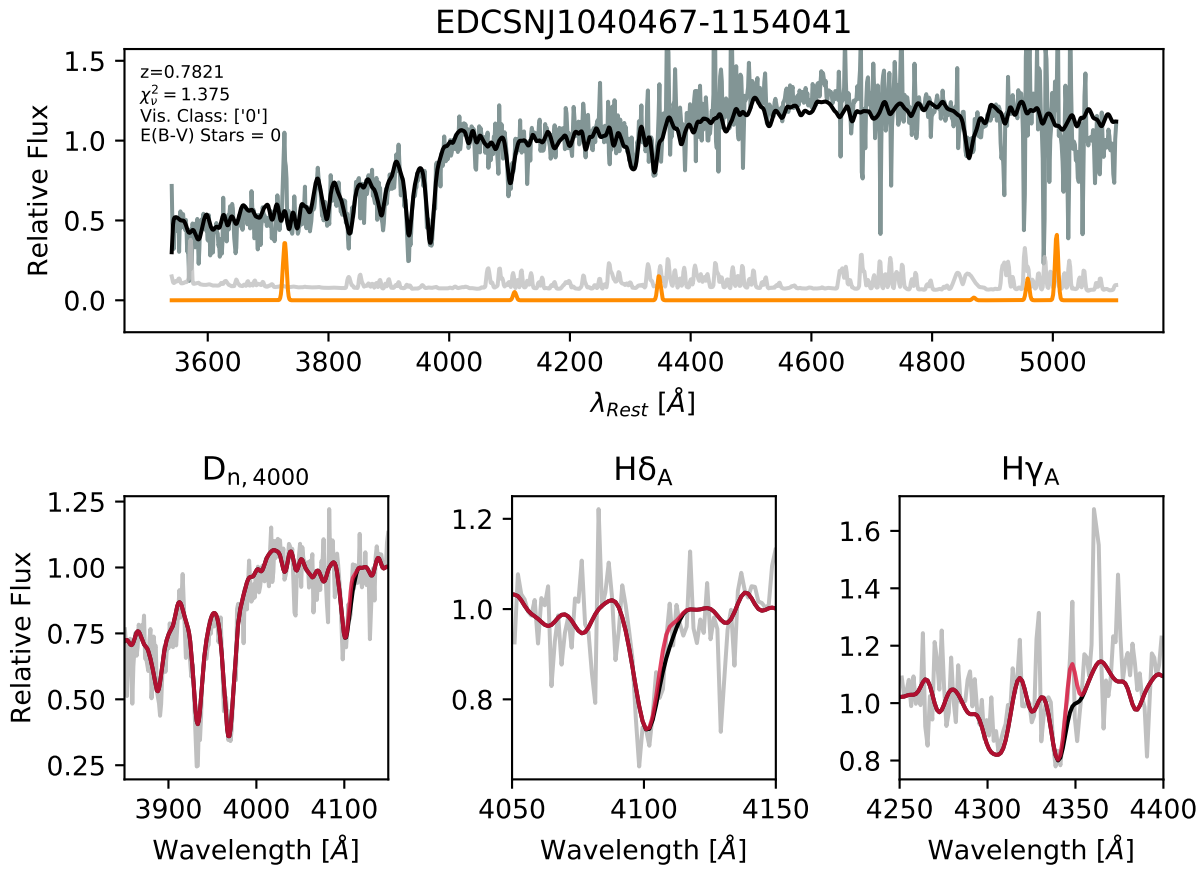
EDCSNJ1040467-1154041
z=0.7821
$\chi^2_\nu = 1.375$
Vis. Class: ['0']
E(B-V) Stars = 0
Relative Flux
λ_{Rest} [Å]
$D_{n,4000}$
$H\delta_A$
$H\gamma_A$
Wavelength [Å]

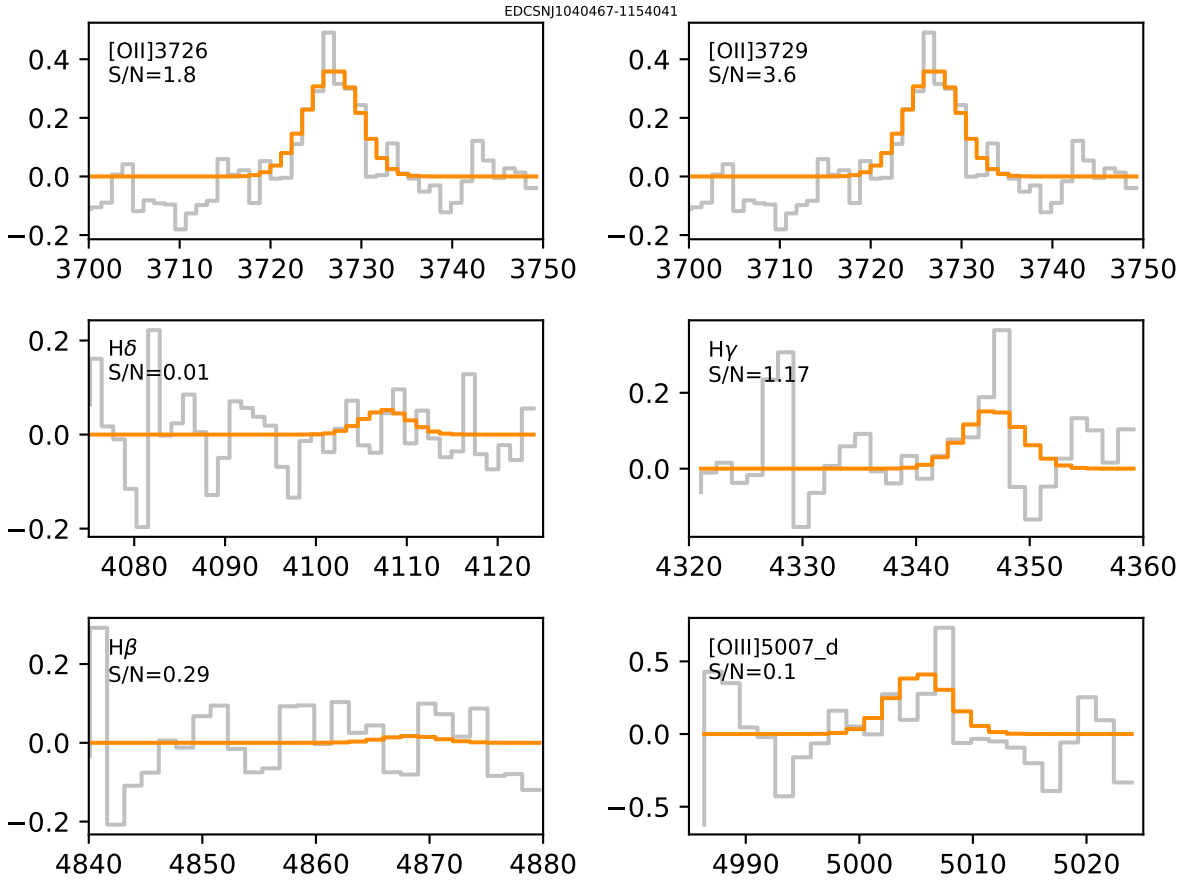
EDCSNJ1040467-1154041
[OII]3726
S/N=1.8
[OII]3729
S/N=3.6
Hδ
S/N=0.01
Hγ
S/N=1.17
Hβ
S/N=0.29
[OIII]5007_d
S/N=0.1

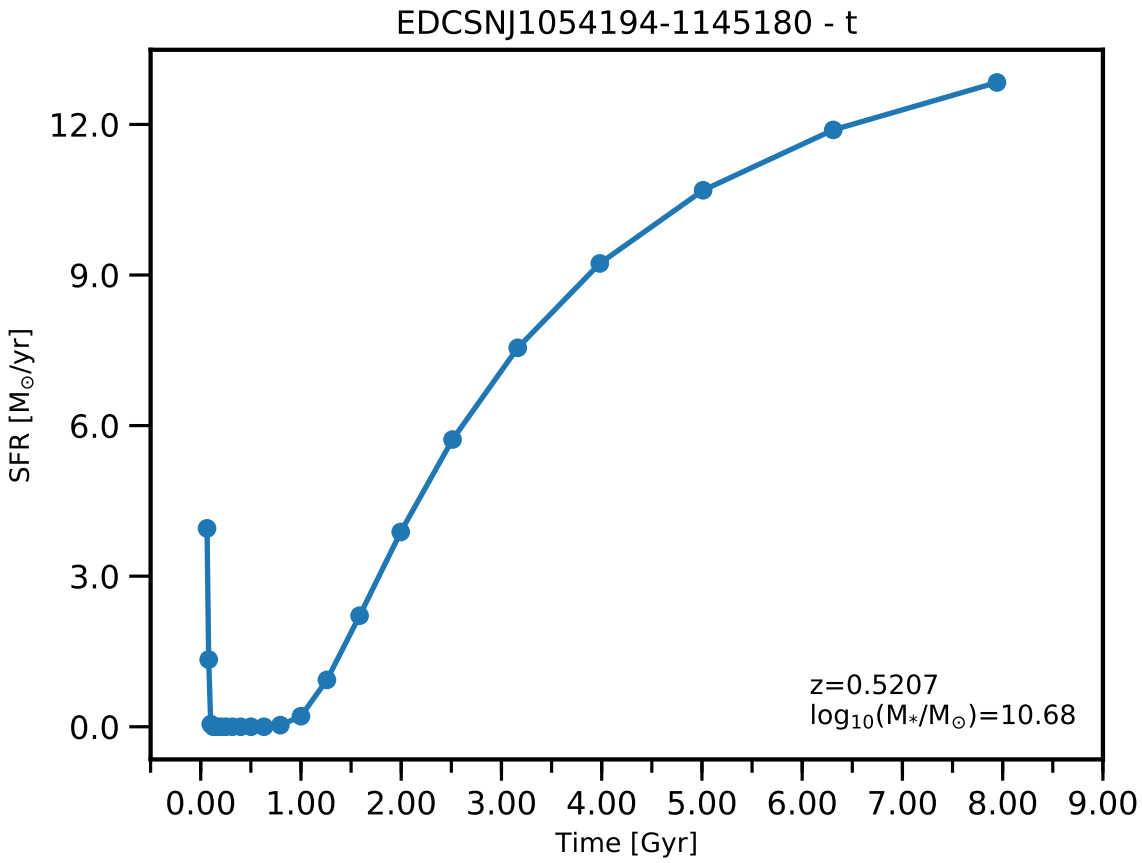
EDCSNJ1054194-1145180 - t
SFR [M⊙/yr]
12.0
9.0
6.0
3.0
0.0
0.00
1.00
2.00
3.00
4.00
5.00
6.00
7.00
8.00
9.00
Time [Gyr]
z=0.5207
log10(M*/M⊙)=10.68

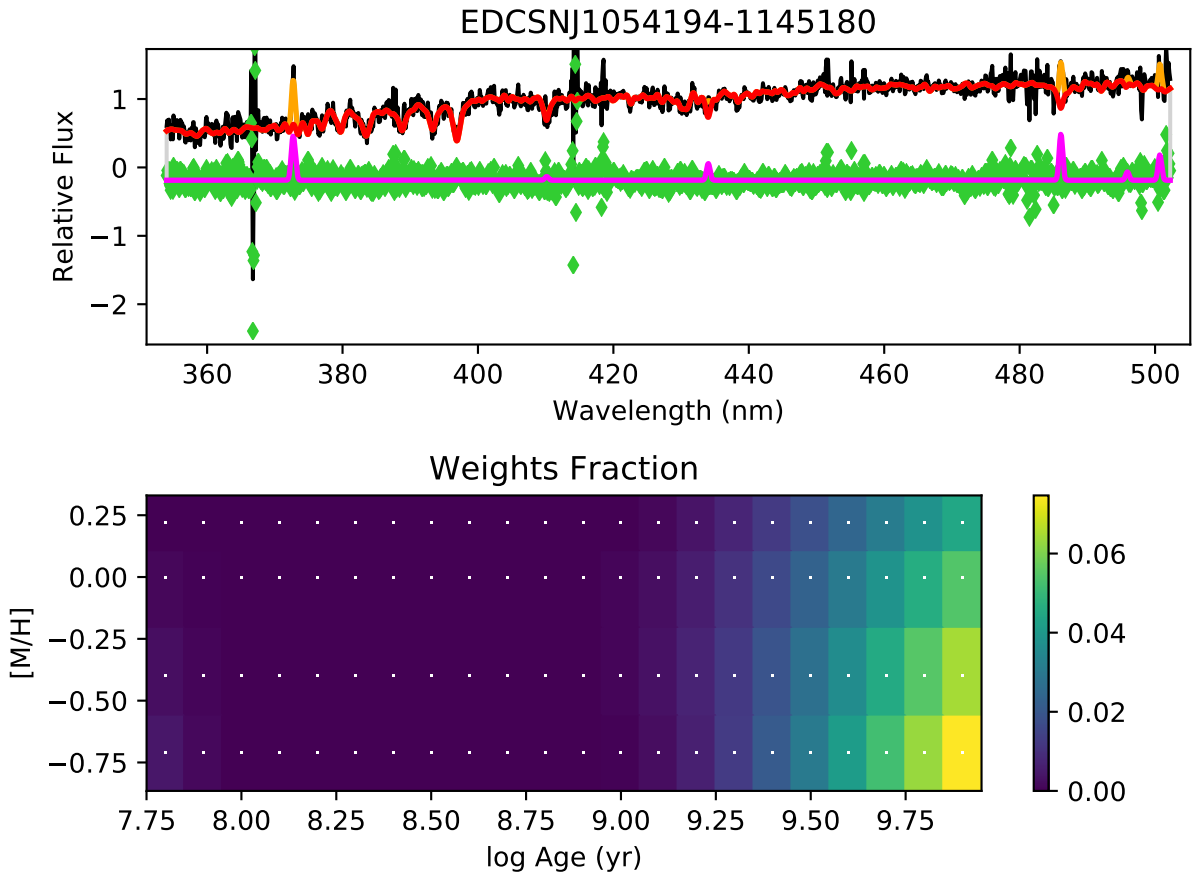
EDCSNJ1054194-1145180
Relative Flux
1
0
−1
−2
360
380
400
420
440
460
480
500
Wavelength (nm)
Weights Fraction
[M/H]
0.25
0.00
−0.25
−0.50
−0.75
7.75
8.00
8.25
8.50
8.75
9.00
9.25
9.50
9.75
log Age (yr)
0.06
0.04
0.02
0.00

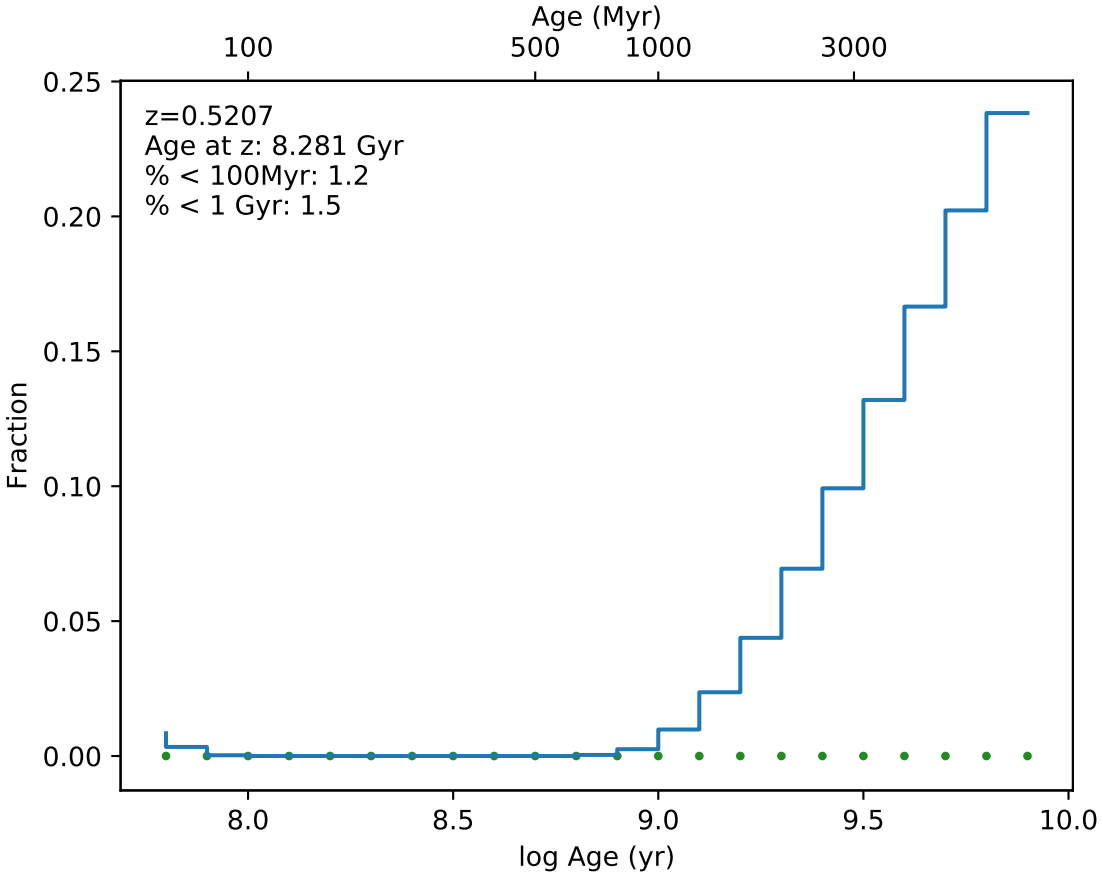
Age (Myr)
100
500
1000
3000
z=0.5207
Age at z: 8.281 Gyr
% < 100Myr: 1.2
% < 1 Gyr: 1.5
Fraction
0.25
0.20
0.15
0.10
0.05
0.00
8.0
8.5
9.0
9.5
10.0
log Age (yr)

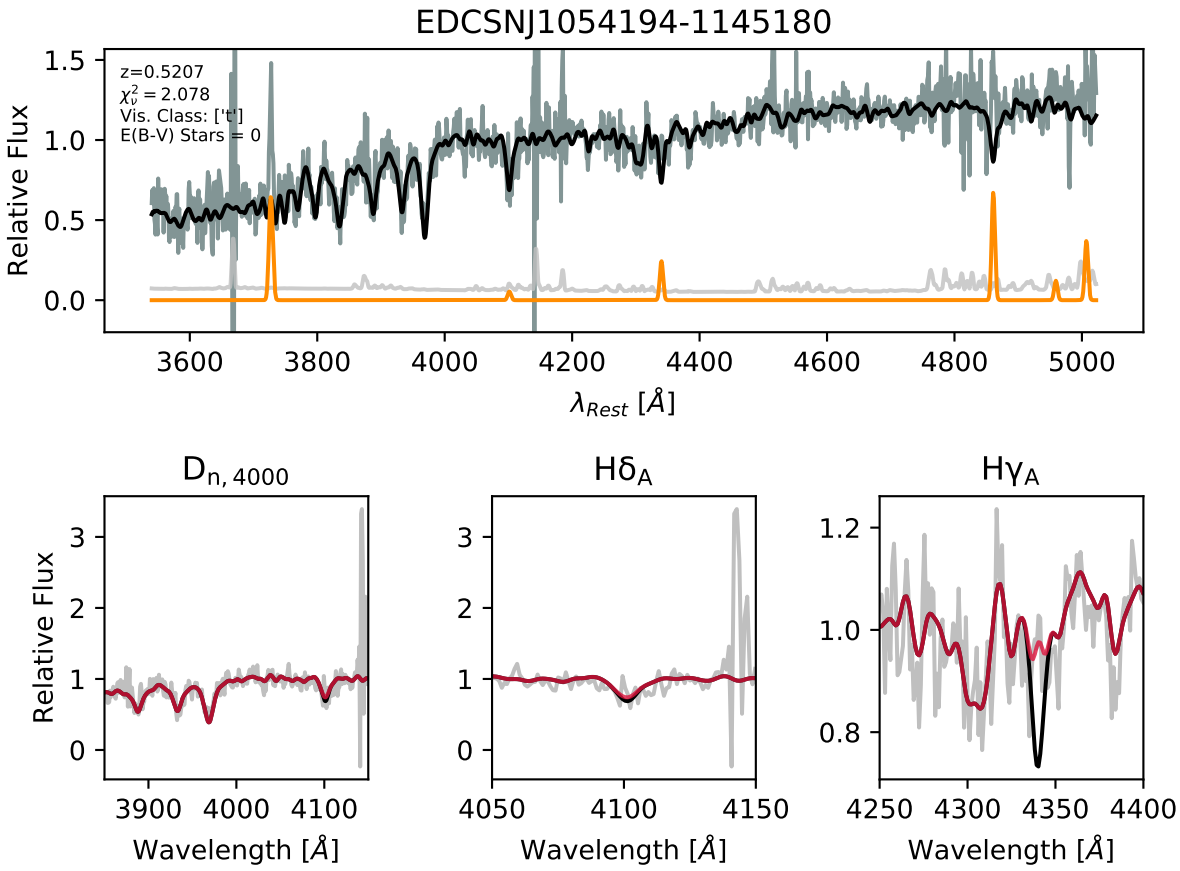
EDCSNJ1054194-1145180
z=0.5207
$\chi^2_\nu = 2.078$
Vis. Class: ['t']
E(B-V) Stars = 0
Relative Flux
λ_{Rest} [Å]
$D_{n,4000}$
$H\delta_A$
$H\gamma_A$
Wavelength [Å]

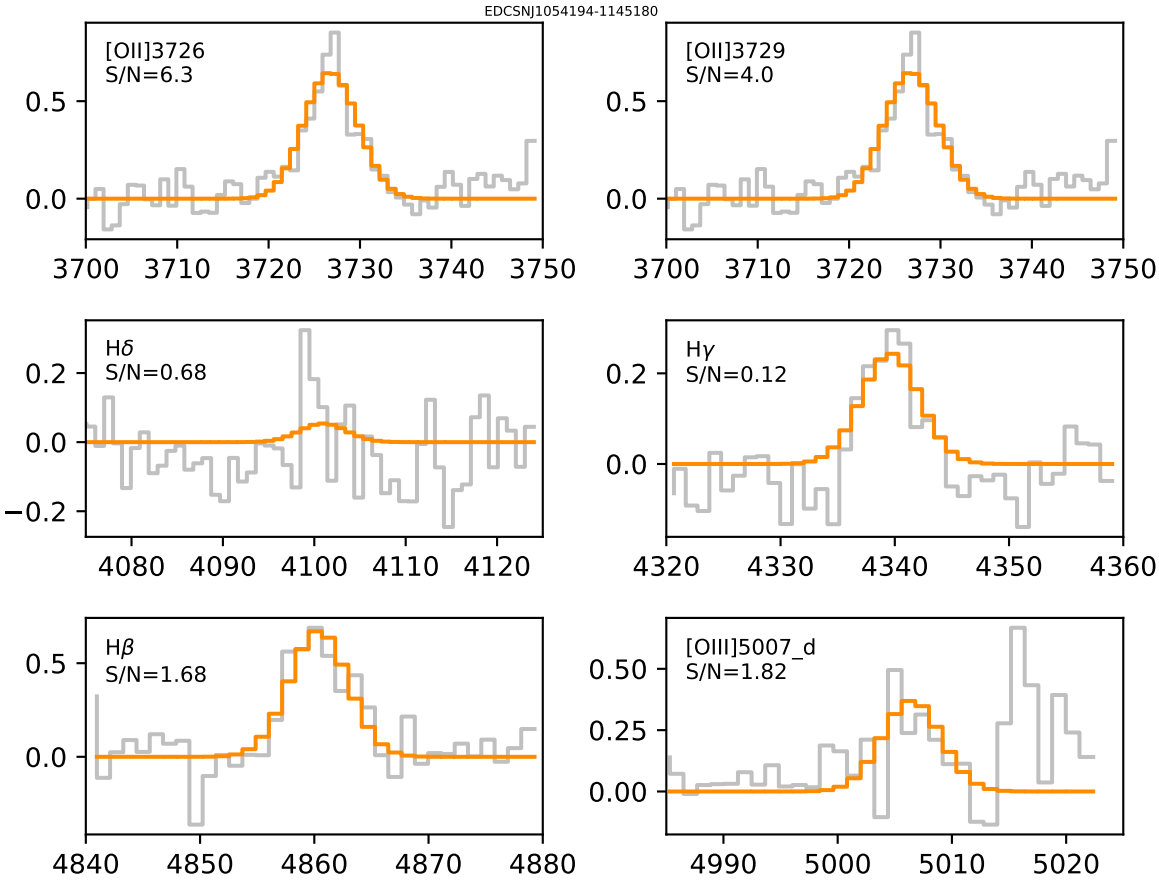
EDCSNJ1054194-1145180
[OII]3726
S/N=6.3
[OII]3729
S/N=4.0
Hδ
S/N=0.68
Hγ
S/N=0.12
Hβ
S/N=1.68
[OIII]5007_d
S/N=1.82

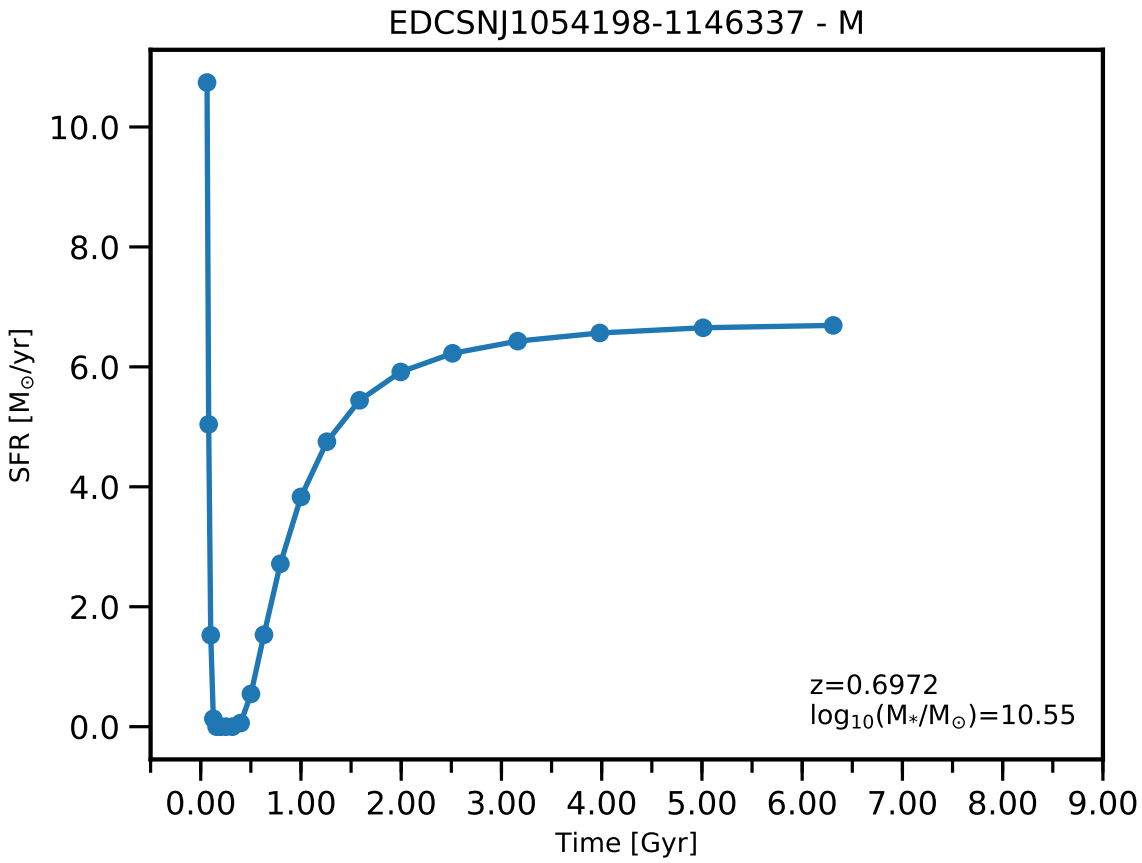
EDCSNJ1054198-1146337 - M
SFR [M⊙/yr]
10.0
8.0
6.0
4.0
2.0
0.0
0.00
1.00
2.00
3.00
4.00
5.00
6.00
7.00
8.00
9.00
Time [Gyr]
z=0.6972
log10(M*/M⊙)=10.55

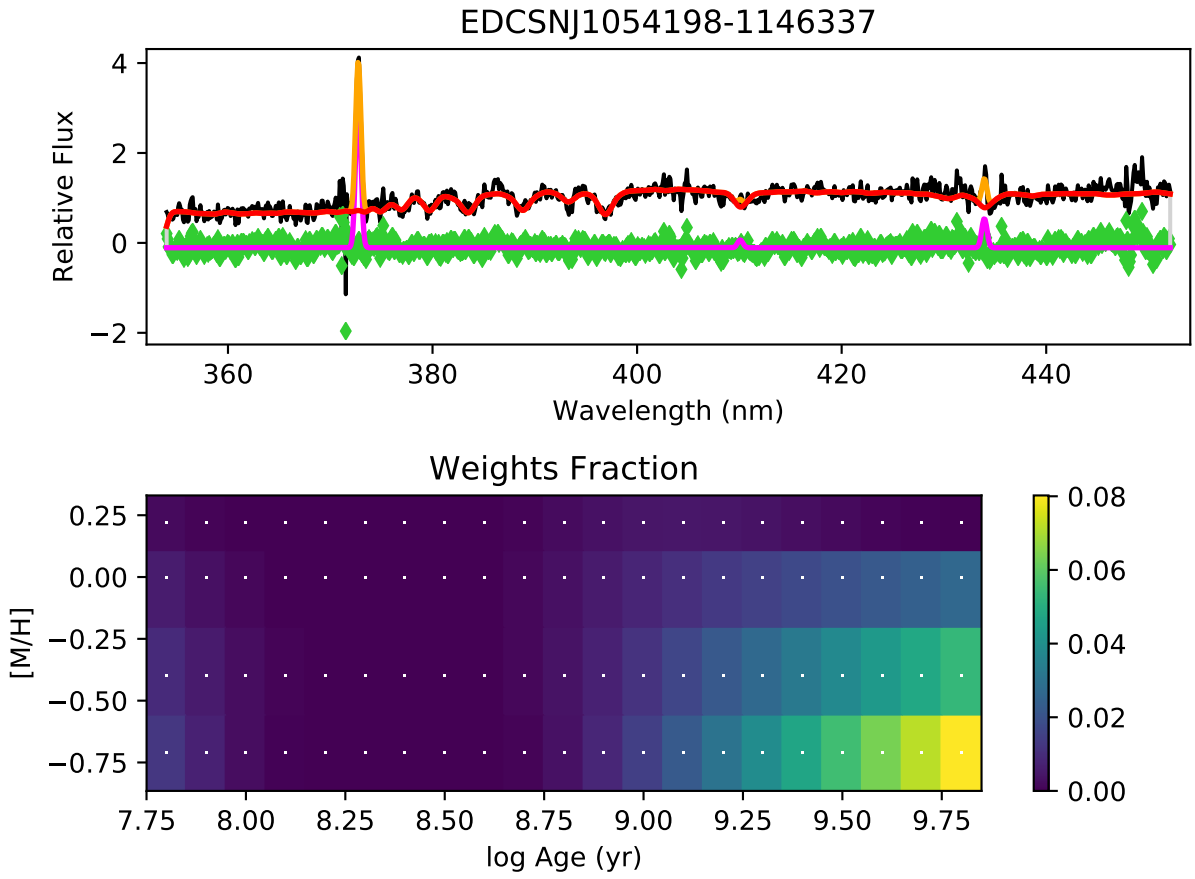
EDCSNJ1054198-1146337
Relative Flux
4
2
0
−2
360
380
400
420
440
Wavelength (nm)
Weights Fraction
[M/H]
0.25
0.00
−0.25
−0.50
−0.75
7.75
8.00
8.25
8.50
8.75
9.00
9.25
9.50
9.75
log Age (yr)
0.08
0.06
0.04
0.02
0.00

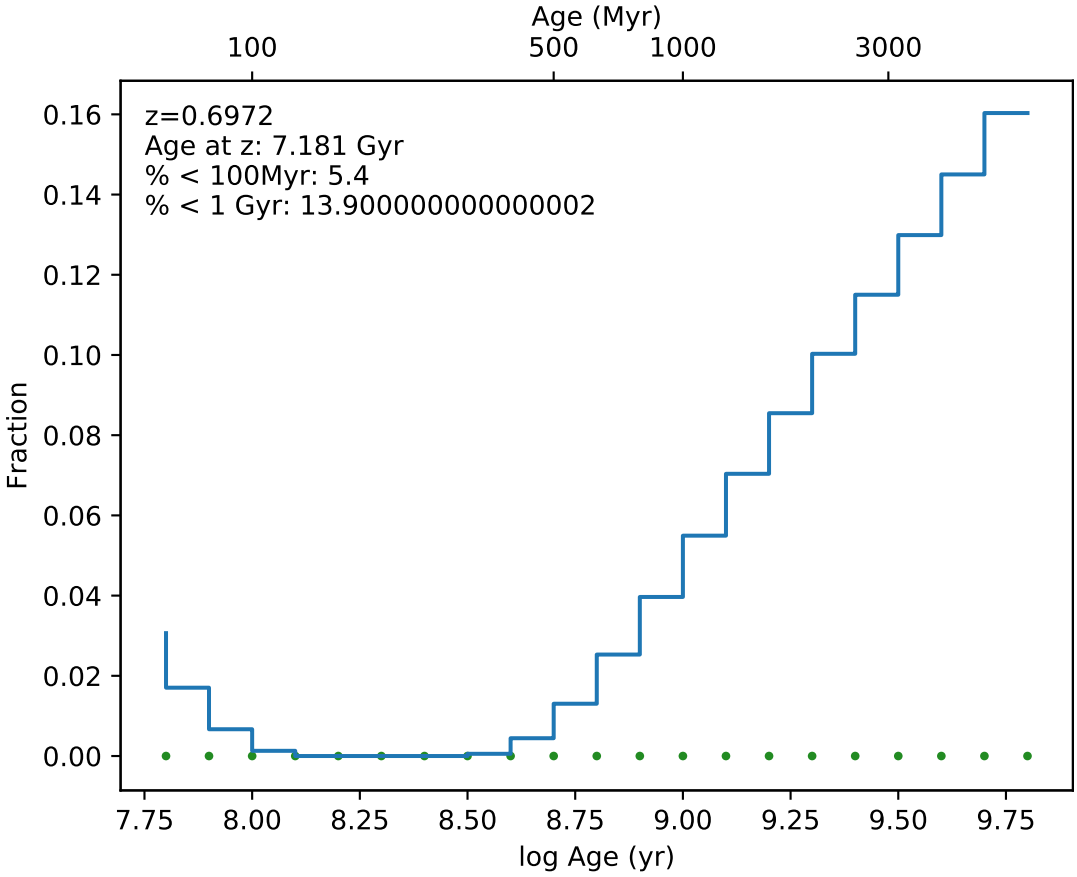
Age (Myr)
100
500
1000
3000
z=0.6972
Age at z: 7.181 Gyr
% < 100Myr: 5.4
% < 1 Gyr: 13.900000000000002
Fraction
0.16
0.14
0.12
0.10
0.08
0.06
0.04
0.02
0.00
7.75
8.00
8.25
8.50
8.75
9.00
9.25
9.50
9.75
log Age (yr)

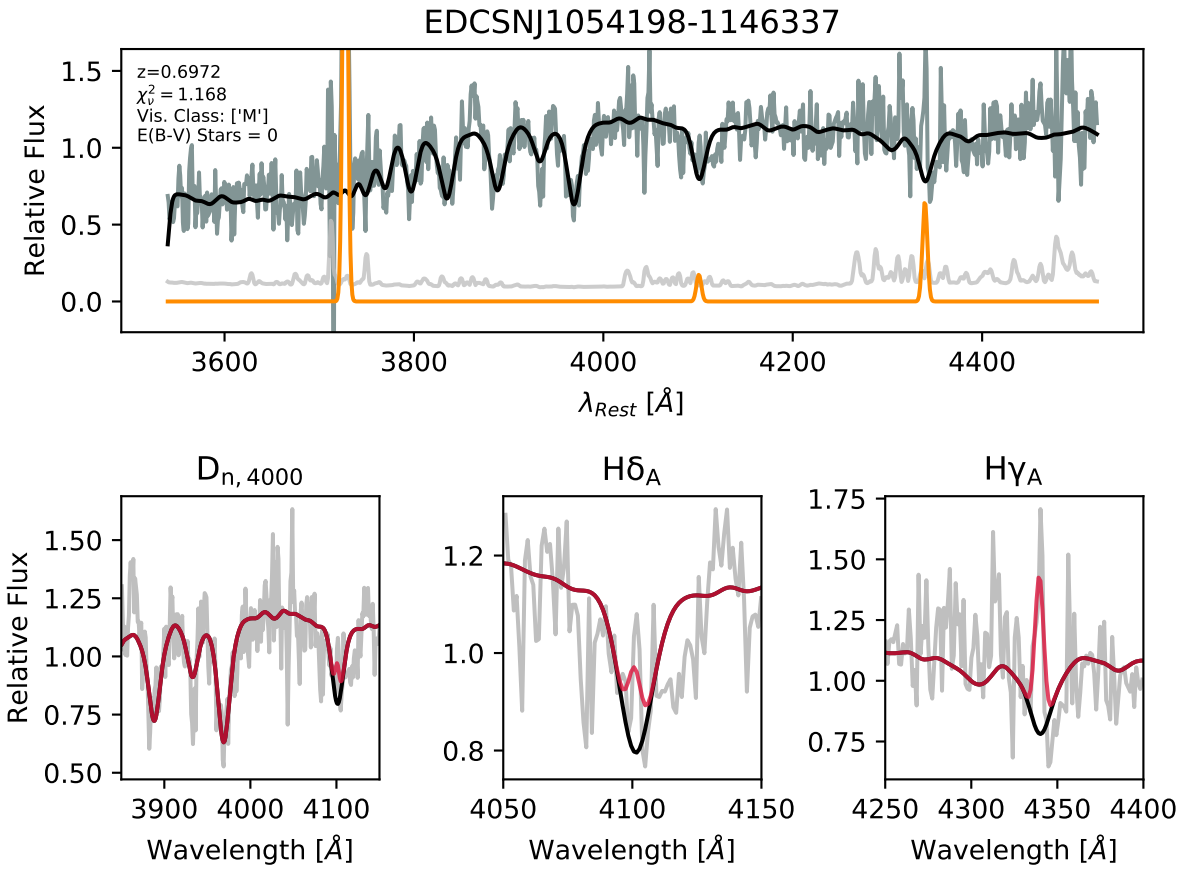
EDCSNJ1054198-1146337
z=0.6972
$\chi^2_\nu = 1.168$
Vis. Class: ['M']
E(B-V) Stars = 0
Relative Flux
λ_{Rest} [Å]
$D_{n,4000}$
$H\delta_A$
$H\gamma_A$
Wavelength [Å]

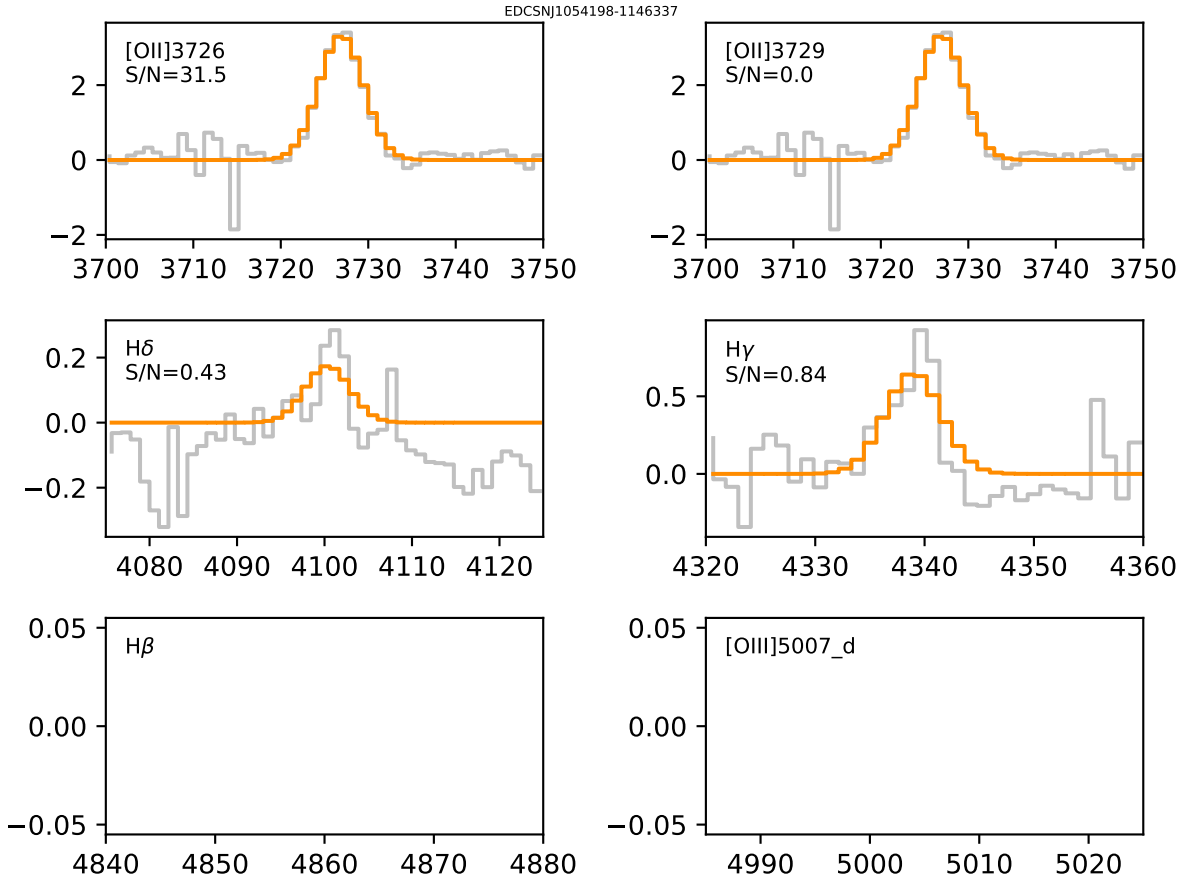
EDCSNJ1054198-1146337
[OII]3726
S/N=31.5
[OII]3729
S/N=0.0
Hδ
S/N=0.43
Hγ
S/N=0.84
Hβ
[OIII]5007_d

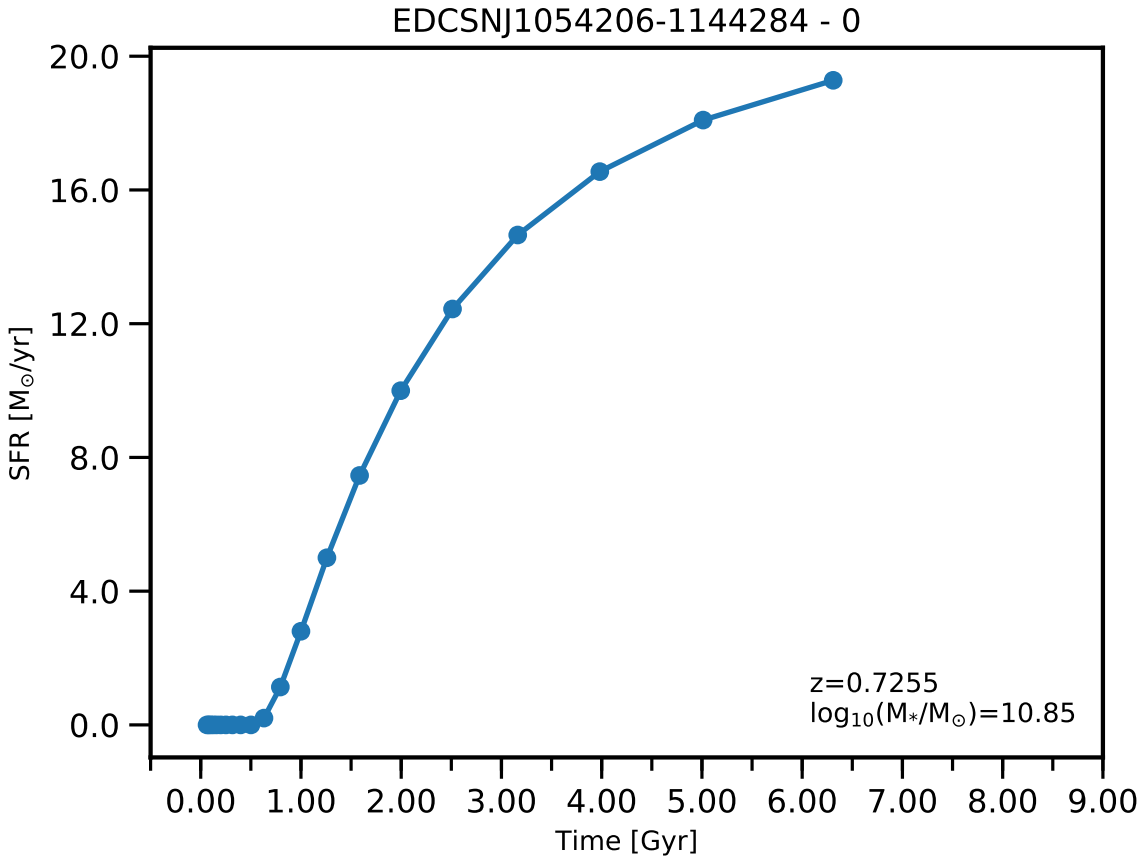
EDCSNJ1054206-1144284 - 0
20.0
16.0
12.0
8.0
4.0
0.0
SFR [M⊙/yr]
0.00
1.00
2.00
3.00
4.00
5.00
6.00
7.00
8.00
9.00
Time [Gyr]
z=0.7255
log10(M*/M⊙)=10.85

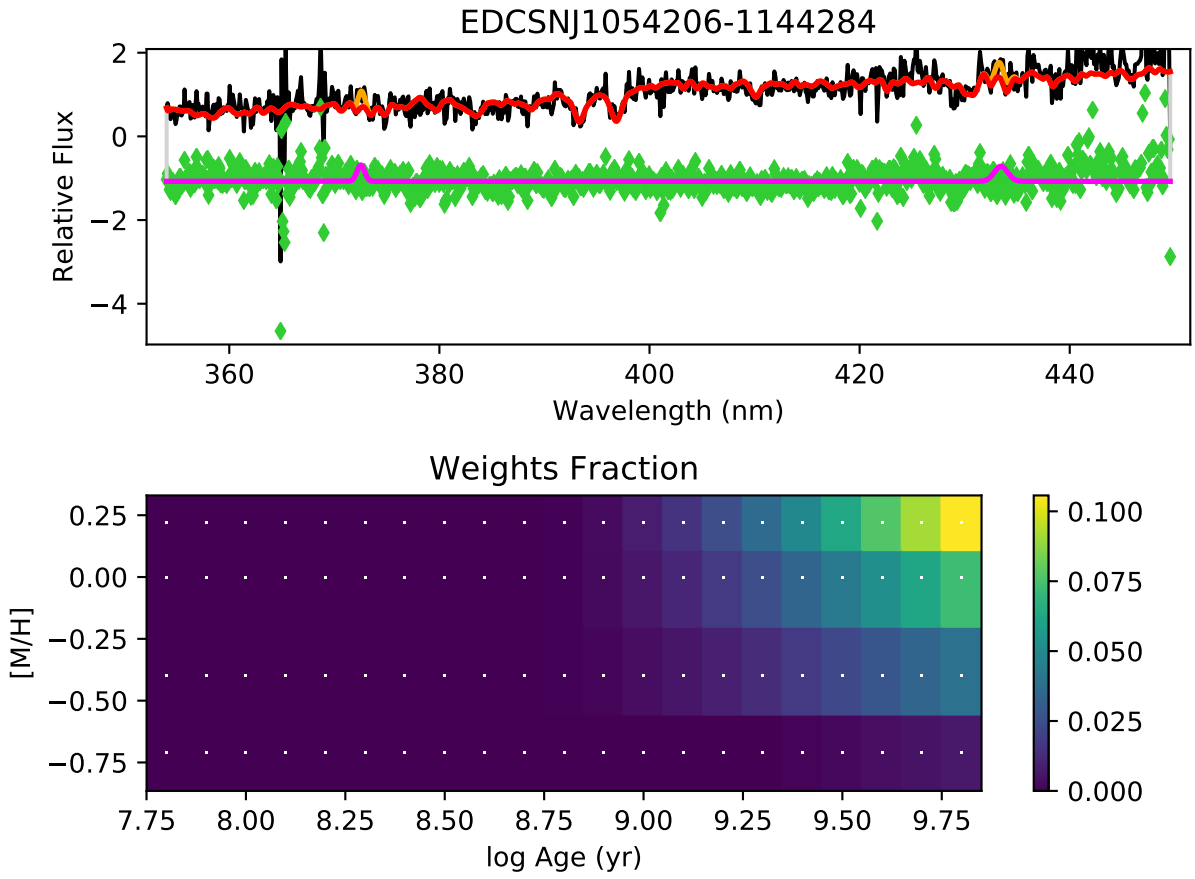
EDCSNJ1054206-1144284
Relative Flux
2
0
−2
−4
360
380
400
420
440
Wavelength (nm)
Weights Fraction
[M/H]
0.25
0.00
−0.25
−0.50
−0.75
7.75
8.00
8.25
8.50
8.75
9.00
9.25
9.50
9.75
log Age (yr)
0.100
0.075
0.050
0.025
0.000

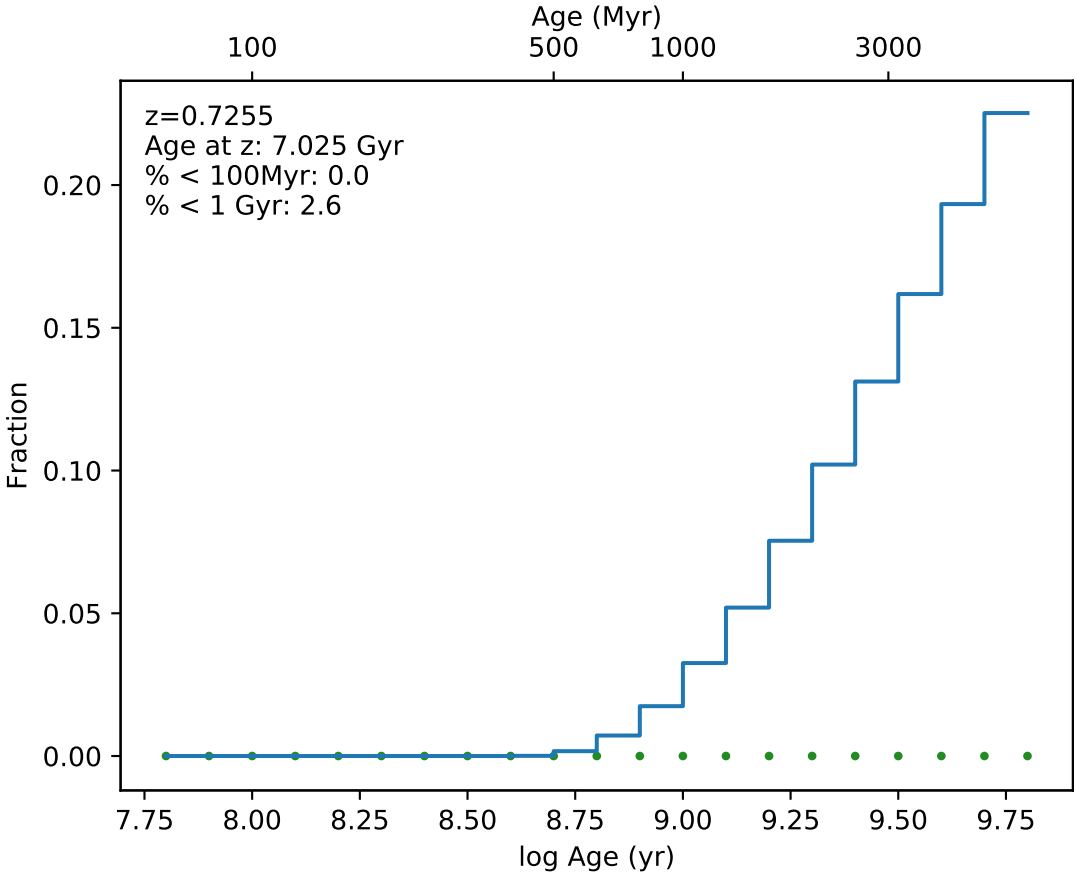
Age (Myr)
100
500
1000
3000
z=0.7255
Age at z: 7.025 Gyr
% < 100Myr: 0.0
% < 1 Gyr: 2.6
Fraction
0.20
0.15
0.10
0.05
0.00
7.75
8.00
8.25
8.50
8.75
9.00
9.25
9.50
9.75
log Age (yr)

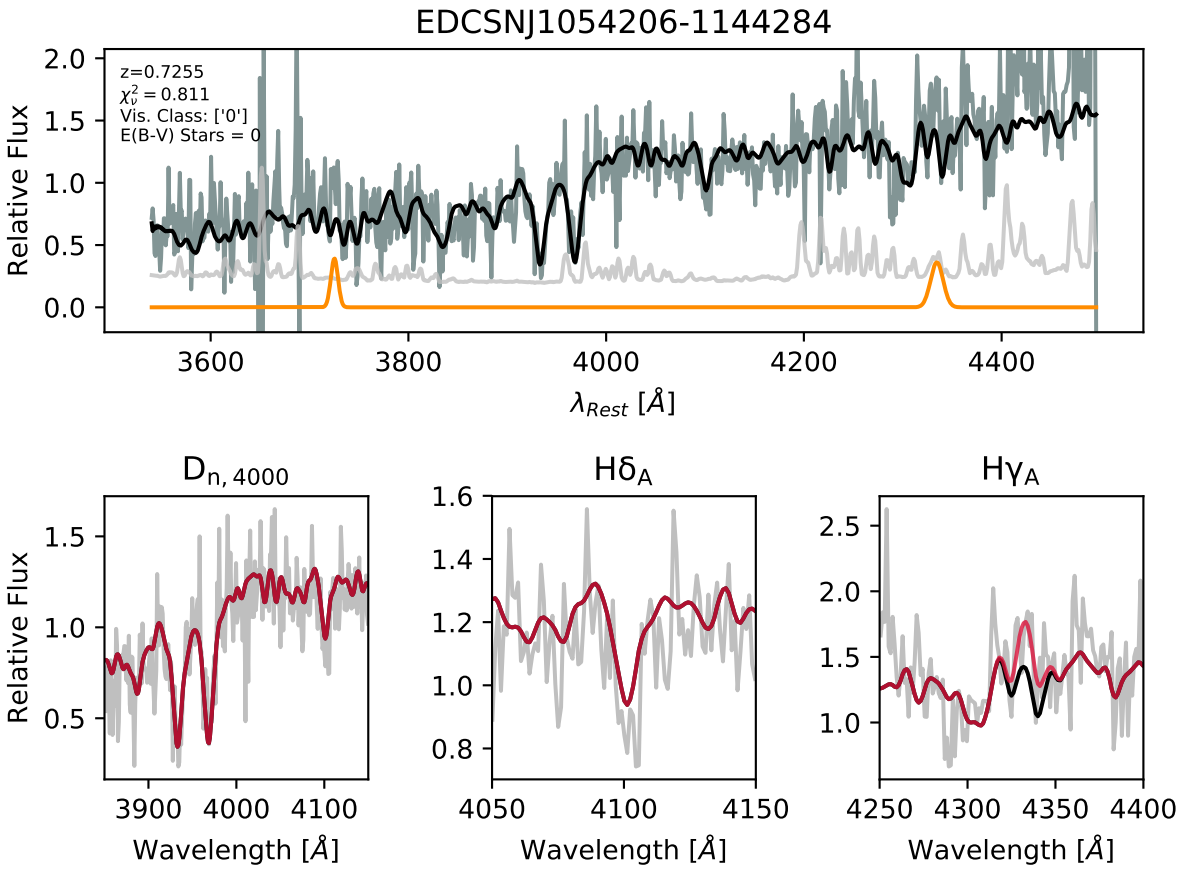
EDCSNJ1054206-1144284
z=0.7255
$\chi^2_\nu = 0.811$
Vis. Class: ['0']
E(B-V) Stars = 0
Relative Flux
λ_{Rest} [Å]
$D_{n,4000}$
$H\delta_A$
$H\gamma_A$
Wavelength [Å]

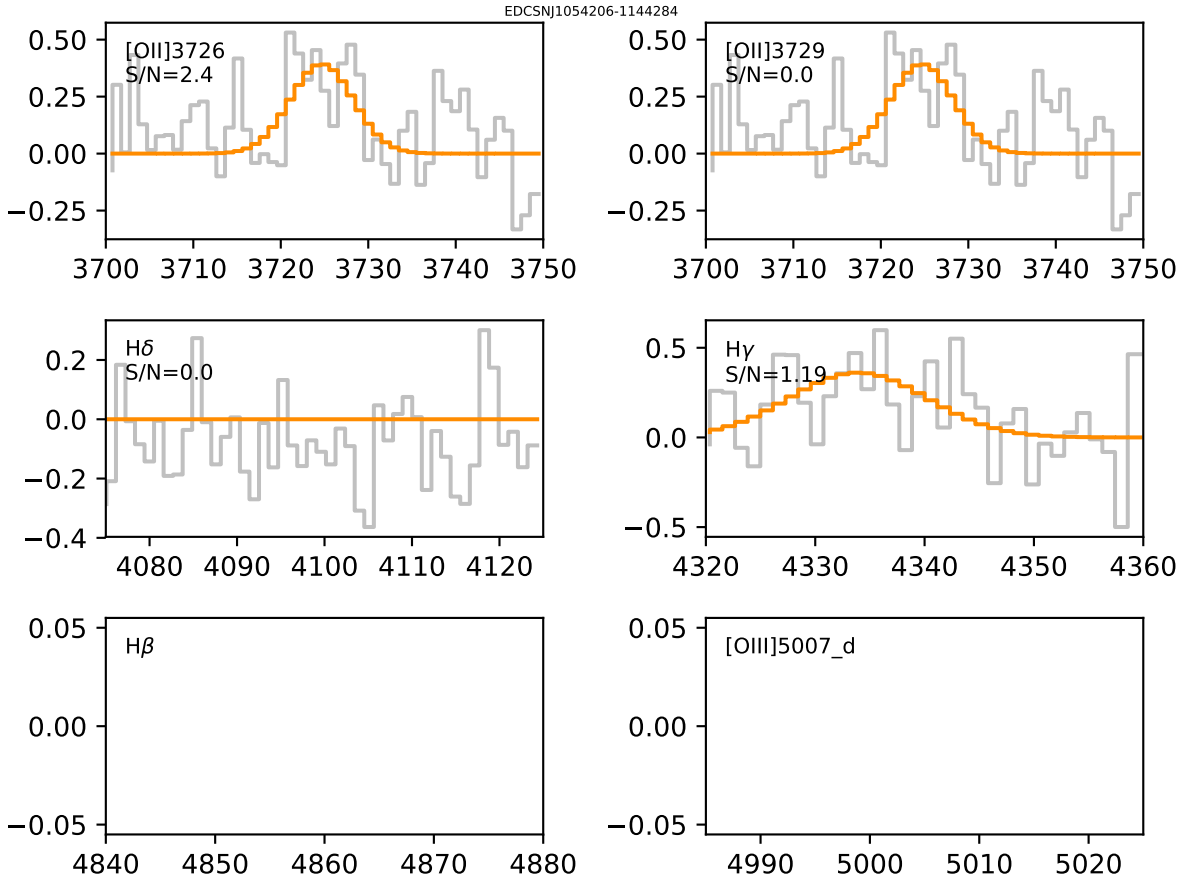
EDCSNJ1054206-1144284
[OII]3726
S/N=2.4
[OII]3729
S/N=0.0
Hδ
S/N=0.0
Hγ
S/N=1.19
Hβ
[OIII]5007_d

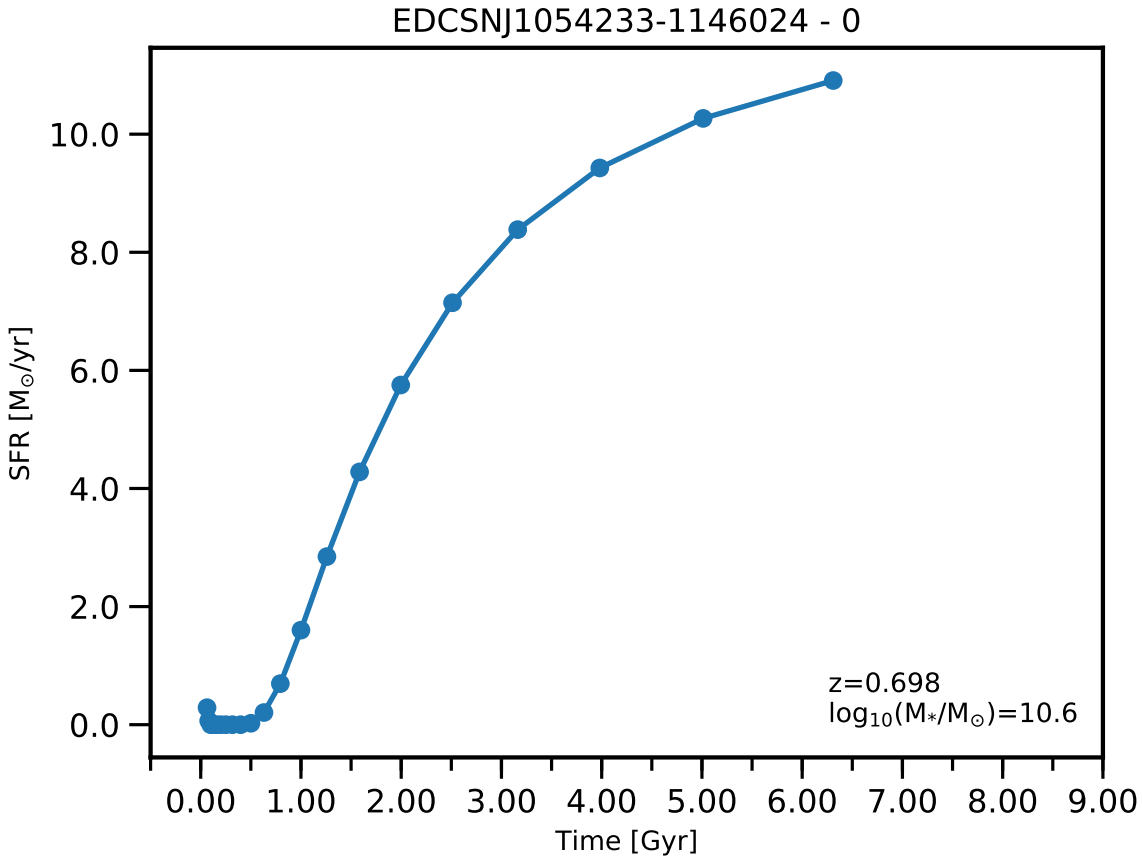
EDCSNJ1054233-1146024 - 0
SFR [M⊙/yr]
10.0
8.0
6.0
4.0
2.0
0.0
0.00
1.00
2.00
3.00
4.00
5.00
6.00
7.00
8.00
9.00
Time [Gyr]
z=0.698
log10(M*/M⊙)=10.6

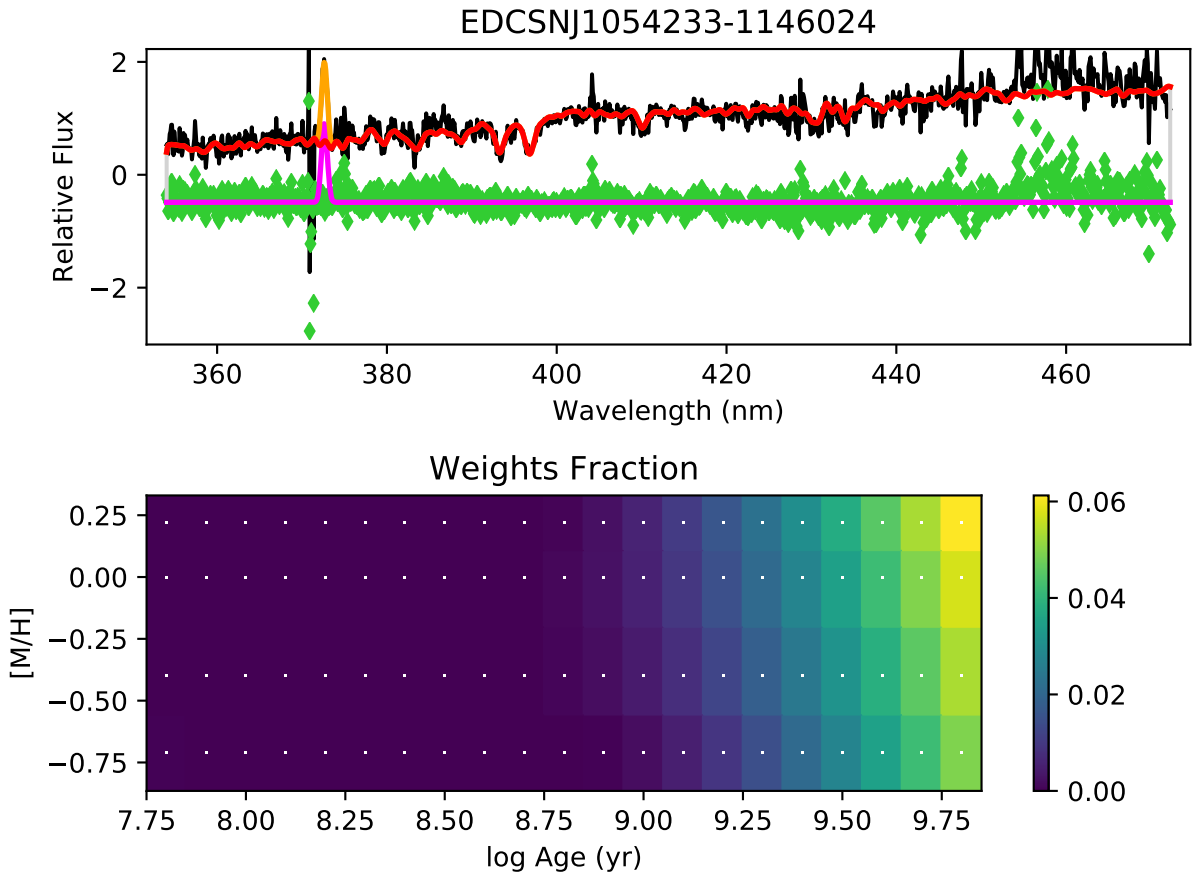
EDCSNJ1054233-1146024
Relative Flux
2
0
−2
360
380
400
420
440
460
Wavelength (nm)
Weights Fraction
[M/H]
0.25
0.00
−0.25
−0.50
−0.75
7.75
8.00
8.25
8.50
8.75
9.00
9.25
9.50
9.75
log Age (yr)
0.06
0.04
0.02
0.00

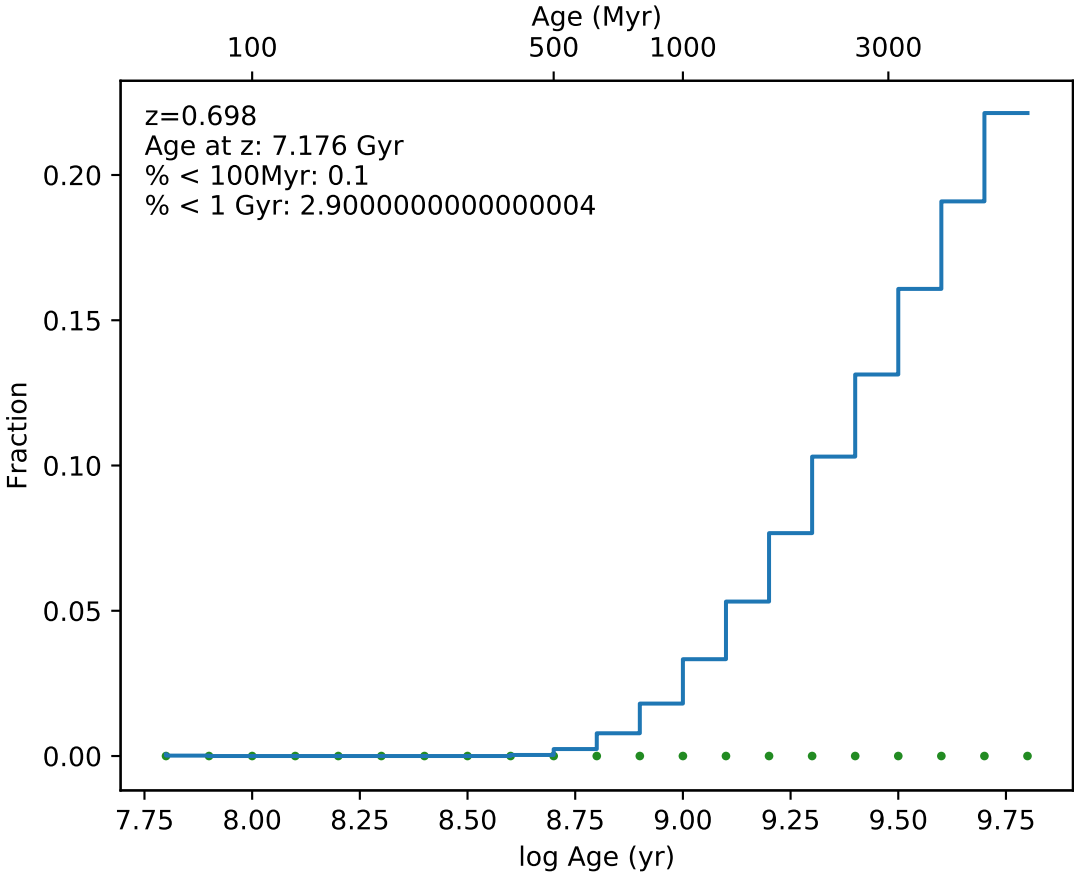
Age (Myr)
100
500
1000
3000
z=0.698
Age at z: 7.176 Gyr
% < 100Myr: 0.1
% < 1 Gyr: 2.9000000000000004
Fraction
0.20
0.15
0.10
0.05
0.00
7.75
8.00
8.25
8.50
8.75
9.00
9.25
9.50
9.75
log Age (yr)

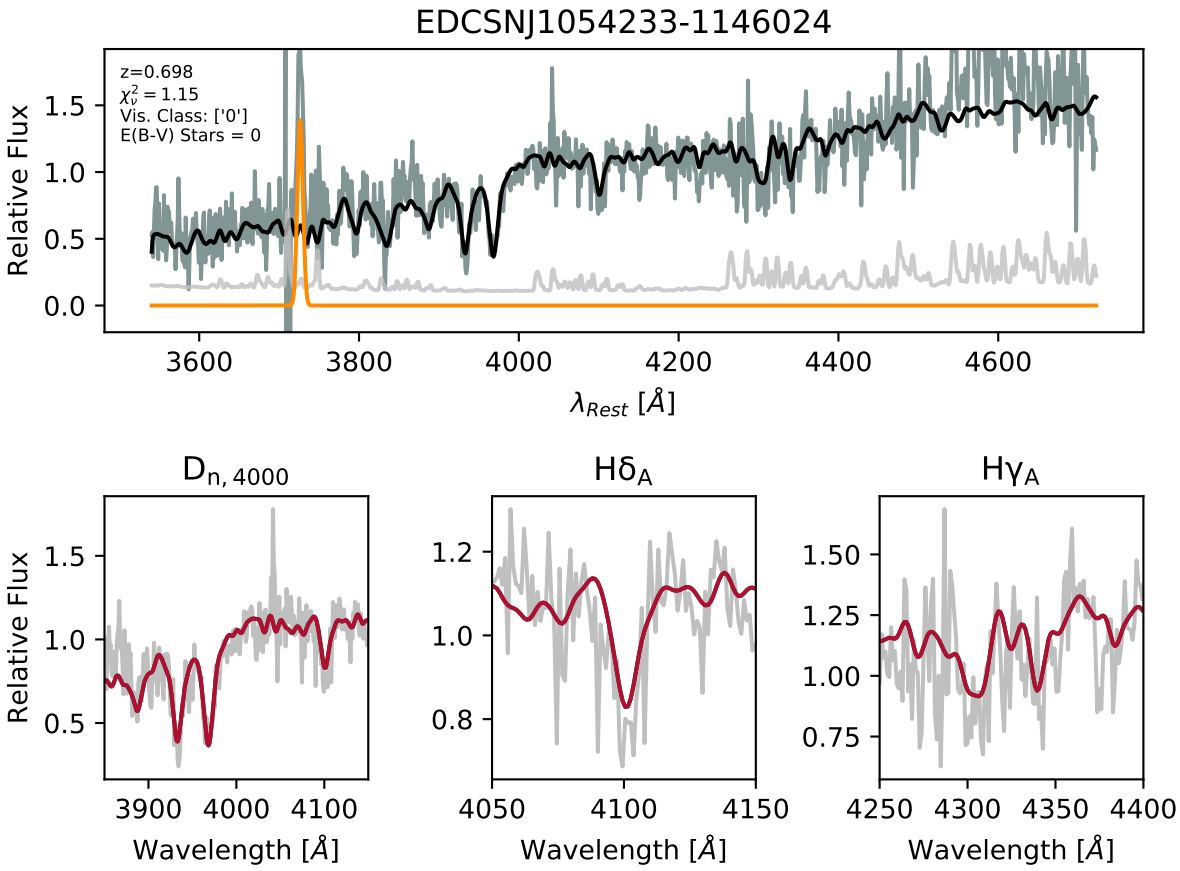
EDCSNJ1054233-1146024
z=0.698
$\chi^2_\nu = 1.15$
Vis. Class: ['0']
E(B-V) Stars = 0
Relative Flux
λ_{Rest} [Å]
$D_{n,4000}$
$H\delta_A$
$H\gamma_A$
Wavelength [Å]

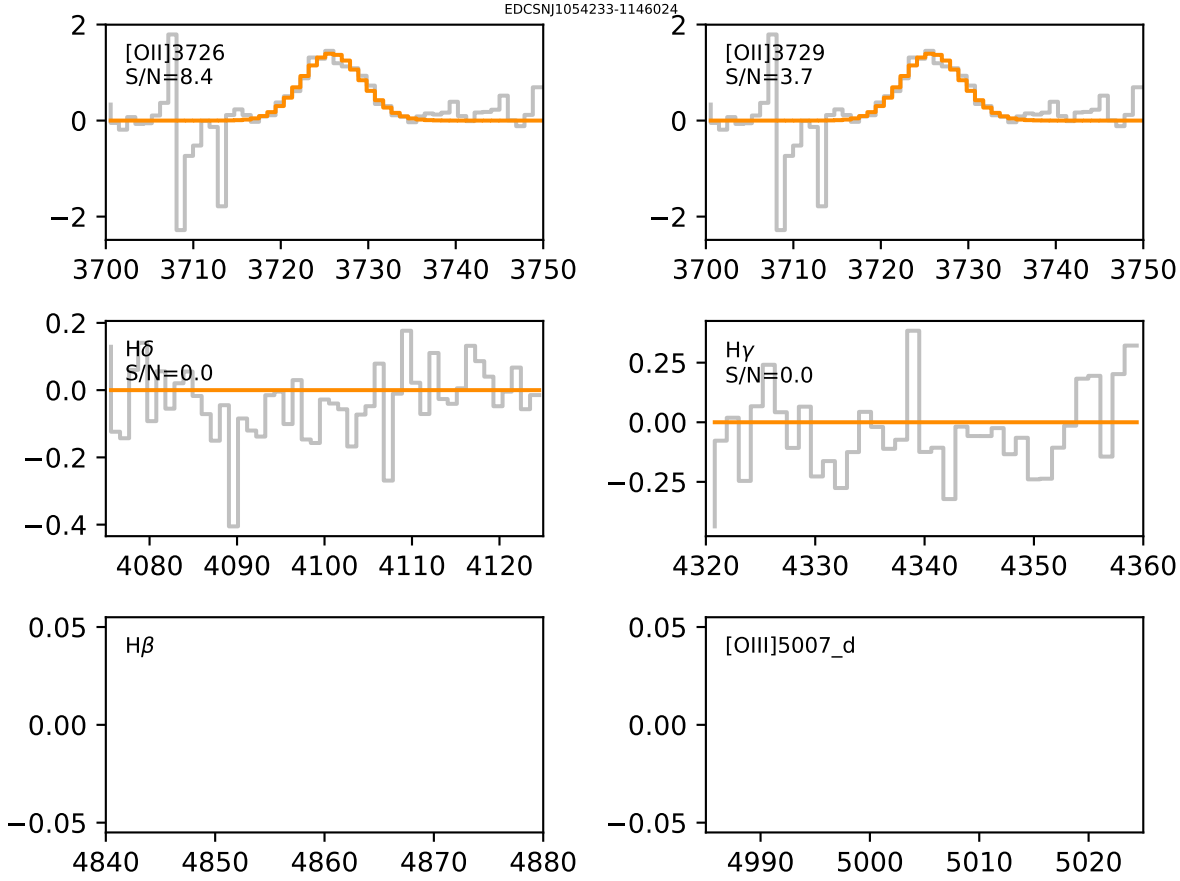
EDCSNJ1054233-1146024
[OII]3726
S/N=8.4
[OII]3729
S/N=3.7
Hδ
S/N=0.0
Hγ
S/N=0.0
Hβ
[OIII]5007_d

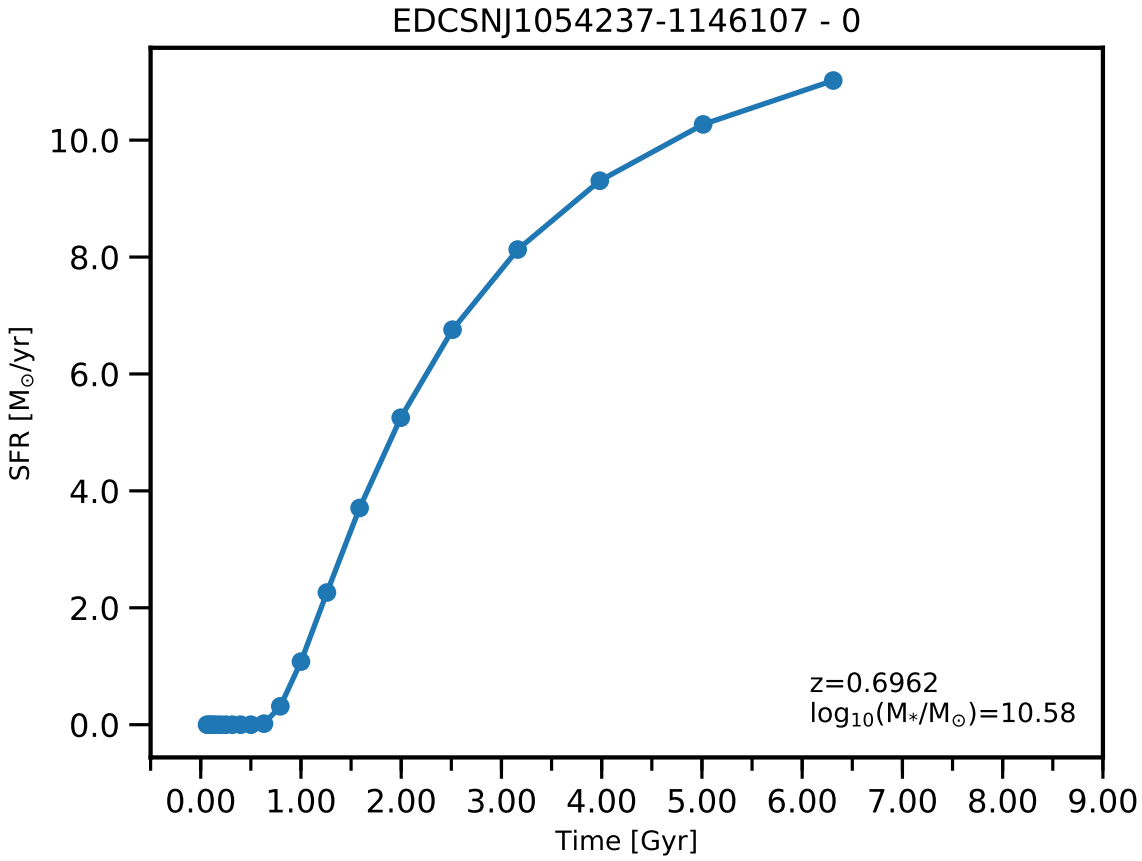
EDCSNJ1054237-1146107 - 0
SFR [M⊙/yr]
10.0
8.0
6.0
4.0
2.0
0.0
0.00
1.00
2.00
3.00
4.00
5.00
6.00
7.00
8.00
9.00
Time [Gyr]
z=0.6962
log10(M*/M⊙)=10.58

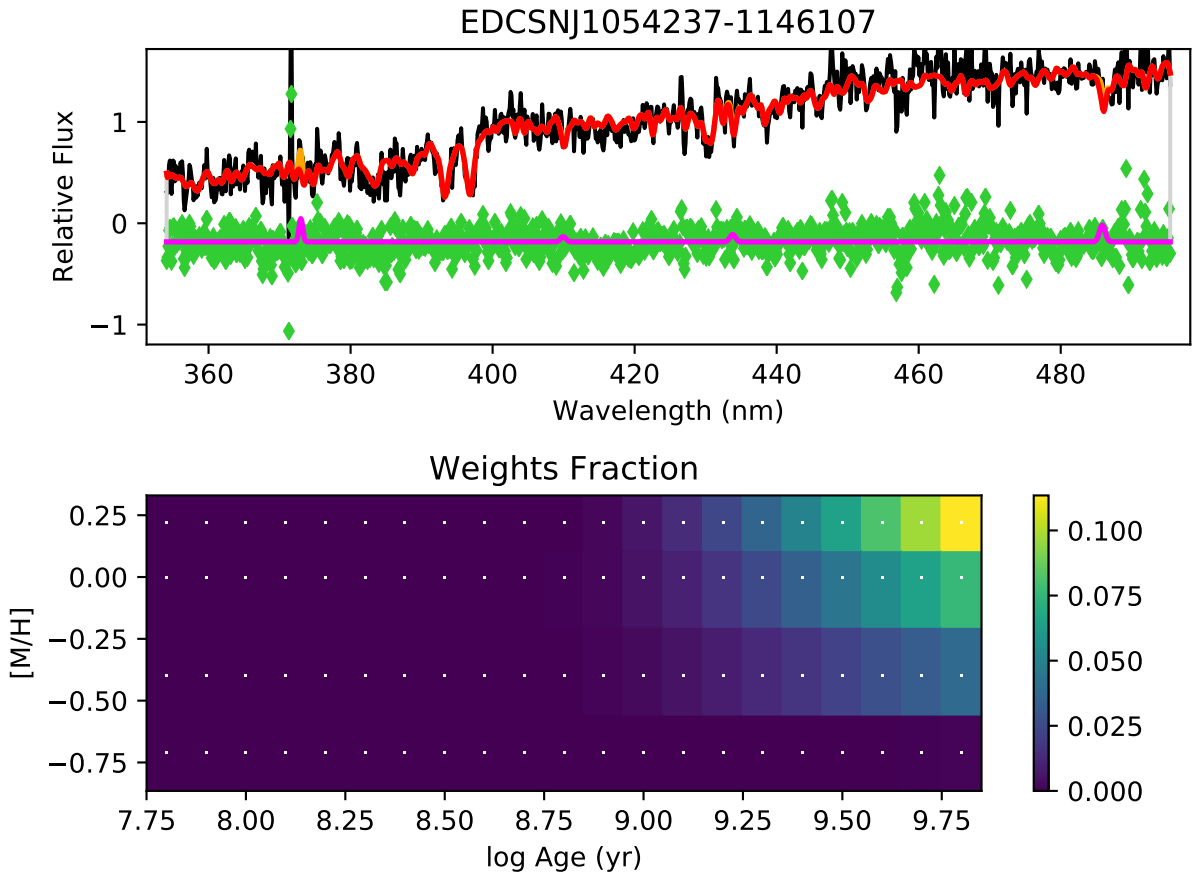
EDCSNJ1054237-1146107
Relative Flux
1
0
−1
360
380
400
420
440
460
480
Wavelength (nm)
Weights Fraction
[M/H]
0.25
0.00
−0.25
−0.50
−0.75
7.75
8.00
8.25
8.50
8.75
9.00
9.25
9.50
9.75
log Age (yr)
0.100
0.075
0.050
0.025
0.000

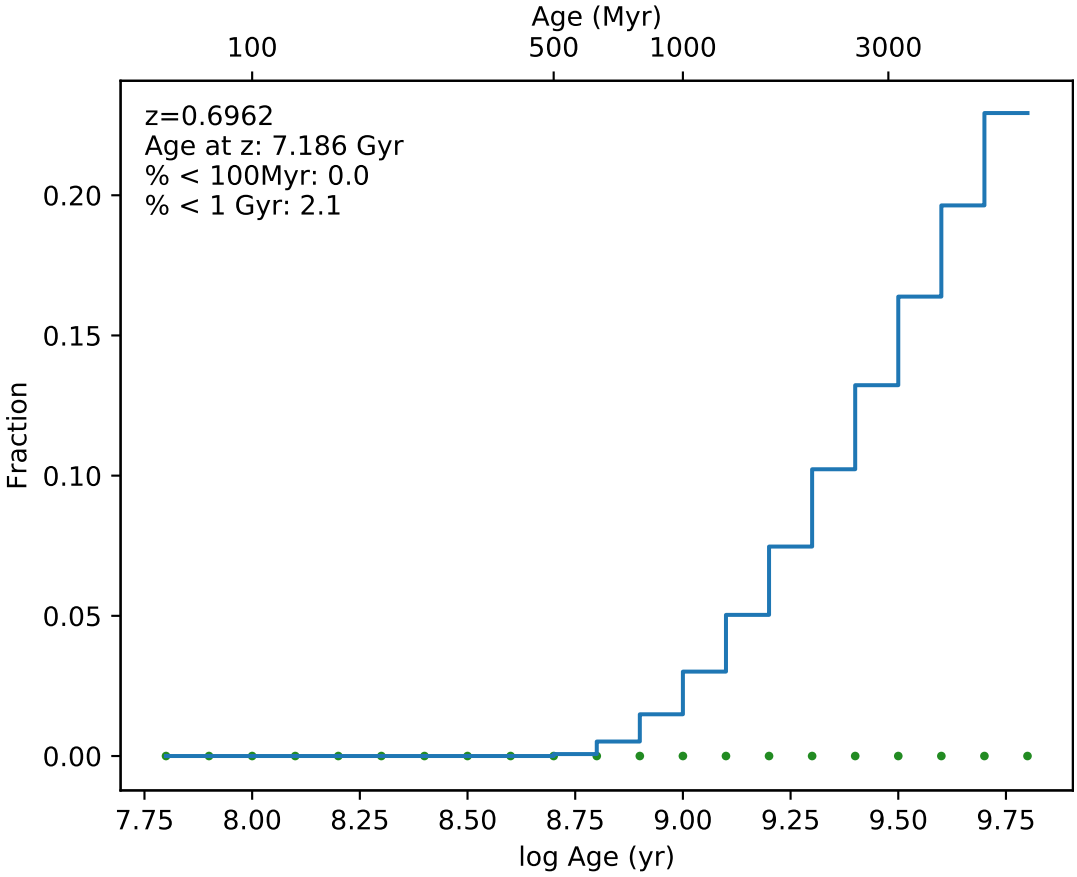
Age (Myr)
100
500
1000
3000
z=0.6962
Age at z: 7.186 Gyr
% < 100Myr: 0.0
% < 1 Gyr: 2.1
Fraction
0.20
0.15
0.10
0.05
0.00
7.75
8.00
8.25
8.50
8.75
9.00
9.25
9.50
9.75
log Age (yr)

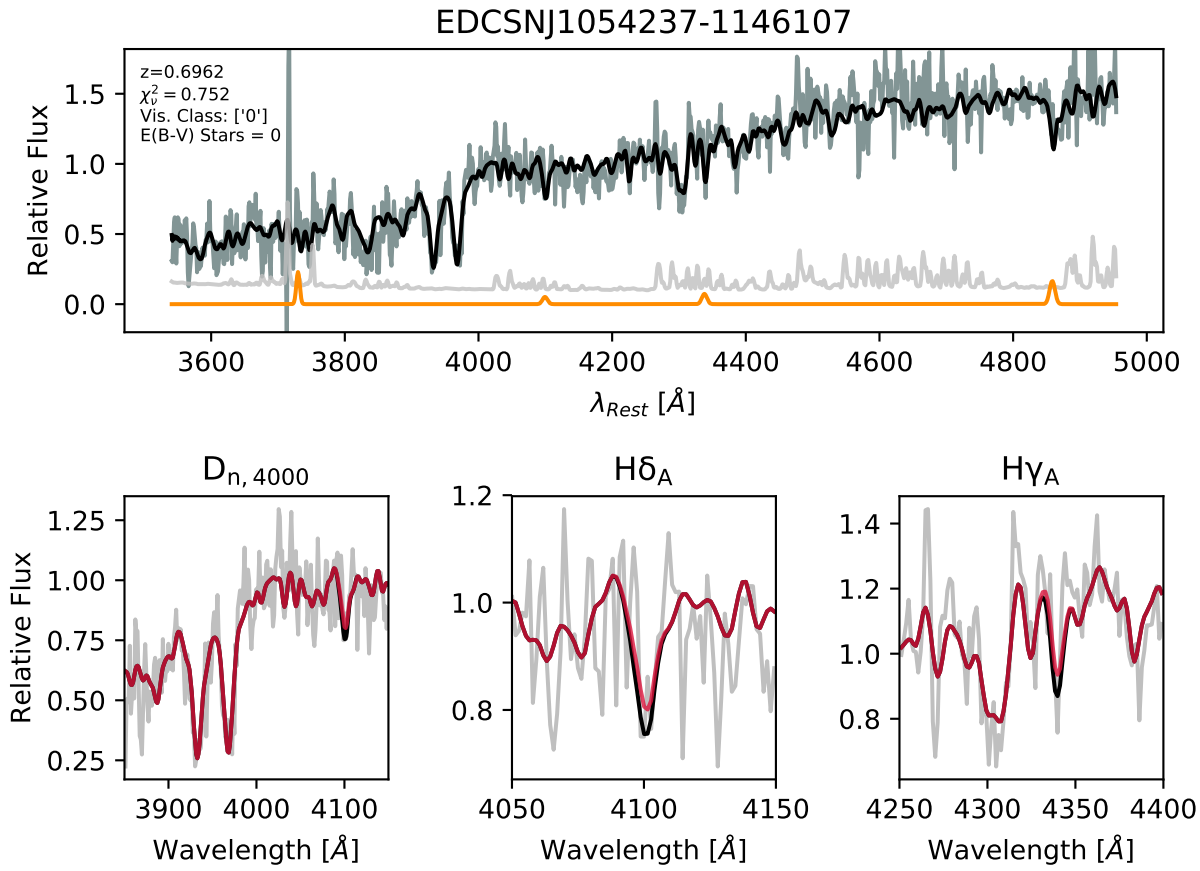
EDCSNJ1054237-1146107
z=0.6962
$\chi^2_\nu = 0.752$
Vis. Class: ['0']
E(B-V) Stars = 0
Relative Flux
λ_{Rest} [Å]
$D_{n,4000}$
$H\delta_A$
$H\gamma_A$
Wavelength [Å]

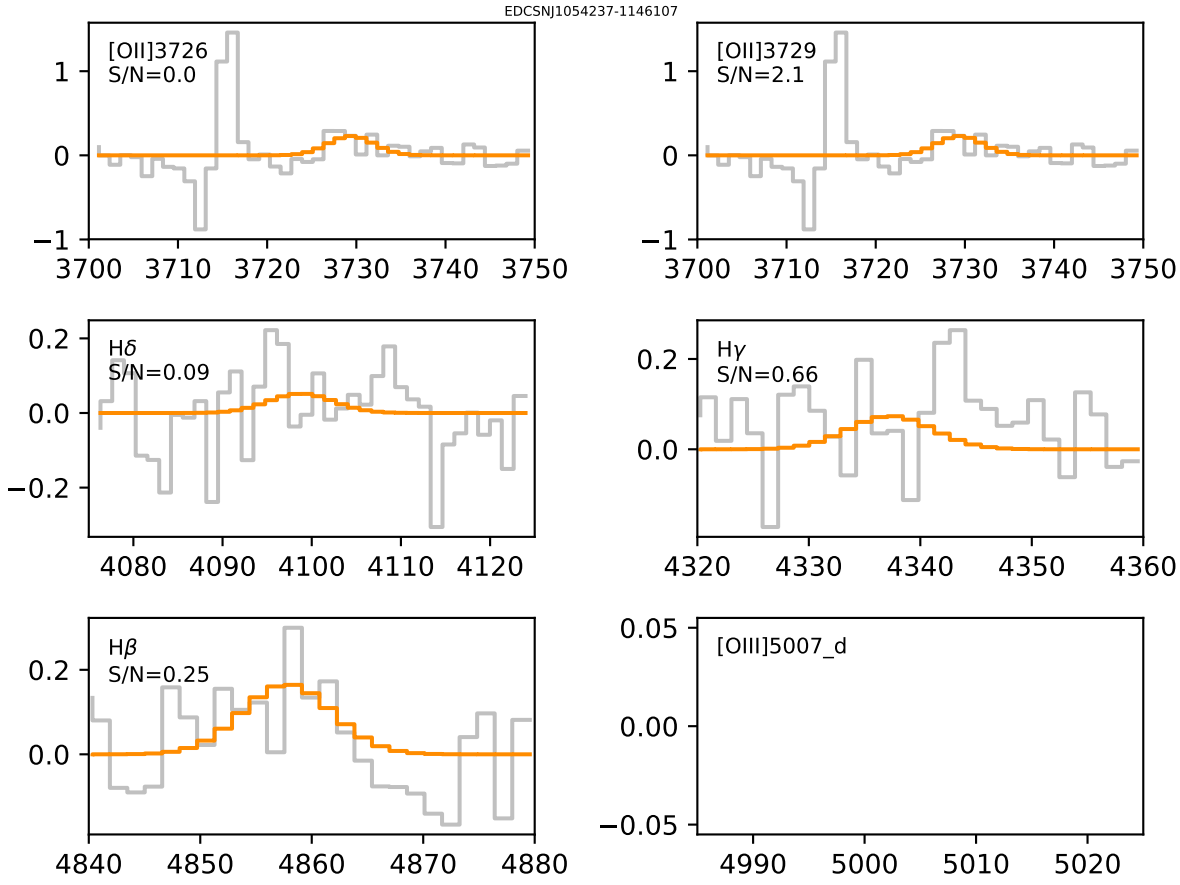
EDCSNJ1054237-1146107
[OII]3726
S/N=0.0
[OII]3729
S/N=2.1
Hδ
S/N=0.09
Hγ
S/N=0.66
Hβ
S/N=0.25
[OIII]5007_d

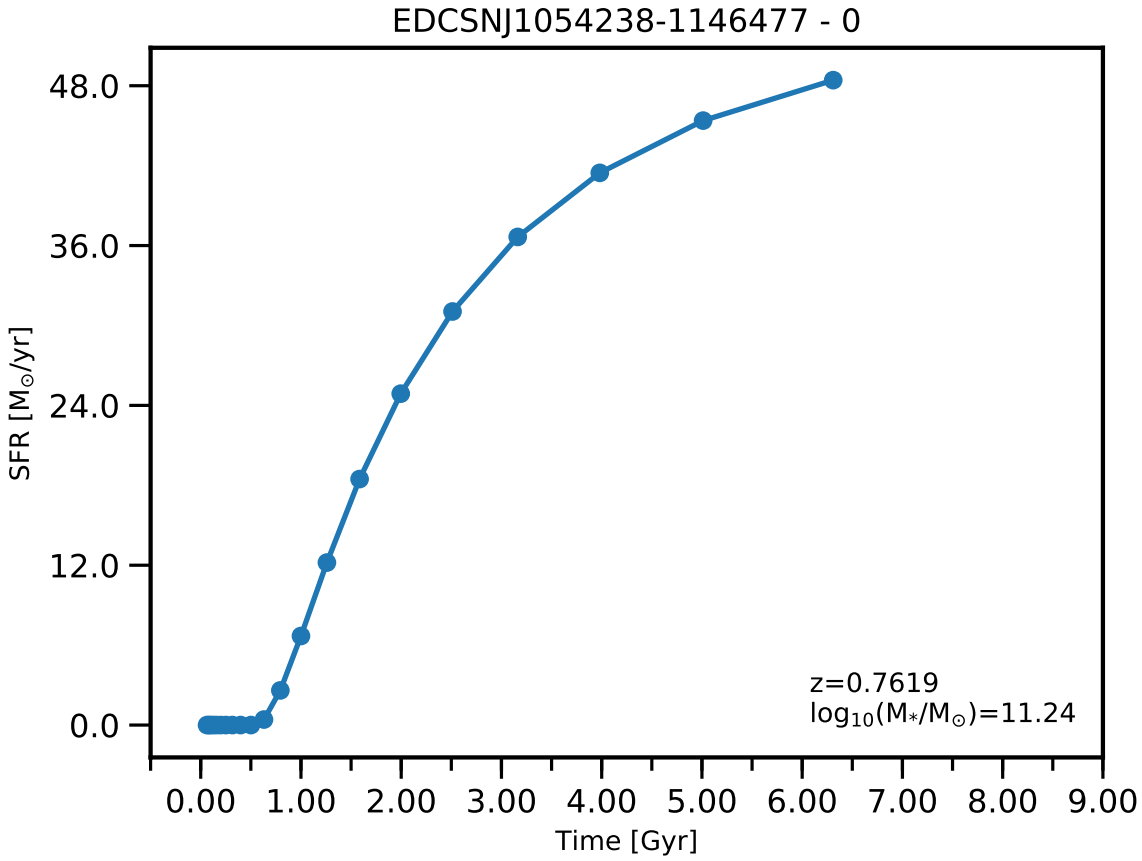
EDCSNJ1054238-1146477 - 0
48.0
36.0
24.0
12.0
0.0
SFR [M⊙/yr]
0.00
1.00
2.00
3.00
4.00
5.00
6.00
7.00
8.00
9.00
Time [Gyr]
z=0.7619
log10(M*/M⊙)=11.24

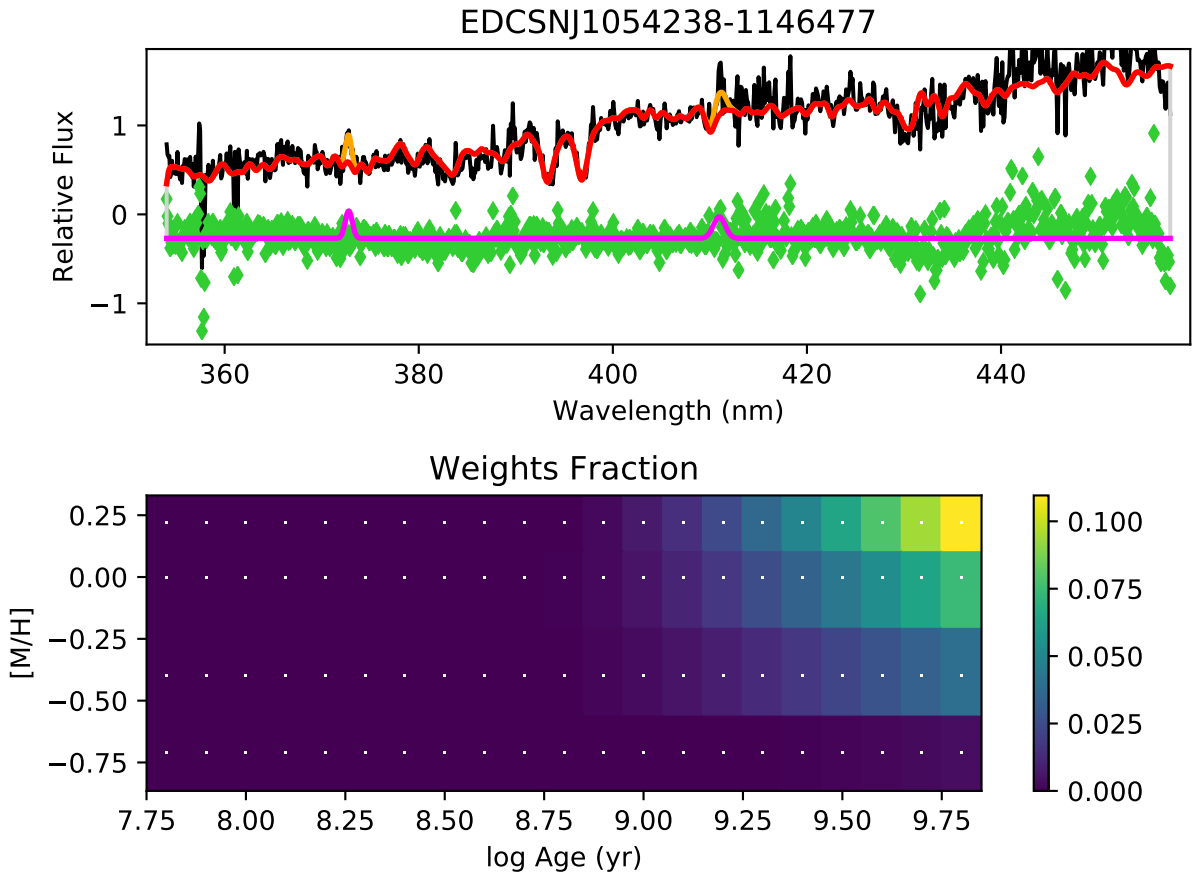
EDCSNJ1054238-1146477
Relative Flux
1
0
−1
360
380
400
420
440
Wavelength (nm)
Weights Fraction
[M/H]
0.25
0.00
−0.25
−0.50
−0.75
7.75
8.00
8.25
8.50
8.75
9.00
9.25
9.50
9.75
log Age (yr)
0.100
0.075
0.050
0.025
0.000

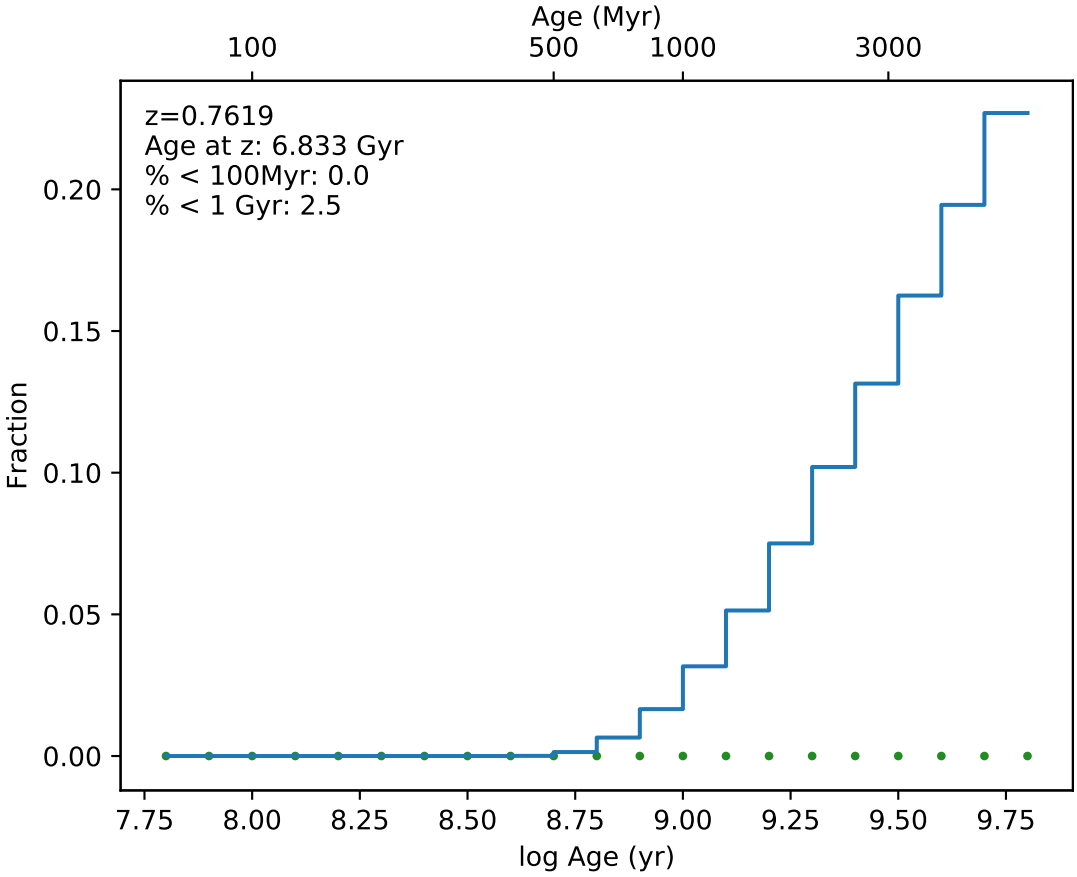
Age (Myr)
100
500
1000
3000
z=0.7619
Age at z: 6.833 Gyr
% < 100Myr: 0.0
% < 1 Gyr: 2.5
Fraction
0.20
0.15
0.10
0.05
0.00
7.75
8.00
8.25
8.50
8.75
9.00
9.25
9.50
9.75
log Age (yr)

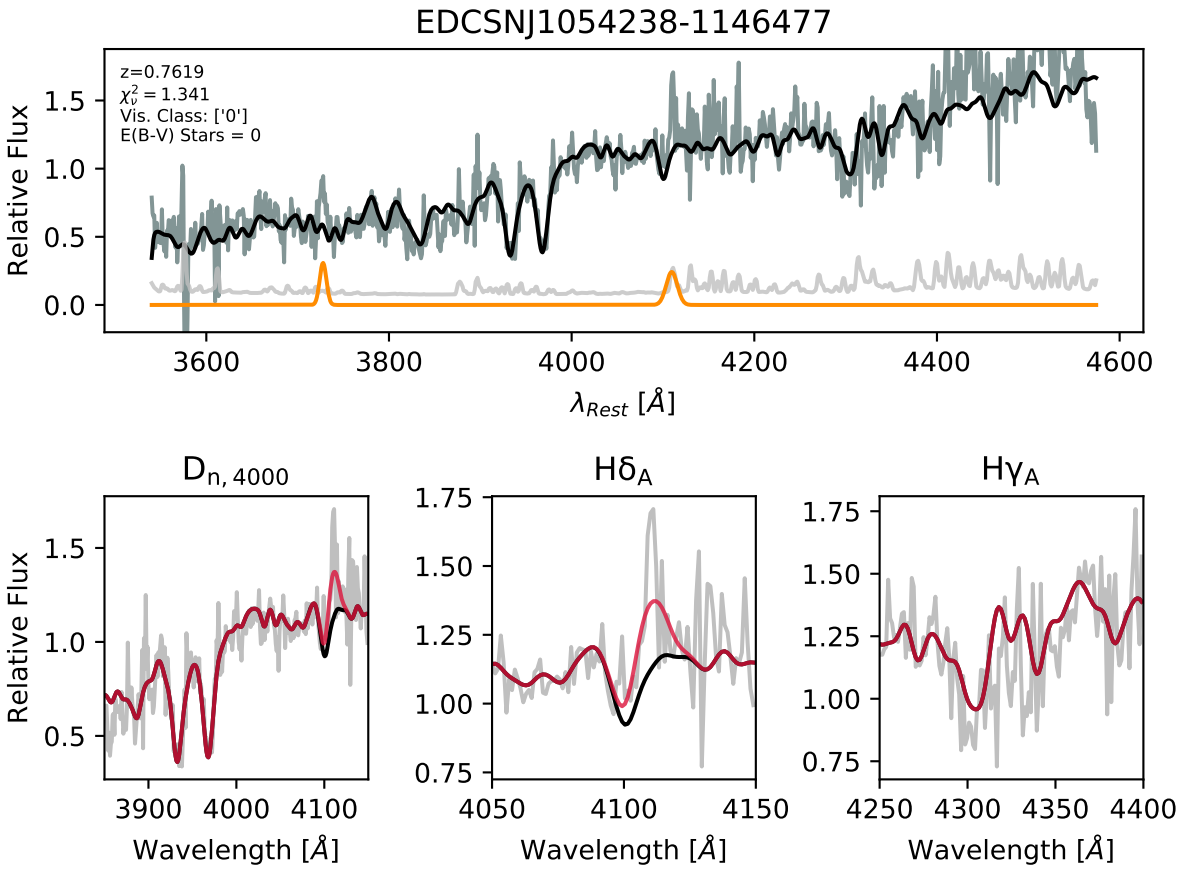
EDCSNJ1054238-1146477
z=0.7619
$\chi^2_\nu = 1.341$
Vis. Class: ['0']
E(B-V) Stars = 0
Relative Flux
λ_{Rest} [Å]
$D_{n,4000}$
$H\delta_A$
$H\gamma_A$
Wavelength [Å]

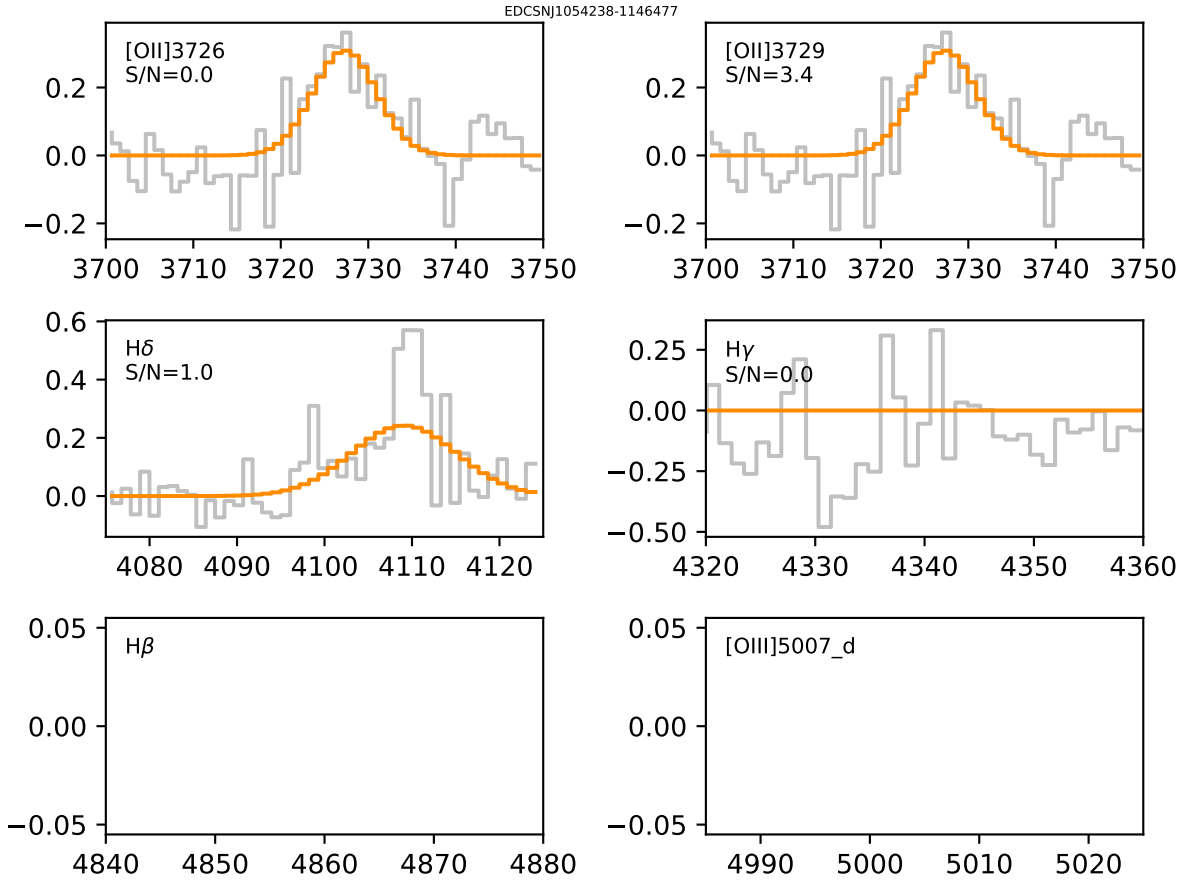
EDCSNJ1054238-1146477
[OII]3726
S/N=0.0
[OII]3729
S/N=3.4
Hδ
S/N=1.0
Hγ
S/N=0.0
Hβ
[OIII]5007_d

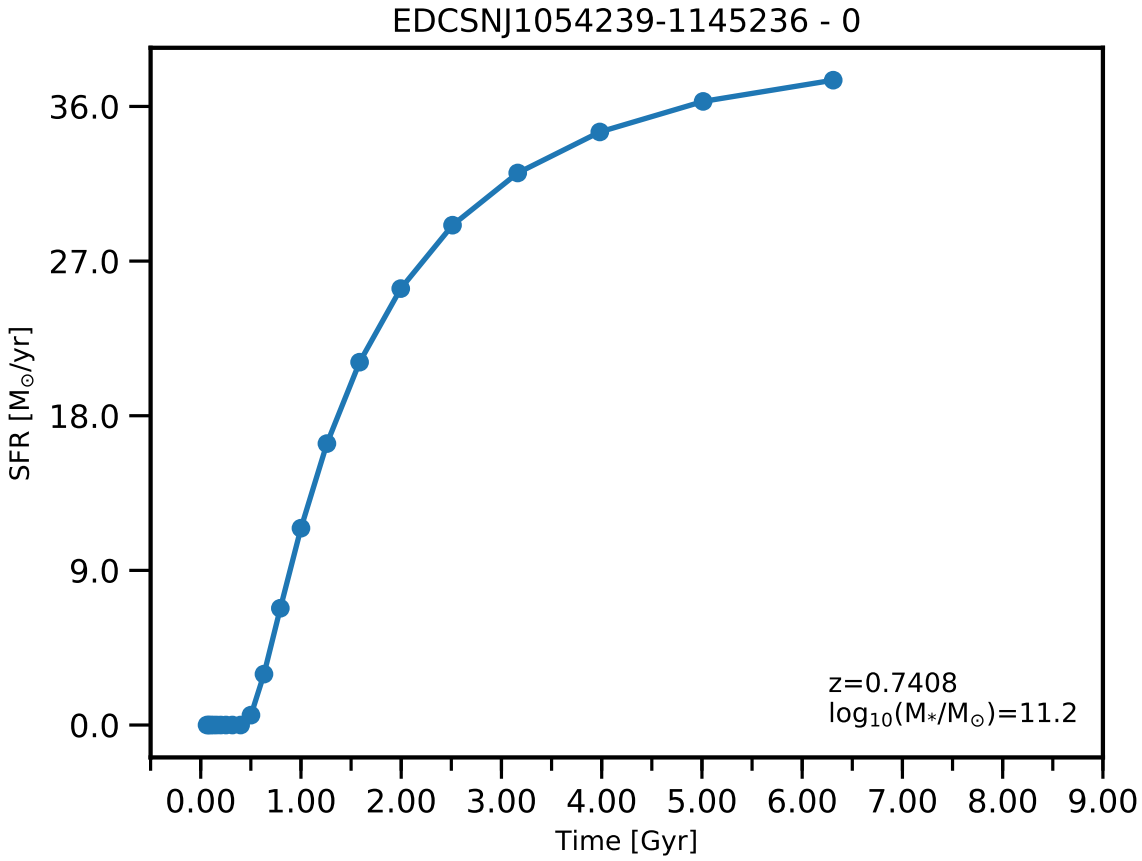
EDCSNJ1054239-1145236 - 0
SFR [M⊙/yr]
36.0
27.0
18.0
9.0
0.0
0.00
1.00
2.00
3.00
4.00
5.00
6.00
7.00
8.00
9.00
Time [Gyr]
z=0.7408
log10(M∗/M⊙)=11.2

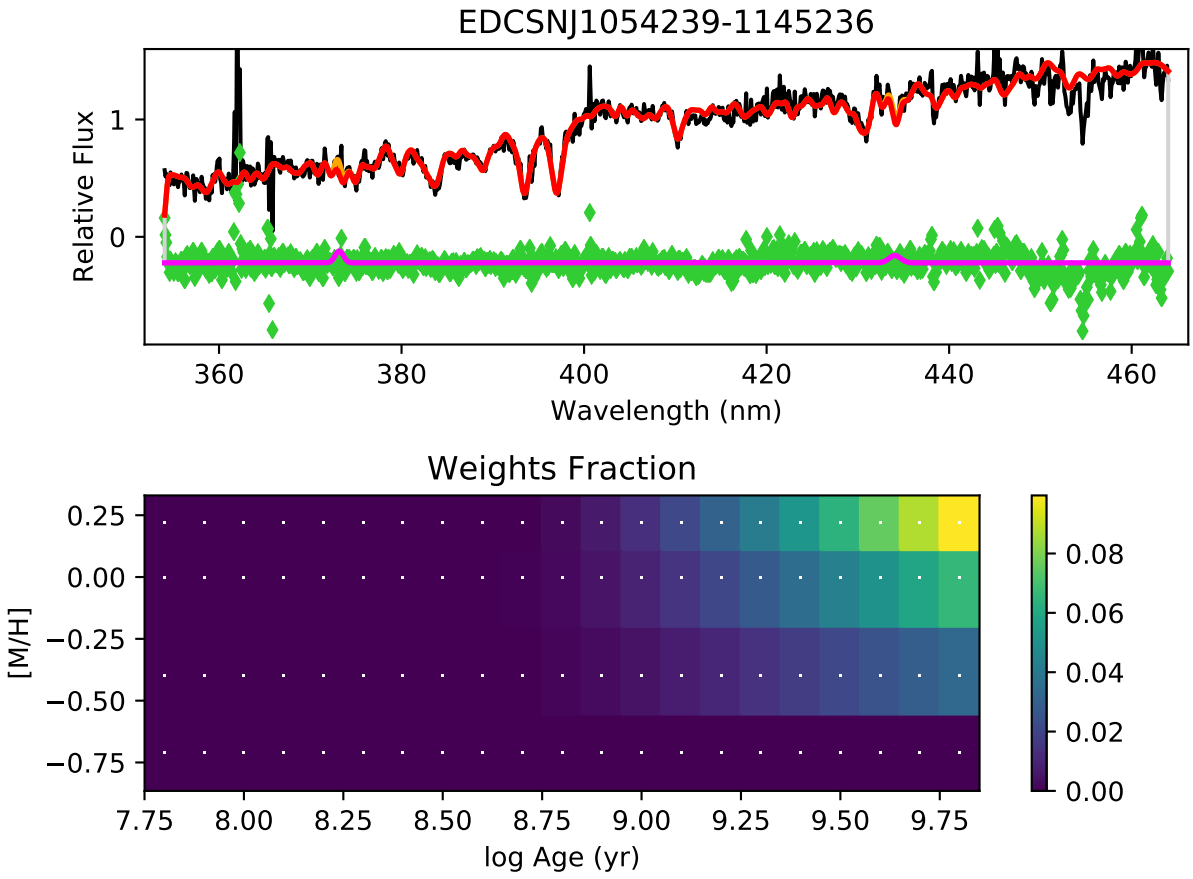
EDCSNJ1054239-1145236
Relative Flux
1
0
360
380
400
420
440
460
Wavelength (nm)
Weights Fraction
[M/H]
0.25
0.00
−0.25
−0.50
−0.75
7.75
8.00
8.25
8.50
8.75
9.00
9.25
9.50
9.75
log Age (yr)
0.08
0.06
0.04
0.02
0.00

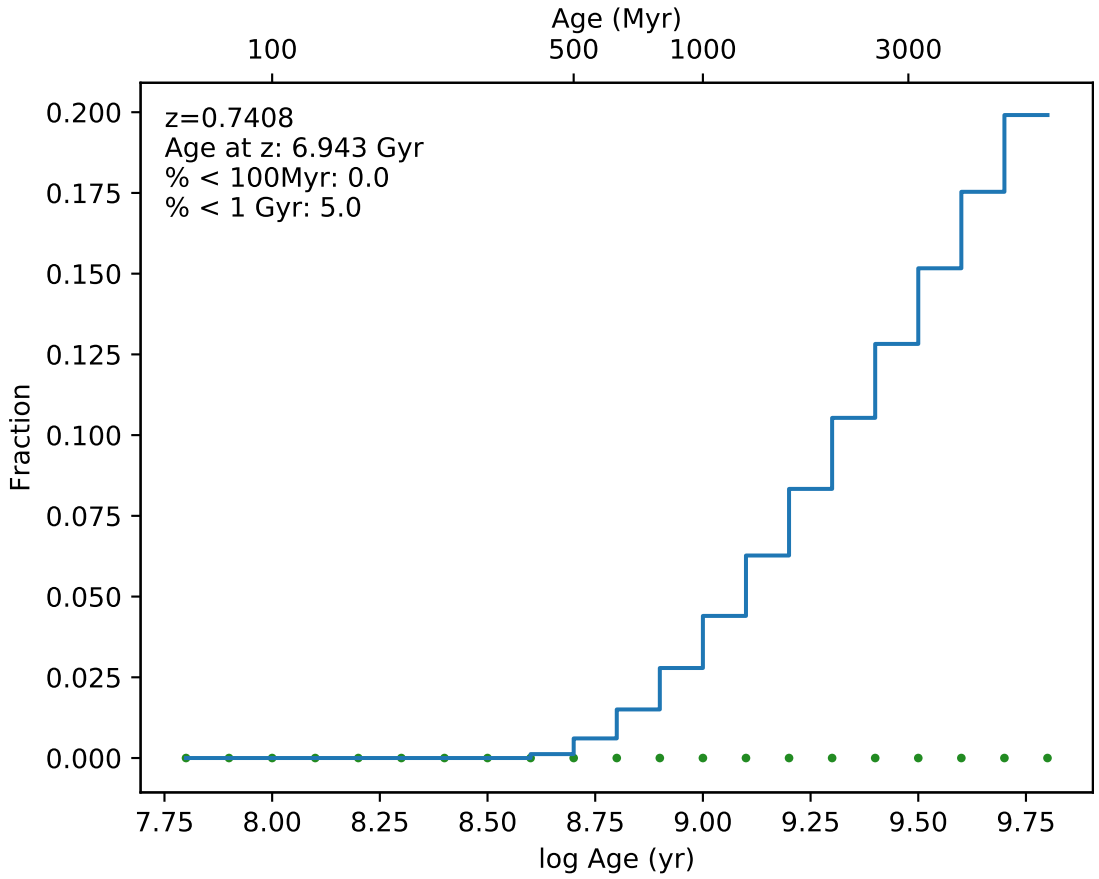
Age (Myr)
100
500
1000
3000
z=0.7408
Age at z: 6.943 Gyr
% < 100Myr: 0.0
% < 1 Gyr: 5.0
Fraction
0.200
0.175
0.150
0.125
0.100
0.075
0.050
0.025
0.000
7.75
8.00
8.25
8.50
8.75
9.00
9.25
9.50
9.75
log Age (yr)

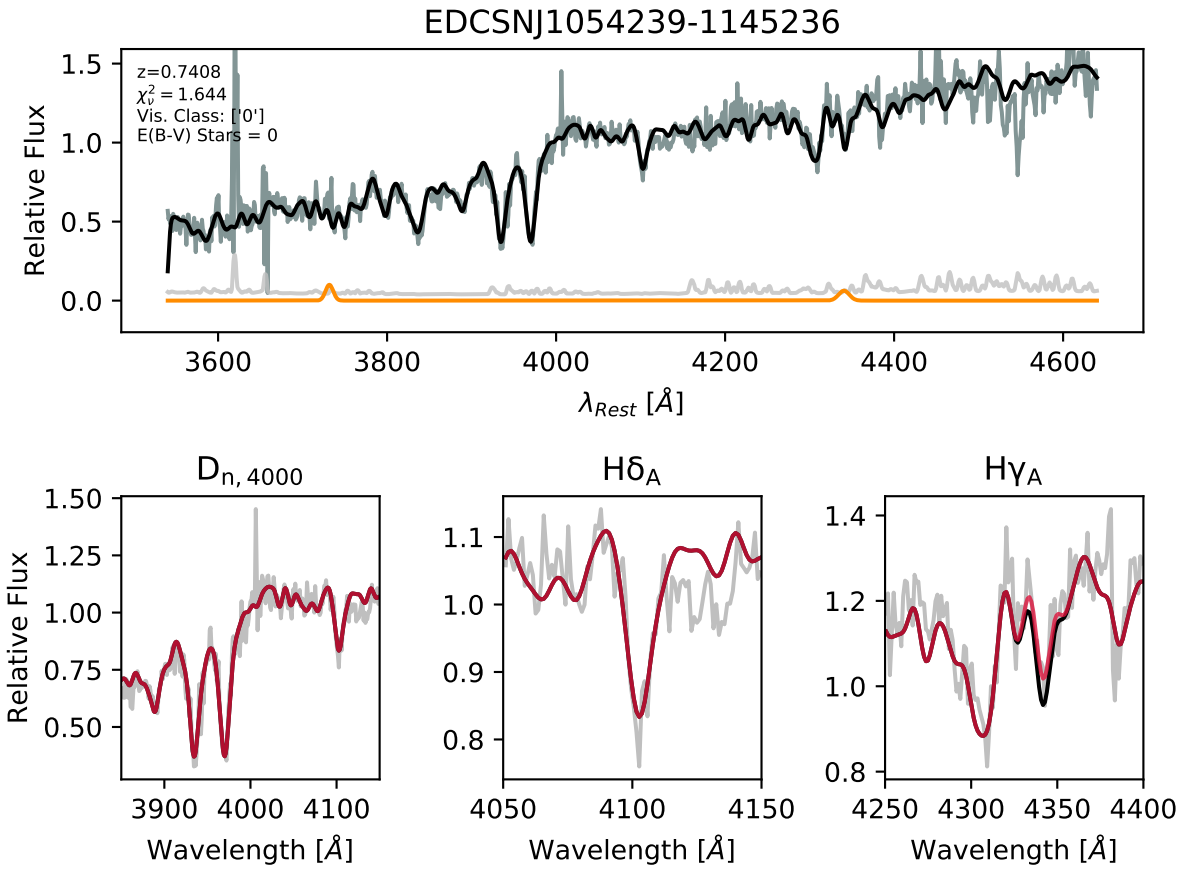
EDCSNJ1054239-1145236
z=0.7408
$\chi^2_\nu = 1.644$
Vis. Class: ['0']
E(B-V) Stars = 0
Relative Flux
λ_{Rest} [Å]
$D_{n,4000}$
$H\delta_A$
$H\gamma_A$
Relative Flux
Wavelength [Å]
Wavelength [Å]
Wavelength [Å]

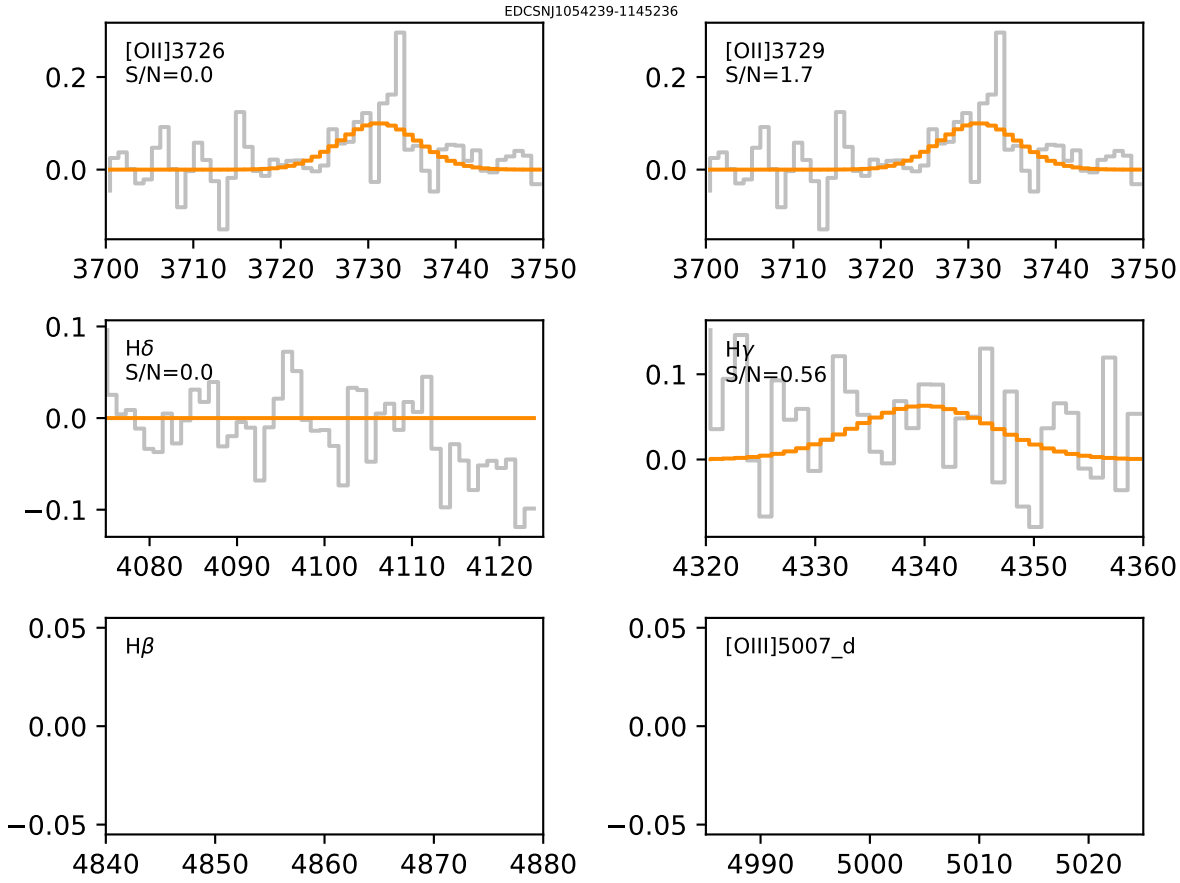
EDCSNJ1054239-1145236
[OII]3726
S/N=0.0
[OII]3729
S/N=1.7
Hδ
S/N=0.0
Hγ
S/N=0.56
Hβ
[OIII]5007_d

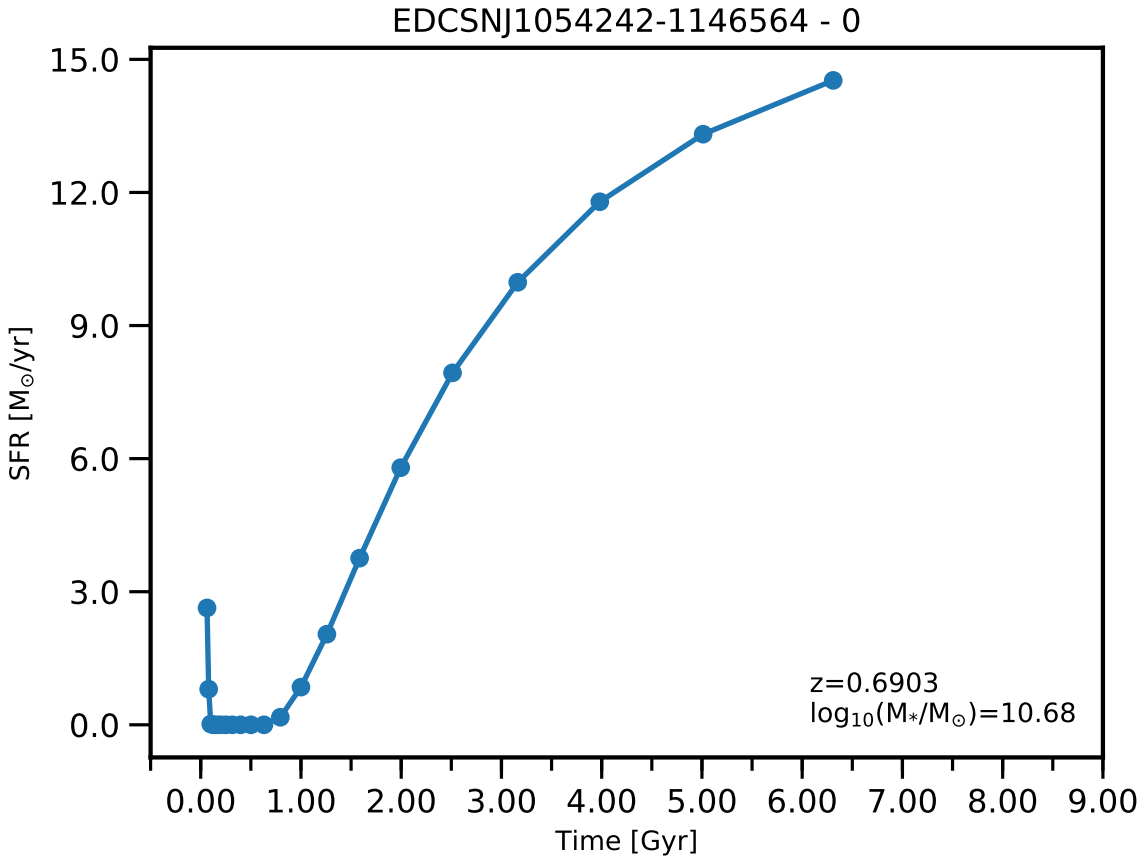
EDCSNJ1054242-1146564 - 0
15.0
12.0
9.0
6.0
3.0
0.0
SFR [M⊙/yr]
0.00
1.00
2.00
3.00
4.00
5.00
6.00
7.00
8.00
9.00
Time [Gyr]
z=0.6903
log10(M*/M⊙)=10.68

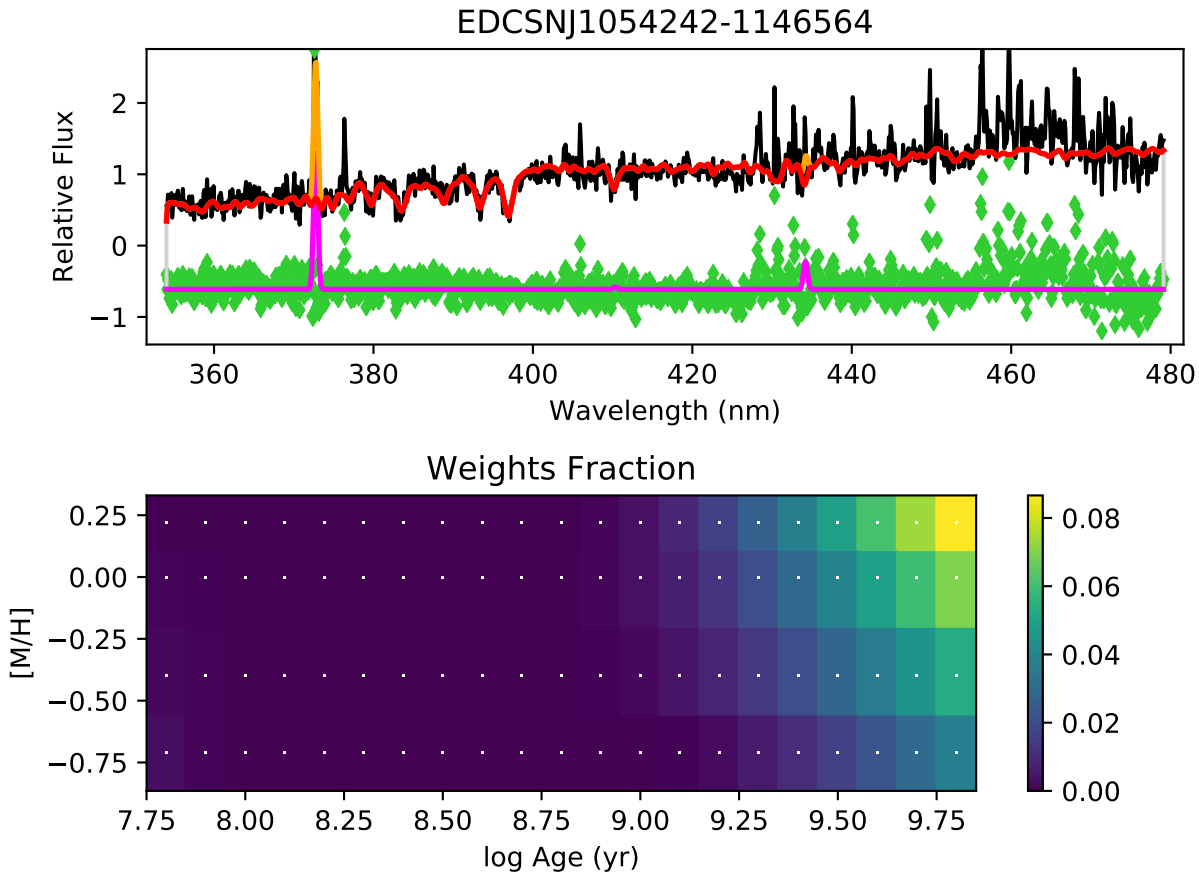
EDCSNJ1054242-1146564
Relative Flux
2
1
0
−1
360
380
400
420
440
460
480
Wavelength (nm)
Weights Fraction
[M/H]
0.25
0.00
−0.25
−0.50
−0.75
7.75
8.00
8.25
8.50
8.75
9.00
9.25
9.50
9.75
log Age (yr)
0.08
0.06
0.04
0.02
0.00

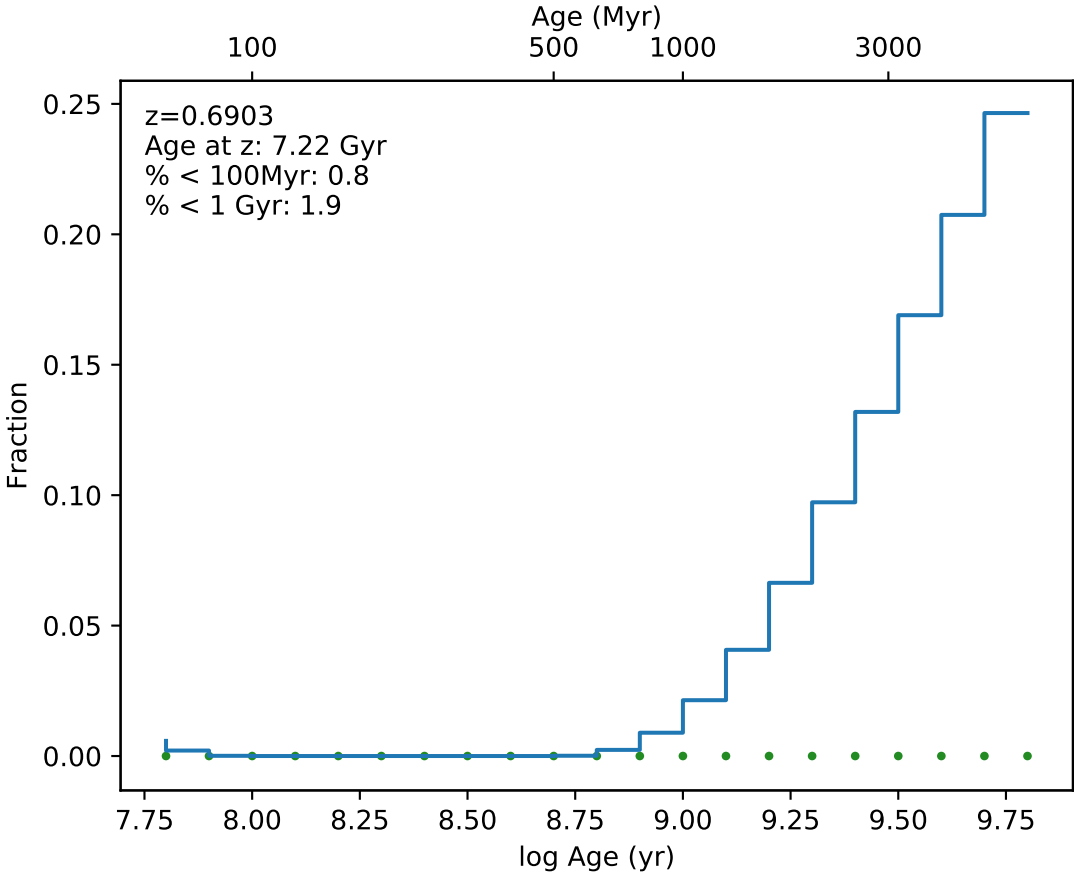
Age (Myr)
100
500
1000
3000
z=0.6903
Age at z: 7.22 Gyr
% < 100Myr: 0.8
% < 1 Gyr: 1.9
Fraction
0.25
0.20
0.15
0.10
0.05
0.00
7.75
8.00
8.25
8.50
8.75
9.00
9.25
9.50
9.75
log Age (yr)

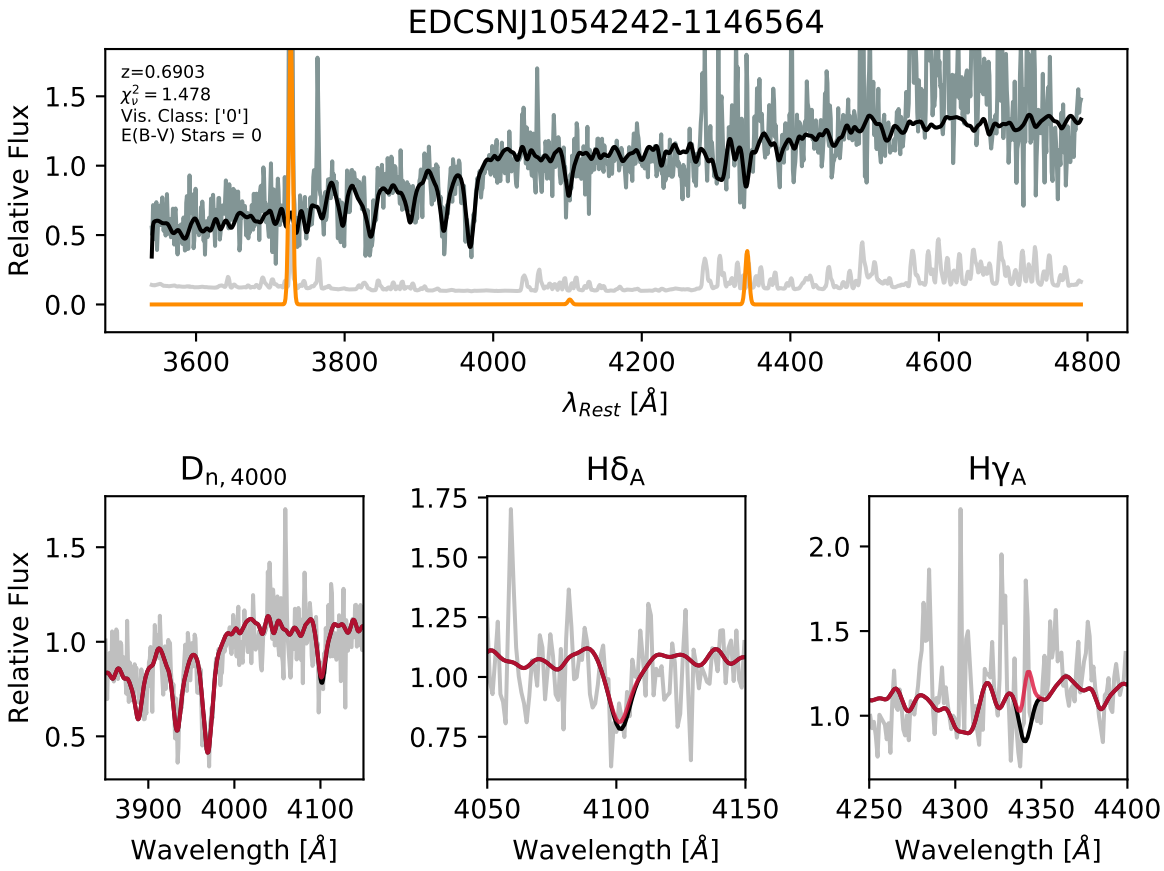
EDCSNJ1054242-1146564
z=0.6903
$\chi^2_\nu = 1.478$
Vis. Class: ['0']
E(B-V) Stars = 0
Relative Flux
λ_{Rest} [Å]
$D_{n,4000}$
$H\delta_A$
$H\gamma_A$
Wavelength [Å]

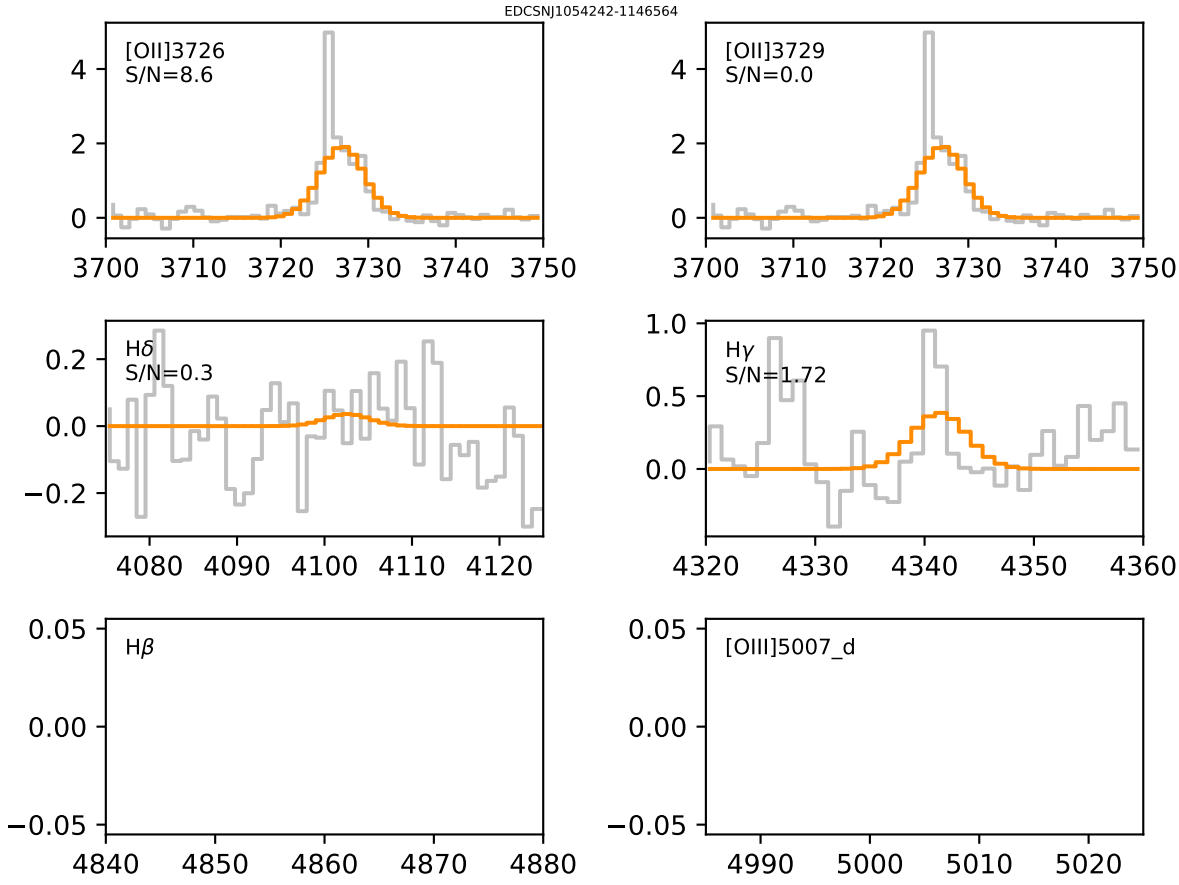
EDCSNJ1054242-1146564
[OII]3726
S/N=8.6
[OII]3729
S/N=0.0
Hδ
S/N=0.3
Hγ
S/N=1.72
Hβ
[OIII]5007_d

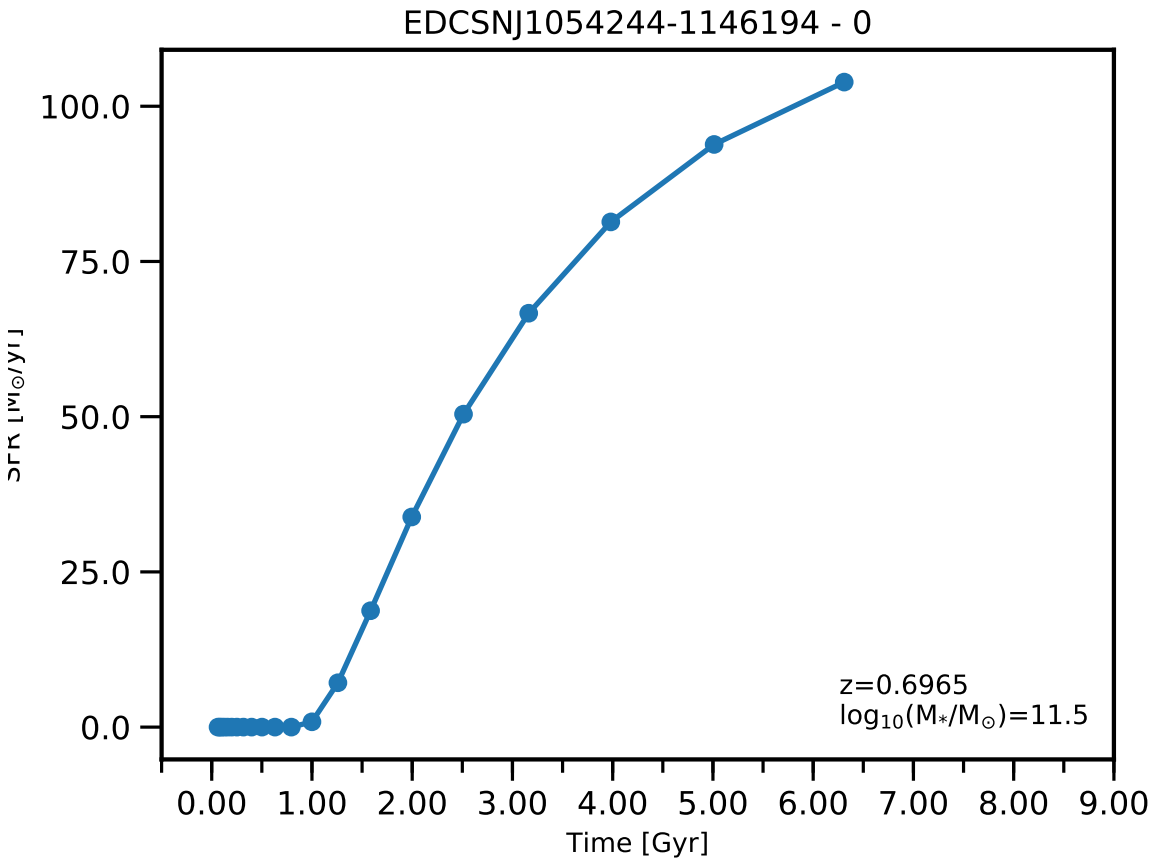
EDCSNJ1054244-1146194 - 0
100.0
75.0
50.0
25.0
0.0
SFR [M⊙/yr]
0.00
1.00
2.00
3.00
4.00
5.00
6.00
7.00
8.00
9.00
Time [Gyr]
z=0.6965
log10(M*/M⊙)=11.5

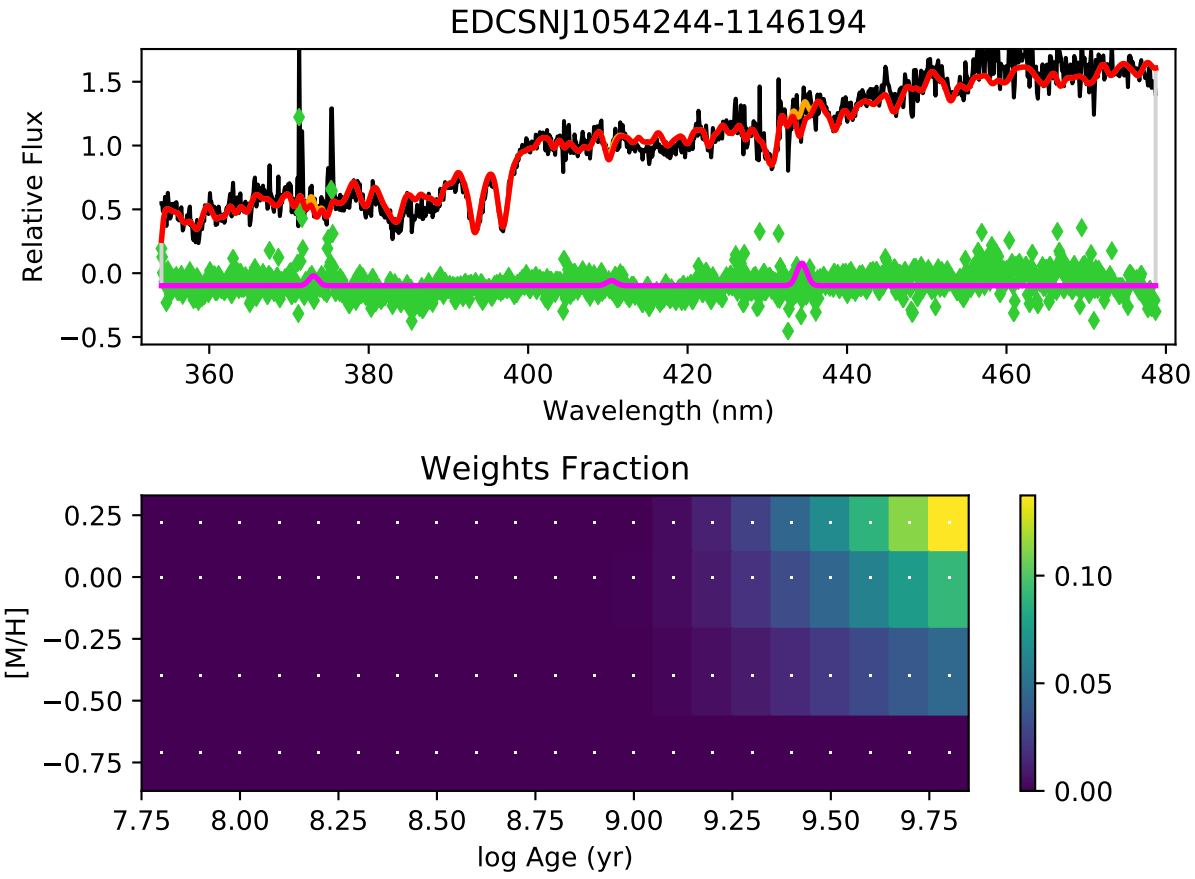
EDCSNJ1054244-1146194
Relative Flux
1.5
1.0
0.5
0.0
−0.5
360
380
400
420
440
460
480
Wavelength (nm)
Weights Fraction
[M/H]
0.25
0.00
−0.25
−0.50
−0.75
7.75
8.00
8.25
8.50
8.75
9.00
9.25
9.50
9.75
log Age (yr)
0.10
0.05
0.00

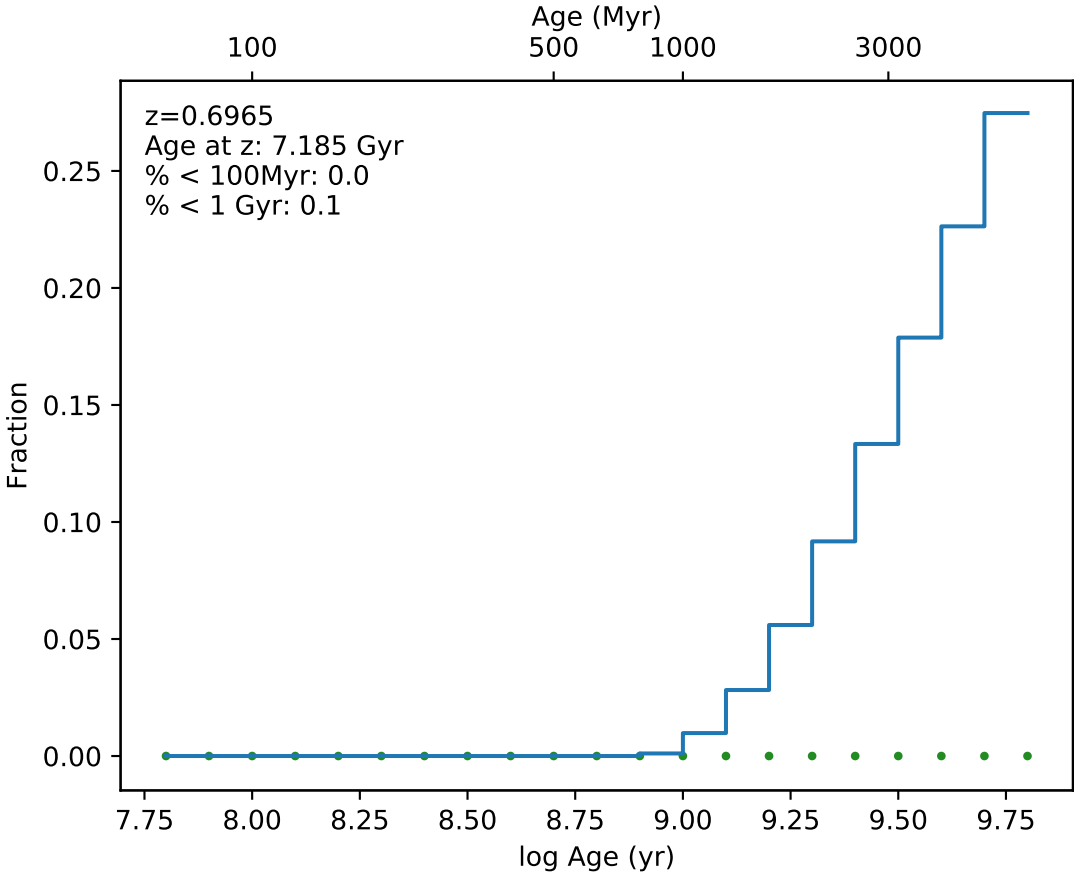
Age (Myr)
100
500
1000
3000
z=0.6965
Age at z: 7.185 Gyr
% < 100Myr: 0.0
% < 1 Gyr: 0.1
Fraction
0.25
0.20
0.15
0.10
0.05
0.00
7.75
8.00
8.25
8.50
8.75
9.00
9.25
9.50
9.75
log Age (yr)

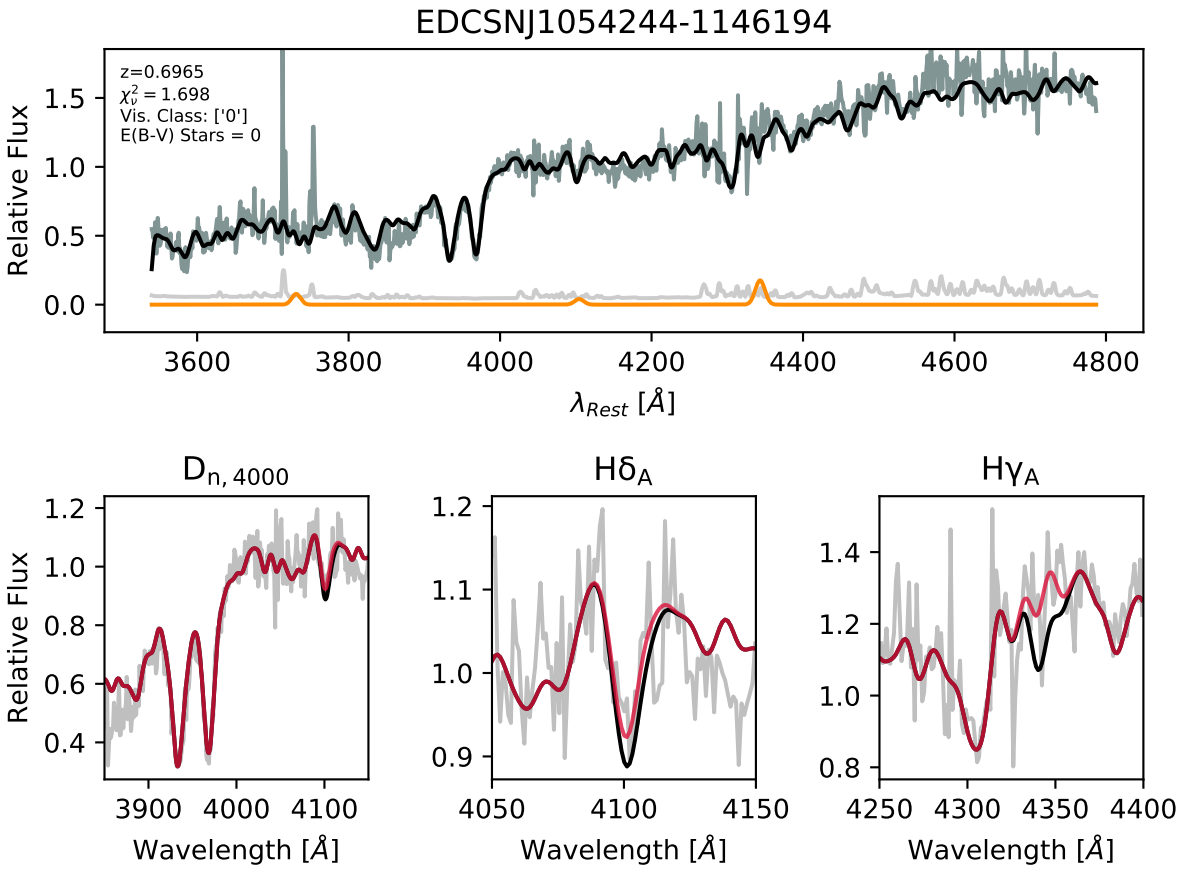
EDCSNJ1054244-1146194
z=0.6965
$\chi^2_\nu = 1.698$
Vis. Class: ['0']
E(B-V) Stars = 0
Relative Flux
λ_{Rest} [Å]
$D_{n,4000}$
$H\delta_A$
$H\gamma_A$
Wavelength [Å]

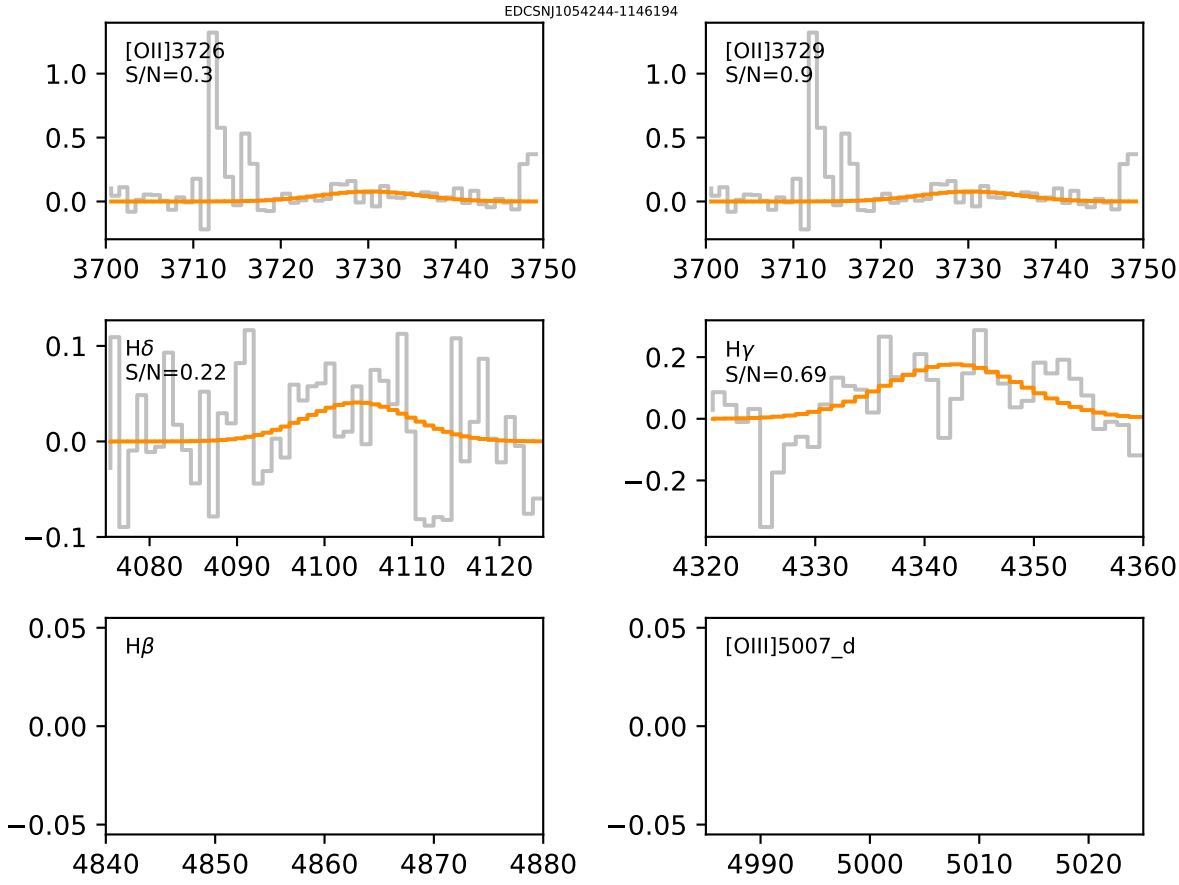
EDCSNJ1054244-1146194
[OII]3726
S/N=0.3
[OII]3729
S/N=0.9
Hδ
S/N=0.22
Hγ
S/N=0.69
Hβ
[OIII]5007_d

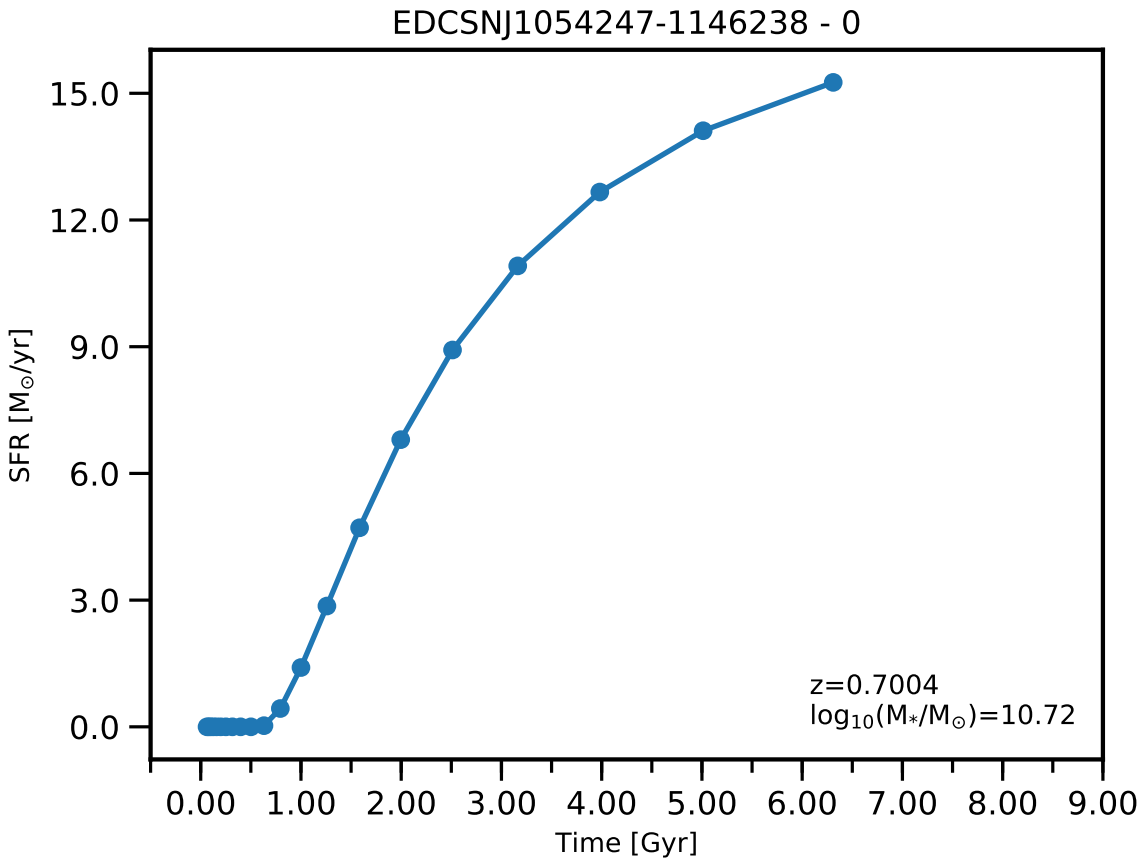
EDCSNJ1054247-1146238 - 0
SFR [M⊙/yr]
15.0
12.0
9.0
6.0
3.0
0.0
0.00
1.00
2.00
3.00
4.00
5.00
6.00
7.00
8.00
9.00
Time [Gyr]
z=0.7004
log10(M*/M⊙)=10.72

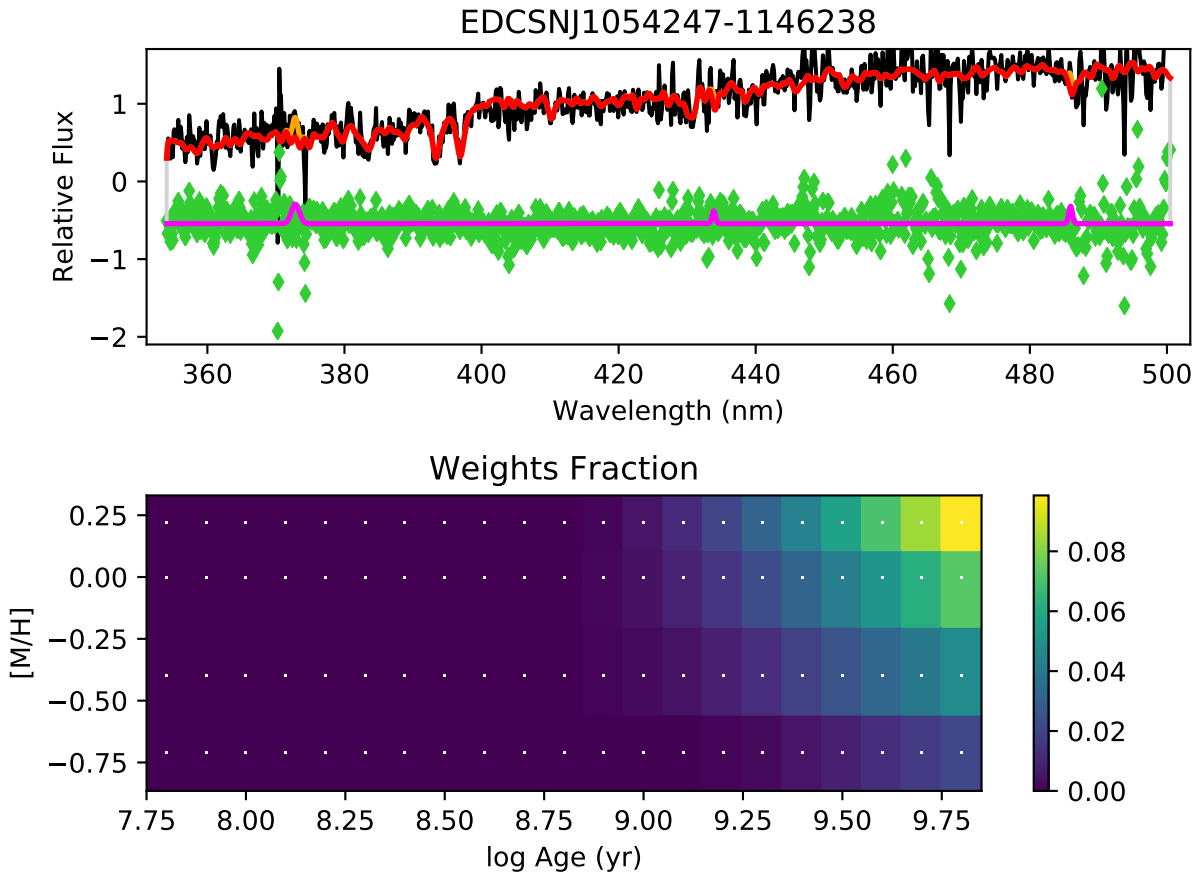
EDCSNJ1054247-1146238
Relative Flux
1
0
−1
−2
360
380
400
420
440
460
480
500
Wavelength (nm)
Weights Fraction
[M/H]
0.25
0.00
−0.25
−0.50
−0.75
7.75
8.00
8.25
8.50
8.75
9.00
9.25
9.50
9.75
log Age (yr)
0.08
0.06
0.04
0.02
0.00

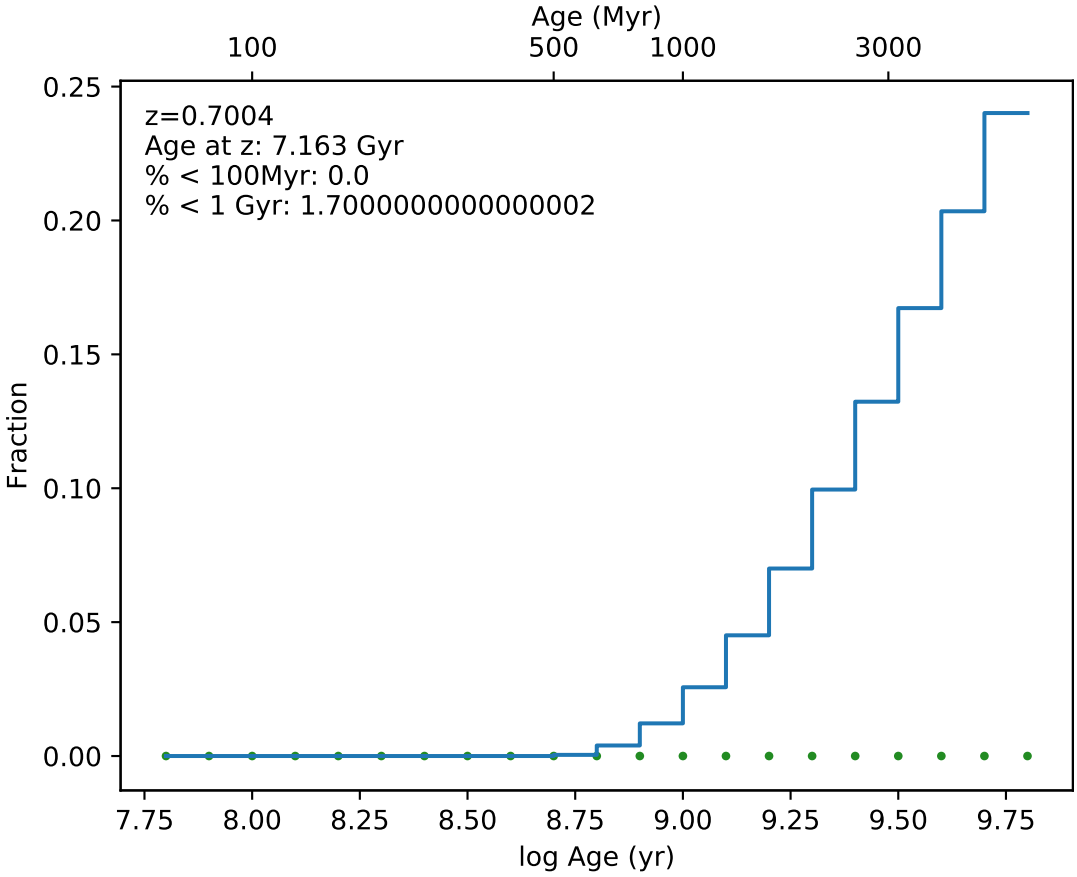
Age (Myr)
100
500
1000
3000
z=0.7004
Age at z: 7.163 Gyr
% < 100Myr: 0.0
% < 1 Gyr: 1.7000000000000002
Fraction
0.25
0.20
0.15
0.10
0.05
0.00
7.75
8.00
8.25
8.50
8.75
9.00
9.25
9.50
9.75
log Age (yr)

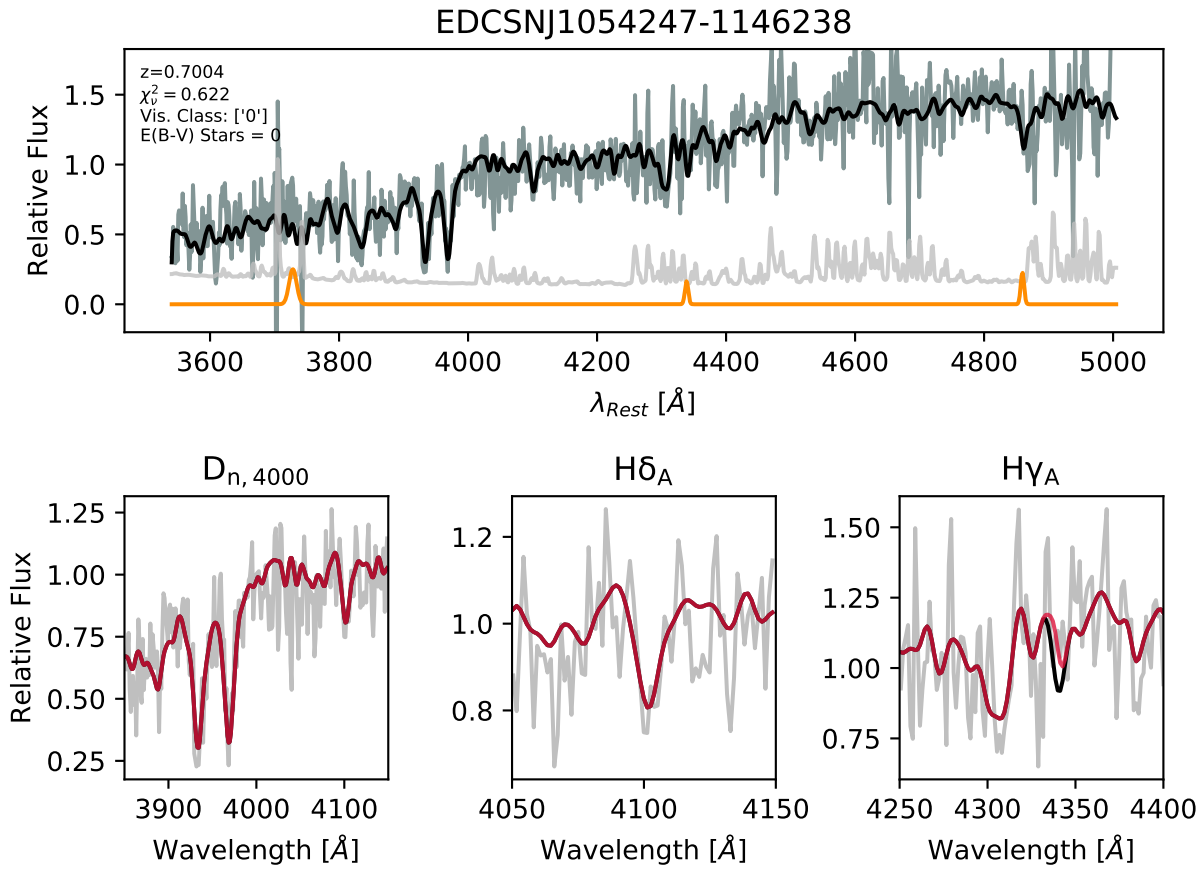
EDCSNJ1054247-1146238
z=0.7004
$\chi^2_\nu = 0.622$
Vis. Class: ['0']
E(B-V) Stars = 0
Relative Flux
λ_{Rest} [Å]
$D_{n,4000}$
$H\delta_A$
$H\gamma_A$
Wavelength [Å]

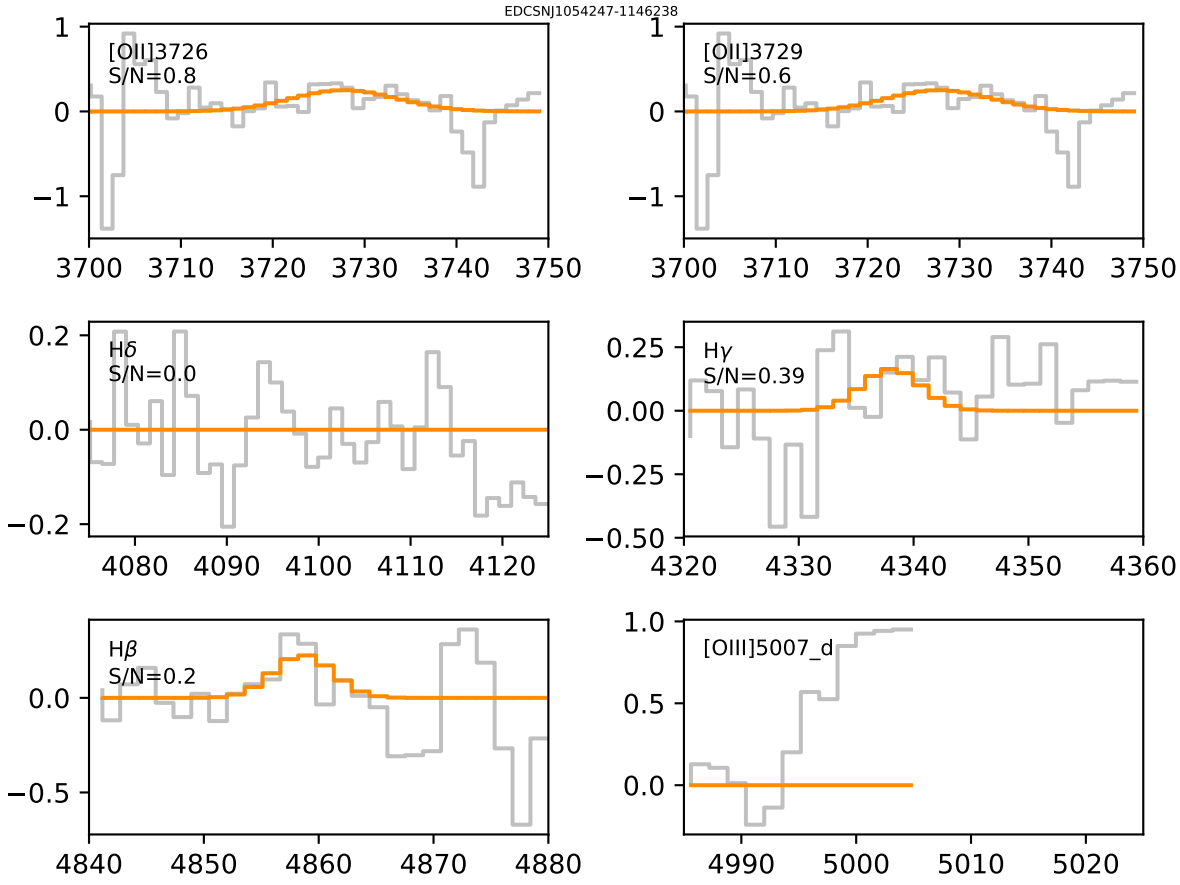
EDCSNJ1054247-1146238
[OII]3726
S/N=0.8
[OII]3729
S/N=0.6
Hδ
S/N=0.0
Hγ
S/N=0.39
Hβ
S/N=0.2
[OIII]5007_d

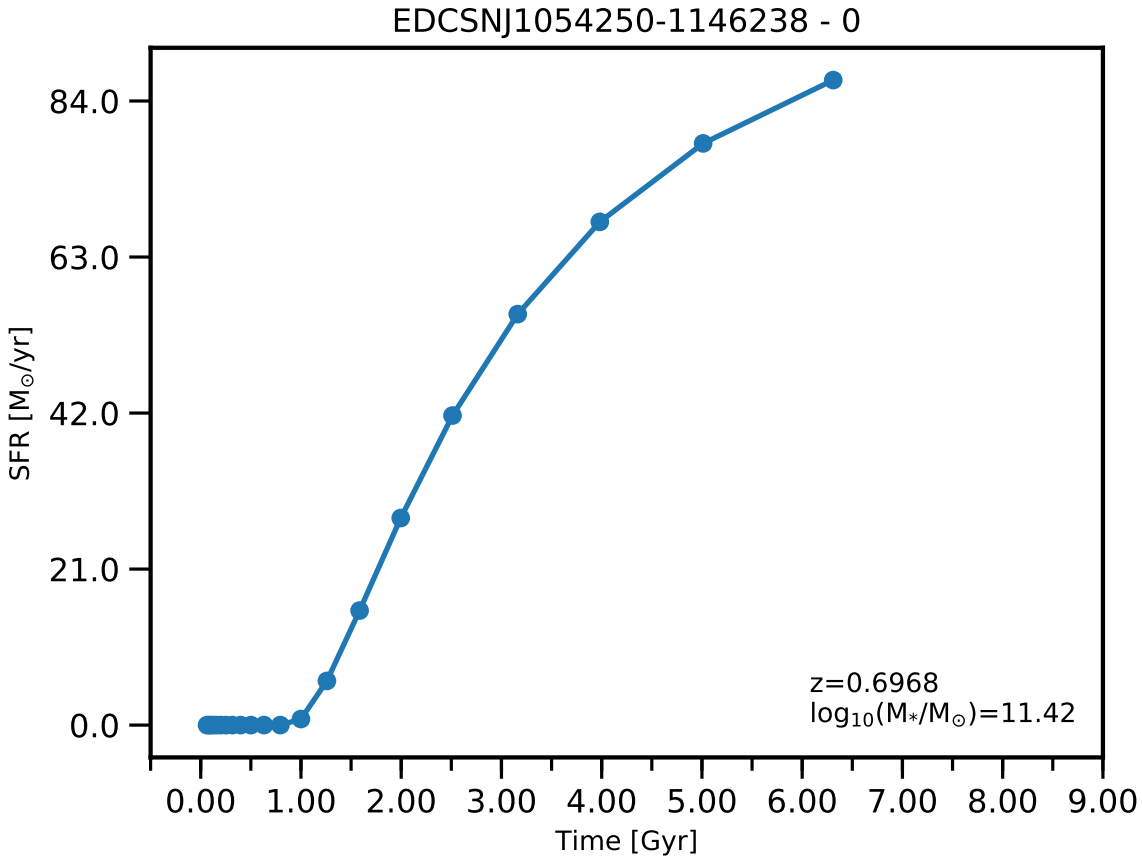
EDCSNJ1054250-1146238 - 0
84.0
63.0
42.0
21.0
0.0
SFR [M⊙/yr]
0.00
1.00
2.00
3.00
4.00
5.00
6.00
7.00
8.00
9.00
Time [Gyr]
z=0.6968
log10(M*/M⊙)=11.42

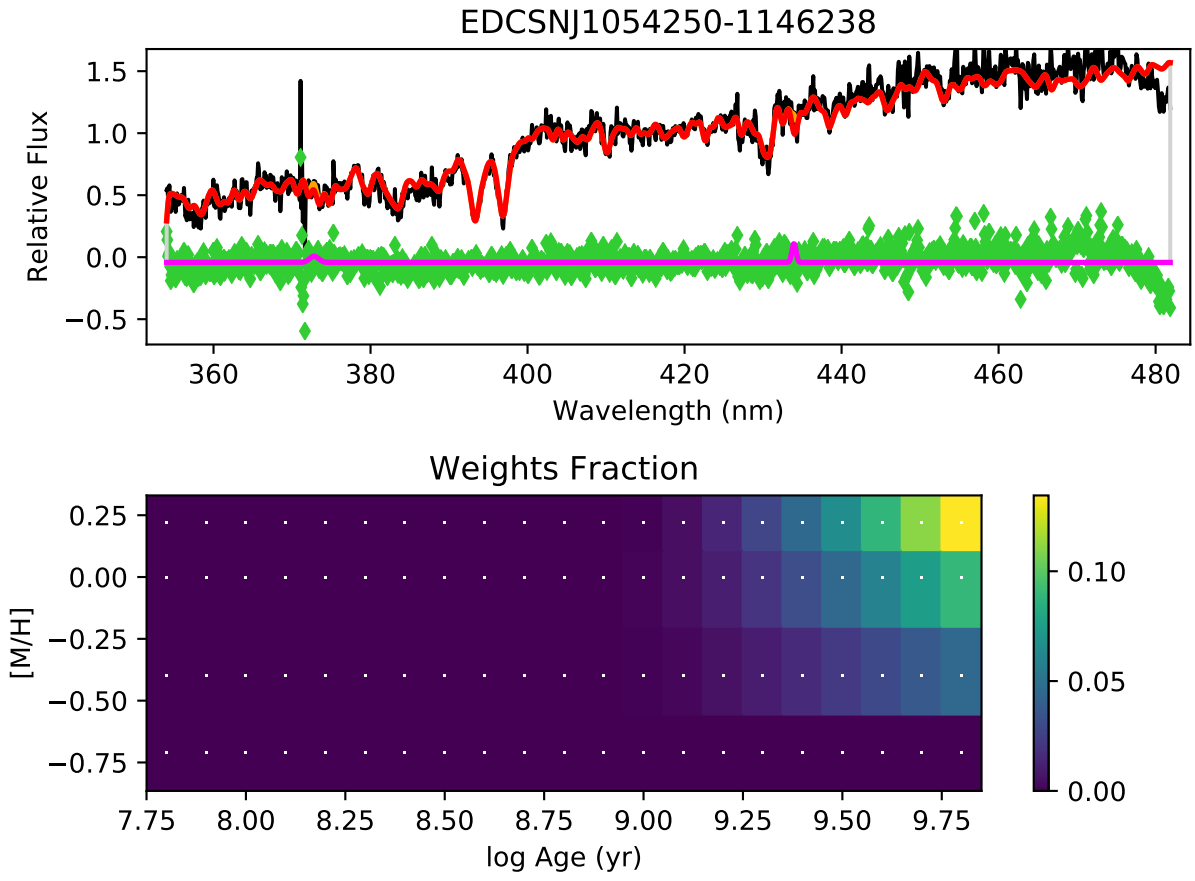
EDCSNJ1054250-1146238
Relative Flux
1.5
1.0
0.5
0.0
−0.5
360
380
400
420
440
460
480
Wavelength (nm)
Weights Fraction
[M/H]
0.25
0.00
−0.25
−0.50
−0.75
7.75
8.00
8.25
8.50
8.75
9.00
9.25
9.50
9.75
log Age (yr)
0.10
0.05
0.00

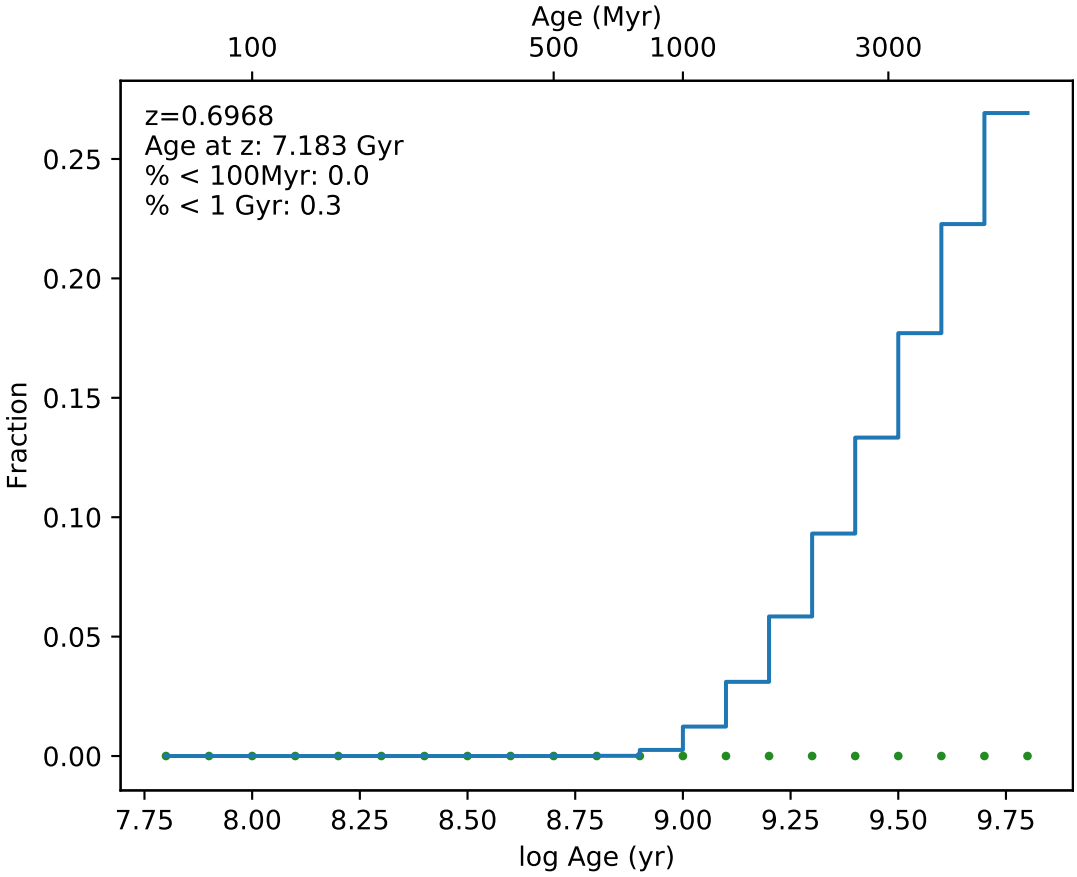
Age (Myr)
100
500
1000
3000
z=0.6968
Age at z: 7.183 Gyr
% < 100Myr: 0.0
% < 1 Gyr: 0.3
Fraction
0.25
0.20
0.15
0.10
0.05
0.00
7.75
8.00
8.25
8.50
8.75
9.00
9.25
9.50
9.75
log Age (yr)

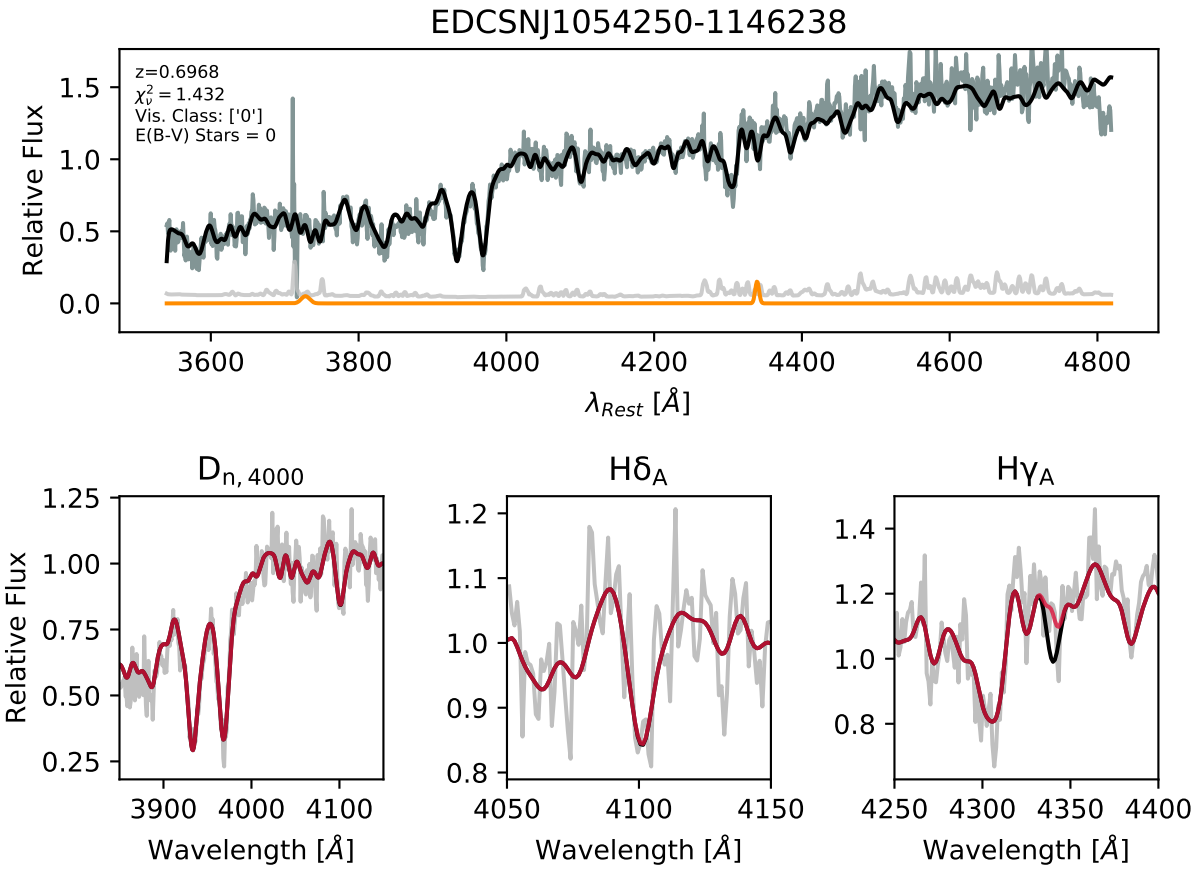
EDCSNJ1054250-1146238
z=0.6968
$\chi^2_\nu = 1.432$
Vis. Class: ['0']
E(B-V) Stars = 0
Relative Flux
λ_{Rest} [Å]
$D_{n,4000}$
$H\delta_A$
$H\gamma_A$
Wavelength [Å]

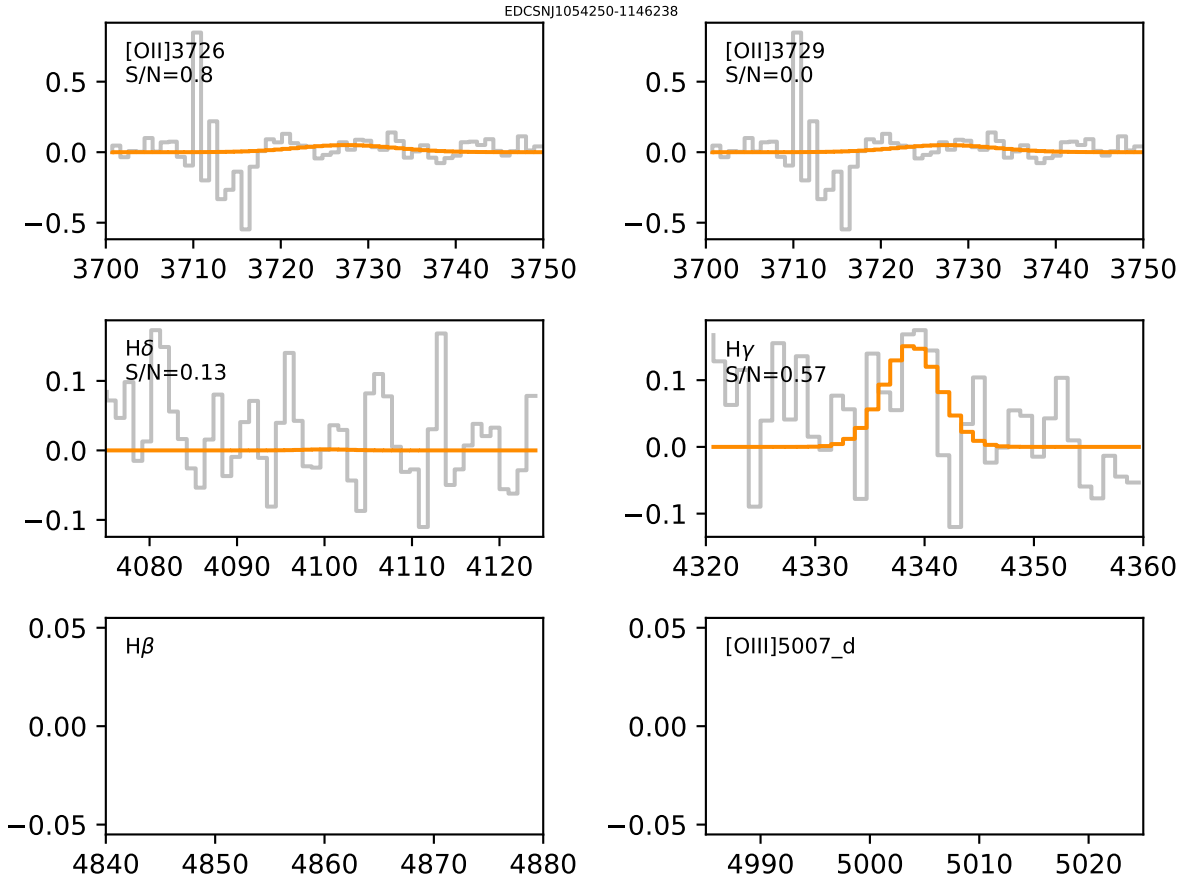
EDCSNJ1054250-1146238
[OII]3726
S/N=0.8
[OII]3729
S/N=0.0
Hδ
S/N=0.13
Hγ
S/N=0.57
Hβ
[OIII]5007_d

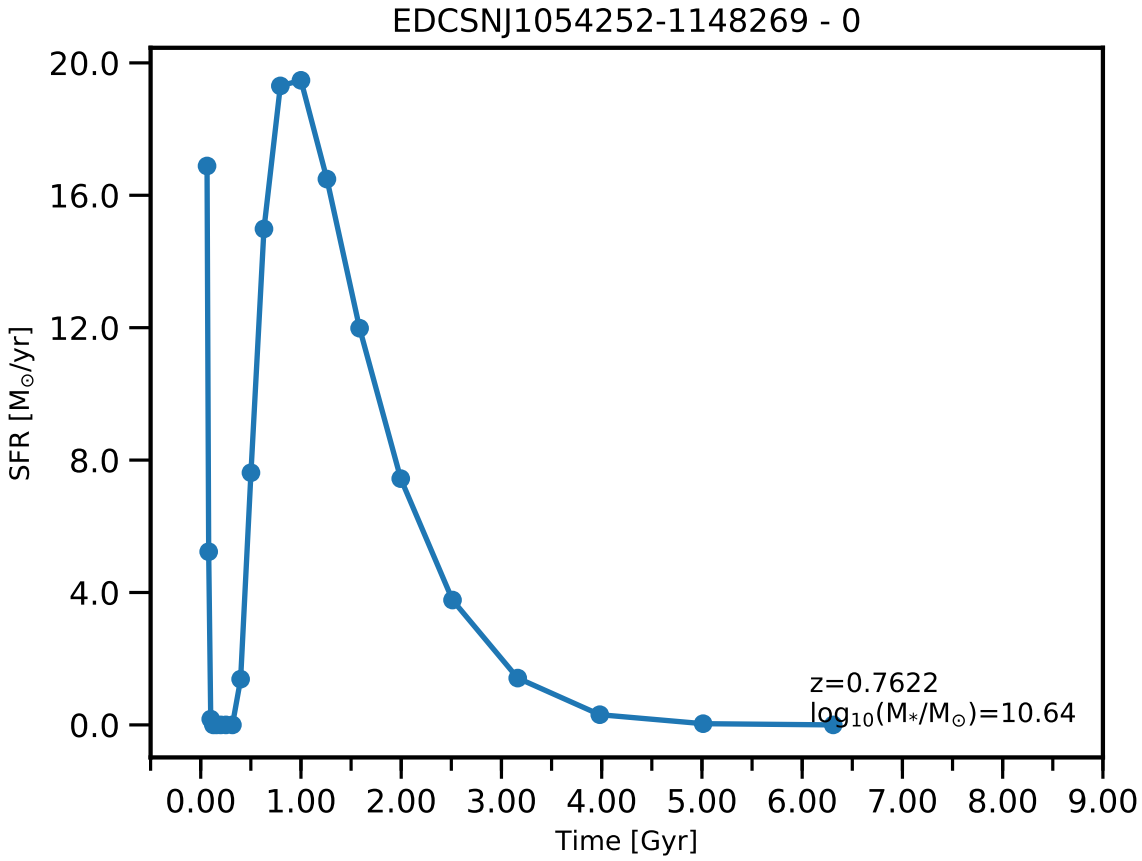
EDCSNJ1054252-1148269 - 0
SFR [M⊙/yr]
Time [Gyr]
z=0.7622
log10(M*/M⊙)=10.64

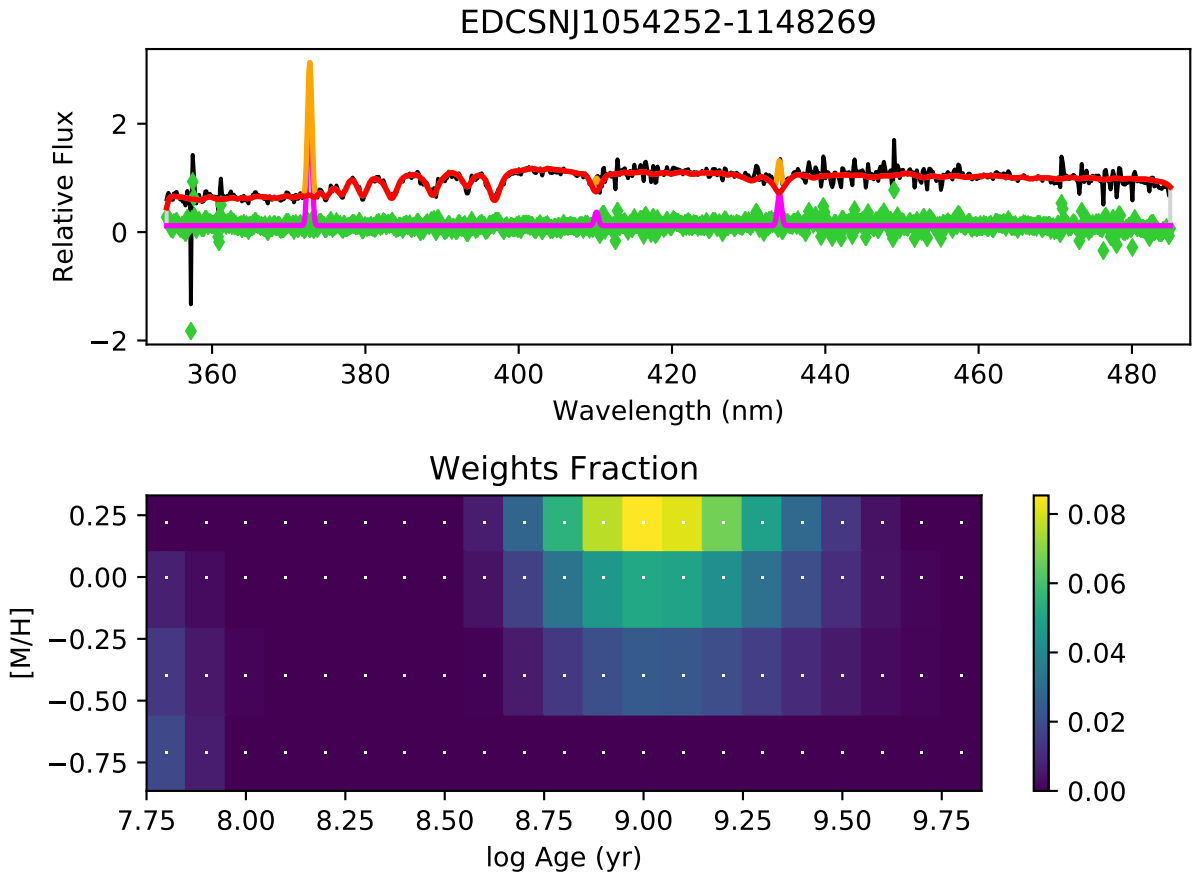
EDCSNJ1054252-1148269
Relative Flux
2
0
−2
360
380
400
420
440
460
480
Wavelength (nm)
Weights Fraction
[M/H]
0.25
0.00
−0.25
−0.50
−0.75
7.75
8.00
8.25
8.50
8.75
9.00
9.25
9.50
9.75
log Age (yr)
0.08
0.06
0.04
0.02
0.00

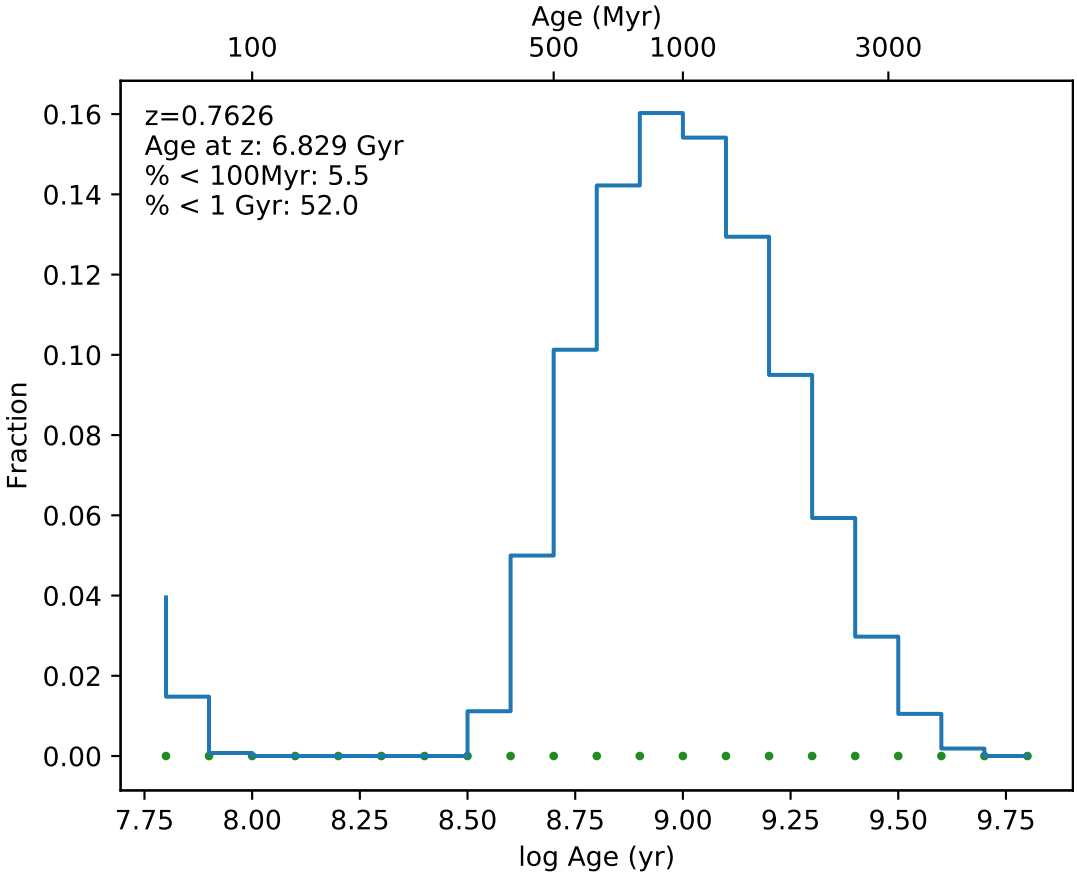
Age (Myr)
100
500
1000
3000
z=0.7626
Age at z: 6.829 Gyr
% < 100Myr: 5.5
% < 1 Gyr: 52.0
Fraction
0.16
0.14
0.12
0.10
0.08
0.06
0.04
0.02
0.00
7.75
8.00
8.25
8.50
8.75
9.00
9.25
9.50
9.75
log Age (yr)

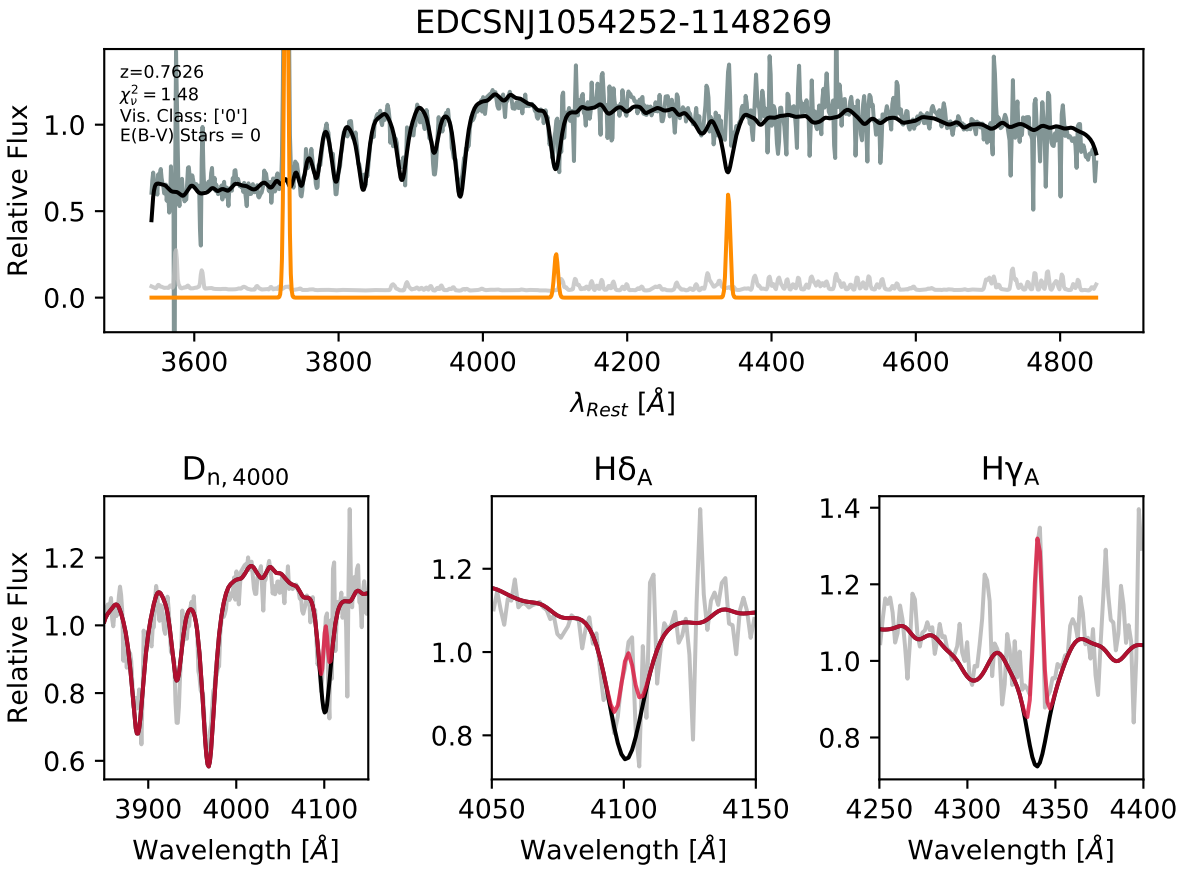
EDCSNJ1054252-1148269
z=0.7626
$\chi^2_\nu = 1.48$
Vis. Class: ['0']
E(B-V) Stars = 0
Relative Flux
λ_{Rest} [Å]
$D_{n,4000}$
$H\delta_A$
$H\gamma_A$
Wavelength [Å]

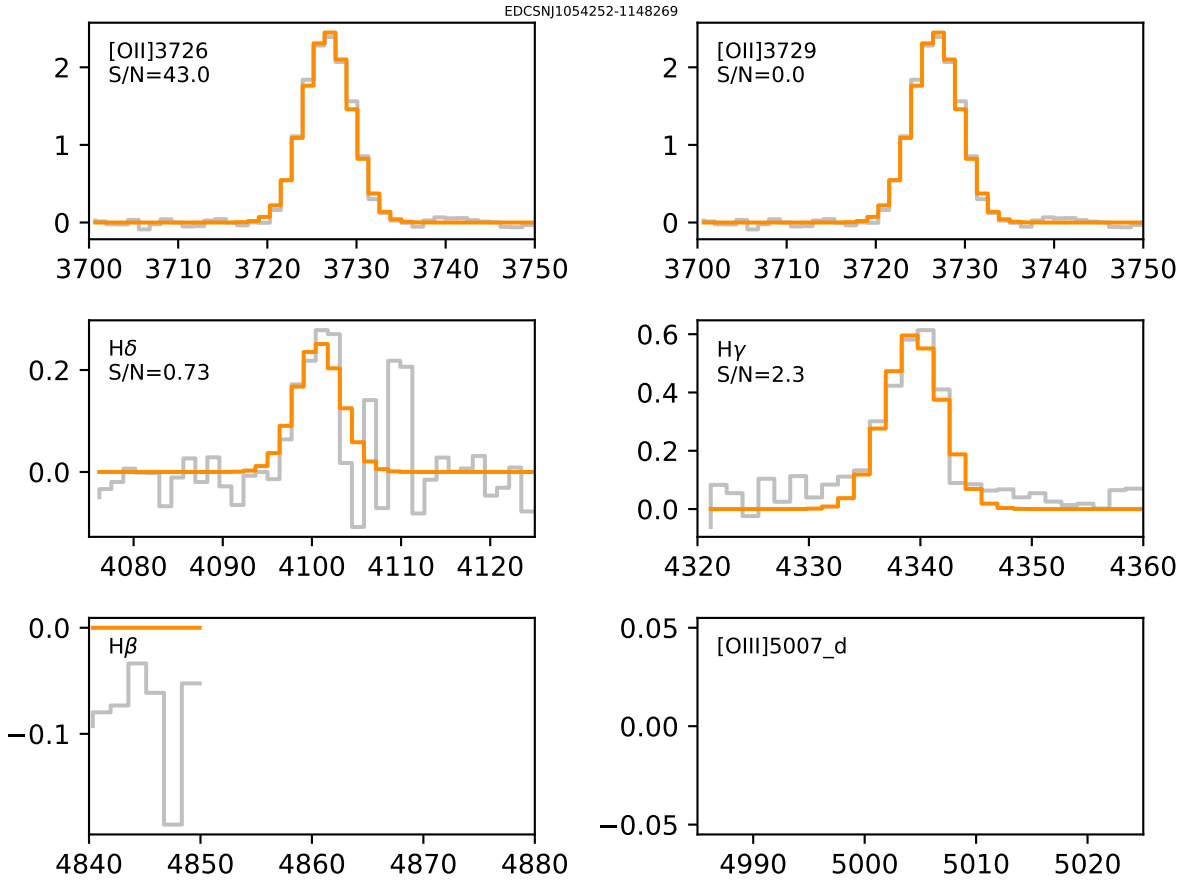
EDCSNJ1054252-1148269
[OII]3726
S/N=43.0
[OII]3729
S/N=0.0
Hδ
S/N=0.73
Hγ
S/N=2.3
Hβ
[OIII]5007_d

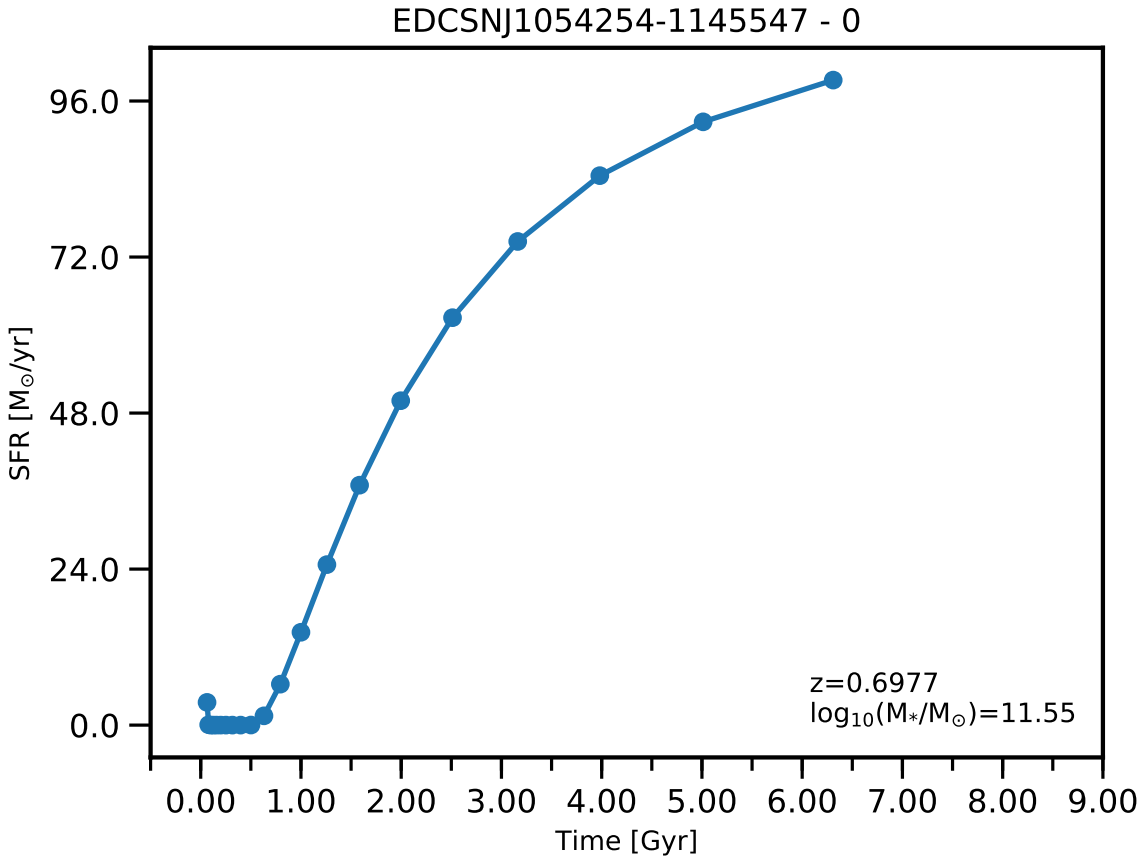
EDCSNJ1054254-1145547 - 0
96.0
72.0
48.0
24.0
0.0
SFR [M⊙/yr]
0.00
1.00
2.00
3.00
4.00
5.00
6.00
7.00
8.00
9.00
Time [Gyr]
z=0.6977
log10(M*/M⊙)=11.55

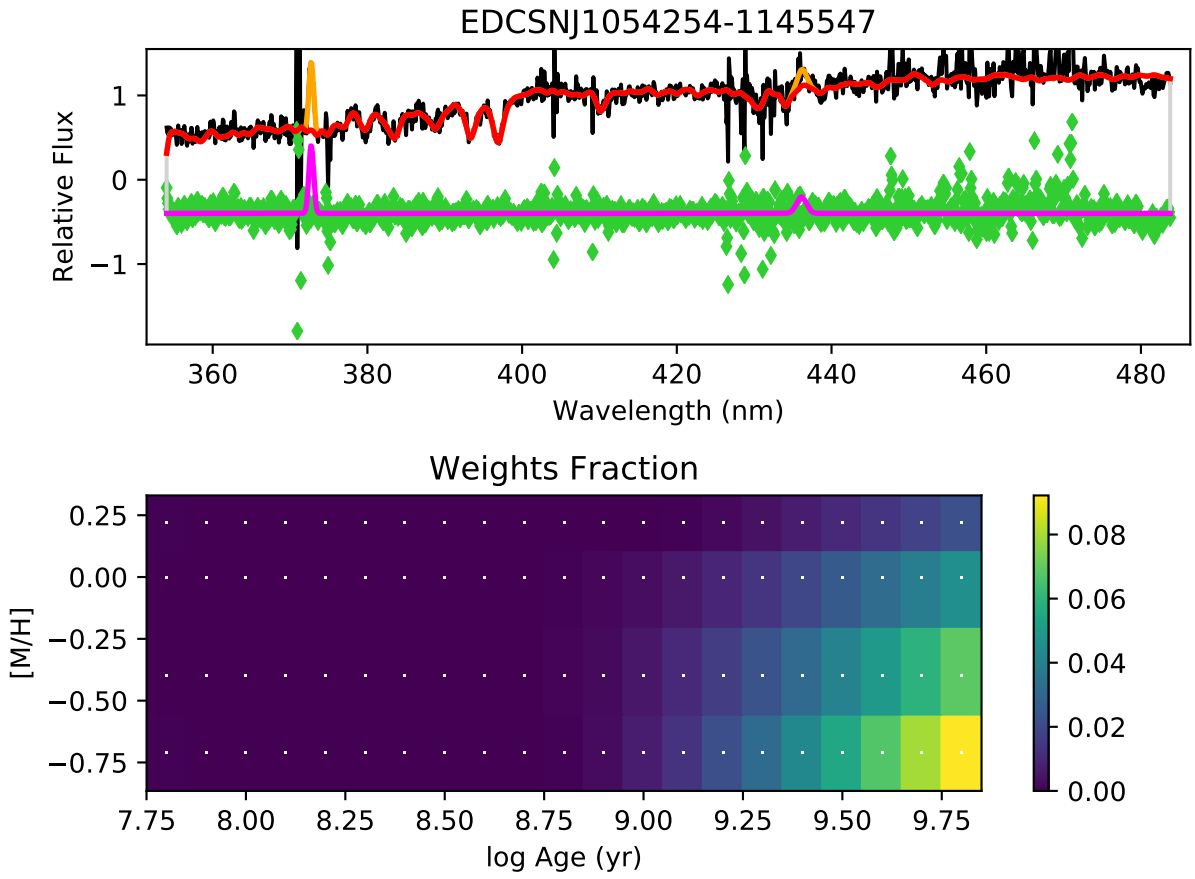
EDCSNJ1054254-1145547
Relative Flux
1
0
−1
360
380
400
420
440
460
480
Wavelength (nm)
Weights Fraction
[M/H]
0.25
0.00
−0.25
−0.50
−0.75
7.75
8.00
8.25
8.50
8.75
9.00
9.25
9.50
9.75
log Age (yr)
0.08
0.06
0.04
0.02
0.00

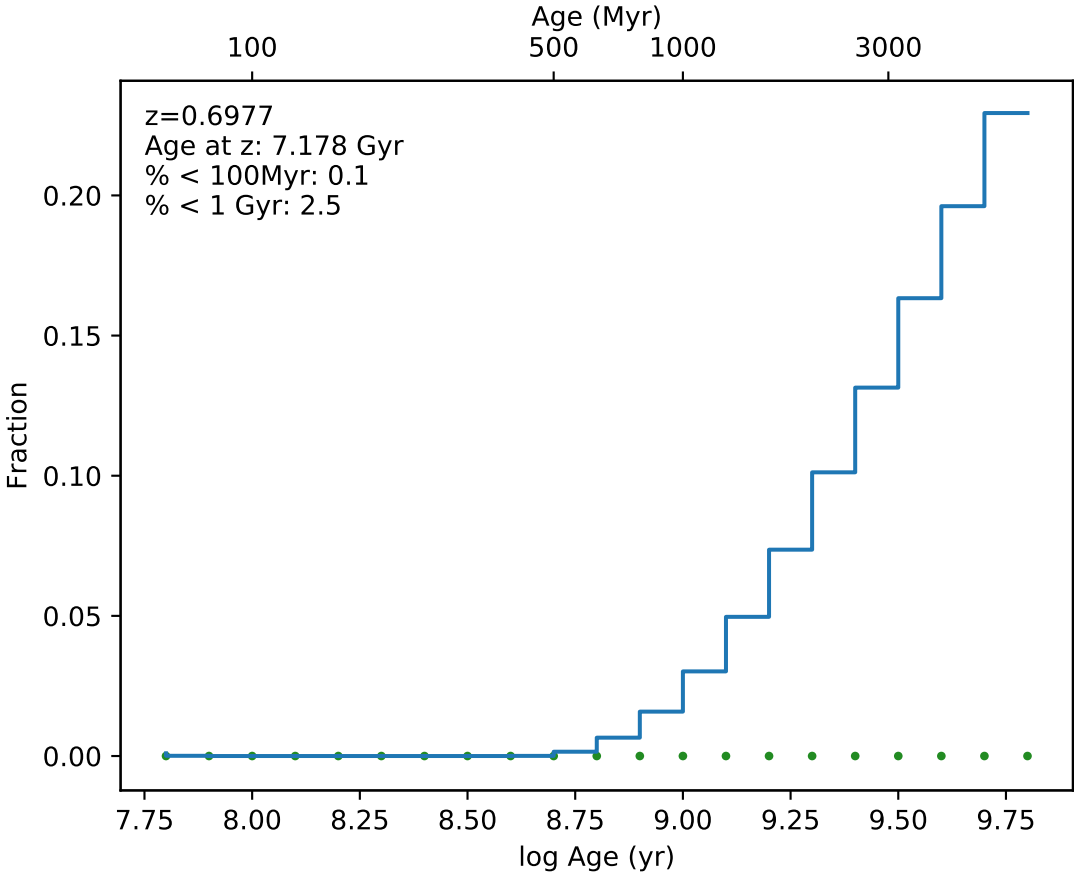
Age (Myr)
100
500
1000
3000
z=0.6977
Age at z: 7.178 Gyr
% < 100Myr: 0.1
% < 1 Gyr: 2.5
Fraction
0.20
0.15
0.10
0.05
0.00
7.75
8.00
8.25
8.50
8.75
9.00
9.25
9.50
9.75
log Age (yr)

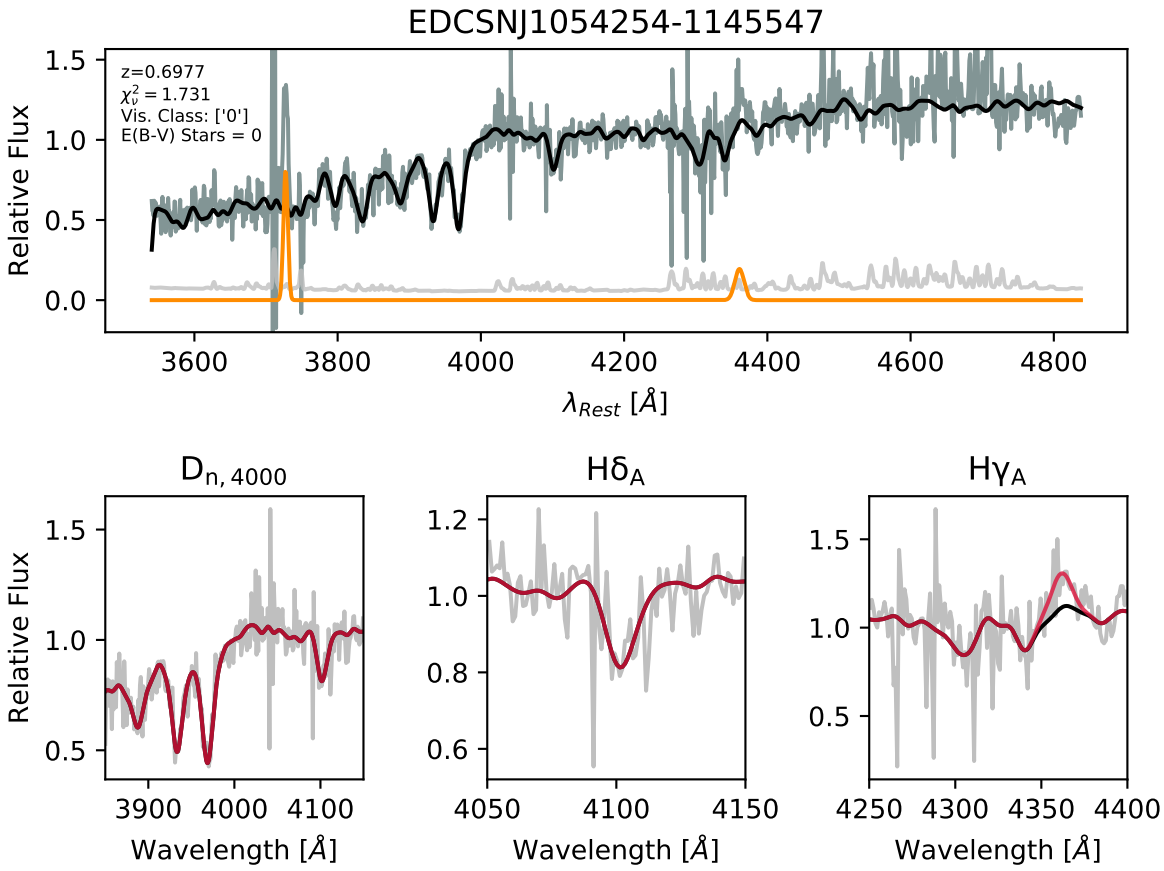
EDCSNJ1054254-1145547
z=0.6977
$\chi^2_\nu = 1.731$
Vis. Class: ['0']
E(B-V) Stars = 0
Relative Flux
λ_{Rest} [Å]
$D_{n,4000}$
$H\delta_A$
$H\gamma_A$
Wavelength [Å]

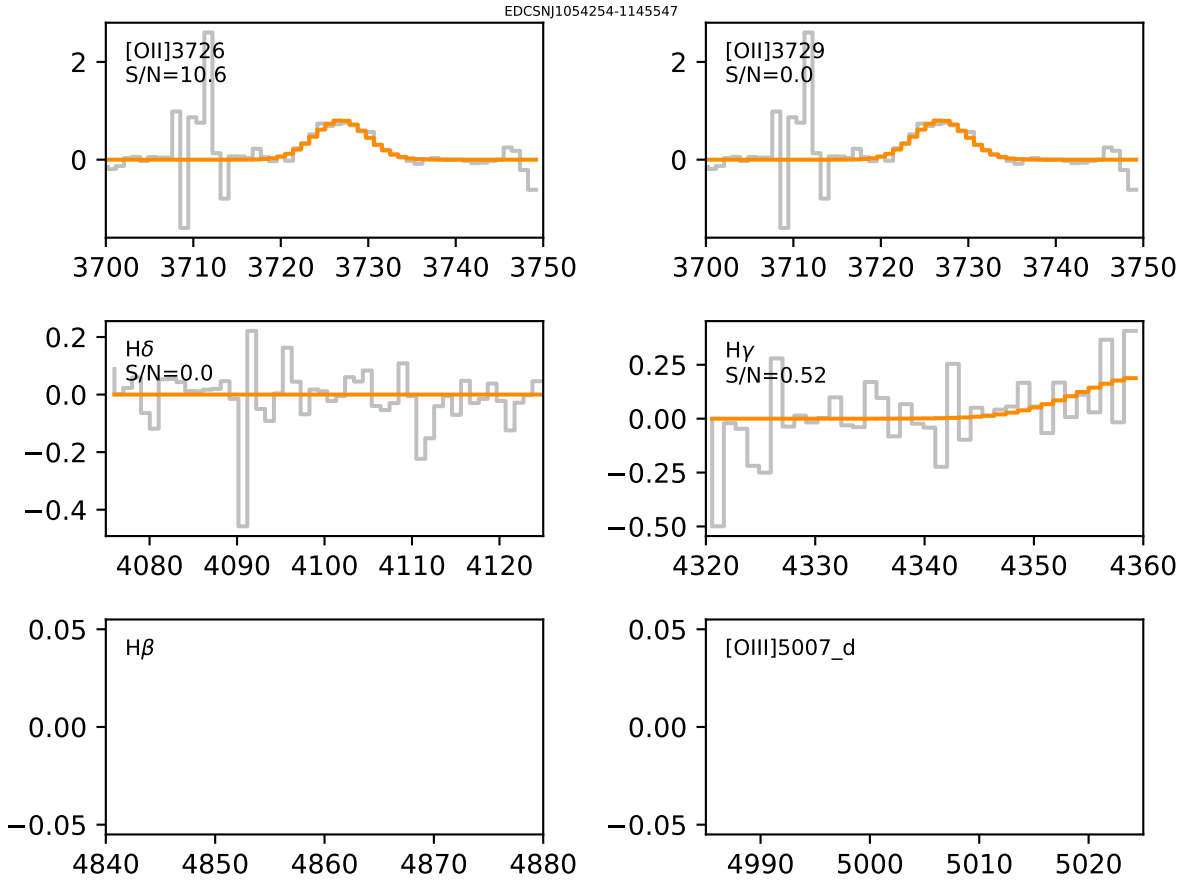
EDCSNJ1054254-1145547
[OII]3726
S/N=10.6
[OII]3729
S/N=0.0
Hδ
S/N=0.0
Hγ
S/N=0.52
Hβ
[OIII]5007_d

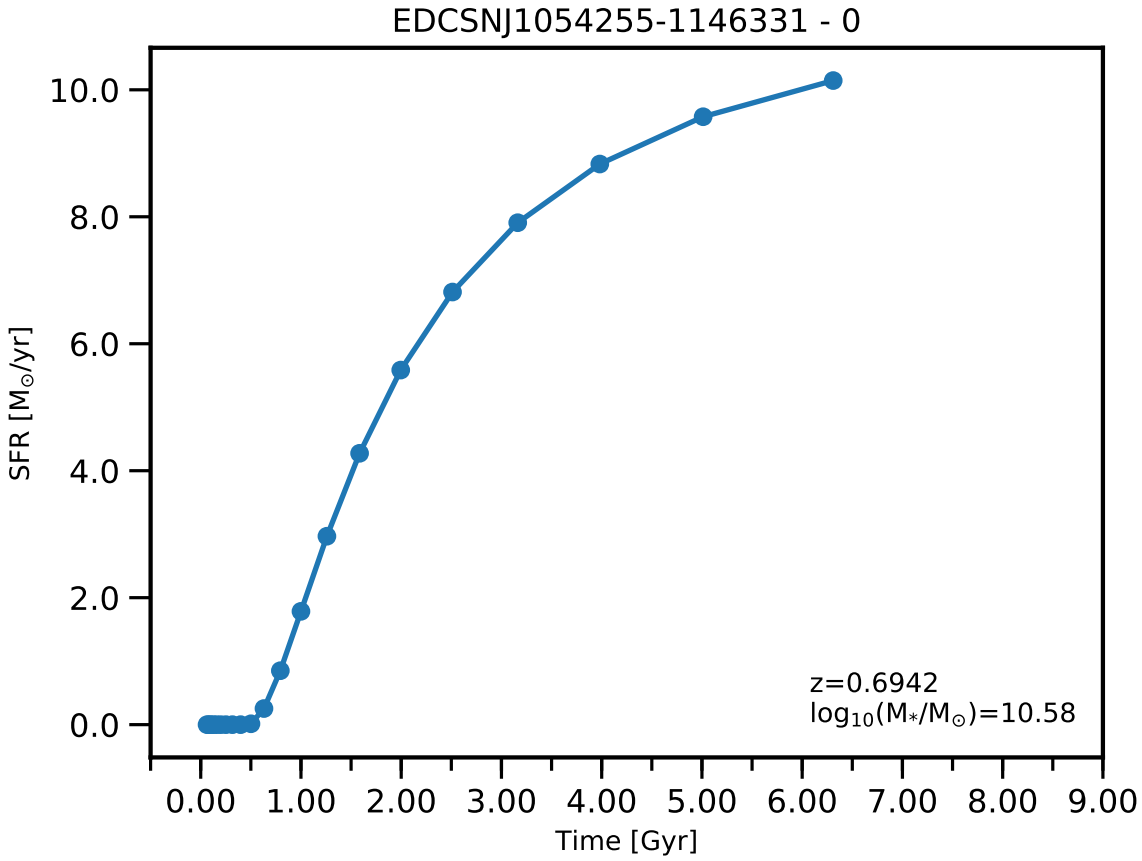
EDCSNJ1054255-1146331 - 0
SFR [M⊙/yr]
10.0
8.0
6.0
4.0
2.0
0.0
0.00
1.00
2.00
3.00
4.00
5.00
6.00
7.00
8.00
9.00
Time [Gyr]
z=0.6942
log10(M*/M⊙)=10.58

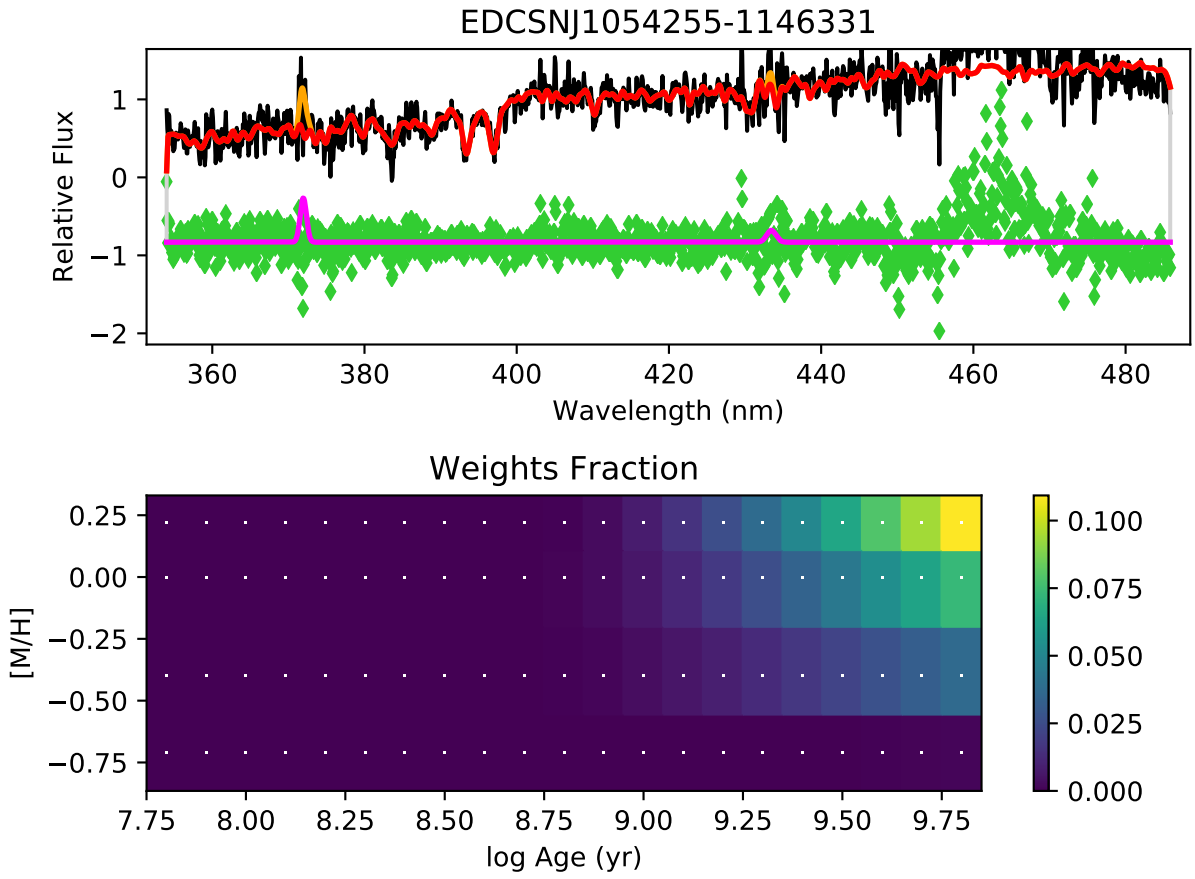
EDCSNJ1054255-1146331
Relative Flux
1
0
−1
−2
360
380
400
420
440
460
480
Wavelength (nm)
Weights Fraction
[M/H]
0.25
0.00
−0.25
−0.50
−0.75
7.75
8.00
8.25
8.50
8.75
9.00
9.25
9.50
9.75
log Age (yr)
0.100
0.075
0.050
0.025
0.000

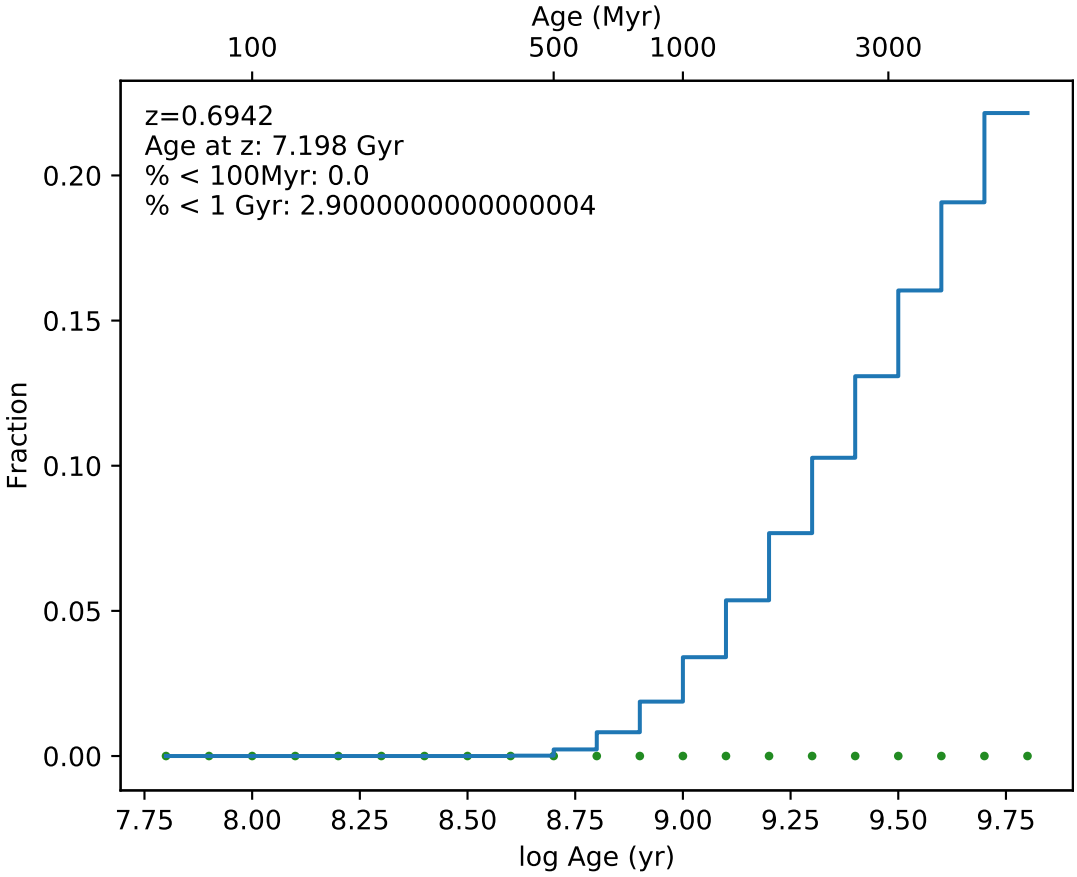
Age (Myr)
100
500
1000
3000
z=0.6942
Age at z: 7.198 Gyr
% < 100Myr: 0.0
% < 1 Gyr: 2.9000000000000004
Fraction
0.20
0.15
0.10
0.05
0.00
7.75
8.00
8.25
8.50
8.75
9.00
9.25
9.50
9.75
log Age (yr)

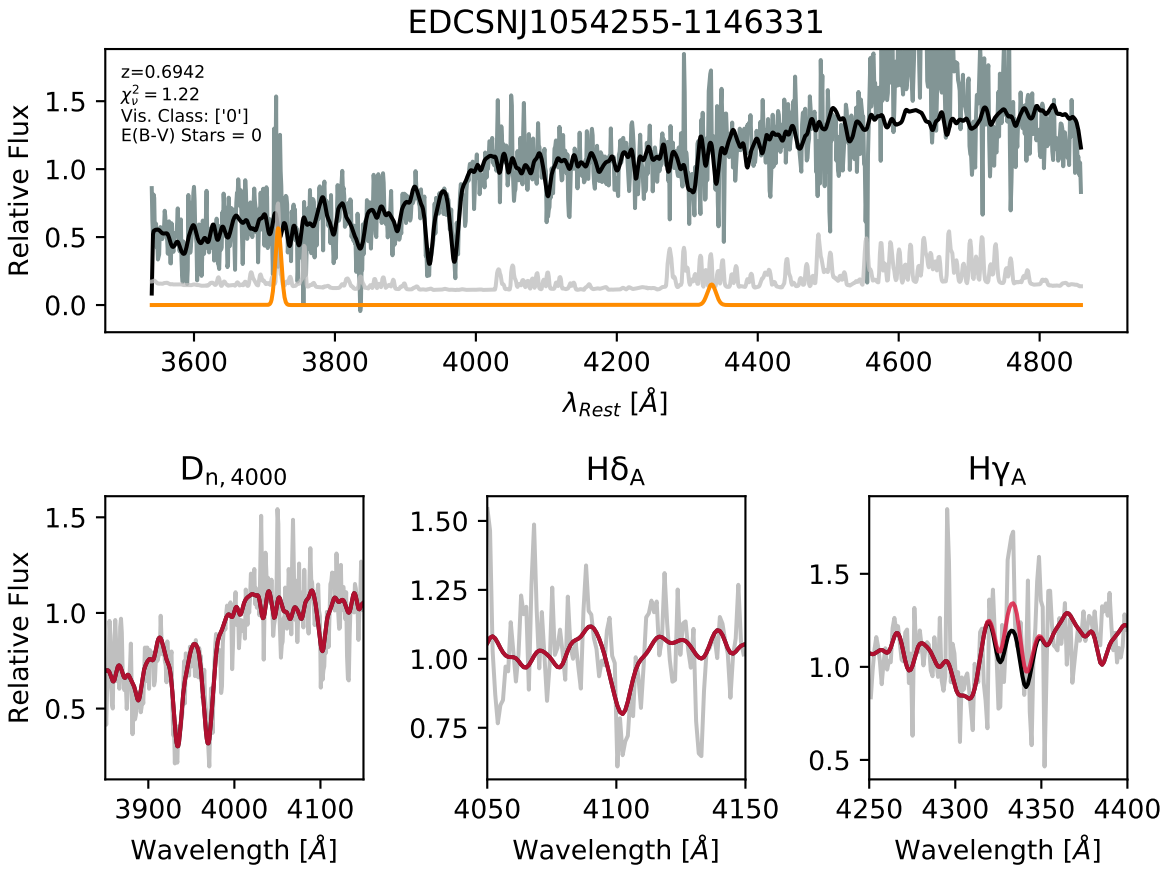
EDCSNJ1054255-1146331
z=0.6942
$\chi^2_\nu = 1.22$
Vis. Class: ['0']
E(B-V) Stars = 0
Relative Flux
λ_{Rest} [Å]
$D_{n,4000}$
$H\delta_A$
$H\gamma_A$
Wavelength [Å]

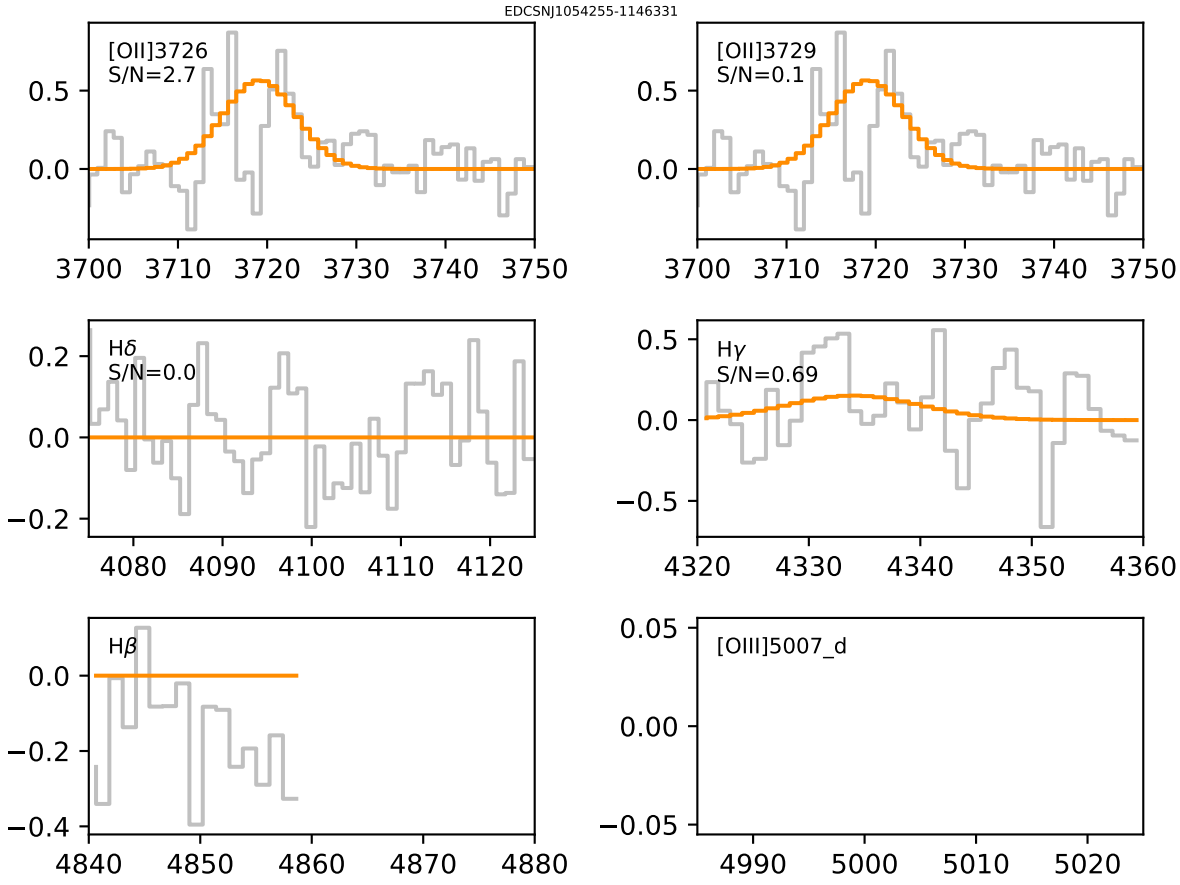
EDCSNJ1054255-1146331
[OII]3726
S/N=2.7
[OII]3729
S/N=0.1
Hδ
S/N=0.0
Hγ
S/N=0.69
Hβ
[OIII]5007_d

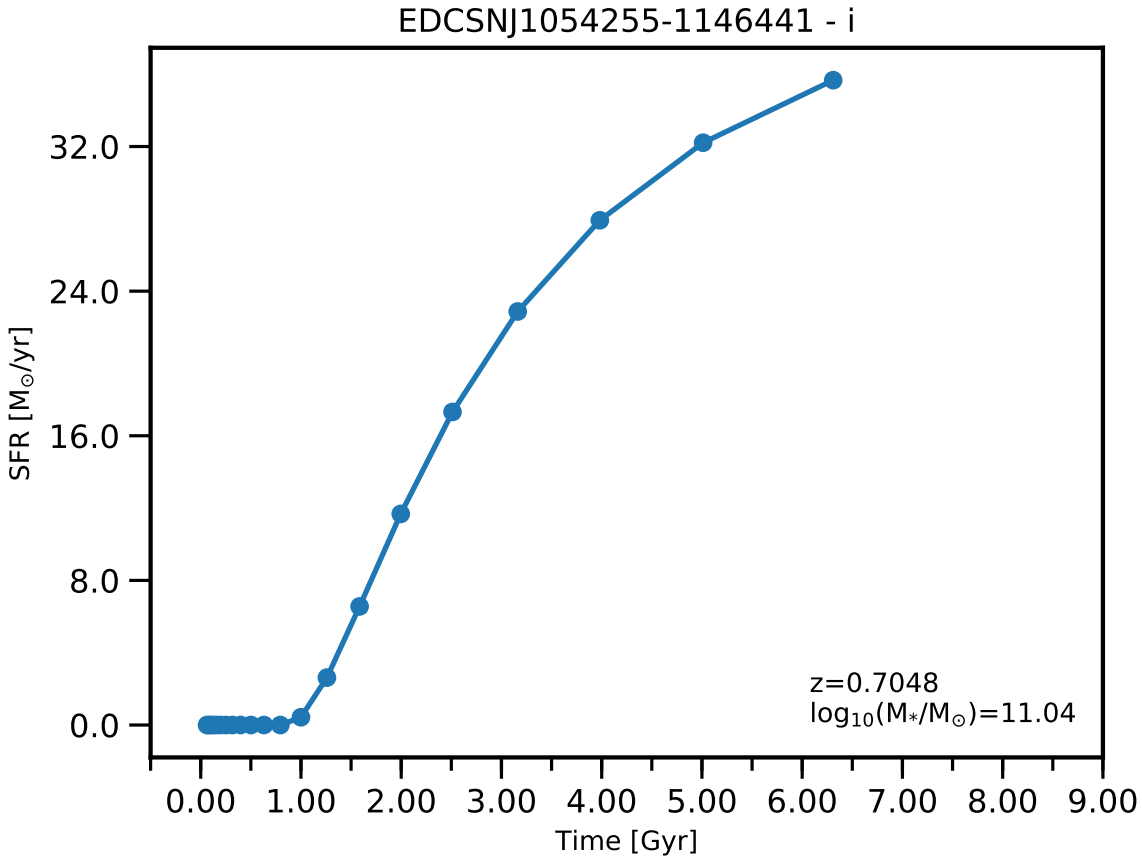
EDCSNJ1054255-1146441 - i
SFR [M⊙/yr]
32.0
24.0
16.0
8.0
0.0
0.00
1.00
2.00
3.00
4.00
5.00
6.00
7.00
8.00
9.00
Time [Gyr]
z=0.7048
log10(M*/M⊙)=11.04

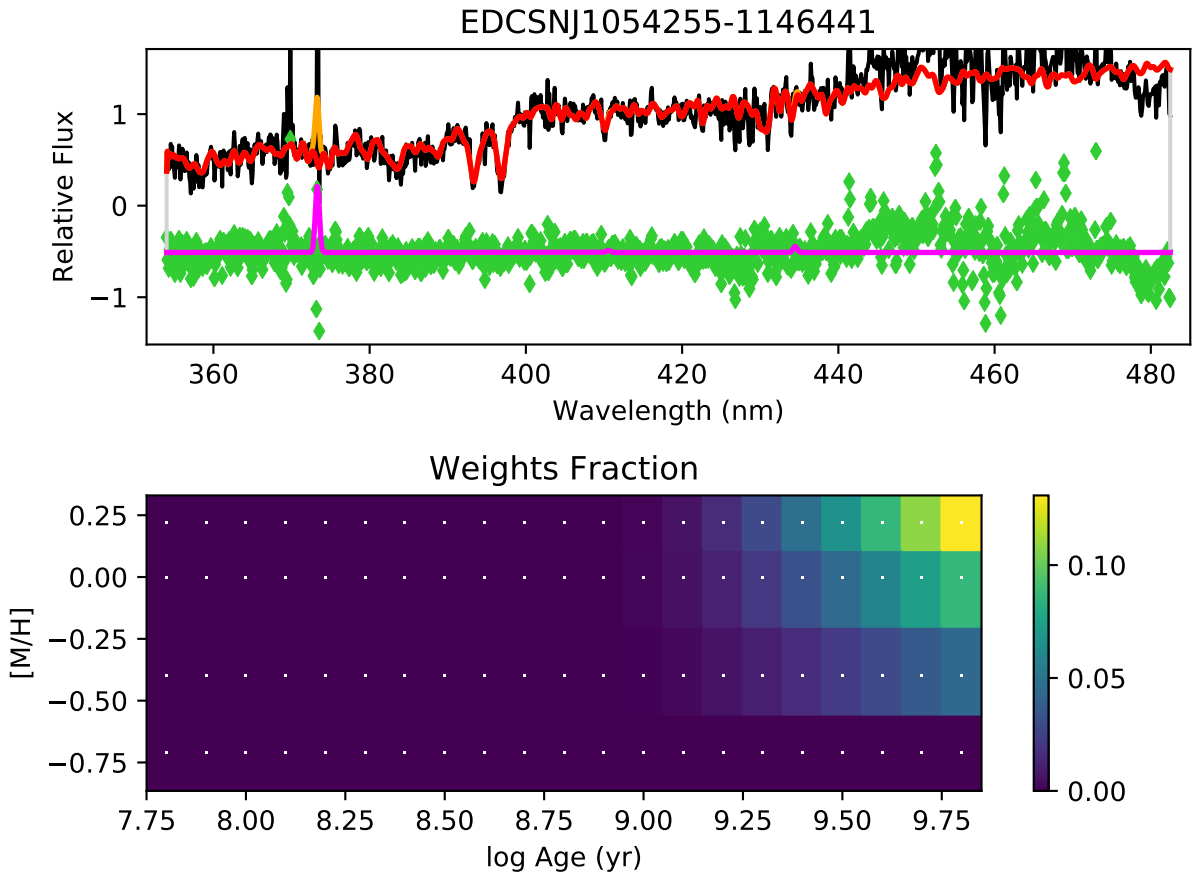
EDCSNJ1054255-1146441
Relative Flux
1
0
−1
360
380
400
420
440
460
480
Wavelength (nm)
Weights Fraction
[M/H]
0.25
0.00
−0.25
−0.50
−0.75
7.75
8.00
8.25
8.50
8.75
9.00
9.25
9.50
9.75
log Age (yr)
0.10
0.05
0.00

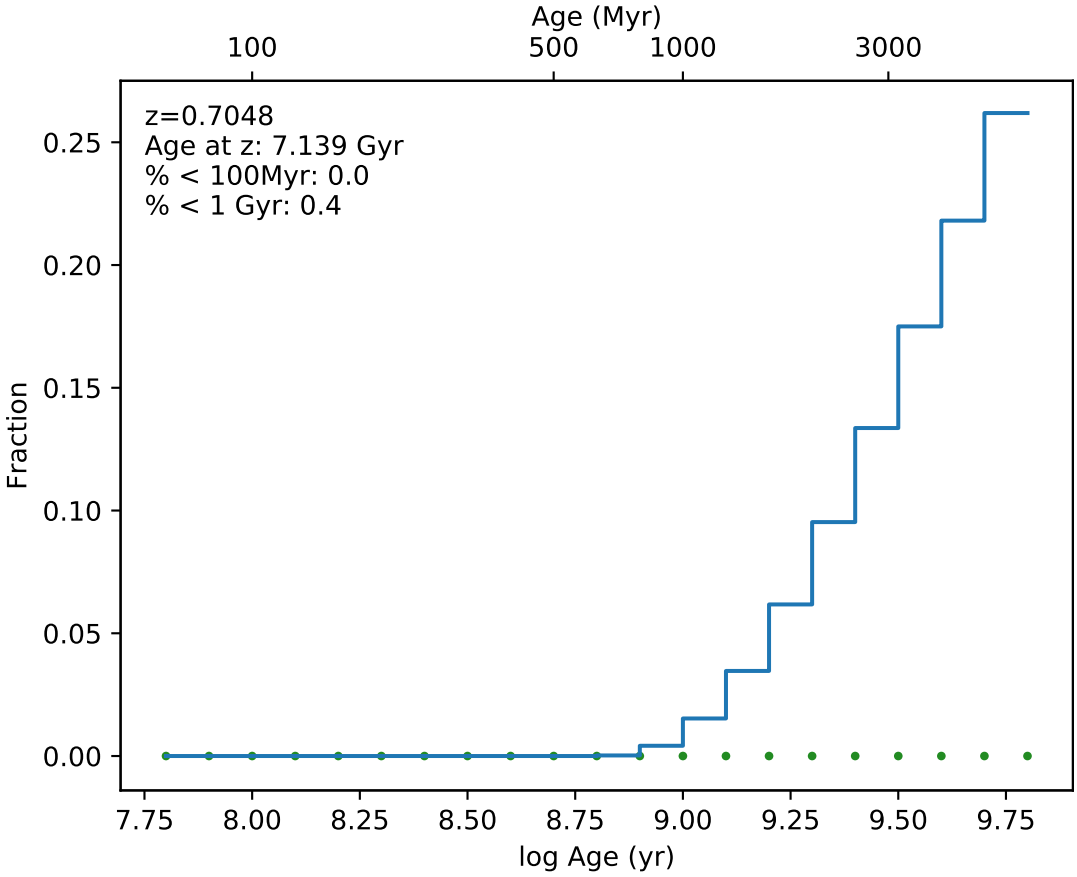
Age (Myr)
100
500
1000
3000
z=0.7048
Age at z: 7.139 Gyr
% < 100Myr: 0.0
% < 1 Gyr: 0.4
Fraction
0.25
0.20
0.15
0.10
0.05
0.00
7.75
8.00
8.25
8.50
8.75
9.00
9.25
9.50
9.75
log Age (yr)

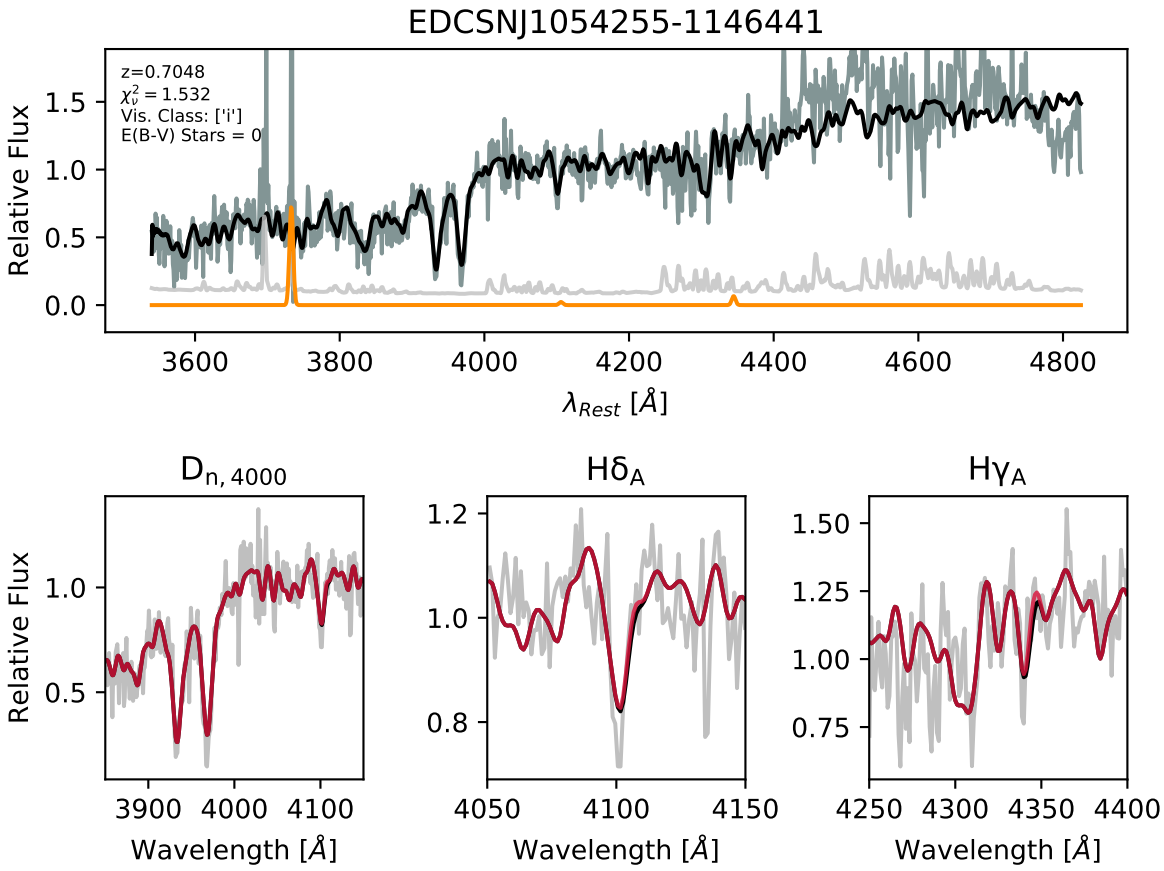
EDCSNJ1054255-1146441
z=0.7048
$\chi^2_\nu = 1.532$
Vis. Class: ['i']
E(B-V) Stars = 0
Relative Flux
λ_{Rest} [Å]
$D_{n,4000}$
$H\delta_A$
$H\gamma_A$
Wavelength [Å]

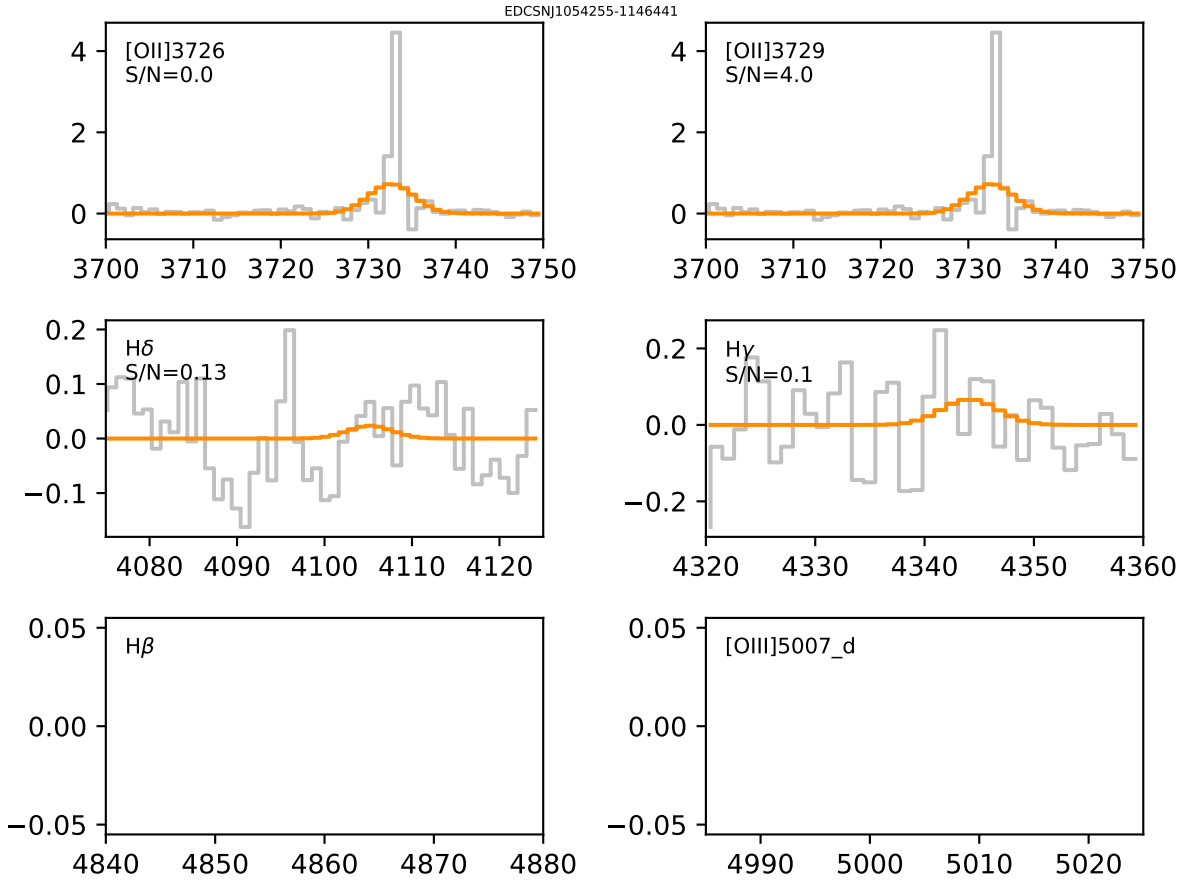
EDCSNJ1054255-1146441
[OII]3726
S/N=0.0
[OII]3729
S/N=4.0
Hδ
S/N=0.13
Hγ
S/N=0.1
Hβ
[OIII]5007_d

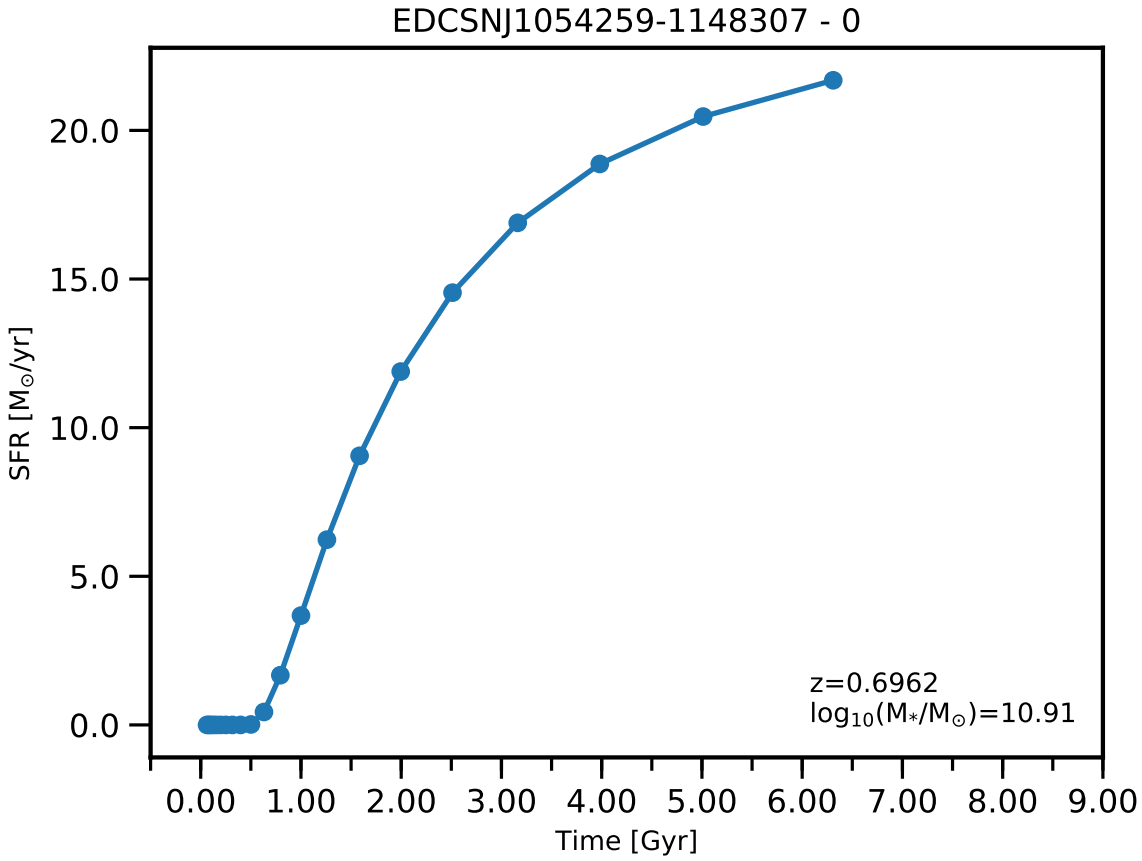
EDCSNJ1054259-1148307 - 0
SFR [M⊙/yr]
20.0
15.0
10.0
5.0
0.0
0.00
1.00
2.00
3.00
4.00
5.00
6.00
7.00
8.00
9.00
Time [Gyr]
z=0.6962
log10(M*/M⊙)=10.91

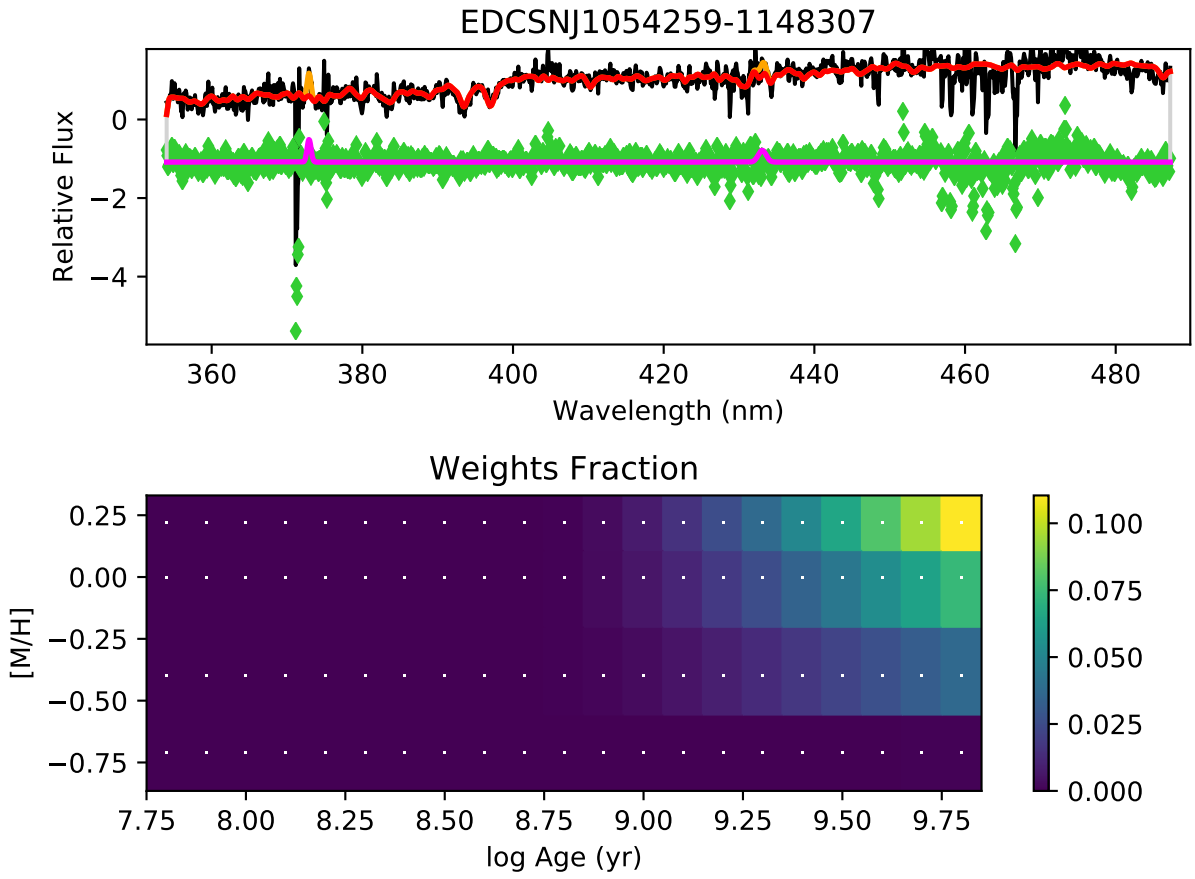
EDCSNJ1054259-1148307
Relative Flux
0
−2
−4
360
380
400
420
440
460
480
Wavelength (nm)
Weights Fraction
[M/H]
0.25
0.00
−0.25
−0.50
−0.75
7.75
8.00
8.25
8.50
8.75
9.00
9.25
9.50
9.75
log Age (yr)
0.100
0.075
0.050
0.025
0.000

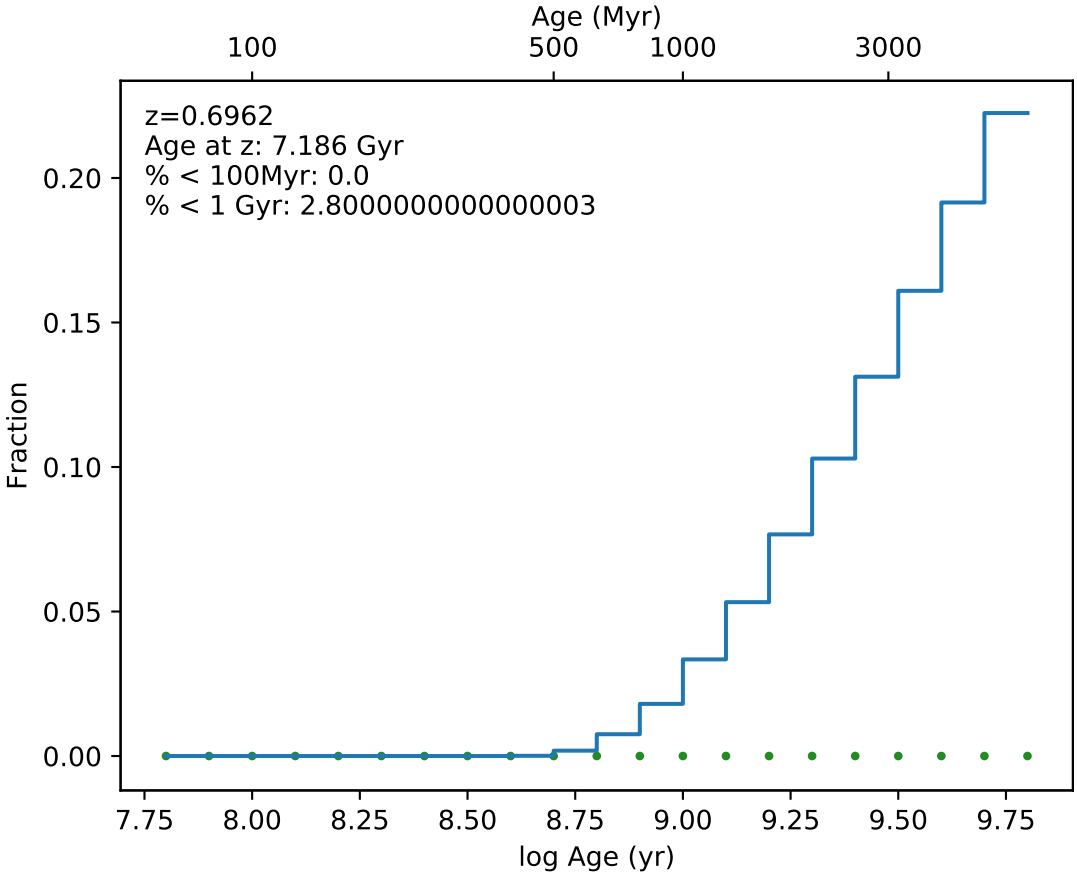
Age (Myr)
100
500
1000
3000
z=0.6962
Age at z: 7.186 Gyr
% < 100Myr: 0.0
% < 1 Gyr: 2.8000000000000003
Fraction
0.20
0.15
0.10
0.05
0.00
7.75
8.00
8.25
8.50
8.75
9.00
9.25
9.50
9.75
log Age (yr)

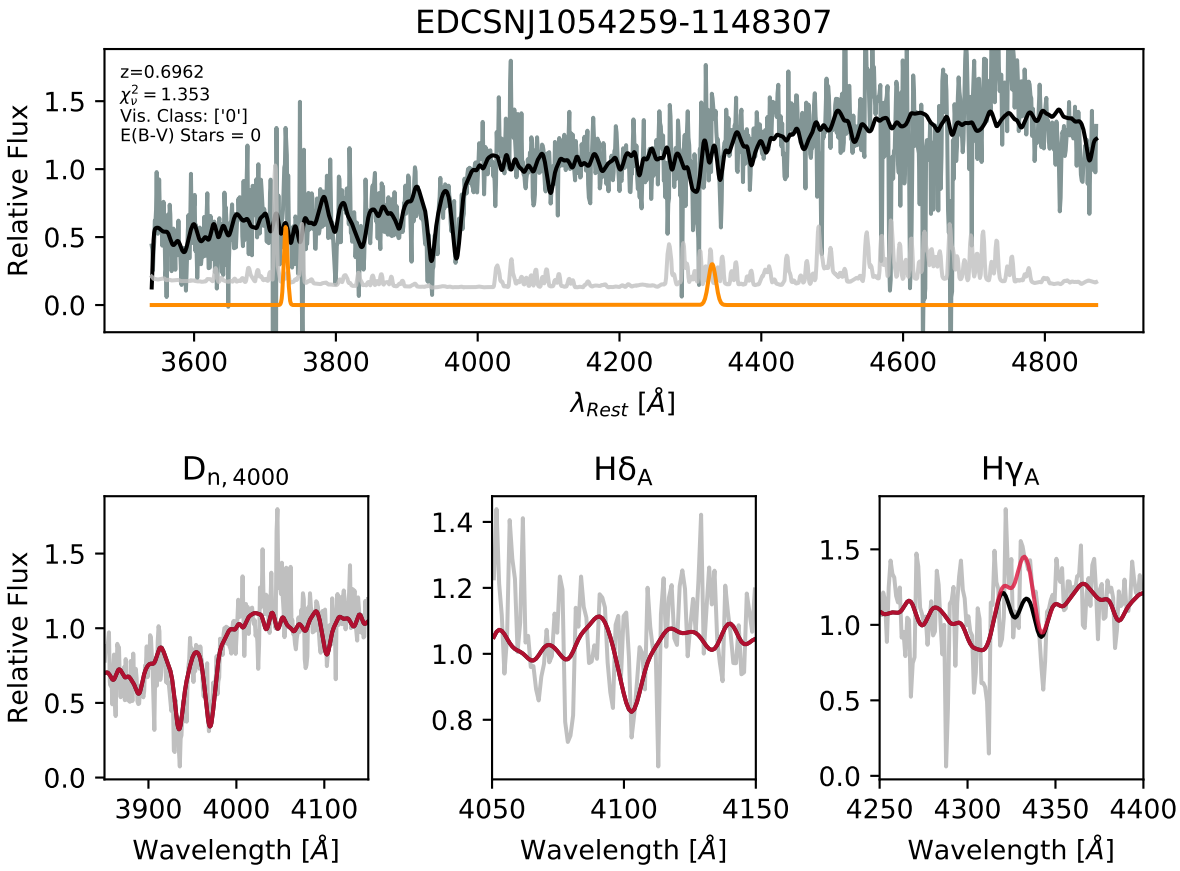
EDCSNJ1054259-1148307
z=0.6962
$\chi^2_\nu = 1.353$
Vis. Class: ['0']
E(B-V) Stars = 0
Relative Flux
λ_{Rest} [Å]
$D_{n,4000}$
$H\delta_A$
$H\gamma_A$
Wavelength [Å]

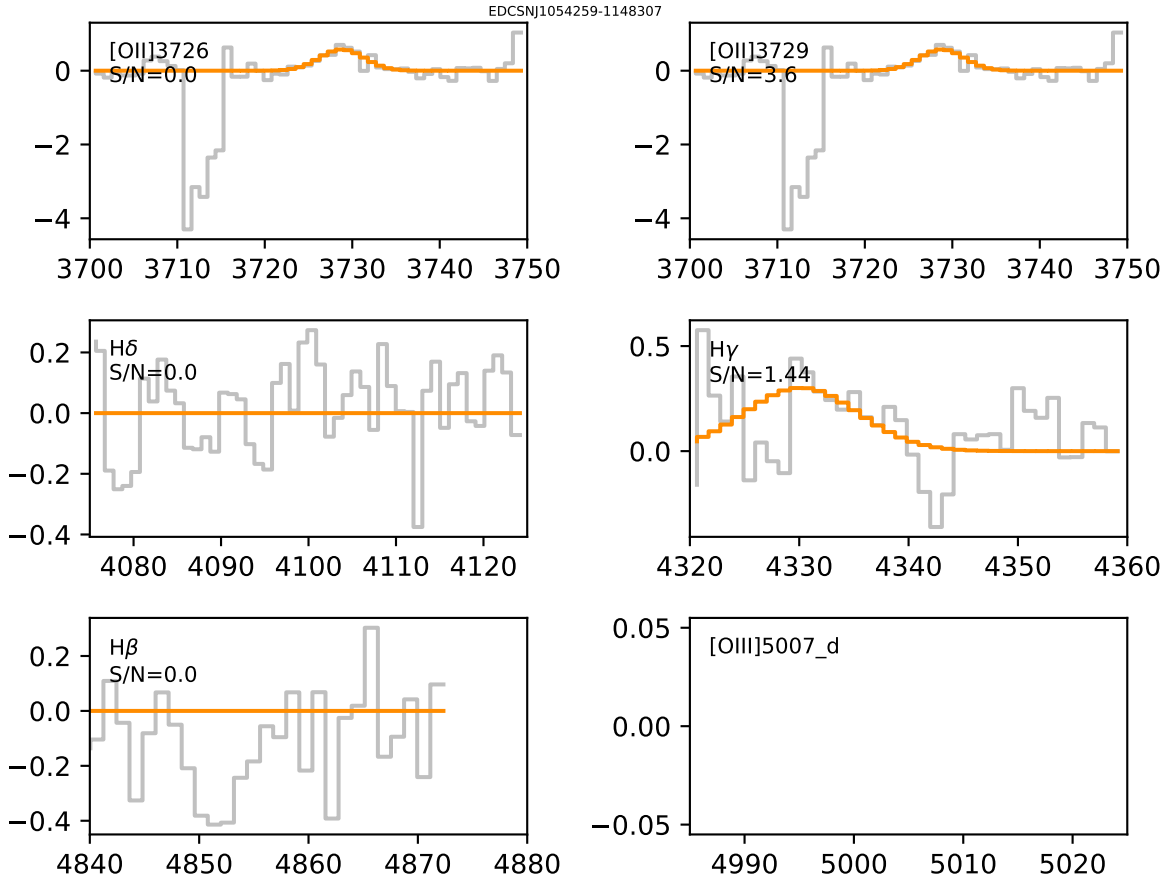
EDCSNJ1054259-1148307
[OII]3726
S/N=0.0
[OII]3729
S/N=3.6
Hδ
S/N=0.0
Hγ
S/N=1.44
Hβ
S/N=0.0
[OIII]5007_d

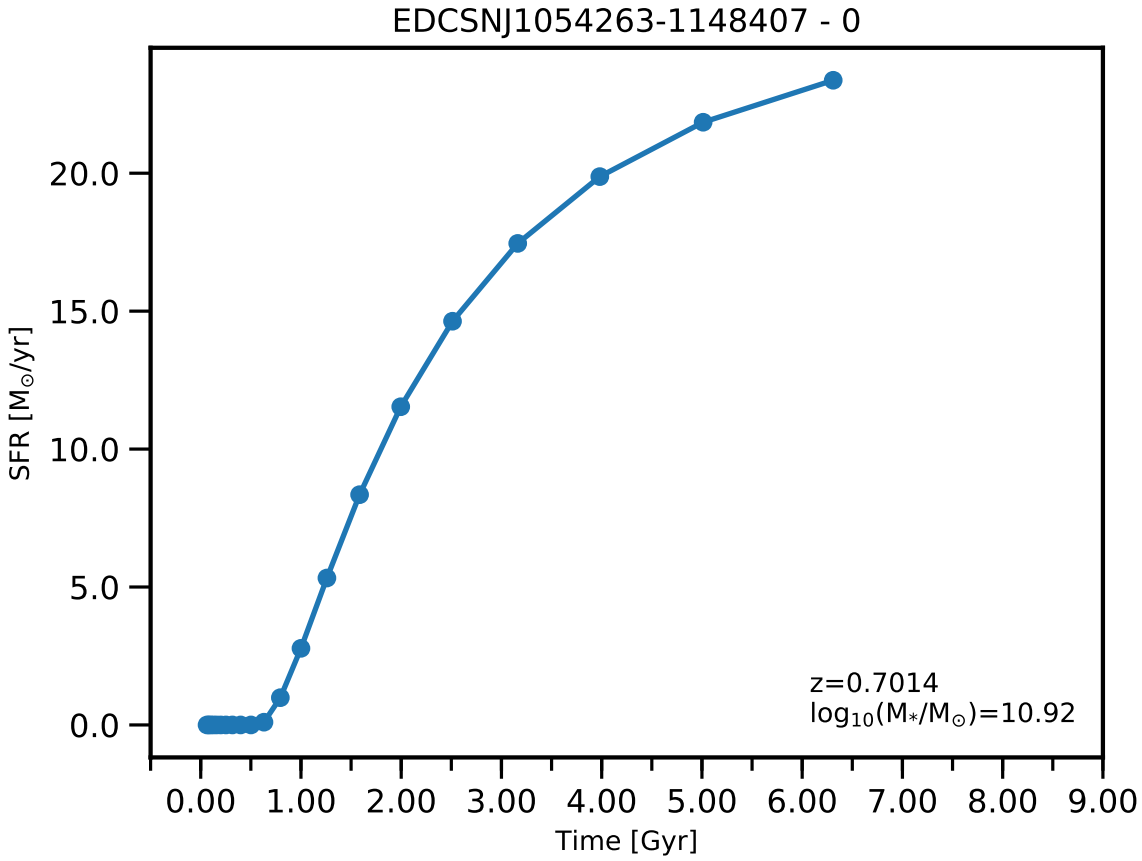
EDCSNJ1054263-1148407 - 0
SFR [M⊙/yr]
20.0
15.0
10.0
5.0
0.0
0.00
1.00
2.00
3.00
4.00
5.00
6.00
7.00
8.00
9.00
Time [Gyr]
z=0.7014
log10(M*/M⊙)=10.92

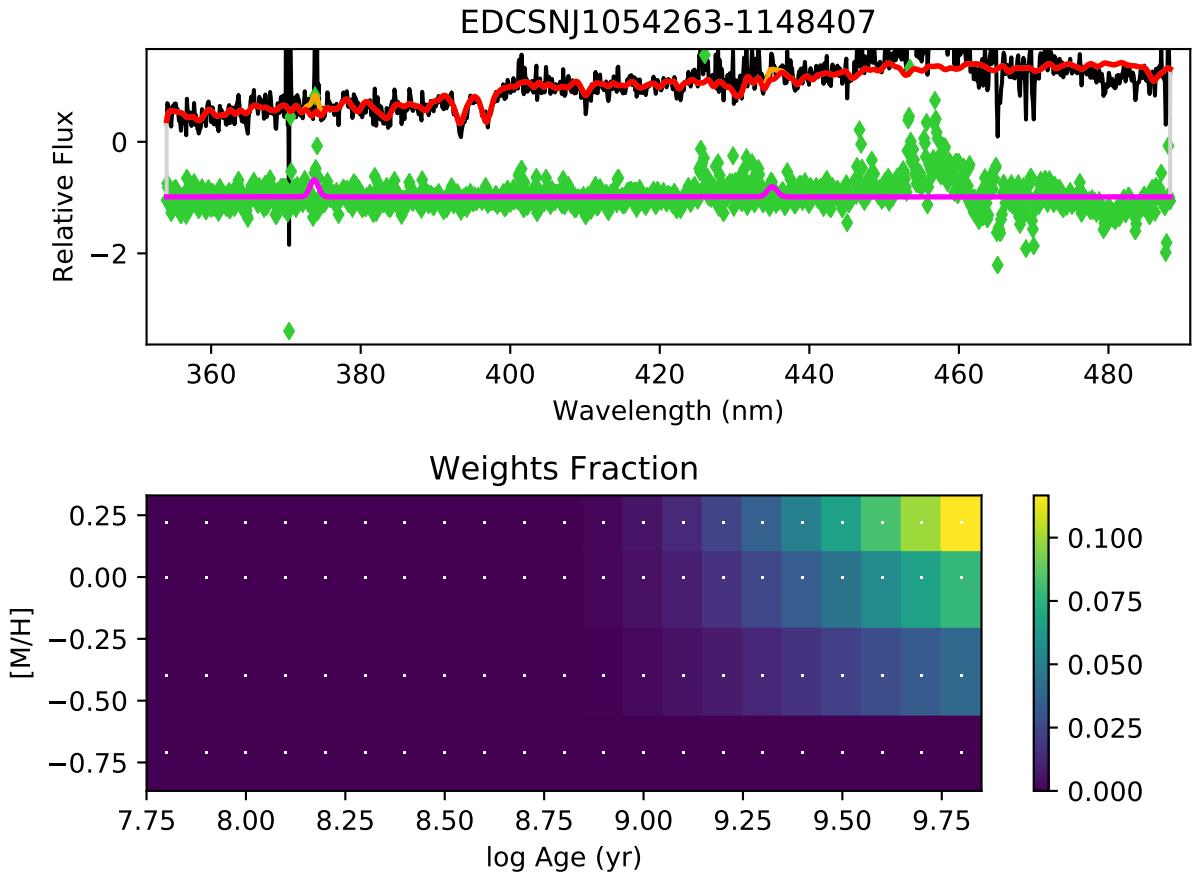
EDCSNJ1054263-1148407
Relative Flux
0
−2
360
380
400
420
440
460
480
Wavelength (nm)
Weights Fraction
[M/H]
0.25
0.00
−0.25
−0.50
−0.75
7.75
8.00
8.25
8.50
8.75
9.00
9.25
9.50
9.75
log Age (yr)
0.100
0.075
0.050
0.025
0.000

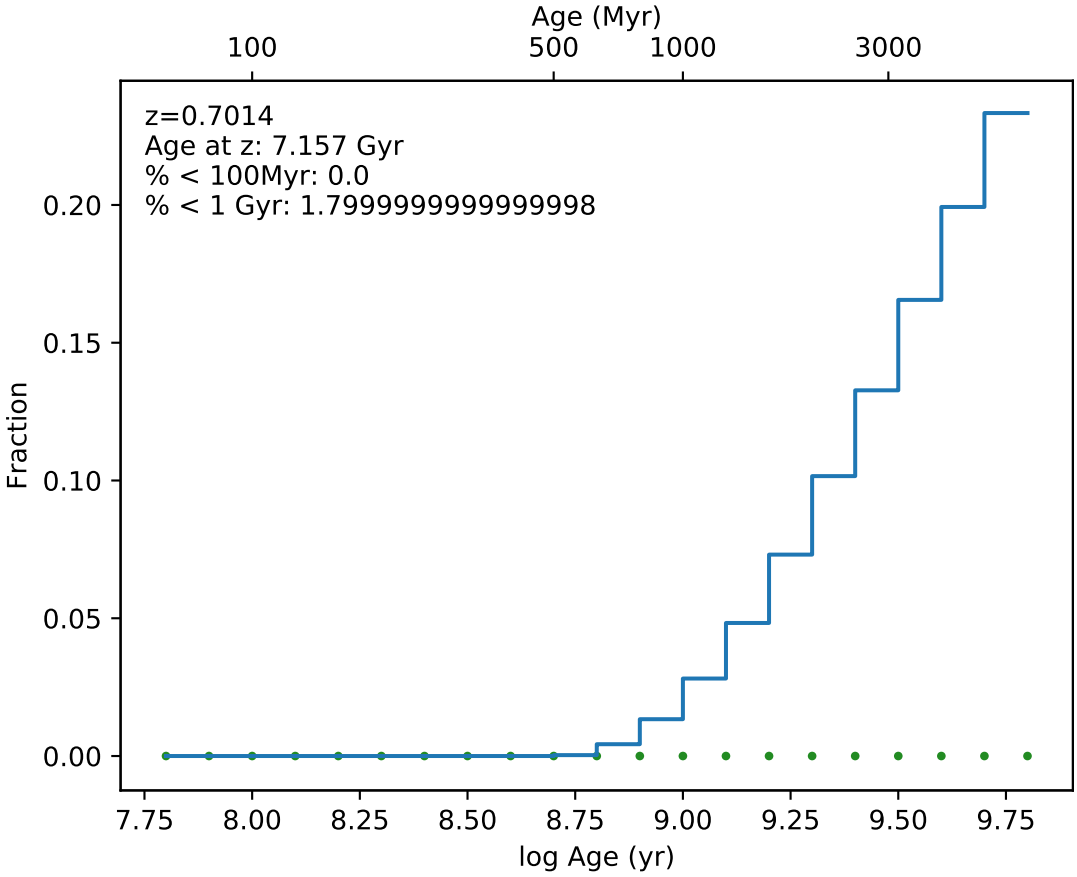
Age (Myr)
100
500
1000
3000
z=0.7014
Age at z: 7.157 Gyr
% < 100Myr: 0.0
% < 1 Gyr: 1.7999999999999998
Fraction
0.00
0.05
0.10
0.15
0.20
7.75
8.00
8.25
8.50
8.75
9.00
9.25
9.50
9.75
log Age (yr)

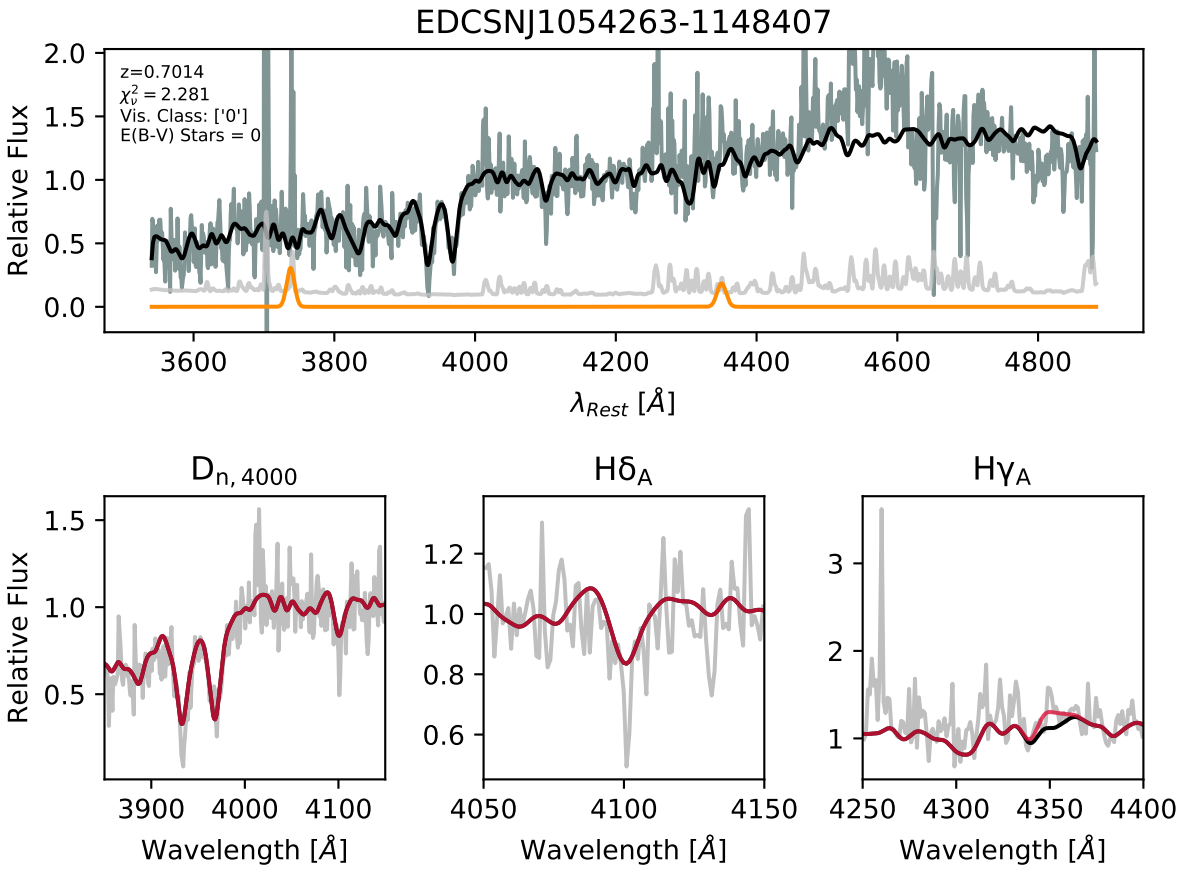
EDCSNJ1054263-1148407
z=0.7014
$\chi^2_\nu = 2.281$
Vis. Class: ['0']
E(B-V) Stars = 0
Relative Flux
λ_{Rest} [Å]
$D_{n,4000}$
$H\delta_A$
$H\gamma_A$
Wavelength [Å]

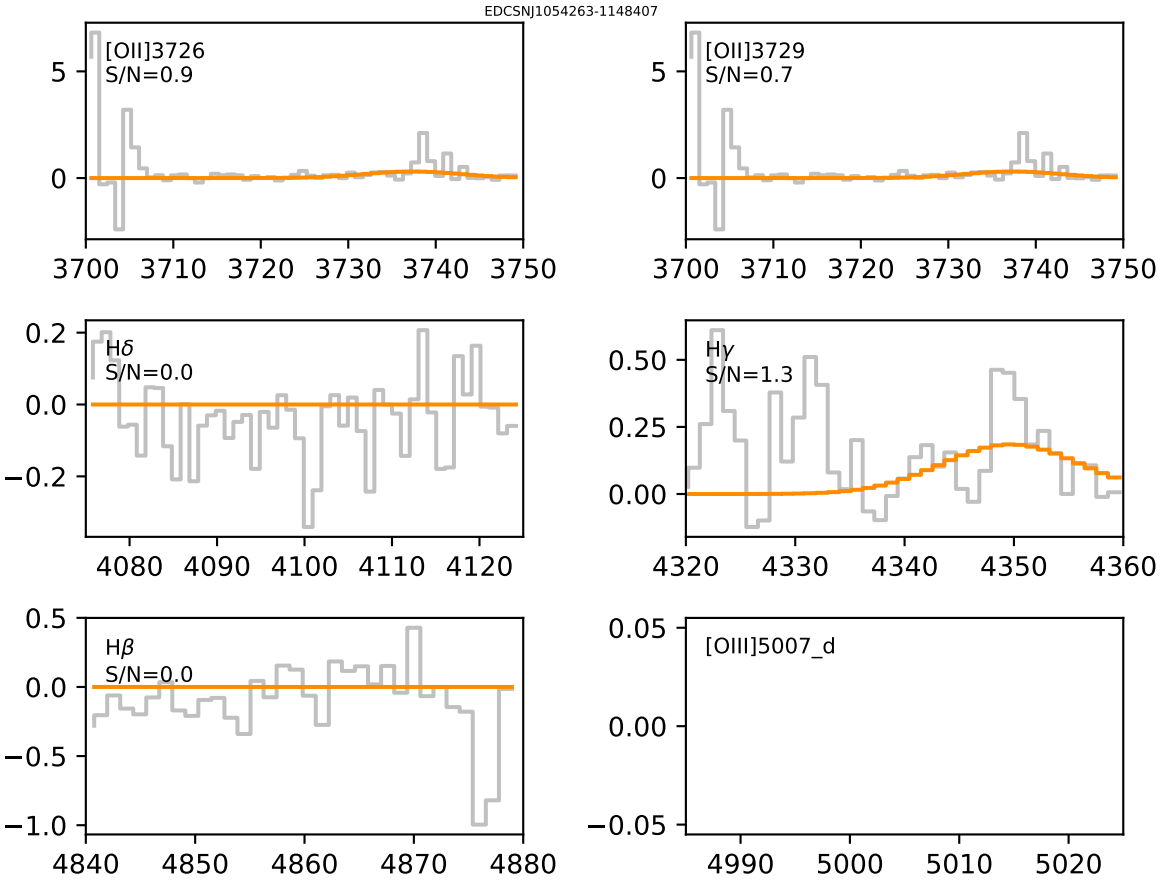
EDCSNJ1054263-1148407
[OII]3726
S/N=0.9
[OII]3729
S/N=0.7
Hδ
S/N=0.0
Hγ
S/N=1.3
Hβ
S/N=0.0
[OIII]5007_d

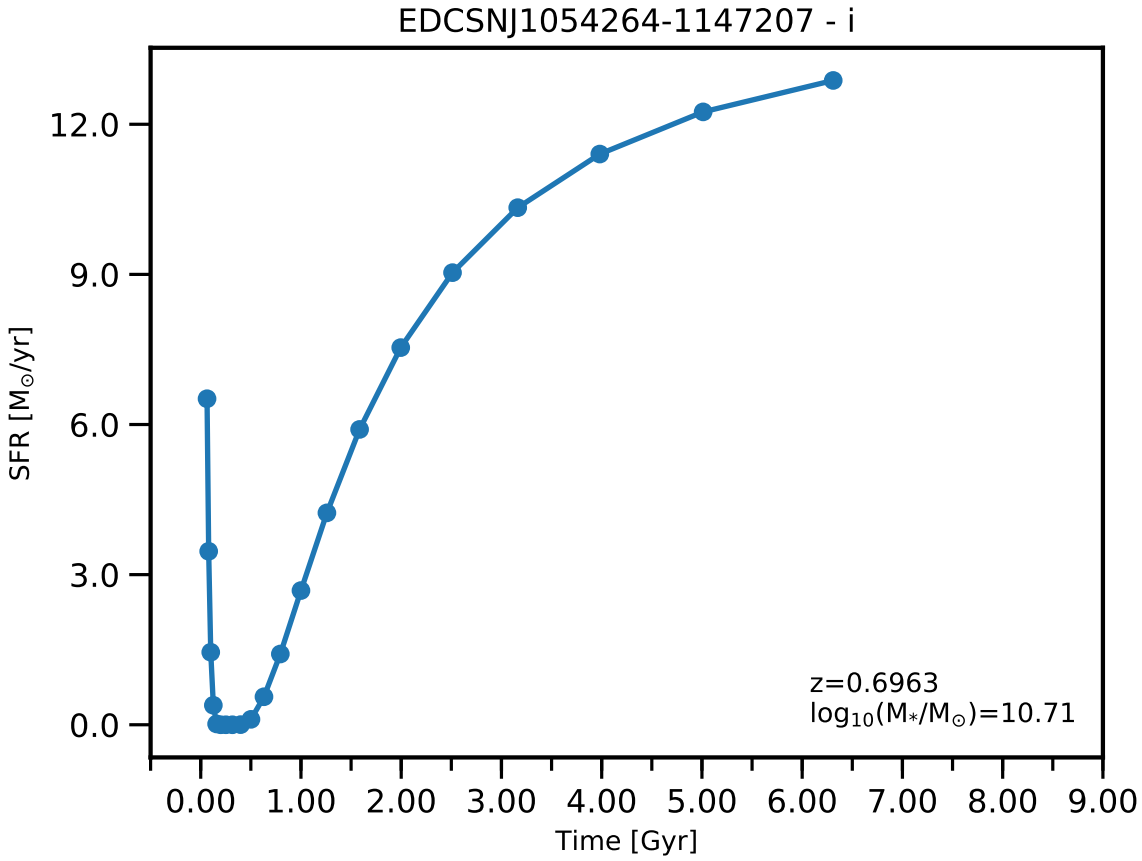
EDCSNJ1054264-1147207 - i
SFR [M⊙/yr]
12.0
9.0
6.0
3.0
0.0
0.00
1.00
2.00
3.00
4.00
5.00
6.00
7.00
8.00
9.00
Time [Gyr]
z=0.6963
log10(M*/M⊙)=10.71

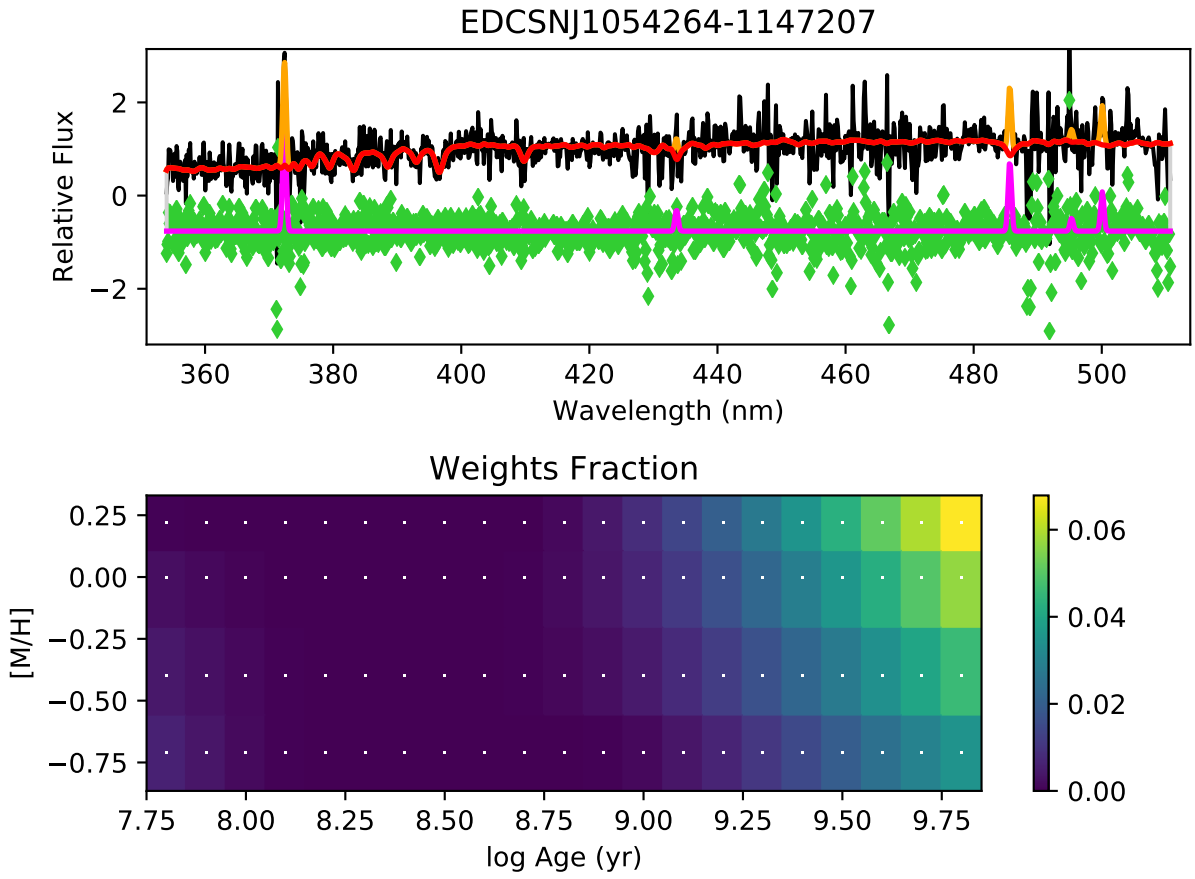
EDCSNJ1054264-1147207
Relative Flux
2
0
−2
360
380
400
420
440
460
480
500
Wavelength (nm)
Weights Fraction
[M/H]
0.25
0.00
−0.25
−0.50
−0.75
7.75
8.00
8.25
8.50
8.75
9.00
9.25
9.50
9.75
log Age (yr)
0.06
0.04
0.02
0.00

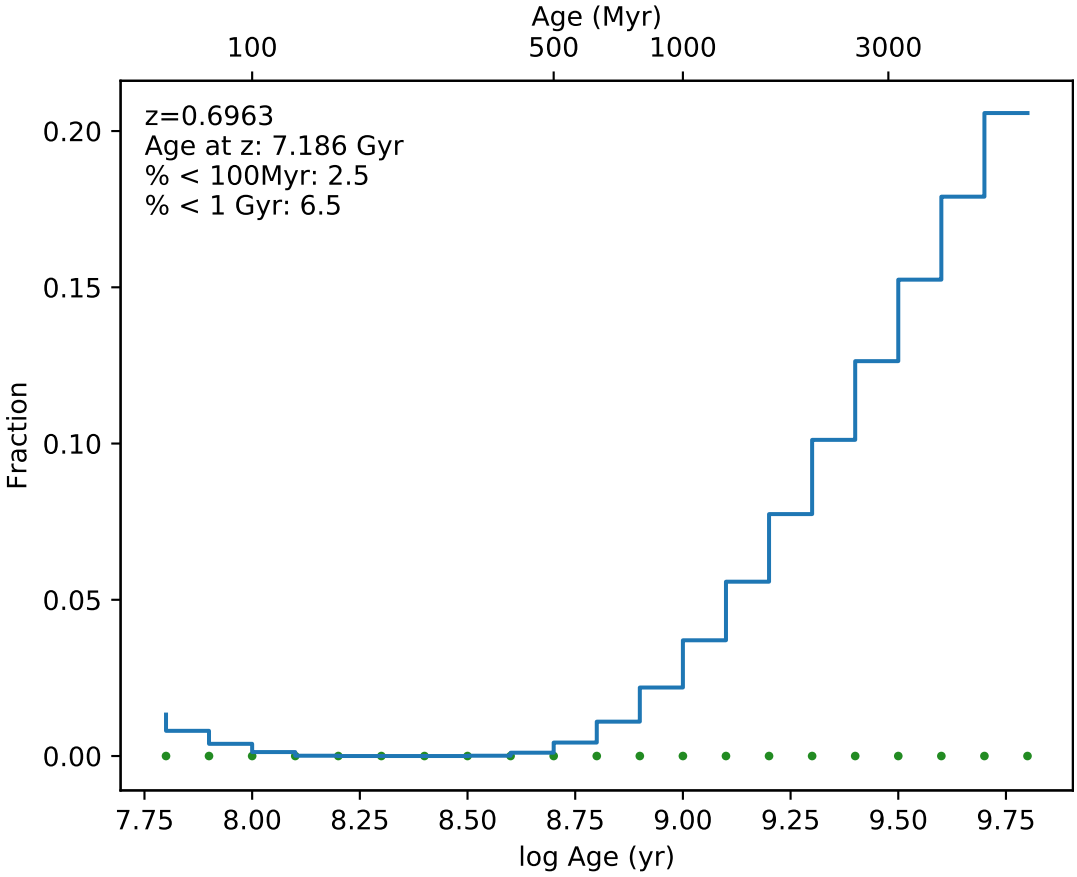
Age (Myr)
100
500
1000
3000
z=0.6963
Age at z: 7.186 Gyr
% < 100Myr: 2.5
% < 1 Gyr: 6.5
Fraction
0.20
0.15
0.10
0.05
0.00
7.75
8.00
8.25
8.50
8.75
9.00
9.25
9.50
9.75
log Age (yr)

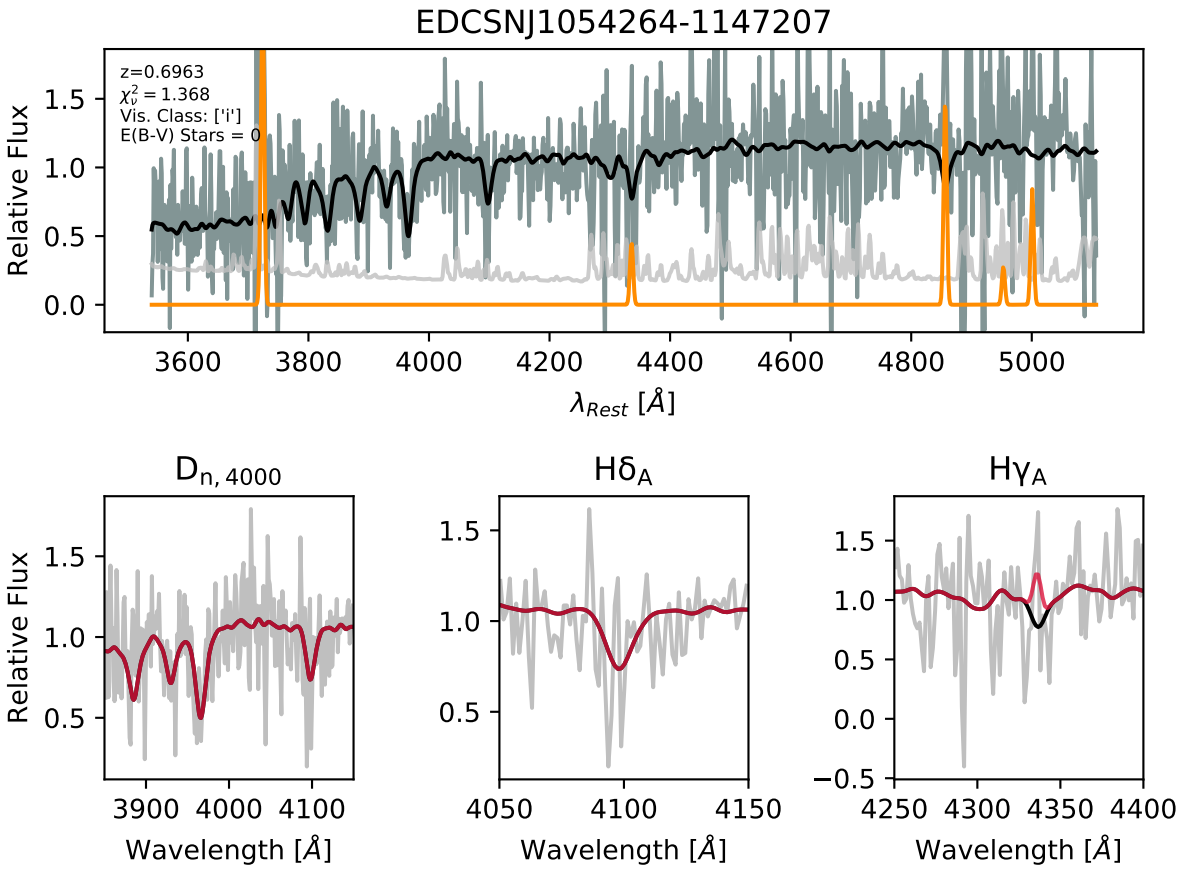
EDCSNJ1054264-1147207
z=0.6963
$\chi^2_\nu = 1.368$
Vis. Class: ['i']
E(B-V) Stars = 0
Relative Flux
λ_{Rest} [Å]
$D_{n,4000}$
$H\delta_A$
$H\gamma_A$
Wavelength [Å]

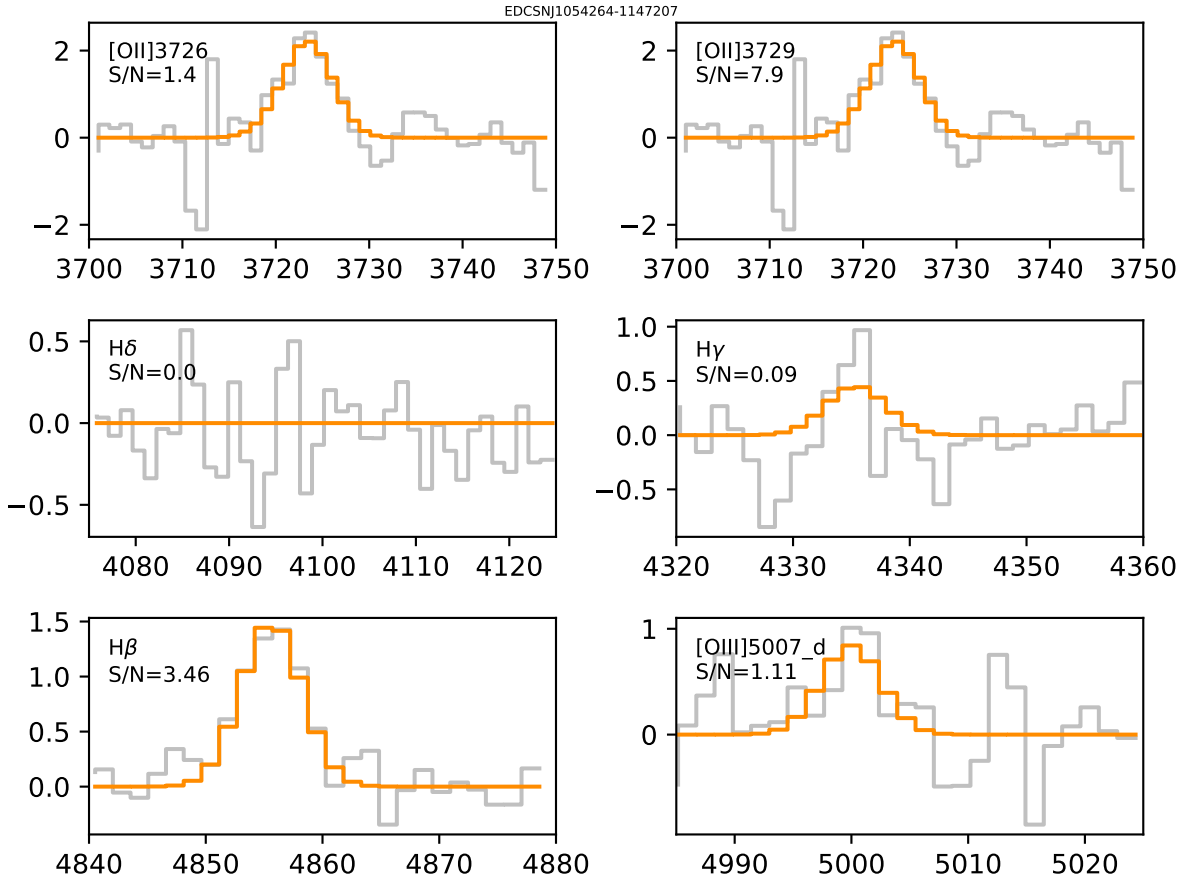
EDCSNJ1054264-1147207
[OII]3726
S/N=1.4
[OII]3729
S/N=7.9
Hδ
S/N=0.0
Hγ
S/N=0.09
Hβ
S/N=3.46
[OIII]5007_d
S/N=1.11

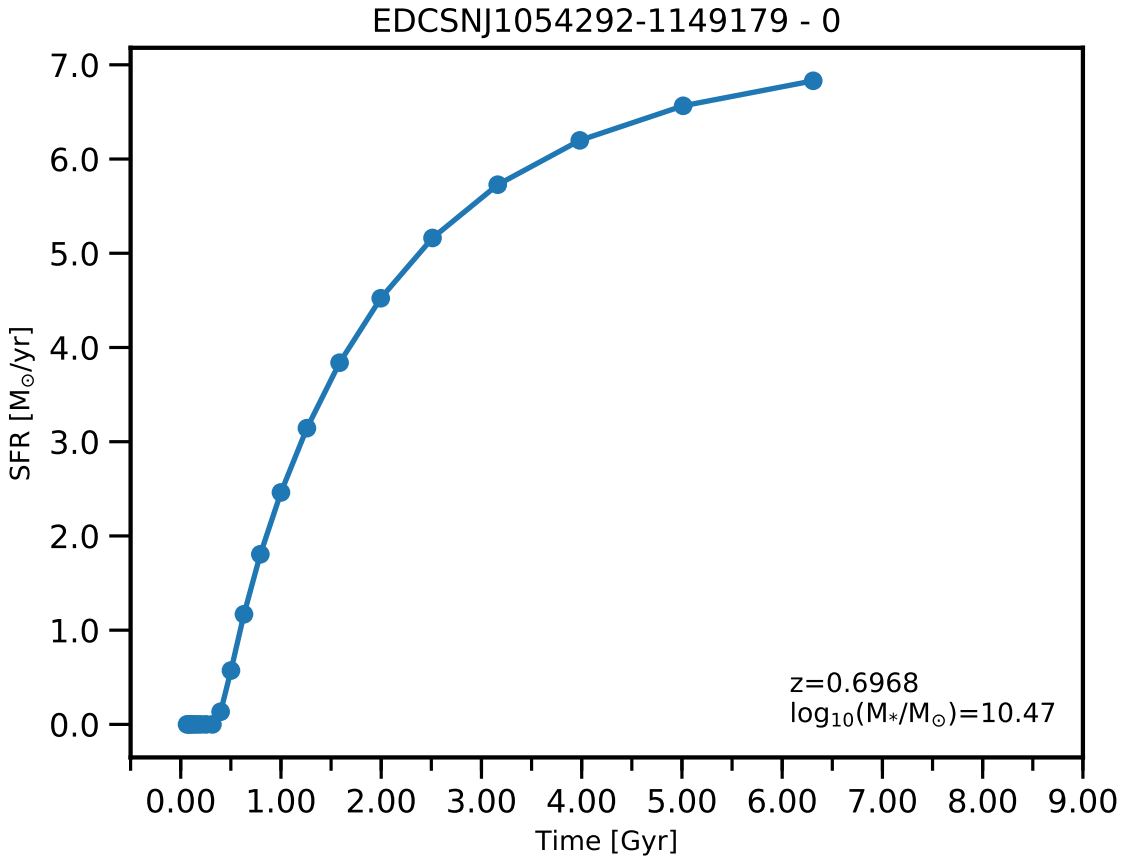
EDCSNJ1054292-1149179 - 0
SFR [M⊙/yr]
Time [Gyr]
z=0.6968
log10(M*/M⊙)=10.47
0.0
1.0
2.0
3.0
4.0
5.0
6.0
7.0
0.00
1.00
2.00
3.00
4.00
5.00
6.00
7.00
8.00
9.00

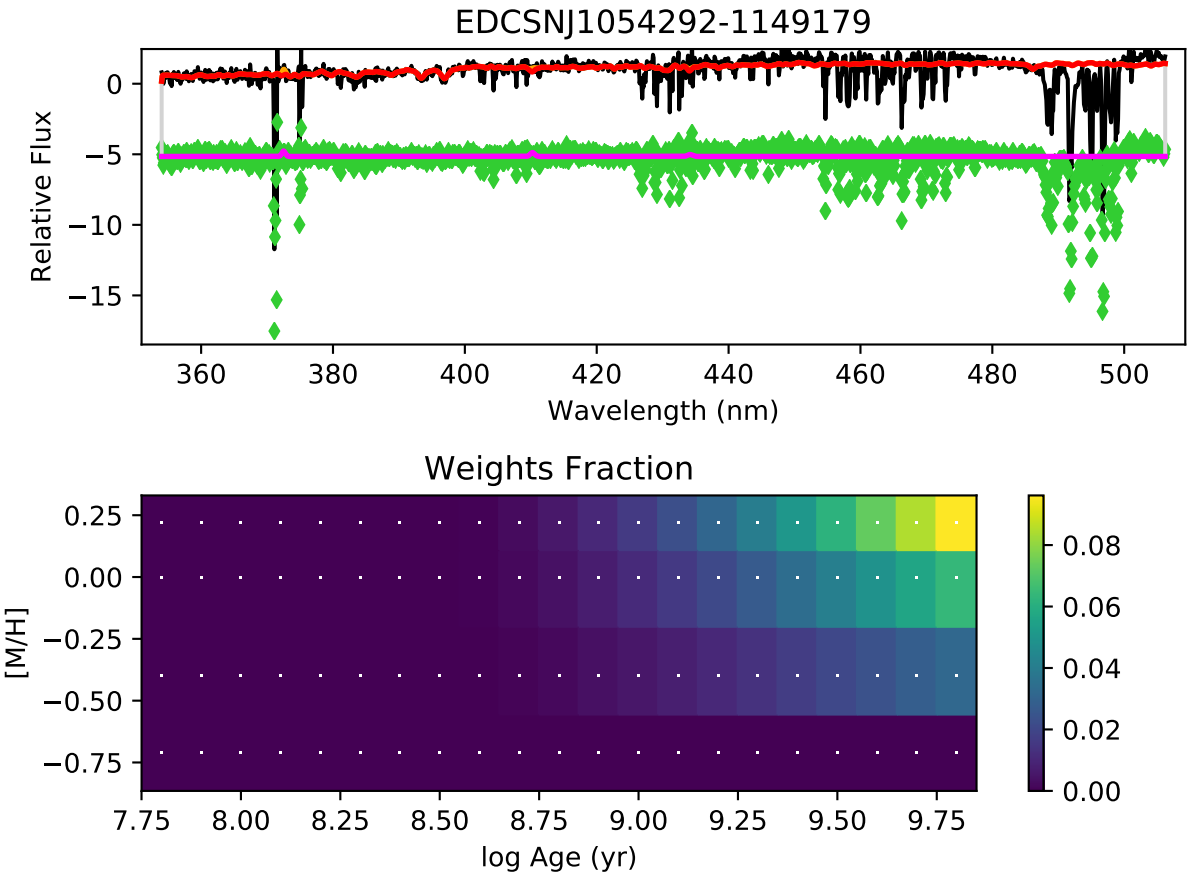
EDCSNJ1054292-1149179
Relative Flux
0
−5
−10
−15
360
380
400
420
440
460
480
500
Wavelength (nm)
Weights Fraction
[M/H]
0.25
0.00
−0.25
−0.50
−0.75
7.75
8.00
8.25
8.50
8.75
9.00
9.25
9.50
9.75
log Age (yr)
0.08
0.06
0.04
0.02
0.00

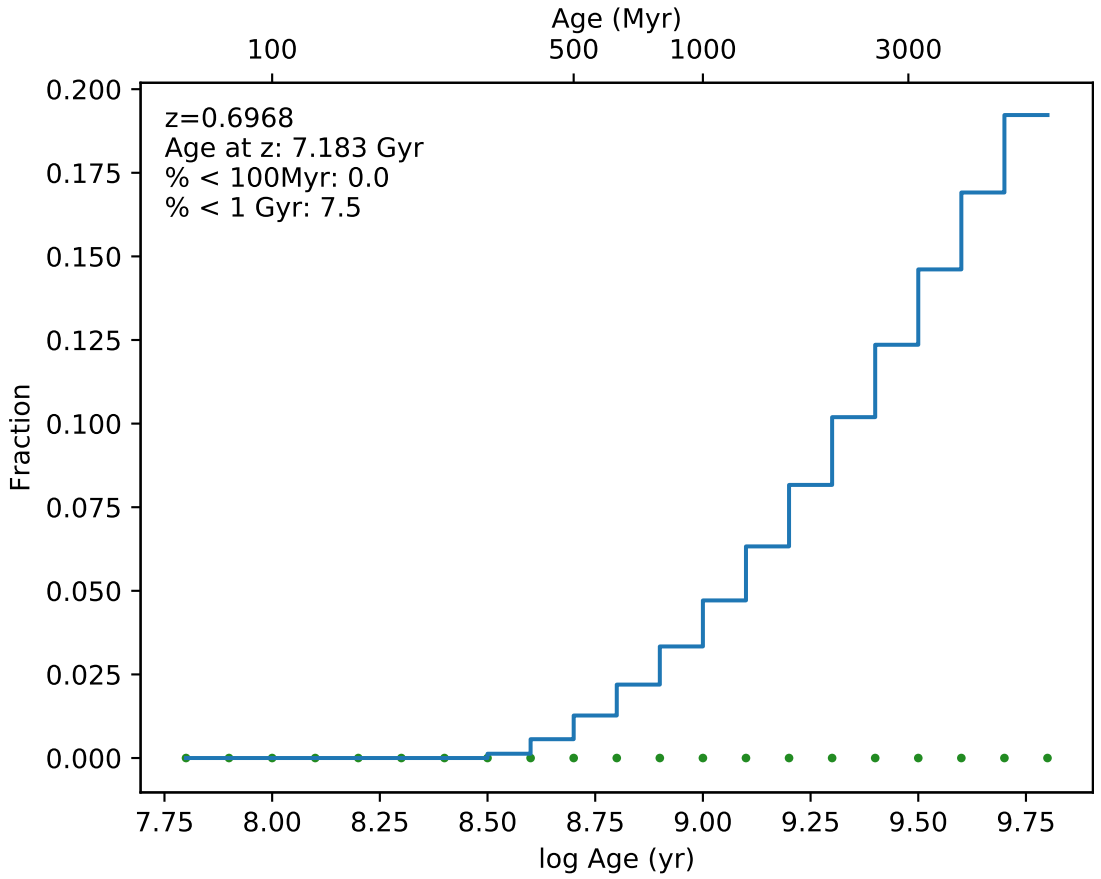
Age (Myr)
100
500
1000
3000
z=0.6968
Age at z: 7.183 Gyr
% < 100Myr: 0.0
% < 1 Gyr: 7.5
Fraction
0.200
0.175
0.150
0.125
0.100
0.075
0.050
0.025
0.000
7.75
8.00
8.25
8.50
8.75
9.00
9.25
9.50
9.75
log Age (yr)

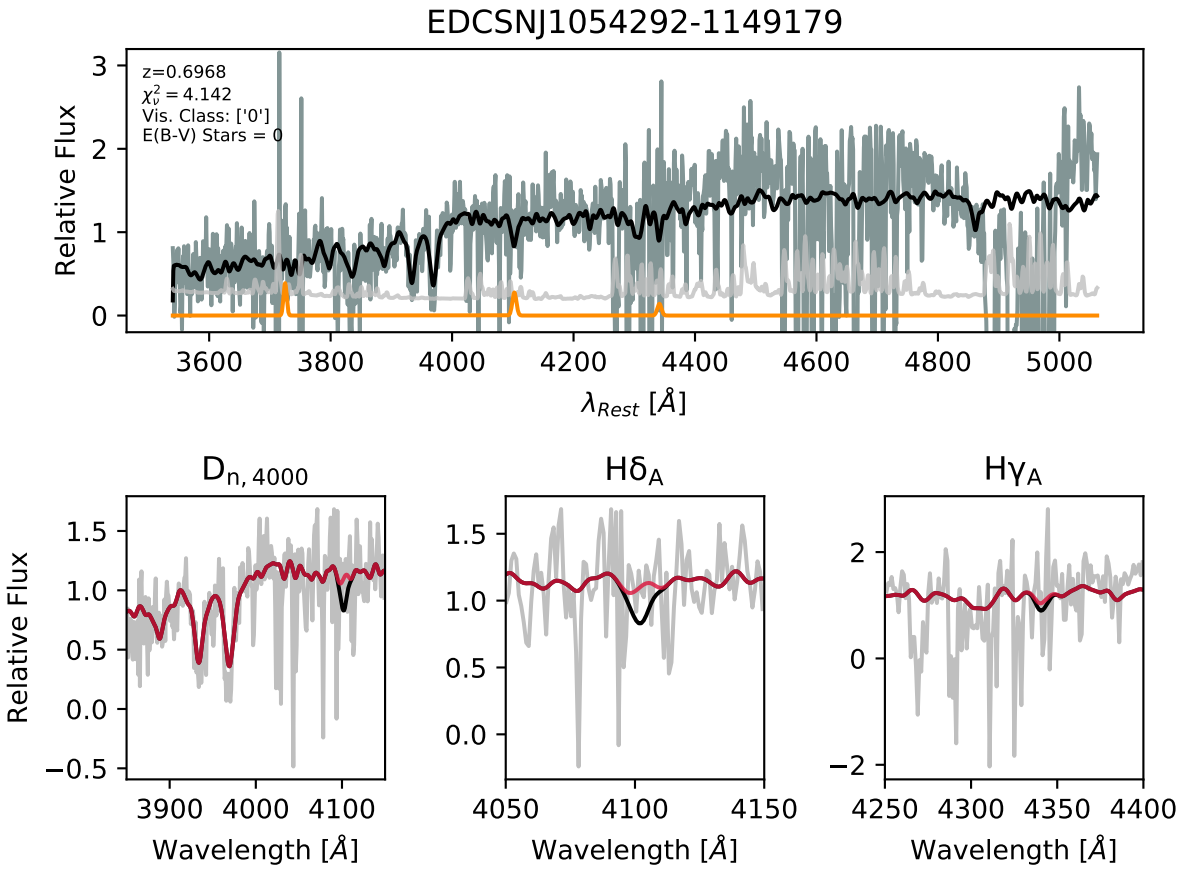
EDCSNJ1054292-1149179
z=0.6968
$\chi^2_\nu = 4.142$
Vis. Class: ['0']
E(B-V) Stars = 0
Relative Flux
λ_{Rest} [Å]
$D_{n,4000}$
$H\delta_A$
$H\gamma_A$
Relative Flux
Wavelength [Å]
Wavelength [Å]
Wavelength [Å]

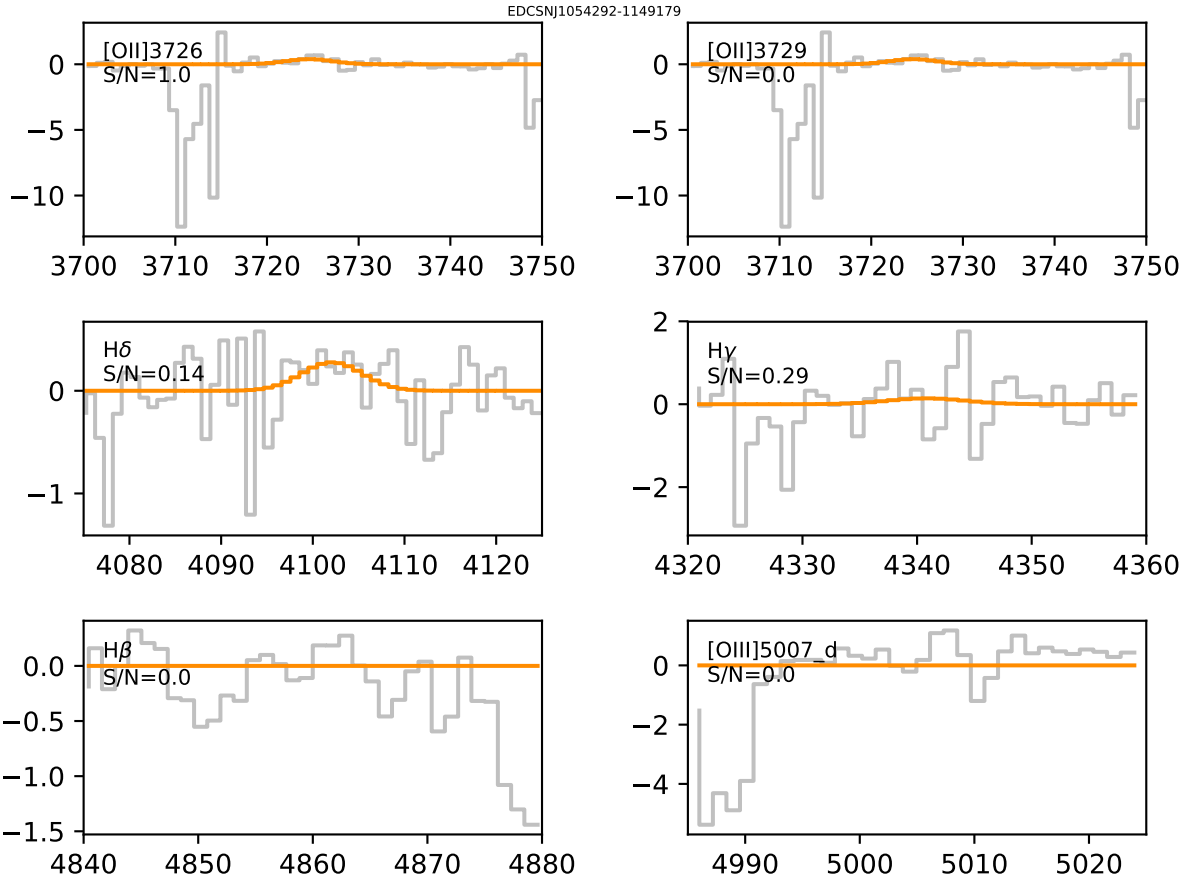
EDCSNJ1054292-1149179
[OII]3726
S/N=1.0
[OII]3729
S/N=0.0
Hδ
S/N=0.14
Hγ
S/N=0.29
Hβ
S/N=0.0
[OIII]5007_d
S/N=0.0

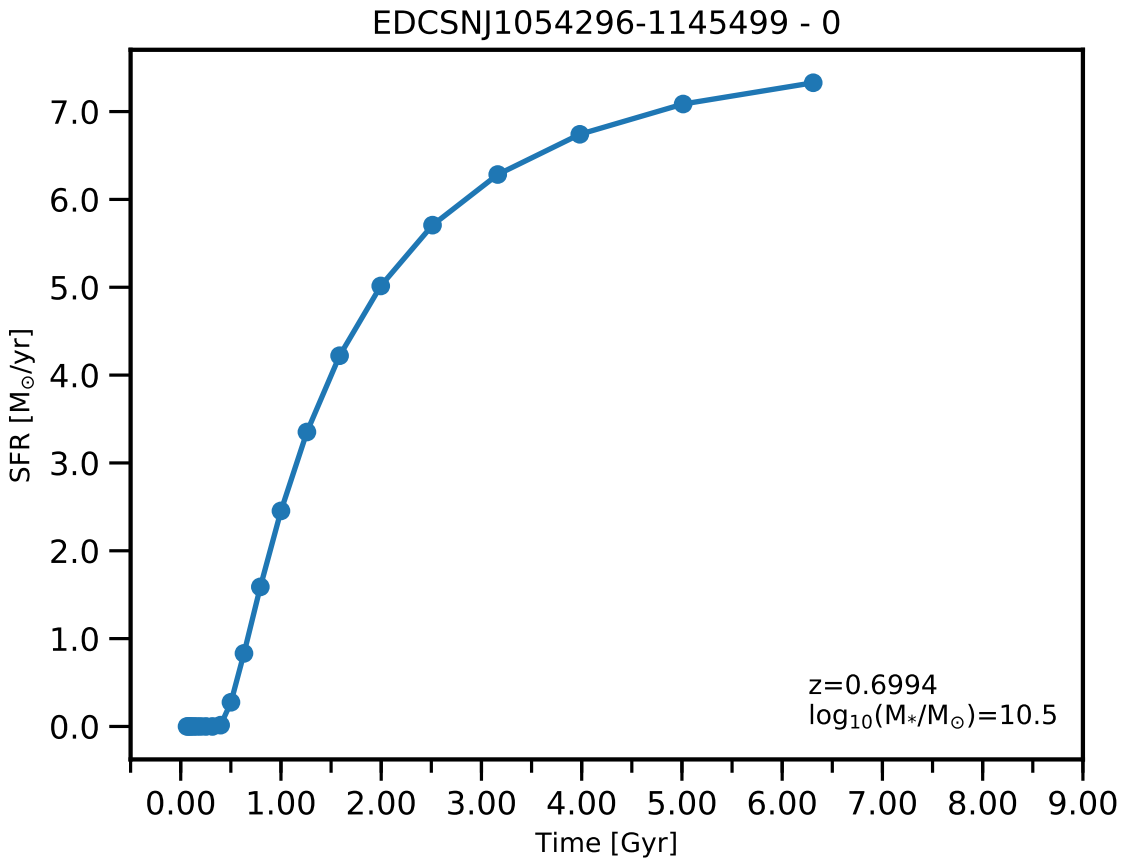
EDCSNJ1054296-1145499 - 0
SFR [M⊙/yr]
Time [Gyr]
z=0.6994
log10(M*/M⊙)=10.5
0.0
1.0
2.0
3.0
4.0
5.0
6.0
7.0
0.00
1.00
2.00
3.00
4.00
5.00
6.00
7.00
8.00
9.00

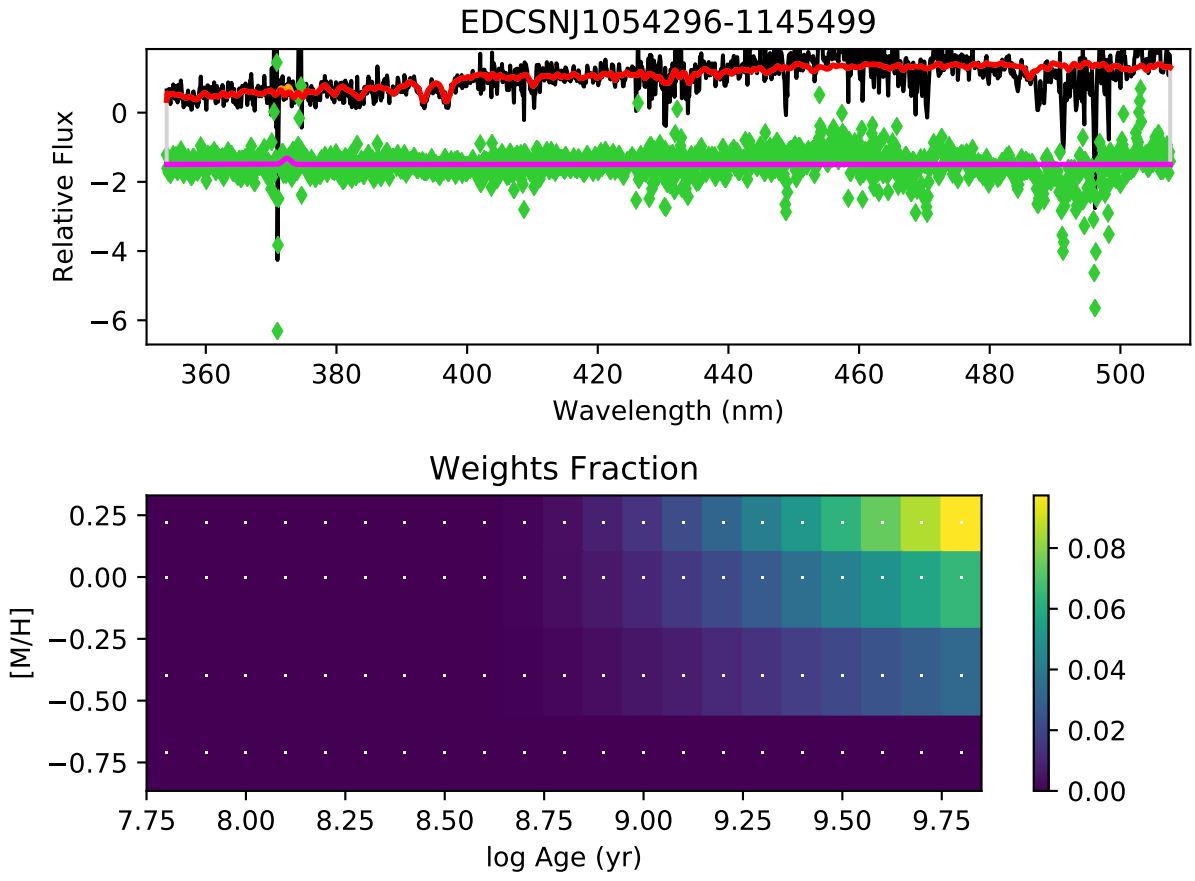
EDCSNJ1054296-1145499
Relative Flux
0
−2
−4
−6
360
380
400
420
440
460
480
500
Wavelength (nm)
Weights Fraction
[M/H]
0.25
0.00
−0.25
−0.50
−0.75
7.75
8.00
8.25
8.50
8.75
9.00
9.25
9.50
9.75
log Age (yr)
0.08
0.06
0.04
0.02
0.00

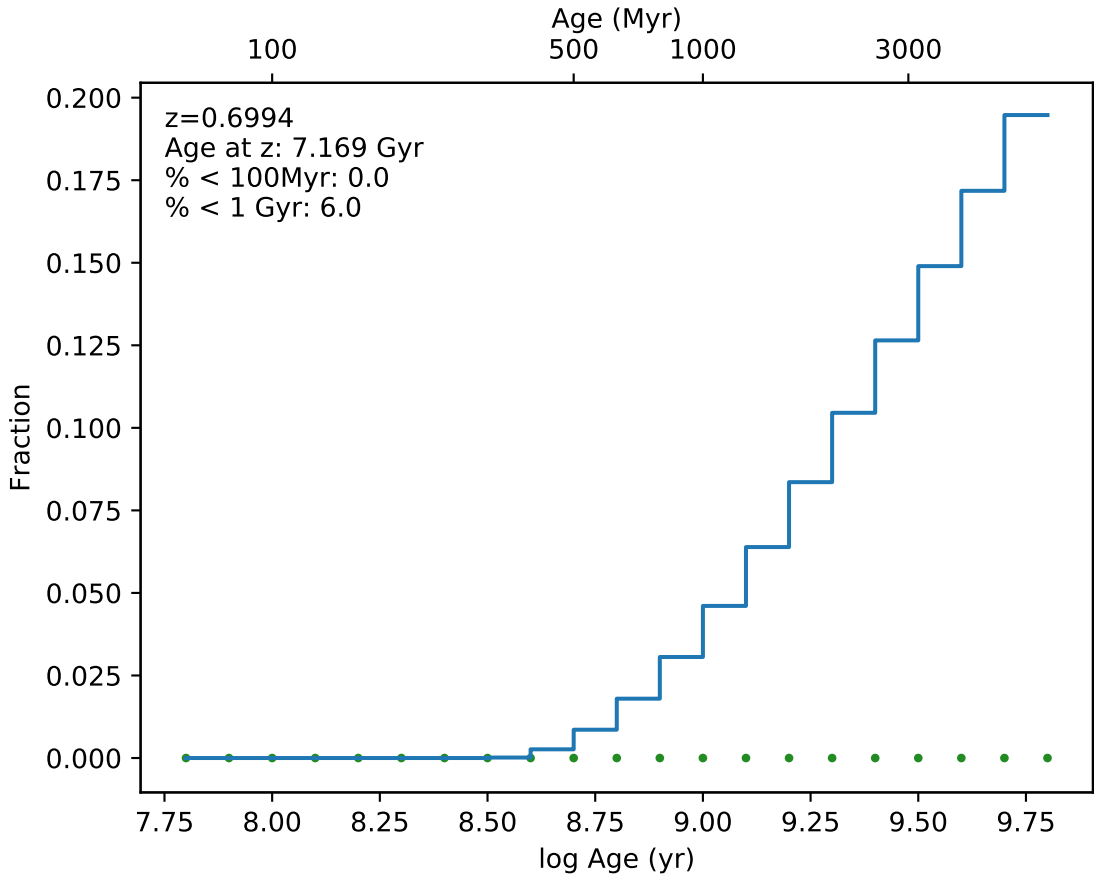
Age (Myr)
100
500
1000
3000
z=0.6994
Age at z: 7.169 Gyr
% < 100Myr: 0.0
% < 1 Gyr: 6.0
Fraction
0.200
0.175
0.150
0.125
0.100
0.075
0.050
0.025
0.000
7.75
8.00
8.25
8.50
8.75
9.00
9.25
9.50
9.75
log Age (yr)

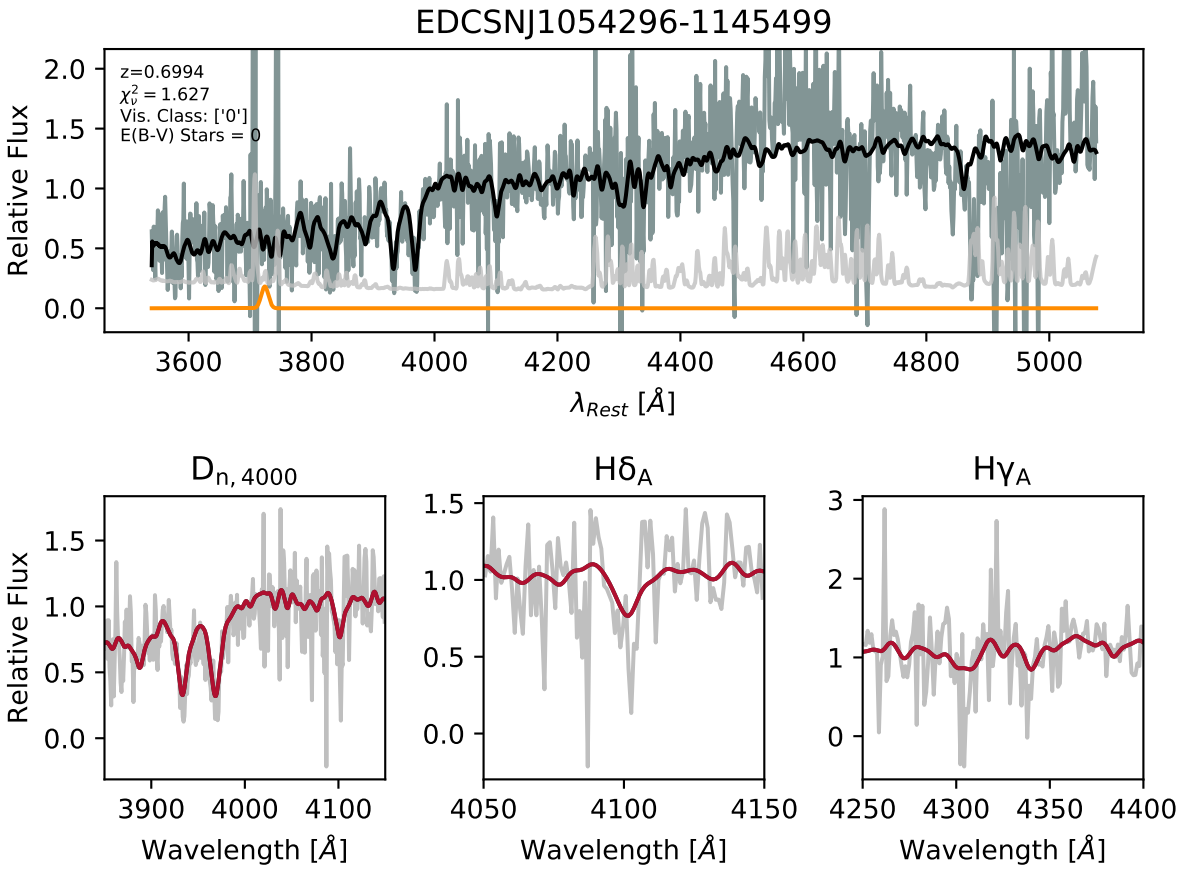
EDCSNJ1054296-1145499
z=0.6994
$\chi^2_\nu = 1.627$
Vis. Class: ['0']
E(B-V) Stars = 0
Relative Flux
λ_{Rest} [Å]
$D_{n,4000}$
$H\delta_A$
$H\gamma_A$
Wavelength [Å]

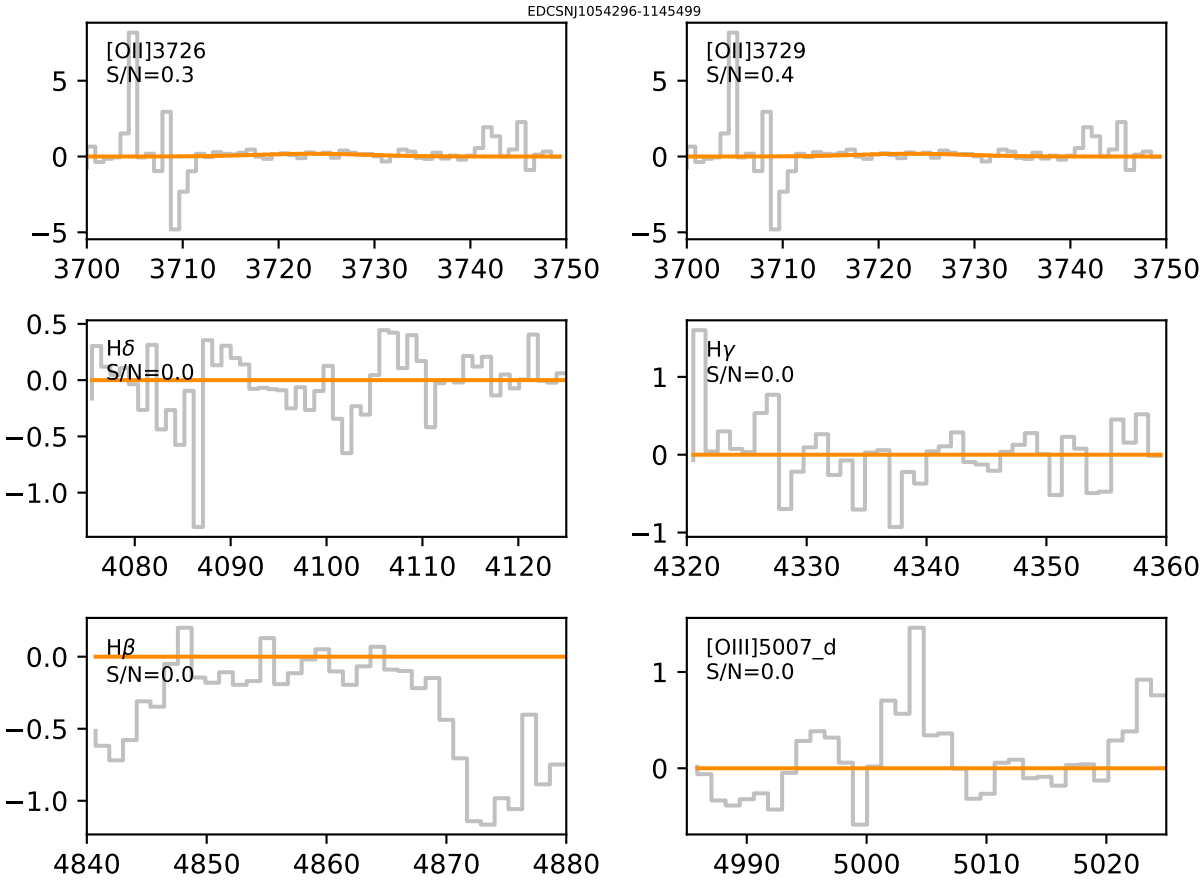
EDCSNJ1054296-1145499
[OII]3726
S/N=0.3
[OII]3729
S/N=0.4
Hδ
S/N=0.0
Hγ
S/N=0.0
Hβ
S/N=0.0
[OIII]5007_d
S/N=0.0

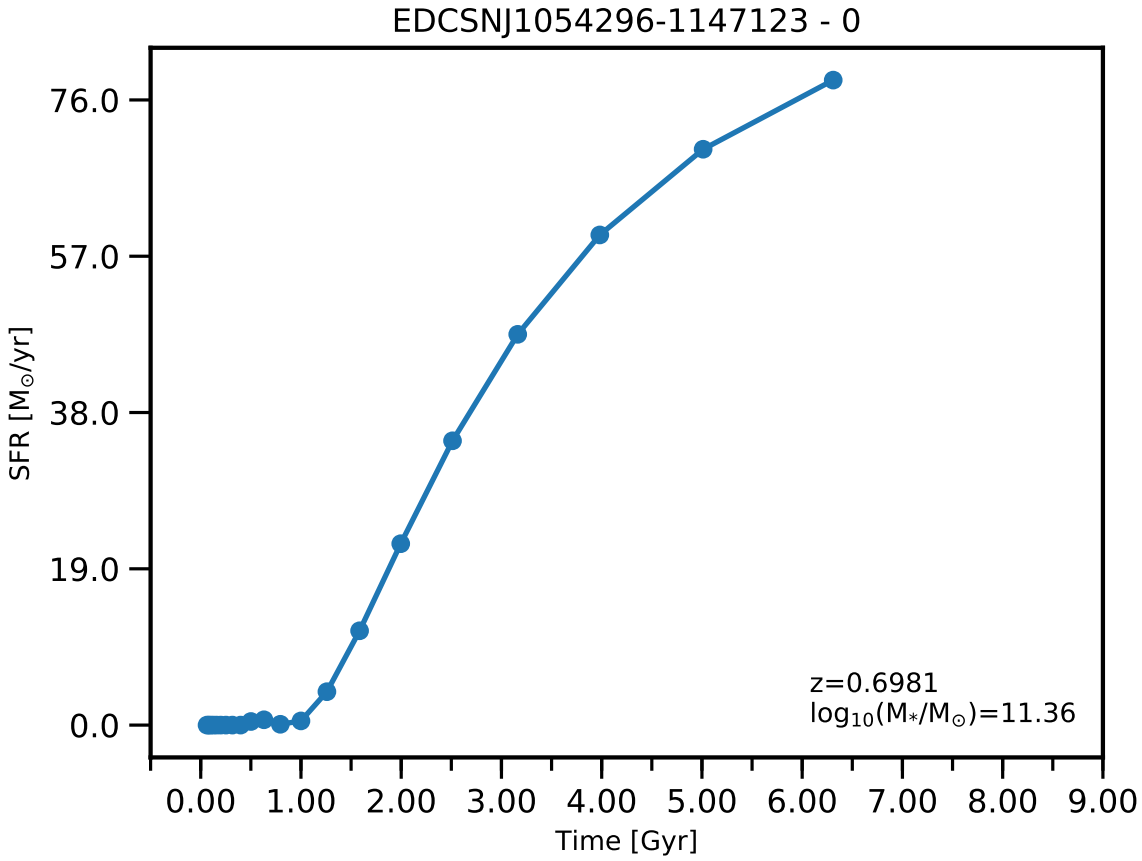
EDCSNJ1054296-1147123 - 0
76.0
57.0
38.0
19.0
0.0
SFR [M⊙/yr]
0.00
1.00
2.00
3.00
4.00
5.00
6.00
7.00
8.00
9.00
Time [Gyr]
z=0.6981
log10(M*/M⊙)=11.36

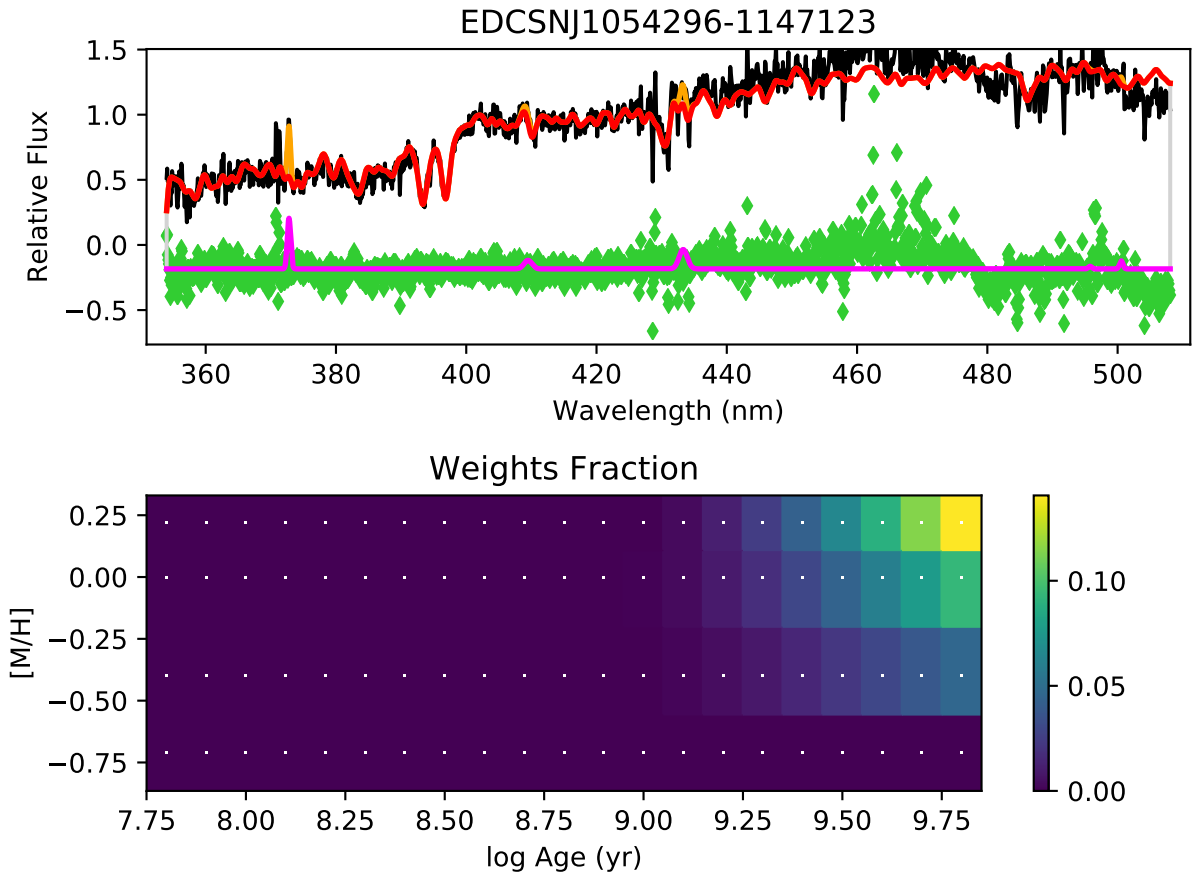
EDCSNJ1054296-1147123
Relative Flux
1.5
1.0
0.5
0.0
−0.5
360
380
400
420
440
460
480
500
Wavelength (nm)
Weights Fraction
[M/H]
0.25
0.00
−0.25
−0.50
−0.75
7.75
8.00
8.25
8.50
8.75
9.00
9.25
9.50
9.75
log Age (yr)
0.10
0.05
0.00

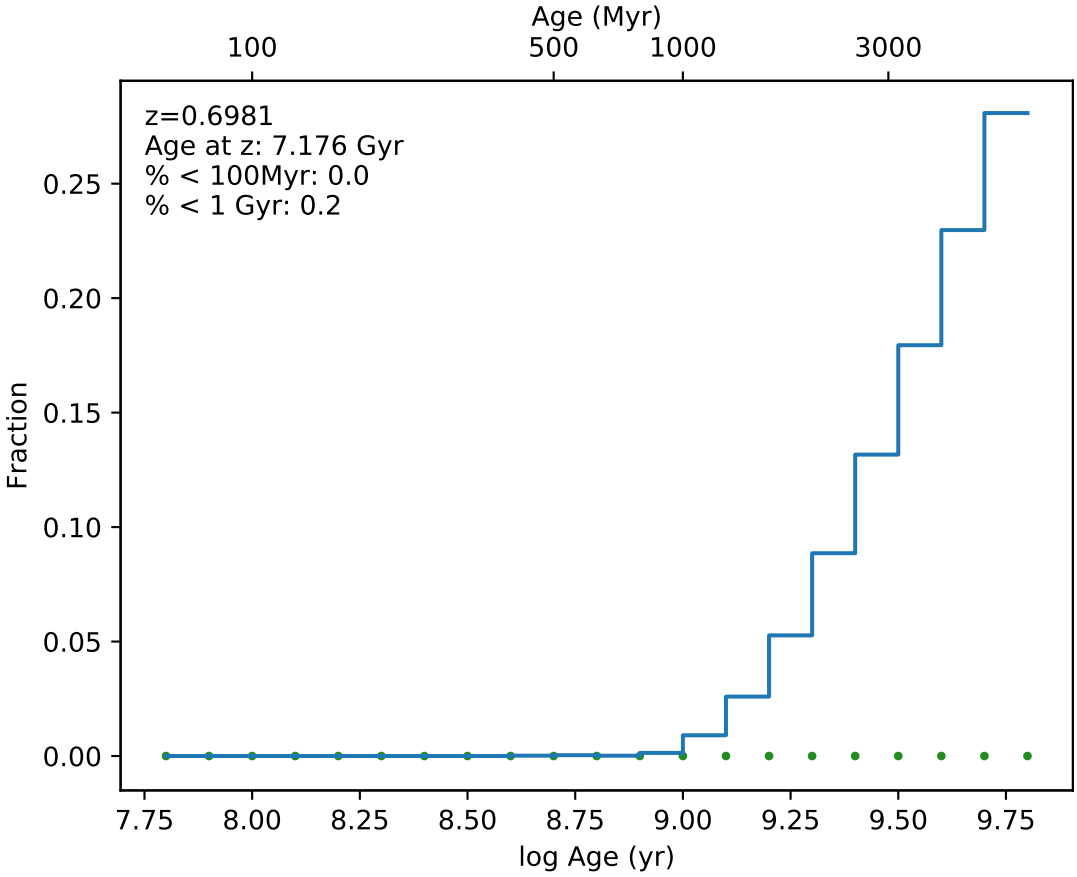
Age (Myr)
100
500
1000
3000
z=0.6981
Age at z: 7.176 Gyr
% < 100Myr: 0.0
% < 1 Gyr: 0.2
Fraction
0.25
0.20
0.15
0.10
0.05
0.00
7.75
8.00
8.25
8.50
8.75
9.00
9.25
9.50
9.75
log Age (yr)

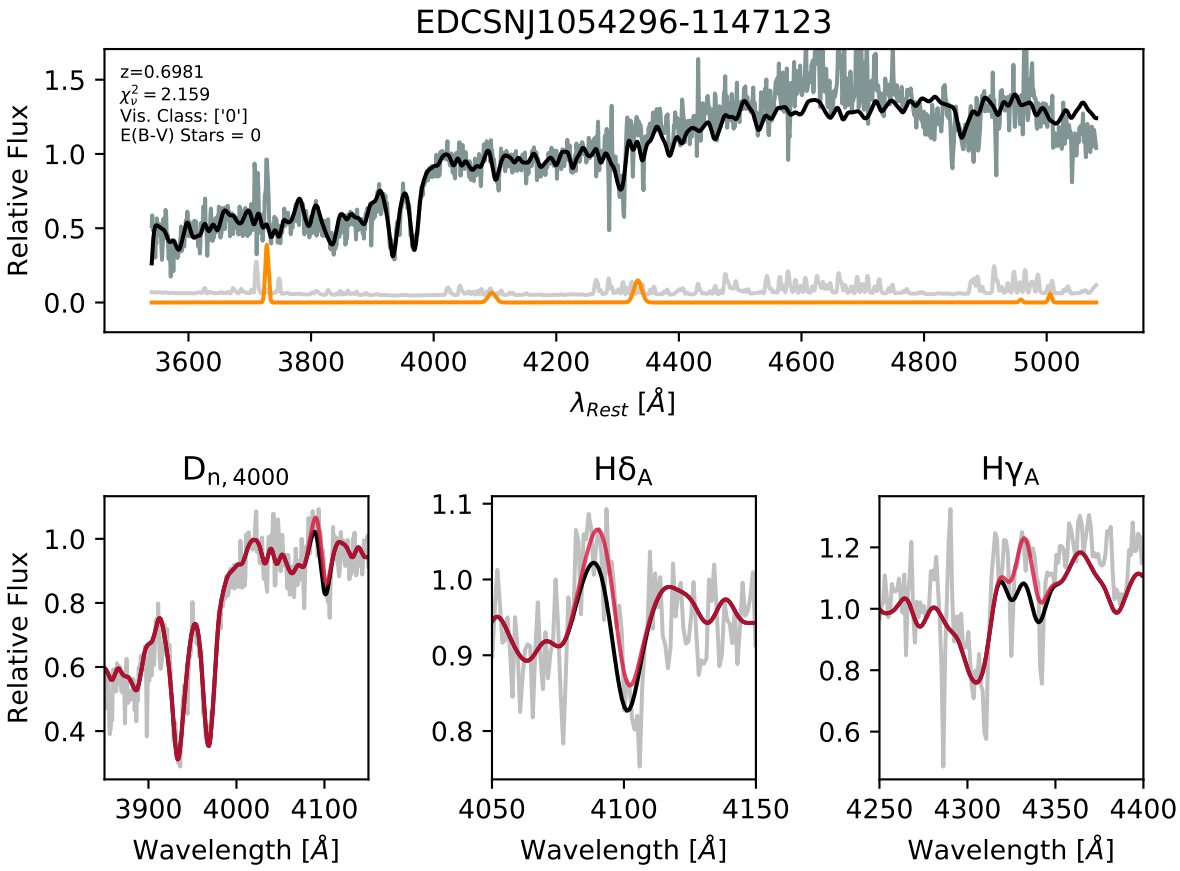
EDCSNJ1054296-1147123
z=0.6981
$\chi^2_\nu = 2.159$
Vis. Class: ['0']
E(B-V) Stars = 0
Relative Flux
λ_{Rest} [Å]
$D_{n,4000}$
$H\delta_A$
$H\gamma_A$
Wavelength [Å]

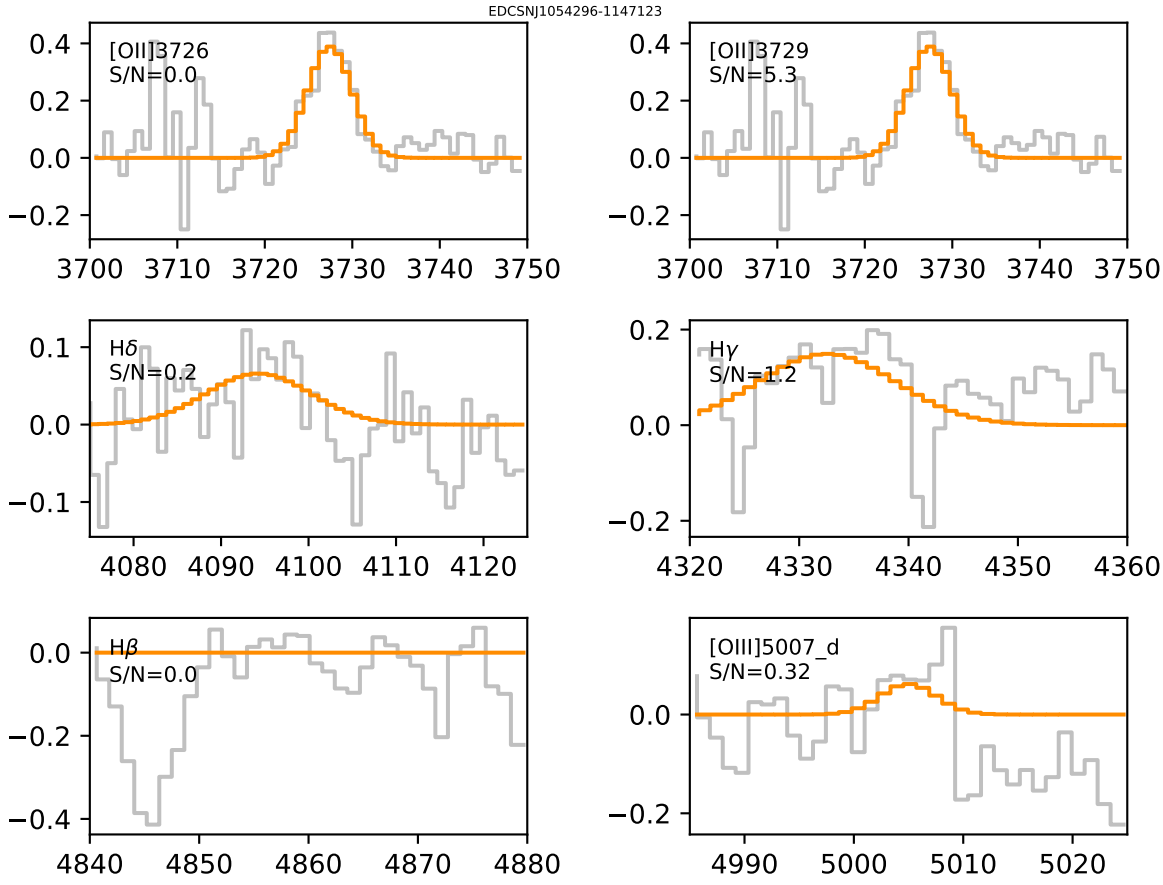
EDCSNJ1054296-1147123
[OII]3726
S/N=0.0
[OII]3729
S/N=5.3
Hδ
S/N=0.2
Hγ
S/N=1.2
Hβ
S/N=0.0
[OIII]5007_d
S/N=0.32

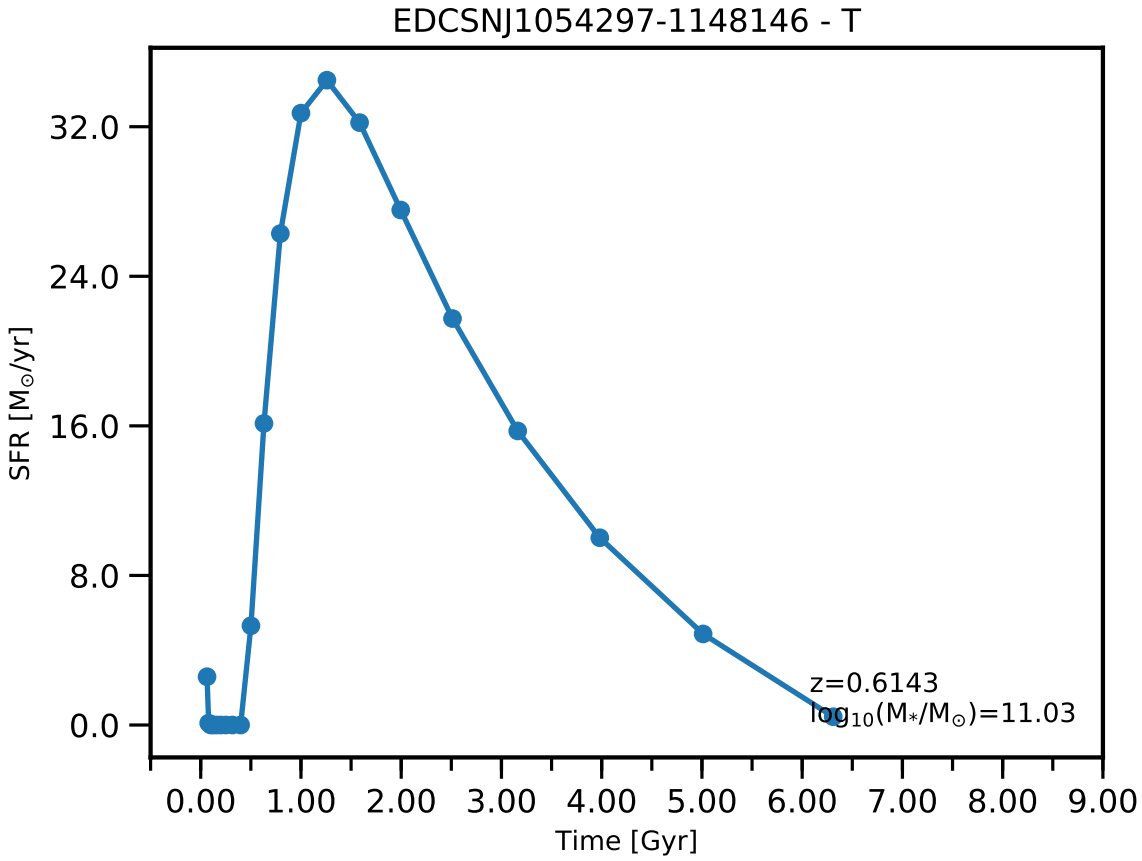
EDCSNJ1054297-1148146 - T
SFR [M⊙/yr]
32.0
24.0
16.0
8.0
0.0
0.00
1.00
2.00
3.00
4.00
5.00
6.00
7.00
8.00
9.00
Time [Gyr]
z=0.6143
log10(M*/M⊙)=11.03

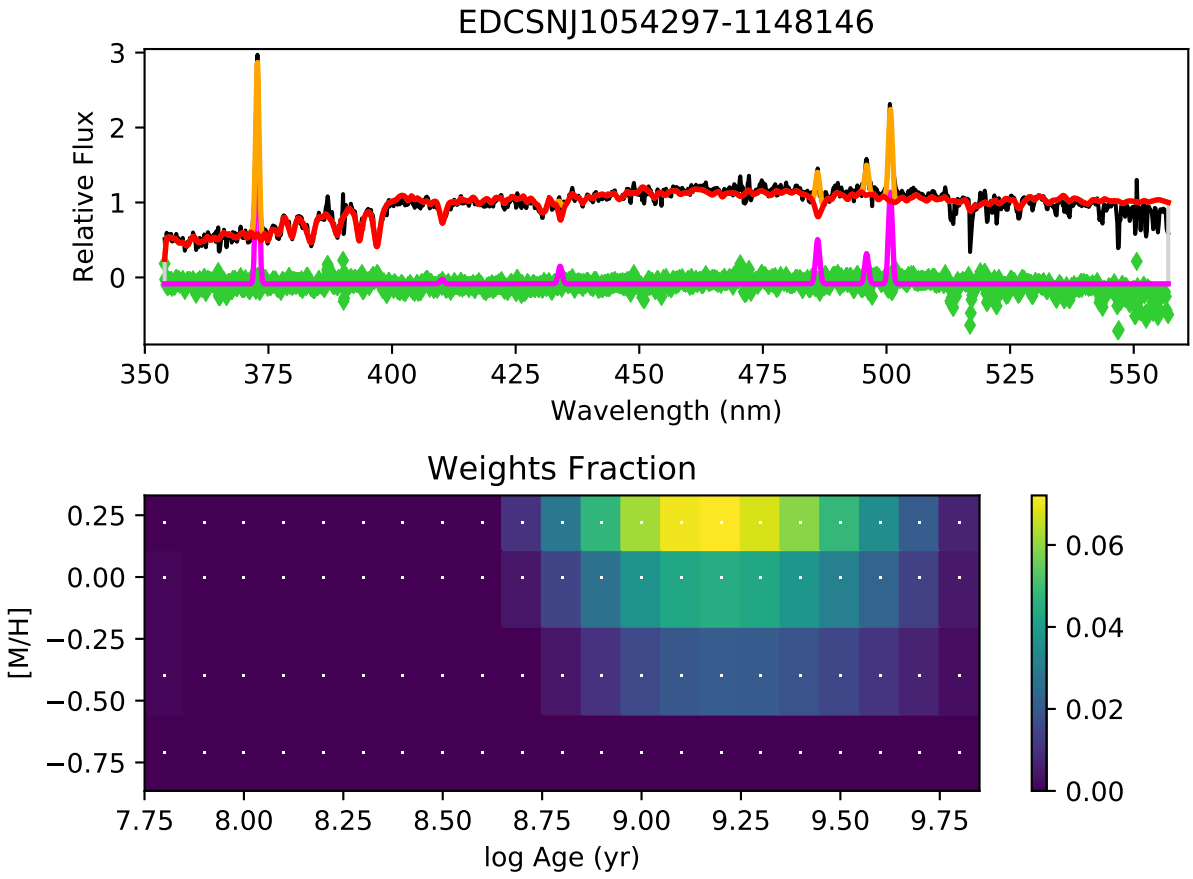
EDCSNJ1054297-1148146
Relative Flux
Wavelength (nm)
Weights Fraction
[M/H]
log Age (yr)

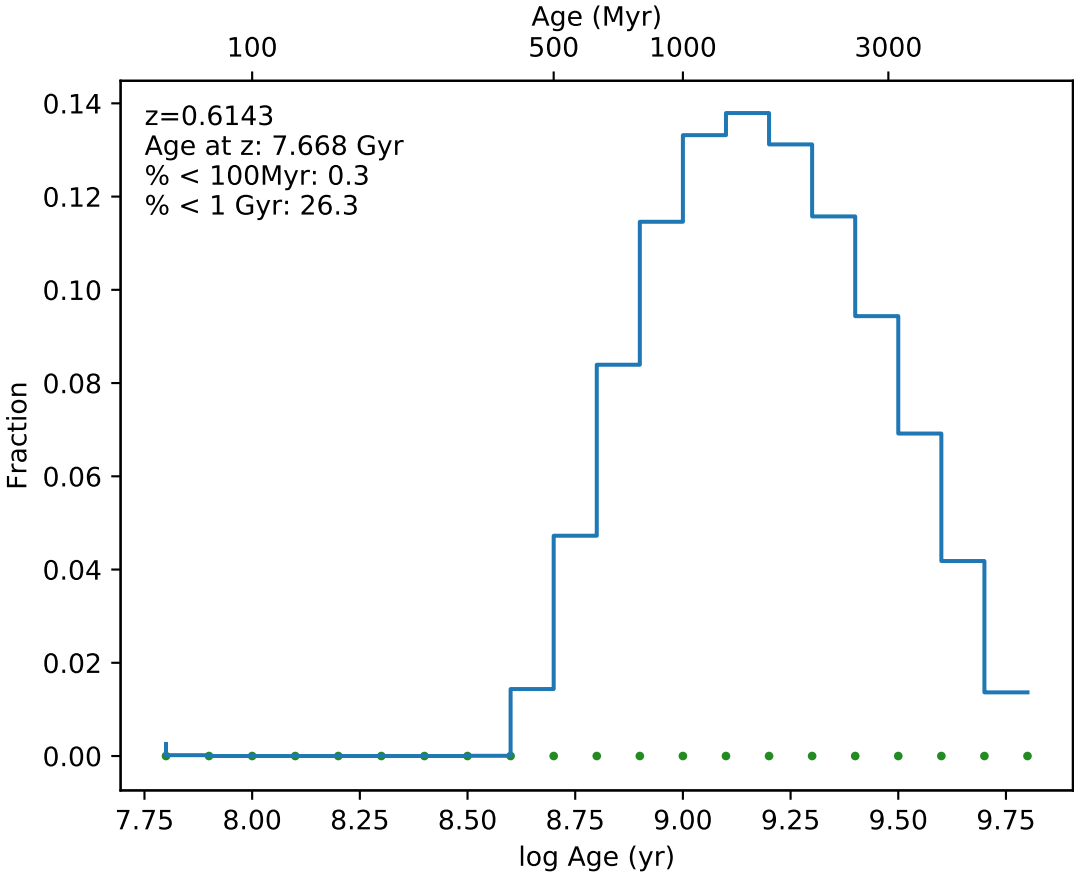
Age (Myr)
100
500
1000
3000
z=0.6143
Age at z: 7.668 Gyr
% < 100Myr: 0.3
% < 1 Gyr: 26.3
Fraction
0.14
0.12
0.10
0.08
0.06
0.04
0.02
0.00
7.75
8.00
8.25
8.50
8.75
9.00
9.25
9.50
9.75
log Age (yr)

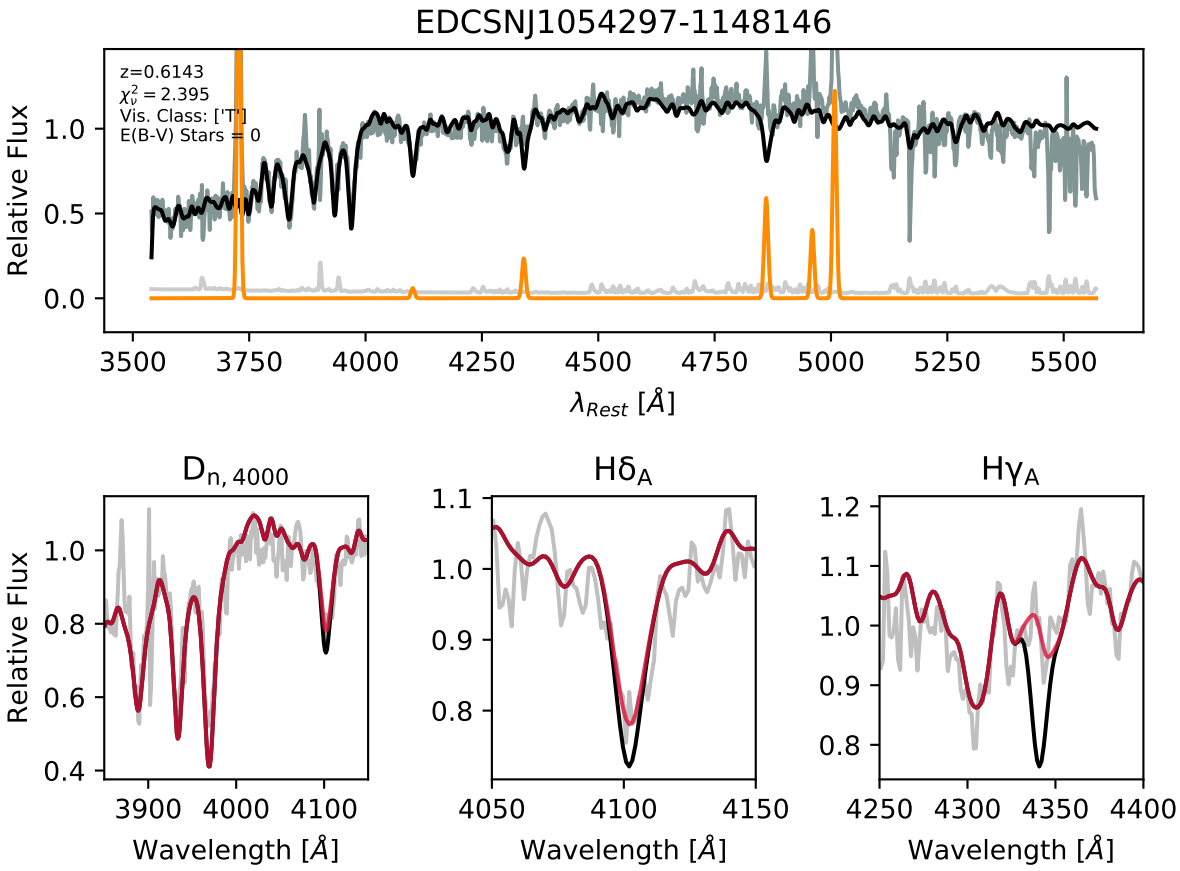
EDCSNJ1054297-1148146
z=0.6143
$\chi^2_\nu = 2.395$
Vis. Class: ['T']
E(B-V) Stars = 0
Relative Flux
λ_{Rest} [Å]
$D_{n,4000}$
$H\delta_A$
$H\gamma_A$
Wavelength [Å]

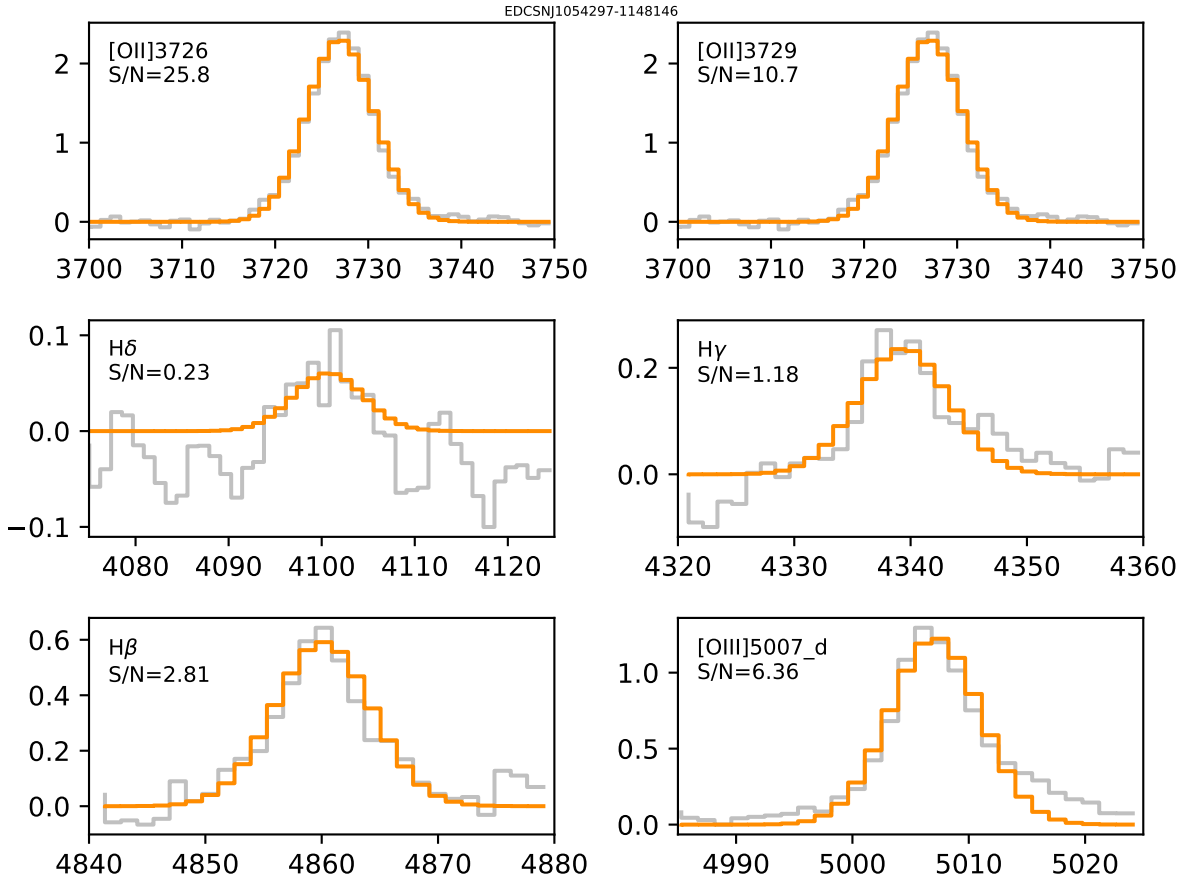
EDCSNJ1054297-1148146
[OII]3726
S/N=25.8
[OII]3729
S/N=10.7
Hδ
S/N=0.23
Hγ
S/N=1.18
Hβ
S/N=2.81
[OIII]5007_d
S/N=6.36

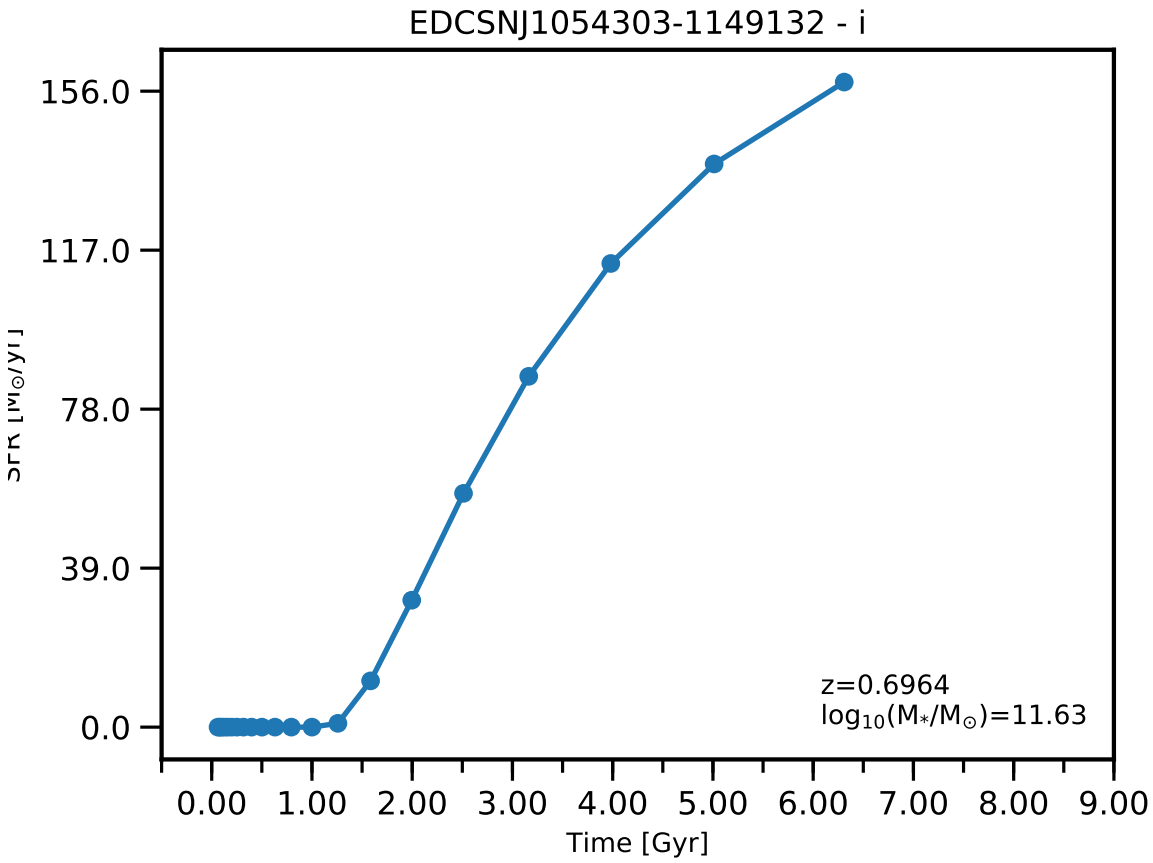
EDCSNJ1054303-1149132 - i
156.0
117.0
78.0
39.0
0.0
SFR [M⊙/yr]
0.00
1.00
2.00
3.00
4.00
5.00
6.00
7.00
8.00
9.00
Time [Gyr]
z=0.6964
log10(M*/M⊙)=11.63

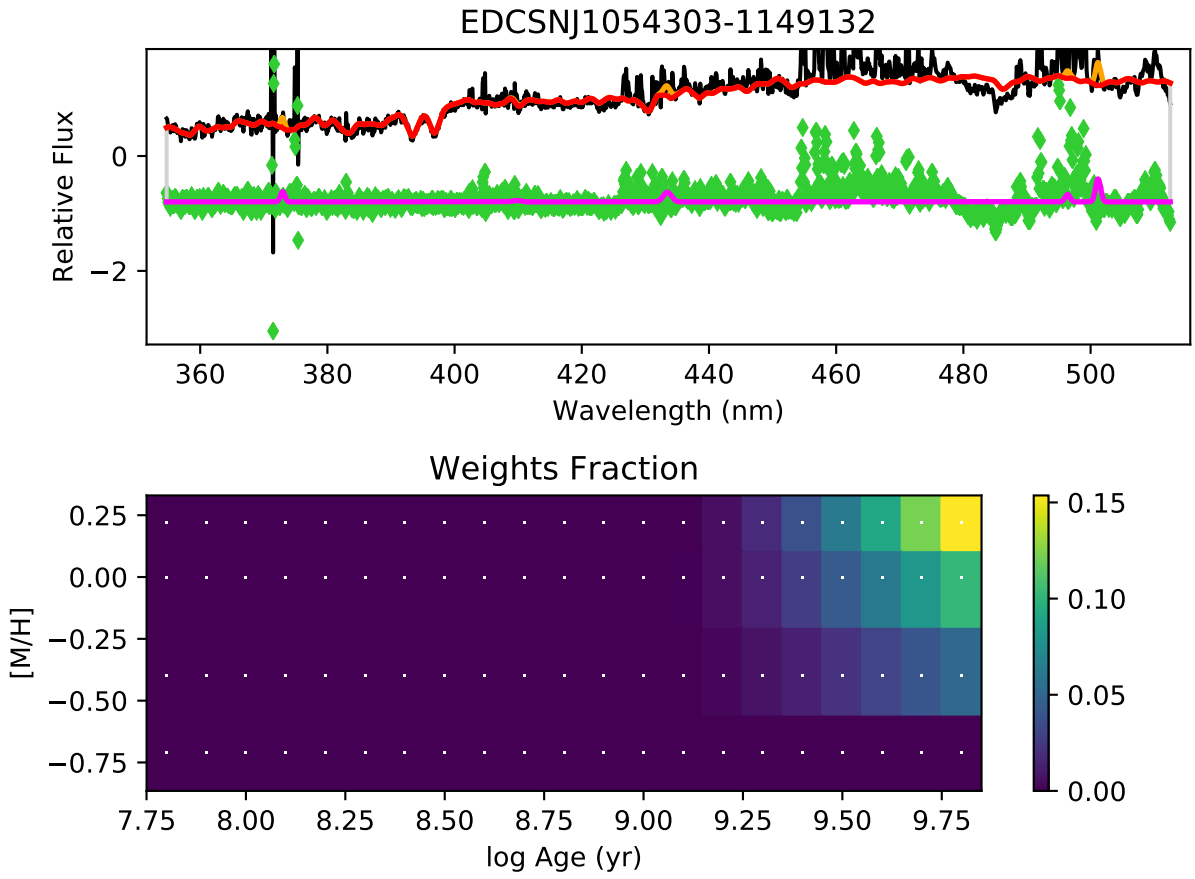
EDCSNJ1054303-1149132
Relative Flux
0
−2
360
380
400
420
440
460
480
500
Wavelength (nm)
Weights Fraction
[M/H]
0.25
0.00
−0.25
−0.50
−0.75
7.75
8.00
8.25
8.50
8.75
9.00
9.25
9.50
9.75
log Age (yr)
0.15
0.10
0.05
0.00

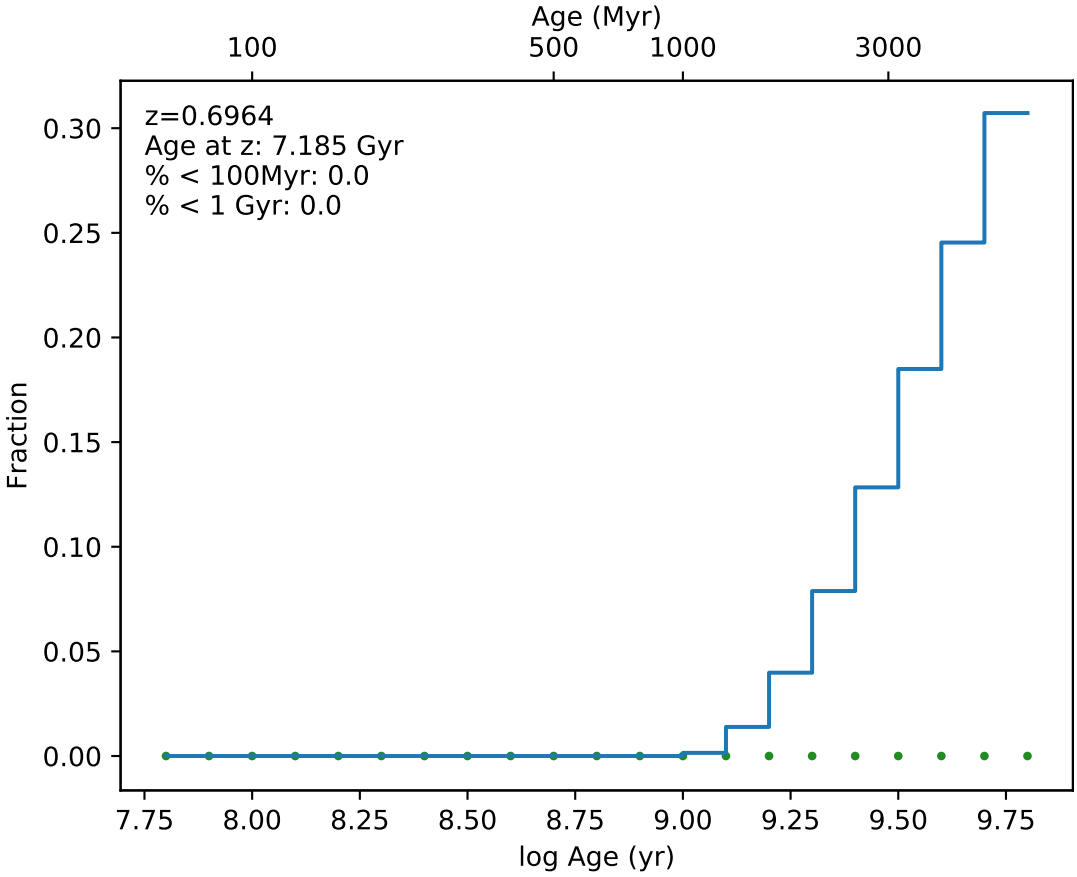
Age (Myr)
100
500
1000
3000
z=0.6964
Age at z: 7.185 Gyr
% < 100Myr: 0.0
% < 1 Gyr: 0.0
Fraction
0.30
0.25
0.20
0.15
0.10
0.05
0.00
7.75
8.00
8.25
8.50
8.75
9.00
9.25
9.50
9.75
log Age (yr)

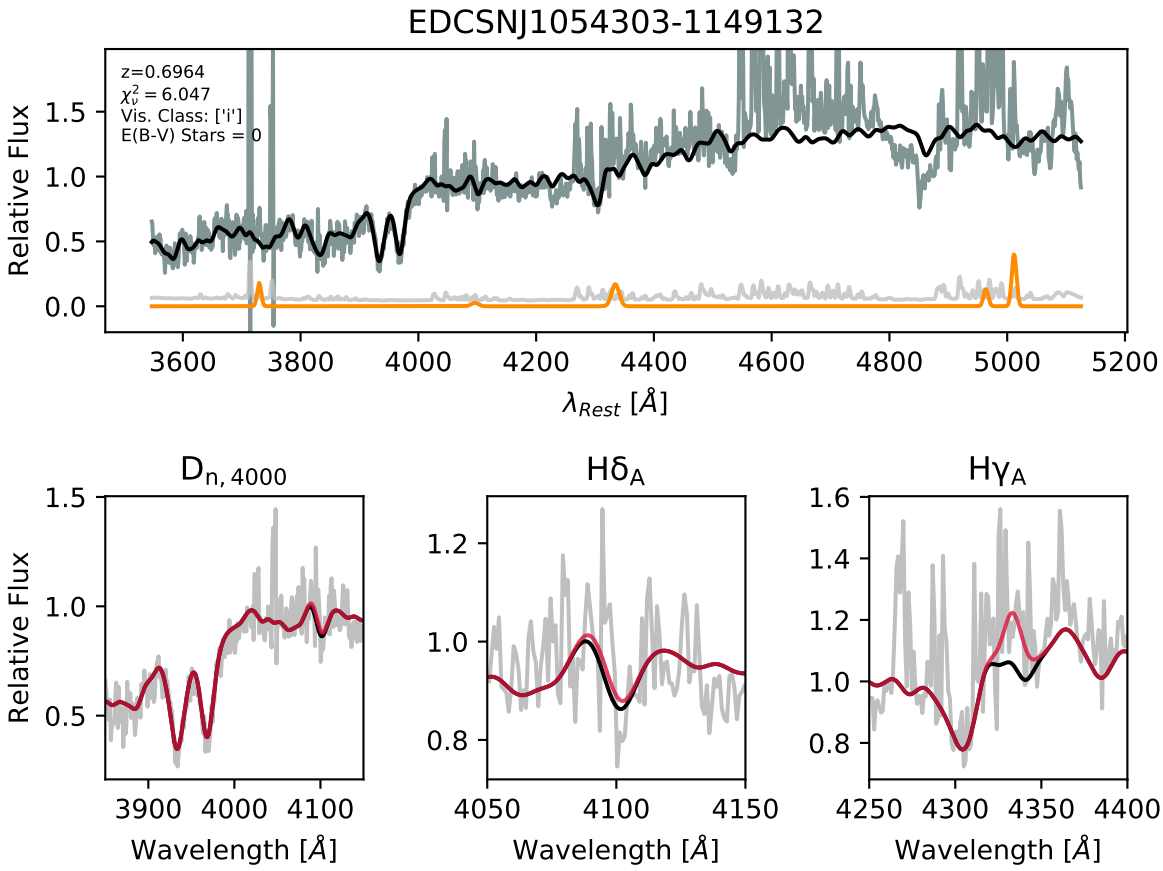
EDCSNJ1054303-1149132
z=0.6964
$\chi^2_\nu = 6.047$
Vis. Class: ['i']
E(B-V) Stars = 0
Relative Flux
λ_{Rest} [Å]
$D_{n,4000}$
$H\delta_A$
$H\gamma_A$
Wavelength [Å]

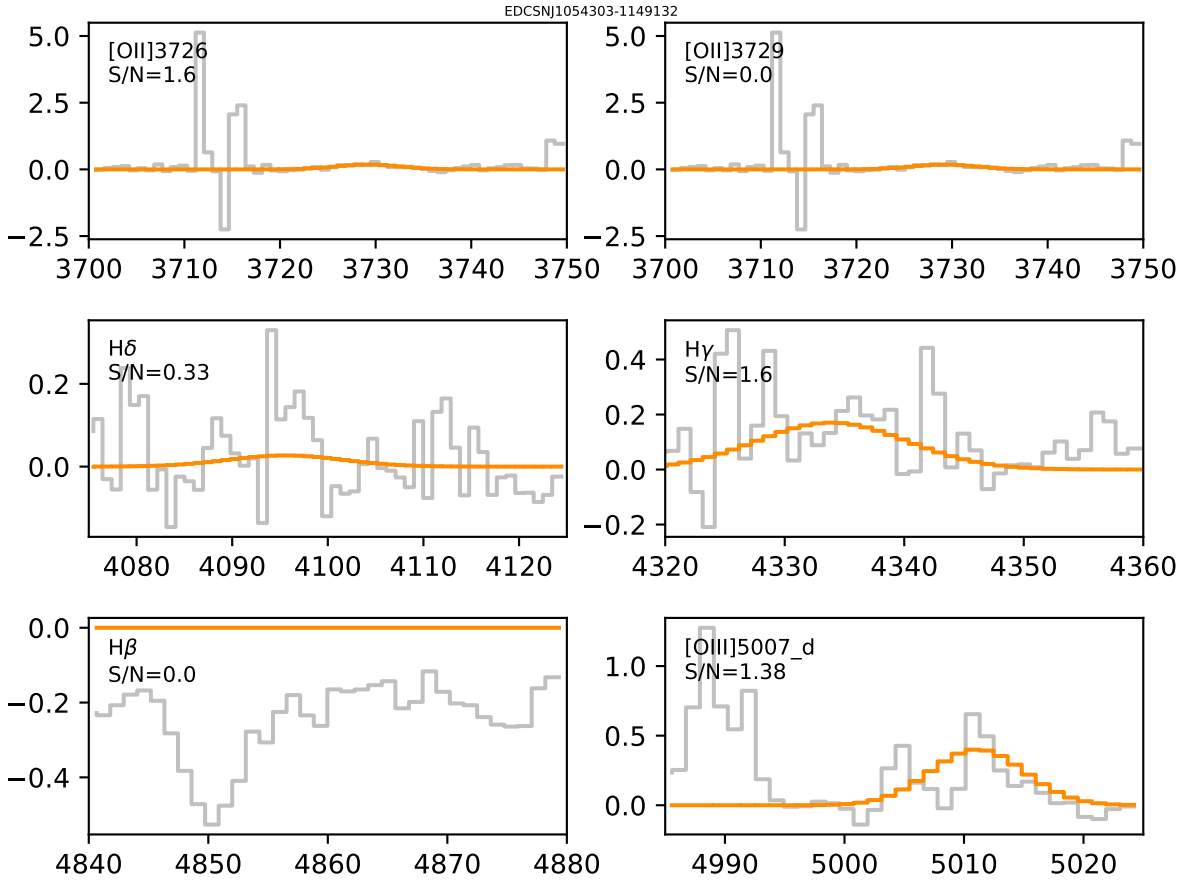
EDCSNJ1054303-1149132
[OII]3726
S/N=1.6
[OII]3729
S/N=0.0
Hδ
S/N=0.33
Hγ
S/N=1.6
Hβ
S/N=0.0
[OIII]5007_d
S/N=1.38

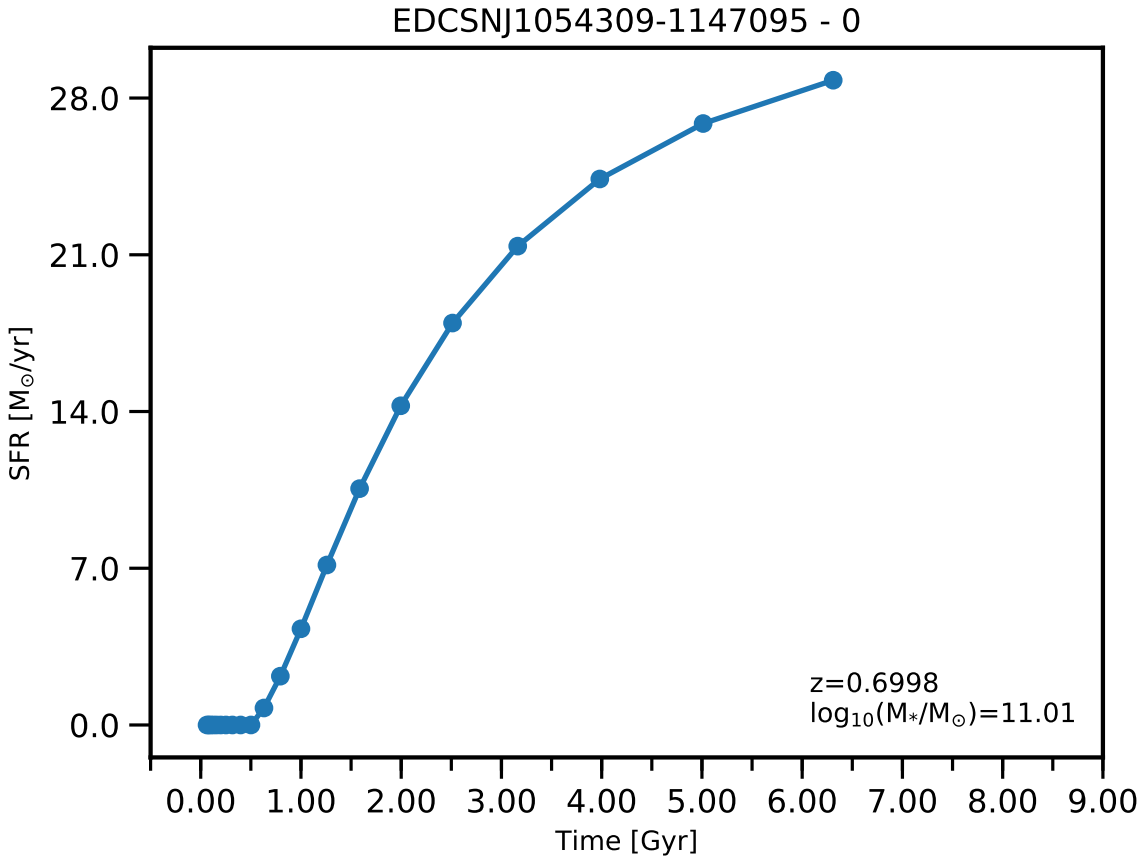
EDCSNJ1054309-1147095 - 0
28.0
21.0
14.0
7.0
0.0
SFR [M⊙/yr]
0.00
1.00
2.00
3.00
4.00
5.00
6.00
7.00
8.00
9.00
Time [Gyr]
z=0.6998
log10(M*/M⊙)=11.01

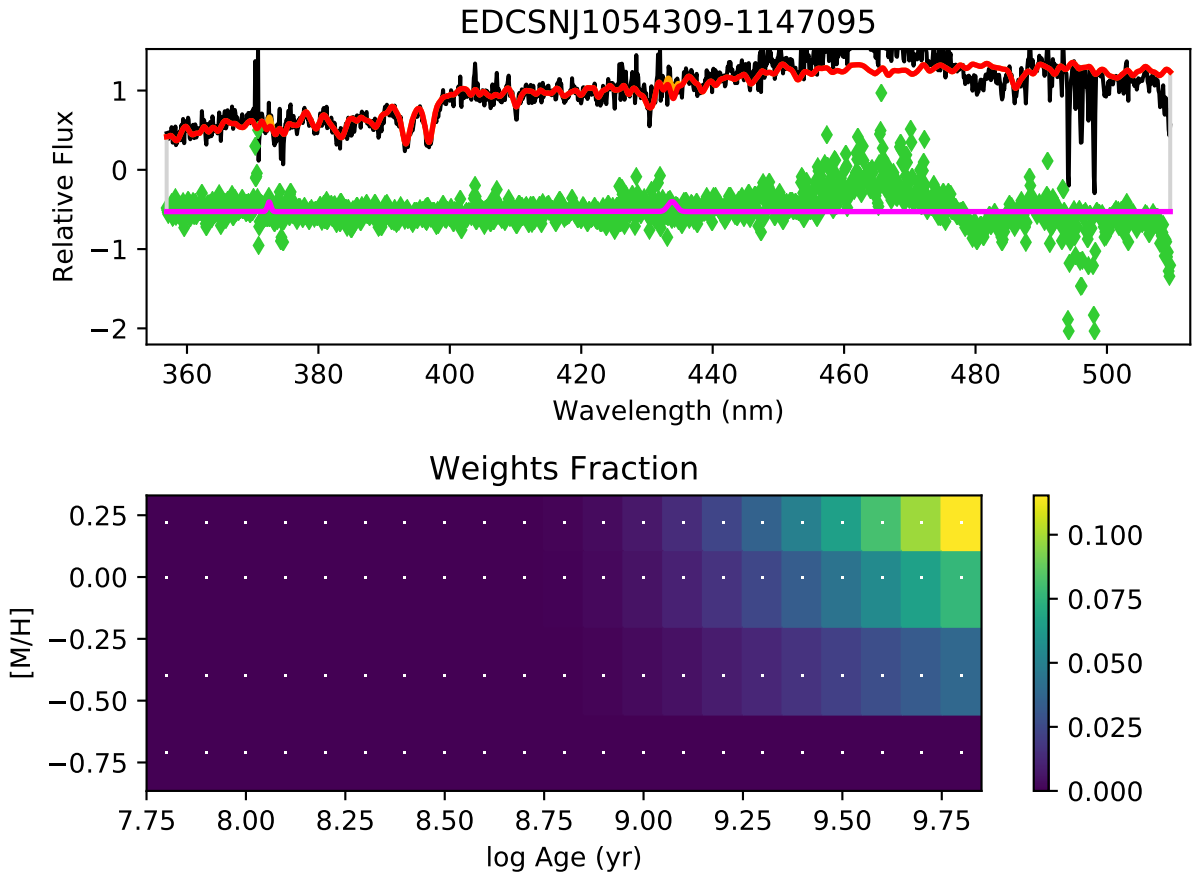
EDCSNJ1054309-1147095
Relative Flux
1
0
−1
−2
360
380
400
420
440
460
480
500
Wavelength (nm)
Weights Fraction
[M/H]
0.25
0.00
−0.25
−0.50
−0.75
7.75
8.00
8.25
8.50
8.75
9.00
9.25
9.50
9.75
log Age (yr)
0.100
0.075
0.050
0.025
0.000

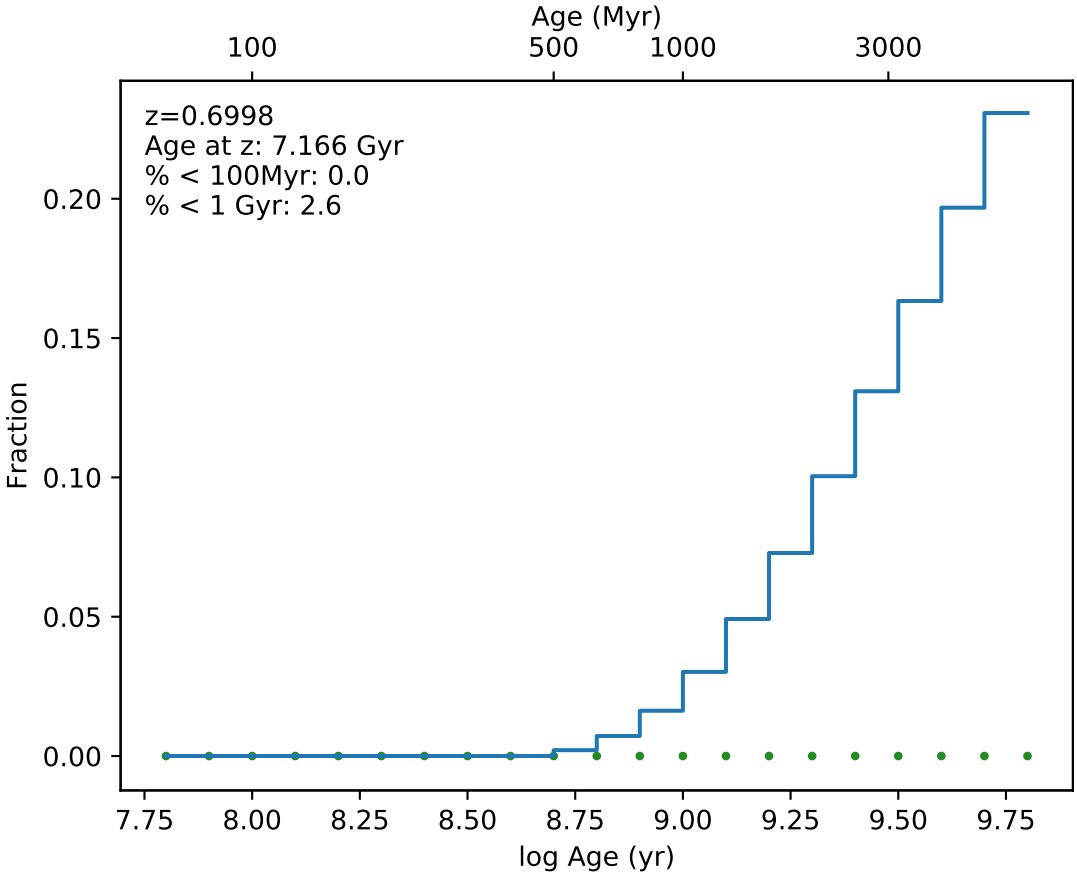
Age (Myr)
100
500
1000
3000
z=0.6998
Age at z: 7.166 Gyr
% < 100Myr: 0.0
% < 1 Gyr: 2.6
Fraction
0.00
0.05
0.10
0.15
0.20
7.75
8.00
8.25
8.50
8.75
9.00
9.25
9.50
9.75
log Age (yr)

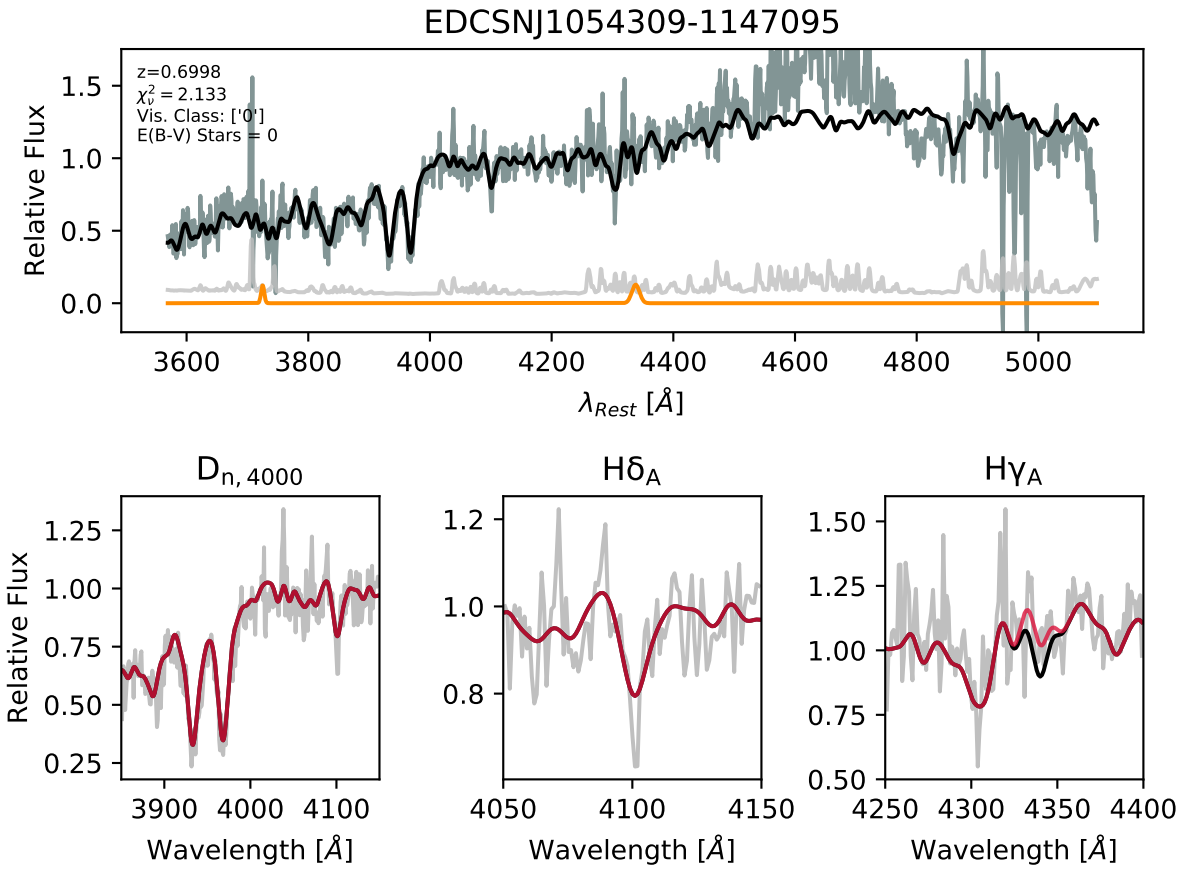
EDCSNJ1054309-1147095
z=0.6998
$\chi^2_\nu = 2.133$
Vis. Class: ['0']
E(B-V) Stars = 0
Relative Flux
λ_{Rest} [Å]
$D_{n,4000}$
$H\delta_A$
$H\gamma_A$
Relative Flux
Wavelength [Å]
Wavelength [Å]
Wavelength [Å]

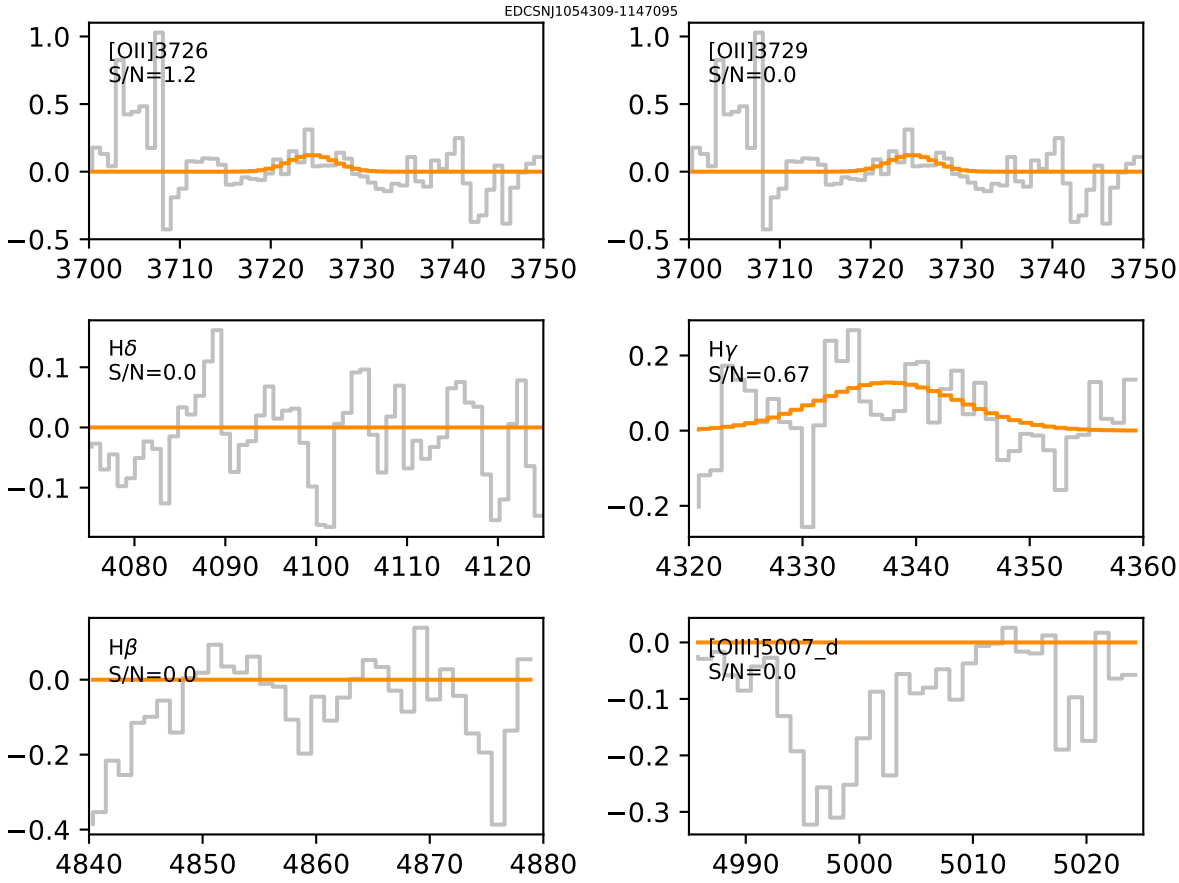
EDCSNJ1054309-1147095
[OII]3726
S/N=1.2
[OII]3729
S/N=0.0
Hδ
S/N=0.0
Hγ
S/N=0.67
Hβ
S/N=0.0
[OIII]5007_d
S/N=0.0

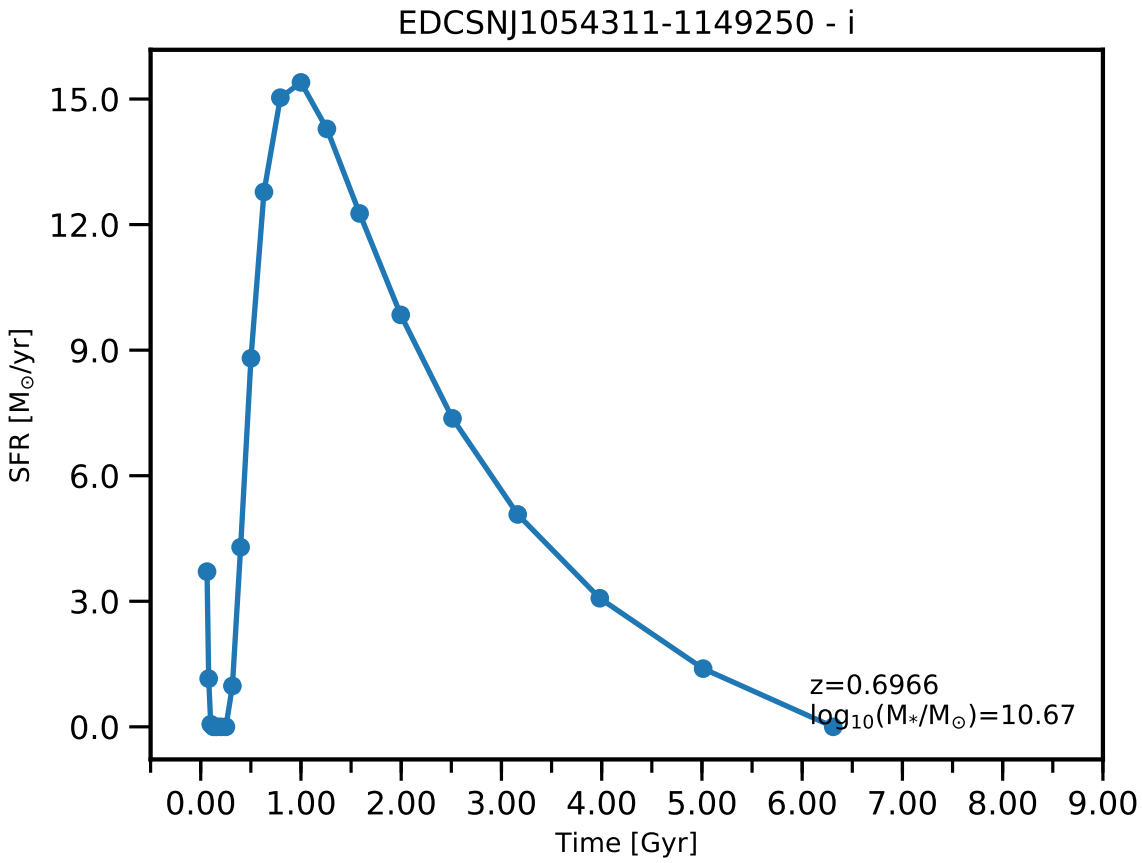
EDCSNJ1054311-1149250 - i
SFR [M⊙/yr]
15.0
12.0
9.0
6.0
3.0
0.0
0.00
1.00
2.00
3.00
4.00
5.00
6.00
7.00
8.00
9.00
Time [Gyr]
z=0.6966
log10(M*/M⊙)=10.67

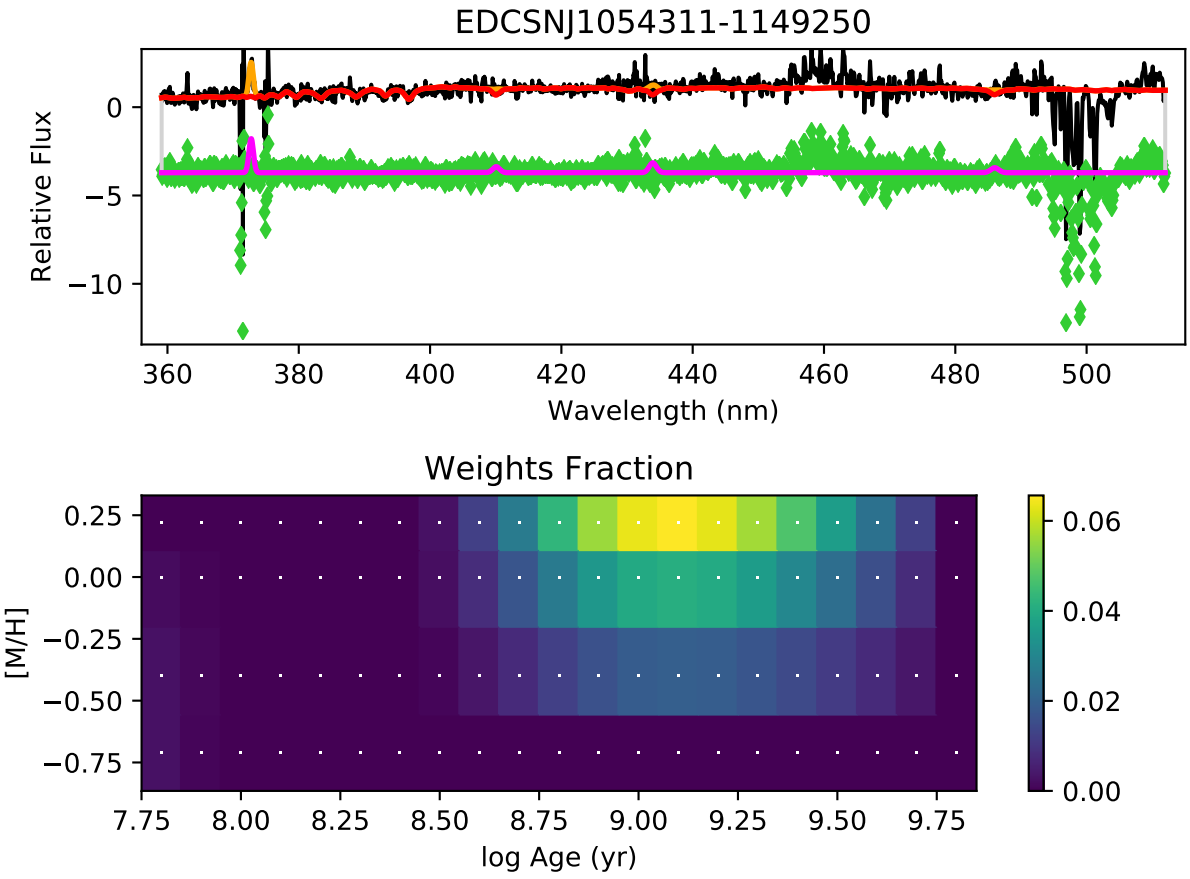
EDCSNJ1054311-1149250
Relative Flux
0
−5
−10
360
380
400
420
440
460
480
500
Wavelength (nm)
Weights Fraction
[M/H]
0.25
0.00
−0.25
−0.50
−0.75
7.75
8.00
8.25
8.50
8.75
9.00
9.25
9.50
9.75
log Age (yr)
0.06
0.04
0.02
0.00

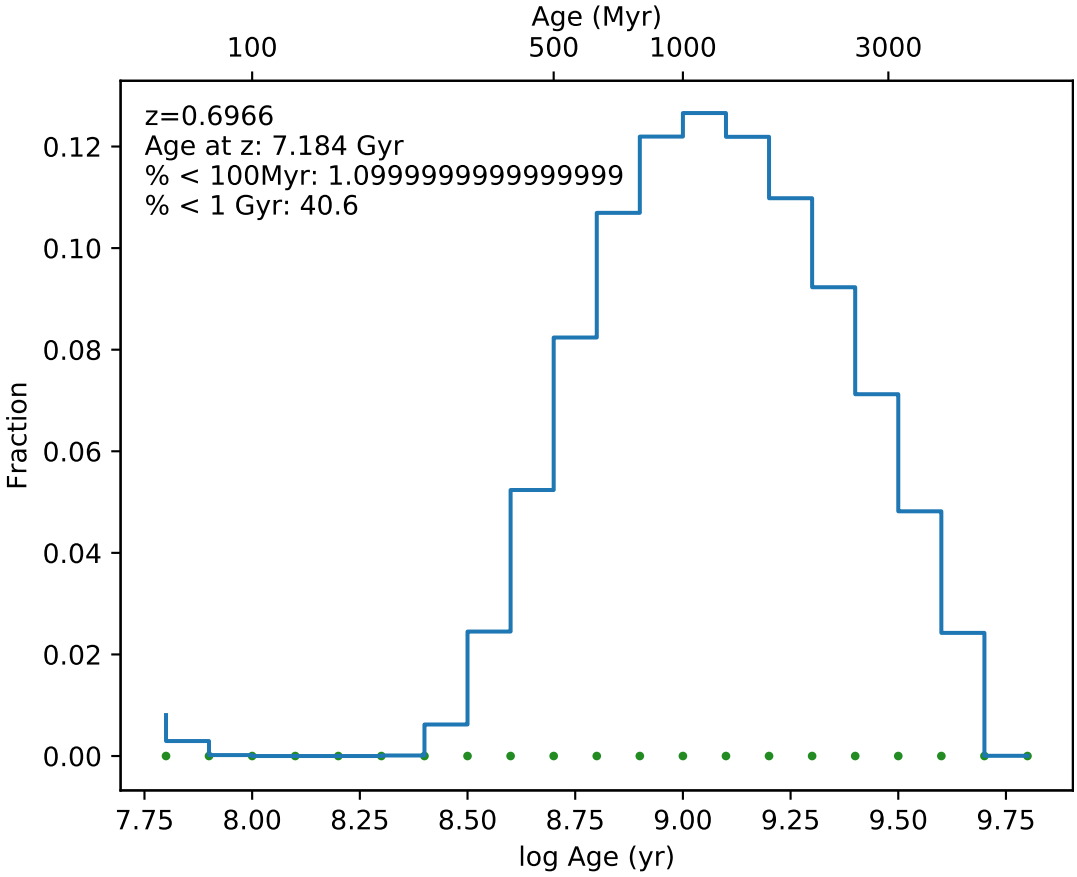
Age (Myr)
100
500
1000
3000
z=0.6966
Age at z: 7.184 Gyr
% < 100Myr: 1.0999999999999999
% < 1 Gyr: 40.6
Fraction
0.12
0.10
0.08
0.06
0.04
0.02
0.00
7.75
8.00
8.25
8.50
8.75
9.00
9.25
9.50
9.75
log Age (yr)

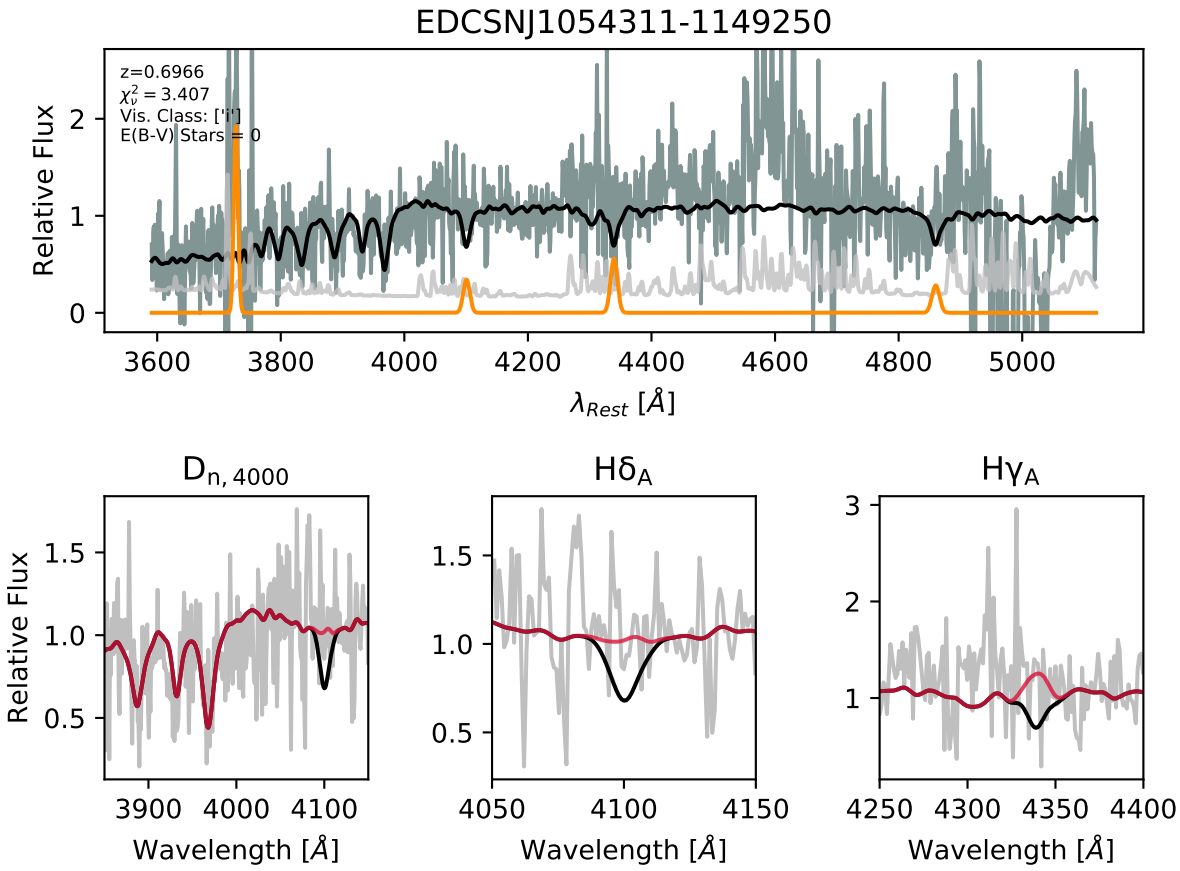
EDCSNJ1054311-1149250
z=0.6966
$\chi^2_\nu = 3.407$
Vis. Class: ['i']
E(B-V) Stars = 0
Relative Flux
λ_{Rest} [Å]
$D_{n,4000}$
$H\delta_A$
$H\gamma_A$
Wavelength [Å]

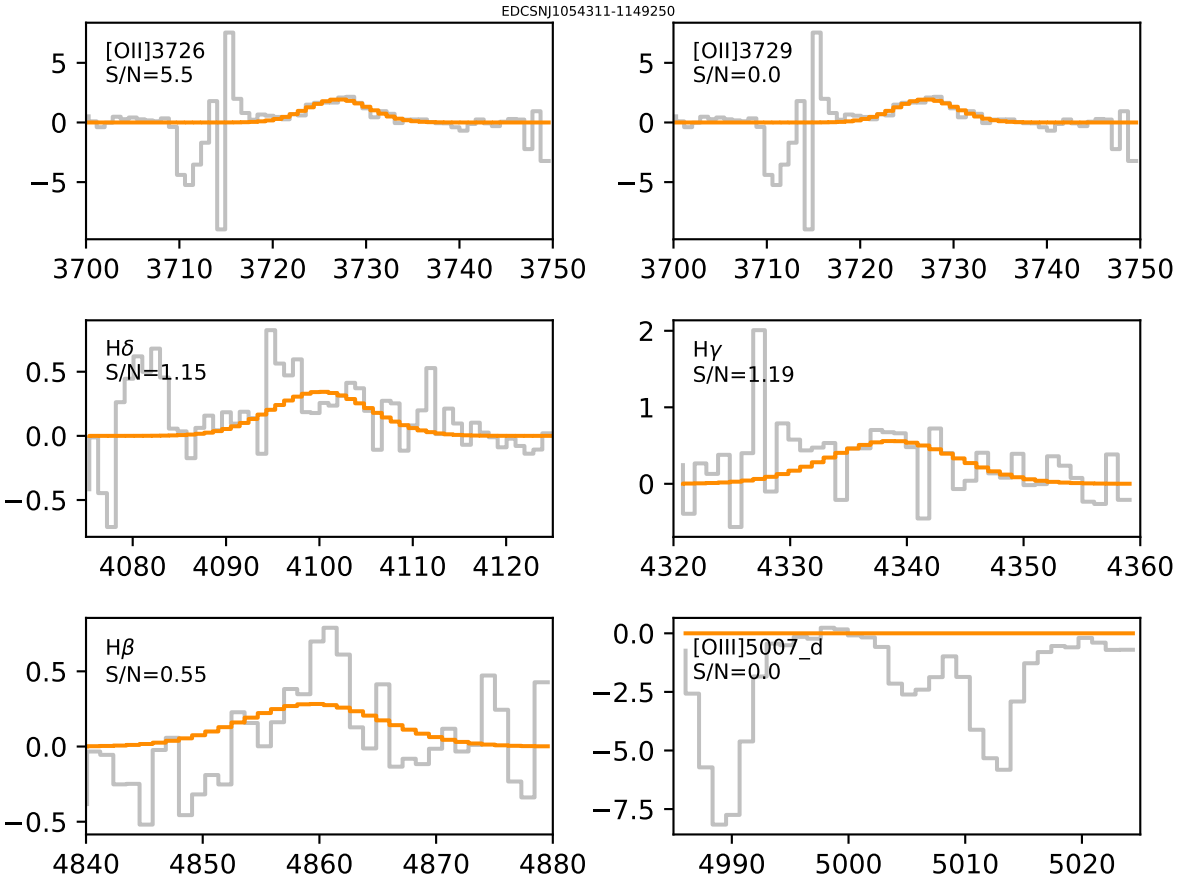
EDCSNJ1054311-1149250
[OII]3726
S/N=5.5
[OII]3729
S/N=0.0
Hδ
S/N=1.15
Hγ
S/N=1.19
Hβ
S/N=0.55
[OIII]5007_d
S/N=0.0

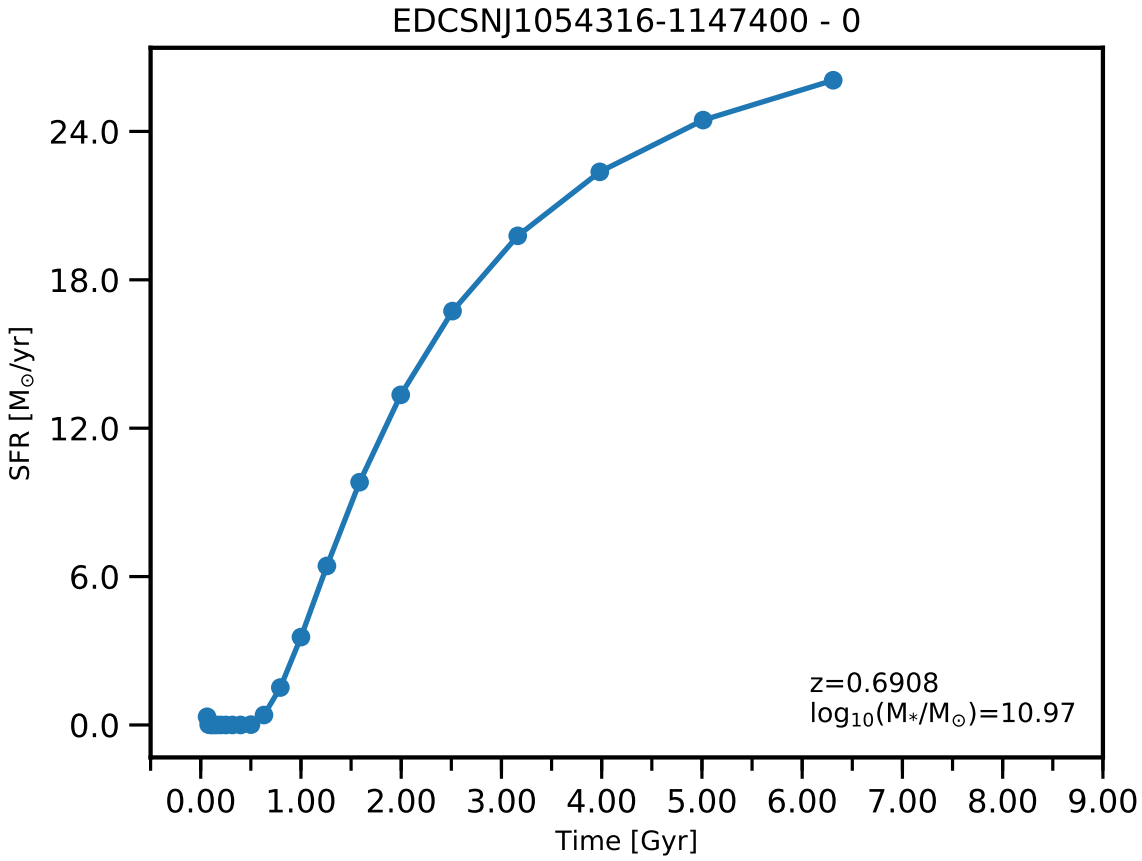
EDCSNJ1054316-1147400 - 0
SFR [M⊙/yr]
24.0
18.0
12.0
6.0
0.0
0.00
1.00
2.00
3.00
4.00
5.00
6.00
7.00
8.00
9.00
Time [Gyr]
z=0.6908
log10(M*/M⊙)=10.97

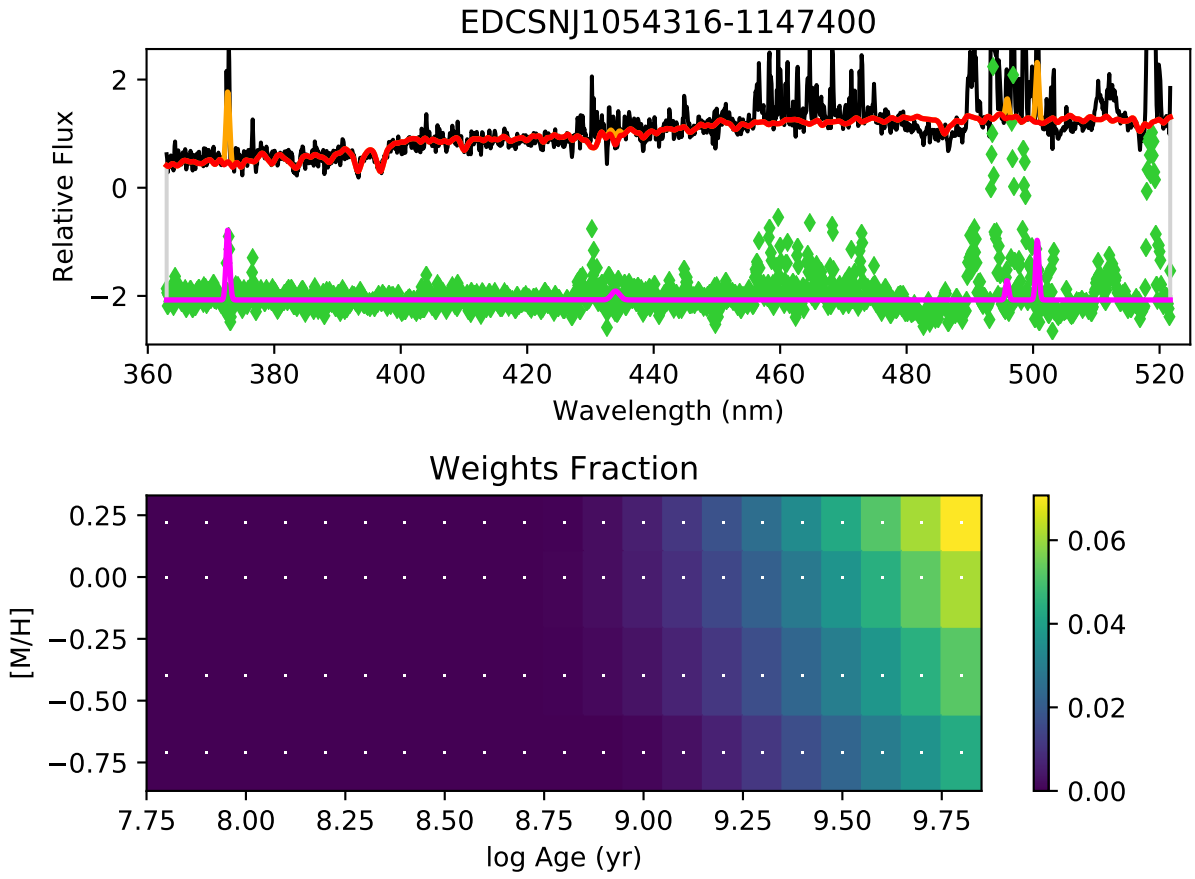
EDCSNJ1054316-1147400
Relative Flux
2
0
−2
360
380
400
420
440
460
480
500
520
Wavelength (nm)
Weights Fraction
[M/H]
0.25
0.00
−0.25
−0.50
−0.75
7.75
8.00
8.25
8.50
8.75
9.00
9.25
9.50
9.75
log Age (yr)
0.06
0.04
0.02
0.00

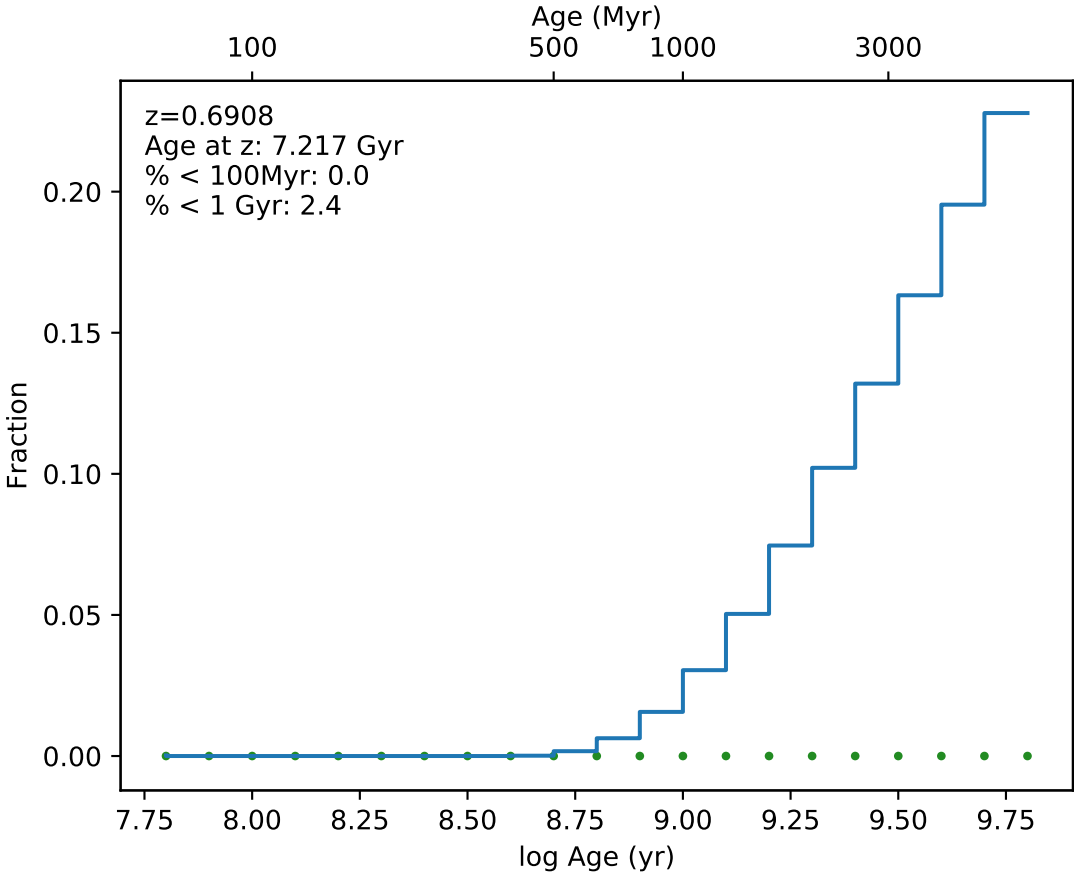
Age (Myr)
100
500
1000
3000
z=0.6908
Age at z: 7.217 Gyr
% < 100Myr: 0.0
% < 1 Gyr: 2.4
Fraction
0.00
0.05
0.10
0.15
0.20
7.75
8.00
8.25
8.50
8.75
9.00
9.25
9.50
9.75
log Age (yr)

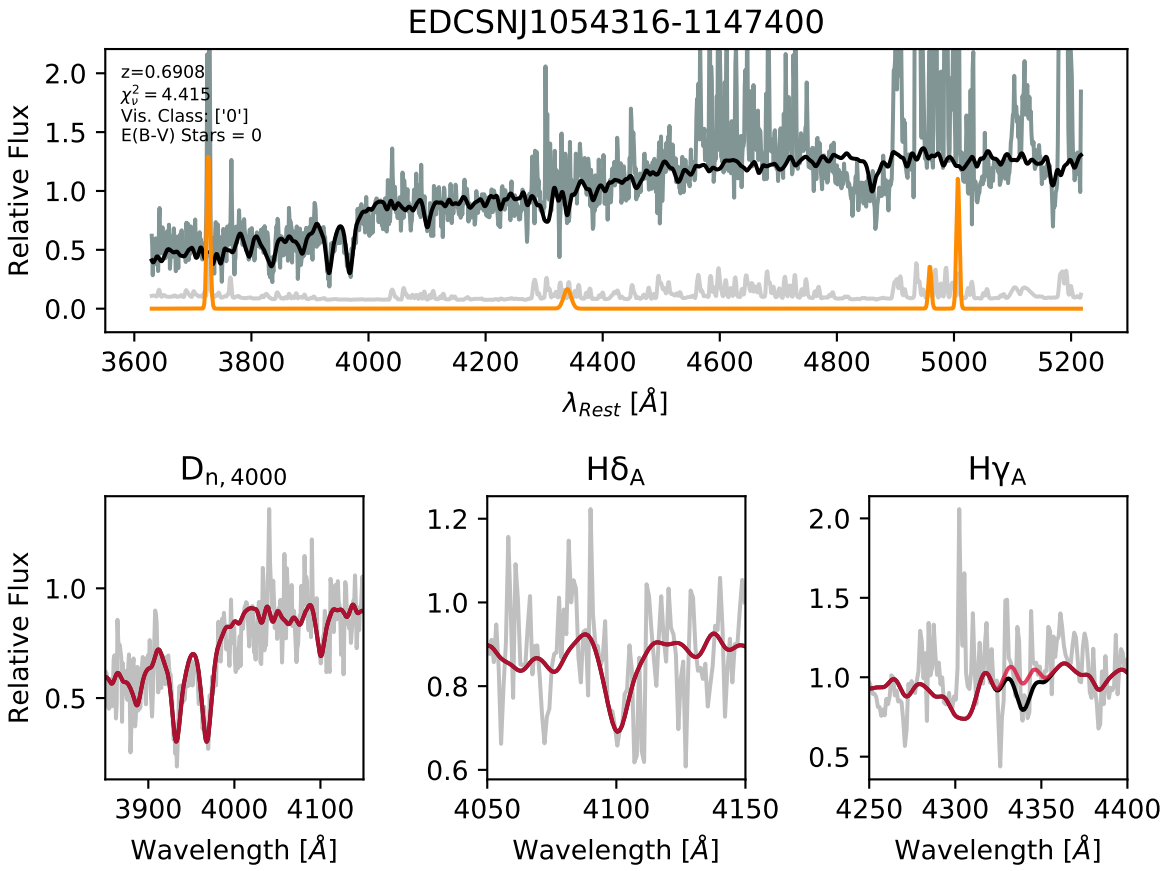
EDCSNJ1054316-1147400
z=0.6908
$\chi^2_\nu = 4.415$
Vis. Class: ['0']
E(B-V) Stars = 0
Relative Flux
λ_{Rest} [Å]
$D_{n,4000}$
$H\delta_A$
$H\gamma_A$
Wavelength [Å]

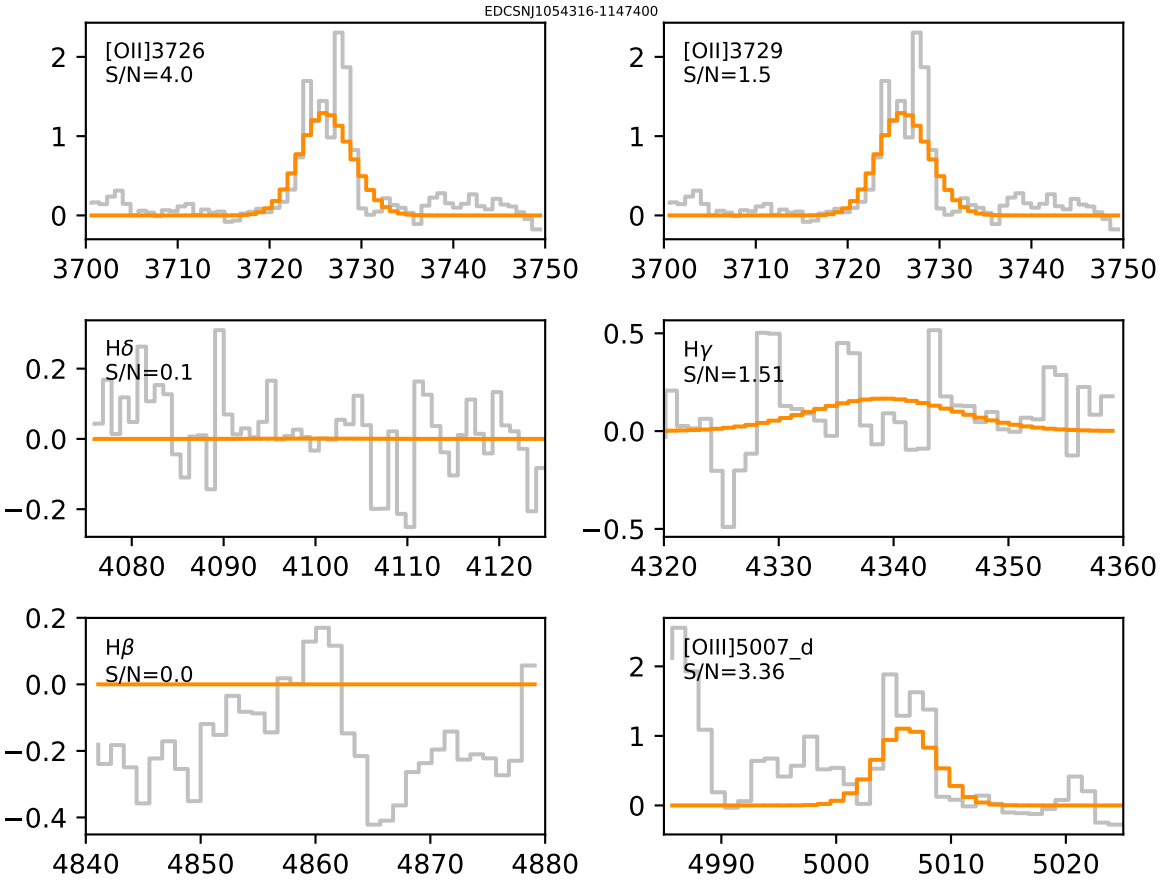
EDCSNJ1054316-1147400
[OII]3726
S/N=4.0
[OII]3729
S/N=1.5
Hδ
S/N=0.1
Hγ
S/N=1.51
Hβ
S/N=0.0
[OIII]5007_d
S/N=3.36

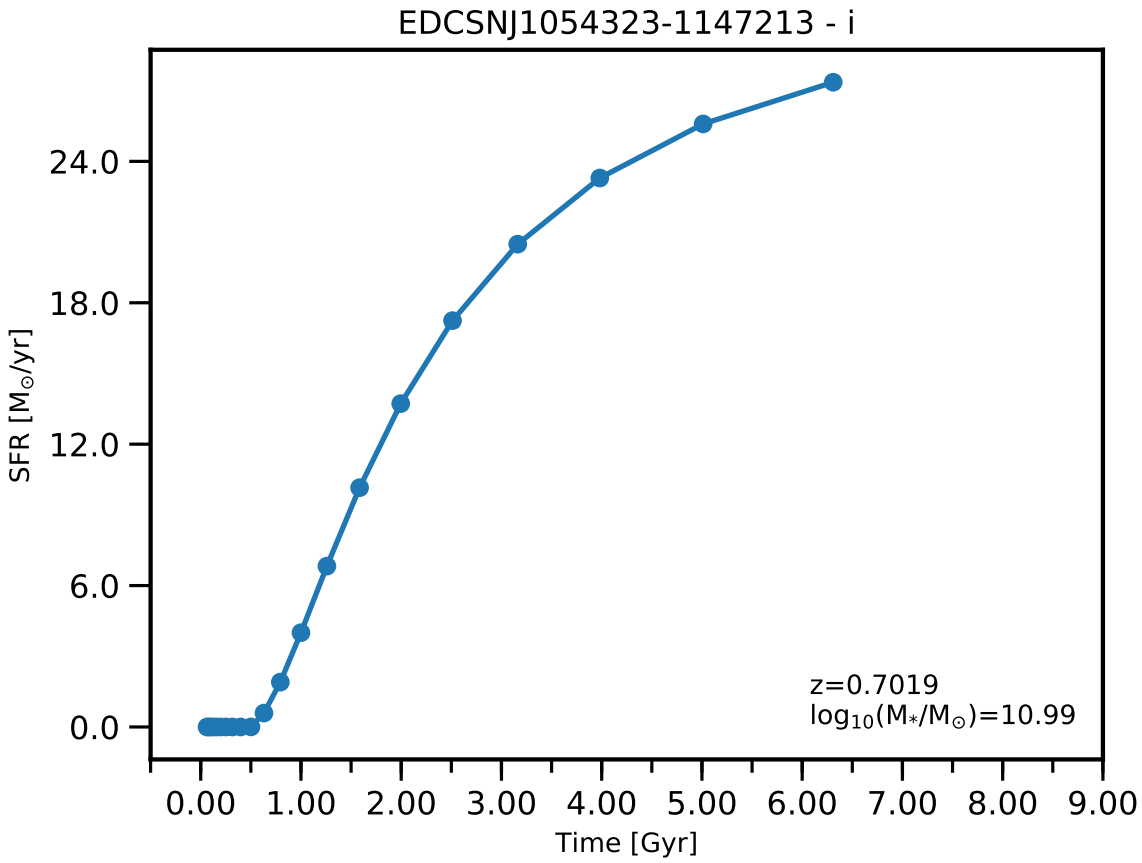
EDCSNJ1054323-1147213 - i
SFR [M⊙/yr]
24.0
18.0
12.0
6.0
0.0
0.00
1.00
2.00
3.00
4.00
5.00
6.00
7.00
8.00
9.00
Time [Gyr]
z=0.7019
log10(M*/M⊙)=10.99

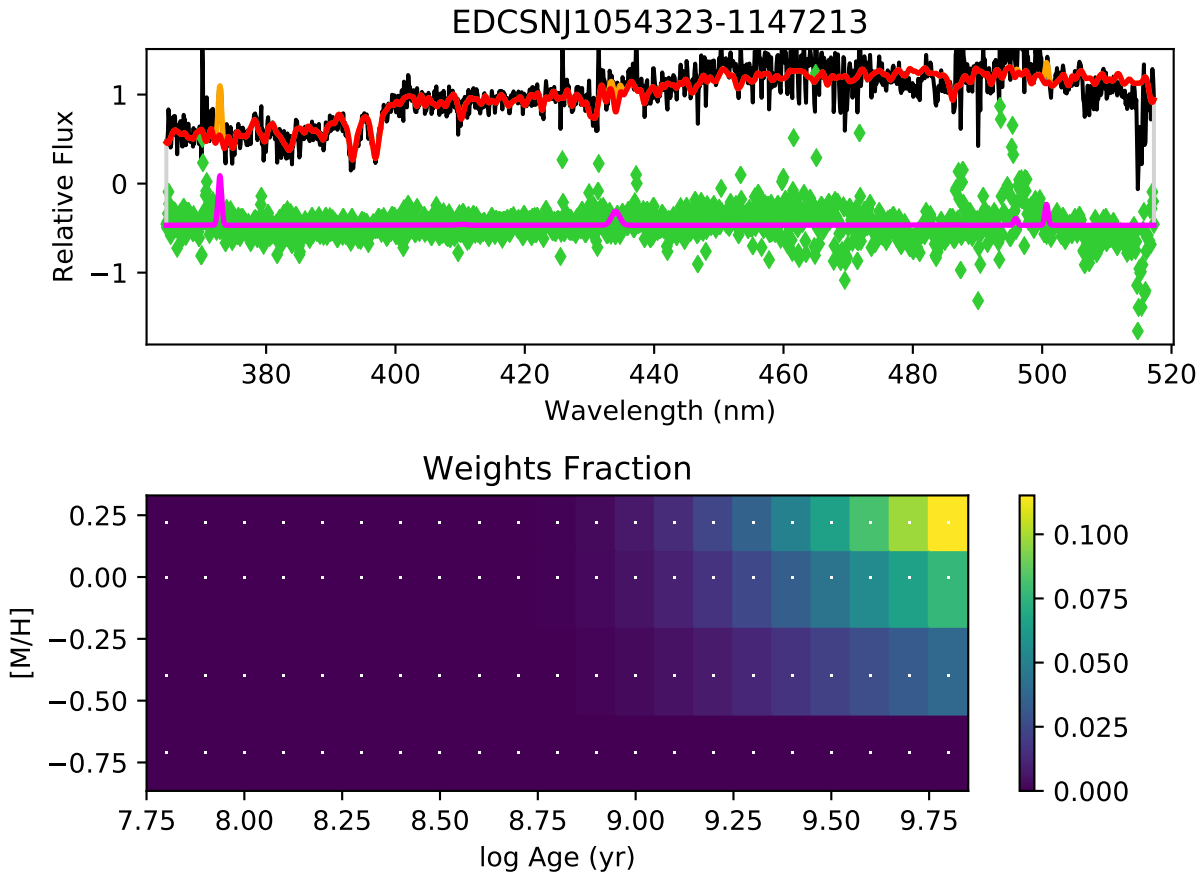
EDCSNJ1054323-1147213
Relative Flux
1
0
−1
380
400
420
440
460
480
500
520
Wavelength (nm)
Weights Fraction
[M/H]
0.25
0.00
−0.25
−0.50
−0.75
7.75
8.00
8.25
8.50
8.75
9.00
9.25
9.50
9.75
log Age (yr)
0.100
0.075
0.050
0.025
0.000

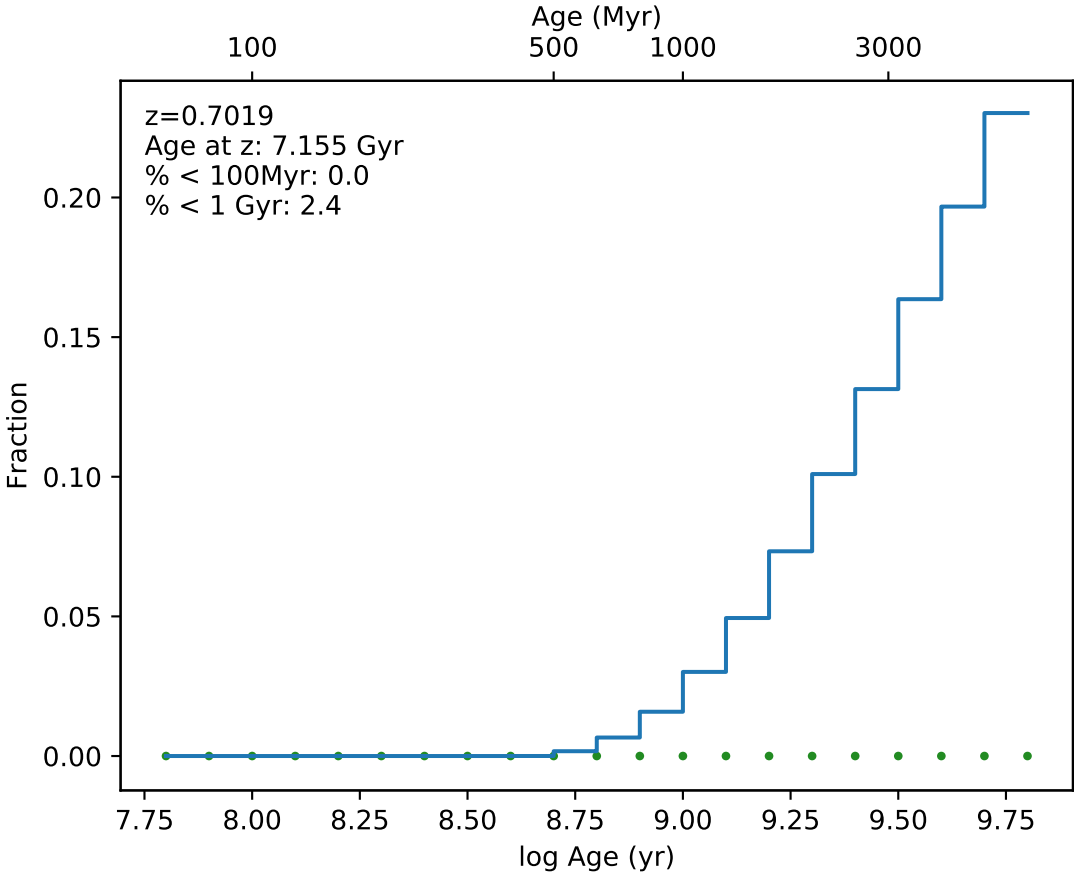
Age (Myr)
100
500
1000
3000
z=0.7019
Age at z: 7.155 Gyr
% < 100Myr: 0.0
% < 1 Gyr: 2.4
Fraction
0.20
0.15
0.10
0.05
0.00
7.75
8.00
8.25
8.50
8.75
9.00
9.25
9.50
9.75
log Age (yr)

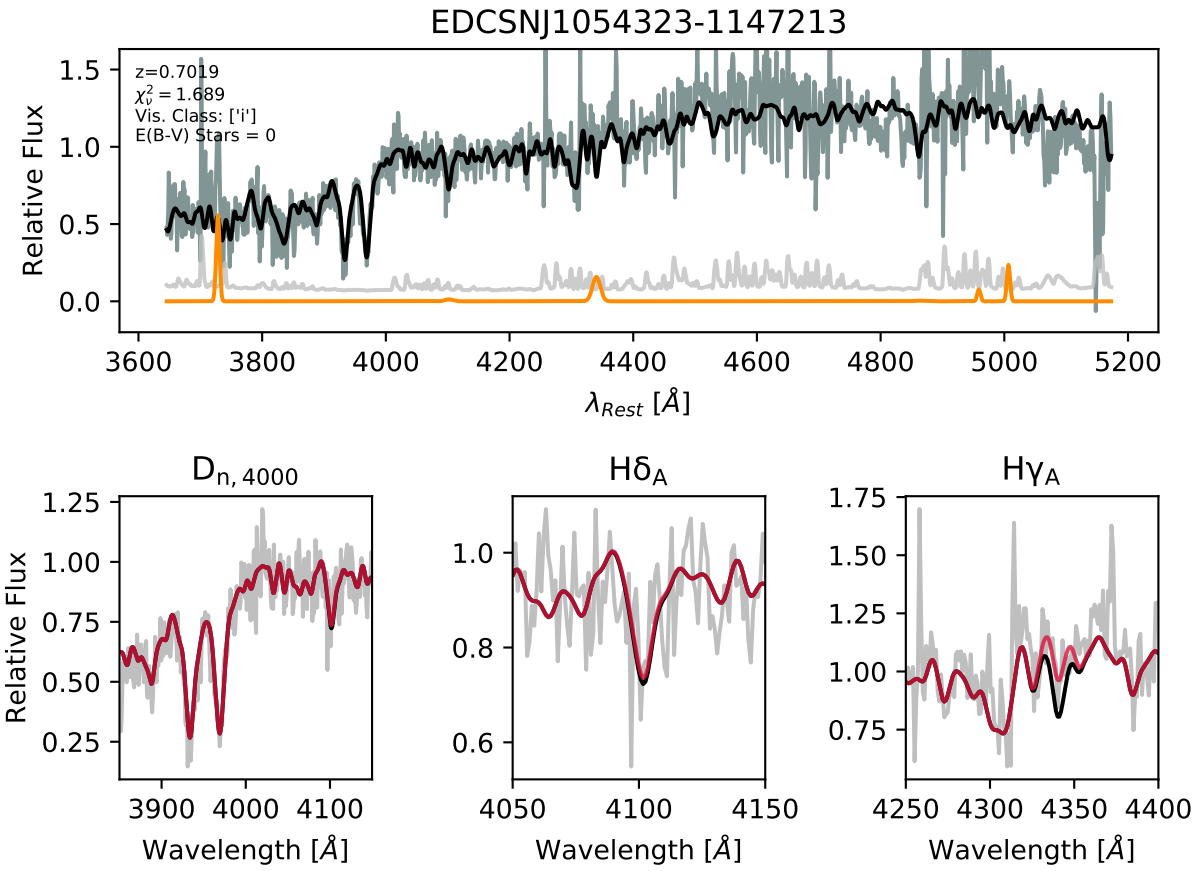
EDCSNJ1054323-1147213
z=0.7019
$\chi^2_\nu = 1.689$
Vis. Class: ['i']
E(B-V) Stars = 0
Relative Flux
λ_{Rest} [Å]
$D_{n,4000}$
$H\delta_A$
$H\gamma_A$
Wavelength [Å]

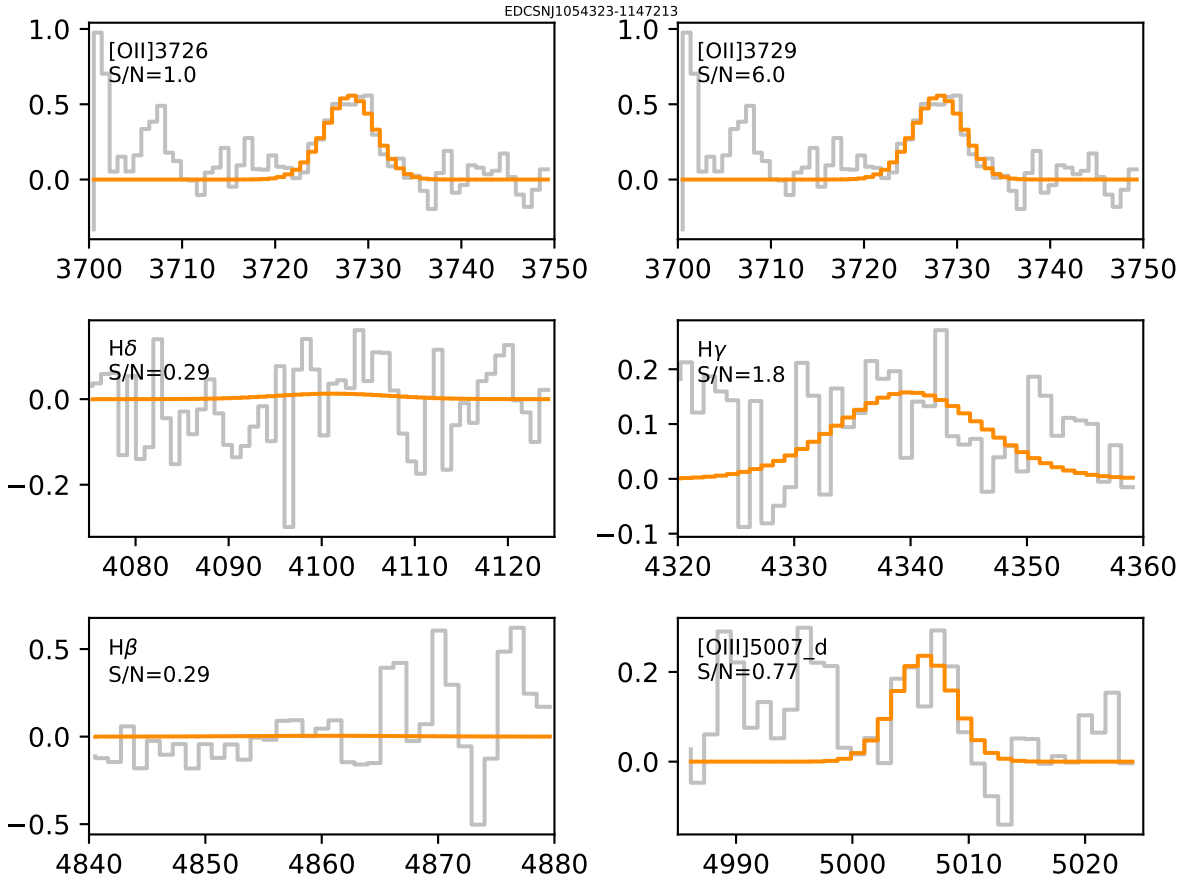
EDCSNJ1054323-1147213
[OII]3726
S/N=1.0
[OII]3729
S/N=6.0
Hδ
S/N=0.29
Hγ
S/N=1.8
Hβ
S/N=0.29
[OIII]5007_d
S/N=0.77

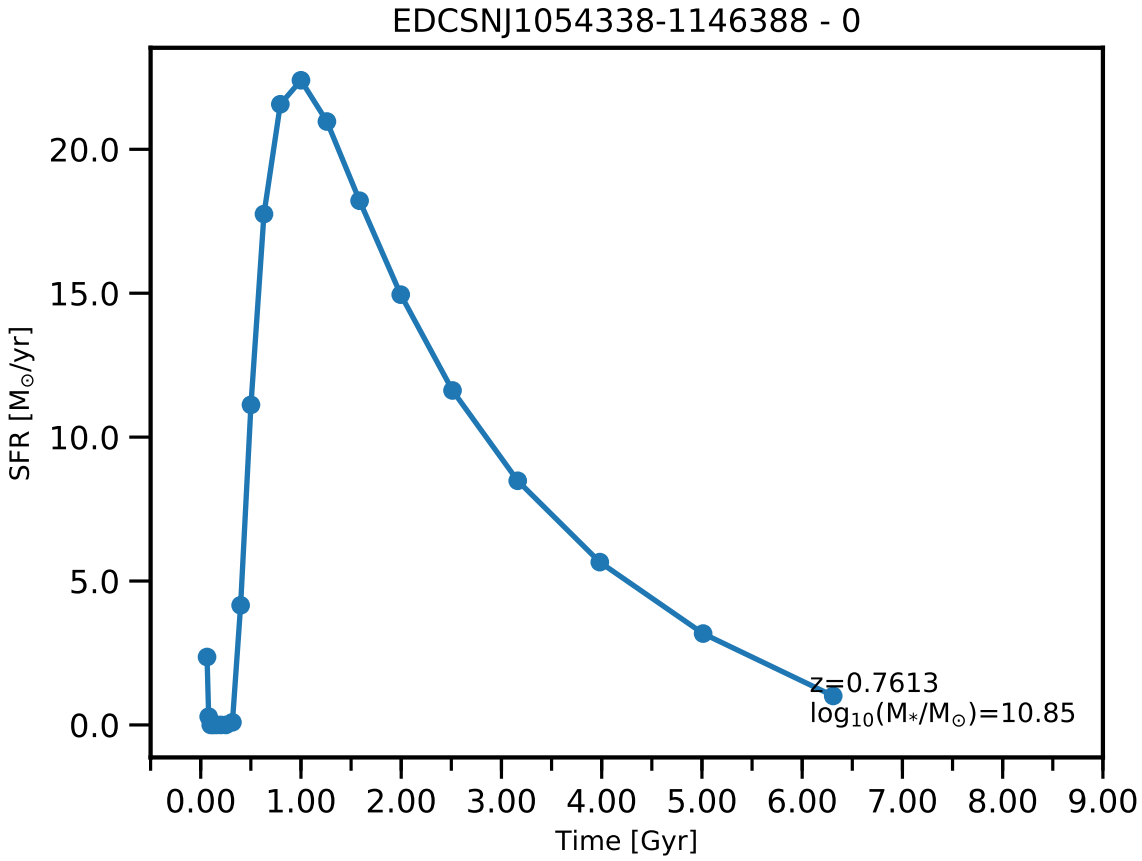
EDCSNJ1054338-1146388 - 0
SFR [M⊙/yr]
20.0
15.0
10.0
5.0
0.0
0.00
1.00
2.00
3.00
4.00
5.00
6.00
7.00
8.00
9.00
Time [Gyr]
z=0.7613
log10(M*/M⊙)=10.85

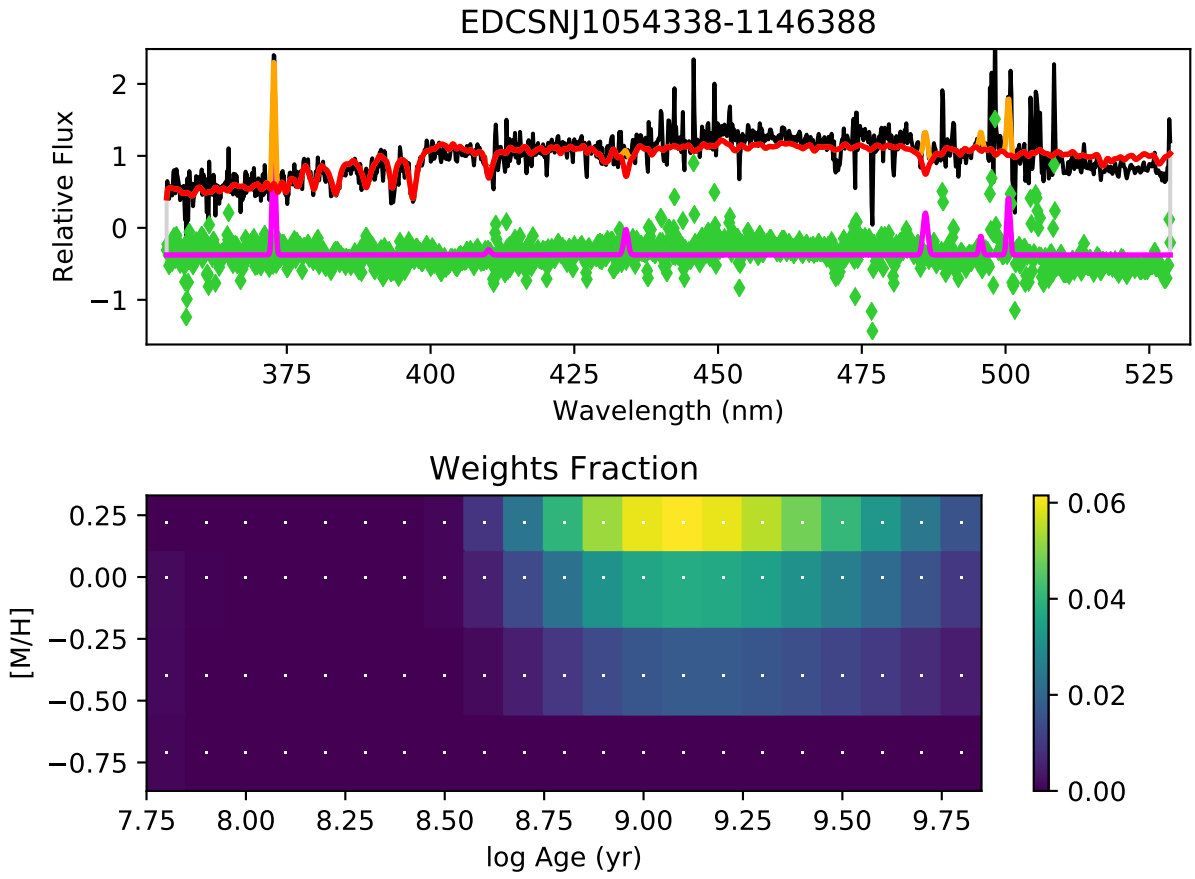
EDCSNJ1054338-1146388
Relative Flux
2
1
0
−1
375
400
425
450
475
500
525
Wavelength (nm)
Weights Fraction
[M/H]
0.25
0.00
−0.25
−0.50
−0.75
7.75
8.00
8.25
8.50
8.75
9.00
9.25
9.50
9.75
log Age (yr)
0.06
0.04
0.02
0.00

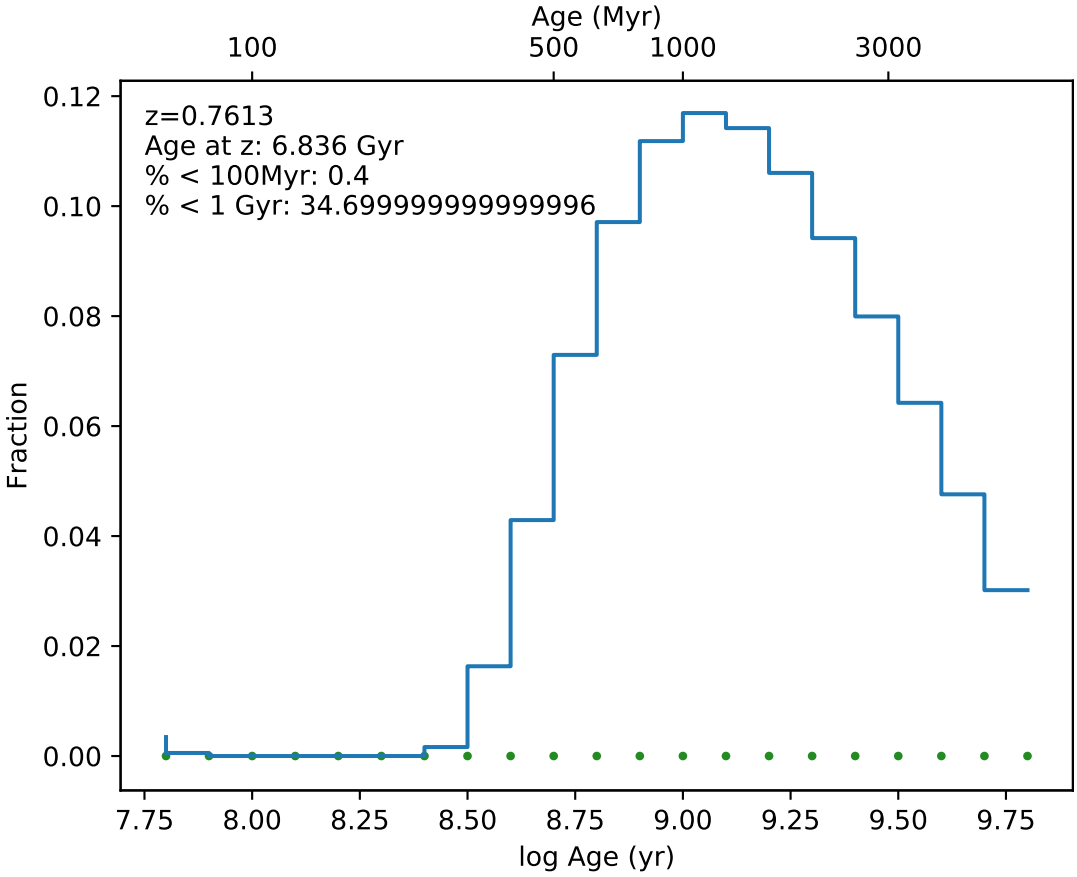
Age (Myr)
100
500
1000
3000
z=0.7613
Age at z: 6.836 Gyr
% < 100Myr: 0.4
% < 1 Gyr: 34.699999999999996
Fraction
0.12
0.10
0.08
0.06
0.04
0.02
0.00
7.75
8.00
8.25
8.50
8.75
9.00
9.25
9.50
9.75
log Age (yr)

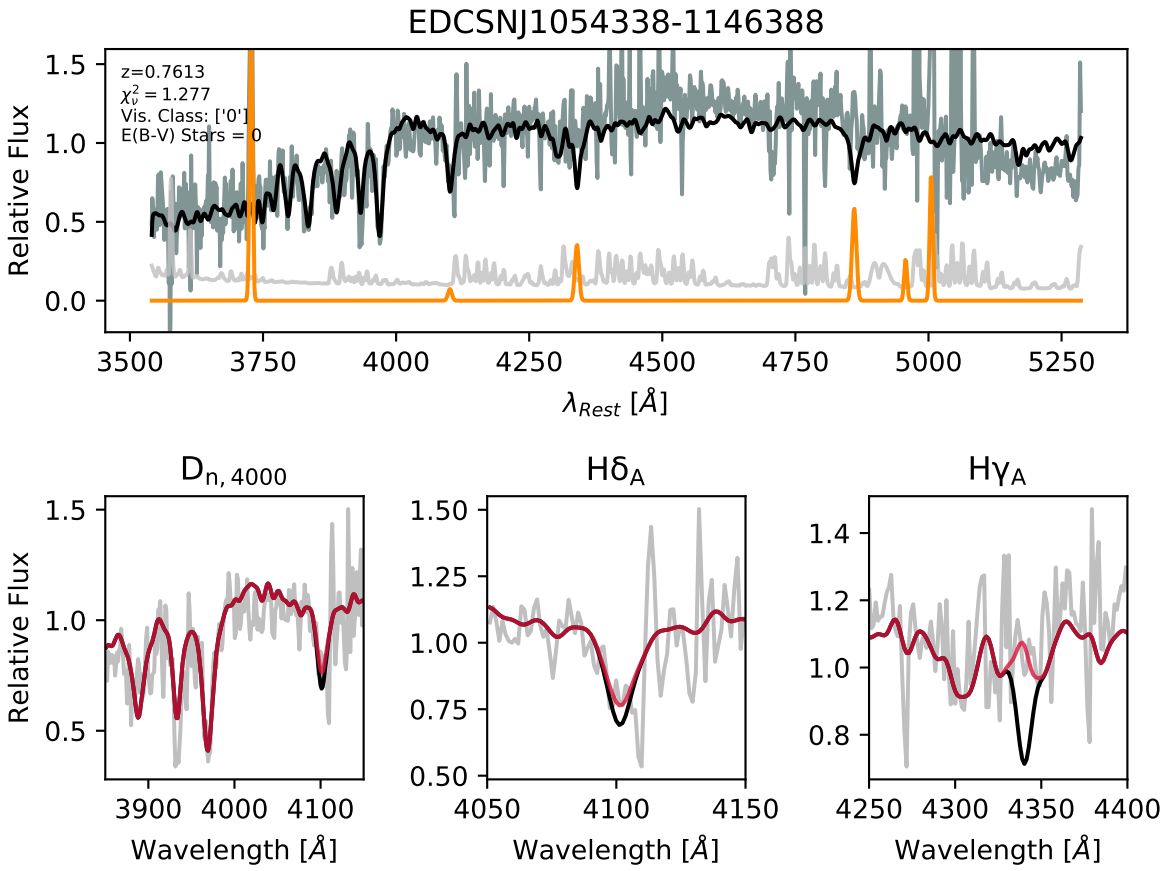
EDCSNJ1054338-1146388
z=0.7613
$\chi^2_\nu = 1.277$
Vis. Class: ['0']
E(B-V) Stars = 0
Relative Flux
λ_{Rest} [Å]
$D_{n,4000}$
$H\delta_A$
$H\gamma_A$
Wavelength [Å]

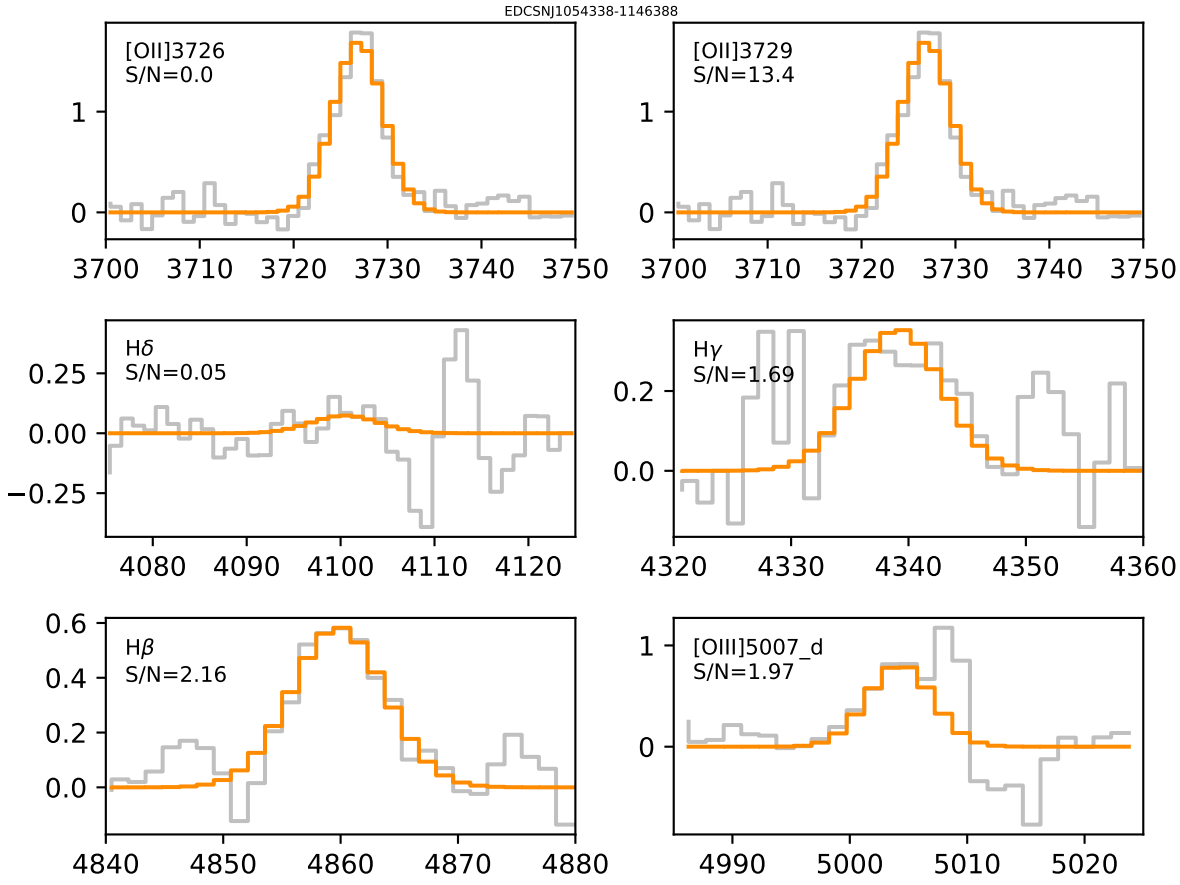
EDCSNJ1054338-1146388
[OII]3726
S/N=0.0
[OII]3729
S/N=13.4
Hδ
S/N=0.05
Hγ
S/N=1.69
Hβ
S/N=2.16
[OIII]5007_d
S/N=1.97

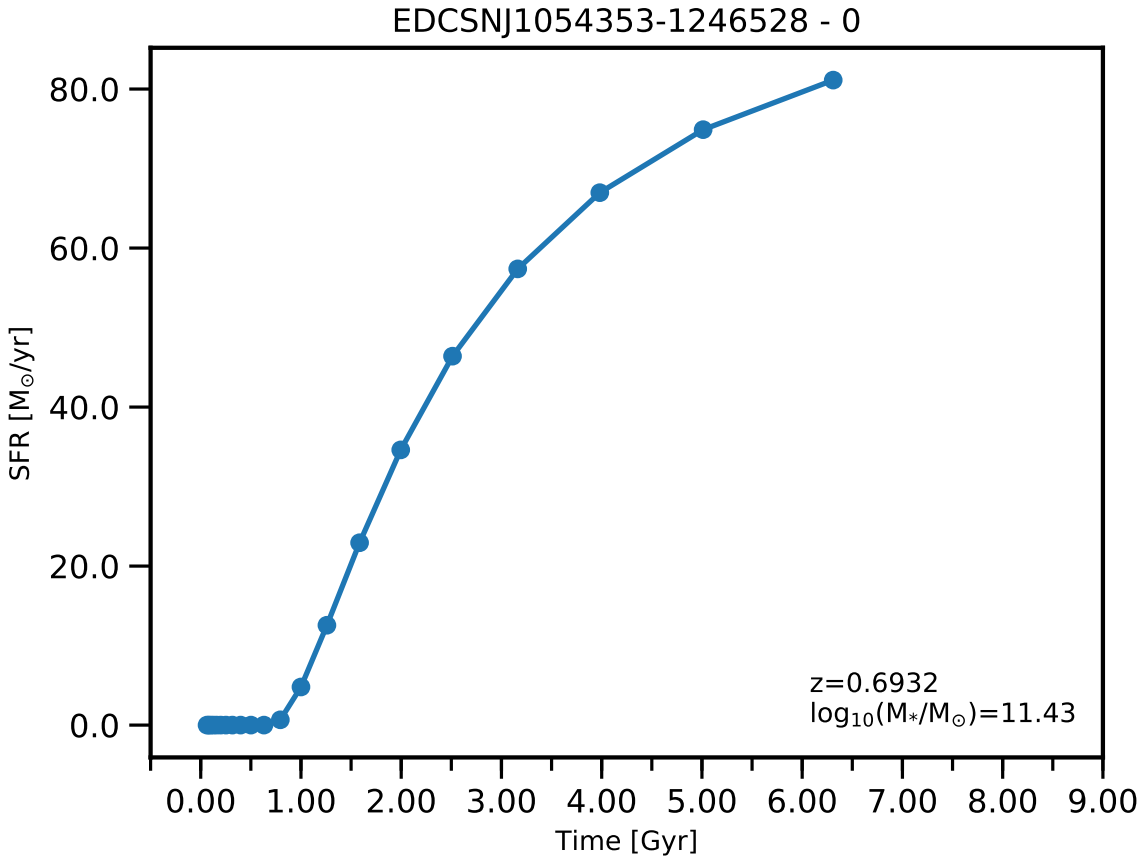
EDCSNJ1054353-1246528 - 0
80.0
60.0
40.0
20.0
0.0
SFR [M⊙/yr]
0.00
1.00
2.00
3.00
4.00
5.00
6.00
7.00
8.00
9.00
Time [Gyr]
z=0.6932
log10(M*/M⊙)=11.43

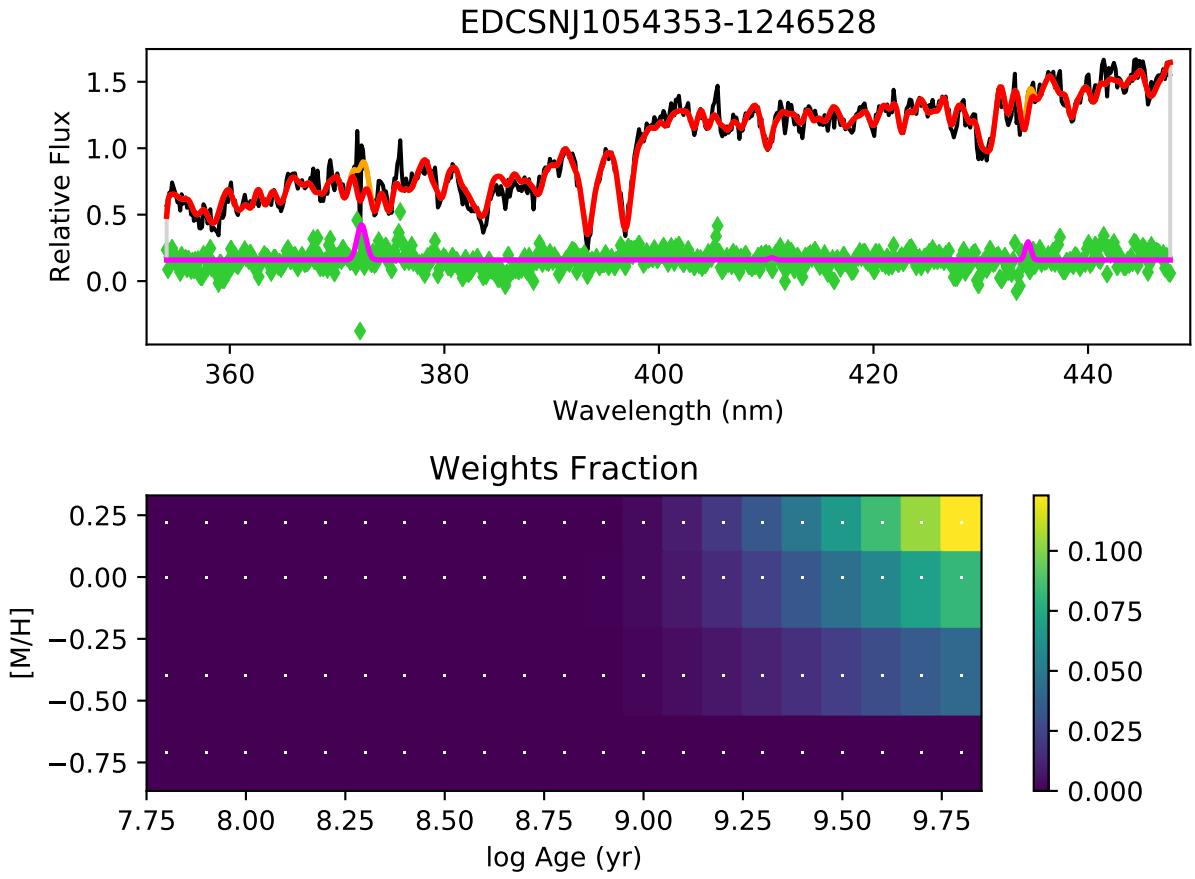
EDCSNJ1054353-1246528
Relative Flux
1.5
1.0
0.5
0.0
360
380
400
420
440
Wavelength (nm)
Weights Fraction
[M/H]
0.25
0.00
−0.25
−0.50
−0.75
7.75
8.00
8.25
8.50
8.75
9.00
9.25
9.50
9.75
log Age (yr)
0.100
0.075
0.050
0.025
0.000

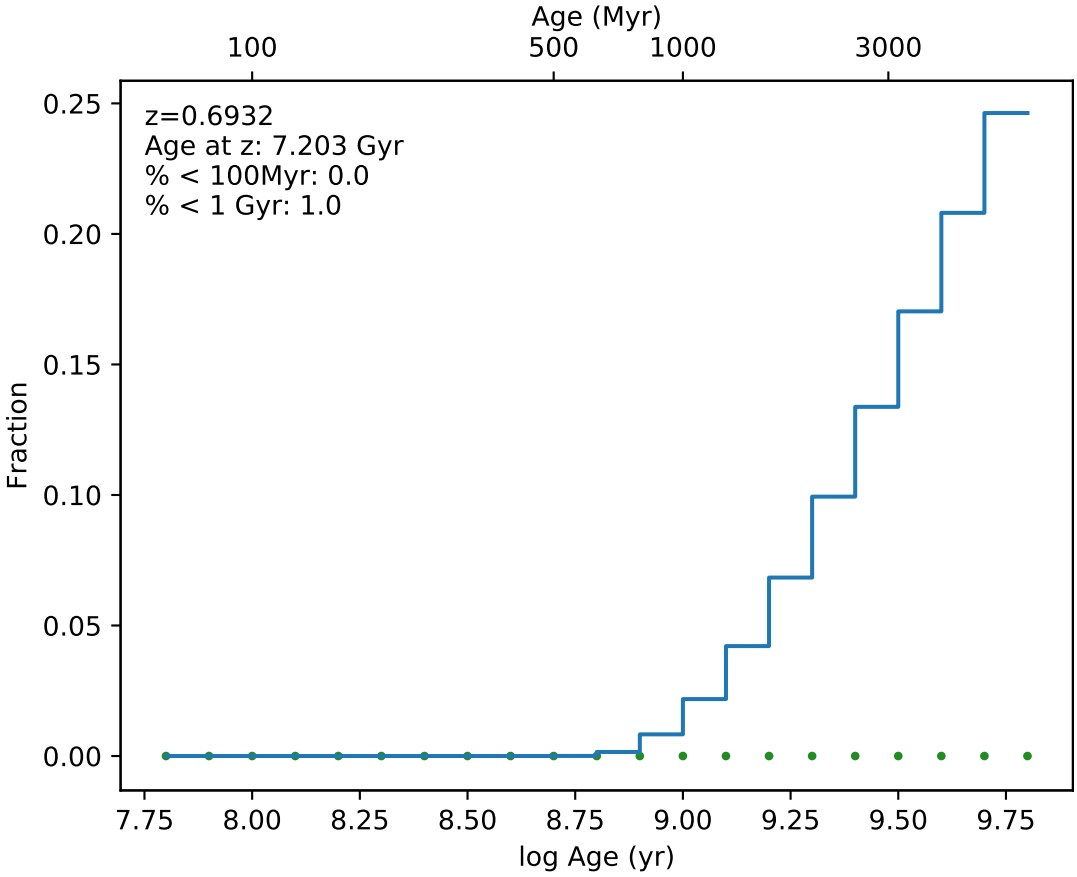
Age (Myr)
100
500
1000
3000
z=0.6932
Age at z: 7.203 Gyr
% < 100Myr: 0.0
% < 1 Gyr: 1.0
Fraction
0.25
0.20
0.15
0.10
0.05
0.00
7.75
8.00
8.25
8.50
8.75
9.00
9.25
9.50
9.75
log Age (yr)

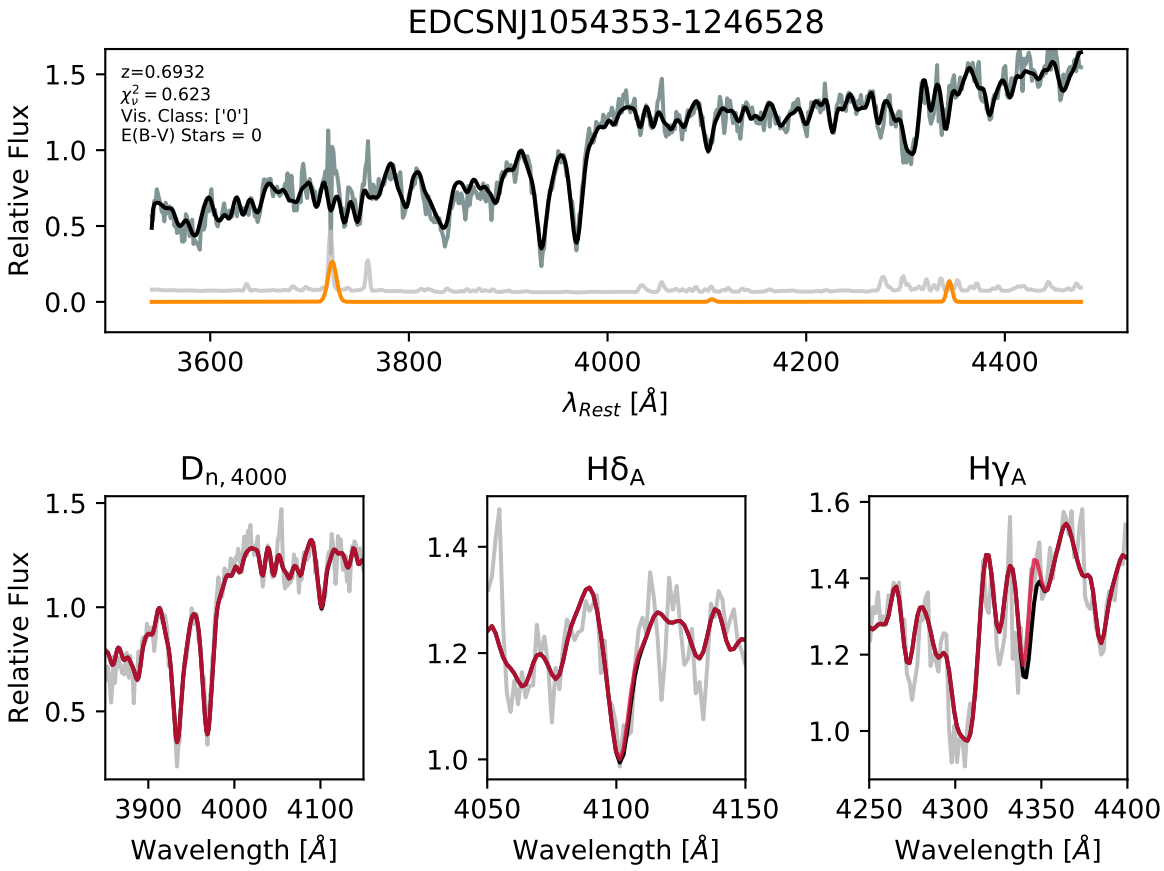
EDCSNJ1054353-1246528
z=0.6932
$\chi^2_\nu = 0.623$
Vis. Class: ['0']
E(B-V) Stars = 0
Relative Flux
λ_{Rest} [Å]
$D_{n,4000}$
$H\delta_A$
$H\gamma_A$
Wavelength [Å]

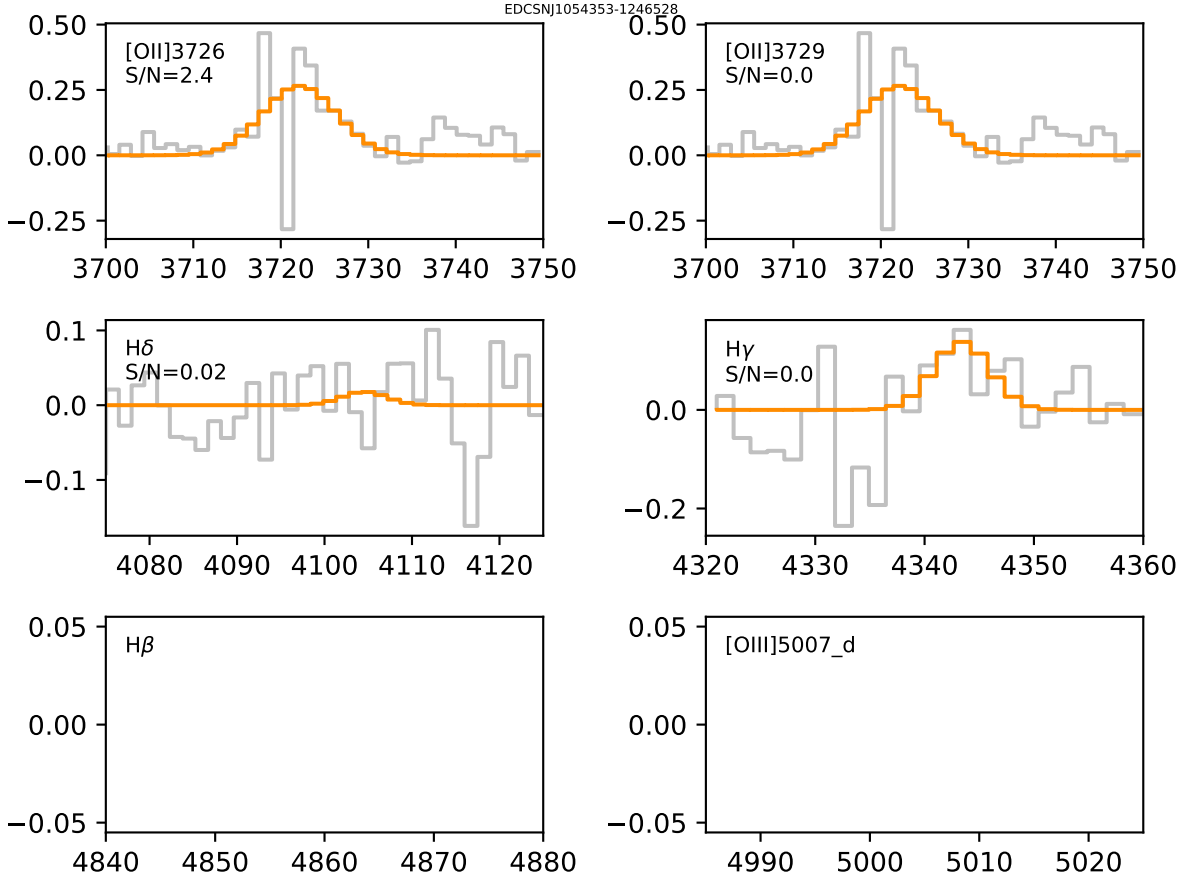
EDCSNJ1054353-1246528
[OII]3726
S/N=2.4
[OII]3729
S/N=0.0
Hδ
S/N=0.02
Hγ
S/N=0.0
Hβ
[OIII]5007_d

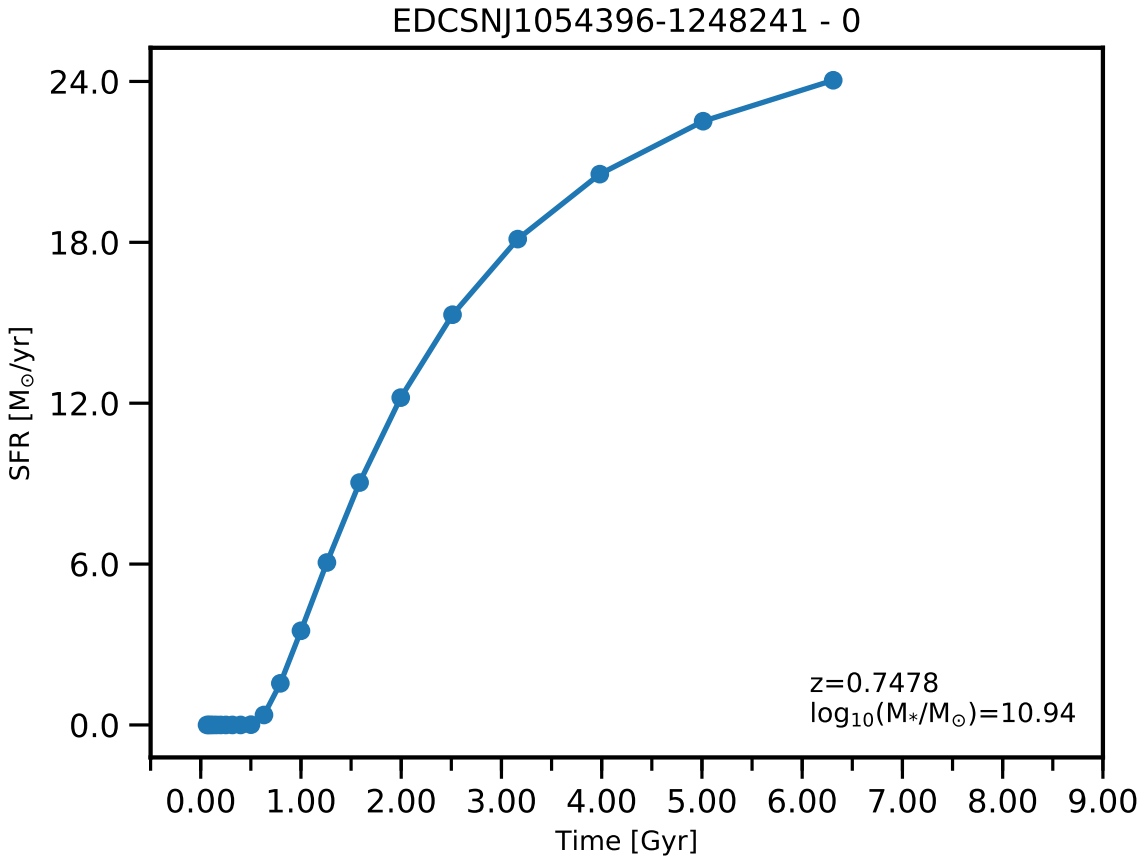
EDCSNJ1054396-1248241 - 0
24.0
18.0
12.0
6.0
0.0
SFR [M⊙/yr]
0.00
1.00
2.00
3.00
4.00
5.00
6.00
7.00
8.00
9.00
Time [Gyr]
z=0.7478
log10(M*/M⊙)=10.94

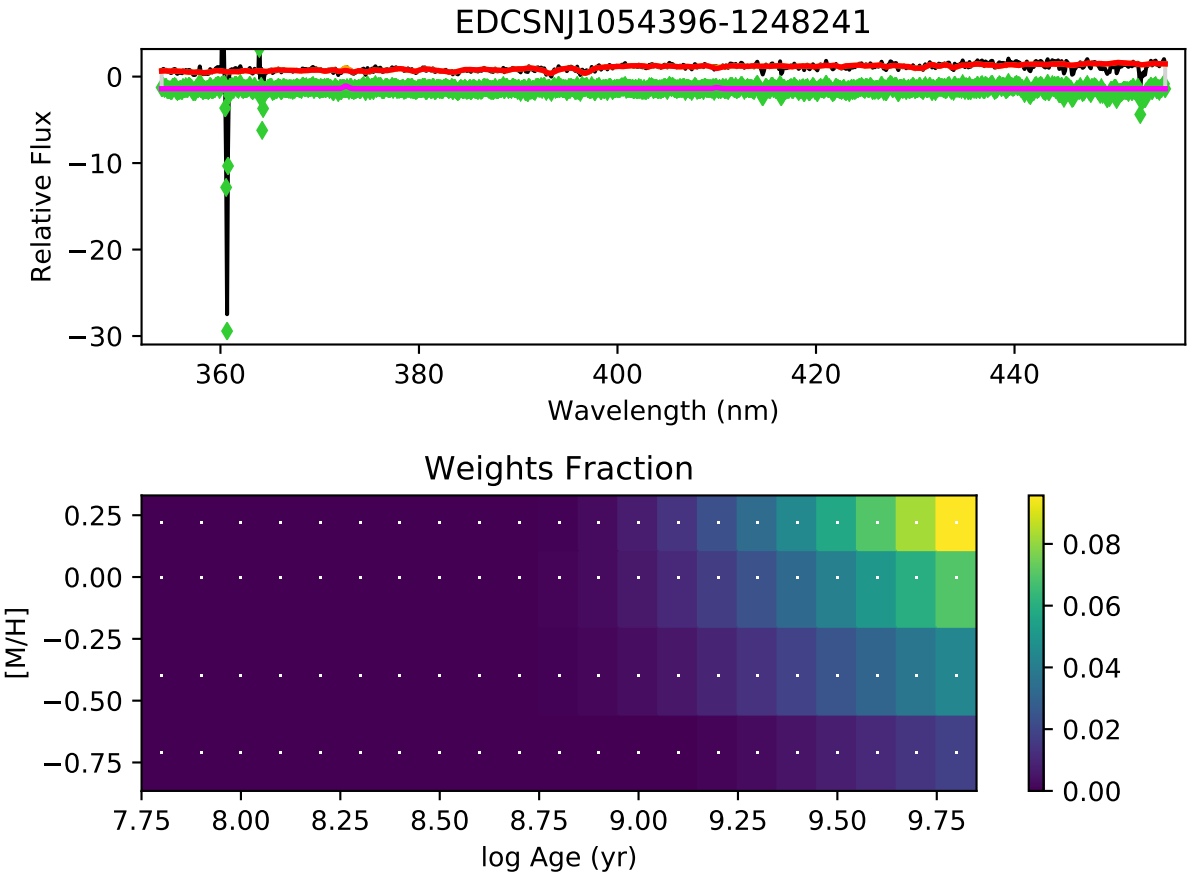
EDCSNJ1054396-1248241
Relative Flux
0
−10
−20
−30
360
380
400
420
440
Wavelength (nm)
Weights Fraction
[M/H]
0.25
0.00
−0.25
−0.50
−0.75
7.75
8.00
8.25
8.50
8.75
9.00
9.25
9.50
9.75
log Age (yr)
0.08
0.06
0.04
0.02
0.00

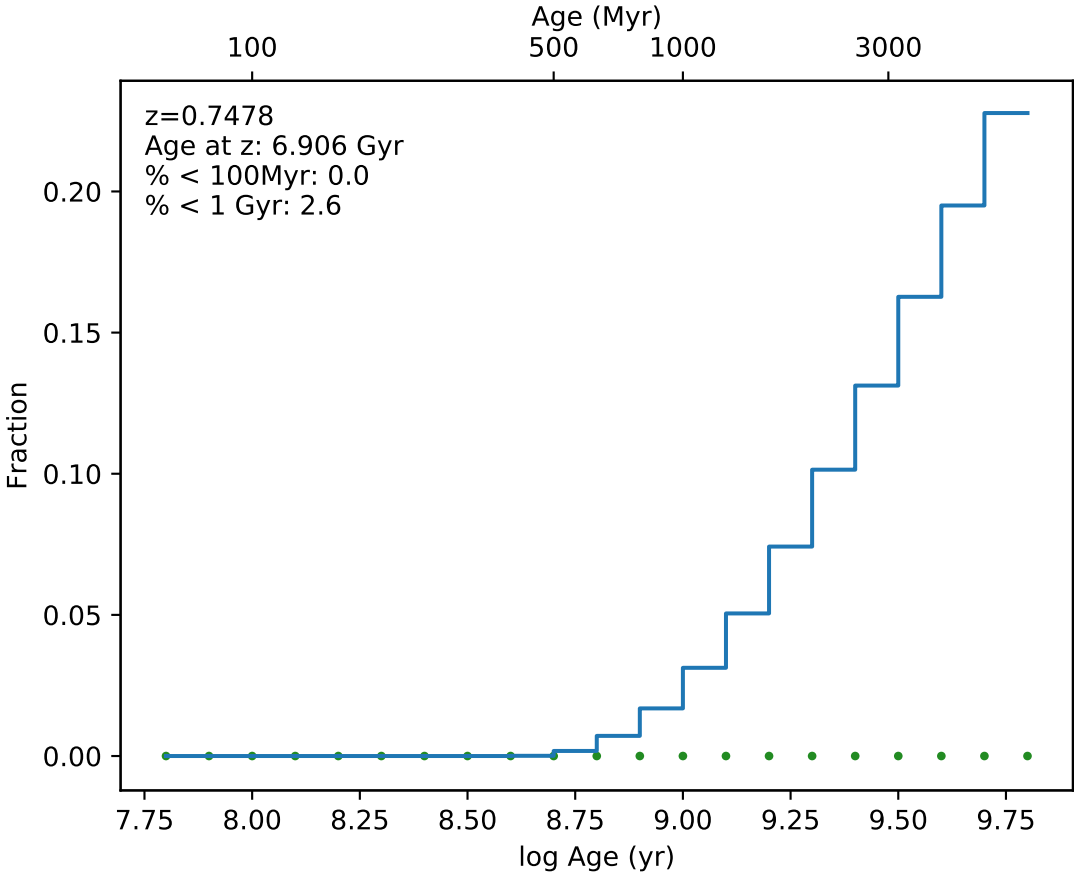
Age (Myr)
100
500
1000
3000
z=0.7478
Age at z: 6.906 Gyr
% < 100Myr: 0.0
% < 1 Gyr: 2.6
Fraction
0.20
0.15
0.10
0.05
0.00
7.75
8.00
8.25
8.50
8.75
9.00
9.25
9.50
9.75
log Age (yr)

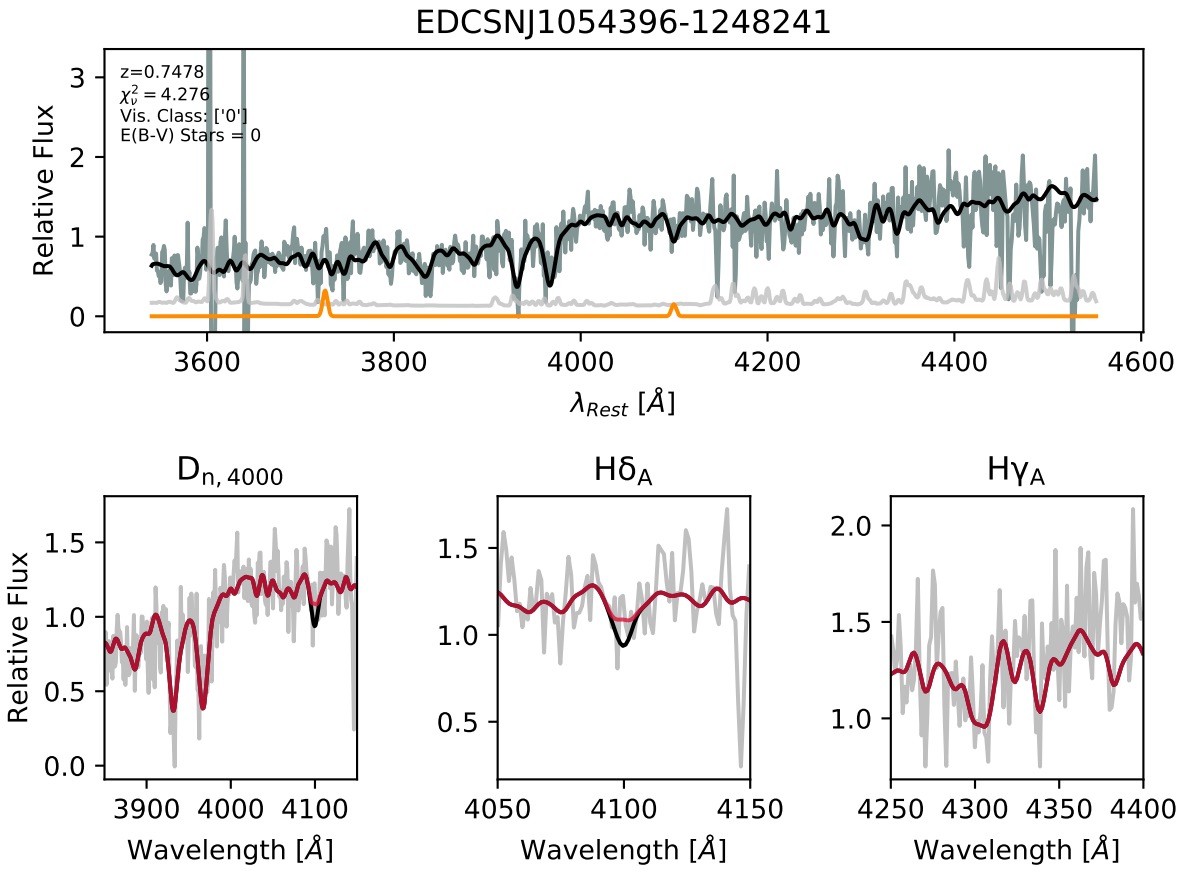
EDCSNJ1054396-1248241
z=0.7478
$\chi^2_\nu = 4.276$
Vis. Class: ['0']
E(B-V) Stars = 0
Relative Flux
λ_{Rest} [Å]
$D_{n,4000}$
$H\delta_A$
$H\gamma_A$
Wavelength [Å]

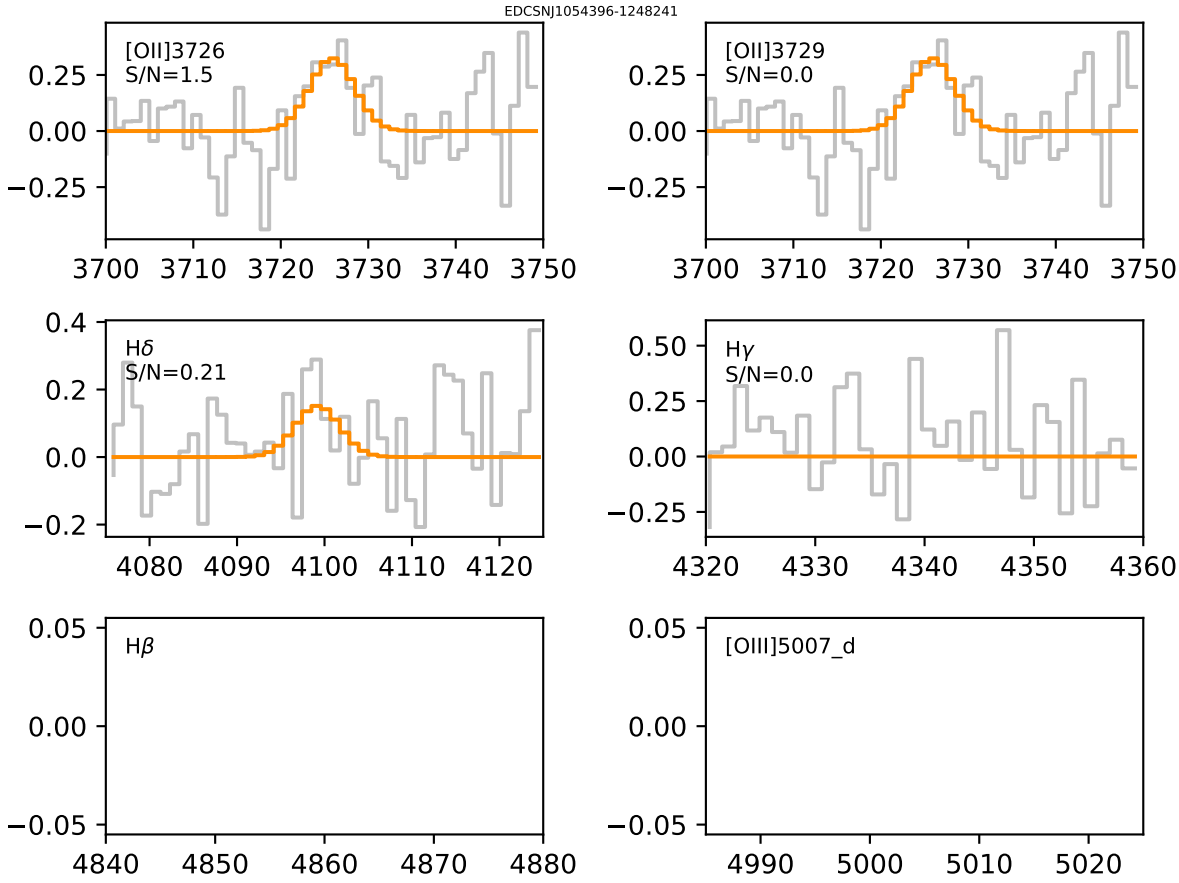
EDCSNJ1054396-1248241
[OII]3726
S/N=1.5
[OII]3729
S/N=0.0
Hδ
S/N=0.21
Hγ
S/N=0.0
Hβ
[OIII]5007_d

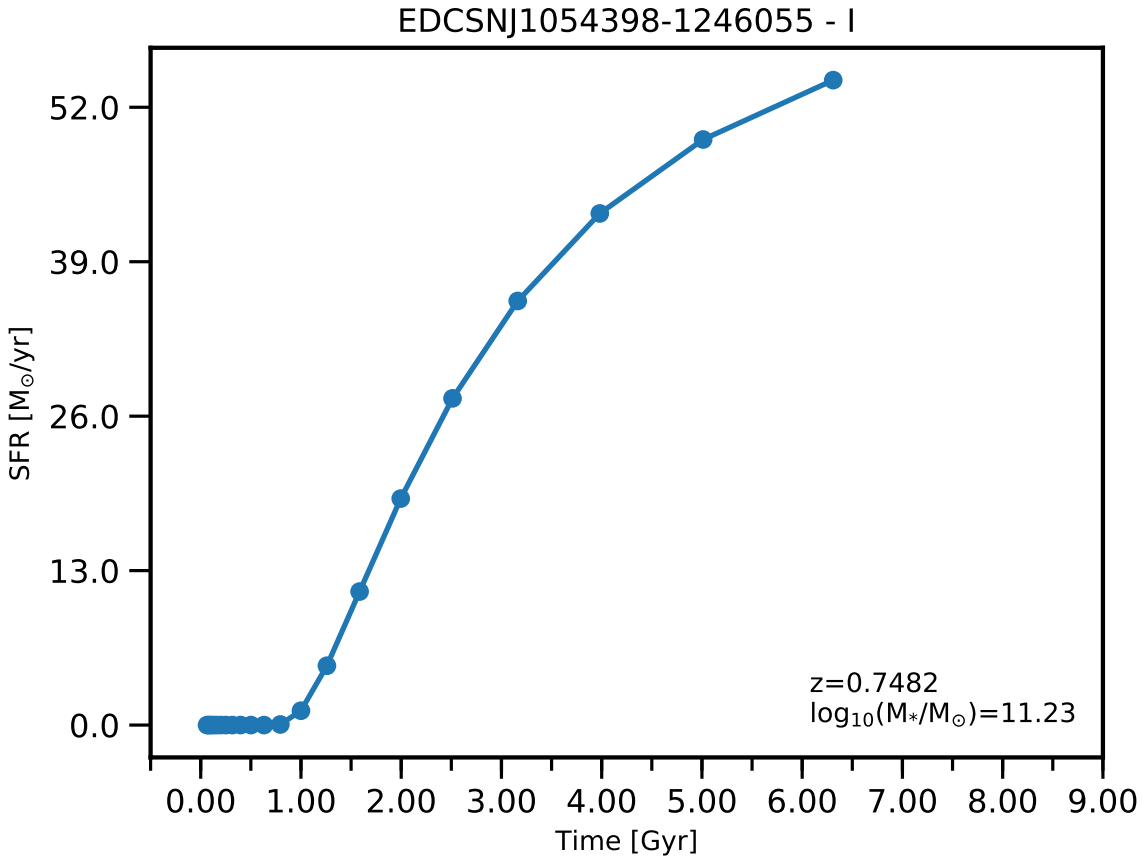
EDCSNJ1054398-1246055 - I
52.0
39.0
26.0
13.0
0.0
SFR [M⊙/yr]
0.00
1.00
2.00
3.00
4.00
5.00
6.00
7.00
8.00
9.00
Time [Gyr]
z=0.7482
log10(M*/M⊙)=11.23

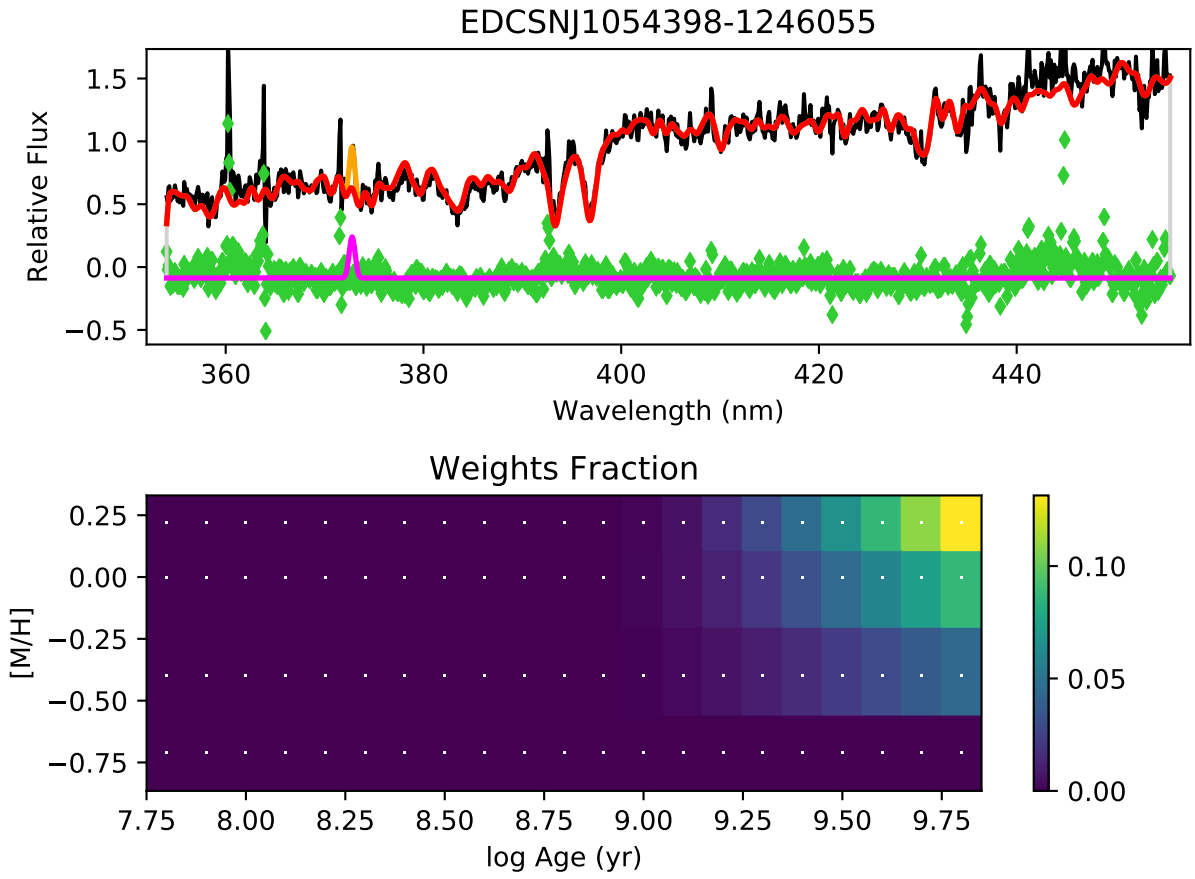
EDCSNJ1054398-1246055
Relative Flux
1.5
1.0
0.5
0.0
−0.5
360
380
400
420
440
Wavelength (nm)
Weights Fraction
[M/H]
0.25
0.00
−0.25
−0.50
−0.75
7.75
8.00
8.25
8.50
8.75
9.00
9.25
9.50
9.75
log Age (yr)
0.10
0.05
0.00

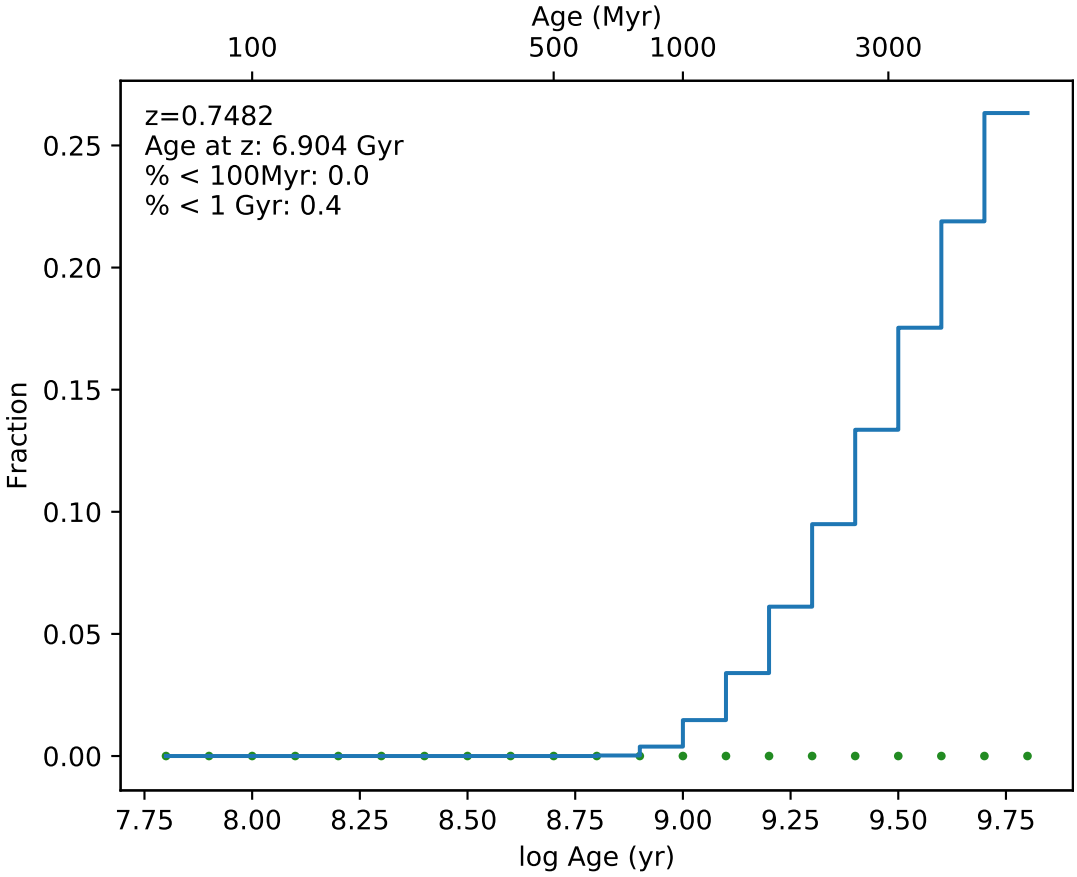
Age (Myr)
100
500
1000
3000
z=0.7482
Age at z: 6.904 Gyr
% < 100Myr: 0.0
% < 1 Gyr: 0.4
Fraction
0.25
0.20
0.15
0.10
0.05
0.00
7.75
8.00
8.25
8.50
8.75
9.00
9.25
9.50
9.75
log Age (yr)

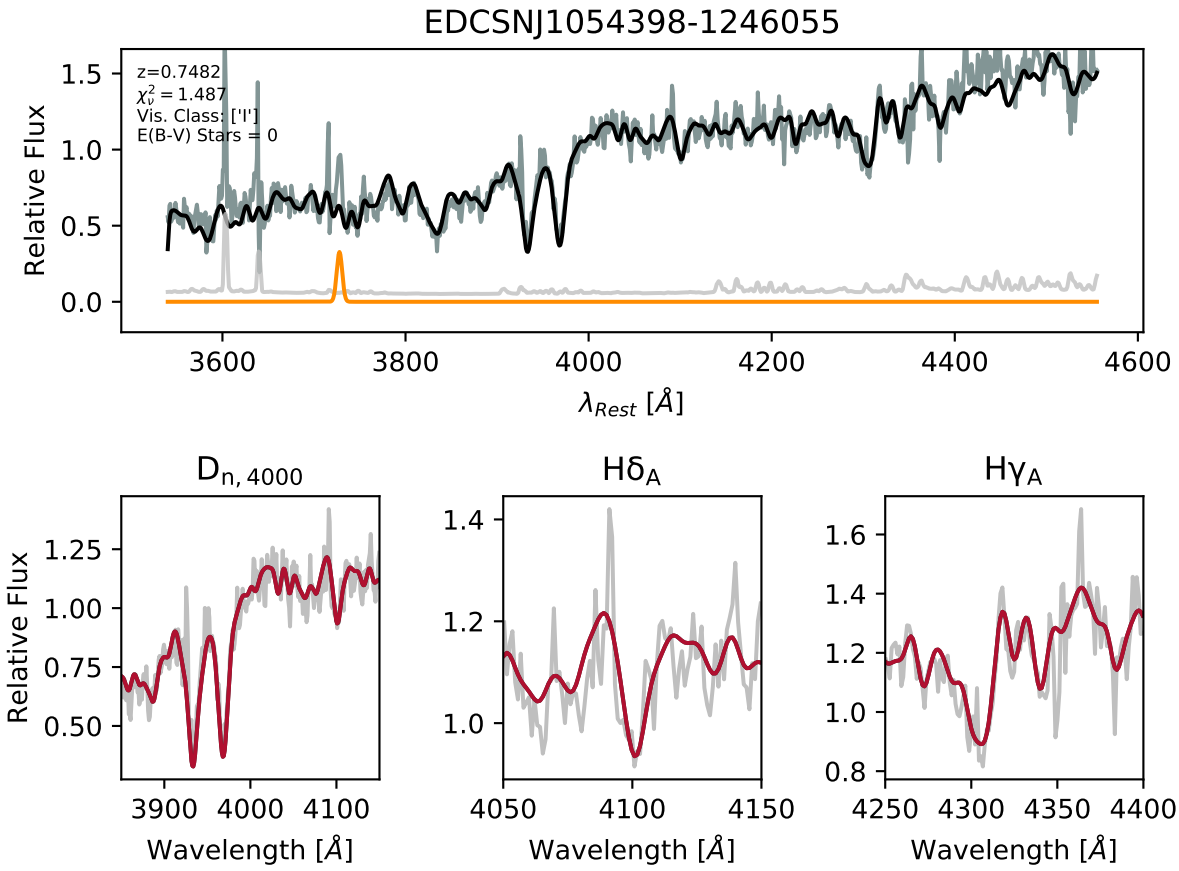
EDCSNJ1054398-1246055
z=0.7482
$\chi^2_\nu = 1.487$
Vis. Class: ['I']
E(B-V) Stars = 0
Relative Flux
λ_{Rest} [Å]
$D_{n,4000}$
$H\delta_A$
$H\gamma_A$
Wavelength [Å]

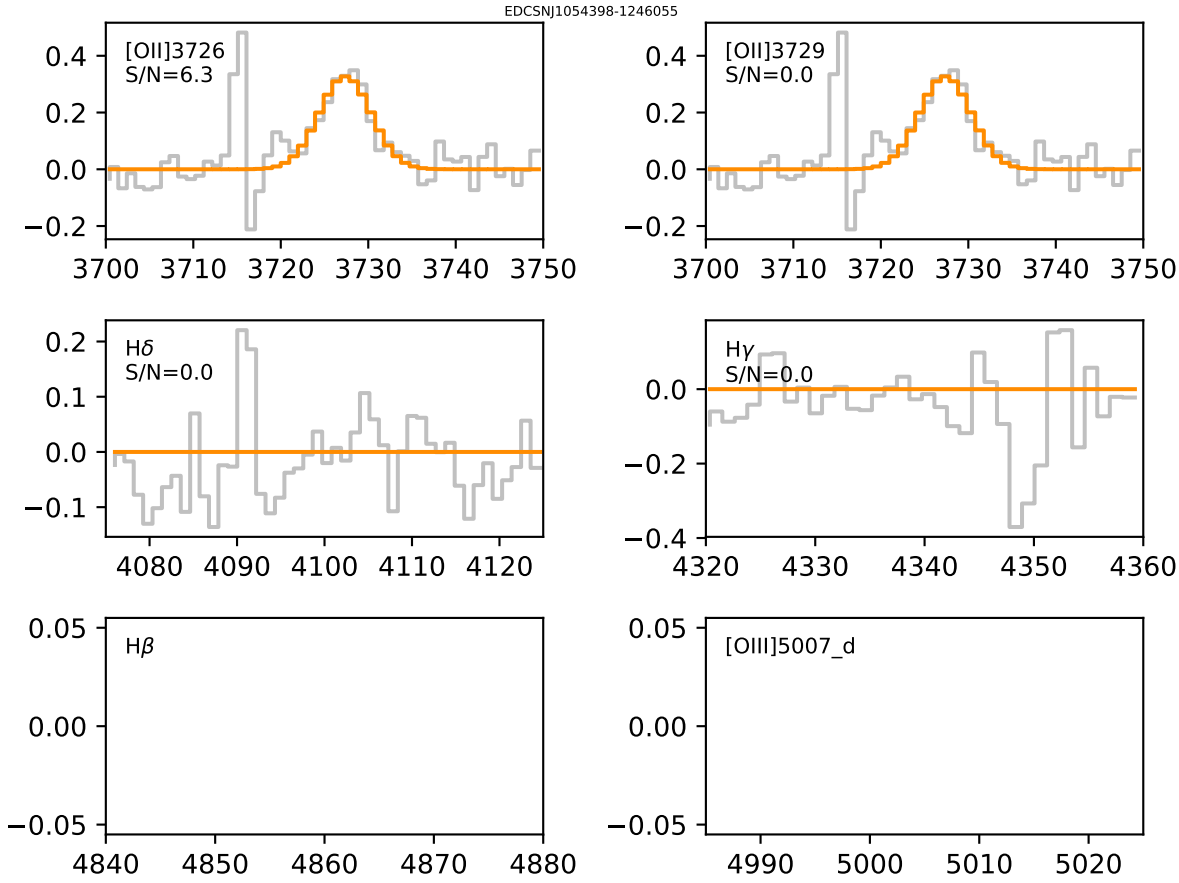
EDCSNJ1054398-1246055
[OII]3726
S/N=6.3
[OII]3729
S/N=0.0
Hδ
S/N=0.0
Hγ
S/N=0.0
Hβ
[OIII]5007_d

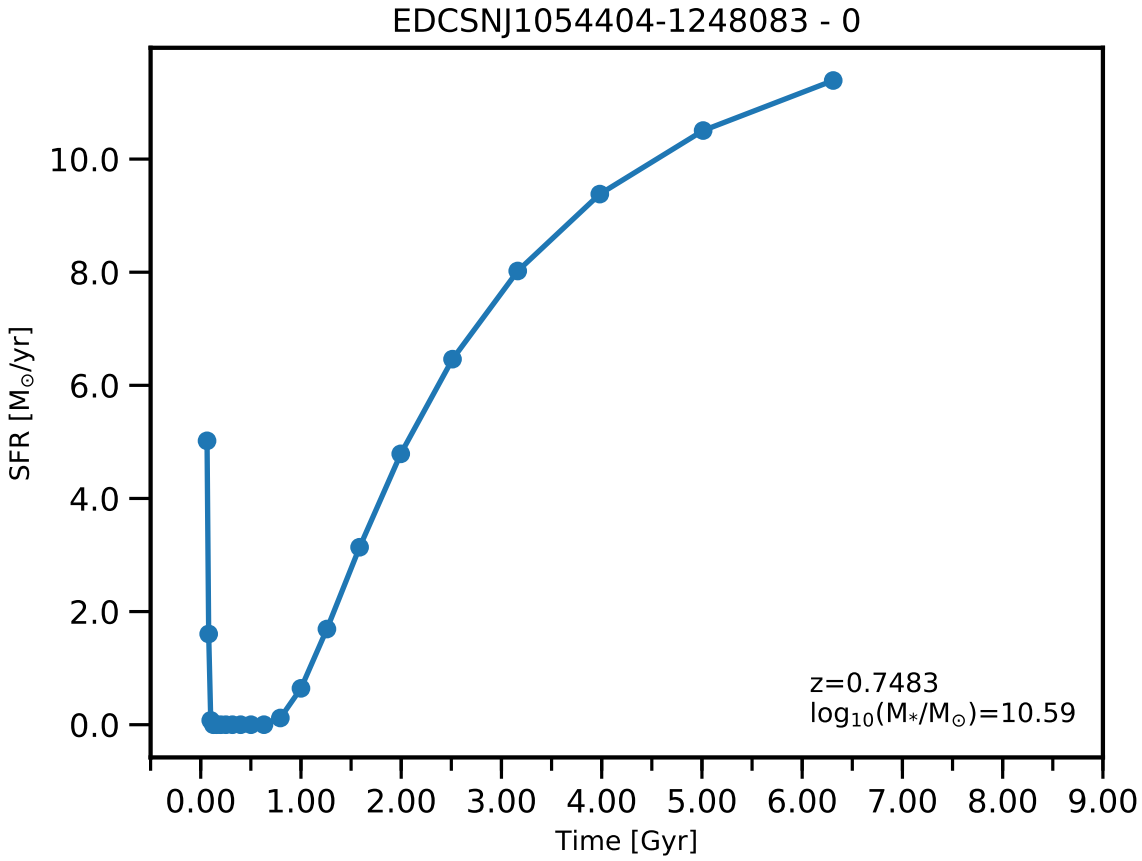
EDCSNJ1054404-1248083 - 0
SFR [M⊙/yr]
10.0
8.0
6.0
4.0
2.0
0.0
0.00
1.00
2.00
3.00
4.00
5.00
6.00
7.00
8.00
9.00
Time [Gyr]
z=0.7483
log10(M*/M⊙)=10.59

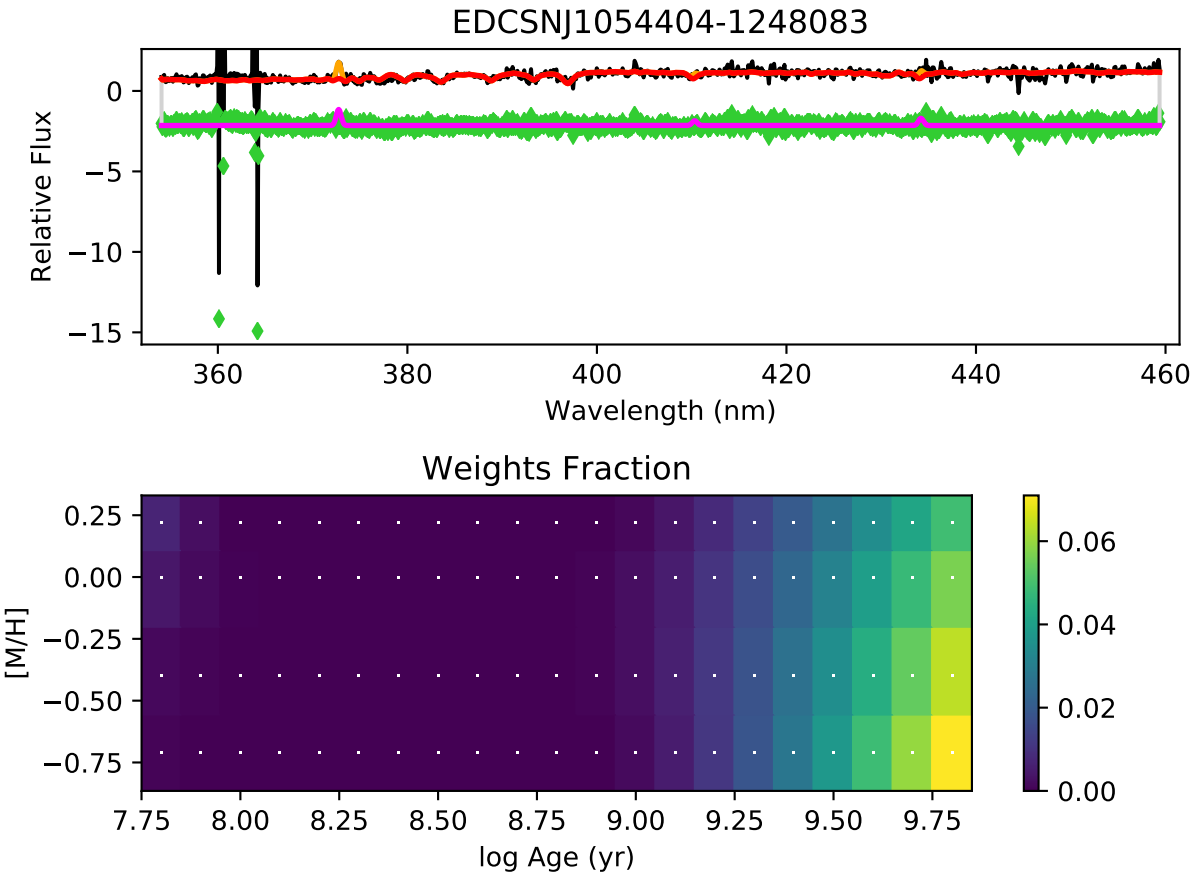
EDCSNJ1054404-1248083
Relative Flux
0
−5
−10
−15
360
380
400
420
440
460
Wavelength (nm)
Weights Fraction
[M/H]
0.25
0.00
−0.25
−0.50
−0.75
7.75
8.00
8.25
8.50
8.75
9.00
9.25
9.50
9.75
log Age (yr)
0.06
0.04
0.02
0.00

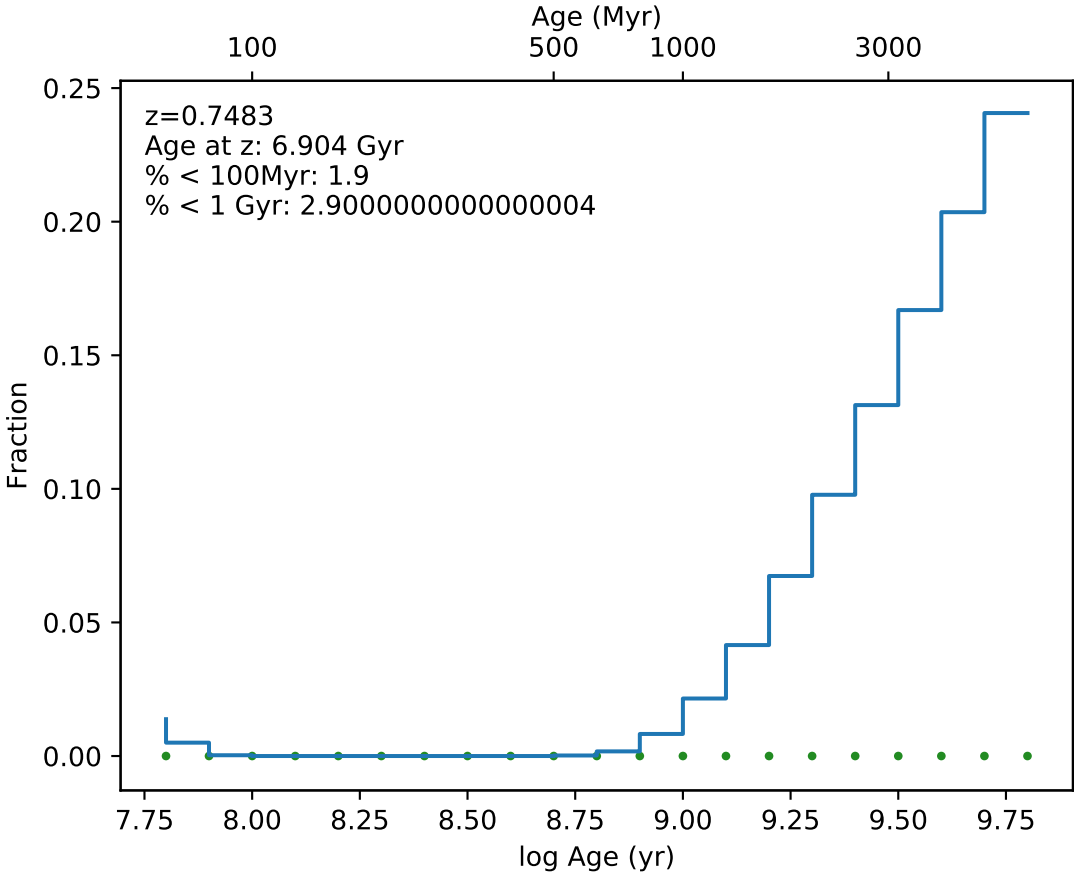
Age (Myr)
100
500
1000
3000
z=0.7483
Age at z: 6.904 Gyr
% < 100Myr: 1.9
% < 1 Gyr: 2.9000000000000004
Fraction
0.25
0.20
0.15
0.10
0.05
0.00
7.75
8.00
8.25
8.50
8.75
9.00
9.25
9.50
9.75
log Age (yr)

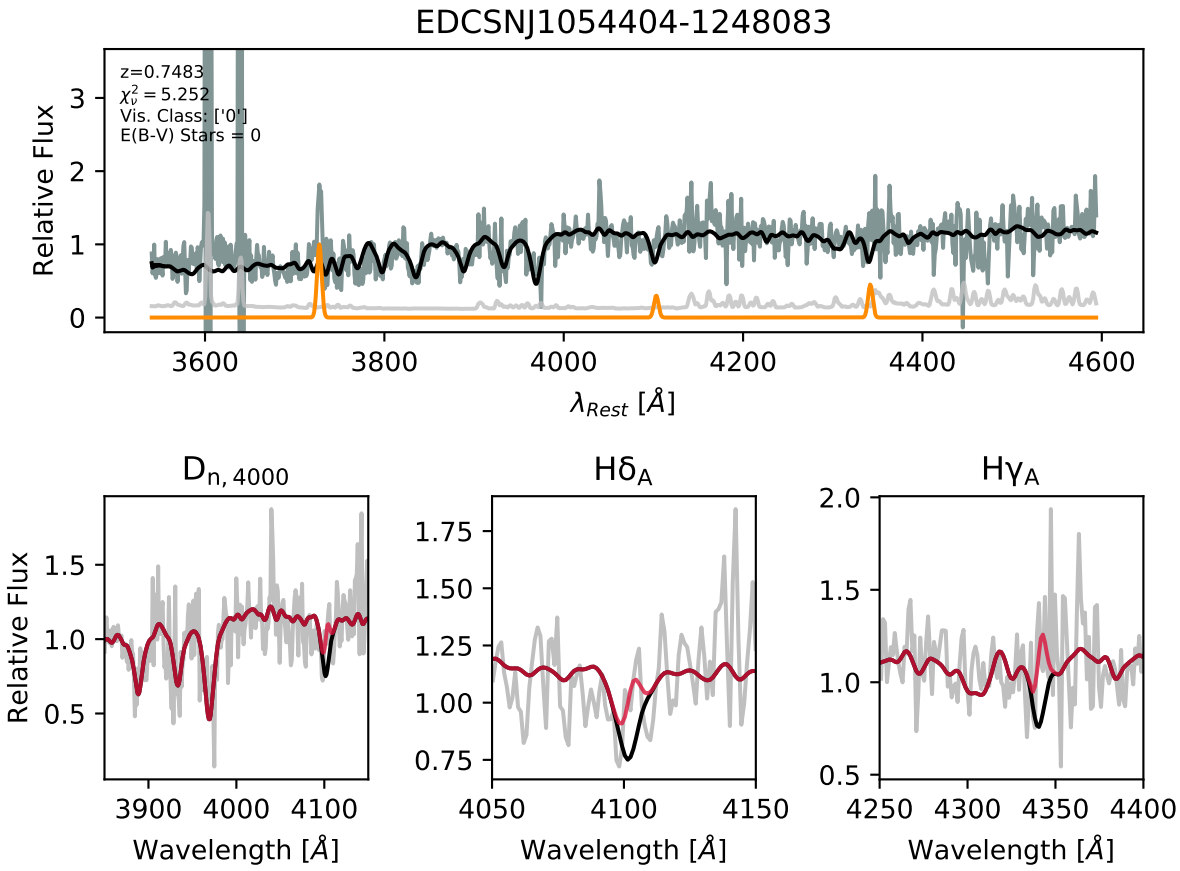
EDCSNJ1054404-1248083
z=0.7483
$\chi^2_\nu = 5.252$
Vis. Class: ['0']
E(B-V) Stars = 0
Relative Flux
λ_{Rest} [Å]
$D_{n,4000}$
$H\delta_A$
$H\gamma_A$
Wavelength [Å]

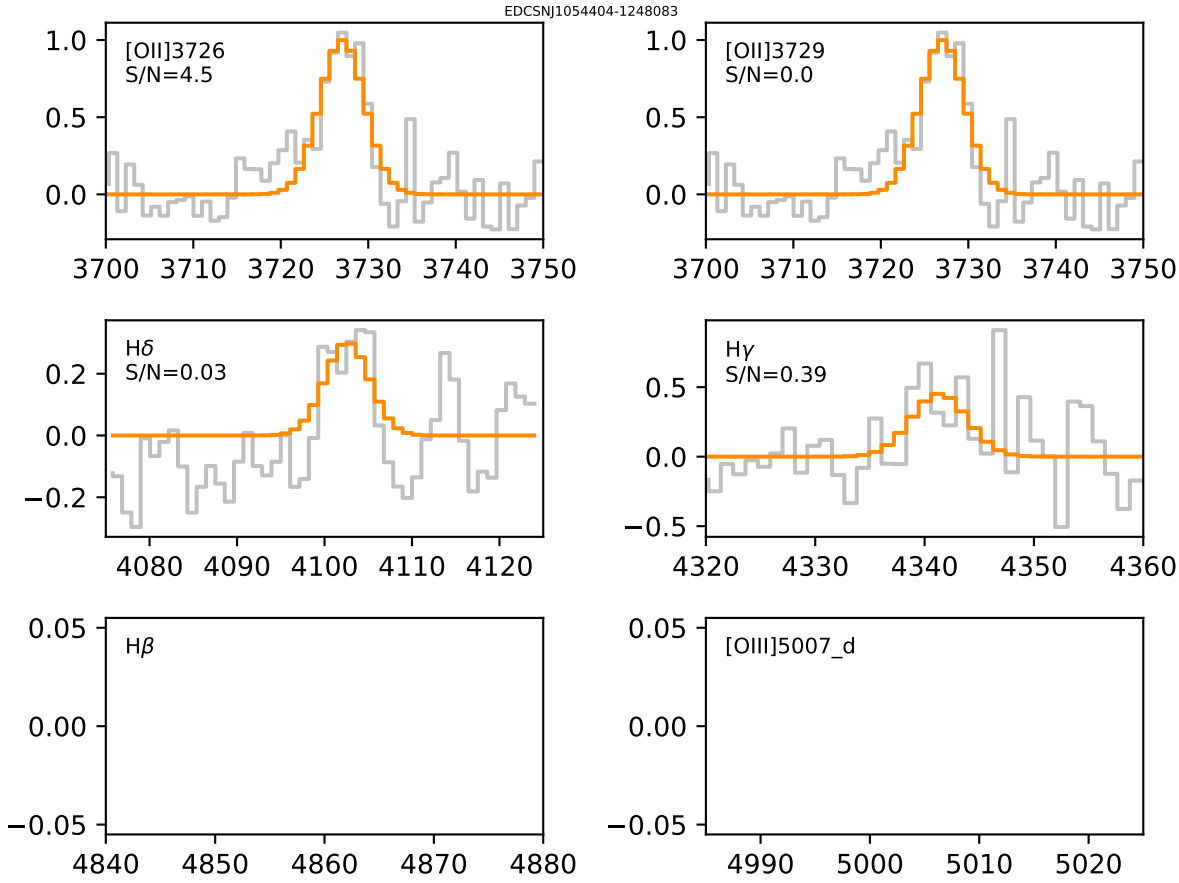
EDCSNJ1054404-1248083
[OII]3726
S/N=4.5
[OII]3729
S/N=0.0
Hδ
S/N=0.03
Hγ
S/N=0.39
Hβ
[OIII]5007_d

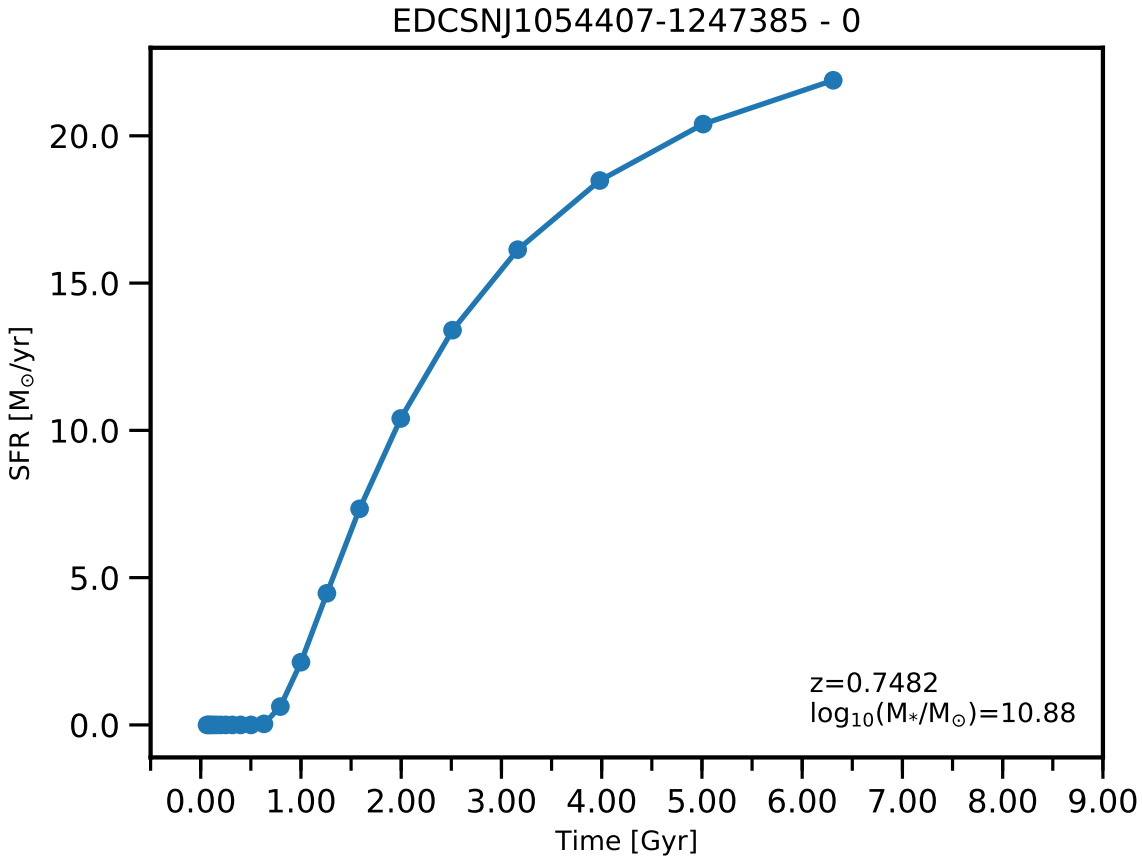
EDCSNJ1054407-1247385 - 0
SFR [M⊙/yr]
20.0
15.0
10.0
5.0
0.0
0.00
1.00
2.00
3.00
4.00
5.00
6.00
7.00
8.00
9.00
Time [Gyr]
z=0.7482
log10(M*/M⊙)=10.88

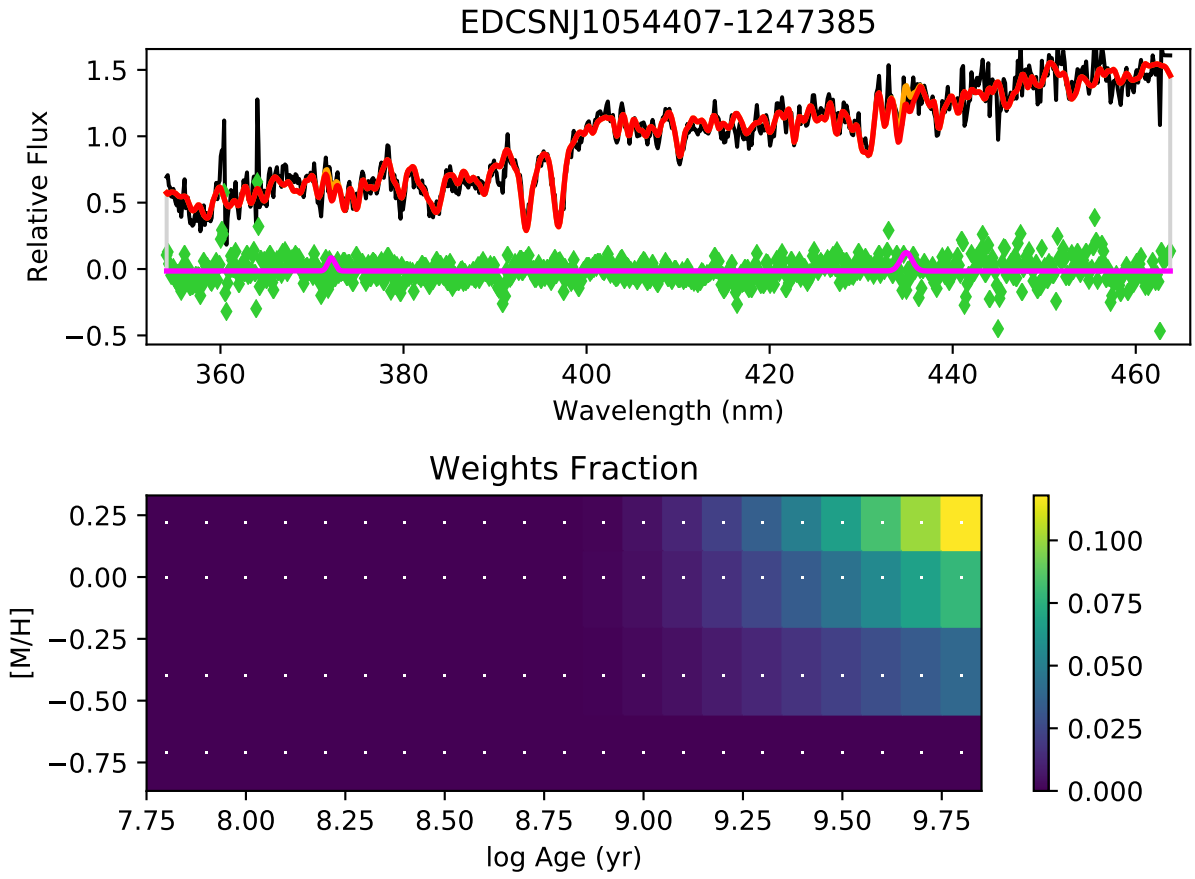
EDCSNJ1054407-1247385
Relative Flux
1.5
1.0
0.5
0.0
−0.5
360
380
400
420
440
460
Wavelength (nm)
Weights Fraction
[M/H]
0.25
0.00
−0.25
−0.50
−0.75
7.75
8.00
8.25
8.50
8.75
9.00
9.25
9.50
9.75
log Age (yr)
0.100
0.075
0.050
0.025
0.000

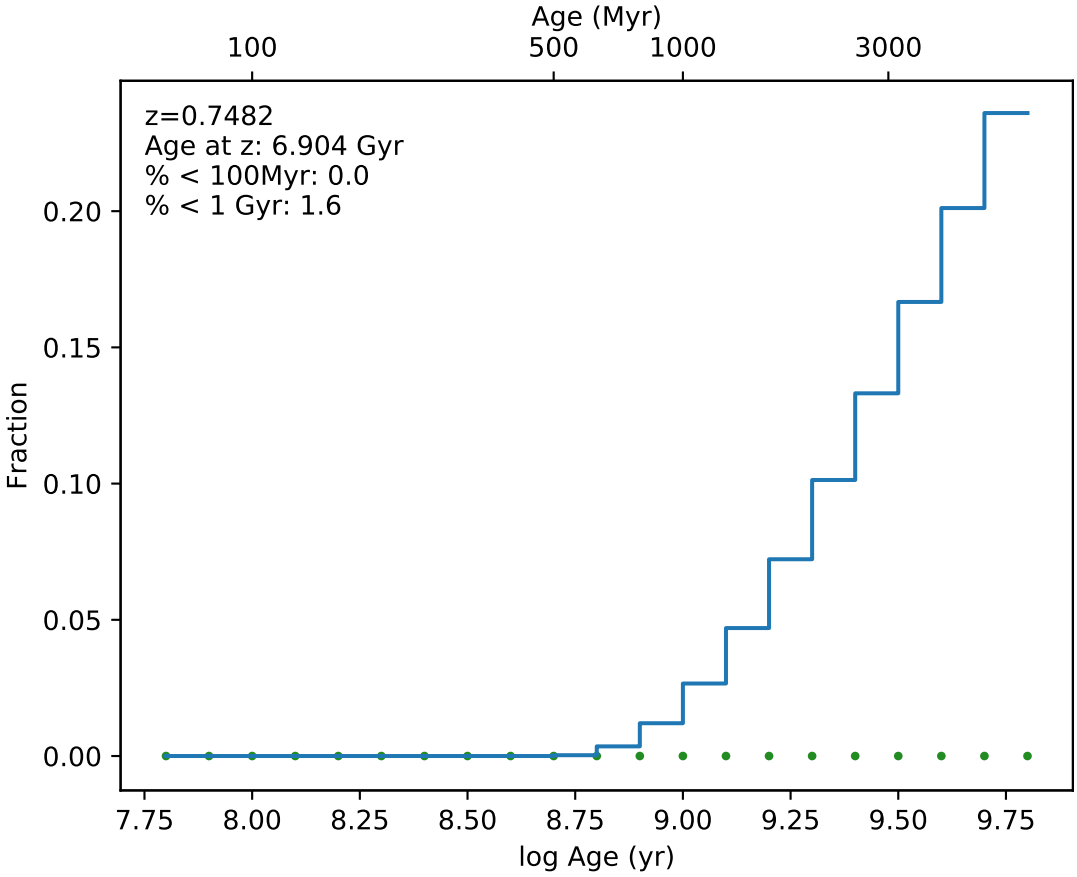
Age (Myr)
100
500
1000
3000
z=0.7482
Age at z: 6.904 Gyr
% < 100Myr: 0.0
% < 1 Gyr: 1.6
Fraction
0.00
0.05
0.10
0.15
0.20
7.75
8.00
8.25
8.50
8.75
9.00
9.25
9.50
9.75
log Age (yr)

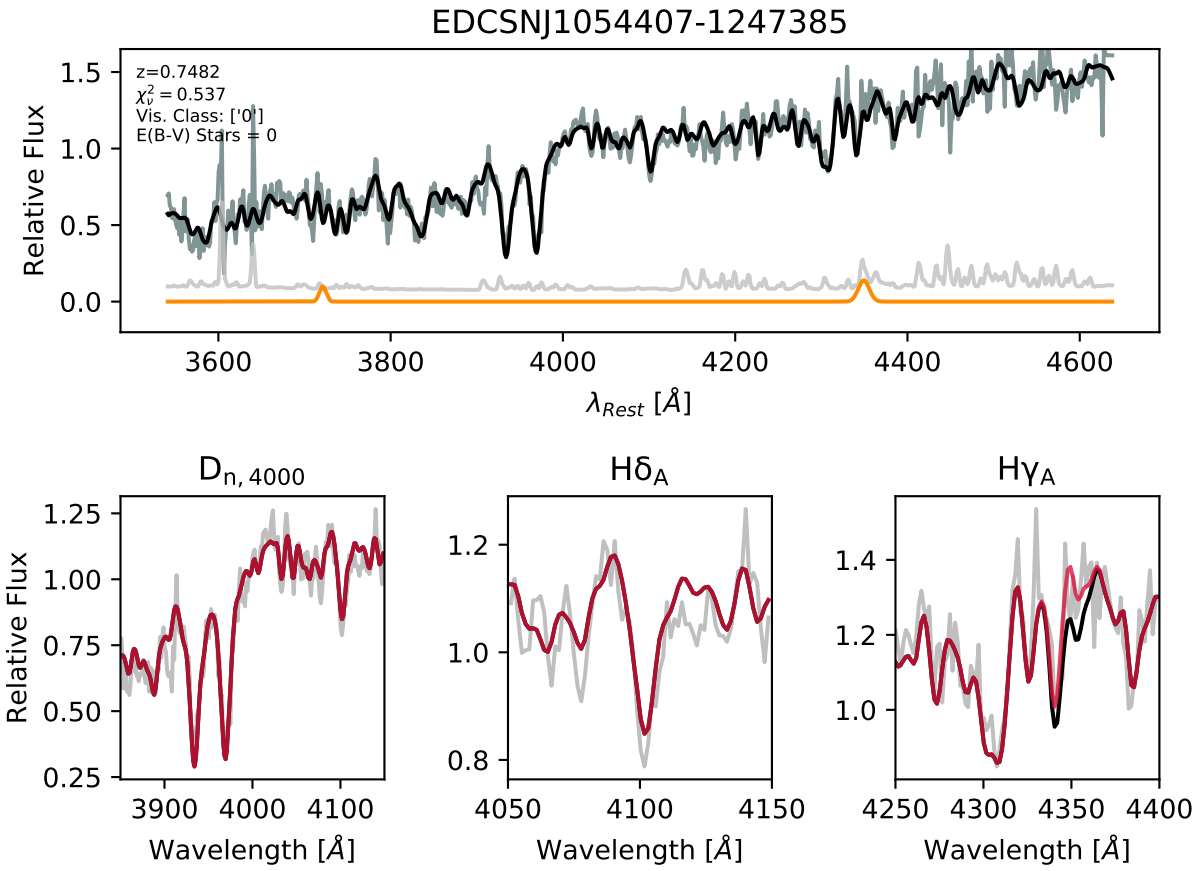
EDCSNJ1054407-1247385
z=0.7482
$\chi^2_\nu = 0.537$
Vis. Class: ['0']
E(B-V) Stars = 0
Relative Flux
λ_{Rest} [Å]
$D_{n,4000}$
$H\delta_A$
$H\gamma_A$
Wavelength [Å]

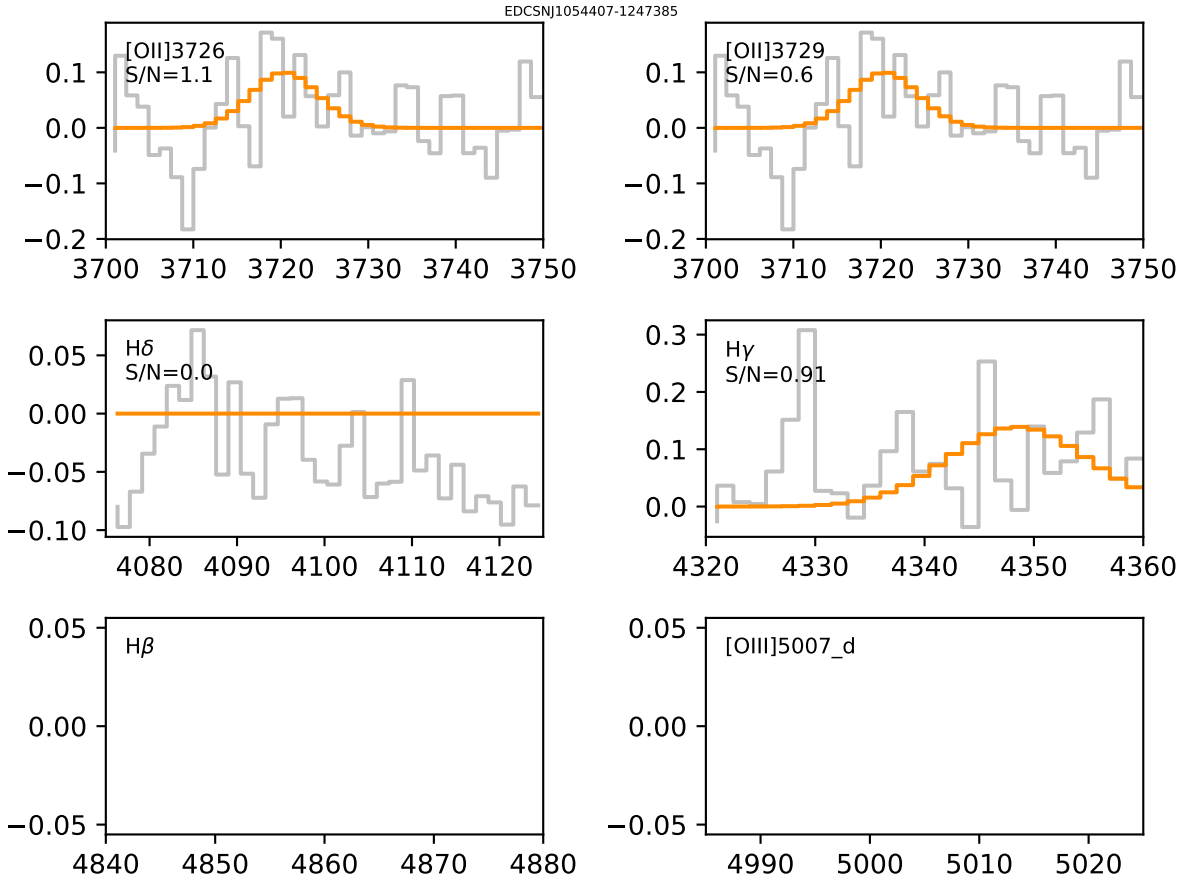
EDCSNJ1054407-1247385
[OII]3726
S/N=1.1
[OII]3729
S/N=0.6
Hδ
S/N=0.0
Hγ
S/N=0.91
Hβ
[OIII]5007_d

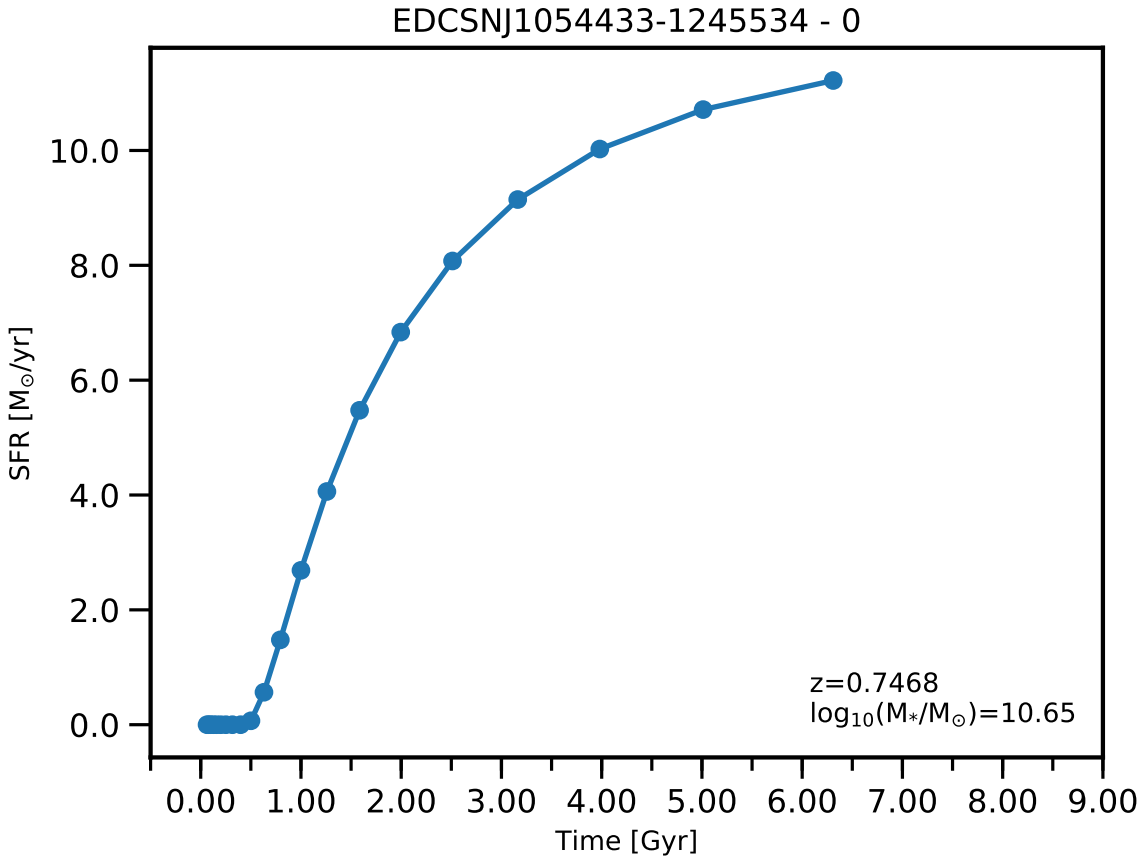
EDCSNJ1054433-1245534 - 0
SFR [M⊙/yr]
10.0
8.0
6.0
4.0
2.0
0.0
0.00
1.00
2.00
3.00
4.00
5.00
6.00
7.00
8.00
9.00
Time [Gyr]
z=0.7468
log10(M*/M⊙)=10.65

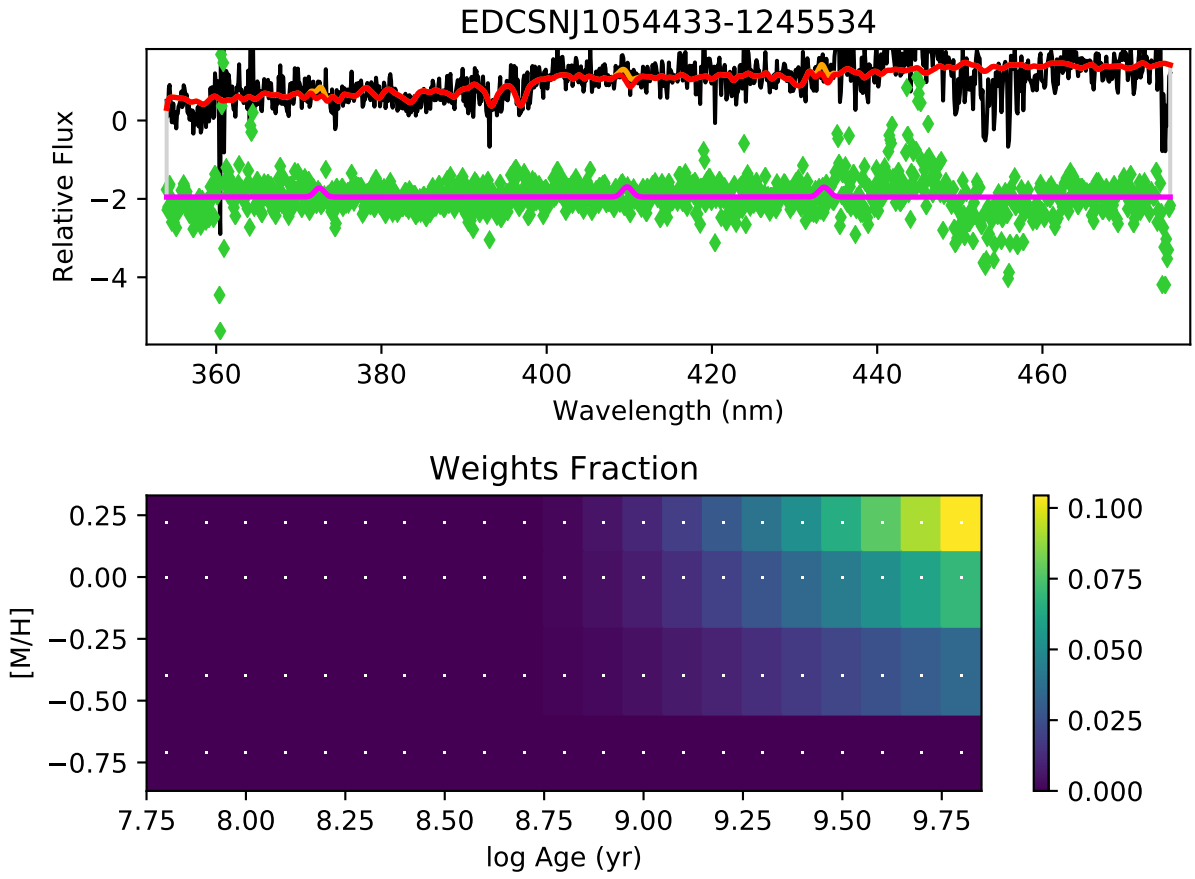
EDCSNJ1054433-1245534
Relative Flux
0
−2
−4
360
380
400
420
440
460
Wavelength (nm)
Weights Fraction
[M/H]
0.25
0.00
−0.25
−0.50
−0.75
7.75
8.00
8.25
8.50
8.75
9.00
9.25
9.50
9.75
log Age (yr)
0.100
0.075
0.050
0.025
0.000

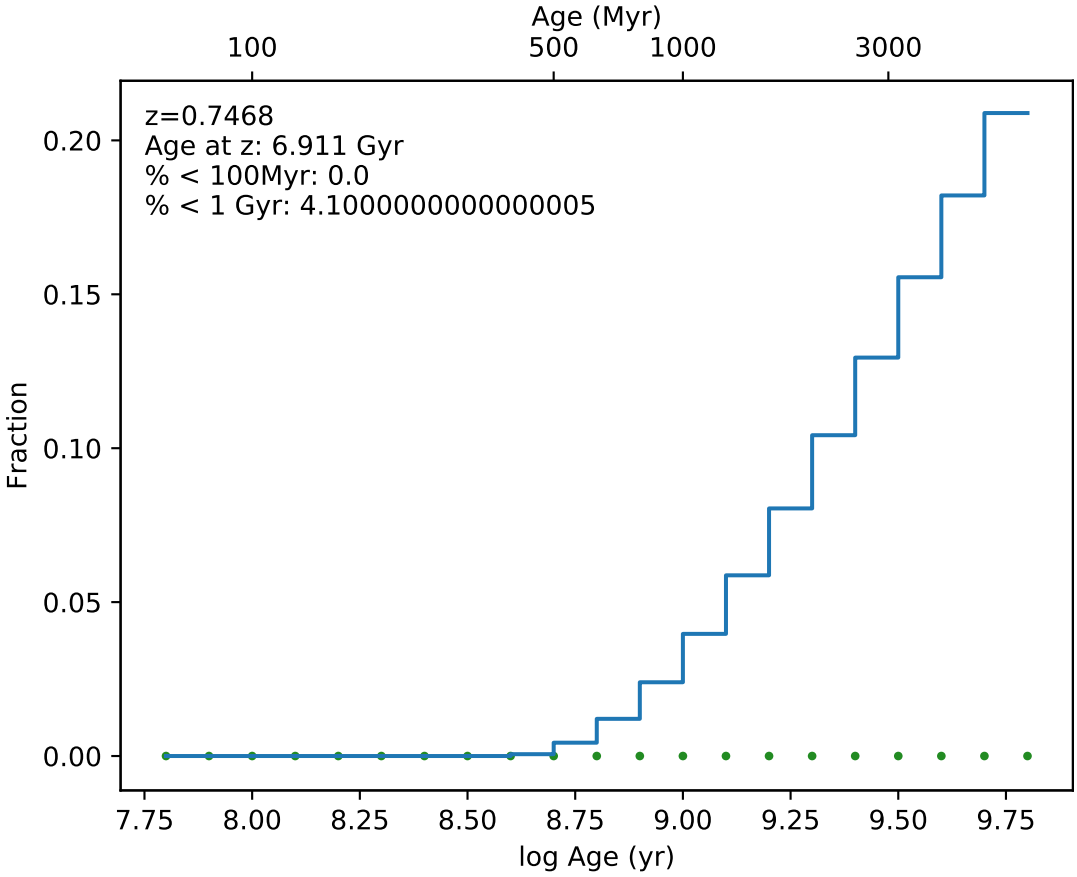
Age (Myr)
100
500
1000
3000
z=0.7468
Age at z: 6.911 Gyr
% < 100Myr: 0.0
% < 1 Gyr: 4.1000000000000005
Fraction
0.20
0.15
0.10
0.05
0.00
7.75
8.00
8.25
8.50
8.75
9.00
9.25
9.50
9.75
log Age (yr)

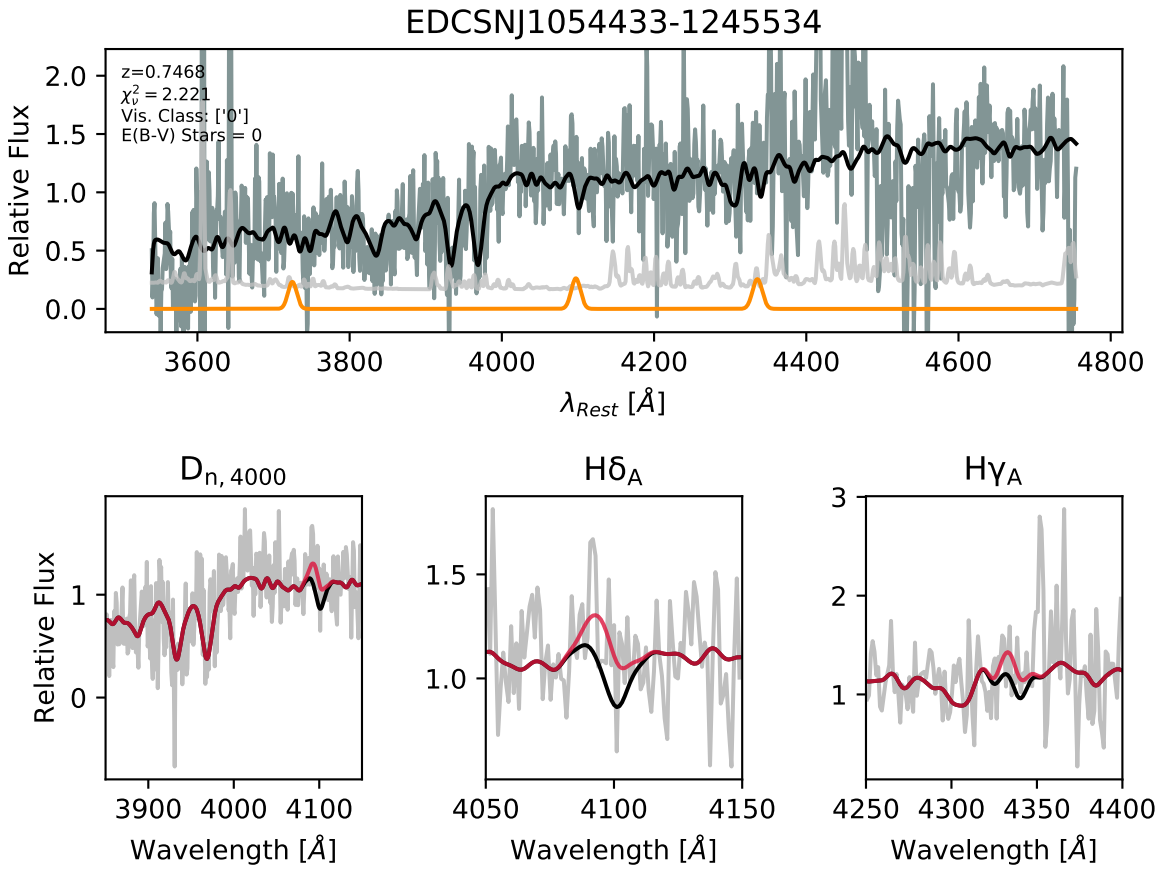
EDCSNJ1054433-1245534
z=0.7468
$\chi^2_\nu = 2.221$
Vis. Class: ['0']
E(B-V) Stars = 0
Relative Flux
λ_{Rest} [Å]
$D_{n,4000}$
$H\delta_A$
$H\gamma_A$
Wavelength [Å]

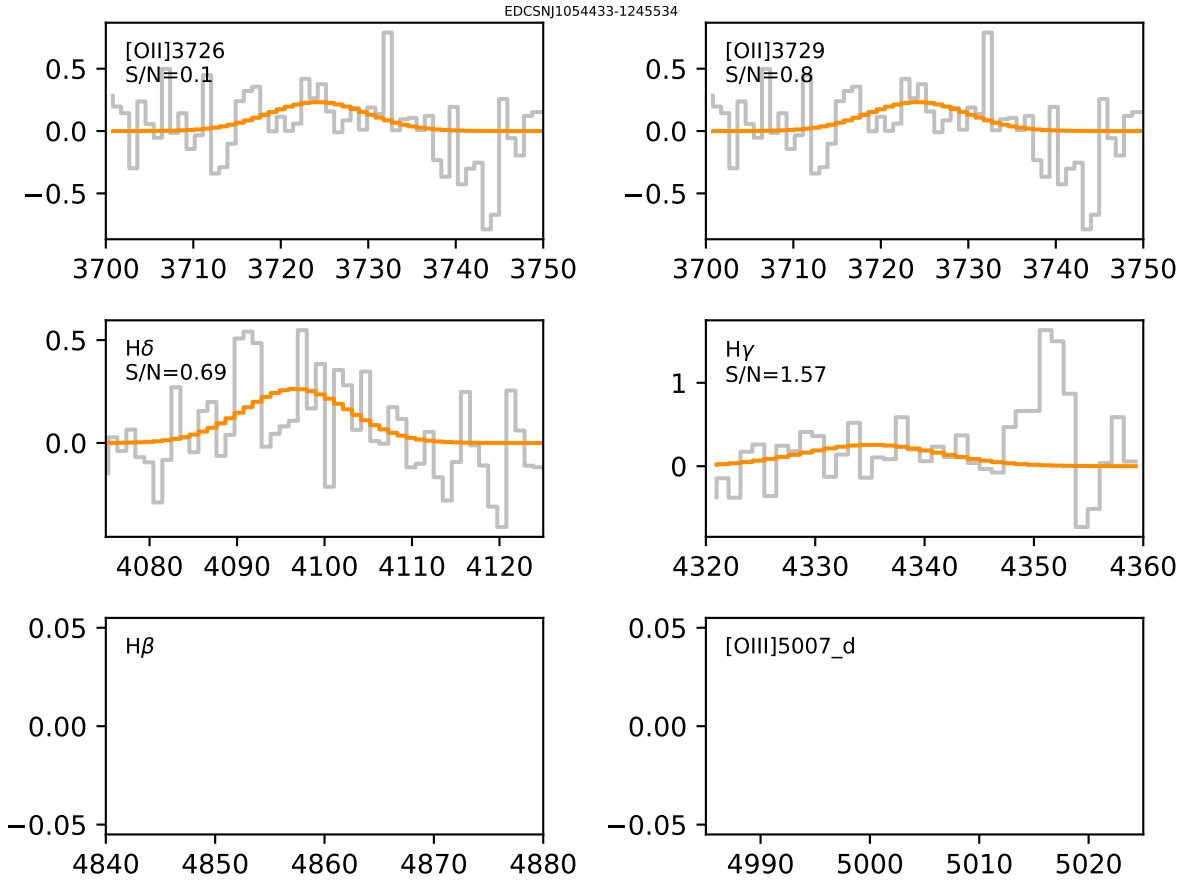
EDCSNJ1054433-1245534
[OII]3726
S/N=0.1
[OII]3729
S/N=0.8
Hδ
S/N=0.69
Hγ
S/N=1.57
Hβ
[OIII]5007_d

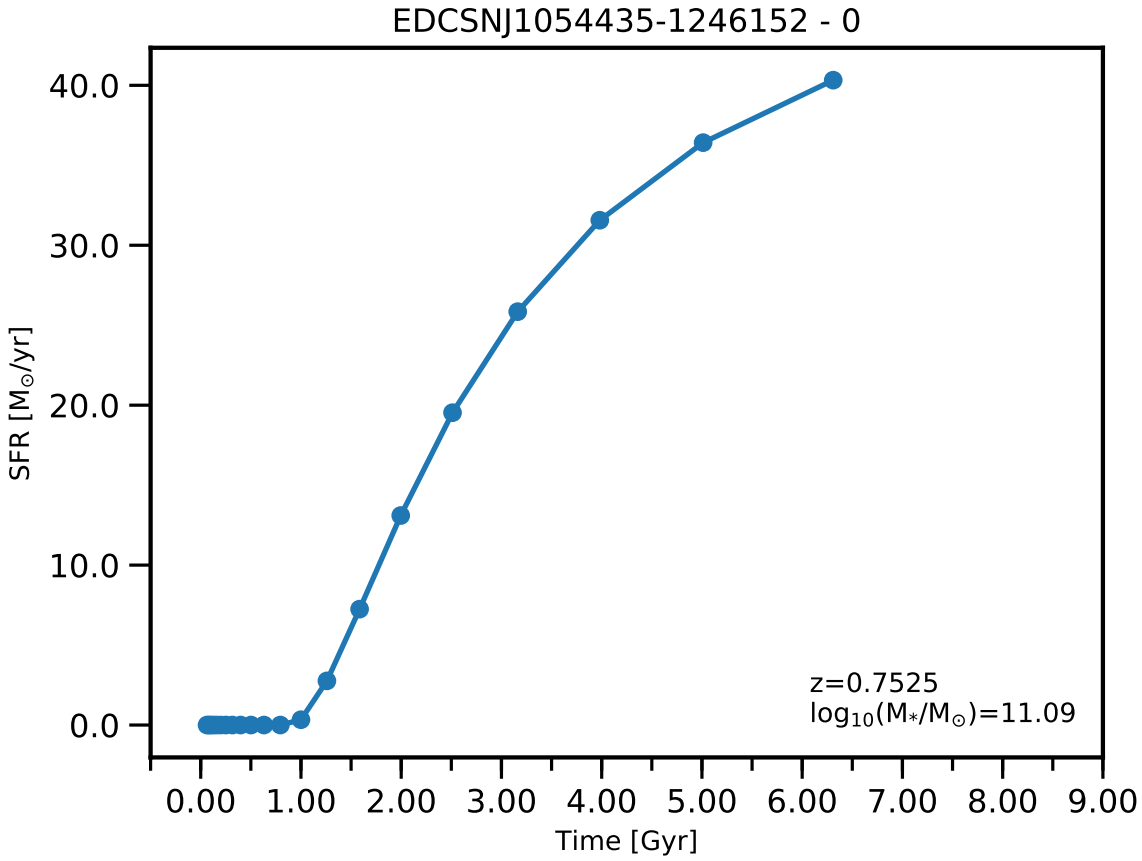
EDCSNJ1054435-1246152 - 0
SFR [M⊙/yr]
40.0
30.0
20.0
10.0
0.0
0.00
1.00
2.00
3.00
4.00
5.00
6.00
7.00
8.00
9.00
Time [Gyr]
z=0.7525
log10(M*/M⊙)=11.09

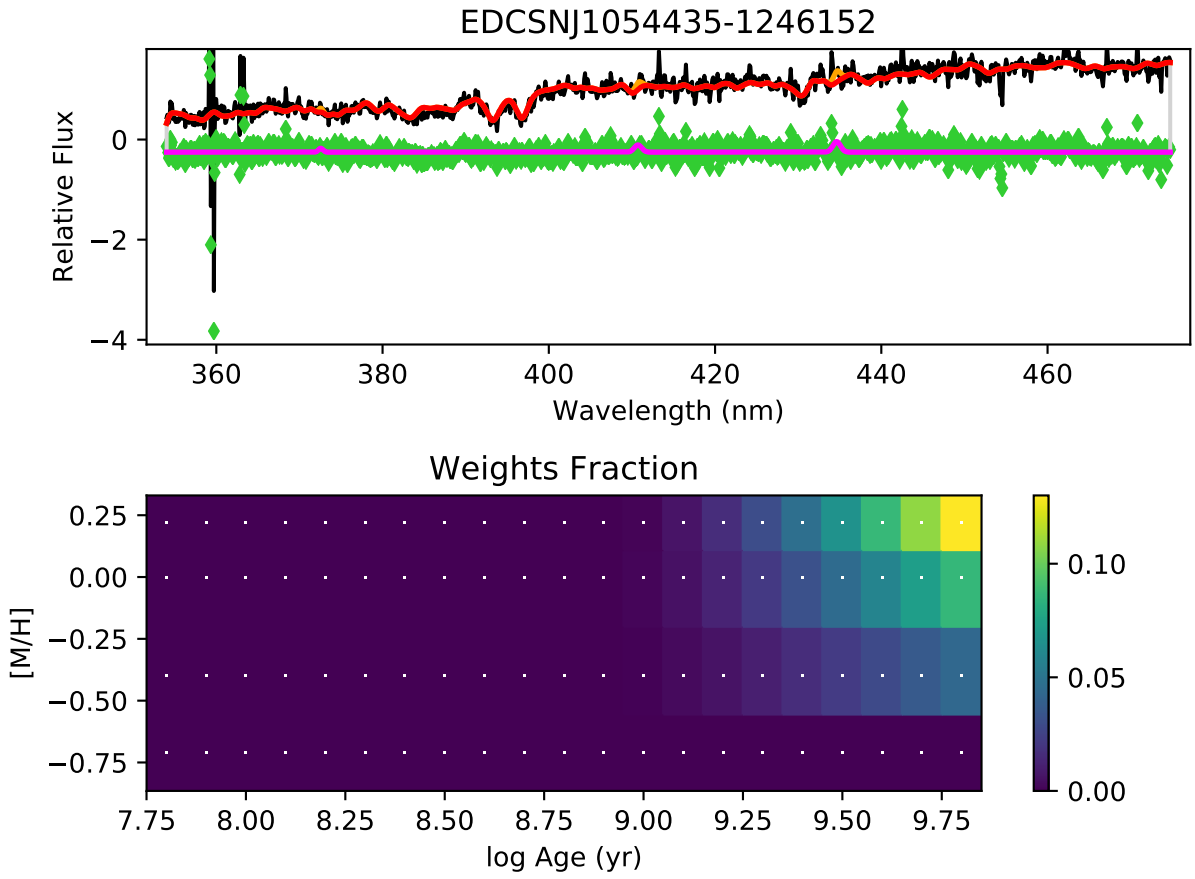
EDCSNJ1054435-1246152
Relative Flux
0
−2
−4
360
380
400
420
440
460
Wavelength (nm)
Weights Fraction
[M/H]
0.25
0.00
−0.25
−0.50
−0.75
7.75
8.00
8.25
8.50
8.75
9.00
9.25
9.50
9.75
log Age (yr)
0.10
0.05
0.00

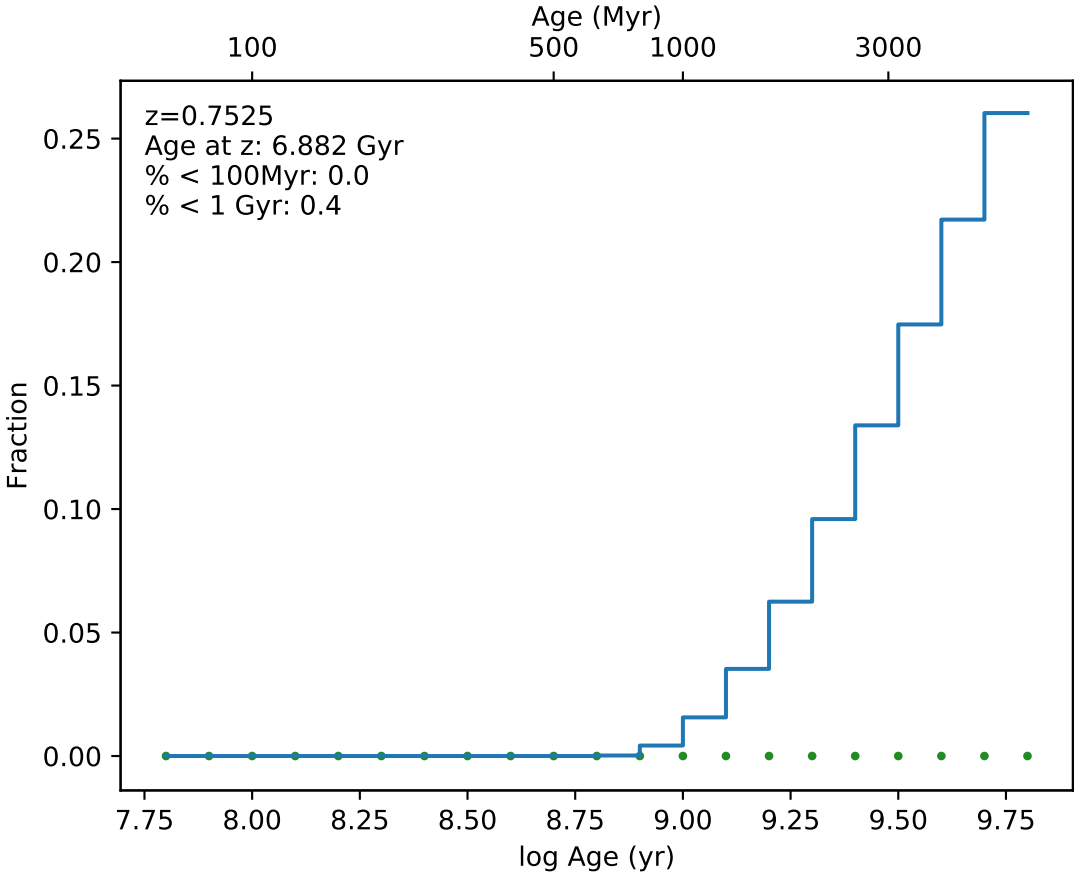
Age (Myr)
100
500
1000
3000
z=0.7525
Age at z: 6.882 Gyr
% < 100Myr: 0.0
% < 1 Gyr: 0.4
Fraction
0.25
0.20
0.15
0.10
0.05
0.00
7.75
8.00
8.25
8.50
8.75
9.00
9.25
9.50
9.75
log Age (yr)

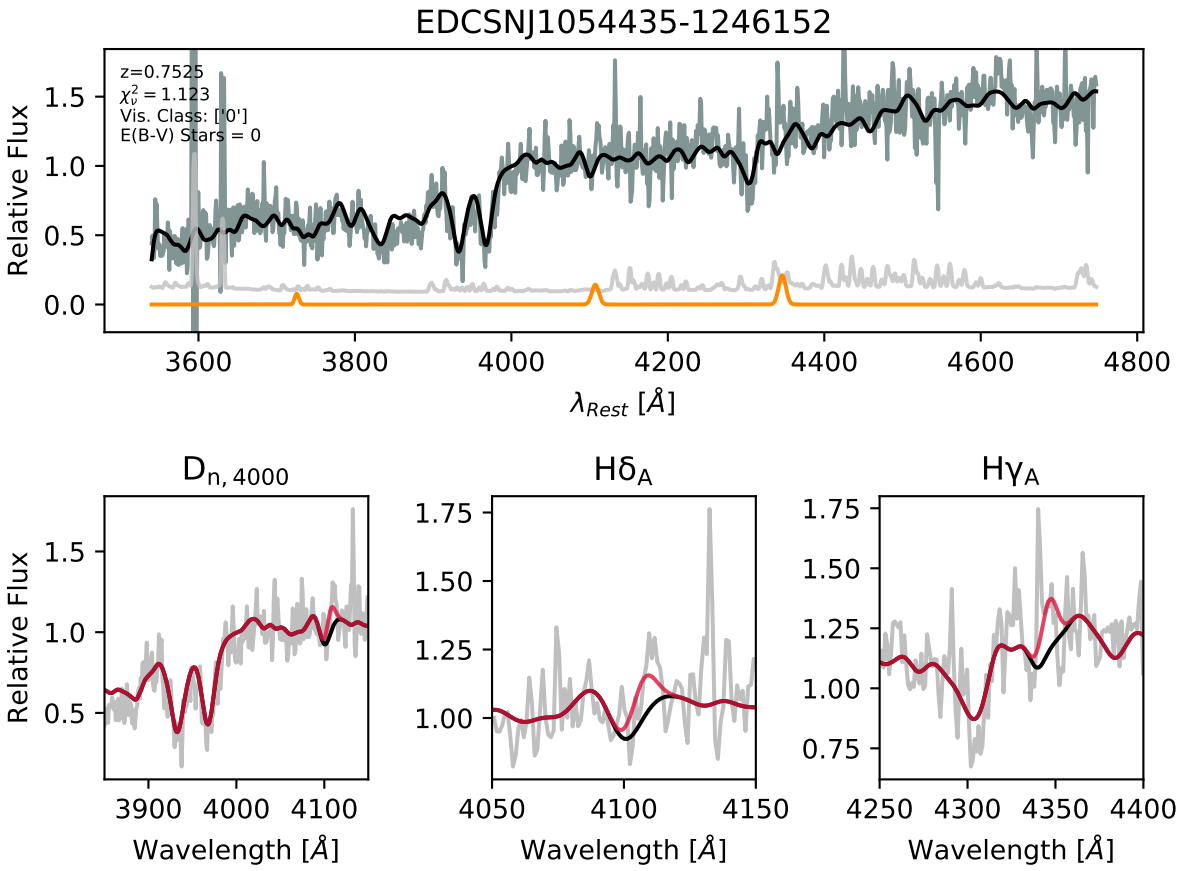
EDCSNJ1054435-1246152
z=0.7525
$\chi^2_\nu = 1.123$
Vis. Class: ['0']
E(B-V) Stars = 0
Relative Flux
λ_{Rest} [Å]
$D_{n,4000}$
$H\delta_A$
$H\gamma_A$
Wavelength [Å]

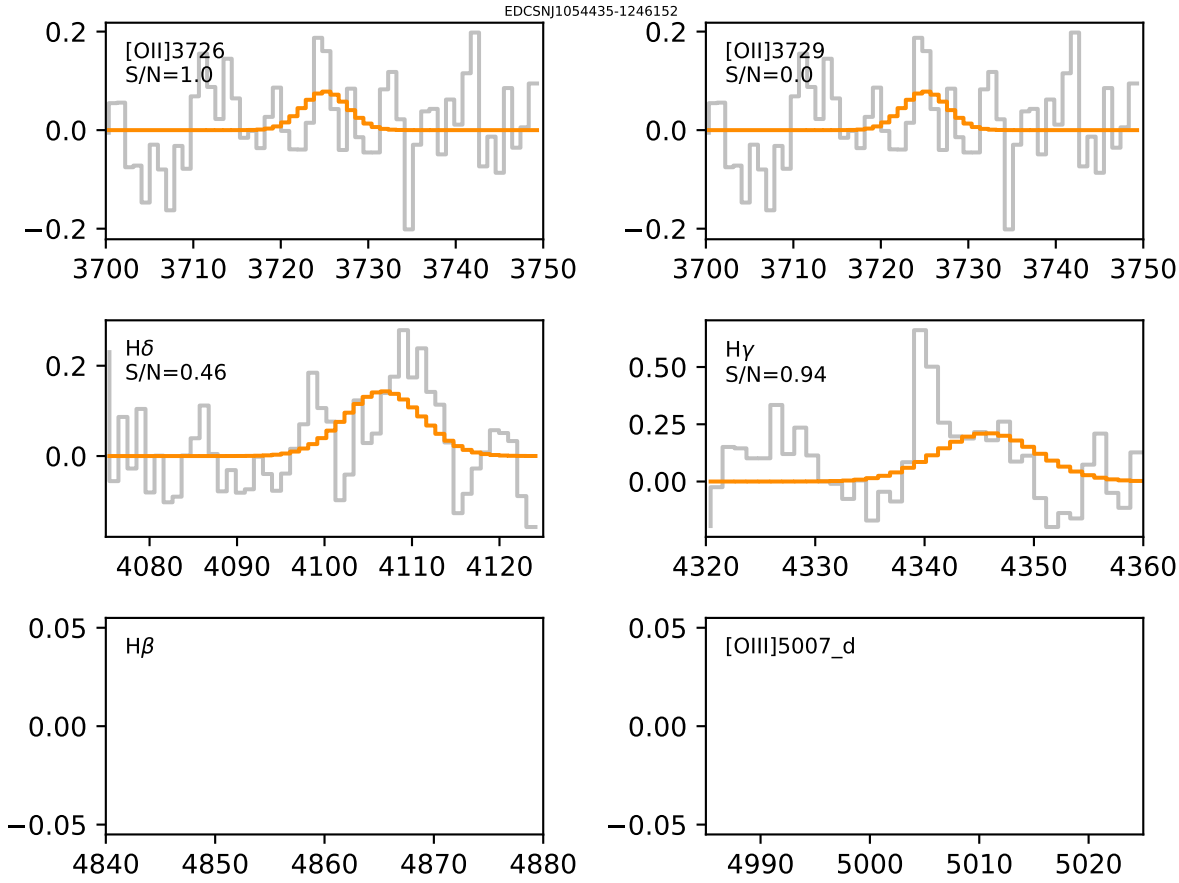
EDCSNJ1054435-1246152
[OII]3726
S/N=1.0
[OII]3729
S/N=0.0
Hδ
S/N=0.46
Hγ
S/N=0.94
Hβ
[OIII]5007_d

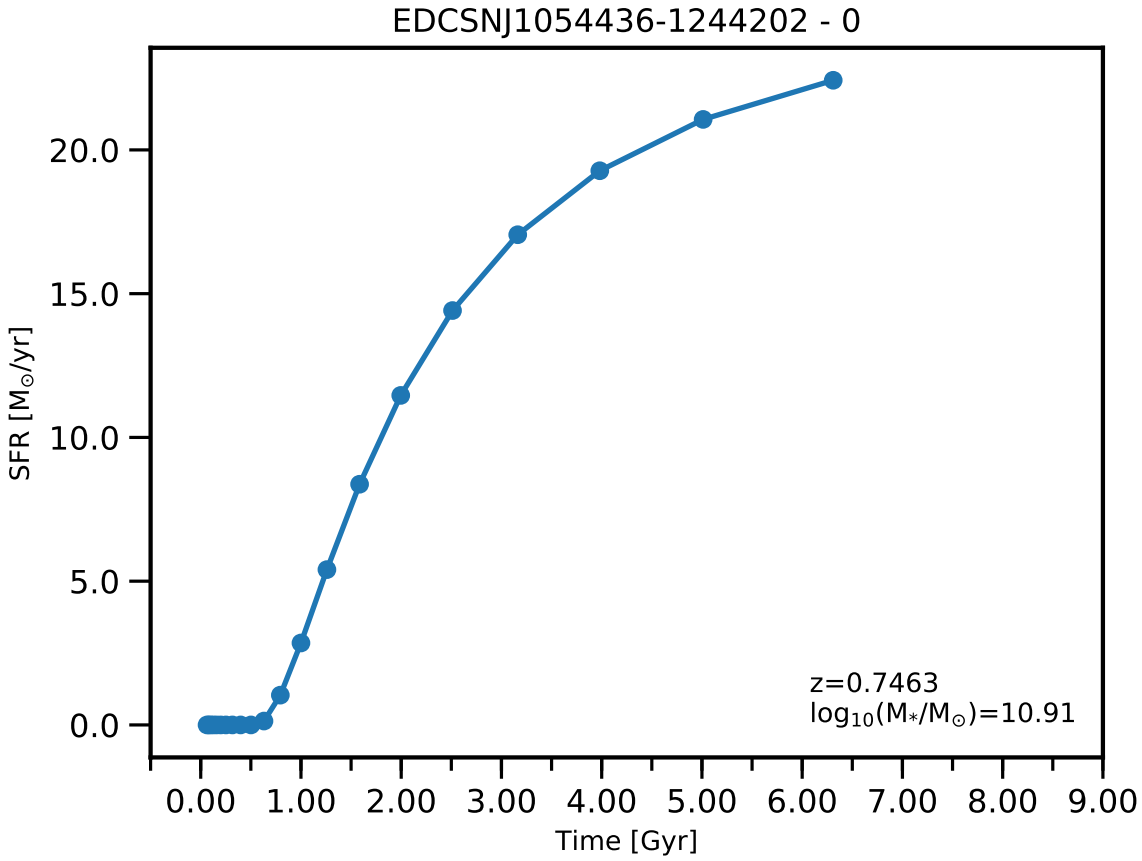
EDCSNJ1054436-1244202 - 0
SFR [M⊙/yr]
20.0
15.0
10.0
5.0
0.0
0.00
1.00
2.00
3.00
4.00
5.00
6.00
7.00
8.00
9.00
Time [Gyr]
z=0.7463
log10(M*/M⊙)=10.91

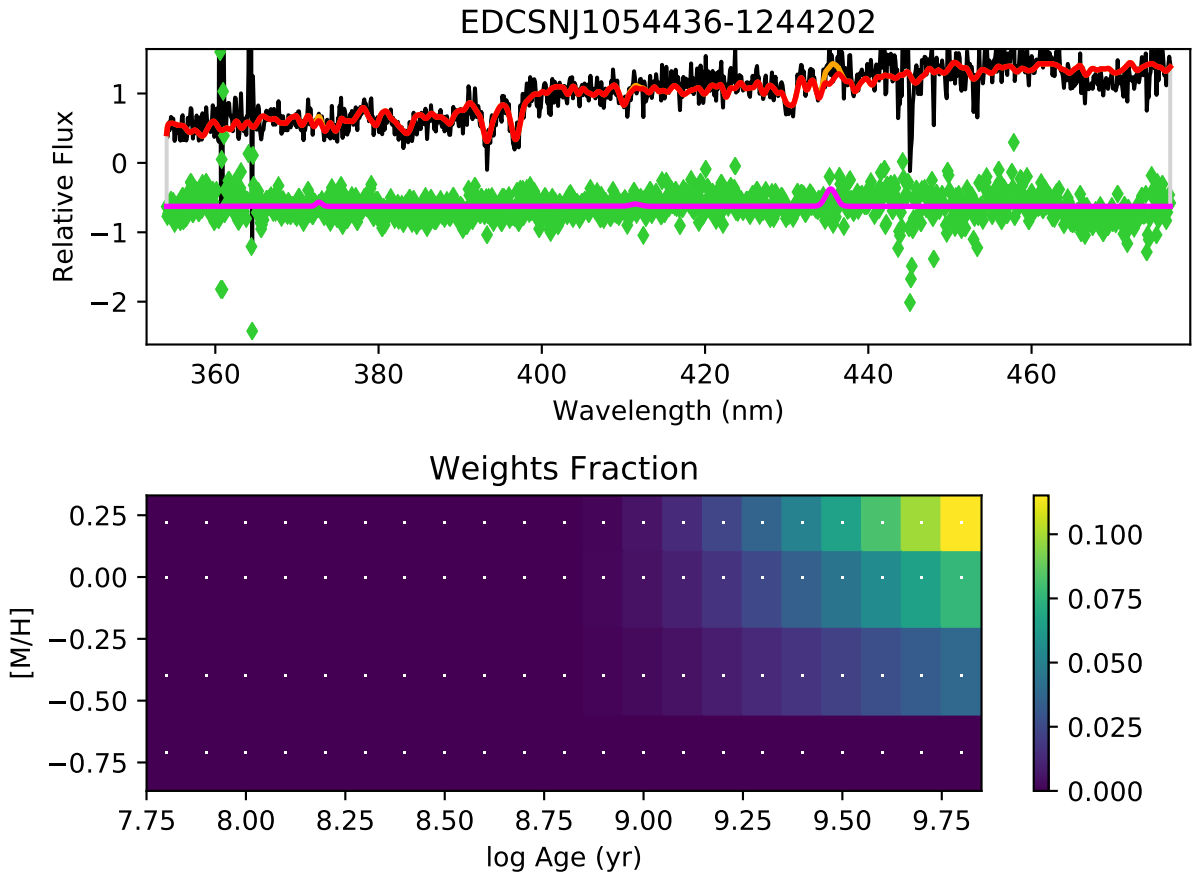
EDCSNJ1054436-1244202
Relative Flux
1
0
−1
−2
360
380
400
420
440
460
Wavelength (nm)
Weights Fraction
[M/H]
0.25
0.00
−0.25
−0.50
−0.75
7.75
8.00
8.25
8.50
8.75
9.00
9.25
9.50
9.75
log Age (yr)
0.100
0.075
0.050
0.025
0.000

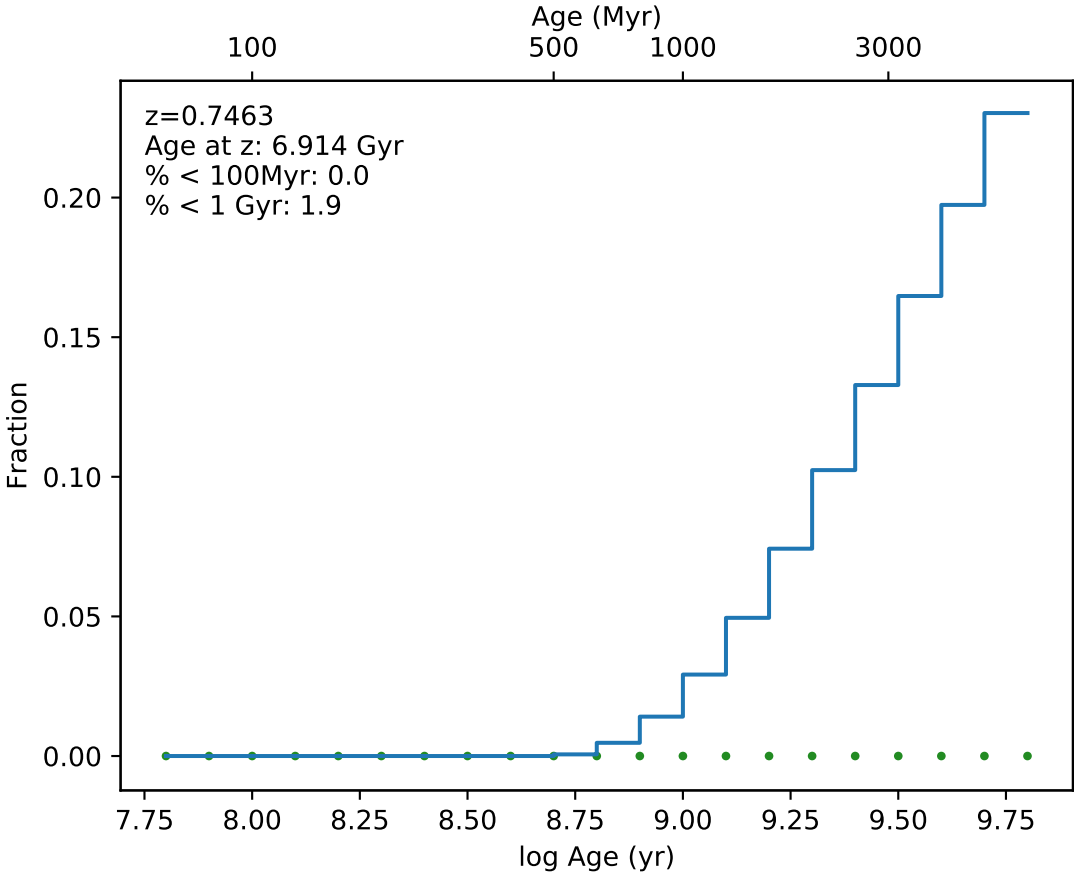
Age (Myr)
100
500
1000
3000
z=0.7463
Age at z: 6.914 Gyr
% < 100Myr: 0.0
% < 1 Gyr: 1.9
Fraction
0.00
0.05
0.10
0.15
0.20
7.75
8.00
8.25
8.50
8.75
9.00
9.25
9.50
9.75
log Age (yr)

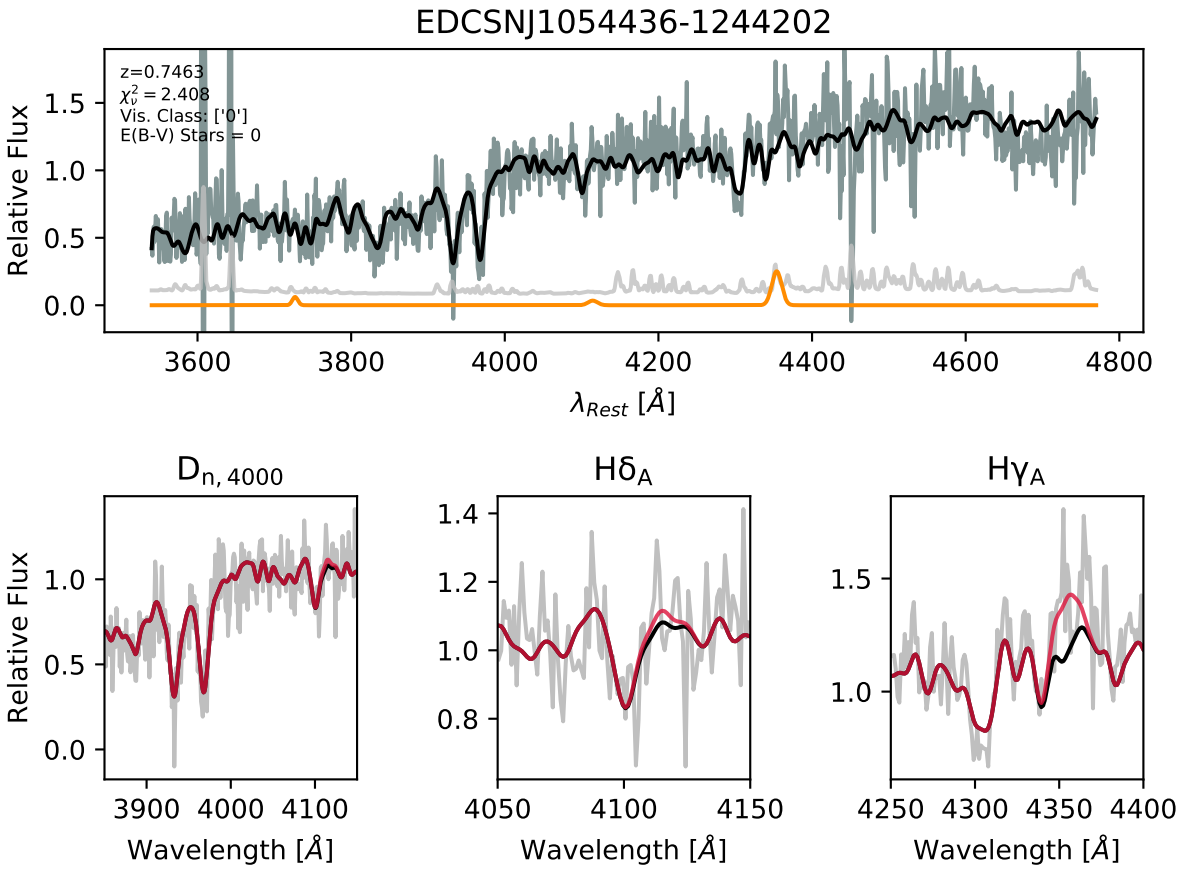
EDCSNJ1054436-1244202
z=0.7463
$\chi^2_\nu = 2.408$
Vis. Class: ['0']
E(B-V) Stars = 0
Relative Flux
λ_{Rest} [Å]
$D_{n,4000}$
$H\delta_A$
$H\gamma_A$
Wavelength [Å]

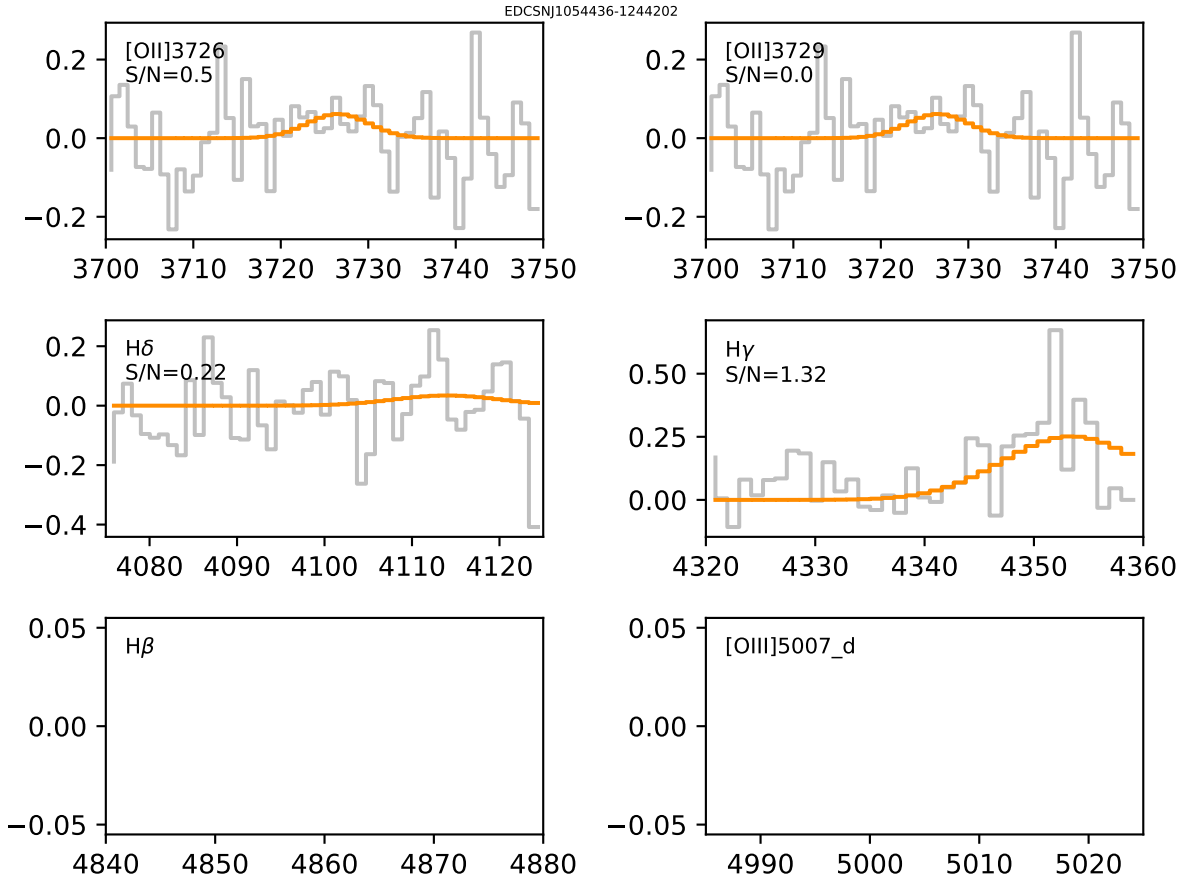
EDCSNJ1054436-1244202
[OII]3726
S/N=0.5
[OII]3729
S/N=0.0
Hδ
S/N=0.22
Hγ
S/N=1.32
Hβ
[OIII]5007_d

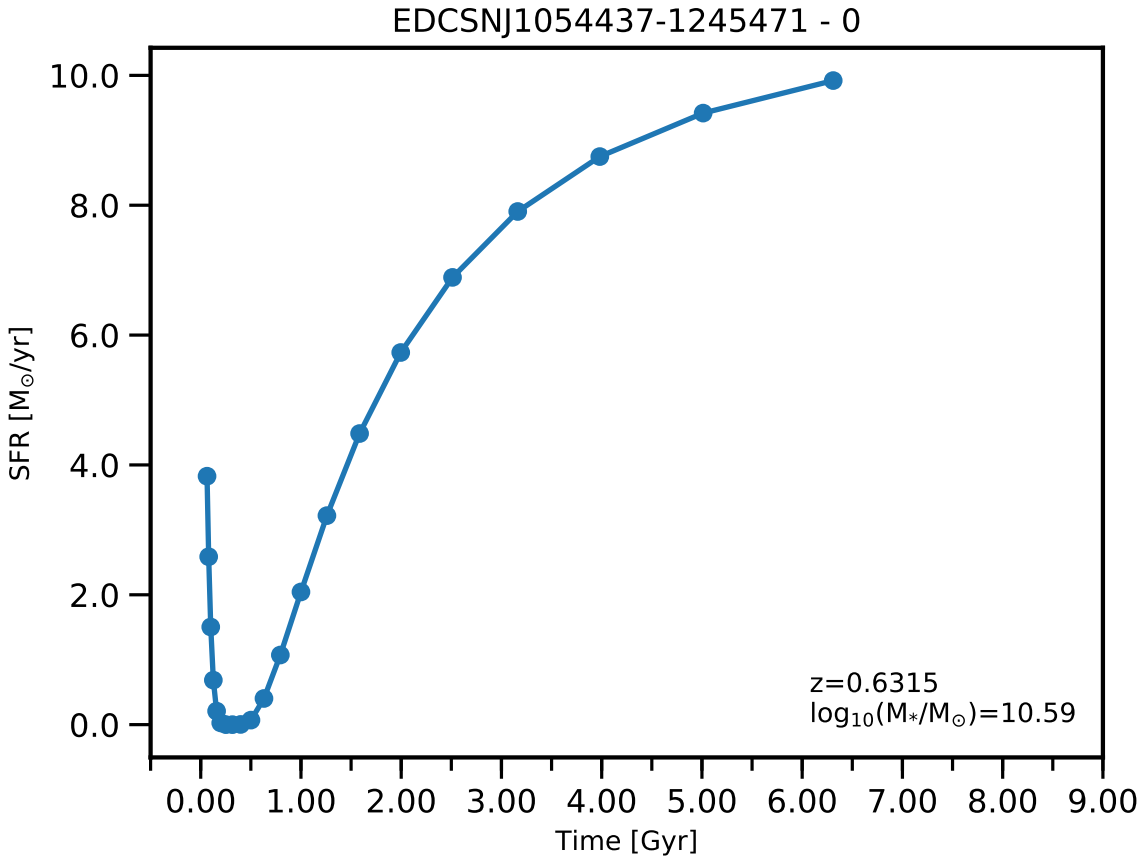
EDCSNJ1054437-1245471 - 0
SFR [M⊙/yr]
Time [Gyr]
z=0.6315
log10(M*/M⊙)=10.59
0.0
2.0
4.0
6.0
8.0
10.0
0.00
1.00
2.00
3.00
4.00
5.00
6.00
7.00
8.00
9.00

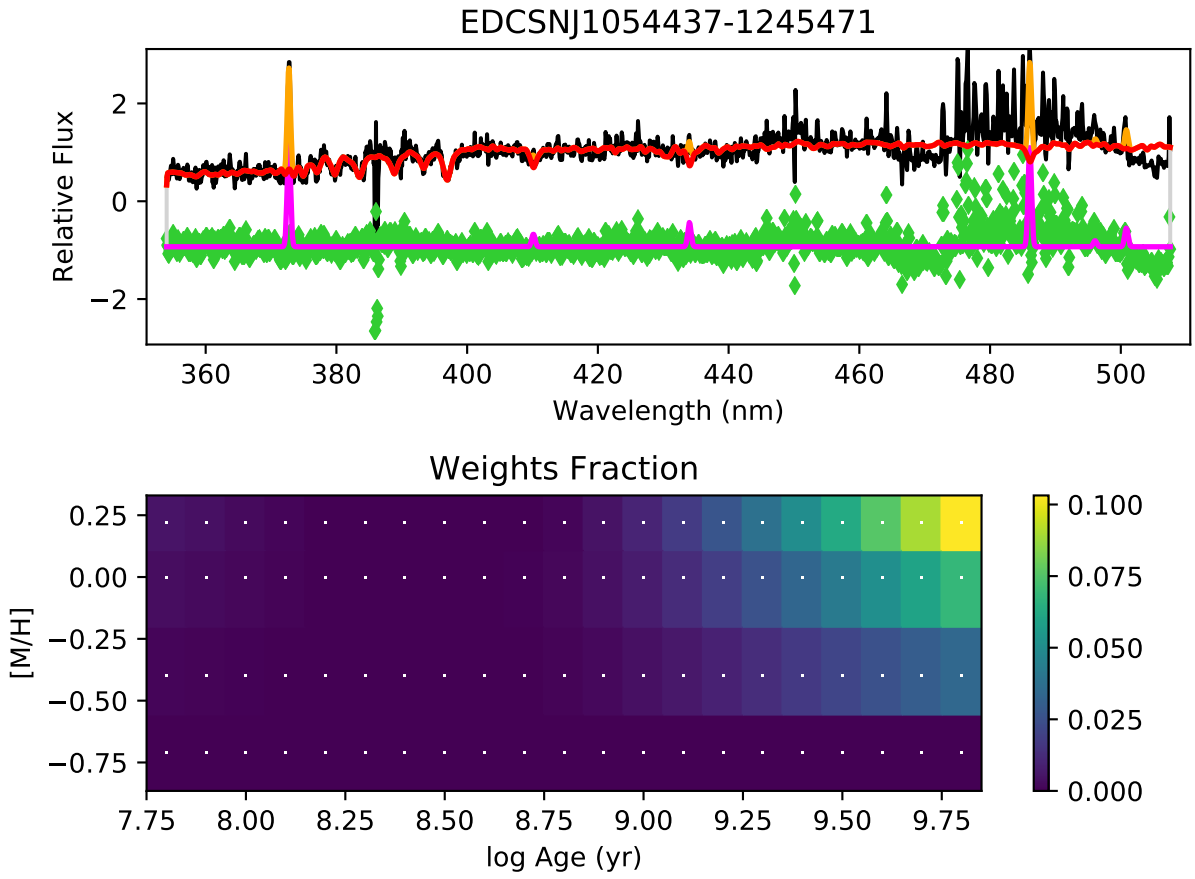
EDCSNJ1054437-1245471
Relative Flux
2
0
−2
360
380
400
420
440
460
480
500
Wavelength (nm)
Weights Fraction
[M/H]
0.25
0.00
−0.25
−0.50
−0.75
7.75
8.00
8.25
8.50
8.75
9.00
9.25
9.50
9.75
log Age (yr)
0.100
0.075
0.050
0.025
0.000

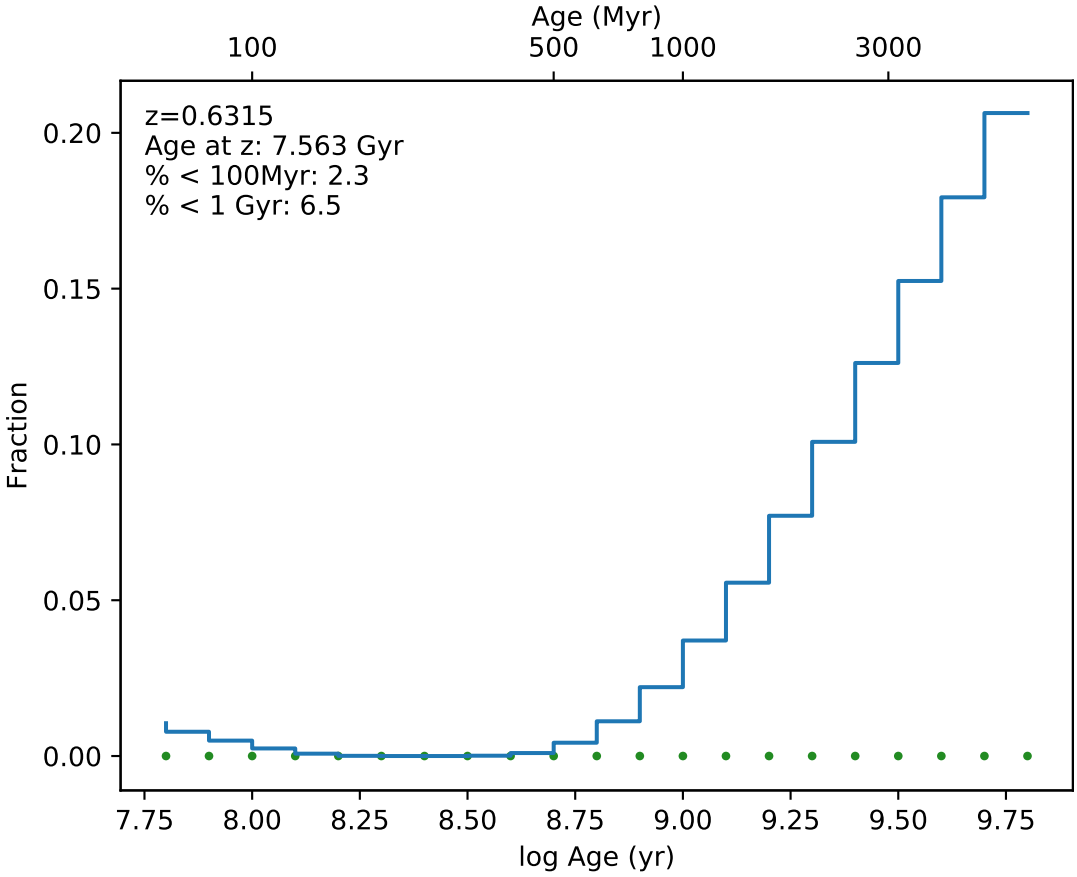
Age (Myr)
100
500
1000
3000
z=0.6315
Age at z: 7.563 Gyr
% < 100Myr: 2.3
% < 1 Gyr: 6.5
0.20
0.15
0.10
0.05
0.00
Fraction
7.75
8.00
8.25
8.50
8.75
9.00
9.25
9.50
9.75
log Age (yr)

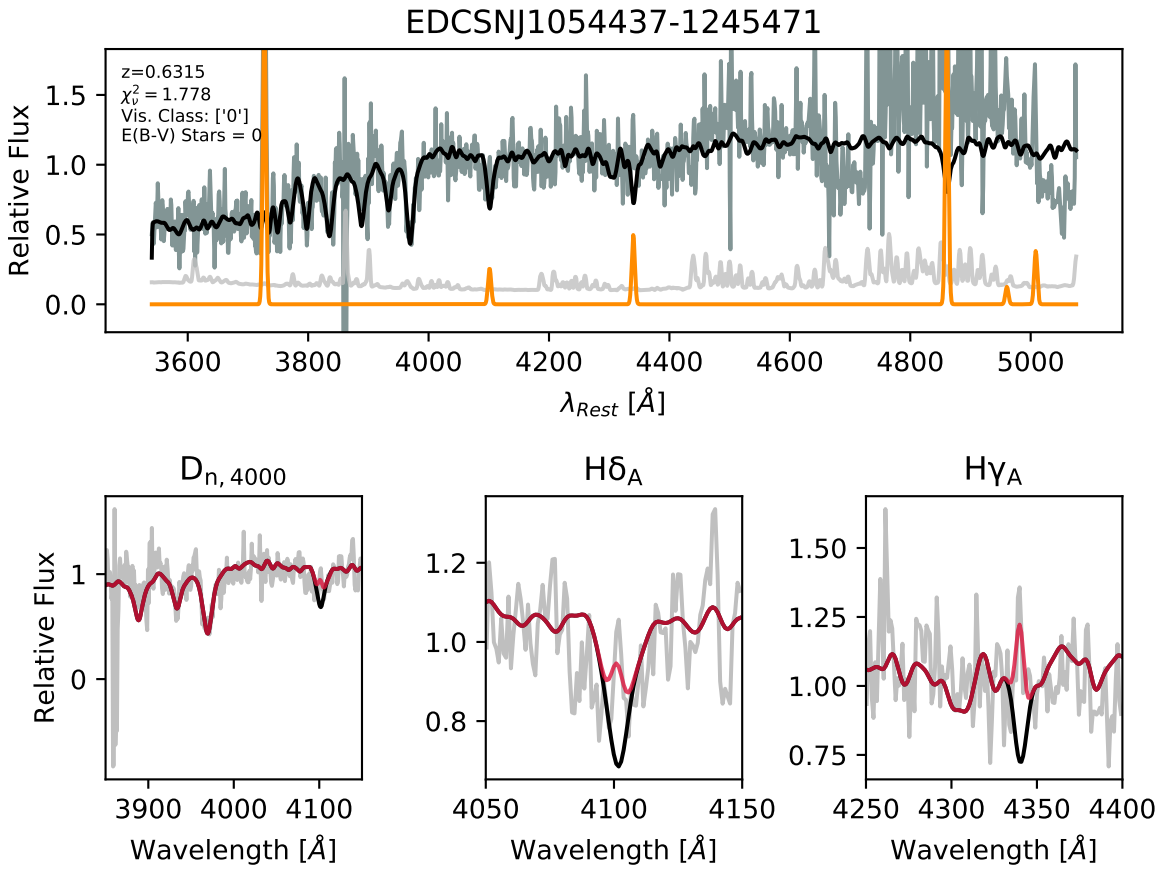
EDCSNJ1054437-1245471
z=0.6315
$\chi^2_\nu = 1.778$
Vis. Class: ['0']
E(B-V) Stars = 0
Relative Flux
1.5
1.0
0.5
0.0
3600
3800
4000
4200
4400
4600
4800
5000
λ_{Rest} [Å]
$D_{n,4000}$
$H\delta_A$
$H\gamma_A$
Relative Flux
1
0
3900
4000
4100
Wavelength [Å]
1.2
1.0
0.8
4050
4100
4150
Wavelength [Å]
1.50
1.25
1.00
0.75
4250
4300
4350
4400
Wavelength [Å]

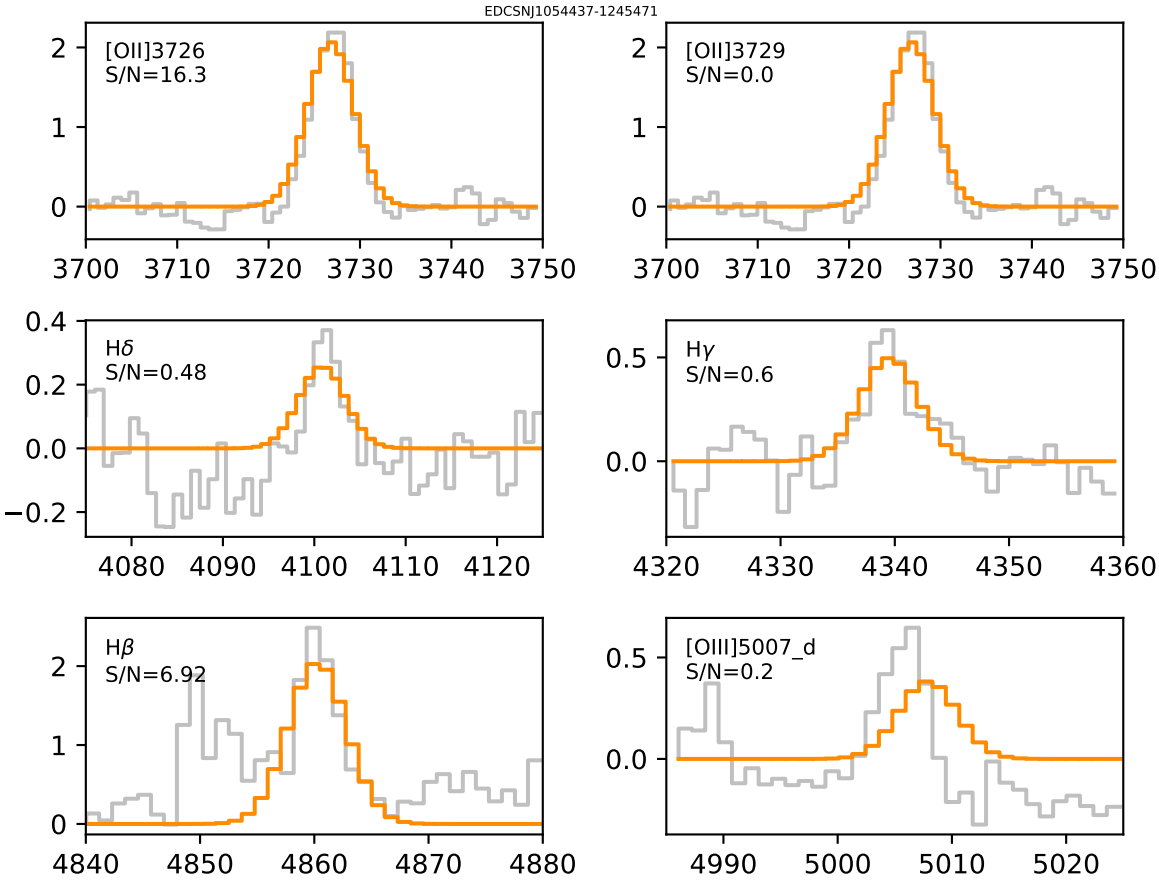
EDCSNJ1054437-1245471
[OII]3726
S/N=16.3
[OII]3729
S/N=0.0
Hδ
S/N=0.48
Hγ
S/N=0.6
Hβ
S/N=6.92
[OIII]5007_d
S/N=0.2

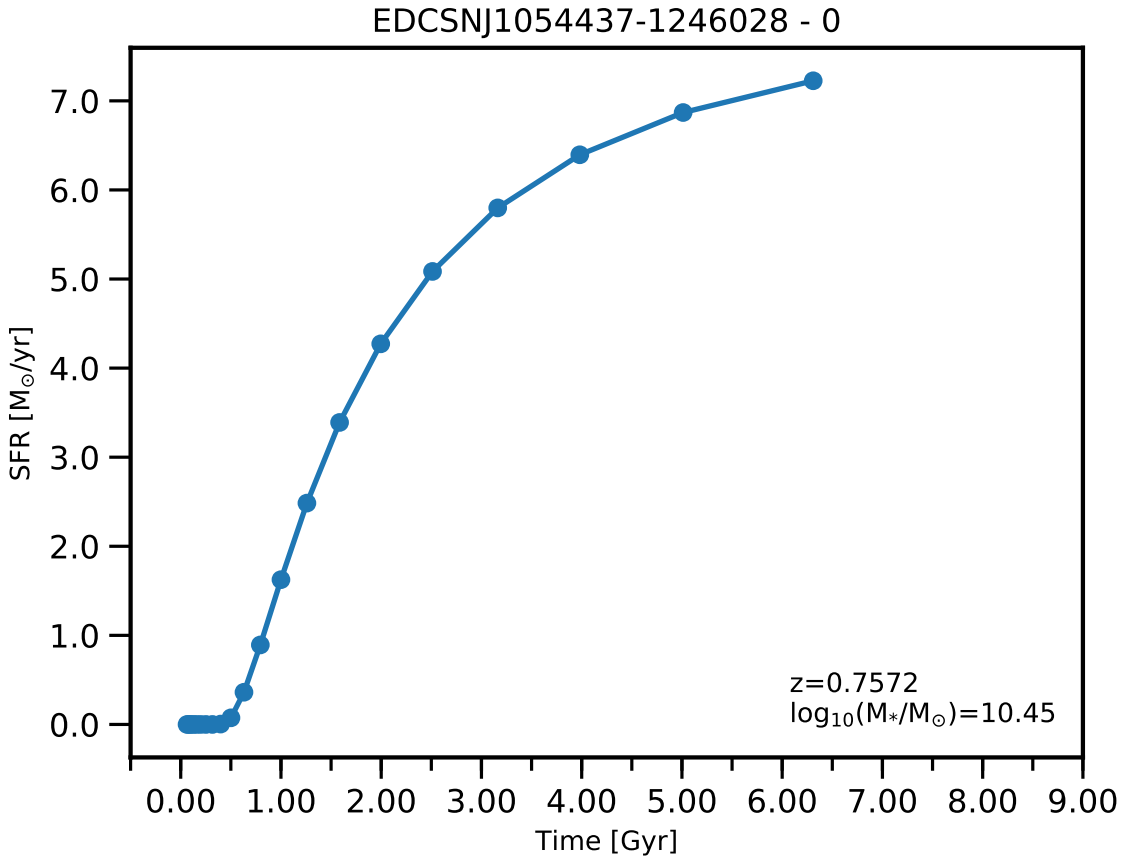
EDCSNJ1054437-1246028 - 0
SFR [M⊙/yr]
7.0
6.0
5.0
4.0
3.0
2.0
1.0
0.0
0.00
1.00
2.00
3.00
4.00
5.00
6.00
7.00
8.00
9.00
Time [Gyr]
z=0.7572
log10(M*/M⊙)=10.45

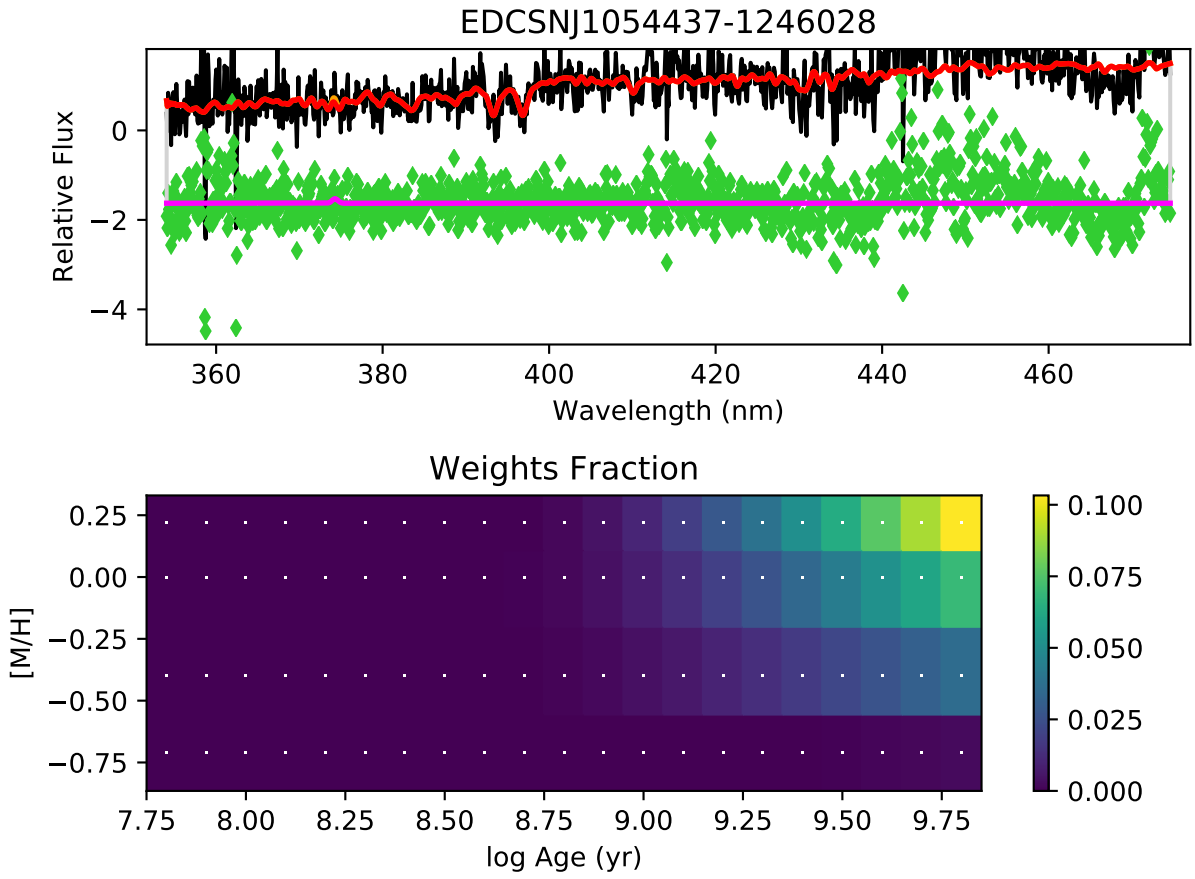
EDCSNJ1054437-1246028
Relative Flux
0
−2
−4
360
380
400
420
440
460
Wavelength (nm)
Weights Fraction
[M/H]
0.25
0.00
−0.25
−0.50
−0.75
7.75
8.00
8.25
8.50
8.75
9.00
9.25
9.50
9.75
log Age (yr)
0.100
0.075
0.050
0.025
0.000

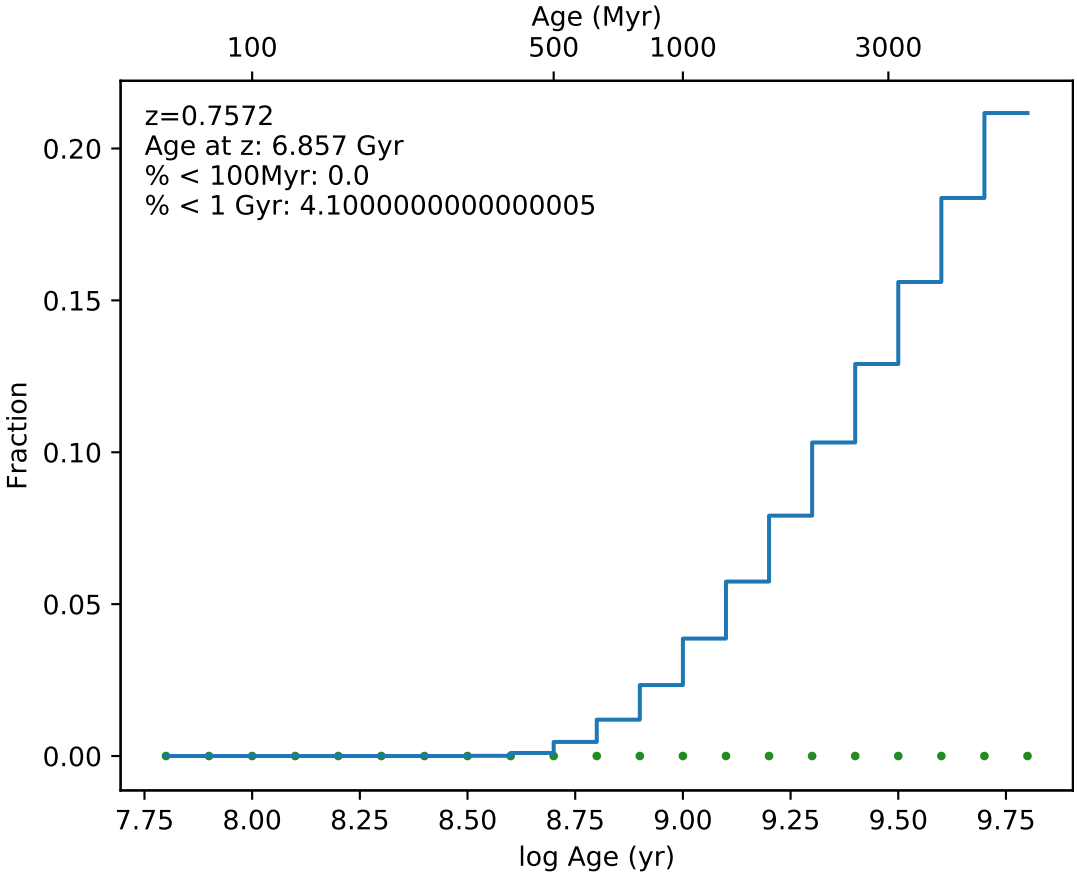
Age (Myr)
100
500
1000
3000
z=0.7572
Age at z: 6.857 Gyr
% < 100Myr: 0.0
% < 1 Gyr: 4.1000000000000005
0.20
0.15
0.10
0.05
0.00
Fraction
7.75
8.00
8.25
8.50
8.75
9.00
9.25
9.50
9.75
log Age (yr)

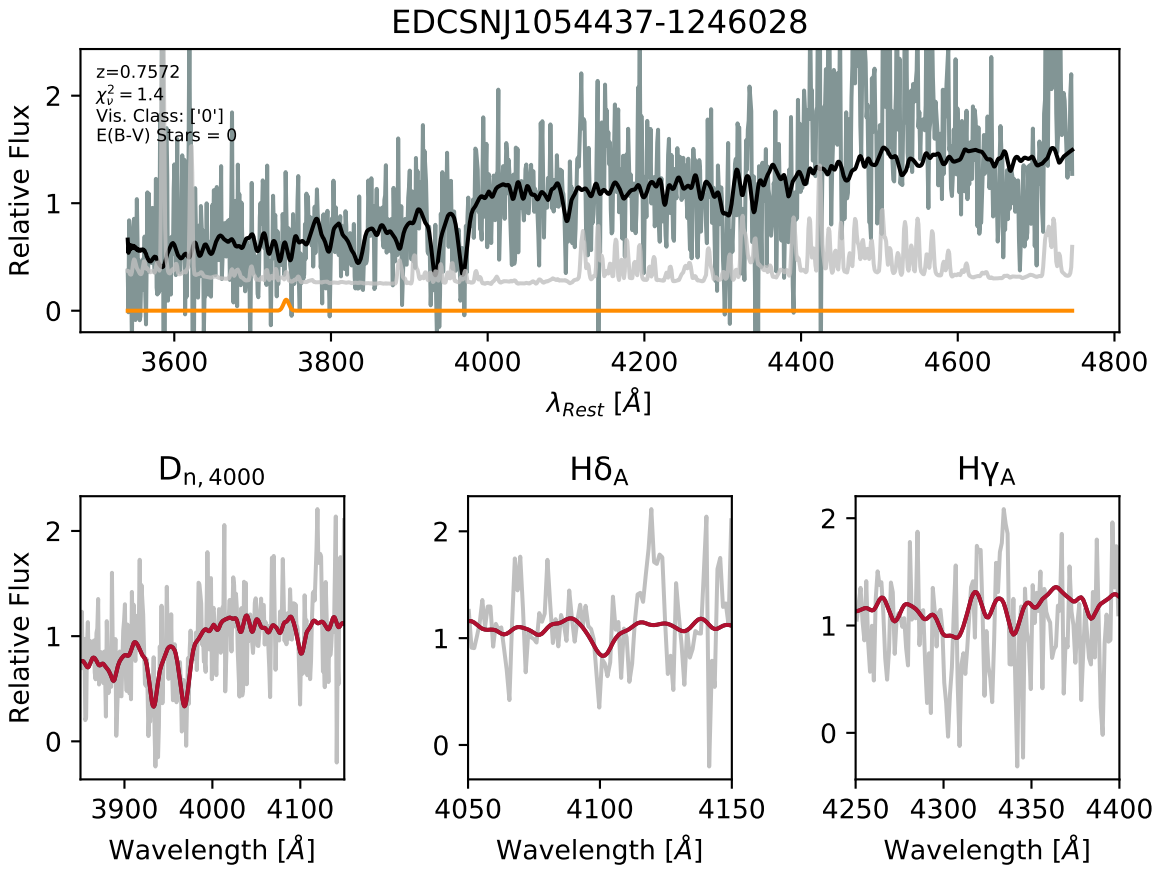
EDCSNJ1054437-1246028
z=0.7572
$\chi^2_\nu = 1.4$
Vis. Class: ['0']
E(B-V) Stars = 0
Relative Flux
λ_{Rest} [Å]
$D_{n,4000}$
$H\delta_A$
$H\gamma_A$
Wavelength [Å]

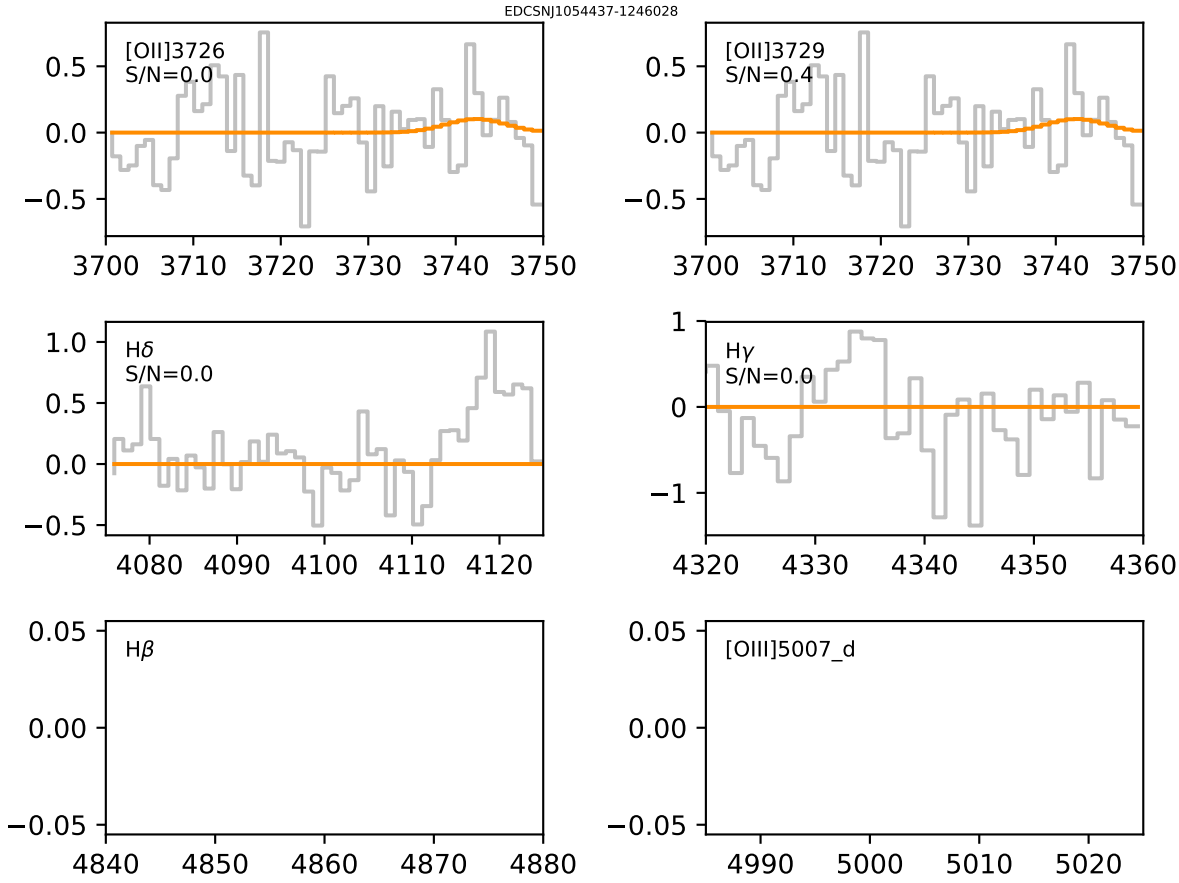
EDCSNJ1054437-1246028
[OII]3726
S/N=0.0
[OII]3729
S/N=0.4
Hδ
S/N=0.0
Hγ
S/N=0.0
Hβ
[OIII]5007_d

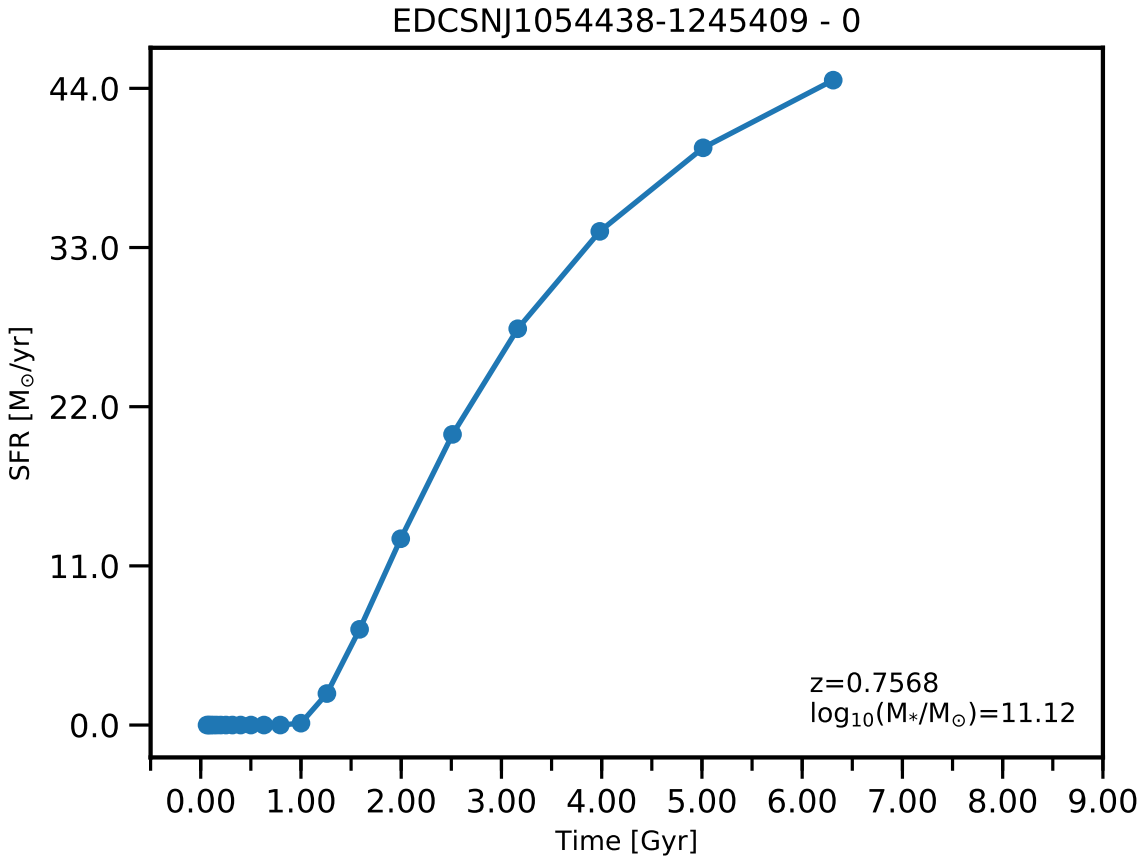
EDCSNJ1054438-1245409 - 0
44.0
33.0
22.0
11.0
0.0
SFR [M⊙/yr]
0.00
1.00
2.00
3.00
4.00
5.00
6.00
7.00
8.00
9.00
Time [Gyr]
z=0.7568
log10(M*/M⊙)=11.12

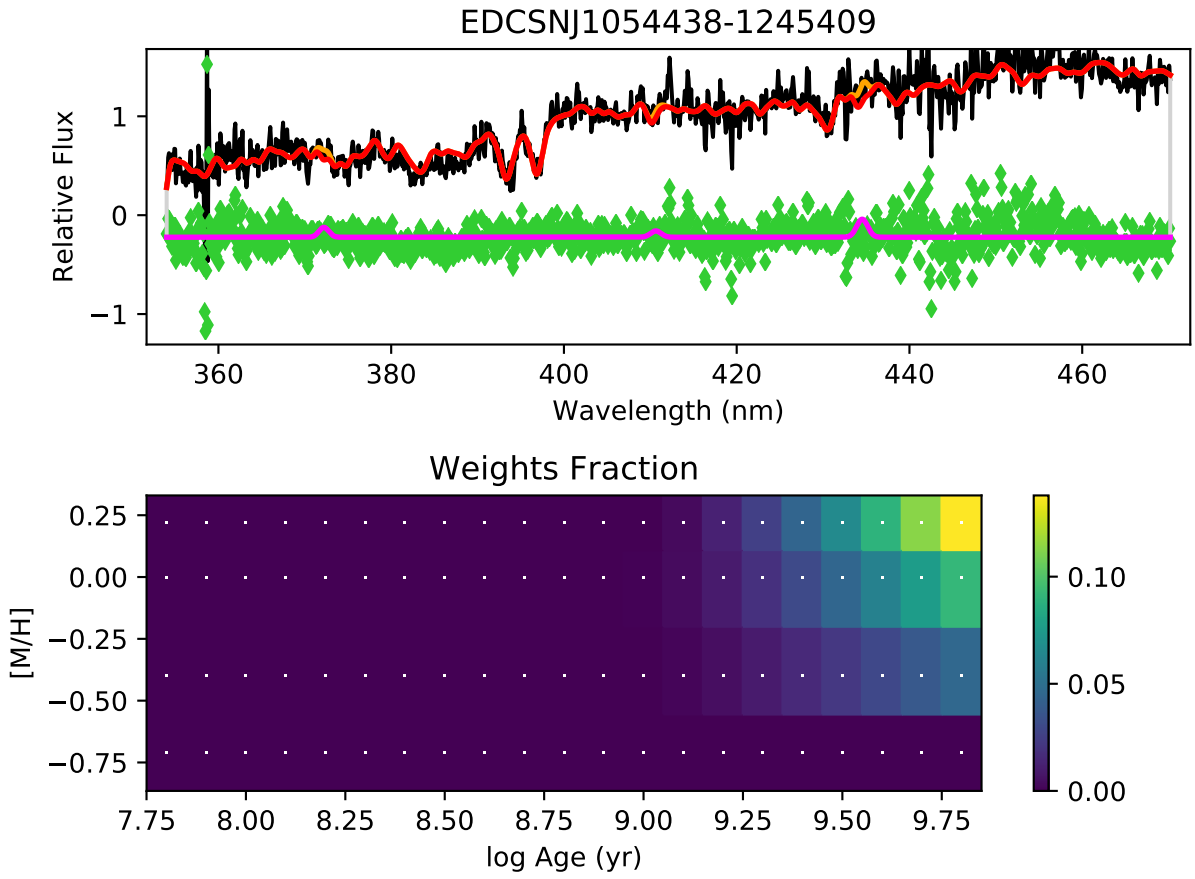
EDCSNJ1054438-1245409
Relative Flux
1
0
−1
360
380
400
420
440
460
Wavelength (nm)
Weights Fraction
[M/H]
0.25
0.00
−0.25
−0.50
−0.75
7.75
8.00
8.25
8.50
8.75
9.00
9.25
9.50
9.75
log Age (yr)
0.10
0.05
0.00

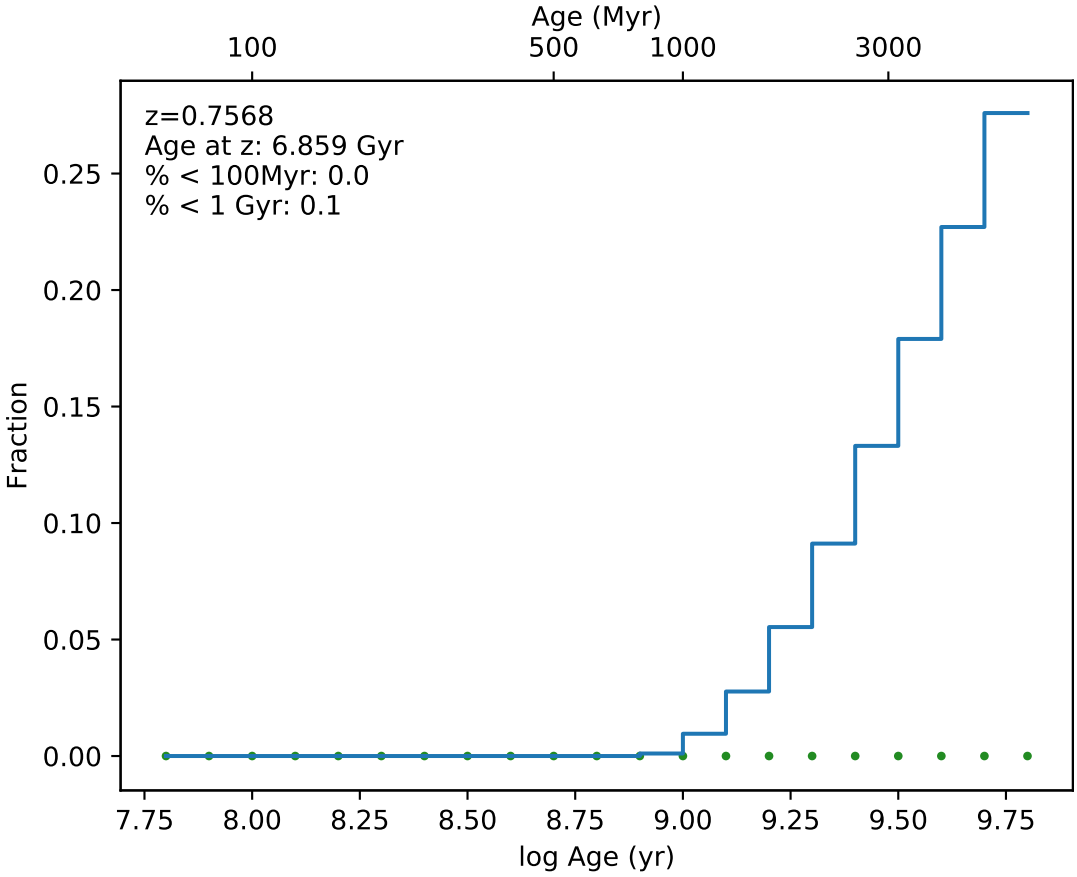
Age (Myr)
100
500
1000
3000
z=0.7568
Age at z: 6.859 Gyr
% < 100Myr: 0.0
% < 1 Gyr: 0.1
Fraction
0.25
0.20
0.15
0.10
0.05
0.00
7.75
8.00
8.25
8.50
8.75
9.00
9.25
9.50
9.75
log Age (yr)

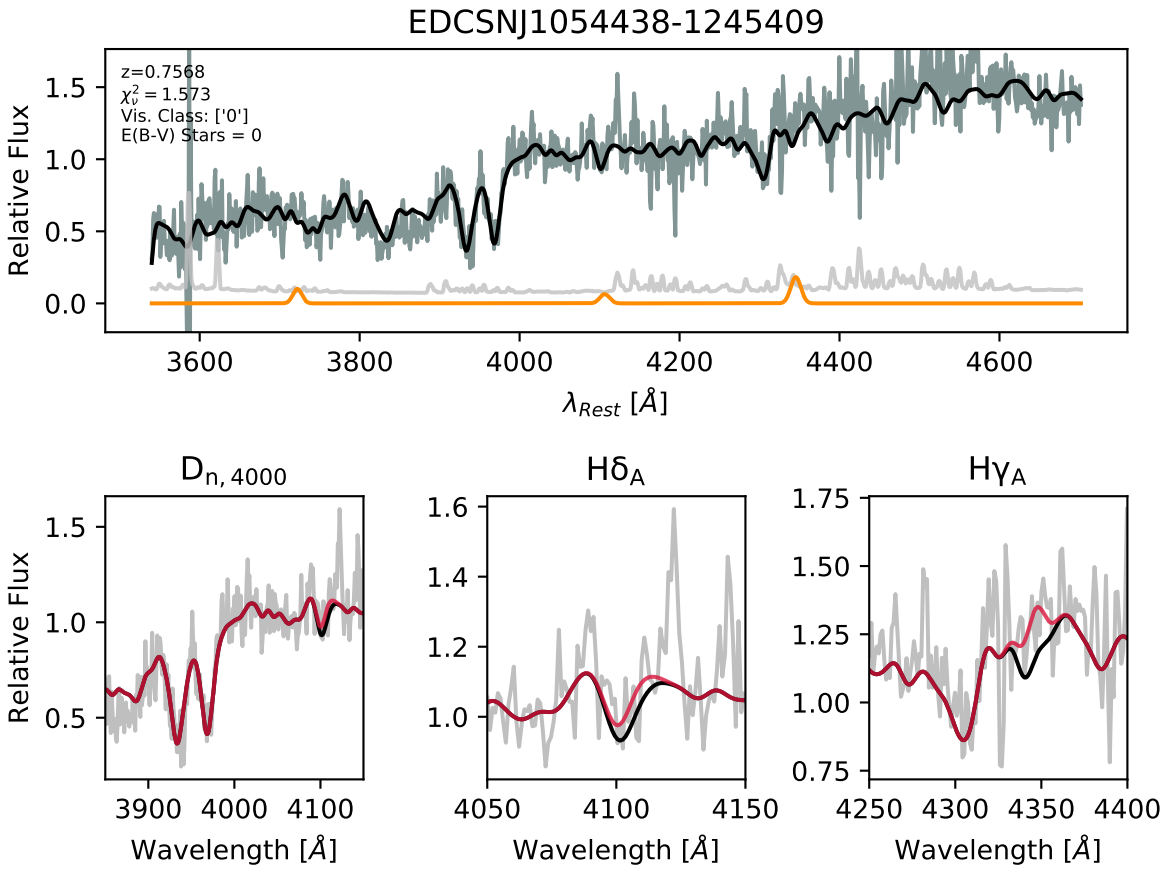
EDCSNJ1054438-1245409
z=0.7568
$\chi^2_\nu = 1.573$
Vis. Class: ['0']
E(B-V) Stars = 0
Relative Flux
λ_{Rest} [Å]
$D_{n,4000}$
$H\delta_A$
$H\gamma_A$
Wavelength [Å]

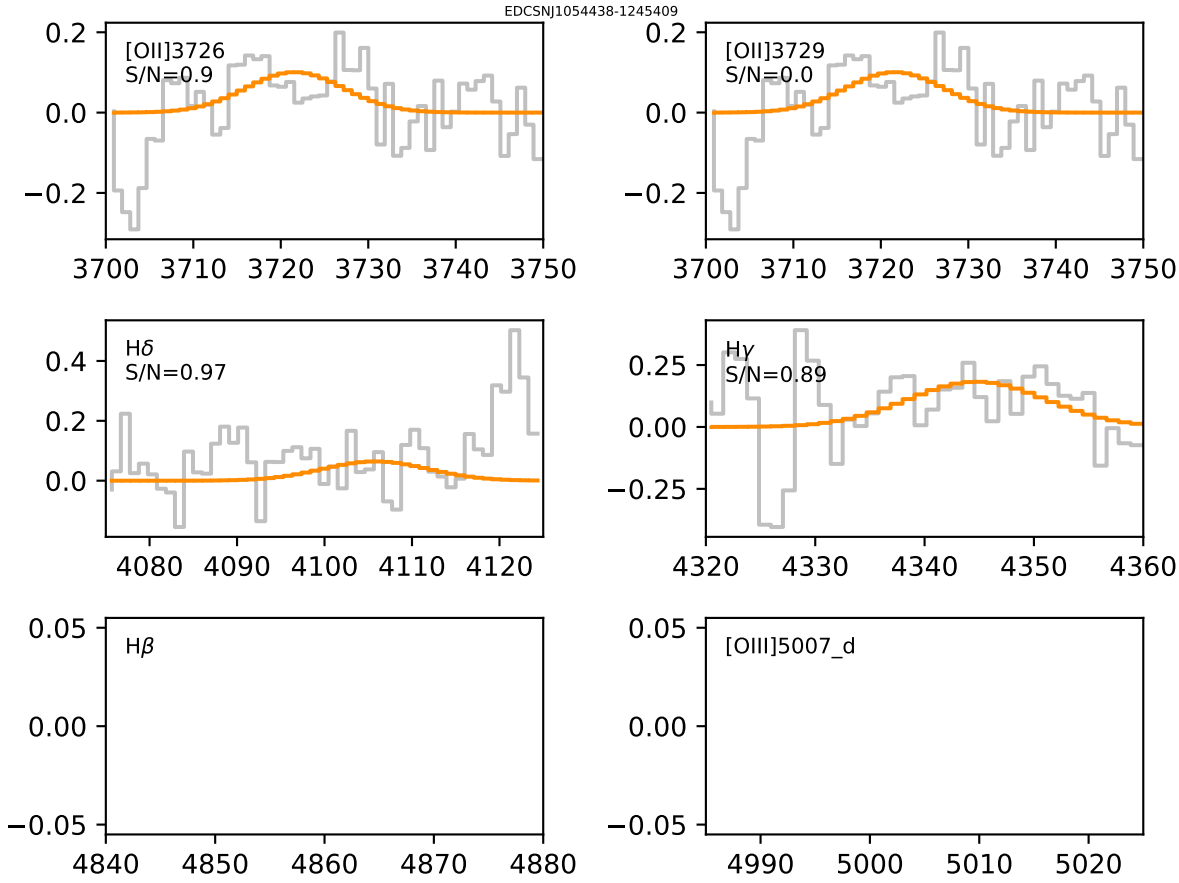
EDCSNJ1054438-1245409
[OII]3726
S/N=0.9
[OII]3729
S/N=0.0
Hδ
S/N=0.97
Hγ
S/N=0.89
Hβ
[OIII]5007_d

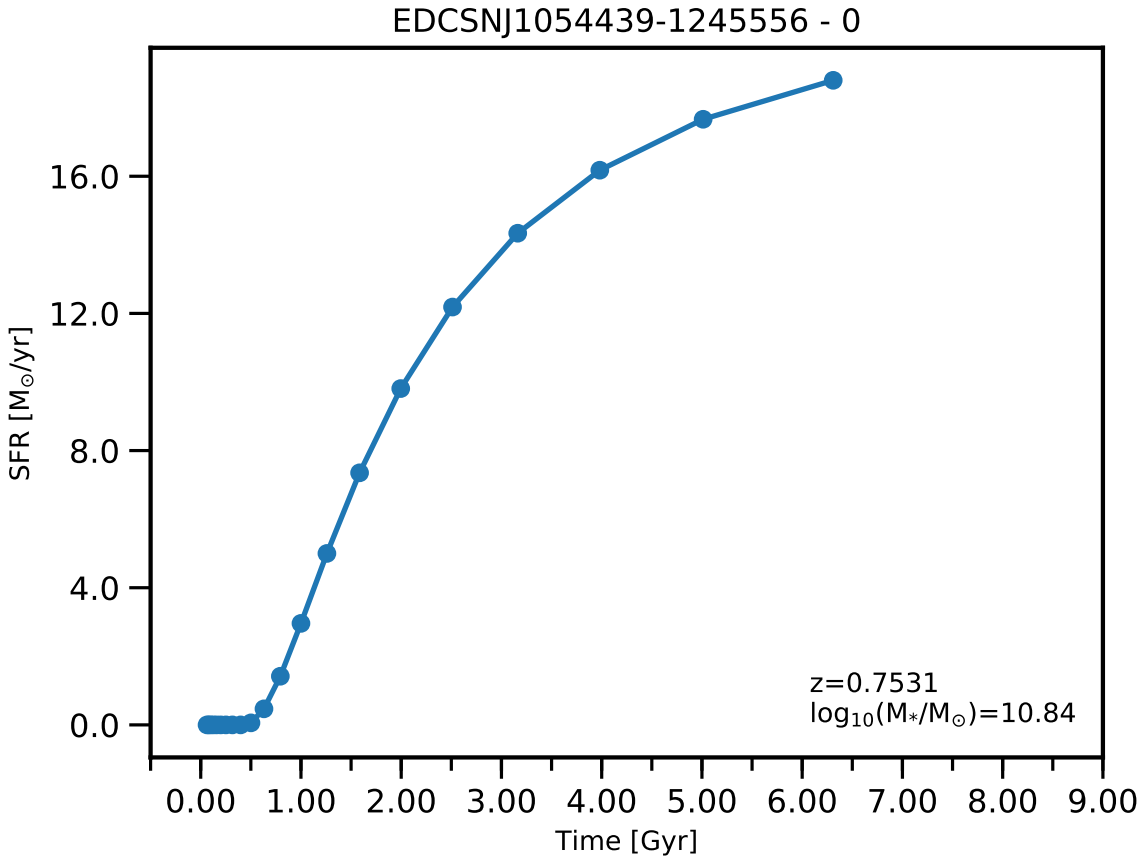
EDCSNJ1054439-1245556 - 0
SFR [M⊙/yr]
16.0
12.0
8.0
4.0
0.0
0.00
1.00
2.00
3.00
4.00
5.00
6.00
7.00
8.00
9.00
Time [Gyr]
z=0.7531
log10(M*/M⊙)=10.84

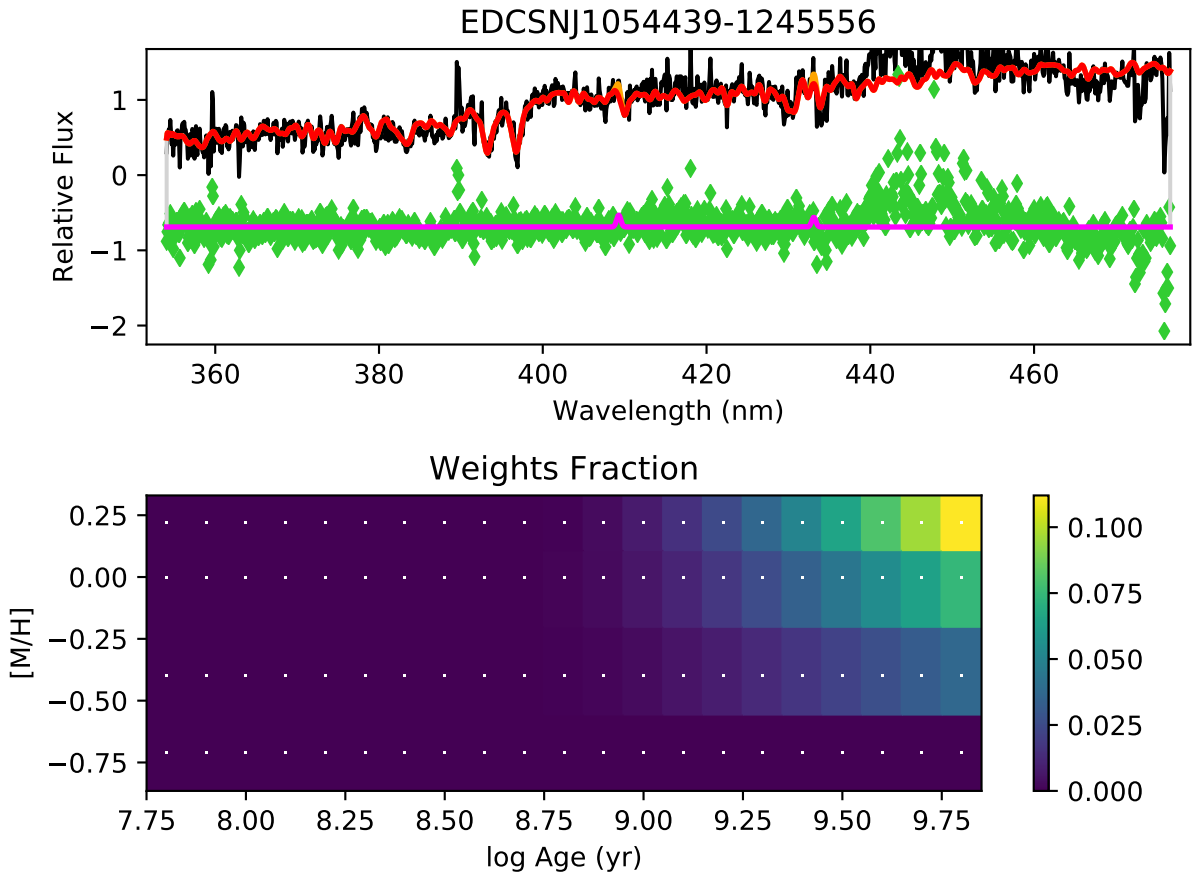
EDCSNJ1054439-1245556
Relative Flux
1
0
−1
−2
360
380
400
420
440
460
Wavelength (nm)
Weights Fraction
[M/H]
0.25
0.00
−0.25
−0.50
−0.75
7.75
8.00
8.25
8.50
8.75
9.00
9.25
9.50
9.75
log Age (yr)
0.100
0.075
0.050
0.025
0.000

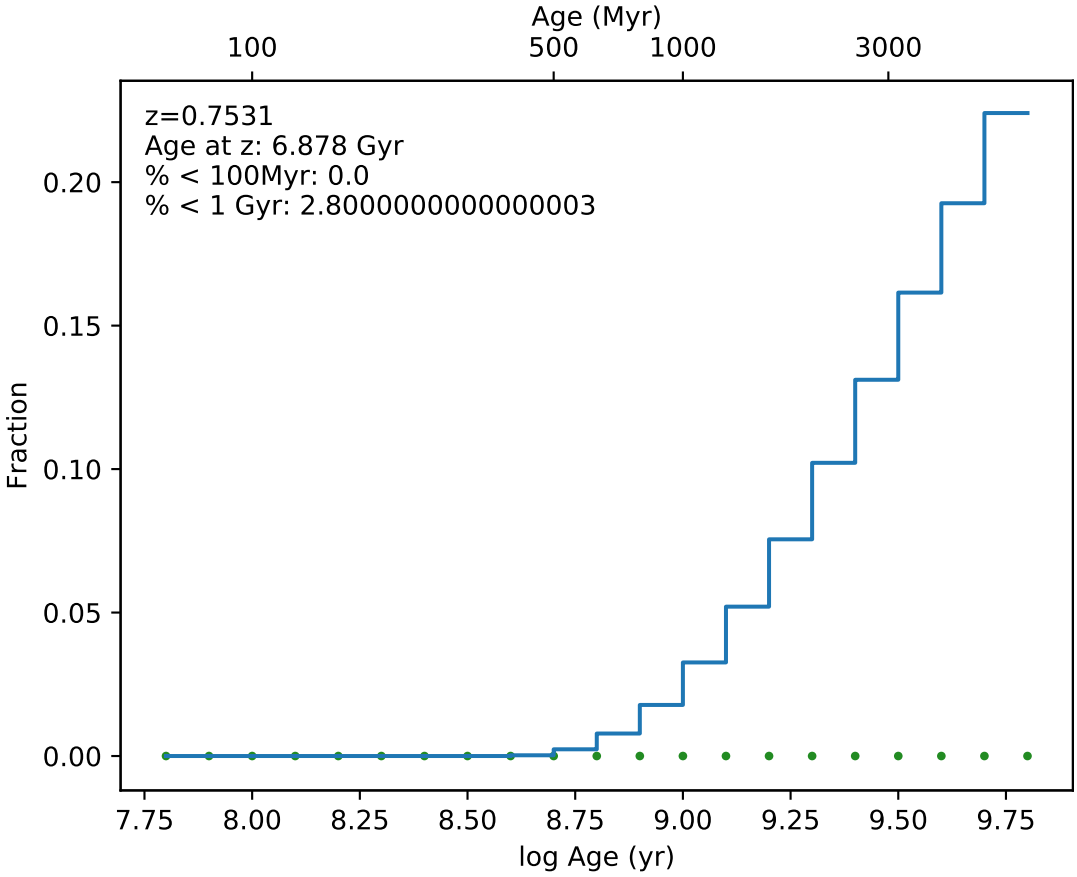
Age (Myr)
100
500
1000
3000
z=0.7531
Age at z: 6.878 Gyr
% < 100Myr: 0.0
% < 1 Gyr: 2.8000000000000003
Fraction
0.20
0.15
0.10
0.05
0.00
7.75
8.00
8.25
8.50
8.75
9.00
9.25
9.50
9.75
log Age (yr)

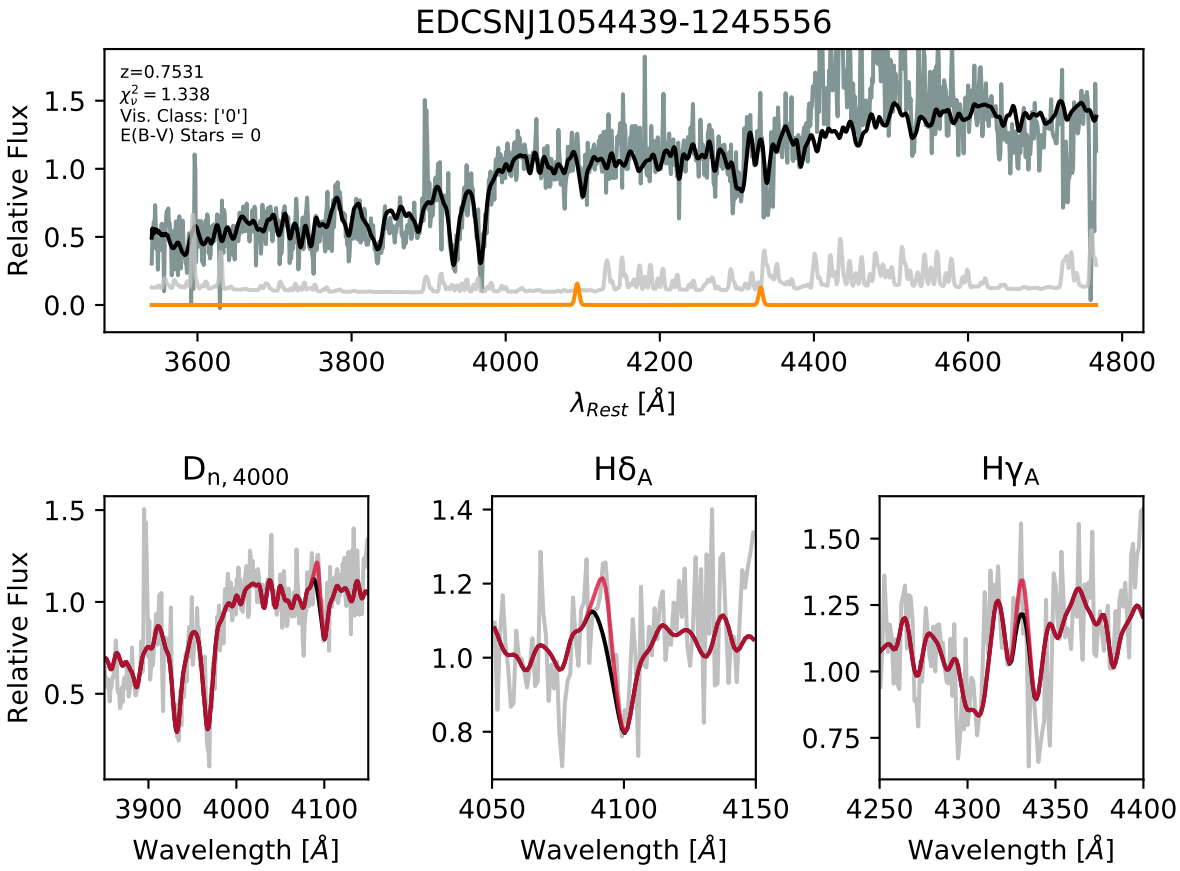
EDCSNJ1054439-1245556
z=0.7531
$\chi^2_\nu = 1.338$
Vis. Class: ['0']
E(B-V) Stars = 0
Relative Flux
λ_{Rest} [Å]
$D_{n,4000}$
$H\delta_A$
$H\gamma_A$
Wavelength [Å]

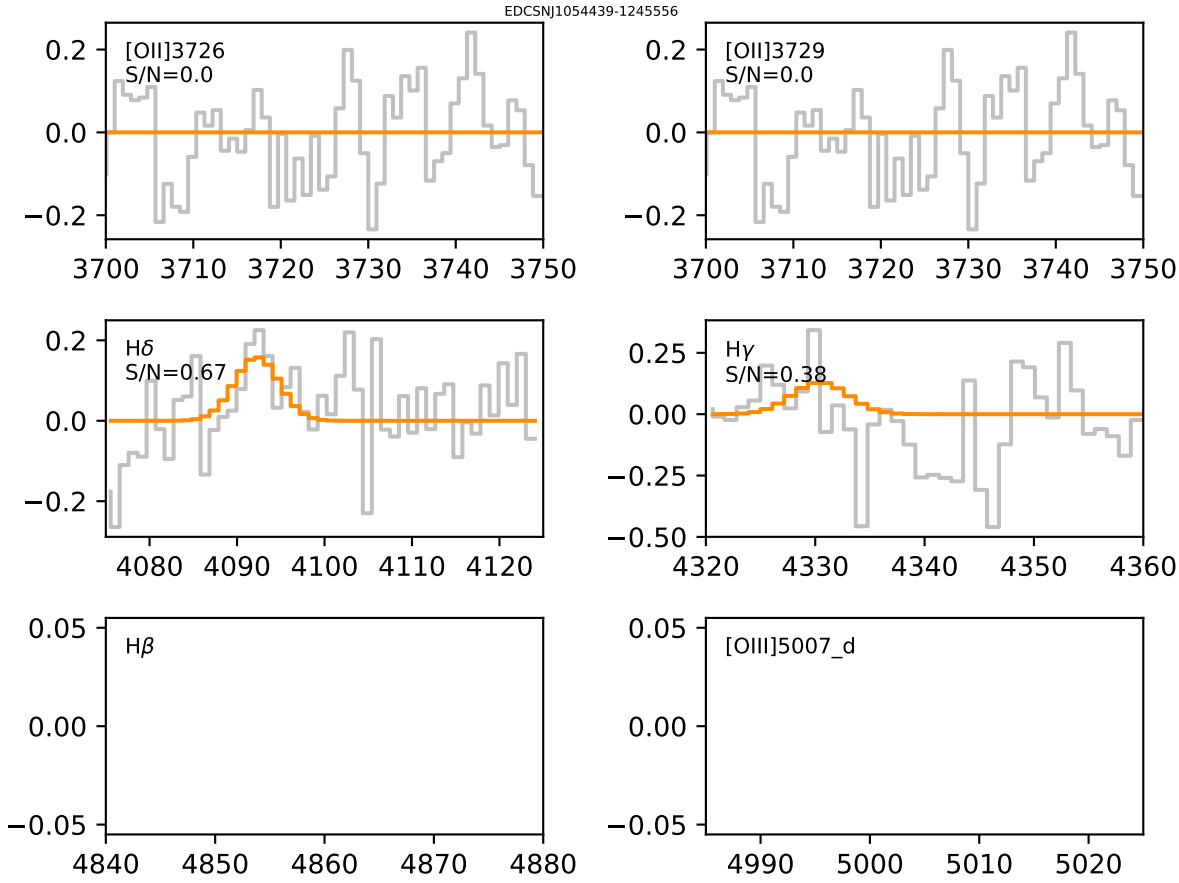
EDCSNJ1054439-1245556
[OII]3726
S/N=0.0
[OII]3729
S/N=0.0
Hδ
S/N=0.67
Hγ
S/N=0.38
Hβ
[OIII]5007_d

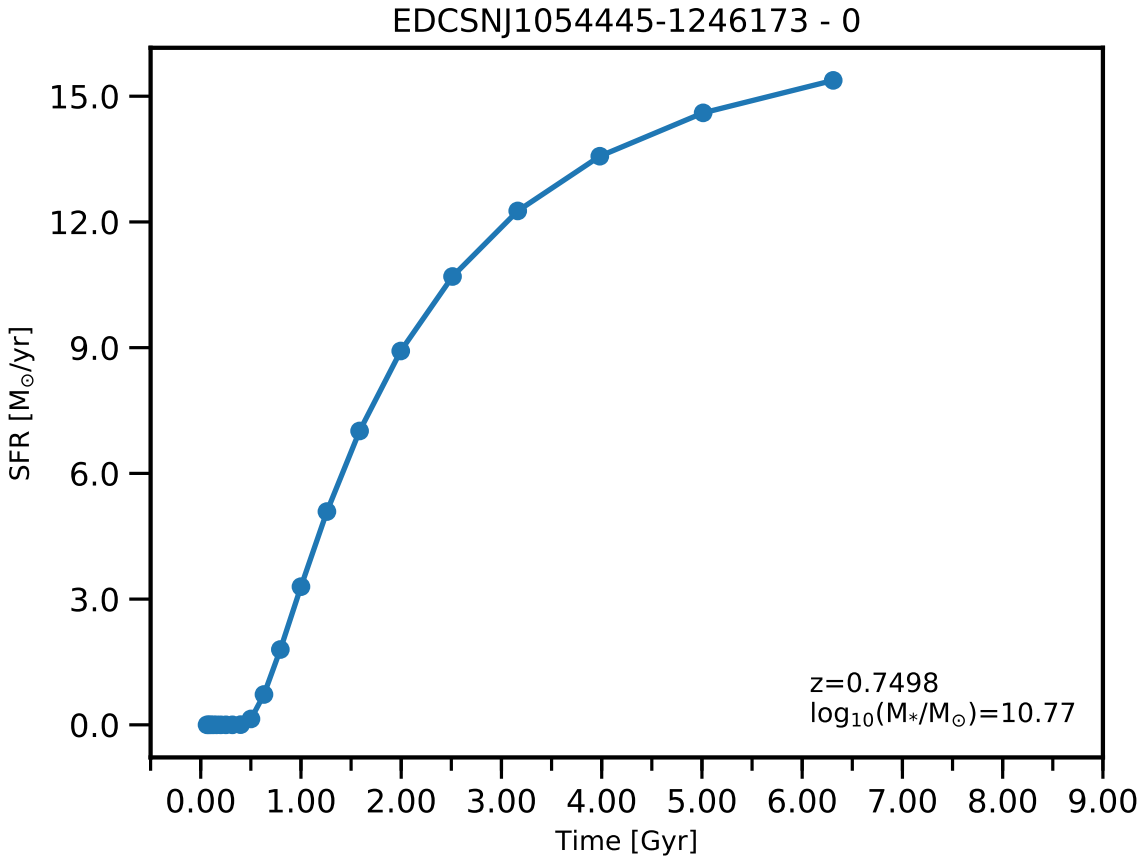
EDCSNJ1054445-1246173 - 0
SFR [M⊙/yr]
15.0
12.0
9.0
6.0
3.0
0.0
0.00
1.00
2.00
3.00
4.00
5.00
6.00
7.00
8.00
9.00
Time [Gyr]
z=0.7498
log10(M*/M⊙)=10.77

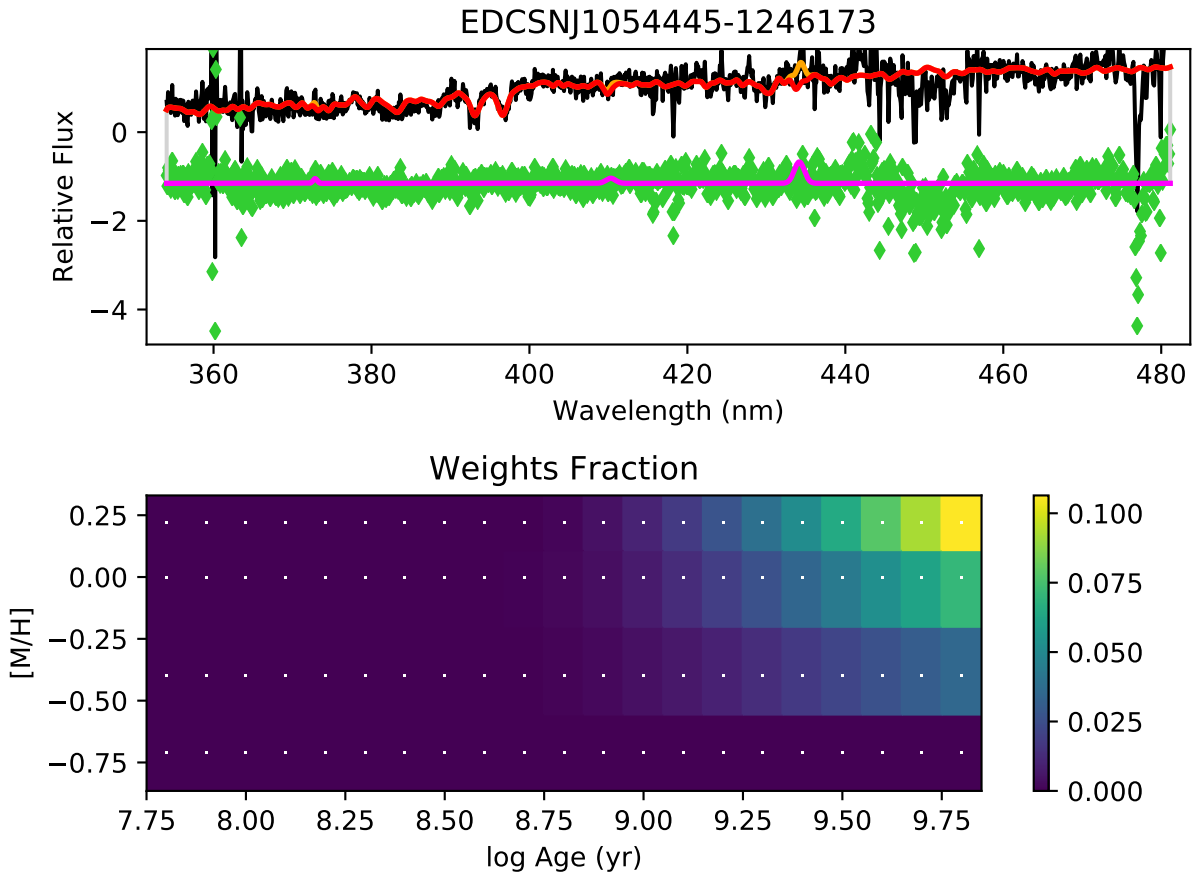
EDCSNJ1054445-1246173
Relative Flux
0
−2
−4
360
380
400
420
440
460
480
Wavelength (nm)
Weights Fraction
[M/H]
0.25
0.00
−0.25
−0.50
−0.75
7.75
8.00
8.25
8.50
8.75
9.00
9.25
9.50
9.75
log Age (yr)
0.100
0.075
0.050
0.025
0.000

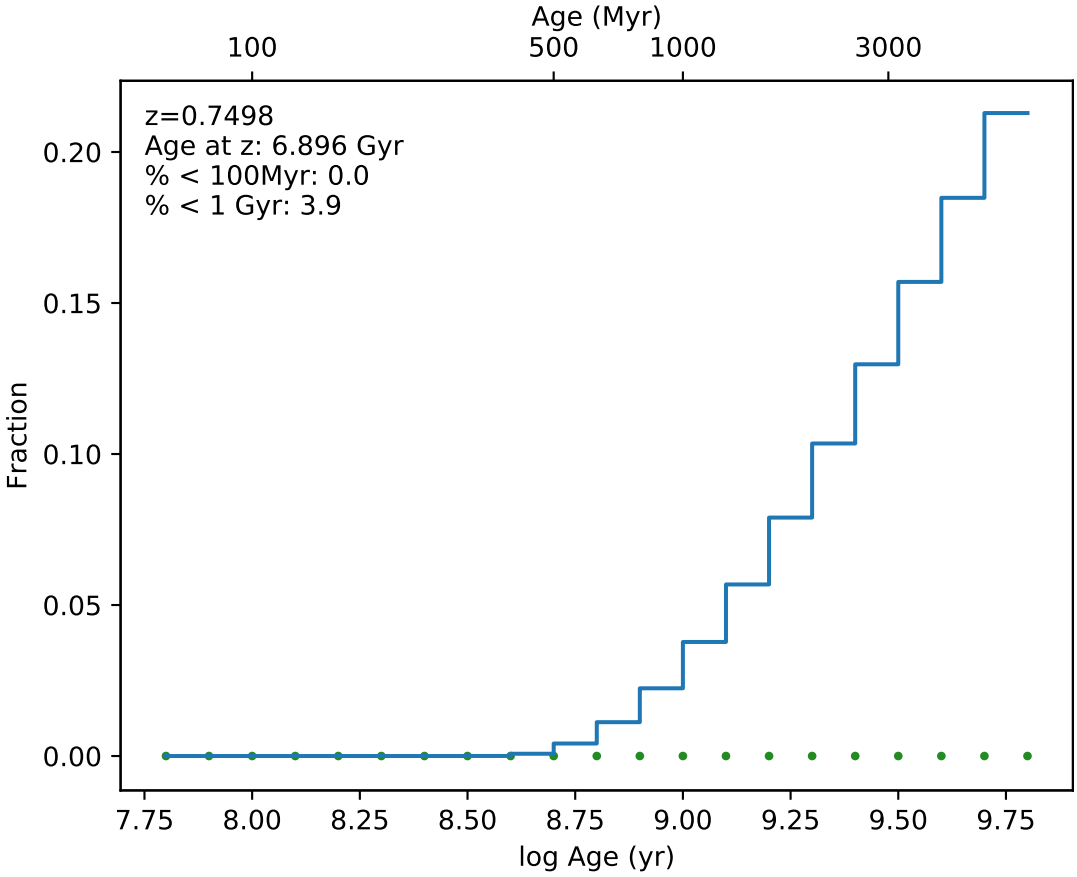
Age (Myr)
100
500
1000
3000
z=0.7498
Age at z: 6.896 Gyr
% < 100Myr: 0.0
% < 1 Gyr: 3.9
0.20
0.15
0.10
0.05
0.00
Fraction
7.75
8.00
8.25
8.50
8.75
9.00
9.25
9.50
9.75
log Age (yr)

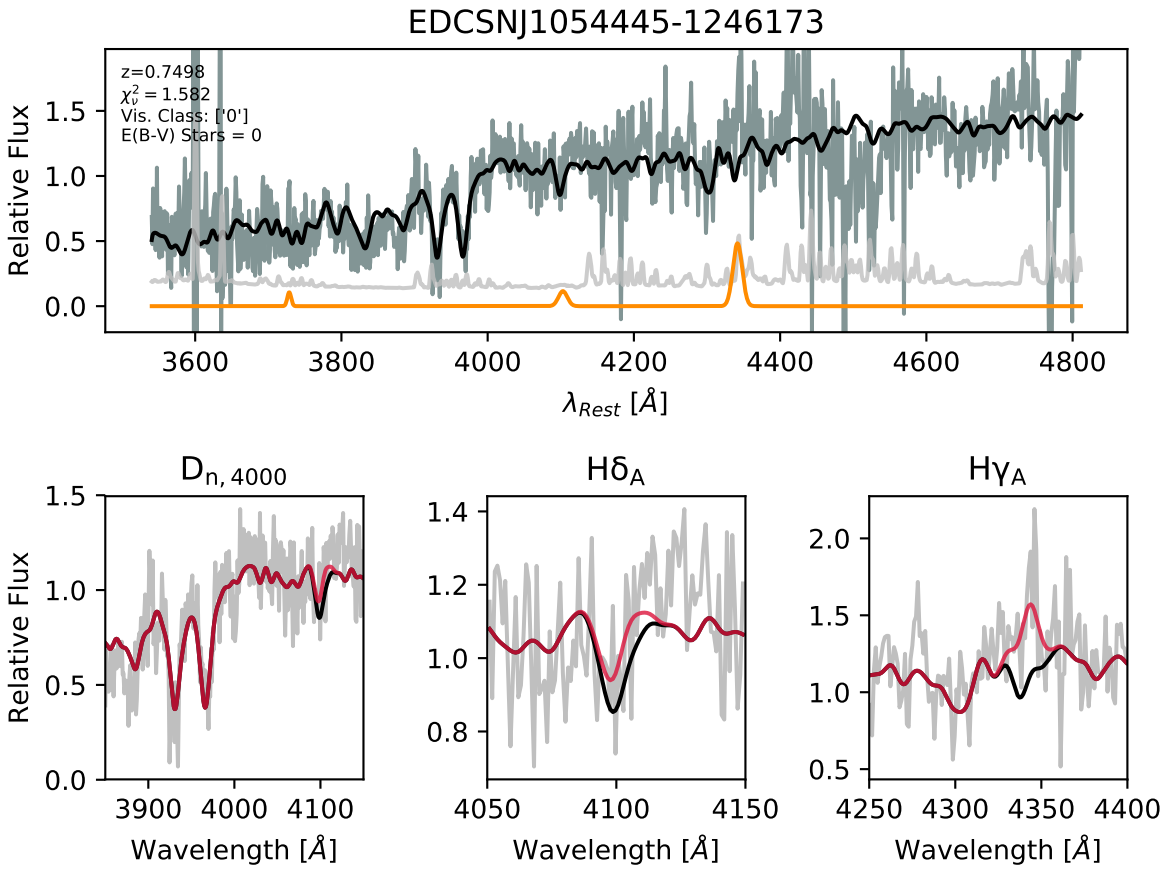
EDCSNJ1054445-1246173
z=0.7498
$\chi^2_\nu = 1.582$
Vis. Class: ['0']
E(B-V) Stars = 0
Relative Flux
λ_{Rest} [Å]
$D_{n,4000}$
$H\delta_A$
$H\gamma_A$
Wavelength [Å]

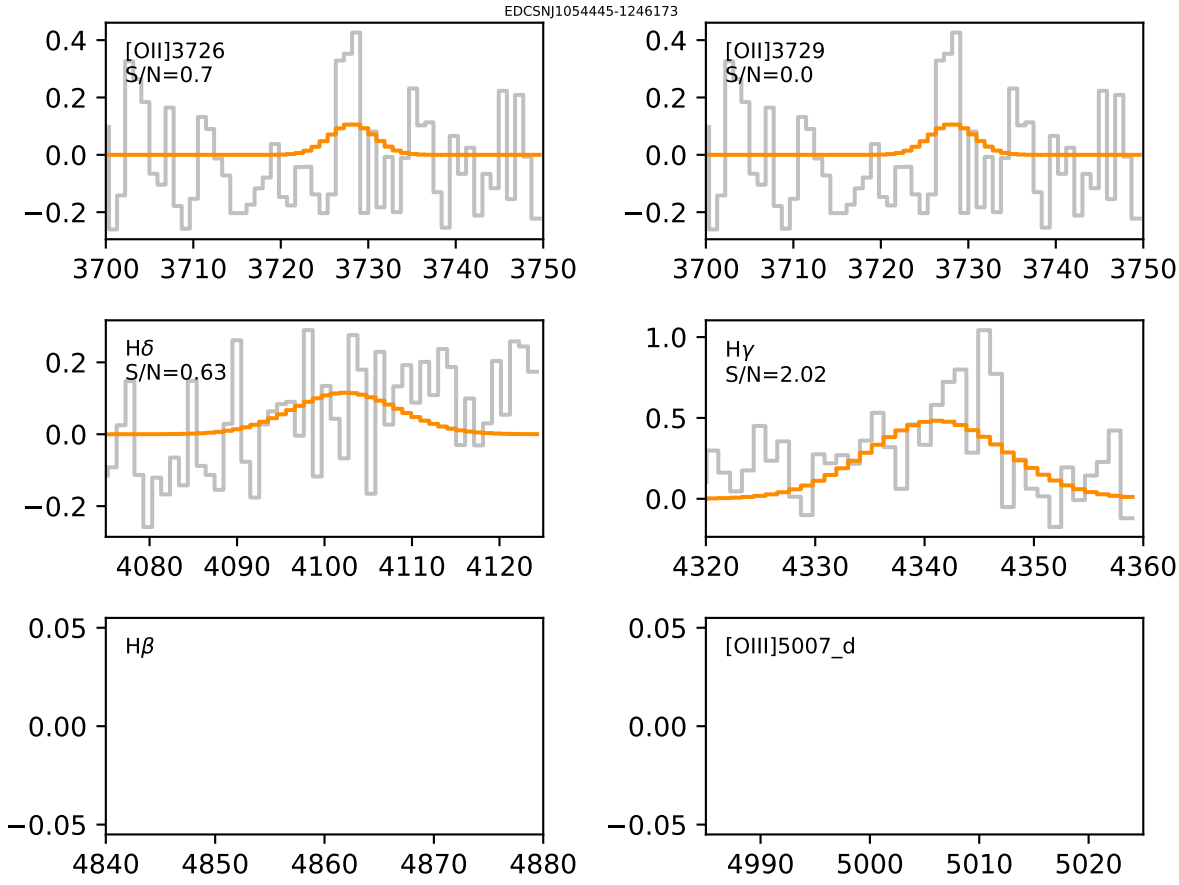
EDCSNJ1054445-1246173
[OII]3726
S/N=0.7
[OII]3729
S/N=0.0
Hδ
S/N=0.63
Hγ
S/N=2.02
Hβ
[OIII]5007_d

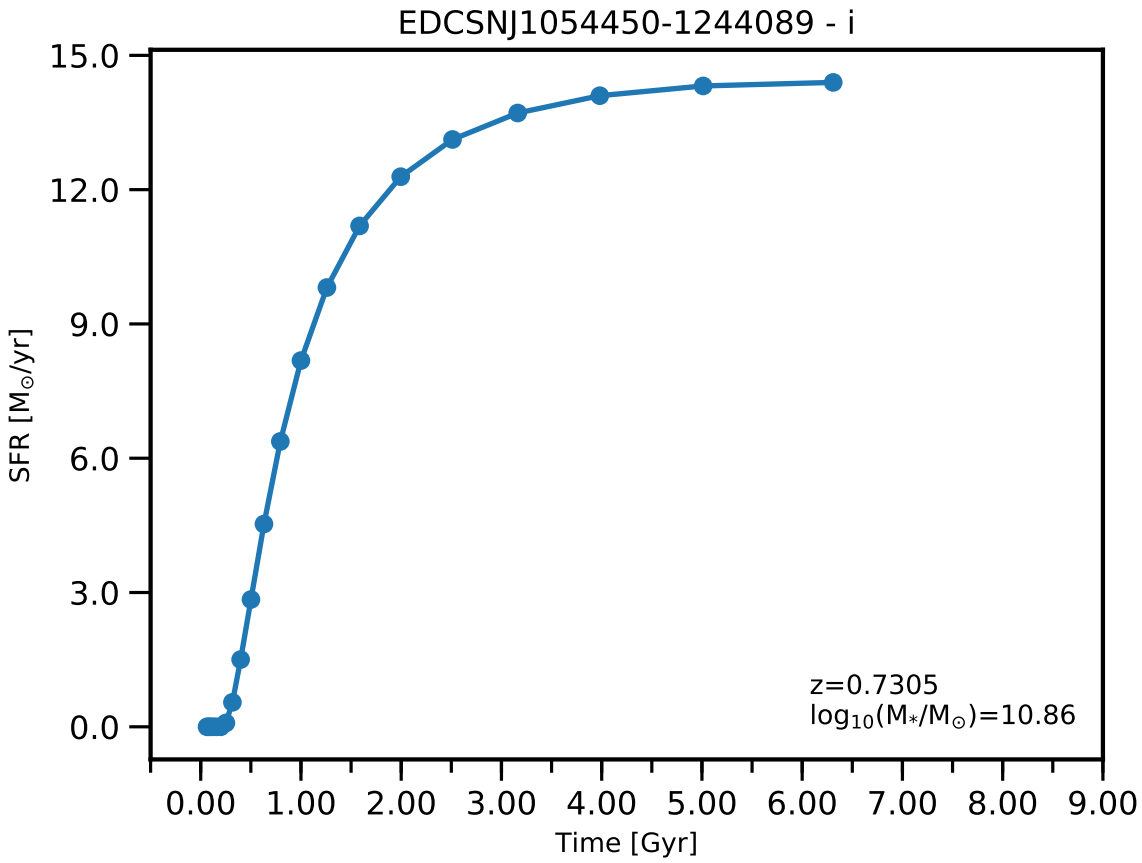
EDCSNJ1054450-1244089 - i
15.0
12.0
9.0
6.0
3.0
0.0
SFR [M⊙/yr]
0.00
1.00
2.00
3.00
4.00
5.00
6.00
7.00
8.00
9.00
Time [Gyr]
z=0.7305
log10(M*/M⊙)=10.86

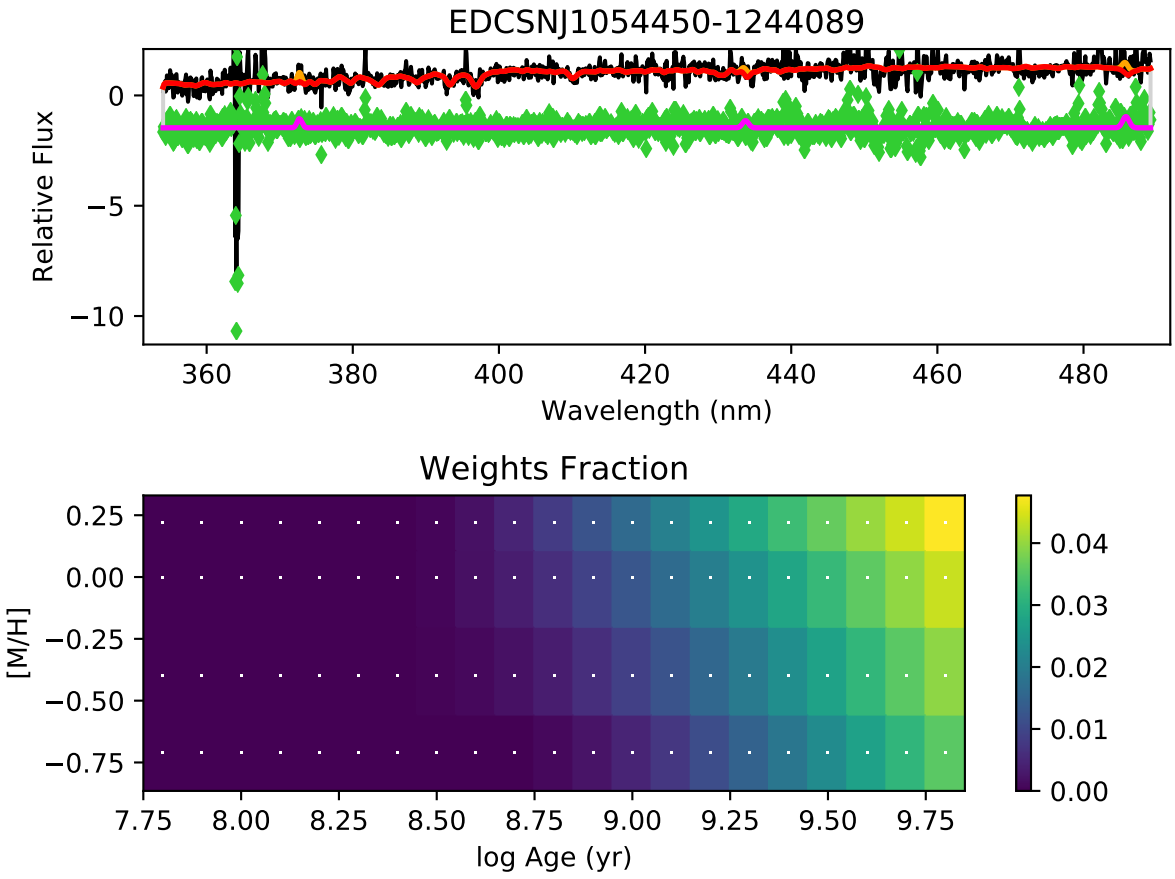
EDCSNJ1054450-1244089
Relative Flux
0
−5
−10
360
380
400
420
440
460
480
Wavelength (nm)
Weights Fraction
[M/H]
0.25
0.00
−0.25
−0.50
−0.75
7.75
8.00
8.25
8.50
8.75
9.00
9.25
9.50
9.75
log Age (yr)
0.04
0.03
0.02
0.01
0.00

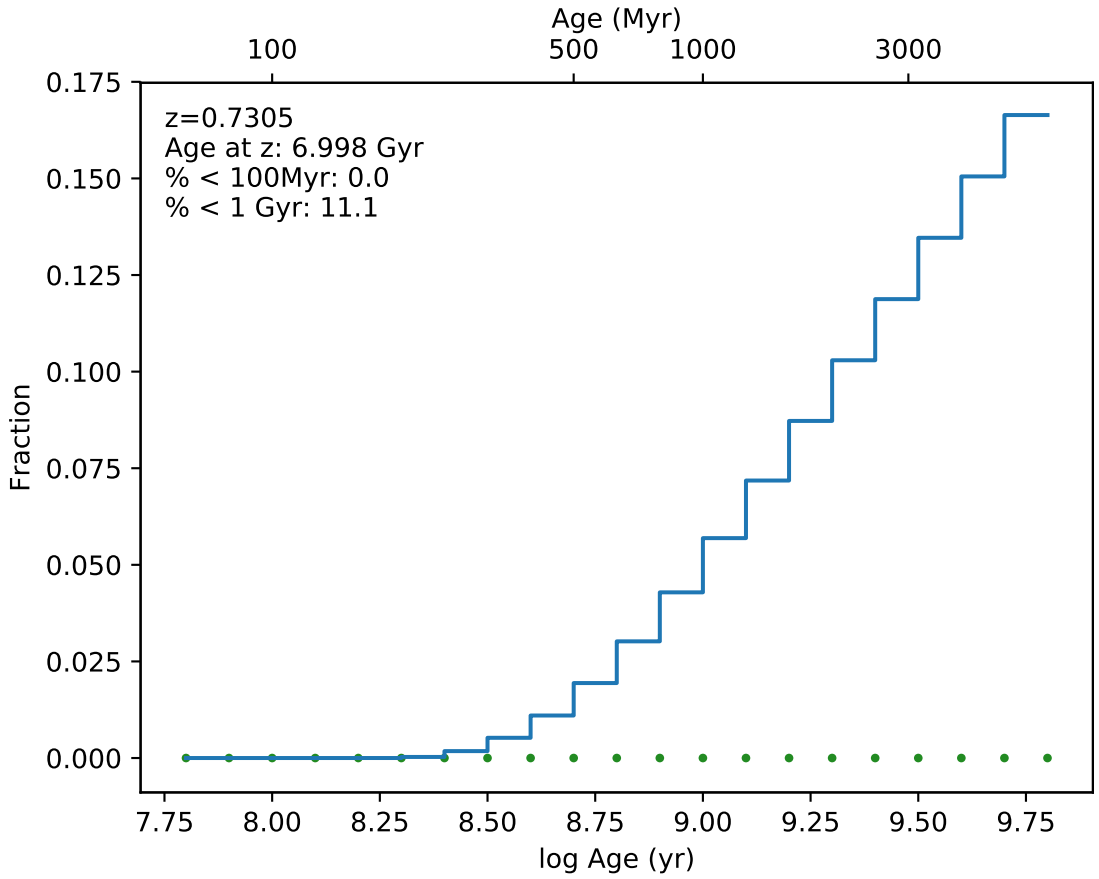
Age (Myr)
100
500
1000
3000
z=0.7305
Age at z: 6.998 Gyr
% < 100Myr: 0.0
% < 1 Gyr: 11.1
Fraction
0.175
0.150
0.125
0.100
0.075
0.050
0.025
0.000
7.75
8.00
8.25
8.50
8.75
9.00
9.25
9.50
9.75
log Age (yr)

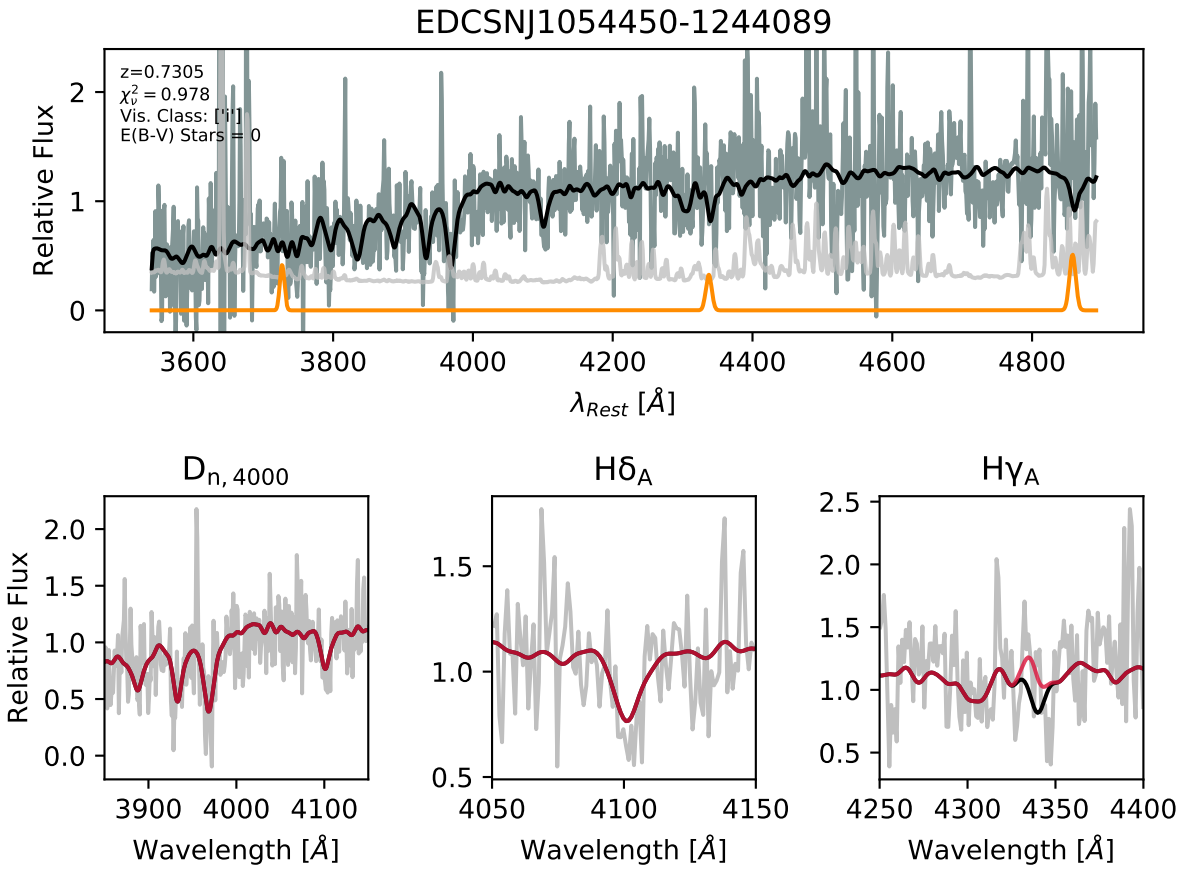
EDCSNJ1054450-1244089
z=0.7305
$\chi^2_\nu = 0.978$
Vis. Class: ['i']
E(B-V) Stars = 0
Relative Flux
λ_{Rest} [Å]
$D_{n,4000}$
$H\delta_A$
$H\gamma_A$
Wavelength [Å]

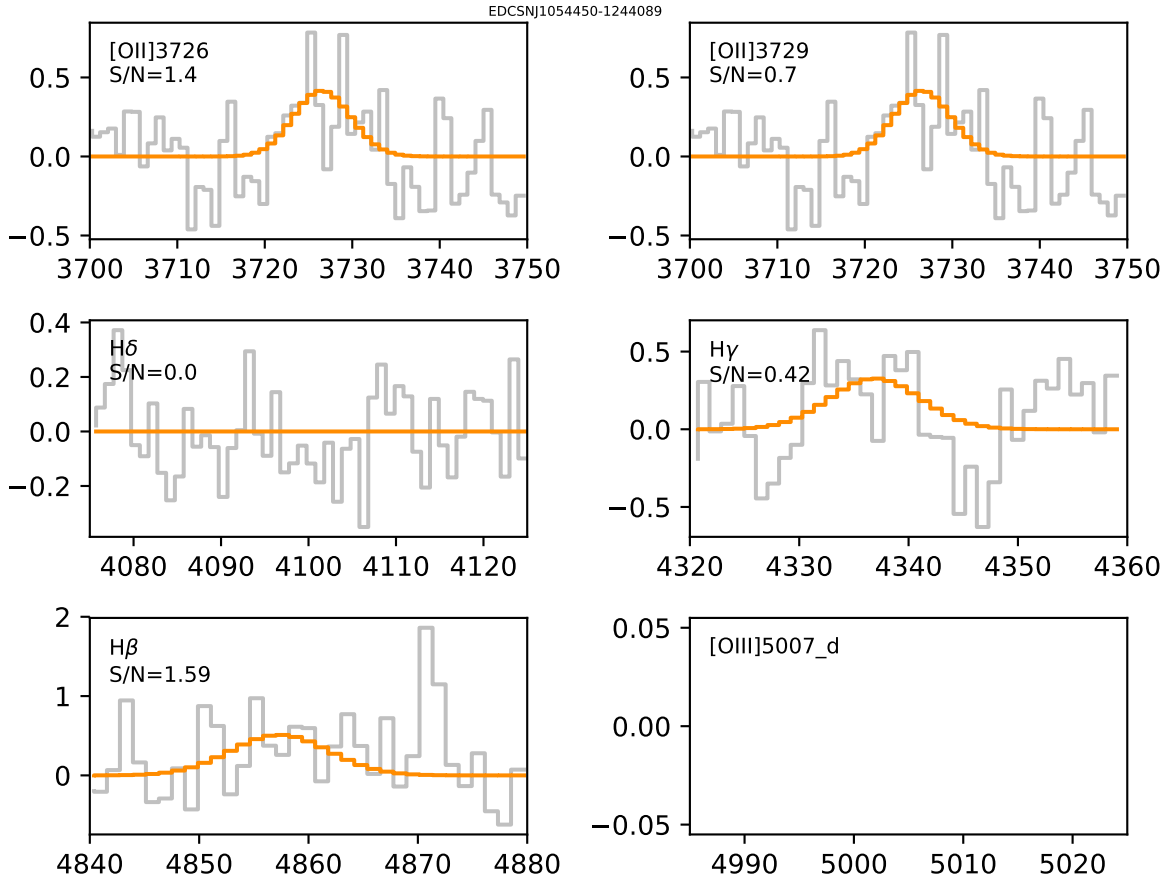
EDCSNJ1054450-1244089
[OII]3726
S/N=1.4
[OII]3729
S/N=0.7
Hδ
S/N=0.0
Hγ
S/N=0.42
Hβ
S/N=1.59
[OIII]5007_d

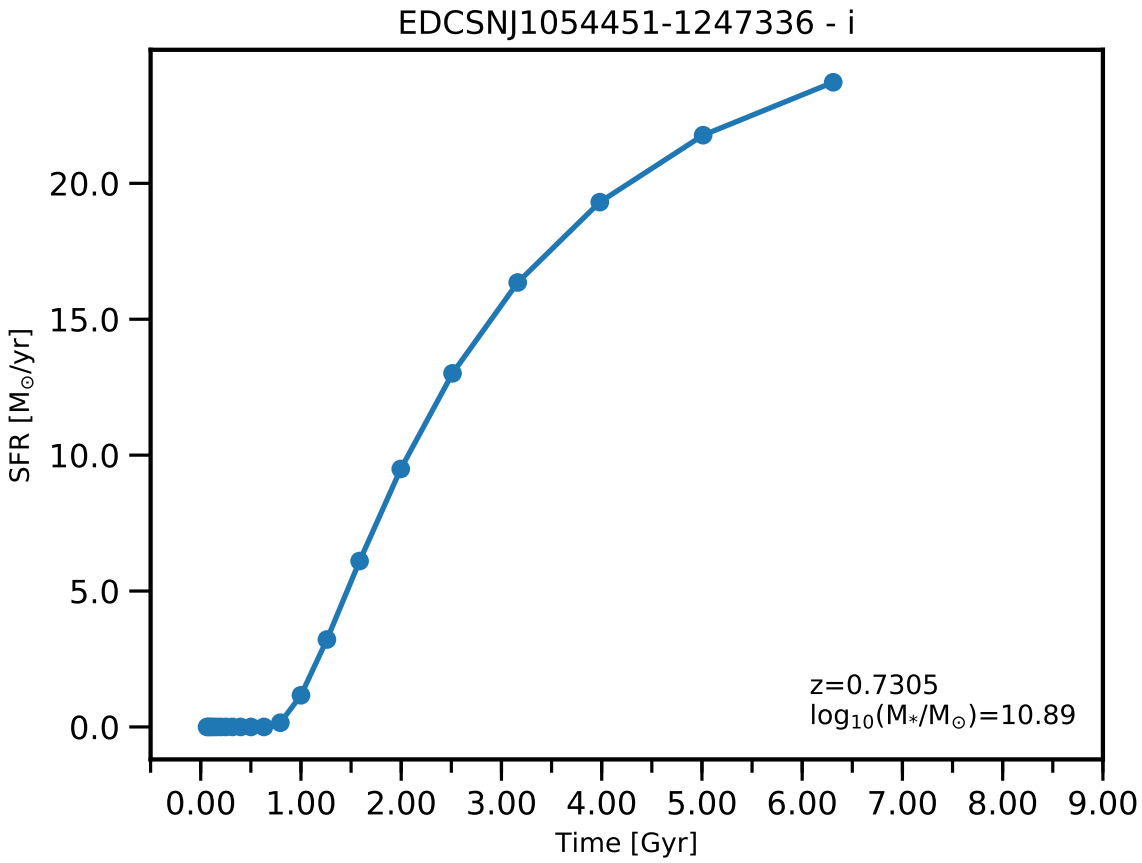
EDCSNJ1054451-1247336 - i
SFR [M⊙/yr]
20.0
15.0
10.0
5.0
0.0
0.00
1.00
2.00
3.00
4.00
5.00
6.00
7.00
8.00
9.00
Time [Gyr]
z=0.7305
log10(M*/M⊙)=10.89

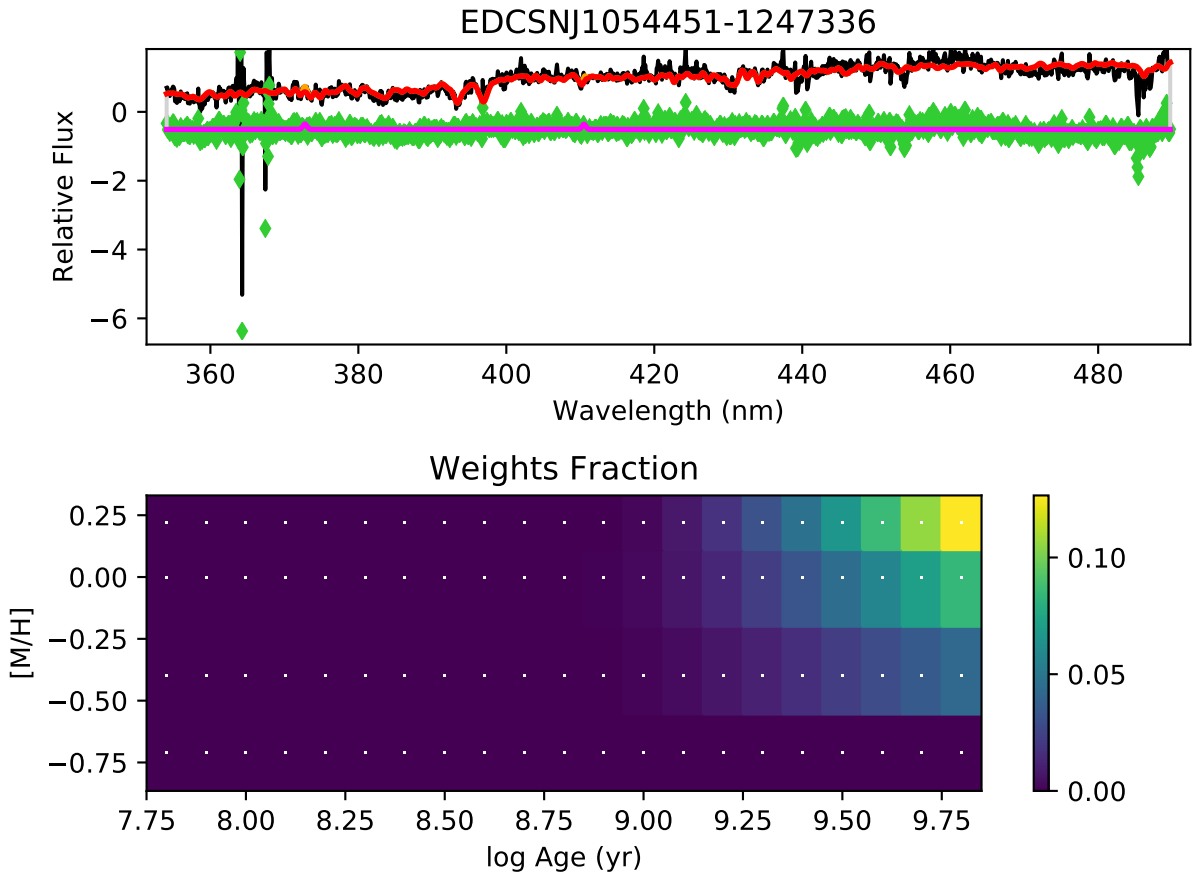
EDCSNJ1054451-1247336
Relative Flux
0
−2
−4
−6
360
380
400
420
440
460
480
Wavelength (nm)
Weights Fraction
[M/H]
0.25
0.00
−0.25
−0.50
−0.75
7.75
8.00
8.25
8.50
8.75
9.00
9.25
9.50
9.75
log Age (yr)
0.10
0.05
0.00

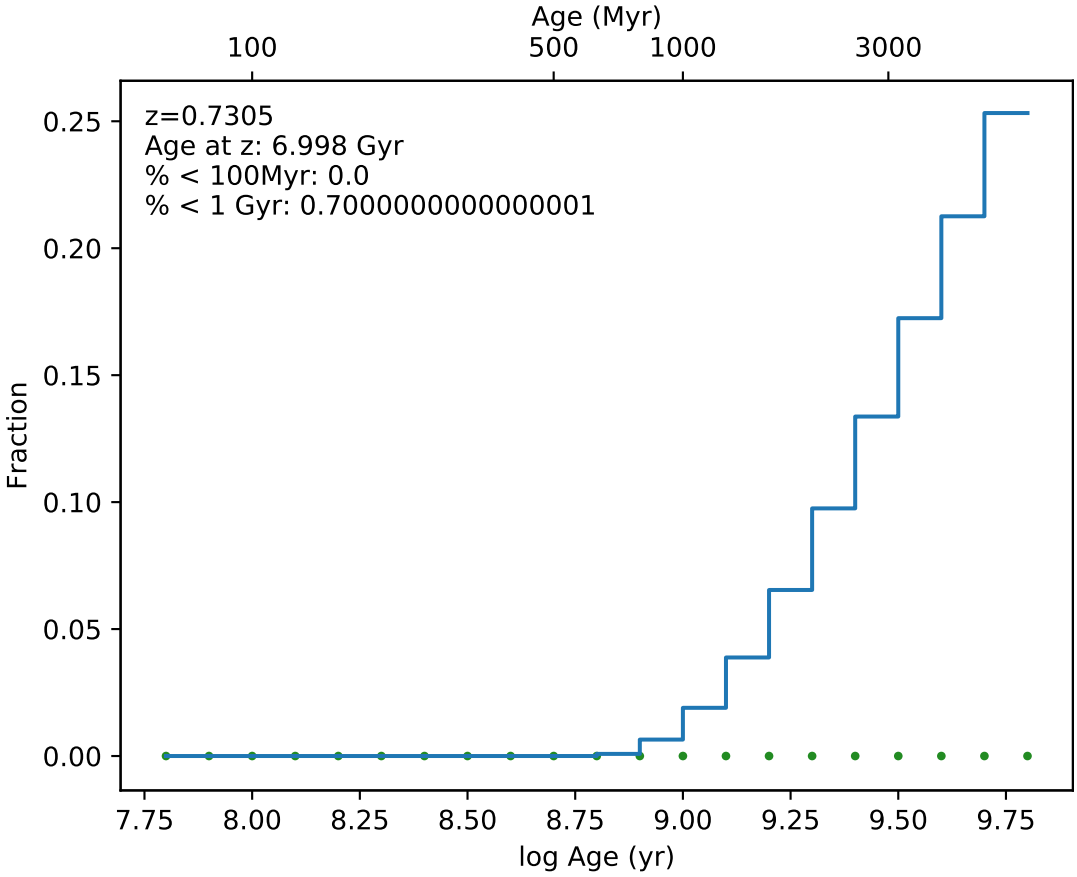
Age (Myr)
100
500
1000
3000
z=0.7305
Age at z: 6.998 Gyr
% < 100Myr: 0.0
% < 1 Gyr: 0.7000000000000001
Fraction
0.25
0.20
0.15
0.10
0.05
0.00
7.75
8.00
8.25
8.50
8.75
9.00
9.25
9.50
9.75
log Age (yr)

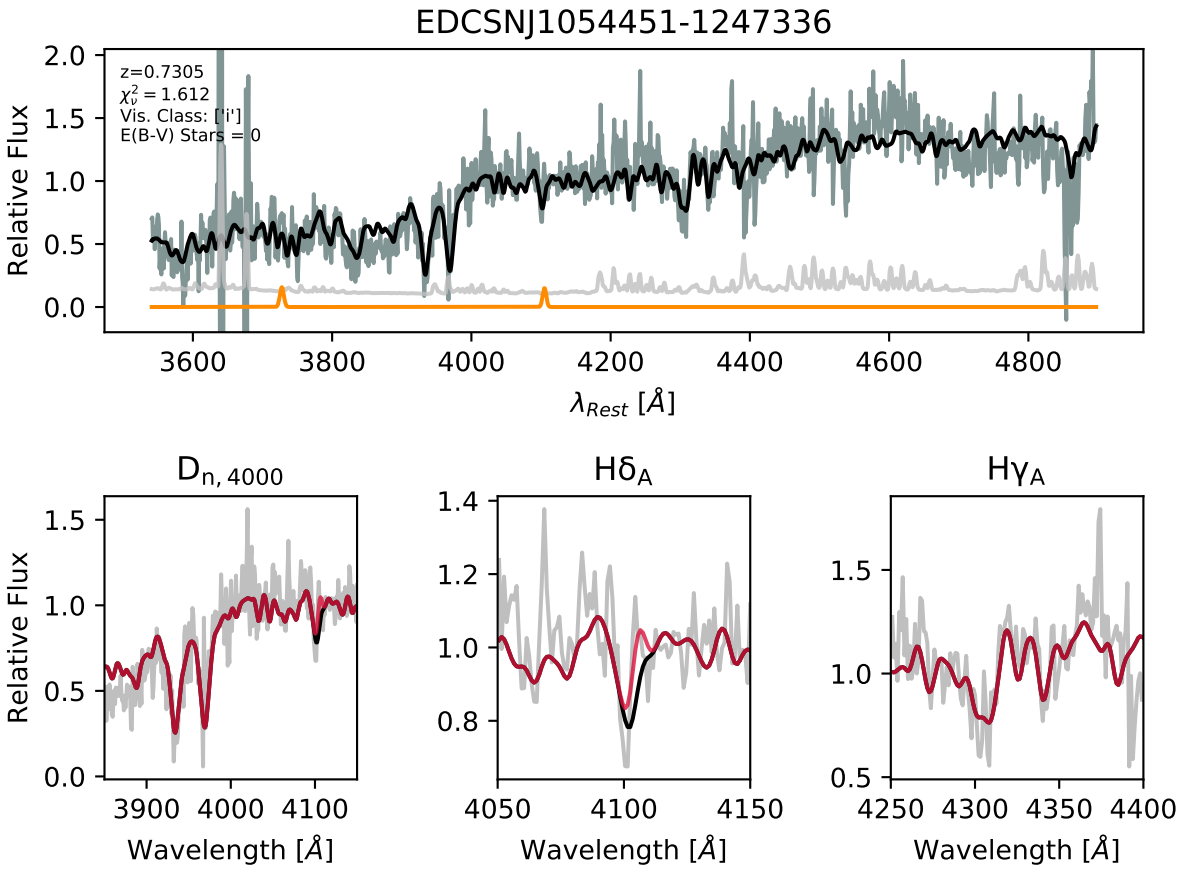
EDCSNJ1054451-1247336
z=0.7305
$\chi^2_\nu = 1.612$
Vis. Class: ['i']
E(B-V) Stars = 0
Relative Flux
λ_{Rest} [Å]
$D_{n,4000}$
$H\delta_A$
$H\gamma_A$
Wavelength [Å]

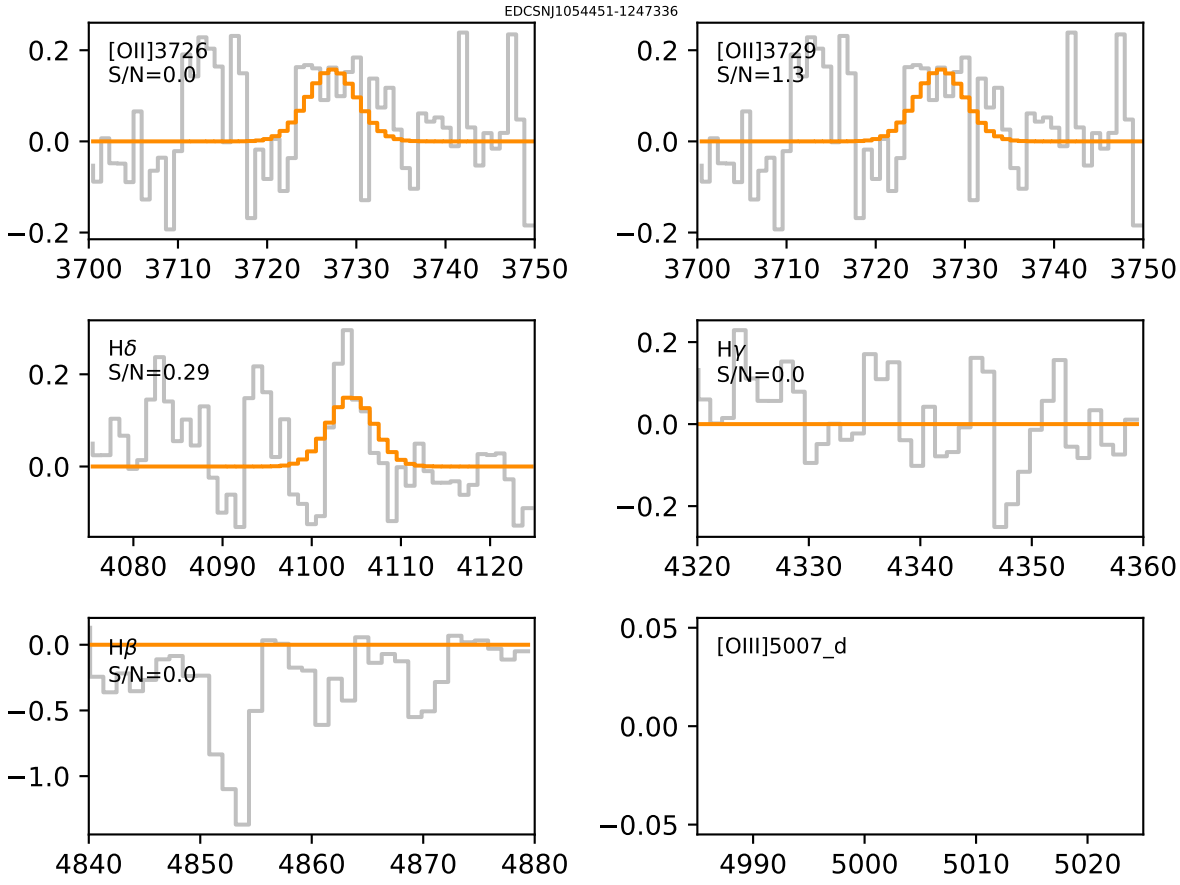
EDCSNJ1054451-1247336
[OII]3726
S/N=0.0
[OII]3729
S/N=1.3
Hδ
S/N=0.29
Hγ
S/N=0.0
Hβ
S/N=0.0
[OIII]5007_d

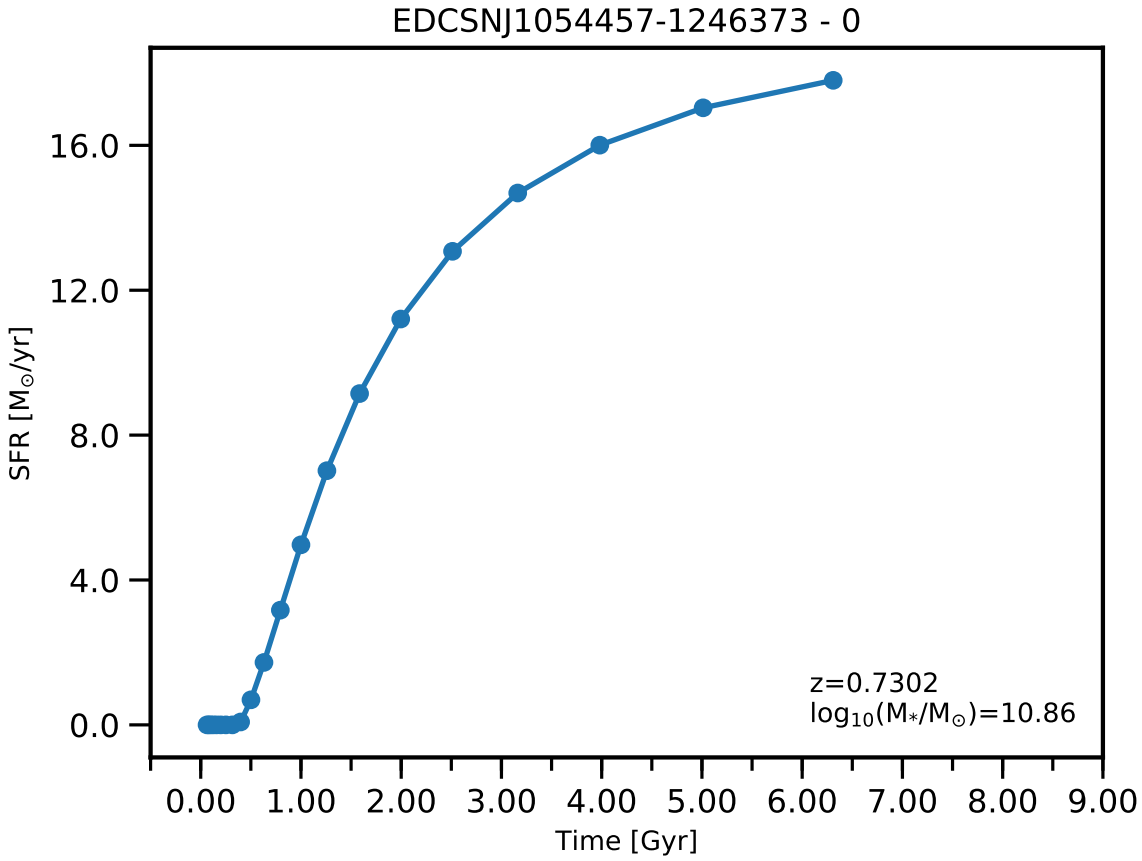
EDCSNJ1054457-1246373 - 0
SFR [M⊙/yr]
16.0
12.0
8.0
4.0
0.0
0.00
1.00
2.00
3.00
4.00
5.00
6.00
7.00
8.00
9.00
Time [Gyr]
z=0.7302
log10(M*/M⊙)=10.86

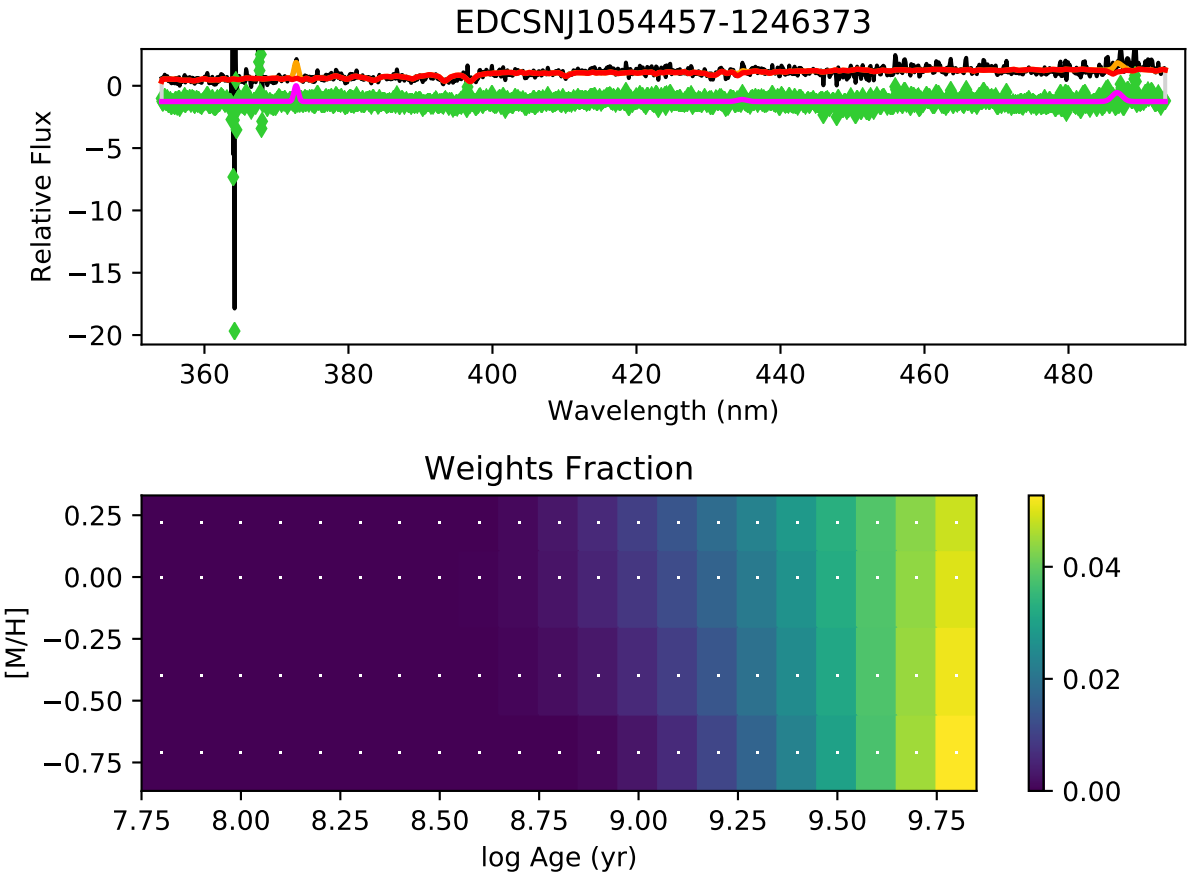
EDCSNJ1054457-1246373
Relative Flux
0
−5
−10
−15
−20
360
380
400
420
440
460
480
Wavelength (nm)
Weights Fraction
[M/H]
0.25
0.00
−0.25
−0.50
−0.75
7.75
8.00
8.25
8.50
8.75
9.00
9.25
9.50
9.75
log Age (yr)
0.04
0.02
0.00

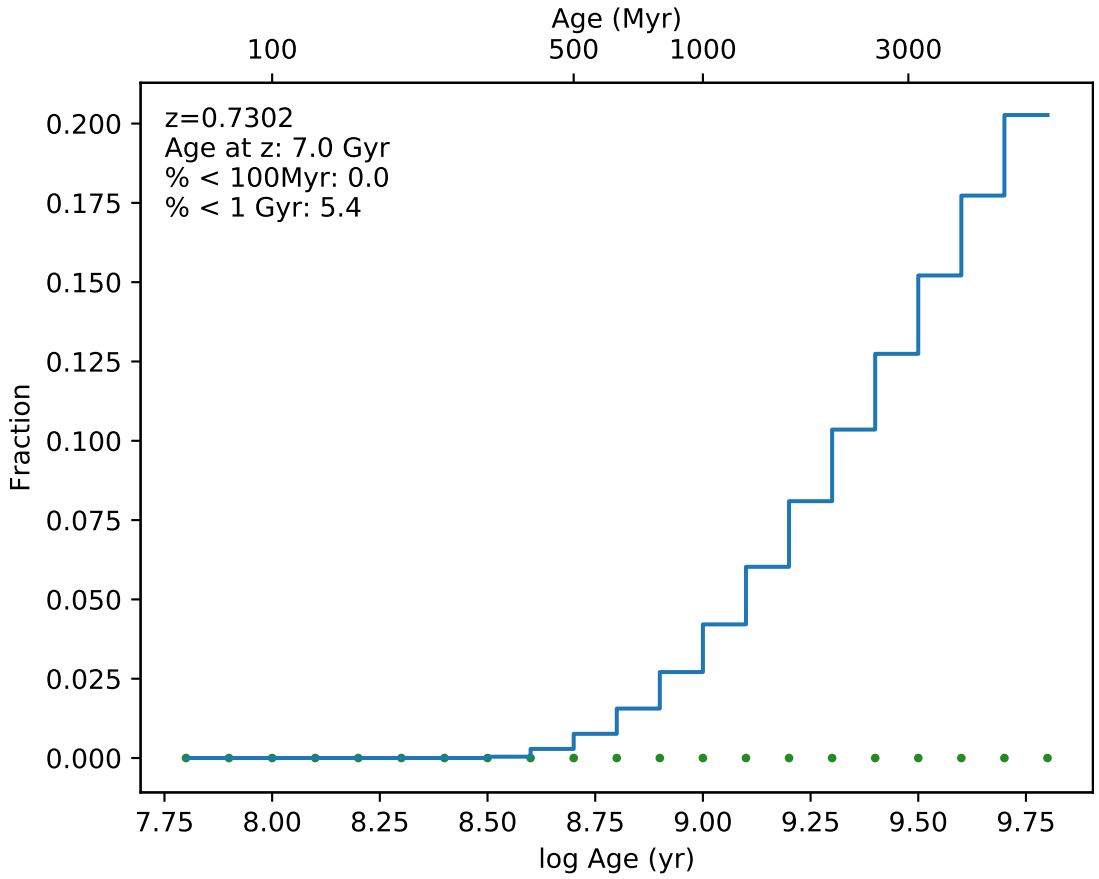
Age (Myr)
100
500
1000
3000
z=0.7302
Age at z: 7.0 Gyr
% < 100Myr: 0.0
% < 1 Gyr: 5.4
Fraction
0.200
0.175
0.150
0.125
0.100
0.075
0.050
0.025
0.000
7.75
8.00
8.25
8.50
8.75
9.00
9.25
9.50
9.75
log Age (yr)

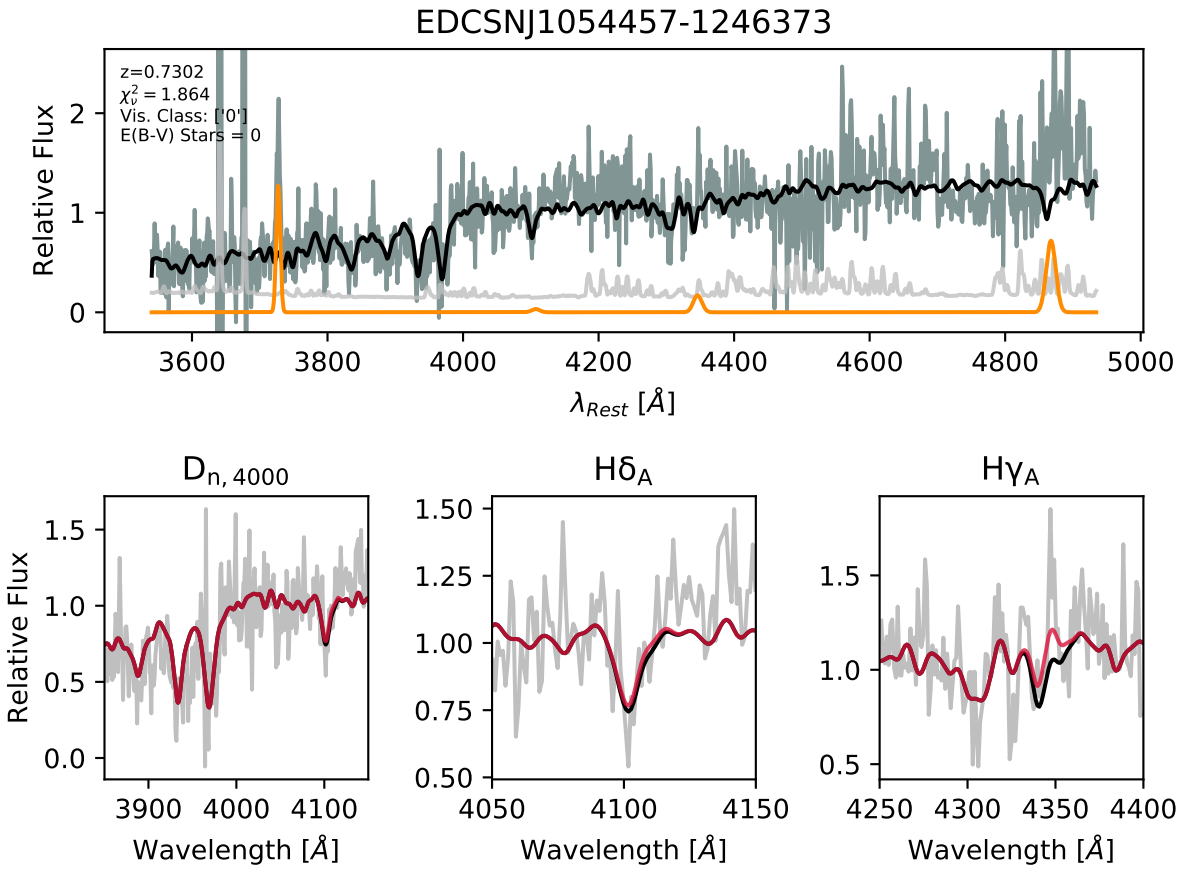
EDCSNJ1054457-1246373
z=0.7302
$\chi^2_\nu = 1.864$
Vis. Class: ['0']
E(B-V) Stars = 0
Relative Flux
λ_{Rest} [Å]
$D_{n,4000}$
$H\delta_A$
$H\gamma_A$
Wavelength [Å]

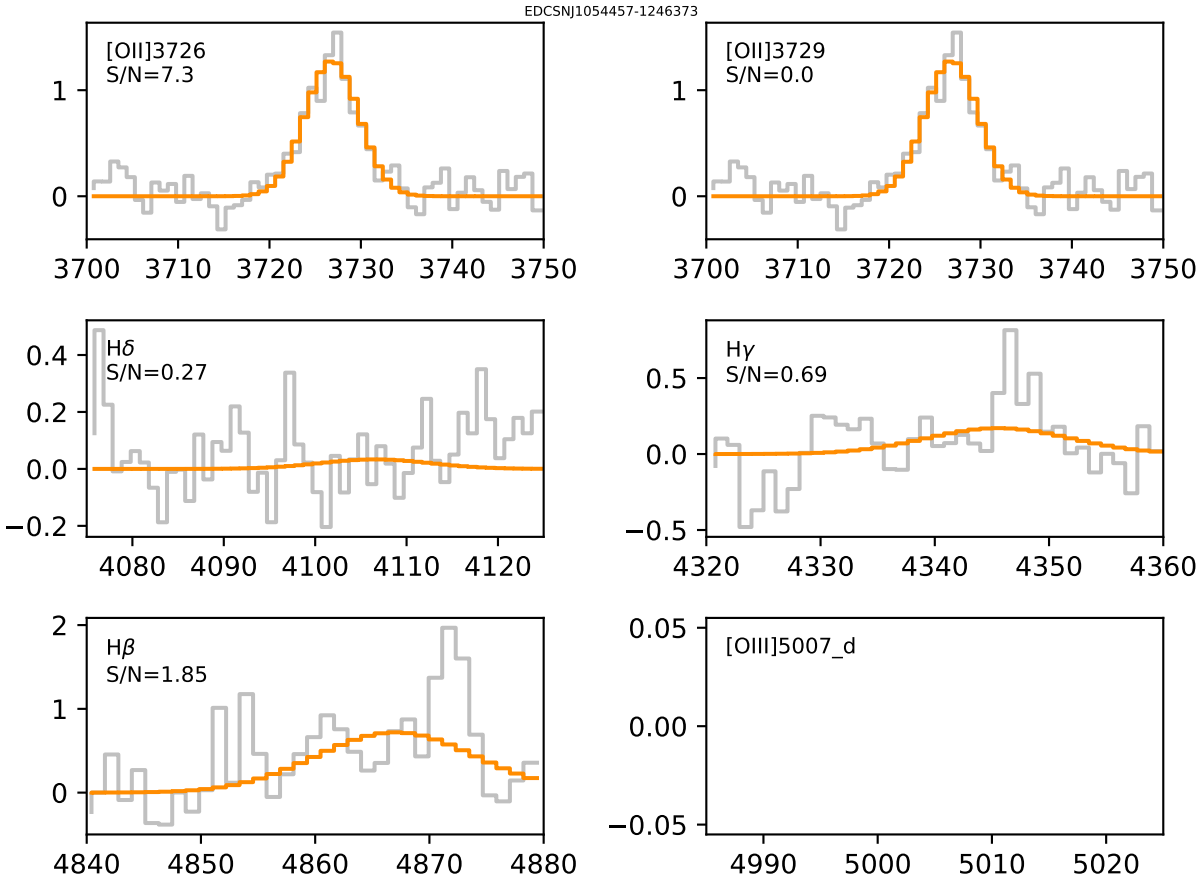
EDCSNJ1054457-1246373
[OII]3726
S/N=7.3
[OII]3729
S/N=0.0
Hδ
S/N=0.27
Hγ
S/N=0.69
Hβ
S/N=1.85
[OIII]5007_d

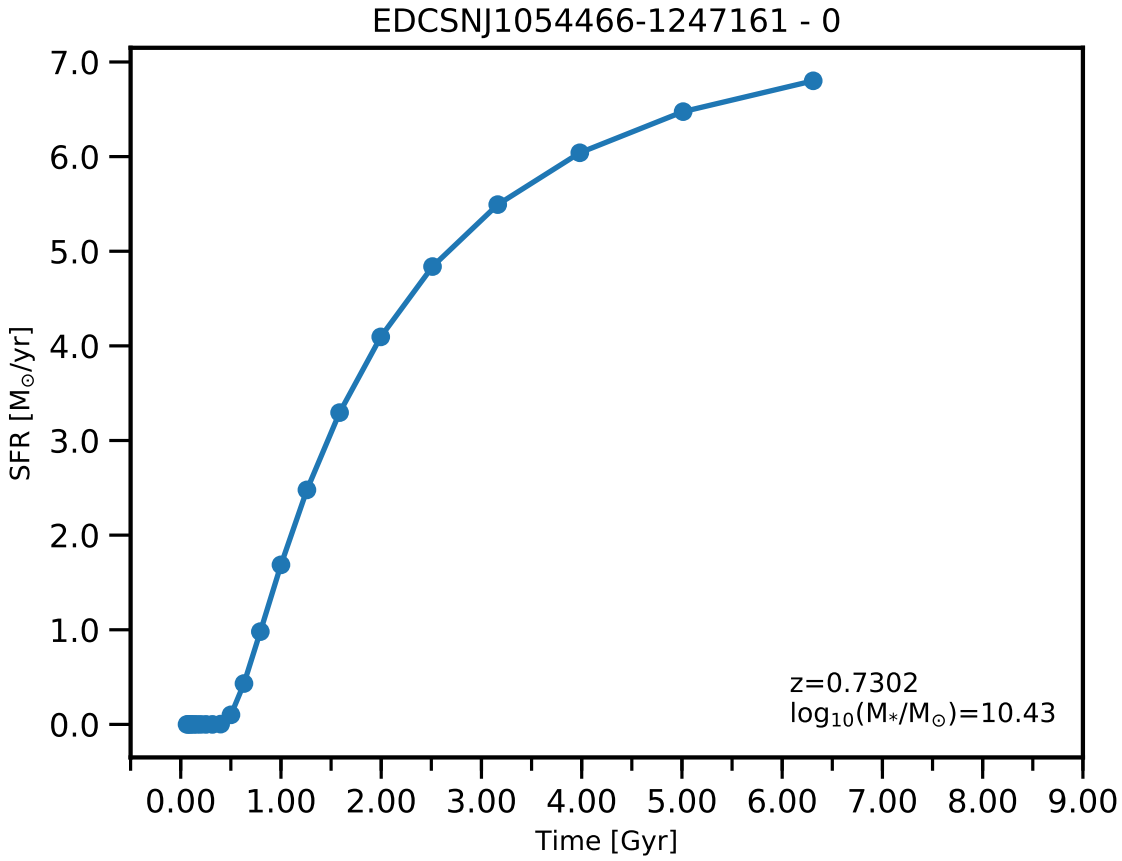
EDCSNJ1054466-1247161 - 0
SFR [M⊙/yr]
Time [Gyr]
z=0.7302
log10(M*/M⊙)=10.43
0.0
1.0
2.0
3.0
4.0
5.0
6.0
7.0
0.00
1.00
2.00
3.00
4.00
5.00
6.00
7.00
8.00
9.00

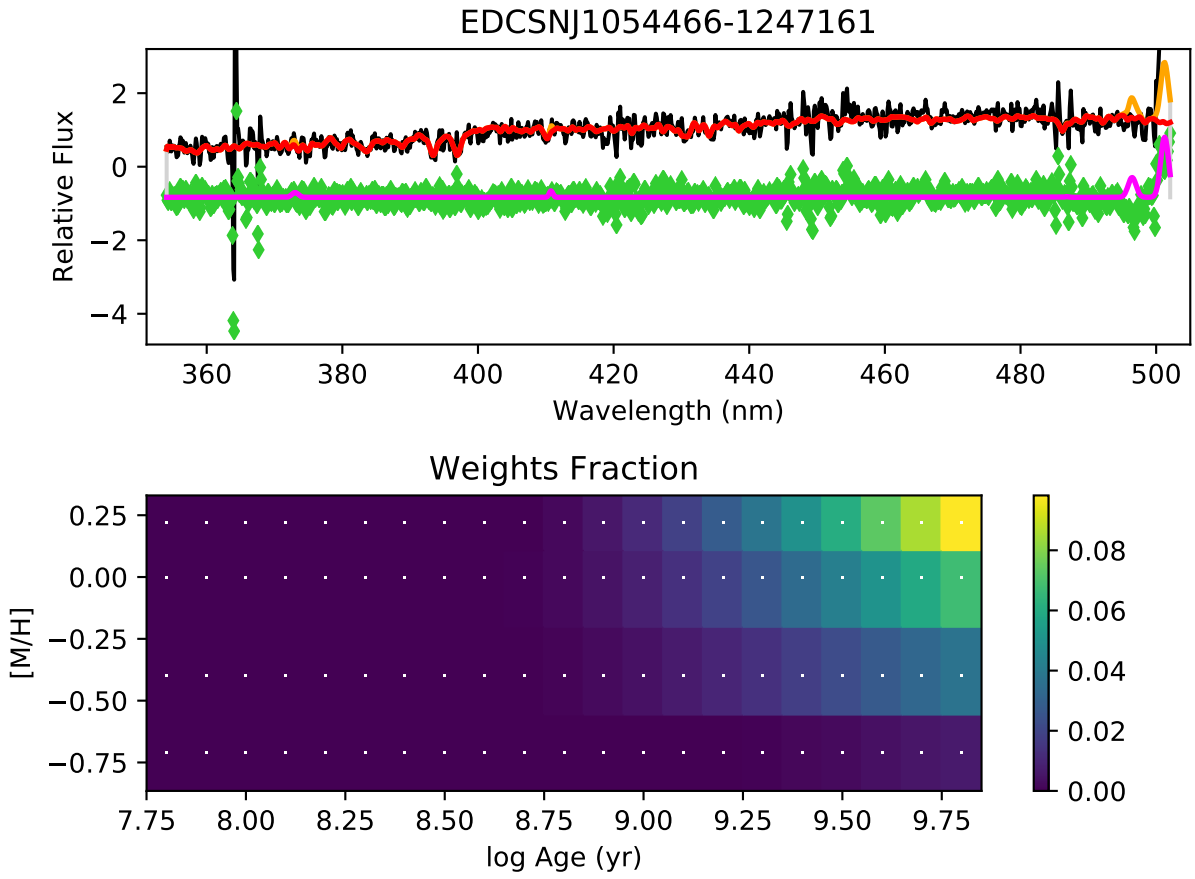
EDCSNJ1054466-1247161
Relative Flux
2
0
−2
−4
360
380
400
420
440
460
480
500
Wavelength (nm)
Weights Fraction
[M/H]
0.25
0.00
−0.25
−0.50
−0.75
7.75
8.00
8.25
8.50
8.75
9.00
9.25
9.50
9.75
log Age (yr)
0.08
0.06
0.04
0.02
0.00

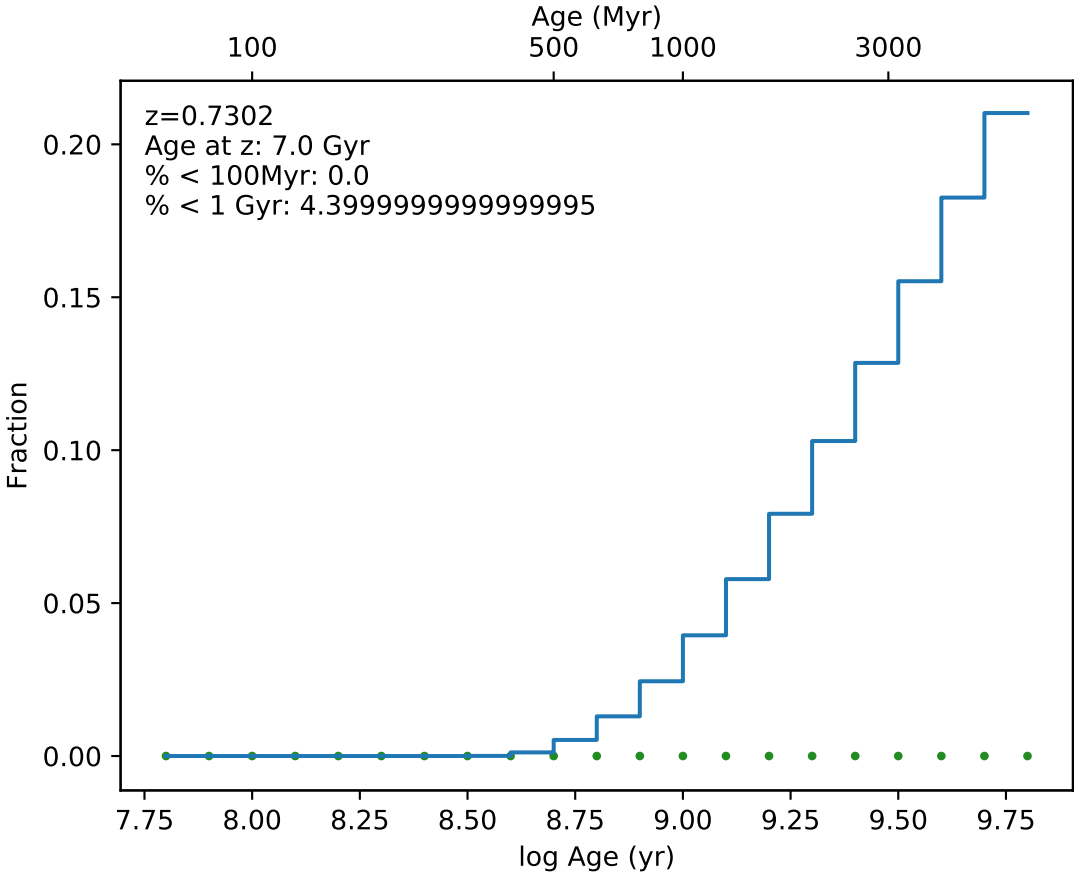
Age (Myr)
100
500
1000
3000
z=0.7302
Age at z: 7.0 Gyr
% < 100Myr: 0.0
% < 1 Gyr: 4.3999999999999995
0.20
0.15
0.10
0.05
0.00
Fraction
7.75
8.00
8.25
8.50
8.75
9.00
9.25
9.50
9.75
log Age (yr)

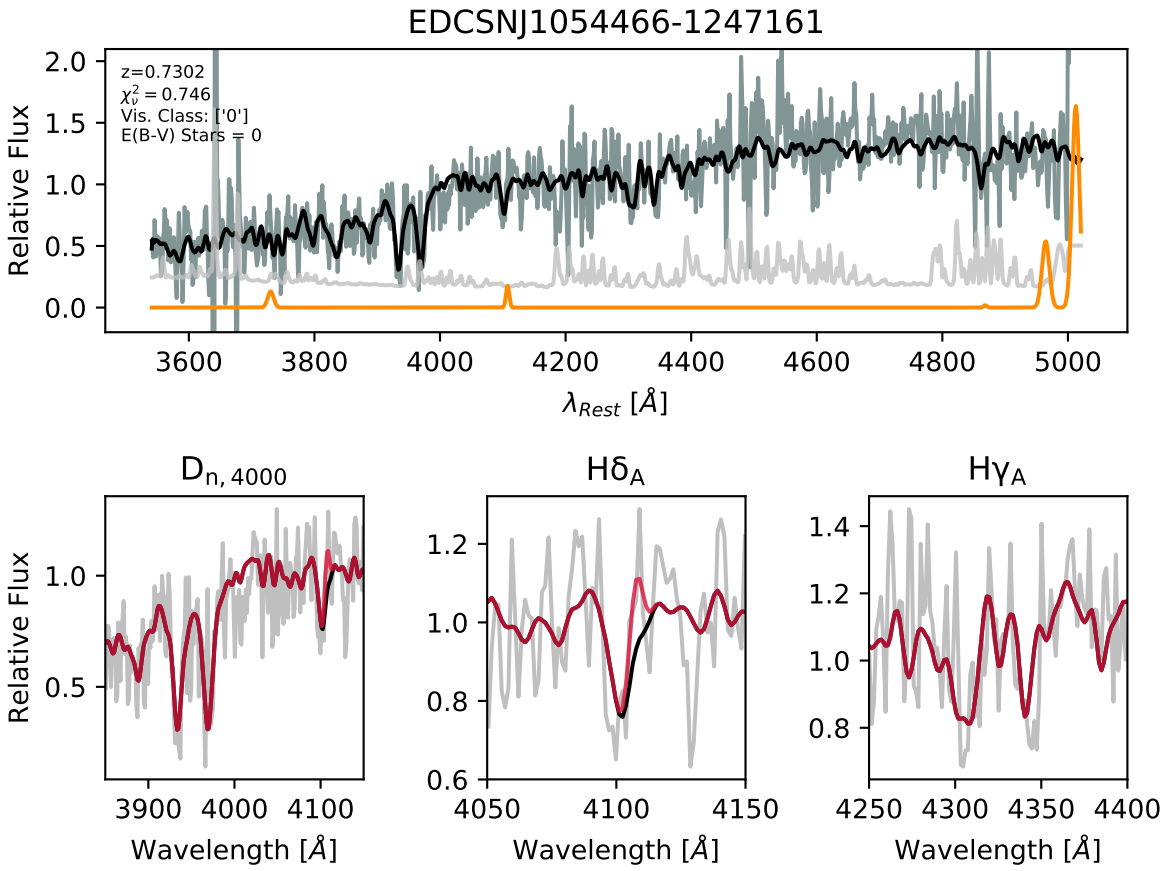
EDCSNJ1054466-1247161
z=0.7302
$\chi^2_\nu = 0.746$
Vis. Class: ['0']
E(B-V) Stars = 0
Relative Flux
λ_{Rest} [Å]
$D_{n,4000}$
$H\delta_A$
$H\gamma_A$
Wavelength [Å]

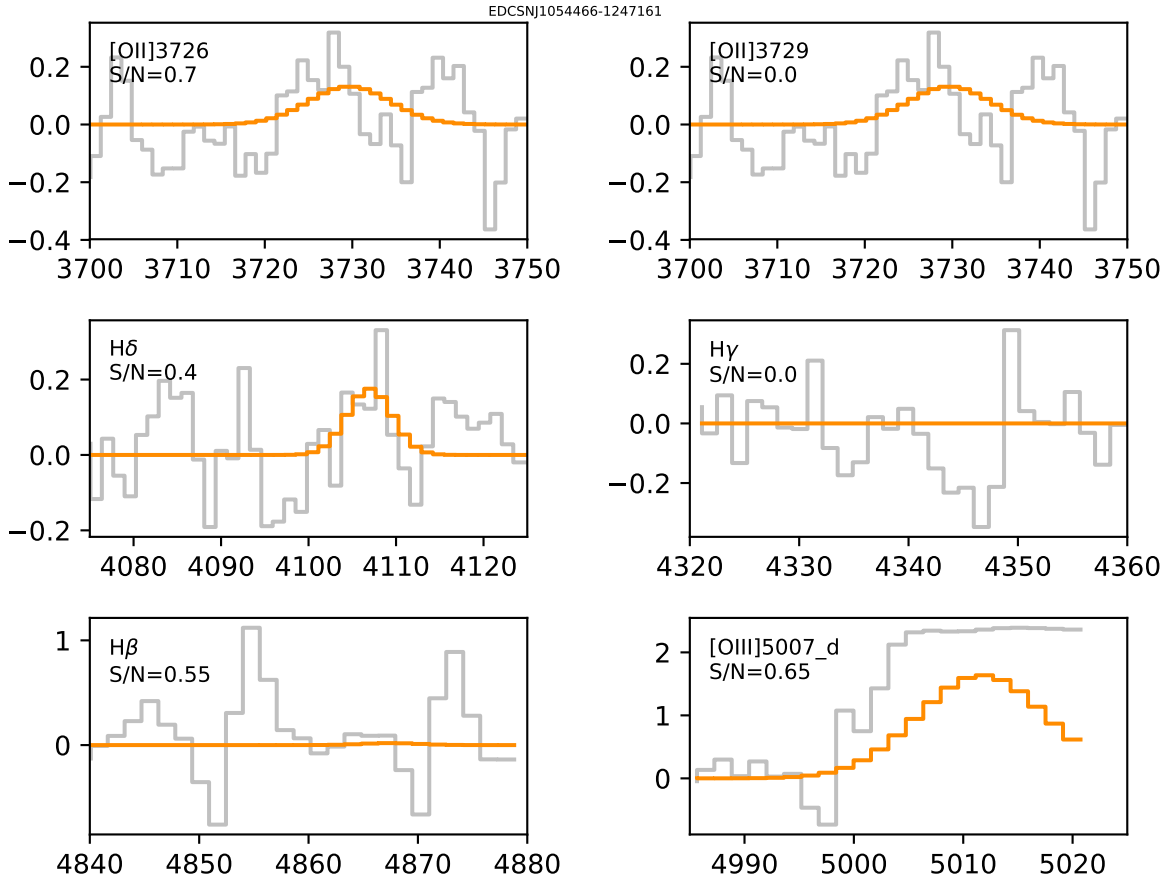
EDCSNJ1054466-1247161
[OII]3726
S/N=0.7
[OII]3729
S/N=0.0
Hδ
S/N=0.4
Hγ
S/N=0.0
Hβ
S/N=0.55
[OIII]5007_d
S/N=0.65

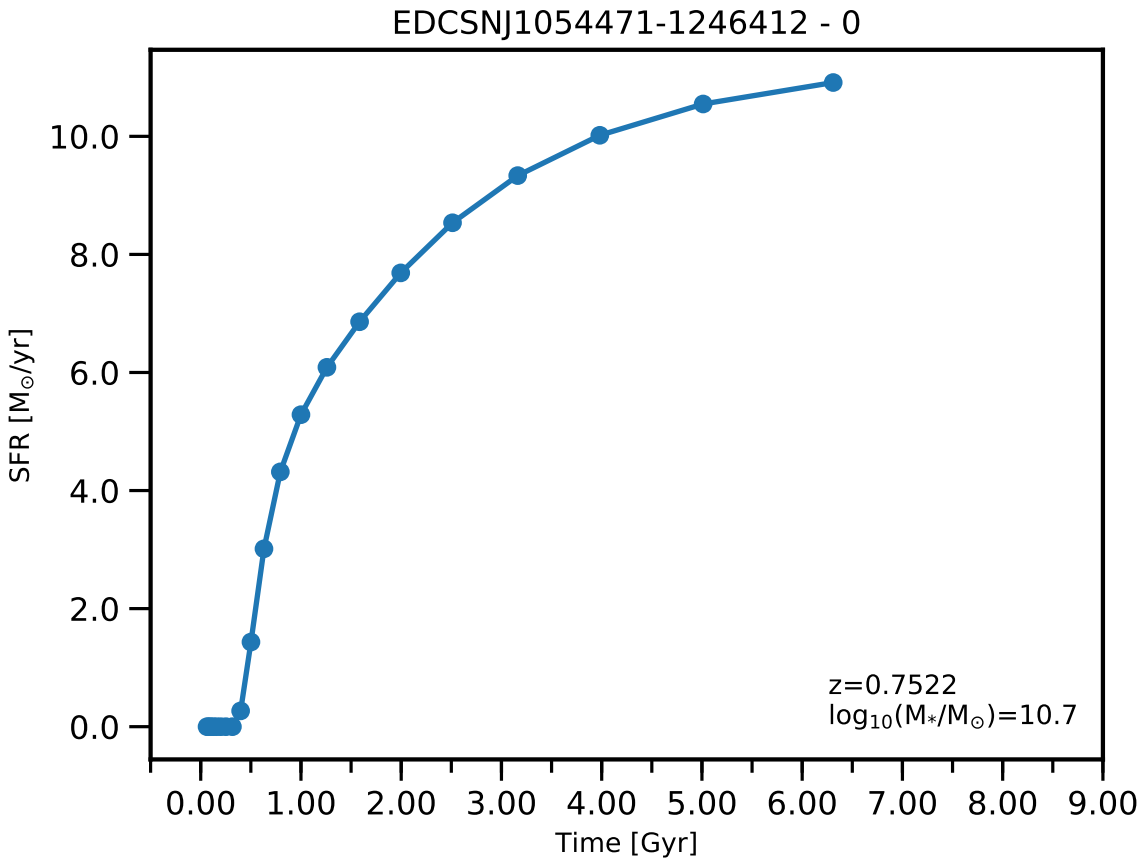
EDCSNJ1054471-1246412 - 0
SFR [M⊙/yr]
10.0
8.0
6.0
4.0
2.0
0.0
0.00
1.00
2.00
3.00
4.00
5.00
6.00
7.00
8.00
9.00
Time [Gyr]
z=0.7522
log10(M∗/M⊙)=10.7

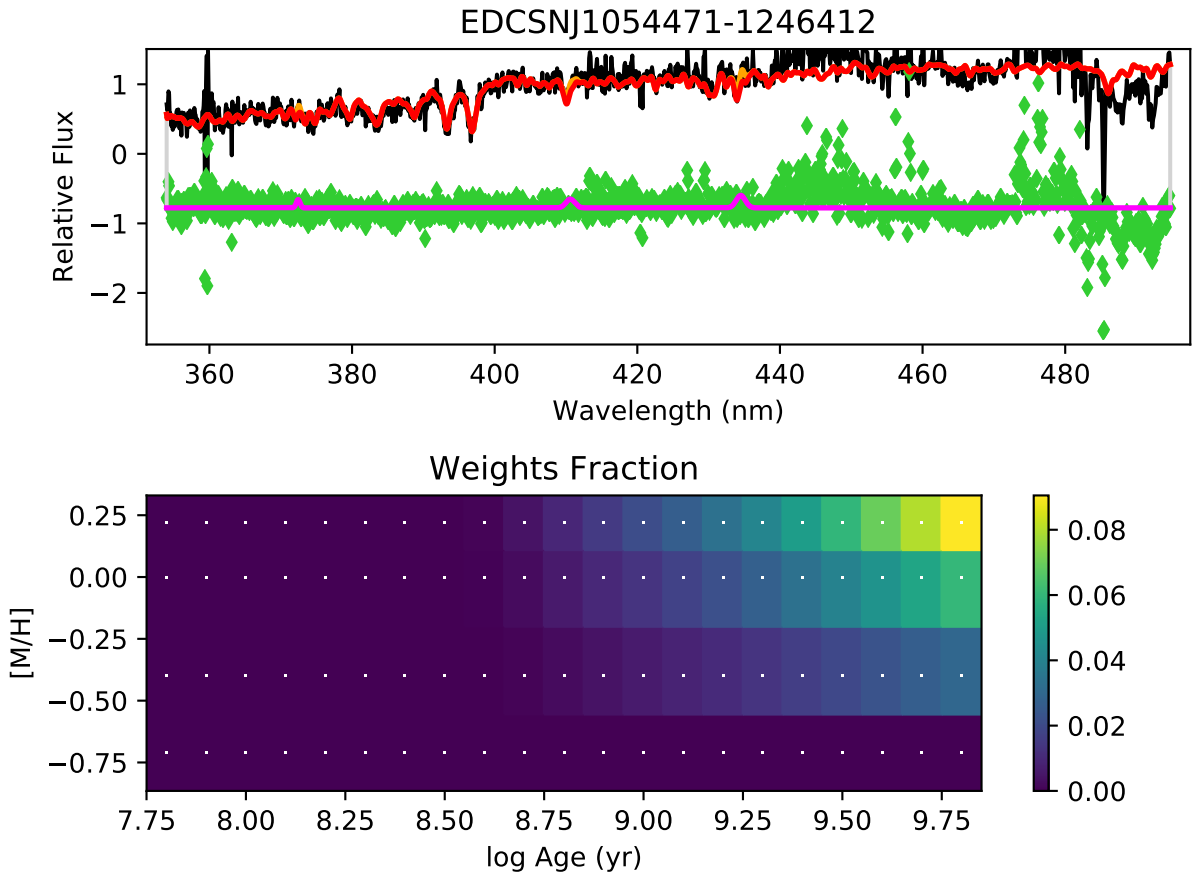
EDCSNJ1054471-1246412
Relative Flux
1
0
−1
−2
360
380
400
420
440
460
480
Wavelength (nm)
Weights Fraction
[M/H]
0.25
0.00
−0.25
−0.50
−0.75
7.75
8.00
8.25
8.50
8.75
9.00
9.25
9.50
9.75
log Age (yr)
0.08
0.06
0.04
0.02
0.00

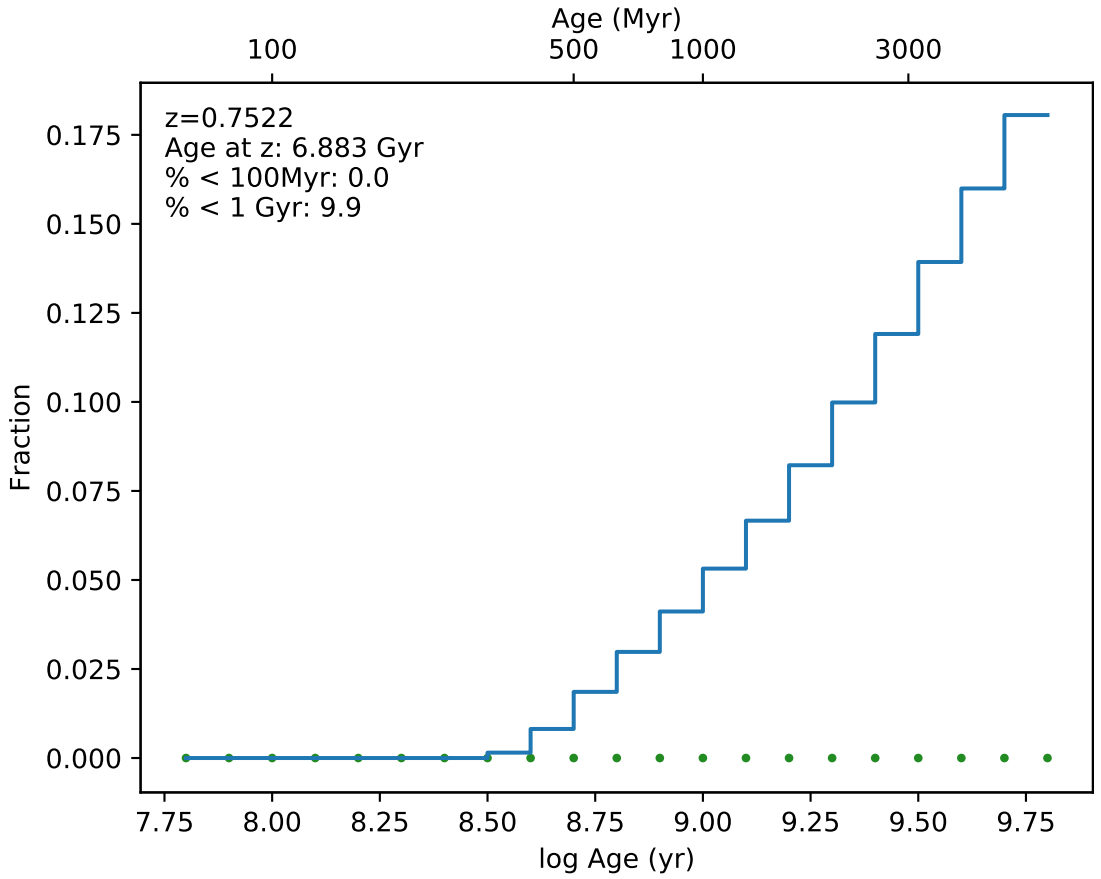
Age (Myr)
100
500
1000
3000
z=0.7522
Age at z: 6.883 Gyr
% < 100Myr: 0.0
% < 1 Gyr: 9.9
Fraction
0.175
0.150
0.125
0.100
0.075
0.050
0.025
0.000
7.75
8.00
8.25
8.50
8.75
9.00
9.25
9.50
9.75
log Age (yr)

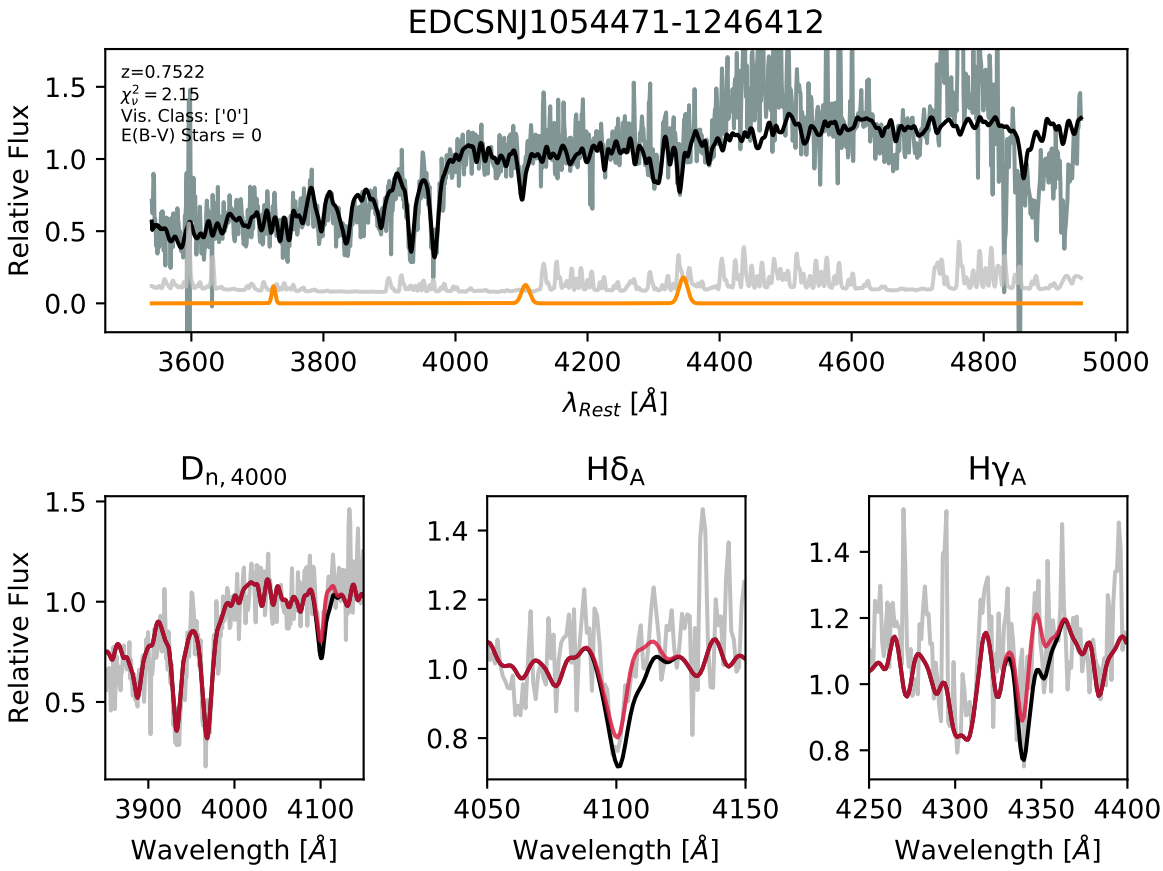
EDCSNJ1054471-1246412
z=0.7522
$\chi^2_\nu = 2.15$
Vis. Class: ['0']
E(B-V) Stars = 0
Relative Flux
λ_{Rest} [Å]
$D_{n,4000}$
$H\delta_A$
$H\gamma_A$
Wavelength [Å]

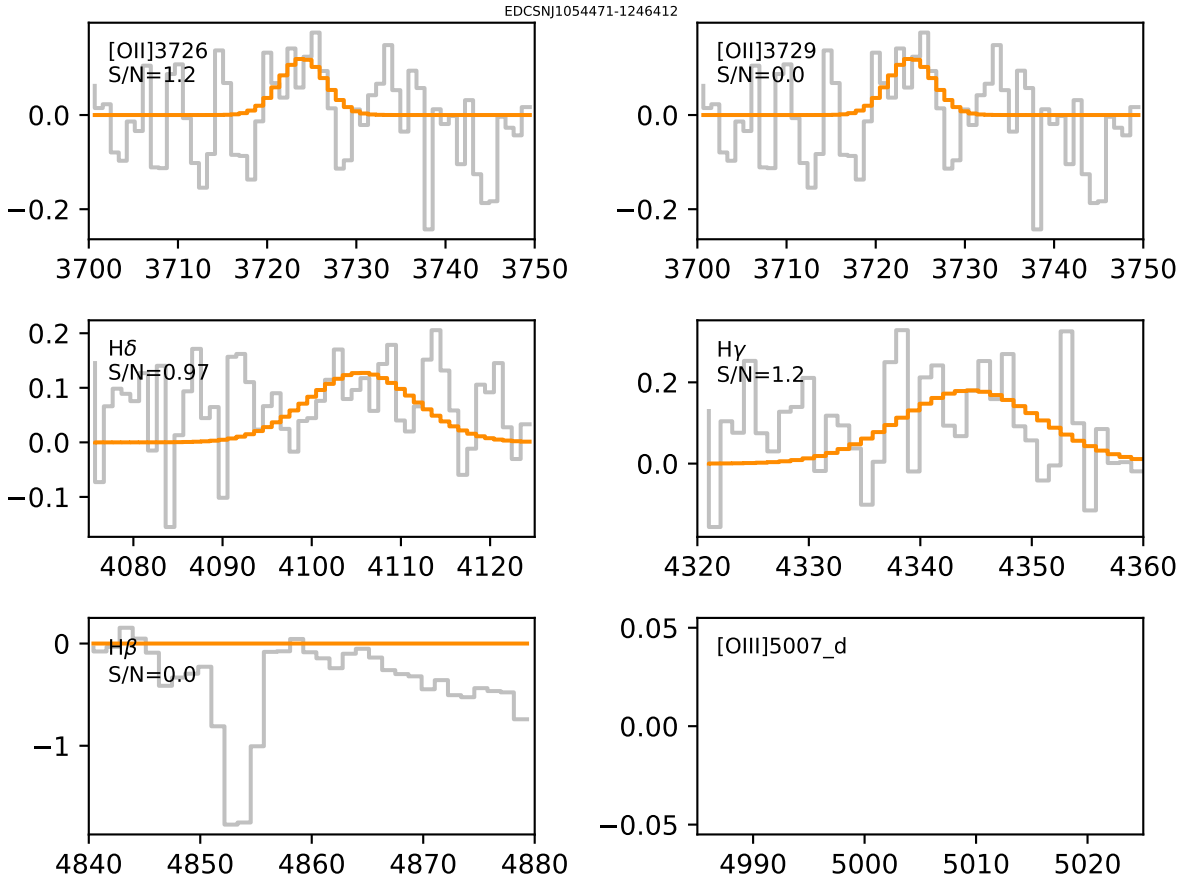
EDCSNJ1054471-1246412
[OII]3726
S/N=1.2
[OII]3729
S/N=0.0
Hδ
S/N=0.97
Hγ
S/N=1.2
Hβ
S/N=0.0
[OIII]5007_d

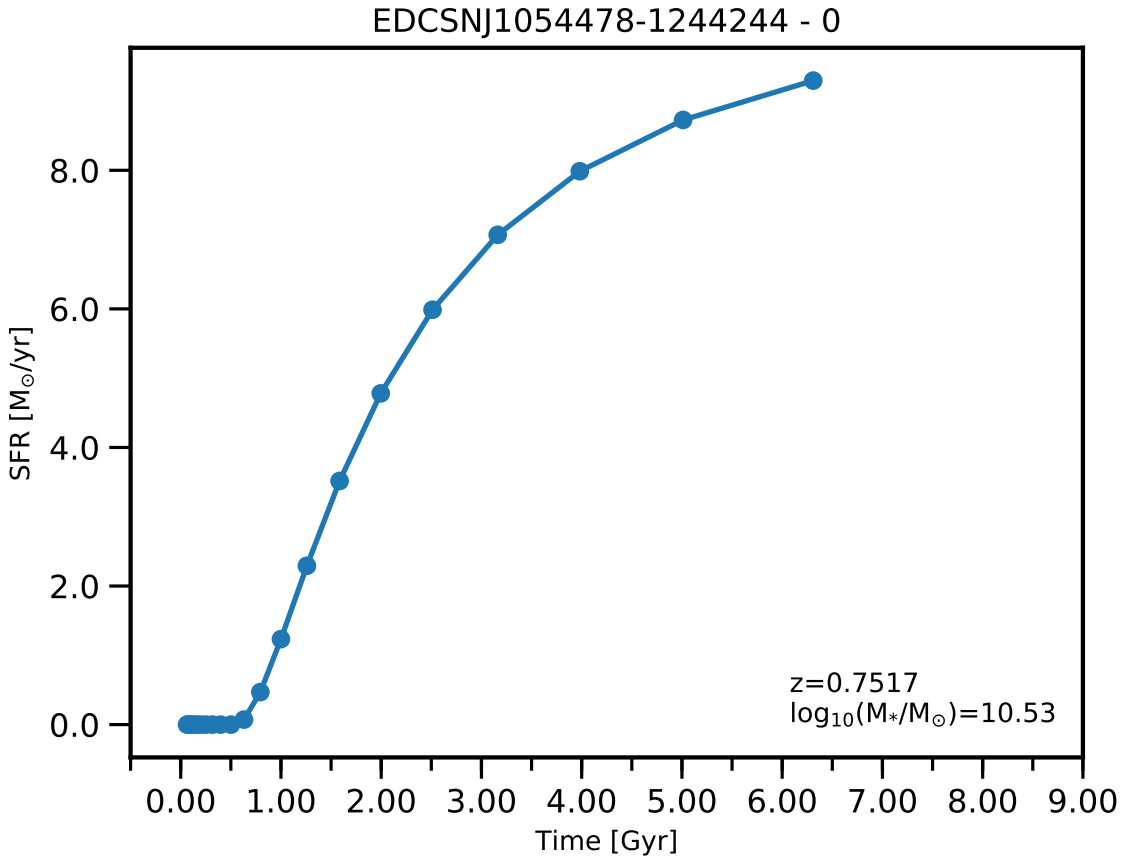
EDCSNJ1054478-1244244 - 0
SFR [M⊙/yr]
0.0
2.0
4.0
6.0
8.0
0.00
1.00
2.00
3.00
4.00
5.00
6.00
7.00
8.00
9.00
Time [Gyr]
z=0.7517
log10(M*/M⊙)=10.53

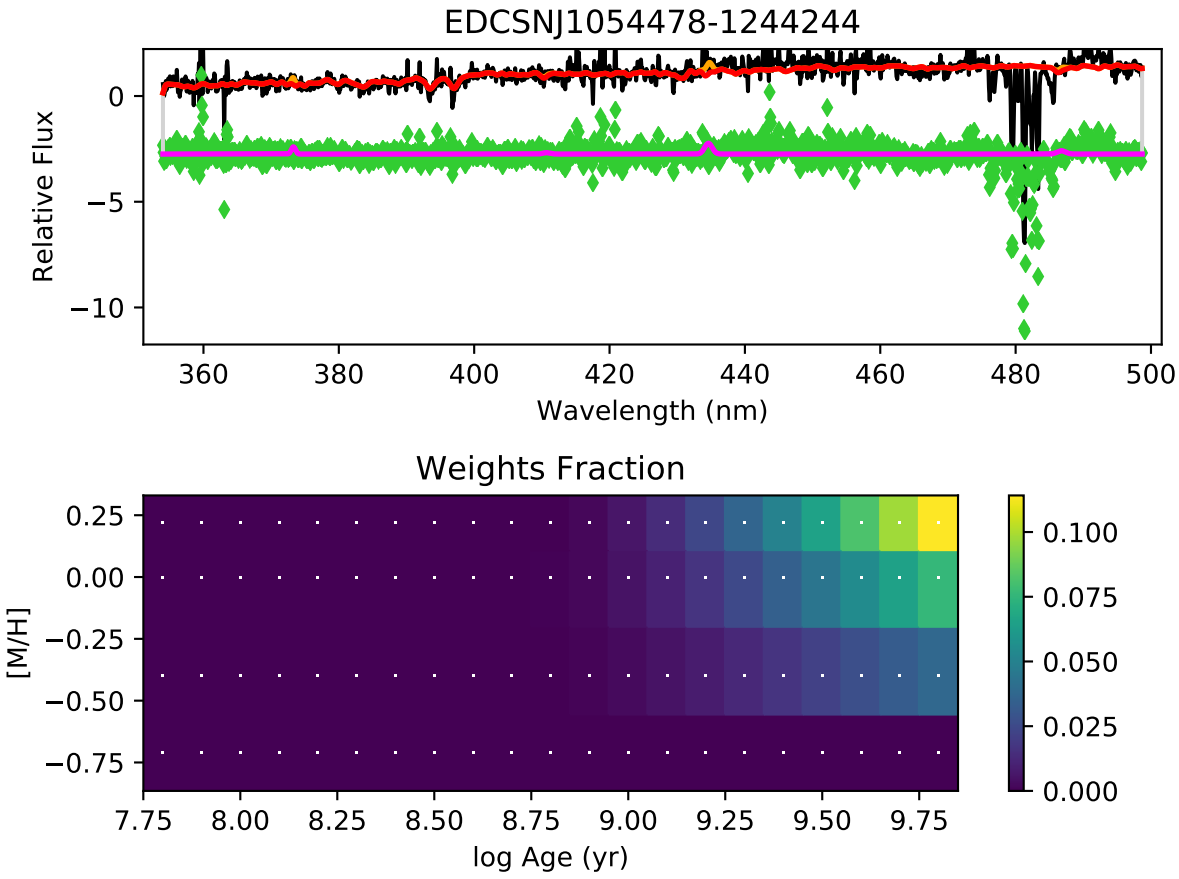
EDCSNJ1054478-1244244
Relative Flux
0
−5
−10
360
380
400
420
440
460
480
500
Wavelength (nm)
Weights Fraction
[M/H]
0.25
0.00
−0.25
−0.50
−0.75
7.75
8.00
8.25
8.50
8.75
9.00
9.25
9.50
9.75
log Age (yr)
0.100
0.075
0.050
0.025
0.000

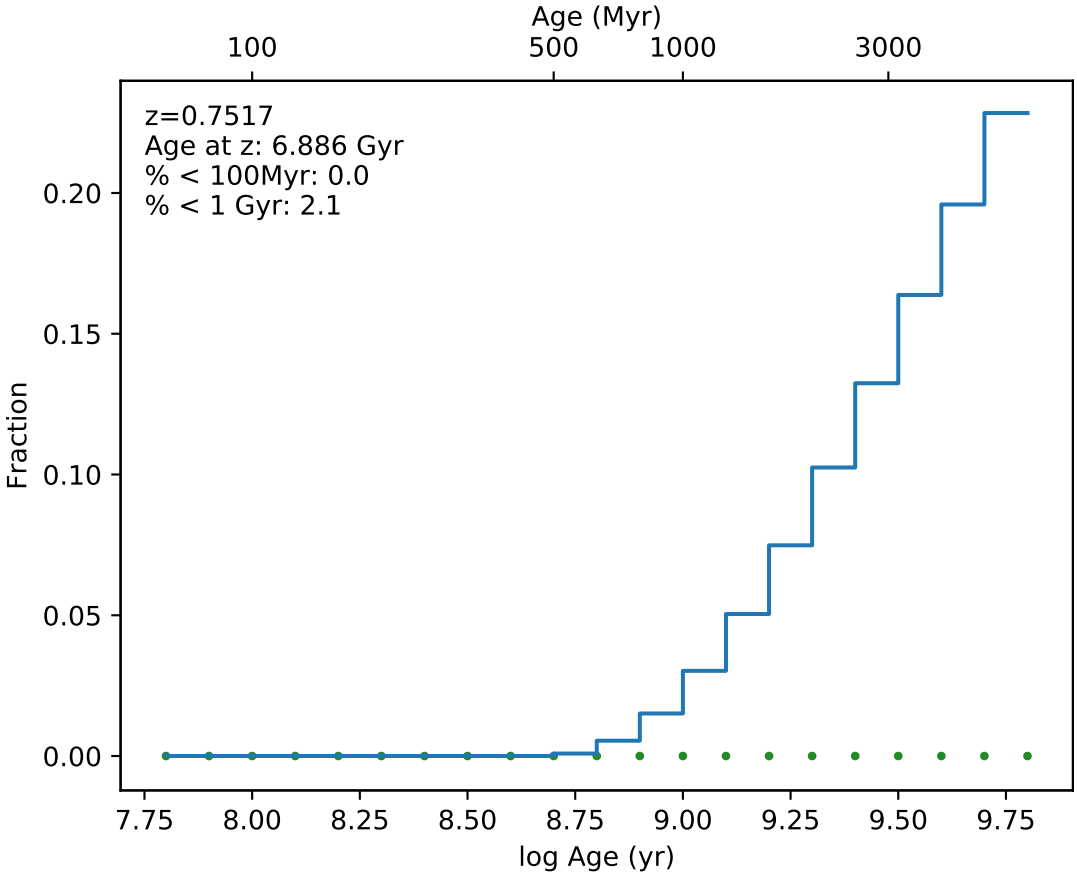
Age (Myr)
100
500
1000
3000
z=0.7517
Age at z: 6.886 Gyr
% < 100Myr: 0.0
% < 1 Gyr: 2.1
Fraction
0.20
0.15
0.10
0.05
0.00
7.75
8.00
8.25
8.50
8.75
9.00
9.25
9.50
9.75
log Age (yr)

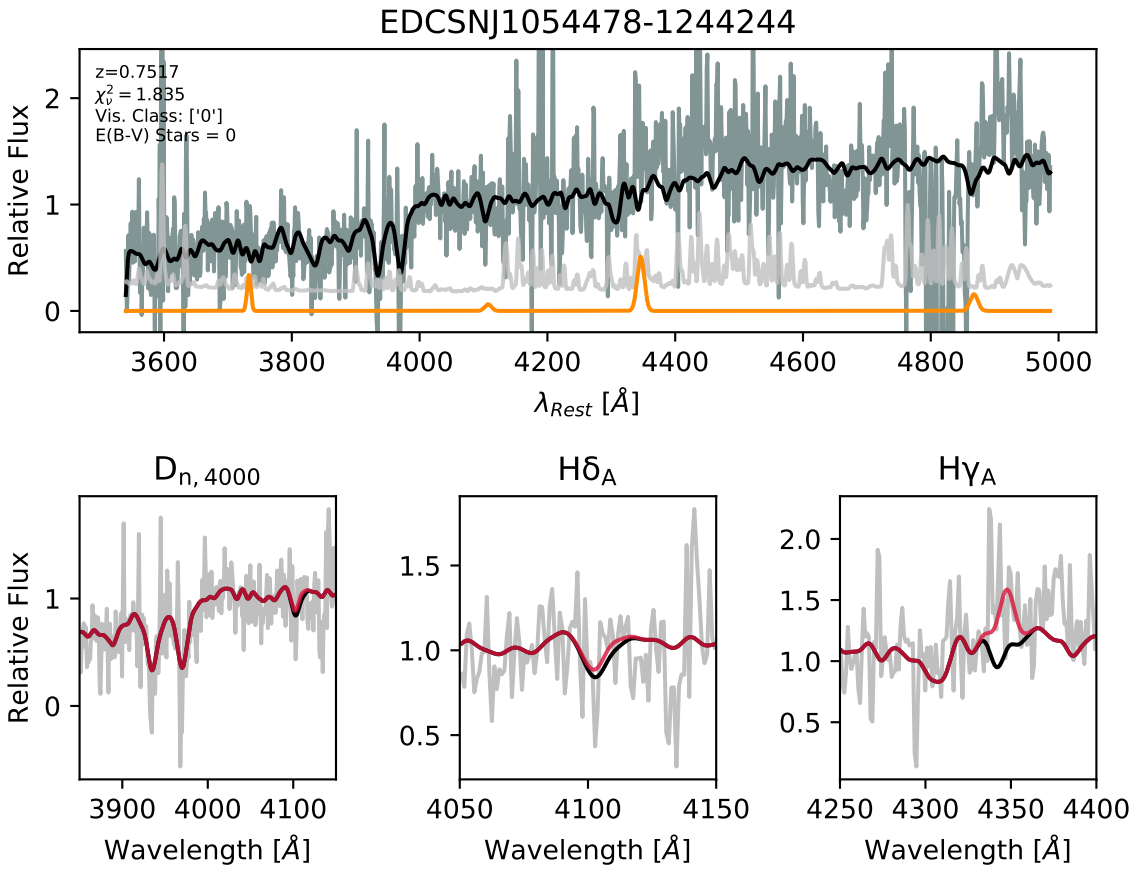
EDCSNJ1054478-1244244
z=0.7517
$\chi^2_\nu = 1.835$
Vis. Class: ['0']
E(B-V) Stars = 0
Relative Flux
λ_{Rest} [Å]
$D_{n,4000}$
$H\delta_A$
$H\gamma_A$
Wavelength [Å]

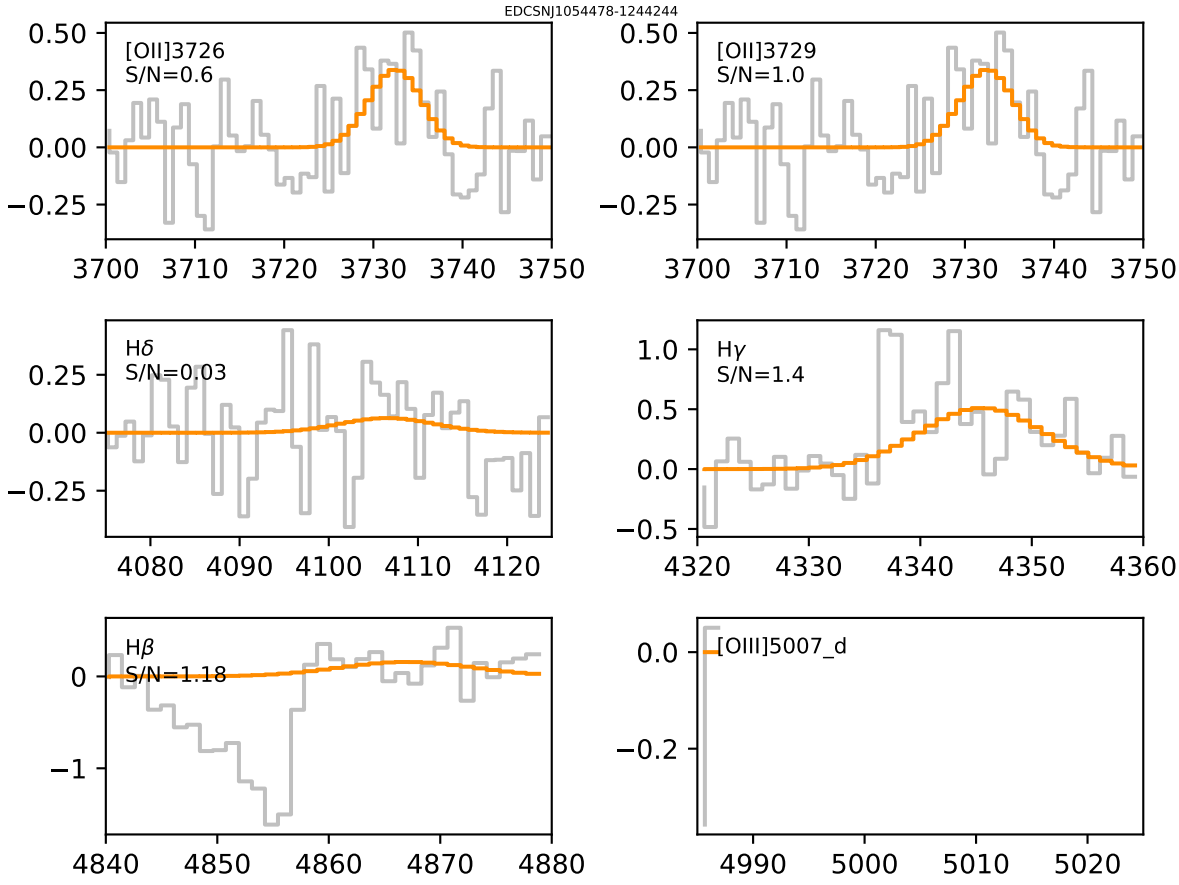
EDCSNJ1054478-1244244
[OII]3726
S/N=0.6
[OII]3729
S/N=1.0
Hδ
S/N=0.03
Hγ
S/N=1.4
Hβ
S/N=1.18
[OIII]5007_d

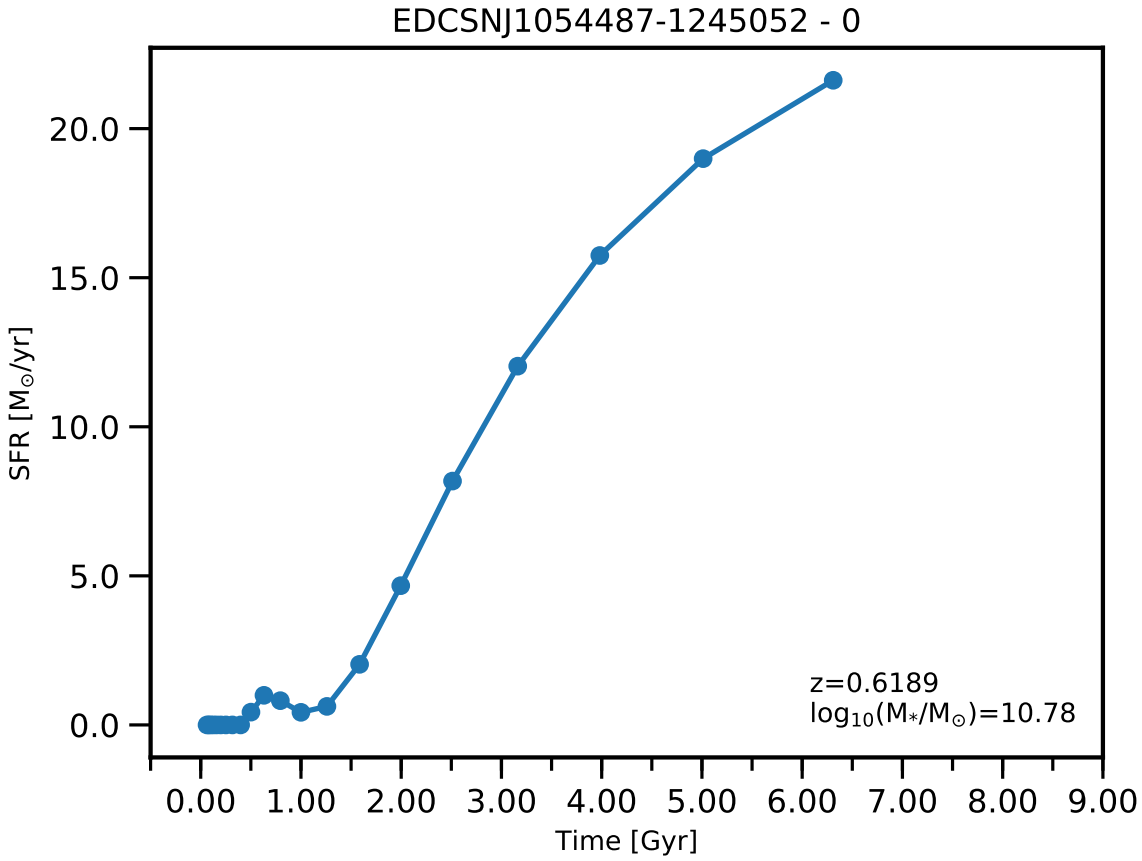
EDCSNJ1054487-1245052 - 0
SFR [M⊙/yr]
20.0
15.0
10.0
5.0
0.0
0.00
1.00
2.00
3.00
4.00
5.00
6.00
7.00
8.00
9.00
Time [Gyr]
z=0.6189
log10(M*/M⊙)=10.78

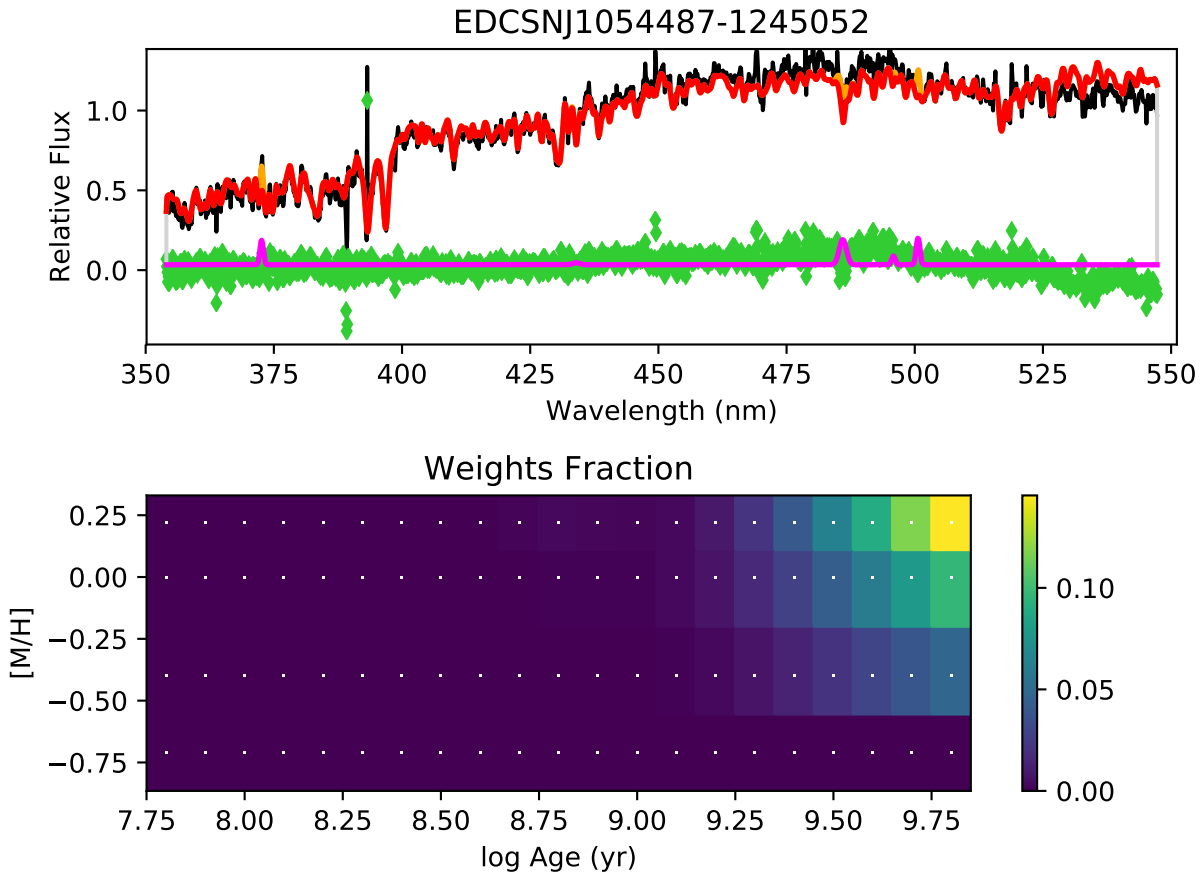
EDCSNJ1054487-1245052
Relative Flux
1.0
0.5
0.0
350
375
400
425
450
475
500
525
550
Wavelength (nm)
Weights Fraction
[M/H]
0.25
0.00
−0.25
−0.50
−0.75
7.75
8.00
8.25
8.50
8.75
9.00
9.25
9.50
9.75
log Age (yr)
0.10
0.05
0.00

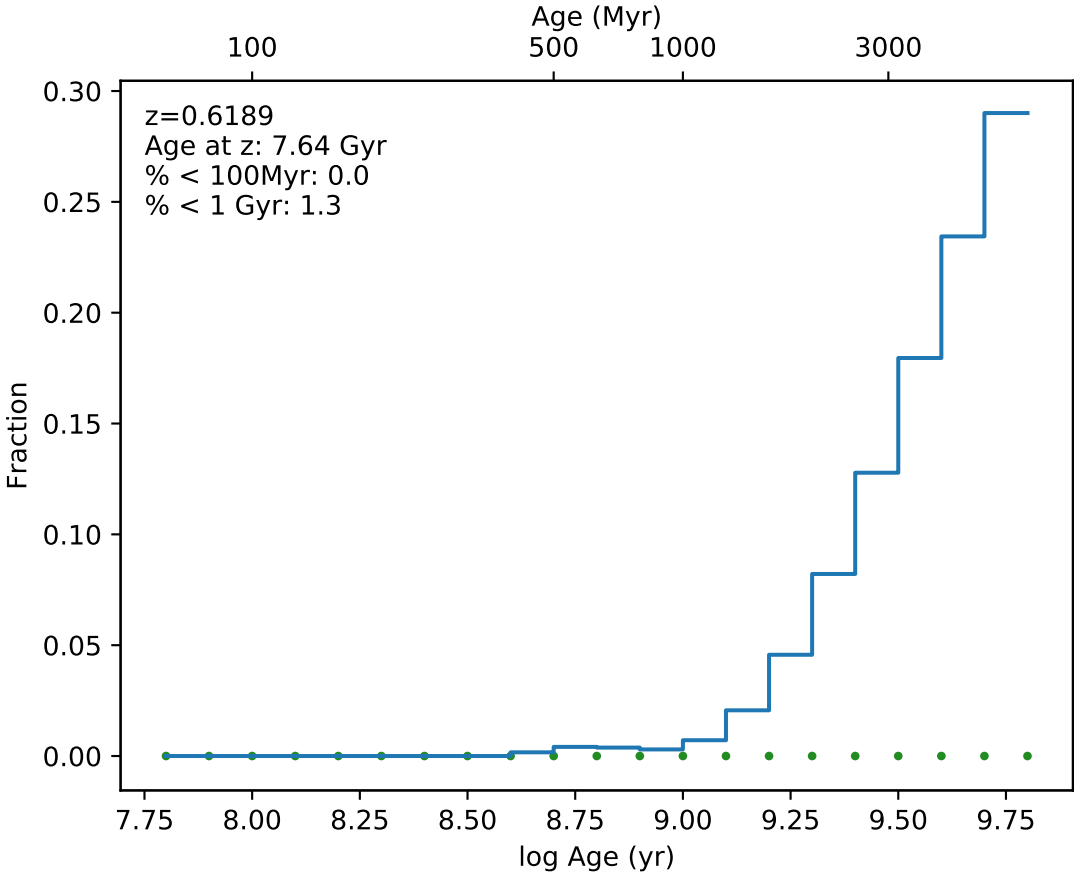
Age (Myr)
100
500
1000
3000
z=0.6189
Age at z: 7.64 Gyr
% < 100Myr: 0.0
% < 1 Gyr: 1.3
Fraction
0.30
0.25
0.20
0.15
0.10
0.05
0.00
7.75
8.00
8.25
8.50
8.75
9.00
9.25
9.50
9.75
log Age (yr)

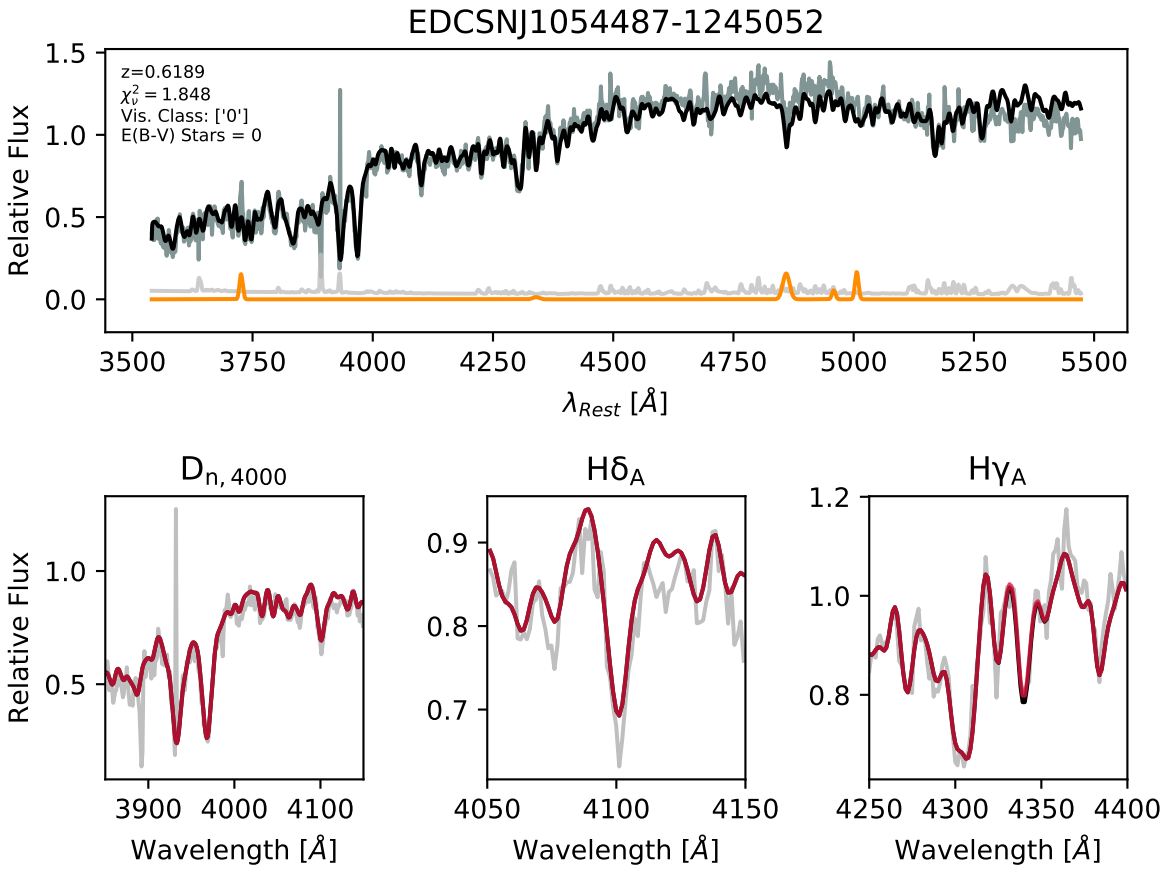
EDCSNJ1054487-1245052
z=0.6189
$\chi^2_\nu = 1.848$
Vis. Class: ['0']
E(B-V) Stars = 0
Relative Flux
λ_{Rest} [Å]
$D_{n,4000}$
$H\delta_A$
$H\gamma_A$
Wavelength [Å]

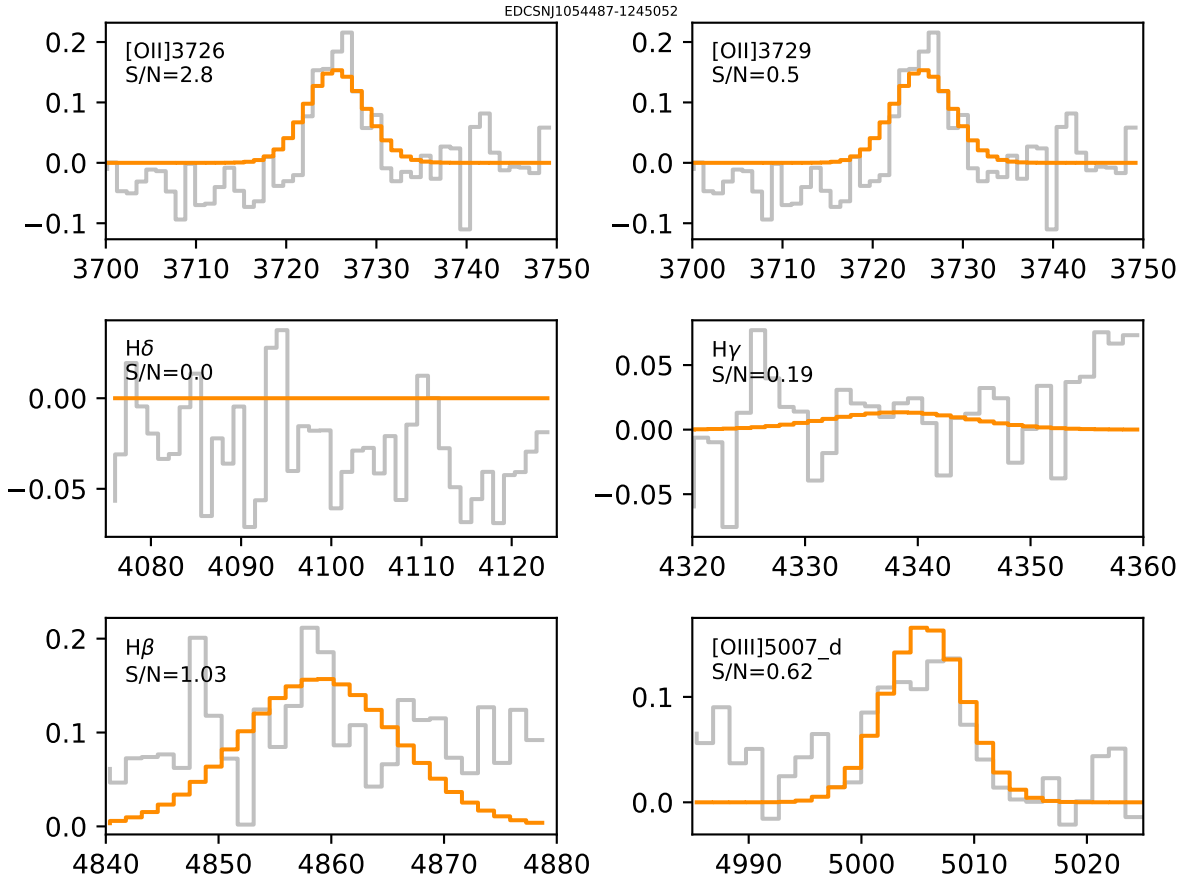
EDCSNJ1054487-1245052
[OII]3726
S/N=2.8
[OII]3729
S/N=0.5
Hδ
S/N=0.0
Hγ
S/N=0.19
Hβ
S/N=1.03
[OIII]5007_d
S/N=0.62

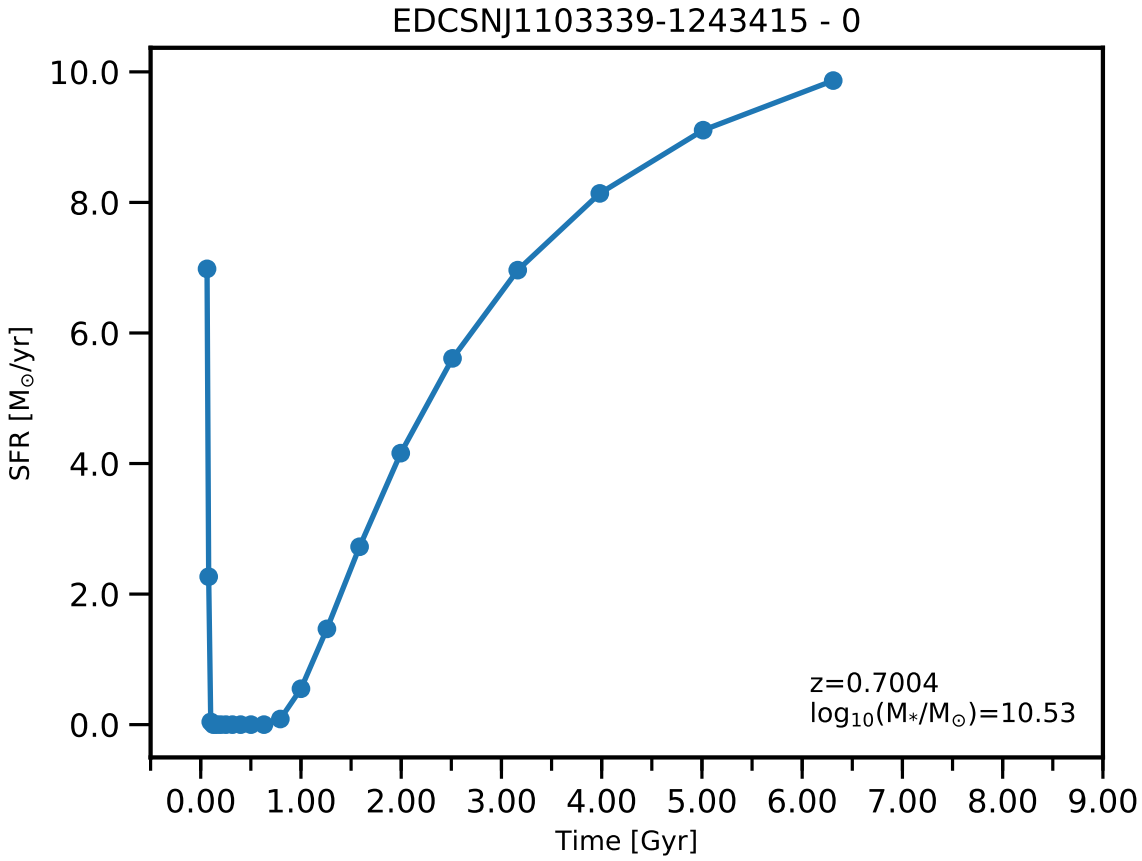
EDCSNJ1103339-1243415 - 0
SFR [M⊙/yr]
Time [Gyr]
z=0.7004
log10(M*/M⊙)=10.53
0.0
2.0
4.0
6.0
8.0
10.0
0.00
1.00
2.00
3.00
4.00
5.00
6.00
7.00
8.00
9.00

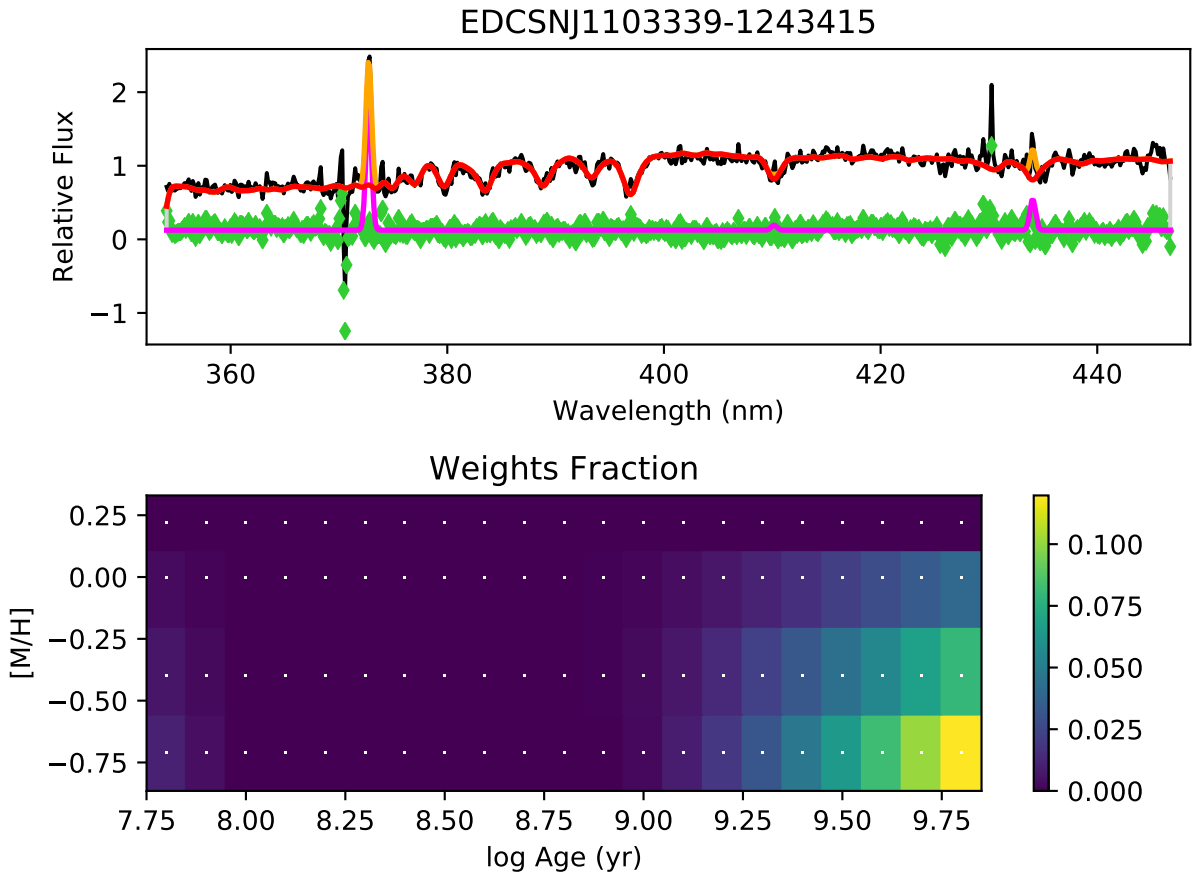
EDCSNJ1103339-1243415
Relative Flux
2
1
0
−1
360
380
400
420
440
Wavelength (nm)
Weights Fraction
[M/H]
0.25
0.00
−0.25
−0.50
−0.75
7.75
8.00
8.25
8.50
8.75
9.00
9.25
9.50
9.75
log Age (yr)
0.100
0.075
0.050
0.025
0.000

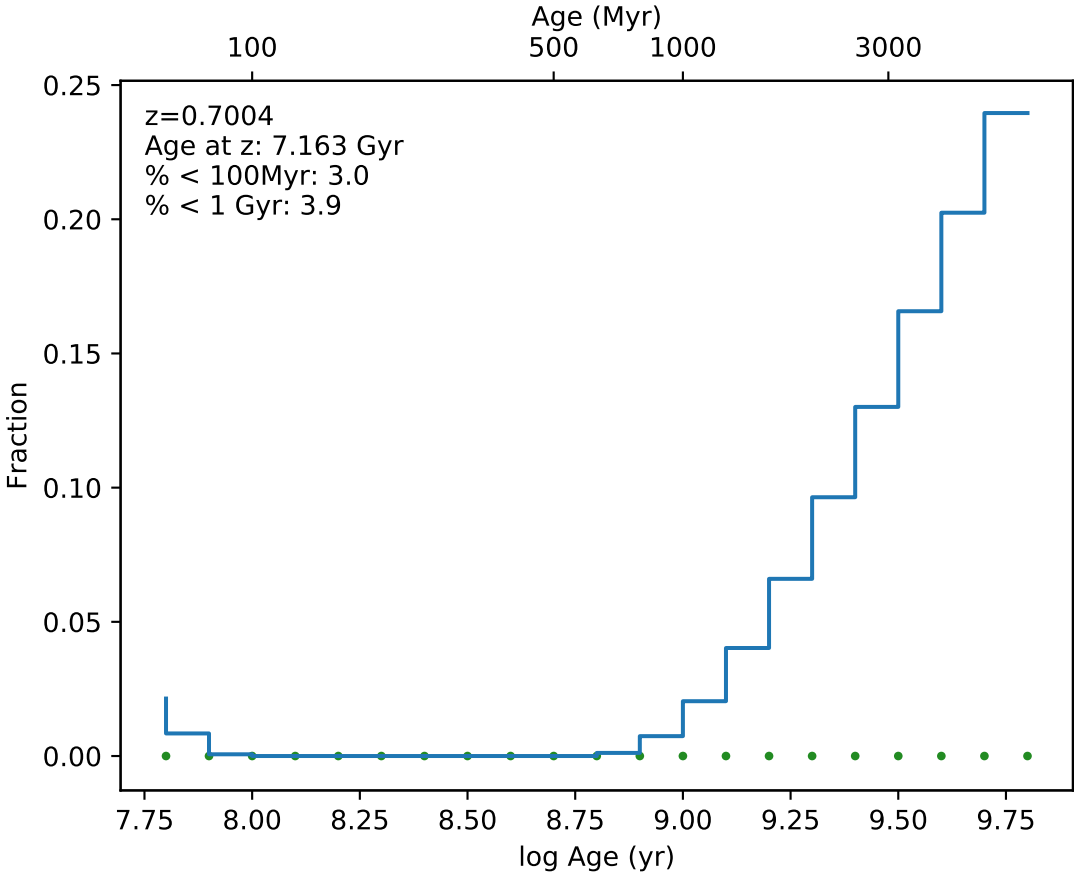
Age (Myr)
100
500
1000
3000
z=0.7004
Age at z: 7.163 Gyr
% < 100Myr: 3.0
% < 1 Gyr: 3.9
Fraction
0.25
0.20
0.15
0.10
0.05
0.00
7.75
8.00
8.25
8.50
8.75
9.00
9.25
9.50
9.75
log Age (yr)

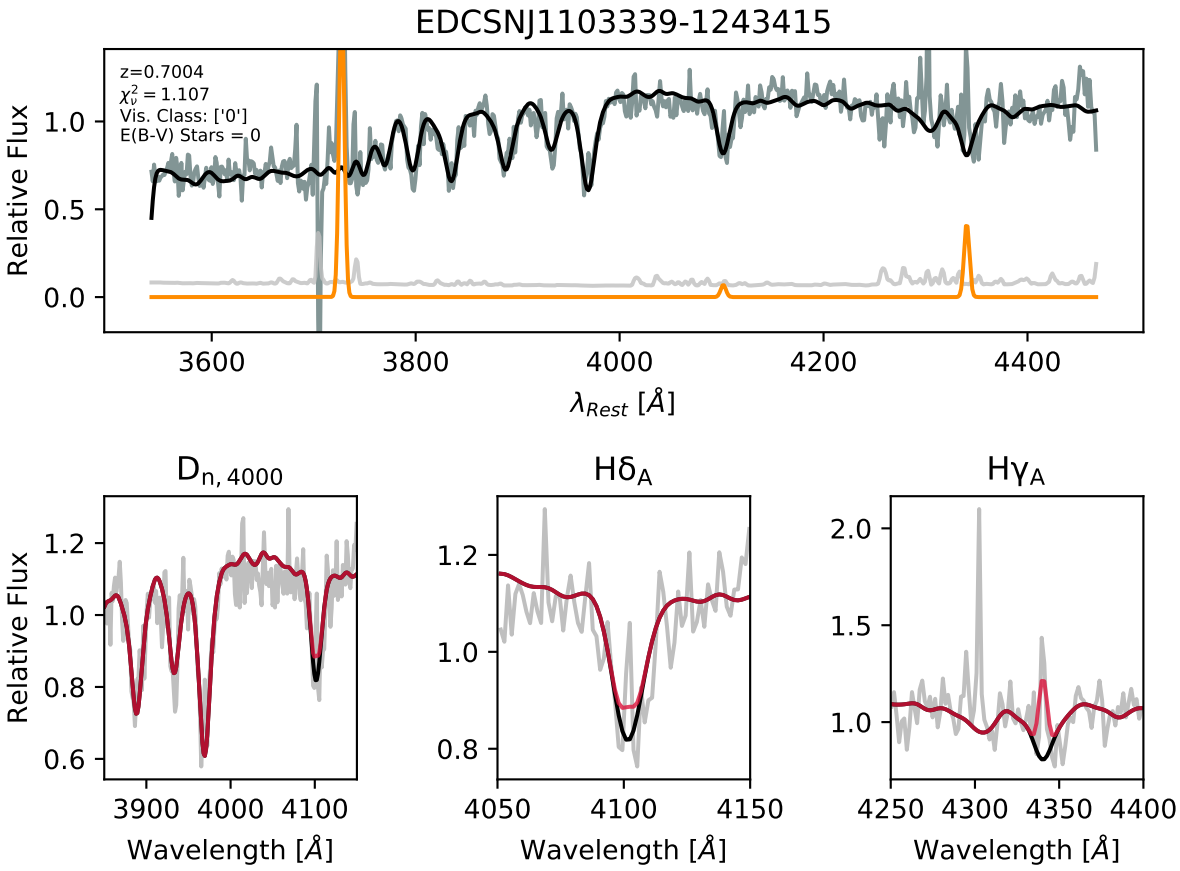
EDCSNJ1103339-1243415
z=0.7004
$\chi^2_\nu = 1.107$
Vis. Class: ['0']
E(B-V) Stars = 0
Relative Flux
1.0
0.5
0.0
3600
3800
4000
4200
4400
λ_{Rest} [Å]
$D_{n,4000}$
$H\delta_A$
$H\gamma_A$
Relative Flux
1.2
1.0
0.8
0.6
3900 4000 4100
Wavelength [Å]
1.2
1.0
0.8
4050 4100 4150
Wavelength [Å]
2.0
1.5
1.0
4250 4300 4350 4400
Wavelength [Å]

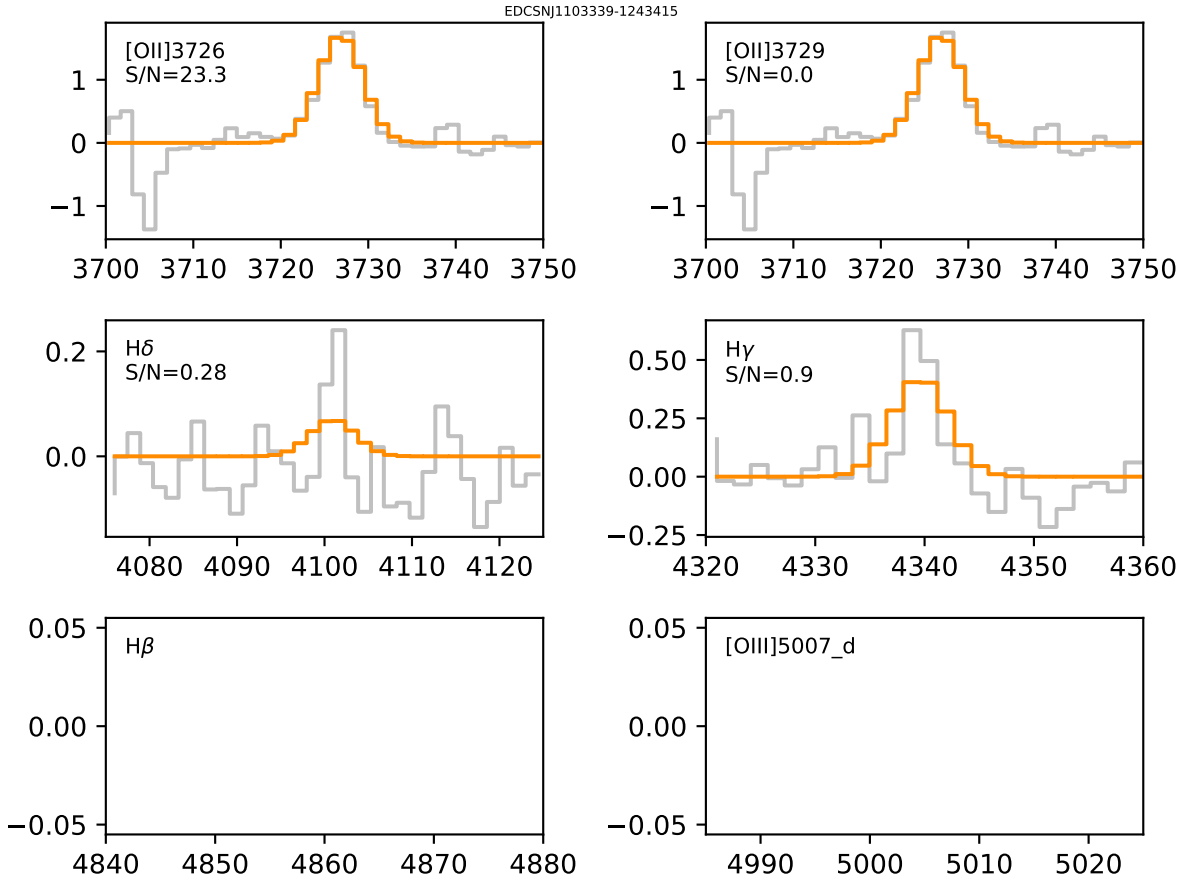
EDCSNJ1103339-1243415
[OII]3726
S/N=23.3
[OII]3729
S/N=0.0
Hδ
S/N=0.28
Hγ
S/N=0.9
Hβ
[OIII]5007_d

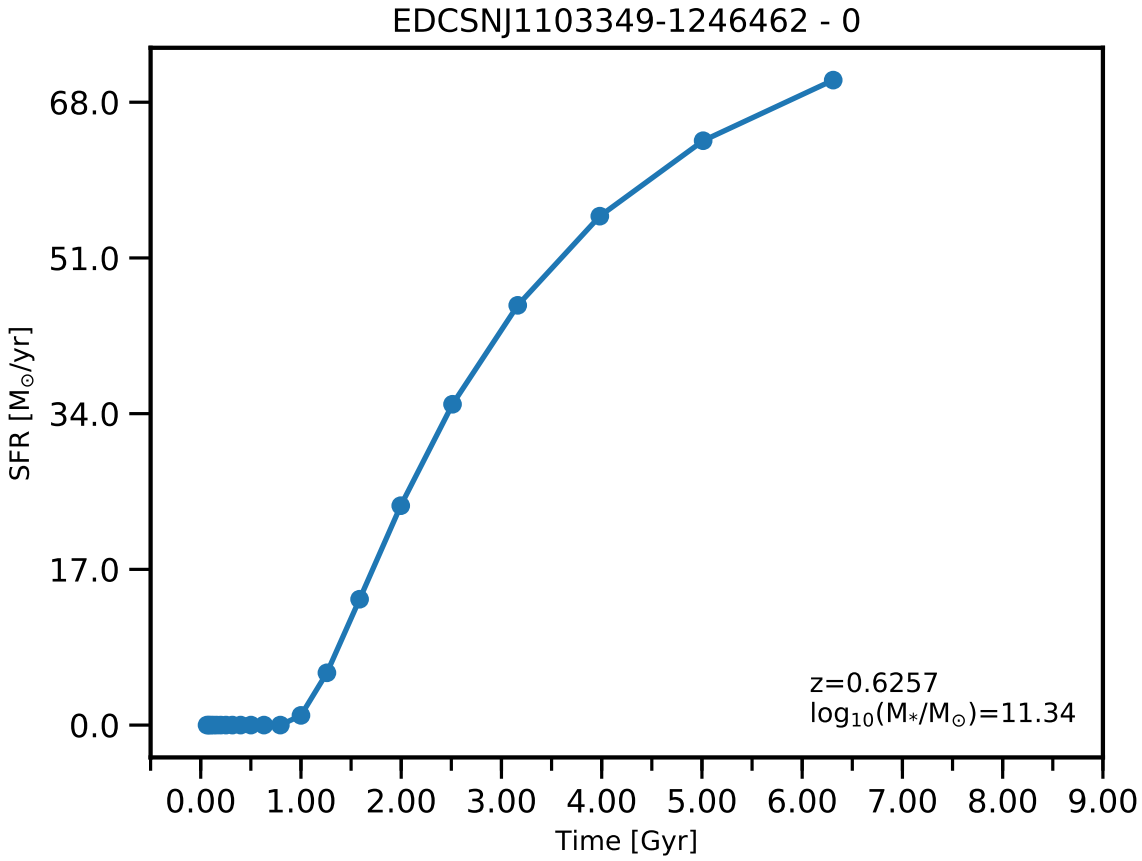
EDCSNJ1103349-1246462 - 0
68.0
51.0
34.0
17.0
0.0
SFR [M⊙/yr]
0.00
1.00
2.00
3.00
4.00
5.00
6.00
7.00
8.00
9.00
Time [Gyr]
z=0.6257
log10(M*/M⊙)=11.34

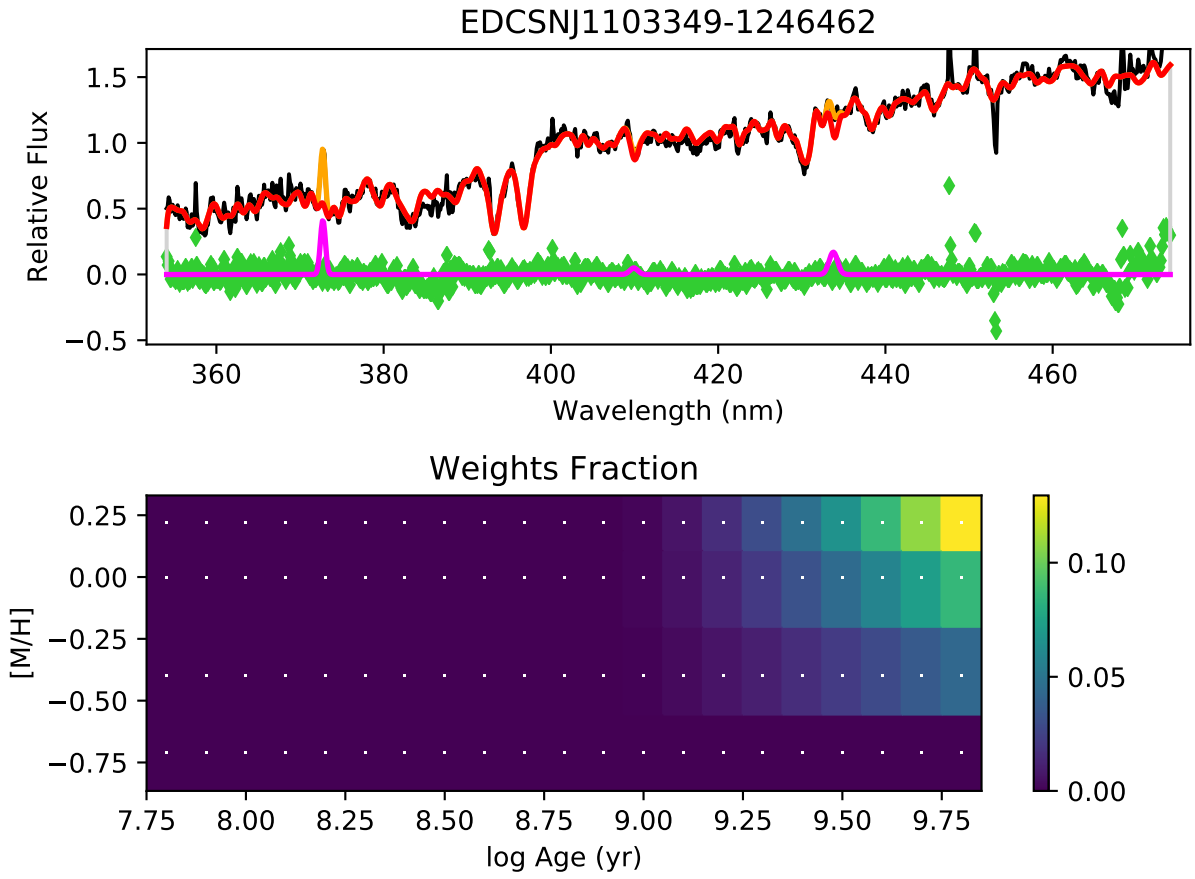
EDCSNJ1103349-1246462
Relative Flux
1.5
1.0
0.5
0.0
−0.5
360
380
400
420
440
460
Wavelength (nm)
Weights Fraction
[M/H]
0.25
0.00
−0.25
−0.50
−0.75
7.75
8.00
8.25
8.50
8.75
9.00
9.25
9.50
9.75
log Age (yr)
0.10
0.05
0.00

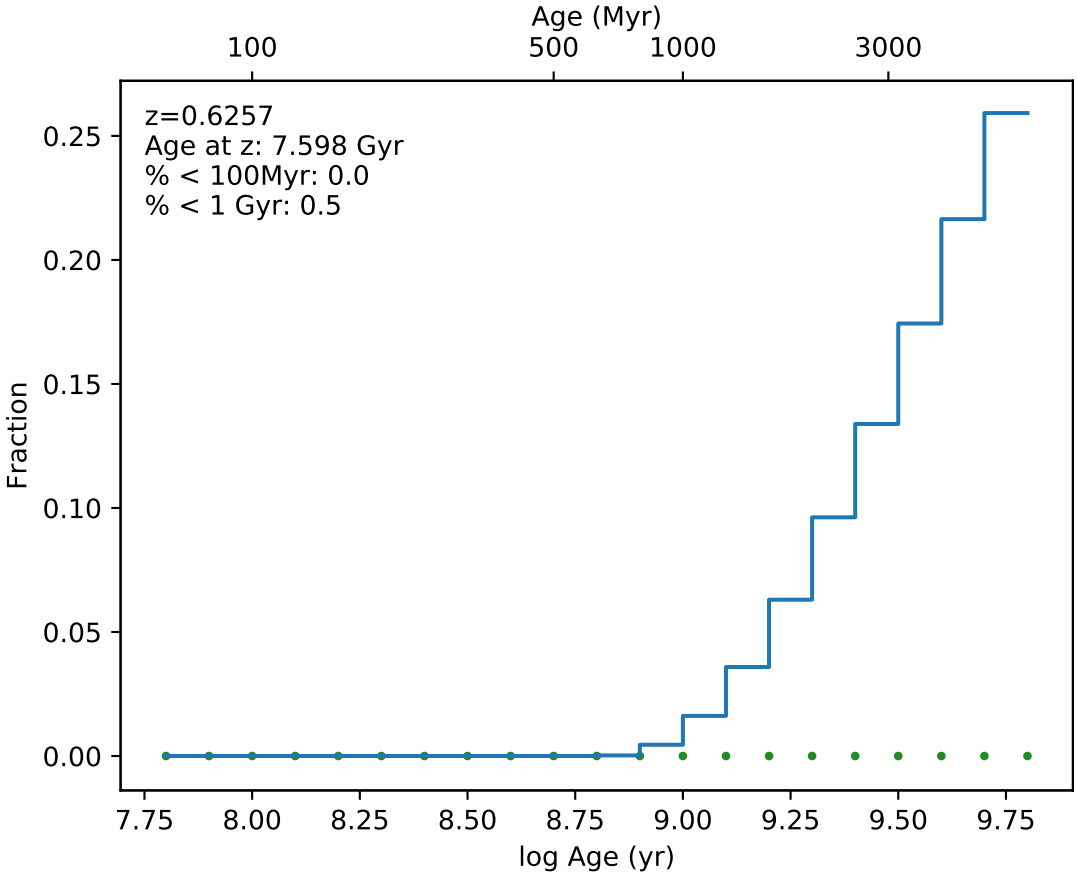
Age (Myr)
100
500
1000
3000
z=0.6257
Age at z: 7.598 Gyr
% < 100Myr: 0.0
% < 1 Gyr: 0.5
Fraction
0.25
0.20
0.15
0.10
0.05
0.00
7.75
8.00
8.25
8.50
8.75
9.00
9.25
9.50
9.75
log Age (yr)

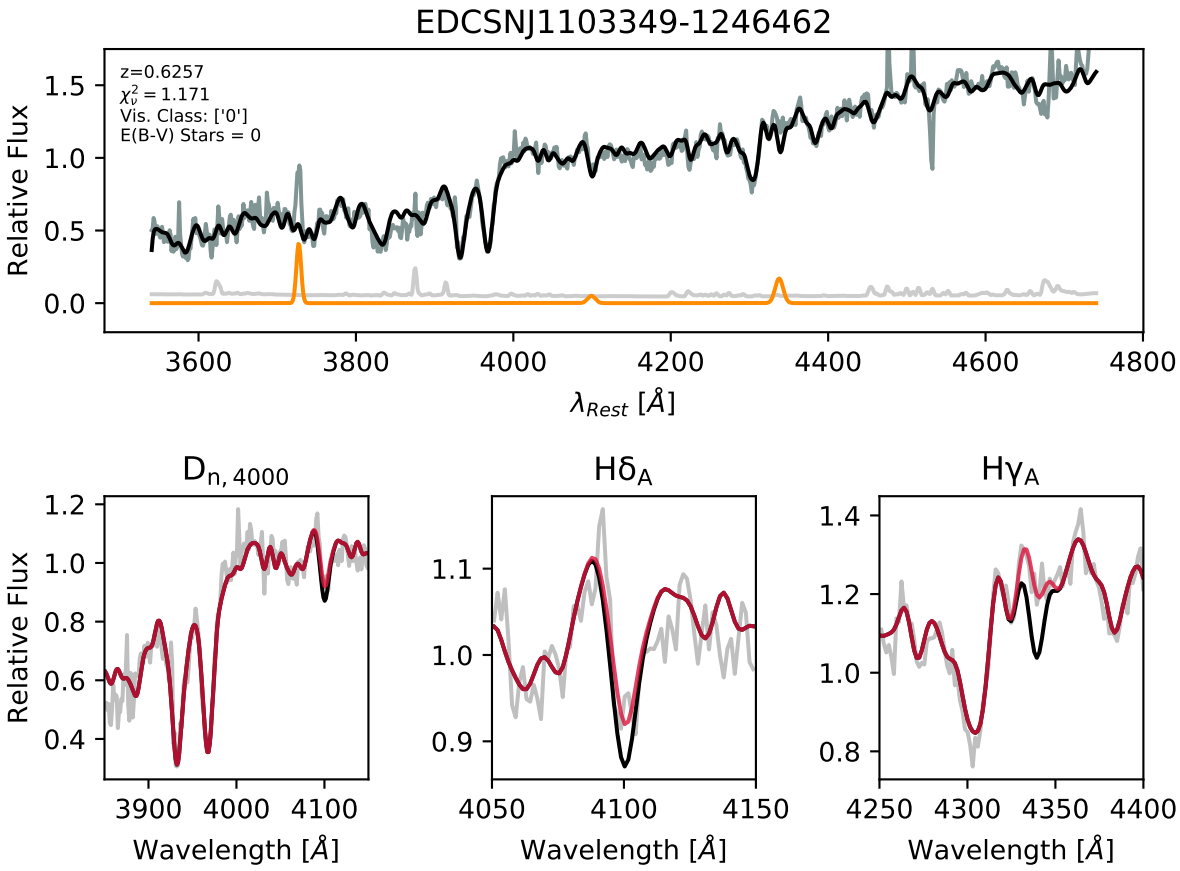
EDCSNJ1103349-1246462
z=0.6257
$\chi^2_\nu = 1.171$
Vis. Class: ['0']
E(B-V) Stars = 0
Relative Flux
λ_{Rest} [Å]
$D_{n,4000}$
$H\delta_A$
$H\gamma_A$
Wavelength [Å]

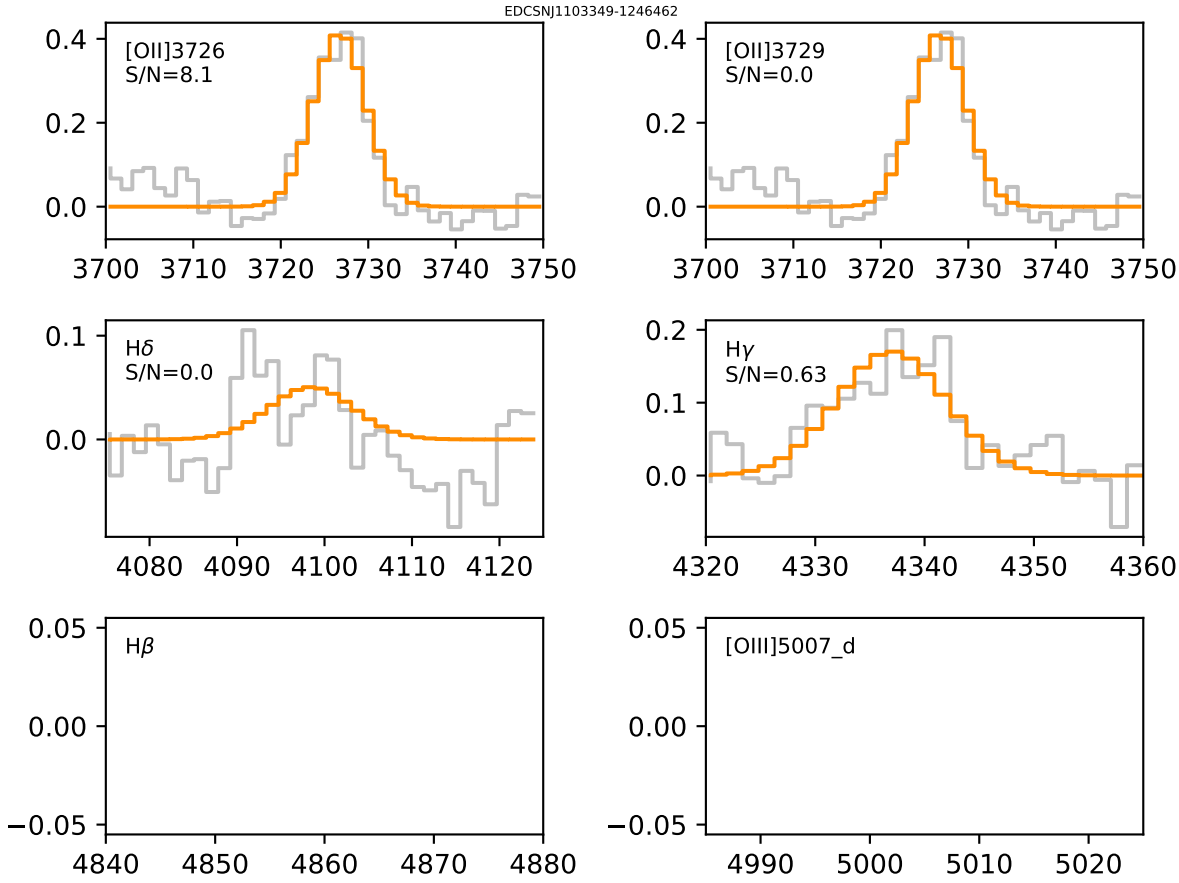
EDCSNJ1103349-1246462
[OII]3726
S/N=8.1
[OII]3729
S/N=0.0
Hδ
S/N=0.0
Hγ
S/N=0.63
Hβ
[OIII]5007_d

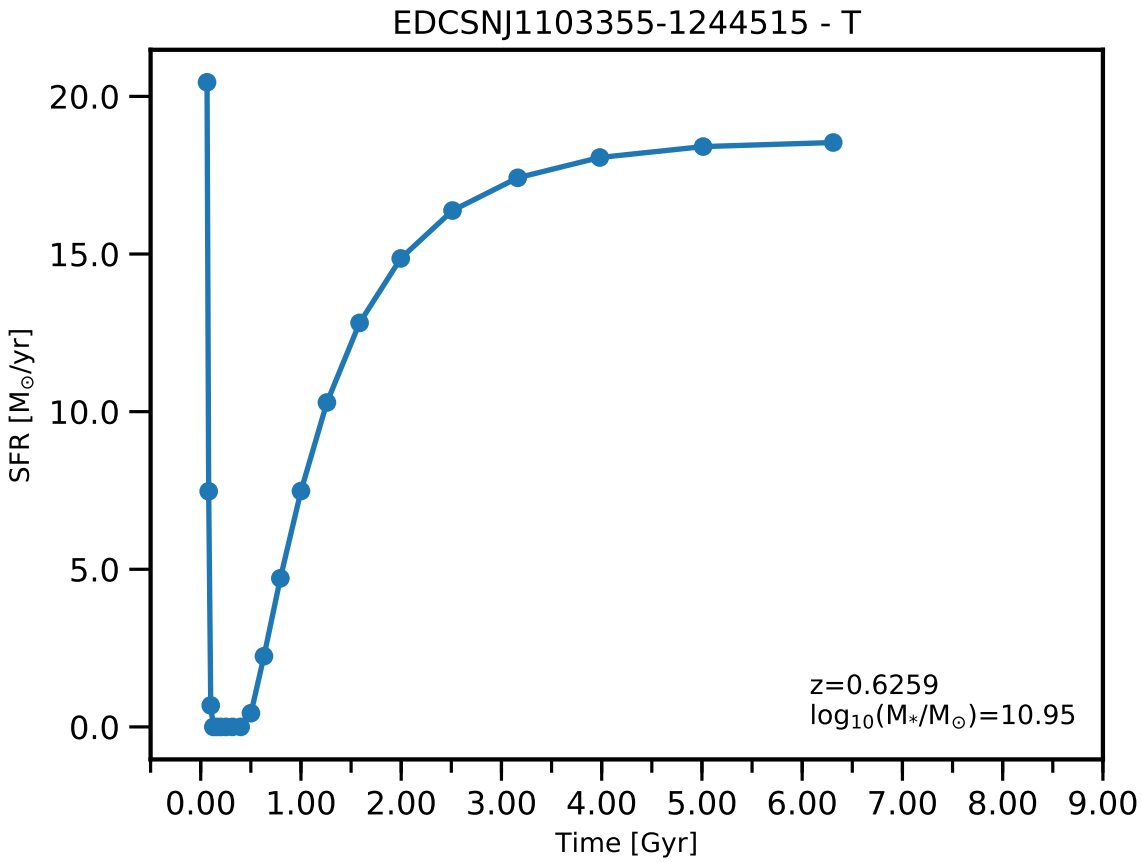
EDCSNJ1103355-1244515 - T
SFR [M⊙/yr]
20.0
15.0
10.0
5.0
0.0
0.00
1.00
2.00
3.00
4.00
5.00
6.00
7.00
8.00
9.00
Time [Gyr]
z=0.6259
log10(M*/M⊙)=10.95

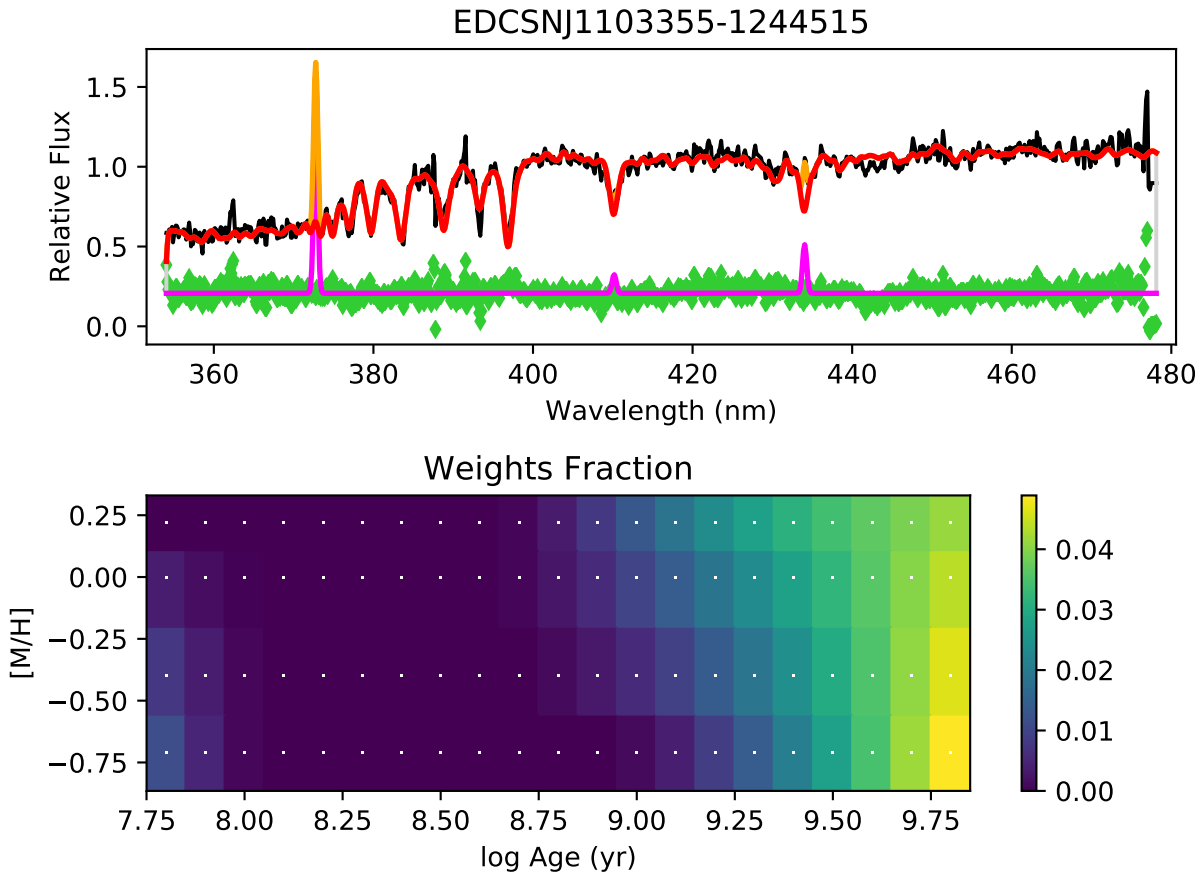
EDCSNJ1103355-1244515
Relative Flux
1.5
1.0
0.5
0.0
360
380
400
420
440
460
480
Wavelength (nm)
Weights Fraction
[M/H]
0.25
0.00
−0.25
−0.50
−0.75
7.75
8.00
8.25
8.50
8.75
9.00
9.25
9.50
9.75
log Age (yr)
0.04
0.03
0.02
0.01
0.00

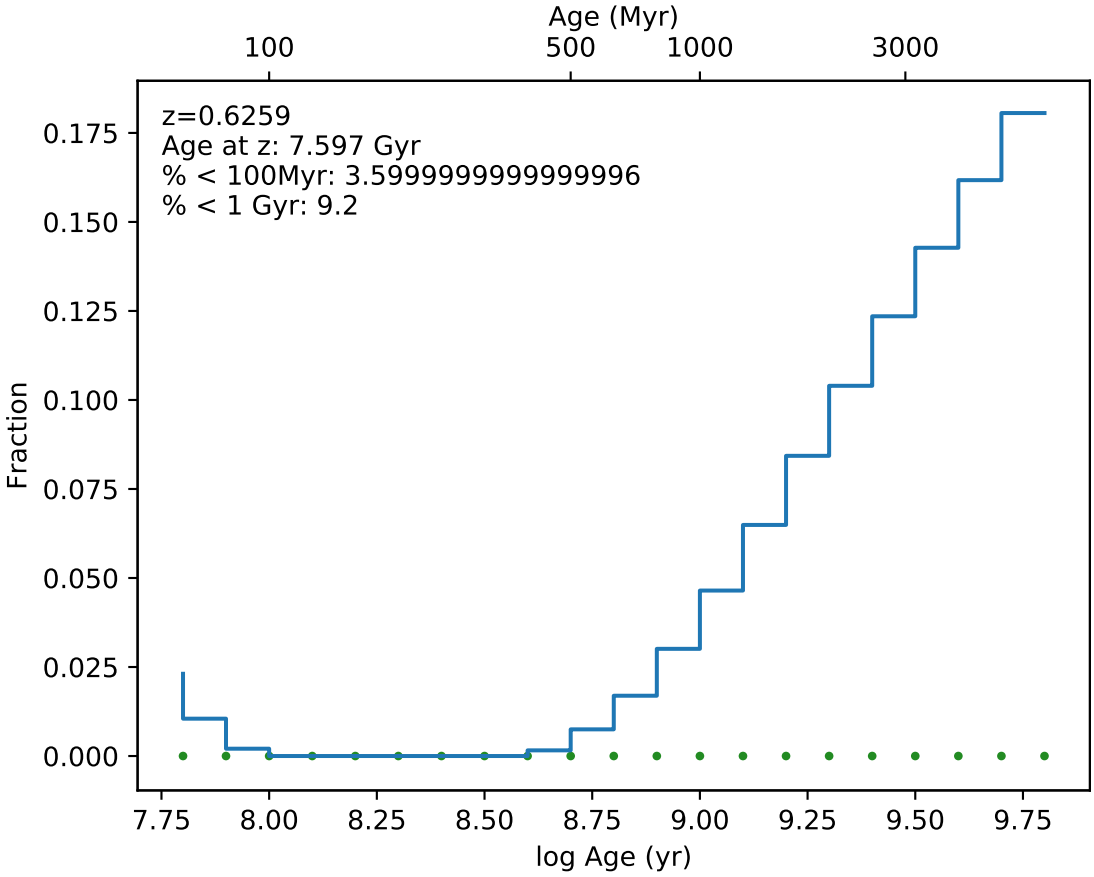
Age (Myr)
100
500
1000
3000
z=0.6259
Age at z: 7.597 Gyr
% < 100Myr: 3.5999999999999996
% < 1 Gyr: 9.2
Fraction
0.175
0.150
0.125
0.100
0.075
0.050
0.025
0.000
7.75
8.00
8.25
8.50
8.75
9.00
9.25
9.50
9.75
log Age (yr)

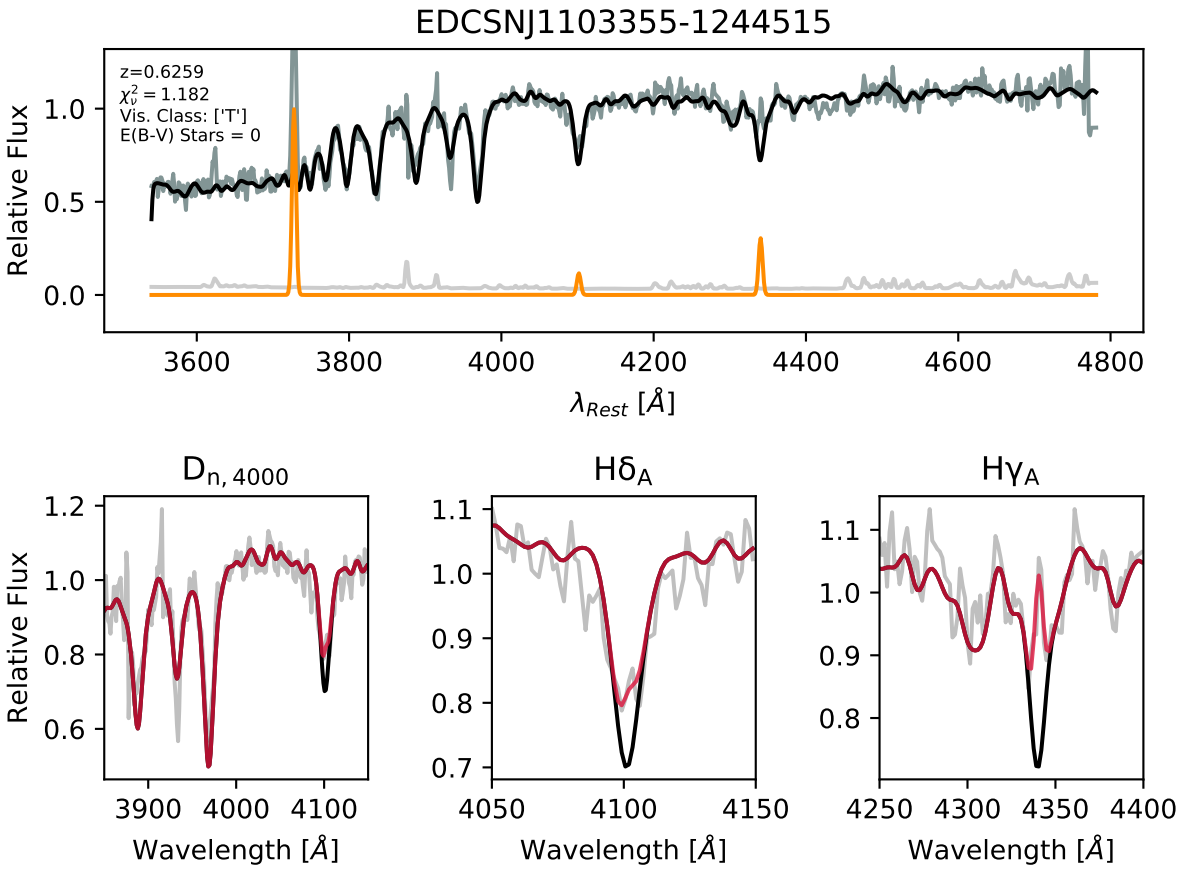
EDCSNJ1103355-1244515
z=0.6259
$\chi^2_\nu = 1.182$
Vis. Class: ['T']
E(B-V) Stars = 0
Relative Flux
1.0
0.5
0.0
3600
3800
4000
4200
4400
4600
4800
λ_{Rest} [Å]
$D_{n,4000}$
$H\delta_A$
$H\gamma_A$
Relative Flux
1.2
1.0
0.8
0.6
3900
4000
4100
Wavelength [Å]
1.1
1.0
0.9
0.8
0.7
4050
4100
4150
Wavelength [Å]
1.1
1.0
0.9
0.8
4250
4300
4350
4400
Wavelength [Å]

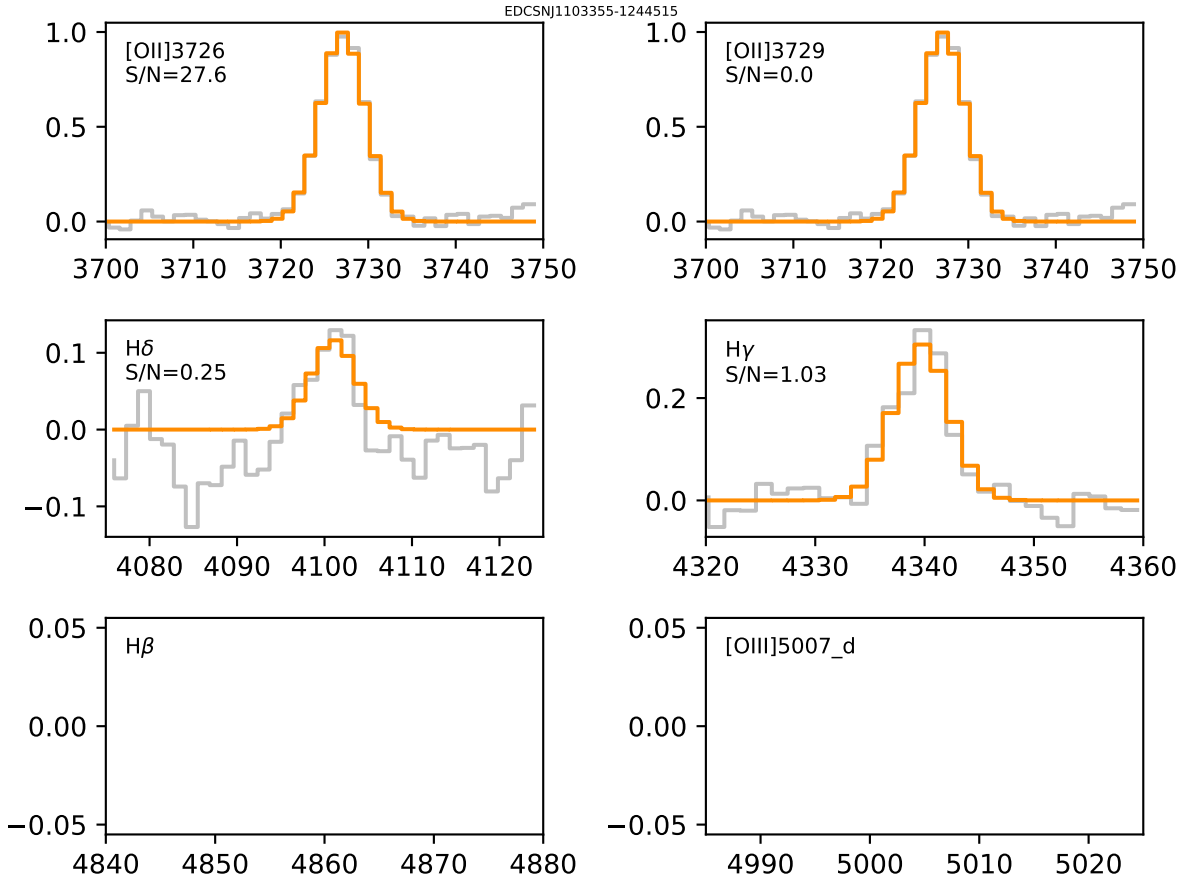
EDCSNJ1103355-1244515
[OII]3726
S/N=27.6
[OII]3729
S/N=0.0
Hδ
S/N=0.25
Hγ
S/N=1.03
Hβ
[OIII]5007_d

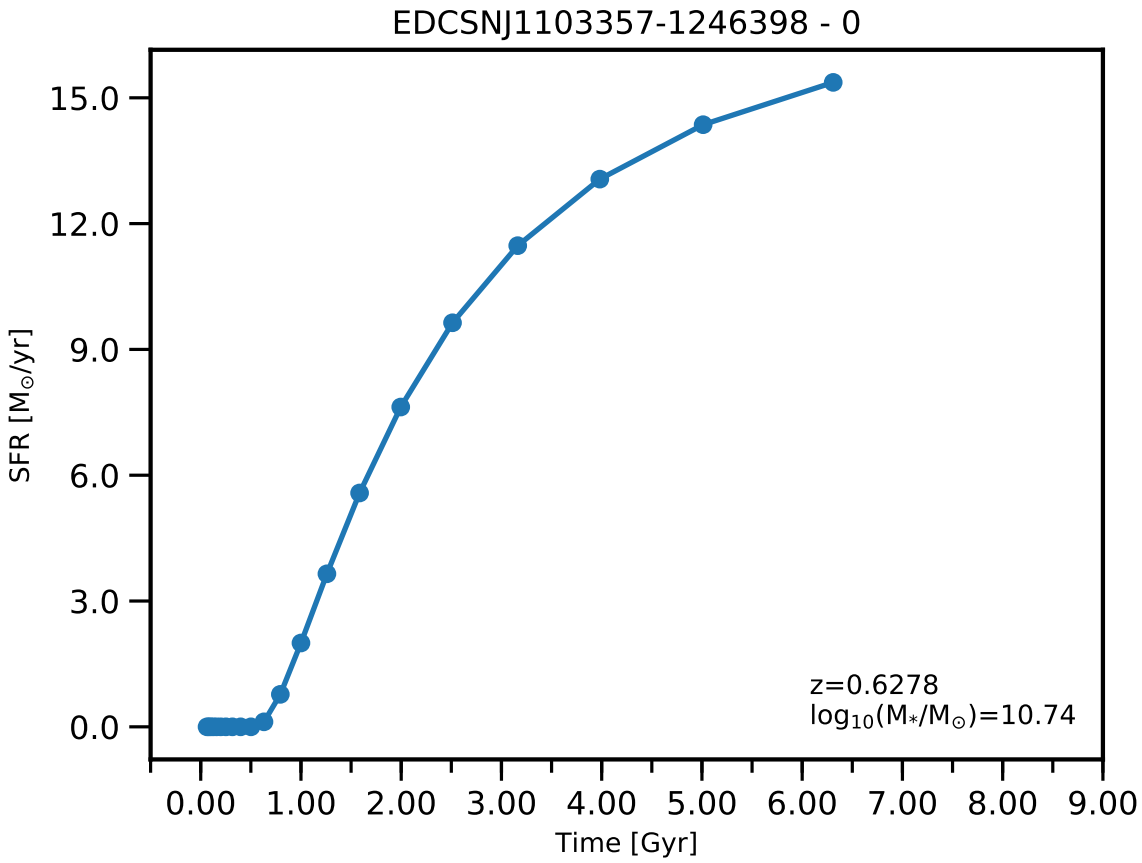
EDCSNJ1103357-1246398 - 0
SFR [M⊙/yr]
15.0
12.0
9.0
6.0
3.0
0.0
0.00
1.00
2.00
3.00
4.00
5.00
6.00
7.00
8.00
9.00
Time [Gyr]
z=0.6278
log10(M*/M⊙)=10.74

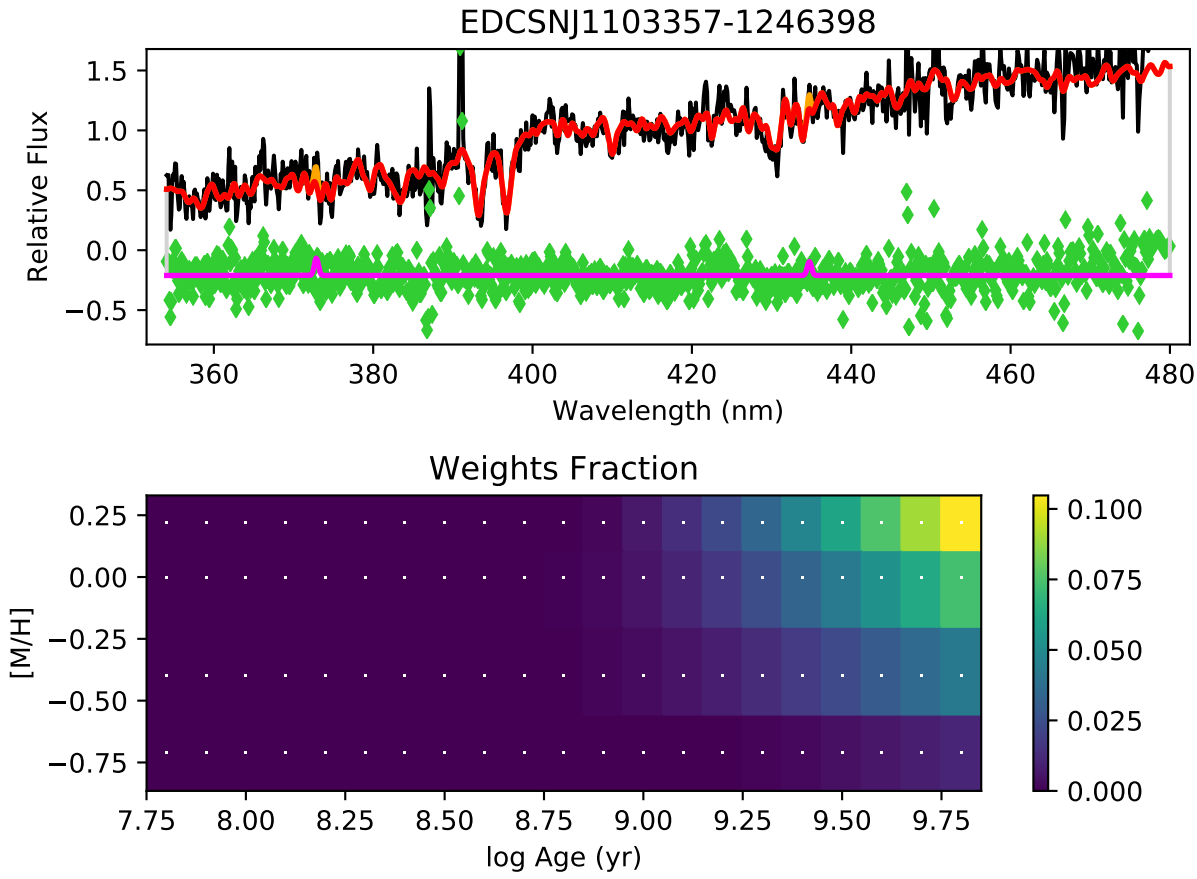
EDCSNJ1103357-1246398
Relative Flux
1.5
1.0
0.5
0.0
−0.5
360
380
400
420
440
460
480
Wavelength (nm)
Weights Fraction
[M/H]
0.25
0.00
−0.25
−0.50
−0.75
7.75
8.00
8.25
8.50
8.75
9.00
9.25
9.50
9.75
log Age (yr)
0.100
0.075
0.050
0.025
0.000

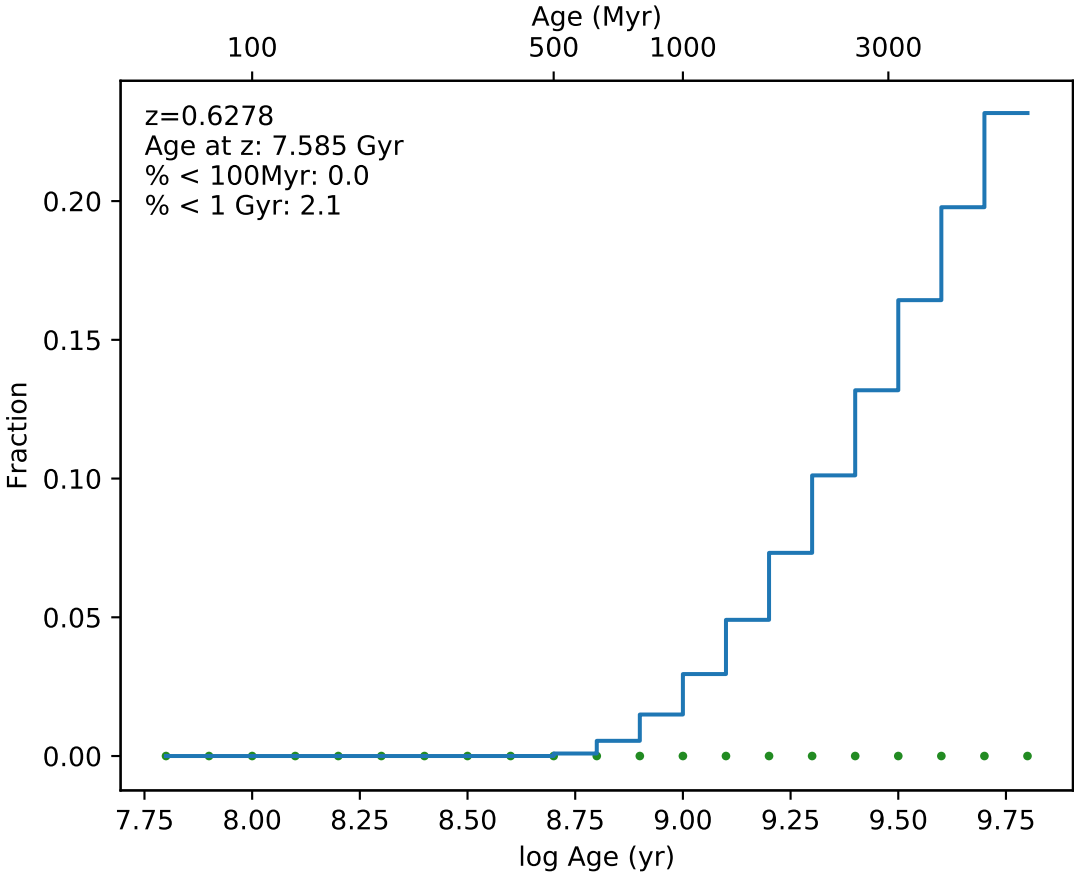
Age (Myr)
100
500
1000
3000
z=0.6278
Age at z: 7.585 Gyr
% < 100Myr: 0.0
% < 1 Gyr: 2.1
Fraction
0.00
0.05
0.10
0.15
0.20
7.75
8.00
8.25
8.50
8.75
9.00
9.25
9.50
9.75
log Age (yr)

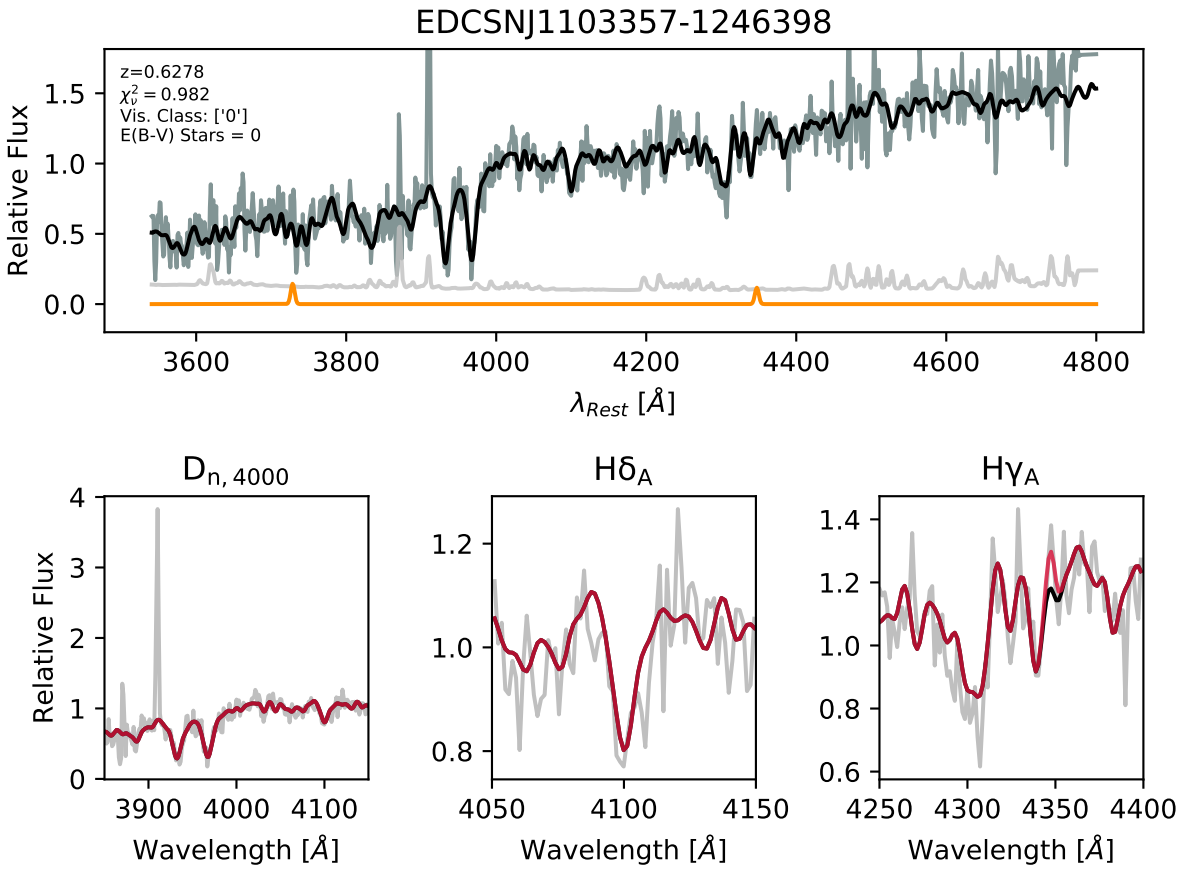
EDCSNJ1103357-1246398
z=0.6278
$\chi^2_\nu = 0.982$
Vis. Class: ['0']
E(B-V) Stars = 0
Relative Flux
λ_{Rest} [Å]
$D_{n,4000}$
$H\delta_A$
$H\gamma_A$
Wavelength [Å]

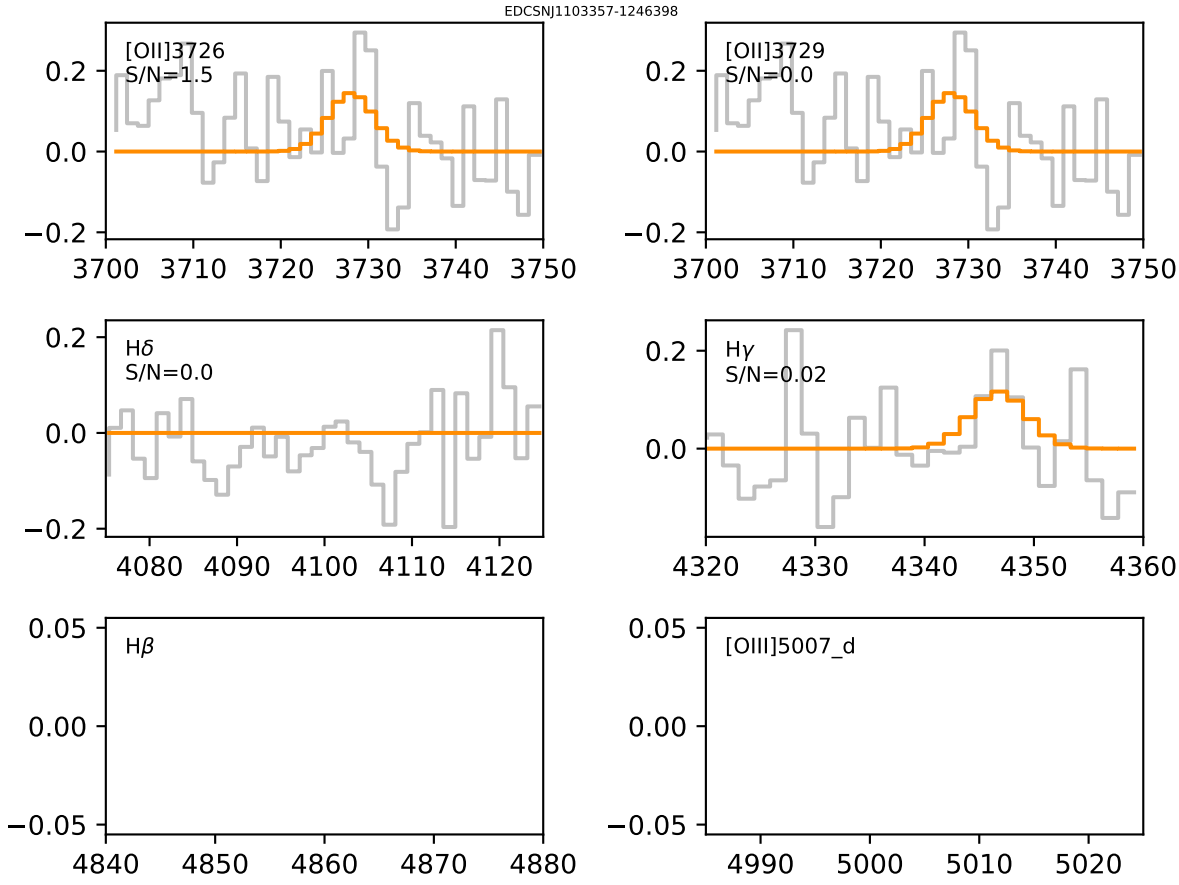
EDCSNJ1103357-1246398
[OII]3726
S/N=1.5
[OII]3729
S/N=0.0
Hδ
S/N=0.0
Hγ
S/N=0.02
Hβ
[OIII]5007_d

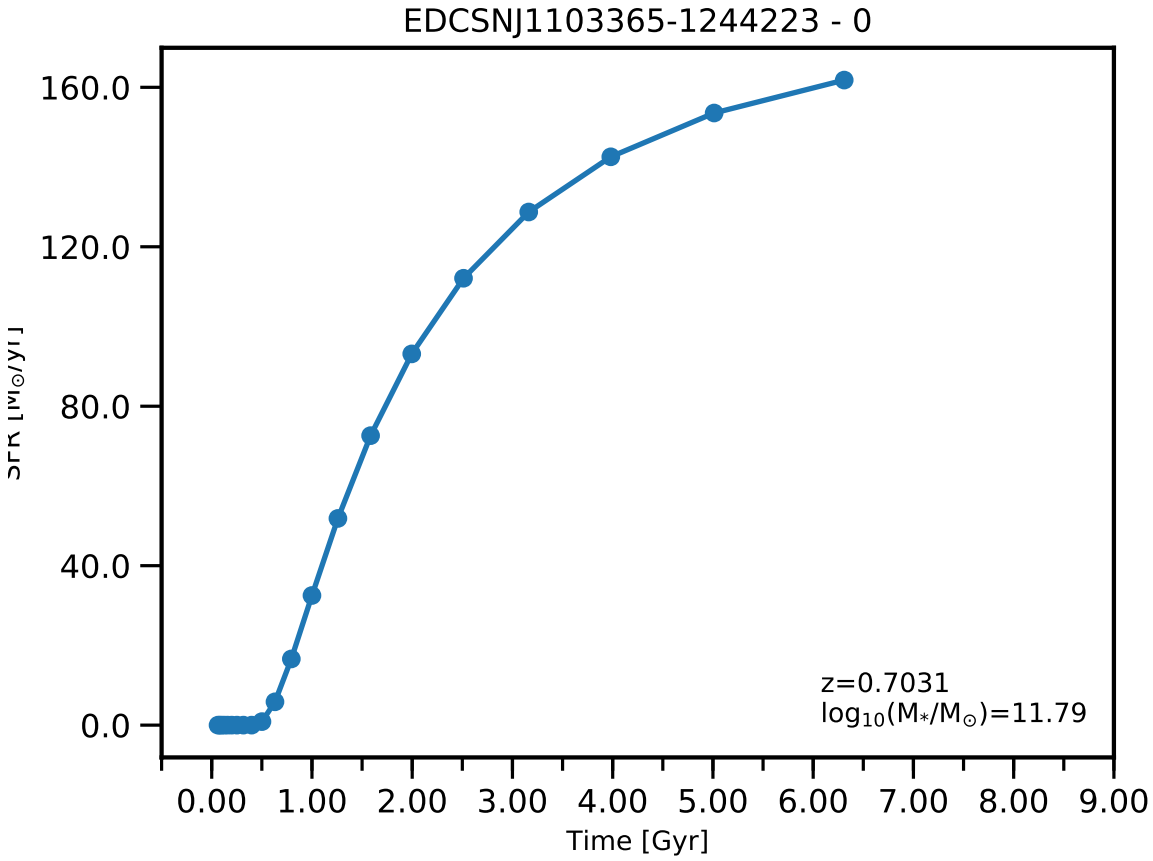
EDCSNJ1103365-1244223 - 0
160.0
120.0
80.0
40.0
0.0
SFR [M⊙/yr]
0.00
1.00
2.00
3.00
4.00
5.00
6.00
7.00
8.00
9.00
Time [Gyr]
z=0.7031
log10(M*/M⊙)=11.79

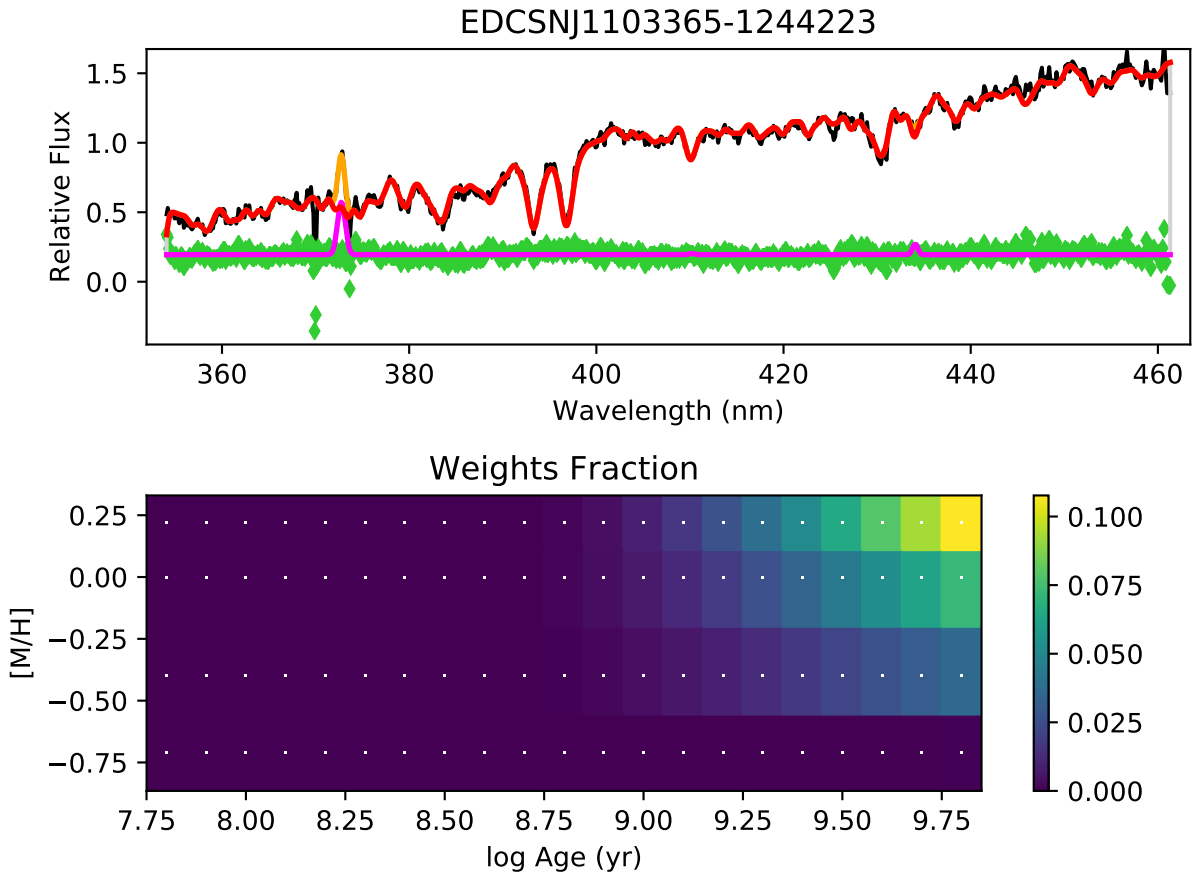
EDCSNJ1103365-1244223
Relative Flux
1.5
1.0
0.5
0.0
360
380
400
420
440
460
Wavelength (nm)
Weights Fraction
[M/H]
0.25
0.00
−0.25
−0.50
−0.75
7.75
8.00
8.25
8.50
8.75
9.00
9.25
9.50
9.75
log Age (yr)
0.100
0.075
0.050
0.025
0.000

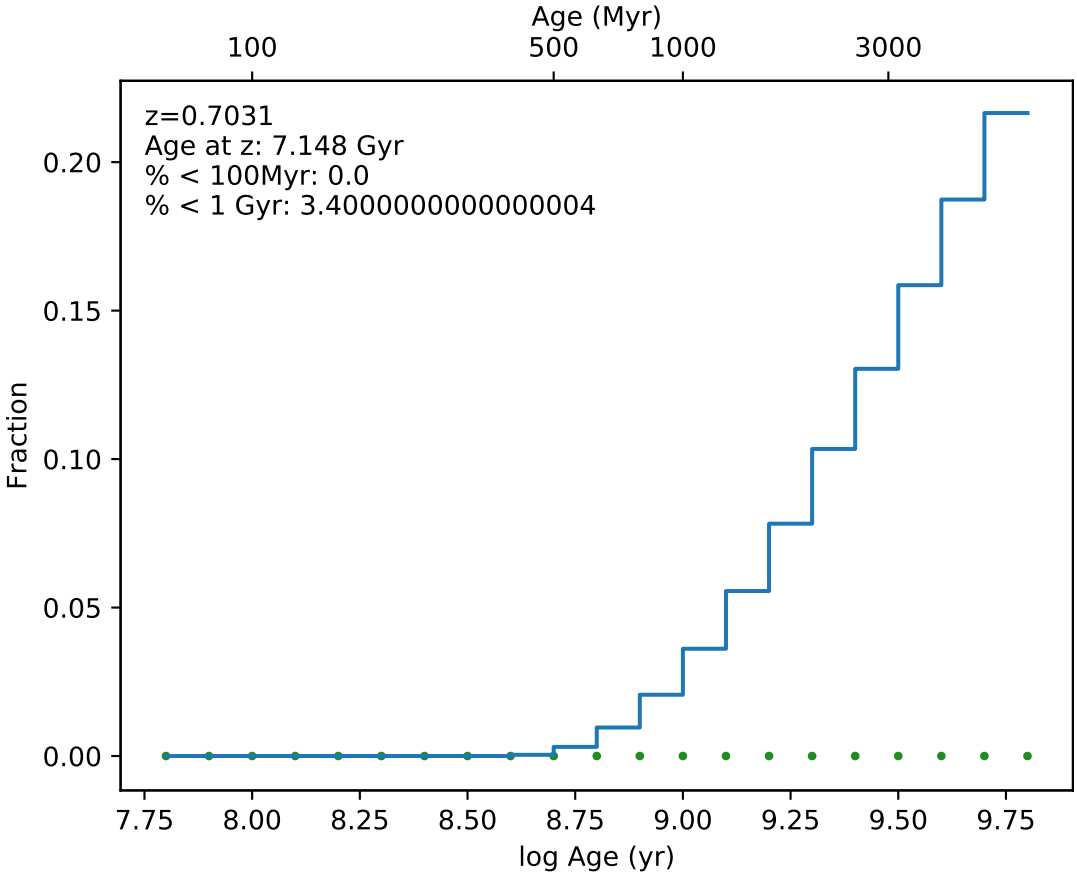
Age (Myr)
100
500
1000
3000
z=0.7031
Age at z: 7.148 Gyr
% < 100Myr: 0.0
% < 1 Gyr: 3.4000000000000004
Fraction
0.00
0.05
0.10
0.15
0.20
7.75
8.00
8.25
8.50
8.75
9.00
9.25
9.50
9.75
log Age (yr)

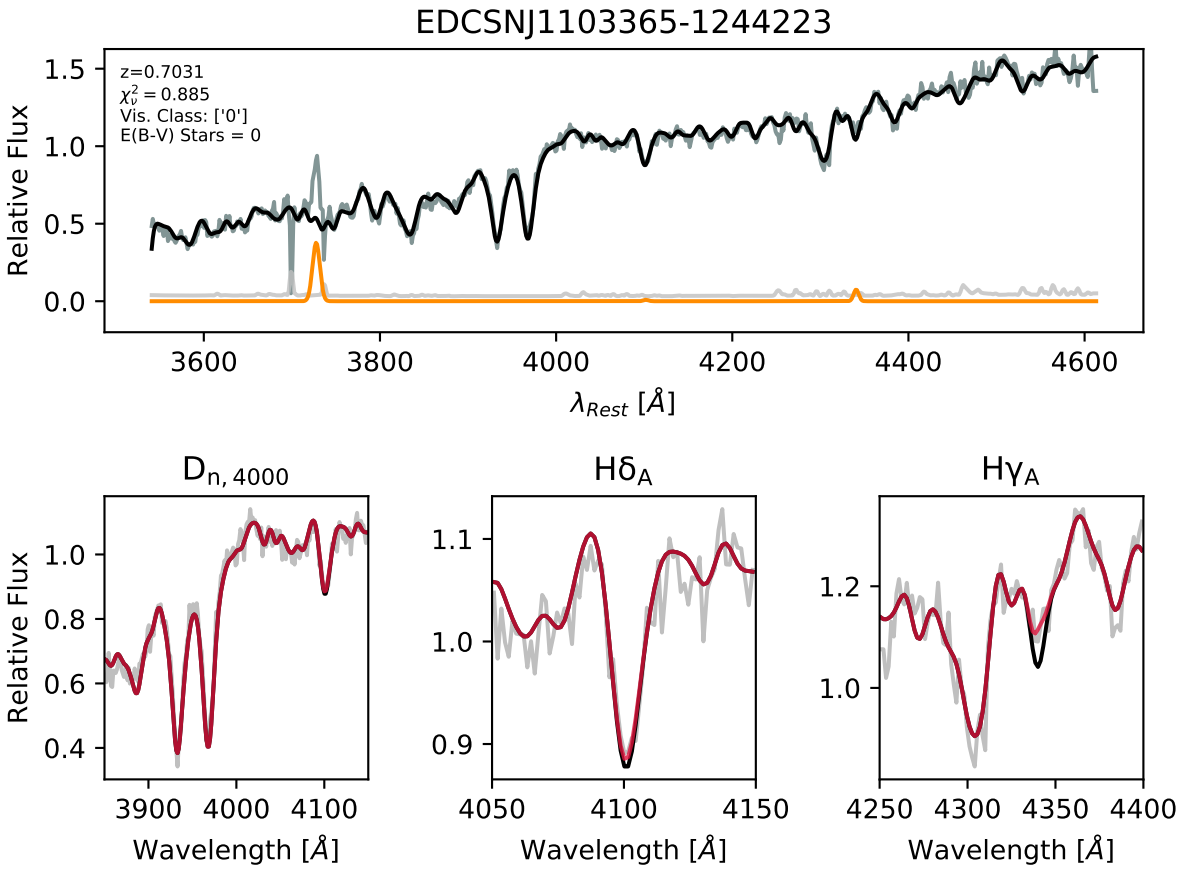
EDCSNJ1103365-1244223
z=0.7031
$\chi^2_\nu = 0.885$
Vis. Class: ['0']
E(B-V) Stars = 0
Relative Flux
1.5
1.0
0.5
0.0
3600
3800
4000
4200
4400
4600
λ_{Rest} [Å]
$D_{n,4000}$
$H\delta_A$
$H\gamma_A$
Relative Flux
1.0
0.8
0.6
0.4
3900
4000
4100
Wavelength [Å]
1.1
1.0
0.9
4050
4100
4150
Wavelength [Å]
1.2
1.0
4250
4300
4350
4400
Wavelength [Å]

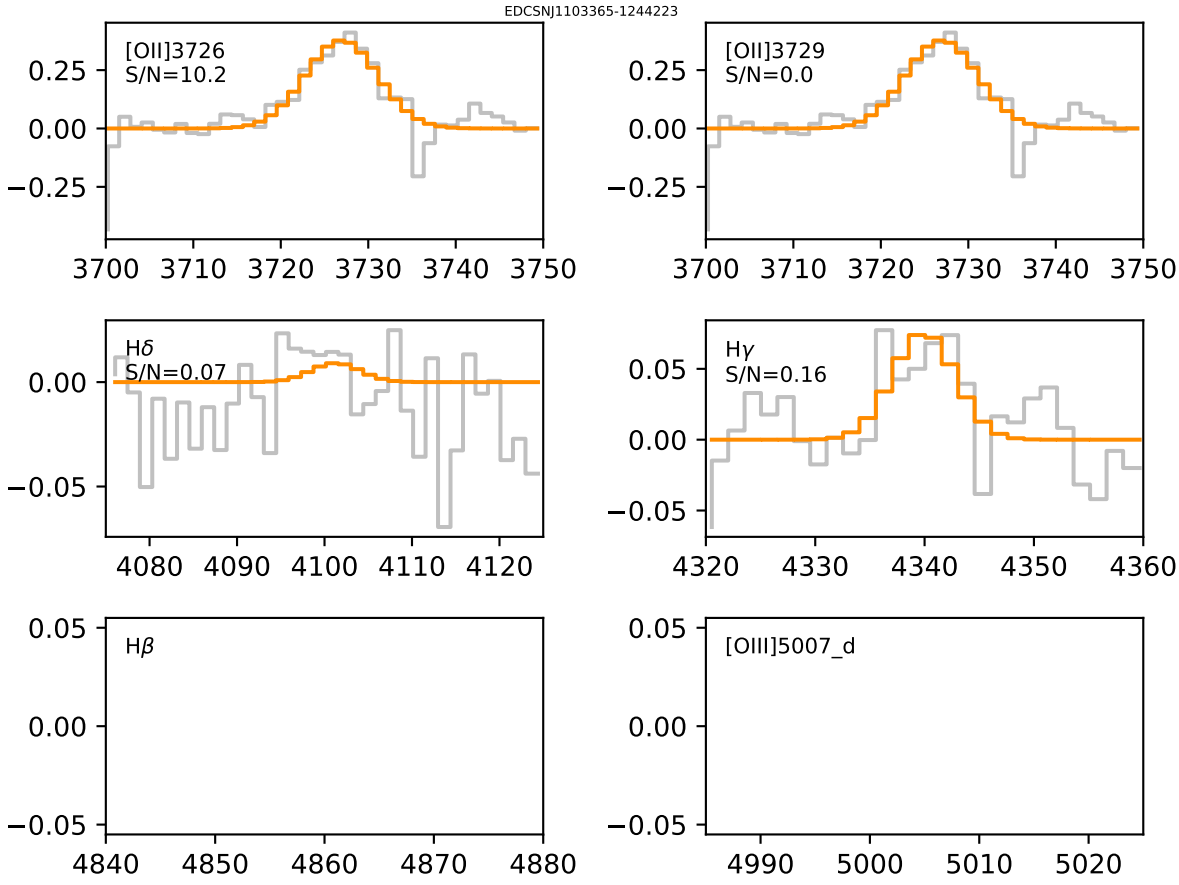
EDCSNJ1103365-1244223
[OII]3726
S/N=10.2
[OII]3729
S/N=0.0
Hδ
S/N=0.07
Hγ
S/N=0.16
Hβ
[OIII]5007_d

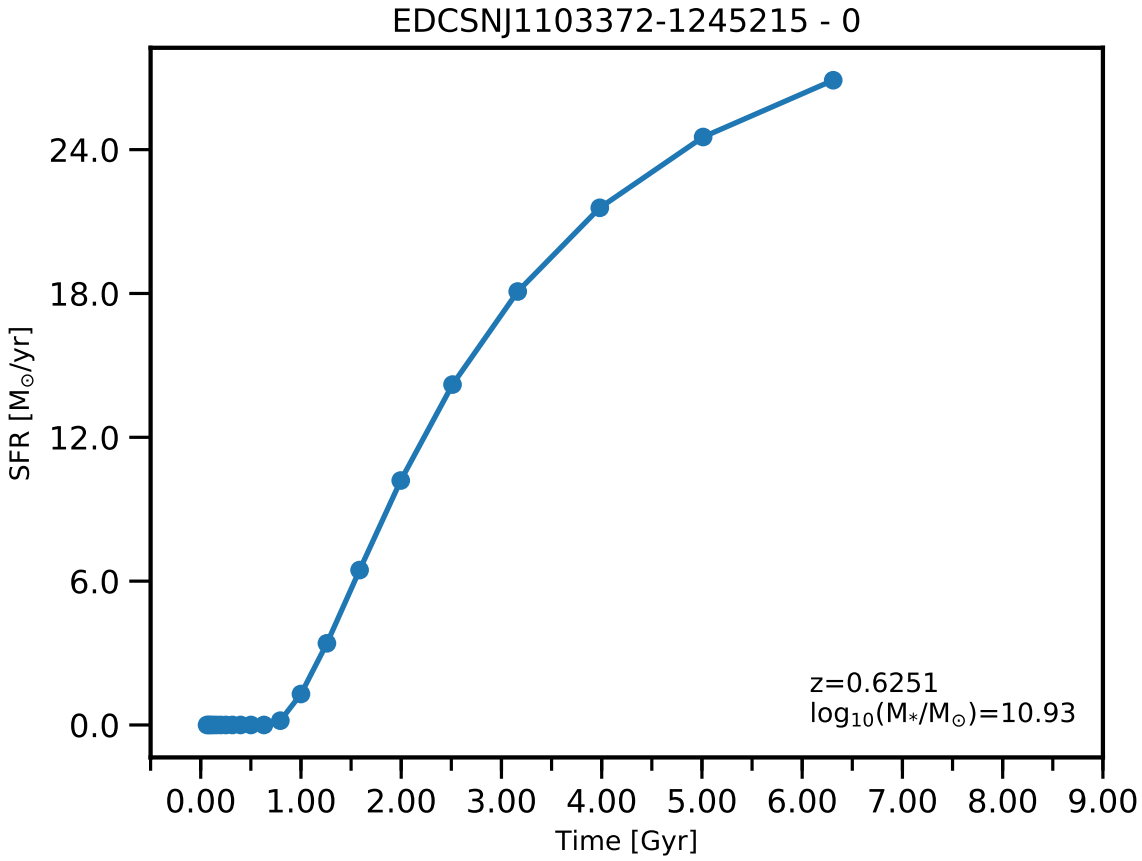
EDCSNJ1103372-1245215 - 0
SFR [M⊙/yr]
24.0
18.0
12.0
6.0
0.0
0.00
1.00
2.00
3.00
4.00
5.00
6.00
7.00
8.00
9.00
Time [Gyr]
z=0.6251
log10(M*/M⊙)=10.93

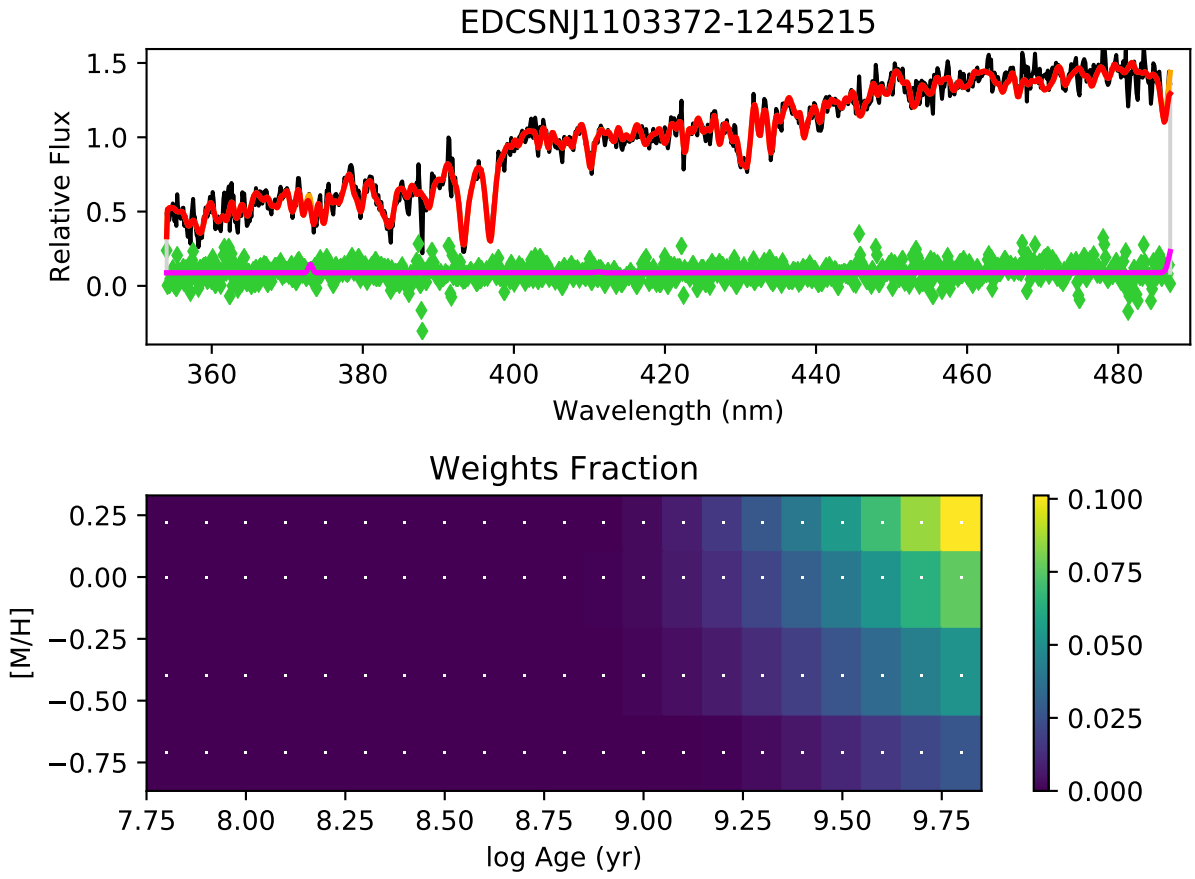
EDCSNJ1103372-1245215
Relative Flux
1.5
1.0
0.5
0.0
360
380
400
420
440
460
480
Wavelength (nm)
Weights Fraction
[M/H]
0.25
0.00
−0.25
−0.50
−0.75
7.75
8.00
8.25
8.50
8.75
9.00
9.25
9.50
9.75
log Age (yr)
0.100
0.075
0.050
0.025
0.000

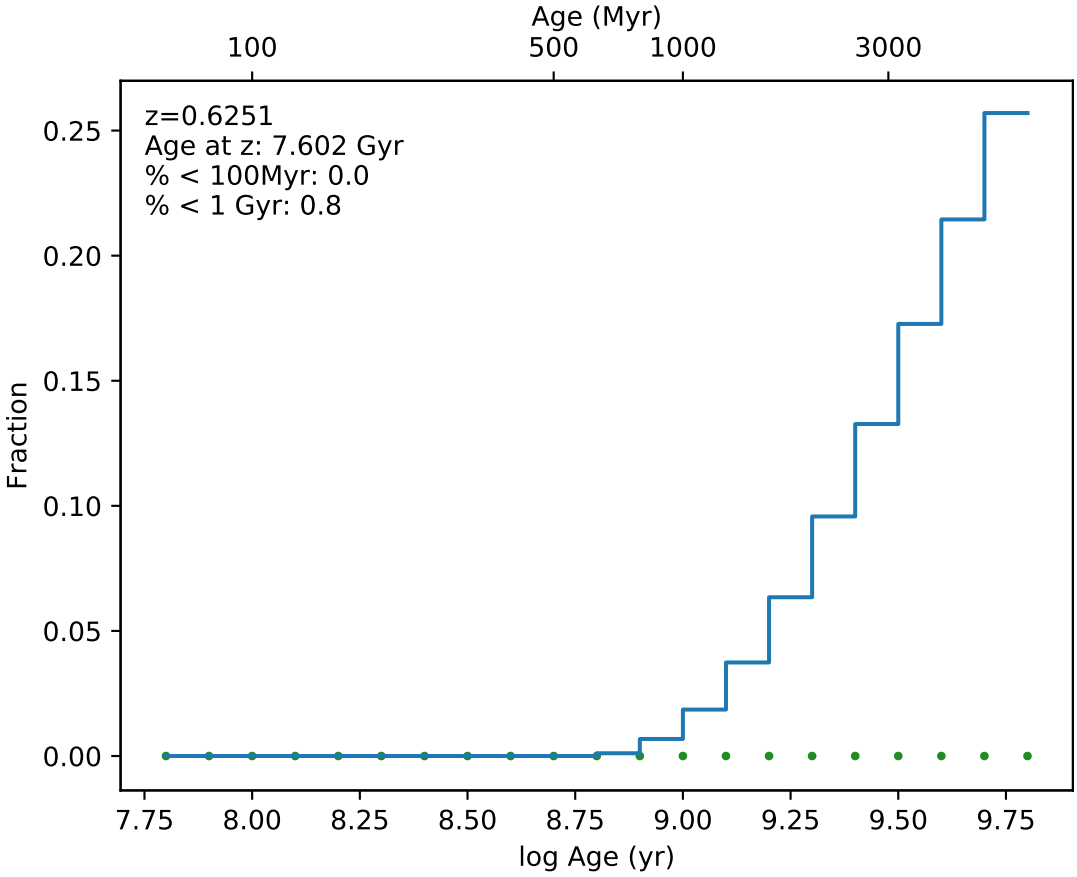
Age (Myr)
100
500
1000
3000
z=0.6251
Age at z: 7.602 Gyr
% < 100Myr: 0.0
% < 1 Gyr: 0.8
Fraction
0.25
0.20
0.15
0.10
0.05
0.00
7.75
8.00
8.25
8.50
8.75
9.00
9.25
9.50
9.75
log Age (yr)

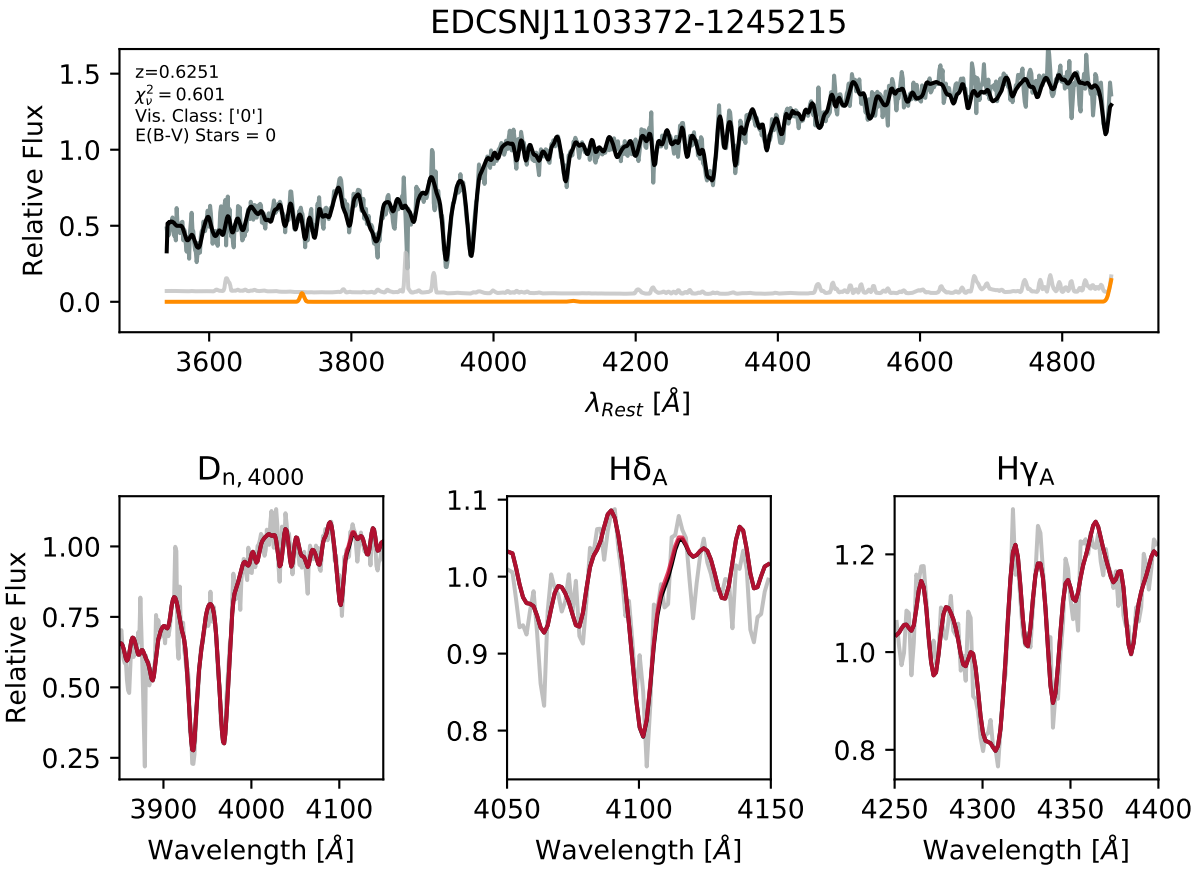
EDCSNJ1103372-1245215
z=0.6251
$\chi^2_\nu = 0.601$
Vis. Class: ['0']
E(B-V) Stars = 0
Relative Flux
λ_{Rest} [Å]
$D_{n,4000}$
$H\delta_A$
$H\gamma_A$
Wavelength [Å]

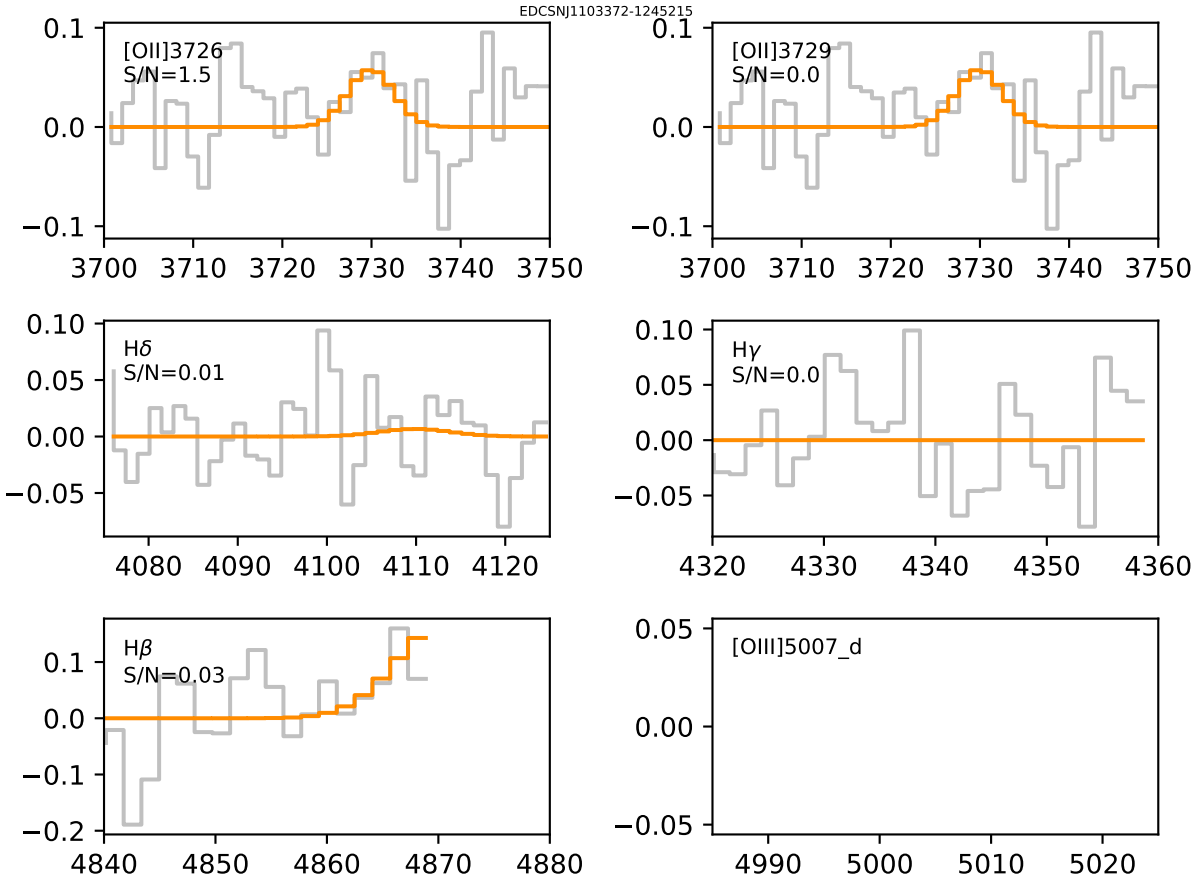
EDCSNJ1103372-1245215
[OII]3726
S/N=1.5
[OII]3729
S/N=0.0
Hδ
S/N=0.01
Hγ
S/N=0.0
Hβ
S/N=0.03
[OIII]5007_d

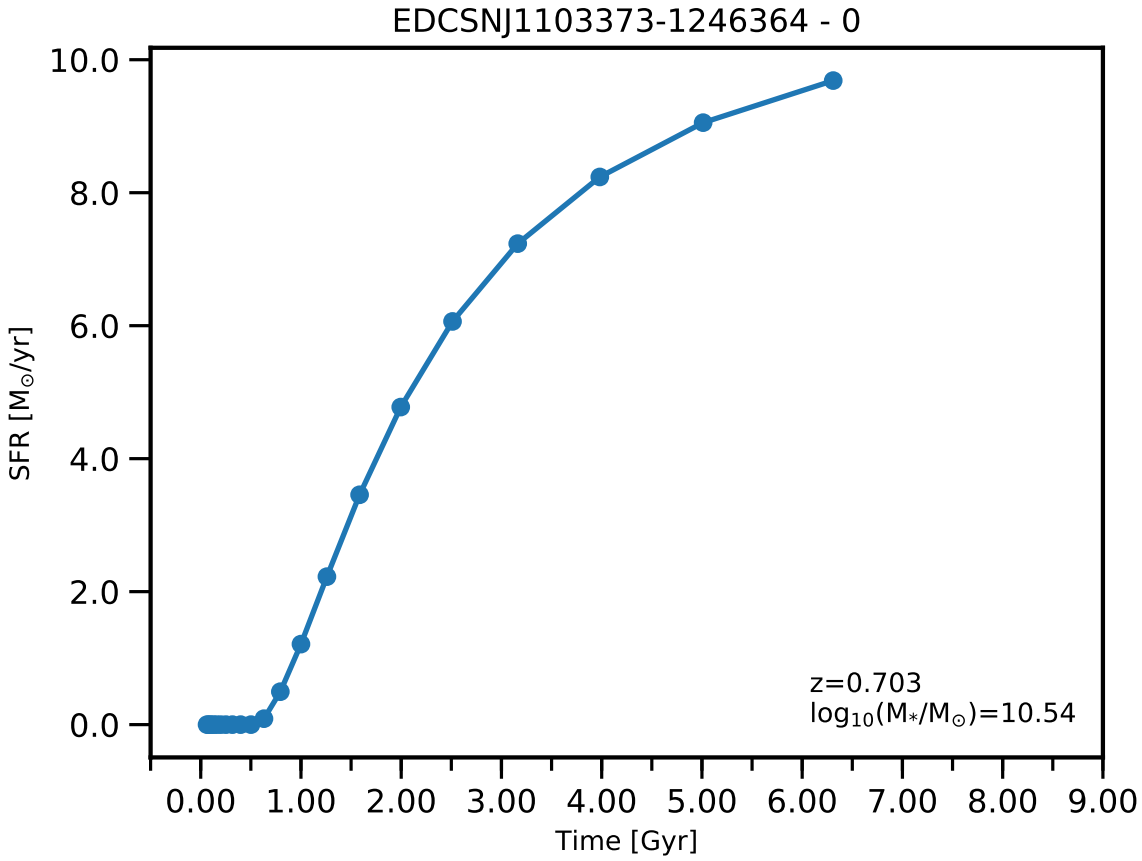
EDCSNJ1103373-1246364 - 0
SFR [M⊙/yr]
Time [Gyr]
z=0.703
log10(M*/M⊙)=10.54
0.0
2.0
4.0
6.0
8.0
10.0
0.00
1.00
2.00
3.00
4.00
5.00
6.00
7.00
8.00
9.00

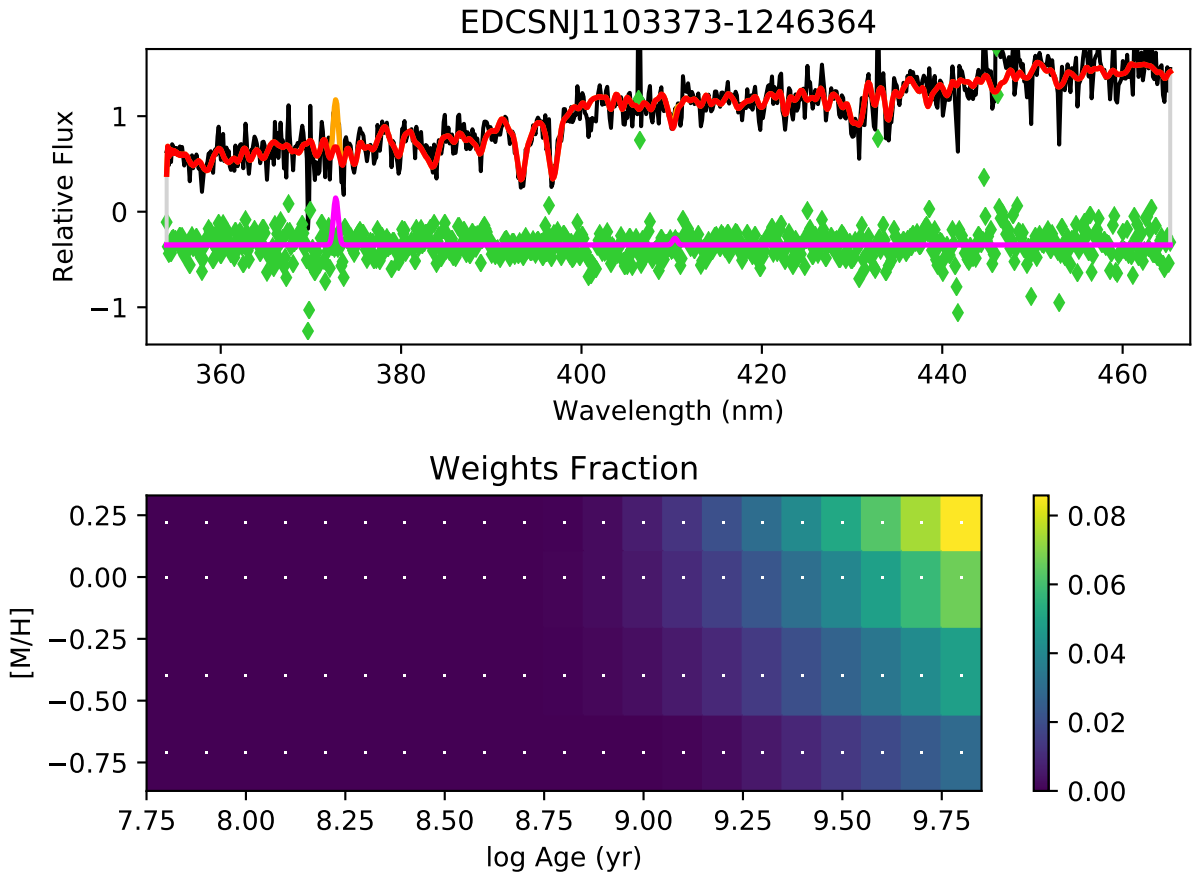
EDCSNJ1103373-1246364
Relative Flux
1
0
−1
360
380
400
420
440
460
Wavelength (nm)
Weights Fraction
[M/H]
0.25
0.00
−0.25
−0.50
−0.75
7.75
8.00
8.25
8.50
8.75
9.00
9.25
9.50
9.75
log Age (yr)
0.08
0.06
0.04
0.02
0.00

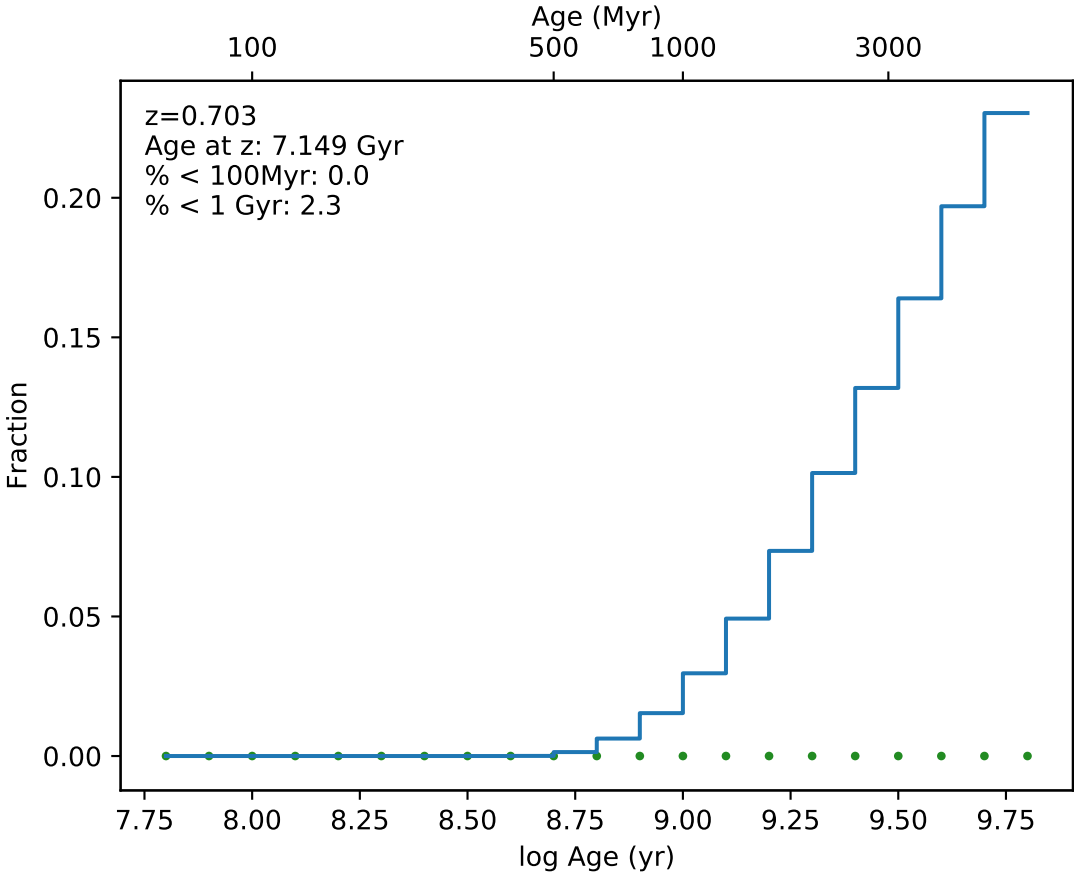
Age (Myr)
100
500
1000
3000
z=0.703
Age at z: 7.149 Gyr
% < 100Myr: 0.0
% < 1 Gyr: 2.3
Fraction
0.00
0.05
0.10
0.15
0.20
7.75
8.00
8.25
8.50
8.75
9.00
9.25
9.50
9.75
log Age (yr)

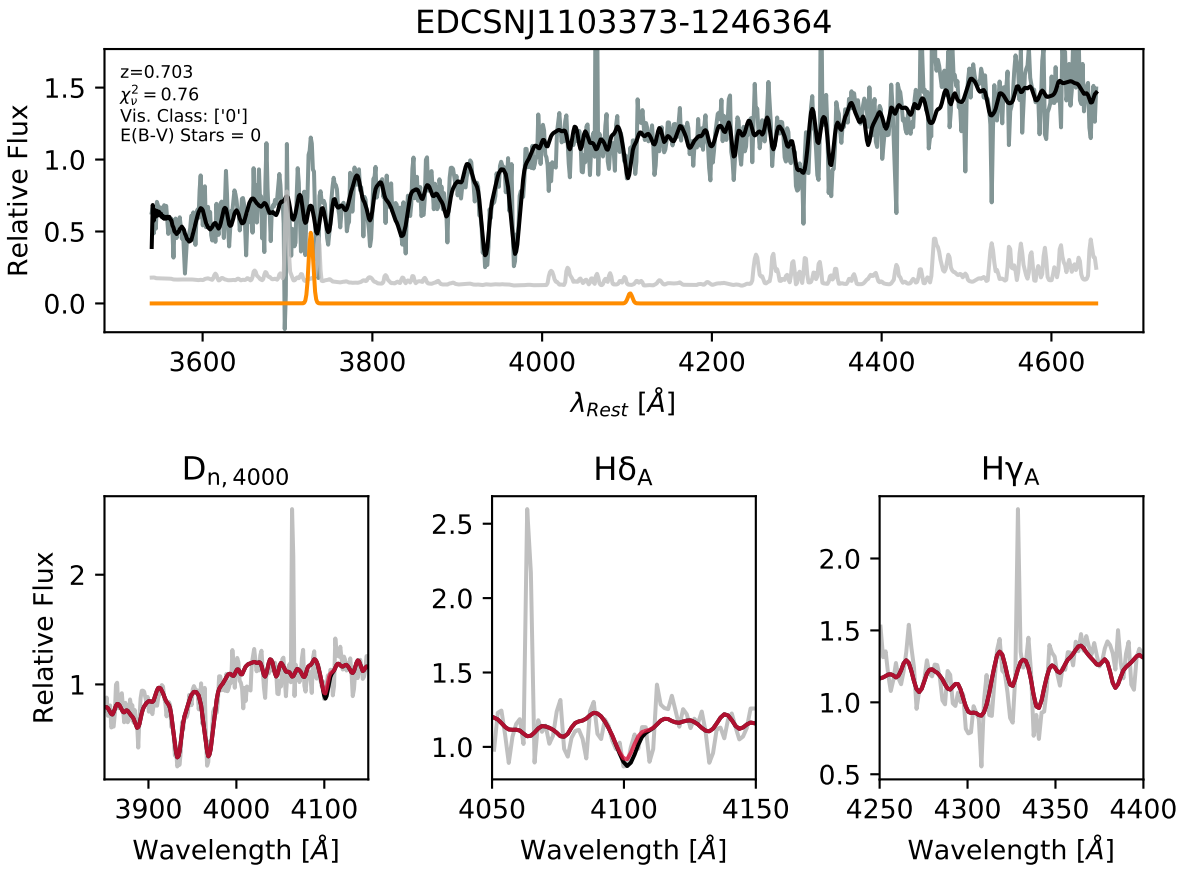
EDCSNJ1103373-1246364
z=0.703
$\chi^2_\nu = 0.76$
Vis. Class: ['0']
E(B-V) Stars = 0
Relative Flux
1.5
1.0
0.5
0.0
3600
3800
4000
4200
4400
4600
λ_{Rest} [Å]
$D_{n,4000}$
$H\delta_A$
$H\gamma_A$
Relative Flux
2
1
3900
4000
4100
Wavelength [Å]
2.5
2.0
1.5
1.0
4050
4100
4150
Wavelength [Å]
2.0
1.5
1.0
0.5
4250
4300
4350
4400
Wavelength [Å]

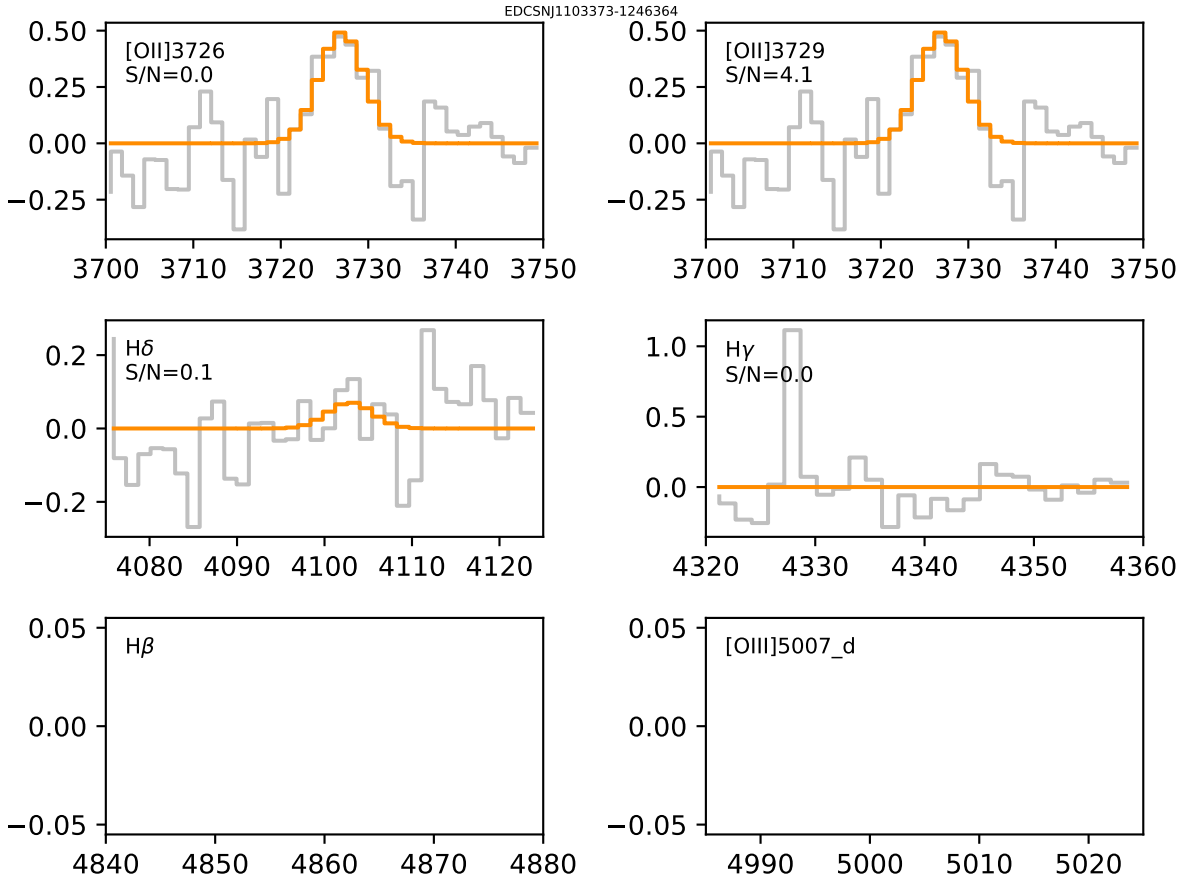
EDCSNJ1103373-1246364
[OII]3726
S/N=0.0
[OII]3729
S/N=4.1
Hδ
S/N=0.1
Hγ
S/N=0.0
Hβ
[OIII]5007_d

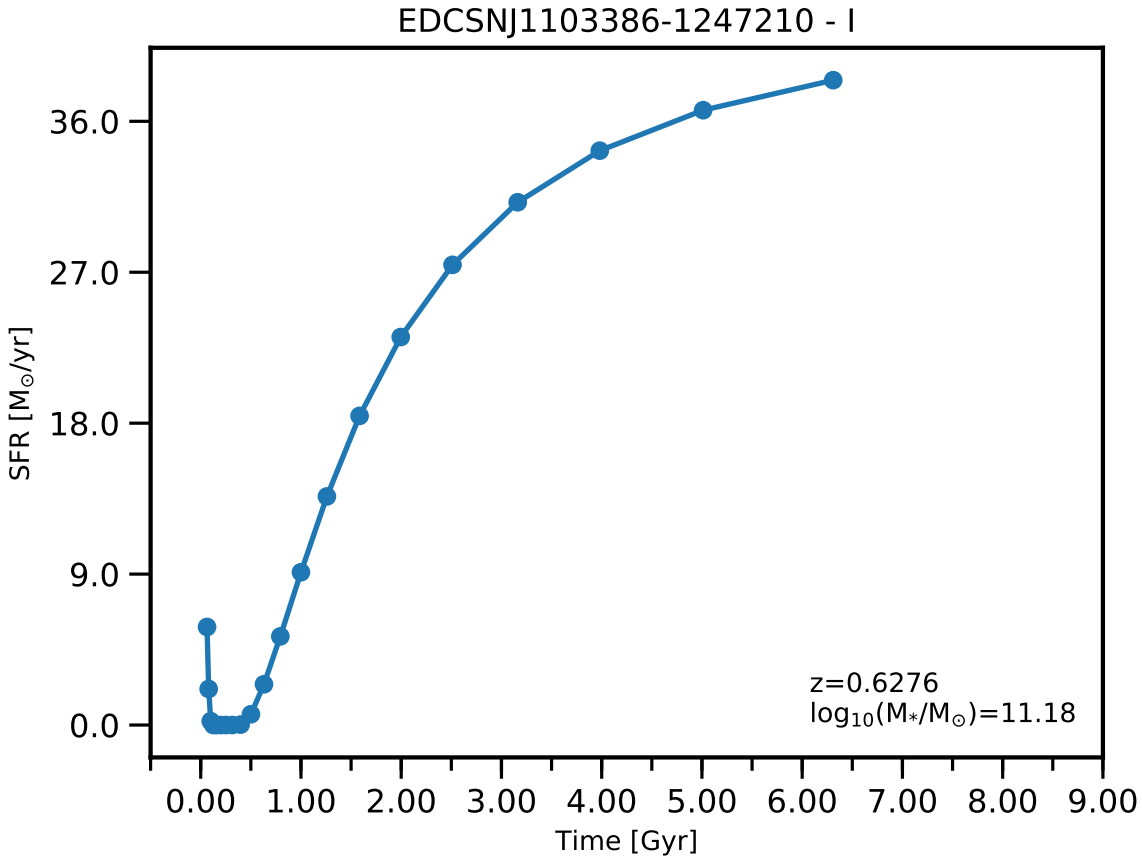
EDCSNJ1103386-1247210 - I
36.0
27.0
18.0
9.0
0.0
SFR [M⊙/yr]
0.00
1.00
2.00
3.00
4.00
5.00
6.00
7.00
8.00
9.00
Time [Gyr]
z=0.6276
log10(M*/M⊙)=11.18

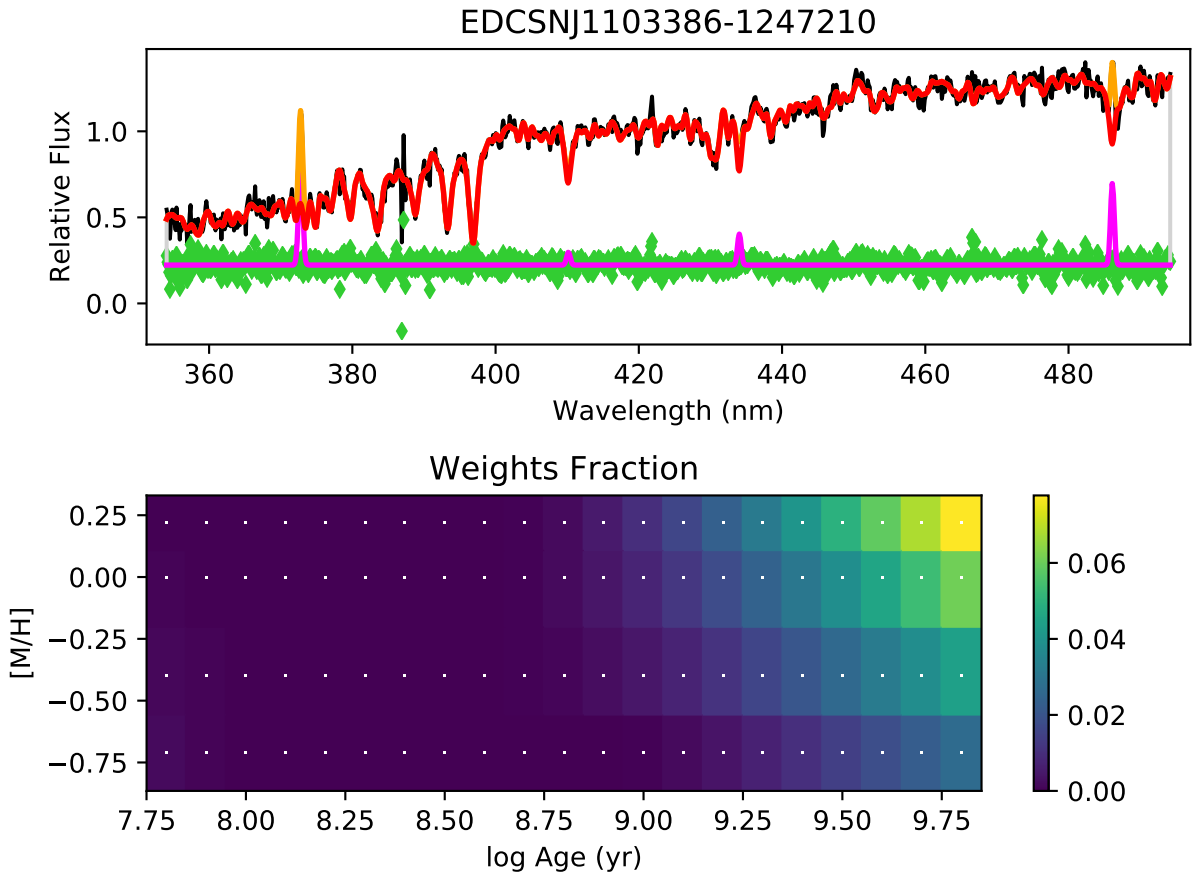
EDCSNJ1103386-1247210
Relative Flux
1.0
0.5
0.0
360
380
400
420
440
460
480
Wavelength (nm)
Weights Fraction
[M/H]
0.25
0.00
−0.25
−0.50
−0.75
7.75
8.00
8.25
8.50
8.75
9.00
9.25
9.50
9.75
log Age (yr)
0.06
0.04
0.02
0.00

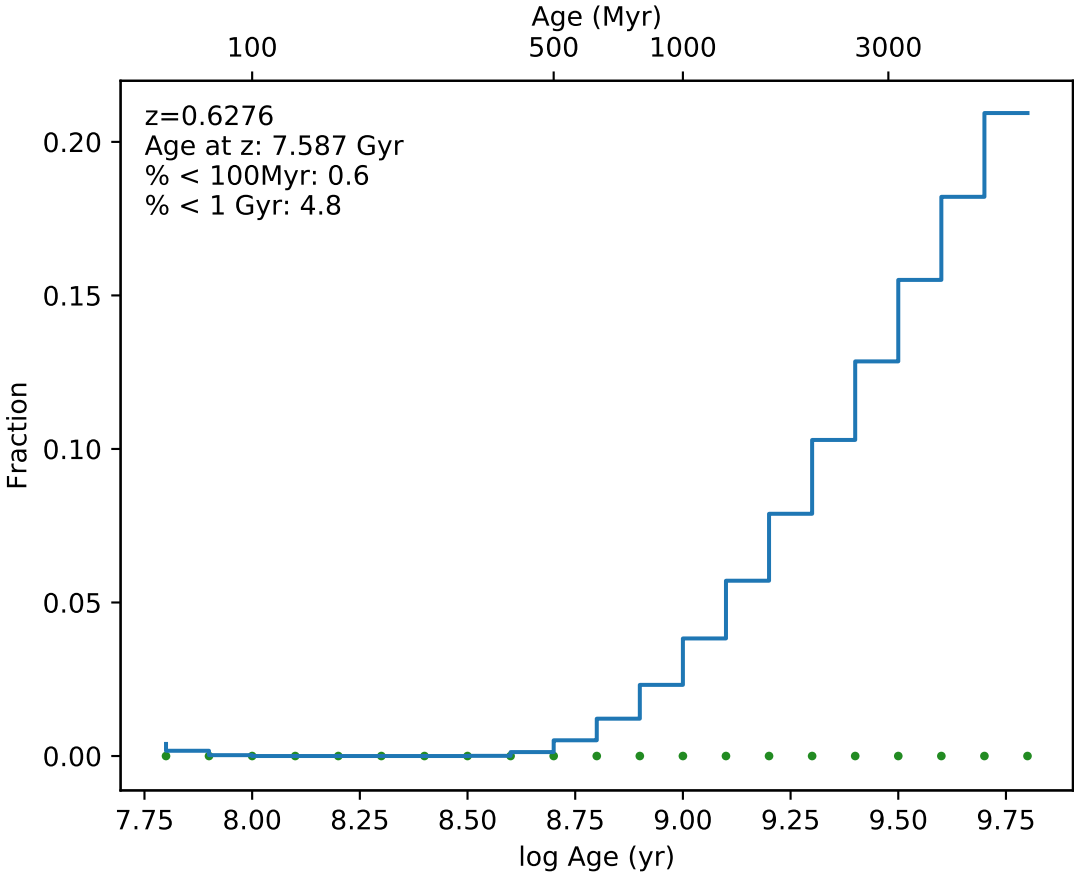
Age (Myr)
100
500
1000
3000
z=0.6276
Age at z: 7.587 Gyr
% < 100Myr: 0.6
% < 1 Gyr: 4.8
0.20
0.15
0.10
0.05
0.00
Fraction
7.75
8.00
8.25
8.50
8.75
9.00
9.25
9.50
9.75
log Age (yr)

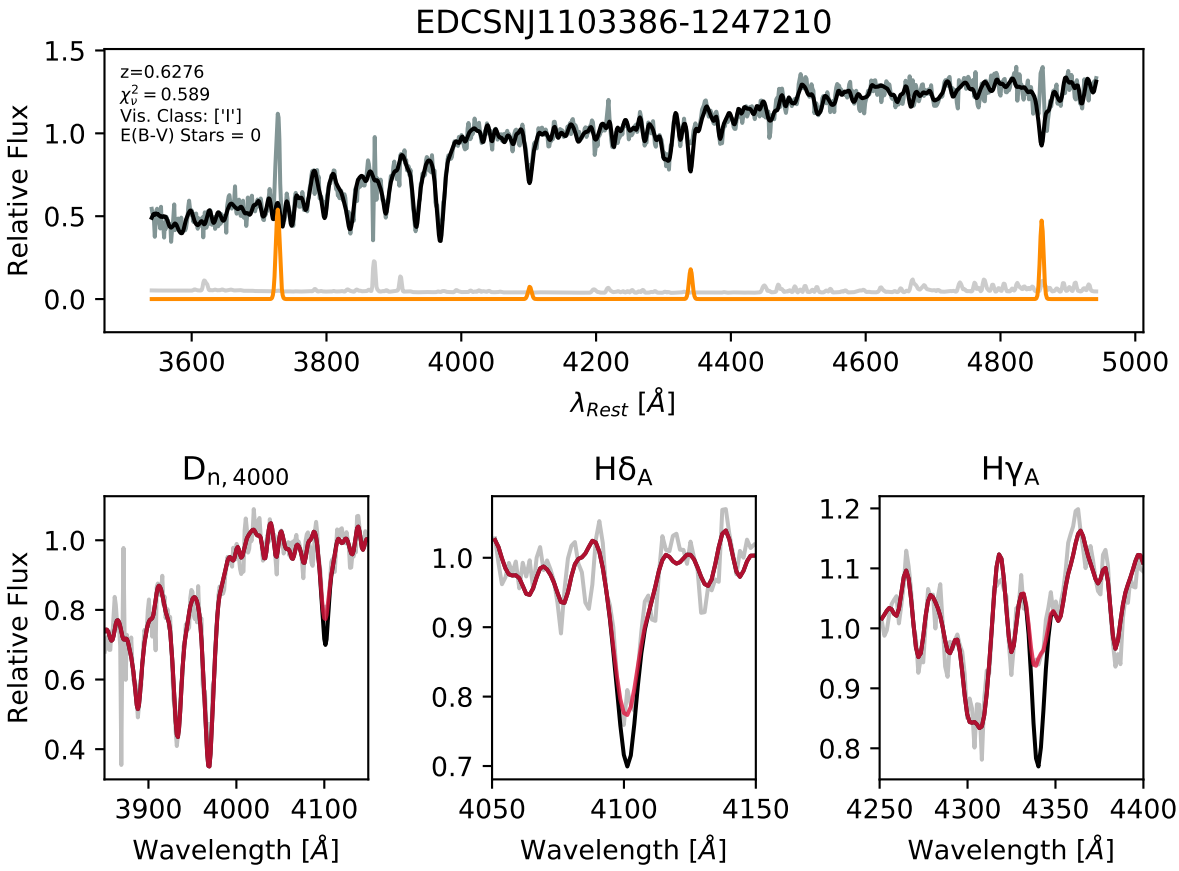
EDCSNJ1103386-1247210
z=0.6276
$\chi^2_\nu = 0.589$
Vis. Class: ['I']
E(B-V) Stars = 0
Relative Flux
λ_{Rest} [Å]
$D_{n,4000}$
$H\delta_A$
$H\gamma_A$
Wavelength [Å]

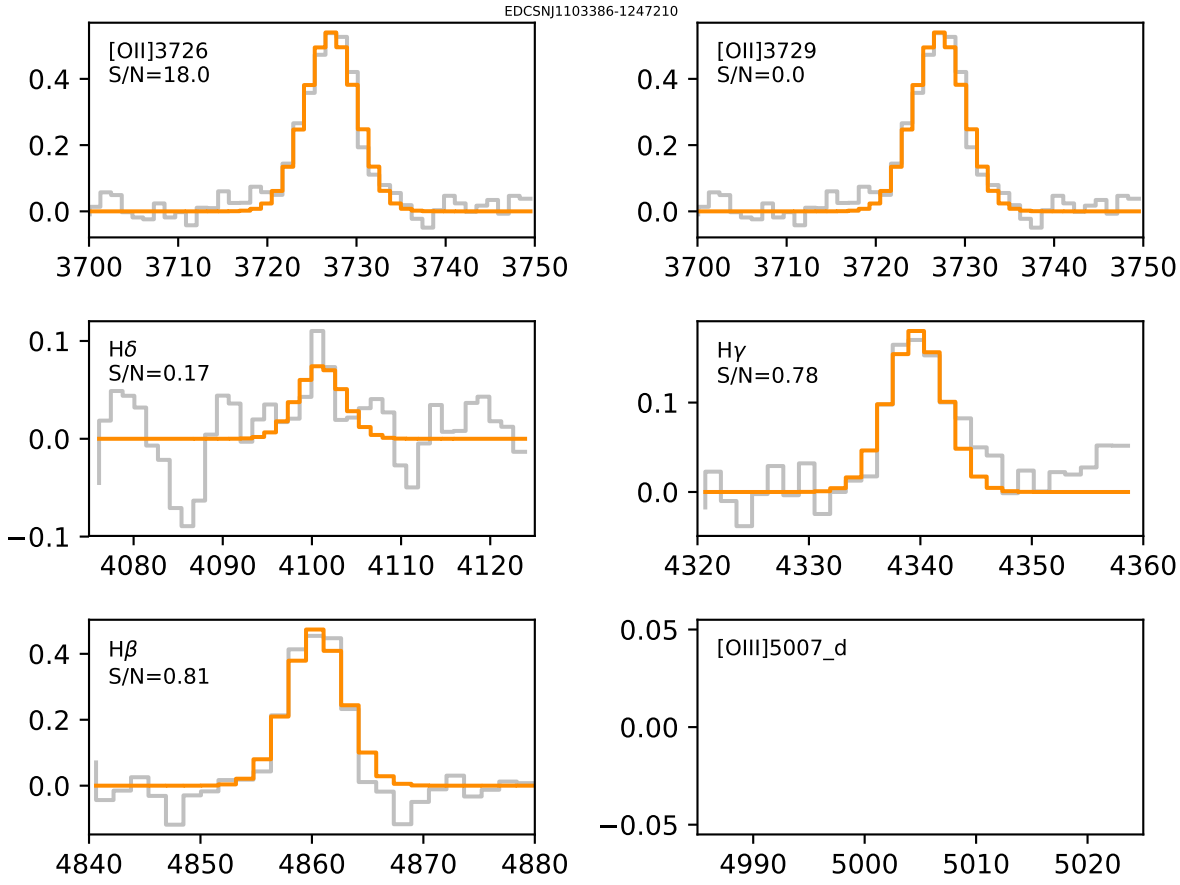
EDCSNJ1103386-1247210
[OII]3726
S/N=18.0
[OII]3729
S/N=0.0
Hδ
S/N=0.17
Hγ
S/N=0.78
Hβ
S/N=0.81
[OIII]5007_d

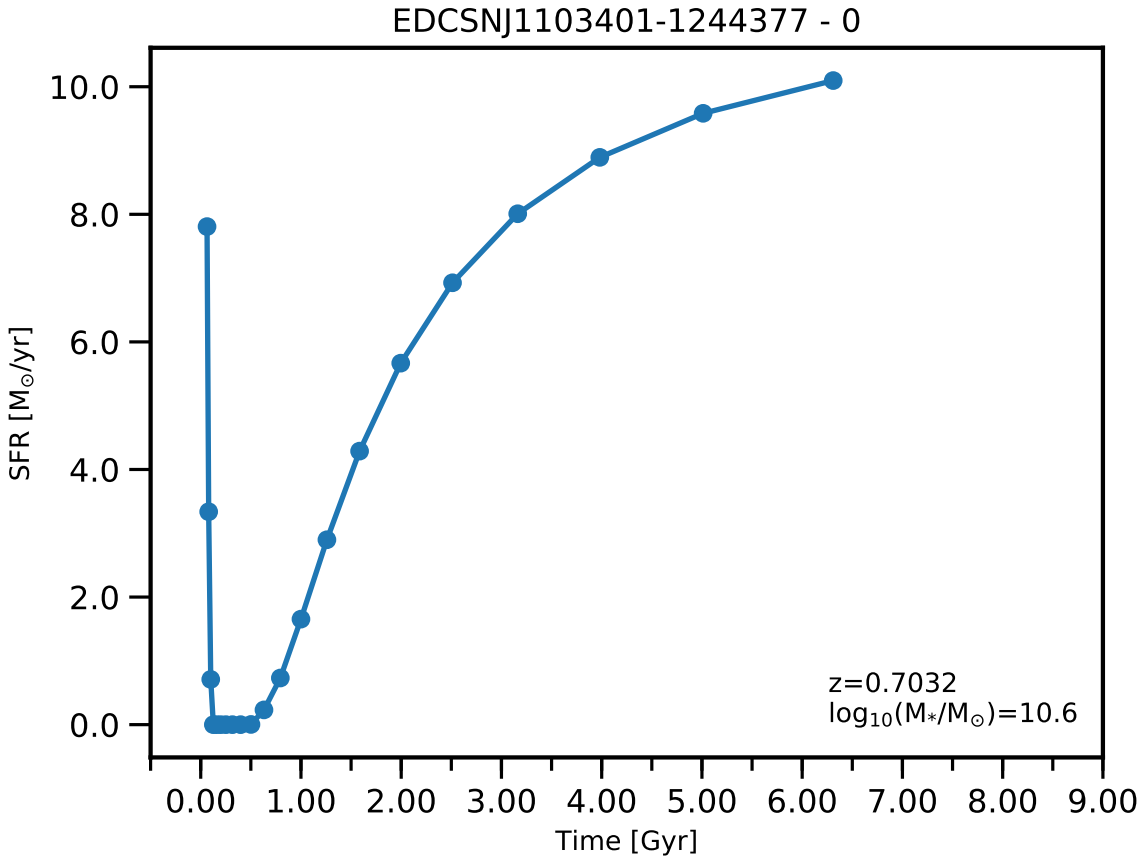
EDCSNJ1103401-1244377 - 0
SFR [M⊙/yr]
10.0
8.0
6.0
4.0
2.0
0.0
0.00
1.00
2.00
3.00
4.00
5.00
6.00
7.00
8.00
9.00
Time [Gyr]
z=0.7032
log10(M*/M⊙)=10.6

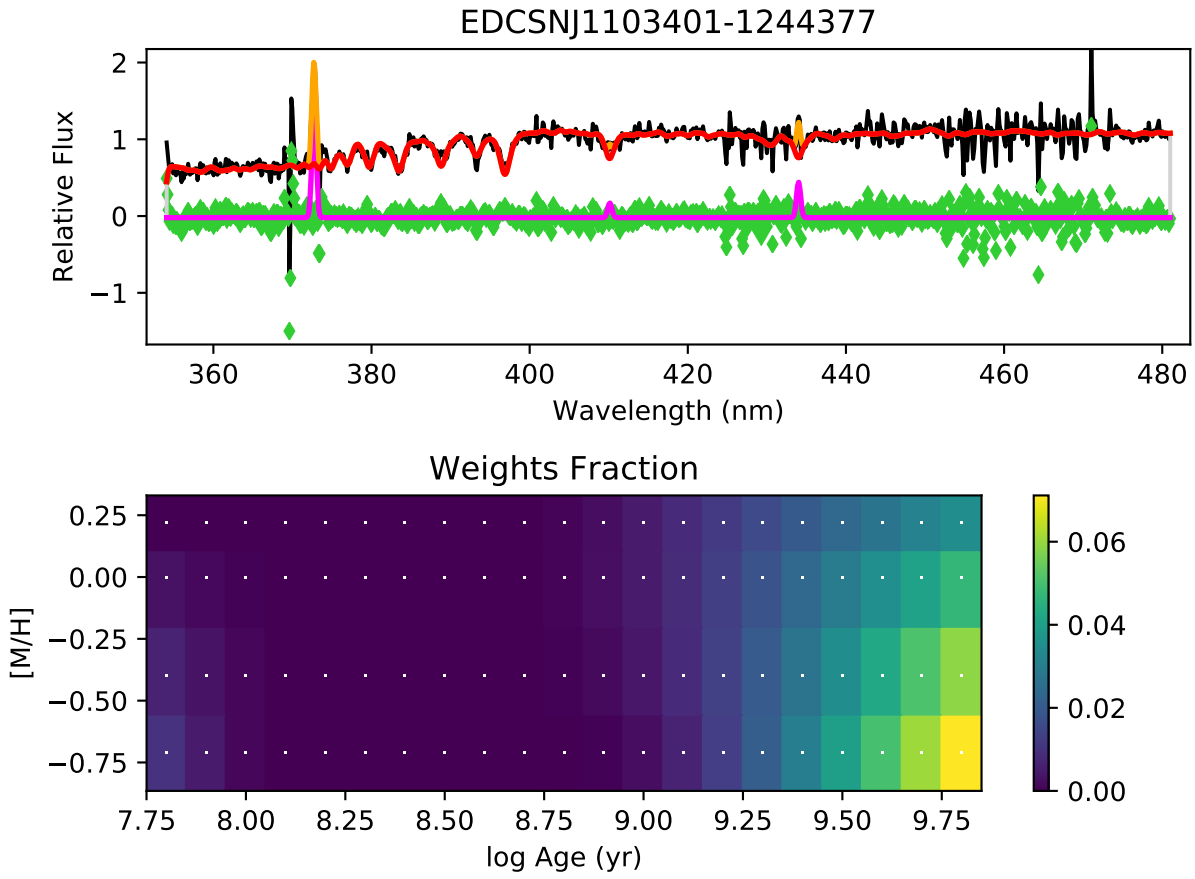
EDCSNJ1103401-1244377
Relative Flux
2
1
0
−1
360
380
400
420
440
460
480
Wavelength (nm)
Weights Fraction
[M/H]
0.25
0.00
−0.25
−0.50
−0.75
7.75
8.00
8.25
8.50
8.75
9.00
9.25
9.50
9.75
log Age (yr)
0.06
0.04
0.02
0.00

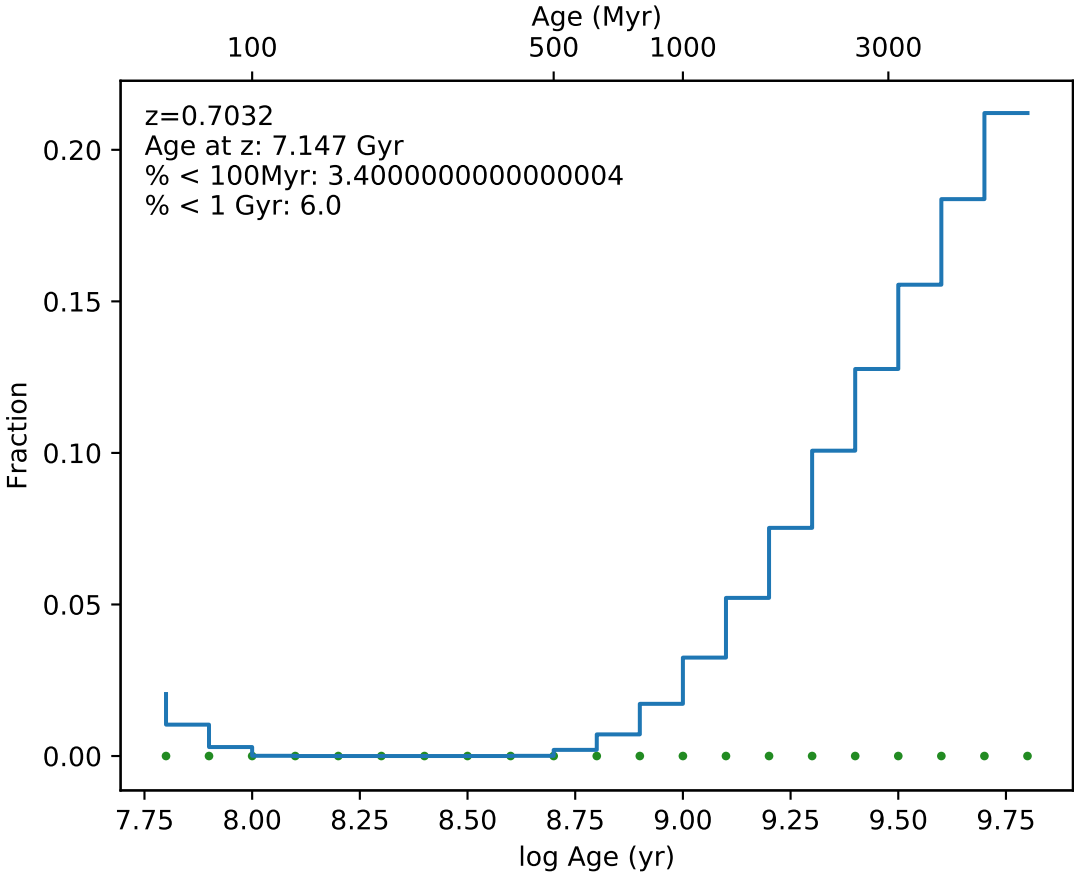
Age (Myr)
100
500
1000
3000
z=0.7032
Age at z: 7.147 Gyr
% < 100Myr: 3.4000000000000004
% < 1 Gyr: 6.0
Fraction
0.20
0.15
0.10
0.05
0.00
7.75
8.00
8.25
8.50
8.75
9.00
9.25
9.50
9.75
log Age (yr)

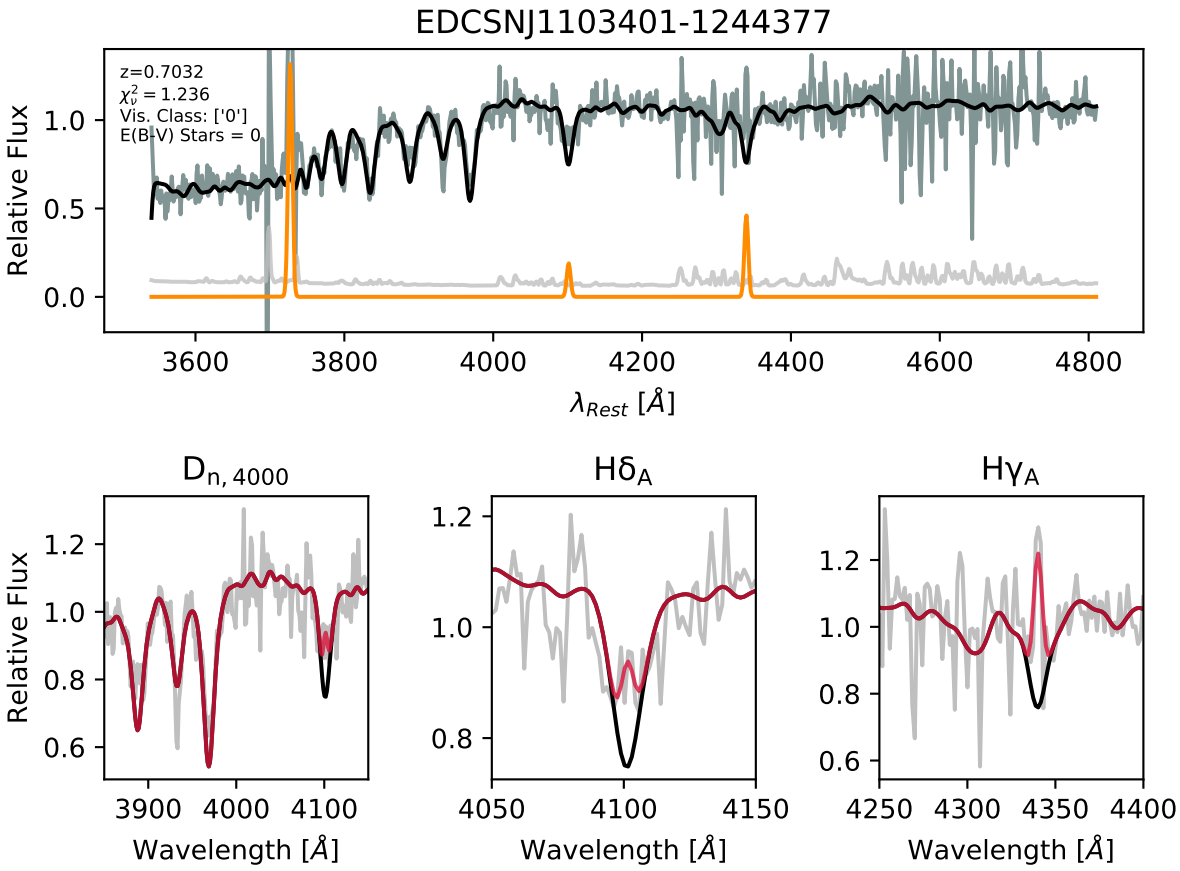
EDCSNJ1103401-1244377
z=0.7032
$\chi^2_\nu = 1.236$
Vis. Class: ['0']
E(B-V) Stars = 0
Relative Flux
1.0
0.5
0.0
3600
3800
4000
4200
4400
4600
4800
λ_{Rest} [Å]
$D_{n,4000}$
$H\delta_A$
$H\gamma_A$
Relative Flux
1.2
1.0
0.8
0.6
3900
4000
4100
Wavelength [Å]
1.2
1.0
0.8
4050
4100
4150
Wavelength [Å]
1.2
1.0
0.8
0.6
4250
4300
4350
4400
Wavelength [Å]

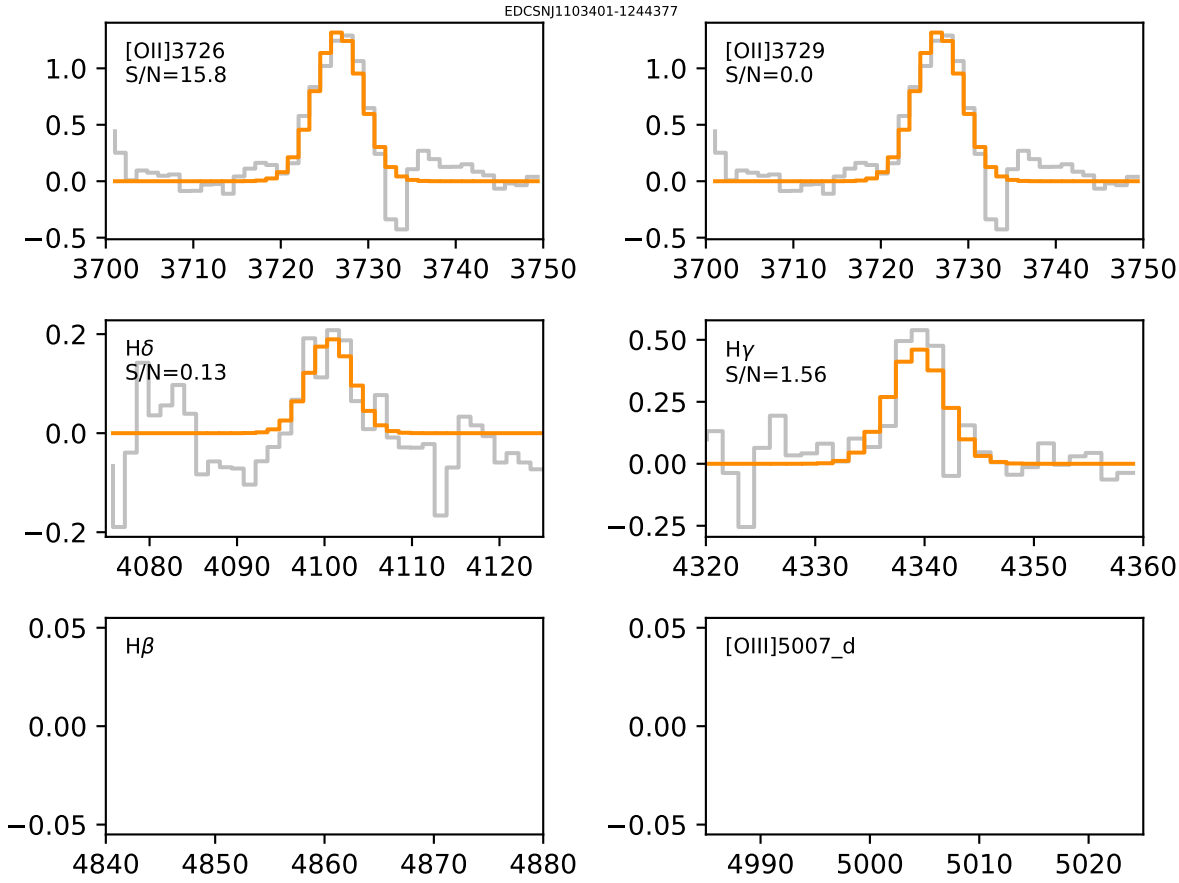
EDCSNJ1103401-1244377
[OII]3726
S/N=15.8
[OII]3729
S/N=0.0
Hδ
S/N=0.13
Hγ
S/N=1.56
Hβ
[OIII]5007_d

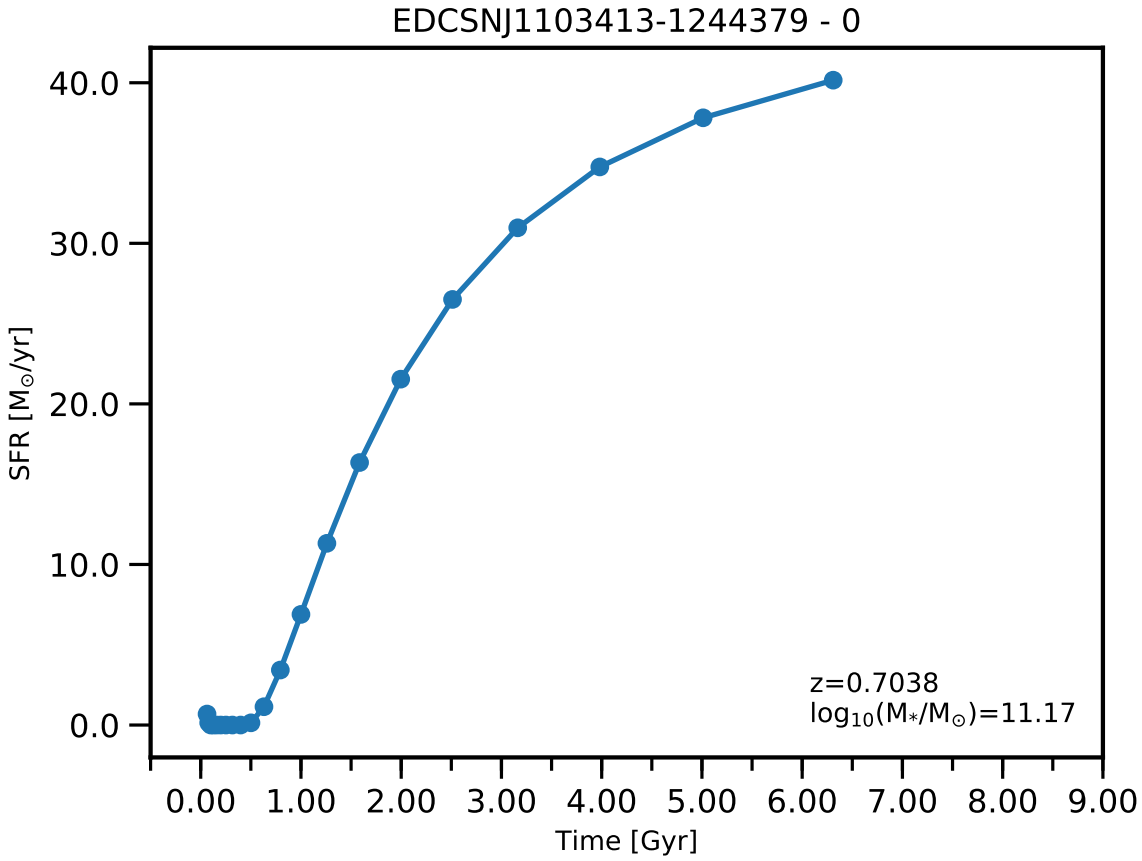
EDCSNJ1103413-1244379 - 0
40.0
30.0
20.0
10.0
0.0
SFR [M⊙/yr]
0.00
1.00
2.00
3.00
4.00
5.00
6.00
7.00
8.00
9.00
Time [Gyr]
z=0.7038
log10(M*/M⊙)=11.17

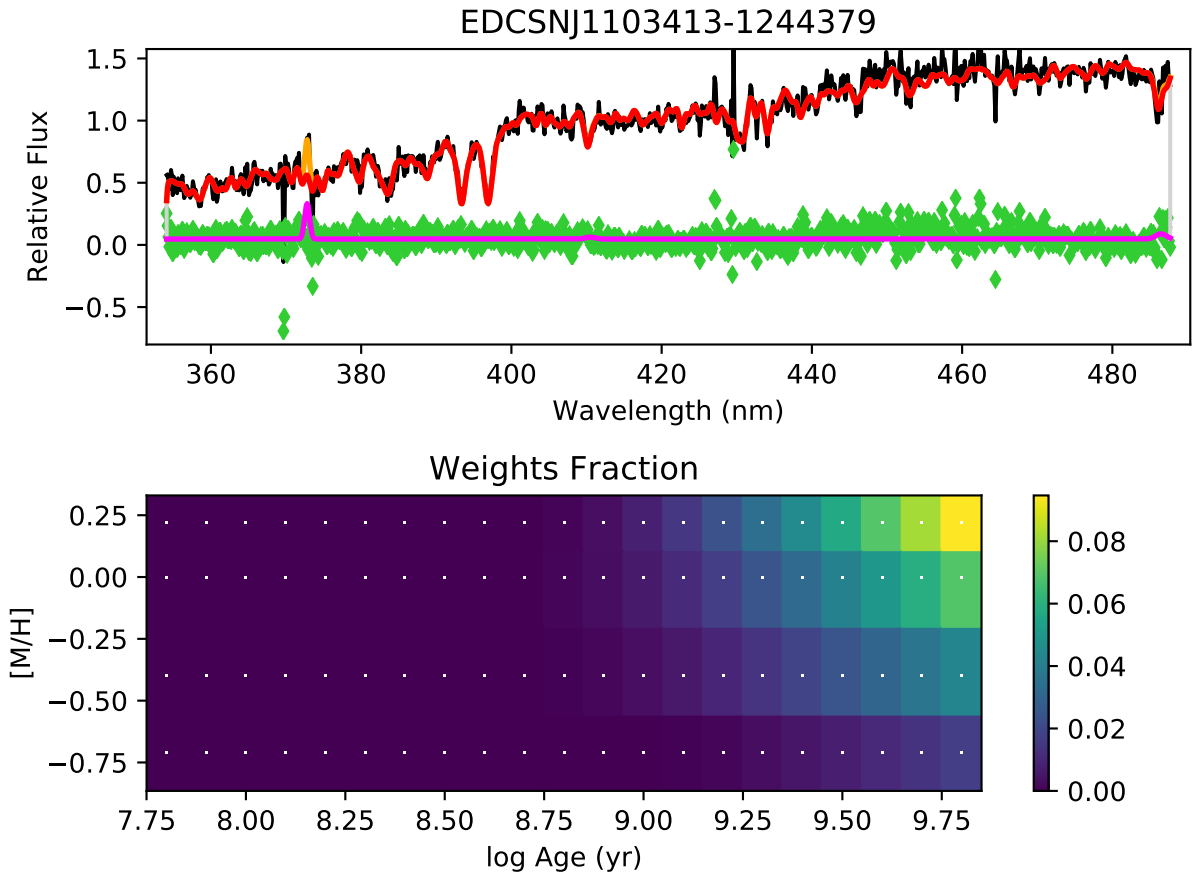
EDCSNJ1103413-1244379
Relative Flux
1.5
1.0
0.5
0.0
−0.5
360
380
400
420
440
460
480
Wavelength (nm)
Weights Fraction
[M/H]
0.25
0.00
−0.25
−0.50
−0.75
7.75
8.00
8.25
8.50
8.75
9.00
9.25
9.50
9.75
log Age (yr)
0.08
0.06
0.04
0.02
0.00

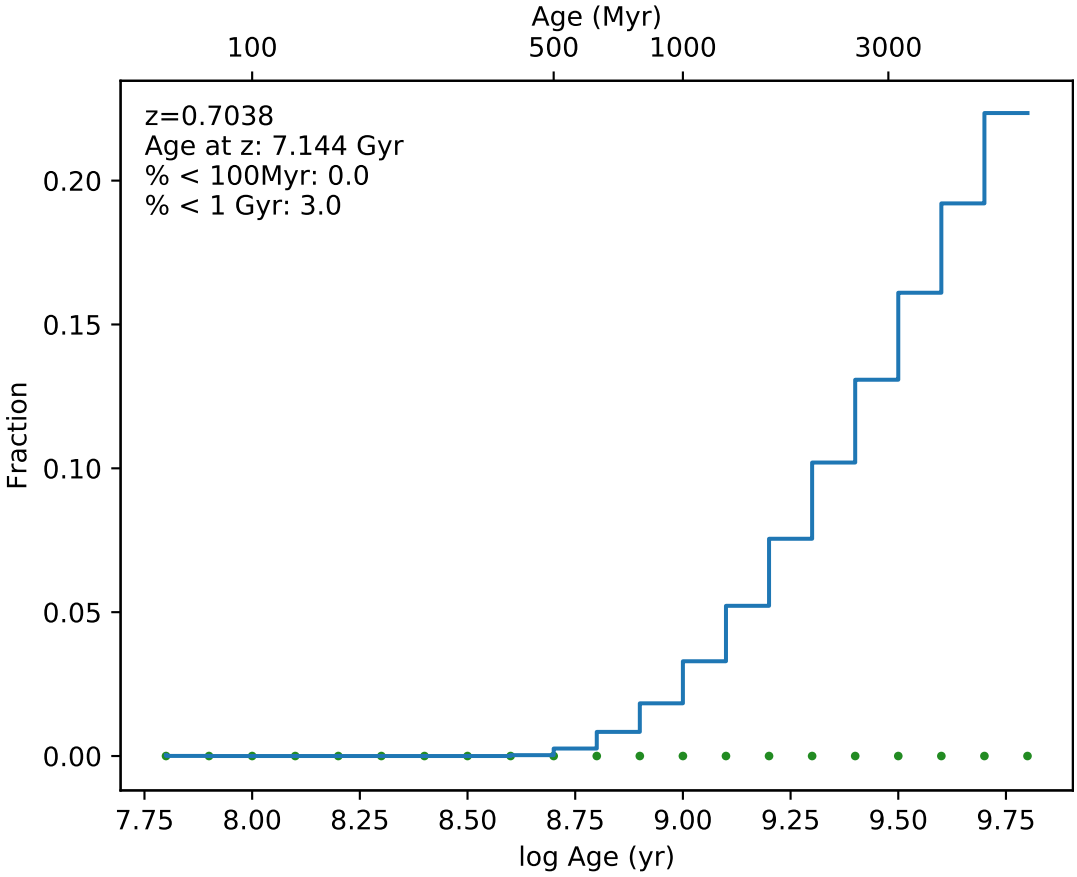
Age (Myr)
100
500
1000
3000
z=0.7038
Age at z: 7.144 Gyr
% < 100Myr: 0.0
% < 1 Gyr: 3.0
Fraction
0.20
0.15
0.10
0.05
0.00
7.75
8.00
8.25
8.50
8.75
9.00
9.25
9.50
9.75
log Age (yr)

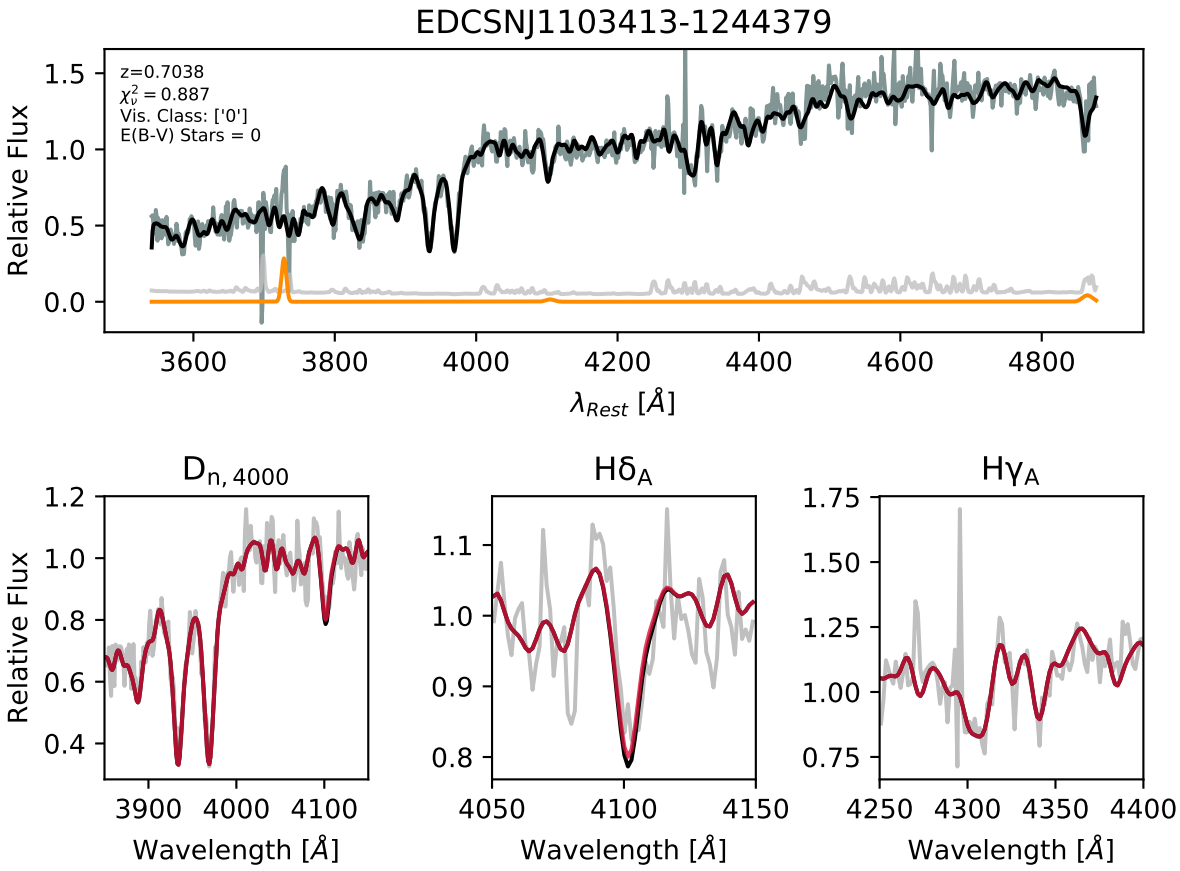
EDCSNJ1103413-1244379
z=0.7038
$\chi^2_\nu = 0.887$
Vis. Class: ['0']
E(B-V) Stars = 0
Relative Flux
λ_{Rest} [Å]
$D_{n,4000}$
$H\delta_A$
$H\gamma_A$
Wavelength [Å]

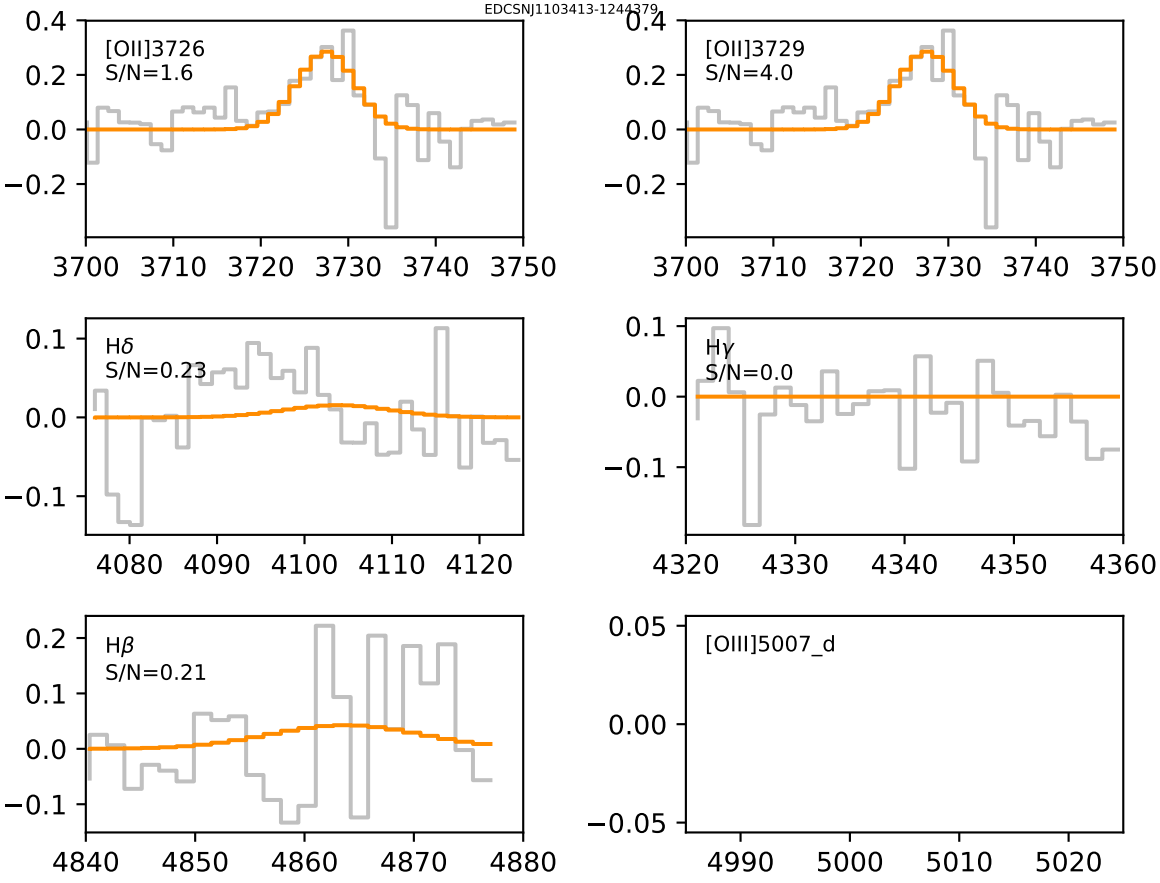
EDCSNJ1103413-1244379
[OII]3726
S/N=1.6
[OII]3729
S/N=4.0
Hδ
S/N=0.23
Hγ
S/N=0.0
Hβ
S/N=0.21
[OIII]5007_d

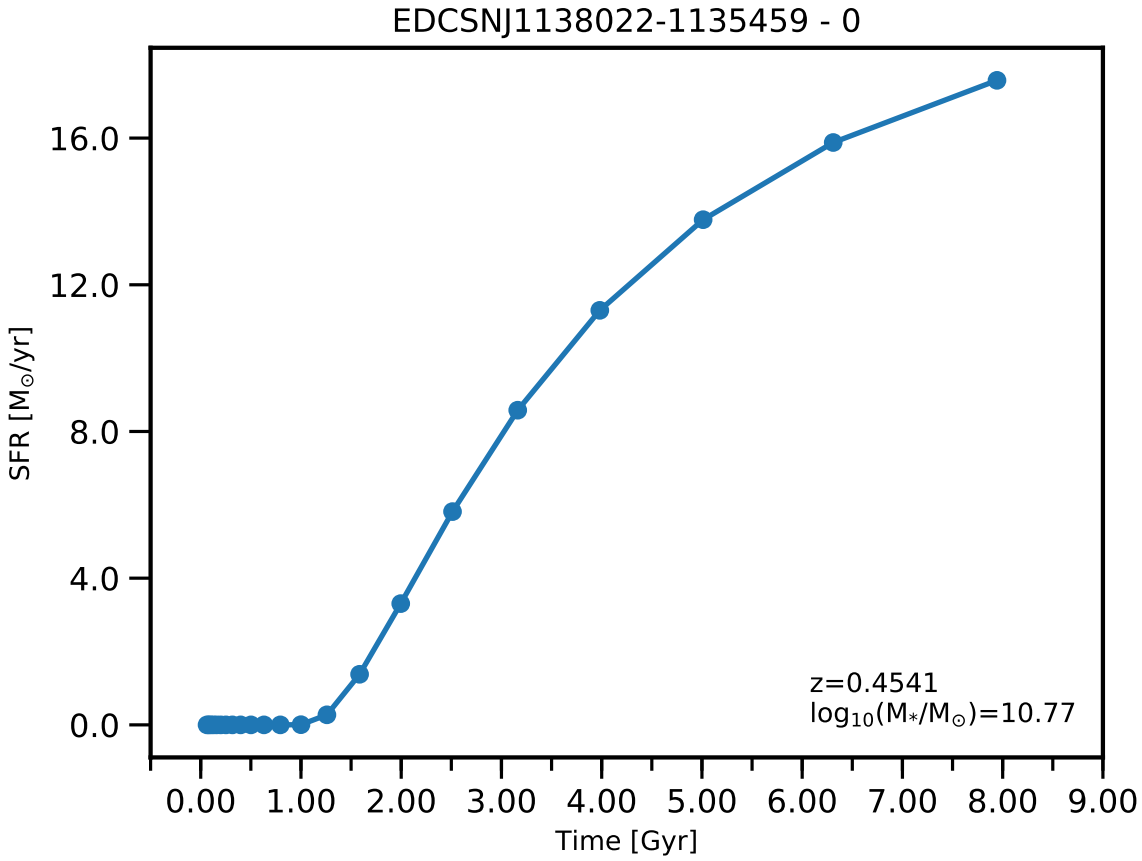
EDCSNJ1138022-1135459 - 0
SFR [M⊙/yr]
16.0
12.0
8.0
4.0
0.0
0.00
1.00
2.00
3.00
4.00
5.00
6.00
7.00
8.00
9.00
Time [Gyr]
z=0.4541
log10(M*/M⊙)=10.77

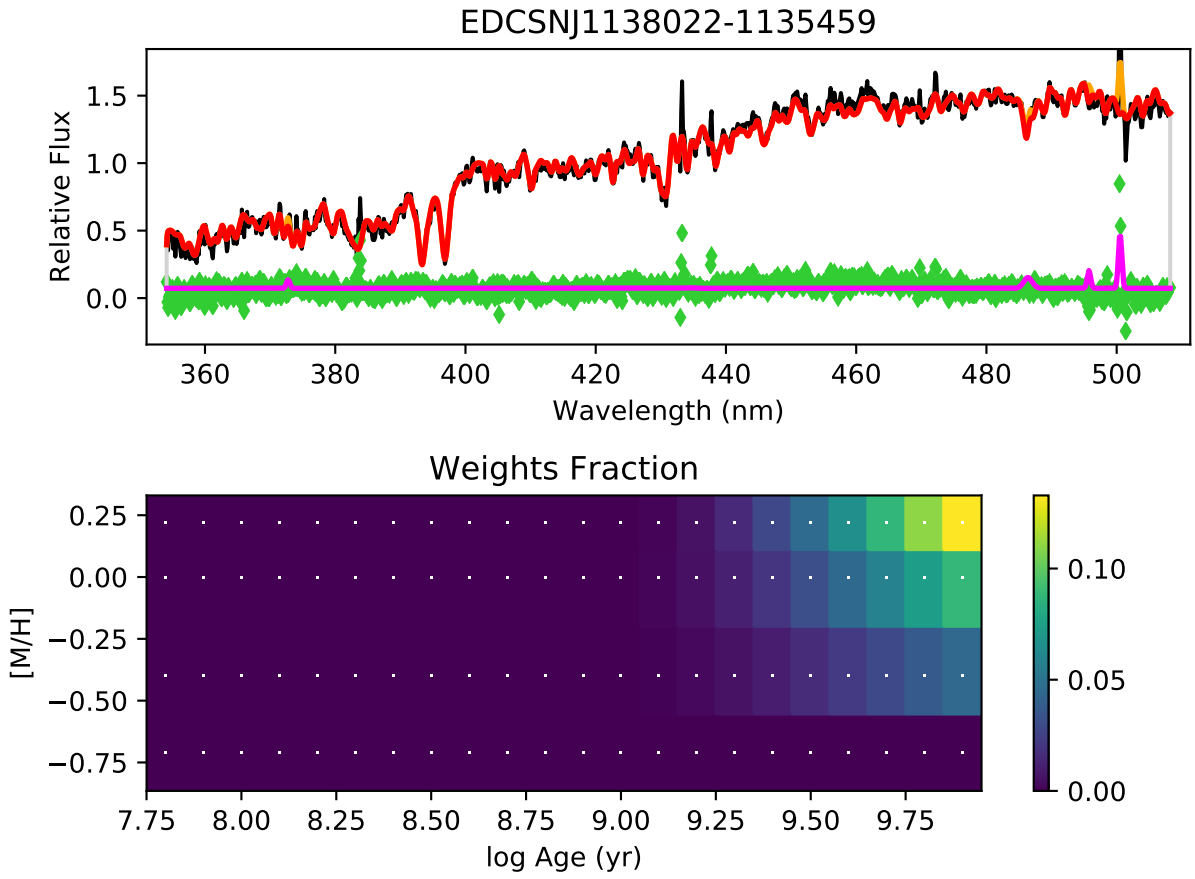
EDCSNJ1138022-1135459
Relative Flux
1.5
1.0
0.5
0.0
360
380
400
420
440
460
480
500
Wavelength (nm)
Weights Fraction
[M/H]
0.25
0.00
−0.25
−0.50
−0.75
7.75
8.00
8.25
8.50
8.75
9.00
9.25
9.50
9.75
log Age (yr)
0.10
0.05
0.00

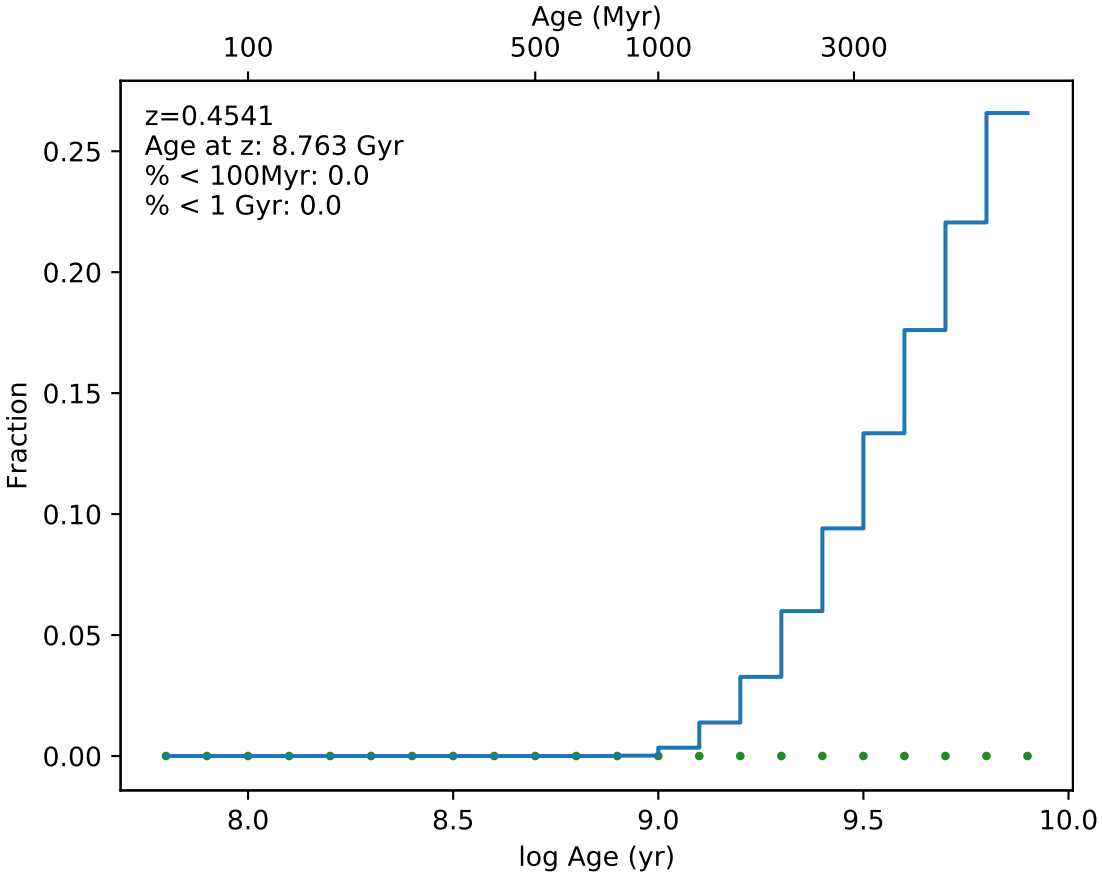
Age (Myr)
100
500
1000
3000
z=0.4541
Age at z: 8.763 Gyr
% < 100Myr: 0.0
% < 1 Gyr: 0.0
Fraction
0.25
0.20
0.15
0.10
0.05
0.00
8.0
8.5
9.0
9.5
10.0
log Age (yr)

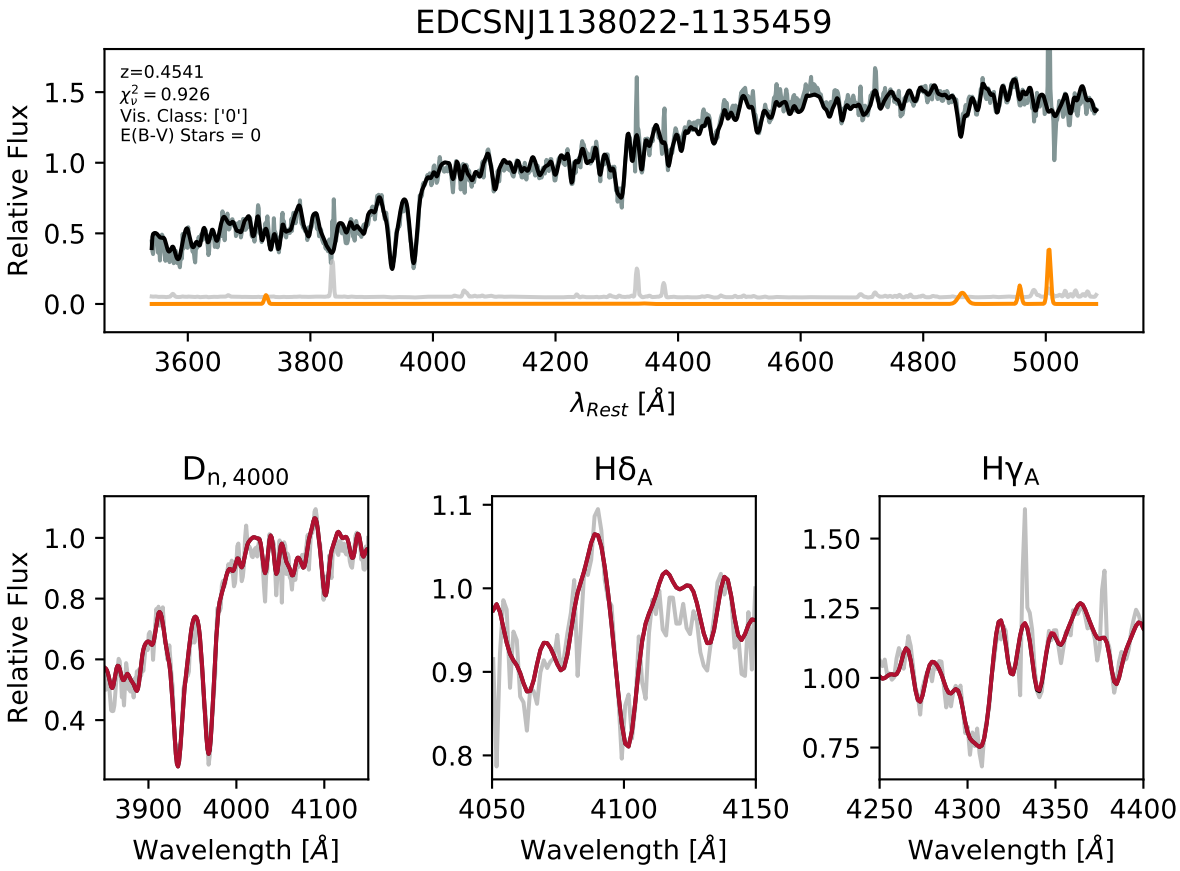
EDCSNJ1138022-1135459
z=0.4541
$\chi^2_\nu = 0.926$
Vis. Class: ['0']
E(B-V) Stars = 0
Relative Flux
λ_{Rest} [Å]
$D_{n,4000}$
$H\delta_A$
$H\gamma_A$
Wavelength [Å]

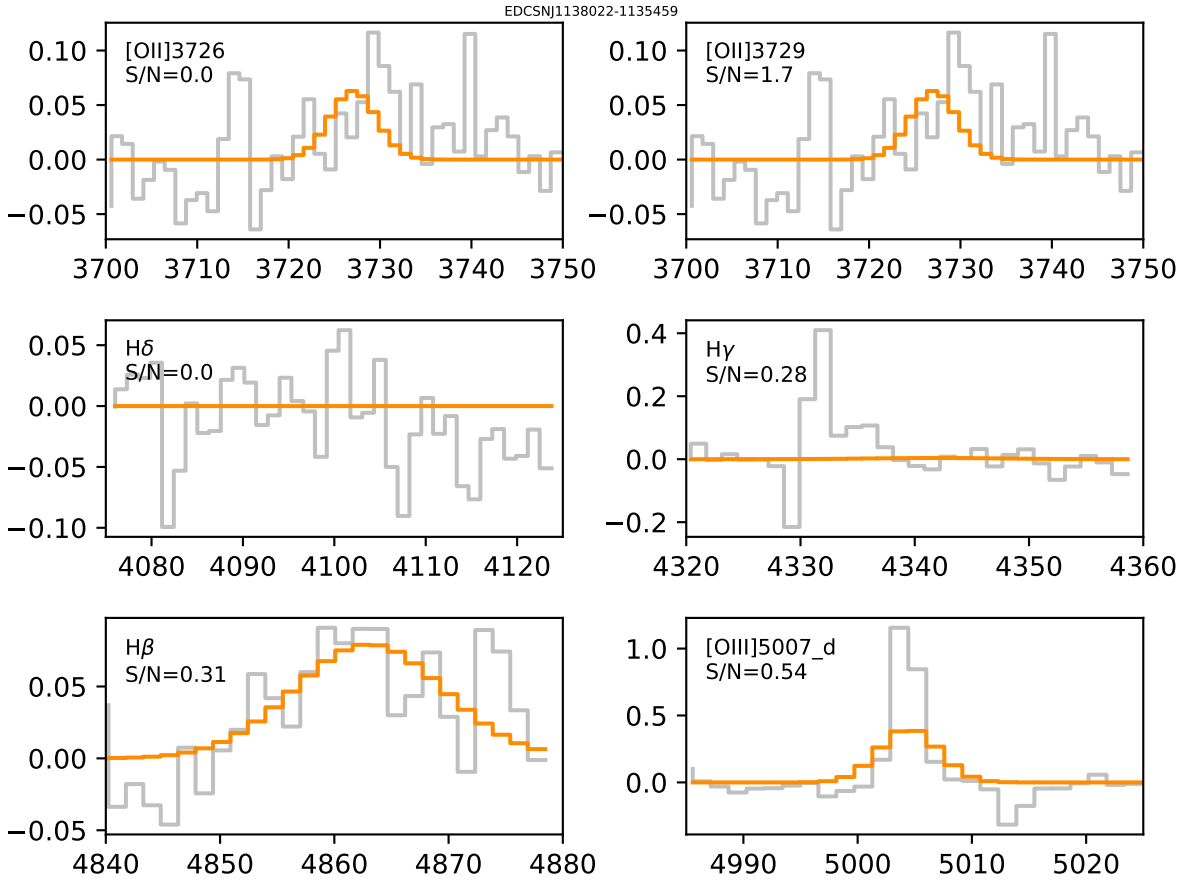
EDCSNJ1138022-1135459
[OII]3726
S/N=0.0
[OII]3729
S/N=1.7
Hδ
S/N=0.0
Hγ
S/N=0.28
Hβ
S/N=0.31
[OIII]5007_d
S/N=0.54

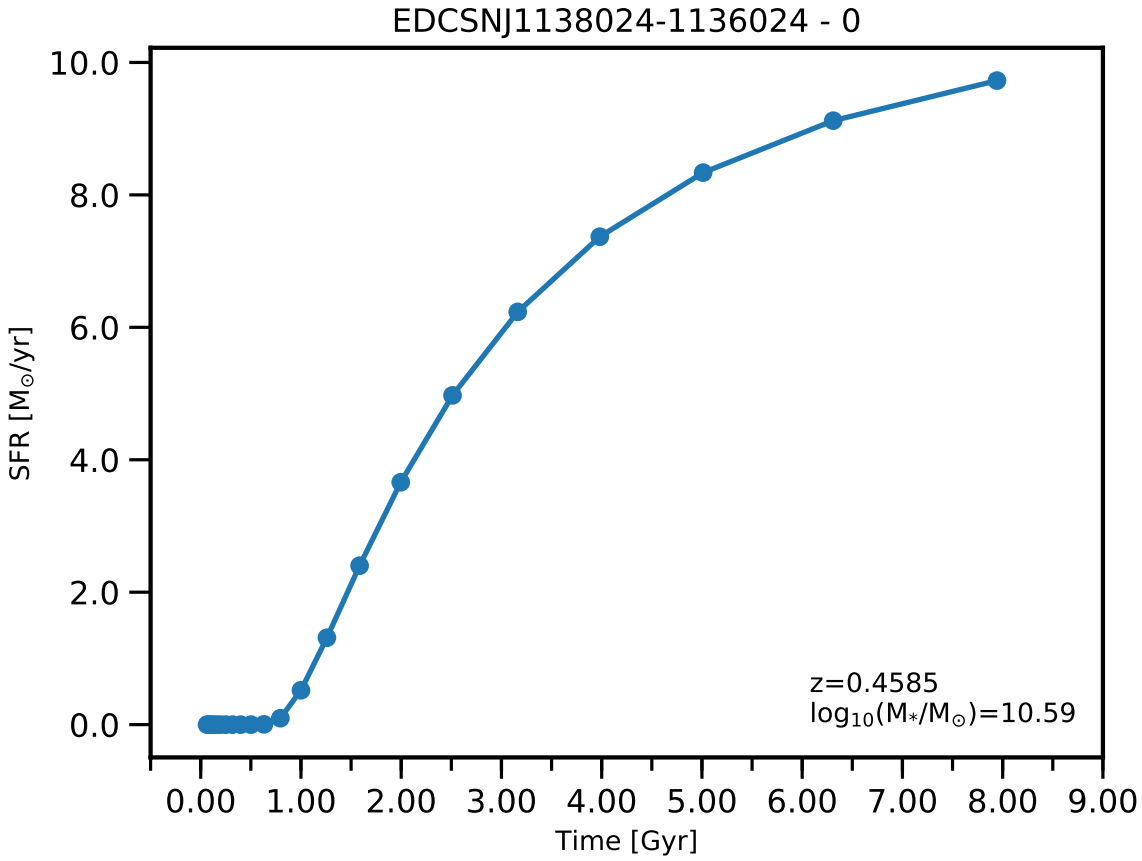
EDCSNJ1138024-1136024 - 0
SFR [M⊙/yr]
Time [Gyr]
z=0.4585
log10(M*/M⊙)=10.59
0.0
2.0
4.0
6.0
8.0
10.0
0.00
1.00
2.00
3.00
4.00
5.00
6.00
7.00
8.00
9.00

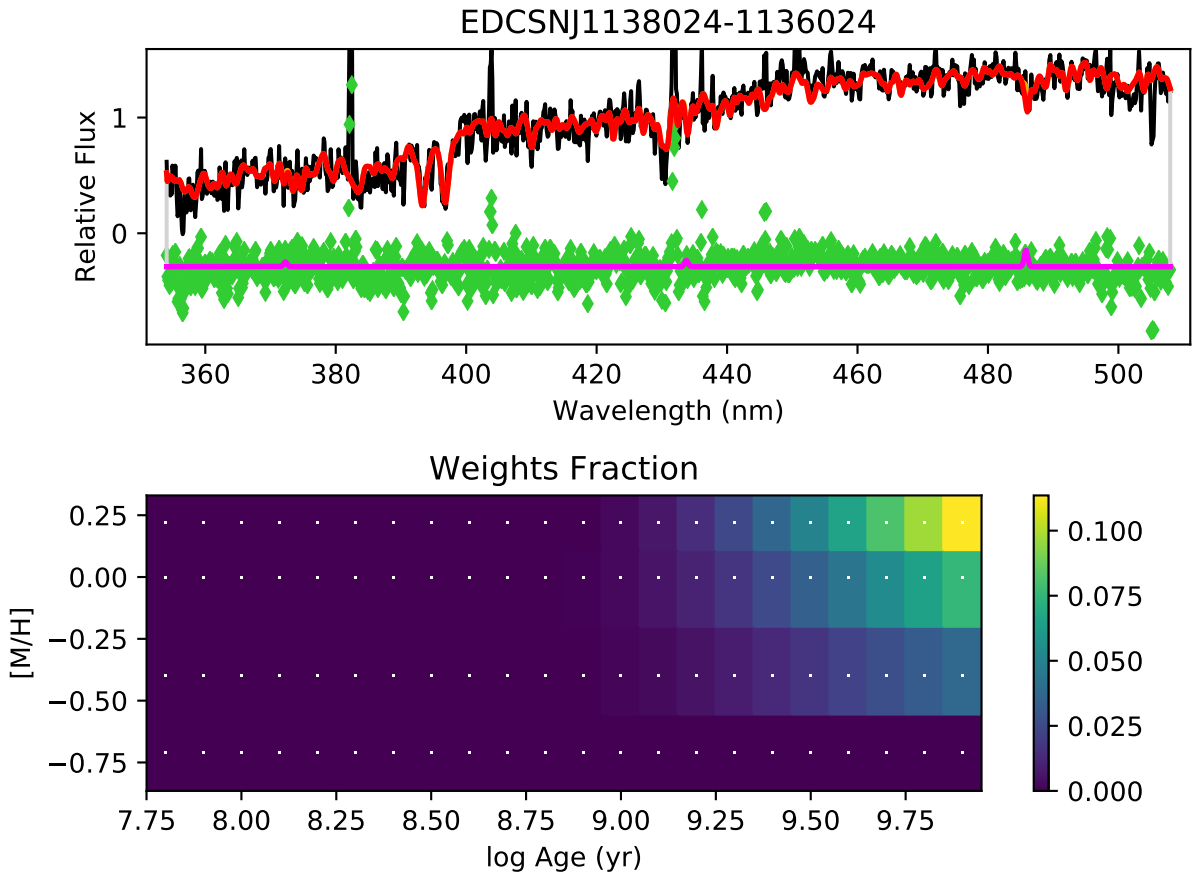
EDCSNJ1138024-1136024
Relative Flux
1
0
360
380
400
420
440
460
480
500
Wavelength (nm)
Weights Fraction
[M/H]
0.25
0.00
−0.25
−0.50
−0.75
7.75
8.00
8.25
8.50
8.75
9.00
9.25
9.50
9.75
log Age (yr)
0.100
0.075
0.050
0.025
0.000

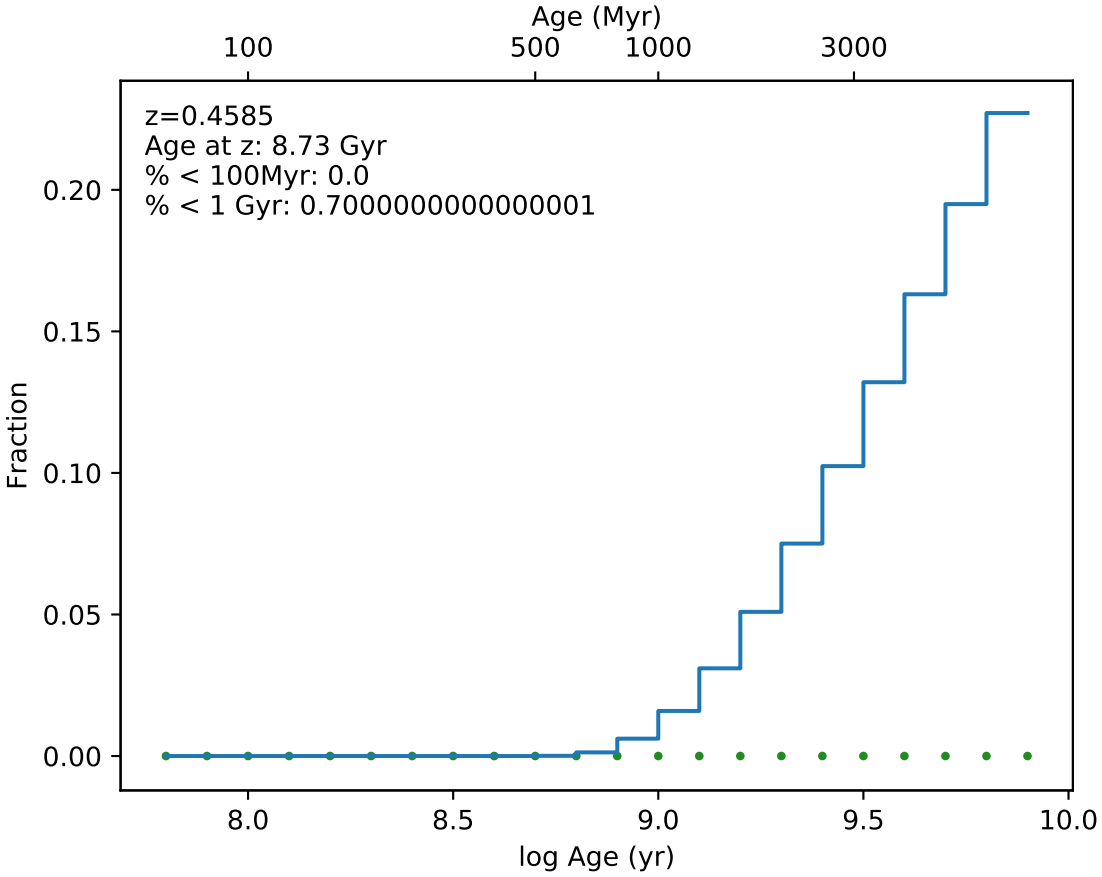
Age (Myr)
100
500
1000
3000
z=0.4585
Age at z: 8.73 Gyr
% < 100Myr: 0.0
% < 1 Gyr: 0.7000000000000001
Fraction
0.20
0.15
0.10
0.05
0.00
8.0
8.5
9.0
9.5
10.0
log Age (yr)

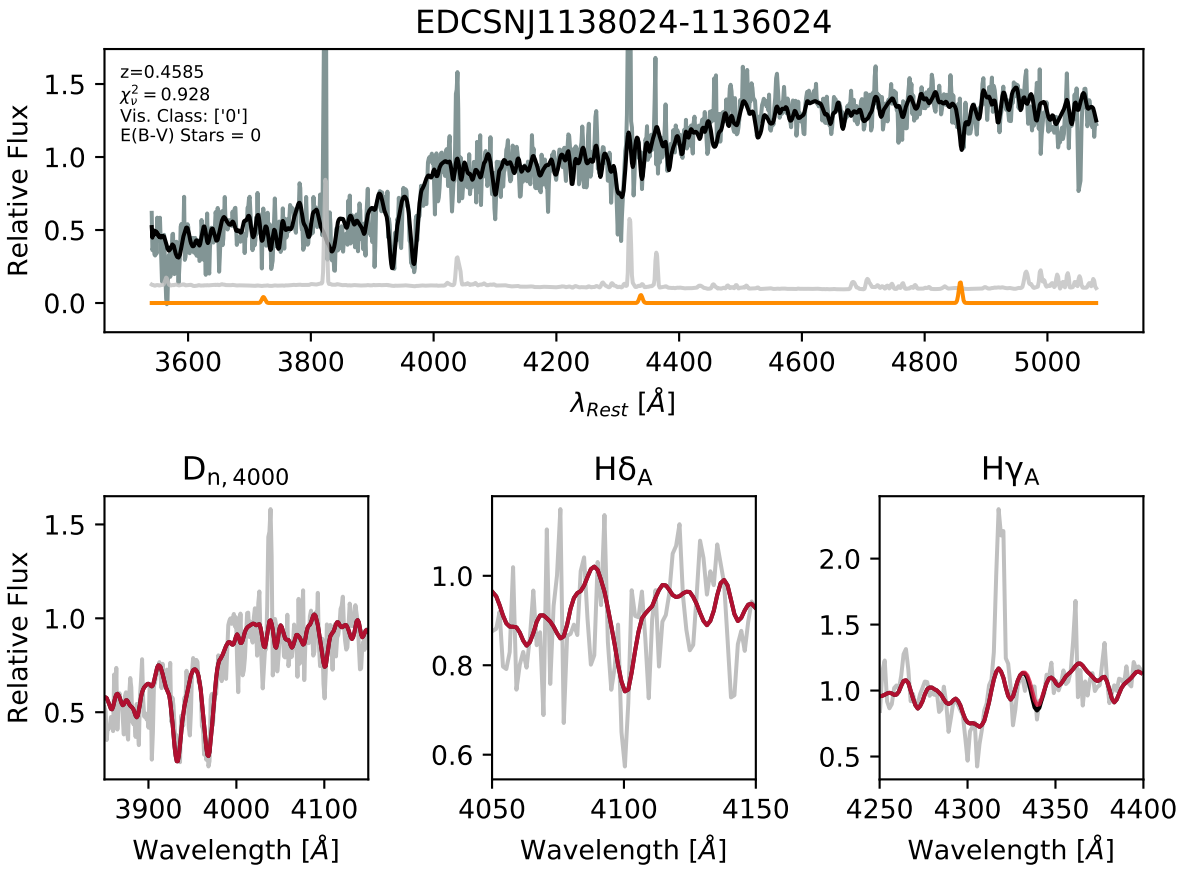
EDCSNJ1138024-1136024
z=0.4585
$\chi^2_\nu = 0.928$
Vis. Class: ['0']
E(B-V) Stars = 0
Relative Flux
λ_{Rest} [Å]
$D_{n,4000}$
$H\delta_A$
$H\gamma_A$
Wavelength [Å]

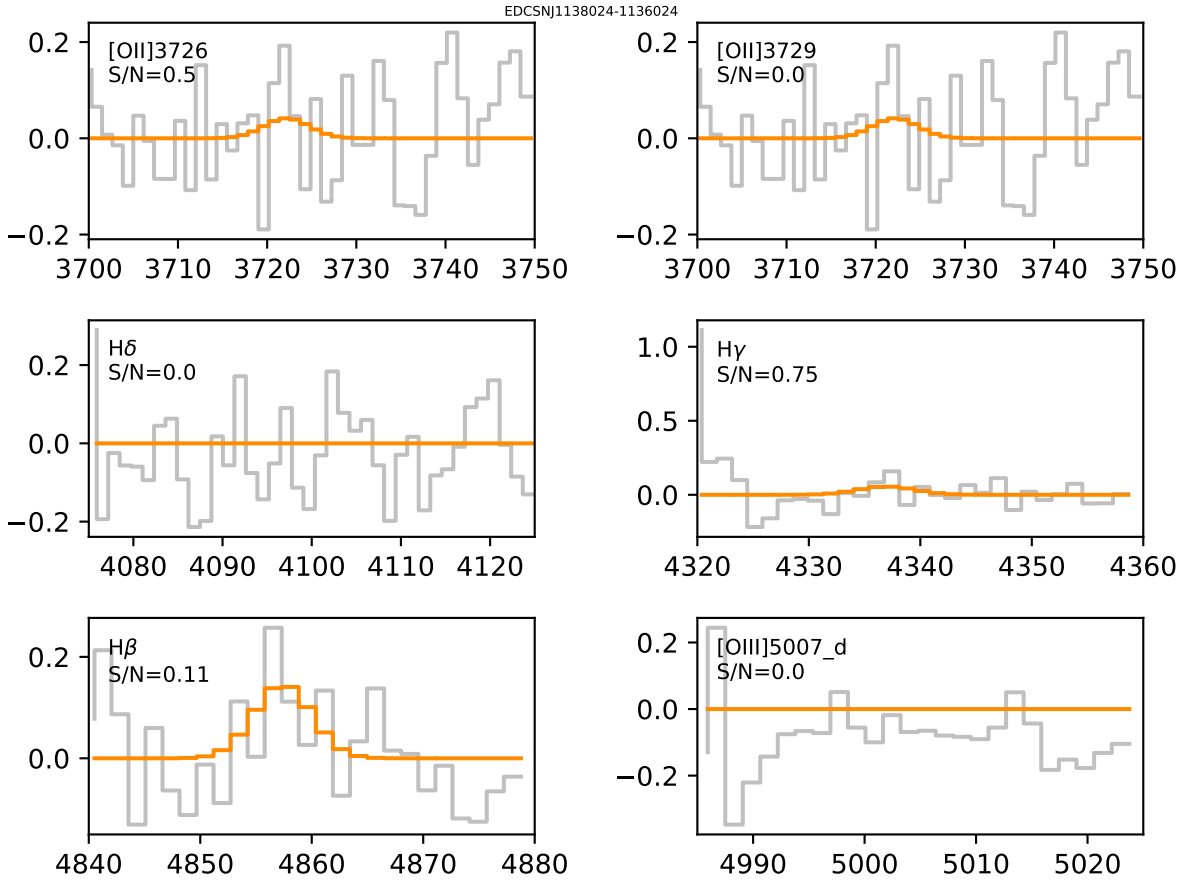
EDCSNJ1138024-1136024
[OII]3726
S/N=0.5
[OII]3729
S/N=0.0
Hδ
S/N=0.0
Hγ
S/N=0.75
Hβ
S/N=0.11
[OIII]5007_d
S/N=0.0

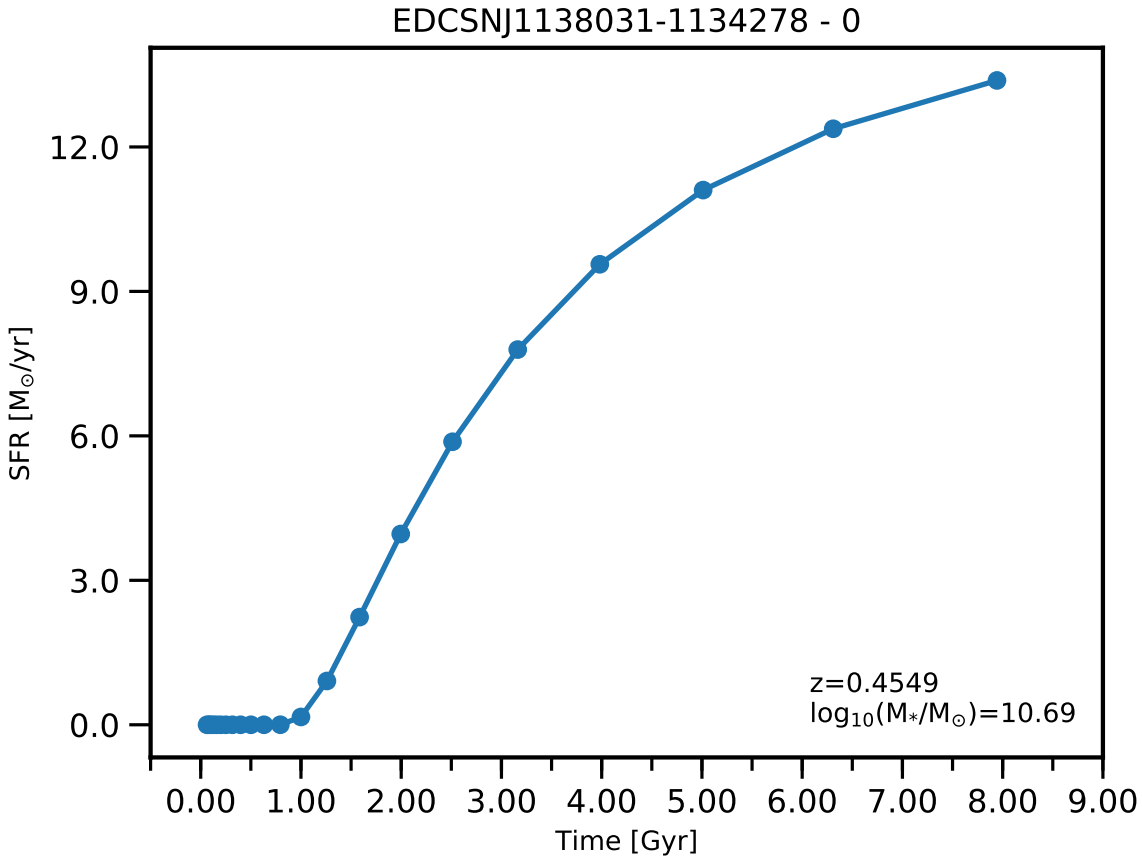
EDCSNJ1138031-1134278 - 0
SFR [M⊙/yr]
12.0
9.0
6.0
3.0
0.0
0.00
1.00
2.00
3.00
4.00
5.00
6.00
7.00
8.00
9.00
Time [Gyr]
z=0.4549
log10(M*/M⊙)=10.69

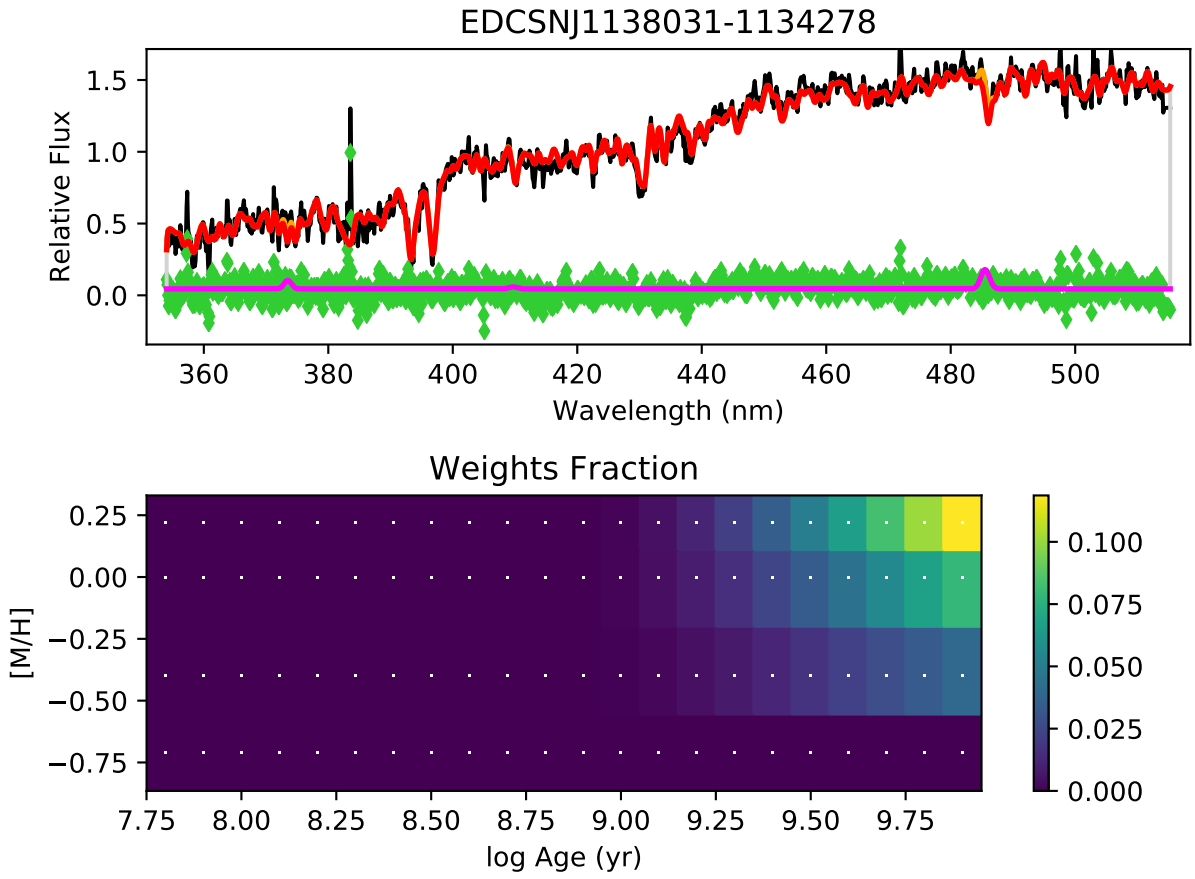
EDCSNJ1138031-1134278
Relative Flux
1.5
1.0
0.5
0.0
360
380
400
420
440
460
480
500
Wavelength (nm)
Weights Fraction
[M/H]
0.25
0.00
−0.25
−0.50
−0.75
7.75
8.00
8.25
8.50
8.75
9.00
9.25
9.50
9.75
log Age (yr)
0.100
0.075
0.050
0.025
0.000

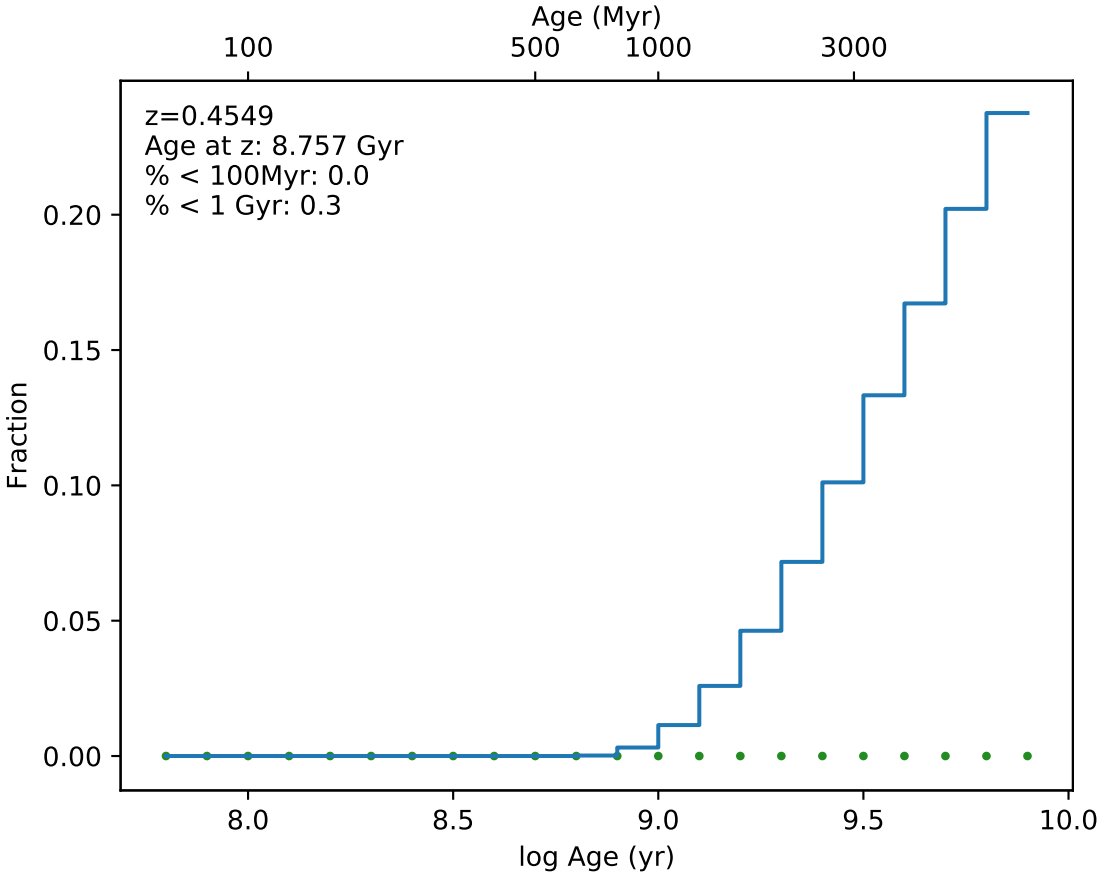
Age (Myr)
100
500
1000
3000
z=0.4549
Age at z: 8.757 Gyr
% < 100Myr: 0.0
% < 1 Gyr: 0.3
0.20
0.15
0.10
0.05
0.00
Fraction
8.0
8.5
9.0
9.5
10.0
log Age (yr)

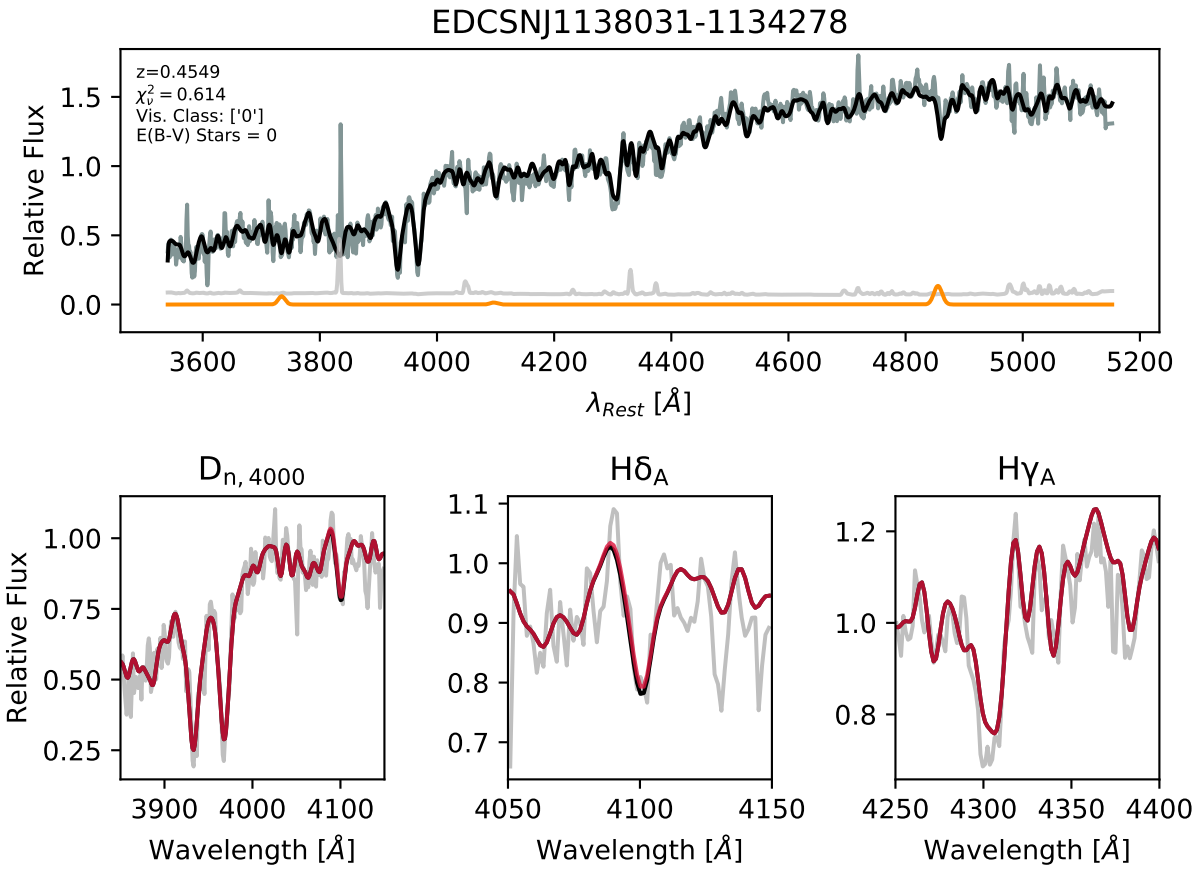
EDCSNJ1138031-1134278
z=0.4549
$\chi^2_\nu = 0.614$
Vis. Class: ['0']
E(B-V) Stars = 0
Relative Flux
λ_{Rest} [Å]
$D_{n,4000}$
$H\delta_A$
$H\gamma_A$
Wavelength [Å]

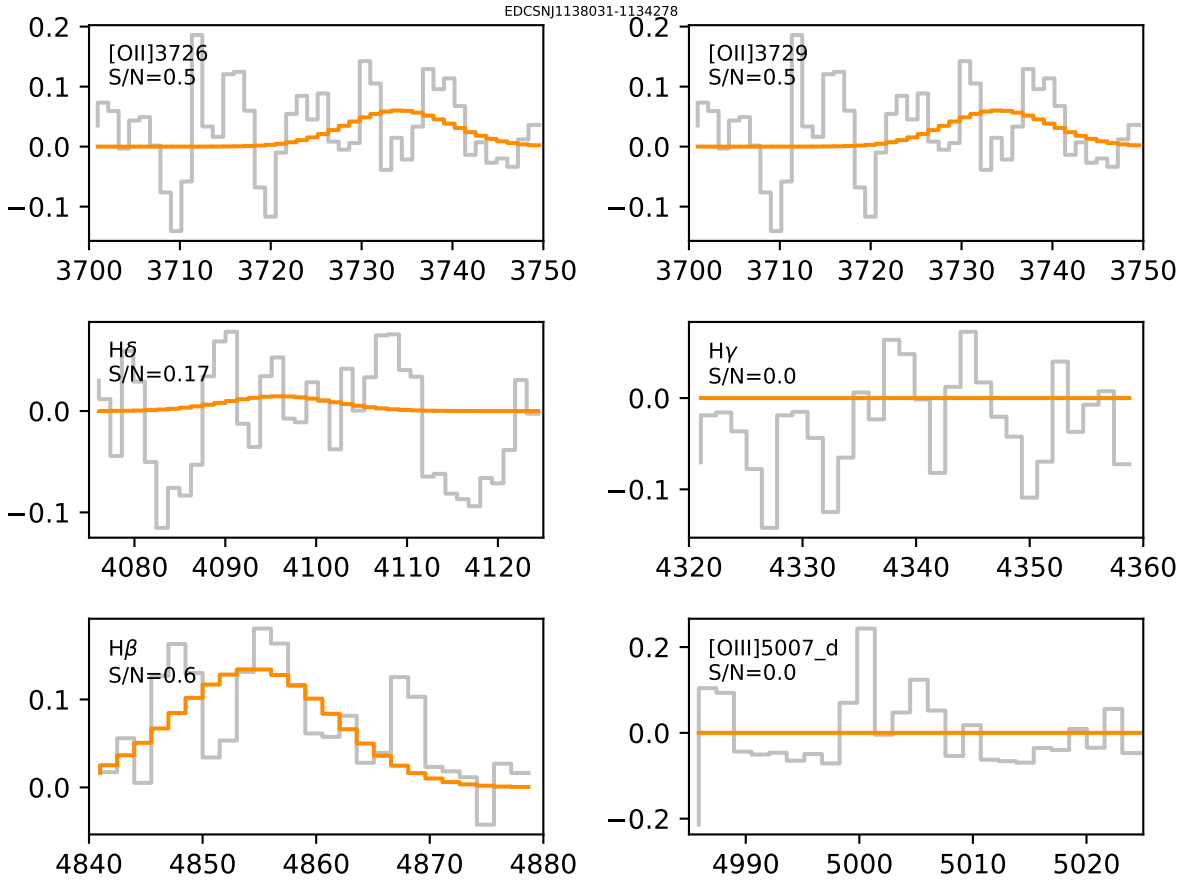
EDCSNJ1138031-1134278
[OII]3726
S/N=0.5
[OII]3729
S/N=0.5
Hδ
S/N=0.17
Hγ
S/N=0.0
Hβ
S/N=0.6
[OIII]5007_d
S/N=0.0

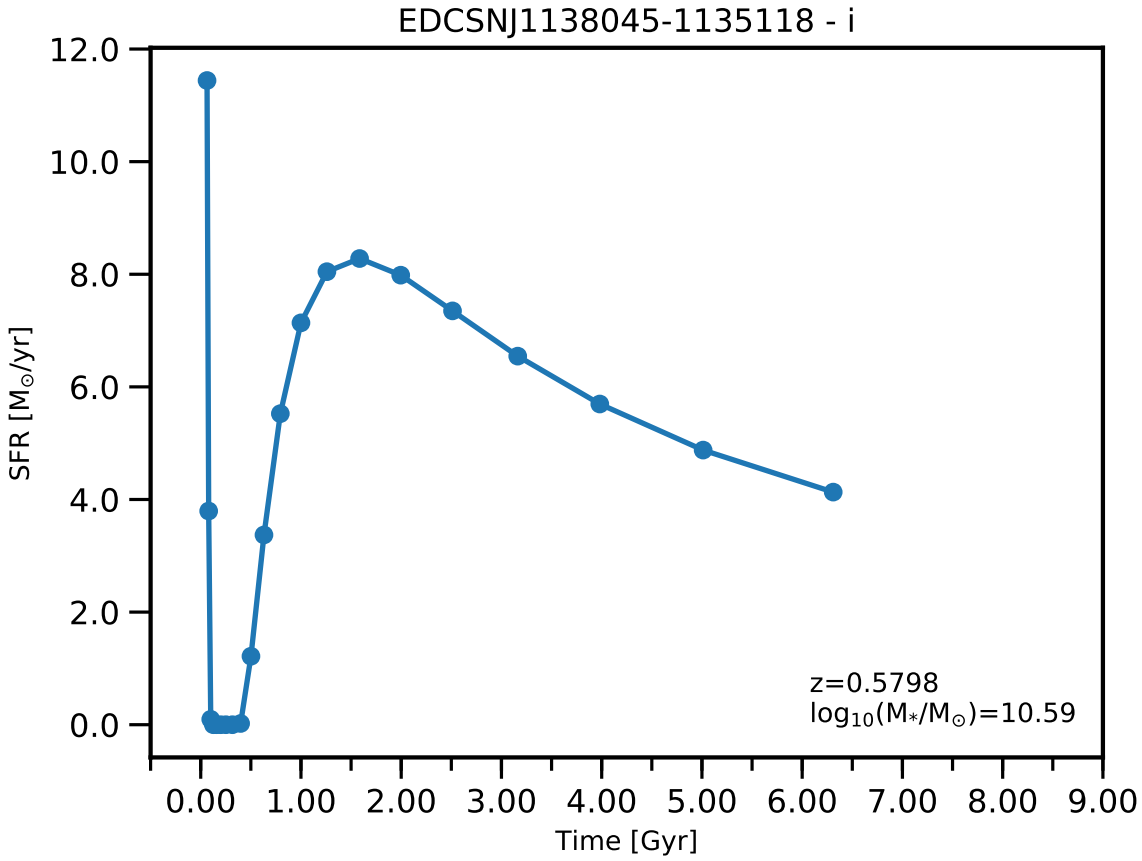
EDCSNJ1138045-1135118 - i
SFR [M⊙/yr]
Time [Gyr]
z=0.5798
log10(M*/M⊙)=10.59
0.0
2.0
4.0
6.0
8.0
10.0
12.0
0.00
1.00
2.00
3.00
4.00
5.00
6.00
7.00
8.00
9.00

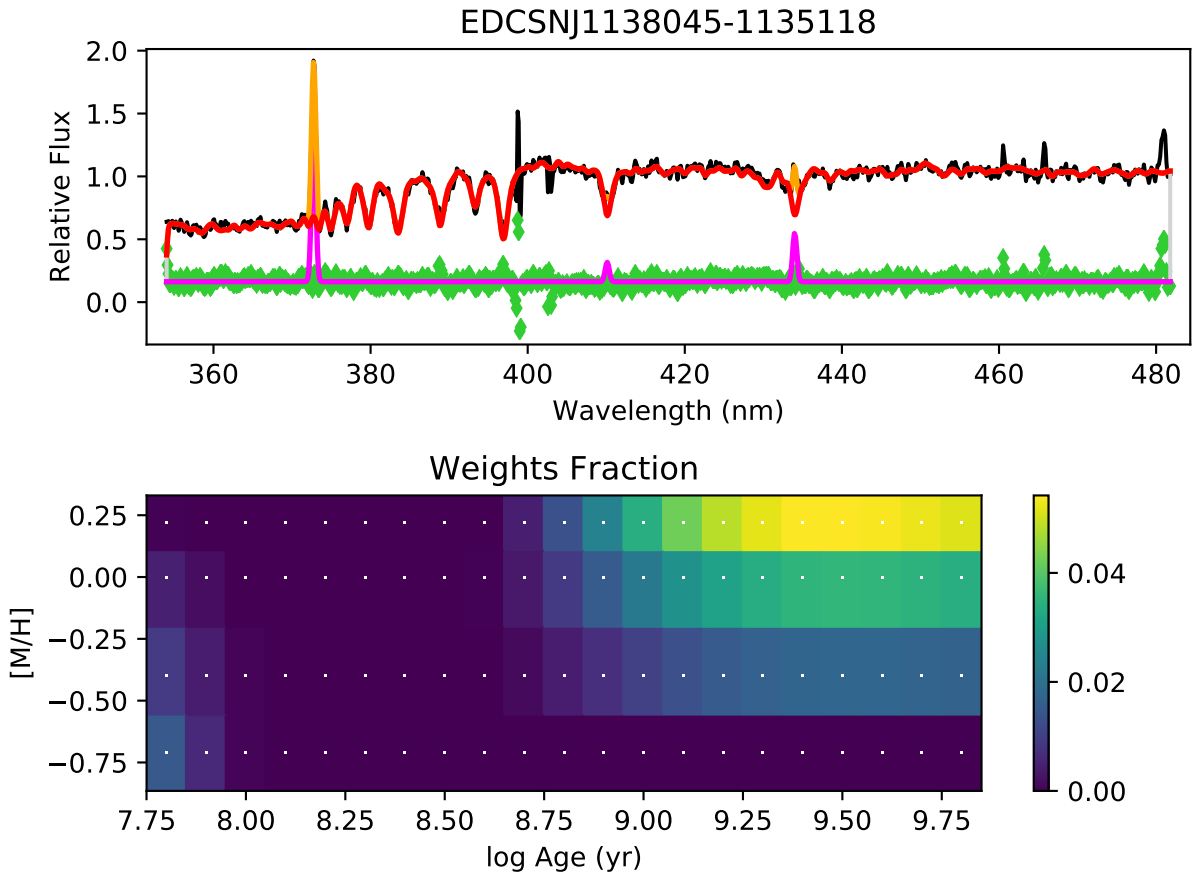
EDCSNJ1138045-1135118
Relative Flux
2.0
1.5
1.0
0.5
0.0
360
380
400
420
440
460
480
Wavelength (nm)
Weights Fraction
[M/H]
0.25
0.00
−0.25
−0.50
−0.75
7.75
8.00
8.25
8.50
8.75
9.00
9.25
9.50
9.75
log Age (yr)
0.04
0.02
0.00

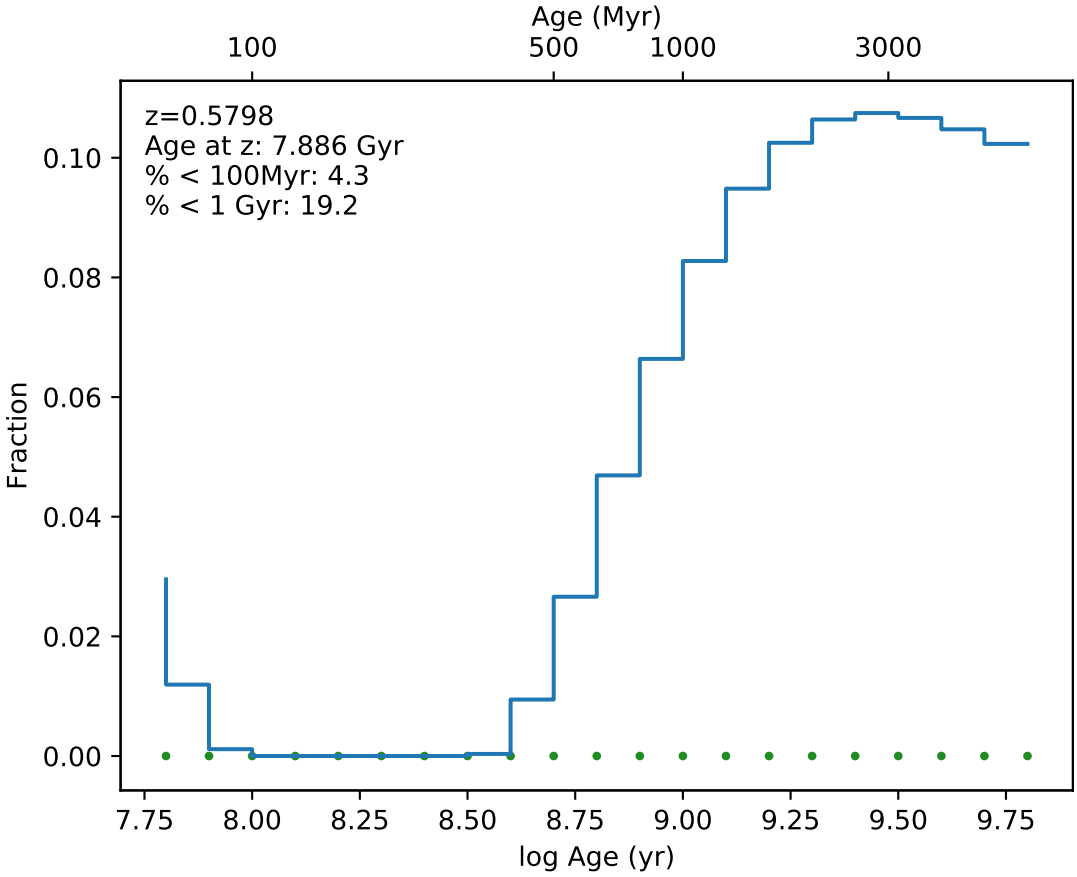
Age (Myr)
100
500
1000
3000
z=0.5798
Age at z: 7.886 Gyr
% < 100Myr: 4.3
% < 1 Gyr: 19.2
Fraction
0.10
0.08
0.06
0.04
0.02
0.00
7.75
8.00
8.25
8.50
8.75
9.00
9.25
9.50
9.75
log Age (yr)

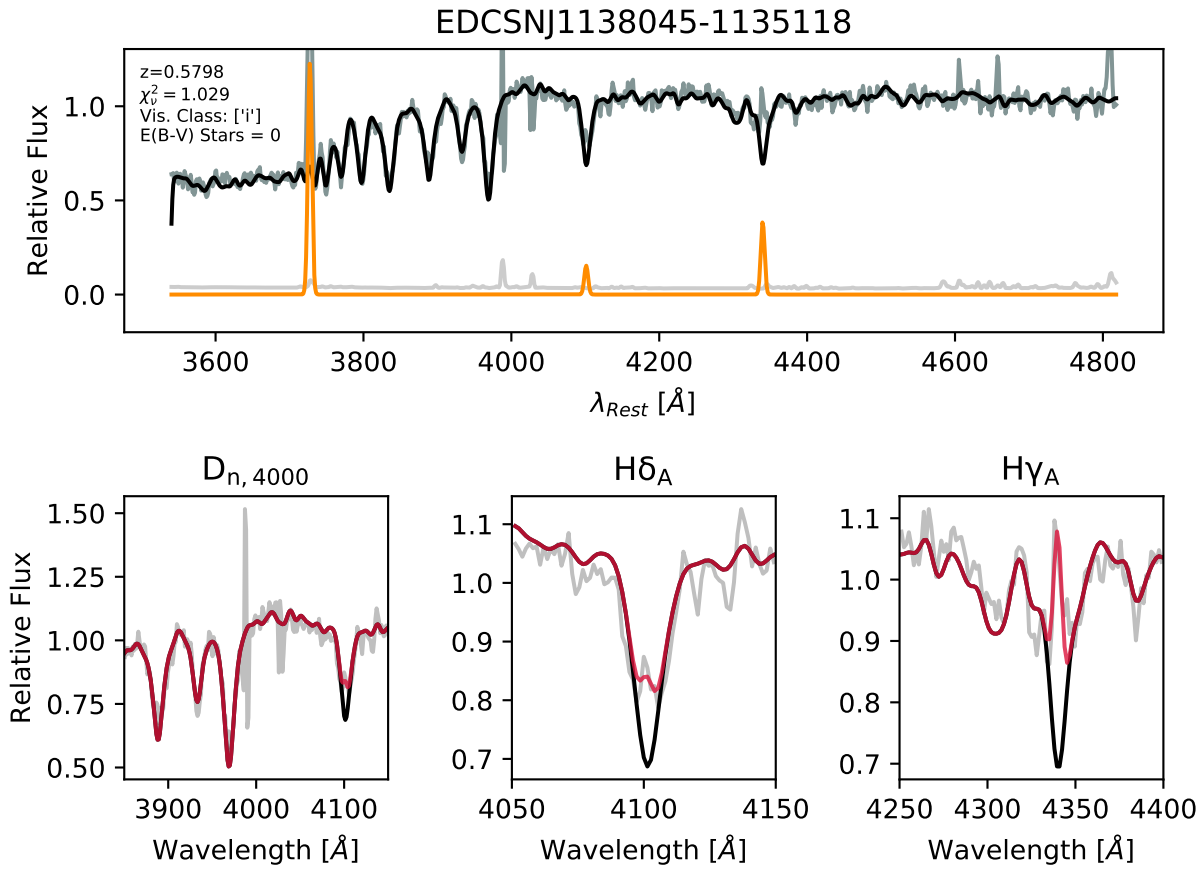
EDCSNJ1138045-1135118
z=0.5798
$\chi^2_\nu = 1.029$
Vis. Class: ['i']
E(B-V) Stars = 0
Relative Flux
1.0
0.5
0.0
3600
3800
4000
4200
4400
4600
4800
λ_{Rest} [Å]
$D_{n,4000}$
$H\delta_A$
$H\gamma_A$
Relative Flux
1.50
1.25
1.00
0.75
0.50
3900
4000
4100
Wavelength [Å]
1.1
1.0
0.9
0.8
0.7
4050
4100
4150
Wavelength [Å]
1.1
1.0
0.9
0.8
0.7
4250
4300
4350
4400
Wavelength [Å]

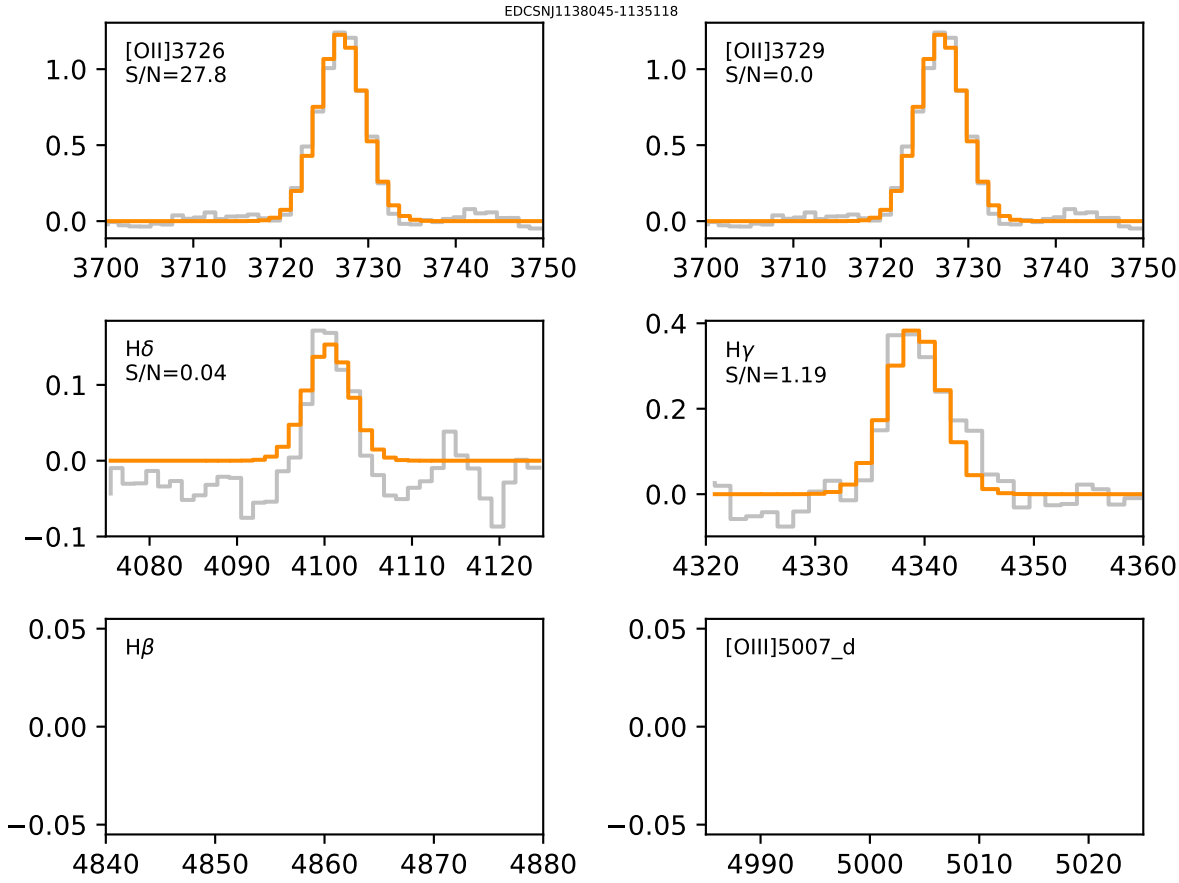
EDCSNJ1138045-1135118
[OII]3726
S/N=27.8
[OII]3729
S/N=0.0
Hδ
S/N=0.04
Hγ
S/N=1.19
Hβ
[OIII]5007_d

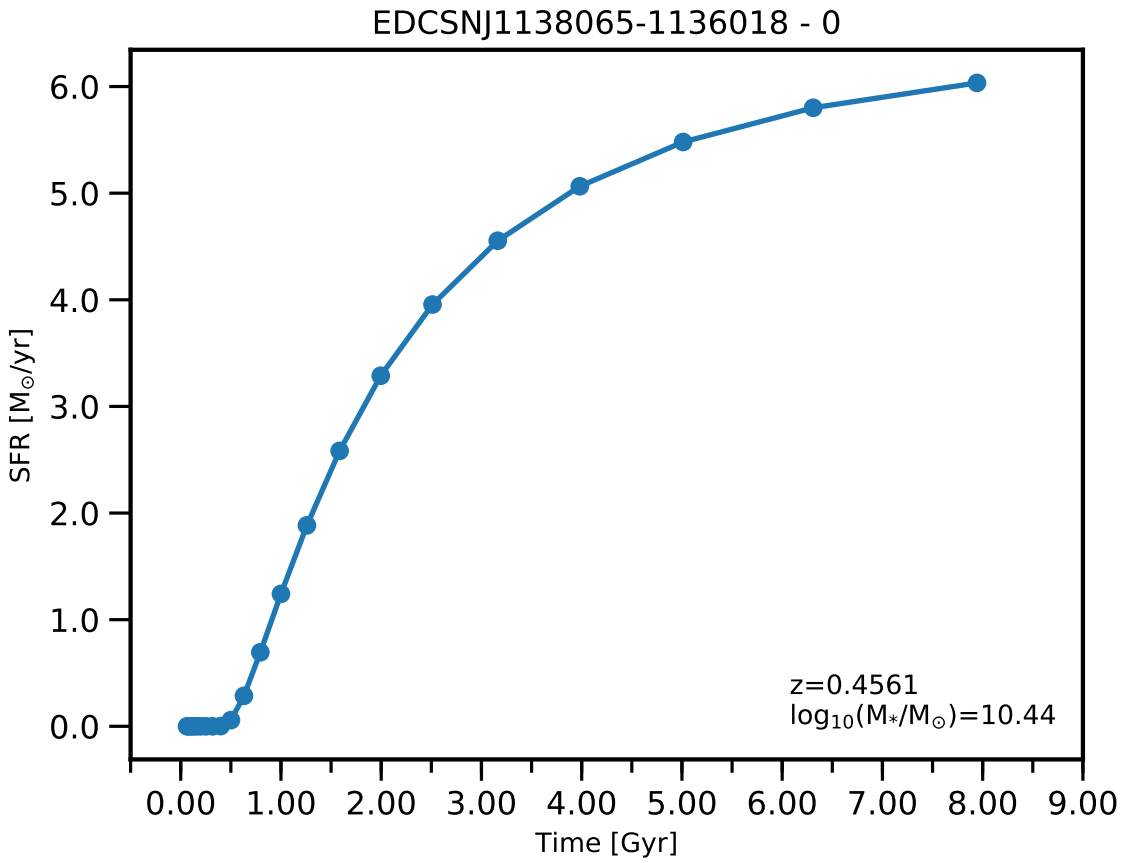
EDCSNJ1138065-1136018 - 0
SFR [M⊙/yr]
Time [Gyr]
z=0.4561
log10(M*/M⊙)=10.44
0.0
1.0
2.0
3.0
4.0
5.0
6.0
0.00
1.00
2.00
3.00
4.00
5.00
6.00
7.00
8.00
9.00

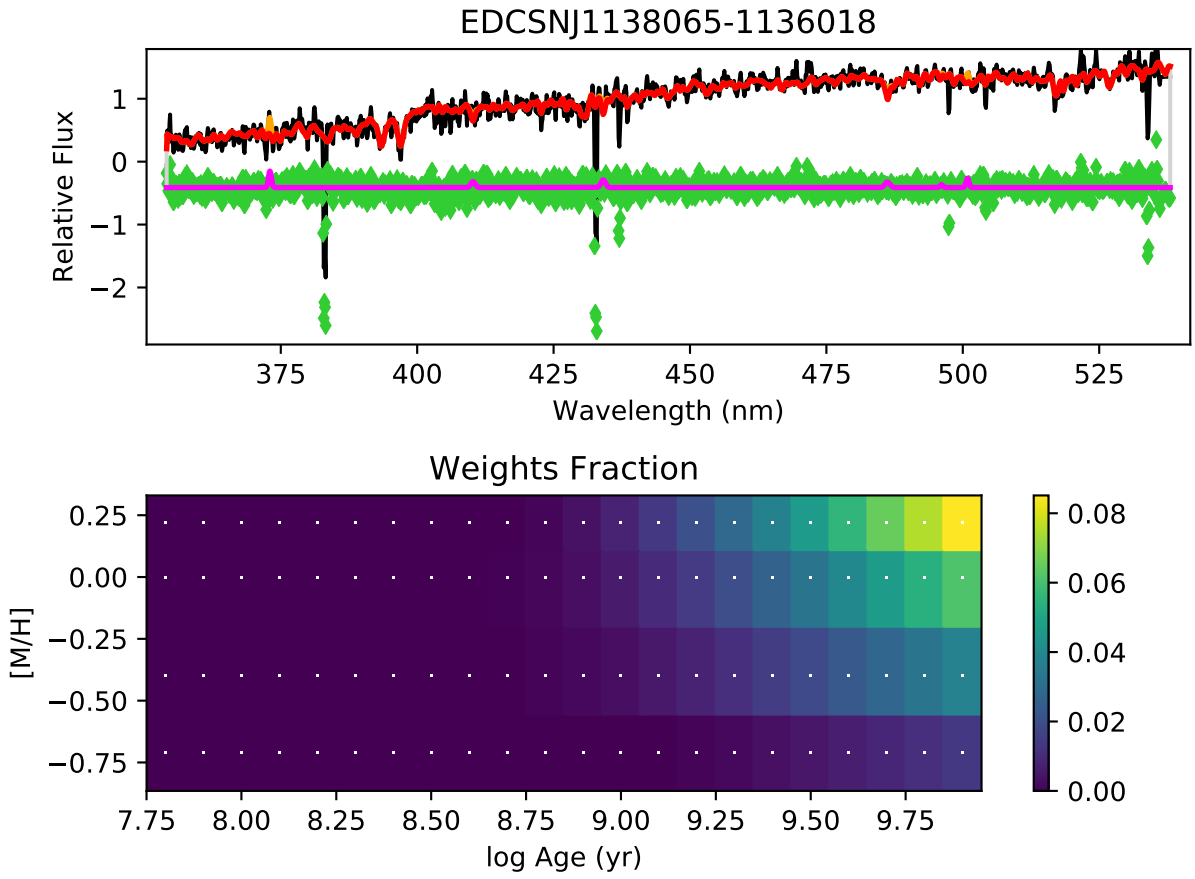
EDCSNJ1138065-1136018
Relative Flux
1
0
−1
−2
375
400
425
450
475
500
525
Wavelength (nm)
Weights Fraction
[M/H]
0.25
0.00
−0.25
−0.50
−0.75
7.75
8.00
8.25
8.50
8.75
9.00
9.25
9.50
9.75
log Age (yr)
0.08
0.06
0.04
0.02
0.00

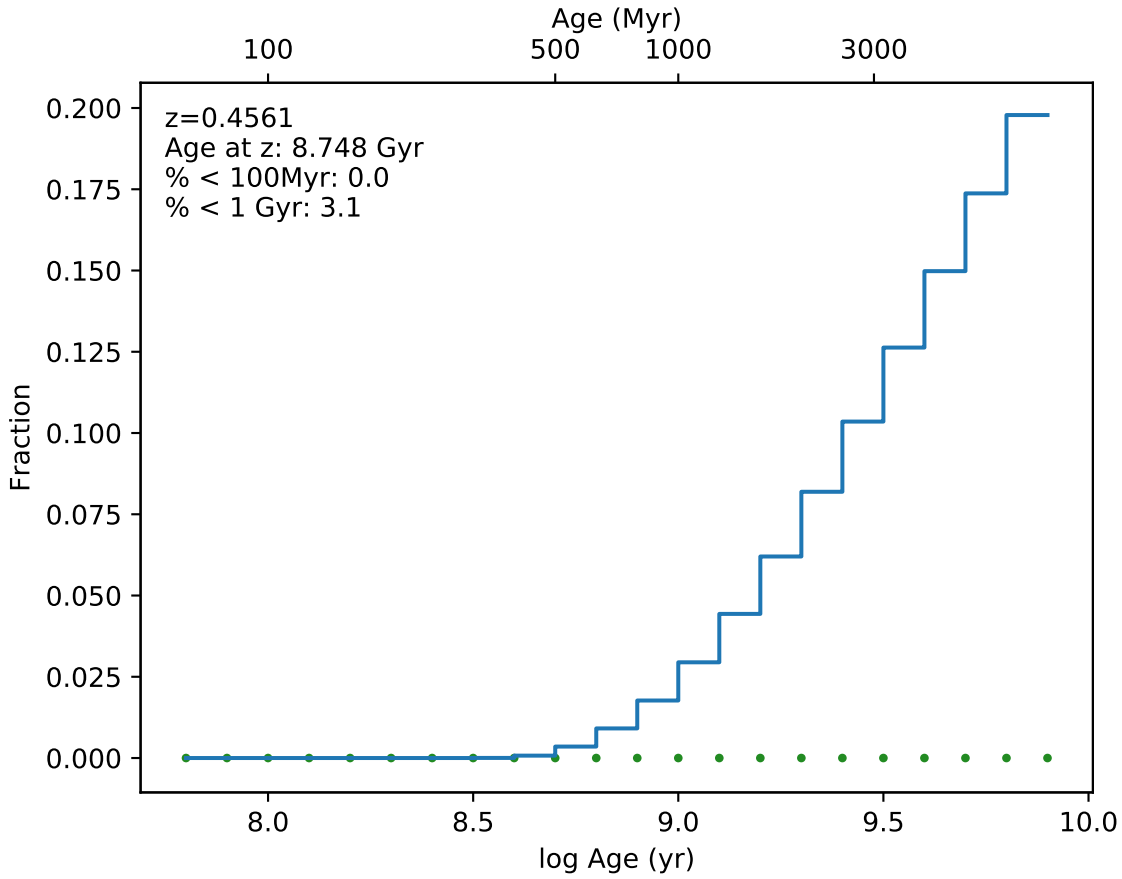
Age (Myr)
100
500
1000
3000
z=0.4561
Age at z: 8.748 Gyr
% < 100Myr: 0.0
% < 1 Gyr: 3.1
Fraction
0.200
0.175
0.150
0.125
0.100
0.075
0.050
0.025
0.000
8.0
8.5
9.0
9.5
10.0
log Age (yr)

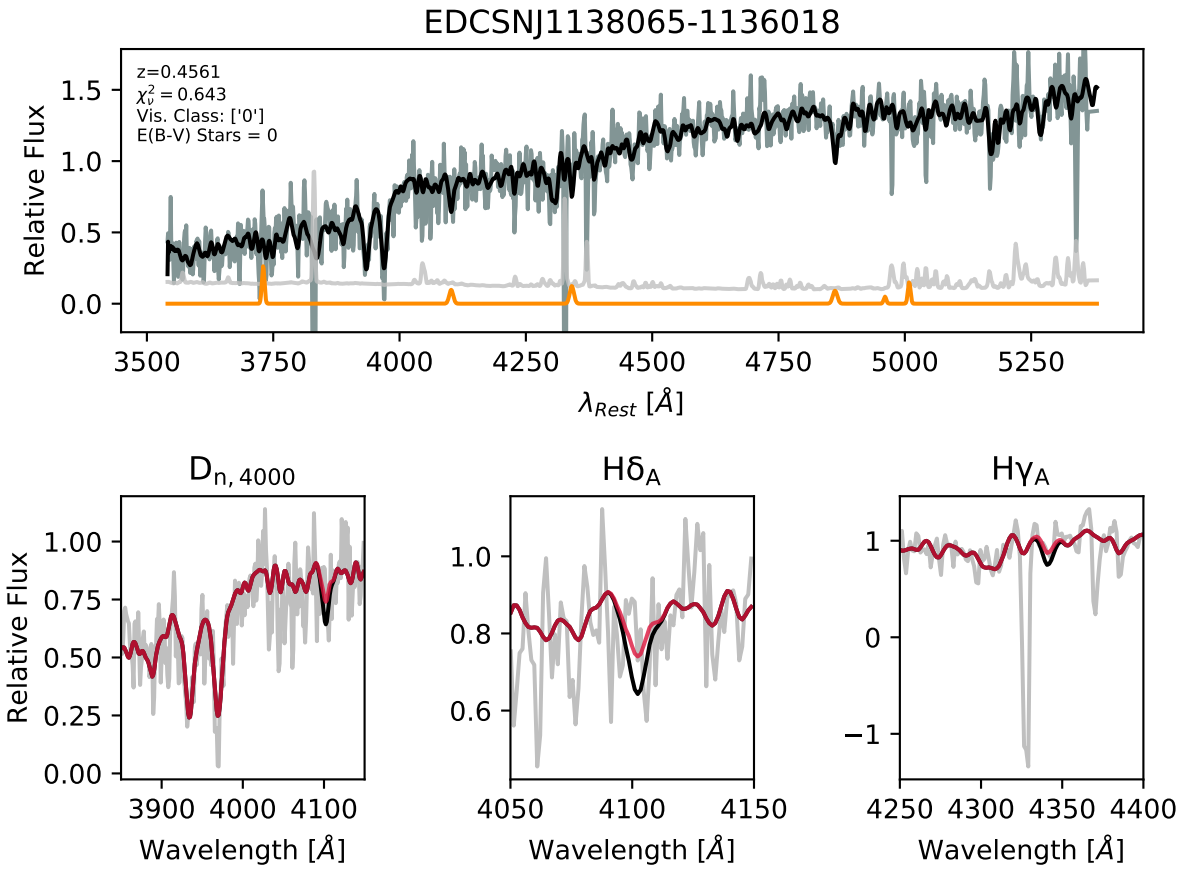
EDCSNJ1138065-1136018
z=0.4561
$\chi^2_\nu = 0.643$
Vis. Class: ['0']
E(B-V) Stars = 0
Relative Flux
λ_{Rest} [Å]
$D_{n,4000}$
$H\delta_A$
$H\gamma_A$
Wavelength [Å]

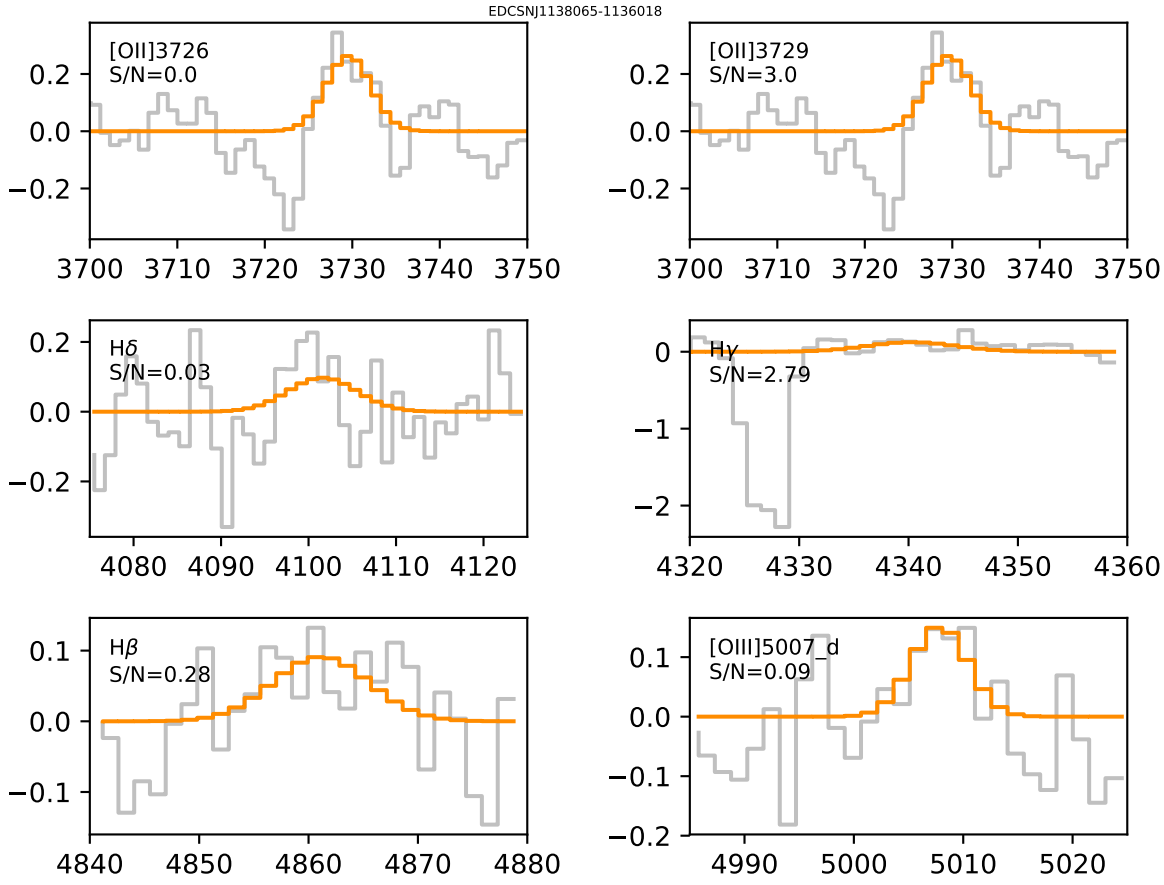
EDCSNJ1138065-1136018
[OII]3726
S/N=0.0
[OII]3729
S/N=3.0
Hδ
S/N=0.03
Hγ
S/N=2.79
Hβ
S/N=0.28
[OIII]5007_d
S/N=0.09

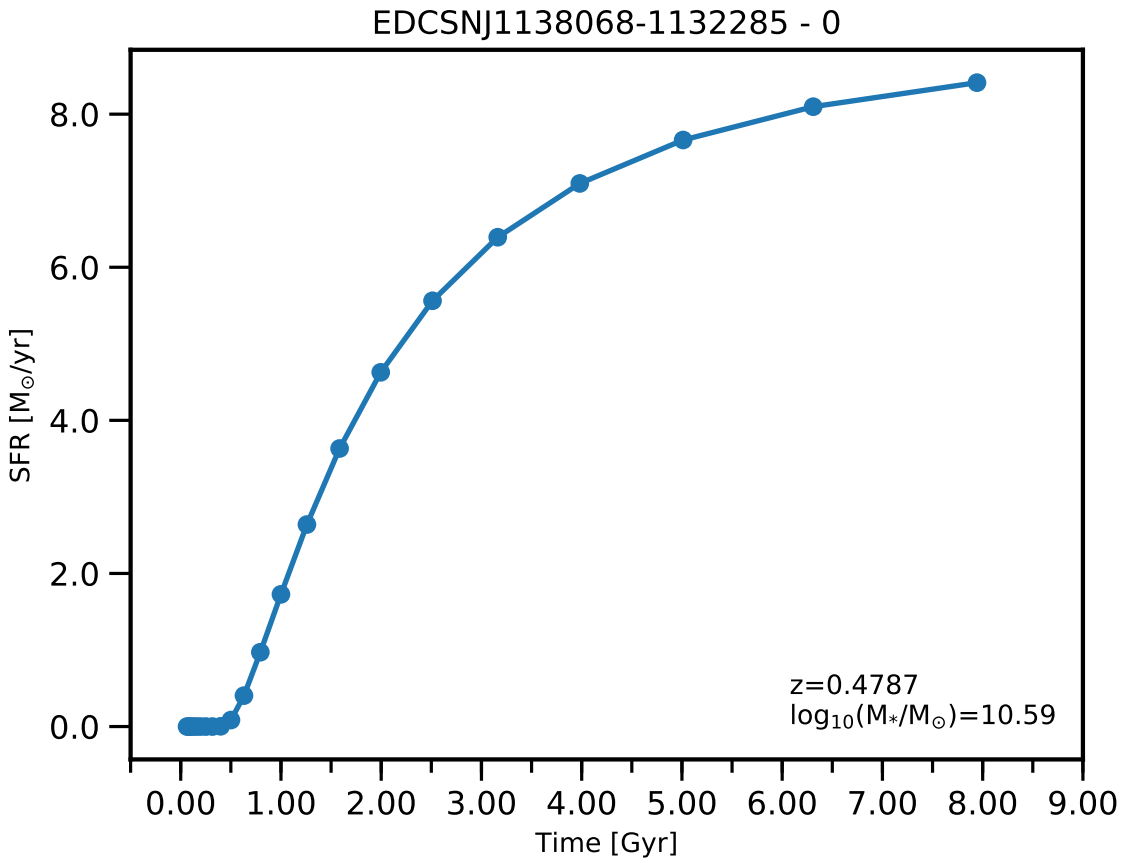
EDCSNJ1138068-1132285 - 0
SFR [M⊙/yr]
8.0
6.0
4.0
2.0
0.0
0.00
1.00
2.00
3.00
4.00
5.00
6.00
7.00
8.00
9.00
Time [Gyr]
z=0.4787
log10(M*/M⊙)=10.59

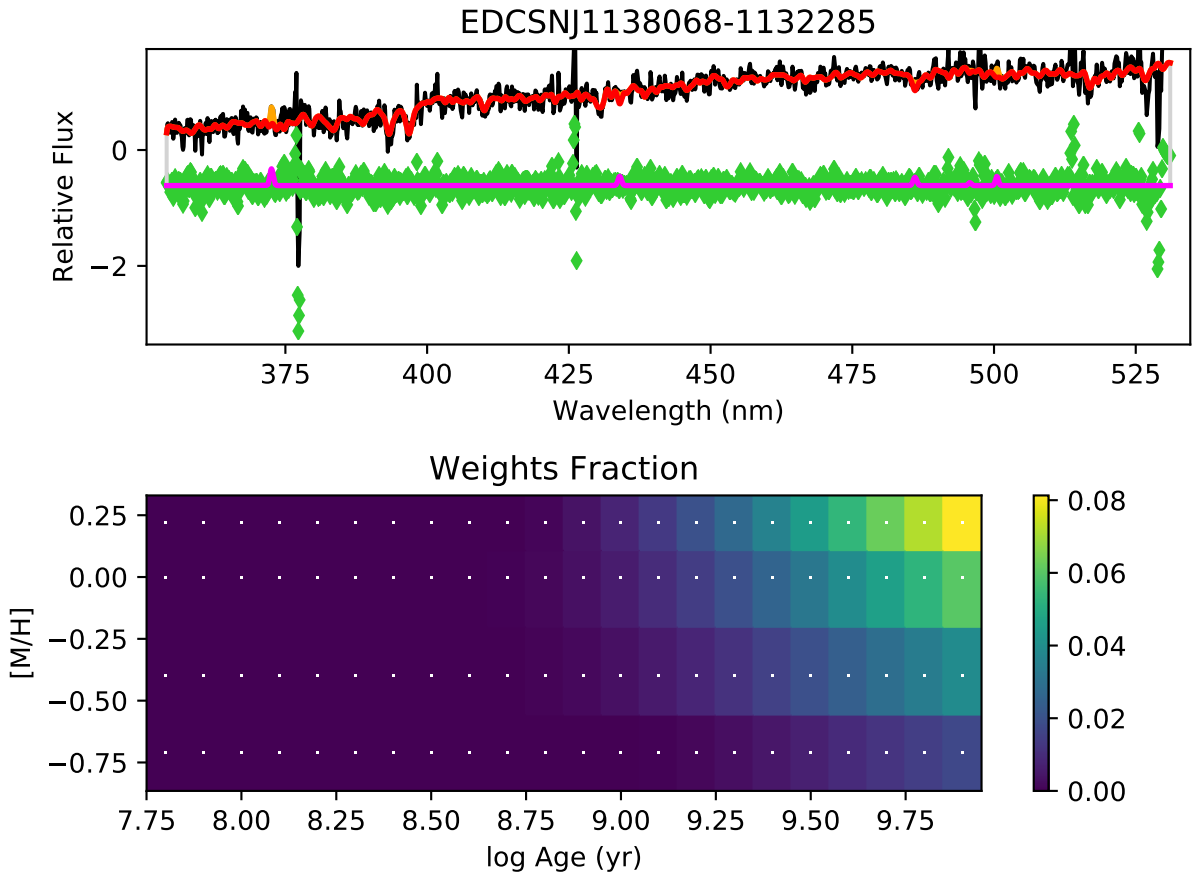
EDCSNJ1138068-1132285
Relative Flux
0
−2
375
400
425
450
475
500
525
Wavelength (nm)
Weights Fraction
[M/H]
0.25
0.00
−0.25
−0.50
−0.75
7.75
8.00
8.25
8.50
8.75
9.00
9.25
9.50
9.75
log Age (yr)
0.08
0.06
0.04
0.02
0.00

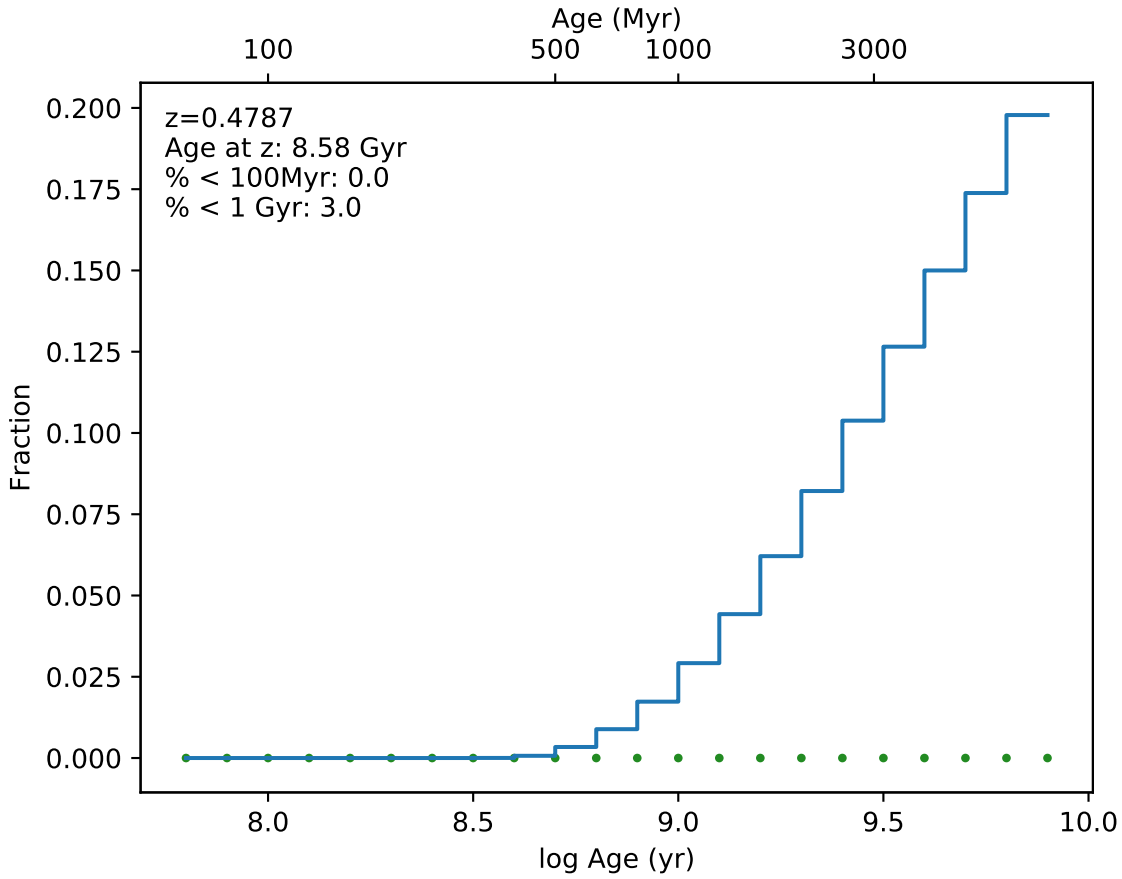
Age (Myr)
100
500
1000
3000
z=0.4787
Age at z: 8.58 Gyr
% < 100Myr: 0.0
% < 1 Gyr: 3.0
Fraction
0.200
0.175
0.150
0.125
0.100
0.075
0.050
0.025
0.000
8.0
8.5
9.0
9.5
10.0
log Age (yr)

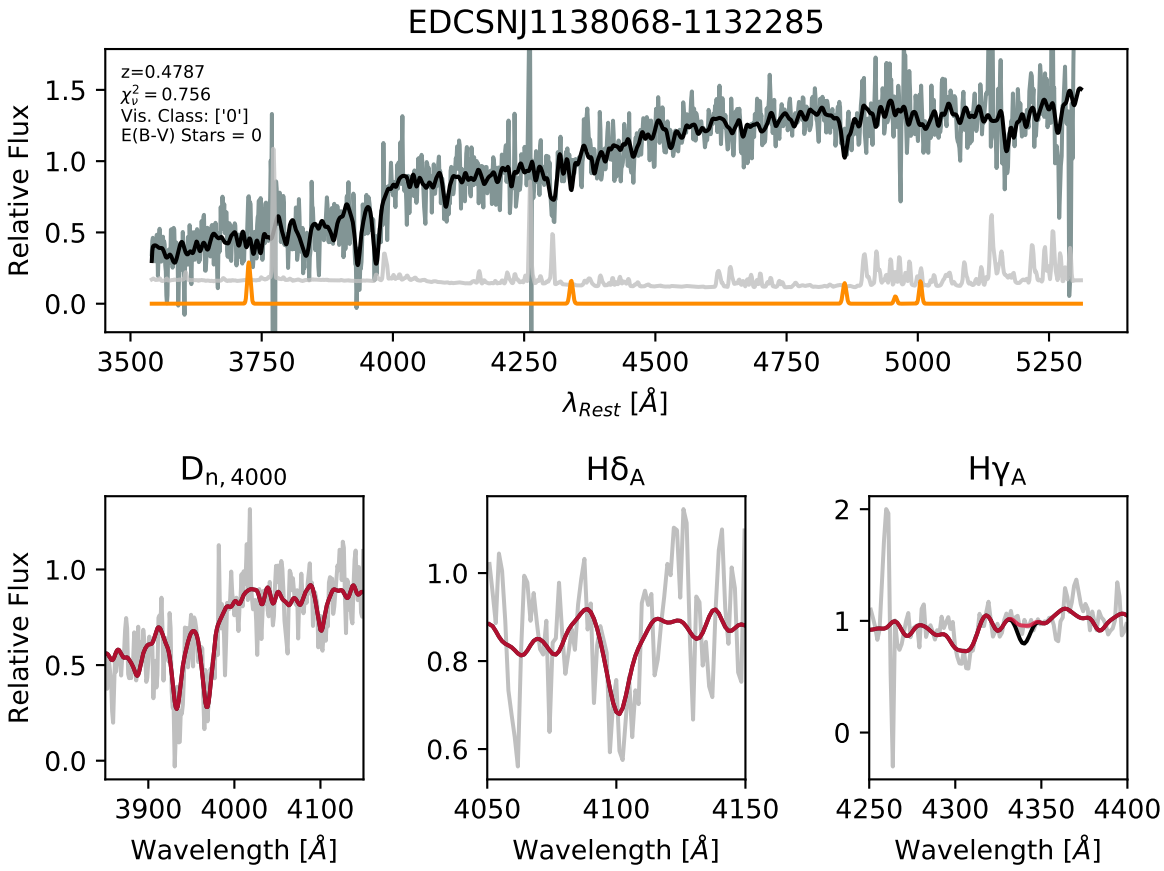
EDCSNJ1138068-1132285
z=0.4787
$\chi^2_\nu = 0.756$
Vis. Class: ['0']
E(B-V) Stars = 0
Relative Flux
λ_{Rest} [Å]
$D_{n,4000}$
$H\delta_A$
$H\gamma_A$
Wavelength [Å]

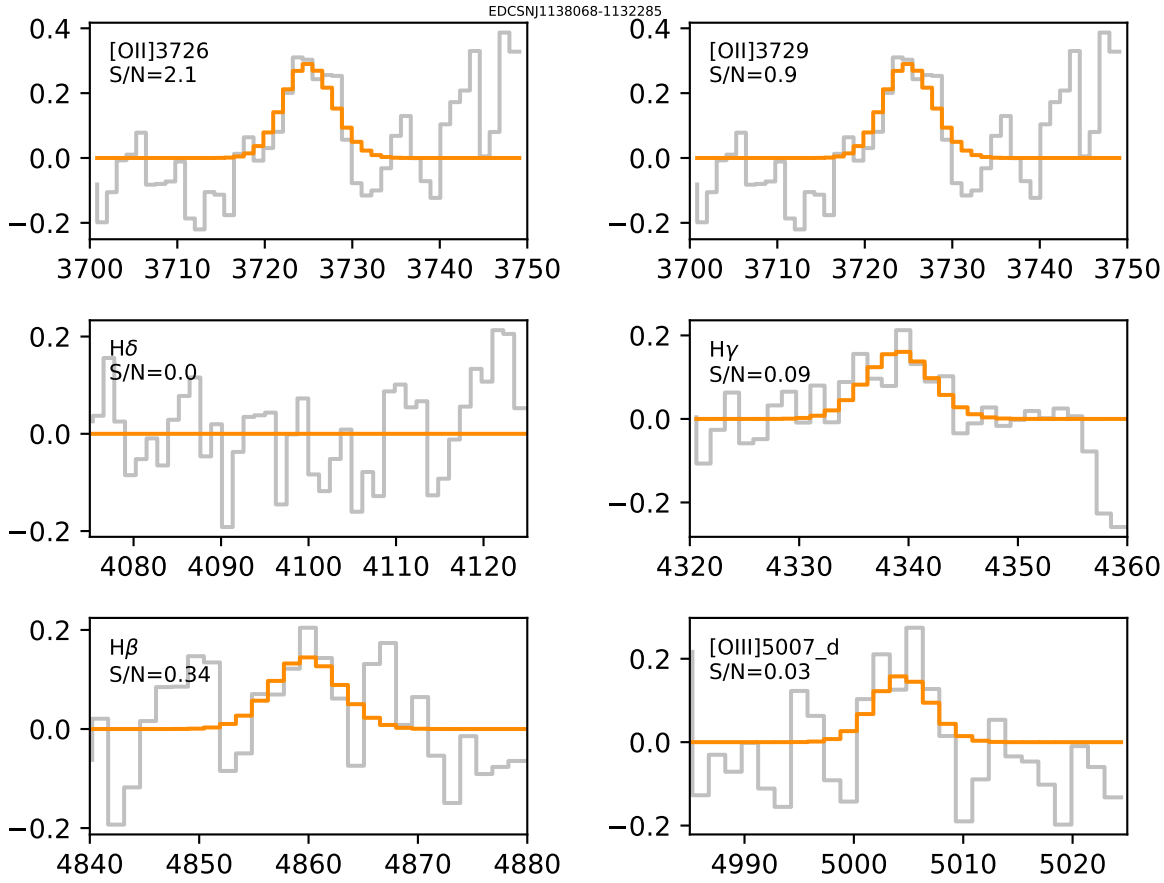
EDCSNJ1138068-1132285
[OII]3726
S/N=2.1
[OII]3729
S/N=0.9
Hδ
S/N=0.0
Hγ
S/N=0.09
Hβ
S/N=0.34
[OIII]5007_d
S/N=0.03

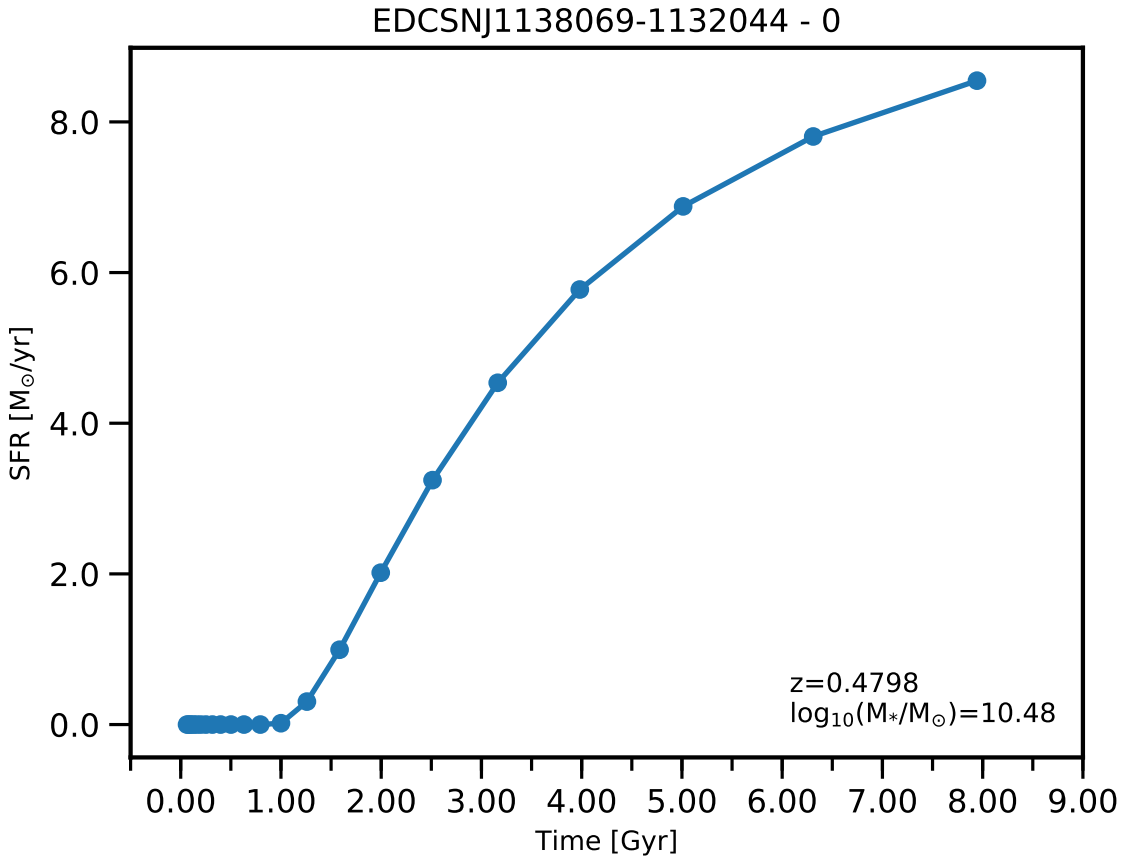
EDCSNJ1138069-1132044 - 0
SFR [M⊙/yr]
Time [Gyr]
z=0.4798
log10(M*/M⊙)=10.48
0.0
2.0
4.0
6.0
8.0
0.00
1.00
2.00
3.00
4.00
5.00
6.00
7.00
8.00
9.00

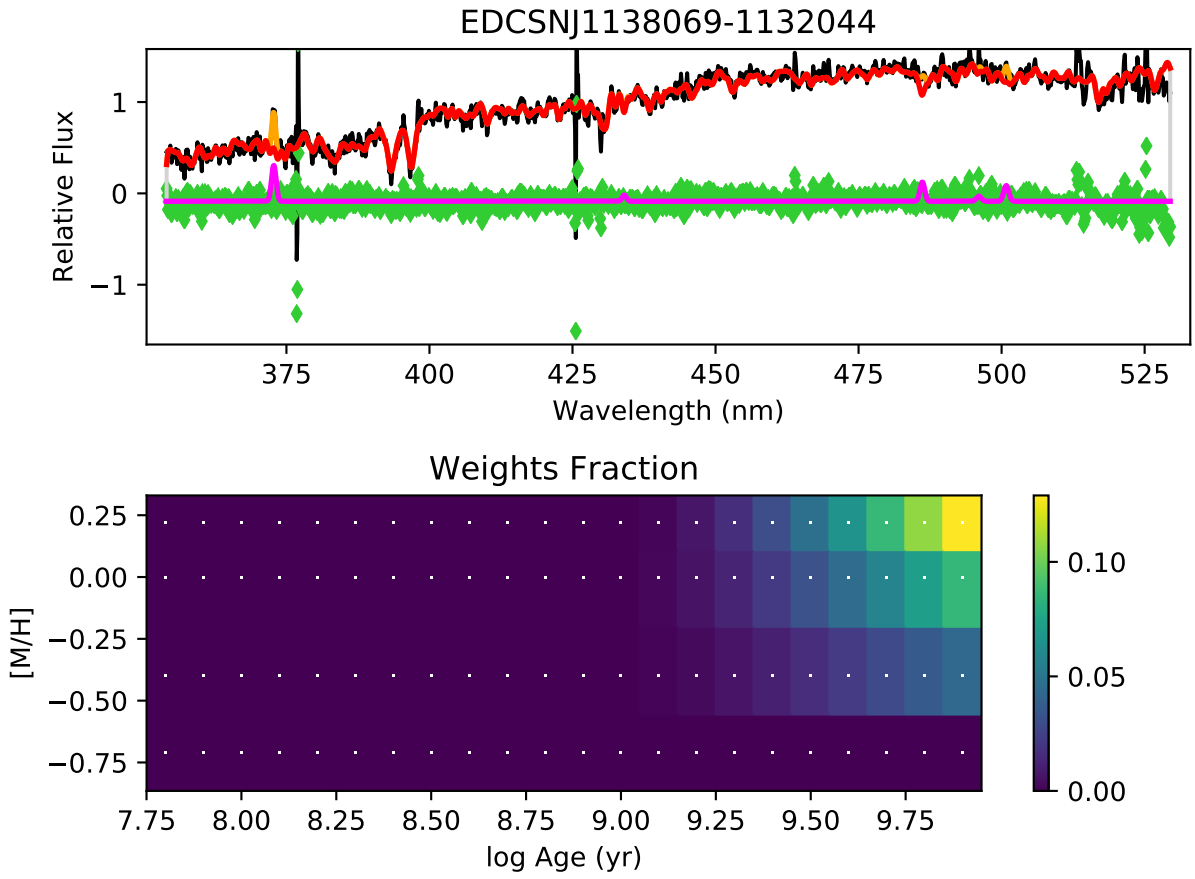
EDCSNJ1138069-1132044
Relative Flux
1
0
−1
375
400
425
450
475
500
525
Wavelength (nm)
Weights Fraction
[M/H]
0.25
0.00
−0.25
−0.50
−0.75
7.75
8.00
8.25
8.50
8.75
9.00
9.25
9.50
9.75
log Age (yr)
0.10
0.05
0.00

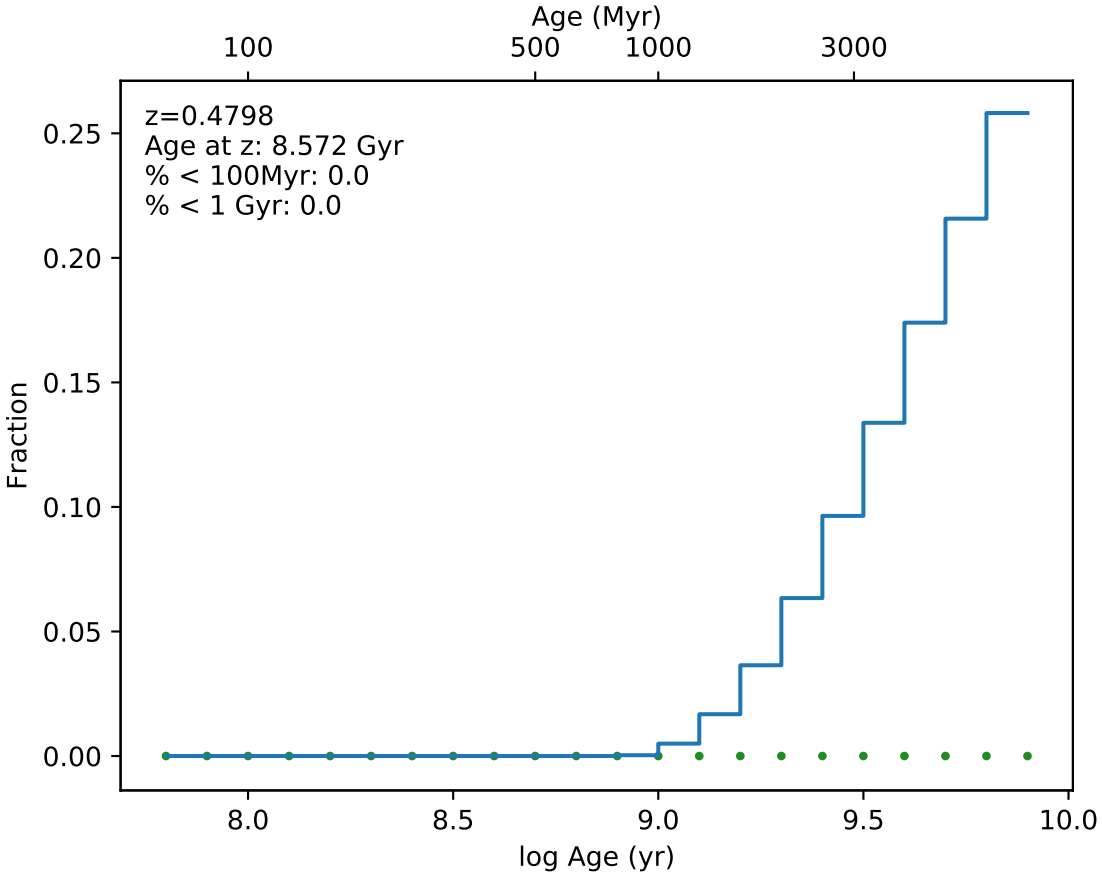
Age (Myr)
100
500
1000
3000
z=0.4798
Age at z: 8.572 Gyr
% < 100Myr: 0.0
% < 1 Gyr: 0.0
Fraction
0.25
0.20
0.15
0.10
0.05
0.00
8.0
8.5
9.0
9.5
10.0
log Age (yr)

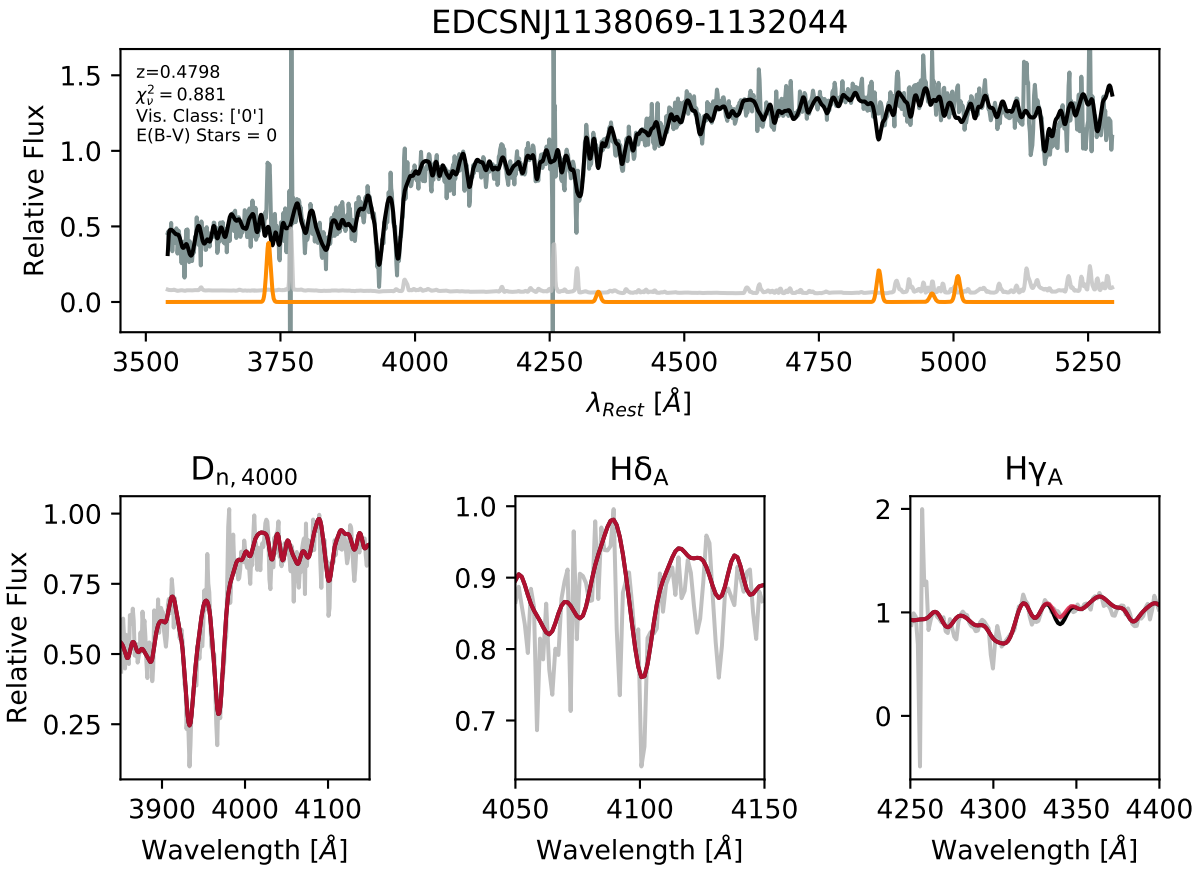
EDCSNJ1138069-1132044
z=0.4798
$\chi^2_\nu = 0.881$
Vis. Class: ['0']
E(B-V) Stars = 0
Relative Flux
λ_{Rest} [Å]
$D_{n,4000}$
$H\delta_A$
$H\gamma_A$
Wavelength [Å]

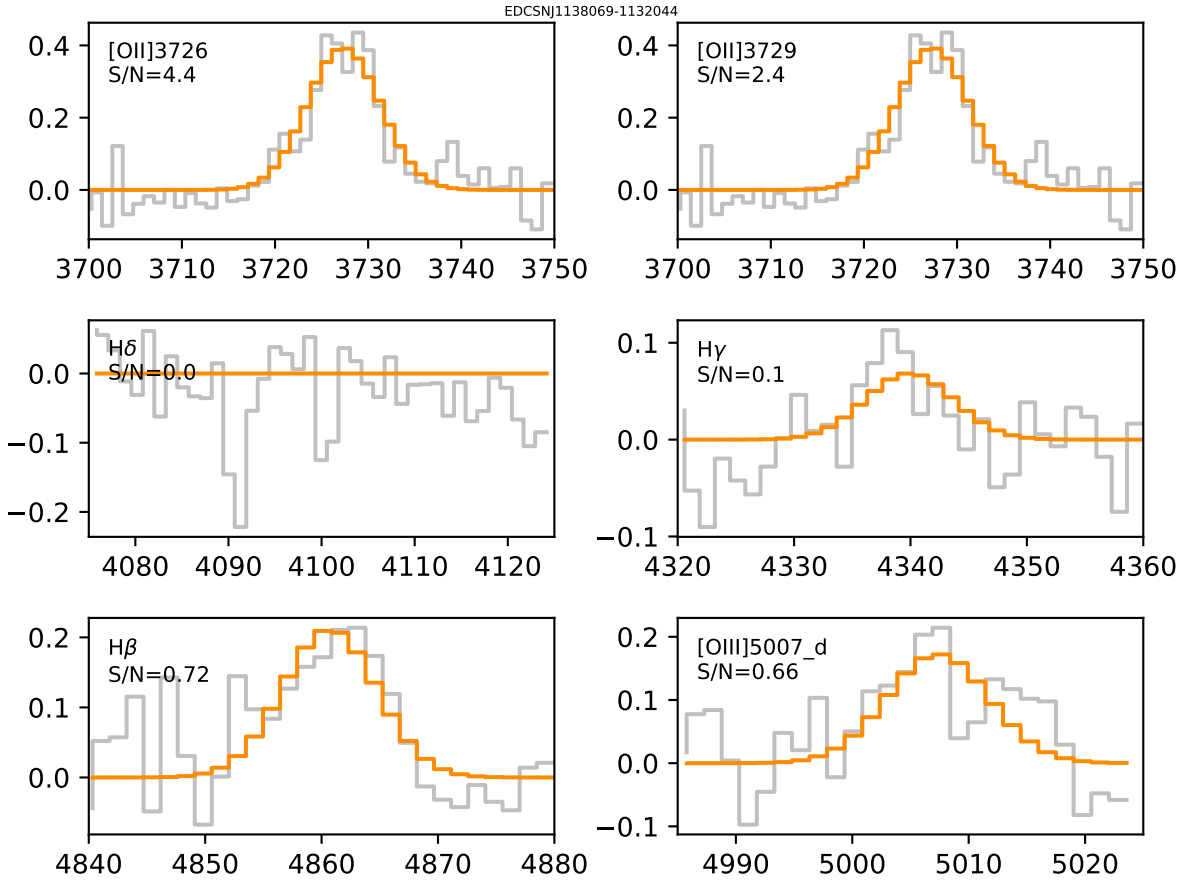
EDCSNJ1138069-1132044
[OII]3726
S/N=4.4
[OII]3729
S/N=2.4
Hδ
S/N=0.0
Hγ
S/N=0.1
Hβ
S/N=0.72
[OIII]5007_d
S/N=0.66

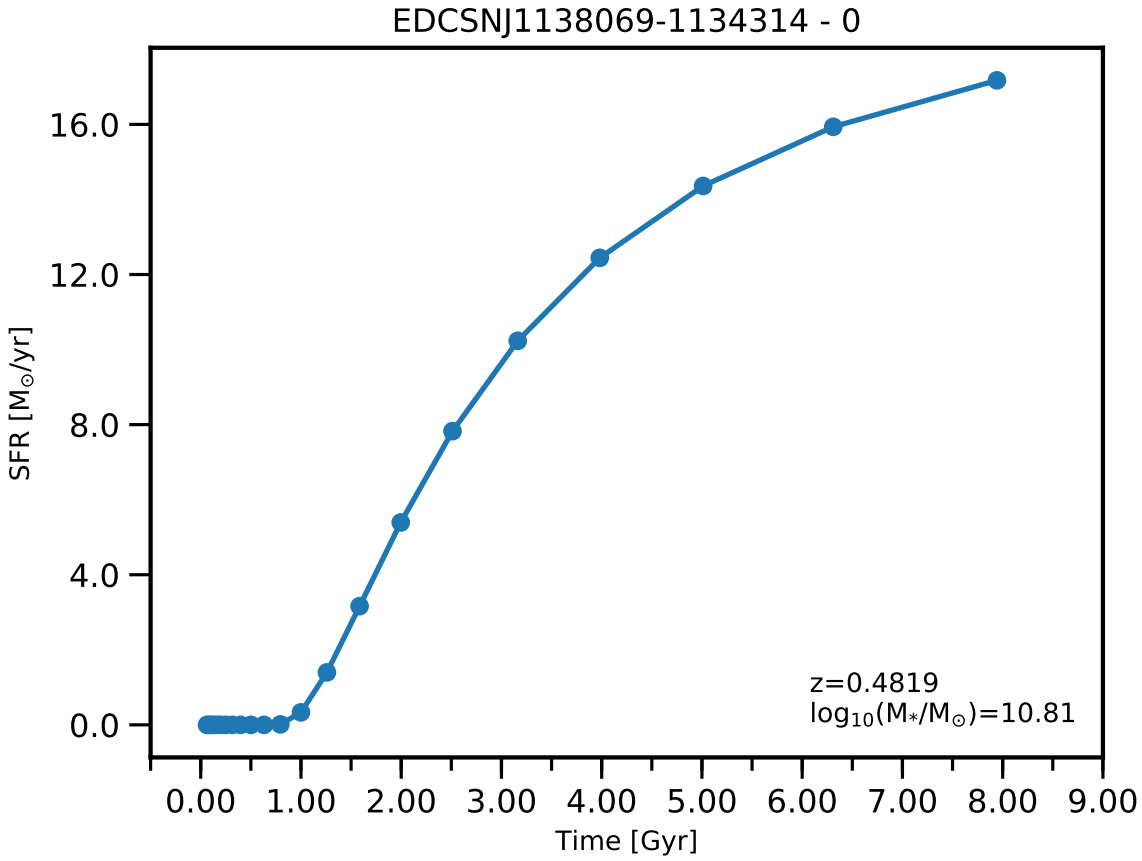
EDCSNJ1138069-1134314 - 0
SFR [M⊙/yr]
16.0
12.0
8.0
4.0
0.0
0.00
1.00
2.00
3.00
4.00
5.00
6.00
7.00
8.00
9.00
Time [Gyr]
z=0.4819
log10(M*/M⊙)=10.81

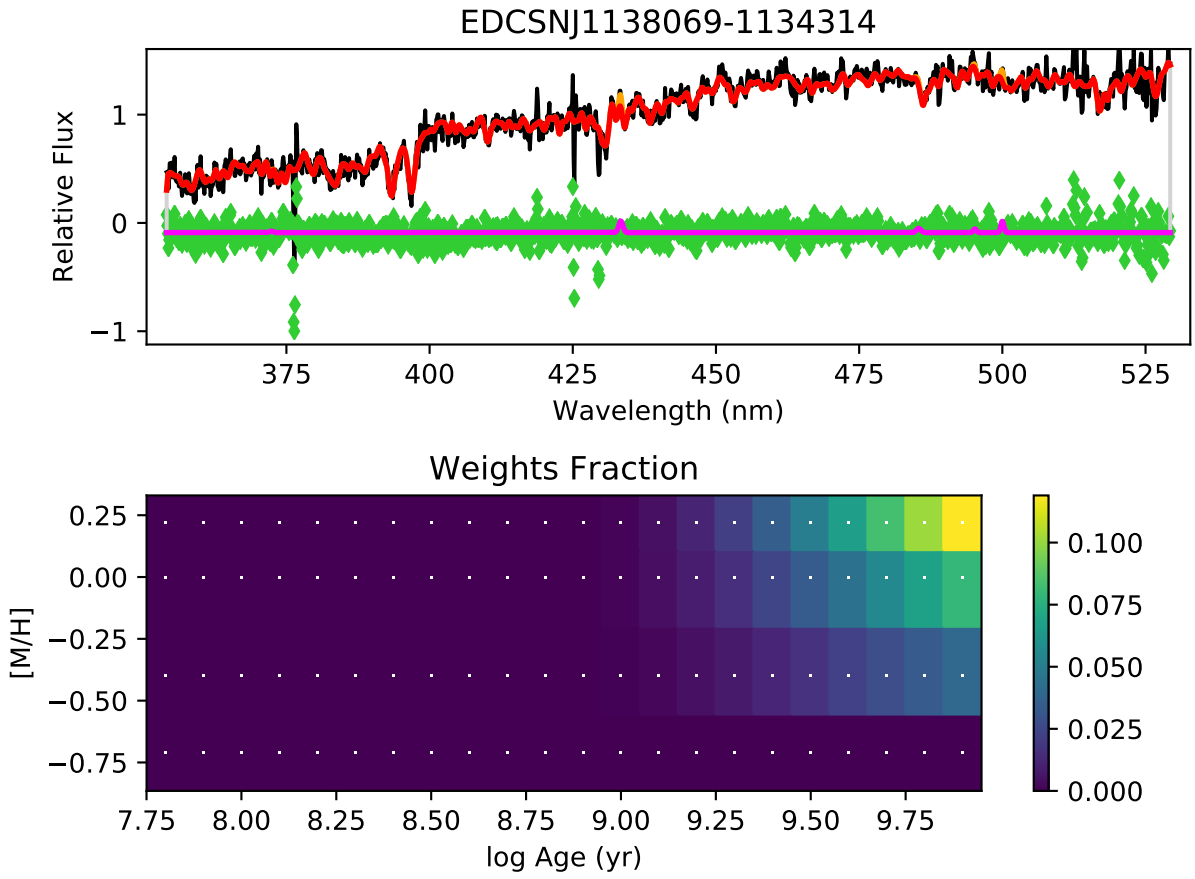
EDCSNJ1138069-1134314
Relative Flux
1
0
−1
375
400
425
450
475
500
525
Wavelength (nm)
Weights Fraction
[M/H]
0.25
0.00
−0.25
−0.50
−0.75
7.75
8.00
8.25
8.50
8.75
9.00
9.25
9.50
9.75
log Age (yr)
0.100
0.075
0.050
0.025
0.000

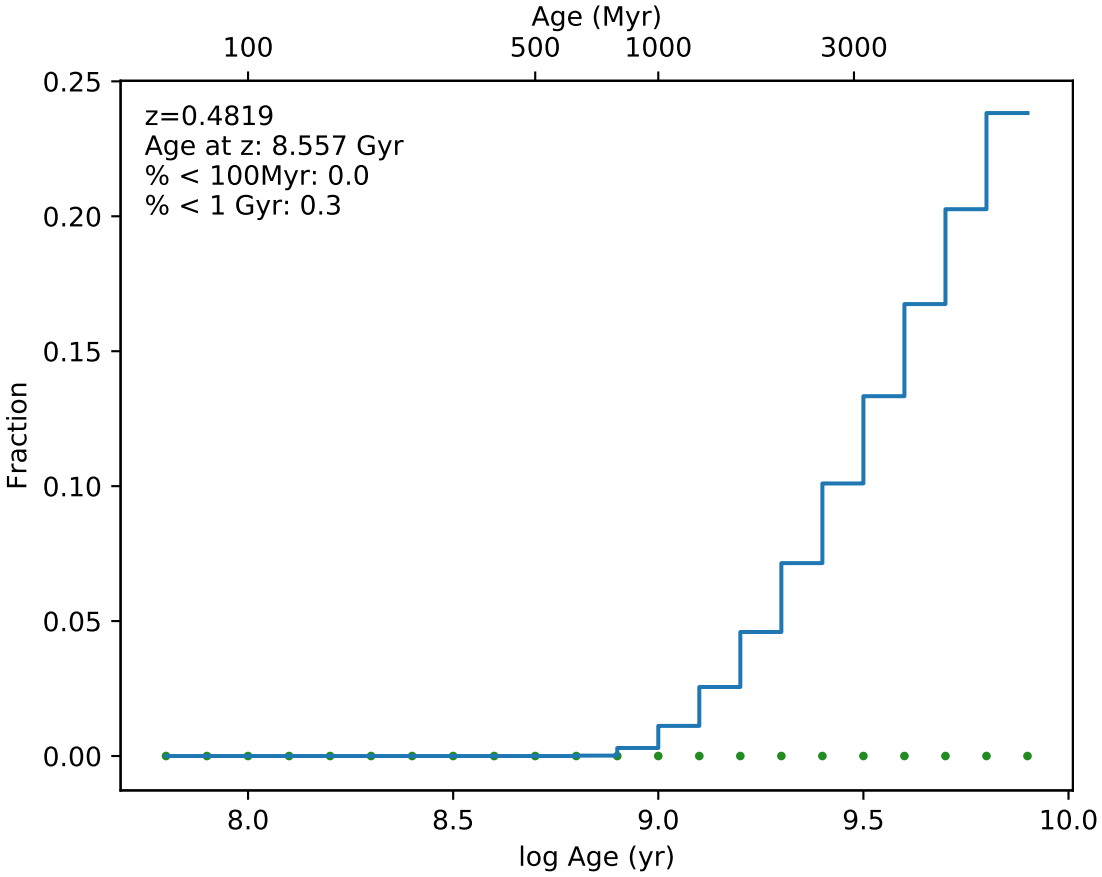
Age (Myr)
100
500
1000
3000
z=0.4819
Age at z: 8.557 Gyr
% < 100Myr: 0.0
% < 1 Gyr: 0.3
Fraction
0.25
0.20
0.15
0.10
0.05
0.00
8.0
8.5
9.0
9.5
10.0
log Age (yr)

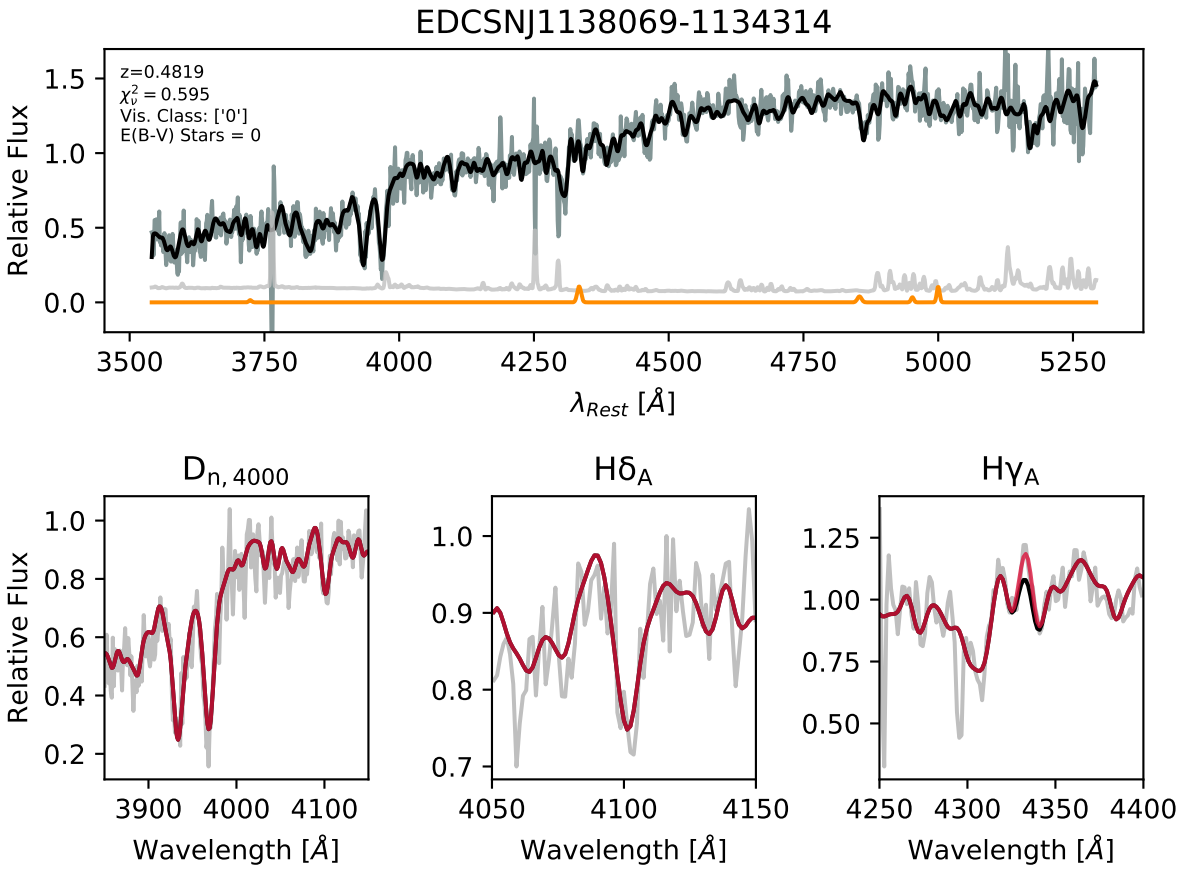
EDCSNJ1138069-1134314
z=0.4819
$\chi^2_\nu = 0.595$
Vis. Class: ['0']
E(B-V) Stars = 0
Relative Flux
λ_{Rest} [Å]
$D_{n,4000}$
$H\delta_A$
$H\gamma_A$
Wavelength [Å]

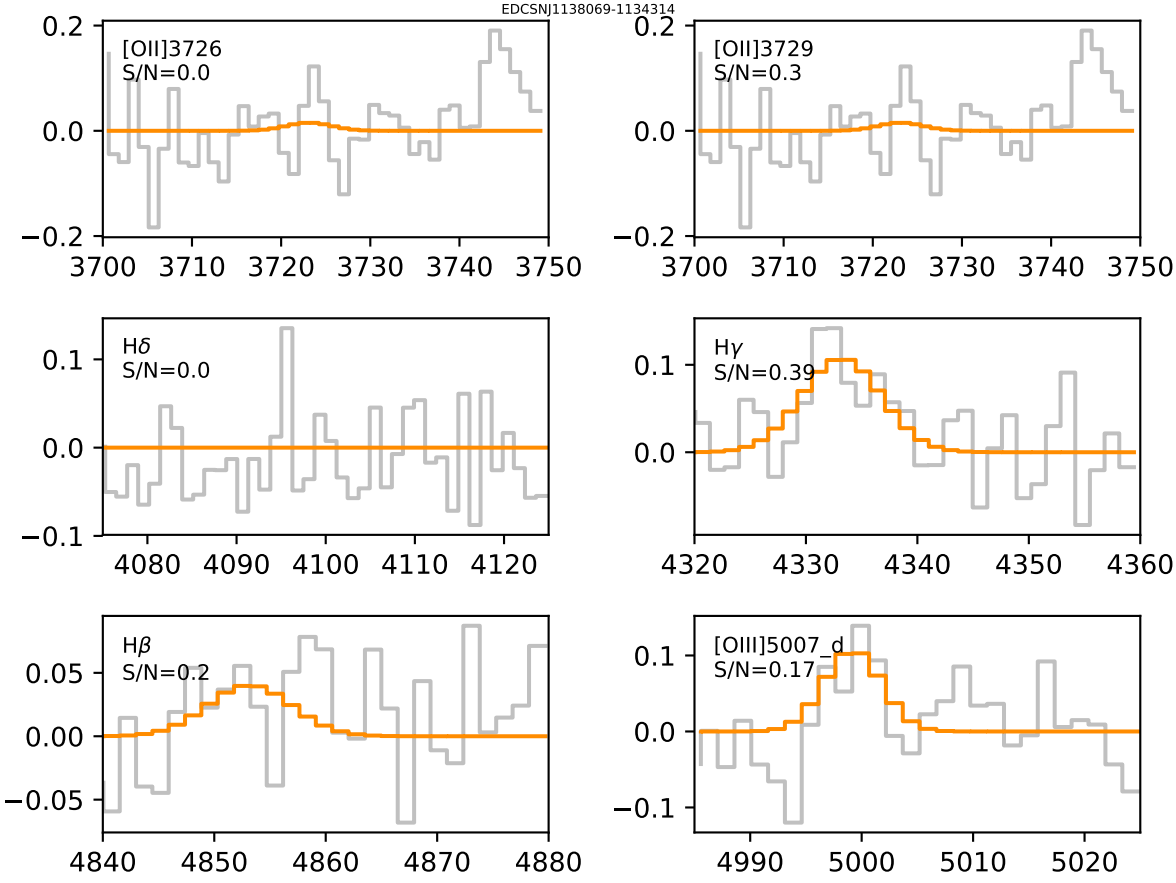
EDCSNJ1138069-1134314
[OII]3726
S/N=0.0
[OII]3729
S/N=0.3
Hδ
S/N=0.0
Hγ
S/N=0.39
Hβ
S/N=0.2
[OIII]5007_d
S/N=0.17

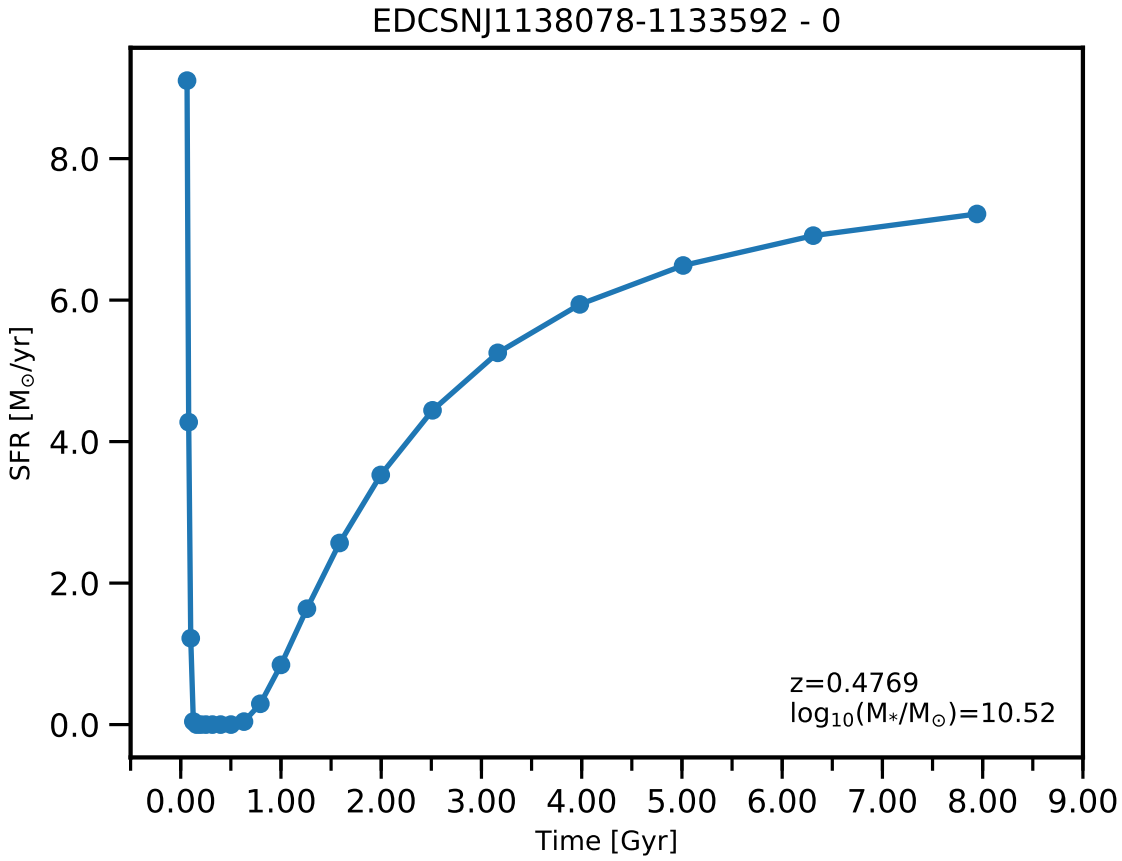
EDCSNJ1138078-1133592 - 0
SFR [M⊙/yr]
8.0
6.0
4.0
2.0
0.0
0.00
1.00
2.00
3.00
4.00
5.00
6.00
7.00
8.00
9.00
Time [Gyr]
z=0.4769
log10(M*/M⊙)=10.52

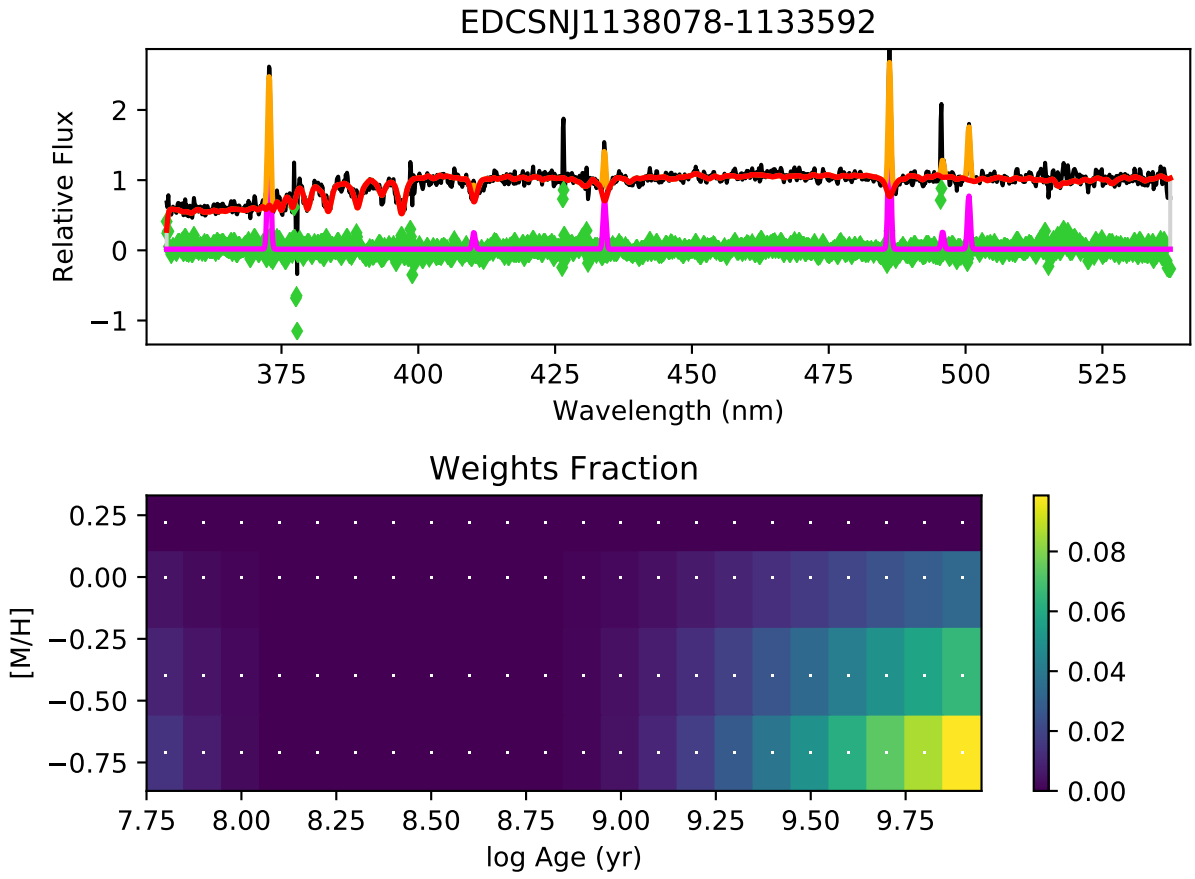
EDCSNJ1138078-1133592
Relative Flux
2
1
0
−1
375
400
425
450
475
500
525
Wavelength (nm)
Weights Fraction
[M/H]
0.25
0.00
−0.25
−0.50
−0.75
7.75
8.00
8.25
8.50
8.75
9.00
9.25
9.50
9.75
log Age (yr)
0.08
0.06
0.04
0.02
0.00

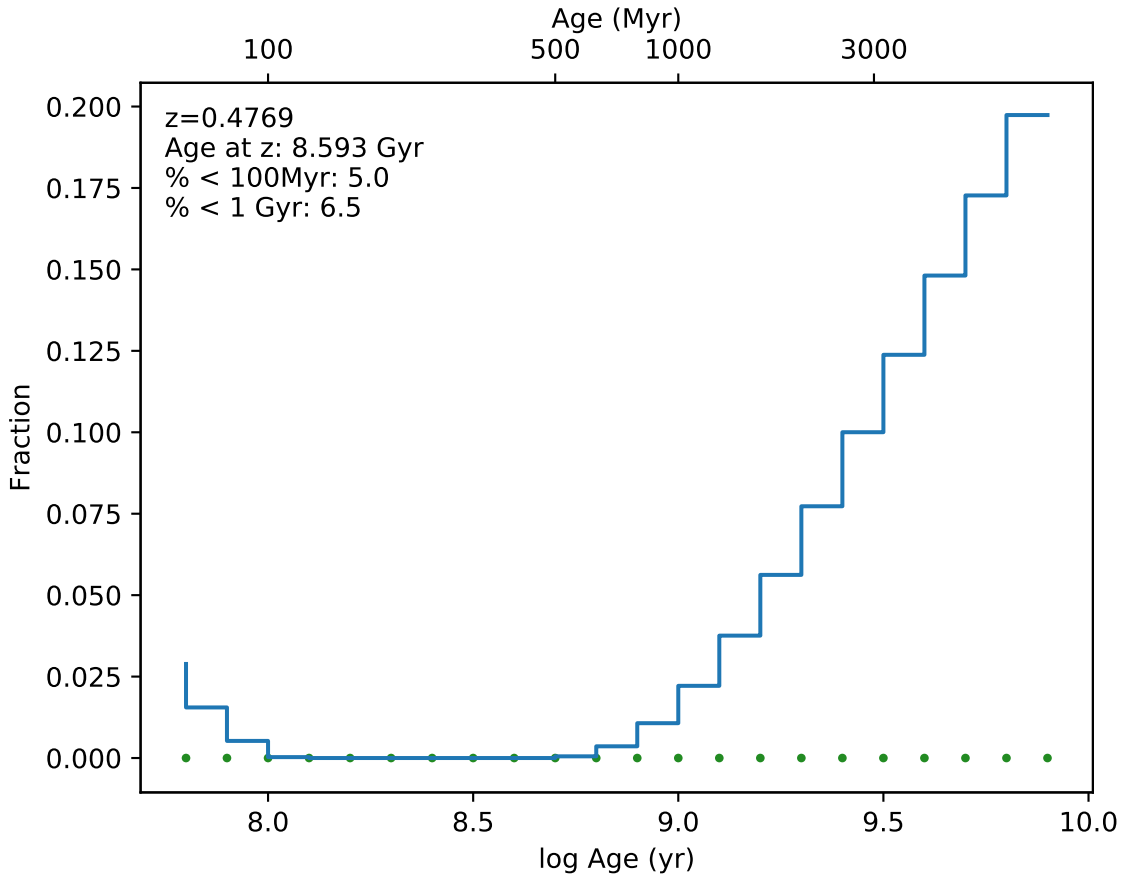
Age (Myr)
100
500
1000
3000
z=0.4769
Age at z: 8.593 Gyr
% < 100Myr: 5.0
% < 1 Gyr: 6.5
Fraction
0.200
0.175
0.150
0.125
0.100
0.075
0.050
0.025
0.000
8.0
8.5
9.0
9.5
10.0
log Age (yr)

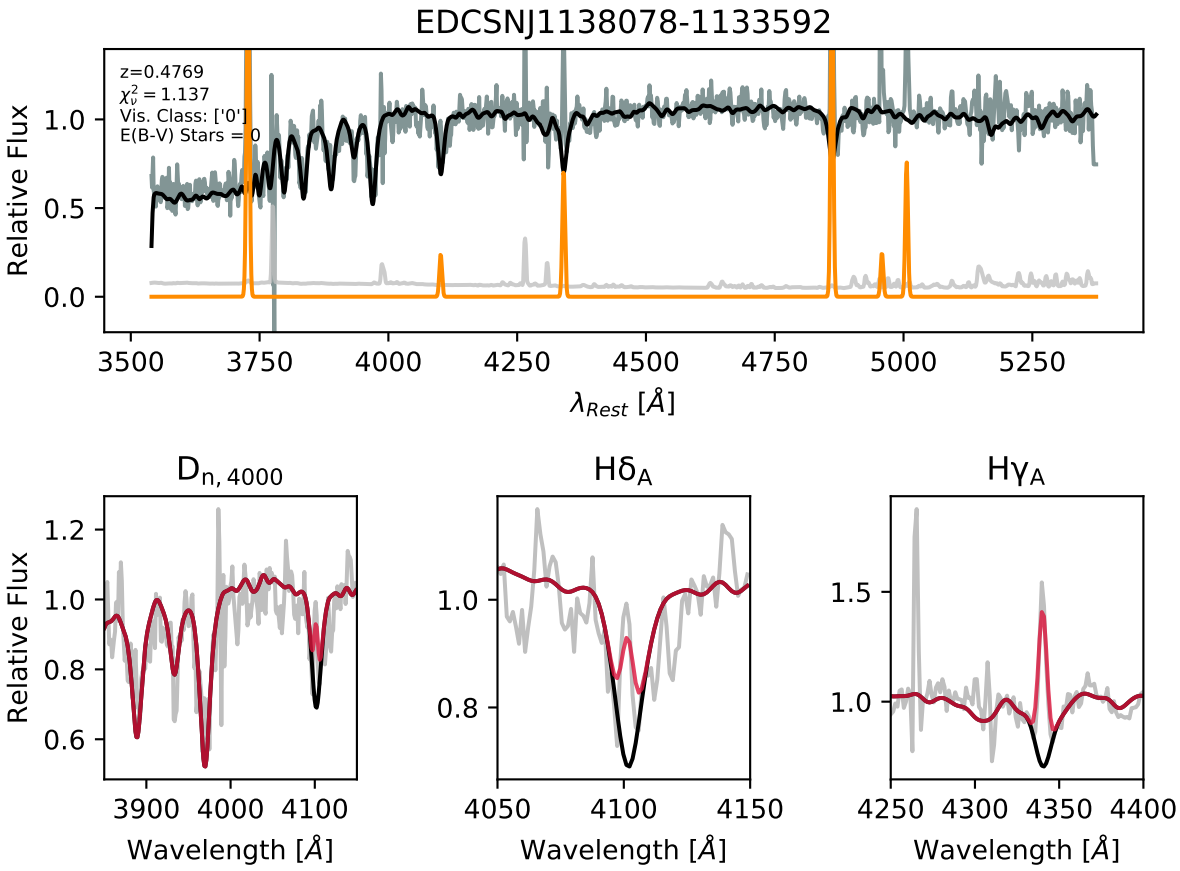
EDCSNJ1138078-1133592
z=0.4769
$\chi^2_\nu = 1.137$
Vis. Class: ['0']
E(B-V) Stars = 0
Relative Flux
1.0
0.5
0.0
3500
3750
4000
4250
4500
4750
5000
5250
λ_{Rest} [Å]
$D_{n,4000}$
$H\delta_A$
$H\gamma_A$
Relative Flux
1.2
1.0
0.8
0.6
3900
4000
4100
Wavelength [Å]
1.0
0.8
4050
4100
4150
Wavelength [Å]
1.5
1.0
4250
4300
4350
4400
Wavelength [Å]

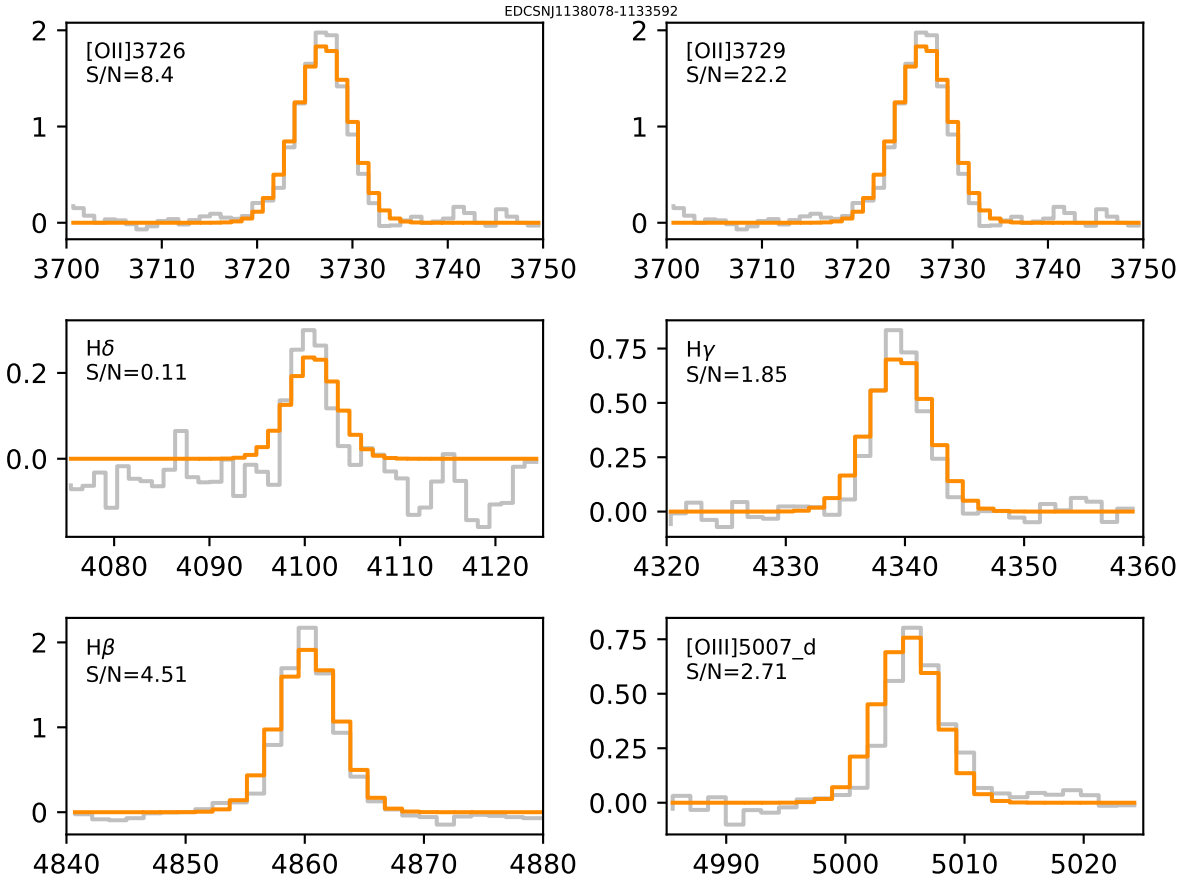
EDCSNJ1138078-1133592
[OII]3726
S/N=8.4
[OII]3729
S/N=22.2
Hδ
S/N=0.11
Hγ
S/N=1.85
Hβ
S/N=4.51
[OIII]5007_d
S/N=2.71

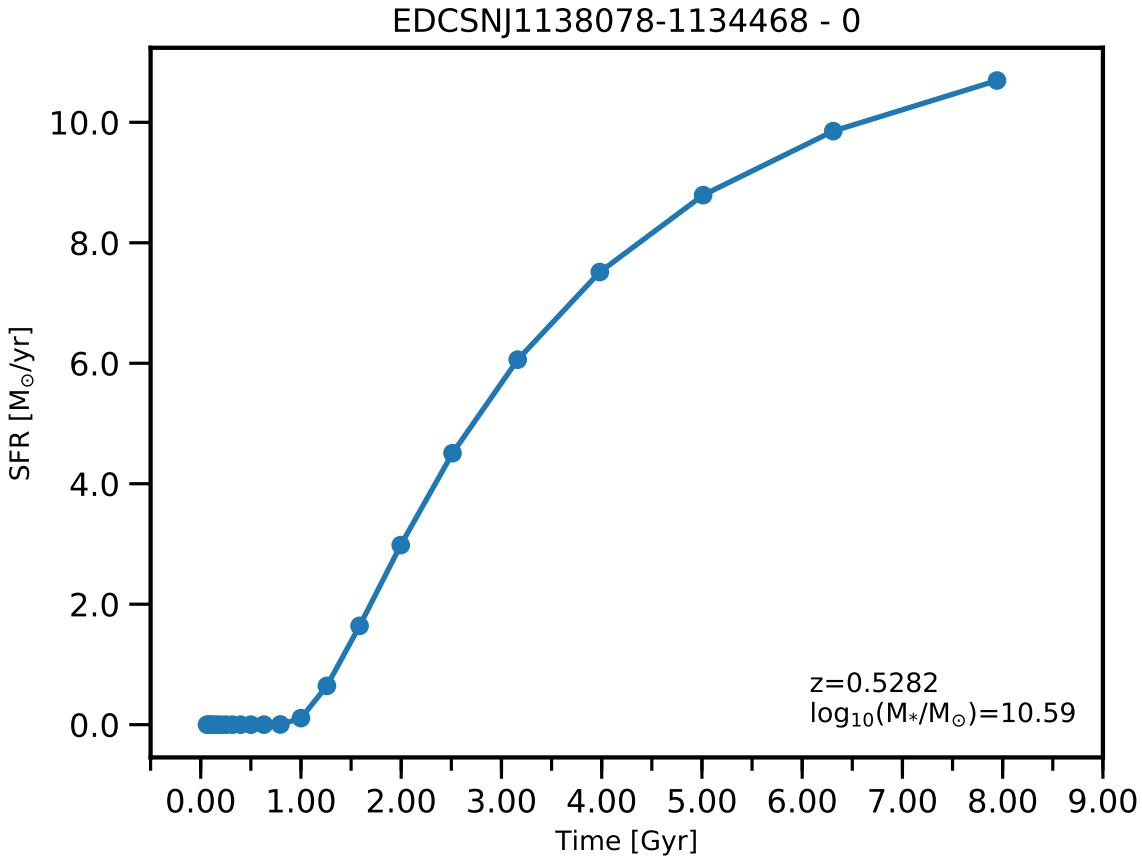
EDCSNJ1138078-1134468 - 0
SFR [M⊙/yr]
10.0
8.0
6.0
4.0
2.0
0.0
0.00
1.00
2.00
3.00
4.00
5.00
6.00
7.00
8.00
9.00
Time [Gyr]
z=0.5282
log10(M*/M⊙)=10.59

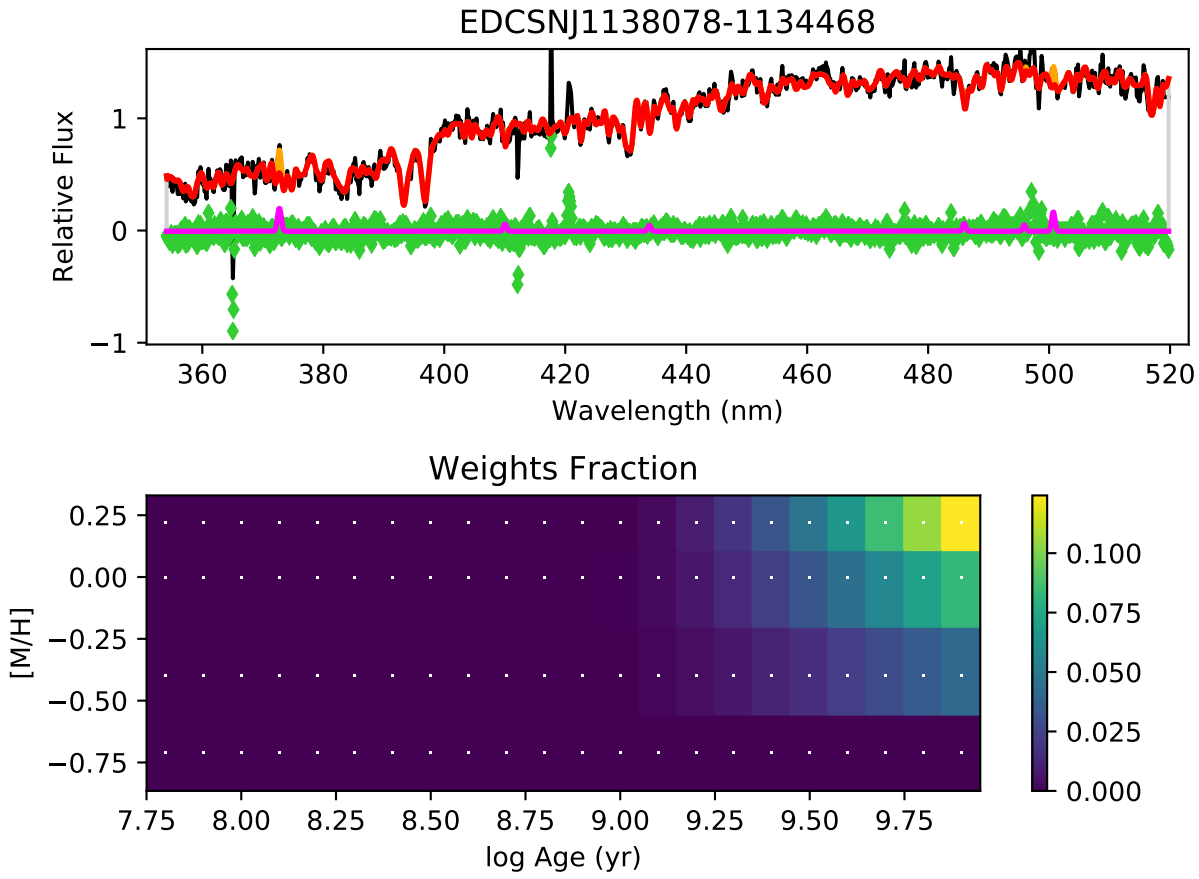
EDCSNJ1138078-1134468
Relative Flux
1
0
−1
360
380
400
420
440
460
480
500
520
Wavelength (nm)
Weights Fraction
[M/H]
0.25
0.00
−0.25
−0.50
−0.75
7.75
8.00
8.25
8.50
8.75
9.00
9.25
9.50
9.75
log Age (yr)
0.100
0.075
0.050
0.025
0.000

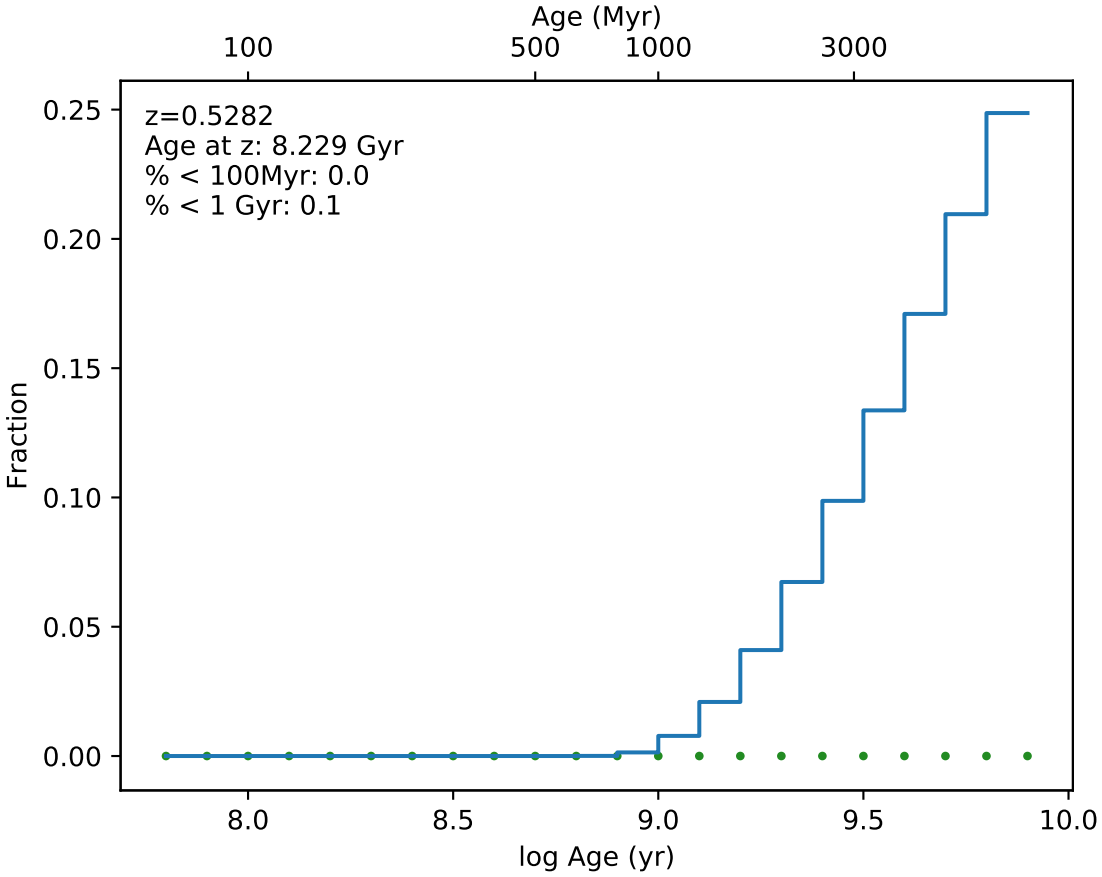
Age (Myr)
100
500
1000
3000
z=0.5282
Age at z: 8.229 Gyr
% < 100Myr: 0.0
% < 1 Gyr: 0.1
Fraction
0.25
0.20
0.15
0.10
0.05
0.00
8.0
8.5
9.0
9.5
10.0
log Age (yr)

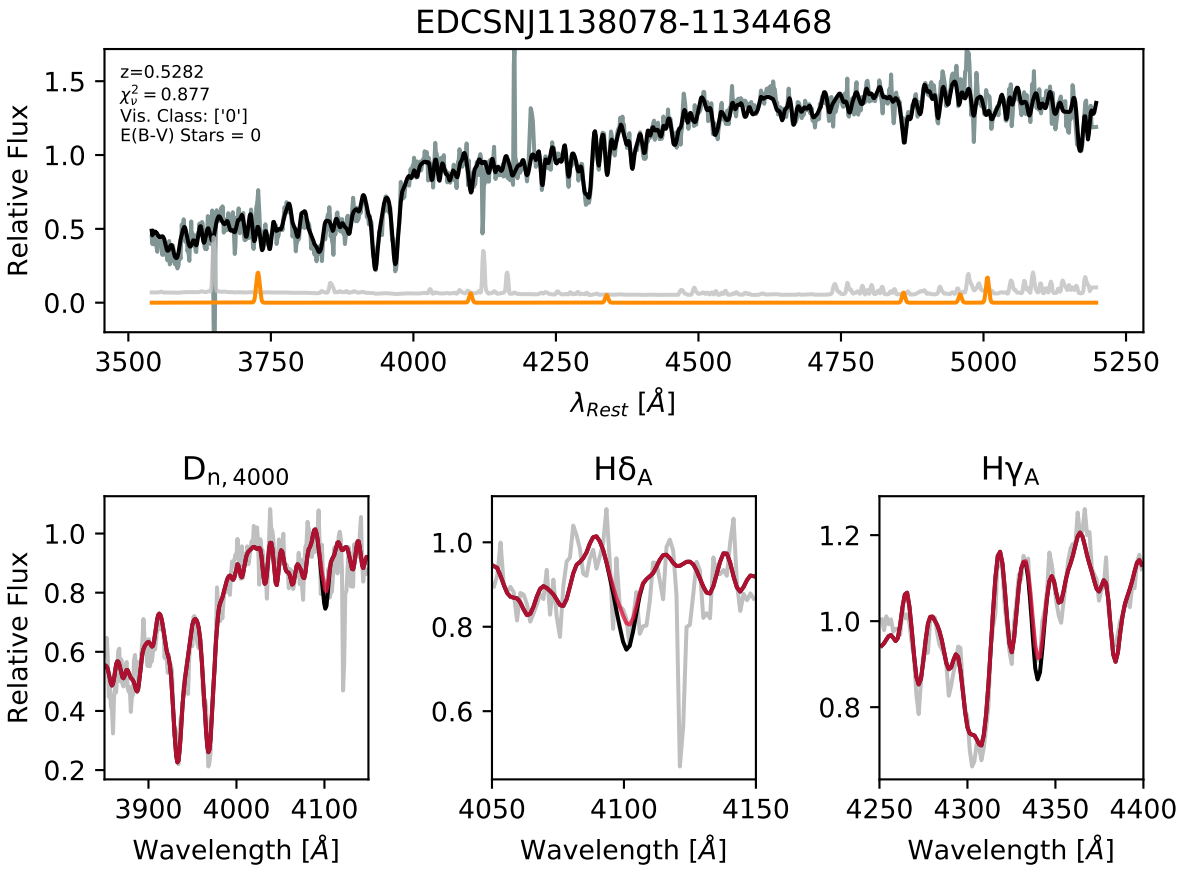
EDCSNJ1138078-1134468
z=0.5282
$\chi^2_\nu = 0.877$
Vis. Class: ['0']
E(B-V) Stars = 0
Relative Flux
λ_{Rest} [Å]
$D_{n,4000}$
$H\delta_A$
$H\gamma_A$
Wavelength [Å]

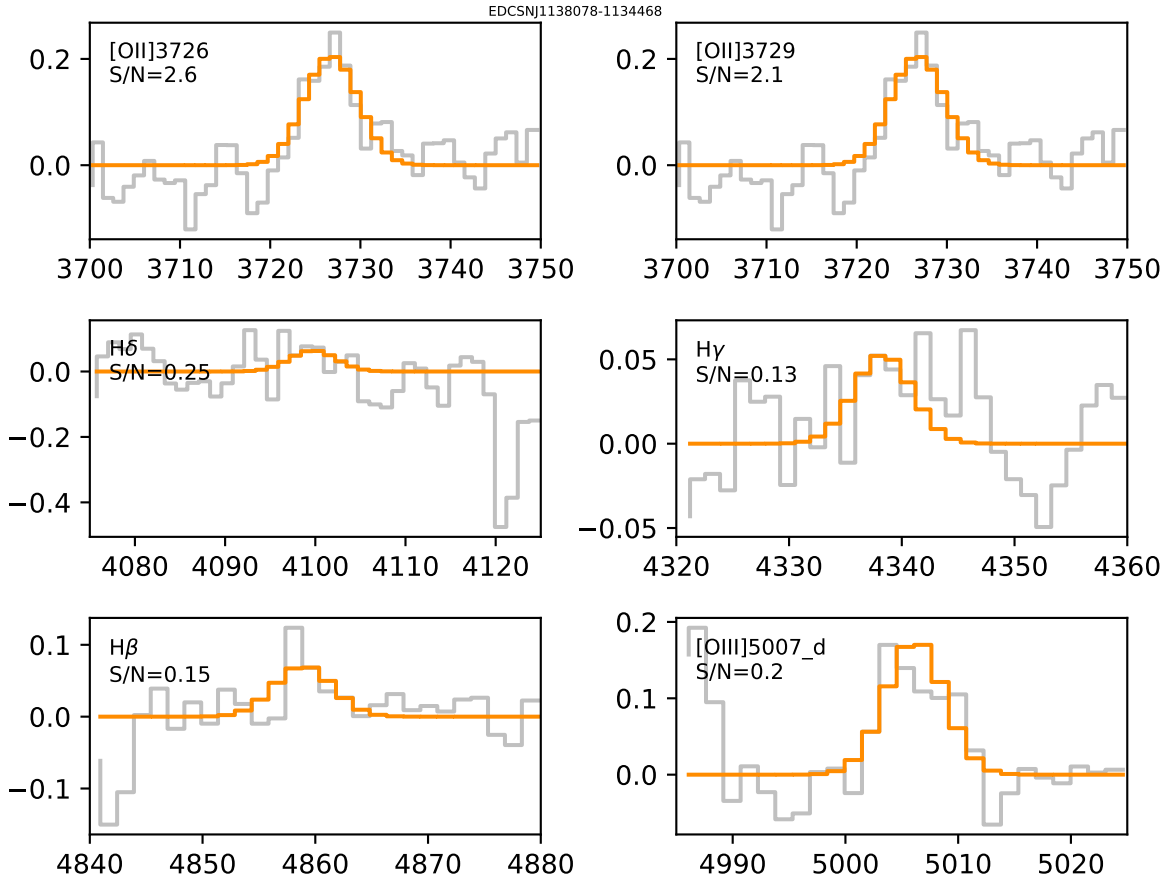
EDCSNJ1138078-1134468
[OII]3726
S/N=2.6
[OII]3729
S/N=2.1
Hδ
S/N=0.25
Hγ
S/N=0.13
Hβ
S/N=0.15
[OIII]5007_d
S/N=0.2

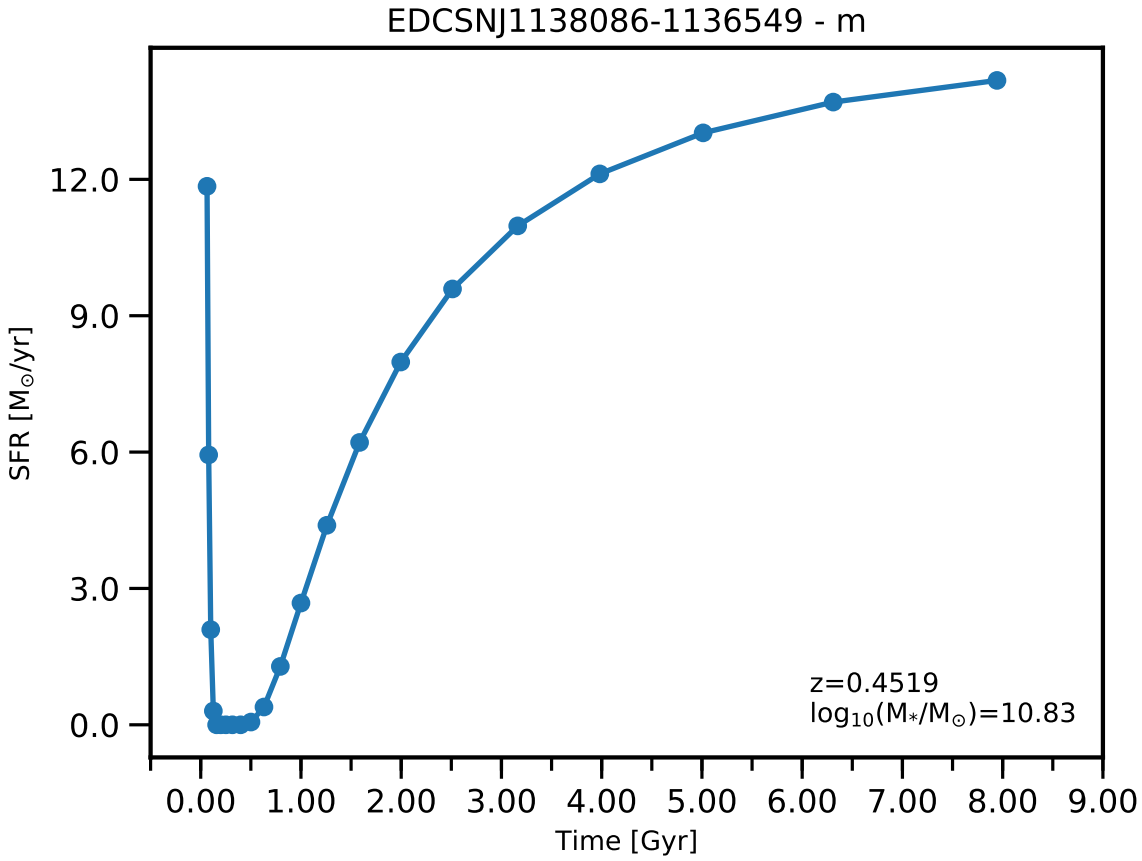
EDCSNJ1138086-1136549 - m
SFR [M⊙/yr]
12.0
9.0
6.0
3.0
0.0
0.00
1.00
2.00
3.00
4.00
5.00
6.00
7.00
8.00
9.00
Time [Gyr]
z=0.4519
log10(M*/M⊙)=10.83

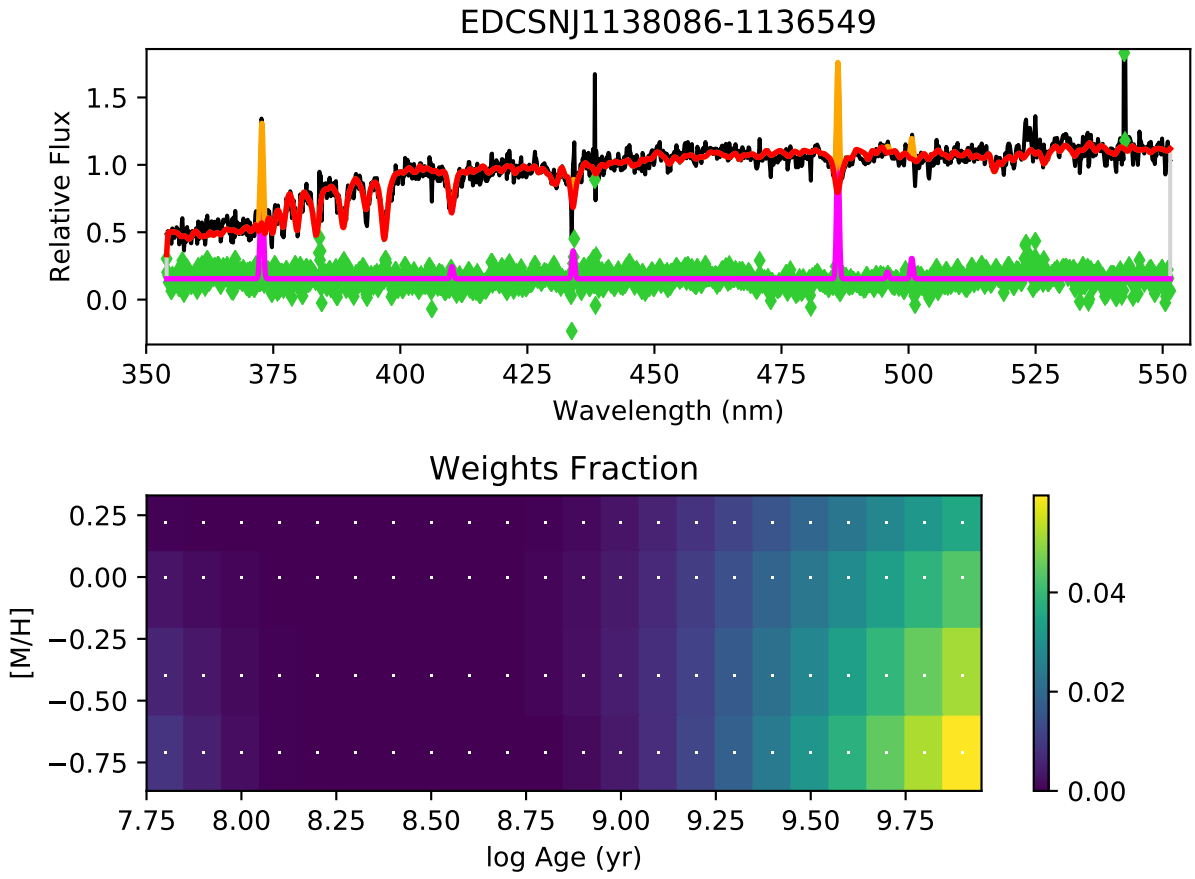
EDCSNJ1138086-1136549
Relative Flux
1.5
1.0
0.5
0.0
350
375
400
425
450
475
500
525
550
Wavelength (nm)
Weights Fraction
[M/H]
0.25
0.00
−0.25
−0.50
−0.75
7.75
8.00
8.25
8.50
8.75
9.00
9.25
9.50
9.75
log Age (yr)
0.04
0.02
0.00

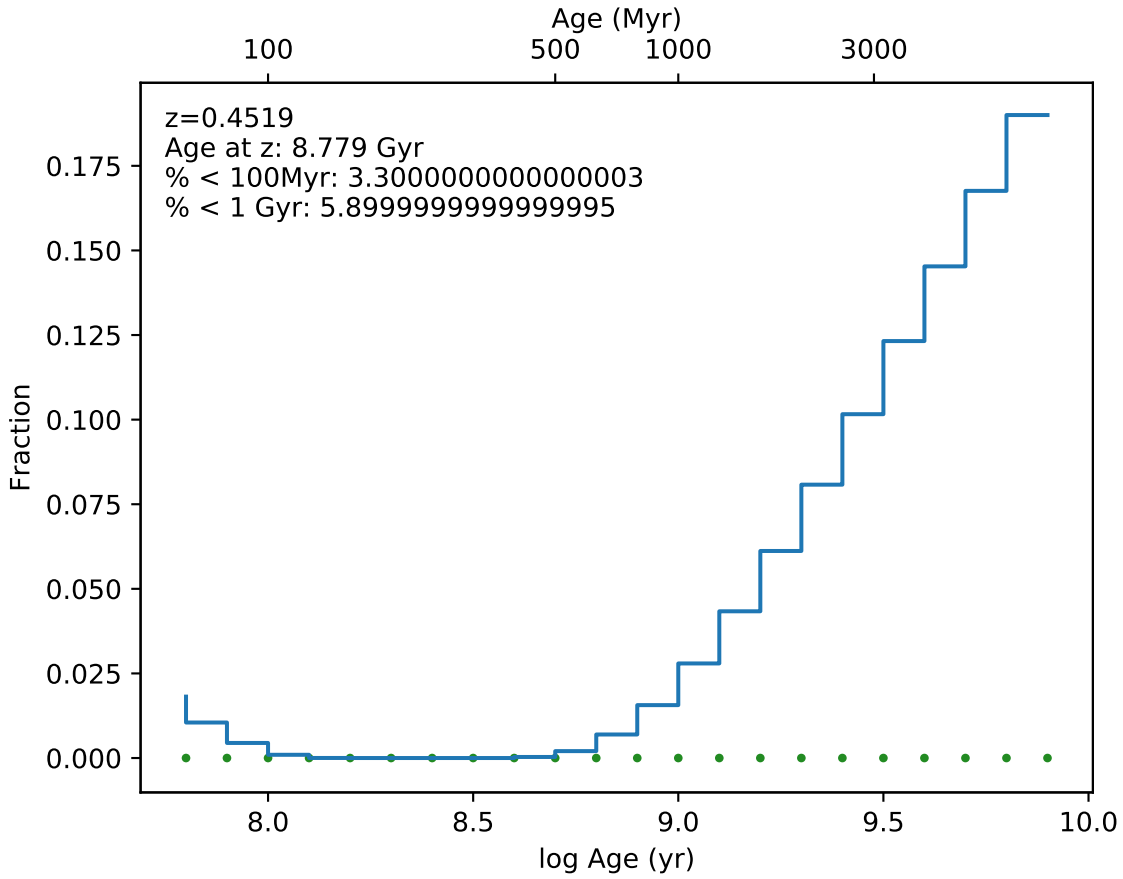
Age (Myr)
100
500
1000
3000
z=0.4519
Age at z: 8.779 Gyr
% < 100Myr: 3.3000000000000003
% < 1 Gyr: 5.8999999999999995
Fraction
0.175
0.150
0.125
0.100
0.075
0.050
0.025
0.000
8.0
8.5
9.0
9.5
10.0
log Age (yr)

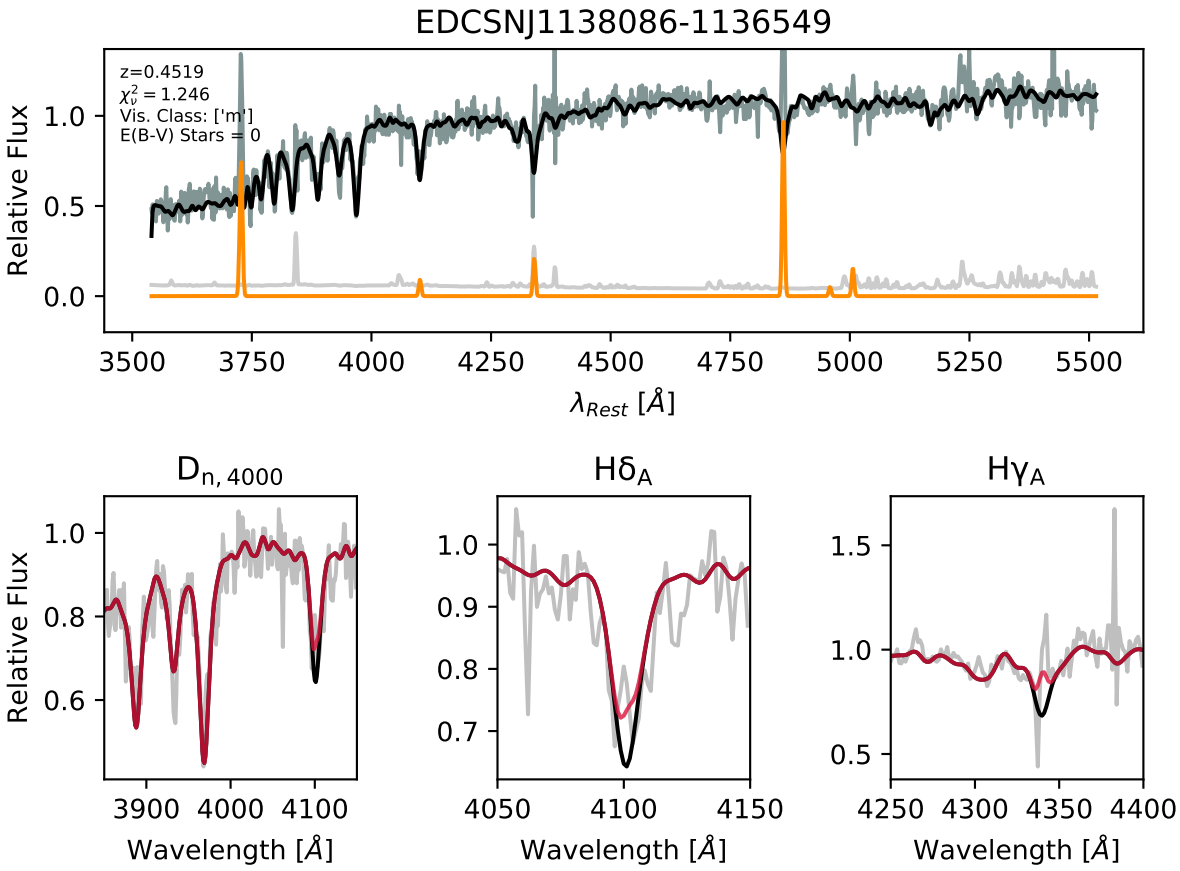
EDCSNJ1138086-1136549
z=0.4519
$\chi^2_\nu = 1.246$
Vis. Class: ['m']
E(B-V) Stars = 0
Relative Flux
1.0
0.5
0.0
3500
3750
4000
4250
4500
4750
5000
5250
5500
λ_{Rest} [Å]
$D_{n,4000}$
$H\delta_A$
$H\gamma_A$
Relative Flux
1.0
0.8
0.6
3900
4000
4100
Wavelength [Å]
1.0
0.9
0.8
0.7
4050
4100
4150
Wavelength [Å]
1.5
1.0
0.5
4250
4300
4350
4400
Wavelength [Å]

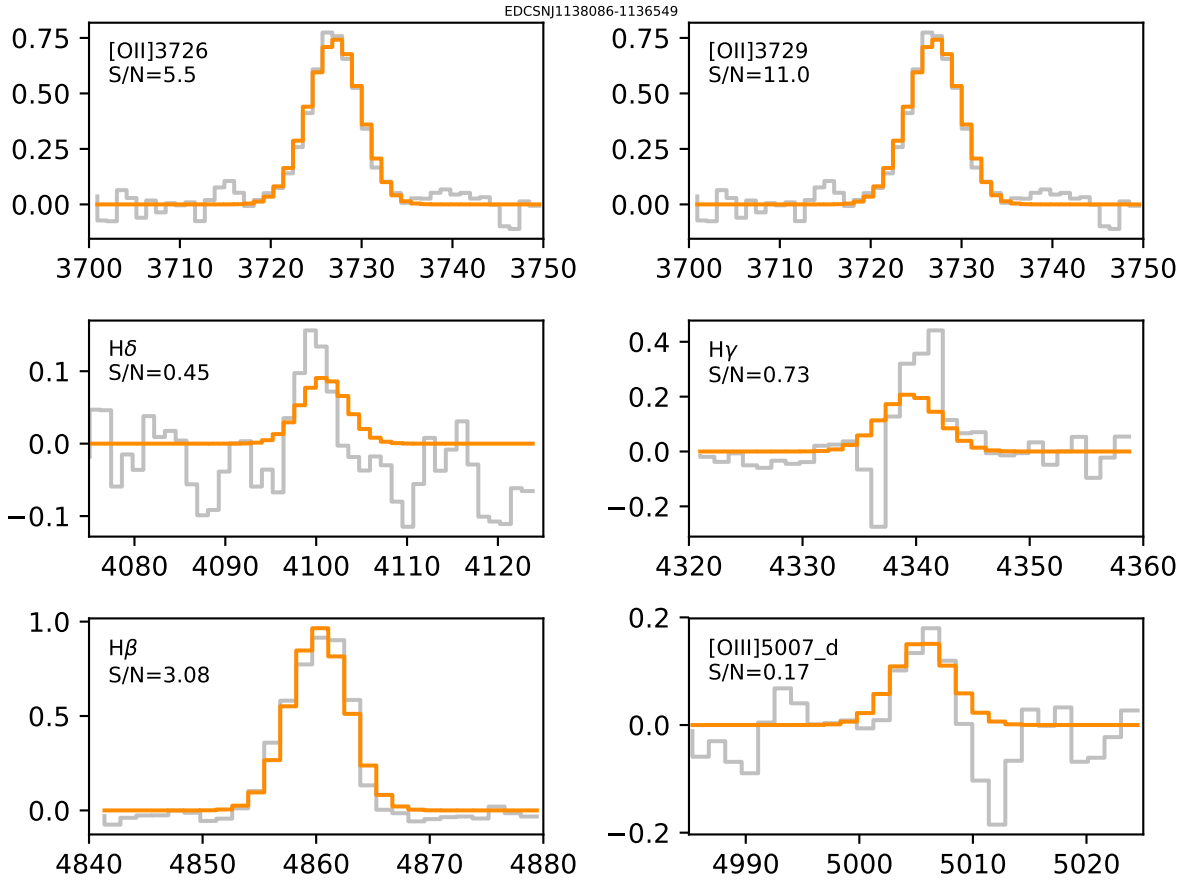
EDCSNJ1138086-1136549
[OII]3726
S/N=5.5
[OII]3729
S/N=11.0
Hδ
S/N=0.45
Hγ
S/N=0.73
Hβ
S/N=3.08
[OIII]5007_d
S/N=0.17

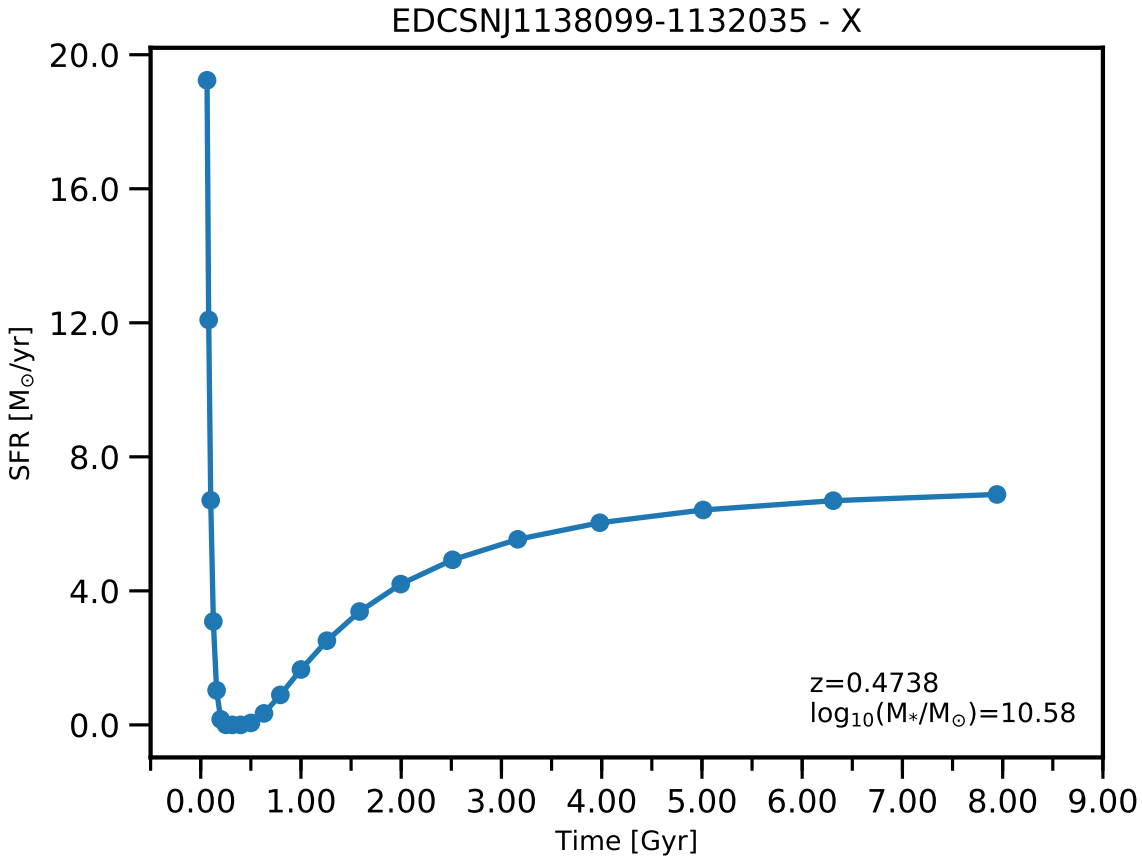
EDCSNJ1138099-1132035 - X
SFR [M⊙/yr]
Time [Gyr]
z=0.4738
log10(M*/M⊙)=10.58
20.0
16.0
12.0
8.0
4.0
0.0
0.00
1.00
2.00
3.00
4.00
5.00
6.00
7.00
8.00
9.00

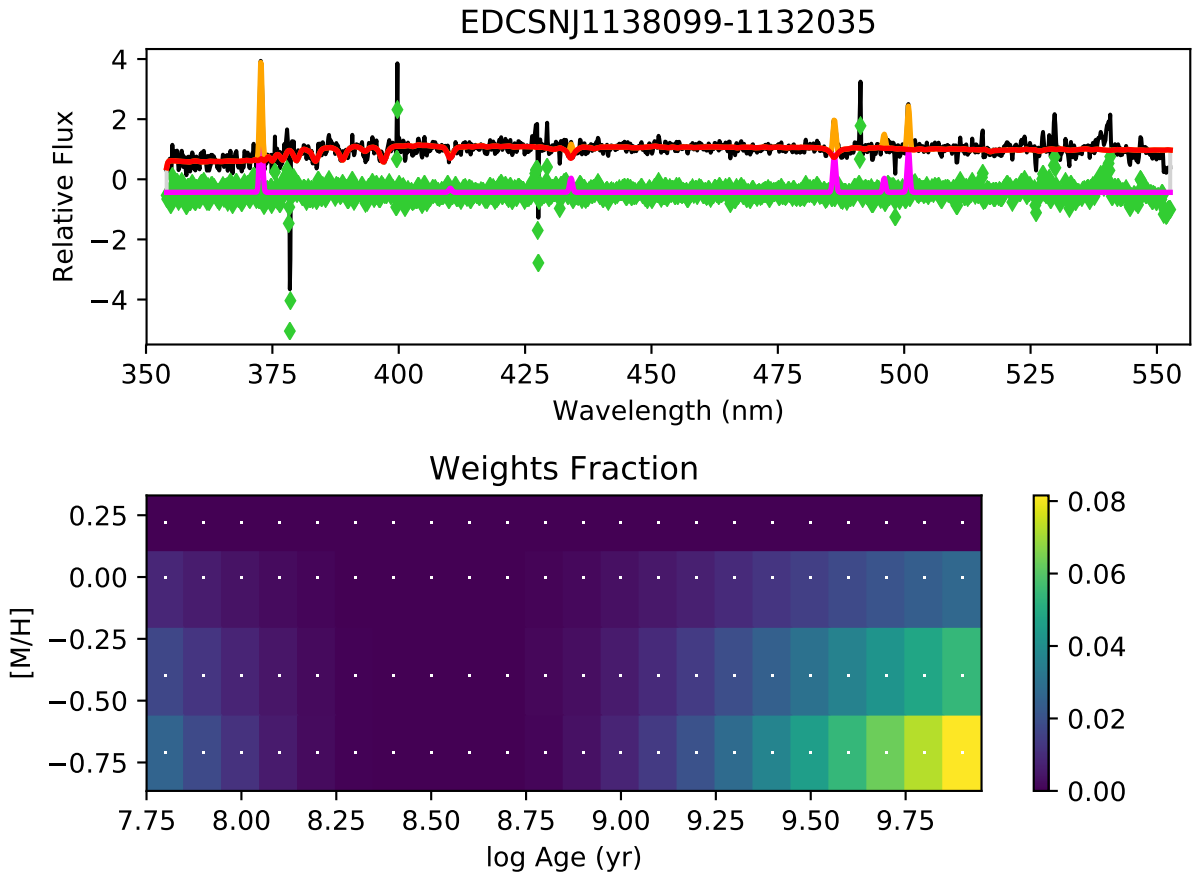
EDCSNJ1138099-1132035
Relative Flux
4
2
0
−2
−4
350
375
400
425
450
475
500
525
550
Wavelength (nm)
Weights Fraction
[M/H]
0.25
0.00
−0.25
−0.50
−0.75
7.75
8.00
8.25
8.50
8.75
9.00
9.25
9.50
9.75
log Age (yr)
0.08
0.06
0.04
0.02
0.00

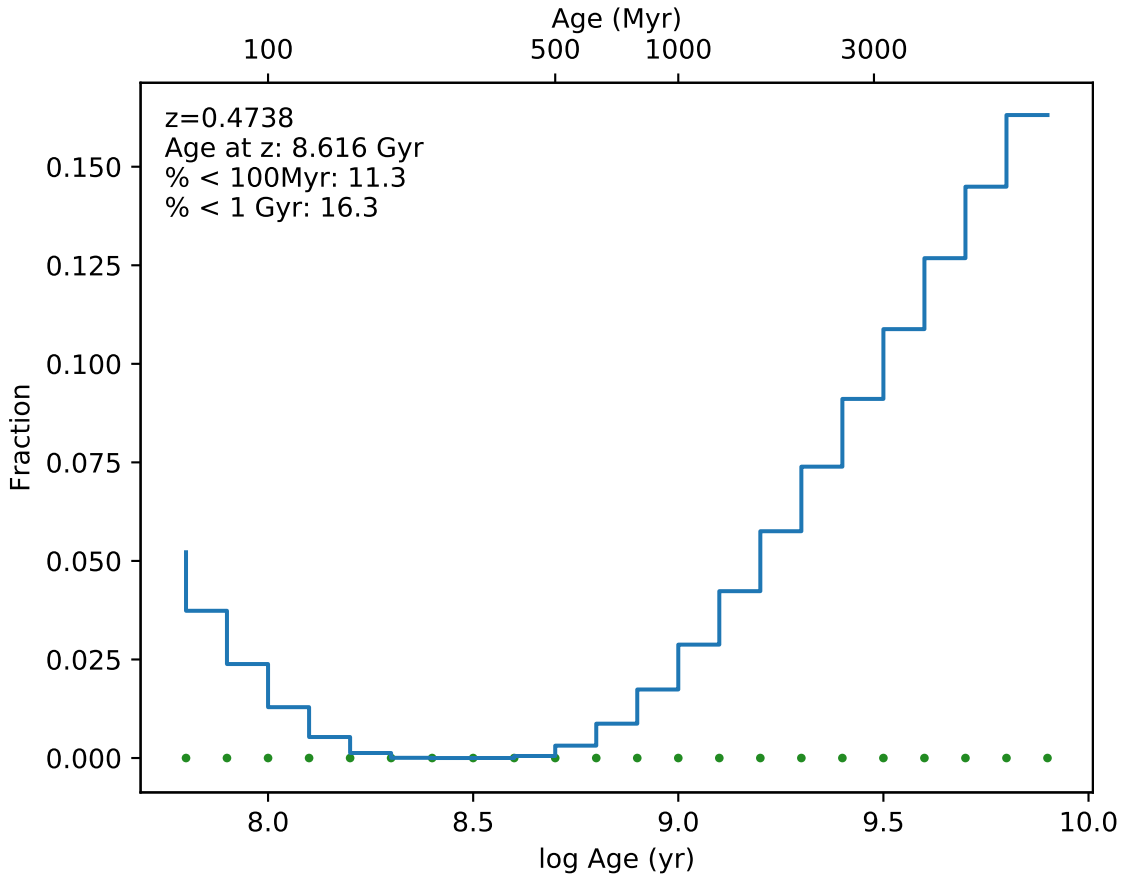
Age (Myr)
100
500
1000
3000
z=0.4738
Age at z: 8.616 Gyr
% < 100Myr: 11.3
% < 1 Gyr: 16.3
0.150
0.125
0.100
0.075
0.050
0.025
0.000
Fraction
8.0
8.5
9.0
9.5
10.0
log Age (yr)

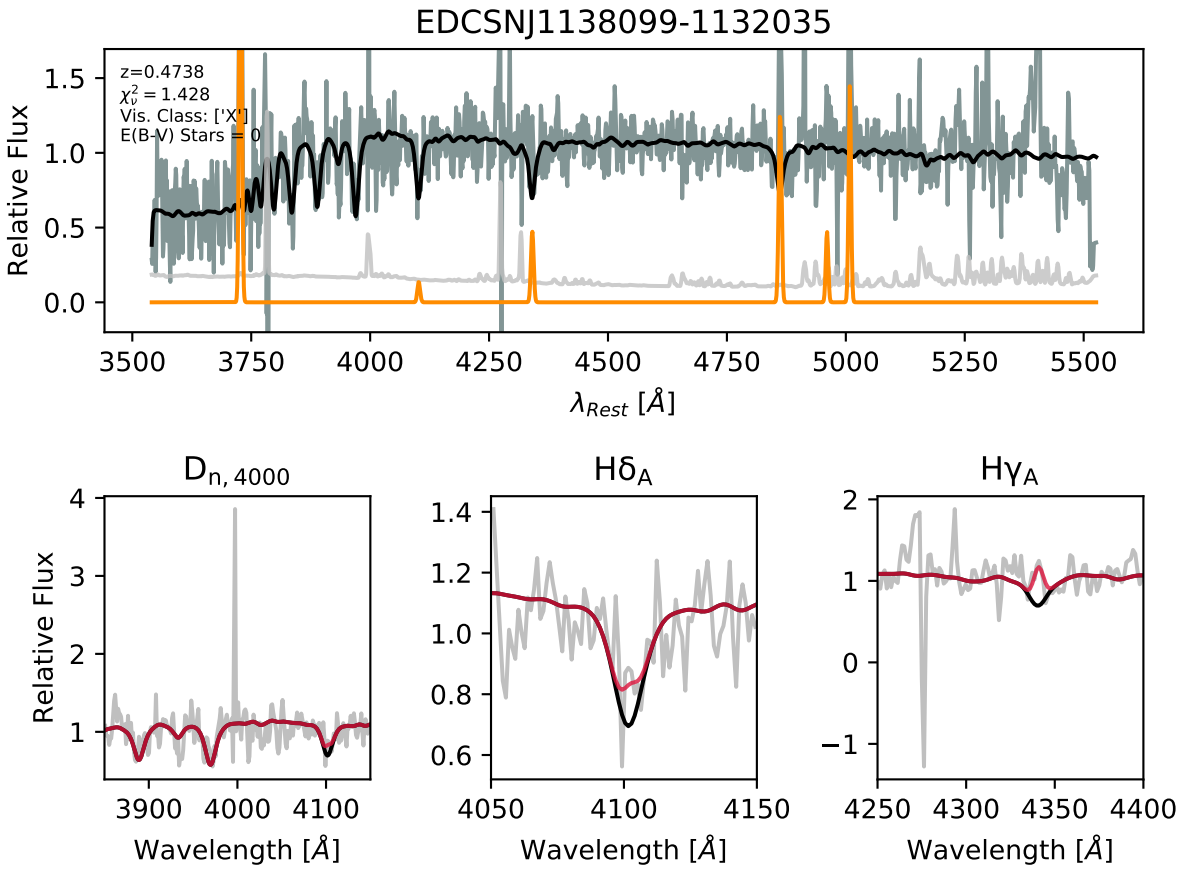
EDCSNJ1138099-1132035
z=0.4738
$\chi^2_\nu = 1.428$
Vis. Class: ['X']
E(B-V) Stars = 0
Relative Flux
λ_{Rest} [Å]
$D_{n,4000}$
$H\delta_A$
$H\gamma_A$
Wavelength [Å]

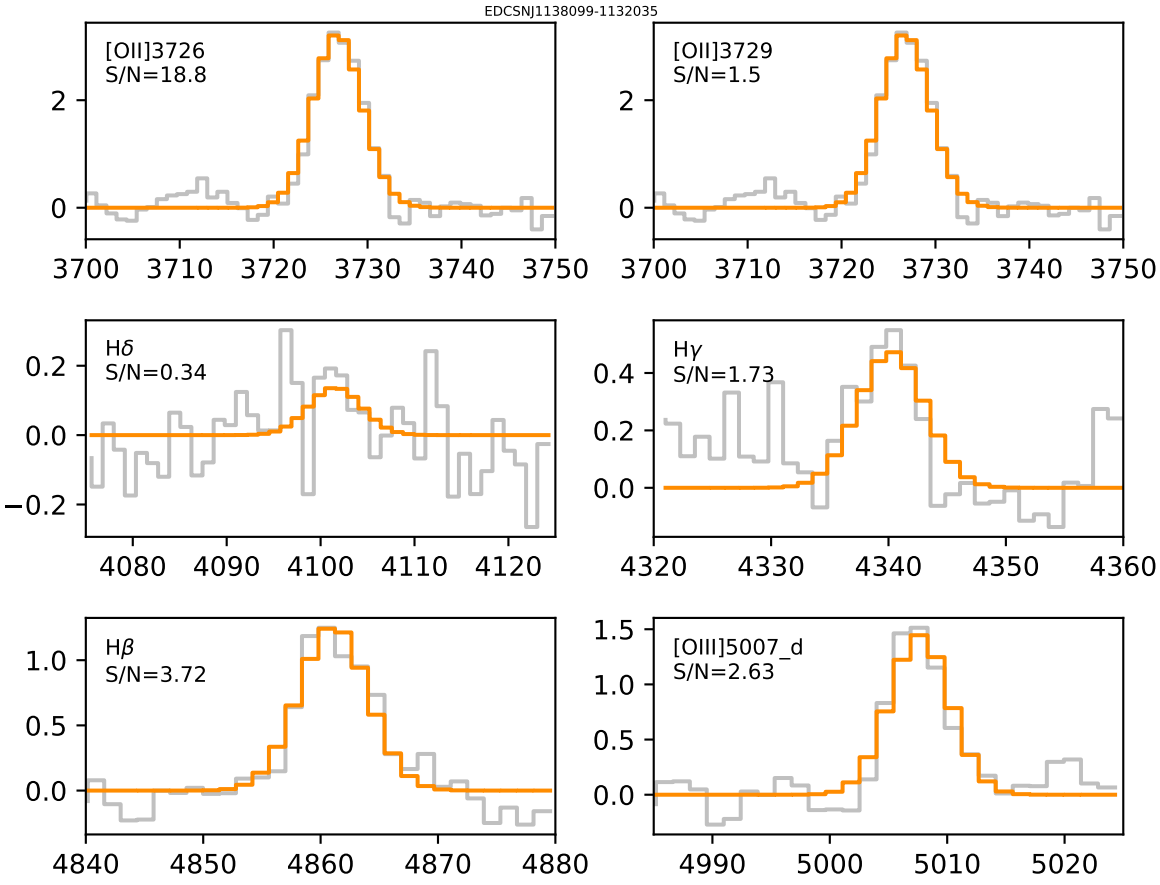
EDCSNJ1138099-1132035
[OII]3726
S/N=18.8
[OII]3729
S/N=1.5
Hδ
S/N=0.34
Hγ
S/N=1.73
Hβ
S/N=3.72
[OIII]5007_d
S/N=2.63

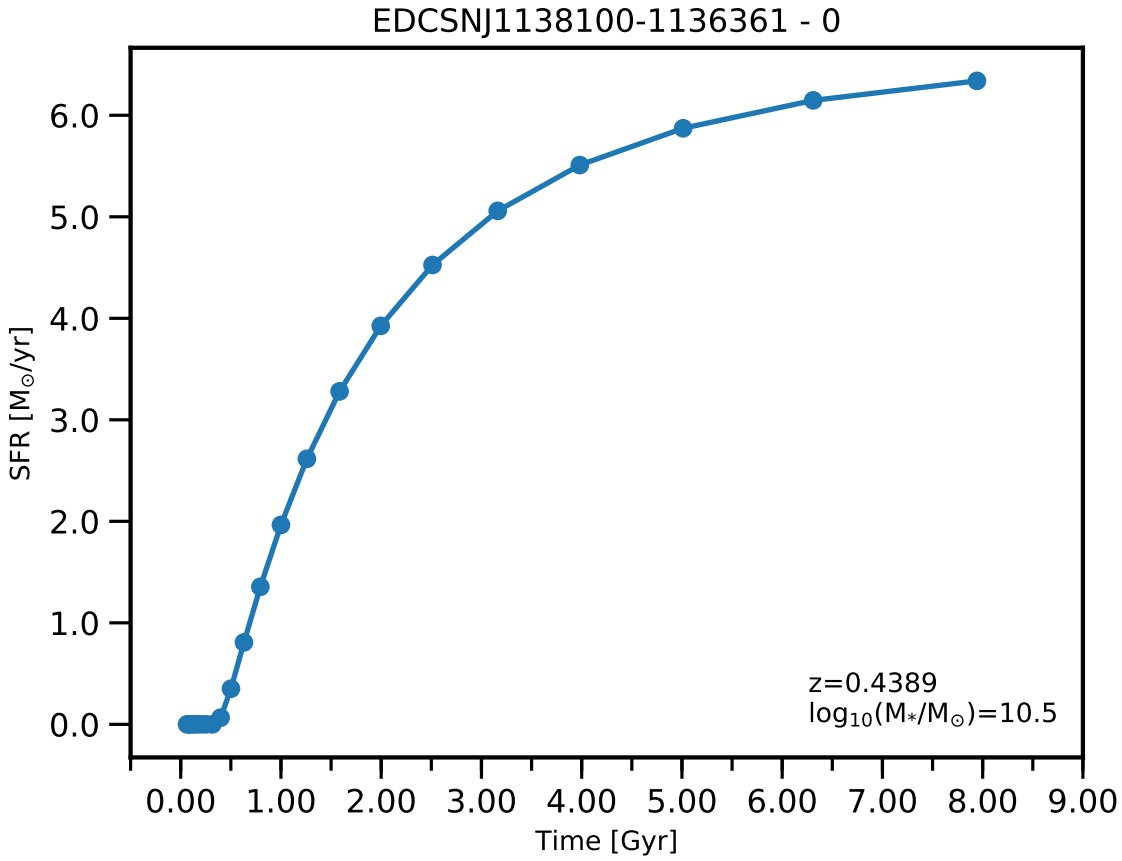
EDCSNJ1138100-1136361 - 0
SFR [M⊙/yr]
Time [Gyr]
z=0.4389
log10(M*/M⊙)=10.5
0.0
1.0
2.0
3.0
4.0
5.0
6.0
0.00
1.00
2.00
3.00
4.00
5.00
6.00
7.00
8.00
9.00

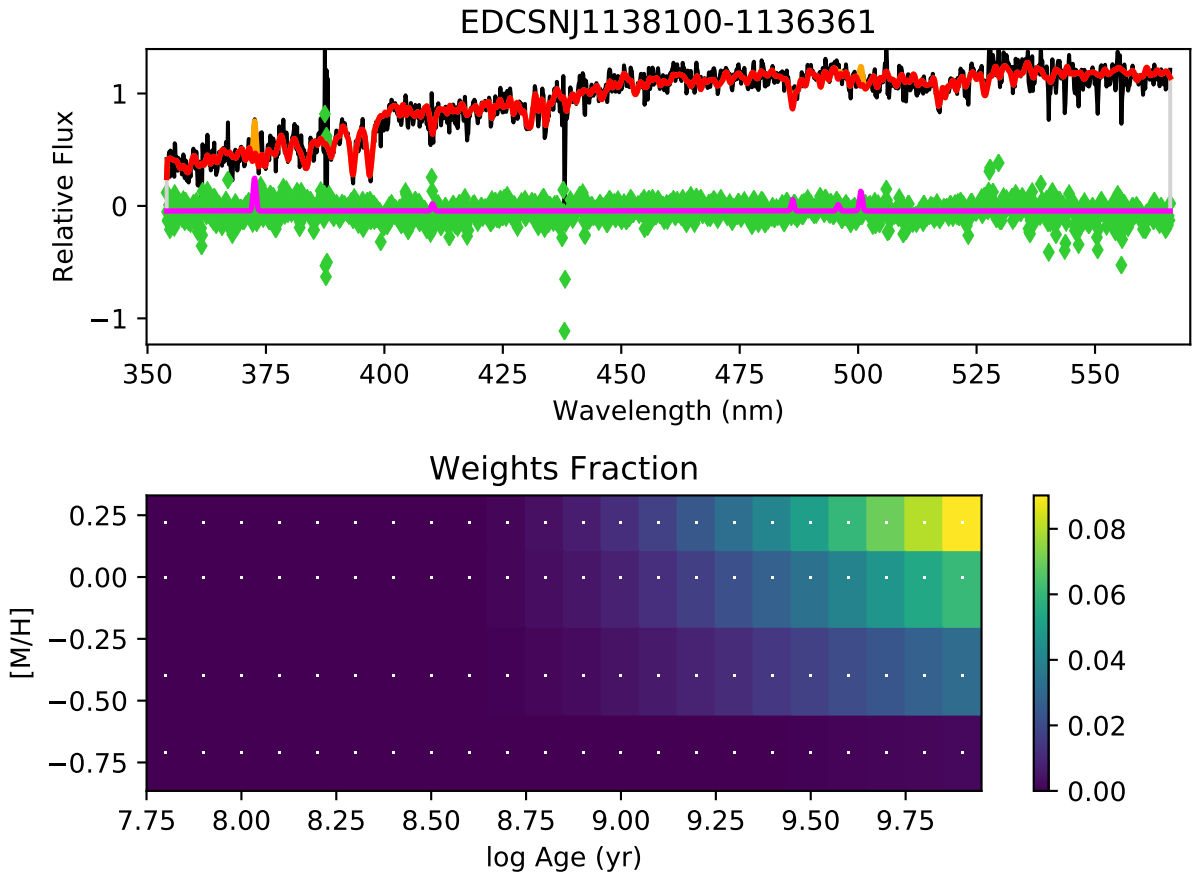
EDCSNJ1138100-1136361
Relative Flux
1
0
−1
350
375
400
425
450
475
500
525
550
Wavelength (nm)
Weights Fraction
[M/H]
0.25
0.00
−0.25
−0.50
−0.75
7.75
8.00
8.25
8.50
8.75
9.00
9.25
9.50
9.75
log Age (yr)
0.08
0.06
0.04
0.02
0.00

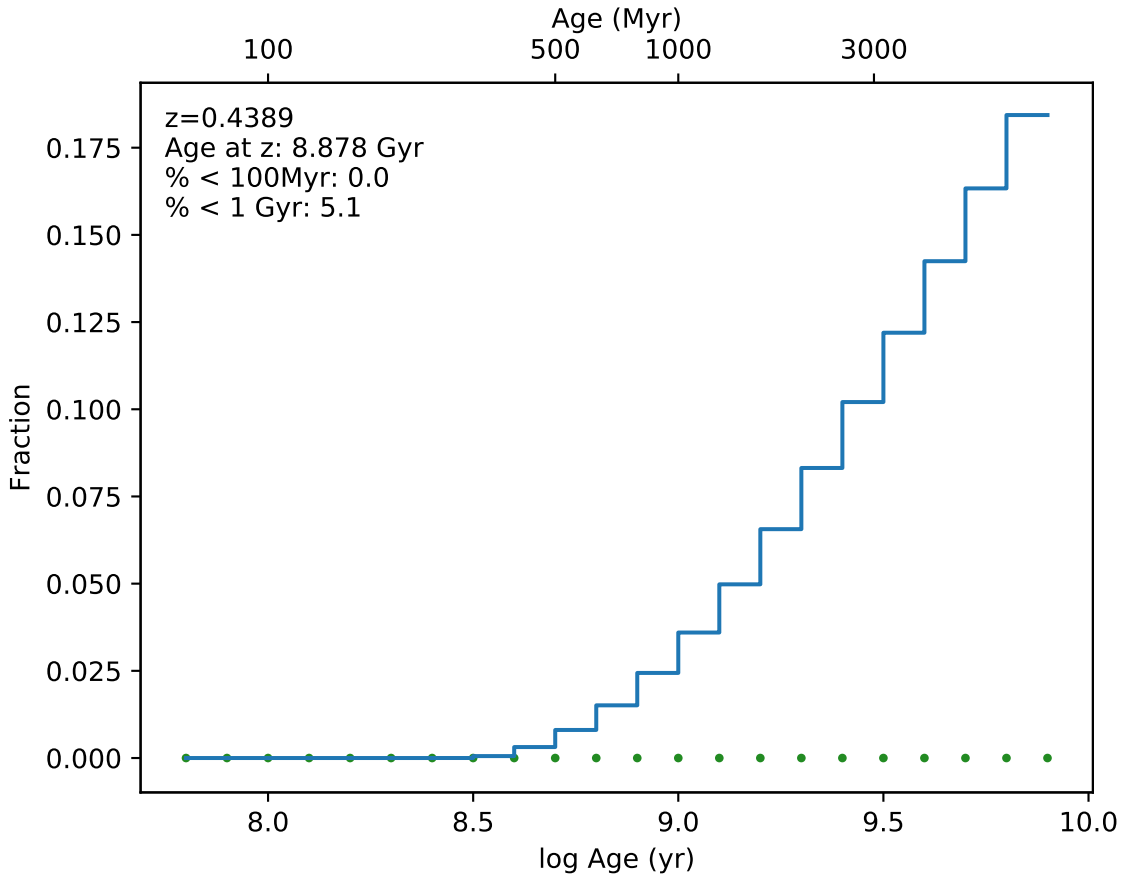
Age (Myr)
100
500
1000
3000
z=0.4389
Age at z: 8.878 Gyr
% < 100Myr: 0.0
% < 1 Gyr: 5.1
Fraction
0.175
0.150
0.125
0.100
0.075
0.050
0.025
0.000
8.0
8.5
9.0
9.5
10.0
log Age (yr)

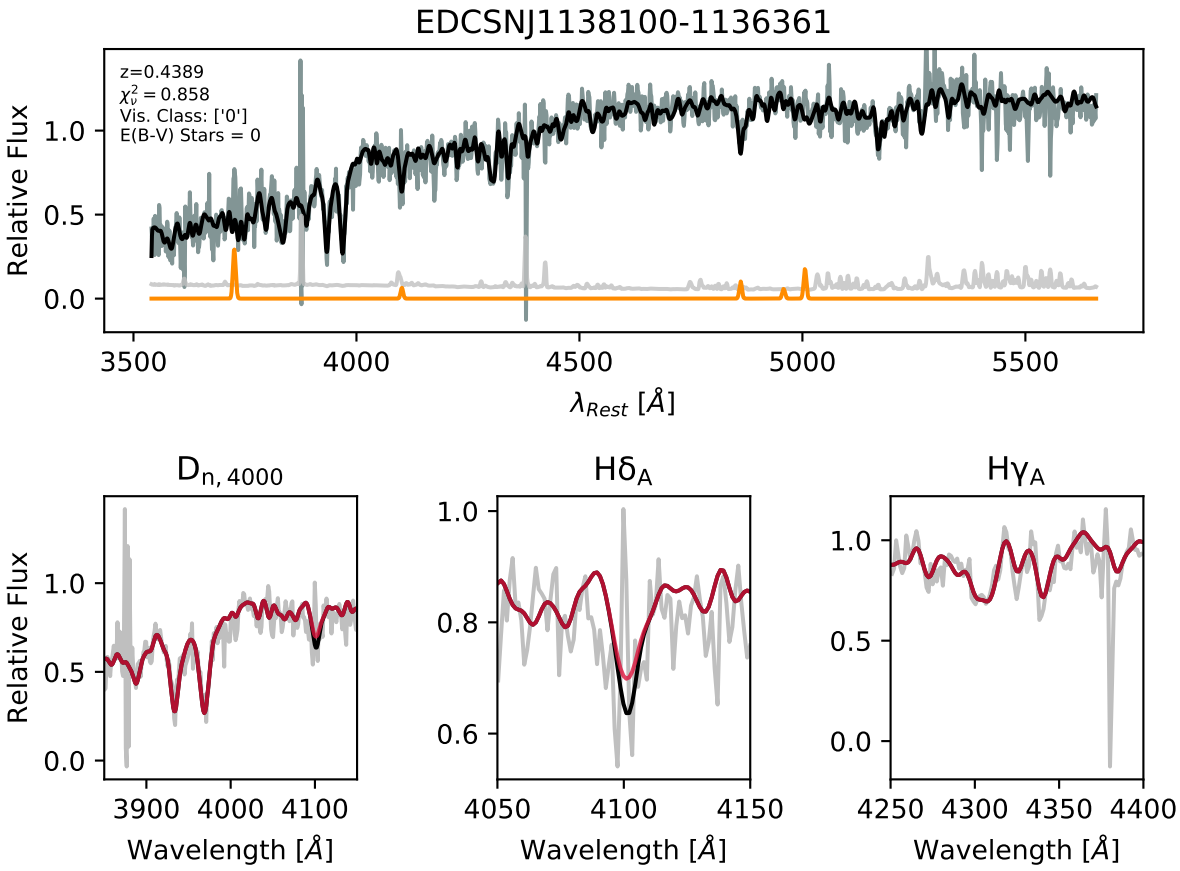
EDCSNJ1138100-1136361
z=0.4389
$\chi^2_\nu = 0.858$
Vis. Class: ['0']
E(B-V) Stars = 0
Relative Flux
1.0
0.5
0.0
3500
4000
4500
5000
5500
λ_{Rest} [Å]
$D_{n,4000}$
$H\delta_A$
$H\gamma_A$
Relative Flux
1.0
0.5
0.0
3900 4000 4100
Wavelength [Å]
1.0
0.8
0.6
4050 4100 4150
Wavelength [Å]
1.0
0.5
0.0
4250 4300 4350 4400
Wavelength [Å]

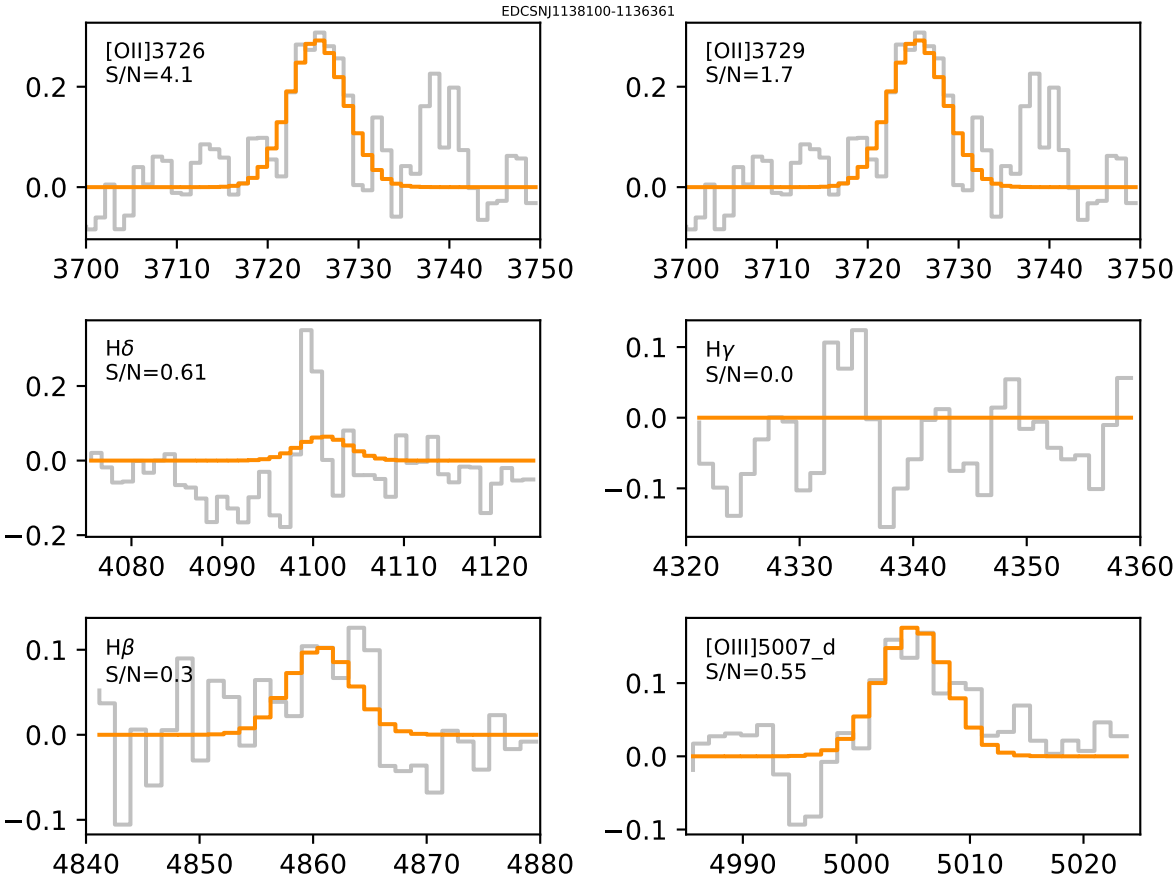
EDCSNJ1138100-1136361
[OII]3726
S/N=4.1
[OII]3729
S/N=1.7
Hδ
S/N=0.61
Hγ
S/N=0.0
Hβ
S/N=0.3
[OIII]5007_d
S/N=0.55

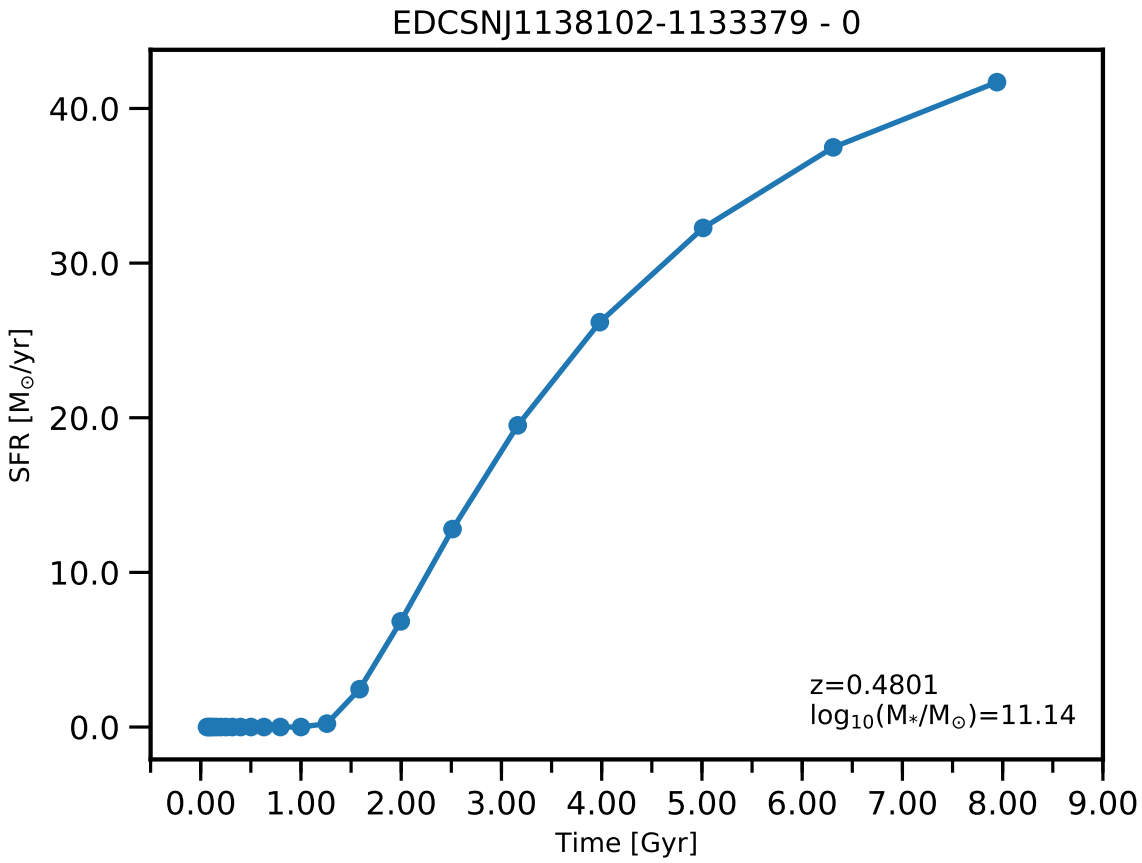
EDCSNJ1138102-1133379 - 0
SFR [M⊙/yr]
40.0
30.0
20.0
10.0
0.0
0.00
1.00
2.00
3.00
4.00
5.00
6.00
7.00
8.00
9.00
Time [Gyr]
z=0.4801
log10(M*/M⊙)=11.14

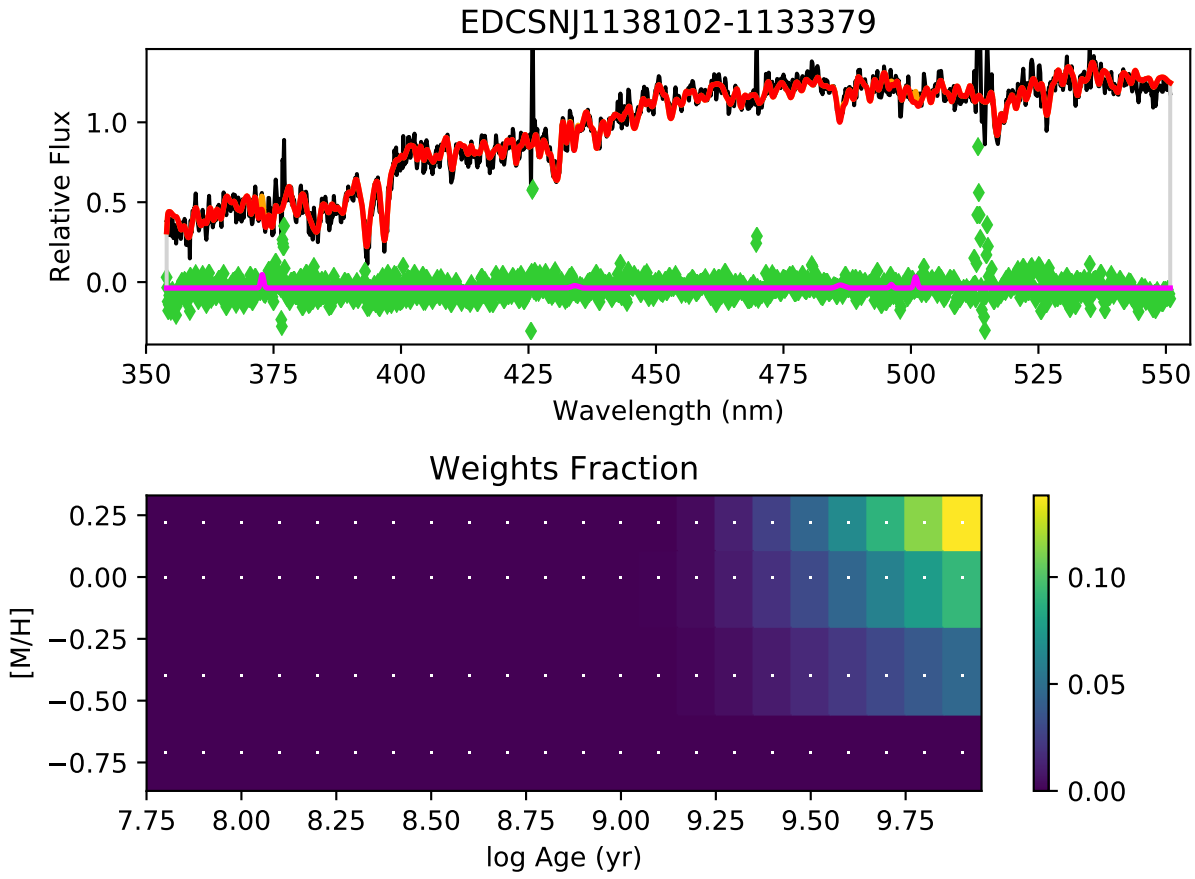
EDCSNJ1138102-1133379
Relative Flux
1.0
0.5
0.0
350
375
400
425
450
475
500
525
550
Wavelength (nm)
Weights Fraction
[M/H]
0.25
0.00
−0.25
−0.50
−0.75
7.75
8.00
8.25
8.50
8.75
9.00
9.25
9.50
9.75
log Age (yr)
0.10
0.05
0.00

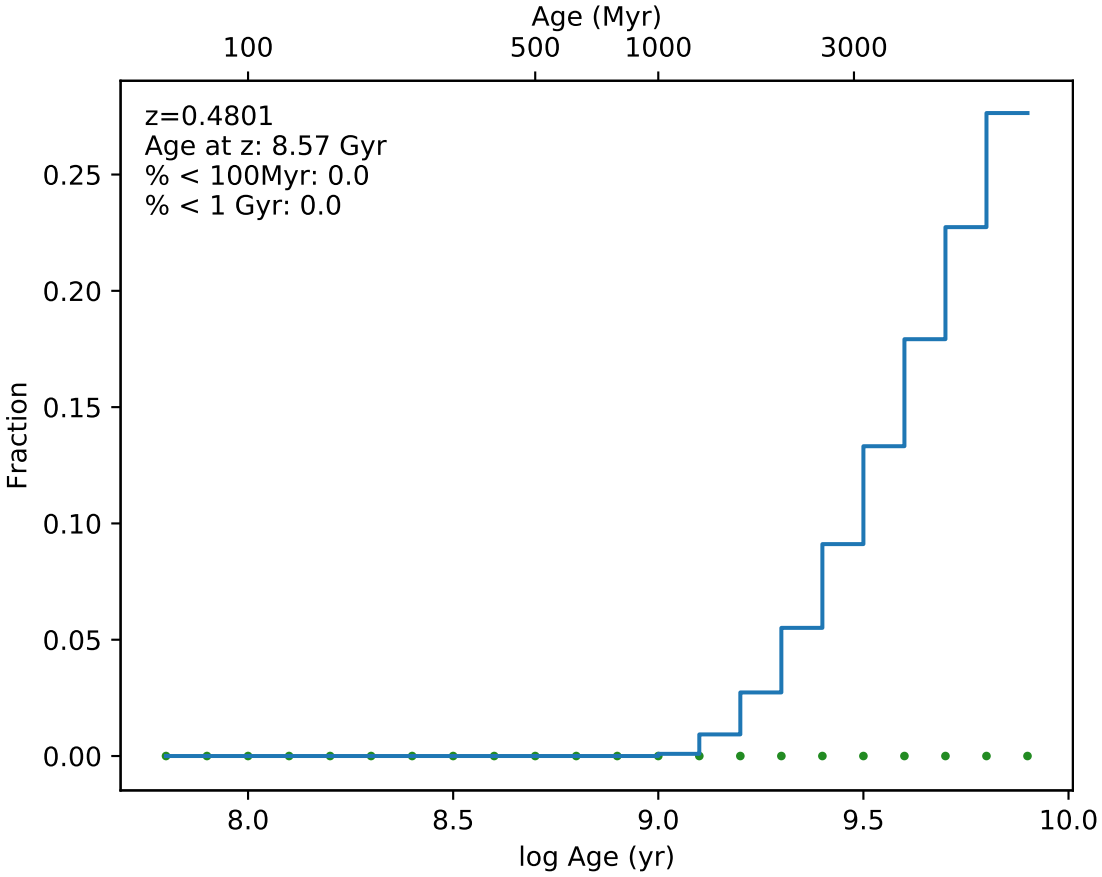
Age (Myr)
100
500
1000
3000
z=0.4801
Age at z: 8.57 Gyr
% < 100Myr: 0.0
% < 1 Gyr: 0.0
Fraction
0.25
0.20
0.15
0.10
0.05
0.00
8.0
8.5
9.0
9.5
10.0
log Age (yr)

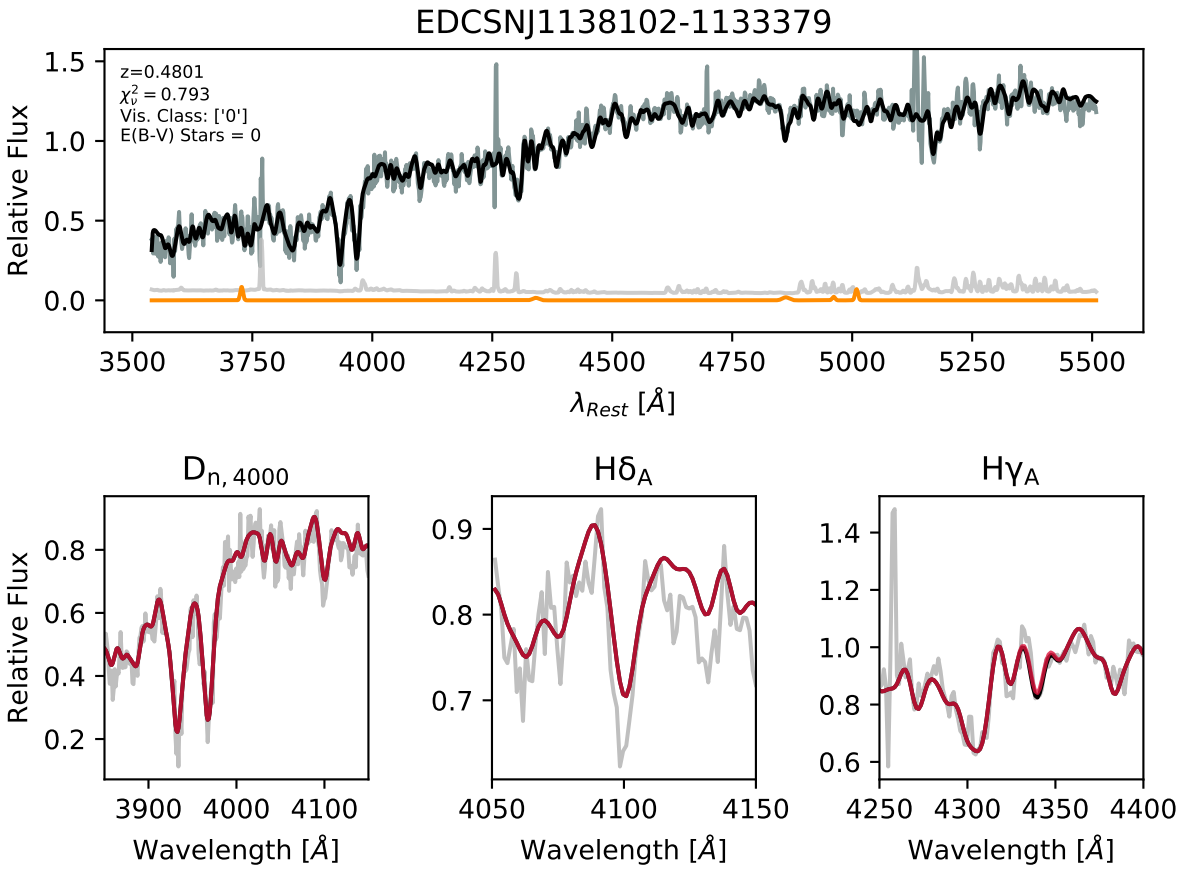
EDCSNJ1138102-1133379
z=0.4801
$\chi^2_\nu = 0.793$
Vis. Class: ['0']
E(B-V) Stars = 0
Relative Flux
λ_{Rest} [Å]
$D_{n,4000}$
$H\delta_A$
$H\gamma_A$
Wavelength [Å]

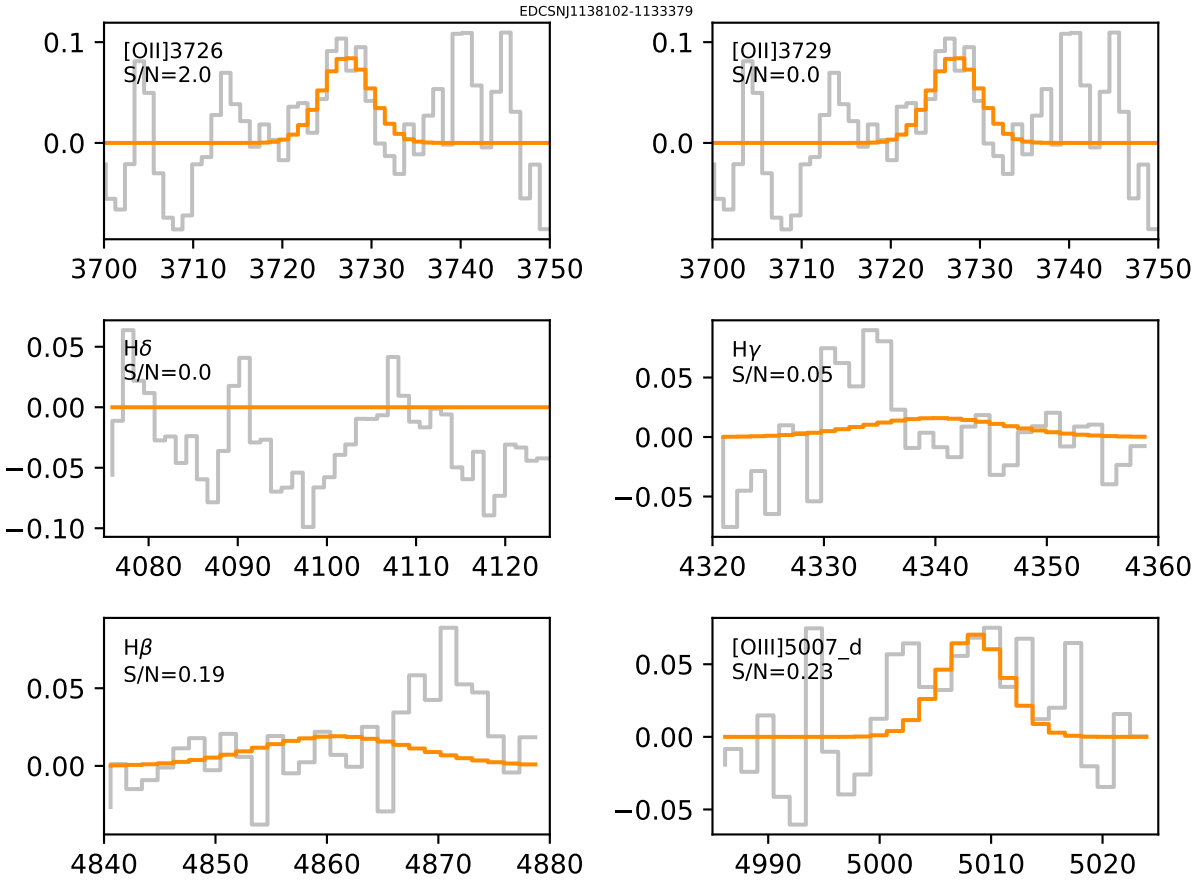
EDCSNJ1138102-1133379
[OII]3726
S/N=2.0
[OII]3729
S/N=0.0
Hδ
S/N=0.0
Hγ
S/N=0.05
Hβ
S/N=0.19
[OIII]5007_d
S/N=0.23

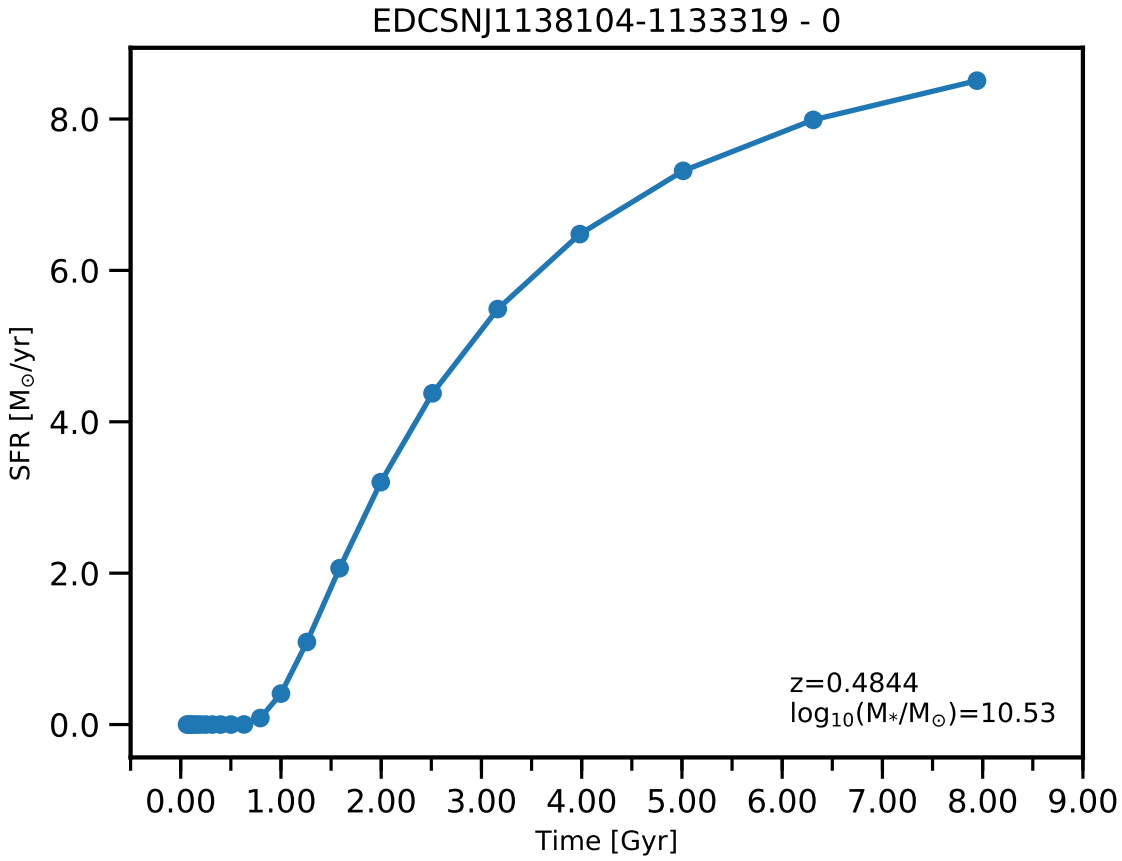
EDCSNJ1138104-1133319 - 0
SFR [M⊙/yr]
8.0
6.0
4.0
2.0
0.0
0.00
1.00
2.00
3.00
4.00
5.00
6.00
7.00
8.00
9.00
Time [Gyr]
z=0.4844
log10(M*/M⊙)=10.53

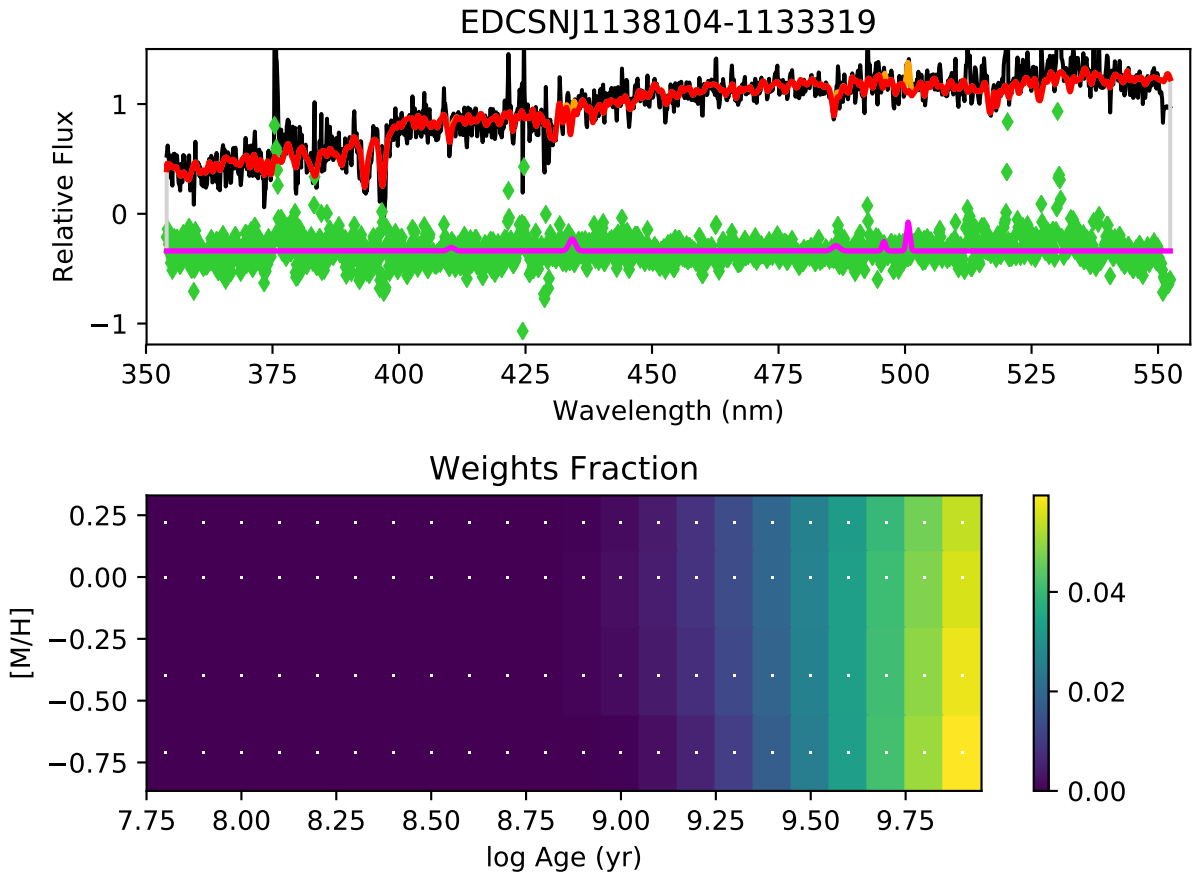
EDCSNJ1138104-1133319
Relative Flux
1
0
−1
350
375
400
425
450
475
500
525
550
Wavelength (nm)
Weights Fraction
[M/H]
0.25
0.00
−0.25
−0.50
−0.75
7.75
8.00
8.25
8.50
8.75
9.00
9.25
9.50
9.75
log Age (yr)
0.04
0.02
0.00

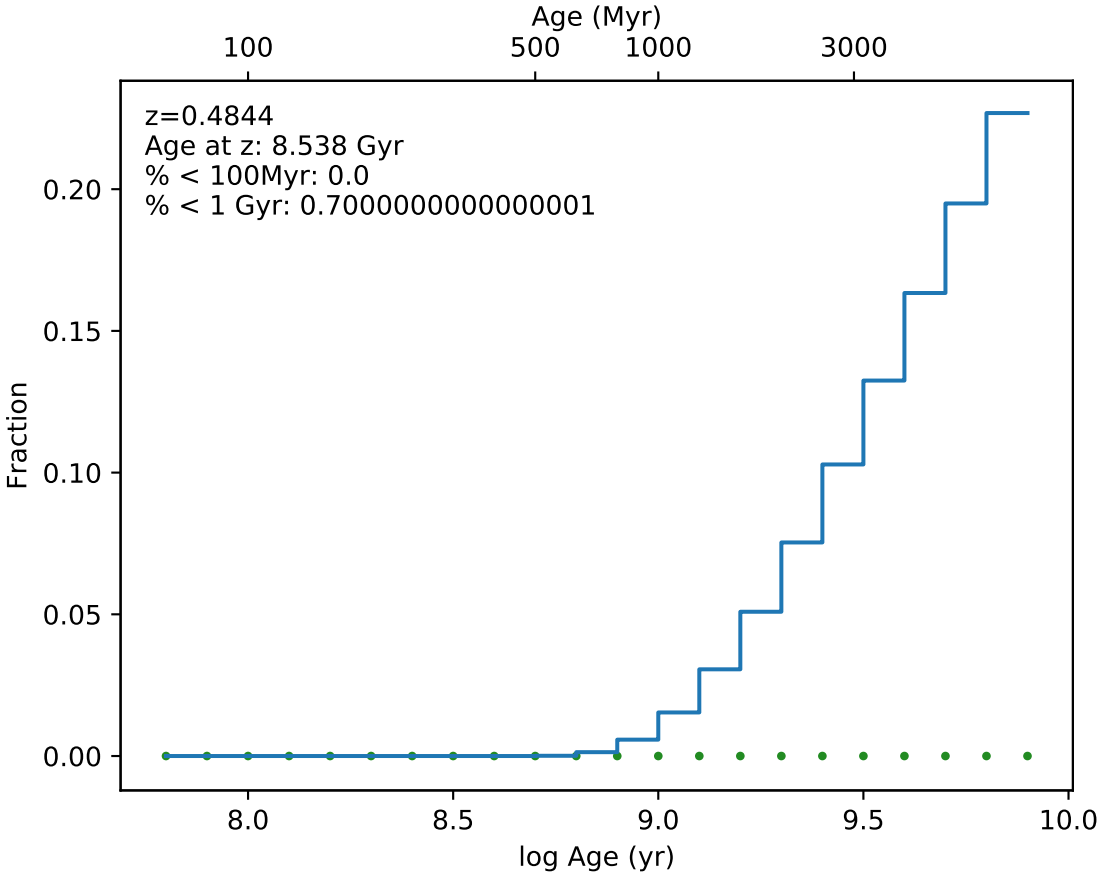
Age (Myr)
100
500
1000
3000
z=0.4844
Age at z: 8.538 Gyr
% < 100Myr: 0.0
% < 1 Gyr: 0.7000000000000001
Fraction
0.20
0.15
0.10
0.05
0.00
8.0
8.5
9.0
9.5
10.0
log Age (yr)

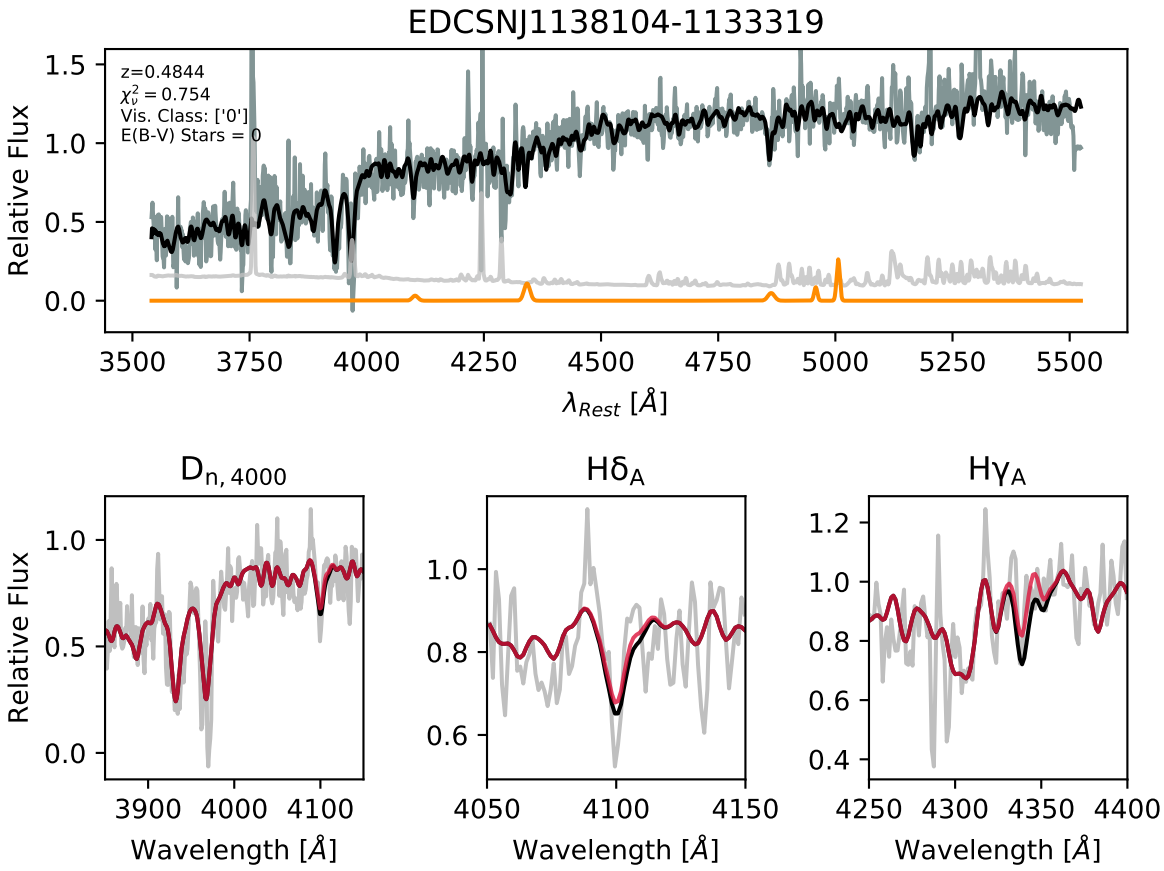
EDCSNJ1138104-1133319
z=0.4844
$\chi^2_\nu = 0.754$
Vis. Class: ['0']
E(B-V) Stars = 0
Relative Flux
λ_{Rest} [Å]
$D_{n,4000}$
$H\delta_A$
$H\gamma_A$
Wavelength [Å]

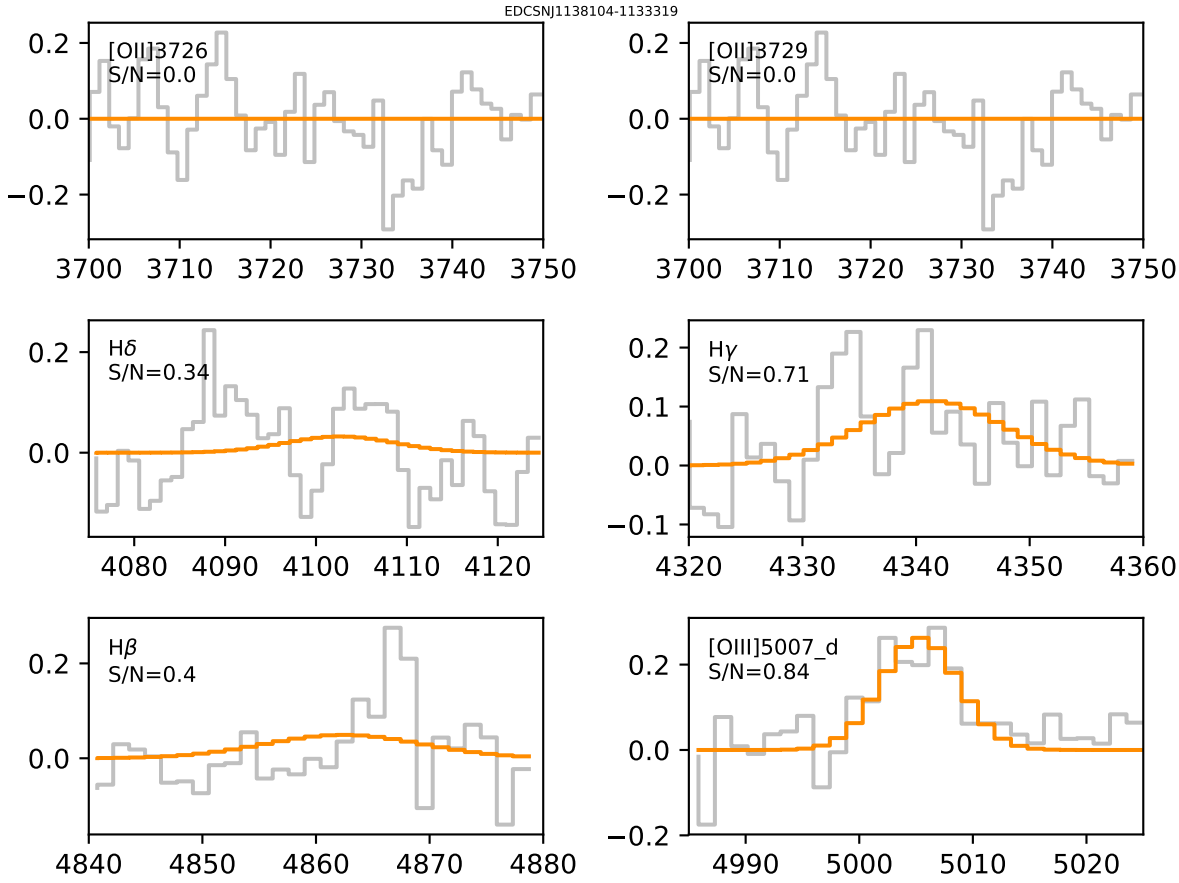
EDCSNJ1138104-1133319
[OII]3726
S/N=0.0
[OII]3729
S/N=0.0
Hδ
S/N=0.34
Hγ
S/N=0.71
Hβ
S/N=0.4
[OIII]5007_d
S/N=0.84

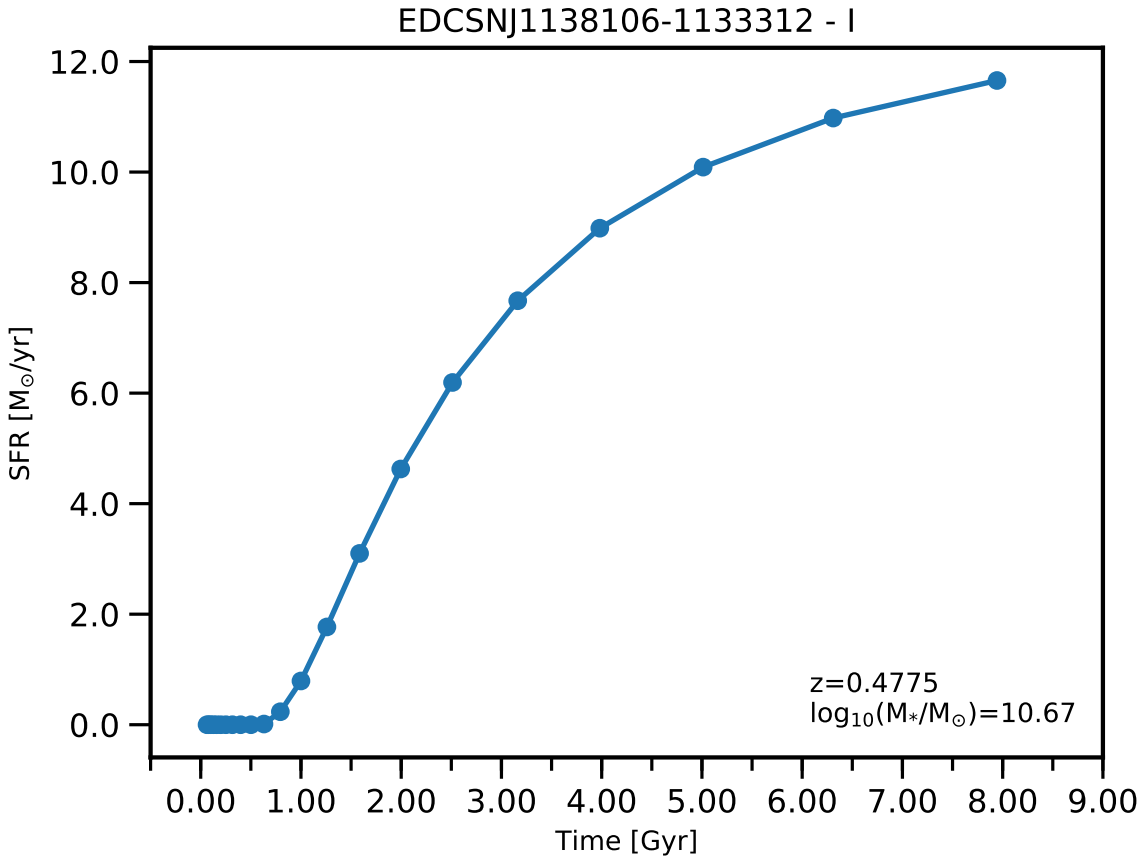
EDCSNJ1138106-1133312 - I
SFR [M⊙/yr]
Time [Gyr]
z=0.4775
log10(M*/M⊙)=10.67
0.0
2.0
4.0
6.0
8.0
10.0
12.0
0.00
1.00
2.00
3.00
4.00
5.00
6.00
7.00
8.00
9.00

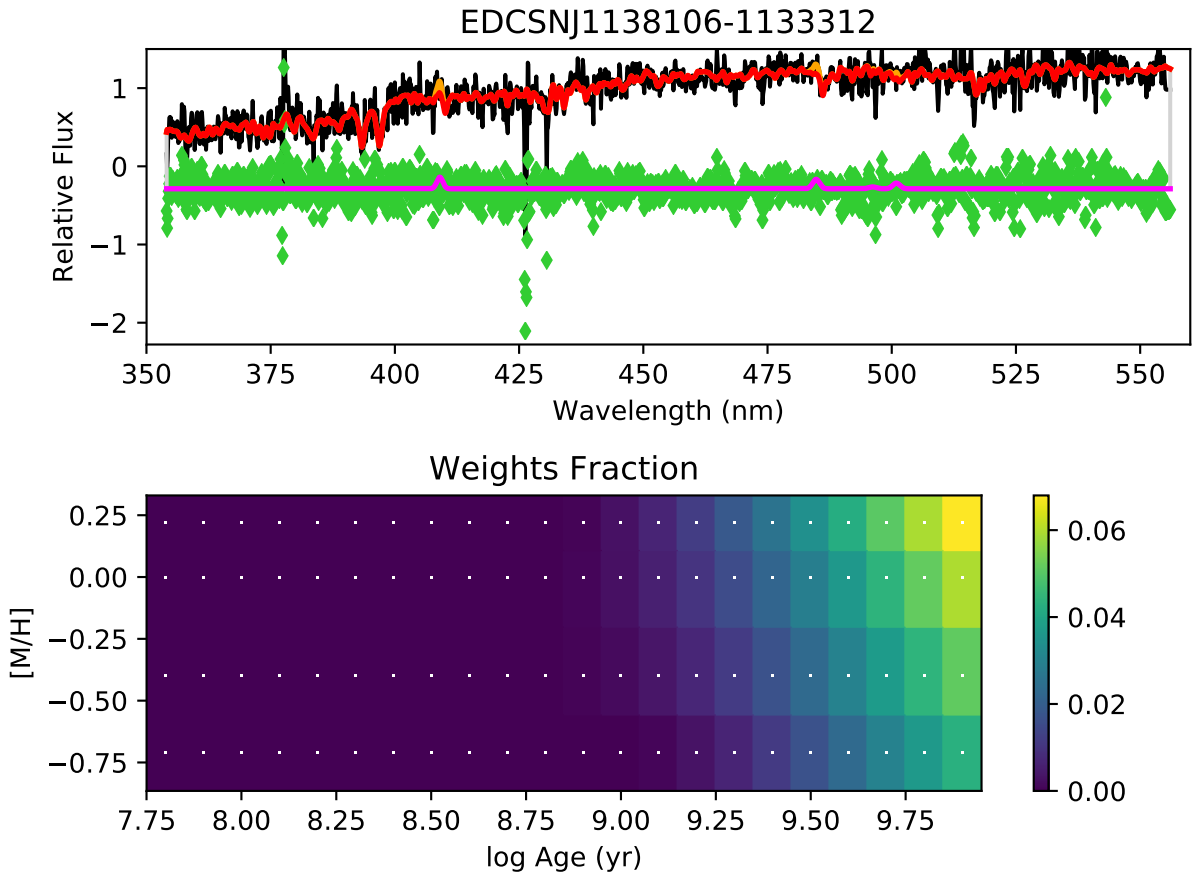
EDCSNJ1138106-1133312
Relative Flux
1
0
−1
−2
350
375
400
425
450
475
500
525
550
Wavelength (nm)
Weights Fraction
[M/H]
0.25
0.00
−0.25
−0.50
−0.75
7.75
8.00
8.25
8.50
8.75
9.00
9.25
9.50
9.75
log Age (yr)
0.06
0.04
0.02
0.00

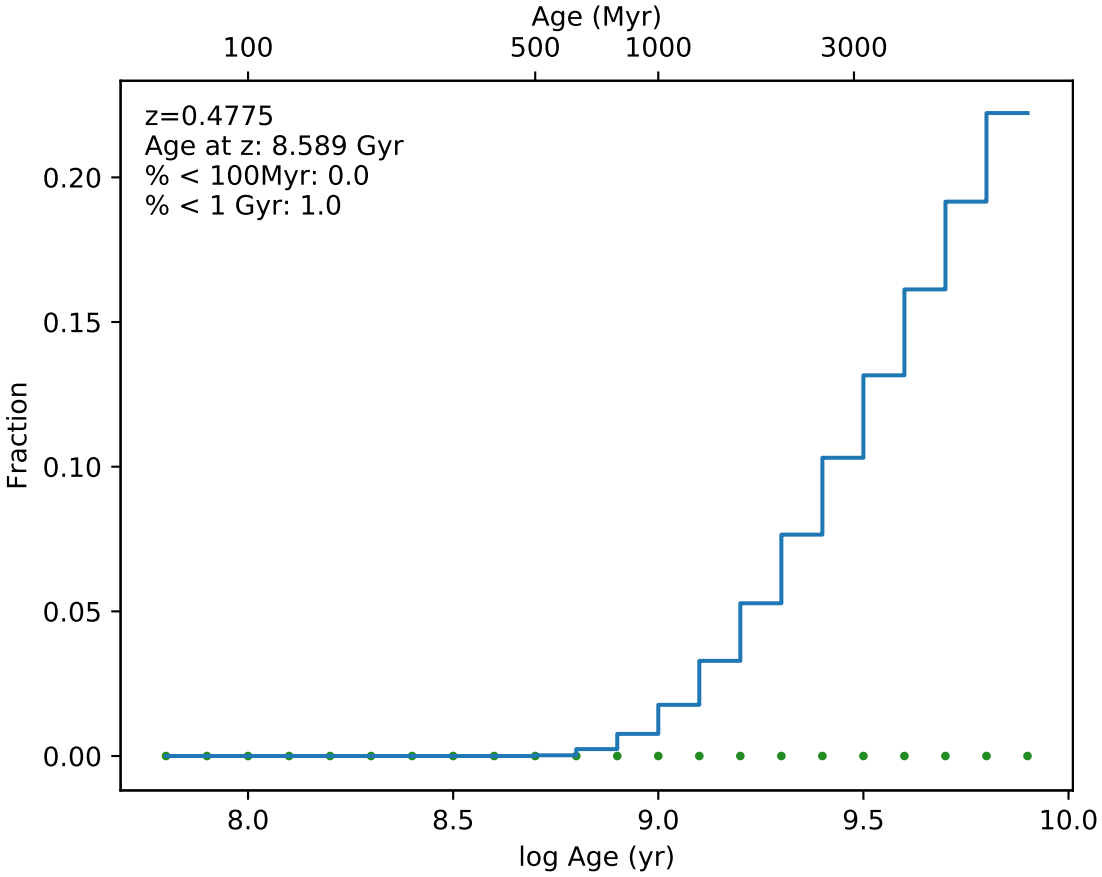
Age (Myr)
100
500
1000
3000
z=0.4775
Age at z: 8.589 Gyr
% < 100Myr: 0.0
% < 1 Gyr: 1.0
Fraction
0.00
0.05
0.10
0.15
0.20
8.0
8.5
9.0
9.5
10.0
log Age (yr)

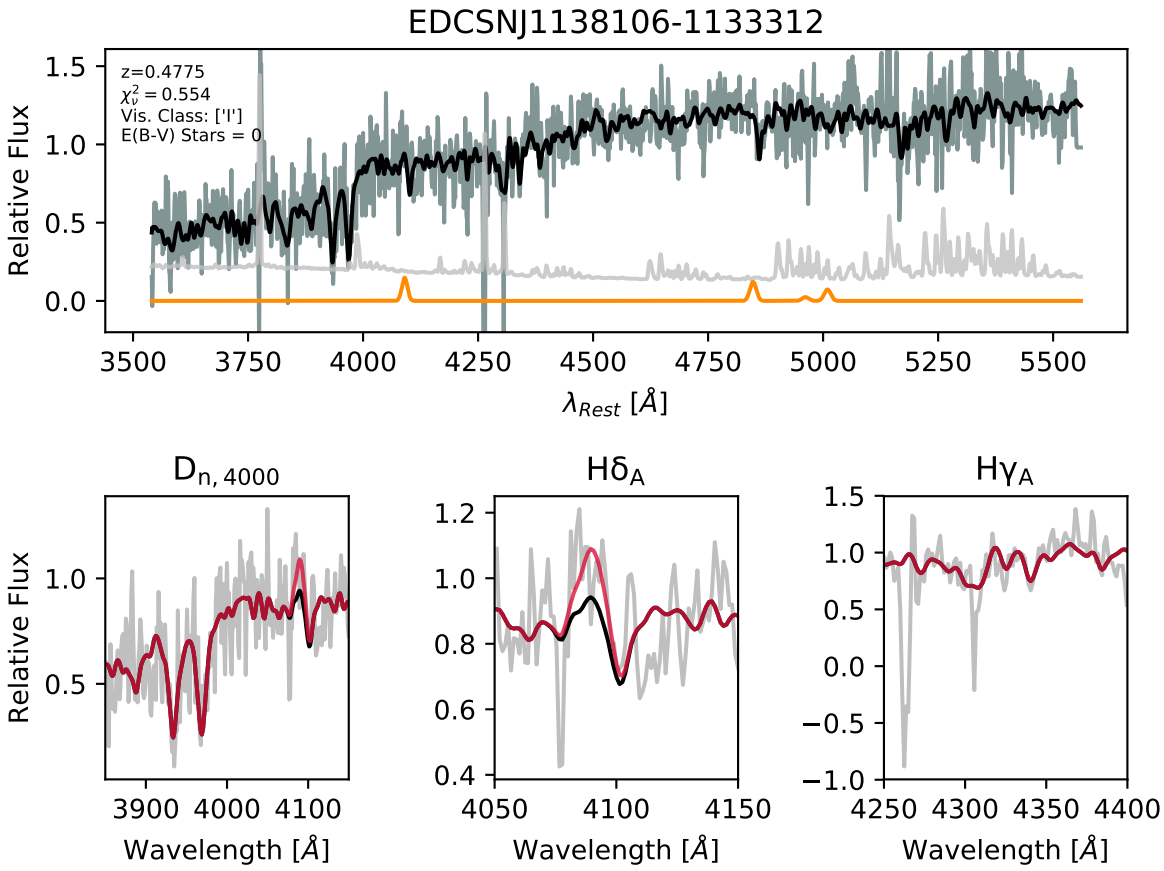
EDCSNJ1138106-1133312
z=0.4775
$\chi^2_\nu = 0.554$
Vis. Class: ['I']
E(B-V) Stars = 0
Relative Flux
λ_{Rest} [Å]
$D_{n,4000}$
$H\delta_A$
$H\gamma_A$
Wavelength [Å]

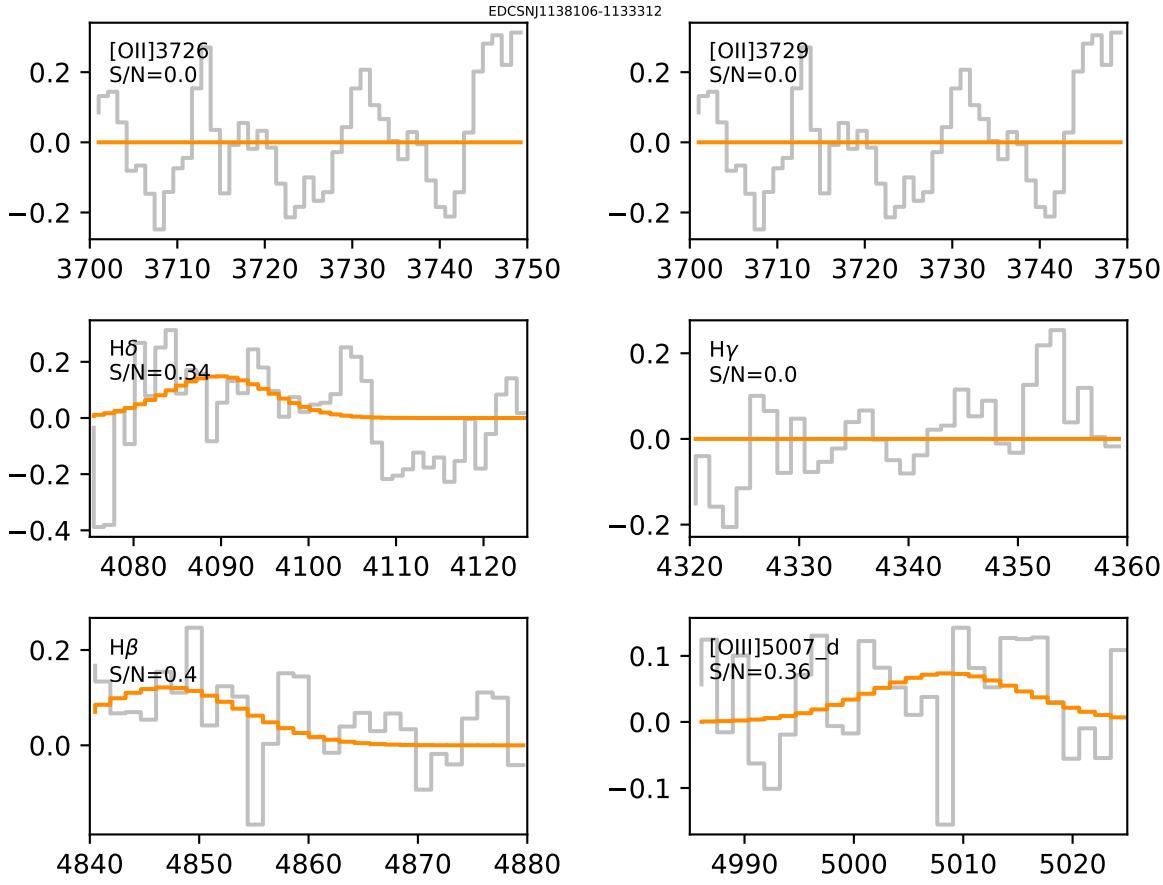
EDCSNJ1138106-1133312
[OII]3726
S/N=0.0
[OII]3729
S/N=0.0
Hδ
S/N=0.34
Hγ
S/N=0.0
Hβ
S/N=0.4
[OIII]5007_d
S/N=0.36

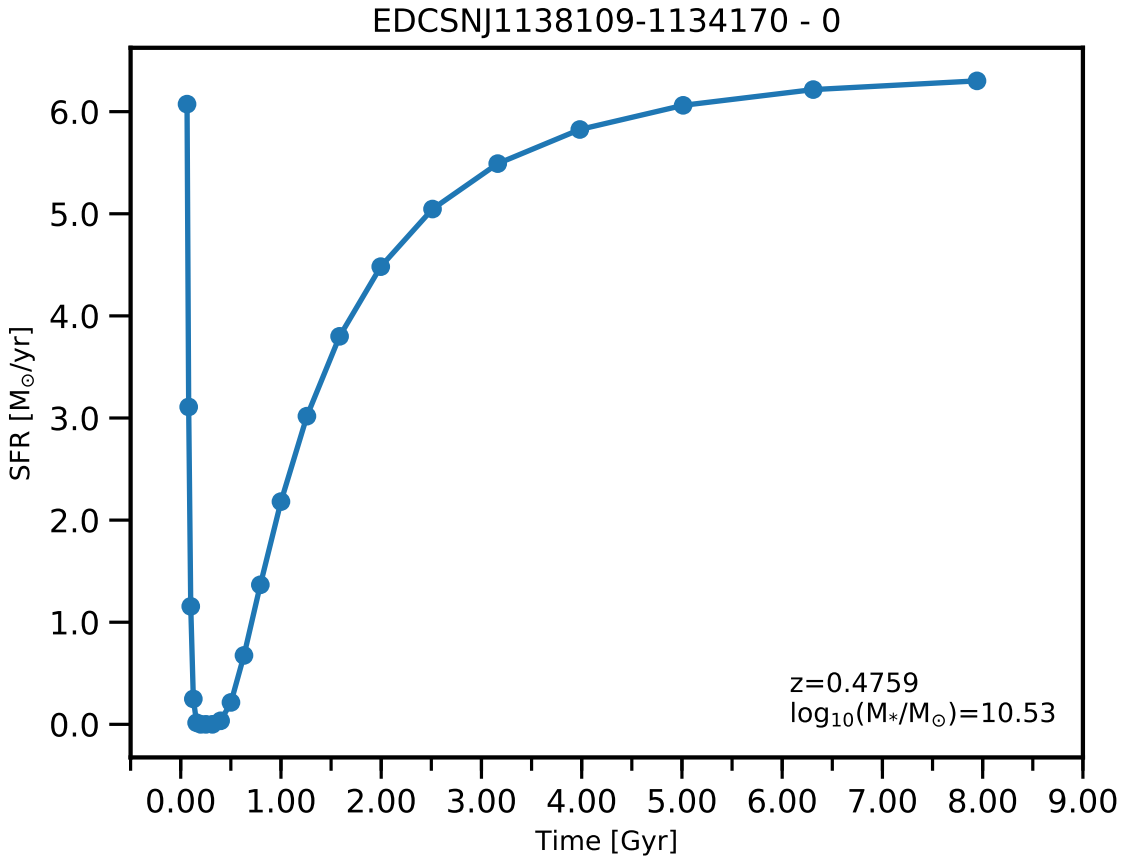
EDCSNJ1138109-1134170 - 0
SFR [M⊙/yr]
Time [Gyr]
z=0.4759
log10(M*/M⊙)=10.53
0.0
1.0
2.0
3.0
4.0
5.0
6.0
0.00
1.00
2.00
3.00
4.00
5.00
6.00
7.00
8.00
9.00

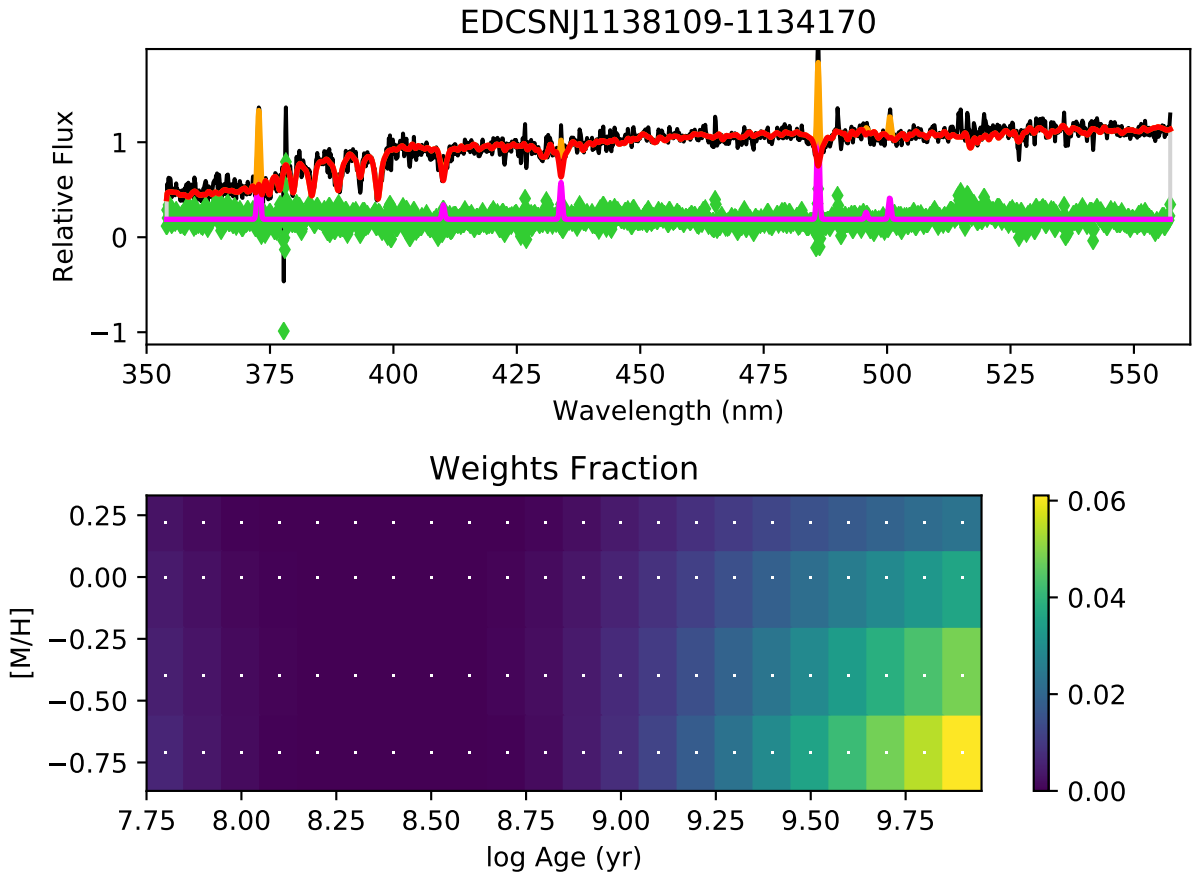
EDCSNJ1138109-1134170
Relative Flux
1
0
−1
350
375
400
425
450
475
500
525
550
Wavelength (nm)
Weights Fraction
[M/H]
0.25
0.00
−0.25
−0.50
−0.75
7.75
8.00
8.25
8.50
8.75
9.00
9.25
9.50
9.75
log Age (yr)
0.06
0.04
0.02
0.00

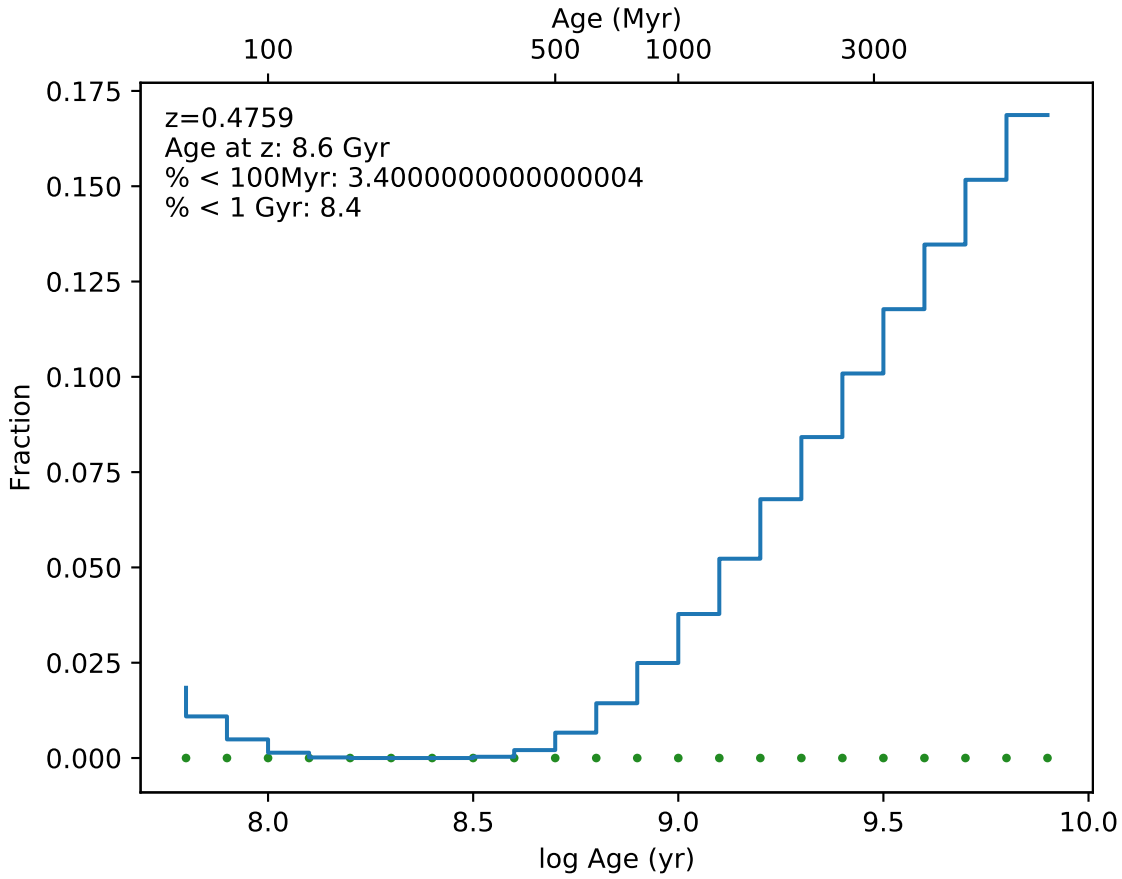
Age (Myr)
100
500
1000
3000
z=0.4759
Age at z: 8.6 Gyr
% < 100Myr: 3.4000000000000004
% < 1 Gyr: 8.4
Fraction
0.175
0.150
0.125
0.100
0.075
0.050
0.025
0.000
8.0
8.5
9.0
9.5
10.0
log Age (yr)

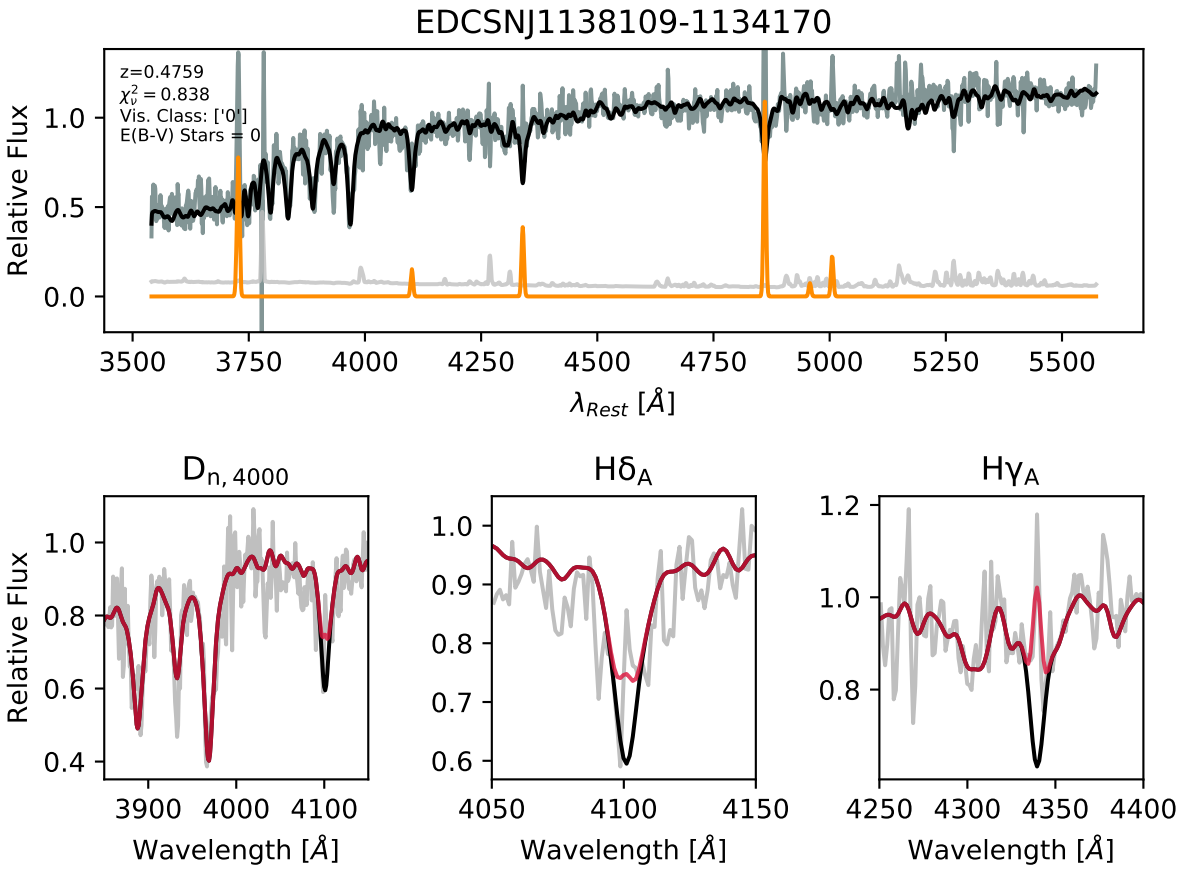
EDCSNJ1138109-1134170
z=0.4759
$\chi^2_\nu = 0.838$
Vis. Class: ['0']
E(B-V) Stars = 0
Relative Flux
λ_{Rest} [Å]
$D_{n,4000}$
$H\delta_A$
$H\gamma_A$
Wavelength [Å]

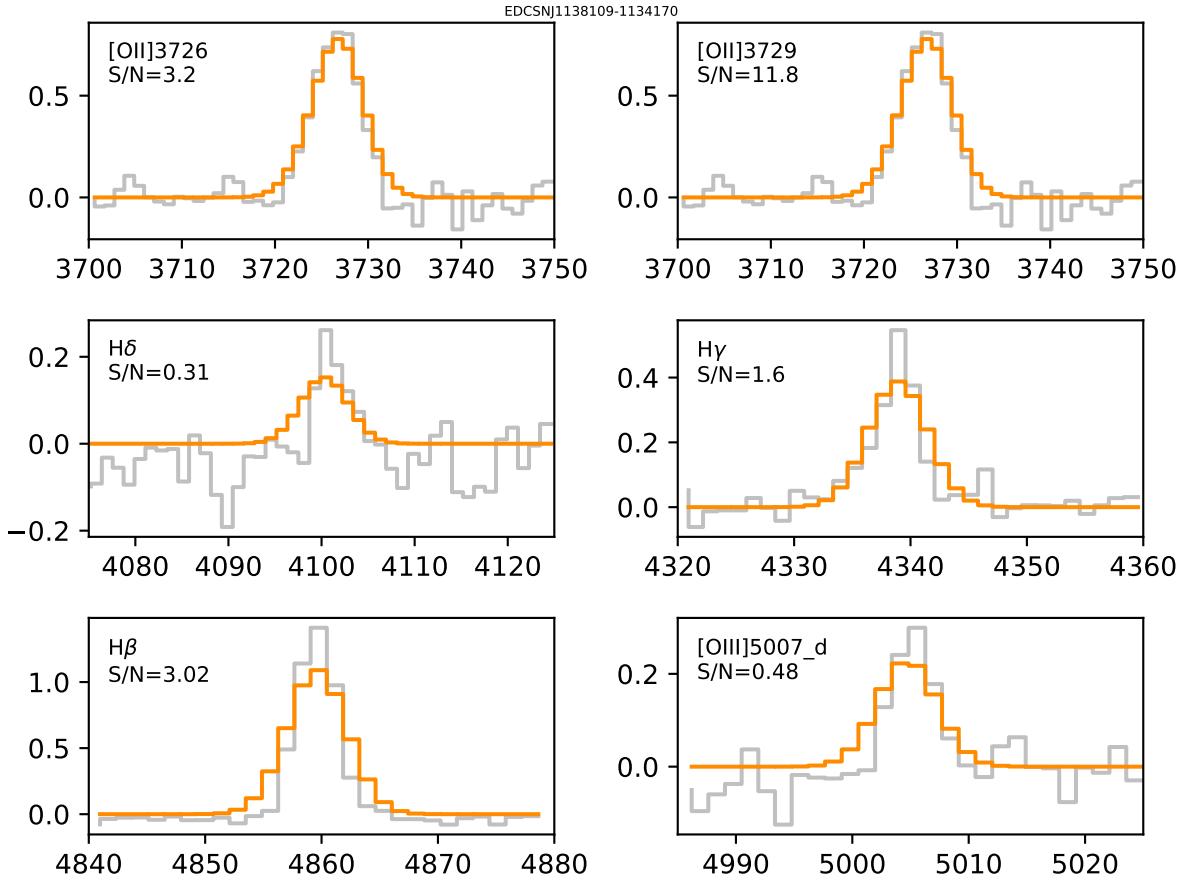
EDCSNJ1138109-1134170
[OII]3726
S/N=3.2
[OII]3729
S/N=11.8
Hδ
S/N=0.31
Hγ
S/N=1.6
Hβ
S/N=3.02
[OIII]5007_d
S/N=0.48

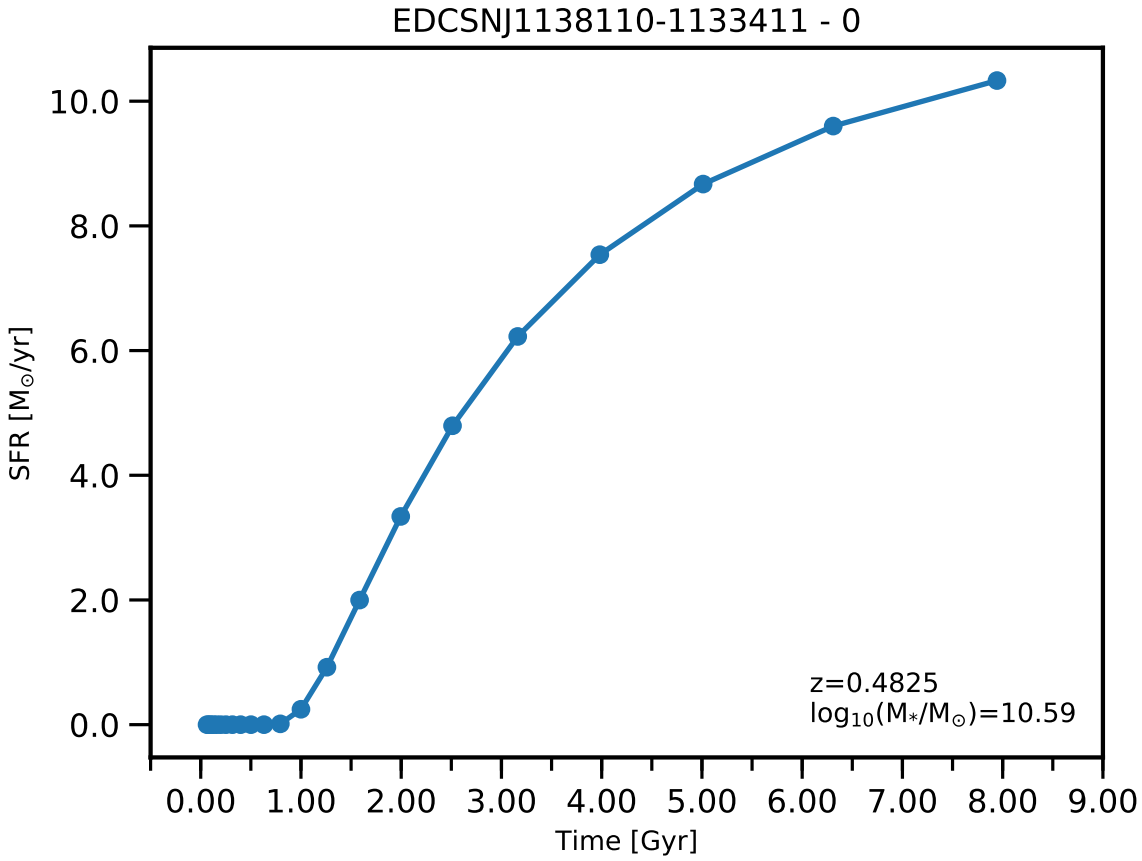
EDCSNJ1138110-1133411 - 0
SFR [M⊙/yr]
10.0
8.0
6.0
4.0
2.0
0.0
0.00
1.00
2.00
3.00
4.00
5.00
6.00
7.00
8.00
9.00
Time [Gyr]
z=0.4825
log10(M*/M⊙)=10.59

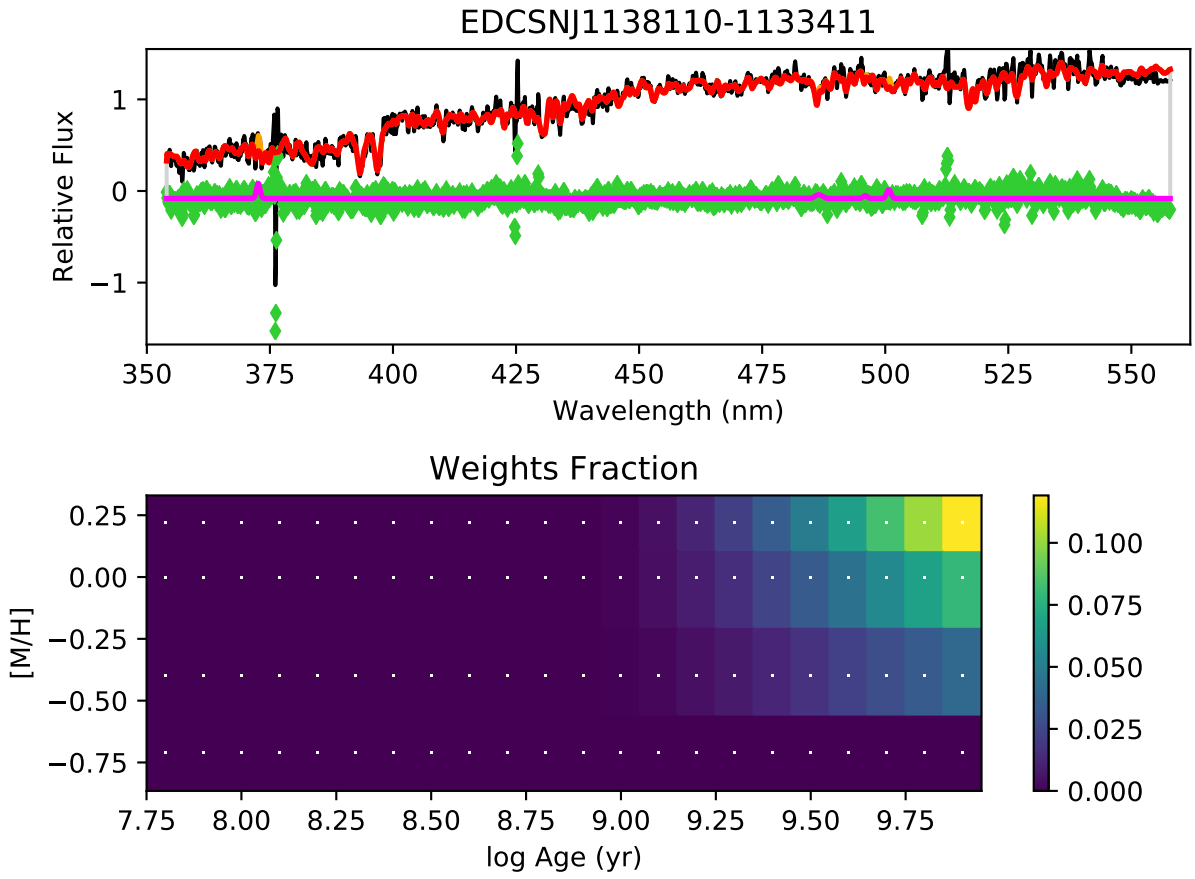
EDCSNJ1138110-1133411
Relative Flux
1
0
−1
350
375
400
425
450
475
500
525
550
Wavelength (nm)
Weights Fraction
[M/H]
0.25
0.00
−0.25
−0.50
−0.75
7.75
8.00
8.25
8.50
8.75
9.00
9.25
9.50
9.75
log Age (yr)
0.100
0.075
0.050
0.025
0.000

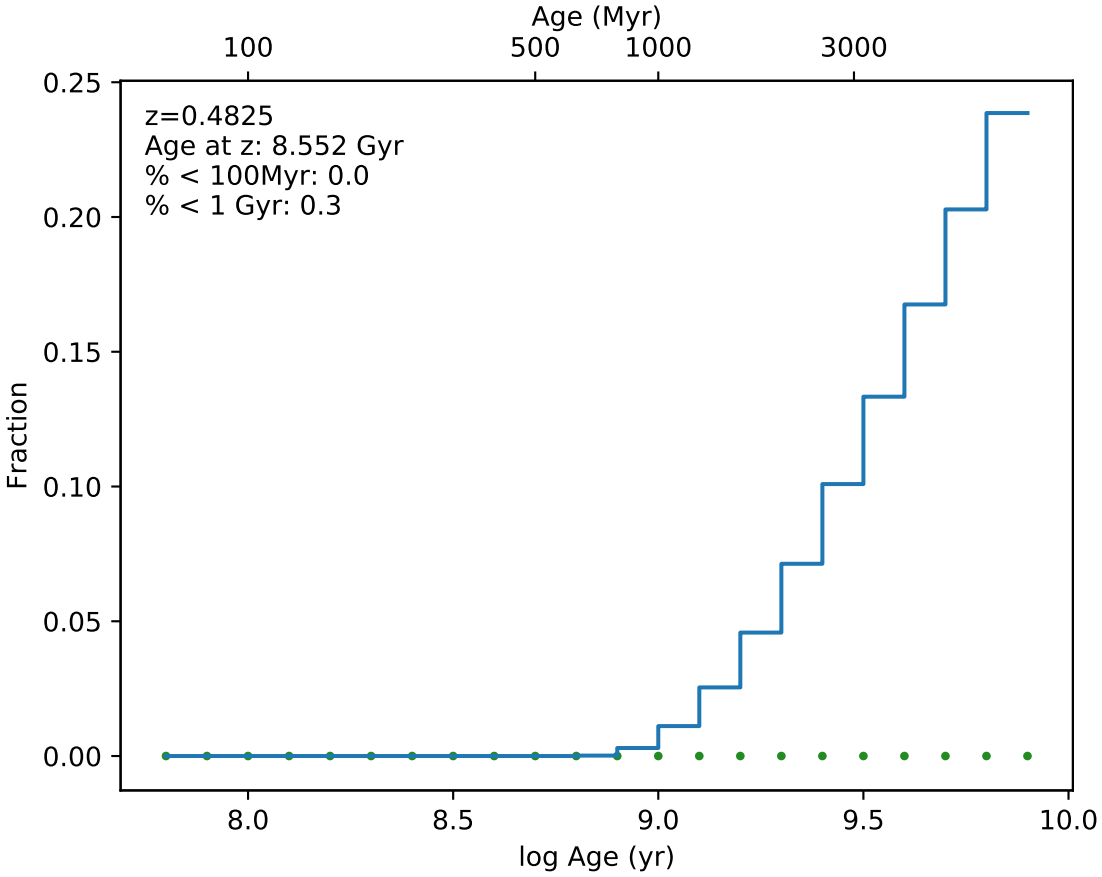
Age (Myr)
100
500
1000
3000
z=0.4825
Age at z: 8.552 Gyr
% < 100Myr: 0.0
% < 1 Gyr: 0.3
Fraction
0.25
0.20
0.15
0.10
0.05
0.00
8.0
8.5
9.0
9.5
10.0
log Age (yr)

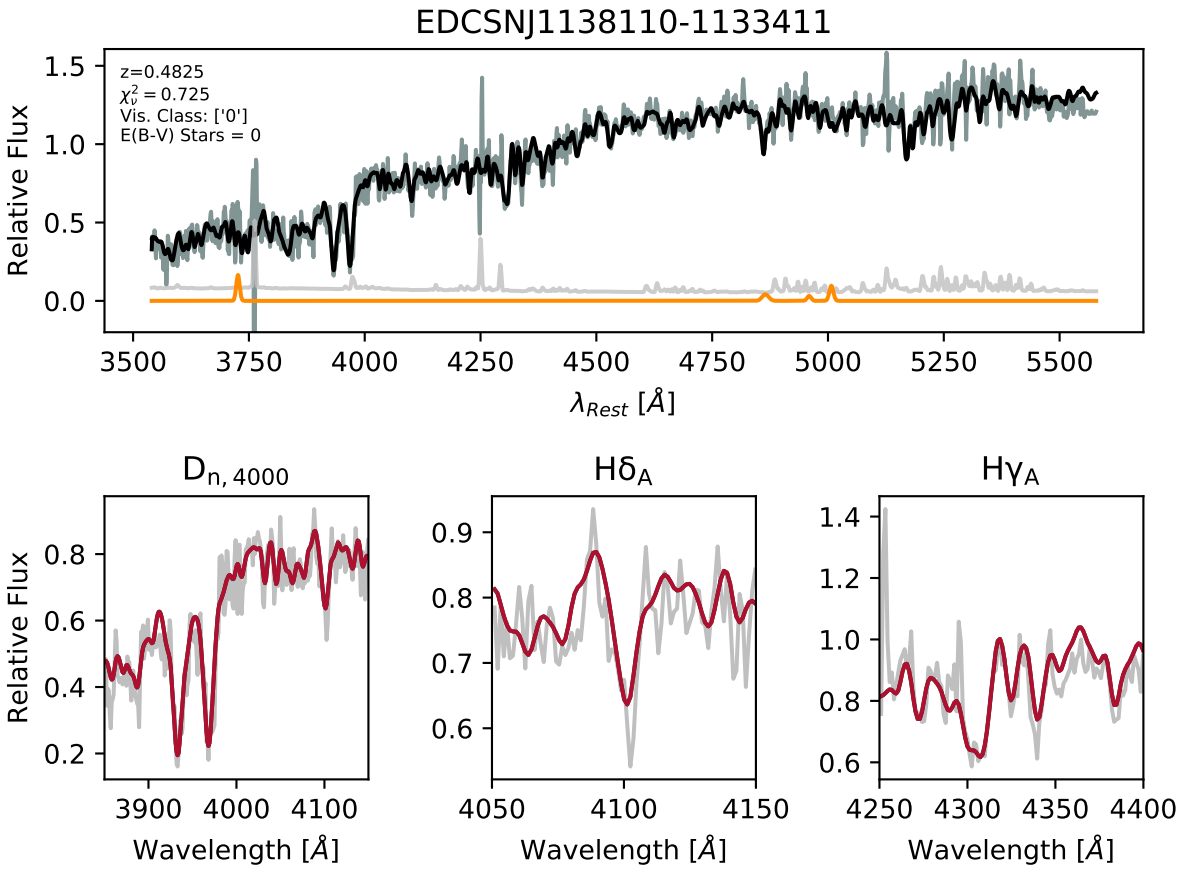
EDCSNJ1138110-1133411
z=0.4825
$\chi^2_\nu = 0.725$
Vis. Class: ['0']
E(B-V) Stars = 0
Relative Flux
λ_{Rest} [Å]
$D_{n,4000}$
$H\delta_A$
$H\gamma_A$
Wavelength [Å]

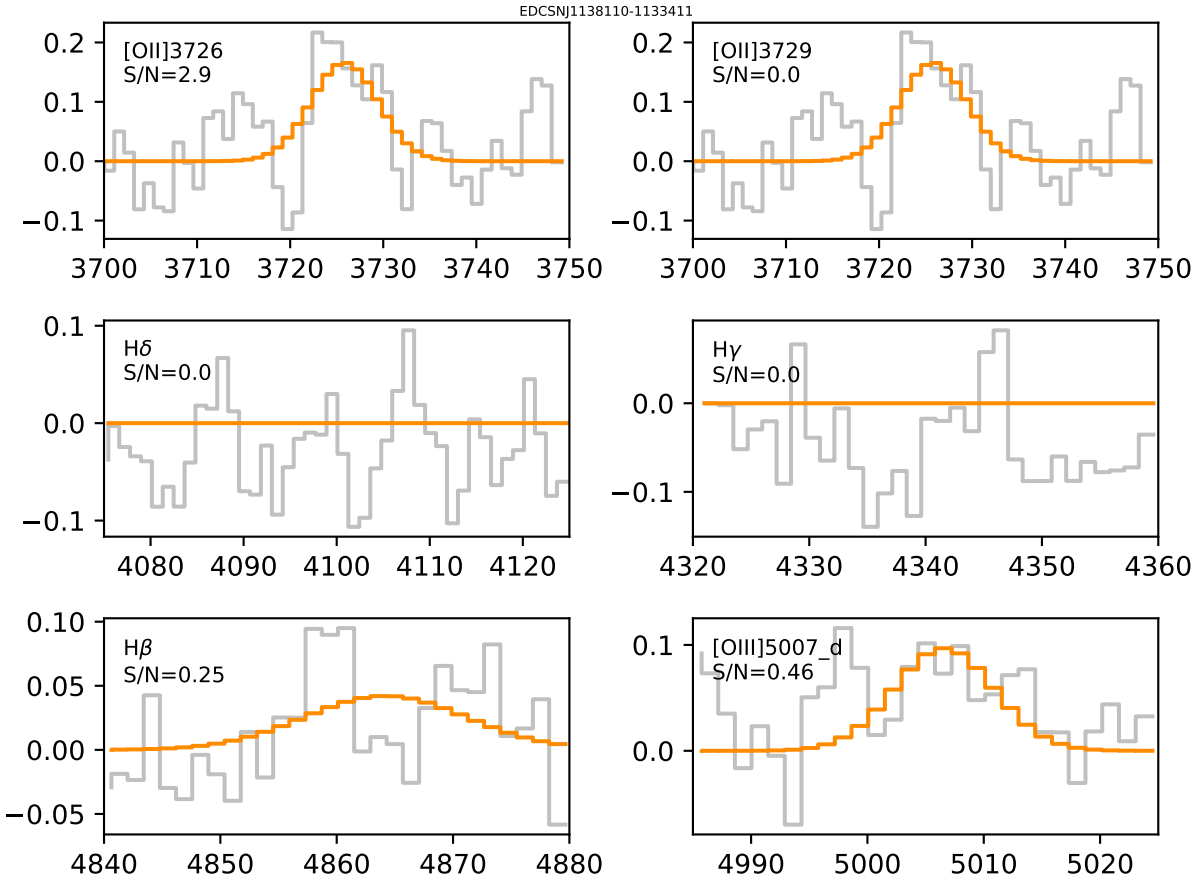
EDCSNJ1138110-1133411
[OII]3726
S/N=2.9
[OII]3729
S/N=0.0
Hδ
S/N=0.0
Hγ
S/N=0.0
Hβ
S/N=0.25
[OIII]5007_d
S/N=0.46

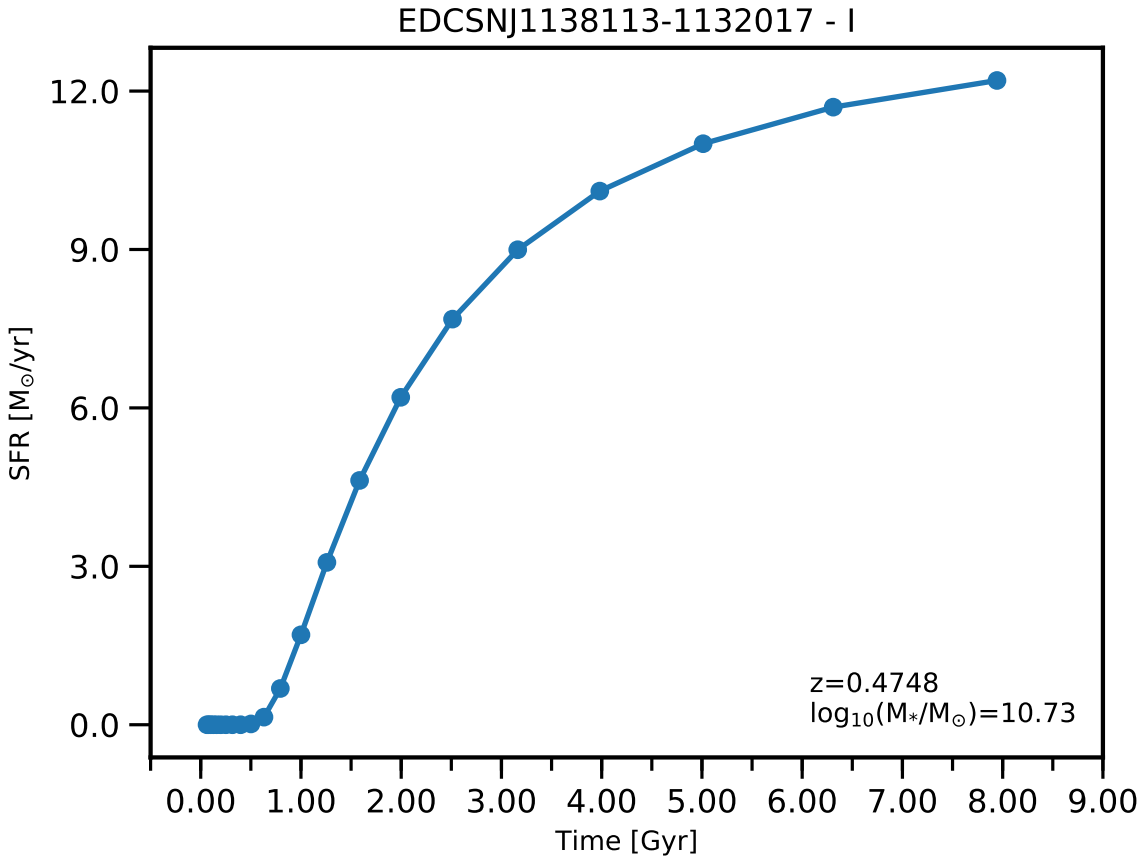
EDCSNJ1138113-1132017 - I
12.0
9.0
6.0
3.0
0.0
SFR [M⊙/yr]
0.00
1.00
2.00
3.00
4.00
5.00
6.00
7.00
8.00
9.00
Time [Gyr]
z=0.4748
log10(M*/M⊙)=10.73

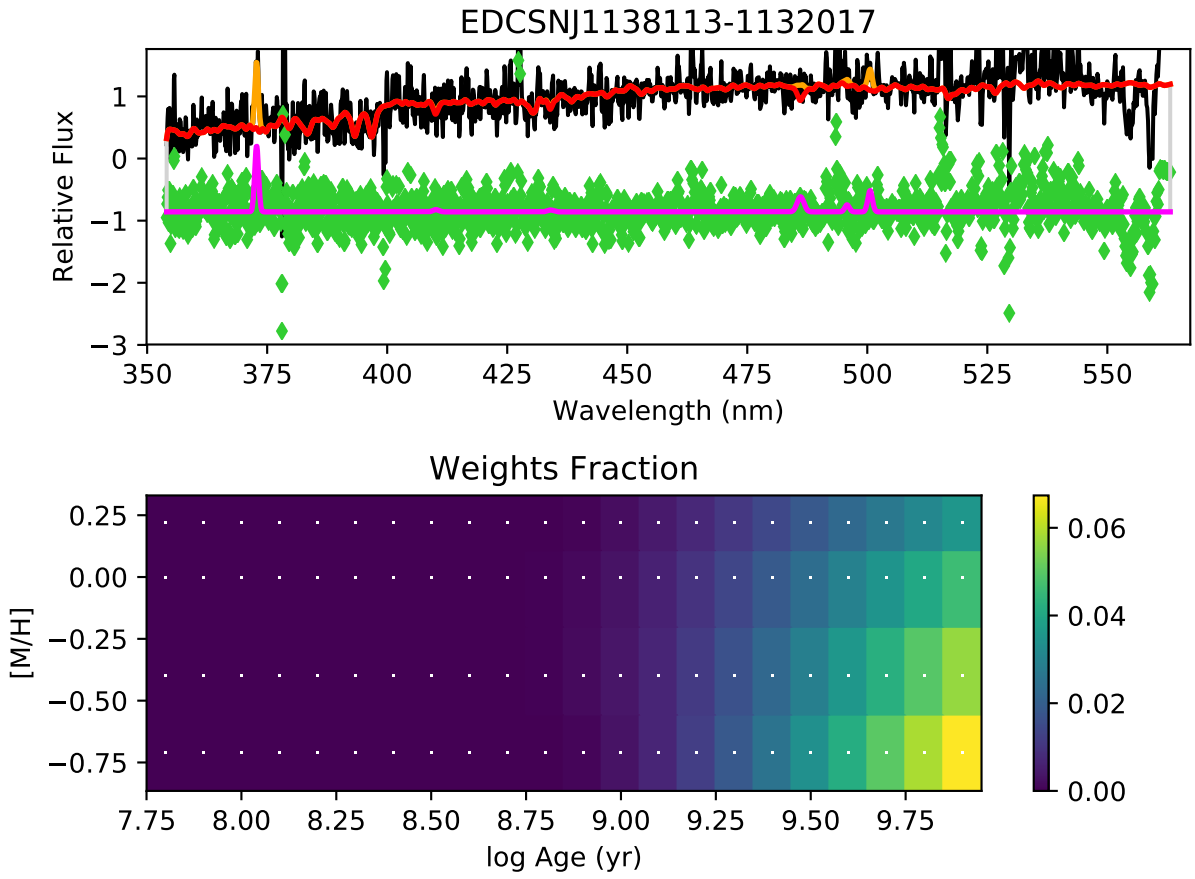
EDCSNJ1138113-1132017
Relative Flux
1
0
−1
−2
−3
350
375
400
425
450
475
500
525
550
Wavelength (nm)
Weights Fraction
[M/H]
0.25
0.00
−0.25
−0.50
−0.75
7.75
8.00
8.25
8.50
8.75
9.00
9.25
9.50
9.75
log Age (yr)
0.06
0.04
0.02
0.00

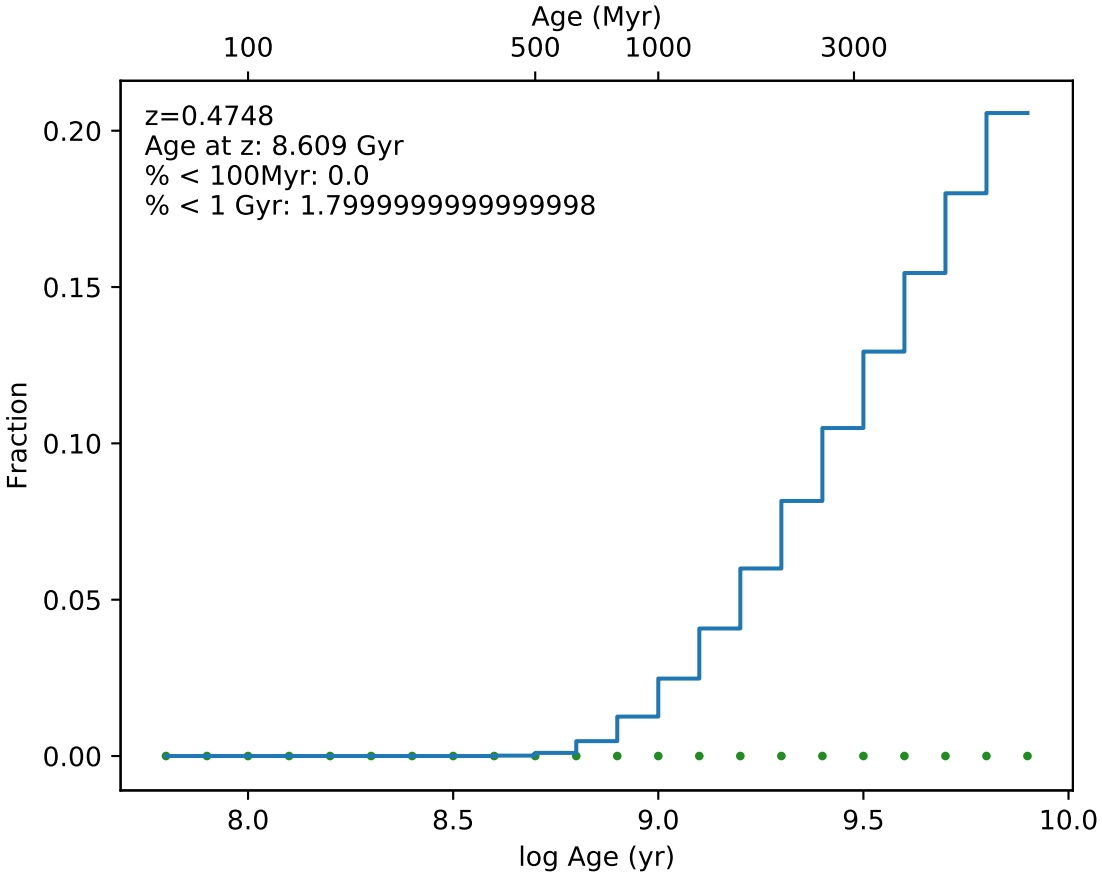
Age (Myr)
100
500
1000
3000
z=0.4748
Age at z: 8.609 Gyr
% < 100Myr: 0.0
% < 1 Gyr: 1.7999999999999998
0.20
0.15
0.10
0.05
0.00
Fraction
8.0
8.5
9.0
9.5
10.0
log Age (yr)

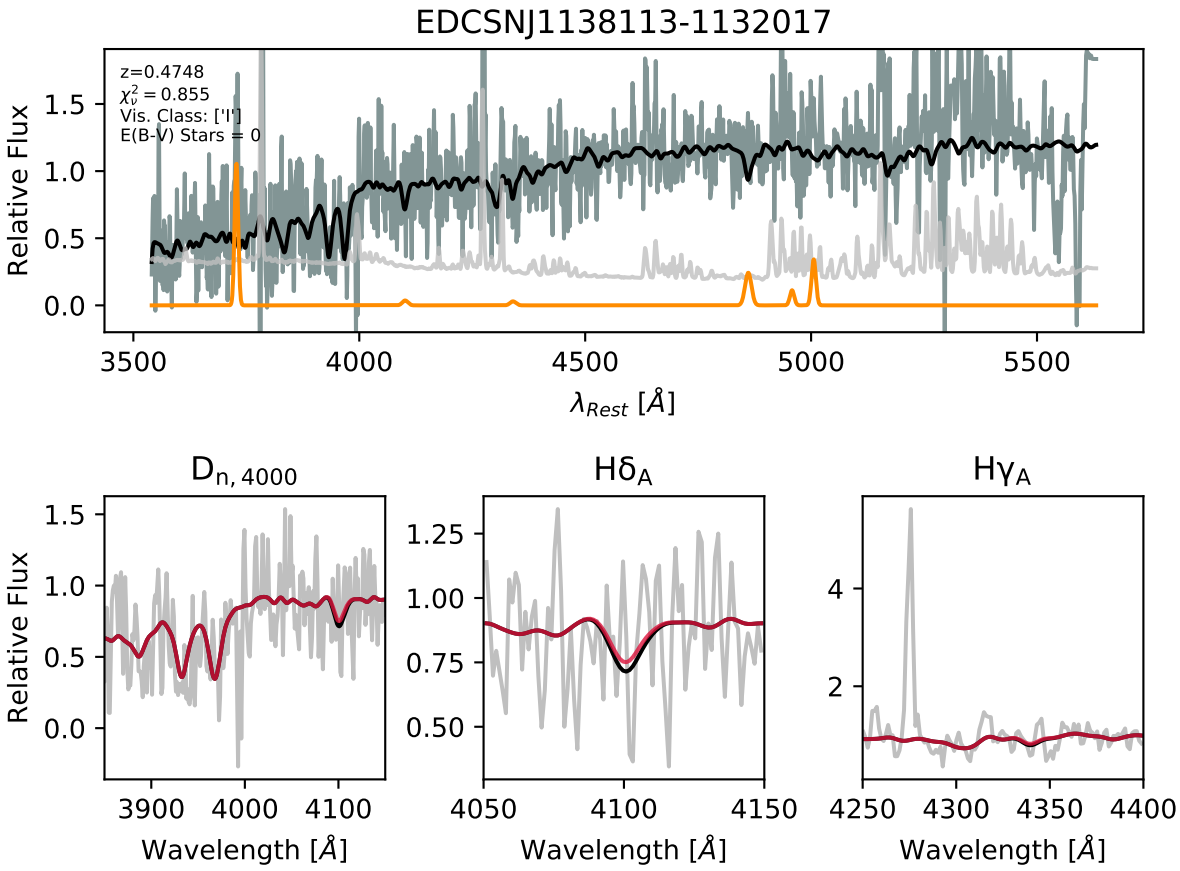
EDCSNJ1138113-1132017
z=0.4748
$\chi^2_\nu = 0.855$
Vis. Class: ['I']
E(B-V) Stars = 0
Relative Flux
λ_{Rest} [Å]
$D_{n,4000}$
$H\delta_A$
$H\gamma_A$
Wavelength [Å]

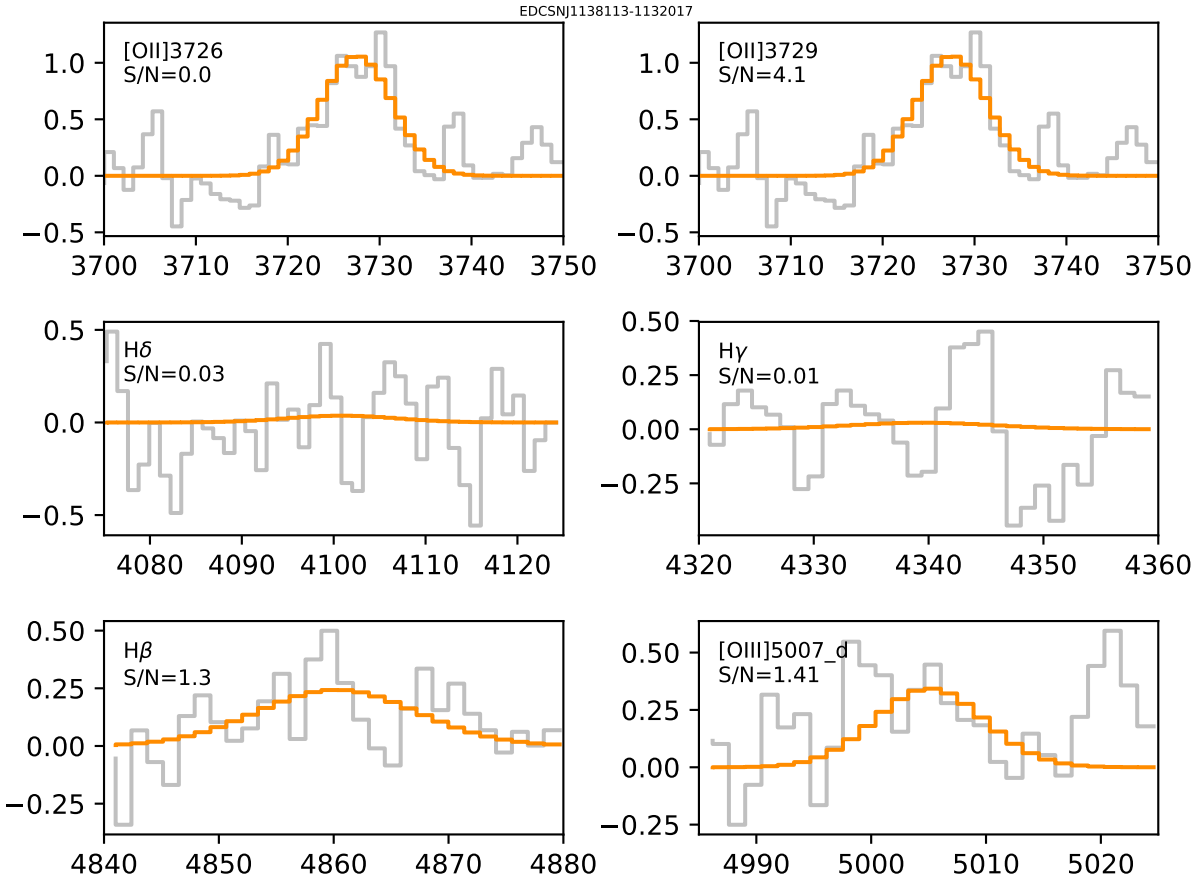
EDCSNJ1138113-1132017
[OII]3726
S/N=0.0
[OII]3729
S/N=4.1
Hδ
S/N=0.03
Hγ
S/N=0.01
Hβ
S/N=1.3
[OIII]5007_d
S/N=1.41

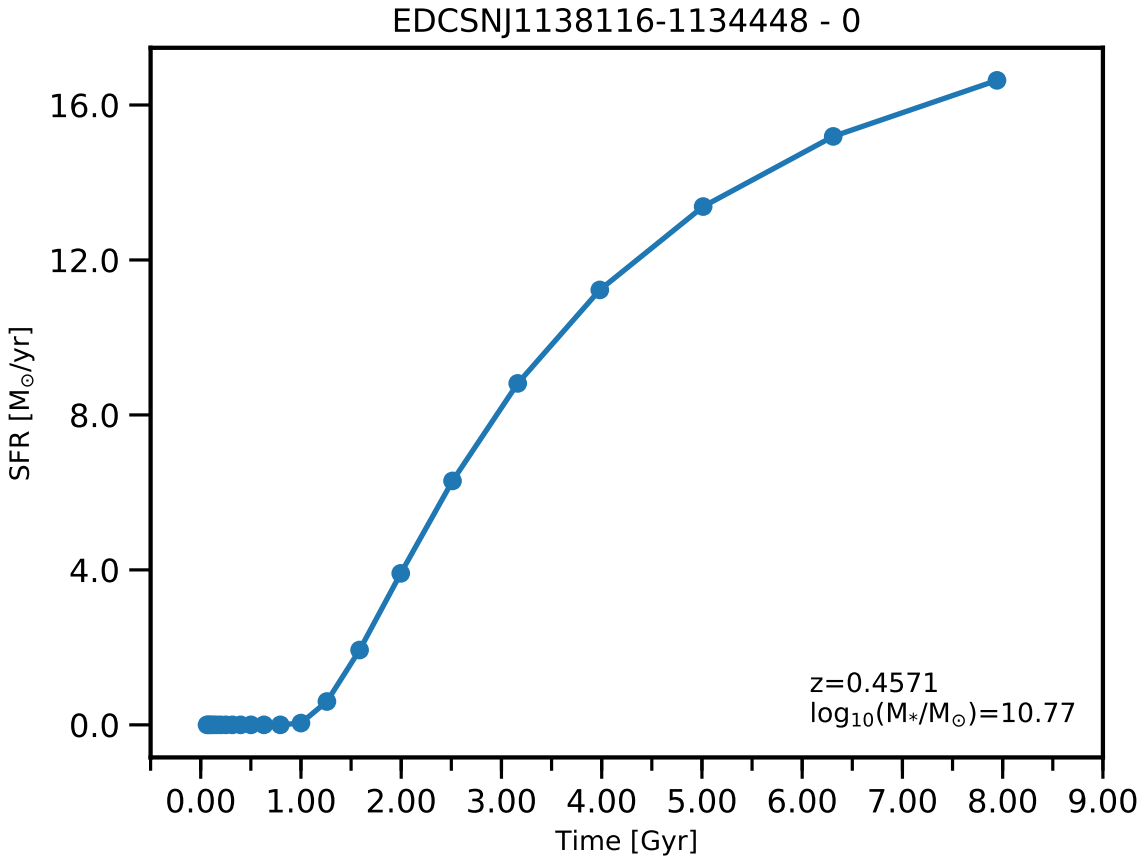
EDCSNJ1138116-1134448 - 0
SFR [M⊙/yr]
16.0
12.0
8.0
4.0
0.0
0.00
1.00
2.00
3.00
4.00
5.00
6.00
7.00
8.00
9.00
Time [Gyr]
z=0.4571
log10(M*/M⊙)=10.77

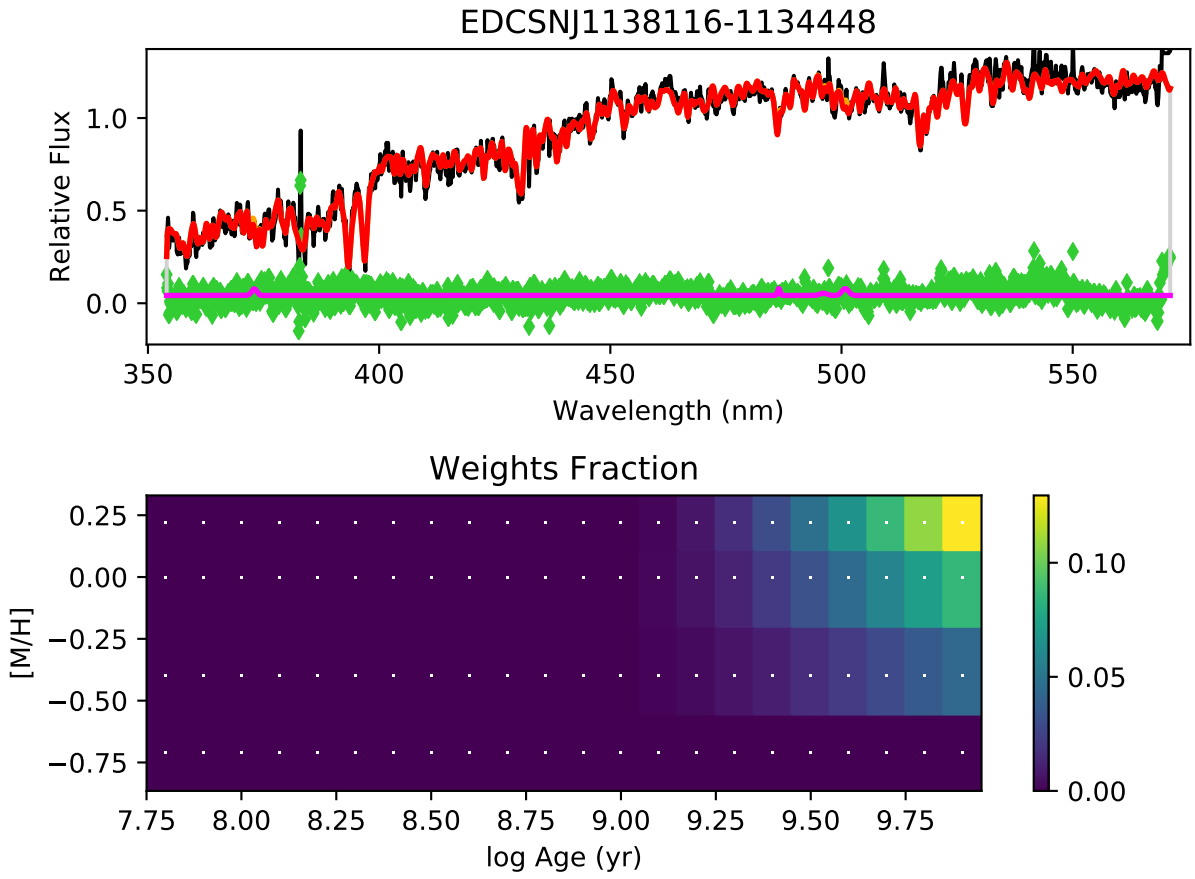
EDCSNJ1138116-1134448
Relative Flux
1.0
0.5
0.0
350
400
450
500
550
Wavelength (nm)
Weights Fraction
[M/H]
0.25
0.00
−0.25
−0.50
−0.75
7.75
8.00
8.25
8.50
8.75
9.00
9.25
9.50
9.75
log Age (yr)
0.10
0.05
0.00

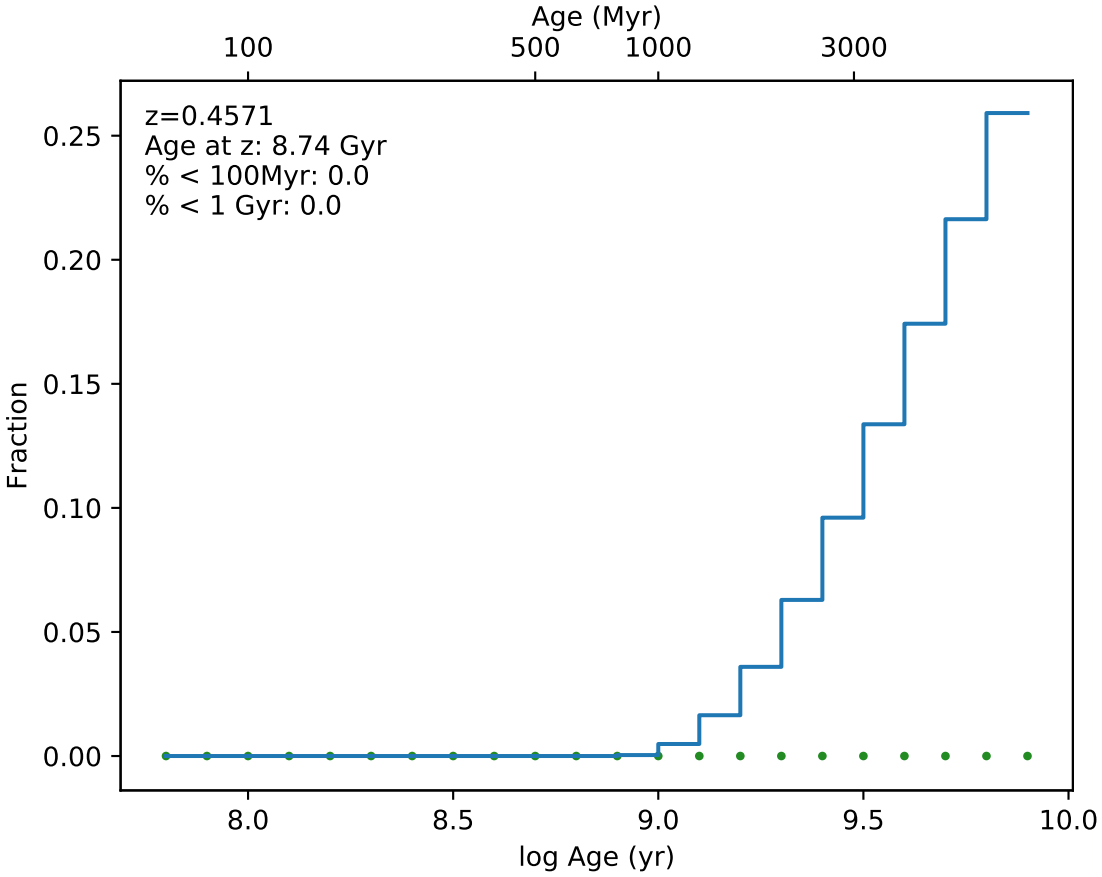
Age (Myr)
100
500
1000
3000
z=0.4571
Age at z: 8.74 Gyr
% < 100Myr: 0.0
% < 1 Gyr: 0.0
Fraction
0.25
0.20
0.15
0.10
0.05
0.00
8.0
8.5
9.0
9.5
10.0
log Age (yr)

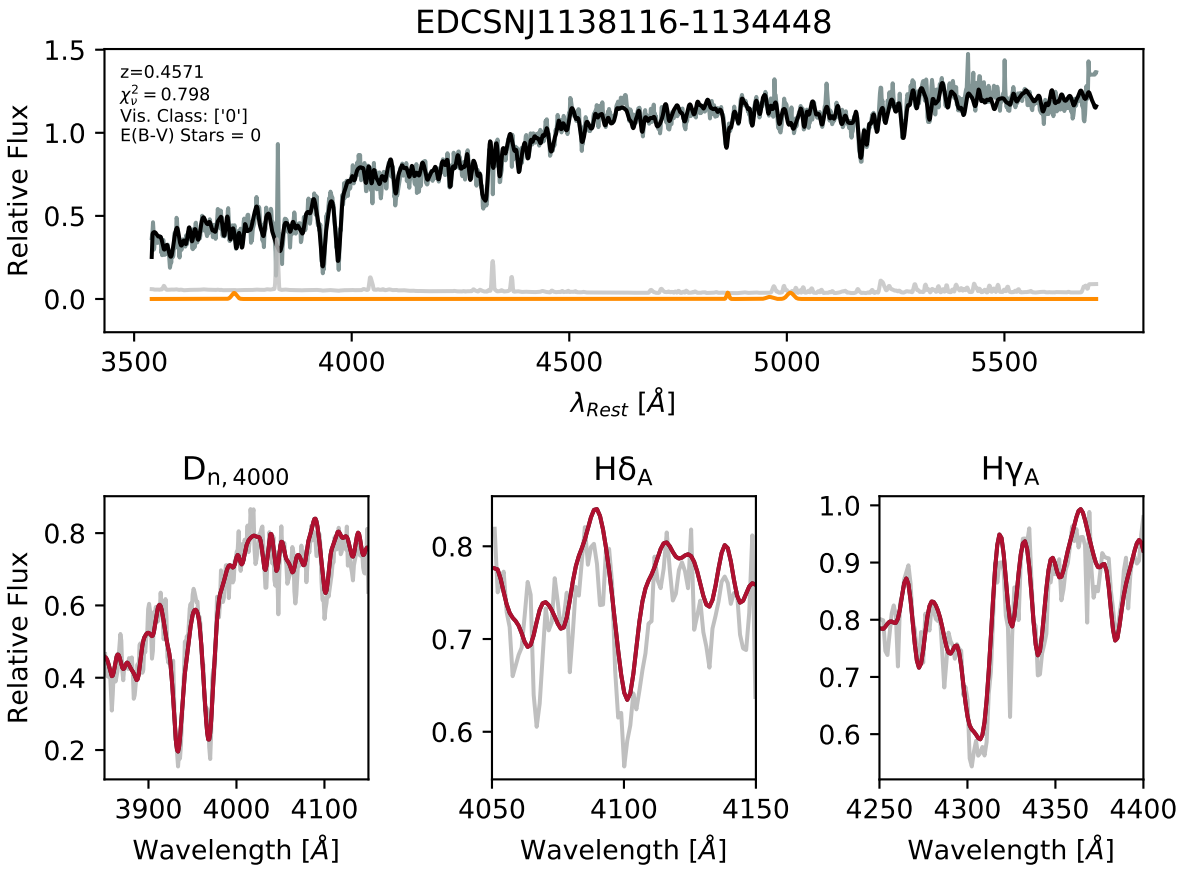
EDCSNJ1138116-1134448
z=0.4571
$\chi^2_\nu = 0.798$
Vis. Class: ['0']
E(B-V) Stars = 0
Relative Flux
λ_{Rest} [Å]
$D_{n,4000}$
$H\delta_A$
$H\gamma_A$
Wavelength [Å]

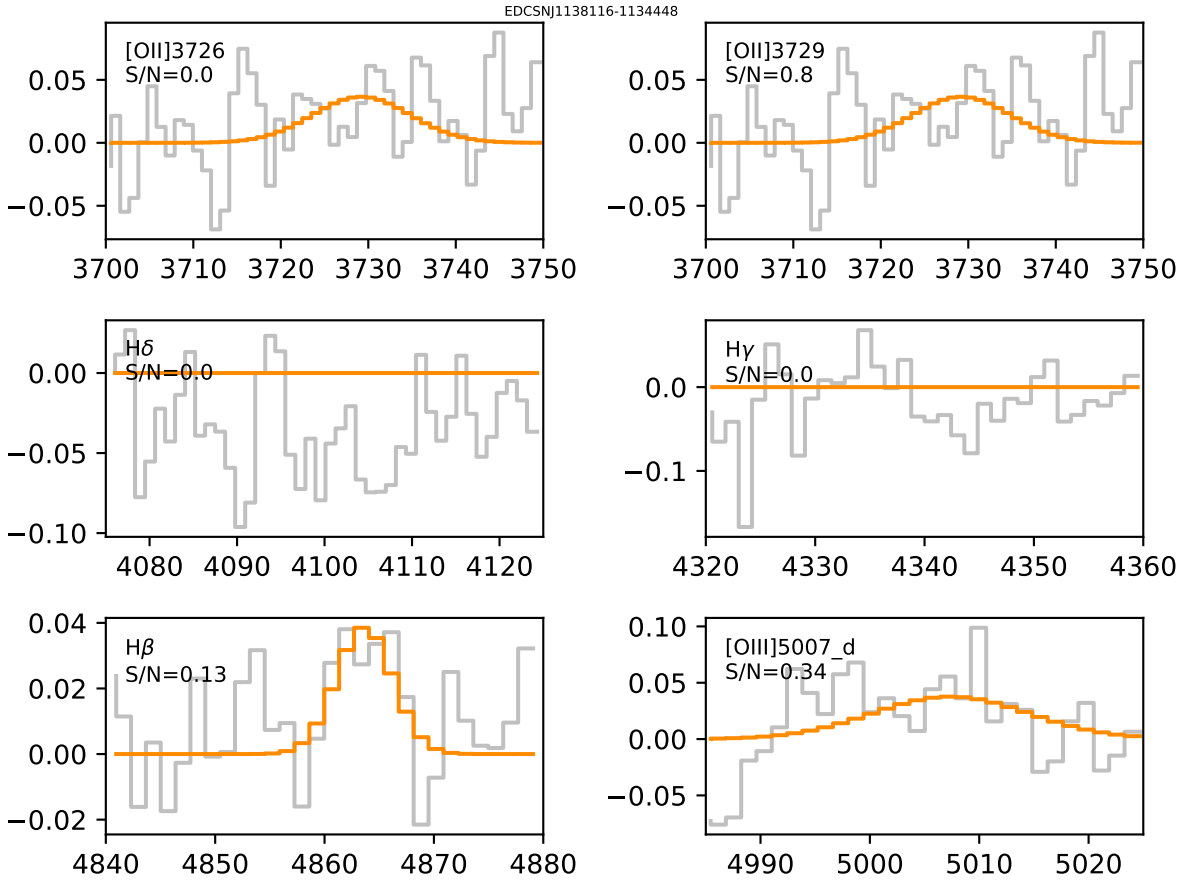
EDCSNJ1138116-1134448
[OII]3726
S/N=0.0
[OII]3729
S/N=0.8
Hδ
S/N=0.0
Hγ
S/N=0.0
Hβ
S/N=0.13
[OIII]5007_d
S/N=0.34

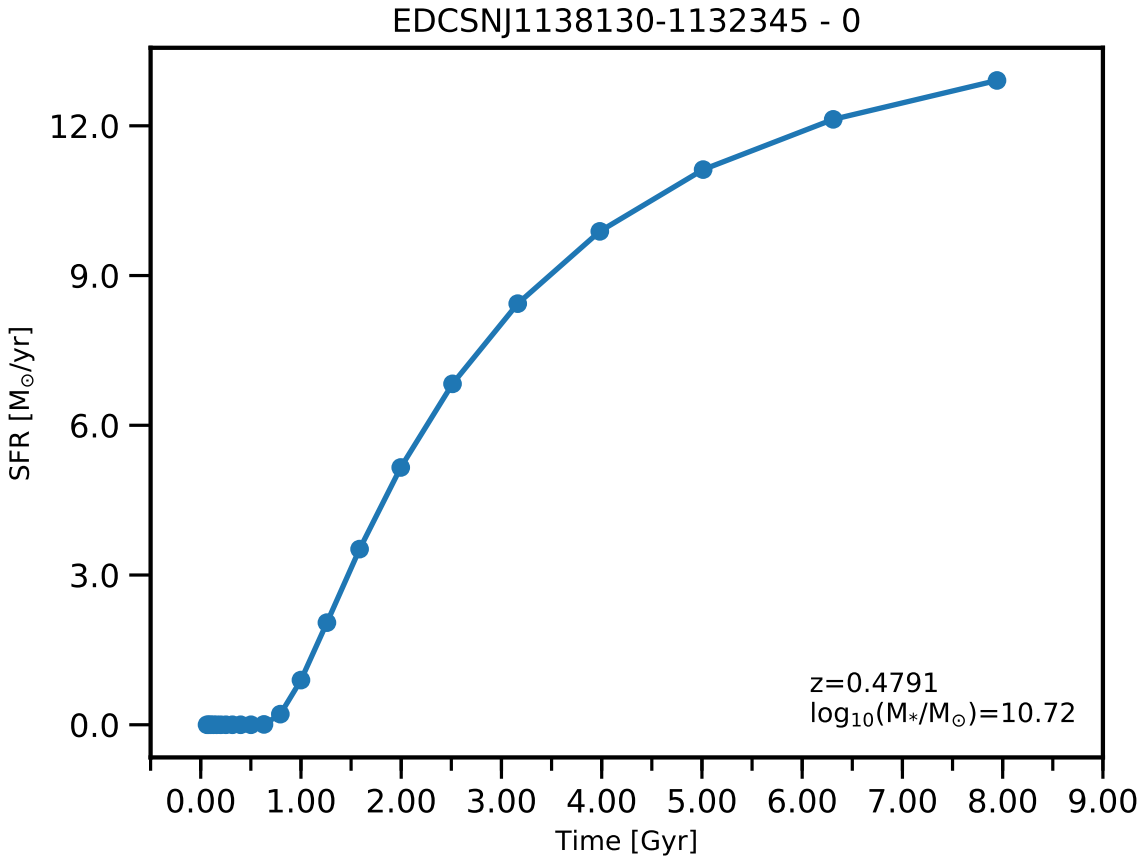
EDCSNJ1138130-1132345 - 0
SFR [M⊙/yr]
12.0
9.0
6.0
3.0
0.0
0.00
1.00
2.00
3.00
4.00
5.00
6.00
7.00
8.00
9.00
Time [Gyr]
z=0.4791
log10(M*/M⊙)=10.72

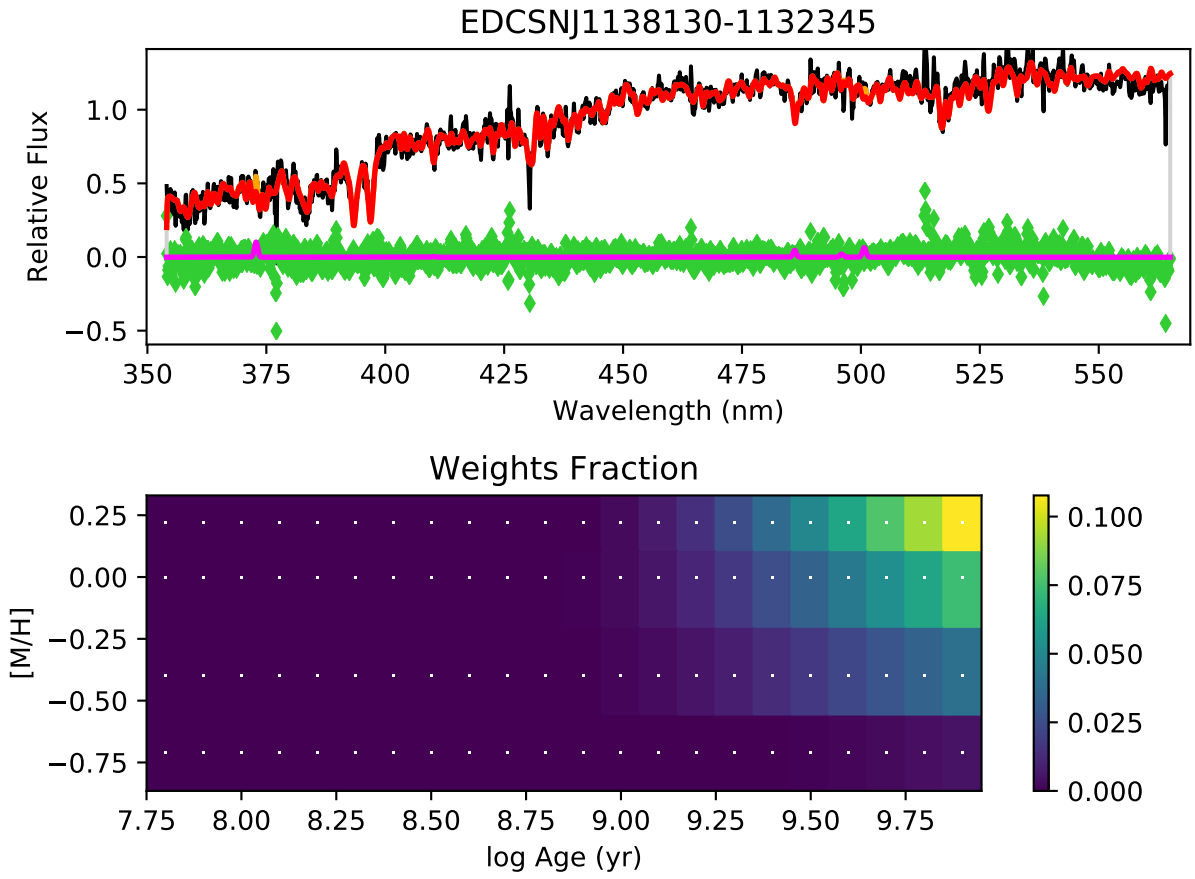
EDCSNJ1138130-1132345
Relative Flux
1.0
0.5
0.0
−0.5
350
375
400
425
450
475
500
525
550
Wavelength (nm)
Weights Fraction
[M/H]
0.25
0.00
−0.25
−0.50
−0.75
7.75
8.00
8.25
8.50
8.75
9.00
9.25
9.50
9.75
log Age (yr)
0.100
0.075
0.050
0.025
0.000

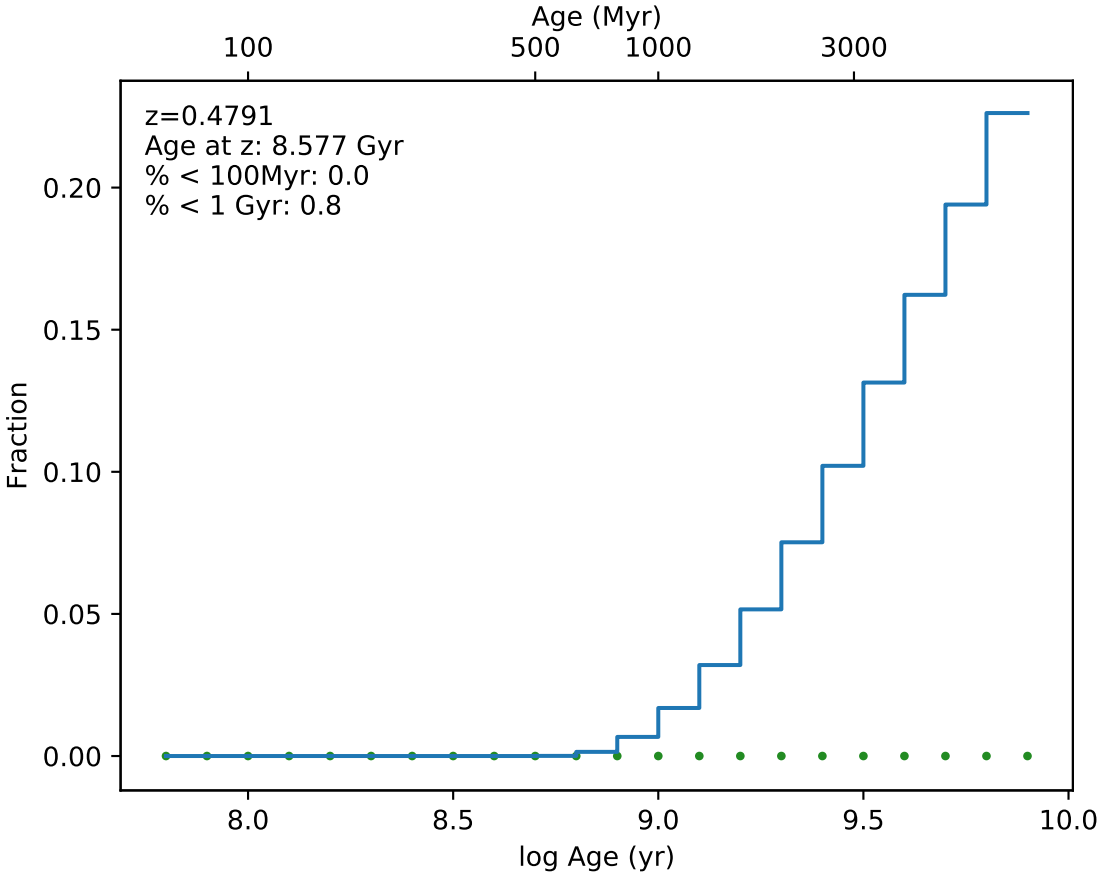
Age (Myr)
100
500
1000
3000
z=0.4791
Age at z: 8.577 Gyr
% < 100Myr: 0.0
% < 1 Gyr: 0.8
Fraction
0.00
0.05
0.10
0.15
0.20
8.0
8.5
9.0
9.5
10.0
log Age (yr)

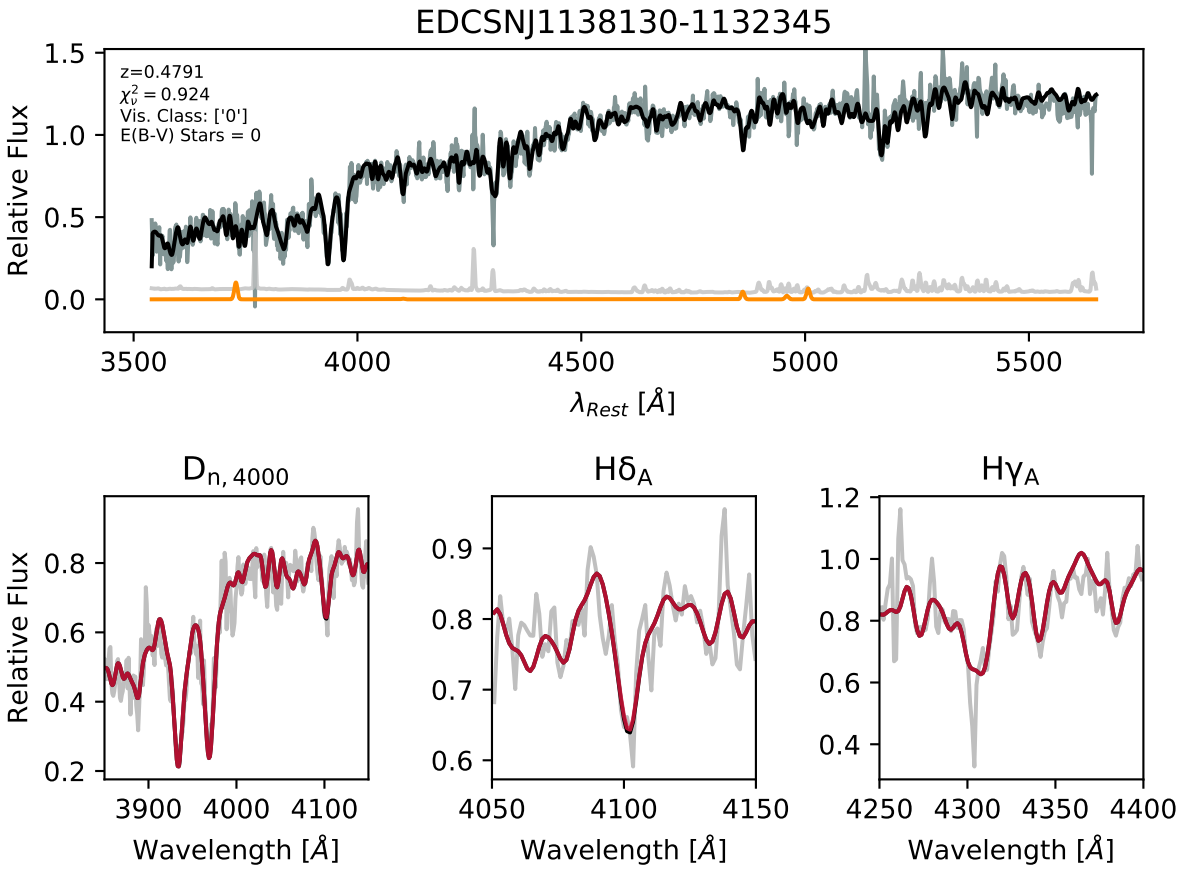
EDCSNJ1138130-1132345
z=0.4791
$\chi^2_\nu = 0.924$
Vis. Class: ['0']
E(B-V) Stars = 0
Relative Flux
λ_{Rest} [Å]
$D_{n,4000}$
$H\delta_A$
$H\gamma_A$
Wavelength [Å]

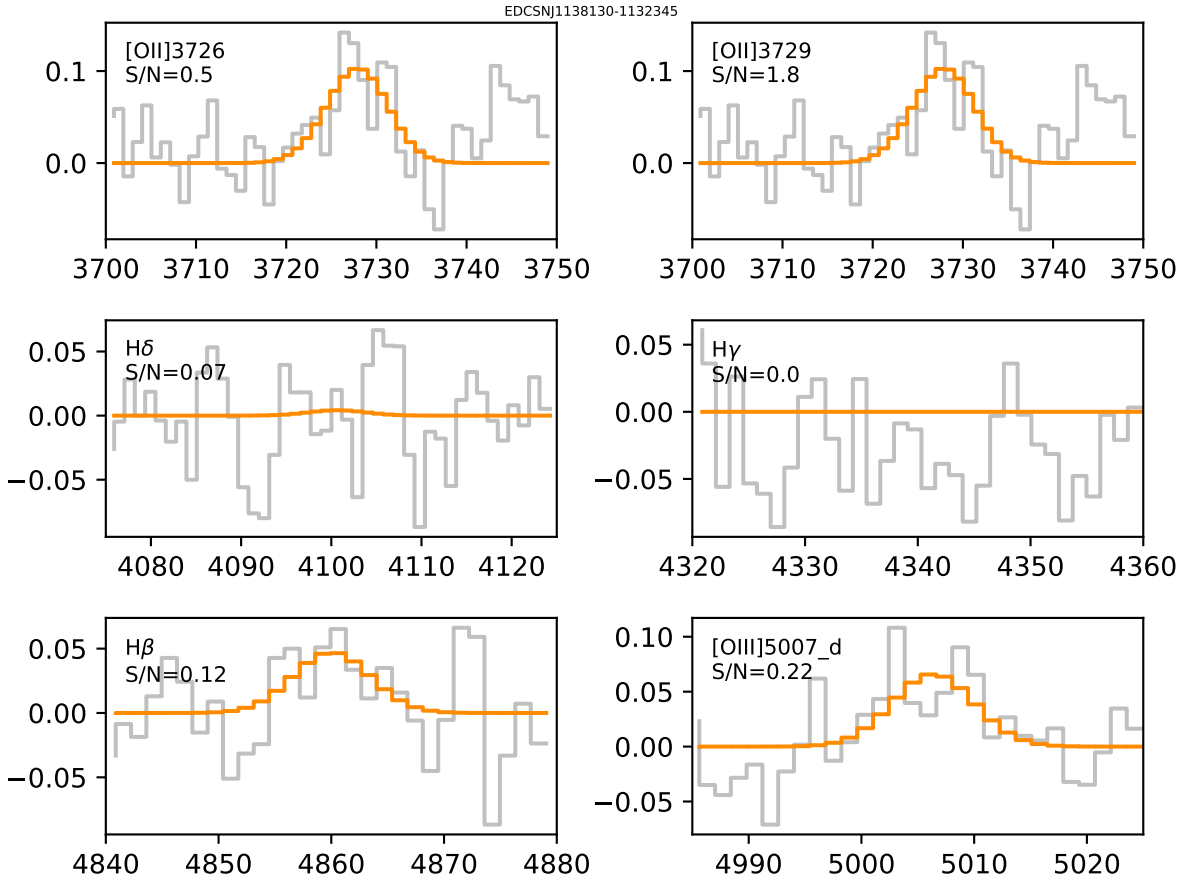
EDCSNJ1138130-1132345
[OII]3726
S/N=0.5
[OII]3729
S/N=1.8
Hδ
S/N=0.07
Hγ
S/N=0.0
Hβ
S/N=0.12
[OIII]5007_d
S/N=0.22

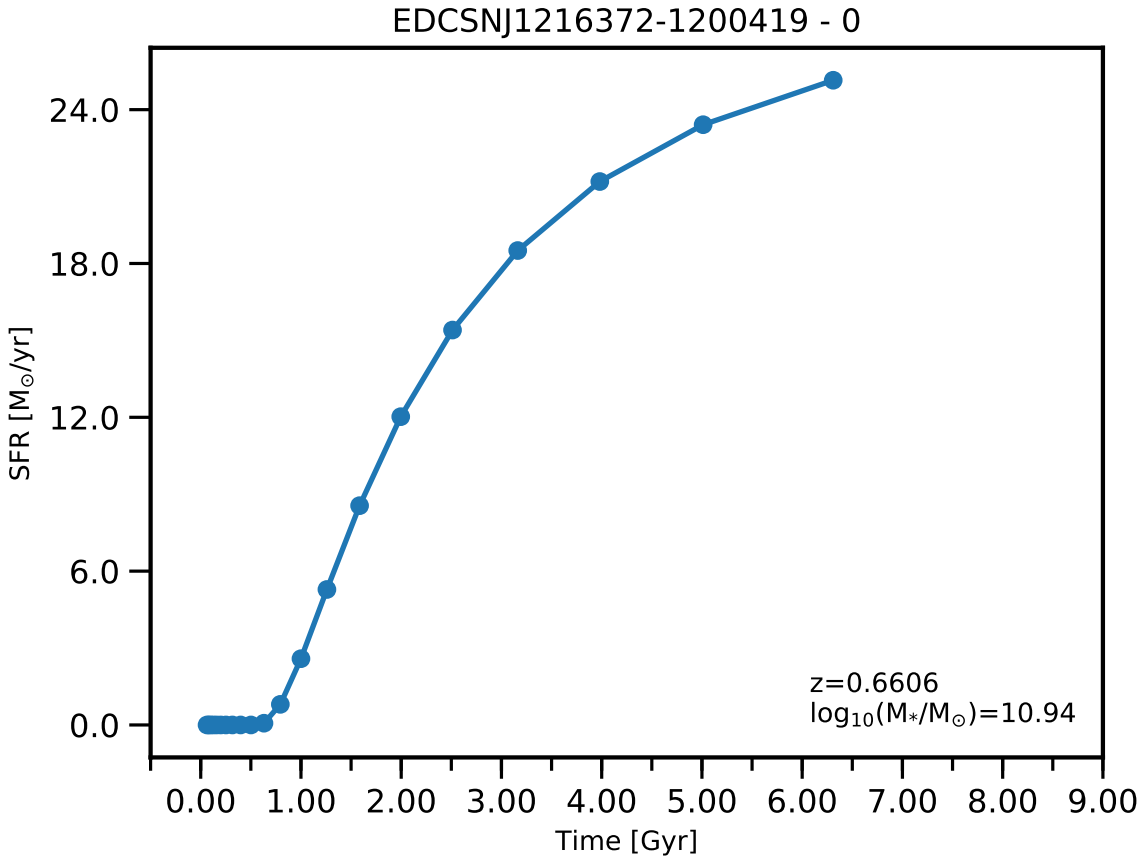
EDCSNJ1216372-1200419 - 0
24.0
18.0
12.0
6.0
0.0
SFR [M⊙/yr]
0.00
1.00
2.00
3.00
4.00
5.00
6.00
7.00
8.00
9.00
Time [Gyr]
z=0.6606
log10(M*/M⊙)=10.94

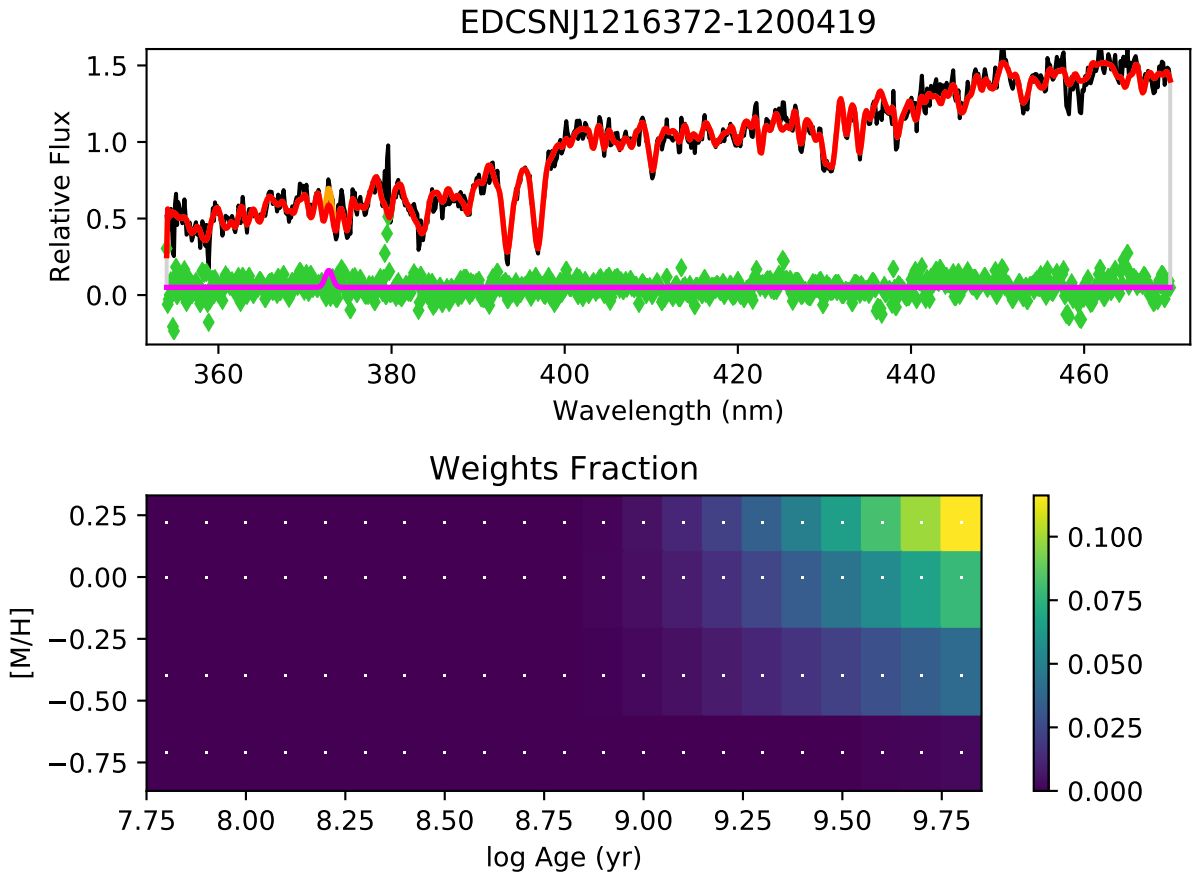
EDCSNJ1216372-1200419
Relative Flux
1.5
1.0
0.5
0.0
360
380
400
420
440
460
Wavelength (nm)
Weights Fraction
[M/H]
0.25
0.00
−0.25
−0.50
−0.75
7.75
8.00
8.25
8.50
8.75
9.00
9.25
9.50
9.75
log Age (yr)
0.100
0.075
0.050
0.025
0.000

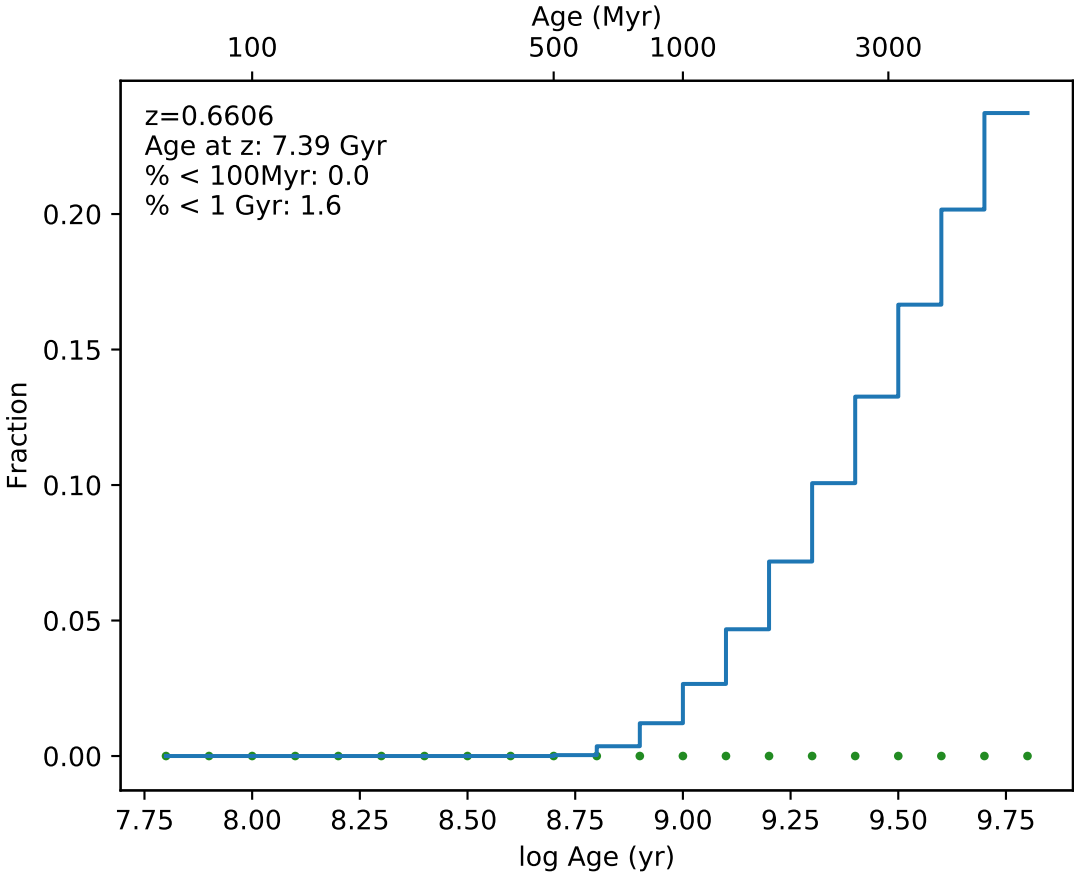
Age (Myr)
100
500
1000
3000
z=0.6606
Age at z: 7.39 Gyr
% < 100Myr: 0.0
% < 1 Gyr: 1.6
Fraction
0.20
0.15
0.10
0.05
0.00
7.75
8.00
8.25
8.50
8.75
9.00
9.25
9.50
9.75
log Age (yr)

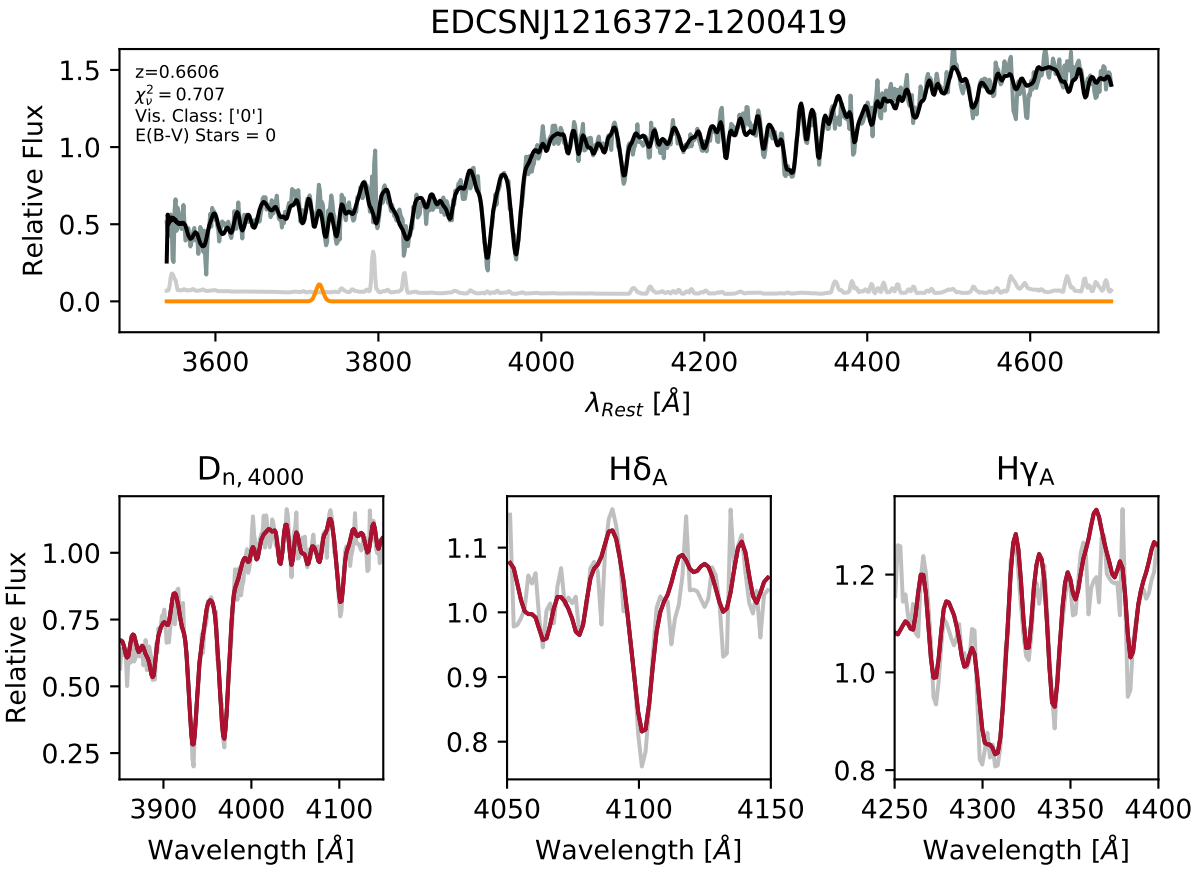
EDCSNJ1216372-1200419
z=0.6606
$\chi^2_\nu = 0.707$
Vis. Class: ['0']
E(B-V) Stars = 0
Relative Flux
λ_{Rest} [Å]
$D_{n,4000}$
$H\delta_A$
$H\gamma_A$
Wavelength [Å]

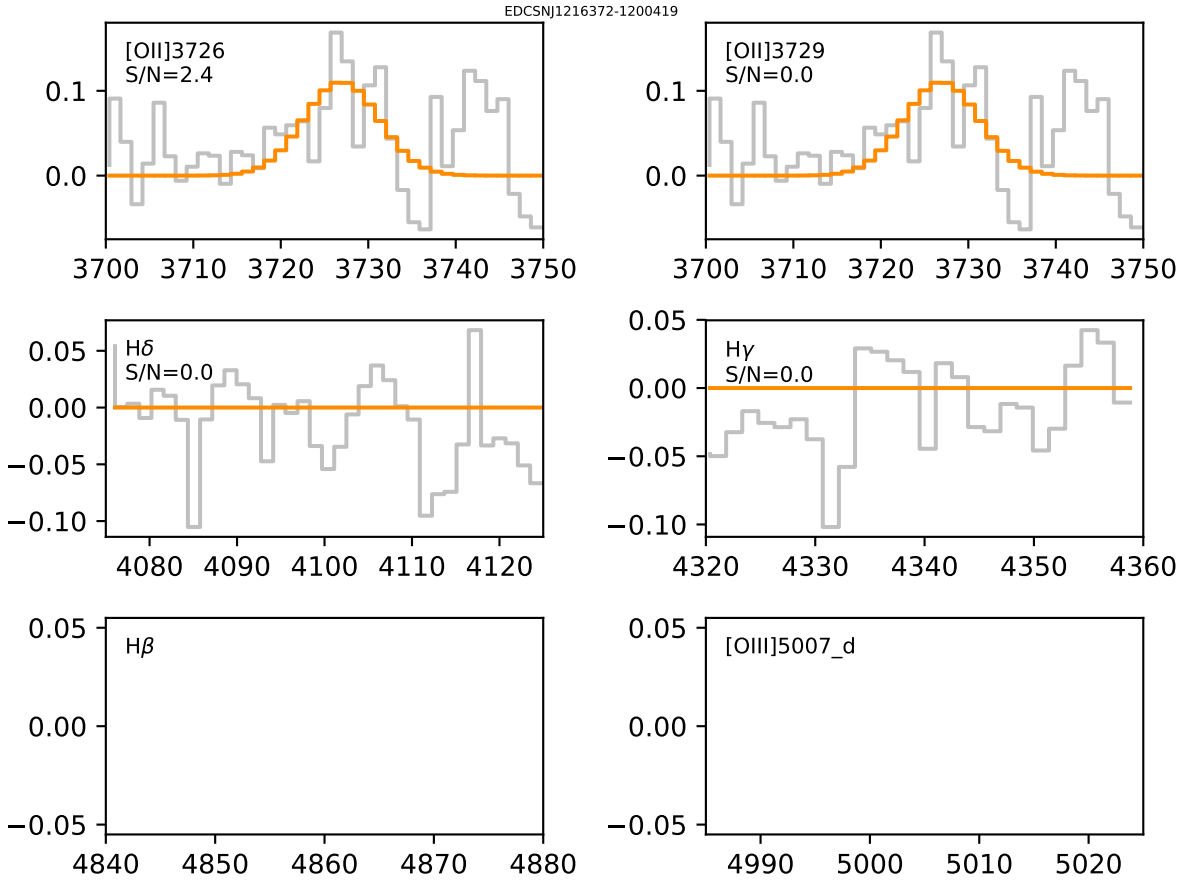
EDCSNJ1216372-1200419
[OII]3726
S/N=2.4
[OII]3729
S/N=0.0
Hδ
S/N=0.0
Hγ
S/N=0.0
Hβ
[OIII]5007_d

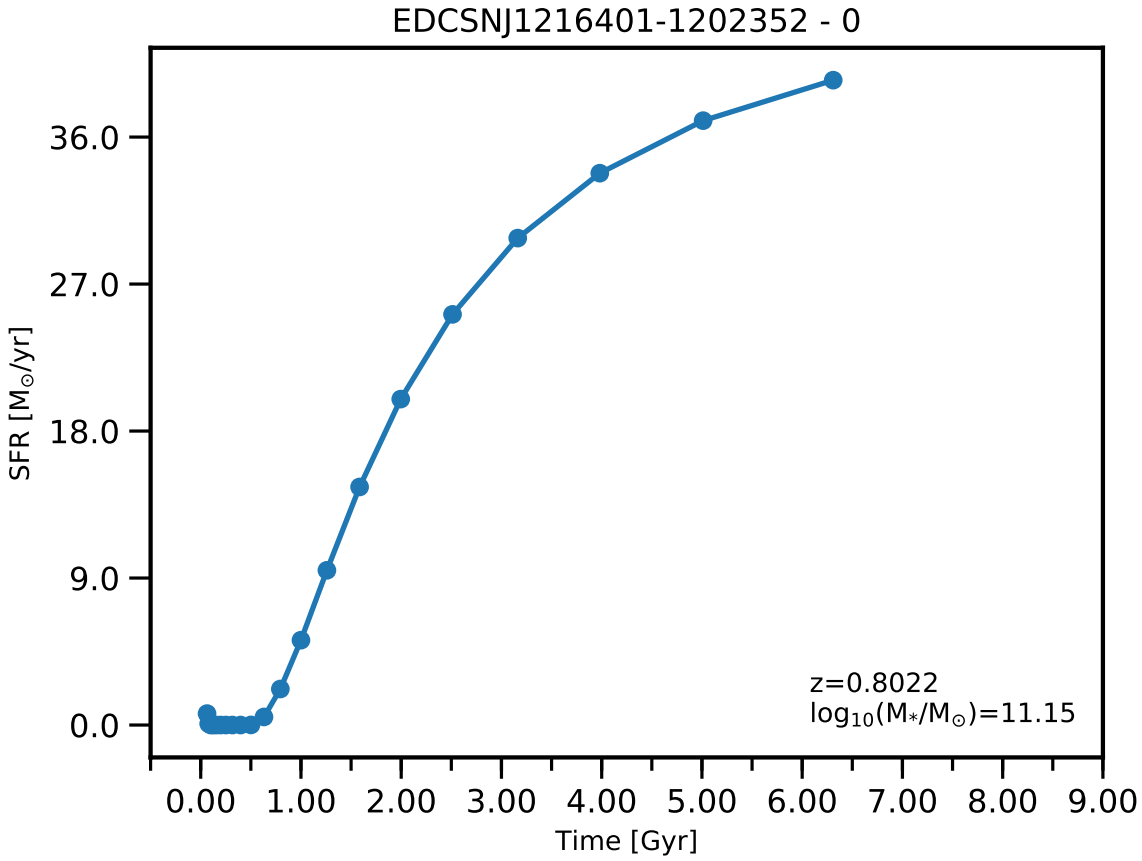
EDCSNJ1216401-1202352 - 0
SFR [M⊙/yr]
36.0
27.0
18.0
9.0
0.0
0.00
1.00
2.00
3.00
4.00
5.00
6.00
7.00
8.00
9.00
Time [Gyr]
z=0.8022
log10(M*/M⊙)=11.15

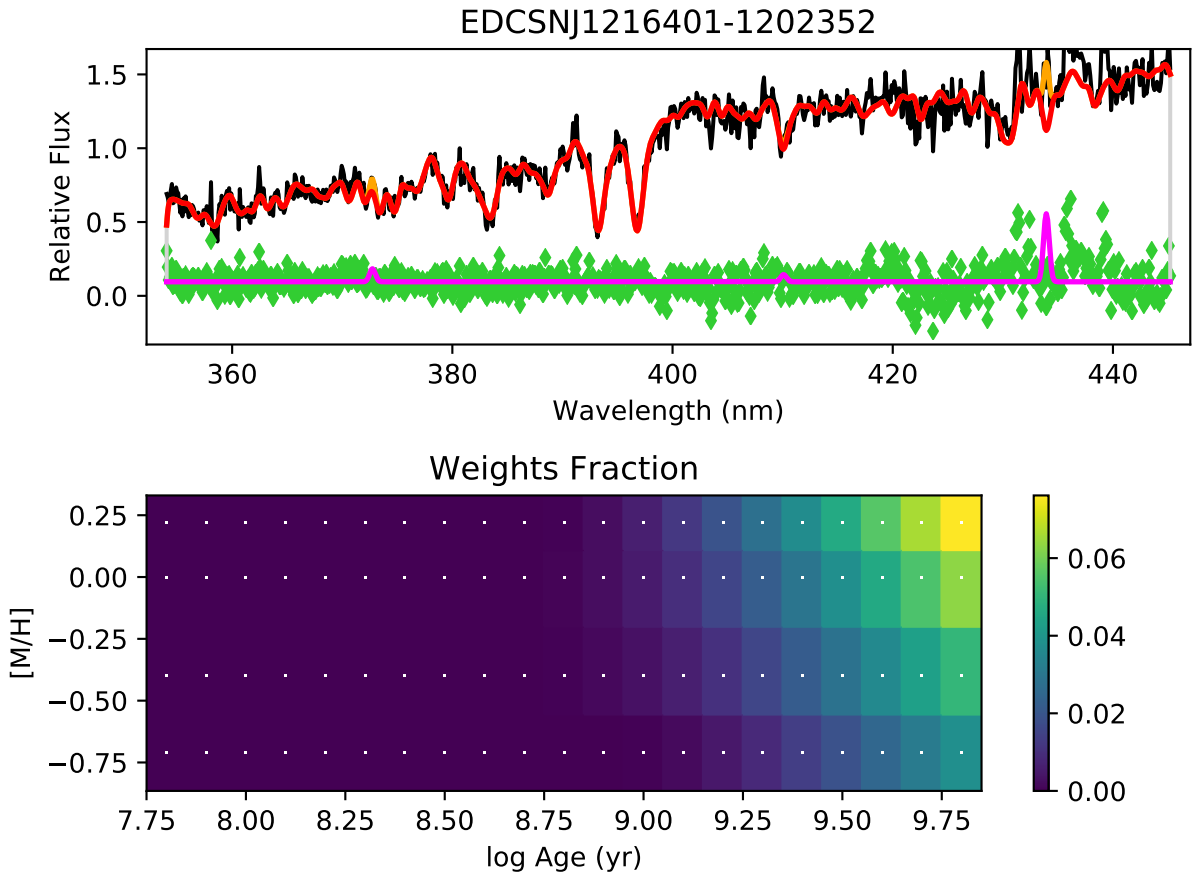
EDCSNJ1216401-1202352
Relative Flux
1.5
1.0
0.5
0.0
360
380
400
420
440
Wavelength (nm)
Weights Fraction
[M/H]
0.25
0.00
−0.25
−0.50
−0.75
7.75
8.00
8.25
8.50
8.75
9.00
9.25
9.50
9.75
log Age (yr)
0.06
0.04
0.02
0.00

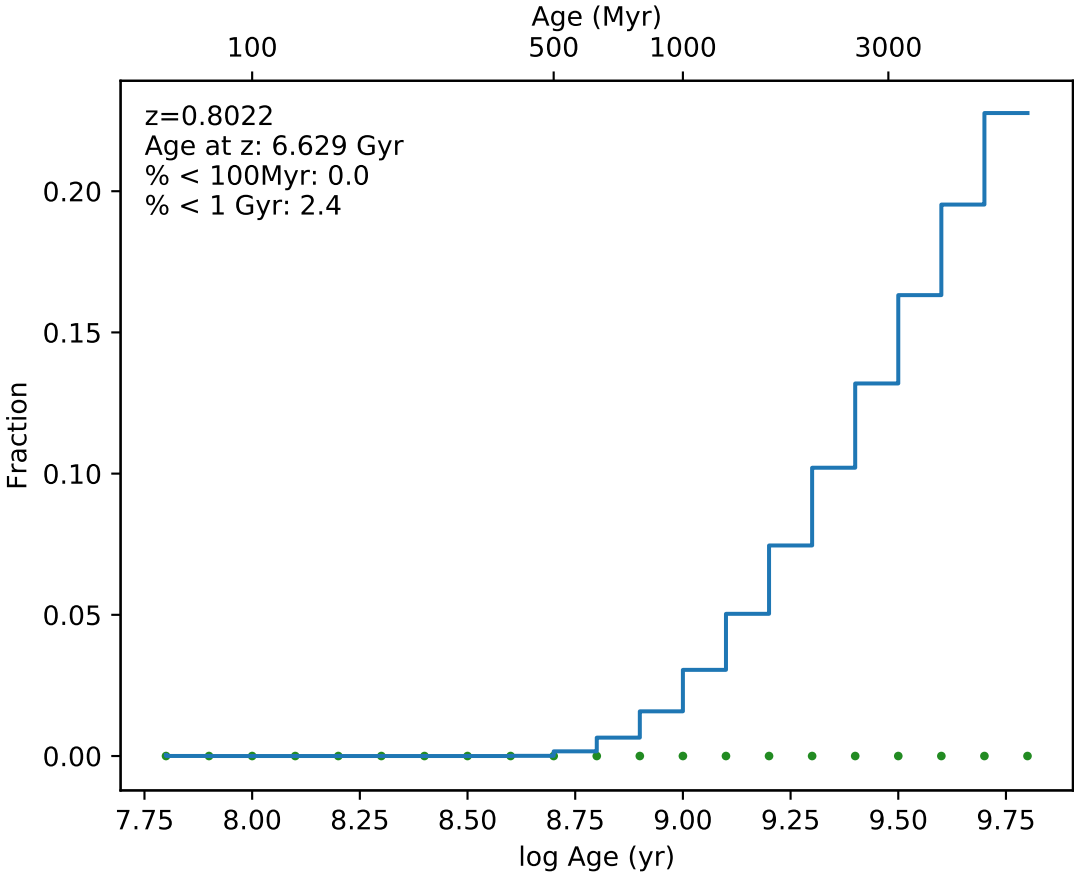
Age (Myr)
100
500
1000
3000
z=0.8022
Age at z: 6.629 Gyr
% < 100Myr: 0.0
% < 1 Gyr: 2.4
Fraction
0.20
0.15
0.10
0.05
0.00
7.75
8.00
8.25
8.50
8.75
9.00
9.25
9.50
9.75
log Age (yr)

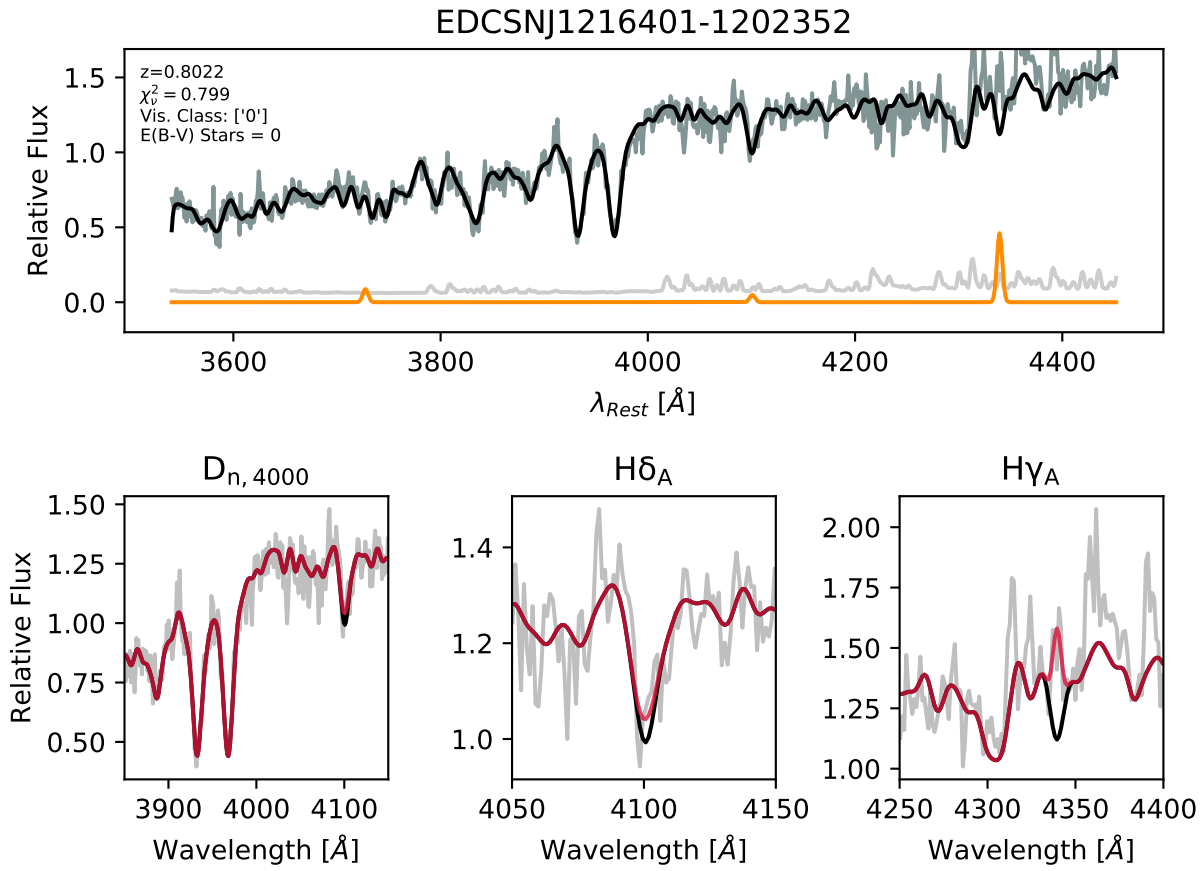
EDCSNJ1216401-1202352
z=0.8022
$\chi^2_\nu = 0.799$
Vis. Class: ['0']
E(B-V) Stars = 0
Relative Flux
λ_{Rest} [Å]
$D_{n,4000}$
$H\delta_A$
$H\gamma_A$
Wavelength [Å]

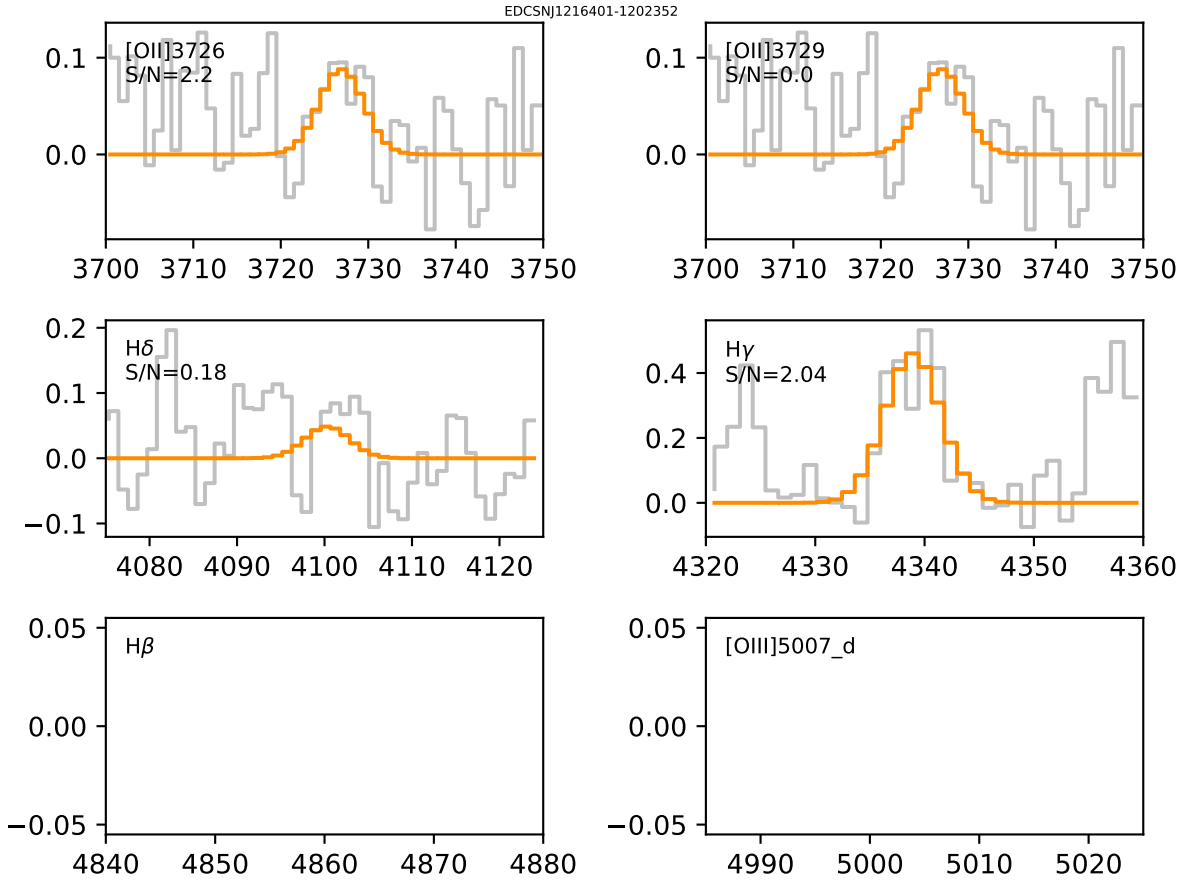
EDCSNJ1216401-1202352
[OII]3726
S/N=2.2
[OII]3729
S/N=0.0
Hδ
S/N=0.18
Hγ
S/N=2.04
Hβ
[OIII]5007_d

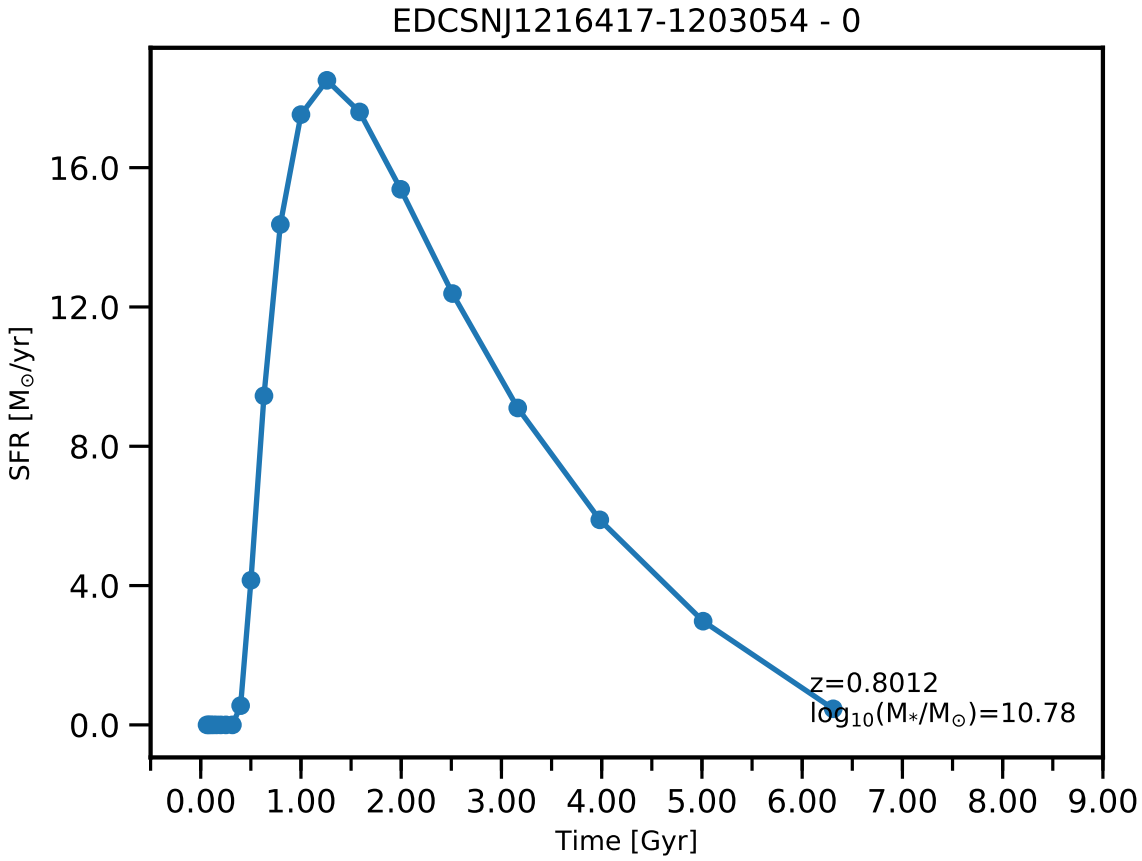
EDCSNJ1216417-1203054 - 0
SFR [M⊙/yr]
16.0
12.0
8.0
4.0
0.0
0.00
1.00
2.00
3.00
4.00
5.00
6.00
7.00
8.00
9.00
Time [Gyr]
z=0.8012
log10(M*/M⊙)=10.78

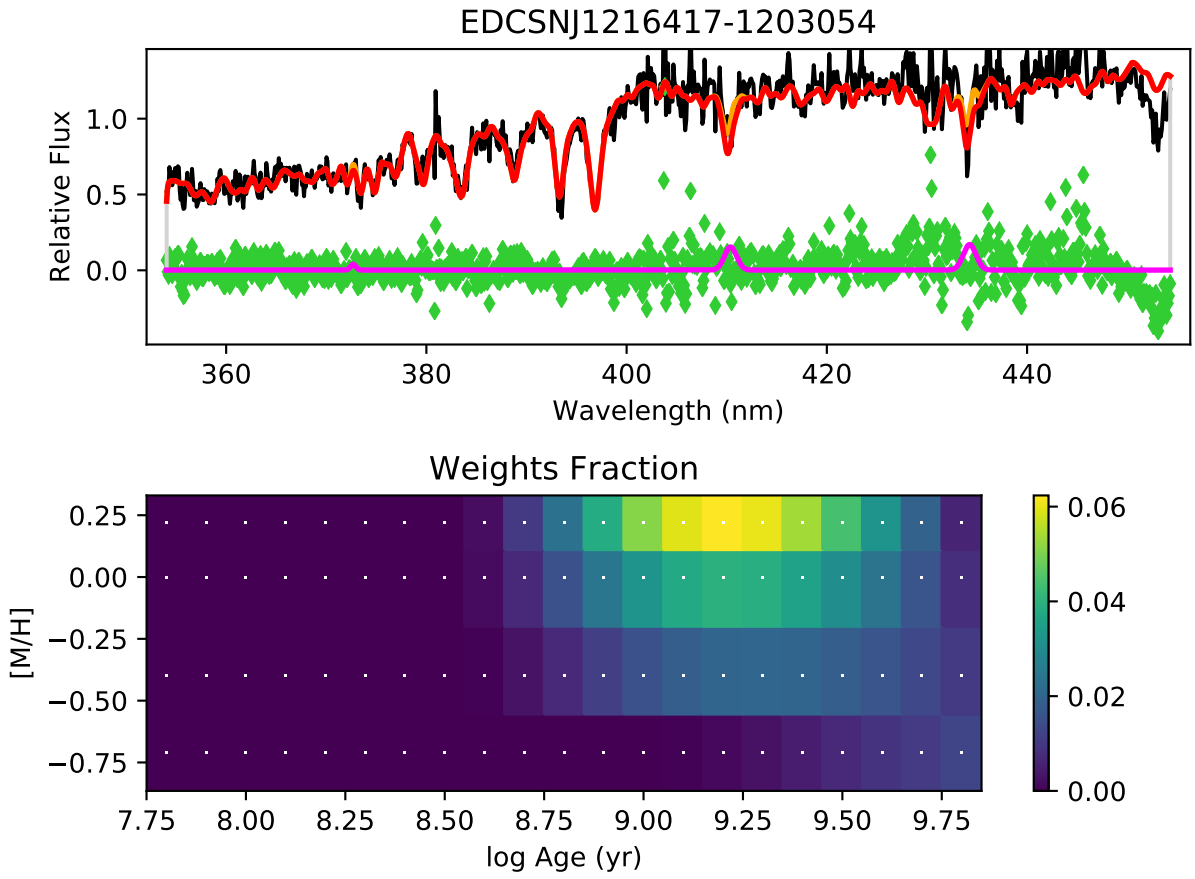
EDCSNJ1216417-1203054
Relative Flux
1.0
0.5
0.0
360
380
400
420
440
Wavelength (nm)
Weights Fraction
[M/H]
0.25
0.00
−0.25
−0.50
−0.75
7.75
8.00
8.25
8.50
8.75
9.00
9.25
9.50
9.75
log Age (yr)
0.06
0.04
0.02
0.00

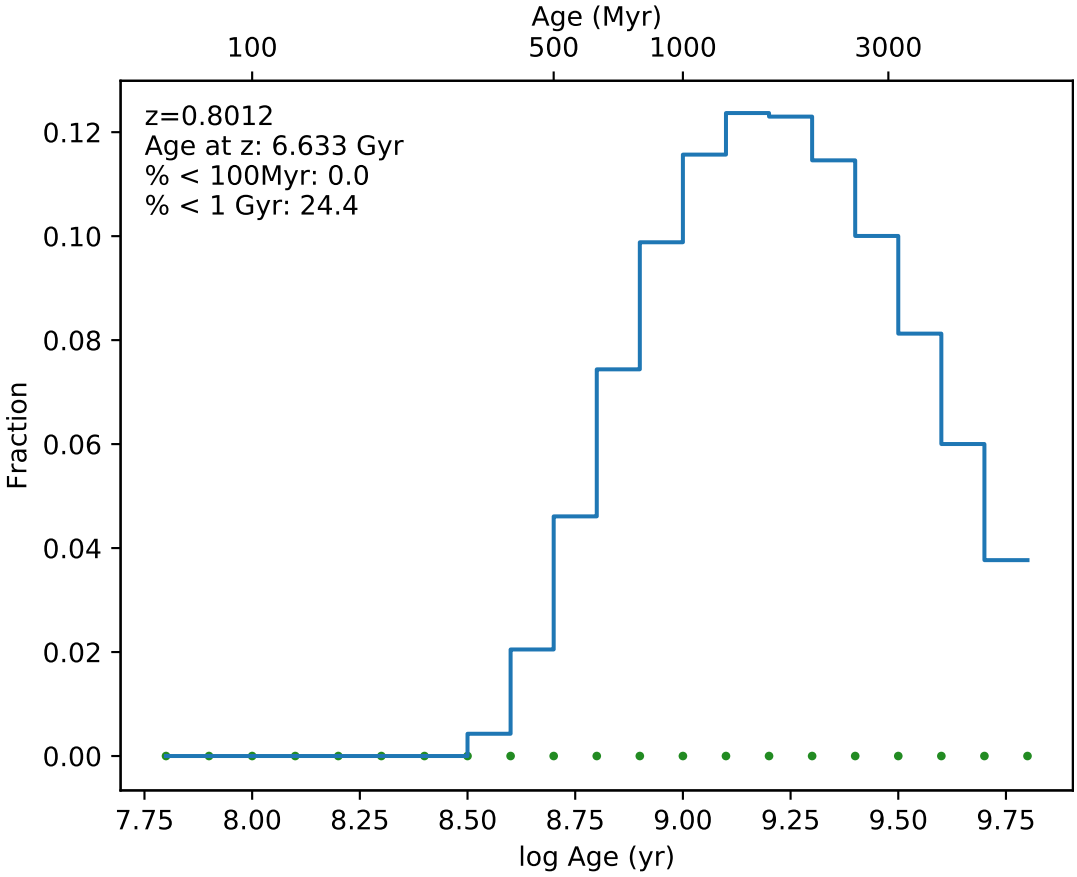
Age (Myr)
100
500
1000
3000
z=0.8012
Age at z: 6.633 Gyr
% < 100Myr: 0.0
% < 1 Gyr: 24.4
Fraction
0.12
0.10
0.08
0.06
0.04
0.02
0.00
7.75
8.00
8.25
8.50
8.75
9.00
9.25
9.50
9.75
log Age (yr)

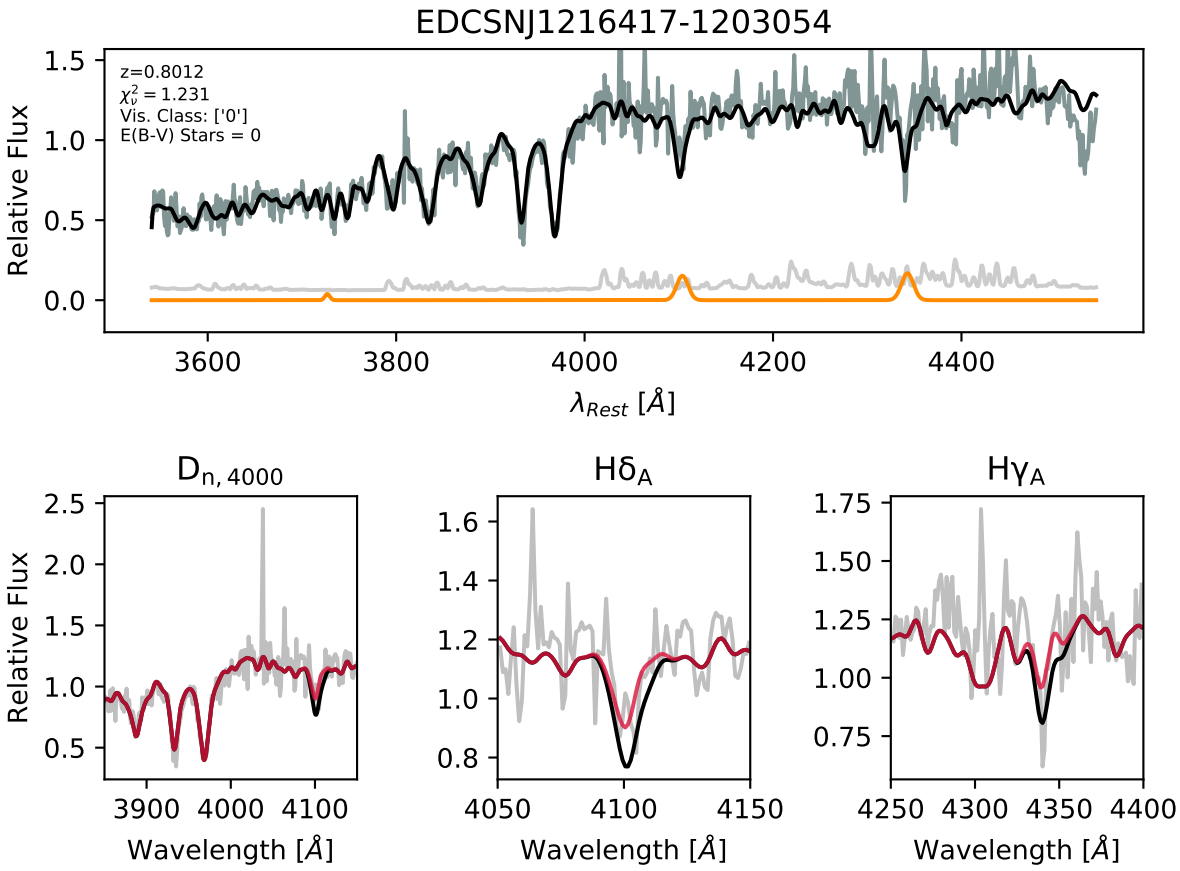
EDCSNJ1216417-1203054
z=0.8012
$\chi^2_\nu = 1.231$
Vis. Class: ['0']
E(B-V) Stars = 0
Relative Flux
λ_{Rest} [Å]
$D_{n,4000}$
$H\delta_A$
$H\gamma_A$
Wavelength [Å]

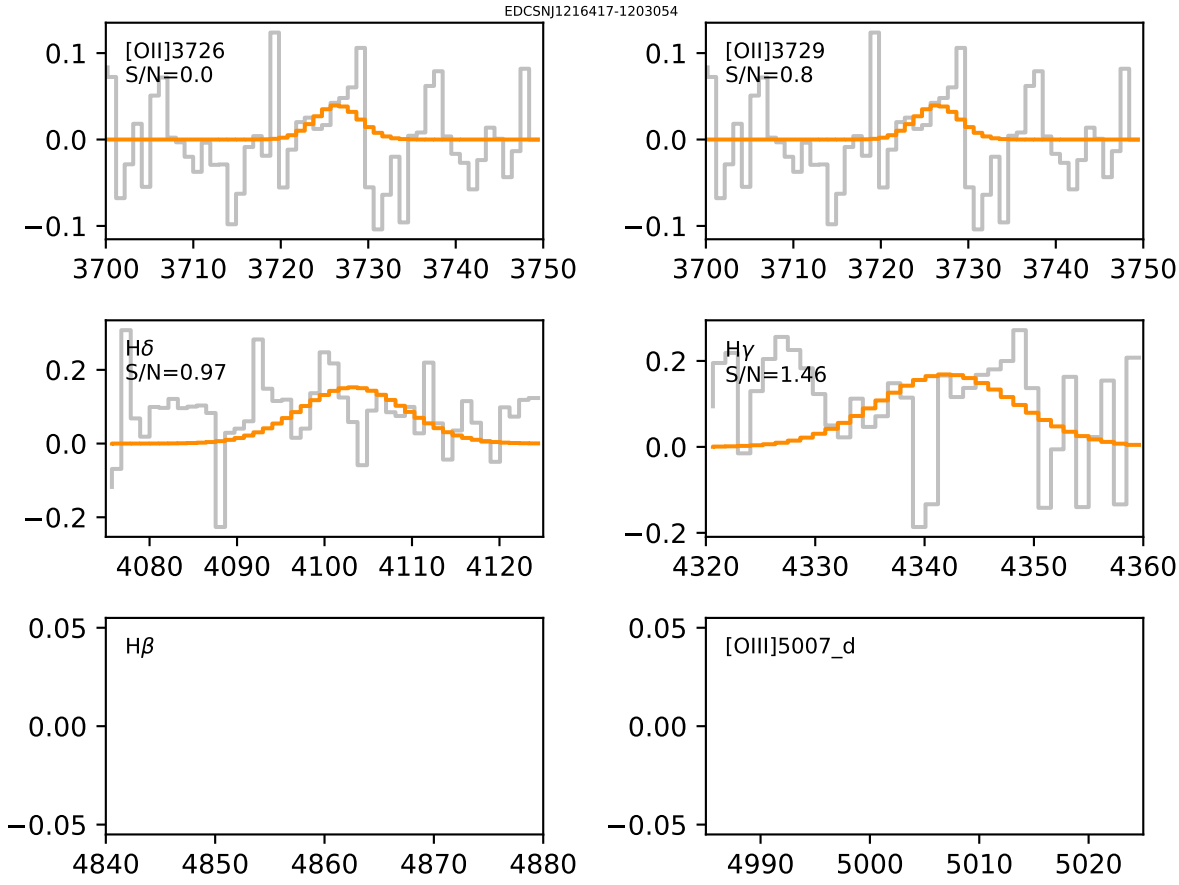
EDCSNJ1216417-1203054
[OII]3726
S/N=0.0
[OII]3729
S/N=0.8
Hδ
S/N=0.97
Hγ
S/N=1.46
Hβ
[OIII]5007_d

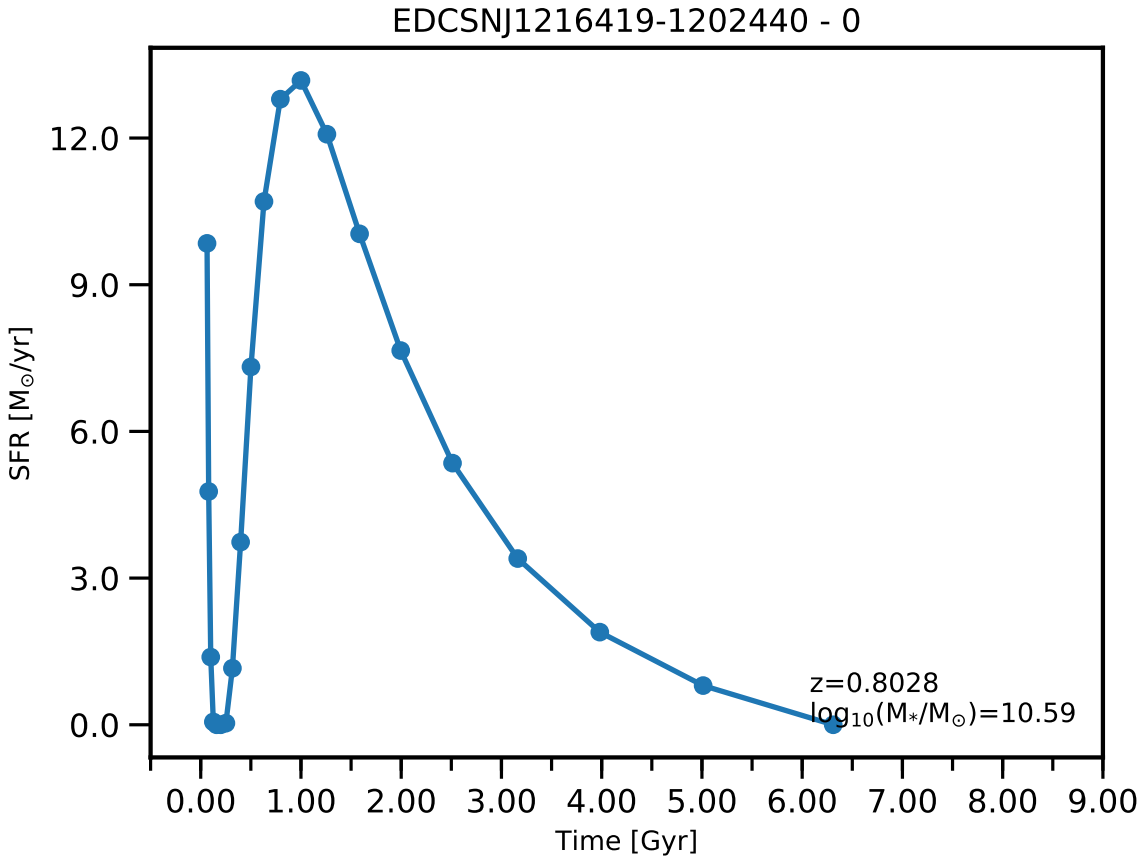
EDCSNJ1216419-1202440 - 0
SFR [M⊙/yr]
12.0
9.0
6.0
3.0
0.0
0.00
1.00
2.00
3.00
4.00
5.00
6.00
7.00
8.00
9.00
Time [Gyr]
z=0.8028
log10(M*/M⊙)=10.59

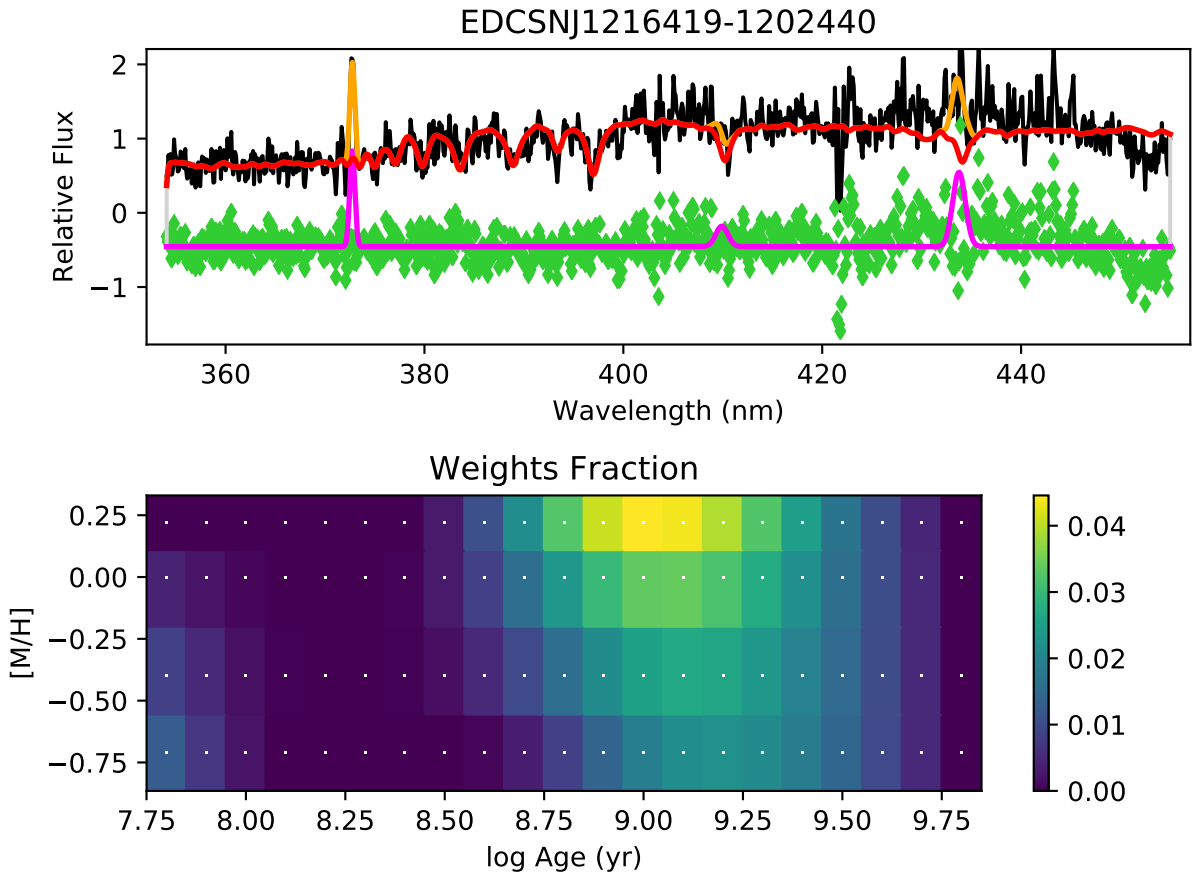
EDCSNJ1216419-1202440
Relative Flux
2
1
0
−1
360
380
400
420
440
Wavelength (nm)
Weights Fraction
[M/H]
0.25
0.00
−0.25
−0.50
−0.75
7.75
8.00
8.25
8.50
8.75
9.00
9.25
9.50
9.75
log Age (yr)
0.04
0.03
0.02
0.01
0.00

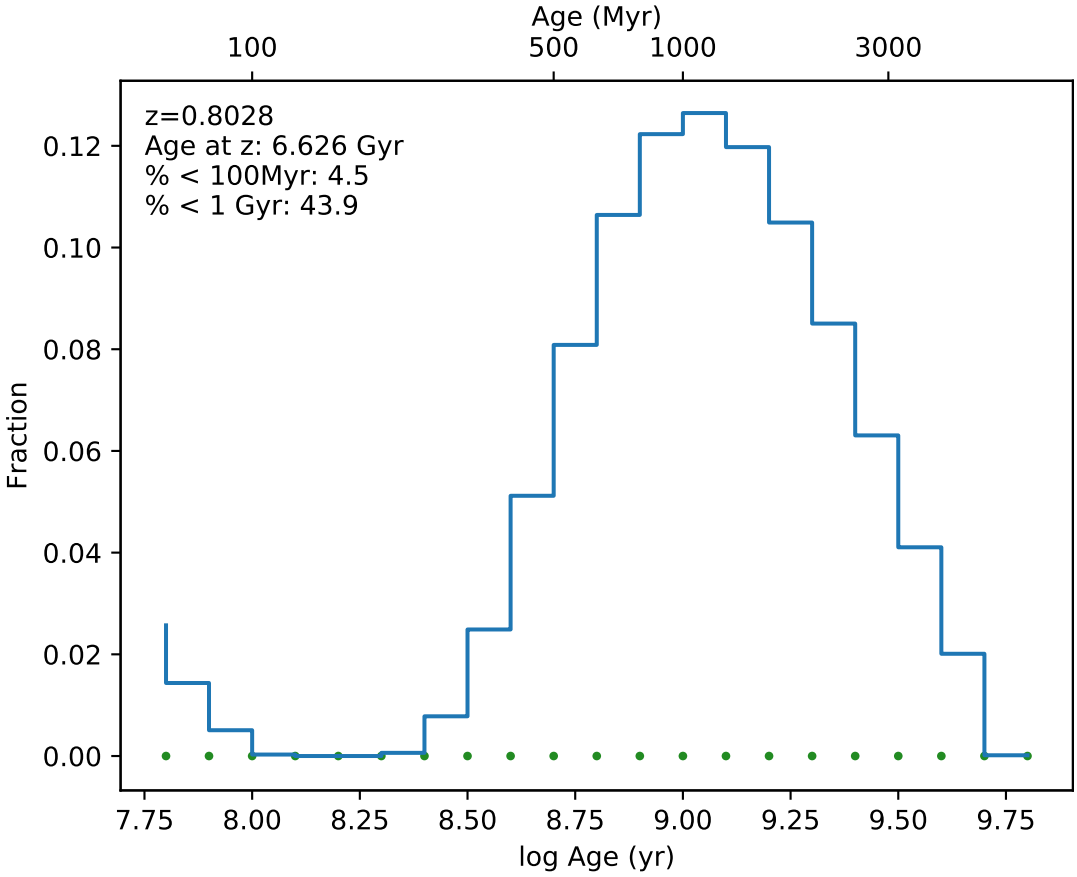
Age (Myr)
100
500
1000
3000
z=0.8028
Age at z: 6.626 Gyr
% < 100Myr: 4.5
% < 1 Gyr: 43.9
Fraction
0.12
0.10
0.08
0.06
0.04
0.02
0.00
7.75
8.00
8.25
8.50
8.75
9.00
9.25
9.50
9.75
log Age (yr)

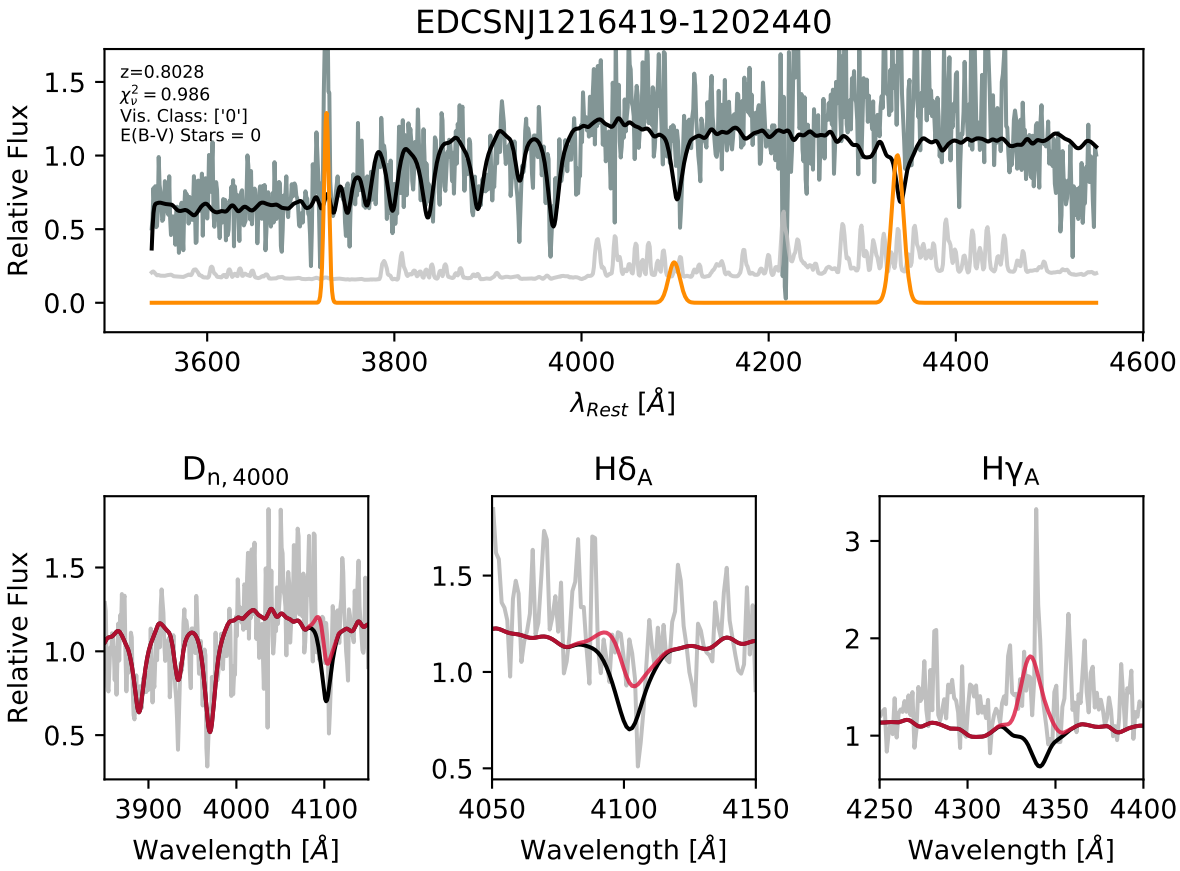
EDCSNJ1216419-1202440
z=0.8028
$\chi^2_\nu = 0.986$
Vis. Class: ['0']
E(B-V) Stars = 0
Relative Flux
λ_{Rest} [Å]
$D_{n,4000}$
$H\delta_A$
$H\gamma_A$
Wavelength [Å]

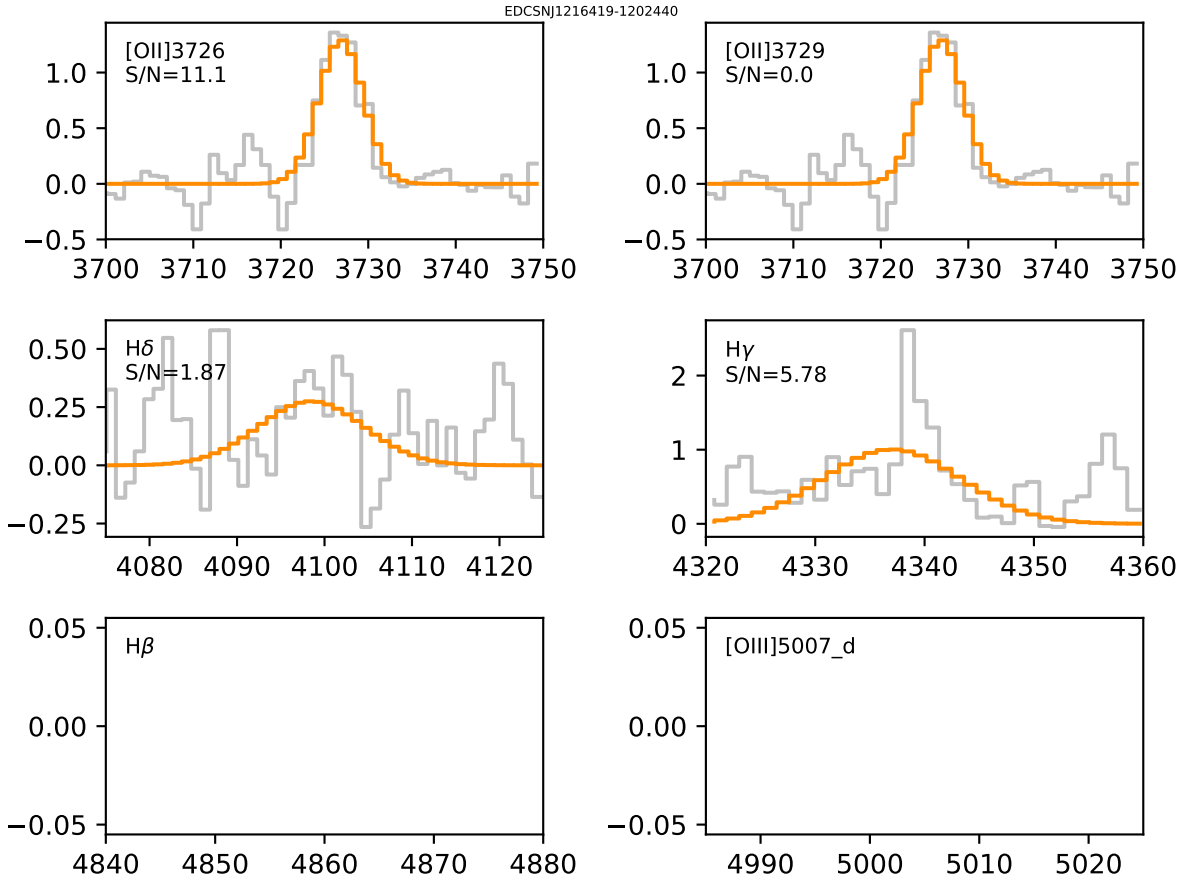
EDCSNJ1216419-1202440
[OII]3726
S/N=11.1
[OII]3729
S/N=0.0
Hδ
S/N=1.87
Hγ
S/N=5.78
Hβ
[OIII]5007_d

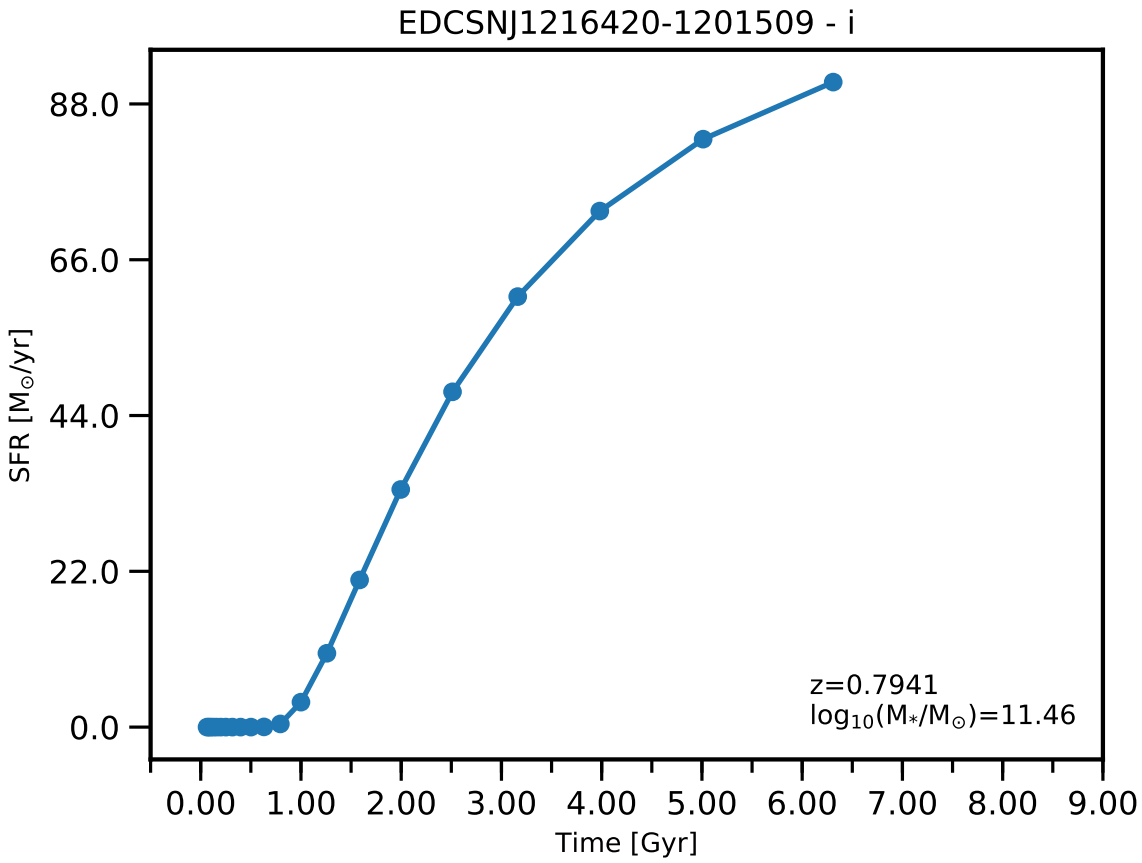
EDCSNJ1216420-1201509 - i
88.0
66.0
44.0
22.0
0.0
SFR [M⊙/yr]
0.00
1.00
2.00
3.00
4.00
5.00
6.00
7.00
8.00
9.00
Time [Gyr]
z=0.7941
log10(M*/M⊙)=11.46

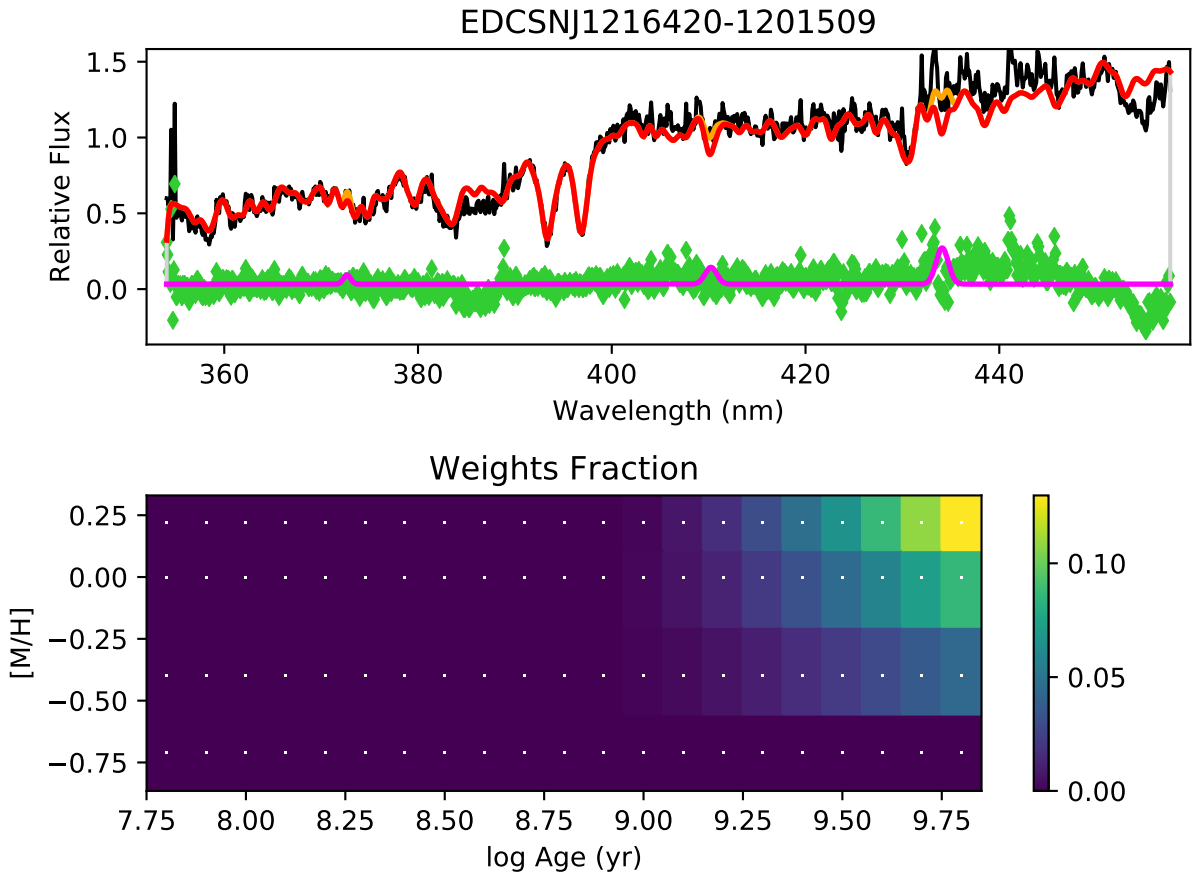
EDCSNJ1216420-1201509
Relative Flux
1.5
1.0
0.5
0.0
360
380
400
420
440
Wavelength (nm)
Weights Fraction
[M/H]
0.25
0.00
−0.25
−0.50
−0.75
7.75
8.00
8.25
8.50
8.75
9.00
9.25
9.50
9.75
log Age (yr)
0.10
0.05
0.00

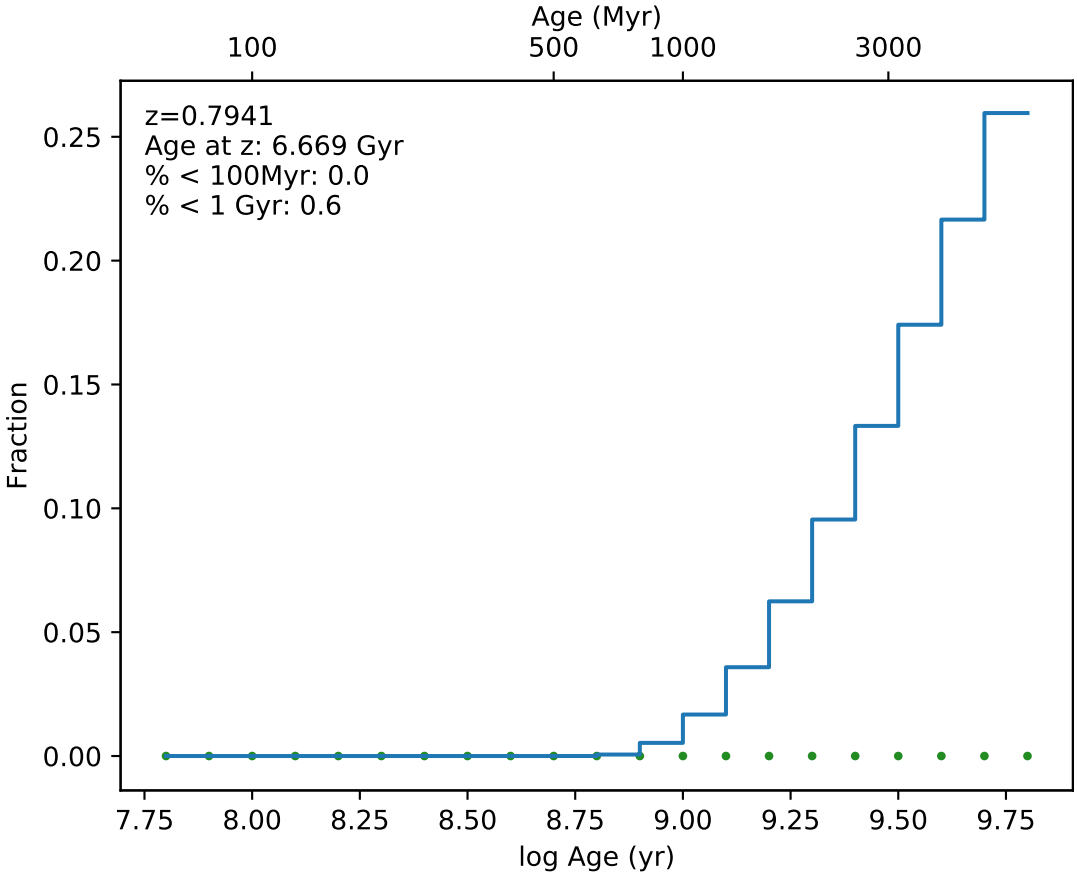
Age (Myr)
100
500
1000
3000
z=0.7941
Age at z: 6.669 Gyr
% < 100Myr: 0.0
% < 1 Gyr: 0.6
Fraction
0.25
0.20
0.15
0.10
0.05
0.00
7.75
8.00
8.25
8.50
8.75
9.00
9.25
9.50
9.75
log Age (yr)

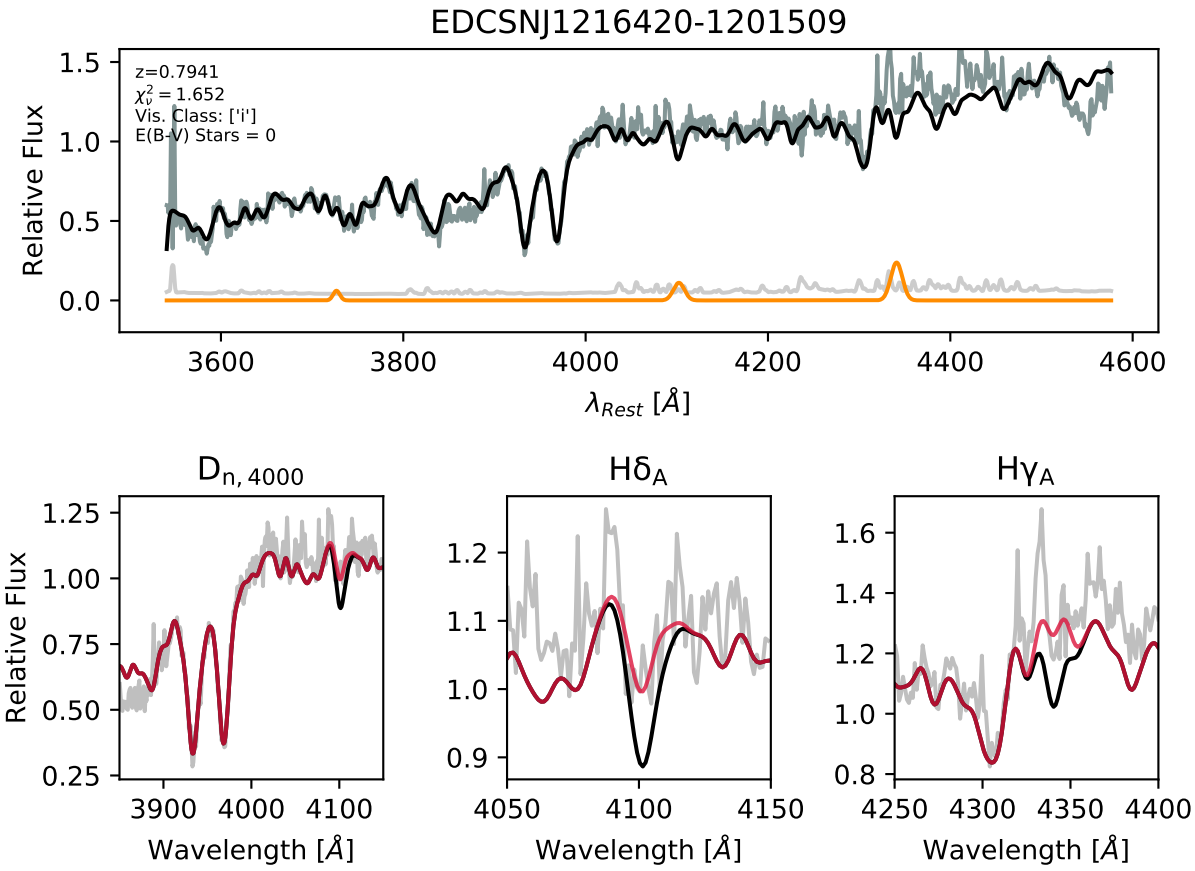
EDCSNJ1216420-1201509
z=0.7941
$\chi^2_\nu = 1.652$
Vis. Class: ['i']
E(B-V) Stars = 0
Relative Flux
λ_{Rest} [Å]
$D_{n,4000}$
$H\delta_A$
$H\gamma_A$
Wavelength [Å]

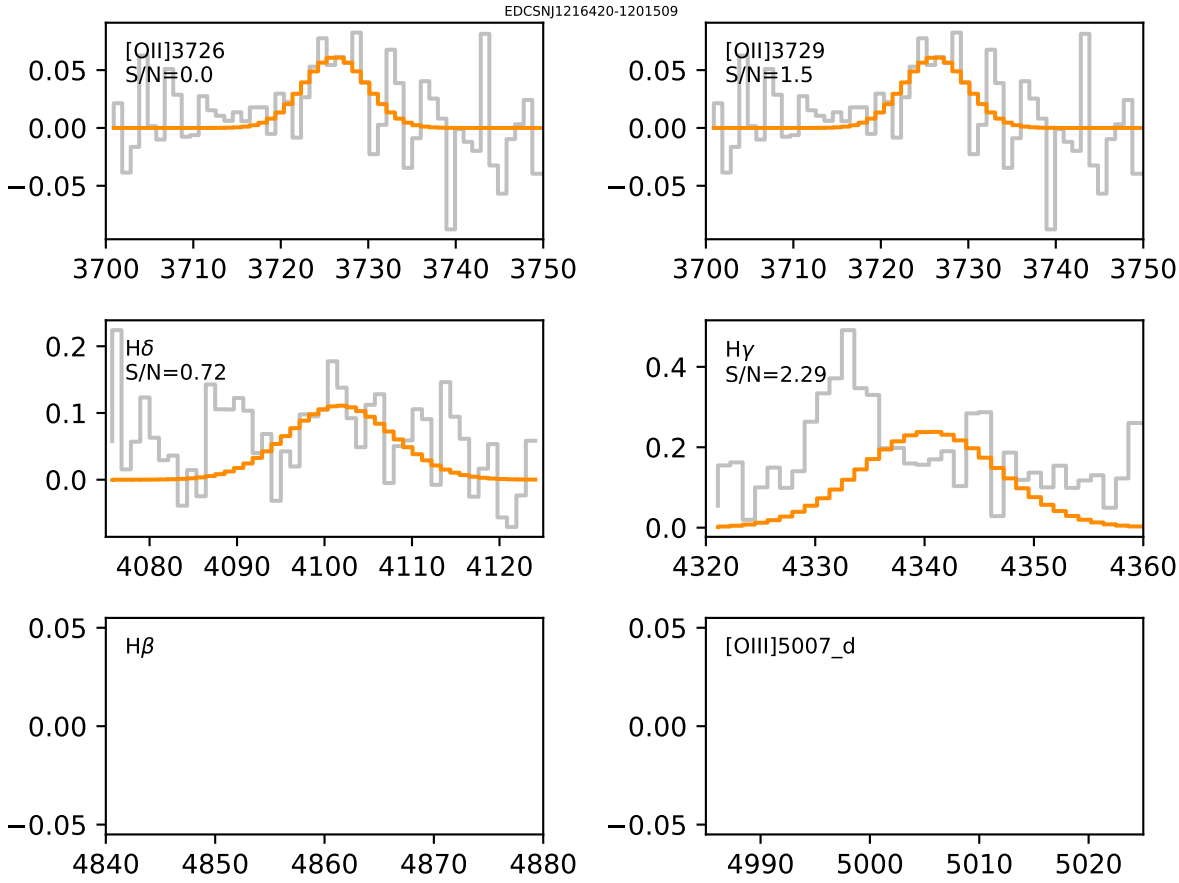
EDCSNJ1216420-1201509
[OII]3726
S/N=0.0
[OII]3729
S/N=1.5
Hδ
S/N=0.72
Hγ
S/N=2.29
Hβ
[OIII]5007_d

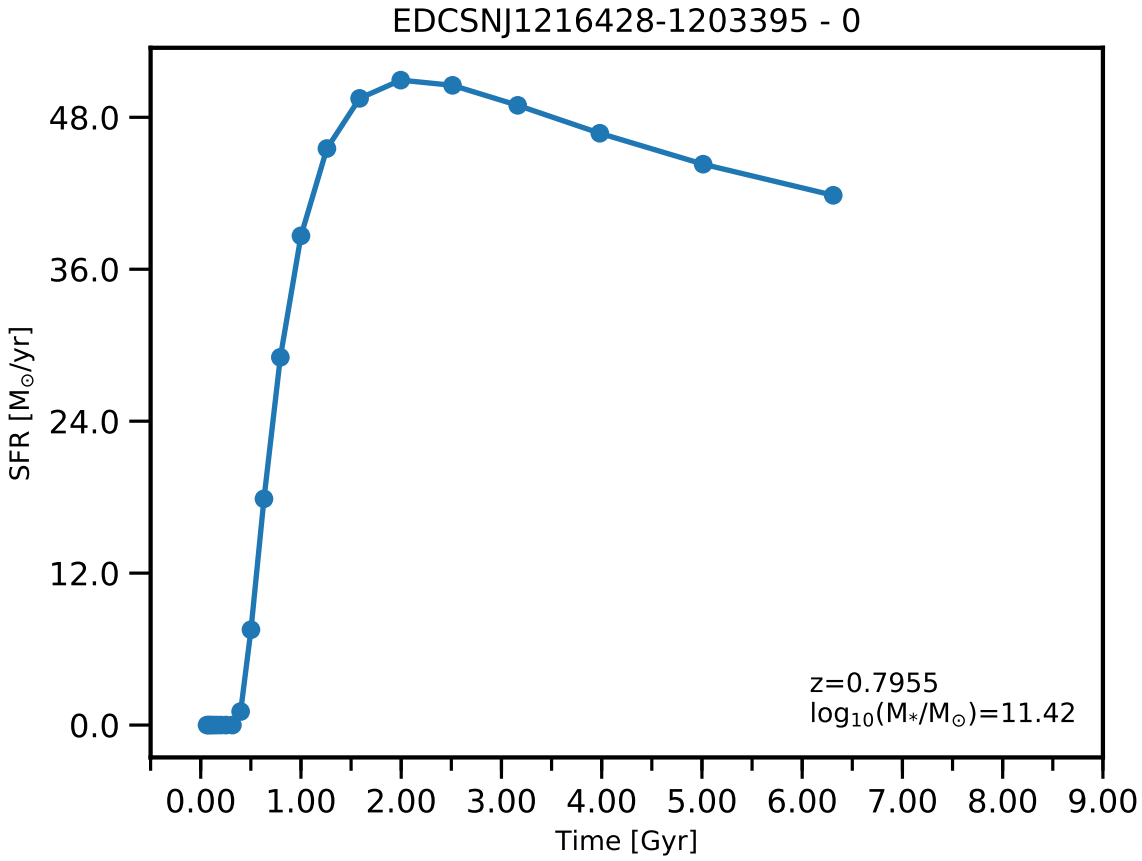
EDCSNJ1216428-1203395 - 0
SFR [M⊙/yr]
48.0
36.0
24.0
12.0
0.0
0.00
1.00
2.00
3.00
4.00
5.00
6.00
7.00
8.00
9.00
Time [Gyr]
z=0.7955
log10(M*/M⊙)=11.42

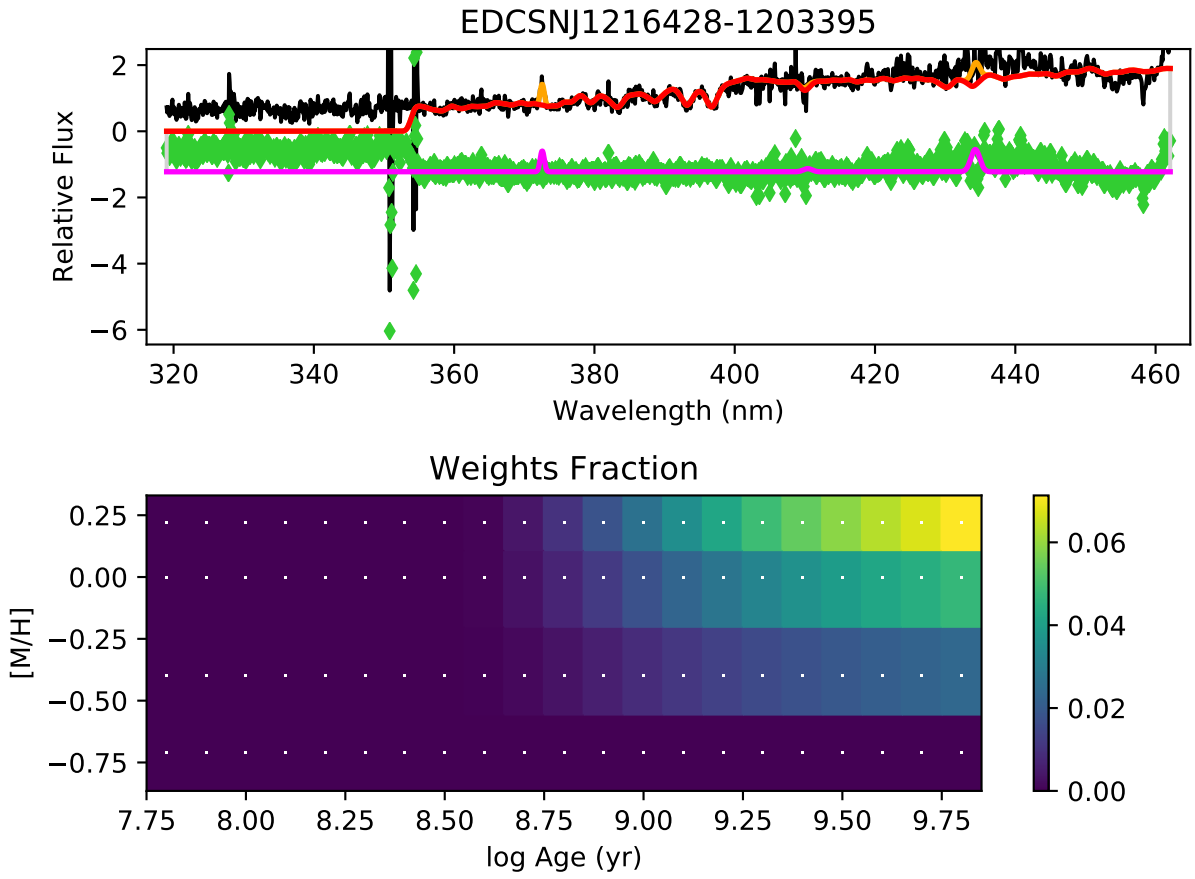
EDCSNJ1216428-1203395
Relative Flux
2
0
−2
−4
−6
320
340
360
380
400
420
440
460
Wavelength (nm)
Weights Fraction
[M/H]
0.25
0.00
−0.25
−0.50
−0.75
7.75
8.00
8.25
8.50
8.75
9.00
9.25
9.50
9.75
log Age (yr)
0.06
0.04
0.02
0.00

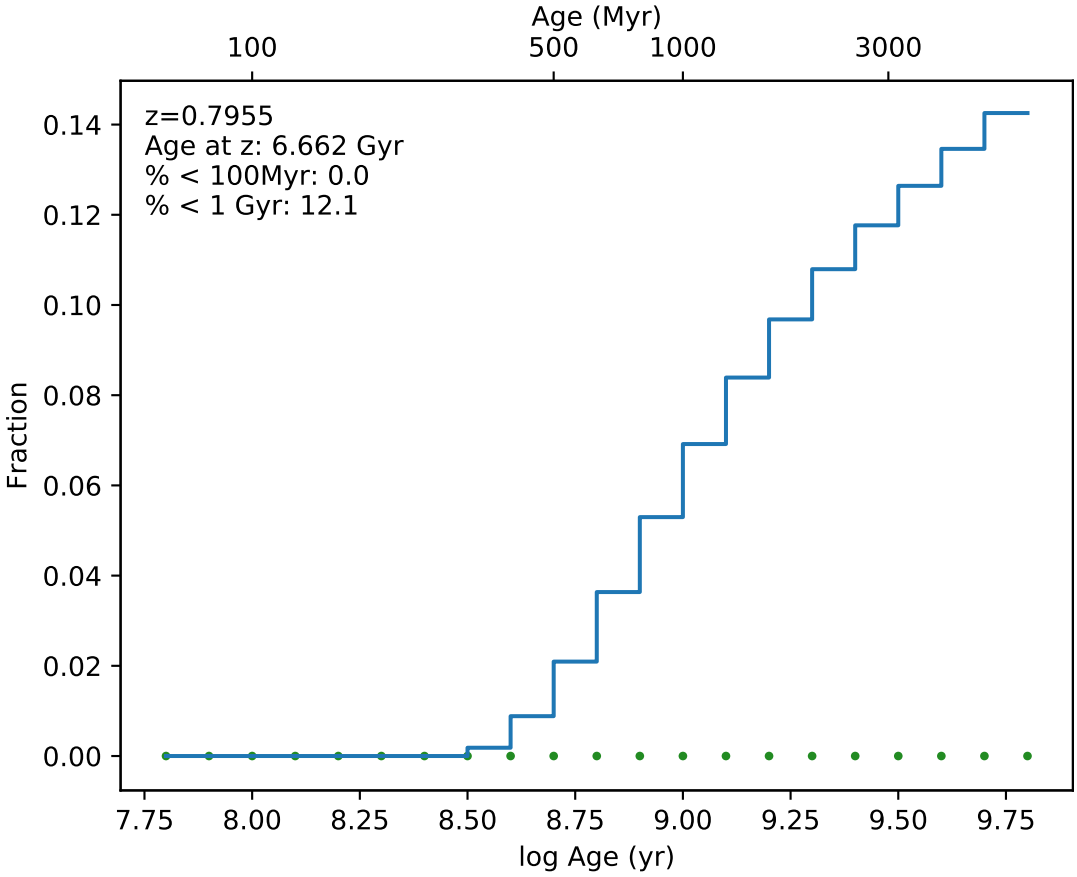
Age (Myr)
100
500
1000
3000
z=0.7955
Age at z: 6.662 Gyr
% < 100Myr: 0.0
% < 1 Gyr: 12.1
Fraction
0.14
0.12
0.10
0.08
0.06
0.04
0.02
0.00
7.75
8.00
8.25
8.50
8.75
9.00
9.25
9.50
9.75
log Age (yr)

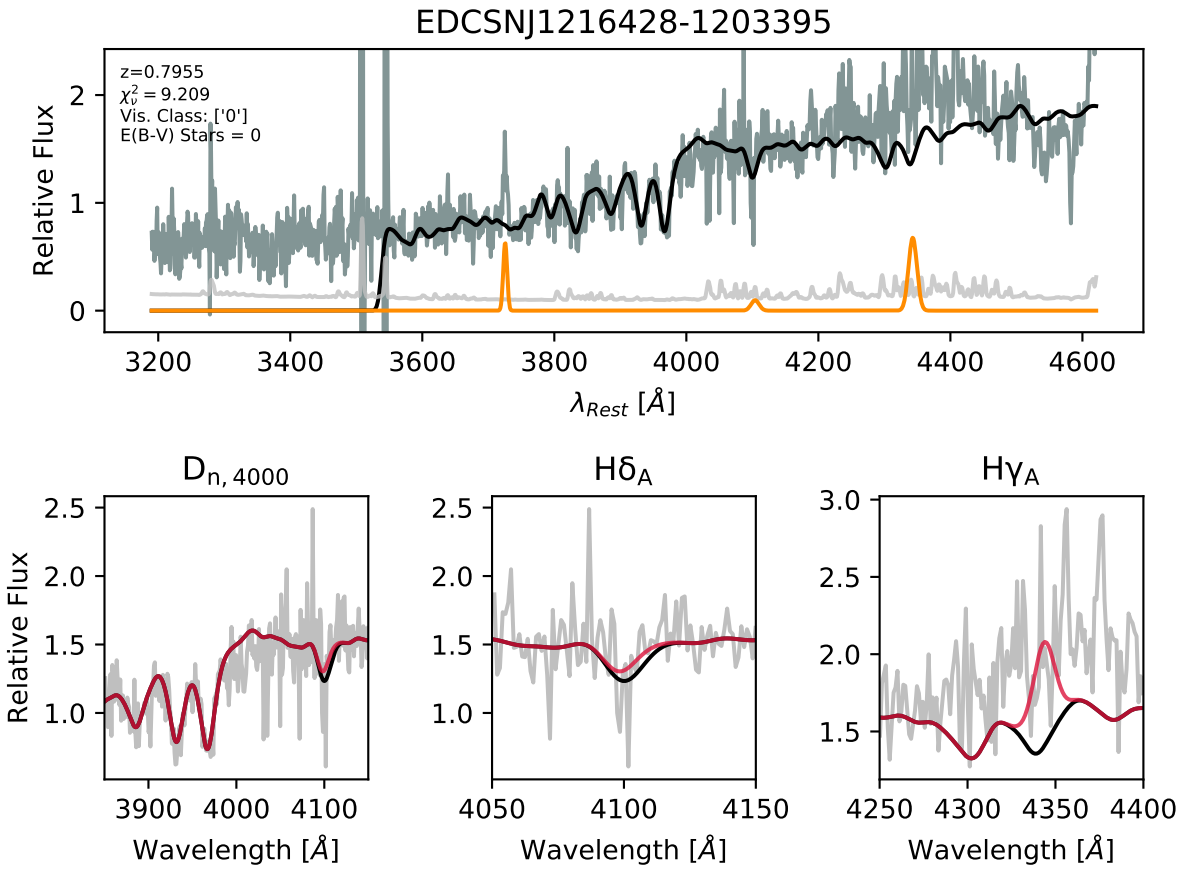
EDCSNJ1216428-1203395
z=0.7955
$\chi^2_\nu = 9.209$
Vis. Class: ['0']
E(B-V) Stars = 0
Relative Flux
λ_{Rest} [Å]
$D_{n,4000}$
$H\delta_A$
$H\gamma_A$
Wavelength [Å]

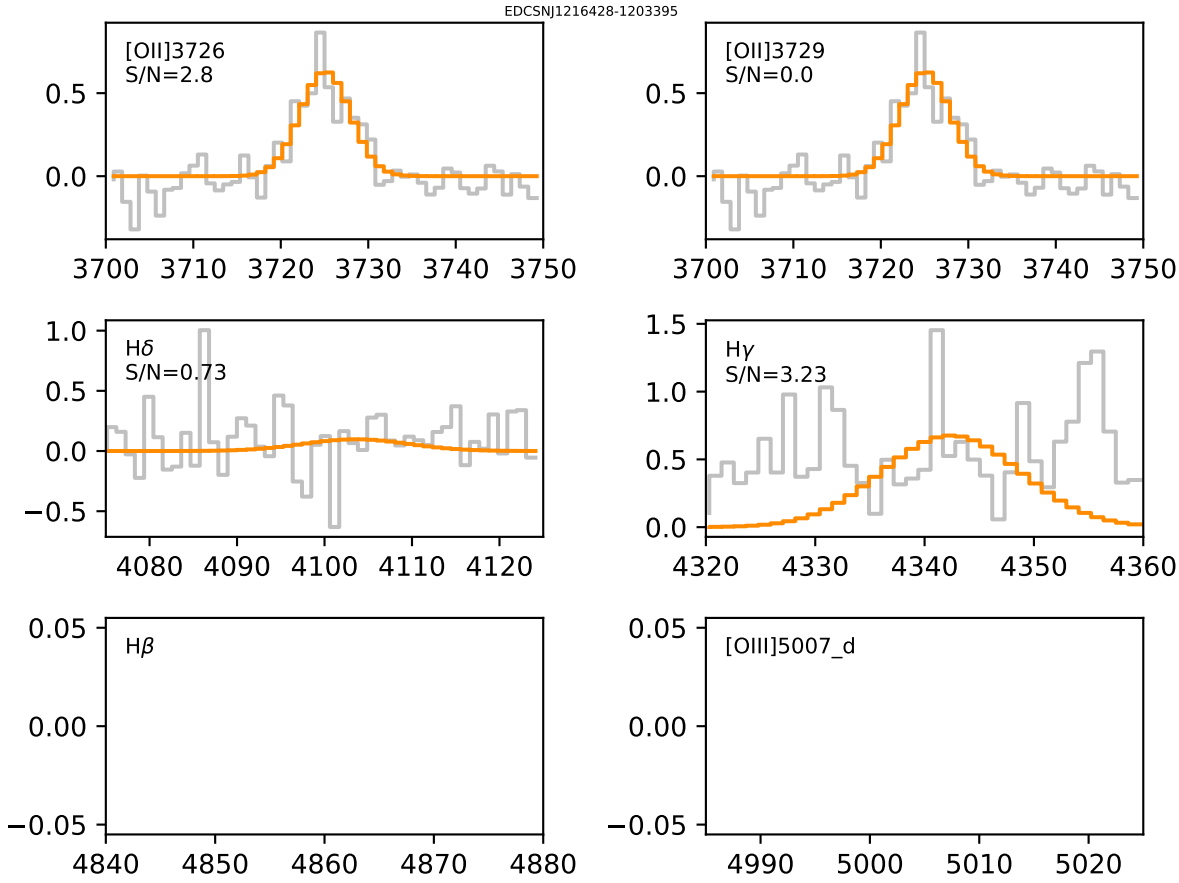
EDCSNJ1216428-1203395
[OII]3726
S/N=2.8
[OII]3729
S/N=0.0
Hδ
S/N=0.73
Hγ
S/N=3.23
Hβ
[OIII]5007_d

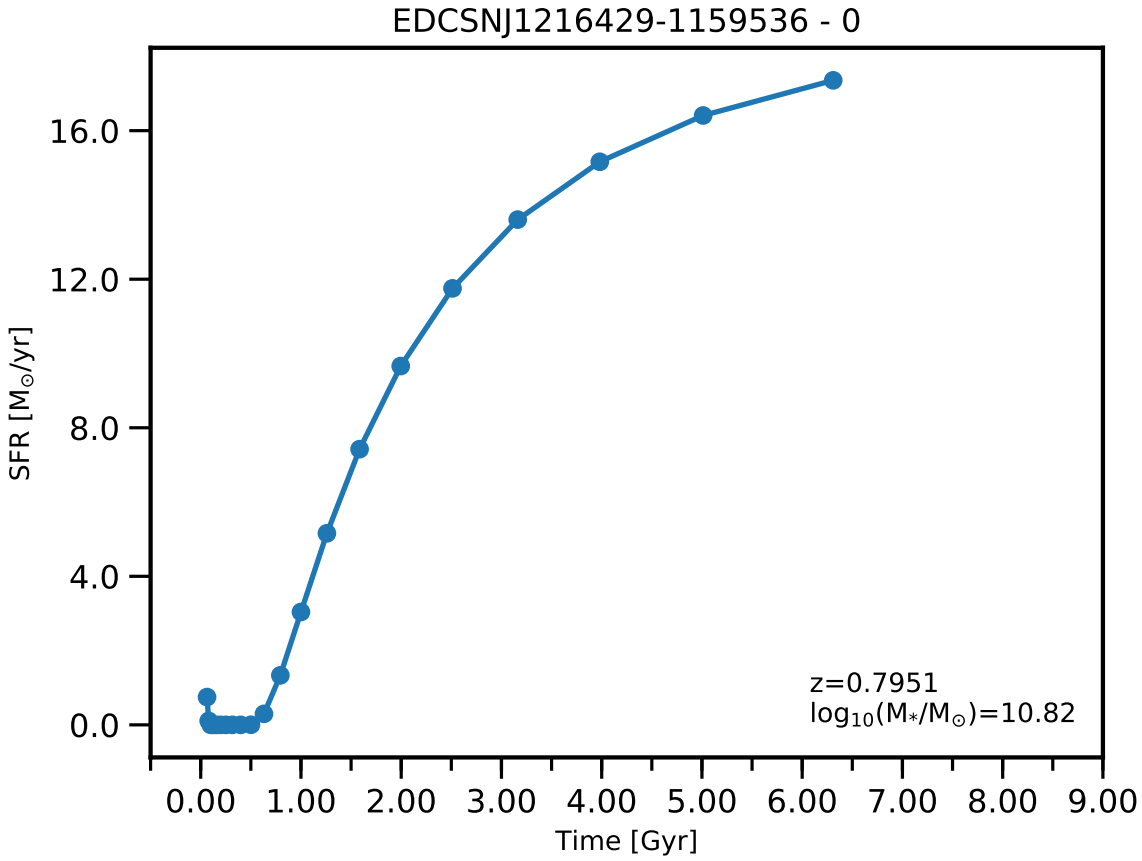
EDCSNJ1216429-1159536 - 0
SFR [M⊙/yr]
16.0
12.0
8.0
4.0
0.0
0.00
1.00
2.00
3.00
4.00
5.00
6.00
7.00
8.00
9.00
Time [Gyr]
z=0.7951
log10(M*/M⊙)=10.82

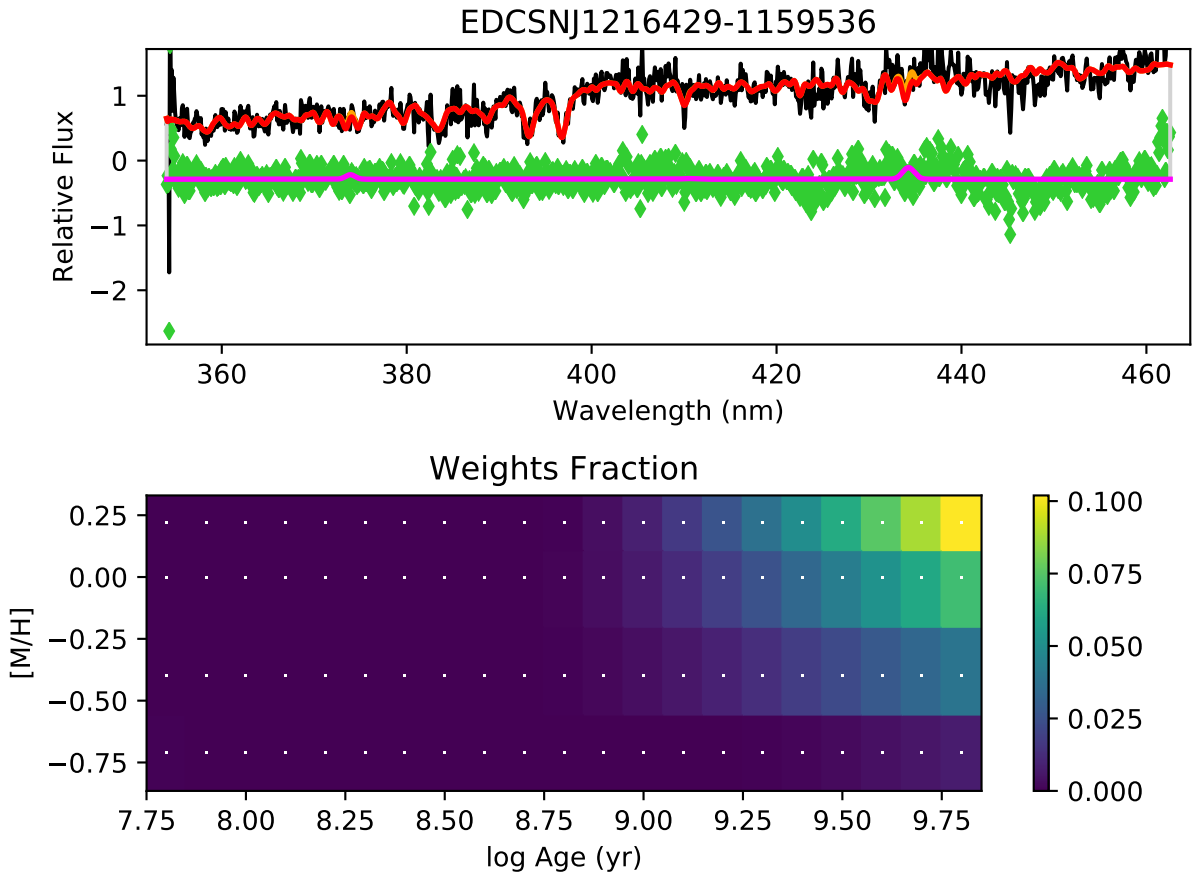
EDCSNJ1216429-1159536
Relative Flux
1
0
−1
−2
360
380
400
420
440
460
Wavelength (nm)
Weights Fraction
[M/H]
0.25
0.00
−0.25
−0.50
−0.75
7.75
8.00
8.25
8.50
8.75
9.00
9.25
9.50
9.75
log Age (yr)
0.100
0.075
0.050
0.025
0.000

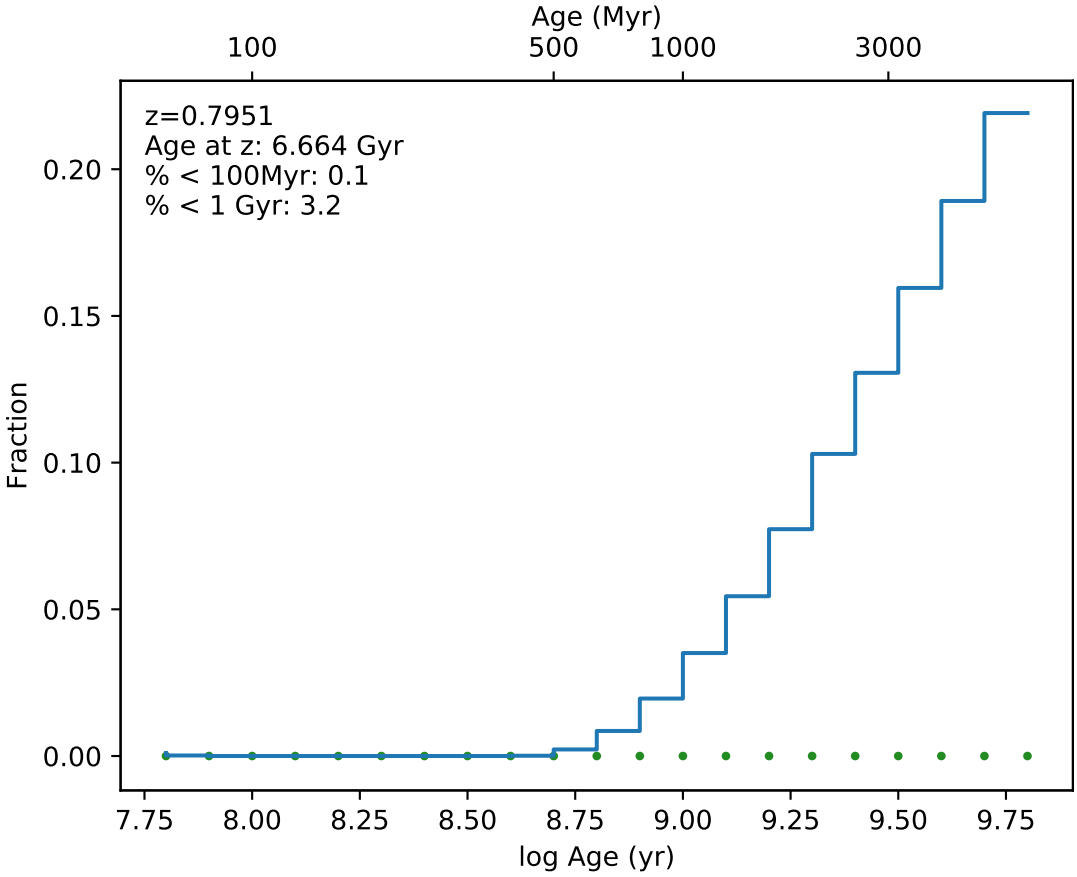
Age (Myr)
100
500
1000
3000
z=0.7951
Age at z: 6.664 Gyr
% < 100Myr: 0.1
% < 1 Gyr: 3.2
Fraction
0.20
0.15
0.10
0.05
0.00
7.75
8.00
8.25
8.50
8.75
9.00
9.25
9.50
9.75
log Age (yr)

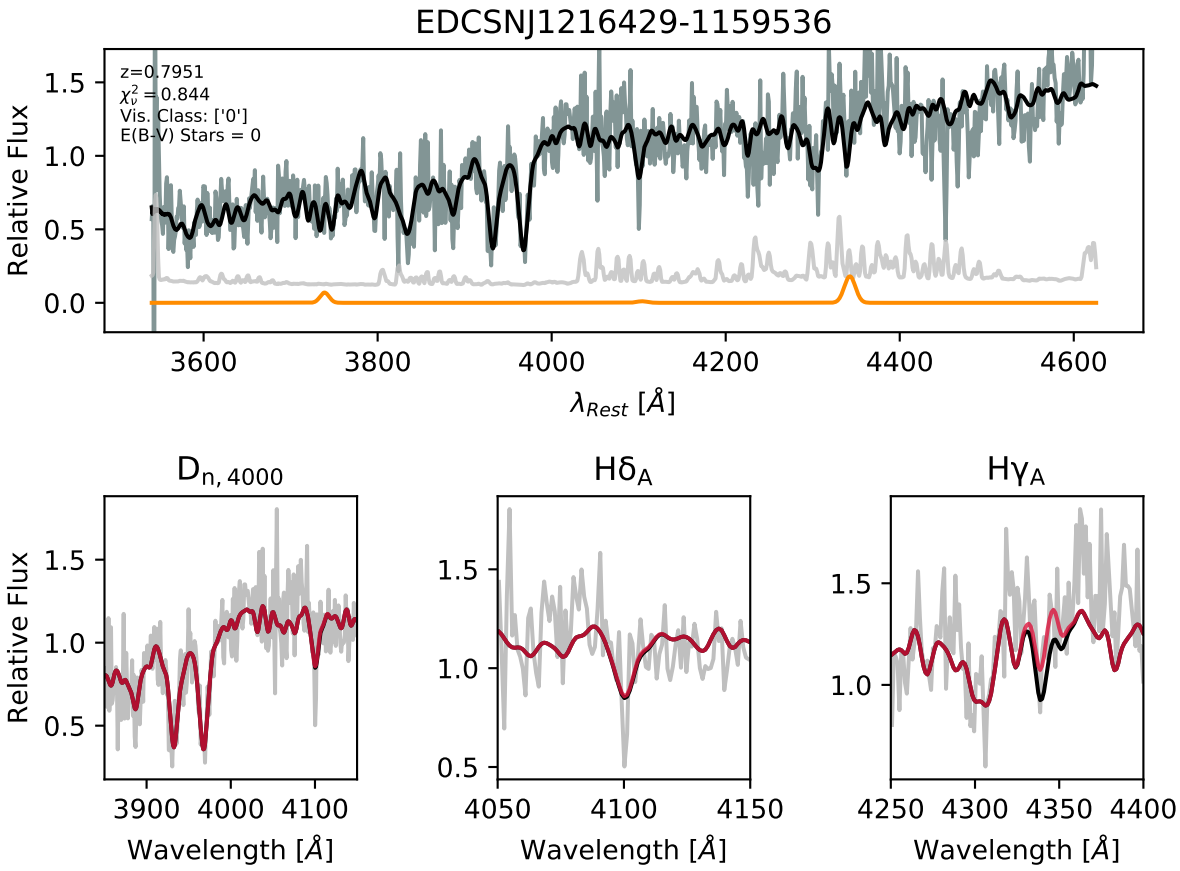
EDCSNJ1216429-1159536
z=0.7951
$\chi^2_\nu = 0.844$
Vis. Class: ['0']
E(B-V) Stars = 0
Relative Flux
λ_{Rest} [Å]
$D_{n,4000}$
$H\delta_A$
$H\gamma_A$
Wavelength [Å]

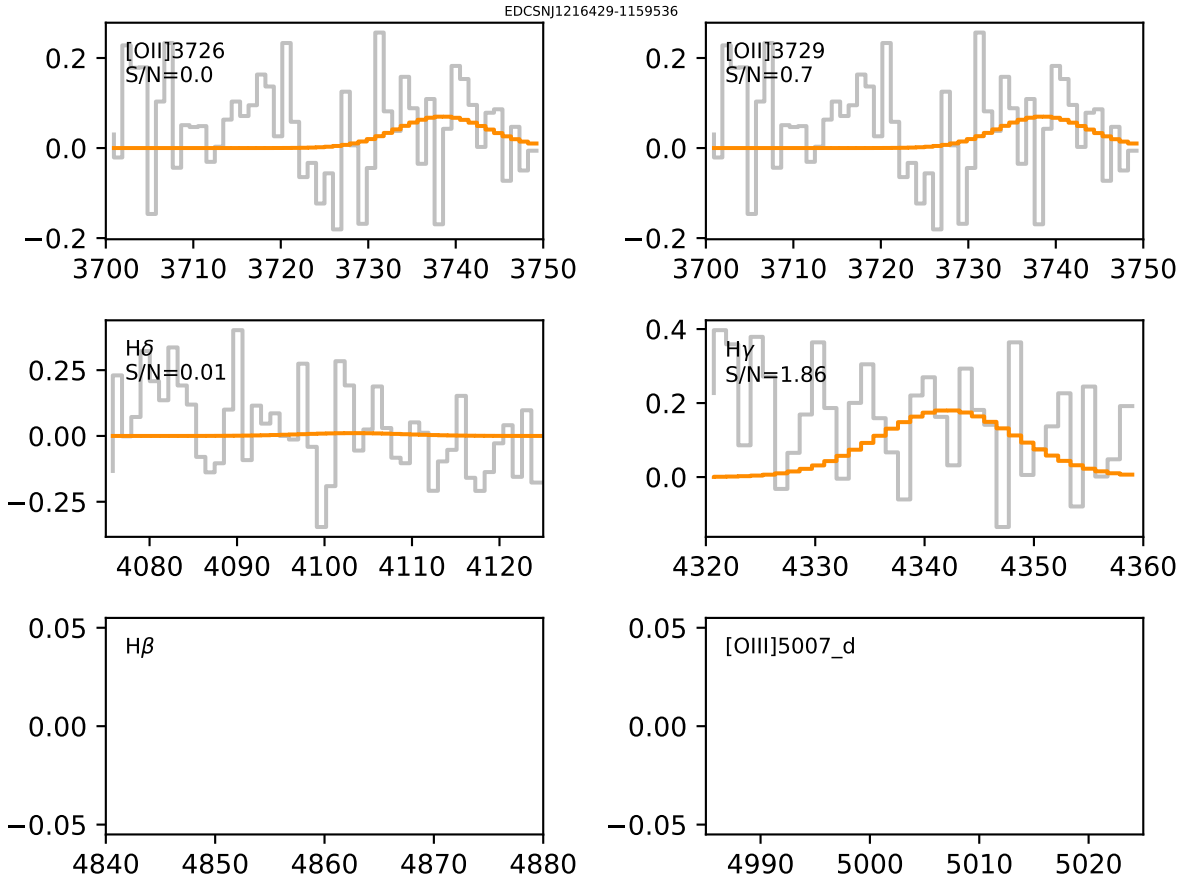
EDCSNJ1216429-1159536
[OII]3726
S/N=0.0
[OII]3729
S/N=0.7
Hδ
S/N=0.01
Hγ
S/N=1.86
Hβ
[OIII]5007_d

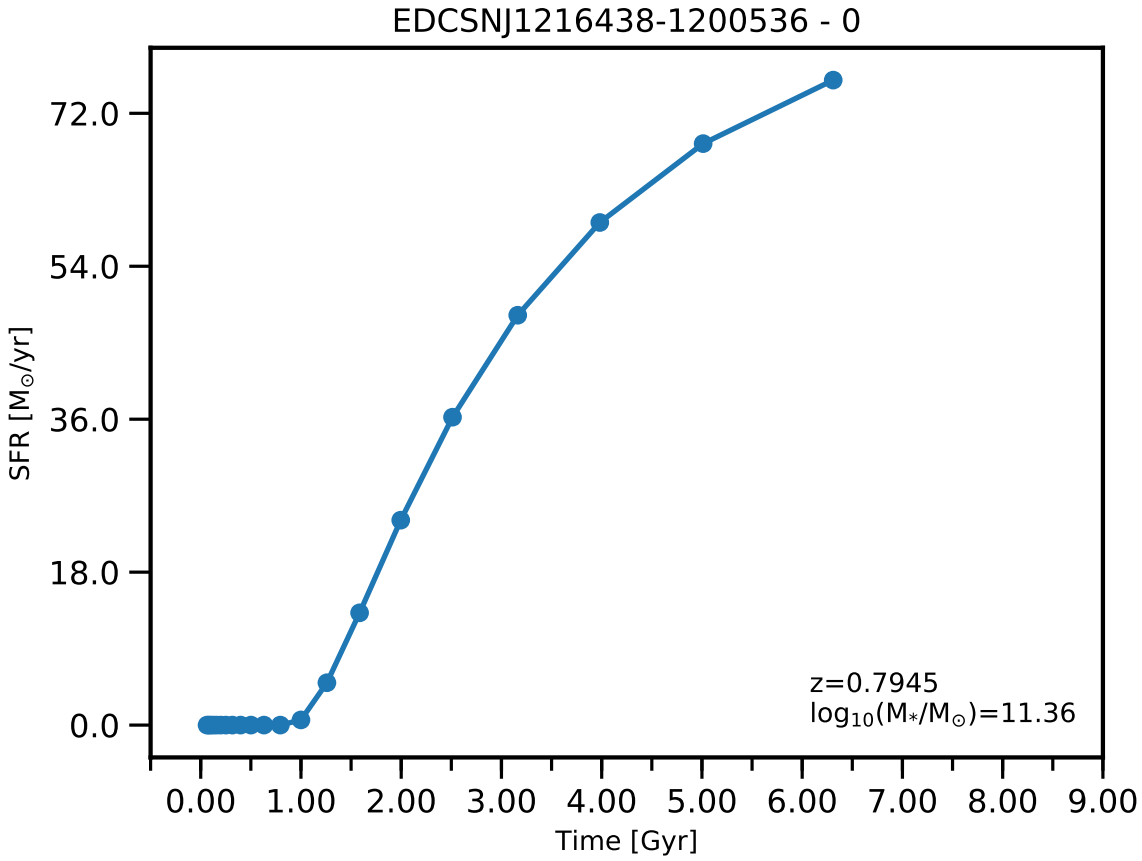
EDCSNJ1216438-1200536 - 0
72.0
54.0
36.0
18.0
0.0
SFR [M⊙/yr]
0.00
1.00
2.00
3.00
4.00
5.00
6.00
7.00
8.00
9.00
Time [Gyr]
z=0.7945
log10(M*/M⊙)=11.36

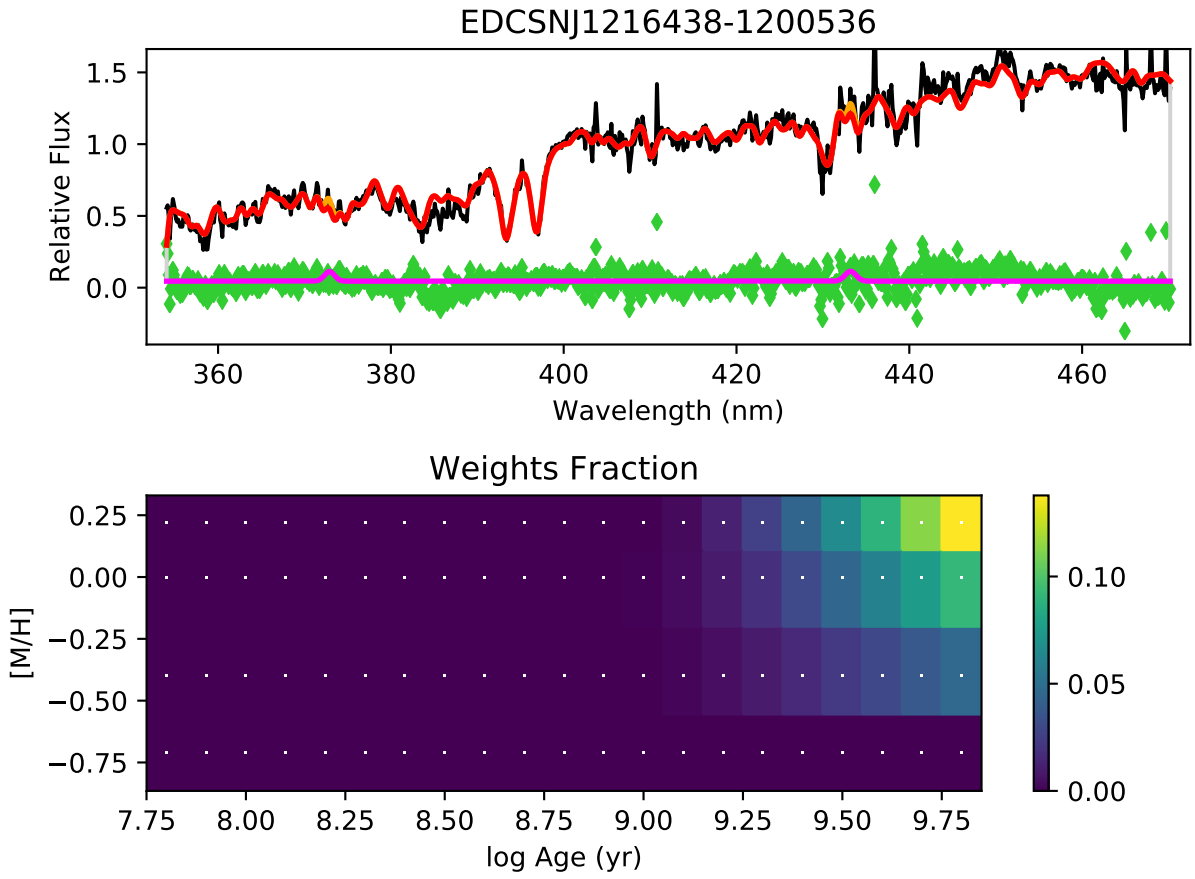
EDCSNJ1216438-1200536
Relative Flux
1.5
1.0
0.5
0.0
360
380
400
420
440
460
Wavelength (nm)
Weights Fraction
[M/H]
0.25
0.00
−0.25
−0.50
−0.75
7.75
8.00
8.25
8.50
8.75
9.00
9.25
9.50
9.75
log Age (yr)
0.10
0.05
0.00

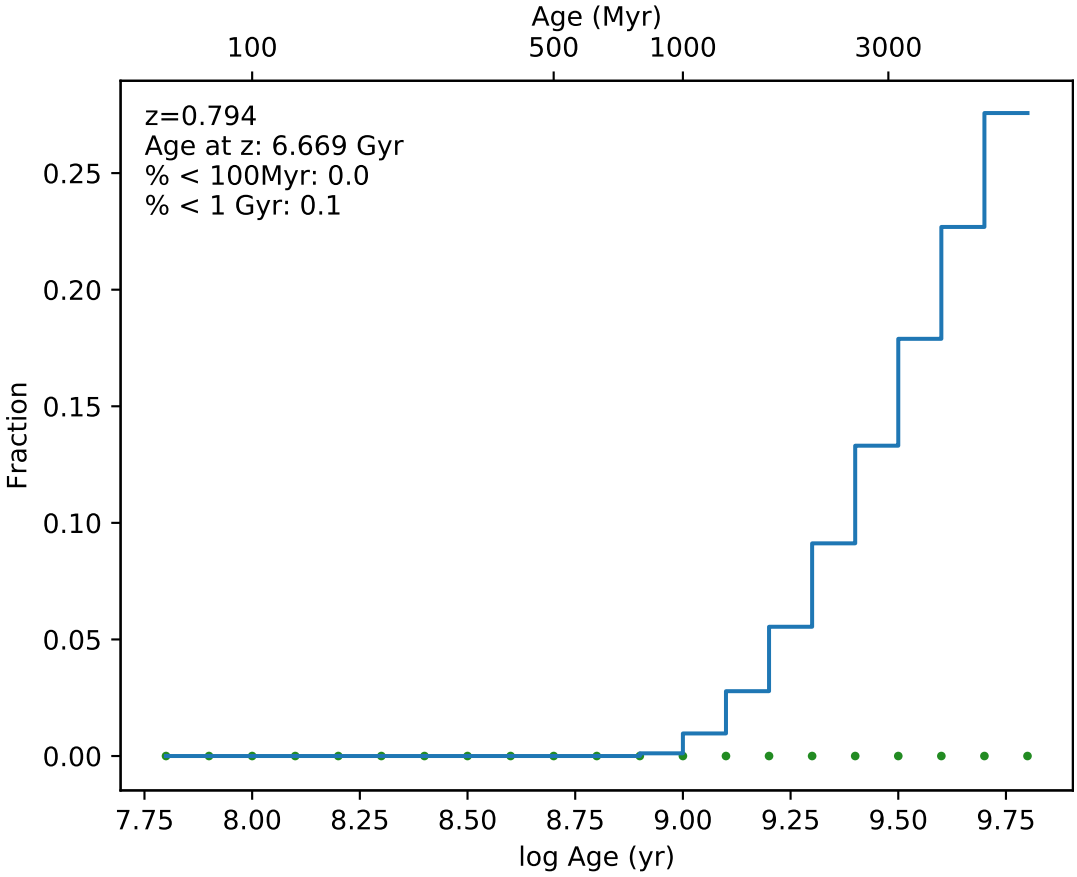
Age (Myr)
100
500
1000
3000
z=0.794
Age at z: 6.669 Gyr
% < 100Myr: 0.0
% < 1 Gyr: 0.1
Fraction
0.25
0.20
0.15
0.10
0.05
0.00
7.75
8.00
8.25
8.50
8.75
9.00
9.25
9.50
9.75
log Age (yr)

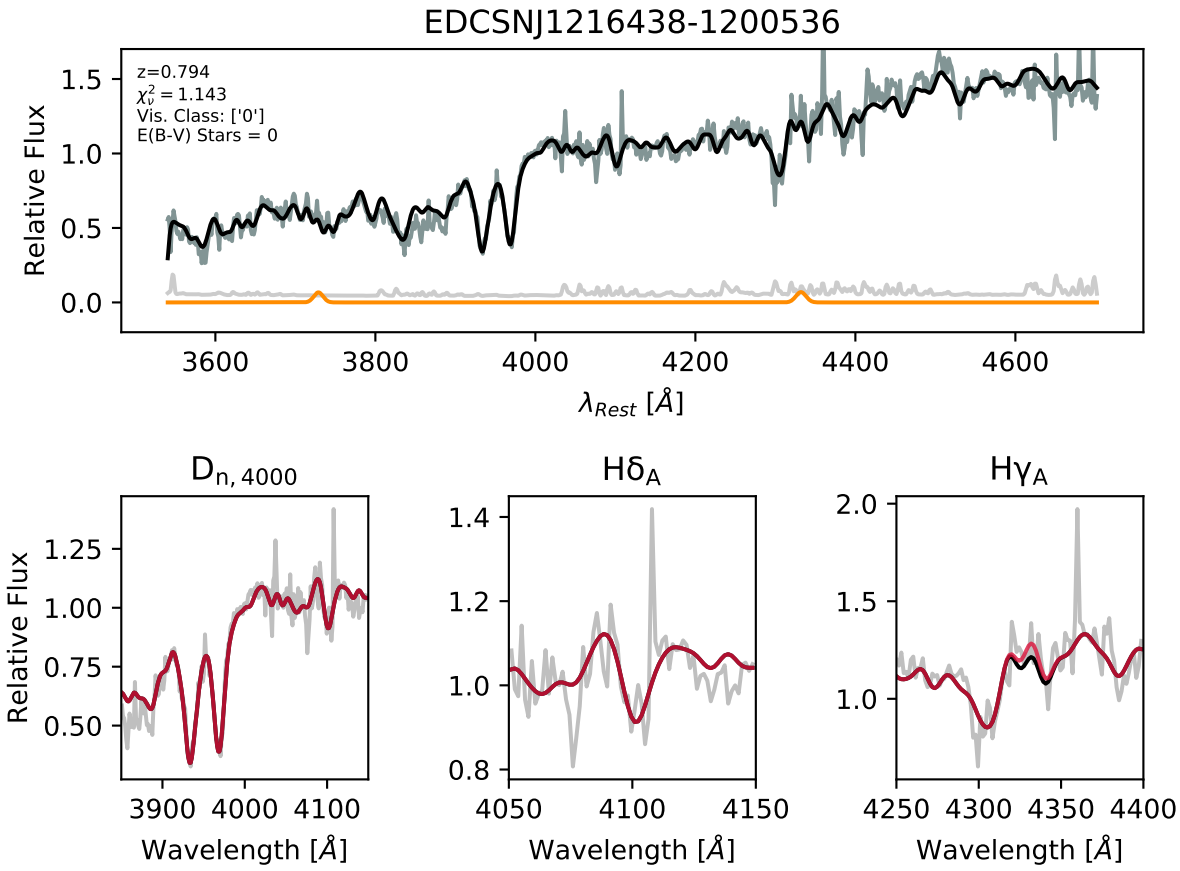
EDCSNJ1216438-1200536
z=0.794
$\chi^2_\nu = 1.143$
Vis. Class: ['0']
E(B-V) Stars = 0
Relative Flux
λ_{Rest} [Å]
$D_{n,4000}$
$H\delta_A$
$H\gamma_A$
Wavelength [Å]

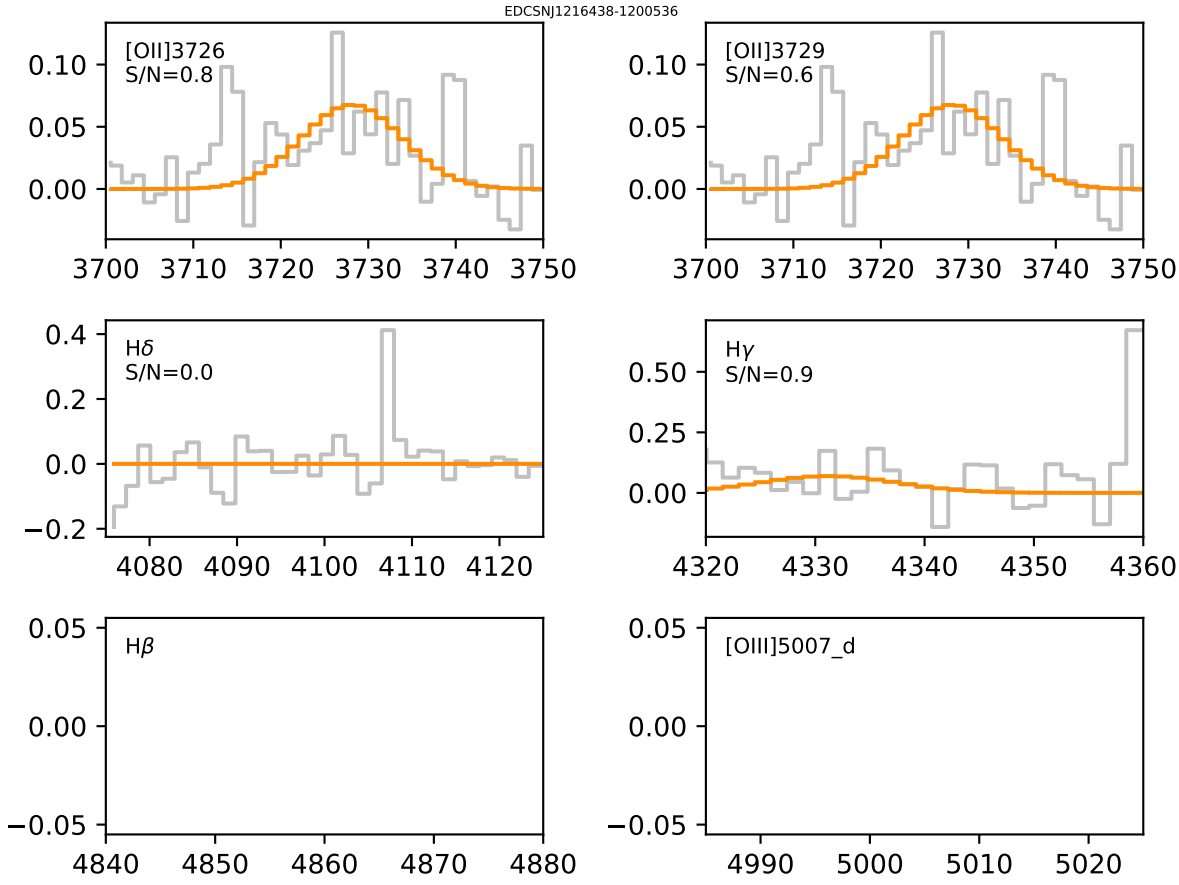
EDCSNJ1216438-1200536
[OII]3726
S/N=0.8
[OII]3729
S/N=0.6
Hδ
S/N=0.0
Hγ
S/N=0.9
Hβ
[OIII]5007_d

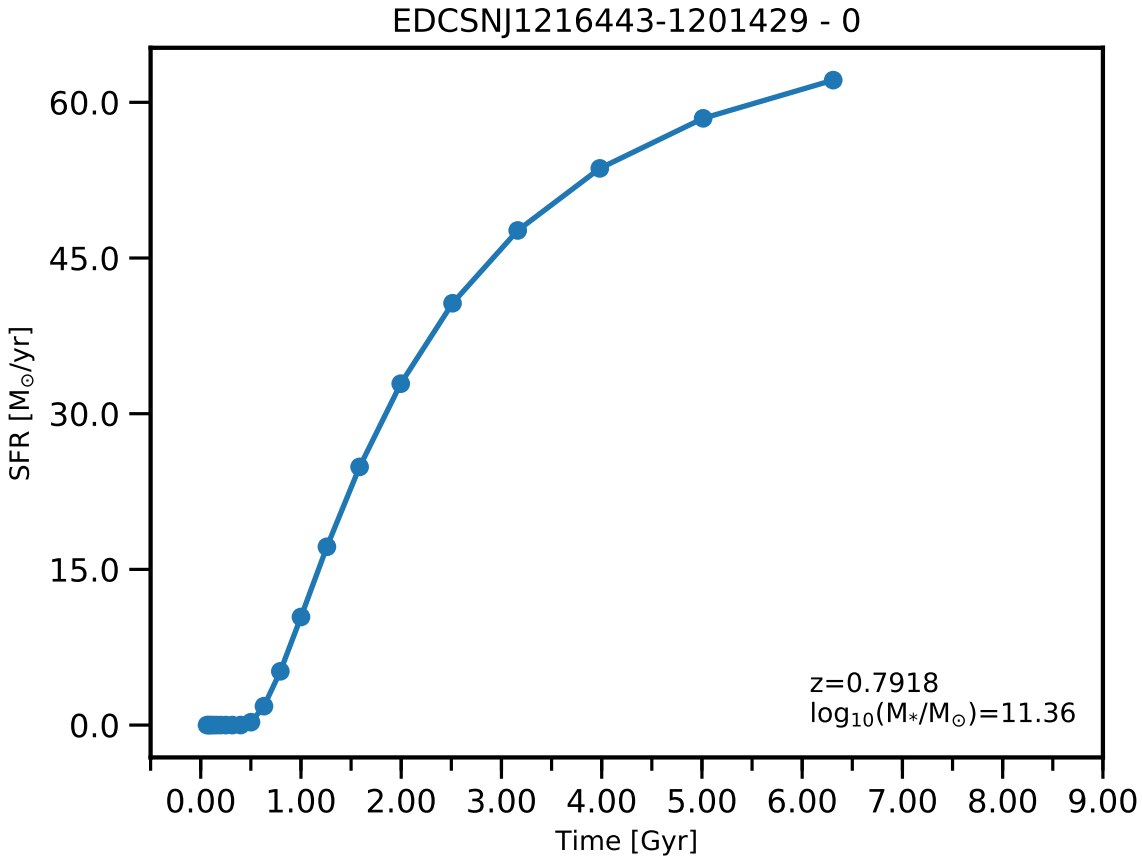
EDCSNJ1216443-1201429 - 0
60.0
45.0
30.0
15.0
0.0
SFR [M⊙/yr]
0.00
1.00
2.00
3.00
4.00
5.00
6.00
7.00
8.00
9.00
Time [Gyr]
z=0.7918
log10(M*/M⊙)=11.36

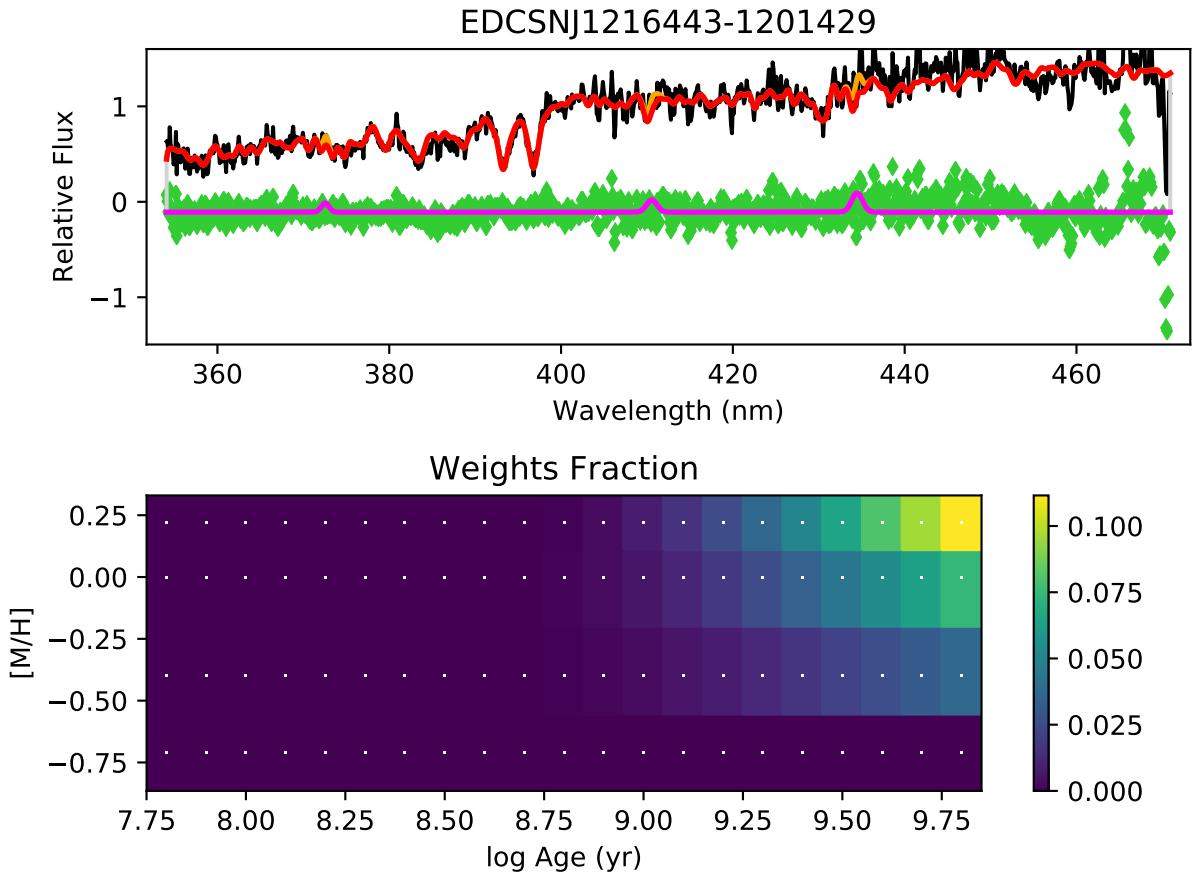
EDCSNJ1216443-1201429
Relative Flux
1
0
−1
360
380
400
420
440
460
Wavelength (nm)
Weights Fraction
[M/H]
0.25
0.00
−0.25
−0.50
−0.75
7.75
8.00
8.25
8.50
8.75
9.00
9.25
9.50
9.75
log Age (yr)
0.100
0.075
0.050
0.025
0.000

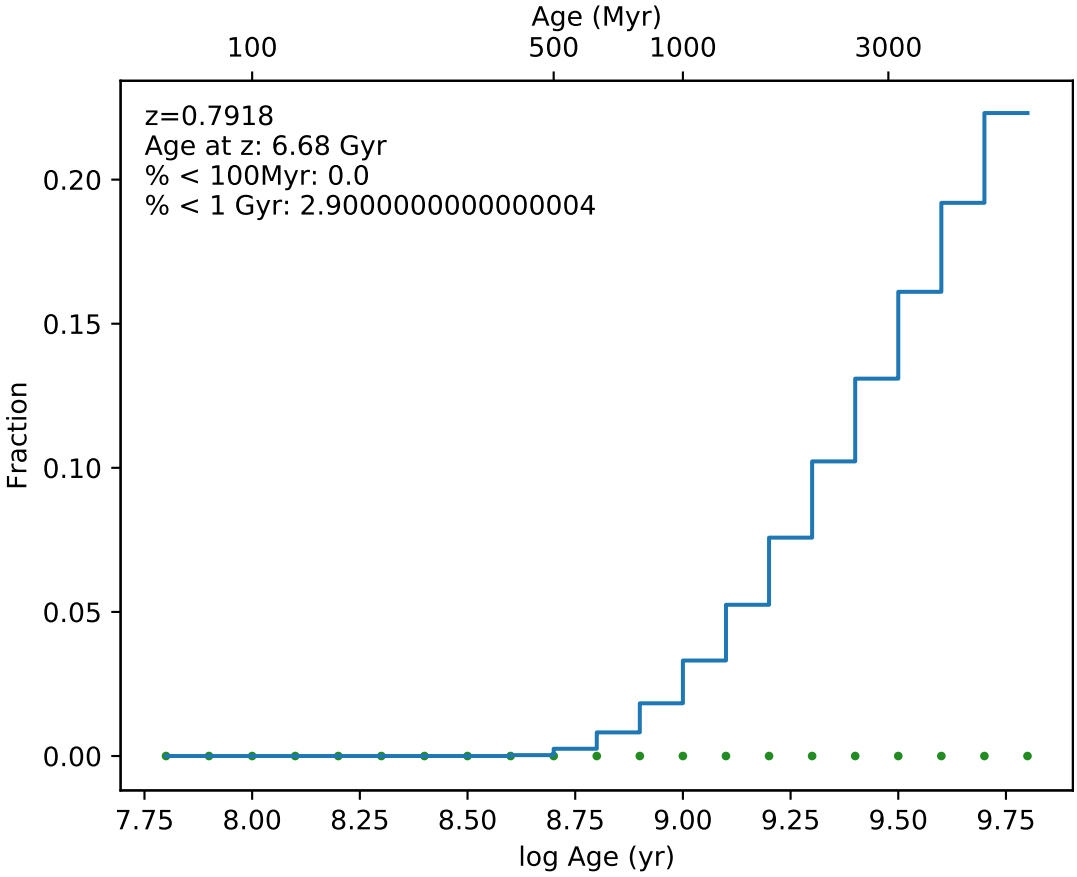
Age (Myr)
100
500
1000
3000
z=0.7918
Age at z: 6.68 Gyr
% < 100Myr: 0.0
% < 1 Gyr: 2.9000000000000004
Fraction
0.20
0.15
0.10
0.05
0.00
7.75
8.00
8.25
8.50
8.75
9.00
9.25
9.50
9.75
log Age (yr)

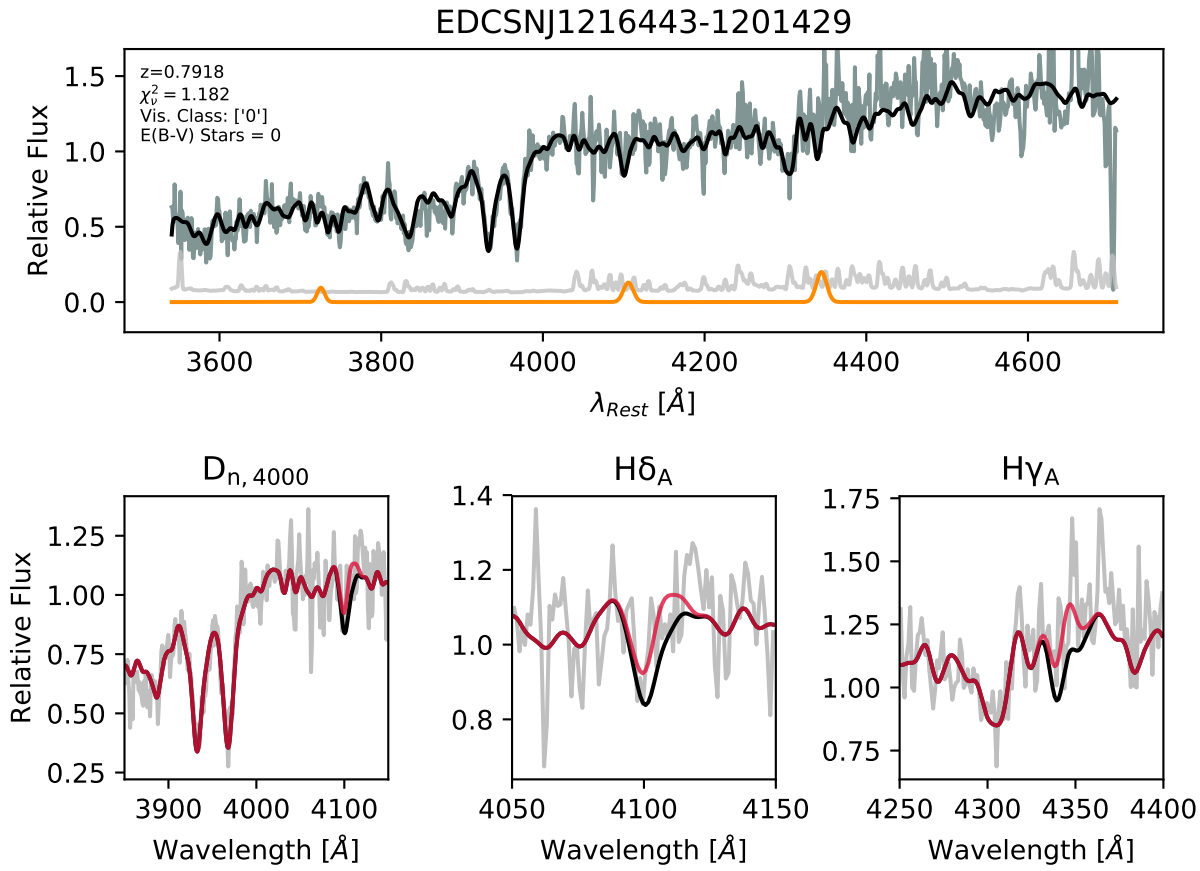
EDCSNJ1216443-1201429
z=0.7918
$\chi^2_\nu = 1.182$
Vis. Class: ['0']
E(B-V) Stars = 0
Relative Flux
λ_{Rest} [Å]
$D_{n,4000}$
$H\delta_A$
$H\gamma_A$
Wavelength [Å]

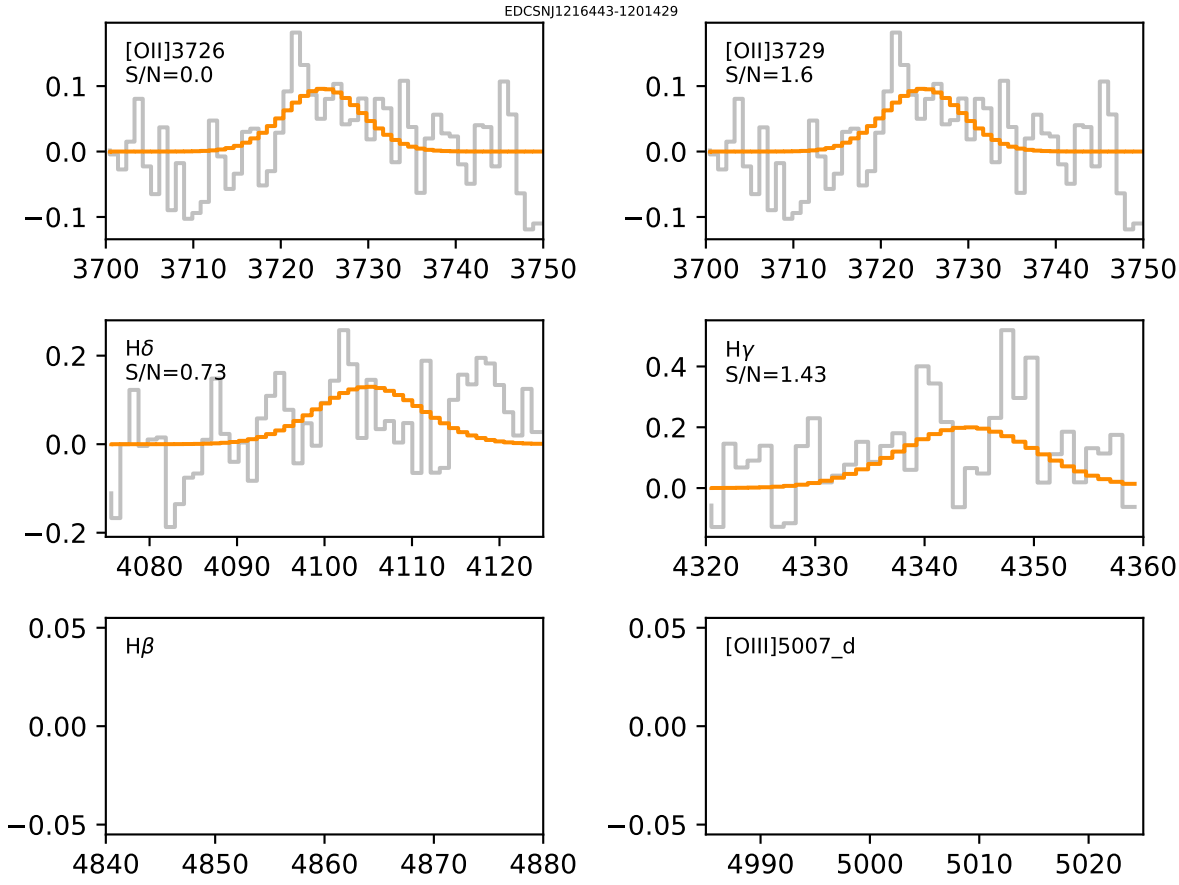
EDCSNJ1216443-1201429
[OII]3726
S/N=0.0
[OII]3729
S/N=1.6
Hδ
S/N=0.73
Hγ
S/N=1.43
Hβ
[OIII]5007_d

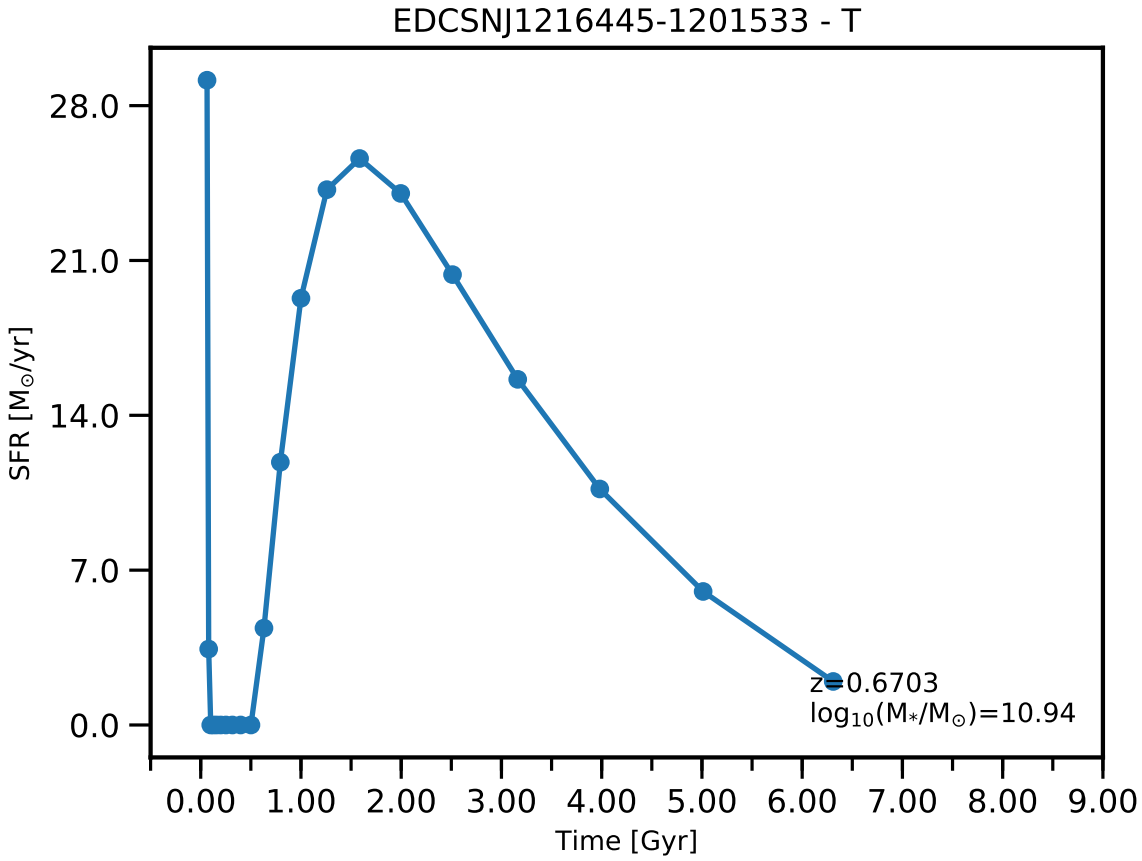
EDCSNJ1216445-1201533 - T
28.0
21.0
14.0
7.0
0.0
SFR [M⊙/yr]
0.00
1.00
2.00
3.00
4.00
5.00
6.00
7.00
8.00
9.00
Time [Gyr]
z=0.6703
log10(M*/M⊙)=10.94

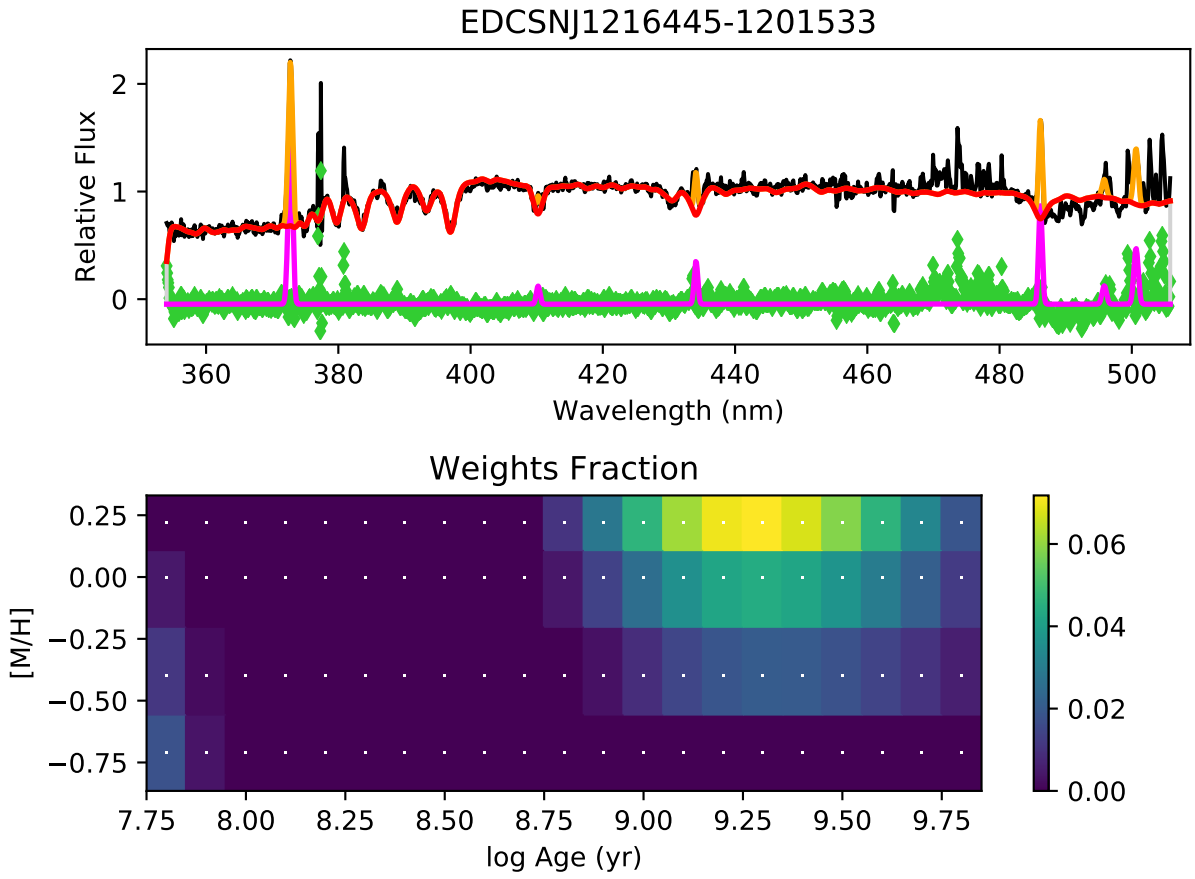
EDCSNJ1216445-1201533
Relative Flux
2
1
0
360
380
400
420
440
460
480
500
Wavelength (nm)
Weights Fraction
[M/H]
0.25
0.00
−0.25
−0.50
−0.75
7.75
8.00
8.25
8.50
8.75
9.00
9.25
9.50
9.75
log Age (yr)
0.06
0.04
0.02
0.00

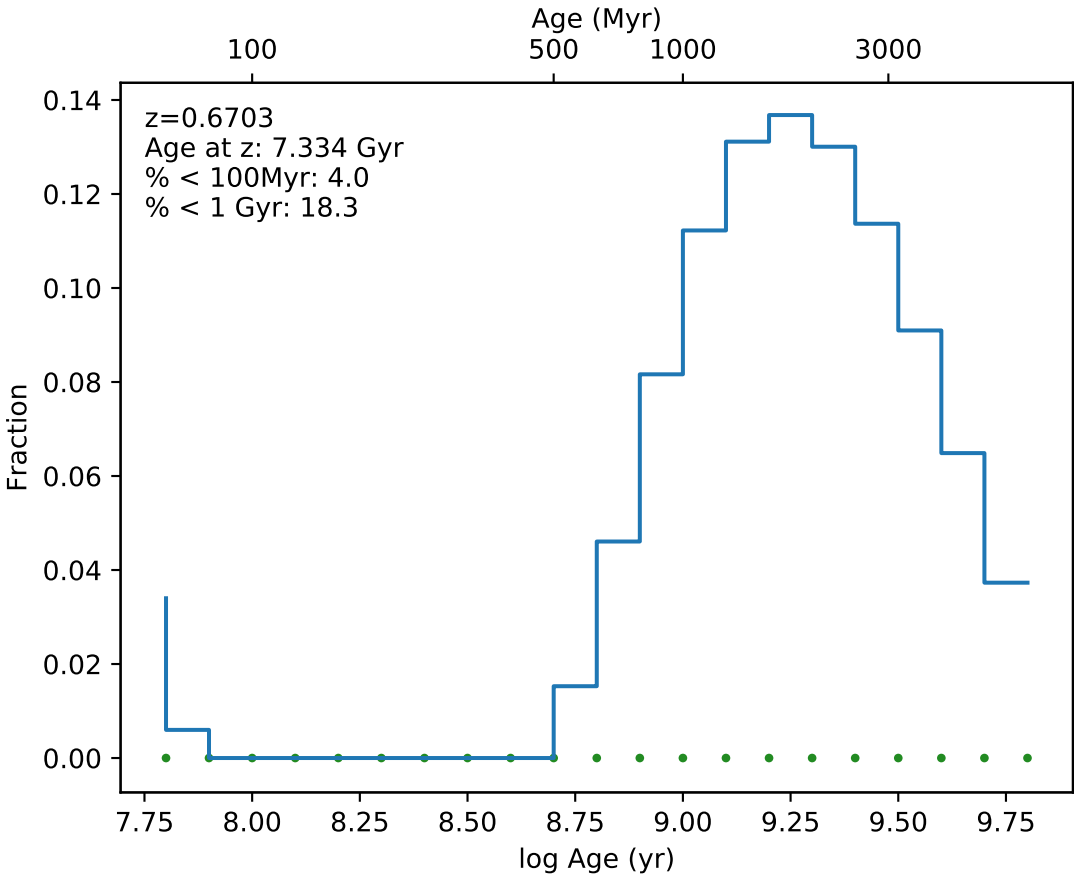
Age (Myr)
100
500
1000
3000
z=0.6703
Age at z: 7.334 Gyr
% < 100Myr: 4.0
% < 1 Gyr: 18.3
Fraction
0.14
0.12
0.10
0.08
0.06
0.04
0.02
0.00
7.75
8.00
8.25
8.50
8.75
9.00
9.25
9.50
9.75
log Age (yr)

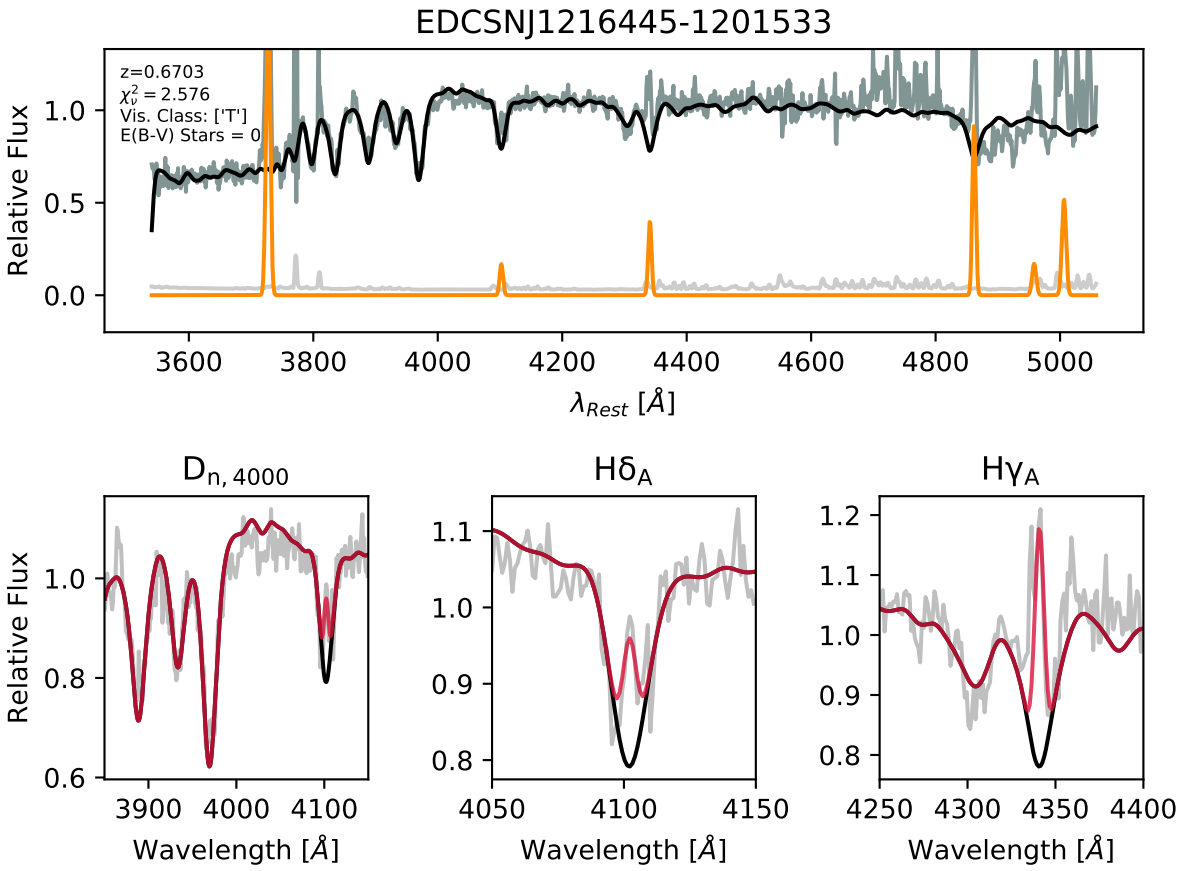
EDCSNJ1216445-1201533
z=0.6703
$\chi^2_\nu = 2.576$
Vis. Class: ['T']
E(B-V) Stars = 0
Relative Flux
1.0
0.5
0.0
3600
3800
4000
4200
4400
4600
4800
5000
λ_{Rest} [Å]
$D_{n,4000}$
$H\delta_A$
$H\gamma_A$
Relative Flux
1.0
0.8
0.6
3900
4000
4100
Wavelength [Å]
1.1
1.0
0.9
0.8
4050
4100
4150
Wavelength [Å]
1.2
1.1
1.0
0.9
0.8
4250
4300
4350
4400
Wavelength [Å]

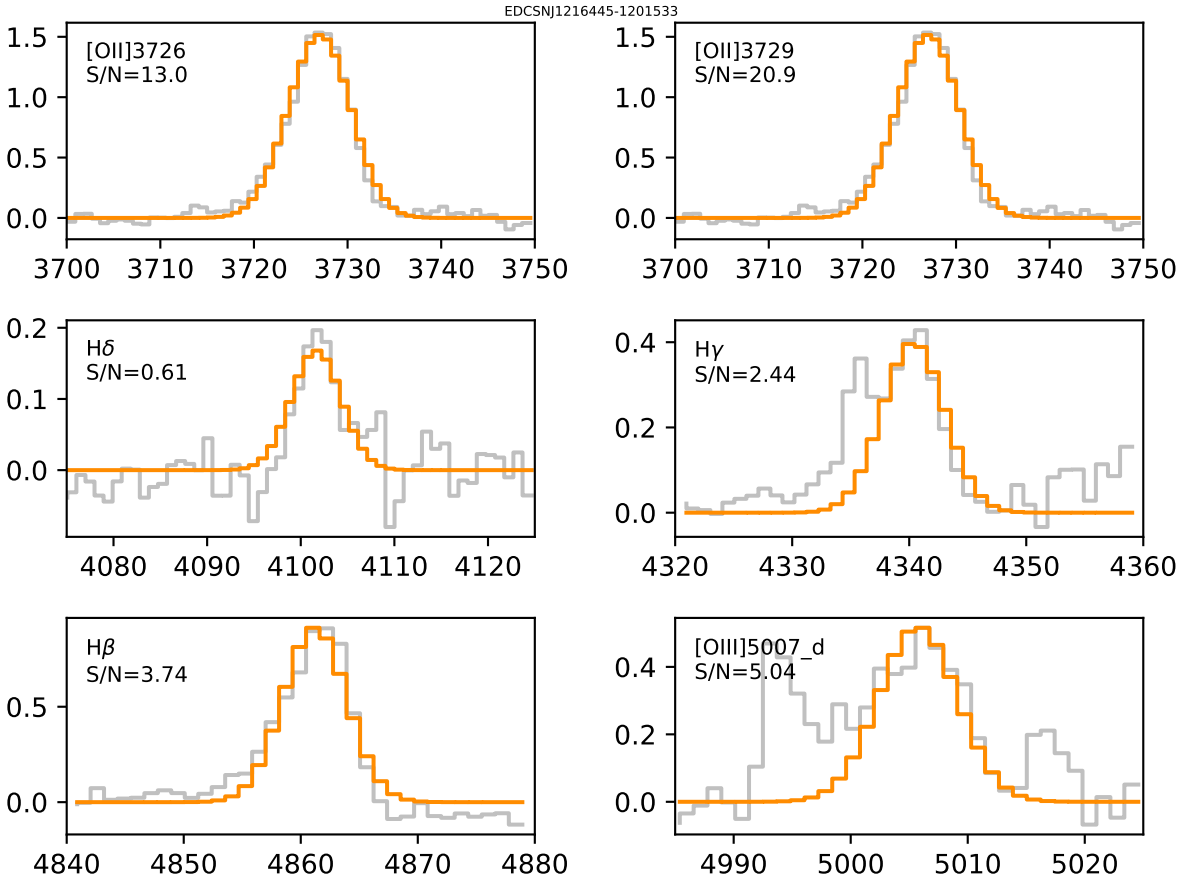
EDCSNJ1216445-1201533
[OII]3726
S/N=13.0
[OII]3729
S/N=20.9
Hδ
S/N=0.61
Hγ
S/N=2.44
Hβ
S/N=3.74
[OIII]5007_d
S/N=5.04

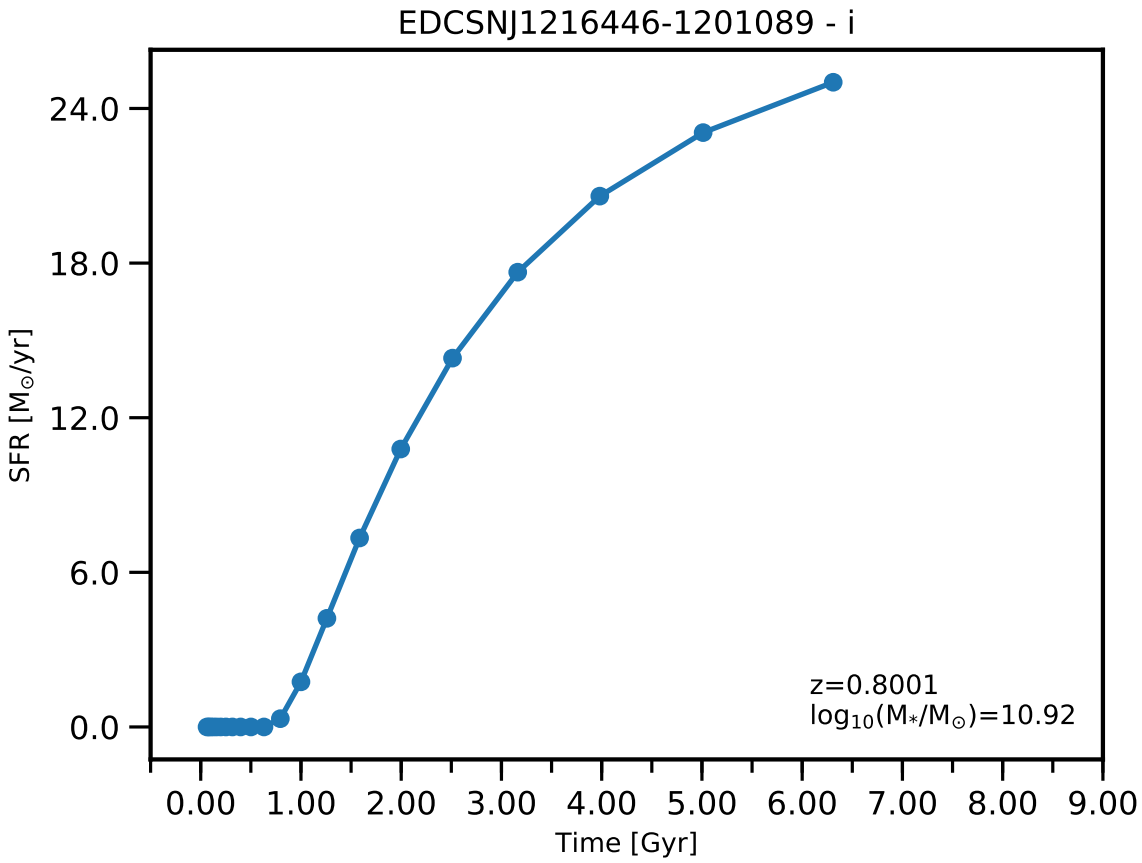
EDCSNJ1216446-1201089 - i
SFR [M⊙/yr]
24.0
18.0
12.0
6.0
0.0
0.00
1.00
2.00
3.00
4.00
5.00
6.00
7.00
8.00
9.00
Time [Gyr]
z=0.8001
log10(M*/M⊙)=10.92

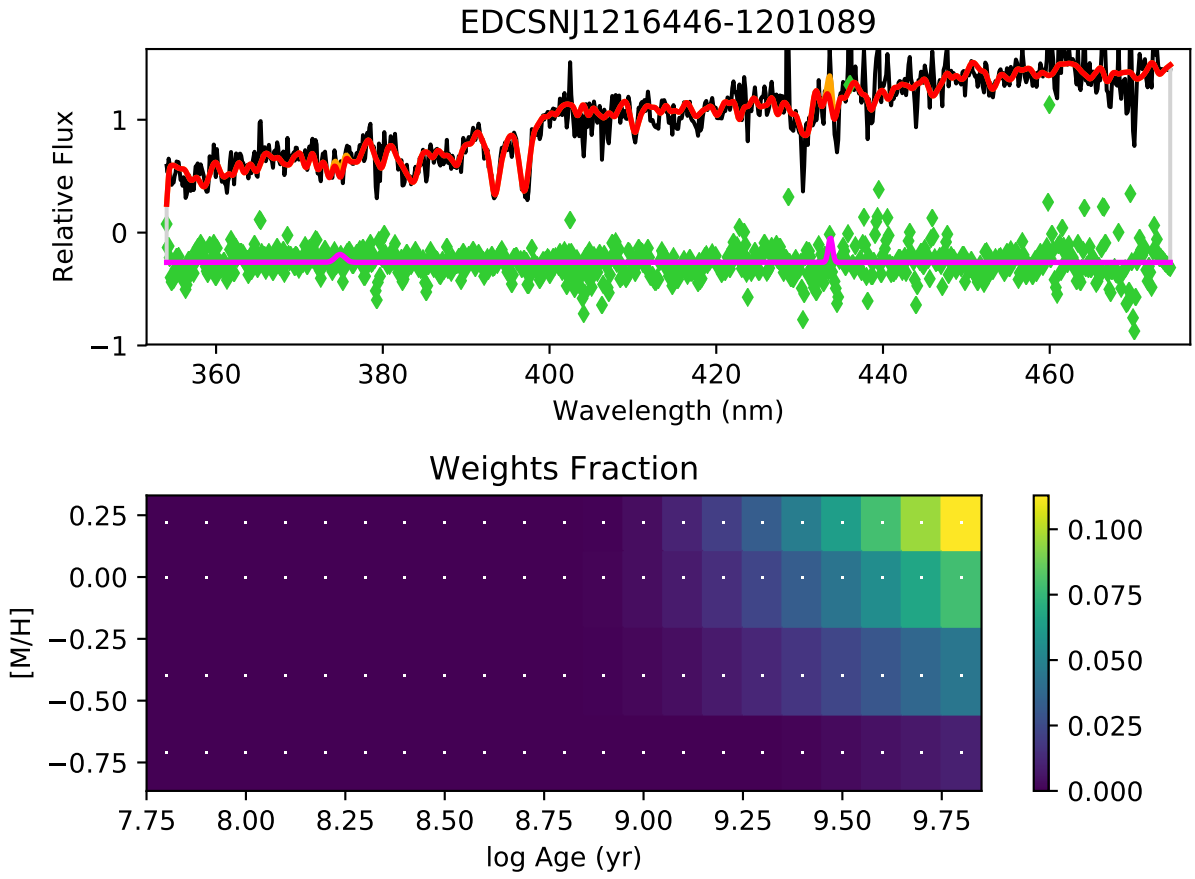
EDCSNJ1216446-1201089
Relative Flux
1
0
−1
360
380
400
420
440
460
Wavelength (nm)
Weights Fraction
[M/H]
0.25
0.00
−0.25
−0.50
−0.75
7.75
8.00
8.25
8.50
8.75
9.00
9.25
9.50
9.75
log Age (yr)
0.100
0.075
0.050
0.025
0.000

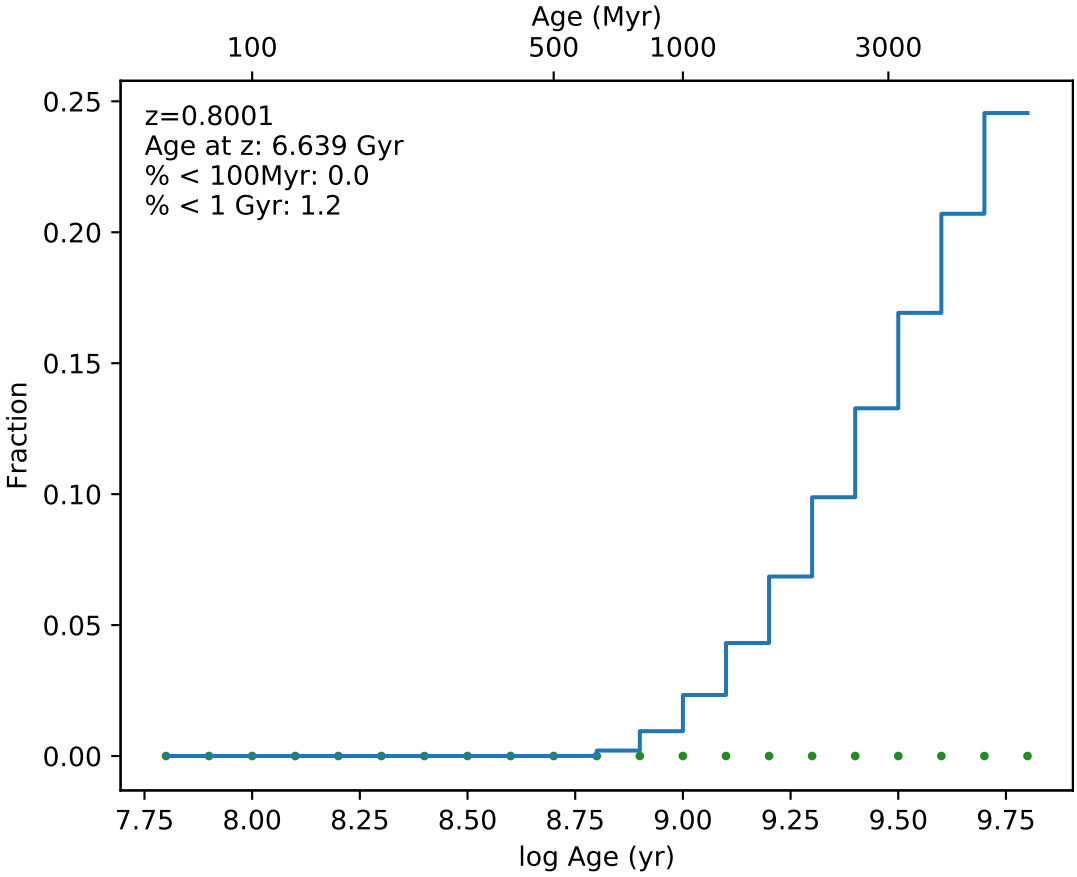
Age (Myr)
100
500
1000
3000
z=0.8001
Age at z: 6.639 Gyr
% < 100Myr: 0.0
% < 1 Gyr: 1.2
Fraction
0.25
0.20
0.15
0.10
0.05
0.00
7.75
8.00
8.25
8.50
8.75
9.00
9.25
9.50
9.75
log Age (yr)

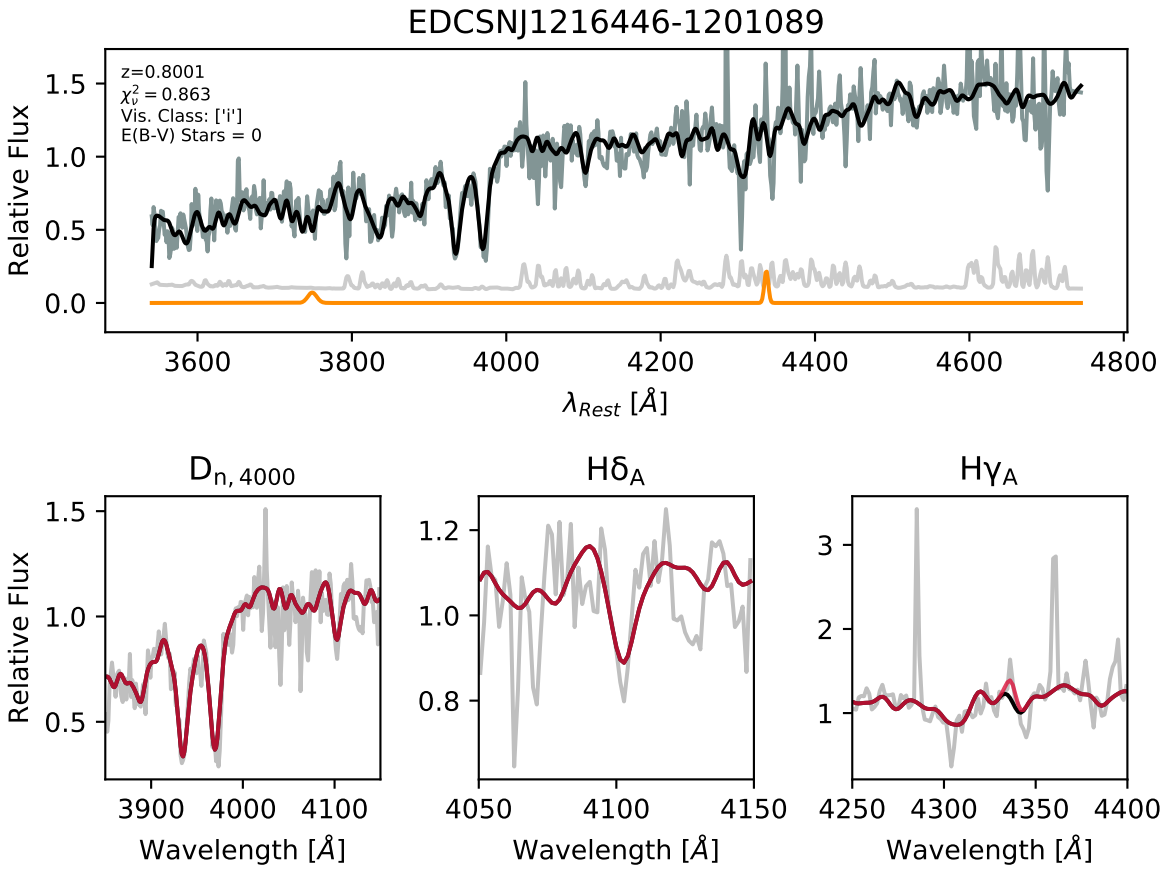
EDCSNJ1216446-1201089
z=0.8001
$\chi^2_\nu = 0.863$
Vis. Class: ['i']
E(B-V) Stars = 0
Relative Flux
λ_{Rest} [Å]
$D_{n,4000}$
$H\delta_A$
$H\gamma_A$
Wavelength [Å]

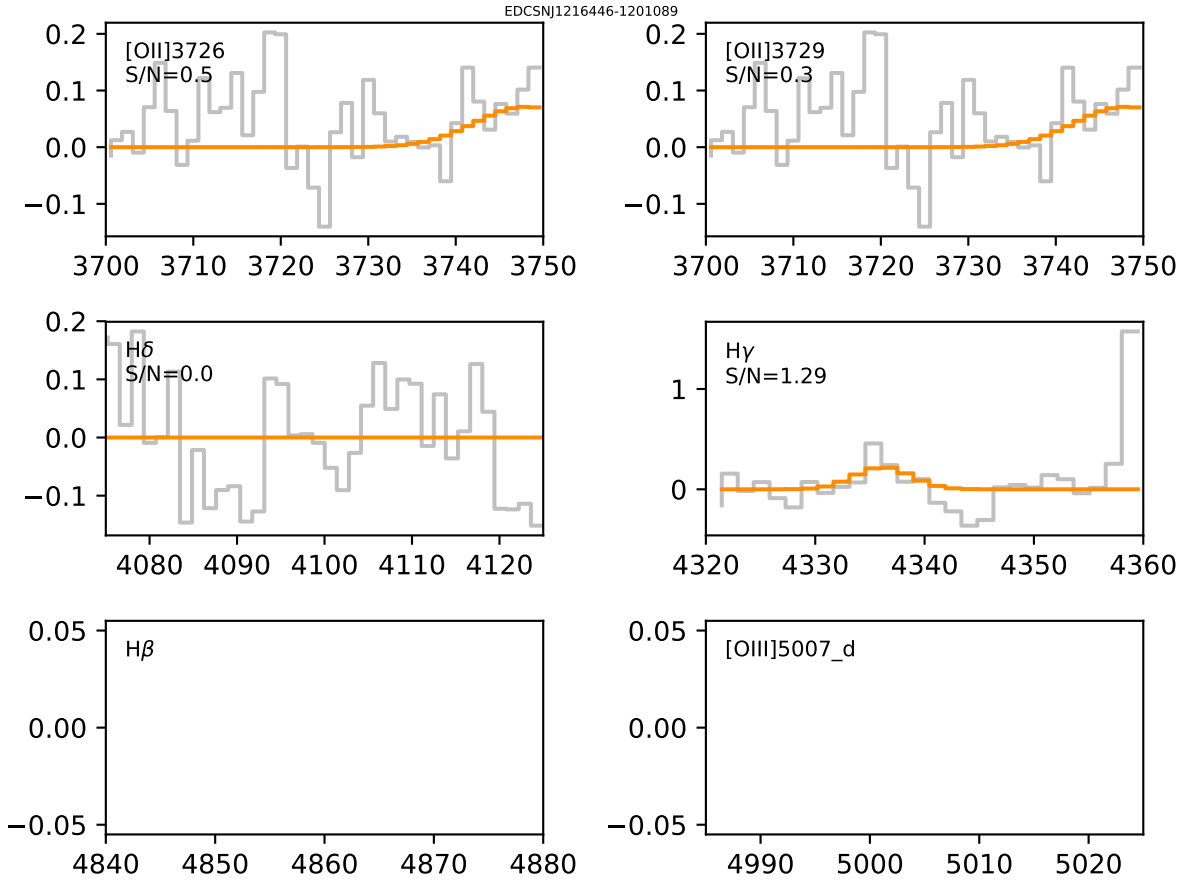
EDCSNJ1216446-1201089
[OII]3726
S/N=0.5
[OII]3729
S/N=0.3
Hδ
S/N=0.0
Hγ
S/N=1.29
Hβ
[OIII]5007_d

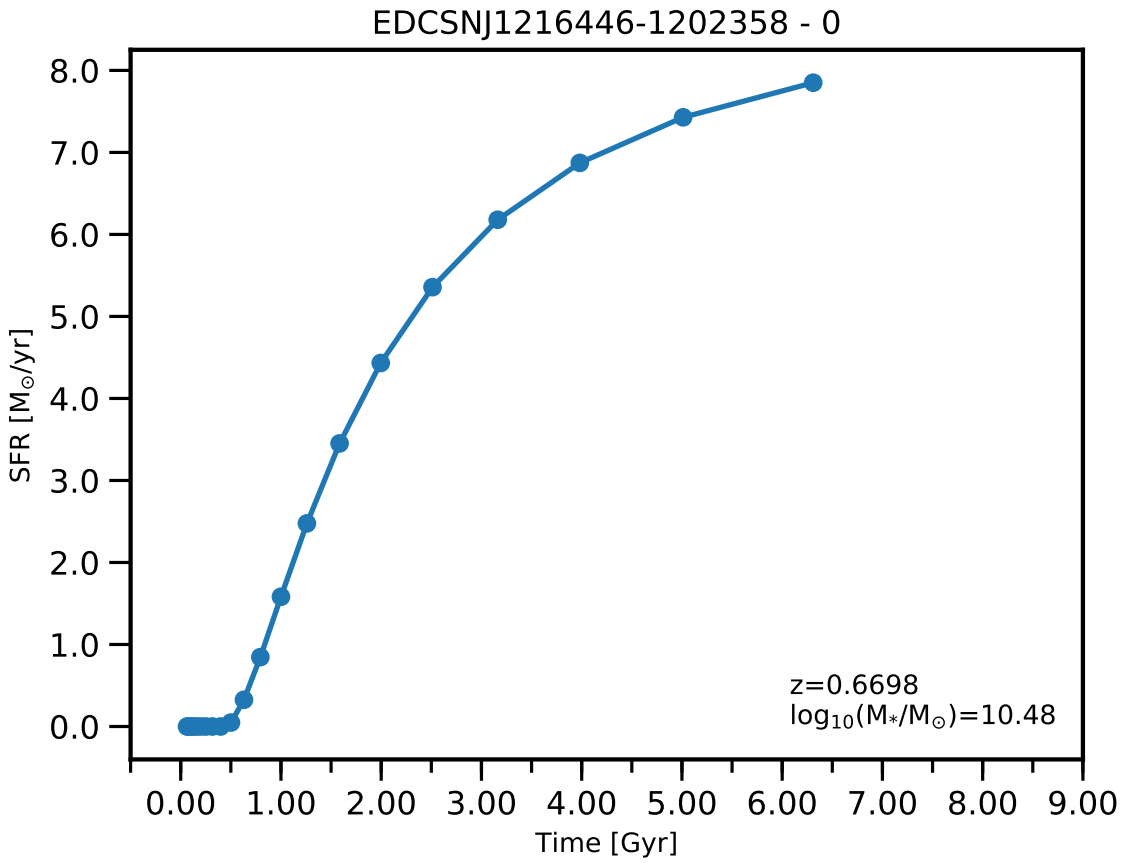
EDCSNJ1216446-1202358 - 0
SFR [M⊙/yr]
Time [Gyr]
z=0.6698
log10(M*/M⊙)=10.48
0.0
1.0
2.0
3.0
4.0
5.0
6.0
7.0
8.0
0.00
1.00
2.00
3.00
4.00
5.00
6.00
7.00
8.00
9.00

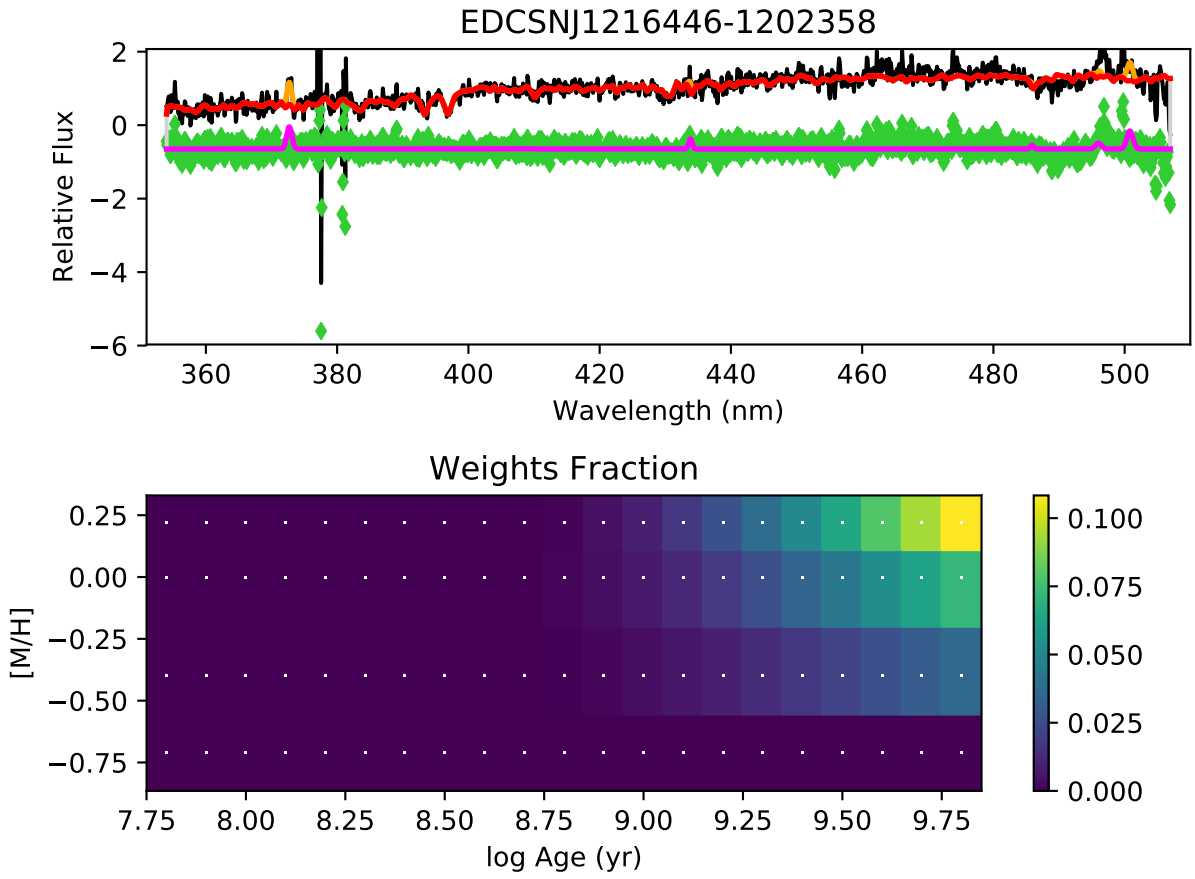
EDCSNJ1216446-1202358
Relative Flux
2
0
−2
−4
−6
360
380
400
420
440
460
480
500
Wavelength (nm)
Weights Fraction
[M/H]
0.25
0.00
−0.25
−0.50
−0.75
7.75
8.00
8.25
8.50
8.75
9.00
9.25
9.50
9.75
log Age (yr)
0.100
0.075
0.050
0.025
0.000

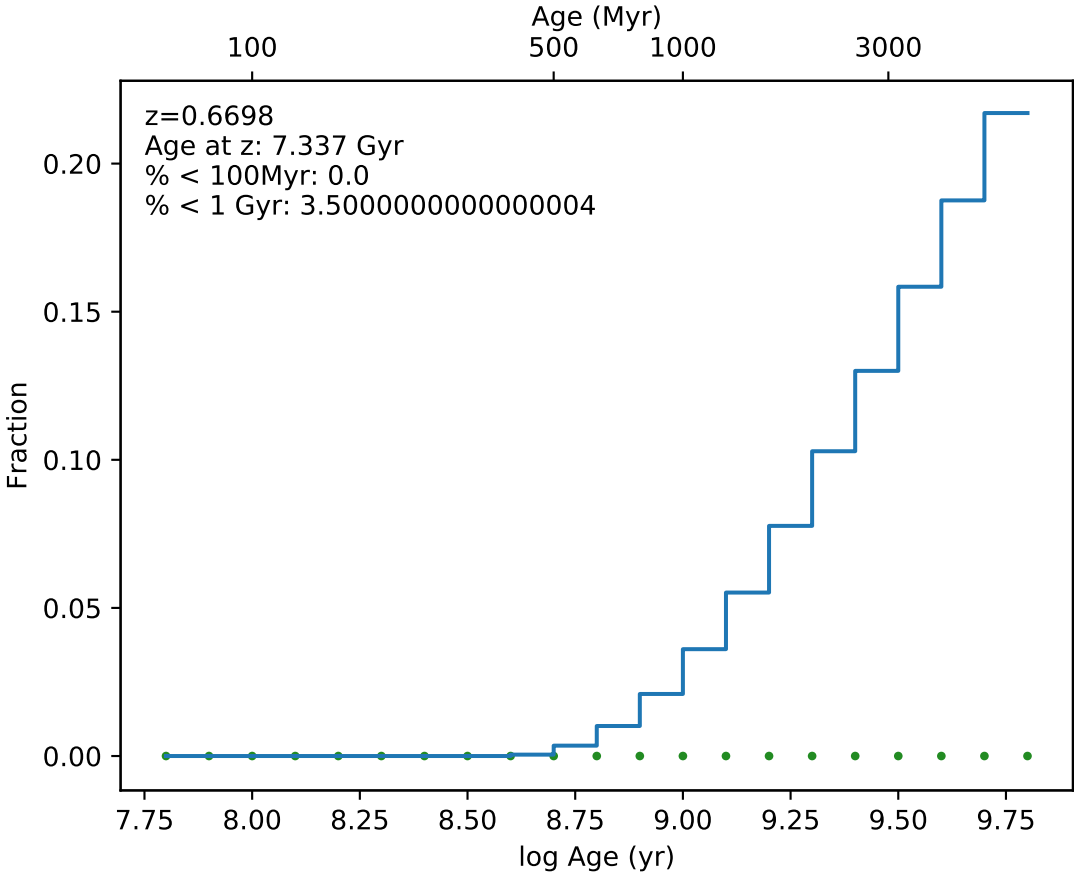
Age (Myr)
100
500
1000
3000
z=0.6698
Age at z: 7.337 Gyr
% < 100Myr: 0.0
% < 1 Gyr: 3.5000000000000004
Fraction
0.20
0.15
0.10
0.05
0.00
7.75
8.00
8.25
8.50
8.75
9.00
9.25
9.50
9.75
log Age (yr)

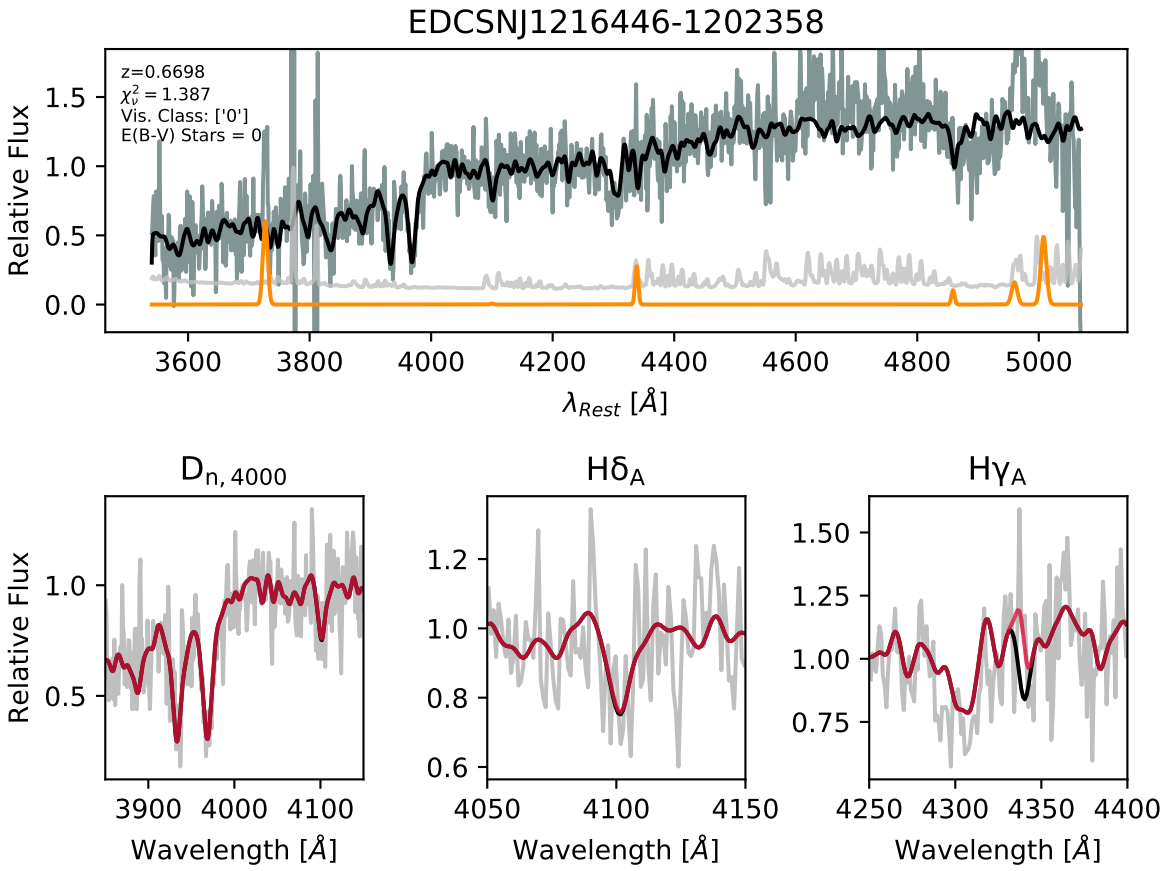
EDCSNJ1216446-1202358
z=0.6698
$\chi^2_\nu = 1.387$
Vis. Class: ['0']
E(B-V) Stars = 0
Relative Flux
λ_{Rest} [Å]
$D_{n,4000}$
$H\delta_A$
$H\gamma_A$
Wavelength [Å]

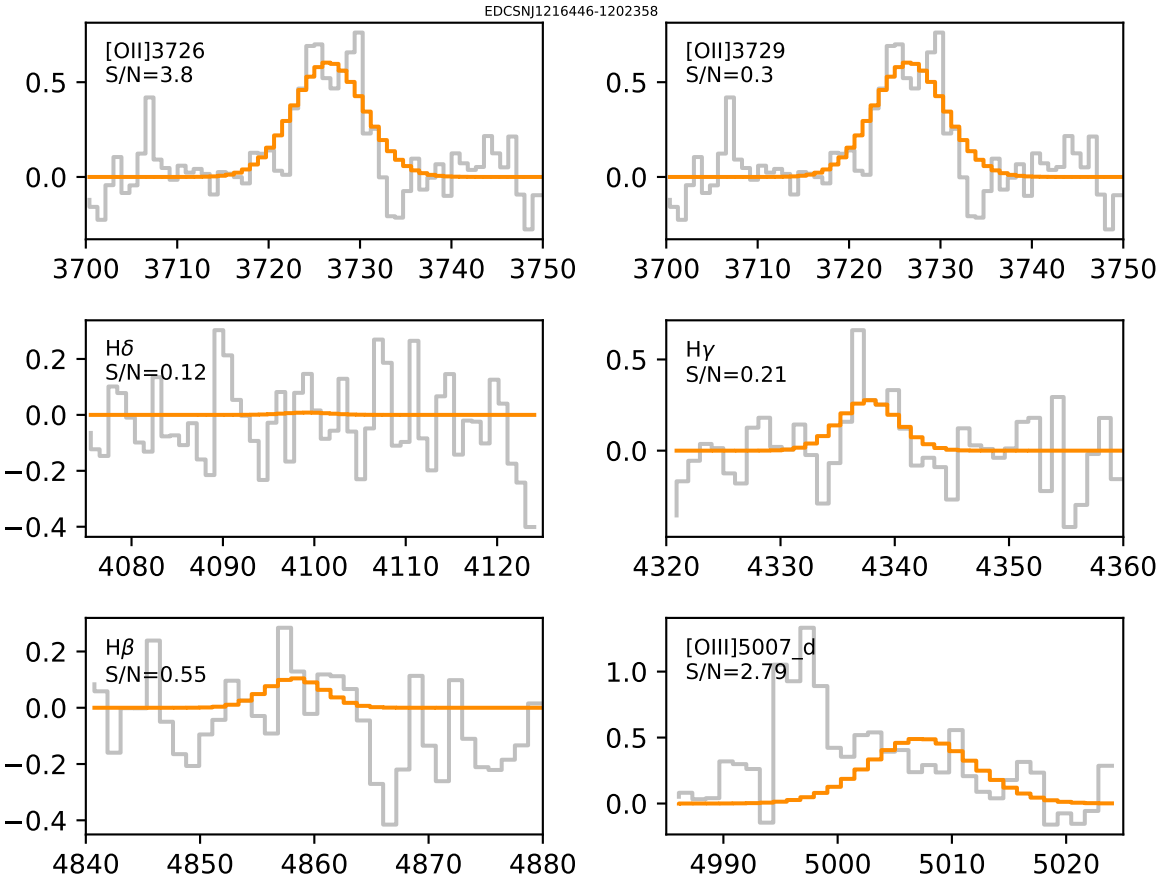
EDCSNJ1216446-1202358
[OII]3726
S/N=3.8
[OII]3729
S/N=0.3
Hδ
S/N=0.12
Hγ
S/N=0.21
Hβ
S/N=0.55
[OIII]5007_d
S/N=2.79

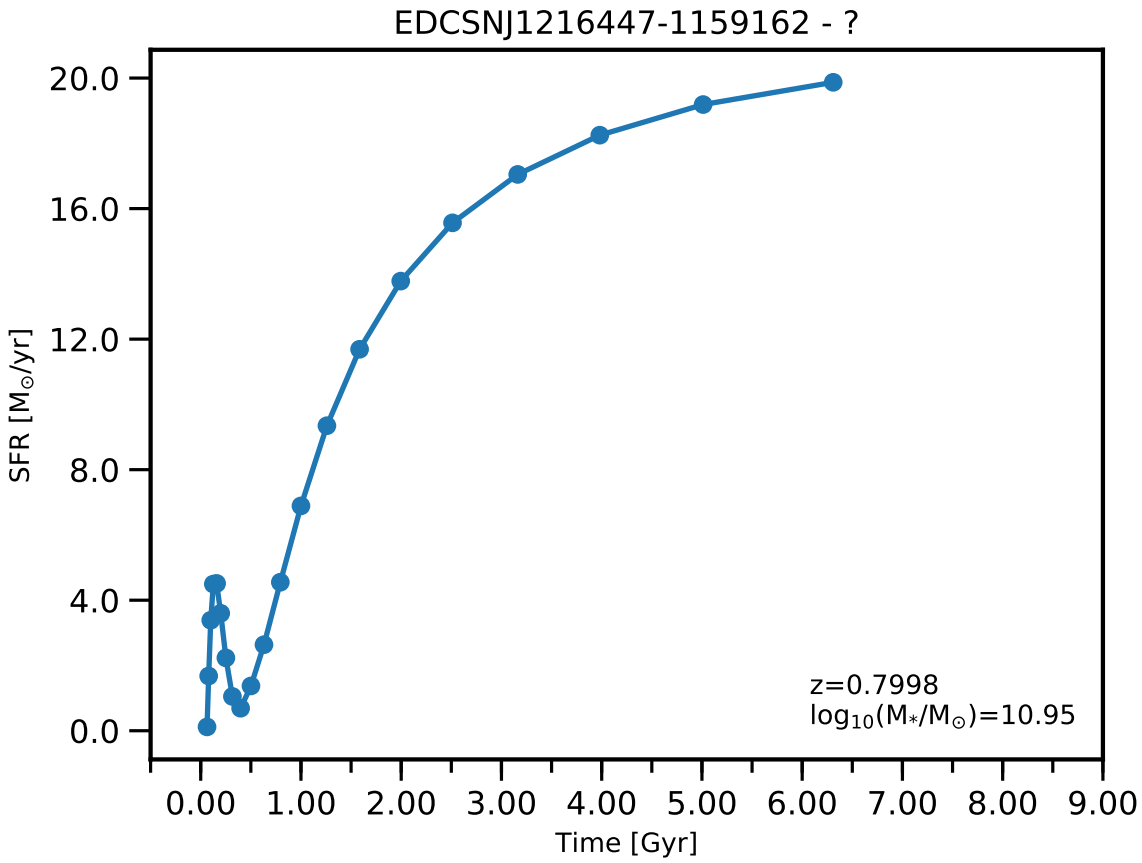
EDCSNJ1216447-1159162 - ?
SFR [M⊙/yr]
20.0
16.0
12.0
8.0
4.0
0.0
0.00
1.00
2.00
3.00
4.00
5.00
6.00
7.00
8.00
9.00
Time [Gyr]
z=0.7998
log10(M*/M⊙)=10.95

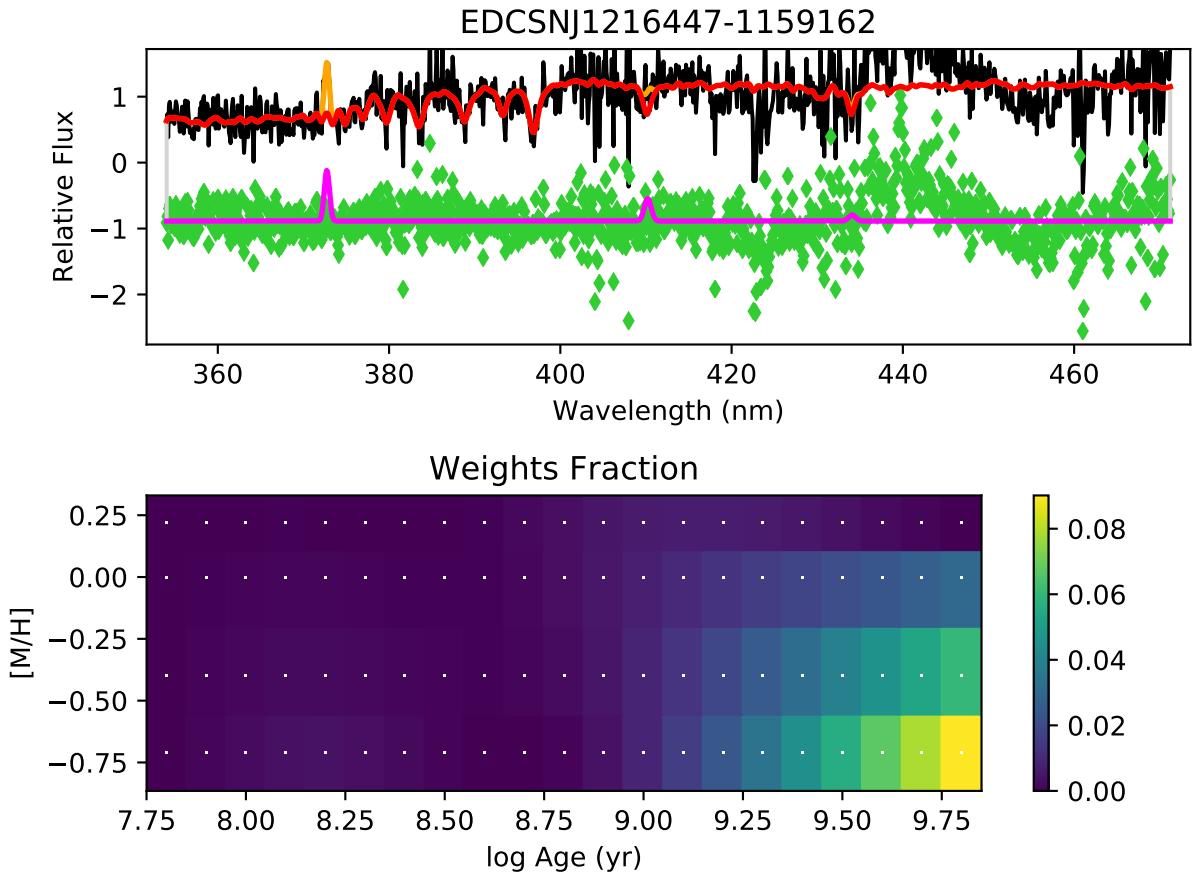
EDCSNJ1216447-1159162
Relative Flux
1
0
−1
−2
360
380
400
420
440
460
Wavelength (nm)
Weights Fraction
[M/H]
0.25
0.00
−0.25
−0.50
−0.75
7.75
8.00
8.25
8.50
8.75
9.00
9.25
9.50
9.75
log Age (yr)
0.08
0.06
0.04
0.02
0.00

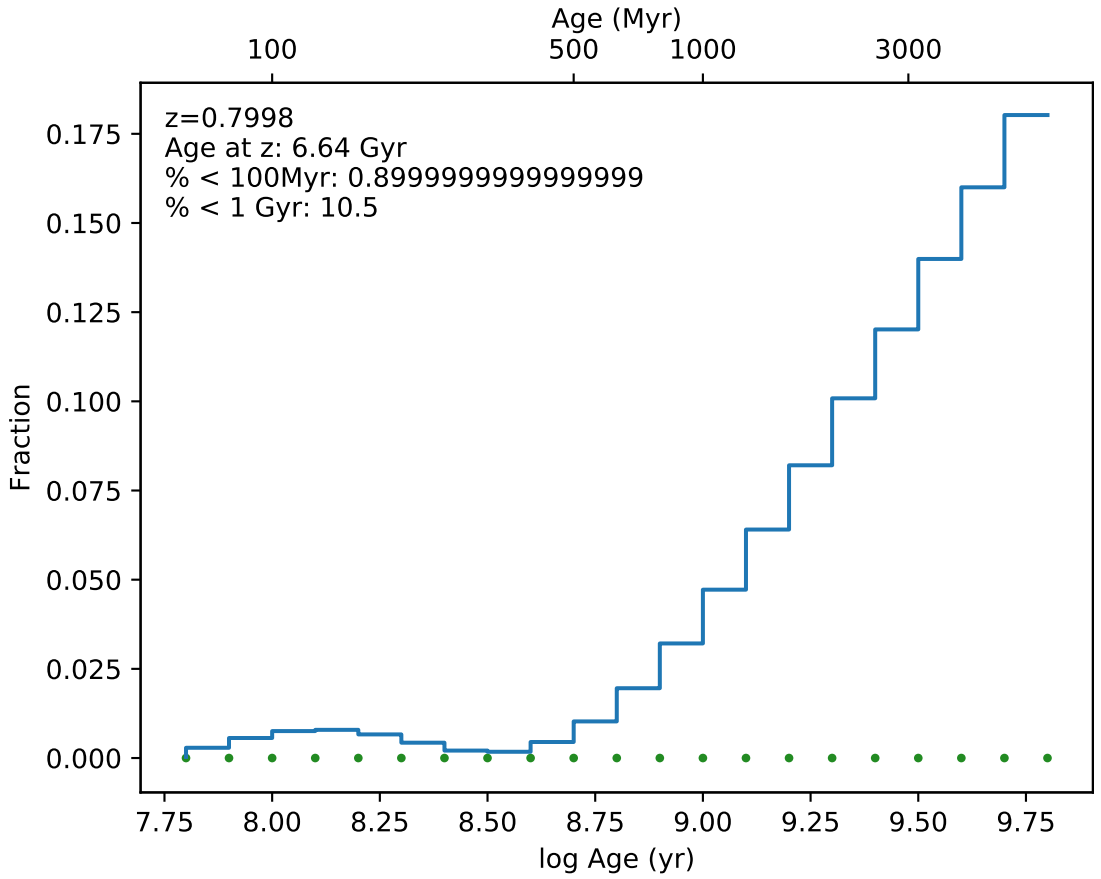
Age (Myr)
100
500
1000
3000
z=0.7998
Age at z: 6.64 Gyr
% < 100Myr: 0.8999999999999999
% < 1 Gyr: 10.5
Fraction
0.175
0.150
0.125
0.100
0.075
0.050
0.025
0.000
7.75
8.00
8.25
8.50
8.75
9.00
9.25
9.50
9.75
log Age (yr)

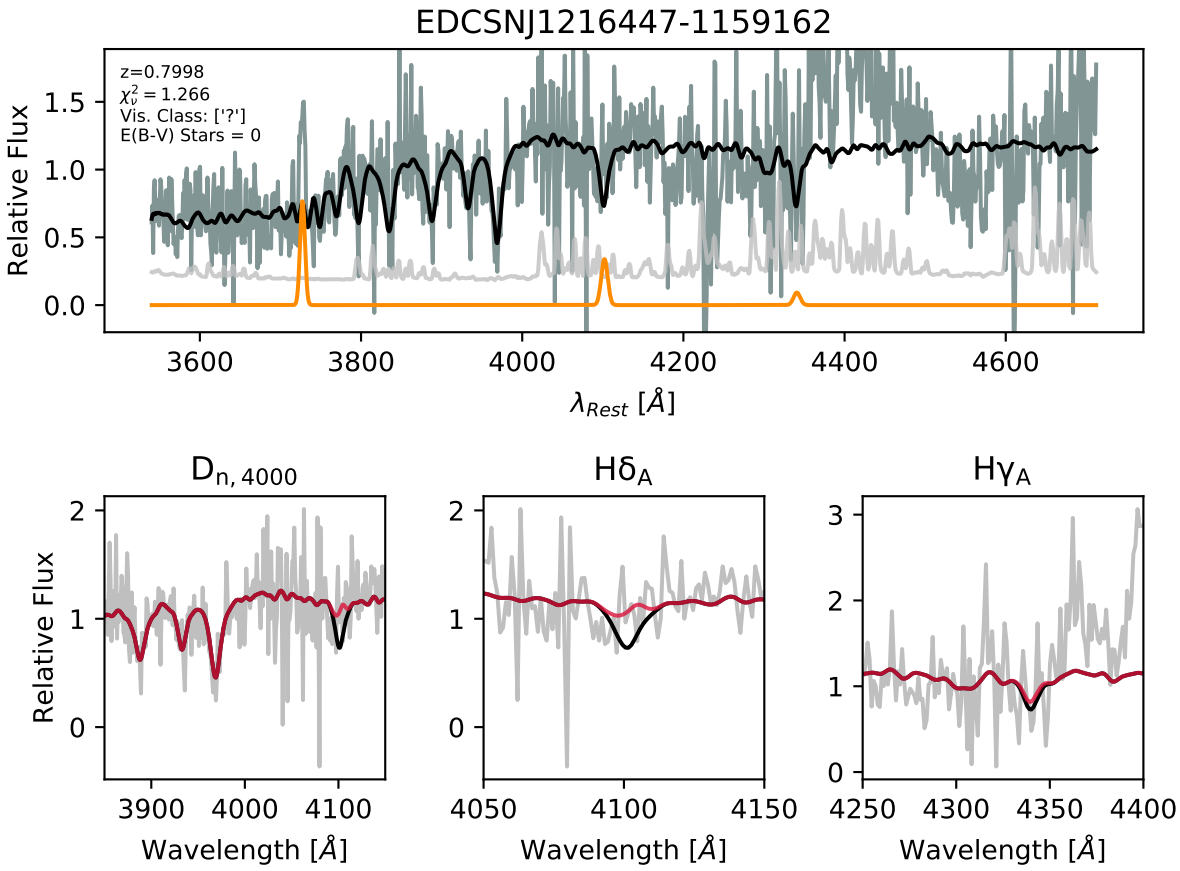
EDCSNJ1216447-1159162
z=0.7998
$\chi^2_\nu = 1.266$
Vis. Class: ['?']
E(B-V) Stars = 0
Relative Flux
λ_{Rest} [Å]
$D_{n,4000}$
$H\delta_A$
$H\gamma_A$
Wavelength [Å]

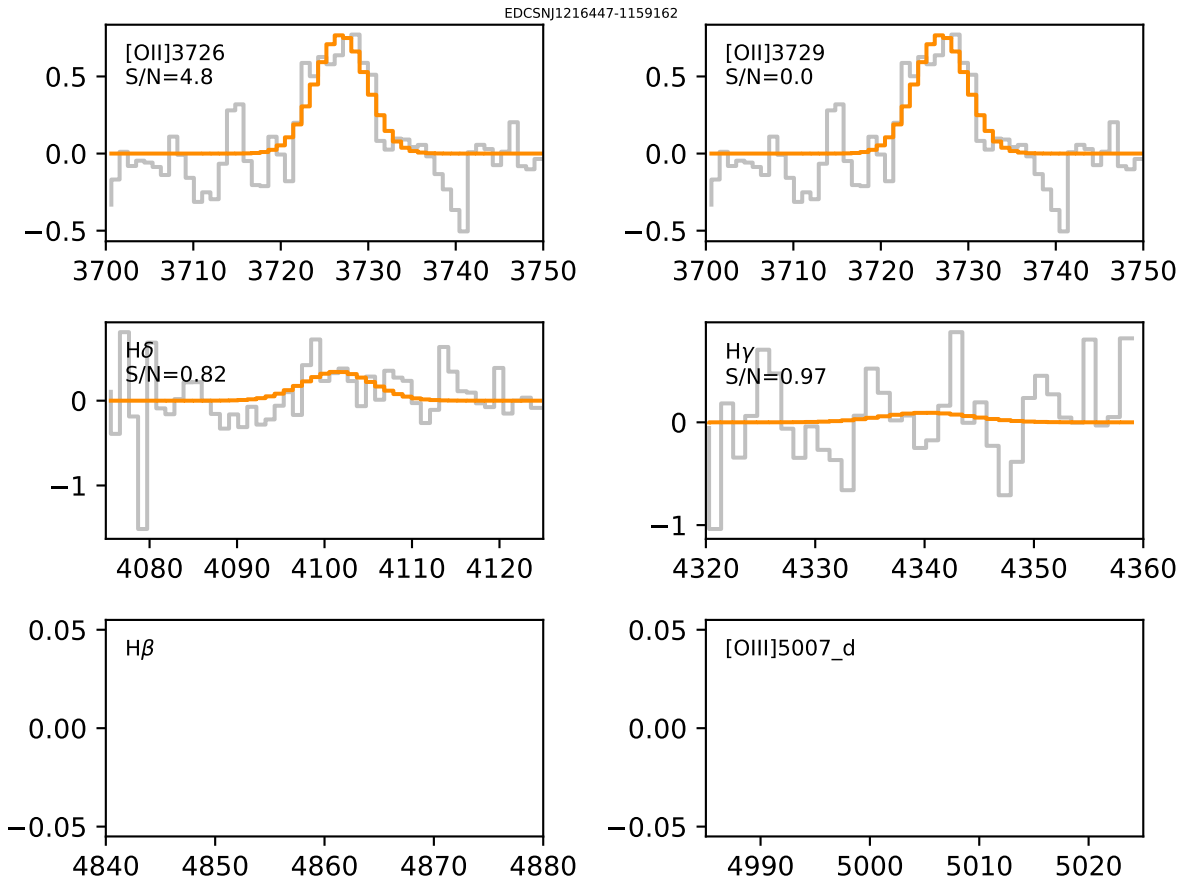
EDCSNJ1216447-1159162
[OII]3726
S/N=4.8
[OII]3729
S/N=0.0
Hδ
S/N=0.82
Hγ
S/N=0.97
Hβ
[OIII]5007_d

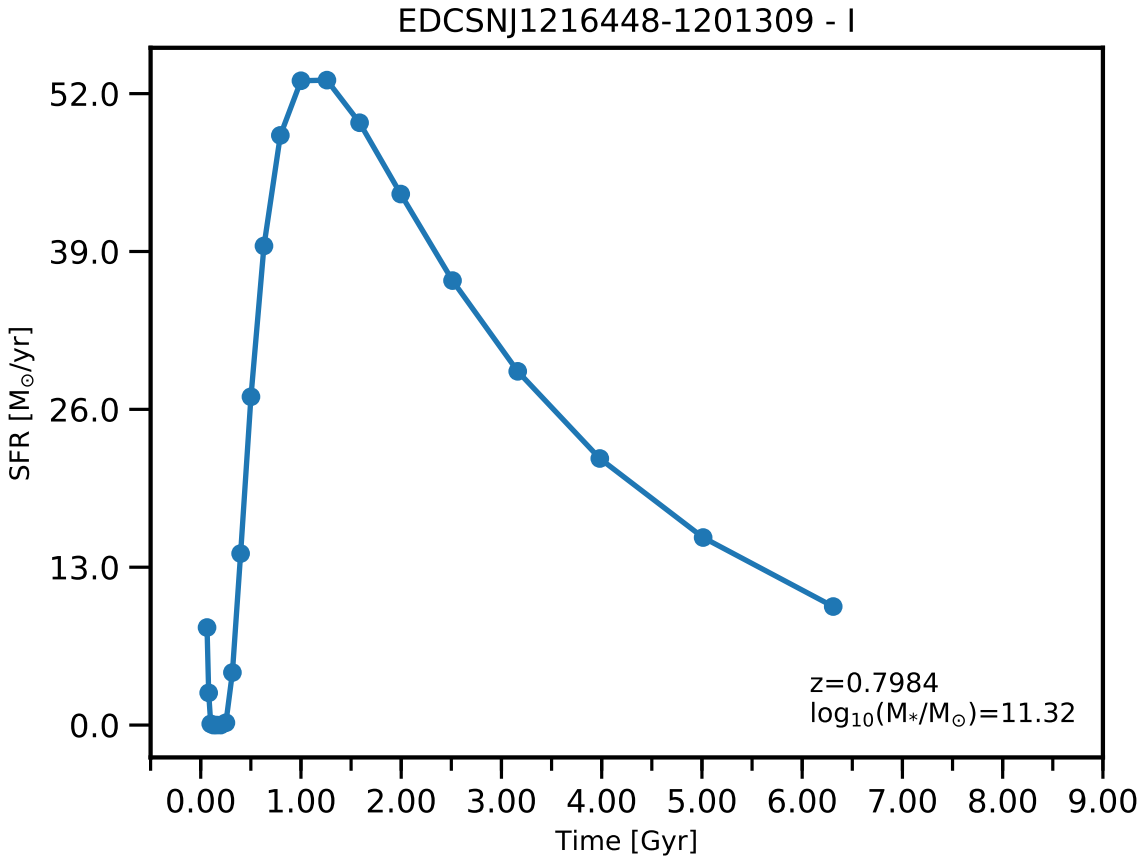
EDCSNJ1216448-1201309 - I
52.0
39.0
26.0
13.0
0.0
SFR [M⊙/yr]
0.00
1.00
2.00
3.00
4.00
5.00
6.00
7.00
8.00
9.00
Time [Gyr]
z=0.7984
log10(M*/M⊙)=11.32

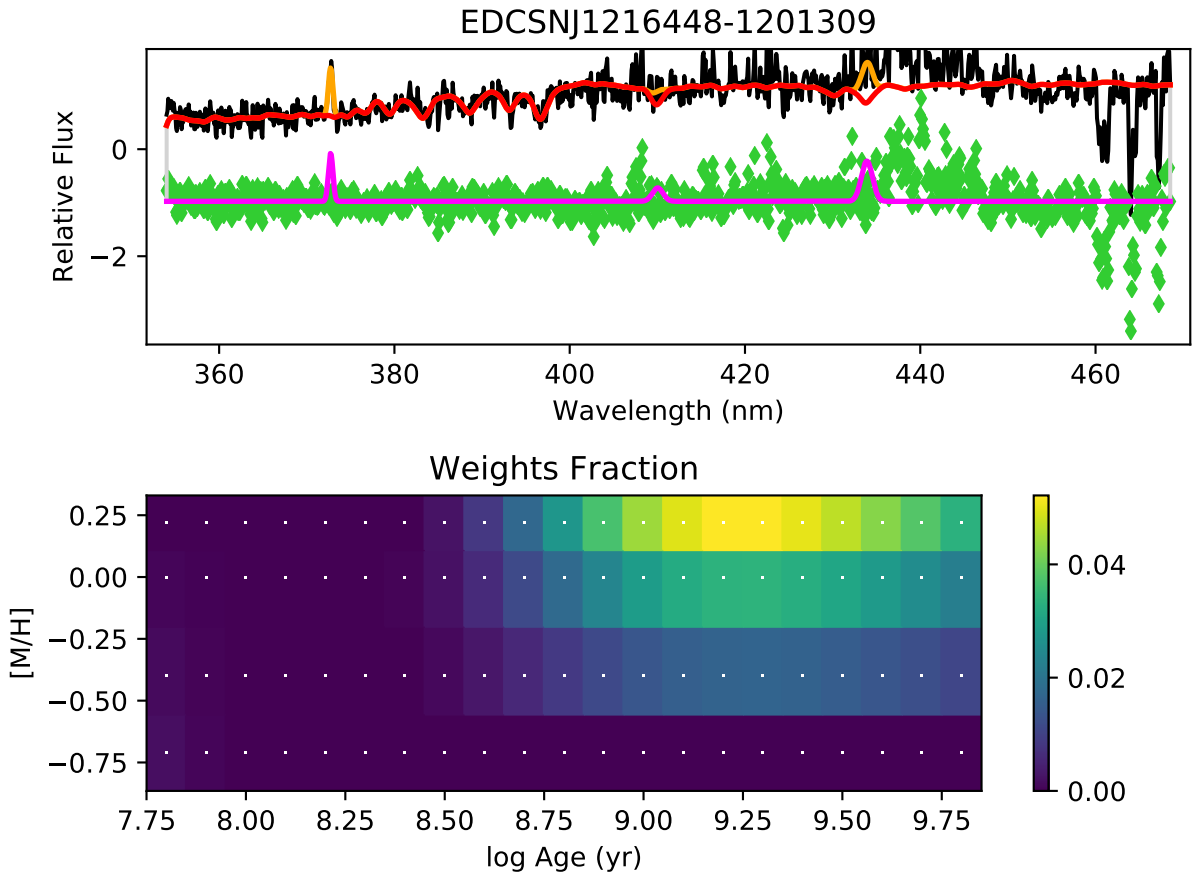
EDCSNJ1216448-1201309
Relative Flux
0
−2
360
380
400
420
440
460
Wavelength (nm)
Weights Fraction
[M/H]
0.25
0.00
−0.25
−0.50
−0.75
7.75
8.00
8.25
8.50
8.75
9.00
9.25
9.50
9.75
log Age (yr)
0.04
0.02
0.00

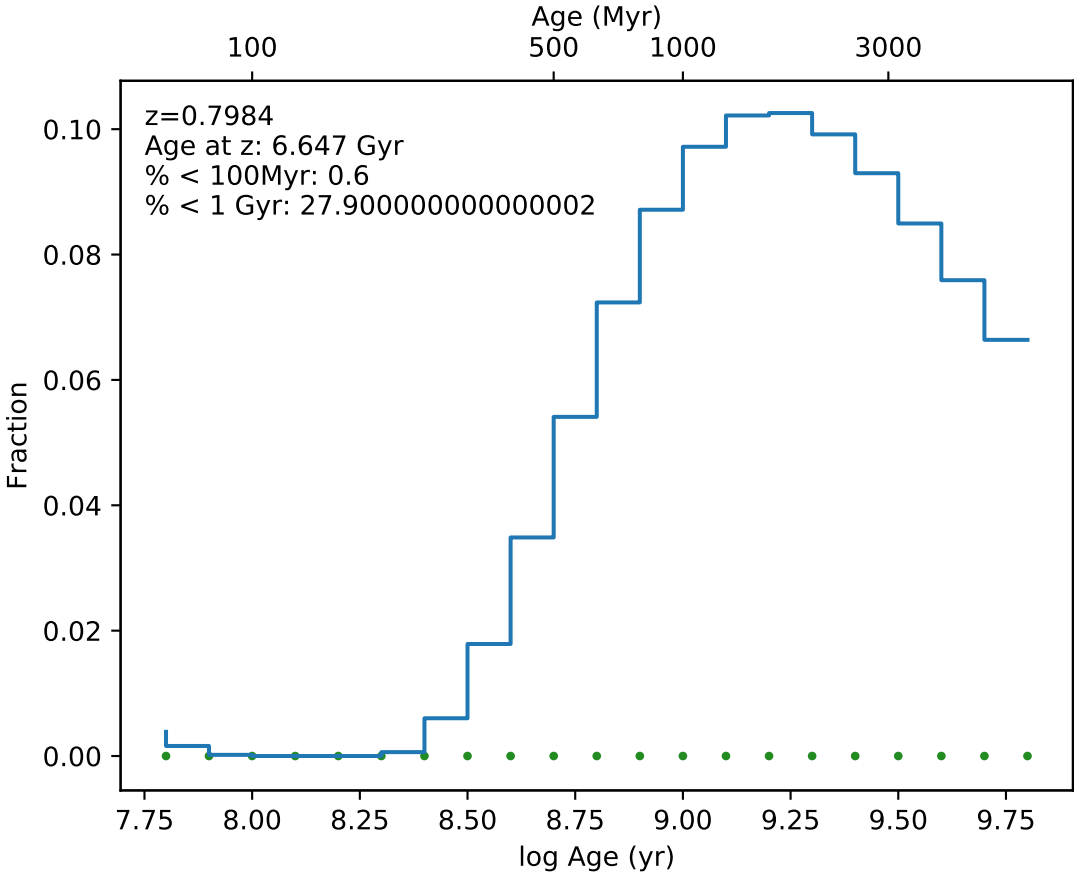
Age (Myr)
100
500
1000
3000
z=0.7984
Age at z: 6.647 Gyr
% < 100Myr: 0.6
% < 1 Gyr: 27.900000000000002
Fraction
0.10
0.08
0.06
0.04
0.02
0.00
7.75
8.00
8.25
8.50
8.75
9.00
9.25
9.50
9.75
log Age (yr)

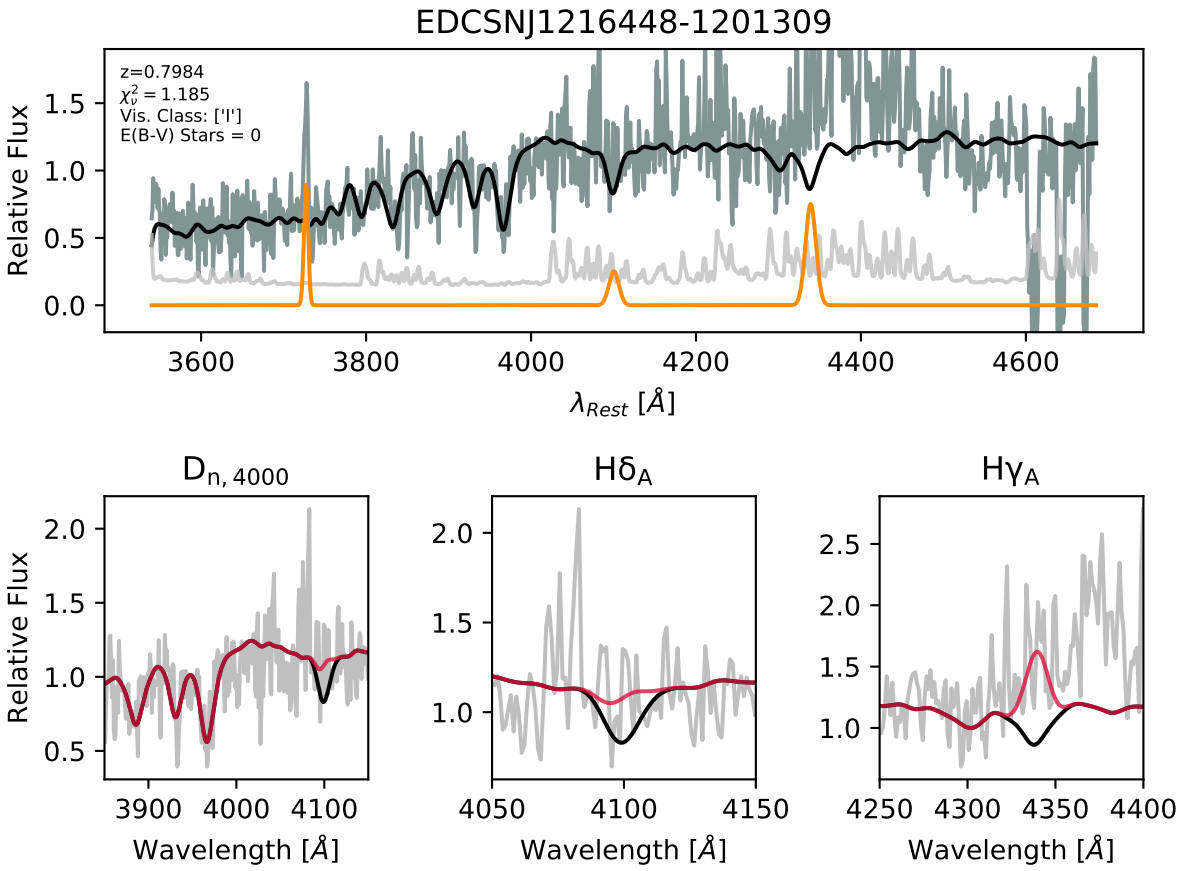
EDCSNJ1216448-1201309
z=0.7984
$\chi^2_\nu = 1.185$
Vis. Class: ['I']
E(B-V) Stars = 0
Relative Flux
λ_{Rest} [Å]
$D_{n,4000}$
$H\delta_A$
$H\gamma_A$
Wavelength [Å]

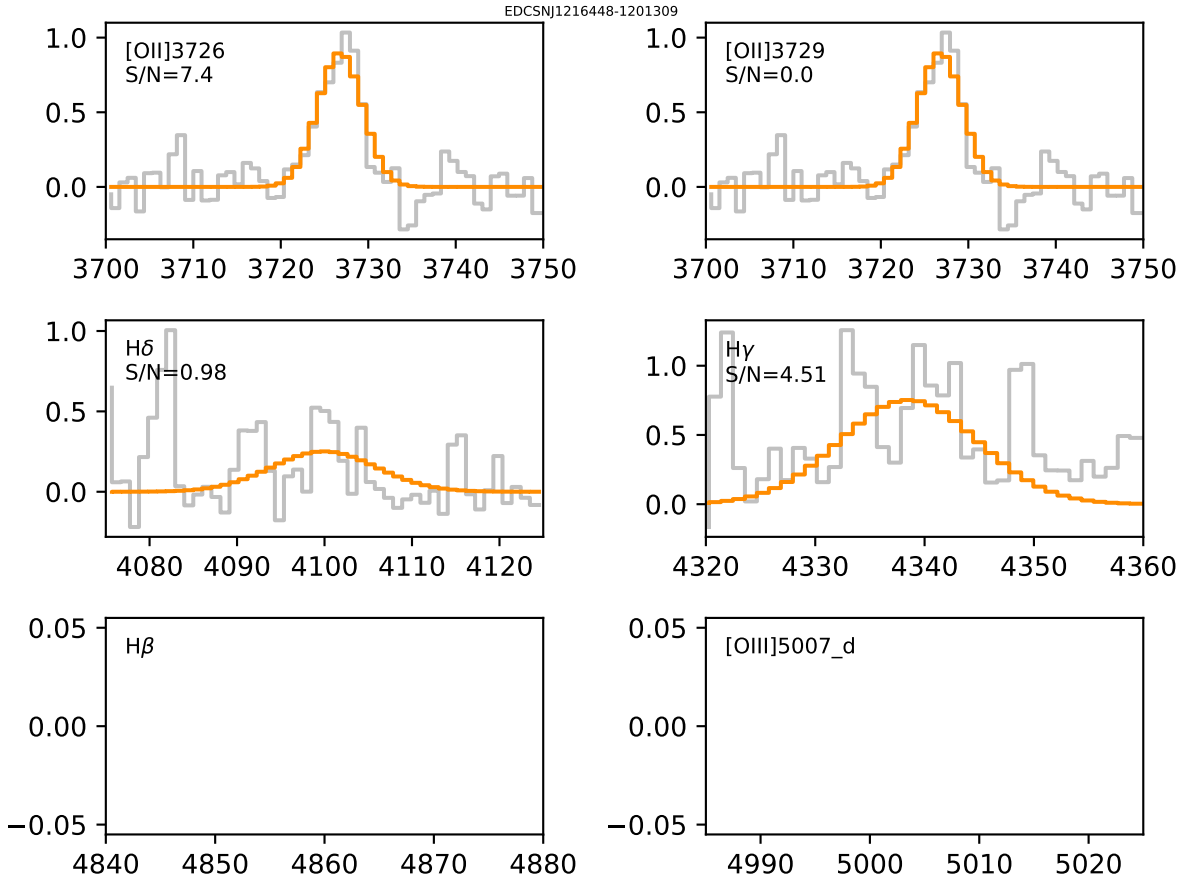
EDCSNJ1216448-1201309
[OII]3726
S/N=7.4
[OII]3729
S/N=0.0
Hδ
S/N=0.98
Hγ
S/N=4.51
Hβ
[OIII]5007_d

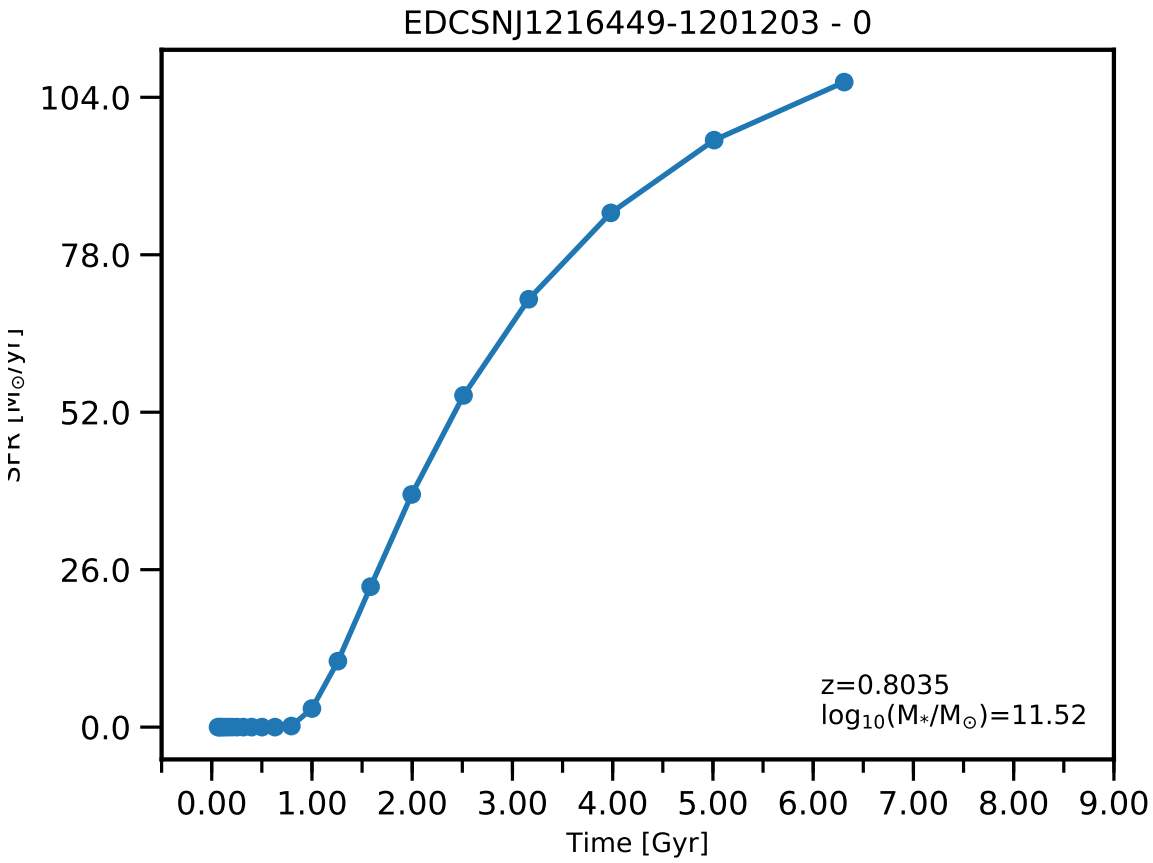
EDCSNJ1216449-1201203 - 0
104.0
78.0
52.0
26.0
0.0
SFR [M⊙/yr]
0.00
1.00
2.00
3.00
4.00
5.00
6.00
7.00
8.00
9.00
Time [Gyr]
z=0.8035
log10(M*/M⊙)=11.52

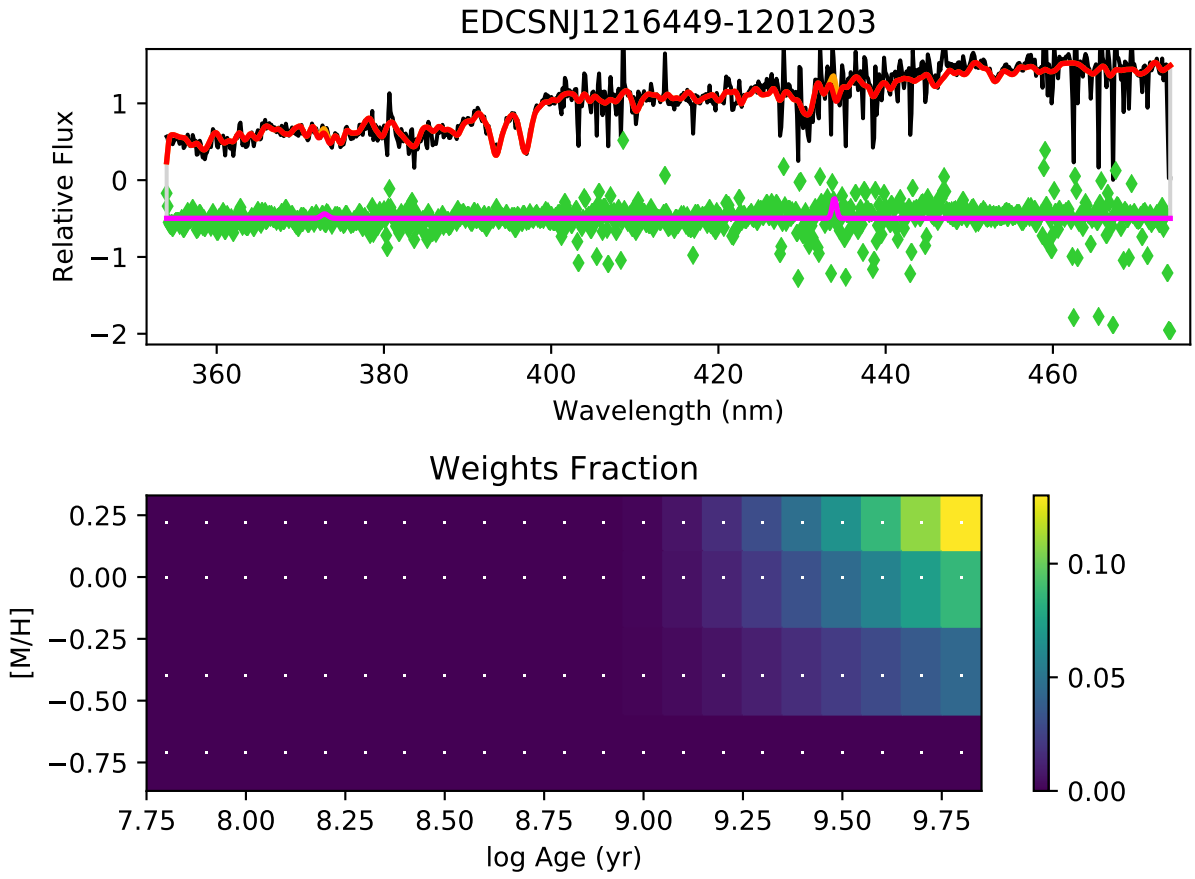
EDCSNJ1216449-1201203
Relative Flux
1
0
−1
−2
360
380
400
420
440
460
Wavelength (nm)
Weights Fraction
[M/H]
0.25
0.00
−0.25
−0.50
−0.75
7.75
8.00
8.25
8.50
8.75
9.00
9.25
9.50
9.75
log Age (yr)
0.10
0.05
0.00

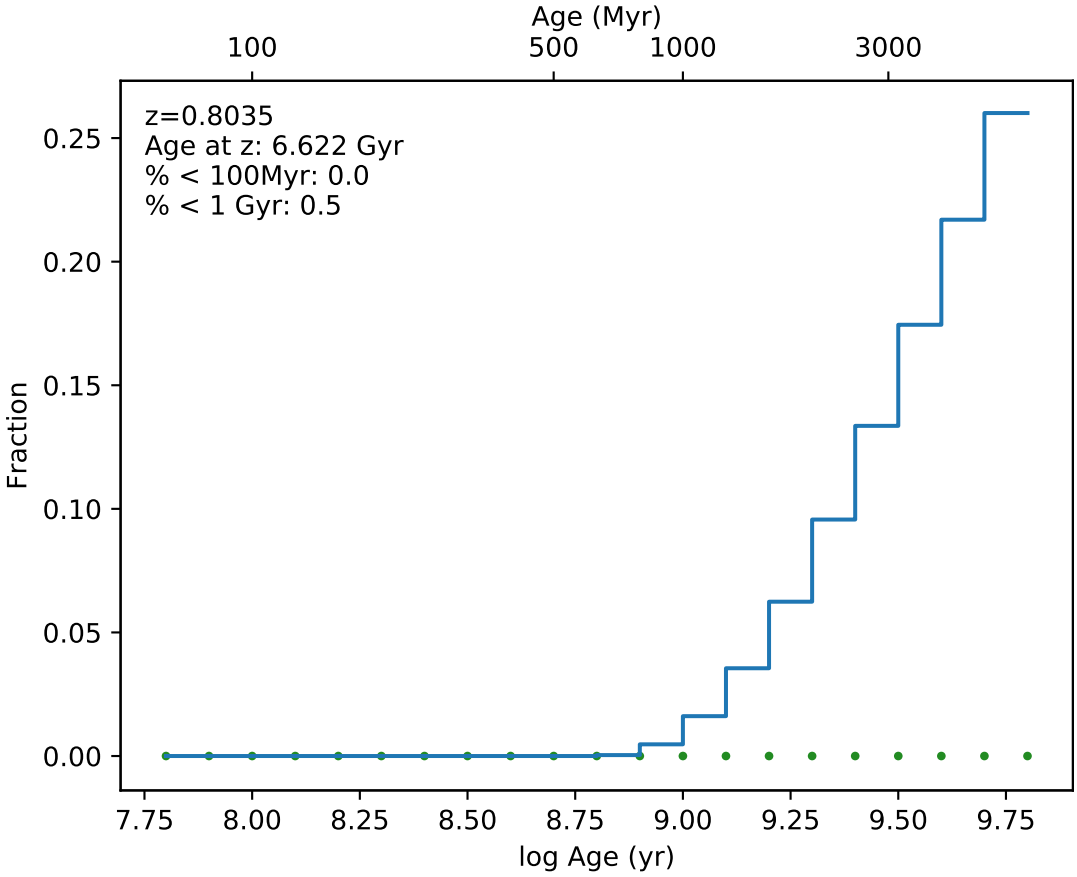
Age (Myr)
100
500
1000
3000
z=0.8035
Age at z: 6.622 Gyr
% < 100Myr: 0.0
% < 1 Gyr: 0.5
Fraction
0.25
0.20
0.15
0.10
0.05
0.00
7.75
8.00
8.25
8.50
8.75
9.00
9.25
9.50
9.75
log Age (yr)

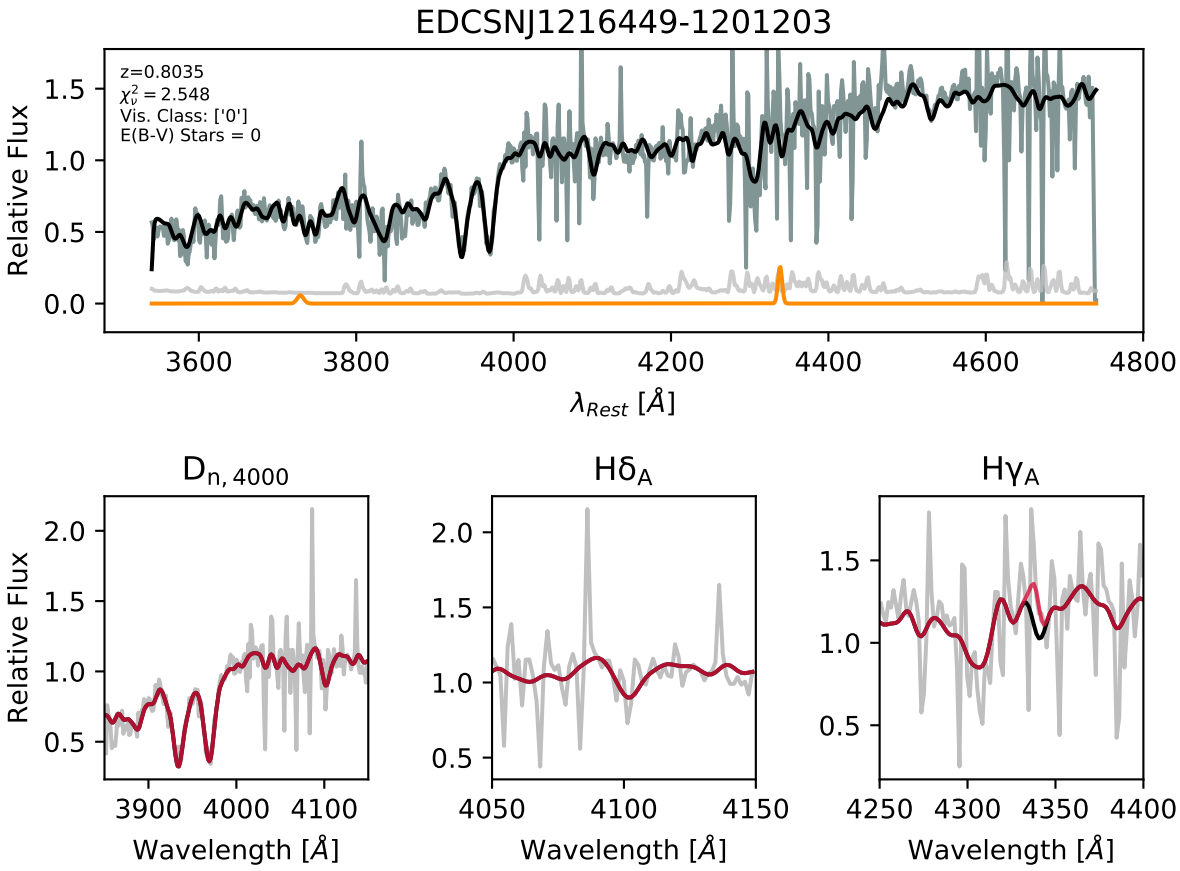
EDCSNJ1216449-1201203
z=0.8035
$\chi^2_\nu = 2.548$
Vis. Class: ['0']
E(B-V) Stars = 0
Relative Flux
λ_{Rest} [Å]
$D_{n,4000}$
$H\delta_A$
$H\gamma_A$
Wavelength [Å]

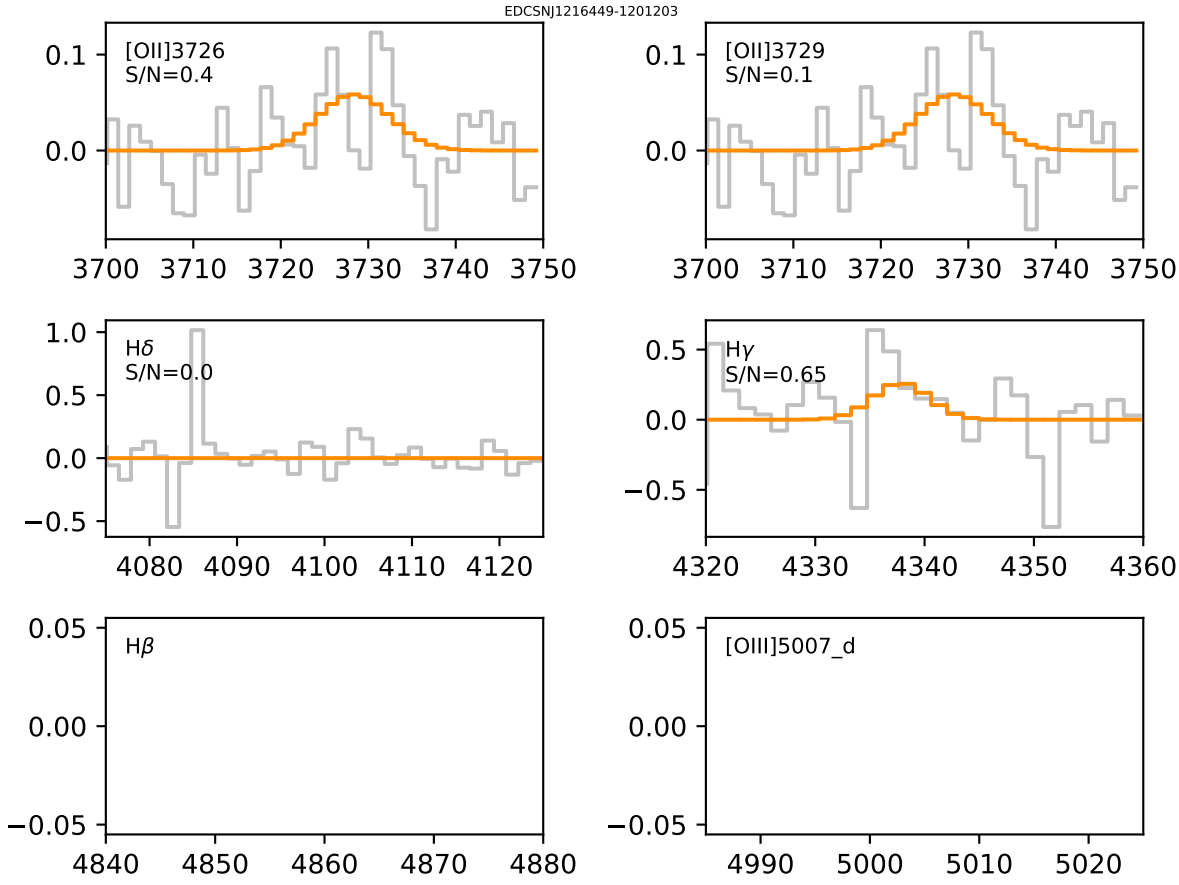
EDCSNJ1216449-1201203
[OII]3726
S/N=0.4
[OII]3729
S/N=0.1
Hδ
S/N=0.0
Hγ
S/N=0.65
Hβ
[OIII]5007_d

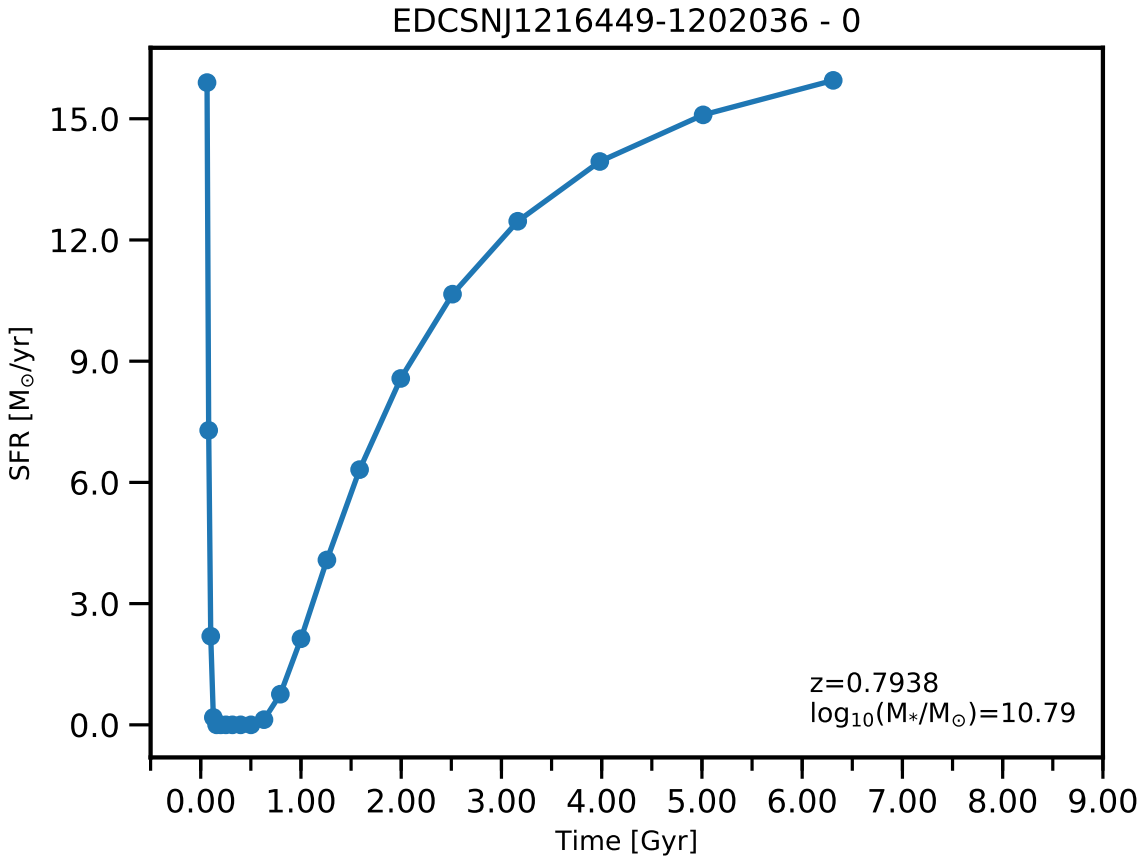
EDCSNJ1216449-1202036 - 0
SFR [M⊙/yr]
15.0
12.0
9.0
6.0
3.0
0.0
0.00
1.00
2.00
3.00
4.00
5.00
6.00
7.00
8.00
9.00
Time [Gyr]
z=0.7938
log10(M*/M⊙)=10.79

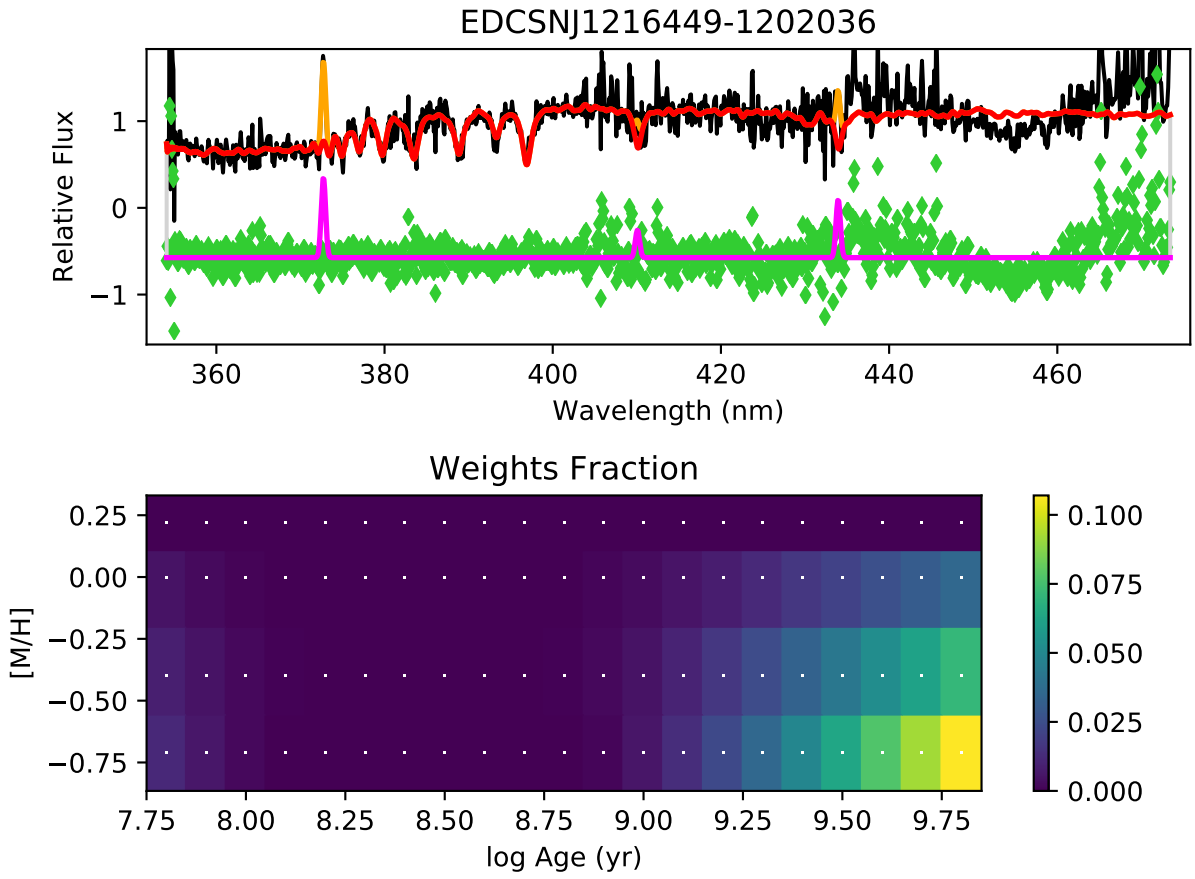
EDCSNJ1216449-1202036
Relative Flux
1
0
−1
360
380
400
420
440
460
Wavelength (nm)
Weights Fraction
[M/H]
0.25
0.00
−0.25
−0.50
−0.75
7.75
8.00
8.25
8.50
8.75
9.00
9.25
9.50
9.75
log Age (yr)
0.100
0.075
0.050
0.025
0.000

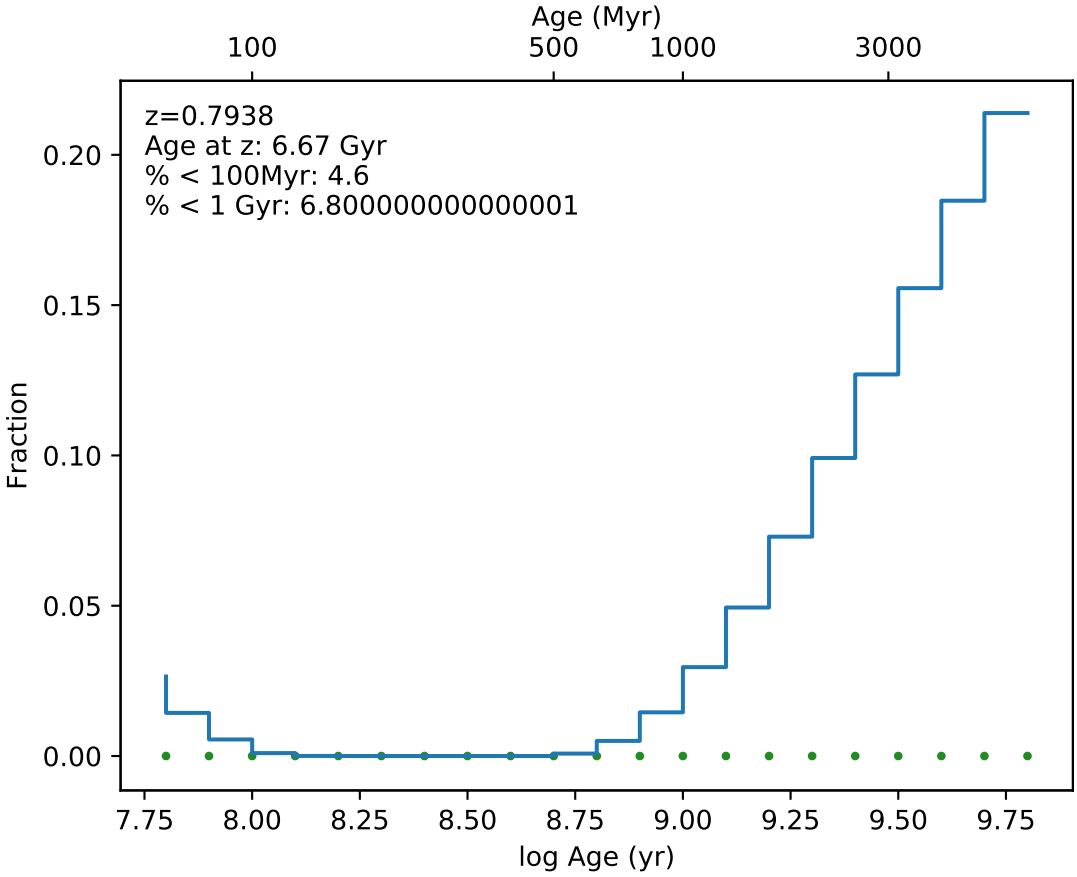
Age (Myr)
100
500
1000
3000
z=0.7938
Age at z: 6.67 Gyr
% < 100Myr: 4.6
% < 1 Gyr: 6.800000000000001
Fraction
0.20
0.15
0.10
0.05
0.00
7.75
8.00
8.25
8.50
8.75
9.00
9.25
9.50
9.75
log Age (yr)

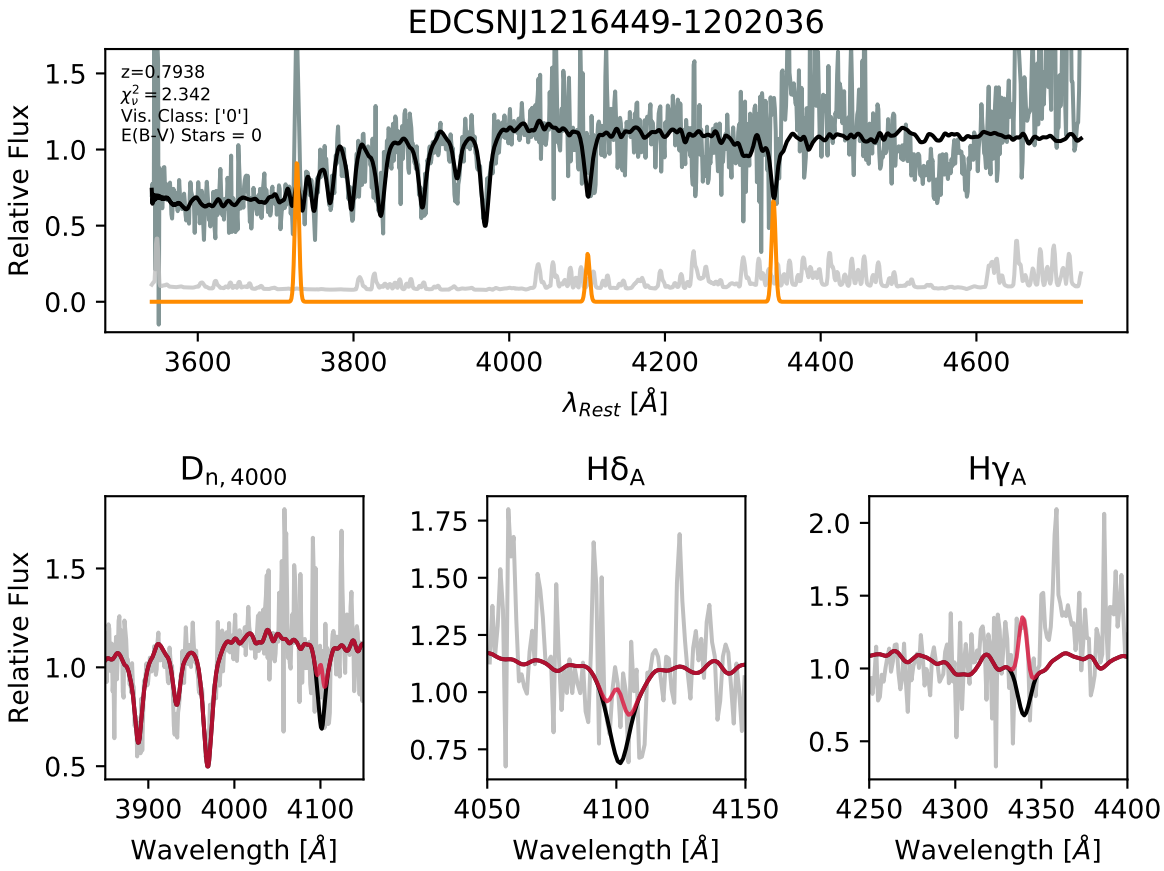
EDCSNJ1216449-1202036
z=0.7938
$\chi^2_\nu = 2.342$
Vis. Class: ['0']
E(B-V) Stars = 0
Relative Flux
λ_{Rest} [Å]
$D_{n,4000}$
$H\delta_A$
$H\gamma_A$
Wavelength [Å]

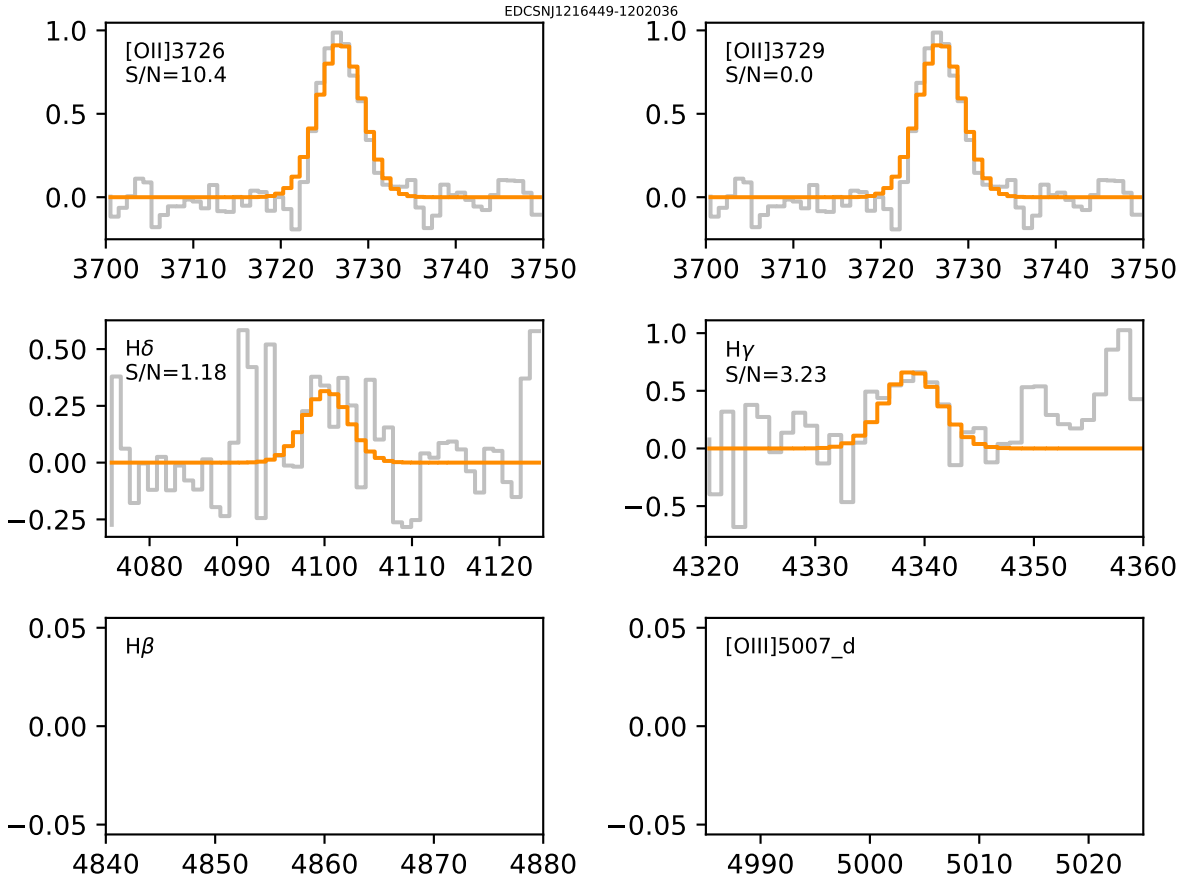
EDCSNJ1216449-1202036
[OII]3726
S/N=10.4
[OII]3729
S/N=0.0
Hδ
S/N=1.18
Hγ
S/N=3.23
Hβ
[OIII]5007_d

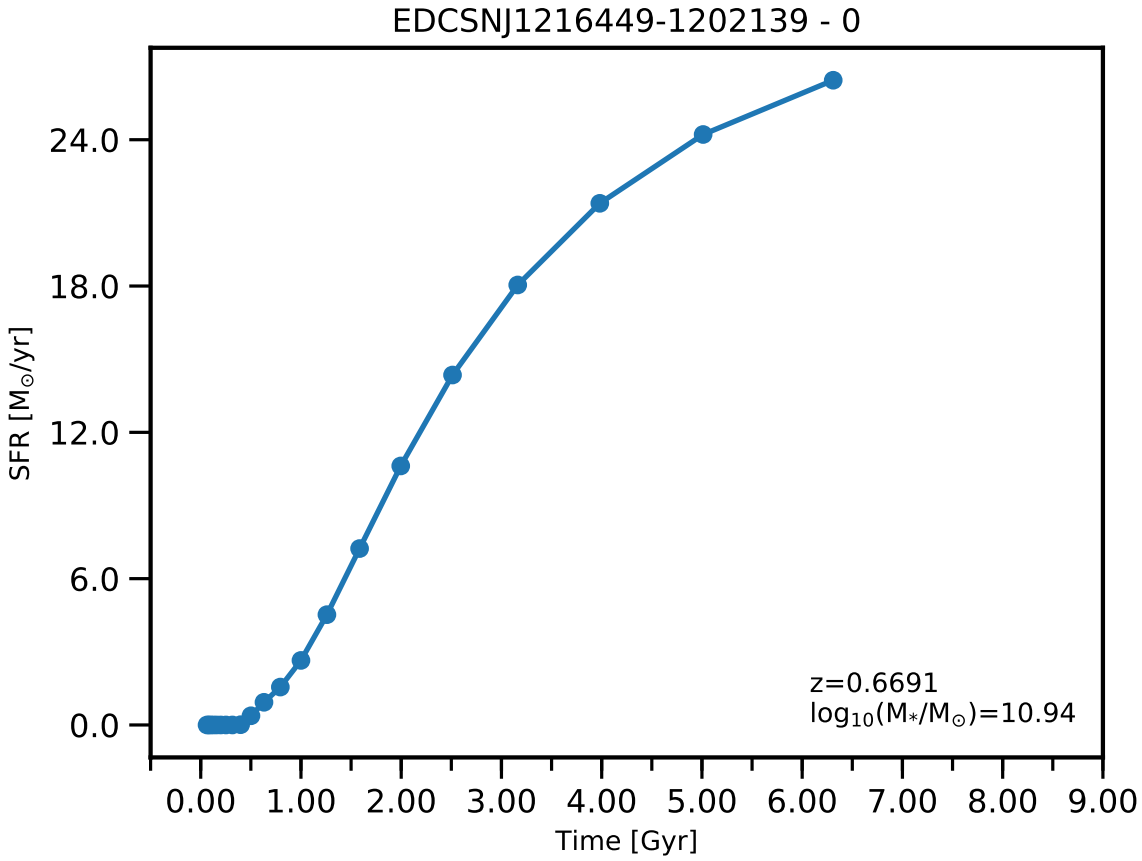
EDCSNJ1216449-1202139 - 0
SFR [M⊙/yr]
24.0
18.0
12.0
6.0
0.0
0.00
1.00
2.00
3.00
4.00
5.00
6.00
7.00
8.00
9.00
Time [Gyr]
z=0.6691
log10(M*/M⊙)=10.94

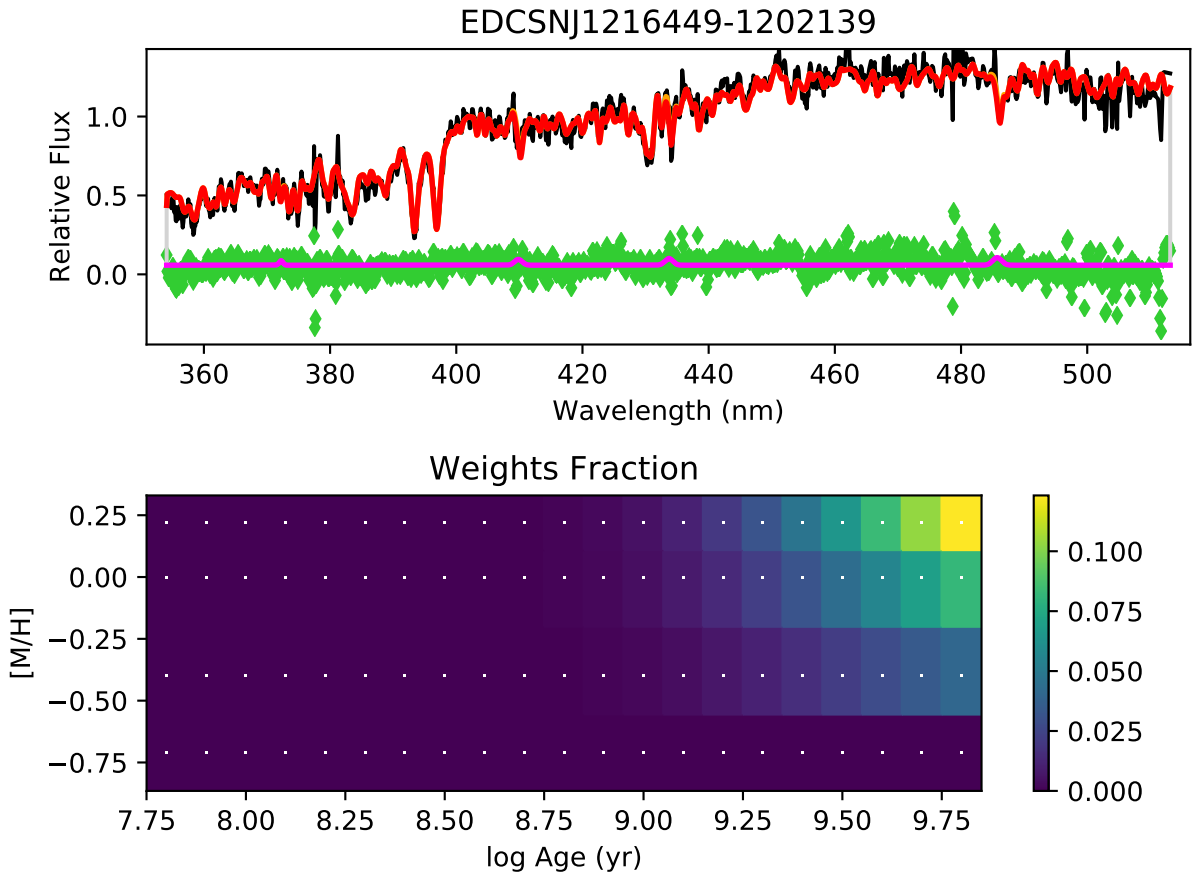
EDCSNJ1216449-1202139
Relative Flux
1.0
0.5
0.0
360
380
400
420
440
460
480
500
Wavelength (nm)
Weights Fraction
[M/H]
0.25
0.00
−0.25
−0.50
−0.75
7.75
8.00
8.25
8.50
8.75
9.00
9.25
9.50
9.75
log Age (yr)
0.100
0.075
0.050
0.025
0.000

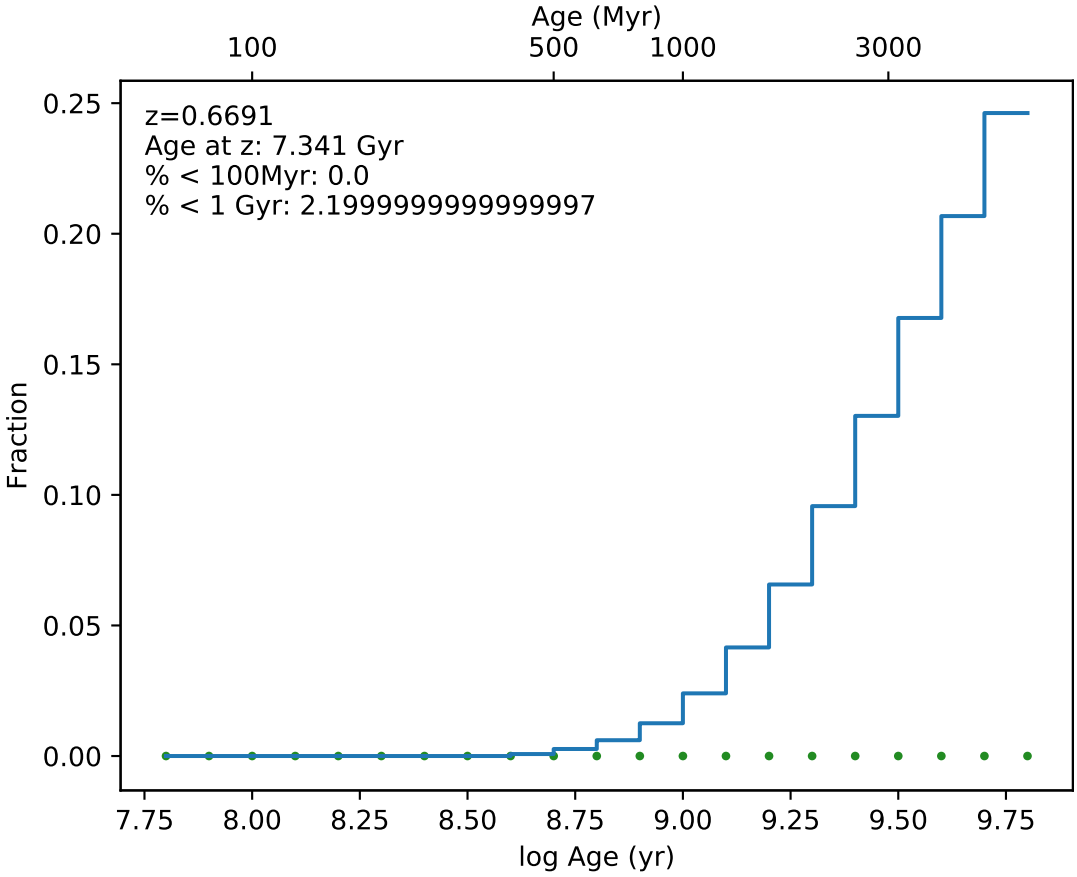
Age (Myr)
100
500
1000
3000
z=0.6691
Age at z: 7.341 Gyr
% < 100Myr: 0.0
% < 1 Gyr: 2.1999999999999997
Fraction
0.25
0.20
0.15
0.10
0.05
0.00
7.75
8.00
8.25
8.50
8.75
9.00
9.25
9.50
9.75
log Age (yr)

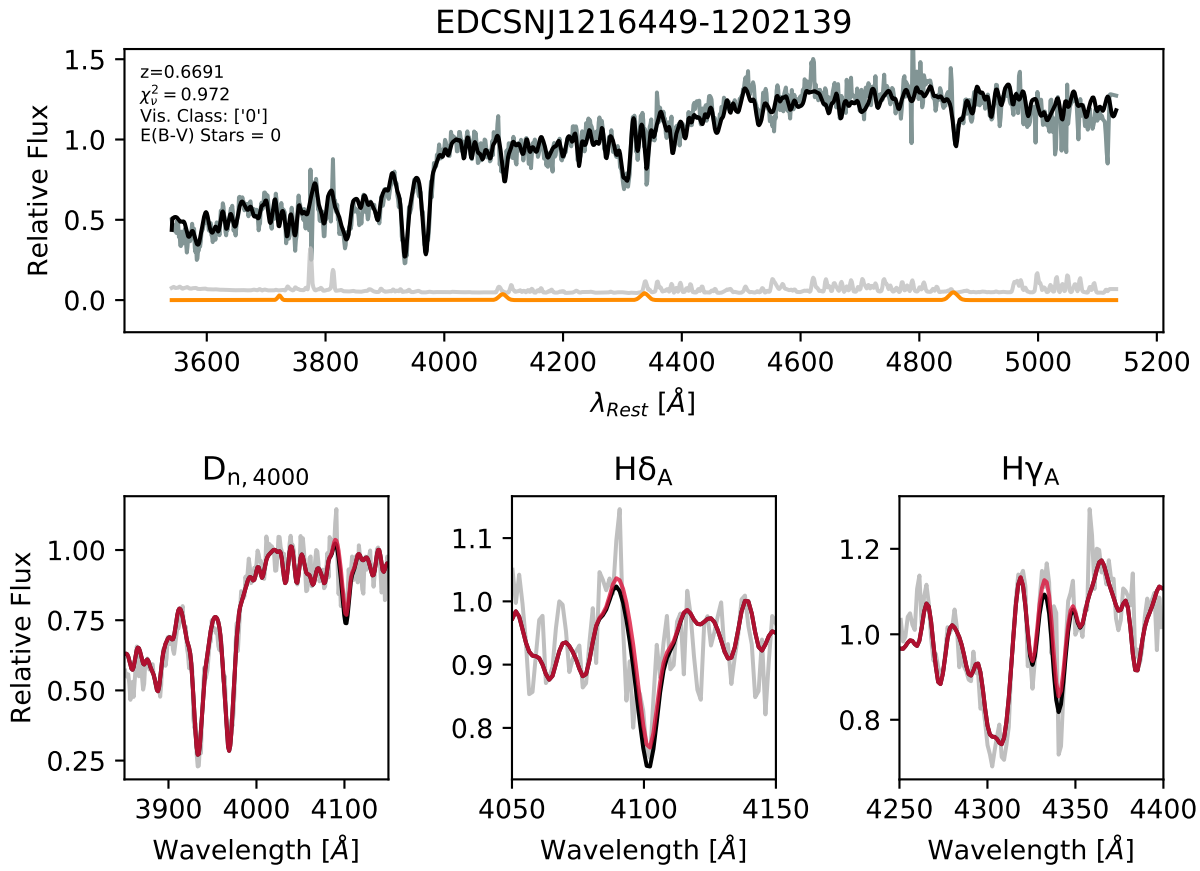
EDCSNJ1216449-1202139
z=0.6691
$\chi^2_\nu = 0.972$
Vis. Class: ['0']
E(B-V) Stars = 0
Relative Flux
λ_{Rest} [Å]
$D_{n,4000}$
$H\delta_A$
$H\gamma_A$
Wavelength [Å]

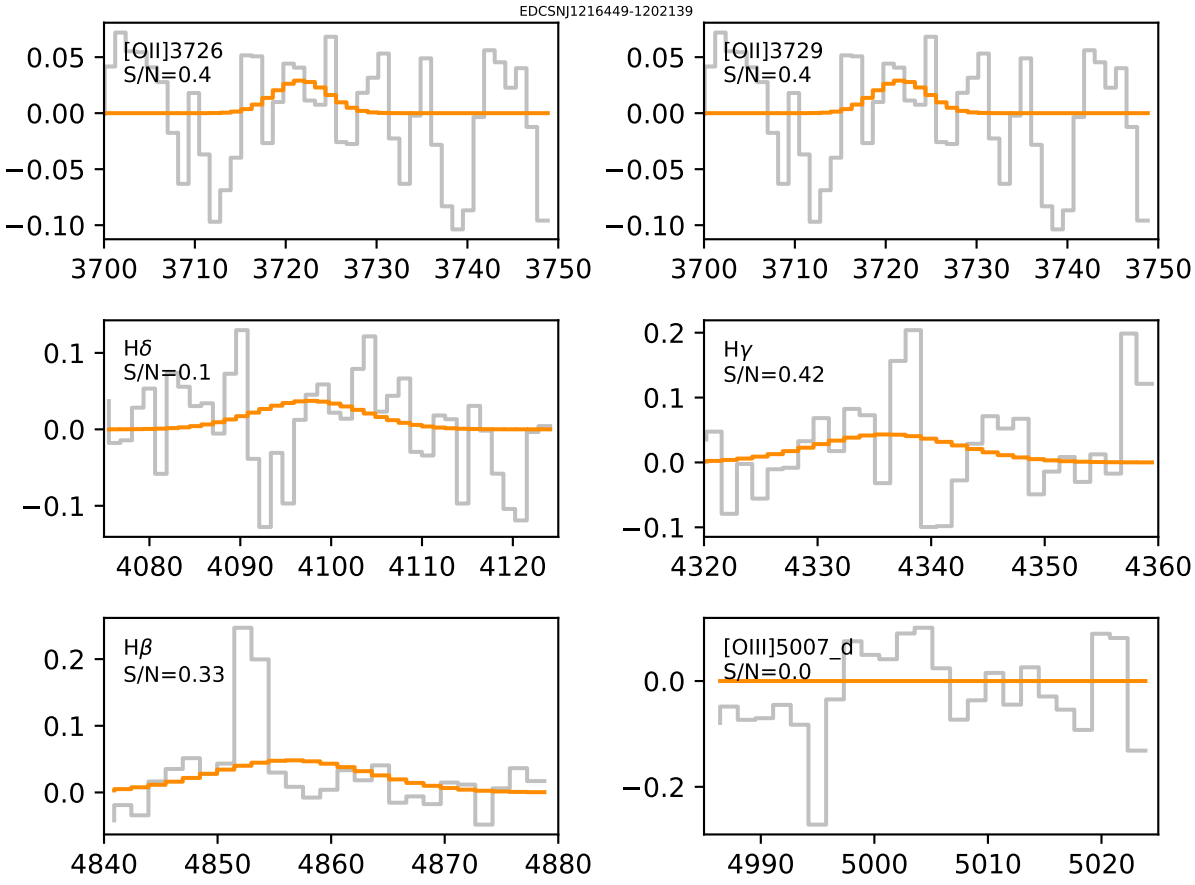
EDCSNJ1216449-1202139
[OII]3726
S/N=0.4
[OII]3729
S/N=0.4
Hδ
S/N=0.1
Hγ
S/N=0.42
Hβ
S/N=0.33
[OIII]5007_d
S/N=0.0

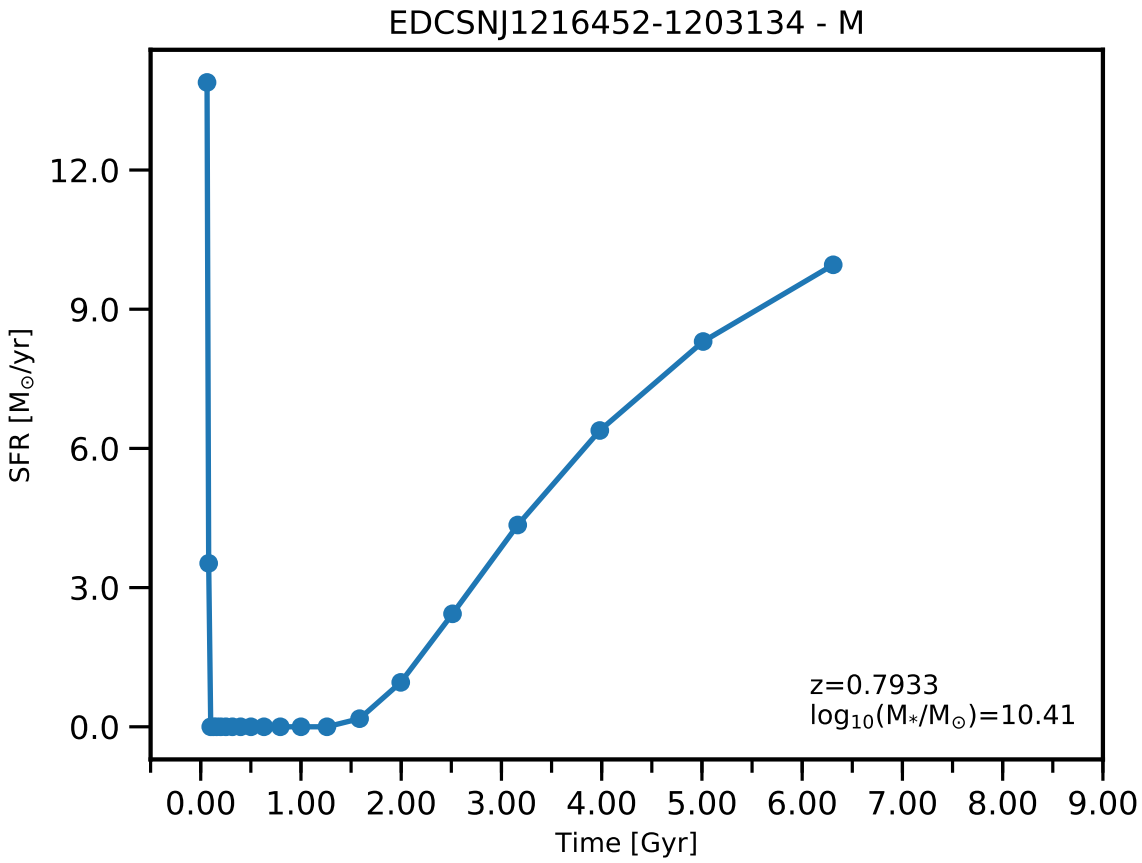
EDCSNJ1216452-1203134 - M
SFR [M⊙/yr]
12.0
9.0
6.0
3.0
0.0
0.00
1.00
2.00
3.00
4.00
5.00
6.00
7.00
8.00
9.00
Time [Gyr]
z=0.7933
log10(M*/M⊙)=10.41

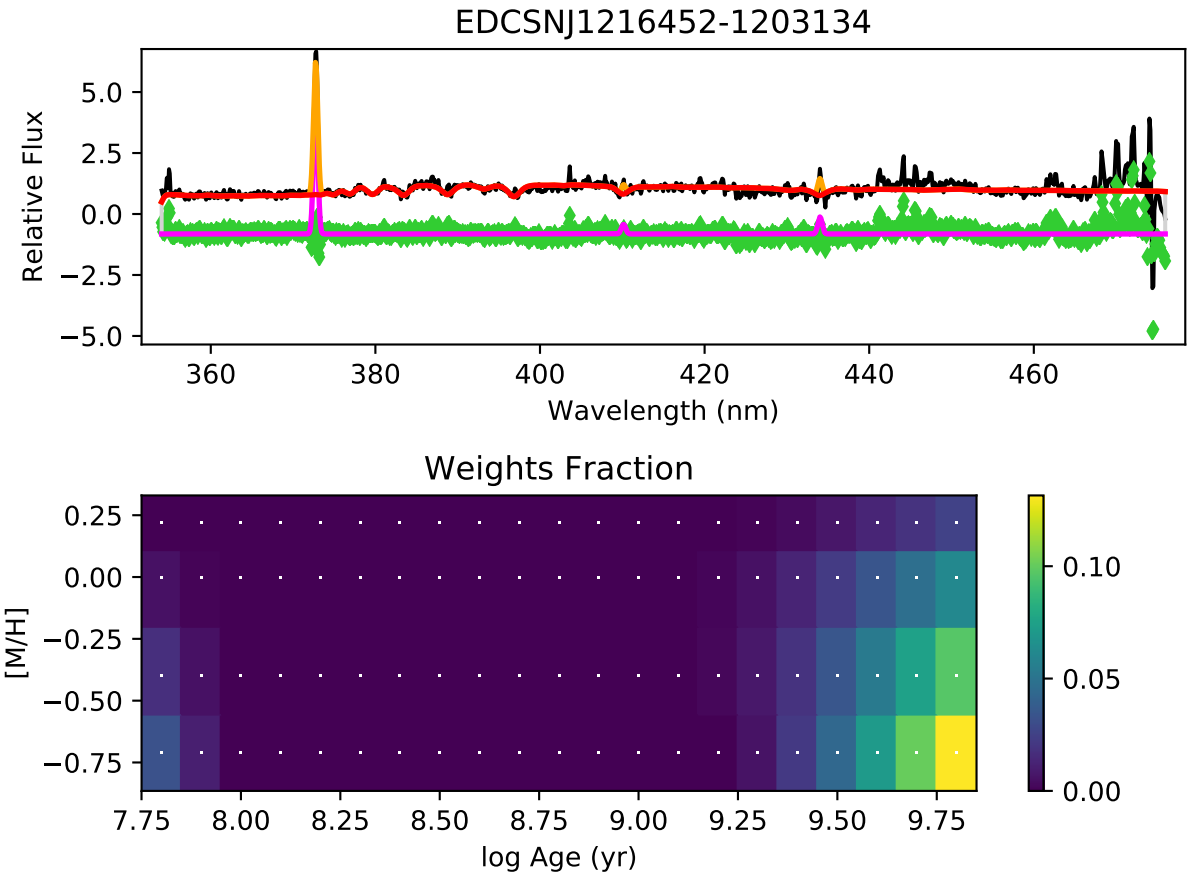
EDCSNJ1216452-1203134
Relative Flux
5.0
2.5
0.0
−2.5
−5.0
360
380
400
420
440
460
Wavelength (nm)
Weights Fraction
[M/H]
0.25
0.00
−0.25
−0.50
−0.75
7.75
8.00
8.25
8.50
8.75
9.00
9.25
9.50
9.75
log Age (yr)
0.10
0.05
0.00

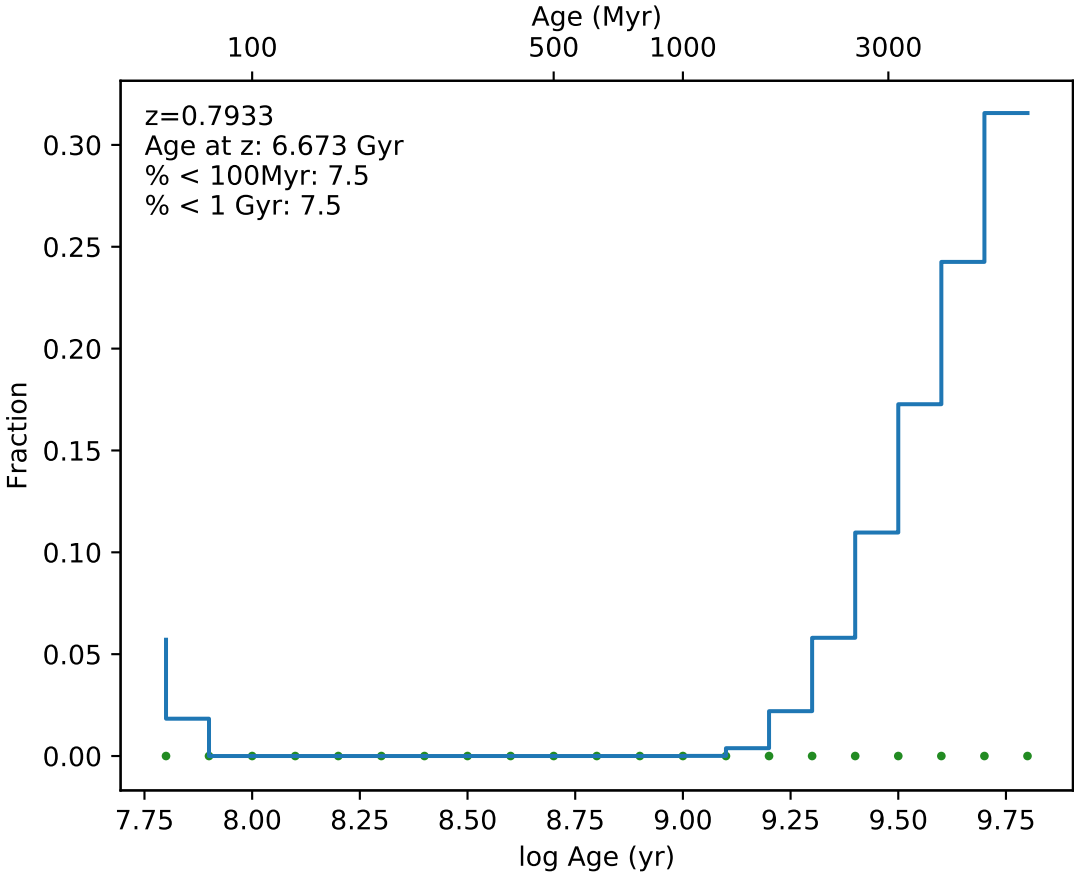
Age (Myr)
100
500
1000
3000
z=0.7933
Age at z: 6.673 Gyr
% < 100Myr: 7.5
% < 1 Gyr: 7.5
Fraction
0.30
0.25
0.20
0.15
0.10
0.05
0.00
7.75
8.00
8.25
8.50
8.75
9.00
9.25
9.50
9.75
log Age (yr)

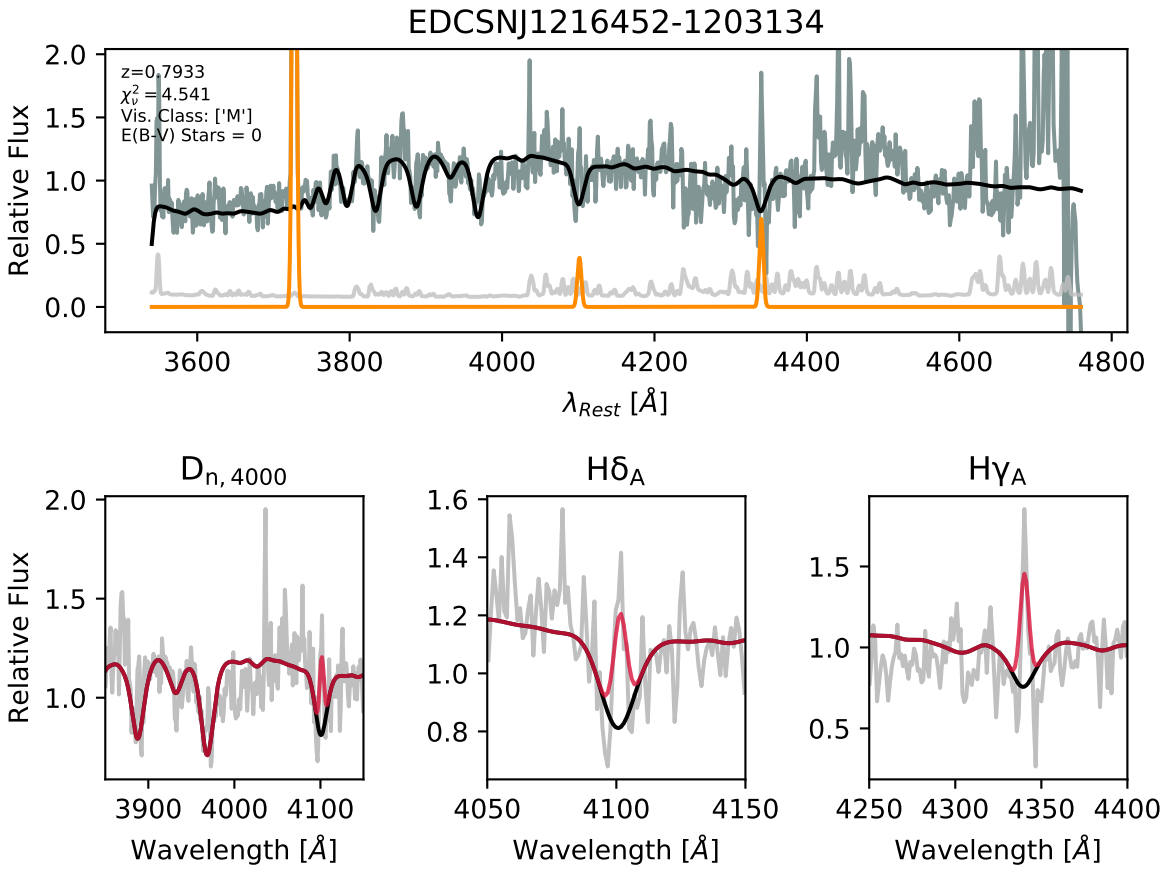
EDCSNJ1216452-1203134
z=0.7933
χ^2_ν = 4.541
Vis. Class: ['M']
E(B-V) Stars = 0
Relative Flux
λ_{Rest} [Å]
$D_{n,4000}$
$H\delta_A$
$H\gamma_A$
Wavelength [Å]

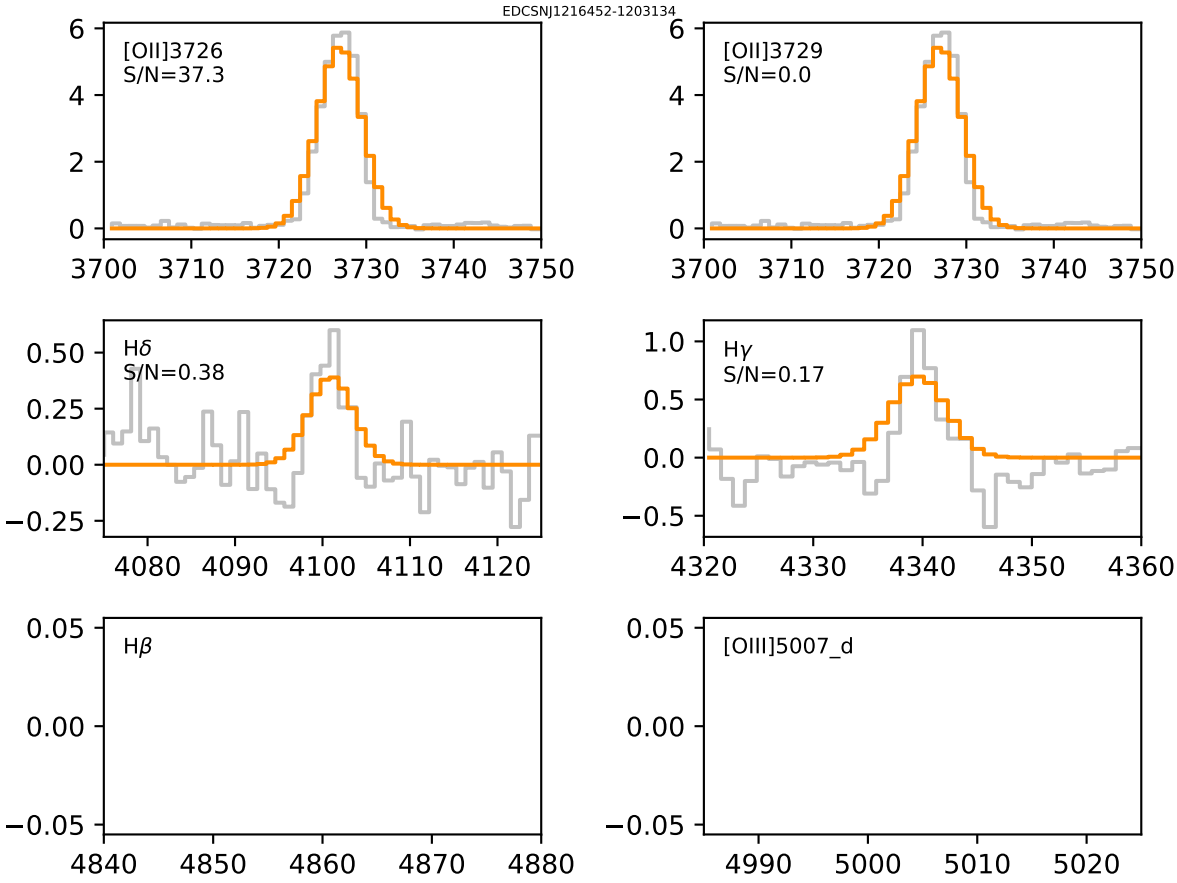
EDCSNJ1216452-1203134
[OII]3726
S/N=37.3
[OII]3729
S/N=0.0
Hδ
S/N=0.38
Hγ
S/N=0.17
Hβ
[OIII]5007_d

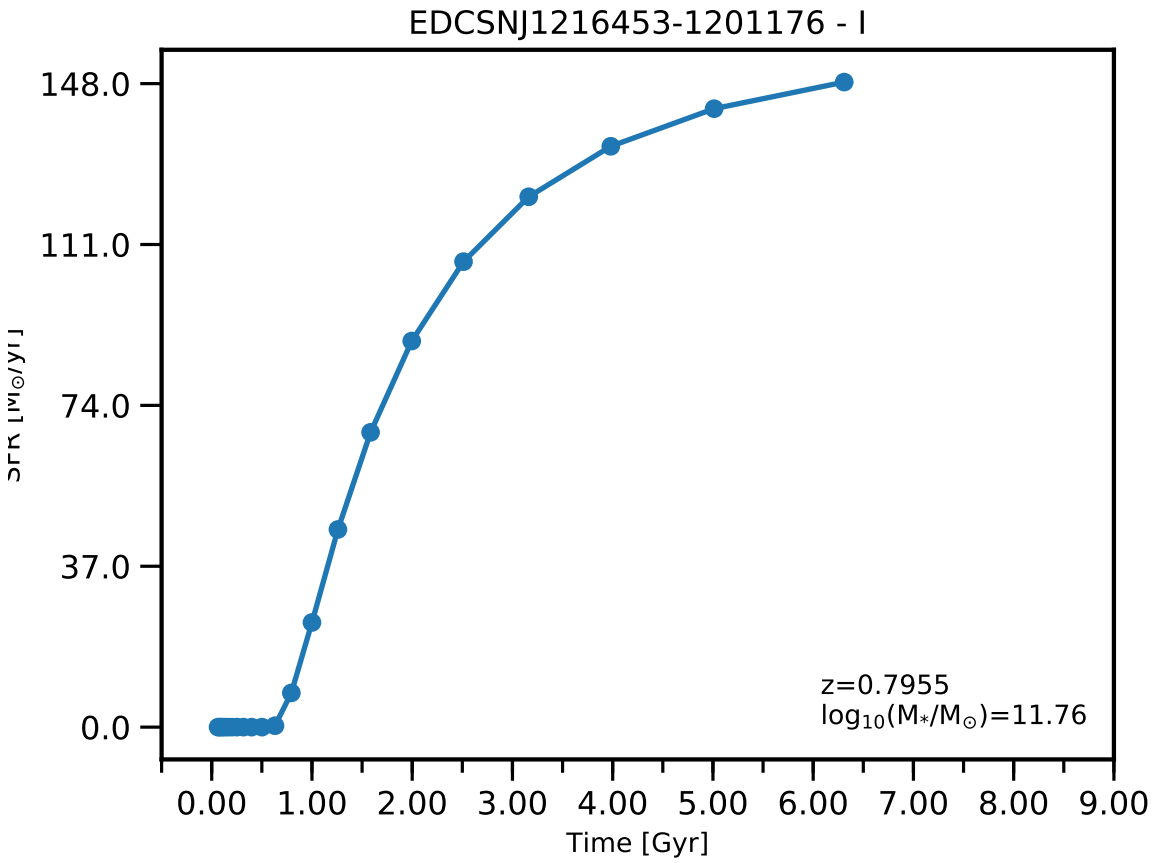
EDCSNJ1216453-1201176 - I
148.0
111.0
74.0
37.0
0.0
SFR [M⊙/yr]
0.00
1.00
2.00
3.00
4.00
5.00
6.00
7.00
8.00
9.00
Time [Gyr]
z=0.7955
log10(M*/M⊙)=11.76

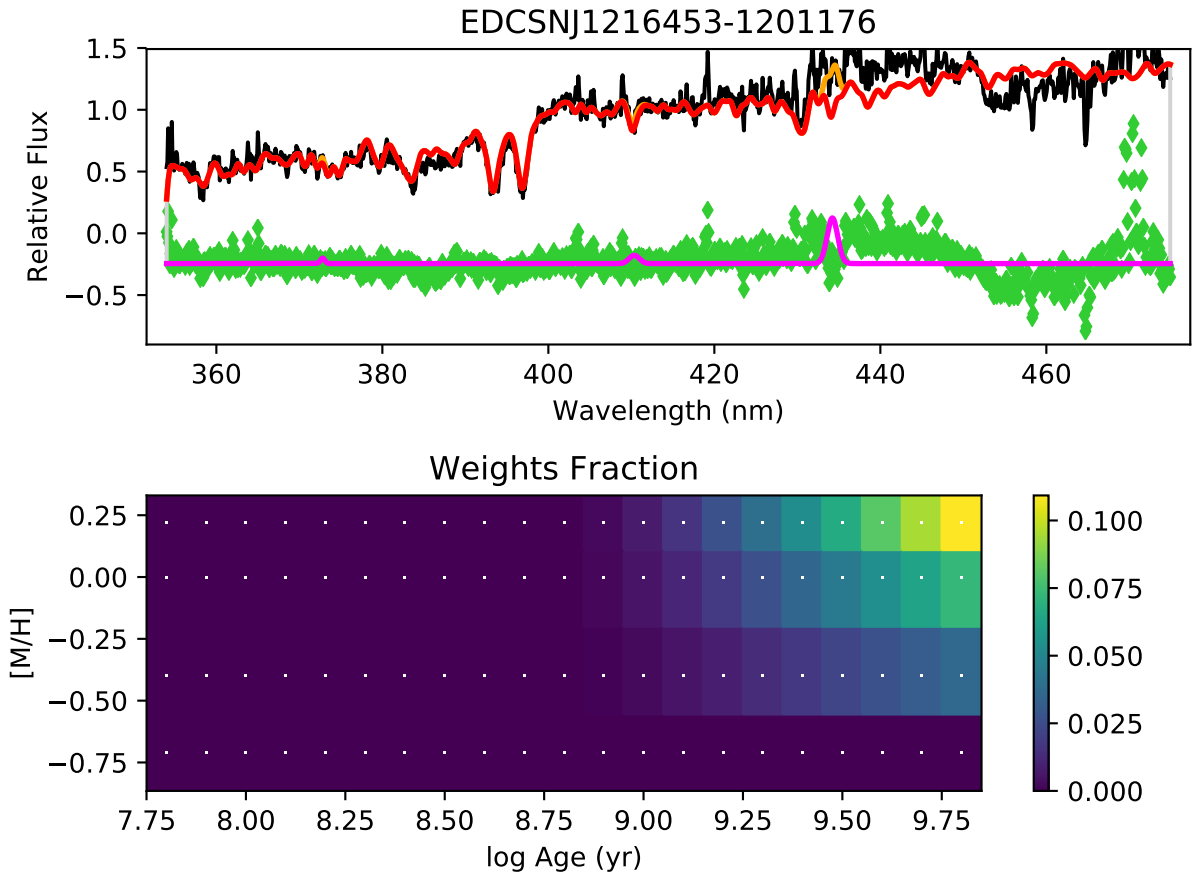
EDCSNJ1216453-1201176
Relative Flux
1.5
1.0
0.5
0.0
−0.5
360
380
400
420
440
460
Wavelength (nm)
Weights Fraction
[M/H]
0.25
0.00
−0.25
−0.50
−0.75
7.75
8.00
8.25
8.50
8.75
9.00
9.25
9.50
9.75
log Age (yr)
0.100
0.075
0.050
0.025
0.000

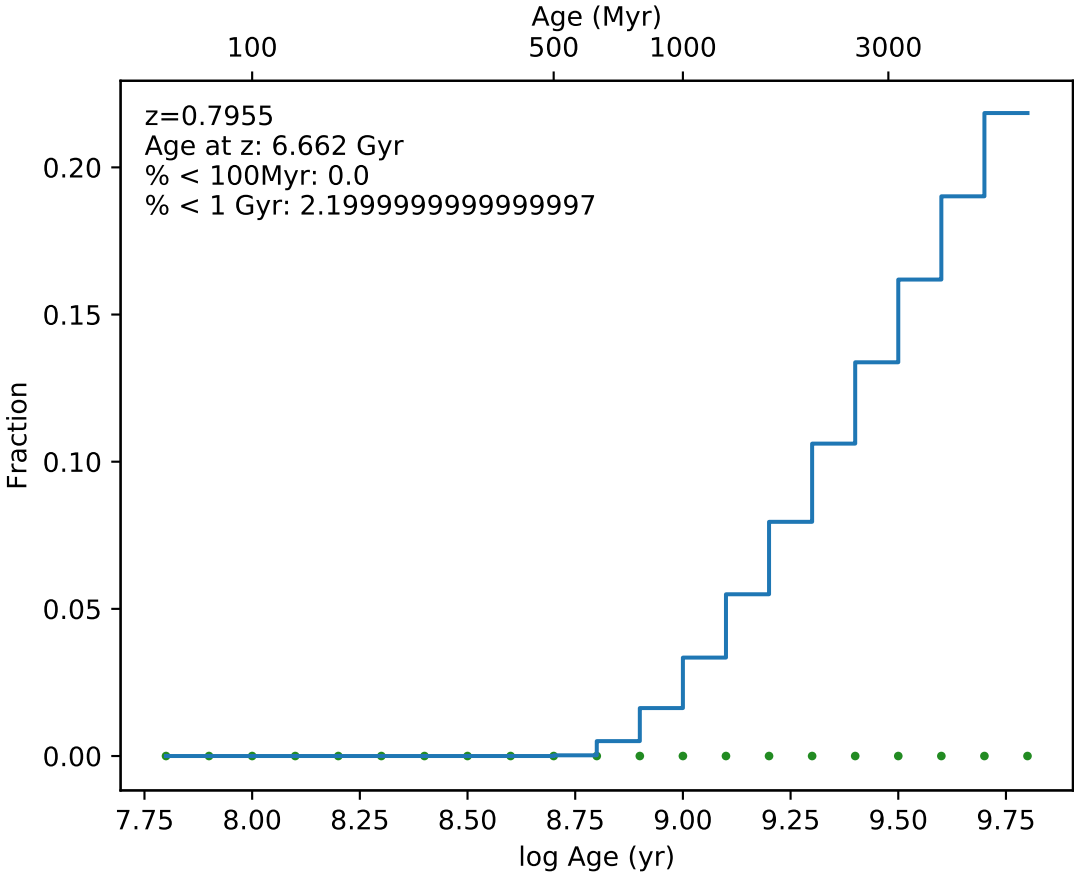
Age (Myr)
100
500
1000
3000
z=0.7955
Age at z: 6.662 Gyr
% < 100Myr: 0.0
% < 1 Gyr: 2.1999999999999997
Fraction
0.00
0.05
0.10
0.15
0.20
7.75
8.00
8.25
8.50
8.75
9.00
9.25
9.50
9.75
log Age (yr)

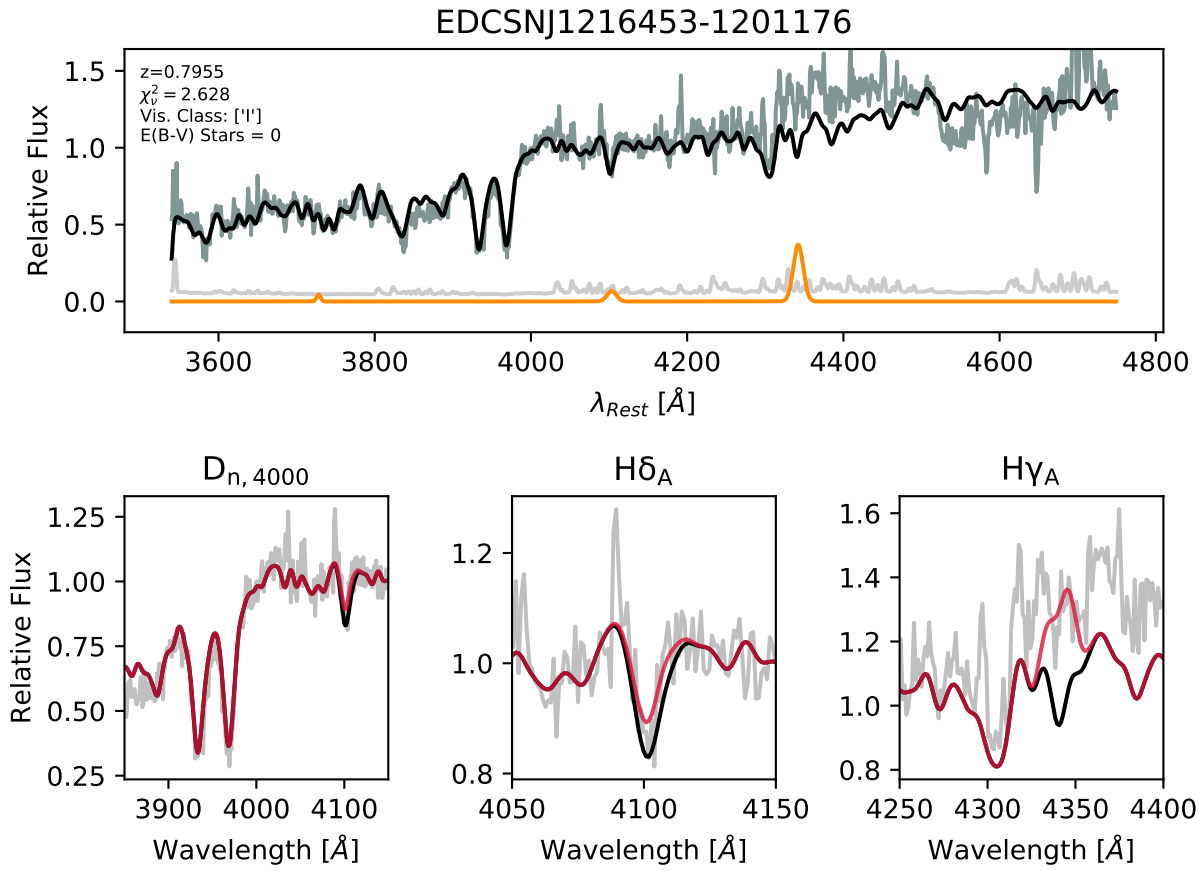
EDCSNJ1216453-1201176
z=0.7955
$\chi^2_\nu = 2.628$
Vis. Class: ['I']
E(B-V) Stars = 0
Relative Flux
λ_{Rest} [Å]
$D_{n,4000}$
$H\delta_A$
$H\gamma_A$
Wavelength [Å]

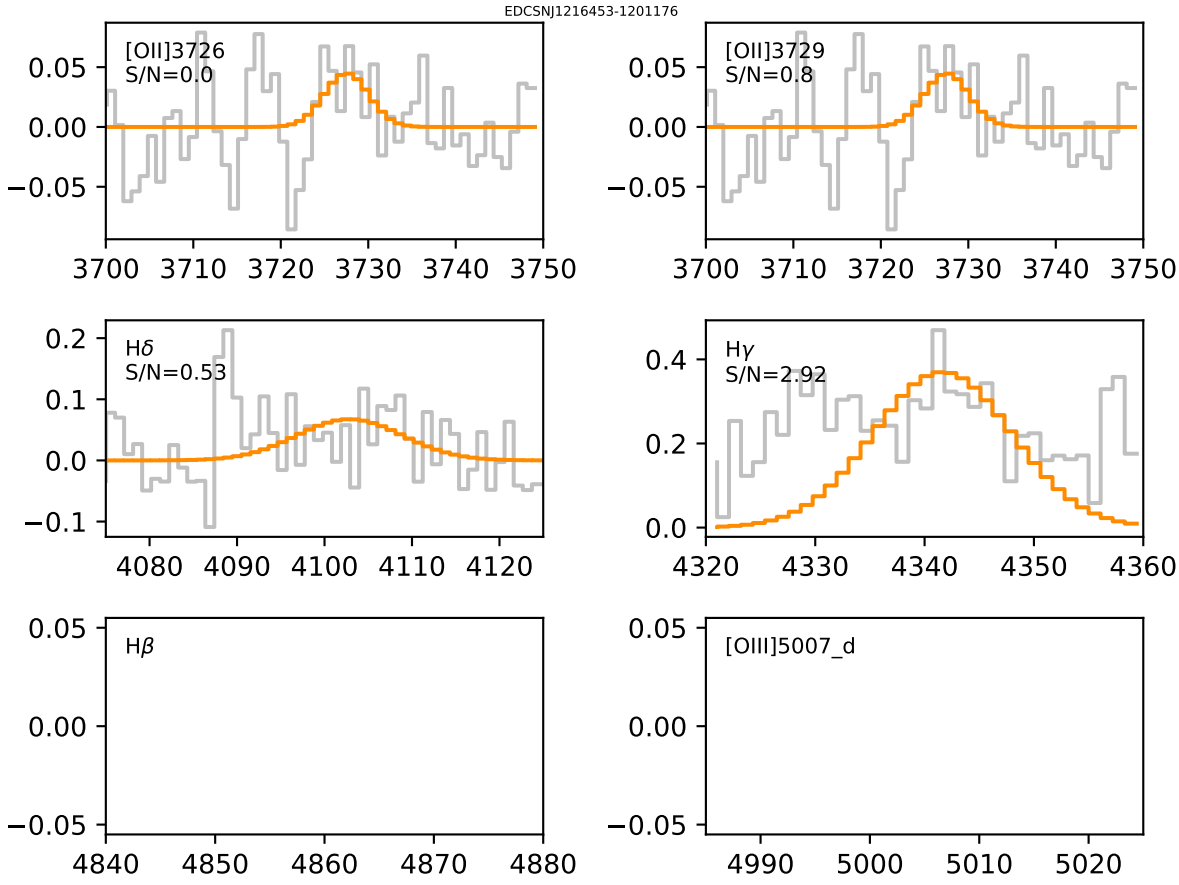
EDCSNJ1216453-1201176
[OII]3726
S/N=0.0
[OII]3729
S/N=0.8
Hδ
S/N=0.53
Hγ
S/N=2.92
Hβ
[OIII]5007_d

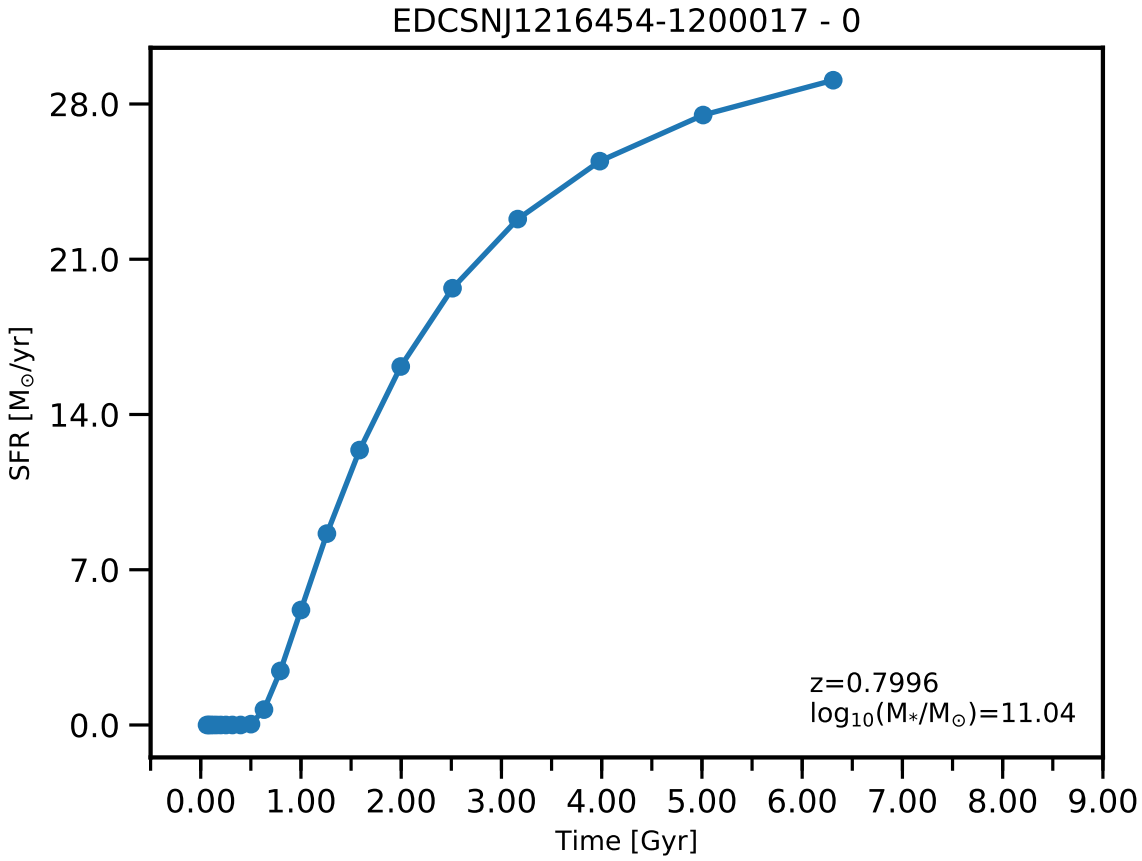
EDCSNJ1216454-1200017 - 0
28.0
21.0
14.0
7.0
0.0
SFR [M⊙/yr]
0.00
1.00
2.00
3.00
4.00
5.00
6.00
7.00
8.00
9.00
Time [Gyr]
z=0.7996
log10(M*/M⊙)=11.04

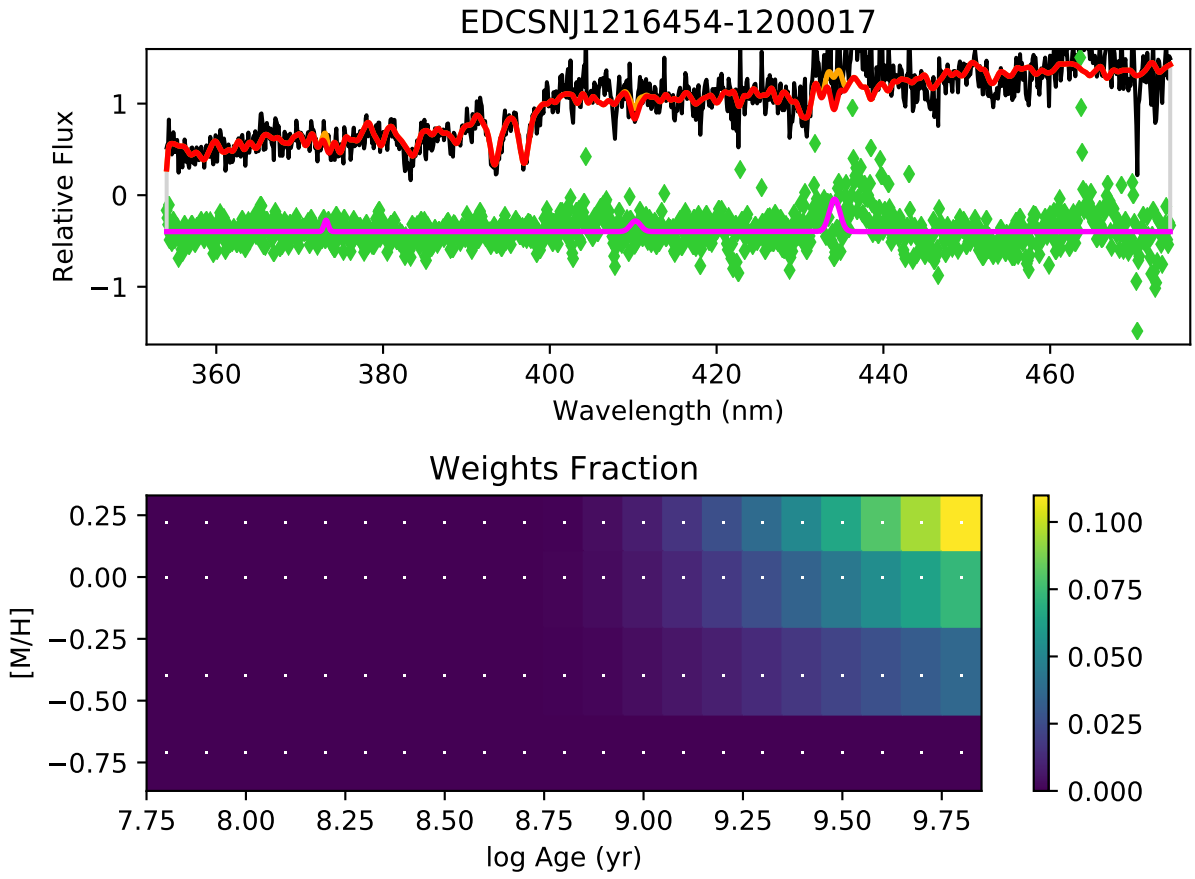
EDCSNJ1216454-1200017
Relative Flux
1
0
−1
360
380
400
420
440
460
Wavelength (nm)
Weights Fraction
[M/H]
0.25
0.00
−0.25
−0.50
−0.75
7.75
8.00
8.25
8.50
8.75
9.00
9.25
9.50
9.75
log Age (yr)
0.100
0.075
0.050
0.025
0.000

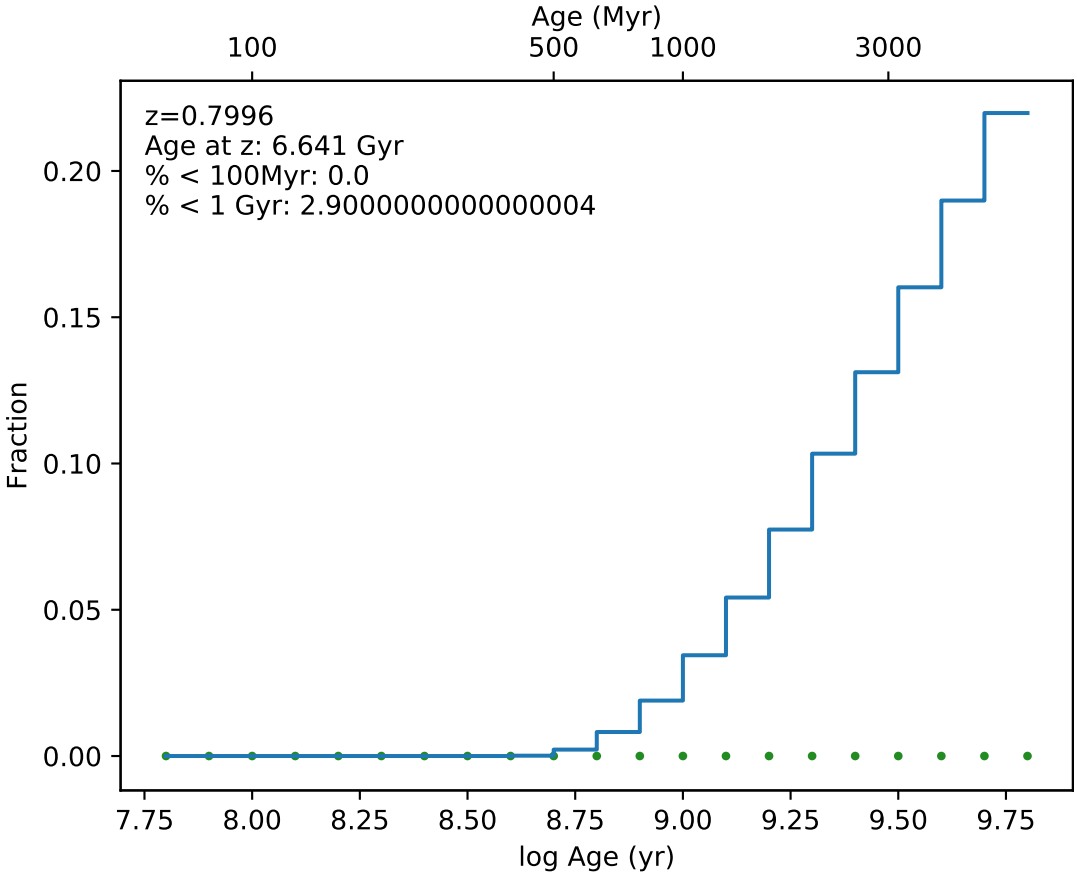
Age (Myr)
100
500
1000
3000
z=0.7996
Age at z: 6.641 Gyr
% < 100Myr: 0.0
% < 1 Gyr: 2.9000000000000004
Fraction
0.20
0.15
0.10
0.05
0.00
7.75
8.00
8.25
8.50
8.75
9.00
9.25
9.50
9.75
log Age (yr)

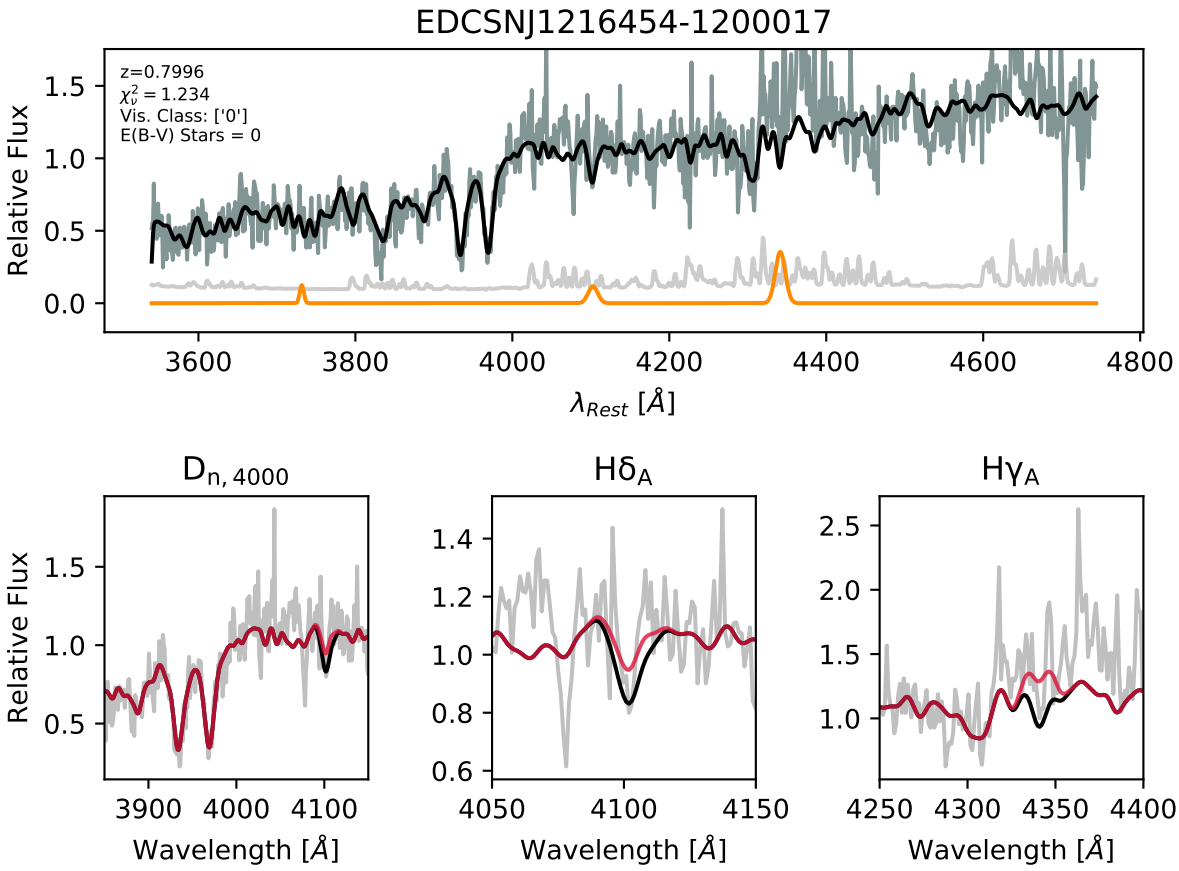
EDCSNJ1216454-1200017
z=0.7996
$\chi^2_\nu = 1.234$
Vis. Class: ['0']
E(B-V) Stars = 0
Relative Flux
λ_{Rest} [Å]
$D_{n,4000}$
$H\delta_A$
$H\gamma_A$
Wavelength [Å]

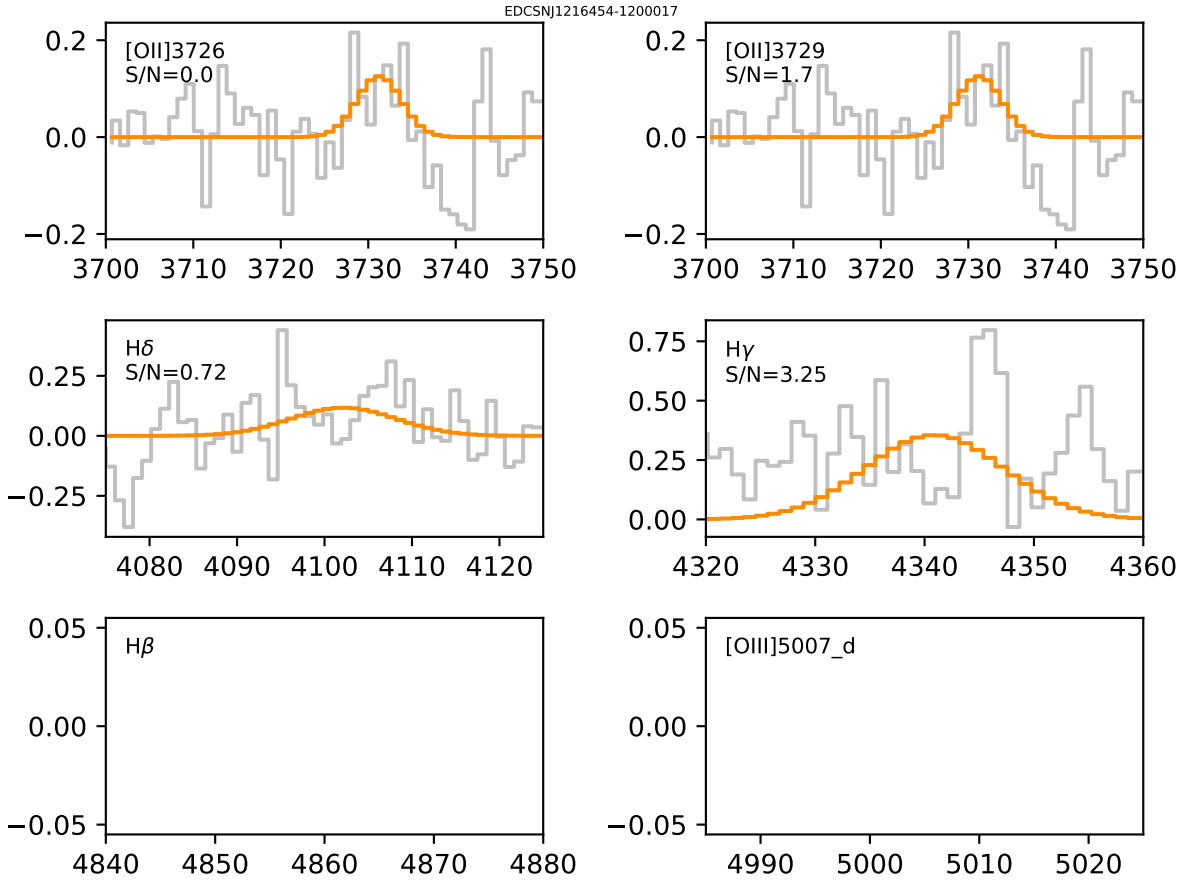
EDCSNJ1216454-1200017
[OII]3726
S/N=0.0
[OII]3729
S/N=1.7
Hδ
S/N=0.72
Hγ
S/N=3.25
Hβ
[OIII]5007_d

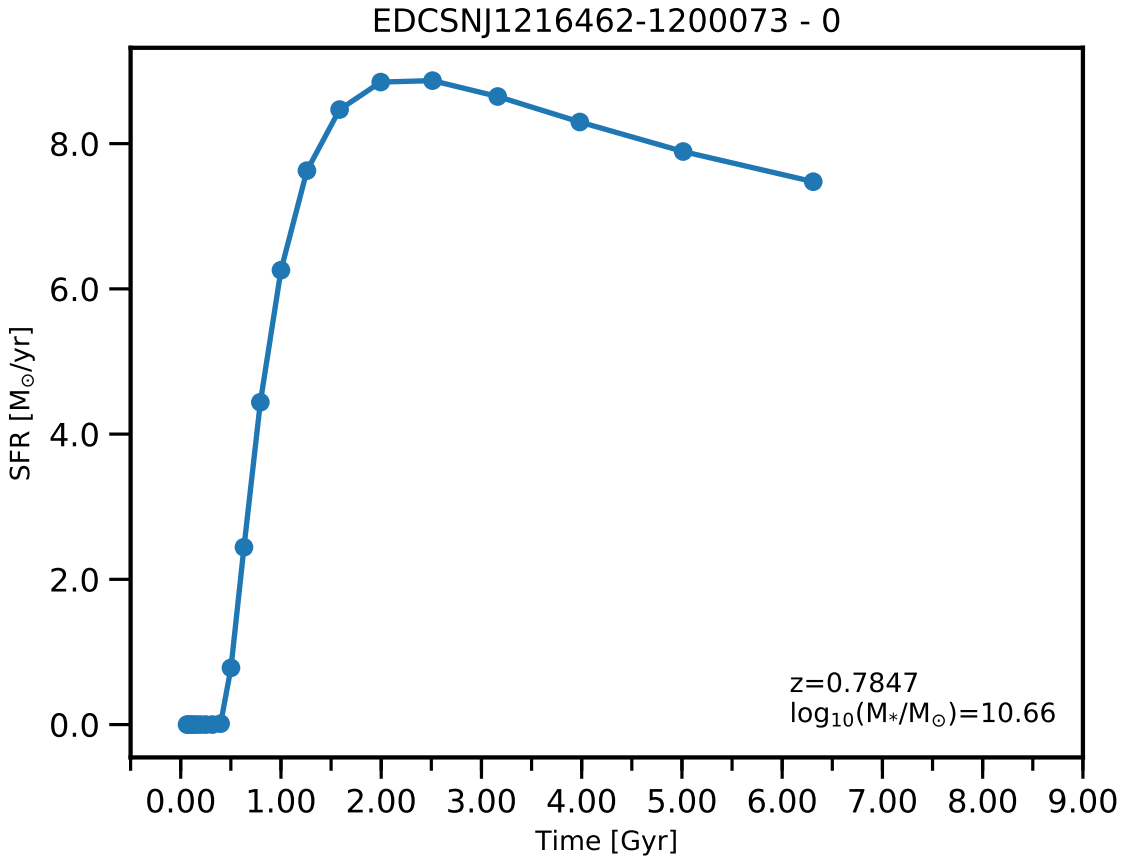
EDCSNJ1216462-1200073 - 0
SFR [M⊙/yr]
0.0
2.0
4.0
6.0
8.0
0.00
1.00
2.00
3.00
4.00
5.00
6.00
7.00
8.00
9.00
Time [Gyr]
z=0.7847
log10(M*/M⊙)=10.66

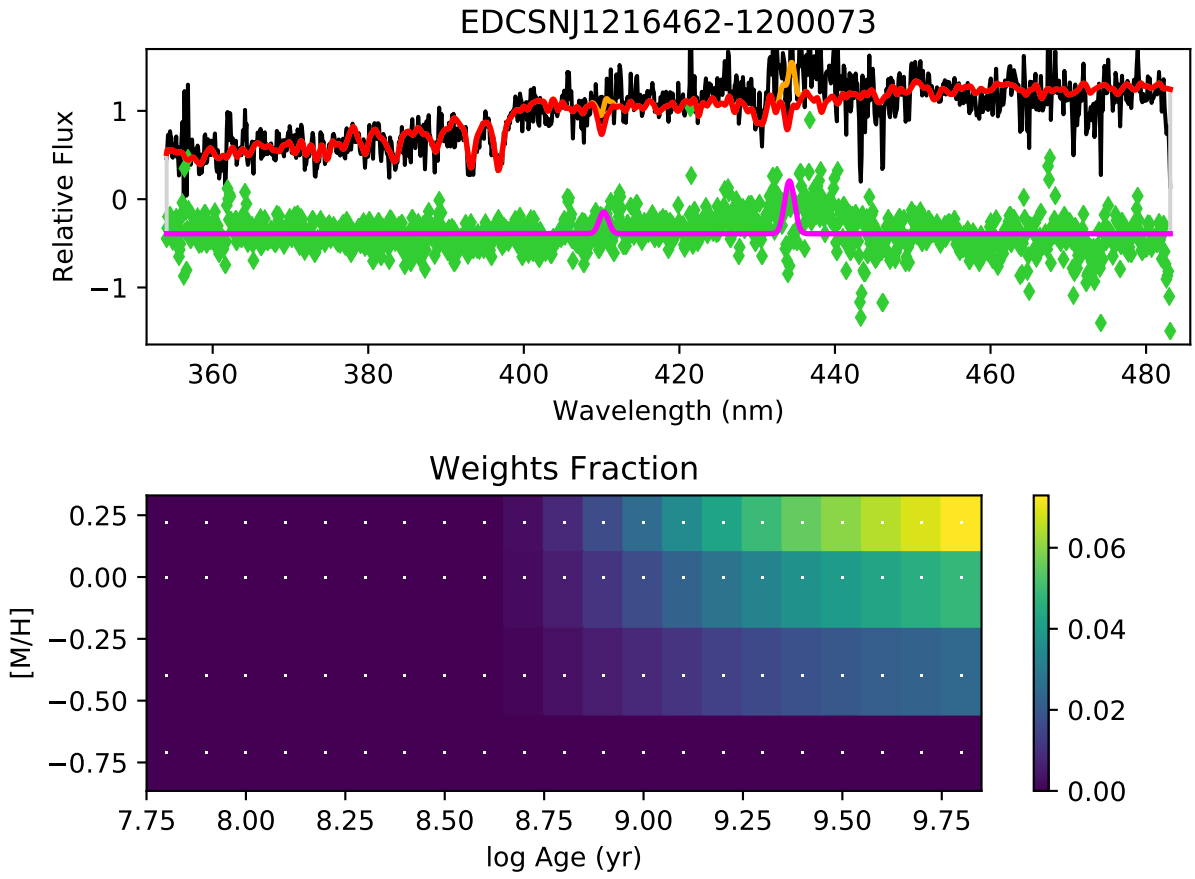
EDCSNJ1216462-1200073
Relative Flux
1
0
−1
360
380
400
420
440
460
480
Wavelength (nm)
Weights Fraction
[M/H]
0.25
0.00
−0.25
−0.50
−0.75
7.75
8.00
8.25
8.50
8.75
9.00
9.25
9.50
9.75
log Age (yr)
0.06
0.04
0.02
0.00

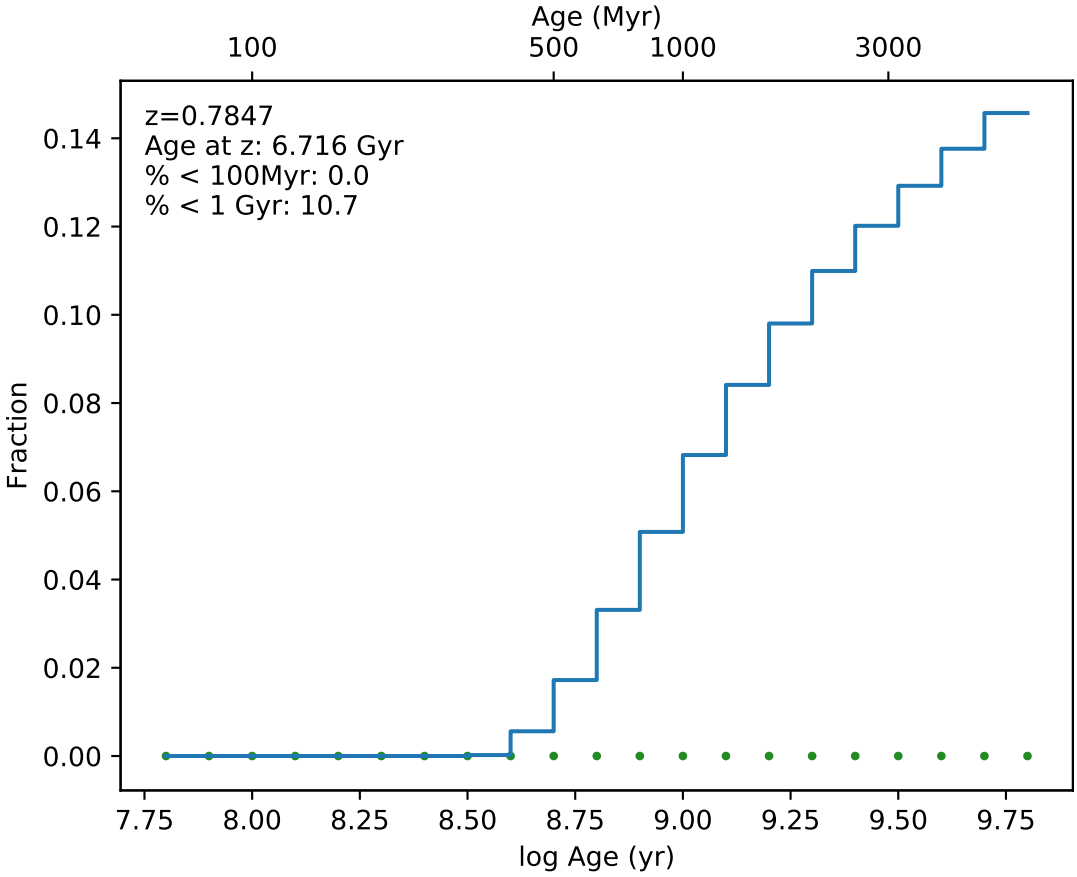
Age (Myr)
100
500
1000
3000
z=0.7847
Age at z: 6.716 Gyr
% < 100Myr: 0.0
% < 1 Gyr: 10.7
Fraction
0.14
0.12
0.10
0.08
0.06
0.04
0.02
0.00
7.75
8.00
8.25
8.50
8.75
9.00
9.25
9.50
9.75
log Age (yr)

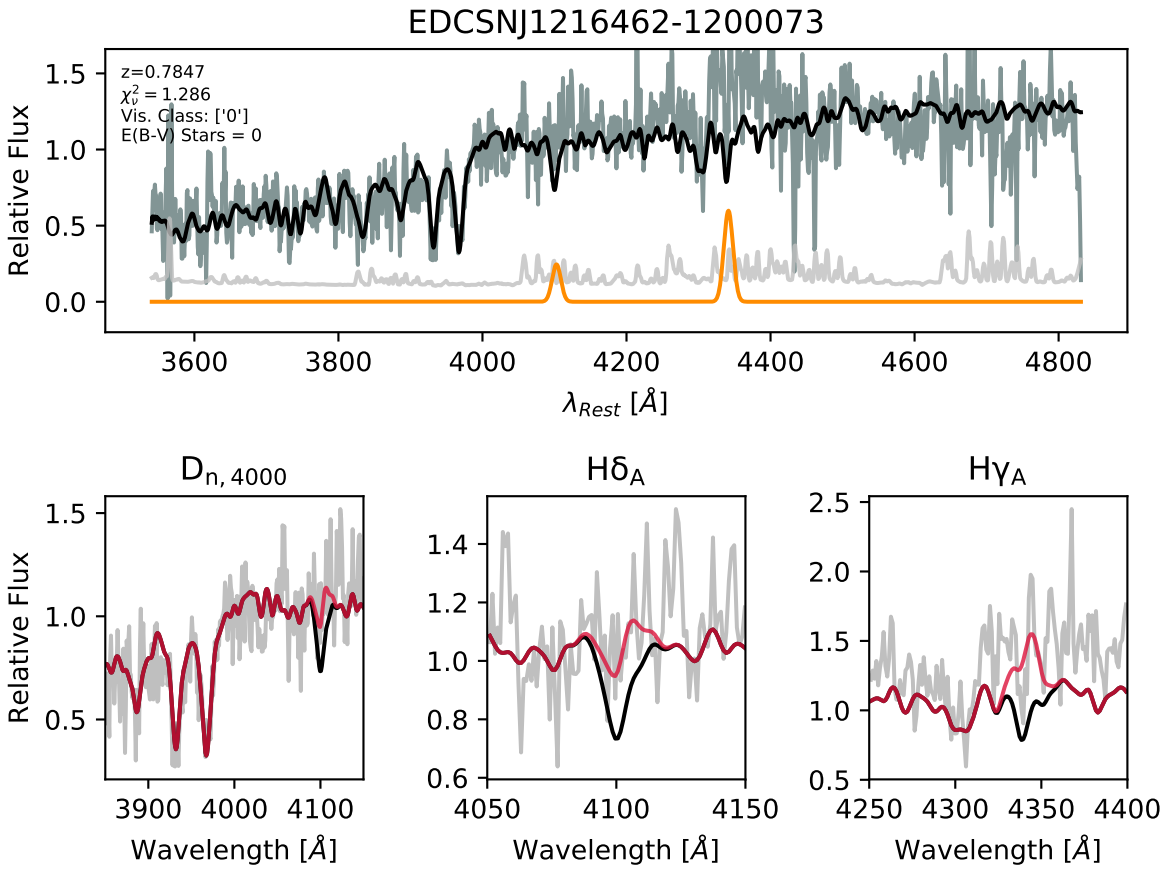
EDCSNJ1216462-1200073
z=0.7847
$\chi^2_\nu = 1.286$
Vis. Class: ['0']
E(B-V) Stars = 0
Relative Flux
λ_{Rest} [Å]
$D_{n,4000}$
$H\delta_A$
$H\gamma_A$
Wavelength [Å]

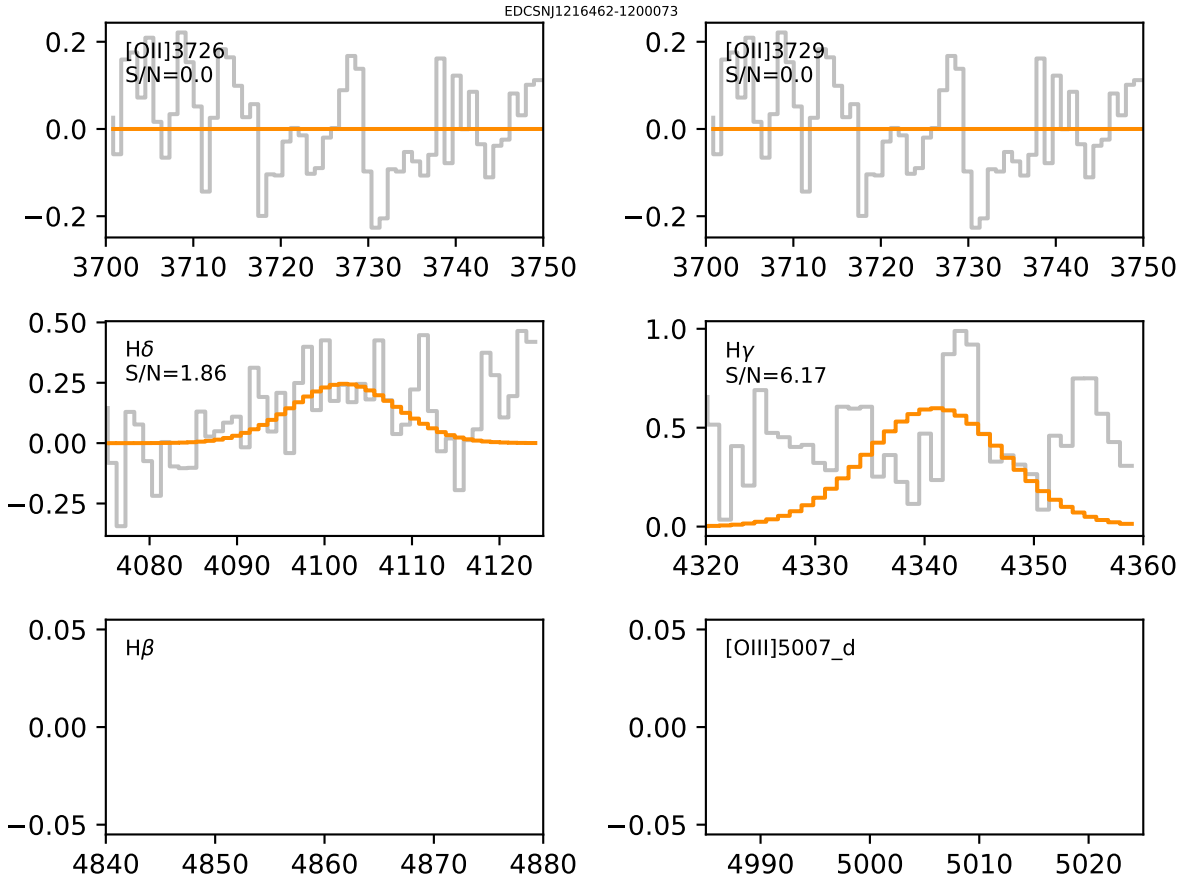
EDCSNJ1216462-1200073
[OII]3726
S/N=0.0
[OII]3729
S/N=0.0
Hδ
S/N=1.86
Hγ
S/N=6.17
Hβ
[OIII]5007_d

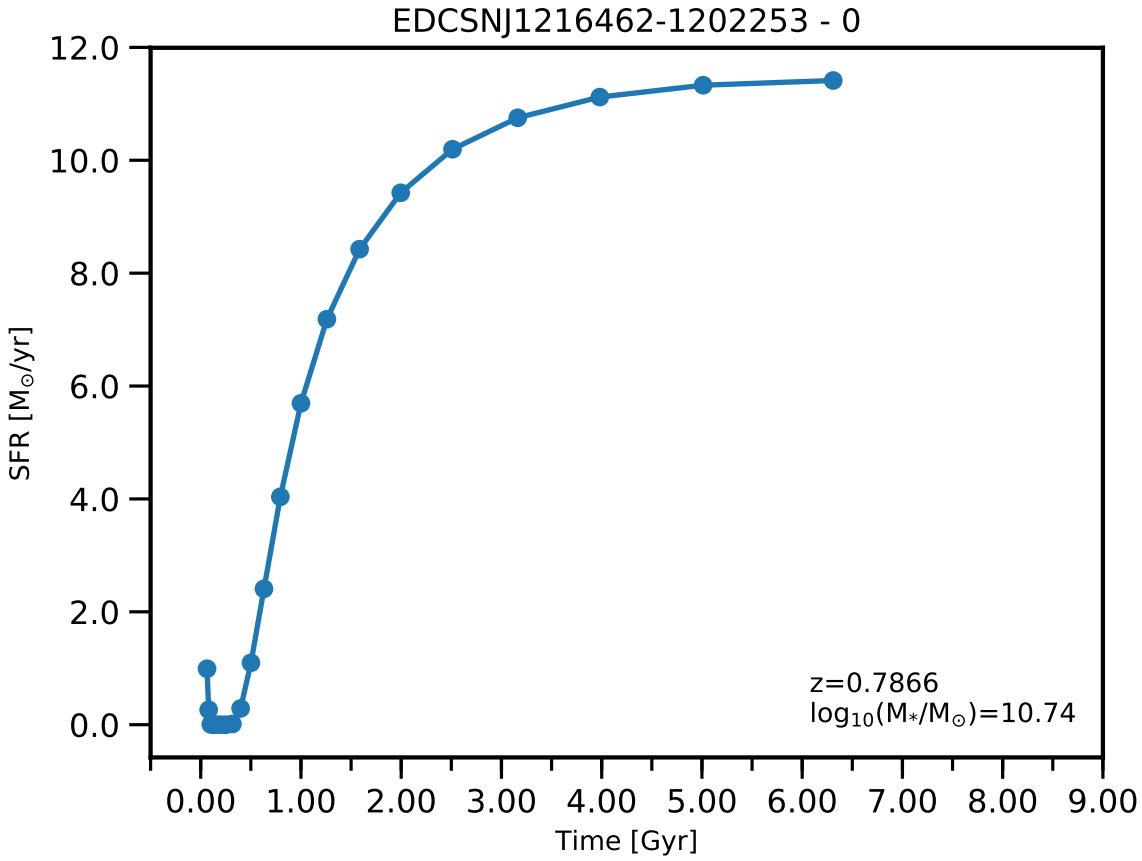
EDCSNJ1216462-1202253 - 0
12.0
10.0
8.0
6.0
4.0
2.0
0.0
SFR [M⊙/yr]
0.00
1.00
2.00
3.00
4.00
5.00
6.00
7.00
8.00
9.00
Time [Gyr]
z=0.7866
log10(M*/M⊙)=10.74

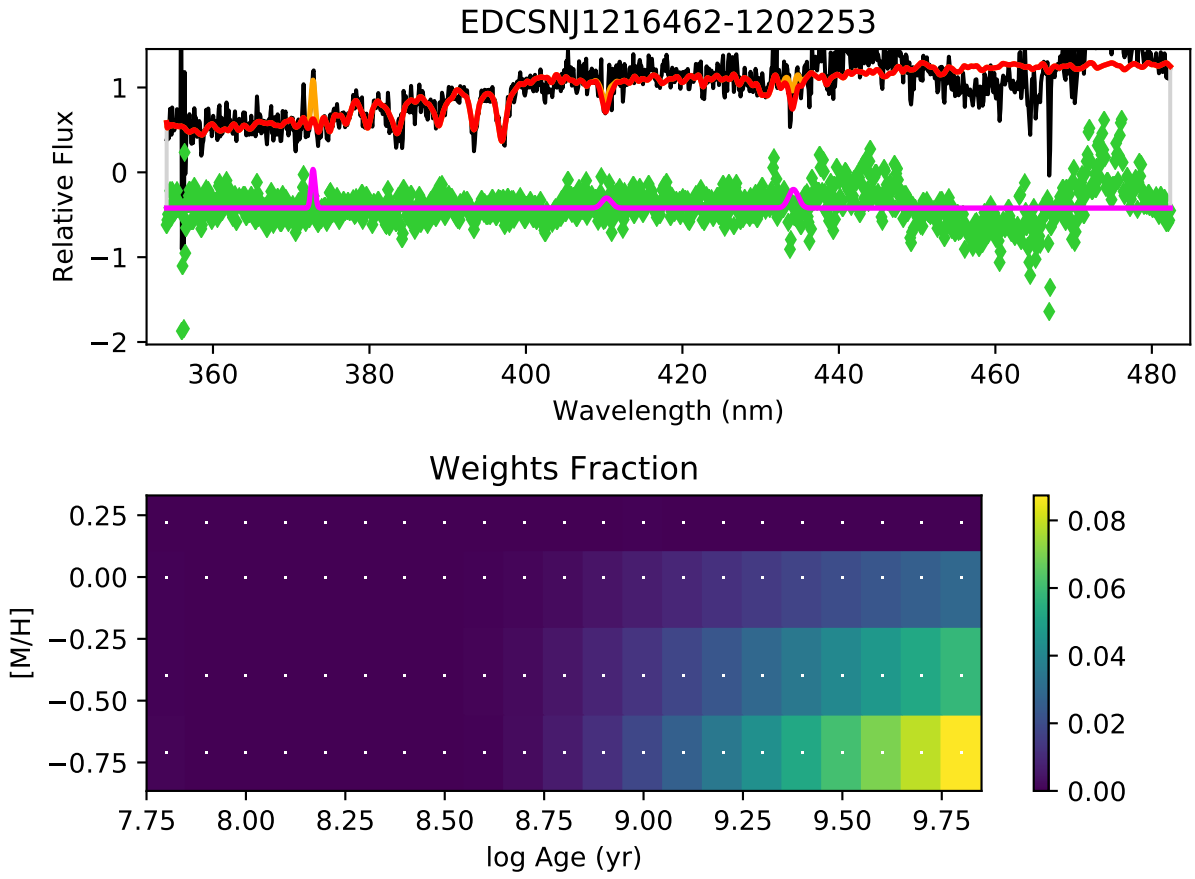
EDCSNJ1216462-1202253
Relative Flux
1
0
−1
−2
360
380
400
420
440
460
480
Wavelength (nm)
Weights Fraction
[M/H]
0.25
0.00
−0.25
−0.50
−0.75
7.75
8.00
8.25
8.50
8.75
9.00
9.25
9.50
9.75
log Age (yr)
0.08
0.06
0.04
0.02
0.00

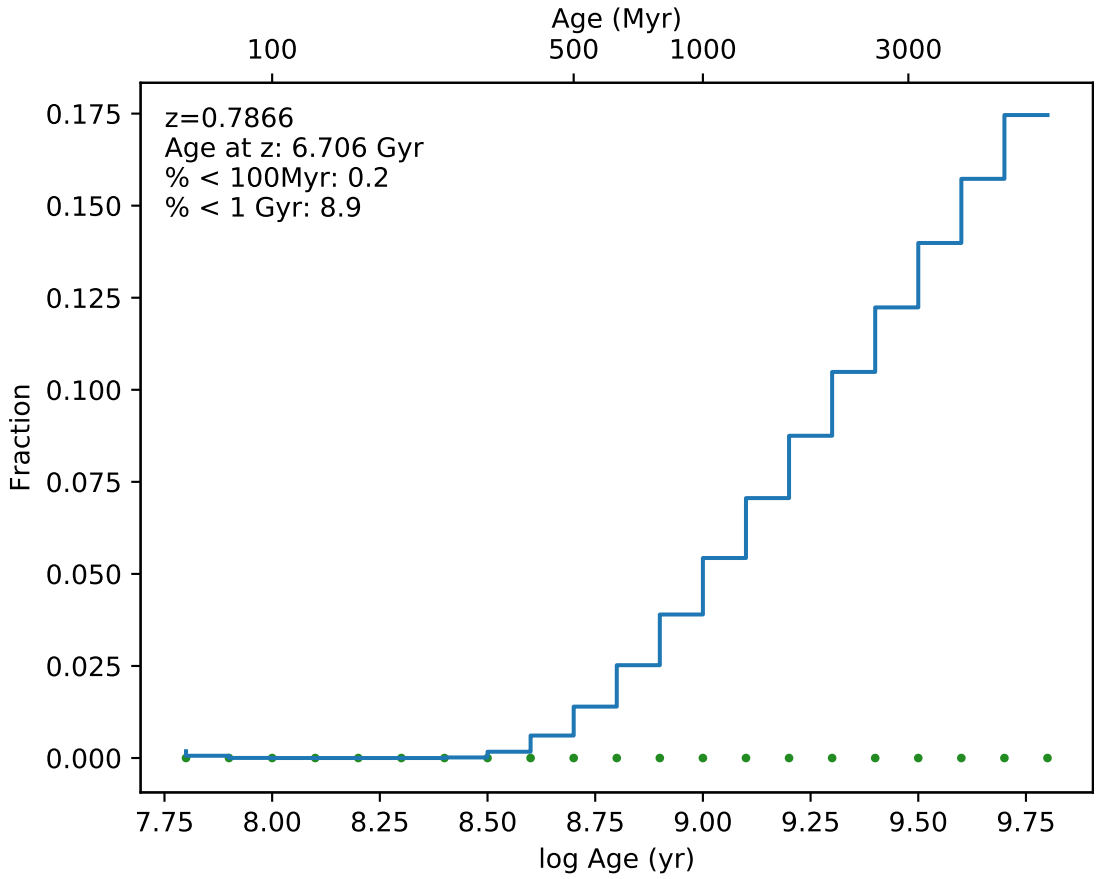
Age (Myr)
100
500
1000
3000
z=0.7866
Age at z: 6.706 Gyr
% < 100Myr: 0.2
% < 1 Gyr: 8.9
Fraction
0.175
0.150
0.125
0.100
0.075
0.050
0.025
0.000
7.75
8.00
8.25
8.50
8.75
9.00
9.25
9.50
9.75
log Age (yr)

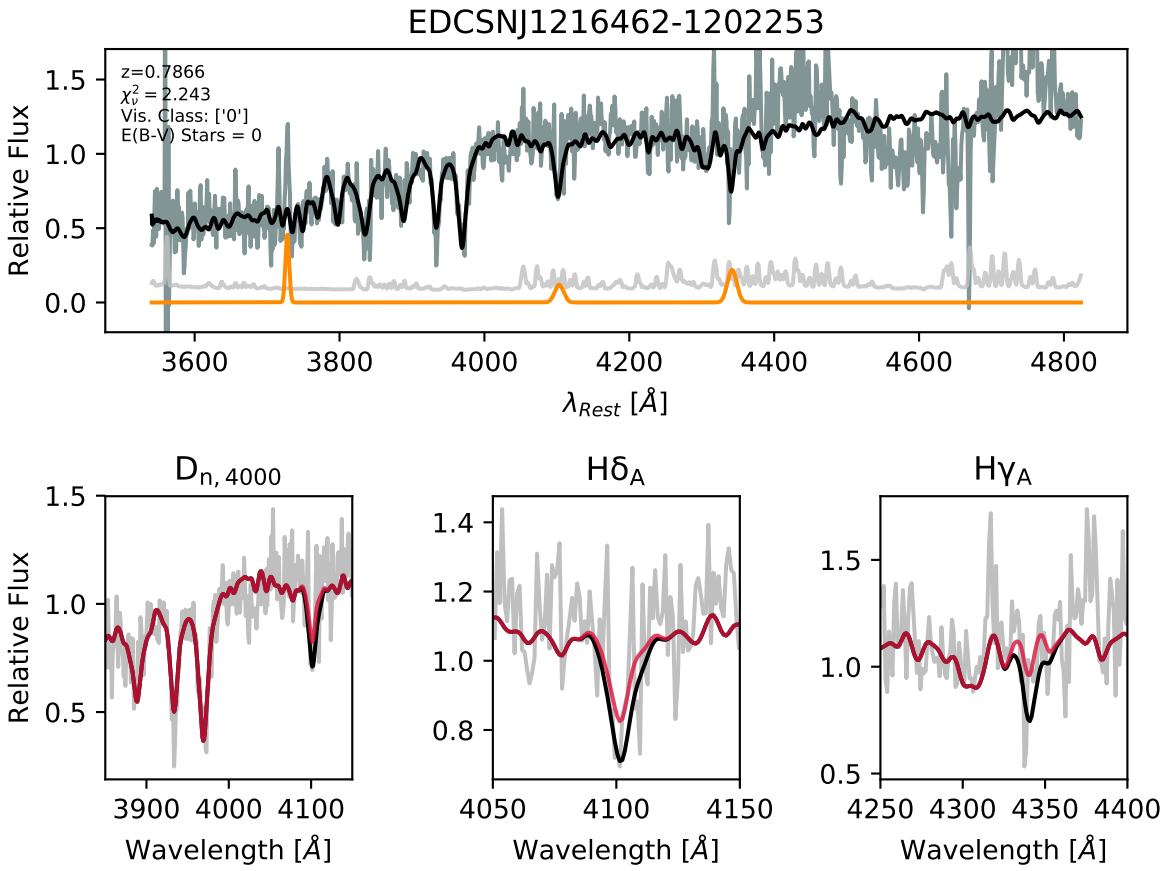
EDCSNJ1216462-1202253
z=0.7866
$\chi^2_\nu = 2.243$
Vis. Class: ['0']
E(B-V) Stars = 0
Relative Flux
λ_{Rest} [Å]
$D_{n,4000}$
$H\delta_A$
$H\gamma_A$
Wavelength [Å]

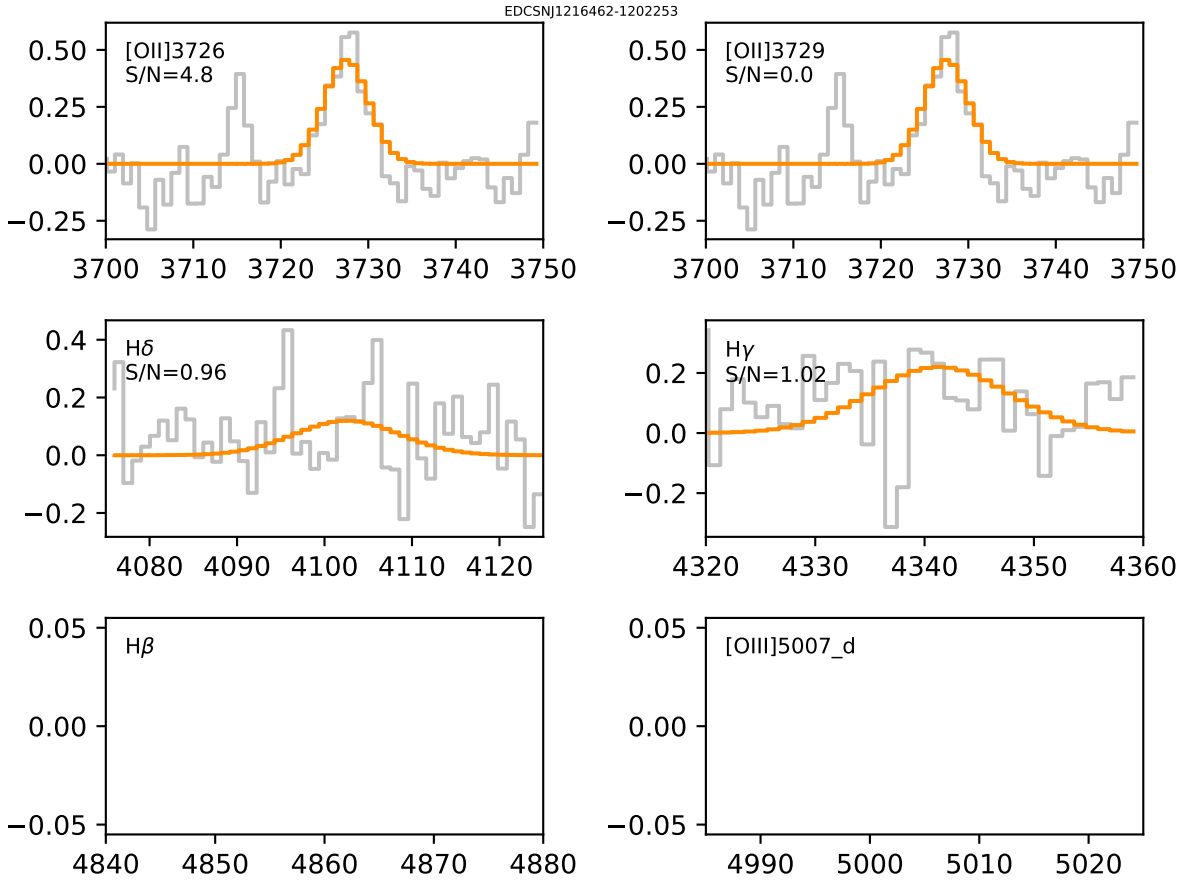
EDCSNJ1216462-1202253
[OII]3726
S/N=4.8
[OII]3729
S/N=0.0
Hδ
S/N=0.96
Hγ
S/N=1.02
Hβ
[OIII]5007_d

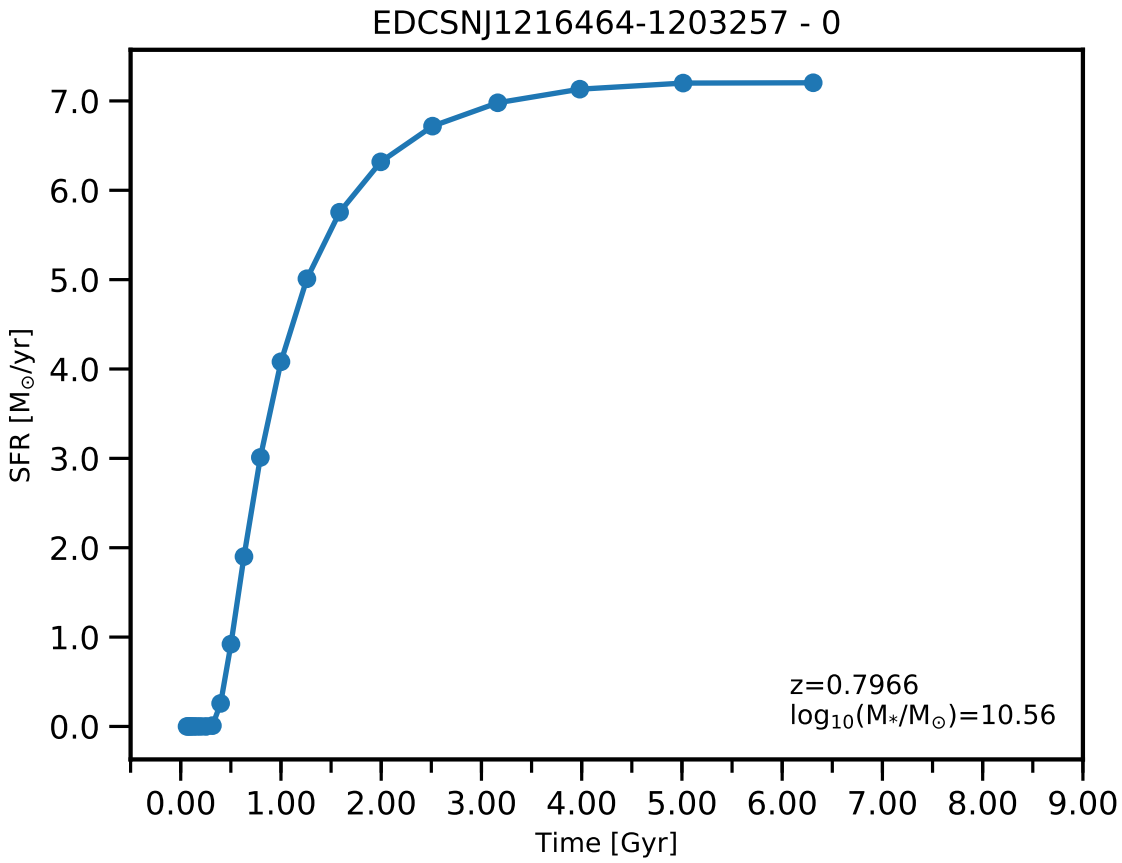
EDCSNJ1216464-1203257 - 0
SFR [M⊙/yr]
0.0
1.0
2.0
3.0
4.0
5.0
6.0
7.0
0.00
1.00
2.00
3.00
4.00
5.00
6.00
7.00
8.00
9.00
Time [Gyr]
z=0.7966
log10(M*/M⊙)=10.56

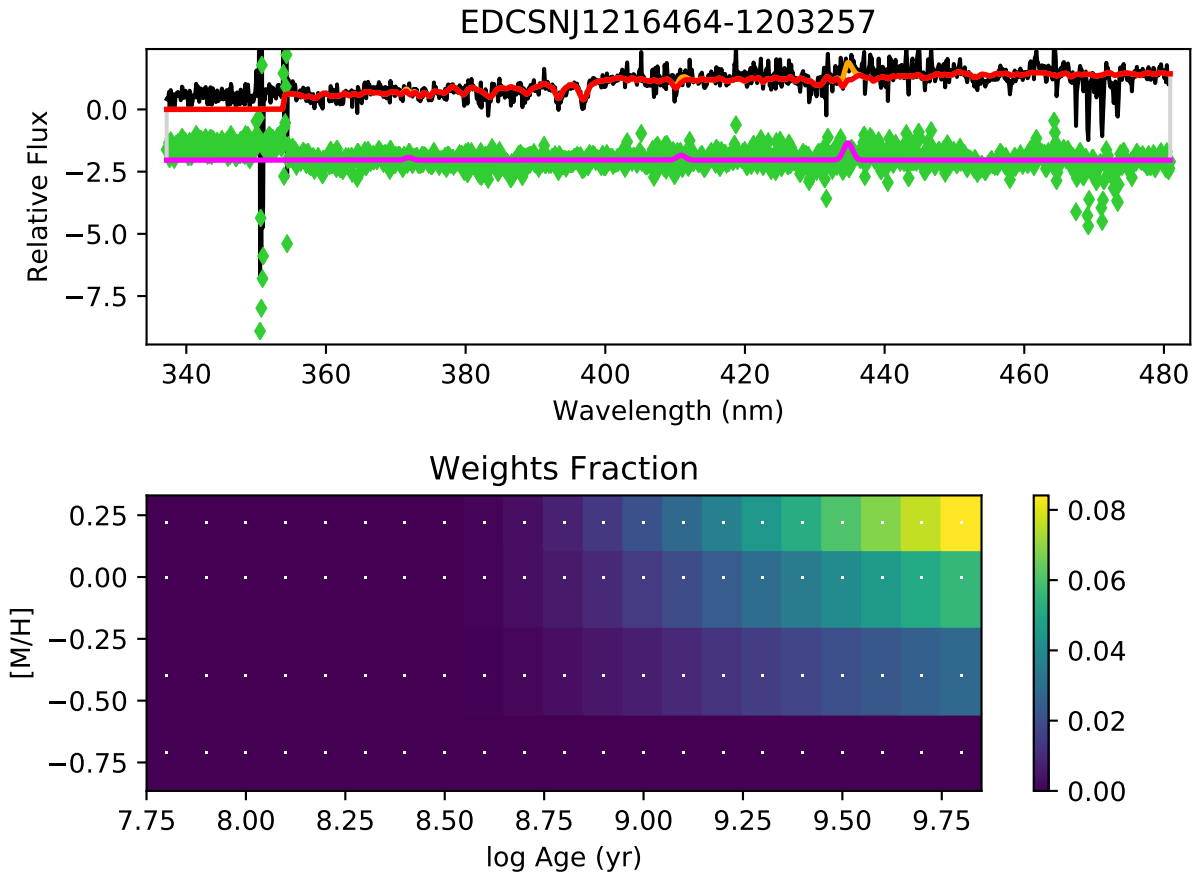
EDCSNJ1216464-1203257
Relative Flux
0.0
−2.5
−5.0
−7.5
340
360
380
400
420
440
460
480
Wavelength (nm)
Weights Fraction
[M/H]
0.25
0.00
−0.25
−0.50
−0.75
7.75
8.00
8.25
8.50
8.75
9.00
9.25
9.50
9.75
log Age (yr)
0.08
0.06
0.04
0.02
0.00

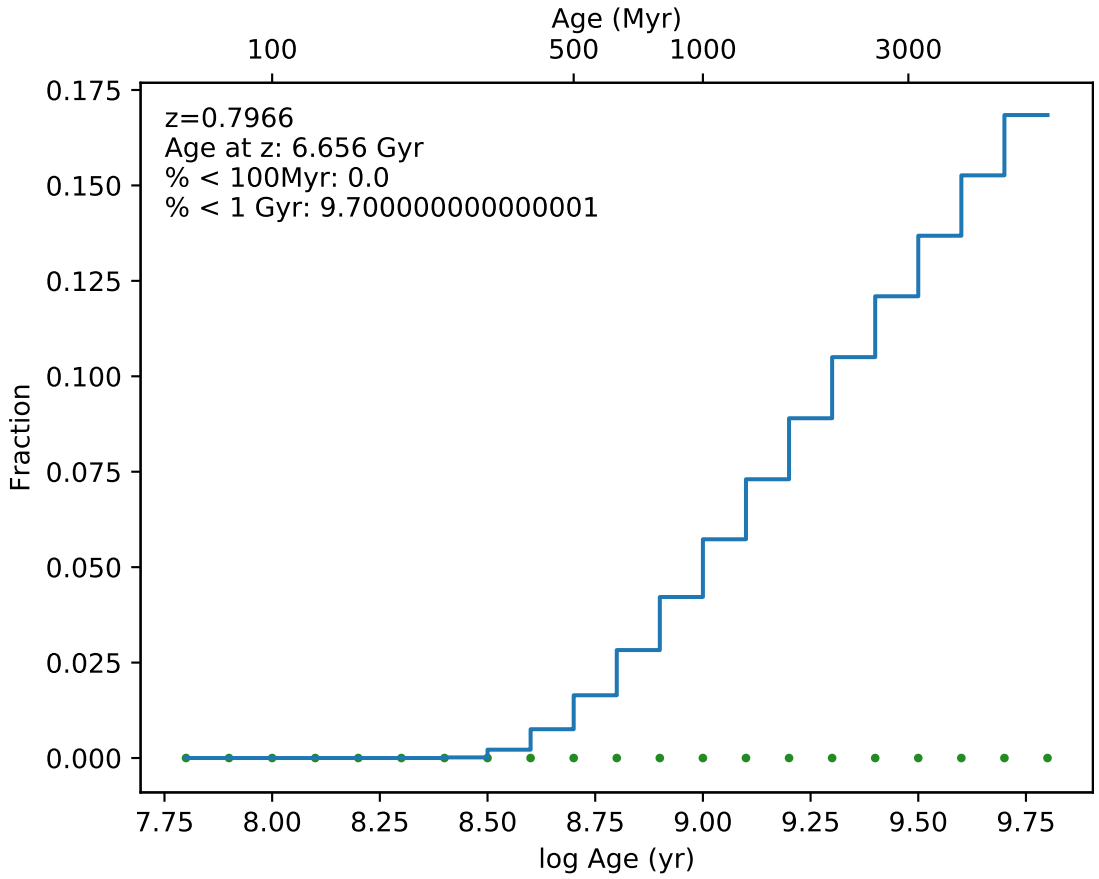
Age (Myr)
100
500
1000
3000
z=0.7966
Age at z: 6.656 Gyr
% < 100Myr: 0.0
% < 1 Gyr: 9.700000000000001
Fraction
0.175
0.150
0.125
0.100
0.075
0.050
0.025
0.000
7.75
8.00
8.25
8.50
8.75
9.00
9.25
9.50
9.75
log Age (yr)

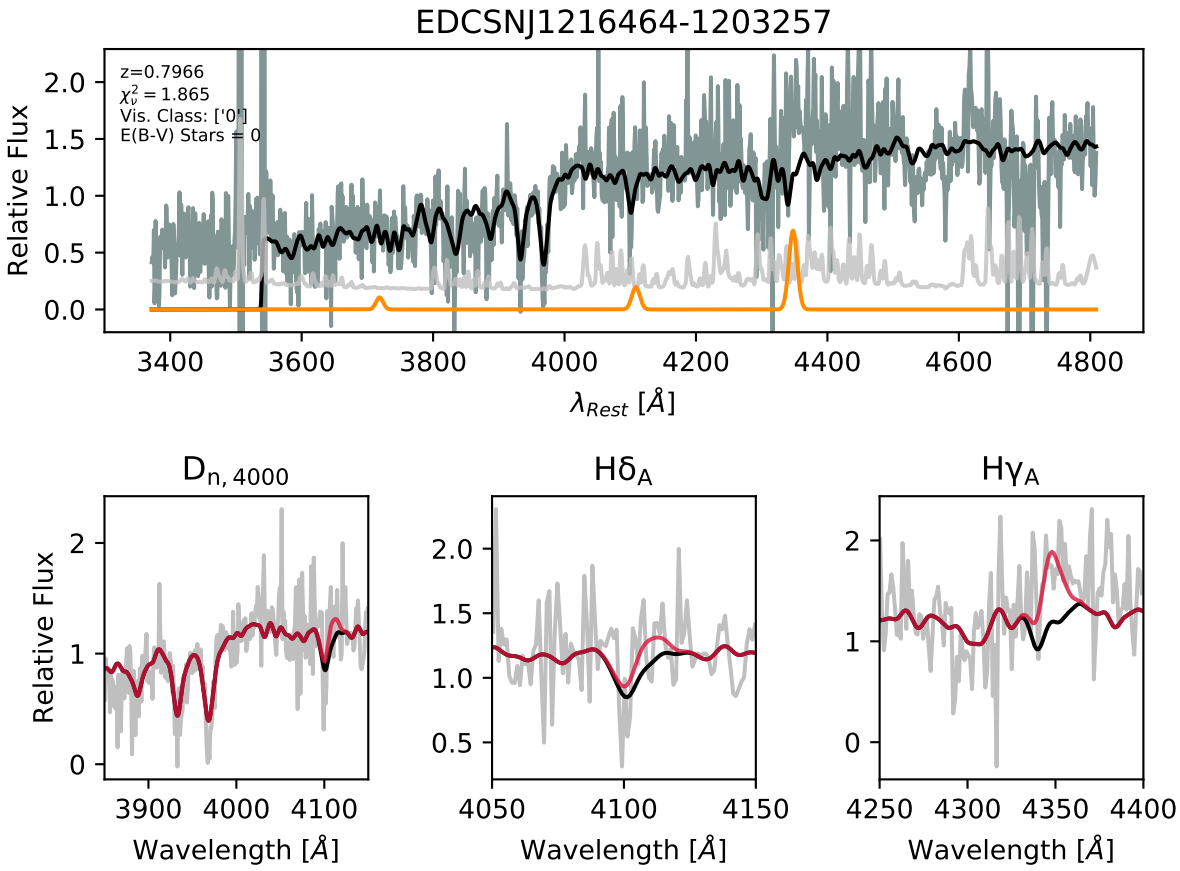
EDCSNJ1216464-1203257
z=0.7966
$\chi^2_\nu = 1.865$
Vis. Class: ['0']
E(B-V) Stars = 0
Relative Flux
λ_{Rest} [Å]
$D_{n,4000}$
$H\delta_A$
$H\gamma_A$
Wavelength [Å]

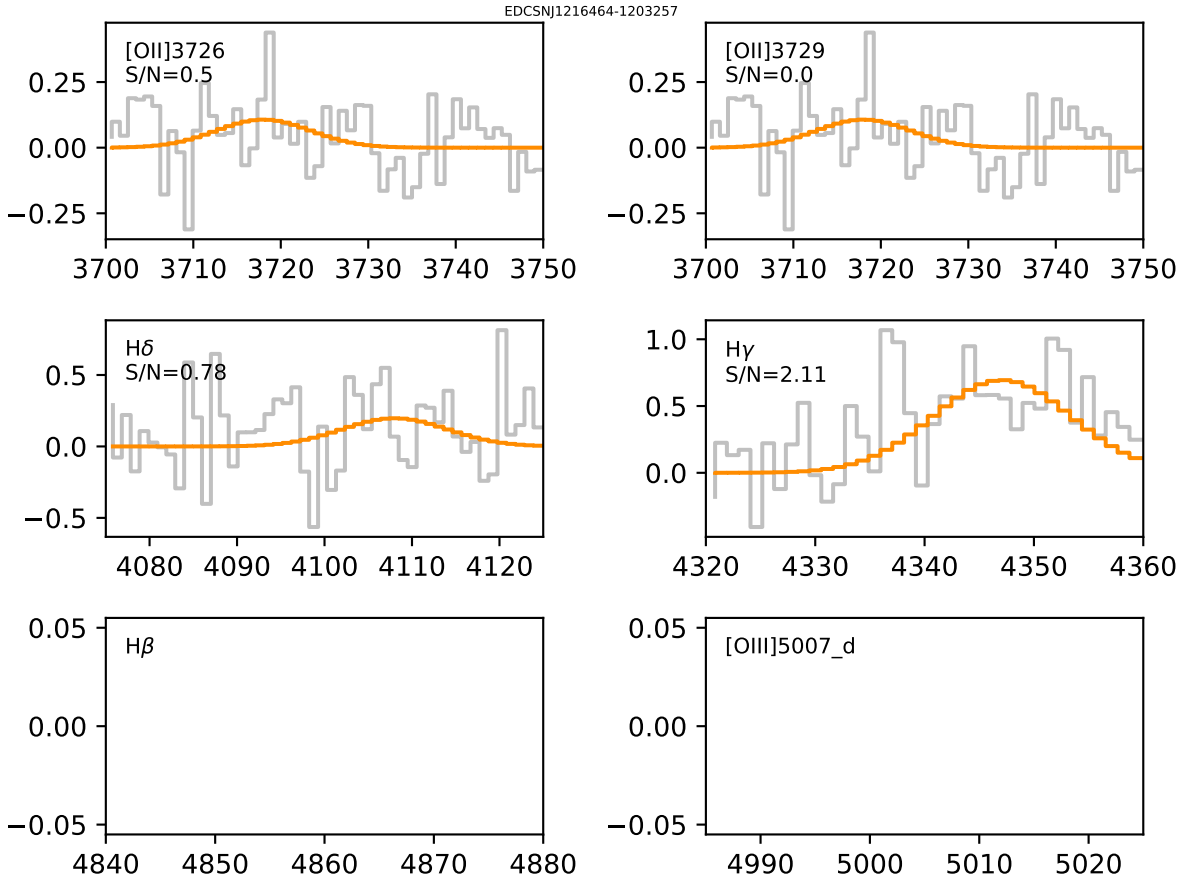
EDCSNJ1216464-1203257
[OII]3726
S/N=0.5
[OII]3729
S/N=0.0
Hδ
S/N=0.78
Hγ
S/N=2.11
Hβ
[OIII]5007_d

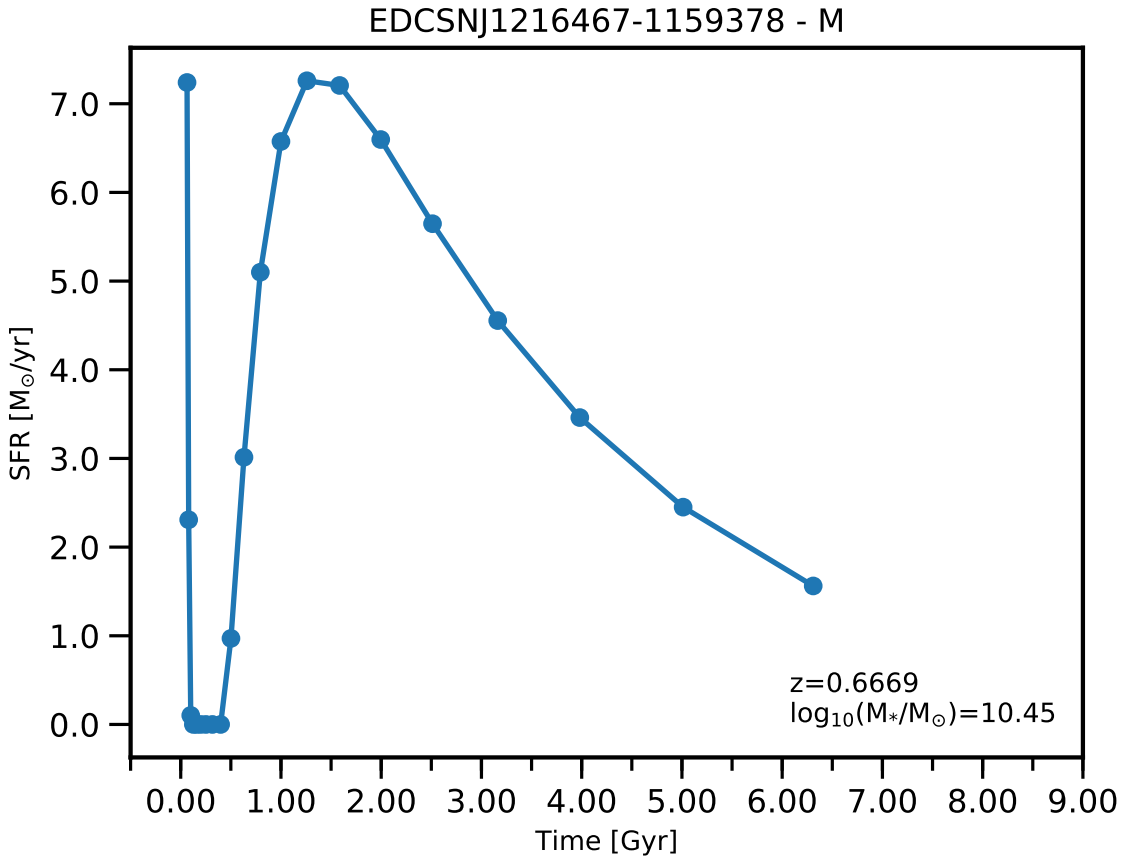
EDCSNJ1216467-1159378 - M
SFR [M⊙/yr]
Time [Gyr]
z=0.6669
log10(M*/M⊙)=10.45
0.0
1.0
2.0
3.0
4.0
5.0
6.0
7.0
0.00
1.00
2.00
3.00
4.00
5.00
6.00
7.00
8.00
9.00

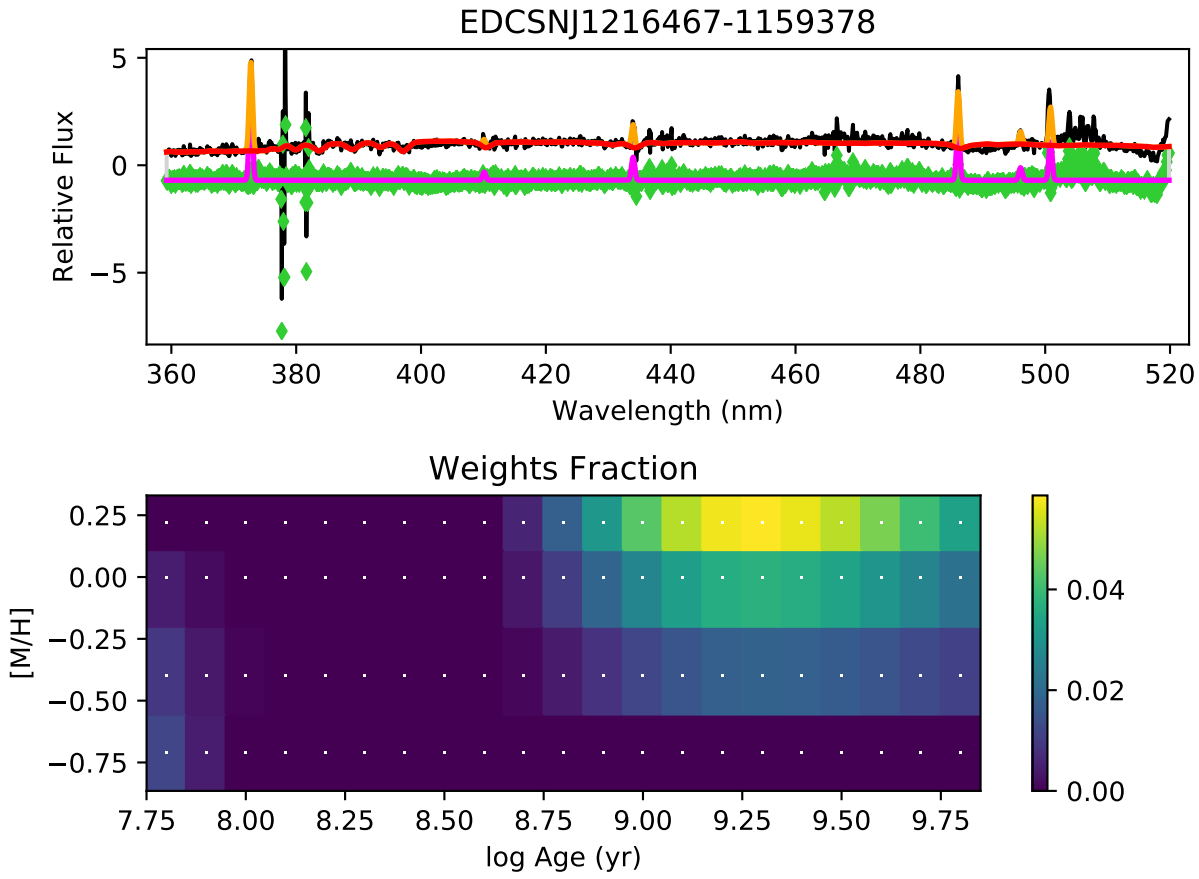
EDCSNJ1216467-1159378
Relative Flux
5
0
−5
360
380
400
420
440
460
480
500
520
Wavelength (nm)
Weights Fraction
[M/H]
0.25
0.00
−0.25
−0.50
−0.75
7.75
8.00
8.25
8.50
8.75
9.00
9.25
9.50
9.75
log Age (yr)
0.04
0.02
0.00

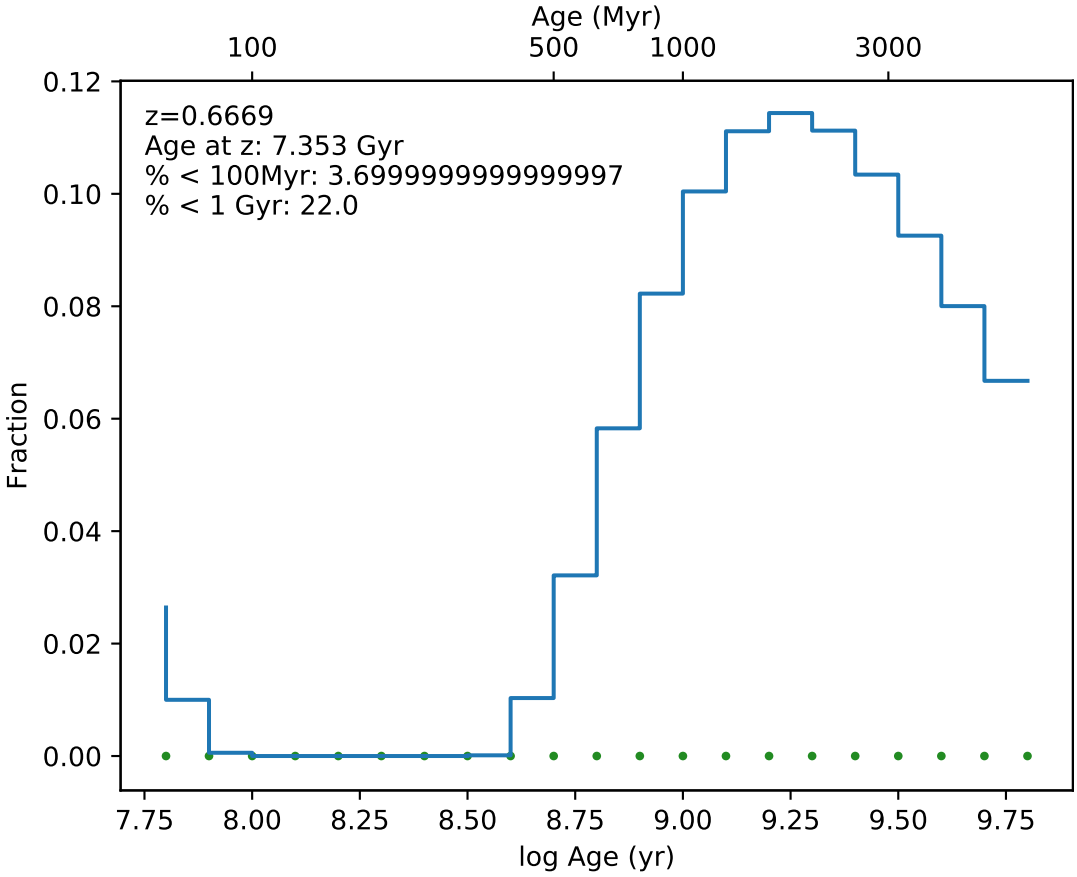
Age (Myr)
100
500
1000
3000
z=0.6669
Age at z: 7.353 Gyr
% < 100Myr: 3.6999999999999997
% < 1 Gyr: 22.0
Fraction
0.12
0.10
0.08
0.06
0.04
0.02
0.00
7.75
8.00
8.25
8.50
8.75
9.00
9.25
9.50
9.75
log Age (yr)

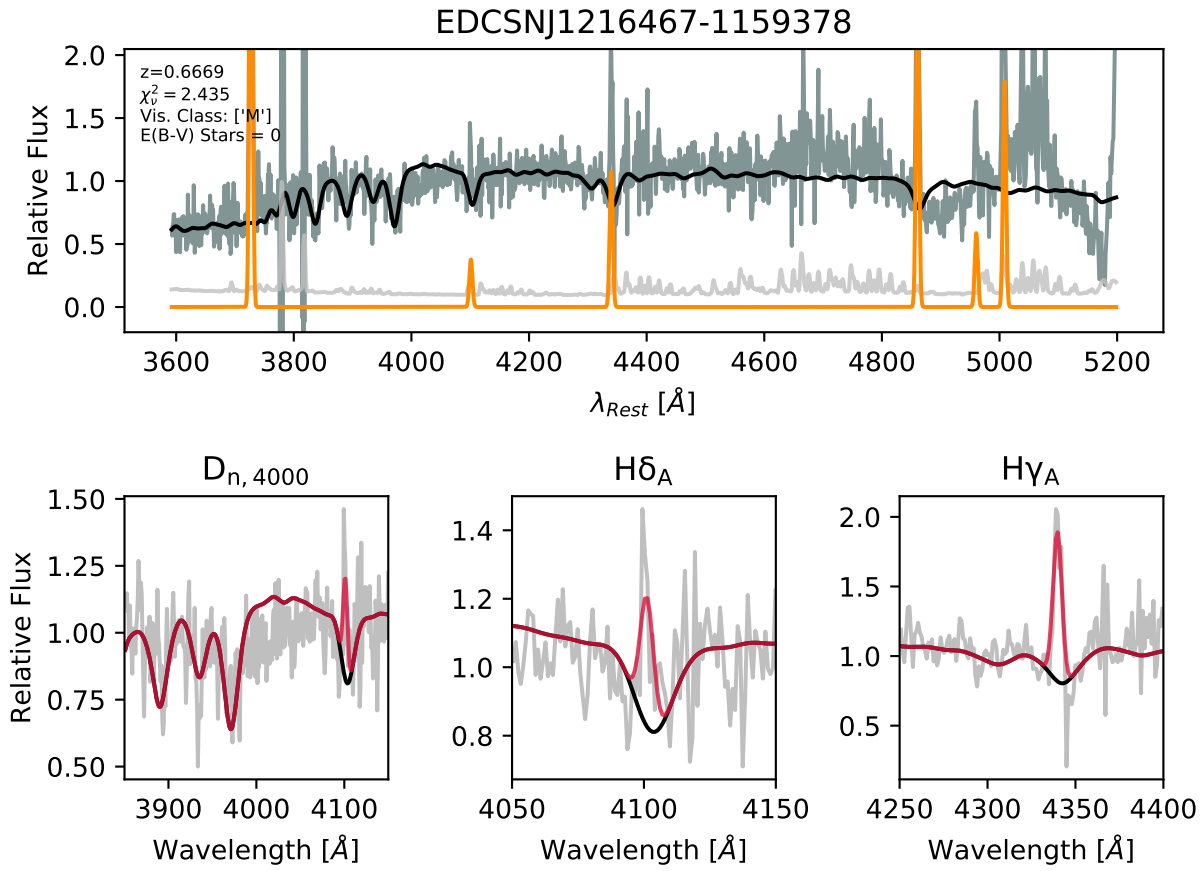
EDCSNJ1216467-1159378
z=0.6669
$\chi^2_\nu = 2.435$
Vis. Class: ['M']
E(B-V) Stars = 0
Relative Flux
λ_{Rest} [Å]
$D_{n,4000}$
$H\delta_A$
$H\gamma_A$
Wavelength [Å]

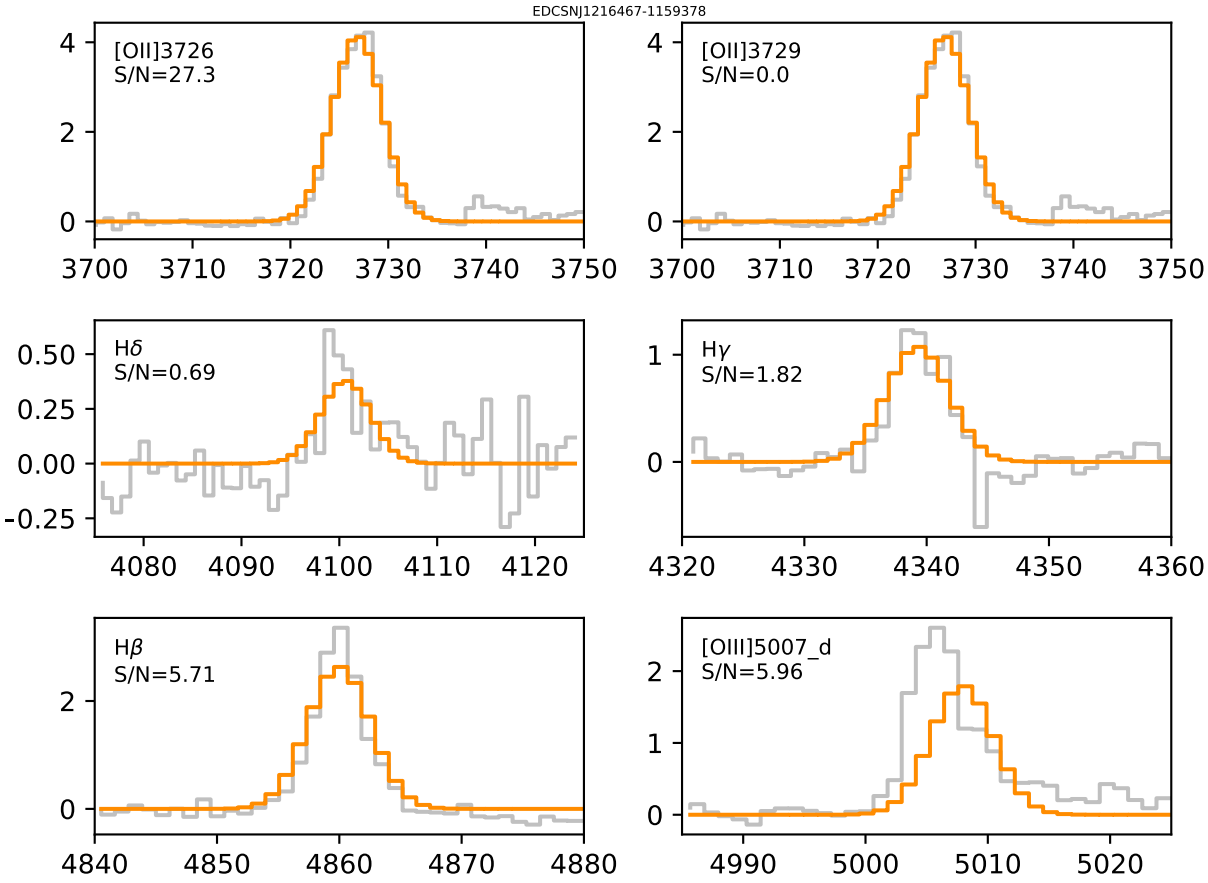
EDCSNJ1216467-1159378
[OII]3726
S/N=27.3
[OII]3729
S/N=0.0
Hδ
S/N=0.69
Hγ
S/N=1.82
Hβ
S/N=5.71
[OIII]5007_d
S/N=5.96

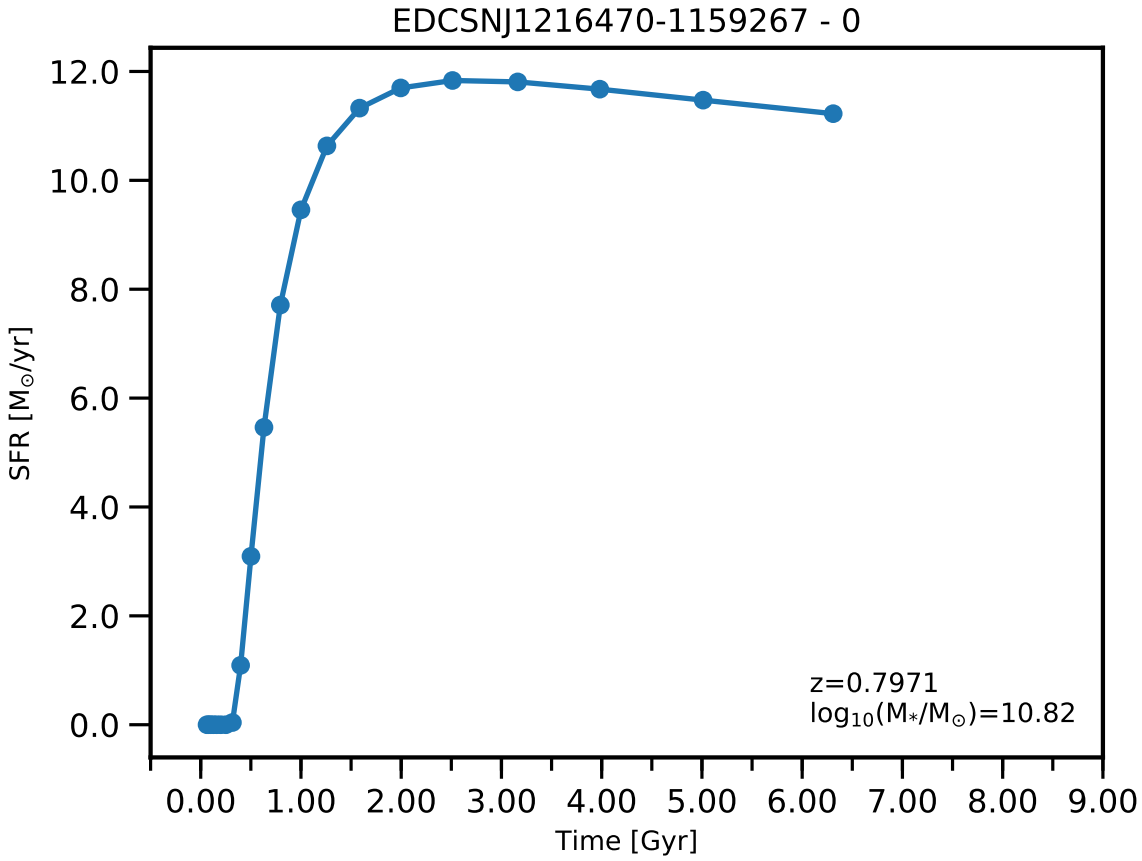
EDCSNJ1216470-1159267 - 0
SFR [M⊙/yr]
Time [Gyr]
z=0.7971
log10(M*/M⊙)=10.82
0.0
2.0
4.0
6.0
8.0
10.0
12.0
0.00
1.00
2.00
3.00
4.00
5.00
6.00
7.00
8.00
9.00

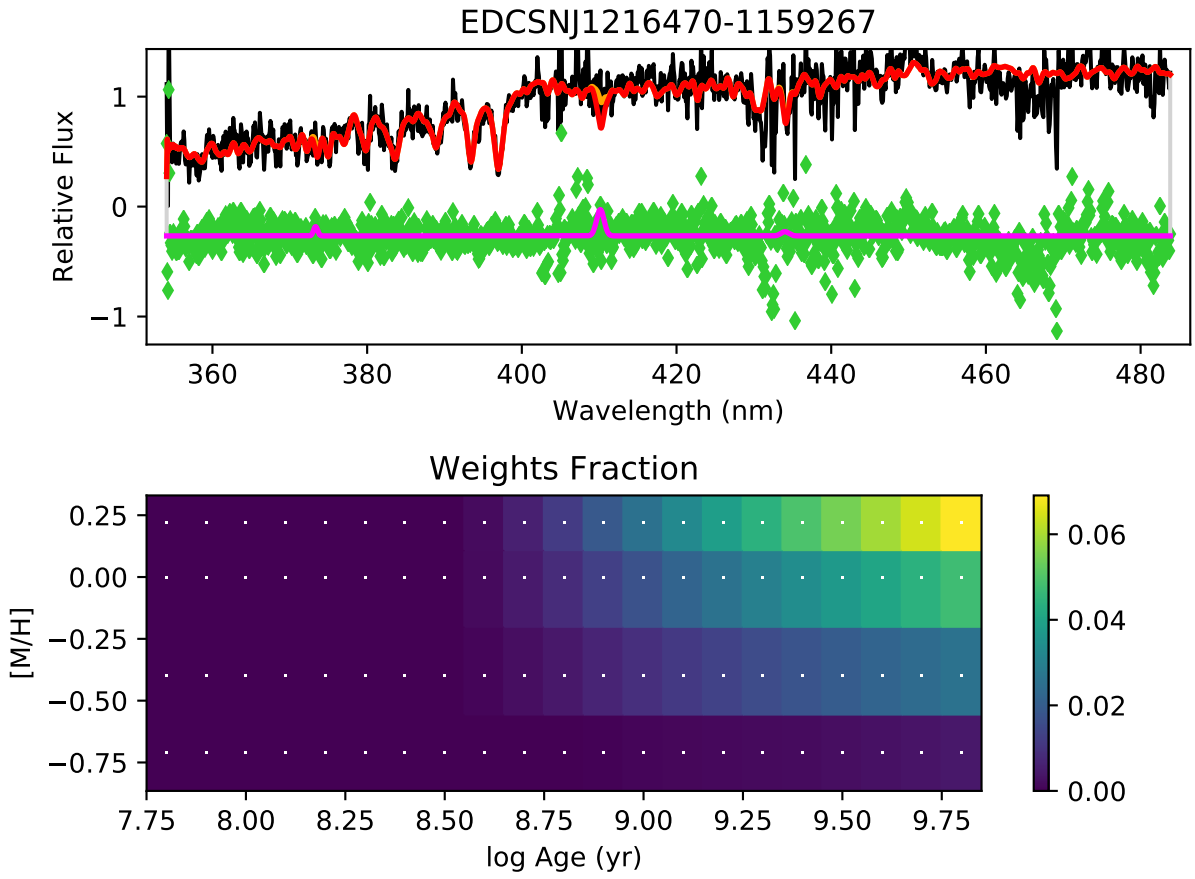
EDCSNJ1216470-1159267
Relative Flux
1
0
−1
360
380
400
420
440
460
480
Wavelength (nm)
Weights Fraction
[M/H]
0.25
0.00
−0.25
−0.50
−0.75
7.75
8.00
8.25
8.50
8.75
9.00
9.25
9.50
9.75
log Age (yr)
0.06
0.04
0.02
0.00

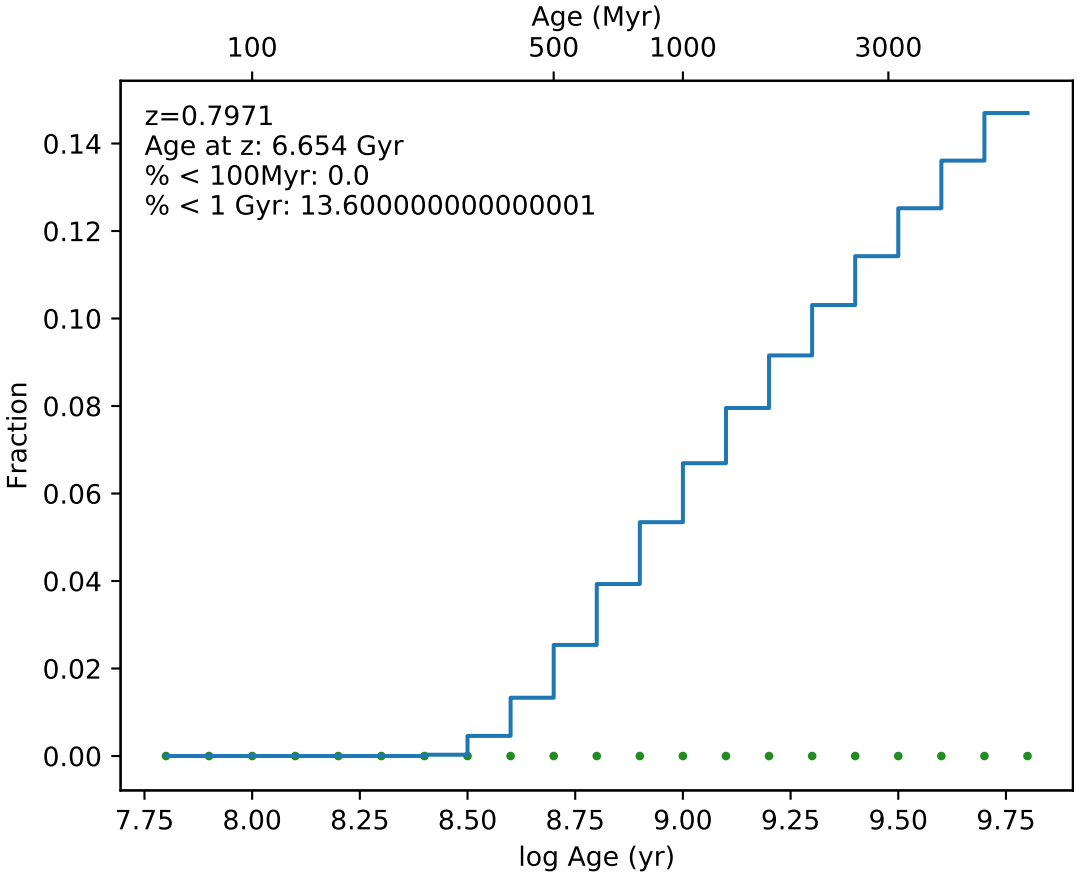
Age (Myr)
100
500
1000
3000
z=0.7971
Age at z: 6.654 Gyr
% < 100Myr: 0.0
% < 1 Gyr: 13.600000000000001
Fraction
0.14
0.12
0.10
0.08
0.06
0.04
0.02
0.00
7.75
8.00
8.25
8.50
8.75
9.00
9.25
9.50
9.75
log Age (yr)

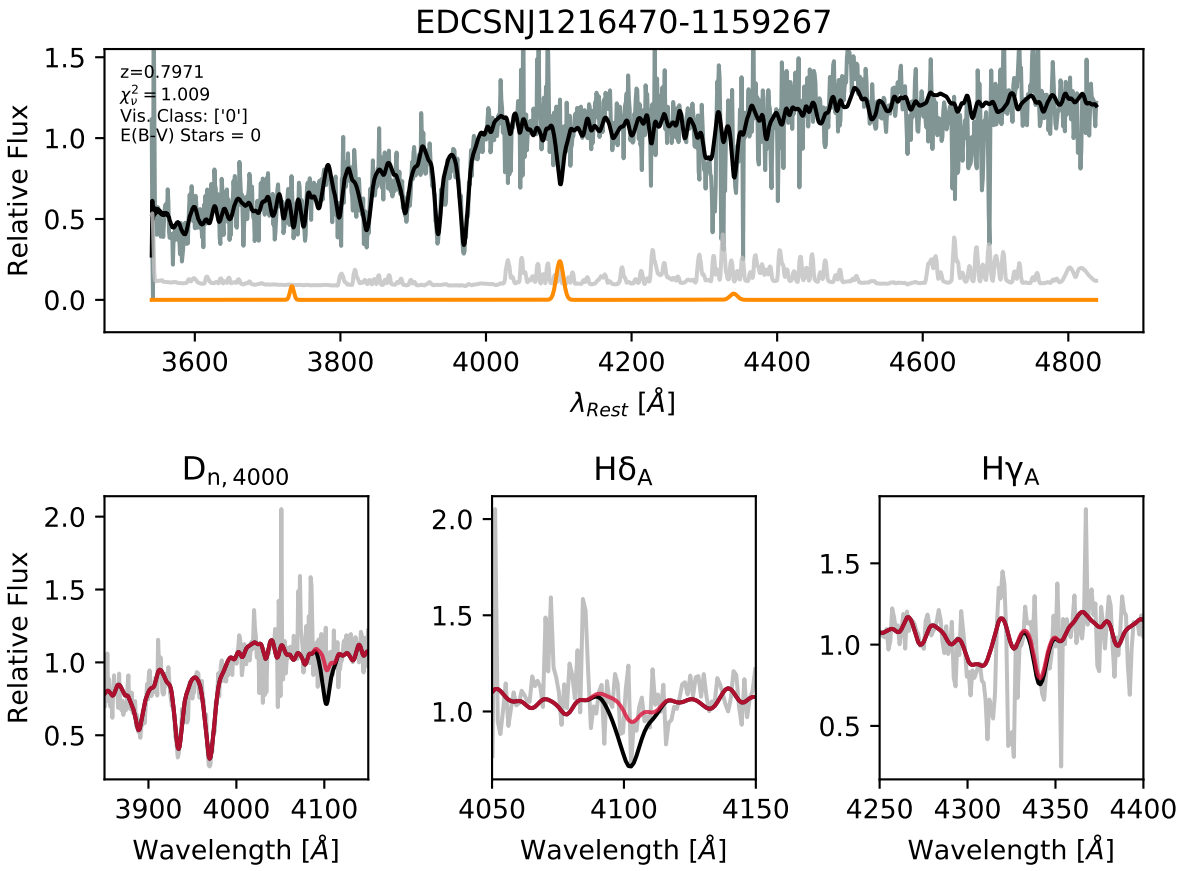
EDCSNJ1216470-1159267
z=0.7971
$\chi^2_\nu = 1.009$
Vis. Class: ['0']
E(B-V) Stars = 0
Relative Flux
λ_{Rest} [Å]
$D_{n,4000}$
$H\delta_A$
$H\gamma_A$
Wavelength [Å]

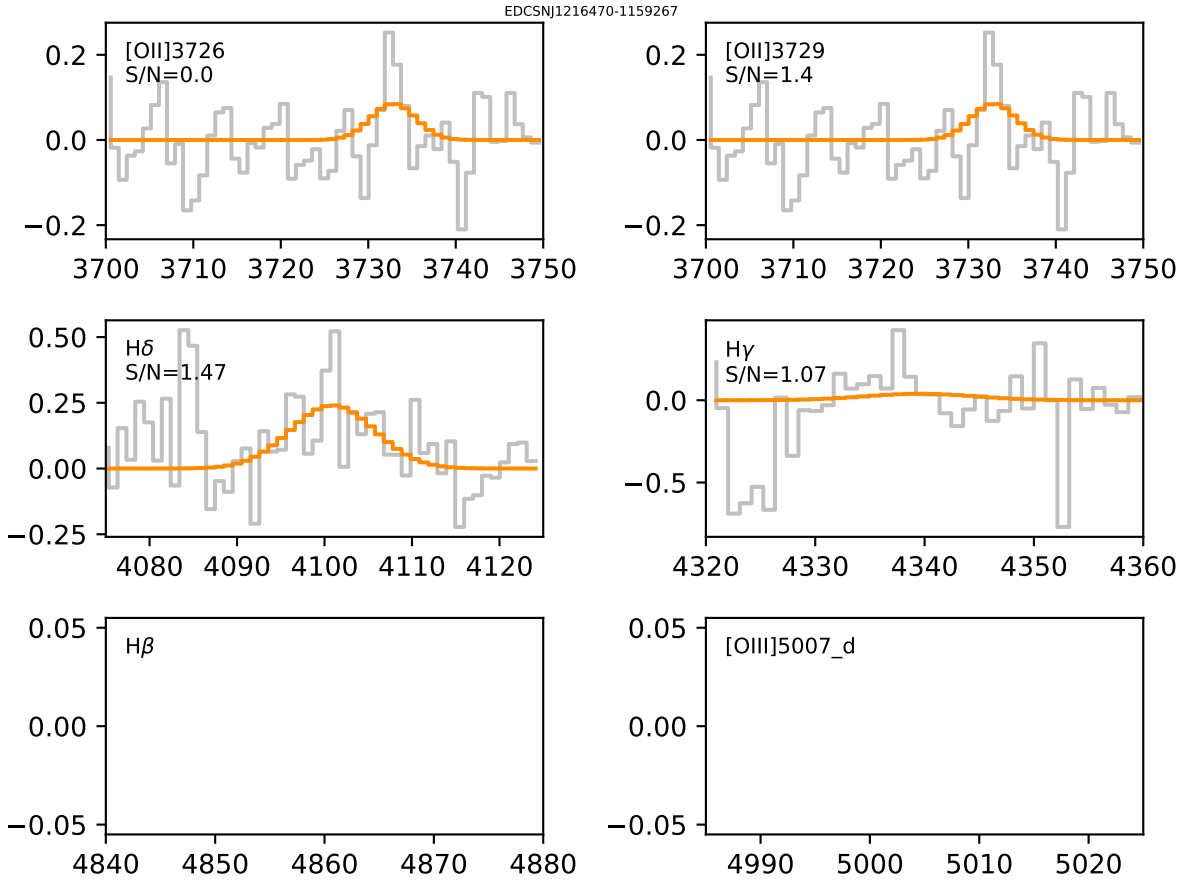
EDCSNJ1216470-1159267
[OII]3726
S/N=0.0
[OII]3729
S/N=1.4
Hδ
S/N=1.47
Hγ
S/N=1.07
Hβ
[OIII]5007_d

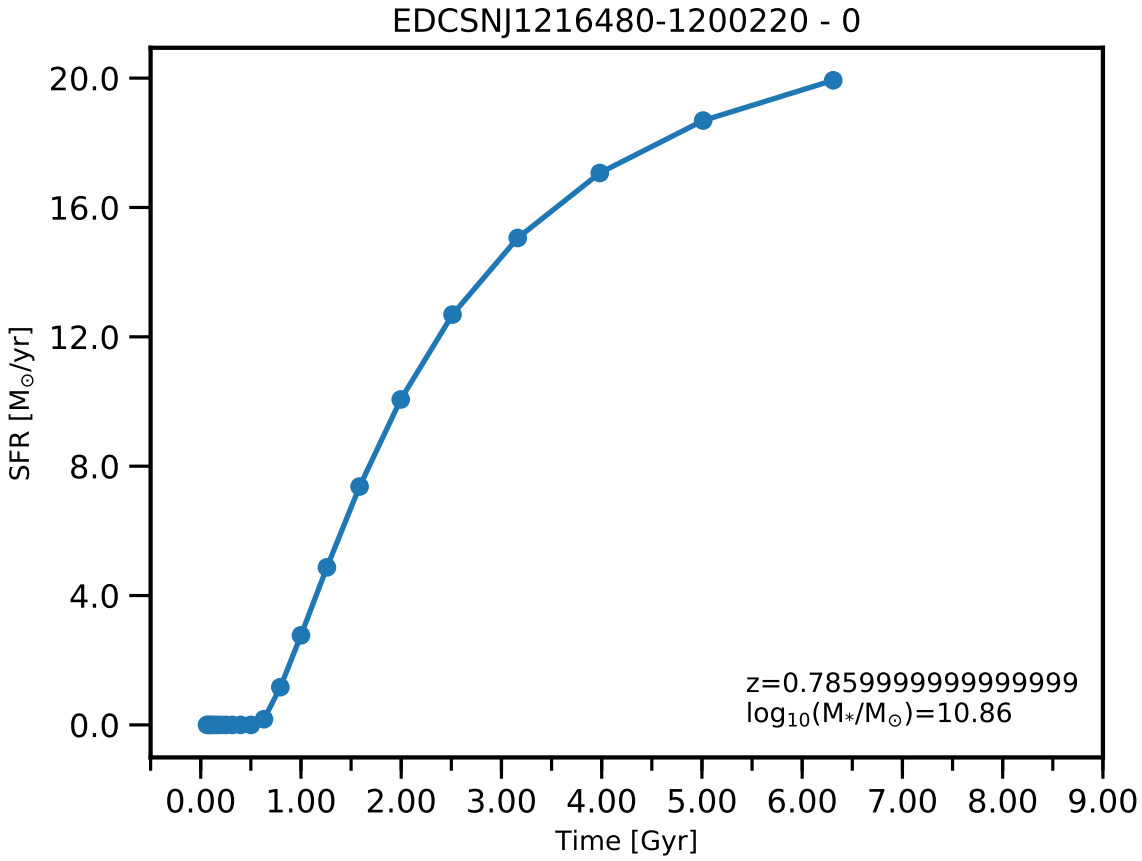
EDCSNJ1216480-1200220 - 0
SFR [M⊙/yr]
20.0
16.0
12.0
8.0
4.0
0.0
0.00
1.00
2.00
3.00
4.00
5.00
6.00
7.00
8.00
9.00
Time [Gyr]
z=0.7859999999999999
log10(M*/M⊙)=10.86

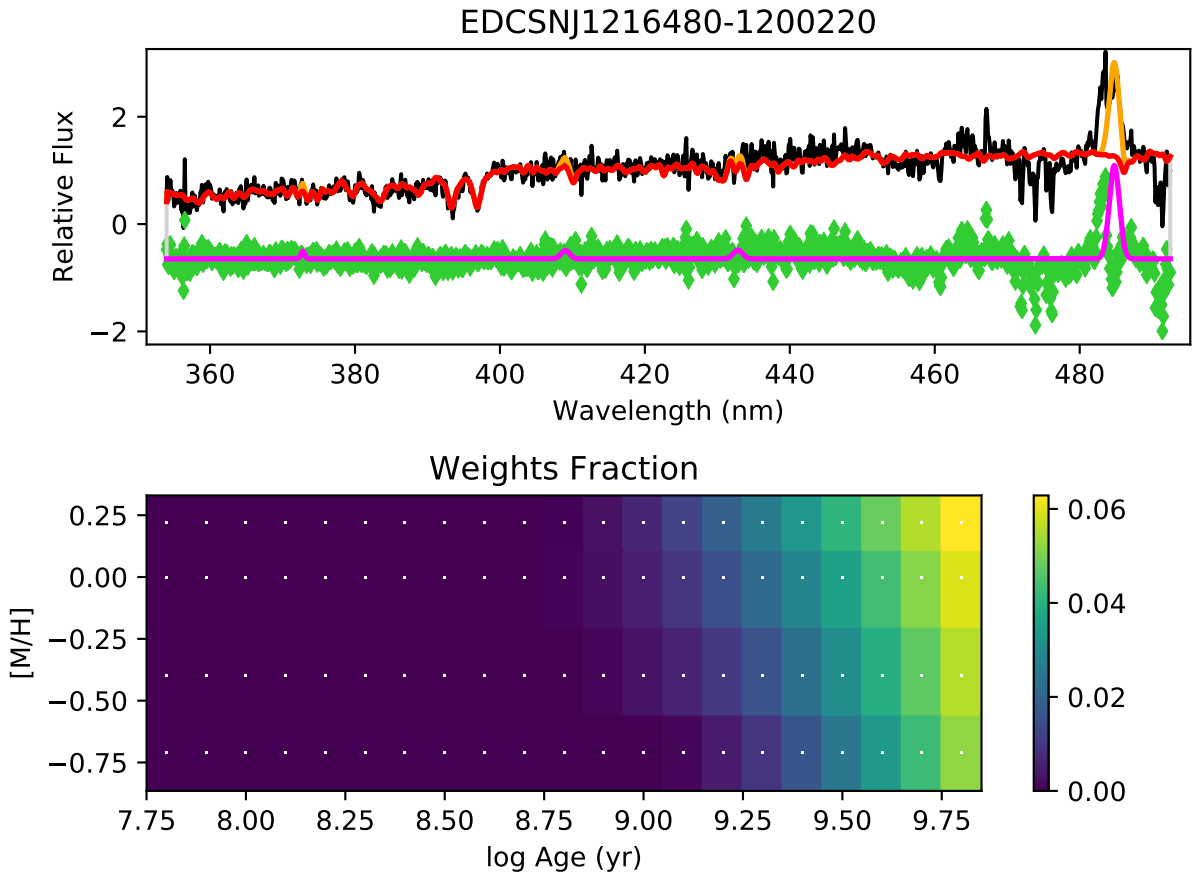
EDCSNJ1216480-1200220
Relative Flux
2
0
−2
360
380
400
420
440
460
480
Wavelength (nm)
Weights Fraction
[M/H]
0.25
0.00
−0.25
−0.50
−0.75
7.75
8.00
8.25
8.50
8.75
9.00
9.25
9.50
9.75
log Age (yr)
0.06
0.04
0.02
0.00

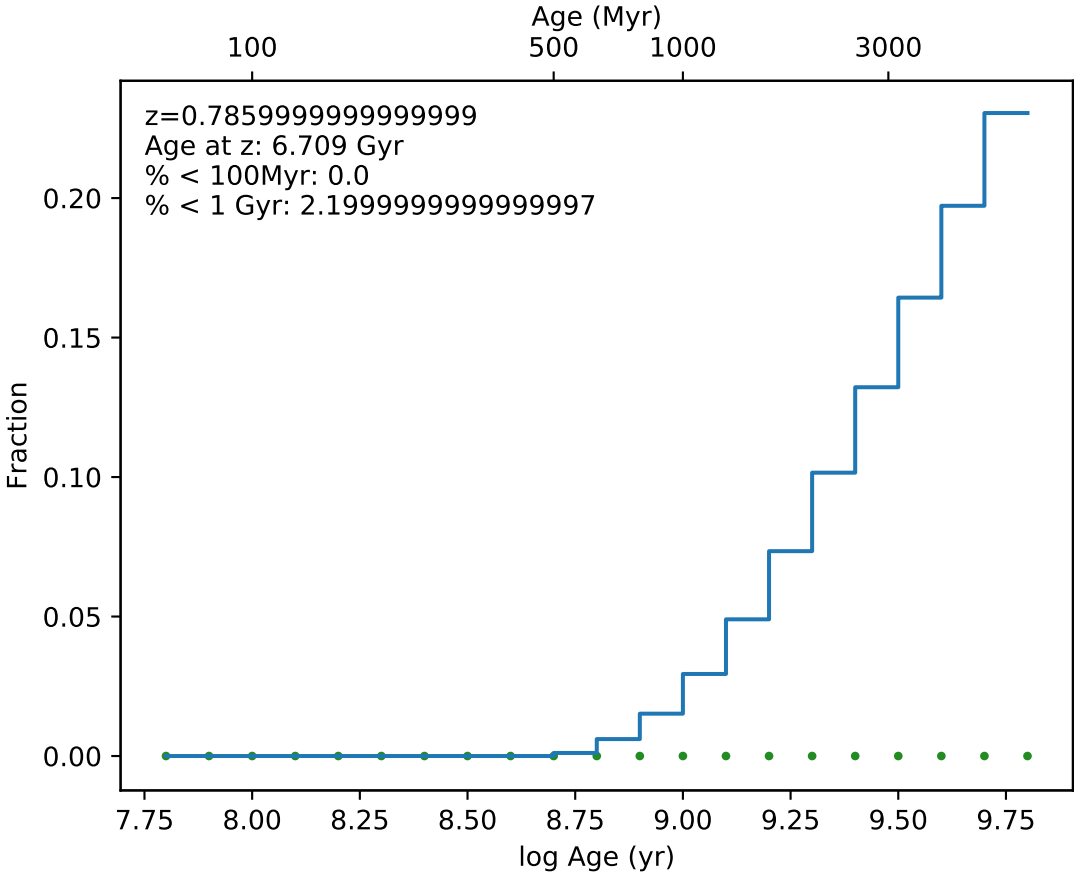
Age (Myr)
100
500
1000
3000
z=0.7859999999999999
Age at z: 6.709 Gyr
% < 100Myr: 0.0
% < 1 Gyr: 2.1999999999999997
Fraction
0.00
0.05
0.10
0.15
0.20
7.75
8.00
8.25
8.50
8.75
9.00
9.25
9.50
9.75
log Age (yr)

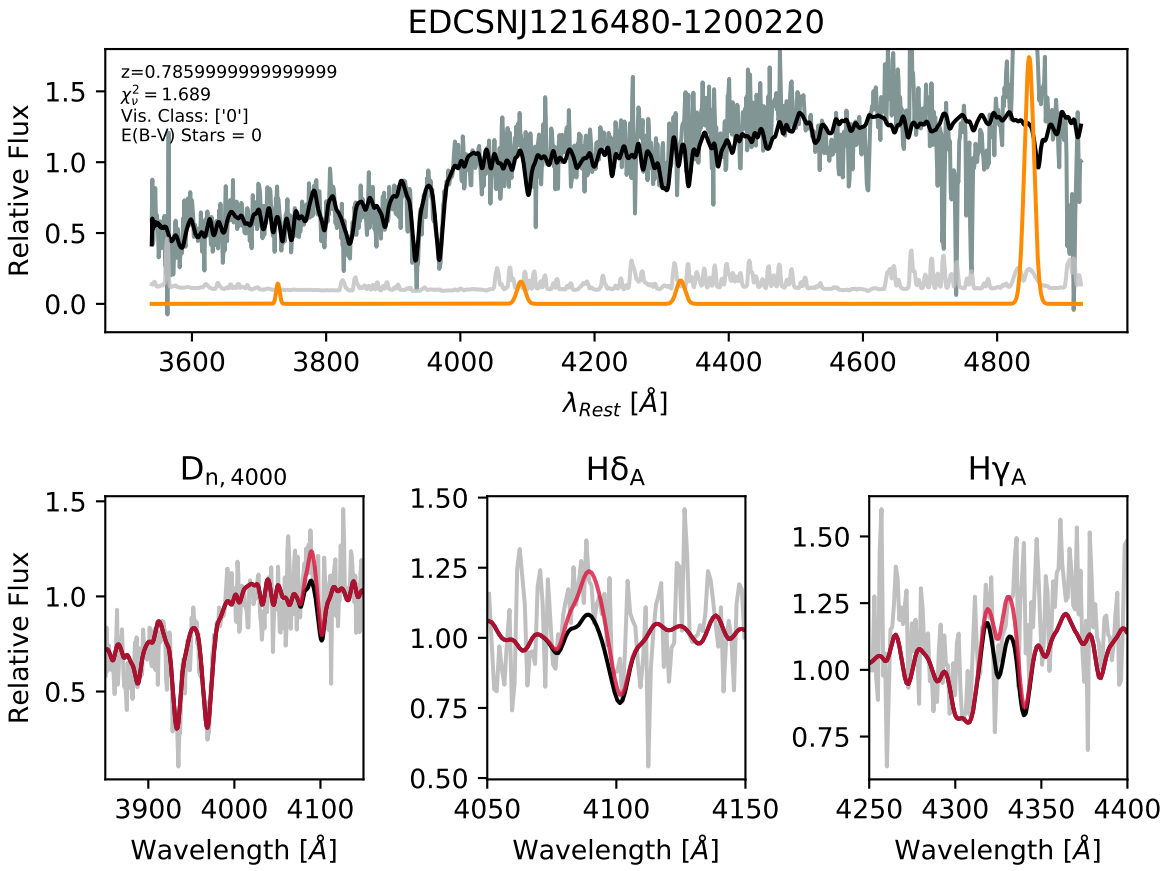
EDCSNJ1216480-1200220
z=0.7859999999999999
$\chi^2_\nu = 1.689$
Vis. Class: ['0']
E(B-V) Stars = 0
Relative Flux
λ_{Rest} [Å]
$D_{n,4000}$
$H\delta_A$
$H\gamma_A$
Wavelength [Å]

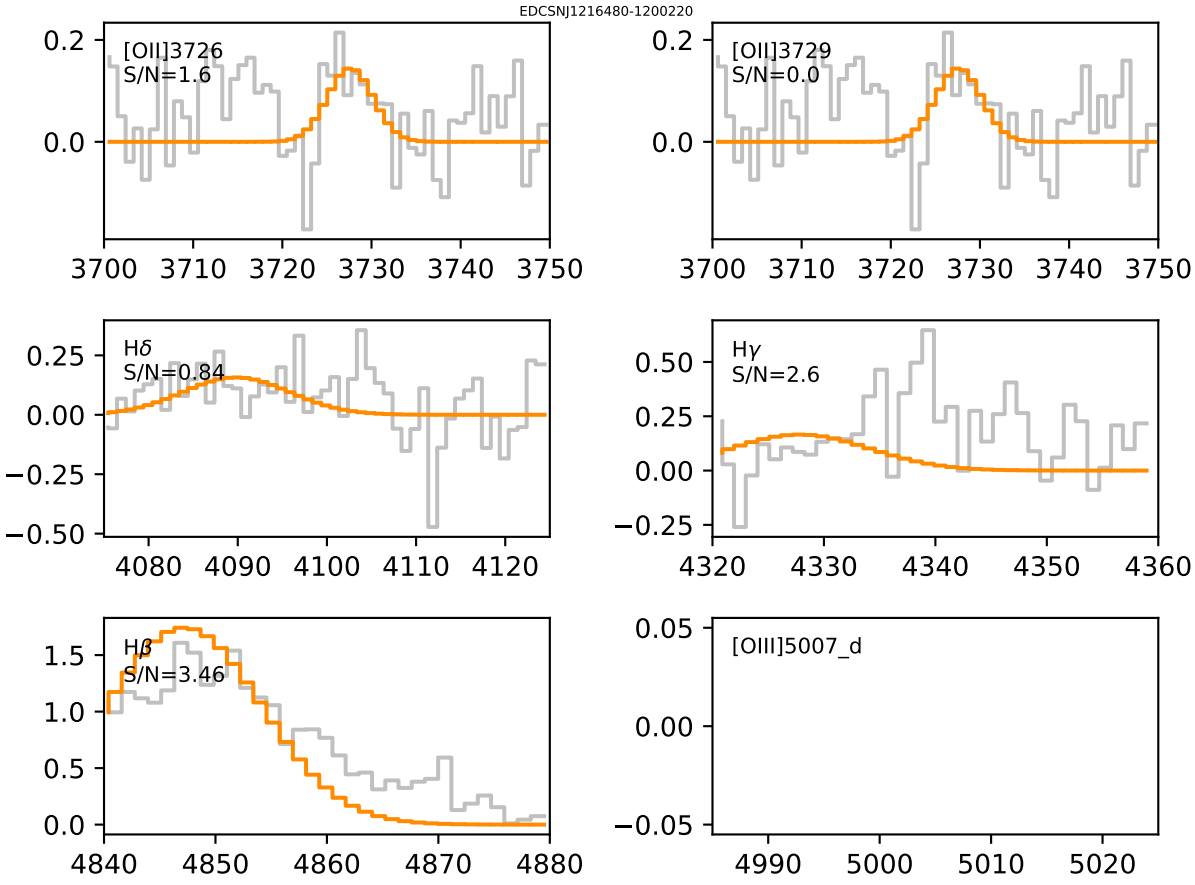
EDCSNJ1216480-1200220
[OII]3726
S/N=1.6
[OII]3729
S/N=0.0
Hδ
S/N=0.84
Hγ
S/N=2.6
Hβ
S/N=3.46
[OIII]5007_d

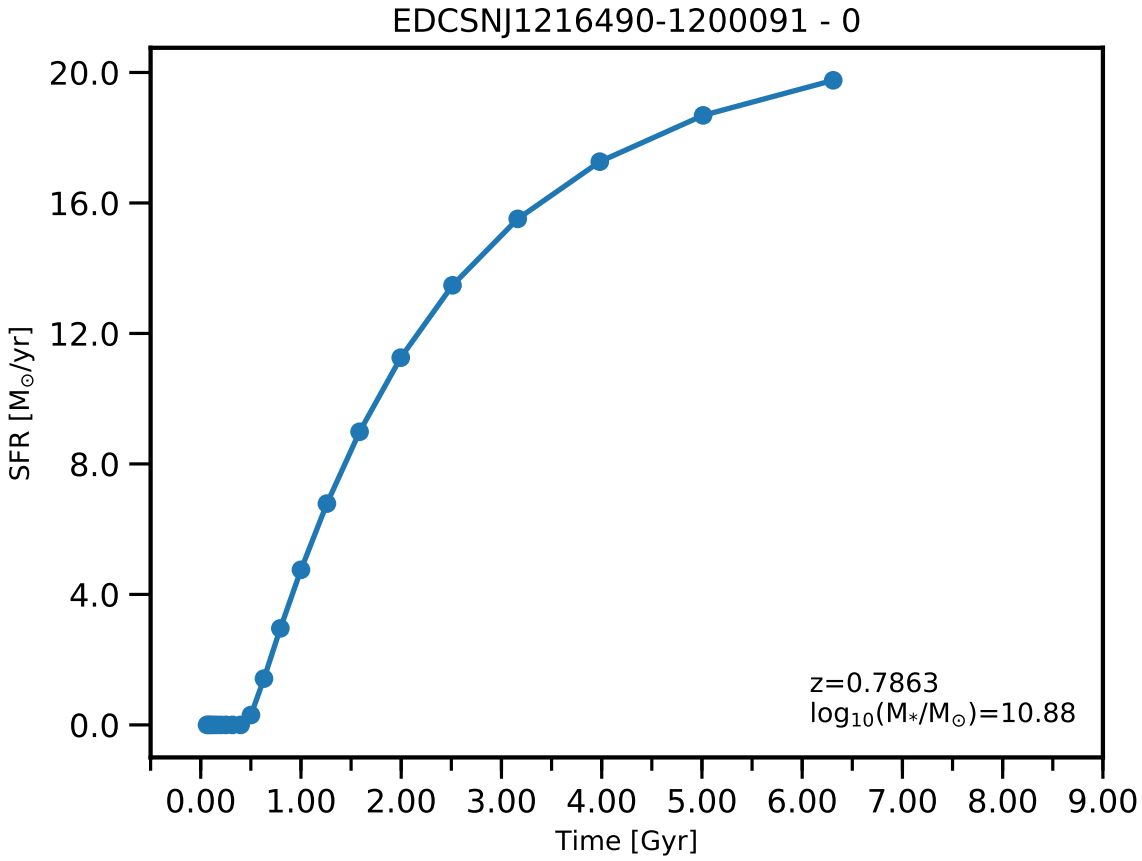
EDCSNJ1216490-1200091 - 0
20.0
16.0
12.0
8.0
4.0
0.0
SFR [M⊙/yr]
0.00
1.00
2.00
3.00
4.00
5.00
6.00
7.00
8.00
9.00
Time [Gyr]
z=0.7863
log10(M*/M⊙)=10.88

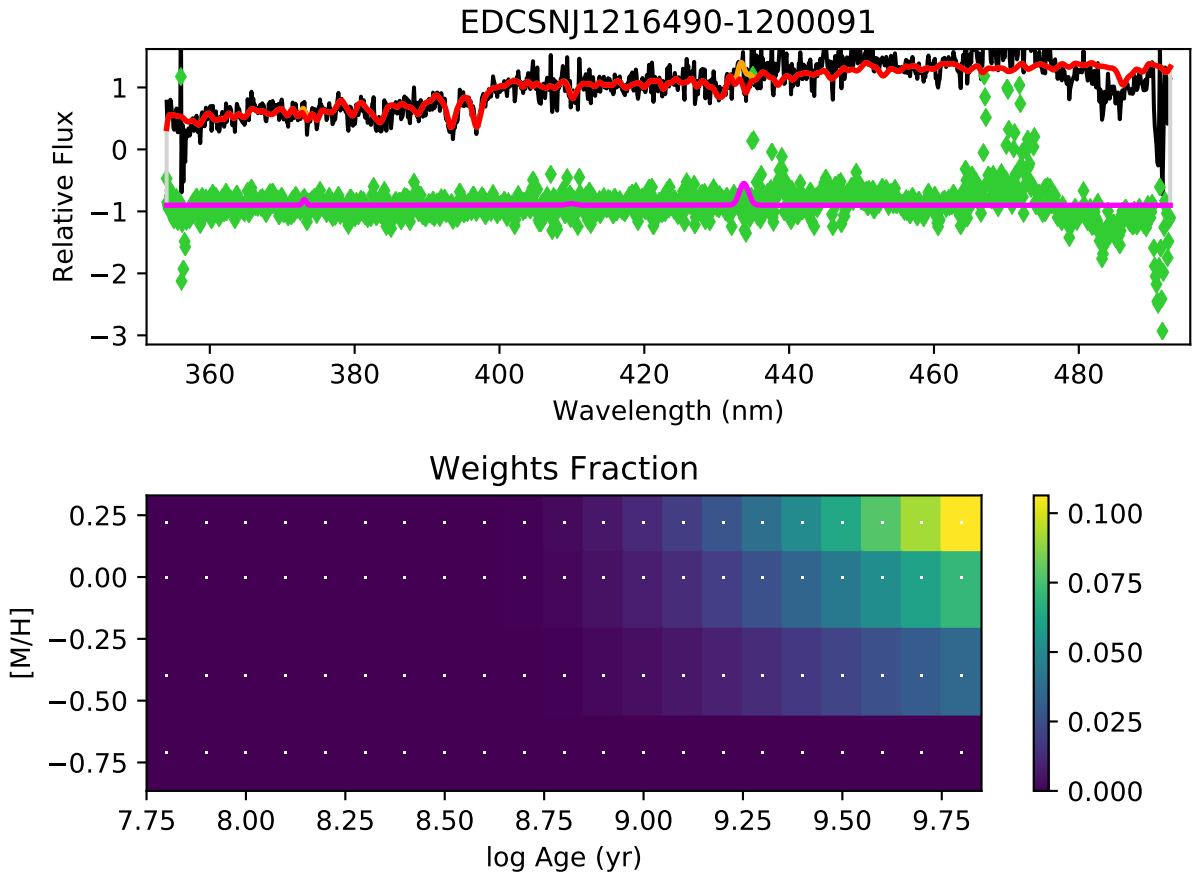
EDCSNJ1216490-1200091
Relative Flux
1
0
−1
−2
−3
360
380
400
420
440
460
480
Wavelength (nm)
Weights Fraction
[M/H]
0.25
0.00
−0.25
−0.50
−0.75
7.75
8.00
8.25
8.50
8.75
9.00
9.25
9.50
9.75
log Age (yr)
0.100
0.075
0.050
0.025
0.000

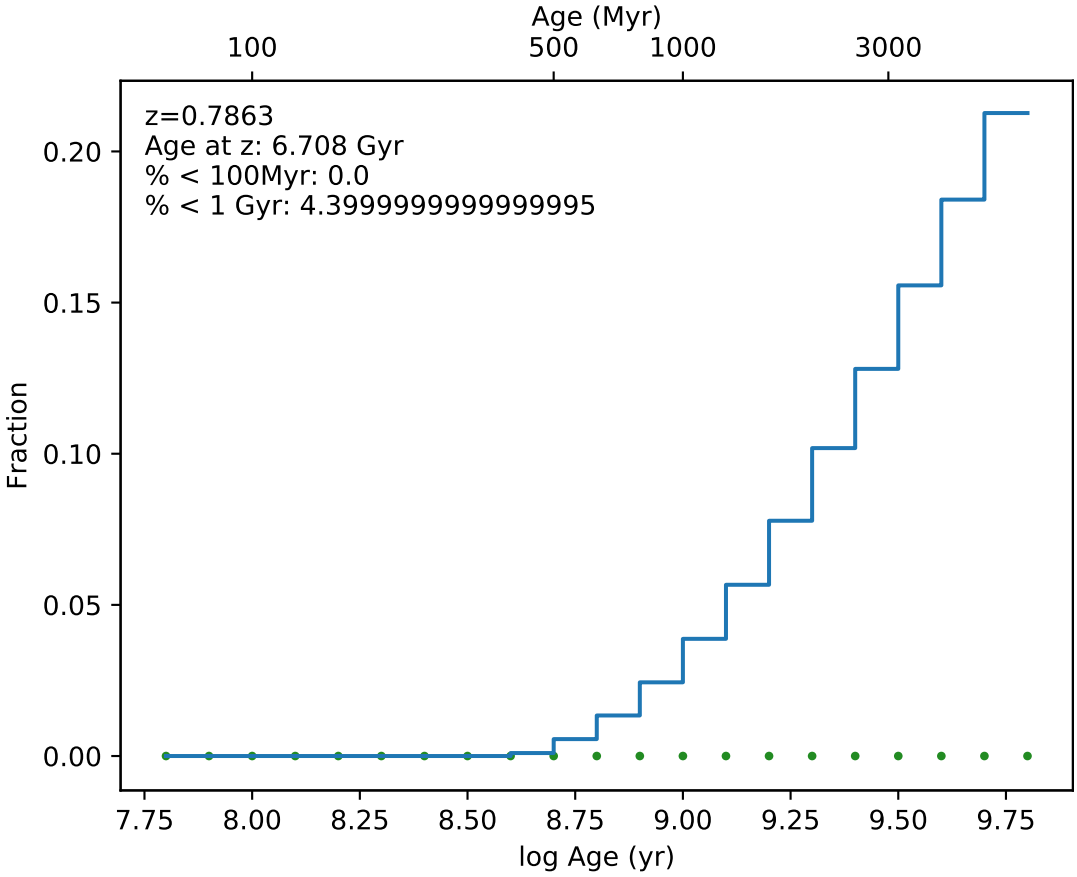
Age (Myr)
100
500
1000
3000
z=0.7863
Age at z: 6.708 Gyr
% < 100Myr: 0.0
% < 1 Gyr: 4.3999999999999995
Fraction
0.20
0.15
0.10
0.05
0.00
7.75
8.00
8.25
8.50
8.75
9.00
9.25
9.50
9.75
log Age (yr)

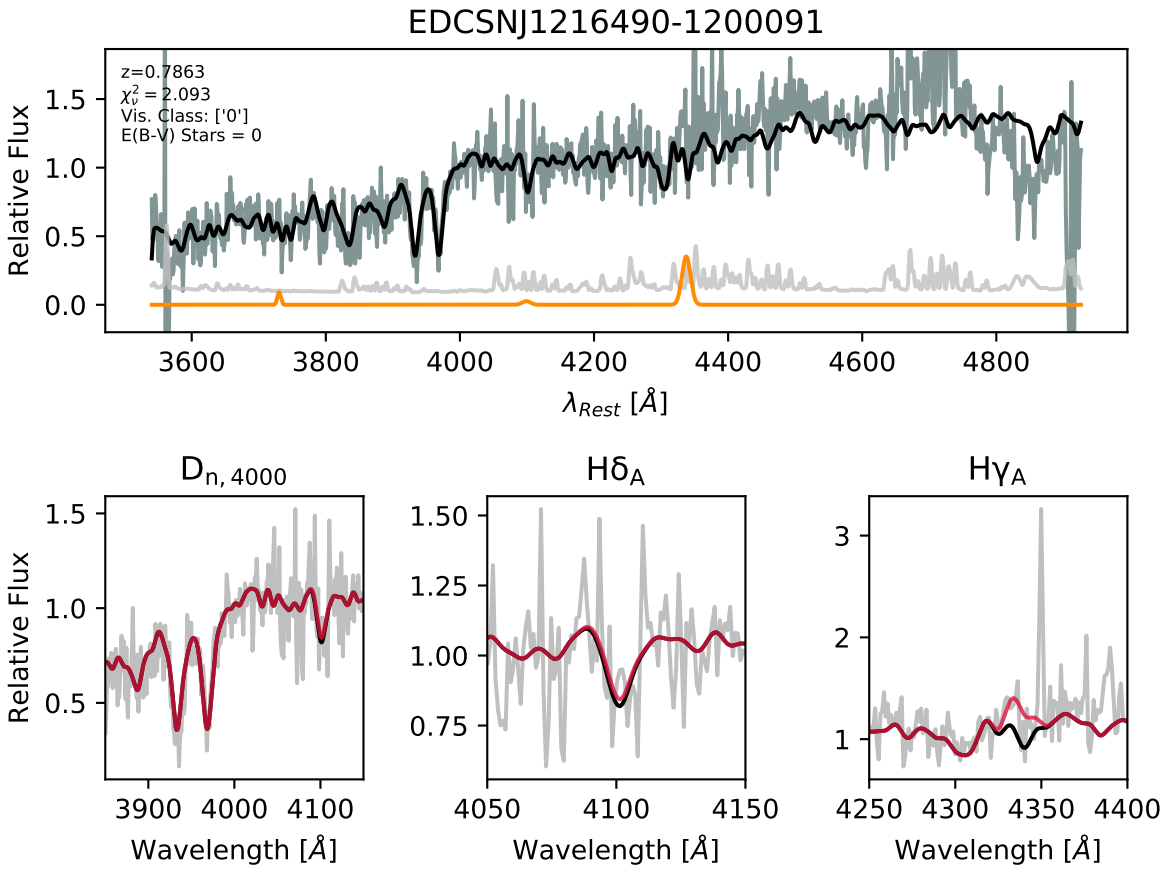
EDCSNJ1216490-1200091
z=0.7863
$\chi^2_\nu = 2.093$
Vis. Class: ['0']
E(B-V) Stars = 0
Relative Flux
λ_{Rest} [Å]
$D_{n,4000}$
$H\delta_A$
$H\gamma_A$
Wavelength [Å]

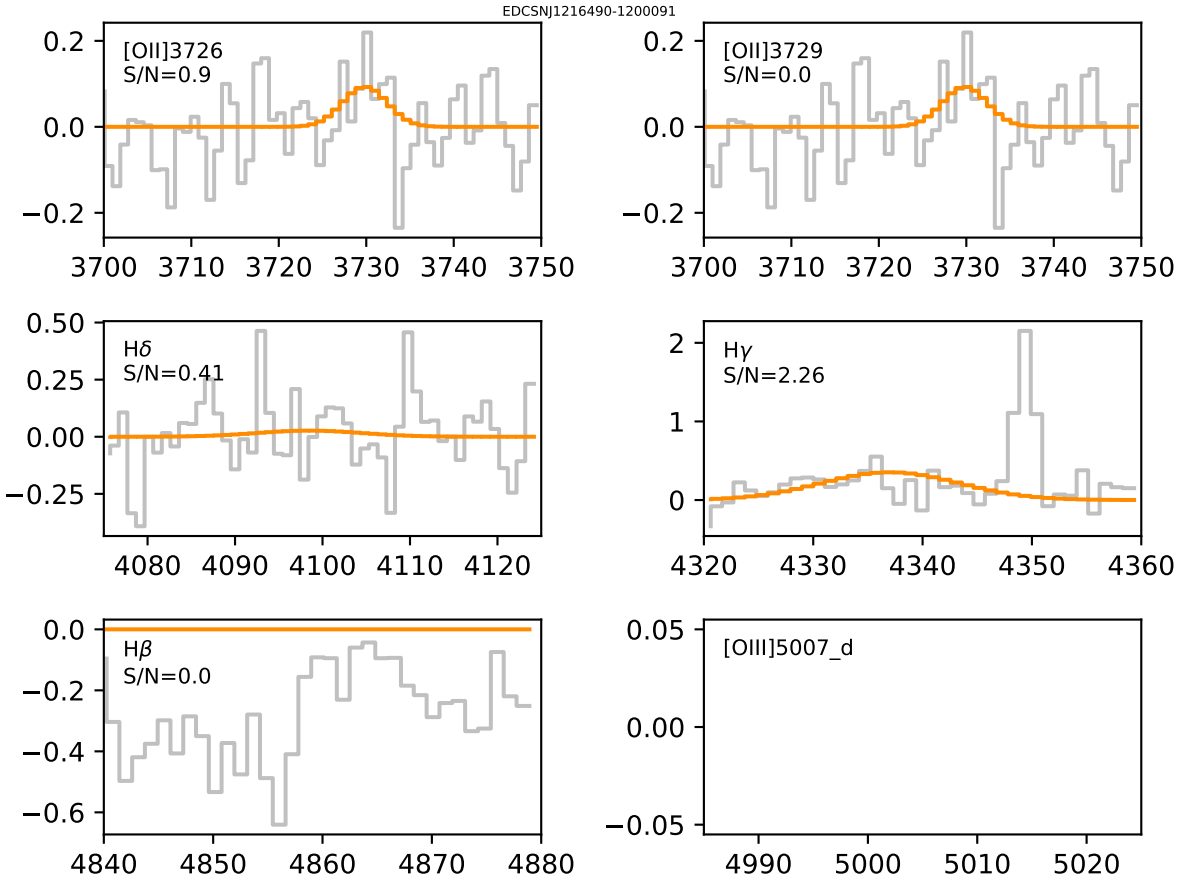
EDCSNJ1216490-1200091
[OII]3726
S/N=0.9
[OII]3729
S/N=0.0
Hδ
S/N=0.41
Hγ
S/N=2.26
Hβ
S/N=0.0
[OIII]5007_d

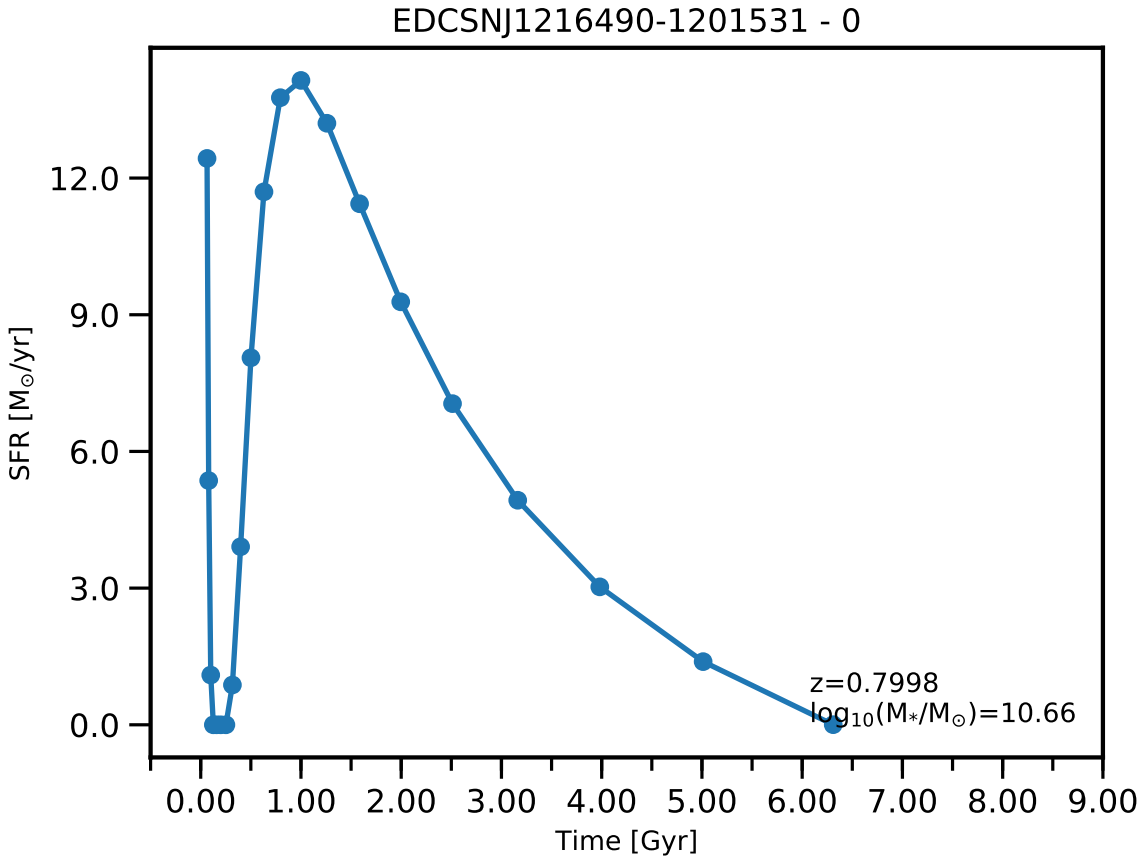
EDCSNJ1216490-1201531 - 0
SFR [M⊙/yr]
12.0
9.0
6.0
3.0
0.0
0.00
1.00
2.00
3.00
4.00
5.00
6.00
7.00
8.00
9.00
Time [Gyr]
z=0.7998
log10(M*/M⊙)=10.66

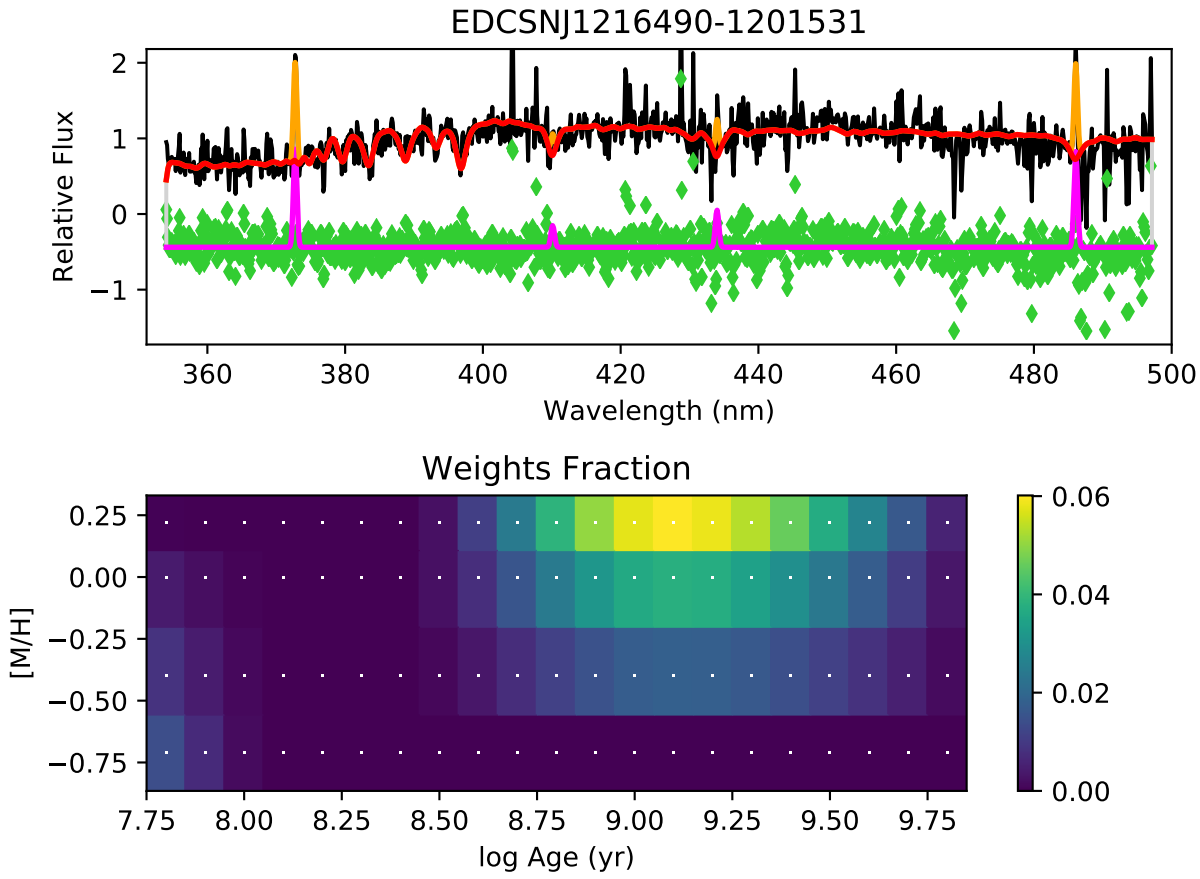
EDCSNJ1216490-1201531
Relative Flux
2
1
0
−1
360
380
400
420
440
460
480
500
Wavelength (nm)
Weights Fraction
[M/H]
0.25
0.00
−0.25
−0.50
−0.75
7.75
8.00
8.25
8.50
8.75
9.00
9.25
9.50
9.75
log Age (yr)
0.06
0.04
0.02
0.00

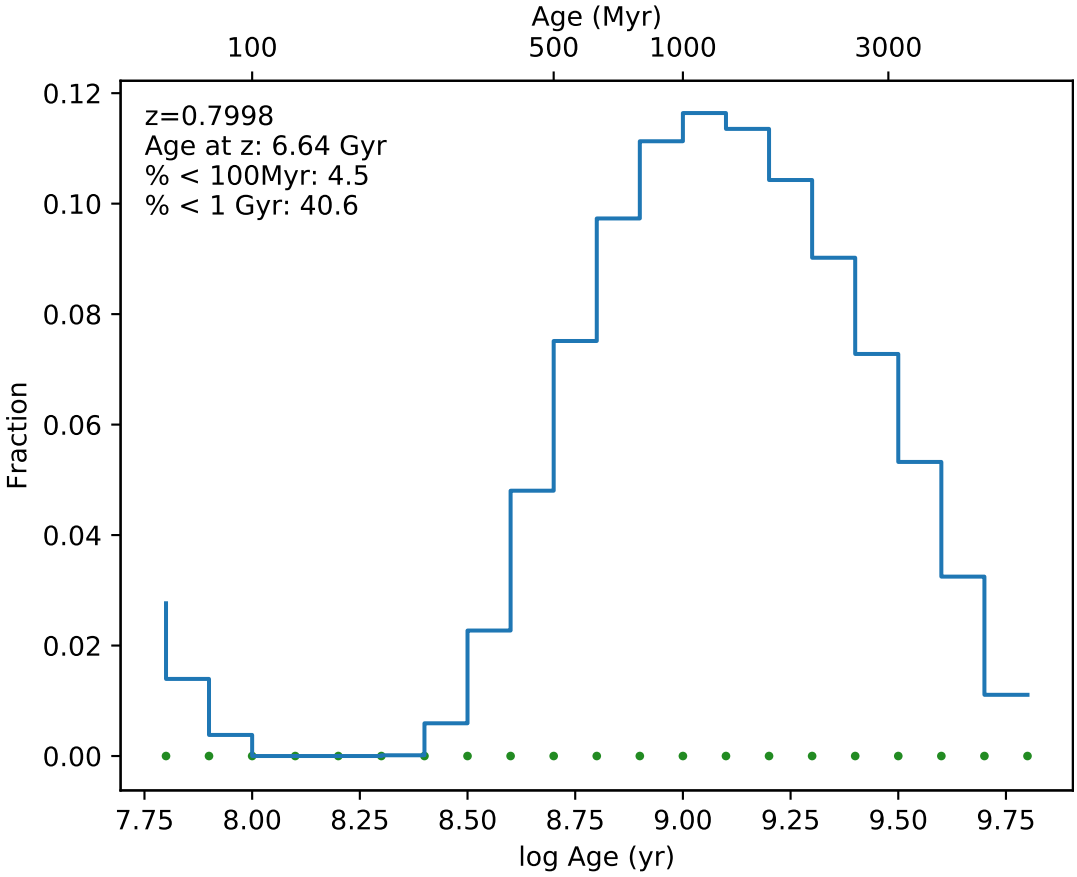
Age (Myr)
100
500
1000
3000
z=0.7998
Age at z: 6.64 Gyr
% < 100Myr: 4.5
% < 1 Gyr: 40.6
Fraction
0.12
0.10
0.08
0.06
0.04
0.02
0.00
7.75
8.00
8.25
8.50
8.75
9.00
9.25
9.50
9.75
log Age (yr)

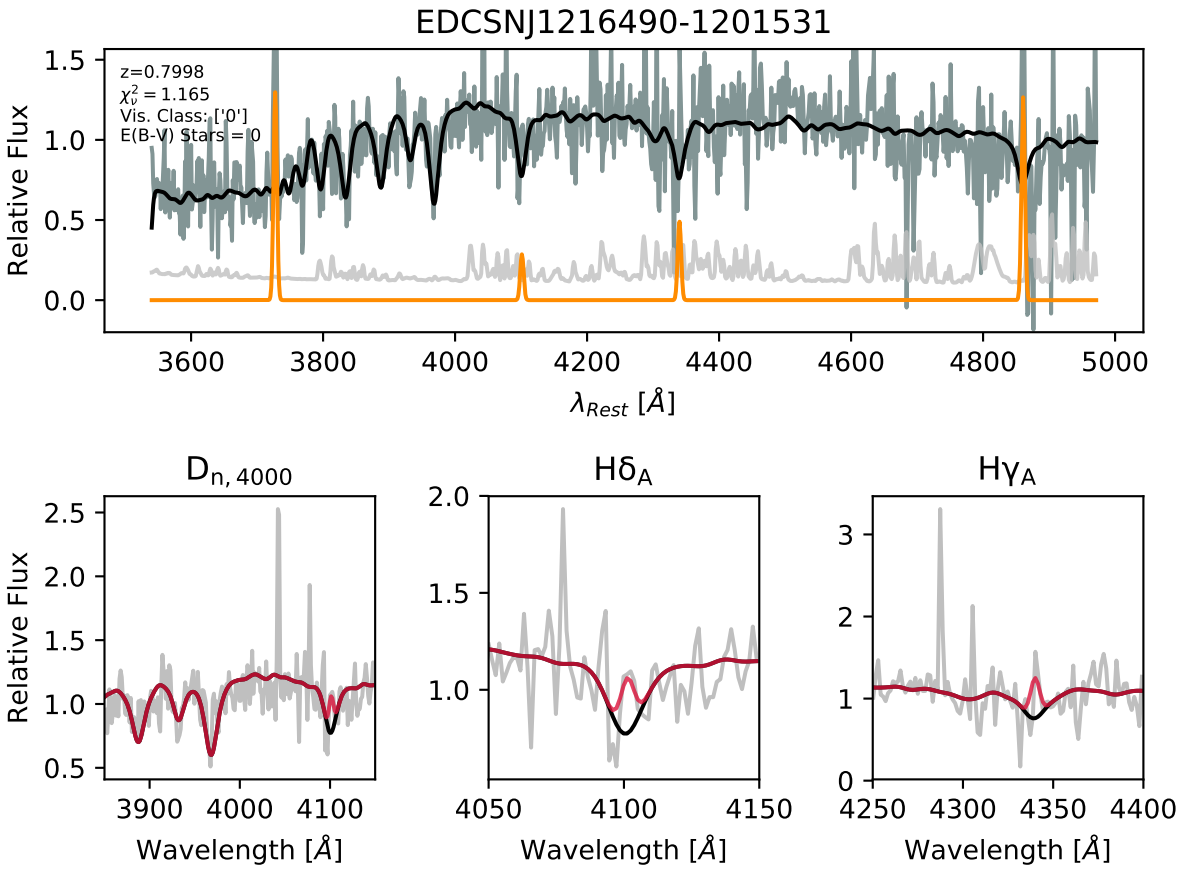
EDCSNJ1216490-1201531
z=0.7998
$\chi^2_\nu = 1.165$
Vis. Class: ['0']
E(B-V) Stars = 0
Relative Flux
λ_{Rest} [Å]
$D_{n,4000}$
$H\delta_A$
$H\gamma_A$
Wavelength [Å]

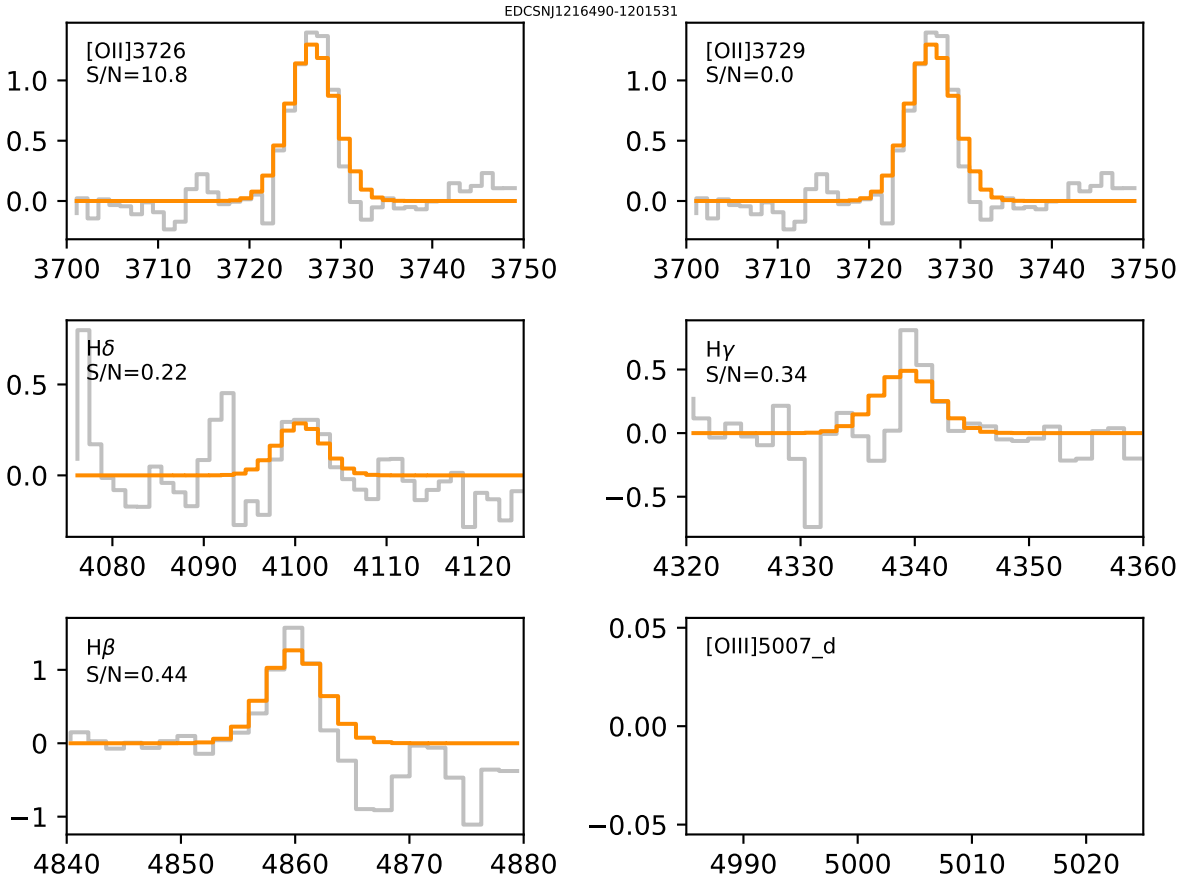
EDCSNJ1216490-1201531
[OII]3726
S/N=10.8
[OII]3729
S/N=0.0
Hδ
S/N=0.22
Hγ
S/N=0.34
Hβ
S/N=0.44
[OIII]5007_d

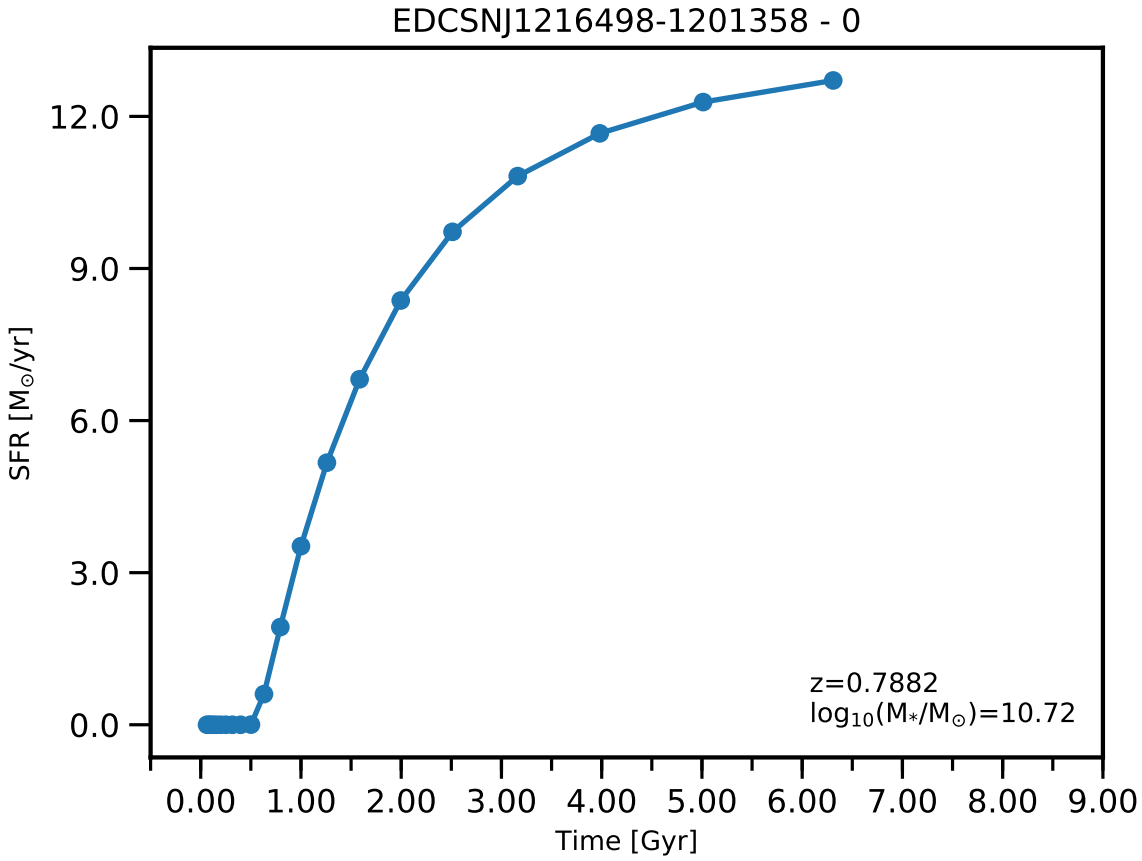
EDCSNJ1216498-1201358 - 0
SFR [M⊙/yr]
12.0
9.0
6.0
3.0
0.0
0.00
1.00
2.00
3.00
4.00
5.00
6.00
7.00
8.00
9.00
Time [Gyr]
z=0.7882
log10(M*/M⊙)=10.72

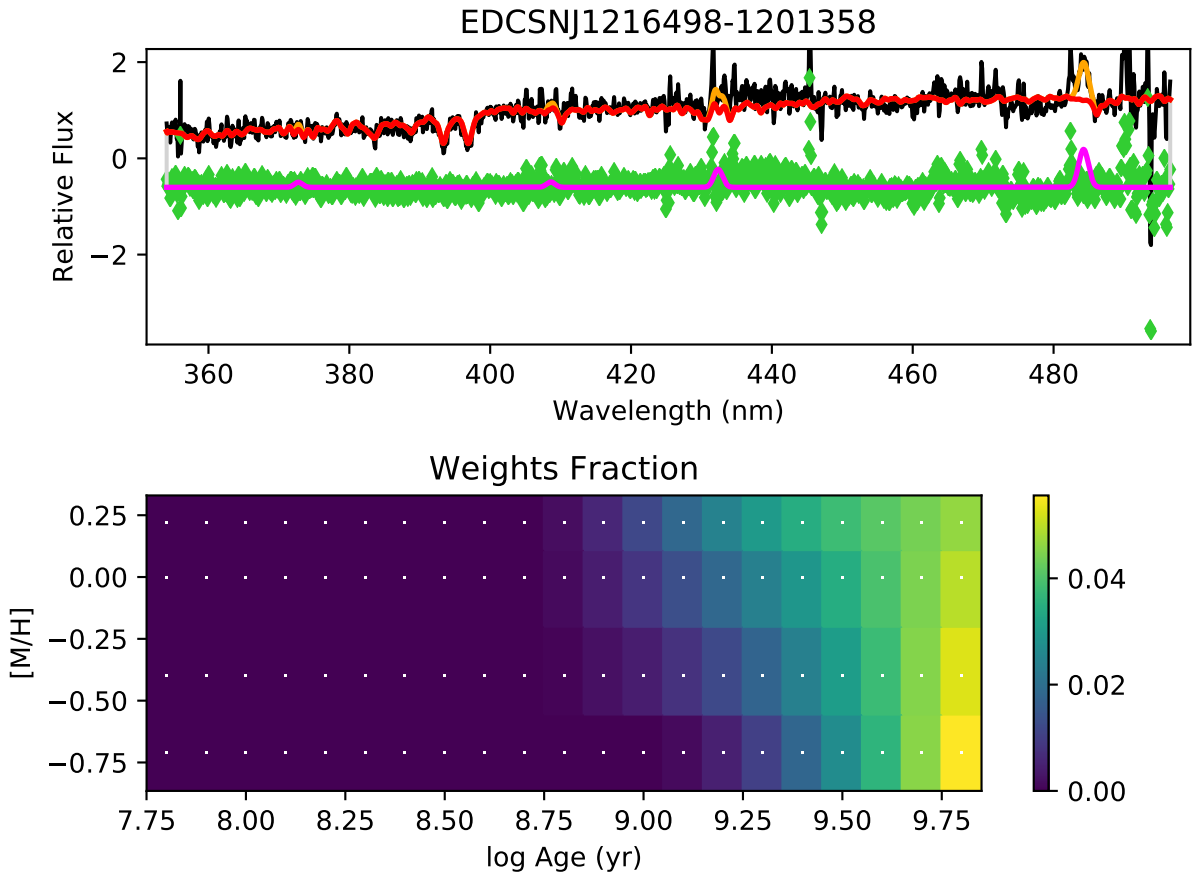
EDCSNJ1216498-1201358
Relative Flux
2
0
−2
360
380
400
420
440
460
480
Wavelength (nm)
Weights Fraction
[M/H]
0.25
0.00
−0.25
−0.50
−0.75
7.75
8.00
8.25
8.50
8.75
9.00
9.25
9.50
9.75
log Age (yr)
0.04
0.02
0.00

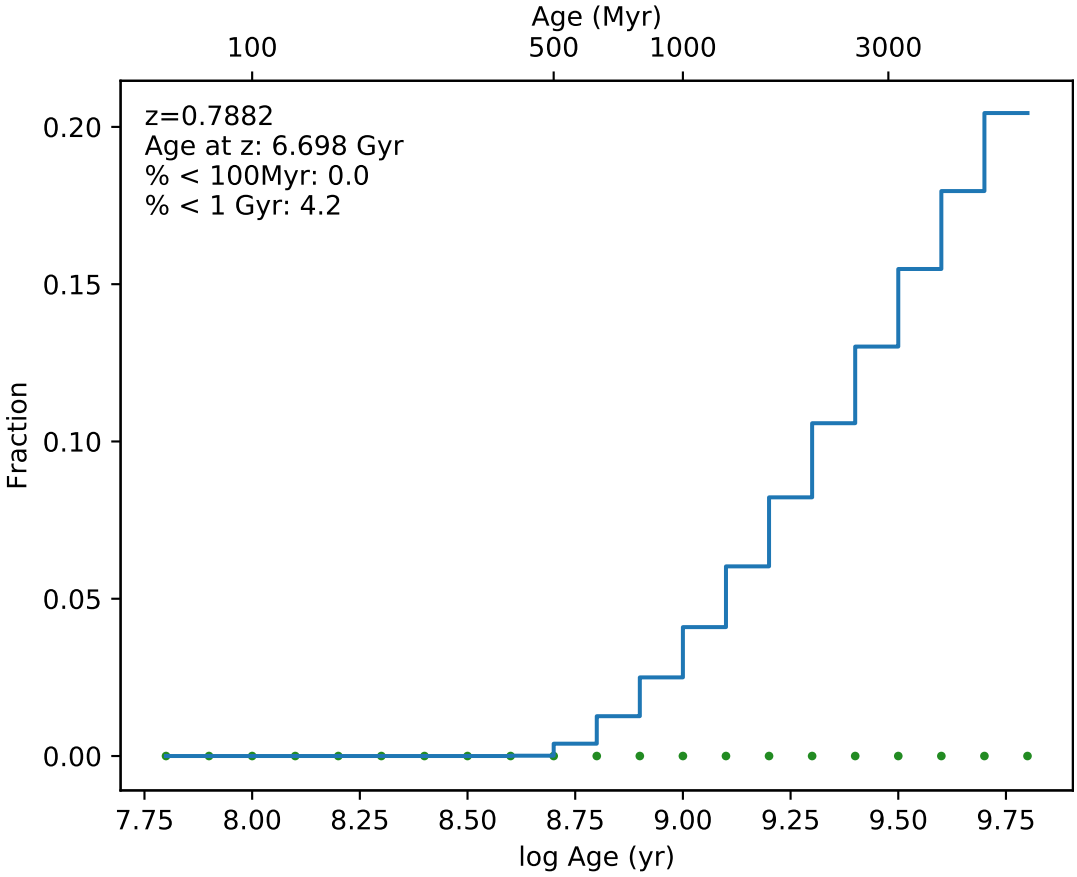
Age (Myr)
100
500
1000
3000
z=0.7882
Age at z: 6.698 Gyr
% < 100Myr: 0.0
% < 1 Gyr: 4.2
Fraction
0.20
0.15
0.10
0.05
0.00
7.75
8.00
8.25
8.50
8.75
9.00
9.25
9.50
9.75
log Age (yr)

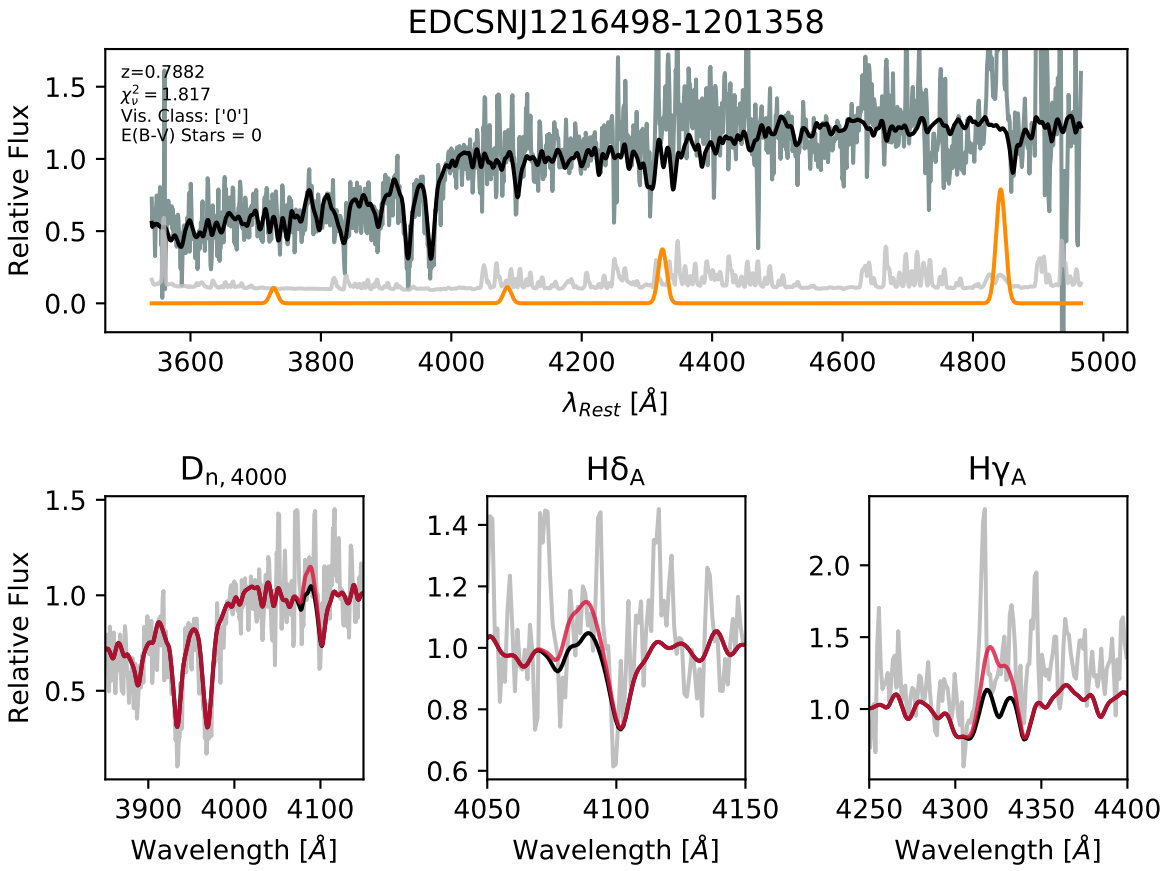
EDCSNJ1216498-1201358
z=0.7882
$\chi^2_\nu = 1.817$
Vis. Class: ['0']
E(B-V) Stars = 0
Relative Flux
λ_{Rest} [Å]
$D_{n,4000}$
$H\delta_A$
$H\gamma_A$
Wavelength [Å]

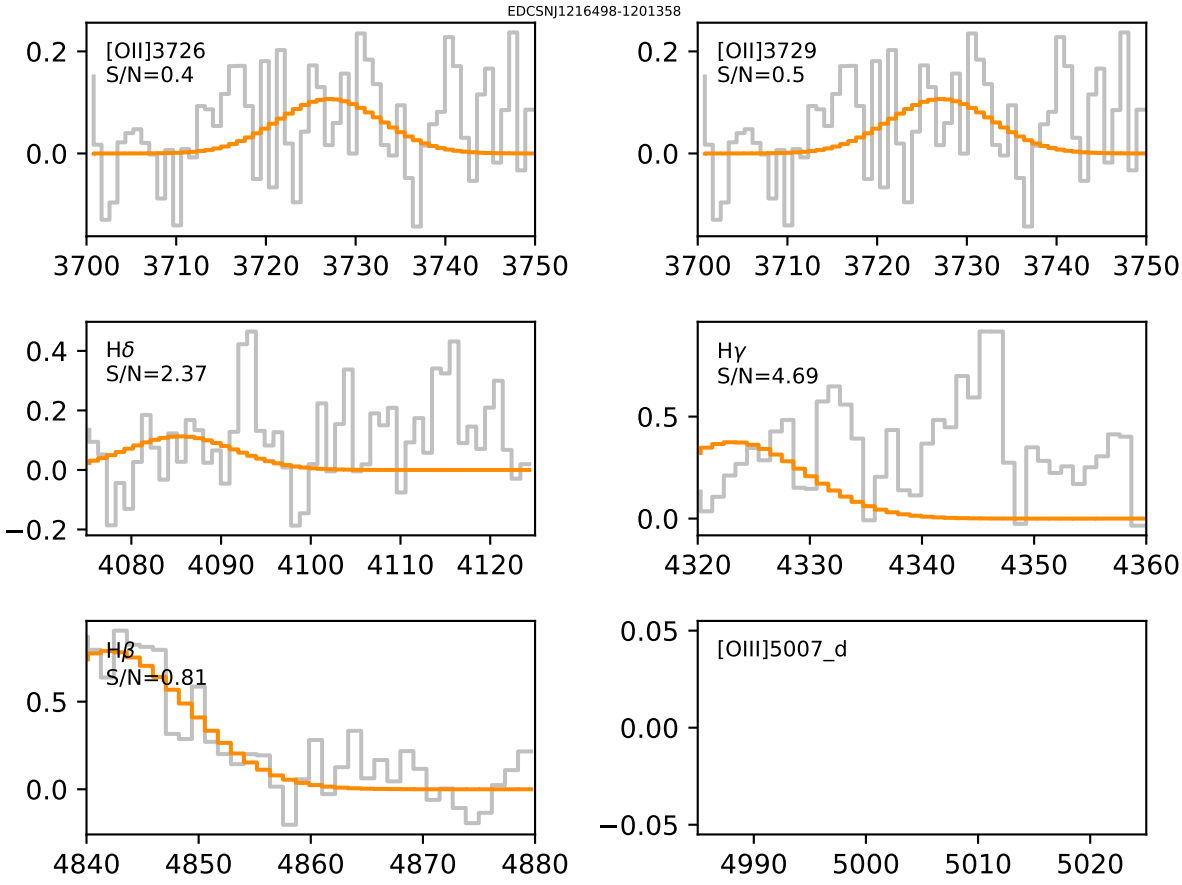
EDCSNJ1216498-1201358
[OII]3726
S/N=0.4
[OII]3729
S/N=0.5
Hδ
S/N=2.37
Hγ
S/N=4.69
Hβ
S/N=0.81
[OIII]5007_d

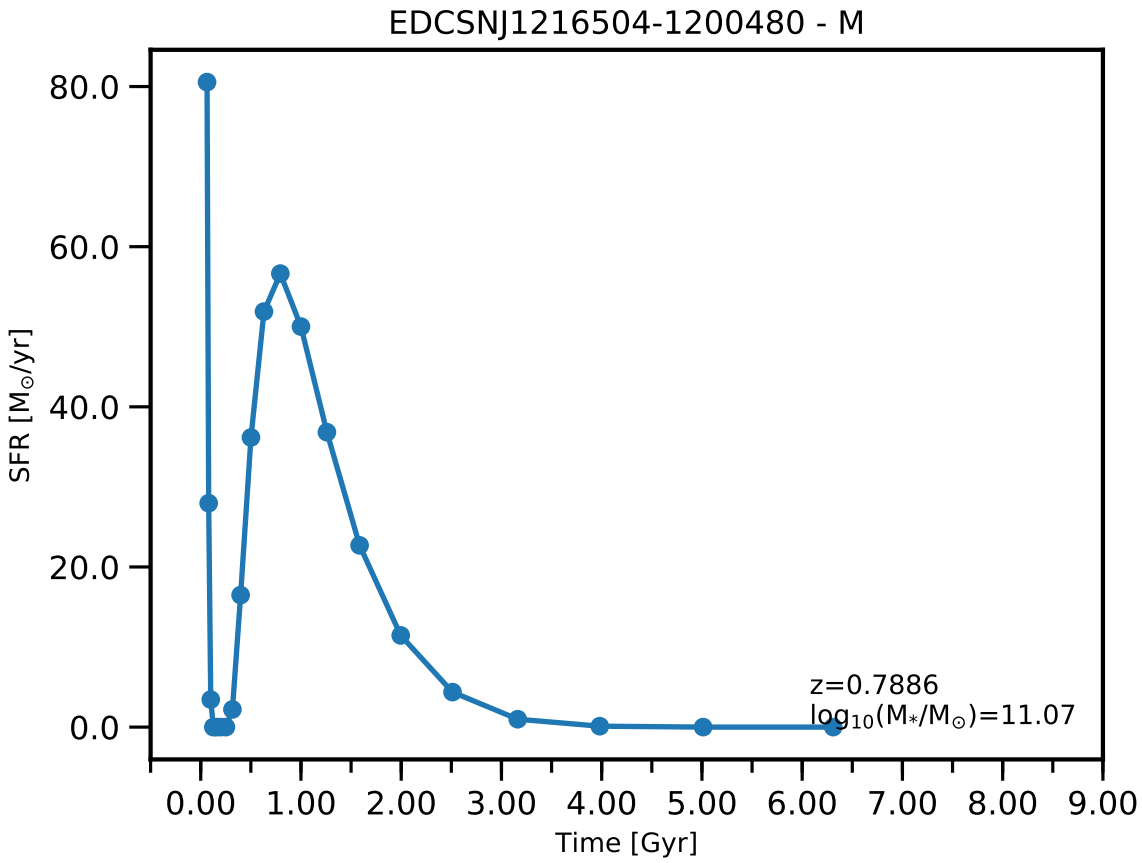
EDCSNJ1216504-1200480 - M
SFR [M⊙/yr]
80.0
60.0
40.0
20.0
0.0
0.00
1.00
2.00
3.00
4.00
5.00
6.00
7.00
8.00
9.00
Time [Gyr]
z=0.7886
log10(M*/M⊙)=11.07

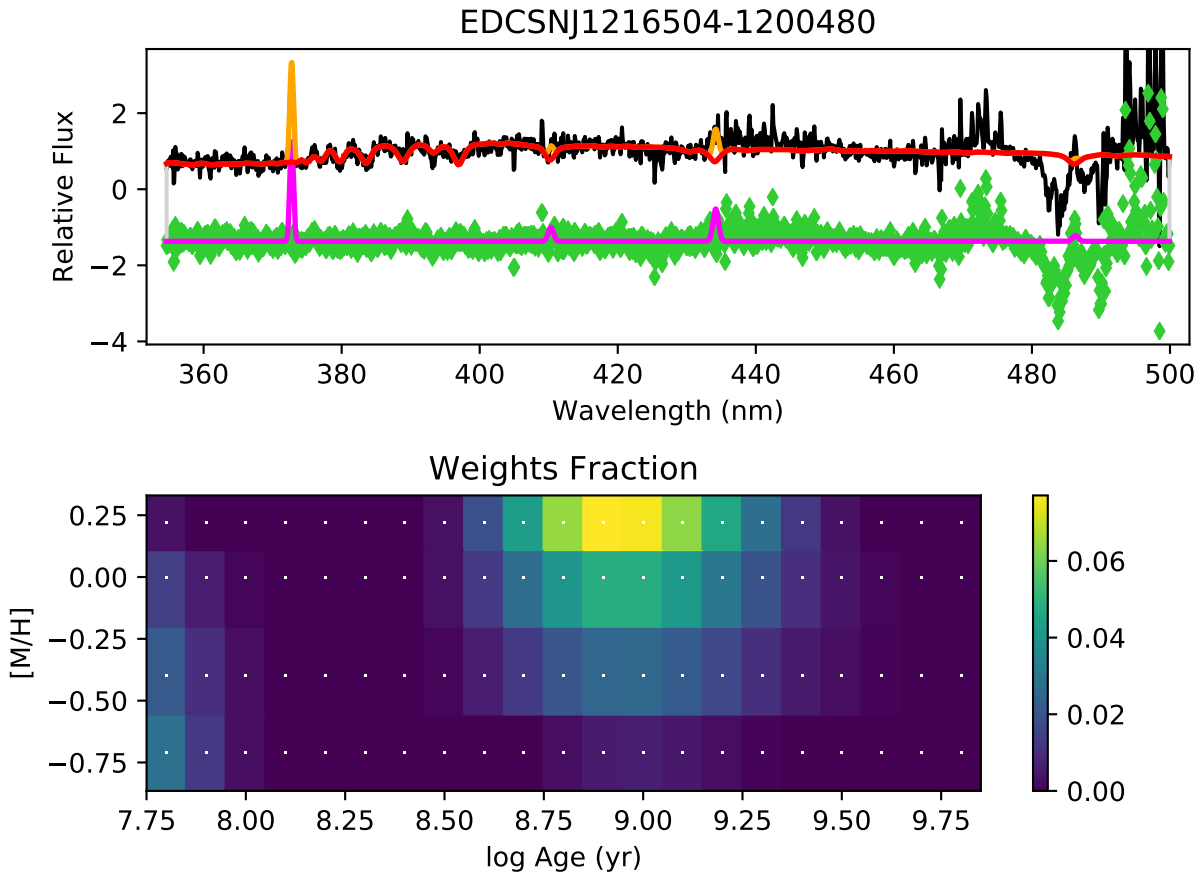
EDCSNJ1216504-1200480
Relative Flux
2
0
−2
−4
360
380
400
420
440
460
480
500
Wavelength (nm)
Weights Fraction
[M/H]
0.25
0.00
−0.25
−0.50
−0.75
7.75
8.00
8.25
8.50
8.75
9.00
9.25
9.50
9.75
log Age (yr)
0.06
0.04
0.02
0.00

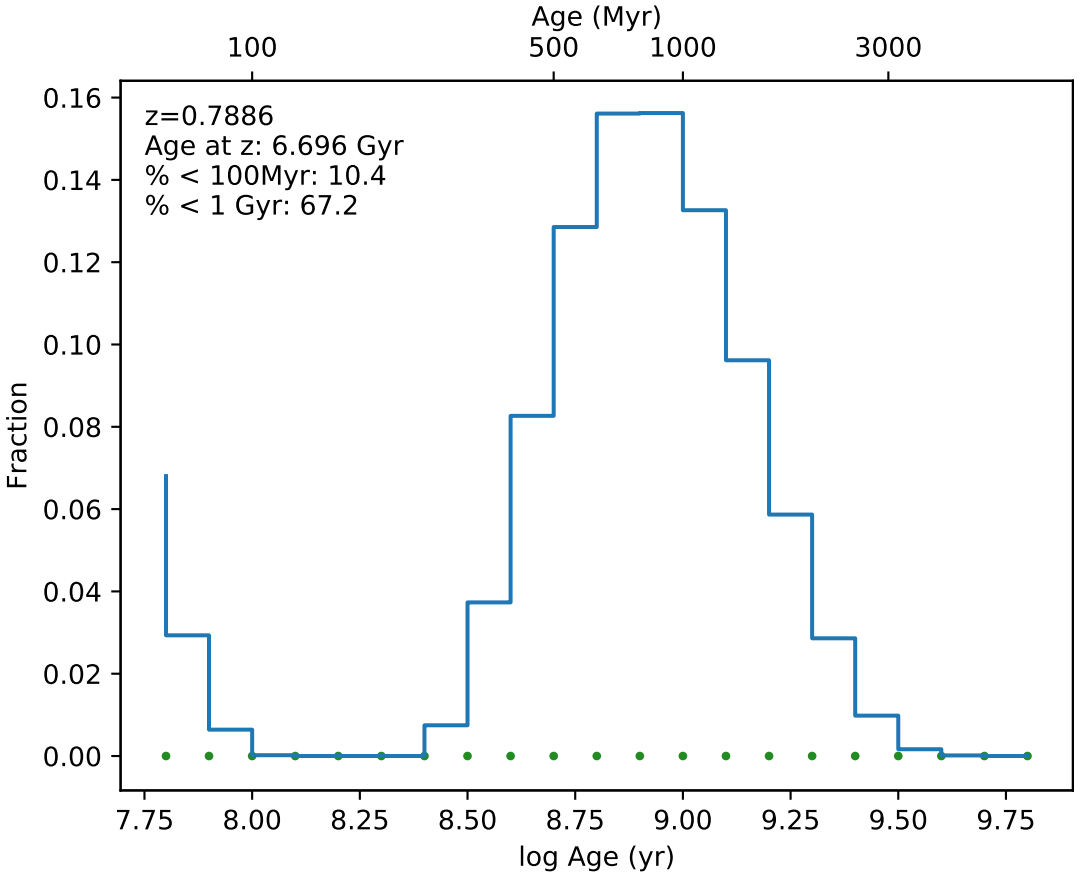
Age (Myr)
100
500
1000
3000
z=0.7886
Age at z: 6.696 Gyr
% < 100Myr: 10.4
% < 1 Gyr: 67.2
Fraction
0.16
0.14
0.12
0.10
0.08
0.06
0.04
0.02
0.00
7.75
8.00
8.25
8.50
8.75
9.00
9.25
9.50
9.75
log Age (yr)

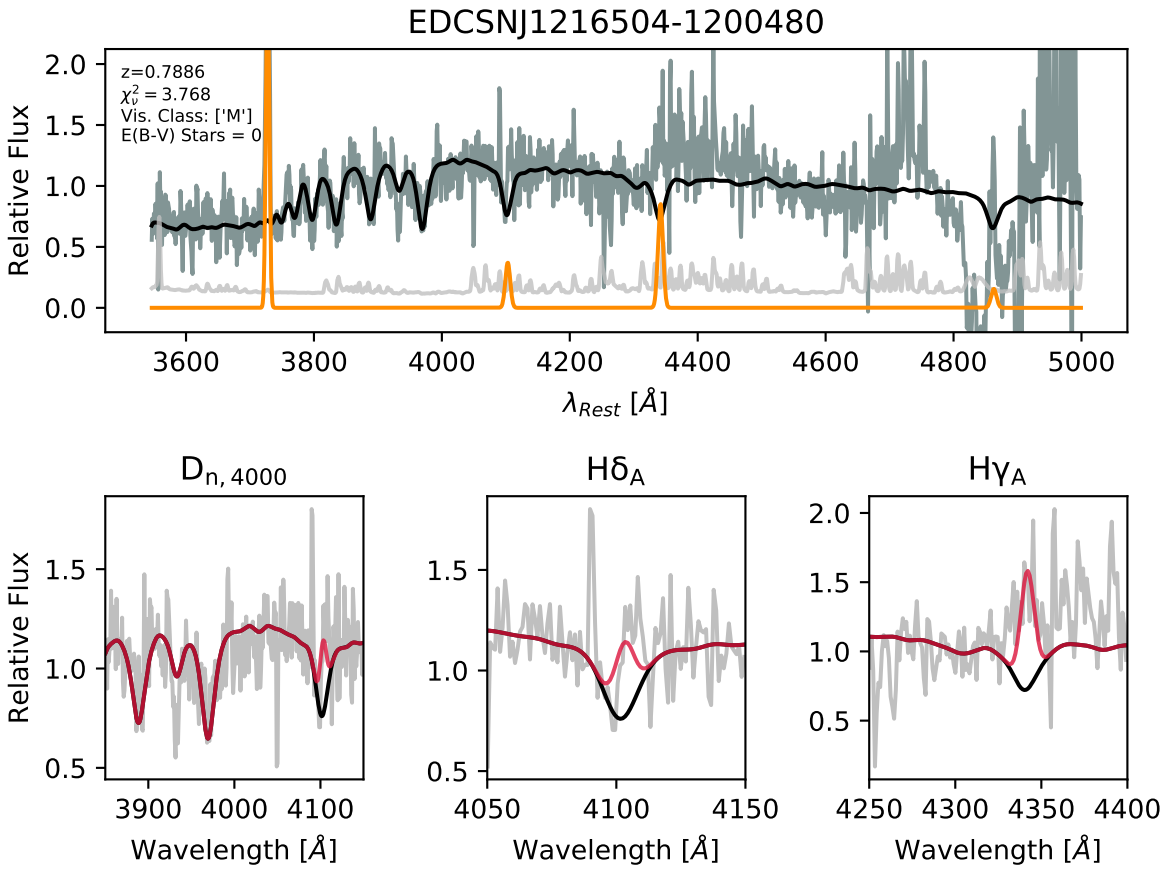
EDCSNJ1216504-1200480
z=0.7886
$\chi^2_\nu = 3.768$
Vis. Class: ['M']
E(B-V) Stars = 0
Relative Flux
λ_{Rest} [Å]
$D_{n,4000}$
$H\delta_A$
$H\gamma_A$
Wavelength [Å]

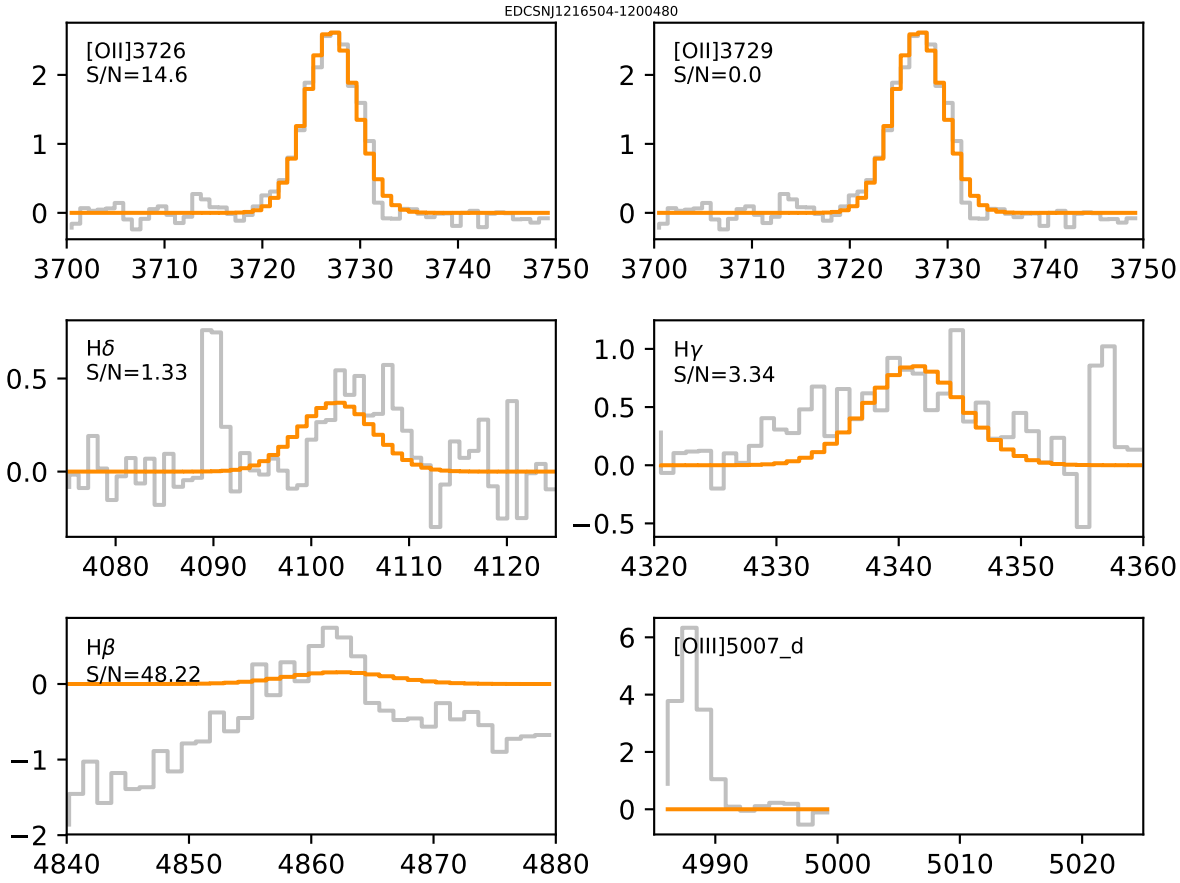
EDCSNJ1216504-1200480
[OII]3726
S/N=14.6
[OII]3729
S/N=0.0
Hδ
S/N=1.33
Hγ
S/N=3.34
Hβ
S/N=48.22
[OIII]5007_d

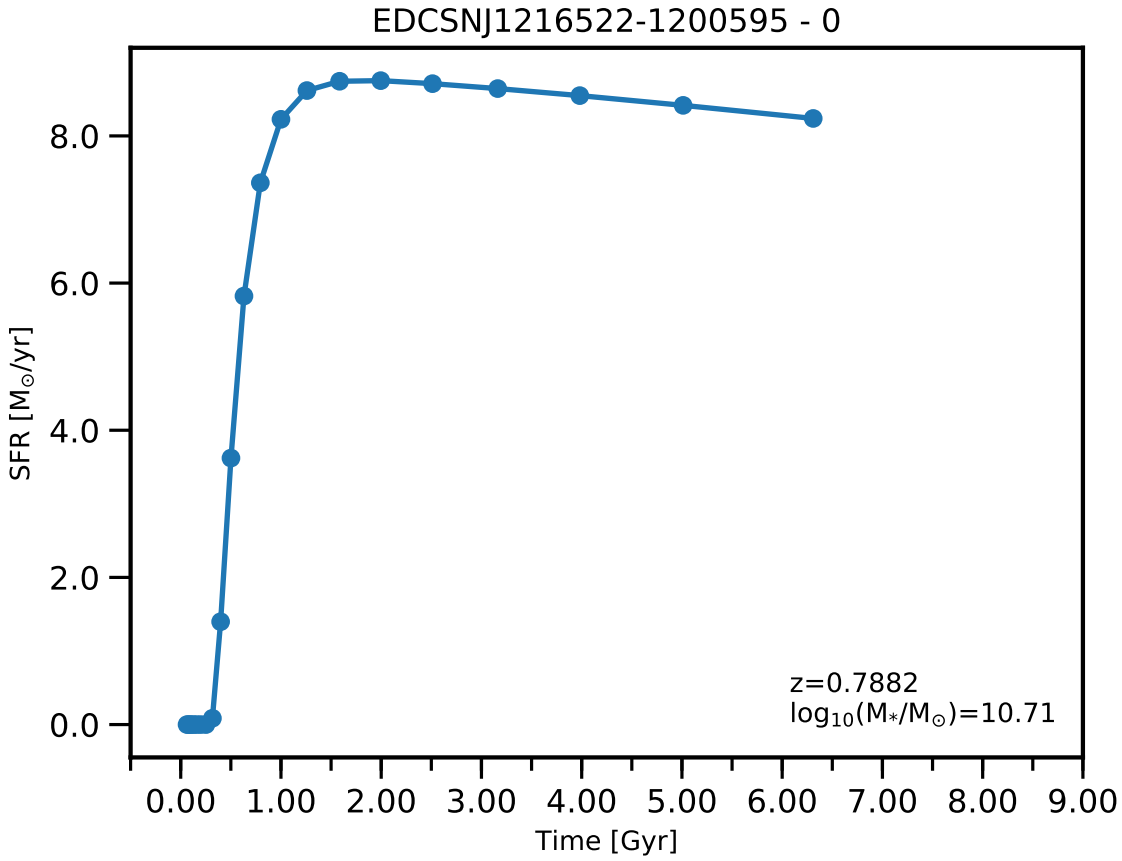
EDCSNJ1216522-1200595 - 0
SFR [M⊙/yr]
0.0
2.0
4.0
6.0
8.0
0.00
1.00
2.00
3.00
4.00
5.00
6.00
7.00
8.00
9.00
Time [Gyr]
z=0.7882
log10(M*/M⊙)=10.71

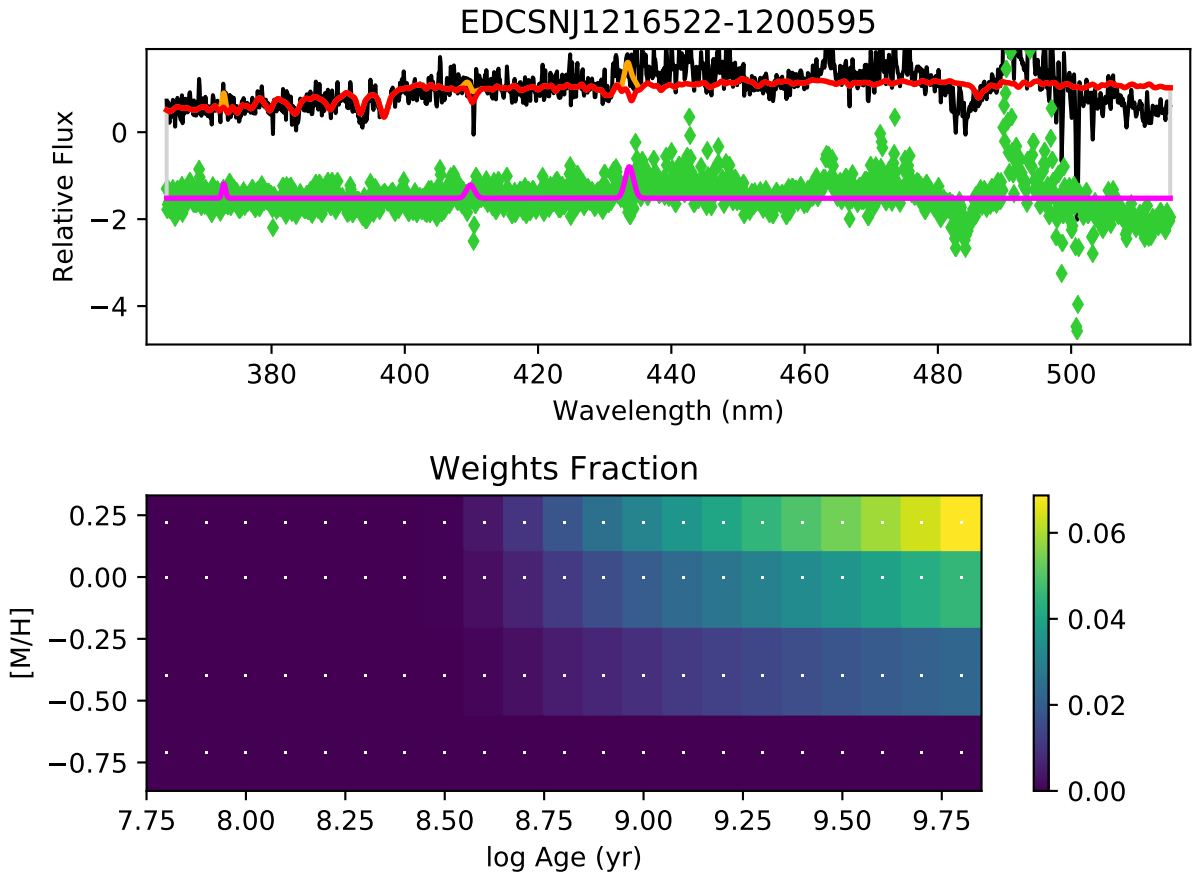
EDCSNJ1216522-1200595
Relative Flux
0
−2
−4
380
400
420
440
460
480
500
Wavelength (nm)
Weights Fraction
[M/H]
0.25
0.00
−0.25
−0.50
−0.75
7.75
8.00
8.25
8.50
8.75
9.00
9.25
9.50
9.75
log Age (yr)
0.06
0.04
0.02
0.00

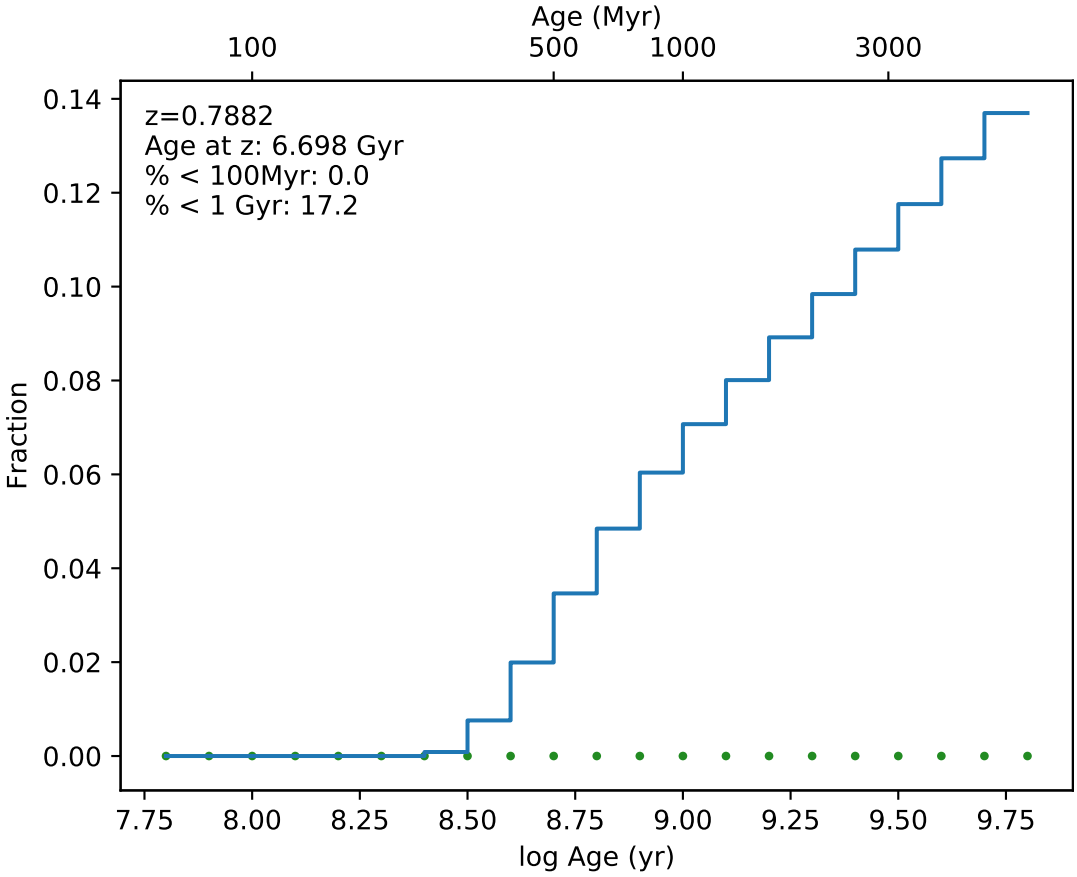
Age (Myr)
100
500
1000
3000
z=0.7882
Age at z: 6.698 Gyr
% < 100Myr: 0.0
% < 1 Gyr: 17.2
Fraction
0.14
0.12
0.10
0.08
0.06
0.04
0.02
0.00
7.75
8.00
8.25
8.50
8.75
9.00
9.25
9.50
9.75
log Age (yr)

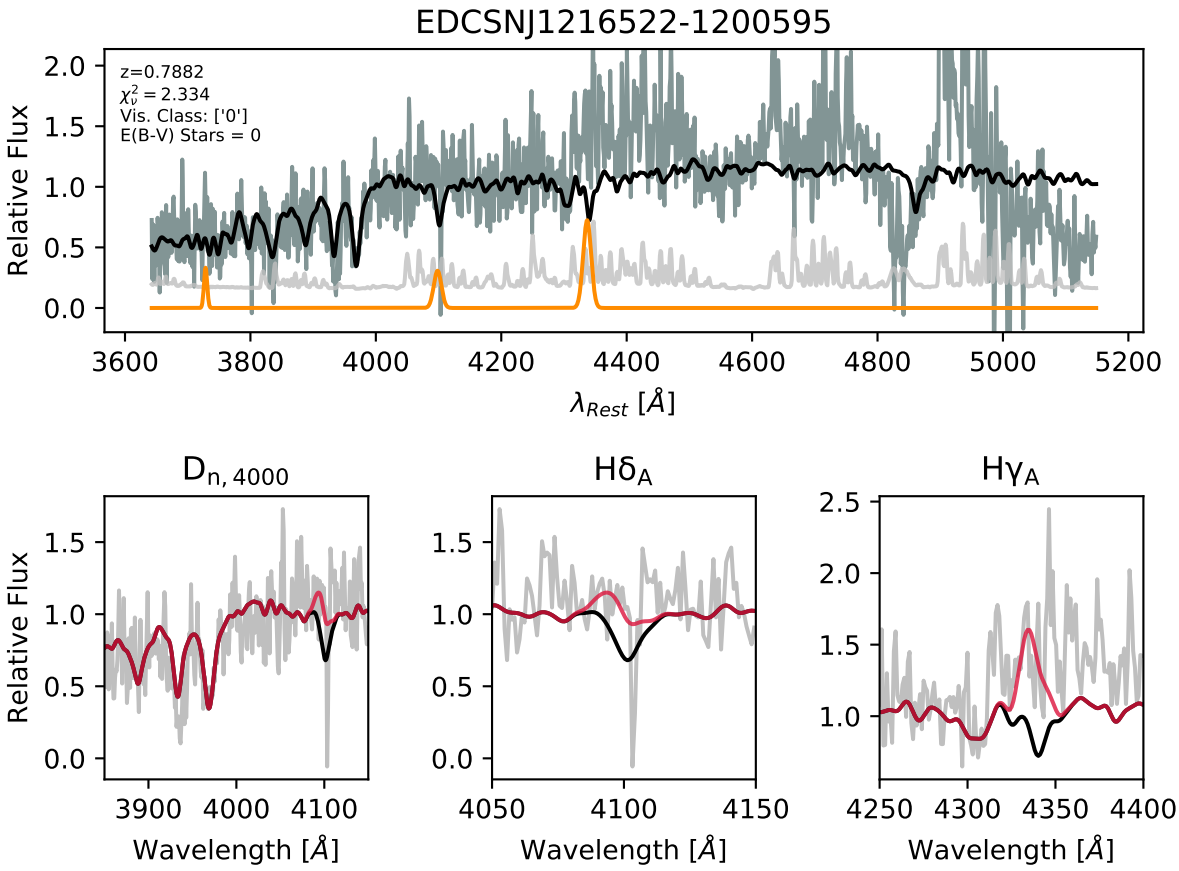
EDCSNJ1216522-1200595
z=0.7882
$\chi^2_\nu = 2.334$
Vis. Class: ['0']
E(B-V) Stars = 0
Relative Flux
λ_{Rest} [Å]
$D_{n,4000}$
$H\delta_A$
$H\gamma_A$
Wavelength [Å]

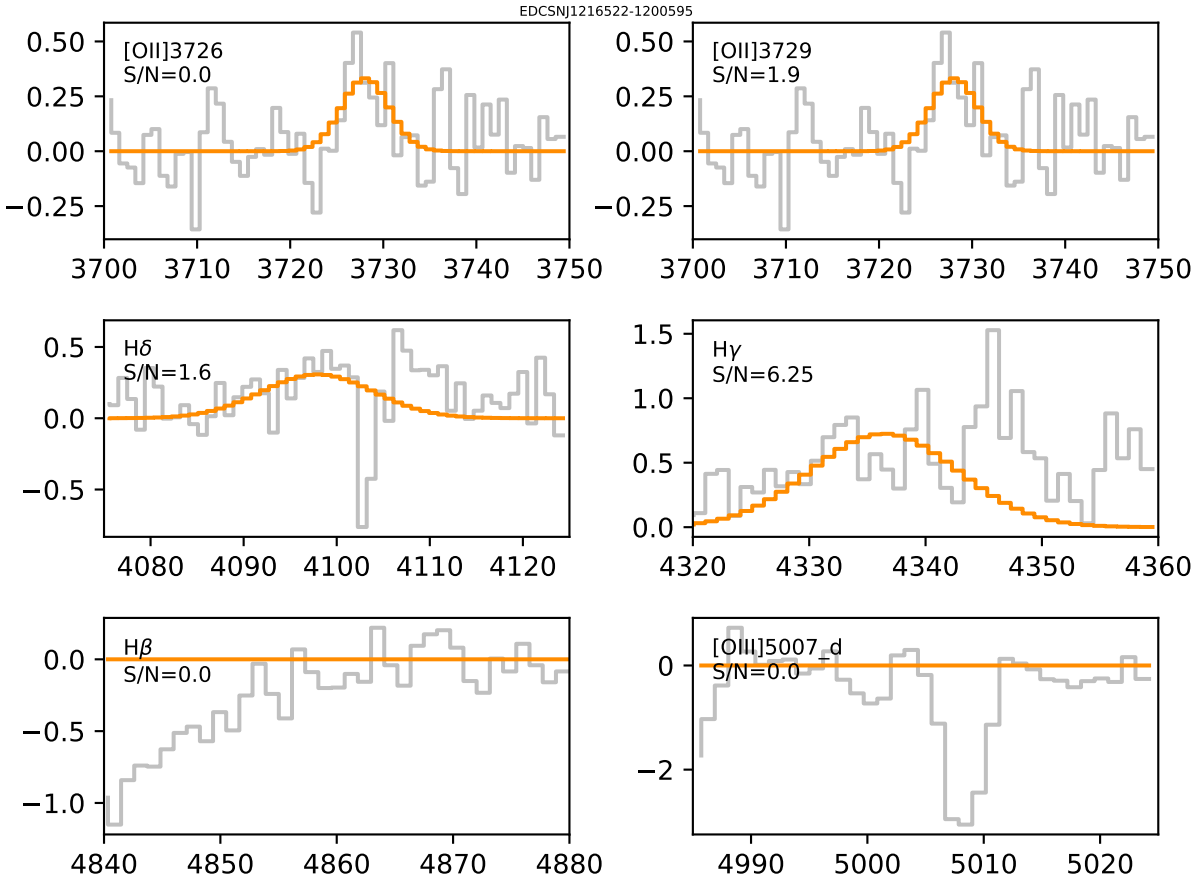
EDCSNJ1216522-1200595
[OII]3726
S/N=0.0
[OII]3729
S/N=1.9
Hδ
S/N=1.6
Hγ
S/N=6.25
Hβ
S/N=0.0
[OIII]5007_d
S/N=0.0

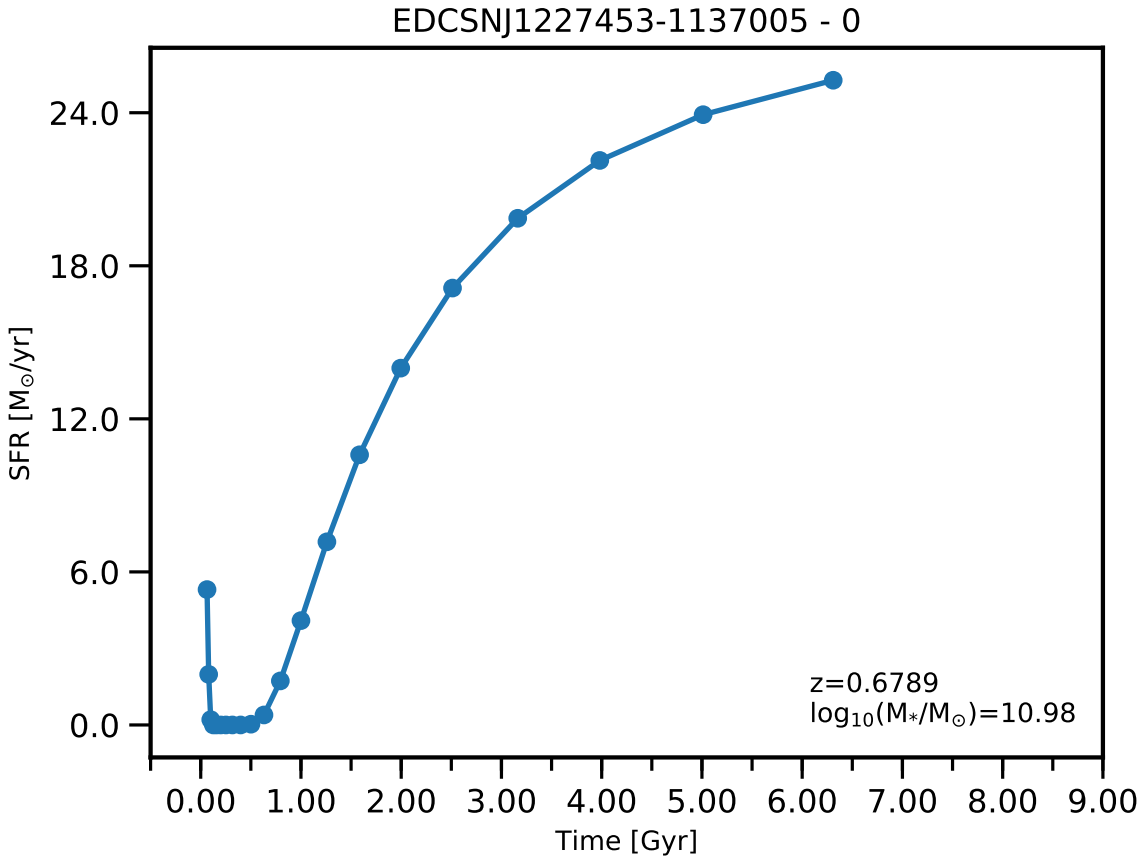
EDCSNJ1227453-1137005 - 0
SFR [M⊙/yr]
24.0
18.0
12.0
6.0
0.0
0.00
1.00
2.00
3.00
4.00
5.00
6.00
7.00
8.00
9.00
Time [Gyr]
z=0.6789
log10(M*/M⊙)=10.98

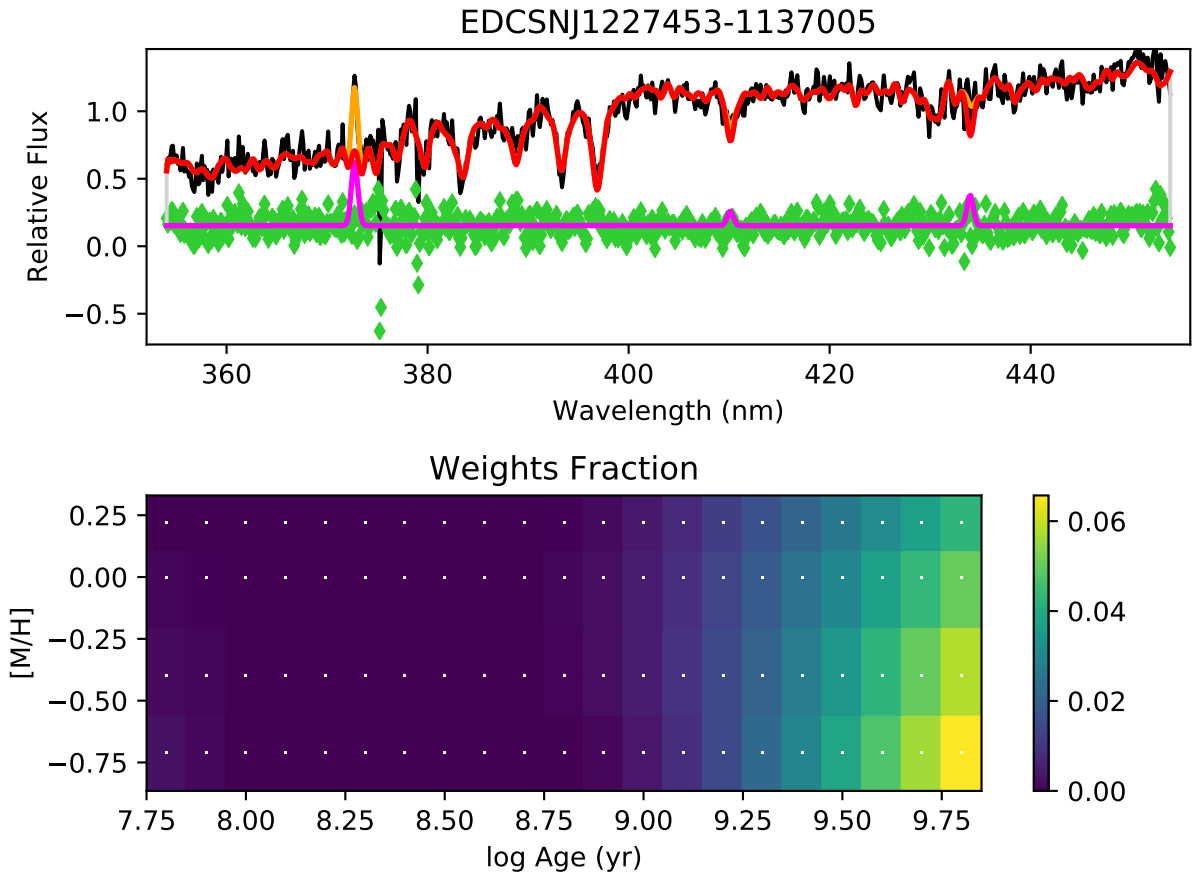
EDCSNJ1227453-1137005
Relative Flux
1.0
0.5
0.0
−0.5
360
380
400
420
440
Wavelength (nm)
Weights Fraction
[M/H]
0.25
0.00
−0.25
−0.50
−0.75
7.75
8.00
8.25
8.50
8.75
9.00
9.25
9.50
9.75
log Age (yr)
0.06
0.04
0.02
0.00

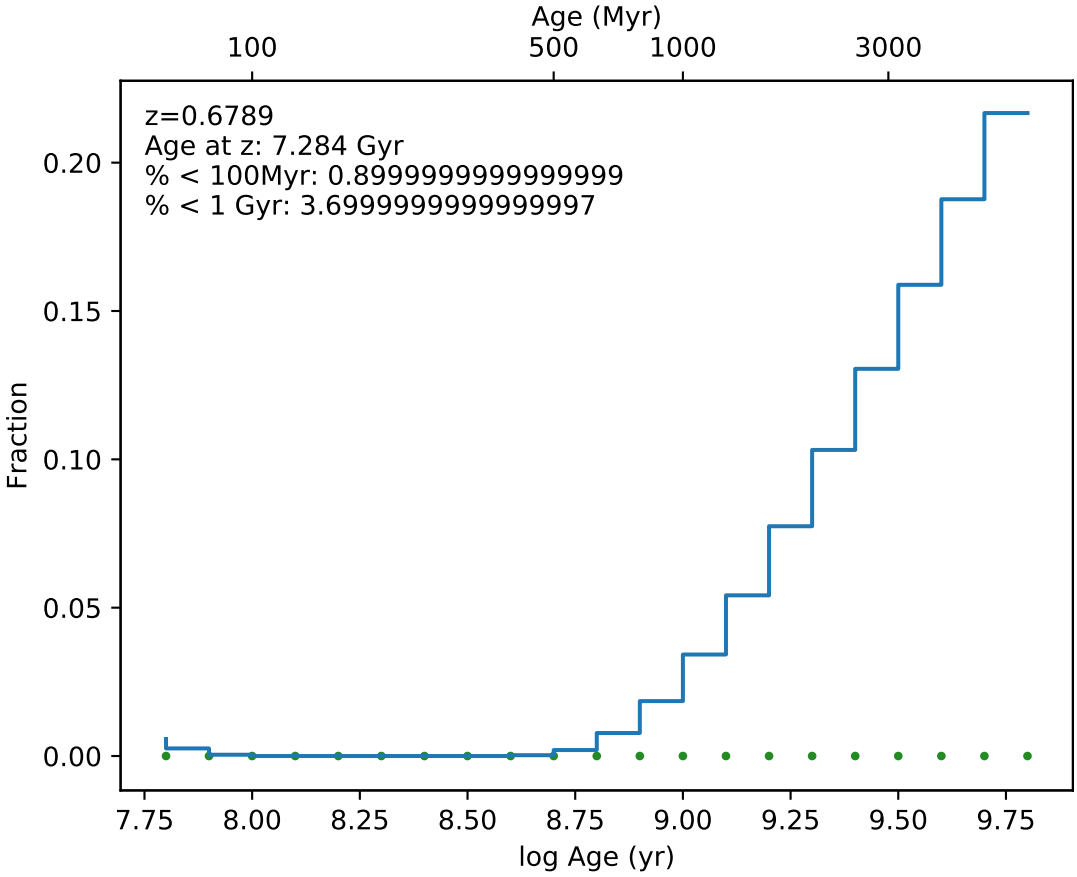
Age (Myr)
100
500
1000
3000
z=0.6789
Age at z: 7.284 Gyr
% < 100Myr: 0.8999999999999999
% < 1 Gyr: 3.6999999999999997
Fraction
0.20
0.15
0.10
0.05
0.00
7.75
8.00
8.25
8.50
8.75
9.00
9.25
9.50
9.75
log Age (yr)

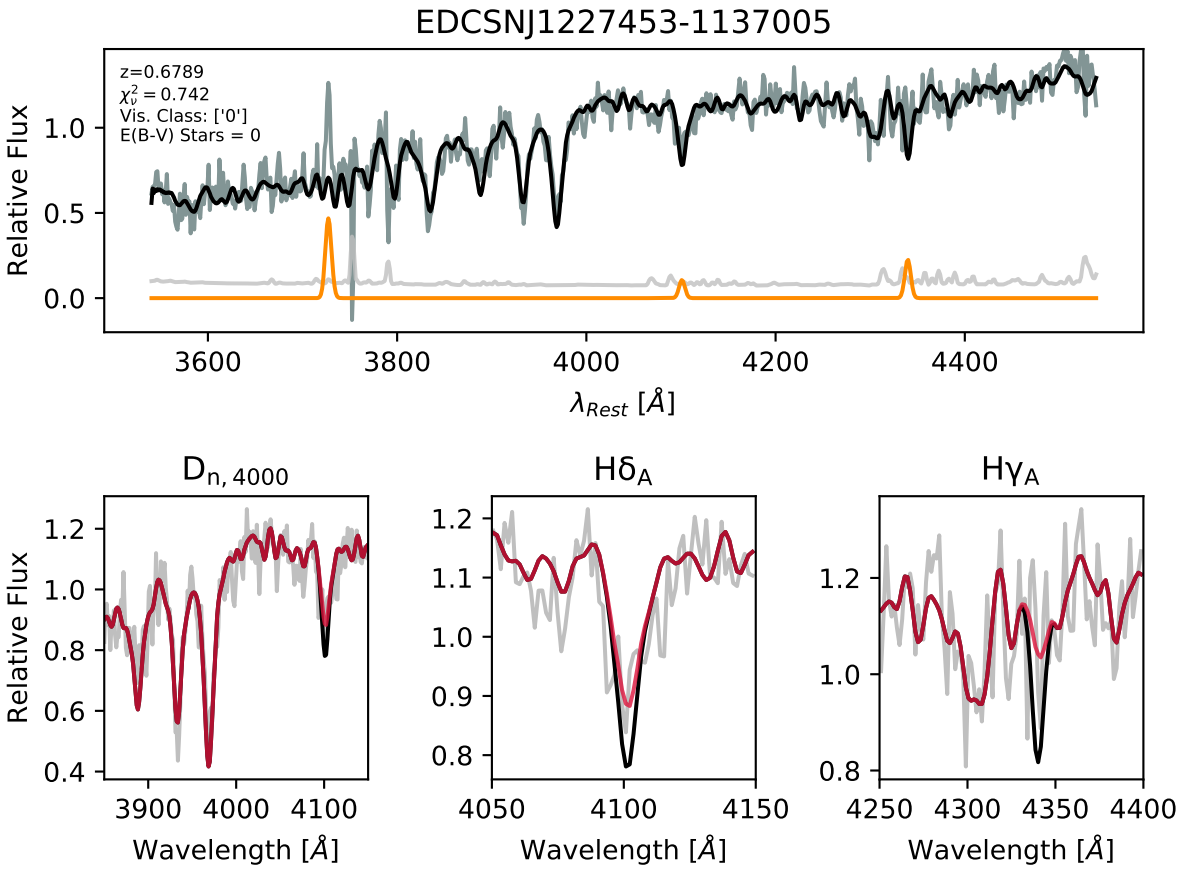
EDCSNJ1227453-1137005
z=0.6789
$\chi^2_\nu = 0.742$
Vis. Class: ['0']
E(B-V) Stars = 0
Relative Flux
λ_{Rest} [Å]
$D_{n,4000}$
$H\delta_A$
$H\gamma_A$
Wavelength [Å]

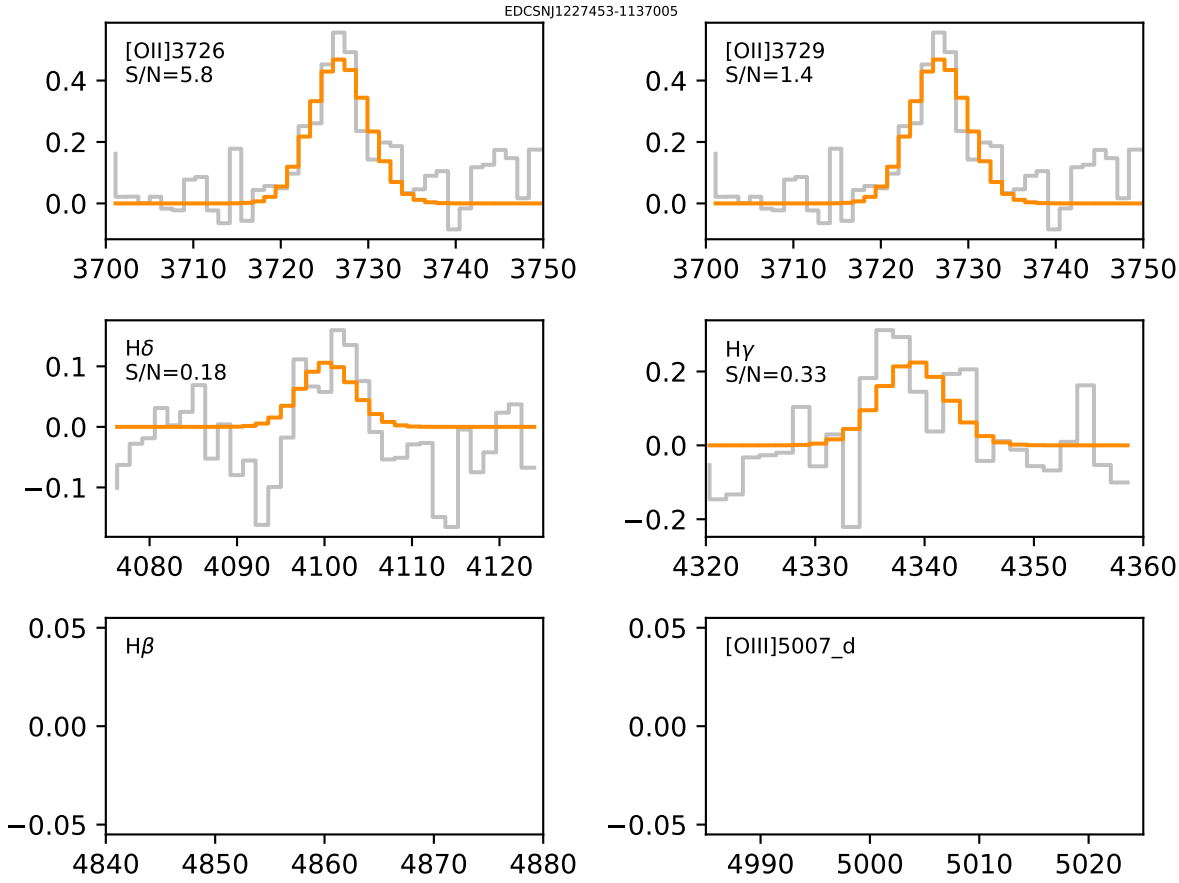
EDCSNJ1227453-1137005
[OII]3726
S/N=5.8
[OII]3729
S/N=1.4
Hδ
S/N=0.18
Hγ
S/N=0.33
Hβ
[OIII]5007_d

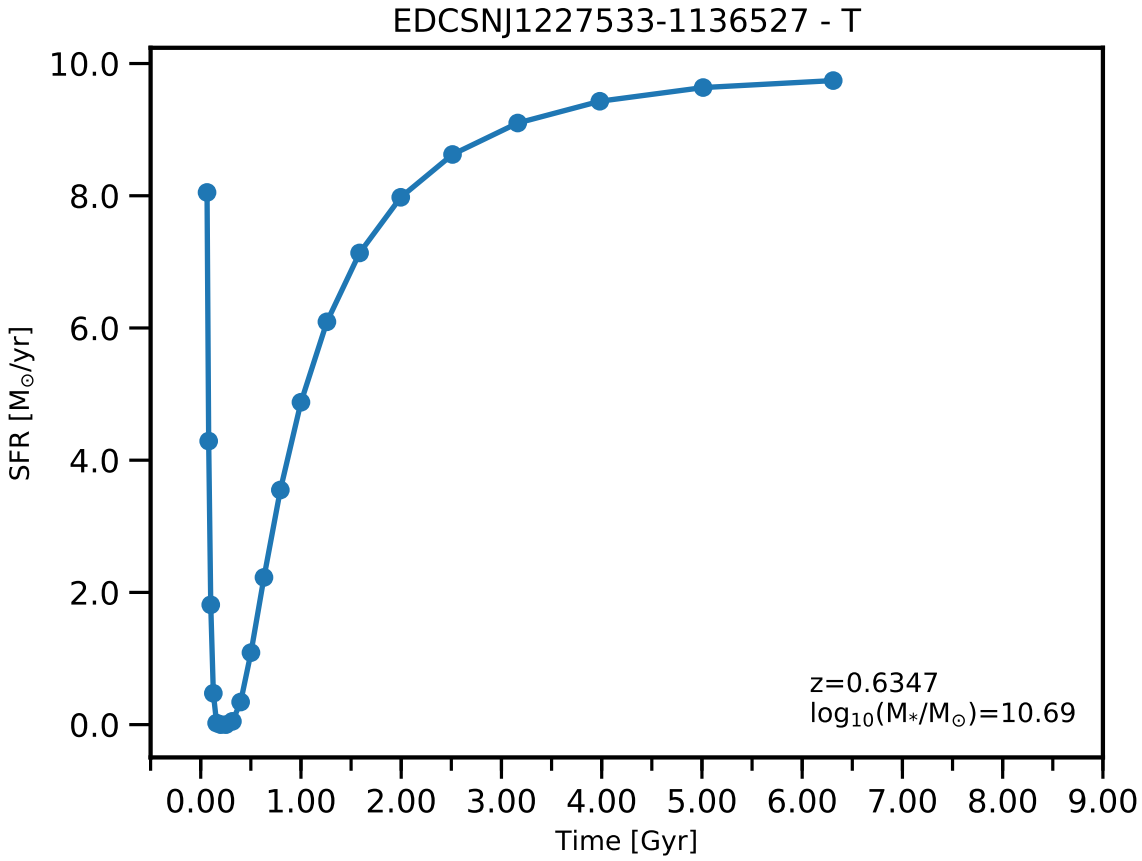
EDCSNJ1227533-1136527 - T
10.0
8.0
6.0
4.0
2.0
0.0
SFR [M⊙/yr]
0.00
1.00
2.00
3.00
4.00
5.00
6.00
7.00
8.00
9.00
Time [Gyr]
z=0.6347
log10(M*/M⊙)=10.69

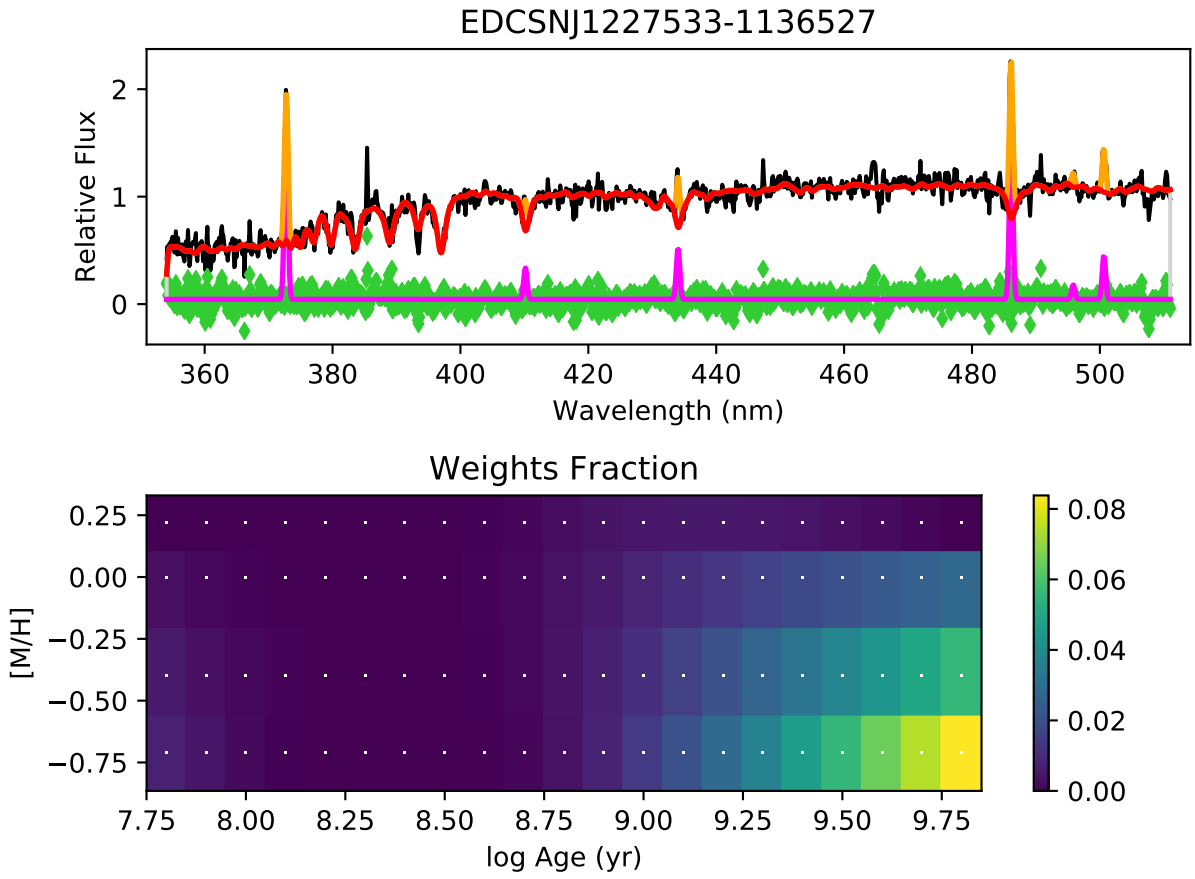
EDCSNJ1227533-1136527
Relative Flux
2
1
0
360
380
400
420
440
460
480
500
Wavelength (nm)
Weights Fraction
[M/H]
0.25
0.00
−0.25
−0.50
−0.75
7.75
8.00
8.25
8.50
8.75
9.00
9.25
9.50
9.75
log Age (yr)
0.08
0.06
0.04
0.02
0.00

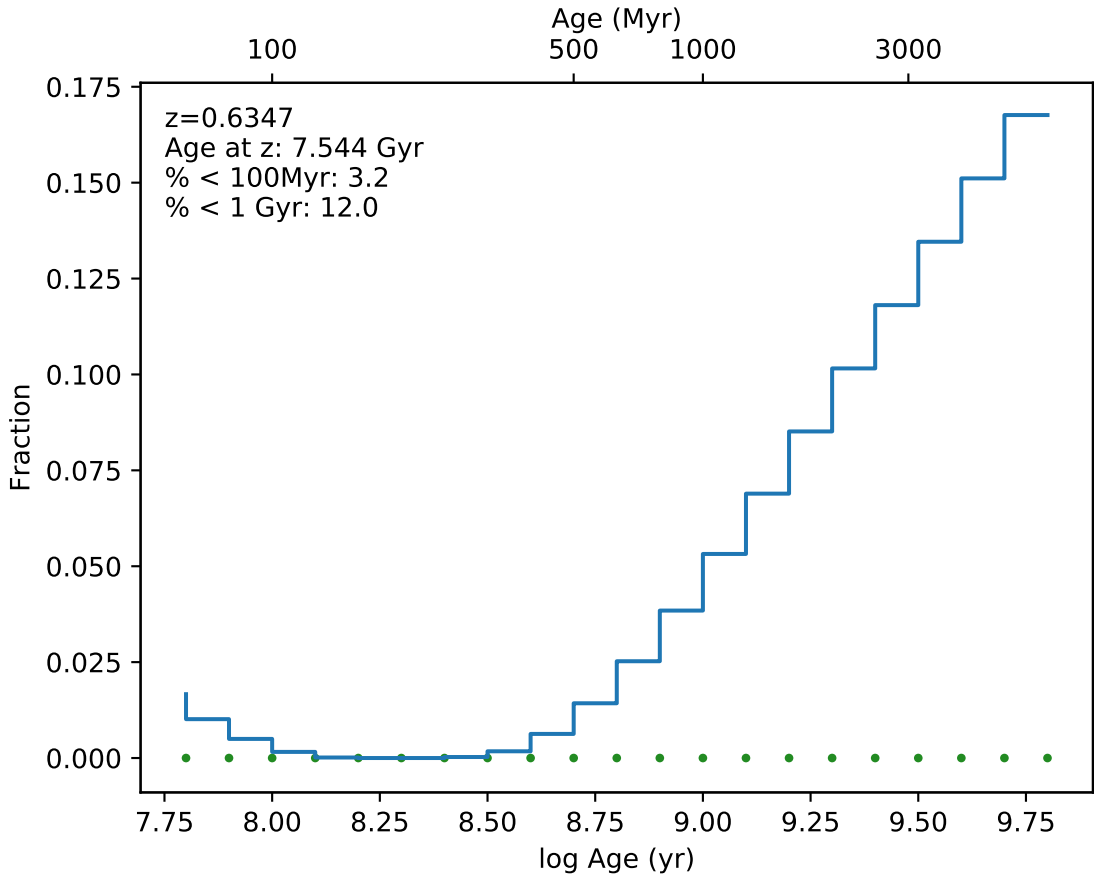
Age (Myr)
100
500
1000
3000
z=0.6347
Age at z: 7.544 Gyr
% < 100Myr: 3.2
% < 1 Gyr: 12.0
Fraction
0.175
0.150
0.125
0.100
0.075
0.050
0.025
0.000
7.75
8.00
8.25
8.50
8.75
9.00
9.25
9.50
9.75
log Age (yr)

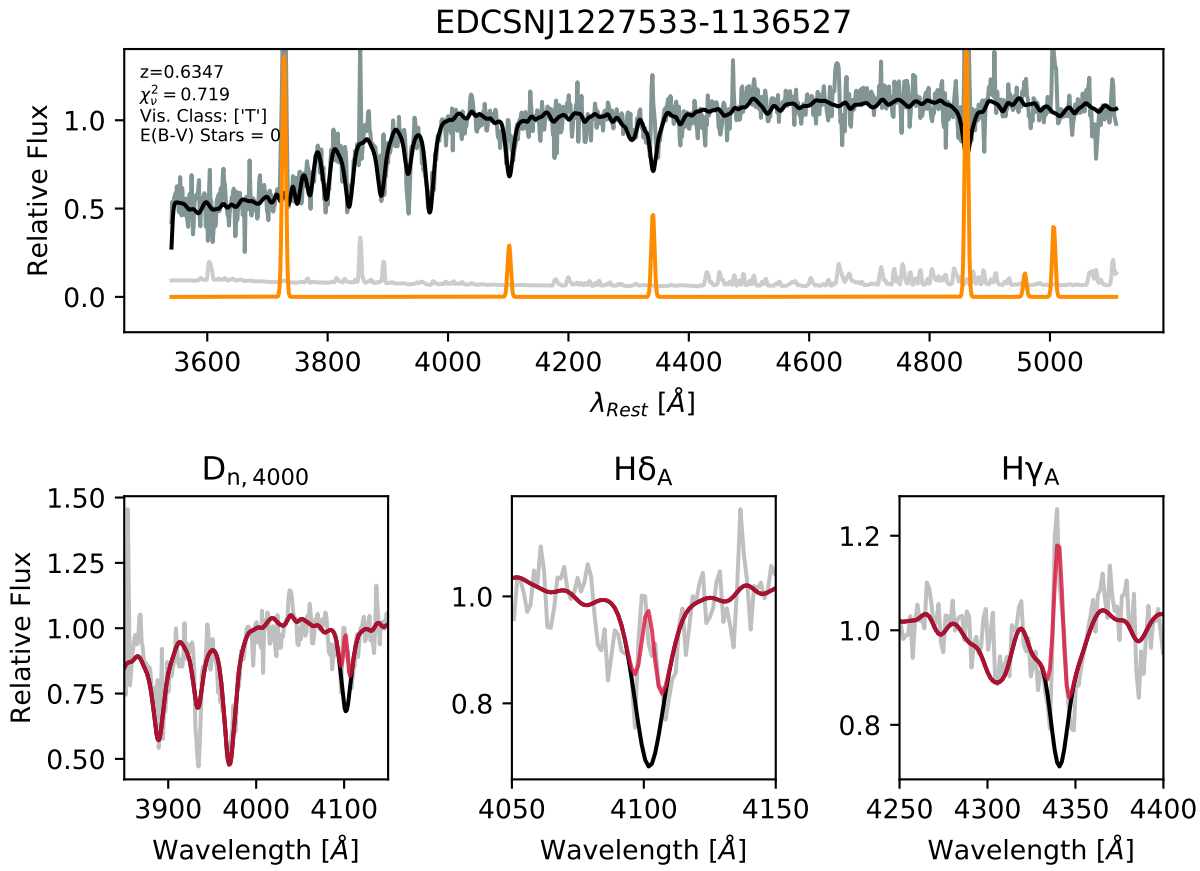
EDCSNJ1227533-1136527
z=0.6347
$\chi^2_\nu = 0.719$
Vis. Class: ['T']
E(B-V) Stars = 0
Relative Flux
1.0
0.5
0.0
3600
3800
4000
4200
4400
4600
4800
5000
λ_{Rest} [Å]
$D_{n,4000}$
$H\delta_A$
$H\gamma_A$
Relative Flux
1.50
1.25
1.00
0.75
0.50
3900
4000
4100
Wavelength [Å]
1.0
0.8
4050
4100
4150
Wavelength [Å]
1.2
1.0
0.8
4250
4300
4350
4400
Wavelength [Å]

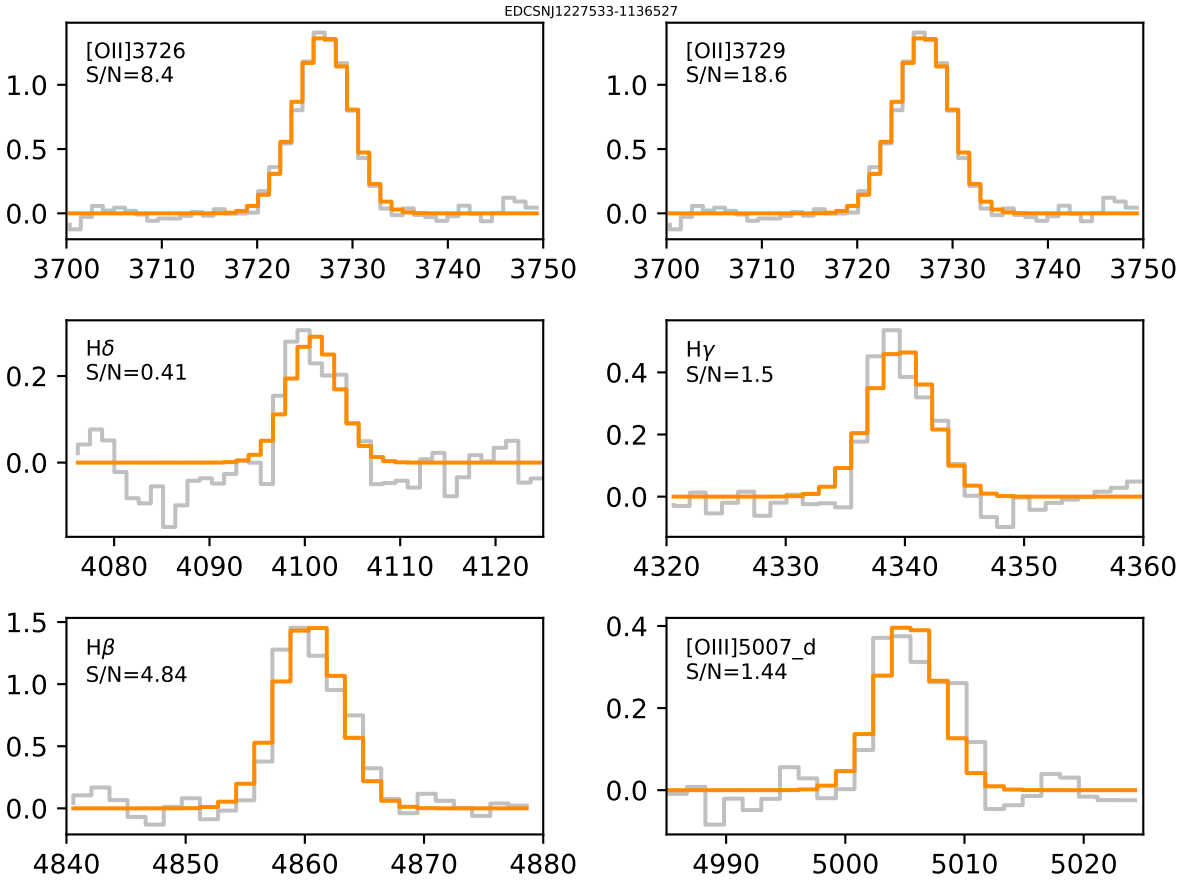
EDCSNJ1227533-1136527
[OII]3726
S/N=8.4
[OII]3729
S/N=18.6
Hδ
S/N=0.41
Hγ
S/N=1.5
Hβ
S/N=4.84
[OIII]5007_d
S/N=1.44

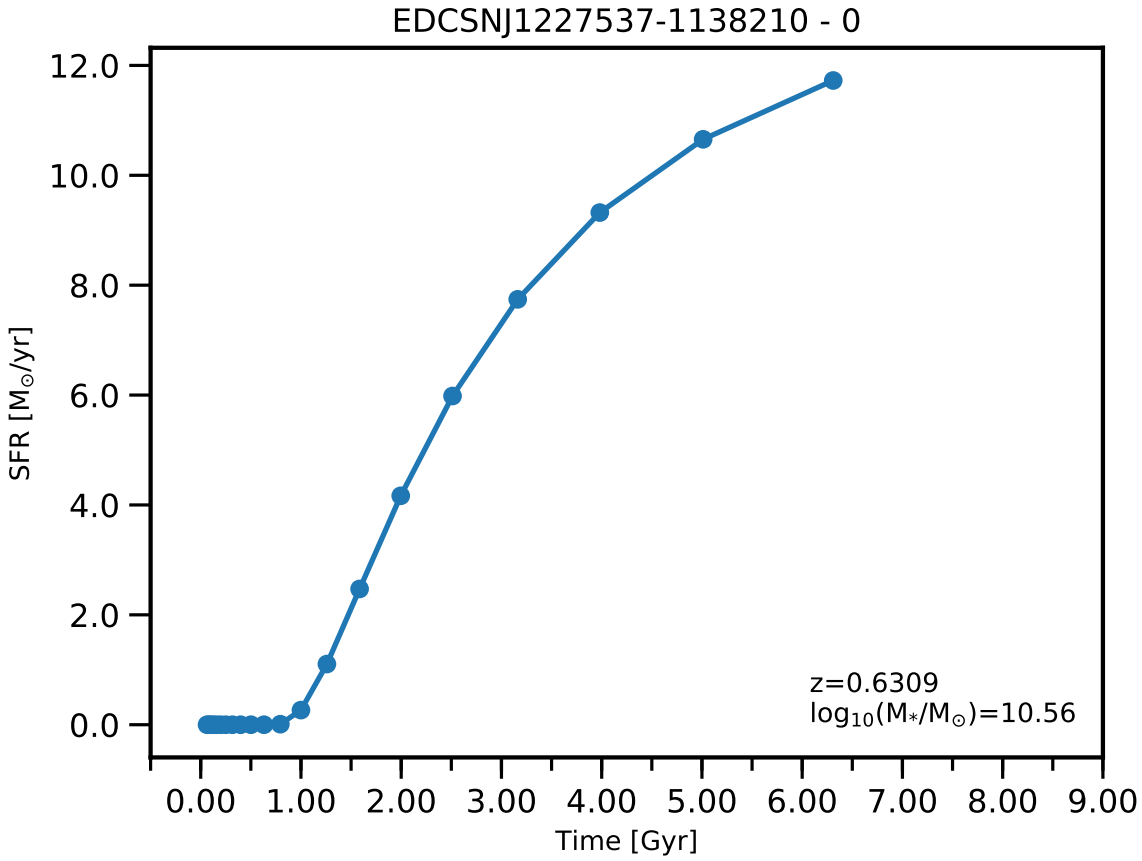
EDCSNJ1227537-1138210 - 0
12.0
10.0
8.0
6.0
4.0
2.0
0.0
SFR [M⊙/yr]
0.00
1.00
2.00
3.00
4.00
5.00
6.00
7.00
8.00
9.00
Time [Gyr]
z=0.6309
log10(M*/M⊙)=10.56

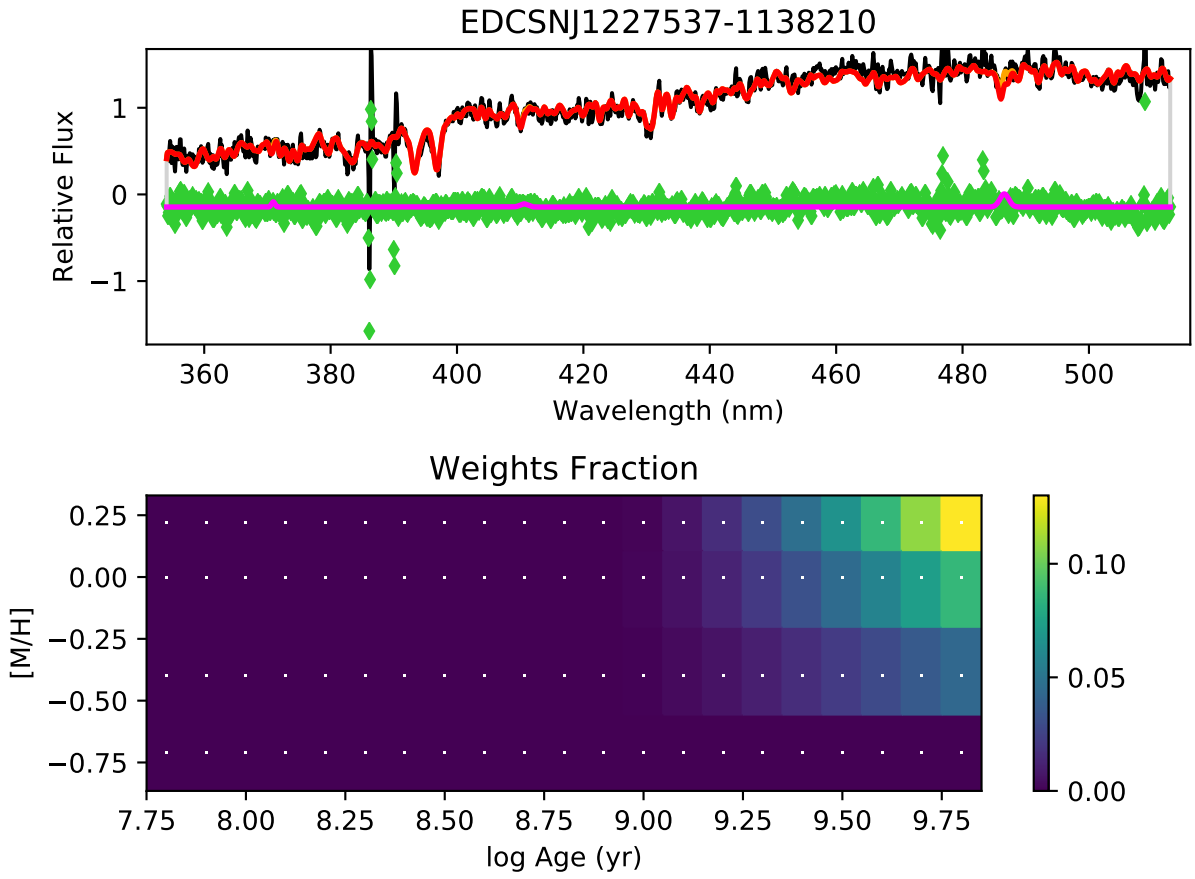
EDCSNJ1227537-1138210
Relative Flux
1
0
−1
360
380
400
420
440
460
480
500
Wavelength (nm)
Weights Fraction
[M/H]
0.25
0.00
−0.25
−0.50
−0.75
7.75
8.00
8.25
8.50
8.75
9.00
9.25
9.50
9.75
log Age (yr)
0.10
0.05
0.00

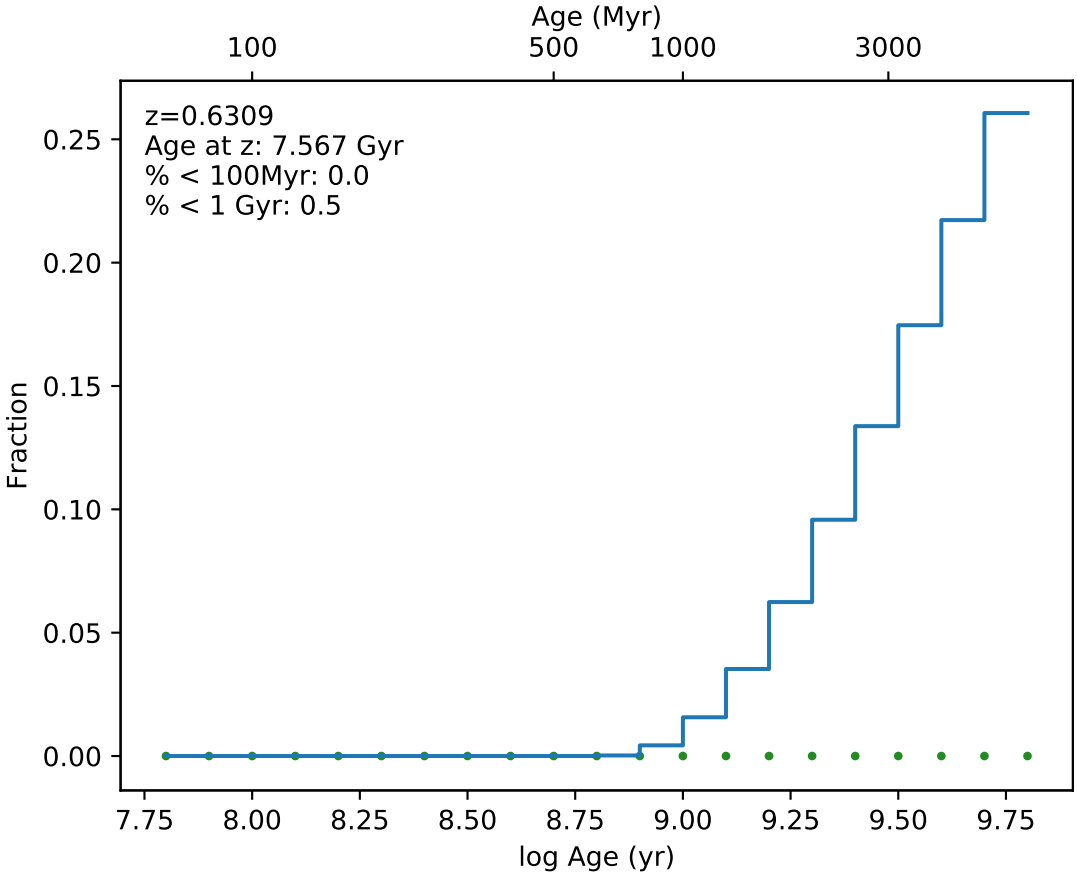
Age (Myr)
100
500
1000
3000
z=0.6309
Age at z: 7.567 Gyr
% < 100Myr: 0.0
% < 1 Gyr: 0.5
Fraction
0.25
0.20
0.15
0.10
0.05
0.00
7.75
8.00
8.25
8.50
8.75
9.00
9.25
9.50
9.75
log Age (yr)

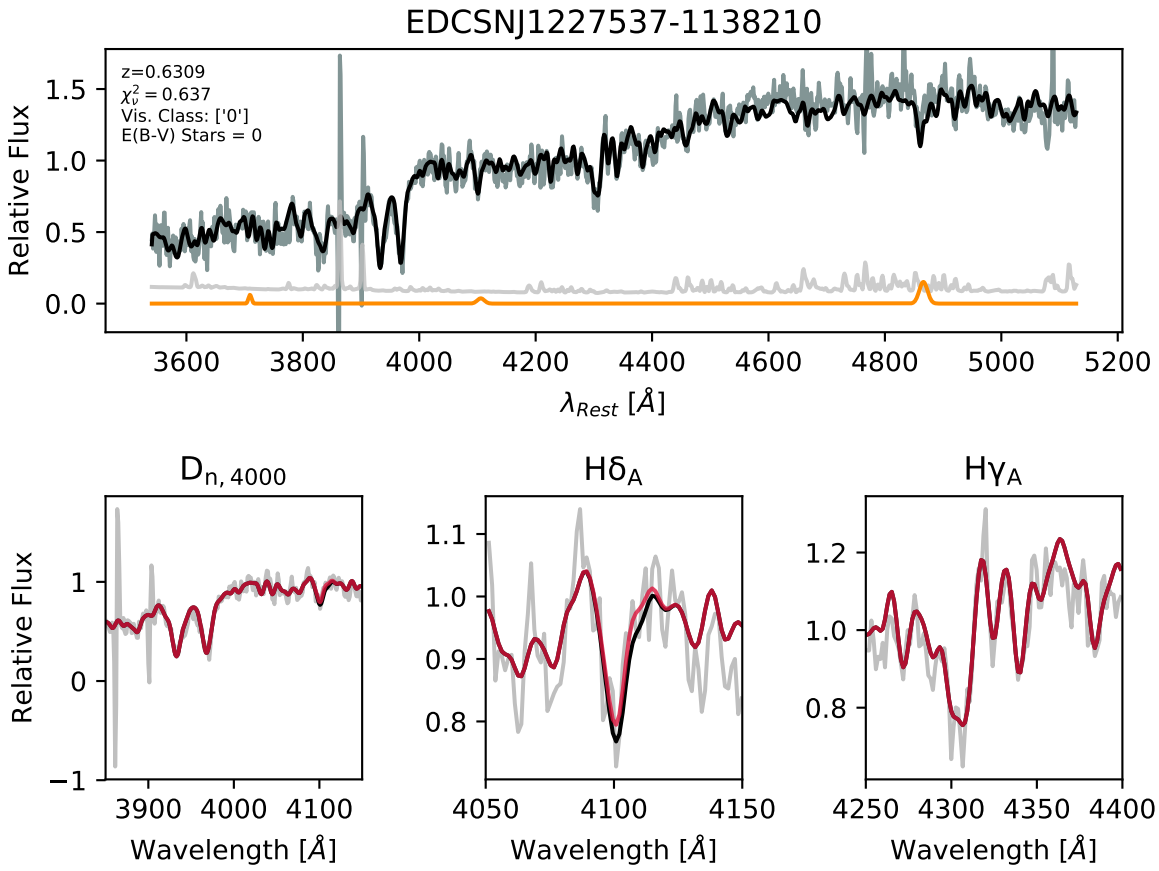
EDCSNJ1227537-1138210
z=0.6309
$\chi^2_\nu = 0.637$
Vis. Class: ['0']
E(B-V) Stars = 0
Relative Flux
λ_{Rest} [Å]
$D_{n,4000}$
$H\delta_A$
$H\gamma_A$
Wavelength [Å]

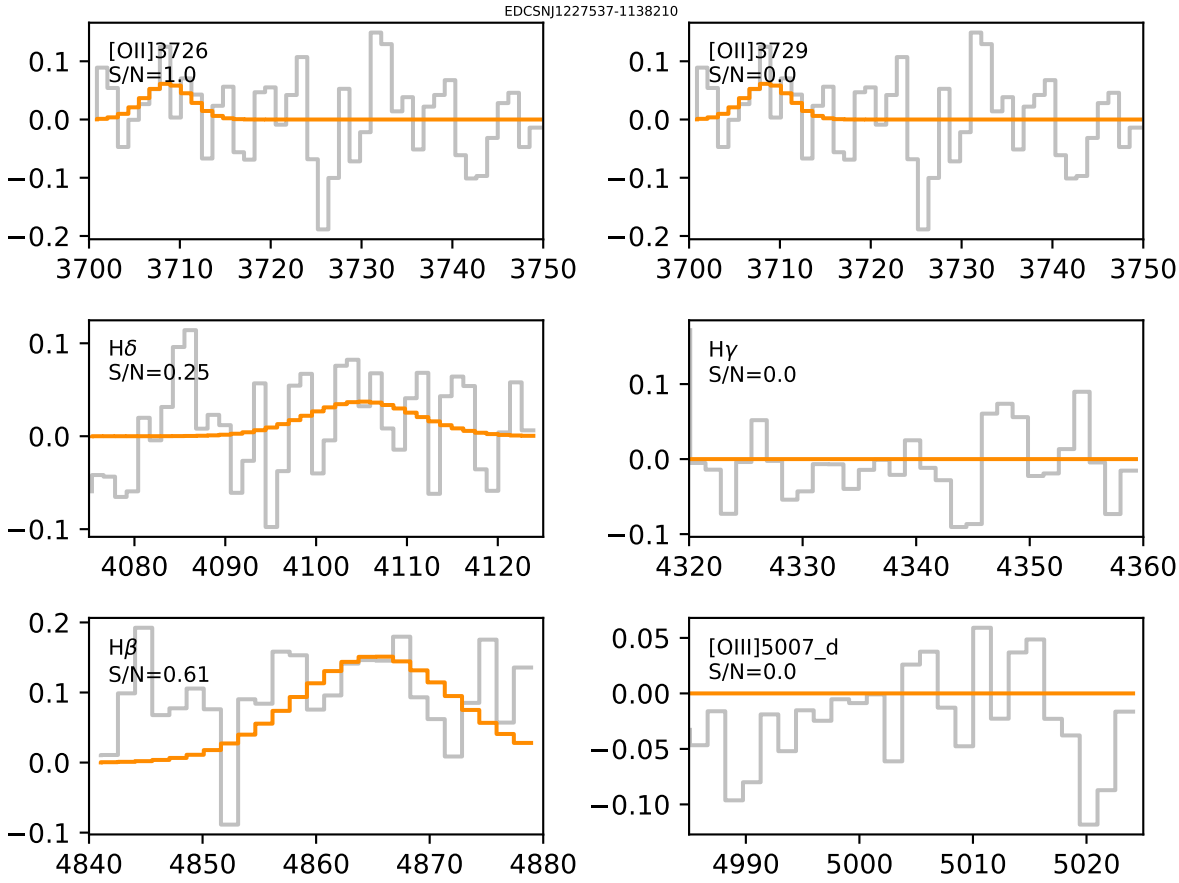
EDCSNJ1227537-1138210
[OII]3726
S/N=1.0
[OII]3729
S/N=0.0
Hδ
S/N=0.25
Hγ
S/N=0.0
Hβ
S/N=0.61
[OIII]5007_d
S/N=0.0

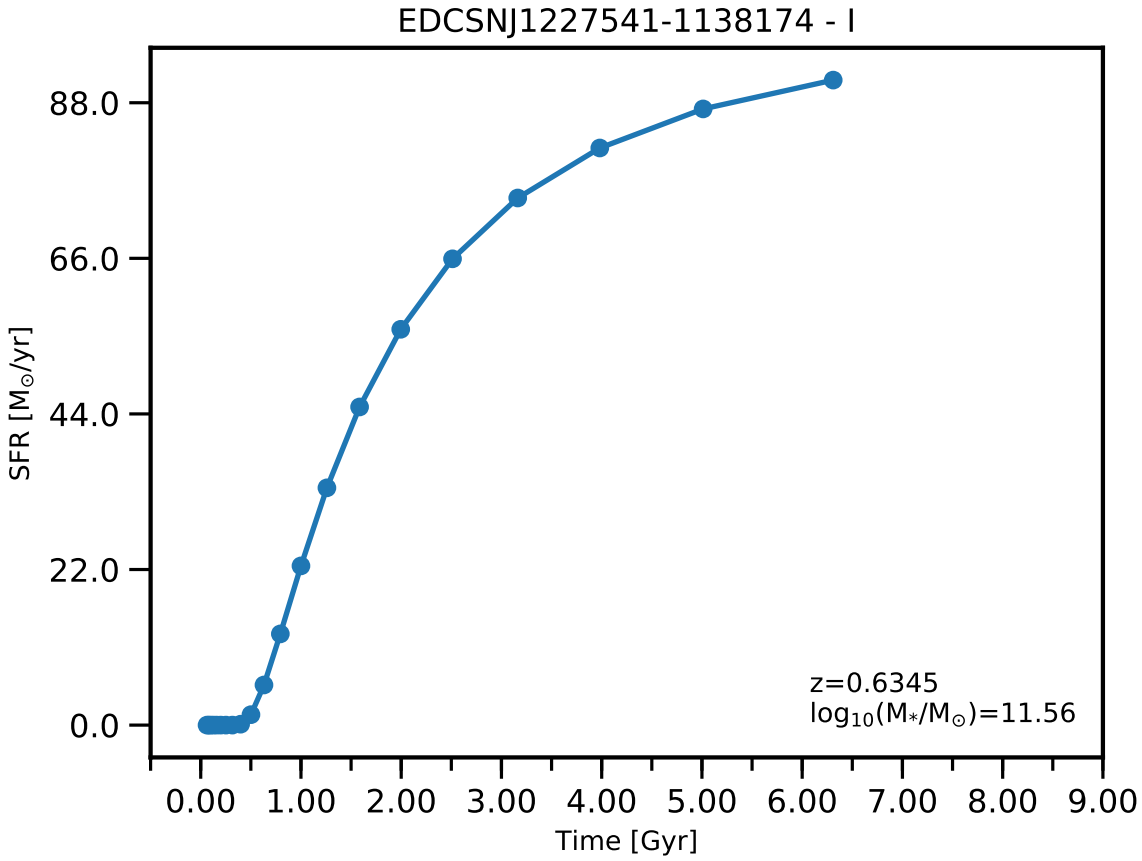
EDCSNJ1227541-1138174 - I
88.0
66.0
44.0
22.0
0.0
SFR [M⊙/yr]
0.00
1.00
2.00
3.00
4.00
5.00
6.00
7.00
8.00
9.00
Time [Gyr]
z=0.6345
log10(M*/M⊙)=11.56

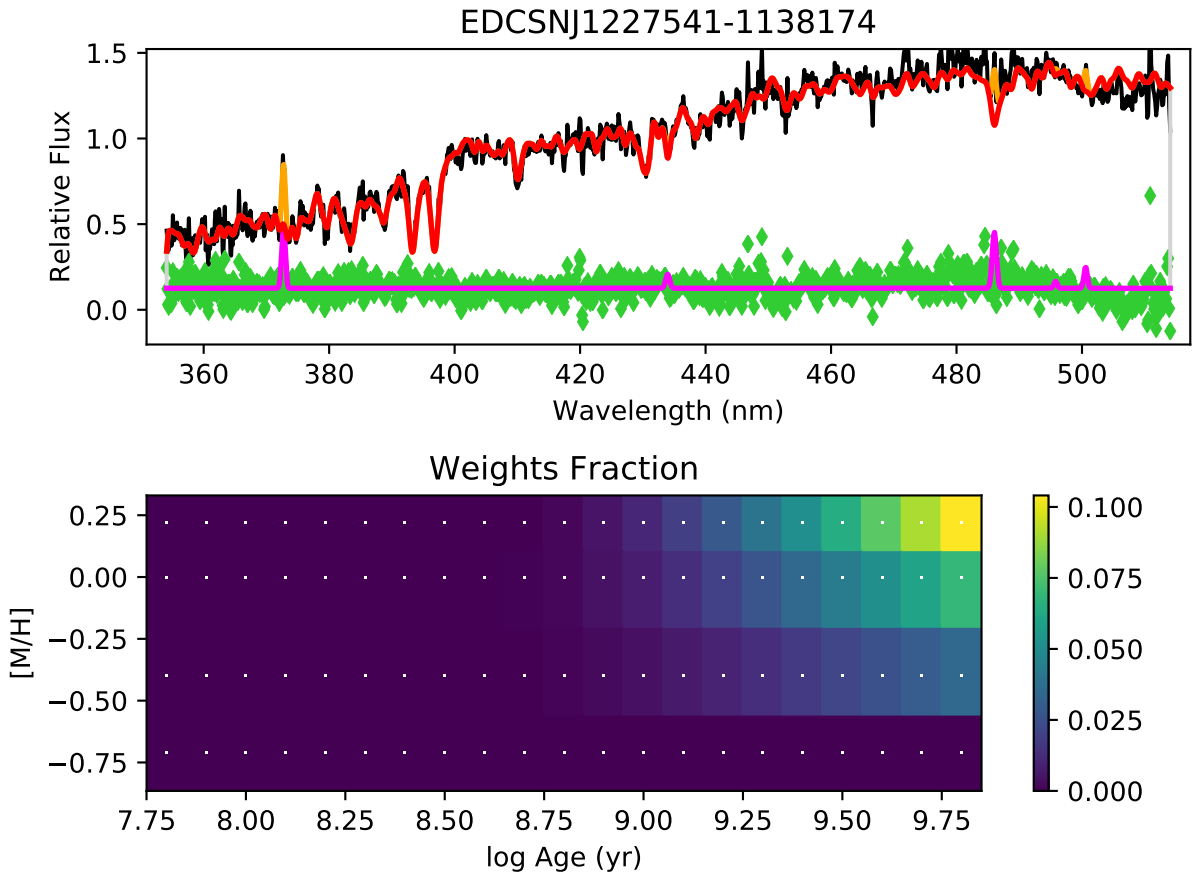
EDCSNJ1227541-1138174
Relative Flux
1.5
1.0
0.5
0.0
360
380
400
420
440
460
480
500
Wavelength (nm)
Weights Fraction
[M/H]
0.25
0.00
−0.25
−0.50
−0.75
7.75
8.00
8.25
8.50
8.75
9.00
9.25
9.50
9.75
log Age (yr)
0.100
0.075
0.050
0.025
0.000

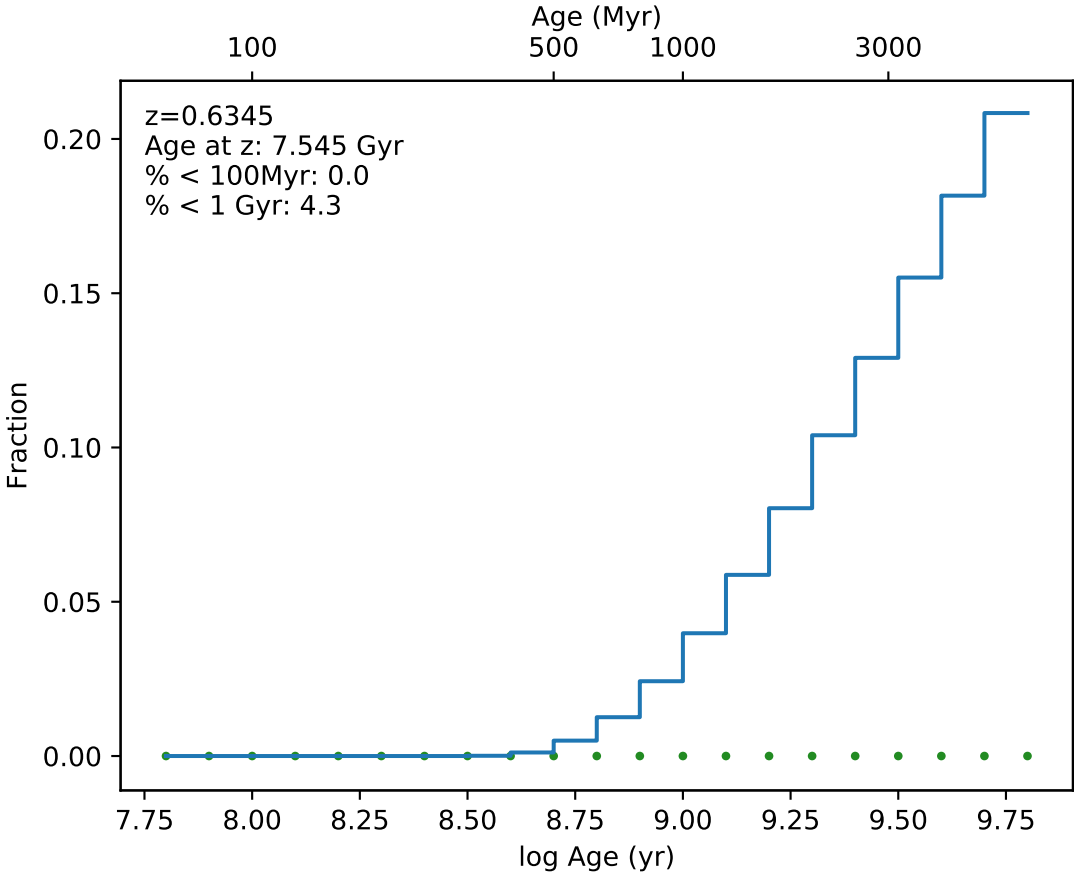
Age (Myr)
100
500
1000
3000
z=0.6345
Age at z: 7.545 Gyr
% < 100Myr: 0.0
% < 1 Gyr: 4.3
Fraction
0.20
0.15
0.10
0.05
0.00
7.75
8.00
8.25
8.50
8.75
9.00
9.25
9.50
9.75
log Age (yr)

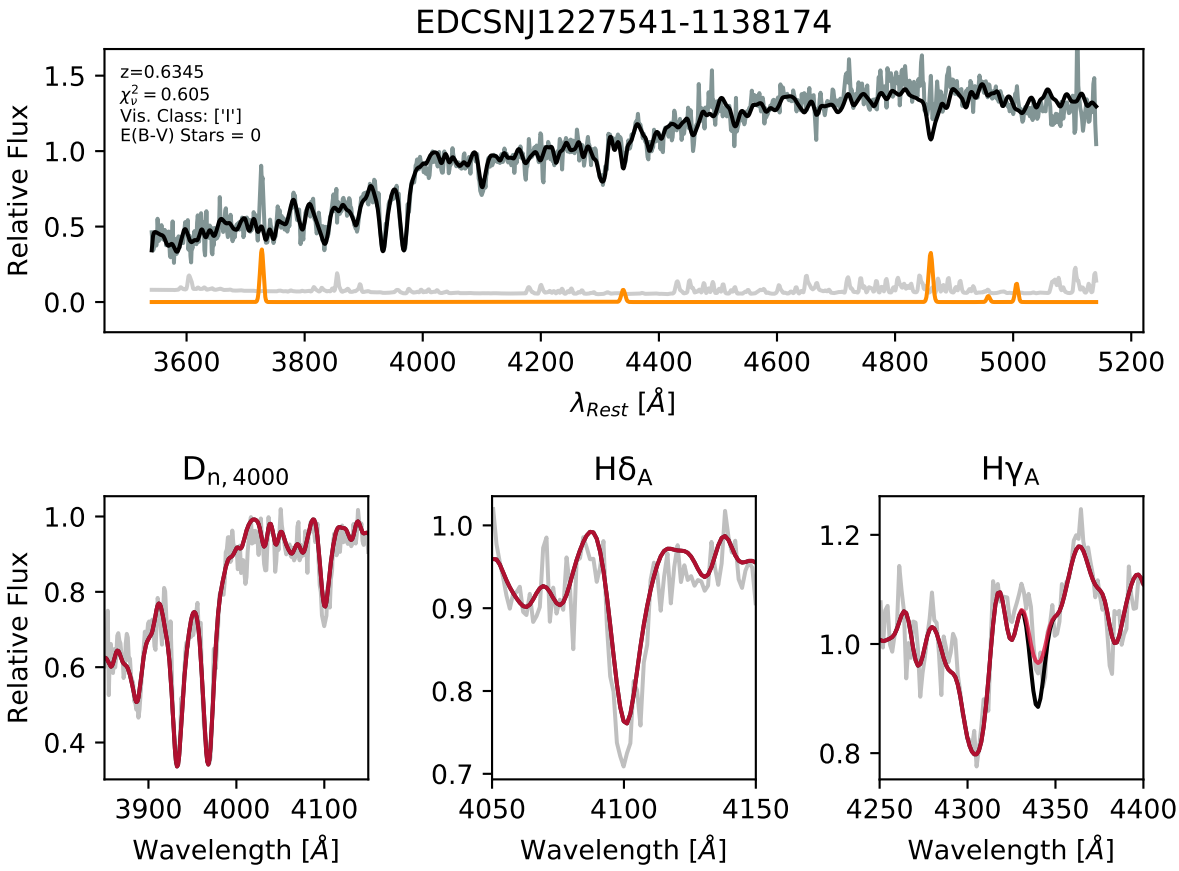
EDCSNJ1227541-1138174
z=0.6345
$\chi^2_\nu = 0.605$
Vis. Class: ['I']
E(B-V) Stars = 0
Relative Flux
λ_{Rest} [Å]
$D_{n,4000}$
$H\delta_A$
$H\gamma_A$
Wavelength [Å]

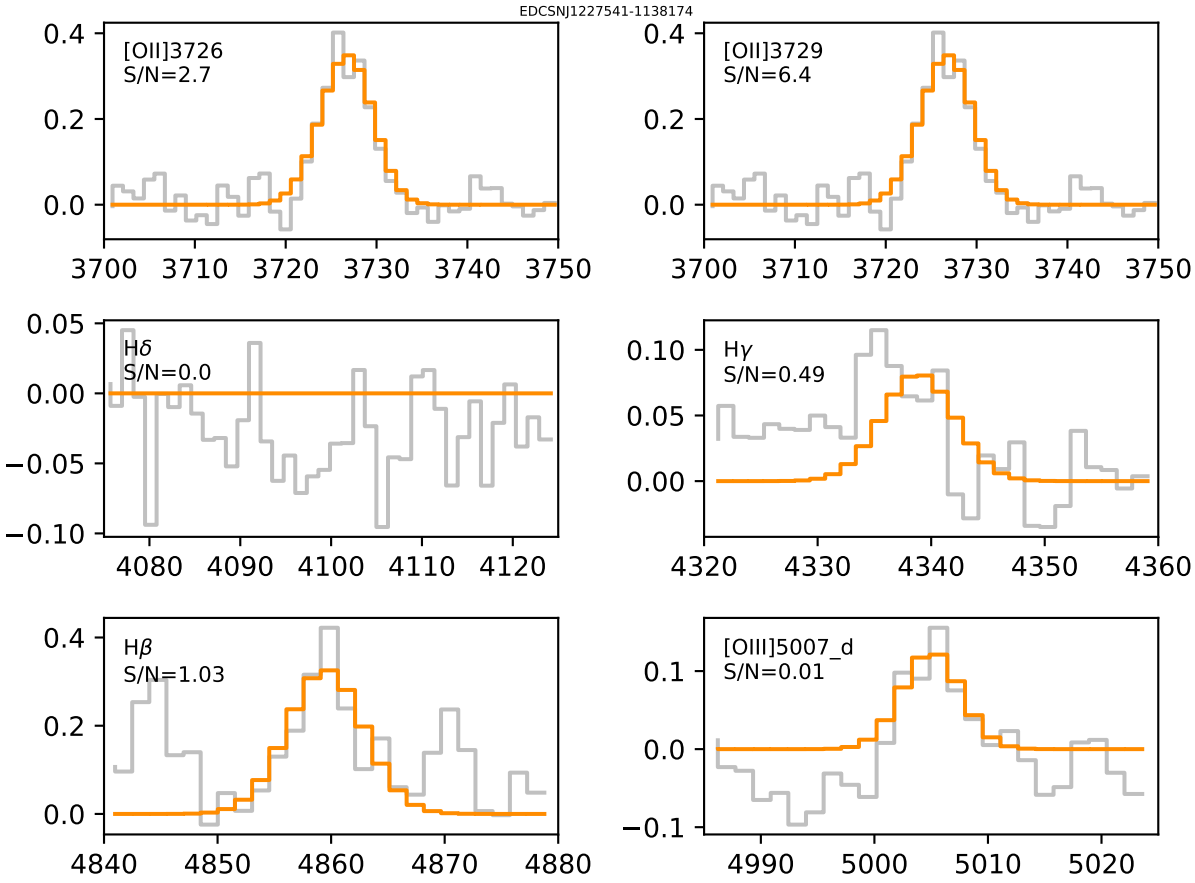
EDCSNJ1227541-1138174
[OII]3726
S/N=2.7
[OII]3729
S/N=6.4
Hδ
S/N=0.0
Hγ
S/N=0.49
Hβ
S/N=1.03
[OIII]5007_d
S/N=0.01

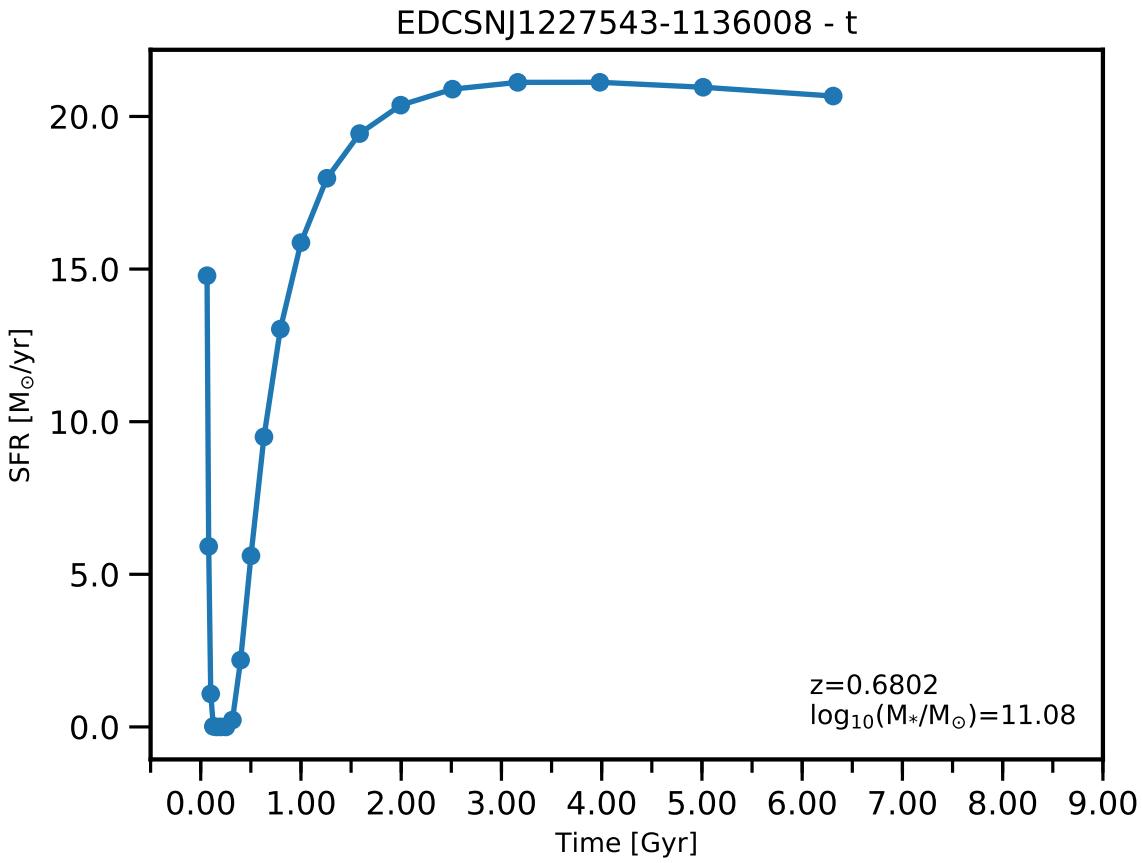
EDCSNJ1227543-1136008 - t
SFR [M⊙/yr]
20.0
15.0
10.0
5.0
0.0
0.00
1.00
2.00
3.00
4.00
5.00
6.00
7.00
8.00
9.00
Time [Gyr]
z=0.6802
log10(M*/M⊙)=11.08

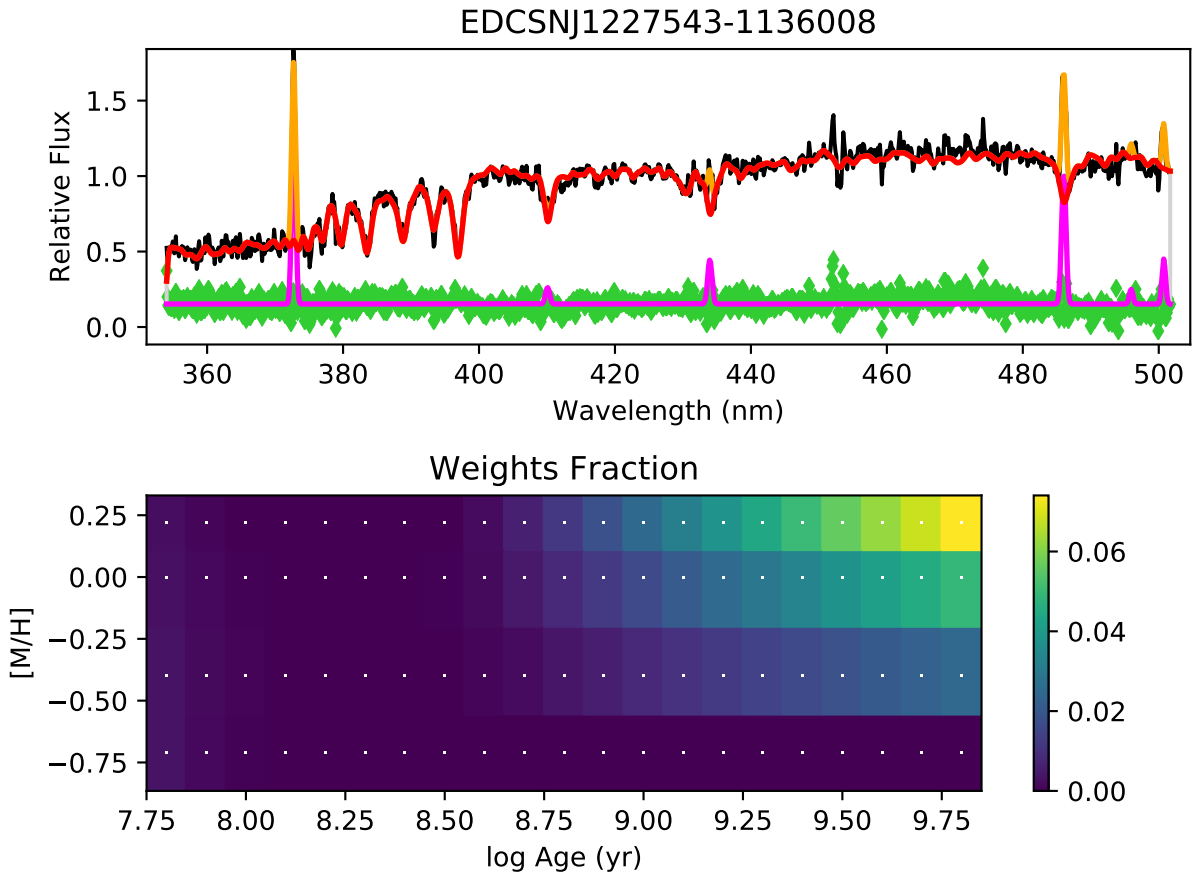
EDCSNJ1227543-1136008
Relative Flux
1.5
1.0
0.5
0.0
360
380
400
420
440
460
480
500
Wavelength (nm)
Weights Fraction
[M/H]
0.25
0.00
−0.25
−0.50
−0.75
7.75
8.00
8.25
8.50
8.75
9.00
9.25
9.50
9.75
log Age (yr)
0.06
0.04
0.02
0.00

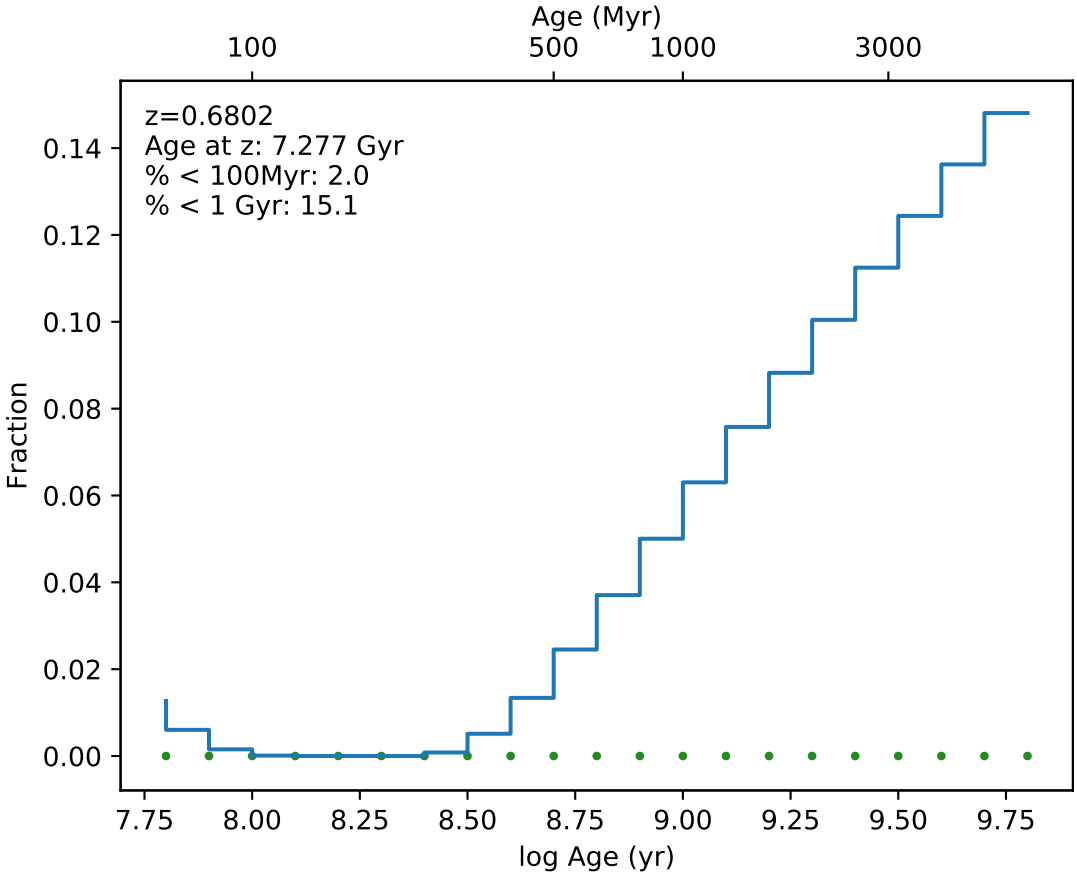
Age (Myr)
100
500
1000
3000
z=0.6802
Age at z: 7.277 Gyr
% < 100Myr: 2.0
% < 1 Gyr: 15.1
Fraction
0.14
0.12
0.10
0.08
0.06
0.04
0.02
0.00
7.75
8.00
8.25
8.50
8.75
9.00
9.25
9.50
9.75
log Age (yr)

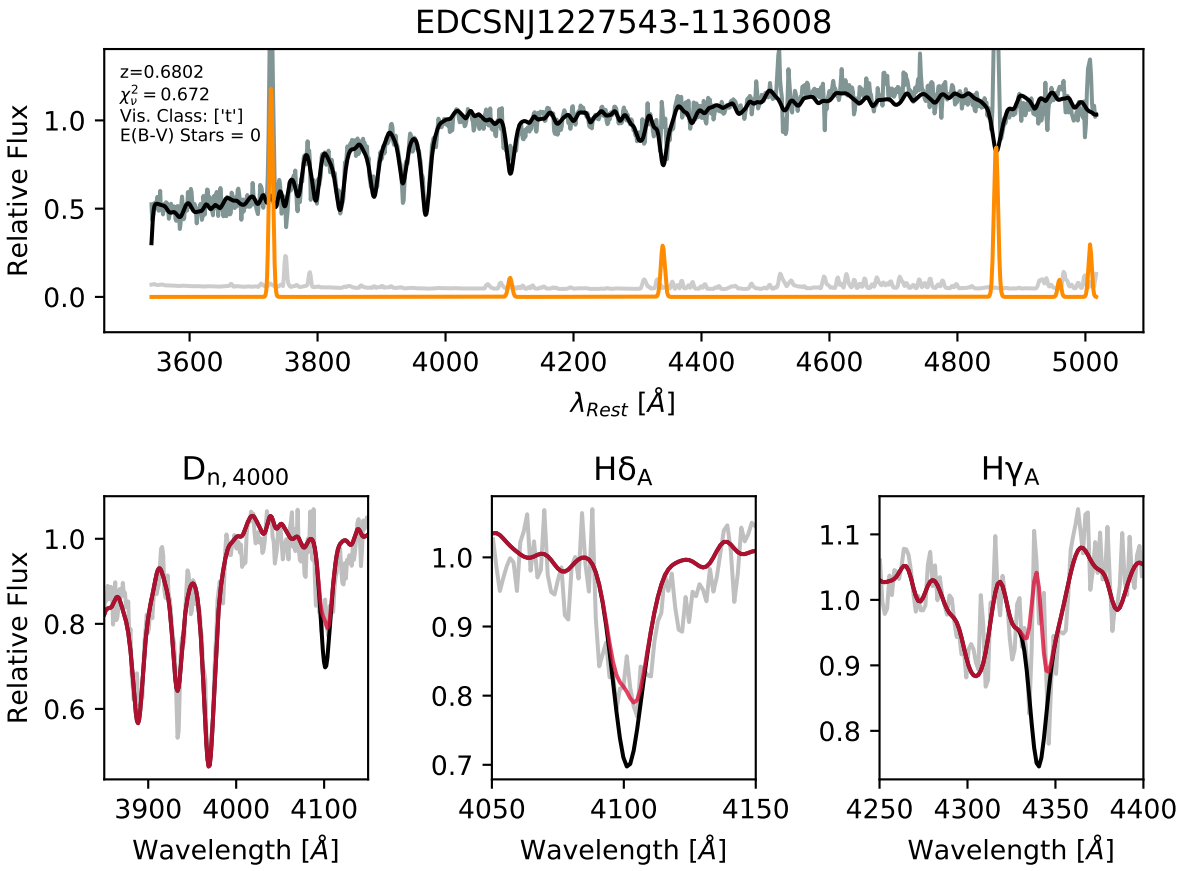
EDCSNJ1227543-1136008
z=0.6802
$\chi^2_\nu = 0.672$
Vis. Class: ['t']
E(B-V) Stars = 0
Relative Flux
1.0
0.5
0.0
3600
3800
4000
4200
4400
4600
4800
5000
λ_{Rest} [Å]
$D_{n,4000}$
$H\delta_A$
$H\gamma_A$
Relative Flux
1.0
0.8
0.6
3900
4000
4100
Wavelength [Å]
1.0
0.9
0.8
0.7
4050
4100
4150
Wavelength [Å]
1.1
1.0
0.9
0.8
4250
4300
4350
4400
Wavelength [Å]

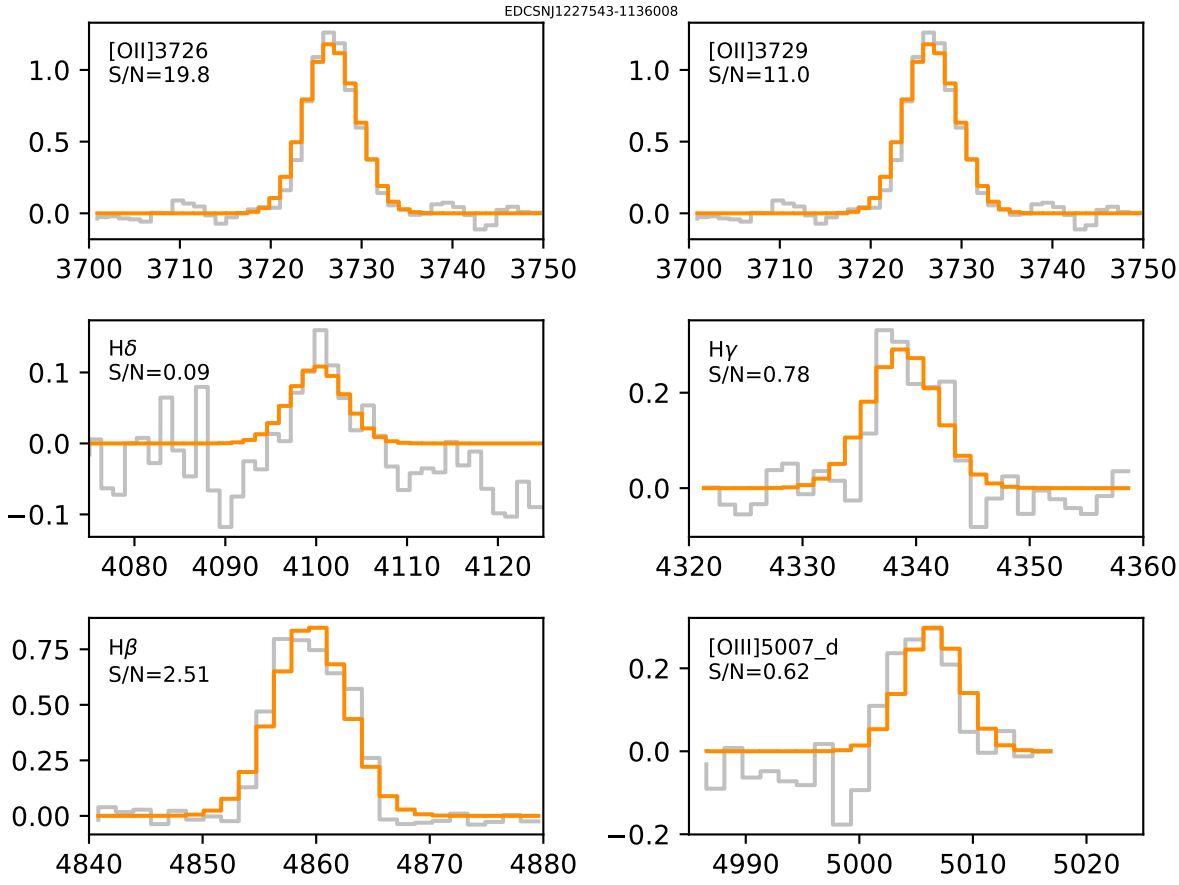
EDCSNJ1227543-1136008
[OII]3726
S/N=19.8
[OII]3729
S/N=11.0
Hδ
S/N=0.09
Hγ
S/N=0.78
Hβ
S/N=2.51
[OIII]5007_d
S/N=0.62

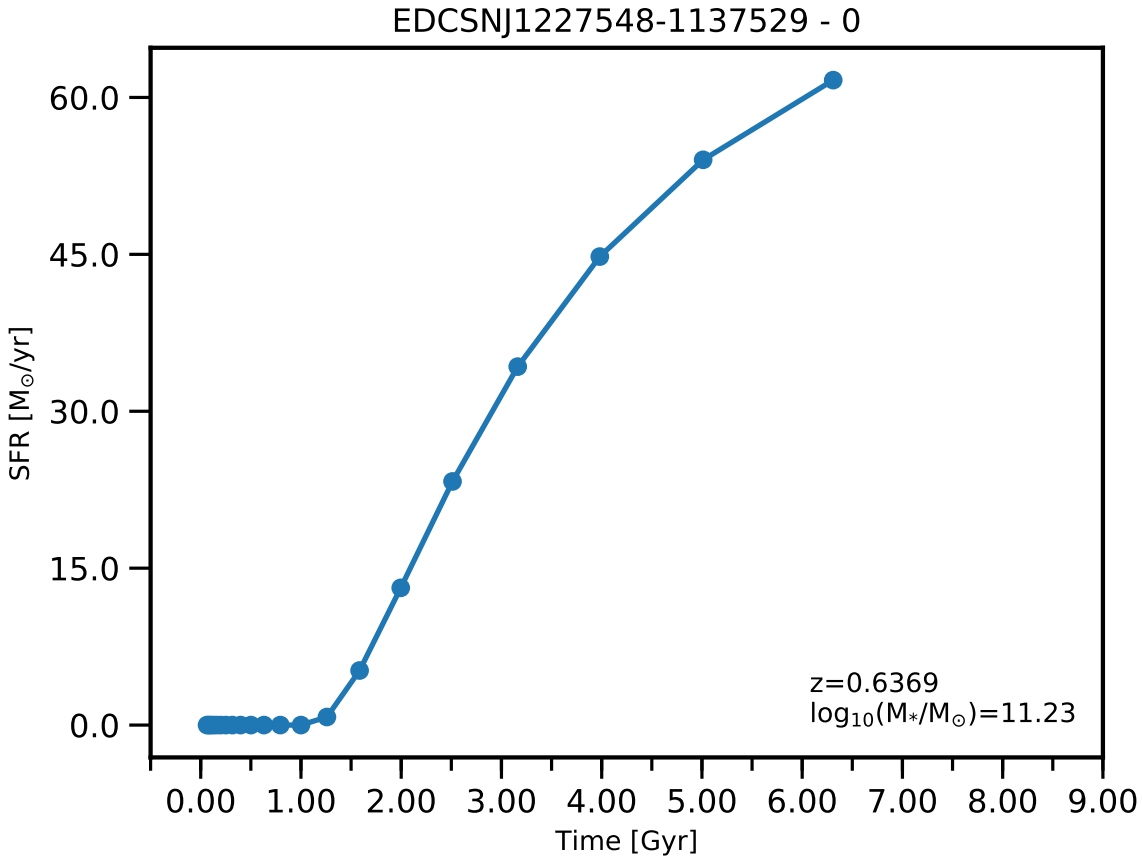
EDCSNJ1227548-1137529 - 0
60.0
45.0
30.0
15.0
0.0
SFR [M⊙/yr]
0.00
1.00
2.00
3.00
4.00
5.00
6.00
7.00
8.00
9.00
Time [Gyr]
z=0.6369
log10(M*/M⊙)=11.23

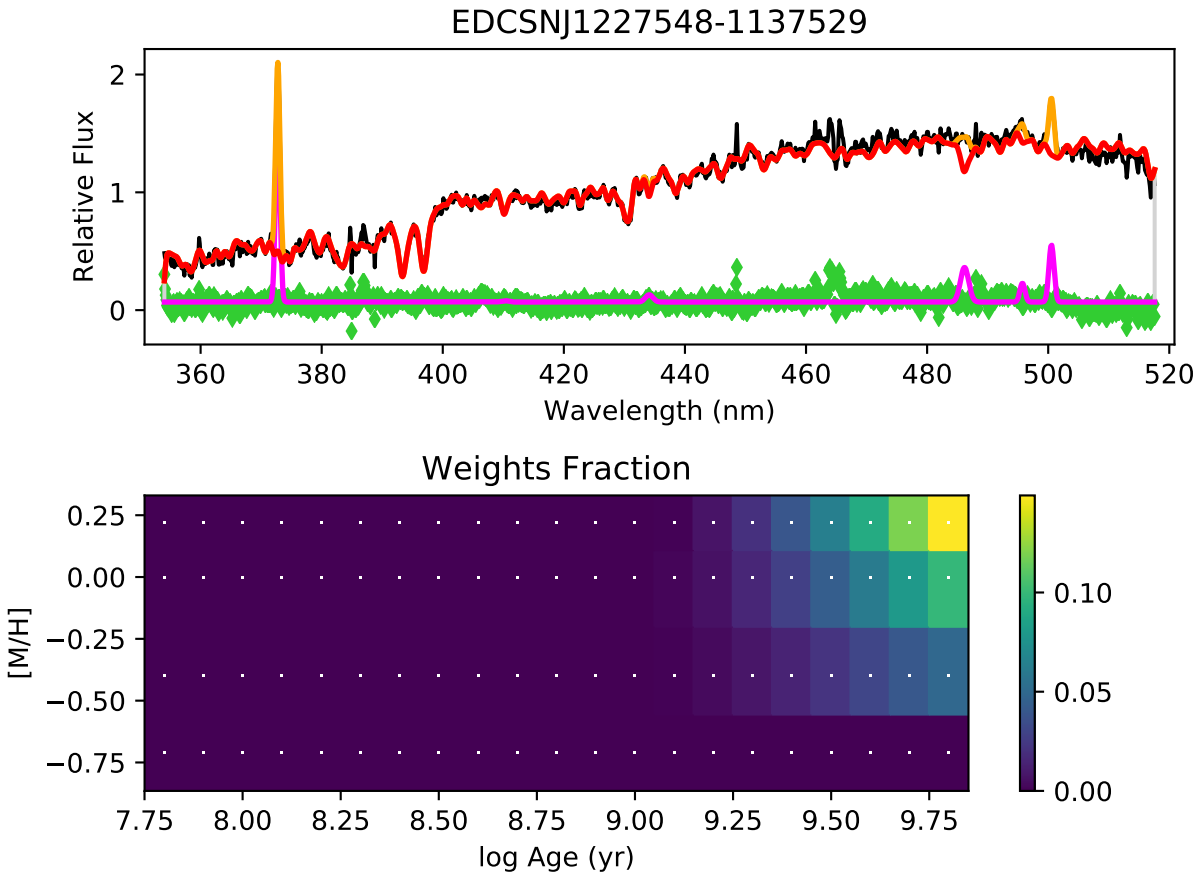
EDCSNJ1227548-1137529
Relative Flux
2
1
0
360
380
400
420
440
460
480
500
520
Wavelength (nm)
Weights Fraction
[M/H]
0.25
0.00
−0.25
−0.50
−0.75
7.75
8.00
8.25
8.50
8.75
9.00
9.25
9.50
9.75
log Age (yr)
0.10
0.05
0.00

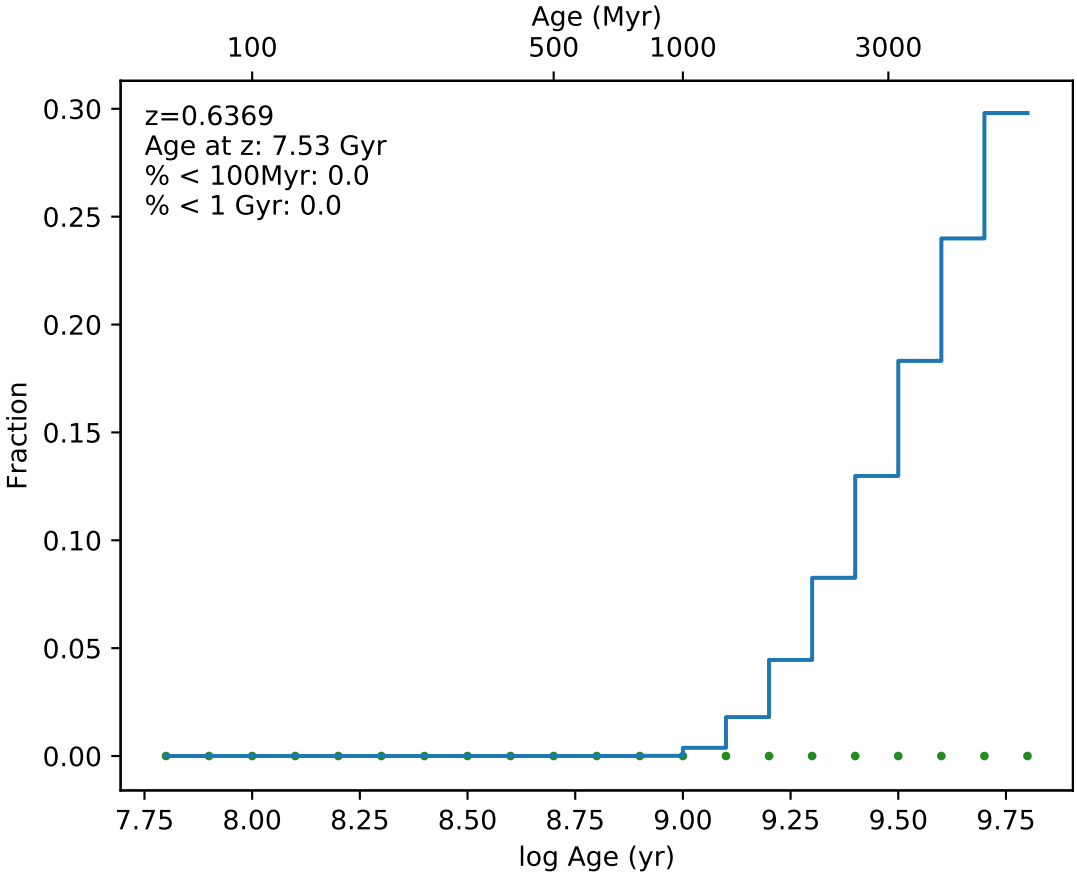
Age (Myr)
100
500
1000
3000
z=0.6369
Age at z: 7.53 Gyr
% < 100Myr: 0.0
% < 1 Gyr: 0.0
Fraction
0.30
0.25
0.20
0.15
0.10
0.05
0.00
7.75
8.00
8.25
8.50
8.75
9.00
9.25
9.50
9.75
log Age (yr)

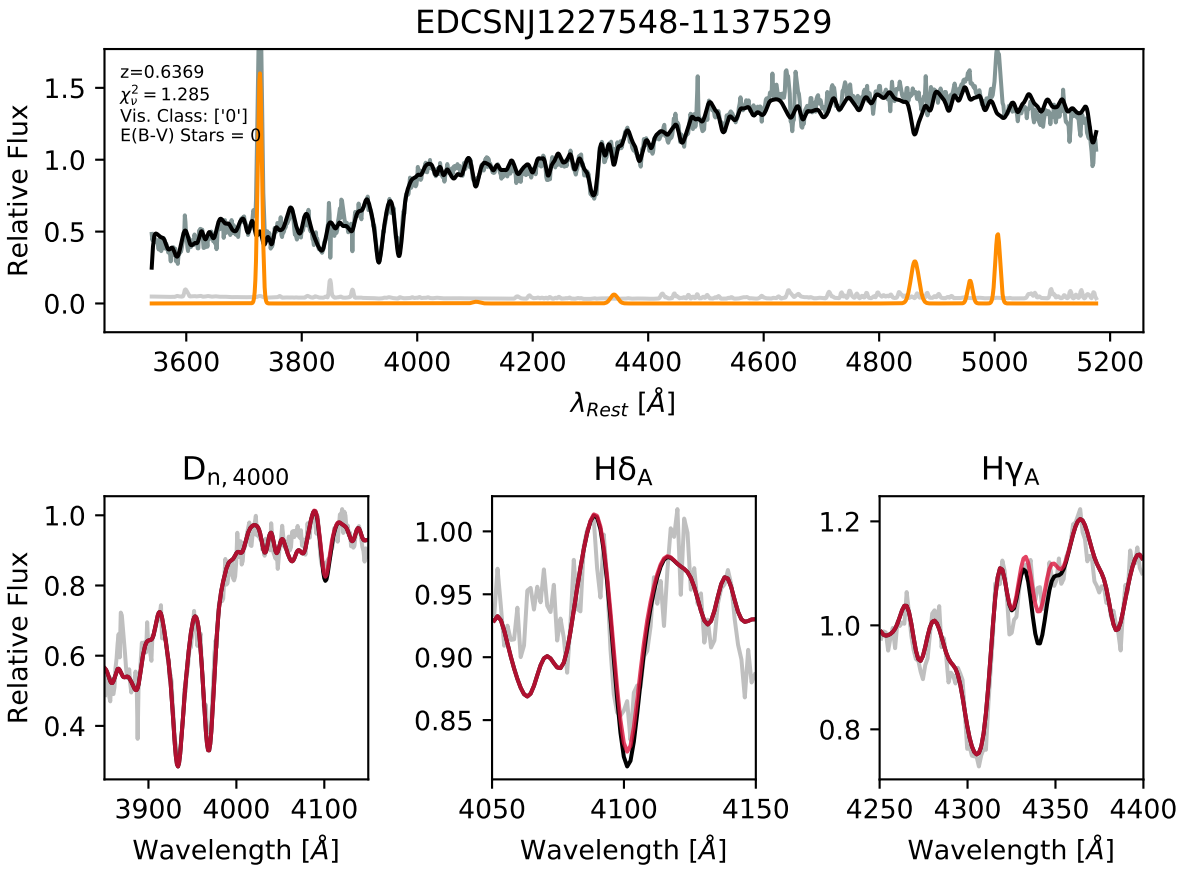
EDCSNJ1227548-1137529
z=0.6369
$\chi^2_\nu = 1.285$
Vis. Class: ['0']
E(B-V) Stars = 0
Relative Flux
λ_{Rest} [Å]
$D_{n,4000}$
$H\delta_A$
$H\gamma_A$
Wavelength [Å]

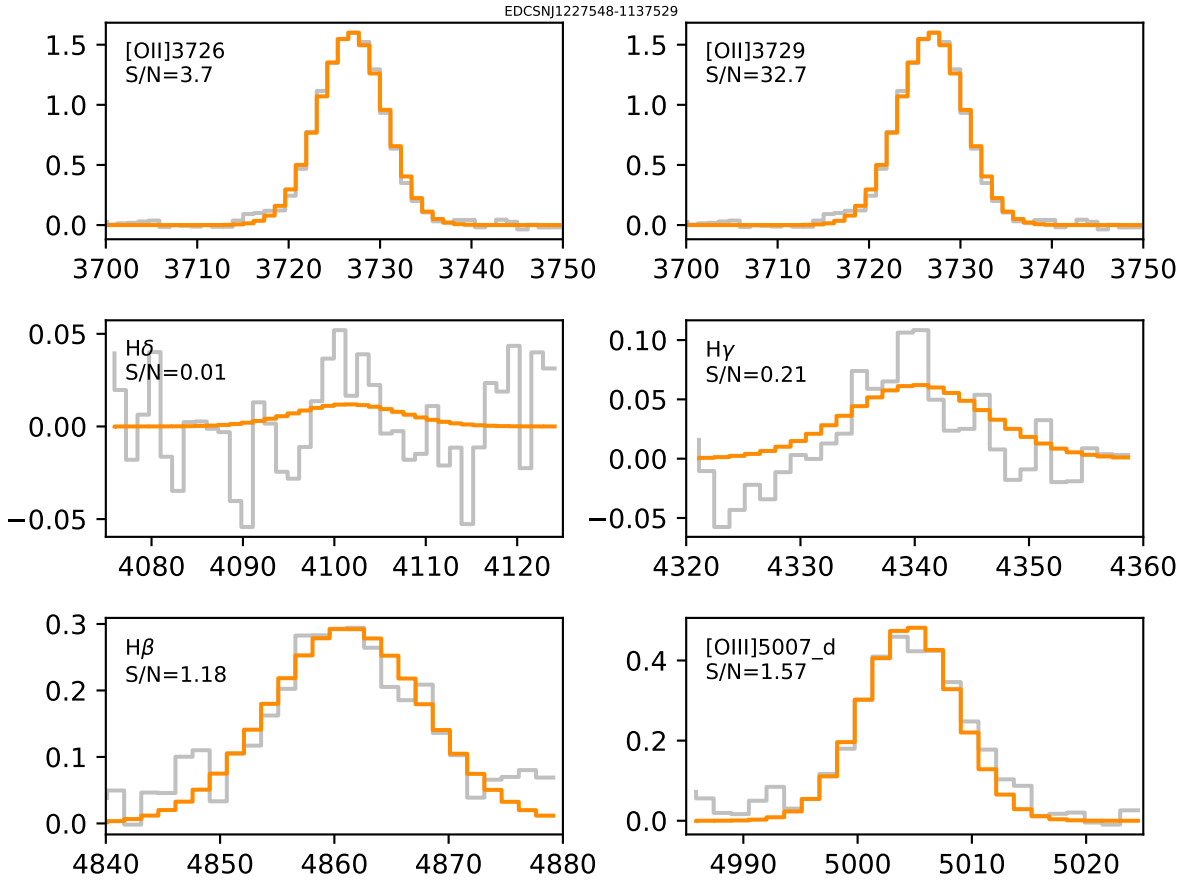
EDCSNJ1227548-1137529
[OII]3726
S/N=3.7
[OII]3729
S/N=32.7
Hδ
S/N=0.01
Hγ
S/N=0.21
Hβ
S/N=1.18
[OIII]5007_d
S/N=1.57

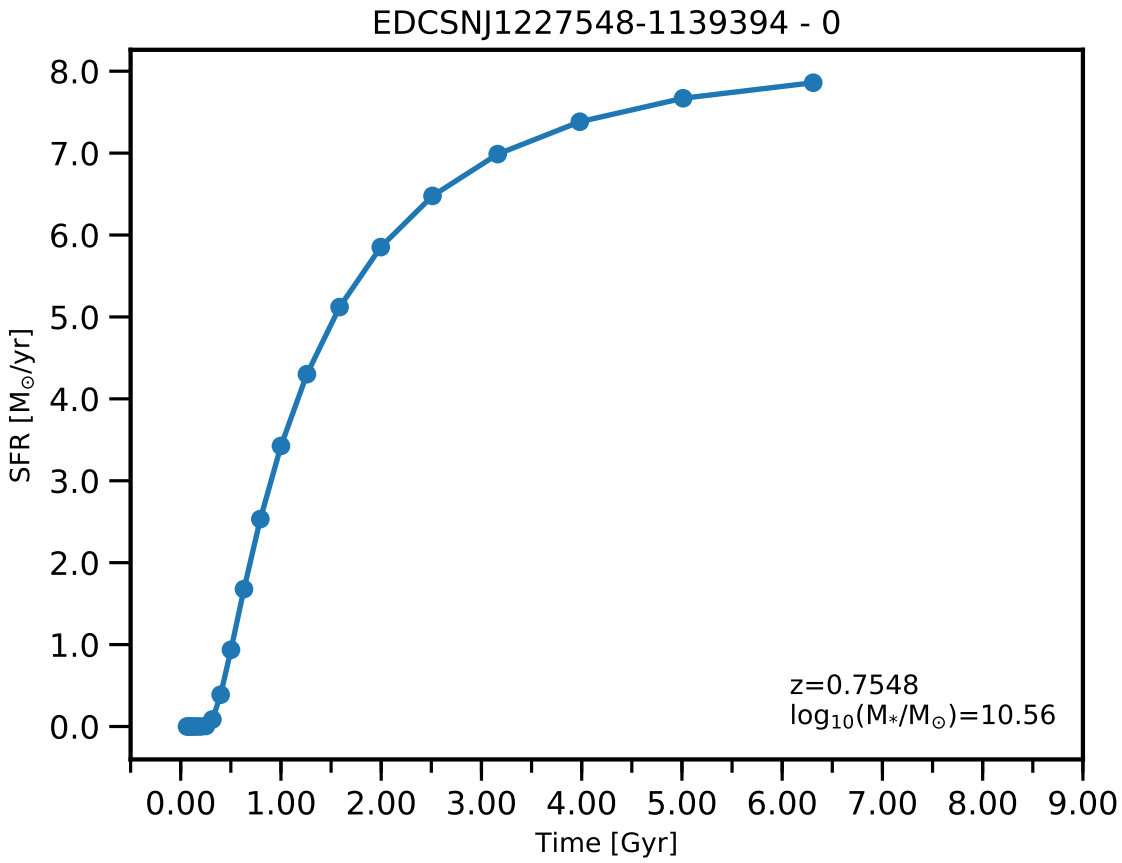
EDCSNJ1227548-1139394 - 0
SFR [M⊙/yr]
Time [Gyr]
z=0.7548
log10(M*/M⊙)=10.56
0.0
1.0
2.0
3.0
4.0
5.0
6.0
7.0
8.0
0.00
1.00
2.00
3.00
4.00
5.00
6.00
7.00
8.00
9.00

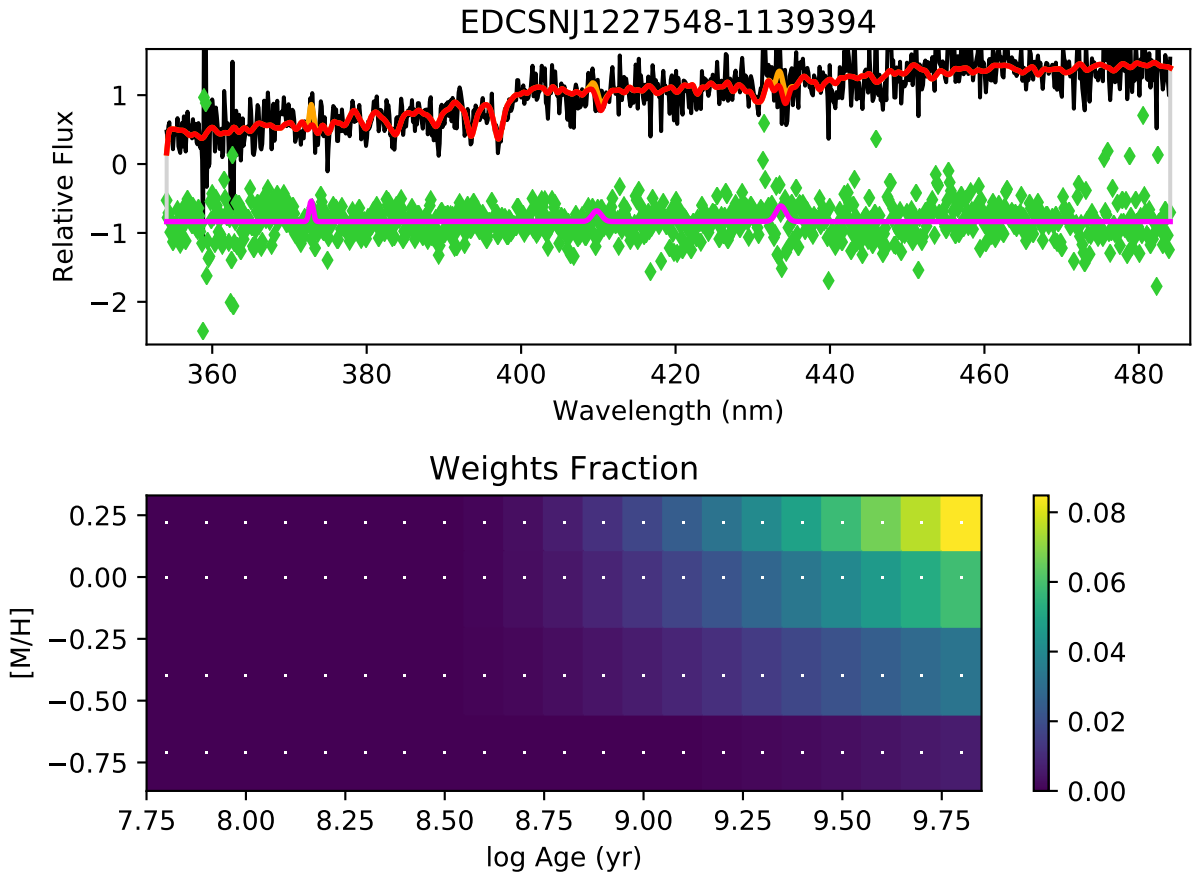
EDCSNJ1227548-1139394
Relative Flux
1
0
−1
−2
360
380
400
420
440
460
480
Wavelength (nm)
Weights Fraction
[M/H]
0.25
0.00
−0.25
−0.50
−0.75
7.75
8.00
8.25
8.50
8.75
9.00
9.25
9.50
9.75
log Age (yr)
0.08
0.06
0.04
0.02
0.00

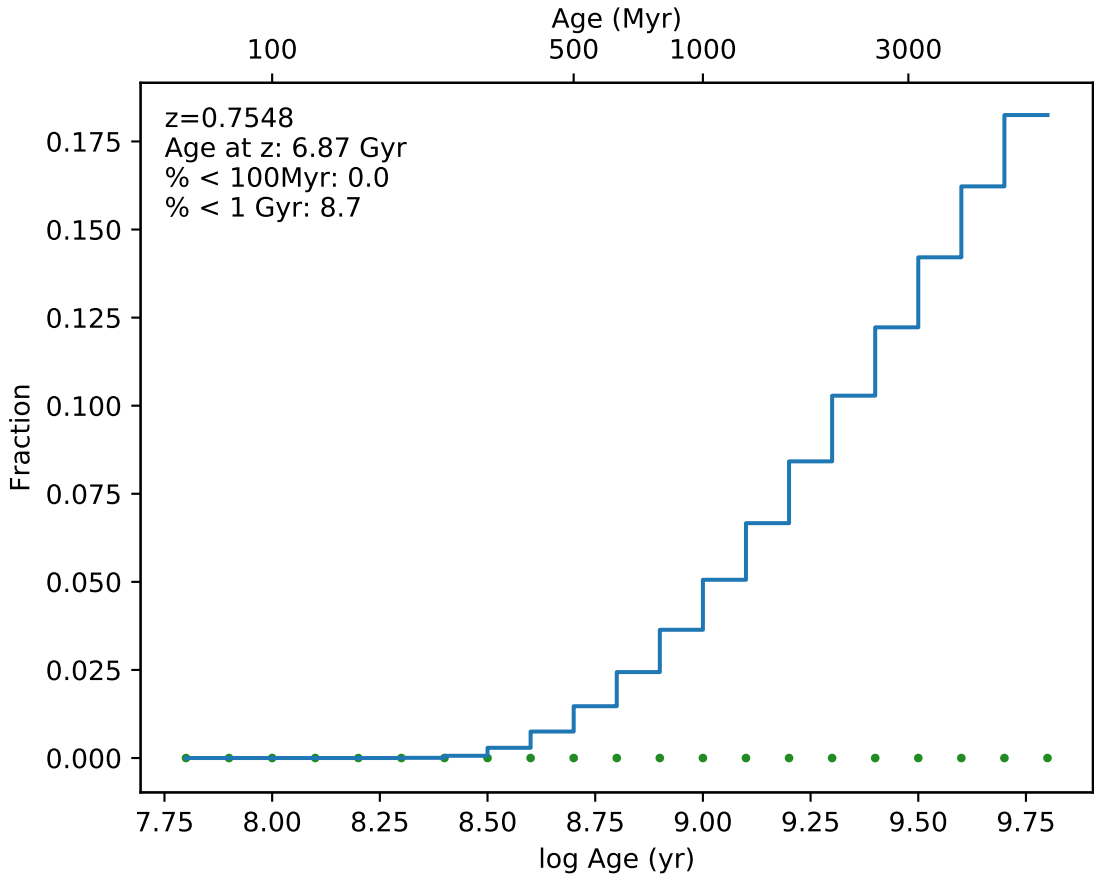
Age (Myr)
100
500
1000
3000
z=0.7548
Age at z: 6.87 Gyr
% < 100Myr: 0.0
% < 1 Gyr: 8.7
Fraction
0.175
0.150
0.125
0.100
0.075
0.050
0.025
0.000
7.75
8.00
8.25
8.50
8.75
9.00
9.25
9.50
9.75
log Age (yr)

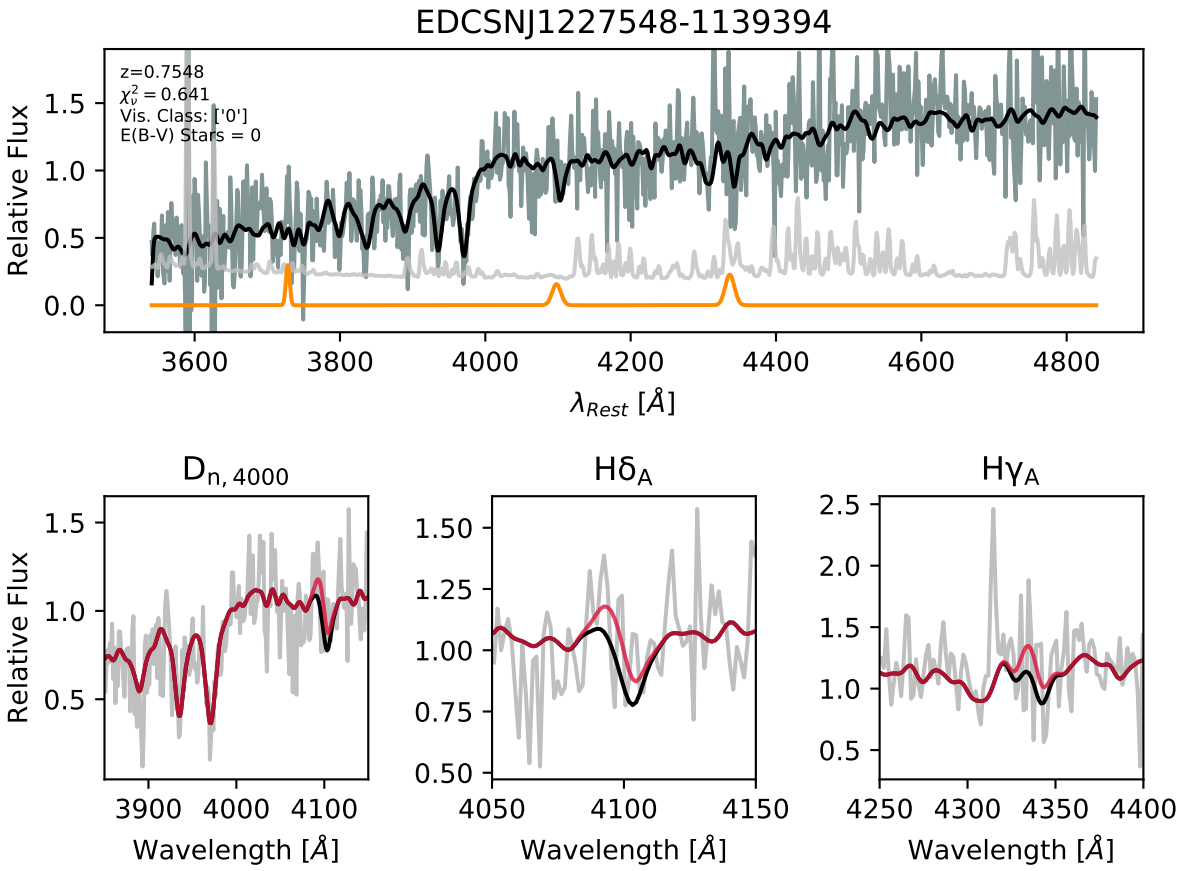
EDCSNJ1227548-1139394
z=0.7548
$\chi^2_\nu = 0.641$
Vis. Class: ['0']
E(B-V) Stars = 0
Relative Flux
λ_{Rest} [Å]
$D_{n,4000}$
$H\delta_A$
$H\gamma_A$
Wavelength [Å]

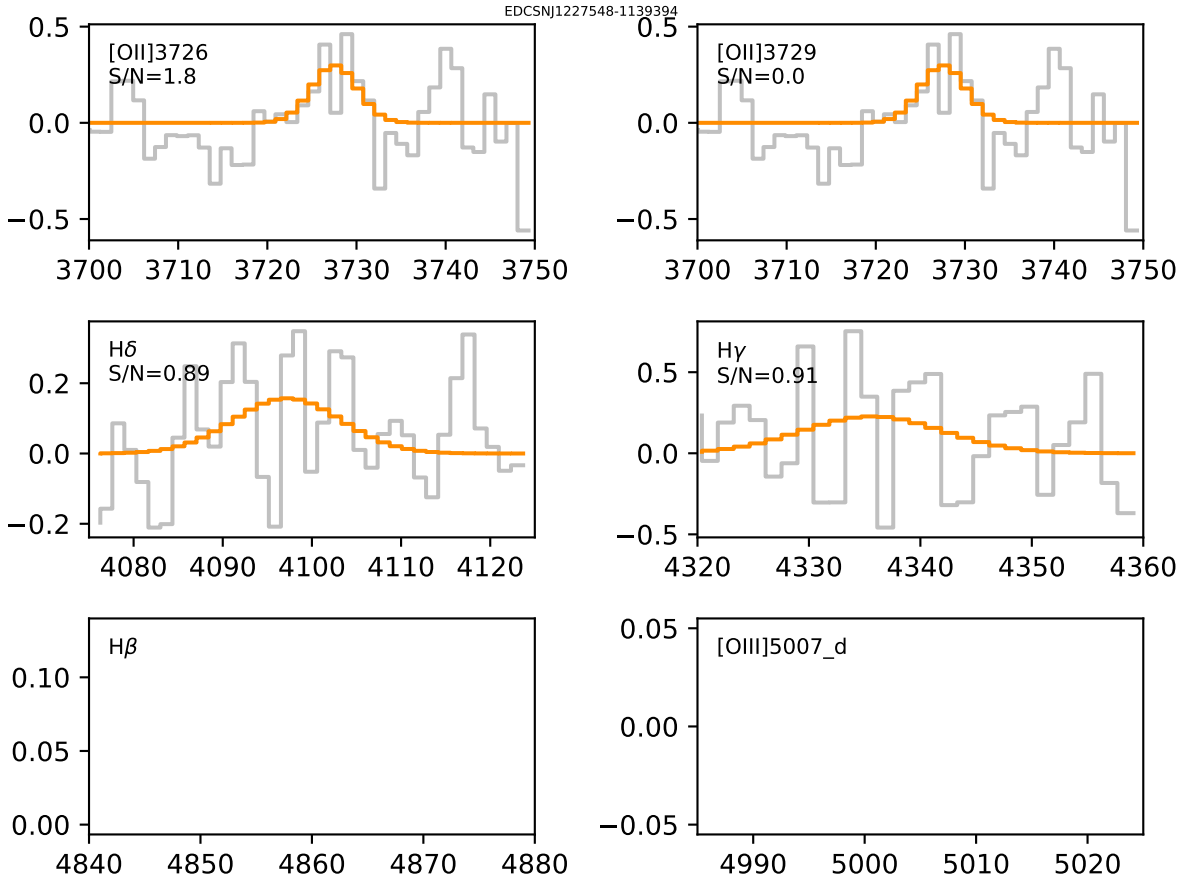
EDCSNJ1227548-1139394
[OII]3726
S/N=1.8
[OII]3729
S/N=0.0
Hδ
S/N=0.89
Hγ
S/N=0.91
Hβ
[OIII]5007_d

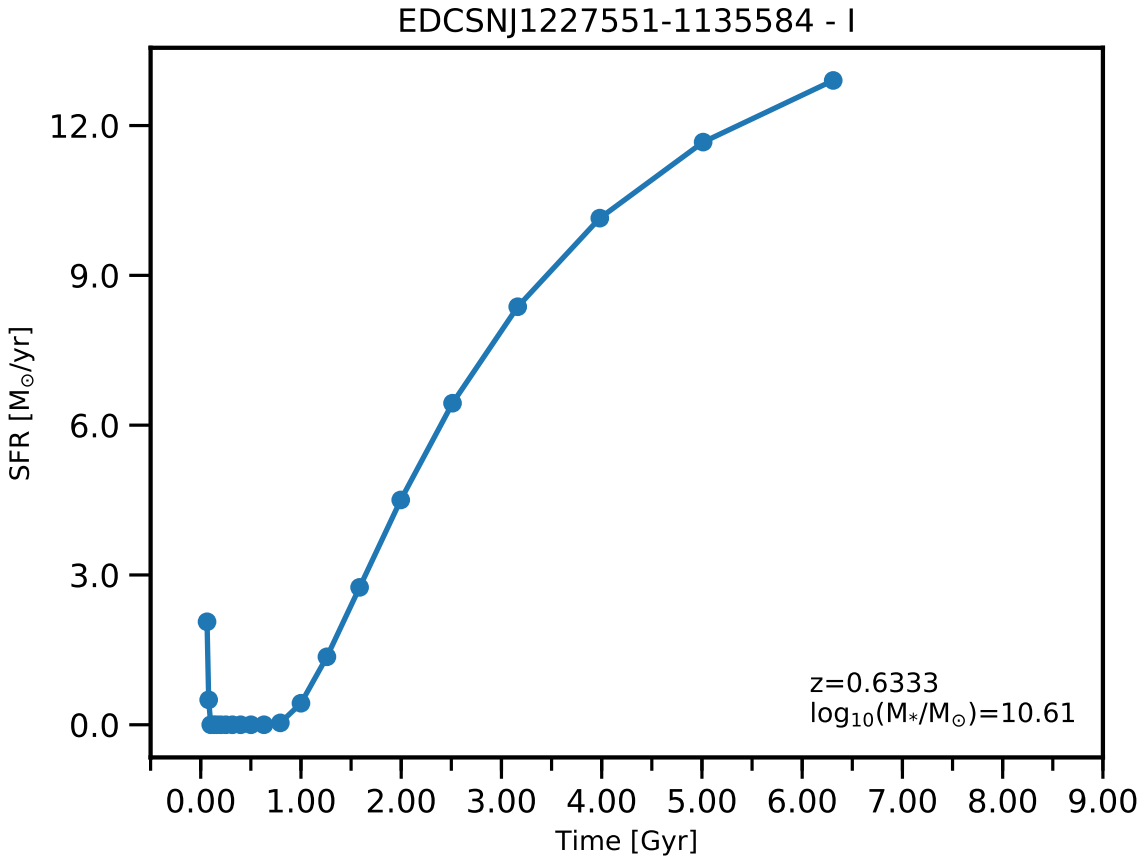
EDCSNJ1227551-1135584 - I
12.0
9.0
6.0
3.0
0.0
SFR [M⊙/yr]
0.00
1.00
2.00
3.00
4.00
5.00
6.00
7.00
8.00
9.00
Time [Gyr]
z=0.6333
log10(M*/M⊙)=10.61

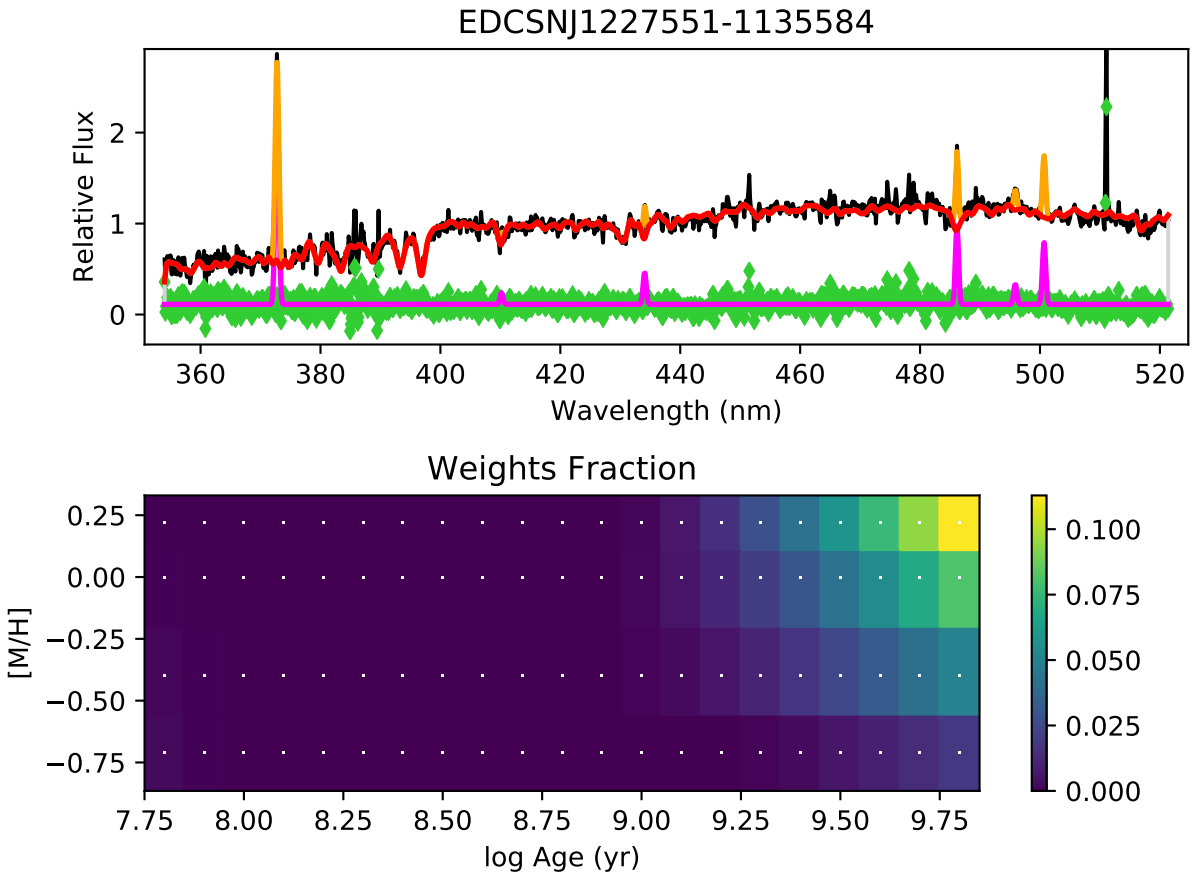
EDCSNJ1227551-1135584
Relative Flux
0
1
2
360
380
400
420
440
460
480
500
520
Wavelength (nm)
Weights Fraction
[M/H]
0.25
0.00
−0.25
−0.50
−0.75
7.75
8.00
8.25
8.50
8.75
9.00
9.25
9.50
9.75
log Age (yr)
0.100
0.075
0.050
0.025
0.000

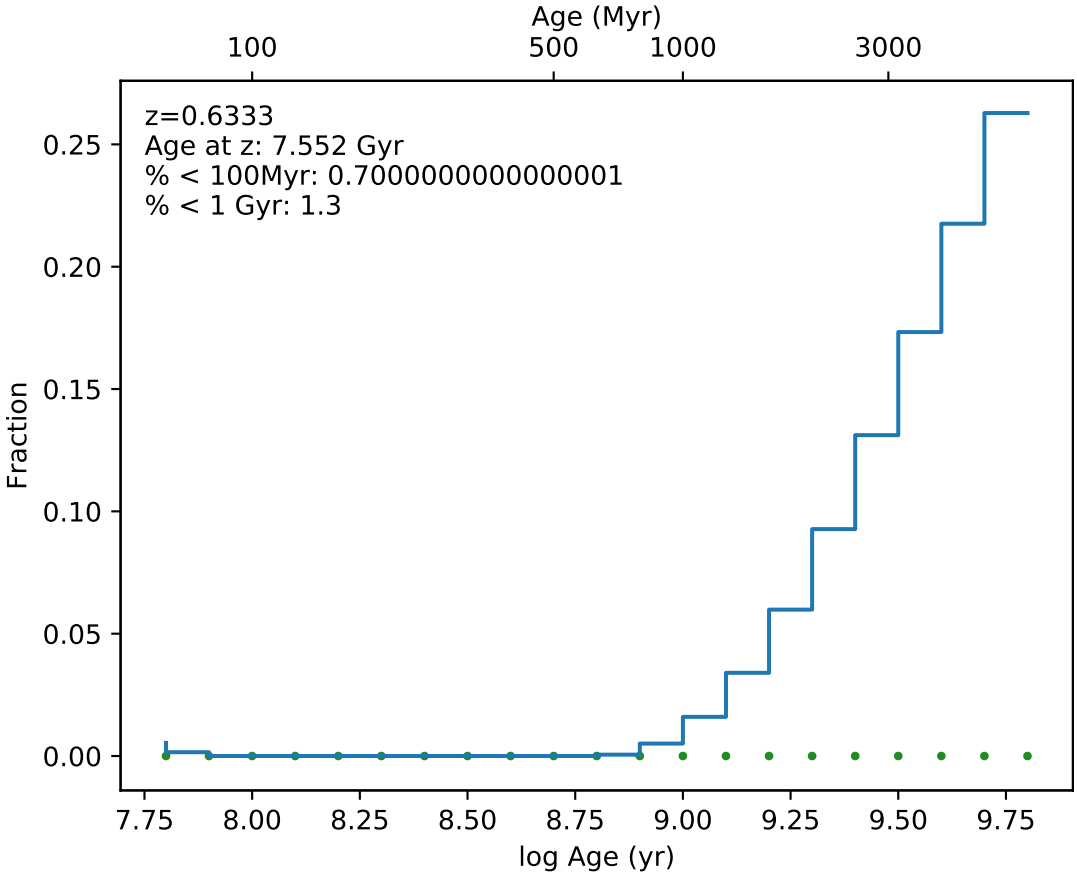
Age (Myr)
100
500
1000
3000
z=0.6333
Age at z: 7.552 Gyr
% < 100Myr: 0.7000000000000001
% < 1 Gyr: 1.3
Fraction
0.25
0.20
0.15
0.10
0.05
0.00
7.75
8.00
8.25
8.50
8.75
9.00
9.25
9.50
9.75
log Age (yr)

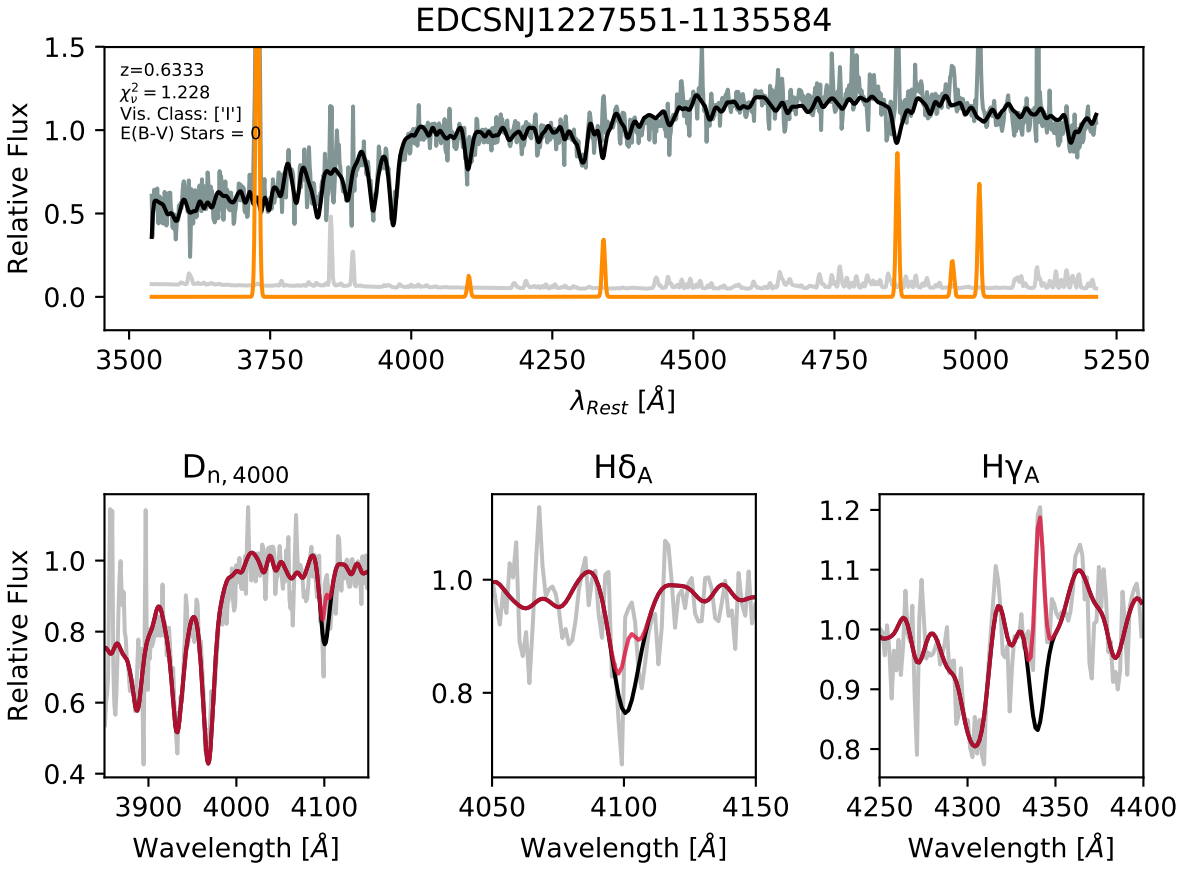
EDCSNJ1227551-1135584
z=0.6333
$\chi^2_\nu = 1.228$
Vis. Class: ['I']
E(B-V) Stars = 0
Relative Flux
λ_{Rest} [Å]
$D_{n,4000}$
$H\delta_A$
$H\gamma_A$
Wavelength [Å]

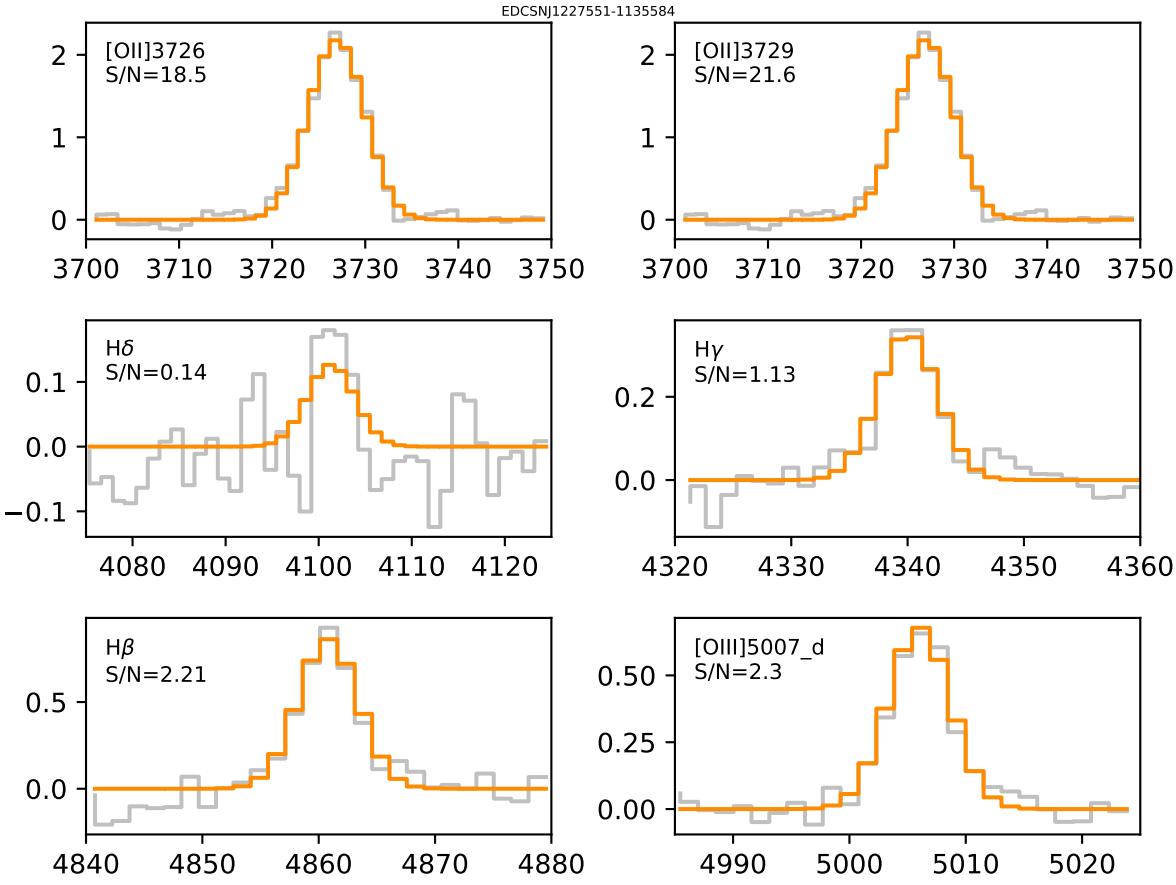
EDCSNJ1227551-1135584
[OII]3726
S/N=18.5
[OII]3729
S/N=21.6
Hδ
S/N=0.14
Hγ
S/N=1.13
Hβ
S/N=2.21
[OIII]5007_d
S/N=2.3

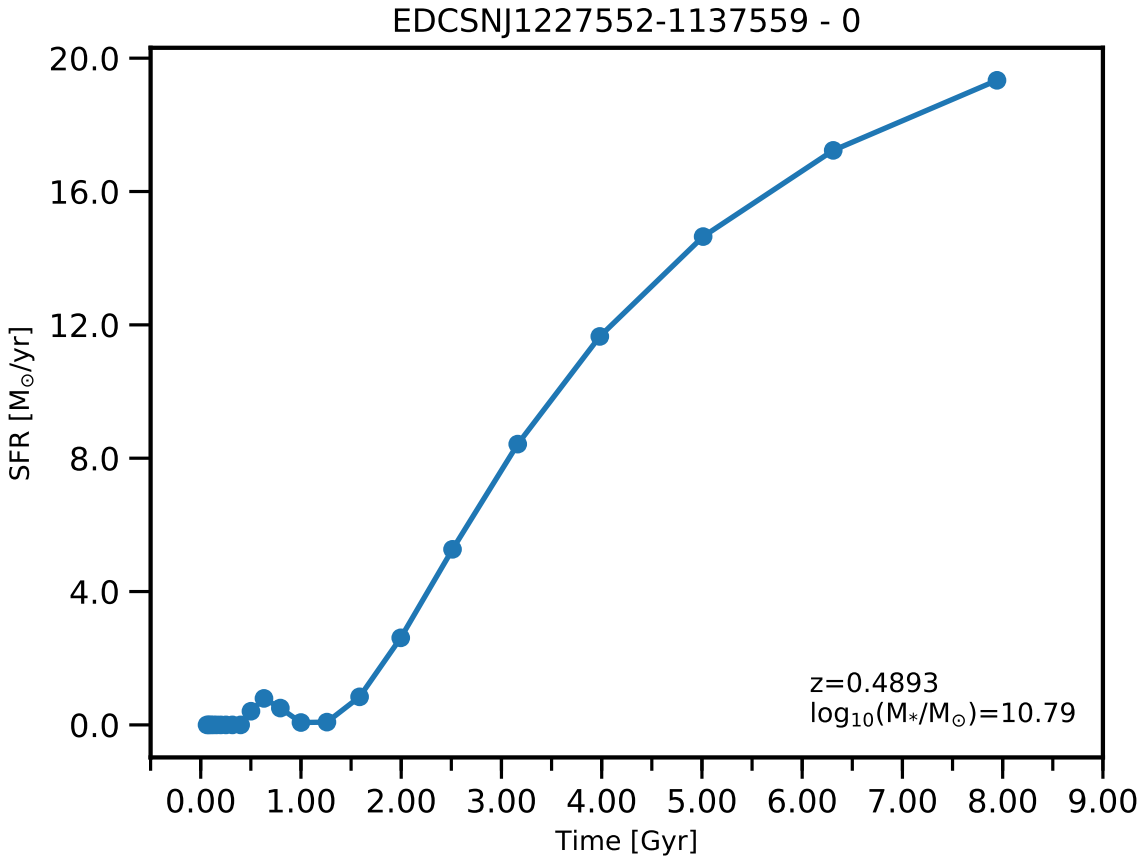
EDCSNJ1227552-1137559 - 0
SFR [M⊙/yr]
Time [Gyr]
z=0.4893
log10(M*/M⊙)=10.79
0.0
4.0
8.0
12.0
16.0
20.0
0.00
1.00
2.00
3.00
4.00
5.00
6.00
7.00
8.00
9.00

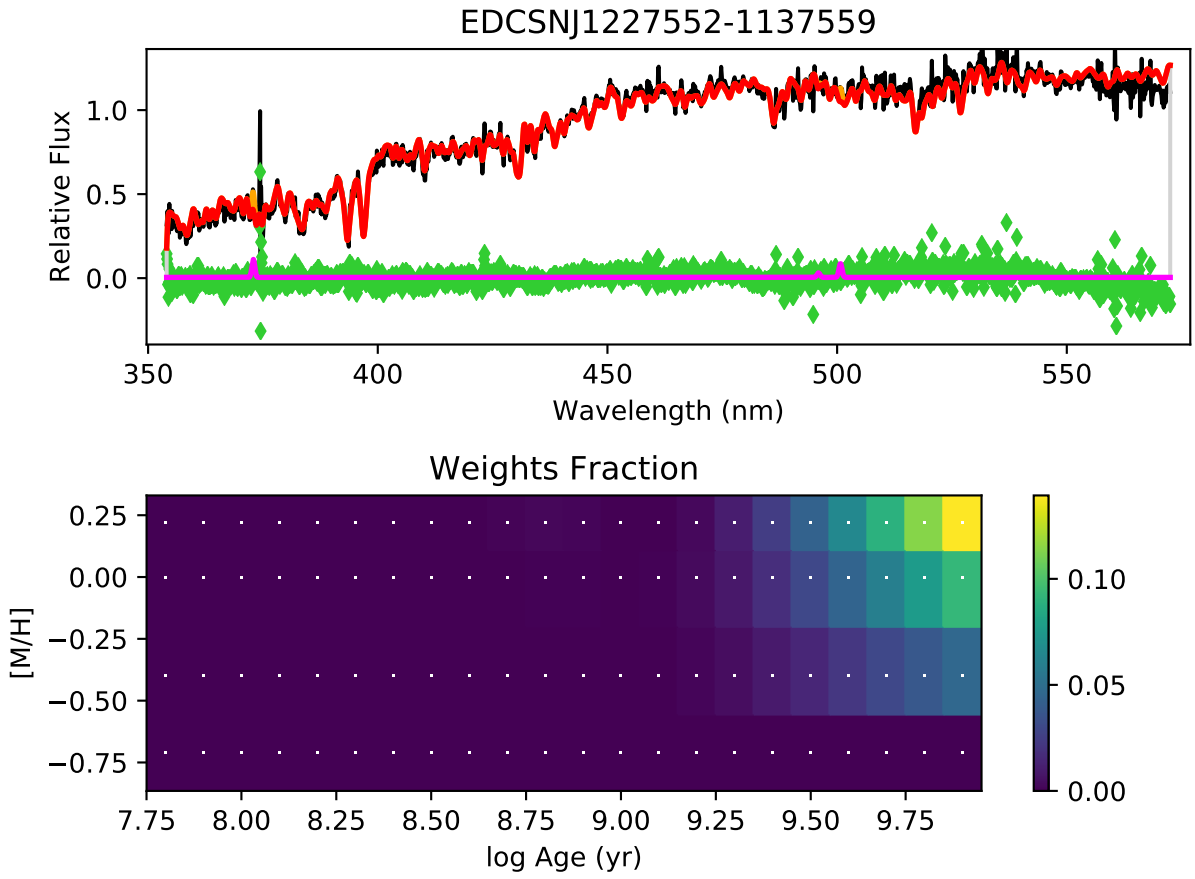
EDCSNJ1227552-1137559
Relative Flux
1.0
0.5
0.0
350
400
450
500
550
Wavelength (nm)
Weights Fraction
[M/H]
0.25
0.00
−0.25
−0.50
−0.75
7.75
8.00
8.25
8.50
8.75
9.00
9.25
9.50
9.75
log Age (yr)
0.10
0.05
0.00

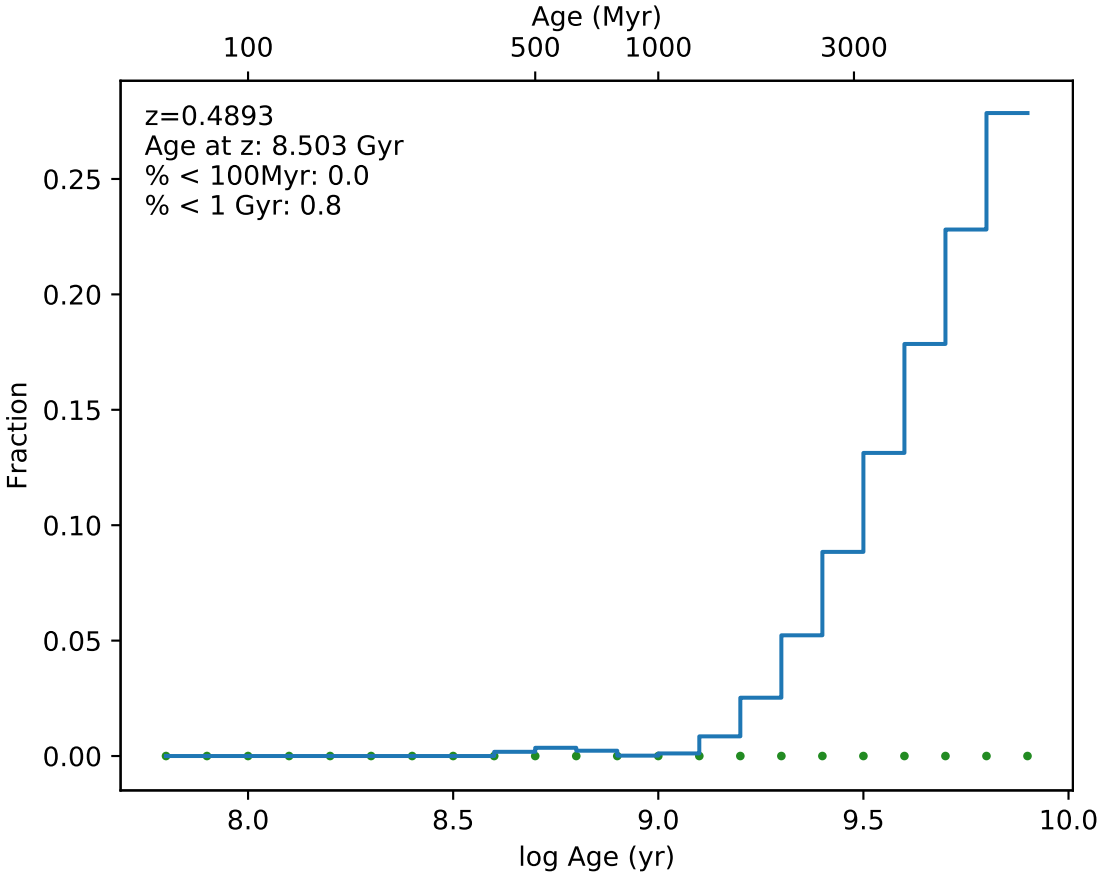
Age (Myr)
100
500
1000
3000
z=0.4893
Age at z: 8.503 Gyr
% < 100Myr: 0.0
% < 1 Gyr: 0.8
Fraction
0.25
0.20
0.15
0.10
0.05
0.00
8.0
8.5
9.0
9.5
10.0
log Age (yr)

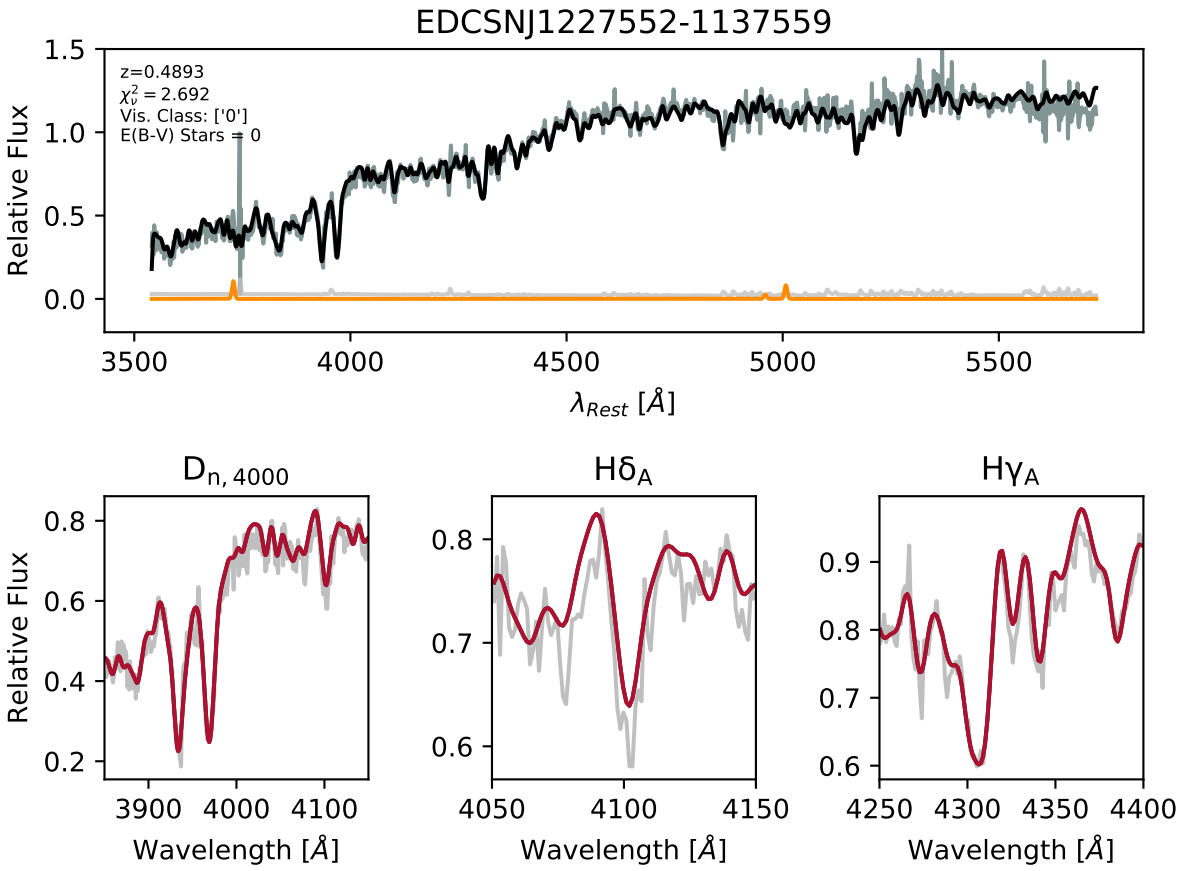
EDCSNJ1227552-1137559
z=0.4893
$\chi^2_\nu = 2.692$
Vis. Class: ['0']
E(B-V) Stars = 0
Relative Flux
λ_{Rest} [Å]
$D_{n,4000}$
$H\delta_A$
$H\gamma_A$
Wavelength [Å]

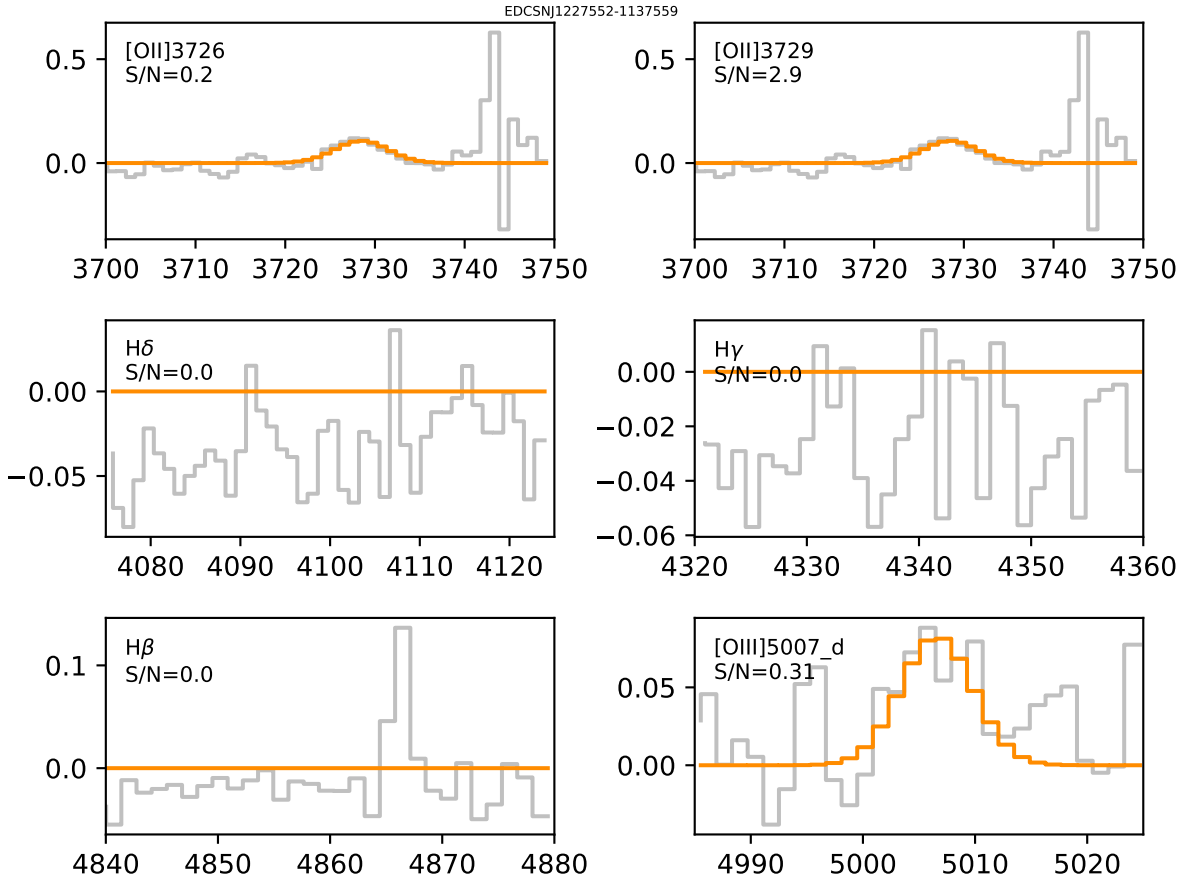
EDCSNJ1227552-1137559
[OII]3726
S/N=0.2
[OII]3729
S/N=2.9
Hδ
S/N=0.0
Hγ
S/N=0.0
Hβ
S/N=0.0
[OIII]5007_d
S/N=0.31

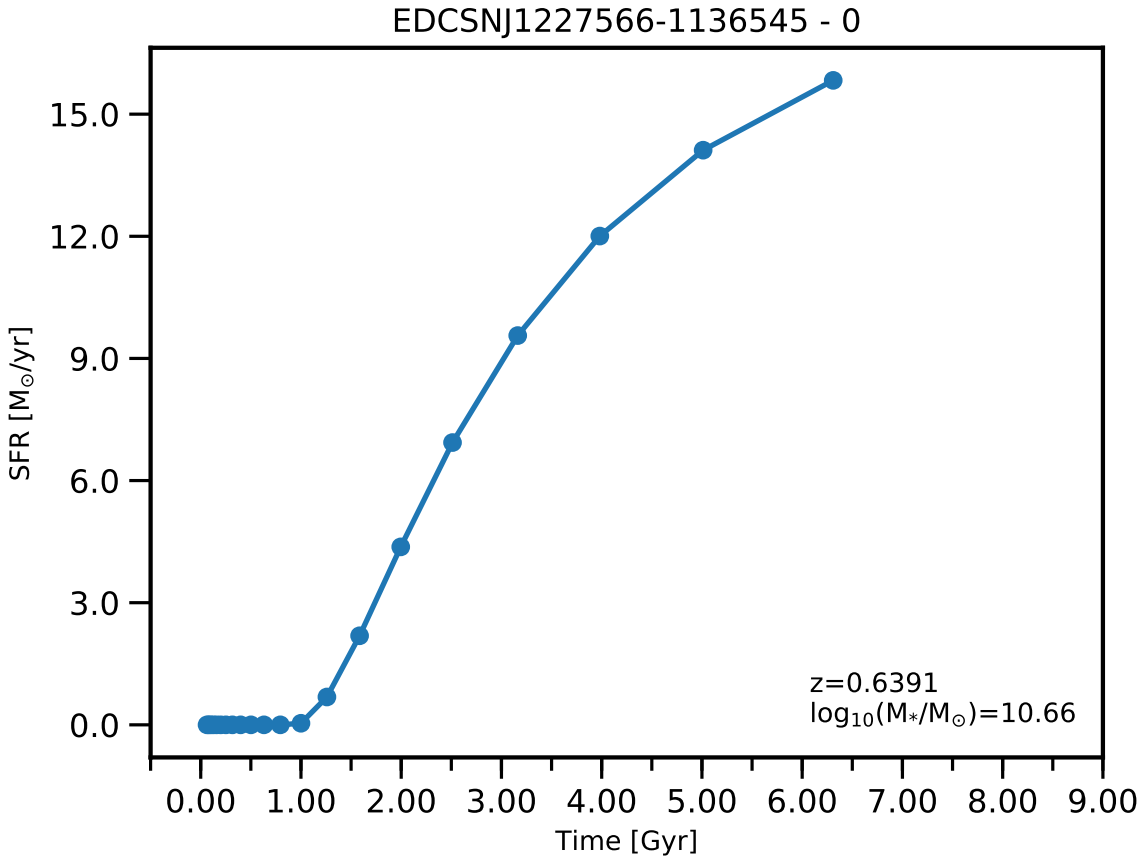
EDCSNJ1227566-1136545 - 0
SFR [M⊙/yr]
15.0
12.0
9.0
6.0
3.0
0.0
0.00
1.00
2.00
3.00
4.00
5.00
6.00
7.00
8.00
9.00
Time [Gyr]
z=0.6391
log10(M*/M⊙)=10.66

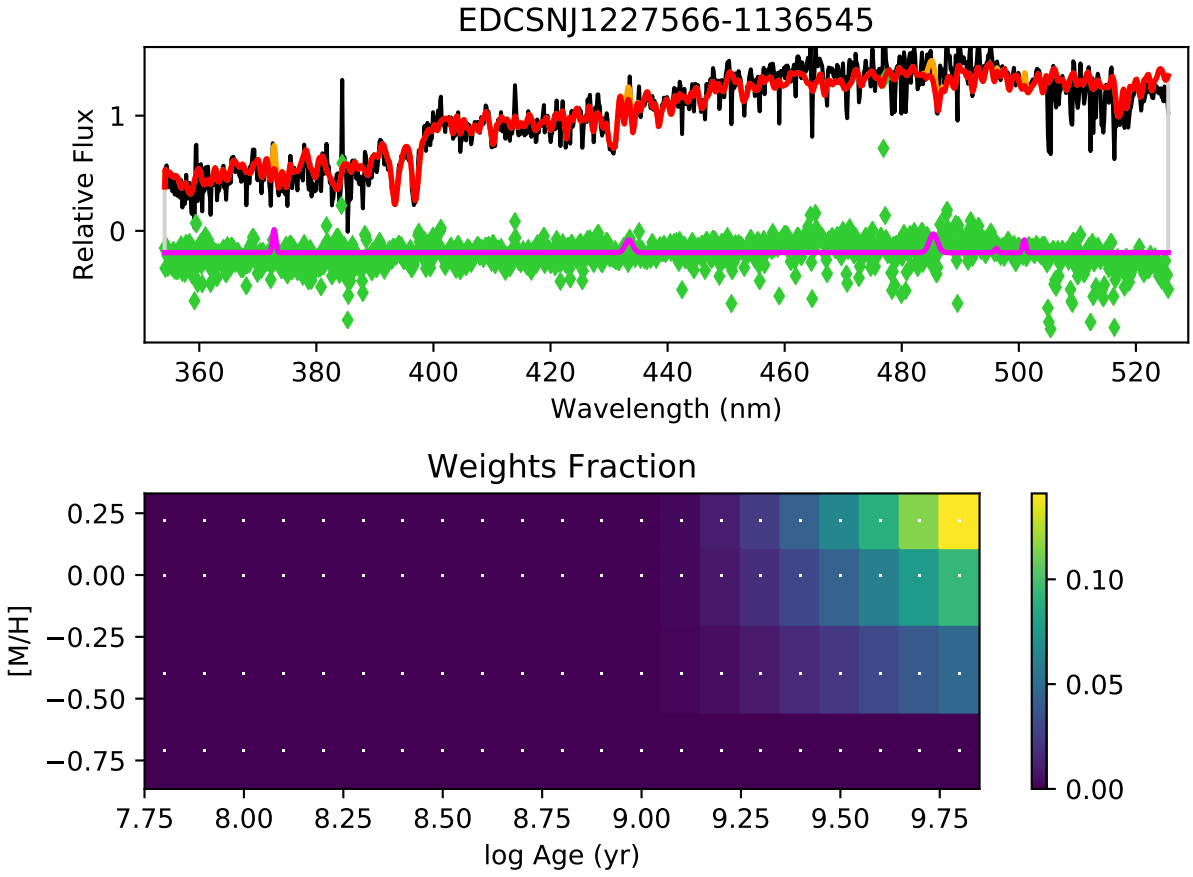
EDCSNJ1227566-1136545
Relative Flux
1
0
360
380
400
420
440
460
480
500
520
Wavelength (nm)
Weights Fraction
[M/H]
0.25
0.00
−0.25
−0.50
−0.75
7.75
8.00
8.25
8.50
8.75
9.00
9.25
9.50
9.75
log Age (yr)
0.10
0.05
0.00

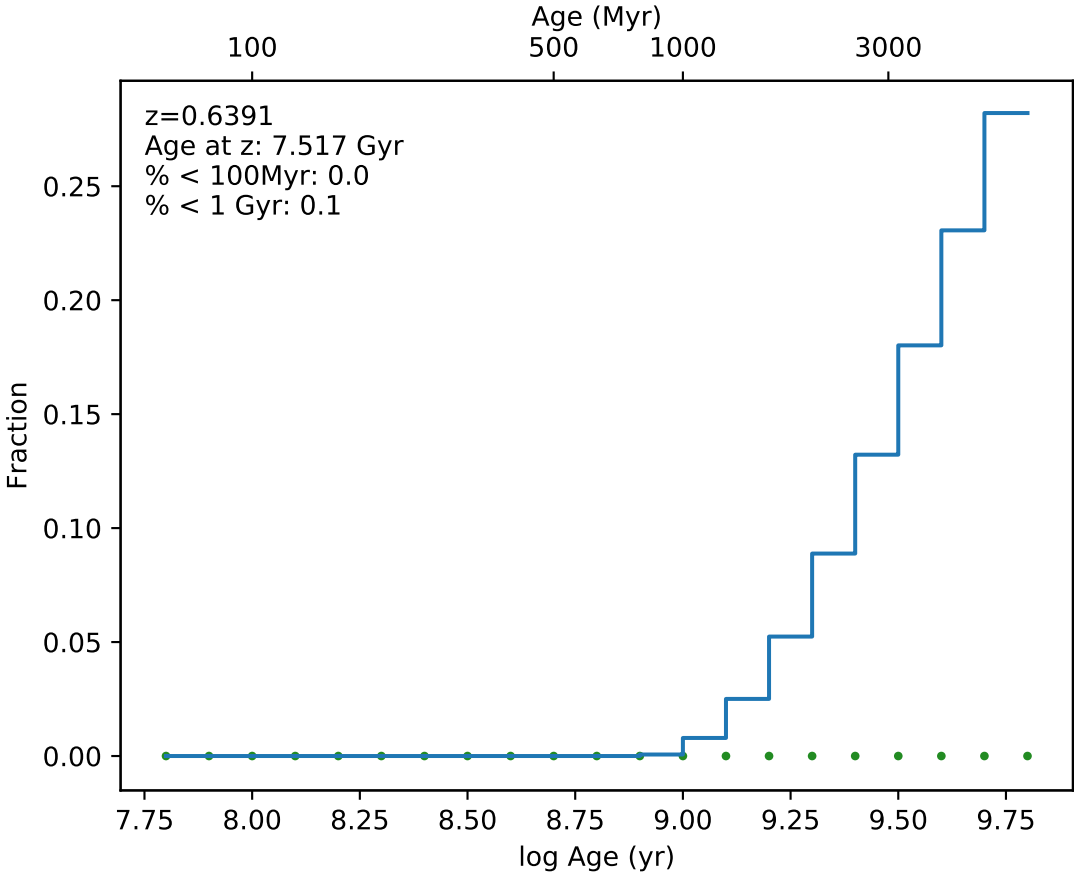
Age (Myr)
100
500
1000
3000
z=0.6391
Age at z: 7.517 Gyr
% < 100Myr: 0.0
% < 1 Gyr: 0.1
Fraction
0.25
0.20
0.15
0.10
0.05
0.00
7.75
8.00
8.25
8.50
8.75
9.00
9.25
9.50
9.75
log Age (yr)

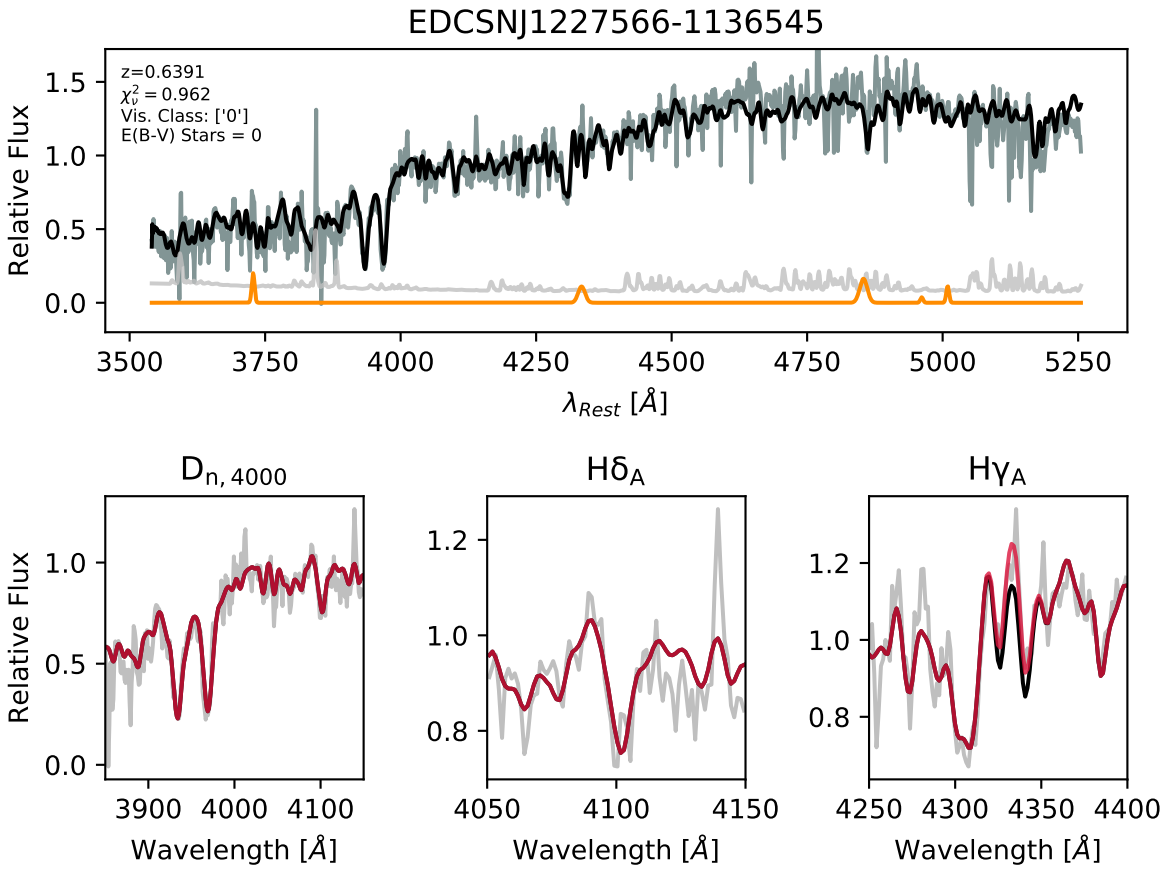
EDCSNJ1227566-1136545
z=0.6391
$\chi^2_\nu = 0.962$
Vis. Class: ['0']
E(B-V) Stars = 0
Relative Flux
λ_{Rest} [Å]
$D_{n,4000}$
$H\delta_A$
$H\gamma_A$
Wavelength [Å]

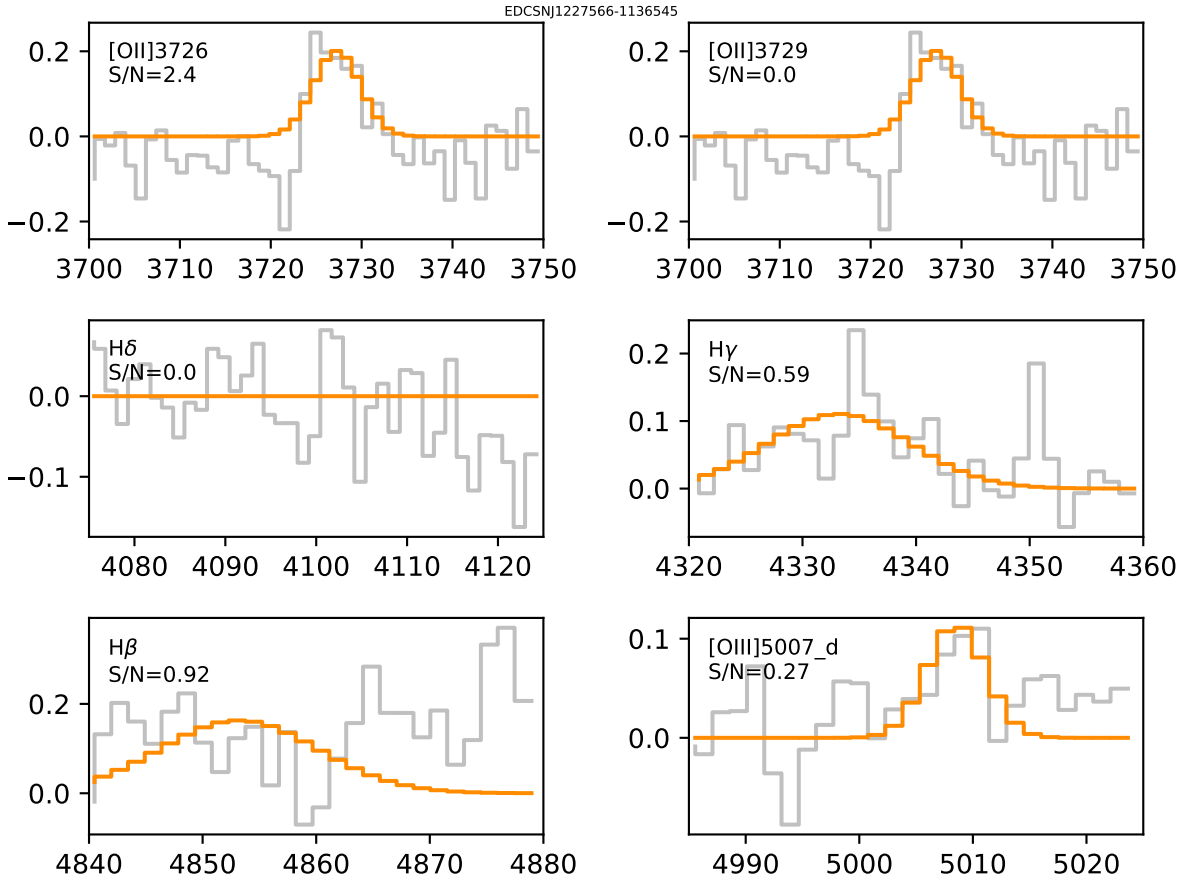
EDCSNJ1227566-1136545
[OII]3726
S/N=2.4
[OII]3729
S/N=0.0
Hδ
S/N=0.0
Hγ
S/N=0.59
Hβ
S/N=0.92
[OIII]5007_d
S/N=0.27

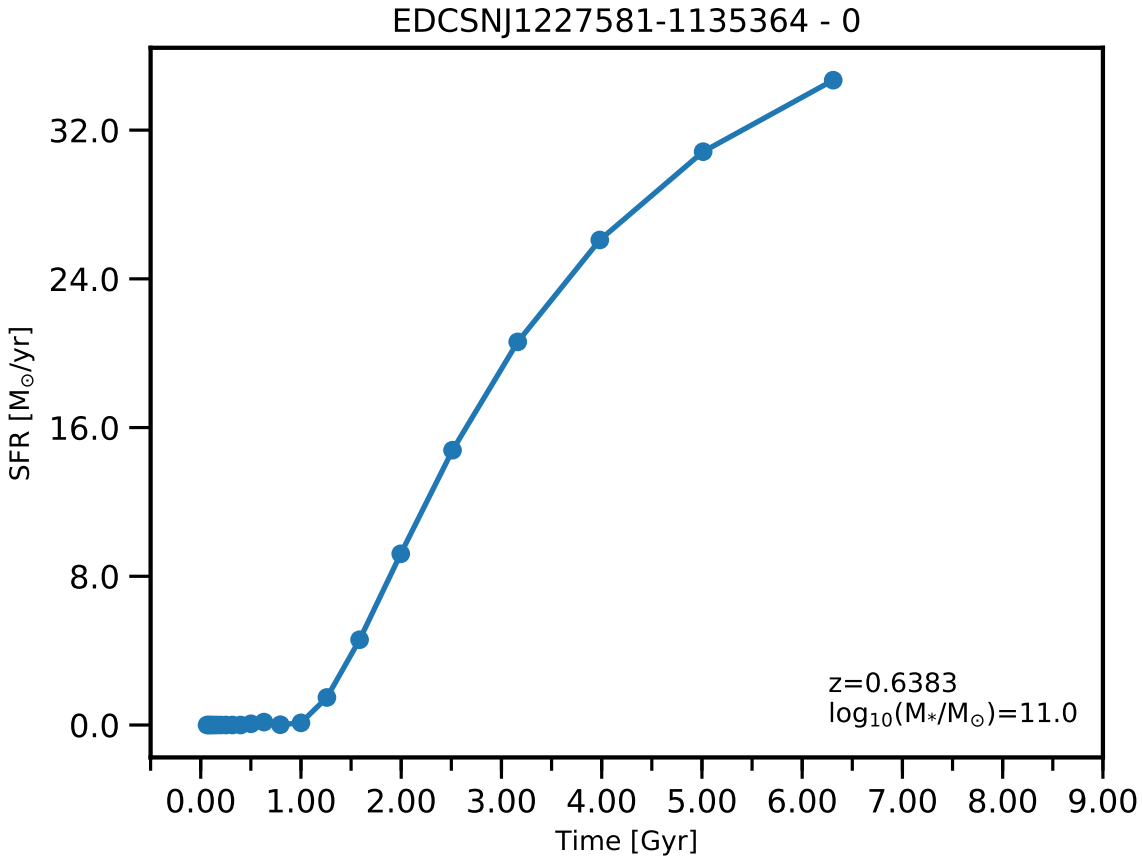
EDCSNJ1227581-1135364 - 0
SFR [M⊙/yr]
32.0
24.0
16.0
8.0
0.0
0.00
1.00
2.00
3.00
4.00
5.00
6.00
7.00
8.00
9.00
Time [Gyr]
z=0.6383
log10(M∗/M⊙)=11.0

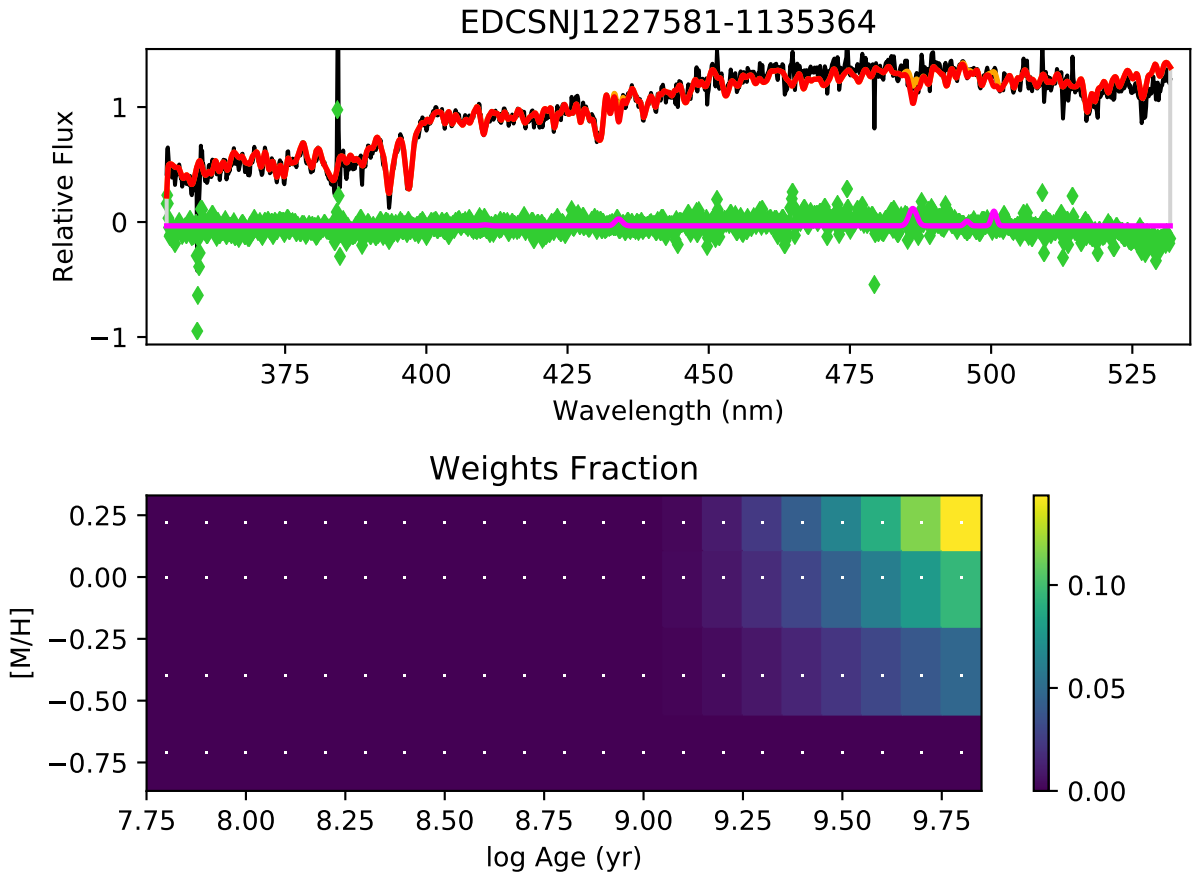
EDCSNJ1227581-1135364
Relative Flux
1
0
−1
375
400
425
450
475
500
525
Wavelength (nm)
Weights Fraction
[M/H]
0.25
0.00
−0.25
−0.50
−0.75
7.75
8.00
8.25
8.50
8.75
9.00
9.25
9.50
9.75
log Age (yr)
0.10
0.05
0.00

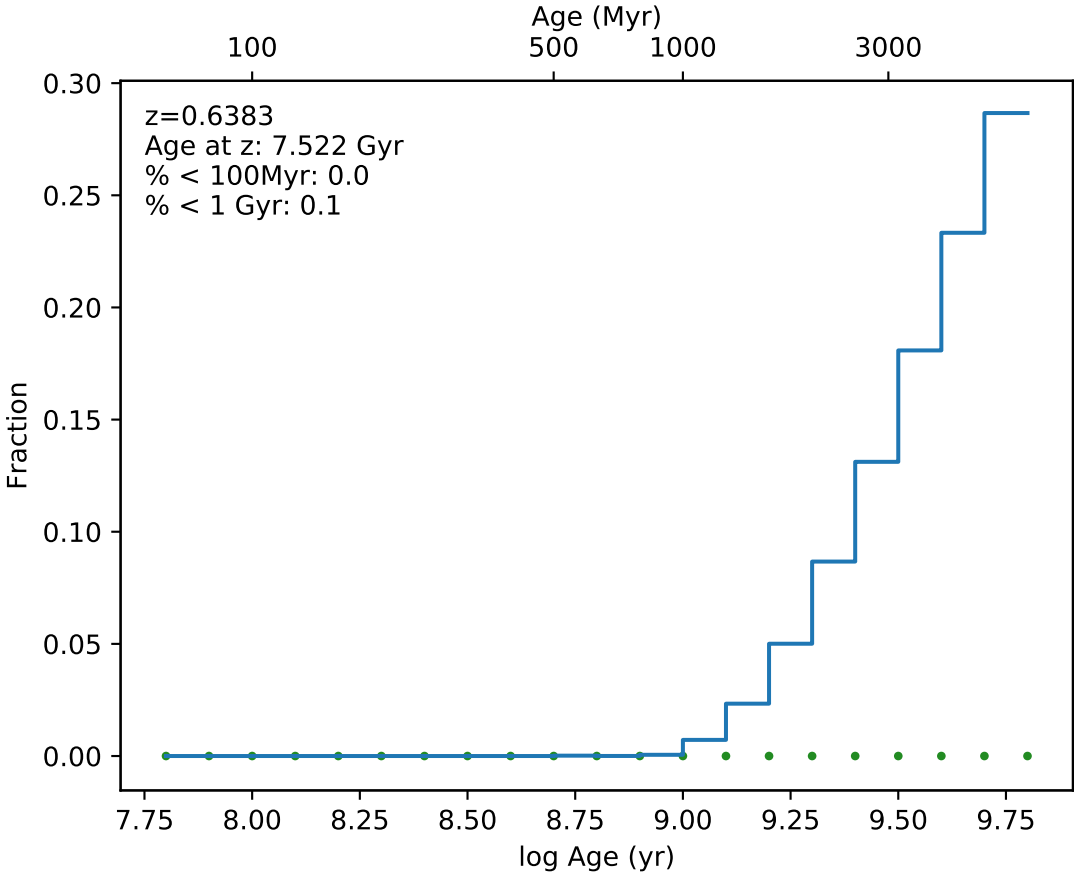
Age (Myr)
100
500
1000
3000
z=0.6383
Age at z: 7.522 Gyr
% < 100Myr: 0.0
% < 1 Gyr: 0.1
Fraction
0.30
0.25
0.20
0.15
0.10
0.05
0.00
7.75
8.00
8.25
8.50
8.75
9.00
9.25
9.50
9.75
log Age (yr)

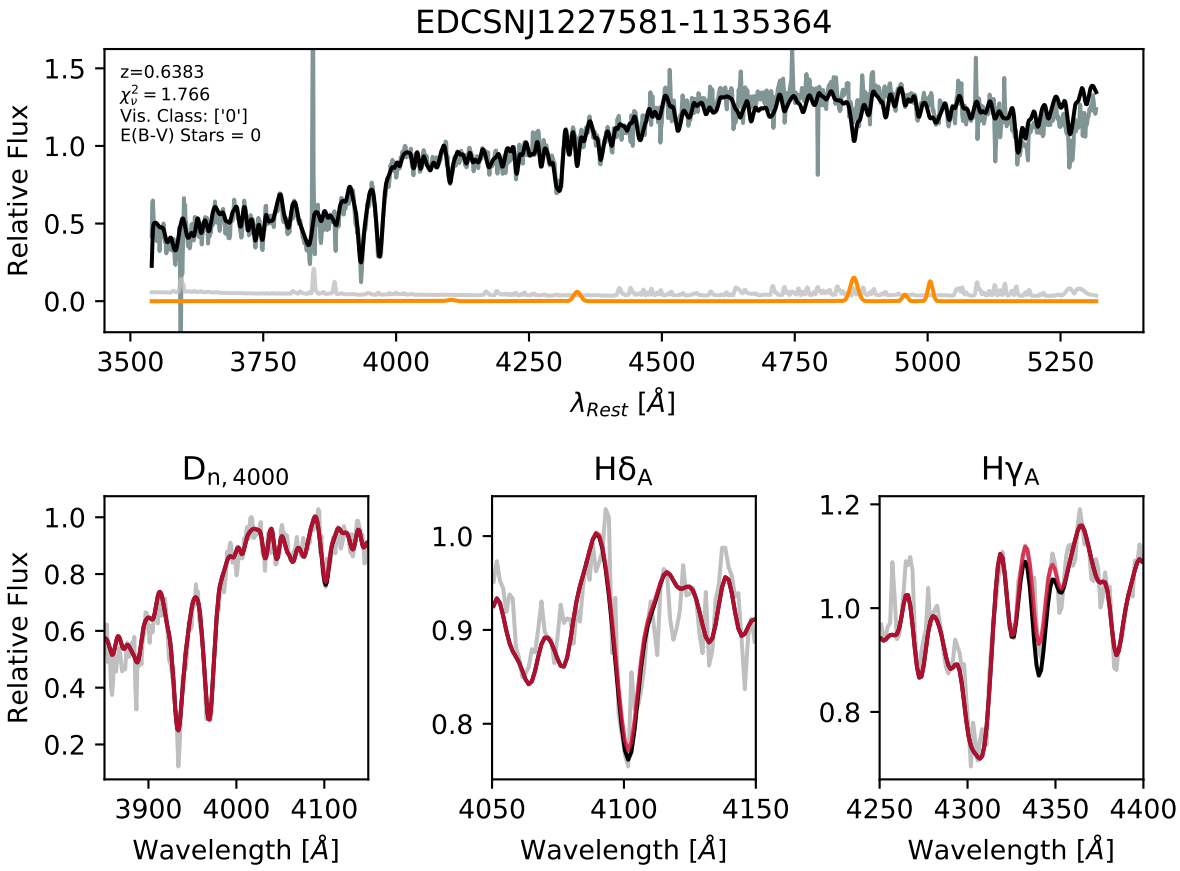
EDCSNJ1227581-1135364
z=0.6383
$\chi^2_\nu = 1.766$
Vis. Class: ['0']
E(B-V) Stars = 0
Relative Flux
λ_{Rest} [Å]
$D_{n,4000}$
$H\delta_A$
$H\gamma_A$
Wavelength [Å]

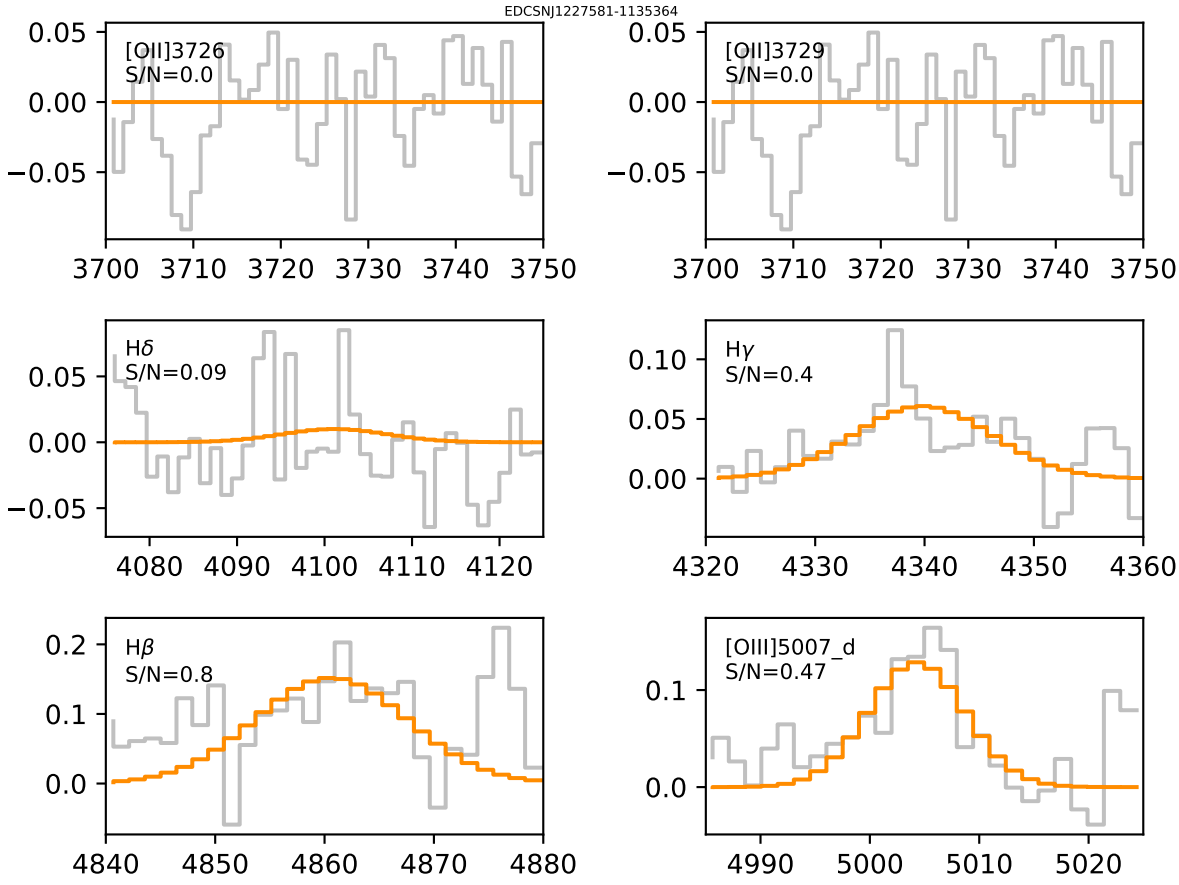
EDCSNJ1227581-1135364
[OII]3726
S/N=0.0
[OII]3729
S/N=0.0
Hδ
S/N=0.09
Hγ
S/N=0.4
Hβ
S/N=0.8
[OIII]5007_d
S/N=0.47

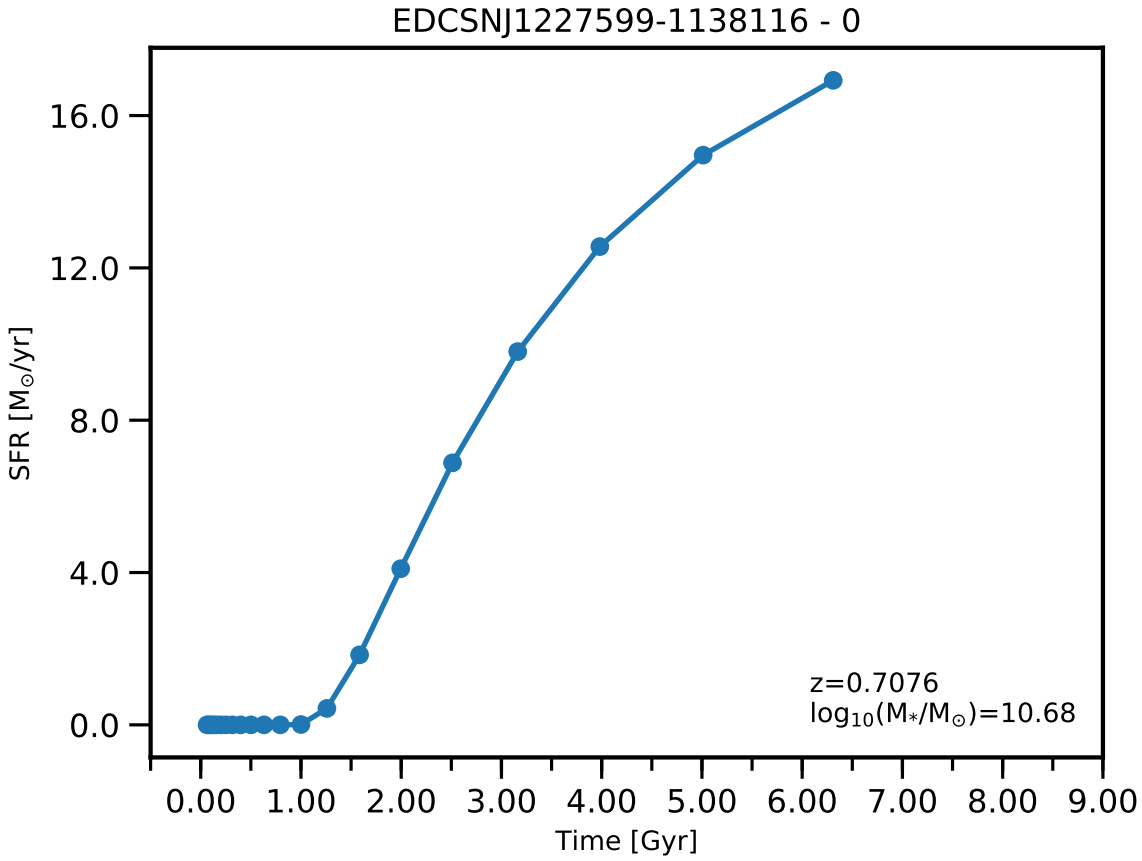
EDCSNJ1227599-1138116 - 0
SFR [M⊙/yr]
16.0
12.0
8.0
4.0
0.0
0.00
1.00
2.00
3.00
4.00
5.00
6.00
7.00
8.00
9.00
Time [Gyr]
z=0.7076
log10(M*/M⊙)=10.68

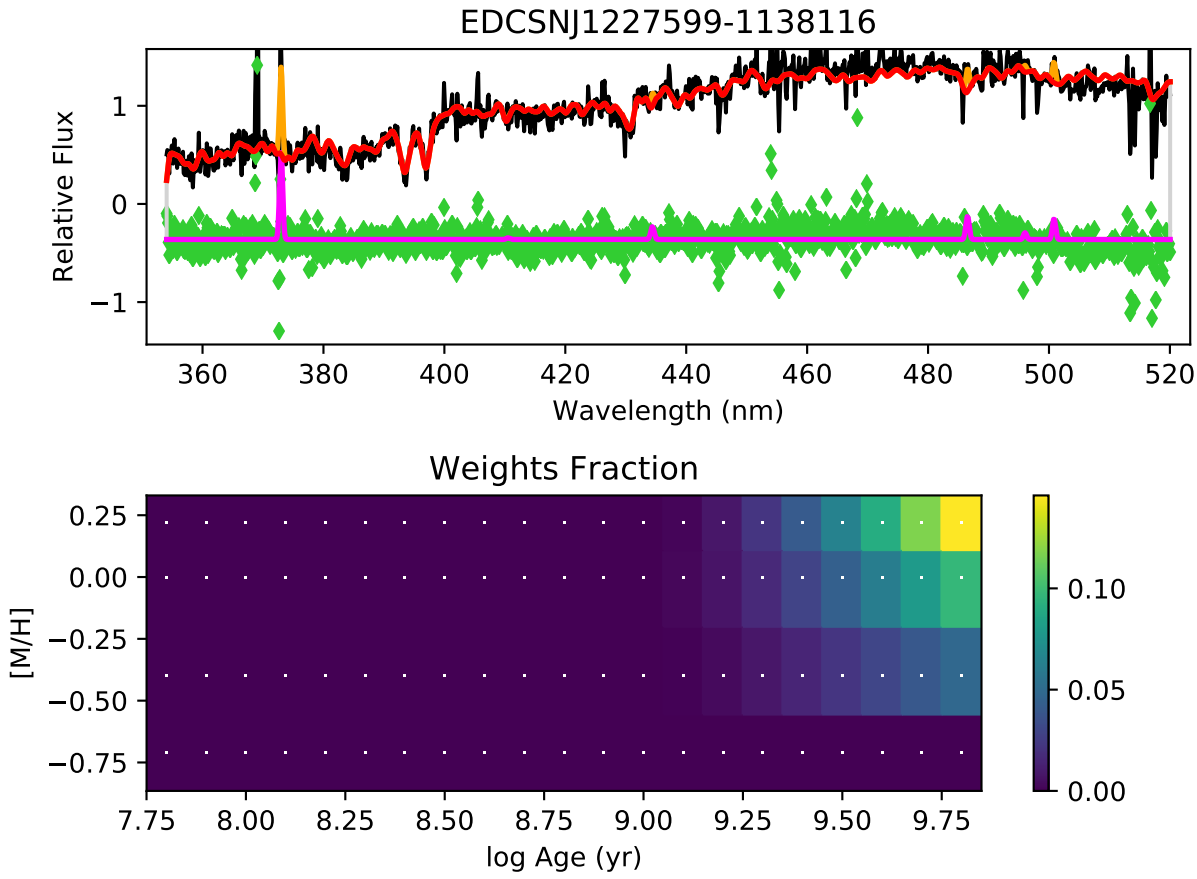
EDCSNJ1227599-1138116
Relative Flux
1
0
−1
360
380
400
420
440
460
480
500
520
Wavelength (nm)
Weights Fraction
[M/H]
0.25
0.00
−0.25
−0.50
−0.75
7.75
8.00
8.25
8.50
8.75
9.00
9.25
9.50
9.75
log Age (yr)
0.10
0.05
0.00

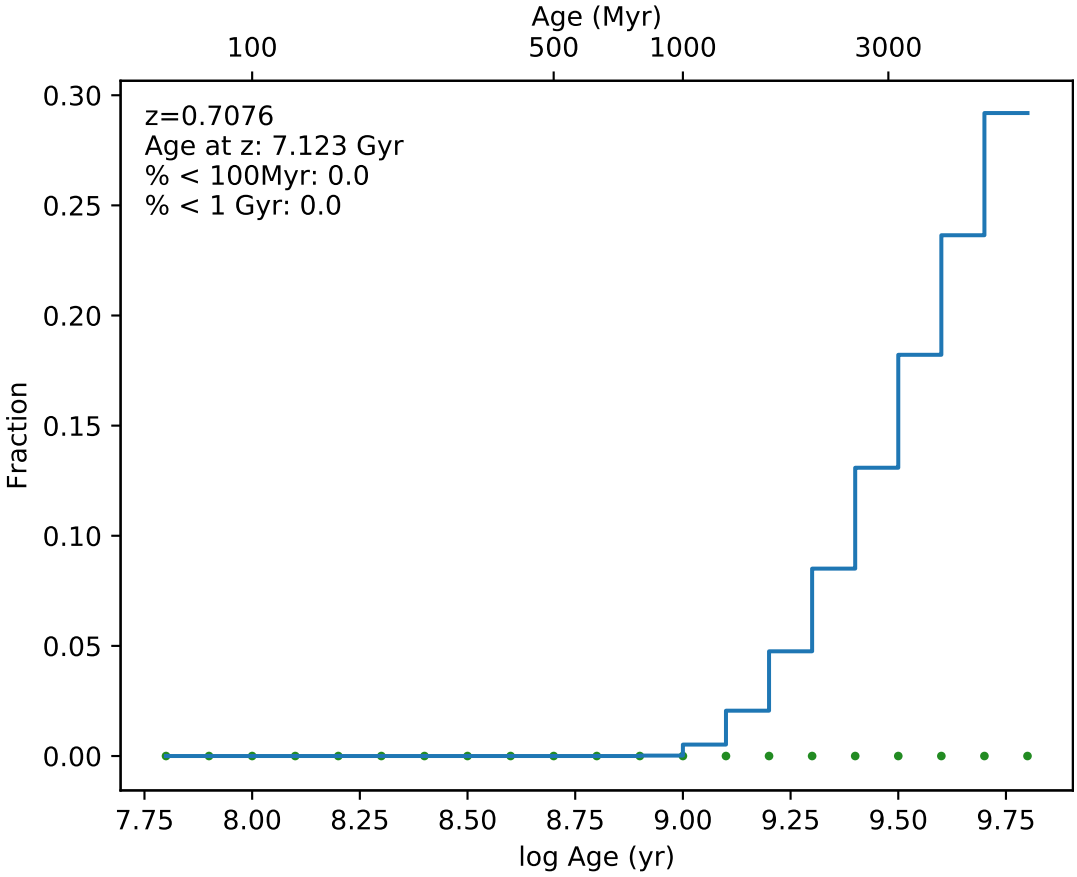
Age (Myr)
100
500
1000
3000
z=0.7076
Age at z: 7.123 Gyr
% < 100Myr: 0.0
% < 1 Gyr: 0.0
Fraction
0.30
0.25
0.20
0.15
0.10
0.05
0.00
7.75
8.00
8.25
8.50
8.75
9.00
9.25
9.50
9.75
log Age (yr)

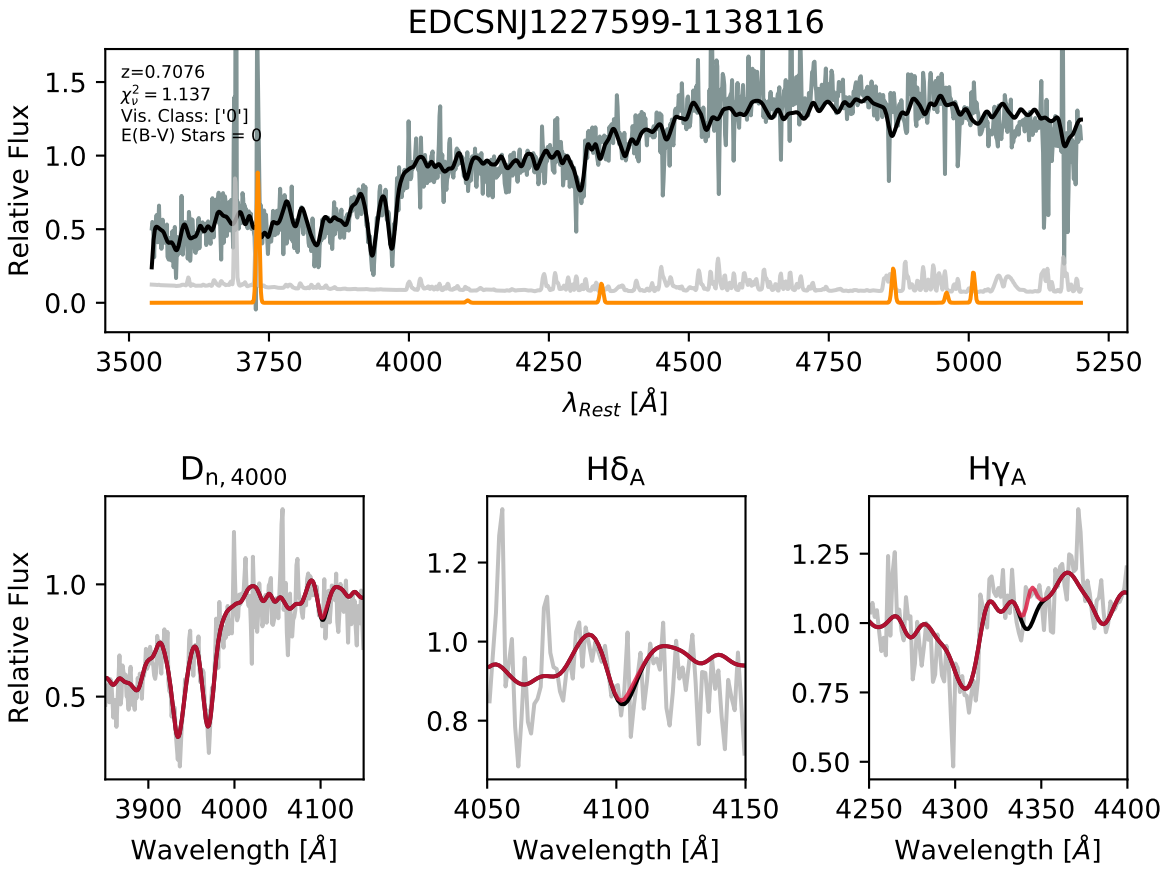
EDCSNJ1227599-1138116
z=0.7076
$\chi^2_\nu = 1.137$
Vis. Class: ['0']
E(B-V) Stars = 0
Relative Flux
λ_{Rest} [Å]
$D_{n,4000}$
$H\delta_A$
$H\gamma_A$
Wavelength [Å]

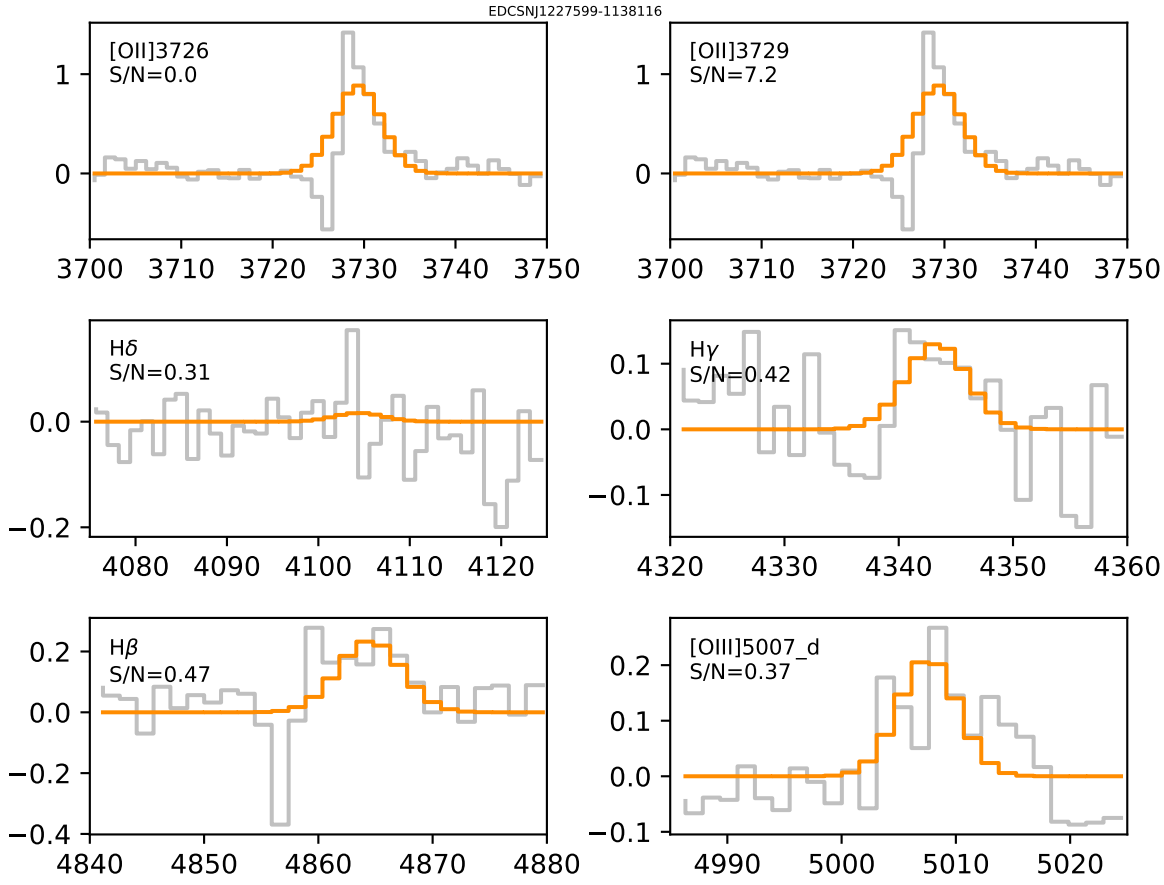
EDCSNJ1227599-1138116
[OII]3726
S/N=0.0
[OII]3729
S/N=7.2
Hδ
S/N=0.31
Hγ
S/N=0.42
Hβ
S/N=0.47
[OIII]5007_d
S/N=0.37

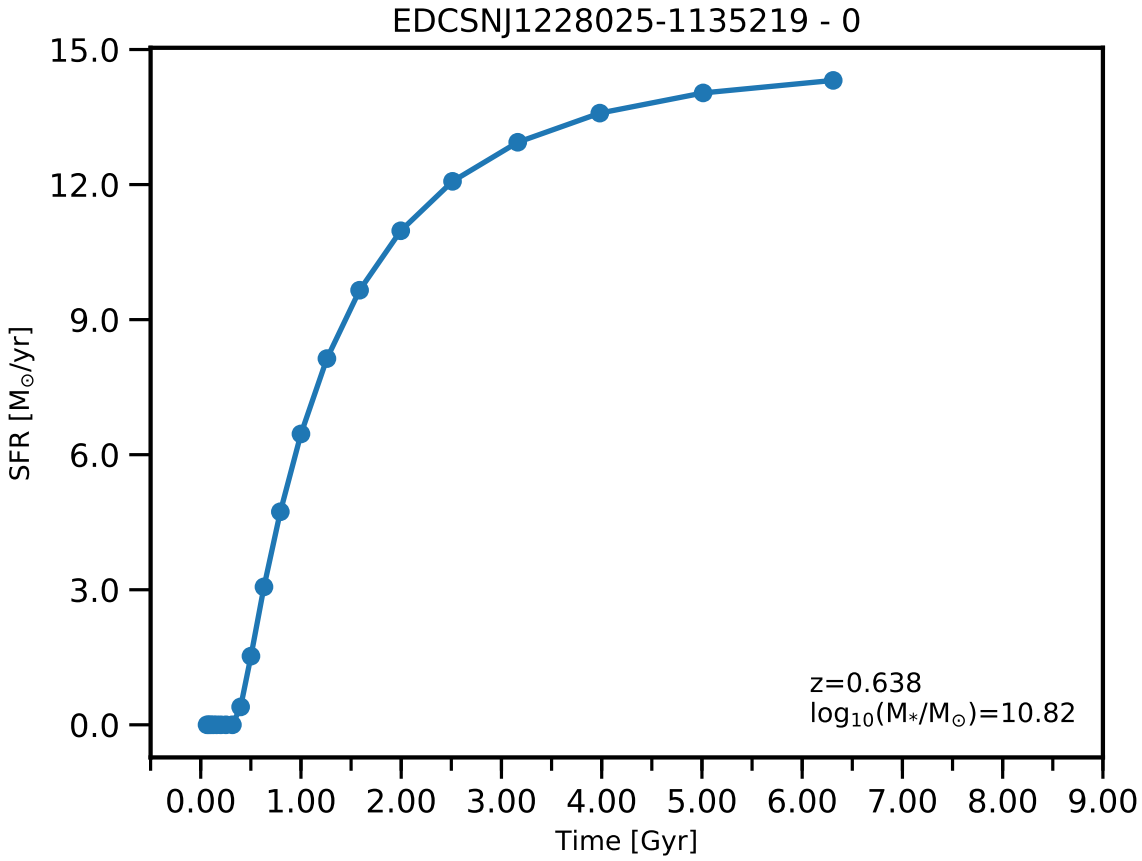
EDCSNJ1228025-1135219 - 0
15.0
12.0
9.0
6.0
3.0
0.0
SFR [M⊙/yr]
0.00
1.00
2.00
3.00
4.00
5.00
6.00
7.00
8.00
9.00
Time [Gyr]
z=0.638
log10(M*/M⊙)=10.82

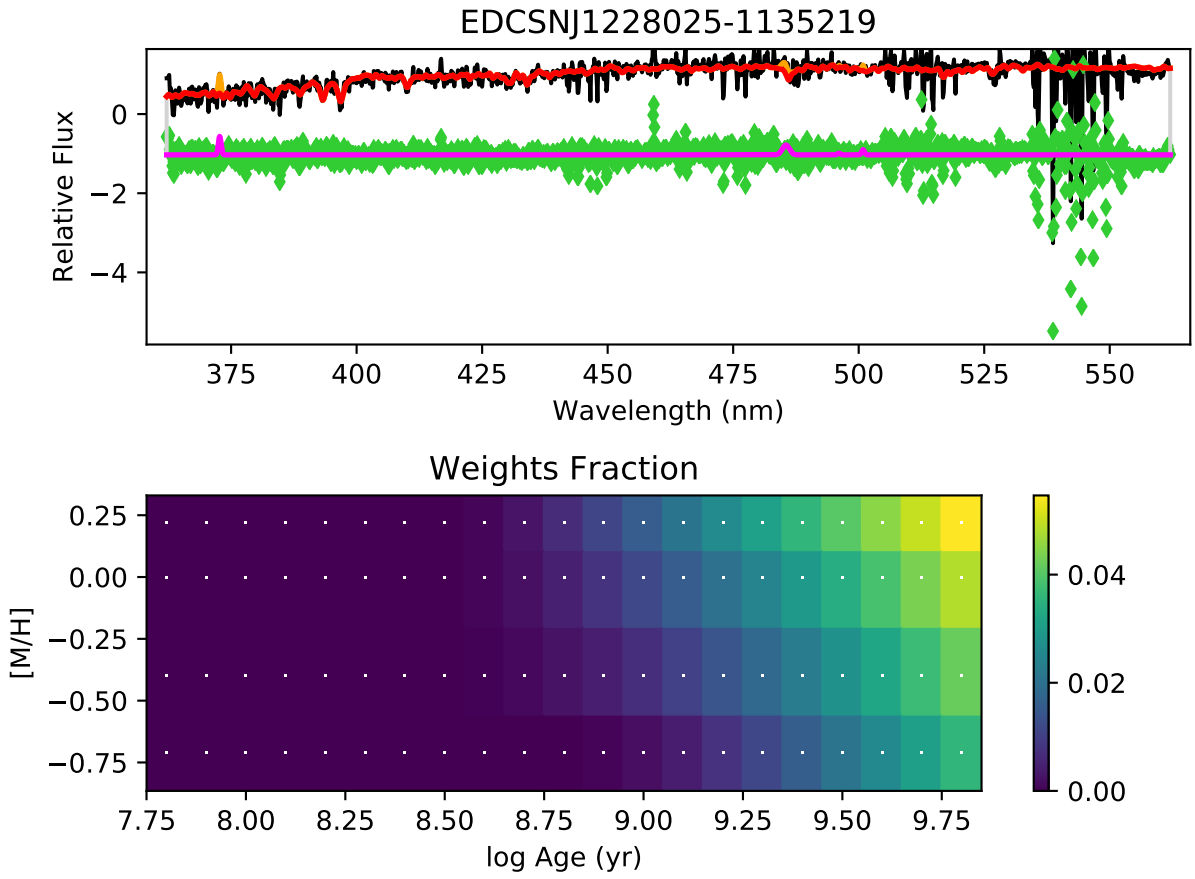
EDCSNJ1228025-1135219
Relative Flux
0
−2
−4
375
400
425
450
475
500
525
550
Wavelength (nm)
Weights Fraction
[M/H]
0.25
0.00
−0.25
−0.50
−0.75
7.75
8.00
8.25
8.50
8.75
9.00
9.25
9.50
9.75
log Age (yr)
0.04
0.02
0.00

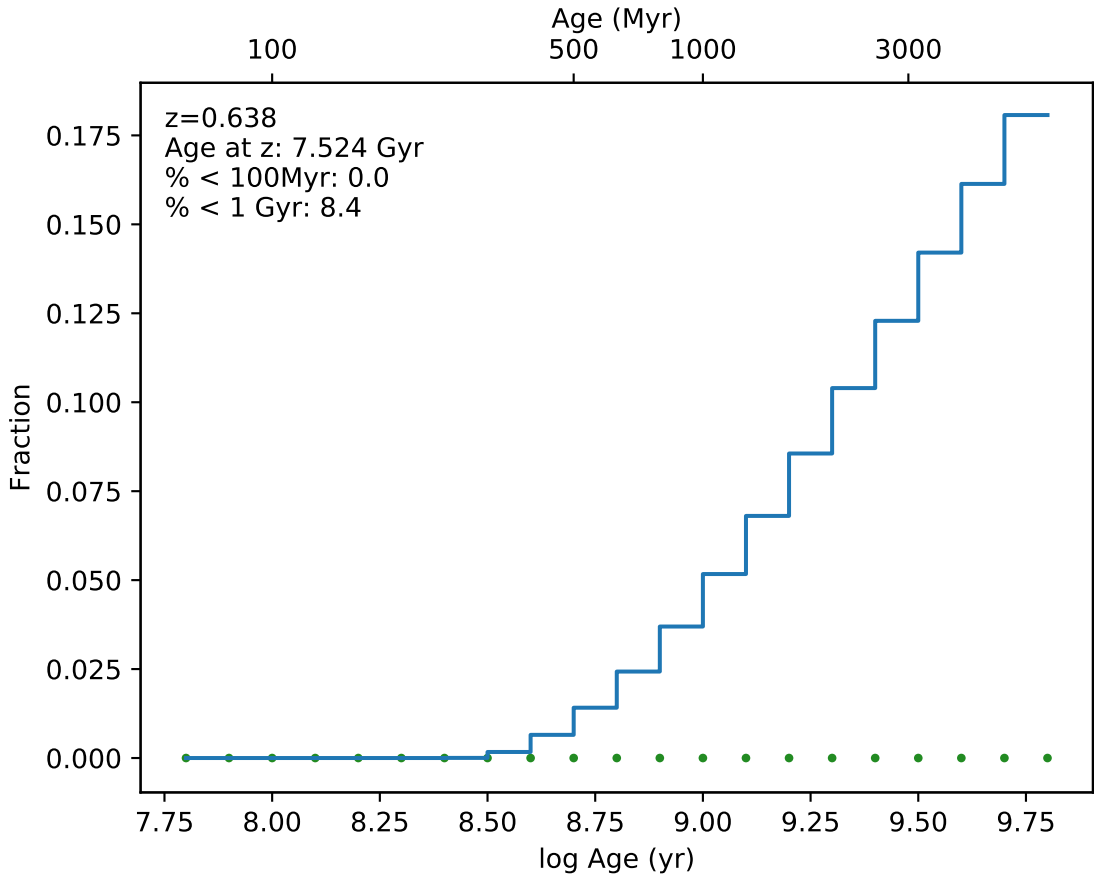
Age (Myr)
100
500
1000
3000
z=0.638
Age at z: 7.524 Gyr
% < 100Myr: 0.0
% < 1 Gyr: 8.4
Fraction
0.175
0.150
0.125
0.100
0.075
0.050
0.025
0.000
7.75
8.00
8.25
8.50
8.75
9.00
9.25
9.50
9.75
log Age (yr)

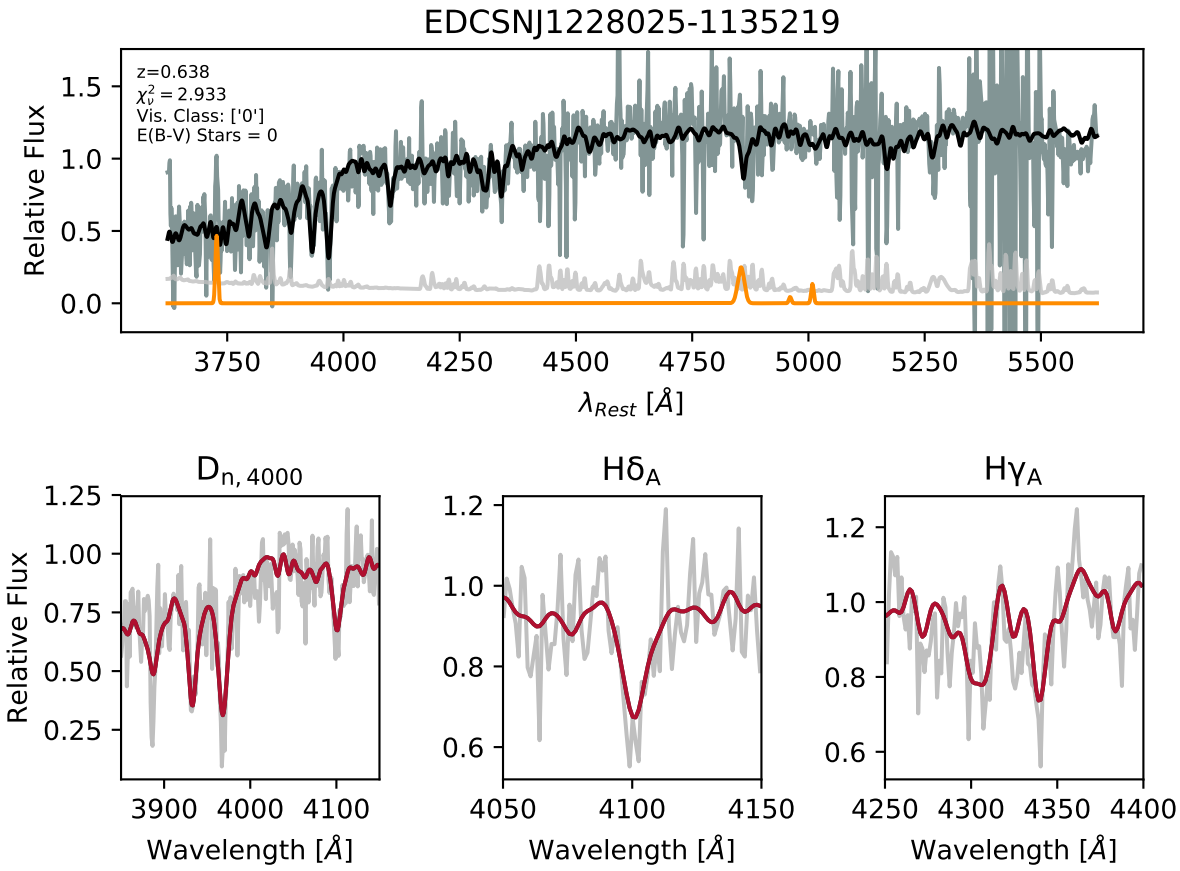
EDCSNJ1228025-1135219
z=0.638
$\chi^2_\nu = 2.933$
Vis. Class: ['0']
E(B-V) Stars = 0
Relative Flux
λ_{Rest} [Å]
$D_{n,4000}$
$H\delta_A$
$H\gamma_A$
Relative Flux
Wavelength [Å]
Wavelength [Å]
Wavelength [Å]

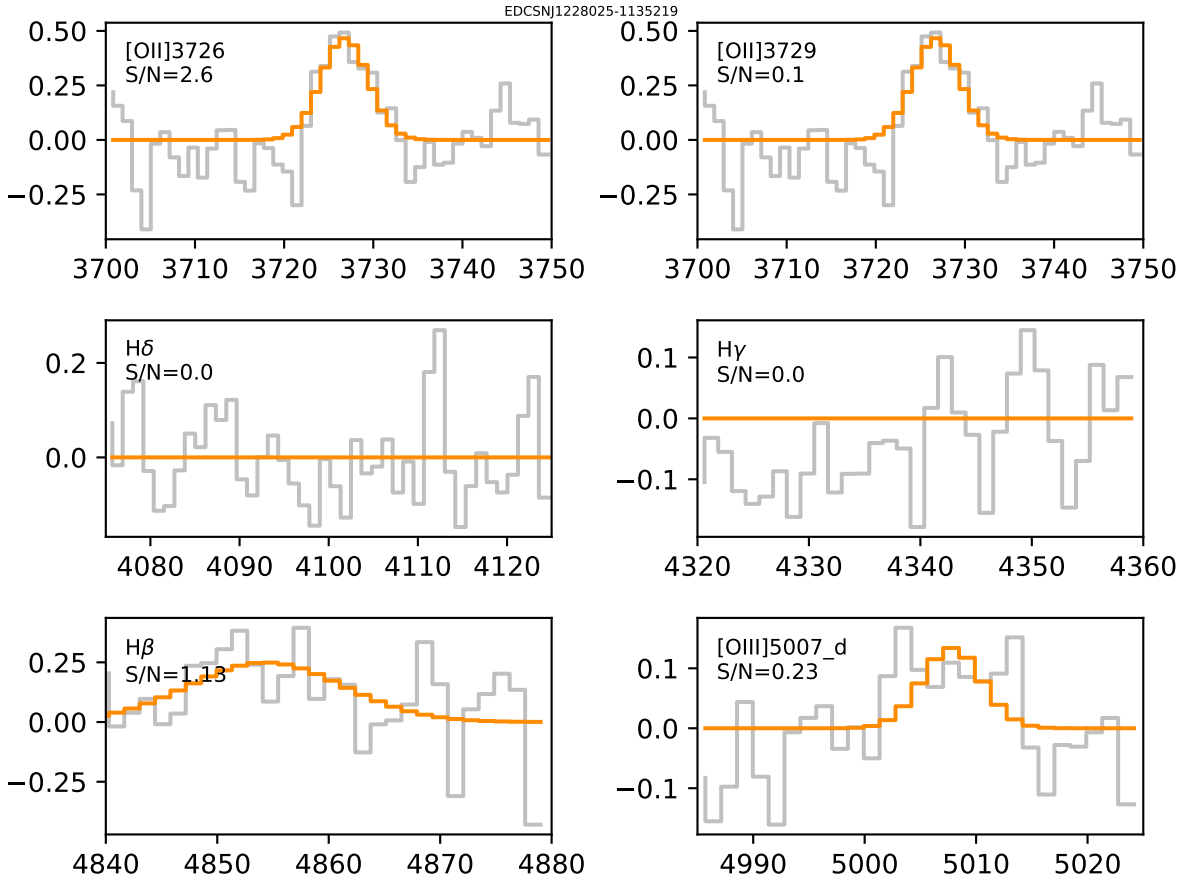
EDCSNJ1228025-1135219
[OII]3726
S/N=2.6
[OII]3729
S/N=0.1
Hδ
S/N=0.0
Hγ
S/N=0.0
Hβ
S/N=1.13
[OIII]5007_d
S/N=0.23

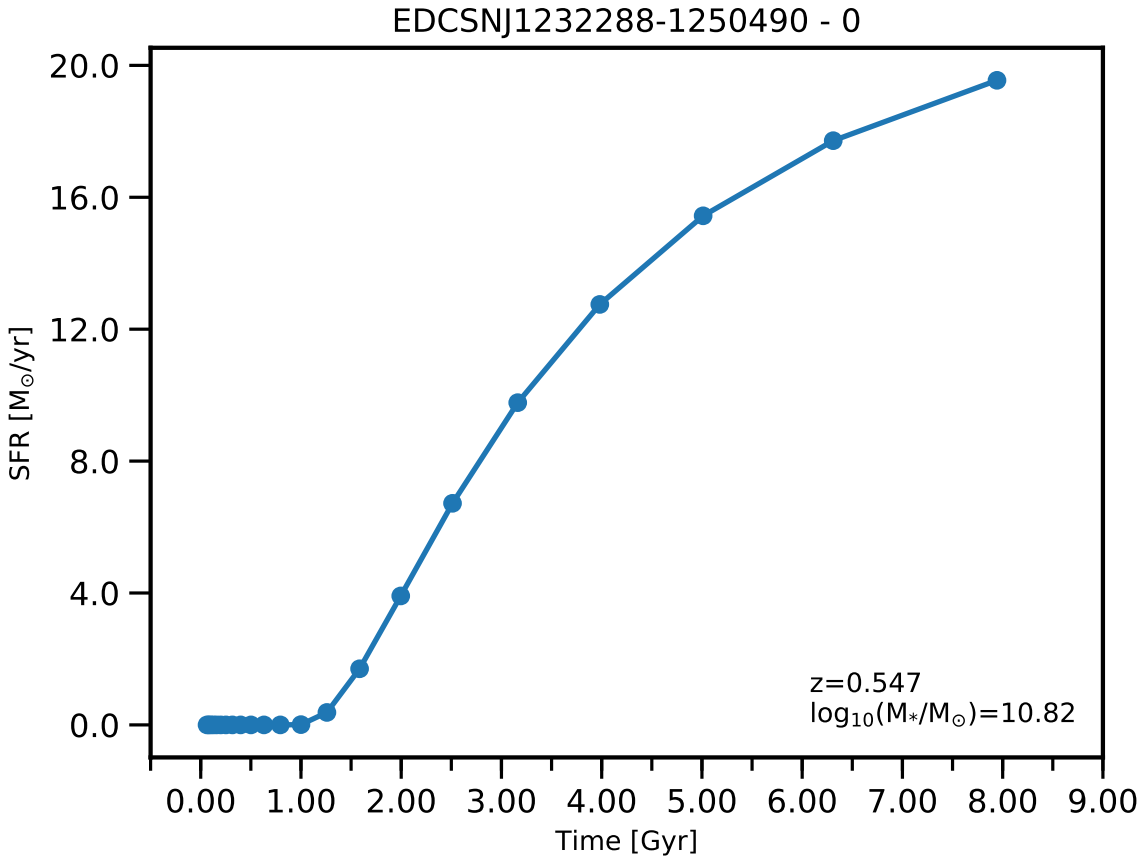
EDCSNJ1232288-1250490 - 0
20.0
16.0
12.0
8.0
4.0
0.0
SFR [M⊙/yr]
0.00
1.00
2.00
3.00
4.00
5.00
6.00
7.00
8.00
9.00
Time [Gyr]
z=0.547
log10(M*/M⊙)=10.82

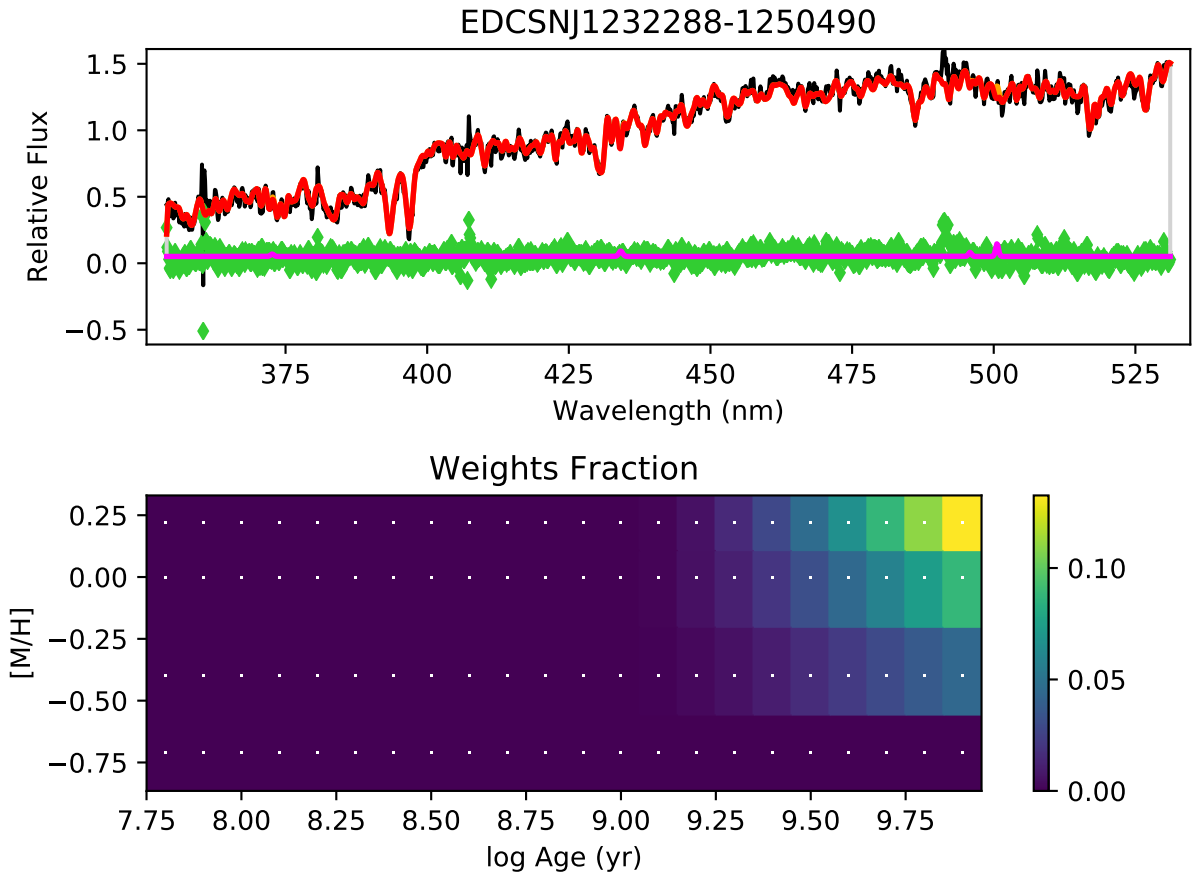
EDCSNJ1232288-1250490
Relative Flux
1.5
1.0
0.5
0.0
−0.5
375
400
425
450
475
500
525
Wavelength (nm)
Weights Fraction
[M/H]
0.25
0.00
−0.25
−0.50
−0.75
7.75
8.00
8.25
8.50
8.75
9.00
9.25
9.50
9.75
log Age (yr)
0.10
0.05
0.00

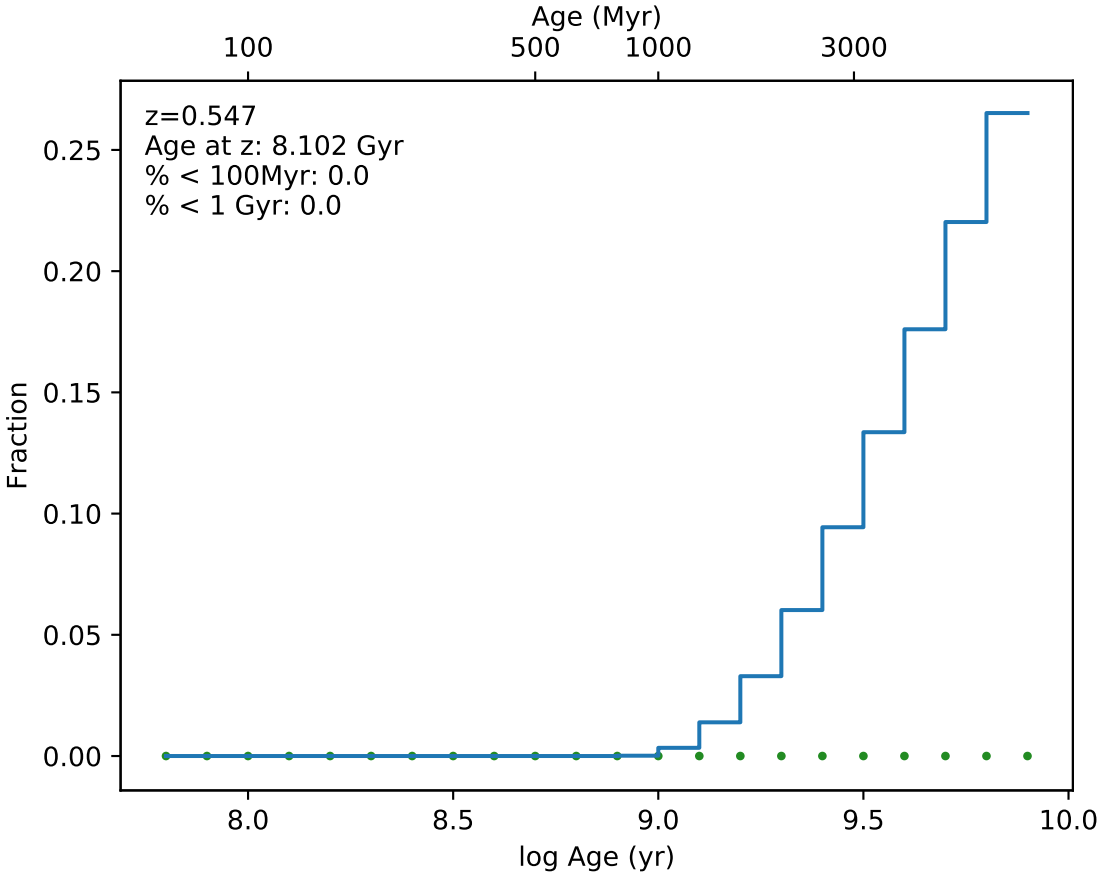
Age (Myr)
100
500
1000
3000
z=0.547
Age at z: 8.102 Gyr
% < 100Myr: 0.0
% < 1 Gyr: 0.0
Fraction
0.25
0.20
0.15
0.10
0.05
0.00
8.0
8.5
9.0
9.5
10.0
log Age (yr)

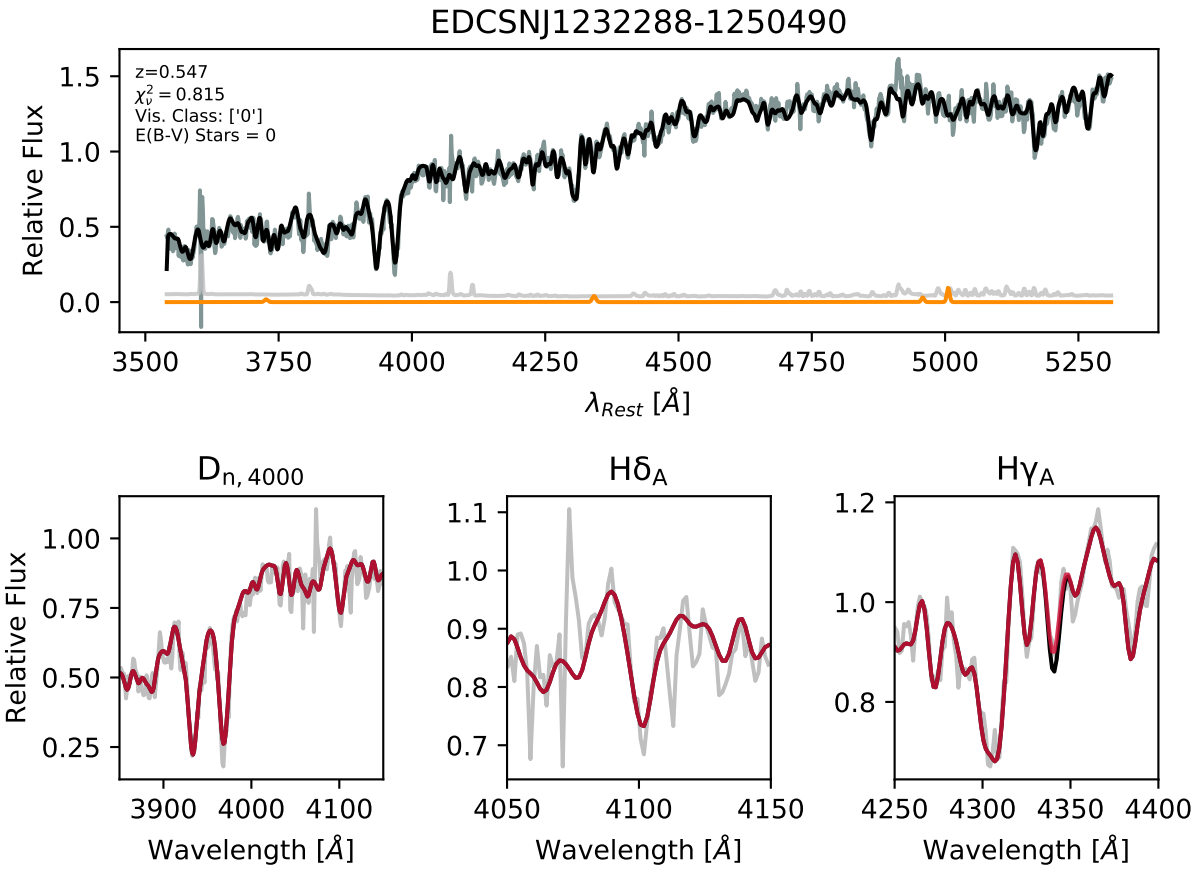
EDCSNJ1232288-1250490
z=0.547
$\chi^2_\nu = 0.815$
Vis. Class: ['0']
E(B-V) Stars = 0
Relative Flux
λ_{Rest} [Å]
$D_{n,4000}$
$H\delta_A$
$H\gamma_A$
Wavelength [Å]

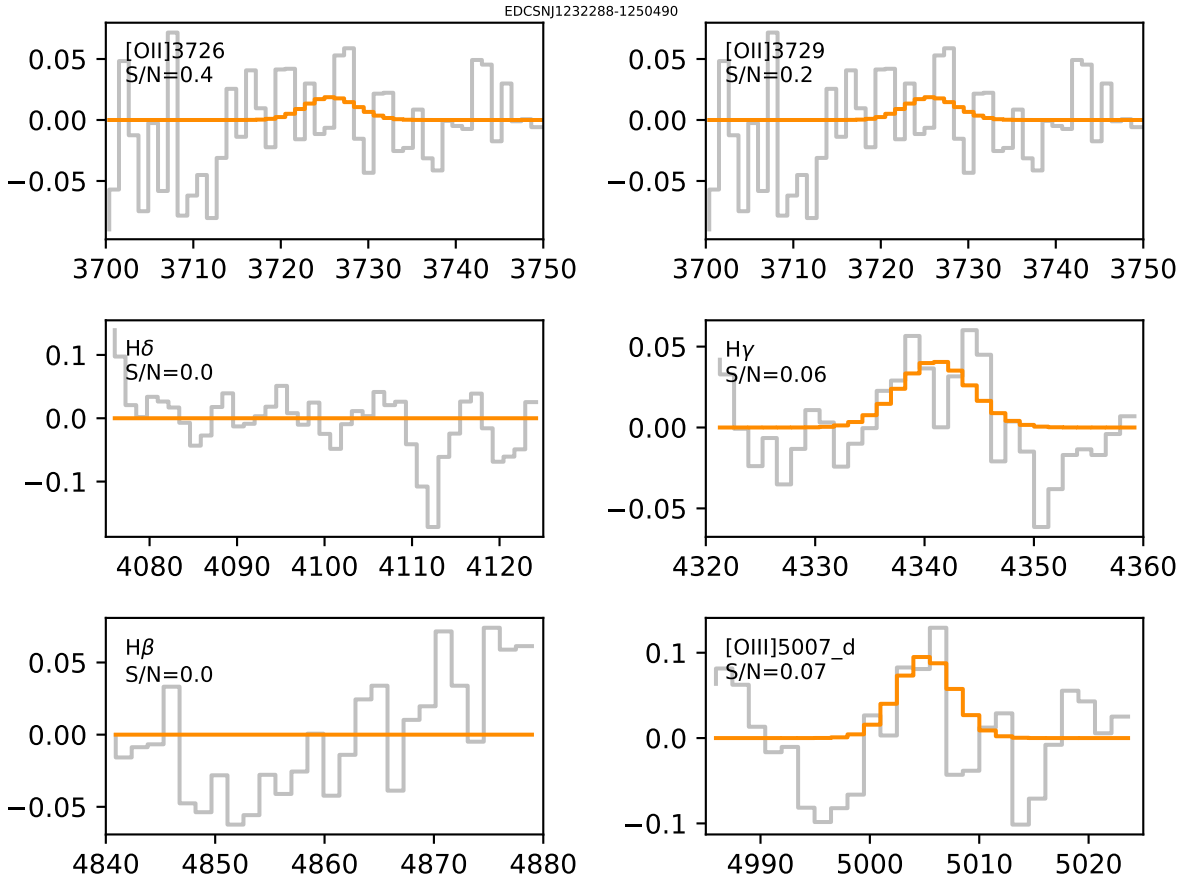
EDCSNJ1232288-1250490
[OII]3726
S/N=0.4
[OII]3729
S/N=0.2
Hδ
S/N=0.0
Hγ
S/N=0.06
Hβ
S/N=0.0
[OIII]5007_d
S/N=0.07

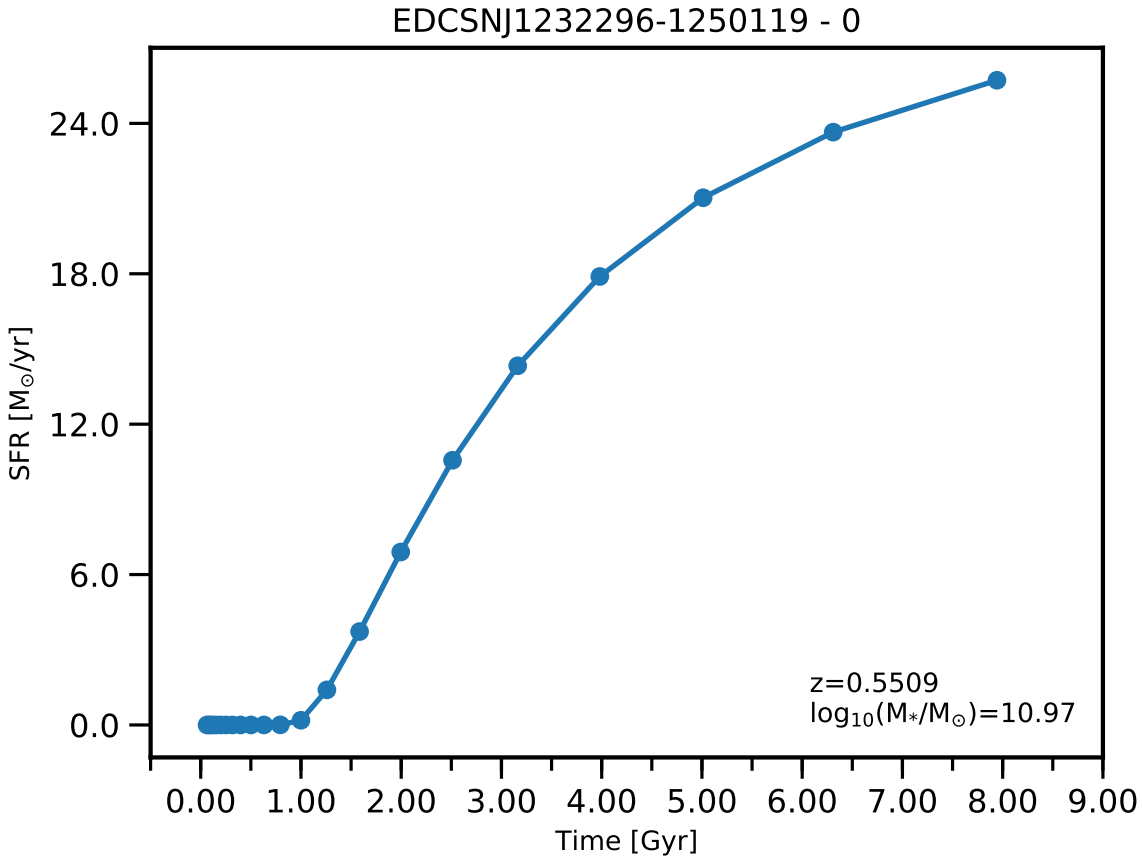
EDCSNJ1232296-1250119 - 0
24.0
18.0
12.0
6.0
0.0
SFR [M⊙/yr]
0.00
1.00
2.00
3.00
4.00
5.00
6.00
7.00
8.00
9.00
Time [Gyr]
z=0.5509
log10(M*/M⊙)=10.97

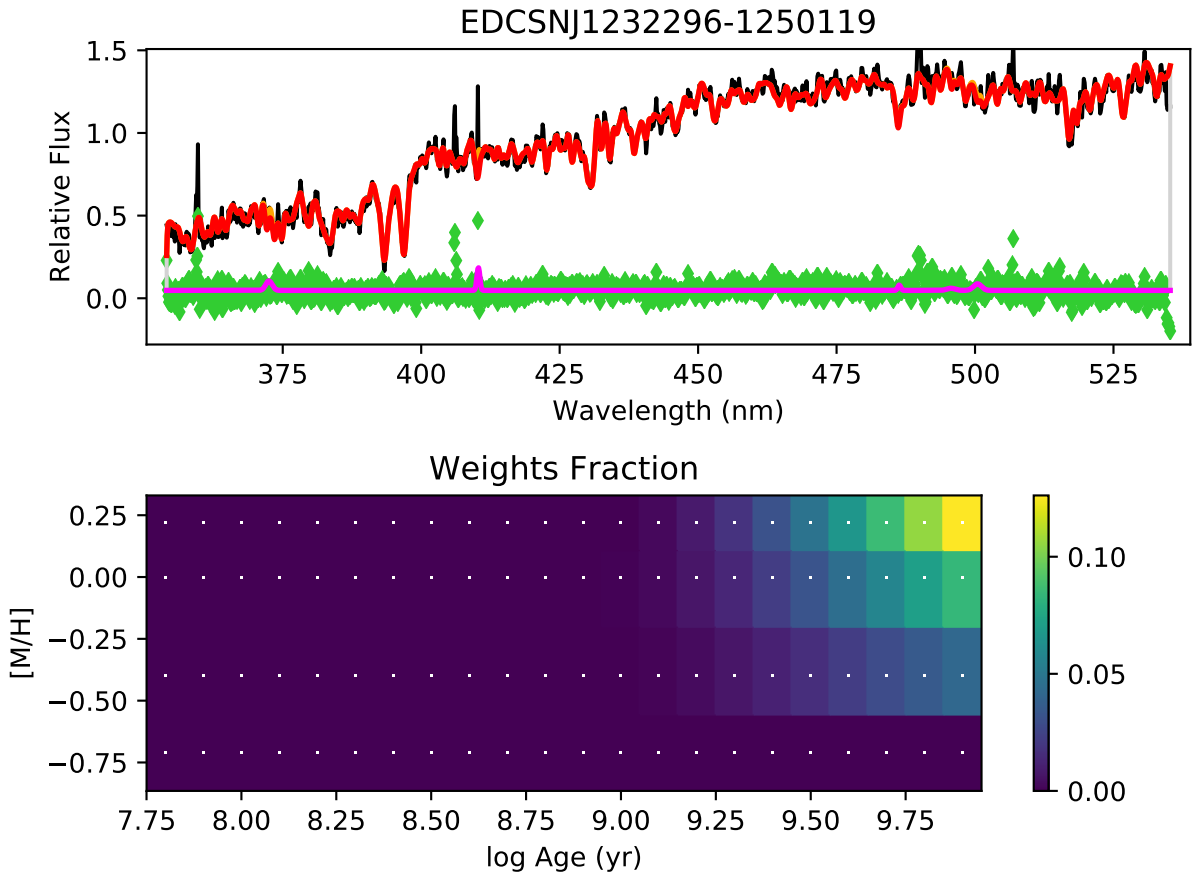
EDCSNJ1232296-1250119
Relative Flux
1.5
1.0
0.5
0.0
375
400
425
450
475
500
525
Wavelength (nm)
Weights Fraction
[M/H]
0.25
0.00
−0.25
−0.50
−0.75
7.75
8.00
8.25
8.50
8.75
9.00
9.25
9.50
9.75
log Age (yr)
0.10
0.05
0.00

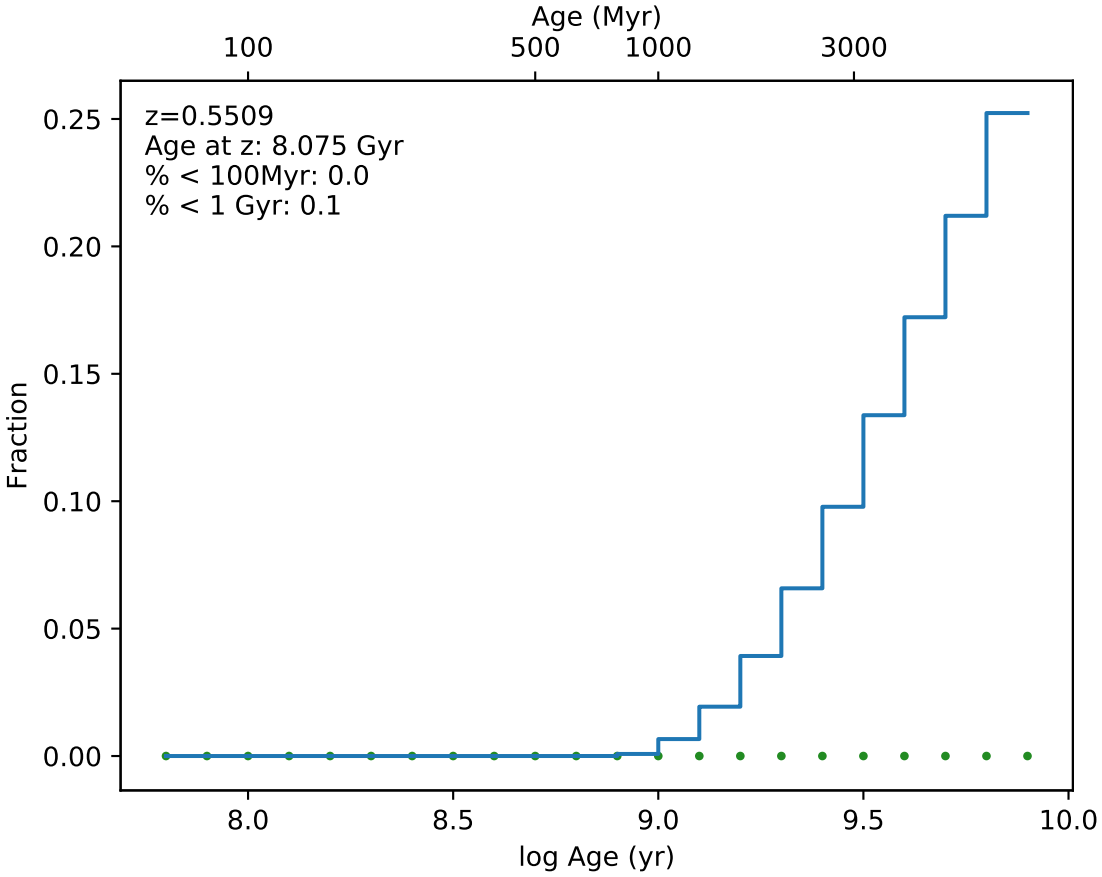
Age (Myr)
100
500
1000
3000
z=0.5509
Age at z: 8.075 Gyr
% < 100Myr: 0.0
% < 1 Gyr: 0.1
Fraction
0.25
0.20
0.15
0.10
0.05
0.00
8.0
8.5
9.0
9.5
10.0
log Age (yr)

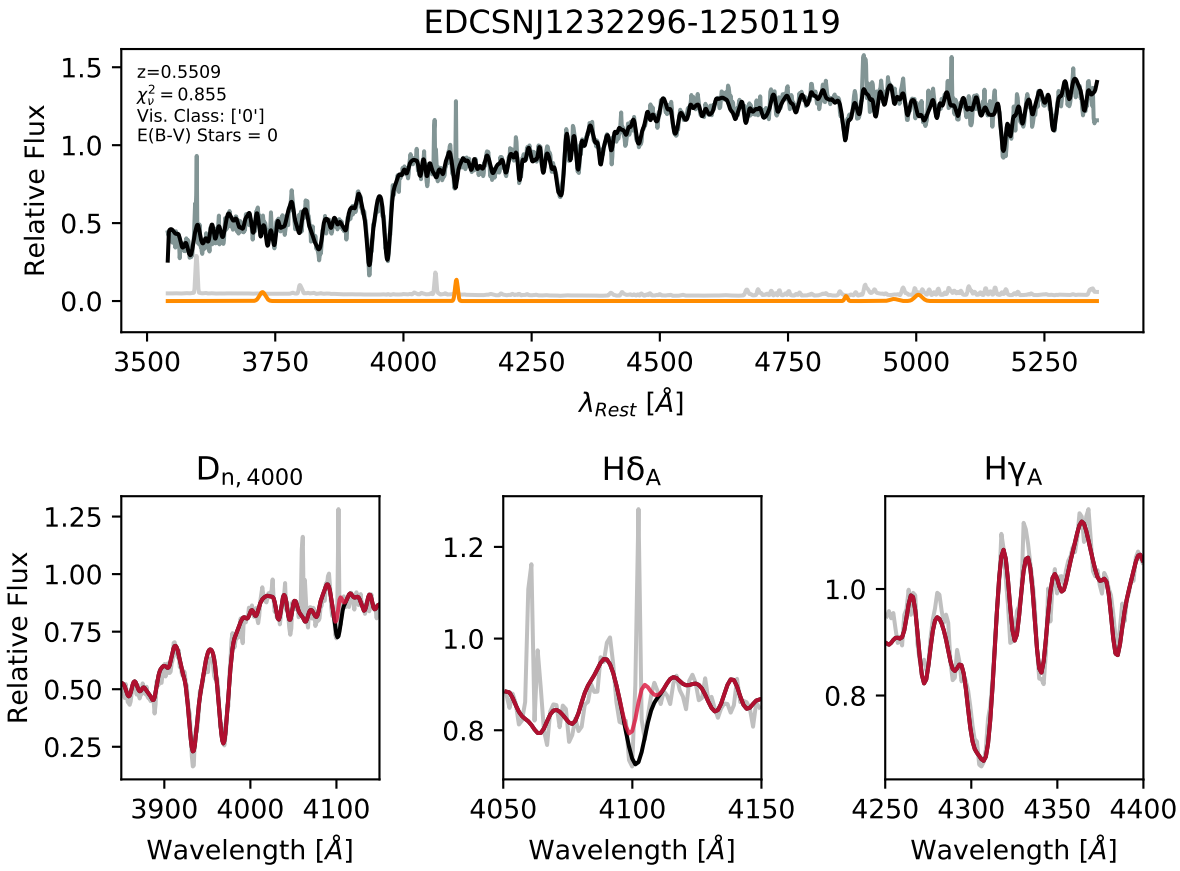
EDCSNJ1232296-1250119
z=0.5509
$\chi^2_\nu = 0.855$
Vis. Class: ['0']
E(B-V) Stars = 0
Relative Flux
λ_{Rest} [Å]
$D_{n,4000}$
$H\delta_A$
$H\gamma_A$
Wavelength [Å]

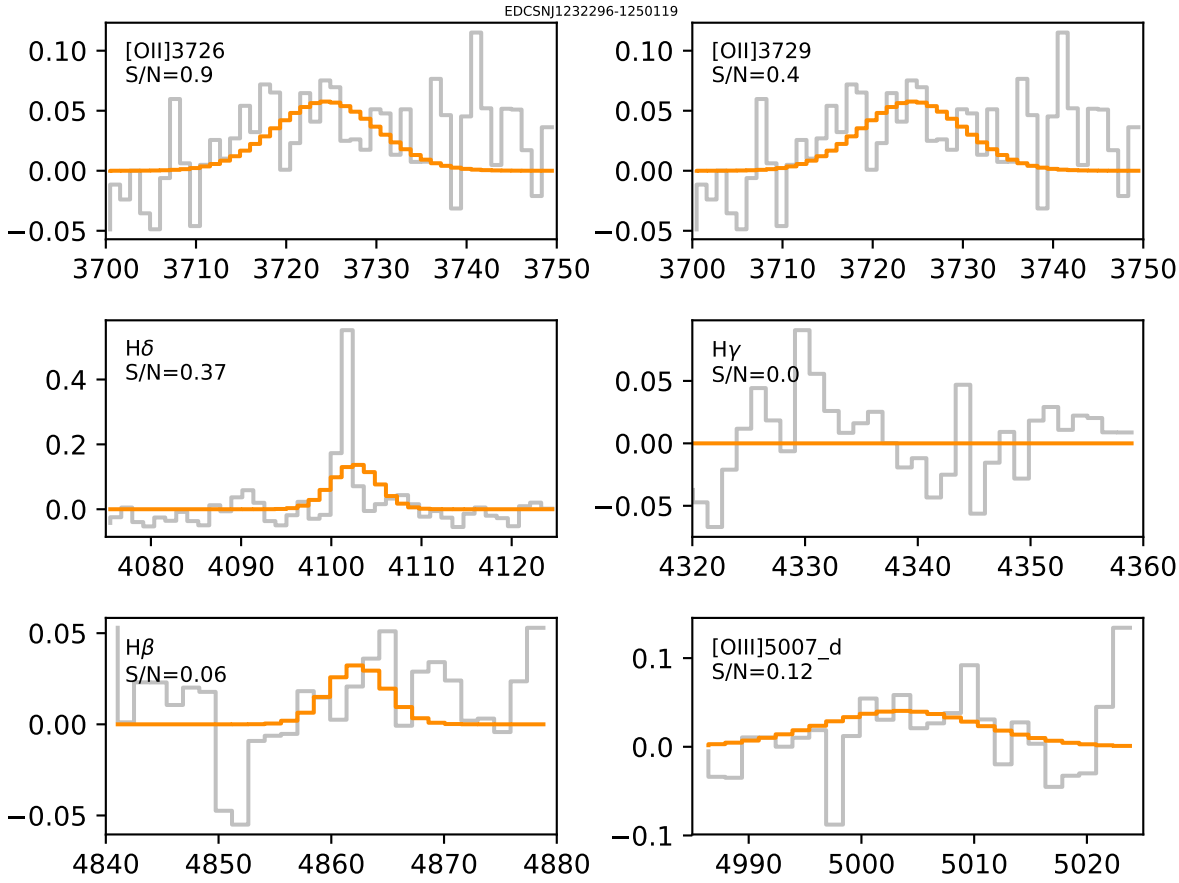
EDCSNJ1232296-1250119
[OII]3726
S/N=0.9
[OII]3729
S/N=0.4
Hδ
S/N=0.37
Hγ
S/N=0.0
Hβ
S/N=0.06
[OIII]5007_d
S/N=0.12

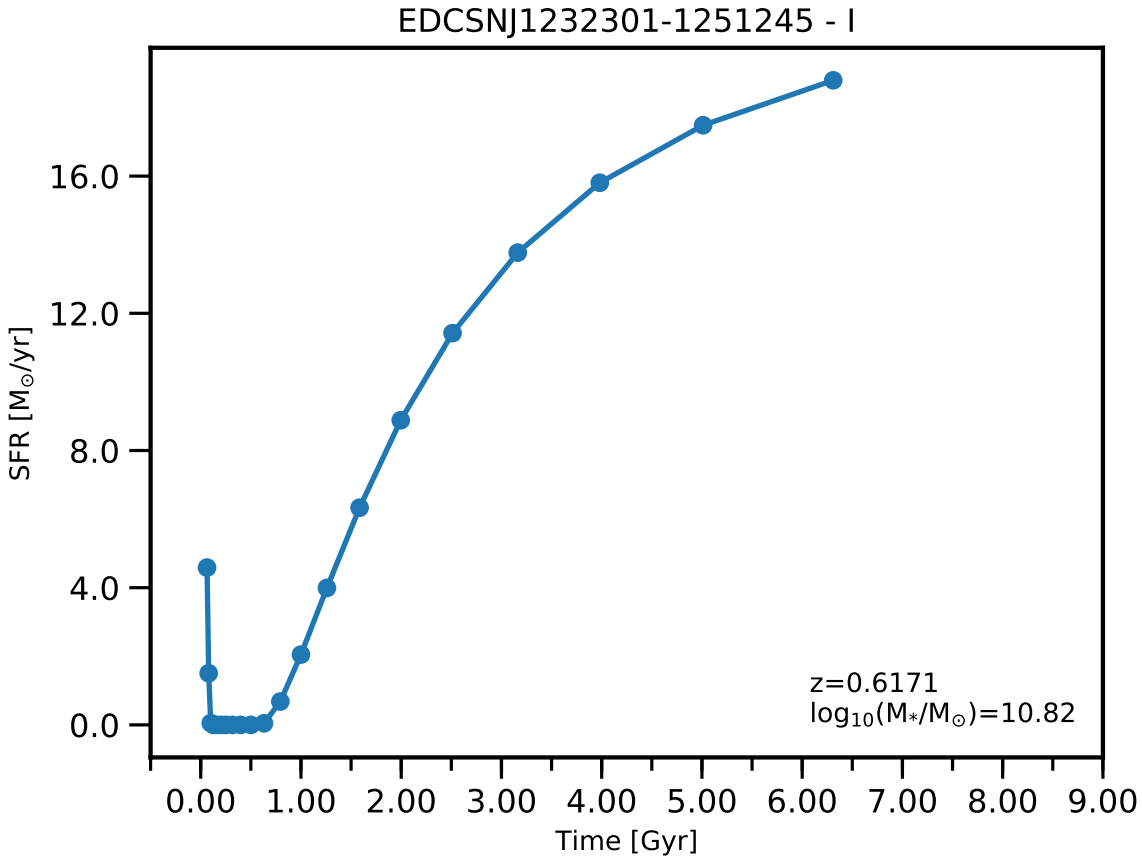
EDCSNJ1232301-1251245 - I
SFR [M⊙/yr]
16.0
12.0
8.0
4.0
0.0
0.00
1.00
2.00
3.00
4.00
5.00
6.00
7.00
8.00
9.00
Time [Gyr]
z=0.6171
log10(M*/M⊙)=10.82

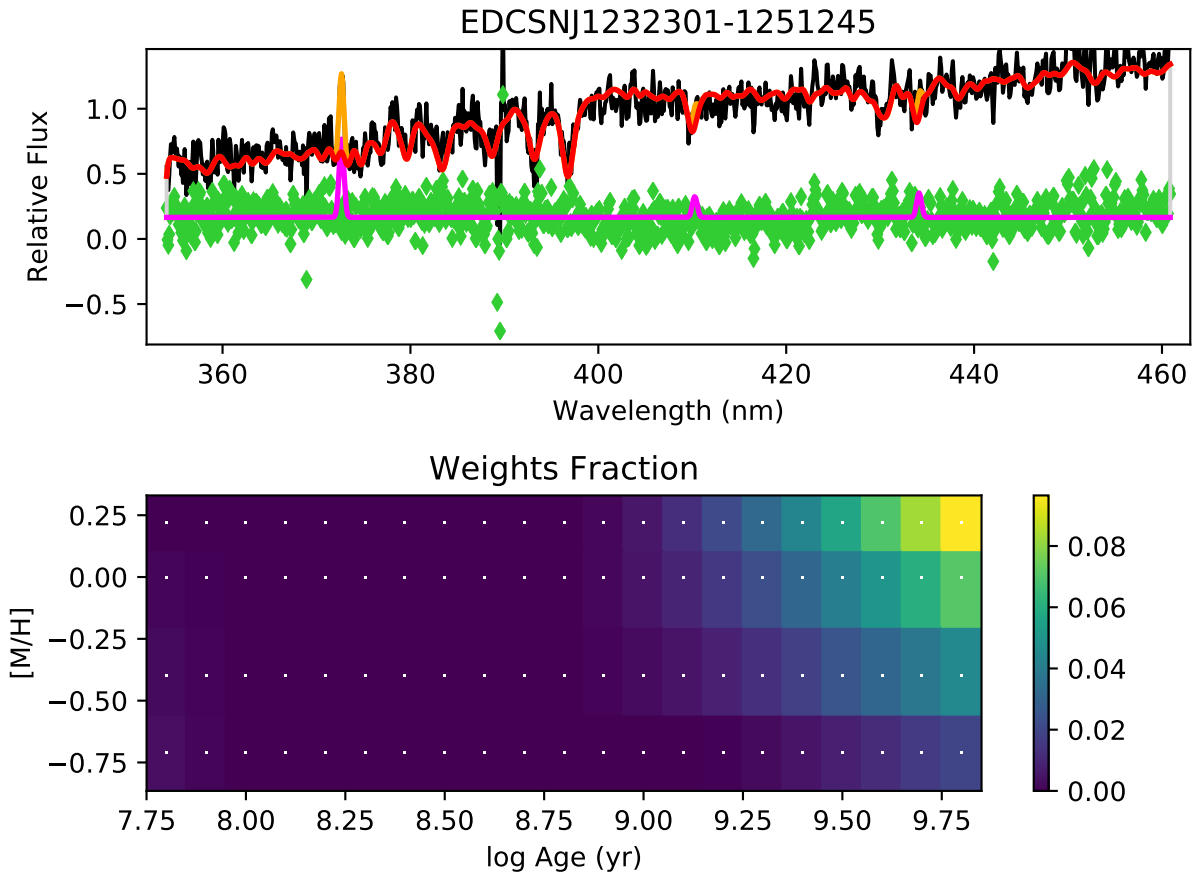
EDCSNJ1232301-1251245
Relative Flux
1.0
0.5
0.0
−0.5
360
380
400
420
440
460
Wavelength (nm)
Weights Fraction
[M/H]
0.25
0.00
−0.25
−0.50
−0.75
7.75
8.00
8.25
8.50
8.75
9.00
9.25
9.50
9.75
log Age (yr)
0.08
0.06
0.04
0.02
0.00

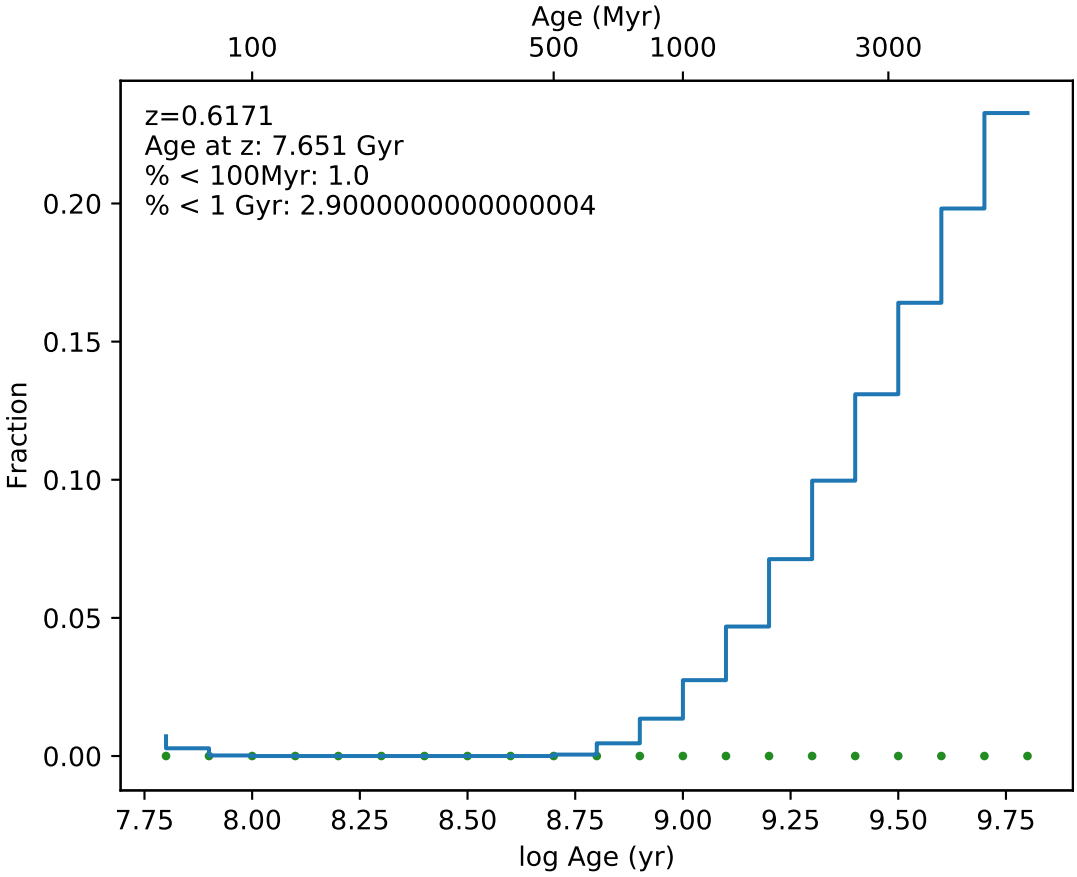
Age (Myr)
100
500
1000
3000
z=0.6171
Age at z: 7.651 Gyr
% < 100Myr: 1.0
% < 1 Gyr: 2.9000000000000004
Fraction
0.20
0.15
0.10
0.05
0.00
7.75
8.00
8.25
8.50
8.75
9.00
9.25
9.50
9.75
log Age (yr)

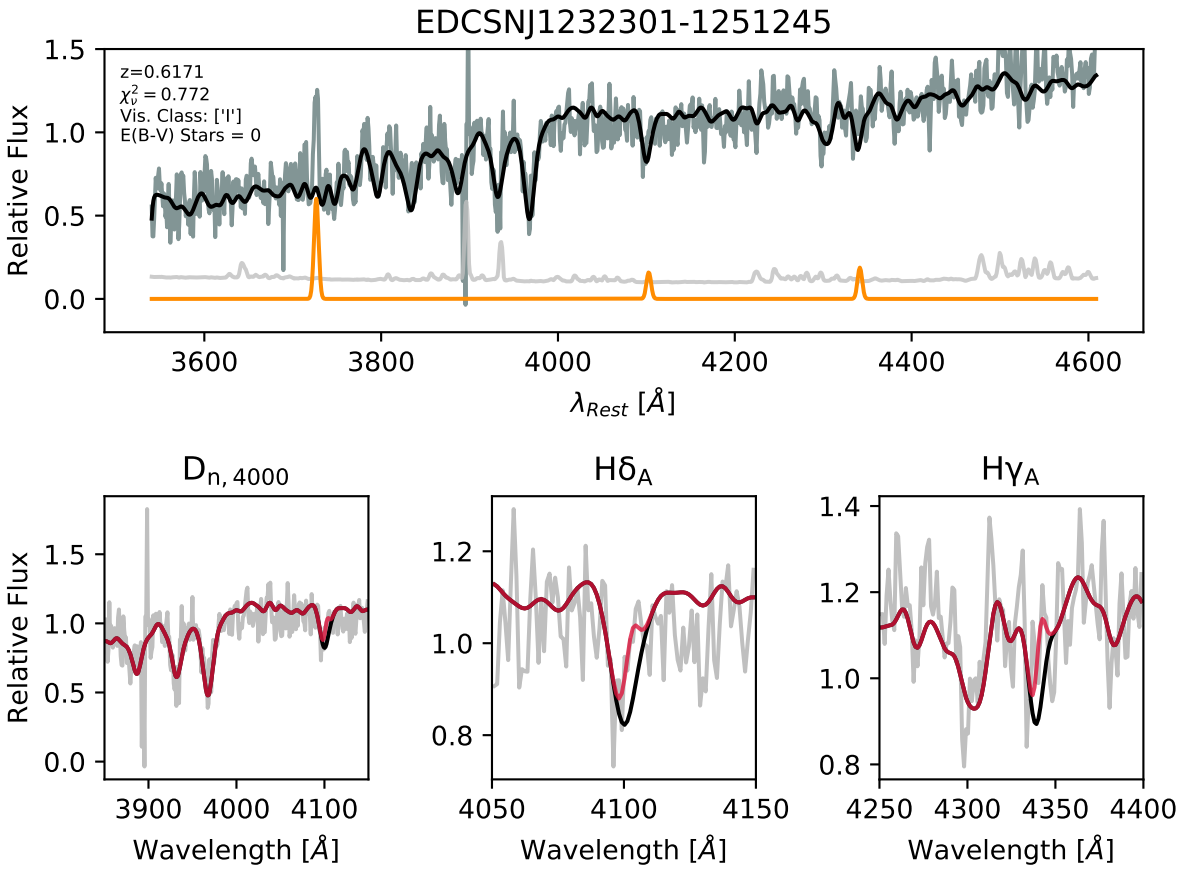
EDCSNJ1232301-1251245
z=0.6171
$\chi^2_\nu = 0.772$
Vis. Class: ['I']
E(B-V) Stars = 0
Relative Flux
λ_{Rest} [Å]
$D_{n,4000}$
$H\delta_A$
$H\gamma_A$
Wavelength [Å]

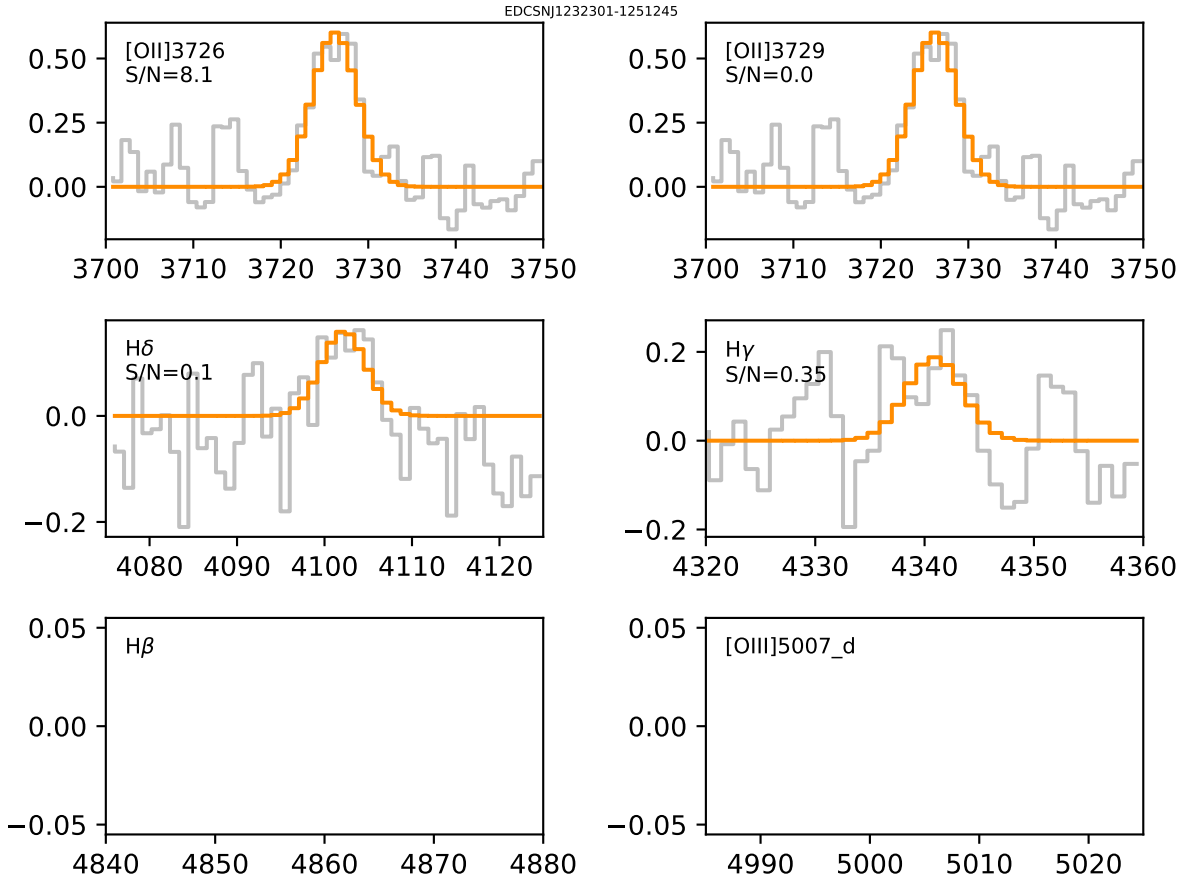
EDCSNJ1232301-1251245
[OII]3726
S/N=8.1
[OII]3729
S/N=0.0
Hδ
S/N=0.1
Hγ
S/N=0.35
Hβ
[OIII]5007_d

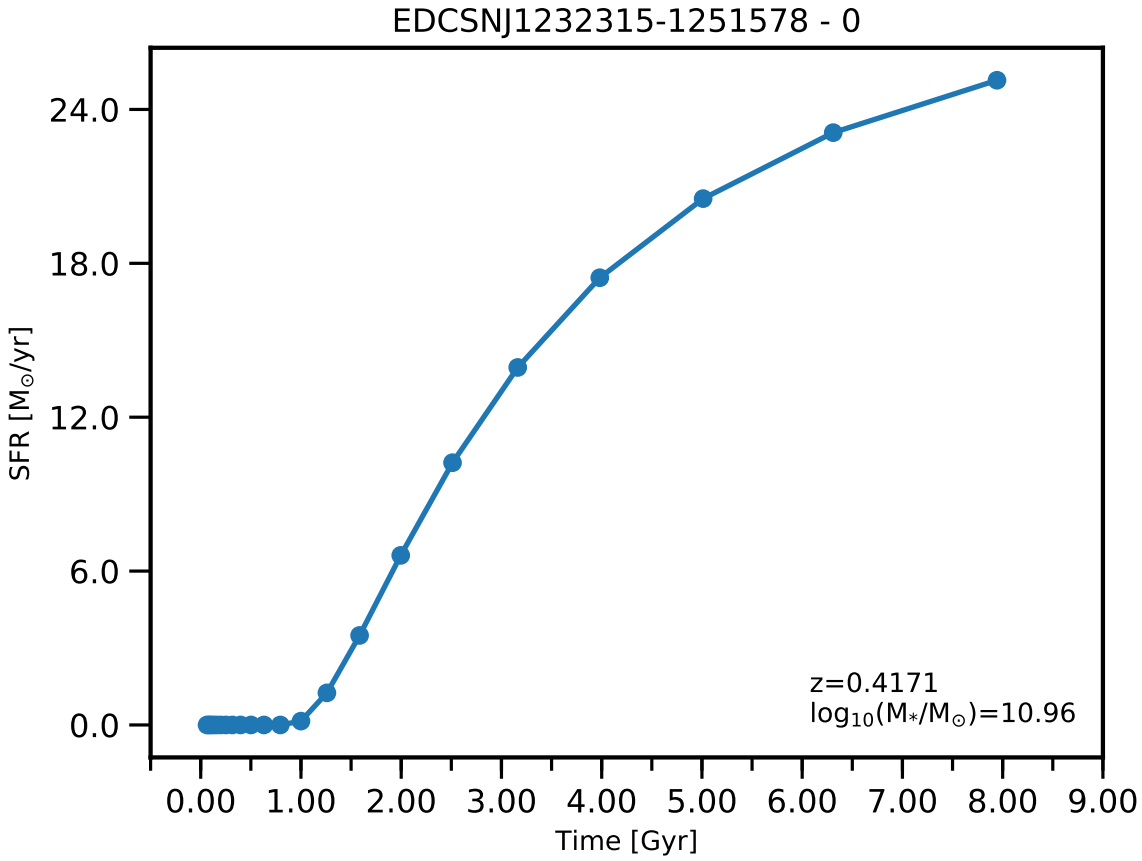
EDCSNJ1232315-1251578 - 0
SFR [M⊙/yr]
24.0
18.0
12.0
6.0
0.0
0.00
1.00
2.00
3.00
4.00
5.00
6.00
7.00
8.00
9.00
Time [Gyr]
z=0.4171
log10(M*/M⊙)=10.96

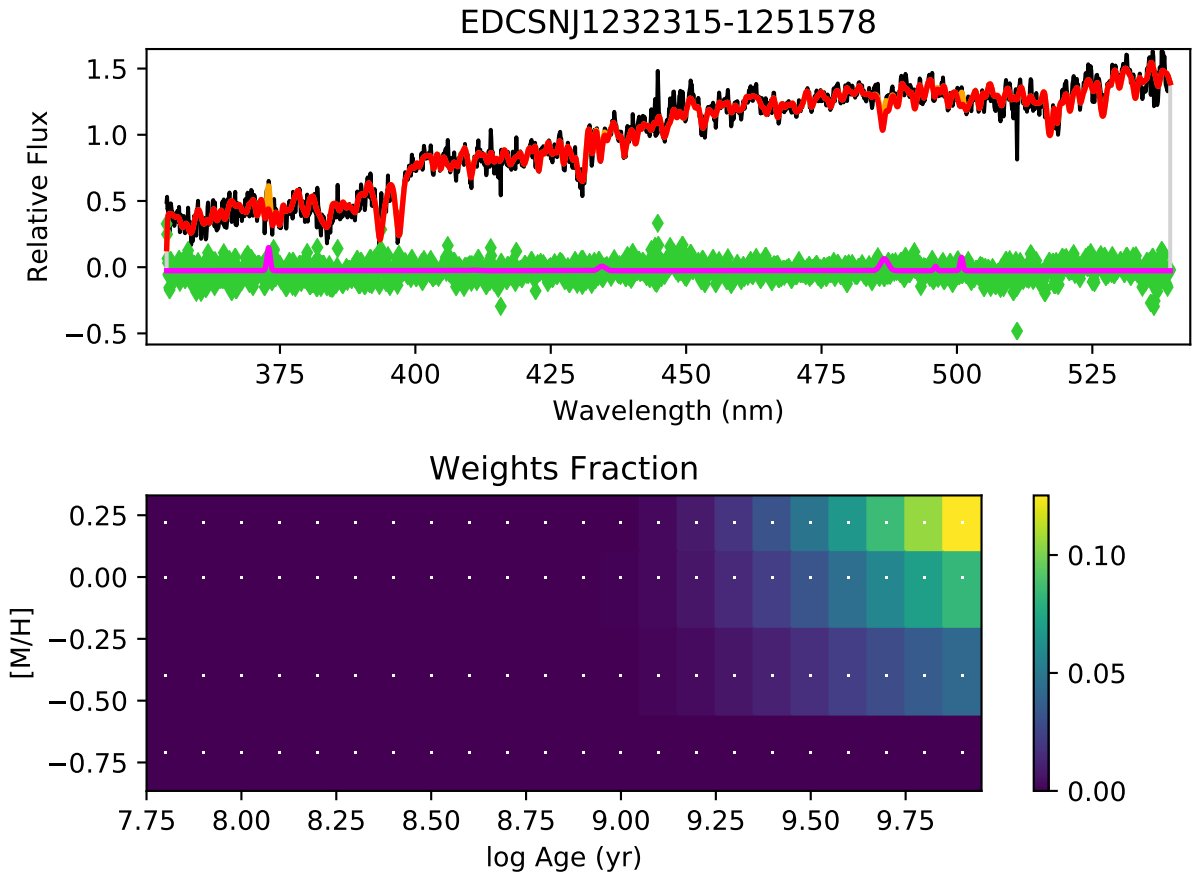
EDCSNJ1232315-1251578
Relative Flux
1.5
1.0
0.5
0.0
−0.5
375
400
425
450
475
500
525
Wavelength (nm)
Weights Fraction
[M/H]
0.25
0.00
−0.25
−0.50
−0.75
7.75
8.00
8.25
8.50
8.75
9.00
9.25
9.50
9.75
log Age (yr)
0.10
0.05
0.00

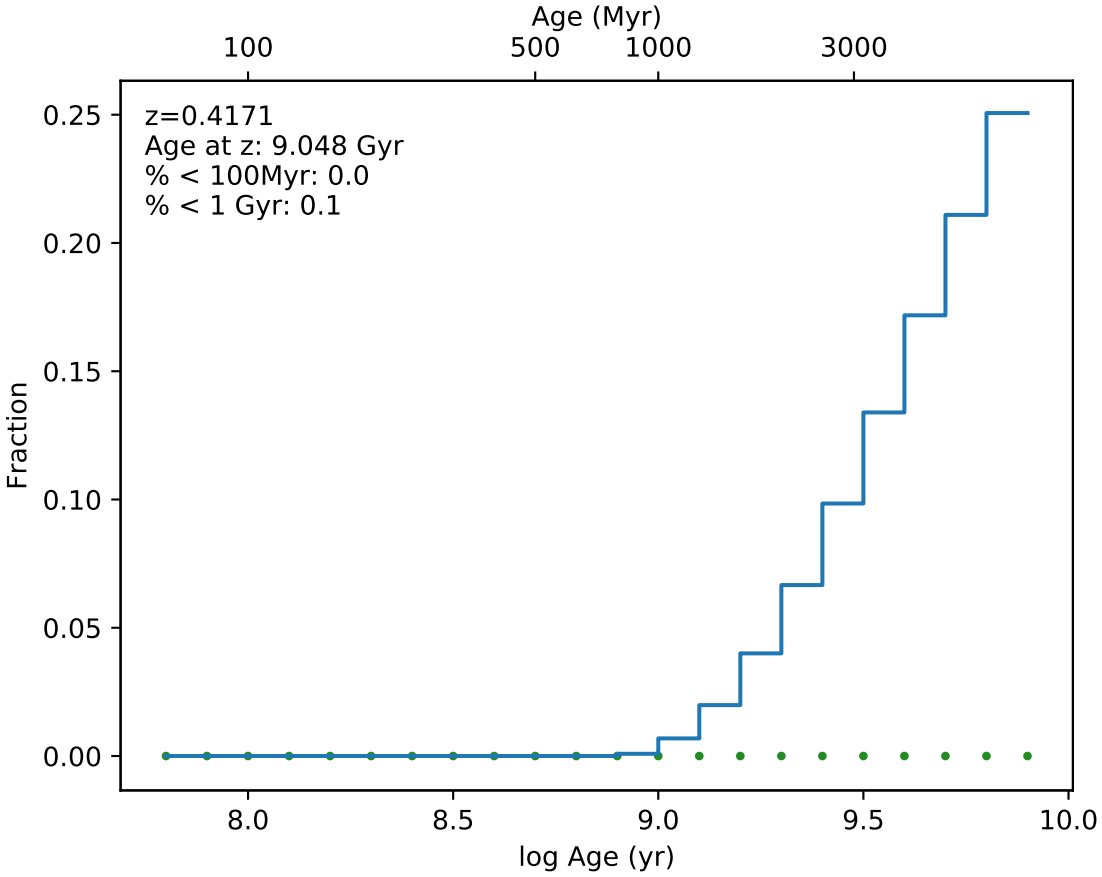
Age (Myr)
100
500
1000
3000
z=0.4171
Age at z: 9.048 Gyr
% < 100Myr: 0.0
% < 1 Gyr: 0.1
Fraction
0.25
0.20
0.15
0.10
0.05
0.00
8.0
8.5
9.0
9.5
10.0
log Age (yr)

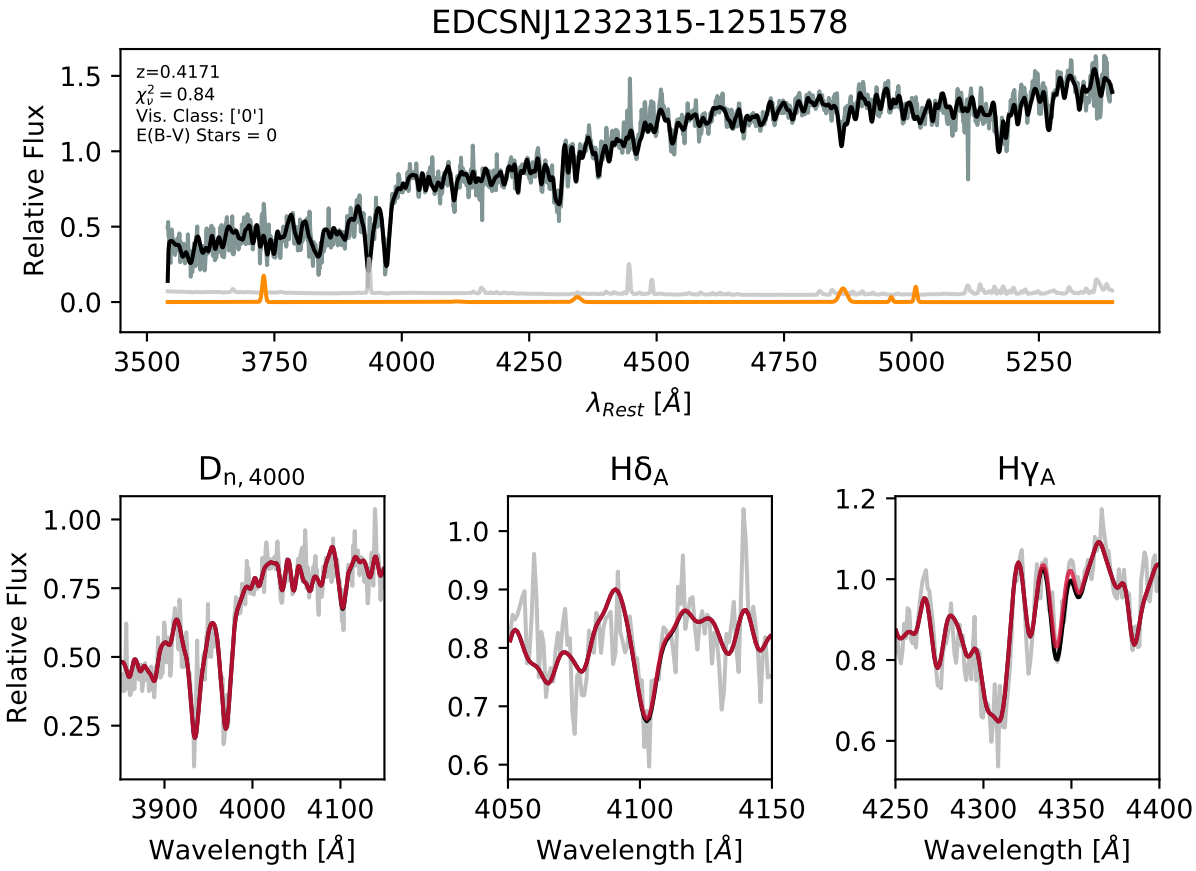
EDCSNJ1232315-1251578
z=0.4171
$\chi^2_\nu = 0.84$
Vis. Class: ['0']
E(B-V) Stars = 0
Relative Flux
λ_{Rest} [Å]
$D_{n,4000}$
$H\delta_A$
$H\gamma_A$
Wavelength [Å]

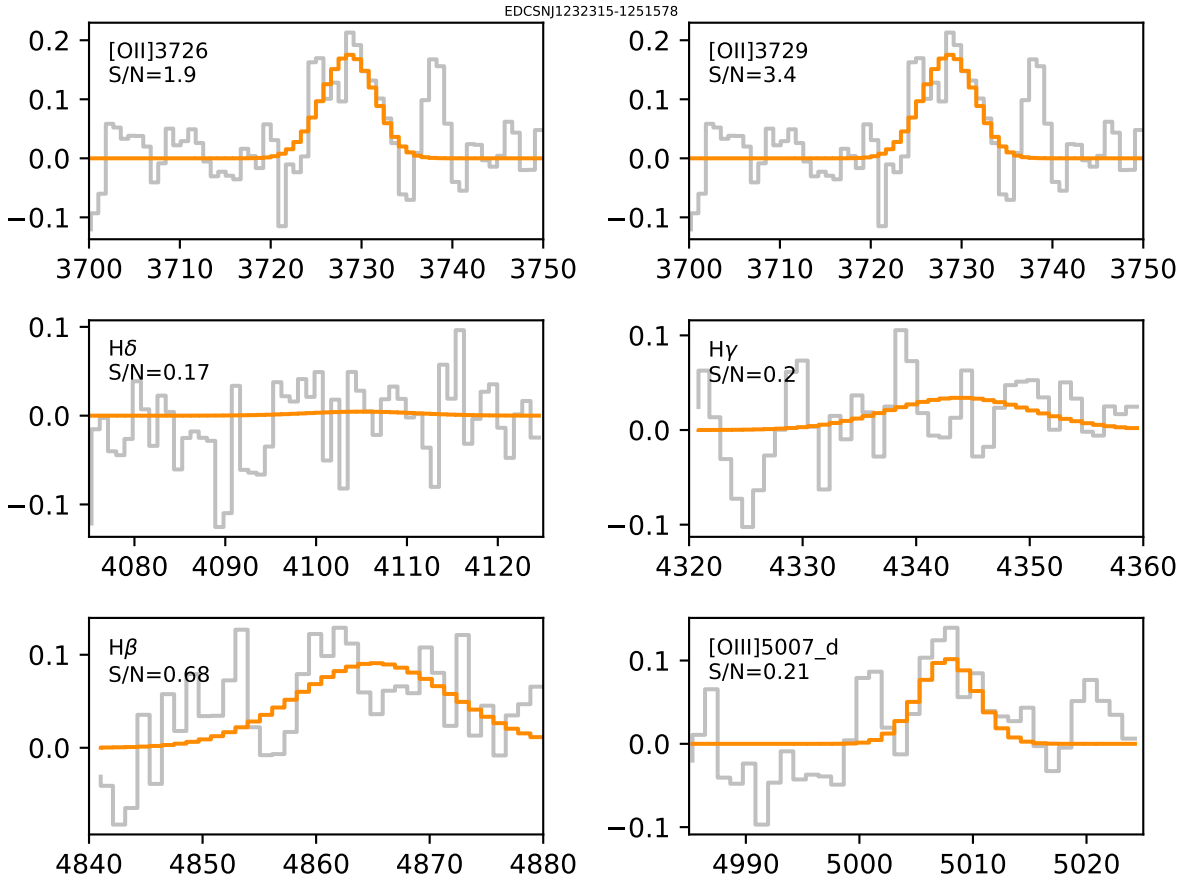
EDCSNJ1232315-1251578
[OII]3726
S/N=1.9
[OII]3729
S/N=3.4
Hδ
S/N=0.17
Hγ
S/N=0.2
Hβ
S/N=0.68
[OIII]5007_d
S/N=0.21

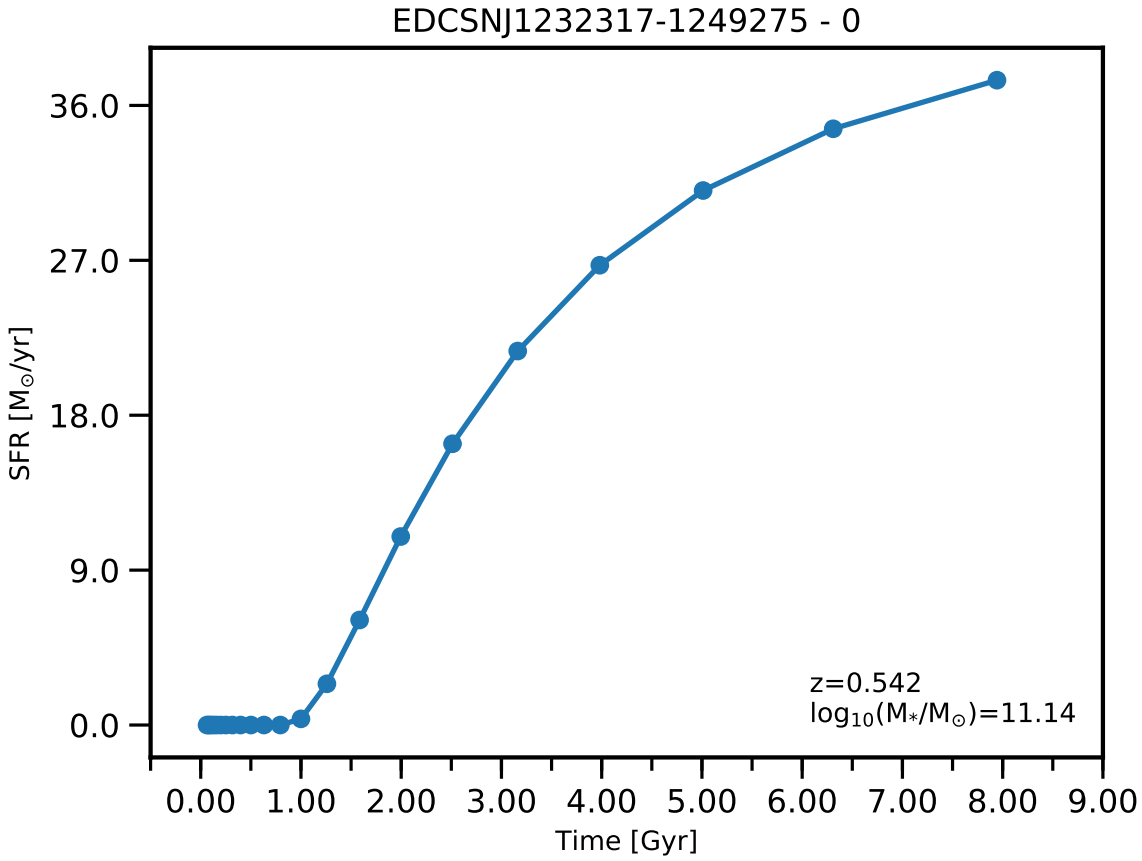
EDCSNJ1232317-1249275 - 0
SFR [M⊙/yr]
36.0
27.0
18.0
9.0
0.0
0.00
1.00
2.00
3.00
4.00
5.00
6.00
7.00
8.00
9.00
Time [Gyr]
z=0.542
log10(M*/M⊙)=11.14

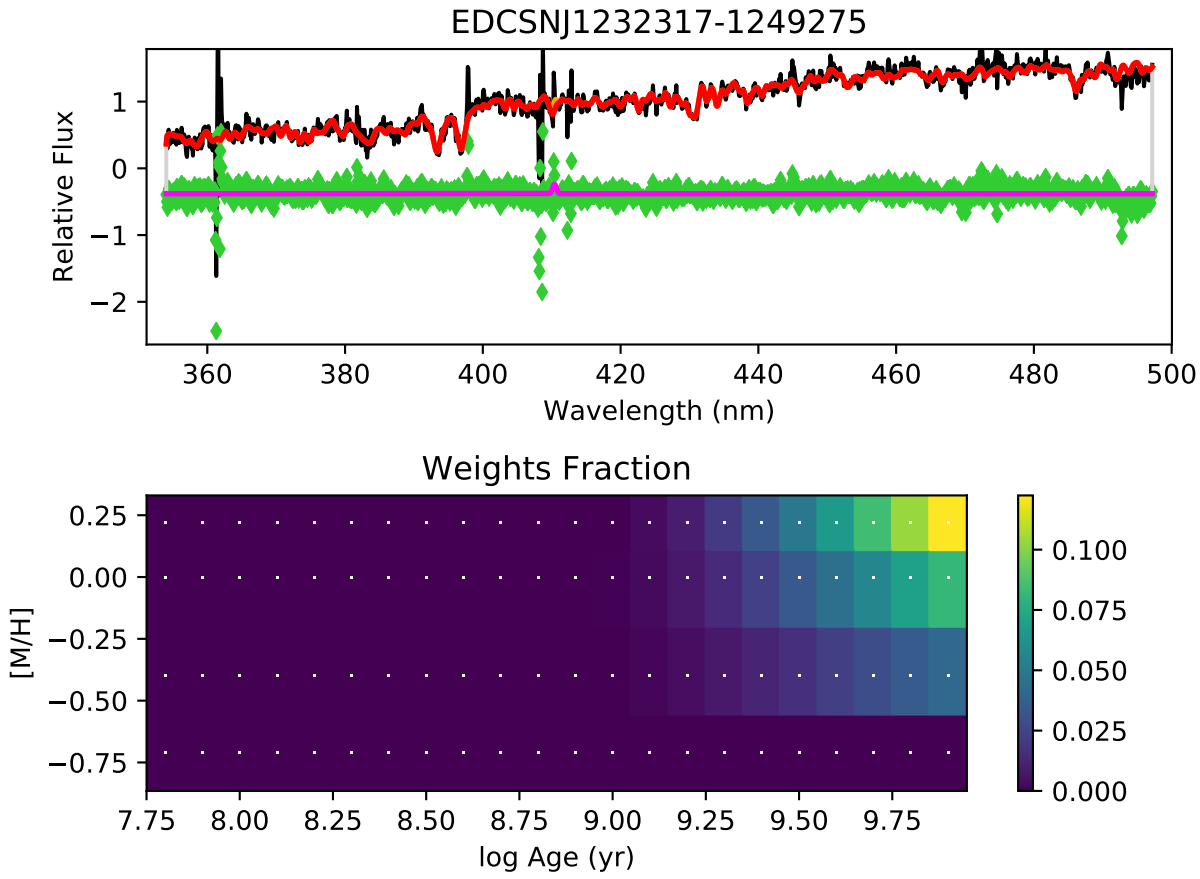
EDCSNJ1232317-1249275
Relative Flux
1
0
−1
−2
360
380
400
420
440
460
480
500
Wavelength (nm)
Weights Fraction
[M/H]
0.25
0.00
−0.25
−0.50
−0.75
7.75
8.00
8.25
8.50
8.75
9.00
9.25
9.50
9.75
log Age (yr)
0.100
0.075
0.050
0.025
0.000

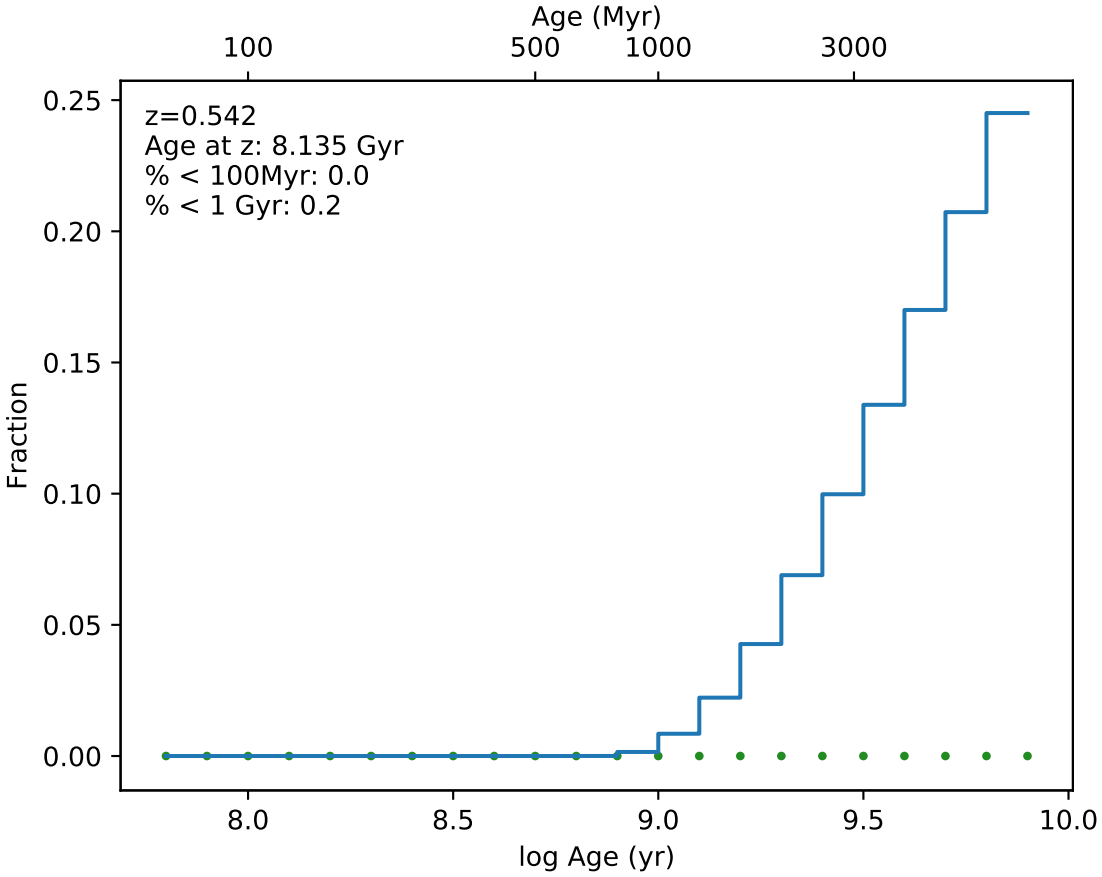
Age (Myr)
100
500
1000
3000
z=0.542
Age at z: 8.135 Gyr
% < 100Myr: 0.0
% < 1 Gyr: 0.2
Fraction
0.25
0.20
0.15
0.10
0.05
0.00
8.0
8.5
9.0
9.5
10.0
log Age (yr)

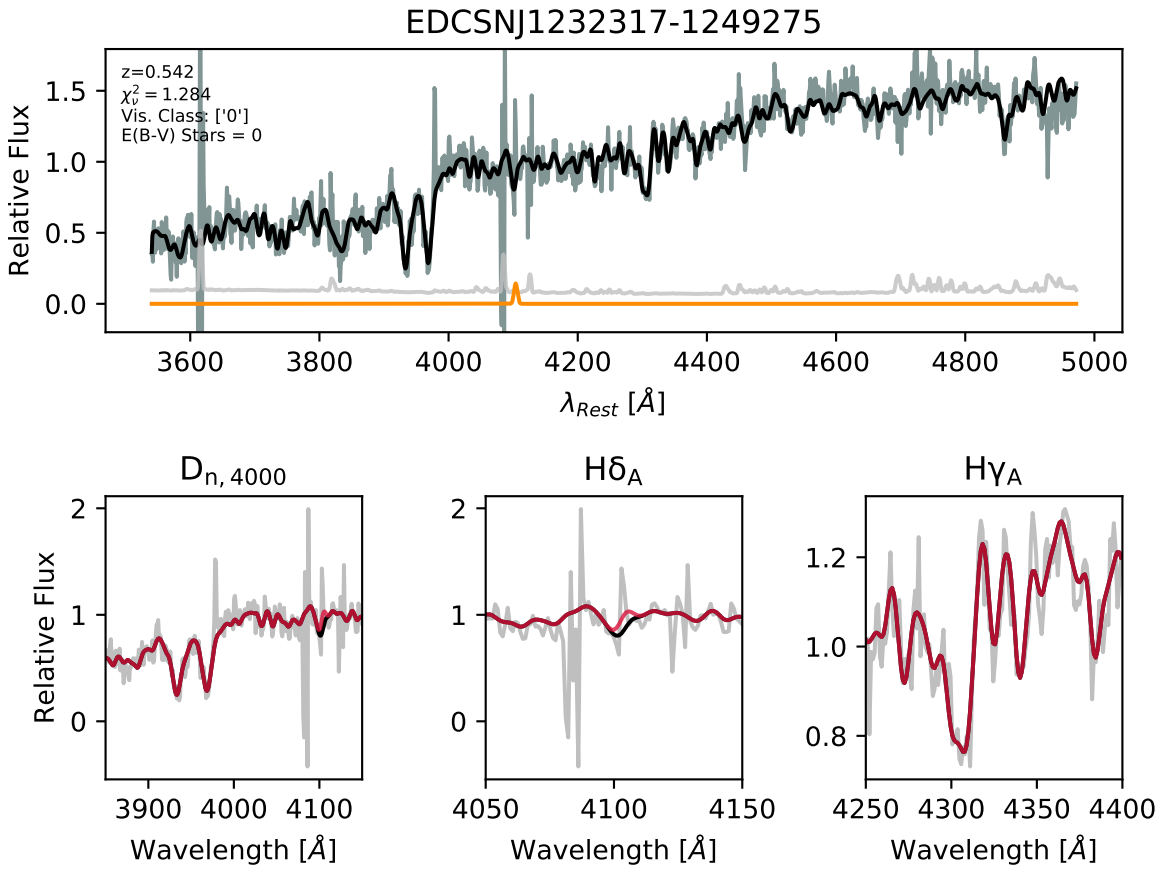
EDCSNJ1232317-1249275
z=0.542
$\chi^2_\nu = 1.284$
Vis. Class: ['0']
E(B-V) Stars = 0
Relative Flux
λ_{Rest} [Å]
$D_{n,4000}$
$H\delta_A$
$H\gamma_A$
Wavelength [Å]

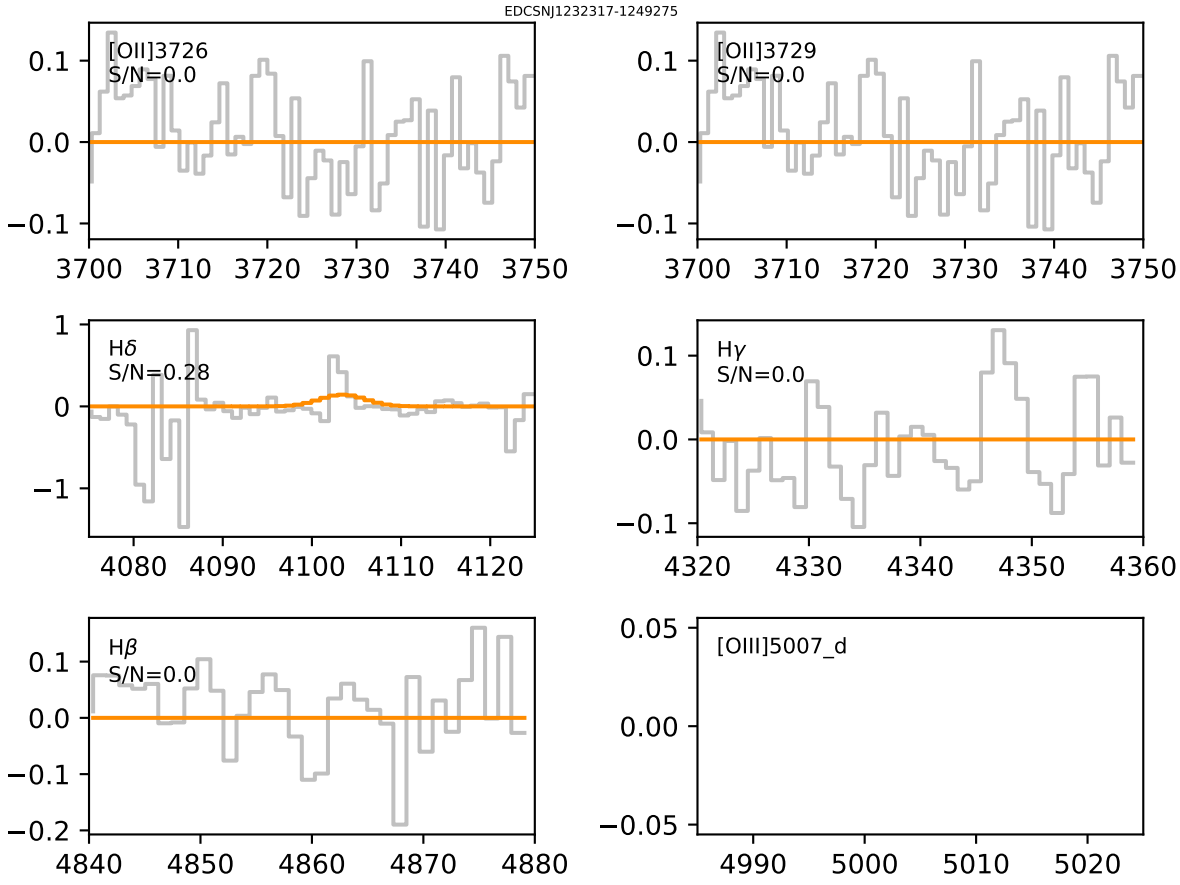
EDCSNJ1232317-1249275
[OII]3726
S/N=0.0
[OII]3729
S/N=0.0
Hδ
S/N=0.28
Hγ
S/N=0.0
Hβ
S/N=0.0
[OIII]5007_d

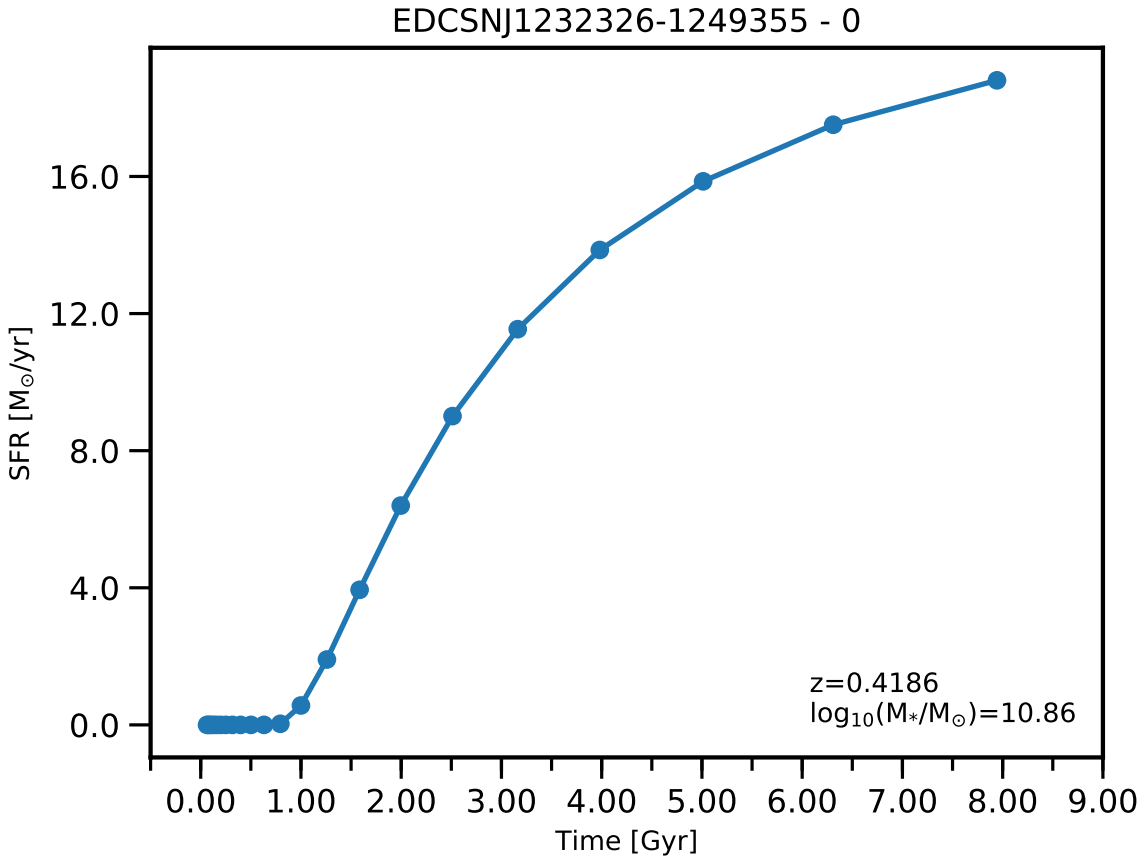
EDCSNJ1232326-1249355 - 0
SFR [M⊙/yr]
16.0
12.0
8.0
4.0
0.0
0.00
1.00
2.00
3.00
4.00
5.00
6.00
7.00
8.00
9.00
Time [Gyr]
z=0.4186
log10(M*/M⊙)=10.86

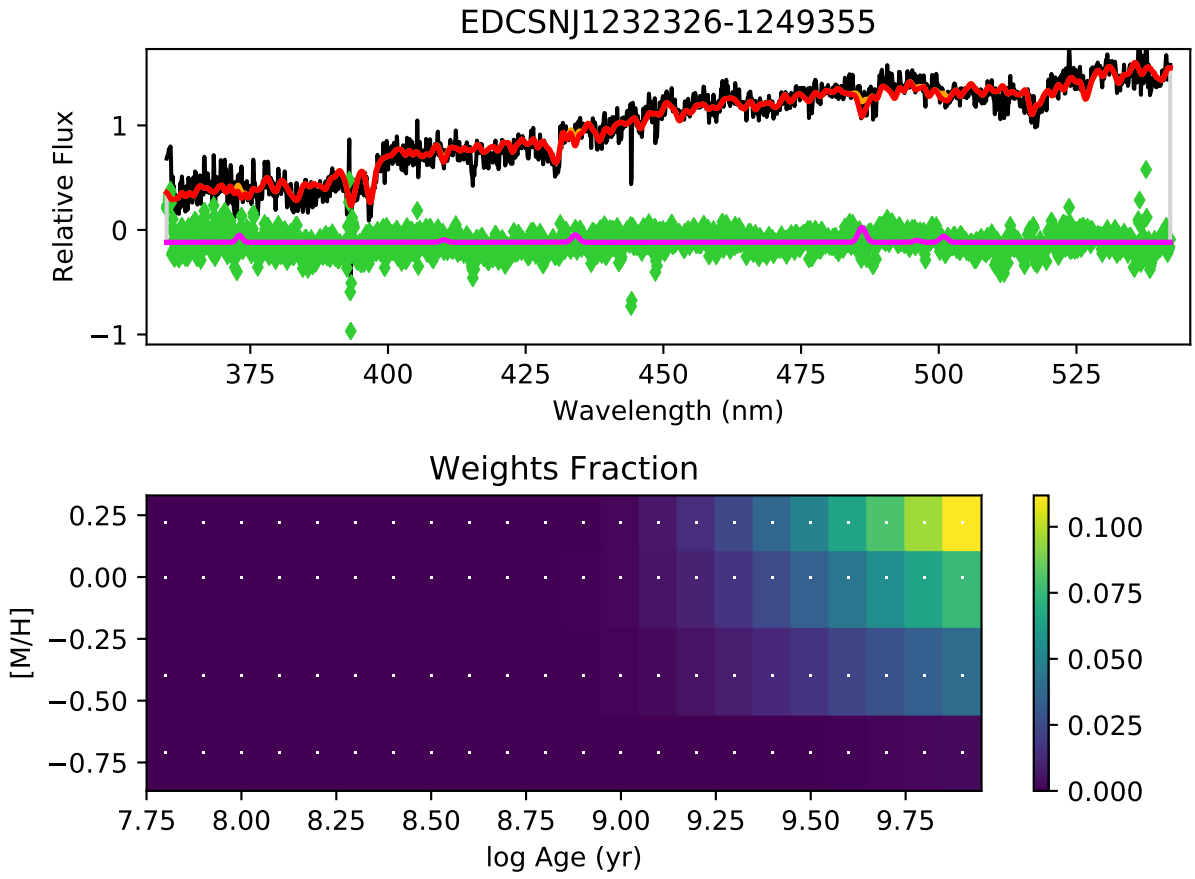
EDCSNJ1232326-1249355
Relative Flux
1
0
−1
375
400
425
450
475
500
525
Wavelength (nm)
Weights Fraction
[M/H]
0.25
0.00
−0.25
−0.50
−0.75
7.75
8.00
8.25
8.50
8.75
9.00
9.25
9.50
9.75
log Age (yr)
0.100
0.075
0.050
0.025
0.000

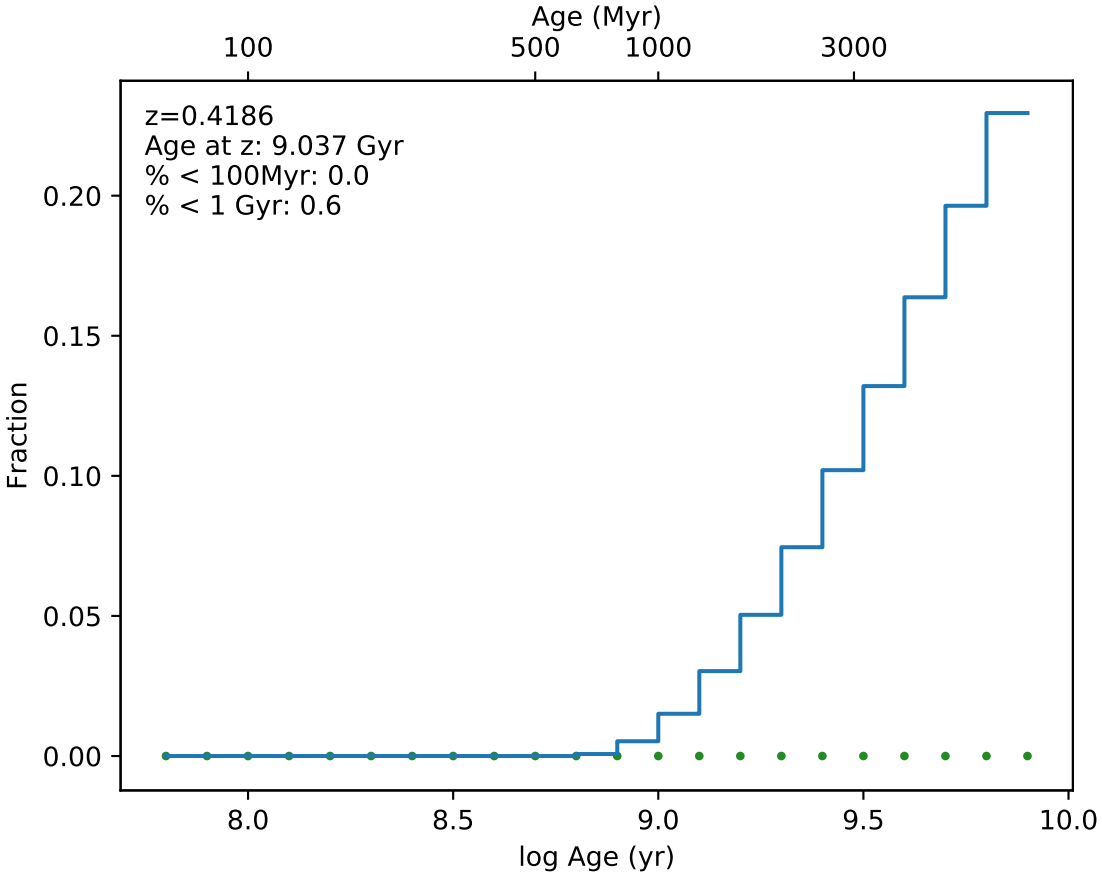
Age (Myr)
100
500
1000
3000
z=0.4186
Age at z: 9.037 Gyr
% < 100Myr: 0.0
% < 1 Gyr: 0.6
0.20
0.15
0.10
0.05
0.00
Fraction
8.0
8.5
9.0
9.5
10.0
log Age (yr)

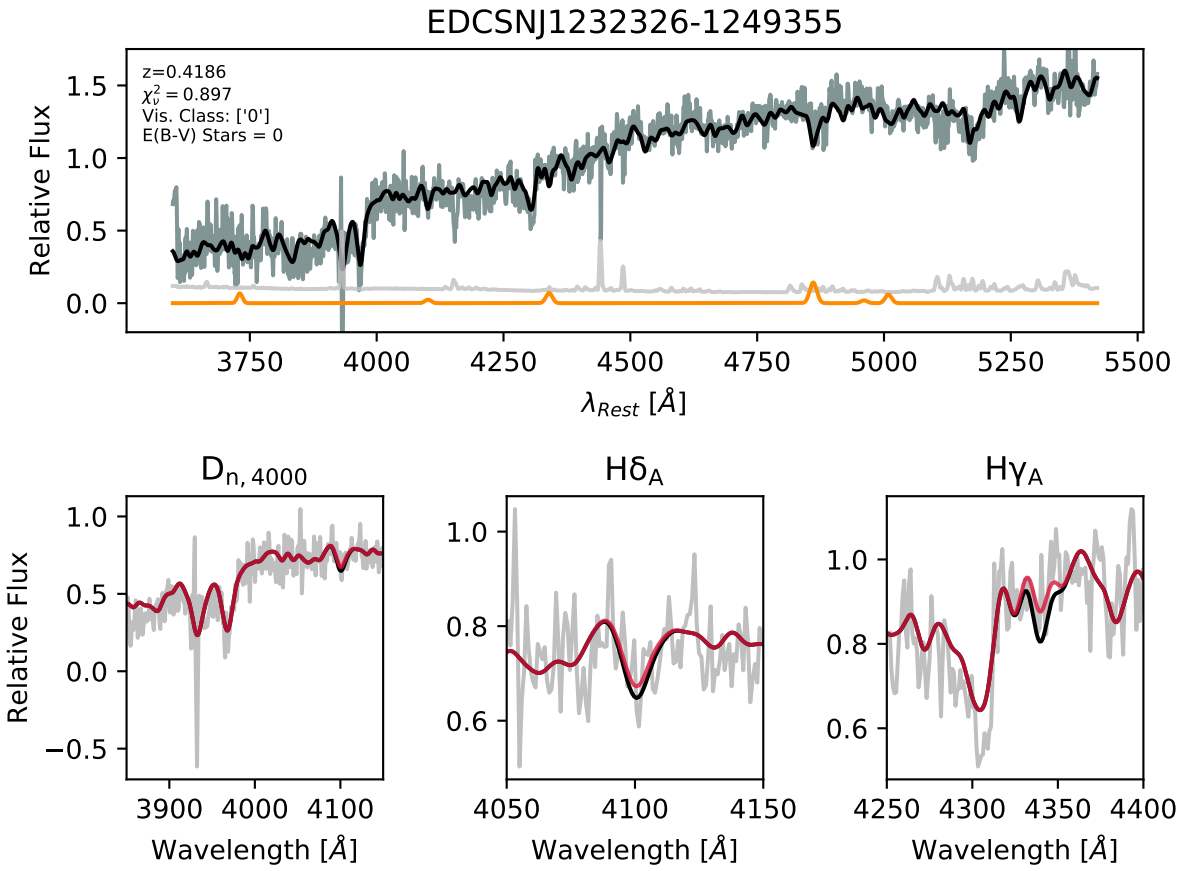
EDCSNJ1232326-1249355
z=0.4186
$\chi^2_\nu = 0.897$
Vis. Class: ['0']
E(B-V) Stars = 0
Relative Flux
1.5
1.0
0.5
0.0
3750
4000
4250
4500
4750
5000
5250
5500
λ_{Rest} [Å]
$D_{n,4000}$
$H\delta_A$
$H\gamma_A$
Relative Flux
1.0
0.5
0.0
−0.5
3900
4000
4100
Wavelength [Å]
1.0
0.8
0.6
4050
4100
4150
Wavelength [Å]
1.0
0.8
0.6
4250
4300
4350
4400
Wavelength [Å]

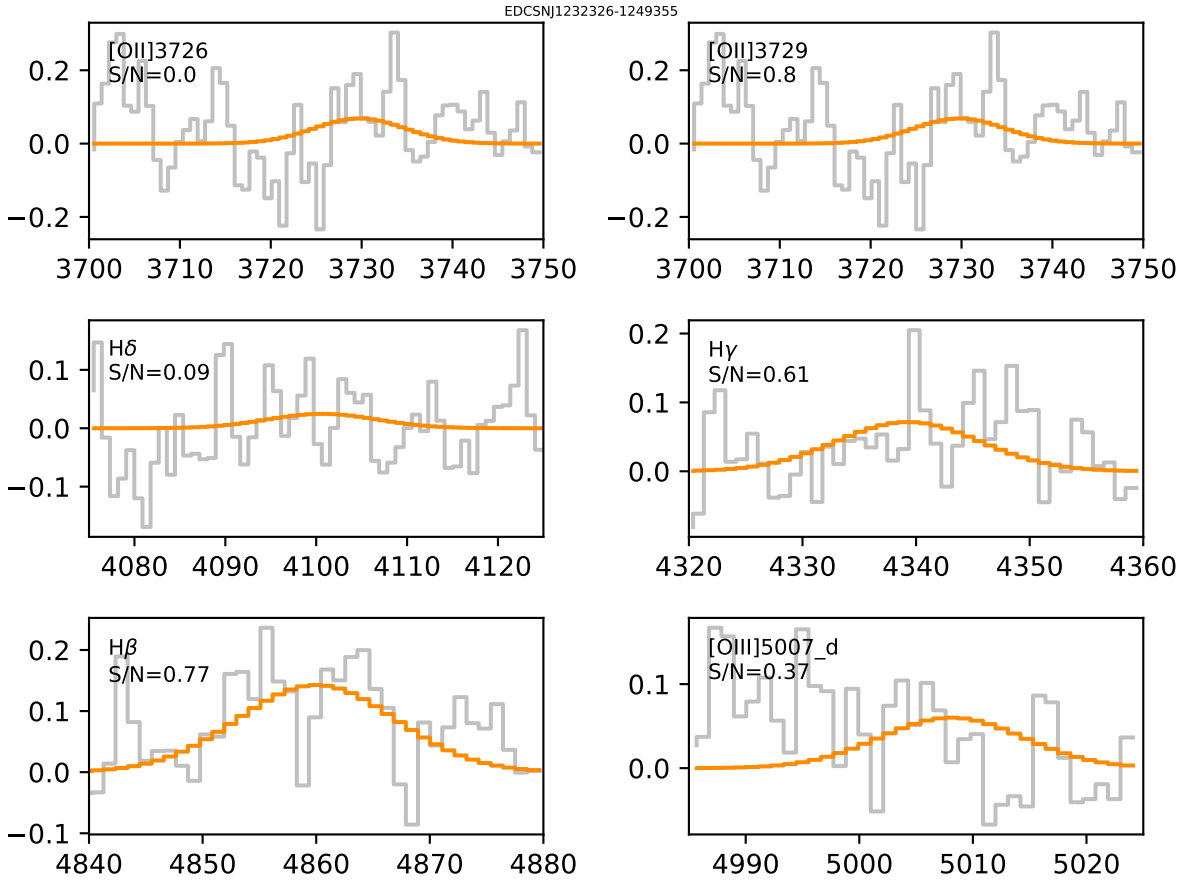
EDCSNJ1232326-1249355
[OII]3726
S/N=0.0
[OII]3729
S/N=0.8
Hδ
S/N=0.09
Hγ
S/N=0.61
Hβ
S/N=0.77
[OIII]5007_d
S/N=0.37

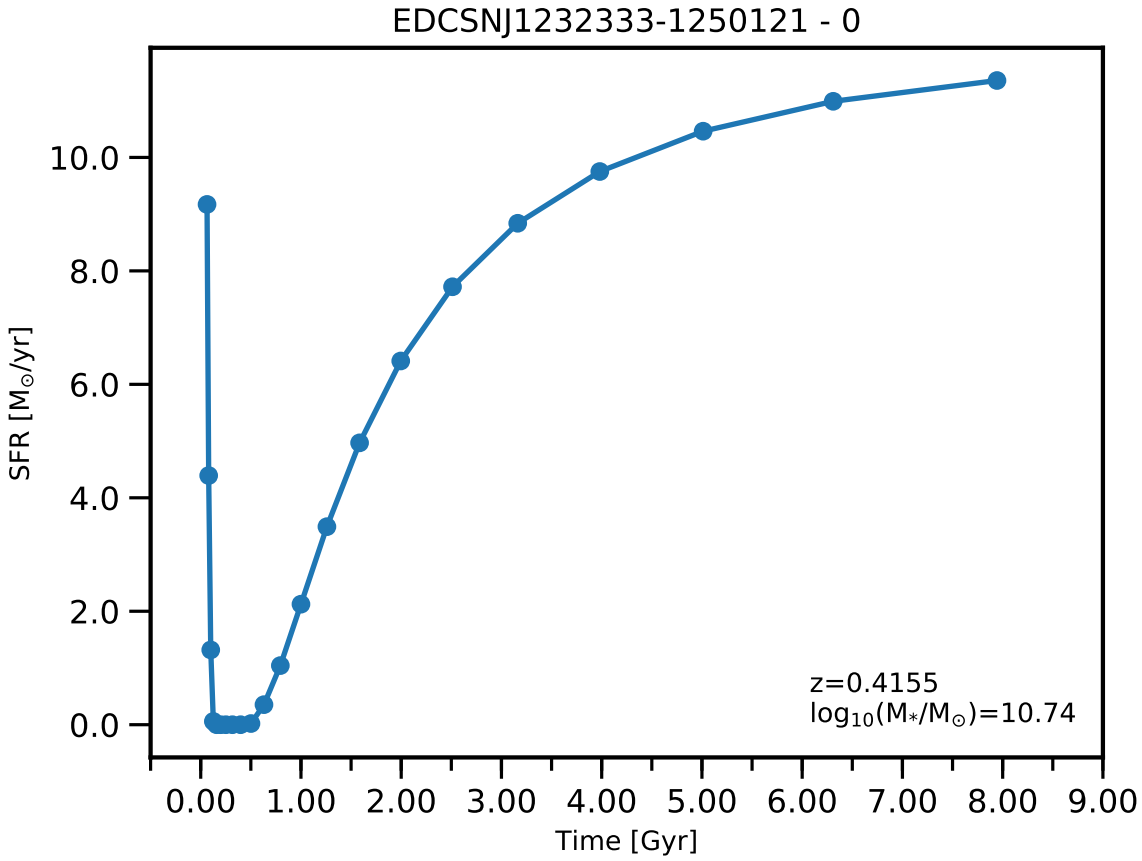
EDCSNJ1232333-1250121 - 0
SFR [M⊙/yr]
10.0
8.0
6.0
4.0
2.0
0.0
0.00
1.00
2.00
3.00
4.00
5.00
6.00
7.00
8.00
9.00
Time [Gyr]
z=0.4155
log10(M*/M⊙)=10.74

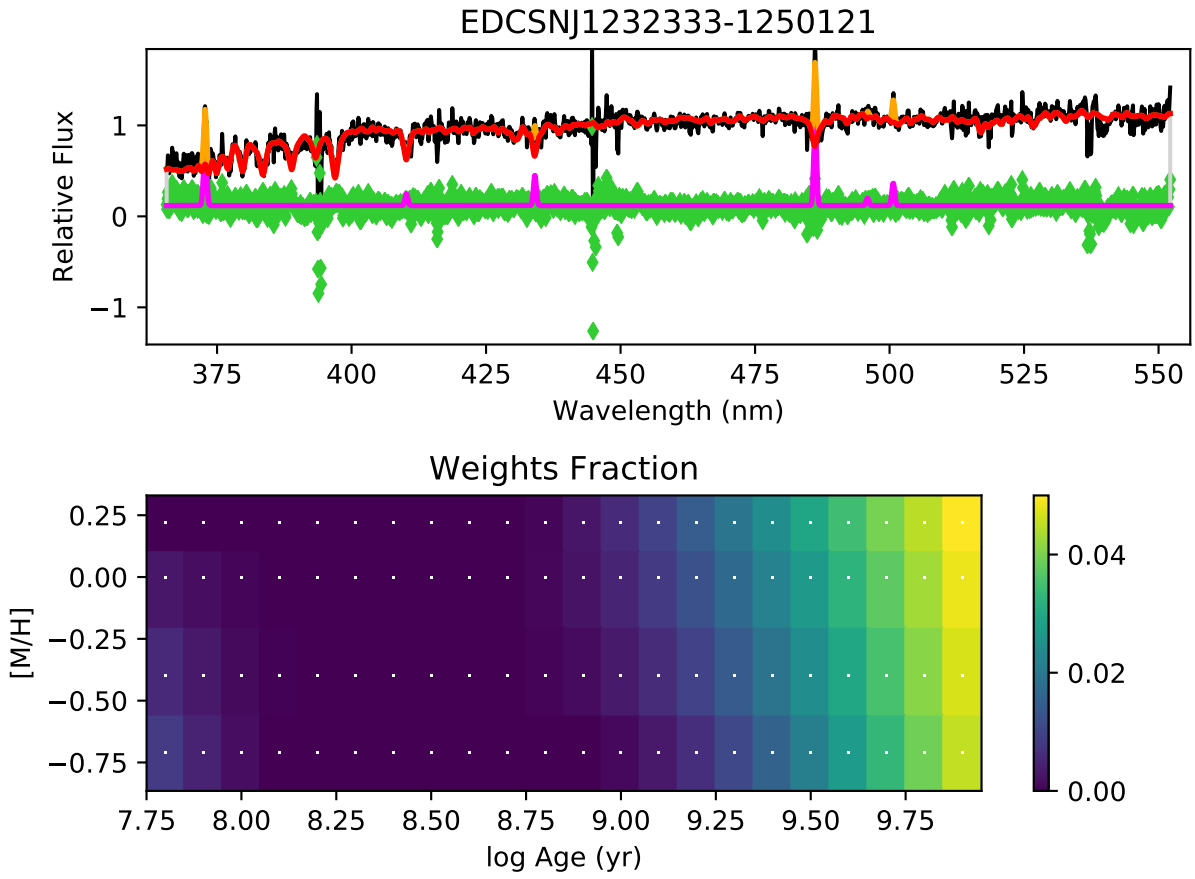
EDCSNJ1232333-1250121
Relative Flux
1
0
−1
375
400
425
450
475
500
525
550
Wavelength (nm)
Weights Fraction
[M/H]
0.25
0.00
−0.25
−0.50
−0.75
7.75
8.00
8.25
8.50
8.75
9.00
9.25
9.50
9.75
log Age (yr)
0.04
0.02
0.00

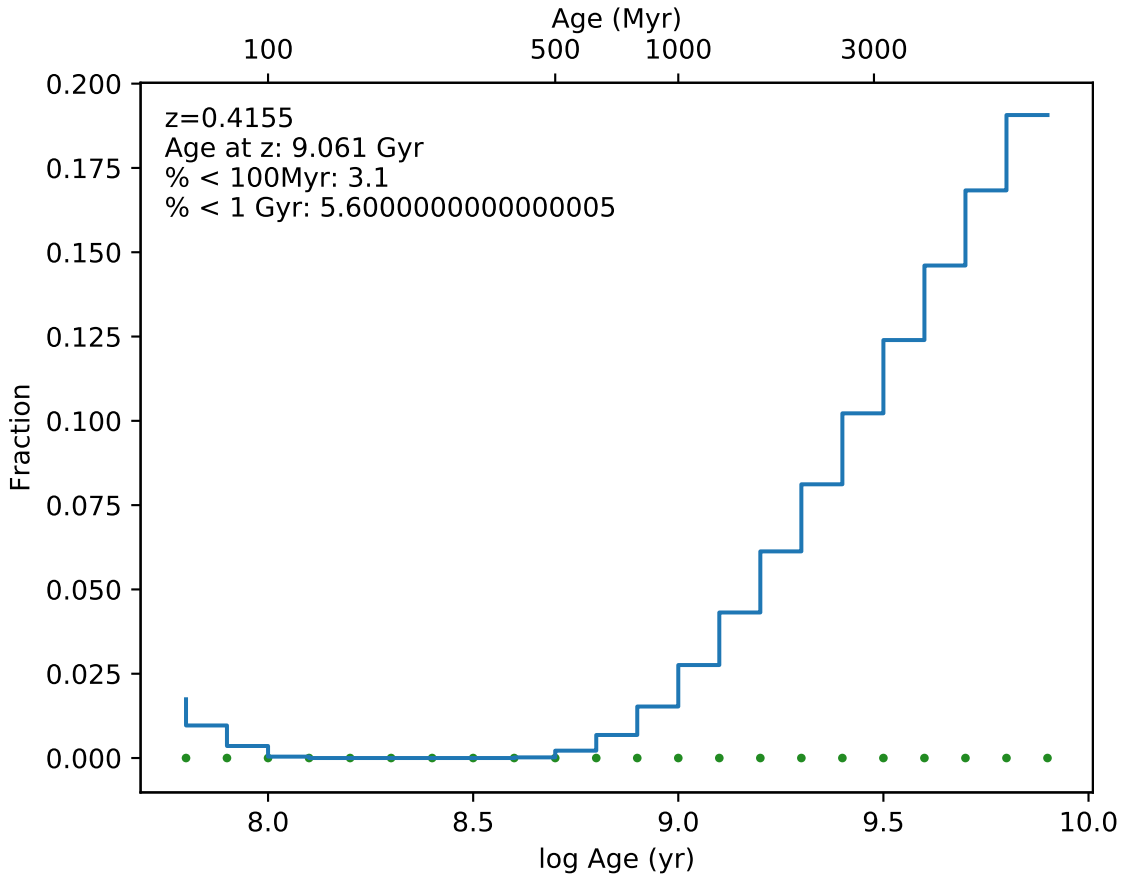
Age (Myr)
100
500
1000
3000
z=0.4155
Age at z: 9.061 Gyr
% < 100Myr: 3.1
% < 1 Gyr: 5.6000000000000005
Fraction
0.200
0.175
0.150
0.125
0.100
0.075
0.050
0.025
0.000
8.0
8.5
9.0
9.5
10.0
log Age (yr)

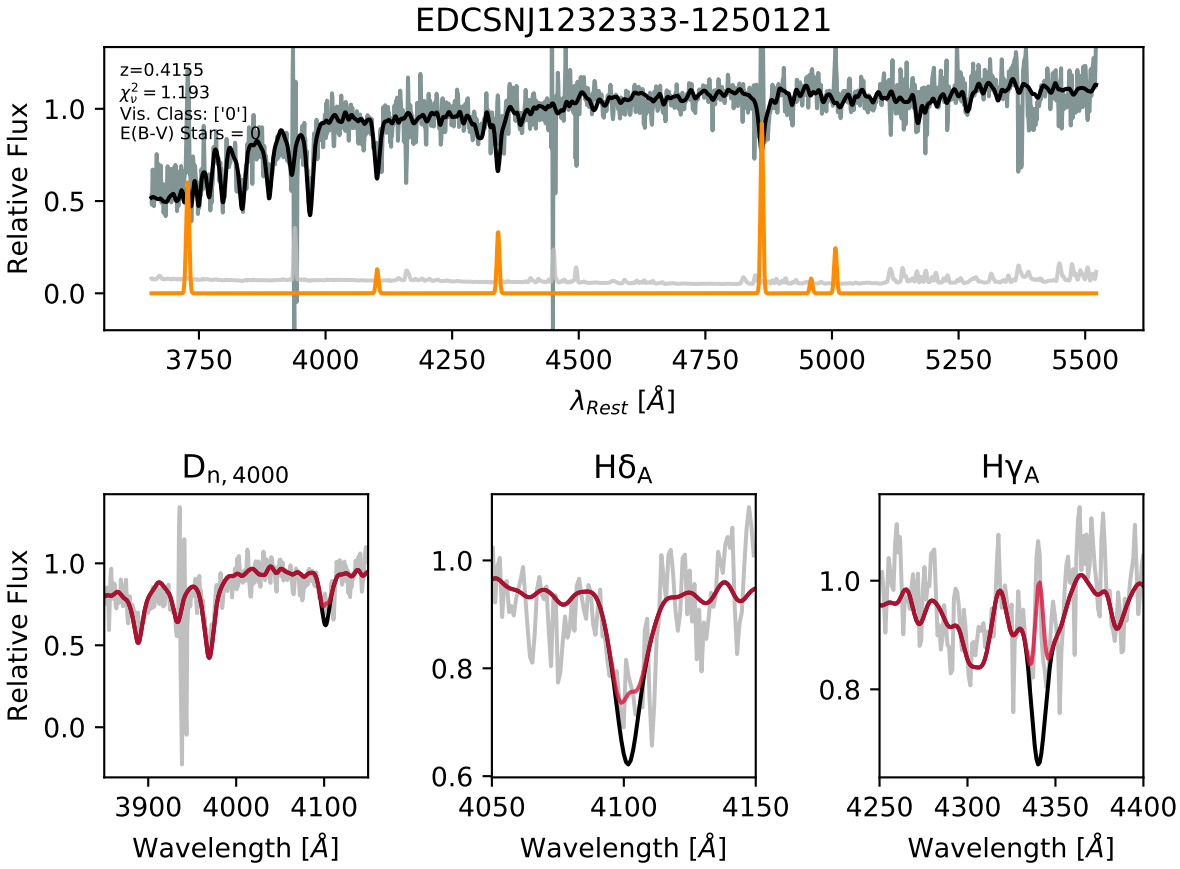
EDCSNJ1232333-1250121
z=0.4155
$\chi^2_\nu = 1.193$
Vis. Class: ['0']
E(B-V) Stars = 0
Relative Flux
1.0
0.5
0.0
3750
4000
4250
4500
4750
5000
5250
5500
λ_{Rest} [Å]
$D_{n,4000}$
$H\delta_A$
$H\gamma_A$
Relative Flux
1.0
0.5
0.0
3900
4000
4100
Wavelength [Å]
1.0
0.8
0.6
4050
4100
4150
Wavelength [Å]
1.0
0.8
4250
4300
4350
4400
Wavelength [Å]

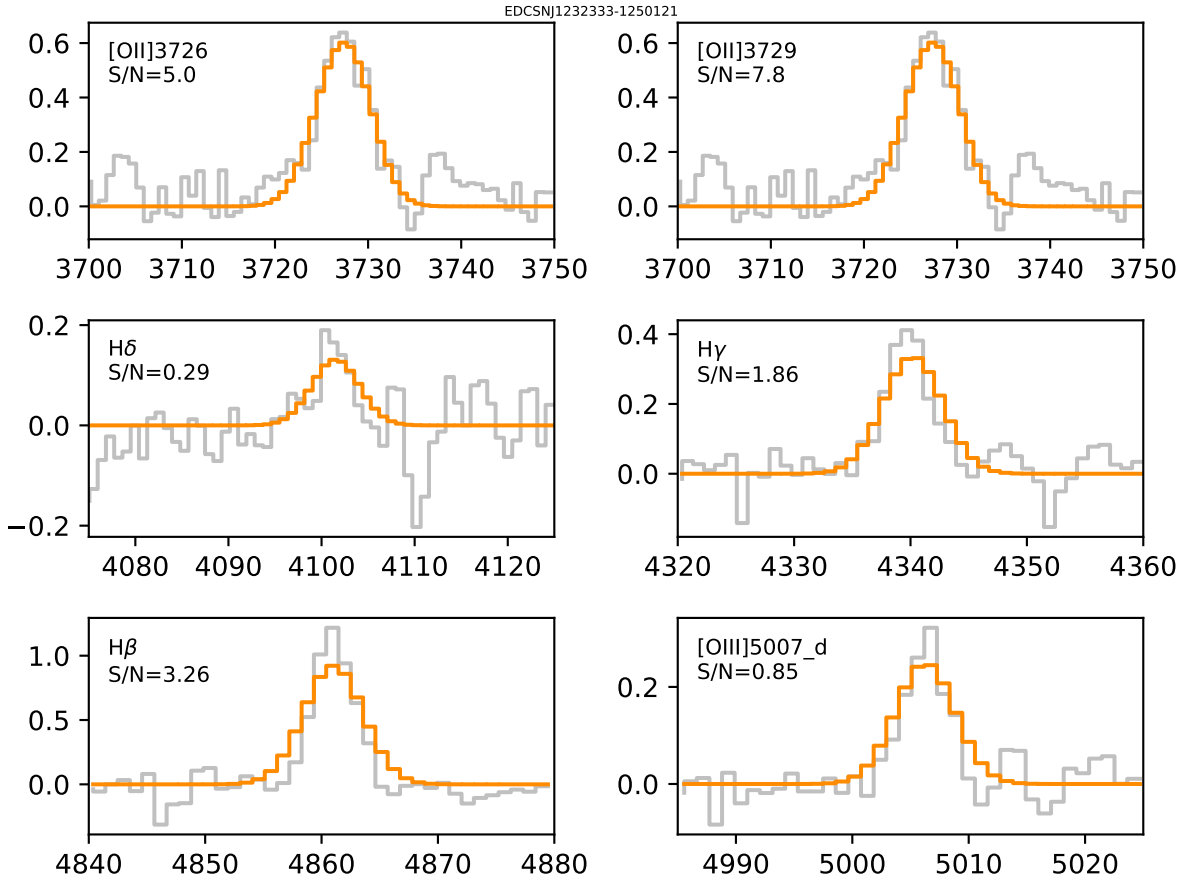
EDCSNJ1232333-1250121
[OII]3726
S/N=5.0
[OII]3729
S/N=7.8
Hδ
S/N=0.29
Hγ
S/N=1.86
Hβ
S/N=3.26
[OIII]5007_d
S/N=0.85

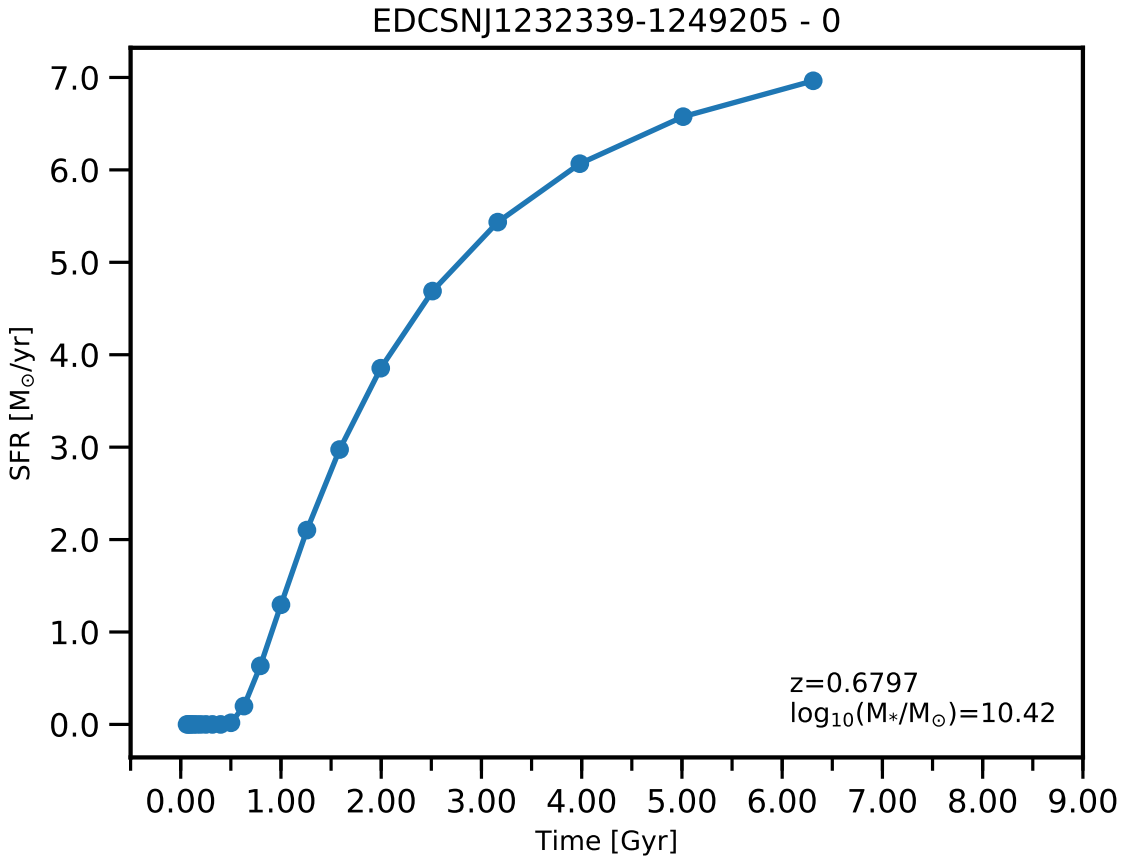
EDCSNJ1232339-1249205 - 0
SFR [M⊙/yr]
Time [Gyr]
z=0.6797
log10(M*/M⊙)=10.42
0.0
1.0
2.0
3.0
4.0
5.0
6.0
7.0
0.00
1.00
2.00
3.00
4.00
5.00
6.00
7.00
8.00
9.00

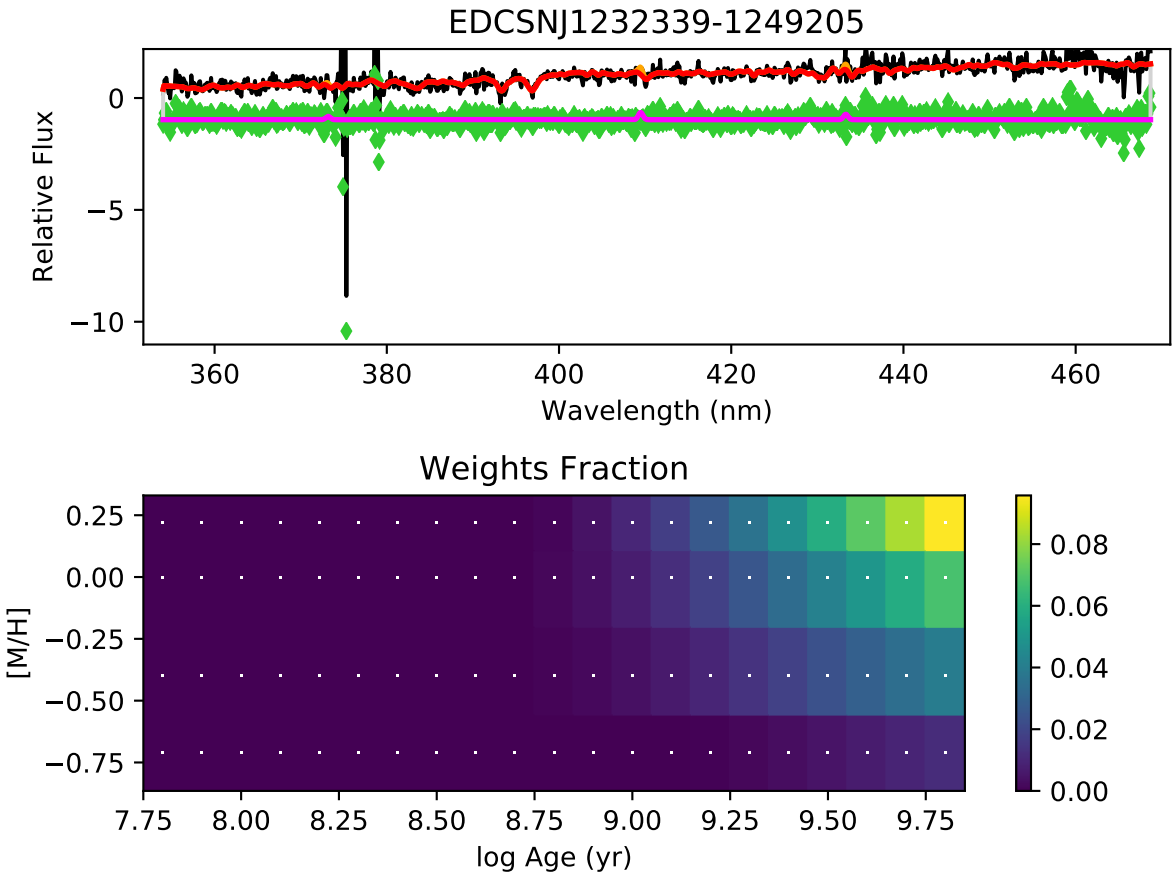
EDCSNJ1232339-1249205
Relative Flux
0
−5
−10
360
380
400
420
440
460
Wavelength (nm)
Weights Fraction
[M/H]
0.25
0.00
−0.25
−0.50
−0.75
7.75
8.00
8.25
8.50
8.75
9.00
9.25
9.50
9.75
log Age (yr)
0.08
0.06
0.04
0.02
0.00

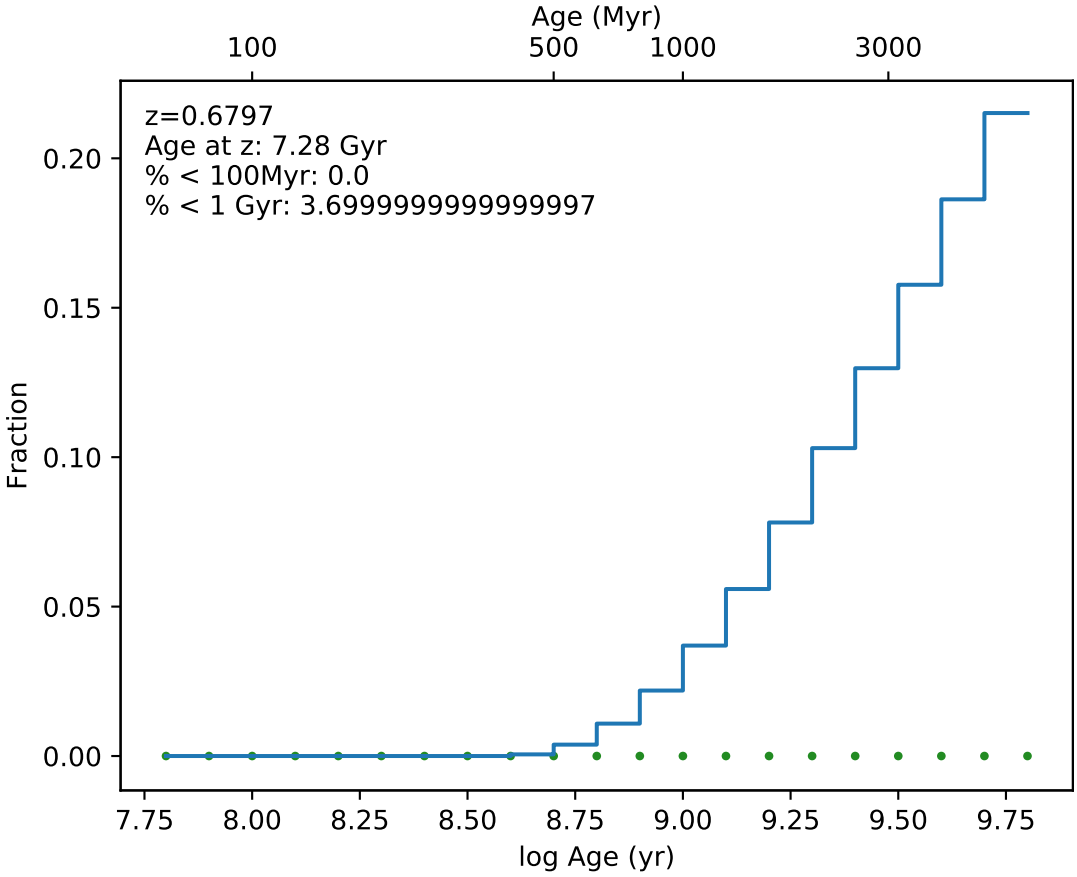
Age (Myr)
100
500
1000
3000
z=0.6797
Age at z: 7.28 Gyr
% < 100Myr: 0.0
% < 1 Gyr: 3.6999999999999997
Fraction
0.20
0.15
0.10
0.05
0.00
7.75
8.00
8.25
8.50
8.75
9.00
9.25
9.50
9.75
log Age (yr)

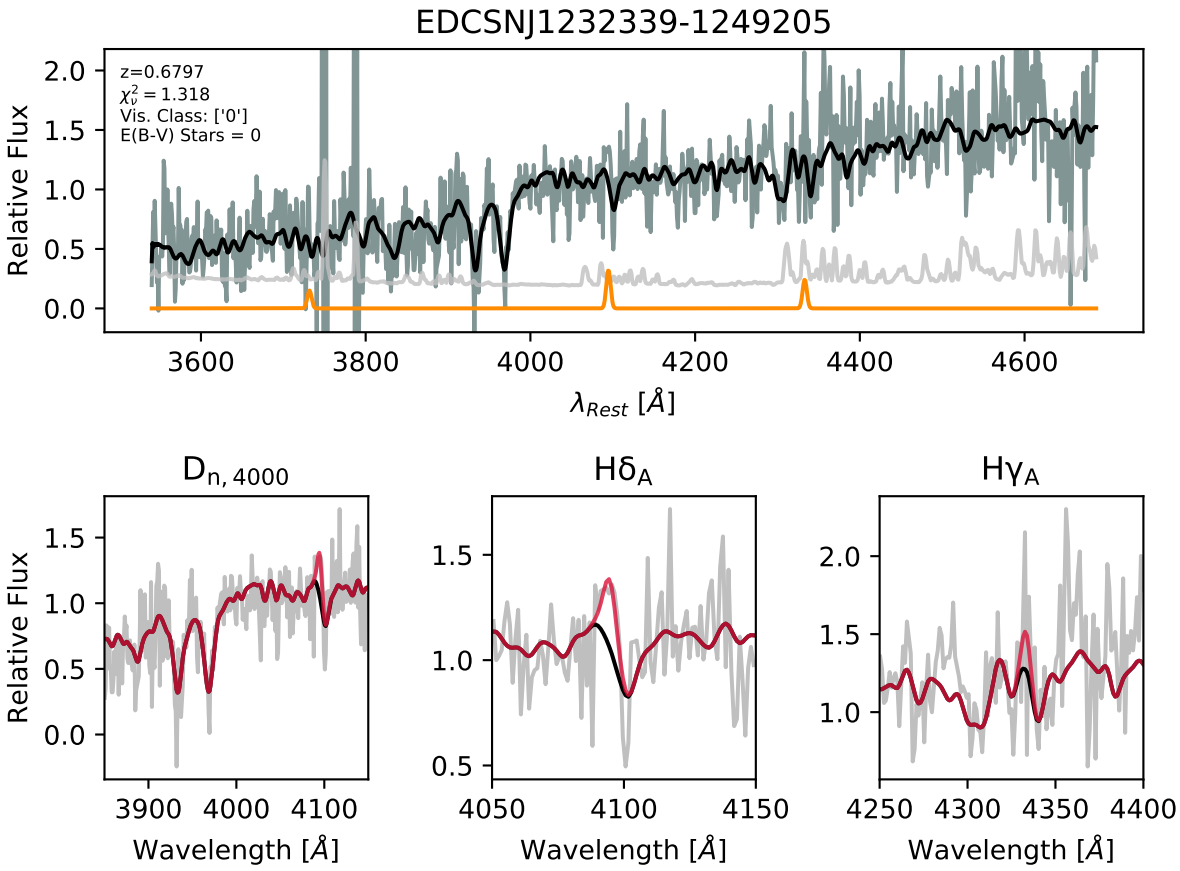
EDCSNJ1232339-1249205
z=0.6797
$\chi^2_\nu = 1.318$
Vis. Class: ['0']
E(B-V) Stars = 0
Relative Flux
λ_{Rest} [Å]
$D_{n,4000}$
$H\delta_A$
$H\gamma_A$
Wavelength [Å]

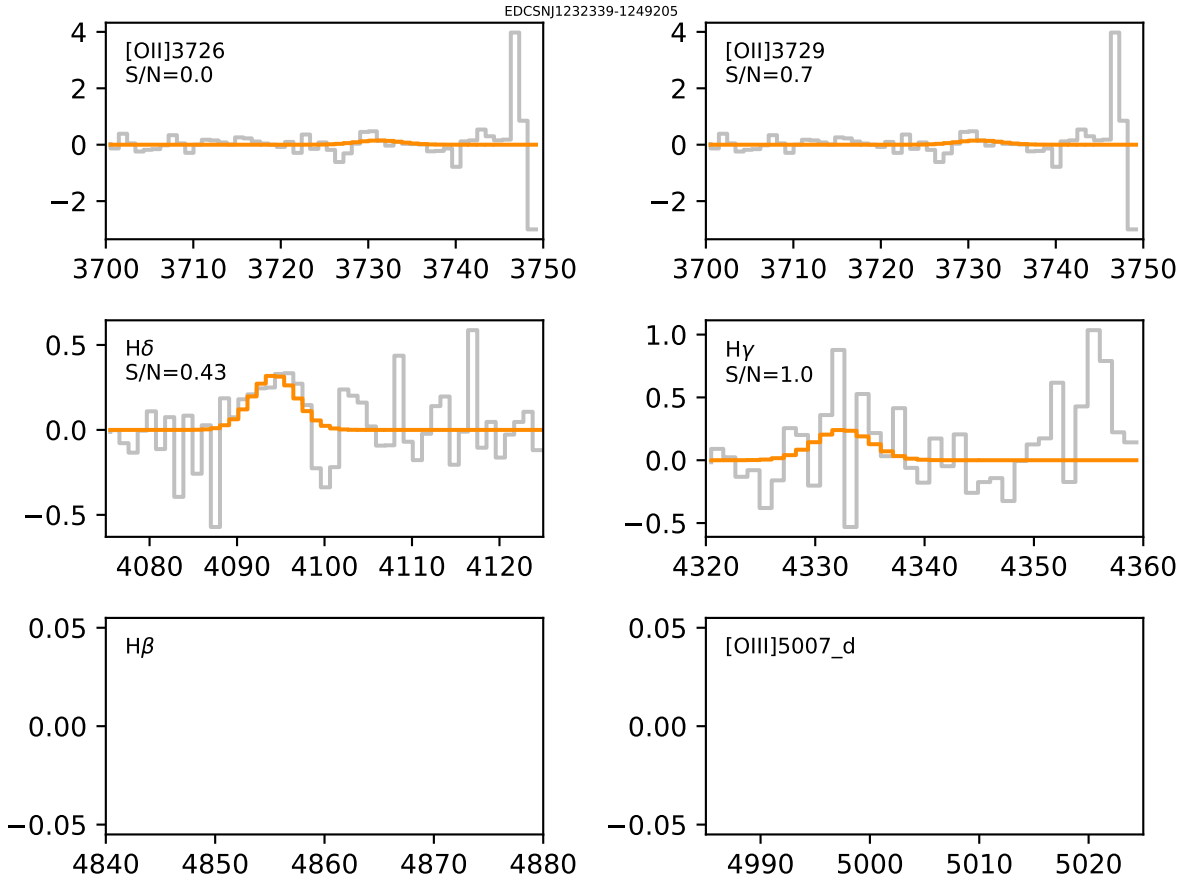
EDCSNJ1232339-1249205
[OII]3726
S/N=0.0
[OII]3729
S/N=0.7
Hδ
S/N=0.43
Hγ
S/N=1.0
Hβ
[OIII]5007_d

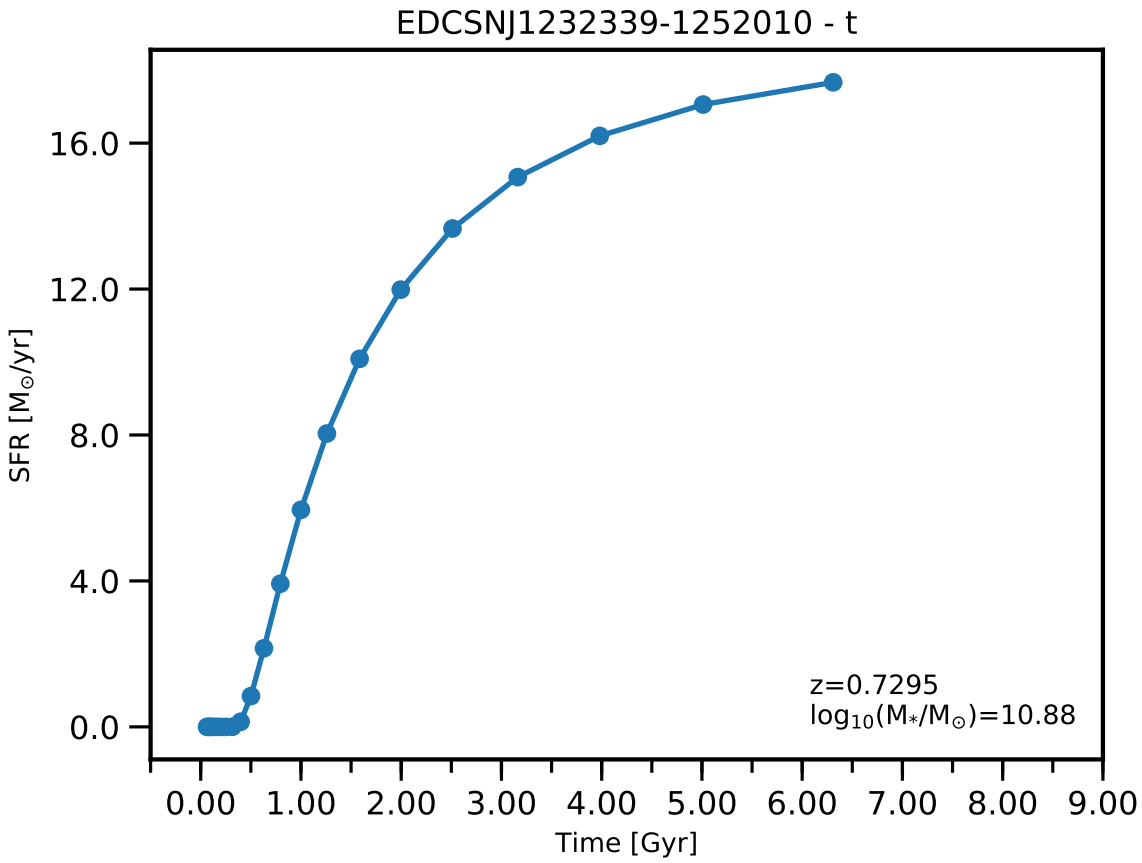
EDCSNJ1232339-1252010 - t
SFR [M⊙/yr]
16.0
12.0
8.0
4.0
0.0
0.00
1.00
2.00
3.00
4.00
5.00
6.00
7.00
8.00
9.00
Time [Gyr]
z=0.7295
log10(M*/M⊙)=10.88

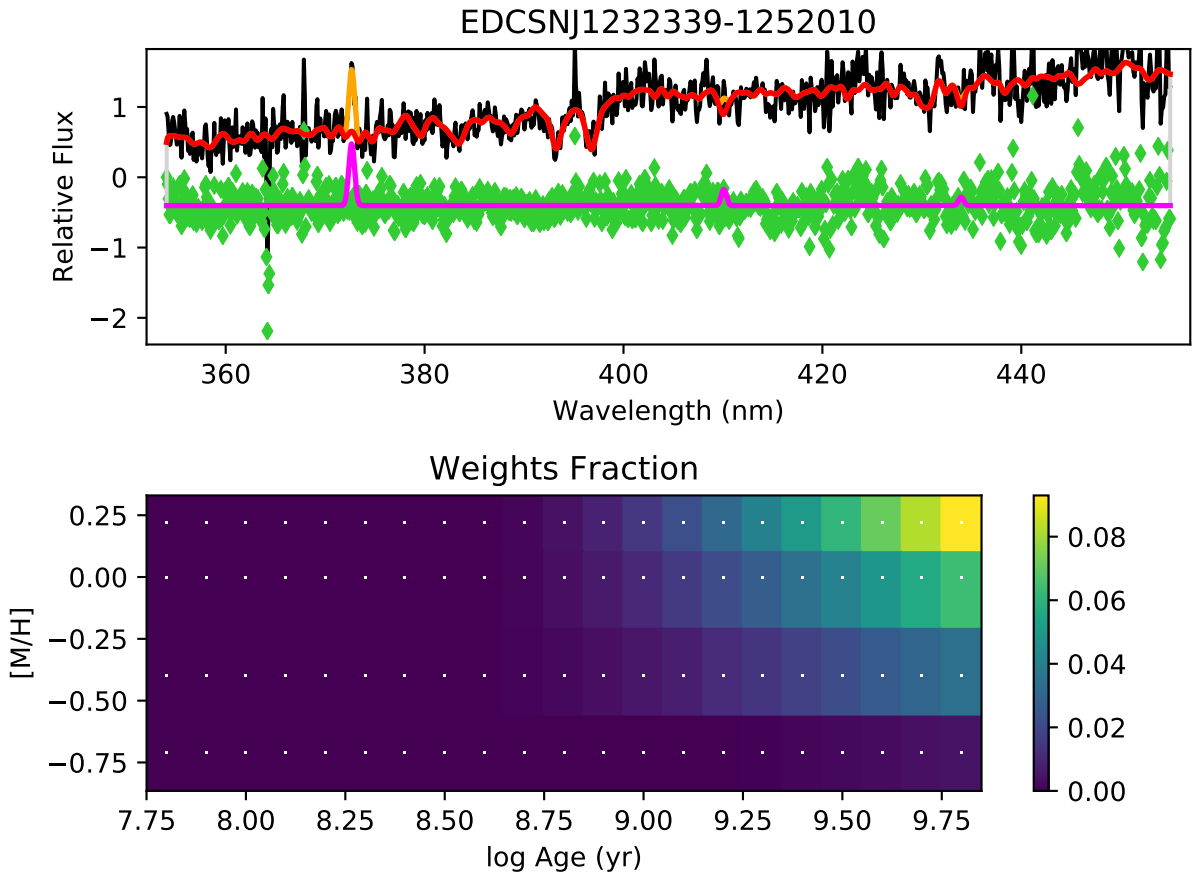
EDCSNJ1232339-1252010
Relative Flux
1
0
−1
−2
360
380
400
420
440
Wavelength (nm)
Weights Fraction
[M/H]
0.25
0.00
−0.25
−0.50
−0.75
7.75
8.00
8.25
8.50
8.75
9.00
9.25
9.50
9.75
log Age (yr)
0.08
0.06
0.04
0.02
0.00

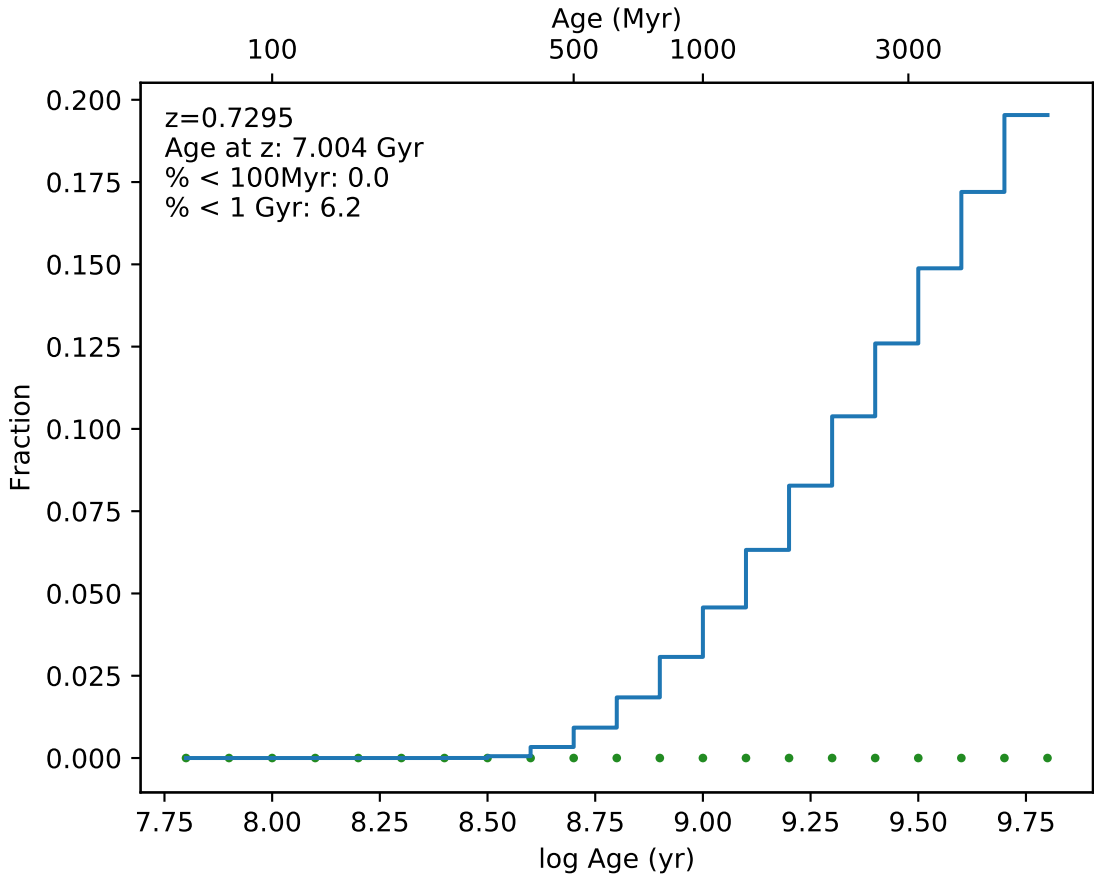
Age (Myr)
100
500
1000
3000
z=0.7295
Age at z: 7.004 Gyr
% < 100Myr: 0.0
% < 1 Gyr: 6.2
Fraction
0.200
0.175
0.150
0.125
0.100
0.075
0.050
0.025
0.000
7.75
8.00
8.25
8.50
8.75
9.00
9.25
9.50
9.75
log Age (yr)

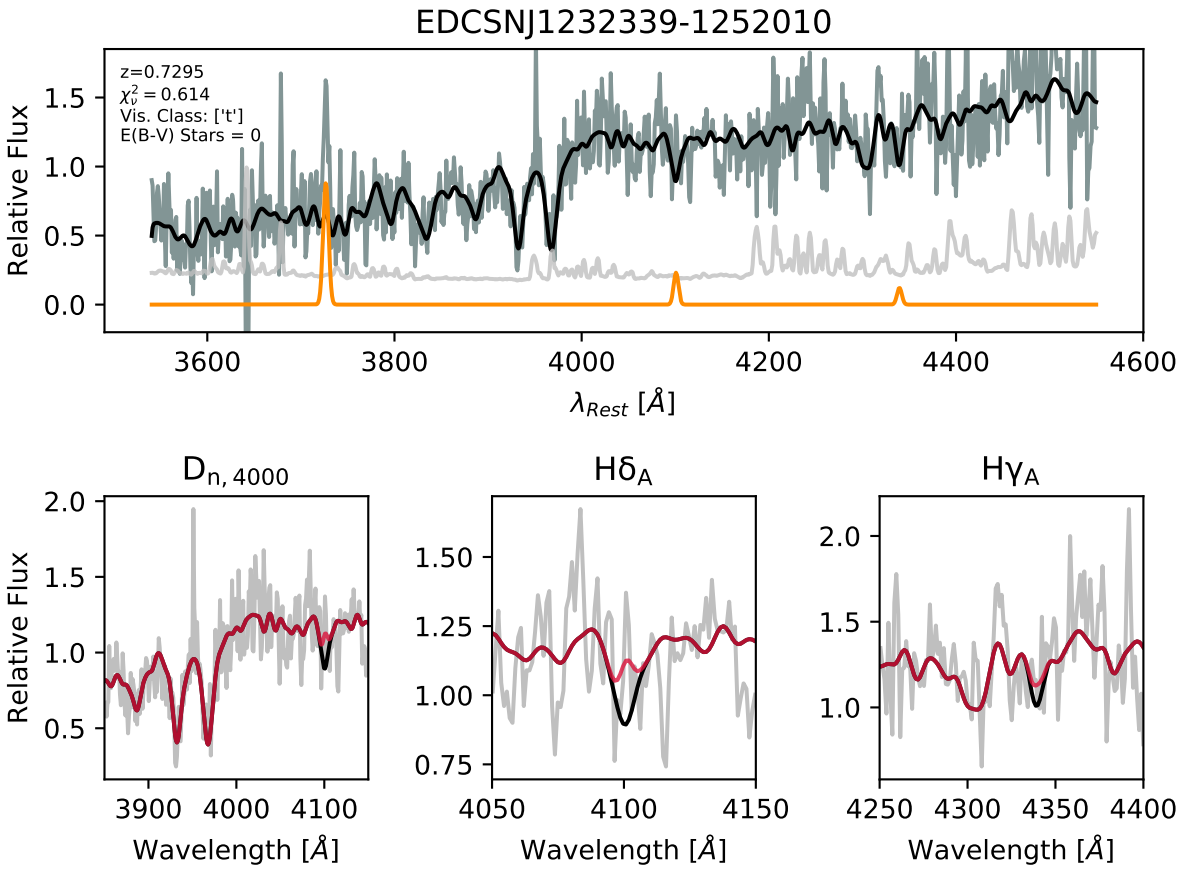
EDCSNJ1232339-1252010
z=0.7295
$\chi^2_\nu = 0.614$
Vis. Class: ['t']
E(B-V) Stars = 0
Relative Flux
λ_{Rest} [Å]
$D_{n,4000}$
$H\delta_A$
$H\gamma_A$
Wavelength [Å]

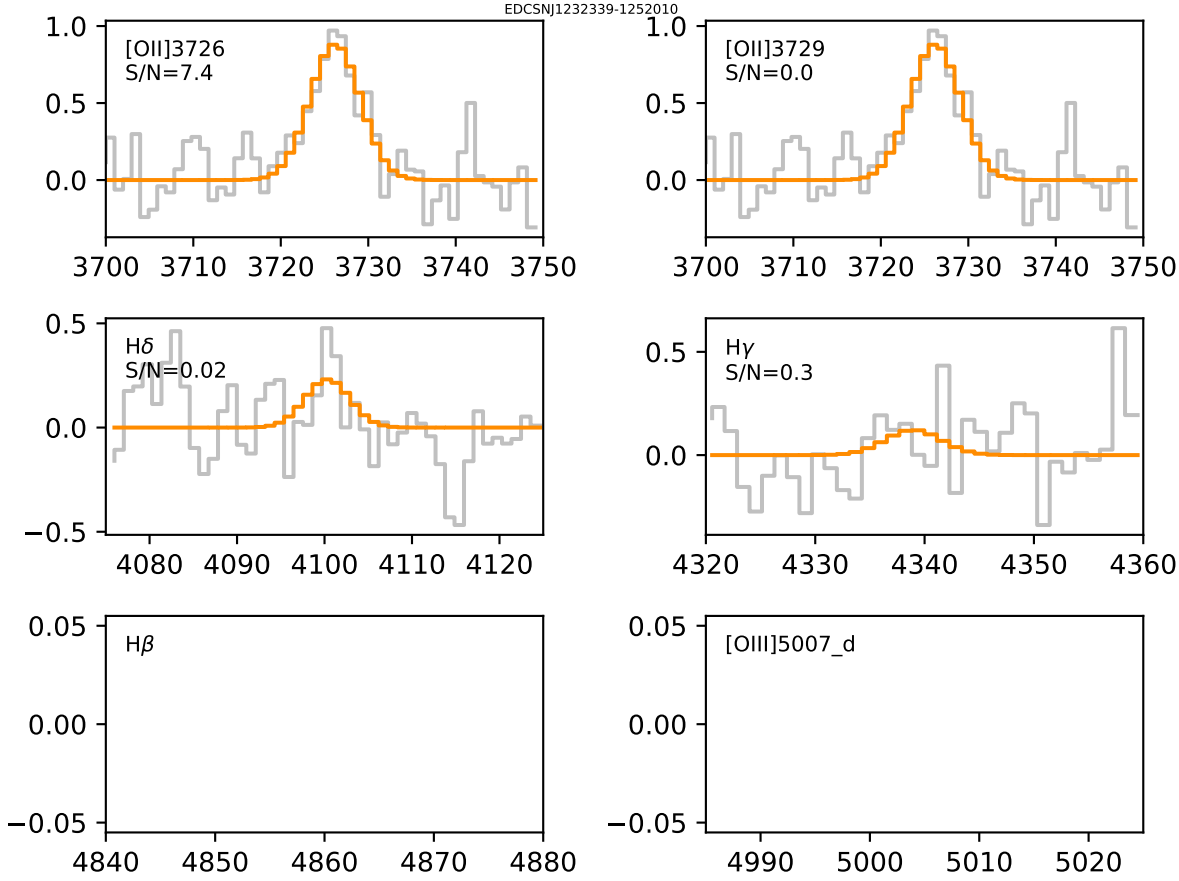
EDCSNJ1232339-1252010
[OII]3726
S/N=7.4
[OII]3729
S/N=0.0
Hδ
S/N=0.02
Hγ
S/N=0.3
Hβ
[OIII]5007_d

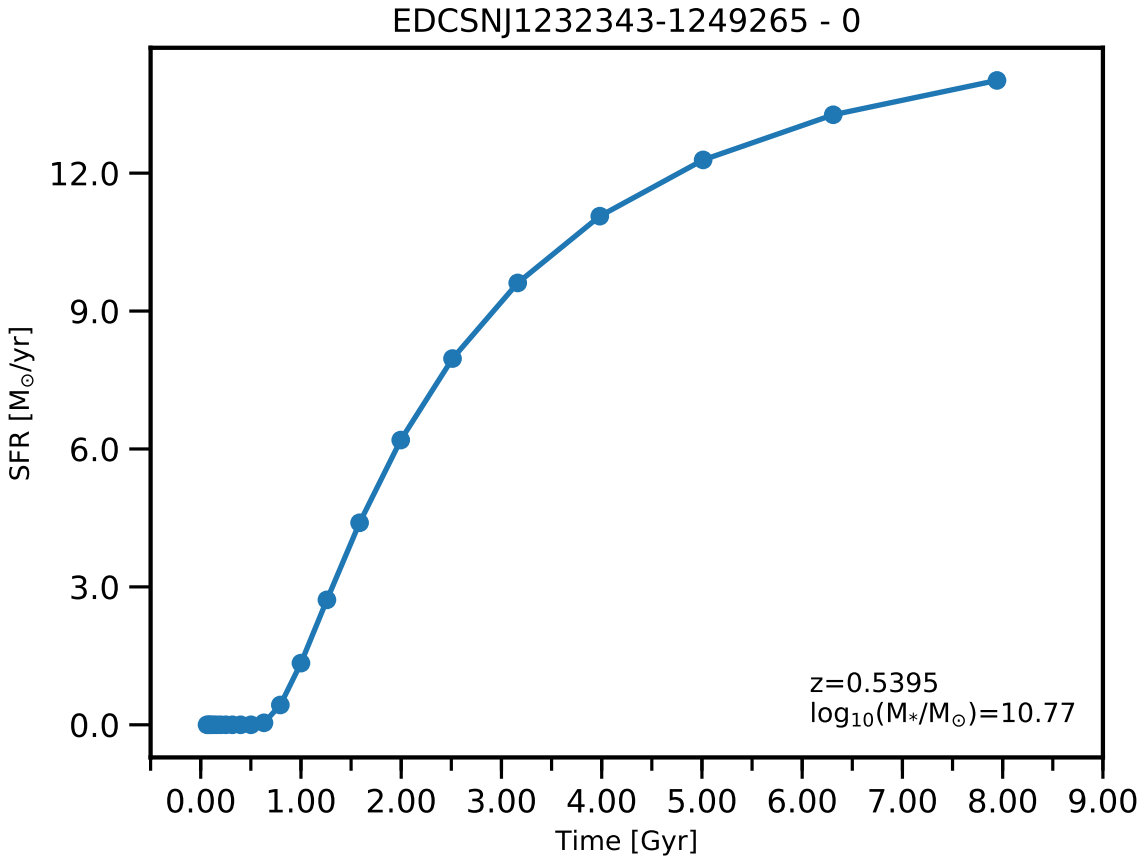
EDCSNJ1232343-1249265 - 0
SFR [M⊙/yr]
12.0
9.0
6.0
3.0
0.0
0.00
1.00
2.00
3.00
4.00
5.00
6.00
7.00
8.00
9.00
Time [Gyr]
z=0.5395
log10(M*/M⊙)=10.77

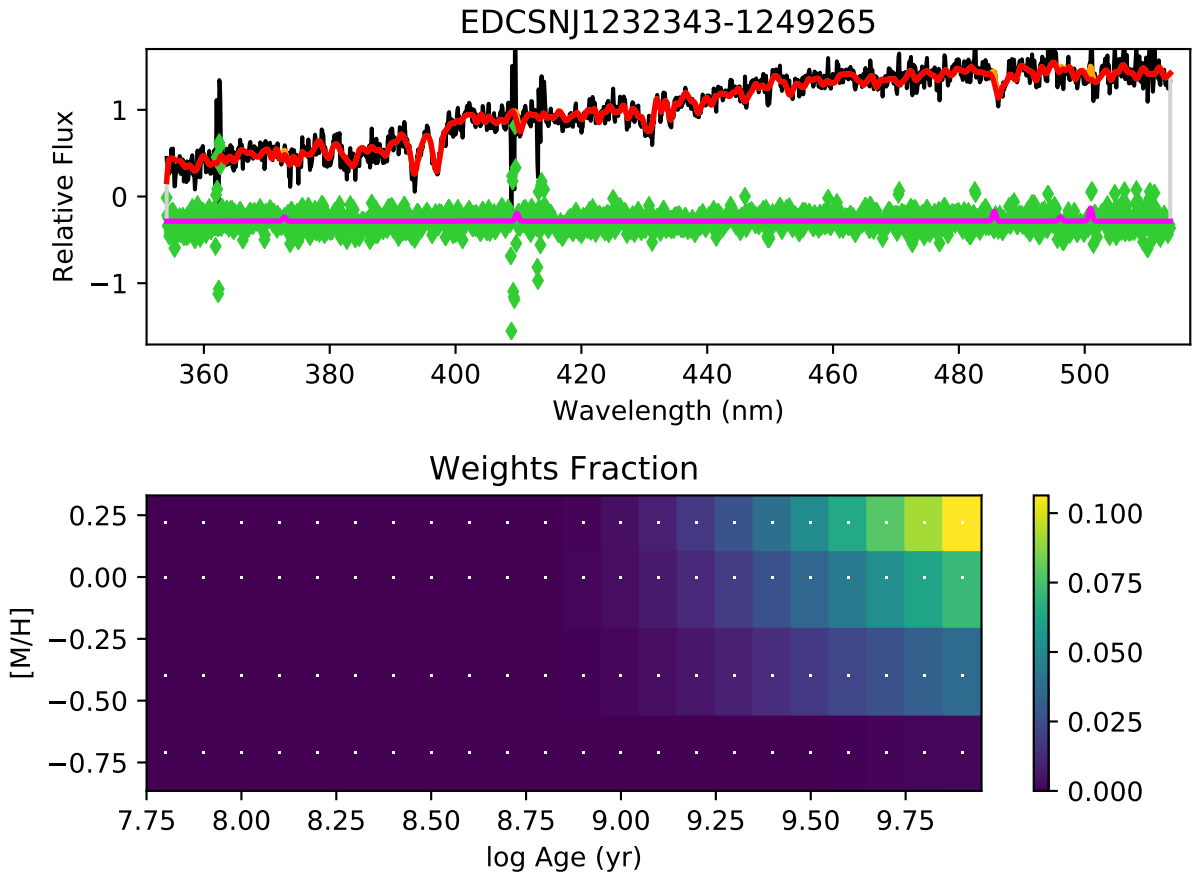
EDCSNJ1232343-1249265
Relative Flux
1
0
−1
360
380
400
420
440
460
480
500
Wavelength (nm)
Weights Fraction
[M/H]
0.25
0.00
−0.25
−0.50
−0.75
7.75
8.00
8.25
8.50
8.75
9.00
9.25
9.50
9.75
log Age (yr)
0.100
0.075
0.050
0.025
0.000

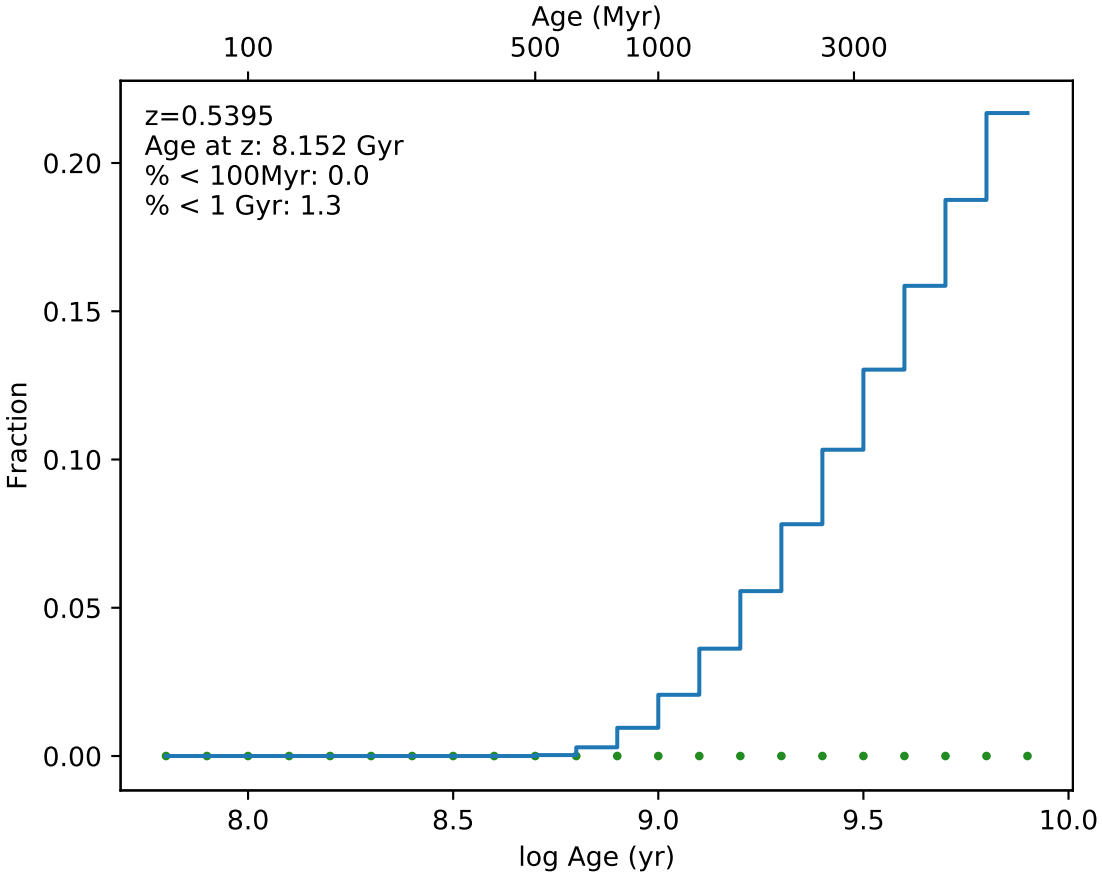
Age (Myr)
100
500
1000
3000
z=0.5395
Age at z: 8.152 Gyr
% < 100Myr: 0.0
% < 1 Gyr: 1.3
0.20
0.15
0.10
0.05
0.00
Fraction
8.0
8.5
9.0
9.5
10.0
log Age (yr)

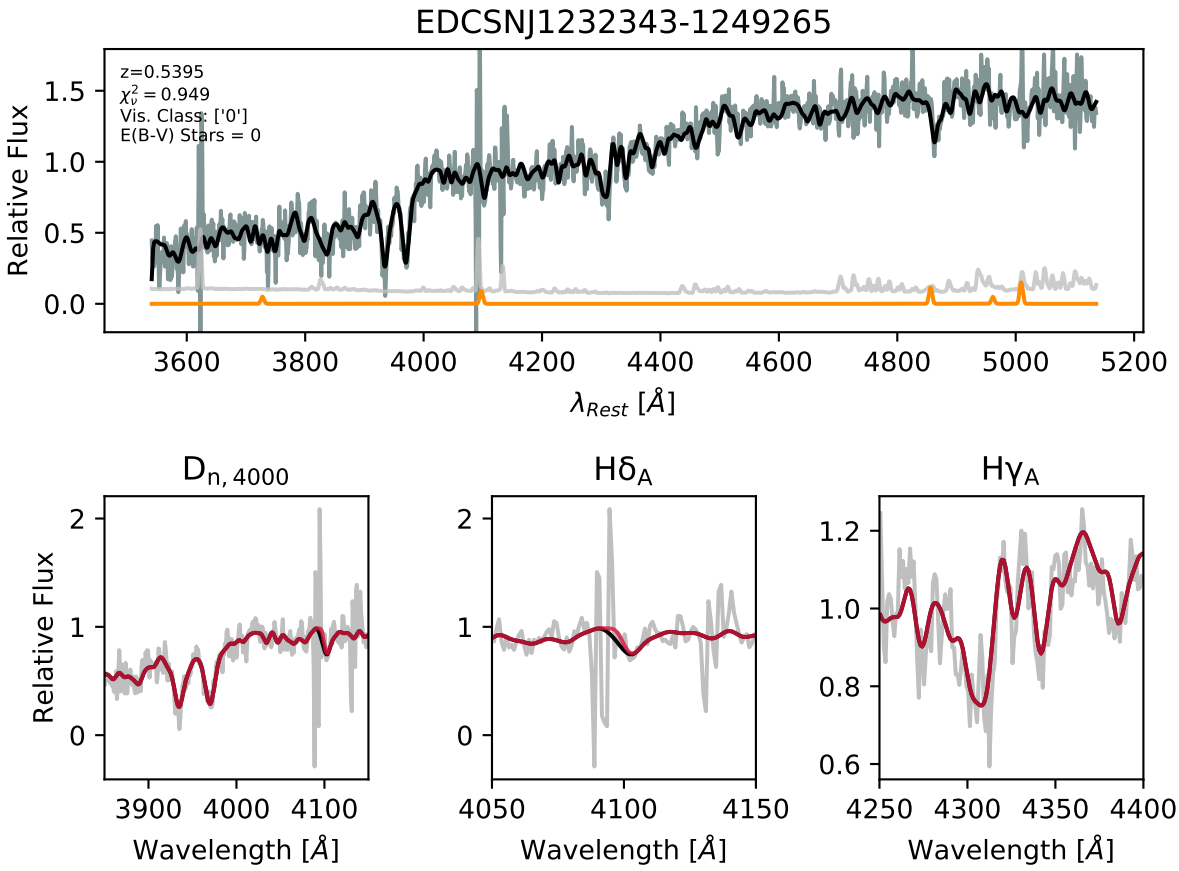
EDCSNJ1232343-1249265
z=0.5395
$\chi^2_\nu = 0.949$
Vis. Class: ['0']
E(B-V) Stars = 0
Relative Flux
λ_{Rest} [Å]
$D_{n,4000}$
$H\delta_A$
$H\gamma_A$
Wavelength [Å]

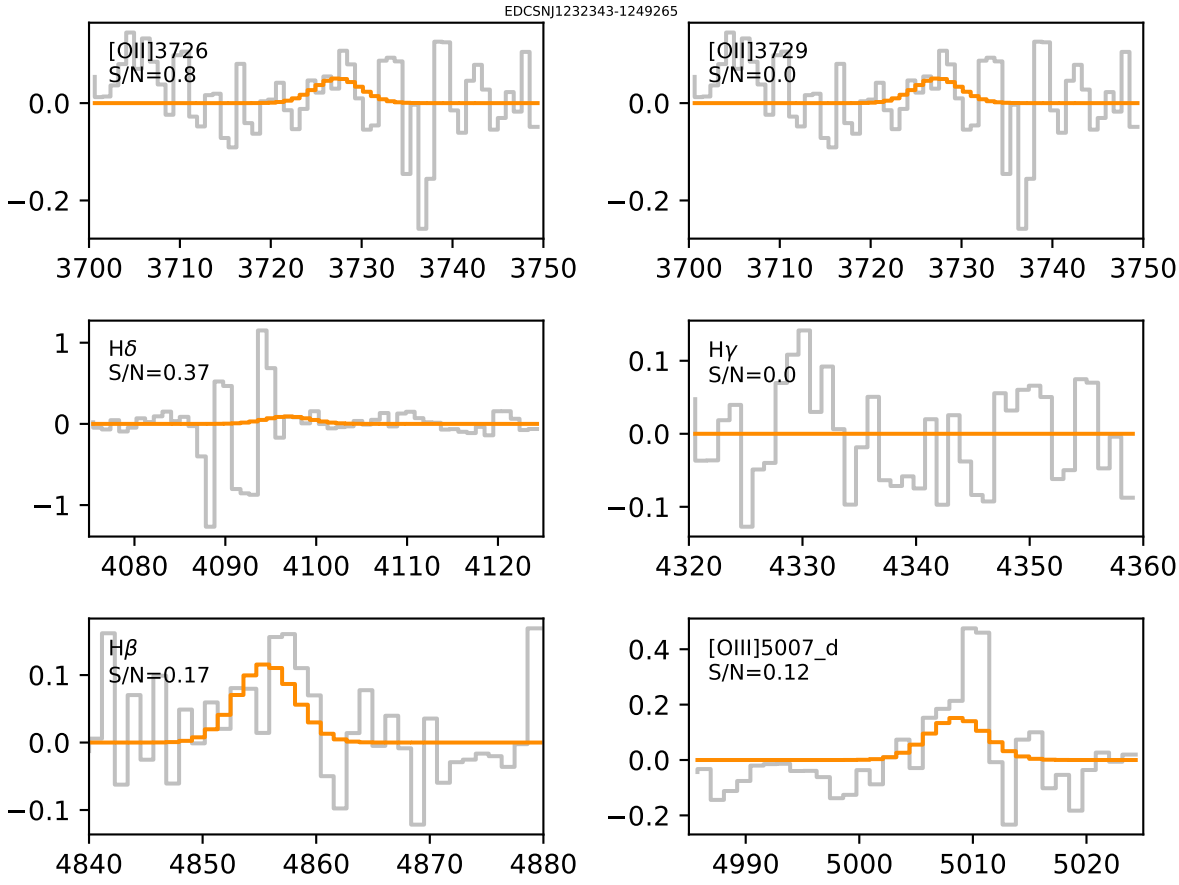
EDCSNJ1232343-1249265
[OII]3726
S/N=0.8
[OII]3729
S/N=0.0
Hδ
S/N=0.37
Hγ
S/N=0.0
Hβ
S/N=0.17
[OIII]5007_d
S/N=0.12

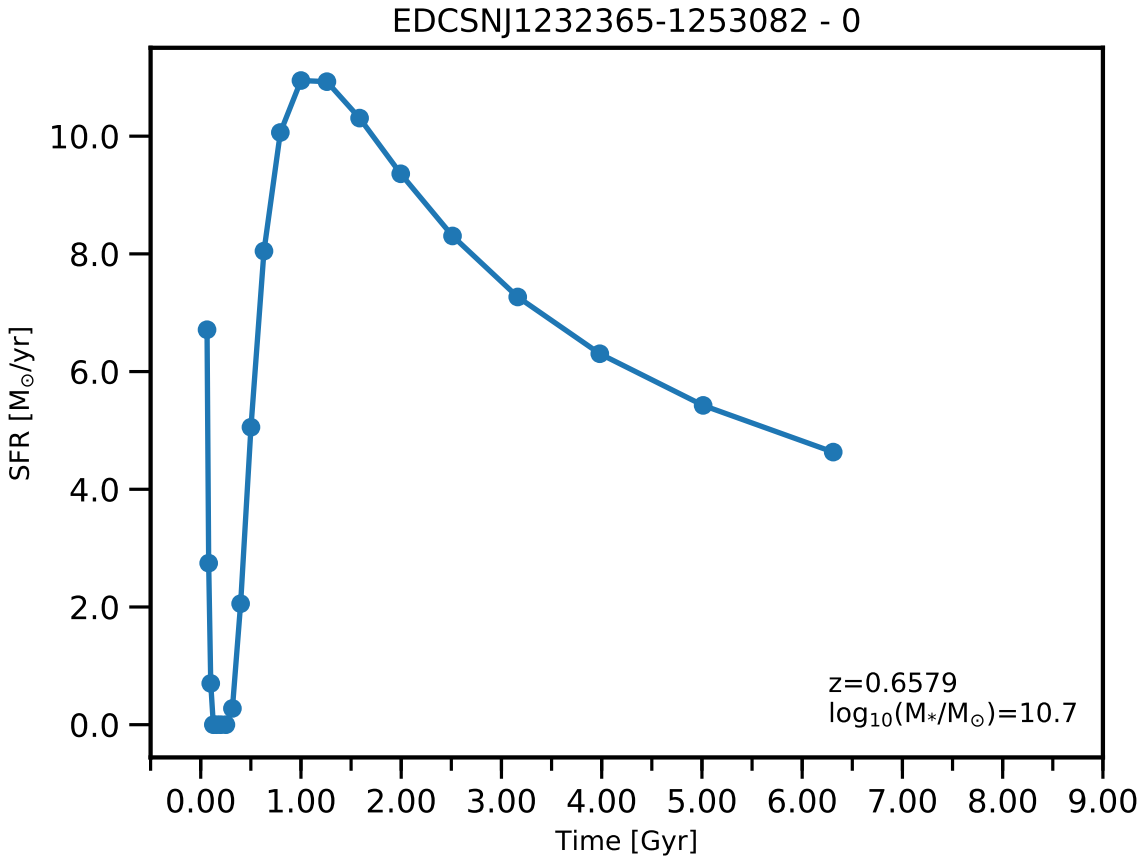
EDCSNJ1232365-1253082 - 0
SFR [M⊙/yr]
10.0
8.0
6.0
4.0
2.0
0.0
0.00
1.00
2.00
3.00
4.00
5.00
6.00
7.00
8.00
9.00
Time [Gyr]
z=0.6579
log10(M∗/M⊙)=10.7

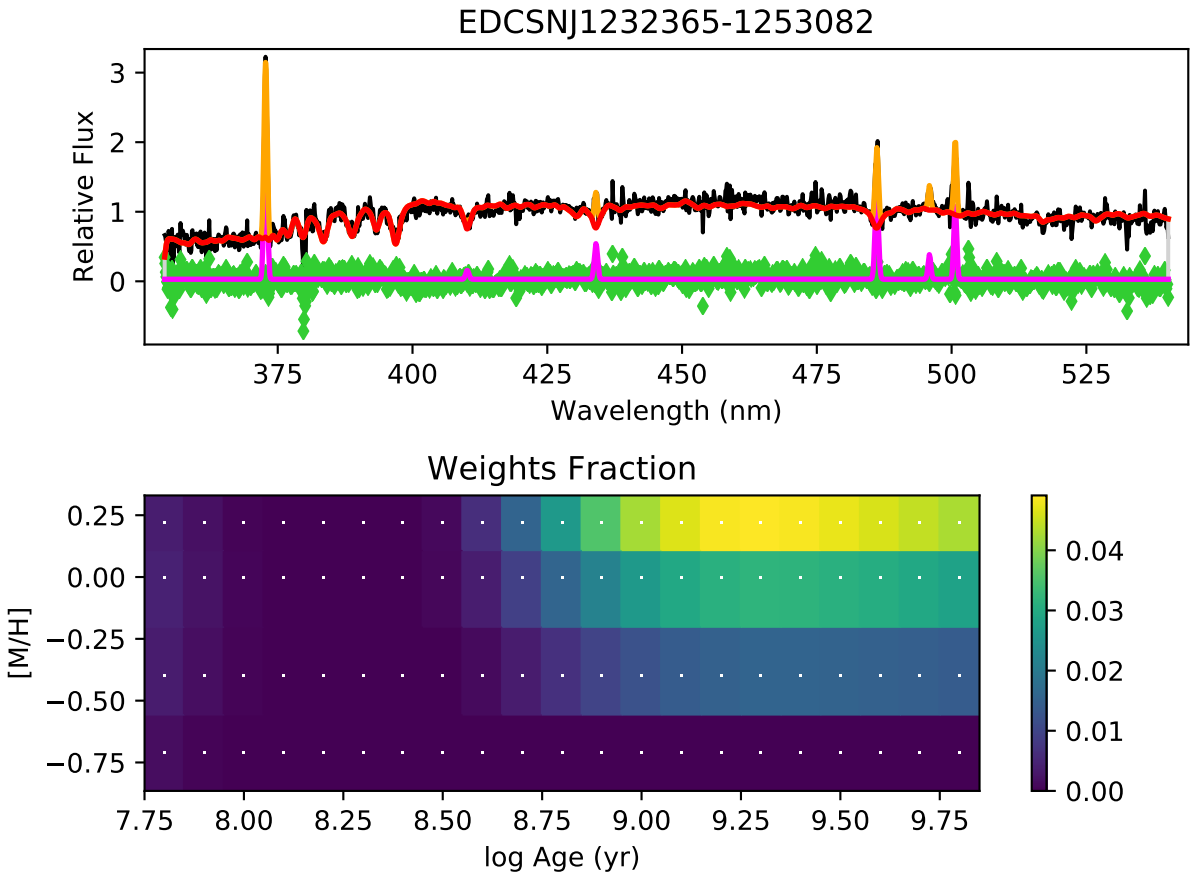
EDCSNJ1232365-1253082
Relative Flux
3
2
1
0
375
400
425
450
475
500
525
Wavelength (nm)
Weights Fraction
[M/H]
0.25
0.00
−0.25
−0.50
−0.75
7.75
8.00
8.25
8.50
8.75
9.00
9.25
9.50
9.75
log Age (yr)
0.04
0.03
0.02
0.01
0.00

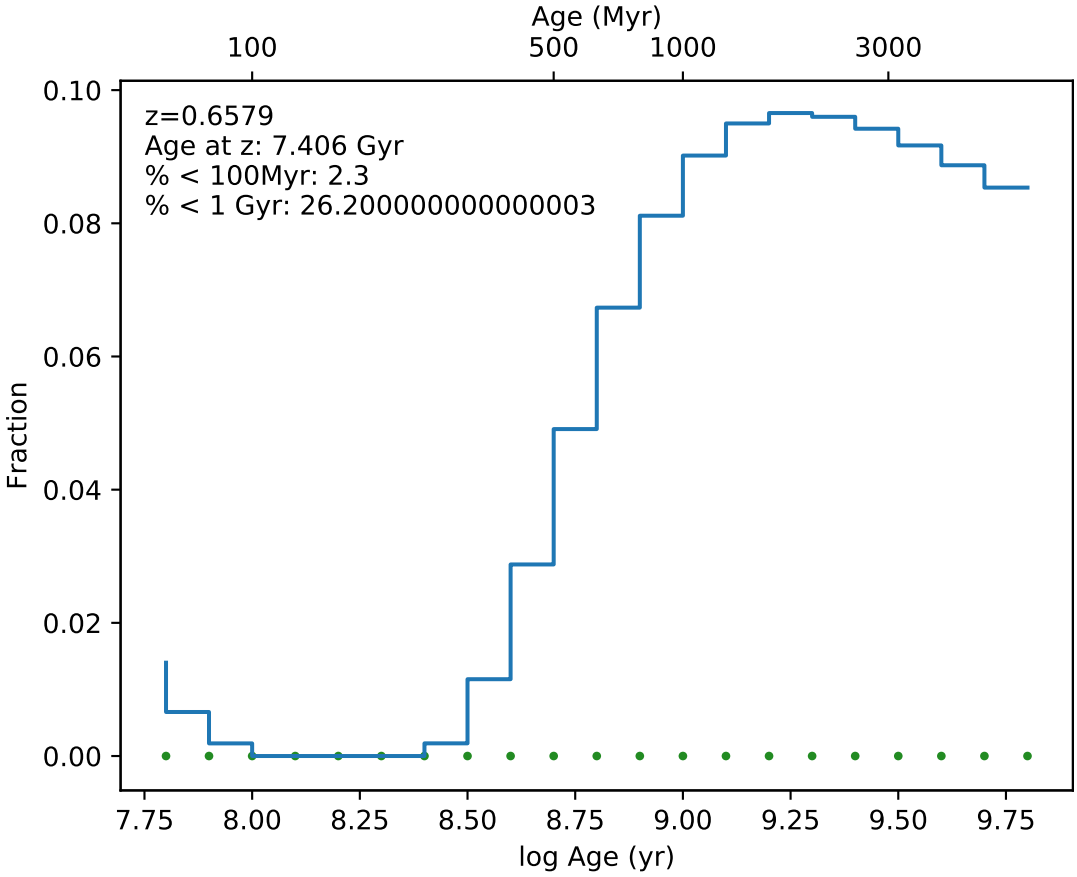
Age (Myr)
100
500
1000
3000
z=0.6579
Age at z: 7.406 Gyr
% < 100Myr: 2.3
% < 1 Gyr: 26.200000000000003
Fraction
0.10
0.08
0.06
0.04
0.02
0.00
7.75
8.00
8.25
8.50
8.75
9.00
9.25
9.50
9.75
log Age (yr)

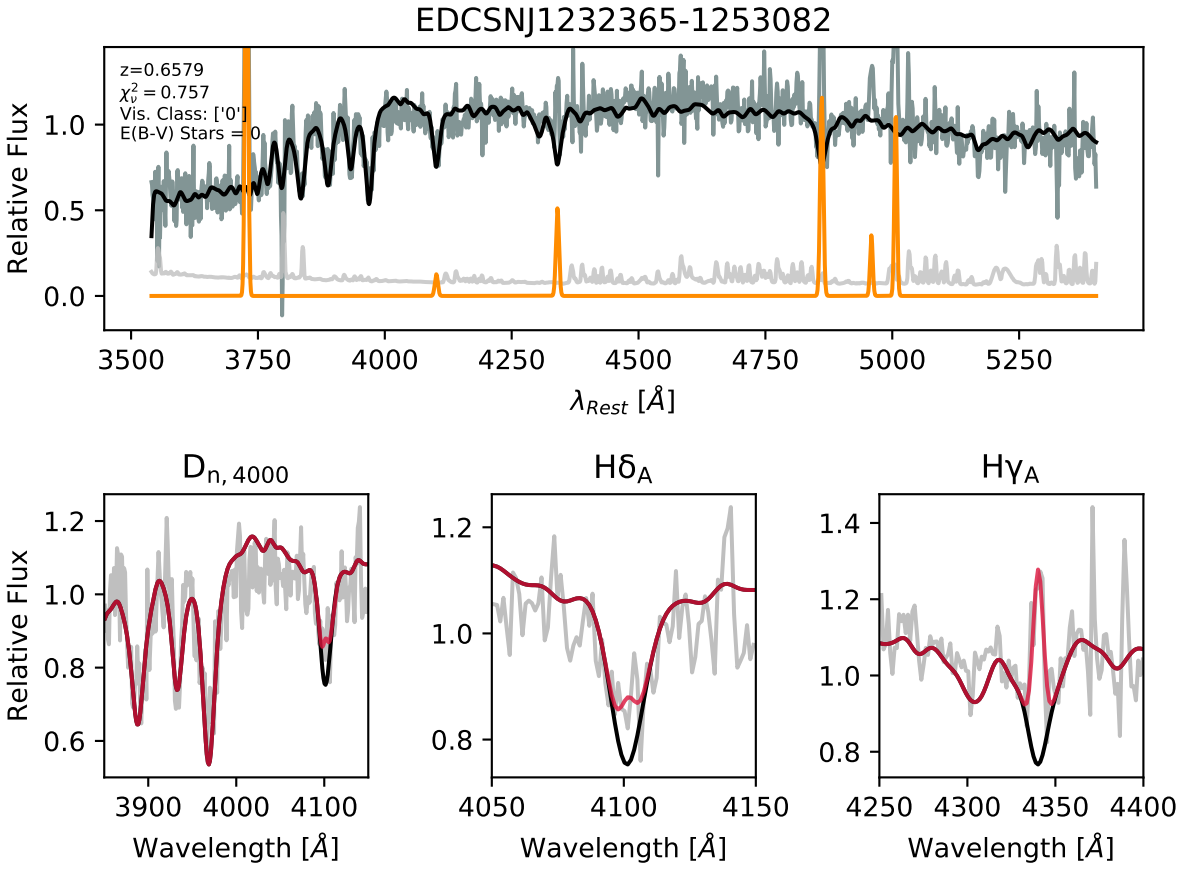
EDCSNJ1232365-1253082
z=0.6579
$\chi^2_\nu = 0.757$
Vis. Class: ['0']
E(B-V) Stars = 0
Relative Flux
λ_{Rest} [Å]
$D_{n,4000}$
$H\delta_A$
$H\gamma_A$
Wavelength [Å]

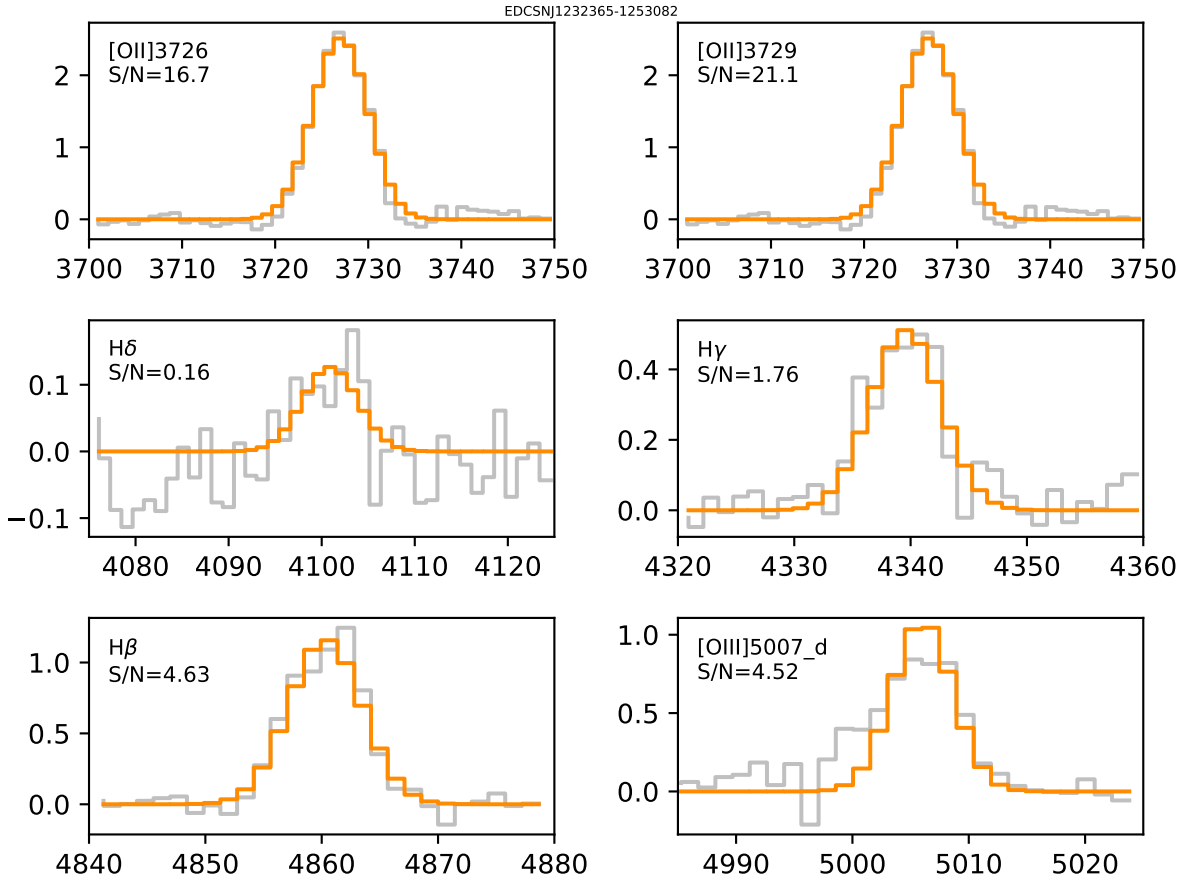
EDCSNJ1232365-1253082
[OII]3726
S/N=16.7
[OII]3729
S/N=21.1
Hδ
S/N=0.16
Hγ
S/N=1.76
Hβ
S/N=4.63
[OIII]5007_d
S/N=4.52

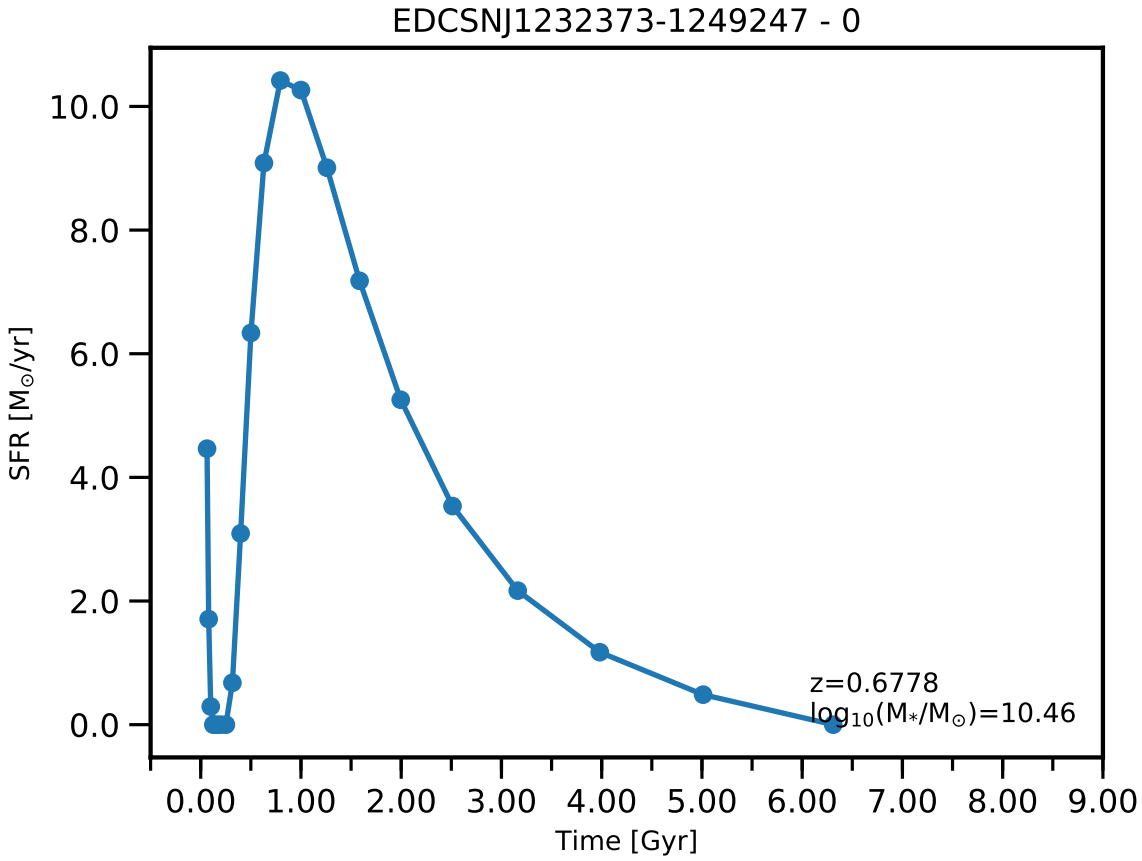
EDCSNJ1232373-1249247 - 0
SFR [M⊙/yr]
10.0
8.0
6.0
4.0
2.0
0.0
0.00
1.00
2.00
3.00
4.00
5.00
6.00
7.00
8.00
9.00
Time [Gyr]
z=0.6778
log10(M*/M⊙)=10.46

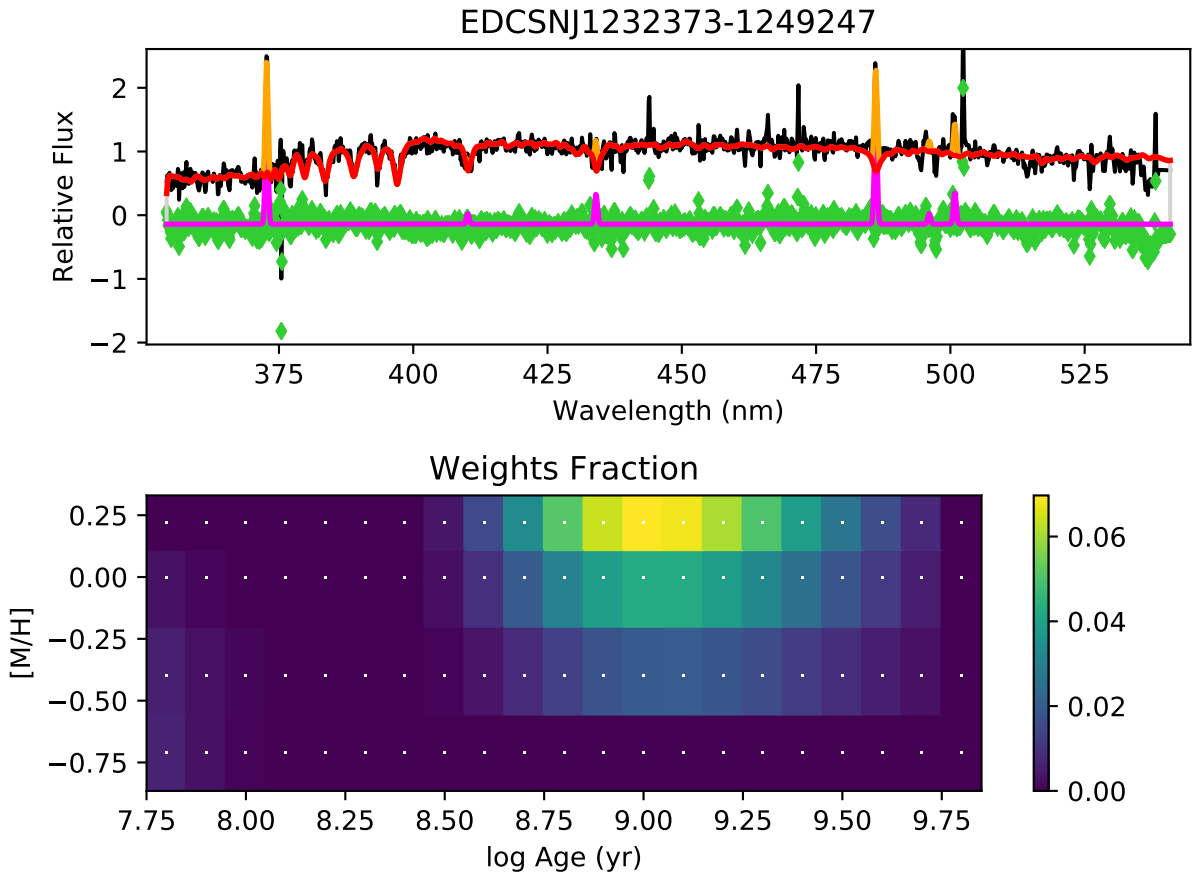
EDCSNJ1232373-1249247
Relative Flux
2
1
0
−1
−2
375
400
425
450
475
500
525
Wavelength (nm)
Weights Fraction
[M/H]
0.25
0.00
−0.25
−0.50
−0.75
7.75
8.00
8.25
8.50
8.75
9.00
9.25
9.50
9.75
log Age (yr)
0.06
0.04
0.02
0.00

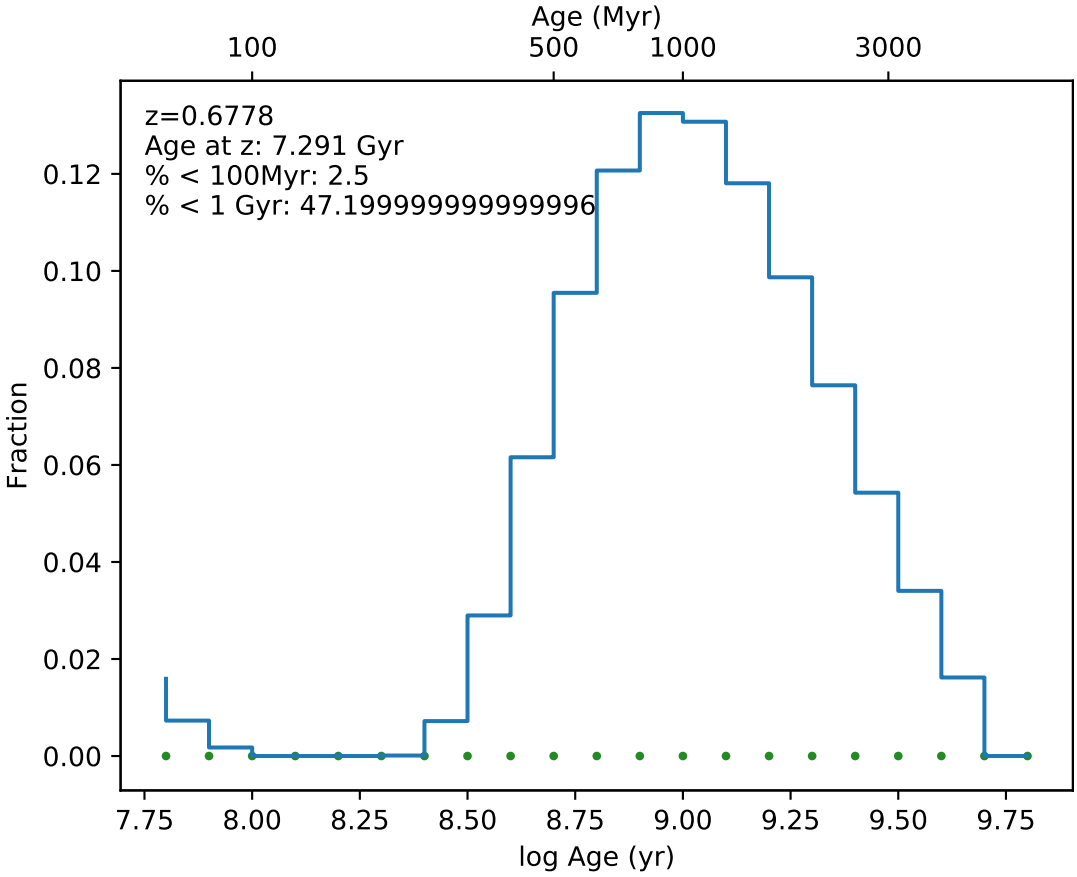
Age (Myr)
100
500
1000
3000
z=0.6778
Age at z: 7.291 Gyr
% < 100Myr: 2.5
% < 1 Gyr: 47.199999999999996
Fraction
0.12
0.10
0.08
0.06
0.04
0.02
0.00
7.75
8.00
8.25
8.50
8.75
9.00
9.25
9.50
9.75
log Age (yr)

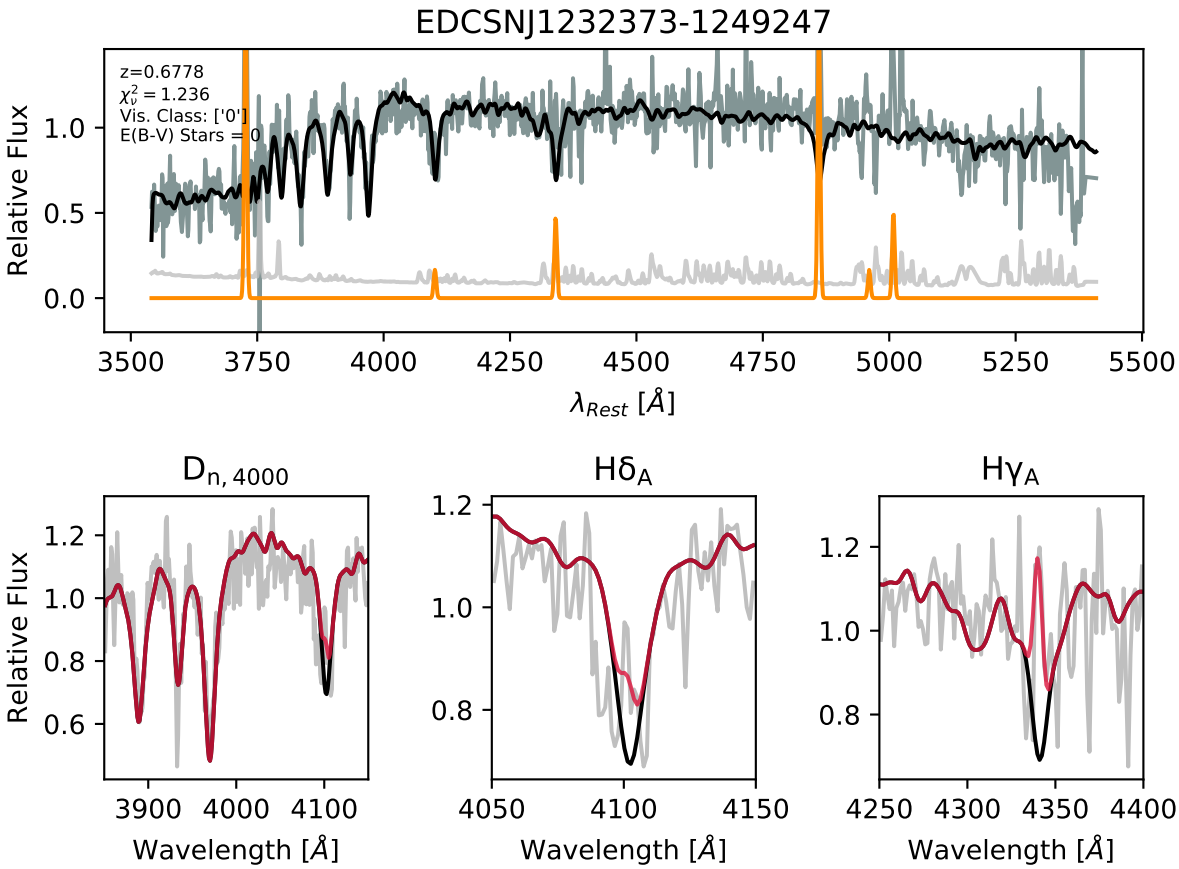
EDCSNJ1232373-1249247
z=0.6778
$\chi^2_\nu = 1.236$
Vis. Class: ['0']
E(B-V) Stars = 0
Relative Flux
λ_{Rest} [Å]
$D_{n,4000}$
$H\delta_A$
$H\gamma_A$
Wavelength [Å]

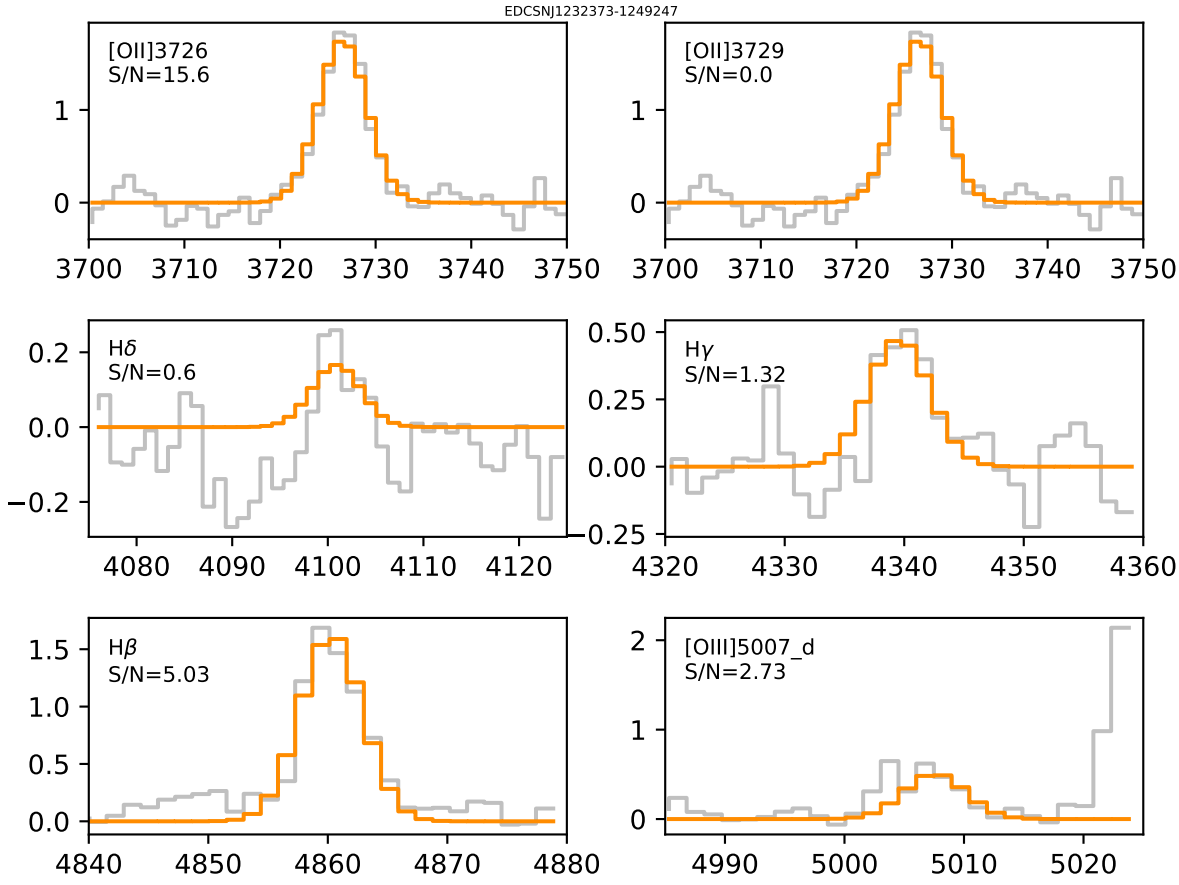
EDCSNJ1232373-1249247
[OII]3726
S/N=15.6
[OII]3729
S/N=0.0
Hδ
S/N=0.6
Hγ
S/N=1.32
Hβ
S/N=5.03
[OIII]5007_d
S/N=2.73

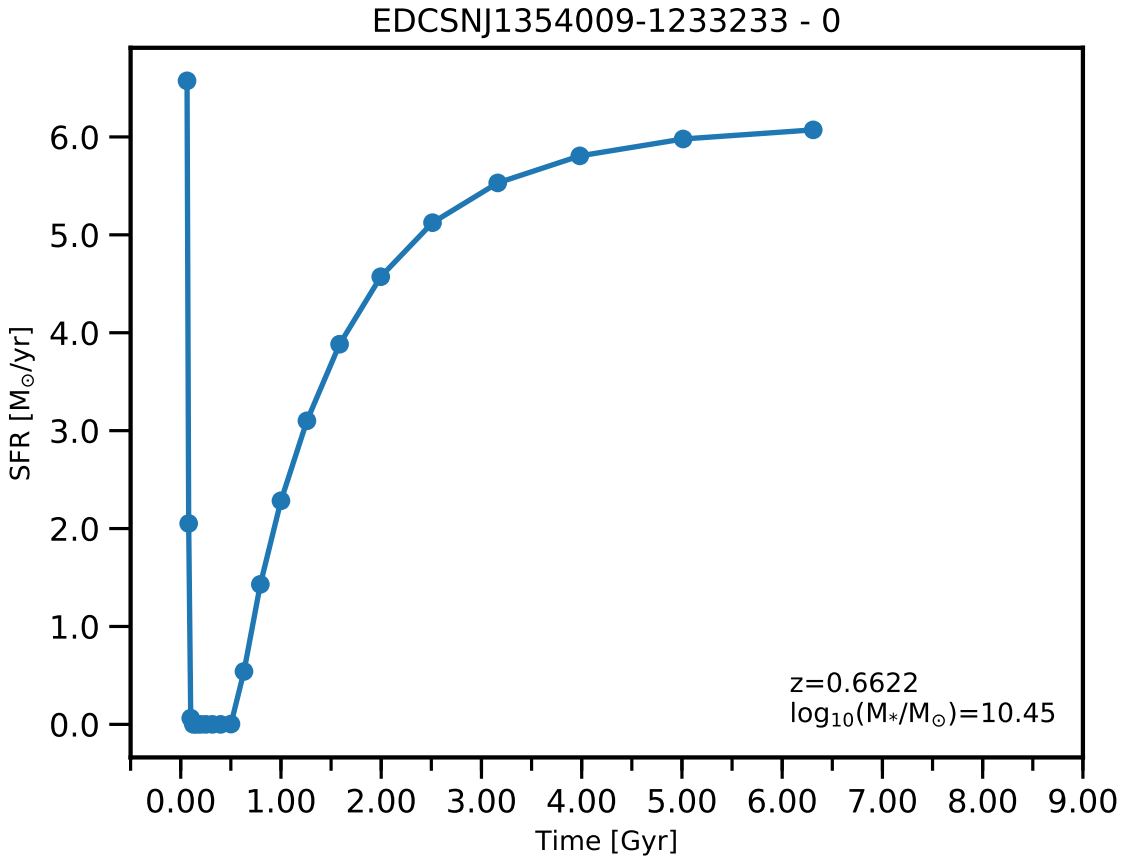
EDCSNJ1354009-1233233 - 0
SFR [M⊙/yr]
0.0
1.0
2.0
3.0
4.0
5.0
6.0
0.00
1.00
2.00
3.00
4.00
5.00
6.00
7.00
8.00
9.00
Time [Gyr]
z=0.6622
log10(M*/M⊙)=10.45

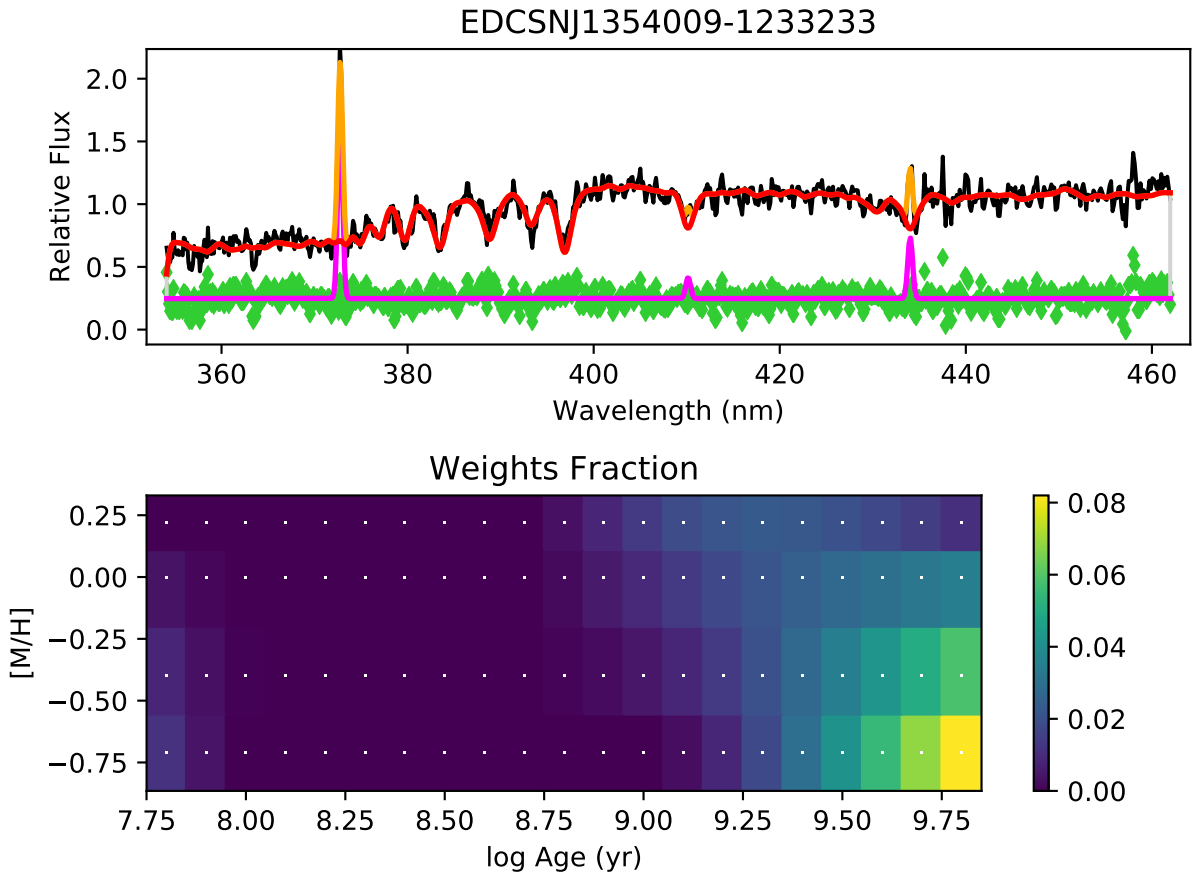
EDCSNJ1354009-1233233
Relative Flux
2.0
1.5
1.0
0.5
0.0
360
380
400
420
440
460
Wavelength (nm)
Weights Fraction
[M/H]
0.25
0.00
−0.25
−0.50
−0.75
7.75
8.00
8.25
8.50
8.75
9.00
9.25
9.50
9.75
log Age (yr)
0.08
0.06
0.04
0.02
0.00

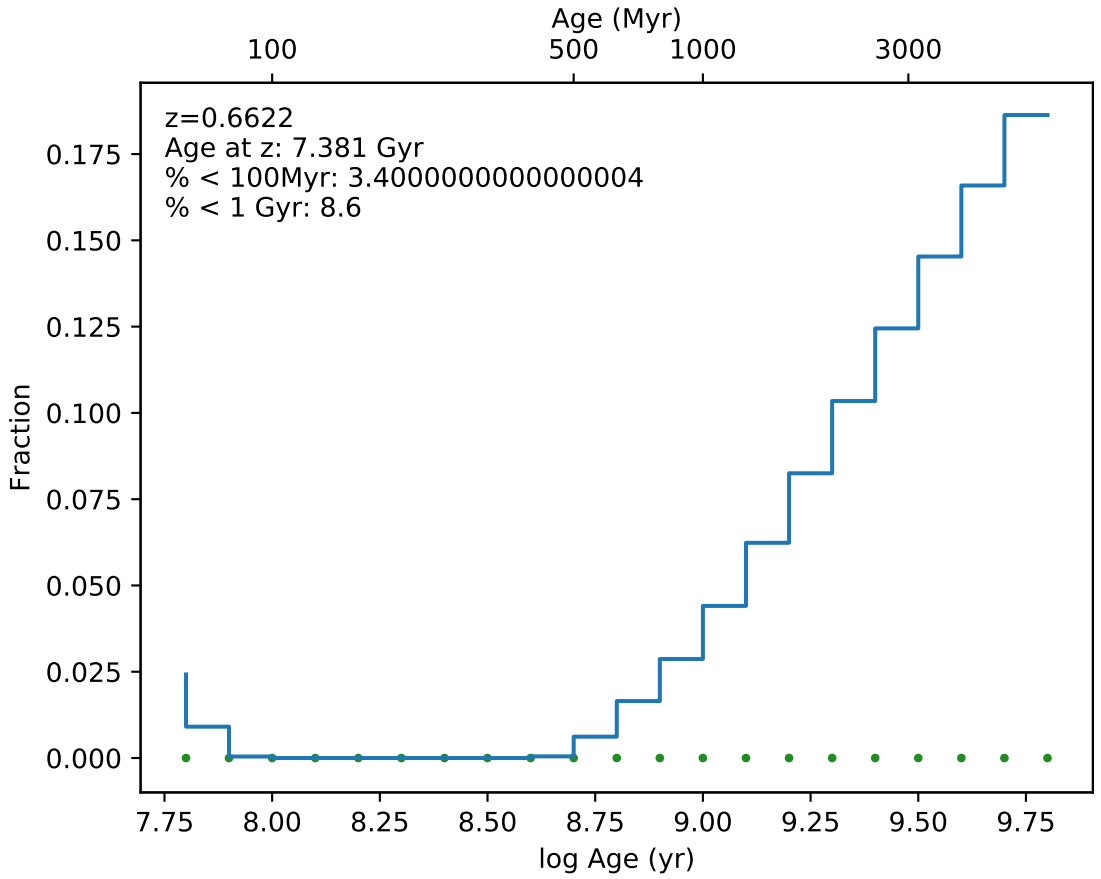
Age (Myr)
100
500
1000
3000
z=0.6622
Age at z: 7.381 Gyr
% < 100Myr: 3.4000000000000004
% < 1 Gyr: 8.6
Fraction
0.175
0.150
0.125
0.100
0.075
0.050
0.025
0.000
7.75
8.00
8.25
8.50
8.75
9.00
9.25
9.50
9.75
log Age (yr)

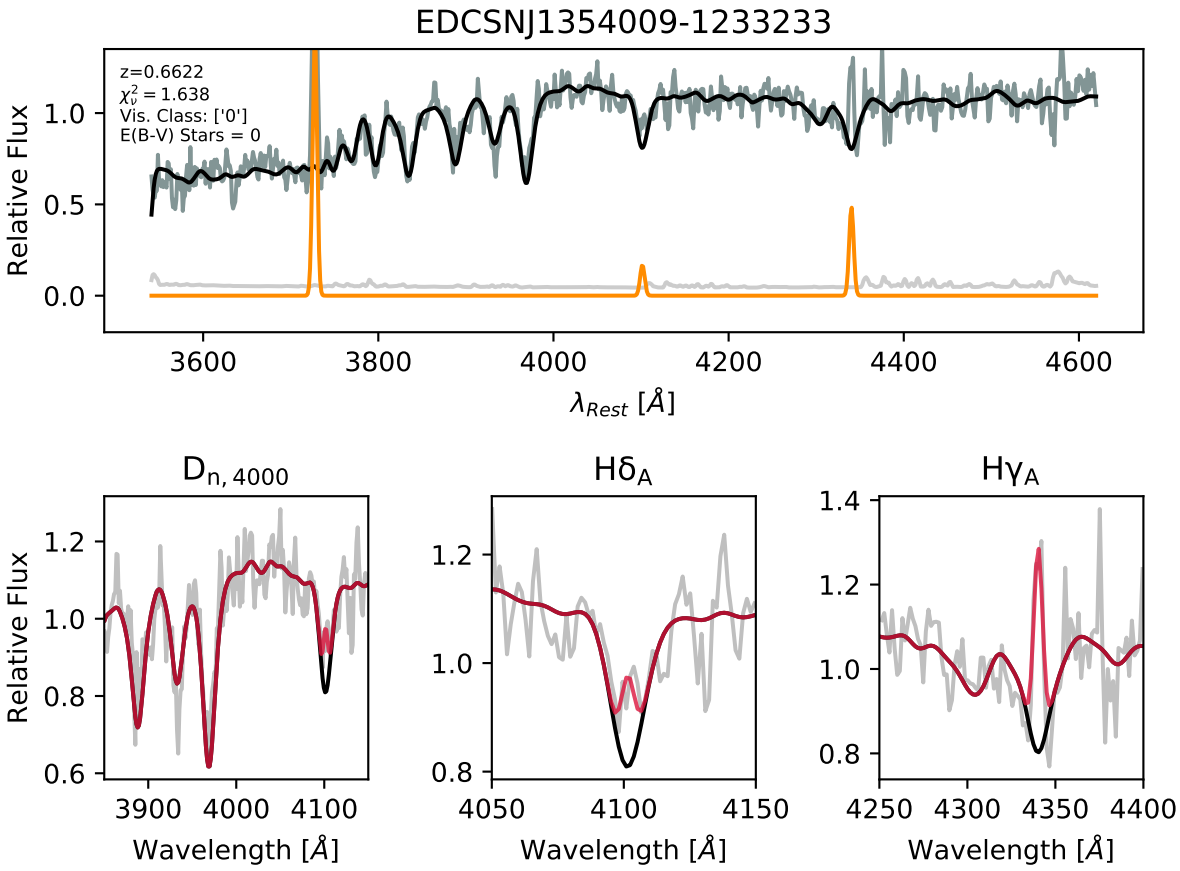
EDCSNJ1354009-1233233
z=0.6622
$\chi^2_\nu = 1.638$
Vis. Class: ['0']
E(B-V) Stars = 0
Relative Flux
1.0
0.5
0.0
3600
3800
4000
4200
4400
4600
λ_{Rest} [Å]
$D_{n,4000}$
$H\delta_A$
$H\gamma_A$
Relative Flux
1.2
1.0
0.8
0.6
3900
4000
4100
Wavelength [Å]
1.2
1.0
0.8
4050
4100
4150
Wavelength [Å]
1.4
1.2
1.0
0.8
4250
4300
4350
4400
Wavelength [Å]

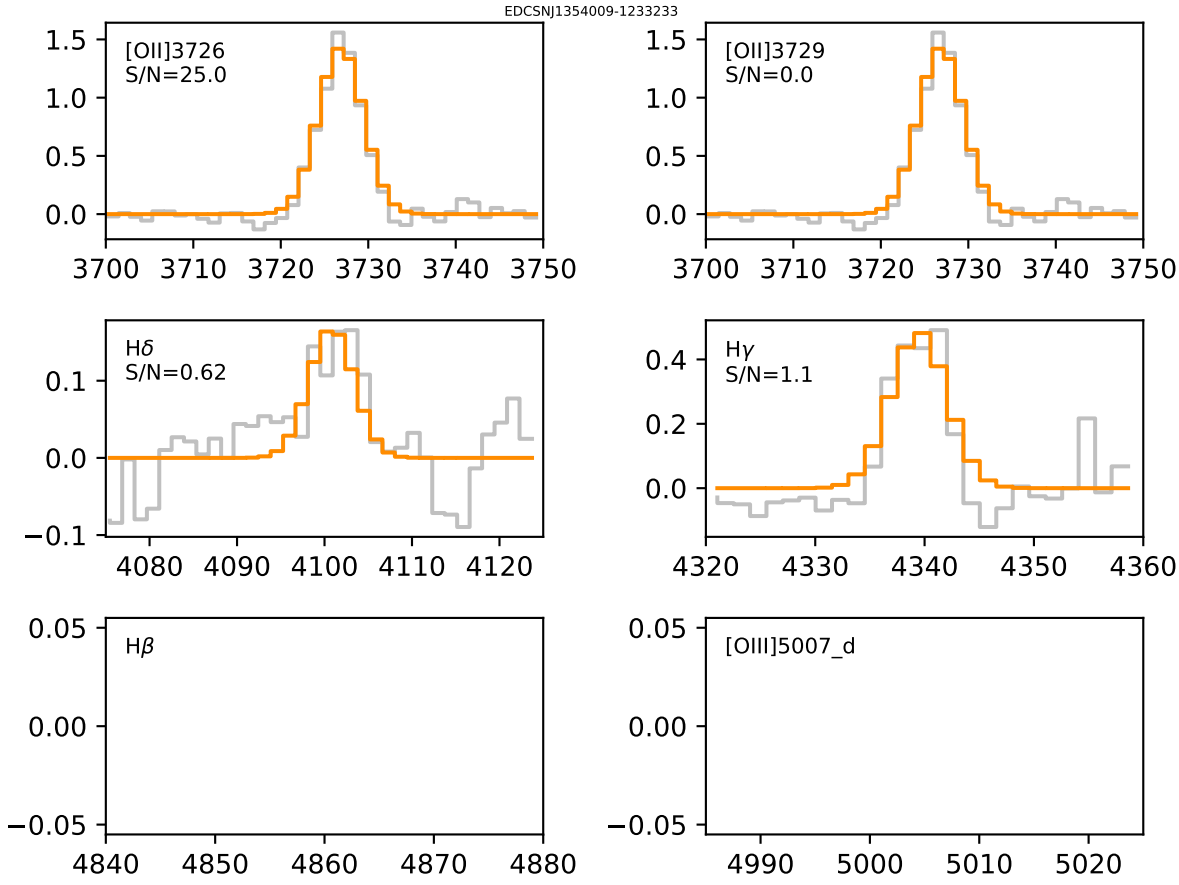
EDCSNJ1354009-1233233
[OII]3726
S/N=25.0
[OII]3729
S/N=0.0
Hδ
S/N=0.62
Hγ
S/N=1.1
Hβ
[OIII]5007_d

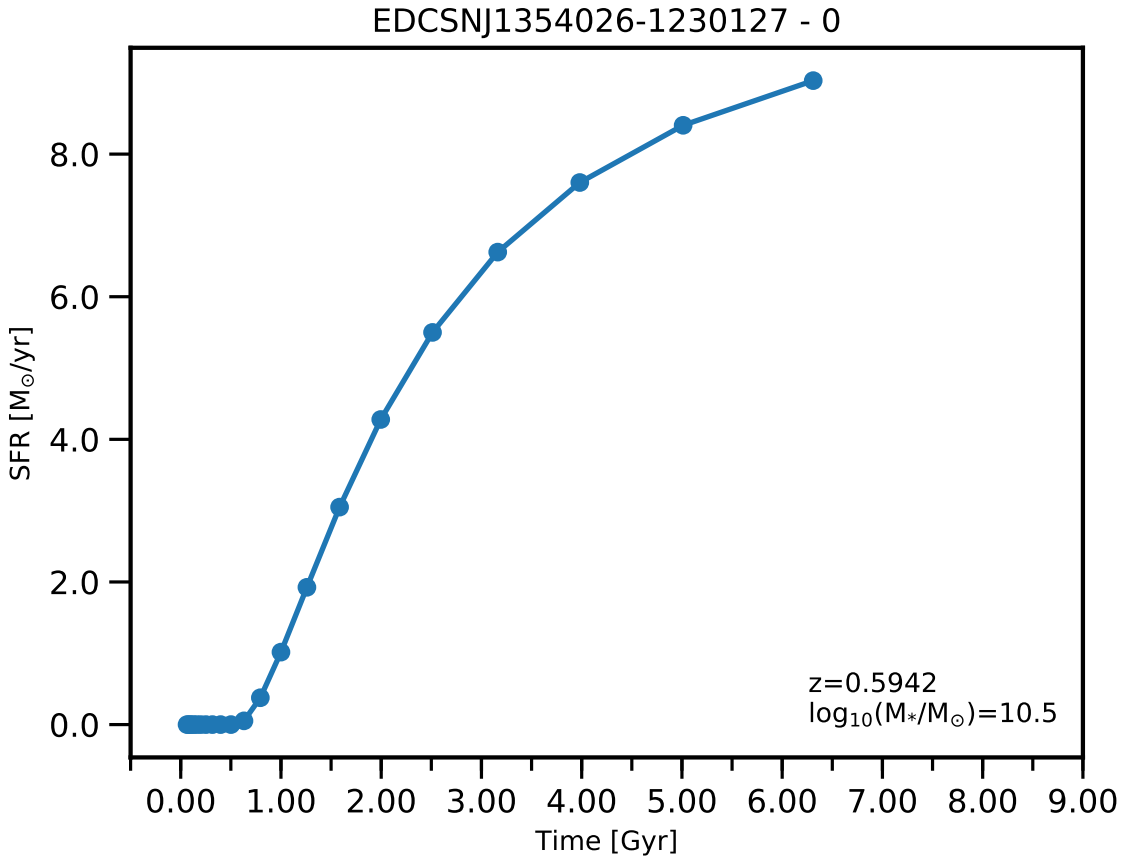
EDCSNJ1354026-1230127 - 0
SFR [M⊙/yr]
0.0
2.0
4.0
6.0
8.0
0.00
1.00
2.00
3.00
4.00
5.00
6.00
7.00
8.00
9.00
Time [Gyr]
z=0.5942
log10(M*/M⊙)=10.5

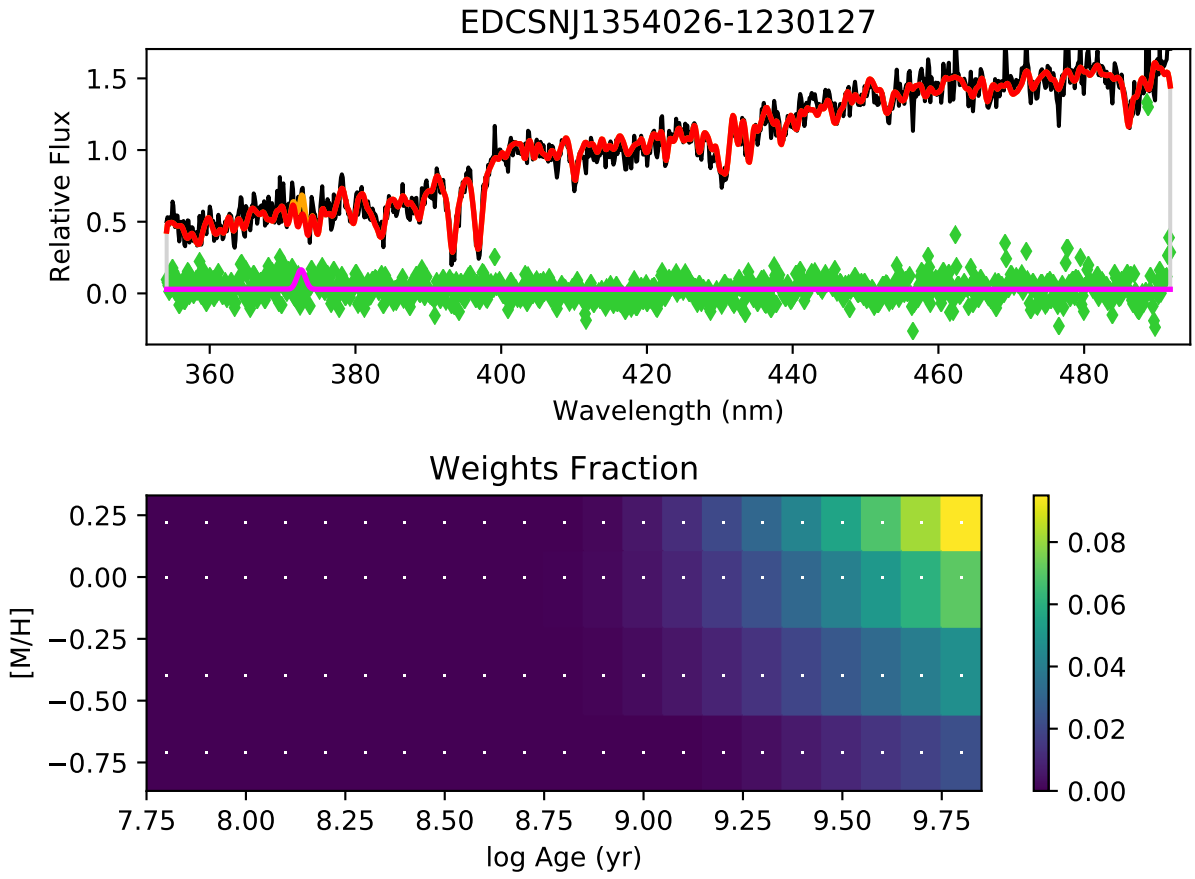
EDCSNJ1354026-1230127
Relative Flux
1.5
1.0
0.5
0.0
360
380
400
420
440
460
480
Wavelength (nm)
Weights Fraction
[M/H]
0.25
0.00
−0.25
−0.50
−0.75
7.75
8.00
8.25
8.50
8.75
9.00
9.25
9.50
9.75
log Age (yr)
0.08
0.06
0.04
0.02
0.00

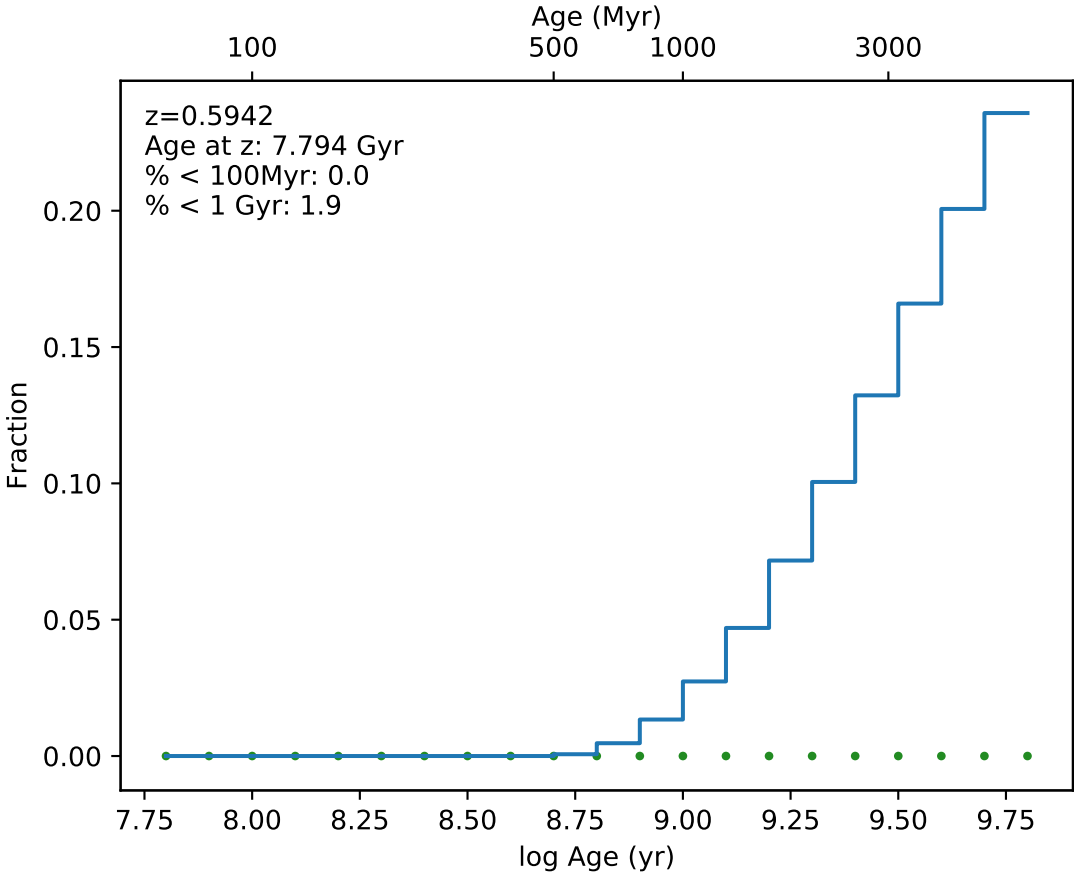
Age (Myr)
100
500
1000
3000
z=0.5942
Age at z: 7.794 Gyr
% < 100Myr: 0.0
% < 1 Gyr: 1.9
Fraction
0.00
0.05
0.10
0.15
0.20
7.75
8.00
8.25
8.50
8.75
9.00
9.25
9.50
9.75
log Age (yr)

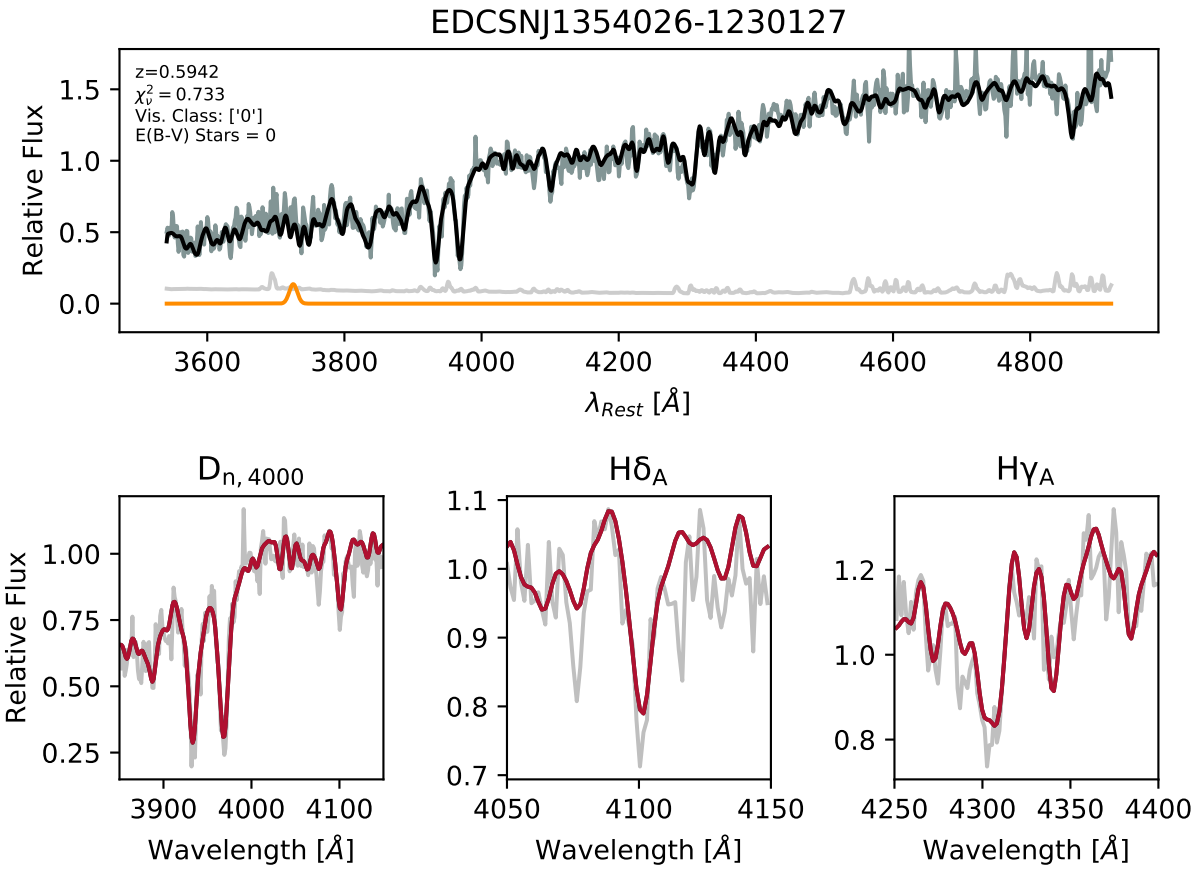
EDCSNJ1354026-1230127
z=0.5942
$\chi^2_\nu = 0.733$
Vis. Class: ['0']
E(B-V) Stars = 0
Relative Flux
λ_{Rest} [Å]
$D_{n,4000}$
$H\delta_A$
$H\gamma_A$
Wavelength [Å]

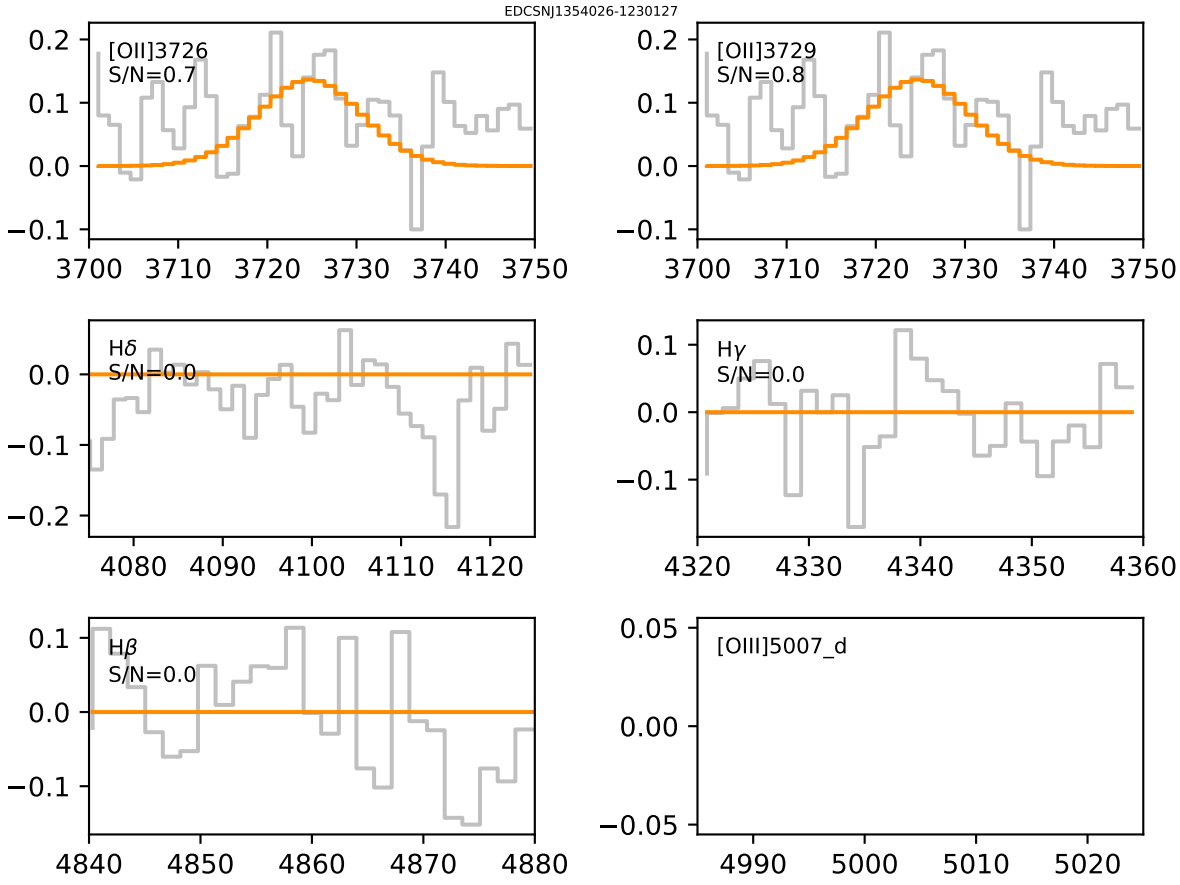
EDCSNJ1354026-1230127
[OII]3726
S/N=0.7
[OII]3729
S/N=0.8
Hδ
S/N=0.0
Hγ
S/N=0.0
Hβ
S/N=0.0
[OIII]5007_d

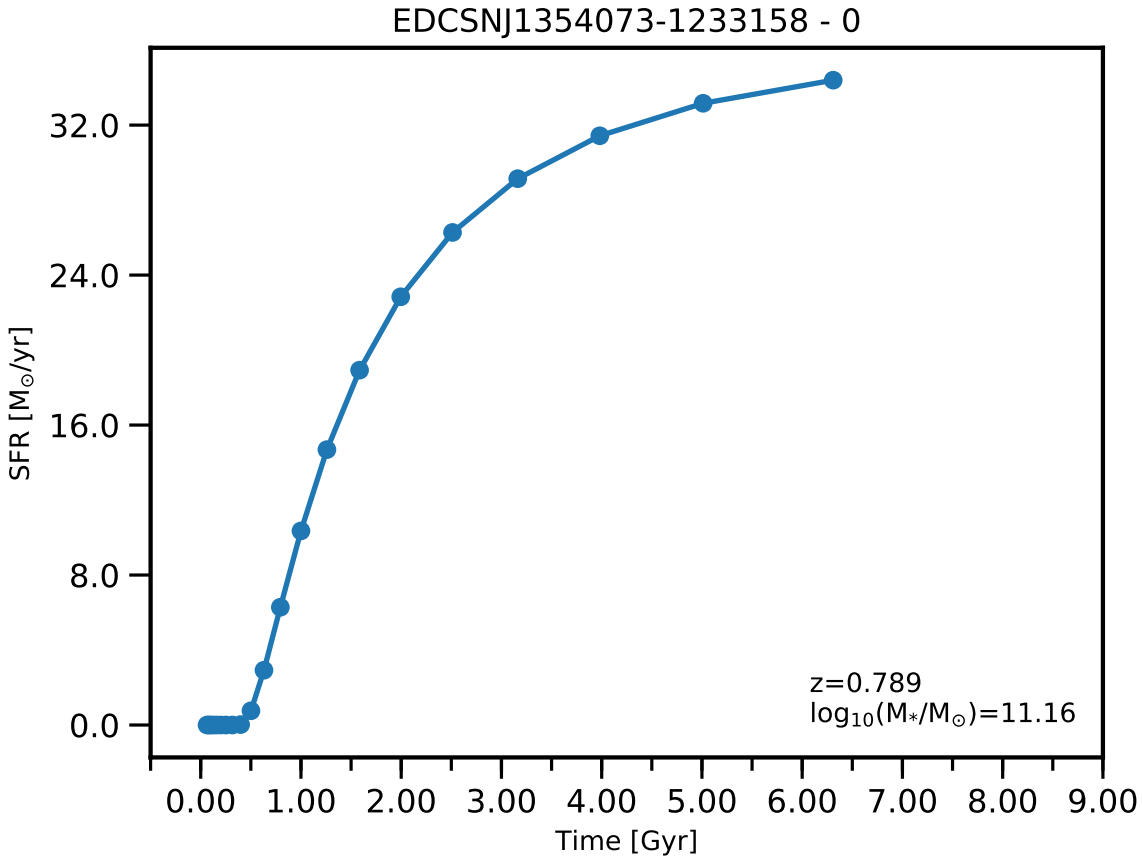
EDCSNJ1354073-1233158 - 0
SFR [M⊙/yr]
32.0
24.0
16.0
8.0
0.0
0.00
1.00
2.00
3.00
4.00
5.00
6.00
7.00
8.00
9.00
Time [Gyr]
z=0.789
log10(M*/M⊙)=11.16

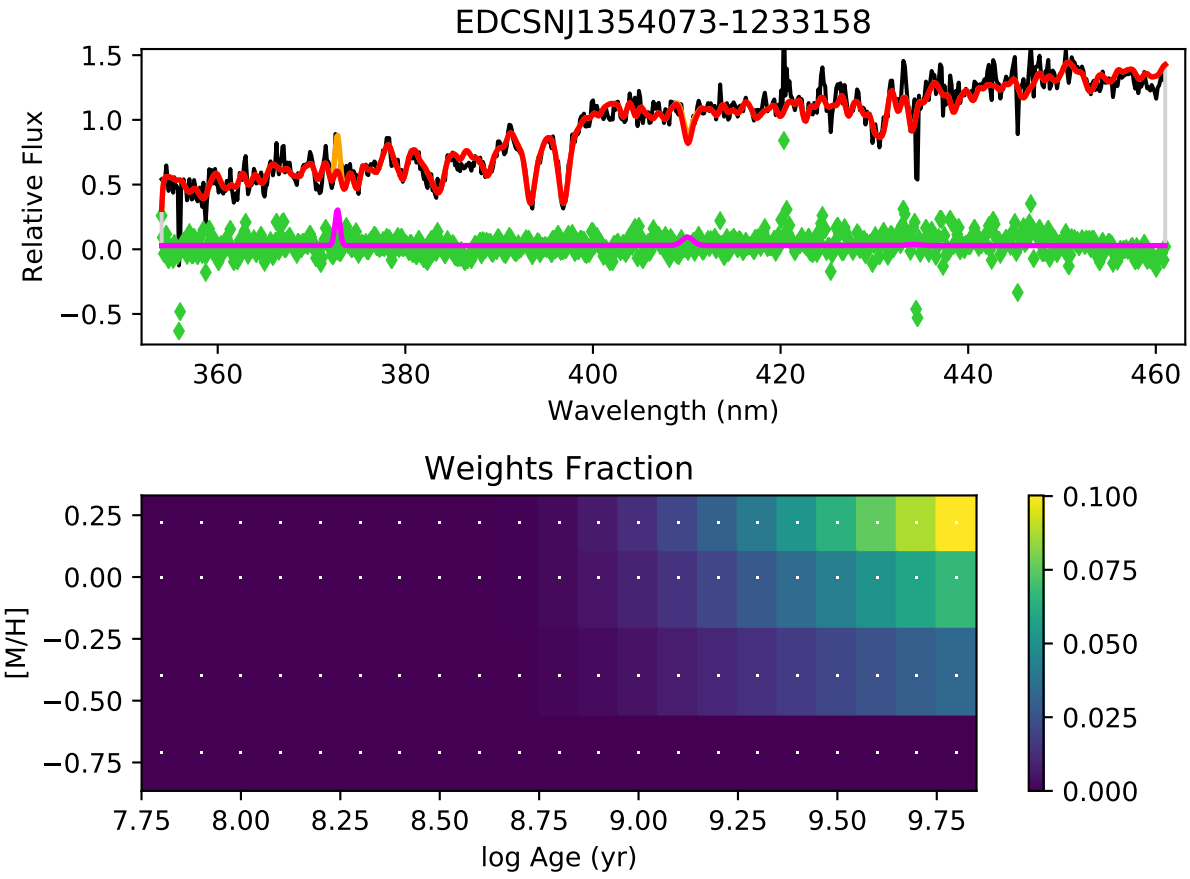
EDCSNJ1354073-1233158
Relative Flux
1.5
1.0
0.5
0.0
−0.5
360
380
400
420
440
460
Wavelength (nm)
Weights Fraction
[M/H]
0.25
0.00
−0.25
−0.50
−0.75
7.75
8.00
8.25
8.50
8.75
9.00
9.25
9.50
9.75
log Age (yr)
0.100
0.075
0.050
0.025
0.000

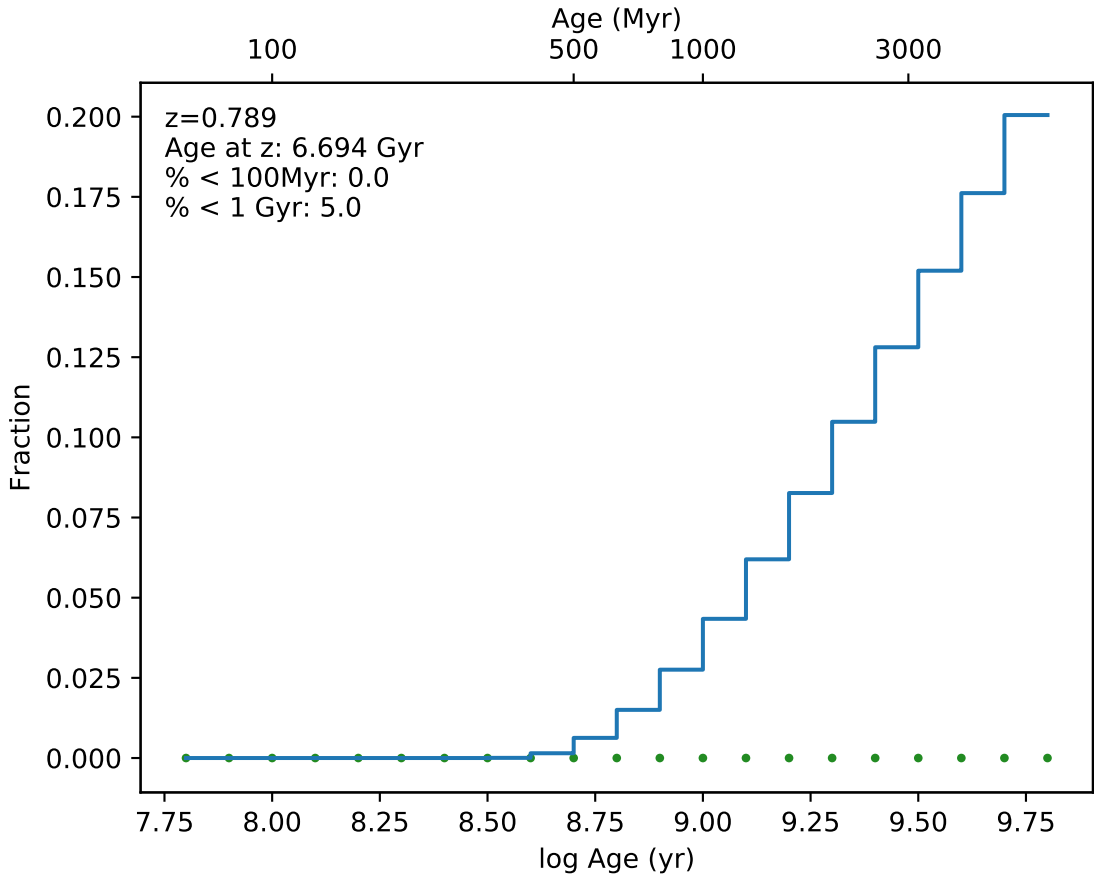
Age (Myr)
100
500
1000
3000
z=0.789
Age at z: 6.694 Gyr
% < 100Myr: 0.0
% < 1 Gyr: 5.0
Fraction
0.200
0.175
0.150
0.125
0.100
0.075
0.050
0.025
0.000
7.75
8.00
8.25
8.50
8.75
9.00
9.25
9.50
9.75
log Age (yr)

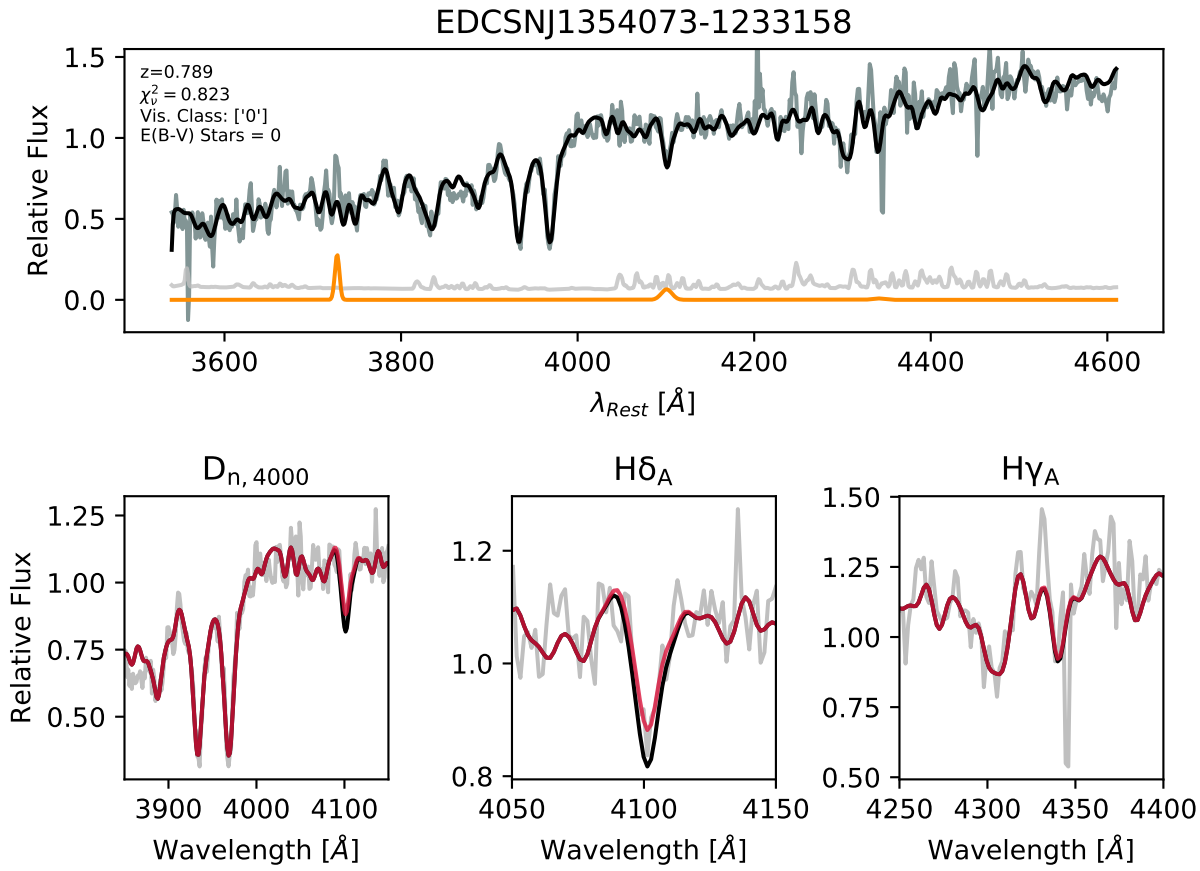
EDCSNJ1354073-1233158
z=0.789
$\chi^2_\nu = 0.823$
Vis. Class: ['0']
E(B-V) Stars = 0
Relative Flux
λ_{Rest} [Å]
$D_{n,4000}$
$H\delta_A$
$H\gamma_A$
Wavelength [Å]

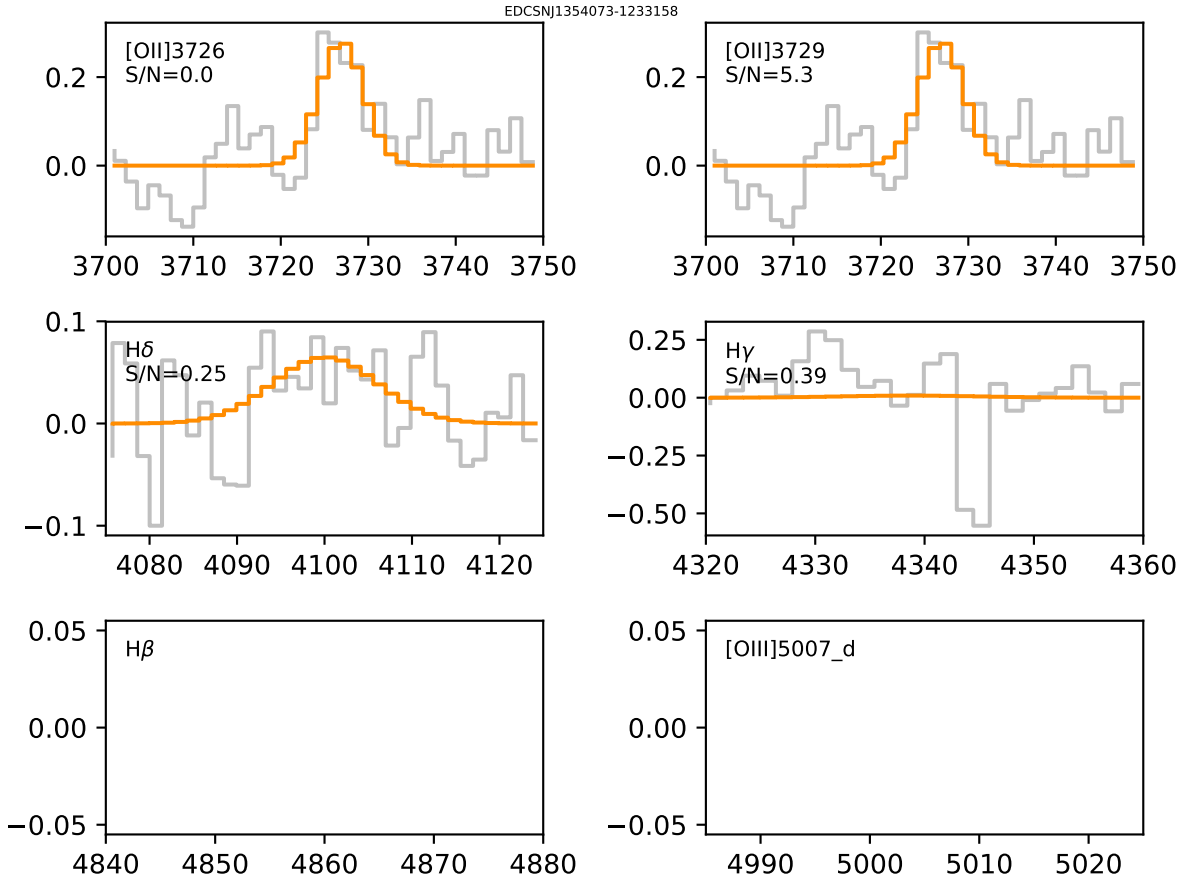
EDCSNJ1354073-1233158
[OII]3726
S/N=0.0
[OII]3729
S/N=5.3
Hδ
S/N=0.25
Hγ
S/N=0.39
Hβ
[OIII]5007_d

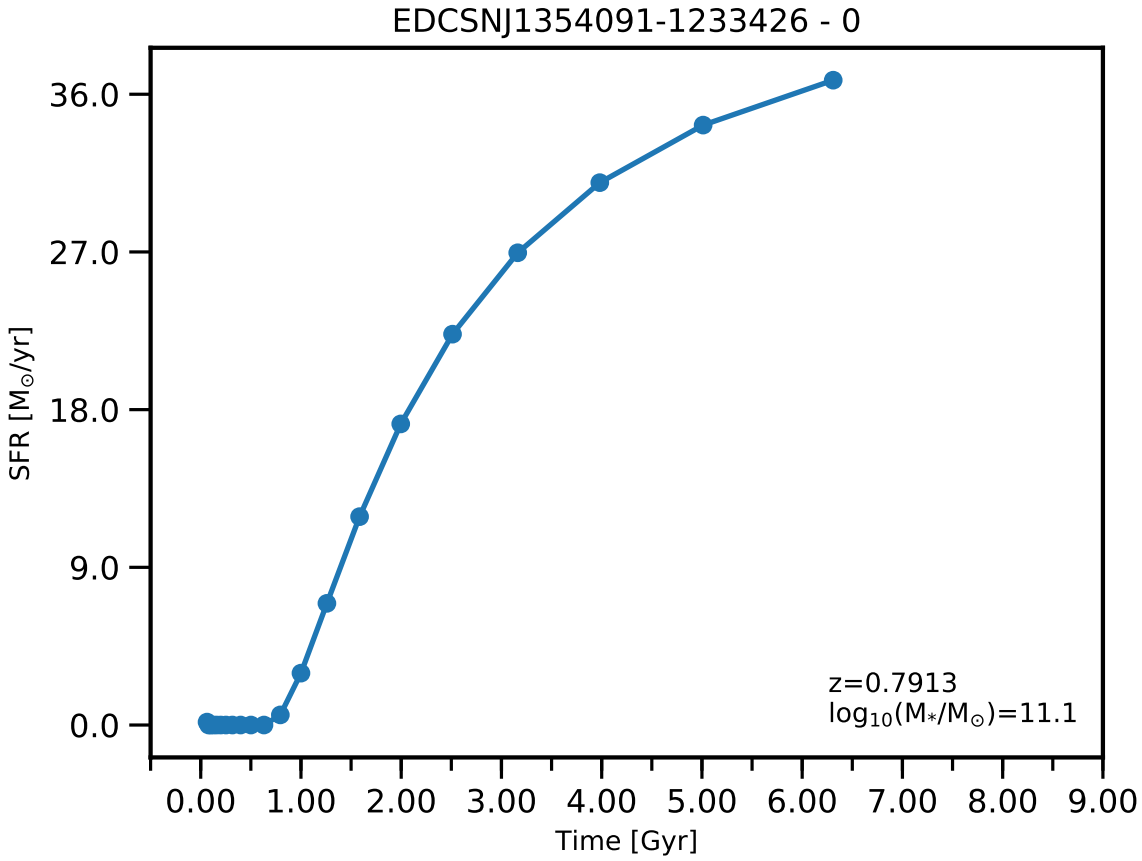
EDCSNJ1354091-1233426 - 0
36.0
27.0
18.0
9.0
0.0
SFR [M⊙/yr]
0.00
1.00
2.00
3.00
4.00
5.00
6.00
7.00
8.00
9.00
Time [Gyr]
z=0.7913
log10(M∗/M⊙)=11.1

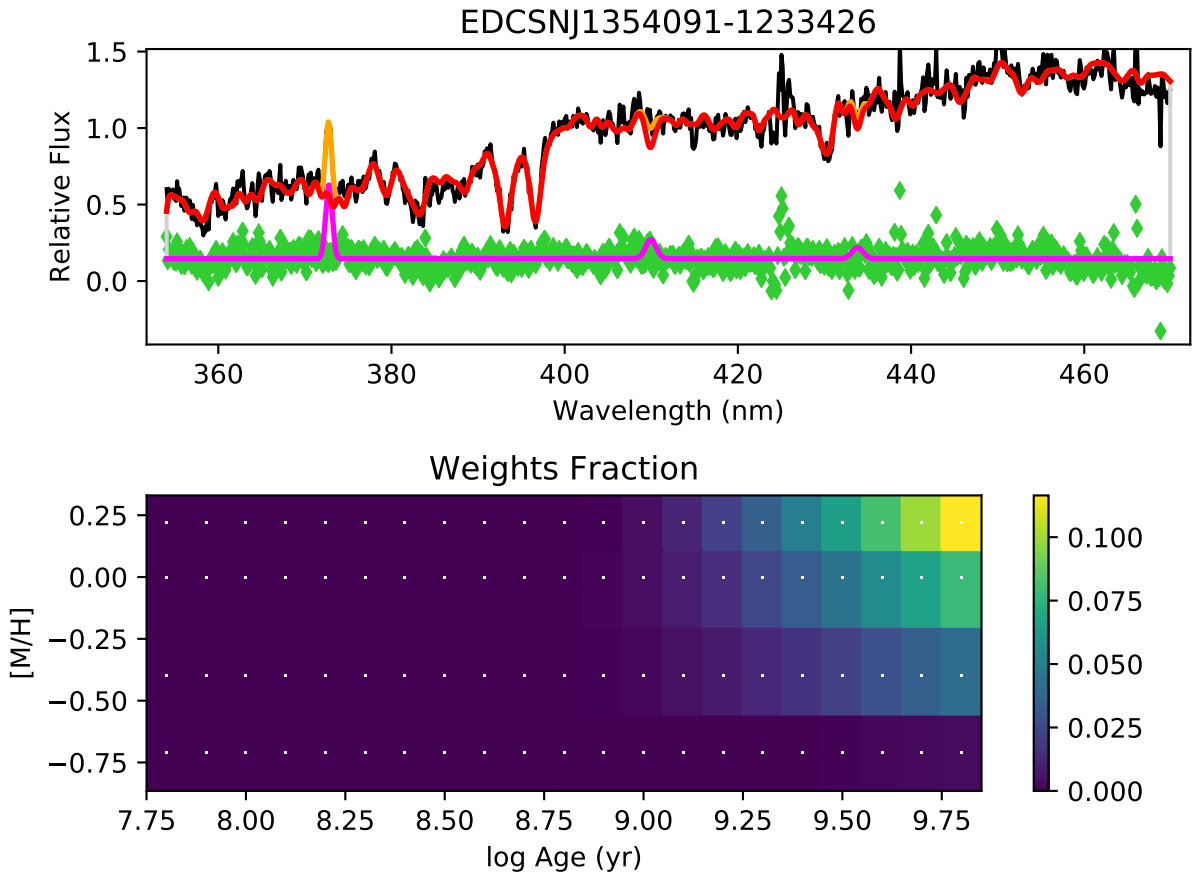
EDCSNJ1354091-1233426
Relative Flux
1.5
1.0
0.5
0.0
360
380
400
420
440
460
Wavelength (nm)
Weights Fraction
[M/H]
0.25
0.00
−0.25
−0.50
−0.75
7.75
8.00
8.25
8.50
8.75
9.00
9.25
9.50
9.75
log Age (yr)
0.100
0.075
0.050
0.025
0.000

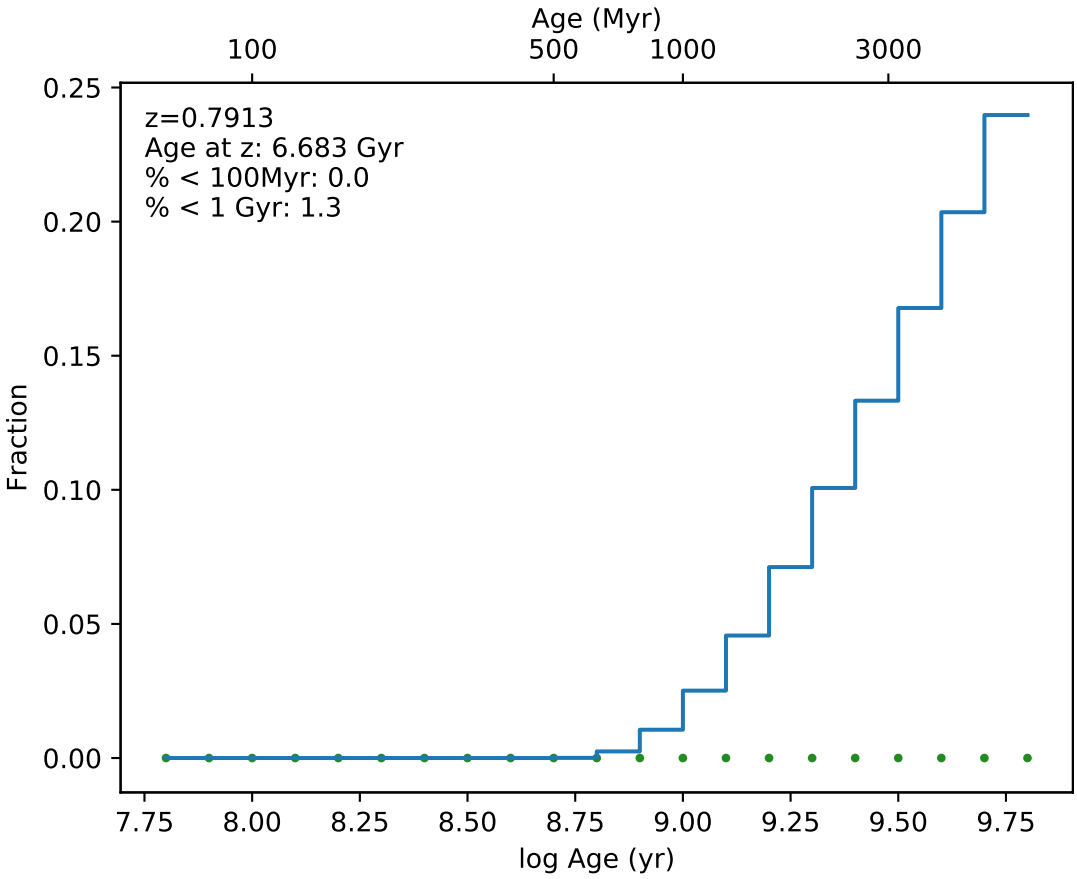
Age (Myr)
100
500
1000
3000
z=0.7913
Age at z: 6.683 Gyr
% < 100Myr: 0.0
% < 1 Gyr: 1.3
Fraction
0.25
0.20
0.15
0.10
0.05
0.00
7.75
8.00
8.25
8.50
8.75
9.00
9.25
9.50
9.75
log Age (yr)

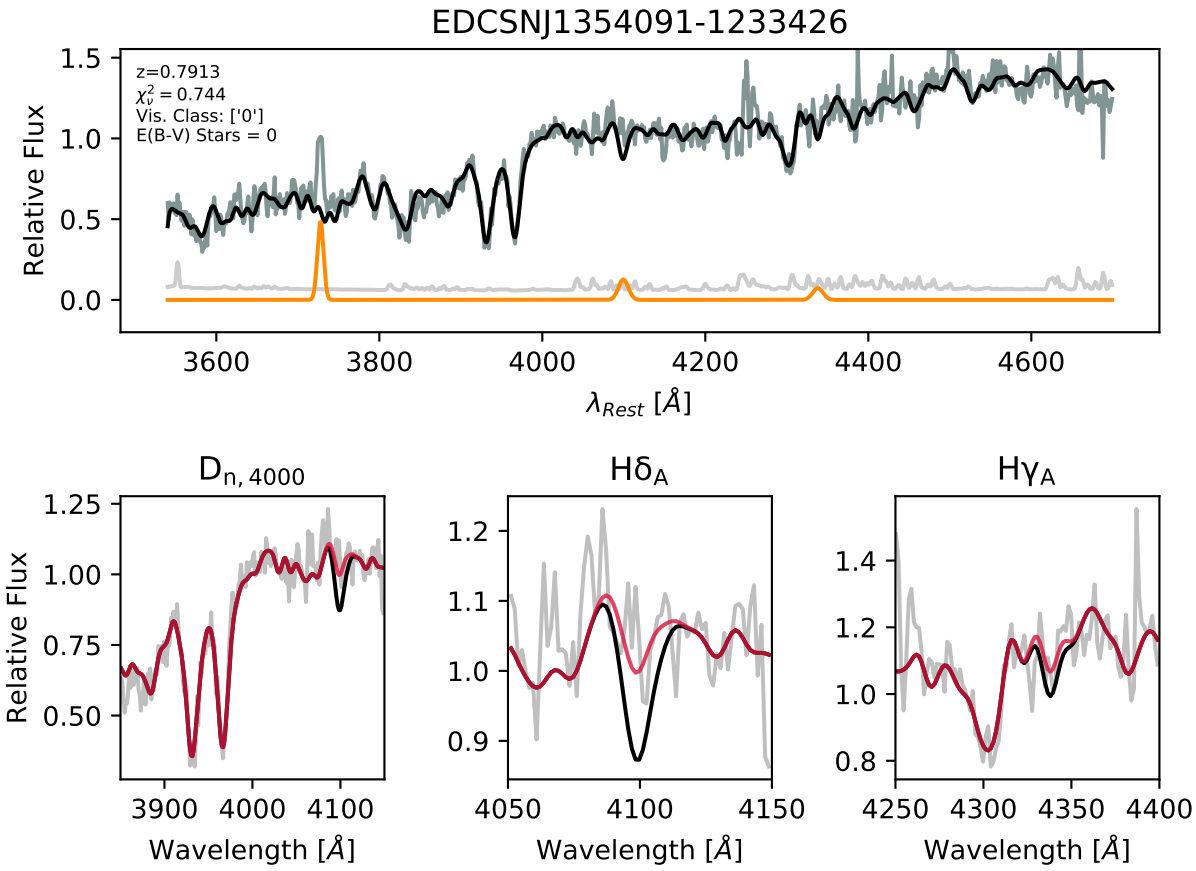
EDCSNJ1354091-1233426
z=0.7913
$\chi^2_\nu = 0.744$
Vis. Class: ['0']
E(B-V) Stars = 0
Relative Flux
λ_{Rest} [Å]
$D_{n,4000}$
$H\delta_A$
$H\gamma_A$
Wavelength [Å]

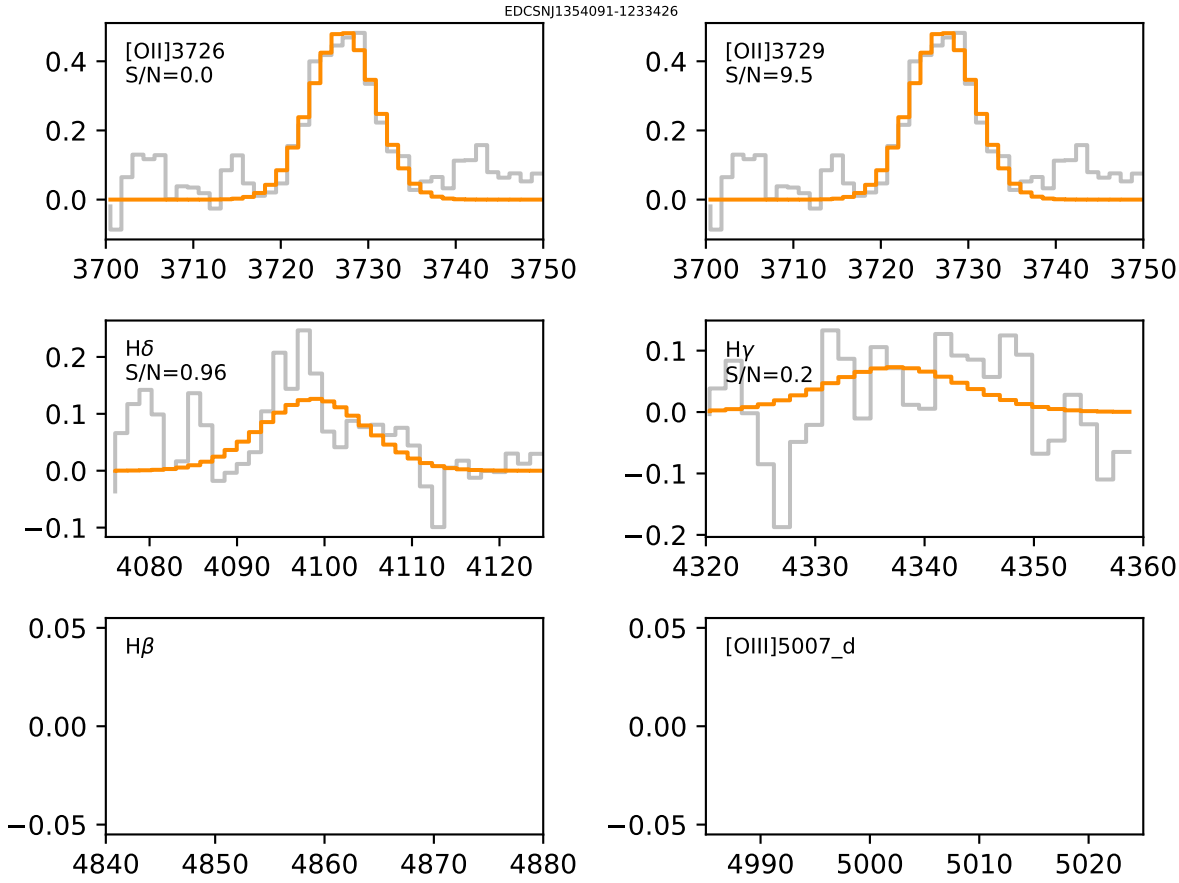
EDCSNJ1354091-1233426
[OII]3726
S/N=0.0
[OII]3729
S/N=9.5
Hδ
S/N=0.96
Hγ
S/N=0.2
Hβ
[OIII]5007_d

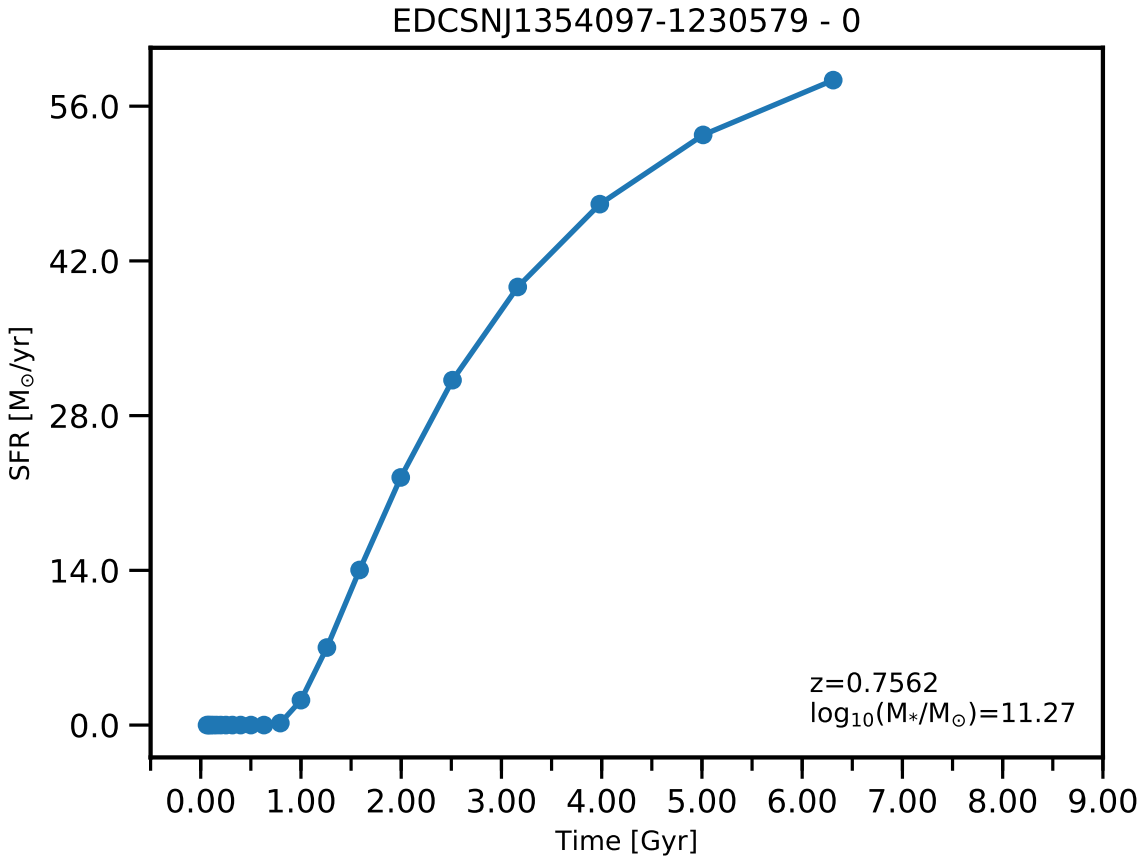
EDCSNJ1354097-1230579 - 0
56.0
42.0
28.0
14.0
0.0
SFR [M⊙/yr]
0.00
1.00
2.00
3.00
4.00
5.00
6.00
7.00
8.00
9.00
Time [Gyr]
z=0.7562
log10(M*/M⊙)=11.27

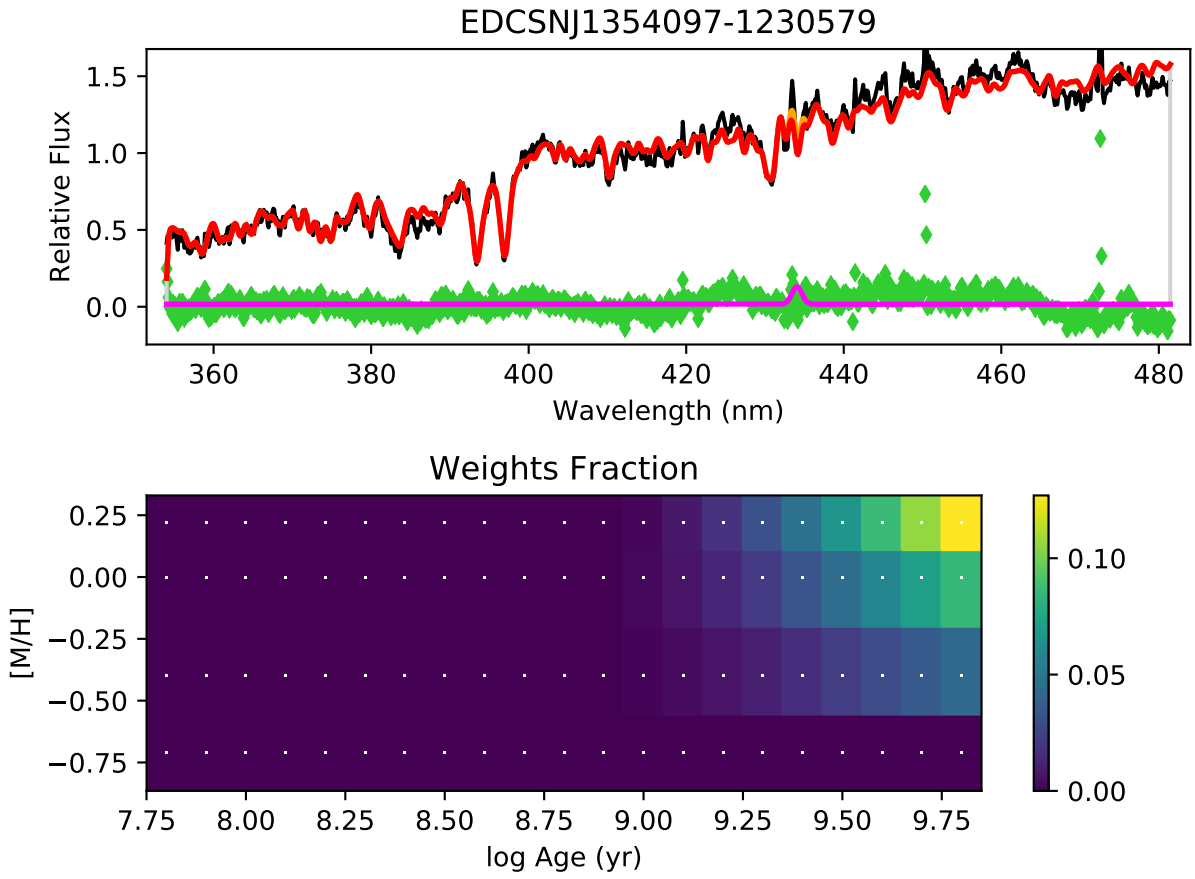
EDCSNJ1354097-1230579
Relative Flux
1.5
1.0
0.5
0.0
360
380
400
420
440
460
480
Wavelength (nm)
Weights Fraction
[M/H]
0.25
0.00
−0.25
−0.50
−0.75
7.75
8.00
8.25
8.50
8.75
9.00
9.25
9.50
9.75
log Age (yr)
0.10
0.05
0.00

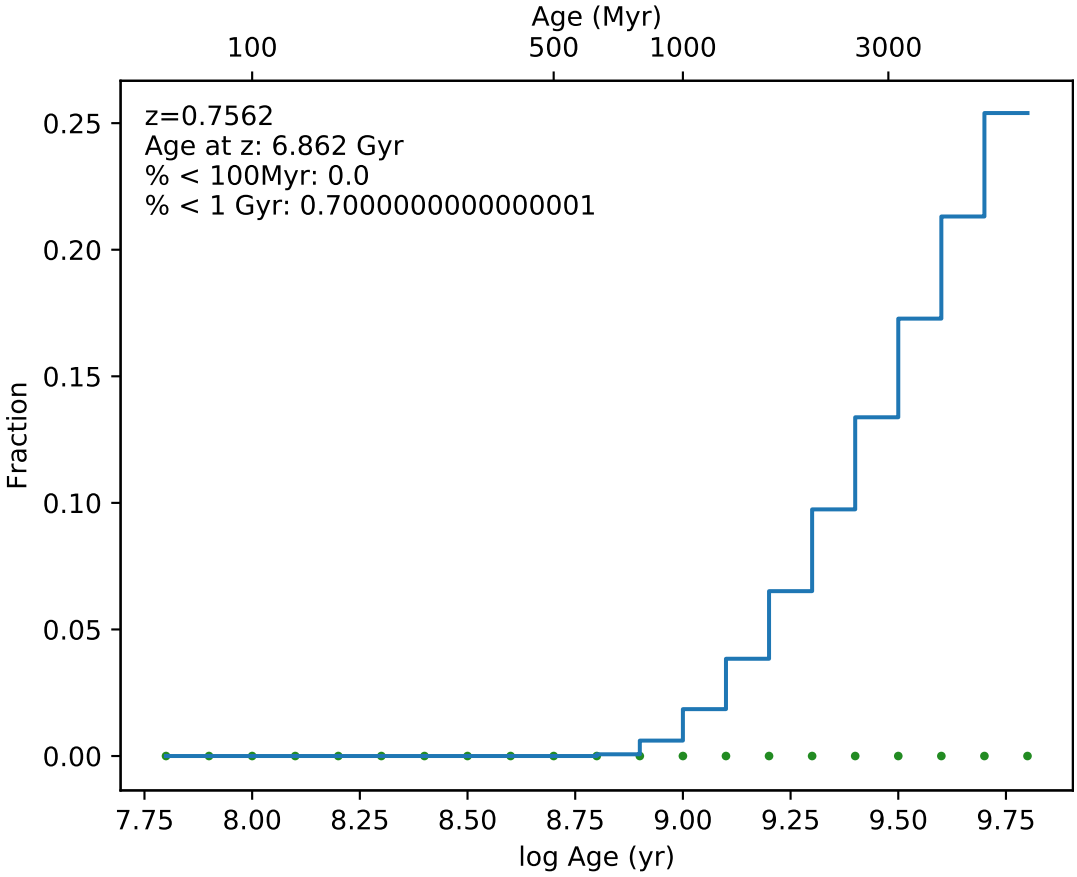
Age (Myr)
100
500
1000
3000
z=0.7562
Age at z: 6.862 Gyr
% < 100Myr: 0.0
% < 1 Gyr: 0.7000000000000001
Fraction
0.25
0.20
0.15
0.10
0.05
0.00
7.75
8.00
8.25
8.50
8.75
9.00
9.25
9.50
9.75
log Age (yr)

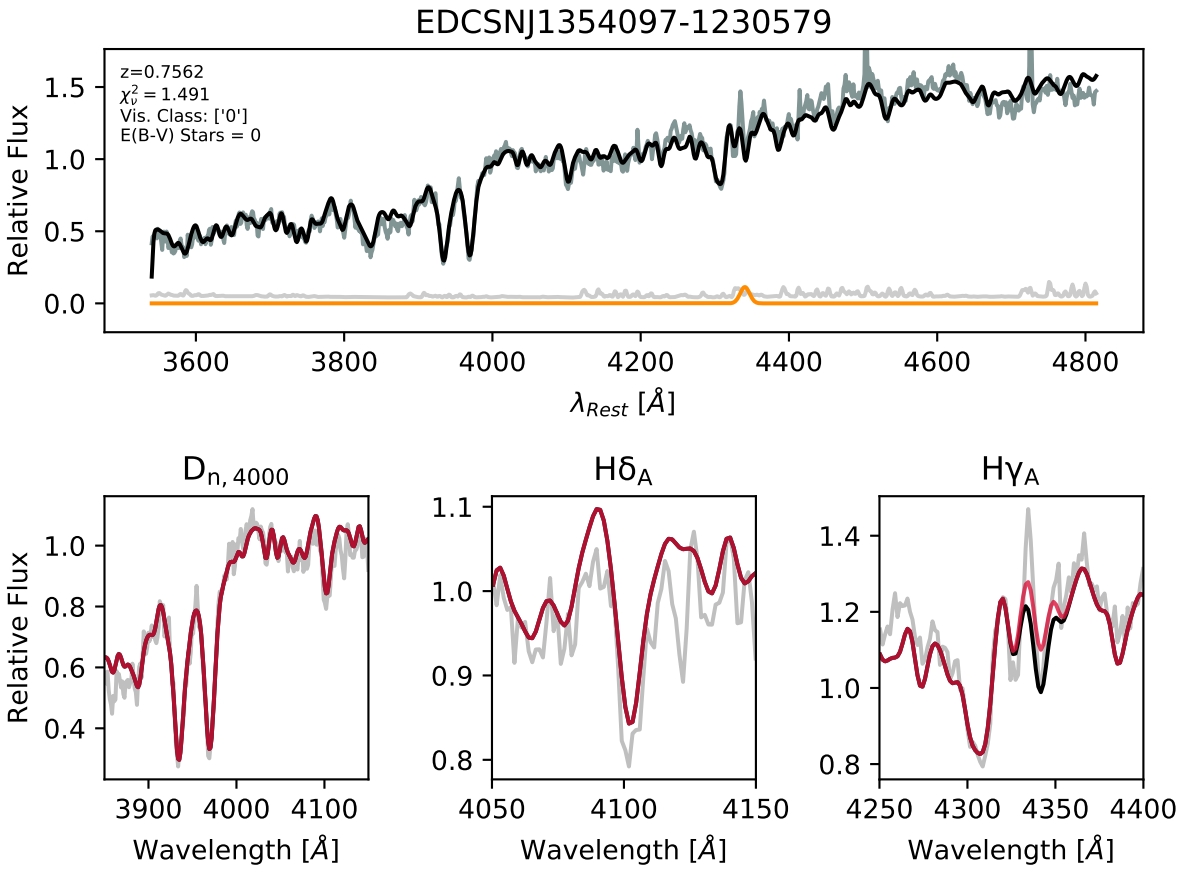
EDCSNJ1354097-1230579
z=0.7562
$\chi^2_\nu = 1.491$
Vis. Class: ['0']
E(B-V) Stars = 0
Relative Flux
λ_{Rest} [Å]
$D_{n,4000}$
$H\delta_A$
$H\gamma_A$
Wavelength [Å]

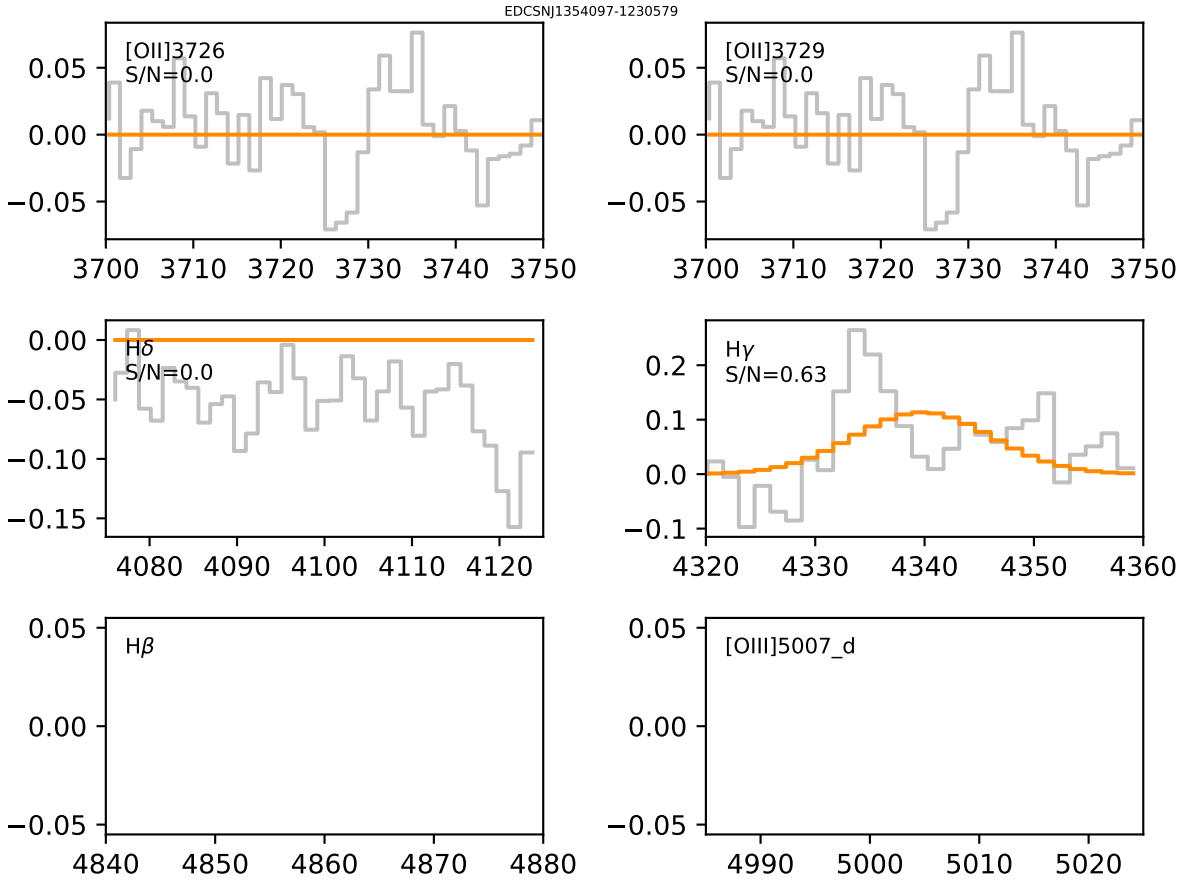
EDCSNJ1354097-1230579
[OII]3726
S/N=0.0
[OII]3729
S/N=0.0
Hδ
S/N=0.0
Hγ
S/N=0.63
Hβ
[OIII]5007_d

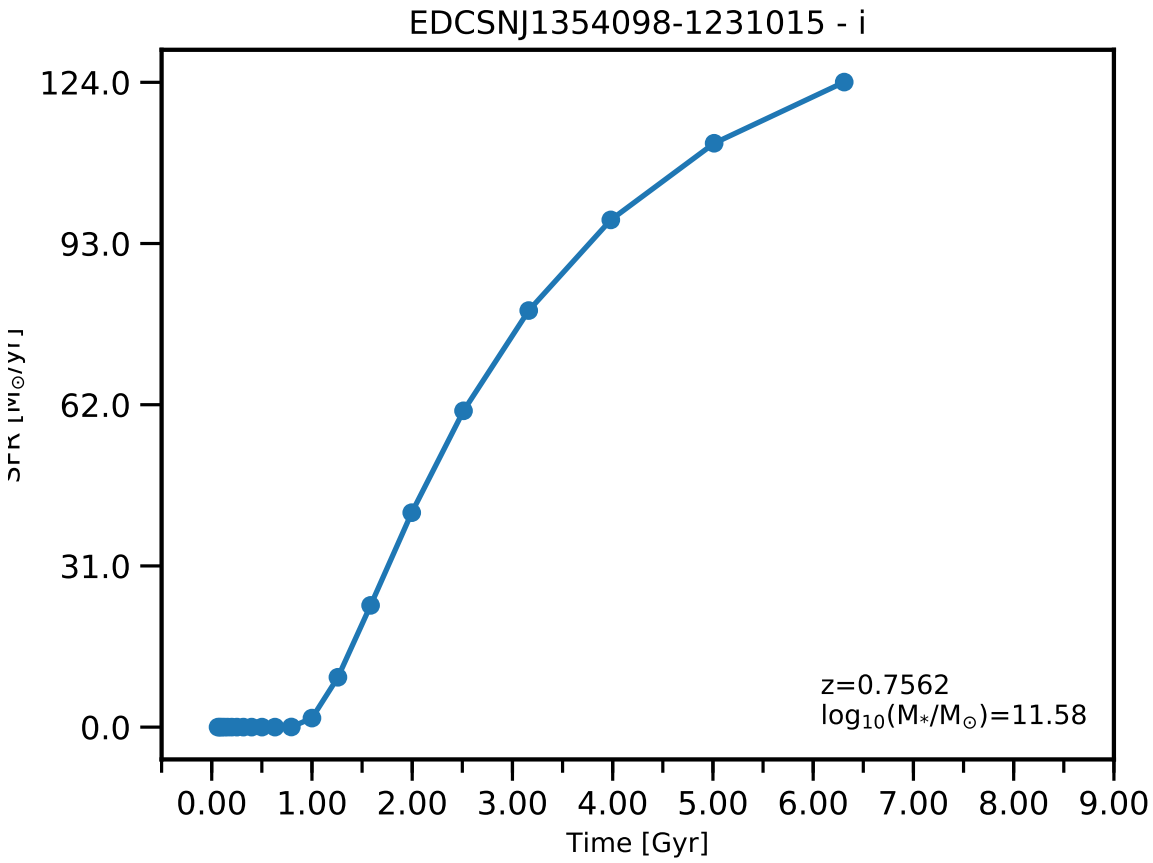
EDCSNJ1354098-1231015 - i
124.0
93.0
62.0
31.0
0.0
SFR [M⊙/yr]
0.00
1.00
2.00
3.00
4.00
5.00
6.00
7.00
8.00
9.00
Time [Gyr]
z=0.7562
log10(M*/M⊙)=11.58

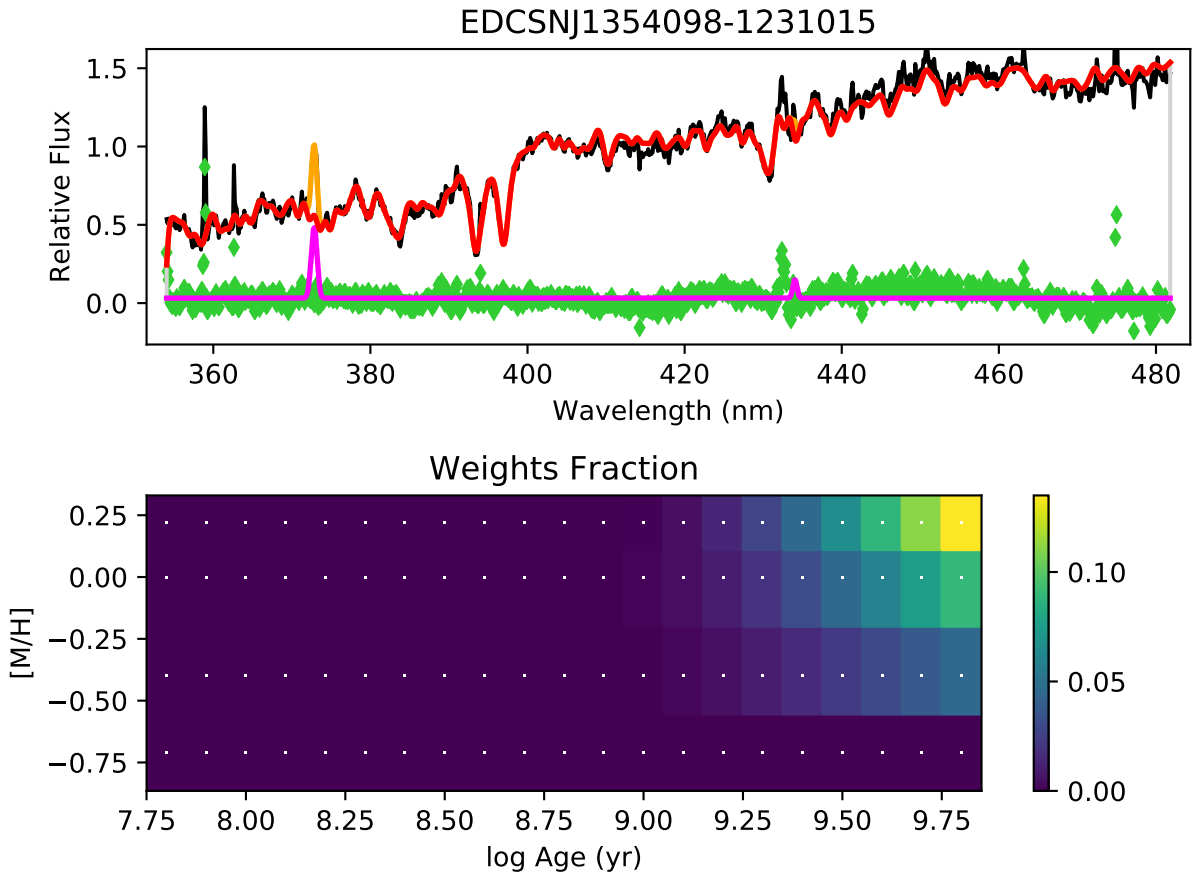
EDCSNJ1354098-1231015
Relative Flux
1.5
1.0
0.5
0.0
360
380
400
420
440
460
480
Wavelength (nm)
Weights Fraction
[M/H]
0.25
0.00
−0.25
−0.50
−0.75
7.75
8.00
8.25
8.50
8.75
9.00
9.25
9.50
9.75
log Age (yr)
0.10
0.05
0.00

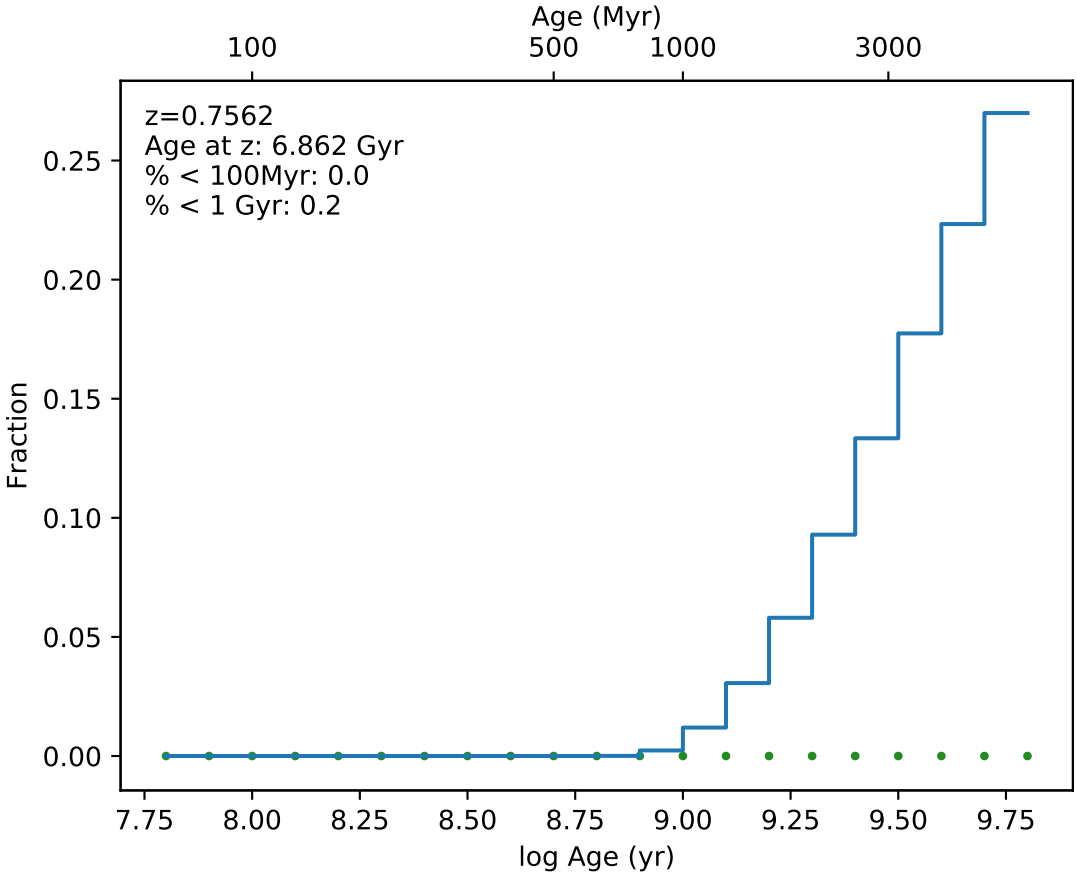
Age (Myr)
100
500
1000
3000
z=0.7562
Age at z: 6.862 Gyr
% < 100Myr: 0.0
% < 1 Gyr: 0.2
Fraction
0.25
0.20
0.15
0.10
0.05
0.00
7.75
8.00
8.25
8.50
8.75
9.00
9.25
9.50
9.75
log Age (yr)

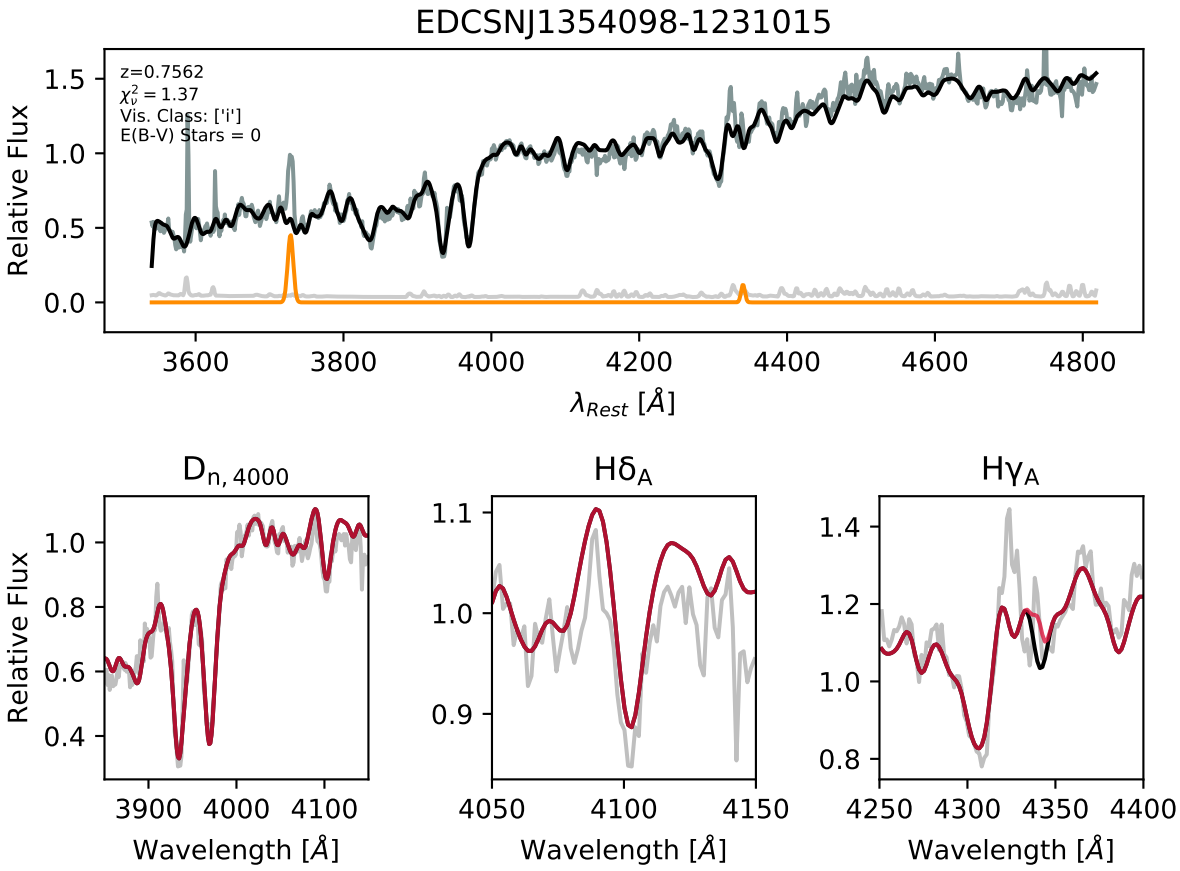
EDCSNJ1354098-1231015
z=0.7562
$\chi^2_\nu = 1.37$
Vis. Class: ['i']
E(B-V) Stars = 0
Relative Flux
λ_{Rest} [Å]
$D_{n,4000}$
$H\delta_A$
$H\gamma_A$
Wavelength [Å]

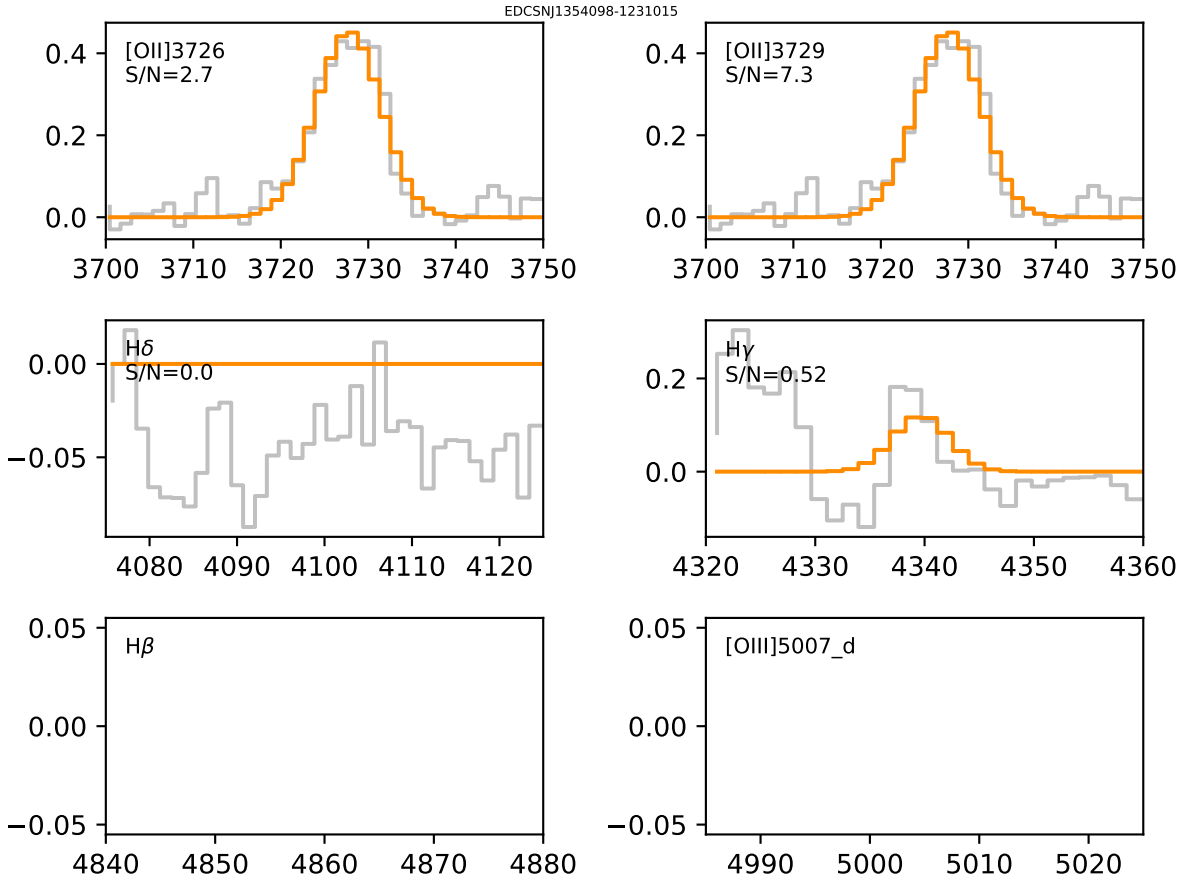
EDCSNJ1354098-1231015
[OII]3726
S/N=2.7
[OII]3729
S/N=7.3
Hδ
S/N=0.0
Hγ
S/N=0.52
Hβ
[OIII]5007_d

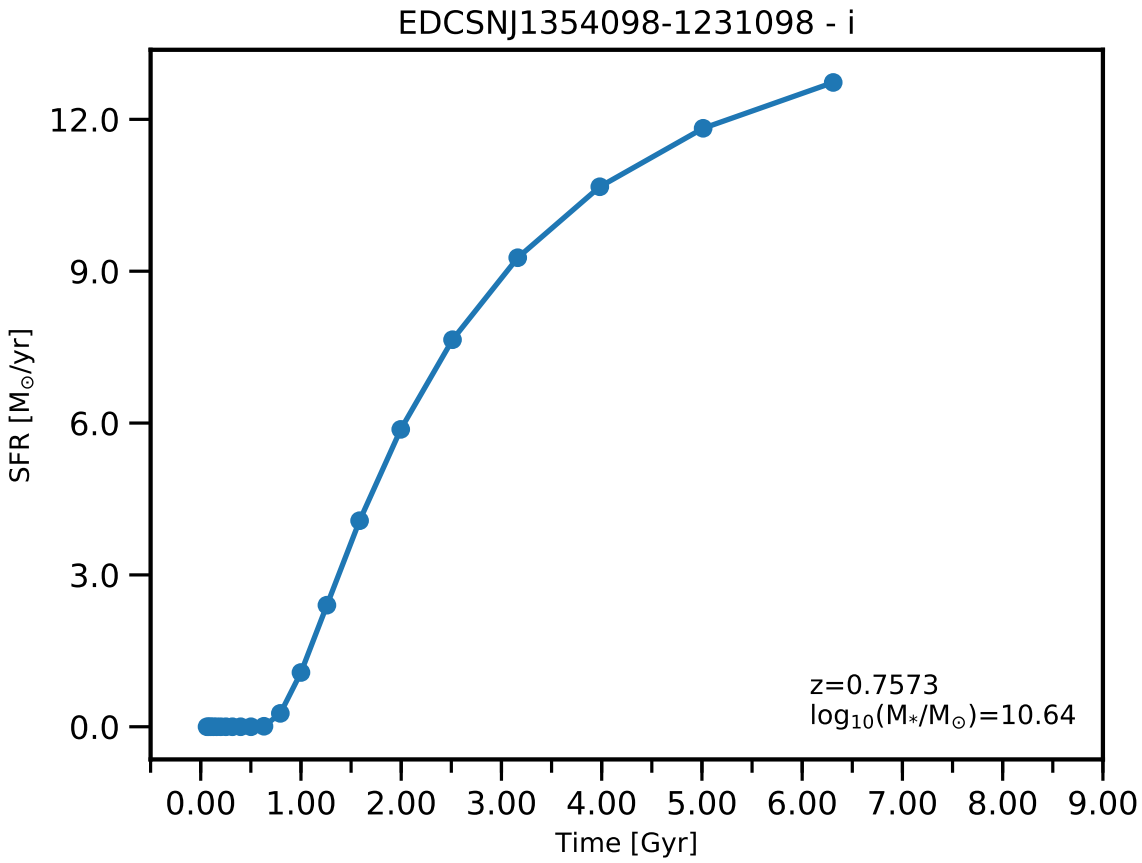
EDCSNJ1354098-1231098 - i
SFR [M⊙/yr]
12.0
9.0
6.0
3.0
0.0
0.00
1.00
2.00
3.00
4.00
5.00
6.00
7.00
8.00
9.00
Time [Gyr]
z=0.7573
log10(M*/M⊙)=10.64

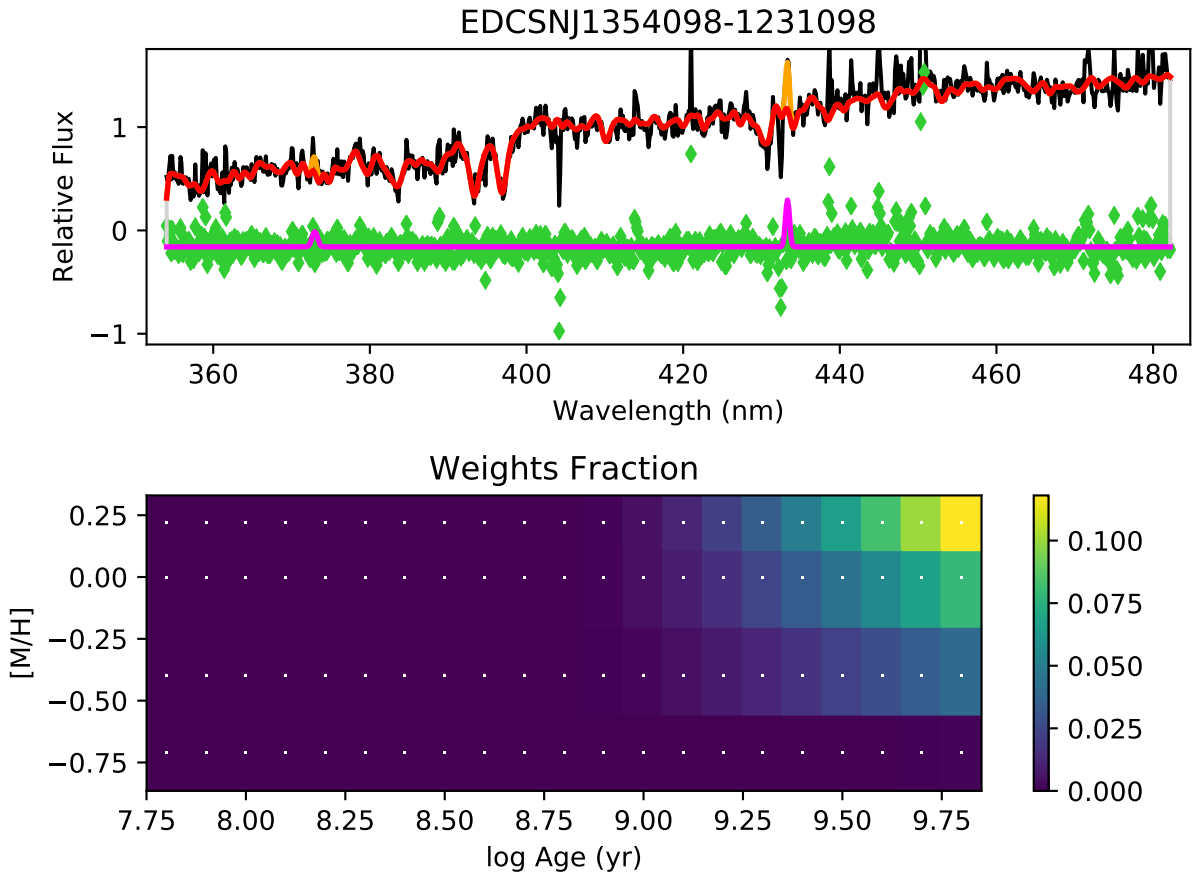
EDCSNJ1354098-1231098
Relative Flux
1
0
−1
360
380
400
420
440
460
480
Wavelength (nm)
Weights Fraction
[M/H]
0.25
0.00
−0.25
−0.50
−0.75
7.75
8.00
8.25
8.50
8.75
9.00
9.25
9.50
9.75
log Age (yr)
0.100
0.075
0.050
0.025
0.000

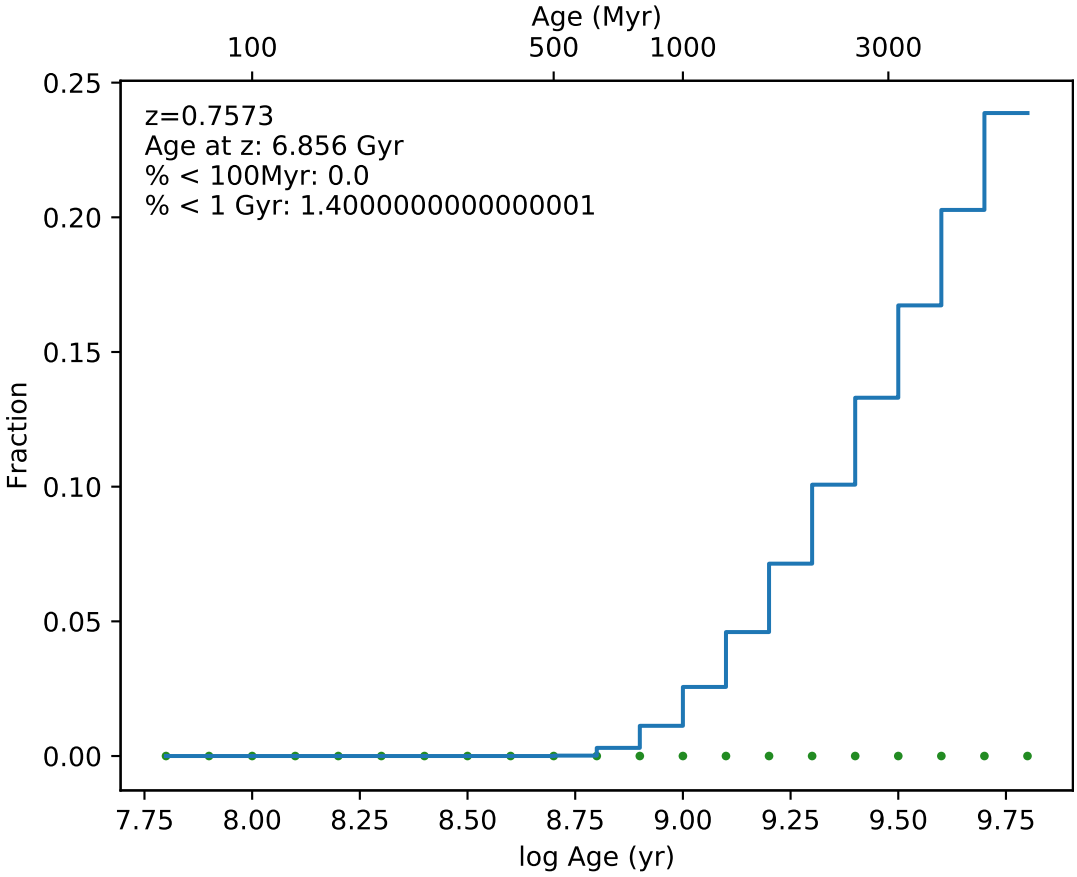
Age (Myr)
100
500
1000
3000
z=0.7573
Age at z: 6.856 Gyr
% < 100Myr: 0.0
% < 1 Gyr: 1.4000000000000001
Fraction
0.25
0.20
0.15
0.10
0.05
0.00
7.75
8.00
8.25
8.50
8.75
9.00
9.25
9.50
9.75
log Age (yr)

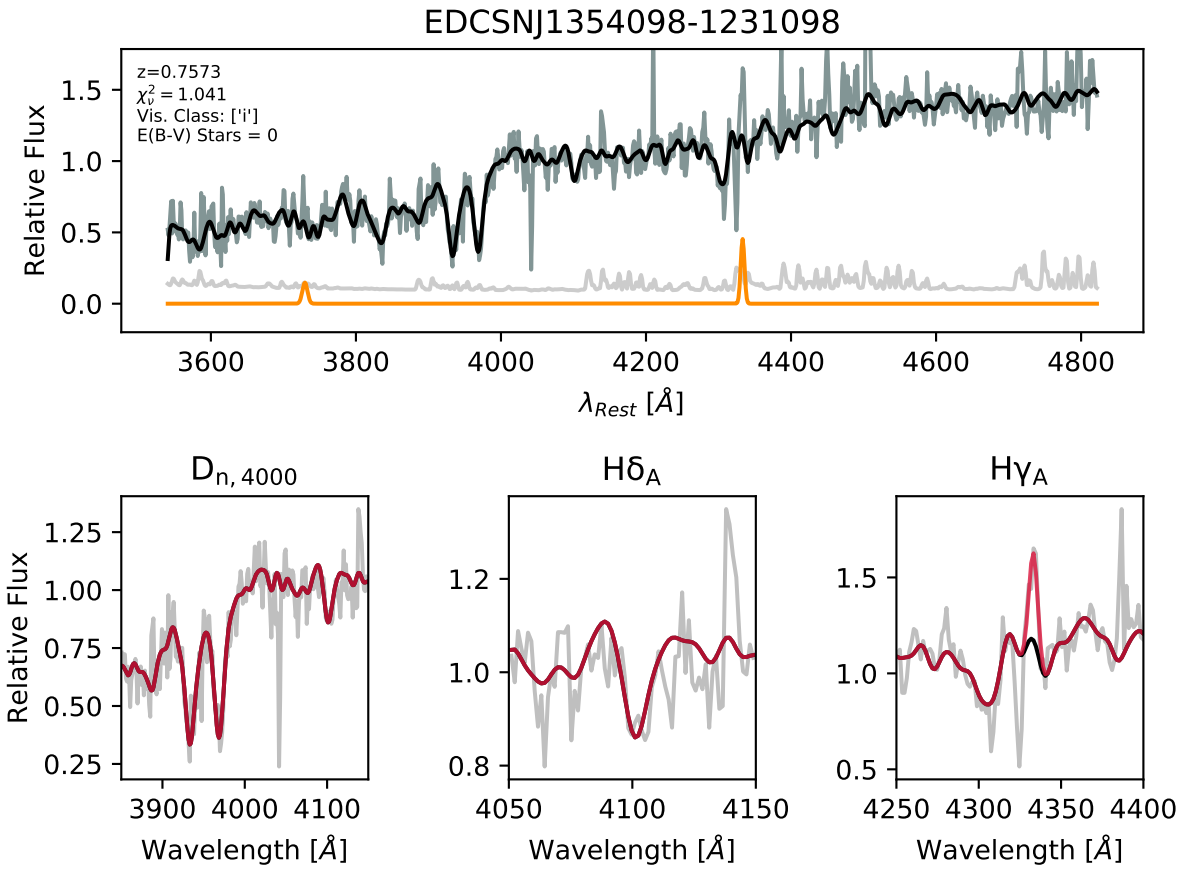
EDCSNJ1354098-1231098
z=0.7573
$\chi^2_\nu = 1.041$
Vis. Class: ['i']
E(B-V) Stars = 0
Relative Flux
λ_{Rest} [Å]
$D_{n,4000}$
$H\delta_A$
$H\gamma_A$
Wavelength [Å]

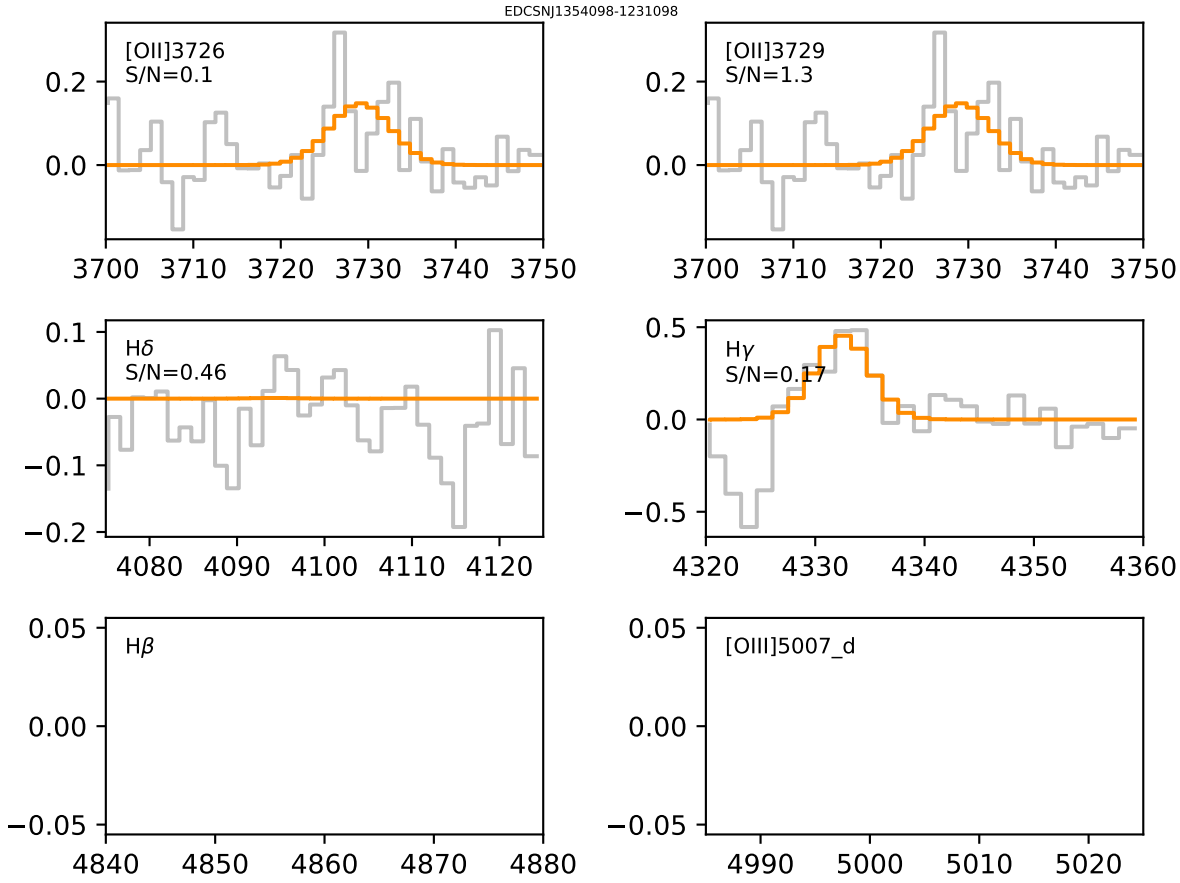
EDCSNJ1354098-1231098
[OII]3726
S/N=0.1
[OII]3729
S/N=1.3
Hδ
S/N=0.46
Hγ
S/N=0.17
Hβ
[OIII]5007_d

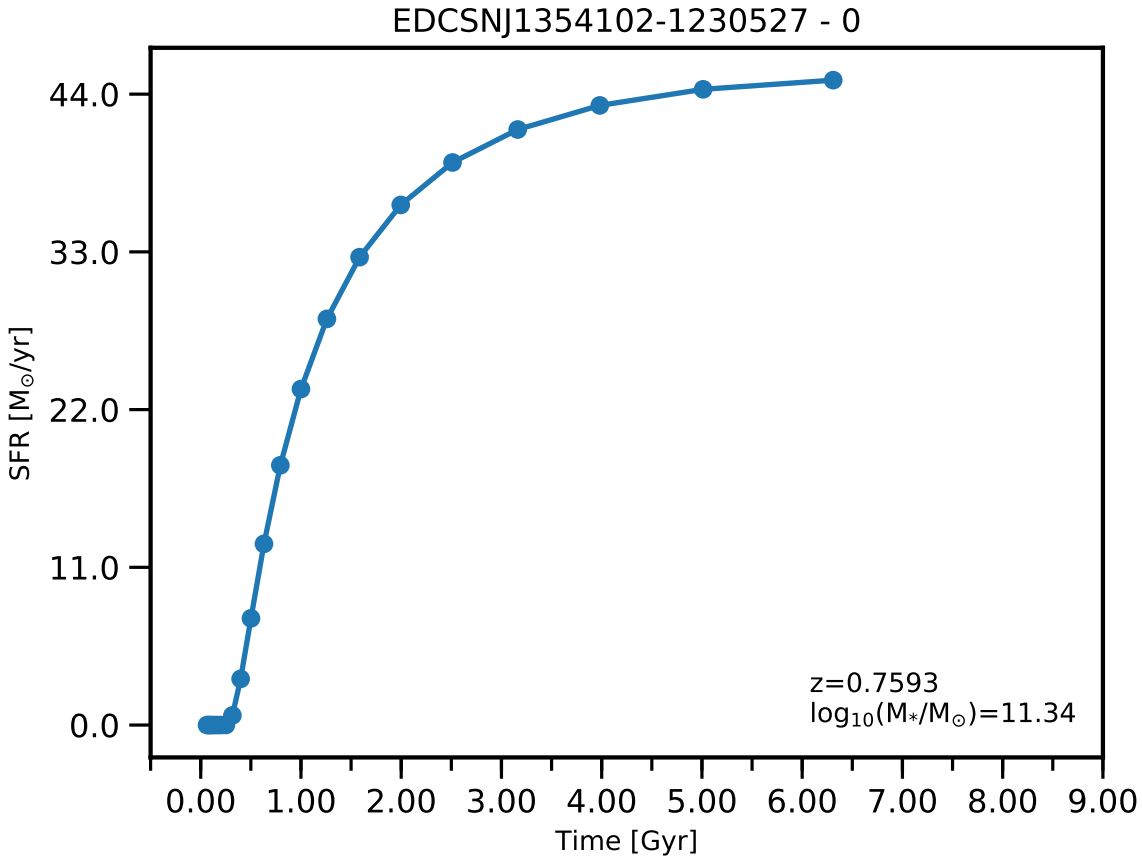
EDCSNJ1354102-1230527 - 0
SFR [M⊙/yr]
44.0
33.0
22.0
11.0
0.0
0.00
1.00
2.00
3.00
4.00
5.00
6.00
7.00
8.00
9.00
Time [Gyr]
z=0.7593
log10(M*/M⊙)=11.34

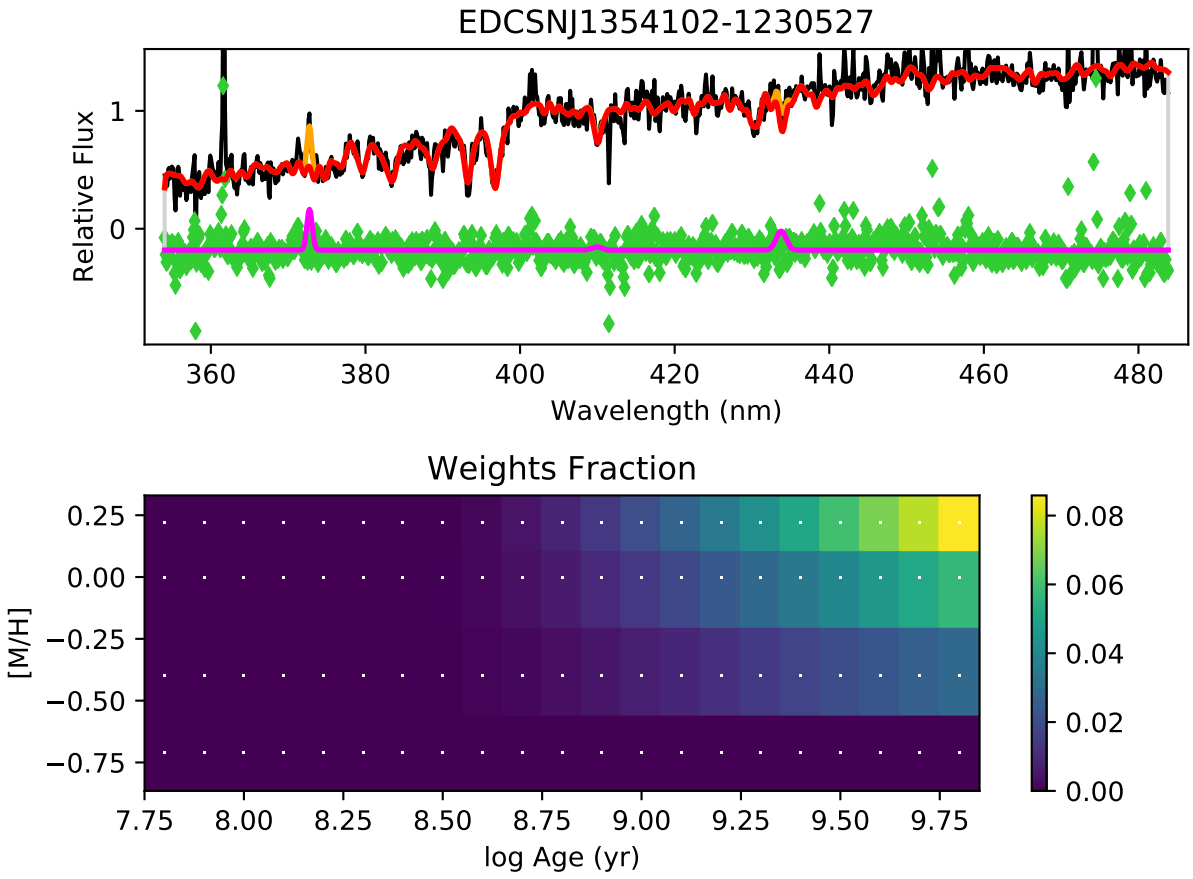
EDCSNJ1354102-1230527
Relative Flux
1
0
360
380
400
420
440
460
480
Wavelength (nm)
Weights Fraction
[M/H]
0.25
0.00
−0.25
−0.50
−0.75
7.75
8.00
8.25
8.50
8.75
9.00
9.25
9.50
9.75
log Age (yr)
0.08
0.06
0.04
0.02
0.00

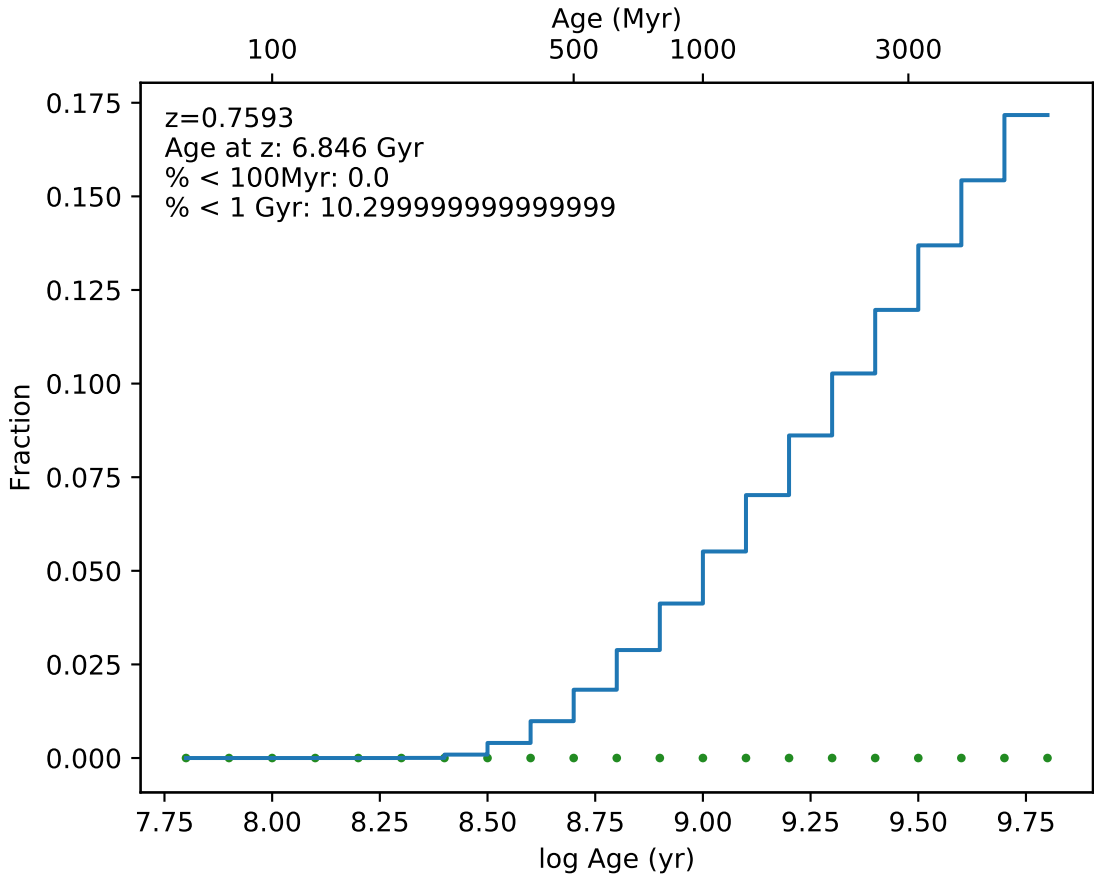
Age (Myr)
100
500
1000
3000
z=0.7593
Age at z: 6.846 Gyr
% < 100Myr: 0.0
% < 1 Gyr: 10.299999999999999
Fraction
0.175
0.150
0.125
0.100
0.075
0.050
0.025
0.000
7.75
8.00
8.25
8.50
8.75
9.00
9.25
9.50
9.75
log Age (yr)

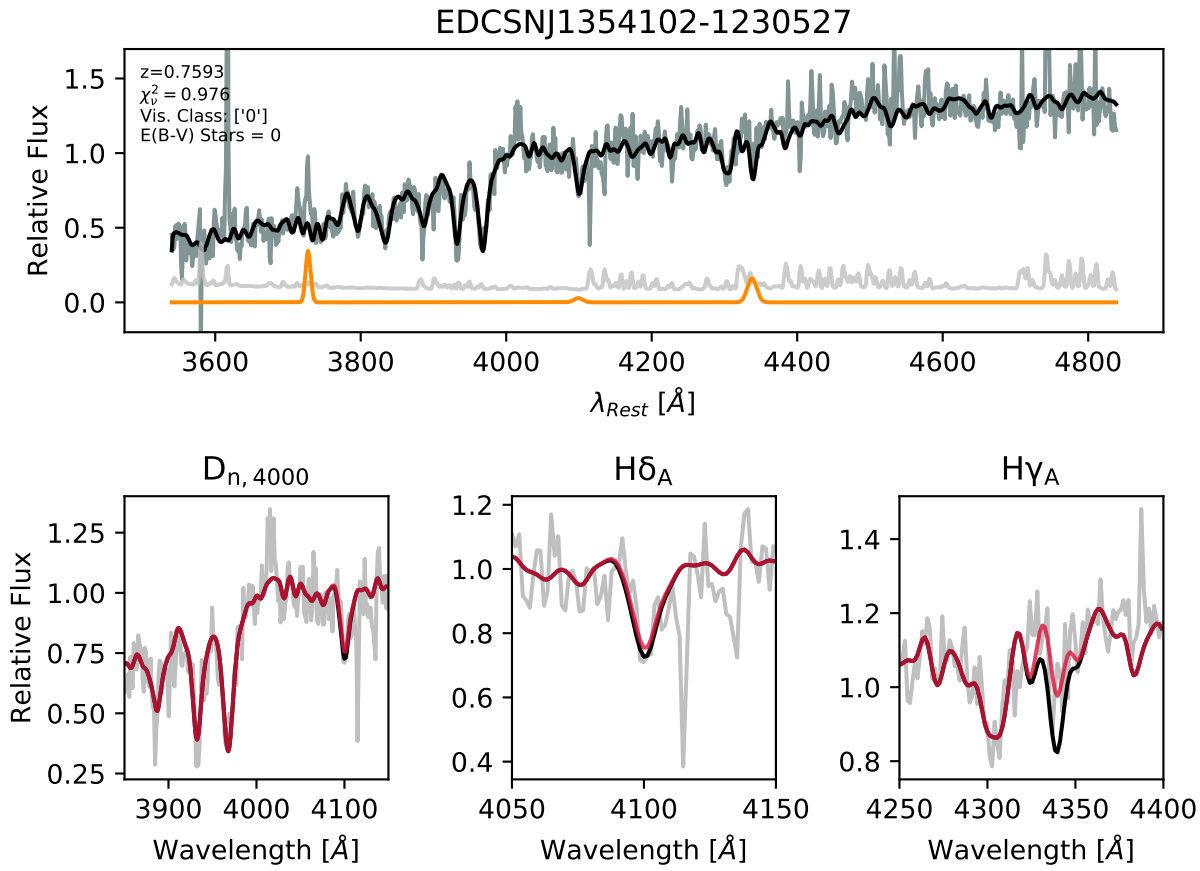
EDCSNJ1354102-1230527
z=0.7593
$\chi^2_\nu = 0.976$
Vis. Class: ['0']
E(B-V) Stars = 0
Relative Flux
λ_{Rest} [Å]
$D_{n,4000}$
$H\delta_A$
$H\gamma_A$
Wavelength [Å]

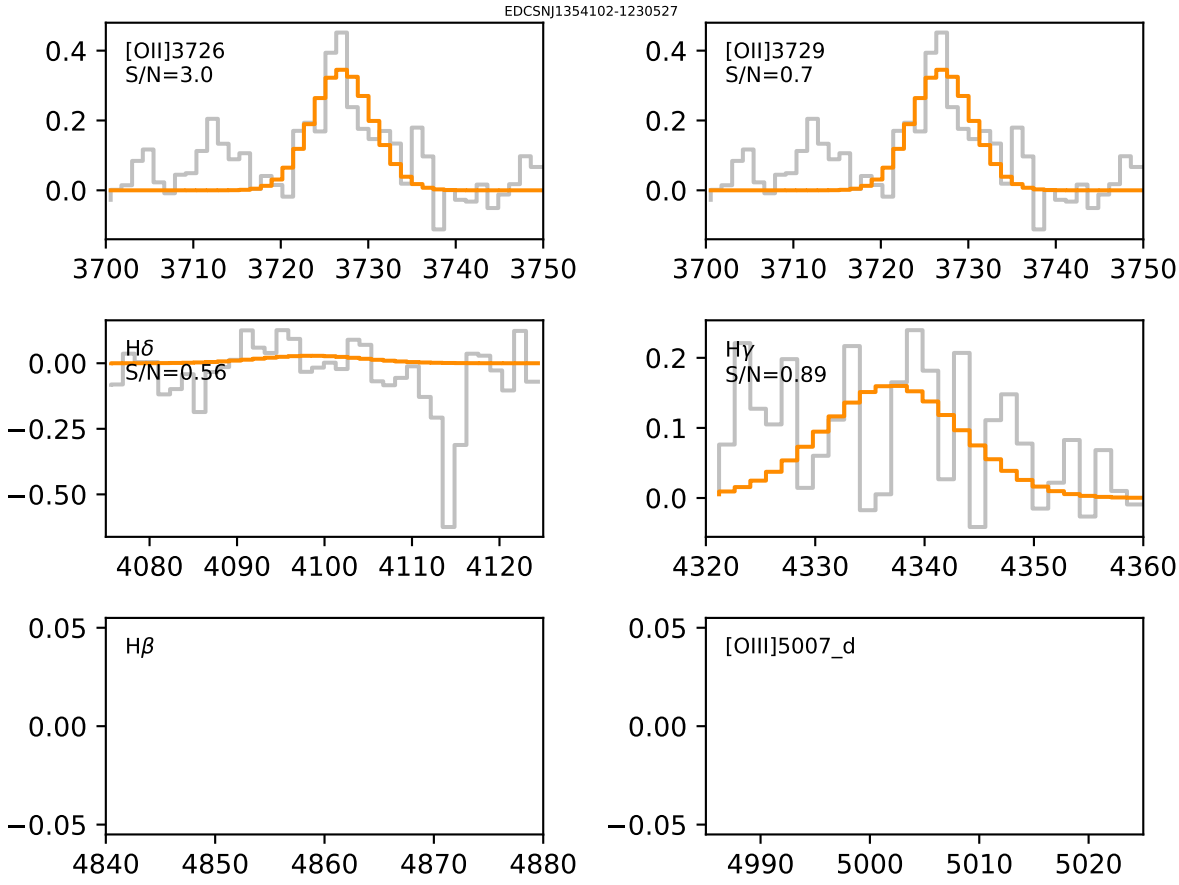
EDCSNJ1354102-1230527
[OII]3726
S/N=3.0
[OII]3729
S/N=0.7
Hδ
S/N=0.56
Hγ
S/N=0.89
Hβ
[OIII]5007_d

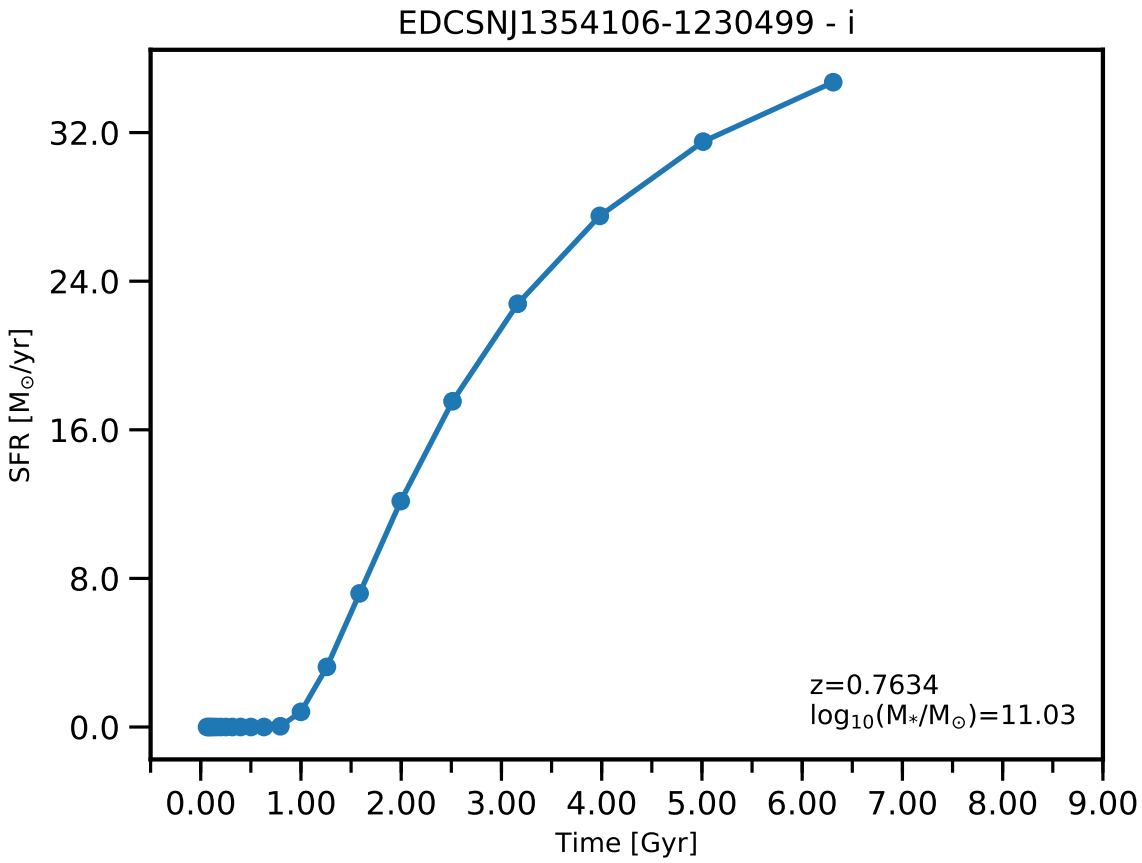
EDCSNJ1354106-1230499 - i
SFR [M⊙/yr]
32.0
24.0
16.0
8.0
0.0
0.00
1.00
2.00
3.00
4.00
5.00
6.00
7.00
8.00
9.00
Time [Gyr]
z=0.7634
log10(M*/M⊙)=11.03

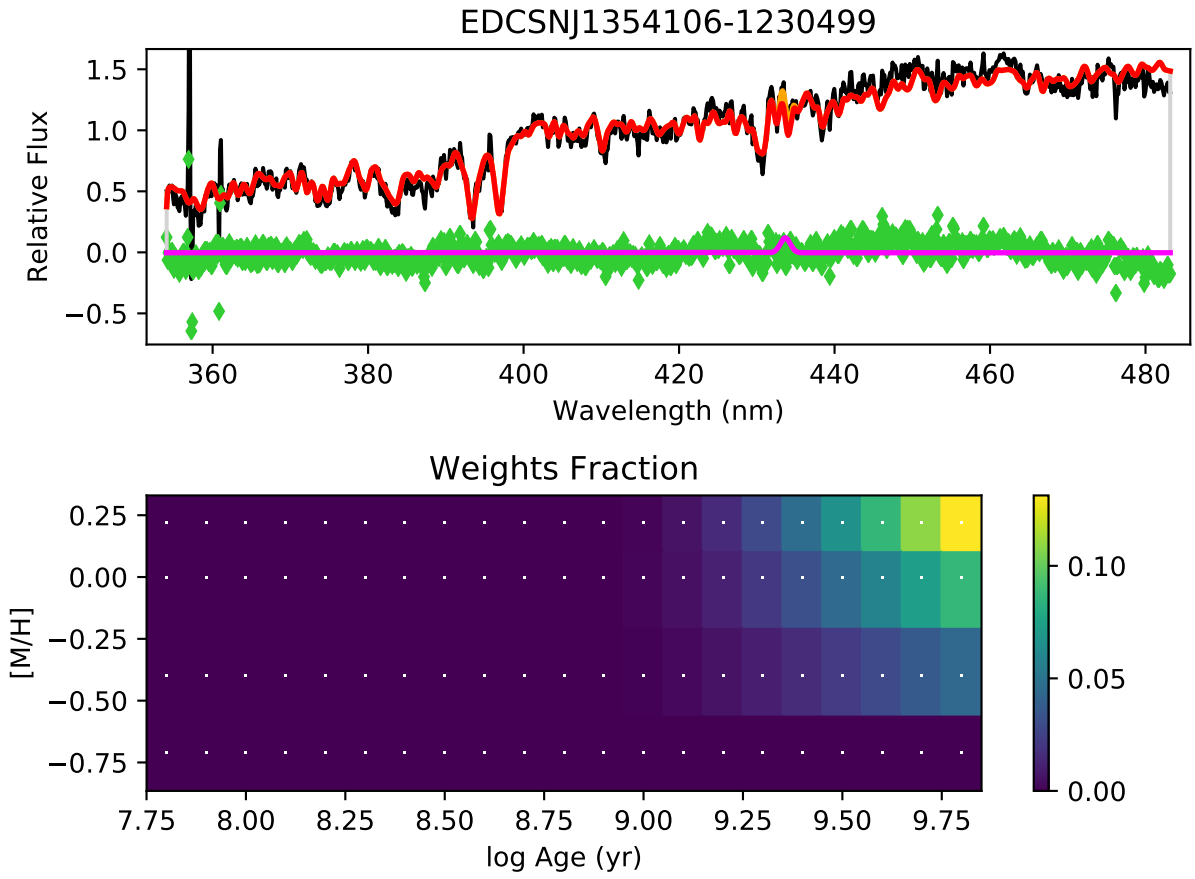
EDCSNJ1354106-1230499
Relative Flux
1.5
1.0
0.5
0.0
−0.5
360
380
400
420
440
460
480
Wavelength (nm)
Weights Fraction
[M/H]
0.25
0.00
−0.25
−0.50
−0.75
7.75
8.00
8.25
8.50
8.75
9.00
9.25
9.50
9.75
log Age (yr)
0.10
0.05
0.00

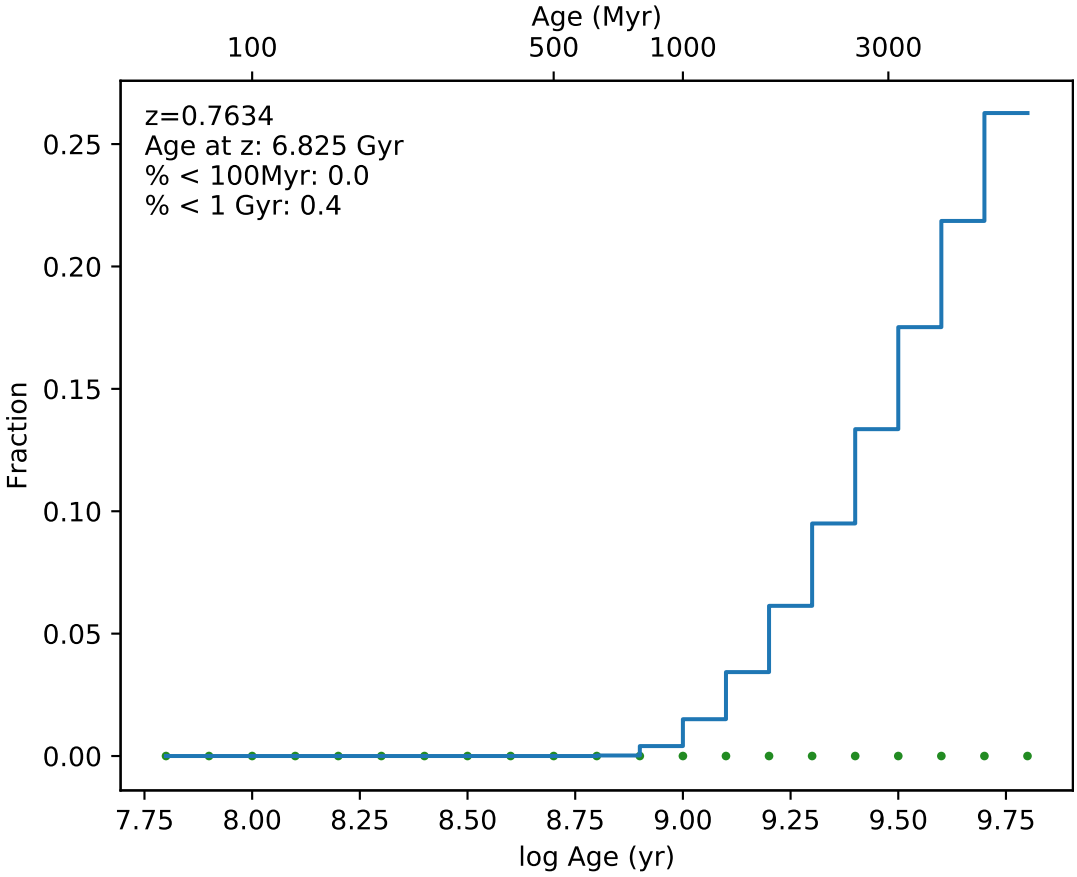
Age (Myr)
100
500
1000
3000
z=0.7634
Age at z: 6.825 Gyr
% < 100Myr: 0.0
% < 1 Gyr: 0.4
Fraction
0.25
0.20
0.15
0.10
0.05
0.00
7.75
8.00
8.25
8.50
8.75
9.00
9.25
9.50
9.75
log Age (yr)

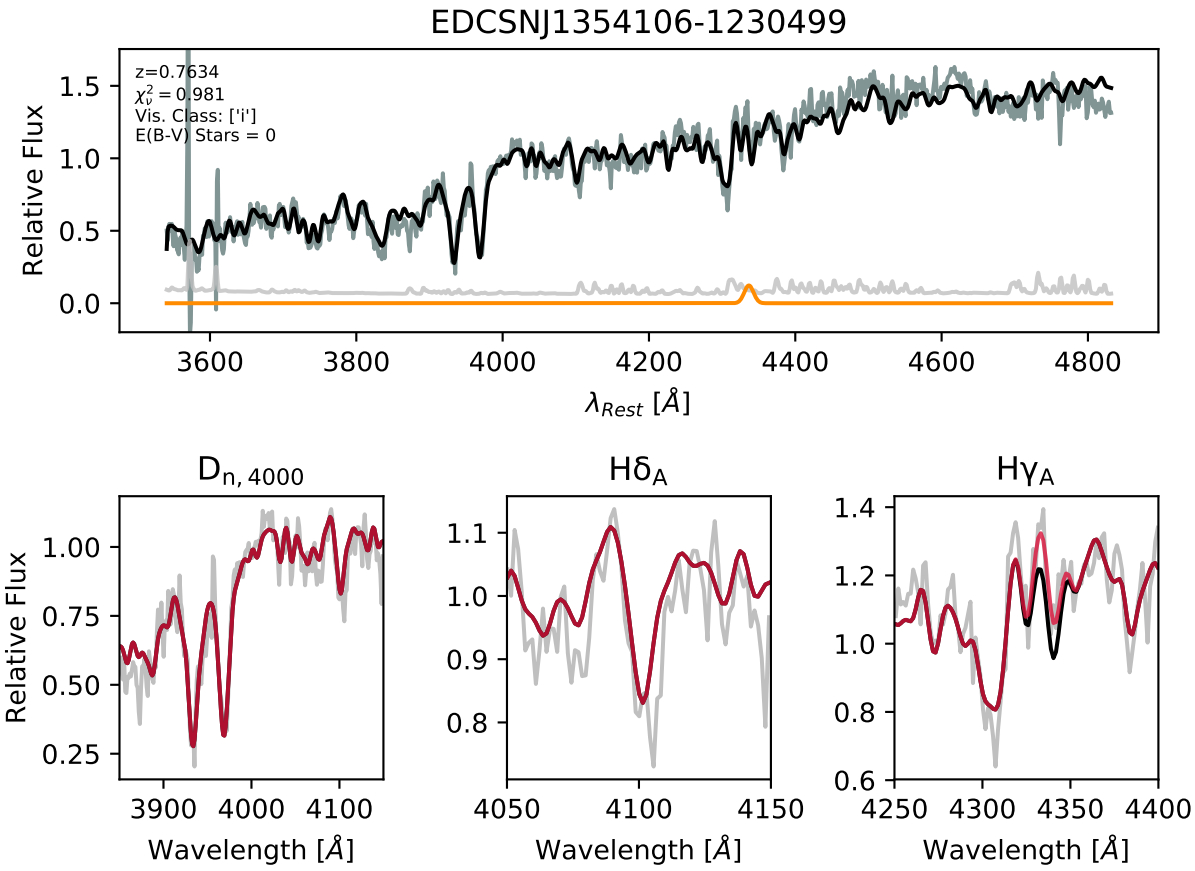
EDCSNJ1354106-1230499
z=0.7634
$\chi^2_\nu = 0.981$
Vis. Class: ['i']
E(B-V) Stars = 0
Relative Flux
λ_{Rest} [Å]
$D_{n,4000}$
$H\delta_A$
$H\gamma_A$
Wavelength [Å]

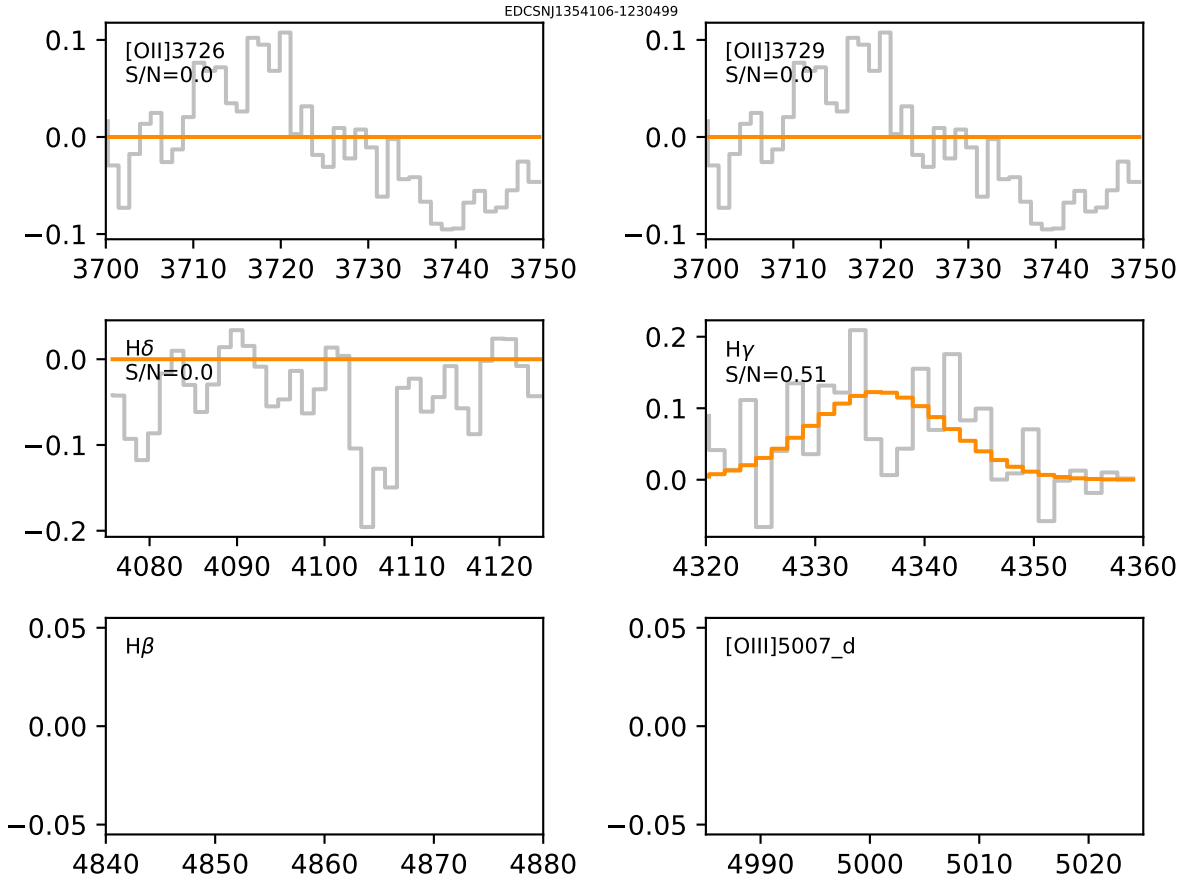
EDCSNJ1354106-1230499
[OII]3726
S/N=0.0
[OII]3729
S/N=0.0
Hδ
S/N=0.0
Hγ
S/N=0.51
Hβ
[OIII]5007_d

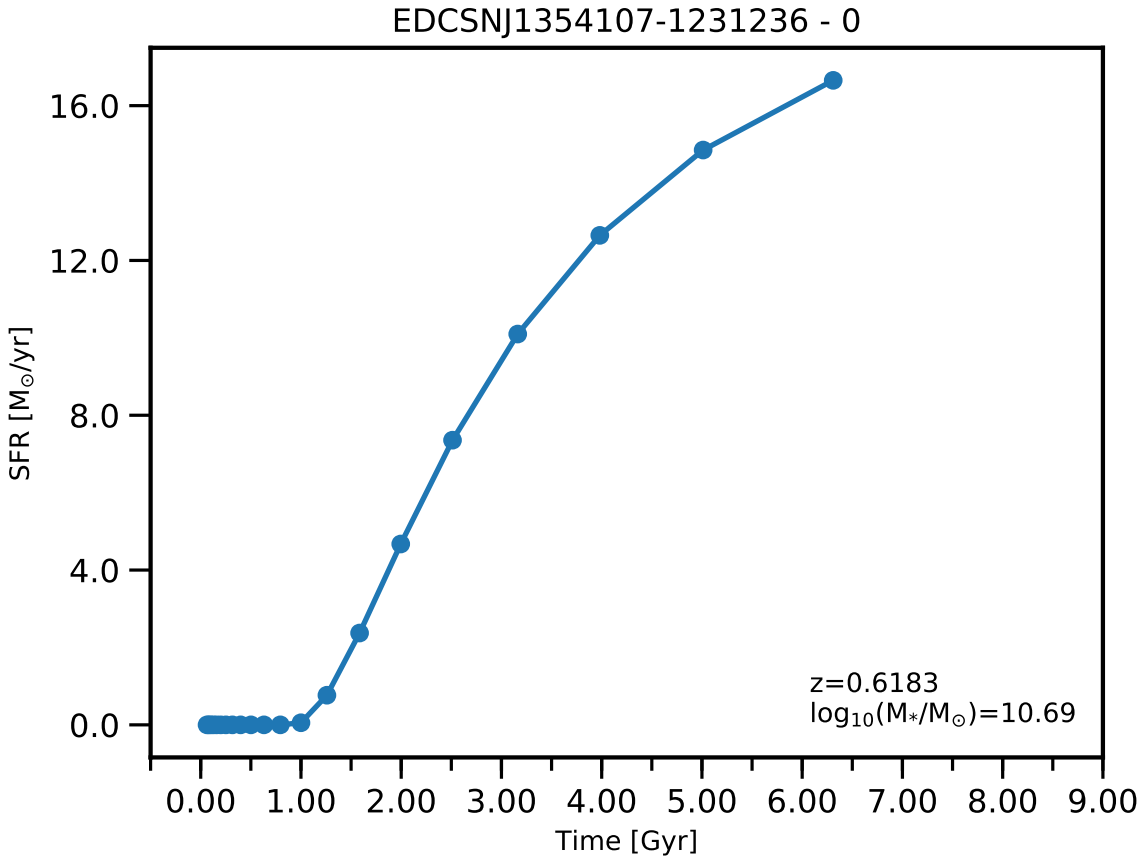
EDCSNJ1354107-1231236 - 0
16.0
12.0
8.0
4.0
0.0
SFR [M⊙/yr]
0.00
1.00
2.00
3.00
4.00
5.00
6.00
7.00
8.00
9.00
Time [Gyr]
z=0.6183
log10(M*/M⊙)=10.69

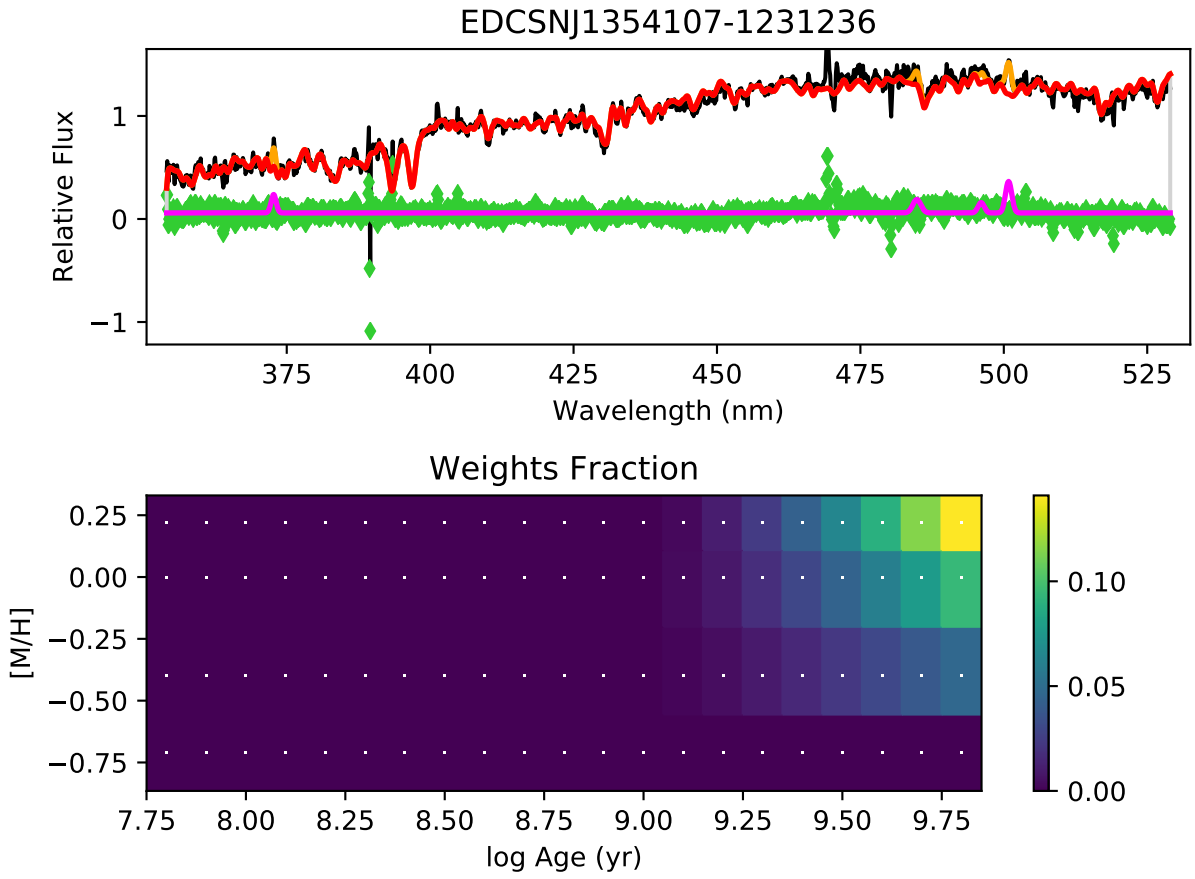
EDCSNJ1354107-1231236
Relative Flux
1
0
−1
375
400
425
450
475
500
525
Wavelength (nm)
Weights Fraction
[M/H]
0.25
0.00
−0.25
−0.50
−0.75
7.75
8.00
8.25
8.50
8.75
9.00
9.25
9.50
9.75
log Age (yr)
0.10
0.05
0.00

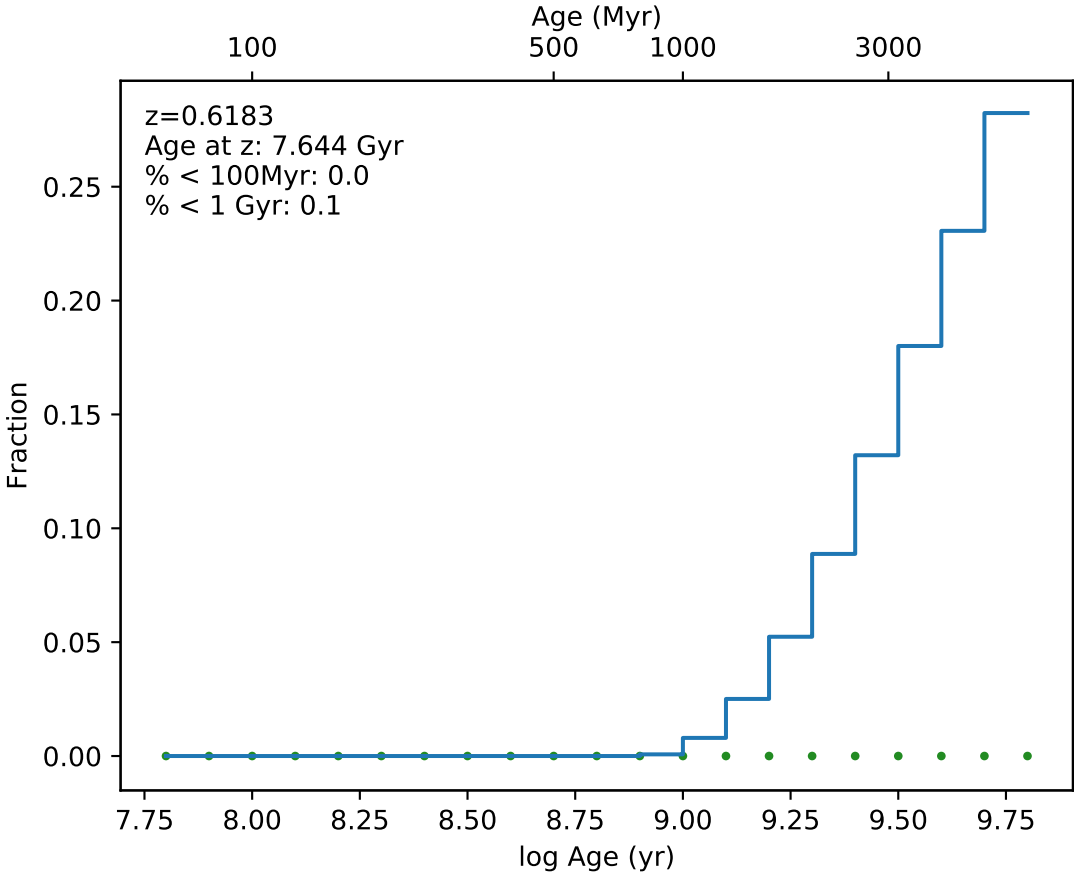
Age (Myr)
100
500
1000
3000
z=0.6183
Age at z: 7.644 Gyr
% < 100Myr: 0.0
% < 1 Gyr: 0.1
Fraction
0.25
0.20
0.15
0.10
0.05
0.00
7.75
8.00
8.25
8.50
8.75
9.00
9.25
9.50
9.75
log Age (yr)

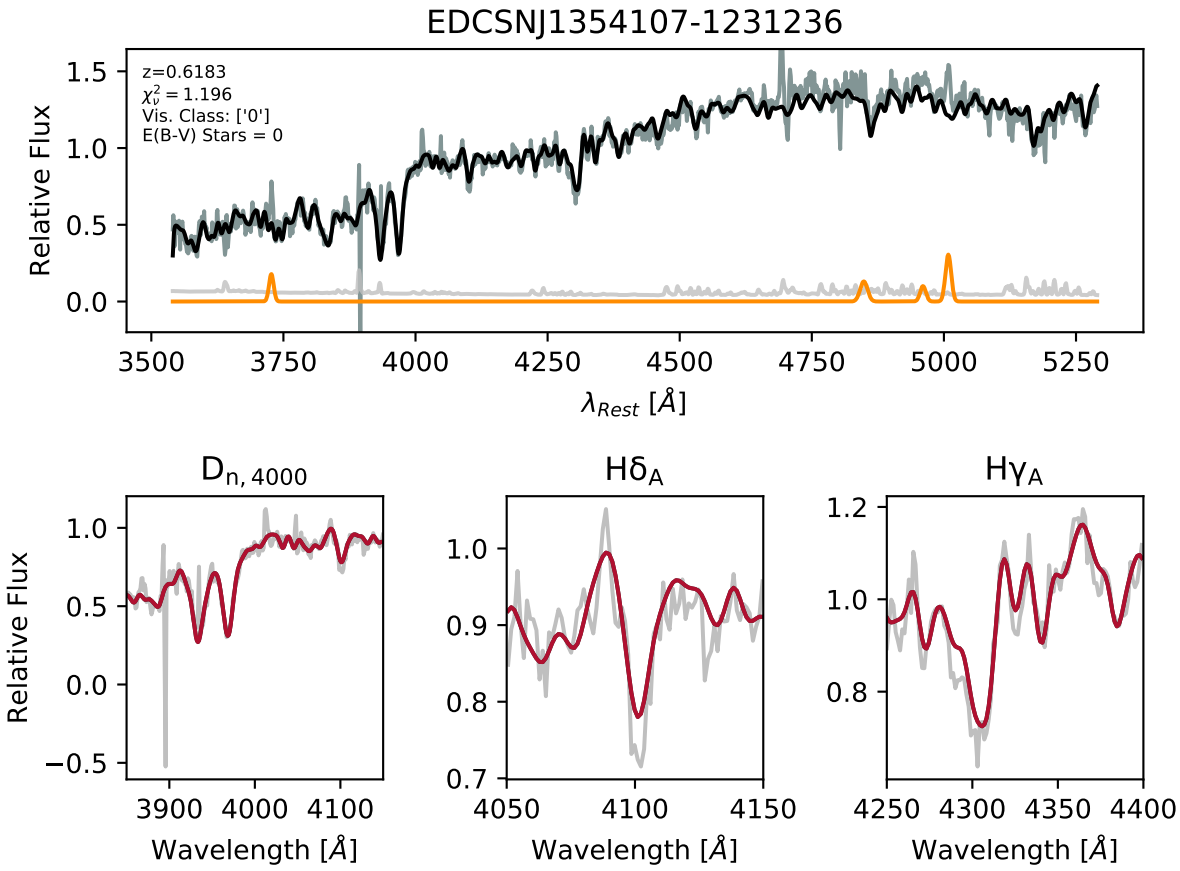
EDCSNJ1354107-1231236
z=0.6183
$\chi^2_\nu = 1.196$
Vis. Class: ['0']
E(B-V) Stars = 0
Relative Flux
λ_{Rest} [Å]
$D_{n,4000}$
$H\delta_A$
$H\gamma_A$
Wavelength [Å]

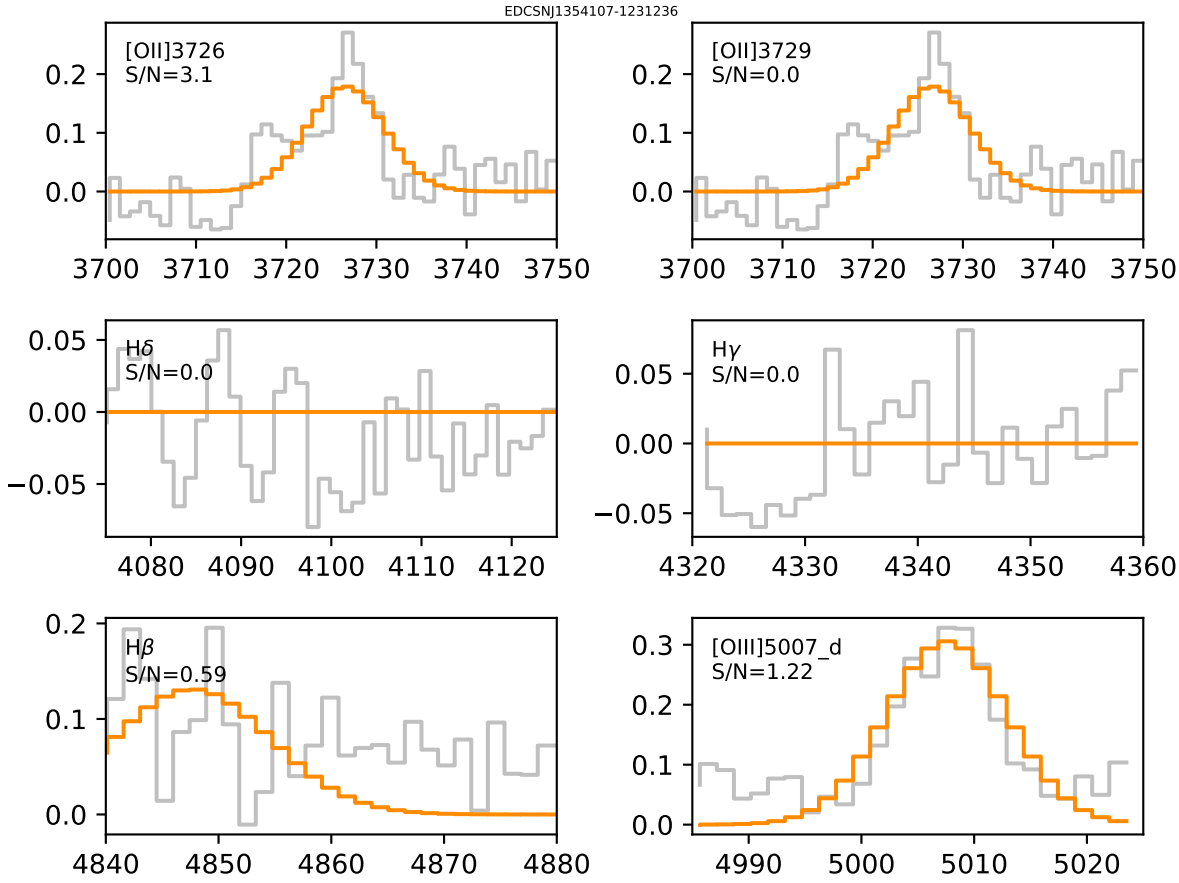
EDCSNJ1354107-1231236
[OII]3726
S/N=3.1
[OII]3729
S/N=0.0
Hδ
S/N=0.0
Hγ
S/N=0.0
Hβ
S/N=0.59
[OIII]5007_d
S/N=1.22

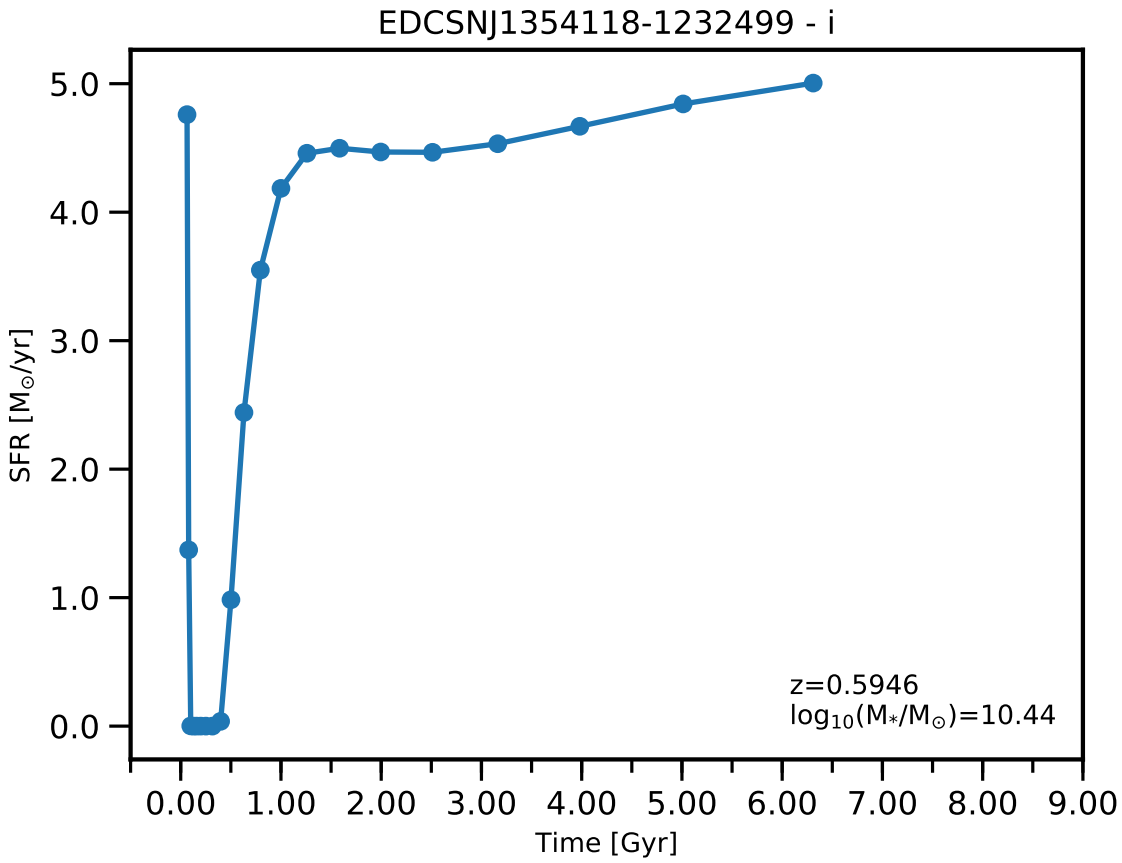
EDCSNJ1354118-1232499 - i
SFR [M⊙/yr]
Time [Gyr]
z=0.5946
log10(M*/M⊙)=10.44
0.0
1.0
2.0
3.0
4.0
5.0
0.00
1.00
2.00
3.00
4.00
5.00
6.00
7.00
8.00
9.00

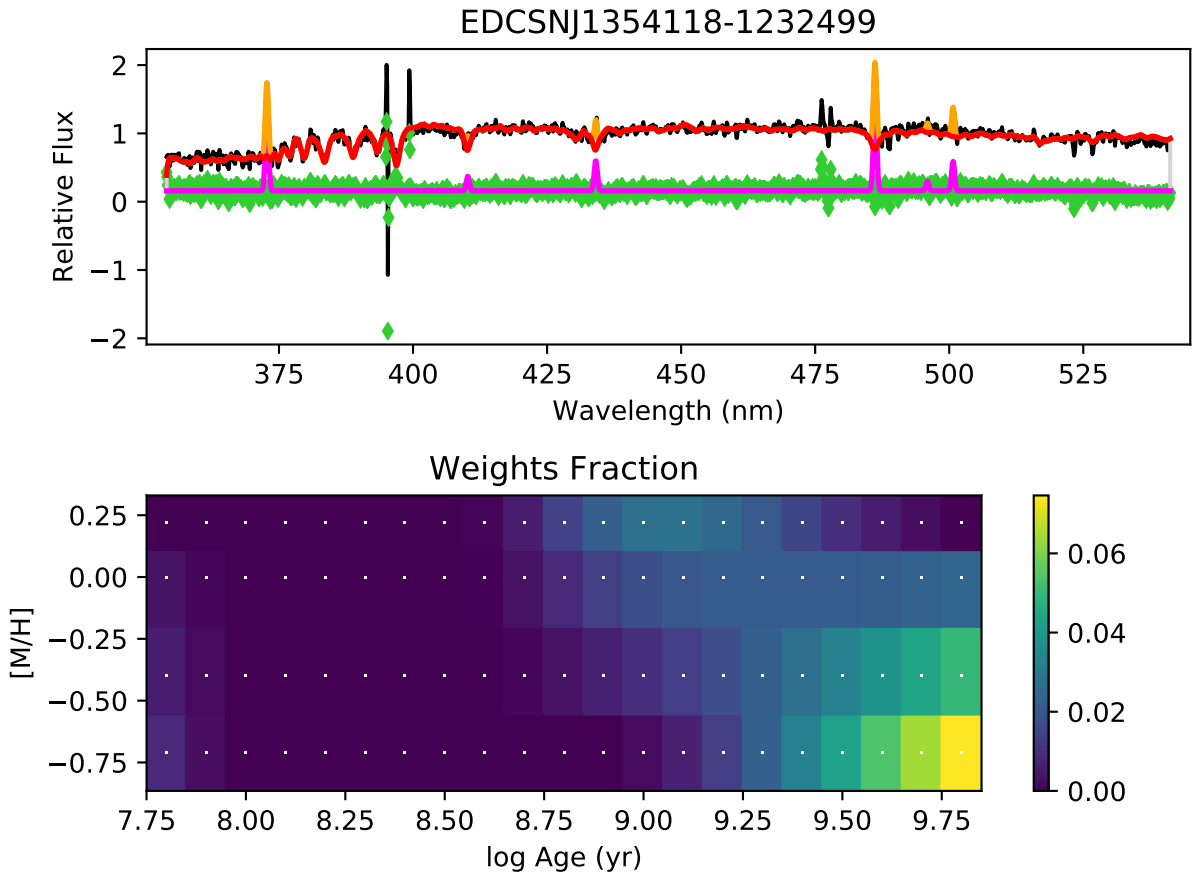
EDCSNJ1354118-1232499
Relative Flux
2
1
0
−1
−2
375
400
425
450
475
500
525
Wavelength (nm)
Weights Fraction
[M/H]
0.25
0.00
−0.25
−0.50
−0.75
7.75
8.00
8.25
8.50
8.75
9.00
9.25
9.50
9.75
log Age (yr)
0.06
0.04
0.02
0.00

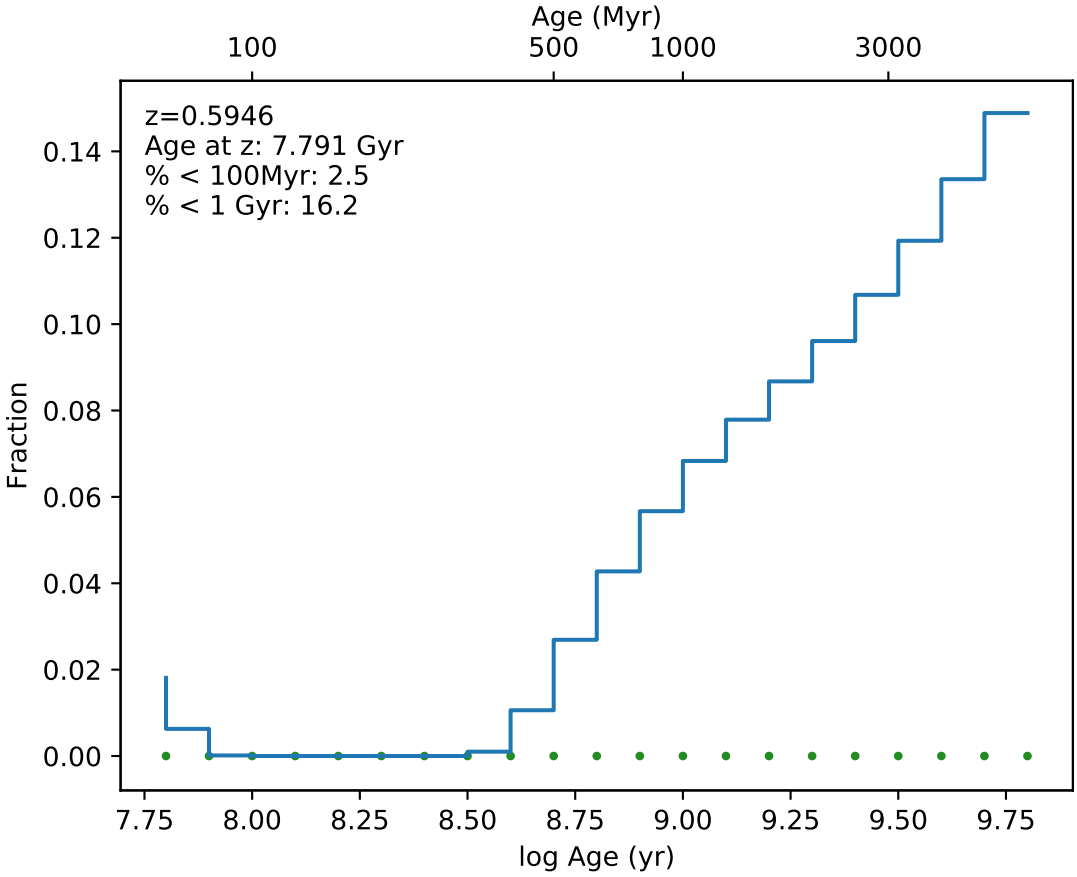
Age (Myr)
100
500
1000
3000
z=0.5946
Age at z: 7.791 Gyr
% < 100Myr: 2.5
% < 1 Gyr: 16.2
Fraction
0.14
0.12
0.10
0.08
0.06
0.04
0.02
0.00
7.75
8.00
8.25
8.50
8.75
9.00
9.25
9.50
9.75
log Age (yr)

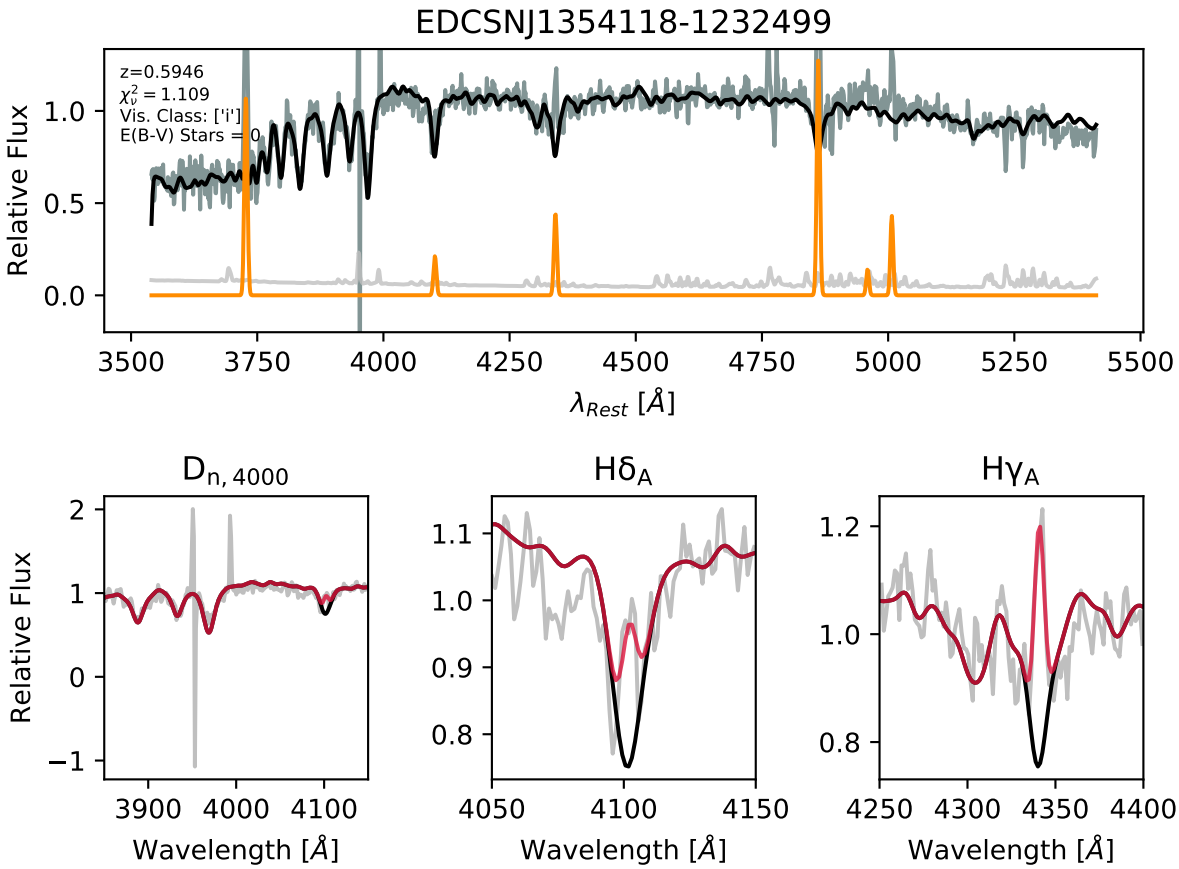
EDCSNJ1354118-1232499
z=0.5946
$\chi^2_\nu = 1.109$
Vis. Class: ['i']
E(B-V) Stars = 0
Relative Flux
λ_{Rest} [Å]
$D_{n,4000}$
$H\delta_A$
$H\gamma_A$
Wavelength [Å]

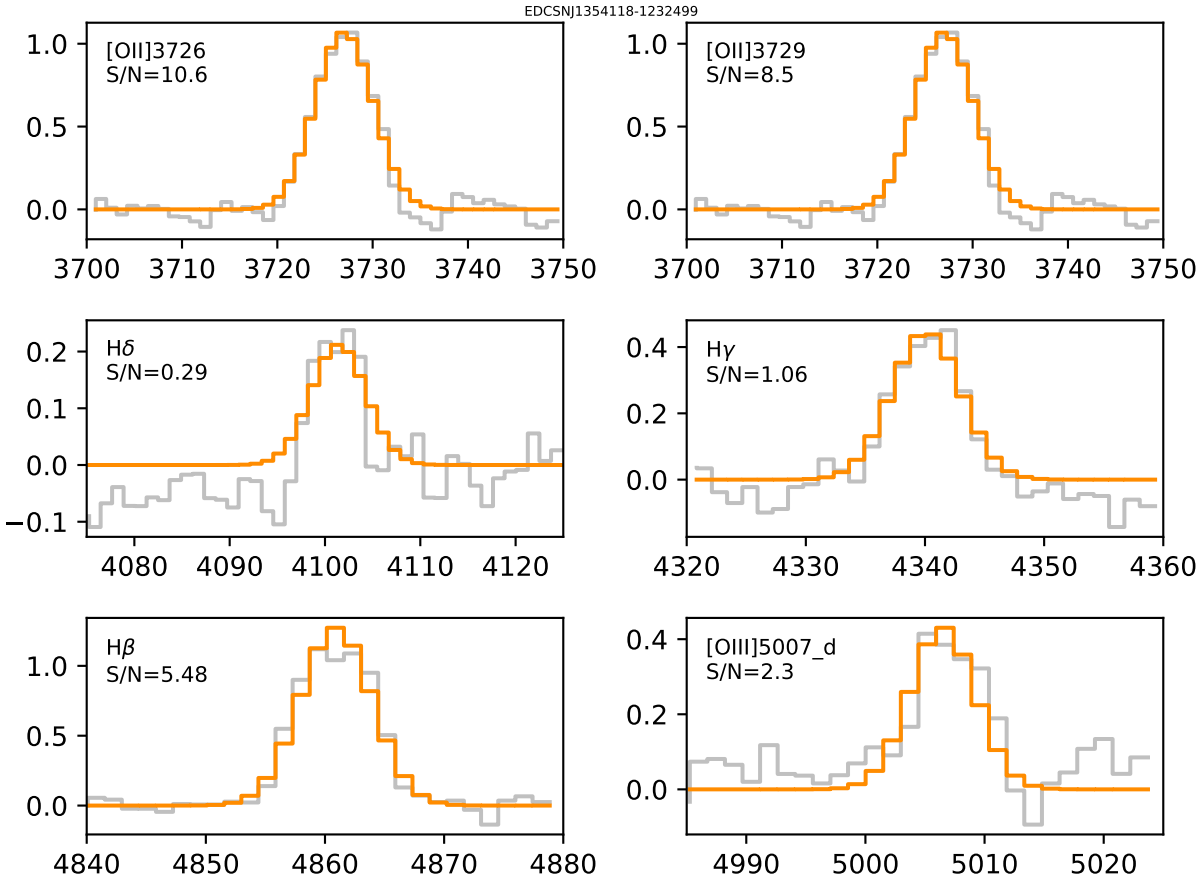
EDCSNJ1354118-1232499
[OII]3726
S/N=10.6
[OII]3729
S/N=8.5
Hδ
S/N=0.29
Hγ
S/N=1.06
Hβ
S/N=5.48
[OIII]5007_d
S/N=2.3

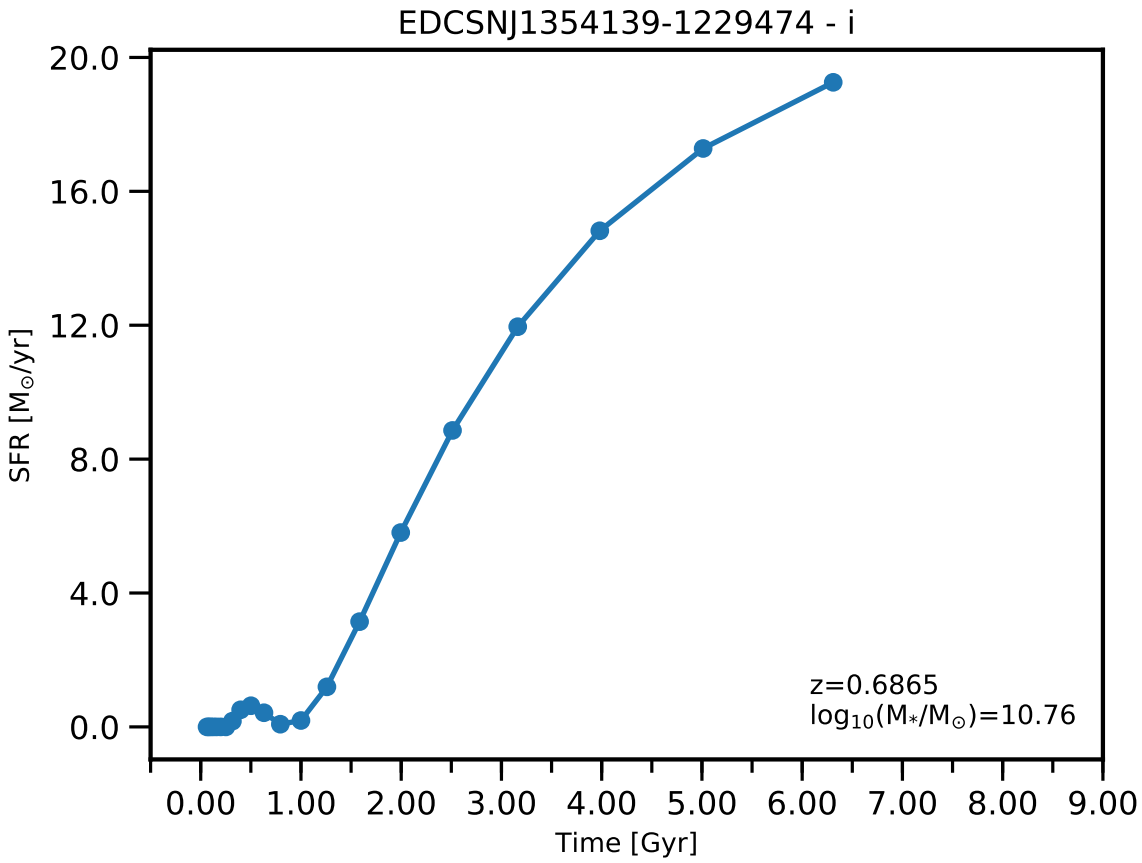
EDCSNJ1354139-1229474 - i
20.0
16.0
12.0
8.0
4.0
0.0
SFR [M⊙/yr]
0.00
1.00
2.00
3.00
4.00
5.00
6.00
7.00
8.00
9.00
Time [Gyr]
z=0.6865
log10(M*/M⊙)=10.76

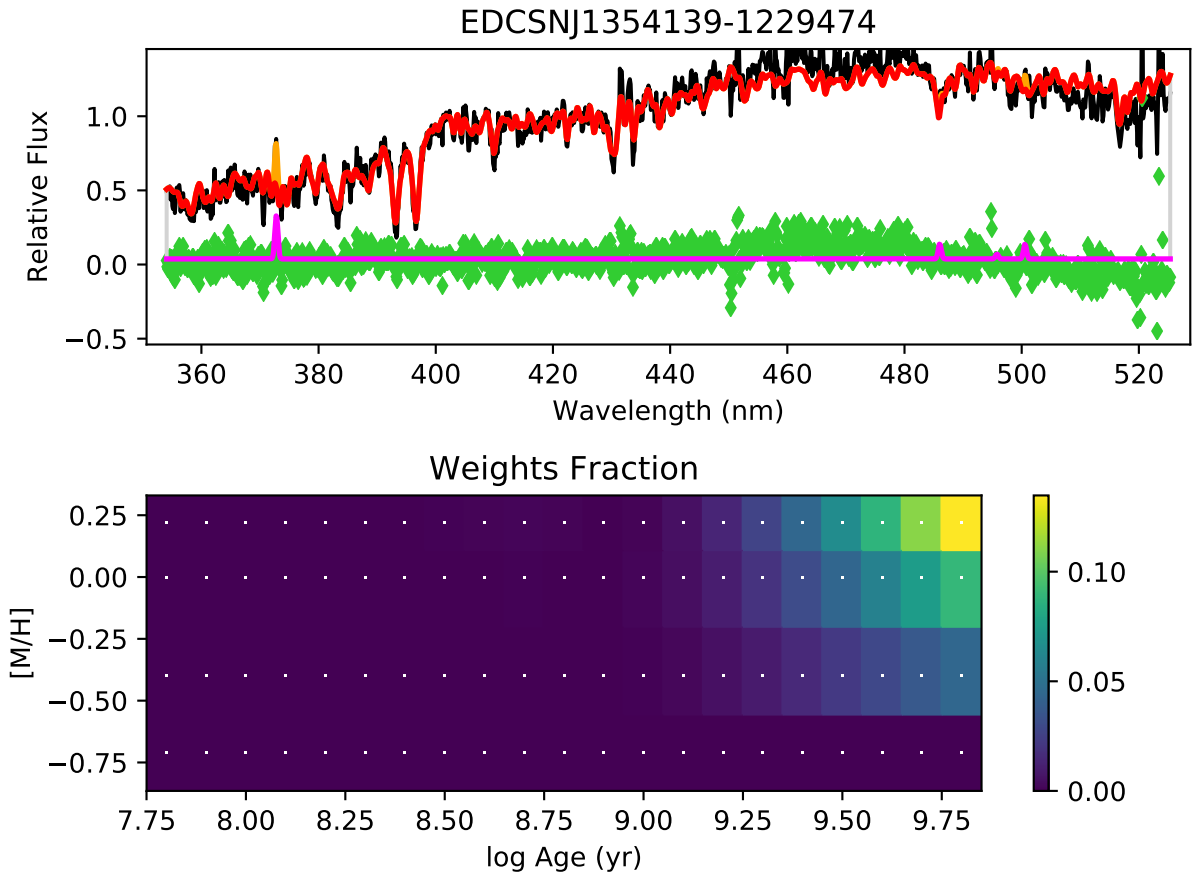
EDCSNJ1354139-1229474
Relative Flux
1.0
0.5
0.0
−0.5
360
380
400
420
440
460
480
500
520
Wavelength (nm)
Weights Fraction
[M/H]
0.25
0.00
−0.25
−0.50
−0.75
7.75
8.00
8.25
8.50
8.75
9.00
9.25
9.50
9.75
log Age (yr)
0.10
0.05
0.00

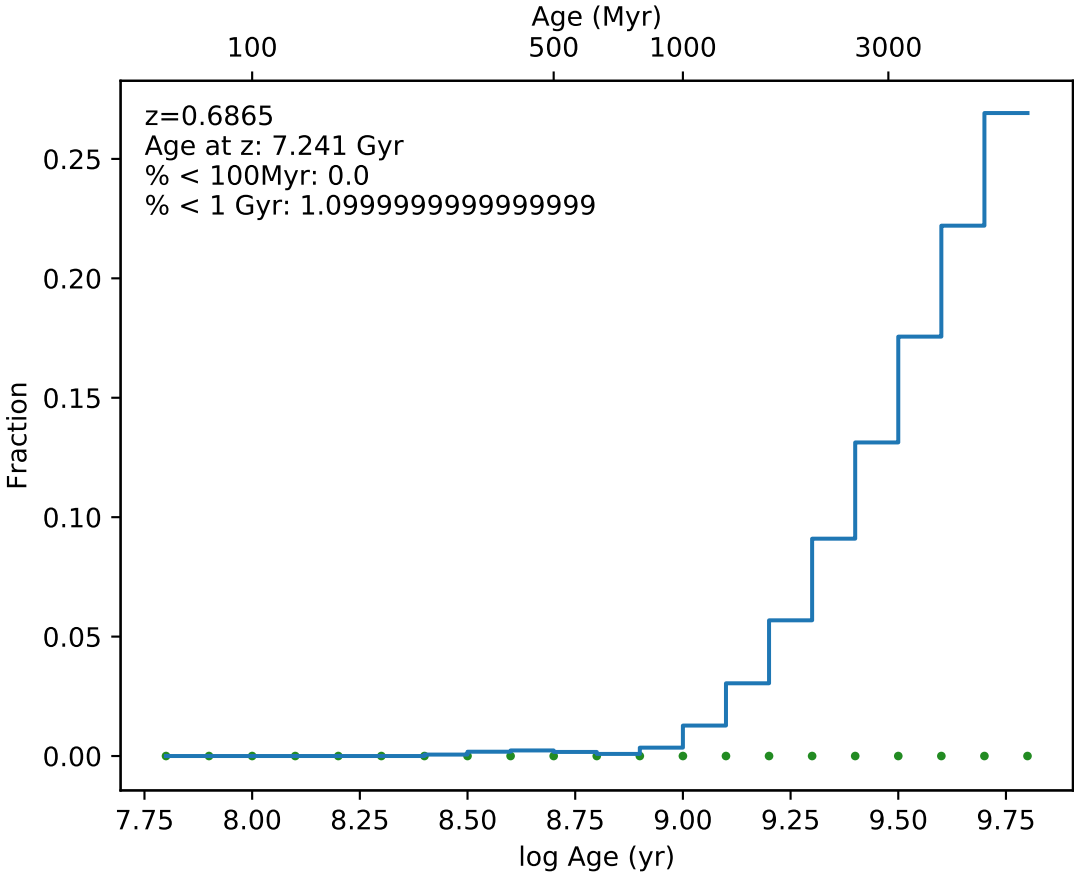
Age (Myr)
100
500
1000
3000
z=0.6865
Age at z: 7.241 Gyr
% < 100Myr: 0.0
% < 1 Gyr: 1.0999999999999999
Fraction
0.25
0.20
0.15
0.10
0.05
0.00
7.75
8.00
8.25
8.50
8.75
9.00
9.25
9.50
9.75
log Age (yr)

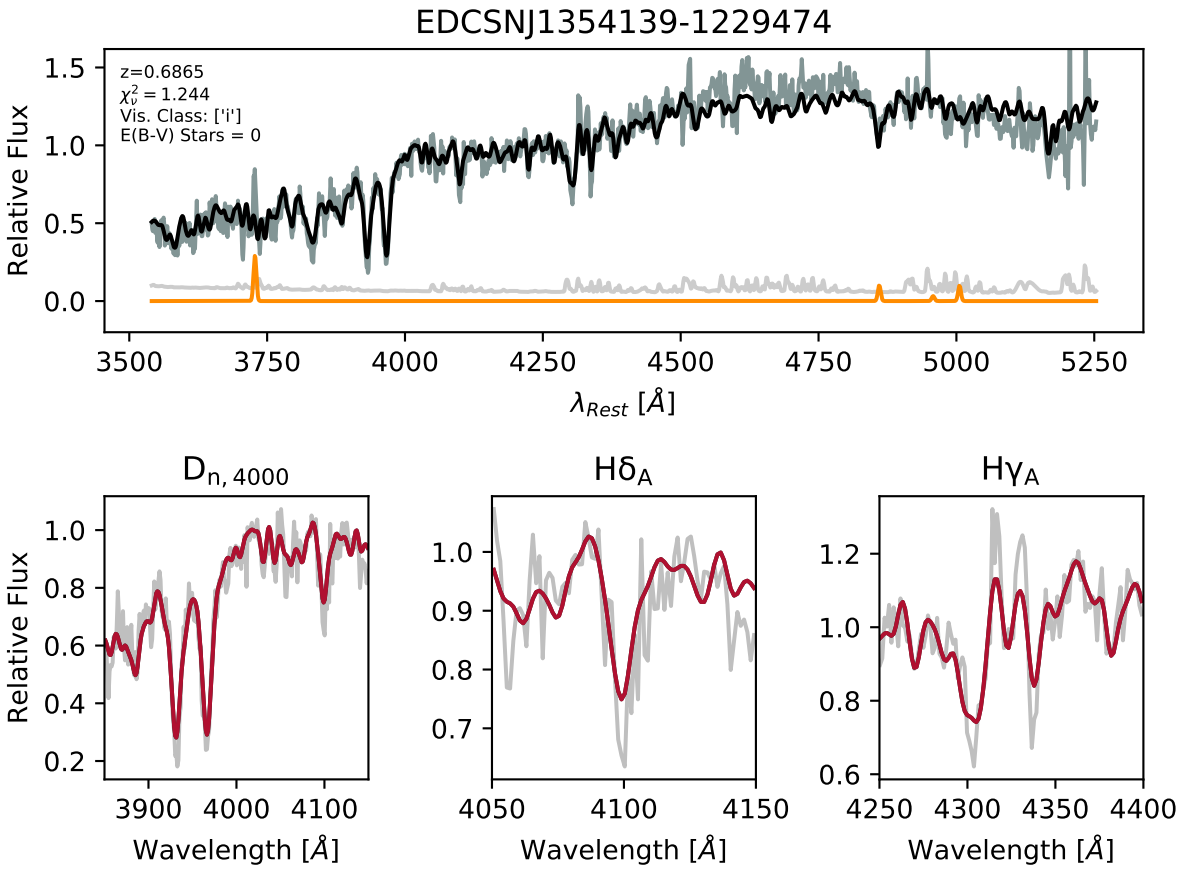
EDCSNJ1354139-1229474
z=0.6865
$\chi^2_\nu = 1.244$
Vis. Class: ['i']
E(B-V) Stars = 0
Relative Flux
λ_{Rest} [Å]
$D_{n,4000}$
$H\delta_A$
$H\gamma_A$
Wavelength [Å]

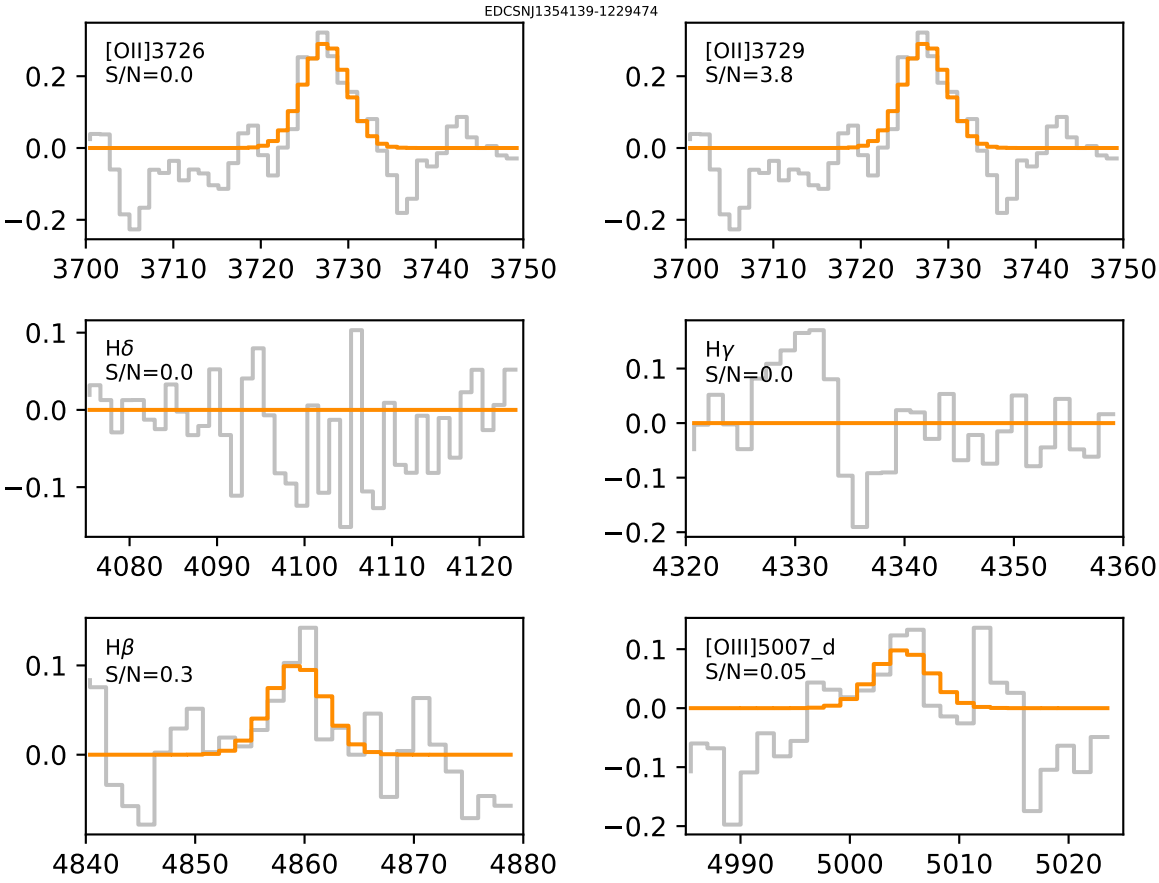
EDCSNJ1354139-1229474
[OII]3726
S/N=0.0
[OII]3729
S/N=3.8
Hδ
S/N=0.0
Hγ
S/N=0.0
Hβ
S/N=0.3
[OIII]5007_d
S/N=0.05

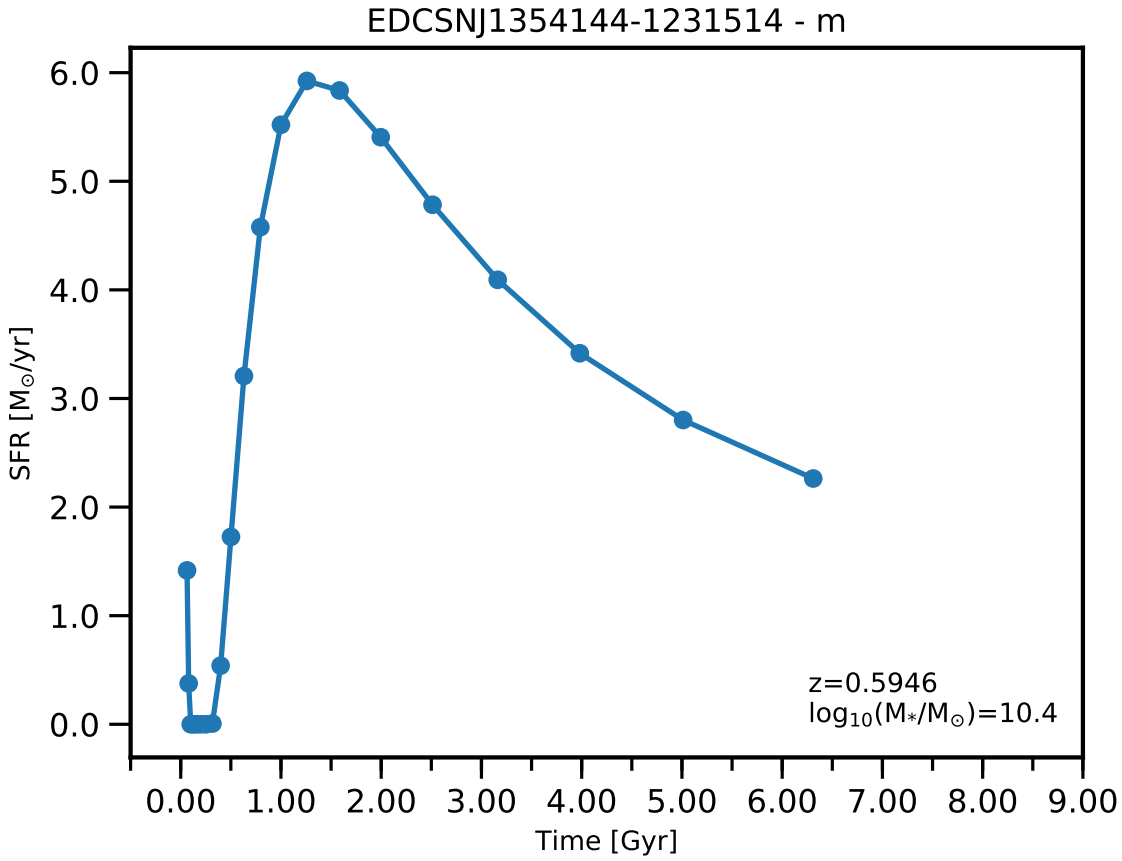
EDCSNJ1354144-1231514 - m
SFR [M⊙/yr]
Time [Gyr]
z=0.5946
log10(M*/M⊙)=10.4
0.0
1.0
2.0
3.0
4.0
5.0
6.0
0.00
1.00
2.00
3.00
4.00
5.00
6.00
7.00
8.00
9.00

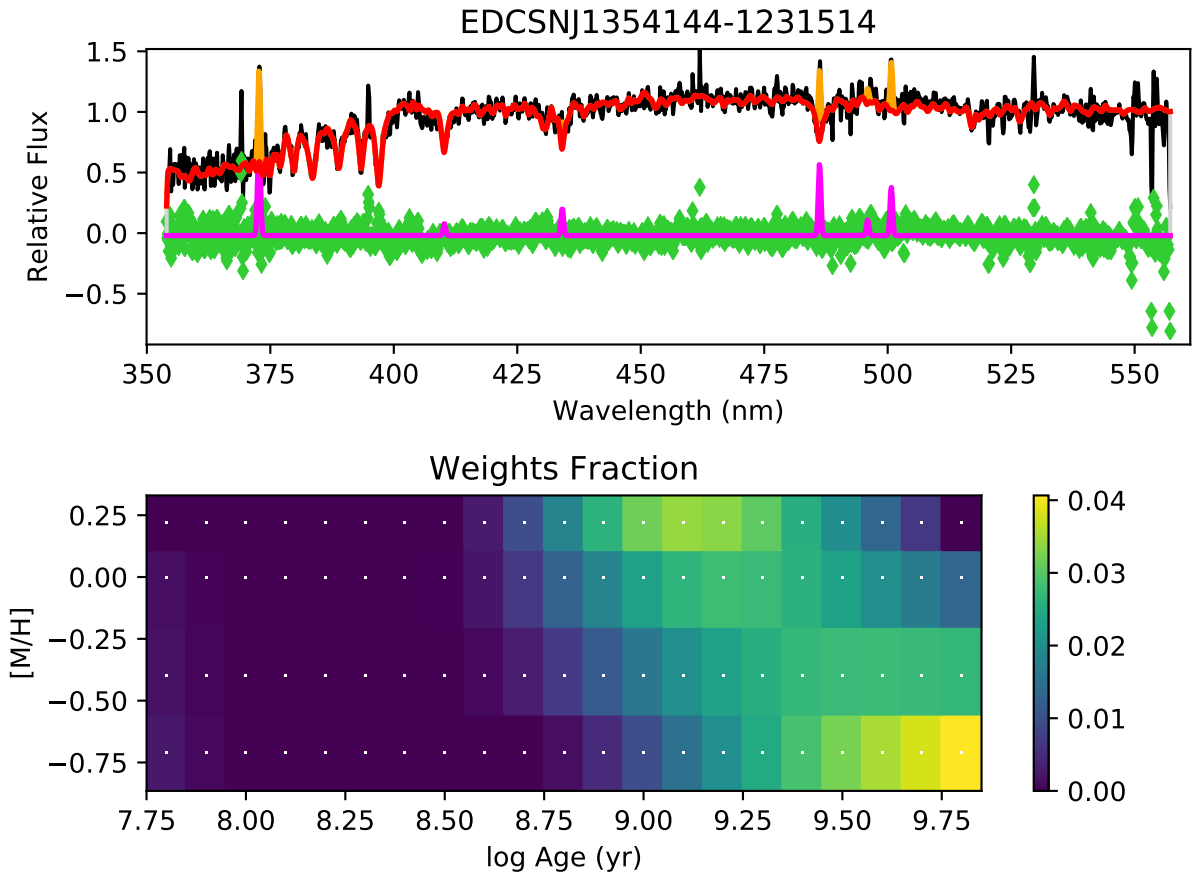
EDCSNJ1354144-1231514
Relative Flux
1.5
1.0
0.5
0.0
−0.5
350
375
400
425
450
475
500
525
550
Wavelength (nm)
Weights Fraction
[M/H]
0.25
0.00
−0.25
−0.50
−0.75
7.75
8.00
8.25
8.50
8.75
9.00
9.25
9.50
9.75
log Age (yr)
0.04
0.03
0.02
0.01
0.00

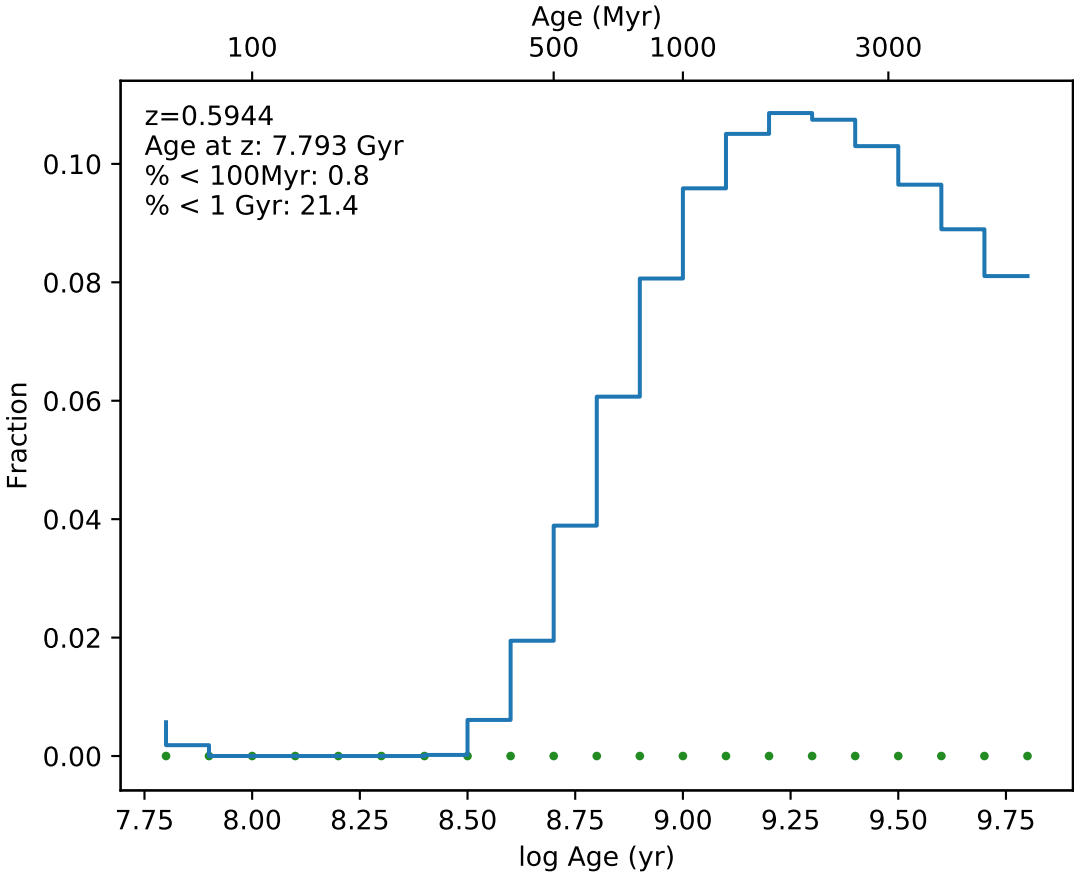
Age (Myr)
100
500
1000
3000
z=0.5944
Age at z: 7.793 Gyr
% < 100Myr: 0.8
% < 1 Gyr: 21.4
Fraction
0.10
0.08
0.06
0.04
0.02
0.00
7.75
8.00
8.25
8.50
8.75
9.00
9.25
9.50
9.75
log Age (yr)

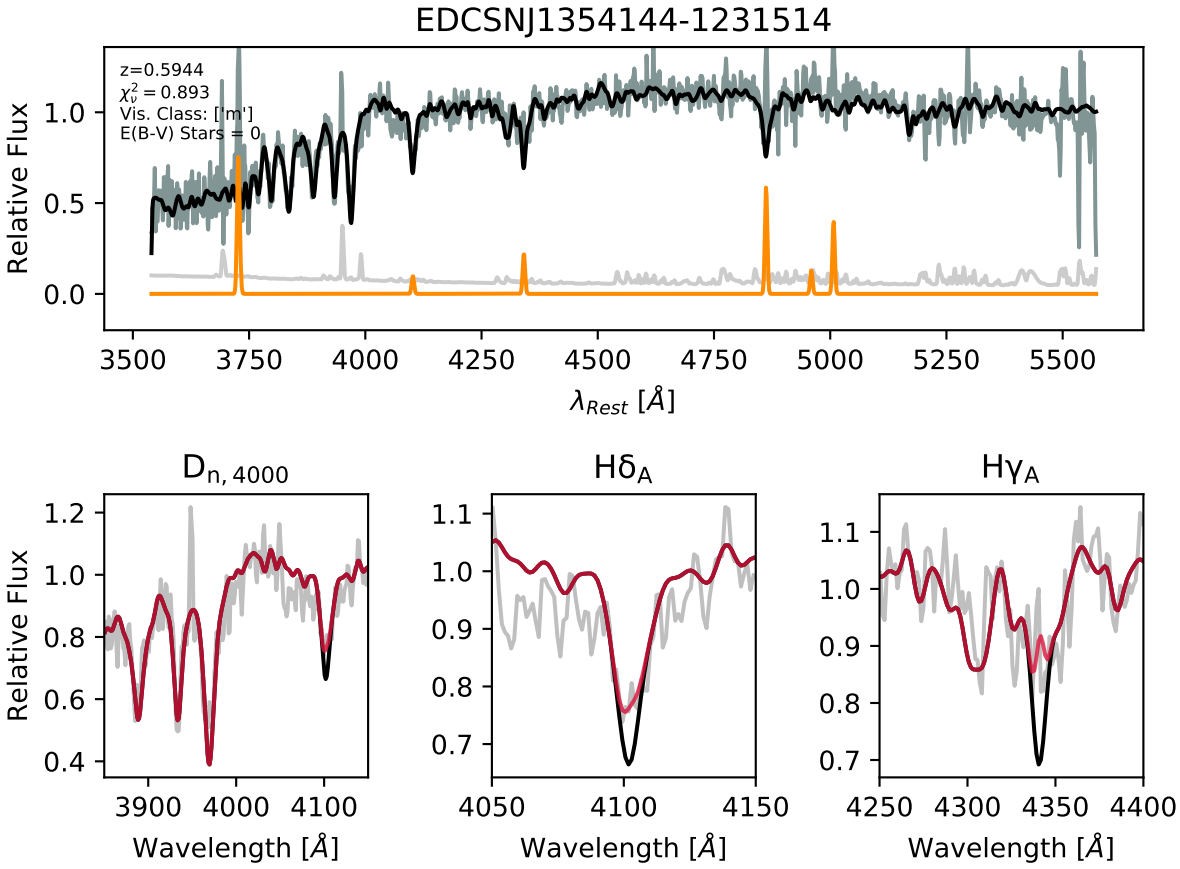
EDCSNJ1354144-1231514
z=0.5944
$\chi^2_\nu = 0.893$
Vis. Class: ['m']
E(B-V) Stars = 0
Relative Flux
λ_{Rest} [Å]
$D_{n,4000}$
$H\delta_A$
$H\gamma_A$
Wavelength [Å]

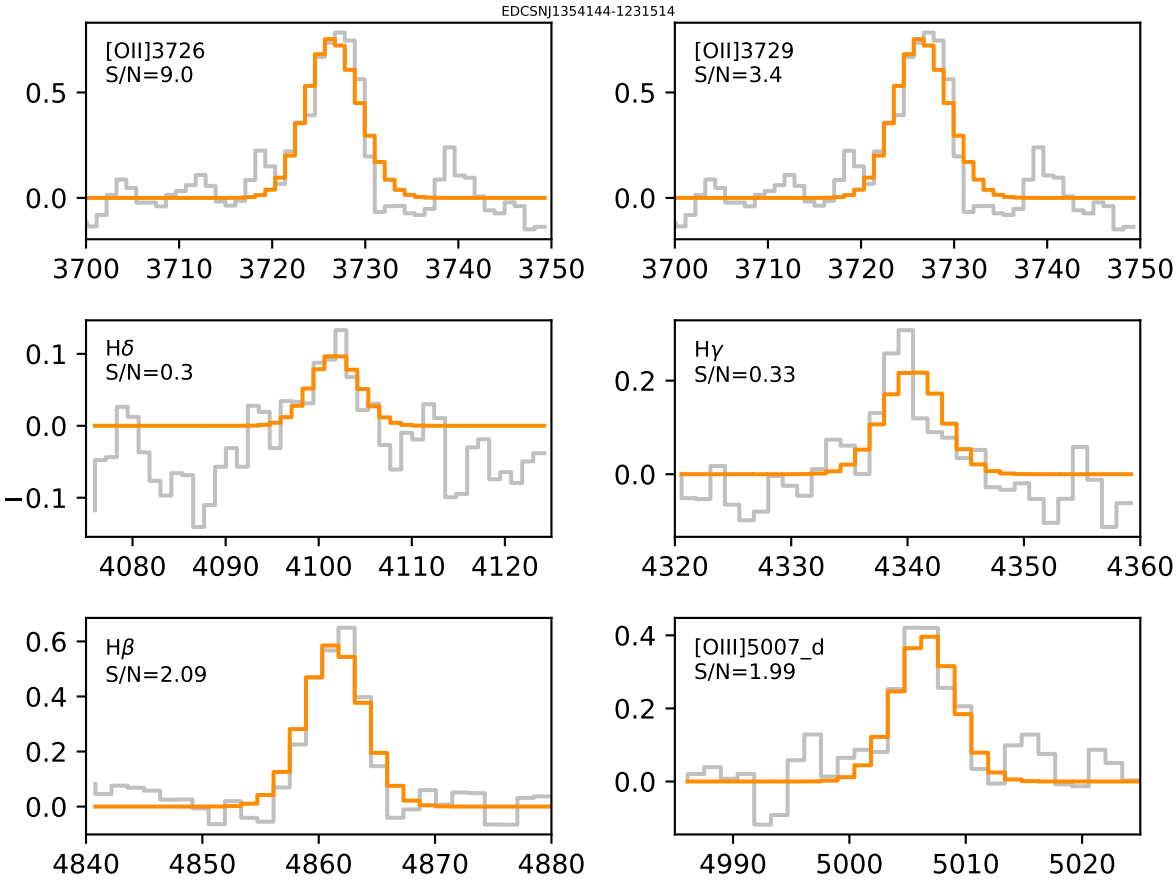
EDCSNJ1354144-1231514
[OII]3726
S/N=9.0
[OII]3729
S/N=3.4
Hδ
S/N=0.3
Hγ
S/N=0.33
Hβ
S/N=2.09
[OIII]5007_d
S/N=1.99

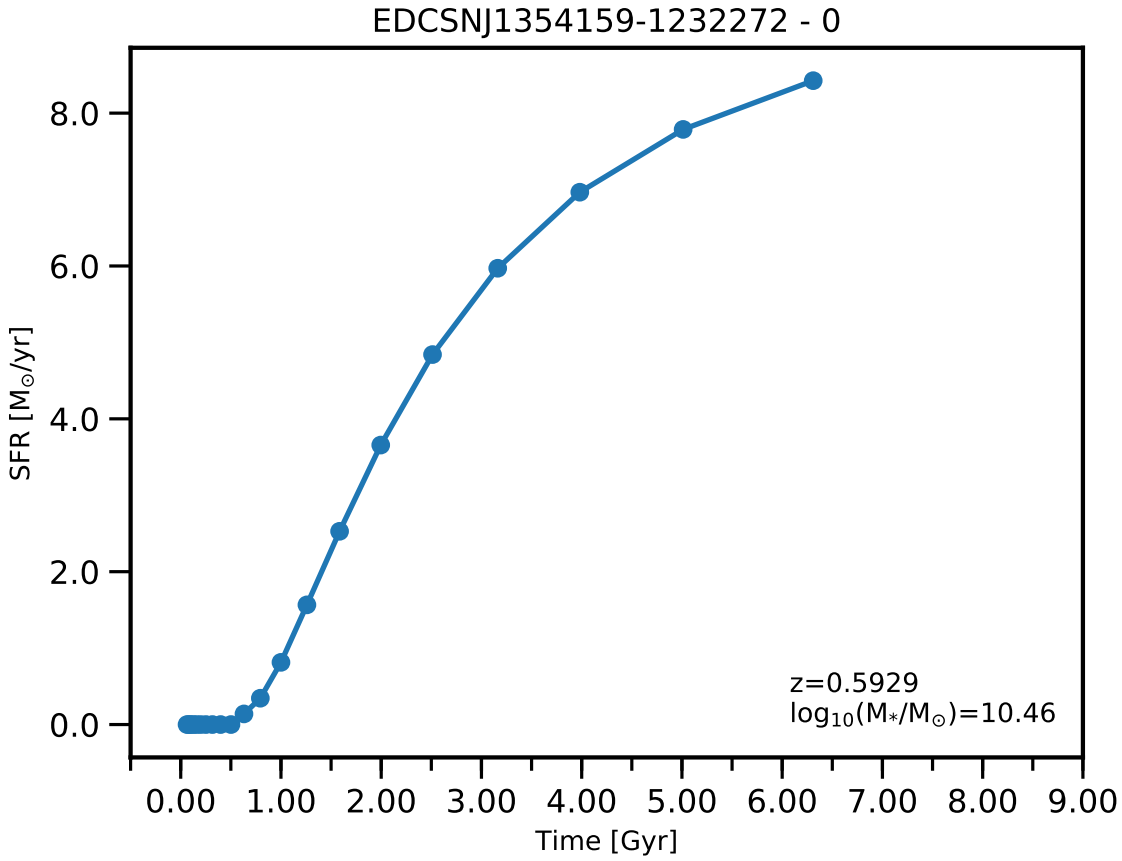
EDCSNJ1354159-1232272 - 0
SFR [M⊙/yr]
8.0
6.0
4.0
2.0
0.0
0.00
1.00
2.00
3.00
4.00
5.00
6.00
7.00
8.00
9.00
Time [Gyr]
z=0.5929
log10(M*/M⊙)=10.46

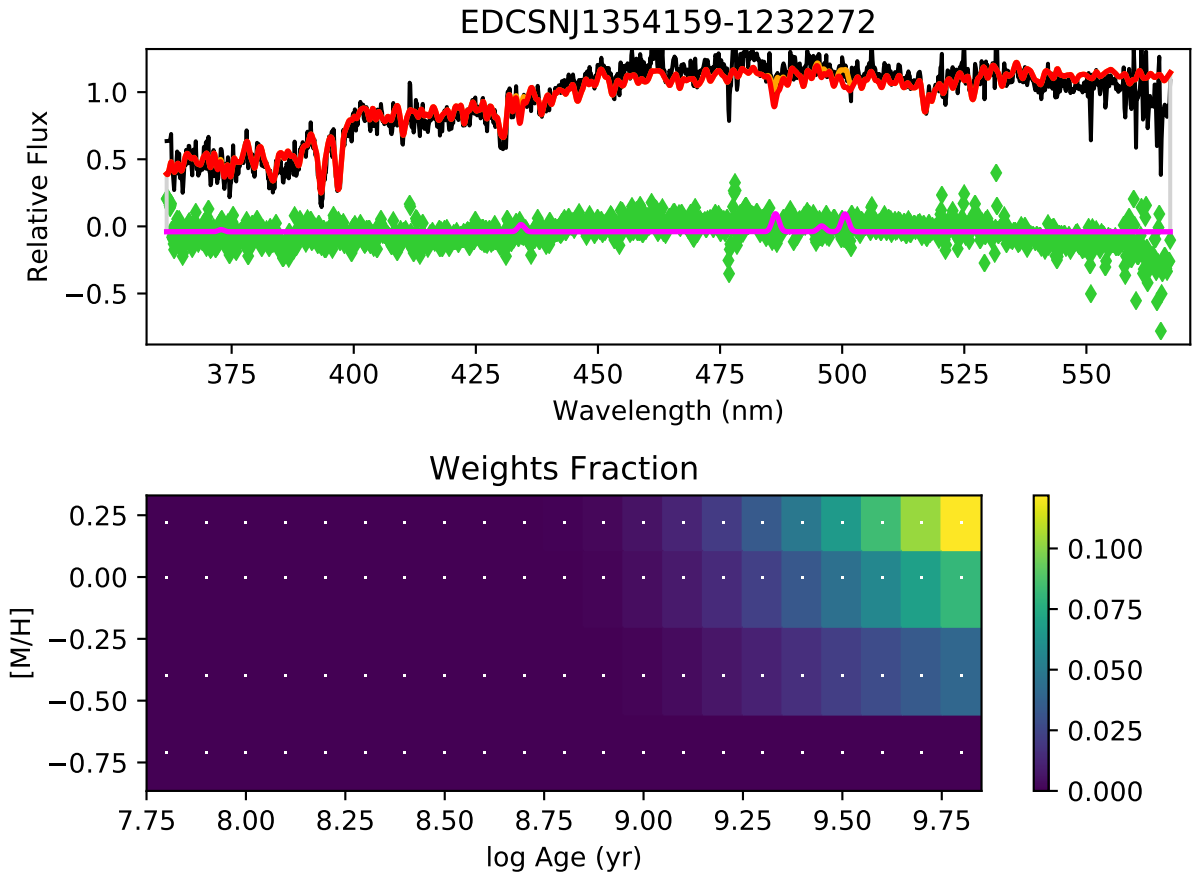
EDCSNJ1354159-1232272
Relative Flux
1.0
0.5
0.0
−0.5
375
400
425
450
475
500
525
550
Wavelength (nm)
Weights Fraction
[M/H]
0.25
0.00
−0.25
−0.50
−0.75
7.75
8.00
8.25
8.50
8.75
9.00
9.25
9.50
9.75
log Age (yr)
0.100
0.075
0.050
0.025
0.000

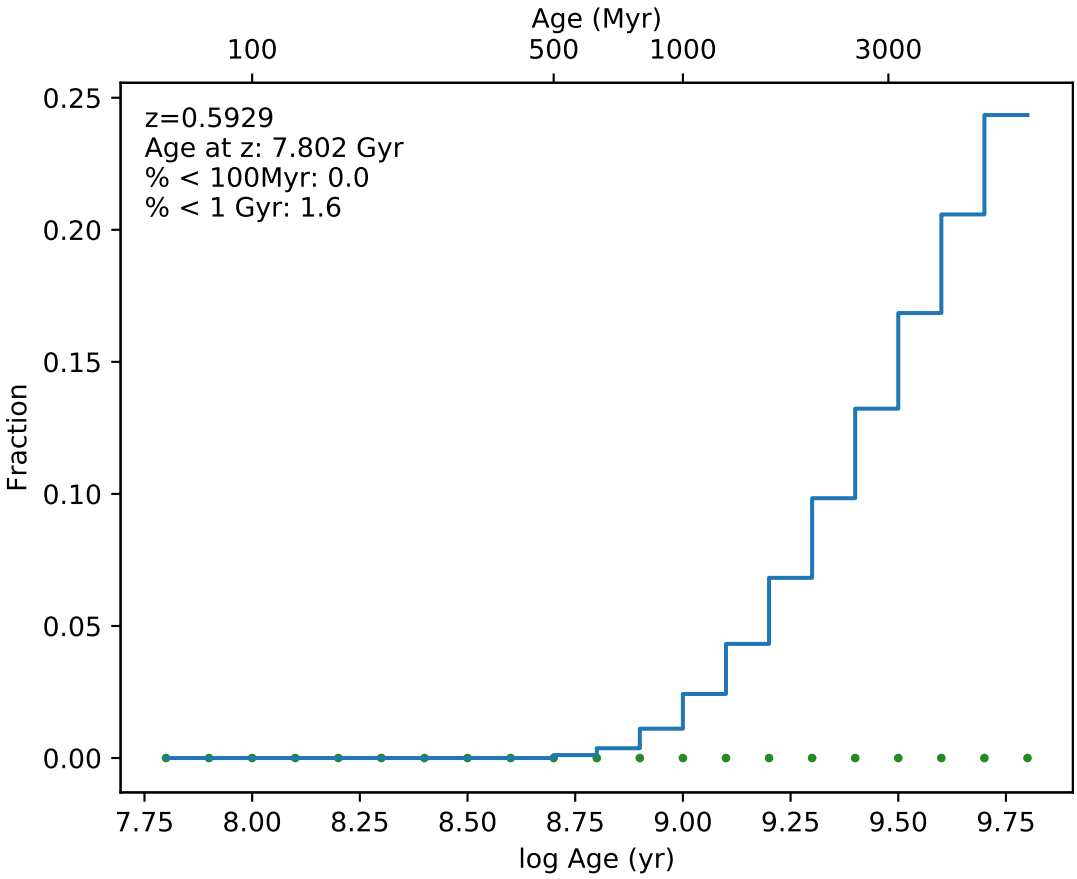
Age (Myr)
100
500
1000
3000
z=0.5929
Age at z: 7.802 Gyr
% < 100Myr: 0.0
% < 1 Gyr: 1.6
Fraction
0.25
0.20
0.15
0.10
0.05
0.00
7.75
8.00
8.25
8.50
8.75
9.00
9.25
9.50
9.75
log Age (yr)

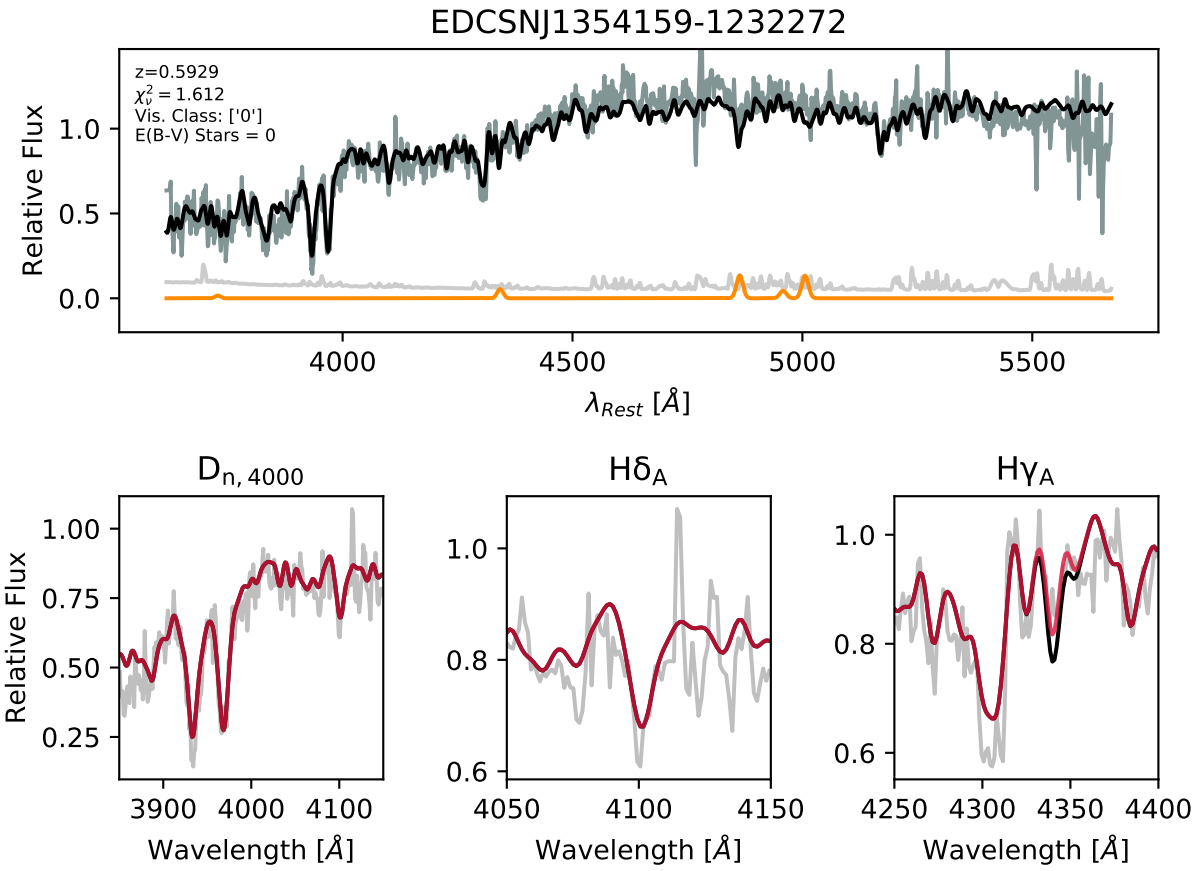
EDCSNJ1354159-1232272
z=0.5929
$\chi^2_\nu = 1.612$
Vis. Class: ['0']
E(B-V) Stars = 0
Relative Flux
1.0
0.5
0.0
4000
4500
5000
5500
λ_{Rest} [Å]
$D_{n,4000}$
$H\delta_A$
$H\gamma_A$
Relative Flux
1.00
0.75
0.50
0.25
3900
4000
4100
Wavelength [Å]
1.0
0.8
0.6
4050
4100
4150
Wavelength [Å]
1.0
0.8
0.6
4250
4300
4350
4400
Wavelength [Å]

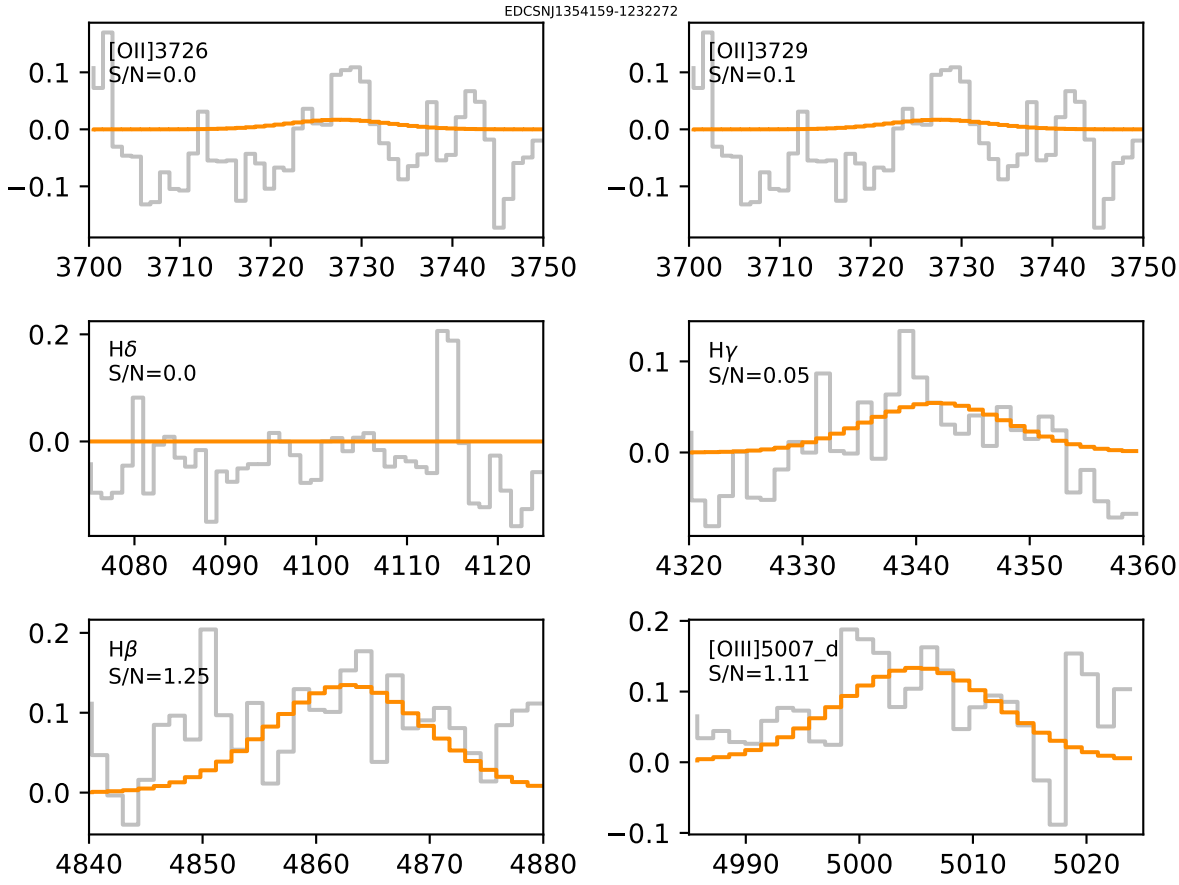
EDCSNJ1354159-1232272
[OII]3726
S/N=0.0
[OII]3729
S/N=0.1
Hδ
S/N=0.0
Hγ
S/N=0.05
Hβ
S/N=1.25
[OIII]5007_d
S/N=1.11

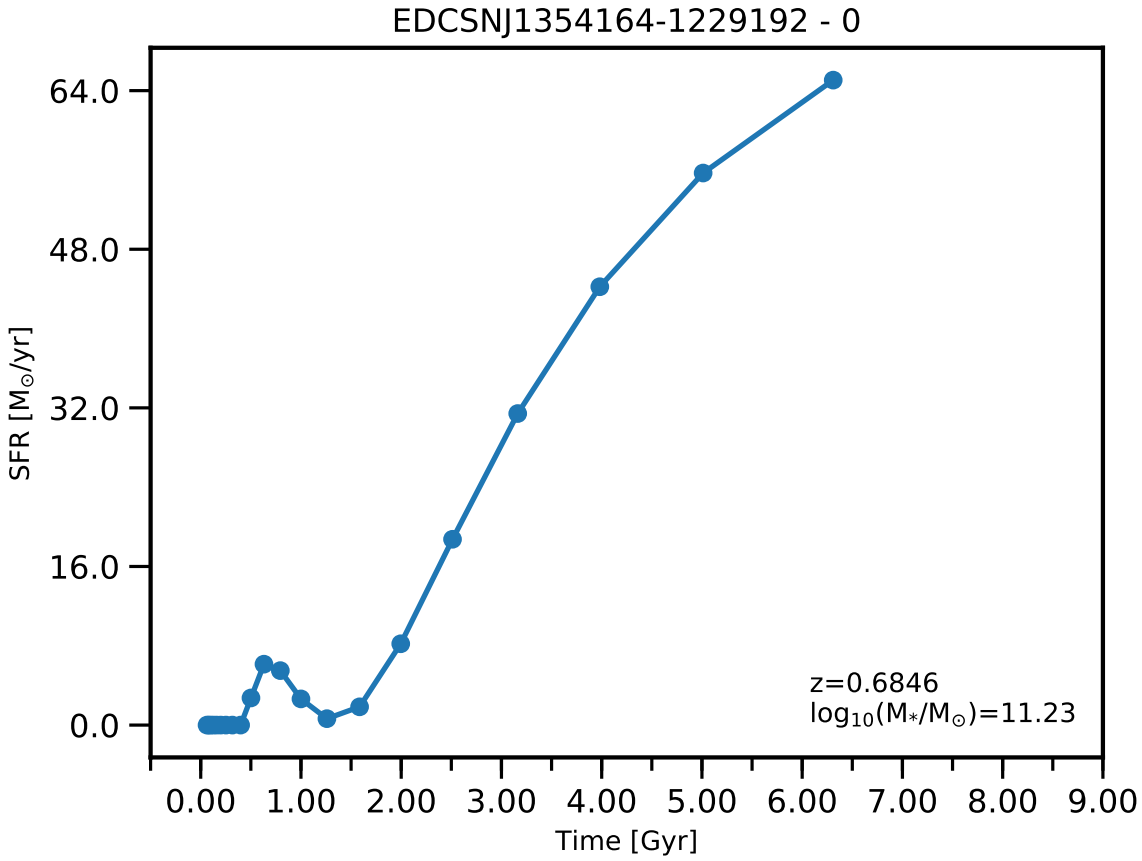
EDCSNJ1354164-1229192 - 0
64.0
48.0
32.0
16.0
0.0
SFR [M⊙/yr]
0.00
1.00
2.00
3.00
4.00
5.00
6.00
7.00
8.00
9.00
Time [Gyr]
z=0.6846
log10(M*/M⊙)=11.23

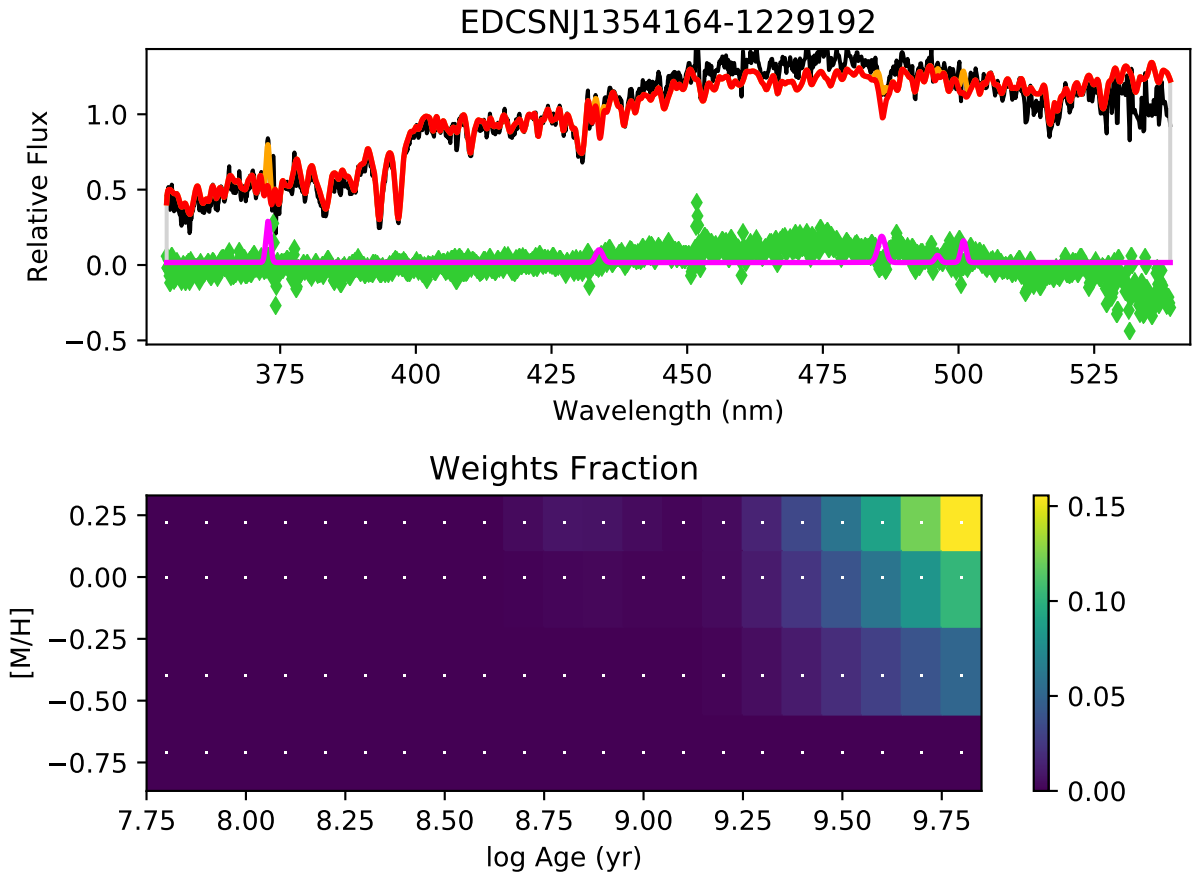
EDCSNJ1354164-1229192
Relative Flux
1.0
0.5
0.0
−0.5
375
400
425
450
475
500
525
Wavelength (nm)
Weights Fraction
[M/H]
0.25
0.00
−0.25
−0.50
−0.75
7.75
8.00
8.25
8.50
8.75
9.00
9.25
9.50
9.75
log Age (yr)
0.15
0.10
0.05
0.00

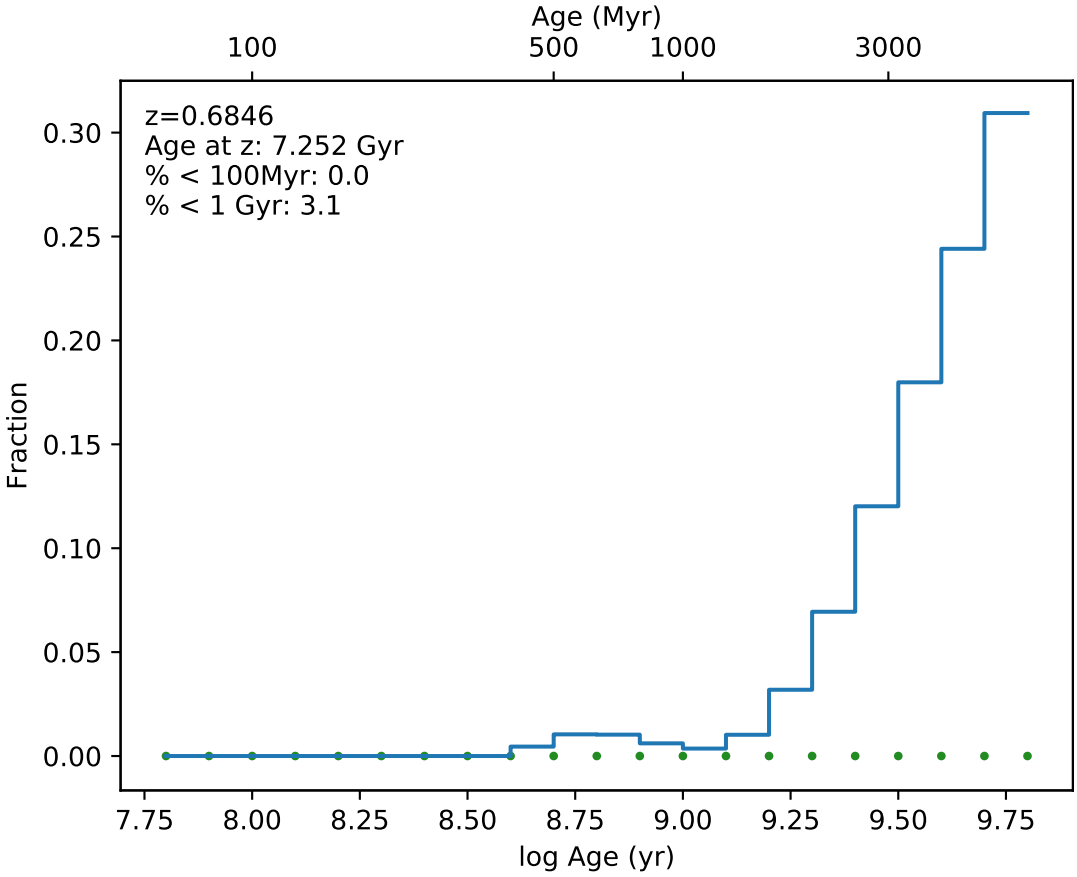
Age (Myr)
100
500
1000
3000
z=0.6846
Age at z: 7.252 Gyr
% < 100Myr: 0.0
% < 1 Gyr: 3.1
Fraction
0.30
0.25
0.20
0.15
0.10
0.05
0.00
7.75
8.00
8.25
8.50
8.75
9.00
9.25
9.50
9.75
log Age (yr)

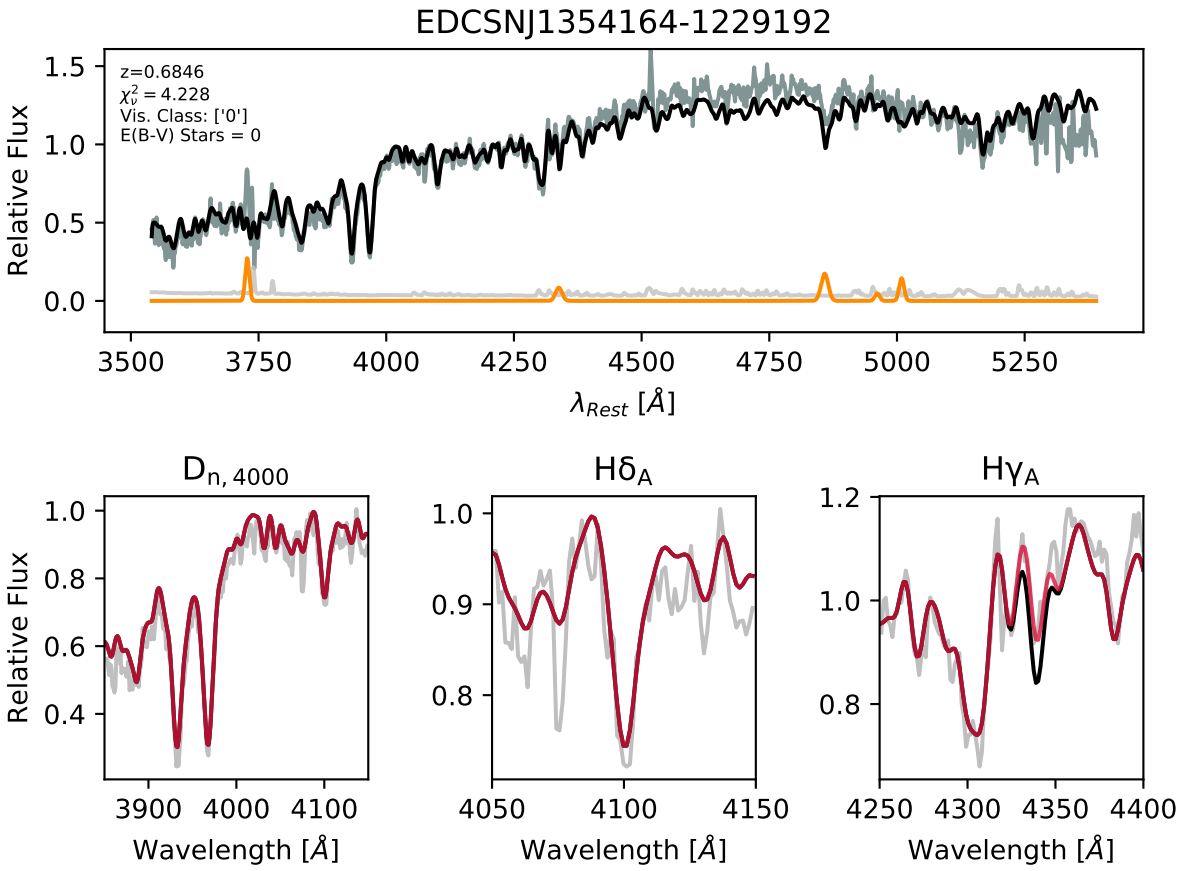
EDCSNJ1354164-1229192
z=0.6846
$\chi^2_\nu = 4.228$
Vis. Class: ['0']
E(B-V) Stars = 0
Relative Flux
λ_{Rest} [Å]
$D_{n,4000}$
$H\delta_A$
$H\gamma_A$
Wavelength [Å]

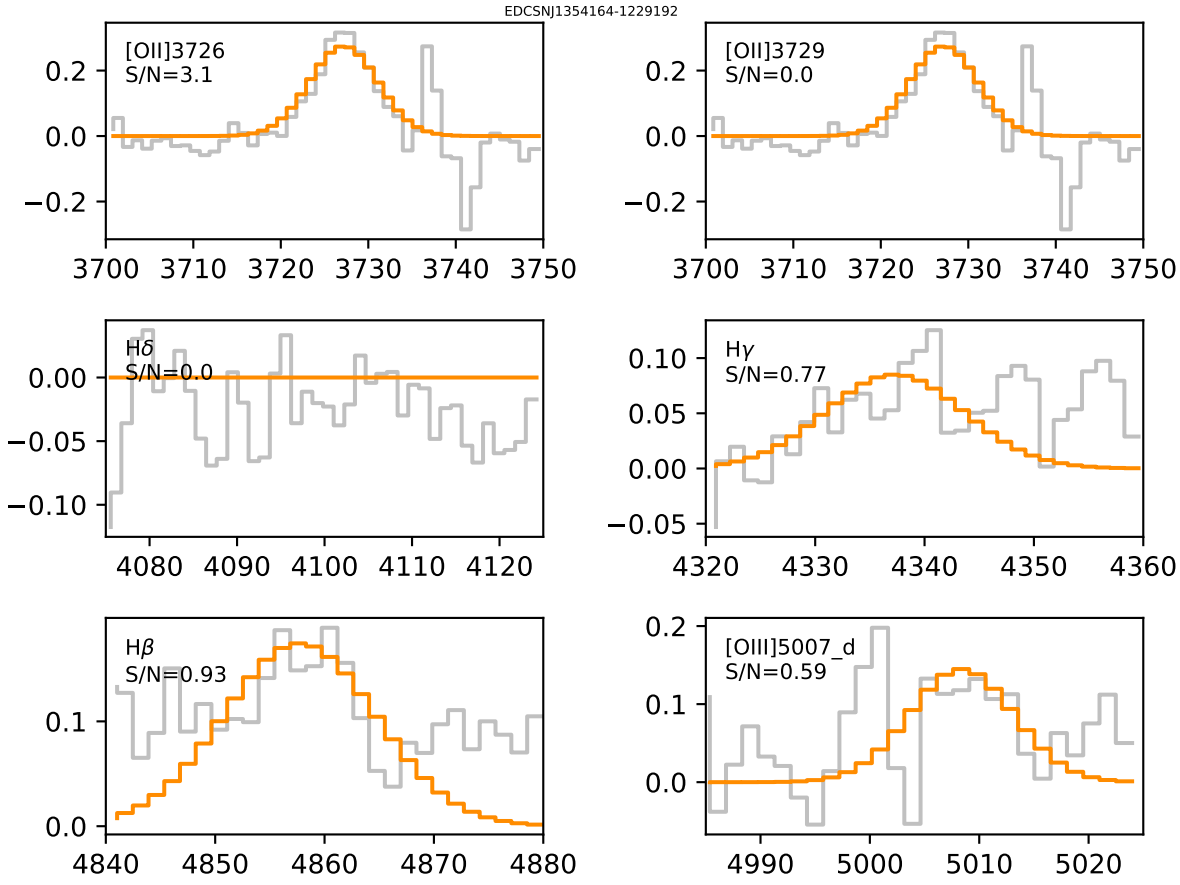
EDCSNJ1354164-1229192
[OII]3726
S/N=3.1
[OII]3729
S/N=0.0
Hδ
S/N=0.0
Hγ
S/N=0.77
Hβ
S/N=0.93
[OIII]5007_d
S/N=0.59

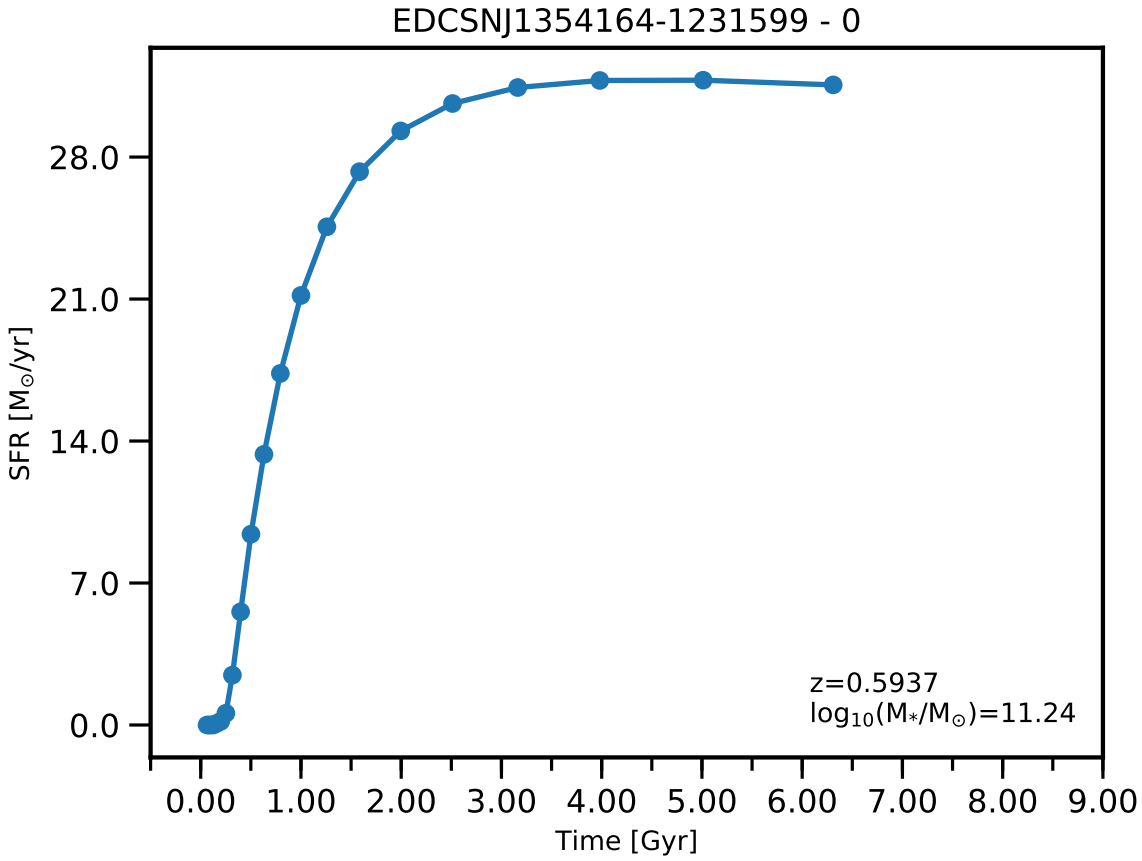
EDCSNJ1354164-1231599 - 0
SFR [M⊙/yr]
28.0
21.0
14.0
7.0
0.0
0.00
1.00
2.00
3.00
4.00
5.00
6.00
7.00
8.00
9.00
Time [Gyr]
z=0.5937
log10(M*/M⊙)=11.24

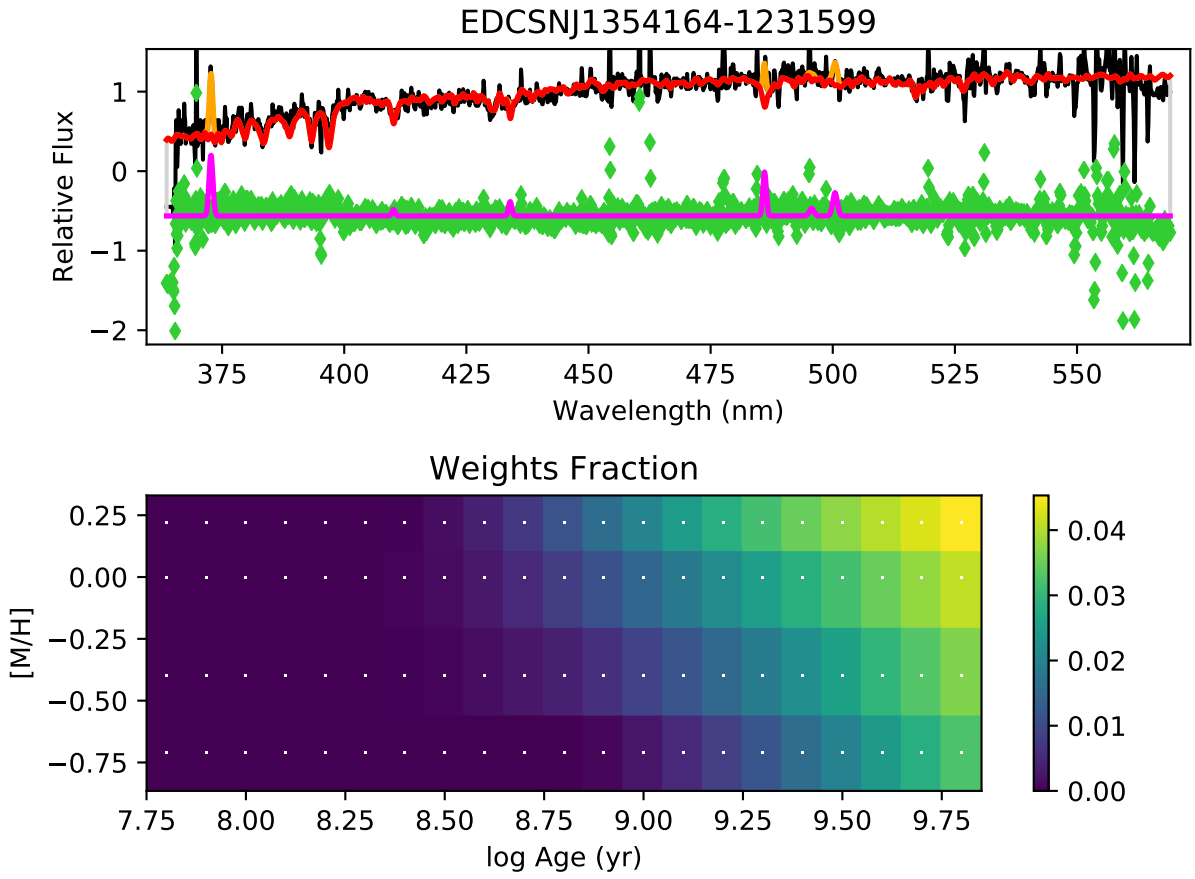
EDCSNJ1354164-1231599
Relative Flux
1
0
−1
−2
375
400
425
450
475
500
525
550
Wavelength (nm)
Weights Fraction
[M/H]
0.25
0.00
−0.25
−0.50
−0.75
7.75
8.00
8.25
8.50
8.75
9.00
9.25
9.50
9.75
log Age (yr)
0.04
0.03
0.02
0.01
0.00

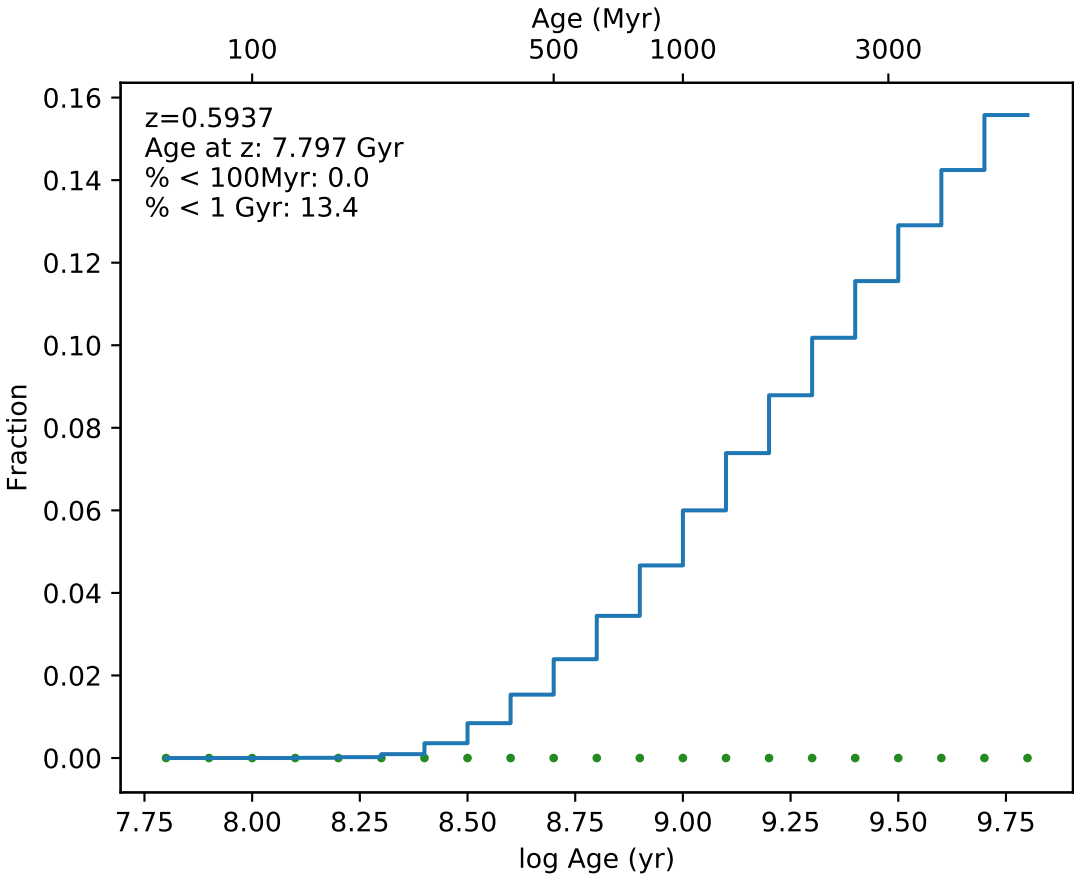
Age (Myr)
100
500
1000
3000
z=0.5937
Age at z: 7.797 Gyr
% < 100Myr: 0.0
% < 1 Gyr: 13.4
Fraction
0.16
0.14
0.12
0.10
0.08
0.06
0.04
0.02
0.00
7.75
8.00
8.25
8.50
8.75
9.00
9.25
9.50
9.75
log Age (yr)

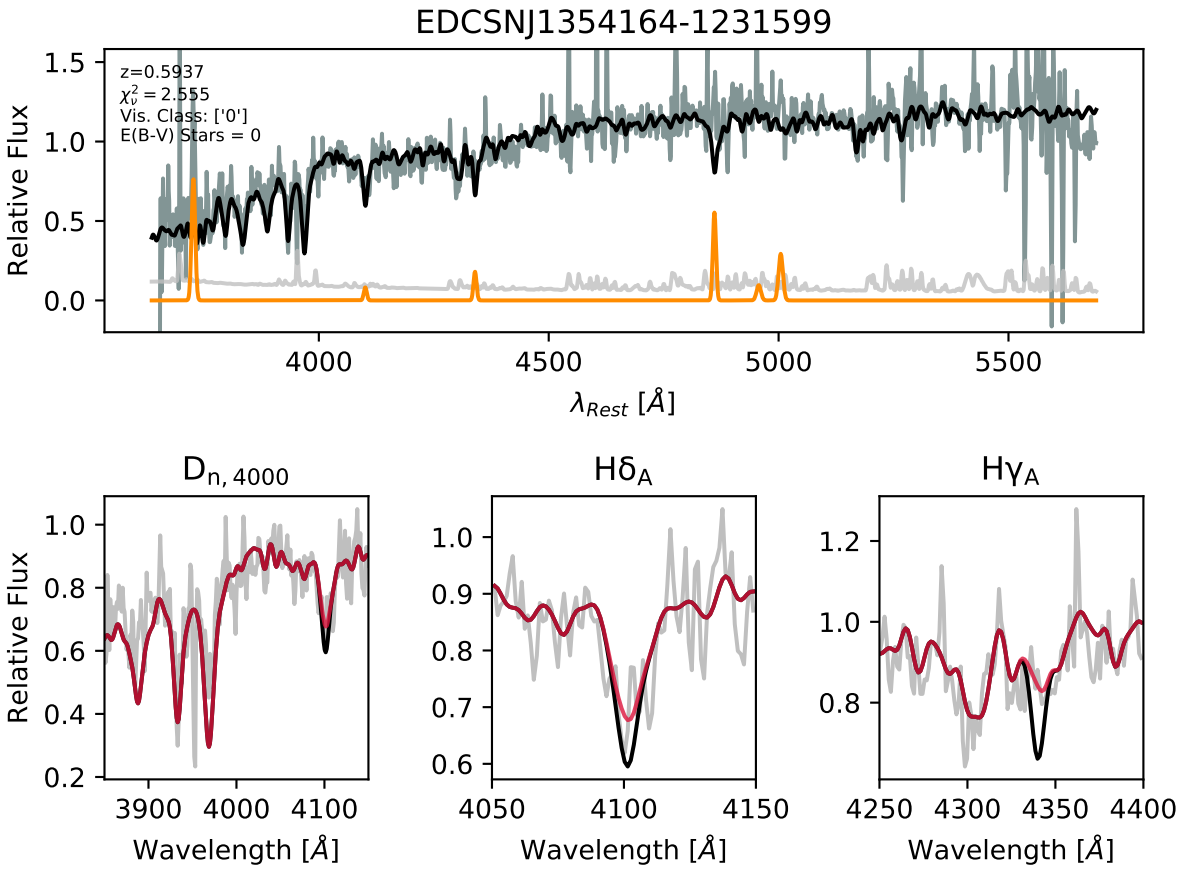
EDCSNJ1354164-1231599
z=0.5937
$\chi^2_\nu = 2.555$
Vis. Class: ['0']
E(B-V) Stars = 0
Relative Flux
λ_{Rest} [Å]
$D_{n,4000}$
$H\delta_A$
$H\gamma_A$
Wavelength [Å]

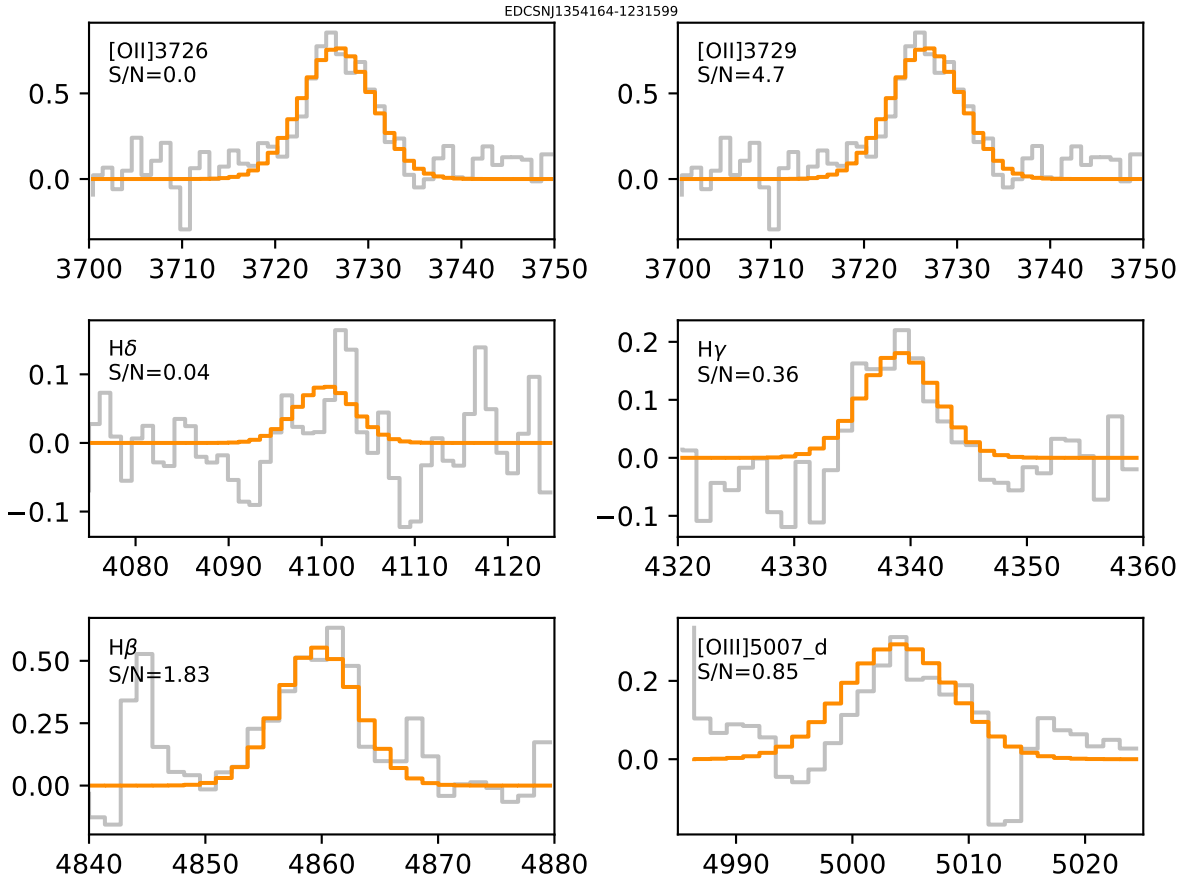
EDCSNJ1354164-1231599
[OII]3726
S/N=0.0
[OII]3729
S/N=4.7
Hδ
S/N=0.04
Hγ
S/N=0.36
Hβ
S/N=1.83
[OIII]5007_d
S/N=0.85

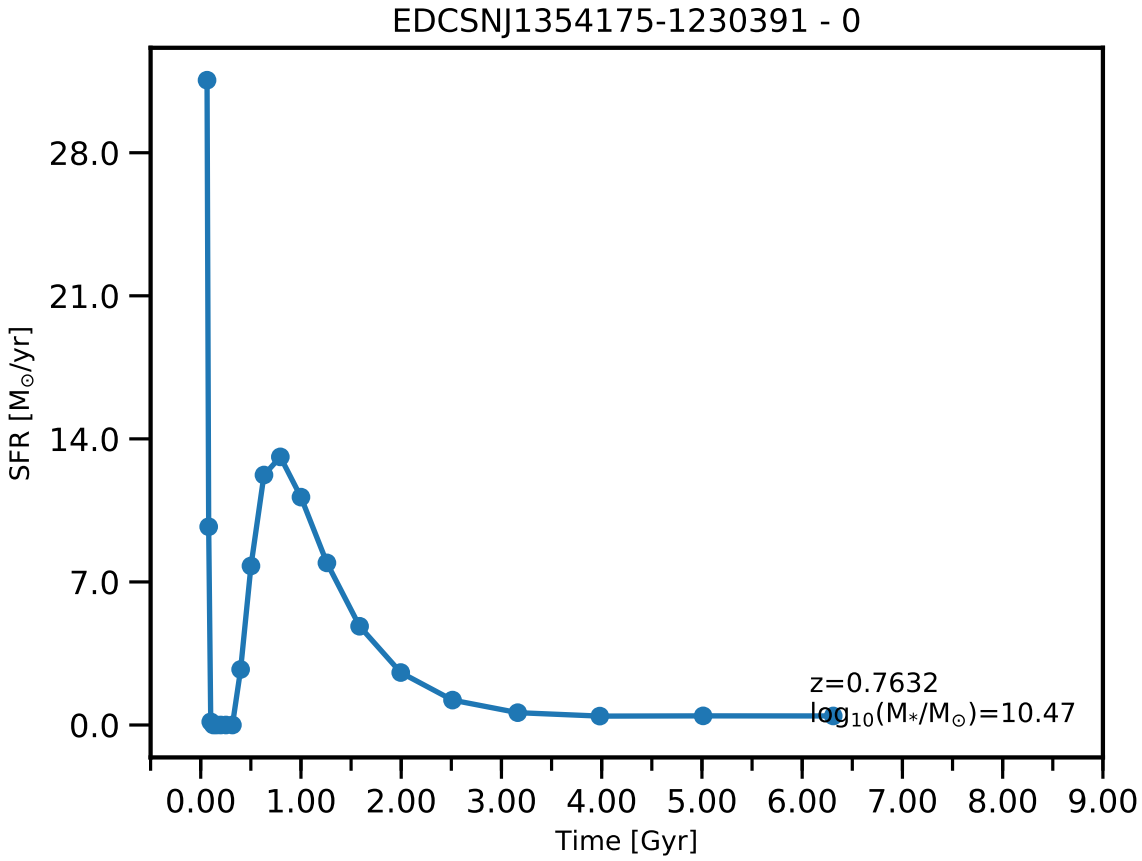
EDCSNJ1354175-1230391 - 0
SFR [M⊙/yr]
28.0
21.0
14.0
7.0
0.0
0.00
1.00
2.00
3.00
4.00
5.00
6.00
7.00
8.00
9.00
Time [Gyr]
z=0.7632
log10(M*/M⊙)=10.47

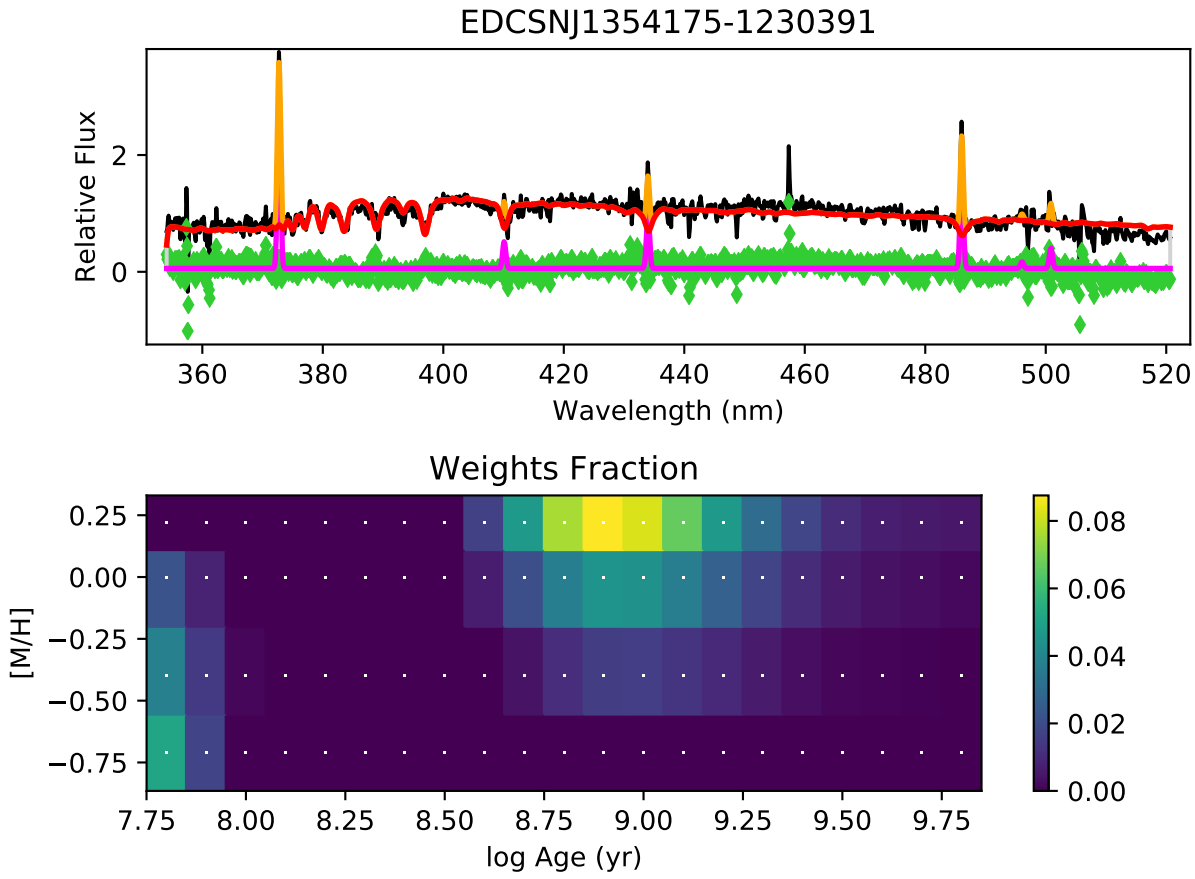
EDCSNJ1354175-1230391
Relative Flux
2
0
360
380
400
420
440
460
480
500
520
Wavelength (nm)
Weights Fraction
[M/H]
0.25
0.00
−0.25
−0.50
−0.75
7.75
8.00
8.25
8.50
8.75
9.00
9.25
9.50
9.75
log Age (yr)
0.08
0.06
0.04
0.02
0.00

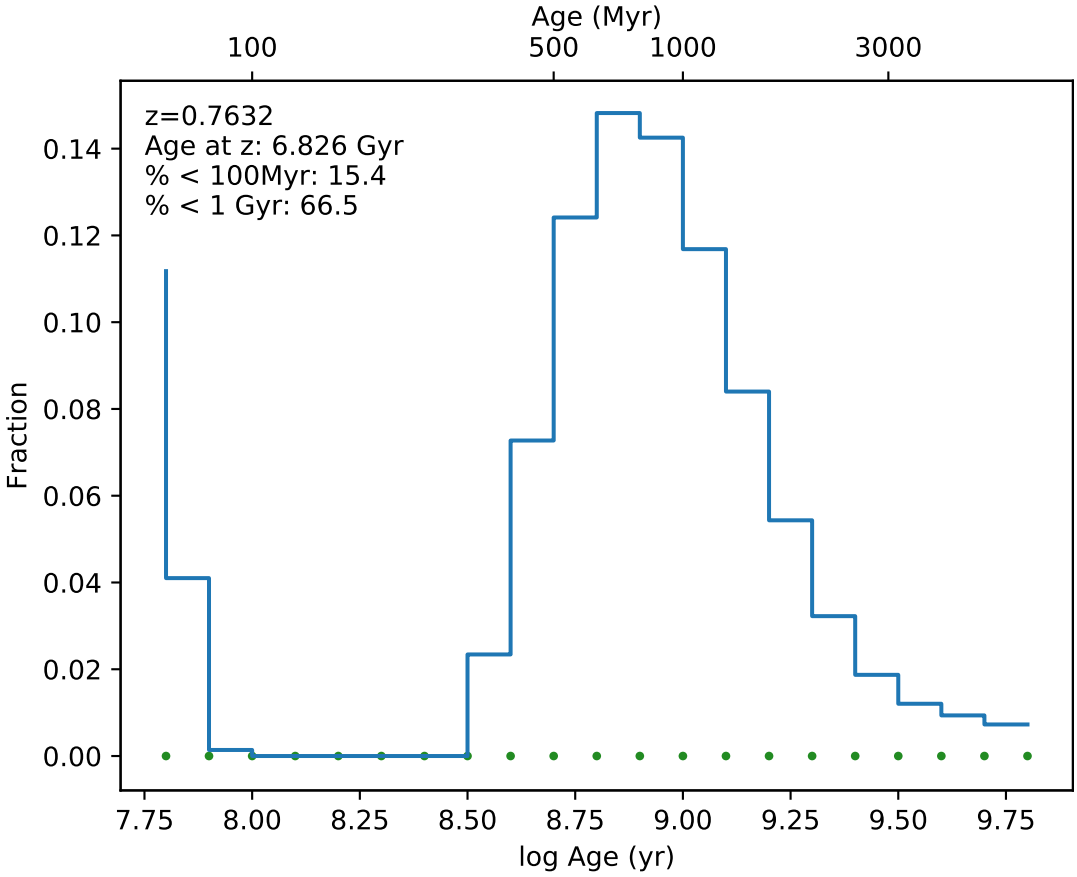
Age (Myr)
100
500
1000
3000
z=0.7632
Age at z: 6.826 Gyr
% < 100Myr: 15.4
% < 1 Gyr: 66.5
Fraction
0.14
0.12
0.10
0.08
0.06
0.04
0.02
0.00
7.75
8.00
8.25
8.50
8.75
9.00
9.25
9.50
9.75
log Age (yr)

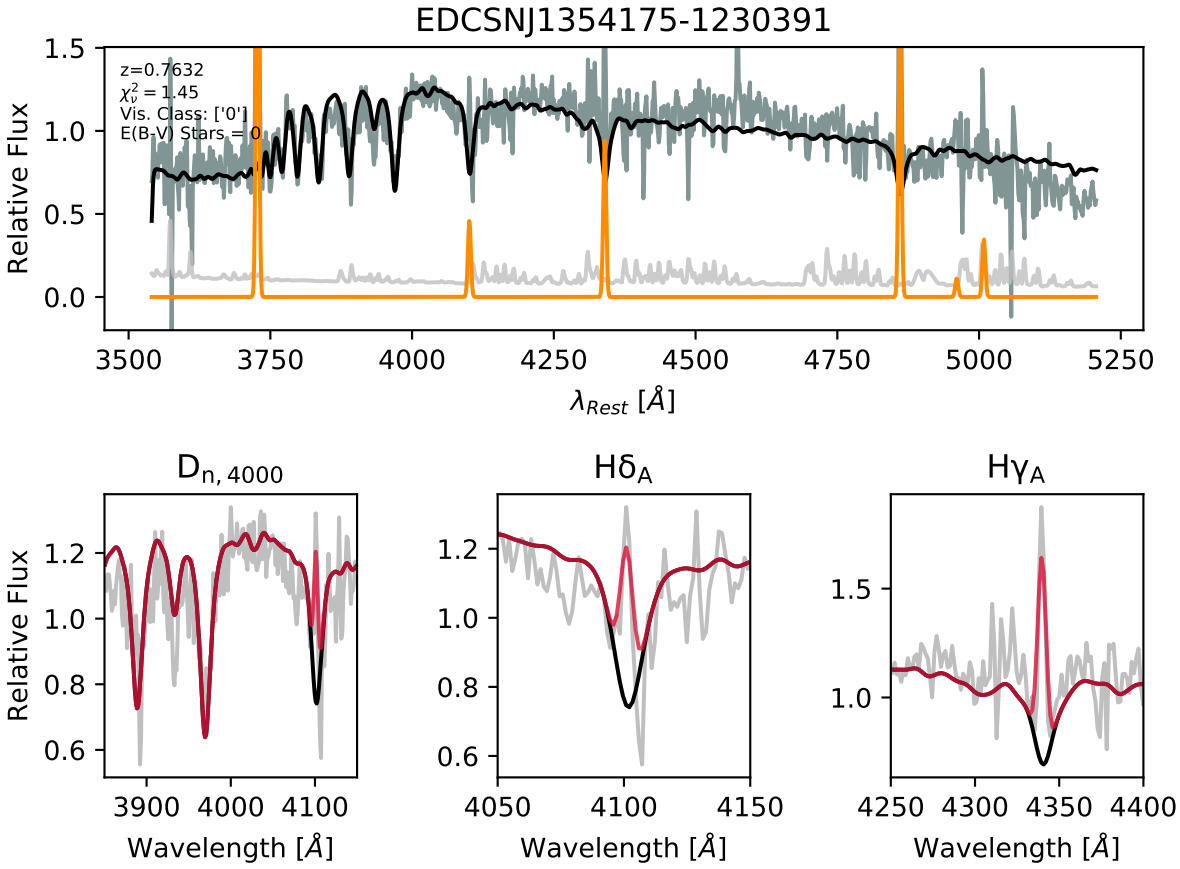
EDCSNJ1354175-1230391
z=0.7632
$\chi^2_\nu = 1.45$
Vis. Class: ['0']
E(B-V) Stars = 0
Relative Flux
λ_{Rest} [Å]
$D_{n,4000}$
$H\delta_A$
$H\gamma_A$
Wavelength [Å]

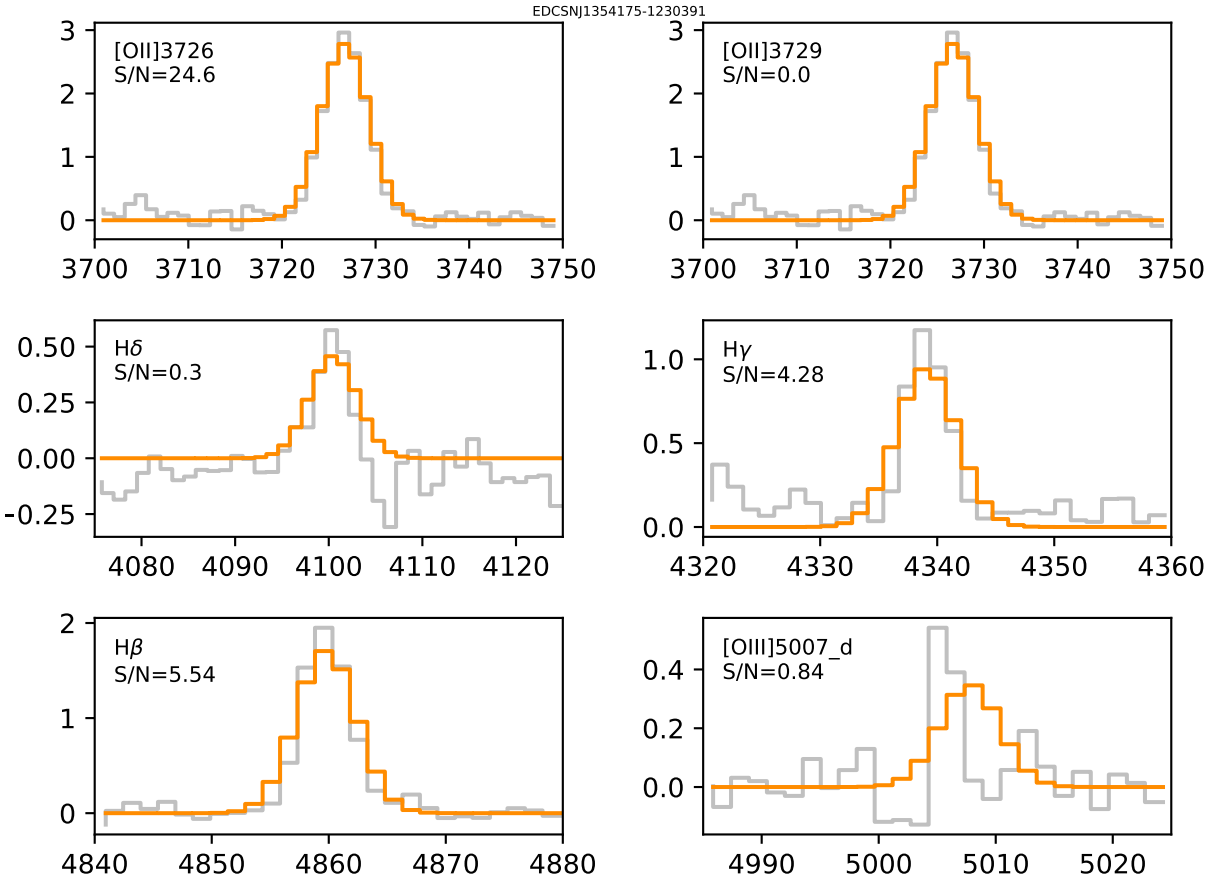
EDCSNJ1354175-1230391
[OII]3726
S/N=24.6
[OII]3729
S/N=0.0
Hδ
S/N=0.3
Hγ
S/N=4.28
Hβ
S/N=5.54
[OIII]5007_d
S/N=0.84

Bibliography

Abazajian, K., Adelman-McCarthy, J. K., Agüeros, M. A., Allam, S. S., Anderson, S. F., Annis, J., Bahcall, N. A., Baldry, I. K., Bastian, S., Berlind, A., Bernardi, M., Blanton, M. R., Blythe, N., Bochanski, John J., J., Boroski, W. N., Brewington, H., Briggs, J. W., Brinkmann, J., Brunner, R. J., Budavári, T., Carey, L. N., Carr, M. A., Castander, F. J., Chiu, K., Collinge, M. J., Connolly, A. J., Covey, K. R., Csabai, I., Dalcanton, J. J., Dodelson, S., Doi, M., Dong, F., Eisenstein, D. J., Evans, M. L., Fan, X., Feldman, P. D., Finkbeiner, D. P., Friedman, S. D., Frieman, J. A., Fukugita, M., Gal, R. R., Gillespie, B., Glazebrook, K., Gonzalez, C. F., Gray, J., Grebel, E. K., Grodnicki, L., Gunn, J. E., Gurbani, V. K., Hall, P. B., Hao, L., Harbeck, D., Harris, F. H., Harris, H. C., Harvanek, M., Hawley, S. L., Heckman, T. M., Helmboldt, J. F., Hendry, J. S., Hennessy, G. S., Hindsley, R. B., Hogg, D. W., Holmgren, D. J., Holtzman, J. A., Homer, L., Hui, L., Ichikawa, S.-i., Ichikawa, T., Inkmann, J. P., Ivezić, Ž., Jester, S., Johnston, D. E., Jordan, B., Jordan, W. P., Jorgensen, A. M., Jurić, M., Kauffmann, G., Kent, S. M., Kleinman, S. J., Knapp, G. R., Kniazev, A. Y., Kron, R. G., Krzesiński, J., Kunszt, P. Z., Kuropatkin, N., Lamb, D. Q., Lampeitl, H., Laubscher, B. E., Lee, B. C., Leger, R. F., Li, N., Lidz, A., Lin, H., Loh, Y.-S., Long, D. C., Loveday, J., Lupton, R. H., Malik, T., Margon, B., McGehee, P. M., McKay, T. A., Meiksin, A., Miknaitis, G. A., Moorthy, B. K., Munn, J. A., Murphy, T., Nakajima, R., Narayanan, V. K., Nash, T., Neilsen, Eric H., J., Newberg, H. J., Newman, P. R., Nichol, R. C., Nicinski, T., Nieto-Santisteban, M., Nitta, A., Odenkirchen, M., Okamura, S., Ostriker, J. P., Owen, R., Padmanabhan, N., Peoples, J., Pier, J. R., Pindor, B., Pope, A. C., Quinn, T. R., Rafikov, R. R., Raymond, S. N., Richards, G. T., Richmond, M. W., Rix, H.-W., Rockosi, C. M., Schaye, J., Schlegel, D. J., Schneider, D. P., Schroeder, J., Scranton, R., Sekiguchi, M., Seljak, U., Sergey, G., Sesar, B., Sheldon, E., Shimasaku, K., Siegmund, W. A., Silvestri, N. M., Sinisgalli, A. J., Sirko, E., Smith, J. A., Smolčić, V., Snedden, S. A., Stebbins, A., Steinhardt, C.,

Stinson, G., Stoughton, C., Strateva, I. V., Strauss, M. A., SubbaRao, M., Szalay, A. S., Szapudi, I., Szkody, P., Tasca, L., Tegmark, M., Thakar, A. R., Tremonti, C., Tucker, D. L., Uomoto, A., Vanden Berk, D. E., Vandenberg, J., Vogeley, M. S., Voges, W., Vogt, N. P., Walkowicz, L. M., Weinberg, D. H., West, A. A., White, S. D. M., Wilhite, B. C., Willman, B., Xu, Y., Yanny, B., Yarger, J., Yasuda, N., Yip, C.-W., Yocum, D. R., York, D. G., Zakamska, N. L., Zehavi, I., Zheng, W., Zibetti, S., & Zucker, D. B. (2003). The First Data Release of the Sloan Digital Sky Survey. *AJ*, 126(4), 2081–2086.

Abell, G. O. (1958). The Distribution of Rich Clusters of Galaxies. *ApJS*, 3, 211.

Abraham, R. G., Tanvir, N. R., Santiago, B. X., Ellis, R. S., Glazebrook, K., & van den Bergh, S. (1996). Galaxy morphology to I=25 mag in the Hubble Deep Field. *MNRAS*, 279, L47–L52.

Abraham, R. G., van den Bergh, S., & Nair, P. (2003). A New Approach to Galaxy Morphology. I. Analysis of the Sloan Digital Sky Survey Early Data Release. *ApJ*, 588, 218–229.

Abramson, L. E., Dressler, A., Gladders, M. D., Oemler, Jr., A., Poggianti, B. M., Monson, A., Persson, E., & Vulcani, B. (2013). The IMACS Cluster Building Survey. V. Further Evidence for Starburst Recycling from Quantitative Galaxy Morphologies. *ApJ*, 777, 124.

Adams, S. M., Zaritsky, D., Sand, D. J., Graham, M. L., Bildfell, C., Hoekstra, H., & Pritchet, C. (2012). The Environmental Dependence of the Incidence of Galactic Tidal Features. *AJ*, 144, 128.

Baldry, I. K., Balogh, M. L., Bower, R. G., Glazebrook, K., Nichol, R. C., Bamford, S. P., & Budavari, T. (2006). Galaxy bimodality versus stellar mass and environment. *MNRAS*, 373, 469–483.

Baldry, I. K., Glazebrook, K., Brinkmann, J., Ivezić, Ž., Lupton, R. H., Nichol, R. C., & Szalay, A. S. (2004). Quantifying the Bimodal Color-Magnitude Distribution of Galaxies. *ApJ*, 600, 681–694.

Balogh, M., Eke, V., Miller, C., Lewis, I., Bower, R., Couch, W., Nichol, R., Bland-Hawthorn, J., Baldry, I. K., Baugh, C., Bridges, T., Cannon, R., Cole, S., Colless, M., Collins, C., Cross, N., Dalton, G., de Propris, R., Driver, S. P., Efstathiou, G., Ellis, R. S., Frenk, C. S., Glazebrook, K., Gomez, P., Gray, A., Hawkins, E., Jackson, C., Lahav, O., Lumsden, S., Maddox, S., Madgwick, D., Norberg, P., Peacock, J. A., Percival, W., Peterson, B. A., Sutherland, W., & Taylor, K. (2004). Galaxy ecology: groups and low-density environments in the SDSS and 2dFGRS. *MNRAS*, 348, 1355–1372.

Balogh, M. L., Morris, S. L., Yee, H. K. C., Carlberg, R. G., & Ellingson, E. (1999). Differential Galaxy Evolution in Cluster and Field Galaxies at z˜0.3. *ApJ*, 527, 54–79.

Barnes, J. E. (2004). Shock-induced star formation in a model of the Mice. *MNRAS*, 350(3), 798–808.

Barnes, J. E. & Hernquist, L. (1996). Transformations of Galaxies. II. Gasdynamics in Merging Disk Galaxies. *ApJ*, 471, 115.

Bekki, K. (1998). Unequal-Mass Galaxy Mergers and the Creation of Cluster S0 Galaxies. *ApJL*, 502(2), L133–L137.

Bekki, K. (2009). Ram-pressure stripping of halo gas in disc galaxies: implications for galactic star formation in different environments. *MNRAS*, 399(4), 2221–2230.

Bekki, K., Couch, W. J., & Shioya, Y. (2002). Passive Spiral Formation from Halo Gas Starvation: Gradual Transformation into S0s. *ApJ*, 577, 651–657.

Blanton, M. R. & Moustakas, J. (2009). Physical Properties and Environments of Nearby Galaxies. *ARA&A*, 47, 159–210.

Bluck, A. F. L., Mendel, J. T., Ellison, S. L., Patton, D. R., Simard, L., Henriques, B. M. B., Torrey, P., Teimoorinia, H., Moreno, J., & Starkenburg, E. (2016). The impact of galactic properties and

environment on the quenching of central and satellite galaxies: a comparison between SDSS, Illustris and L-Galaxies. *MNRAS*, 462(3), 2559–2586.

Bolzonella, M., Miralles, J.-M., & Pelló, R. (2000). Photometric redshifts based on standard SED fitting procedures. *A&A*, 363, 476–492.

Boquien, M., Burgarella, D., Roehlly, Y., Buat, V., Ciesla, L., Corre, D., Inoue, A. K., & Salas, H. (2019). CIGALE: a python Code Investigating GALaxy Emission. *A&A*, 622, A103.

Boselli, A. & Gavazzi, G. (2006). Environmental Effects on Late-Type Galaxies in Nearby Clusters. *PASP*, 118(842), 517–559.

Boselli, A. & Gavazzi, G. (2014). On the origin of the faint-end of the red sequence in high-density environments. *A&A Rv*, 22, 74.

Boselli, A., Roehlly, Y., Fossati, M., Buat, V., Boissier, S., Boquien, M., Burgarella, D., Ciesla, L., Gavazzi, G., & Serra, P. (2016). Quenching of the star formation activity in cluster galaxies. *A&A*, 596, A11.

Bridge, C. R., Carlberg, R. G., & Sullivan, M. (2010). The CFHTLS-Deep Catalog of Interacting Galaxies. I. Merger Rate Evolution to z = 1.2. *ApJ*, 709(2), 1067–1082.

Brinchmann, J., Charlot, S., White, S. D. M., Tremonti, C., Kauffmann, G., Heckman, T., & Brinkmann, J. (2004). The physical properties of star-forming galaxies in the low-redshift Universe. *MNRAS*, 351, 1151–1179.

Brinchmann, J. & Ellis, R. S. (2000). The Mass Assembly and Star Formation Characteristics of Field Galaxies of Known Morphology. *ApJL*, 536(2), L77–L80.

Bruzual, G. & Charlot, S. (2003). Stellar population synthesis at the resolution of 2003. *MNRAS*, 344, 1000–1028.

Bruzual A., G. (1983). Spectral evolution of galaxies. I - Early-type systems. *ApJ*, 273, 105–127.

Bundy, K., Ellis, R. S., & Conselice, C. J. (2005). The Mass Assembly Histories of Galaxies of Various Morphologies in the GOODS Fields. *ApJ*, 625(2), 621–632.

Bundy, K., Fukugita, M., Ellis, R. S., Kodama, T., & Conselice, C. J. (2004). A Slow Merger History of Field Galaxies since z $\sim$1. *ApJL*, 601(2), L123–L126.

Bundy, K., Fukugita, M., Ellis, R. S., Targett, T. A., Belli, S., & Kodama, T. (2009). The Greater Impact of Mergers on the Growth of Massive Galaxies: Implications for Mass Assembly and Evolution since z sime 1. *ApJ*, 697(2), 1369–1383.

Bundy, K., Scarlata, C., Carollo, C. M., Ellis, R. S., Drory, N., Hopkins, P., Salvato, M., Leauthaud, A., Koekemoer, A. M., Murray, N., Ilbert, O., Oesch, P., Ma, C.-P., Capak, P., Pozzetti, L., & Scoville, N. (2010). The Rise and Fall of Passive Disk Galaxies: Morphological Evolution Along the Red Sequence Revealed by COSMOS. *ApJ*, 719, 1969–1983.

Burkey, J. M., Keel, W. C., Windhorst, R. A., & Franklin, B. E. (1994). Galaxy Pairs in Deep HST Images: Evidence for Evolution in the Galaxy Merger Rate. *ApJL*, 429, L13.

Butcher, H. & Oemler, Jr., A. (1978). The evolution of galaxies in clusters. I - ISIT photometry of C1 0024+1654 and 3C 295. *ApJ*, 219, 18–30.

Calzetti, D., Armus, L., Bohlin, R. C., Kinney, A. L., Koornneef, J., & Storchi-Bergmann, T. (2000). The Dust Content and Opacity of Actively Star-forming Galaxies. *ApJ*, 533, 682–695.

Cantale, N., Courbin, F., Tewes, M., Jablonka, P., & Meylan, G. (2016a). Firedec: a two-channel finite-resolution image deconvolution algorithm. *A&A*, 589, A81.

Cantale, N., Jablonka, P., Courbin, F., Rudnick, G., Zaritsky, D., Meylan, G., Desai, V., De Lucia, G., Aragón-Salamanca, A., Poggianti, B. M., Finn, R., & Simard, L. (2016b). Disc colours in field and cluster spiral galaxies at $0.5 \lesssim z \lesssim 0.8$. *A&A*, 589, A82.

Cappellari, M. (2017). Improving the full spectrum fitting method: accurate convolution with Gauss-Hermite functions. *MNRAS*, 466, 798–811.

Cappellari, M. & Emsellem, E. (2004). Parametric Recovery of Line-of-Sight Velocity Distributions from Absorption-Line Spectra of Galaxies via Penalized Likelihood. *PASP*, 116, 138–147.

Carlberg, R. G., Cohen, J. G., Patton, D. R., Bland ford, R., Hogg, D. W., Yee, H. K. C., Morris, S. L., Lin, H., Hall, P. B., Sawicki, M., Wirth, G. D., Cowie, L. L., Hu, E., & Songaila, A. (2000). Caltech Faint Galaxy Redshift Survey. XI. The Merger Rate to Redshift 1 from Kinematic Pairs. *ApJL*, 532(1), L1–L4.

Christlein, D. & Zabludoff, A. I. (2004). Can Early-Type Galaxies Evolve from the Fading of the Disks of Late-Type Galaxies? *ApJ*, 616, 192–198.

Conselice, C. J. (2003). The Relationship between Stellar Light Distributions of Galaxies and Their Formation Histories. *ApJS*, 147, 1–28.

Conselice, C. J. (2014). The Evolution of Galaxy Structure Over Cosmic Time. *ARA&A*, 52, 291–337.

Cooper, M. C., Newman, J. A., Madgwick, D. S., Gerke, B. F., Yan, R., & Davis, M. (2005). Measuring Galaxy Environments with Deep Redshift Surveys. *ApJ*, 634, 833–848.

Cortese, L., Gavazzi, G., Boselli, A., Franzetti, P., Kennicutt, R. C., O'Neil, K., & Sakai, S. (2006). Witnessing galaxy preprocessing in the local Universe: the case of a star-bursting group falling into Abell 1367. *A&A*, 453, 847–861.

Couch, W. J., Barger, A. J., Smail, I., Ellis, R. S., & Sharples, R. M. (1998). Morphological Studies of the Galaxy Populations in Distant "Butcher-Oemler" Clusters with the Hubble Space Telescope. II. AC 103, AC 118, and AC 114 at Z = 0.31. *ApJ*, 497(1), 188–211.

Couch, W. J., Ellis, R. S., Godwin, J., & Carter, D. (1983). Spectral energy distributions for galaxies in high redshift clusters.I. Methods and application to three clusters with $0.22 \leq z \leq 0.31$. *MNRAS*, 205, 1287–1312.

Couch, W. J., Ellis, R. S., Sharples, R. M., & Smail, I. (1994). Morphological Studies of the Galaxy Populations in Distant "Butcher-Oemler" Clusters with HST. I. AC 114 at Z = 0.31 and Abell 370 at Z = 0.37. *ApJ*, 430, 121.

Couch, W. J. & Sharples, R. M. (1987). A spectroscopic study of three rich galaxy clusters at zeta=0.31. *MNRAS*, 229, 423–456.

Cox, T. J., Jonsson, P., Primack, J. R., & Somerville, R. S. (2006). Feedback in simulations of disc-galaxy major mergers. *MNRAS*, 373, 1013–1038.

Cox, T. J., Jonsson, P., Somerville, R. S., Primack, J. R., & Dekel, A. (2008). The effect of galaxy mass ratio on merger-driven starbursts. *MNRAS*, 384(1), 386–409.

Crowl, H. H. & Kenney, J. D. P. (2008). The Stellar Populations of Stripped Spiral Galaxies in the Virgo Cluster. *AJ*, 136(4), 1623–1644.

Daddi, E., Dickinson, M., Morrison, G., Chary, R., Cimatti, A., Elbaz, D., Frayer, D., Renzini, A., Pope, A., Alexander, D. M., Bauer, F. E., Giavalisco, M., Huynh, M., Kurk, J., & Mignoli, M. (2007). Multiwavelength Study of Massive Galaxies at z˜2. I. Star Formation and Galaxy Growth. *ApJ*, 670, 156–172.

de Vaucouleurs, G. (1948). Recherches sur les Nebuleuses Extragalactiques. *Annales d'Astrophysique*, 11, 247.

Deger, S., Rudnick, G., Kelkar, K., Aragón-Salamanca, A., Desai, V., Lotz, J. M., Jablonka, P., Moustakas, J., & Zaritsky, D. (2018). Tidal Interactions and Mergers in Intermediate-redshift EDisCS Clusters. *ApJ*, 869, 6.

Desai, V., Dalcanton, J. J., Aragón-Salamanca, A., Jablonka, P., Poggianti, B., Gogarten, S. M., Simard, L., Milvang-Jensen, B., Rudnick, G., Zaritsky, D., Clowe, D., Halliday, C., Pelló, R., Saglia, R., & White, S. (2007). The Morphological Content of 10 EDisCS Clusters at $0.5 < z < 0.8$. *ApJ*, 660, 1151–1164.

Dickinson, H., Fortson, L., Lintott, C., Scarlata, C., Willett, K., Bamford, S., Beck, M., Cardamone, C., Galloway, M., Simmons, B., Keel, W., Kruk, S., Masters, K., Vogelsberger, M., Torrey, P., & Snyder, G. F. (2018). Galaxy Zoo: Morphological Classification of Galaxy Images from the Illustris Simulation. *ApJ*, 853(2), 194.

Dressler, A. (1980). Galaxy morphology in rich clusters - Implications for the formation and evolution of galaxies. *ApJ*, 236, 351–365.

Dressler, A. & Gunn, J. E. (1983). Spectroscopy of galaxies in distant clusters. II. The population of the 3C 295 cluster. *ApJ*, 270, 7–19.

Dressler, A., Oemler, Jr., A., Couch, W. J., Smail, I., Ellis, R. S., Barger, A., Butcher, H., Poggianti, B. M., & Sharples, R. M. (1997). Evolution since z = 0.5 of the Morphology-Density Relation for Clusters of Galaxies. *ApJ*, 490, 577–591.

Dressler, A., Oemler, Jr., A., Poggianti, B. M., Gladders, M. D., Abramson, L., & Vulcani, B. (2013). The IMACS Cluster Building Survey. II. Spectral Evolution of Galaxies in the Epoch of Cluster Assembly. *ApJ*, 770, 62.

Dressler, A., Oemler, Augustus, J., Butcher, H. R., & Gunn, J. E. (1994). The Morphology of Distant Cluster Galaxies. I. HST Observations of CL 0939+4713. *ApJ*, 430, 107.

Elbaz, D., Daddi, E., Le Borgne, D., Dickinson, M., Alexander, D. M., Chary, R.-R., Starck, J.-L., Brandt, W. N., Kitzbichler, M., MacDonald, E., Nonino, M., Popesso, P., Stern, D., & Vanzella, E. (2007). The reversal of the star formation-density relation in the distant universe. *A&A*, 468, 33–48.

Farouki, R. T. & Shapiro, S. L. (1982). Simulations of merging disk galaxies. *ApJ*, 259, 103–115.

Fasano, G., Poggianti, B. M., Couch, W. J., Bettoni, D., Kjærgaard, P., & Moles, M. (2000). The Evolution of the Galactic Morphological Types in Clusters. *ApJ*, 542, 673–683.

Finn, R. A., Desai, V., Rudnick, G., Poggianti, B., Bell, E. F., Hinz, J., Jablonka, P., Milvang-Jensen, B., Moustakas, J., Rines, K., & Zaritsky, D. (2010). Dust-obscured Star Formation in Intermediate Redshift Galaxy Clusters. *ApJ*, 720, 87–98.

Freeman, P. E., Izbicki, R., Lee, A. B., Newman, J. A., Conselice, C. J., Koekemoer, A. M., Lotz, J. M., & Mozena, M. (2013). New image statistics for detecting disturbed galaxy morphologies at high redshift. *MNRAS*, 434, 282–295.

Fujita, Y. (2004). Pre-Processing of Galaxies before Entering a Cluster. *PASJ*, 56, 29–43.

Gehrels, N. (1986). Confidence limits for small numbers of events in astrophysical data. *ApJ*, 303, 336–346.

Genel, S., Genzel, R., Bouché, N., Naab, T., & Sternberg, A. (2009). The Halo Merger Rate in the Millennium Simulation and Implications for Observed Galaxy Merger Fractions. *ApJ*, 701(2), 2002–2018.

Genel, S., Vogelsberger, M., Springel, V., Sijacki, D., Nelson, D., Snyder, G., Rodriguez-Gomez, V., Torrey, P., & Hernquist, L. (2014). Introducing the Illustris project: the evolution of galaxy populations across cosmic time. *MNRAS*, 445(1), 175–200.

Gerke, B. F., Newman, J. A., Faber, S. M., Cooper, M. C., Croton, D. J., Davis, M., Willmer, C. N. A., Yan, R., Coil, A. L., Guhathakurta, P., Koo, D. C., & Weiner, B. J. (2007). The DEEP2 galaxy redshift survey: the evolution of the blue fraction in groups and the field. *MNRAS*, 376, 1425–1444.

Gómez, P. L., Nichol, R. C., Miller, C. J., Balogh, M. L., Goto, T., Zabludoff, A. I., Romer, A. K., Bernardi, M., Sheth, R., Hopkins, A. M., Castander, F. J., Connolly, A. J., Schneider, D. P., Brinkmann, J., Lamb, D. Q., SubbaRao, M., & York, D. G. (2003). Galaxy Star Formation as a Function of Environment in the Early Data Release of the Sloan Digital Sky Survey. *ApJ*, 584, 210–227.

Gonzalez, A. H., Zaritsky, D., Dalcanton, J. J., & Nelson, A. (2001). The Las Campanas Distant Cluster Survey: The Catalog. *ApJS*, 137, 117–138.

Gunn, J. E. & Gott, III, J. R. (1972). On the Infall of Matter Into Clusters of Galaxies and Some Effects on Their Evolution. *ApJ*, 176, 1.

Guo, Q. & White, S. D. M. (2008). Galaxy growth in the concordance ΛCDM cosmology. *MNRAS*, 384(1), 2–10.

Halliday, C., Milvang-Jensen, B., Poirier, S., Poggianti, B. M., Jablonka, P., Aragón-Salamanca, A., Saglia, R. P., De Lucia, G., Pelló, R., Simard, L., Clowe, D. I., Rudnick, G., Dalcanton, J. J., White, S. D. M., & Zaritsky, D. (2004). Spectroscopy of clusters in the ESO Distant Cluster Survey (EDisCS). Redshifts, velocity dispersions and substructure for 5 clusters. *A&A*, 427, 397–413.

Hausman, M. A. & Ostriker, J. P. (1978). Galactic cannibalism. III - The morphological evolution of galaxies and clusters. *ApJ*, 224, 320–336.

Hogg, D. W., Blanton, M. R., Brinchmann, J., Eisenstein, D. J., Schlegel, D. J., Gunn, J. E., McKay, T. A., Rix, H.-W., Bahcall, N. A., Brinkmann, J., & Meiksin, A. (2004). The Dependence on Environment of the Color-Magnitude Relation of Galaxies. *ApJL*, 601, L29–L32.

Holmberg, E. (1958). A photographic photometry of extragalactic nebulae. *Meddelanden fran Lunds Astronomiska Observatorium Serie II*, 136, 1.

Hopkins, A. M. & Beacom, J. F. (2006). On the Normalization of the Cosmic Star Formation History. *ApJ*, 651(1), 142–154.

Hoyos, C., Aragón-Salamanca, A., Gray, M. E., Maltby, D. T., Bell, E. F., Barazza, F. D., Böhm, A., Häußler, B., Jahnke, K., Jogee, S., Lane, K. P., McIntosh, D. H., & Wolf, C. (2012). A new automatic method to identify galaxy mergers - I. Description and application to the Space Telescope A901/902 Galaxy Evolution Survey. *MNRAS*, 419, 2703–2724.

Hubble, E. P. (1926). Extragalactic nebulae. *ApJ*, 64, 321–369.

Hubble, E. P. (1936). *Realm of the Nebulae*.

Johnson, H. L. & Morgan, W. W. (1953). Fundamental stellar photometry for standards of spectral type on the Revised System of the Yerkes Spectral Atlas. *ApJ*, 117, 313.

Johnston, E. J., Aragón-Salamanca, A., & Merrifield, M. R. (2014). The origin of S0s in clusters: evidence from the bulge and disc star formation histories. *MNRAS*, 441, 333–342.

Just, D. W., Zaritsky, D., Sand, D. J., Desai, V., & Rudnick, G. (2010). The Environmental Dependence of the Evolving S0 Fraction. *ApJ*, 711, 192–200.

Karim, A., Schinnerer, E., Martínez-Sansigre, A., Sargent, M. T., van der Wel, A., Rix, H. W., Ilbert, O., Smolčić, V., Carilli, C., Pannella, M., Koekemoer, A. M., Bell, E. F., & Salvato, M. (2011). The Star Formation History of Mass-selected Galaxies in the COSMOS Field. *ApJ*, 730(2), 61.

Kartaltepe, J. S., Mozena, M., Kocevski, D., McIntosh, D. H., Lotz, J., Bell, E. F., Faber, S., Ferguson, H., Koo, D., Bassett, R., Bernyk, M., Blancato, K., Bournaud, F., Cassata, P., Castellano, M., Cheung, E., Conselice, C. J., Croton, D., Dahlen, T., de Mello, D. F., DeGroot, L., Donley, J., Guedes, J., Grogin, N., Hathi, N., Hilton, M., Hollon, B., Koekemoer, A., Liu, N., Lucas, R. A., Martig, M., McGrath, E., McPartland, C., Mobasher, B., Morlock, A., O'Leary, E., Peth, M., Pforr, J., Pillepich, A., Rosario, D., Soto, E., Straughn, A., Telford, O., Sunnquist, B., Trump, J., Weiner, B., Wuyts, S., Inami, H., Kassin, S., Lani, C., Poole, G. B., & Rizer, Z. (2015). CANDELS Visual Classifications: Scheme, Data Release, and First Results. *ApJS*, 221(1), 11.

Kartaltepe, J. S., Sanders, D. B., Scoville, N. Z., Calzetti, D., Capak, P., Koekemoer, A., Mobasher, B., Murayama, T., Salvato, M., Sasaki, S. S., & Taniguchi, Y. (2007). Evolution of the Frequency of Luminous (>=L^*_V) Close Galaxy Pairs at z $<$ 1.2 in the COSMOS Field. *ApJS*, 172, 320–328.

Kauffmann, G., Heckman, T. M., White, S. D. M., Charlot, S., Tremonti, C., Brinchmann, J., Bruzual, G., Peng, E. W., Seibert, M., Bernardi, M., Blanton, M., Brinkmann, J., Castander, F., Csábai, I., Fukugita, M., Ivezic, Z., Munn, J. A., Nichol, R. C., Padmanabhan, N., Thakar, A. R., Weinberg, D. H., & York, D. (2003). Stellar masses and star formation histories for 10^5 galaxies from the Sloan Digital Sky Survey. *MNRAS*, 341, 33–53.

Kauffmann, G., White, S. D. M., Heckman, T. M., Ménard, B., Brinchmann, J., Charlot, S., Tremonti, C., & Brinkmann, J. (2004). The environmental dependence of the relations between stellar mass, structure, star formation and nuclear activity in galaxies. *MNRAS*, 353, 713–731.

Kawata, D. & Mulchaey, J. S. (2008). Strangulation in Galaxy Groups. *ApJL*, 672, L103.

Kelkar, K., Gray, M. E., Aragón-Salamanca, A., Rudnick, G., Milvang-Jensen, B., Jablonka, P., & Schrabback, T. (2017). The effect of the environment on the structure, morphology and star formation history of intermediate-redshift galaxies. *MNRAS*, 469, 4551–4564.

Kriek, M., van Dokkum, P. G., Labbé, I., Franx, M., Illingworth, G. D., Marchesini, D., & Quadri, R. F. (2009). An Ultra-Deep Near-Infrared Spectrum of a Compact Quiescent Galaxy at z = 2.2. *ApJ*, 700, 221–231.

Kronberger, T., Kapferer, W., Ferrari, C., Unterguggenberger, S., & Schindler, S. (2008). On the influence of ram-pressure stripping on the star formation of simulated spiral galaxies. *A&A*, 481(2), 337–343.

Kroupa, P. (2001). On the variation of the initial mass function. *MNRAS*, 322, 231–246.

Larson, R. B. & Tinsley, B. M. (1978). Star formation rates in normal and peculiar galaxies. *ApJ*, 219, 46–59.

Larson, R. B., Tinsley, B. M., & Caldwell, C. N. (1980). The evolution of disk galaxies and the origin of S0 galaxies. *ApJ*, 237, 692–707.

Lavery, R. J. & Henry, J. P. (1986). Spectroscopy of Three Butcher-Oemler Clusters of Galaxies at a Redshift of 0.2. *ApJL*, 304, L5.

Le Floc'h, E., Papovich, C., Dole, H., Bell, E. F., Lagache, G., Rieke, G. H., Egami, E., Pérez-González, P. G., Alonso-Herrero, A., Rieke, M. J., Blaylock, M., Engelbracht, C. W., Gordon, K. D., Hines, D. C., Misselt, K. A., Morrison, J. E., & Mould, J. (2005). Infrared Luminosity Functions from the Chandra Deep Field-South: The Spitzer View on the History of Dusty Star Formation at 0 <∼z <∼1. *ApJ*, 632(1), 169–190.

Leja, J., Johnson, B. D., Conroy, C., van Dokkum, P. G., & Byler, N. (2017). Deriving Physical Properties from Broadband Photometry with Prospector: Description of the Model and a Demonstration of its Accuracy Using 129 Galaxies in the Local Universe. *ApJ*, 837(2), 170.

Lewis, I., Balogh, M., De Propris, R., Couch, W., Bower, R., Offer, A., Bland-Hawthorn, J., Baldry, I. K., Baugh, C., Bridges, T., Cannon, R., Cole, S., Colless, M., Collins, C., Cross, N., Dalton, G., Driver, S. P., Efstathiou, G., Ellis, R. S., Frenk, C. S., Glazebrook, K., Hawkins, E., Jackson, C., Lahav, O., Lumsden, S., Maddox, S., Madgwick, D., Norberg, P., Peacock, J. A., Percival, W., Peterson, B. A., Sutherland, W., & Taylor, K. (2002). The 2dF Galaxy Redshift Survey: the environmental dependence of galaxy star formation rates near clusters. *MNRAS*, 334, 673–683.

Lilly, S. J., Le Fevre, O., Hammer, F., & Crampton, D. (1996). The Canada-France Redshift Survey: The Luminosity Density and Star Formation History of the Universe to Z approximately 1. *ApJL*, 460, L1.

Lotz, J. M., Davis, M., Faber, S. M., Guhathakurta, P., Gwyn, S., Huang, J., Koo, D. C., Le Floc'h, E., Lin, L., Newman, J., Noeske, K., Papovich, C., Willmer, C. N. A., Coil, A., Conselice, C. J., Cooper, M., Hopkins, A. M., Metevier, A., Primack, J., Rieke, G., & Weiner, B. J. (2008a). The Evolution of Galaxy Mergers and Morphology at $z < 1.2$ in the Extended Groth Strip. *ApJ*, 672, 177–197.

Lotz, J. M., Jonsson, P., Cox, T. J., Croton, D., Primack, J. R., Somerville, R. S., & Stewart, K. (2011). The Major and Minor Galaxy Merger Rates at z < 1.5. *ApJ*, 742(2), 103.

Lotz, J. M., Jonsson, P., Cox, T. J., & Primack, J. R. (2008b). Galaxy merger morphologies and time-scales from simulations of equal-mass gas-rich disc mergers. *MNRAS*, 391, 1137–1162.

Lotz, J. M., Jonsson, P., Cox, T. J., & Primack, J. R. (2010a). The effect of gas fraction on the morphology and time-scales of disc galaxy mergers. *MNRAS*, 404, 590–603.

Lotz, J. M., Jonsson, P., Cox, T. J., & Primack, J. R. (2010b). The effect of mass ratio on the morphology and time-scales of disc galaxy mergers. *MNRAS*, 404, 575–589.

Lotz, J. M., Primack, J., & Madau, P. (2004). A New Nonparametric Approach to Galaxy Morphological Classification. *AJ*, 128, 163–182.

Madau, P. & Dickinson, M. (2014). Cosmic Star-Formation History. *ARA&A*, 52, 415–486.

Madau, P., Pozzetti, L., & Dickinson, M. (1998). The Star Formation History of Field Galaxies. *ApJ*, 498(1), 106–116.

Mahajan, S., Mamon, G. A., & Raychaudhury, S. (2011). The velocity modulation of galaxy properties in and near clusters: quantifying the decrease in star formation in backsplash galaxies. *MNRAS*, 416, 2882–2902.

Margoniner, V. E. & de Carvalho, R. R. (2000). Photometric Properties of 48 Clusters of Galaxies. I. The Butcher-Oemler Effect. *AJ*, 119(4), 1562–1578.

Margoniner, V. E., de Carvalho, R. R., Gal, R. R., & Djorgovski, S. G. (2001). The Butcher-Oemler Effect in 295 Clusters: Strong Redshift Evolution and Cluster Richness Dependence. *ApJL*, 548(2), L143–L146.

Milvang-Jensen, B., Noll, S., Halliday, C., Poggianti, B. M., Jablonka, P., Aragón-Salamanca, A., Saglia, R. P., Nowak, N., von der Linden, A., De Lucia, G., Pelló, R., Moustakas, J., Poirier,

S., Bamford, S. P., Clowe, D. I., Dalcanton, J. J., Rudnick, G. H., Simard, L., White, S. D. M., & Zaritsky, D. (2008). Spectroscopy of clusters in the ESO distant cluster survey (EDisCS). II.. Redshifts, velocity dispersions, and substructure for clusters in the last 15 fields. *A&A*, 482, 419–449.

Moore, B., Lake, G., & Katz, N. (1998). Morphological Transformation from Galaxy Harassment. *ApJ*, 495, 139–151.

Mori, M. & Burkert, A. (2000). Gas Stripping of Dwarf Galaxies in Clusters of Galaxies. *ApJ*, 538(2), 559–568.

Mortlock, A., Conselice, C. J., Bluck, A. F. L., Bauer, A. E., Grützbauch, R., Buitrago, F., & Ownsworth, J. (2011). A deep probe of the galaxy stellar mass functions at z 1-3 with the GOODS NICMOS Survey. *MNRAS*, 413(4), 2845–2859.

Moustakas, J., Coil, A. L., Aird, J., Blanton, M. R., Cool, R. J., Eisenstein, D. J., Mendez, A. J., Wong, K. C., Zhu, G., & Arnouts, S. (2013). PRIMUS: Constraints on Star Formation Quenching and Galaxy Merging, and the Evolution of the Stellar Mass Function from z = 0-1. *ApJ*, 767, 50.

Naab, T. & Burkert, A. (2003). Statistical Properties of Collisionless Equal- and Unequal-Mass Merger Remnants of Disk Galaxies. *ApJ*, 597, 893–906.

Noeske, K. G., Weiner, B. J., Faber, S. M., Papovich, C., Koo, D. C., Somerville, R. S., Bundy, K., Conselice, C. J., Newman, J. A., Schiminovich, D., Le Floc'h, E., Coil, A. L., Rieke, G. H., Lotz, J. M., Primack, J. R., Barmby, P., Cooper, M. C., Davis, M., Ellis, R. S., Fazio, G. G., Guhathakurta, P., Huang, J., Kassin, S. A., Martin, D. C., Phillips, A. C., Rich, R. M., Small, T. A., Willmer, C. N. A., & Wilson, G. (2007). Star Formation in AEGIS Field Galaxies since z=1.1: The Dominance of Gradually Declining Star Formation, and the Main Sequence of Star-forming Galaxies. *ApJL*, 660(1), L43–L46.

Ostriker, J. P. & Tremaine, S. D. (1975). Another evolutionary correction to the luminosity of giant galaxies. *ApJL*, 202, L113–L117.

Pelló, R., Rudnick, G., De Lucia, G., Simard, L., Clowe, D. I., Jablonka, P., Milvang-Jensen, B., Saglia, R. P., White, S. D. M., Aragón-Salamanca, A., Halliday, C., Poggianti, B., Best, P., Dalcanton, J., Dantel-Fort, M., Fort, B., von der Linden, A., Mellier, Y., Rottgering, H., & Zaritsky, D. (2009). Photometric redshifts and cluster tomography in the ESO Distant Cluster Survey. *A&A*, 508, 1173–1191.

Poggianti, B. M., Aragón-Salamanca, A., Zaritsky, D., De Lucia, G., Milvang-Jensen, B., Desai, V., Jablonka, P., Halliday, C., Rudnick, G., Varela, J., Bamford, S., Best, P., Clowe, D., Noll, S., Saglia, R., Pelló, R., Simard, L., von der Linden, A., & White, S. (2009). The Environments of Starburst and Post-Starburst Galaxies at z = 0.4-0.8. *ApJ*, 693, 112–131.

Poggianti, B. M., Desai, V., Finn, R., Bamford, S., De Lucia, G., Varela, J., Aragón-Salamanca, A., Halliday, C., Noll, S., Saglia, R., Zaritsky, D., Best, P., Clowe, D., Milvang-Jensen, B., Jablonka, P., Pelló, R., Rudnick, G., Simard, L., von der Linden, A., & White, S. (2008). The Relation between Star Formation, Morphology, and Local Density in High-Redshift Clusters and Groups. *ApJ*, 684, 888–904.

Poggianti, B. M., Smail, I., Dressler, A., Couch, W. J., Barger, A. J., Butcher, H., Ellis, R. S., & Oemler, Augustus, J. (1999). The Star Formation Histories of Galaxies in Distant Clusters. *ApJ*, 518(2), 576–593.

Poggianti, B. M., von der Linden, A., De Lucia, G., Desai, V., Simard, L., Halliday, C., Aragón-Salamanca, A., Bower, R., Varela, J., Best, P., Clowe, D. I., Dalcanton, J., Jablonka, P., Milvang-Jensen, B., Pello, R., Rudnick, G., Saglia, R., White, S. D. M., & Zaritsky, D. (2006). The Evolution of the Star Formation Activity in Galaxies and Its Dependence on Environment. *ApJ*, 642, 188–215.

Postman, M., Franx, M., Cross, N. J. G., Holden, B., Ford, H. C., Illingworth, G. D., Goto, T., Demarco, R., Rosati, P., Blakeslee, J. P., Tran, K.-V., Benítez, N., Clampin, M., Hartig, G. F., Homeier, N., Ardila, D. R., Bartko, F., Bouwens, R. J., Bradley, L. D., Broadhurst, T. J., Brown, R. A., Burrows, C. J., Cheng, E. S., Feldman, P. D., Golimowski, D. A., Gronwall, C., Infante, L., Kimble, R. A., Krist, J. E., Lesser, M. P., Martel, A. R., Mei, S., Menanteau, F., Meurer, G. R., Miley, G. K., Motta, V., Sirianni, M., Sparks, W. B., Tran, H. D., Tsvetanov, Z. I., White, R. L., & Zheng, W. (2005). The Morphology-Density Relation in z ˜ 1 Clusters. *ApJ*, 623, 721–741.

Quilis, V., Moore, B., & Bower, R. (2000). Gone with the Wind: The Origin of S0 Galaxies in Clusters. *Science*, 288, 1617–1620.

Rakos, K. D. & Schombert, J. M. (1995). Color Evolution from Z = 0 to Z = 1. *ApJ*, 439, 47.

Richstone, D. O. (1976). Collisions of galaxies in dense clusters. II - Dynamical evolution of cluster galaxies. *ApJ*, 204, 642–648.

Roberts, M. S. & Haynes, M. P. (1994). Physical Parameters along the Hubble Sequence. *ARA&A*, 32, 115–152.

Robertson, B., Bullock, J. S., Cox, T. J., Di Matteo, T., Hernquist, L., Springel, V., & Yoshida, N. (2006). A Merger-driven Scenario for Cosmological Disk Galaxy Formation. *ApJ*, 645, 986–1000.

Rodighiero, G., Daddi, E., Baronchelli, I., Cimatti, A., Renzini, A., Aussel, H., Popesso, P., Lutz, D., Andreani, P., Berta, S., Cava, A., Elbaz, D., Feltre, A., Fontana, A., Förster Schreiber, N. M., Franceschini, A., Genzel, R., Grazian, A., Gruppioni, C., Ilbert, O., Le Floch, E., Magdis, G., Magliocchetti, M., Magnelli, B., Maiolino, R., McCracken, H., Nordon, R., Poglitsch, A., Santini, P., Pozzi, F., Riguccini, L., Tacconi, L. J., Wuyts, S., & Zamorani, G. (2011). The Lesser Role of Starbursts in Star Formation at z = 2. *ApJL*, 739(2), L40.

Rodriguez-Gomez, V., Sales, L. V., Genel, S., Pillepich, A., Zjupa, J., Nelson, D., Griffen, B., Torrey, P., Snyder, G. F., Vogelsberger, M., Springel, V., Ma, C.-P., & Hernquist, L. (2017). The role of mergers and halo spin in shaping galaxy morphology. *MNRAS*, 467(3), 3083–3098.

Rodriguez-Gomez, V., Snyder, G. F., Lotz, J. M., Nelson, D., Pillepich, A., Springel, V., Genel, S., Weinberger, R., Tacchella, S., Pakmor, R., Torrey, P., Marinacci, F., Vogelsberger, M., Hernquist, L., & Thilker, D. A. (2019). The optical morphologies of galaxies in the IllustrisTNG simulation: a comparison to Pan-STARRS observations. *MNRAS*, 483(3), 4140–4159.

Roediger, E. & Hensler, G. (2005). Ram pressure stripping of disk galaxies. From high to low density environments. *A&A*, 433(3), 875–895.

Rudnick, G., Franx, M., Rix, H.-W., Moorwood, A., Kuijken, K., van Starkenburg, L., van der Werf, P., Röttgering, H., van Dokkum, P., & Labbé, I. (2001). A K-band-Selected Photometric Redshift Catalog in the Hubble Deep Field South: Sampling the Rest-Frame V Band to z =3. *AJ*, 122, 2205–2221.

Rudnick, G., Jablonka, P., Moustakas, J., Aragón-Salamanca, A., Zaritsky, D., Jaffé, Y. L., De Lucia, G., Desai, V., Halliday, C., Just, D., Milvang-Jensen, B., & Poggianti, B. (2017). Determining the Halo Mass Scale Where Galaxies Lose Their Gas. *ApJ*, 850, 181.

Rudnick, G., Rix, H.-W., & Kennicutt, Jr., R. C. (2000). Lopsided Galaxies, Weak Interactions, and Boosting the Star Formation Rate. *ApJ*, 538, 569–580.

Rudnick, G., von der Linden, A., Pelló, R., Aragón-Salamanca, A., Marchesini, D., Clowe, D., De Lucia, G., Halliday, C., Jablonka, P., Milvang-Jensen, B., Poggianti, B., Saglia, R., Simard, L., White, S., & Zaritsky, D. (2009). The Rest-frame Optical Luminosity Function of Cluster Galaxies at $z < 0.8$ and the Assembly of the Cluster Red Sequence. *ApJ*, 700, 1559–1588.

Sales, L. V., Vogelsberger, M., Genel, S., Torrey, P., Nelson, D., Rodriguez-Gomez, V., Wang, W., Pillepich, A., Sijacki, D., Springel, V., & Hernquist, L. (2015). The colours of satellite galaxies in the Illustris simulation. *MNRAS*, 447, L6–L10.

Sandage, A. (1961). *The Hubble Atlas of Galaxies*.

Sandage, A. (2005). The Classification of Galaxies: Early History and Ongoing Developments. *ARA&A*, 43(1), 581–624.

Schawinski, K., Thomas, D., Sarzi, M., Maraston, C., Kaviraj, S., Joo, S.-J., Yi, S. K., & Silk, J. (2007). Observational evidence for AGN feedback in early-type galaxies. *MNRAS*, 382(4), 1415–1431.

Schawinski, K., Urry, C. M., Simmons, B. D., Fortson, L., Kaviraj, S., Keel, W. C., Lintott, C. J., Masters, K. L., Nichol, R. C., Sarzi, M., Skibba, R., Treister, E., Willett, K. W., Wong, O. I., & Yi, S. K. (2014). The green valley is a red herring: Galaxy Zoo reveals two evolutionary pathways towards quenching of star formation in early- and late-type galaxies. *MNRAS*, 440, 889–907.

Schiminovich, D., Ilbert, O., Arnouts, S., Milliard, B., Tresse, L., Le Fèvre, O., Treyer, M., Wyder, T. K., Budavári, T., Zucca, E., Zamorani, G., Martin, D. C., Adami, C., Arnaboldi, M., Bardelli, S., Barlow, T., Bianchi, L., Bolzonella, M., Bottini, D., Byun, Y. I., Cappi, A., Contini, T., Charlot, S., Donas, J., Forster, K., Foucaud, S., Franzetti, P., Friedman, P. G., Garilli, B., Gavignaud, I., Guzzo, L., Heckman, T. M., Hoopes, C., Iovino, A., Jelinsky, P., Le Brun, V., Lee, Y. W., Maccagni, D., Madore, B. F., Malina, R., Marano, B., Marinoni, C., McCracken, H. J., Mazure, A., Meneux, B., Morrissey, P., Neff, S., Paltani, S., Pellò, R., Picat, J. P., Pollo, A., Pozzetti, L., Radovich, M., Rich, R. M., Scaramella, R., Scodeggio, M., Seibert, M., Siegmund, O., Small, T., Szalay, A. S., Vettolani, G., Welsh, B., Xu, C. K., & Zanichelli, A. (2005). The GALEX-VVDS Measurement of the Evolution of the Far-Ultraviolet Luminosity Density and the Cosmic Star Formation Rate. *ApJL*, 619(1), L47–L50.

Schweizer, F. (1982). Colliding and merging galaxies. I. Evidence for the recent merging of two disk galaxies in NGC 7252. *ApJ*, 252, 455–460.

Sérsic, J. L. (1963). Influence of the atmospheric and instrumental dispersion on the brightness distribution in a galaxy. *Boletin de la Asociacion Argentina de Astronomia La Plata Argentina*, 6, 41.

Somerville, R. S., Primack, J. R., & Faber, S. M. (2001). The nature of high-redshift galaxies. *MNRAS*, 320(4), 504–528.

Sparke, L. S. & Gallagher, John S., I. (2007). *Galaxies in the Universe: An Introduction*.

Springel, V. & Hernquist, L. (2005). Formation of a Spiral Galaxy in a Major Merger. *ApJL*, 622, L9–L12.

Strateva, I., Ivezić, Ž., Knapp, G. R., Narayanan, V. K., Strauss, M. A., Gunn, J. E., Lupton, R. H., Schlegel, D., Bahcall, N. A., Brinkmann, J., Brunner, R. J., Budavári, T., Csabai, I., Castander, F. J., Doi, M., Fukugita, M., Győry, Z., Hamabe, M., Hennessy, G., Ichikawa, T., Kunszt, P. Z., Lamb, D. Q., McKay, T. A., Okamura, S., Racusin, J., Sekiguchi, M., Schneider, D. P., Shimasaku, K., & York, D. (2001). Color Separation of Galaxy Types in the Sloan Digital Sky Survey Imaging Data. *AJ*, 122, 1861–1874.

Tasca, L. A. M., Kneib, J.-P., Iovino, A., Le Fèvre, O., Kovač, K., Bolzonella, M., Lilly, S. J., Abraham, R. G., Cassata, P., Cucciati, O., Guzzo, L., Tresse, L., Zamorani, G., Capak, P., Garilli, B., Scodeggio, M., Sheth, K., Zucca, E., Carollo, C. M., Contini, T., Mainieri, V., Renzini, A., Bardelli, S., Bongiorno, A., Caputi, K., Coppa, G., de La Torre, S., de Ravel, L., Franzetti, P., Kampczyk, P., Knobel, C., Koekemoer, A. M., Lamareille, F., Le Borgne, J.-F., Le Brun, V., Maier, C., Mignoli, M., Pello, R., Peng, Y., Perez Montero, E., Ricciardelli, E., Silverman, J. D., Vergani, D., Tanaka, M., Abbas, U., Bottini, D., Cappi, A., Cimatti, A., Ilbert, O., Leauthaud, A., Maccagni, D., Marinoni, C., McCracken, H. J., Memeo, P., Meneux, B., Oesch, P., Porciani, C., Pozzetti, L., Scaramella, R., & Scarlata, C. (2009). The zCOSMOS redshift survey: the role of environment and stellar mass in shaping the rise of the morphology-density relation from z ˜ 1. *A&A*, 503, 379–398.

Toomre, A. & Toomre, J. (1972). Galactic Bridges and Tails. *ApJ*, 178, 623–666.

Tran, K.-V. H., Franx, M., Illingworth, G., Kelson, D. D., & van Dokkum, P. (2003). The Nature of E+A Galaxies in Intermediate-Redshift Clusters. *ApJ*, 599(2), 865–885.

Tran, K.-V. H., Franx, M., Illingworth, G. D., van Dokkum, P., Kelson, D. D., & Magee, D. (2004). Field E+A Galaxies at Intermediate Redshifts (0.3 < z < 1). *ApJ*, 609(2), 683–691.

Urquhart, S. A., Willis, J. P., Hoekstra, H., & Pierre, M. (2010). An environmental Butcher-Oemler effect in intermediate-redshift X-ray clusters. *MNRAS*, 406, 368–381.

Vazdekis, A., Koleva, M., Ricciardelli, E., Röck, B., & Falcón-Barroso, J. (2016). UV-extended E-MILES stellar population models: young components in massive early-type galaxies. *MNRAS*, 463, 3409–3436.

Vijayaraghavan, R. & Ricker, P. M. (2013). Pre-processing and post-processing in group-cluster mergers. *MNRAS*, 435, 2713–2735.

Vogelsberger, M., Genel, S., Springel, V., Torrey, P., Sijacki, D., Xu, D., Snyder, G., Nelson, D., & Hernquist, L. (2014). Introducing the Illustris Project: simulating the coevolution of dark and visible matter in the Universe. *MNRAS*, 444(2), 1518–1547.

Vollmer, B., Balkowski, C., Cayatte, V., van Driel, W., & Huchtmeier, W. (2004). NGC 4569: Recent evidence for a past ram pressure stripping event. *A&A*, 419, 35–46.

Vollmer, B., Cayatte, V., Balkowski, C., & Duschl, W. J. (2001). Ram Pressure Stripping and Galaxy Orbits: The Case of the Virgo Cluster. *ApJ*, 561(2), 708–726.

Vulcani, B., Poggianti, B. M., Aragón-Salamanca, A., Fasano, G., Rudnick, G., Valentinuzzi, T., Dressler, A., Bettoni, D., Cava, A., D'Onofrio, M., Fritz, J., Moretti, A., Omizzolo, A., & Varela, J. (2011). Galaxy stellar mass functions of different morphological types in clusters, and their evolution between z= 0.8 and 0. *MNRAS*, 412(1), 246–268.

Vulcani, B., Poggianti, B. M., Finn, R. A., Rudnick, G., Desai, V., & Bamford, S. (2010). Comparing the Relation Between Star Formation and Galaxy Mass in Different Environments. *ApJL*, 710, L1–L6.

Whitaker, K. E., Labbé, I., van Dokkum, P. G., Brammer, G., Kriek, M., Marchesini, D., Quadri, R. F., Franx, M., Muzzin, A., Williams, R. J., Bezanson, R., Illingworth, G. D., Lee, K.-S., Lundgren, B., Nelson, E. J., Rudnick, G., Tal, T., & Wake, D. A. (2011). The NEWFIRM Medium-band Survey: Photometric Catalogs, Redshifts, and the Bimodal Color Distribution of Galaxies out to z ∼3. *ApJ*, 735(2), 86.

Whitaker, K. E., van Dokkum, P. G., Brammer, G., & Franx, M. (2012). The Star Formation Mass Sequence Out to z = 2.5. *ApJL*, 754, L29.

White, S. D. M. (1976). Dynamical friction in spherical clusters. *MNRAS*, 174, 19–28.

White, S. D. M., Clowe, D. I., Simard, L., Rudnick, G., De Lucia, G., Aragón-Salamanca, A., Bender, R., Best, P., Bremer, M., Charlot, S., Dalcanton, J., Dantel, M., Desai, V., Fort, B., Halliday, C., Jablonka, P., Kauffmann, G., Mellier, Y., Milvang-Jensen, B., Pelló, R., Poggianti, B., Poirier, S., Rottgering, H., Saglia, R., Schneider, P., & Zaritsky, D. (2005). EDisCS - the ESO distant cluster survey. Sample definition and optical photometry. *A&A*, 444, 365–379.

Williams, R. J., Quadri, R. F., Franx, M., van Dokkum, P., & Labbé, I. (2009). Detection of Quiescent Galaxies in a Bicolor Sequence from Z = 0-2. *ApJ*, 691, 1879–1895.

Wilman, D. J., Oemler, Jr., A., Mulchaey, J. S., McGee, S. L., Balogh, M. L., & Bower, R. G. (2009). Morphological Composition of z ˜ 0.4 Groups: The Site of S0 Formation. *ApJ*, 692, 298–308.

Wuyts, S., Förster Schreiber, N. M., Lutz, D., Nordon, R., Berta, S., Altieri, B., Andreani, P., Aussel, H., Bongiovanni, A., Cepa, J., Cimatti, A., Daddi, E., Elbaz, D., Genzel, R., Koekemoer, A. M., Magnelli, B., Maiolino, R., McGrath, E. J., Pérez García, A., Poglitsch, A., Popesso,

P., Pozzi, F., Sanchez-Portal, M., Sturm, E., Tacconi, L., & Valtchanov, I. (2011). On Star Formation Rates and Star Formation Histories of Galaxies Out to z ˜ 3. *ApJ*, 738, 106.

Wuyts, S., Labbé, I., Franx, M., Rudnick, G., van Dokkum, P. G., Fazio, G. G., Förster Schreiber, N. M., Huang, J., Moorwood, A. F. M., Rix, H.-W., Röttgering, H., & van der Werf, P. (2007). What Do We Learn from IRAC Observations of Galaxies at $2 < z < 3.5$? *ApJ*, 655, 51–65.

Zabludoff, A. I. & Mulchaey, J. S. (1998). The Properties of Poor Groups of Galaxies. I. Spectroscopic Survey and Results. *ApJ*, 496, 39–72.

Zabludoff, A. I., Zaritsky, D., Lin, H., Tucker, D., Hashimoto, Y., Shectman, S. A., Oemler, A., & Kirshner, R. P. (1996). The Environment of "E+A" Galaxies. *ApJ*, 466, 104.